# The 9th International Concrete Conference 2016

Jones, Martyn; Newlands, Moray; Halliday, Judith; Csetenyi, Laszlo; Zheng, Li; McCarthy, Michael

*Publication date:*
2016

*Document Version*
Publisher's PDF, also known as Version of record

# The 9th International Concrete Conference 2016

## Environment, Efficiency and Economic Challenges for Concrete

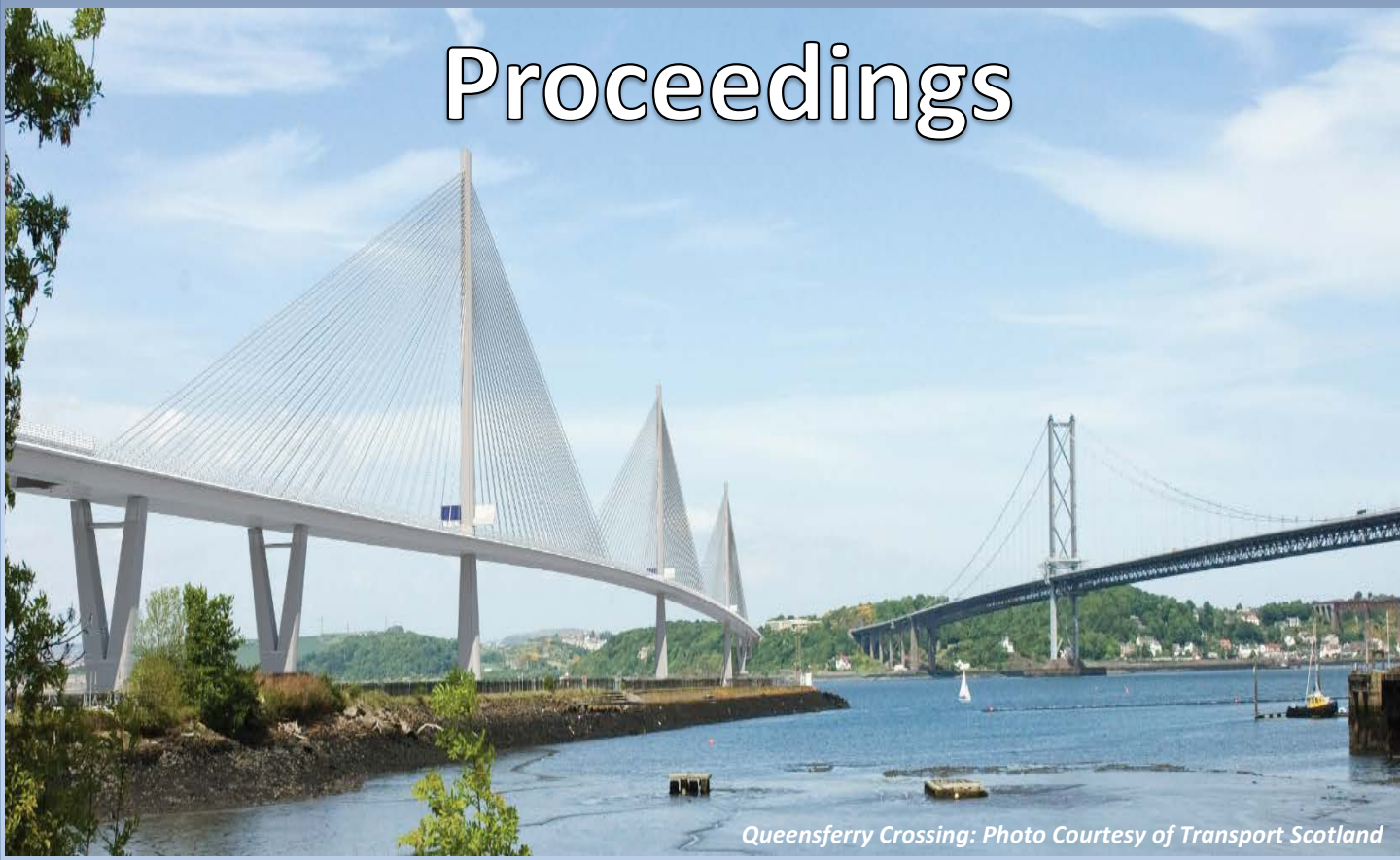

# Proceedings

*Queensferry Crossing: Photo Courtesy of Transport Scotland*

## Sponsored by

## Exhibitors

ISBN 9780957326316

**9th International Concrete Conference 2016**

# Environment, Efficiency and Economic Challenges for Concrete

**4-6 July 2016**
**Dundee, Scotland, UK**

**Edited by**


## M Roderick Jones
*Director,* Concrete Technology Unit
University of Dundee

## Moray D Newlands
*Senior Lecturer,* Concrete Technology Unit
University of Dundee

## Judith E Halliday
*Research/Teaching Fellow,* Concrete Technology Unit
University of Dundee

## Laszlo J Csetenyi
*Research/Teaching Fellow,* Concrete Technology Unit
University of Dundee

## Li Zheng
*Research/Teaching Fellow,* Concrete Technology Unit
University of Dundee

## Michael J McCarthy
*Reader,* Concrete Technology Unit
University of Dundee

## Thomas D Dyer
*Lecturer,* Concrete Technology Unit
University of Dundee

## ABOUT THE EDITORS

**Professor M Roderick Jones** is the Director of the Concrete Technology Unit at the University of Dundee. A renowned practitioner in the field of concrete technology, he is a member of numerous national and international technical committees and has published extensively on many aspects of concrete technology, cement science and sustainable construction.

**Dr Moray D Newlands** is a Senior Lecturer within the Concrete Technology Unit at the University of Dundee. His research focusses on balancing sustainability and durability performance in concrete construction, as well as the use of novel materials and the development of test methods for assessing concrete.

**Dr Judith E Halliday** is a Research/Teaching Fellow within the Concrete Technology Unit at the University of Dundee. She has been involved in numerous projects relating to sustainable and environmental issues of recycling materials in concrete construction. She has now shifted her focus on the awareness of the depletion of natural resources and the impact of their use in construction as a whole.

**Dr Laszlo J Csetenyi** is a Research/Teaching Fellow in the Concrete Technology Unit at the University of Dundee. His main areas of interest include cement and concrete science and technology with emphasis on waste stabilisation/solidification and practical use of these materials in construction.

**Dr Li Zheng** is a Research/Teaching Fellow within the Concrete Technology Unit at the University of Dundee. His current work is concerned with concrete durability, recycling aggregates, foamed concrete, fly ash recovery and beneficiation, cement hydration and temperature rise modelling and mix design/optimisation with novel cement combinations.

**Dr Michael J McCarthy** is a Reader in the Concrete Technology Unit at the University of Dundee. He has carried out research in the field of concrete technology for the last 20 years. Much of his work has been concerned with the use of fly ash in various construction applications, deterioration of concrete in various exposure conditions and aspects of concrete construction technology. He has been involved in many projects and has published widely on his work.

**Dr Thomas D Dyer** is a Lecturer in the Concrete Technology Unit at the University of Dundee. His research has primarily involved investigation of interactions of by-products with cement. He is also involved in applying life-cycle assessment techniques to construction. Recently his work has extended to include imprinting of biomimetic microstructures in construction materials, and interactions of brownfield contaminants with fresh concrete.

*Cover Photo: Queensferry Crossing, Scotland, Courtesy of Transport Scotland*

Details of all publications from the University of Dundee - Concrete Technology Unit are available from:
Concrete Technology Unit, University of Dundee, Dundee, DD1 4HN, UK
Tel: 01382 384498, m.r.jones@dundee.ac.uk

Published by University of Dundee – Concrete Technology Unit, 2016

Requests to copy any part of this publication should be made to:
Concrete Technology Unit, University of Dundee, Dundee, DD1 4HN, UK
Tel: 01382 384498, m.r.jones@dundee.ac.uk

ISBN 978-0-9573263-1-6

The major themes of this year's conference draw heavily on the need to constantly improve sustainability in the concrete industry. There has been significant progress on issues including, $CO_2$ and $NO_x$ emissions from raw materials, manufacture, construction, operation and end of use. The industry is developing innovative solutions with low energy cements and by-product materials, and through the use of recycled and secondary aggregates. However, there is still work to be done to balance overall resource efficiency with concrete performance requirements for economic construction.

The demands on concrete are changing emphasis, and beyond the proven engineering advantages other properties are being exploited, for example its high thermal mass, which can help to regulate building temperatures and minimise energy consumption. Off-site prefabricated concrete can offer improved vibration, sound insulation and acoustic performance. At a broader scale, climate change presents a major challenge for infrastructure reliability and resilience and concrete is capable of resisting damage and recovering rapidly from extreme weather events. With increasing traffic, concrete road base/blacktop wearing course composites will be important in achieving road pavement design lives. Energy mixes in most countries are changing from fossil to increasing renewable and low emission production. Wind farm sites have proved popular but are being moved offshore and into deeper waters, and concrete foundations and sub-structures can offer more cost effective solutions for the majority of soils and water depths. New nuclear power stations are being planned and again high performance concrete will be a requirement.

Over the next decade digital design and structural engineering technologies will become de facto and it will be imperative that there is a close working relationship between the research, design, industry and standards communities. Innovative thinking and adoption of practical research and development must be utilised to their full potential for the sector to prosper, which Dundee has championed for many years.

The Concrete Technology Unit organised this Conference to address these challenges, continuing its established series of events, namely, Concrete in the Low Carbon Era, 2012; Concrete: Construction's Sustainable Option, 2008; Global Construction: Ultimate Concrete Opportunities, 2005; Challenges of Concrete Construction, 2002; Creating with Concrete, 1999; Concrete in the Service of Mankind, 1996; Economic and Durable Concrete Construction Through Excellence, 1993 and Protection of Concrete, 1990.

Under the theme of Environment, Efficiency and Economic Challenges for Concrete, the Conference consisted of six Events: *(i) Recycling and Reuse, (ii) Waste Minimisation and Resource Efficiency, (iii) Low Carbon Cements and Concrete, (iv) Novel, Smart and Multi-Functional Concrete, (v) Durability, Serviceability and Reliability, (vi) Advances in Structural Modelling.* In all, over 110 papers were presented from over 40 countries.

The Opening Addresses were given by Professor Sir Peter Downes, Principal and Vice-Chancellor of the University of Dundee, and Professor Rod Jones, Conference Chairman, University of Dundee. The Conference Opening Paper was presented by Professor Tom Robl of the University of Kentucky, USA. The Closing Summary Paper was presented by Professor Peter Hewlett, Visiting Professor at the University of Dundee and Director of Research to the David Ball Group.

The support of International Professional Institutions and Sponsoring Organisations was a major contribution to the success of the Conference. Exhibitors, representing both global and local industry as well as instrument manufacturers and a research centre, formed an integral part of the event. The work of the Conference was an immense undertaking and all of those involved are gratefully acknowledged, in particular, the members of the Organising Committee for managing the event from start to finish; members of the Scientific and Technical Committee for advising on the selection and reviewing of papers; the Authors and the Chairmen of Technical Sessions for their invaluable contributions to the proceedings.

**Professor Roderick Jones, Conference Chairman, 4 July 2016**

# ORGANISING COMMITTEE

**Professor M R Jones**
*Conference Chairman*

**Dr M D Newlands**
*Conference Secretary*

**Dr M J McCarthy**

**Dr T D Dyer**

**Dr J E Halliday**

**Dr L J Csetenyi**

**Dr L Zheng**

**Dr L Chernin**

**Professor P C Hewlett,**
*David Ball Group, UK*

**Professor T A Harrison,**
*Independent Consultant, UK*

**Professor P Chana**
*Mineral Products Association, UK*

**Mr Raman Mangabhai**
*Mangabhai Consulting, UK*

**Dr David Dunne**
*AECOM, UK*

# SCIENTIFIC AND TECHNICAL COMMITTEE

**Prof M Thomas**
University New Brunswick, Canada
**Prof C Shi**
China Building Materials Academy, China, China
**Prof J Qian**
Chongqing University, China
**Dr S Caliskan**
Saudi Aramco, Saudi Arabia
**Prof S P Singh**
NIT Jalandhar, India
**Prof M Ganesh**
VIT Vellore, India
**Prof U Dave**
Nirma University, India
**Prof M Alexander**
UCT, South Africa
**Dr E Kearsley**
University of Pretoria, South Africa
**Prof P Sukontasukkul**
King Mongkut University of Technology-North Bangkok, Thailand
**Prof M Sugiyama**
Hokkai Gakuen University, Japan
**Prof B H Oh**
Seoul National University, Korea

**Prof R I Gilbert**
University of New South Wales, Australia
**Prof P Helene**
Brazilian Concrete Institute, Brazil
**Prof K Curtis**
Georgia Tech, USA
**Prof I Papayianni**
Aristotle University of Thessaloniki, Greece
**Prof K van Breugel**
Delft University of Technology, Netherlands
**Mr C Heidrich**
ADAA, Australia
**Dr C Clear**
MPA, UK
**Dr K Paine**
University of Bath, UK
**Dr V Baroghel-Bouny**
IFSTTAR, France
**Prof F Hunkeler**
TFB, Switzerland
**Prof S Hanehara**
Iwate Universtiy, Japan
**Mr C Shaw**
independent consultant, UK
**Dr A Yerramala**
Madanapalle Institute of Technology and Science, India

# SPONSORING ORGANISATIONS

**The Institute of Concrete Technology, UK**

**RILEM**

**The Institute of Materials Minerals and Mining, UK**

**Dundee and Angus Convention Bureau**

**University of Dundee**

# EXHIBITORS

**banahCEM**

**BASF – The Chemical Company**

**Dundee and Angus Convention Bureau / Dundee City Council**

**Elkem Silicon Materials**

**Hanson Cement**

**Jet Materials Ltd**

**Quantachrome UK**

**Surface Measurement Systems UK**

**TA Instruments**

**University of Kentucky Center for Applied Energy Research**

# SUPPORTING INSTITUTIONS

**China Civil Engineering Society**

**Chinese Institute of Engineers (Taiwan)**

**Concrete Society, UK**

**Polish Concrete Producers Association**

**Spanish Precast Concrete Association – ANDECE**

**Taiwan Concrete Institute**

# CONTENTS

**Please enter page number into your pdf reader page navigator to go to paper**

## THEME 2 WASTE MINIMISATION AND RESOURCE EFFICIENCY



## THEME 3 LOW CARBON CEMENTS AND CONCRETE

# Theme 1

# Recycling and Reuse

**Keynote Paper**

# SUSTAINABILITY IN THE PRODUCTION OF RECYCLED CONCRETE AGGREGATES

**K Weimann**

**C Adam**

Federal Institute for Materials Research and Testing

Germany

**ABSTRACT.** Concrete is one of the most widely used construction materials and, accordingly, the concrete industry is an important stakeholder in the field of sustainable construction. Therefore various approaches have been implemented to increase the sustainability of concrete. Besides reducing $CO_2$-emissions during cement production, increasing the energy efficiency of buildings and extending their life span, the end-of-life performance of concrete is also an essential aspect of sustainability. Reusing concrete as a secondary building material meets the requirements of sustainability in several ways: the extended time availability of primary raw materials and, thereby, the protection of natural resources as well as conserving landfill site. Furthermore, the production of recycled concrete aggregates (RCA) is a good example for closed-loop recycling. However, regarding the use of RCA as a substitute for natural aggregates in concrete, attention must be paid to all issues of sustainability: this means that environmental, economic and social aspects have to be considered. Since RCA generally have inferior building material properties, such as higher porosity and lower density, the implementation of closed-loop recycling of concrete only makes sense if the technical quality assurance is secured. This paper focusses on the implementation of techniques for the deconstruction/demolition of buildings and the subsequent treatment of concrete rubble in order to improve the building material properties of RCA with regard to the requirements of sustainability and also technical rules and standards.

**Keywords:** CDW (Construction and demolition waste), RCA (Recycled concrete aggregates), Gypsum, Selective dismantling, CDW treatment

**Karin Weimann** works as a scientist for the Federal Institute for Materials Research and Testing in Germany, Division 4.4, Thermochemical Residues Treatment and Resource Recovery in the field recycling of construction waste. She is member of several technical committees and has also a wide experience as a construction site manager in the fields of foundation engineering and soil decontamination.

**Christian Adam** is the head of the Division 4.4, Thermochemical Residues Treatment and Resource Recovery of the Federal Institute for Materials Research and Testing. His field of research is recycling technologies for inorganic solid residues with focus on thermochemical processing.

## INTRODUCTION

Regarding the growing importance of conserving natural resources, the resource potential of building materials is of particular interest. This is due to the high consumption of raw materials and the large quantities of construction and demolition waste in the construction industry [1, 2]. Therefore various approaches have been made to decrease the environmental impacts in the construction industry.

A promising approach towards environmental friendly buildings is the extension of the life time of buildings and building materials. This can be achieved e.g. by an improvement of the durability of building materials as well as by extending the service life time of buildings. Restoration, renovation and modernization instead of demolition and rebuilding and also flexible designs of interior fittings for different potential uses may prolong a buildings life time [2-4].

For a number of years a development towards low energy houses and even zero-energy houses could be observed [5, 6]. Houses with a high insulation level, green heating systems and housing technologies for the use of alternative energies have been designed and realized. However, based on the predominant use of concrete in the building sector, its application is also evaluated with regard to sustainability. As stated in the European Commission Construction Products Regulation, construction works need to be designed, built and demolished whilst maintaining sustainable use of natural resources [7]. Accordingly, construction works need to be durable, the raw and secondary materials used need to be environmentally compatible and the materials and demolition wastes of construction works need to be recyclable.

The utilization of used or recycled building materials as secondary building materials can meet the requirements of positive environmental impacts in several aspects: the extended time availability of primary raw materials and the related protection of natural resources as well as the saving of landfill site. Therefore a reduction of construction and demolition waste (CDW) can be environmentally advantageous. Since concrete is the most widely used building material worldwide and its production raises significant environmental impacts, concrete is often in the centre of attention when the issue sustainability arises [1, 8].

## INCREASING THE SUSTAINABILITY OF CONCRETE

Regarding concrete, the focus is on the consumption of cement. Cement manufacturing is a high volume process, with large quantities of substances turned into commercial products. It is one of the most material and energy-intensive industrial processes, and also $CO_2$ emissions-intensive. Accordingly various attempts have been made to reduce the environmental impacts of cement production like the use of secondary raw materials or alternative fuels during the cement production [9].

Furthermore special concrete formulations were developed with regard to a preferably low proportion of cement. The replacement of cement clinker with pulverised fuel ash (PFA) is one example of saving cement in concrete respectively of the reduction of $CO_2$ emissions in concrete production. Also the cement substitution with granulated blast furnace slag (GBFS) or limestone powder (LP) showed promising results e.g. for Ultra-High Performance Concrete (UHPC).

The calculated embedded $CO_2$ emission of concretes showed advantages compared to conventional concretes with comparable building material properties. Moreover in some investigations also the amount of required water was lower. [10-12]

Regarding the growing importance of conserving natural resources, the resource potential of CDW is of particular interest as well. The large quantities of CDW and also the high consumption of raw materials in the construction industry, point out the importance of the reuse of building materials for an improvement of resource efficiency. The utilization of used or recycled building materials as secondary building materials can meet the requirements of positive environmental impacts in several aspects: the extended time availability of primary raw materials and the related protection of natural resources as well as the saving of landfill site. Therefore a reduction of CDW can be environmentally advantageous as well.

## CONCRETE RECYCLING

The use of recycled concrete aggregates as secondary building material is only possible if the specific technical functionality of the certain material is secured. Hence many studies investigated the building material properties of recycled concrete aggregates. In general RCA have inferior building material properties like higher porosity and lower density that are caused by adherent old cement paste in crushed concrete. Several studies have also shown that the purity of the recycled fractions is an important prerequisite for an efficient and environmentally friendly reuse of secondary building materials [13]. Quality requirements for various possible applications have been elaborated and were implemented in technical rules and standards. These regulations for the use of RCA apply several requirements with regard to the material composition. A minimum percentage of concrete or rather natural aggregates is required and furthermore impurities and contaminants like wood, plastics or organic substances and heavy metals are limited [14].

Besides the composition of the construction, the quality of the recycled concrete is influenced by two main processing steps: the demolition or dismantling of the construction and the subsequent treatment of the concrete rubble. The effects of different techniques for demolition or selective dismantling and of processing methods for the improvement of the building material properties of the treated CDW have been investigated in several studies [15, 16].

### Separation and Recycling of Impurities

Unwanted substances can be removed during demolition and/or deconstruction of buildings by using techniques for selective dismantling or by subsequent treatments of the construction and demolition waste. The use of techniques for selective dismantling allows the separation of different building materials before blending with other building materials. The key for a successful selective dismantling is a careful planning and preparation of the chronological processing steps – based on the inventory of the building, impurities and contaminants have to be located and identified. In contrast to conventional demolition, usually less expenditure for the subsequent treatment of the concrete rubble is necessary.

However, depending on the specific deconstruction site it can be more effective and/or more environmentally compatible to remove impurities and harmful substances by treating the concrete rubble in a stationary CDW processing plant after conventional demolition.

The main processing steps for a treatment of CDW are comminution and grading of the material. For the reduction of impurities further processing steps like second crushing and/or sorting steps can be useful. In specific cases a wet treatment may be necessary for the reduction of certain harmful substances, but usually a dry processing is sufficient. However, it should be noted that the implementation of these dismantling and/or processing steps usually causes additional environmental impacts e.g. by energy consumption. Table 1 summarizes advantages and disadvantages of both approaches.

Table 1 Advantages (↑) and disadvantages (↓) of conventional demolition and selective dismantling

| CONVENTIONAL DEMOLITION | SELECTIVE DISMANTLING |
|---|---|
| mixed CDW ↓ | sorted materials ↑ |
| lower space requirements ↑ | greater space requirements ↓ |
| comparatively fast ↑ | longer duration of the work ↓ |
| increased disposal costs ↓ | lower disposal costs ↑ |
| environmental impacts ? | environmental impacts ? |

## Environmental Aspects in the Production of RCA

Since almost all working and processing steps are associated with environmental impacts, the benefits of reusing CDW as secondary building materials and the correlated environmental costs for further dismantling or processing steps have to be calculated and evaluated carefully [16]. Several studies already have been conducted to analyse the environmental impacts of the RCA production. Preferably used impact categories for an environmental evaluation of RCA are energy consumption and the related category global warming, land use and abiotic depletion, acidification, eutrophication, ozone layer depletion and photochemical oxidation [17, 18]. Several LCA compared the environmental impacts of RCA and natural aggregates and also of recycled aggregate concrete and of concrete made of natural aggregates. Since various parameters may influence the specific example, e.g. transportation distances are an important factor, it is necessary to evaluate the investigated scenarios carefully.

A German investigation focused on the production of RCA [15]. According to European Standards (CEN/TC 350), the end-of-life-phase of buildings “C stage” was investigated [19]. This evaluation included the working steps demolition/selective dismantling (C1), related transports (C2), CDW processing (mobile or stationary) (C3) and final disposal/landfilling of residues (C4). The process flows for the model scenarios were estimated, data were taken from manufacturers for building machines or tools and also from the life cycle inventory (LCI) database ecoinvent data 2.2 [20]. Using the impact assessment model CML 2002-method, the categories climate change, land consumption, ozone depletion potential, eutrophication potential and acidification potential were evaluated. All environmental impacts were calculated in relation to the production of one ton of RCA as the functional unit. The results showed less environmental impacts for the scenarios of selective dismantling in all investigated categories and for all three building types.

Since the environmental impacts were related to the production of one ton of RCA, most of the values for the building type “one-family-dwelling” were higher than for the other building types because of its brick content and accordingly a comparable lower proportion of concrete.

The utilization of a secondary product should be environmentally advantageous compared to the use of the primary product. In that context a comparative environmental evaluation is a common procedure for the verification of the sustainability of the aimed substitution. Therefore the results were also compared with data for natural aggregates likewise from ecoinvent data 2.2. To exclude regional influences and the related transport distances for RCA and natural aggregates, the environmental impacts of material transports were not taken into account.

In this investigation significant differences between recycled aggregates and natural aggregate could only be determined in the impact category land consumption. Nevertheless, the substitution of natural aggregates by RCA could help saving natural resources by reducing land consumption. Figure 1 shows the results of the comparison of the production of one ton natural gravel and one ton RCA from a one-family dwelling and from a multiple-dwelling-unit in the impact categories climate change and land consumption.

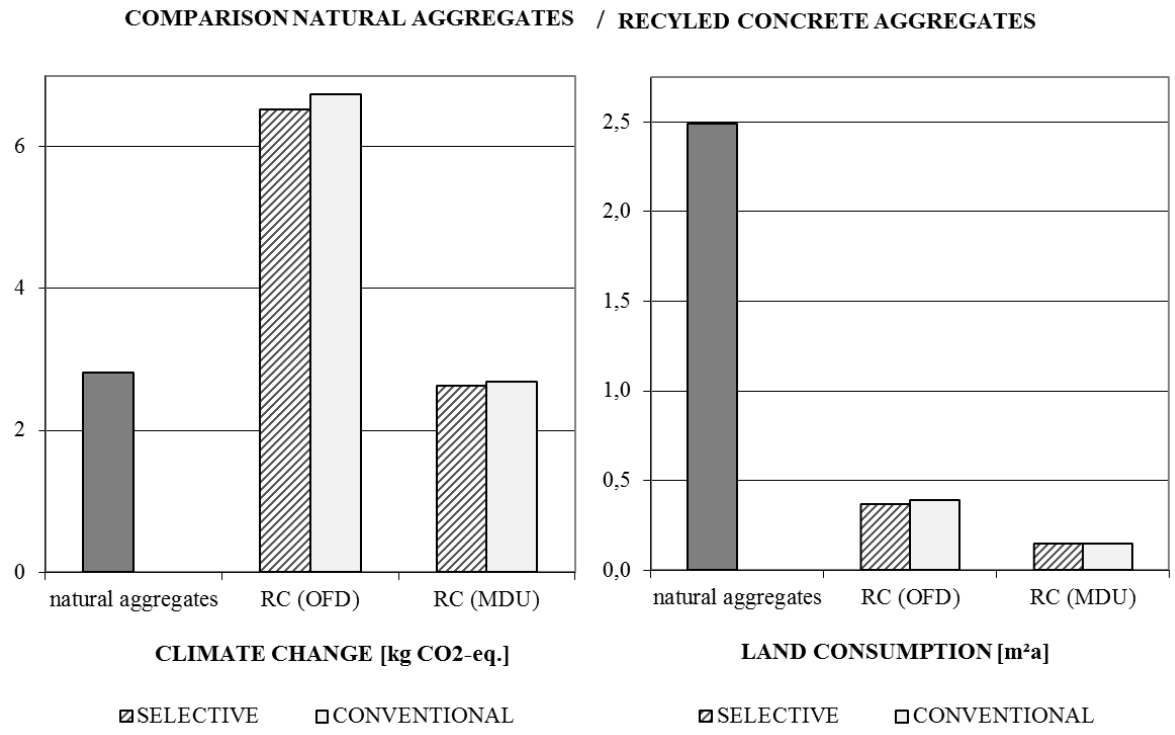


Figure 1 Environmental impacts of the production of 1 t natural aggregates compared with RCA from the selective dismantling resp. conventional demolition of a one-family dwelling (OFD) and a Multiple Dwelling Unit (MDU) [15]

## GYPSUM IN CDW

In recent years the content of gypsum in CDW received growing attention. Two reasons have to be mentioned: the utilization of gypsum containing building materials increased strongly in the last decades in many industrialized countries (Figure 2).

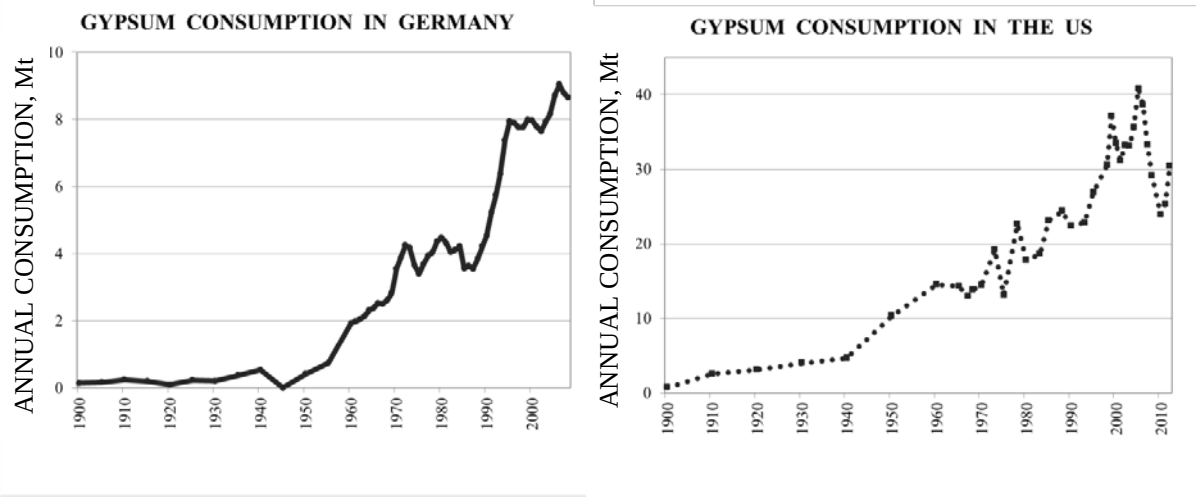


Figure 2 Gypsum consumption in Germany (left) and the United States (right) in Mt, 1900 – 2010/2012 [21-23]

Because of the growing gypsum stock in buildings an increase of gypsum in future CDW has to be expected. Gypsum is unwanted in RCA because of its content of sulfates. Under certain conditions sulfates might damage concrete by the formation of voluminous mineral phases, particularly ettringite but also thaumasite, resulting in cracking, expansion or a loss of bond between cement paste and aggregate [24]. Furthermore, sulfates can also impair the setting behaviour of fresh concrete. Accordingly technical standards and guidelines restrict sulfates in secondary building materials and an increasing proportion of gypsum in CDW should be paid particular attention.

Table 2 summarises actual data from the last decade of potentially recyclable gypsum in CDW in selected European countries per annum.

To develop strategies for the reduction of gypsum resp. sulfates in CDW it is necessary to distinguish between the specific gypsum building components. Gypsum in construction waste usually originates from different interior fittings. Some of these building components can be removed relatively easily by manual labour or by using mechanical equipment during the selective dismantling or as part of preliminary work. These components include e.g. gypsum walls, dry screeds or plasterboards. In some cases floor screeds can be removed by milling, but nevertheless, bonded gypsum screeds and also plaster are usually quite difficult to remove during the deconstruction process. A subsequent treatment in a stationary CDW processing plant for sulfate reduction include manual labour like manual sorting of gypsum wall blocks as well as mechanical treatments like intensive crushing.

Table 2 Recyclable gypsum waste in CDW in selected European countries [25]

| RECYCABLE GYPSUM WASTE IN CDW IN SELECTED EUROPEAN CONTRIES | |
|---|---|
| Country | Amount, Mg |
| France | 363,000 |
| Great Britain | 352,000 |
| Germany | 242,000 |
| Spain | 110,000 |
| Italy | 82,000 |
| Netherlands | 46,000 |
| Sweden | 45,000 |
| Belgium | 36,000 |
| Austria | 35,000 |
| Finland | 32,000 |
| Denmark | 25,000 |
| Switzerland | 13,000 |
| Selected European Countries | 1,381,000 |

**Gypsum Recycling**

In general recycling strategies aim at reusing materials in closed loops (i.e. material recycled as or nearly as the same product as the original) and to utilize as much of the contents of the material as possible [26]. Regarding the environmental evaluation of the production of RCA, it would be also advantageous to recycle separated gypsum residues in two aspects: on one hand the reduction of landfilling and on the other hand conservation of natural gypsum resources.

For a reuse of recycled gypsum as a substitution for natural gypsum in gypsum production, several requirements for the material quality have to be met. Important technical parameters for the processing refer to the content of: free moisture, calcium sulfate dehydrate, water-soluble salts of potassium, magnesium and sodium, chlorides and TOC (total organic carbon). Furthermore, regarding ecological and human-toxicological risks additional requirements are set for heavy metals and organic components.

Plasterboards are most suitable for gypsum recycling, because of their good sortability during the deconstruction. Therefore the purity of the gathered gypsum residues is comparably high and good to recycle. Furthermore the amount of installed components e.g. in Germany is comparably high [15]. In Europe mobile and stationary recycling plants are operated [27]. The used techniques include different steps of comminution and classifying and also sorting, aiming at the production of gypsum powder that could be used in gypsum production.

In a current project the environmental impacts of the recycling of gypsum residues are investigated with regard to a closed loop recycling of gypsum. This includes collecting as well as transportation and the processing steps of recycling the material in a gypsum recycling plant. Furthermore a comparison with the environmental impacts of the exploitation of natural gypsum is included. Regarding the sustainability in the production of RCA this will be a further step towards a sustainable development of the construction industry.

## CONCLUSIONS

The growing necessity to save material and energy resources, together with an increasing concern for environmental issues is of particular importance for the construction industry. Since concrete is one of the most widely used building materials, various approaches have been implemented to increase the sustainability of concrete.

- The sustainability of concrete respectively concrete production can be increased by using recycled concrete aggregates.
- Several technical standards have been implemented for the use of RCA. An important factor is the reduction of impurities in the recycled material. This can be achieved by using techniques for selective dismantling as well as by further treatment of the CDW.
- The use of techniques for selective dismantling can be environmental advantageous for the production of RCA. Since there are many influencing parameters, the calculation of the environmental impacts of RCA recycling has to be made carefully.
- As a result of the increasing amount of installed interior fittings in buildings in the last decades, a growing amount of gypsum in CDW has to be expected. Therefore the recycling of gypsum will become more important in the upcoming years.
- Techniques for the recycling of gypsum already exist but an optimisation of the whole processing, including collecting, transportation and recycling will be useful. With regard to the sustainability of the production of RCA, an evaluation of the treatment of the gypsum containing residues is of particular interest.

## ACKNOWLEDGEMENTS

We thank the Federal Ministry for the Environment, Nature Conservation and Nuclear Safety and the Federal Environment Agency, Germany, for funding the research for reducing gypsum in C&D waste in the project No. Ufoplan 3709 33 317 and the investigations of the environmental impacts of gypsum plasterboard recycling in the project No. Ufoplan 3715 343 200.

## REFERENCES

1. JIN R., CHEN Q. and SOBOYEJO A. Survey of the current status of sustainable concrete production in the U.S. Resources Conservation and Recycling, Vol. 105 2015, pp. 148–159.

2. MARIE I. and QUIASRAWI H. Closed-loop recycling of recycled concrete aggregates. Journal of Cleaner Production, Vol. 37, 2012, pp. 243–248.

3. MATEUS R., NEIVA S.D.O., BRAGANÇA L., MENDONÇA P. and MACIEIRA M. Sustainability assessment of an innovative lightweight building technology for partition walls - Comparison with conventional technologies. Building and Environment, Vol. 67, 2013, pp. 147–159.

4. RAUF A. and CRAWFORD R.H. Building service life and its effect on the life cycle embodied energy of buildings. Energy, Vol. 79, 2015, pp. 140–148.

5. PINEAU D., RIVIÈRE P., STABAT P., HOANG P. and ARCHAMBAULT V. Performance analysis of heating systems for low energy houses. Energy and Buildings, Vol. 65, 2013, pp. 45–54.

6. RODRIGUEZ-UBINAS E., RODRIGUEZ S., VOSS K. and TODOROVIĆ M.S. Energy efficiency evaluation of zero energy houses. Energy and Buildings, Vol. 83, 2014, pp. 23–35.

7. EUROPEAN PARLIAMENT, Construction Products Regulation (CPR), in Construction Products Regulation (CPR) No 305/2011, European Commission, Editor 2011, Official Journal of the European Union, Brussels, 39 p.

8. MEYER C. The greening of the concrete industry. Cement & Concrete Composites, Vol. 31, No. 8, 2009, pp. 601–605.

9. EUROPEAN COMMISSION, Best Available Techniques (BAT) Reference Document for the Production of Cement, Lime and Magnesium Oxide, 2013, Brussels.

10. PROSKE T., HAINER S., REZVANI M. and GRAUBNER C-A. Eco-friendly concretes with reduced water and cement contents - Mix design principles and laboratory tests. Cement and Concrete Research, Vol. 51, 2013, pp. 38–46.

11. YU R., SPIESZ P. and BROUWERS H.J.H. Development of an eco-friendly Ultra-High Performance Concrete (UHPC) with efficient cement and mineral admixtures uses. Cement & Concrete Composites, Vol. 55, 2015, pp. 383–394.

12. PURNELL P. and BLACK L. Embodied carbon dioxide in concrete: Variation with common mix design parameters. Cement and Concrete Research, Vol. 42, No. 6, 2012, pp. 874–877.

13. POON C.S. and CHAN D. The use of recycled aggregate in concrete in Hong Kong. Resources Conservation & Recycling, Vol. 50, No. 3, 2007, pp. 293–305.

14. DIN-DEUTSCHES INSTITUT FÜR NORMUNG E.V., DIN EN 12 620 Aggregates for concrete; German version EN 12620:2002+A1:2008 2008, Beuth Verlag, Berlin, 58 p.

15. WEIMANN K., MATYSCHIK J., ADAM C., SCHULZ T, LINß E. and MÜLLER A. Optimization of demolition/dismantling of buildings for the recovery and treatment of building materials considering the reduction of harmful substances (in particular sulphates) in the recycled building material and aspects of life-cycle analyses, Federal Environment Agency, Editor 2012, Bundesanstalt für Materialforschung und -prüfung and Bauhaus-Universität Weimar, Germany, Dessau, Germany, 225 p.

16. BRITE/EURAM, Construction recycling technologies for high quality cement and concrete - Task 5 Cement production, 2000, Berlin, Barcelona, 52 p.

17. SERRES N., BRAYMAND S. and FEUGEAS F. Environmental evaluation of concrete made from recycled concrete aggregate implementing life cycle assessment. Journal of Building Engineering, Vol. 5, 2016, pp. 24–33.

18. BLENGINI G.A. and GARBARINO E. Resources and waste management in Turin (Italy): the role of recycled aggregates in the sustainable supply mix. Journal of Cleaner Production, Vol. 18, Nos. 10-11, 2010, pp. 1021–1030.

19. CEN, Sustainability of construction works, in CEN/TC 350, Technical Committee 350 of the European Committee for Standardization, Editor 2011.

20. ECOINVENT CENTRE, Database ecoinvent data v2.2 - life cycle inventory (LCI) data, 2011, St. Gallen, Switzerland.

21. US GEOLOGICAL SURVEY (USGS). Gypsum Statistics. 2014 [cited 2015], Available from: http://minerals.usgs.gov/ds/2005/140/ds140-gypsu.pdf.

22. STATISTISCHES BUNDESAMT (Federal Statistical Office), Statistisches Jahrbuch 2010, 2010, Wiesbaden, Germany, 745 p.

23. BUNDESVERBAND BAUSTOFFE - STEINE UND ERDEN E.V., Aufgaben, Themen und Ziele 2010/2011 - Jahresbericht der Baustoffindustrie, 2010, bbs: Berlin. 21 p.

24. RAHMAN M.M. and BASSUONI M.T. Thaumasite sulfate attack on concrete: Mechanisms, influential factors and mitigation. Construction and Building Materials, Vol. 73, 2014, pp. 652–662.

25. POLYTECHNIC UNIVERSITY OF MADRID (UPM Team), GtoG: From production to recycling: a circular economy for the European Gypsum Industry with the Demolition and Recycling Industry, 2013, 332 p.

26. THORMARK C. Conservation of energy and natural resources by recycling building waste. Resources Conservation & Recycling, Vol. 33, No. 2, 2001, pp. 113–130.

27. EUROGYPSUM, Gypsum at the heart of sustainable construction. 2011 [cited 2016 2016/01/19], Available from: http://www.eurogypsum.org/.

# CARBONATION EFFECT ON SANDCRETE-TALC COMPOSITE MORTAR MORPHOLOGY

**M Abdullahi**

The Federal Polytechnic, Bida

**J O Odigure A S Kovo A S Abdulkareem**

Federal University of Technology, Minna

Nigeria

**ABSTRACT.** The increasing investigation of atmospheric $CO_2$ and greenhouse gases in global warming has necessitated the need to research its effects on early cement minerals hydration chemistry and morphology of hydrates. This paper seeks to investigate the mechanism and effect of carbonation on the sandcrete-talc composite microstructure development at an early age. Standard experimental techniques and analytical equipments were used in the investigations. The results showed that the presence of talc during carbonation process of cement-based material significantly influenced the hydration mechanism of the cement minerals and their hydrates. The EDS, XRD, TGA and SEM results are consistent and confirm the influence on cement minerals hydrates of talc. Early age carbonation of sandcrete led to visible change in the hydrated minerals microstructures and reduced porosity of the matrix. The disappearance of portlandite and calcium silicate to more stable calcite peak in both EDS and XRD are indication of morphological changes induced by talc to the cement mineral hydrates microstructure. The morphology of hydrates produced is dependent on the talc percentage used and temperature. It was observed that S-T matrix composites unlike the control without talc, showed a more densified morphology with a foil-like appearance of C-S-H phase.

**Keywords:** Sandcrete, Carbon dioxide, Morphology, Carbonation, Composite

**J O Odigure** is a Professor of Chemical Engineering at the Federal University of Technology, Minna.

**Dr Abdulkareem A. Saka** is a senior Lecturer in the Department of Chemical Engineering, Federal University of Technology, Minna.

**Dr Kovo Abdulsalam Sanni** is presently a Senior Lecturer in the Department of Chemical Engineering, Federal University of Technology, Minna.

**Dr M Abdullahi** has just completed is PhD degree from the University of Technology, Minna, Nigeria. He is currently a senior lecturer in the department of Chemical Engineering, the Federal Polytechnic, Bida.

## INTRODUCTION

Cement-based materials such as sandcrete adsorb carbon dioxide ($CO_2$) through a process known as carbonation. There are two different categories of carbonation: the early age carbonation and the weathering carbonation [1]. The early age carbonation takes place instantly in a fresh sandcrete mix at an early age and ends prior to when accelerated curing stops while the weathering carbonation, is pertinent to mature concrete over a prolonged period of time when it is exposed to the atmosphere.

Sandcrete is widely used in Nigeria and in almost all African countries for infrastructure development and plays tremendous role in modern building industry [2]. One of the key durability indicators of sandcrete is the degree of carbonation. Understanding sandcrete micro-structure as it affects durability is the hallmark for most sandcrete researchers [3]. Sandcrete and sandcrete related materials microstructure could be characterized using SEM, EDS and XRD analyses.

The degree of porosity, pore types and size, pore connectivity and their distributions coupled with mineral crystals sizes and arrangement in the solid matrix significantly affect physicochemical properties of cement-based materials [4]. The carbonation of cement-based material is highly dependent on the porosity and level of pore saturation. Shah [5] in his study explicates that during carbonation process, the decrease in porosity and water supply greatly affects the diffusion coefficient and water penetrability of the cement-based material.

Silva *et al.*[6] studied the effect of microstructural changes in carbonated concrete. They reported that the total porosity for carbonated concrete was lower when compared with the controlled non-carbonated concrete.

Rostami *et al.*[1] studied microstructure of cement paste subject to early age carbonation curing with the aim of understanding the mechanism of concrete carbonation through microstructure development. They found out that early carbonation curing could accelerate strength gain and increases durability of concrete.

Research has shown that the three polymorphs (Calcite, Aragonite or Vaterite) of calcium carbonate could be formed during carbonation as $CO_2$ ingress into the concrete. The microstructure of calcite formed during carbonation is characterised by small, closely crammed crystals of a circular shape with particle size of less than 3 μm [6].

Different methodologies and technologies have been developed for the sequestration of atmospheric carbon dioxide [7]. However, $CO_2$ capture and sequestration using sandcrete blend is probably the best short-to-long term solution for the reduction of atmospheric acidic emissions in developing nations. The effects of admixture on sandcrete carbonation have not been highlighted by most researchers. Significant knowledge gap exits. This work presents a study on the microstructure development of sandcrete-talc composite subjected to 9 hours of carbonation curing at varying temperatures in an attempt to understand the degree of carbon dioxide sequestration and the formation of calcite at an early age.

## EXPERIMENTAL METHODOLOGY

### Materials

A performance-based approach for early age microstructural development in standard sandcrete (S-S) and S-T (10, 30 and 50 %) composites was studied. The performance of the composite mixture was compared with standard sandcrete (control) [8]. Ordinary Portland Cement (OPC) with ISO 9001: 2008 and siliceous sharp sand conforming to American Standard for Testing and Measurement (ASTM C33) were used for the investigation. The sand has a specific gravity of 2.66, an average moisture content of 0.92 % and coefficient of uniformity of 2.95. The composition of the talc used is presented in Figure 1 while the potable water conformed to NIS 554: 2007.

The starting materials (Natural talc, Cement and Sharp Sand) required for the research work were analyzed using X-ray Diffractometer (XRD) (Model: DY614 Empyrean by Panalytical), Scanning Electron Microscopy (SEM) (Field Emission Gun Nova NanoSEM 230), Elemental Diffraction Spectrometer (EDS) (Oxford X-Max Detector using INCA Software) and Energy Dispersive X-ray Fluorescence (EDXRF) (Model: MiniPal4 embedded with X'pert HighScore Plus Software) to determine the mineralogical compositions, micro-structural changes, elemental and oxides compositions respectively.

### Sandcrete Mortar Preparation

Two sets of different air entrained mortar specimens designated as "A" and "B" of the same workability per set were produced. The first set "A" constitute the control and consists of nine (9) different samples labelled $A_1$ to $A_9$ with a constant standard mix design proportion based on Nigeria Industrial Standard [8].

The second set "B" unlike "A" had varying percentages of talc substituting the siliceous sharp sand. Set B is subdivided into three (3) subsets namely: $B_{11} - B_{19}$, $B_{31} - B_{39}$ and $B_{51} - B_{59}$. Each subset consists of 3 specimens made up of 10, 30 and 50 % partial replacement of siliceous sharp sand with talc. The mix design proportion is presented in Table 1. All the mortar samples were prepared using a fixed cement-to-sand ratio of 1:6 [2,8,9] a water-to-cement ratio (W/C) of 0.5 [2,8,9,10] and potable water.

Table 1 Mixed Design Proportion for Standard Mortar (reference) and Sandcrete-talc (S-T)

| MIX DESIGNATION | $A_1$-$A_9$ | $B_{11}$-$B_{19}$ | $B_{31}$-$B_{39}$ | $B_{51}$- $B_{59}$ |
|---|---|---|---|---|
| Temperature, $^oC$ | 30 – 45 | 30 – 45 | 30 – 45 | 30 – 45 |
| Replacement, % | - | 10 | 30 | 50 |
| Cement, g | 33.71 | 33.71 | 33.71 | 33.71 |
| Sand, g | 202.29 | 182.06 | 141.60 | 101.145 |
| Talc, g | - | 20.23 | 60.69 | 101.145 |
| Water, g | 16.85 | 16.85 | 16.85 | 16.85 |
| Curing Age, hrs | 1-9 | 1-9 | 1-9 | 1-9 |
| Water/Cement | 0.5 | 0.5 | 0.5 | 0.5 |

## Specimen Production

The samples were weighed separately and placed on a non-porous metal sheet. Hand mixing was employed using hand trowel. Water in the ratio of 0.5 (cement: water) in mass was added to the raw sample. The mortar samples were poured into clean 50 mm cylindrical mould (Model No.: H-2820m) rammed, compacted and smoothed in the mould. In order to remove excess trapped air in the sandcrete mortar, the specimens were fully compacted accordingly [8].

## Accelerated Carbonation Curing

Set $A_1$-$A_9$ was placed in the carbonation chamber immediately after demoulding. 99.5 % carbon dioxide gas at 3 atm pressure was injected to the chamber. The carbonation chamber was equipped with thermo-regulator, hydrometer (SE126 digital SOLEX Model No. K68734) and $CO_2$ gas regulator. The temperatures in the chamber were maintained at 30, 35, 40 and 45 $^oC$ varying from 1-9 hours accordingly. Hourly, a sample ($A_1$) was removed from the chamber to determine the degree of carbonation as $CO_2$ ingress into the samples. The samples were crushed, collected for quantitative, XRD, TGA, SEM and porosity analysis.

## Quantitative Analysis

The calcium carbonate ($CaCO_3$) formed as carbonation reaction progresses for 1-9 hours for all carbonated specimens were determined using quantitative analysis. 157 g of pulverised carbonated sandcrete specimen was weighed into a volumetric flask. 20 mls of 0.1 M HCl acid was added and shaken thoroughly for $CO_2$ to effervesce. After effervesce has stopped, distilled water was added to make it up to 1 $dm^3$. 0.5 M NaOH was used to titrate against the standard solution of carbonated sandcrete to neutralize the HCl acid using phenolphthalein indicator.

## Characterization of Carbonated Sandcrete Specimens

The mineralogical compositions, micro-structural changes and oxide compositions of the carbonated samples were analysed using XRD, SEM, EDS and XRF (ASTM D4326) respectively. Pulverized carbonated samples were examined foe carbonatable constituent (Portlandite) using thermogravimetric analysis (TGA). PerKinElmer, TGA4000 was used in examine the samples. The experiment was carried out under a Nitrogen flux of 20 ml/min, starting from ambient thermal condition and increasing by 10 $^oC$/min up to 1000 $^oC$.

## Determination of Porosity

The method adopted by [11] was used for porosity determination. The porosity was calculated using the expression:

$$\varepsilon = (V_{void} / V_{total}) \times 100\%$$

The same procedure was repeated for samples $A_2$-$A_9$ and $B_{11} - B_{19}$, $B_{31} - B_{39}$ and $B_{51} - B_{59}$ respectively.

## RESULTS AND DISCUSSION

### Chemical, Mineralogical and Morphological Characterization of Sandcrete Materials

The EDS analysis shown in Table 2 for cement suggests the presence of major amount of calcium (Ca) and oxygen (O), while the sand and talc showed the existence of silicon and oxygen in high quantities. The presence of high quantity of magnesium shown by EDS analysis distinguished talc from other sandcrete materials. The XRD analysis shown in Figure 1 indicates heterogeneous compositions with peaks of graphite, magnesium silicate, rutile, nacaphite and calcium oxide silicate. Forsterite ($Mg_2SiO_4$) was identified as the primary phase while the pozzolanic nature of talc is attributed to the silica content.

Table 2 EDS analysis of sandcrete composites

| ELEMENT | CEMENT | TALC | SAND |
|---|---|---|---|
| O | 44.41 | 44.59 | 48.2 |
| Al | 1.14 | - | 1.3 |
| Si | 4.72 | 32.87 | 35.2 |
| Ca | 34.16 | 4.85 | - |
| Fe | 1.34 | - | 0.99 |
| Mg | - | 14.62 | - |
| C | 12.76 | 3.07 | 14.02 |
| S | 1.48 | - | - |

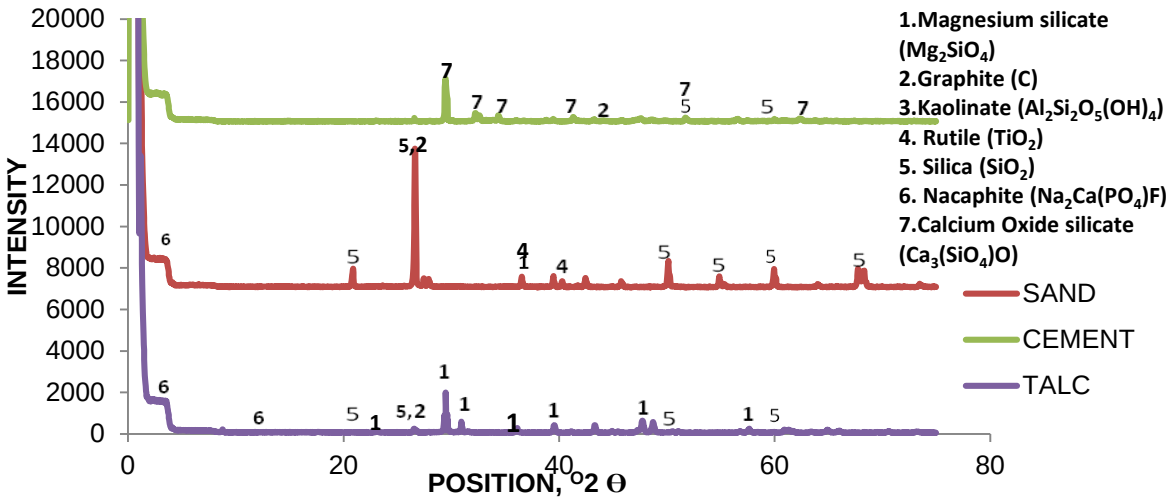


Figure 1 Comparative XRD analysis of all sandcrete constituents' porosity

The porosities of S-S (control) and S-T composites (10, 30 and 50 %) are presented together in Figure 2 at varying thermal conditions and age. The porosity decreases as carbonation advanced with age and temperature for all the samples investigated.

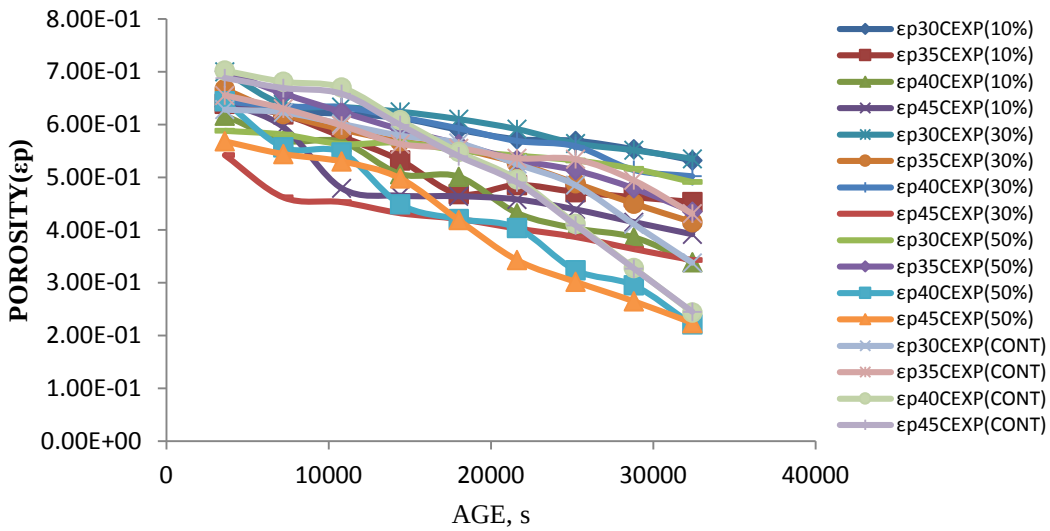


Figure 2 Porosities for 10, 30, 50 % partial replacement of siliceous sharp sand with talc and the control sample (S-S) at varying temperatures (30 – 45 $^{o}$C)

Quantitatively, for 10 % S-T composite, the porosities decreased from initial value of 0.634 – to 0.532, 0.639 – 0.453, 0.617 – 0.339 and 0.643 – 0.392 at 30, 35, 40 and 45 $^{o}$C after 9 hours of carbonation. The same patterns were observed for 30 % S-T (0.70 - 0.535, 0.667 – 0.415, 0.644 – 0.502, and 0.542 – 0.343) and 50 % S-T (0.588 – 0.491, 0.701 – 0.435, 0.644 – 0.221 and 0.568 - 0.224) composites at 30, 35, 40 and 45 $^{o}$C respectively. The control samples porosity decreased from 0.628 – 0.338, 0.655 – 0.431, 0.702 – 0.244 and 0.688 – 0.245 for the same temperature range after 9 hours of carbonation.

Unlike the control, the S-T composites matrix experienced decreased porosities. The densification of S-T composites irrespective of percentage of talc in the mix could be attributed to increased carbonation rate of mineral talc dissolution and hydrated cement products ($Ca(OH)_2$, C-S-H and C-A-H) as depicted in the Equations (1) to (6) [3,5,12,13,14].

$H_2O + CO_2 \longrightarrow H_2CO_3$ (Dissolution of $CO_2$ in pore solution) (1)

$Mg_3Si_4O_{10}(OH)_2 + 5H_2CO_3 + 3CaO.2SiO_2.3H_2O \longrightarrow Mg(HCO_3)_2 + 2Mg(OH)_2 + 3CaCO_3 + 6SiO_2 + 6H_2O$ (Dissolution of talc in acidic solution and subsequent reaction with cement hydrated product) (2)

$Mg(HCO_3)_2 + 2Ca(OH)_2 \longrightarrow 2CaCO_3 + Mg(OH)_2 + 2H_2O$ (Reaction between talc dissolution product with portlandite) (3)

$Mg_3Si_4O_{10}(OH)_2 + CO_2 \longrightarrow 3MgCO_3 + 4SiO_2 + H_2O$ (Direct sequestration ) (4)

$Ca(OH)_2 + H_2CO_3 \longrightarrow CaCO_3 + 2H_2O$ (Reaction between cement hydrated product with hydrated carbon dioxide) (5)

$3CaO.2SiO_2.3H_2O + 3CO_2 \longrightarrow 3CaCO_3 + 2SiO_2 + 3H_2O$ (Sequestration of dissolved carbon dioxide with cement binding gel) (6)

Research has shown that, the characteristic properties of talc and other clay minerals strongly depend on the exposed atoms [14]. Talc releases amorphous $SiO_2$ to the reaction medium on carbonation. The cement minerals hydrates also carbonate increasing the overall composite density with age [15]. The significant decrease in porosity of sample containing talc maybe attributed to either: that the presence of talc enhanced the conversion of hydrated cement minerals to other polymorphic form or increased mass of the carbonates produced according to Equations 1- 6. It is important to note that the researchers are more interested in the calcite formation as the composite materials interact.

**EDS Analysis**

The EDS results for 10, 30 and 50 % S-T composites and the control sample at 30 and 45 $^oC$ are presented in Table 3. It is consistent with earlier observed increased carbonate formation in S-T composites; high carbon (C), calcium (Ca) and oxygen (O) intensities. The high content of the designated elements indicates the presence of dissociating silicate hydrates (C-S-H) during 9 hours carbonation period. There was a complete absence of carbon in the EDS analysis for the control sample (S-S). This could be attributed to slower rate of carbonate formation in the sandcrete matrix; hence an overall high porosity after 9 hours of carbonation when compared to S-T composites. The high oxygen intensity for the control and S-T hydrated sample indicates the presence of portlandite generated as cement hydrates in the samples matrix.

Table 3 EDS Analyses for 10, 30 and 50 % S-T composite and standard sandcrete at varying temperatures

| COMPOSITES | ELEMENT | | | | | | | | |
|---|---|---|---|---|---|---|---|---|---|
| | C | O | Mg | Si | Ca | Al | S | K | Fe |
| S-T (10%) 30$^o$C | 18.78 | 48.78 | 6.81 | 1.98 | 23.65 | - | - | - | - |
| S-T (10%) 45$^o$C | 18.12 | 46.43 | 2.33 | 5.78 | 26.45 | 0.89 | - | - | - |
| S-T (30%) 30$^o$C | 21.92 | 43.19 | 2.59 | 13.25 | 18.29 | - | 0.75 | - | - |
| S-T (30%) 45$^o$C | 21.05 | 47.75 | 4.15 | 12.02 | 15.04 | - | - | - | - |
| S-T (50%) 30$^o$C | 16.37 | 48.50 | 0.49 | 2.20 | 32.43 | - | - | - | - |
| S-T (50%) 45$^o$C | 20.06 | 49.03 | - | 1.21 | 29.70 | - | - | - | - |
| S-S (30$^o$C) | - | 54.64 | - | 13.08 | 26.98 | 2.72 | - | 0.50 | 2.06 |
| S-S (45$^o$C) | - | 55.74 | 0.84 | 3.40 | 39.06 | 0.96 | - | - | - |

**XRD Results**

Figures 3-5 show the XRD patterns of 10, 30, 50 % S-T composites and the control sample at various temperatures. Comparison of the XRD patterns of S-S, 10, 30 and 50 % S-T composites showed that the portlandite, calcite, calcium silicate and dolomite concentrations decreased with increasing talc concentration with the formation of new polymeric form of calcium silicates. This is also evident from the peaks sizes and diversion as indicated in Figures 3 to 5. In addition, a noticeable increase in calcite peak numbers as portlandite intensity reduces irrespective of temperature variations in both S-T and S-S composites.

The presence of residual portlandite in both carbonated samples (S-T and S-S) might be due to isolation of the portlandite crystals by the carbonate formation in the composite matrix, a phenomenon observed by other researchers [1, 16].

A noticeable increase in calcite peaks for 50 % S-T composite was observed when compared to 10 and 30 % S-T composites. However, reduced calcite and portlandite peak intensities were observed for S-S. This might be attributed to the absent of pozzolans and poor decalcification of C-S-H gel.

Comparing S-T composites at varying temperatures, the results suggest increase in carbonate peak intensities as temperature increases from 30 to 45 $^{o}$C as depicted in Figures 3 to 5. The increase might be due to increase ionic activities as mineral talc and cement hydrate. The changes in peak intensity are indicative of reaction of the magnesium from the talc. However, the unconverted portlandite in S-S appears as hexagonal crystals as depicted by the scanning electron microscopy analysis shown in Figure 12.

Figures 6 – 11 showed the micrographs of 10, 30 and 50 % S-T composites at 30 and 45 $^{o}$C after 9 hours of carbonation. The micrographs showed increased densification of morphology as more carbonates, calcium silicates hydrates, calcites and others are precipitated in the matrix. Comparative analyses of the S-S and samples containing talc clearly showed the influence on changing the morphology of the matrix from distinct crystalline grains to cloudy foil-like appearance. The hydrates are more closely inter-grown with lesser pore space within the solid phases in presence of talc. This confirms the observed significant change in the hydration chemistry in presence of talc in the carbonation process of cement mineral.

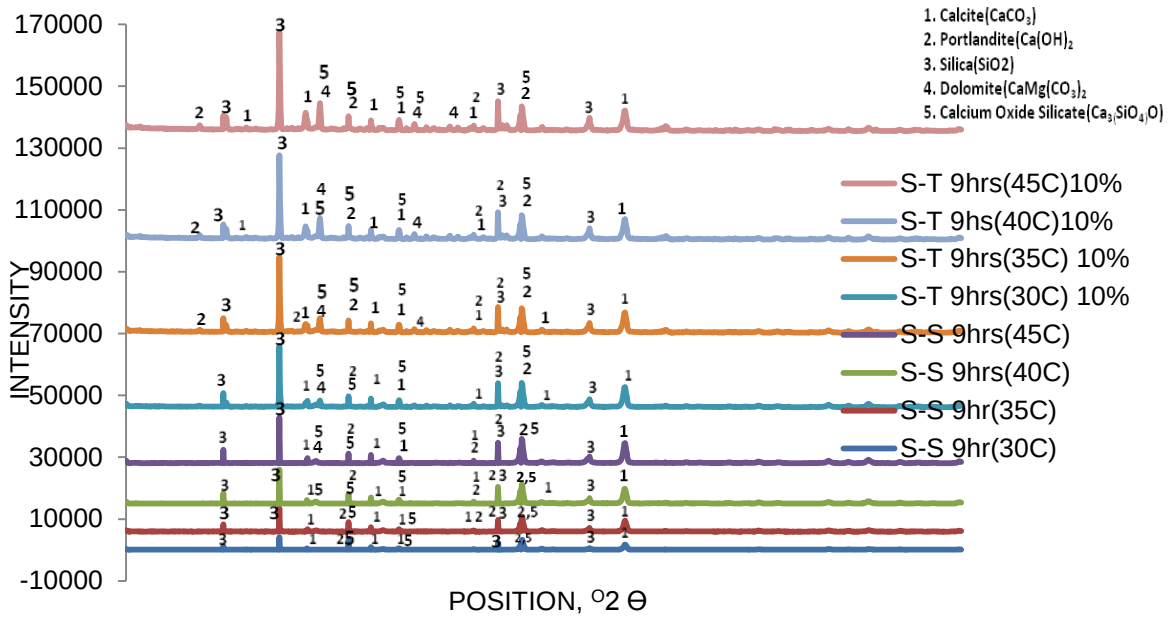


Figure 3 Comparative XRD analysis for 10 % S-T and S-S matrix composite at varying temperature (30 – 45 $^{o}$C)

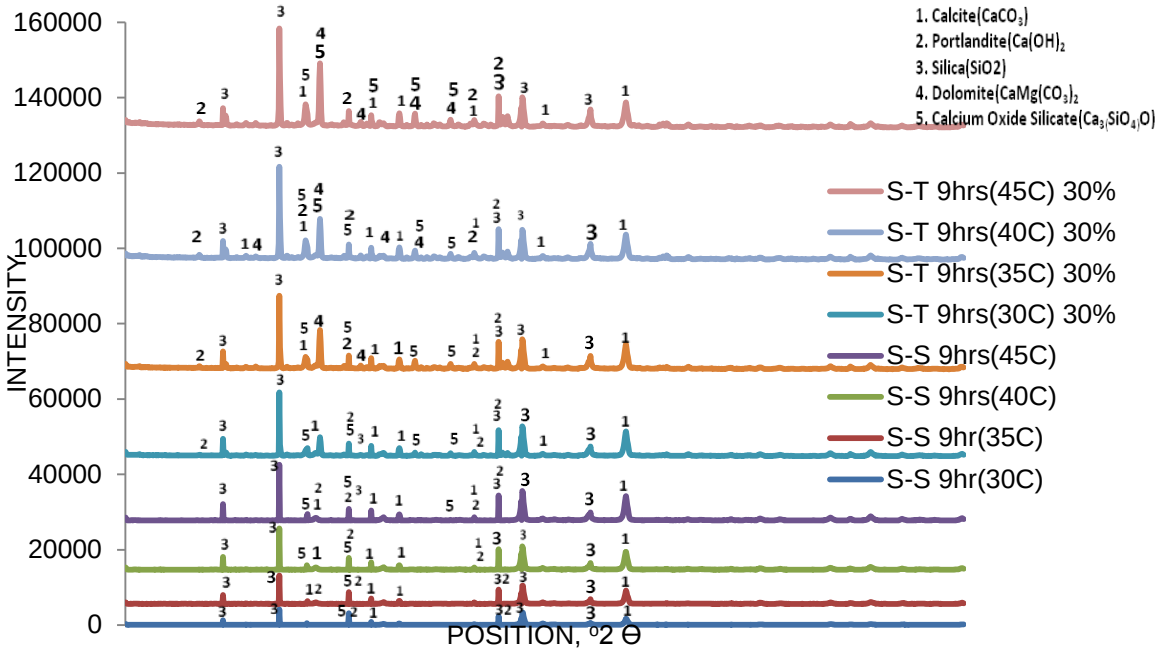


Figure 4 Comparative XRD analysis for 30 % S-T and S-S matrix composite at varying temperature (30 °C– 45 °C)

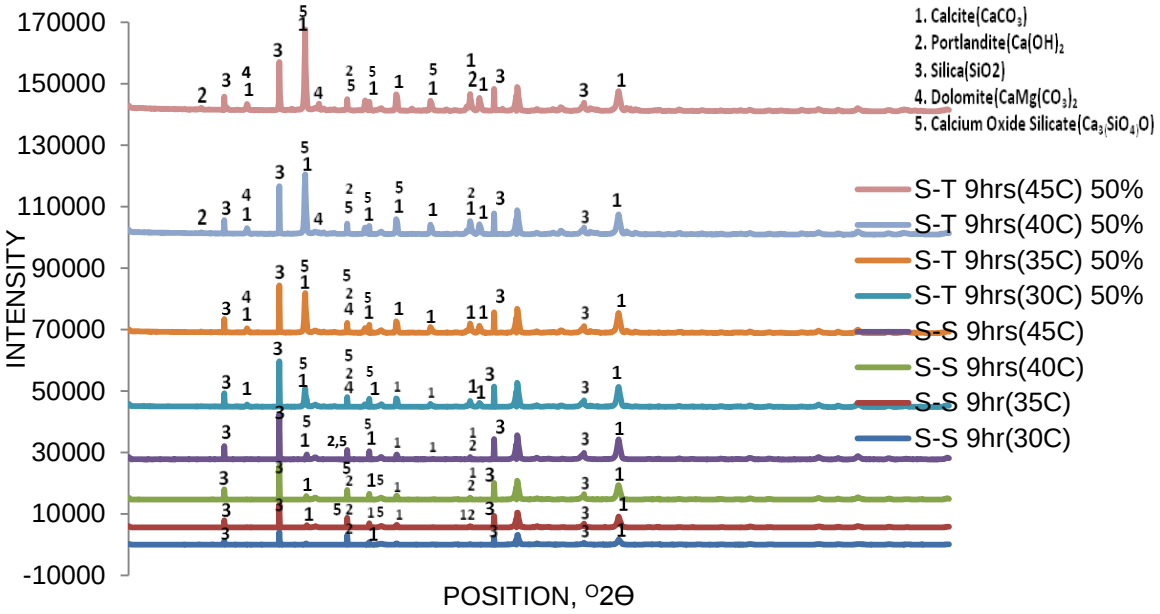


Figure 5 Comparative XRD analysis for 50 % S-T and S-S matrix composite at varying temperature (30 – 45 °C)

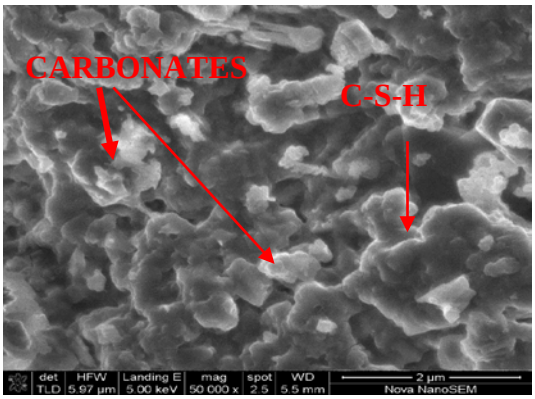


Figure 6: SEM Photomicrograph for 10 % S-T at 30 $^{o}$C after 9 hours carbonation

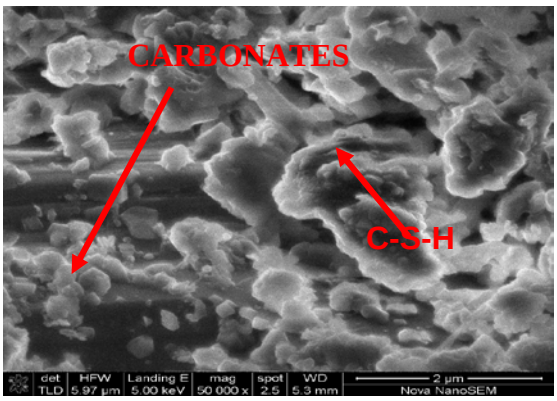


Figure 7: SEM Photomicrograph for 10 % S-T at 45 $^{o}$C after 9 hours carbonation

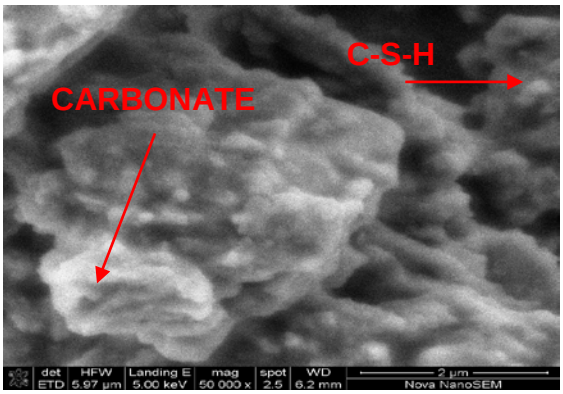


Figure 8: SEM Photomicrograph for 30 % S-T at 30 $^{o}$C after 9 hours carbonation

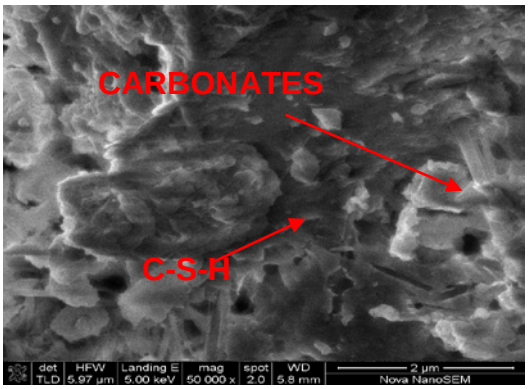


Figure 9: SEM Photomicrograph for 30 % S-T at 45 $^{o}$C after 9 hours carbonation

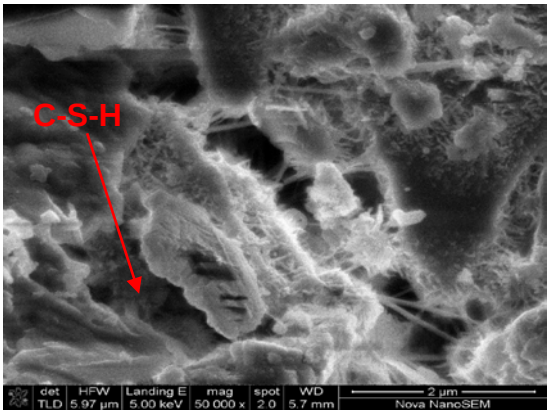


Figure 10: SEM Photomicrograph for 50 % S-T at 30 $^{o}$C after 9 hours carbonation

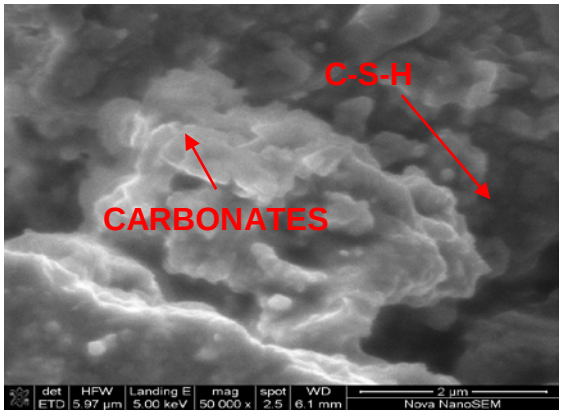


Figure 11: SEM Photomicrograph for 50% S-T at 45 $^{o}$C after 9 hours carbonation

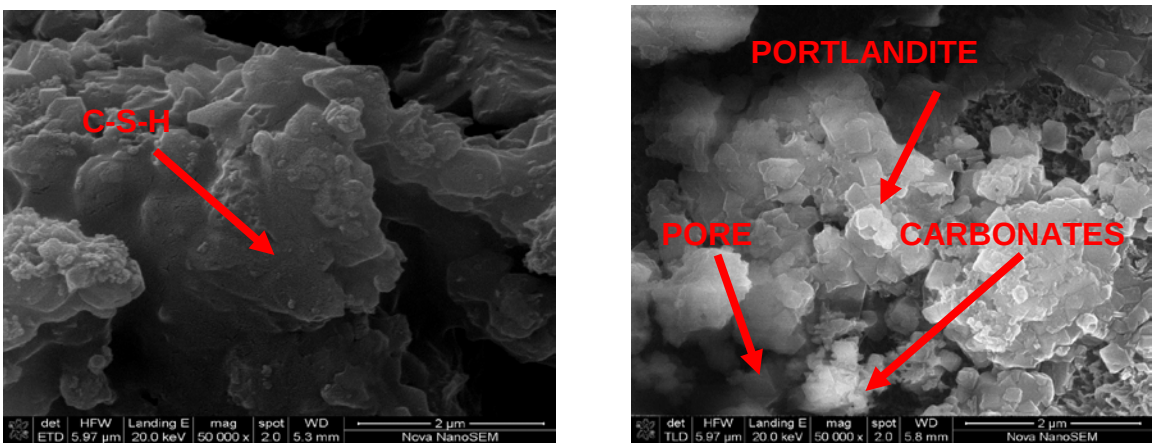


(a) (b)

Figure 12 (a and b): SEM micrograph for control sample at 30 and 45 $^{o}$C after 9 hours carbonation

## TGA

Figure 13 shows an enlarge thermogravimetric curves for carbonated S-T (10, 30 and 50 %) and S-S composites after 9 hours of carbonation. A general mass loss between 100 and 150 $^{o}$C is apparent for all carbonated samples indicating C-S-H dehydration. However, the reference sample (S-S) showed a steeper curve indicates high loss of moisture due to high porosity and poor carbonation. A low rate of mass loss attributable to portlandite decomposition at 460 to 600 $^{o}$C was observed for all the carbonated samples. The loss of mass after 620$^{o}$C is attributed to decarbonation, hence the loss of bonded carbon dioxide [1].

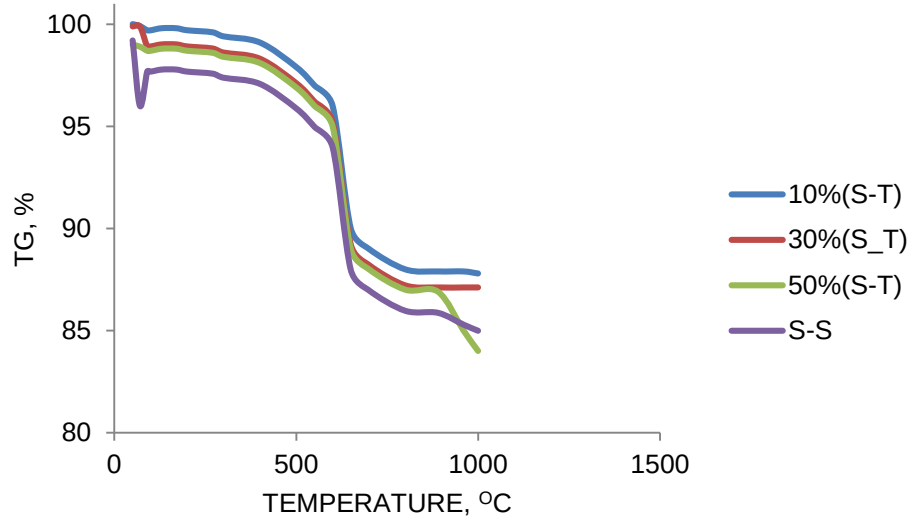


Figure 13 Typical TGA curves for carbonated S-T ($B_{19}$, $B_{39}$ and $B_{59}$) and S-S composites

## CONCLUSIONS

The presences of talc during carbonation process of cement-based material significantly influence the hydration mechanism of the minerals and their hydrates. Early age carbonation of sandcrete led to visible change in the hydrated minerals micro-structures and reduced porosity of the matrix. The EDS, XRD and SEM results are consistent and confirm the

influence on cement minerals hydrates of talc. The disappearance of portlandite and calcium silicate to more stable calcite peak in TGA, EDS and XRD are indication of morphological changes induced by talc to the cement mineral hydrates microstructure. The morphology of the hydrated S-T composites produced is dependent on the talc percentage used and temperature.

## ACKNOWLEDGEMENTS

Authors wish to acknowledge the Tertiary Education Trust Fund TETFund for providing the grant TETFUND/FUTMINNA/2014/18 and TETFUND/FUTMINNA/2014/21 for this research.

## REFERENCES

1. ROSTAMI, V., SHAO, Y., BOYD, A. J., HE, Z. Micro-structure of paste subject to early carbonation curing. Cement and concrete research, Vol. 42, 2012, pp 186 – 193.

2. ANOSIKE M. N., OYEBADE A. A. Concrete blocks and quality management in Nigeria building industry. J. Eng. Proj. Prod. Manag. Vol. 2, 2012, pp 37–46.

3. ODIGURE J. O. Deterioration of long-serving Cement-based Structures in Nigeria. Cem. and Concr. Res., Vol. 32, 2002, pp 1451 – 1455.

4. NAIK, T. R., KUMAR, R. Global warming and cement-based materials. UWM centre for by-products utilization, Milwaukee, Wisconsin, USA, 2010, pp 1 – 70.

5. SHAH, T. C. $CO_2$ Sequestration in concrete. Master of Science in Engineering Thesis, 2005, University of Wisconsin-Milwaukee, USA.

6. FERNANDEZ B. M., SIMONS S., HILLS C., CAREY P. A review of accelerated carbonation technology in the treatment of cement-based materials and sequestration of $CO_2$. Journal of Hazardous Materials, Vol. 112, No. 3, 2004, pp 193–205.

7. SUNHO, C., JEFFREY, H. D., CHRISTOPHER, W. J. Adsorbent Materials for Carbon Dioxide Capture from large anthropogenic point sources. ChemSusChem, Vol. 2, 2009, pp 796 – 854.

8. THE NIGERIA INDUSTRIAL STANDARD (NIS) Draft Code of Practice for Sandcrete Blocks, 2007, Federal Ministries of Industries, Lagos, Nigeria.

9. OMOREGIE A. Impact of Vibration Time on Compressive Strength of Hardened Sandcrete Building Blocks. Buildings, Vol. 2, 2012, pp 153-172.

10. OYEKAN G. L., KANIYO O. M. A study on the Engineering Properties of Sandcrete blocks produced with rice husk ash blended Cement. Journal of Engineering and Technology, Vol. 3, No. 3, 2011, pp 88 – 98.

11. TURCRY, PH., OKSRI-NELFIA, L., YOUNSI, A., AÏT-MOKHTAR, A. Analysis of an Accelerated Carbonation Test with Severe Preconditioning. Cement and Concrete Research, Vol. 57, 2014, pp 70 – 78.

12. VASBURD, A. M., SABNIS, G. M., EMMONS, P. H. Concrete carbonation-A fresh look. Indian Concrete Journal, Vol. 67, No. 5, 1997, pp 215-220.

13. NAIK, T. R., CHUN, Y-M., KRAUS, R. N. Carbon dioxide sequestration in Concrete in different curing environments. Proceedings of the International Conference on Sustainable Construction Materials and Technologies, 2007, Coventry U.K.

14. LIMA-DE-FARIA, J. Talc, in Structural Mineralogy-an Introduction. Kluwer: The Netherlands, 1994, pp 227 – 228.

15. YOUNSI, A., TURCRY, PH., AÏT-MOKHTAR, A., STAQUET, S. Accelerated Carbonation of Concrete with High Content of Mineral Additions: Effect of Interactions between Hydration and Drying. Cement and Concrete Research, Vol. 43, 2013, pp 25–33.

16. VILLAIN, G., PLATRET, G. Two experimental methods to determine carbonation profile in concrete. ACI Material Journal, Vol. 103, 2006, pp 265 – 271.

# FEASIBLE USE OF BIOMASS BOTTOM ASH IN THE MANUFACTURE OF CEMENT-BASED MATERIALS

**F Agrela Sainz** **J Rosales Garcia** **M Cabrera Montenegro**

**A M Velasco Moreno** **J Ayuso**

University of Cordoba

**C Dorado**

I.E.S. Nuestra Señora de la Cabeza

Spain

**ABSTRACT.** Different types of recycled materials have been extensively studied for the manufacture of Cement-based materials, such as recycled aggregates, used tyres, etc. However, new waste from the combustion of biomass as bottom ash has been less used in the manufacture of Cement-based materials. The subject of this research is to evaluate the use of BBA in the manufacture of Cement-based materials with different cement contents. The materials were subjected to standard laboratory tests and the effect of compaction was proved in different tested samples. For that, their physical properties were determined according to standard laboratory procedures and their mechanical behaviour was analysed according to the following parameters: compressive strength, splitting tests and dimensional changes. From the obtained results, it can be stated that the use of BBA in Cement-based materials is feasible with a replacement rate of 10% in most cases. Thus, recycled Cement-based materials can be applied in sub-base of roads manufactured with 3-6.5% of cement and as pavement when the percentage of cement used increases to 10%.

**Keywords:** Bottom ash, Biomass, Cement-based materials, Civil infrastructures, Mechanical properties, Durability properties.

**Prof Francisco Agrela Sainz** is a Professor of Construction Engineering at the University of Cordoba, Spain.

**Julia Rosales Garcia** is an Architect, Civil Engineer and PhD student at the University of Cordoba.

**Manuel Cabrera Montenegro** is an Civil Engineer and PhD student at the University of Cordoba.

**Antonio Manuel Velasco Moreno** is a Technician in the development of urban projects and surveying operations. Collaborator student in the Department of Rural Engineering of the University of Cordoba.

## INTRODUCTION

Renewable energy is an emerging sector because in recent years there has been an increase in environmental consciousness which leads to replace conventional energy sources with renewable sources. To date, the main natural sources used for power generation are the sun and wind. However, other types of energy are applied in order to reuse the waste generated by other industries. In recent years, the use of biomass to generate heat and electrical energy has increased substantially in the European Community. According to the EU's energy predictions, the contribution of this energy is expected to grow to 236–255 Mtep by 2030, an increase of up to 210% in its current market share [1]. In Spain, biomass represents 5.21% of the total energy consumed [2].

In Andalusia (Spain), there is an important industry focused on the agrifood sector. Specifically, industrial production derived from olive oil generates residues as olive pruning and other elements, which are used in power generation from combustion [3]. This waste is known as biomass.

Ash produced by the process of biomass combustion can be divided into bottom (BBA) and fly ash (BFA). Biomass Bottom Ash is produced on the grate in the first combustion chamber of the boiler. This portion of the ash is often mixed with impurities from the biomass, such as sand, stone, and dirt [4].

Fly ash is produced by dragging ash from the base of the furnace. It gathers primarily in multi-cyclones placed behind the combustion unit and in electrostatic, ceramic, or bag filters, which are usually placed behind the cyclones [5].

Biomass ashes properties would depend on the characteristics of the plants, type of pruning waste, temperature and time process; and the procedure for its final disposal [6].

In most countries the biomass ashes are transported to landfills. Based on both the physical and the chemical properties of biomass ash, bottom ash could be used. These ashes have been extensively studied for their use as fertilizer and for agriculture and forestry [7, 8].

Recently, industrial by-products have been extensively studied for its use in cement-based materials [9, 10]. However, very little of this research treats the effect of the bottom ash from biomass on these materials. Some studies have shown the possibility of using BBA in cement production [11], as a substitute for aggregates in concrete mixtures [12] and its application in based-cement materials [13]. Previous researchers have demonstrated the satisfactory application of biomass wastes in road pavements and building blocks because of its pozzolanic and mechanical properties [14, 5].

Since using these by-products reduces cost and minimizes the environmental impact, the aim of this work is to evaluate the feasible use of BBA as a partial replacement of natural aggregates (NA) in cement-based materials with 3% and 6.5% percentage of cement for its use in sub-base of roads and with 10% percentage of cement for its use in pavements. To achieve this objective, the physical properties of BBA from the combustion of olive tree pruning and NA were studied; then applied in the manufacture of recycled cement-based materials. Mechanical (compressive strength and splitting test) and durability properties (shrinkage) of recycled cement-based materials manufactured with different replacement percentages of cement, natural aggregates and BBA were studied.

This paper presents a comparative of mechanical and durability properties between mixtures manufactured with BBA, NA and different percentages of cement for possible use in road base and subbase.

## MATERIALS

### Cement

Ordinary Portland Cement type CEM-I 52.5 with rapid hardening and a characteristic strength of 52.5 MPa were used in this work, according to ASTM C150. This cement is pure clinker grey cement without additions which is resistant to chemical attack by sulphates. Its properties are summarized in Table 1.

Table 1 Properties of cement

| BULK OXIDE COMPSITION, % | | | | | | | | Granul. 45 µm | Granul. 32 µm | Blaine E. S. | Loss of ignition |
|---|---|---|---|---|---|---|---|---|---|---|---|
| $SiO_2$ | $Al_2O_3$ | $Fe_2O_3$ | CaO | MgO | $SO_3$ | $K_2O$ | $Na_2O$ | % | % | $cm^2/g$ | % |
| 20.18 | 4.14 | 4.51 | 63.75 | 0.91 | 3.24 | 0.75 | 0.31 | 6.2 | 16.1 | 3701 | 1.44 |

### Natural Aggregate and Biomass Bottom Ash

The natural aggregate used for the manufacture of mixtures came from a quarry located in the north of the province of Córdoba (Spain). It was composed mainly of silica and limestone. Three types of natural aggregates were used in the manufacture of cement-based materials: natural coarse gravel (CG), natural medium gravel (MG) and natural sand (NS).

Biomass Bottom Ash (BBA) from the thermal plant located in Puente Genil, Córdoba (Spain) was used. Power generation with biomass-based products produces solid residue ash, a result of thermochemical degradation. These thermochemical processes include combustion, pyrolysis, and incineration of woody biomass. The BBA may vary in properties due to the different types of biomass available, operating conditions and the type of system used.

Physical properties as water absorption and saturated surface dry density: SDD-Density (according to standard UNE-EN 1097-6, 2001), the particle size distribution (UNE-EN 933-3, 1997), Los Angeles (L.A.) coefficient (UNE-EN 1097-2, 2010) and friability coefficients (UNE 83-115, 1989), were measured. In addition, chemical properties the BBA as elemental content, organic matter and sulphate soluble are included in the present study. Table 2 summarizes the physical and chemical characterization of both materials.

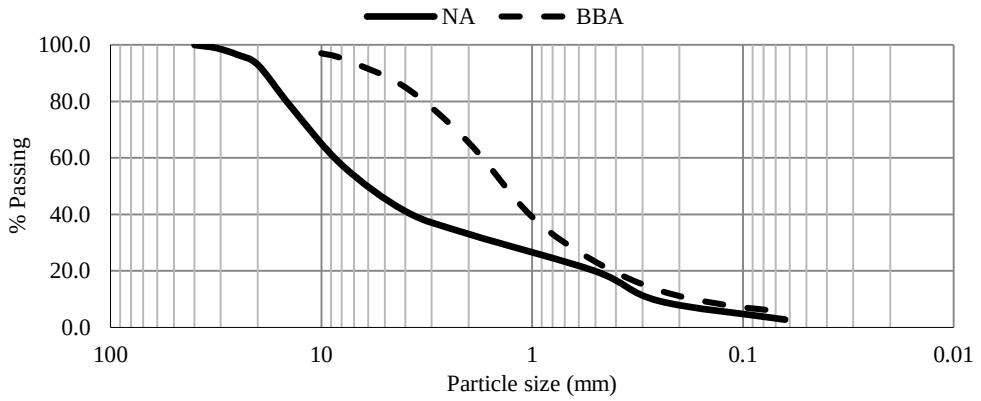


Figure 1 Particle size distribution

The grain size distribution of used materials is presented in Figure 1. The granulometric analysis showed that grain size distribution of NA presented a higher fines content (<0.063 mm) and the particle size distribution of BBA varies from fine gravel to sand.

Table 2 physical and chemical properties of materials used

| PROPERTIES | | NA | BBA | TEST METHOD |
|---|---|---|---|---|
| Density-SSD, kg/m³ | | | | UNE - EN 1097 - 01 |
| | 0-4 mm | 2.57 | 1.86 | |
| | 4-31.5 mm | 2.61 | - | |
| Water absorption, % | | | | |
| | 0-4 mm | 2.5 | 24 | |
| | 4-31.5 mm | 0.93 | - | |
| Los Angeles, % | | 26 | - | |
| Friability ratio, % | | - | 31.8 | UNE 83-115 |
| Plasticity | | Non plastic | Non plastic | UNE 103103 & UNE 103104 |
| Organic matter, % | | < 0.1 | 4.12 | UNE 103204 |
| Water-soluble sulphate, $\%SO_3$ | | <0.01 | 0.36 | UNE - EN 1744-1 |
| Acid-soluble sulfate, $\%SO_3$ | | <0.01 | 0.42 | UNE - EN 1744-1 |
| Elemental content, % | Si | | 22.18 | UNE 80-215 |
| | Ca | | 16.85 | |
| | K | | 14.2 | |
| | Mg | | 2.58 | |
| | Fe | | 1.73 | |
| | Al | | 0.75 | |
| | Na | | 0.29 | |
| | Ti | | 0.15 | |

As it is showed in Table 2, BBA presented a low density compared to NA (1.86 kg/dm³). In relation to water absorption capacity, BBA obtained a high value (24%). Regarding chemical properties, it is highlighted the high organic content (4.12%) and silica and calcium content.

### Water-Reducing Admixture

A super-plasticiser additive (SP), type BASF Rheobuild 1222, was used. The objective was to reduce the mixing water and allow the concrete to be manufactured with a low effective water/cement ratio (w/c) because of its high water reduction.

### Mixtures Materials and Dosage

For the study of Cement-based materials with BBA, six batches were made by applying different percentage of cement and added BBA (Table 3). Batches, called "CONV." were made with natural aggregates in order to be the reference Cement-based material. 3 batches of conventional types were performed, depending on the percentage of cement used (3, 6.5 and 10%). To assess the conventional Cement-based material made with a BBA, 3 batches were produced substituting 10% of natural aggregate mass in each by BBA. Due to the low density of BBA and since the substitution is made in weight, mixed with 10%, BBA have a substitution of about 25% by volume relative to the total amount of aggregate.

The substitution of NA by BBA was according to particle size distribution of both materials. BBA was replaced with the medium and fine fraction of the NA.

Table 3 Cement-based mix proportions (kg/m³)

| MIX | AG | | | BBA | CEM | WATER | ADDITIVE |
|---|---|---|---|---|---|---|---|
| | CG | MG | NS | | | | |
| CONV 10%CEM | 417 | 618 | 1019 | - | 250 | 150 | 2.7 |
| 10BBA 10%CEM | 417 | 550 | 882 | 205 | 250 | 150 | 3.2 |
| CONV 6.5%CEM | 459 | 681 | 1123 | - | 162.5 | 97.5 | 2.9 |
| 10BBA 6.5%CEM | 459 | 606 | 972 | 226 | 162.5 | 97.5 | 3.3 |
| CONV 3%CEM | 502 | 745 | 1227 | - | 75 | 45 | 3.1 |
| 10BBA 3%CEM | 502 | 662 | 1062 | 247 | 75 | 45 | 3.6 |

The effective w/c ratio was 0.6 for all cases. The amount of additive was modified to maintain the same w/c ratio in all batches and to obtain the same slump (8–9 cm) for all manufactured cement-based materials. Materials were pre-saturated, as required by the regulations. This pre-saturation water compensates for increased water absorption possessing BBA respect to NA. The Bolomey method was used to calculate the mixture proportions shown in Table 3.

### Manufacturing Concrete

The methodology used for the manufacture of the mixtures was the same for all Cement-based materials. First, the coarse and medium aggregate was introduced to the mixer, followed by the fine aggregate and 50% of the total water. The mixture was homogenised for 5 min of mixing. Later, the cement and the additive dissolved in the remaining water were added and mixed for 5 min. Finally, the specimens were manufactured, and after 24 h, the specimens were removed from their moulds. Then, the specimens were cured in the curing room at an ambient temperature of 20°C and 100% relative humidity.

## EXPERIMENTAL TEST RESULTS

After exposure to the physical characterization, the mix proportions dosage and method of manufacture, the results for all mechanical and durability properties of cement-based materials are shown here.

The experimental tests of hardened cement-based materials are presented as follows.

### Workability

The consistency of fresh concrete was measured by the slump in the Abrams cone (EN 12350-2), providing the values displayed in Table 4.

Due to the incorporation of BBA as a substitute of medium and fine fraction of natural aggregates, it was necessary to apply different amounts of super-plasticiser in order to obtain similar workability in all the lightweight concrete manufactured (Table 3). All concretes showed similar consistency due to the execution of previous studies of consistency.

### Compressive Strength

The compressive strength was applied using a hydraulic press with a maximum capacity of 2000 kN, which was applied at a constant speed load. The compressive strength was applied using the standard EN 12390-3 on cubic specimens with 100 mm sides, for 7 and 28 days. Table 4 shows the results for the compressive strength of the Cement-based materials manufactured.

Table 4 Physical and mechanical properties of cement-based materials

| PROPERTY | AGE days | CONV 10%CEM | 10BBA 10%CEM | CONV 6.5%CEM | 10BBA 6.5%CEM | CONV 3%CEM | 10BBA 3%CEM |
|---|---|---|---|---|---|---|---|
| Workability, mm | 28 | 8.5 | 9 | 9 | 8 | 8 | 8.5 |
| Compressive strength, MPa | 7 | 17.63 | 14.44 | 13.45 | 14.54 | 7.42 | 6.45 |
| | 28 | 21.74 | 20.36 | 17.81 | 16.29 | 9.09 | 8.03 |
| Splitting test, MPa | 28 | 3.98 | 3.72 | 2.85 | 2.81 | 1.87 | 1.56 |

An increase is observed according to the curing age as expected by Katz [15]. Similarly, approximately 75% of the compressive strength at 28 days was obtained at only 7 days for the entire series, as obtained by Kou et al. [16]. Replacing BBA by NA presented low compressive strength loss. In batch with 10% cement the strength loss was about 5%, 6.5% 10BBA CEM showed a resistance decrease of about 8% compared to control and finally, batch with 3.5% for CEM replacing BBA by NA showed a loss compressive strength of about 12%. This low compressive strength loss by replacing NA by BBA is due to high content of Si and Ca presented by BBA [17]. This composition provides hardening capacity for the mix.

## Splitting Test

This test (UNE EN 12390-6), often referred to as the split-cylinder test, indirectly measures the tensile strength by compressing a cylinder through a line load applied along its length. This test can be completed in a standard concrete compression testing machine, with only one special requirement: the hinged bearing that loads the specimen. It is observed that splitting test results show approximate values between 15 - 20% compared to the compressive strength values for all series.

## Drying Shrinkage Test

To study the durability of the cement-based materials, drying shrinkage measurements were obtained on the concrete prisms measuring 100 mm × 100 mm × 500 mm, according to ASTM C157. The specimens were exposed to conditions of 50% relative humidity and 20°C, and the measurements were taken for 1, 4, 7, 14, 28 and 56 days.

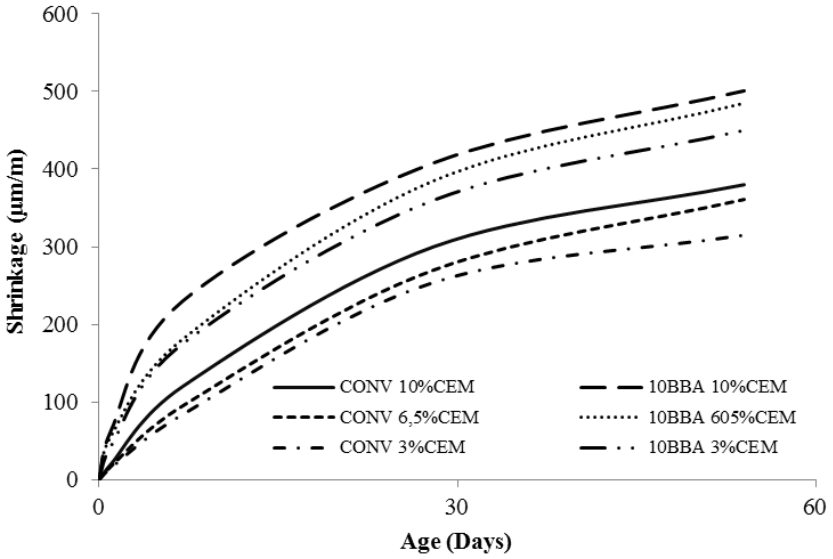


Figure 2 Evolution of shrinkage

Shrinkage to different age was reflected in Figure 2, where higher values for cement-based materials shrinkage are observed with BBA. It is observed that 7 days old concrete with BBA obtained significant differences from the Control and at 28 days these differences were more relevant. However, 56 days old stabilization is observed in increased shrinkage, increasing from that date less than in previous ages.

## CONCLUSIONS

This study present a technical assessment of biomass bottom ash (BBA) as material for construction in road bases and sub-bases, proving that it is possible to apply these materials in cement-based materials.

The following particular conclusions can be identifying:

- The low density of BBA caused a 25% increasing of percentage of replacement of aggregates in volume.

- Replacing NA by BBA in all batches with different percentages of cement resulted in a low decrease of compressive strength. This is due to high content of Si-Ca having the BBA that provides hardening properties to the mixture.

- Splitting test results are directly correlated to the compressive strength, ranging between 25 and 30% compared to the values of compressive strength at 28 days.

- The batch manufactured with 12% cement and 10% of BBA complies with Spanish regulations for its use as structural concrete. Batches with less amount of cement may be used as infill concrete, vibrated concrete, etc.

The present study has demonstrated the mechanical ability of BBA used as material construction in civil infrastructures. The valorisation of this industrial by-product instead of exploiting the natural resources can eliminate the negative impact associated with the indiscriminate disposal of this by-product in landfill.

## REFERENCES

1. CAPROS, P., MANTZOS, L., TASIOS, N., DE VITA, A., & KOUVARITAKIS, N. «EU Energy Trends to 2030: Update 2009.» Publications Office of the European Union, 2010.

2. ASSOCIATION, EUROPEAN BIOMASS. «Annual Statistical Report .» 2011.

3. ROSÚA, J. M., & PASADAS, M. «Biomass potential in Andalusia, from grapevines, olives, fruit trees and poplar, for providing heating in homes.» Renewable and Sustainable Energy Reviews, 2012: 16, 4190-4195.

4. BIEDERMANN, F., & OBERNBERGER, I. «Ash-related problems during biomass combustion and possibilities for a sustainable ash utilization.» Austrian Bioenergy Centre GmbH & BIOS Bioenergiesysteme. Graz, Austria, 2005

5. CARRASCO, B., CRUZ, N., TERRADOS, J., CORPAS, F. A., & PÉREZ, L. « An evaluation of bottom ash from plant biomass as a replacement for cement in building blocks.» Fuel, 2014: 118, 272-280.

6. S.V. VASSILEV, D. BAXTER, L.K. ANDERSEN, C.G. VASSILEVA. « An overview of the composition and application of biomass ash. Part 1. Phase–mineral and chemical composition and classification.» Fuel, 2013: 105, 40-76.

7. PELS, J. R., DE NIE, D. S., & KIEL, J. H. «Utilization of ashes from biomass combustion and gasification.» 14th European Biomass Conference & Exhibition. París, France, 2005. 17-21

8. AHMARUZZAMAN, M. «A review on the utilization of fly ash.» Progress in Energy and Combustion Science, 2010: 36, 327-363.

9. RAJAMMA, R., BALL, R. J., TARELHO, L. A., ALLEN, G. C., LABRINCHA, J. A., & FERREIRA, V. M. «Characterisation and use of biomass fly ash in cement-based materials.» Journal of hazardous materials, 2009: 172, 1049-1060

10. MASCHIO S, TONELLO G, PIANI L, FURLANI E. «Fly and bottom ashes from biomass combustion as cement replacing components in mortars production: Rheological behaviour of the pastes and materials compression strength. .» Chemosphere, 2011: 85, 666-671.

11. AJIWE, V. I. E., OKEKE, C. A., & AKIGWE, F. C. « A preliminary study of manufacture of cement from rice husk ash.» Bioresource Technology, 2000: 73, 37-39

12. MARTIN MORALES, M., CUENCA, J., LOPEZ, P., RODRIGUEZ, J., ZAMORANO, M., & VALVERDE, P. I. «Self-compacting concrete with biomass fly ash: preliminary results.» 13 International Waste Management and Landfill Symposium. Cagliari, 2011.

13. CABRERA, M., AGRELA, F., AYUSO, J., GALVIN, A. P., & ROSALES, J. «Materials and Structures,.» Feasible use of biomass bottom ash in the manufacture of cement treated recycled materials, 2015: 1-12.

14. TORALDO, E., SAPONARO, S., CAREGHINI, A., & MARIANI, E. «Use of stabilized bottom ash for bound layers of road pavements.» Journal of environmental managemen, 2013: 121, 117-123

15. KATZ, A. (2003). « Properties of concrete made with recycled aggregate from partially hydrated old concrete.» Cement and concrete research, 2003: 33, 703-711.

16. KOU, S. C., POON, C. S., & WAN, H. W. « Properties of concrete prepared with low-grade recycled aggregates. .» Construction and Building Materials, 2012: 36, 881-889.

17. CABRERA, M., GALVIN, A. P., AGRELA, F., CARVAJAL, M. D., & AYUSO, J. «Characterisation and technical feasibility of using biomass bottom ash for civil infrastructures.» Construction and Building Materials, 2014: 58, 234-244.

# VAPOUR SORPTION PROPERTIES OF BUILDING MATERIALS USING GRAVIMETRIC SORPTION INSTRUMENTATION

**D Cattaneo**

**D Burnett A R Garcia**

**M Naderi M Acharya**

Surface Measurement Systems Ltd

United Kingdom

**ABSTRACT.** Dynamic Vapour Sorption (DVS) has long been used for investigating the interaction of water and organic vapours with solid materials. The versatility and impact of DVS has particular importance in the study of building materials. This paper describes the use of DVS for cement.

**Keywords :** Dynamic Vapour Sorption, Cement, Moisture, Kinetics

**Dr Damiano Cattaneo** obtained his PhD in chemistry (material science) at the University of St Andrews (UK) in December 2015. Damiano has a Master's degree in Medicinal Chemistry (Pharmaceutical Chemistry and Technologies) from Università degli Studi di Milano (IT). During the last year he joined the scientists team of Surface Measurement Systems Ltd., U.K., as an instrument scientist working on the application of dynamic vapor sorption (DVS) and inverse gas chromatography surface energy analyzer (IGC SEA).

**Ms Manaswini Archarya** holds a dual Masters degree, MS and M.Tech, from Indian Institute of Technology, Delhi, India in Advanced Chemistry. She has been working at Surface Measurement Systems Ltd., U.K., since 2002 and has in-depth expertise across a spectrum of products like DVS and IGC-SEA .

**Dr Dan Burnett** is the Director of Science Strategy for Surface Measurement Systems, Ltd. located at the North American headquarters in Allentown, PA. His team works on research studies and science applications for many prominent companies.

**Dr Majid Naderi** received his Ph.D. degree in Physical Chemistry from the University of Manchester Institute of Science and Technology (U.M.I.S.T.), Manchester, U.K., in 1998, and since 2002 has been working as a Principal Scientist and Laboratory Manager at Surface Measurement Systems Ltd., U.K.

**Armando R. Garcia** graduated from Union College New Jersey in 1980 with an Associate in Applied Science degree in Chemical Technology. Upon graduation Armando worked for Exxon Research and Engineering Co. in New Jersey as an NMR Spectroscopist. He received a B.S. in Computer Science from Moravian College, Bethlehem PA in 1999 and worked for Air Products and Chemicals from 1998 to 2003.

## INTRODUCTION

The interactions of water vapour (moisture) with solid materials have impact over a wide range of industries and materials including pharmaceuticals [1] foods [2, 3], fuel cell membranes [4], and polymers [5]. In particular to building materials [6], moisture sorption has significant implications for cements [7], woods [8], insulation materials [9], and fibres [10]. Moisture damage is a significant factor limiting a building's lifespan [11]. As well, moisture infusion through a building's outer structure can have a significant effect on indoor air quality and air-conditioning loads [11]. The use of automated gravimetric vapour sorption instruments has become standard practice in many industries for investigating the vapour sorption properties of solid materials. This overview paper outlines how Dynamic Vapour Sorption (DVS) instruments can be used to investigate several different types of materials used in the building industry. This study examines use of DVS in cement.

## METHOD

A schematic of the DVS-Advantage instrument is shown in Figure 1. The instrument measures the uptake and loss of vapour gravimetrically using the SMS UltraBalance. The SMS UltraBalance comes in two configurations: (1) one gram capacity with a mass resolution of at least 0.1 μg and (2) four gram capacity with a mass resolution of at least 1.0 μg. The vapour partial pressure around the sample is generated by mixing saturated and dry carrier gas streams using electronic mass flow controllers. The DVS- Advantage instrument has the unique capability to actively measure and control the concentration of water and a wide range of organic vapours.

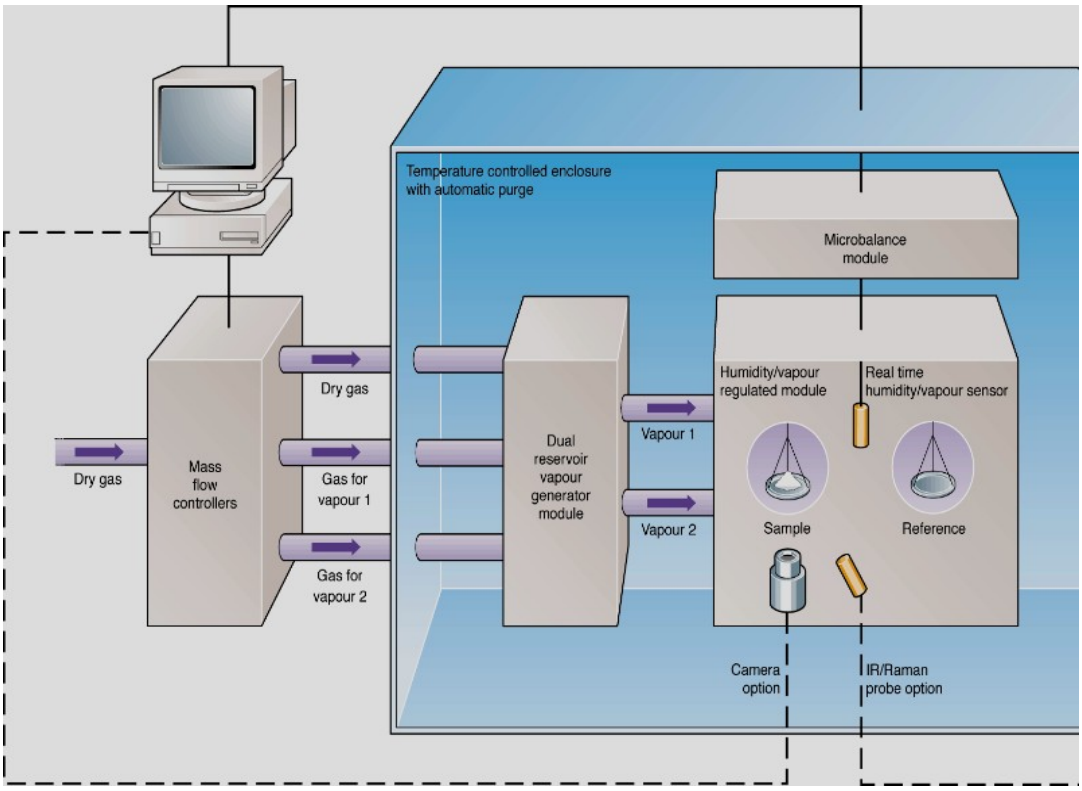


Figure 1 Schematic overview of the SMS DVS- Advantage instrument

## RESULTS AND DISCUSSION

This is accomplished by utilising a proprietary optical sensor which is specifically tuned for a wide range of solvents. This technology allows the instrument to measure and control organic vapour concentrations in real time. The DVS-Intrinsic instrument has similar balance configurations (1 gram or 4 gram capacity), but is designed for water vapour only.

Studying the moisture transport behaviour in porous building materials, like cements, is essential to improving their performance [11]. For these materials, vapour concentration and temperature are considered to be the principal driving principals in understanding moisture transfer. For concrete and reinforced concrete structures, degradation pathways, such as; carbonation, chloride or sulphate ingress, freezing and thawing cycles, and alkali-silica reaction, are all dependent on moisture [12,13]. For instance, there is a critical relative humidity range where carbonation is favoured, which is important for accelerated carbonation tests.

Additionally, water has the ability to impair the mechanical durability of reinforced concrete structures. Also, hardened cement paste is known to be a dynamic system with regards to moisture content [14]. Further, water sorption isotherms have been used to study the hardening processes of cement[15]. Water sorption-desorption isotherms are essential parameters for durability evaluation and prediction [12]. For these reasons, water sorption studies on cements or cement components using gravimetric sorption instrumentation has been used many researchers [14, 15, 16, 17,18].

Figure 2 shows the dehydration kinetics (a.) and resulting desorption isotherm (b.) for a cement paste sample at 25 °C. The desorption isotherm in Figure 2b shows evidence of dehydration occurring in several steps. There is rapid mass loss above 90% RH, most likely due to loss of loosely bound water. There is gradual mass loss between 90% and 40% RH followed by a sharper mass loss at 30% RH, which may be due to loss of internal or hydrated water. There is another sharp drop in mass as the sample is fully dried at 0% RH.

The sorption kinetics for two different cement samples has been studied previously in SMS Application Note 09 [19]. In this study two different dry cement powders were exposed to 95% RH at 40 °C and the mass was monitored over time (see Figure 3). The Cement 1 sample rapidly increases in mass initially, followed by a more gradual increases over time. In contrast, the Cement 2 sample shows a very small mass increase initially, followed by a large increase in mass after nearly 24 hours of exposure to 95% RH conditions.

Therefore, the Cement 2 sample might have a longer storage lifetime compared to the Cement 1 sample. These two simple studies illustrate how gravimetric moisture sorption experiments can be used to study cement-based materials. Experiments could be expanded to include a wide range of samples (i.e. cement components, wood-cement composites, synthetic cements) and a wide range of conditions (up to 85 °C with the correct instrument configuration).

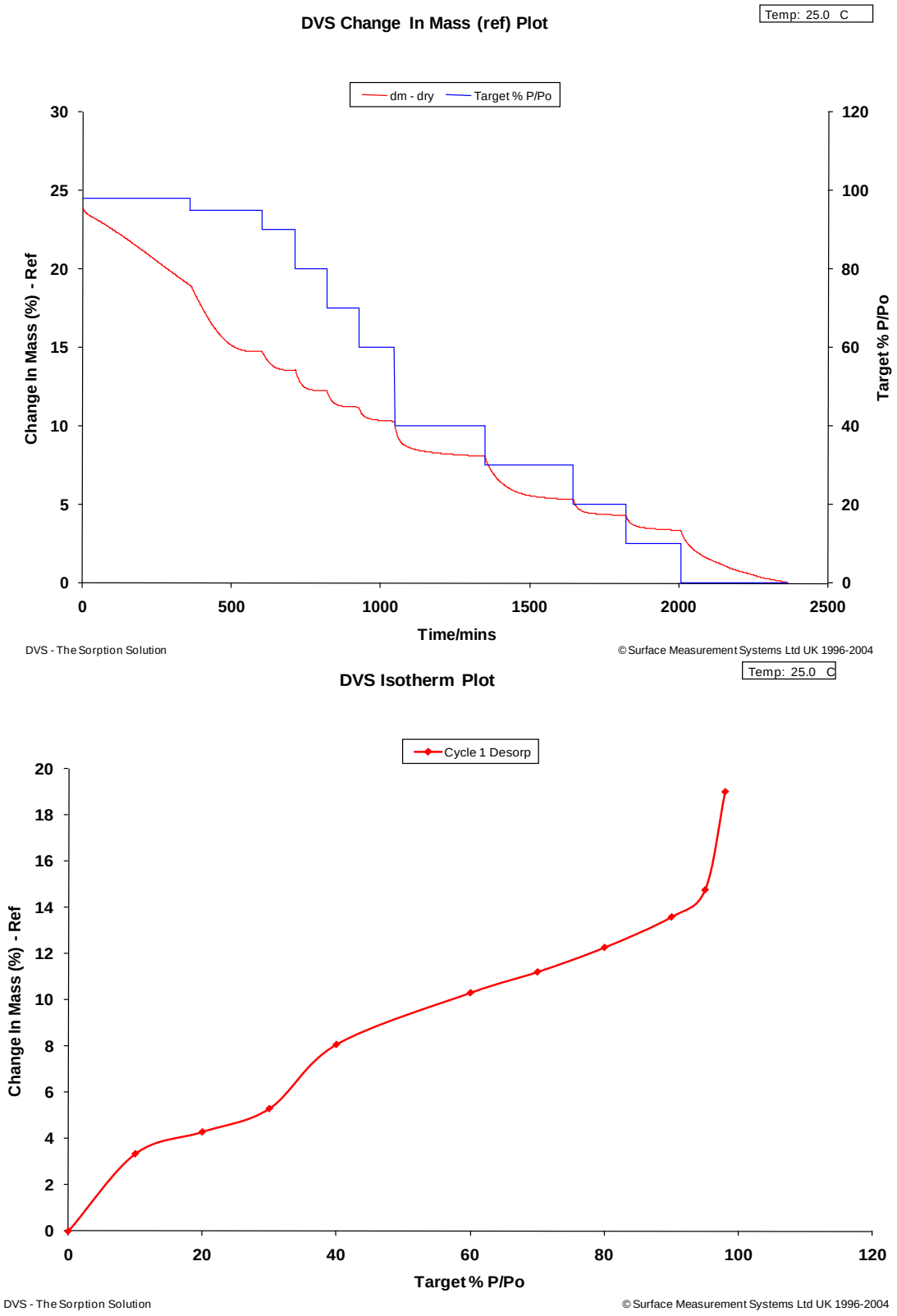


Figure 2 (a, top) Drying kinetics and (b, bottom) desorption isotherm for a cement paste sample at 25.0 °C.

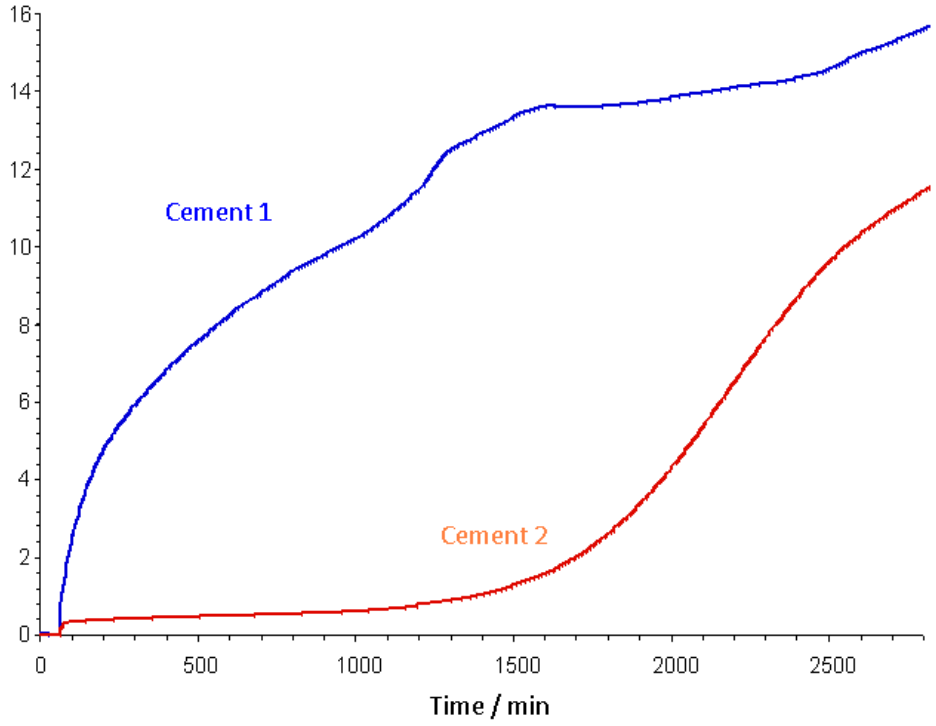


Figure 3 Moisture sorption kinetics for two dry cement powders at 40°C

## CONCLUSIONS

Utilizing the functionality of DVS instrumentation for the study of building materials allows the vapour sorption characteristics to be studied on wood, paint, insulation, cement, asphalt, and textiles. Water sorption on these materials can be vital in understanding and controlling mould growth, material stability, inter-material adhesion, and exterior weathering. Organic vapour sorption studies allow the study of material surface energetics, VOC sorption capacity, and herbicide/insecticide retention behaviour. This overview application note only summarizes a handful of these applications, but hopefully illustrates how DVS technology could be applied to a wide range of building-related materials and problems.

## ACKNOWLEDGEMENTS

We would like to acknowledge Dr Dan Burnett, Dr Majid Naderi for their contribution on this paper.

## REFERENCES

1. KHANKARI, R.K. AND ZOGRAFI, G., Sorption of water by solids. In: Brittain H.G., editor. Physical Characterization of Pharmaceutical Solids. New York: Marcel Dekker, Inc., pp 387-418.

2. FENNEMA, O.R. Food Chemistry, Marcel Dekker: New York, 1985.

3. CHIRAFE, J. AND BEURA, M.D., 1996. Critical Reviews in Food Science and Nutrition, 36, 465-513.

4. ZAWODZINSKI, T.A., NEEMAN, M., SILLERUD, L.O., AND SHIMSHON, G., 1991. J. Phys. Chem., 95, 6040-4044.

5. LEVOGUER, C. AND WILLIAMS, D., 1998. Medical Device Techn., 9, 14.

6. LIEFF, M. AND TRECHSEL, HR, editors, *Moisture Migration in Buildings*, ASTM: PA, 1982.

7. MAEKAWA, K., ISHIDA, T., AND KISHI, T., 2003. J. of Advanced Concrete Technology, 1, 91-126.

8. SKAAR, C., *Wood-Water Relations*, Springer-Verlag: Berlin, 1998.

9. MARCHAND, R.G. AND KUMARAN, M.K., Journal of Thermal Insulation and Building Envelopes, 1994. 17, 362-367.

10. OKUBAYASHI, S., GRIESSER, U.J., AND BECHTOLD, T., Journal of Applied Polymer Science, 2005. 97, 1621-1625.

11. QIN, M., BELARBI, R., AIT-MOKHTAR, A., AND NILSSON, L-O., 2009. Construction and Building Materials, 23, 967-975.

12. BAROGHEL-BOUNY, V., Cement and Concrete Research, 2007. 37, 414-437.

13. NIKKEN, M.R. AND HOOTON, R.D., Cement Concrete and Aggregates, 2002. 24, 20-24.

14. ADOLPHS, J., Materials and Structures, 2005. 38, 443-448.

15. ROBENS, E., BENZLER, B., REICHERT, H., AND UNGER, K.K., Journal of Thermal Analysis and Calorimetry, 2000. 62, 435-44.

16. ADOLPHS, J., Applied Surface Science, 2007. 253, 5645-5649.

17. TADA, S. AND WATANABE, K., Cement and Concrete Research, 2005. 35, 2271-2277.

18. ROBENS, E., DAROWSKI, A., AND KUTAROV, V.V., Journal of Thermal Analysis and Calorimetry, 2004. 76, 647-657.

19. SMS Application Note 09,

# ANALYSIS OF MECHANICAL PROPERTIES AND DURABILITY OF CONCRETE WITH FLY ASH

**D A A Silva**

**A E B Cabral**

Federal University of Ceará

Brazil

**ABSTRACT.** The use of fly ash in the composition of the composites cementitious material makes it more sustainable. This study reports the characterization of two ashes coming from the burning of coal from two different thermoelectric to analyse the similarity between the ashes and concrete was produced by replacing part of the Portland cement by fly ash. The ashes were named CTP – I and CTP – II. The ashes were characterized in their physical, chemical, mineralogical and morphological properties. We observed, through testing, that just one of fly ashes were pozzolanic, the CTP - II, making possible the substitution of fly ash for cement. The other ash, CTP – I, presented a $SO_3^-$ concentration of approximately 12% and so it was used as fine material in the production of mortar to analyse the material by leaching and solubilization tests to determine if there is dangerousness waste in the production or waste in these mortars. It establishes the reference concrete and the cement was replacement by ash was made by volume, where it replaces 7,5% and 15% Portland cement by fly ash, in three ratios of 0,4, 0,5 and 0,6. The work analysed the durability, mechanical and physical properties of the reference concrete and the concrete with ashes. The results of analyses of concretes indicate a technical viability of replacing Portland cement by fly ash.

**Keywords:** Fly ash, Concrete, Coal thermoelectric

**David Alison Araujo Silva** is a graduate in Civil Engineering from the Federal University of Ceará (2014), Master in Civil Engineering (Construction). Author and Co-author of technical articles published in national congresses.

**Professor Antonio Eduardo Bezerra Cabral** congresses He graduated in Civil Engineering from the Federal University of Ceará (1997), master's degree in Civil Engineering (Construction), Federal University of Rio Grande do Sul (2000), doctorate in Environmental Engineering Sciences, University of São Paulo (2007), with internship abroad (Universiy of Technology, Sydney - Australia) and post-doctoral training at the Universitat Politècnica de Catalunya (UPC-Barcelona, Spain, 2012). He is currently Assistant Professor, Department of Structural Engineering and Construction (DEECC) of the Federal University of Ceará (UFC). It operates in undergraduate education in Civil Engineering and the Graduate Program in Civil Engineering: Structures and Construction (PEC) of the UFC.

## INTRODUCTION

The concept of sustainability is understood in its broadest sense, reconciling environmental concerns with economic and social. Currently, the environmental aspects have a greater impact, both in the media and in marketing strategies, indeed quite disturbing in a country with social and economic problems such as Brazil. Environmental factors - economy - society, should be considered in an integrated manner, otherwise there will be no sustainable development. One way to apply the concept of sustainability is the use of mineral admixtures in cementitious material composition that aims to reduce the extraction of raw materials for the production of Portland cement, reducing the emission of carbon dioxide into the atmosphere, and to target the agri-products-industrial which are usually treated as mere waste [1].

The environmental impact of the production of cement is inversely proportional to the added mineral content incorporated in the composition of the cementitious material. Therefore, the CP type III, 70% of blast furnace slag has the best performance among environmental produced in Brazil, followed cement IV CP, 50% fly ash [2].

The production of coal has increased in recent years, according to the Brazilian Mineral Summary published by the National Department of Mineral Production [3], also according to the document, the gross production of coal has grown since 2011, and it was observed also, an increase in the apparent energy consumption of coal, or coal used for firing power plants. Figure 1 below shows the production of coal processed for energy and apparent energy consumption of coal in Brazil.

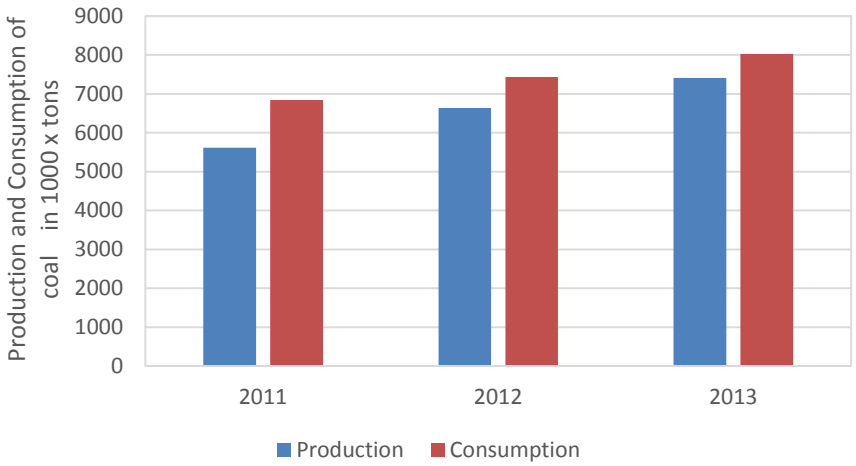


Figure 1 Energy production and consumption of coal

It can be seen in Figure 1 an average consumption of 7.4 million tons of coal for burning in power plants, the burning of coal produces bottom ash and fly ash, with very different characteristics. The bottom ash, with defined and low reactivity crystal structure is used as fine aggregate for various purposes such as blocks, mortars, among others. Fly ash, for its pozzolanic activity is used as a mineral addition in the production of Portland cement [4].
According to Hoppe Filho [5] (2008), it is estimated that 50% of fly ash generated is used by the cement industry and a complementary part, not yet determined, is used by concrete core.
The study using mineral admixtures in the concrete gives reinforces the importance that has to reuse the waste generated by industries and specifically the thermal.

So besides the environmental importance, reuse waste with high value creation while minimizing environmental impacts and contributing to sustainable construction, there is also an importance on knowledge about the characterization of fly ash, pozzolanic activity and their influence on hydrated matrix cement system - fly ash, makes the study of this issue of paramount importance thus justifying the present work.

The goal of the present study is to analyze the ashes from the burning of coal, making sure that the ashes are characterized as fly ash, and verify the potential use of the ash in cement composites. For this characterization of the ash were made using the technique of X-ray fluorescence (XRF), scanning electron microscopy (SEM), laser granulometry, thermogravimetry and physical tests using Portland cement and calcium hydroxide.

## EXPERIMENTAL PROCEDURE

### Conditions for Pozzolanic Materials

The standard NBR 12.653[6] (ABNT, 2014) establishes certain requirements for pozzolanic materials classification. According to the norm, pozzolanic materials can be classified into three classes: Class N, or Class C and Class E

- Class N: Any natural or artificial pozzolan, which comply with the standard requirements, such as volcanic materials acid petrographic character, siliceous cherts, diatomaceous earth and calcined clays.
- Class C: fly ash produced by coal-fired power plants that fulfil the requirements of the standard.
- Class E: Any pozzolan, not included in the N and C class, which comply with the requirements of the standard.

In addition, the standard also establishes physical requirements for classification as ash fly ash. Table 1 shows the chemical requirements of the two ashes analysed and several authors. The chemical characteristics were obtained by XRF, thermogravimetry and specific tests contained in the NBR 12.653.

Table 1 Chemical Characteristics, %

| FLY ASH | OXIDE (Si, Fe, Al) | $SO_3$ | $Na_2O$ | CaO | LOI[1] |
|---|---|---|---|---|---|
| CTP – I | 51,99 | 10,77 | 0,75 | 31,06 | 18,56 |
| CTP – II | 84,03 | 1,64 | 1,37 | 6,76 | 2,07 |
| Bentz et al. (2015)[7] | 92,70 | 0,02 | 1,78 | 0,70 | 0,80 |
| Bui et al. (2015)[8] | 90,67 | 0,36 | 1,20 | 1,26 | 2,80 |
| Görhan (2015)[9] | 76,50 | 1,54 | 2,45 | 6,34 | 3,26 |
| Kabay et al. (2015)[10] | 88,11 | 0,95 | - | 1,90 | 1,69 |
| Mejía et al. (2015)[11] | 79,70 | 0,60 | 2,20 | 0,80 | 14,80 |
| Shaikh and Supit (2015)[12] | 91,20 | 0,21 | 0,99 | 1,61 | 0,50 |
| NBR 12653 – C | $\geq 70$ | $\leq 5$ | $\leq 1,5$ | - | $\leq 10$ |

[1] LOI = Loss on Ignition (950 ºC)

It can be seen from the table that the CTP - I did not show chemical characteristics compatible with the chemical requirements of the standard, already CTP - II met all the chemical requirements of the NBR 12654 qualifying ash as pozzolan. One can observe a similarity between the various aforementioned fly ash, which characterize a certain homogeneity in the fly ash generated in different thermoelectric, with the exception of ash CTP – I. Table 2 shows the physical properties of the fly ash.

Table 2 Physical Characteristics

| FLY ASH | $D_{50}$ (µm) | DENSITY (kg/m³) | SPECIFIC AREA Blaine (cm²/g) | SPECIFIC AREA BET (cm²/g) |
|---|---|---|---|---|
| CTP – I | 13,1 | 2330 | 8220 | - |
| CTP – II | 1,44 | 2360 | 3760 | - |
| Bentz et al. (2015) | 18,4 | 2490 | - | 12800 |
| Bui et al. (2015) | - | 2210 | 3290 | - |
| Hoppe Filho (2008) | 44,25 | 2380 | 6780 | 36300 |
| Kabay et al. (2015) | - | 2210 | 3545 | - |
| Mejía et al. (2015) | 19,5 | 2216 | - | - |
| Shaikh e Supit (2015) | 10,0 | 2600 | - | - |

The following Figure 2 show the image of the sly ash obtained by SEM analysis of fly ash CTP – I and CTP – II. It can be seen that both ashes have spherical shapes, typical of this waste.

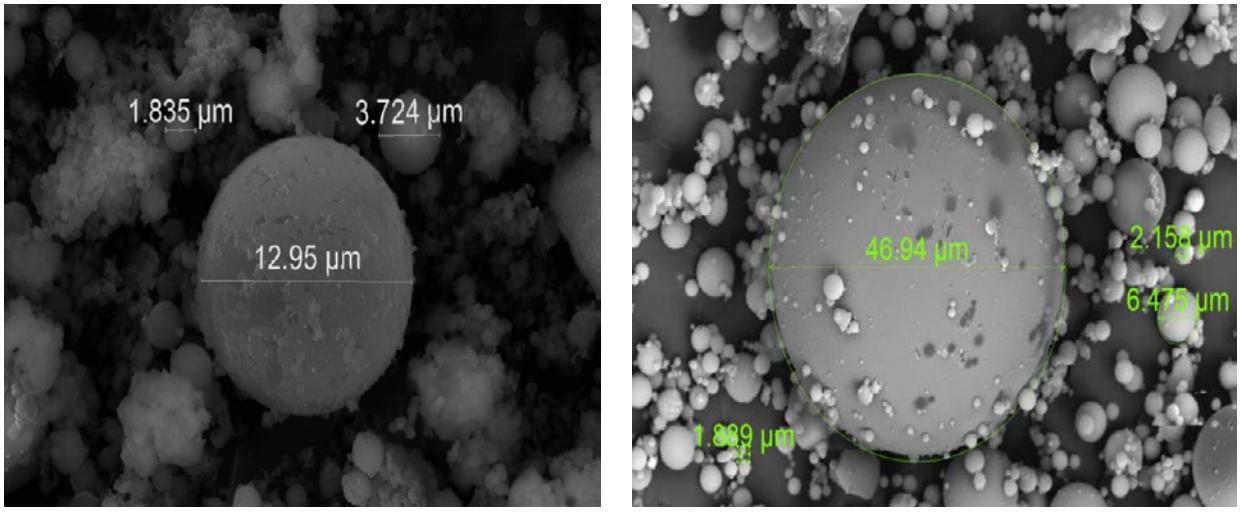


Figure 2 SEM CTP - I and II

It is observed that some results as a specific area Blaine, differ slightly from the limits given by some authors, showing that there is greater variability in the physical characteristics of the ashes. Table 3 shows the physical requirements of the fly ash analysed here. For physical analysis references mortars were produced with only Portland cement, and mortars with ash, replacing part of the Portland cement for ashes. It was also produced mortars with lime to pozzolanic activity, or pozzolanicity, all test according to NBR 12653 (ABNT, 2014) and standards contained in NBR 12653.

Table 3 Mechanical characteristics of mortar

| MIXTURE | COMPRESSIVE STRENGTHS (MPa) | IAP | POZZOLANICITY (MPa) |
|---|---|---|---|
| Cement Mortar | 26,76 | - | - |
| Cement + CTP – I Mortar | 26,90 | 100,5% | - |
| Cement + CTP – II Mortar | 28,31 | 105,8% | - |
| Lime + CTP – I | - | - | 6,50 |
| Lime + CTP - II | - | - | 7,61 |
| NBR 12653 - C | - | ≥ 90% | ≥ 6,00 |

## RESULTS

### Production of Concrete With Fly Ash

After the characterization of the ash, it was observed that CPT - II has been characterized chemically and physically as fly ash, and it was used for concrete production. It was established the reference concrete and replacing the Portland cement by fly ash in amounts of 7.5% to 15% by volume, in three ratio w/c different, 0,4, 0,5 and 0,6. It was analyzed the concrete properties in fresh and hardened condition.

### Concrete characteristics in the fresh condition

Table 4 shows the concrete mix used in this study and Figure 3 shows the concrete characteristics in the fresh condition.

Table 4 Mixture proportions for the nine concretes mixtures (kg/m³)

| MIXTURE | CEMENT | FLY ASH | FINE AGG | COARSE AGG | WATER | ADDITIVE | SLUMP TEST |
|---|---|---|---|---|---|---|---|
| 0,4 – Ref | 450 | - | 663 | 1029,6 | 180 | 1,60 | 10 |
| 0,4 – 7,5% | 416,25 | 26,55 | 663 | 1029,6 | 180 | 1,85 | 9,5 |
| 0,4 – 15% | 382,5 | 53,12 | 663 | 1029,6 | 180 | 2,28 | 10 |
| 0,5 – Ref | 360 | - | 693,6 | 1077,1 | 180 | 1,48 | 8,5 |
| 0,5 – 7,5% | 333 | 21,24 | 693,6 | 1077,1 | 180 | 1,54 | 9,5 |
| 0,5 – 15% | 306 | 42,48 | 693,6 | 1077,1 | 180 | 1,49 | 9,5 |
| 0,6 – Ref | 300 | - | 714 | 1108,8 | 180 | 0,70 | 9,5 |
| 0,6 – 7,5% | 277,5 | 17,7 | 714 | 1108,8 | 180 | 0,81 | 8,5 |
| 0,6 – 15% | 255 | 35,4 | 714 | 1108,8 | 180 | 0,85 | 9,5 |

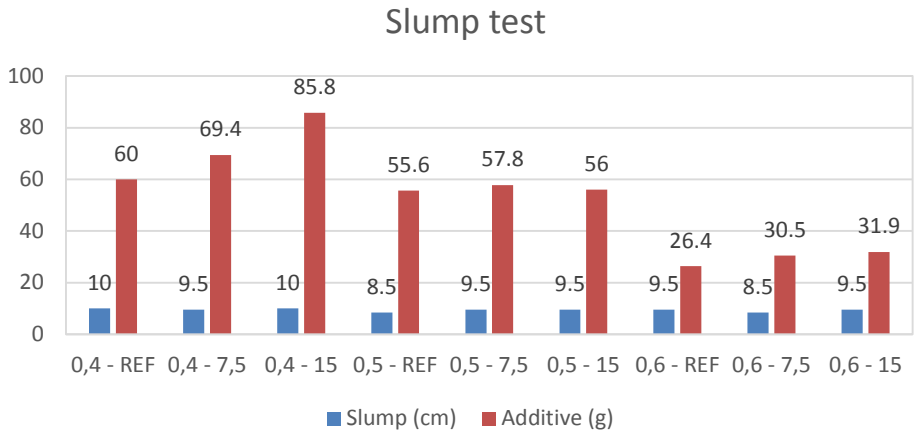


Figure 3 Slump test of concrete

Observed an increase in consumption of fly ash to the average has increased to the fly ash content in replacement of Portland cement, this is due to the fact that fly ash is finer than the Portland cement, generating a high specific surface. We opted for the volumetric replacement of Portland cement with fly ash, to assess the behavior of concrete mixtures at constant volumes. Another factor was the ratio preserved Vc / Vw, because the cement has specific mass greater than the fly ash, thus, would then disproportionate thus their disproportion between the water particles and particle agglomerate. It can be seen that, in general, increasing the fly ash content led to a demand plasticizer additive. Typically, due to the spherical ash particles, there is a decrease in the use of plasticizing additives, however the particles of ash are very thin and this effect may have contributed to an increased demand additive.

**Concrete characteristics in the hardened condition.**

The Figure 4 below shows the compressive strength of the concrete at the ages of 3, 7, 28 and 91 days.

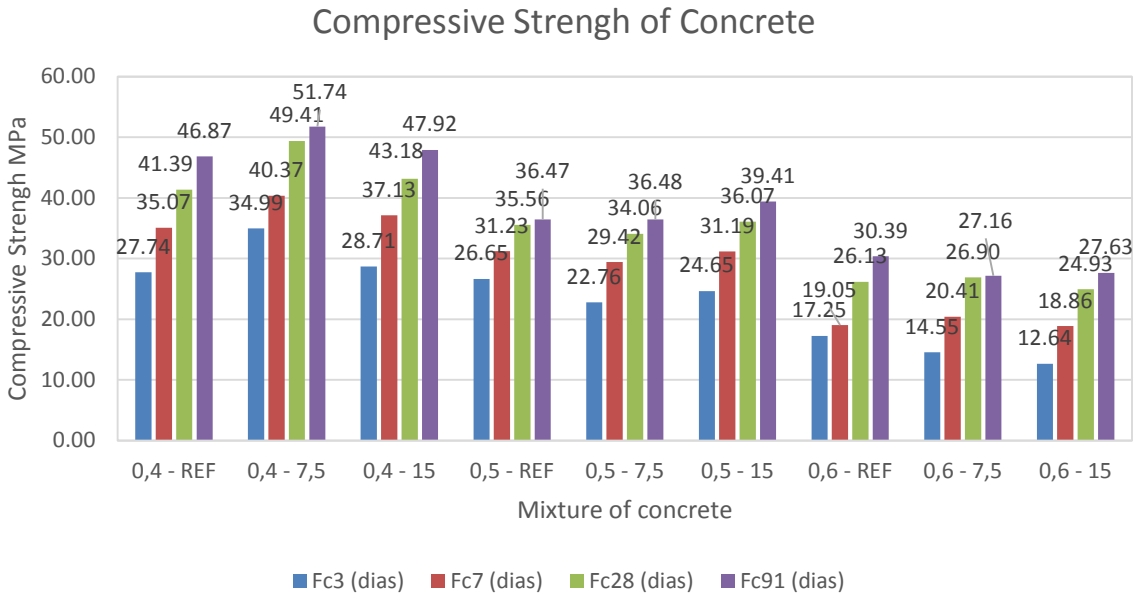

Figure 4 Compressive Strength of Concrete

In the early ages, 3 and 7 days, there was an increase in resistance was used as fly ash for concrete production. It can be seen fly ash had little effect on the mixtures w/c = 0,5 and 0,6, where the resistance in the respective ages were almost constant. The effect of fly ash developed better in the mixture of w/c = 0,4, specifically in the mix 0,4 – 7,5, which had the best mechanical performance. The effect of the fly ash can be better performed at mix 0,4 due to the low ratio a/c of the same, generate less gaps consequently a greater degree of packing.

## CONCLUSIONS

- It can be seen that the ash CTP – I, although not chemically classified as fly ash, presents increments of resistance in cementitious composites. They are made leaching and dissolution tests in order to evaluate whether the use is no risk that ash in the composites, because it presents a sulfur content of SO3 significant.

- The ash CTP - II has been classified chemically and physically fulfilling all the requirements of the NBR 12653, can be used as replacement Portland cement for pozzolan in concrete.

- It was observed that mechanical resistance of the mixes fly ash was practically the same as the reference concretes, in the ratio w/c = 0,5 and 0,6, while in w/c = 0,4 there was a significant increase in resistance mix 0,4 – 7,5.

- Although there was no significant increase in strength in all mixtures, the use of fly ash is important sustainable point of view, since the mixtures fly ash less Portland cement and keeps approximately the same reference concrete strength

- It is extremely important that researchers seek to give a suitable destination to the residues generated in the industry, however, several analysis must be made in order to ensure the safety and good performance in reuse of this waste.

## REFERENCES

1. ISAIA, G. C., & GASTALDINI, A. L. (agosto de 2004). Perspectivas ambientais e econômicas do concreto com altos teores de adições minerais: um estudo de caso. Associação Nacional de Tecnologia do Ambiente Construído, 4(2), 19-30.

2. CARVALHO, J. (2002). Análise do ciclo de vida ambiental aplicada a construção civil - Estudo de caso: comparação de cimento portland com adição de resíduos. Dissertação, Universidade de São Paulo (USP), São Paulo.

3. DNPM - Departamento Nacional de Produção Mineral. (2014). Sumário Mineral 2014. Ministério de Minas e Engergia, Departamento Nacional de Produção Mineral. Brasília: Departamento Nacional de Produção Mineral. Fonte: www.dnpm.gov.br.

4. CHIES, F., SILVA, N. I., & ZWONOK, O. (2003). Desenvolvimento de blocos e tijolos a partir de cinzas de fundo de carvão - CIPECAL. Em J. C. Rocha, & V. M. John (Eds.), Utilização de Resíduos na Construção Habitacional (Vol. 4, p. 272). Porto Alegre: Associação Nacional de Tecnologia do Ambiente Construído - ANTAC.

5. HOPPE FILHO, J. (2008). Sistemas cimento, cinza volante e cal hidratada: Mecanismo de hidratação, microestrutura e carbonatação do concreto. Universidade de São Paulo, São Paulo.

6. ASSOCIAÇÃO BRASILEIRA DE NORMAS TÉCNICAS. (2014). NBR 12653: Materiais Pozolânicos - Requisitos. Rio de Janeiro.

7. BENTZ, D. P., JONES, S. Z., & SNYDER, K. A. (Março de 2015). Design and performance of ternary blend high-volume fly ash concretes of moderate slump. Construction and Building MATERIALS, 409-415.

8. BUI, P. T., OGAWA, Y., NAKARAI, K., & KAWAI, K. (Julho de 2015). A study on pozzolanic reaction of fly ash cement paste activated by an injection of alkali solution. Construction and Building MATERIALS, 28-34.

9. KABAY, N., TUFEKCI, M. M., KIZILKANAT, A. B., & OKTAY, D. (Março de 2015). Properties of concrete with pumice powder and fly ash as cement replacement materials. Construction and Building MATERIALS, 1-8.

10. MEJÍA, J. M., RODRÍGUEZ, E., GUTIÉRREZ, R. M., & GALLEGO, N. (Maio de 2015). Preparation and characterization of a hybrid alkaline binder based on a fly ash with no commercial value. Construction and Building MATERIALS, 346-352.

11. SHAIKH, F. U., & SUPIT, S. W. (Março de 2015). Compressive strength and durability properties of high volume fly ash (HFVA) concretes containing ultrafine fly ash (UFFA). Construction and Building MATERIALS, 192-205.

# STRENGTH AND DURABILITY STUDIES OF QUATERNARY BLENDED CONCRETES USING MINERAL ADMIXTURES

**G. Sree Lakshmi Devi**

**P Srinivasa Rao**

Jawaharlal Nehru Technology University

**Srikanth Devi**

MREC

India

**ABSTRACT.** Extensively used material in the construction industry is concrete in the world. The utilization of SCM's (Supplementary Cementitious Material) in concrete has become more popular these days and increased along with the development of concrete industry, due to the consideration of problems associated with the manufacture of cement like extraction of raw material and carbon dioxide emission. These effects brought pressures to reduce cement consumption by the use of supplementary materials such as fly ash, micro silica, rice husk ash (RHA), GGBS, etc., use of these byproducts facilitates sustainable development. A lot of research shown different Properties of concrete were improved with addition of SCM's i.e. binary blending .Incorporating of high volume of single type of SCM may have negative impacts on concrete properties. To overcome negative impacts, researchers explored the incorporation of two types of SCM's in concrete i.e. ternary blending concrete. By using quaternary blending which may further improve properties of concrete. In this paper attempt has been made to study the compressive strength properties and durability properties by cubes immersion in 5% $H_2SO_4$, 5%HCL and 5%$Na_2SO_4$, using pond test of quaternary blended concrete made with various percentage of replacement to cement with the fly ash, micro silica and GGBS for various W/B ratios of 0.55 & 0.35 at 28 and 90 days.

**Keywords:** Quaternary blended concrete, Ternary blended concrete, Binary blended concrete Silica, Fly ash, GGBS, Durability.

**G Sree Lakshmi Devi** is a Research Scholar in JNTU Hyderabad, Specialized in Structural Engineering. Research interests are concrete technology, special concretes, self-compacting concrete and use of micro silica, flyash in concrete.

**Dr P Srinivasa Rao** is working as Professor & Vice Principal in Jawaharlal Nehru Technology University, Hyderabad, Specialized in Structural Engineering with 25-Years of teaching, research and consultancy experience. Research interests are concrete technology, structural designs, special concretes, high performance concrete, self-compacting concrete and use of micro silica, metakaolin, high volumes of fy ash in concrete.

**Srikanth Devi** is working as Assistant Professor in MREC Hyderabad, Specialized in Structural Engineering. He has 5 years of academic, research and industrial experience.

## INTRODUCTION

As the usage of concrete is inevitable, pre-emptive measures should be taken to reduce the usage of cement in concrete while maintaining the same engineering properties. To address this cause, research has been carried out on various constituents and parameters of concrete which lead to the realization of new construction materials and practices. The addition of pozzolanic materials is an alternative practice in construction industry. The use of mineral admixtures will be increased over the coming few decades to provide more sustainability in the concrete construction which results to maximize the production of mineral admixtures which leads to their effectiveness with regards to environmental impacts, cost and performance.

By addition of these admixtures as partial replacement of cement not only improves the properties of concrete but also reduces the cement content in concrete. The reduction of cement content means it minimize the environment impacts caused in cement production process and most of these materials are industrial by-products, problems with disposal also can be solved.

Admixtures are added to batch immediately or during mixing to modify one or more of the properties of concrete in fresh and hardened state. The use of mineral admixture as partial replacement to cement in concrete is common practice in modern concrete technology[10].

Fly ash; one of the by-products of thermal power plants is utilized as a pozzolanic material in cement worldwide. The Fly ash replacement level varies from a minimum percentage to maximum of 60% for mass concrete constructions. It improves durability but the drawback is early age strength. The early age strength development of fly ash binary blend shows poor performance than ordinary concrete.

By adding super fine admixture like micro silica to binary blended concrete of fly ash improves early age performance of concrete and fly ash improves the properties at the later age [1]. GGBS is the by-product obtained in iron manufacture in blast furnace heated iron ore. Partial replacement of GGBS to cement, makes concrete more durable than conventional concrete.

## EXPERMENTAL INVESTIGATIONS

The objective of this investigation was to study the compressive strength and durability of blended concretes made with fly ash, GGBS and micro silica. It's a detailed study about the blending of admixtures in concrete with different combinations with different percentages. Total 12 combinations were used. In this, the blending was done basically with binary, ternary and quaternary with water binder ratio of 0.55 and 0.35. These 12 mix results were compared with ordinary concrete at 28 days and 90 days for strength and durability, these mix proportions are designed according to IS 10262-2009 and details are tabulated in Tables 1 and 2.

Table 1 Material required for $1m^3$of concrete for W/B ratio 0.55

| NO | MIX | CEMENT | | MICRO SILICA | | FLY ASH | | GGBS | | FINE AGG | COARSE AGG | WATER |
|---|---|---|---|---|---|---|---|---|---|---|---|---|
| | | % | kg/m³ | % | kg/m³ | % | kg/m³ | % | kg/m³ | kg/m³ | kg/m³ | Ltr |
| 1 | M0 | 100 | 320 | 0 | - | 0 | - | 0 | - | 762 | 1157 | 176 |
| 2 | M11 | 50 | 160 | 0 | - | 50 | 160 | 0 | - | 762 | 1157 | 176 |
| 3 | M12 | 50 | 160 | 0 | - | 0 | - | 50 | 160 | 762 | 1157 | 176 |
| 4 | M21 | 75 | 240 | 5 | 16.2 | 20 | 64.8 | 0 | - | 762 | 1157 | 176 |
| 5 | M22 | 70 | 224 | 10 | 32.4 | 20 | 64.8 | 0 | - | 762 | 1157 | 176 |
| 6 | M23 | 50 | 160 | 0 | - | 25 | 80 | 25 | 80 | 762 | 1157 | 176 |
| 7 | M24 | 65 | 208 | 5 | 16 | 0 | - | 30 | 96 | 762 | 1157 | 176 |
| 8 | M25 | 60 | 192 | 10 | 32 | 0 | - | 30 | 96 | 762 | 1157 | 176 |
| 9 | M31 | 40 | 128 | 10 | 32 | 25 | 80 | 25 | 80 | 762 | 1157 | 176 |
| 10 | M32 | 25 | 80 | 10 | 32 | 25 | 80 | 40 | 128 | 762 | 1157 | 176 |
| 11 | M33 | 15 | 48 | 10 | 32 | 25 | 80 | 50 | 160 | 762 | 1157 | 176 |
| 12 | M34 | 25 | 80 | 10 | 32 | 40 | 128 | 25 | 80 | 762 | 1157 | 176 |
| 13 | M35 | 15 | 48 | 10 | 32 | 50 | 160 | 25 | 80 | 762 | 1157 | 176 |

Table 2 Material required for 1 $m^3$ concrete for W/B ratio 0.35

| NO | MIX | CEMENT | | MICRO SILICA | | FLY ASH | | GGBS | | FINE AGG | COARSE AGG | WATER | SUPER PLASTICIZER |
|---|---|---|---|---|---|---|---|---|---|---|---|---|---|
| | | % | kg/m³ | % | kg/m³ | % | kg/m³ | % | kg/m³ | kg/m³ | kg/m³ | Ltr | ml |
| 1 | M0 | 100 | 469 | 0 | - | 0 | - | 0 | - | 725 | 1101 | 164 | 2213 |
| 2 | M11 | 50 | 234.5 | 0 | - | 50 | 234.5 | 0 | - | 725 | 1101 | 164 | 2321 |
| 3 | M12 | 50 | 234.5 | 0 | - | 0 | - | 50 | 234.5 | 725 | 1101 | 164 | 2135 |
| 4 | M21 | 75 | 351.75 | 5 | 23.45 | 20 | 93.8 | 0 | - | 725 | 1101 | 164 | 2798 |
| 5 | M22 | 70 | 328.3 | 10 | 46.9 | 20 | 93.8 | 0 | - | 725 | 1101 | 164 | 3132 |
| 6 | M23 | 50 | 234.5 | 0 | - | 25 | 117.25 | 25 | 117.25 | 725 | 1101 | 164 | 2315 |
| 7 | M24 | 65 | 304.85 | 5 | 23.45 | 0 | - | 30 | 140.7 | 725 | 1101 | 164 | 2536 |
| 8 | M25 | 60 | 281.4 | 10 | 46.9 | 0 | - | 30 | 140.7 | 725 | 1101 | 164 | 3130 |
| 9 | M31 | 40 | 187.6 | 10 | 46.9 | 25 | 117.25 | 25 | 117.25 | 725 | 1101 | 164 | 3128 |
| 10 | M32 | 25 | 117.25 | 10 | 46.9 | 25 | 117.25 | 40 | 187.6 | 725 | 1101 | 164 | 3115 |
| 11 | M33 | 15 | 70.35 | 10 | 46.9 | 25 | 117.25 | 50 | 234.5 | 725 | 1101 | 164 | 3135 |
| 12 | M34 | 25 | 117.25 | 10 | 46.9 | 40 | 187.6 | 25 | 117.25 | 725 | 1101 | 164 | 3124 |
| 13 | M35 | 15 | 70.35 | 10 | 46.9 | 50 | 234.5 | 25 | 117.25 | 725 | 1101 | 164 | 3129 |

Mix nomenclature: M0 is Ordinary concrete, M11 to M12 are Binary mixes, M21 to M25 are Ternary mixes and M31 to M35 are Quaternary mixes.

**Materials**

**Cement:** Ordinary Portland cement of 53 grade was used and it confirming to IS: 12269

**Admixtures:** In the present investigation Fly Ash, Micro Silica and Ground Granulated Blast Furnace Slag (GGBS) are used as partial replacement of cement.

**Fine Aggregates:** Locally available river sand was used as fine aggregate. It is free from clayey matter, Silt and organic impurities. The sand is tested for various properties like bulk density, specific gravity and fineness modules in accordance with IS 2386-1963.
**Coarse Aggregates:** 20 mm nominal size of Machine crushed angular granite metal is used as coarse aggregate.
**Water:** Portable water was used for mixing and curing and it is free from injurious amounts that may be deleterious to concrete.
**Super Plasticizer:** CONPLAST 430 was used as water reducing admixture.

## TESTS CONDUCTED

Compressive testing was conducted as shown in Figure 1 at 28, 90 and 180 days of curing period to determine the compressive strength. For the durability study, mass loss of 100×100×100 mm size cubes were determined at 28 and 90 days. These cubes were immersed in 5 % $H_2SO_4$, HCl and $Na_2SO_4$ solutions as shown in Figure 2 and 4. Figure 3 and 6 shows the cubes after 28 days of pond testing for the durability study.

Figure1 Compressive strength of concrete Specimen under testing

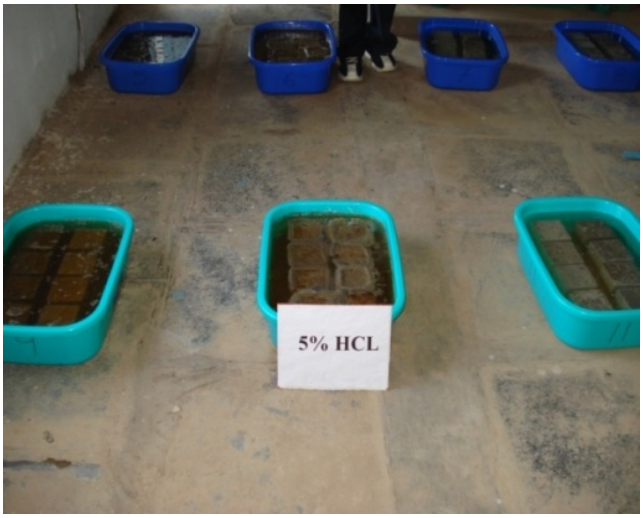


Figure 2 Concrete immersed in 5%HCl Acid solution


Figure 3 Cubes after 5% Hcl Acid immersion

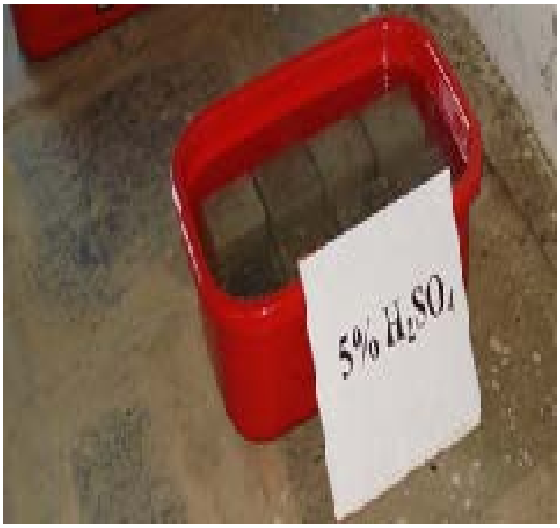


Figure 4 Cubes in 5% $H_2SO_4$ Acid solution

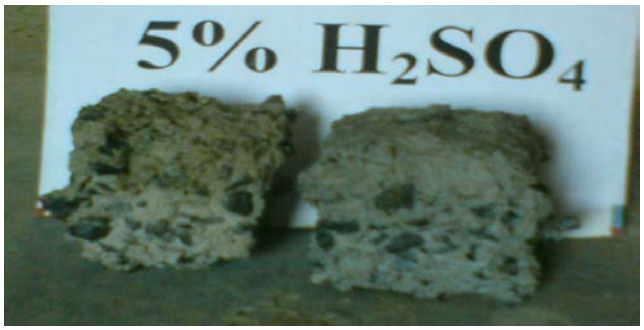


Figure 5 Cubes after 5% $H_2SO_4$ Acid immersion after 28 days of pond curing

## DISCUSSION OF TEST RESULTS

Compressive strengths of ordinary, binary, ternary and quaternary blended concrete were tabulated in tables 3 and 4. Percentage of Weight losses of Ordinary, Binary, Ternary and Quaternary Blended concretes at 28 and 90 days for w/b ratio 0.55 & 0.35 were tabulated in tables 5 and 6.

The compressive strength development of binary mix in w/b ratio of 0.55 replacement of cement with fly ash is comparable with GGBS replacement. When it comes to w/b ratio 0.35 the development of strength is reduced at the age of 90, 180 days.

The compressive strength development of ternary mix, all ternary mix shows comparable except M23 mix achieved very low strength irrespective of w/b ratio.

Quaternary mix M31 only shows comparable strength with ternary mixes. Other quaternary mixes show reduction in strength development due high volume replacement.

Table 3 Compressive strengths of Ordinary, Binary, Ternary and Quaternary Blended concretes at age of 28, 90 and 180 days for w/b ratio 0.55.

| S.NO | W/B RATIO | MIX | COMPRESSIVE STRENGTH ($N/mm^2$) | | | PERCENTAGE OF INCREASE IN COMPRESSIVE STRENGTH ($N/mm^2$) w.r.t 28 days | |
|---|---|---|---|---|---|---|---|
| | | | 28 days | 90days | 180 days | 90 days | 180days |
| 1 | | M0 | 35.60 | 38.89 | 42.63 | 9.24 | 19.75 |
| 2 | | M11 | 25.78 | 27.31 | 29.93 | 5.93 | 16.10 |
| 3 | | M12 | 27.78 | 30.65 | 33.16 | 10.33 | 19.37 |
| 4 | | M21 | 38.47 | 41.45 | 46.61 | 7.75 | 21.16 |
| 5 | | M22 | 34.10 | 37.13 | 40.85 | 8.89 | 19.79 |
| 6 | | M23 | 23.43 | 26.42 | 29.24 | 12.76 | 24.80 |
| 7 | 0.55 | M24 | 38.69 | 43.23 | 49.81 | 11.73 | 28.74 |
| 8 | | M25 | 39.54 | 43.01 | 48.42 | 8.78 | 22.46 |
| 9 | | M31 | 33.46 | 35.74 | 40.23 | 6.81 | 20.23 |
| 10 | | M32 | 31.36 | 34.72 | 39.02 | 10.71 | 24.43 |
| 11 | | M33 | 29.36 | 32.78 | 36.63 | 11.65 | 24.76 |
| 12 | | M34 | 30.37 | 32.91 | 37.55 | 8.36 | 23.64 |
| 13 | | M35 | 28.63 | 29.87 | 34.12 | 4.33 | 19.18 |

Table 4: Compressive strengths of Ordinary, Binary, Ternary and Quaternary Blended concretes at age of 28, 90 and 180 days for w/b ratio 0.35.

| S. NO | W/B RATIO | MIX | COMPRESSIVE STRENGTH ($N/mm^2$) | | | PERCENTAGE OF INCREASE IN COMPRESSIVE STRENGTH ($N/mm^2$) w.r.t 28 days | |
|---|---|---|---|---|---|---|---|
| | | | 28 days | 90days | 180 days | 90 days | 180days |
| 1 | | M0 | 62.10 | 69.25 | 77.62 | 11.51 | 24.99 |
| 2 | | M11 | 48.12 | 50.25 | 54.25 | 4.43 | 12.74 |
| 3 | | M12 | 51.16 | 57.25 | 62.35 | 11.90 | 21.87 |
| 4 | | M21 | 69.88 | 74.47 | 83.48 | 6.57 | 19.46 |
| 5 | | M22 | 61.30 | 65.82 | 73.75 | 7.37 | 20.31 |
| 6 | | M23 | 52.36 | 57.62 | 63.64 | 10.05 | 21.54 |
| 7 | 0.35 | M24 | 71.25 | 77.25 | 86.87 | 8.42 | 21.92 |
| 8 | | M25 | 74.16 | 80.15 | 91.18 | 8.08 | 22.95 |
| 9 | | M31 | 60.63 | 65.65 | 76.32 | 8.28 | 25.88 |
| 10 | | M32 | 59.68 | 64.35 | 76.87 | 7.83 | 28.80 |
| 11 | | M33 | 57.45 | 63.25 | 70.89 | 10.10 | 23.39 |
| 12 | | M34 | 58.78 | 61.31 | 68.93 | 4.30 | 17.27 |
| 13 | | M35 | 54.25 | 56.25 | 62.19 | 3.69 | 14.64 |

Table 5 Percentage of Weight losses of Ordinary, Binary, Ternary and Quaternary Blended concretes at 28 and 90 days for w/b ratio 0.55.

| S.NO | W/B RATIO | MIX | PERCENTAGE DECREASE IN WEIGHT LOSS | | | | | |
|---|---|---|---|---|---|---|---|---|
| | | | $H_2SO_4$ | | HCl | | $Na_2SO_4$ | |
| | | | 28 days | 90 days | 28 days | 90 days | 28 days | 90 days |
| 1 | | M0 | 4.84 | 10.53 | 1.21 | 1.89 | 0.15 | 0.78 |
| 2 | | M11 | 6.37 | 17.06 | 1.79 | 2.54 | 0.45 | 1.35 |
| 3 | | M12 | 5.69 | 11.79 | 1.56 | 2.23 | 0.37 | 1.27 |
| 4 | | M21 | 5.53 | 11.69 | 1.52 | 1.91 | 0.36 | 1.36 |
| 5 | | M22 | 5.10 | 11.16 | 1.53 | 1.89 | 0.22 | 1.22 |
| 6 | | M23 | 7.06 | 17.65 | 1.90 | 2.65 | 0.65 | 1.55 |
| 7 | 0.55 | M24 | 4.98 | 11.43 | 1.21 | 1.92 | 0.20 | 0.90 |
| 8 | | M25 | 4.88 | 11.16 | 1.23 | 1.90 | 0.18 | 0.85 |
| 9 | | M31 | 5.25 | 11.60 | 1.31 | 2.06 | 0.21 | 0.89 |
| 10 | | M32 | 5.45 | 16.06 | 1.42 | 2.25 | 0.43 | 1.24 |
| 11 | | M33 | 5.69 | 18.21 | 1.53 | 2.32 | 0.49 | 1.29 |
| 12 | | M34 | 6.75 | 19.76 | 1.56 | 2.41 | 0.55 | 1.45 |
| 13 | | M35 | 7.41 | 21.12 | 1.61 | 2.46 | 0.59 | 1.59 |

Table 6 Percentage of Weight losses of Ordinary, Binary, Ternary and Quaternary Blended concretes at 28, 90 days for w/b ratio 0.35.

| S.NO | W/B RATIO | MIX | PERCENTAGE DECREASE IN WEIGHT LOSS | | | | | |
|---|---|---|---|---|---|---|---|---|
| | | | $H_2So_4$ | | HCl | | $Na_2So_4$ | |
| | | | 28 days | 90 days | 28 days | 90 days | 28 days | 90 days |
| 1 | | M0 | 4.67 | 12.56 | 1.15 | 1.78 | 0.21 | 0.89 |
| 2 | | M11 | 6.34 | 17.34 | 1.45 | 2.35 | 0.79 | 1.54 |
| 3 | | M12 | 5.56 | 16.35 | 1.37 | 2.27 | 0.56 | 1.23 |
| 4 | | M21 | 5.34 | 14.34 | 1.26 | 2.36 | 0.52 | 0.91 |
| 5 | | M22 | 5.39 | 14.54 | 1.22 | 2.22 | 0.53 | 0.89 |
| 6 | | M23 | 6.89 | 17.97 | 1.65 | 2.55 | 0.90 | 1.65 |
| 7 | 0.35 | M24 | 5.12 | 13.60 | 1.20 | 1.90 | 0.21 | 0.92 |
| 8 | | M25 | 5.09 | 13.55 | 1.18 | 1.85 | 0.23 | 0.90 |
| 9 | | M31 | 5.18 | 13.86 | 1.21 | 1.89 | 0.31 | 1.06 |
| 10 | | M32 | 5.87 | 15.23 | 1.43 | 2.24 | 0.42 | 1.25 |
| 11 | | M33 | 6.12 | 15.67 | 1.49 | 2.29 | 0.53 | 1.32 |
| 12 | | M34 | 6.38 | 16.21 | 1.55 | 2.45 | 0.56 | 1.41 |
| 13 | | M35 | 6.67 | 16.56 | 1.59 | 2.59 | 0.61 | 1.46 |

## CONCLUSIONS

This study shows that high volume mineral admixtures can be used to replace cement in concrete. 60% replacement of OPC with three mineral additive components, i.e. fly ash, GGBS and micro silica produce comparable compressive strength and durable concrete with 40% replacement with two mineral additive components (GGBS and micro silica) and 30% replacement with two mineral additive components (fly ash and micro silica).

- The resistance to chemical attack of M31 mix is same as Ternary Blended and Ordinary Concrete mixes. Even though the cement content is replaced up to 60%.
- But whereas the cement content reduced to 70% and 85% the resistance to chemical attack has been reduced drastically in Quaternary Blended mixes.
- The use of mineral admixtures to concrete will improve the performance of conventional concrete in fresh state and reduces the super plasticizer quantity.
- Mechanical properties of blended concretes had shown significant results as that of ordinary concrete and significant strength has been obtained for concrete having micro silica.
- M25 had shown significant results as it contains 40% of cement replacement and showed significant results over ordinary concrete.
- The mix M31 performed the best of all ages and at all w/b ratios studied in compressive strengths and acid attacks among the four quaternary combinations studied.
- Since M31 is more economical compared to M25 because it contains 60% of cement replacement and has given comparable strengths as that of ternary blended and ordinary concrete mix.

## REFERENCES

1. BOUZUOBBA NABILI "Development of Ternary Blends for High Performance Concrete" ACI Material Journal No.1 101(2004)19-29

2. ALI REZA BAGHERI,HAMED ZANGANESH, MOHAMAD MEHDI MOALEMI "Mechanical and durability properties of ternary concretes containing silica fume and low reactivity blast furnace slag" Cement and Concrete Composites 34(2012) page no 663-670.

3. GIACCIA GM ,MALHOTRA VM," Concrete incorporating high volumes of ASTM class F flyash ", ASTM cement concrete aggregates 1988;10:88-95.

4. A.K. MULLICK. “Performance of Concrete with Binary and Ternary cement blends”. The Indian Concrete Journal, January 2007.

5. P.SRINIVASA RAO, SESHADRI .T AND P. SRAVANA. “Durability Studies on glass Fibre SCC “The Indian Concrete Journal, October 2009.

6. M.D.A. THOMASS, M.H. SHEHATA, S.G. SHAISHIPRAKASH, D.S.HOPKINS, K.CAIL. “Use of Ternary cementitious system containing Silica fume and Fly ash in Concrete”. Cement and concrete Research 29(1999) Pg 1207-1214.

7. TAHIR KEMAL ERDEM, ONDER KLRCA. “Use of Binary and Ternary Blended in high strength concrete”. Construction and Building materials 22(2008) Pg 1477-1483.

8. S.P. PANDEY, A.K.SINGH, R.L.SHARMA, A.K.TIWARI. “Studies on high-performance blended/ multi blended cements and their Durability characteristics “.Cement and concrete Research 33(2003) Pg 1433-1436.

9. S.K.ANTIOHOS, V.G.PAPADAKIS, E.CHANIOTAKIS, S.TSIMAS. ” Improving the Performance of Ternary Blended Cements by mixing different types of fly ashes”. Cement and Concrete Research 37(2007) Pg 877-885.

10. G. SREE LAKSHMI DEVI, P. SRINIVASA RAO, SRIKANTH DEVI “Review On Blended Concretes” International Journal of Research in Engineering and Technology Volume: 04 Issue: 03 Mar-2015.

# RECYCLED CONCRETE AGGREGATE USE IN CONCRETE PAVEMENTS AND ITS PERFORMANCE IN THE US

**F Reza**

**W J Wilde**

Minnesota State University

United States of America

**ABSTRACT.** A review of literature and surveys of the various State Departments of Transportation in the US reveal that there was a period of time between the 1970s and 1990s when several test sections of concrete pavement containing recycled concrete aggregate (RCA) were created. In general, the performance was said to be satisfactory; however, Michigan placed a moratorium on new construction with RCA because of some noted distresses. In subsequent studies, the cause was found to be flaws in design rather than problems with the material. Since that time; there has not been a significant number of new projects built using RCA in the concrete. Most states allow the use of RCA in base layers and it is in widespread use in this application. Several allow the use of RCA in concrete pavement but it is not widely practiced. Several recent research projects seem to show a renewed interest in using RCA in concrete. In this paper, first a review of the literature and state of practice is performed for both the US and Europe; next the performance of pavements using RCA built in Minnesota is analyzed based on historical data of ride quality and distress indices and compared with similar concrete pavements built with conventional aggregate. The results show that the average service life of RCA pavements was less than that of pavements made with conventional aggregates.

**Keywords**: Recycled, Secondary, Aggregates, Concrete, Pavements.

**Dr Farhad Reza** is a professor in the Department of Mechanical & Civil Engineering at Minnesota State University, Mankato, USA. His research interests include concrete materials science, structural health monitoring, and nondestructive evaluation.

**Dr W James Wilde** is a professor and Director of the Center for Transportation Research and Implementation at Minnesota State University, Mankato, USA. His research interests include pavement design and analysis, concrete durability, and pavement-related research and implementation.

## INTRODUCTION

The principles of sustainability dictate that materials should be recycled and reused whenever possible. In fact, the American Society of Civil Engineers' Code of Ethics requires sustainability to be considered in design. Coupled with the fact that natural aggregate resources are dwindling in some major urban areas, it becomes imperative to consider the recycling and reuse of old concrete as crushed aggregates. Indeed, the practice of recycling old concrete pavements and using it as aggregates for the base course in a new pavement is widespread in the US with at least 38 states (out of 50) adopting this practice [1]. However; there is a notion that recycled concrete aggregates (RCA) possess sufficiently good properties to be used in an application requiring higher quality aggregate than base courses, namely in the concrete pavement structure itself. In this paper, an assessment of the current state of the practice in the US regarding the use of RCA as aggregates in new concrete pavements is performed utilizing the results of various surveys. The vast amount of literature in both the US and Europe concerning RCA use in new concrete is reviewed. The long-term performance of pavements built with RCA in Minnesota are then compared to the long-term performance of pavements built with conventional concrete.

## STATE SURVEYS

One of the pioneering studies was conducted around 1996 by Mark Snyder and others under a Federal Highway Administration (FHWA) sponsored study. Portions of this study have been presented at various conferences [2-3] as well as published in a Master's Thesis [4] and a study conducted for the Department of Transportation (DOT) of Washington [5]. In the survey, eleven states are identified which built trial projects of Portland cement concrete (PCC) pavements using RCA. A total of 98 projects were listed. The state with the most number of trials was Michigan with 30, followed by Wisconsin 17, Iowa 16, and Minnesota 14. In general, most of the states observed good performance in pavements with RCA except for Michigan which in fact issued a moratorium on the use of RCA in pavements in 1991. Michigan noted a number of failures on their jointed reinforced concrete pavement (JRCP) built with RCA due to mid-slab transverse cracking. Failure was attributed to a number of factors that included the small size of the aggregate (19 mm) which did not resist the cracking, high amounts of mortar, which detracted from the abrasion resistance, insufficient slab thickness, and incompatible joint spacing (12.5 m).

In 2004, the FHWA conducted a survey to determine the extent and types of transportation-related applications of RCA [1]. It was found that forty-one states recycle concrete as aggregate, thirty-eight states use RCA as aggregate base, and only eleven use RCA in PCC. Five states were selected for a more in-depth review. Among the results noted were that Texas reported that the use of RCA created problems with mix workability due to the high absorption of aggregate and the difficulty in maintaining a consistent and uniform SSD condition of RCA aggregate. The contractors overcame this hurdle by improving their process control program and heightened their awareness of the need to water stockpiles and to conduct frequent testing of aggregate for moisture content. Increases in creep and shrinkage were noted. Initially there were issues with lower compressive strength, which was attributed to RCA fines and a limit of 20% fines was established. Minnesota noted that since the year 2000, they use a 60-year pavement design life on high-volume freeways and a 35-year design life on all other highways.

These factors have contractors shying away from its use in the concrete pavement since the belief is that aggregate washing would be required to produce useable aggregates. This increase in cost may be a key issue to using RCA in PCC as coarse aggregate.

In 2006, the Washington DOT conducted a follow-up survey with a limited number of states, mainly those previously identified as having used RCA in PCC, and then again in 2009 only with those states deemed to be most active in their trials of RCA [5]. It identified only a very few number of additional projects that had been built since the original 1994 survey. Some additional information was noted from the respondents. Illinois reported that a 20-year performance evaluation of only one project, a continuously reinforced concrete pavement (CRCP) built with RCA showed it was performing equivalent to other CRCP pavements of the same age built with virgin aggregates. They suggested moist curing to prevent premature cracking. South Carolina built one project in 2003-04 with no RCA fine aggregates. The concrete mix met or exceeded strength, air, and slump requirements and was performing well. Texas used both coarse and fine RCA with no virgin aggregates on one CRCP project in 1995. Approximately 30% old mortar was attached to the RCA. The compressive and tensile strengths were lower for the RCA concrete than conventional concrete. The density was lower and the water absorption was higher. Moisture control was difficult and they resorted to watering the stockpiles. The pavement was performing well but for future construction a limit of 20% RCA fines would be implemented. Wyoming had used RCA in 8-11 projects as of 2006 all of which were JPCP. The RCA coarse aggregate was limited to 60% with the remainder virgin aggregates. RCA fines were limited to 15%. The cement content requirement increased by ½ sack (21 kg corresponding to a volume of 0.014 $m^3$).

In 2011, Iowa State University conducted a survey to assess the use of RCA in PCC mixtures [6]. Based on the results of the survey, some states showed interest in learning more about how to use RCA in new concrete paving mixtures. Barriers (obstacles and misperceptions) that limited the use of RCA in new concrete paving mixtures could be grouped as compliance, quality, or production related. Compliance barriers included the inability for RCA to meet state specifications for aggregate soundness, abrasion, gradation, and strength. In addition, there was a concern expressed that alkali-silica reaction (ASR) would be a problem. Barriers associated with quality included maintaining consistency and the perception that RCA is a waste material not worthy of use in new concrete paving mixtures. Production barriers included storage, workability, supply, debris removal, and location of processing equipment.

In 2012, the California Transportation Department (Caltrans) sponsored a study to learn about different states' practices, policies and research related to concrete recycling [7]. The survey showed that among the 30 state respondents, 10 allowed the use of crushed concrete as aggregate for new concrete pavements. About half of the respondents discussed problems in using crushed concrete as aggregates, including high pH levels related to the alkali-silica reaction (ASR) and groundwater leaching; high absorption of crushed asphalt concrete; and debris and contamination. Fewer than half of the respondents have considered expanding the use of crushed concrete as aggregate, with several citing availability as a barrier to expanded use of RCA as aggregate.

In summary, through the various surveys a total of 23 states have indicated that they have used RCA in PCC. Upon further inspection it can be found that many of them may allow the use of RCA in PCC pavements but have never built one or else have built a limited number (often just one) project. It appears that in the time period between the late 1970's to the mid

1990's many projects (more than 100) were built, but this activity has significantly slowed down since. Tracking the history of the states who were most active in building projects we find that Michigan (who built the most number of projects) placed a moratorium on using RCA in PCC pavements in 1991. It is now only allowed in lower-risk applications such as curb and gutter, sidewalks, barriers etc. Michigan experienced some problems with mid-slab transverse cracking, but most of this was attributed to design features rather than the RCA itself. In Wisconsin, contractors are electing to use RCA in the base and shoulders, not in the pavements. Iowa indicated the majority of their trial projects were built by counties rather than the DOT. They noted some mid-slab transverse cracking, and now the RCA is mainly used in the base. Among the most active states in using RCA in PCC pavements it might be said that Minnesota currently has the most favorable outlook. Among the issues noted by Minnesota, were the extra cost of washing the aggregates, and maintaining a water-cement ratio of 0.40. Minnesota built trial sections of composite RCA pavements using the two-lift approach at the MnROAD test facility in 2010.

## LITERATURE REVIEW

A large amount of work conducted in one of the earlier studies was documented in an unpublished report in 2006 and is reproduced in [5]. Other comprehensive literature reviews include European studies [8] and other international work [6]. Some physical properties and characteristics of RCA from [5] are given in Table 1.

Table 1 Properties and characteristics of RCA versus virgin aggregates

| PROPERTIES | VIRGIN AGGREGATES | RCA |
|---|---|---|
| Shape and texture | Well rounded, smooth (gravels) to angular, rough (crushed rock) | Angular with rough surface |
| Absorption capacity | 0.8 – 3.7 % | 3.7 – 8.7 % |
| Specific gravity | 2.4 – 2.9 | 2.1 – 2.4 |
| LA abrasion loss | 15 – 30 % | 20 – 45 % |
| Sodium sulfate soundness loss | 7 – 21 % | 18 – 59 % |
| Magnesium sulfate soundness loss | 4 – 7 % | 1 – 9 % |
| Chloride content | 0 – 1.2 kg/m$^3$ | 0.6 – 7.1 kg/m$^3$ |

Soundness tests are performed on aggregates to provide an indication of an aggregate's resistance to weathering and other environmental effects. RCA commonly fail the sodium sulfate soundness test while passing the magnesium sulfate soundness test as indicated in Table 1 [5]. This contradiction between the results of the two test methods brings into question if they are applicable to RCA. Many agencies waive soundness testing on RCA. Pavements with long-term exposure to deicing salts may produce RCA with high levels of sodium chloride. There is concern that RCA with high chloride contents may affect the durability of the new concrete and the corrosion of steel in new concrete. If there is a concern it is suggested that the fine aggregate be washed and that epoxy-coated steel or other corrosion resistant steels be used for reinforcement [5]. European standards for test methods to qualify RCA for use in new concrete mixtures recommend using a magnesium solution for testing RCA durability in freeze-thaw environments [6]. It has been reported that absorption testing for RCA requires more time for accuracy [9-11]. The process for determining gradation may affect the accuracy of the results because the shaking during sieving causes mortar particles to separate from the original aggregates. Instead, it has been recommended

by the Swedish National Testing and Research Institute, the Foundation of Scientific and Industrial Research at Norwegian Institute of Technology, and the Icelandic Building Research Institute to test several smaller samples. The order in which gradation and abrasion testing is done with the same sample affects the results. For abrasion testing or fracture resistance, it is recommended that the sample be tested as a unit [11].

Concrete mixtures with both coarse and fine recycled aggregates can be very harsh and difficult to work due to the highly angular and rough surface of the RCA. Additional water is required in order to obtain the same degree of workability as a mix containing conventional aggregates, especially when both coarse and fine recycled aggregates are used [5]. Increasing the water content will necessitate an increase in the cement content to produce a cement paste that is equivalent to mixes made with conventional aggregates. The result is a costlier mix design. Workability can be improved by reducing (down to about 30%) or eliminating the amount of recycled fines in favor of natural fines, using water reducers, adding fly ash or a combination of all three. Using fly ash alone may not provide a workable mix and a reduction in the percentage or elimination of the recycled fines may be necessary. Slump loss is commonly observed for mixtures containing RCA due to its high absorption characteristics. Solutions include presoaking the aggregates or pre-wetting the stockpile. The higher and more variable absorption capacity of RCA also makes it difficult to determine the water content which in turn leads to variation in the strength of the hardened concrete. Higher and more variable air contents are common in fresh concrete made with RCA. This is due to the higher porosity of the recycled aggregates themselves and to the entrained air in the original mortar. Therefore, the target air content of mixtures containing RCA must be higher to achieve the same durability as conventional mixes [5].

As is the case for new concrete mixtures with virgin aggregates, the w/cm ratio should be optimized for placement and performance. Some research simply suggests that new concrete mixtures with RCA require additional water and cement. However, in order to achieve a workable mix that is strong and durable for paving applications, new concrete mixtures with RCA should be engineered to include chemical and mineral admixtures that minimize the need for additional water and cement [12-14]. Research in New Zealand resulted in a method for determining trial batch proportions based on a series of strength curves developed for a range of w/cm ratios for both RCA and virgin aggregate mixes [15]. RCA is more absorptive than natural aggregate because of its recycled mortar content. This makes it less dense and it requires more attention to mix design since each batch of recycled aggregate requires a unique adjustment to satisfy the absorption of the aggregates [8]. The absorption of both coarse and fine natural aggregate is around 1% or less. In order to not compromise the workability of the concrete some suggest simply wetting the aggregate or adding a little more water to the concrete mix. At a concrete batch plant or even onsite, the aggregate could be tested ahead of time to determine the absorption. If such testing is not feasible then sprinkling the RCA for 48 h before incorporating it in a concrete mix ensures that each aggregate batch is fully saturated [8].

As more RCA is used in place of virgin aggregate for the same mixture design, noticeable differences in concrete properties such as strength, workability, and durability become apparent. Research has shown that, when replacing virgin aggregate with RCA, there is a limit at which, when all other mix constituents (e.g., cement, water, air content) are held constant, concrete properties such as strength and durability are affected. In Austria, it is reported that virgin coarse aggregate can be replaced with up to 20% RCA [16]. In Australia, up to 30% of virgin coarse aggregate can be replaced by RCA, but only in new concrete

mixtures for curbs and sidewalks [17]. Research in the UK supports the use of 30% replacement of coarse aggregate with RCA and reports that there is little to no effect on concrete properties [18]. Research in Japan concludes that up to 20% coarse aggregate can be replaced with RCA without affecting concrete properties and that maximum aggregate size should be limited to a range of 16-20 mm [12]. RCA as a fine aggregate is not typically used in new concrete mixtures. It has been reported that RCA fine material contains increased amounts of contaminants that adversely affect concrete properties [19, 20]. Fine RCA may cause increased shrinkage, reduced strength, and reduced workability. Therefore, most specifications currently in existence that address the use of RCA in new concrete mixtures do not allow the use of RCA as a substitute for fine aggregate.

Compressive strengths of concrete containing RCA are generally slightly lower than that of concretes made with natural aggregates. Some studies cite two to ten percent lower compressive strengths, others report similar and sometimes higher strengths depending upon the water-cement ratios for the mixes. The higher air content normally found in mixes containing RCA may also lead to lower strength values [5]. Reduced concrete strength when RCA is used in place of virgin aggregates is attributed to the mortar fraction around the original aggregate. It has been shown that when a new concrete mixture has a higher *w/cm* and includes RCA with a strong transition zone between the original aggregate and the old concrete mortar fraction, the new concrete will exhibit strengths similar to that of the same mix if virgin aggregate were used. If the w/cm is low and the RCA transition zone is weak, the concrete will have lower strengths than if virgin aggregates were used in the same mix [21]. Reports indicate that the use of recycled coarse aggregate reduces the flexural strength by up to eight percent at the same water-cement ratio, and that this reduction increases if recycled fines are also used. The quality of the concrete used to produce the RCA has a strong influence on flexural strength, which relies most heavily on the paste-aggregate bond strength [5].

Hardened concrete containing RCA generally has a lower modulus of elasticity [14, 22]. The stiffness or modulus of elasticity of concretes made with RCA is 20 to 40 percent lower than that of conventional concrete at the same water-cement ratio. This reduction can be even greater when recycled fines are also used. The reduction in modulus of elasticity is due to the fact that recycled aggregates typically have lower elastic moduli than natural aggregates. A reduction in modulus of elasticity in pavement applications is not a serious concern from a fatigue standpoint, as the lower modulus should result in lower tensile stresses in the slab. On the deflection side, the lower modulus may result in increased corner deflections, which could result in more pumping and faulting at joints [5]. Hardened concrete containing RCA generally has a higher coefficient of thermal expansion (CTE) [14, 22]. Bond strength reductions between concrete and steel have not been noted when only coarse RCA is used; however, when recycled fines are used reductions have been reported. The additional water required to produce a workable mix in concretes using recycled fines is blamed for this reduced bond strength [5].

Various users have reported increased freeze-thaw resistance due to the higher entrained air contents that result from the air entrainment contained in the RCA aggregate. RCA should be tested prior to use to determine the potential for each particular source. In general, the D-cracking susceptibility of RCA is less because the aggregate that is susceptible is crushed to a smaller size in producing the RCA. The addition of fly ash has also been shown to reduce the D-cracking potential by increasing the workability of the mix which allows the use of less

water, thereby rendering the mix less permeable. Using natural sands rather than recycled sands also has been shown to be effective in reducing the D-cracking potential [5].

Alkali-silica reaction (ASR) potential is higher in mixtures that use RCA because more aggregate surfaces are exposed for the reaction by the crushing operation. This can be combated by using low alkali, Type II cement, blending the RCA with quality conventional aggregates, and using fly ash in the mix to reduce the expansion of the recycled concrete pavement [5]. A joint research effort between four universities was primarily focused on laboratory investigation of ASR in RCA [23,24]. Overall it was found that modifications to standard aggregate testing and characterization standards were necessary for testing RCA. It was found that the potential for ASR did exist for new concrete containing RCA. RCA with a higher content of reactive coarse or fine aggregate (compared to paste fraction) exhibited greater reaction and would therefore require higher levels of mitigation [23]. Generally, as the replacement level of RCA was reduced, the amount of supplementary cementitious material (SCM) needed to control deleterious ASR also decreased. Ternary blends containing metakaolin resulted in the most significant decrease in expansions compared to the mixtures with no SCMs. The amount of adhered mortar can affect the level of reactivity in an aggregate, and subsequently may affect the efficacy of an SCM to mitigate ASR [24].

The creep potential of concrete is generally proportional to the paste content of the mix. RCA mixtures, which contain more paste than conventional mixes, have a 20 to 40 percent higher creep potential. Creep is generally not a major concern in highway pavements [5]. Hardened concrete containing RCA generally experiences more drying shrinkage [14, 22]. Drying shrinkage in concrete is dependent upon the amount of excess water present in the fresh cement paste and the ability of the aggregate to restrain the paste from shrinking. Higher water-cement ratios, higher paste contents, and lower coarse aggregate contents will all tend to increase shrinkage. Mixtures with RCA have higher paste contents and thus have increased shrinkage. Mix designs that use both coarse and fine aggregates have the highest drying shrinkage [5].

## LONG-TERM PERFORMANCE OF RCA PAVEMENTS

From the vast amount of literature reporting on the laboratory-based investigations of both RCA itself as well as concrete made with RCA, it might be assumed that the field performance of concrete pavements made with RCA would be worse than that of pavements made with conventional aggregates. Studies on the actual performance of RCA pavements in the field tend to be limited in scope to distress evaluation and petrographic analyses of just a few sections, for example [25]. The long-term performance of RCA pavements based on a relatively large database has apparently not been evaluated. The relatively large network of RCA pavements in Minnesota and available historical performance records provided a good opportunity to evaluate the long-term performance of RCA pavements.

The pavement performance measures used by the Minnesota Department of Transportation (MnDOT) include the International Roughness Index (IRI), Ride Quality Index (RQI), Surface Rating (SR), and Pavement Quality Index (PQI). The IRI provides an objective measure of the roughness of the pavement. It simulates a standard vehicle traveling down the roadway and is equal to the total anticipated vertical movement of this vehicle accumulated over the length of the section. The IRI is typically reported in units of m/km (vertical meters of movement per km traveled) or inches/mile. The higher the IRI is, the rougher the roadway.

The IRI is correlated to the typical road-user's perception of the level of comfort in driving over a pavement section by means of a regression equation and this is called the RQI. The RQI is on a scale of 0 to 5 with 5 being excellent. Pavements are normally designed for a terminal RQI of 2.5. Once the RQI has reached 2.5, this generally signifies that a major Concrete Pavement Rehabilitation (CPR) must be performed. The RQI is used as the primary indicator of the condition of MnDOT's pavements in its Pavement Condition Annual Report, and is also the basis for predicting the remaining service life of a pavement.

The Surface Rating (SR) is used as the indicator for pavement distress. It varies between 0 to 4 with 4 being excellent. For jointed concrete pavement, the distresses which are considered include transverse joint spalling, longitudinal joint spalling, faulted joints, cracked panels, broken panels, faulted panels, overlaid panels, patched panels, and D-cracked panels. The percentage of each distress in a 152 m (500 ft) sample is determined and multiplied by a weighting factor to give a weighted percentage. The weighting factors are higher for higher severity levels of the same distress and higher for distress types that indicate more serious problems exist in the roadway such as alligator cracking and broken panels. The Pavement Quality Index (PQI) is the index that attempts to provide an overall condition rating based on both ride quality and distress. It ranges between 0 to 4.5 with 4.5 being excellent. The PQI can be calculated using:

$$PQI = \sqrt{RQI \times SR} \qquad (1)$$

A dataset of approximately 341 km (212 miles) of RCA pavements was analyzed. Figure 1 shows the average index value by years for RQI, SR, and PQI for RCA sections. As expected there is a trend of deterioration i.e. the values decrease with time; however, after about 23 years or so, the data show an increase. This is due to the influence of a large enough number of major CPR taking place and improving the index value, thus causing the average to move higher. It can also be observed that RQI is the lowest of the curves, and thus on average it can be expected that more CPR decisions will be triggered by RQI reaching the terminal value rather than the other indexes. For this reason, it was decided to mainly focus on RQI for forecasting and studying the difference in performance between RCA and conventional (non-RCA) concrete. It should also be noted that sometimes, corridor-wide improvements may take place, and even a pavement seemingly not in need of rehabilitation may be repaired.

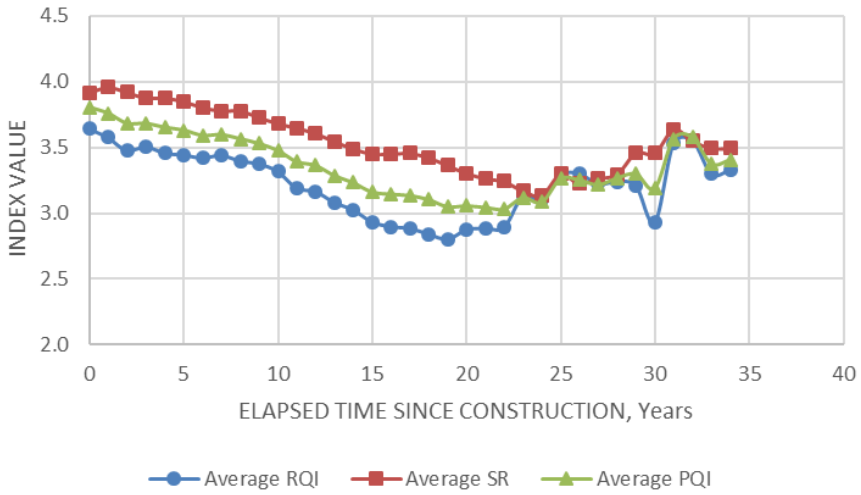


Figure 1 Average index values of RQI, SR, and PQI for RCA sections over time

To provide a comparison with the RCA pavements, a similar dataset of non-RCA concrete pavements was evaluated. Filtering was performed to consider only new construction in the 1980's and 1990's (to match the timeframe of the RCA sections) and similar range of Average Annual Daily Traffic (about 2000 to 90,000). Since the resulting database was still large, random sampling using the RAND() function in Excel was used to obtain a dataset of 341 km (212 miles) equalling the size for the RCA dataset.

The datasets were examined to establish the service life of the pavements. Since fluctuations can occur, the failure point was taken as the time for a pavement section to reach RQI of 2.5 for at least three years in a row. In the cases where a pavement had not reached the RQI of 2.5 during the period of record, or when a pavement had been rehabilitated before its time, it became necessary to forecast the time it would have taken to reach the terminal RQI. Two models were examined, namely the Holt-Winters triple exponential smoothing method and the Autoregressive Integrated Moving Average (ARIMA) model. A conservative approach was used by taking the smaller of the two predictions as the controlling one.

The triple exponential smoothing approach for forecasting can be summarized by:

$$s_t = \alpha \frac{x_t}{c_{t-L}} + (1-\alpha)(s_{t-1} + b_{t-1}) \quad (2)$$

$$b_t = \beta (s_t - s_{t-1}) + (1-\beta) b_{t-1} \quad (3)$$

$$c_t = \gamma \frac{x_t}{s_t} + (1-\gamma) c_{t-L} \quad (4)$$

$$F_{t+m} = (s_t + m b_t) c_{t-L+m} \quad (5)$$

where $x$ is the observation, $s$ is the smoothed observation, $b$ is the trend factor, $c$ is the seasonal index, $F$ is the forecast at $m$ periods ahead, $t$ is an index denoting a time period, $L$ is the number of periods in a season, and $\alpha$, $\beta$, $\gamma$ are constants (that typically range from 0.1 to 0.3) that must be estimated to minimize the mean squared errors.

ARIMA models are generally denoted as ARIMA(p,d,q) where $p$ is the number of autoregressive terms, $d$ is the number of nonseasonal differences needed for stationarity, and $q$ is the number of lagged forecast errors in the prediction equation. First let $y$ denote the $d^{th}$ difference of $Y$. This means

If d = 0: $y_t = Y_t$ (7)

If d = 1: $y_t = Y_t - Y_{t-1}$ (8)

If d = 2: $y_t = (Y_t - Y_{t-1}) - (Y_{t-1} - Y_{t-2})$ (9)

Then the general forecasting equation is given by

$$\hat{y}_t = a_t + \phi_1 y_{t-1} + \ldots + \phi_p y_{t-p} - \theta_1 a_{t-1} \ldots - \theta_q a_{t-q} \quad (10)$$

where $\hat{y}_t$ is the forecasted value, $y$ is the differenced value of the original data $Y$, $\phi$ are the autoregressive parameters, $\theta$ are the moving average parameters taken here to be negative following the Box-Jenkins convention, $a_t$ are the error or noise terms, $t$ is an index denoting

time and $p$ and $q$ are as defined previously. The modeling process usually begins by examining the degree of differencing required to remove non-stationarity. Next, some decision about the number of autoregressive and/or moving parameters required is made. This can be done by examining the autocorrelation and partial autocorrelation functions, in addition to observing the goodness of fit which can be obtained from software. For this study, the statistics software SYSTAT was used for both the exponential smoothing and ARIMA modeling and the ARIMA(2,1,1) model was found to adequately model the behavior.

The frequency distribution and probability density functions for both datasets appeared to approximate a normal distribution. The results are summarized in Table 2. For RCA sections, the time to reach major CPR i.e. RQI of 2.5 or less for at least 3 years ranged between 8 and 60 with a mean of 27. Using the one sided *z*-test for large samples with the sample mean as an estimator of the population mean, and standard deviation of the sample as an estimator for the standard deviation of the population; we are 95% confident that the true mean (population mean) of RCA pavements is larger than 26. We are 95% confident that the true mean is less than 28. Using the two-sided *z*-test, we are 95% confident that the true mean lies between 26 and 28. For non-RCA sections, the service life ranged between 5 and 60 with a mean of 32, Using the one-sided *z*-test, we are 95% confident that the true mean is larger than 30 and less than 33. Using the two-sided *z*-test, we are 95% confident that the true mean lies between 30 and 33.

Table 2 Summary Statistics for Service Life (in Years) for RCA and non-RCA Sections

| STATISTIC | RCA SECTIONS | NON-RCA SECTIONS |
|---|---|---|
| Sum of miles | 211.934 | 211.752 |
| Number of observations | 231 | 245 |
| Maximum service life | 60 | 60 |
| Minimum service life | 8 | 5 |
| Mean service life by observations | 27 | 30 |
| Variance by observations | 90 | 152 |
| Standard deviation by observations | 9 | 12 |
| Mean service life by miles | 27 | 32 |
| Variance by miles | 91 | 148 |
| Standard deviation by miles | 10 | 12 |
| Lower 95% confidence limit (one-sided) by miles | 26 | 30 |
| Upper 95% confidence limit (one-sided) by miles | 28 | 33 |
| Lower 95% confidence limit (two-sided) by miles | 26 | 30 |
| Upper 95% confidence limit (two-sided) by miles | 28 | 33 |

Tests were conducted to check if the difference between the population means of RCA and non-RCA sections are real or statistically significant. Using the *z*-test, we are 95% confident that the difference in means ($\mu_{\text{non-RCA}} - \mu_{\text{RCA}}$) will be more than 2.35 years. We are 95% confident that the difference in means will be less than 6.51 years. Both interval limits are positive, so this implies that the non-RCA sections have a higher time to reach major CPR i.e. perform better than RCA sections. Finally, hypothesis testing was performed. The null hypothesis was that there is no difference between the population means.

The *z*-test statistic resulted in 4.2. Since this exceeds $z_{0.025}$ which is 1.96, we can reject the null hypothesis at the 5% significance level. That is, the evidence suggests that the difference between the means is real, and the RCA sections performance is worse compared to that of the non-RCA sections.

## SUMMARY AND CONCLUSIONS

A review of literature and surveys of the various State DOT's in the US reveal that there was a period of time between the 1970s and 1990s when several test sections of concrete pavement containing RCA were created, primarily by four different states. Since that time, the activity has slowed significantly perhaps influenced by Michigan's moratorium on the use of RCA in new concrete. A growing number of recent research reports seems to show a renewed interest in this aspect. A vast amount of literature exists on lab-based investigations of physical and mechanical properties of RCA as an aggregate as well as of concrete made with RCA. In general, the results show inferior properties for the RCA and concrete made with RCA. In this paper, the long-term performance of concrete pavements made with RCA were compared with that of similar pavements made with conventional aggregates. The mean time to reach the condition of major CPR (i.e. RQI of 2.5) for RCA sections was found to be 27 years and for non-RCA sections was 32 years. The difference in means was found to be statistically significant, i.e. the RCA sections have a shorter service life than the non-RCA sections.

One possible reason for the differences seen may be the large absorption and variable levels of saturation in the RCA aggregate during construction which may have prompted additional water to be used to maintain workability. A second reason may be the inclusion of RCA fines which is essentially mortar. This could be less durable under abrasion. Finally, the top size aggregate is typically smaller in the crushed RCA which could result in poorer aggregate interlock. Sustainability practices dictate that the use of RCA still be considered when possible. One recent development in the US is the evaluation of the two-lift method where concrete with RCA could be used in the lower lift, and a thinner lift with more durable aggregate could be used on the top.

## ACKNOWLEDGEMENTS

This research was partially funded by a grant from the Minnesota Department of Transportation under Agreement No. 05309. The contents of this paper reflect the views of the authors and do not necessarily reflect the official views and policies of the Minnesota Department of Transportation or the Federal Highway Administration.

## REFERENCES

1. FEDERAL HIGHWAY ADMINISTRATION (FHWA) Transportation Applications of Recycled Concrete Aggregate, FHWA State of the Practice National Review, Federal Highway Administration, McLean, Virginia, September 2004.

2. GRESS, D L, SNYDER, M B, STURTEVANT, J R. Performance of Rigid Pavements Containing Recycled Concrete Aggregate – 2006 Update, Annual Meeting of the Transportation Research Board, Washington, D.C. January 2008.
3. SNYDER, M B. Performance of Concrete Pavements Constructed Using Recycled Concrete Aggregate – FHWA Study Update, Minnesota Concrete Conference, St Paul, MN. February 14, 2008.
4. STURTEVANT, J. Performance of Rigid Pavements Containing Recycled Concrete Aggregates, M.S. Thesis, University of New Hampshire. 2007.
5. ANDERSON, K W, UHLMEYER, J S, RUSSELL, M. Use of Recycled Concrete Aggregate in PCCP: Literature Search, Washington DOT Research Report WA-RD 726.1. June 2009.
6. GARBER, S, RASMUSSEN, R, CACKLER, T, TAYLOR, P, HARRINGTON, D, FICK, G, SNYDER, M, VAN DAM, T, LOBO, C. Development of a Technology Deployment Plan for the Use of Recycled Concrete Aggregate in Concrete Paving Mixtures, FHWA DTFH61-06-H-00011, work plan 27. June 2011.
7. CTC & ASSOCIATES. Concrete Recycling: Reuse of Returned Plastic Concrete and Crushed Concrete as Aggregate, Preliminary Investigation for Caltrans Division of Research and Innovation by CTC & Associates LLC. September 7, 2012.
8. VANCURA, M, KHAZANOVICH, L, TOMKINS, D. Reappraisal of Recycled Concrete Aggregate as Coarse Aggregates in Concretes for Rigid Pavements, Transportation Research Record No. 2113, pp. 149-155, 2009.
9. MEINHOLD, U, MELLMANN, G, MAULTZSCH, M. Performance of High-Grade Concrete with Full Substitution of Aggregates by Recycled Concrete, Third CANMET/ACI International Symposium on Sustainable Development of Cement and Concrete, ISBN 0-87031-041-0, 2001.
10. GOMEZ, J, AGULLO, L, VAZQUEZ, E. Repercussions on Concrete Permeability Due to Recycled Concrete Aggregate, Third CANMET/ACI International Symposium on Sustainable Development of Cement and Concrete, ISBN 0-87031-041-0, 2001.
11. SCHOUENBORG, AURSTAD, J, PETERSSON, P. Test Methods Adapted to Alternative Aggregates, Conference on the Use of Recycled Materials in Building and Structures, Abstract 253, Barcelona, Spain, 2004.
12. DOSHO, Y. Development of a Sustainable Concrete Waste Recycling System: Application of Recycled Concrete Aggregate Concrete Produced by Aggregate Replacing Method, Tokyo Electric Power Company (TEPCO), Tokyo, Japan, 2007.
13. HANSEN T, NARUD, H. Strength of Recycled Concrete Made from Crushed Coarse Aggregate, Concrete International, January Edition, Farmington Hills, Michigan, 1983.
14. BURKE, T, COHEN, M, SCHOLER, C. Synthesis Study on Use of Concrete Recycled from Pavement and Building Rubble in the Indiana Highway System, Joint Highway Research Program, Purdue University, West Lafayette, Indiana, 1992.
15. ZHANG W, INGHAM, J. Using Recycled Concrete Aggregates in New Zealand Ready-Mix Concrete Production, Journal of Materials in Civil Engineering, ASCE, Vol. 22, No. 5, 2010.

16. SOMMER, H. Recycling of Concrete for the Construction of the Concrete Pavement of the Motorway Vienna – Salzburg, 7th International Symposium on Concrete Roads, Vienna, 1994.
17. CCA. Use of Recycled Aggregates in Construction, Cement Concrete & Aggregates Australia, on-line, 2008.
18. LIMBACHIYA M, KOULOURIS, A, ROBERTS, J, FRIED, A. Performance of Recycled Aggregate Concrete, RILEM International Symposium on Environmental-Conscious Materials and Systems for Sustainable Development, Print-ISBN: 2-912143-55-1, RILEM Publications SARL, 2004.
19. RILEM. Specifications for Concrete with Recycled Aggregates, International Union of Laboratories and Experts in Construction Materials, Systems, and Structures (RILEM), Materials and Structures, Vol. 27, 2004.
20. SMITH J, TIGHE, S, NORRIS, J, KIM E, and XU, X. Coarse Recycled Aggregate Concrete Pavements – Design, Instrumentation, and Performance, Recycled Materials and Recycling Process for Sustainable Infrastructure Session, Conference of the Transportation Association of Canada, Toronto, Ontario.
21. OTSUKI, N, MIYAZATO, S, YODSUDJAI, W. Influence of Recycled Aggregate on Interfacial Transition Zone, Strength, Chloride Penetration and Carbonation of Concrete, Journal of Materials in Civil Engineering, 2003.
22. ACPA. Recycling Concrete Pavements, American Concrete Pavement Association, Skokie, Illinois, 2009.
23. IDEKER, J H, ADAMS, M P, TANNER, J, JONES, A. Durability Assessment of Recycled Concrete Aggregates for Use in New Concrete Phase I – Revised, Oregon Transportation Research and Education Consortium Research Report OTREC-RR-11-09 Revision 1. October 2013.
24. IDEKER, J H, ADAMS, M P, TANNER, J, JONES, A. Durability Assessment of Recycled Concrete Aggregates for Use in New Concrete Phase II Report, Oregon Transportation Research and Education Consortium Research Report OTREC-RR-13-01. June 2014.
25. CUTTELL, G D, SNYDER, M B, VANDENBOSSCHE, J M, WADE, M J. Performance of Rigid Pavements Containing Recycled Concrete Aggregates, Transportation Research Record 1574. Transportation Research Board, Washington, D.C. 1997.

# ENGINEERING PROPERTIES OF CONCRETE MADE WITH BRICK DUST WASTE

**J E Oti**

**J M Kinuthia**

University of South Wales

United Kingdom

**ABSTRACT.** This research work reports the potential of using Brick Dust Waste (BDW) as a partial substitute for Portland Cement (PC) in the development of concrete. BDW is a recycled waste materials that is sourced from the demolishing of fired clay brick buildings or the discarded by-product materials from the cutting of fired clay bricks into shape and sizes for the construction of chimneys, and other uses needing the use of fired bricks. This results in the disposal of BDW as an environmental problem of concern. BDW has pozzolanic properties that enables it play an important role in the strength and durability of concrete, its use in concrete will alleviate the increasing challenges of scarcity and high cost of cement and will help to strike a balance between the sustainability of the environment and the demand on construction due to the increase in population growth worldwide. In order to investigate the Cement replacement potential of BDW, four types of mixes were designed at varying BDW replacement levels—10%, 20%, 30% and 40% with a water binding ratio of 0.6 and tested at 7, 14, and 28 days. The testing programme included material characterisation, the determination of slump value and compressive strength.

**Keywords:** Brick dust waste, Concrete; Sustainability, Cement; strength.

**Dr Jonathan E Oti** is a Senior Lecturer in Civil Engineering and the MSc Course leader at the University of South Wales. A renowned practitioner in the field sustainable construction material technology, he is a member of numerous national and international technical committees and has published extensively on many aspects of concrete technology, cement science and unfired clay masonry bricks.

**Prof John M Kinuthia** is a Professor of Innovation and Engagement in Civil Engineering and Head of the Centre for Engineering, Research and Environmental Applications (CEREA) at the University of South Wales. He has published extensively on many aspects of concrete technology, cement science and unfired clay masonry bricks.

## INTRODUCTION

There has been a rise in the construction of civil infrastructure worldwide, leading to an increase in the use of concrete. This results in the consumption of billions of tons of conventional aggregate and cement by the construction industry. Previous work by Mehta and Monteiro [1] estimated the annual concrete production to be about 11 billion metric tons, out of which, around 10–15% is cementitious binder and the majority of the cementitious binder used in concrete is based on Portland Cement (PC) clinker, which is an energy-intensive process, about one ton of PC production is responsible for one ton of carbon dioxide ($CO_2$) emission [2]. Several environmental concerns are being raised regarding the high energy usage and $CO_2$ emission in the PC production process. In order to mitigate against this concern, a push towards the use of pozzolanic materials such as pulverised Fuel Ash [3], marble dust [4], fly ash/quarry dust [5] and agricultural wastes such as palm kernel shell and ash [6] in PC replacement is required.

Baronio and Binda [7] reported that, the Greeks used of pozzolans in construction. When the Romans took over, they refined the practice and discovered brick dust as a new pozzolanic material which they mixed with lime to obtain a strong, durable binding material. Another work by Bektas [8] reported that kaolin clay demonstrates a high pozzolanic activity when used as PC replacement material. A Study carried out by O'Farell et al [9], reported an increased resistance of mortar mixture to sulphate attack when ground bricks is been added to the mixture. A recent research carried out by Toledo Filho et al [10] reported on the potentials of using crushed waste calcined-clay brick as a supplementary cementitious material in Brazil.

This research reports on the results of the investigation on the slump value and strength of concrete made by partially replacing 10%, 20%, 30% and 40% of the PC in conventional concrete with Brick Dust Waste (BDW). The use of a cement replacement material such as BDW in the production of concrete will increase environmental sustainability, by the reducing the high energy usage and $CO_2$ emission during cement production process, it will also help to reduce the problems associated with the demolition of fire clay building or discarded by-product materials from cutting of fired clay bricks.

## MATERIALS

### Brick Dust Waste

The Brick Dust Waste (BDW) used for this research was supplied by Brick Fabrication Ltd., Gemini Works, Pontypool, South wales, UK. Some engineering properties of the material and its oxide/mineralogical compositions can be seen in Table 1.

### Portland Cement

The Portland cement (PC) used throughout this research was manufactured in accordance with BS 197-1 [11] and supplied by Lafarge Cement UK. The minimum compressive strength of the PC is 32.5 $N/mm^2$. The physical properties and Oxide/chemical composition of the PC are shown in Table 2.

### Limestone Aggregates

The limestone aggregate used throughout this investigation was size 10/4. The aggregate was supplied by a local quarry and complied with the requirements of PD 6682-1 [12] and BS EN 12620 [13]. Some geometrical, mechanical and physical properties of the limestone aggregate in compliance with BS EN 1097-6 [14], BS EN 933-4 [15] and BS 812-112 [16] are shown in Table 3. The results of sieve analysis of the limestone aggregate performed in accordance with BS EN 933-1: [17] are also given in Table 4.

### Sand

The sand used throughout this study was natural sea-dredged sand from the Bristol Channel. Some geometrical, mechanical and physical properties of the sand in compliance with BS EN 1097-6 [14], BS EN 933-4 [15] and BS 812-112 [16] are also are given in Table 3.The results of sieve analysis of the sand performed in accordance with BS EN 933-1: [17] are given in Table 4.

Table 1 Some engineering properties and oxide/mineralogical compositions of BDW

| **Properties** | |
|---|---|
| Specific gravity | 2.5 |
| Bulk density (kg/m$^3$) | 1837 |
| Maximum Dry Density (MDD)(Mg/m$^3$) | 1.5 |
| Optimum moisture content (OMC) (%) | 17 |
| Colour | Brick red |
| **Oxide** | % |
| $SiO_2$ | 52 |
| $Al_2O_3$ | 41 |
| $Fe_2O_3$ | 0.7 |
| CaO | 4.32 |
| MgO | 0.12 |
| $K_2O$ | 0.53 |
| $SO_3$ | 0.33 |
| $TiO_2$ | 0.65 |
| $Na_2O$ | 0.05 |
| L.O.I | 2.01 |
| **Compound** | |
| Kaolinite | 54% |
| Aunite | 5% |
| Quartz | 41% |

Table 2 The physical properties and Oxide/chemical composition of the PC

| **Properties** | |
|---|---|
| Insoluble Residue | 0.5 |
| Bulk Density (kg/m³) | 1400 |
| Relative Density | 3.1 |
| Blaine fineness ($m^2$/kg) | 365 |
| Colour | Grey |
| **Oxide** | **%** |
| $SiO_2$ | 20.00 |
| $Al_2O_3$ | 6.00 |
| $Fe_2O_3$ | 3.00 |
| MgO | 4.21 |
| MnO | 0.03 - 1.11 |
| $SO_3$ | 2.30 |
| Loss on Ignition | 0.8 |
| **Chemical (%)** | |
| Cl | 0.03 |
| Free lime | 1.32 |
| **Bogue's composition** | |
| Tricalcium aluminate ($C_3A$) | 6.48 |
| Tricalcium silicate ($C_3S$) | 70.58 |
| Dicalcium silicate ($C_2S$) | 6.09 |
| Tetracalcium alumunate-ferrite ($C_4AF$) | 6.45 |

Table 3 Some geometrical, mechanical and physical properties of the limestone aggregate

| PROPERTY | SAND | LIMESTONE 10/4. |
|---|---|---|
| Water absorption (%) | 0.85 | 1.5 |
| Saturated density ($Mg/m^3$) | 2.82 | 2.68 |
| Dry density ($Mg/m^3$) | 2.71 | 2.57 |
| Shape index (%) | – | 12 |
| Impact value (%) | – | 23 |

## METHODOLOGY

### Mix Design

The control mix (MC) was a RC28 concrete strength type designed in accordance with BS 8500-2:2015, target slump range of 100-150mm, water cement ratio of 0.6, binder: fine aggregate: coarse aggregate portion of 1: 2: 3. Based on the control mix for the concrete, the

current investigation developed four mixes, by using BDW to replace the Portland Cement PC in the control mix, the various combinations as shown in Table 5. The first mix was referred as MC1 which is the mix produced by replacing 10% of the PC in the control mix with BDW. For the second mix (MC2), 20% of the PC in the control concrete mix was replaced with BDW. The third mix was designated MC3 and the mix was produced by replacing 30% of the PC in the control concrete mix with BDW. The final mix was designated MC4 and the mix was produced by replacing 40% of the PC in the control concrete mix with BDW.

**Sample preparation and testing**

Cube (100 mm × 100 mm × 100 mm) test specimens were used in the production of all the concrete. For all mix compositions, the test specimens, were prepared in accordance with BS EN 206 [18], BS EN 12350-1[19] and BS EN 12390-1 [20]. The consistency of the fresh concrete was measured using slump test in accordance with BS EN 12350-2 [21]. De-moulding of the test specimens was done after 24 hours. The curing of the test specimens were carried out in accordance with BS EN 12390-2 [22]. All the cube specimens were tested for 7, 14 and 28 -day compressive strength in accordance with BS EN 12390-3 [23] and BS EN 12390-4 [24]. For all mix compositions, the results reported are the average obtained from five individual specimens for compressive strength

Table 4 Sieve analysis of the limestone aggregate and sand

| SIEVE SIZES (mm) | SAND | LIMESTONE 10/4. |
|---|---|---|
| 31.5 | 100 | 100 |
| 16 | 100 | 100 |
| 8 | 100 | 77 |
| 4 | 100 | 2 |
| 2 | 83 | 0.3 |
| 1 | 54 | 0.28 |
| 0.5 | 21.8 | 0.19 |
| 0.25 | 6 | 0.14 |
| 0.125 | 1.2 | 0.1 |

Table 5 The various combinations

| MIX CODE | % REPLACEMENT | WEIGHT OF VARIOUS MIX MATERIALS (KG) | | | | |
|---|---|---|---|---|---|---|
| | | PC | BDW | Sand | Limestone | Water |
| MC (Control) | 0 | 6.0 | 0.0 | 12 | 12 | 3.6 |
| MC 1 | 10 | 5.4 | 0.6 | 12 | 12 | 3.6 |
| MC 2 | 20 | 4.8 | 1.2 | 12 | 12 | 3.6 |
| MC 3 | 30 | 4.2 | 1.8 | 12 | 12 | 3.6 |
| MC 4 | 40 | 3.6 | 2.4 | 12 | 12 | 3.6 |
| **Note** | PC = Portland Cement; BDW = Brick Dust Waste | | | | | |

## RESULTS

### Slump

Figure 1 shows the results of the slump test for all mixes. The target slump was only achieved with MC1, MC4 and the control. It was not possible to achieve this target slump for the concrete mixes where the PC in the concrete control mix was replaced with 20% and 30% BDW. The Highest slump value was observed for the control mix. The lowest slump value was observed for Mix MC3 (the mix where 30% of the PC in the control concrete was replaced with BDW). Overall, there was a gradual reduction in slump value with the addition of BDW, the only exception was mix MC4 (the mix where 40% of the PC in the control concrete was replaced with BDW). No segregation was observed for all the mixes.

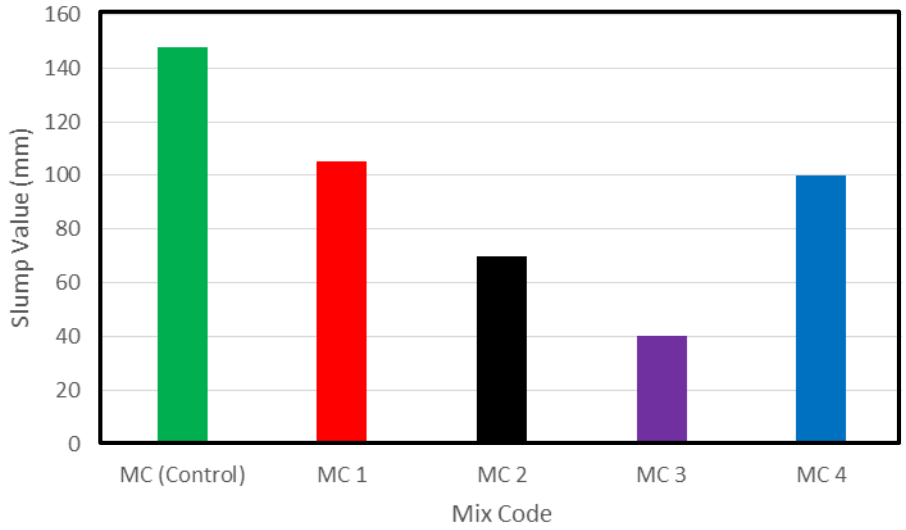


Figure 1 The Slump values for all mixes

### Compressive Strength

Figure 2 shows the results of the compressive strength for 7, 14 and 28 days. There was a progressive increase in strength values for all the mix compositions with age. The compressive strengths for Mixes MC1, MC2 and the control were all well above the targeted strength of 28N/mm$^2$.There was an initial slow increase in strength for MC1, but the mix rapidly gained more strength after 14 days of curing to achieve the highest strength at 28 days of curing. The lowest Compressive strength value was observed for mix MC4, this was the mix produced by replacing 40% of the PC in the control mix with BDW.

## DISCUSSION

There were some observed variations in the slump values of the various mixes with the addition of BDW. It appears that a continual trend of reduction in slump values was developed for every percentage increase in the amount of BDW in the concrete mix, the only exception is mix MC4, this is the mix where 40% of the PC in the control mix was replace with BDW. This trend is line with the findings from previous researches carried out by O'Farrel et al [9] and Bektas [8] which reports that there was a gradual reduction in the slump values for every percentage increase in ground clay bricks replacement with PC. A similar research carried out by Golaszweski et al [25] on the influence of ground brick on the physical properties of mortar

and concrete also confirms that the slump values of concrete made by replacing PC with BDW varies with the addition of BDW. This is believed to be due to the complex mechanisms associated with the degree at which ground bricks absorbs more water in the mix, which varies in a non-systematic manner from one mix composition to another. The use of ground clay bricks as partial PC replacement increases the water demand due to the increase in fineness of BDW compared to PC.

The variations observed with regards to the compressive strength was a progressive increase in strength values for each mix composition as the curing age increases. Mix MC1 which has a 10% replacement of ordinary PC with BDW attained a higher strength at 28 days. This higher strength gain might be due to the gradual formation of the calcium silicate hydrate gel (C-S-H gel) in the hydration process due to a 62% increase in silicon dioxide ($SiO_2$), which BDW has over ordinary PC, making it possess more dicalcium silicate ($C_2S$), which is responsible for the strength gain at the later days age. This also explains the continuous increase in strength over a prolonged curing age [9].

According to Bektas et al (2007), this behaviour of a higher gain in strength as experienced in this current research is well expected, since BDW is known to be a pozzolanic material that produces more secondary C-S-H gels. There was an early strength gain for the control mix, at 7 and 14 days curing age. This might be due to a high amount of tricalcium silicate ($C_3S$) present within the PC, which is responsible for early strength gained and forms the bulk of the C-S-H gel and calcium hydroxide ($Ca(OH)_2$) produced during hydration. The 20% replacement of BDW is considered as the optimum replacement level in the research, previous work by Toledo et al [10], reported no detrimental effect in terms of strength up to 20% replacement of ground clay bricks in concrete

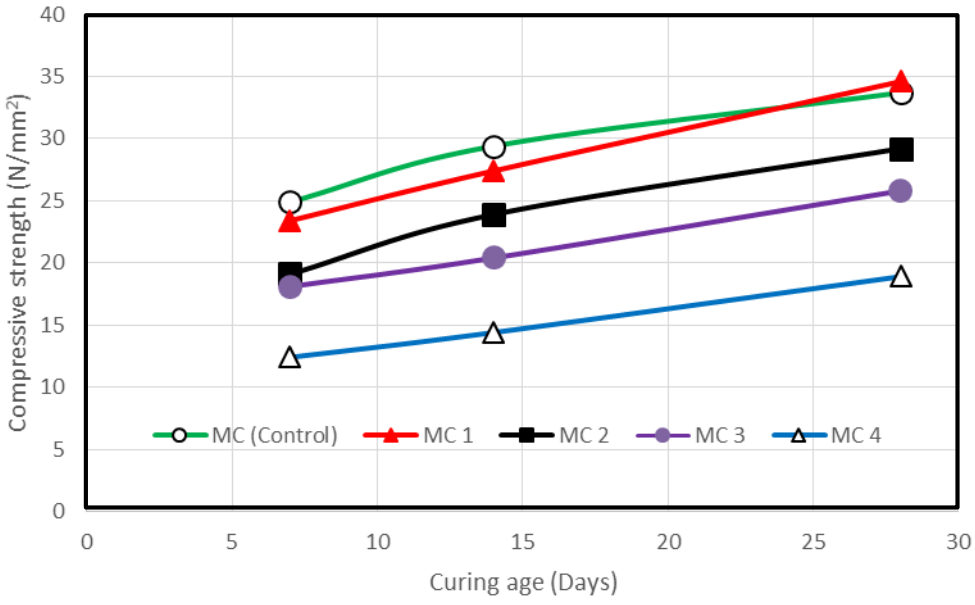


Figure 2 Compressive strength for all mixes

## CONCLUSIONS

The investigation carried out in the current study has demonstrated the potential of replacing up to 40% PC with BDW. The key conclusions that can be drawn from this investigation are summarised in the following list.

1) There was variation in the slump values of the concretes with the addition of BDW. The highest slump value was observed from the control mix while the lowest slump value was observed from mix MC3, this is the mix where 30% of the PC in the control mix was replace with BDW.
2) The results of the compressive strength test showed that the highest strength value was obtained for mix MC1, which is the mix produced by replacing 10% PC in the control mix with BDW. The lowest strength was obtained from the concrete where 40% of the PC in the control concrete was replaced with BDW.

## REFERENCES

1. MEHTA, PK, MONTEIRO, PJM. Concrete - Microstructure, Properties, and Materials, 3rd edition, 2006, New York, NY: McGraw Hill.

2. World Business Council for Sustainable Development (2005). The cement Sustainability initiative: Progress report, 2005. Available at: http://www.wbcsdcement.org/ pdf/csi_progress_report_2005.pdf, (Accessed 28th June, 2015).

3. OTI J. E, KINUTHIA J.M, ROBINSON R, DAVIES P. Heating and Cooling Scenario of Blended Concrete Subjected to 780 Degrees Celsius. World Academy of Science, Engineering and Technology, International Science Index 100, International Journal of Civil, Environmental, Structural, Construction and Architectural Engineering 2015, 9(4), 407 – 413.

4. ALIABDO, A.A, ELMOATY, M.A, AUDA, E.M. Re-use of waste marble dust in the production of cement and concrete. Construction and Building Materials 2014, 50, pp. 28–41.

5. SHAKIR, A.A, NAGANATHAN, S, MUSTAPHA K.N. Properties of bricks made using fly ash, quarry dust and billet scale. Construction and building materials 2013, 41, pp. 131–138

6. OTI J, KINUTHIA J, ROBINSON R, DAVIES P. The Use of Palm Kernel Shell and Ash for Concrete Production. World Academy of Science, Engineering and Technology, International Science Index 99, International Journal of Civil, Environmental, Structural, Construction and Architectural Engineering 2015, 9(3), 263 – 270.

7. BARONIO G. AND BINDA L. (1997). Study of the pozzolanicity of some bricks and clays. Construction and Building Materials 1997, 11(1), pp.41-46.

8. BEKTAS F. Use of ground clay brick as a supplementary cementitious material in concrete hydration characteristics, mechanical properties and ASR durability. Phd Thesis 2007, Iowa State University.

9. O' FARRELL M., WILD S., SABIR B. B. Pore size distribution and compressive strength of waste clay brick mortar. Cement & Concrete Composites 2001, 23(1), pp.82.

10. TOLEDO FILHO R. D., GONCALVES J. P, AMERICANO B. B., FAIRBAIRN E. M. R. Potential for use of crushed waste calcined-clay brick as a supplementary cementitious material in Brazil. Cement & Concrete Research 2007, 37(9), pp.1357-1365

11. BS EN 197-1: 2011. Cement - Part 1: Composition, Specification and Conformity Criteria for Common Cements

12. PD 6682-1:2009+A1:2013. Aggregates – Part 1: Aggregates for concrete – Guidance on the use of BS EN 12620

13. BS EN 12620:2002 +A1:2008. Aggregates for concrete

14. BS EN 1097-6:2013- Tests for mechanical and physical properties of aggregates Part 6: Determination of particle density and water absorption

15. BS EN 933-4:2008. Tests for geometrical properties of aggregates Part 4: Determination of particle shape — Shape index

16. BS 812-112: 1990. Testing aggregates — Part 112: Methods for determination of aggregate impact value (AIV)

17. BS EN 933-1:2012-Tests for geometrical properties of aggregates Part 1: Determination of particle size distribution — Sieving method

18. BS EN 206:2013-Concrete. Specification, performance, production and conformity

19. BS EN 12350-1:2009. Testing fresh concrete Part 1: Sampling.

20. BS EN 12390-1:2009.Testing hardened Concrete. Part 1: Shape, dimensions and other requirements of specimens and moulds

21. BS EN 12350-2:2009. Testing fresh concrete Part 2: Slump-test.

22. BS EN 12390-2:2009.Testing hardened Concrete. Part 2: Making and curing specimens for strength tests.

23. BS EN 12390-3:2009.Testing hardened Concrete. Part 3: Compressive strength of test specimens.

24. BS EN 12390-4:2009.Testing hardened Concrete. Part 4: Compressive strength - Specification for testing machines.

25. GOLASZEWSKI, J. SUCHON, S SZWABOWSKI, J. O'FARRELL, M. SABIR, B. B, WILD S. The Influence of Ground Brick on the Physical Properties of Mortar and Concrete - Modern Concrete Materials: Binders, Additions and Admixtures. January 1999, p 119-130

# STONE-INTERLOCKING CONCRETE: MECHANISM, EXPERIMENT AND APPLICATION ON PHC TUBULAR PILE

**W Shen**

**X Chen J Bai**

**H Yang C Li X Li**

Wuhan University of Technology

China

**ABSTRACT.** The high extra mortar and paste content in the cement concrete leads to separation in the spun casting prestress high concrete（PHC）tubular pile. Scattering-filling coarse aggregate (SFCA) is employed to fabricate the PHC tubular pile by adding 5~15% of coarse aggregate in the concrete to prepare a type of coarse aggregate interlocking concrete (CAIC) PHC tubular pile on factorial manufacture. The experimental results show that the extra coefficient of cement paste in SFCA is much lower than the ordinary one; strength of SFCA concrete increases and its cementitious materials consumption is significantly reduced; and the volume of coarse aggregate is higher than the ordinary concrete, so the coarse aggregate can interlock with each other firmly, the mortar lay in the tubular pile can be restricted below 5mm, the inner structure of tubular pile becomes more integrity therefore higher impacting resistance is obtained. The SFCA reduced the cost and the environmental impact of tubular pile and increased the ratio of finished product, so SFCA has a promising application prospect.

**Keywords**: PHC tubular pile, Spun casting, SFCA, Environmental impact, Application prospect

**Weiguo Shen** is a Professor at State Key Laboratory of Silicate Materials for Architecture, Wuhan University of Technology. Where he received his BS, MS and Ph.D. He is an executive director of WUT-UC Berkeley Joint Laboratory on Concrete Science and Technology, vice director of International Cooperation Base on Environment Friendly Materials, Council Member of Portland cement branch of Chinese Ceramic Society Chairman of China Concrete Canoe Race Committee. He was a visiting scholar of Northwestern University and a visiting Professor of UC Berkeley. His research interests include low carbon cement and concrete, Life Cycle Assessment of carbon footprint of cement materials, nano structure of cement materials and solid waste cementitious materials.

## INTRODUCTION

Concrete is arguably the most widely used manufactured materials in the world. The production processes of concrete result in tremendous environmental impact as cement is the most remarkable ingredient in the concrete which has the largest resource consumption, energy intensity, green house gases and acid rain gases emission [1-3]. The manufacture of Portland cement (PC) is responsible for up to 10% of anthropogenic $CO_2$ emissions worldwide. To prepare qualified concrete with low cement content is a very effective approach to reduce the total environment impact of the concrete and even the human activity $CO_2$ emission.

The concrete is a three phased material: aggregate particles, interfacial transitional zone (ITZ) and cement paste matrix [4]. The coarse aggregate is the strength framework of the plain concrete and it is the structure unit with highest strength, volume stability, durability and lowest cost in the most concrete [5, 6]. As a composition material, the concrete's hydration heat, shrinkage, permeability and creep will decrease, whereas the strength, elasticity modulus and anti-cracking will increase with the increase of coarse aggregate content [7-9]. The conventional plastic or fluidal concrete is prepared by mixing the binders (cement and mineral admixture), fine aggregate, coarse aggregate and water together then placing and vibrating the mixture to fabricate a consolidated matrix. In order to keep the fresh mixture a reasonable flowability and avoid gravity segregation, the aggregate content in the conventional concrete (especially those high strength high performance concrete) keeps relatively low [10]. The total aggregate volume fraction in high performance concrete is around 65% [11] and the coarse aggregate volume ratio is around 40%, so the aggregates can't act fully as the matrix structure of the concrete. The high volume fraction of cement paste increases the permeability, creep and drying shrinkage of the concrete [11]. To address this, Shen, et al [12-14] developed a new concrete placing process named scattering-filling stone method: adding 10~30% (by the volume of the finished concrete) of coarse aggregate while the concrete is being poured, paved or placed, then vibrating the matrix to form a consolidated concrete as illustrated in Figure 1.

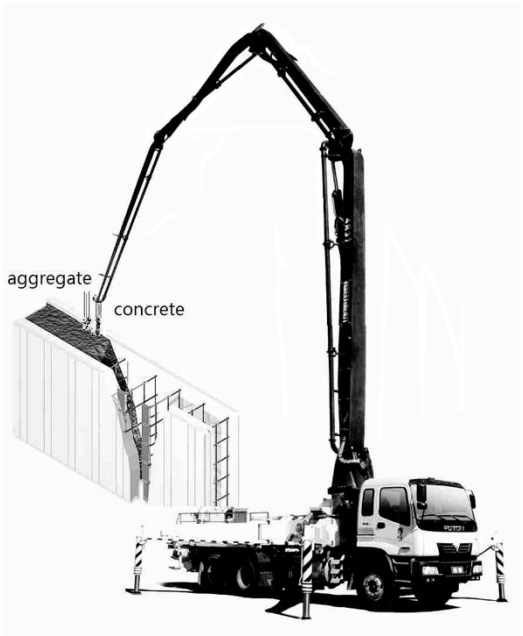


Figure 1 Schematic diagram of the scattering-filling concrete placing process

The concrete produced with this technology contains 10~30% less cement content than the conventional made concrete so it is a typical low carbon concrete. In this paper, the mechanism of this concrete is revealed, and the experiment and engineering utilization of this technology is reported.

## THE MECHANISM OF THE COARSE AGGREGATE INTERLOCKING CONCRETE

As illustrated in Figure 2, with the increase of coarse aggregate in the concrete, its workability will become worse. To keep a reasonable workability, the w/c ratio need to be increased, therefor the strength of concrete will reduce. Whereas the increase of the coarse aggregate increased the strength, modules of concrete, it reduced the permeability, shrinkage, creep, and hydration heat. In general, the increase of coarse aggregate makes the workability worse but makes the service performance better.

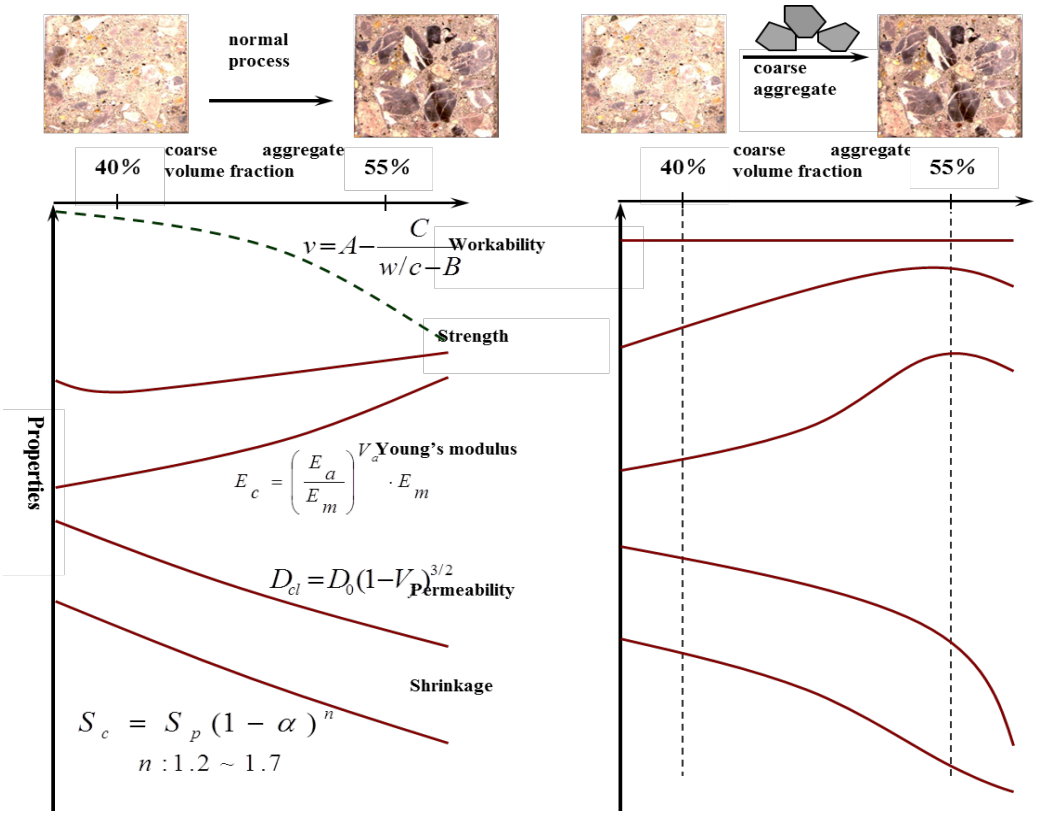


Figure 2 The mechanism of Scattering-Filling Stone Concrete

This new SFS process is a solution to this dilemma. The concrete is designed, mixed and ship with traditional method, so the fresh concrete keep the workability of itself. When the concrete is cast, the coarse aggregate (stone, it can be coarser than the original coarse aggregate in the concrete) is scattered in, therefore, the finished concrete has high coarse aggregate content, thus the service performance increased. First of all, the coarse aggregate volume fraction increases dramatically in this type of concrete when more than 20% of coarse aggregate is scattered in the mixture. The coarse aggregates can interlock with each other and the friction

forces among the aggregate contribute to the strength enhance in a certain extent. The second, the coarse aggregate distributes more evenly in this kind of concrete than the concrete prepared with conventional process. With the vibration, the segregation of the coarse aggregate toward the bottom of the formwork and the cement paste toward the top may result in the conventional concrete [17], so the surface of the concrete will be very weak. When scatting-filling process is applied, the coarse aggregate will fill evenly at the top of the form. The third, the addition of extra amount of air dry coarse aggregates acts as somewhat water reducer, not only reduces the W/C of the paste close to the aggregate and make the paste stronger, so the ITZ of the concrete is enhanced. With the volume fraction of the aggregate increasing, as a composite material, the concrete will become stronger and stiffer.

## EXPERIMENTAL STUDY

The conventional tubular pile concretes with strength grade of C80 are prepared with 5-25mm coarse aggregate, river sand with fineness modulus of 3.1, P ‖ 52.5R cement, fine quartz filler, naphthalene water reducer and drinking water. The mixing proportions and the properties of the tubular pile concrete with different content of adding coarse aggregate are listed in Table 1. The concrete was formed in mould with size of 100×100×100mm$^3$, the N serial concrete specimens are preparing with ordinary method, the C specimens are prepared with CFSC process, the mothed is reported elsewhere [13, 14].

Table 1 The mixing properties and properties of tubular pile concrete

| No. | MIXING PROPORTION (kg/m$^3$) | | | | | | ADDING AGGREGATE* | SLUMP (mm) | CURING METHOD | $f_{cc}$（MPa） |
|---|---|---|---|---|---|---|---|---|---|---|
| | Cement | Quartz filler | Crushed stone | Sand | FDN | water | | | | |
| $N_{000}$ | 310.0 | 140.0 | 1225.0 | 683.0 | 12.0 | 135.0 | 0 | 75 | Steam | 53.8 |
| | | | | | | | | | Autoclave | 95.2 |
| $N_{050}$ | 294.5 | 133.0 | 1163.8 | 648.9 | 11.4 | 128.3 | 5% | 0 | Steam | 54.2 |
| | | | | | | | | | Autoclave | 95.8 |
| $C_{050}$ | 294.5 | 133.0 | 1163.8 | 648.9 | 11.4 | 128.3 | 5% | 75 | Steam | 54.3 |
| | | | | | | | | | Autoclave | 96.1 |
| $C_{075}$ | 286.7 | 129.5 | 1133.1 | 631.8 | 11.1 | 124.9 | 7.5% | 75 | Steam | 54.7 |
| | | | | | | | | | Autoclave | 97.4 |
| $C_{090}$ | 282.1 | 127.4 | 1114.8 | 621.5 | 10.9 | 122.9 | 9% | 75 | Steam | 54.6 |
| | | | | | | | | | Autoclave | 99.8 |
| $C_{120}$ | 272.8 | 123.2 | 1078.0 | 601.0 | 10.6 | 118.8 | 12% | 75 | Steam | 55.4 |
| | | | | | | | | | Autoclave | 103.8 |
| $C_{150}$ | 263.5 | 119.0 | 1041.3 | 580.6 | 10.2 | 114.7 | 15% | 75 | Steam | 56.6 |
| | | | | | | | | | Autoclave | 100.9 |

Note: the volume percentage of adding coarse aggregate in the finish concrete by volume.

It can be found that the strength of the concrete increased with the content of adding coarse aggregate, and reach a peak value when 12% of aggregate was added and filled in. After the peak value, the strength reduced a little but was still higher than the control group. It is easy to find that concretes with 100 MPa can be prepared with only 263.5 Kg/$m^3$ of cement and 119 Kg/$m^3$of filler, which can be never achieved with the conventional concrete placing process. The scattering-filling stone can prepare concrete with very high coarse aggregate, although the "pre-placed aggregate" concrete process [16] can prepare concrete with as low cement dosage as this process, but it can only prepare low or middle strength concrete. The scattering-filling stone method can produce higher strength and performance at the same time. The decrease on cement dosage not only give the concrete good cost competitive but also good environmental harmonization. If the coarse aggregate (5% by volume) is added directly in before mixing, the strength can improve obviously but the fresh concrete has no slump and the workability is poor.

## THE UTILIZATION OF SCATTERING-FILLING STONE CONCRETE IN PHC TUBULAR PILE

The scattering-filling stone concrete was used in the prestress high strength tubular pile concrete in a factory of Yangjiang, Guangdong China. The mix proportion of the original concrete is listed in Table 1 as control group. Around 10-12% of Scattering-Filling Stone Aggregate is added in the mould of the tubular pile, then the fresh concrete is cast in, after the low speed centrifugal process, high speed centrifugal process and curing, tubular pile is prepared, the appearance is just the same as the pile prepared with normal process. The cross section of tubular piles is shown at Figure 3.


a) The pile made with normal process(A, B) b) pile made with CFSC process (C, D)

Figure 3 The cross section of tubular pile with difference process

Form Figure 3, it is very clear that, in the normal PHC tubular pile, the coarse aggregate enriches at the outer wall of the pile, the cement paste enriches at the inner wall, around 20mm paste can be found at the inner wall. Because the paste has lower modules and higher shrinkage than the concrete, when the pile is push in the soil foundation, the paste will be broken and scaled and the loading ability reduced significantly. Adding aggregate by SFSC process can prepare concrete with higher content of coarse aggregate, and the coarse aggregates interlock together and build a framework of aggregates. Therefore, the inner structure of tubular pile become more uniform, having higher strength and less shrinkage.

The tubular pile concrete is a dry concrete and has relatively low cementitious content. About 10~15% of cement can be saved when SFSC is used to produce tubular pile. It is well known that the tubular pile has very low slump and compacted by centrifugal force, there are nearly no mortar more than needed in this kinds of concrete, whereas, this SFC process can be used and get good technical and economic benefit. If we can invent an equipment to fulfil the scattering- filling stone process in the flowing especially the pumping concrete, much more aggregate can be scattered and filled in the mixes, and thus much more cement can be saved and the performance of concrete can be improved more remarkably. This process can be used to produce nearly all types of concrete mixes except that roll compact and no fine mixes. Once this concrete produce technology have the opportunity to be applied in all the possible concrete project, more than 15% of cement could be saved and around 1% of the anthropogenic $CO_2$ could be reduced, i.e. nearly 0.3 billion tonnes of $CO_2$ could be reduced annually. Therefore, it is promising to be a low carbon solution to the concrete industry.

## CONCLUSIONS

This paper presents a new type of SFSC process developed by the first author. The mechanism, experimental study and engineering application of this process in manufacture of prestress high strength concrete tubular pile are reported. The following conclusions can be drawn:

1. The increase of coarse aggregate volume fraction increases the service performances but reduces the workability of fresh concrete in conventional concrete, however, the use of SFSC increases the volume fraction of coarse aggregate without influence on the workability of the original concrete.

2. With the increasing of adding aggregate, the strength of concrete increased and reached a peak volume around 12% of coarse aggregate addition.

3. The application of SFSC in prestress high strength tubular pile indicates this process can be successfully used, the strength of the tubular pile increased and 10-12% cement saved.

## ACKNOWLEDGMENTS

The author acknowledges the funding support of Hubei Highway Bureau and the independent innovation foundation of State key laboratory of Silicate Materials for Architecture, Wuhan University of Technology.

## REFERENCES


1. MEHTA P K. Concrete technology for sustainable development. Concrete Intern 1999; 21(11): 47-53.
2. MIZUGUCHI H. A review of environmentally friendly concrete. Concrete Intern. 1998; 36(1): 9-12.
3. VAN OSS H G, PADOVANI A C. Cement Manufacture and the Environment, Part II: Environmental Challenges and Opportunities. J Industr Ecol. 2003; 7, (1): 93-126.
4. A.U. NILSEN, P.J.M MONTEIRO. Concrete: A Three Phase Material. Cement and Concrete Res.1993. 23(2): 147-151.
5. ÖZTURAN T, ÇEÇEN C. Effect of coarse aggregate type on mechanical properties of concretes with different strengths. Cement Concrete Res. 1997; 27(2): 165-170.
6. BESHR H, ALMUSALLAM A. A, MASLEHUDDIN M. Effect of coarse aggregate quality on the mechanical properties of high strength concrete. Constr Build Mater 2003; 17(2): 97-103.
7. STOCK A F, HANNANT D J, WILLIAMS R I T. The effect of aggregate concentration upon the strength and modulus of elasticity of concrete. Mag Concrete Res 1979; 31(2): 225– 234.
8. COUNTO U.J. The effect of elastic modulus of the aggregate on the elastic modulus, creep and creep recovery of concrete. Mag Concrete Res. 1964; 16(2): 129.
9. HIRSCH, T.J. Modulus of elasticity of concrete affected by elastic module of cement paste matrix and aggregate. ACI Mater J 1962; 59(3): 427–451.
10. ALEXANDERSON J. The influence of the properties of Cement and aggregates on the consistency of concrete. Proc. RILEM Seminar 1971; 23(2): 12-22 .
11. MEHTA P K, MONTEIRO P J M. Concrete: Microstructure, Properties, and Materials. New York, McGraw-Hill, 1993.
12. SHEN W, ZHANG T , ZHOU M, ET AL. Investigation on the scattering-filling stone self-consolidating concrete. Materials and structures, 2010,43 (10):1343–1350.
13. SHEN W, DONG R, LI J ET AL. A study on the coarse aggregate interlocking concrete. Construction and building material, 2010,24(11) 2312–2316.
14. SHEN W, CAI Z, ZHOU M. High Strength Coarse Aggregate Interlocking Concrete: Preparation And Properties, 8th International sympsum on utilization of High-strength and High performance concrete (fib), 2008, Tokyo, 188-192.
15. BESTE U, JACOBSON S. Micro scale hardness distribution of rock types related to rock drill wear, Wear 2003,254 (5):1147–1154.
16. NEVILLE A.M. Properties of concrete. London, Pitman publishing limited, 1981.
17. MINDESS S, YOUNG J F, DAVID D. Concrete (Second Edition), New Jersey. Pearson Education, Inc. 2003.

# EVALUATING THE FLEXURAL FATIGUE PERFORMANCE OF CONCRETE MADE WITH COARSE RECYCLED CONCRETE AGGREGATES

**S P Singh**

**S Arora**

Dr B R Ambedkar National Institute of Technology

India

**ABSTRACT.** Results of an investigation conducted to evaluate the flexural fatigue performance of concrete made with Coarse Recycled Concrete Aggregates (RCA) are presented. The replacement of Coarse Natural Aggregates (NA) with RCA was kept at 50% and 100%. Concrete beams made with 100% NA were also tested for comparison purpose. The flexural fatigue performance of concrete beams made with RCA has been assessed in terms flexural fatigue life distributions and two-million cycle endurance limit. Experiments were conducted to obtain the flexural fatigue lives of concrete beams made with RCA and NA tested under different stress levels. Specimens of size 100 mm × 100 mm × 500 mm were tested under four point flexural fatigue loads applied at a frequency of 10 Hz using 100 kN MTS Servo-controlled Actuator. It has been shown that the fatigue life distributions of concrete made with RCA and NA can approximately be modelled by the two-parameter Weibull distribution. The results indicated higher variability in the distribution of fatigue lives of concrete made with RCA viz. a viz. concrete made with NA. The two-million cycles endurance limit for concrete made with RCA has been found to be lower than that of concrete made with NA.

**Keywords:** Coarse recycled concrete aggregates (RCA), Natural aggregates (NA), Flexural fatigue performance, Two-million cycles fatigue strength.

**S P Singh** is a Professor of Civil Engineering at Dr B R Ambedkar National Institute of Technology Jalandhar, India. His research interests are fatigue behaviour of concrete composites and recycling of materials in concrete.

**S Arora** is a Research Scholar in Department of Civil Engineering at Dr B R Ambedkar National Institute of Technology, Jalandhar (Pb.), India.

## INTRODUCTION

Concrete industry is the largest consumer of natural resources at global level with a consumption of 12.6 billion tonnes of raw materials per annum [1]. By the end of 2015, the global market for construction aggregates is expected to increase 48.3 billion tonnes [2]. In USA, the Environmental Protection Agency [3] estimated that the generation of debris, from construction, demolition, and renovation of residential and non-residential buildings in 2003, was close to 170 million tonnes. As per Eurostat [4], the total amount of waste generated in the European Union, in 2010, was over 2.5 billion tonnes, of which almost 860 million tones belonged to construction and demolition activities. Out of 48 million tonnes of solid waste generated in India, annual C & D waste makes up 25% [5]. Dumping of C&D waste requires lot of space which is gradually causing serious environmental issues. Since maintenance and protection of environment is vital for the survival of human race, the strategy of converting this C&D waste into valuable coarse aggregates can be of suitable choice. This can be achieved by breaking or crushing the concrete waste materials into suitable sizes as per requirements. Adopting this particular approach would automatically preserve the accumulation of waste on an open land and would help preserving the space.

The amount of coarse aggregates required for concrete production make up nearly 65% of total raw materials. Production of one tonne of NA and RCA respectively results in the emission of 4600 tonnes and 2400 tonnes of carbon. Keeping in view the consumption rate of aggregates at 10 billion per year, one can easily calculate the carbon emissions for NA as well as for RCA [6].

The utilization of RCA as coarse aggregates has been explored over last few decades so that sustainability of concrete be maintained [7]. The mechanical properties of concrete containing 100% RCA have been investigated in previous studies, keeping the various parameters same such as water–cement ratio, volume of aggregates and with same amount of cement and water as used in concrete made with NA. Due to high variability observed for the characteristic properties of RCA, a large number of experiments need to be conducted so that a suitable mix can be achieved for obtaining the desired requirements of concrete made with RCA [8].

A few investigations have been carried out to estimate the mechanical performance of concrete made with RCA under static loadings by replacing NA partially and fully with RCA [9]. A previous study has concluded that the compressive strength of concrete containing RCA is lower than that of concrete containing NA at same W/C ratio, and this behavior has been attributed to the dissimilar fracture process in concrete containing RCA and concrete containing NA [10]. The strength behavior of concrete containing RCA has been correlated to the microstructural features using scanning electron microscopy, wherein loose hydration products were observed in interfacial transition zone (ITZ) of normal strength concrete and relatively dense hydration products in ITZ of high performance concrete [11]. Concrete containing 100% RCA usually gives lower strengths (1-15%), lower modulus of elasticity (13-18%) and reduction in the fracture energy (27-45%) when compared with concrete containing 100% NA [12]. Density of RCA is generally less than that of NA due to the low density of adhered mortar than the underlying rocks [13]. With bulk densities of 2394 $Kg/m^3$ and 2890 $Kg/m^3$ observed for RCA and NA respectively, researchers have reported a density difference of about 17% between the two [14]. Limbachiya et al. have reported the density of RCA to be 7-9% lower than that of NA [15]. The water absorption of RCA and NA has been reported to be 4.9-5.2% and 1.0-2.5% respectively. The gradation curves for RCA lie in the range which is required for aggregates to be accepted for use in the concrete production [16]. Amount of

adhered mortar signifies the strength features of source concrete, effectiveness of crushing procedure, crushing method and particle size of RCA. It has been found that the presence of adhered mortar degrades the quality of RCA and the RCA surface becomes rough with an irregular shape due to the presence of adhered mortar [17]. When compared to NA, RCA exhibits poor mechanical properties such as low crushing strength, low impact resistance and low abrasion resistance than natural aggregate [14, 15, 18]. Consequently, the quality and quantity of RCA used in concrete strongly affects the strength properties of concrete.

Vast literature is available on the rheological properties of fresh and mechanical properties of hardened concrete containing RCA under statically applied loads. Utilization of RCA as partial or complete replacement of NA in concrete production would offer huge number of benefits to the construction industry in terms of cost reduction and solving the issues of waste disposal. RCA can be applied in making bridge decks & piers, precast structural elements, pavements, high rise buildings, etc. These structures are usually subjected to dynamic loadings, therefore, there is a need to investigate the performance of concrete containing RCA under fatigue loading. Undoubtedly, a fair amount of studies have been carried out in order to investigate the fatigue behavior of concrete containing NA. For instance, the fatigue behavior of concrete containing NA has been investigated by testing 462 cylindrical specimens under static and dynamic compression [19, 20]. Empirical expressions between the stress level (S), number of cycles (N) and probability of failure ($P_f$), S-N-$P_f$ relationships, were derived on the basis of fatigue strength results [19]. The effect of variable stress levels on the fatigue behavior of concrete containing NA was investigated under flexure loading and it was reported that the Palmgren-Miner hypothesis might give conservative or unsafe predictions of the fatigue strength, depending on the loading schemes [20, 21]. Unfortunately, few studies have been carried out on the fatigue performance of concrete containing RCA. These studies have shown that the fatigue life decreases as the percentage of RCA is increased in replacement with NA [7, 22]. Due to the significant spread observed in the fatigue test data of concrete containing RCA, efforts have been made to apply the probabilistic approach to predict its flexural fatigue strength. The wide potential of RCA as quality aggregate prompted the authors to work in this direction and to carry out the present study to evaluate the flexural fatigue behavior of concrete beam specimens containing 100% RCA.

## RESEARCH SIGNIFICANCE

In depth review of literature reported indicates that good amount of research has been conducted to investigate the flexural fatigue behavior of concrete containing NA. Regarding RCA, only the mechanical properties of concrete containing RCA under statically applied loads have been the subject of interest for past few years. Lack of information on the flexural fatigue characteristics of concrete containing RCA motivates the one to analyse the same so that suitability of RCA can be effectively realised in concrete production and application. Thus, the present investigation was designed to evaluate the flexural fatigue performance of concrete containing 100% RCA and concrete containing 50% RCA, and to compare the same with concrete containing 100% NA. Two-parameter Weibull distribution has been verified at different stress levels to establish the probability distributions of concrete made with RCA and NA respectively. Further, the two-million cycles fatigue strength/endurance limit of concrete made with RCA has been estimated from the S–N diagrams.

## EXPERIMENTAL PROCEDURE

In the study, 96 beam specimens of size 100 mm × 100 mm × 500 mm were tested for their flexural fatigue and 72 specimens of size 100 mm × 100 mm × 500 mm were tested for their static flexural strength under four point flexural loading. The quality of concrete made in each batch was also checked by conducting compressive strength tests on concrete cubic specimens of size 150 mm × 150 mm × 150 mm for the respective batch, after 28 days of curing.

### Materials and Mix Proportions

Grade 43, Ordinary Portland Cement (PC) has been used in this study. Well-graded RCA with maximum size of 12.5 mm obtained by crushing the concrete specimens available in the Concrete Laboratories of this Institute were used. The specific gravity of RCA is 2.46 and water absorption value of 5.39. Natural Aggregates (NA) with same grading was procured from local market. The grading of RCA and NA was purposely made nearly similar to each other as it was proposed to compare the results of concrete made with RCA and concrete made with NA. Figure-1 shows the grading of RCA and NA used in current study.

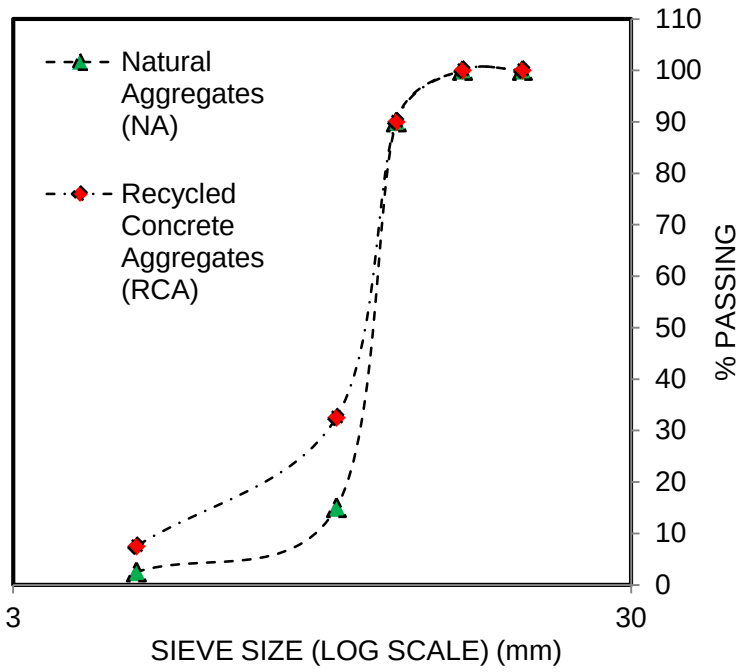


Figure 1 Sieve analysis of RCA and NA used in current study

Locally available coarse sand was used as fine aggregates. Class F fly ash was used as partial replacement of PC at 30% by weight of cementitious materials. A polycarboxylic ether (PCE) based superplasticizer (SP) was used as chemical admixture in suitable dosages to obtain the required workability of concrete mixes containing RCA and NA. The mix proportions for different concrete mixes containing 100% RCA (M1), 100% NA (M2) and 50% RCA & 50% NA (M3) are shown in Table-1.

Table 1 Mix proportions per cum of concrete made with RCA and NA

| AGGREGATE USED | CEMENT (kg) | FLY ASH (kg) | FINE AGGREGATES (kg) | COARSE AGGREGATES (kg) | WATER (liters) |
|---|---|---|---|---|---|
| RCA | 343 | 148 | 762 | 935 | 206 |
| NA | 343 | 148 | 762 | 1003 | 206 |
| RCA + NA | 343 | 148 | 762 | 468 + 501 | 206 |

**Casting of Specimens**

In this investigation, slump test was performed to control the workability of all the mixes and obtained slump was in the range of 65 mm to 90 mm. Batch-wise casting of specimens was carried out wherein each batch consisted of three cube specimens (size 150 mm × 150 mm × 150 mm) for determining 28- days compressive strength and seven standard beam specimens (size 100 mm × 100 mm × 500 mm) for static flexure and flexural fatigue tests. Mixing was done in a drum mixer and the fresh pastes were poured into the standard molds. The filled molds were compacted using vibration at 3600 r.p.m. The specimens were demoulded after 24 hours of casting and kept in water for curing at standard temperature of $27\pm2^0$C until tested for flexure or compression. The average compressive strengths obtained for 28 days cured mixes M1, M2 and M3 were 31.70 MPa, 41.77 MPa and 34.23 MPa respectively. Batch-wise compressive strength of M1, M2 and M3 after 28 days of curing is summarized in Table-2. The beam specimens were water cured under laboratory conditions for 90 days and stored in the laboratory environment for another 60 days in order to avoid possible increase in the strength during the fatigue tests.

Table 2 Compressive strength and static flexural strength test results of concrete made with RCA and NA (Present Investigation)

| BATCH NO. | 28 DAYS COMPRESSIVE STRENGTH (MPa) | | | STATIC FLEXURAL STRENGTH (MPa) | | |
|---|---|---|---|---|---|---|
| | RCA | NA | RCA + NA | RCA | NA | RCA + NA |
| 1 | 30.24 | 35.40 | 34.90 | 4.59 | 5.95 | 5.32 |
| 2 | 32.09 | 40.69 | 35.29 | 4.84 | 4.90 | 5.41 |
| 3 | 34.52 | 36.83 | 30.91 | 4.17 | 5.29 | 3.84 |
| 4 | 32.87 | 46.24 | 33.19 | 4.89 | 4.45 | 5.22 |
| 5 | 31.66 | 41.54 | 36.32 | 4.66 | 4.89 | 5.19 |
| 6 | 31.10 | 44.37 | 33.09 | 4.29 | 5.22 | 4.28 |
| 7 | 30.56 | 47.62 | 35.62 | 3.98 | 5.05 | 5.44 |
| 8 | 30.47 | 41.44 | 34.53 | 4.79 | 5.02 | 4.39 |
| AVERAGE | 31.7 | 41.77 | 34.23 | 4.53 | 5.1 | 4.89 |

### Flexural Fatigue Testing

Static flexural tests were carried out for each mix (i.e. mixes M1, M2 and M3) prior to fatigue tests in order to determine the maximum and minimum load limits to be applied during flexural fatigue tests on the specimens. At least three specimens from each batch were tested to determine the static flexural strength of that batch. The average value of static flexural strengths obtained for concrete mixes M1, M2 and M3 were 4.53 MPa, 5.1 MPa and 4.89 MPa respectively, and the same has been tabulated batch-wise in Table-2. The remaining four specimens from a particular batch were tested for flexural fatigue once the static flexural strength was evaluated for each batch. The static flexural and flexural fatigue tests were conducted on a 100 kN Servo-controlled Actuator. The loading points in flexural fatigue tests were kept the same as in static flexural tests. The flexural fatigue tests were conducted at different stress levels S ($S = f_{max}/f_r$), ranging from 0.85 to 0.55. The fatigue stress ratio R ($R = f_{max}/f_{min}$) was kept constant at 0.10 throughout the investigation. All the tests were conducted at constant amplitude in the form of sinusoidal loads applied at a frequency of 10 Hz. The cycle counter of the flexural testing machine displayed the number of cycles to the failure of each specimen under fatigue loading. In the present investigation, an upper limit of $2 \times 10^6$ cycles of fatigue loading was chosen as the number of specimens to be tested was large [23, 24, 25]. As soon as the failure of the beam specimen occurred or it reached the fixed upper limit of two million cycles, the test was terminated. Table-3 shows the number of specimens tested at each stress level and the corresponding flexural fatigue results of mixes M1, M2 and M3.

## RESULTS AND DISCUSSION

### Fatigue Life Distributions

To analyse the Weibull Distribution Parameters in the present investigation, three methods have been employed i.e. Graphical Method, Method of Moments and Method of Maximum Likelihood. The results obtained for the different concrete mixes at various stress levels using these methods are discussed below.

### Graphical method

Firstly the graphical method has been employed to verify that the fatigue life data of concrete mixes M1, M2 and M3 can be modelled by the two-parameter Weibull distribution at a given stress level. Subsequently, the graphical method, method of moments and method of maximum likelihood have been used to determine the parameters of the Weibull distribution.

The reliability function $L_N\ (n)$ of the two-parameter Weibull distribution may be written as follows [24 – 28]:

$$L_N(n) = exp\left[\frac{n}{u}\right]^{\alpha} \qquad (1)$$

Where $n$ is the specific value of random variable N; $\alpha$ = Shape parameter at stress level S; $u$= characteristic life at stress level S.

Table 3 Laboratory fatigue life data (number of cycles to failure N, in ascending order) for concrete made with RCA and NA (Present Investigation)

| FATIGUE LIFE DATA 'N' | | | | | |
|---|---|---|---|---|---|
| STRESS LEVEL S → | SPECIMEN NO. | 0.85 | 0.75 | 0.65 | 0.55 |
| RCA | 1 | 567 | 192[a] | 67225 | 478640[b] |
| | 2 | 789 | 4353 | 68738 | 567390[b] |
| | 3 | 1054 | 5615 | 88969 | 763984[b] |
| | 4 | 1188 | 9382 | 90371 | 1167919[b] |
| | 5 | 1345 | 9792 | 120805 | ---- |
| | 6 | 1765 | 12829 | 189763 | ---- |
| | 7 | 1897 | 13702 | 249867 | ---- |
| | 8 | 2098 | 14045 | 261009 | ---- |
| | 9 | 2156 | 23020 | 319551 | ---- |
| | 10 | 2354 | 26079 | 409876 | ---- |
| RCA+NA | 1 | 688 | 7261 | 86887 | ---- |
| | 2 | 982 | 9762 | 138405 | ---- |
| | 3 | 1041 | 10172 | 163781 | ---- |
| | 4 | 1128 | 12674 | 220108 | ---- |
| | 5 | 1429 | 16554 | 347947 | ---- |
| | 6 | 1673 | 20673 | 361778 | ---- |
| | 7 | 1931 | 23752 | 374560 | ---- |
| | 8 | 2176 | 29401 | 396702 | ---- |
| | 9 | 2294 | 32963 | 595673 | ---- |
| | 10 | 2567 | 39675 | ---- | ---- |
| NA | 1 | 444[a] | 10781 | 100801 | ---- |
| | 2 | 1137 | 13879 | 142054 | ---- |
| | 3 | 1367 | 18489 | 187623 | ---- |
| | 4 | 1678 | 21945 | 220075 | ---- |
| | 5 | 1945 | 25467 | 260685 | ---- |
| | 6 | 2271 | 31256 | 323068 | ---- |
| | 7 | 2605 | 36543 | 360845 | ---- |
| | 8 | 2647 | 42842 | 456944 | ---- |
| | 9 | 3096 | 46951 | 512089 | ---- |
| | 10 | 3987 | 51348 | 558973 | ---- |

[a]Rejected as outlier by Chauvenet's Criterion, not included in analysis.
[b]Used for S-N curves only.

Taking the logarithm twice on both sides of Equation (1):

$$l_n\left[l_n\left(\frac{1}{L_N}\right)\right] = \alpha l_n n - \alpha l_n u \quad (2)$$

or;

$$Y = \alpha X - \beta \quad (3)$$

where, $Y = ln[ln(1/ L_N)]$, $X = ln\ (n)$, and $\beta = \alpha\ ln\ u$.

Equation (2) represents a linear relationship between $ln[ln(1/L_N)]$ and $ln(n)$, which can be used to verify the suitability of the two-parameter Weibull distribution for the description of fatigue life data of concrete mix M1, M2 and M3. To do so, the fatigue life data at a given stress level must be first arranged in ascending order and the empirical survivorship function $L_N$ is then obtained from the following expression [24 – 27, 29]:

$$L_N = 1 - \frac{i}{k+1} \quad (4)$$

Where, $i$ = failure order number, and $k$ = number of fatigue data points at a given stress level S. A graph is plotted between the $ln[ln(1/ L_N)]$ and $ln(N)$and if the test data, at a particular stress level, follows approximately straight line, it can be observed that two-parameter Weibull distribution is a reasonable assumption for the description of fatigue test data at that stress level. Fig.-2(a), Fig.-2(b) and Fig.- 2(c) show the plot of the fatigue life data of M1, M2 and M3, at stress levels (S = 0.85). It can be observed that the data points fall approximately along a straight line, indicating that the two-parameter Weibull distribution is reasonably valid for the distribution of fatigue life of concrete mixes M1, M2 and M3 at the considered stress level. The corresponding values of the correlation coefficient, $C_c$, observed from the graphical method are 0.989, 0.982 and 0.957 for M1; 0.99, 0.994 and 0.996 for M2; and 0.988, 0.983 and 0.982 for mix M3 at stress levels 0.85, 0.75 and 0.65 respectively. The values of the Weibull parameters obtained by this method are $\alpha$ = 2.090 & $u$ = 1761 [30]; $\alpha$ = 2.442 and $u$ = 2619; and $\alpha$ = 2.287 and $u$ = 1822 for mix M1, M2 and M3 at stress level, $S$ = 0.85.

**Method of moments**

Shape parameter $\alpha$ and scale parameter $u$ can also be calculated using the following relationships [24 -26, 29]:

$$\alpha = (COV)^{-1.08} \quad (5)$$

and,

$$u = \frac{\mu}{\Gamma\left(\frac{1}{\alpha}+1\right)} \quad (6)$$

where, $\mu$ is the sample mean of the fatigue life data at a given stress level, COV (= $\sigma/\mu$, $\sigma$ is standard deviation of data sample) is the coefficient of variation of the data, and $\Gamma$ is the gamma function.

The parameters obtained by the method of moments for concrete mix M1, M2 and M3 are $\alpha$ = 2.6458 & $u$ = 1716 [30]; $\alpha$ = 2.7711 and $u$ = 2540 [30]; and $\alpha$ = 2.6917 and $u$ = 1754 respectively at stress level $S$ = 0.85.

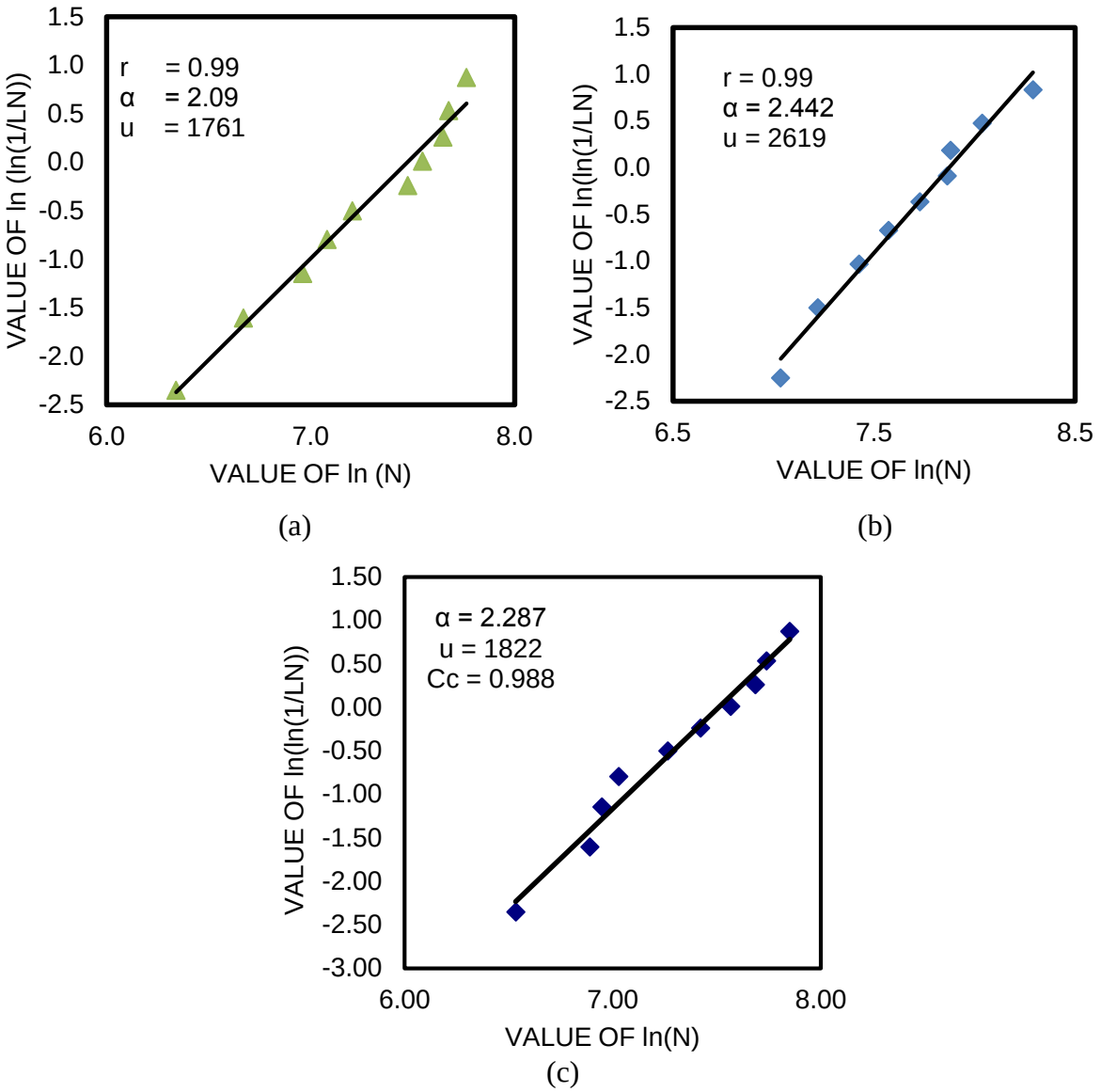


Figure 2 Graphical analysis of fatigue life data of concrete made with (a) 100% RCA at stress levels S = 0.85 (b) 100% NA at stress levels S = 0.85. (c) 50% RCA and 50% NA at stress levels S = 0.85.

**Method of maximum likelihood estimation**

The probability density function of Weibull distribution may be written as follows:

$$f_N(n) = \frac{\alpha}{\theta} n^{\alpha-1} \, exp\left[\frac{n^\alpha}{\theta}\right] \quad (7)$$

in which;

$$\theta = u^\alpha \quad (8)$$

The maximum likelihood function may be then expressed as:

$$\frac{\sum_{i=1}^{k}\left(n_i{}^{\alpha^*} l_n(n_i)\right)}{\sum_{i=1}^{k} n_i{}^{\alpha^*}} - \frac{1}{\alpha^*} = \frac{1}{k}\sum_{i=1}^{k} l_n n_i \quad (9)$$

$$\theta^* = \frac{1}{k}\sum_{i=1}^{k} n_i{}^{\alpha^*} \quad (10)$$

Where, $\alpha^*$ and $\theta^*$ are the maximum likelihood estimators of '$\alpha$' and '$\theta$' respectively. The parameter '$\alpha$' may now be obtained from Eq. (9) by a simple computer program based on iterative procedure. The parameter '$u$' is then estimated from the Eq. (6); i.e., $u = \theta^{1/\alpha}$.

The values evaluated, for concrete mix M1 from the method of maximum likelihood are $\alpha$ = 2.934 and $u$ = 1711 at stress level $S$ = 0.85. Similarly, with the same method, obtained values of Weibull distribution parameters for mix M2 are $\alpha$ = 2.9505 and $u$ = 2587 at stress level $S$ = 0.85 [30]. The values of parameters for mix M3 are $\alpha$ = 2.9365 and $u$ = 1790. The values of the parameters estimated by various methods for the three concrete mixes M1, M2 and M3 at all the stress levels are listed in Table-4 along with their average values.

A comparison of parameters obtained in the present investigation for concrete made with 100% RCA (M1) has been made with that of the concrete made with 100% NA (M2)and the concrete made with 50% RCA & 50% NA (M3). The comparisons are shown in Table-4. The results of the on static flexural strength of concrete mixes M1, M2 and M3 are plotted in Fig.-3 for the purpose of comparison.

Table 4 Values of shape parameters $\alpha$ and characteristic life $u$ for the fatigue life data of concretes made with RCA and NA

| AGGREGATES USED | METHODS | S = 0.85 | | S = 0.75 | | S = 0.65 | |
|---|---|---|---|---|---|---|---|
| | | α | u | α | u | A | u |
| RCA | Graphical Method | 2.09 | 1761 | 1.647 | 15395 | 1.424 | 218895 |
| | Method of Moments | 2.646 | 1715 | 1.898 | 14888 | 1.620 | 210449 |
| | Maximum Likelihood | 2.934 | 1712 | 2.055 | 14971 | 1.752 | 210922 |
| | Average | 2.556 | 1729 | 1.867 | 15085 | 1.598 | 213422 |
| NA | Graphical Method | 2.442 | 2619 | 1.8810 | 34794 | 1.760 | 362629 |
| | Method of Moments | 2.7711 | 2540 | 2.2491 | 33801 | 2.0879 | 349097 |
| | Maximum Likelihood | 2.9505 | 2587 | 2.4405 | 33909 | 2.2515 | 353990 |
| | Average | 2.7212 | 2582 | 2.1902 | 34168 | 2.0331 | 355239 |
| RCA + NA | Graphical Method | 2.287 | 1822 | 1.71 | 23490 | 1.572 | 350521 |
| | Method of Moments | 2.6917 | 1754 | 1.9395 | 22897 | 1.96 | 333572 |
| | Maximum Likelihood | 2.9365 | 1790 | 2.0950 | 23029 | 2.1 | 337905 |
| | Average | 2.6384 | 1789 | 1.9148 | 23139 | 1.8802 | 340666 |

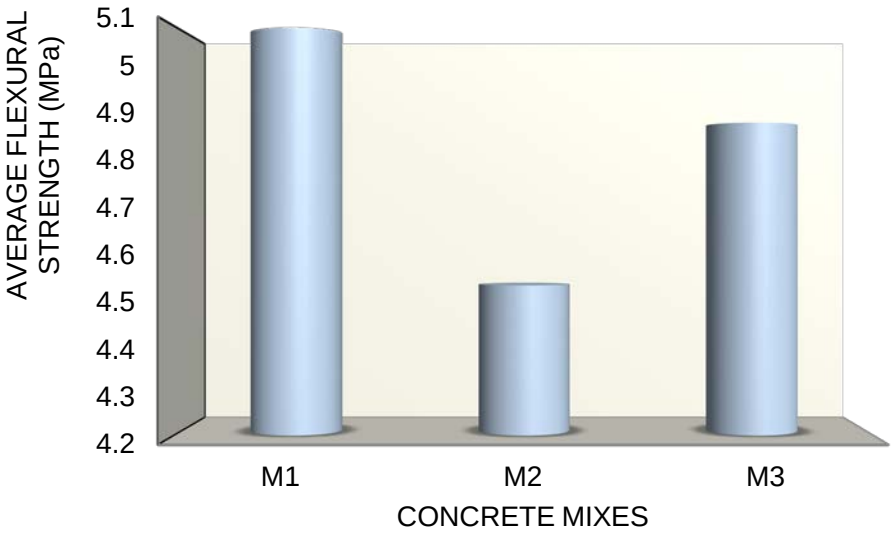


Figure 3 Comparison of average static flexural strength of concrete mixes M1, M2 and M3.

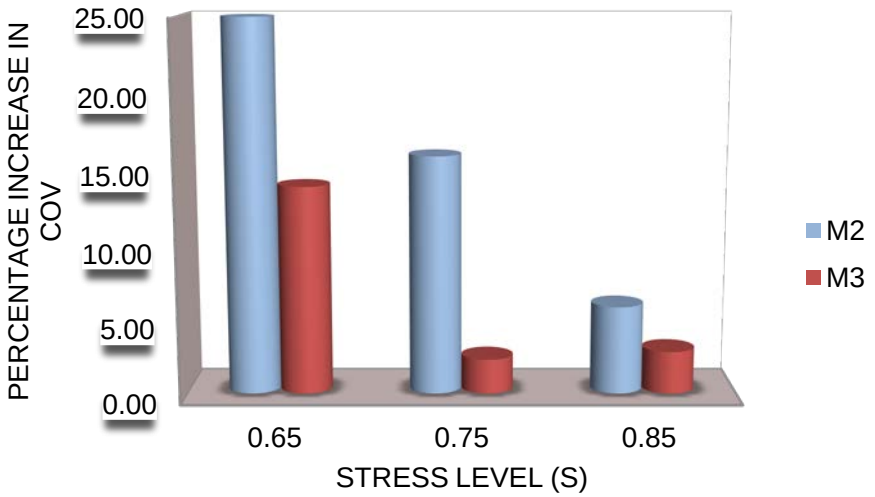


Figure 4 Percentage increase in coefficient of variation (COV) of concrete mix M1 with respect to the concrete mixes M2 and M3 respectively.

In the present investigation, the values of the Coefficient of Variation (COV) of the fatigue life data of concrete made with RCA (M1) has been found to be 41.93%, 56.10% and 64.77% at stress levels 0.85, 0.75 and 0.65 respectively [30]. Similarly COV values of the fatigue life data of concrete mixes M2 and M3 are calculated at each stress level and the same are given in Table-5 for the purpose of comparison. The corresponding increase in COV of the fatigue life data of concrete mix M1 is plotted and compared with that of mix M2 and M3 in Fig.-4. This indicates that concrete made with 100% RCA (M1) has higher variability in the distribution of fatigue life at different stress levels as compared to concrete containing 100% NA (M2) and concrete containing 50% RCA & 50% NA (M3).

Table 5 Comparison of COV values for the fatigue life of concrete mixes M1, M2 and M3.

| STRESS LEVEL 'S' | M1 | M2 | M3 |
|---|---|---|---|
| | COV (%) | COV (%) | COV (%) |
| 0.85 | 41.93 | 39.58 | 40.73 |
| 0.80 | ---- | ---- | ---- |
| 0.75 | 56.11 | 48.39 | 54.80 |
| 0.70 | ---- | ---- | ---- |
| 0.65 | 64.77 | 51.84 | 55.73 |

**Goodness-of-Fit Test**

The present investigation shows that Weibull distribution can be used to describe the distribution of fatigue life of concrete made with RCA. To supplement it further, Goodness- of – Fit Test has also been performed, apart from the graphical method. For this purpose, Kolmogorov – Smirnov Test (Kennedy and Neville 1986) has been applied, which can be conducted by defining a parameter D by using the following expression:

$$D = {}_{i=1}^{k}max[|F^*(x_i) - F_N(x_i)|] \quad (11)$$

in which $F^*(x_i) = i/k$ = observed cumulative histogram; $i$ = failure order number of the data point; $k$ = total number of data points in the sample under consideration at a given stress level. A maximum difference ($D_1$) of 0.1108, 0.1208 and 0.1437 is observed in the case of concrete made with 100% RCA (M1), 100% NA (M2) and 50% RCA & 50% NA (M3) respectively. The critical value for n = 10 and 5 percent significance level is found to be 0.41 from the Kolmogorov – Smirnov table. Thus, the applied model must be accepted at the 5 percent level of significance.

The Kolmogorov – Smirnov test was also conducted for other stress levels i.e. 0.75 and 0.65 and it was found that the model is acceptable at 5% level of significance.

**Two-Million Cycles Endurance Limit**

The previous section showed the probability distributions for the fatigue life of concretes mixes M1, M2 and M3 at various fatigue stress levels. The results show that there is increase in the variability in the distribution of fatigue life of concrete mix M1 (i.e, 100% RCA) compared to concrete mixes M2 and M3. A linear regression analysis has been carried out for each set of data and plotted in the semi-logarithmic format in the form of S-N curves to determine the two million fatigue strength. Fig.-5 represents the S-N relationship for the concrete mixes M1, M2 and M3, in which the ordinate represents the maximum fatigue stress expressed as a percentage of the corresponding static flexural strength.

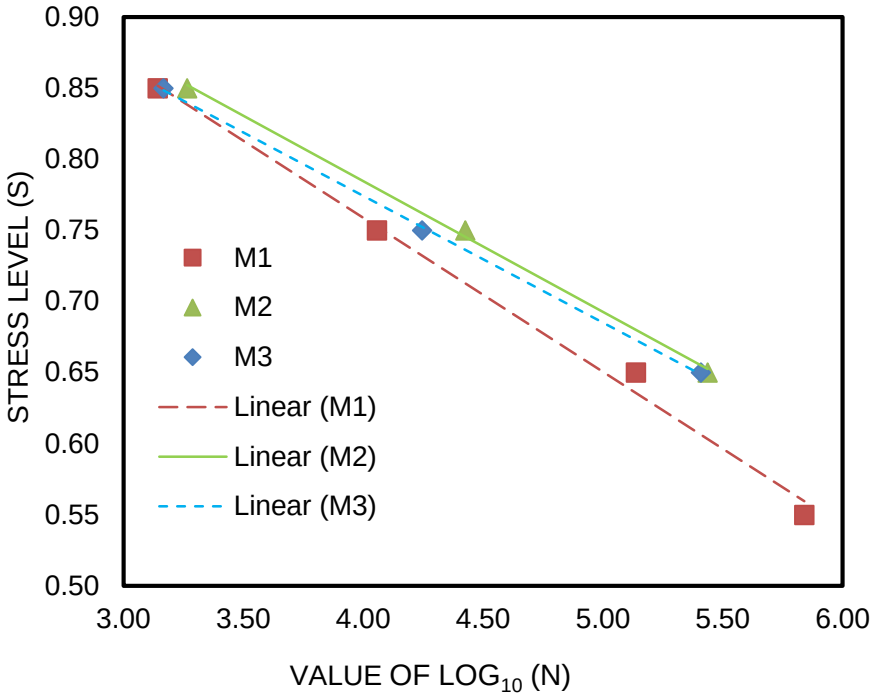


Figure 5 Comparison of endurance limit of concrete mixes M1, M2 and M3.

Assuming conservatively that the test duration of two-million cycles represents safe life, the fatigue strength of concrete mixes M1, M2 and M3 can be evaluated from the S-N curves given in Fig.-5. The two-million cycles fatigue strength for concrete mix M1 (i.e. 100% RCA) has been found to be about 50% of the corresponding static flexural strength. Similarly the two million fatigue strength of concrete mixes M2 and M3 was found to be 58% and 56% of the corresponding static flexural strength respectively. The two million cycles endurance limit for concrete made with 100% NA (M2 in the present study) has been justified from the previous studies [24, 28, 29, 31] which have reported the same value i.e. approximately 58% of the static flexural strength. Whereas concrete containing 50% RCA and 50% NA performs equally well as concrete containing 100% NA.

Thus concrete made with 100% RCA has been found to perform weakly compared to concrete made with 100% NA and concrete made with 50% RCA and 50% NA, necessitating the need for improving its flexural fatigue performance of concrete made with RCA. The work is in progress in the Authors' Institute towards the enhancement of the flexural fatigue performance of concrete containing 100% RCA by adding suitable amount of some mineral admixtures into the concrete mix.

## CONCLUSION

Flexural fatigue tests were conducted on three concrete mixes M1 (100% RCA), M2 (100% NA) and M3 (50% RCA & 50% NA) so as to evaluate their flexural fatigue performance. Further, the fatigue performance has also been analysed in terms of fatigue life data and two million cycles endurance limit for these mixes. Obtained results show that probabilistic distribution of fatigue life of the three concrete mixes, at a particular stress level S, can be approximately modeled by the two-parameter Weibull distribution. Least value of the shape

parameter for fatigue life were obtained for mix M1 whereas highest values were obtained in case of mix M2, with mix M3 lying in between these two mixes. This clearly depicts highest variability in the flexural fatigue life distribution of mix M1. The maximum increase in the COV of fatigue life data of M1 with respect to mix M2 and M3 has been found to be 24.94% and 13.95% at a stress level of 0.65. Incorporation of RCA as half or complete replacement of NA in concrete resulted in poor fatigue performance in terms of two million cycles fatigue strength. The two million cycle endurance limit for mix M1 has been found to be approximately 50% of the static flexural strength, which is nearly 8% and 6% lesser than the endurance limit of mix M2 and M3.

## ACKNOWLEDGEMENTS

The authors would like to gratefully acknowledge the support of the staff of Structures Testing Laboratory at Dr B R Ambedkar National Institute of Technology, Jalandhar, India during the experimentation work reported in the paper. The financial support from MHRD to carry out the present research work is gratefully acknowledged.

## REFERENCES

1. MEHTA, P K. Reducing the environmental impact of concrete, Concrete International, Vol. 23, 2001, pp 61-66.

2. EPA. Environmental Protection Agency. Available in: <http://www.epa.gov>[accessed January 2014].

3. Eurostat. Waste statistics in Europe. Available in: <http://epp.eurostat.ec.europa.eu/> [accessed in July 2014].

4. Freedonia. World construction aggregates. Industry Study No. 2838: The Freedonia Group; 2012, pp 334.

5. http://www.waste-management-world.com/articles/print/volume-12/issue5/features/rebuilding-c-d-waste-recycling-efforts-in-india.html.

6. PIMPLIKAR, S. Use of recycled aggregate in concrete, International Journal of Engineering Research & Technology, Vol. 2, 2013, pp 1-9.

7. HEERALAL, M, RATHISH, P K, RAO, Y V. Flexural Fatigue Characteristics of Steel Fiber Reinforced Recycled Aggregate Concrete (SFRRAC), Architecture and Civil Engineering, Vol. 7, No. 1, 2009, pp 19–33.

8. LIN, Y H, TYAN, Y Y, CHANG, T P, CHANG, C Y. An assessment of optimal mixture for concrete made with recycled concrete aggregates. Cement and Concrete Research, Vol. 34, 2004, pp 1373–1380.

9. ZAHARIEVA, R, BUYLE-BODIN, F, SKOCZYLAS, F, WIRQUIN, E. Assessment of the surface permeation properties of recycled aggregate concrete, Cement & Concrete Composites, Vol. 25, 2003, pp 223–232.

10. YANG, J, DU, Q, BAO, Y. Concrete with recycled concrete aggregate and crushed clay bricks, Construction and Building Materials, Vol. 25, 2011, pp 1935–1945.

11. POON C S, SHUI Z H, LAM, L. Effect of microstructure of itz on compressive strength of concrete prepared with recycled aggregates, Construction and Building Materials, Vol. 18, 2004, pp 461–468.

12. CASUCCIO, M, TORRIJOS, M C, GIACCIO, G, GIACCIO, R. Failure mechanism of recycled aggregate concrete. Construction and Building Materials, Vol. 22, 2008, pp 1500–1506.

13. MCNEIL, K, KANG, T H K. Recycled concrete aggregates: A Review, International Journal of Concrete Structures and Materials, Vol. 7, 2013, pp. 61-69.

14. SAGOE-CRENTSIL, K K, BROWN, T, TAYLOR, A H. Performance of concrete made with commercially produced coarse recycled concrete aggregate, Cement and Concrete Research, Vol. 31, 2001 pp 701–712.

15. LIMBACHIYA, M C, LEELAWAT, T, & DHIR, R K. Use of recycled concrete aggregate in high-strength concrete, Materials and Structures, Vol. 33, 2000, pp 574–580.

16. SHAYAN, A, & XU, A. Performance and properties of structural concrete made with recycled concrete aggregate, ACI Materials Journal, Vol. 100, 2003, pp 371–380.

17. BEHERA, M, BHATTACHARYYA, S K, MINOCHA, A K, DEOLIYA, R, MAITI, S. Recycled aggregates from C& D waste and its use in concrete – A breakthrough towards sustainability in construction sector: A review, Construction and Building Materials, Vol. 68, 2014, pp 501-516.

18. HANSON, T C editor, Recycling of demolished concrete and masonary, Oxfordshire, UK: 1992, Taylor and Francis.

19. HOLMEN, J O. Fatigue of concrete by constant and variable amplitude loading, NTH-Trondheim: Division of Concrete Structures, Bulletin No. 79-1, 1979, 218.

20. HILSDORF, H K, KESLER, C E. Fatigue strength of concrete under varying flexural stresses, ACI Joural, Vol. 63, 1966, pp 1059–76.

21. WEIGLER, H, KLAUSEN, D. Fatigue behaviour of concrete effect of loading in the fatigue strength range Betonwerk Fertigteil-Technik, 1979), Heft 4.

22. XIAO, J, LI, H, YANG, Z. Fatigue behavior of recycled aggregate concrete under compression and bending cyclic loading, Construction and Building Materials, Vol. 38, 2013, pp 681-688.

23. SINGH, S P, KAUSHIK, S K. Fatigue strength of steel fibre reinforced concrete in flexure, Cement and Concrete Composites, Vol. 25, 2003, pp 779-786.

24. MOHAMMADI, Y, KAUSHIK, S K. Flexural fatigue-life distributions of plain and fibrous concrete at various stress levels, Journal of Materials in Civil Engineering, ASCE, Vol. 17, No. 6, 2005, pp 650-658.

25. GOEL, S, SINGH, S P. Fatigue performance of plain and steel fibre reinforced self compacting concrete using S–N relationship, Engineering Structures, Vol. 74, 2014, pp 65-73.

26. WIRSCHING, P H, YAO, J T P. Statistical Methods in Structural Fatigue, Proceedings, ASCE100, No. ST6, 1970, pp 1201-1219.

27. OH, B H. Fatigue analyses of plain concrete in flexure, Journal of Structural Engineering – ASCE Vol. 112, issue 2, 1986, pp 273–88.

28. OH, B H. Fatigue life distribution of concrete for various stress levels, ACI Materials Journal, Vol. 88, No. 2, 1991, pp 122-128.

29. GOEL, S, SINGH, S P, SINGH, P. Flexural fatigue strength and failure probability of self compacting fibre reinforced concrete beams, Engineering Structures, Vol. 40, 2012, pp 131-140.

30. ARORA, S, SINGH, S P. Analysis of flexural fatigue failure of concrete made with 100% coarse recycled concrete aggregates, Construction and Building Materials, Vol. 102, 2016, pp 782-791.

31. SHI, X P, FWA, T F, TAN, S A. Flexural fatigue strength of plain concrete, ACI Materials Journal Vol. 90, No. 5, 1993 pp 435–440.

# DEVELOPMENT OF CONCRETE MIXES WITH RECYCLED AGGREGATES: FROM THE LABORATORY TO THE FIELD

**G A Benítez**

National Institute of Industrial Technology (INTI)

**P Carreño R Verna**

Fenomix SA

Argentina

**ABSTRACT.** Sustainability is an interesting challenge for the ready-mixed concrete industry in Argentina. The use of aggregates from concrete demolition industry has been more a theoretical approach than a real application up to the present. The economic and technical difficulties related to designing an adequate and efficient process delayed the application of this practice. A ready-mixed concrete local company has recently installed a modern crushing and classifying plant in order to introduce these sustainable concretes into the market. The Concrete Technology Laboratory (INTI) has joined in the project assessing the feasibility and giving technical support to the initiative. The present paper deals with the development in the laboratory of concrete mixes using recycled aggregates originated by concrete demolition waste and the production at an industrial scale. The mixes designed consisted in 0, 25, 50, 75 and 100 % of natural aggregate replacement, with a medium and high range plasticizers in order to reproduce a standard workability. The properties assessed were: compressive cylindrical strength, splitting tensile test, modulus of elasticity and density. Durability parameters measured were air (kT) and oxygen (kO) permeability coefficients, water penetration under pressure, capillary sorptivity rate, accelerated carbonation penetration depth and the ability to resist chloride ion penetration. The results obtained were analyzed against the reference mix in order to recommend an optimum replacement which may result in an adequate performance and cost:benefit equation. The recycled concrete mixes are being produced at the moment for not severe environmental exposure conditions contributing to the more sustainable development of the ready-mixed industry in our country.

**Keywords:** Sustainability, Recycling, Aggregates, Demolition, Waste.

**Eng. Alejandra Benitez** is the Head of the Concrete Technology Unit at the National Institute of Industrial Technology. Practitioner in the field of concrete technology, she participates in many technical standards committees, teaches at Buenos Aires University and has published many papers on concrete technology and sustainable construction.

**Mr P Carreño** and **R Verna** work for the ready-mixed concrete company, Fenomix SA.

## INTRODUCTION

The introduction of sustainable concretes in the local market encounters many difficulties in spite of the wide international experience. The use of recycled aggregates from concrete demolition as partial replacement of natual aggregates, mainly those coming from crushed concrete is supported by the need of environmental improvement, non-renewable resources conservation and cost reductions. Besides it requires standardization and performance assessment before the users are willing to choose this technology. The process of including the recycled aggregates in the current natural aggregates national standard is under development at present. That is the main reason why a well-known ready-mixed concrete company undertook the present studies so that the market gets confident on the final product. The replacement proposed was to use the recycled fractions of aggregates obtained from the crushing and classifying plant in replacement of the corresponding natural coarse aggregates. Fenomix SA has recently purchased an impact crusher and screening plant which permits the crushing of 1200 ton/day of hardened C30 mainly from pavements. Depending on the screens, it is possible to obtain different gradings. Some of them are used in concrete, some in fluid grout mixtures and additionally for soils stabilization. Figure 1 shows the mobile crusher in operation.


Figure 1 Mobile impact crusher and screening plant

In order to assess the general performance of concrete mixes similar to the current mixes, the Concrete Technology Laboratory (INTI) was required to develop a research program using the 6-20 mm commercial fraction.

### Main objective

Assessment of fresh and hardened properties of concrete mixes with partial replacement of natural by recycled aggregates against a current mix with the same design parameters.

### Characterization of materials

The coarse aggregate used was a combination of crushed stone 6-20 mm with gravel (CS 6-20+G). The fine aggregate consisted of natural siliceous sand (S). The crushed concrete waste (CCW) used was 6-20 mm. The results of the tests performed according to ASTM standards are included in Table 1.

Table 1 Aggregates characterization

| PROPERTY | AGGREGATE | | |
|---|---|---|---|
| | CCW 6-20 | CS 6-20+G | S |
| Oven Dry Bulk Specific Gravity, kg/dm$^3$ | 2,41 | 2,55 | 2,60 |
| Saturated Surface Dry Specific Gravity, kg/dm$^3$ | 2,51 | 2,61 | 2,61 |
| Water Absorption, % | 4,02 | 1,81 | 0,12 |
| Los Angeles Abrasion Resistance, % | 30,7 | 20,5 | --- |
| Material finer than 75 µm, % | 0,3 | | |
| Flakiness, % | 7 | | |
| Soundness ($SO_4Na_2$ Immersion), % | 97 | | |

Figure 2 shows the aggregates grading curves and the different combinations. The limit grading curves adopted are included in IRAM Standard 1627.

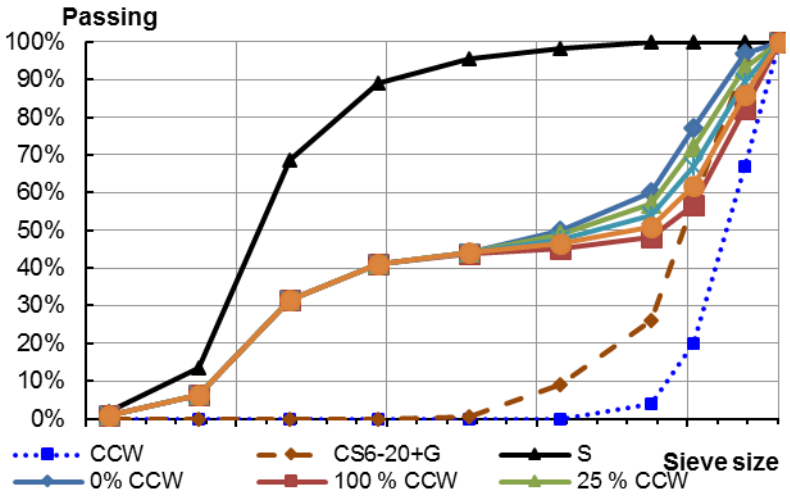


Figure 2 Gradings for the different percentages of replacement

The petrographic examination showed no potential reactive minerals. The CCW consisted in concrete particles with granitic coarse aggregates and fine cuarcitic sand. The mortar showed good adherence and variable porosity. 10 % of the particles are original crushed granite, 38 % consisted of mortar and the rest were mixed particles. The shapes were 92% irregular and 8 % flat. Low quantity of ettringite and calcite was found in the mortar. Figure 3 shows the aspect of the CCW.

Figure 3 Crushed Concrete Waste

## Cement characterization

A blended cement with the addition of a limestone (LL) and ground granulated blast furnace slag (S) of current use in the local market was used. The cement may be classified as a CEM IIA(S,LL)42,5 according to the EN197-1. The parameters determined are included in Table 2.

Table 2 Physical and mechanical properties of cement

| PROPERTY | | CPC 40 (with S and limestone LL) | SPECIFICATION IRAM STANDARD 50000 CPC40 |
|---|---|---|---|
| Composition range | | 76 %<Clinker+gypsum< 82 %<br>12% < S < 16%<br>6 % < Limestone LL < 9 %<br>18 % < S+LL < 24 % | 65 < Clinker+gypsum < 94<br>6 < S+LL < 35 % |
| Density, kg/dm$^3$ ASTM C188 | | 2,97 | --- |
| Specific surface (Blaine), m$^2$/kg EN-196-3 | | 400 | ≥ 250 |
| Compressive strength, MPa EN-196-1 | 2 days<br>7 days<br>28 days | 22,0 ± 0,6<br>38,6 ± 0,4<br>52,5 ± 0,7 | min 10<br>--<br>min. 40 - max. 60 |

## Design of concrete mixes

The natural aggregate was replaced at 0, 25, 50, 75 and 100% replacement levels and Table 3 describes the main parameters of design (note that it is a mix with pumping properties). The mixes identification with their description is shown in Table 4. The mixing was performed with a horizontal mixer of 250 dm$^3$ effective mixing capacity following a standard procedure. The tests in Table 5 were carried put on fresh concrete. Then, cylinders were cast for all the mechanical, physical and durability testing (shown in Table 6). Concrete was cured in water at 23 ± 2 ºC (ASTM C192) until test age shown.

Table 3 Mix design

| CRITERIA | |
|---|---|
| Characteristic compressive strength | 30 MPa |
| Cement Content | 340 kg/m$^3$ |
| Maximum Aggregate Size | 19 mm |
| % S / (% S + % coarse aggregate) | 46 % |
| Plasticizer | 0,8 % mass of cement |
| Superplasticizer | 0,65 % mass of cement |
| a/mc (Relationship water/cementitious material: calculated considering total amount of mixing water and the total amount of cementitious material) | 0,47 |

Table 4 Mix identification

| ID NO | COMMERCIAL IDENTIFICATION | REPLACEMENT LEVEL, % (CCS 6-20 + G) |
|---|---|---|
| # 1 - R 0 | H30-15 Pumped 6-20 | 0 |
| # 2 – R 25 | | 25 |
| # 3 – R 50 | | 50 |
| # 4 – R 75 | | 75 |
| # 5 – R 100 | | 100 |

Table 5 Properties of fresh concrete

| MIX | PROPERTY | | |
|---|---|---|---|
| | Slump, cm ASTM C143 | Unit weight, kg/m$^3$ ASTM C136 | Air content, % ASTM C231 |
| #1R0 | 18,0 | 2340 | 3,8 |
| #2R25 | 18,0 | 2314 | 3,7 |
| #3R50 | 16,0 | 2316 | 3,8 |
| #4R75 | 19,0 | 2325 | 2,8 |
| #5R100 | 19,0 | 2320 | 3,9 |

Table 6. Number of cylinders and tests performed

| CYLINDER DIMENSIONS, mm | NUMBER OF SPECIMENS | TEST | AGE, days |
|---|---|---|---|
| 100 x 200 | 3 | Compressive strength | 2 |
| 100 x 200 | 3 | Compressive strength | 7 |
| 100 x 200 | 3 | Compressive strength | 14 |
| 100 x 200 | 3 | Compressive strength | 28 |
| 150 x 300 | 3 | Modulus of elasticity | 28 |
| 100 x 200 | 3 | Splitting tensile strength | 28 |
| 100 x 200 | 3 | Oxygen Permeability<br>Air permeability<br>Water penetration | According to equipment availability |
| 100 x 200 | 3 | Capillary sorptivity, density and absorption | |
| 100 x 200 | 3 | Depth carbonation<br>Chloride penetration | |

## Mechanical and elastic properties

The compressive tests were carried out with unbounded elastomeric pads on the bases of the cylinders according to ASTM C 123 and ASTM C39. Figure 3 shows the compressive strength ($\sigma_{c\,m}$) evolution.

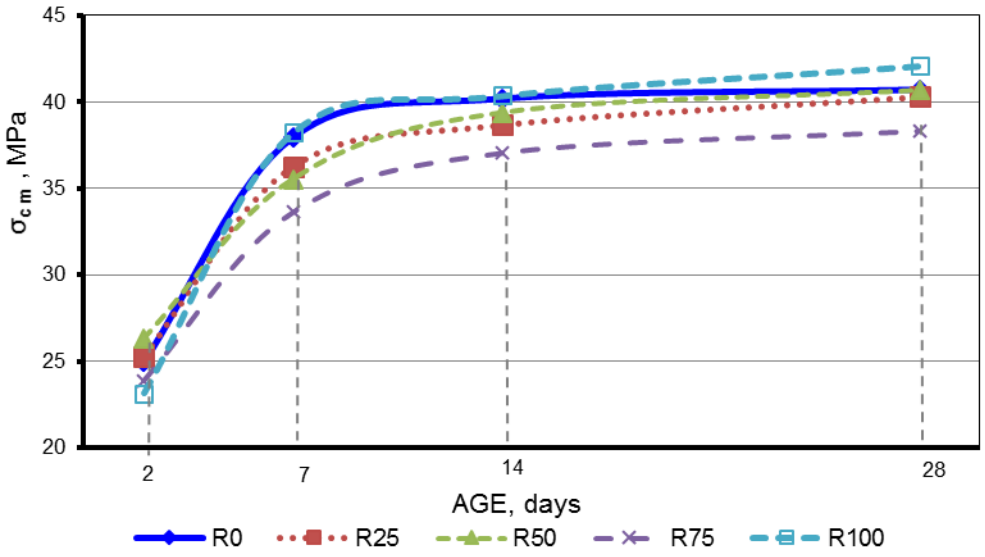


Figure 3 Compressive strength development

Table 7 includes the results for the Static Modulus of Elasticity (E) according to ASTM C469 and splitting tensile strength ($\sigma_{t,m}$ ) (ASTM C496).

Table 7 Modulus of elasticity and splitting tensile strength

| MIX | AGE, days | E, GPa | $\sigma_{t,m,}$ MPa |
|---|---|---|---|
| #1R0 | 28 | 39,5 | 4,4 |
| #2R25 | 28 | 39,4 | 3,5 |
| #3R50 | 28 | 38,5 | 4,0 |
| #4R75 | 28 | 37,0 | 3,5 |
| #5R100 | 28 | 35,8 | 3,7 |

**Physical properties: density and absorption**

The specimens indicated in Table 6 were split in two (using a stihl saw) of 100 x 100 mm. The tests were performed according to UNE EN 12390-7 and UNE EN 1916/F. The values of dry density ($\delta_s$), saturated surface dry density ($\delta_{sss}$) and absorption (Abs) can be seen in Table 9.

Table 9 Density and absorption results

| MIX | AGE, days | PROPERTY | | |
|---|---|---|---|---|
| | | $\delta_{s\ m,}$ kg/m$^3$ | $\delta_{sss\ m,}$ kg/m$^3$ | Abs $_{m,}$ % |
| #1R0 | 28 | 2250 | 2380 | 5,7 |
| #2R25 | 28 | 2230 | 2360 | 5,8 |
| #3R50 | 28 | 2230 | 2360 | 5,8 |
| #4R75 | 28 | 2210 | 2350 | 6,5 |
| #5R100 | 28 | 2220 | 2350 | 6,1 |

**Durability properties**

The penetrability properties of concrete may be particularly important when the aggregates consist of recycled concrete from demolition waste, as this type of crushed concrete waste presents high absorption compared to natural normal weight aggregates. This has to be studied and taken into account when designing mixes for structures subject to severe exposure conditions. The proposed methods to assess the durability performance of the mixes were:

- Air permeability. Torrent Method.(Darcy´s Law) SIA 262/1-E(2003) [1,2,3,4]
- Oxygen Permeability. Cembureau Recommendation. Rilem 116-PCD. (Hagen-Poiseville Modified Formula) [5]
- Water penetration. DIN 1048, EN 12390-8 [6,7]
- Capillary sorptivity. (Jury´s Law) IRAM 1871, similar to SIA 262/1-B [8]
- Chloride penetration. (Ficks´s Law) ASTM C 1202 [9,10]
- Carbonation Depth. Accelerated INTI method based on the 1$^{st}$ Fick´s Law

These methods are well known and can be consulted in the bibliography. A summary of the results obtained can be seen in Tables 10 and 11.

Table 10 Permeability results

| MIX | AGE, days | PROPERTY | | | |
|---|---|---|---|---|---|
| | | Average Air permeability kT [x $10^{-16}$], $m^2$ [3] | Average Oxygen permeability kO [x $10^{-16}$], $m^2$ [5] | Average / maximum water penetration depth, mm [6] | Capillary Sorptivity Rate [$g/m^2.s^{1/2}$] IRAM 1871[8] |
| #1R0 | 70 | 0,065 | 0,19 | 28,4 / 48,5 | 1,39 |
| #2R25 | 90 | 0,097 | 0,23 | 44,2 / 57,0 | 3,34 |
| #3R50 | 130 | 0,035 | (*) | 29,3 / 43,0 | 1,69 |
| #4R75 | 150 | 0,012 | (*) | 35,0 / 21,1 | 2,13 |
| #5R100 | 165 | 0,035 | (*) | 20,1 / 39,0 | 0,73 |

(*) The values could not be determined due to a failure of the equipment at the moment of the test.

Table 11 Chloride penetration test results

| MIX | AGE, days | PROPERTY | | | |
|---|---|---|---|---|---|
| | | Charge (Q), Coulombs [9] | Penetration depth $X_d$ Average, mm [9] | Non-steady state migration coefficient $Cm_{ne,}$ $m^2/s$[10] | Penetration Rate $V_{p,}$ mm/V.h[10] |
| #1R0 | 56 | 2506 | 12,23 | 12,22 | 0,034 |
| #2R25 | 56 | 2710 | 14,60 | 14,77 | 0,041 |
| #3R50 | 56 | 2916 | 16,73 | 17,05 | 0,046 |
| #4R75 | 56 | 2755 | 17,17 | 17,46 | 0,048 |
| #5R100 | 56 | 2964 | 13,27 | 13,32 | 0,037 |

In the case of the accelerated carbonation test, the method was developed at INTI based on the ASTM Standard. The specimens were moist cured for 56 days, oven dried for 7 days, stored under controlled conditions until the age of testing when they were put into the carbonation chamber with the $CO_2$ atmosphere for 14 days. After that they were split to measure the carbonation depth and calculate $K_N$ constant applying 1st Fick´s Law. Table 12 shows the results.

Table 12 Carbonation test results (INTI Method)

| MIX | AGE, mm | CARBONATION DEPTH $X_{CO2\ promedio,}$ mm | $K_{N\ promedio,}$ $mm/año^{1/2}$ |
|---|---|---|---|
| #1R0 | 270 | 4,88 | 4,00 |
| #2R25 | 270 | 6,72 | 5,51 |
| #3R50 | 270 | 6,15 | 5,04 |
| #4R75 | 270 | 6,37 | 5,22 |
| #5R100 | 270 | 6,36 | 5,21 |

## CONCLUSIONS

The specimens were kept in the curing chamber until they were applied the different tests treatments. It has to be considered that hydration keeps going on with age when they are cured under saturated conditions.

Compressive strength does not show significant variation for the mixes with aggregate replacement, which may be due to the influence of the hydration of the paste. The tensile strength and modulus of elasticity was found to be lower for mixes using recycled aggregates. This was to be expected as the interface may have been under stress before.

The density of recycled concrete was found to be lower than the reference concrete, mainly due to a lower density of recycled aggregates.

Absorption was found to be higher for the mixes with aggregate replacement, and this may be due to the presence of mortar attached to the recycled aggregates, and also the recycled aggregate having higher absorption values.

Alkali-Silica Reaction is not expected to be a problem since the recycled aggregates showed no presence of potentially reactive minerals.

Air and oxygen coefficients for the 25, 50, 75 and 100 % replacement were determined at higher age than for the reference mix.

According to kO and kT it can be concluded that the 5 mixes classify as “Good” quality [1].

The air and oxygen permeability coefficients (kO, kT) showed an acceptable correlation to the bilbiography data [2].

For 50, 75 y 100 % of replacement the air permeability coefficient was lower compared to the reference mix. This also could be explained by the grade of hydration of the paste.

Capillary sorptivity rate obtained were below the requirements specified by the CIRSOC 201:2005 [11].

Water penetration test results were not acceptable for concretes to be used under severe exposure conditions according to the Building Code Requirements for Structural Concrete [1]. This type of mixes could be used for concretes that are not required to undergo such extreme conditions.

Chloride ion penetration shows increased with aggregate replacement increase. This can be seen by an increase in the charge measured (Q), except for the 75% considered an anomalous value. In spite of this the ion choride penetrability was moderate for all the mixes [9]. The non-steady state migration coefficient and the penetration rate increase with the replacement percentage, except for the 100 % which was considered anomalous. The presence of aggregates in the measurement point may difficult the measurement of the penetration depth.

Carbonation depth showed an increase with increasing recycled aggregates replacement.

The 25 % of replacement could be adopted considering exposure conditions according to Table 2.5 and article 2.2.11 CIRSOC 201:2005[11].

Durability parameters should be object of further research to confirm the results.

The present experience will contribute to the update of the current standards.

## ACKNOWLEDGEMENTS

To María José Fernandez Sturla and Erica Köber who belong to the Chemistry Area of INTI Construcciones and performed the chloride penetration and carbonation test sharing their expertise in the subject.

## REFERENCES

1. TORRENT, R. und FRENZER, G., Methoden zur Messung und Beurteilung der Kennwerte des Überdeckungsbetons auf der Baustelle, Holcim Report RMP 95/3430/D, Okt. 1995, 106 p.

2. TORRENT R. J., FRENZER, G., A method for the rapid determination of the coefficient of permeability of the covercrete, International Symposium Non-Destructive Testing in Civil Engineering (NDT-CE), 1995, pp. 985-992.

3. SWISS STANDARD SIA 262/1 (2003), Construction en béton – Spécifications complémentaires", Annexe A: 'Perméabilité à l'eau'. Annex E: Air-Permeability on the Structures.

4. SWISS STANDARD SIA 262/1:2013, Betonbau – Ergänzende Festlegungen (Concrete Structures - Supplementary Specifications); Annex E: Luftpermeabilität am Bauwerk (Air-permeability on site).

5. KOLLEK, J.J., The determination of the permeability of concrete to oxygen by the Cembureau method – a recommendation, Materials and Structures, 1989, 225-230.

6. DIN 1048 Part 5, Testing concrete; testing of hardened concrete, water permeability

7. EN 12390-8:2000, "Testing hardened concrete - Part 8: Depth of penetration of water under pressure", 5 p

8. IRAM STANDARD 1871 "Hormigón. Método de ensayo para determinar la capacidad y la velocidad de succión capilar de agua del hormigón endurecido. Concrete. Test method for determination the water capacity and the capillary suction speed of the hardened concrete"

9. ASTM STANDARD C1202-12 Standard test method for electrical indication of concrete's ability to resist chloride ion penetration.

10. NT BUILD 492 1999-11 Chloride migration coefficient from non-steady-state migration experiments.

11. CIRSOC 201-2005 "Reglamento Argentino de Estructuras de Hormigón Armado" (Building Code Requirements for Structural Concrete).

# ALKALI-ACTIVATED SLAG AND FLY ASH CEMENT MORTARS PREPARED WITH RECYCLED CONSTRUCTION AND DEMOLITION WASTE AGGREGATE: BEHAVIOUR AND DURABILITY

**M M Alonso F Puertas**

Eduardo Torroja Institute for Construction Sciences (IETcc-CSIC)

**A Rodríguez**

Technical Universtiy of Madrid

Spain

**ABSTRACT.** The reuse of construction and demolition waste (C&DW) as an aggregate in mortar and concrete has entailed a significant reduction in raw material consumption. Such recycled aggregate has been used for many years in Portland cement mortars and concretes. Very little information has been published on the application of this waste to prepare alkaline slag and fly ash cement mortars, however. This study explores the technological feasibility of such use, ascertaining the mechanical and microstructural behaviour as well as the durability of the resulting materials. Mortars were prepared with an aggregate/binder ratio of 2/1. The binders used were Portland cement (OPC), vitreous blast furnace slag alkali-activated with a waterglass solution (4% $Na_2O$ by mass of slag and a $SiO_2/Na_2O$= 1.2) (AAS) and fly ash alkali-activated with a solution consisting in 85 wt% 10-M NaOH and 15 wt% waterglass (AAFA). Normalised siliceous sand and two types of recycled concrete aggregate were used in the mixes in a proportion 80/20 in weight. The findings showed that water demand was higher in mortars prepared with recycled than with conventional aggregate. Partial replacement of conventional aggregate with the recycled material was also observed to yield mortars with high mechanical strength, although total porosity also rose. The microstructural and durability studies conducted indicated that alkaline cement mortars prepared with recycled aggregated exhibit acceptable performance.

**Keywords:** Portland cement Mortars; Alkali activated slag mortars; Alkali activated fly ash mortars; Construction and demolition waste (C&DW) aggregates; Mechanical performance; Durability

**Dr M M Alonso** heads the cement chemistry laboratories at the Eduardo Torroja Institute, Madrid. She has published papers and communications on her areas of expertise, chemical admixtures and alkaline cements.

**A Rodríguez** is chemical engineer at the Technical University of Madrid.

**Professor F Puertas** is research professor with the Eduardo Torroja Institute**,** Madrid**.** She sits on several national and international committees and has published over 130 papers on cement and concrete technology. She is Editor-in-Chief of the journal *Materiales de Construcción*.

## INTRODUCTION

Construction industry is an important activity that entails a sizeable environmental problem. On the one hand, the associated quarrying of raw materials for ordinary Portland cement (OPC) and natural aggregate (NA) for concrete leaves unsightly scars on the landscape. Moreover, large quantities of greenhouse gases are emitted in concrete manufacture [1]. Also high rates of housing and infrastructure remodelling have led to the generation of large amounts of construction and demolition waste (C&DW) [2], which is stockpiled in landfills. Actions are therefore needed to ensure resource conservation and construction industry sustainability [3]. The avenues for attaining that objective include shrinking the amount of waste generated and furthering the reuse of stockpiled industrial by-products.

The development of alkaline cements or geopolymers (alkali-activated materials, AAMs) [4-5] lies within this second line of action. AAM mortars and concretes are known to feature high mechanical strength, which varies essentially with the starting aluminosilicate, activator composition and concentration, curing conditions and preparation [6, 7]. Another possible sustainability measure is to reuse C&DW to produce recycled aggregate (RA) as a partial or total replacement for natural aggregate (NA) in concrete manufacture [8]. The properties of recycled aggregate differ depending on the origin of the waste and its majority constituent (demolished concrete structures, concrete with clay-based materials, clay-based construction materials, asphalt or similar). Recycled aggregate is apt for a variety of applications, from road sub-bases, precast concrete, pavements and masonry mortars [9, 10]. As a rule, RA is believed to lower portland cement mortar and concrete mechanical strength [8, 11, 12] due essentially to its higher water demand and the weaker bonds formed with the cementitious matrix by recycled than natural aggregate. The possible combination of alkaline cements or geopolymers and recycled construction waste aggregate would constitute a further step toward sustainability. However, little has been published to date on the use of such waste as an aggregate in alkaline slag or fly ash cement mortars and concretes and in some cases contradictory.

Moreover, the effect of recycled construction and demolition waste aggregate on AAS and AAFA mortar and concrete mechanical strength is not the only knowledge gap that must be addressed: its effect on mortar and concrete microstructure and other properties must also be ascertained. This study therefore addressed the mechanical strength, drying shrinkage, microstructure and durability of alkaline cement mortars containing 20 % recycled aggregate consisting in construction and demolition waste OPC mortars were used as a control.

## EXPERIMENTAL

### Materials

Table 1 gives the chemical composition of the three materials used, CEM I 52.5R cement (OPC), blast furnace slag (S) and fly ash (FA), determined on a PHILIPS PW-1004 X-ray fluorescence (XRF) spectroscope. The blast furnace slag had a 99 % vitreous content and the fly ash comprised 45 % reactive silica. The Blaine specific surface values for OPC, S and FA were 425, 325 and 202 $m^2$/kg, respectively. Of the three types of fine aggregate used in this study, one was siliceous (AN) while the other two (R and H) (Figure 1) were sourced from recycled construction and demolition waste (C&DW). Their chemical composition is listed in Table 2.

Table 1 Chemical composition of OPC, S and FA (wt%)

| | OPC | S | FA |
|---|---|---|---|
| CaO | 63.22 | 38.52 | 2.72 |
| $SiO_2$ | 18.90 | 38.27 | 54.44 |
| $Al_2O_3$ | 4.41 | 11.80 | 27.51 |
| $K_2O$ | 0.82 | 0.46 | 3.13 |
| $Na_2O$ | 0.10 | 0.40 | 0.52 |
| $Fe_2O_3$ | 3.91 | 1.04 | 6.38 |
| MgO | 1.68 | 8.31 | 1.51 |
| $TiO_2$ | 0.25 | 0.39 | 1.27 |
| $P_2O_5$ | 0.09 | | 0.31 |
| $SO_3$ | 3.30 | 0.99 | |
| MnO | | 0.26 | 0.08 |
| LoI | 2.35 | - | 2.10 |
| Free CaO | 1.40 | | |

Table 2 Chemical composition of fine aggregates AN, R and H (wt%)

| | AN | R | H |
|---|---|---|---|
| $SiO_2$ | 96.8 | 15.7 | 6.1 |
| $Al_2O_3$ | 1.5 | 4.4 | 1.7 |
| $Fe_2O_3$ | 0.4 | 1.8 | 0.7 |
| CaO | 0.1 | 30.6 | 31.1 |
| $K_2O$ | 0.6 | 0.8 | 0.3 |
| MgO | | 8.1 | 16.7 |
| $TiO_2$ | | 0.2 | 0.1 |
| $P_2O_5$ | | 0.1 | |
| $SO_3$ | | 5.3 | 0.7 |
| SrO | | 0.2 | < 0.1 |
| LOI | 0.6 | 32.7 | 42.6 |
| Soluble $SO_3$ | - | 6.1 | 1.5 |
| Cl- | | 0.05 | 0.02 |

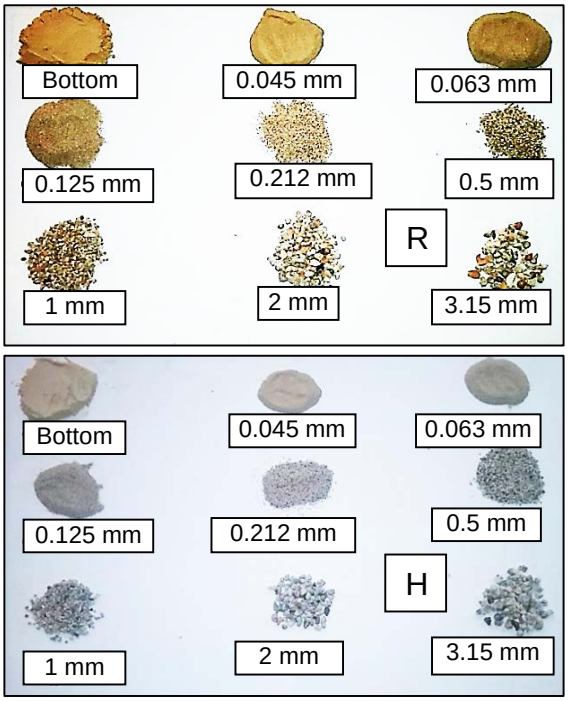


Figure 1 Aggregate R and H particles

The mineralogical composition of the fines, determined on a Philips PW1710 X-ray diffractometer, and the respective Rietveld analysis are given in Table 3. Further to the data in Table 3, aggregate AN was siliceous, with over 98 % quartz in its composition. Aggregate R comprised mostly calcite and dolomite, although smaller percentages of basanite, quartz and muscovite were also identified. Aggregate H consisted essentially of dolomite (around 80 % of the total) and calcite (16%), with quartz and muscovite as minority phases. The physical characteristics of the three types of aggregate used to prepare the mortars are summarised in Table 4. Their particle size distribution is plotted in Figure 2.

Table 3 Quantitative mineralogical composition of fines (wt%)

| | AN | R | H |
|---|---|---|---|
| Quartz | 98.3 | 7.6 (1) | 2.7 (1) |
| Microcline | 1.7 | - | - |
| Calcite | - | 35.6 (2) | 16.1 (2) |
| Dolomite | - | 36.5 (2) | 79.9 (1) |
| Basanite | - | 12.8 (2) | - |
| Muscovite | - | 7.4 (3) | 1.3 (3) |

Table 4 Physical properties of the aggregates [13]

| | AN | R | H |
|---|---|---|---|
| Humidity (%) | 0.1 | 7.1 | 4.5 |
| Water absorption (%) | 0.1 | 3.7 | 3.3 |
| Density (g/mL) | 2.6 | 2.5 | 2.6 |

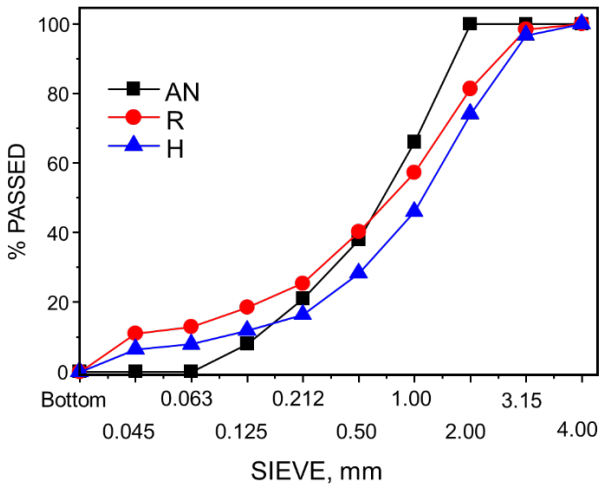


Figure 2 Particle size distribution for aggregates AN, R and H

## Mortar Preparation and Tests Conducted

Portland cement (OPC) and alkali-activated slag (AAS) and fly ash (AAFA) mortars were prepared at an aggregate/binder ratio of 2/1. Thee mortars were prepared with each binder: one with 100 % siliceous sand (AN) and the other two with 80 % AN and 20 % recycled aggregate R or H. The liquid/solid ratios for the mortars were determined further to Spanish standard UNE 83-811-92 [14] to ensure the same consistency in all the materials.

The OPC mortars were water-hydrated and cured at 99 % RH and 20±2 °C for 24 h. The specimens were subsequently removed from the moulds and stored in a climatic chamber (99 % RH and 20±2 °C Tª), submerged in water, until the test age. The slag was activated with a waterglass solution (Wg) ($Na_2O$ n$SiO_2$ mH2O + NaOH) containing 4% $Na_2O$ by slag mass and a $SiO_2/Na_2O$ ratio of 1.2 (cured at 99 % RH and 20±2 °C for 24 h). After removal from the moulds, these specimens were stored in the same climatic chamber until tested. The AAFA

mortars were activated with a 10 M solution of NaOH containing 15 % Wg. Here the specimens were cured in an oven at 85 °C and 99 % relative humidity for the first 20 hours. They were subsequently removed from the moulds and stored in a climatic chamber in the same conditions as the AAS mortar specimens. Table 5 lists the OPC, AAS and AAFA mortars prepared.

Mechanical strength was found for the 2, 7 and 28 day mortar specimens (4x4x16 cm) in a IBERTEST press. Total porosity and pore size distribution were found in the 7 day specimens on a Micromeritics 9320 porosimeter.

AAS mortar shrinkage was studied on prismatic specimens measuring 2.5x2.5x28.7 cm. These specimens were cured as described above for the first 24 hours and subsequently stored in climatic chambers at 22±2 °C and at either 99 or 45 % RH. Three-centimetre cubic specimens were prepared for the AAFA fire resistance tests. After curing for 28 days in the conditions described above, they were kept in a kiln at 50 °C for 24 h to eliminate any residual moisture. They were subsequently heated to 200, 400, 600, 800 and 1000 °C, ramping at a rate of 6 °C/min and holding the temperature constant for 1 h at each plateau. Specimen weight and compressive strength were determined.

Table 5 OPC, AAS and AAFA mortar batching

| BINDER | FINE AGGREGATE (% WEIGHT) | | | SAMPLE NAME |
|---|---|---|---|---|
| | AN | R | H | |
| OPC | 100 | | | OPC100AN |
| | 80 | 20 | | OPC80:20AN/R |
| | 80 | | 20 | OPC80:20AN/H |
| AAS | 100 | | | AAS100AN |
| | 80 | 20 | | AAS80:20AN/R |
| | 80 | | 20 | AAS80:20AN/H |
| AAFA | 100 | | | AAFA100AN |
| | 80 | 20 | | AAFA80:20AN/R |
| | 80 | | 20 | AAFA80:20AN/R |

## RESULTS AND DISCUSSION

Table 6 gives the liquid/solid ratios used for the mortars, based on slump test results. This table shows that the replacement of aggregate AN with 20 % R or H called for raising the l/s ratio in OPC and AAFA by 7 and 25 %, respectively. No differences were observed between aggregates R and H, despite the higher water absorption (Table 4) and greater fineness (Figure 2) in the former. The presence of recycled aggregate in mortars is known to raise the liquid demand, which as a rule rises with the aggregate replacement rate. [15]. Corinaldesi and Moriconi [16], studying the amount of water needed to prepare OPC mortars with different types of recycled aggregate, observed that at 100 % replacement, the l/s ratio climbed by 19 to 52 %. Conversely, other authors who maintained the same l/s ratio observed that mortar slump values declined more steeply when more recycled aggregate was used. This effect depends on the nature of the recycled aggregate, its water absorption and shape, particularly in clay-based aggregate [15, 17].

Table 6 Liquid/solid ratio for OPC, AAS and AAFA mortars

| SAMPLE NAME | L/S |
|---|---|
| OPC100AN | 0.41 |
| OPC80:20AN/R | 0.44 |
| OPC80:20AN/H | 0.44 |
| AAS100AN | 0.49 |
| AAS80:20AN/R | 0.50 |
| AAS80:20AN/H | 0.49 |
| AAFA100AN | 0.42 |
| AAFA80:20AN/R | 0.53 |
| AAFA80:20AN/R | 0.52 |

The l/s ratio was not observed to grow when recycled C&DW aggregate was added to AAS mortars, however (see Table 6). While the liquid required in these mortars was greater than in the OPC and AAFA materials, no clear explanation could be given for the absence of any change in the liquid/solid ratio when 20 % of the AN was replaced with recycled aggregate. Further research is called for in this respect, although this finding may be associated with the aggregate replacement ratio and the nature and properties of the activating solution.

The compressive strength for OPC, AAS and AAFA mortars is shown in Figures 3a, 3b and 3c, respectively. Figure 3 shows that, generally speaking, in all the mortars tested (OPC, AAS and AAFA) and at all ages, replacing siliceous aggregate AN with 20 % of recycled aggregate induced a decline in mechanical strength, even in AAS mortars where the liquid content was unaffected by the replacement.

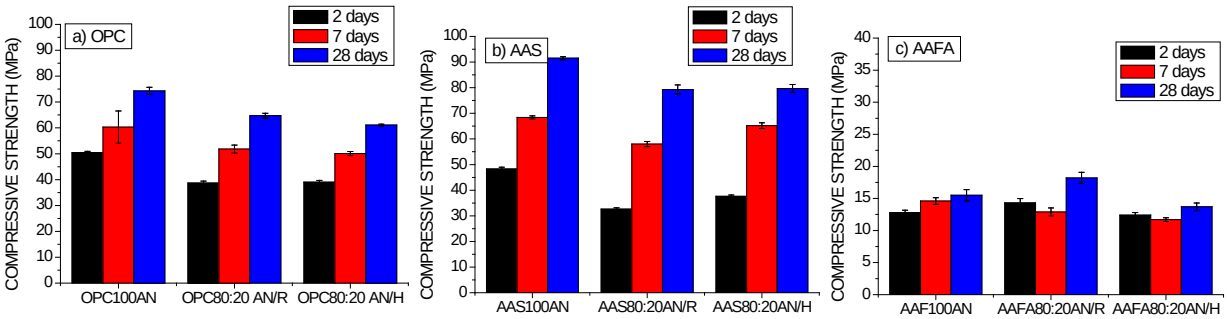


Figure 3 OPC, AAS and AAFA mortar compressive strength

Strength grew in all the OPC mortars (Figure 3a) with test time. Partial (20 %) replacement of aggregate AN lowered 7 and 28 day strength by around 15 %. That may be attributable to the higher water demand in the mortars with recycled aggregate, which would concur with earlier reports [8, 11]. Note that the percentage decline in mechanical strength was lower than the aggregate replacement rate applied (20 % of AN). A number of authors have reported that the replacement of natural with recycled aggregate in OPC concrete induced a downturn of 5 to 76 % in mechanical strength for replacement ratios of 100 % [12, 17]. Such a wide variation would be due to the host of factors that affect strength in concrete bearing recycled aggregate, including l/s ratio; nature, particle size distribution and shape of the aggregate; number of reuses; replacement ratio; and type of aggregate replaced. In mortars in which sand was replaced, behaviour was also found to vary widely, particularly when the finest fraction was involved [15].

As in the OPC mortars, compressive strength in AAS mortars (Figure 3b) was observed to rise with test time. Moreover, both the 7 and 28 day strength values were higher in all the AAS mortars than in the respective OPC materials, a finding likewise consistent with prior studies [18]. Seven-day mechanical strength declined by 15 and 5 % when the standardised aggregate was partially replaced with 20 % R and H, respectively. In the 28 day materials, the decline evened out at around 13 % for both types of aggregate. Again as in OPC mortars, the slide in compressive strength was less steep than the aggregate replacement ratio, affording proof of the viability of using recycled aggregate in these AAS mortars. Since the liquid/solid ratio was not observed to change, however, these declines may be associated with alterations in mortar microstructure and compactness.

Lastly, Figure 3c shows mechanical performance in mortar AAFA. Strength was much lower in these mortars than in the other two at all the ages studied. In the 7 day specimens mechanical strength dipped by 15 % with both types of recycled aggregate; the 28 day values were comparable or even slightly greater than in the mortars with standardised aggregate.

Table 7 Total porosity and pore size distribution in OPC, AAS and AAFA mortars

| SAMPLE | PORE DIAMETER (μm) (%) | | | | TOTAL POROSITY (%) |
|---|---|---|---|---|---|
| | >10 | 10-0.05 | 0.05-0.01 | <0.01 | |
| OPC100AN | 0.69 | 6.30 | 4.73 | 0.11 | 11.83 |
| OPC80:20AN/R | 0.82 | 10.55 | 3.95 | 0.18 | 15.50 |
| OPC80:20AN/H | 1.58 | 14.57 | 1.70 | 0.14 | 17.99 |
| AAS100AN | 1.16 | 3.48 | 1.29 | 0.69 | 6.62 |
| AAS80:20AN/R | 1.04 | 3.56 | 1.52 | 2.10 | 8.22 |
| AAS80:20AN/H | 1.68 | 4.61 | 1.57 | 0.83 | 8.69 |
| AAFA100AN | 2.05 | 12.75 | 0.14 | 0.15 | 15.09 |
| AAFA80:20AN/R | 1.00 | 15.03 | 2.09 | 0.16 | 18.28 |
| AAFA80:20AN/H | 1.41 | 9.20 | 3.94 | 0.11 | 14.66 |

Total porosity and pore size distribution were determined for the 7 day mortars. The findings are given in Table 7. Total porosity climbed in the OPC mortars with the replacement of AN by R and H; while the rise was greater with aggregate H than R, the l/s ratio was the same in both. The especially steep rise observed in air pores (>10 μm) and macropores (10-0.05 μm) with 20 % replacements may explain the decline in compressive strength in the mortars prepared with aggregates R and H. In the AAS mortars, despite the flat l/s ratio, total porosity was observed to rise, with increases in the percentages of macropores (10-0.05 μm) and mesopores (0.05-0.01 μm) in the mortars containing aggregates R and H. The mortar bearing 20 % aggregate H exhibited the highest porosity. Lastly, despite the 25 % higher liquid demand in the AAFA mortars with 20 % replacement, porosity values rose only slightly or not at all.

The graph in Figure 4 plots the 7 day values for the three variables studied (compressive strength, l/s ratio and porosity) in the OPC, AAS and AAFA mortars. As the graph shows, since the starting materials (OPC, S and FA) differed widely, the resulting mortars occupied different regions in space

- In OPC mortars the 20 % replacement of aggregate AN with aggregates R and H raised the liquid demand by 5 % and induced a 15 % decline in mechanical strength. The upturn in the l/s ratio also led to higher mortar porosity (30-55 %). Here, the dip in strength and rise in porosity appeared essentially to be the result of the higher amount of liquid needed in mortars containing recycled aggregate.

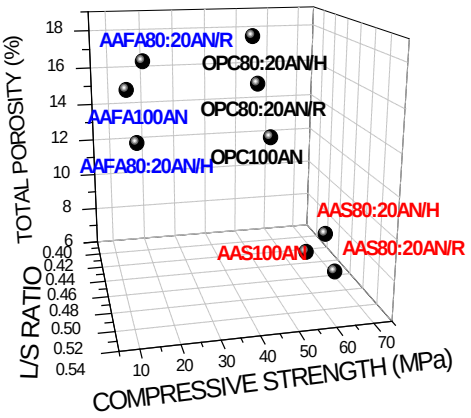


Figure 4 L/s ratio, compressive strength and total porosity in OPC, AAS and AAFA mortars

- In AAS mortars, although the 20 % replacement of aggregate AN induced no change in the l/s ratio, strength decreased by 15 %, nearly the same value as observed in OPC mortars. Although the liquid demand did not rise, porosity climbed by 25-32 %, with no significant differences between the mortars bearing aggregates R and H. Here the downswing in strength was not the result of the amount of liquid used, but rather appeared to be related to the compositional differences between the siliceous AN and the calcareous R and dolomitic H and the nature of the activating solution.

- In AAFA mortars the presence of 20 % aggregate R or H raised the l/s ratio by 25 % and lowered compressive strength at a rate equivalent to the declines recorded for the OPC and AAS mortars. In addition, porosity rose by 20 % in the mortar with aggregate R. One possible interpretation of these results would be that despite the greater amount of liquid needed by aggregates R and H (25 %), the N-A-S-H gel generated by ash activation was able to absorb or take up the excess liquid into its three-dimensional structure, whereby the effects on porosity and mechanical strength were not as great as would be expected.

The results of the shrinkage tests conducted at 99 and 45 % RH on AAS mortars containing only siliceous (AN) aggregate or AN with 20 % aggregate R or H are shown in Figure 5. Note that when the test was conducted at 99 % RH, the AAS mortar specimens exhibited similar behaviour regardless of the type of aggregate used, with slightly higher shrinkage than observed in prior studies [18]. The drying shrinkage values (test conducted at 45 % RH) were higher than found for autogenous shrinkage [18, 19]. The poorest performance was observed for mortar AAS80:20AN/H, with total shrinkage of 0.65 %, 15 % higher than mortars AAS100AN and AAS80:20AN/R. AAS80:20AN/H was also the most porous AAS mortar (see Table 7). Further to these findings, the inclusion of 20 % construction and demolition waste aggregate did not reduce drying shrinkage in these mortars.

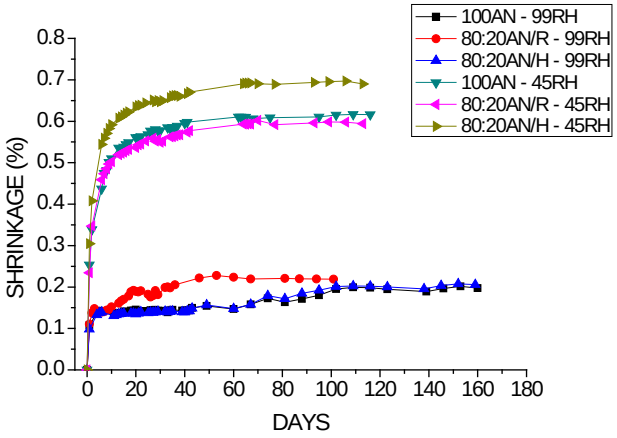


Figure 5 Drying shrinkage in AAS mortars after during at 99 % RH and 45 % RH

Lastly, Table 8 gives the percentage of weight loss in AAFA mortars after exposure to high temperatures in the durability test. The photographs in Figure 6 depict the AAFA100AN, AAFA80:20AN/R and AAFA80:20AN/H specimens after testing at 200-1000 °C.
The AAFA100AN specimens were in best condition, with fewest cracks and least weight loss. Their colour also darkened more than in the other two materials. The AAFA80:20AN/H specimens were in the poorest condition, with lowest density and the highest detachment rate

Table 8 Weight loss (%) after exposure to heat

| | TEMPERATURE (ºC) | | | | | |
|---|---|---|---|---|---|---|
| | 50 | 200 | 400 | 600 | 800 | 1000 |
| 100AN | 2.34 | 2.35 | 3.08 | 3.10 | 3.21 | 5.80 |
| 80:20AN/R | 2.32 | 3.16 | 6.60 | 8.47 | 11.22 | 11.46 |
| 80:20AN/H | 2.46 | 3.19 | 4.28 | 6.13 | 10.1 | 10.90 |

Such greater loss in mortars AAFA80:20AN/R and AAFA80:20AN/H was due in all likelihood to the calcareous nature of the replacement aggregates. At temperatures of over 600 °C these aggregates lost a substantial portion of their mass due to thermal decomposition.

The three types of mortar tested for durability exhibited similar compressive strength patterns (Figure 7). At 50 °C, strength was 16 % lower in the mortars bearing aggregates R and H than in mortar AAFA100AN. Strength values rose in all three mortars at 200 °C, due to higher activation of fly ash, and then declined until reaching 600 °C to subsequently climb through the end of the test.

This increase in mechanichal strength is due to changes in pore size distribution with temperature [20]. At 200 °C strength climbed by 52 % in mortar AAFA100AN but only by 25 % in the mortars with 20 % aggregate replacement. By the same token, 600 °C strength dropped in mortar AAFA100AN to values comparable to 50 °C. In the recycled aggregate,

however, strength was 40 % lower than at 50 °C. Lastly, at 1000 °C mortars AAFA100AN and AAFA80:20AN/R reverted to the 200 °C values, whereas the mortar with 20 % aggregate H barely attained its initial strength

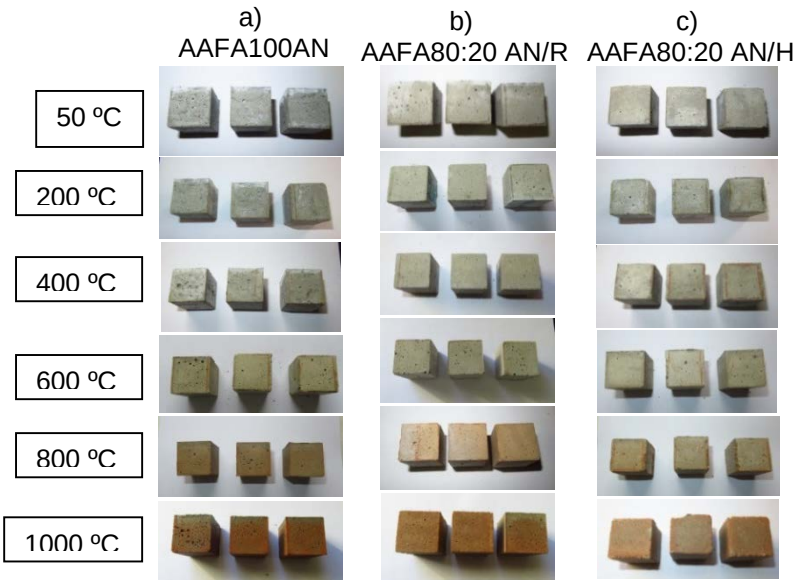


Figure 6 AAFA mortar specimens after exposure to high temperatures: a) AAFA100AN; b) AAFA80:20AN/R; and c) AAFA80:20AN/H

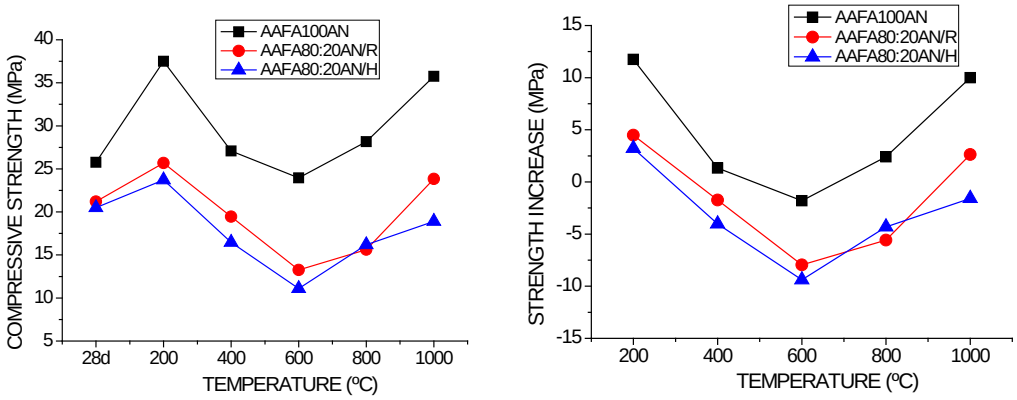


Figure 7 Compressive strength in AAFA specimens: a) versus high temperature; b) fluctuation relative to 28 day AAFA specimens

## CONCLUSIONS

- The replacement of silicieous aggregate (AN) with 20 % of recycled aggragate called for raising the l/s ratio in OPC and AAFA mortars. The l/s ratio was not observed to grow when recycled C&DW aggregate was added to AAS mortars.

- In OPC, AAS and AAFA mortars the percentage decline in mechanical strength was lower than the aggregate replacement rate applied (20% of AN aggregate by RA).

- The inclusion of 20 % construction and demolition waste aggregate on AAS mortars did not induce significant changes on shrinkage in these mortars.

- AAFA mortar specimens with 20% replacement, presented higher loss of mass after exposure to high temperatures than AAFA mortars with AN aggregate. Mechanical performances were worse in AAFA mortars with recycled aggregates.

## ACKNOWLEDGEMENTS

This research was funded by the Spanish Ministry of the Economy under project BIA2013-47876-C2-1-P.

## REFERENCES

1. PACHECO-TORGAL, F, LABRINCHA, LA. Review: The future of construction materials research and the seventh UN Millennium Development Goal: A few insights, Construction and Building Materials Vol 40,2013, pp 729–737
2. PUERTAS, F, SANTOS, R, ALONSO, MM, DEL RÍO, M. Alkali-activated cement mortars containing recycled clay-based construction and demolition waste, Ceramics Silikáty vol 59, No 3, 2015, pp 202-210.
3. MÜLLER, HS, HAIST, M, VOGEL, M. Assessment of the sustainability potential of concrete and concrete structures considering their environmental impact, performance and lifetime, Construction Building Materials vol 67, 2014, pp 321-337.
4. PALOMO, A, KRIVENKO, P, GARCIA-LODEIRO, I, KAVALEROVA, E, MALTSEVA, O, FERNÁNDEZ-JIMÉNEZ, A. A review on alkaline activation: new analytical perspectives, Mater. Construcc. vol 64, No 315, 2014, e022
5. PROVIS, JL, PALOMO, A, SHI, C. Advances in understanding alkali-activated materials, Cement and Concrete Research, volume 78, 2015, pp 110-125
6. FERNÁNDEZ-JIMÉNEZ, A, PUERTAS, F. Alkali-activated slag cements: Kinetic studies, Cement and Concrete Research, vol 27, No 3, 1997, pp 359-368
7. PUERTAS, F, PALACIOS, M, MANZANO, H, DOLADO, JS, RICO, A, RODRÍGUEZ, J. A model for the C-A-S-H gel formed in alkali-activated slag cements, Journal of European Ceramic Society, vol 31, No 12, 2011, pp 2043-2056
8. MARTÍN MORALES, M. El residuo de construcción y demolición (RCD) como árido en la elaboración de prefabricados no estructurales, PhD thesis, UG, Spain, 2013.
9. VEGAS, I, IBAÑEZ, JA, LISBONA, A, SÁEZ DE CORTAZAR, A, FRÍAS, M. Pre-normative research on the use of mixed recycled aggregates in unbound road sections. Construction and Building Materials, vol 25, No 5, 2011, pp 2674–2682.
10. FERNÁNDEZ-LEDESMA, E, JIMÉNEZ, JR, AYUSO, J, CORINALDESI, V, IGLESIAS-GODINO, FJ. A proposal for the maximum use of recycled concrete sand in masonry mortar design. Mater Construcc, vol 66, No 321, 2016, e075.
11. SHI, XS, COLLINS, FG, ZHAO, XL, WANG, QY. Mechanical properties and microstructure analysis of fly ash geopolymeric recycled concrete, Journal Hazard Mater , vol 237-238, 2012, pp 20-29

12. BEHERA, M, BHATTACHARYYA, SK, MINOCHA, AK, DEOLIYA, R, MAITI, S. Recycled aggregate from C&D waste & its use in concrete. A breakthrough towards sustainability in construction sector. A review, Construction Building Materials, vol 68, 2014, pp 501–516.
13. UNE- EN 1097-6:2001/A1:2006 Tests for mechanical and physical properties of aggregates Part 6: Determination of particle density and water absorption
14. UNE 83-811-1992. Morteros frescos: determinación de la consistencia: mesa de sacudidas : método de referencia. (In Spanish)
15. SILVA, RV, DE BRITO, J, DHIR RK. Performance of cementitious renderings and masonry mortars containing recycled aggregates from construction and demolition wastes Construction and Building Materials, vol 105, No 15, 2016, pp 400-415
16. CORINALDESI, V, MORICONI, G. Behaviour of cementitious mortars containing different kinds of recycled aggregate, Construction Building Materials, 23, 1, 2009, 289– 294
17. YILDIRIM, ST, MEYER, C, HERFELLNER, S. Effects of internal curing on the strength, drying shrinkage and freeze–thaw resistance of concrete containing recycled concrete aggregates, Construction Building Materials, vol 91, 2015, pp 288-296.
18. PALACIOS, M. Empleo de aditivos orgánicos en la mejora de las propiedades de cementos y morteros de escoria activada alcalinamente, PhD thesis, UAM, Spain, 2006
19. PALACIOS, M, PUERTAS, F. Effect of shrinkage-reducing admixtures on the properties of alkali-activated slag mortars and pastes Cement and Concrete Research vol 37, 2007, pp 691–702
20. MARTIN, A, PASTOR, JY, PALOMO, A, FERNÁNDEZ JIMÉNEZ, A. Mechanical behaviour at high temperature of alkali-activated aluminosilicates (geopolymers) Construction and Building Materials, vol 93, 2015, pp 1188-1196

# MECHANICAL CHARACTERISTICS OF USED BENT REBARS AS A FACTOR LIMITING THEIR REUSE

**J Domski**

**J Katzer**

**M Zakrzewski**

Koszalin University of Technology

Poland

**ABSTRACT.** Ribbed rebars of different diameters were tested and several mechanical properties were established after ranging numbers of bends. There are available several testing methods of ribbed rebars. Keeping in mind the possible re-use of used bend rebars there was utilized testing method described in ISO 7801:1984. This method is based on bending rebars several times. Thermographic photography was utilized to follow heat development in bended area. Achieved relations allowed to define safe practices for reusing rebars while maintaining their mechanical properties.

**Keywords:** Rebars, Reuse, Reinforcement, Steel, Bending

**Jacek Domski** is an assistant professor of Koszalin University of Technology and Director of Laboratory of Materials Strength and Civil Building Structures at Koszalin University of Technology. He is a successful Ph.D. M.Sc. B.Sc. qualified scientist, highly experienced engineer of concrete structures. He has wide experience as a concrete researcher, mix designer, quality controller of concrete production (both ready-mix and precast elements) and concrete structures lecturer.

**Jacek Katzer** is a professor of Koszalin University of Technology. He is Director of Department of Housing Engineering and Construction Materials. He is a successful D.Sc. Ph.D. M.Sc. B.Sc. qualified, highly experienced technologist of concrete. He has wide expertise as a concrete researcher, mix designer, quality controller of concrete production (both ready-mix and precast elements) and concrete technology lecturer.

**Mateusz Zakrzewski** is a scientist in Laboratory of Materials Strength and Civil Building Structures at Koszalin University of Technology. M.Sc. B.Sc. He is experienced as reinforcing materials researcher.

## INTRODUCTION

Since the invention of reinforced concrete in mid-19$^{th}$ century, steel, in different forms (bars, fibres, wires, nets, meshes etc.) was used as reinforcement. Steel rebars quickly proved to be the most efficient and thus became the most popular type of concrete reinforcement. Global production of concrete has been rising every year and it has recently reached the volume of 1m$^3$ per person per year [1]. Along with the growing concrete consumption there is a proportional increase in rebar consumption.

In a vast majority of cases, while preparing reinforcement cages, rebars are bent in one way or another. Some reinforcement cages are very dense and rebars are bent several times to get desired geometrical shapes. Some of the prepared cages and bent rebars are not used due to changes in building design, quality control issues, halted constructions, payment problems etc. Steel, being expensive is often reused (infringing multiple national and international codes and regulations) - rebars are straightened and cages are folded back. Steel bars achieved in this way are bend again according to a new design. Such reuse practises are very common and seen as sustainable, but they are associated with multiple technological and structural problems. Bend and straightened rebars are not as perfectly straight as the new ones and they are characterized by different mechanical properties [2]. Safety of structural elements cast with reused rebars is questionable and their real strength unknown.

On the other hand reusing materials or using recycled materials in civil and structural engineering is becoming very common [3] and excluding rebars from these sustainable practices is not logical. The knowledge about properties of bend rebars would be also valuable for analysis of low-cycle fatigue degradation of rebars [4]. Taking into account these considerations Authors conducted a research programme to enable safe reuse of the already bend rebars.

## RESEARCH PROGRAMME

Research programme was focused on testing chosen properties of rebars after bending. There were used steel ribbed rebars characterized by diameter (#) of 8 mm, 10 mm and 12 mm and made out of steel 34GS. According to the Polish Standard PN-B-03264:2002 this steel is hard weldable and characterized by yield strength $f_{yk}$ of 410 MPa and characteristic computational $f_{yd}$ of 350 MPa. According to Eurokod 2 it can be classified as steel class C. There are available several testing methods of ribbed rebars including those described in EN ISO 15630-1:2010 [5] and ASTM E290:2014 [6].

Keeping in mind the possible re-use of used bend rebars there was utilized testing method described in ISO 7801:1984 [7]. This method is based on bending rebars several Times. The length of specimens was equal to 420 mm. The first stage of the research programme covered the bending the rebar specimens. The bending was conducted over a cylindrical support with radius of 20 mm, 25 mm and 30 mm for rebar #8 mm, #10 mm and #12 mm respectively. The test was conducted according to ISO 7801:1984 [7] (one bending was performed during 2 seconds with a constant speed). A schematic diagram of rebar specimen being bend over a cylindrical support and used apparatus are presented in Figure 1. The specimens were bend until ultimate failure. In case of rebars #10 mm and #12 mm the specimens were ultimately destroyed after 4$^{th}$ bend. Rebars #8 mm were ultimately destroyed after 6$^{th}$ bend.

This knowledge allowed to prepare right number of specimens of specific diameter. It was planned to test tensile strength (EN ISO 6892-1 [8]) and conduct analysis of strain of bend six rebar specimens of each type after each bend.

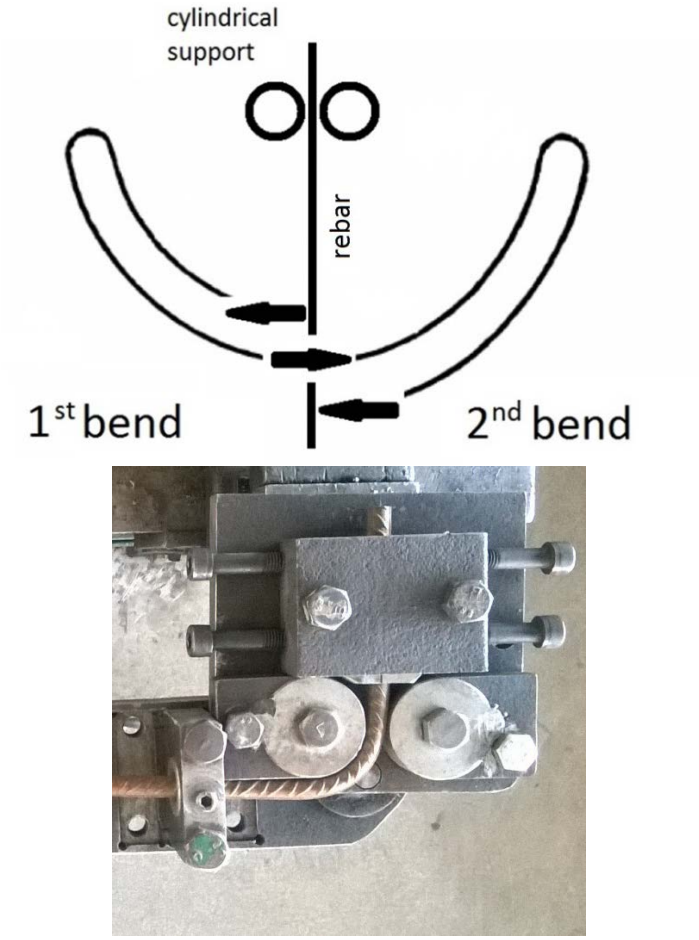


Figure 1 Schematic diagram of rebar bending over a cylindrical support and used apparatus

The second stage of the research programme consisted of strength tests of specimens after specific number of bends. These tests were accompanied by thermographic analysis. After each bend specimens were photographed using handheld thermal imaging camera (TIC). The pictures were taken in temperature of +23˚C which is inside a range of TIC operating temperature (from -15°C to +40 °C). The used TIC was equipped with wide-angle lens 32° · 25 and 640 pixels · 480 pixels detector. It was characterized by thermal sensitivity NETD < 100 mK, spectral range from 8 μm to 14 μm and refresh rate from 8 Hz to 15 Hz.

The pictures were digitally created using pseudo-colour to clearly visualize temperature differences. Exemplary thermal images of tested #8 mm rebar are presented in Figure 2. While analysing these pictures one has to keep in mind that accuracy of TIC is ±2 °C or ±2 % of reading (whichever is the greater).

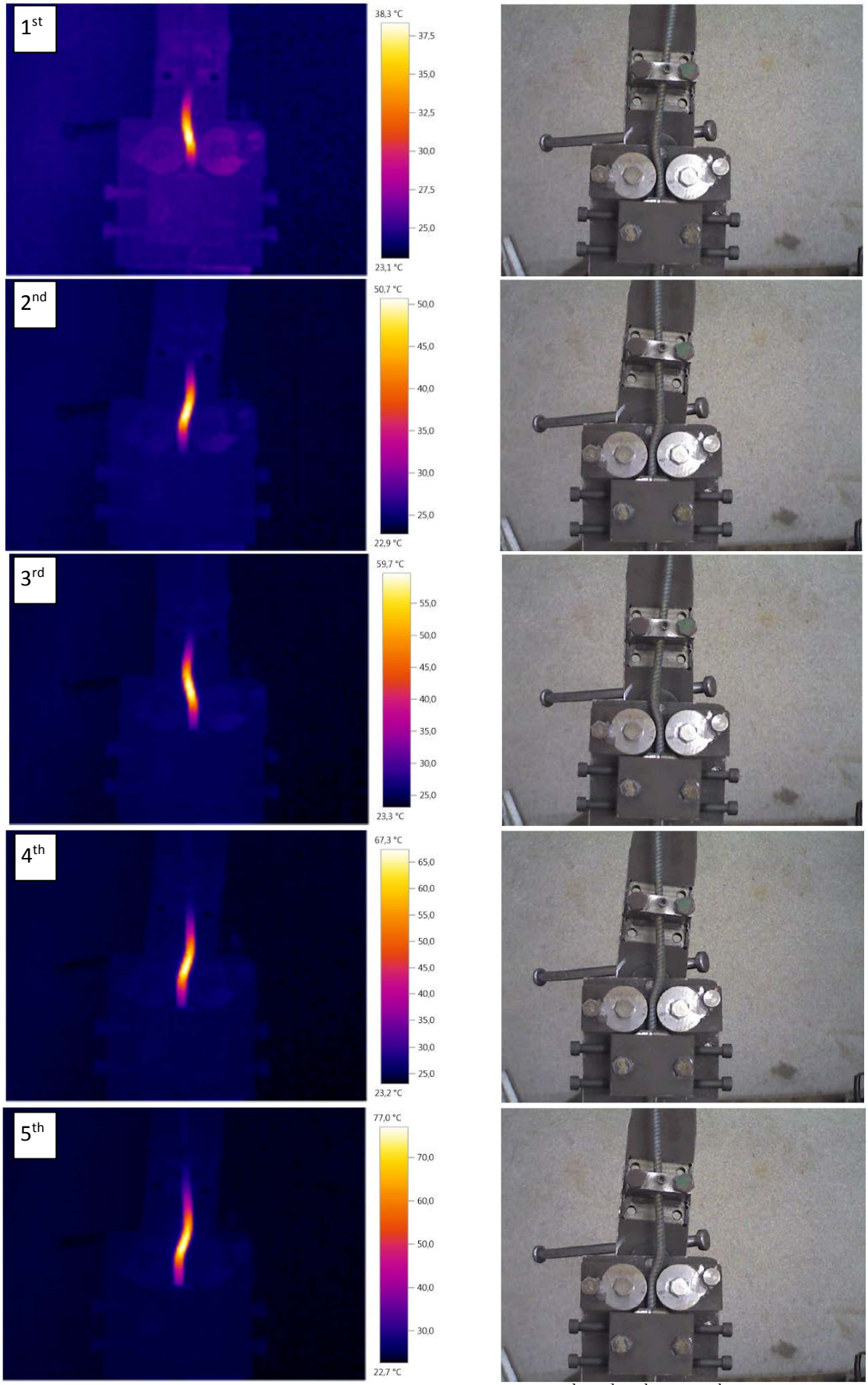


Figure 2 Temperature of rebar #8 mm after 1st, 2nd, 3rd, 4th and 5th bend and shape of bend rebar

## RESULTS

In Figure 2 exemplary temperature distribution in rebar #8 mm after 1st, 2nd, 3rd, 4th and 5th bend and shape of bend rebar are presented. The highest registered temperature were of special interest after each bend. The shape of bend rebar was important for analysis of tensile force – specimen elongation relations discussed in the further part of the paper. The significant rise of temperature was noted during the rebar bending test. In case of rebar #8 mm after first bend the maximum observed temperature was equal to +38°C. The temperature rose to +77°C after 5th bend. Rebars #10 mm and #12 mm were characterized by higher temperatures during bending than rebar #8 mm. After the 1st bend of rebars #10 mm and #12 mm the maximum temperature was equal to +42°C and +43°C respectively. After the 3rd bend of rebars #10 mm and #12 mm the maximum temperature was equal to +67°C and +70°C respectively. All recorded temperatures after specific number of rebar bends are presented in Figure 3. One can see that apart from rising temperature after each bend, thicker rebras are characterized by higher temperatures. This phenomenon is caused by larger amount of energy "transferred" into a rebar during bending. The thicker the rebar the bigger the work required for its bending.

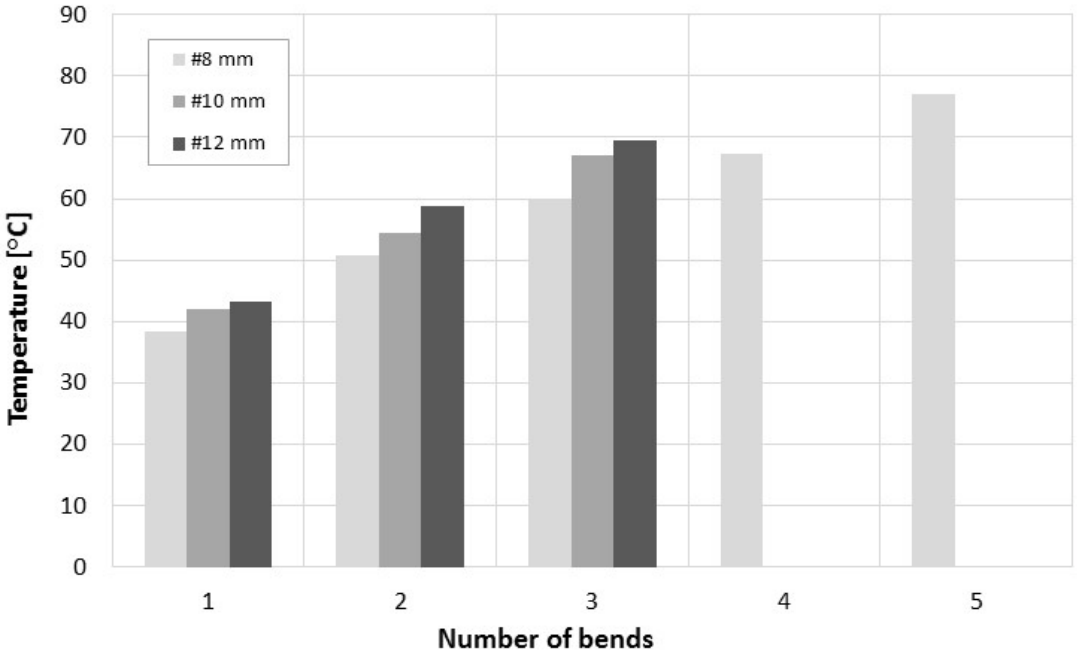


Figure 3 Temperature of tested rebars after specific number of bends

The tested rebars were characterized by very clear yield strength. In the Figure 4 the tensile force – elongation of a rebar specimens relations are presented for rebars #12 mm. In case of rebar with no bends the yield strength is very clearly visible for elongation over 1 mm (force = 50 kN). After 1st bend the yield strength part of the relation is missing, but overall elongation in the first part of the test is larger. This phenomenon is associated with the shape of bend rebars and their straitening during tensile strength test. The elongation of tested rebars was getting smaller and smaller after each bend. For the 3rd bend the elongation is over 8 mm shorter than in case of no bends.

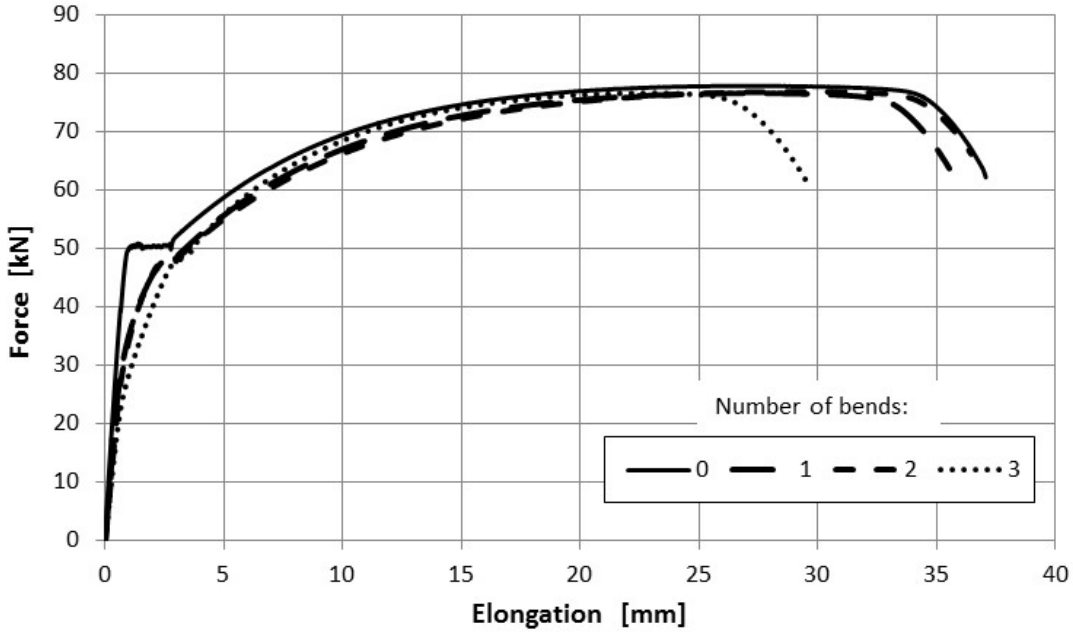


Figure 4 Force – elongation relations for bended rebars #12 mm

The influence of bending rebars on their tensile strength was presented in Figure 5. One can see that after first two bends, in case of rebars #10 mm and #12 mm, and three bends, in case of rebars #8 mm, tensile strength decreased from 1% to 3%. Such small differences are difficult to be realibly asses due to testing accuracy. For rebars #10 mm and 12 mm, significant decrease in tensile strength was achieved after three bends and was equal to 7% and 12% respectively. Rebars #8 mm were characterized by tensile strength decrease of 8% and 10% after fourth and fifth bend. Such differences in tensile strength of rebars affect load carrying ability of a reinforced concrete structure.

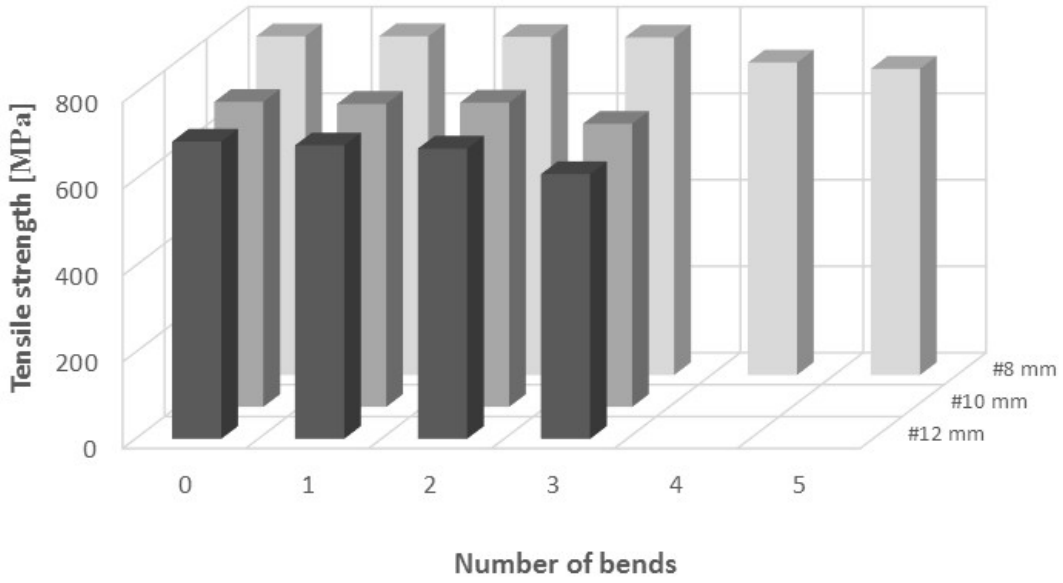


Figure 5 Tensile strength of rebars after specific number of bends

## CONCLUSIONS

According to EN 1992-1-1 [9] rebars should be able to bend and re-bend fulfilling the requirements of EN ISO 15630-1 [5] (and EN 10080). Ability of rebar to be "safely" bend is achieved if there are no visible cracks on rebar surface after first bend. During the research programme the surfaces of rebars were thoroughly inspected after first bend and no crack were observed. However, the test was conducted according to ISO 7801:1984 [7] and this standard allows multiple bends of tested steel wires. Achieved results prove that influence of single bend of a rebar is unnoticeable while taking into account change of tensile strength and value of elongation. For rebars #10 mm and 12 mm the third bend is critical (for rebars #8 mm the fourth bend is critical) when strength decrease and value of elongation are becoming significant. One can also compare the achieved results with results of similar tests conducted on steel fibres [10]. The conducted research programme gives introductionary data for mechanical modelling [11, 12] of concrete elements reinforced by reused and previously bend rebars. Future research effort, apart from testing large populations of different types of steel bars should be also focused on utilizing X-ray computed tomography [13] to assess the behaviour of the reused rebars in a loaded concrete element.

## REFERENCES

1. MALHORTA, V M, MEHTA, P K. High-Performance High-Volume Fly Ash Concrete. Ottawa, SCMSD Inc., 2005.

2. WARSIANTO, H, NARAYUDHA, M. Bending of reinforcing bars testing method and influence on structures. Technik, 2009, vol. 30, pp 79-82 (4p). ISSN: 0852-1697.

3. ŁAPKO, A, GRYGO, R. Effectiveness of the use of recycling aggregate concrete for sustainable building structures. Rocznik Ochrona Środowiska, 2014, 16:627-638.

4. KASHANI, M M, BARMI, A K, MALINOVA, V S. Influence of inelastic buckling on low-cycle fatigue degradation of reinforcing bars. Construction and Building Materials, vol. 94, 2015, pp 644-655

5. EN ISO 15630-1:2010, Steel for the reinforcement and prestressing of concrete. Test methods. Part 1: Reinforcing bars, wire rod and wire.

6. ASTM E290:2014, Standard Test Methods for Bend Testing of Material for Ductility.

7. ISO 7801:1984, Metallic materials. Wire. Reverse bend test.

8. EN ISO 6892-1:2009, Metallic materials. Tensile testing. Part 1: Method of test at room temperature.

9. EN 1992-1-1:2008, Design of concrete structures. Part 1-1: General rules and rules for buildings.

10. KATZER, J, DOMSKI J. Quality and mechanical properties of engineered steel fibre used as reinforcement for concrete. Construction and Building Materials, 2012, 36:243-248.

11. CICHOCKI, K, ADAMCZYK, R, RUCHWA, M. Material modelling for structures subjected to impulsive loading. Computer Assisted Mechanics and Engineering Sciences. Poland, Polish Academy of Sciences, vol. 6, 1999, pp 231-244 (14 p). ISSN 2299-3649.

12. VESELY, V, FRANTIK, P. Reconstruction of fracture process zone during tensile failure of quasi-brittle materials. Applied and Computational Mechanics. Pilsen (Czech): University of West Bohemia, vol. 4, 2011, pp 237-250 (14 p). ISSN 1802-680X.

13. PONIKIEWSKI, T, GOŁASZEWSKI, J, RUDZKI, M,. BUGDOL, M. Determination of steel fibres distribution in self-compacting concrete beams using X-ray computed tomography. Archives of Civil and Mechanical Engineering. Elsevier, vol. 15, 2015, pp 558-568. ISSN: 1644-9665.

# Theme 2

# Waste Minimisation and Resource Efficiency

# CONSTRUCTION EFFICIENCY WITH GYPSUM-BASED FLOWING SCREEDS: A DRYING CHARACTERISTICS STUDY

**L J Csetenyi**
University of Dundee
United Kingdom

**ABSTRACT.** Efficiency of the construction process depends on the various stages running in parallel or following each other in a logical manner, avoiding delays. From this aspect, time consuming steps, such as drying, are worthy of attention to save on overall project costs, calculated by a complex analysis of elements of the construction process alongside procurement data. It is often the case that selecting a more expensive material or construction method proves to be the most beneficial after all. In current work, drying characteristics of slabs of gypsum-based levelling screed were measured by standard air pocket and direct moisture content tests. Results were plotted for 40, 50, 65 and 75 mm slab thicknesses and the minimum drying periods determined so that different permeation floor covers could be laid down safely, without the risk of mould or odour formation. Correlation was found between the test methods applied, which may simplify the assessment of screeds if there is limited experience with the use of a given material.

**Keywords:** Screeds, Floor, Gypsum, Drying, Air pocket.

**Laszlo J Csetenyi** is a Research Fellow at the University of Dundee. His areas of research interest cover cement and concrete science, binder technology, the use of secondary and by-products to increase recycled material content in building materials and to improve sustainability of the construction process as a whole.

## INTRODUCTION

Efficiency of construction starts with a well thought out design plan, where the choice of construction materials and methods considered have a major effect on the project, irrespective of further adjustments and savings down the line. Complex analysis of each element of the construction process is needed alongside with procurement data. It well may be that selecting a more expensive material or construction method proves to be the most beneficial after all. Current study looks at a gypsum-based levelling screed and provides information on its drying characteristics measured by different methods. The feasibility of using this particular material for a cost-effective floor solution hinges on the time required to wait before floor covers can be laid. If the drying time is too long, it may cost precious time, causes damage to flooring or risks unwanted mould formation between the floor and applied cover (e.g. carpet, laminate or linoleum). Remediation in such cases is clearly the last scenario to wish for, but sufficiently dry status is also important for good adhesion [1].

In order to provide reliable information on the likely performance of the screed, test pours before the actual large-scale operation may prove to be useful, especially if there is limited experience with the material in the given circumstances e.g. substrate structural element. It has to be stressed though that in-situ monitoring and validating test data is indispensable should there be dispute on performance later on.

## CRITERIA AND METHODS OF TESTING

The speed of drying is affected by environmental conditions (temperature, relative humidity, air movement), but in the main governed by the nature of the actual screed material and its thickness applied. Screed product descriptions shall state the drying characteristic of the material, as determined by standard methods [2-4]. Typical values at which it would be permissible to lay moisture sensitive floor finishes on a calcium sulfate based screed are given as either <75% relative humidity (air pocket method) or 0.5% w/w moisture content for impermeable floors and 1.0% w/w moisture content for more permeable finishes such as carpet tiles (direct moisture testing).

Test were carried out to assess drying characteristics of this gypsum-based screed material, supplied by a local manufacturer as 600 mm × 600 mm slabs, poured in thicknesses of 40, 50, 65 and 75 mm. The periods required to achieve moisture contents satisfactorily low to apply various floor coverings are reported.

## TEST METHODOLOGY

Test specimens were kept in a drying chamber, operating at 20±2°C and 50±5% relative humidity, but sheltering them from forced air movement. Moisture contents of the various thickness slabs were determined on a regular basis by the ‘hygrometer in the air pocket’ standard method, as described in BS 8201:2011 Code of practice for installation of flooring of wood and wood-based panels [3] and also by taking cores from counterpart specimens and determining their moisture contents by drying at 40°C until constant mass (Figure 1). The hygrometer (model AZ-8711, humidity. range: 5-95% RH, accuracy: ±3% RH, resolution: 0.1% RH) was calibrated above saturated salt solutions (MgCl: 33%; NaCl: 75.5% at 20°C) before commencing the test series.


Figure 1 Insulated air pocket with humidity probe (top), slab surface after removal of air pocket (middle) and cored slab surface (bottom)

When the relative humidity of the pocket of air entrapped between the impervious, thermally insulated housing and the surface of the screed becomes 75% or lower, the material can be declared sufficiently dry to apply floor coverings.

## RESULTS BY THE AIR POCKET METHOD (STANDARD PROCEDURE)

Tests using the air pocket method indicate that, as expected, the thinnest (40 mm) layer went below the maximum 75% RH limit first, after 7 weeks, whereas the 50, 65 and 75 mm layers required 11, 15 and 17 weeks to achieve this, respectively (Table 1).

Table 1 Measured humidity values in the air pocket at equilibrium

| TIME SINCE CASTING, days (weeks) | SLAB THICKNESS, mm | | | |
|---|---|---|---|---|
| | 40 | 50 | 65 | 75 |
| | RH at equilibrium, % | | | |
| 21 (3) | 85.6 | 86.5 | 87.7 | 88.2 |
| 28 (4) | 79.3 | 80.8 | 82.7 | 83.1 |
| 35 (5) | 76.7 | 78.5 | 80.8 | 81.3 |
| 42 (6) | 75.8 | 77.5 | 79.5 | 80.1 |
| 49 (7) | 75.1 | 76.8 | 78.8 | 79.2 |
| 56 (8) | 74.7 | 76.3 | 78.0 | 78.5 |
| 63 (9) | 74.4 | 75.8 | 77.5 | 78.0 |
| 70 (10) | 74.0 | 75.4 | 77.1 | 77.6 |
| 77 (11) | 73.6 | 75.0 | 76.7 | 77.3 |
| 83 (12) | 73.3 | 74.6 | 76.3 | 76.9 |
| 91 (13) | 73.0 | 74.3 | 75.9 | 76.5 |
| 98 (14) | 72.7 | 74.0 | 75.5 | 76.2 |
| 105 (15) | 72.3 | 73.6 | 75.0 | 75.6 |
| 112 (16) | 71.8 | 73.2 | 74.7 | 75.2 |
| 119 (17) | 71.4 | 72.8 | 74.2 | 74.8 |
| 126 (18) | 70.8 | 72.1 | 73.5 | 74.1 |
| 133 (19) | 70.2 | 71.3 | 72.7 | 73.4 |
| 140 (20) | 69.8 | 70.8 | 72.2 | 72.8 |
| 147 (21) | 69.4 | 70.3 | 71.6 | 72.2 |

## RESULTS BY DETERMINING MOISTURE CONTENTS OF CORES

Based on recommendations in BS 8204-7:2003 [1] for calcium sulfate based screeds i.e. 0.5% w/w moisture content for impermeable floors and 1.0% w/w for more permeable finishes such as carpet tiles, it can be advised that the 40, 50, 65 and 75 mm thick layers reached the 1.0%/0.5% thresholds after 7/13, 11/17, 17/20 and 19/21 weeks, respectively. Table 2 shows the applicable drying period ranges in colour.

Table 2 Measured moisture contents of cores

| TIME SINCE CASTING, days (weeks) | SLAB THICKNESS, mm | | | |
|---|---|---|---|---|
| | 40 | 50 | 65 | 75 |
| | Loss on drying at 40°C until constant mass, % | | | |
| 28 (4) | 1.97 | – | – | – |
| 35 (5) | 1.56 | – | – | – |
| 42 (6) | 1.26 | 1.62 | – | – |
| 49 (7) | 0.98 | 1.39 | 2.54 | – |
| 56 (8) | 0.84 | 1.24 | 2.31 | 2.64 |
| 63 (9) | 0.77 | 1.13 | 2.08 | 2.41 |
| 70 (10) | 0.74 | 1.03 | 1.96 | 2.25 |
| 77 (11) | 0.63 | 0.94 | 1.91 | 2.15 |
| 83 (12) | 0.56 | 0.87 | 1.82 | 2.06 |
| 91 (13) | 0.50 | 0.82 | 1.73 | 1.98 |
| 98 (14) | 0.44 | 0.74 | 1.64 | 1.91 |
| 105 (15) | 0.39 | 0.65 | 1.47 | 1.75 |
| 112 (16) | 0.30 | 0.56 | 1.26 | 1.55 |
| 119 (17) | 0.23 | 0.50 | 1.00 | 1.32 |
| 126 (18) | 0.20 | 0.39 | 0.80 | 1.07 |
| 133 (19) | 0.18 | 0.33 | 0.65 | 0.85 |
| 140 (20) | 0.15 | 0.29 | 0.50 | 0.67 |
| 147 (21) | 0.14 | 0.26 | 0.42 | 0.50 |

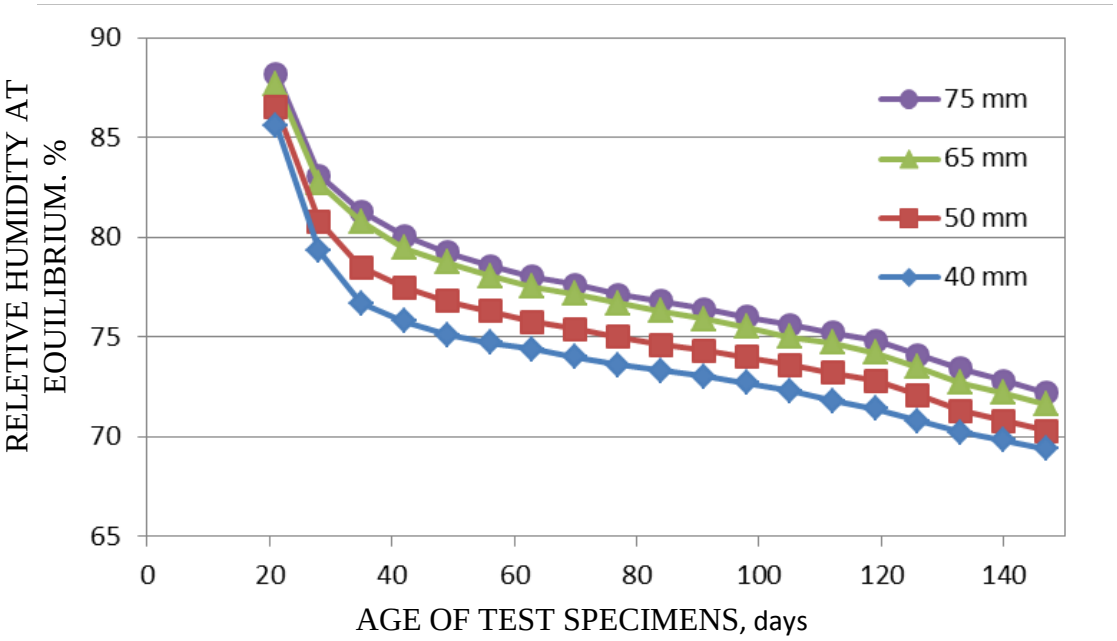


Figure 2 Relative humidity in the air pocket above the specimens

## CONCLUSIONS AND PERSPECTIVE

The detected drying characteristics show that the results based on cores are more conservative than for the standard (air pocket) method, which are in turn closer to the general expectation suggesting a 1 day/mm slab thickness drying rate. Nonetheless, the direct moisture level assessment method appears to be attractive in development stages of new composition screeds given the avoidance of using large specimens and several air pocket boxes. Laboratory space requirements are also lower. It has to be noted though that site conditions as opposed to a draft-free laboratory may allow more air movement and even quicker drying, which adds a safety margin to the findings.

## REFERENCES

1. BS 8204:2003. Screeds, bases and in situ floorings — Part 7: Pumpable self-smoothing screeds — Code of practice, British Standards Institution, London, UK.

2. BS 5325:2001. Installation of textile floor coverings — Code of practice, British Standards Institution, London, UK.

3. BS 8201:2011. Code of practice for installation of flooring of wood and wood-based panels, British Standards Institution, London, UK.

4. BS 8203:2001 +A1:2009. Code of practice for installation of resilient floor coverings, British Standards Institution, London, UK.

# EVALUATION OF PROPERTIES OF NO-AGGREGATE CONCRETE BY INCORPORATION OF FIBRES

**C N Gajera**

**U V Dave**

Nirma University

India

**ABSTRACT.** In this study, the attempt has been made to evaluate the mechanical properties of No-Aggregate Concrete with and without fibres. Two No-aggregate concrete mixes were prepared using nominal cement content of 320 kg/m$^3$. The fly ash and gypsum were also added. Polycarboxylate ether based chemical admixture was used. No coarse aggregates as well as the fine aggregates were used. Fibres used were polypropylene (PP) fibre of 12 mm length and having the density of 1000 kg/m$^3$. The proportion of the PP fibres was of 0.4% of the volume of concrete. Effectiveness of addition of the PP fibres on the compressive strength, flexure strength and split tensile strength was evaluated at the end of 28 days of water curing for No-aggregate concrete with the PP fibres (NACPF) and No-aggregate concrete without fibres (NAC). The modulus of elasticity and bond strength were also evaluated for both concrete mixes. Other important properties for the fibre reinforced concrete like impact energy and abrasion resistance were further investigated and the results were compared. As per the provision of IS: 456-2000, the minimum cement content of 320 kg/m$^3$ is required for control concrete in order to acquire the compressive strength of 20 MPa. However in the present investigation, both concrete mixes have exhibited the compressive strength in vicinity of 50 MPa at equivalent cement content. Test results revealed that the incorporation of the PP fibres enhanced the splitting tensile strength and the flexural strength. Significant enhancement was observed in the impact strength and the abrasion resistance due to incorporation of the fibres in the concrete. At par performance was observed for both concrete mixes in case of the compressive strength, modulus of elasticity and bond strength. Also enhancement in the ductility was observed in concrete due to the inclusion of the PP fibres.

**Keywords:** No-aggregate concrete, Mechanical properties, Polypropylene fibres.

**Chintan Gajera** is a Post Graduate Student in Computer Aided Structural Analysis and Design at the Nirma University of Ahmedabad, India.

**Dr Urmil Dave,** BE (Civil), ME (Structures), PhD (Civil), is a Professor at Nirma University, Ahmedabad. He has 19 years of teaching experience. His research areas are concreting materials and techniques, non-destructive testing of structures & repair and rehabilitation of structures. He has published number of papers at National and International conferences and journals.

## INTRODUCTION

India is one of the fastest growing economy in which infrastructure growth is at its peak level. This ultimately leads to increase in demand of construction materials. Out of all the construction materials, demand of cement is costliest and energy intensive component of concrete. Production of cement releases large amount of carbon-dioxide in the air. It also uses large part of limestone which is available in a limited quantity. Fly ash which is the major by-product of all the thermal power stations need to be dumped which adds to the cost. Leading towards the greener world, many cement manufactures have started using fly ash in manufacturing of cement.

To reduce the cement content in the concrete will pose difficulty in achieving the desired strength. So, to overcome such problem requires such material which can replace cement without any loss in strength. One of the alternatives to produce more environmental friendly concrete is to replace the amount of Portland cement in concrete by fly ash. Here comes a new type of material known as No-Aggregate Concrete (NAC) [1]. As the very name suggests, it is devoid of aggregates, neither coarser nor fines but having the engineering properties compatible to a structural concrete in addition to high strengths. NAC contains low cement (OPC) content of 320 kg/m$^3$, but rendering grade strength equivalent to 50 MPa. In this concrete, fly ash contributes to 75% of cementitious materials and remaining 25% by cement.

This type of concrete has very good flow-ability characteristics. It is cheaper compared to control concrete because fly ash is the major constituent which is available at cheap price and also as no aggregates are used for making the same. Experimental work in this study comprises of preliminary investigation on No-aggregate concrete with addition of polypropylene fibres.

## NEED OF STUDY

No-aggregate concrete has high compressive strength which leads to its brittle failure without giving any warning. It suddenly ruptures and burst under bending loads [2 and 3]. To arrest the propagation of cracks and sudden failure, use of polypropylene fibre is attempted to check whether the improvement in properties of no-aggregate concrete takes place or otherwise. Therefore, main objective of the present investigation is to improve performance of No-aggregate concrete by adding the polypropylene fibres.

## EXPERIMENTAL STUDY

### Materials

Physical and chemical properties of Ordinary Portland Cement utilized for the production of no-aggregate concrete mixes is shown in Table 1.

Table 1 Physical and chemical properties of Portland cement

| PHYSICAL AND CHEMICAL PROPERTIES OF PORTLAND CEMENT | | | |
|---|---|---|---|
| Parameters | Unit | Portland cement | Specification As per IS: 12269-1987 [4] |
| 28 days compressive strength | MPa | 55.19 | 53 (min) |
| Fineness | $m^2/kg$ | 309 | 225 (min) |
| Initial setting time | minutes | 125 | 30 (min) |
| Final setting time | minutes | 218 | 600 (max) |
| Le-chatelier soundness | mm | 1 | 10 (max) |
| Loss on ignition | % | 1.87 | 4 (max) |
| Magnesia | % | 3.6 | 6 (max) |
| Chloride content | % | 0.05 | 0.1 (max) |
| Lime saturation factor | % | 0.92 | 0.8 to 1.02 |
| Alumina iron ratio | % | 1.25 | 0.66 (max) |

Physical and chemical properties of class F fly ash given by the supplier and utilized for the production of no-aggregate concrete mixes is shown in Table 2.

Table 2Physical and chemical properties of fly ash

| PHYSICAL AND CHEMICAL PROPERTIES OFFLY ASH | | | |
|---|---|---|---|
| Parameters | Unit | Result | Specification As per IS: 3812 (part-1)-2003 [5] |
| Fineness Specific Surface by Blain | $m^2/kg$ | 416.36 | Min. 320.0 |
| Passing on 45 Micron Sieve (Wet Sieving) | % | 82.37 | Min. 66.0 |
| Retention on 45 Micron Sieve (Wet Sieving) | % | 17.63 | Max. 34.0 |
| Pozzolanic Activity Index | % | 88.23 | Min. 80.0 |
| Total Sulphur as Sulphur Trioxide ($SO_3$) | % | 0.56 | Max. 3.0 |
| Available Alkali as Sodium Oxide ($Na_2O$) | % | 0.62 | Max. 1.5 |
| Silicon Dioxide as $SiO_2$ | % | 61.40 | Min. 35.0 |
| $SiO_2 + Al_2O_3 + Fe_2O_3$ | % | 93.02 | Min. 70.0 |
| Reactive Silica | % | 34.36 | Min. 20.0 |
| Magnesium Oxide (MgO) | % | 1.42 | Max. 5.0 |
| Total Chlorides | % | 0.03 | Max. 0.05 |
| Loss on Ignition | % | 1.05 | Max. 5.0 |
| Moisture | $m^2/kg$ | 0.10 | Max. 2.0 |

Physical properties of polypropylene fibres utilized for the production of No-aggregate concrete mixes is shown in Table 3 and polypropylene fibres used for the investigation are as shown in Figure 1.

Table 3 Physical properties of polypropylene fibres

| PHYSICAL PROPERTIES OF POLYPROPYLENE FIBRES | | | |
|---|---|---|---|
| Name of fibre | Length (L) (mm) | Diameter (d) micron | Density (kg/m$^3$) |
| Polypropylene fibres | 12 | 35 | 1000 |

Figure 1 Polypropylene fibres

## Mix Proportions

To investigate the effect of fibre on No-aggregate concrete, mechanical properties of two concrete mixes were designed with constant water to cementitious material ratio of 0.172 and cement content of 320 kg/m$^3$. Mineral admixtures like fly ash and gypsum were utilized at the rate of 1242 kg/m$^3$ and 26 kg/m$^3$ respectively. Based on different trial tests, the proportion of polycarboxylate ether based admixture was selected such that the concrete could flow. Final dosage for admixture was adopted of 6.21 litre/m$^3$. Water utilized for the mix was of 272.7 litre/m$^3$. Mix proportions for both the mix were kept same except for the fibres used in the mix were 0.4% by the concrete volume for fibre mix [6]. No-aggregate concrete is represented as NAC and No-aggregate concrete with fibre is represented as NACPF in this paper.

## Specimen Preparation and Curing

Power driven revolving pan mixer with the capacity of 150 kg was used to mix the concretes as shown in Figure 2.

Figure 2 Pan mixture for NAC and NACPF

Weighing & batching of all necessary ingredients of NAC and NACPF such as cement, fly ash, gypsum, water and chemical admixture was donebefore starting the mixing process. Half of total fly ash was added in themixer machine to start the mixing process. Gypsum was added

alongwith cement in the mixer. Water and admixture is added at regularintervals in the mixer till a viscous paste is obtained. After this, remaining fly ash was added in the mixer along with remaining amount ofwater and admixture at regular intervals. Polypropylene fibres were mixed at the end after the concrete has gained the fluid nature.Fresh concrete was poured into steel moulds after thorough mixing. The specimens were kept in casting room for 24 hours at room temperature &were de-moulded and cured in water for 28 days.

## TESTING PROCEDURE

### Compressive Strength

Compression test was conducted with respect to IS: 516-1959 [7] on 150 × 150 × 150- mm cube specimens using compression testing machine of 2000 kN capacity. Three specimens were cast and tested after 28 days of water curing.

### Flexure Strength

Flexure strength was determined by testing plain concrete beams of dimension 100 mm × 100 mm × 500 mm as per IS: 516-1959 [7].Three specimens were cast and tested after water curing of 28 days.

### Split Tensile Strength

Cylinder of size Φ150 × 300-mm was tested in accordance with the test procedures given in IS: 5816- 1999 [8].Three specimens were cast and tested after water curing of 28 days.

### Modulus of Elasticity

Cylinder specimen of Φ150 × 300-mm was used for finding out the modulus of elasticity of concrete as per the test procedure given in IS: 516-1959 [7] using compression testing machine.Three specimens were cast and tested after water curing of 28 days.

### Bond Strength

Bond strength test was conducted as per IS: 2770-1969 [9]. The test specimen consisted of concrete cubes of 150 mm × 150 mm × 150 mm with a single reinforcing bar embedded vertically along a central axis in each specimen. Three specimens were casted and tested for taking the average values on the $28^{th}$ day. The bar shall project down for a distance of about 10 mm from the bottom face of the cube as cast, and shall project upward from the top face.The test specimen is mounted in a universal testing machine in such a manner that the bar is pulled axially from the cube. The loading shall be continued and the readings of the movement recorded at appropriate intervals until the yield point of the reinforcing bars has been reached, concrete has failed or minimum slippage if 2.5 mm has occurred at the loaded end. The test set-up is shown in Figure 3.

Figure 3 Bond strength test

## Impact Strength

The impact test was performed using drop weight impact testing machine according to ACI: 554.2R-1989 [10]using cylinder ofΦ152 × 63.5-mm size as given in Figure 4.Three specimens were cast and tested for taking the average values of the result after 28 days of curing. The test consisted of repeated application of impact load in the form of blows, using a 4.45 kg hammer falling from 457 mm height on the steel ball of 63.5 mm diameter, placed at the centre of the top surface of disc. Number of blows (n1) and (n2) that caused the first visible crack and failure respectively are noted as first crack strength and the failure strength of the sample.

Figure 4 Drop-weight test equipment

## Abrasion Resistance

The abrasion resistance test was performed in a Dorry abrasion testing machine on the 86 mm × 50 mm × 32mm prism according to BS: 812-1969 [11] as shown in Figure 5. Four specimens were casted and tested for taking the average values on the 28$^{th}$ day.The weight specimens were made to press on the top of disc with a pressure of total 2000 gram with sample tray. The disc is revolved through 500 revolutions at a speed of about 30 rpm, i.e., nearly for 18 minutes. The standard silica sand at least all passing 0.85mm and 75% passing 0.6mm sieve and retained on 0.3mm sieve was used. The specimens were taken out and weighted again. The percentage loss in weight was calculated.

Figure 5 Dorry abrasion test

## TEST RESULTS AND DISCUSSION

### Compressive Strength

Compressive strength = $\frac{P \times 10^3}{A} = \frac{113.26 \times 10^3}{150 \times 150} = 50.34$ N/mm$^2$
(Sample calculation)

Where P (kN) and A (mm$^2$) are maximum load and area of the cube specimen, respectively.

Compressive strength test results obtained from cube specimens are given in Table 4.

Table 4 28 days Compressive Strength

| 28 DAYS COMPRESSIVE STRENGTH | | | | |
|---|---|---|---|---|
| Specimen | NAC | Avg. compressive strength (MPa) | NACPF | Avg. compressive strength (MPa) |
| 1 | 50.34 | | 54.96 | |
| 2 | 50.29 | 49.87 | 52.73 | 53.86 |
| 3 | 48.98 | | 53.88 | |

It was observed that the increment in strength due to incorporation of fibres was 7.99% which is almost at par with the results observed for NAC. The reason for such observation is that the fibres arrest the crack which ultimately leads to enhancement in strength. Brittle failure was avoided due to fibres as shown in Figure 6 for both categories of concrete mixes.

Figure 6 Failed specimens of NAC (left) and NACPF (right)

**Flexure Strength**

Flexure strength = $\frac{P \times l \times 10^3}{b \times d^2} = \frac{11.33 \times 450 \times 10^3}{100 \times 100^2} = 5.01$ MPa
(Sample calculation)

Where P (kN), l (mm), b (mm) and d (mm) are failure load, length, width and depth of beam, respectively.

Test results presented in Table 5 indicates that the flexure strength of NACPF increased significantly by 64.26% as compared to that of NAC. The probable reason behind such observation is that polypropylene fibres are small in size and large in numbers. The fibres prevent the propagation of cracks and change the direction of cracks. This behaviour leads to increase in load carrying capacity of NACPF until the failure takes place. Brittle failure was avoided due to fibres as shown in Figure 7 for both concrete mixes.

Table 5 Flexure strength

| FLEXURE STRENGTH | | | | |
|---|---|---|---|---|
| Specimen | NAC | Avg. flexure strength (MPa) | NACPF | Avg. flexure strength (MPa) |
| 1 | 5.01 | | 8.28 | |
| 2 | 4.98 | 5.04 | 7.92 | 8.27 |
| 3 | 5.12 | | 8.62 | |

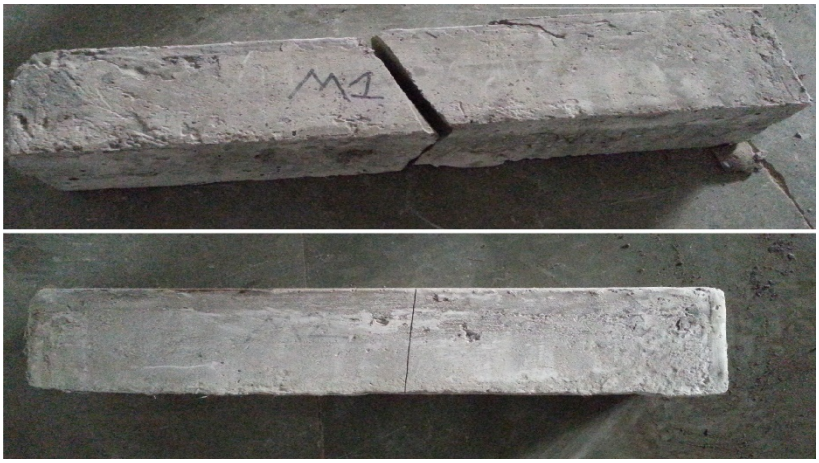

Figure 7 Failed specimens of NAC (top) and NACPF (bottom)

**Split Tensile Strength**

Split tensile strength = $\frac{2 \times P \times 10^3}{\Pi \times l \times d} = \frac{2 \times 299.56 \times 10^3}{3.14 \times 300 \times 150} = 4.24$ MPa
(Sample calculation)

Where P (kN), l (mm) and d (mm) are failure load, height and diameter of cylinder respectively.

Test results presented in Table 6 indicate that the splitting tensile strength of NACPF increased by 27.46% as compared to that of NAC. Here also, fibres contributed similar type of role. NAC mix showed brittle failure, whereas NACPF mix did not exhibit brittle failure as shown in Figure 8.

Table 6 Split tensile strength

| SPLIT TENSILE STRENGTH | | | | |
|---|---|---|---|---|
| Specimen | NAC | Avg. split tensile strength (MPa) | NACPF | Avg. split tensile strength (MPa) |
| 1 | 4.24 | | 5.67 | |
| 2 | 4.39 | 4.26 | 5.38 | 5.43 |
| 3 | 4.15 | | 5.24 | |

Figure 8 Failed specimens of NAC (left) and NACPF (right)

**Modulus of Elasticity**

The load was applied continuously and displacement was measured at equal load intervals as per codal provisions. Stress vs. Strain relationship for concrete mixes was prepared. Slope of the curve by the tangent modulus method presented the modulus of elasticity.The modulus of elasticity obtained from stress strain relationship is as shown in Figure 9.

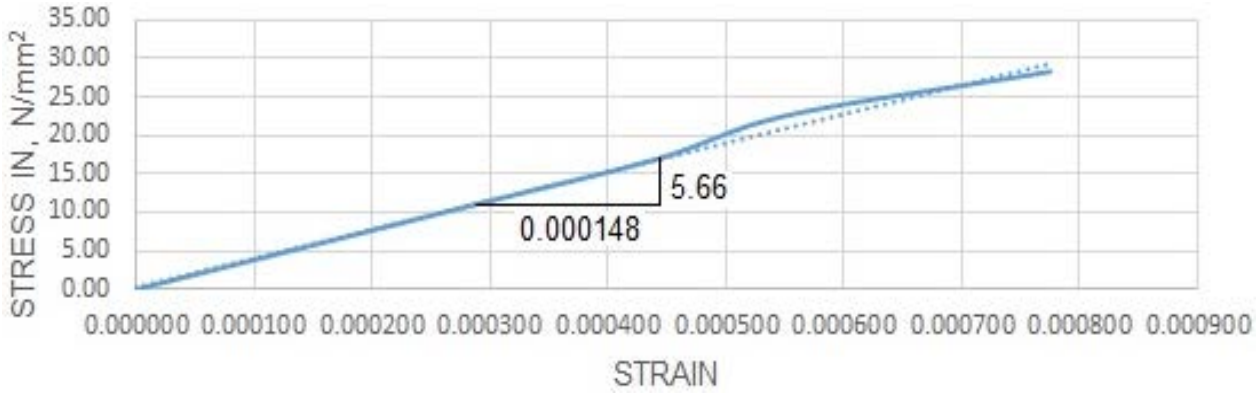


Figure 9 Stress strain curve

Modulus of elasticity = Stress = 5.66 = 38338.66 MPa
(Sample calculation) Strain 0.000148

Elastic modulus was obtained from cylindrical specimens are given in Table 7.Modulus of elasticity of NACPF was found to be 5.84% higher than that of NAC. The increment in modulus of elasticity was almost at par with that of NAC.

Table 7 Modulus of elasticity

| MODULUS OF ELASTICITY | | | | |
|---|---|---|---|---|
| Specimen | NAC | Avg. M.O.E (MPa) | NACPF | Avg. M.O.E (MPa) |
| 1 | 32587.86 | | 36421.72 | |
| 2 | 35143.77 | 34413.51 | 34504.79 | 36421.72 |
| 3 | 35508.90 | | 38338.36 | |

**Bond Strength**

Bond strength (Sample calculation) $= \frac{\text{Failure load}}{\text{Embedded surface area of bar}} = \frac{P \times 10^3}{\pi \times l \times d} = \frac{54.93 \times 10^3}{\pi \times 150 \times 12} = 9.72$ MPa

Where P (kN), l (mm) and d (mm) are failure load, embedded length and diameter of bar respectively.

Test results presented in Table 8 indicate that the bond strength increased with the inclusion of fibre. The increment in strength was of 6.41% which was at par with the bond strength observed for NAC.

Table 8 Bond strength

| BOND STRENGTH | | | | |
|---|---|---|---|---|
| Specimen | NAC | Avg. bond strength (MPa) | NACPF | Avg. bond strength (MPa) |
| 1 | 9.72 | | 10.85 | |
| 2 | 10.67 | 10.30 | 11.28 | 10.96 |
| 3 | 10.50 | | 10.76 | |

**Impact Energy**

Impact Energy (Sample calculation) $= \frac{n_1 \times m \times v^2}{2} = \frac{3 \times 0.00453 \times 2994.38^2}{2} = 61.01$ kN.mm

Where,
$n_1$ = numbers of blows
g = 9810 N/mm$^2$
m = mass of hammer = $\frac{w}{g} = \frac{44.5}{9810} = 0.00453$ kg
H= Height of hammer = 457 mm
t = time required for hammer to fall from a ht. of 457 mm = $\sqrt{\frac{2 \times H}{g}} = \sqrt{\frac{2 \times 457}{9810}} = 0.3052$ s
v = velocity of hammer at impact = g × t = 9810 × 0.3052 = 2994.38 mm/s

Impact energy results presented in Table 9 show that the first crack observedfor NAC at lesser number of blows as compared to that of NACPF. Also, the number of blows required for the complete failure of specimens was also low for NAC as that of NACPF. Results clearly showed that, the impact energy due to incorporation of the PP fibres in No-aggregate concrete had

increased the impact energy significantly as compared to that of NAC. Once again, brittle failure was avoided due to incorporation of fibres as shown in Figure 10.

Table 9 Impact energy results

| IMPACT ENERGY RESULTS | | | | | | | | |
|---|---|---|---|---|---|---|---|---|
| Specimen | NAC | | | | NACPF | | | |
| | First Crack (n1) | First Crack Energy (kN.mm) | Final Crack (n2) | Final Crack Energy (kN.mm) | First Crack (n1) | First Crack Energy (kN.mm) | Final Crack (n2) | Final Crack Energy (kN.mm) |
| 1 | 4 | | 7 | | 14 | | 124 | |
| 2 | 3 | 61.01 | 6 | 122.02 | 16 | 284.71 | 138 | 2582.74 |
| 3 | 3 | | 5 | | 13 | | 119 | |
| Round Avg. | 3 | - | 6 | - | 14 | - | 127 | - |

Figure 10 Failed specimens of NAC (left) and NACPF (right)

**Abrasion Resistance**

Percentage weight loss = $\frac{(A - B) \times 100}{A} = \frac{(252.32 - 194.39) \times 100}{252.32} = 22.96\ \%$
(Sample calculation)

Where, A = Weight of specimen before testing and B = Weight of specimen after testing.

Test results presented in Table 10 clearly suggesting that NAC has lesser resistance to abrasion as compared to that of NACPF.

Table 10 Weight loss of concrete mixes in abrasion test

| WEIGHT LOSS OF CONCRETE MIXES IN ABRASION TEST | | | | | | |
|---|---|---|---|---|---|---|
| | NAC | | | NACPF | | |
| Specimen | Initial Wt. (A) (gram) | Final Wt. (B) (gram) | Wt. loss (%) | Initial Wt. (A) (gram) | Final Wt. (B) (gram) | Wt. loss (%) |
| 1 | 252.32 | 194.39 | 22.96 | 258.92 | 218.34 | 15.67 |
| 2 | 254.93 | 203.43 | 20.20 | 254.51 | 224.43 | 11.82 |
| 3 | 261.17 | 206.83 | 20.81 | 259.12 | 219.56 | 15.27 |
| 4 | 253.74 | 196.21 | 22.67 | 255.76 | 223.87 | 12.47 |
| Avg. | 255.54 | 200.22 | 21.65 | 257.08 | 221.55 | 13.83 |

NACPF showed higher abrasion resistance in form of reduced percentage of weight loss due to the abrasion. NACPF showed higher resistance to abrasion of 36.16% as compared to that of NAC.

## CONCLUSIONS

Based on the experimental results presented herewith, the following conclusions are drawn:

1. The minimum cement content of 320 kg/m$^3$ is required for control concrete inorder to acquire the compressive strength of 20 MPa [12].However in the present investigation, both concrete mixes have exhibited the compressive strength in vicinity of 50 MPa at same cement content in presence of fly ash and admixture.
2. Marginal increase in compressive strength, modulus of elasticity and bond strength has been observed for NACPF as compared to that of NAC.
3. Significant enhancement in flexure strength and split tensile strength has been observed for NACPF at 28days as compared to that of NAC.
4. Increment has been observed in abrasion resistance and impact energy for NACPF as compared to that of NAC.
5. The failure of NACPF was gradual and ductile as compared to that of NAC due to the addition of the polypropylene fibres in the concrete.

It has been observed in the present investigation that the combination of use of OPC, and fly ash has been able to furnish an impressive compressive strength in spite of absence of the aggregates. Also the incorporation of the polypropylene fibres has been able to yield a significant amount of ductility in the concrete mixes.

## ACKNOWLEDGEMENTS

We are thankful to Mr. N. Kalidas & Dr. Bhanumatidas, Directors, Institute for Solid Waste Research & Ecological Balance (INSWAREB), Visakhapatnamfor providing the guidance and support for making the No-aggregate Concrete. We are also thankful to the Director, Institute of Technology, Nirma University, Ahmedabad for giving necessary permission for conducting the work.

## REFERENCES

1. KALIDAS N., BHANUMATHIDAS N., Advanced concrete technology-A Tool for durability, Proceedings of International Conference of National Academy of Construction, 2002.

2. KANUGA H. and DAVE U., Study of mechanical properties of no-aggregate concrete, Proceedings ofUK India Education and Research Initiative (UKIERI) Concrete Congress: Concrete Research Driving Profit and Sustainability, 2015, pp 1-15.

3. DADHANIA P. and DAVE U., Evaluation of mechanical properties of fibre reinforced no-aggregate concrete, Proceedings ofUK India Education and Research Initiative (UKIERI) Concrete Congress: Concrete Research Driving Profit and Sustainability, 2015,pp 1-14.

4. BUREAU OF INDIAN STANDARDS,Specification for 53 grade ordinary Portland cement, No. 12269, 1987.

5. BUREAU OF INDIAN STANDARDS, Specification for fly ash for use as pozzolana and admixture, No. 3812, 2003.

6. NILI M. and AFROUGHSABET V., The effects of silica fume and polypropylene fibers on the impact resistance and mechanical properties of concrete. Construction and building materials, Vol. 24, 2010, pp 927-933.

7. BUREAU OF INDIAN STANDARDS,Methods of tests for strength of concrete, No. 516, 1959.

8. BUREAU OF INDIAN STANDARDS, Splitting tensile strength of concrete method of test, No. 5816, 1999.

9. BUREAU OF INDIAN STANDARDS, Methods of Testing Bond in reinforced concrete Part-1 Pull-out test, No. 2770 (Part-1), 1965.

10. AMERICAN CONCRETE INSTITUE COMMITTEE, Measurement of properties of fibre reinforced concrete, No. 544.2R, 1989.

11. CONCRETE SOCIETY,Testing aggregates, Method for determination of aggregateabrasion value (AAV), No. 812-113, 1990.

12. BUREAU OF INDIAN STANDARDS, Plain and Reinforced concrete code of practice, No. 456, 2000.

# RELATIONSHIP BETWEEN 28-DAYS COMPRESSIVE STRENGTH AND COMPRESSIVE TOUGHNESS FACTOR OF ULTRA HIGH PERFORMANCE USING DESIGN OF EXPERIMENTS

**M A Mosaberpanah**

**O Eren**

Eastern Mediterranean University

Cyprus

**ABSTRACT.** Higher strength of material is not always showing the higher structural strength performance while higher energy absorber material (toughness) express higher structural strength performance when failure happens. This study goals to find the relation between 28-days compressive strength and compressive toughness factor of Ultra High Performance Concrete (UHPC) using vary range of five variables; Steel Fibre, Silica fume (SF), , Cement 42.5, Superplasticizer (SP), and water cement ratio (w/c) by Design of Experiments (DOE) methodology. The results shows the significant relation of compressive toughness factor and 28 days compressive strength of UHPC, The model are valid for the mixes made with 1.0 sand, 0.15-0.30 silica fume amount, 0.70-1.30 cement amount, 0.10- 0.20 steel fibre, 0.04- 0.08 superplasticizer (all values are by aggregate weight mass) and 0.18- 0.32 water cementitious ratio.

**Keywords:** DOE, Compressive toughness, UHPC, 28-day compressive strength

**Mr Mohammad Ali Mosaberpanah** is the Research Assistant and PhD Candidate in Civil Engineering at the Eastern Mediterranean University. He is a member of ASCE and his research interests are High strength Concrete, Ultra High performance concrete, Statistical modelling, Design of Experiments.

**Professor Özgür Eren** received all of his degrees in Civil Engineering as BEng degree from Eastern Mediterranean University, MSc degree from the University of Leeds, and PhD degree from Eastern Mediterranean University. He has been teaching courses on Civil Engineering materials, material sciences, and concrete repair and maintenance at the undergraduate and graduate levels since February 2000. Professor Eren has published research articles on fibre reinforced concrete, natural building stones, recycling of concrete, assessment of buildings, high strength of concrete, and use of pozzolans in cement. He supervised many MSc and PhD theses. Currently, he is the chair of Civil Engineering Department, Eastern Mediterranean University.

## INTRODUCTION

Ductility is defined as a measure of how much materials deform plastically before fracture [1]. Because a material is ductile will not make it tough. The point to toughness is a good combination of strength and ductility [2, 3]. A material with high strength and high ductility will have more energy absorption than a material with low strength and high ductility that it will be useful for structure purposes. Compressive toughness is equal by calculating the area under the load- deflection curve from a compression test. This value is simply called "compression toughness" and it has units of works [4, 5].

Brittleness of high strength concrete is one of the most disadvantages of this type of concrete. In the past many research have been done in order to finding a solution the brittleness of concrete [6, 7, 8]. Ultra High Performance Concrete (UHPC) is the one of the latest advanced composite material which is covering this defect with having unique durability and mechanical properties [9]. The main parameters to produce Ultra High Performance Concrete is are using well graded fine aggregate, using large amount of cement in order to decreasing the porosity, proper curing, accurate compaction, increasing workability by adding the superplaticizer, increasing the ductility by the fibre adding which cause to confine the materials [10, 11, 12].

Higher strength of material is not always showing the higher structural strength performance while higher energy absorber material (toughness) express higher structural strength performance when failure happens [13, 14, 15]. Therefore UHPC as superior material decreases differences between material strength and structural strength. This study tried to find the relation between these two important factors by using five different variables.

Few researches are exist that works on compressive toughness and compressive toughness factor. The researches were focused to see the effect of only fibre properties on compressive toughness. For example, Marar et al. [16] investigated on compression specific toughness of normal strength steel fibre reinforced concrete and high strength steel fibre concrete or Bhargava et al [17] studied on stress- strain behaviour of small scale steel fibre high strength concrete cylinder.

### Research Significance

28-day compressive strength test and stress- strain behavior of UHPC in order to find compressive toughness factor in different mix design under compression were carried out. The objective was to consider if there is any relation between 28 compressive strength and compressive toughness factor of UHPC.

### Material Properties

Forty five different mixes with five variables were used to find the relation between 28-day compressive and compressive toughness factor. The variables were silica fume, steel fibre, cement, superplasticizer, and w/c ratio. The materials properties are: 42.5N Portland sulfate resistance slag cement, type 2, which controlled by European standard EN 197-1 [18] cement composition. Clinker and Slag amount for manufactured cement in Cyprus were between 65-79% and 21-35%, limestone aggregate with Dmax 5 mm, ordinary tap water, superplasticizer was a polycarboxylic ether based with high range water reducing new generation superplasticizer admixture developed.

The diameter and length of used steel fibre was 0.55 mm and 13 mm with young modulus of 210 GPa and the tensile strength of 1345 MPa,a white undensified silica fume with more than 95% purity of silicon dioxide was used with particle sizes between 0.1-1 μm.

The variables range are as follow: 0.70-1.30 cement amount, 0.10- 0.20 steel fibre, 0.04- 0.08 superplasticizer, 0.15-0.30 silica fume amount by aggregate weight mass and 0.18- 0.32 water cementitious ratio.

## Experimental Design

Design of experiment was done by full factorial method. In this study the relation of 28-day compressive strength and compressive toughness factor of UHPC was analyzed and the best model with highest $R^2$ offered.

## Methodology

In this study, relationship between 28-day compressive strength and compressive toughness factor was studied with consideration five variables as SF (A), superplasticizer content (B), steel fibre content (C), cement content (D), w/c ratio (E). Based on previous studies and literature review, the range of variables are as follow: SF amount is from 15 to 30 percent of sand mass, the superplasticizer content is from 4 to 8 percent of sand mass, the steel fibre content is from 10 to 20 percent of sand mass, the cement amount is from 70 to 130 percent of sand mass, and w/c ratio from 0.18 to 0.32. The variables with their level limitation are given in Table 1.

Table 1 The variables with their levels

| VARIABLES | CODE | LOW LEVEL -1 | LEVELS INTERMEDIATE 0 | HIGH LEVEL +1 |
|---|---|---|---|---|
| Silica fume | A | 15% | 25% | 30% |
| Superplasticizer | B | 4% | 6% | 8% |
| Fibre | C | 10% | 15% | 20% |
| Cement | D | 70% | 100% | 130% |
| w/c | E | 0.18 | 0.225 | 0.32 |

**Percentages are based on aggregate mass used*

## Specimen preparation and test specimen

The specimen preparation were as follow steps; first premix which included dry materials (aggregate, cement, silica fume) except steel fibre were mixed in determined proportion for five minutes, then proportional amount of superplasticizer was added to determined water within adding steel fibre, thereafter, water mix was added to premixed mixture and mixed to obtain homogeneous paste. Three 100*100mm cubes were casted for 28-day compressive strength determination and three 100*200 mm cylinder wee casted for stress-strain curve.

After casting, all samples were compacted by vibration table and kept in the moist curing room for 24 hours. They were then molded out and transferred to the curing water tank at 23 ± 2 °C until testing.

**Compressive strength test**

To determine compressive strength of specimens, 100*100 mm UHPC cubes were tested. Concrete compression machine based on ASTM C109 [19] with 3000 kN in capacity was used. Three samples were tested and the average was calculated. The compressive strength of specimens was measured from 47 to 110 MPa for 28-day.

**Compressive toughness factor**

According to Japan society of civil engineering (JSCE) standard SF-5 [20], the compressive toughness is equal to the area under load-deflection curve till deformation reaches to 0.75 mm for cylindrical samples with dimensions of 100*200 mm as shown in Figure 1. The unit of compressive toughness is the unit of works.

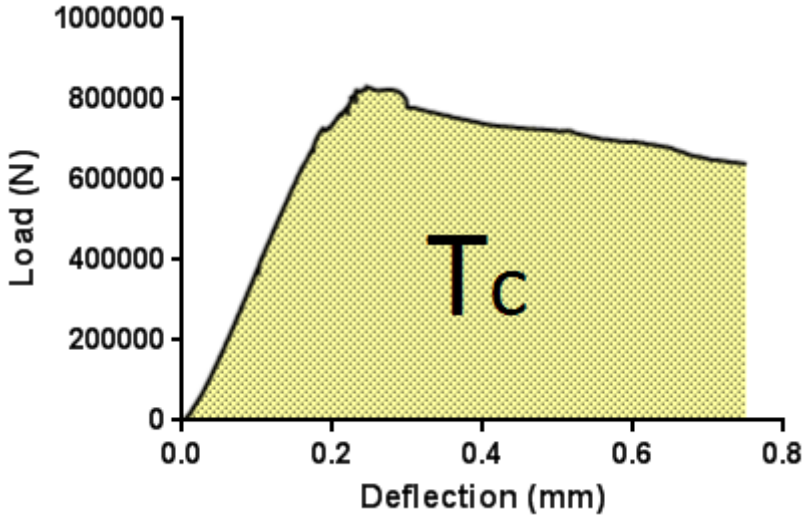


Figure 1 Load- deformation curve of sample in compression

The compressive toughness factor indicate the post matrix cracking residual compressive strength of UHPC without distinguishing the pre-peak and post-peak behaviors deformation corresponding to 0.75 mm. Compressive toughness factor is defined as

$$\overline{\sigma} = \frac{T_c}{A.\delta_{tc}} \qquad (1)$$

Where
$\bar{\sigma}$= compressive toughness factor
$T_c$= compressive toughness (Nm)
$\delta_{tc}$= deformation corresponding to 0.75 percent converted to strain (mm)
A= Surface area of specimen

## RESULTS AND DISCUSSION

Tables 2 and 3 gives the batch weights of each mix and the results of 28-days compressive strength and compressive toughness factor using different variables. Each result was derived by average of 3 specimens.

Compressive toughness factor and 28- day compressive strength range were between 31.0 and 90.4 Mpa and 47.0 and 110.0 MPa, respectively. Figure 2 shows the relation between compressive toughness factor and 28-day compressive strength. The Figure express the significance of structural stress in UHPC. By increasing the 28-day compressive strength, the compressive toughness factor of ultra high performance concrete is increasing with constant slope. It can be said, there is direct relation between 28-compressive strength and compressive toughness factor. Many types of function like polynomial, logarithmic, logit, exponential, and power and linear were tested to find the best $R^2$. The best curve with highest $R^2$ of 0.7082 was obtained by using linear function with the equation of Y= 0.9442X- 32.241 was calculated.

Table 2a Batch weights and responses of UHPC

| MIX | CONSTITUENT, kg | | | | | | 28-DAYS COMP STRENGTH, MPa | COMP TOUGHNESS FACTOR, MPa |
|---|---|---|---|---|---|---|---|---|
| | Sand | Silica Fume | Super-plasticizer | Steel Fibre | Cement | Water | | |
| 1 | 50 | 7.5 | 4 | 5 | 35 | 13.6 | 74.0 | 54.27 |
| 2 | 50 | 15.0 | 2 | 5 | 65 | 25.6 | 49.0 | 34.67 |
| 3 | 50 | 15.0 | 2 | 10 | 35 | 9.0 | 103.2 | 77.33 |
| 4 | 50 | 10.0 | 3 | 10 | 50 | 13.5 | 98.0 | 73.33 |
| 5 | 50 | 15.0 | 2 | 5 | 35 | 9.0 | 97.0 | 66.00 |
| 6 | 50 | 10.0 | 3 | 7.5 | 50 | 10.8 | 102.0 | 69.87 |
| 7 | 50 | 7.5 | 4 | 5 | 35 | 7.6 | 100.0 | 66.67 |
| 8 | 50 | 15.0 | 2 | 10 | 65 | 14.4 | 98.0 | 70.00 |
| 9 | 50 | 7.5 | 3 | 7.5 | 50 | 12.9 | 106.0 | 58.67 |
| 10 | 50 | 7.5 | 2 | 10 | 35 | 13.6 | 85.0 | 56.13 |
| 11 | 50 | 10.0 | 2 | 7.5 | 50 | 13.5 | 83.4 | 54.67 |
| 12 | 50 | 15.0 | 4 | 5 | 65 | 25.6 | 77.0 | 48.40 |
| 13 | 50 | 10.0 | 3 | 7.5 | 65 | 16.8 | 86.0 | 52.13 |
| 14 | 50 | 15.0 | 2 | 10 | 35 | 16.0 | 57.3 | 35.87 |
| 15 | 50 | 15.0 | 2 | 10 | 65 | 25.6 | 47.0 | 36.27 |
| 16 | 50 | 7.5 | 2 | 5 | 65 | 23.2 | 81.5 | 41.20 |
| 17 | 50 | 10.0 | 3 | 7.5 | 50 | 19.2 | 85.0 | 57.07 |
| 18 | 50 | 7.5 | 2 | 10 | 65 | 23.2 | 71.7 | 42.53 |
| 19 | 50 | 7.5 | 2 | 5 | 65 | 13.0 | 104.5 | 70.80 |
| 20 | 50 | 10.0 | 3 | 7.5 | 50 | 13.5 | 75.0 | 56.00 |
| 21 | 50 | 15.0 | 2 | 5 | 35 | 16.0 | 63.6 | 31.20 |
| 22 | 50 | 10.0 | 3 | 7.5 | 50 | 13.5 | 86.0 | 56.67 |
| 23 | 50 | 7.5 | 4 | 5 | 65 | 23.2 | 84.0 | 53.33 |
| 24 | 50 | 15.0 | 4 | 10 | 65 | 14.4 | 93.0 | 69.60 |

Table 3 Batch weights and responses of UHPC

| MIX | CONSTITUENT, kg | | | | | | 28-DAYS COMP STRENGTH, MPa | COMP TOUGHNESS FACTOR, MPa |
|---|---|---|---|---|---|---|---|---|
| | Sand | Silica Fume | Super-plasticizer | Steel Fibre | Cement | Water | | |
| 25 | 50 | 15.0 | 4 | 10 | 65 | 25.6 | 70.8 | 50.80 |
| 26 | 50 | 7.5 | 4 | 10 | 35 | 7.6 | 82.9 | 46.93 |
| 27 | 50 | 7.5 | 2 | 10 | 65 | 13.0 | 106.5 | 80.67 |
| 28 | 50 | 7.5 | 2 | 10 | 35 | 7.6 | 110.0 | 90.40 |
| 29 | 50 | 15.0 | 4 | 5 | 35 | 9.0 | 99.0 | 59.73 |
| 30 | 50 | 15.0 | 4 | 10 | 35 | 16.0 | 85.0 | 63.07 |
| 31 | 50 | 7.5 | 2 | 5 | 35 | 7.6 | 108.0 | 81.20 |
| 32 | 50 | 15.0 | 4 | 10 | 35 | 9.0 | 87.0 | 67.73 |
| 33 | 50 | 15.0 | 2 | 5 | 65 | 14.4 | 95.7 | 59.07 |
| 34 | 50 | 7.5 | 2 | 5 | 35 | 13.6 | 68.9 | 42.67 |
| 35 | 50 | 15.0 | 4 | 5 | 65 | 14.4 | 88.0 | 64.00 |
| 36 | 50 | 7.5 | 4 | 10 | 65 | 23.2 | 87.0 | 41.47 |
| 37 | 50 | 7.5 | 4 | 10 | 35 | 13.6 | 79.0 | 57.47 |
| 38 | 50 | 7.5 | 4 | 5 | 65 | 13.0 | 93.9 | 57.20 |
| 39 | 50 | 15.0 | 4 | 5 | 35 | 16.0 | 86.0 | 45.33 |
| 40 | 50 | 10.0 | 4 | 7.5 | 50 | 13.5 | 86.0 | 52.67 |
| 41 | 50 | 15.0 | 3 | 7.5 | 50 | 14.6 | 95.0 | 56.00 |
| 42 | 50 | 10.0 | 3 | 7.5 | 35 | 10.1 | 83.0 | 54.67 |
| 43 | 50 | 10.0 | 3 | 5 | 50 | 13.5 | 95.2 | 56.00 |
| 44 | 50 | 10.0 | 3 | 7.5 | 50 | 13.5 | 82.0 | 57.33 |
| 45 | 50 | 7.5 | 4 | 10 | 65 | 13.0 | 91.3 | 63.60 |

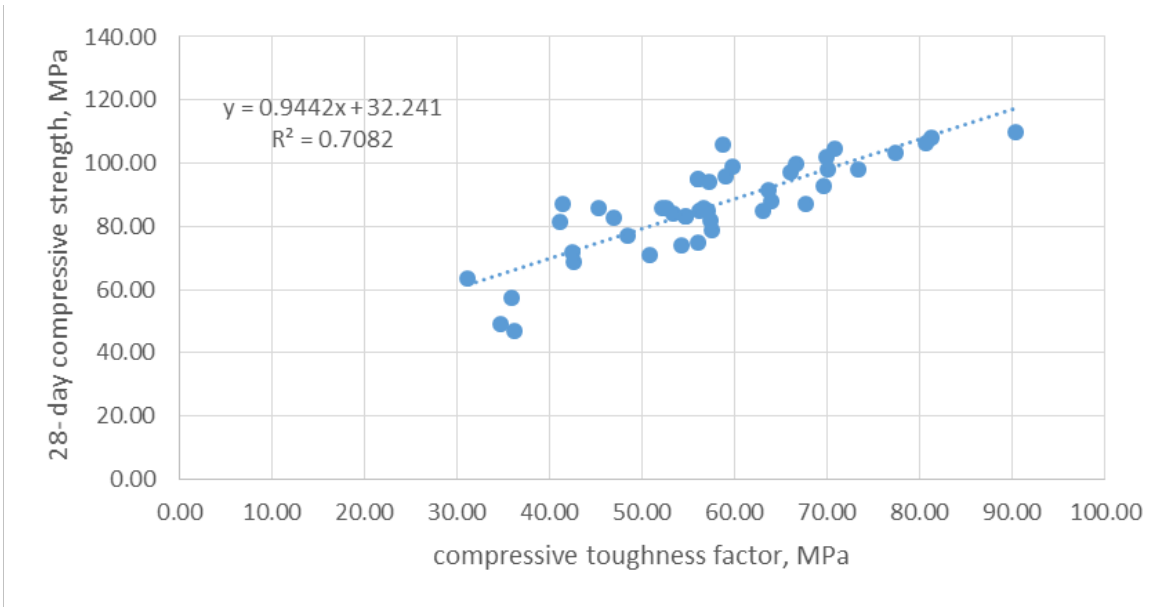


Figure 2 28-day Compressive Strength versus compressive toughness strength

## CONCLUSIONS

Relationship between 28-day compressive strength and compressive toughness factor by considering the effect of five independent variables (amount of silica fume, amount of steel fibres, amount of cement, amount of superplasticizer, and w/c ratio) was studied. In this experimental study forty five batches were produced to create a model. The most important findings of the study are as given as: The linear model is the best function type to compressive toughness factor by having 28-day compressive strength. Compressive toughness factor of ultra high performance concrete can be predicted by using 28-day compressive strength. Linear predication model of compressive toughness factor offered by $R^2$ of 0.7082.

## REFERENCES

1. ASHBY, M.F., The deformation of plastically non-homogeneous materials. Philosophical Magazine, 21(170), 1970, pp.399-424.

2. PAPKOV, D., ZOU, Y., ANDALIB, M.N., GOPONENKO, A., CHENG, S.Z. AND DZENIS, Y.A., Simultaneously strong and tough ultrafine continuous nanofibres. ACS nano, 2013, 7(4), pp.3324-3331.

3. CHENG, Q., JIANG, L. AND TANG, Z., Bioinspired layered materials with superior mechanical performance. Accounts of chemical research, 47(4), 2014, pp.1256-1266.

4. SHAH, A.A. AND RIBAKOV, Y., Recent trends in steel fibreed high-strength concrete. Materials & Design, 32(8), 2011, pp.4122-4151.

5. AHMED, A. AND STURGES, J., Materials Science in Construction: An Introduction. Routledge, 2014

6. MOHAMMED, H., Mechanical Properties Of Ultra High Strength Fibre Reinforced Concrete (Doctoral dissertation, The University of Akron), 2015.

7. PYO, S., Characteristics of ultra high performance concrete subjected to dynamic loading (Doctoral dissertation, University of Michigan), 2014.

8. MOBASHER, B., Mechanics of fibre and textile reinforced cement composites. CRC press, 2011

9. RESPLENDINO, J. AND TOULEMONDE, F., Designing and Building with UHPFRC. John Wiley & Sons, 2013

10. PARK, S.H., KIM, D.J., RYU, G.S. AND KOH, K.T., Tensile behavior of ultra high performance hybrid fibre reinforced concrete. Cement and Concrete Composites, 34(2), 2012, pp.172-184.

11. AÏTCIN, P.C., High performance concrete. CRC Press, 2011.

12. KANG, S.T., LEE, Y., PARK, Y.D. AND KIM, J.K., Tensile fracture properties of an Ultra High Performance Fibre Reinforced Concrete (UHPFRC) with steel fibre. Composite Structures, 92(1), 2010, pp.61-71.

13. CAMPBELL, F.C., Structural composite materials. ASM international, 2010.

14. XINCHENG, P., Super-High-Strength High Performance Concrete. CRC Press, 2012.

15. AGRAWAL, J.P., High energy materials: propellants, explosives and pyrotechnics. John Wiley & Sons, 2010.

16. MARARA, K., ERENB, Ö. AND YITMENA, İ., Compression specific toughness of normal strength steel fibre reinforced concrete (NSSFRC) and high strength steel fibre reinforced concrete (HSSFRC). Materials Research, 14(2), 2011, pp.239-247.

17. BHARGAVA, P., SHARMA, U.K. AND KAUSHIK, S.K., Compressive stress-strain behavior of small scale steel fibre reinforced high strength concrete cylinders. Journal of advanced concrete technology, 4(1), 2006, pp.109-121.

18. EN, T., 2012. 197-1. Cement–Part 1: Composition, specifications and conformity criteria for common cements. Ankara: Turkish Standard Institution.

19. ASTM C109/C109M, 1999. Standard Test Method for Compressive Strength of Hydraulic Cement Mortars (Using 2-in. or [50-mm] Cube Specimens).

20. JSCE. JSCE-SF5 Method of Test for Compressive Strength and Compressive Toughness of Steel Fibre-Reinforced Concrete. Concrete library of JSCE; 1984.

# THERMAL ACTIVATION OF LOW CARBON PRECAST CONCRETE

**J Reddy**

Ecocem

Ireland

**M Soutsos**

Queen's University Belfast

United Kingdom

**ABSTRACT.** Global Portland cement consumption is projected to rise to over 5000 Mt per annum over the next few years. Its manufacture is massively energy and carbon intensive and approximately 900 kg of $CO_2$ is produced per tonne of Portland cement manufactured. Replacing Portland cement with 50% ground granulated blast-furnace slag (GGBS) in precast concrete can reduce its embodied carbon footprint by 45% and play a major role in sustainability by reducing global $CO_2$, but also create a significant technical challenge arising from lower early strength development at standard curing conditions. However, GGBS can be thermally activated to significantly enhance early age strength development and make it suitable for use in precast manufacture. Experimental work on this is presented here. Thermal activation techniques of hot mixing water at 80$^o$C, accelerated curing regimes and insulation measures to protect against heat loss were used. Strength predictions were made using maturity functions. Thermally activated low carbon precast concrete was produced at three manufacturing facilities with early age strength meeting manufacturing requirements. Low carbon concrete in prestressed units achieved 20 MPa in 18 hours, two hours earlier than the Portland cement control. Early hydration of GGBS was evident at 20$^o$C when a secondary heat source was applied and no heat loss was evident. Maturity functions like the Nurse-Saul have been investigated to determine their applicability to concrete mixes with GGBS. GGBS can be incorporated in precast concrete manufacture at 50% replacement to Portland cement when thermally activated. This will enhance the finish and make concrete more durable and much more sustainable. Precast manufacturers can reduce their $CO_2$ impact by 45% and contribute to national and international objectives in spite of increasing cement consumption.

**Keywords:** Low carbon, hot water, thermal activation, GGBS/GGBFS/Slag, precast concrete, sustainability

**John Reddy** is the Technical Development Manager of Ecocem Ireland. He holds an MSc in Advanced Concrete Technology, Queen's University and is a Corporate Member of the Institute of Concrete Technology. He sits on national technical committees and is responsible for technical, quality, environmental and innovation functions of Ecocem Ireland.

**Marios Soutsos** is a Professor at the School of Planning, Architecture and Civil Engineering at Queen's University Belfast. His main interests are in concrete technology and civil engineering. He is an active member on several RILEM committees.

## INTRODUCTION

Worldwide Portland cement consumption grew by 10% from 2012 to 2014 with total cement output reaching 4.18 billion tonnes in 2014 [1] and demand is projected to rise steadily over the next 3 years. Portland cement manufacture is massively energy and carbon intensive and accounts for 7% of anthropogenic global $CO_2$, making it the second most $CO_2$ emitting industry after coal burning power generation [2]. Approximately 900 kg of $CO_2$ is produced per tonne of cement manufactured with $CO_2$ emissions coming from the calcining process and the burning of fossil fuels [3]. In 2014, global cement manufacture released 3.76 billion tonnes of $CO_2$ into our atmosphere. Ground Granulated Blastfurnace Slag (GGBS) is a by-product of the steel industry and requires less than one-fifth of the energy to be processed and only has a carbon footprint of around 5% of that of Portland cement. It can be used in concrete at up to 80% replacement of Portland cement that brings enhanced strength, durability, aesthetics and sustainability to concrete. Its use in precast concrete at 50% can reduce $CO_2$ per $m^3$ of concrete up to 270 kg of and play a major role in reducing global $CO_2$.

Precast concrete has many advantages and offers cost savings on cast in-situ concrete. Its use is growing as we move towards fast track construction. The early age strength of concrete is critical to the economics of precast manufacture and any delays to manufacturing schedule are undesirable. For this reason, CEM I of the highest strength class and the shortest setting time available is generally used in precast concrete. Introducing 50% GGBS in precast concrete represents a significant technical challenge as its early strength development at standard curing conditions (20°C) is slower than Portland cement. However, there are indications that GGBS can be thermally activated which can significantly enhance early age strength development. The presence of new a peak, Peak S, associated with GGBS hydration was found during isothermal conduction calorimetry (ICC) studies [4, 5].

The effect of increasing the curing temperature was observed across other ICC studies [6, 7, 8] where Peak S, associated with GGBS hydration, merged with Peak II, associated with $C_3S$ hydration indicating thermal activation at temperatures as low as 30°C. Many precast concrete manufacturers have existing thermal activation methods through accelerated curing regimes [9]. The principle of using hot mixing water in concrete is known for many years and is typically used in cold weather concreting [10]. The mixing water is the easiest and most practical concrete constituent to heat. It is also the most effective as water can store about five times as much heat as solid materials of the same weight. The method of thermal activation by hot mixing water at 80°C is the main focus of this study. A specific mixing sequence [11] ensured the homogeneity of the mix so that no flash set or balling of cement occurred in the mixer.

Numerous maturity functions have been developed to predict the in-situ strength of concrete. The reliability of these maturity functions should be investigated as to their accuracy in predicting the in-situ strength for given conditions before they are used. When verified by temperature matched curing, a maturity method becomes a valuable method in determining appropriate times for stripping of formwork, demoulding, removal of props, de-stressing or the application of load [12]. The main aim of this study is to produce thermally activated precast concrete with 50% GGBS that has sufficient early age (18-24 hours) strength to keep pace with normal manufacturing schedules. The secondary aim of this study is to provide estimates of early age concrete strengths using recorded temperature time history and different maturity methods and to determine their accuracy against measured temperature matched curing cube strength results.

Experimental development work was designed over four phases of this study. Each phase has its own aim and objectives that develop through the phases of the study. Only by successful completion of the aim and objectives of each phase could progress be made towards ultimate achievement of the main aim of this study of producing thermally activated precast concrete with 50% GGBS. If the early age strength issue of using GGBS in precast concrete can be overcome using thermal activation then using 50% GGBS will make precast concrete more durable, lighter in colour and much more sustainable.

## MATERIALS AND METHODS

Standard mortars [13] and concretes [14] were cast during this study. Concrete for ordinary reinforced precast concrete and prestressed concrete was considered using a variation of three cementitious binders. The workability of concrete cast was high slump, namely S4 (160 to 210 mm) and self-compacting concrete. The designed materials used varied across the phases of the experimental work.

Standard GGBS [15] manufactured by Ecocem Ireland was used in the experimental work of this study. The Blaine value of the GGBS is 450 $m^2/kg$ and the $D_{50}$ value is 11 µm. The chemical composition of GGBS used is given in Table 1. The $Al_2O_3$ content below 14% guarantees the durability performance of Ecocem GGBS. The use of GGBS is generally limited to 15 to 36% in precast concrete due to its low early age strength development at 20°C.

Table 1 GGBS Chemical Composition

| GGBS CHEMICAL COMPOSITION | | | | | | | | | | |
|---|---|---|---|---|---|---|---|---|---|---|
| $SiO_2$ | $Al_2O_3$ | $Fe_2O_3$ | CaO | MgO | MnO | $TiO_2$ | Sr | Cl | S | $Na_2O_{eq}$ |
| 36.5 | 10.4 | 0.7 | 42.4 | 8.1 | 0.4 | 0.5 | 0.1 | 0.01 | 0.7 | 0.5 |

CEM I of the highest strength class and of the most rapid strength development available is generally used in precast concrete to achieve the highest possible early age strength for the quickest turnaround time on units for optimal manufacturing. Two classifications of CEM I [16] were used in this study, CEM I 42.5R [16] and CEM I 52.5R [16].

CEM III/A 52.5L Blastfurnace cement [16] was used in Phase IV of the development work. The designation ‘L’ refers to low early age strength and is undesirable for use in precast concrete. It is a factory blend of 50% CEM I 42.5R and 50% GGBS. By consequence of having a high level of GGBS, CEM III/A 52.5L has a low carbon footprint and excellent durability characteristics. A CEM III/A equivalent can also be made at the concrete manufacturing plant by mixing GGBS with CEM I and this was done in Phases I, II and III of the experimental work. 50% GGBS was selected as the target GGBS content for use in CEM III/A or CEM III/A equivalent to produce low carbon precast concrete in this study.

Standard mortars to EN 196-1 and concrete to EN 206-1 were cast in the development work. The fineness of GGBS was measured [17] and the $D_{50}$ was determined using laser analysis. Chemical analysis of GGBS was determined [18]. Concrete was sampled [19] and tested for workability using the slump test [19] and the slump flow test [21]. Concrete strength was assessed by testing cubes made [22] [23].

## DEVELOPMENT OF TERMALLY ACTIVATED LOW CARBON PRECAST CONCRETE

The experimental development of thermally activated low carbon precast concrete was carried out over four phases. Only by successful completion of the aim and objectives of each phase could progress be made towards ultimate achievement of producing thermally activated precast concrete with 50% GGBS.

### Phase I – Initial Mortar Trials

The aim of Phase I of the experimental development work was to determine if there is a thermal activation effect from adding hot mixing water at 80°C to the early age strength of mortars containing 30% and 50% GGBS. The effect was measured by assessing the early age strength of GGBS mortars and by monitoring the in-situ temperature profiles.

Two trials using 0%, 30% and 50% GGBS with CEM I 52.5R were conducted in the lab at ambient temperature (20 ± 2°C). Standard mortars to EN 196-1 were subsequently cast using water at 20°C and 80°C. Mixing water was heated using a kettle and then cooled to 80°C with cold water addition. The sand and cementitious materials were added to the mixer first with the water added to the dry mix.

Precautions taken to prevent early age heat loss resulted in higher fresh mortar temperatures in Lab Test 2 from Lab Test 1. The recorded in-situ temperatures in Figure 1 show no early age heat loss and a dormant period of four hours. The additional strength gain at 1 day measured for both PI/30%/80°C and PI/50%/80°C in comparison to the companion 20°C mixes confirms the thermal activation of GGBS by the addition of hot mixing water at 80°C.

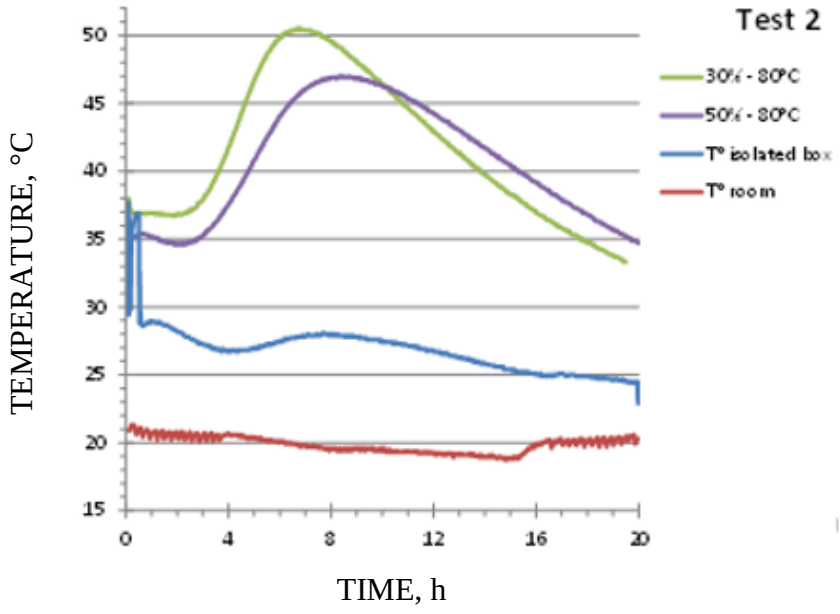


Figure 1 – In-situ temps from Phase I lab trial 2

Table 2 Phase I Lab Test 2 Results

| | PHASE I LAB TEST 2 RESULTS | | | | |
|---|---|---|---|---|---|
| Reference | PI/Control | PI/30%/20°C | PI/30%/80°C | PI/50%/20°C | PI/50%/80°C |
| Water | 20°C | 20°C | 80°C | 20°C | 80°C |
| GGBS | 0% | 30% | 30% | 50% | 50% |
| 1 day strength | 28.0 | 18.2 | 22.6 | 11.4 | 16.5 |
| Fresh mortar in moulds | 18°C | 19°C | 38°C | 18°C | 36°C |

Phase I of the experimental work confirmed thermal activation of GGBS in mortars by using hot mixing water at 80°C. Observations from Phase I showed the importance of protecting against early age heat loss on early age strength gain and how the second casting using hot water was higher than the first from the residual heat.

**Phase II – Initial Concrete Trial**

The aim of Phase II was to determine if there is a thermal activation effect from adding hot mixing water to the early age strength of SCC concrete used in precast containing 36% and 50% GGBS to meet a 14 MPa lifting requirement at 20 hours. Four concrete mixes were cast in this phase of the experimental work with mixes given in Table 3.

Table 3 Phase II Mix design

| | PHASE II MIX DESIGN, SSD WEIGHTS/m³ | | | |
|---|---|---|---|---|
| Reference | PII/Control | PII/36%/20°C | PII/36%/67°C | PII/50%/67°C |
| CEM I 42.5R | 450 kg/m$^3$ | 288 kg/m$^3$ | 288 kg/m$^3$ | 225 kg/m$^3$ |
| GGBS | - | 162 kg/m$^3$ | 162 kg/m$^3$ | 225 kg/m$^3$ |
| Limestone Filler | 150 kg/m$^3$ | 150 kg/m$^3$ | 150 kg/m$^3$ | 150 kg/m$^3$ |
| 10 mm | 940 kg/m$^3$ | 940 kg/m$^3$ | 940 kg/m$^3$ | 940 kg/m$^3$ |
| Sand | 700 kg/m$^3$ | 700 kg/m$^3$ | 700 kg/m$^3$ | 700 kg/m$^3$ |
| Water | 180 l | 180 l | 180 l | 180 l |
| *Added Water 20°C | 135 l | 135 l | - | - |
| *Added Water 67°C | - | - | 135 l | 135 l |
| SP | 4.5 l | 4.5 l | 4.5 l | 4.5 l |

Four mock up trial reinforced architectural precast panels (1500 mm × 1500 mm × 150 mm) were cast in timber moulds. Each batch size was 0.34m$^3$ of concrete. A prototype hot water system was developed to heat the water to a target of 80°C. Maximum water temperature was 67°C with a flow rate of 5.5 l/min. Fresh hot mixing water self-compacting concrete was placed in the moulds with companion test cubes cast. Thermocouple cables were placed in the units and the in-situ concrete temperatures were recorded. Plastic sheeting was placed over the units after casting to cure the concrete and to act as a very crude method of insulation to reduce heat loss. Companion cubes for each trial were cured alongside the trial units and tested for early age strength at 20 hours and 24 hours. Temperature matched curing (TMC) was used to determine the early age strength of concrete in mix PII/50%/67°C. Concrete cores for all trial units were taken at 48 hours to determine the early age in-situ strength as it is feasible that units could be dispatched to site at two days.

Figure 2 shows very minimal temperature loss over the first four hours in mix PII/50%/67ºC. This demonstrated the good insulating properties of the timber form. The dormant period matched the four hours observed in Phase I. Temperature rise was evident from hours 4 – 8, representing hydration and activation.

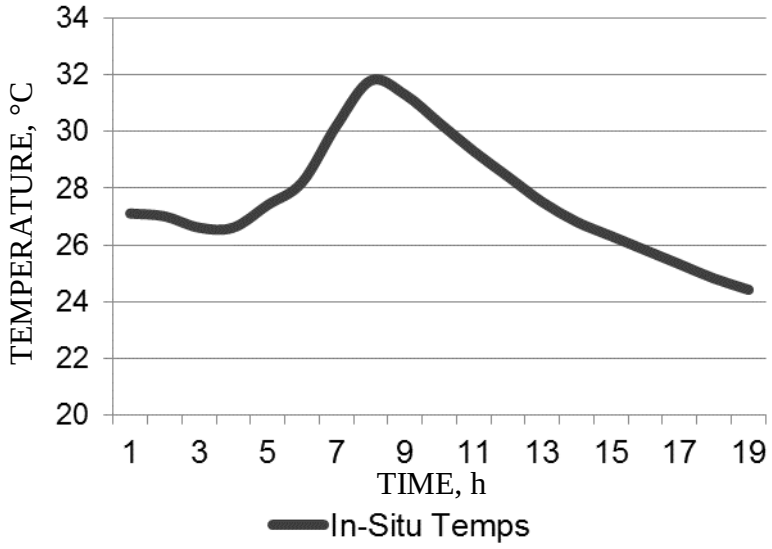


Figure 2 In-situ temps from Phase II

The early age strength requirement for lifting units in Phase II is 14 MPa and early age strength results are presented in Table 4.

Table 4 Phase II Results

| PHASE II RESULTS | | | | |
|---|---|---|---|---|
| Reference | PII/50%/67ºC | PII/36%/67ºC | PII/36%/20ºC | PII/Control |
| Water | 67ºC | 67ºC | 17ºC | 17ºC |
| GGBS | 50% | 36% | 36% | 0% |
| Fresh Concrete | 26.5ºC | 27.1ºC | 20.2ºC | 19.6ºC |
| 20 h TMC Cube Strength, MPa | 23 | - | - | - |
| 20 h Air Cube Strength, MPa | 14 | 17 | 12 | 19 |
| 24 h TMC Cube Strength, MPa | 31 | - | - | - |
| 24 h Air Cube Strength MPa | 17 | 24 | 16 | 30 |
| 48 h Core Strength, MPa | 52 | 55 | 31 | 58 |

The cube results at 20 hours show that the lifting strength of 14 MPa is met by PII/Control; PII/36%/67ºC and PII/50%/67ºC as determined by cubes cured alongside the test units. The effect of thermal activation of GGBS by using 67ºC mixing water is evident as the 20 hour strength of PII/36%/67ºC (17 MPa) is 5 MPa higher than PII/36%/20ºC (12 MPa). The TMC cube result of 23 MPa for mix PII/50%/67ºC is higher than PII/Control and is far in excess of the lifting requirement. This demonstrates how companion cubes cured alongside give a poor representation of in-situ strength and proves the benefit of using TMC to measure in-situ strengths.

The cube results at 24 hours show that the lifting strength of 14 MPa is met by all four mixes as determined by cubes cured alongside the test units. The 24 hour strength of PII/36%/67ºC (24 MPa) is now 8 MPa higher than PII/36%/20ºC (16 MPa). This gives further evidence of the effect of thermal activation of GGBS by using 67ºC mixing water as the rate of strength gain is more pronounced for PII/36%/67ºC (7 MPa increase from 20 – 24 hours) compared to PII/36%/20ºC (4 MPa increase from 20 – 24 hours). The TMC cube result at 24 hours has risen to 31 MPa for mix PII/50%/67ºC and is more than double the lifting strength requirement.

The core results at 48 hours show that mixes PII/Control; PII/36%/67ºC and PII/50%/67ºC met the 50 MPa requirement at two days. Mix PII/36%/20ºC did not meet the 50 MPa requirement. The core results are direct measures of in-situ strength. The fact that the hot water mixes of PII/36%/67ºC and PII/50%/67ºC met the 50 MPa requirement and the normal water mix PII/36%/20ºC did not meet the 50 MPa reaffirms the thermal activation of GGBS by hot mixing water at 67ºC at two days.

Phase II of the experimental development work clearly demonstrated the thermal activation effect of GGBS in precast concrete. The recorded temperature curve had a similar dormant period as in Phase I. This could be reduced with further thermal activation from an external heat source and better insulation to prevent heat loss. TMC is proven to accurately determine in-situ early age strengths.

## Phase III – Manufacturing Unit Trial

The aim of Phase III of the experimental work was to produce sufficient hot water at 80ºC that was dischargeable at a flow rate to meet normal manufacturing demands for bigger batches of concrete. Lifting strength requirement was 16 MPa for the rollover unit cast. A mobile hot water unit capable of heating 1000L of water to 80ºC and a discharging rate of 100L per minute was developed for this trial. The unit has a flow meter to accurately discharge the required amount of added water to the mix. A designed 50N10 self-compacting concrete mix used by Carlow Precast in reinforced “rollover” retaining wall units was cast for this phase of the experimental work. 1.16m$^3$ of concrete was batched for the mix. Full mix design is given in Table 5. The mobile hot water unit was used to heat mixing water to 80ºC that resulted in fresh concrete temperature of 25.5ºC. Fresh concrete was discharged into a skip and delivered to the “rollover” mould by fork truck in two drops. Early age strength of concrete was assessed at 21 hours by testing cubes that were cured in the concrete lab and TMC cubes. In-situ temperatures were also recorded.

Table 5 Phase III Mix design

| PHASE III MIX DESIGN, SSD WEIGHTS/m$^3$ | |
|---|---|
| Reference | PIII/50%/80ºC |
| CEM I 42.5R | 190 kg/m$^3$ |
| GGBS | 190 kg/m$^3$ |
| Limestone filler | 200 kg/m$^3$ |
| 10 mm | 700 kg/m$^3$ |
| Sand | 910 kg/m$^3$ |
| Water | 180 l |
| *Added Water 80ºC | 125 l |
| SP | 4.7 l |

Figure 3 shows that no temperature loss was observed during this phase of the experimental work. Temperature rise was flat for two hours and rose thereafter indicating hydration and activation.

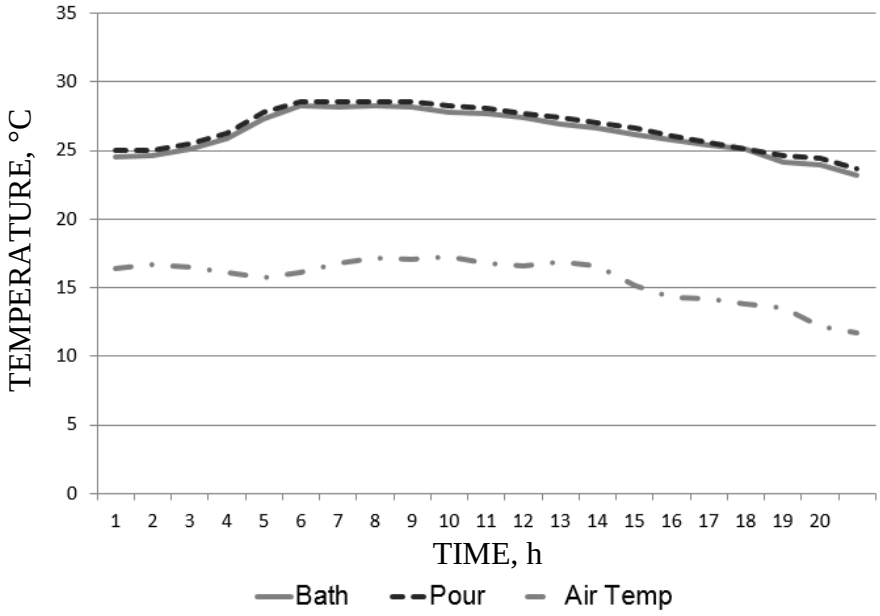


Figure 3 In-situ temps from Phase III

Figure 4 demonstrates how TMC strength for PIII/50%/80$^{o}$C resulted in 19 MPa at 21 hours which met the required lifting strength requirement of 16MPa. The standard cured cube did not meet the lifting requirement.

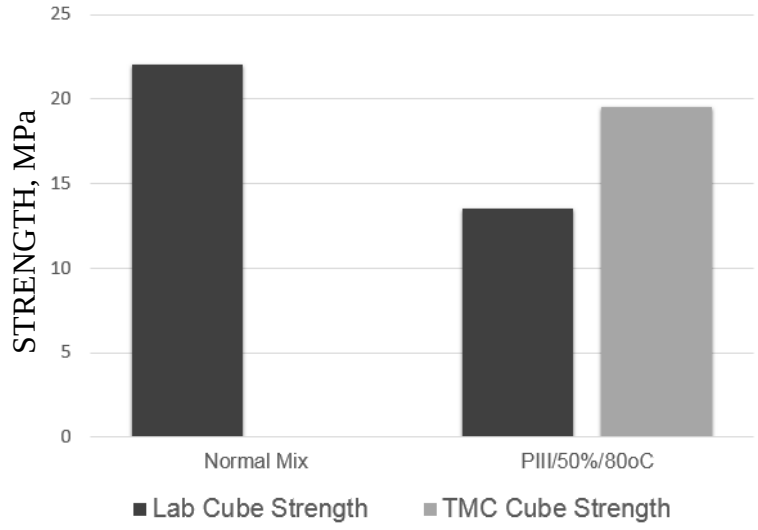


Figure 4 Phase III Cube Results

No temperature loss was observed in this trial indicating activation of GGBS at 25$^{o}$C. 50% GGBS was used in precast manufacture of “Rollover” retaining wall units when thermally activated by hot mixing water at 80$^{o}$C. The observation of how companion cubes cured in the lab give a poor representation of in-situ strength when compared to TMC was noted again.

## Phase IV – Full Scale Manufacturing Trials

The aim of Phase IV was to produce thermally activated precast concrete with 50% GGBS in prestressed units (6000 mm × 1400 mm × 90 mm) with compressive strength of 20 MPa at 18 - 20 hours. Units were assessed for in-situ temperatures and early age strength to determine the effect of different thermal activation methods of 50% GGBS in prestressed concrete.

A designed 50N20 concrete mix used in prestressed wide slab flooring units was cast for this phase of the experimental work. The slump category of the concrete was S4. A control mix using CEM I 42.5R (PIV/Control) was cast in Trial 1. From trials 2-6, mix PIV/CEM3/80$^{o}$C, using CEM III/A 52.5L and hot mixing water at 80$^{o}$C was used. Full mix designs are given in Table 6.

Table 6 Phase IV Mix design

| PHASE IV MIX DESIGN, SSD WEIGHTS/m³ | | |
|---|---|---|
| Reference | PIV/Control | PIV/CEM3/80$^{o}$C |
| CEM I 42.5R | 400 kg/m$^3$ | - |
| CEM III/A 52.5L | - | 400 kg/m$^3$ |
| Limestone filler | 125 kg/m$^3$ | 125 kg/m$^3$ |
| 20 mm | 550 kg/m$^3$ | 550 kg/m$^3$ |
| 10 mm | 400 kg/m$^3$ | 400 kg/m$^3$ |
| Sand | 750 kg/m$^3$ | 750 kg/m$^3$ |
| Water | 160 l | 160 l |
| *Added Water 20$^{o}$C | 115 l | - |
| *Added Water 80$^{o}$C | - | 115 l |
| SP | 3.0 l | 3.0 l |

90 mm deep prestressed floor units with varying width from 1.4 m to 800 mm were cast in Trial 6. Thermal activation was by hot mixing water at 80$^{o}$C, beds were heated for two hours before casting, and a thermal blanket was used. Early age strength assessment was by TMC cubes. Fresh concrete temperatures were consistently at 25$^{o}$C for the duration of the pour. A total of 5.9 m$^3$ of hot water concrete was poured in nine drops in the 50 m long bed. The thermal blanket was put in place after casting. Temperature matched cured cube strengths were measured from 17 to 20 hours. In-situ temperatures were measured at the centre point of the slab.

Figure 5 shows that the in-situ temperature rose immediately during this trial indicating hydration and activation and no dormant period.

Figure 6 demonstrates that the target early age strength of 20 MPa required for de-stressing and lifting was measured at 18 hours.

Thermally activated low carbon concrete was produced in prestressed precast manufacture of slender wide floor slab units. Strength requirement was met at 18 hours which is two hours ahead of normal manufacturing schedule. Thermal activation of GGBS was evident when fresh concrete temperature was elevated to 24$^{o}$C using hot mixing water at 80$^{o}$C together with the complementary methods of a heated bed and thermal blanket.

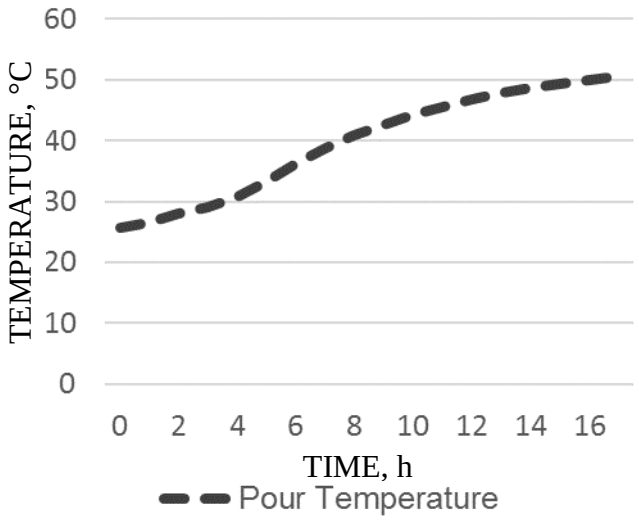


Figure 5 In-situ temps from Phase IV

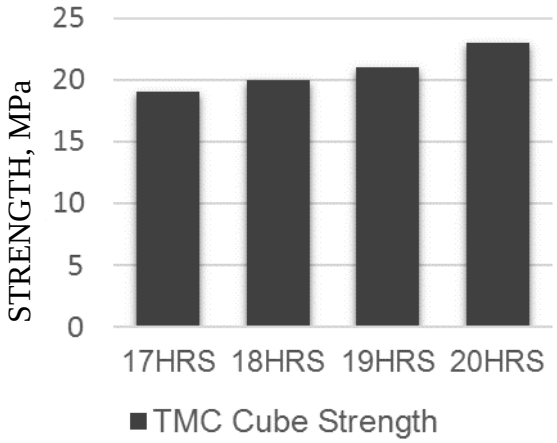


Figure 6 In-situ temps from Phase IV

## STRENGTH PREDICTIONS

Strength predictions were made using the in-situ recorded temperatures from Phase IV and PC45 constants obtained from similar mixes in the past. The Nurse Saul [24] the Freiesleben, Hansen & Pedersen (FHP) [25] and the Weaver Sadgrove [26] functions were used to assess the accuracy of strength predictions/estimates.

The Three Parameter Equation (TPE) [27] was used as the relationship between concrete strength and age/maturity.

The constants needed for the calculation of the different maturity functions were sourced from another study [28] and are assumed to be representative of the C40/50 50% GGBS cast in Phase IV. The assumed constants are given in Table 7.

Table 7 Constants for Maturity Functions

| CONSTANTS FOR MATURITY FUNCTIONS | | |
|---|---|---|
| Mixes | PC45 | 50% GGBS |
| Activation Energy $E_a$, kJ/mol | 34.879 | 45.339 |
| $T_o$, datum Temperature, $^oC$ | -11 | -11 |
| $S_\infty$, MPa | 64.334 | 66.563 |
| $\tau$, h | 36.72 | 97.224 |

Assumptions given in Table 7 have been made on the strength development curves to 28 days as only early age strengths were assessed during the experimental development work.

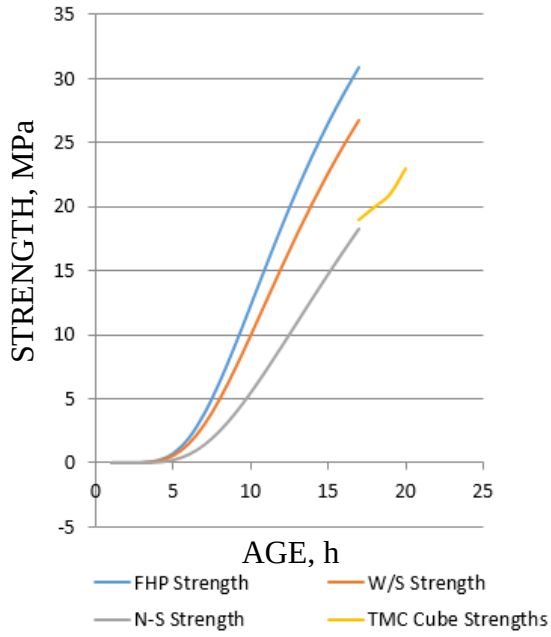


Figure 7 PC45 Predictions

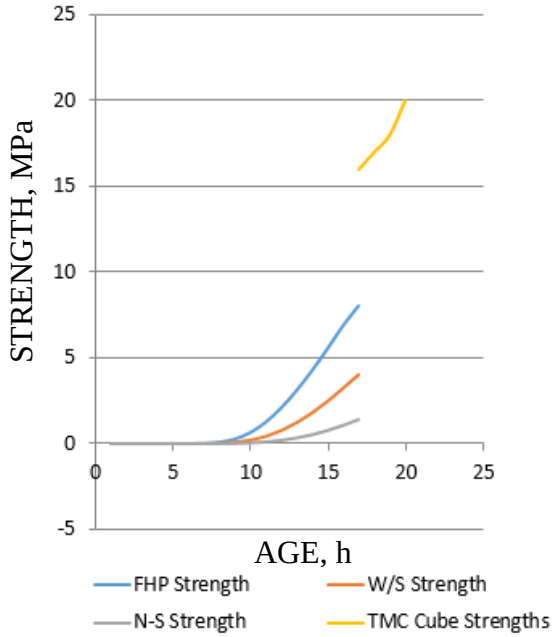


Figure 8 50% GGBS Predictions

Figure 7 shows that the Nurse Saul function, using assumed PC45 constants, estimated relatively well the strength development at elevated curing temperatures, whereas, the FHP and the Weaver Sadgrove both overestimated strength. However, Figure 8 shows that all three maturity functions failed to estimate accurately the strength development of 50% GGBS concretes at elevated curing temperatures.

The use of constants from a similar mix investigated in the past may have led to these inaccuracies. Constants for use in maturity functions must be determined for the particular mix they are intended for. Nonetheless, concerns have been expressed [29] of the applicability of maturity functions, originally developed for Portland cement, for concretes containing GGBS and other supplementary cementitious materials.

## CONCLUSIONS

1. Concrete with 50% GGBS cast in prestressed units achieved 20 MPa in 18 hours when thermally activated by hot mixing water at 80ºC, preheated beds and the use of a thermal blanket after placing.

2. Precast concrete with 50% GGBS reduces its embodied carbon by 45%, making it low carbon concrete.

3. Thermally activated low carbon precast concrete was produced with sufficient early age strength to meet manufacturing requirements. The following points are noted:

    I. It is critical to protect against early age heat loss when using thermal activation techniques.

    II. Thermal activation of GGBS was evident at 25ºC when no heat loss was evident and a secondary heat source was applied.

4. Temperature Matched Curing (TMC) has been shown to accurately determine in-situ early age strengths whereas standard cured cubes or cubes cured alongside consistently underestimated the actual early age strength.

5. The Nurse Saul function accurately predicted the strength of thermally activated low carbon precast concrete with only Portland cement but failed to give accurate predictions/estimates for 50% GGBS. The applicability of maturity functions, originally developed for Portland cement, for concretes containing GGBS needs to be investigated.

## REFERENCES

1. ARMSTRONG T. The Global Cement Report, Trade Publications, 11th Edition, 2015.

2. IPCC, Sources of $CO_2$, Intergovernmental Panel on Climate Change Special Report on Carbon Dioxide Capture and Storage, 2005.

3. TRIANTAFYLLOU G. and KOMINTSAS K. Cement industry towards sustainability, Proceedings of Conference of Advances in Mineral Resources Management and Environmental Geotechnology, Crete, 2004, pp. 299–304.

4. BLAND C.H. and SHARP J.H. A Conduction Calorimetric study of gasifier slag-Portland cement blends, Cement and Concrete Research, Vol. 21, Nos. 2-3, 1991, pp. 359–367.

5. UTTON C., HAYES M., HILL J., MILESTONE N. and SHARP J.H. Effect of temperatures up to 90ºC on the early hydration of Portland-Blastfurnace slag cements' Journal of the American Ceramic Society, Vol. 91, No. 3, 2008, pp. 948–954.

6. ESCALANTE J.I. and SHARP J.H. The effect of temperature on the early age hydration of Portland cement and blended cements, Advances in Cement Research, Vol. 12, No. 3, 2000.

7. MA W., SAMPLE D., MARTIN R., BROWN P.W. Calorimetric study of cement blends containing fly-ash, silica fume and slab at Elevated temperatures, Cement, Concrete and Aggregates, Vol. 16, No. 2, 1994.

8. WU X., JIANG W., ROY D.M. Early activation and properties of slag cement, Cement and Concrete Research, Vol. 20, No. 6, 1990, pp. 961–974.

9. VOLLENWEIDER B. Various methods of accelerated curing for precast concrete applications, and their impact on short and long term compressive strength CE 241: Concrete Technology, http://ce.berkeley.edu, 2004.

10. NRMCA, Maturity Methods to Estimate Concrete Strength, CIP 36, NRMCA, USA, 2006.

11. ACI 306R, Guide to Cold Weather Concreting' American Concrete Institute Committee 306, 2010.

12. REDDY J. A decision making tool for striking of formwork to GGBS concretes, Institute of Concrete Technology, Camberly, UK, 2008.

13. EN 196-1:2005, Methods of testing cement – Part 1: Determination of strength.

14. I.S. EN 206-1:2002, Concrete – Part 1: Specification, performance, production and conformity.

15. EN 15167-1:2006, Ground granulated Blastfurnace slag for use in concrete, mortar and grout – Part 1: Definitions, specifications and conformity data.

16. I.S. EN 197-1: 2011, Cement - Part 1: Composition, specifications and conformity criteria for common cements.

17. EN 196-5:2005, Methods of testing cement – Part 5: Determination of fineness.

18. EN 196-2:2005, Methods of testing cement – Part 1: Chemical Analysis of Cement.

19. EN 12350-1:2000, Testing fresh concrete - Part 1: Sampling.

20. EN 12350-1:2000, Testing fresh concrete - Part 2: Slump Test.

21. EN 12350-1:2000, Testing fresh concrete - Part 8: SCC – Slump flow test.

22. EN 12390-2:2009, Testing hardened concrete – Part 2: Making and curing specimens for strength tests.

23. EN 12390-3:2009, Testing hardened concrete – Part 3: Compressive strength of test specimens.

24. SAUL, A G, Principles Underlying the Steam Curing of Concrete at Atmospheric Pressure, Magazine of Concrete Research, Vol. 2, No. 6, March 1951, pp. 127–140.

25. FREIESLEBEN P.F. and PEDERSEN E.J. Maturity Computer for Controlled Curing and Hardening of Concrete, Journal of the Nordic Concrete Federation, No. 1, 1977, pp. 21–25.

26. WEAVER J. and SADGROVE B.N. Striking Times of Formwork—Tables of Curing Periods to Achieve Given Strengths, Construction Industry Research and Information Association, London, 1971, 76 p.

27. CARINO N. J. The Maturity Method', in Handbook on Non-destructive Testing of Concrete, Eds. VM Malhotra and NJ Carino, CRC Press, Boca Raton, FL, 1991, pp. 101–146.

28. TURU'ALLO G. Early age strength of GGBS concrete cured under different temperatures, Thesis submitted in accordance with the requirements for a degree of Doctor of Philosophy, University of Liverpool, 2013.

29. BARNETT S.J., SOUTSOS M.N., MILLARD S.G. and BUNGEY J.H. Strength development of mortars containing ground granulated blast-furnace slag: Effect of curing temperature and determination of apparent activation energies'. Cement and Concrete Research, Vol. 36, 2006, pp. 434–440.

# IMPROVEMENT OF SILTSTONE AND SANDSTONE MIXTURES BY THE ADDITION OF CALCAREOUS FLY ASH FOR THE CONSTRUCTION OF HARDCORE DAM IN AMFILOCHIA, GREECE

**M Papachristoforou**

**I Papayianni**

Aristotle University of Thessaloniki

**I Drymonitou**

SOFIOS Consultans SA

Greece

**ABSTRACT.** In the hardcore dam projects, the use of local stony materials is a cost effective solution if their suitability has been properly testified. The Calcareous Fly ash (CFA) is produced at power stations of the Ptolemaida basin, around 250 km from Amphilochia where the hardcore dam will be constructed. This CFA has been used successfully in soil stabilization and could also be used as hydraulic binder to bound aggregates according to EN 13282:2. The work done for testing CFA siltstone-sandstone mixtures followed two stages. At the first stage, the siltstone and sandstone crushed material were petrologically analyzed (by thin section analysis) and other properties of fine and coarse fragments were determined such as PI, LL limits, flakiness index, water absorption, resistance to fragmentation and volume stability (including soundness to magnesium sulfate attack and freezing-thawing according to EN 12620:2002 and EN 13242:2002). In parallel, the characteristics of CFA were also determined based on EN 13282:2000. At the second one, different mixtures bound with CFA were tested to determine the optimum moisture content and max density (by the modified Proctor test method) and CBR values (by CBR test method). Furthermore, compressive strength of the compacted mixtures were determined as well as expansion due to the immersion in water. The required mean strength (fm) of the mixtures should be around 6 MPa at 90 days. Based on the results, the addition of 10-15% by mass of CFA to the siltstone-sandstone mixture seems to meet the requirements for the construction of the Hardcore Dam.

**Keywords:** Hardcore Dam, CFA, Sandstone, Siltstone

**Dr Michalis Papachristoforou** is post-doctoral researcher at the Laboratory of Building Materials of the Civil Engineering Department of Aristotle University of Thessaloniki. His research actions aim towards the utilization of by products in concrete for specific applications. **Ioanna Drymonitou** is a civil engineer, member of consultancy Group Sofios Engineering Consultants SA. **Professor Ioanna Papayianni** is the Director of the Laboratory of Building Materials at the Department of Civil Engineering, at Aristotle University of Thessaloniki. She is a specialist in concrete technology and sustainable development.

## INTRODUCTION

The construction of a dam is a large infrastructure project that influences the local environment as well as the economic development of the region [1]. The selection of the place of a dam depends on the topography of the region and geotechnical characteristics of the ground on which the dam will be supported. Among the other types of dams (Rockfill,Earthen) the hardcore or hard fill one is the most advantageous for the economy of the amount of excavated and transported material and significant reduction (about 50%) of the time needed for finishing the dam [2]. Furthermore, the hardcore dams do not need the strong foundation and present low heat evolution in comparison to the RCC dams.

The best section of the dam is the symmetric one with a jacket of impervious material [3] that behaves better in earthquakes. The geotechnical study of the region made with drilling showed that the rocky material of the area is consisted of siltstone and sandstone rocks. Therefore, the suitability of them separately and in combination for the dam construction should be tested. Taking into account the previous experience in using the local calcareous fly ash (CFA) in stabilizing earthen materials [4],[5] as well as the low heat evolution potential of CFA [6] it was decided to use CFA for hydraulically bound mixtures of it with crushed rock filling materials.

The paper focuses on the testing of crushed rock materials as aggregates and development of hydraulically bound mixtures by the addition of calcareous fly ash for the construction of two dams in Amfilochia.

A number of this type dams have been constructed in Greece from the decade of 90’s and after earthquake history their behavior was sufficient [7]. Amfilochia is in prefecture of Aitoloakarnanias in West Greece bordering the Ionian Sea and the Gulf of Patras. The area is very rich in water resources such as rivers and lakes and it has been selected for the construction of hydraulic projects. The whole project study has been undertaken by SOFIOS Consultants S.A. The testing of the rock materials and the development of hydraulically bound mixtures for hardcore dams was entrusted to the Laboratory of Building Materials, AUTH.

## EXPERIMENTAL PROGRAMME

According to geology of the hydraulic project’s area (see Fig.1) [1], the lithology consists of siltstone formations with thin sandstone layers and two types of sandstone formations one compact with fine conglomerates and another with large conglomerate fragments. Samples of local materials were taken from excavations at two places Agios George and Pyrgos, three times summing up an amount around 450 kg. The samples of crushed rocks were transferred to Laboratory AUTH. Then, a furthermore crushing of the stone materials was carried out to meet the granulometry required for testing, where it was necessary.

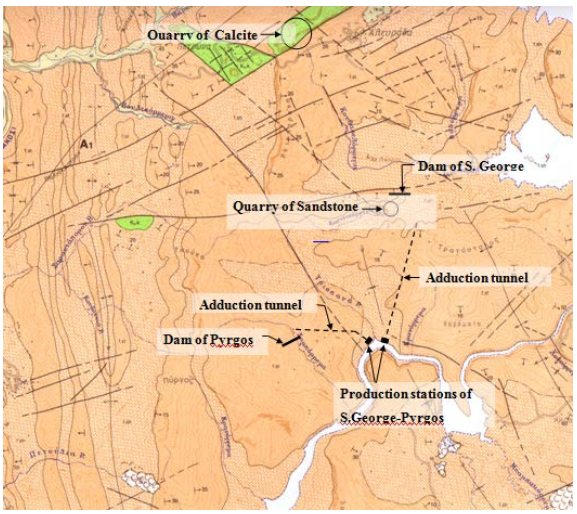


Figure 1 Geological map of Amfilochia region

In the preliminary design phase the different types of stony excavated material were described geologically by thin section polarizing microscopic analysis (Figure 2 and 3). The physical properties of the stones (specific gravity, porosity, and absorption) as well as their compressive strength were determined in a representative number of samples cut from the stone. The results are shown in Table 1.

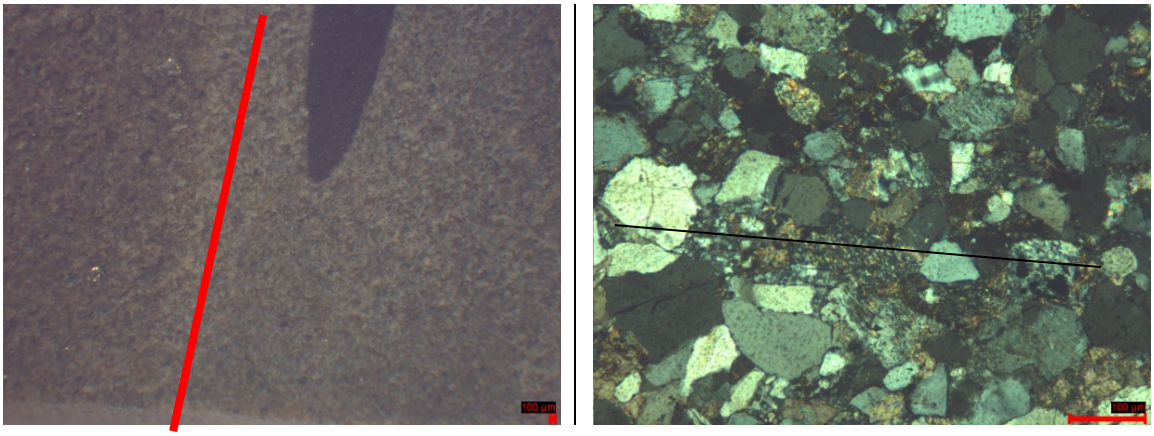

Figure 2 Thin section of sandstone samples by polarizing microscope

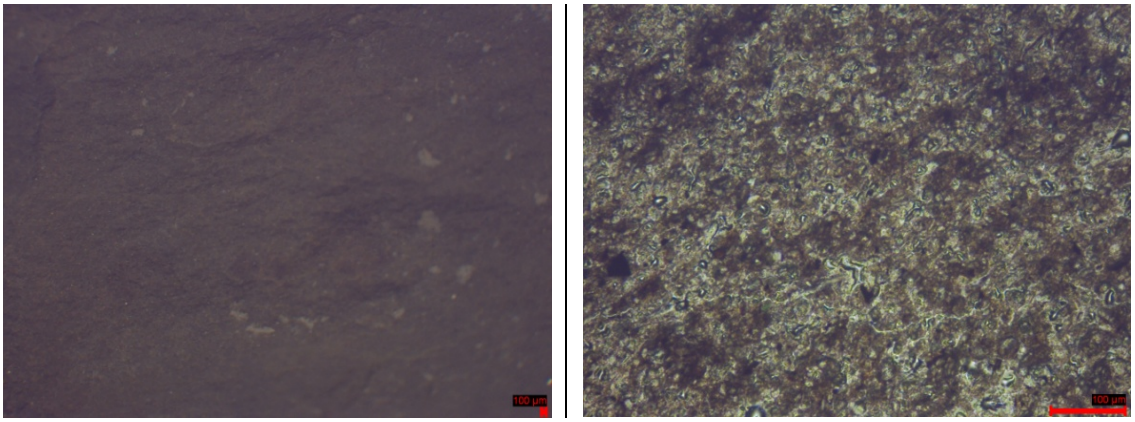

Figure 3 Thin section of siltstone sample by polarizing microscope

Table 1 Physical properties and compressive strength of materials taken from excavations

| Material/ excavated area | | Specific gravity | Porosity | Absorption after 2h boiling | Compressive strength cubes 10x10x10 cm (MPa) |
|---|---|---|---|---|---|
| Siltstone/ Excavation A | | */- | */- | */- | 3-9.5 |
| Sandstone/Excavation A + B | quality 1 | 2.59-2.54 | 1.80-3.60 | 0.72-1.37 | 45-105 |
| | quality 2 | 2.38-2.37 | 6.85-8.10 | 3.45-3.70 | 55-65 |

*Siltstone samples are diluted in the water

**Testing siltstone and siltstone-CFA mixtures**

Testing siltstone since the geological formations comprise a significant amount of siltstone of low compressive strength 3-10 MPa an effort made to improve it by adding local calcareous fly ash (CFA) from Ptolemaida, basin 250 km far from Amfilochia. The characteristics of CFA used are indicated in Table 2. There was previous experience about the good performance of CFA in stabilizing soils. Therefore, the mineralogical composition of the siltstone was found by XRD analysis (Fig.4) showing that the main constituents are quartz, moscovite and calcite. The Atterberg limits were also determined WL=28, WP=20.5, PI=7.5 proving a material of low plasticity.

Table 2 Characteristics of CFA used as hydraulic binder

| CONSTITUENTS | % BY MASS |
|---|---|
| $CaO_{free}$ | 4.96 |
| $SiO_2$ | 34.8 |
| $Al_2O_3$ | 14.83 |
| $Fe_2O_3$ | 2.40 |
| CaO | 31.34 |
| MgO | 1.39 |
| $SO_3$ | 2.37 |
| $Na_2O$ | 4.95 |
| $K_2O$ | 2.88 |
| Loss of Ignition | 4.55 |
| Moisture content % | 0.24 |
| App. Specific gravity | 2.38 |
| Fineness Retained on 45μm sieve | 0.43 |

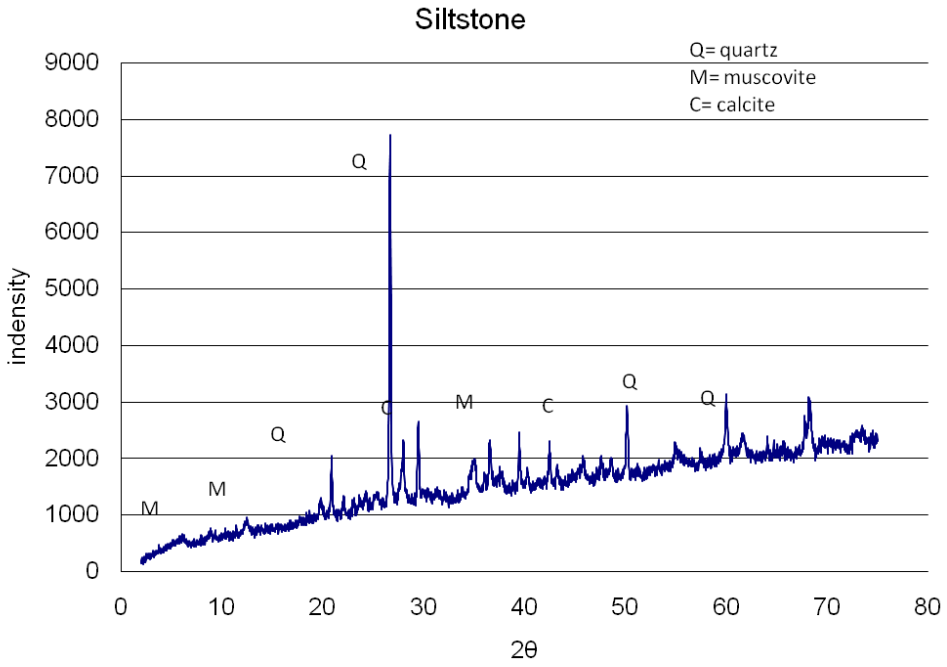


Figure 4 XRD-diagram of siltstone

Then, crushed siltstone (0-4mm) mixtures with addition of CFA at 0, 5, 10 and 15% by mass were tested to find the optimum moisture and max dry density according to modified Proctor method ASTM D1557 and determine the California Bearing Capacity Ratio (CBR) following ASTM D1883-99 method. Expansion under confined immersion of CBR samples was also measured. A compilation of the results is shown in Table 3.

Table 3 Compilation of the results of Proctor and CBR tests concerning mixtures of siltstone with CFA

| Mixtures | Natural moisture (%) | Optimal moisture (%) | Maximum dry density Proctor (gr/cm$^3$) | CBR (%) | Expansion at 10/30/65 drops (mm) |
|---|---|---|---|---|---|
| Siltstone - 0% CFA | 2.5 | 7.8 | 2.17 | 15 | 0.10/0.55/0.20 |
| Siltstone - 5% CFA | 2.5 | 8.0 | 2.10 | 108 | 0.80/0.55/0.20 |
| Siltstone - 10% CFA | 2.5 | 11.6 | 2.05 | 289 | 0 |
| Siltstone - 15% CFA | 2.5 | 11.7 | 1.99 | 200 | 0.53/0.39/0.33 |

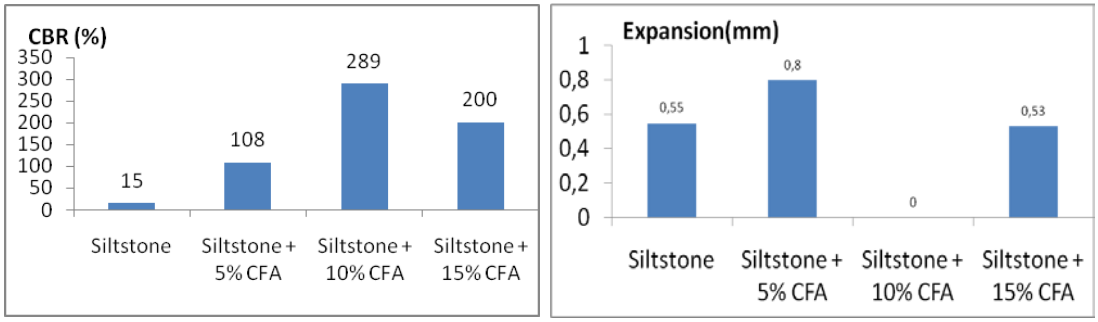


Figure 5 CBR values and expansion of siltstone-CFA mixtures in water under confined conditions

Figure 6 Disintegration of siltstone-CFA mixtures in water without confinement (a)Mixture Siltstone+10%CFA, (b) Mixture net Siltstone

## Testing sandstone

The two types of sandstones (compact and with large conglomerates) after crushing were mixed and tested as coarse aggregates for hardcore filling and concrete as well. The granulometry and content in fines are shown in Figure 7. The flakiness index was evaluated (according to EN 933-3 while for the resistance to fragmentation (Los Angeles test (ASTM C131) the sieved material passing 12.5 mm and retained on 9 mm aperture and that passing the 19 mm and retained on 12.5 mm aperture were tested.
The material passing the sieve of 1.7mm aperture was 31.26% for the two first excavations and 57.3% for the sandstone of the third excavation. The soundness of sandstone aggregates was measured at the mixed sandstone of the first two excavations and the sandstone of the third excavation according to EN 1367-2. The results are shown in Table 4 in which all relevant characteristics concerning the use of sandstone as aggregates for hardcore dam and concrete are summarized.

Table 4 Properties of crushed sandstone aggregates

| Sandstone | Los Angeles (%) | Flakiness Index (%) | Soundness (%) | ASTM C1260-01 Alkali aggregate expansion (%) |
|---|---|---|---|---|
| 1st and 2nd excavation | 31.26 | 29.83 | 20.51 | 20.6 |
| 3rd excavation | 57.3 | - | 36.65 | - |

## Testing mixtures of sandstone with CFA and sandstone-siltstone-CFA ternary systems

The crushed sandstone was mixed with 10% and 15% of CFA by mass. Then the Proctor and CBR tests were applied and the measured optimum moisture, maximum density and CBR are given in Table 5 and Figure 8. Since it is very possible during excavations for the construction of the projects to have actually ternary sandstone-siltstone-CFA systems some complementary mixtures were made and tested. These are as follows: (sandstone:siltstone:CFA) >> (90:10:10), (90:10:15), (80:20:10), (80:20:15) where the numbers in brackets correspond to percentages by mass of the constituents of the mixtures.

The measured parameters for each of the four mixtures in relation to Proctor and CBR tests are depicted in Table 6 and Figure 9.

Table 5 Results of Proctor and CBR tests concerning sandstone-CFA mixtures

| Mixtures | Optimal moisture (%) | Maximum dry density Proctor (gr/cm$^3$) | CBR (%) | Expansion at 10/30/65 drops (mm) |
|---|---|---|---|---|
| Sandstone - 10% CFA | 7.4 | 2.13 | 160 | 0.05/0.05/0.05 |
| Sandstone - 15% CFA | 7.3 | 2.116 | 310 | 0.05/0.05/0 |

Table 6 Results of Proctor and CBR tests concerning ternary mixtures (sandstone-siltstone-CFA)

| Mixtures (Sandstone:Siltstone: CFA) | Optimal moisture (%) | Maximum dry density Proctor (gr/cm$^3$) | CBR (%) | Expansion at 10/30/65 drops (mm) |
|---|---|---|---|---|
| 90:10:10 | 7.9 | 2.10 | 140 | 0.1/0.1/0.1 |
| 90:10:15 | 8.4 | 2.07 | 145 | 0.1/0.1/0.07 |
| 80:20:10 | 9.2 | 2.08 | 100 | 0.1/0.07/0.12 |
| 80:20:15 | 9.5 | 1.841 | 122 | 0.2 |

## Compressive strength of the mixtures

The mixtures tested for finding CBR values were reproduced and similarly compacted in the 15 cm diameter cylinders. The specimens were cured for 7, 28 days and their compressive strength was measured by crushing in compression. For the mixtures of siltstone with CFA the compressive strength developed was around 0.5 MPa at 7 days and 1.0 MPa at 28 days. For sandstone-CFA mixtures the strength development was around 1.5 MPa and 3.0 MPa at 7 days and 28 days respectively. The ternary sandstone-siltstone-CFA systems showed 7-d strength around 1.0 MPa and 28-d strength around 1.5 MPa.

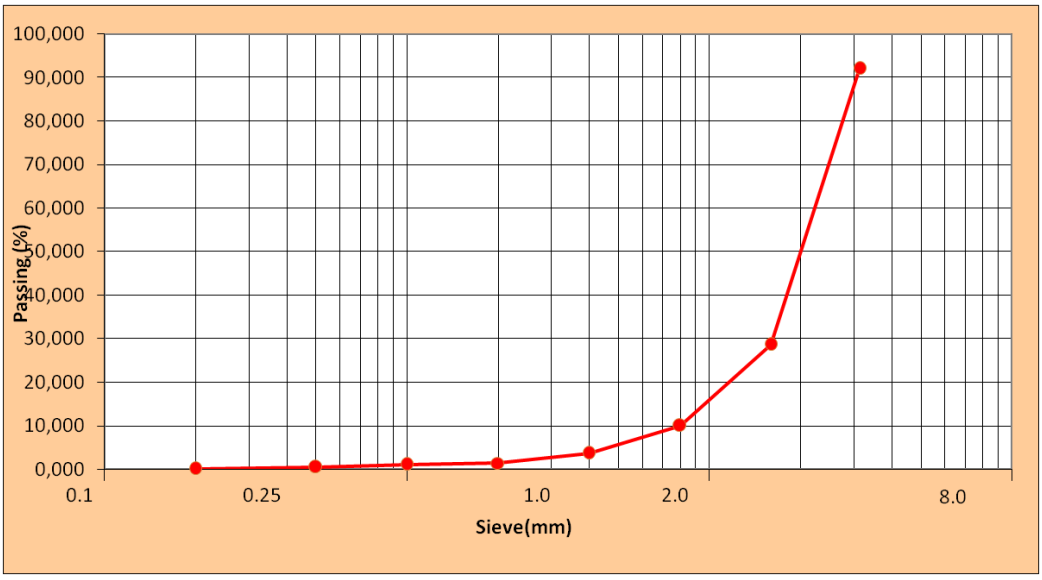


Fig. 7 Granulometric curve of crushed sandstone aggregates

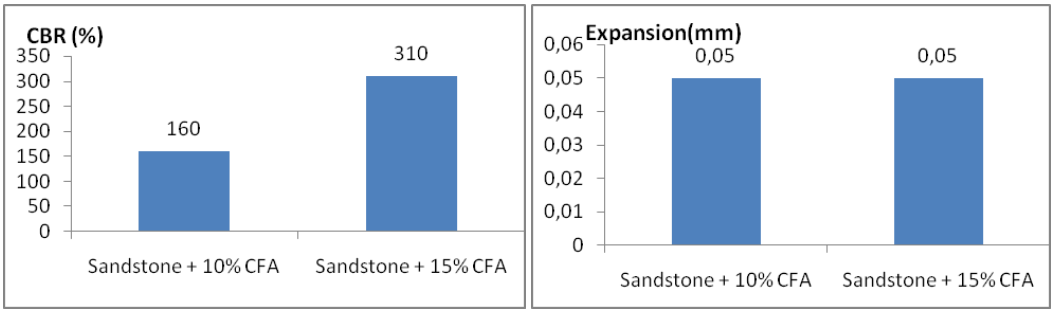


Figure 8 CBR values and expansion in water under confinement of Sandstone-CFA mixtures

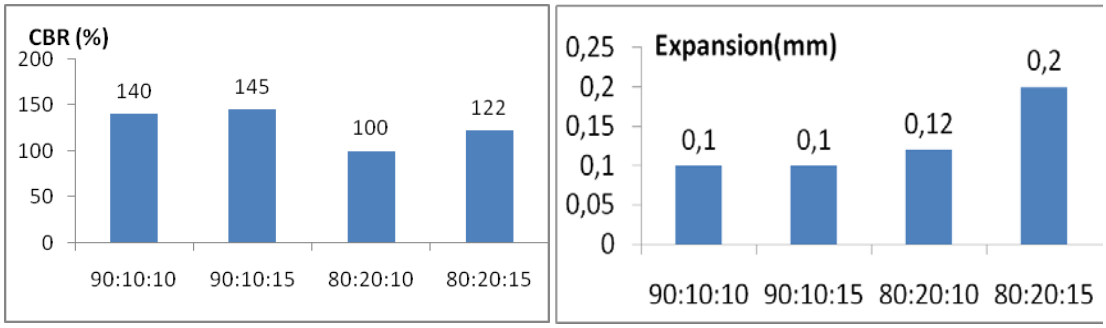


Figure 9 CBR values and expansion in water under confinement of ternary system

## DISCUSSION AND CONCLUSIONS

After the examination of the excavated materials it seems that siltstone is not itself a stable material since it possesses very low strength and is deteriorated in water without confinement. Sandstone samples differ very much. The most compact without large agglomerations and zones of siltstone are of the higher strength but samples with large fragments showed low strength lower than 50% of the sound sandstone samples. Therefore, the low strength sandstone is crushed easier and renders to higher Los Angeles values. Taken into account this possibility stabilization with hydraulic binder is suggested as well as the compaction of the material to be carried out with relatively low capacity vibrators (such as 8-10t) and more passes on the sandstone layers.

The addition of CFA in siltstone mixtures improves significantly the CBR values (from 15 to 280%) and compressive strength (from 0.2 to 0.7 MPa at 7-days) and helps in the volume stability in water. With the addition of CFA (10%, 15%) in sandstone mixtures, CBR values from 160 to 310% have been achieved the best ones with 15% added CFA. The compressive strength developed ranges from 2.0 to 3.0 MPa at 28 days. Based on previous experience with CFA(s), it is considered that the 90-d strength will reach the required one ($f_m$) of 6 MPa. The volume stability or expansion in water is also very low.

In the ternary mixtures (sandstone-siltstone-CFA) in which sandstone content varies from 80% to 90% the CBR values range from 1.0 tp 1.5 MPa with adequate volume stability.

Among excavated materials the sandstone materials seems to meet better the requirements for hard core dam construction. The addition of CFA as hydraulic binder improves spectacularly the CBR values and compressive strength. By adding 15% CFA to sandstone a compressive

strength around 3.0 MPa was achieved with good volume stability. Even in the worst case of excavated material being a mixture of sandstone with zones of siltstone a compressive strength of 1.5 MPa can be achieved. Taking into account that the cost of CFA is actually its transportation cost (current price 2.75 euros per ton) the perspective of adding CFA as stabilizer for hard core mixtures seems feasible and cost effective.

## REFERENCES

1. MOUTAFIS N.I. “Hardfill Dams”, http://www.eeft.gr/pl.pdf

2. COUMOULOS D.G., KORNALOS T.P.(2003) Lean RCC dams Laboratory testing methods and Quality control during Construction” Proceedings 4th International Symposium on RCC Dams, Madrid November 2003, pp 233-238

3. GUILLEMOT TH., LINO MICHAEL, “Design and Construction advantages of Hardfill Symmetrical Dams-Case Study SAFSAF DAM IN EASTERN ALGERIA”, Proceedings of 6th International Symposium on RCC DAMS, Zaragoza 23-25 October 2012

4. PAPAYIANNI I, PAPACHRISTOFOROU M, STAVRIDAKIS E, “Use of calcareous fly ash for improving mechanical and physical characteristics of soils”, Proceedings of EUROCOALASH 2012 Conference, Thessaloniki September 25-27, 2012

5. PAPAYIANNI I., High calcium fly ash applications in Engineering field, CD Proc. Of the 11th Int. conference on Advances in Concrete Technology and Sustainable Development, 9-12 May 2010, Jinan, China

6. STEFANAKOS I., TSIKNAKOU P.,“Technical, Economic and Environmental experiences and conclusions from the use Processed fly ash for the construction of Platanovrisi Dam on the River Nestos”, EVIPAR 1st Hellenic Conference, 24-26 November 2005, Thessaloniki

7. www.eeft.gr/fragmataElladas201311.pdf , Proceedings of the 2nd Hellenic Conference on Dams, November 2013

8. SOFIOS CONSULTANTS SA, Archives:”Preliminary study about the Construction of Hardcore Dam in Amfilochia”

# LOW-CARBON CEMENTS IN BRAZIL: A REVIEW ON THE USE OF METAKAOLIN AS SCM

**A Caldas e Silva**
Universidade Federal Rural Pernambuco (UFRPE)
**S Marden Torres** (UFPB)
Universidade Federal da Paraíba
Brazil
**S Barnett**
University of Portsmouth
United Kingdom

**ABSTRACT.** The use of Portland cement in the world has grown exponentially in recent years. There is a relationship between this material and the economic and social development, especially in development countries, like Brazil and other BRICS. The predictions are that consumption will be 40 billion tons per year in 2040, leading to consequences for the environment, including emissions of $CO_2$ arising from clinker production. One of the supplementary cementitious materials (SCM) used in Brazil is derived from natural or calcined clays. In this way, metakaolin (MK) represented a good option to cement replacement in the Northeast of Brazil. The aim of this paper is to present a review on MK as a SCM and its behaviour to prevent concrete durability issues.

**Keywords:** Low-carbon cements (LCC), Supplementary cementitious materials (SCM), Regional raw-materials, Novel cements.

**Aluizio Caldas e Silva** is M.Sc. (USP, 2002), PhD Student (UFPB, 2014-2017), Researcher Visiting (University of Portsmouth, 2015-2016), Civil Engineer (CHESF, 2005-present) and Lecturer (UFRPE, 2014-present). He is manager of R&D+I projects in AAR and pathologies in the concrete structures of the dams in the hydropower plants of the CHESF.

**Sandro Marden Torres** is PhD (University of Sheffield, 2004), Senior Lecturer at the Department of Engineering Materials (UFPB, 2008-present). He is a respected researcher in Alkaline Activation and Hybrid Cements and microstructure techniques applied to the study of micromechanics and durability of cementitious systems. He is supervisor of 11 masters and 14 PhD projects, and manager of the R&D+I project supported by CHESF.

**Stephanie Barnett** is PhD (Staffordshire University), Senior Lecturer in civil engineering materials (University of Portsmouth, 2010-present) after working as a researcher in cement chemistry and concrete technology for 11 years at the Universities of Aberdeen and Liverpool. She is respected researcher in fibre reinforced concrete, including investigation of the blast and impact resistance of ultra high performance FRC and durability issues affecting concrete.

## INTRODUCTION

In spite of Brazil being a major iron minerals producer, steel structures still have relatively high costs in construction in the country, related to lack of skilled labor and manufactured steel parts cost.

For these reasons, reinforced concrete is the main material used to produce structures in the Brazilian construction industry and its use is related to the need to improve housing and public facilities infrastructure conditions. Thus, the use of Portland cement, the main raw material of Portland Cement Concrete (PCC), is growing and its use as the primary binder is diffused in all regions of the country.

Figure 1 shows the increase of Portland cement use over the last 40 years [1]. In 2012, the Brazilian utilization of Portland cement represented around 2% of the global amount. It is important to highlight the relationship between the higher consumption of PORTLAND CEMENT and the economic improvement of the country. This is because there is a direct relationship between the growth of the economy with the performance of the construction industry which represents almost 6% of Brazil's GDP [1].

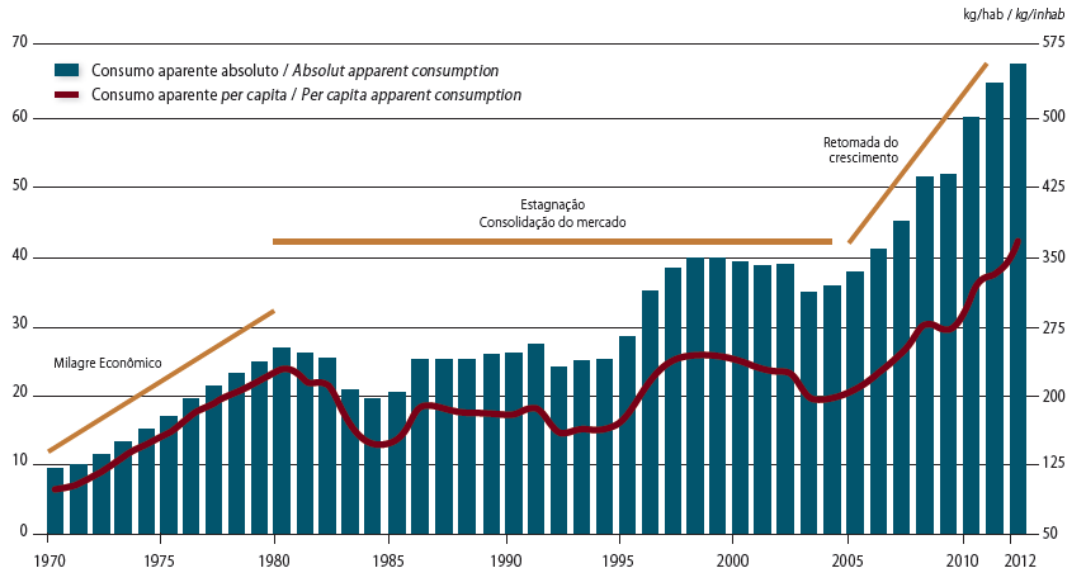


Figure 1 Apparent consumption of Portland cement in Brazil (millions of tonnes) [1]

Due to this importance of Portland-clinker-based hydraulic cements and considering their negative sustainability aspects, in recent years much research has been developed in Brazil and around the world. Researchers are studying new raw materials to develop environmentally sustainable oxide-mineral-based hydraulic binders for general use in construction [2].

These oxides are called Supplementary Cementitious Material (SCM). They can be used to produce novel cements (addition to or replacement of Portland cement either fully or partially) and even improve its behaviour, making them a good alternative to conventional Portland cement. There are several benefits of the use of SCM, besides the environmental aspects already mentioned. Their use could provide cementitious systems which are more durable under attack of the most common pathologies of concrete, including alkali aggregate reaction (AAR). This is feasible considering the pozzolanic activity of some sorts of SCM, such as rice-husk-ash, fly-ash and metakaolin (MK).

However, for these novel potential binders to become viable, the cost and availability of raw materials must be evaluated, since these are the reasons for the widespread use of Portland cement in civil construction [2]. Therefore, the development of SCM from regional raw materials could be the drive towards to making these novel cements viable alternatives to Portland cement.

This variable offer is most important in some countries like Brazil, with continental dimensions, where there is a wide distribution of these raw materials around different regions. For example, rice-husk-ash and fly-ash are available only in the Brazilian South and Southeast, due to the existence of thermoelectric generation from coal and rice cultivation. The transport cost of raw materials for use in areas distant from local production can cripple widespread use.

On the other hand, in the Northeast region these raw materials are not available to be used as SCM. There is also no blast furnace slag (BFS), because the regional steel industry converts pig iron to steel, generating only steel slag and this cannot be used as a cementitious binder.

In this way, calcined clays are the main raw material for replacement and addition as SCM in Portland cement systems in the Northeast of Brazil, because they are available at accessible costs.

The aim of this paper is to present a review on specific calcined clay, Metakaolin (MK) and its potential to be used as SCM in the Northeast of Brazil. The main focuses are issues about availability, its activation and hydration and its use at high levels. Its mineral composition and the resulting influence on the binder behaviour, including concrete durability, are also discussed.

## SUSTAINABILITY IN THE SYSTEMS BASED ON PORTLAND CEMENT

### Environmental Impact From Portland Cement Industry

Carbon dioxide ($CO_2$) is one of the greenhouses gases (GHG). These GHG are believed to be responsible for Earth's heating and increase of the average global surface temperatures over recent years. In the Portland cement manufacturing process, limestone and clays are calcined to sinter Portland clinker, the main input of Portland cement. During firing, limestone dissociates into calcium oxide (CaO) and $CO_2$, according to the stoichiometric balance.

For each 1 ton of limestone, 440 kg of carbon dioxide are emitted. When the fuel related to both the process and the distribution of Portland cement is added, the value reaches around 830 kg per tonne of Portland cement [3].

In spite of this considerable amount, some researchers report these amounts as low in relation to other materials used in civil construction. Other arguments are used to support the idea about the lowest Portland cement industry impacts in relation to the other civil construction industries. They are related to the fact that Portland cement is used mainly in concrete and mortar applications where it is mixed with other low environmental impact materials as the aggregates and water [2]. Table 1 shows some examples of $CO_2$ emissions from different industries.

Table 1 $CO_2$ emissions per 1 tonne of different construction material industries [2]

| $CO_2$ EMISSIONS | |
|---|---|
| Industrial Sector | $CO_2$ (kg/1000 kg) |
| Portland Cement | 830 |
| Steel | 3,000 |
| Aluminium | 15,000 |

However, even considering the arguments on low relative values, the authors recognize the necessity of acting to reduce the reliance on Portland cement, since despite the above, the Portland cement industry still accounts for 5 % of all carbon dioxide emitted by human activities [4], because the widespread use of concrete around the world puts its global production at about 10 $km^3$ per year.

For these reasons, a great deal of research has been developed to find alternatives and mitigate environmental impact from use of Portland clinker based systems. The different approaches of these researchers will be highlighted in the next section.

## APPROACHES TO IMPROVE SUSTAINABILITY

There are different approaches to reduce the $CO_2$ emission from hydraulic systems based on Portland clinker. In a simplified way, it is possible to divide into two views: (a) rationalization of cement and concrete use, e.g. through use of admixtures and optimization of concrete structural design; (b) use of novel cements, based on sustainable raw materials to replace Portland clinker partially or fully.

It is important to highlight that these actions are not exclusive and should be adopted together, because the issue of $CO_2$ emission is not a problem only to the civil construction industry, but to global sustainability.

### The concrete in focus - Efficiency in cement use

The first approach is in the production of more efficient concretes, those manufactured from improved techniques that allow a more efficient use of Portland cement. This alternative allows improvement of concrete performance through changes in concrete composition through the use of additives and fine particles (filler) to increase the compacity of concrete. In this way, it could be feasible to achieve higher strength even at lower cement consumption.

There is research on this subject in progress that measures the environmental impact of concrete through use of indices. They are nominated by: *(a) binder intensity (BI)* and *(b) carbon intensity (CI)*. These indices represent: *(a) the necessary amount of cement to achieve per 1 MPa of concrete strength* and *(b) the amount of $CO_2$ emission per 1 MPa of concrete strength* [5].

### The binder in focus – Novel cements based on sustainable raw materials

In the second approach, the focus to reduce the $CO_2$ emission is not in the concrete, but in the change of the binder composition. The research aims to reduce the percentage of Portland

clinker in the binder systems through more sustainable raw material use, such as SCM with pozzolanic activity. In the same way, they look to adopt the use of renewable fuels and improve the energy efficiency in the cement manufacturing process.

## LOW-CARBON CEMENT – WHAT IS IT?

Low-carbon cements (LCC) seems a good definition applied to describe the new cements developed in research that uses SCM. It is acceptable because this term is currently used to describe binders that emit reduced $CO_2$ content during the production process.

Besides studies about cements made with SCM replacing Portland cement, there are other works trying to develop binders without Portland clinker and they could be called LCC too. The principal examples of these systems containing 0% clinker are geopolymers and binders based on activated blast furnace slag.

The term low carbon concrete has been used in the literature in the context of both concrete containing low carbon cement and concrete utilising techniques to improve efficiency of cement use. In this paper, the term refers only to concrete manufactured with low carbon cement.

## LCC BASED ON METAKAOLIN

Besides the environmental considerations, sustainable novel cements need to be produced with reasonable cost to become feasible. This depends on the viability and availability of their raw-materials. Pozzolans are one class of these materials.

As well known, originally the term pozzolana was associated with naturally formed volcanic ashes which react with lime in the presence of water. Nowadays the term has been extended to cover all siliceous/aluminous materials which will react chemically with calcium hydroxide to form compounds that possess cementitious properties [16]. SCM is a more embracing term for any material that is used as replacement or addition to Portland cement

### Metakaolin as SCM

Considering the general classification, pozzolanic material can be classified as: (a) *natural (i.e.: volcanic ashes, some types of natural clays),* (b) *artificial through industrial process (i.e.: fly ashes, silica fume, calcined clays)* or (c) *derived from industrial wastes (i.e.: sugar cane bagasse ash, rice husk ash).*

Among the various sorts of artificial pozzolanic materials found to replace Portland cement, MK is a good option as a SCM. MK is artificial and produced by industrial process where the clay is exposed to a heat treatment.

Uses of MK as SCM in cement-based systems are still aimed at concrete strength increase and improvement of its durability. In addition, depending on the calcining temperature and the clay type, it is also possible to obtain enhancement in strength during the early stages of curing, due to a combination of the filler effect and accelerated cement hydration [16].

## What is Metakaolin?

MK is a kind of SCM based on oxide minerals and obtained from some calcined clays. The raw material is mainly based on hydrated aluminum silicate ($Al_2Si_2O_5(OH)_4$) and during the calcination the hydroxyl ions are lost, then becoming metakaolinite ($Al_2Si_2O_7$) [6].

The process consists of heating kaolinitic clay between 600ºC and 850ºC through industrial production. This destroys the crystalline structure of the clay minerals which then become one amorphous material. The material is then finely ground. In relation to calcination temperature, a correct level is required to cause disruption of the clay mineral, making the oxides (silicon, aluminium and iron) quite reactive and with high specific surface area [9]. A recent study confirms that calcination temperature is optimal in the end of dehydroxylation and the beginning of recrystallization and uses an interval between 600-800 ºC in its experiments [7].

In this way, we can say that the MK is a sort of calcined clay with high reactivity. Better reactivity occurs due to selection of raw material (specific kaolinitic clays), controlled process of manufacturing, including burn temperature and milling level. The term is used to differentiate the raw materials with high reactivity of the common pozzolans from calcined clays [18].

## Hydration and Beneficial Effects

As in Portland clinker, MK contains $SiO_2$ (silica) and $Al_2O_3$ (alumina), but needs an external calcium supply to react and produce hydraulic compounds such as C-S-H (calcium silicate hydrate). In this way, during the hydration of systems based on Portland clinker, the reaction between the MK and the $Ca(OH)_2$ (calcium hydroxide, called portlandite) released by the cement reaction and C-S-H is formed. The precipitation of these compounds contributes to the mechanical properties of the hydrated paste. There is too a refinement of the pore system that results from this precipitation and the physical effect from the pozzolan fine fraction.

Other beneficial effects are: (a) *decreasing of the hydration rate, which is particularly important for mass concrete*; (b) *mitigation of the alkali-aggregate reaction (AAR);* and (c) *improvement of the concrete properties at later ages* [8].

## Pozzolanic Activity

The disordered nature of the alumina-silicate structure is the reason for the pozzolanic activity of MK [7]. The pozzolanic activity efficiency is related to level of crystallization of its raw material, the original kaolinitic clay [6].

In addition, reactivity can be influenced by variables like specific surface area, alkalinity of medium, temperature, pressure and availability of calcium ions in solution [8] [9]. The amount of cement replacement depends on the fineness of MK. By increasing the fineness of the calcined clay it is possible to increase the level of replacement of cement. Usual values of Blaine fineness are around 7700 $cm^2/g$ [7].

## CONSIDERATION OF MK'S USE IN BRAZIL

### Historical Use of Calcined Clays In Brazil

Unlike other countries such as Chile, Italy and Germany, use of natural pozzolans is not common in Brazil because there is no recent volcanic activity in the Brazilian continent. For this reason, pozzolans from clays are artificial.

The first reported use of calcined clays in Brazil dates from the 1970's in the state of Mato Grosso do Sul, in the west center region of Brazil. This pozzolan was used in concrete to build Jupiá's Dam, considering that all aggregates available were potentially susceptible to the effects of AAR. Since then, their use in mass concrete is widespread in a lot of construction of dams (i.e.: Ilha Solteira/MS, Capivara/SP, Água Vermelha/MG).

Since 1975, Portland pozzolan cement has been produced in Brazil using calcined clays as raw material. Nowadays, beyond several producers of calcined clays used in cement production, there already exist specific manufacturers of MK at industrial scale using the calcination in rotating kilns followed by milling.

## REGIONAL DISTRIBUTION OF SCM

Brazil is a continental country with territorial area around 8.5 million $km^2$. This represents almost half of the total area of South America (17.8 million $km^2$). Therefore, the choice of pozzolan types to be used as SCM must consider geographical conditions. Otherwise, transports costs can prohibit the potential use of pozzolans as SCM. Table 2 presents cement types currently produced in Brazil according to actual standards.

Table 2 – Portland Cement Types manufactured in Brazil and kinds of additions.

| CEMENT | CLINKER + SULPHATES | BFS | POZZOLANIC MATERIALS | CARBONATE FILLER |
|---|---|---|---|---|
| CPI | 100 | 0 | 0 | 0 |
| CPI-S | 95-99 | 1-5 | 1-5 | 1-5 |
| CPII-E (with addition BFS) | 56-94 | 6-34 | - | 0-10 |
| CPII-Z (with addition POZ) | 76-97 | - | 3-14 | 0-10 |
| CPII-F (with addition limestone Filler) | 90-94 | - | - | 6-10 |
| CPIII – (BFS cement) | 25-65 | 35-70 | - | 0-5 |
| CPIV – (pozzolanic cement) | 45-85 | - | 15-50 | 0-5 |
| CPV – ARI (High initial strength) | 95-100 | - | - | 0-5 |

Nowadays, the most common cements are CPII-E and CPIII because of the availability of their main raw material (BFS) and its lower cost (US$ 40/ton) in comparison to Portland cement (US$ 125/ton) [19]. However, BFS generation (from pig iron plants) is mainly available near the Southeast, supplying the market of that region and those nearby (South and East-Centre). On the other hand, for the distant regions, like North and Northeast (which are less industrially developed), in several cases the BFS is imported from other countries such as Russia and China by ship.

This started a trend in the Brazilian Northeast: the opening of new cement plants called milling plants, with a cost 10 times cheaper than a full plant (US$ 250 millions). This industry imports

clinker and BFS which are then mixed, ground and bagged. However, considering the different suppliers, there is not a consistent final product over time and this can cause problems related to the characteristics and properties of the concrete.

Therefore, it is important to have other options to produce cements with additions. Unlike BFS cement, the pozzolanic cements (CPII-Z and CPIV) are available in all Brazilian regions because there is a wider choice of raw materials.

The difference between regions is in the type of pozzolan used. While in the South fly ash is the most common addition, kaolinitic clays are widespread around territory. For this reason, calcined clay is used in the North and Northeast, where no other pozzzolans are available [18]. Figure 2 presents composition of the cements available in Brazil.

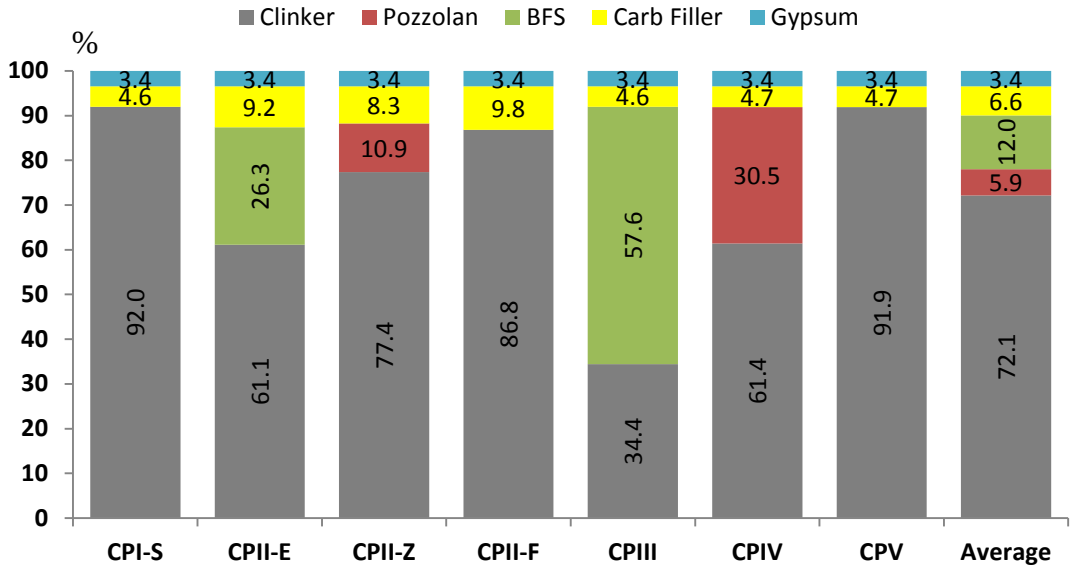


Figure 2 Average composition of Brazilian cements (%) [18]

## CHARACTERISTICS AND REQUIREMENTS OF BRAZILIAN MK

MK is derivate of kaolinitic raw material or a mix between kaolin and smectite (in minor proportion). Quartz can be found also, but if present in high levels reduces the quality of raw material to produce MK [17]. Many samples of Brazilian MK have a red color, due to strong presence of iron minerals in the original raw material.

The standard methods in Brazil applicable to evaluate pozzolanic materials in general are available since 1992 [11], but in 2010 new standards were created to specifically evaluate and establish requirements of MK [12] [13] [14].

The ABNT (Brazilian Association of Technical Standards) defined chemical requirements and their ranges for MK, based on stoichiometric balance, commercial product characteristics and Brazilian specificity. The main aim was to establish limits and define the difference between other common calcined clays and MK, a different pozzolan due its high reactivity [6]. Table 3 contains these limits.

Table 3 Chemical requirements in accord to the Brazilian standards (%).

| COMPONENT | RANGE | METHOD |
|---|---|---|
| $SiO_2$ | $44 \leq SiO_2 \leq 65$ | NBR 14.656 [20] |
| $Al_2O_3$ | $32 \leq Al_2O_3 \leq 46$ | NBR 14.656 [20] |
| CaO + MgO | $\leq 1.5$ | NBR 14.656 [20] |
| $SO_3$ | $\leq 1.0$ | NBR NM 16 [21] |
| $NaO_2$ | $\leq 0.5$ | NBR NM 17 [23] |
| Loss on ignition | $\leq 4.0$ | NBR NM 18 [24] |
| Humidity | $\leq 2.0$ | NBR NM 24 [24] |

Beyond the chemical and mineralogical composition, reactivity of MK depends of the Surface Specific Area. Thus, physical requirements are related with fineness of material. It is important highlight that Blaine's Test is the most used essay to measure fineness of Portland cement and their related materials in Brazil. But its accuracy is not enough to quantify the whole superficial area of the porous system of the powder material. Table 4 contain the standardised values.

Table 4 Physical requirements in accord to the Brazilian standards.

| ANALYSIS | RANGE | METHOD |
|---|---|---|
| Remaining fraction #45µm | $\leq 10\%$ | NBR 15894 [12] |
| Surface Specific Area (B.E.T) [optional] | $\geq 15\ m^2/g$ | ASTM C-1069 [25] |

There are different criteria to measure pozzolanic reactivity. The most common method is according to the ASTM C311 [10], with the compressive strength test on a mix of cement-pozzolanic material (used to evaluate fly-ash). This test is indirect and analyzes just mechanical properties (including the physical effect's influence) and it does not give any information about the pozzolanic material itself [8].

Among the several indirect methods, there are other tests applied to measure pozolanic activity indirectly as X-ray diffractometry and thermogravimetry. However, maybe a better way to find pozolanic activity is related to criteria of chemistry when the calcium consumption is measured in a standard solution. One of the most popular methods to direct determination of calcium consumption is the Chapelle´s test.

The Chapelle's test is standardized by NBR 15895 [15] developed by ABNT. It is being applied to natural and artificial pozzolans, but it is not used on the different types of slags (steel and blast furnace). Tests are commonly applied by the construction materials laboratory of Instituto de Pesquisas Tecnológicas (IPT).

It is an accelerated method where a suspension of pozzolan/lime (1g/1g) and a blank of lime are kept reacting at 90°C for 16 hours; the lime consumed is calculated by the difference between the added and the remaining lime and pozzolanic activity is determined as the amount of calcium hydroxide fixed [6] [8]. The indices required, in compliance with Brazilian standards, the quantity of calcium hydroxide consumed must be $\geq$ 750 mg per gram of pozzolan.

## PERFORMANCE OF SAMPLE OF MK AND OTHER SCM FROM BRAZIL

In a recent paper [8], using the Chapelle's test, researchers show the evaluation of the pozzolanic activity of different SCMs available in Brazil, including FA, SCBA, RHA, MK and SF. The aim was to understand the influence of CaO concentration in the reaction and the tests were carried out comparing amount CaO in solution (1g or 2g) and the conclusions were validated by ANOVA analysis (with 95% confidence). Results are presented in Table 5.

Table 5 Calcium consumption of different SCM (g of CaO/g of pozzolanic material)

SCBA (sugar cane bagasse ash); RHA (rice husk ash); FA (fly ash); MK (metakaolin); SF (silica fume) [8]

| | FA | | SCBA | | RHA | | MK | | SF | |
|---|---|---|---|---|---|---|---|---|---|---|
| | 1g | 2g | 1g | 2g | 1g | 2g | 1g | 2g | 1g | 2g |
| Mean value | 269 | 403 | 279 | 298 | 622 | 864 | 656 | 842 | 755 | 1089 |
| Minimum value | 174 | 286 | 146 | 143 | 255 | 559 | 579 | 752 | 394 | 967 |
| Maximum value | 378 | 489 | 468 | 568 | 867 | 1080 | 804 | 1015 | 858 | 1153 |
| Standard deviation | 97 | 91 | 106 | 145 | 141 | 179 | 50 | 101 | 117 | 71 |
| Number of materials | 4 | 4 | 7 | 13 | 16 | 6 | 17 | 8 | 16 | 5 |
| ANOVA (1g x2g ) | Equal | | equal | | Different | | Different | | Different | |

Considering 1g concentration solution, just the SF achieved the value of 750 mg required by ABNT 15895 [15]. The increase of CaO concentration had no statistical significance to FA and SCBA samples. On the other hand, use of 2g of calcium oxide enhances the CaO consumption in the case of RHA, MK and SF.

The authors suggest that these materials have vitreous phases whose nature or amount are such that they do not react completely when only 1g of CaO is added, requiring a higher lime concentration. Use of industrial production methods was considered important to keep the homogeneous characteristics of SCM considering the importance of the control conditions of temperature and time of burn. Otherwise, the composition of the ash and content of vitreous phase may vary, an idea reinforced by a wide variation in the results [8].

## RESEARCH NEEDS

Considering potential of MK as SCM material and as strategy for AAR mitigation [26], it is important develop different approaches in studies for its use. In spite of the existing research, there are some gaps that need to be studied.

Differently from other industrial by-products, MK has greater compositional and structural variations as it depends on the raw material weathering processes. A different percentage of the main components and presence of guest minerals can influence MK behaviour and consequently the C-S-H phases formed [28].

Also, more studies are needed on the type of calcium aluminates and other interactions regarding structural performance as well as durability issues, mainly AAR, considering its effects in K+ and Na+ concentrations in pore solution.

Performance of admixtures with high levels of MK is not clear. It presents rheological problems and it poses workability problems to concretes.

Among other topics, also needed are more fundamental studies on variations of the Silicate-Aluminate chains with temperature, because its pozzolanicity property varies with activation temperature.

## FINAL REMARKS

This paper discussed the importance of Low-carbon cements, a terminology used to describe the cements based on SCM and that are more sustainable from an environmental point of view. LCCs are a trend to help reduce earth's heating and the increase of average global surface temperatures, considering damage caused by Portland cement production related to high levels of $CO_2$ emissions.

In developing countries such as Brazil, use of Portland cement based materials is growing to supply infrastructure and reduce housing deficit. This implies the need to study and develop new SCM to be used in replacement or addition to Portland cement.

Due the widespread availability of kaolinitic clays in all regions of the country and the high pozzolanic activity of MK, this material seems the best option among the viable SCM. Unlike other SCM based on residues that are not produced by an industrial process, MK is a manufactured material under both time and temperature controlled conditions. In addition, it is also an available commercial product. The sum of these reasons contributes to the offer of a possible homogeneous material (considering an adequate kaolinitic phases in raw materials) with high reactivity in comparison to the common calcined clays.

There are already specific standards to evaluate the chemical, physical and reactivity criteria to guarantee the quality of the MK offered. One the most important of the methods available is the Chapelle's Test that measured the consumption of the CaO when this reacted with MK in solution.

Research is being developed on the benefits of MK use, including its contribution to improve concrete mechanical properties and its durability, its use to mitigate AAR, besides studies about admixture techniques. The use of high levels of MK (upper 50% of addition) could reduce significantly the clinker amount in Portland cement. This subject must be focused in a short time.

Further research is still needed to permit understanding of the microstructure of the modified C-S-H produced and influence of aluminate levels.

## ACKNOWLEDGEMENTS

ACS wishes to thank the School of Civil Engineering and Surveying of the University of Portsmouth, especially to Dr Dominic Fox and Dr Stephanie Barnett for enabling his year as a visiting researcher in the institution. This work was developed by CHESF, UFPB and The University of Portsmouth and supported by CHESF and CNPq.

## REFERENCES


1. SNIC - Sindicato Nacional da indútria do cimento. Relatório anual 2012/2013. Technical Report, 2013, p 08.
2. GARTNER, E; MACPHEE, D. A physico-chemical basis for novel cementitious binders. Cement and Concrete Research, Vol. 41, 2011, pp 736-749.
3. GIELEN, D.; TANAKA, K. Energy efficiency and CO2 emission reduction potentials and policies in the cement industry: towards a plan of action. Proceedings of the IEA/WBCSD: Workshop on Energy Efficiency and CO2 Emission Reduction Potentials and Policies in the Cement Industry. International Energy Agency, 2007.
4. CEMBUREAU - Association Européenne du Ciment. The European Cement association. The role of cement in the 2050 low carbon economy. Technical Report, 2014, p 05.
5. DAMINELI, B. L.; KEMEID, F. M.; AGUIAR, P. S. JOHN, V. M. Measuring the eco-efficiency of cement use. Cement & Concrete Composites, Vol. 32, 2010, pp 555-562.
6. MEDINA, E. A. Pozolanicidade do metacaulim em sistemas binaries com cimento Portland e hidróxido de cálcio, Master thesis, 2011, Department of Construction Engineering, University of São Paulo, São Paulo, Brazil, 134p.
7. SAMET, B.; MNIF, T.; CHAABOUNI, M. Use of a kaolinitic clay as a pozzolanic material for cements: Formulation of blended cement. Cement & Concrete Composites, Vol. 29, 2007, 741–749.
8. QUARCIONI, V. A. ; CHOTOLI, F. F.; COELHO, A. C. V.; CINCOTTO, M. A. Indirect and direct Chapelle's methods for the determination of lime consumption in pozzolanic materials. IBRACON: Structures and Materials Journal, Vol. 8, 2015, 1-7.
9. ZAMPIERI, V. A. Mineralogia e mecanismos de ativação e reação das pozolanas de argilas calcinadas. Master thesis, 1989, Institute of Geosciences, University of São Paulo, São Paulo, Brazil, 209p.
10. ASTM C 311- American Society for Testing and Materials. Standard methods for sampling and testing fly ash in natural pozzolans for use as a mineral admixture in Portland cement concrete. Annual Book of ASTM Standards, ASTM International, West Conshohocken, PA, 2007.
11. ABNT - Associação Brasileira de Normas Técnicas. NBR 12653: Materiais Pozolânicos. Rio de Janeiro, Brazil, 1992.
12. ABNT - Associação Brasileira de Normas Técnicas. NBR 15894-1: Metacaulim para uso com cimento Portland em concreto, argamassa e pasta – Parte 1: Requisitos. São Paulo, Brazil, 2010.
13. ABNT - Associação Brasileira de Normas Técnicas. NBR 15894-2: Metacaulim para uso com cimento Portland em concreto, argamassa e pasta – Parte 2: Determinação do índice de desempenho com cimento aos sete dias. São Paulo, Brazil, 2010.
14. ABNT - Associação Brasileira de Normas Técnicas. NBR 15894-3: Metacaulim para uso com cimento Portland em concreto, argamassa e pasta – Parte 3: Determinação da finura por meio da peneira de 45 □m. São Paulo, Brazil, 2010.

15. ABNT- Associação Brasileira de Normas Técnicas. NBR 15895: Materiais pozolânicos - Determinação do teor de hidróxido de cálcio fixado - Método Chapelle modificado. São Paulo, Brazil, 2010.

16. SABIR, B.B.; WILD, S.; BAI, J. Metakaolin and calcined clays as pozzolans for concrete: a review. Cement & Concrete Composites, Vol. 23, 2001, pp 441-454.

17. ZAMPIERI, V. A. Cimento Portland aditivado com pozolanas de argilas calcinadas: fabricação, hidratação e desempenho. PhD thesis, 1993, Institute of Geosciences, University of São Paulo, São Paulo, Brazil, 233p.

18. MUNHOZ, F. A. C. Efeito das adições ativas na mitigação das reações álcali-sílica e álcali-silicato. Master thesis, 2007, Department of Construction Engineering, University of São Paulo, São Paulo, Brazil, 166p.

19. CALDAS E SILVA, A. Estudo da durabilidade de compósitos reforçados com fibras de celulose. Master Thesis, 2002, Department of Construction Engineering, University of São Paulo, São Paulo, Brazil, 145p.

20. ABNT- Associação Brasileira de Normas Técnicas. NBR 14656: Cimento Portland e matérias-primas - Análise química por espectrometria de raios X - Método de ensaio. São Paulo, Brazil, 2001.

21. ABNT- Associação Brasileira de Normas Técnicas. NBR NM 16: Cimento Portland - Análise química - Determinação de anidrido sulfúrico. São Paulo, Brazil, 2012.

22. ABNT- Associação Brasileira de Normas Técnicas. NBR NM 17: Cimento Portland - Análise química - Método de arbitragem para a determinação de óxido de sódio e óxido de potássio por fotometria de chama. São Paulo, Brazil, 2012.

23. ABNT- Associação Brasileira de Normas Técnicas. NBR NM 18: Cimento Portland - Análise química - Determinação de perda ao fogo. São Paulo, Brazil, 2012.

24. ABNT- Associação Brasileira de Normas Técnicas. NBR NM 24: Materiais pozolânicos - Determinação do teor de umidade. São Paulo, Brazil, 2012.

25. ASTM C 1069- American Society for Testing and Materials. Standard Test Method for Specific Surface Area of Alumina or Quartz by Nitrogen Adsorption. Annual Book of ASTM Standards, ASTM International, West Conshohocken, PA, 2009.

26. CHANG, L.; IDEKER, J. H.; DRIMALAS, T. The Efficacy of Calcined Clays on Mitigating Alakli-Silica Reaction (ASR) in Mortar and Its Influence on Microstructure. Proceedings of the 1st International Conference on Calcined Clays for Sustainable Concrete. RILEM Bookseries, 2014, pp. 211-217.

27. DAI, Z.; TRAN, T. T.; SKIBSTED, J. Aluminum Incorporation in the C–S–H Phase of White Portland Cement–Metakaolin Blends Studied by $^{27}$Al and $^{29}$Si MAS NMR Spectroscopy. Journal of American Ceramic Society, Vol. 97, 2014, pp. 2662–2671.

28. ANDERSEN, M. D.; JAKOBSEN, H. J.; SKIBSTED, J. Characterization of white Portland cement hydration and the C-S-H structure in the presence of sodium aluminate by $^{27}$Al and $^{29}$Si MAS NMR spectroscopy. Cement and Concrete Research, Vol. 34, 2004, pp. 857–868.

# STUDY ON CONSTRUCTION MANAGEMENT EDUCATION IN JAPAN AND THE UK

**H Mihara T Hojo**

Institute of Technology

**T Yoshida**

Kogakuin University

Japan

**ABSTRACT.** The development of CM education in universities is of significant interest both for academia and practitioners. The comparison of CM education between countries may provide insights into development in different places. The purpose of this research is to consider the contextual differences in construction management (CM) taught education between UK and Japan. Curricula in the two countries were compared. Interviews were carried out in UK universities to learn more about UK CM education. UK curricula were found to be heavily influenced by partnerships with British professional institutions. In contrast, the curricula of Japanese higher education institutions are restricted by the Ministry's requirement in relation to professional licenses. This raises interesting questions about how each institutional context influenced the development of different kinds of skill. In the United Kingdom (UK), construction management at risk (CMr) education at the university level is carried out within the context of partnerships with construction-related organizations, such as the Chartered Institute of Building (CIOB) and the Royal Institution of Chartered Surveyors (RICS), which are also involved in the design of construction management (CM) curricula. In Japan, education relating to professional qualifications such as Registered Architect “kenchikushi”, Registered Operation and Management Engineer “sekō kanri gishi”, and Registered Surveyor “sokuryō-shi” is carried out at the university level, and Japanese students intending to become building and construction engineers in the future must take subjects set by the Ministry of Land, Infrastructure, Transport and Tourism (MLIT) within university curricula that are managed by the Ministry of Education, Culture, Sports, Science and Technology (MEXT). In contrast, Japanese government’s control over the curricula is aimed at developing wider architectural and engineering skills. The intention of this paper is to promote dialogue between British and Japanese institutions for the wider development of CM education.

**Keywords:** Partnerships, Curriculum, Education, Employment, Institutional force, Professional institution, Professional license.

**Hitoshi Mihara** is a Professor in the Department of Construction, Institute of Technology, Japan. **Takuro Yoshida** is Emeritus Professor in the School of Architecture, Kogakuin University, Japan. **Tetsuo Hojo** is Emeritus Professor in the Department of Construction, Institute of Technology, Japan.

## INTRODUCTION

Construction management (CM) education has developed in different ways in different countries. Since the curricula differ, it may be possible to transfer learning between countries about how CM education is defined and constituted in different places. Such a task requires prudence, taking into account the major differences in the way that construction is organized in the two nations. The purpose of this paper is to consider the differences in CM curricula between two countries, to ascertain the extent of these differences and the reasons for such differences. The premise of this research is that various industrial contexts are connected to systematic issues about how curricula are designed and controlled. For example, differences between CM programmes in higher education in Japan and UK may variously be related to contextual industry practice, to professional infrastructures or to the way that universities are regulated and managed. The broader aim of this research is to develop a conversation between British and Japanese academics, professional institutions and civil servants about what constitutes CM and how it may be developed in both countries, while respecting the crucial contextual differences in each country.

## LITERATURE REVIEW

Some scholars advocate that higher education (HE) CM curricula need to reflect practical knowledge of the industry. One way to tackle this problem is to seek to bridge the gap between HE and industry. Some articles suggest that this might be beneficial for both constituencies. Gann (2001) studied construction firms' capabilities to take up and implement the outcome of academic research from UK universities. He found that professional institutions play a major role as repositories of knowledge. He also noted the role of government as a sponsor of academic research, particularly the low level of investment in R&D in the construction sector. This implies that the institutional contexts that influence academic practice are different in each country.

For example, the influence of the government is much stronger in Japan than in the UK. Significantly, Cieszyński et al. (2006) studied graduate CM programmes offered by the UK HE institutions to provide insights into the required qualification in Poland. They noted the importance of the role of accreditation bodies in the UK, which have a big influence on the design of CM programmes. They developed a matrix-categorization of the various disciplines of knowledge required in CM in order to provide insights into the development of CM programmes in Poland. However, they did not further explore professional bodies' influence on the HE institutions' programmes.

In the UK, there seems to be a clear understanding about how to constitute a CM programme. This includes factors such as the needs of students in relation to their employability, the needs of government as a sponsor of academic research and the needs of the industry such as the development of soft skills. In the UK, such programmes have evolved over decades of interaction between industry, professions and both further education and HE establishments. In the absence of such a history, countries like Japan have been seeking how to develop CM programmes that are contextually appropriate. For the purpose of providing insights into the potential for CM education in Japan, a first step is to understand such contextual differences. The specific focus of this research is on educational institutions' concerns about the wider context that influences their design of the CM curriculum in UK and Japan.

## METHODS

This paper builds on previous research that involved analysing and summarizing Japanese HE curricula (Mihara et al. 2013). To develop an overview of UK universities' approaches, their curricula were studied and interviews were conducted with academic staff in September 2013. Based on our discussions, as experienced UK and Japanese academics, interview questions were developed and sent to interviewees prior to the interviews. The questions included the following: (1) types of CM programmes offered, (2) distinct features of the university's programmes, (3) constraints and requirements of curriculum design, (4) industry's involvement in curriculum design, (5) graduate destinations and (6) contents of subjects provided. Each interview lasted from one to two hours. In parallel with the interviews, the curricula and the aims of the programme were collected from the universities' websites and brochures, as well as through direct contact with university administrators.

Four universities were targeted due to their reputation in the CM area, which have been anonymized and are referred to as A, B, C and D. Interviewees were selected from those who were engaged in the design of CM programmes. The access to these interviewees was gained through personal contacts. Due to the availability of interviewees during the first author's visit in the UK, the positions and numbers of the interviewees vary in each university. In University A, the interviewee was in charge of designing MSc programme as well as teaching undergraduate students. In University B, the interview was conducted with three personnel; the Director of Research, a BSc programme leader and a Higher National Certificate (HNC) programme leader. In University C, the interview was conducted with the Head of School, who provided answers with regard to the operation of the school. In University D, the interviewee was involved in curriculum development as well as teaching undergraduate students.

The interview data was analysed to explore participants' major concerns in relation to the curriculum design. The specific analytical method was to code interview transcripts to seek common themes. The themes sought were those that would help to understand the wider context that influences their design of the CM curriculum. Following the analysis of the UK universities, the curricula of three higher education institutions in Japan were compared with what was learned in the UK. The three Japanese institutions were selected as their curricula had previously been collected and reported (Mihara et al. 2013). Specifically, the inclusion and emphasis of each subject was compared between Japanese and UK curricula. Finally, additional clarifications were sought through questionnaires distributed to academic staff in Japanese institutions through email. The comments gained from these questionnaires are used to discuss the future development of CM education in Japan. The selected Japanese academic staff were all in charge of curriculum design.

An interview survey and literature review were conducted concerning the involvement of the CIOB and RICS in university curricula relating to CMr. Interviews were conducted with educators at CIOB, Bracknell at 11:00 AM on August 29, 2014. Later, at 2:00 PM on September 2, 2014, a remote interview was conducted by teleconference with RICS educators. For the literature review, a variety of analyses were carried out on materials including (1) "The Education Framework for Undergraduate Programmes"; (2) "CIOB's Professionalism: An Inclusive Definition of Construction Management"; (3) the Quality Assurance Agency for Higher Education 2008 (QAA); (4) "Policy and Procedures for Accredited Courses (2009)"; (5) the "Checklist For Accreditation Visits" (RICS); (6) "RICS Asia Accreditation Template"; (7) "Operational Standards for Curriculum Certification

Relating to Examination for the Qualification of First-Class Architect" ("Ikkyū kenchikushi no juken shikaku ni kakaru kyōiku katei nintei no un'yō kijun") (MLIT, April 2003 revision); (8) MLIT Notification No. 740; (9) "(Sample) Considerations for Judgment in Confirmation Examinations for Specified Subjects" ("Shitei kamoku no kakunin shinsa ni okeru hantei no ryūi-ten (reiji) ni tsuite") (MLIT); (10) "Confirmation Screening Criteria for Specified Subjects" ("Shitei kamoku kakunin shinsa kijun") (MLIT); "(Guidance to) Prior Confirmation of Eligibility Requirements for the Architect Qualification Exam (Academic Requirements: Specified Subjects)" ("Kenchikushi shiken no juken shikaku yōken (gakureki yōken: Shitei kamoku) no jizen kakunin ni tsuite (go an'nai)") (MLIT); (12) the MLIT website; and (13) the MEXT website.

## FINDINGS

### CM Education in the UK

The interviewees' answers varied depending on their roles in curriculum development and the scales of the university. For example, University B's answers mainly focused on the differences between programmes (HNC, BSc and MSc) as the three staff were interested in discussed these differences with each other during the interview. In University B, the detailed content of subjects was not explained as the interviewee was in charge of overall programme design. In contrast, University D's answers were mainly related to how to teach students as the staff had a close relationship with a small number of undergraduate students in a teaching process.

The analysis of the interview data gained from the UK resulted in the identification of UK universities' main concerns about the industrial context. First, there were concerns about the relationship with professional bodies such as Royal Institution of Chartered Surveyors (RICS) and Charted Institute of Building (CIOB). Second was their concern about graduates' employability. The close relation between these two concerns marks the distinctive features and aims of curriculum design.

This is because the accreditation of these professional bodies (e.g. RICS, RIBA) is significant in recruiting students who have certain vocations in mind (e.g. quantity surveyors, architects). Graduates who have taken accredited courses are exempt from further professional exams for membership of professional institutions, which is often a requirement for employability. In order to gain and retain accreditation, professional bodies visit accredited HE institutions every five years to check that their curriculum complies with contemporary professional needs.

Table 1 Features of the UK Universities' CM education

| | UNIVERSITY A | UNIVERSITY B | UNIVERSITY C | UNIVERSITY D |
|---|---|---|---|---|
| Identified features of the design of CM programme | Integration of broad areas of construction management | Distinction between programmes in relation to the balance of theory and practice | Two masters courses aimed for domestic and international markets | Emphasis on construction techniques |
| Partnership with professional bodies | CIOB/RICS | CIOB/RICS | CIOB/RICS | CIOB/ABE |
| Entry requirement | 360 UCAS points | 320 UCAS points | 260-300 UCAS points | 240 UCAS points |
| Graduate employment | Consultancy, construction companies | Consultancy, construction companies | Consultancy, construction companies, subcontractors | Regional construction companies, subcontractors |

## CM Education in Japan

The curricula of Japanese HE CM education reveal marked differences from the UK. The study of these curricula was augmented with an emailed questionnaire sent to the participating universities for clarification of specific points. The three participating institutions have been anonymized and are referred to as E, F and G. The questions included: (1) particular features of CM education, (2) industry needs and (3) partnerships with industry.

The institutions encompass CM curricula in the Department of Architecture. This is because there is no HE education in CM outside of architecture schools. In Japanese, the term, Kenchiku, has an approximate translation as architecture. However, the term is much wider than this translation would imply, as it infers the whole non-civil engineering sector, including the process of building. This can lead to much confusion in making detailed comparisons.

The kenchiku curriculum is mainly designed under the influence of the Ministry of Education, Culture, Sports, Science and Technology (MECSST). Significantly, the Ministry sets the requirements for the curriculum in HE as eligibility requirements in relation to examinations for attaining a professional licenses include first class architect (kenchikushi) license and Engineering Operation Management Engineer certificate. Students mainly aim to attain the license of first-class kenchikushi, which is of significant importance for career development.

The selected institutions have particular features in terms of CM education. Based on the study of UK universities, Table 2 summarizes the features of Japanese HE institutions in relation to the background institutions and graduate employment.

Table 2 Features of Japanese higher education institutions' CM education

| | UNIVERSITY E | UNIVERSITY F | INSTITUTE G |
|---|---|---|---|
| Emphasis of the programme | Large proportion of management and planning | Architecture | Construction techniques |
| Background institution | MECSST | MECSST | MECSST |
| Graduate employment | Construction, housing, architecture, real estate | Construction, housing, architecture, real estate | Construction, builder architecture, real estate |

**Details of Principal Qualification Awarding Bodies for CMr and Engineers**

To begin with, a table was drawn up comparing the respective professional organizations, government courses, and the subject certification status involved in educational curricula for CMr in the UK and building and construction engineers in Japan.

Next, a comparison was undertaken to identify points of respective differences in education for CMr and building and construction engineers, followed by the compilation of details relating to the educational content considered necessary in each country.

At the CIOB, in order to carry out the verification necessary to certify university courses and subjects for which certification applications are submitted, it is necessary to visit universities in order to perform certifications. With regard to the details and methods of verification, face-to-face interviews are held with students taking the course and supervising faculty members, and, after a final confirmation of other details such as the status of the facilities and teaching instruction, certification is granted to the graduate school, or for a particular program (or course). Specified subjects are required at both the general and specialist levels. The content for general courses is detailed in a "Subject benchmark statement" specified by the QAA, while content for specialist courses is discussed in the CIOB framework. The CIOB partners with universities to provide accreditation in accordance with university courses and programs after a documentary review.

Chances for employment become greater with membership, and bachelor's or master's degree certification levels are available for those qualified. Documents are provided through participation in various construction industry events and online activities. After graduation, and following three years of related employment, graduates may become certified members. Furthermore, there is a subsequent professional review that is necessary for achieving the highest grade. As for the RICS, visits to educational institutions are normally carried out three times over a five-year period in accordance with the provisions of the QAA. After ascertaining the state of university facilities and holding dialogues with university officials, the RICS coordinates with the universities in the creation or modification of certified curricula. In addition, in order to provide educational institutions with the most up-to-date construction industry requirements, the RICS creates and implements client management teams. The framework for specified subjects is provided as per the QAA.

Table 4 Details of principal qualification awarding bodies for CMr and engineers in accredited university courses and subjects related to building and construction

| | CIOB | RICS | MILT (Ministry of Land, Infrastructure and Transport) | | |
|---|---|---|---|---|---|
| | | | Registered Architects "kenchikushi" | Registered Operation and Management Engineers "sekō kanri gishi" | Registered Surveyors "sokuryō-shi" |
| unofficial or government office | unofficial | unofficial | government office | government office | government office |
| qualification | CIOB member (each grade) | RICS member (each grade) | First-Class kenchikushi<br>Second-Class kenchikushi<br>mokuzō kenchikushi | First-Class sekō kanri gishi<br>Second-Class sekō kanri gishi | sokuryō-shi |
| qualified number | 46,000 | 100,000 | 352,453 (First-Class)<br>742,122 (Second-Class)<br>17,203 (mokuzō) | 255,810 (First-Class)<br>395,841 (Second-Class) | 228,747 |
| history | since 1836 | since 1792 | since 1951 | since 1983 | since 1949 |
| low | — | — | low of kenchikushi | low of construction | low of registered surveyors |
| definition of CM | Definition (John Bale) | Red Book & Brack Book | — | — | — |
| Framework of education | The education framework for undergraduate progrumees | APC (Assessment of Professional Competence) | MILT<br>MEXT | MILT<br>MEXT | MILT<br>MEXT |
| accredited university courses and subjects related to building and construction | facilities management, design management, construction management, other | construction survey,<br>building survey,<br>PM,<br>building evaluation,<br>real estate appraisal, other | certification of university courses and departments (e.g., architecture, architectural engineering, and construction), certification is also carried out for specific course subjects | certification of university courses and departments (e.g., architecture, architectural engineering, and construction), certification is also carried out for specific course subjects | certification of university courses and departments (e.g., surveying, civil engineering, and construction), certification is also carried out for specific course subjects |
| procedures for certification | documentary examination<br>site audit | documentary examination<br>site audit | Based on the School Education Act, for each accredited subject offered by architecture-related departments at MEXT-affiliated universities, the MLIT (through the Japan Architectural Education and Information Center) ascertains whether the compulsory and elective courses required for qualification as a registered architect conform to the respective subjects and content specifications. | Based on the School Education Act, for each accredited subject offered by architecture-related departments at MEXT-affiliated universities, the MLIT ascertains whether the compulsory and elective courses required for qualification as a registered architect conform to the respective subjects and content specifications. | Based on the School Education Act, for each accredited subject offered by architecture-related departments at MEXT-affiliated universities, the MLIT ascertains whether the compulsory and elective courses required for qualification as a registered architect conform to the respective subjects and content specifications. |
| framework of the specified subjects | Subject benchmark statement<br>CIOB Framework | QAA | the subjects related to architecture specified by the MILT | the subjects related to architecture specified by the MILT | the subjects related to architecture specified by the MILT |
| relationship with universities | partnership relationship | partnership relationship | relationship of top-down | relationship of top-down | relationship of top-down |
| Advantages of member or qualification | Chances for employment become greater with membership, and bachelor's or master's degree certification levels are available for those qualified.<br>Documents are provided through participation in various construction industry events and online activities.<br>After graduation, and following three years of related employment, graduates may become certified members. | Membership arouses personal confidence and pride, and allows members to find employment at a higher level.<br>This further enables members to maintain a professional ethical standard in the construction industry.<br>Prospective members must undergo an APC process after graduating from an accredited university.<br>The APC process involves various procedures, which include registration and structured training. | Registered Architects "kenchikushi" are licensed by the state to offer exclusive business services "kenchikushi" are subdivided into three grades that correspond to building scale, specifically "First-Class Architect" ("ikkyū kenchikushi"), "Second-Class Architect" ("nikyū kenchikushi"), and "Registered Architect for Wooden Buildings" ("mokuzō kenchikushi").<br>Professionals qualified to use the title of "Registered Architects" are allowed to perform design, construction supervision, and other services that relate to buildings. | Registered Operation and Management Engineers "sekō kanri gishi" are licensed by the state to offer exclusive business services. "sekō kanri gishi" are subdivided into "First-Class" and "Second-Class" grades that correspond to the contract amount and scale of buildings as well as civil engineering structures.<br>Professionals qualified to use the title of "Registered Operation and Management Engineer" can carry out construction supervision and other services that relate to buildings and civil engineering structures, but not design work. | Registered Surveyors "sokuryō-shi" are licensed by the state to offer exclusive business services. Professionals qualified to use the title of "Registered Surveyor" can be involved in, or carry out, the production of plans relating to surveying work performed by surveying contractors. In general, survey technicians engaged in basic surveying work or public surveying work being carried out by surveying contractors must be registered surveyors pursuant to the provisions of the Survey Act. "Surveying work" includes site surveying, river surveying, road surveying, and reference point surveying. |

A partnership relationship exists among the universities, the RICS, and the construction industry, and graduates are provided with accreditation in accordance with university courses and programs after a documentary review. Membership arouses personal confidence and pride, and allows members to find employment at a higher level. This further enables members to maintain a professional ethical standard in the construction industry. Prospective members must undergo an APC process after graduating from an accredited university. The APC process involves various procedures, which include registration and structured training.

Japanese building and construction engineers can be categorized into the four following types:

A) Registered Architects "kenchikushi" are licensed by the state to offer exclusive business services, and are subdivided into three grades that correspond to building scale, specifically "First-Class Architect" ("ikkyū kenchikushi"), "Second-Class Architect" ("nikyū kenchikushi"), and "Registered Architect for Wooden Buildings" ("mokuzō kenchikushi"). Professionals qualified to use the title of "Registered Architects" are allowed to perform design, construction supervision, and other services that relate to buildings.

   However, while they are able to carry out design work, unlike in certifications systems for architects in Europe and North America, the title "Registered Architect" refers to an engineering qualification in Japan. In addition to certification of university courses and departments (e.g., architecture, architectural engineering, and construction), certification is also carried out for specific course subjects. Upon graduation, students become eligible to sit for a professional examination. Graduates that pass their respective Registered Architect Examination are able to become registered architects.

   Based on the School Education Act, for each accredited subject offered by architecture-related departments at MEXT-affiliated universities, the MLIT (through the Japan Architectural Education and Information Center) ascertains whether the compulsory and elective courses required for qualification as a registered architect conform to the respective subjects and content specifications. Procedures are updated on an annual basis. The framework for specified subjects requires students to take the architecture-related courses specified by the MLIT. This is a top-down relationship, with the MLIT certifying subjects and course content that universities determine to be necessary for qualification as a registered architect, subject to documentary review.

B) Registered Operation and Management Engineers "sekō kanri gishi" are licensed by the state to offer exclusive business services, and are subdivided into "First-Class" and "Second-Class" grades that correspond to the contract amount and scale of buildings as well as civil engineering structures.

   Professionals qualified to use the title of "Registered Operation and Management Engineer" can carry out construction supervision and other services that relate to buildings and civil engineering structures, but not design work. With regard to the procedures for specified subjects, while the content of the specialist subjects differs in each field, the remainder are identical to those required for registered architects.

C) Registered Surveyors "sokuryō-shi" are licensed by the state to offer exclusive business services. Professionals qualified to use the title of "Registered Surveyor" can be involved

in, or carry out, the production of plans relating to surveying work performed by surveying contractors. In general, survey technicians engaged in basic surveying work or public surveying work being carried out by surveying contractors must be registered surveyors pursuant to the provisions of the Survey Act. “Surveying work” includes site surveying, river surveying, road surveying, and reference point surveying. With regard to procedures for specified subjects, while the content of the specialist subjects differ in each field, the remainder are identical to those required for registered architects.

D) Registered Engineer (“gijutsu-shi”) are licensed by the state to offer exclusive business services. Professionals qualified to use the title of “Registered Engineer” can engage in activities related to planning, research, design, analysis, testing, evaluation or guidance thereof, on matters that require advanced and adaptive expertise in science and technology.

There are twenty-one fields of specialization for registered engineers, including the construction sector, the water and sewerage sector, the mechanical sector, and the electrical and electronic sector. Registered engineers may perform work in the installation fields of “architecture” and “civil works” that are excluded from the business sector exclusive to registered architects, particularly with reference to the design and management of public works. As they are not subject to university certification, this section limits itself to introducing registered engineers as one of Japan’s technical qualifications.

## DISCUSSION

### Difference in the background institution

It was found that the professional bodies and graduate destinations play a major role in the way that universities design their programmes. The key difference between the two nations is related to requirements for entering a professional career. The direct government control of the relevant profession is seen in Japan, by comparison with self-regulation of UK professions.

In Japan, the development of the CM curricula is restrained by the requirements for the professional kenchikushi license set by the Ministry. Although the number of subjects related to the management area has been increasing in a few HE institutions, these subjects are merely optional.

The development of the professional skills of architects is seen as more important. Construction companies employ graduates without practical skills as they educate new employees in their own systems (interview with University E). Therefore, there is not so much motivation for both the academia and industry to develop the partnership (interview with University F). Clearly, this background context does not motivate the development of CM education.

The accreditation of professional bodies is significant in influencing the curriculum in the UK. Students aim to attain membership of the professional bodies as a result of their education in the Universities. The professional institutions tend to restrict entry to the professions to suitably qualified graduates.

The particular benefit of this partnership is that this allows the curriculum to be updated according to contemporary industry needs (interview with University B). This is mutually beneficial for HE institutions and practitioners, as the industry is left to the market in the UK (interview with University C). The lack of motivation for the partnership as well as government control over the curriculum makes this updating mechanism difficult to develop in Japan.

## CONCLUSIONS

In this research, the concerns of UK academics in designing CM curricula were investigated. Their main concerns about the partnership with professional bodies and graduate employment were found to have a huge influence on the design of the curriculum. The inclusion and emphasis of subjects were compared between Japan and the UK in relation to these concerns.

The relation between HE institutions and professional institutions was found to contribute to the design of CM curricula around meeting contemporary industry needs in the UK. In contrast, the relationship between Japanese higher education institutions and the Ministry was found to develop architects' broader skills as well as restrict the development of CM education in Japan. The key finding is that, in both countries, those who regulate admission to a professional career are the most significant in terms of the impact on the content of curricula.

This research provides insights into the study of curriculum design in relation to the institutional context. Previous research typically focused on either specific subjects in curriculum or on market needs. This study suggests that it is useful to relate the institutional context to specific subjects, in order to develop a better understanding of the academic-industrial partnership. Also, this study can be applied to investigate CM education in other countries. As a future direction of this research, the way that professional bodies influence curriculum design in the UK will be further investigated. This is expected to benefit the discussion on how to develop CM education in Japanese higher education institutions.

Finally, discussions were carried out concerning future challenges.

Partnerships between professional organizations and universities in the UK, within the scope of the QAA, have a high degree of freedom and allow a flexible curriculum structure, whereas the top-down relationship between MLIT and Japanese universities only allows for an effective curriculum structure within the range set by the MLIT and MEXT. This confirms both the truth and the practicality of the fact that, in the UK, coordinating organizations in the construction industry like the CIOB and RICS are able make demands on employee training as well as provide materials in response to the needs of the construction industry.

However, in Japan, it was found that the extreme difficulty of making changes to specified subjects (which must be accomplished through legal processes) can cause problems such as preventing the rapid incorporation of new technology and skills in the construction industry, while also adversely affecting the certification of qualifications for Japan's building and construction engineers.

In addition, since it is extremely difficult for engineers qualified as registered architects to function fully as architects and construction management engineers, the result is a qualification system unique to Japan that differs completely from that enjoyed by architects and CMr in the UK.

Since there is a need for universities to incorporate flexibility into their existing construction techniques and systems in education for CM engineers, and for students to have access to the latest information, it would conceivably be effective for universities to enter into partnerships with construction organizations in the private sector and to extend this involvement to curriculum development. In the future, I hope to continue analysing these differences between the features of educational frameworks in the UK and Japan, and to undertake investigations that will help to effectively implement programs for CMr, engineering, and architectural education.

## ACKNOWLEDGEMENTS

The authors acknowledge the support of the UK and Japanese universities who kindly offered their data and participation.

## REFERENCES

1. MIHARA H., KUROKAWA M., HUGHES W. and HOJO T. The comparison of Construction Management curricula in universities between the UK and Japan. In: Raiden, A B and Aboagye-Nimo, E (Eds), Proceedings of the 30th Annual ARCOM Conference, 1-3 September 2014, Association of Researchers in Construction Management (ARCOM2014), Portsmouth, England, 2014, pp. 1443–1452.

2. MIHARA H., YOSHIDA T., SUZUKI K. and HOJO T. A Study on New Construction Techniques and Skills Training with Focus on the Plastering Subcontractor in Japan. Proceedings of the 26th Annual Conference. Association of Researchers in Construction Management (ARCOM 2012), Edinburgh, Scotland, 2012, pp. 223–233.

3. GANN D. Putting academic ideas into practice: technological progress and the absorptive capacity of construction organizations. Construction Management and Economics, Vol. 19, No. 3, 2001, pp. 321–330.

4. MIHARA H., YOSHIDA T., URAE M. and SUZUKI K. A study on the internship education of the subcontractors at the architectural department of the university in Japan - A study on new method for training building work process supervisors through internships in Japan. Proceedings of 29th Symposium on Building Construction and Management of Projects, Architectural Institute of Japan, Part 2, 2013, pp. 9–14.

5. ARDITI D. Graduate education in construction management. Construction Management and Economics, Vol. 2, No. 3, 1984, pp. 193–199.

6. CIESZYŃSKI K., MINASOWICZ A. and TEIXEIRA J.C. Management learning for construction professionals: Inquiries benchmarks and experiences from Poland, United Kingdom and Portugal, Technological and Economic Development of Economy, Vol. 12, No. 2, 2006, pp. 134–145.

7. DEVANEY S. and ROBERTS D. Who gets the jobs? Factors influencing the employability of property and construction graduates in the UK. Construction Management and Economics, Vol. 30, No. 3, 2012, pp. 233–246.

8. MIHARA H., YOSHIDA T. and URAE M. A Study on a New Method for Training Building Work Process Supervisors through Internships in Japan. Proceedings of the 17th International Symposium on Advancement of Construction Management and Real Estate (CRIOCM 2012), CM6-1, Shenzhen, China, 2012, pp. 1–12.

9. MIHARA H., YOSHIDA T., URAE M. and HOJO T. A Study on the New Method to Educate Construction Engineers of Subcontractors and General Contractors through Internships in Japan. The CRIOCM International Symposium on “Advancement of Construction Management and Real Estate (CRIOCM2013) CM07-1, Xi’an Jiaotong University, 2013.

# DEVELOPMENT OF SUSTAINABLE, INNOVATIVE AND ENERGY-EFFICIENT CONCRETE, BASED ON THE INTEGRATION OF ALL-WASTE MATERIALS: SUS-CON PANELS FOR BUILDING APPLICATIONS

**R Vinai** **M Soutsos**
Queen's University Belfast, UK
**A Largo** **A Attanasio**
CETMA, Italy
**I Larraza** **V Chozas**
ACCIONA, Spain
**A Gupta**
BASF, Germany

**ABSTRACT.** The building sector requires the worldwide production of 4 billion tonnes of cement annually, consuming more than 40% of global energy and accounting for about 8% of the total $CO_2$ emissions. The SUS-CON project aimed at integrating waste materials in the production cycle of concrete, for both ready-mixed and pre-cast applications, resulting in an innovative light-weight, ecocompatible and cost-effective construction material, made by all-waste materials and characterized by enhanced thermal insulation performance and low embodied energy and $CO_2$. Alkali activated "cementless" binders, which have recently emerged as eco-friendly construction materials, were used in conjunction with lightweight recycled aggregates to produce sustainable concrete for a range of applications. This paper presents some results from the development of a concrete made with a geopolymeric binder (alkali activated fly ash) and aggregate from recycled mixed plastic. Mix optimisation was achieved through an extensive investigation on production parameters for binder and aggregate. The mix recipe was developed for achieving the required fresh and hardened properties. The optimised mix gave compressive strength of about 7 MPa, flexural strength of about 1.3 MPa and a thermal conductivity of 0.34 W/mK. Fresh and hardened properties were deemed suitable for the industrial production of precast products. Precast panels were designed and produced for the construction of demonstration buildings. Mock-ups of about 2.5 m × 2.5 m × 2.5 m were built at a demo park in Spain both with SUS-CON and Portland cement concrete, monitoring internal and external temperatures. Field results indicate that the SUS-CON mock-ups have better insulation. During the warmest period of the day, the measured temperature in the SUS-CON mock-ups was lower.

**Keywords:** Sustainable concrete, recycled aggregate, geopolymeric binder, precast concrete, mock-up monitoring.

**Raffaele Vinai** is currently Research Fellow at the School of Planning, Architecture and Civil Engineering, Queen's University Belfast, UK. **Professor Marios N Soutsos** is Professor of Structures/Materials in Queen's University Belfast, UK. **Alessandro Largo** is the Project Manager of the SUS-CON project. **Agnese Attanasio** is currently Researcher at CETMA in Materials and Structures Eng. Dept., Diagnostic and Civil Engineering group. **Íñigo Larraza** is currently CEO of Gnanomat, a nanomaterials based start-up company. **Valle Chozas Ligero** is R&D senior researcher. **Anoop Gupta** is currently working as a lab team leader at BASF construction solutions GmbH, Germany.

## INTRODUCTION

According to data from United Nations Environmental Programme (UNEP) reported in [1], building and construction sector employs about 111 million people around the world, consuming 20% of water and between 25% and 40% of energy, while producing between 30% and 40% of solid waste and 30 and 40% of global greenhouse gases (GHGs).

Interventions in the field of sustainable, alternative building materials are essential for achieving the international targets set for stopping the global warming and for a sustainable development. For this reason, European Commission defined an ambitious agenda where the development of innovative, green building materials is a priority. In this context, the 7$^{th}$ Framework Programme (FP7) launched the call EeB.NMP.2011-1 "Materials for new energy efficient building components with reduced embodied energy".

The SUS-CON (SUStainable, innovative and energy-efficient CONcrete, based on the integration of all-waste materials) project, funded under that call, aimed at developing new concepts and technology routes to integrate secondary materials in the production of concrete, for both ready-mixed and pre-cast applications, resulting in an innovative, eco-compatible and cost-effective construction material, characterised by:

- light-weight;
- low embodied energy;
- low $CO_2$ footprint;
- improved thermal and acoustic insulation performance (multi-functionality).

The focus of the project was on waste materials largely available across Europe that are not currently recycled, investigating aggregate and binder from secondary materials and in turn developing a 100% recycled concrete. Whereas aggregates were obtained from lightweight materials (such as waste tyres, MPW, WEEE and rigid polyurethane foams), binders were developed from aluminosilicate-rich precursors (such as coal ash, metallurgical slag, perlite tailings) and alkali materials as activators.

Some details on the project activities can be found in published literature [2, 3] and on the project website [4]. The project was successfully completed in 2015, with the industrial production of panels, blocks and ready-mix floor screed with selected recipes of SUS-CON materials. Three demonstration sites have been set up in Europe (Spain, Turkey and Romania) with SUS-CON and Portland cement concrete reference buildings.

In this paper, some results from the development of a concrete made with a geopolymeric binder (alkali activated fly ash) and aggregate from recycled mixed plastic for the production of precast panels are presented. The mix recipe was developed for achieving the required fresh and hardened properties. Precast panels were designed and produced for the construction of the demonstration buildings. Mock-ups of about 2.5 m × 2.5 m × 2.5 m were built at a demo park in Spain both with SUS-CON and Portland cement concrete, monitoring internal and external temperatures.

## MATERIALS AND METHODS

### Recycled Aggregate Development

Mixed Plastic Wastes (MPW), resulting from the sorting process of plastic recycling, were explored in this study to assess the viability to process them into lightweight concrete aggregates. A technological process to produce innovative lightweight aggregates was developed in collaboration with an Italian company working in material recycling sector (Centro Riciclo Vedelago). Plastic scraps, used as raw material, mainly consist of polyethylene (PE) and polypropylene (PP), but also include residuals of polyethylene terephthalate (PET) and minimal other impurities. The production process basically consists of an extrusion and an expansion stages, resulting in two different aggregate types. The process parameters have been accurately optimized taking also into consideration product quality and production costs. Lightweight aggregates, hereafter referred as Remix (RX), with different density were produced (RX HD – densified flakes with higher density – and RX LD – expanded granules with lower density), see Figure 1. RX HD aggregates are produced by processing the raw material into an extruder, where plastic is melted and densified, then it is cooled and reduced in suitable sizes. RX LD aggregates are obtained by a patented foaming process, using foaming agents also from waste, applied on densified flakes (European Patent EP1598164A1).

In order to assess the suitability of the produced aggregates for concrete manufacturing, these have been fully characterized in terms of physical, mechanical and chemical properties according to specific standards, as reported in Table 1. Remix aggregates, both densified and expanded type, have shown particle density lower than 2000 kg/m$^3$, therefore they can be classified as lightweight aggregates according to EN 206-1 [5]. Moreover, results of chemical tests confirmed their compliance with the standards' requirements and according to HSE (Health, Safety and Environment) assessments the developed aggregates can be classified as non-hazardous.

Table 1 Overview of mixed plastic (Remix - RX) aggregates properties according to specific standards

| RX AGGREGATES PROPERTIES* | | | | | | | | | |
|---|---|---|---|---|---|---|---|---|---|
| | Geometrical | Physical | | | Mechanical | Chemical | | | |
| | EN 933-1 | EN 1097-3 | EN 1097-6 | | EN 13055-1 | EN 1744-1 | | | |
| Aggregate typology | Particle size, mm | Loose bulk density, kg/m$^3$ | Particle density, kg/m$^3$ | Water absorption, % | Compressive strength, N/mm$^2$ | Sulphates, % | Chloride salts, % | Sulphur, % | Organic impurities |
| RX HD (densified) | 0-2 | - | - | - | - | - | - | - | - |
| | 3-7 | 290 | 810 | 10 | 250 | 0.01 | 0.13 | 0.03 | - |
| RX LD (expanded) | 8-12.5 | 359 | 660 | 22 | 215 | 0.15 | 0.02 | 1.06 | absent |

* The standards applied are not specific for the tested materials (recycled mixed plastic). This led to some variability in the results. Moreover, some standards should be applied for size lower than 4 mm, so not all the aggregates sizes were tested.


Figure 1 Mixed plastic scraps (a) used as raw materials for RX aggregates production: densified flakes (b) and expanded granules (c)

**Alkali Activated Binder**

Fly ash (PFA) was supplied by Power Minerals Ltd., Drax Power Station, North Yorkshire, UK. The average dimension ($d_{50}$) of the powder particle was 18 µm. The mineralogical composition was assessed through X-ray diffraction (XRD) with the following setting: pure copper-K-Alpha 1 radiation with wavelength 1.54 Å, X-ray generator @ 40 kV and 40 mA, angular range 5° to 70° (2θ) with a step close to 0.017°. The Rietveld method, adding and blending 20% in weight of corundum ($Al_2O_3$) as internal standard, allowed a quantitative estimation of the amorphous and crystalline fractions. The amorphous content was found to be 86%, whereas quartz (4.6%), mullite (8.1%), hematite (0.5%) and magnetite (0.8%) were the main crystalline phases detected.

Commercial chemicals were used for the activation: solid NaOH of commercial grade (99% purity) and sodium silicate solution with $SiO_2$:$Na_2O$ mass ratio = 2. Mass composition of the commercial sodium silicate solution, provided by Woellner GmbH & Co KG, Ludwigshafen, Germany, with trade name "Betol 52", was $Na_2O$ = 15%, $SiO_2$ = 30%, $H_2O$ = 55%, in weight. NaOH solution was prepared by dissolving solid NaOH in tap water (300 g of NaOH dissolved in 700 g of tap water).
The proportions of these two alkalis and their concentrations were defined as follows:

- Alkali dosage (M+): mass ratio of total sodium oxide ($Na_2O$) in the activating solution of PFA;
- Alkali modulus (AM): mass ratio of sodium oxide to silica in the activating solution.

A previous study on the effect of chemical dosage on the reaction development in a PFA-based system [6] indicated that the mechanical strength of mortar increases with the increase of the AM until an optimum value that was found to be in the range 0.95 – 1.25. Subsequently, it decreases until a residual value, due presumably to the reduced amount of available silica. The effect of the M+ increase was also associated with an increase in the compressive strength of mortars, with a maximum of about 60 MPa for values in the range 11 to 12%, but the incremental gain narrowed when M+ was higher than 9.5%. Moreover, higher dosages were found to trigger fast setting behaviour, besides implying high production costs and higher environmental burden. As a compromise between these conflicting trends, alkali dosages were fixed at M+ = 7.5% and AM = 1.25, ensuring a compressive strength (measured on mortar) of about 25 – 30 MPa. Some details can also be found in [7]. The water/solids ratio was defined as the ratio between total mass of water (i.e. tap water + water in the alkali solutions) and the total solid mass (i.e. mass of PFA + mass of alkali solids).

The water/solid ratio was kept in the range 0.35 – 0.37 as PFA-based geopolymers are very sensitive to water content. PFA-based systems require heat curing for the development of the reaction. The proposed curing regime was 7 days @ 70°C.

### Development of a Suitable Mix Design for Façade Panels and Material Characterisation

The following requirements were set by industrial partners for a mix suitable for façade panel production: slump in the range 9-20 cm, density of about 1100 kg/m$^3$, compressive strength in the range 5-20 MPa. A mix design able to fulfil such requirements was developed and extensively investigated for its full characterisation. Mechanical (compressive strength, Young's modulus, Poisson's ratio, flexural strength, UPV) and thermal (thermal conductivity, thermal expansion coefficients, heat capacity, thermal storage capacity) properties were measured.

## RESULTS AND DISCUSSION

### Suitability of Recycled Aggregate in Ordinary Portland Cement Concrete

Previous experimental activities demonstrated the feasibility of recycling mixed plastic scraps to obtain sustainable aggregates in the form of Remix HD and LD. The following step was the validation of their potential to be used for lightweight concretes. Therefore, their compatibility with traditional binder (ordinary Portland cement, PC) has been evaluated. The specific target was to develop concrete formulations suitable for precast building components such as panels for façades (or part of them). During the trials the following requirements had been targeted for such concrete components: density 350-1700 kg/m$^3$, workability S4-SCC and compressive strength 5-24 MPa. For this, different concrete mixes were designed and produced combining RX aggregates, natural aggregates and PC (Type I 42.5 R, density 3.1 kg/m$^3$). The formulations were optimized to get the target properties and their performance assessed both on the fresh (density, workability, air content) and hardened state (mechanical performance, thermal insulation properties, ultrasonic investigations), according to specific standards.

Different optimisation steps were implemented on the lab scale. Initially, compatibility evaluations of RX aggregates were carried out, i.e. preliminary concrete mixtures were produced and inspected whilst in the fresh state. The use of RX aggregates within concrete mixtures resulted in some undesirable effects, mainly swelling phenomena. This behaviour was related to a possible effect of residual impurities in the raw material used for aggregate production. In subsequent experiments cleaner aggregates were used and such problem was solved. The next step consisted in a systematic experimental programme, carried out in two different labs, for the identification of the best RX based concretes for the target application and for the assessment of their reproducibility. During the first experimental session several mix design parameters (i.e. water/cement, aggregates/paste and aggregates proportioning) were properly adjusted to obtain concretes with suitable density, consistency and mechanical performance. The best performing formulations produced during this phase are shown in Table 2.

Figure 2 Fresh (a) and hardened concrete samples (b, c) based on RX and OPC

Table 2 Optimization of RX based concretes (1st step): design parameters and performance

| RX BASED CONCRETES (1st OPTIMISATION TRIALS) | | | | | | | | |
|---|---|---|---|---|---|---|---|---|
| Design parameters | | | | Fresh performance | | Hardened performance (28 days) | | |
| Mix code | Cement, kg/m$^3$ | w/c | RX aggregate, % vol. | Density, kg/m$^3$ | Slump class | Density, kg/m$^3$ | Compressive strength, MPa | Thermal conductivity @10°C, W/mK |
| | | | | EN 12350-6 | EN 12350-2 | | EN 12390-3 | EN 12664 |
| Mix1 | 400 | 0.45 | 80% | 1102 | S4 | 1054 | 5.6 | - |
| Mix2 | 400 | 0.45 | 70% | 1172 | S4 | 1120 | 5.9 | 0.25 |

Based on the results achieved, a further optimisation step was performed by a second lab. Using Mix 2 as reference, a more detailed study was carried out which monitored the effect of specific design parameters (i.e. RX aggregate percentage, water/cement ratio and cement content) on the final concrete performance. Therefore different RX aggregate volumes were incorporated (from 70% up to 100%), three different water/cement ratios (0.37, 0.40 and 0.45) and two different cement amounts (400 and 450 kg/m$^3$) tested; one of the above mentioned parameters was changed in each trial. The results summarized in Table 3 are the most representative concretes produced during this experimental session.

All the concretes based on RX aggregates showed a good reproducibility as well as a good compatibility with conventional mixing procedures. The density of all the concretes developed was suitable for the target application. The use of different percentage of RX aggregates did not affect the concrete workability (consistency class S4 in all the tests). As expected, higher plastic aggregate amounts resulted in lower compressive strength concretes. Using 400 kg/m$^3$ of cement and w/c 0.45 the compressive strength target is achieved only with 70% of RX, while incorporating more cement (450 kg/m$^3$) and reducing w/c (0.40) all the formulations are suitable for panels fabrication.

Table 3 Optimization of RX based concretes (2nd step): design parameters and performance

| RX BASED CONCRETES (2nd OPTIMISATION TRIALS) | | | | | | | | |
|---|---|---|---|---|---|---|---|---|
| | Design parameters | | | Fresh performance | | Hardened performance (28 days) | | |
| Mix code | Cement, kg/m$^3$ | w/c | RX aggregate, % vol. | Density, kg/m$^3$ | Slump class | Density, kg/m$^3$ | Compressive strength, MPa | Thermal conductivity @10°C, W/mK |
| | | | | EN 12350-6 | EN 12350-2 | | EN 12390-3 | EN 12664 |
| Mix3 | 400 | 0.45 | 70% | 1102 | S4 | 1063 | 5.5 | - |
| Mix4 | 400 | 0.45 | 80% | 910 | S4 | 896 | 3.1 | - |
| Mix5 | 400 | 0.45 | 90% | 860 | S4 | 819 | 3.1 | - |
| Mix6 | 400 | 0.45 | 100% | 734 | S4 | 710 | 2.0 | - |
| Mix7 | 450 | 0.40 | 70% | 1191 | S4 | 1183 | 8.9 | - |
| Mix8 | 450 | 0.40 | 80% | 1115 | S4 | 1076 | 8.3 | 0.25 |
| Mix9 | 450 | 0.40 | 90% | 1108 | S4 | 1097 | 9.0 | - |
| Mix10 | 450 | 0.40 | 100% | 908 | S4 | 881 | 5.3 | - |

**Development of Mix Design with Recycled Aggregate and Geopolymeric Binder**

The optimisation of the mix design was initially investigated varying the paste and the fine aggregate fraction proportions. The 0/2 mm RX aggregate was not used as it was found to cause heat formation, quick drying and swelling of the concrete, presumably due to the presence of residual impurities (such as metallic Al) in the aggregate. The fine fraction was therefore replaced with natural sand. Paste proportion at 50% (mix RX1) was found to be too low for incorporating the aggregate, and therefore it was increased to 60%. Natural sand was dosed at 20% (mix RX2) and 30% (mix RX3) of the total aggregate volume. However, bleeding and segregation phenomena were observed. The flow was observed to be high and therefore a reduction in the w/s ratio was adopted for subsequent investigations.

Compressive strength was measured at 6 days for a quick assessment of its development. Mixes with 60% paste were found to satisfy the requirements (> 5 MPa), although concrete density was found to be slightly higher than the target value (i.e. 1100 kg/m$^3$). Two further mixes (RX4 and RX5) similar to RX3 were cast with the aim of reducing the water content and therefore further increasing the strength, minimising possible bleeding and segregation phenomena. Mix RX4 was prepared with less paste (55%) with the aim of increasing the volume of aggregates incorporated. The sand content was kept equal to 30% of the total aggregate volume.

It was observed that, even with a water content reduction, the workability of the mixes was still compliant with the requirements. However, some bleeding was still observed during the execution of the spread test. The 28-day strength was confirmed to be satisfactory (> 5MPa).

While workability and strength were in line with technical requirements, measured density was found to exceed the suggested value. However, it was judged satisfactory for façade panel production by industrial partners. Therefore, the mix RX4 was chosen for such application.

Table 4 Optimisation of RX + PFA concretes: design parameters and performance

| MIX DESIGN OPTIMISATION | | | | | | |
|---|---|---|---|---|---|---|
| Mix No. | Paste prop., % | Sand, % | RX 3/7, % | Slump, mm | Hardened density, kg/m$^3$ | Compressive strength, MPa |
| RX1 | 50 | 20 | 80 | (collapse) | 1413 [a] | 3.6 [a] |
| RX2 | 60 | 20 | 80 | 210 | 1474 [a] | 5.0 [a] |
| RX3 | 60 | 30 | 70 | 250 | 1605 [a] | 5.8 [a] |
| RX4 | 55 | 30 | 70 | 170 | 1429 [b] | 5.9 [b] |
| RX5 | 60 | 30 | 70 | 270 | 1432 [b] | 5.6 [b] |

[a] measured at 6 days of age, [b] measured at 28 days of age

## Assessment of Mechanical and Thermal Properties

Once the mix design was chosen, a comprehensive characterisation of mechanical and thermal properties of the SUS-CON concrete was carried out. Results from laboratory tests on RX4 mixes (carried out following relevant standards) are shown in Table 5. Fresh properties, compressive strength and hardened density were confirmed to be satisfactory and data were obtained for the thermal performance of the mix. Compressive strength, Young modulus and Poisson ratio were assessed by Magnetti Building (industrial project partner).

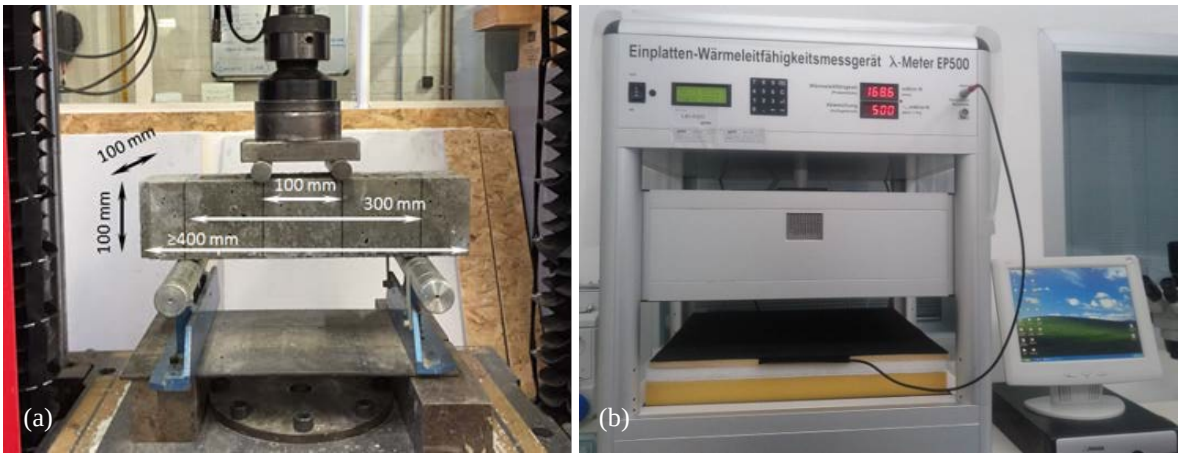


Figure 3 (a) Flexural test set up. (b) Hot plate apparatus for thermal conductivity evaluation

Table 5 Results of laboratory tests

| MECHANICAL AND THERMAL FEATURES OF SELECTED RX MIX | | | |
|---|---|---|---|
| Parameter | Standard | u.o.m. | value |
| Slump | EN 12350-2 | cm | 23 |
| Fresh density | | $kg/m^3$ | 1636 |
| Density (28 days) | EN 12350-6 | $kg/m^3$ | 1440 |
| Compressive strength (28 days) | EN 12390-3 | MPa | 6.8 |
| Flex. strength (28 days) | EN 12390-5 | MPa | 1.3 |
| UPV | EN 12504-4 | m/s | 1613.32 |
| Young modulus | UNI 6556 | GPa | 1.0 |
| Poisson ratio | | - | 0.05 |
| Thermal conductivity (10°C) | EN 12664 | W/mK | 0.344 |
| Heat capacity | | J/g·°C | 1.275 |
| Thermal storage capacity | | $kWh/m^3$ | 7.577 |
| Coefficient of linear expansion (70°C) | | $°C^{-1}$ | -3.36E-05 |

## Panel Production and Mock-up Structure and Monitoring System

In order to demonstrate the feasibility of the SUS-CON products on full scale buildings and their real performance in terms of energy efficiency, 2 mock-ups were built with panel components (one with SUS-CON panels and a second one with Portland cement based-reference panel components). The mock-ups were constructed at ACCIONA Demo-Park (ACCIONA Central Workshop Facilities) in San Sebastián de los Reyes, Madrid.

Magnetti Building was in charge for the design and production of the prefabricated elements. A sandwich structure was chosen for the panel, with two external layers of SUS-CON concrete and an inner layer of EPS100. The panel design was defined for keeping the same weight and thermal transmittance of Portland cement based concrete panels typically produced in the facility. Panels were cast in Magnetti Building premises in Italy (see Figure 4) and shipped to Spain.


Figure 4 (a) SUS-CON panels demoulding, (b) cast panels (courtesy of Magnetti Building)

The dimensions of the mock-ups were 2.5 m each side, provided with a door and a window. The doors were located in the north wall and the windows in the east wall of the mock-ups. The internal walls of the mock-ups were coated with an insulating mortar and their external side was coated with a waterproof grey paint.

In order to monitor the thermal performance of the mock-ups, several probes were installed: two probes for indoor temperature (T1, T2), one temperature probe for indoor temperature on the walls (T3), one heat flux probe on the south wall (T5), one temperature probe for external temperature (T8) and one temperature probe for external temperature on the walls (T9). The windows were covered with a reflective aluminium layer in order to avoid direct irradiation on the probes and therefore overheating. The monitoring results presented in this paper correspond to the values recorded for 53 days (August/October 2015). Figure 5 shows the mock-ups during construction.


Figure 5 (a) SUS-CON panels mock-up, (b) reference panels mock-up, (c) two panels mock-ups finalized (front in the picture: SUS-CON; on the back: reference)

**Mock-up Temperature Monitoring Results**

In order to analyse the energy efficiency of the built mock-ups, different charts of temperature versus time and different charts of heat flux versus time were obtained.

As far as the results on panel mock-ups are concerned, it can be observed that during the day the indoor temperature is 0.5ºC lower in the SUS-CON panels mock-up, and overnight the indoor temperature inside the SUS-CON panels mock-up is 1.0-1.5ºC higher than the reference panels' mock-up. Both of these are considered positive from an energy efficiency point of view. Almost the same temperature oscillations between SUS-CON and reference panels mock-up were recorded. EPS layer in the panel may have had a relevant effect in the insulating properties, leading to quite similar results between SUS-CON and reference concrete. The heat flux in the SUS-CON panel mock-up resulted in slightly higher heat flux than the one obtained in the reference panel mock-up.

Figure 6 shows the trends of indoor temperature (T2) in the reference panels and SUS-CON panel mock-ups versus time.

The thermal inertia of the SUS-CON material was found to be lower than those of the reference construction material. This has obvious advantages from an energy efficiency point of view.

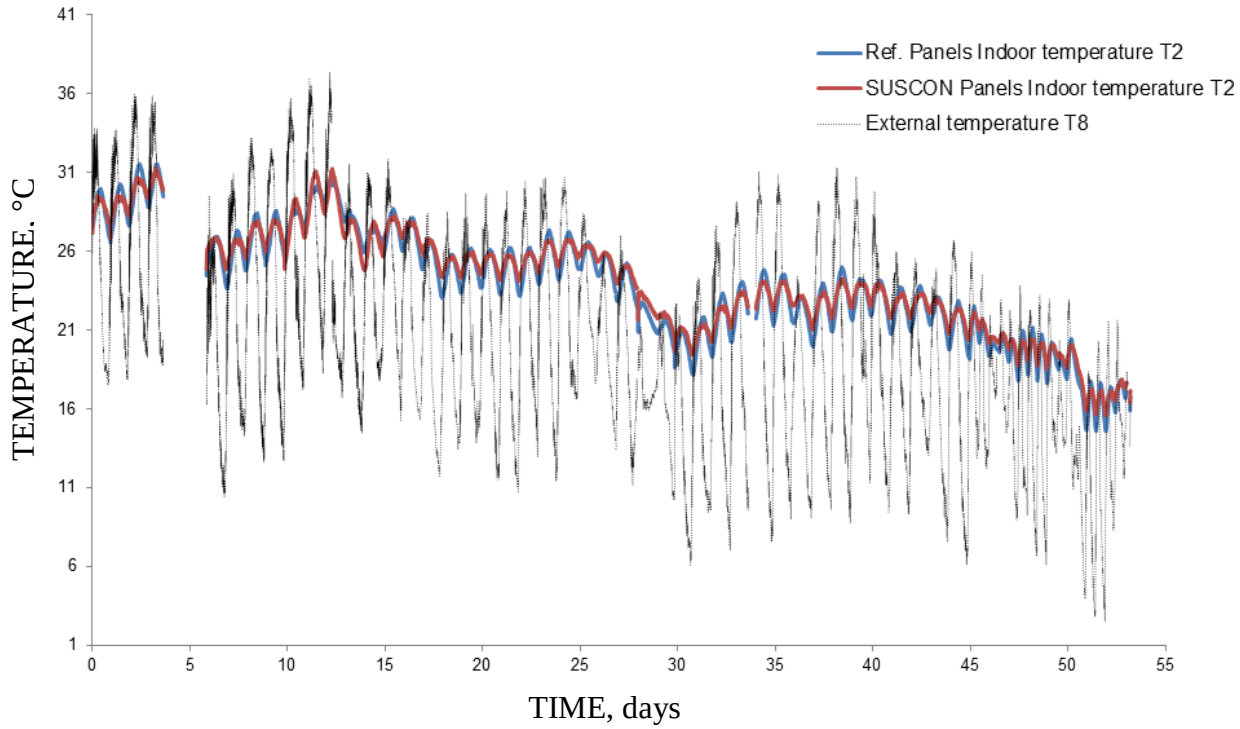


Figure 6 Temperature trends measured for at the demo site in Spain. The gap around day 5 was due to a loss of electricity

## CONCLUSIONS

The SUS-CON project was funded under an FP7 call with the objective of developing new approaches to integrate secondary resource streams in the production of building materials, for both ready-mixed and pre-cast concrete. The project was successfully completed at the end of 2015, with the construction of mock-ups in three demonstration sites in Europe. Life Cycle Analysis and Life Cycle Costs analysis pointed out that the developed material fulfils the requirements of reduced carbon footprint, reduced embodied energy, and reduced cost. Practical applications of the developed materials are building blocks, façade panels and floor screed.

In this paper, some of the results obtained with a combination of aggregate from Mixed Plastic Waste and binder from fly ash were described. Aggregates were developed and their suitability in concrete was assessed through extensive testing with Portland cement. A PFA-based alkali activated binder was developed and the compatibility of the two components (binder + aggregate) was assessed. A mix design fulfilling the technical requirements set by industrial project partners for the production of façade panels was developed, with a compressive strength of about 7 MPa, flexural strength of about 1.3 MPa and a thermal conductivity of 0.34 W/mK. Panels for the installation of a 2.5 m x 2.5 m x 2.5 m mock-up were designed and produced by Magnetti Building. SUS-CON mock-up and reference mock-up (made with Portland cement based concrete) were assembled in a demonstration park in Spain by ACCIONA and monitored over a time span of more than 50 days. Measurements of the internal and external temperature on site showed that SUS-CON material had good insulation properties, with lower thermal inertia than the reference construction materials. The industrial production of SUS-CON panels proved to be feasible with no major changes required from the current Portland cement based concrete production.

## ACKNOWLEDGEMENTS

This research was carried out in the framework of the SUS-CON "Sustainable, Innovative and Energy-Efficient Concrete, based on the Integration of All-Waste Materials" project, which has received funding from the European Union Seventh Framework Programme (FP7/2007-2013) under Grant Agreement No. 285463 (Call FP7-2011-NMP ENV-ENERGY-ICT-EeB).

## REFERENCES

1. JU C., NING Y. and PAN W. A review of interdependence of sustainable building, Environmental Impact Assessment Review, No. 56, 2016, pp. 120–127.

2. CORVAGLIA P., LARGO A. and SOUTSOS M. Sustainable, innovative and energy-efficient concrete, based on the integration of all-waste materials: the SUS-CON project International Conference on Sustainable Built Environment for Now and the Future. Hanoi, 26 - 27 March 2013.

3. VISSER J., BIGAJ A.J. and LARGO A. Editorial to the Special Issue on Sustainable concrete, HERON, Vol. 60, 2016, pp. 1–4.

4. https://www.sus-con.eu/ (visited on January 6th 2016)

5. EN 206-1 Concrete – Part 1: Specification, performance, production and conformity, European standard elaborated by the CEN/TC 104 "Concrete and related products" technical committee.

6. SOUTSOS M., BOYLE A., VINAI R., HADJIERAKLEOUS A. and BARNETT S. Factors influencing the compressive strengths of pulverised fuel ash based geopolymers, Construction and Building Materials, 2016, DOI : 10.1016/j.conbuildmat.2015.11.045

7. RAFEET A., VINAI R., SHA W. and SOUTSOS M. Alkali activated fuel ash and slag mixes: optimization study from paste to concrete building blocks, 34th Cement and Concrete Science Conference, Paper Number 179, pp. 14–17 September 2014, University of Sheffield (UK)

# ALKALI-SALINE SOIL-FLY ASH COMPOSITE MATERIALS AND ITS MECHANICAL PROPERTIES

**Haiyan Yu** **Chengshou He**

Tianjin Chengjian University

China

**L Zheng**

University of Dundee

United Kingdom

**ABSTRACT.** Saline soils, which are mainly found in the arid/semi-arid climatic areas and coastal regions, are widespread all of the world, having limited potential for cultivation. This paper presents a study explored an alternative way by using alkali activated saline soil combined with fly ash to form geopolymer to develop the building materials with ultra-low embodied energy and $CO_2$ for sustainable construction. The properties of the alkali-activated geopolymer made with saline soil – fly ash combination were evaluated. With the study on the effects of the mix proportions and process technics, the production of the geopolymer was optimised. The study indicates that the ideal conditions for the dissolution of $SiO_2$ and $Al_2O_3$ were 10M NaOH at 60°C for 24 hours. The saline soil – fly ash combination has good physical and mechanical properties and durability, which were increased with the fly ash content from 20% to 60%. XRD, FT-IR and SEM were applied to analyse the reaction mechanism and microstructures of the alkali-activated saline soil – fly ash system. After alkali-activation, depolymerisation and reconstruction of the activated silicate and aluminate formed zeolite-liked gel products and generated aluminium silicate network structures, which is the key for the performance of the material obtained. The microstructure of product varied with the fly ash content in the system, affecting the density of the products.

**Keywords:** Geopolymer, Saline soil, Fly ash, Alkali-activation, Properties.

**Dr Haiyan Yu** is Associate Dean and Professor of School of Materials Science and Engineering, Tianjin Chengjian University, Tianjin, China. His research interesting is on developing sustainable construction materials, mainly on new-type wall materials and utilization of solid wastes. He has published 21 papers in different scientific journals including 5 papers retrieved by SCI over the last 10 years.

**Dr Li Zheng** is a Research Fellow in the Concrete Technology Unit, University of Dundee.

**Mr Chengshou He** was an MSc student at School of Materials Science and Engineering, Tianjin Chengjian University, Tianjin 300384, China.

## INTRODUCTION

Saline soils, which are mainly found in the arid/semi-arid climatic areas and coastal regions, are widespread all of the world, having limited potential for cultivation [1]. While the study of the agriculture researchers focused on the cultivation issues [2, 3], the study of the civil engineers was mainly on its stabilisation in situ for infrastructure constructions [4]. Recently, researches on saline soils treated with Portland cement (PC) to improve unconfined compression strength [5] was reported. In our previous study [6], stabilised compressed earth bricks (SCEB) with high strength and water resistance were successfully produced using saline soil with proper activation pretreatment mixed with PC. The use of saline soil to produce SCEB utilises uncultivable soil thus provides a way to mitigate the farmland destruction and reduce non-renewable resources consumption. Its environmental benefits also include reduced energy consumption and $CO_2$ emission in production [7, 8]. However, as PC is a high energy consumption and $CO_2$ emission material, further reduction in embodied energy and $CO_2$ for its earth products is limited. Therefore, this study explored an alternative way by using alkali activated saline soil combined with fly ash to form geopolymer to develop the earth products with ultra-low embodied energy and $CO_2$ for sustainable construction.

## EXPERIMENTAL DETAILS

The aim of this study was to use the waste saline soil as a soil resource to produce earth products for sustainable construction through the geopolymer route. For this purpose, firstly the saline soil along the coastal area of Tianjin, China was collected and its physical and chemical properties characterised. Secondly, alkali activation of the saline soil was studied to determine a range of ideal activate conditions. Based on this, alkali activated saline soil-fly ash composite materials were produced and their properties evaluated.

### Materials

### Saline soil

The saline soil was collected along the coastal area of Tianjin, China. The samples were taken from the undisturbed layer under the surface. Stones and plant residues were removed before it was sealed in the plastic bags and brought back to the laboratory for the characterisation. The chemical compositions of the saline soil are given in Table 1. It can be seen that the oxides of the saline soil are rich in silica and alumina, which indicates that it has potential to be used as an alumina-silicate source material for the synthesis of geopolymer. Concentrations of various ions of the soluble salts of the samples were measured. The total soluble salts content ranged from 2.20% to 2.73%, in which the chloride around 1.5% and sulphate around 0.6%. According to GB50021-2009, the samples can be catalogued as medium class sub-chloride saline soil.

### Fly ash

Low-calcium fly ash obtained from Tianjin First Thermoelectric Power Station, Tianjin, China was used in this study. The chemical compositions of the fly ash are also given in Table 1. It is also rich in silica and alumina. Much research has been done on fly ash to investigate the possibilities to use it as one of the source material for Geopolymer binder [9].

Table 1 Bulk oxide composition of the saline soil and fly ash

| SAMPLE | BULK OXIDE COMPOSITION, % by mass | | | | | | | LOI, % by mass |
|---|---|---|---|---|---|---|---|---|
| | $SiO_2$ | $Al_2O_3$ | $Fe_2O_3$ | MgO | CaO | $K_2O$ | $Na_2O$ | |
| Saline Soil | 65.40 | 12.44 | 6.15 | 2.09 | 3.56 | 2.58 | 2.89 | 3.00 |
| Fly Ash | 52.32 | 32.18 | 1.57 | 1.01 | 1.67 | 0.98 | 0.38 | 3.94 |

**Alkaline solution**

Sodium hydroxide (NaOH) supplied by Tianjin Jiangtian Chemical Engineering and Technology Ltd. was in pearl form with 96% purity. It was used to prepare solutions in concentration of 5M, 10M and 15M.

Sodium silicate solution ($Na_2SiO_3$) with modulus (Ms) = 3.1-3.4, $SiO_2 \geqq 26\%$, $Na_2O \geqq 8.2\%$, and solid content 45%) supplied by Tianjin Ruitian Chemical Engineering Ltd. was used to prepare the combined alkaline solution. The ratios of sodium hydroxide and sodium silicate were 0.5, 1.0, 2.0, and 3.0 by mass.

## RESULTS AND DISCUSSION

**Alkali Activation of Saline Soil**

**Dissolution of saline soil in NaOH solution**

The nature of the reactions occurring in geopolymerisation can be summarized in three basic steps [10]: (i) Dissolution of the aluminosilicate solids to form a solution of silicate, aluminate and aluminosilicate species; (ii) Gel formation; and (iii) Polycondensation. Therefore, the increased dissolution rate of $SiO_2$ and $Al_2O_3$ from precursors will be beneficial to get the increased rate of geopolymer formation [11].

Dissolution of silicate and aluminate ions from the saline soil in 5M, 10M and 15M NaOH solutions at temperatures from 20° to 80°C, at time of 1, 6, 12 and 24 hours was measured and the results are shown in Figures 1 and 2 respectively.

The dissolution of $Si^{4+}$ and $Al^{3+}$ from the saline soil is not only relevant to is soluble contents of Si-$O_4$ and Al-$O_4$ tetrahedron but also relevant to the alkali-activating conditions, such as alkali concentration, temperature and time.

The $Si^{4+}$ dissolution increased significantly with NaOH concentration, temperature, and time in most conditions. The maximum $Si^{4+}$ dissolution reached 57mg/L with 10M NaOH treatment at both 60°C and 80°C for 24 hours. Since at 80°C the $Si^{4+}$ concentration decreased with 15M NaOH treatment from 12 to 24 hours (Figure 1d) while at 60°C it increased significantly with 10M NaOH treatment from 12 to 24 hours (Figure 1c), the ideal alkali treatment condition was thought to be 10M NaOH, 60°C for 24 hours. The $Al_2O_3$ content in saline soil was relative low compared to fly ash used (Table 1). As a result, the $Al^{3+}$ dissolution was low and the maximum

observed was 4.7mg/L with 10M NaOH treatment at both 20°C for 24 hours. $Al^{3+}$ content was found decreased with an increase in temperature, which may not reflect a reduced dissolution but most probably been consumed by the geopolymerisation reactions.

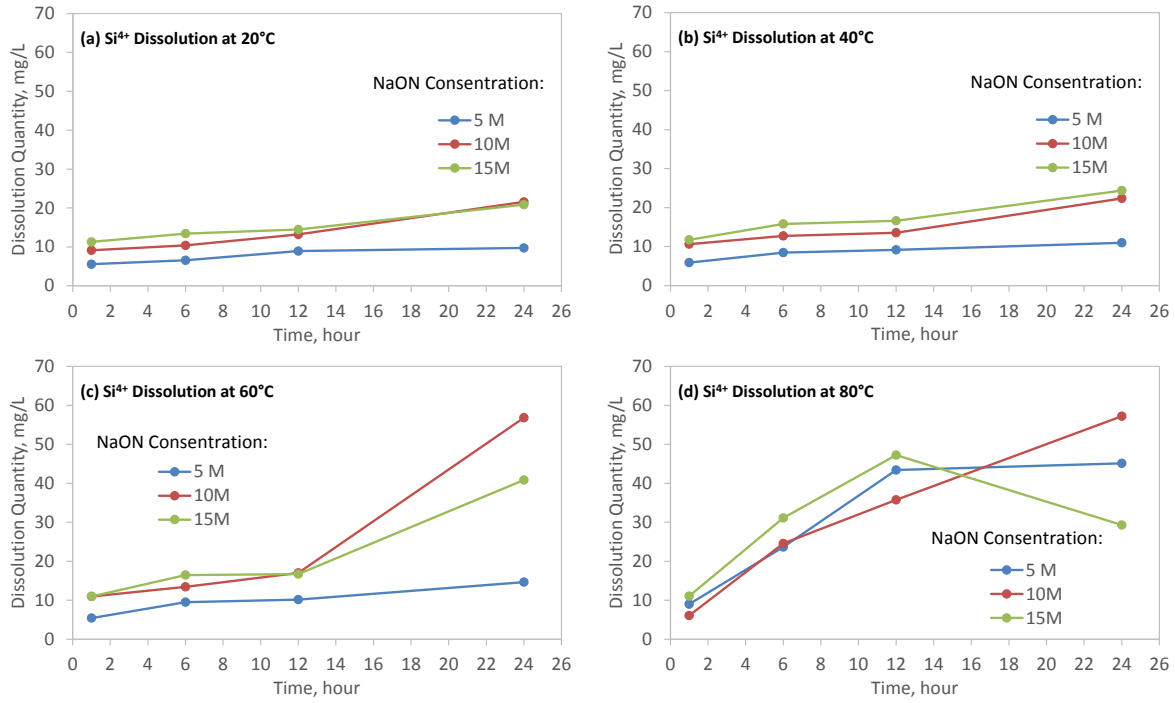


Figure 1 Effect of NaOH concentration and temperature on $Si^{4+}$ Dissolution

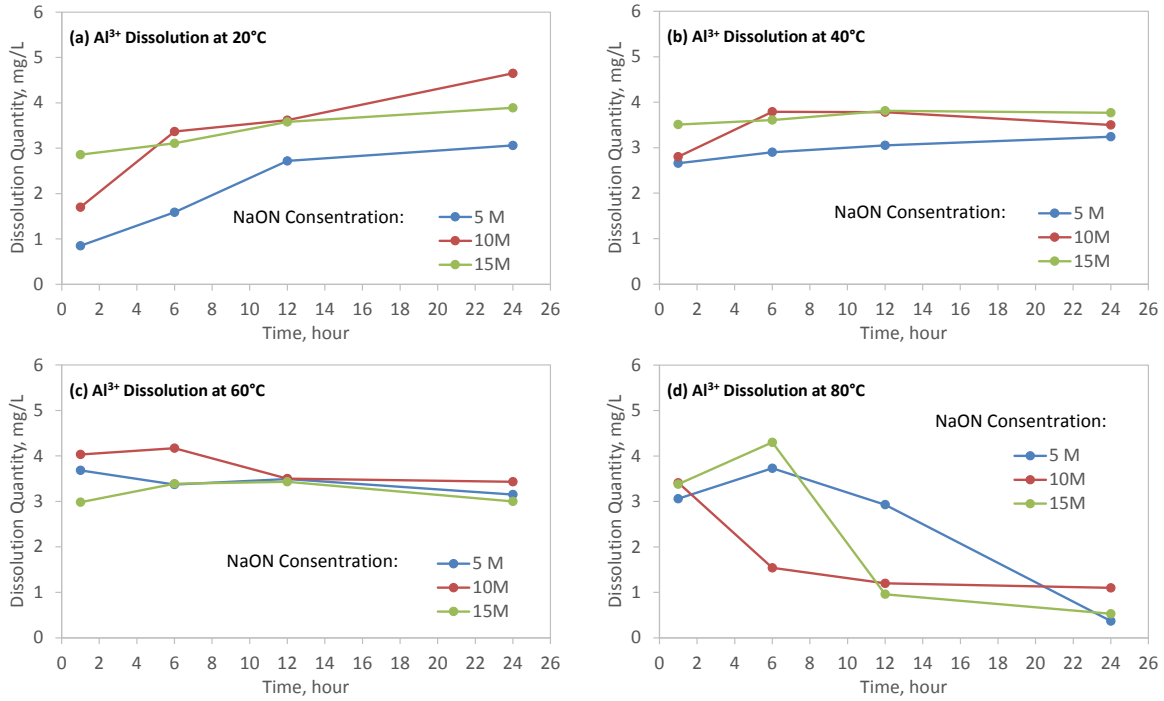


Figure 2 Effect of NaOH concentration and temperature on $Al^{3+}$ Dissolution

## XRD and FTIR analyses of saline soil after NaOH treatment

XRD diagrams for the saline soil treated for 24 hours at different temperature (with 10M NaOH) and with different NaOH concentration (at 60°C) are shown in Figure 3. The main phases of the saline soil are Quartz, Plagioclase, Calcite and Halite (NaCl). It can be seen that the peaks for Quartz, Plagioclase and Calcite decreased with increasing temperature and NaOH concentration, which indicate that these phases were damaged under the NaOH corrosion. On the other hand, the peak of NaCl increased with increasing temperature and NaOH concentration. This may due to the decomposition of Plagioclase, mainly its Albite ($NaAlSi_3O_8$) part, released extra $Na^+$ combined with $Cl^-$ released from other minerals in the saline soil to form NaCl crystal phase during sample drying. So this NaCl peak can also be thought as an indication of the effectiveness of the alkali activation. It can be seen that this NaCl peak reached the highest at 60°C with 10M NaOH. Another reason for reduced NaCl peak at 80°C and 15M NaOH may be related to the formation of $Na^+$-$OAl(OH)_3^-$ monomer, which consumed $Na^+$ in the solution. It was also observed the reduction of $Al^{3+}$ dissolution at that condition as shown in Figure 2d.

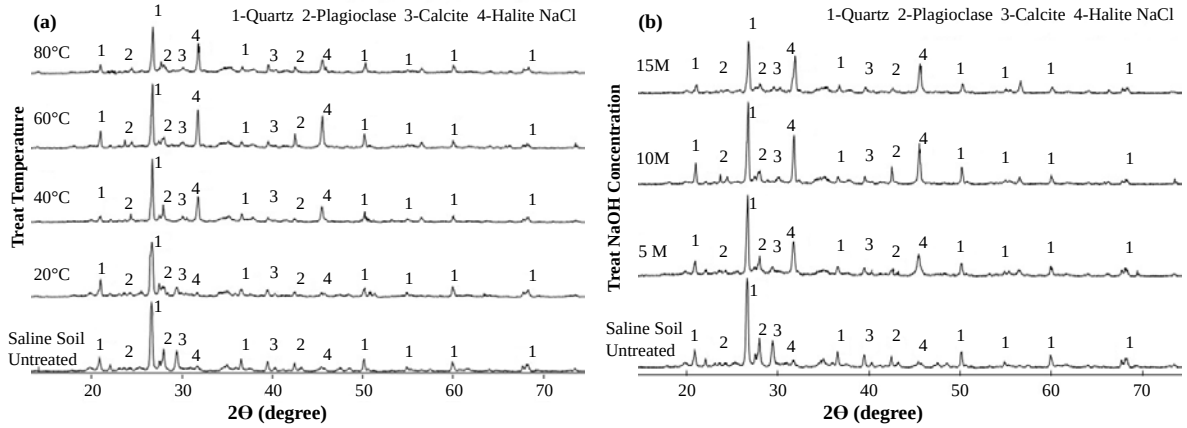


Figure 3 XRD diagrams of the saline soil treated for 24 hours (a) at different temperature with 10M NaOH, and (b) with different NaOH concentration at 60°C.

FTIR analysis was also carried out to evaluate the effects of temperature and NaOH concentration on the alkali activation of saline soil. The FTIR spectra of the saline soil treated for 24 hours at different temperature with 10M NaOH and with different NaOH concentration at 60°C are shown in Figure 4. The main absorption bands observed are at around 3630, 1620, 1440, 1005, 770 and 470 $cm^{-1}$.

The absorption band at around 3630 $cm^{-1}$ could be assigned to the OH stretching vibrations of the hydroxyls in the soil. The peak tends to vanish with the temperature increased above 40°C (Figure 4a) which indicates the decomposition of the crystalline hydroxyls in the soil structure. In Figure 4b, this peak reached minimum with 10M NaOH treatment, indicating the maximum decomposition, which is in line with the results from both dissolution test and XRD analysis.

The band observed at around 1620 $cm^{-1}$ could be H-O-H bending of binding water, which also reached minimum at 60°C with 10M NaOH treatment. Bend at 1440 $cm^{-1}$ is also due to the OH bending vibrations.

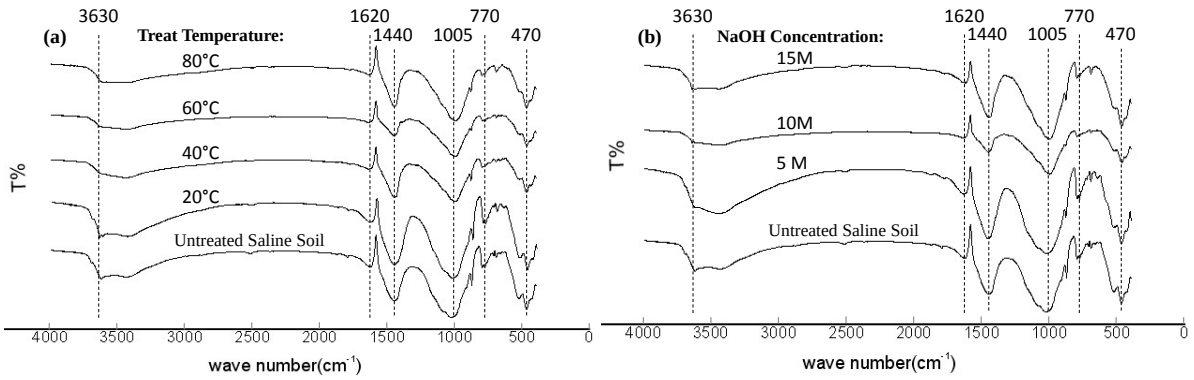


Figure 4 FTIR spectra of of the saline soil treated for 24 hours (a) at different temperature with 10M NaOH, and (b) with different NaOH concentration at 60°C.

The peak around 1005 $cm^{-1}$ is attributed to Si-O-Si(Al) asymmetric stretching vibration in $SiO_4$ molecules, which vanished after geopolymerisation reaction. The minimum of this peak was observed at 60°C with 10M NaOH treatment again.

The peaks around 770 $cm^{-1}$ and 470 $cm^{-1}$ are generated by the symmetric stretching and bending vibrations of Si-O quartz respectively. Changes of these peaks with temperature and NaOH concentration are found similar to that of quartz peaks in XRD analysis as shown in Figure 3.

It can be concluded that the mineralogical components of the saline soil decomposed with the alkali activation. The Si-O and Al-O bonds break in the reaction with $OH^-$ in the following process to form $SiO_4^{4-}$ and $AlO_4^{5-}$ [12]:

$$-Si-O-Si- \xrightarrow{OH^-} Si-O- + -Si-OH \quad (1)$$

$$-Si-O- + OH^- \longrightarrow -O-Si-OH \quad (2)$$

And similar reaction processes would also happen for Al-O-Al and Si-O-Al bonds. Therefore, it is demonstrated that the saline soil can be used as part of the precursor aluminosilicate materials for making geopolymer. It much increases the resource efficiency in use of saline soil to produce earth products for construction. The ideal conditions for the dissolution of $SiO_2$ and $Al_2O_3$ from saline soil were 10M NaOH at 60°C for 24 hours.

However, it is not like other silica and alumina precursors as metakaolin and fly ash which have been extensively studied [9, 10], the reactivity of saline soil as a precursor on its own is low. It is necessary to combine it with other silica and alumina precursors to produce the products with required mechanical properties. At present, saline soil combined with fly ash to form geopolymer was studied. Several factors affecting the reactivity of saline soil – fly ash combination as a precursor for geopolymer earth concrete product have been investigated. These include the effect of alkaline solutions and fly ash content in saline soil – fly ash combination on the properties of produced geopolymer products.

## Alkali Activated Saline Soil-Fly Ash Combination

40×40×160mm prisms were prepared following GB/T17671 (idt ISO 679) [14] for evaluation of the effects of alkaline solution and fly ash content on the strength and water resistance properties of the saline soil – fly ash combination. Alkaline solutions used are mixtures of sodium hydroxide and sodium silicate solution which demonstrated more effective than using NaOH alone in the initial trials and it is also widely used in geopolymer production [9, 10, and 13]. The NaOH/$Na_2SiO_3$ ratio by mass were controlled 0.5:1, 1:1 and 2:1. The mixture to alkali solution ratio is controlled 0.55:1 by mass. All samples were sealed with cling film, cured at 60°C for 24 hours and thereafter continued cured at room temperature to the test ages. Compressive strength of 3, 7 and 28 days in room dry condition was measured according to GB/T17671.

## Effect of alkaline solution

Effect of alkaline solution on strength of alkali activated saline soil are shown in Figure 5. It can be seen that the NaOH/$Na_2SiO_3$ combined alkaline solution was more effective for alkali activation than NaOH only solution. At 28 days, 2:1 NaOH/$Na_2SiO_3$ activated sample obtained compressive strength 2.3 times as that of reference sample.

In all cases, the strength developed with age. Significant strength increases were observed with the NaOH concentration increased from 5M to 10M. However, only minor strength increases were observed with the NaOH increased from 10M to 5M and in some cases decreases were observed.

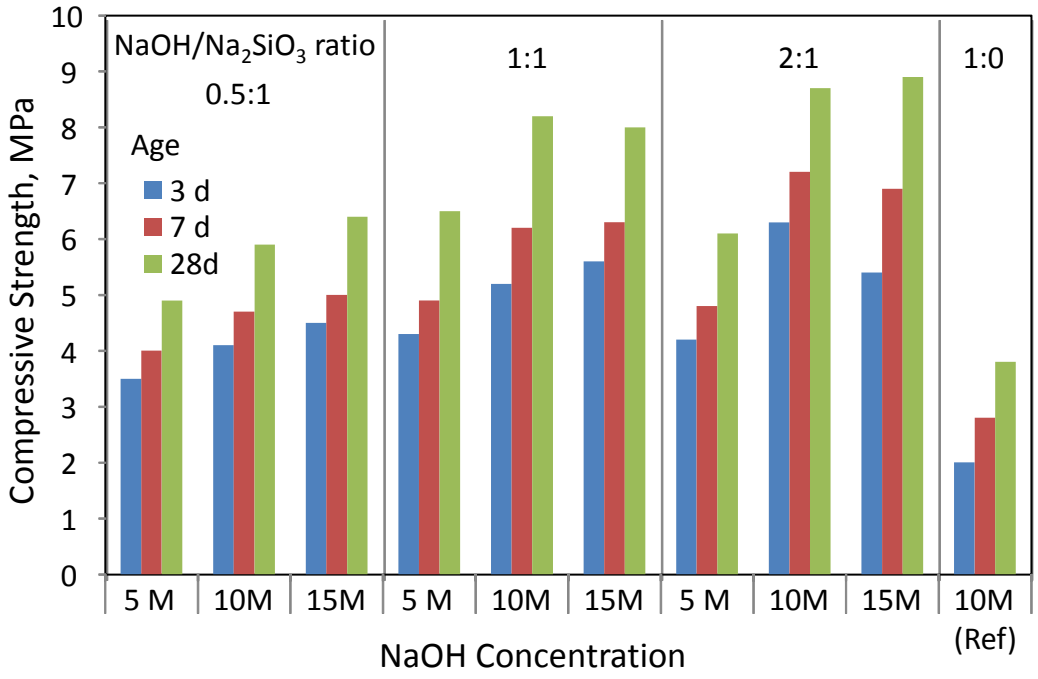


Figure 5 Effect of alkaline solution on strength of alkali activated saline soil.

The $NaOH/Na_2SiO_3$ ratio also affected the strength of alkali activated saline soil. The strength increased with increasing $NaOH/Na_2SiO_3$ ratio from 0.5:1 to 1:1, however, it only had a minor changes with the ratio increased from 1:1 to 2:1. As the consistence of the paste decreased with increasing $NaOH/Na_2SiO_3$ ratio from 1:1 to 2:1, ideal ratio for this material is suggested as 1:1.

**Effect of fly ash content**

Based on the above study, alkali activated saline soil – fly ash combination mixtures were prepared to enhance its strength and water resistance qualified for the production of earth concrete products, such as earth bricks. Fly ash in the mixtures were 0%, 20%, 40%, 60% and 100%. Conditions for alkali activation were 10M NaOH, with 1:1 $NaOH/Na_2SiO_3$ ratio, 60°C curing for 24 hours.

Wet-compressive strength after 28 days curing and then 24 hours water saturation was measured to evaluate the water resistance, which is an important property of earth concrete products [6]. Softening coefficient, *S*, was calculated as follows according to GB/T2542 [15]:

$$S = \frac{f}{F} \tag{3}$$

Where, *f* is the water saturated compressive strength after 24 hours in water saturation and *F* compressive strength in room dry condition. The strength and softening coefficient results are shown in Figure 6.

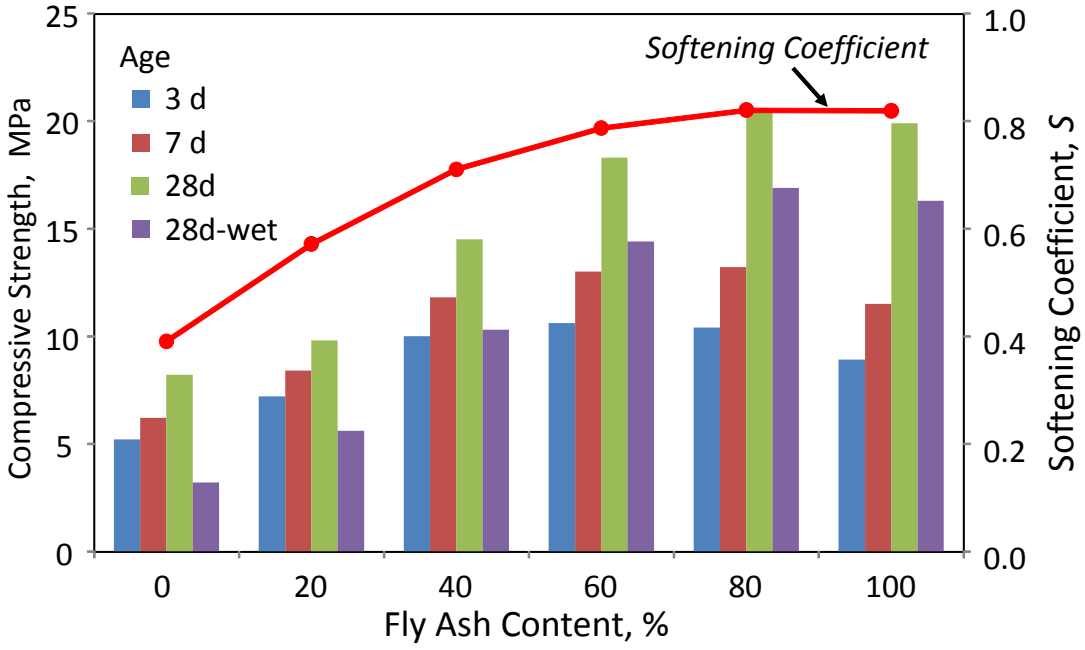


Figure 6 Effect of fly ash content on compressive strength and softening coefficient of alkali activated saline soil – fly ash combination ($NaOH/Na_2SiO_3$ ratio = 1:1)

It can be seen that single alkali activated saline soil has relative low strength ($F$ < 10 MPa at 28 days) and low water resistance ($S$ < 0.4). With the combination of fly ash, both strength and water resistance significantly increased. With 40% fly ash, the strength reached 15 MPa with the wet strength above 10 MPa and softening coefficient, $S$ > 0.7, which meet the basic requirement for earth products used in light humidity environment for non-load bearing walls and comparable to that of saline soil, lime and PC mixtures [6]. The strength, especially late age strength, and water resistance further increased with fly ash content and reached the maximum at 80% fly ash content. As the objective of this study is to maximize the use of saline soil as a resources, 40% fly ash is a proper one, which reached the similar wet strength of saline soil, lime and PC mixture, with 20% of 1:1 lime and PC [6], and clearly has much lower embodied $CO_2$ than the later.

**Microstructure of alkali activated saline soil-fly ash combination**

Microstructures of alkali activated saline soil-fly ash combinations were observed with SEM as shown in Figure 7. The observed microstructures show the raw material particles bound together by depolymerisation and reconstruction of the activated silicate and aluminate formed zeolite-liked gel products and generated aluminium silicate network structures, which is the key for the performance of the material obtained. The microstructure of product varied with the fly ash content in the system, affecting the density of the products.

In the SEM micrograph of alkali activated saline soil sample (Figure 7a), a few fibre-like crystals are identified. The microstructure shows a relative coarsening along with a high number of micro-cracks, which are probably the results of shrinkage and thermal cracking during high-temperature curing. Figure 7b shows the microstructure of alkali activated 60% saline soil and 40% fly ash combination. It can be seen that small raw material particles of different sizes and shapes are embedded in amorphous geopolymers. The microstructure is quite sound with less micro-crack in comparison with Figure 7a, which correspond to increased strength and water resistance. An image of alkali activated fly ash only is shown in Figure 7c. Unreacted sphere fly ash particles can be observed. It is a gel-bonded ash composite and amorphous geopolymers can be seen on the surface of the particles.

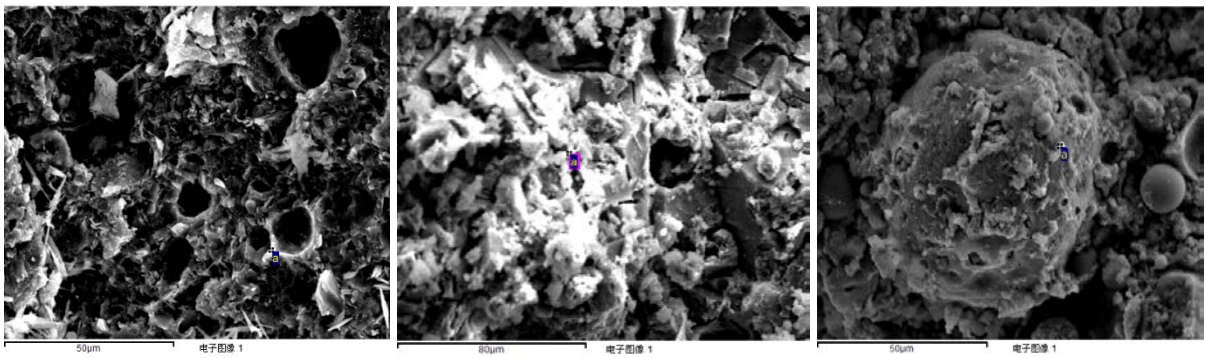

(a) 100% Saline Soil (b) 60% Saline Soil/40% Fly Ash (c) 100% Fly Ash

Figure 7 SEM images of alkali activated saline soil – fly ash combination

## CONCLUSIONS

Saline soil along the coastal area of Tianjin, China has having limited potential for cultivation, however, it can be used as a resource for the production of earth concrete products. This study explored a way to develop alkali activated saline soil – fly ash combinations for building materials with ultra-low embodied energy and $CO_2$ for sustainable construction. The results demonstrated that the saline soil has certain reactivity in alkali activation, which means it be used as part of the precursor aluminosilicate materials for making geopolymer, therefore it much increases the resource efficiency in use of saline soil to produce earth products for construction.

The ideal conditions for the dissolution of $SiO_2$ and $Al_2O_3$ from saline soil were 10M NaOH at 60°C for 24 hours. It was also demonstrated that the NaOH/$Na_2SiO_3$ combined alkaline solution was more effective than just use NaOH only. Proper NaOH/$Na_2SiO_3$ ratio in this study was 1:1. However, the reactivity of saline soil as a precursor on its own is low. It is necessary to combine it with other silica and alumina precursors to produce the products with required mechanical properties. Saline soil – fly ash combination as a precursor was proved to be a solution. Both strength and water resistance significantly increased with the addition of fly ash. With 40% fly ash, the strength and water resistance reached the basic requirements for earth concrete products used in light humidity environment for non-load bearing walls and comparable to that of saline soil, lime and PC mixtures with 20% lime+PC, much reduced the embodied $CO_2$ of the products.

Though the exact comparison of energy consumption and $CO_2$ emission are not available at the moment due to the lack of the data, it is generally accepted that the geopolymeric cement generates 5–6 times less $CO_2$ than PC [16]. Therefore, the use of geopolymer technology to make earth concrete products no doubt will be beneficial for sustainable construction with its ultra-low embodied energy and $CO_2$ characteristics.

## ACKNOWLEDGEMENTS

The support is gratefully acknowledged from Chinese National Science and Technology Supporting Programme No. 2014BAL03B03.

## REFERENCES

1. DRIESSEN P, DECKERS J. World Soil Resources Reports 94: Lecture notes on the major soils of the world. Food and Agriculture Organization of the United Nations; 2001.

2. LIU F, HUANG Z. Observations of the syngenesis and dynamic changes of coastal solonchak vegetation at Jiangsu. Acta Botanica Sinica, Vol. 22, No. 1, 1980, pp 63-66.

3. DEHAA R L, TAYLOR G R. Field-derived spectra of salinized solids and vegetation as indicators of irrigation-induced soil salinization. Remote sensing of Environment, Vol. 80, 2002, pp 406-418.

4. GAO J, WANG Y. Research progress in engineering and mechanical properties of the saline soil, Mechanics in Engineering, 2011:33(4):1-7.

5. CHEN D, LIAO Y, JIANG C, FENG X. The mechanical properties of coastal soil treated with cement. Journal of Wuhan University of Technology-Materials Science, Vol. 28, No. 6, 2013, pp 1155-60.

6. YU H, ZHENG L, YANG J, YANG L. Stabilised compressed earth bricks made with coastal solonchak. Construction and Building Materials, Vol. 77, 2015, pp 409-418.

7. OTI J E, KINUTHIA J M. Stabilised unfired clay bricks for environmental and sustainable use. Applied Clay Science, Vol.58, 2012, pp 52-59.

8. MIQUELEIZ L, RAMIREZ F, SECO A, NIDZAM R M, KINUTHIA J M, TAIR A A, GARCIA R. The use of stabilised Spanish clay soil for sustainable construction materials. Engineering Geology, Vol. 133-134, 2012, pp 9–15.

9. RATTANASAK U, CHINDAPRASIRT P. Influence of NaOH solution on the synthesis of fly ash geopolymer, Minerals Engineering, Vol. 22, 2009, pp 1073–1078.

10. DUXSON P, FERNÁNDEZ-JIMÉNEZ A, PROVIS J L, LUKEY G C, PALOMO A, VAN DEVENTER J S J. Geopolymer technology: the current state of the art. Journal of Materials Science, Vol. 42, No. 9, 2007, pp 2917-2933.

11. KONG D L Y, SANJAYAN J G. Damage behavior of geopolymer composites exposed to elevated temperatures. Cement and Concrete Composites, Vol. 30, pp 986–991.

12. XU Y Z. Salinized soil foundation. Beijing: China Construction Industry Press,1993.

13. AHMED M F, NURUDDIN M F, SHAFIQ N. Compressive Strength and Workability Characteristics of Low-Calcium Fly ash-based Self-Compacting Geopolymer Concrete, International Science Index, Vol. 5, No. 2, 2011, waste.org/Publication/3527.

14. NATIONAL QUALITY AND TECHNICAL SUPERVISION ADMINISTRATION OF THE PEOPLE'S REPUBLIC OF CHINA. GB/T17671-1999 (idt ISO 679:1989). Method of testing cements–Determination of strength. Standards Press of China; 1999.

15. GENERAL ADMINISTRATION OF QUALITY SUPERVISION, INSPECTION AND QUARANTINE OF THE PEOPLE'S REPUBLIC OF CHINA. GB/T2542-2012, Test methods for wall bricks. Beijing: Standards Press of China; 2013.

16. DAVIDOVITS J. Geopolymer chemistry & sustainable development, The Poly(sialate) terminology: a very useful and simple model for the promotion and understanding of green-chemistry, J. Davidovits (Ed.), Proceedings of the World Congress Geopolymer, Saint Quentin, France, 28 June–1 July, 2005, pp. 9–15.

# THE SUPPLY AND USE OF ELKEM MICROSILICA IN SPRAYED CONCRETE APPLICATIONS FOR CROSSRAIL PROJECTS

**J Finch**

Elkem

United Kingdom

**ABSTRACT**. Microsilica is specified globally in a wide variety of applications in order to achieve a wide variety of performance parameters. This Paper considers the implications of using a slurrified Microsilica material for use as a sprayed concrete lining within the Crossrail project. The supplying of the material, the logistics and in situ performance are considered together with the service levels expected and required. Elsewhere we consider the development and use of the "dry silo" concept and the advantages this provided on this and future projects.

**Keywords:** Rail, Silica fume, Production, Concrete

**John Finch** has held a variety of Sales Management roles during his 35 plus years in the Construction Industry. Formerly working in the sealant, grouts and waterproofing industry with Fosroc Expandite, a period was spent with Tarmac ready mix and their Special Products Division before joining Elkem in 2000. Having worked in the Oil-Well and Fibre Cement Divisions of the business, John has always been responsible for "Concrete" sales in Western Europe embracing some 8 countries. Major projects form a major part of his focus, commencing with specification activity, logistics, product supply, trials and meeting service level expectations."

## INTRODUCTION

### Introduction to Crossrail

Most people will perhaps be aware of the Crossrail project to link Reading, Berkshire in the West, with Shenfield, Essex in the East. Although such a plan was mooted as long ago as the 1940's the proposal for Crossrail as we now know it started in earnest in 2009 for completion in 2019. In between its Essex and Berkshire termination points – Crossrail comprises of some 40 stations – including 10 new ones - requiring upgrading or in some cases fully rebuilding in order to accommodate the project. In some cases existing structures have had to allow the new line to pass within 1 metre of existing infrastructure, pipework, tunnels or shafts.

At a cost of circa £15.9 billion, some 73 miles in length with some 26 miles of tunnels running through the centre of London and south toward Woolwich / Abbeywood. 8 TBM's were used tunnelling 24/7. However this brings its own issues with regard to the provision of material and Sprayed Concrete Lining.

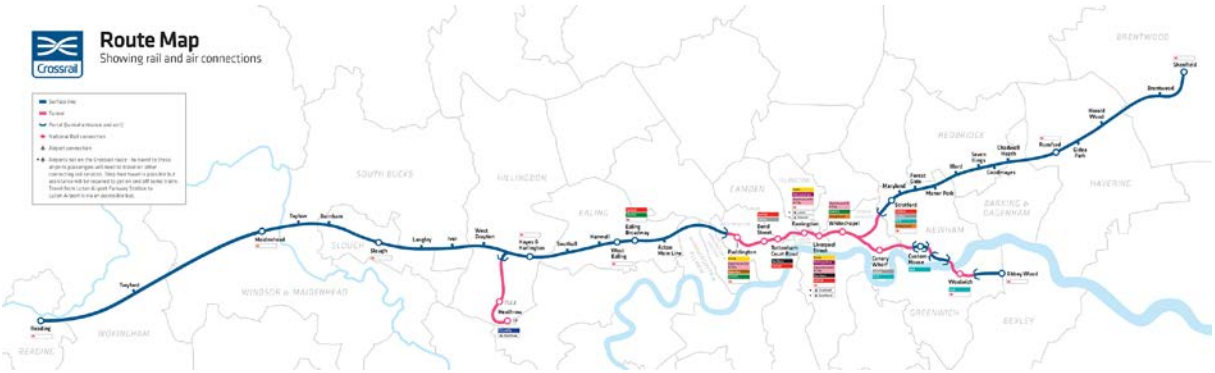


Figure 1 Map of Crossrail

## DIFFICULTIES

The provision of Microsilica into the sprayed concrete lining (SCL) is not likely to be an early issue for the Main Contractor to consider – however once on site and detailed planning starts, the sourcing of product to the specification, storing product into tanks, approved trucks, and finding a producer capable of all the above becomes a priority. The supply of product in FOR's compliant trucks with fully trained and approved drivers was an initial challenge for contractor BBMV who were the first to set up site at the eastern end of the project. Plus choosing a supplier who could meet the expected challenges of turning around orders in very swift (<24 hours in some instances) when supply was always going to be critical to achieve a continuous SCL production and installation.

The provision of a suitable >30,000 ltr storage tank to ensure easy, capable deliveries, combined with sufficient truck space is often not straightforward within some Inner London sites with an already restricted space full of production plant and waste discharge.

The sourcing of in excess of 8,000/mt of Emsac Microsilica slurry is not straightforward. Firstly the production is linked to silicon furnaces and whilst the current global market (for silicon) is strong, this can change. Market demand can fall away and other global projects can eat away at residual stock in the system. Its imperative projects give detailed outlines of what is required in order to secure volumes against a backdrop of potential market production variance – especially with high demand projects in Europe and The Middle East – stock and material availability can change very quickly and ring-fencing supply is paramount.

The supply of Emsac is from our Norwegian Plants is by ship into Boston Lincolnshire. Here we have a tank farm where the material is stored and monitored on a weekly basis - from Boston, the haulier, with dedicated 20,000 ltr capacity trucks, transfer the product to site, timed delivery slots with contractors like (BBMV) Balford Beatty Morgan Vinci ensure full compliance to Inner London route delivery restrictions. Elsewhere on the project ready mixed SCL was via Hanson ready mix in Canary Wharf / Greenwich. However site production restrictions apply to many sites leaving the only option to use a dry silo mix as backup.

## PRODUCT OFFER – DRY SILO

Some 5 years previously, Elkem had set up trial product development programme with CPI Mortars who – having recognised the potential need for having a dry silo Sprayed Concrete Lining product offer, had commenced trials. Such product development however is complex, detailed, complex and time consuming. Issues like Microsilica product type, (Densified or Undensified), flow and pumping characteristics, BET, particle size, Particle Size Distribution, rheology characteristics, settlement and segregation during material transfer, combined with final product in-situ performance - all had to be resolved. Hence it was some 2/3 years before a viable product was available.

This comprises of a sand/cement and aggregate mix + the Microsilica, compliant with EN13263, this time in powder form, ( plus other additives like steel fibres ) delivered in a silo – or the silo filled on site by truck as required. Issues such as flow characteristics, rheology, slump, strength gain are all critical with the final, as sprayed, product. In short it had to match the performance of a site mixed material (in the case of BBMV) or that supplied by a ready mix supplier the likes of Hanson (in the case of BFK). For us, as the producer of the Microsilica, the main issues were the same source supply, regularity of supply/stock, regular particle size distribution, bulk density and a were all essential in the Microsilica and our plant in Iceland was chosen as the best source of our 920ED product .

This concept is ideal for those sites – most of them – in Central London, or indeed any restricted site where access and noise restrictions apply. Since the CPI product introduction Cemex have followed suit and this concept is attracting interest in other countries and markets where such site restrictions apply.

## PRODUCT OFFER – EMSAC MICROSILICA SLURRY

Meanwhile the Microsilica slurry content saw a requirement from BFK for circa 110,000 $m^3$ of sprayed primary concrete lining, and 60,000 $m^3$ of sprayed concrete lining. This order was placed with Hanson Ready Mix with further requirements of 29,000 $m^3$ @ Farringdon and 17,500 $m^3$ @ Stepney Green with 13,500 $m^3$ @ Limmo, again Primary and secondary linings.

This mix required supply 24/7 and 363 days a year ( Christmas Day/Boxing day apart ) but even then I'm assured with full support staff still in place, "just in case". In peak production phase the Hanson plants were providing 150-225 $m^3$ per 12 hour shifts – typically spraying 3 tunnel faces at any one time.

Physically, the mix consisted of 420kg/$m^3$ of CEM1 with 12% by wet weight of Microsilica – importantly this also had a strict requirement of > 15 degrees for the mix as delivered. Results were best at an average of 18 degrees. During some cold periods this was found to be difficult to achieve so mild heating arrangements we placed in the site storage tanks in order to raise the ambient Emsac temperature. Extreme care has to be taken in order to maintain a regular pH of the material when under these storage conditions,

## SPECIFICATION AND SUPPLY.

The specification was a Microsilica to EN13263. In slurry form this calls for the producer to supply a material analysis every two weeks. Elkem Emsac slurry is produced to this specification in Norway, transferred by ship to Boston in Lincolnshire. Held in storage tanks, it's rechecked for compliance on receipt and a analysis forwarded to regular users for use within their QA monitoring system. Likewise material is delivered in dedicated trucks with trained drivers. Trucks and drivers were appraised and approved within the FORS system – deliveries were typically 24 / 36 hours after notification and from 4.00 a.m. onwards to scheduled requirements from site.

## SUPPLIER INVOLVEMENT

Elkem's involvement, as with every supplier, was never at a distance. Meetings over the period, initially in the early stages of supply, were some 12 – 20 in number. Main contractor and planning staff we contacted and, as the contract moved on, this increased with circa 10 further meetings covering aspects like, tanks, storage, delivery scheduling, delivery expectations, driver capability, material handling in cold weather, technical queries, load queries. The whole process is interactive between material supplier, contractor, sub-contractor haulier, buyer, regional production manager and technical staff.

## CONCLUSIONS

Three years in and material supply has been correct with no interruption to supply. Technical queries have been nil and the product supplied to specification throughout with no variation in source or type.

As the main element of the tunnelling construction comes to an end, additional works including Bank Station for example, see a need for further sprayed concrete applications. Both dry silo and ready mixed options remain in place and further works/projects like Northern Line upgrade works and Crossrail 2.

If any aspect of the above were to be improved upon, an earlier engagement with contracting teams would be beneficial allowing more planning time for production trials, plant trails and distribution contractor engagement.

# Theme 3

# Low Carbon Cements and Concrete

*Keynote Paper*

# USE OF CALCIUM ALUMINATE CEMENTS IN $H_2S$ BIOGENIC ENVIRONMENTS

**F Saucier**

**J Herisson**

Kerneos

France

**ABSTRACT.** $H_2S$ biogenic corrosion is a growing problem for sewer owners. Recent developments in water usage tend to increase the potential for $H_2S$ production. Rehabilitation with polymer linings such as epoxy is a popular option but the failure rates observed, by many operators, is pushing them to search for an alternative solution. Calcium aluminate cement-based mortar or concrete is one such alternative. This paper presents a broad review of the $H_2S$ biogenic corrosion process and the reasons explaining the exceptional durability of calcium aluminate cement to this deterioration process. In the absence of a standard test method, field track records remain the most reliable source of data to evaluate the biogenic corrosion of repair materials, and such references are reviewed.

**Keywords:** Calcium aluminate cement, $H_2S$, biogenic corrosion, sewer, durability.

**François Saucier** is a civil engineer working as the Senior Business Unit Director at Kerneos (formerly Lafarge) for Waste Water and Technical Concretes. He has PhD. from Laval University, Québec, Canada, on the durability of the bonding of concrete repairs. He won the 1992 ACI Wason Medal for Materials Research. After founding a concrete consulting company in Canada, he joined Lafarge in France in 1996 and has worked since then in different positions related to concrete technology.

**Jean Herisson** is an R&D engineer at the Kerneos Central Research centre near Lyon, France. He has worked on the bio deterioration of sewer networks for the past 6 years through a PhD thesis conducted at the Ifsttar (French Institute of Science and Technology for Transport, Development and Nnetworks) and now at Kerneos. He is in charge of research for subjects associated with the interaction between micro-organisms and materials.

## INTRODUCTION

Modern sewer networks are buried underground and most people do not realize the size and the complexity of this "invisible grid" spreading under each single house of a city down to sewerage treatment plants. These infrastructures are submitted to various conditions like soil movements, tree root infiltration, or corrosion. Regular maintenance is required to ensure continuous service. One condition very specific to municipal sewers is the "biogenic corrosion" due to bacteria oxidizing in sulphuric acid, the $H_2S$ gas released by the effluent.

There are several options to address biogenic corrosion problems; either upstream, by impairing $H_2S$ formation, or downstream, by venting out the $H_2S$ or using building materials resistant to biogenic corrosion. However, even within a well-designed sewer network, a rule of thumb in the industry suggests that 5% of the total length may/will suffer from biogenic corrosion. In these areas where the favourable conditions are gathered, $H_2S$- related biogenic corrosion can deteriorate metal or several millimetres per year of concrete.

Because biogenic corrosion involves an acidic attack, one option to repair corroding concrete infrastructures is to apply an acid-proof material like an epoxy or other resin-based liners. Although appealing at first sight, the application of these hydrophobic and volatile organic compound (VOC)-containing materials on confined underground moist concrete is a great challenge. Too often the practical service life of such liners is below expectations. This is why greater attention has been paid recently to the biogenic corrosion resistance of calcium aluminates cement-based concretes and mortars to rehabilitate and/or to protect sewer infrastructures.

This paper explains why calcium aluminate concrete resists biogenic corrosion while classical concrete deteriorates. After a short summary of historical evidences of field performance, the key academic studies are presented, putting in evidence the benefit of 100% calcium aluminate-based mortar to maximize biogenic corrosion resistance. Typical application methods, practical considerations and some references are presented to conclude.

## STAKES

In most European countries, the average age of sewer networks is around 50 years old and needs huge rehabilitation works; 10% of networks are above 60 years old while they have been built for 60 to 80 years [1]. Concrete remains the largest utilized building materials. The size of these assets is quite astonishing: for the UK alone, the length of sewers totals 624 200 kilometres, servicing domestic, municipal and industrial users, with about 96% of the population connected to a network. According to a 2009 study from the American Environmental Protection Agency (EPA), the 2009 expense in the USA for sewer rehabilitation was around 3.3 billion USD, which was about 50% of the worldwide market.

With greater attention being given today to water saving and quality, several highly visible mega-projects are being done – like for instance the Thames Tideway Scheme – to capture and direct all waste water to new sewerage treatment plants to reduce or eliminate rejection of untreated water in rivers. But such new projects should not hide the fact that the vast majority of the network is old and aging. Moreover, between the water saving campaigns, the more efficient house appliances and the gradual separation of rain water and septic water, the aggressiveness of the conditions have been increasing in several networks and biogenic

corrosion is seen today in locations where it has been absent for decades. As the existing asset is just too considerable to be replaced, sewer owners have no other choice than to rehabilitate corroding sewers, and choosing both durable and affordable solution is the true challenge.

## H2S BIOGENIC CORROSION PRINCIPLES

The biogenic corrosion process in a sceptic sewer is the result of a two steps ecosystem that is summarized in Figure 1. The sceptic effluent by itself is not corrosive in the absence of industrial waste: typical pH is around 7. However, it contains plenty of sulphated organic matters that could feed bacteria, causing deterioration.

The first step takes place in locations where the effluent is deprived of oxygen, allowing some strains of anaerobic bacteria to use the sulphur as their source of energy by reducing it. One result of this metabolic action is hydrogen sulphide gas (H2S). When transition times are long (little slope, low volume of effluent), some anaerobic bacteria will produce enough H2S to saturate the water and some H2S gas will be released into the air above the effluent, especially in turbulent areas like at flow direction change in manholes, wet-wells or pumping stations. As H2S gas is heavier than air, it tends to stay within the sewer system.

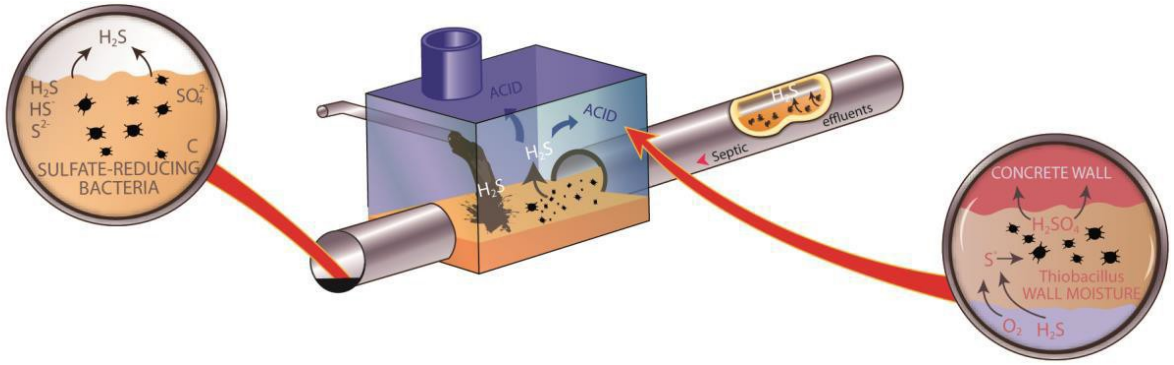


Figure 1 Principle of the biogenic corrosion ecosystem in a septic sewer

The second step takes place in the aerial part of the sewer, where other strains of aerobic bacteria develop on the moist surfaces and are using the sulphur as a source of energy by oxidizing it. The result of this oxidation is sulphuric acid ($H_2SO_4$). There are different bacteria strains which are able to oxidize the sulphur but the most deleterious are the acidophilic strains (which need acidic conditions to grow in).

New concrete surfaces have a natural pH around 12-13. At this alkaline level, micro-organisms cannot survive. Under the action of atmospheric $CO_2$, the concrete surface is gradually carbonated and when the pH reaches values around 9, some fungus and bacteria are able to start developing. Each strain of bacteria has its own ideal conditions of growth and they are able to modify their environment to get closer to these ideal conditions. In the case of colonizing concrete, bacteria try to reduce the surficial pH as a pH of 9 is quite aggressive for them.

According to the ecosystem evolution model commonly proposed in the literature [2] (Figure 2), each strain of bacteria has its own preferred pH range for growth. *Starkeya novella* (formerly

*tThiobacillus novellus*) is the first strain of bacteria to colonize the surface. It will produce some acidic metabolites that will start to decrease the surface pH. This will then permit a second strain, *Halothiobacillus neapolitanus* (formerly *Thiobacillus neapolitanus*), to start developing and lowering further the surface pH. The third strain involved is *Thiomonas intermedia* (formerly *Thiobacillus intermedius*). When the surface pH reaches values around 4-5, *Acidithiobacillus thiooxidans* (formerly *Thiobacillus thiooxidans*) can start to thrive. This bacteria, that was once named as *Thiobacillus concretivorus* [3] because of its capacity to "eat away" the concrete, will produce sulphuric acid until the surface reaches a pH of 1-2, its ideal growth conditions.

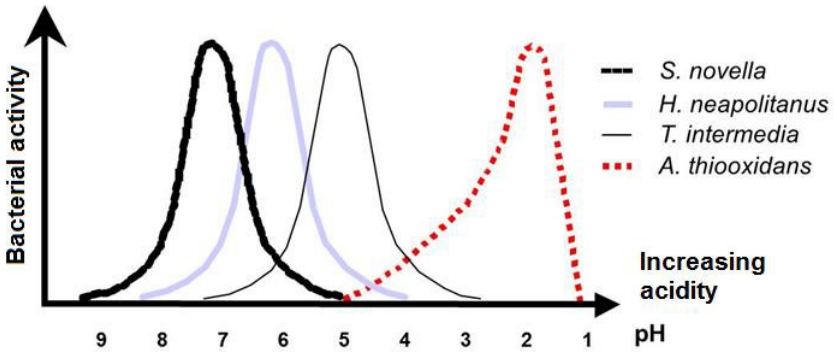


Figure 2 pH ranges for activity of bacteria of the former genus Thiobacilli [2]

Such a low pH is clearly well below what concrete and metal can withstand, and severe corrosion will occur. As long as acidophilic bacteria are supplied with nutrients, $H_2S$ and moisture, they will produce acid. The reaction of sulphuric acid with the ordinary Portland cement (PC) concrete is the dissolution of the cement paste and its re- precipitation as a soft and loose gypsum layer. Figure 3 illustrates how severe biogenic corrosion can be; the picture shows an PC concrete manhole in Egypt only 10 years after being put in service. Even if the corrosion rate is slower in less favourable conditions, the process remains the same.

Figure 3 Biogenic corrosion damage to an PC concrete manhole in Egypt after 10 years in service

It is interesting to notice that biogenic corrosion is only a surface attack. The sulphuric acid from the biofilm is immediately neutralized on contact with the alkaline cement paste, so it cannot penetrate deep in the cement paste.

When the aggregates are of a siliceous nature, only the cement paste is attacked by acid, leading to very uneven surfaces with protruding aggregates that will pull out at some point. This acid attack mechanism is quite different from the usual concrete chemical attack by chloride ions or sulphates ions that are able to penetrate within the porosity of the concrete to create pathologies inside the concrete matrix at a later time. As a matter of fact, some authors suggest that the sulphates from the gypsum formed during the biogenic corrosion process can get into solution at a later stage and then penetrate the concrete porosity to trigger further sulphate attack.

The aggressiveness of the biogenic corrosion ecosystem depends of several parameters, the most important being:

1. **Presence of anaerobic areas** allowing $H_2S$ to form. This condition happens in the sediments accumulating at the bottom of the sewer. It also happens in long pressure pumping pipes, where the available oxygen is consumed by aerobic bacteria to the point that the effluent becomes anaerobic;
2. **The concentration of the effluent**. As waste water needs to be processed nowadays, the trend is to separate the sceptic and rain waters to minimize the volume to be processed, this leads to more concentrated effluent with more organic "food" and less dissolved oxygen, allowing anaerobic conditions to develop more quickly. Reduction of parasite waters involves a reduction of the flow rate, allowing more sedimentation and thus more $H_2S$-forming zones;
3. **Long retention time**. As $H_2S$ is formed only in anaerobic conditions, slow flow and a long retention time gives more time for aerobic bacteria to consume all the available dissolved oxygen in the water, creating anaerobic conditions. The flatter the land, the less slope can be given to the sewer network, and this favours slower flow and more pumping;
4. **A favourable temperature** for bacteria growth. The temperature inside a sewer depends not only on the ambient climate but also on the temperature of the waste water which is heated by the users (shower, washing, cooking, etc.). Although a warm climate is a favourable parameter, biogenic corrosion ecosystems develop also in countries with cold climates;
5. **Moisture**: bacteria needs water to develop and cannot grow on a dry surface of concrete. Inside a sewer, since the waste water temperature is warmer than the soil around the sewer most of the time, moisture condensation is quite likely to occur in most of the aerial parts, allowing the biofilm to develop.

## $H_2S$ BIOGENIC CORROSION: A GROWING PROBLEM FOR OWNERS

When designing a sewer, the engineer considers the slopes, the diameters and the flow rates to minimise the transit time and to ensure good self-curing. Such design aims at minimizing as much as possible the $H_2S$ formation, and there are several reasons for this. For one, $H_2S$ is a deadly gas and its presence complicates the sewer maintenance operation by workers. $H_2S$ is also characterized by a strong "rotten eggs" smell triggering complaints from citizens when it escapes the network through manholes and sewer drains. Finally, $H_2S$ feeds the biogenic corrosion ecosystem, so the less $H_2S$ available, the less corrosion will develop. For all those reasons, one might believe that $H_2S$ biogenic corrosion of sewers is a well understood and mastered topic.

However, according to the author's experience, $H_2S$ biogenic corrosion appears today as a growing problem for numerous sewer owners in urban areas around the world. The same contributing factors seem to apply together in many instances:

1. To start with, the volume of water flowing in the sewers tends to reduce steadily over the years, in sewers that were built to accommodate an increasing flow over time. One reason is the efficiency of the water saving campaigns: citizens are reducing their water consumption either because of their environmental pride and/or the fact that water-meter taxation has become more common. Modern household appliances have also become much more water efficient: showers are equipped with flow reducing devices, washing machines and dishwashers use half the water they did 10 years ago. Also, because communities have to pay for cleaning the waste water and want to avoid overflow due to rain, infiltrations are being fixed and new house developments often have distinctly separate septic and rain water networks. All these efforts result in a decrease of the flow rate in sewers: this reduces the self- curing, i.e. facilitates the sedimentation of sludge (where anaerobic bacteria form $H_2S$). Lower flow rates also imply lower water levels, leaving a larger aerial part where acidophilic bacteria can thrive. All these factors contribute to a larger production of $H_2S$;
2. A second reason comes from urban sprawl. In several cities, the $H_2S$ issue was addressed for decades by a natural ventilation of the sewer system, allowing $H_2S$ to escape into the atmosphere rather than feeding the bacteria. But as a city grows, new houses are built close to the natural vents; citizens complain of foul sewer odour and the simplest solution is to seal the nearby vents. To solve people's odour complaints, $H_2S$ is kept inside the sewer and increases the biogenic corrosion potential;
3. Another consequence of the urban sprawl is the choice to close small local sewerage treatment plants (STP) and to collect and transport all the sewerage water tos mega-STPs far from the city centre. This longer displacement of the sewerage water often involves pumping in long pressurized mains where the water is rapidly deprived of oxygen and permits the formation of $H_2S$ during transportation. When pumped water arrives at the release point, $H_2S$ is released in quantity.

There are no two sewer systems identical and these contributing factors combine in different ways in each location. But the same global trend seems to emerge in many countries: more severe biogenic corrosion is observed today than in previous decades.

One option to fix biogenic corrosion problems is to repair the corroding concrete with an acid-proof lining. Different polymers, like epoxy and polyurethane, can be sprayed or applied inside a corroding sewer to stop the damage from the bacteria-borne sulphuric acid. Although these materials can resist pure sulphuric acid, they are hydrophobic materials and it is at least a great challenge to obtain a flawless lining with durable bonding onto moist concrete. Applying the appropriate concrete drying protocol in the harsh environment of a live sewer is often just not possible, and ensuring an acid-tight membrane with not a single flaw requires a great deal of care. As a result, the rate of failure observed by many owners is too high to be acceptable.

As shown in Figure 4, typical polymer lining failure comes either from debonding or from the presence of flaws in the membrane (pin-holes, bubbles, cracks, breaks, leaking joints) permitting the ingress of bacteria-borne sulphuric acid to the substrate. As the bacteria are able to lower the pH to as low as 1, it is literally pure acid coming in contact with metal and concrete, creating rapid, disruptive corrosion. The reaction of sulphuric acid with Portland cement paste creates the formation of wet gypsum which swells with enough pressure to burst the membrane.

Figure 4 Example of polymer lining failures under $H_2S$ biogenic corrosion conditions. Top left: debonded lining inside a pumping station (USA); top right: damage to an epoxy coated inlet channel (Australia); bottom left: polymer lining perforated in many locations by swelling concrete underneath (Australia); bottom right: polymer lining having failed to protect a manhole from $H_2S$ corrosion (USA)

Hopefully, there are other strategies to address $H_2S$ biogenic corrosion beyond the epoxy and inert linings:

- A chemical reactant, such as calcium nitrate, can be continuously added to the sewerage water to impair the formation of $H_2S$;
- Active ventilation through odour treatment units;
- Injection of compressed air in pressurized mains to prevent the anaerobic condition developing.

These three methods are efficient but they involve the continuous operation of mechanical equipment which requires energy and consumable supplies.

It is in that context that attention is being given today to calcium aluminate cement because of its exceptional resistance to $H_2S$ biogenic corrosion. Calcium aluminate cement is a speciality material utilized largely for making "technical mortars" and also in the refractory world, but its biogenic corrosion resistance properties are still little known. It is expounded and explained hereafter.

## CALCIUM ALUMINATE RESISTANCE TO $H_2S$ BIOGENIC CORROSION: HISTORICAL REMINDER

Calcium aluminate cement (CAC) was first patented in 1908 by Lafarge and sold under the brand "Ciment Fondu®". Today there is a complete range of CACs covering a broad spectrum of chemical composition. In a nutshell, CACs are speciality cements with a different chemistry and mineralogy to ordinary Portland cement (PC), and this difference in composition implies also quite different properties, often little known in the building industry [4, 5]. One of these properties is resistance to $H_2S$ biogenic corrosion. The first mention of CAC utilized in sewers is dated 1933 in Malaysia and Singapore.

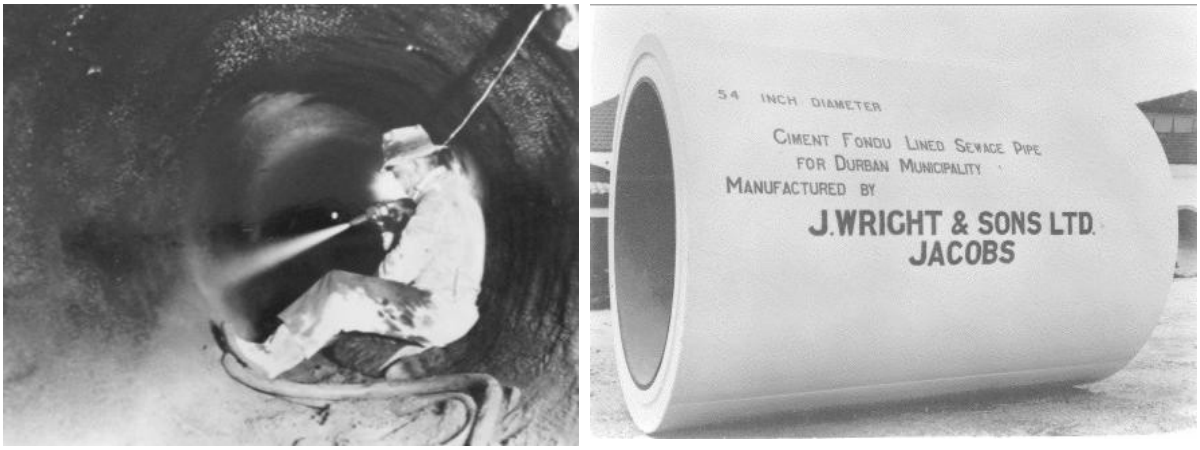


Figure 5 Left: Sewer relined with gunited Ciment Fondu® in Perth (Australia). Right: Precast concrete sewer pipe made in Durban (South Africa) in the 1960s

Figure 5 left shows on-going repairs of a sewer in the Perth area, Australia, where Ciment Fondu® mortar is being applied by dry shotcrete inside a sewer to protect the underlying concrete. The estimated date is in the 1950s. Although not much detailed information can be found for such old applications, Robson [6] mentioned already in 1962 that CAC is regularly utilized to coat concrete pipes or to repair biogenic corrosion-damaged sewers.

Figure 5 right shows a precast concrete sewer pipe made in South Africa in the 1960s. The internal diameter is 1350 mm and it is protected from biogenic corrosion by a 25 mm internal coating of Ciment Fondu® mortar. Around 30 km of such pipes were installed between 1955 and 1964 in the Durban area. An inspection conducted 31 years after commissioning has shown no evidence of corrosion.

In 1977, the French ductile iron pipe maker Saint-Gobain Pont-à-Mousson decided to introduce pipes specifically for sewerage, with a calcium aluminate mortar lining inside (Figure 6). This created a new standard and the current European Standard EN-598 permits only the use of either calcium aluminate mortar or of epoxy for ductile iron sewer pipes.

Figure 6 Saint-Gobain Pont-à-Mousson (France) pipes dedicated for sewerage transport with calcium aluminate mortar lining inside

In 1991, a new step was reached with the commercialization of a 100% calcium aluminate mortar. It was introduced in the USA under the brand SewperCoat® as a repair material to rehabilitate sewer infrastructures severely damaged by $H_2S$ biogenic corrosion. Contrary to the previous sewer applications, where calcium aluminate cement was combined with natural aggregates, this new class of material is composed only of calcium aluminate Calcium aluminate cement is combined with calcium aluminate aggregates to achieve a 100% calcium aluminate material. Figure 7 shows a typical calcium aluminate clinker block that is either milled to make cement or crushed to make aggregates. By combining these two fraction sizes, a unique type of repair material is obtained.

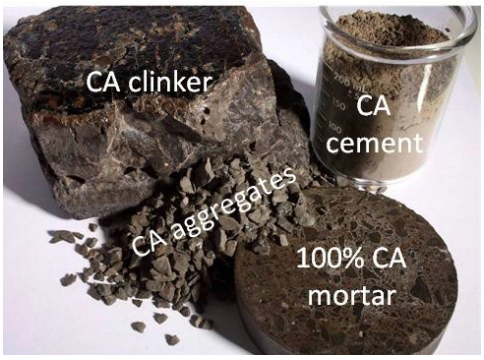


Figure 7 Raw materials used to create a 100% calcium aluminate mortar

## THE SCIENCE BEHIND CALCIUM ALUMINATE'S RESISTANCE TO BIOGENIC CORROSION

The academic study of $H_2S$ biogenic corrosion is quite challenging because it is about observing and understanding a microscopic living ecosystem. Moreover, the interaction between this ecosystem and the building materials requires a pluri-disciplinary approach.

Hamburg Simulation Chamber

One important contribution has been made by the team of Professor Bock of Hamburg University, in the 1990s. This team developed a biogenic simulation chamber where the sewer ecosystem was reproduced in order to test building material specimens in comparable conditions.

Figure 8 shows the principle of the Hamburg simulation chamber. It is a sealed volume of about 1 $m^3$ where the air is saturated with moisture and the temperature is maintained at 30°C. Concrete specimens are introduced into the chamber, a variety of bacteria found in sewers are sprayed on the specimens and then $H_2S$ starts to be fed along with nutrients for the bacteria. Even with ideal conditions, it takes a few months to develop severely corroding conditions because bacteria need first to colonize the specimen's surface to start decreasing the pH.

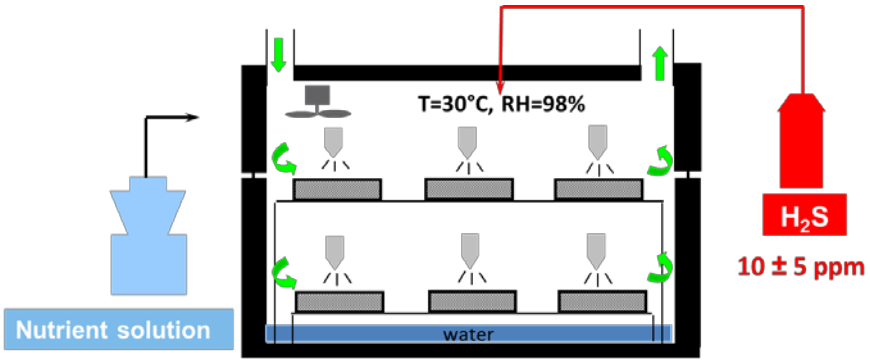


Figure 8 Schematic representation of the Hamburg chamber

The Hamburg simulation chamber permitted various building materials to be exposed to a very severe but realistic cycle of biogenic corrosion. A typical test cycle lasted one year. A comparison with companion specimens exposed in a live corroding sewer in the Hamburg area gave the correlation that one year in the Hamburg Simulation Chamber was equivalent to 24 years of exposure in the live reference sewer.

Figure 9 compares the weight loss over time for four series of mortar specimens exposed in the Hamburg chamber [7]. The first two series, made of CEM I and CEM III, were completely corroded within one year in the simulation chamber. The third series, made of calcium aluminate cement with natural sand, shown a weight loss around 45% after the same year of exposure. The fourth series, made of 100% calcium aluminate mortar, i.e. calcium aluminate cement combined with calcium aluminate aggregates, exposed to the very same conditions, showed only 16% of weight loss after one year. This set of result shows that there is a drastic difference of behaviour between PC and CAC concretes when exposed to the same $H_2S$ deleterious environment.

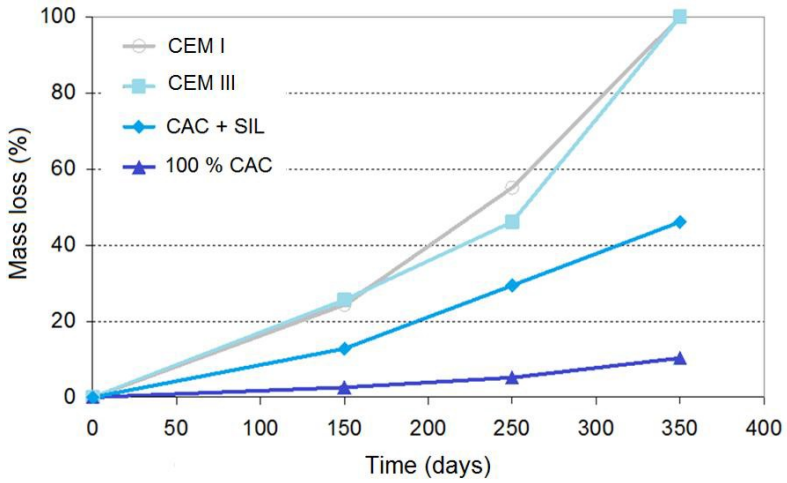


Figure 9 Weight loss over time of four cementitious materials exposed in the Hamburg Simulation Chamber for one year

In parallel with the monitoring of weight loss, each specimen's pH was also measured. Figure 10 shows the surface pH evolution over time for the same specimens shown in Figure 9. It can be seen that for the PC specimens, the bacterial activity lowers the pH to nearly 2 within 6 months and reaches 1 after one year. The behaviour on the CAC based specimens is quite different. For those made with silica sand, which lost 45% weight in one year, the pH remains at 3 for a few months before decreasing to 2. For the specimens made with 100% of calcium aluminates, which lost only 16% weight in one year in the Hamburg Simulation Chamber, the pH reached 3 after 6 months but then did not get any lower. In fact, this stabilization of the pH at around 3 is very characteristic of the capacity of calcium aluminate to interfere with the bacteria metabolism to stop the production of sulphuric acid. This mechanism is detailed hereafter.

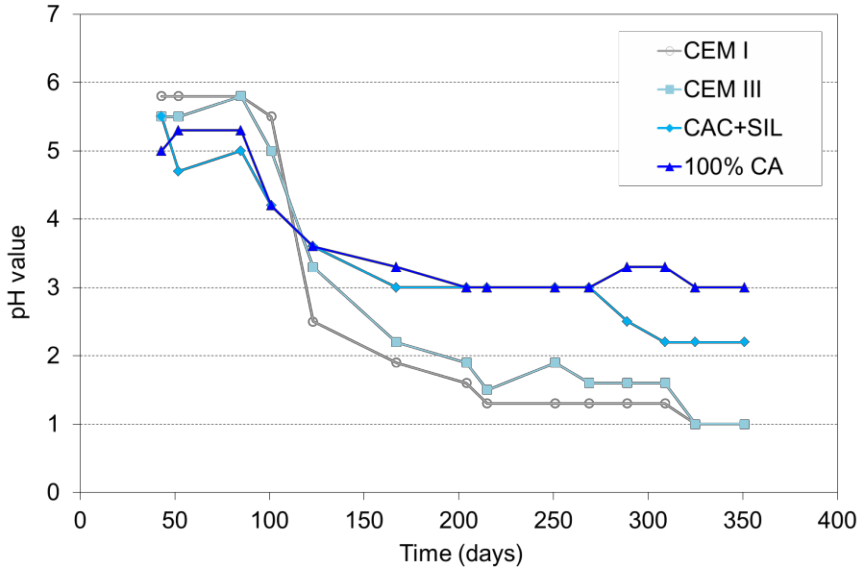


Figure 10 Surface pH evolution over time of four cementitious materials exposed in the Hamburg Simulation Chamber for one year

The reason for the drastic difference between PC and CAC exposed to biogenic corrosion lies in the difference of chemical composition. With CAC, at least 3 different mechanisms contribute to the much better resistance to biogenic corrosion:

1. The first barrier is the **larger neutralization capacity** of CAC vs. PC; one gram of CAC can neutralize around 40% more acid than a gram of PC. This means that for a given production of acid by the biofilm, a CAC concrete will last longer. Moreover, when the concrete is 100% calcium aluminate, the whole matrix neutralizes acid, and not only the cement part (siliceous aggregates are inert to sulphuric acid). The higher neutralization capacity is a positive factor for durability, but it does not explain fully the differences shown in Figures 9 and 10;
2. The second barrier is due to the **precipitation of a layer of alumina gel** ($AH_3$ in cement chemistry notation) when the surface pH get below 10. At that pH, the calcium aluminate hydrates dissociates: on one hand the calcium reacts with the sulphuric acid to form some gypsum; on the other hand, aluminate precipitates as alumina gel. $AH_3$ is a stable compound down to a pH of 4 and it will form an acid-resistant barrier as long as the surface pH is not lowered below 3-4 by the bacterial activity;
3. The third barrier is the **bacteriostatic effect** locally activated when the surface reaches pH values less than 3-4. At this level, the alumina gel is no longer stable and will dissolve, liberating aluminium ions. These aluminium ions will accumulate in the thin biofilm. Once the concentration reaches the 300-500 ppm level, it will produce a bacteriostatic effect on bacterial metabolism, i.e. bacteria will reach a "stasis" state and will stop being active. In other word, bacteria will stop oxidizing the sulphur from the $H_2S$ to produce more acid, and the pH will stop decreasing. This third barrier – the bacteriostatic effect - is the most important and it explains largely the calcium aluminate's capacity to resist severe biogenic corrosion. Rather than trying to resist a continuous flow of acid, a calcium aluminate surface stops the production of acid, putting the corrosion process on hold.

This triple barrier mechanism does mean that some calcium aluminate hydrates are used up in the process, but the rate is slow enough to permit a long lasting performance. What Figures 9 and 10 are showing is that the mechanism is much more efficient when the whole surface presents a uniform chemistry, i.e. when both the cement paste and the aggregates are of the same chemistry. A possible explanation is that, at the scale of bacteria, sand grains (which are not liberating aluminium ions) are acting like "virgin islands" where they can produce sulphuric acid without being slowed down by the bacteriostatic effect. The sulphuric acid produced at the sand grain surface can then run off onto the surrounding cement paste and corrode it. As it was explained, calcium aluminate is not acid-proof, so if pure acid runs off, it will corrode CAC. But because 100% calcium aluminate concrete has the same chemistry throughout, there are no "virgin islands" where the bacteria can produce sulphuric acid without being stopped when the pH reaches the 3-4 threshold. It is this capacity to stop acid production that is the key mechanism.

Strasbourg University Study

A study run at the Strasbourg University in 2006-2007 [8] looked at the impact of aluminium ions on the metabolism of *Acidithiobacillus thiooxidans*. In fact, while aluminium ions are known for their metabolic effect on several bacteria strains, it was not established if *Acidithiobacillus thiooxidans* was sensitive to this specific ion.

Bacteria were grown in different culture mediums and then were exposed to a large range of aluminium ions concentrations. With one culture medium, the threshold to observe the bacteriostatic effect was around 350 ppm. With a second culture medium, the threshold was 600 ppm. Such a concentration can seem quite high but it must be kept in mind that the bacteria live at the surface of concrete in a very thin biofilm (not visible to the naked eye). Thus the quantity of aluminium ions required to reach the bacteriostatic threshold inside the biofilm remains very limited.

IFSTTAR Study

From 2010 to 2013, a four year research program about biogenic corrosion in sewers was run at the French institute IFSTTAR (formerly Laboratoire des Ponts et Chaussées (LCPC)). It provided new findings highlighting the difference between PC and CAC exposed to biogenic corrosion [9]. For instance, abiotic tests (i.e. chemical tests without bacteria) were run to study the $H_2S$ affinity with cement. It has been shown [9-11] that a calcium aluminate surface has a lower chemical affinity with $H_2S$ than an PC surface. Thus, for a given time of exposure, less sulphur deposit forms on a CAC surface. As it is the sulphur that bacteria oxidize, less sulphur results in less acid formation.

The IFSTTAR study was also able to make additional measurements, on *in situ* specimens, of the aluminium threshold that inhibits bacteria growth [9, 10, 12]. The mortar specimens were hung in the sewer by hollow PVC tubes that filled with water from condensation, and this water was in contact with the mortar. Every four months, specimens were inspected, and the condensed water inside the tubes was analysed for the activity of bacteria and aluminium ions content. Figure 11 shows this relationship between the ATP content – a tracker of bacteria activity – and the aluminium content. With that data set, the threshold for bacteriostatic effect is around 350 ppm, confirming the results obtained by the study at Strasbourg University.

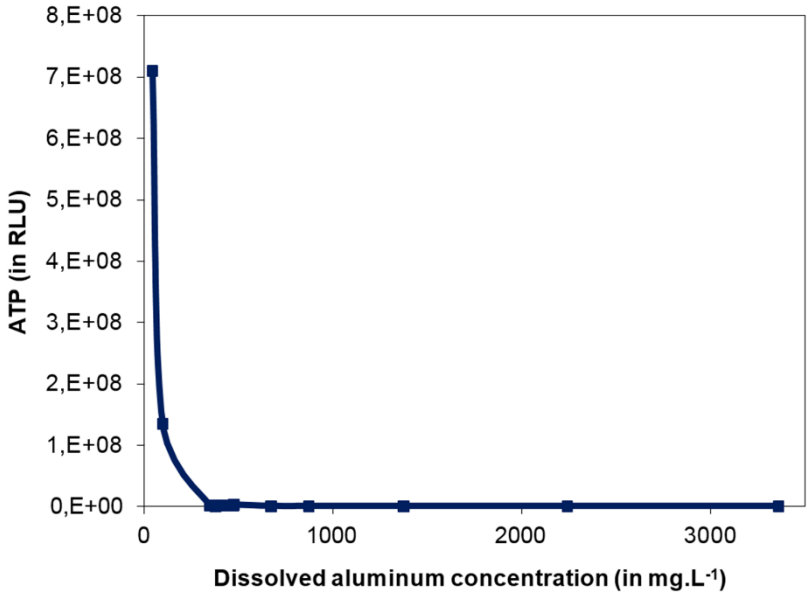


Figure 11 Bacterial activity in relation to total dissolved aluminium concentration

During the IFSTTAR study, specimens exposed to biogenic corrosion were observed with scanning electron microscopy [9,10] (Figure 12). This showed that calcium aluminate specimens were covered with a dense and smooth layer of a mineral compound, which proved to be $AH_3$ once analysed. The presence of this $AH_3$ layer confirms the mechanism described previously and gives a better understanding of how the alumina gel can clog the porosity and reduce the penetration of aggressive compounds into the cement matrix. Also, the smooth appearance of this layer led to the conclusion that it is not favourable for good bonding of the bacteria biofilm. While the key role of the $AH_3$ layer is to cause the bacteriostatic effect, it probably contributes in several ways to the overall excellent biogenic corrosion resistance.

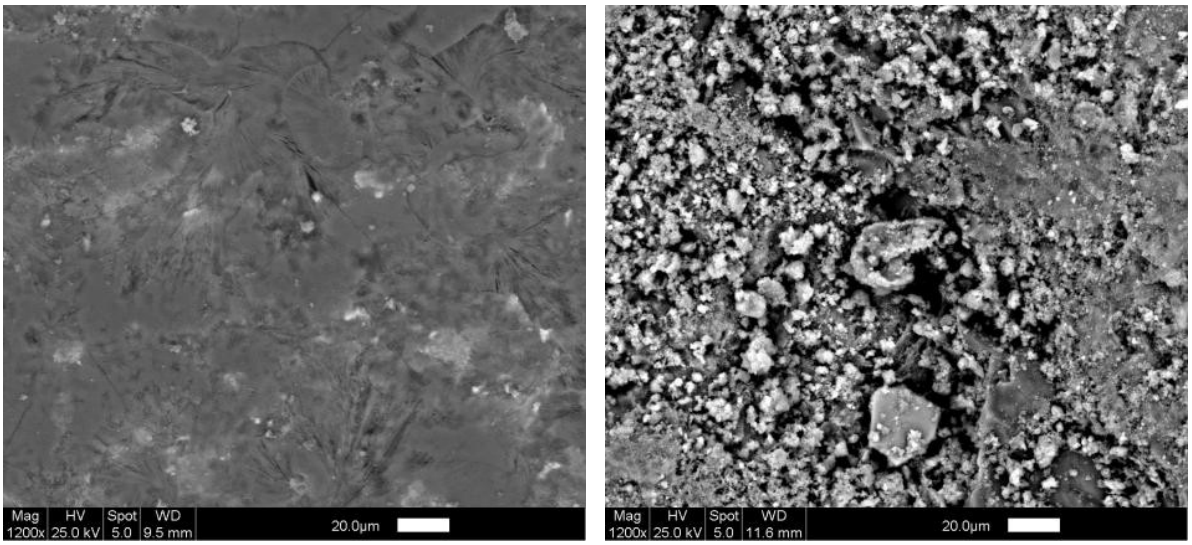


Figure 12: Scanning Electron Microscope observation of specimens exposed to biogenic corrosion: left: Surface of a 100% CA mortar smoothed by the $AH_3$ layer; right: surface of PC mortar specimens showing a typical asperous surface

Study of the deterioration layer

As seen before, biogenic acid attack leads to the formation of a deterioration layer composed mainly of gypsum. A recent study [13] conducted on pipes based on Blast Furnace Slag cement (BFSC) and CAC cement associated with siliceous sand show a clear difference between these two materials after an exposure to their Biogenic Acid Concrete Test (BAC-Test).

This BAC-test consists in inoculating real pipes segments with an activated sludge coming from an urban wastewater treatment plant and trickling a feeding solution containing a safe reduced sulphur source over the inoculated surface in order to select sulphur-oxidizing activity. After 107 days of exposure a clear difference between the two materials was observed (Table 1) in terms of deterioration depth, of acid production and of composition of the deterioration layer. The first two parameters confirm that acid production is slower on CAC surface and the last one gives new facets of the mechanism. Interestingly, secondary ettringite is observed on BFSC in association with cracks while there are no cracks and apparently no secondary ettringite on CAC lining but instead a presence of $AH_3$. In that experiment, absence of gypsum is attributed to a too low residence time of the trickling solution. Another experiment carried out with another sulphur source and with zones not saturated with water enabled higher sulphuric acid production and gypsum formation.

Table 1 Main conclusions after 107 days of exposure to the BAC-test [13].

| | BFSC LINING WITH SILICEOUS SAND | CAC LINING WITH SILICEOUS SAND |
|---|---|---|
| Deterioration depth after 107 days of exposure | 700 µm | 150 µm |
| Observed acid production | 135 µm/mol$H^+$/$m^2$ | 32 µm/mol$H^+$/$m^2$ |
| Description of the surface exposed to biogenic acid | Intense cracking of the outer zone of the paste layer because of the precipitation of secondary ettringite | Observation of an amorphous layer on the surface of the material. Surface was decalcified, enriched in sulphur and mainly composed of $AH_3$ |
| Composition of the sound material | Ettringite, portlandite, C-S-H, anhydrous phases ($C_3S$ and merwinite) | Typical anhydrous (CA, $C_{12}A_7$) and hydrated ($C_3AH_6$, $AH_3$) crystallized phases |
| Composition of the deteriorated layer | Secondary ettringite, calcite, residual anhydrous grains ($C_3S$ and merwinite) | $AH_3$ (crystallized and amorphous forms) |

Mortar specimens exposed *in situ* during the IFSTTAR study were observed with a scanning electron microscope after an exposure of four years to characterize the deterioration layer formed. Specimen based on PC with siliceous sand had lost a mass of around 35%.

Deteriorated surface (Figure 13) is mainly composed of swelling gypsum (in violet/blue on the right part of Figure 13), under which a decalcified layer (in pink on the right part of Figure 13) is observed with a presence of secondary ettringite inside the matrix.

The numerous cracks inside the matrix are most probably generated by the crystallization pressure of this secondary ettringite. Observations are consistent with the description of mechanisms done in literature [14, 15].

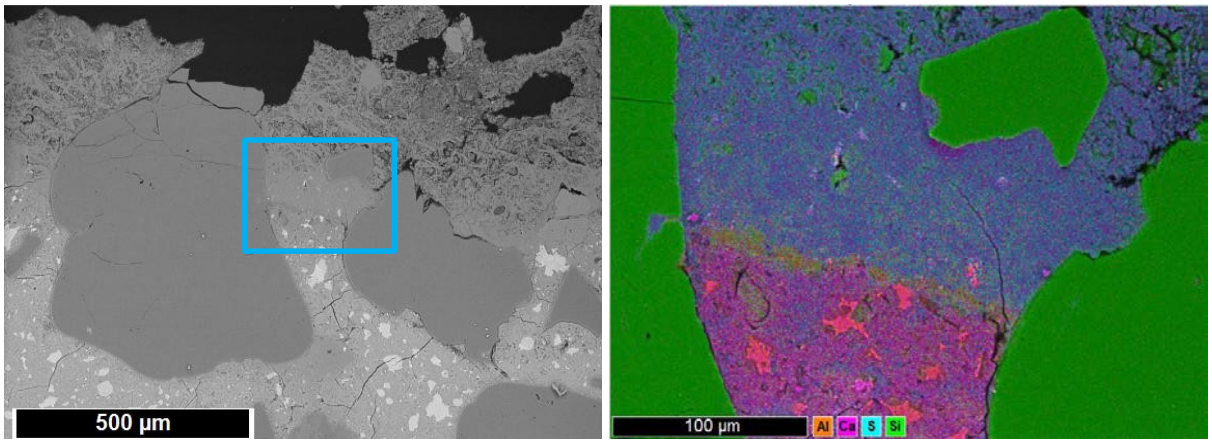


Figure 13 Scanning electron microscopic observation of the surface of an PC mortar exposed during four years in a real sewer network and elemental mapping associated to the identified selection. Initial surface is located on top.

Deterioration layer formed on mortar based on CAC with siliceous sand (Figure 14) is composed of a mix of gypsum (in violet/blue on the right part of Figure 14) and $AH_3$ (in light brown on the right of Figure 14) that have cohesive properties. There are very few cracks located at the surface only and no secondary ettringite observed.

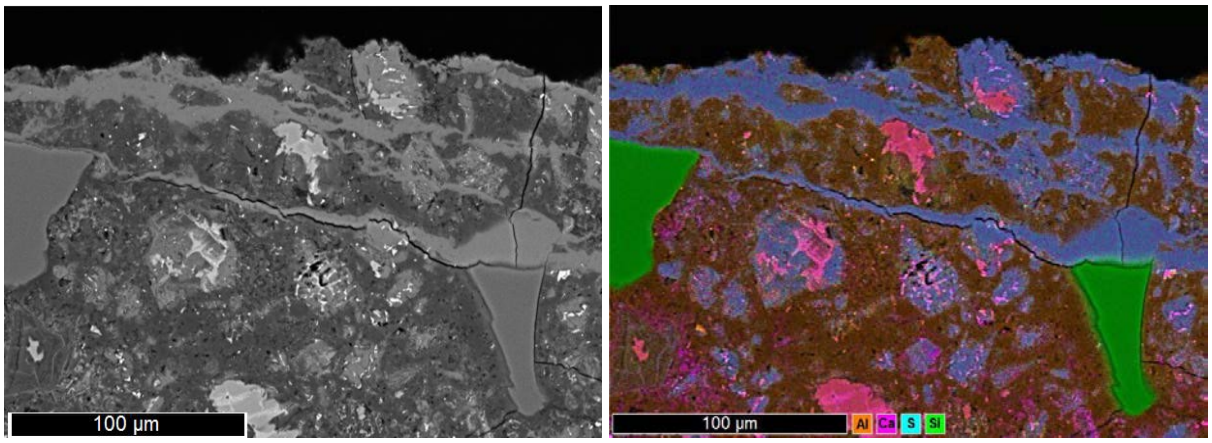


Figure 14 Scanning electron microscopic observation of the surface of a CAC mortar exposed during four years in a real sewer network, and elemental mapping associated. Initial surface is located on top.

The main difference between the two mortars is the cohesiveness of the deterioration layer. While a fluffy and soft layer is seen on the PC material, for the CAC based specimen, due to the precipitation of $AH_3$, the surface stays dense and cohesive, limiting the access to biogenic acid. Interlacing of $AH_3$ and gypsum (Figure 15) acts as reservoir of aluminium ions in the interaction with microorganisms. This association maintains the biostatic effect of the deterioration layer formed with CAC based mortars.

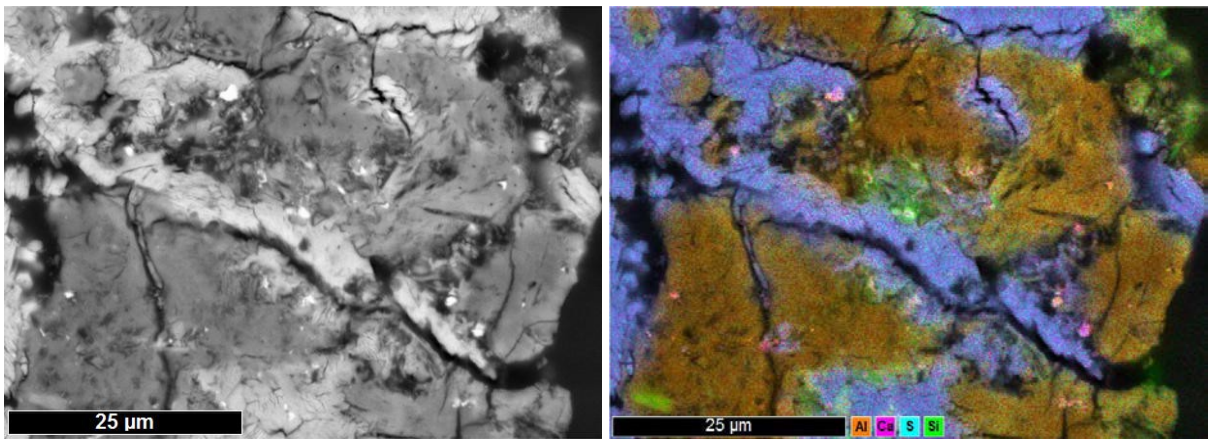


Figure 15 Observation of the good intermingling of $AH_3$ and gypsum in the deterioration layer of CAC mortar exposed during four years in a real sewer network.

As there is no secondary ettringite formed in CAC material when exposed to biogenic acid environment, there is no constrains generated and so no cracks leading to deterioration. Deterioration products are formed on the surface only and the precipitation of $AH_3$ densify the material surface and limit the penetration of biogenic acid formed inside the biofilm.

## THE DIFFICULTY OF TESTING BIOGENIC CORROSION RESISTANCE OF BUILDING MATERIALS

Even if the $H_2S$ biogenic corrosion process is well understood today, there is not yet a representative standard test method to give a realistic evaluation of the biogenic corrosion resistance of a given building material.

Pickle Jar Test Method

What is most found in the literature and in the industry are “pure acid tests” [16, 17], where specimens of materials are immersed in pure acid - for instance sulphuric acid at pH 1 – and weight loss is monitored over time. Such tests are often designed as “pickle jar test”. It is simple to do, and it is based on a simplistic assumption: “since the pH inside a sewer can go as low as 1, let’s test the material’s capacity to withstand a pH of one”. With a pure acid test, polymer materials show good resistance while cementitious materials deteriorate. This is why it has been extensively utilized by polymer material suppliers to prove the value of their products.

Pure acid tests are misleading as they do not take into account the complexity of the biogenic corrosion ecosystem. As shown in Figures 9 and 10, calcium aluminate mortar gives excellent resistance to biogenic corrosion. If you submit the same specimens to a pure acid test at pH 1, they will gradually dissolve and it will be rejected as non-resistant material. In order to make sound choices, the design engineer needs standard test methods that are not only reproducible, but that provide a relative ranking representative of real-life behaviour.

To get closer to this double goal of “reproducibility” and “realistic ranking”, several test methods have been proposed in the literature.

Heidelberg Test Method

The method proposed by Heidelberg University [18, 19], despite the fact that it involved bacteria, was still a pure acid test. The procedure was to cultivate *A. thiooxidans* in a fermenter with a pH around 3.5. The specimens are placed in a reactor and the bacteria solution is pumped over the specimens for 5 minutes every hour. This procedure combined two aggressions. The first one is a pure chemical attack, as specimens are immersed in a low pH solution for 5 min per hour. As the volume of acidic solution is large, the alumina released under the acid attack cannot reach the threshold for bacteriostatic effect. Between the immersion cycles, bacteria are present on the surface of the specimen, but no equilibrium will be reached since the acidic nutrient solution is provided for 55 minutes. With this test procedure, it was shown that PC mortars are 10 times less resistant to biogenic deterioration than CAC mortars.

Gent University Test Method

Another attempt has been made by Belgian researchers from Gent University [20, 21]. The aim of that team was to design a simple test gathering the worst conditions met on site. One test cycle lasts 17 days and involves different steps: exposure to 250 ppm $H_2S$ gas for 3 days; immersion in a solution enriched with *Thiobacillus* inside a rotary shaker for 10 days; washing for 2 days; and finally drying for 2 days. Up to 3 cycles are made before measuring mass loss and mechanical strength. Despite the fact that this test uses microorganisms, the conditions were far from realistic. Actually, the immersion for 10 days in the acidic culture medium is in fact a pure acid attack. Moreover, the use of a drying episode in the cycle of deterioration limits the growth of microorganisms; hence it impacts on the acid concentration.

Virginia Experimental Sewer

In South Africa, the precast pipe manufacturing industry developed, in the 1980s, a very pragmatic approach to study biogenic corrosion that remains unmatched today [22, 23] In the Virginia area, at a location known for its intense biogenic corrosion, a 65 metre long sewer was built with 900 mm diameter industrial pipes made of 9 different types of concrete. This section was doubled with a by-pass line allowing diversion of the water flow on demand, for regular inspection. The Virginia Experimental Sewer was commissioned in 1989. Inspections and measurements were done after 5, 12 and 14 years. At the $14^{th}$ year, some PC concrete sections were so badly corroded that they had to be removed before they collapsed. The removed sections were replaced by a new set of specimens of shorter length, allowing the testing of new concrete compositions. In 2014, 25 years after its commissioning, the experimental sewer was still being monitored as part of an ongoing PhD project at Cape Town University. What is unique with this project is the exposure of full size industrially made concrete pipes in the completely realistic conditions of a live sewer.

Using the data gathered from the Virginia Experimental Sewer, Goyns & Alexander [24] proposed an improved version of the "Life Factor Method" (LFM) developed by Pomeroy and Pakhurst [25]. While the original LFM only considered the alkalinity of concrete, the Virginia Experimental Sewer results gave a sound base to take into consideration the whole influence of the material through a "Material Factor" to be added in the LFM method. The South African pipe manufacturing industry published these results, the improved LFM and the material factor proposed value in a Sewer Design Manual published in 2008 [26] (Figure 16).

| Cement/ Aggregate | 5 year estimate | | 12 year estimate | | 14 year measured | | Material factor*** |
|---|---|---|---|---|---|---|---|
| | total | average | total | average | total | average | |
| PC/SIL | >30 | >6,0 | >64 | >6,0 | > 105 | > 7.5 | 1.000 |
| PC/DOL | 10 – 15 | 2 – 3 | 20 – 30 | 1,7 – 2,5 | 43 | 3.1 | 0.410 |
| CAC/SIL | 5 – 10 | 1 – 2 | 10 – 15 | 0,8 – 1,2 | 26 | 1.9 | 0.250 |
| FC | 10 - 12 | 2 + | 20 - 25 | 1,7 – 2,1 | | | 0.270 |
| CAC/DOL * | 3,0 | 0,6 | 7,2 | 0,6 | 8,4 | 0,6 | 0.085 |
| CAC/ALM ** | | | | | | | 0.025 |

*Values estimated on the basis of other materials and performance of UCT samples in sewer
**Much less than CAC/DOL – no mass loss 17 months in sewer and pH on surface >6,4
***Average of maximum loss at side divided by corresponding value for PC/SIL.

Figure 16 Table 15 of the Sewer Design Manual [26]

In the Sewer Design Manual Table 15, the Material Factor proposed for conventional concrete based on PC and siliceous aggregates (PC/SIL) is 1, meaning that the corrosion rate proposed by the Pomeroy equation is unchanged. However, if PC is replaced with CAC (CAC/SIL), the Material Factor proposed is 0.25, meaning that the corrosion rate proposed by the Pomeroy equation needs to be divided by 4 to fit real-life behaviour of CAC concrete pipes. In the same way, the Material Factor proposed for a concrete made with both calcium aluminate cement and calcium aluminate aggregates (CAC/ALM) is 0.025, i.e. the expected corrosion rate will be 10 times lower than with only calcium aluminate cement concrete (CAC/SIL).

Although one can argue that longer observation time would be required to define more accurately the Material Factor values, the fact is that calcium aluminate based concretes, exposed in a live sewer for up to 14 years, have shown drastically different resistance to $H_2S$ biogenic corrosion, in line with Hamburg University's findings.

Ongoing works to develop a biogenic corrosion standard test

Although providing high credible real-life data, the Virginia Experimental Sewer program is not a standard test method that can be reproduced elsewhere. Considering the growing problems of biogenic corrosion in France, the French institute IFSTTAR started working in 2010 on a test method that could be a candidate for a standard test method, based on the Hamburg Simulation Chamber.

The results were interesting enough to trigger the launch in 2014 of a larger 4 million Euros, 4 year program partly funded by the French government – labelled DURANET and involving the main industry players – to improve the biogenic corrosion resistance of sewer materials. One expected result should be a test method that could be proposed as a reproducible, representative and accelerated Standard Test Method.

For the sewer owner who must choose the most appropriate materials to maintain/rehabilitate the infrastructure, and considering the lack of a standard test method, field track records remain today the single most valuable source of information about the actual biogenic corrosion resistance of repair materials.

## FIELD EVIDENCE OF 100% CALCIUM ALUMINATE MORTAR DURABILITY

Figures 9, 10 and 16 show published data underlining the large gap of durability between conventional PC concrete and 100% calcium aluminate mortar/concrete. Another valuable source of information is the monitoring over years of real-life rehabilitation made with 100% calcium aluminate mortars. Three different sets of data are presented here.

Monterey Waste Water Treatment Plant

In California, USA, the Monterey Waste Water Treatment Plant grid chamber was initially coated with an epoxy liner. Within 18 months, the epoxy liner showed severe distress and the concrete started to corrode badly. In order to choose a repair material able to withstand the severe corroding conditions, a benchmarking test was organized. Cylinder specimens (50x100 mm) were made with several candidate repair mortars, and they were hung within the grit chamber in November 1995. The average $H_2S$ level was reported to be in the 30-50 ppm range for a period of 6 months. Visual observations and pH measurements were made after 10 months and after 2 years. Even if this study is empirical, the results are clear. Figure 17 shows the state, after two years of exposure, of 100% CA mortar specimen and of an PC mortar specimen. The difference in performance is obvious with the 100% CA mortar specimen showing almost no sign of deterioration after 2 years in an environment that was able to corrode completely a 50 mm PC mortar cylinder.

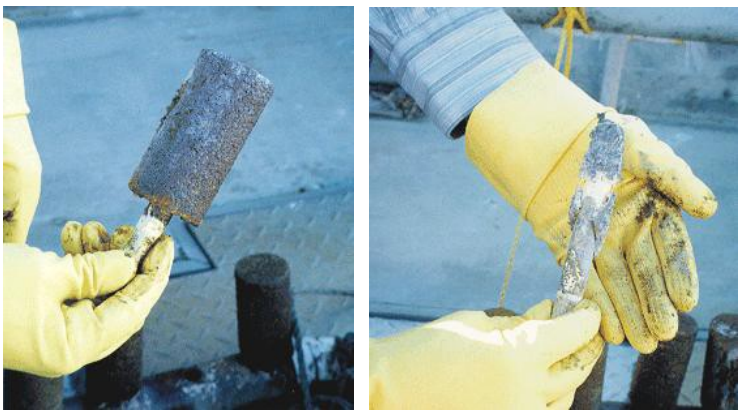

Figure 17 *In situ* specimens exposed for two years in the grit chamber of Monterey waste water treatment plant. Left: 100% CAC mortar. Right: PC mortar

Hampton Roads Sanitation District

The first rehabilitation with a 100% calcium aluminate mortar in the USA took place in 1991 in Virginia, in a split chamber of the Hampton Roads Sanitation District. A very severe process of $H_2S$ biogenic corrosion was on- going, with 75 mm of concrete lost over a 7-year period. Surface pH measurements as low as 1.5 were reported. The chamber was rehabilitated by rebuilding the lost concrete with a dry shotcrete 100% calcium aluminate mortar. This repair was then monitored five times over a period of 11 years through visual inspection, hammer sounding, and surface pH measurement.

Pictures in Figure 18 were taken during this inspection. In Figure 18 left, the inspector is hammering the 100% CA mortar surface, which was found to be hard and sound; note that the manhole cast iron ring, which was protected with epoxy, is showing severe corrosion signs. Figure 18 right shows the pH measured after 11 years both on the cast iron manhole ring, and on the 100% CA mortar. On the epoxy surface, the pH is 1, showing that the biofilm has colonized the surface and is actively producing acid that has damaged the cast iron, despite the presence of an epoxy liner. On the 100% CA mortar, exposed to the same environment, the pH is at 4, the same value that was recorded after 3, 6 and 9 years. This real-life observation illustrates well that the bacteriostatic effect of calcium aluminate has impaired the bacteria to lower the pH below 4 for over 11 years. At the same time, only a few centimetres away, the biofilm without a barrier was able to lower the pH to 1. Note that the 100% CA mortar is not showing any sign of distress after 11 years is such a harsh environment.

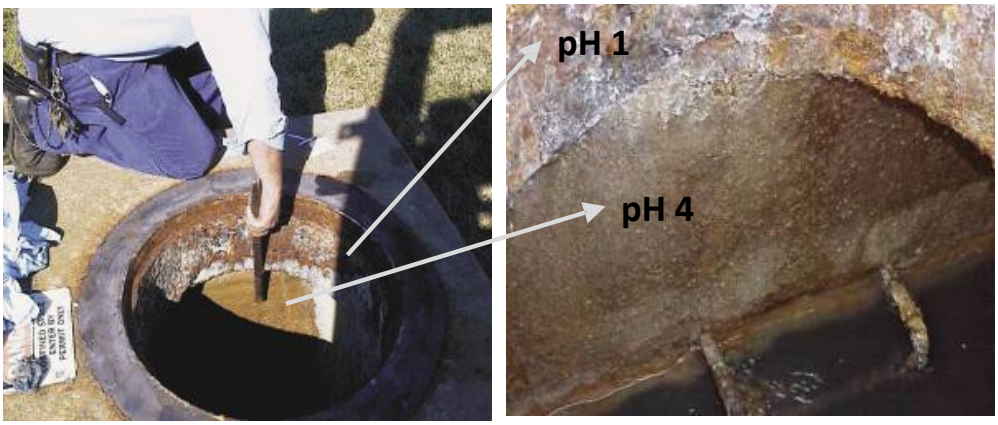


Figure 18 Manhole at Hampton Road Sanitation District rehabilitated with 100% CAC mortar. Left: Inspection of the rehabilitated surface. Right: pH measurements done after 11 years in service

Ayer Rajah Discharge Chamber

In Singapore, the flat topography combined with the tropical climate is very favourable for $H_2S$ biogenic corrosion in the sewer system. Figure 19 shows the state of decay of the Ayer Rajah discharge chamber in 2008, before its rehabilitation: concrete was badly corroded with rebars exposed and corroded. PUB, the Singapore's national water agency, decided to rehabilitate this chamber using 100% calcium aluminate mortar. The other option would have been to by-pass the flow for several weeks to rebuild a new discharge chamber, but this would have been much more expensive and troublesome for the citizens. The rehabilitation was done by rebuilding the missing concrete using the dry spray process in March 2008. A first inspection took place 2 years later, in August 2010 and the 100% CA mortar was found to be sound and solid, despite being stained by a yellowish compound showing an active deposit of sulphur. On the basis of this excellent performance, PUB authorized 100% CA mortar to be utilized for the regular maintenance of its sewer infrastructures. Since then, 100% CA technology is utilized on a monthly basis in Singapore.

Figure 19 Manhole of Ayer Rajah Discharge Chamber. Left: Corrosion damages before rehabilitation. Right: Application of 100% calcium aluminate mortar by dry spray process

## PRACTICAL BUILDING CONSIDERATION

Main application of CAC in sewers

The biogenic corrosion resistance of calcium aluminate cement is utilized today in three main applications:

1) **Ductile Iron Pipes** (DIP) for waste water have an internal lining made of calcium aluminate cement mortar;

2) **Concrete pipes** for sewers (seen mostly in Asia) are made either with full mass CAC concrete or with an internal liner of CAC mortar;

3) **Rehabilitation** of man-accessible sewer infrastructures with 100% CA mortar.

DIP and concrete pipes are standardized products covered by national standards. Thus our attention here will be about the practical consideration for rehabilitation works.

Application methods for 100% CA mortar

For rehabilitation works with 100% CA mortar, three installation methods are possible, depending on the job site constraints:

- **Low pressure wet spray:** this method is the most common because it does not produce dust and virtually no material is lost by rebound. It utilizes a classical facade rotor pump, easily available in the market. The main drawback is the limited pumping distance that cannot exceed 75 metres.

- **Spinning head wet spray:** this method is similar to the first but the manual spraying is replaced by a spinning head projecting the mortar. It is fast and especially suited for cylindrical chambers like manholes. When a structure is so severely corroded that man-entry is a risk, spinning head application permits an un-manned application to a manhole.

- **High pressure dry spray:** this method, also called shotcrete or gunite, allows a faster rate of rehabilitation, and also makes a thicker application in a single pass. The main reason to use dry shotcrete is the capacity to pump the mortar over a long distance and this is needed when the access points are distant. The longest dry shotcrete distance the authors are aware of is a job site in Australia where 100% CA mortar was air transported over 800 metres before being sprayed. The main drawback with dry shotcrete is the generation of dust and rebound; these could be limited by appropriate means (pre-moisture ring, adapted aggregate grading, experienced nozzleman).

Whatever the application method chosen, the first step is a thorough cleaning of the corroded concrete to remove loose material and contaminants in order to expose a sound, rough and clean substrate. Depending on the concrete condition and contamination, the cleaning can range from simple high pressure jet water cleaning (200 bar) up to real hydro-demolition (2000 bars). One method to ensure that sound concrete is exposed is to verify that the pH is greater than 10. As for any concrete repair, the state-of-the-art rules must be followed.

100% Calcium Aluminate Mortar & Conversion

When biogenic corrosion has removed several centimetres of concrete, the owner may want the rehabilitation not only to protect a structure from further deterioration, but also to restore the structural capacity. As calcium aluminate cement is subject to the conversion phenomenon, this should be taken into account when structural capacity is required.

The conversion phenomenon is specific to calcium aluminate cement: the meta-stable hydrates formed initially will transform over time into denser stable hydrates. Thus, the initial strength (1 day – 1 month) may be higher than the long term stable strength. Conversion phenomenon is an inevitable thermodynamic process and – for design purpose - only the long term stable strength must be taken into account. As for other hydraulic cement, the strength of calcium aluminate concrete is proportional to the water/cement ratio. The long term stable strength can be evaluated by an accelerated test, as described in the Annex 1 of the EN 14647 Standard [27].

In the specific case of 100% calcium aluminate mortar utilized for water infrastructure rehabilitation, the water/cement is typically moderate as good adhesion to the walls or the ceiling of the repaired structures is required. A combination of the positive effect of a moderate W/C ratio, and the good bonding between the calcium aluminate aggregate with the calcium aluminate cement paste, a long term stable strength of 40 MPa is typically obtained.

Protection vs Consolidation

Depending on the progress of biogenic corrosion damage, a given structure may need only to be protected from further damage, or it may need to be consolidated to ensure long term stability. When only protection is needed, a 100% CA mortar can be applied with a typical thickness ranging from 15 to 25 mm. When the corrosion has already removed several centimetres of concrete, the owner may want to re-build the missing thickness in order to restore the structural capacity of the structure. Depending on the constraints specific to the given job site, two choices are possible:

1) To rebuild the missing thickness with 100% CA mortar, eventually in a single pass, as it permits a shorter intervention;
2) To rebuild the missing thickness with classical PC concrete, and then to protect this conventional concrete with a protection layer of 100% CA mortar.

The choice between options 1 and 2 really depends on the costs involved in a given location. While 100% CA mortar is more expensive than plain PC concrete, the capacity to make the rehabilitation in a single pass and to return to service within a few hours may prove to be cheaper than having to come twice to install structural PC concrete first and then later a 100% CA mortar protection layer. The choice really depends on the constraints and cost structure of each repair.

Robustness to Moisture

When a sewer needs to be rehabilitated, it is safe to assume that the underground concrete structure is either moist or water saturated. Good bonding of the rehabilitation material must take this reality into account. With polymer liners like epoxy, because of the hydrophobic nature of these materials, the concrete surface needs to be dry enough to permit satisfactory bonding. Achieving a proper surface dryness in a sewer is, at least, a challenge. Conversely, hydraulic cement based mortars – like 100% CA mortars - need the concrete substrate to be either moist or even saturated-surface-dry to develop good bond during hydration. Moreover, to ensure good hydration of the mortar, moist curing is required and typically the ambient air in a sewer is quite humid. In other words, there is a “good fit” with the moist environment of a sewer, and rehabilitation in a live sewer is possible with a 100% CA mortar. However, if $H_2S$ is present, forced ventilation is needed during the working shift, this may reduce the ambient air moisture and active curing actions may still be required to achieve good curing of the cementitious mortar.

Time for Return to Service

To proceed with a sewer rehabilitation, it may be necessary to retain or divert the flow during the repair. The cost of by-passing a sewer flow can be easily the largest expense for a given operation. Thus the time to return to service after the repair is a non-negligible parameter. One property of calcium aluminate cement is a normal setting time followed by a fast strength development, within few hours. Typical 100% CA mortar, which is formulated to ensure good pumpability and good bonding to the substrate, will start setting within 3 to 5 hours, and can be put back in service after 8 hours.

In some circumstances, the time available is shorter than that. For instance, for some large collectors, diverting the flow can prove to be uneconomically and the rehabilitation takes place at night when the sewer flow is lowest. The working window can be as short as 6 hours to clean the surface, proceed with the rehabilitation, let the material harden and return to service. When needed, it is possible to accelerate the 100% CA mortar hardening by applying a lithium based accelerator; the hardening then starts within 30 minutes and the accelerated surface may allowt exposure to live water as soon as 1 hour after the accelerator application. The application of a lithium based accelerator is also a simple way seal the 100% CA mortar surface to ensure proper curing.

## CONCLUSIONS

$H_2S$ biogenic corrosion is a growing problem for sewer owners as the increase in water usage tends to increase the production of $H_2S$. This paper has presented a broad review of the $H_2S$ biogenic corrosion process and the reasons explaining the exceptional durability of calcium aluminate cement to this deterioration process. The historical use of calcium aluminate in sewers has been briefly reviewed.

There are several possibilities to protect or to rehabilitate a sewer exposed to biogenic corrosion. The application of a polymer protection lining, like epoxy, is one option but the failure rate observed over years by many operators is pushing them to search for an alternative solution with better reliability. Calcium aluminate mortar or concrete is such an alternative, its main weakness it to be little known in the engineering community.

While conventional PC concrete can be severely corroded by bacteria-borne sulphuric acid, calcium aluminate concrete will resist it much better because of its capacity to induce a bacteriostatic effect, stopping the production of acid by bacteria. It has been shown in academic studies and from field track records that this resistance is at a maximum when the material is made entirely of calcium aluminates, i.e. that both the cement and the aggregates are made of calcium aluminate.

One missing element for the engineering community is a standard test method that would permit the evaluation of the concrete repairs material's resistance to $H_2S$ biogenic corrosion. The paper shows why current methods like the "pure acid test" do not provide realistic results. There is on-going work toward a standard test method proposal in a near future.

For the time being, actual field performance remains the most reliable source of data to evaluate the biogenic corrosion of repair materials. There is today a large body of evidences showing that calcium aluminate-based materials present an exceptional resistance to $H_2S$ biogenic corrosion.

## REFERENCES

1. SATIN M, SELMI B, Guide technique de l'assainissement : Moniteur reference technique. Paris: Edition du moniteur, 2010, 660 p., ISBN 2-281-11239-X.

2. LAMBERET S, GUINOT D, LEMPEREUR E, TALLEY, J, ALT C, Field investigations of high performance calcium aluminate mortar for wastewater applications – Calcium aluminate Cements, proceedings of the centenary Conference, Avignon, 30 June – 2 July 2008, pp. 269-277. Fentiman C H, Mangabhai R J and Scrivener K L. (editors). IHS BRE Press, 2008, EP94. ISBN 978-1-84806-045-6.

3. PARKER C D, Species of Sulphur Bacteria Associated with the Corrosion of Concrete, *Nature*, Vol. 159, 1947, pp. 439-440.

4. CALCIUM ALUMINATE CEMENT. InChemistry of cement and concrete, 4th Edition, Chapter 13: Lea F, edited by Hewlett, P C, 1988, ISBN: 0750662565, Publisher: Elsevier Science & Technology Books, Pub. Date: January 2004, pp. 713-782.

5. CALCIUM ALUMINATE CEMENT. Advanced Concrete Technology: Constituent Materials Volume 1, Chapter 2: edited by Newman j B and Choo B S, 2003, ISBN: 9780750651035, Publisher: Elsevier Science & Technology Books, Pub. Date: September 2003.

6. ROBSON .D, High-Alumina Cements and Concretes, Wiley, New York, U.S.A., 1962, pp. 145-159.

7. EHRICH S, HELARD L, LETOURNEAUX R, WILLOCQ J, BOCK E, Biogenic and Chemical Sulfuric Acid Corrosion of Mortars, *Journal of Materials in Civil Engineering*, Vol. 11, 1999, pp. 340-344.

8. GEOFFROY V A, BACHELET M, CROVISIER J-L, AOUAD G, DAMIDOT D, Evaluation of Aluminium Sensitivity on a Biodegrading Bacteria *Acidithiobacillus Thiooxidans*: Definition of a Specific Growth Medium – Calcium aluminate Cements, proceedings of the centenary Conference, Avignon, 30 June – 2 July 2008, pp. 309-319. Fentiman CH, Mangabhai RJ and Scrivener KL. (editors). IHS BRE Press, 2008, EP94. ISBN 978-1-84806-045-6.

9. HERISSON J, VAN HULLEBUSCH E D, GUÉGUEN-MINERBE M, CHAUSSADENT T, Biogenic corrosion mechanism: study of parameters explaining calcium aluminate cement durability - Calcium aluminate: Proceedings of the International Conference, Avignon, 18-21 May 2014, pp. 633-644. Fentiman CH, Mangabhai RJ and Scrivener KL. (editors). IHS BRE Press, 2014, EP104. ISBN 978-1-84806-316-7.

10. HERISSON J, "Biodétérioration des matériaux cimentaires dans les réseaux d'assainissement – Etude comparative du ciment d'aluminate de calcium et du ciment Portland" (Biodeterioration of cementitious materials in sewers networks – comparative study of calcium aluminate cement and ordinary Portland cement). PhD thesis, Ifsttar, Université Paris-Est, Marne-la-Vallée, France, pp.233.

11. HERISSON J, VAN HULLEBUSCH E D, MOLETTA-DENAT M, TAQUET P, CHAUSSADENT T, Toward an Accelerated Biodeterioration Test to Understand the Behavior of Portland and Calcium Aluminate Cementitious Materials in Sewer Networks, *International Biodeterioration & Biodegradation*, Vol. 84, 2013, pp. 236-243.

12. HERISSON J, GUÉGUEN-MINERBE M, VAN HULLEBUSCH E D, CHAUSSADENT T, Behaviour of Different Cementitious Material Formulations in Sewer Networks, *Water Science & Technology*, Vol. 69, 2014, pp 1502–1508.

13. PEYRE-LAVIGNE M, BERTRON A., BOTANCH C, AUER L, HERNANDEZ-RAQUET G, COCKX A, FOUSSARD JN, ESCADEILLAS G, PAUL E, Innovative approach to simulating the biodeterioration of industrial cementitious products in sewer environment. Part II: validation on CAC and BFSC linings, *Cement and Concrete Research*, Vol. 79, 2016, pp. 409-418.

14. ISLANDER RL, DEVINNY JS, MANSFELD F, POSTYN A, SHIH H, Microbial ecology of crown corrosion in sewers, *Journal of Environmental Engineering*, Vol. 117, 1991, pp. 751-770.

15. ROBERTS DJ, NICA D, ZUO G, DAVIS JL, Quantifying microbially induced deterioration of concrete: initial studies, *International Biodeterioration & Biodegradation*, Vol. 49, 2002, 227-234.

16. Greenbook Standard Specifications for Public Works Construction, 2009 Edition, published by Building News, Los Angeles, CA.

17. ASTM C 267-01, Standard Test Methods for Chemical Resistance of Mortars, Grouts, and Monolithic Surfacings and Polymer Concretes, ASTM International, 100 Barr Harbor Drive, PO Box C700, West Conshohocken, PA 19428-2959. United States.

18. HORMANN K, HOFMANN, F, SCHMIDT M, Stability of Concrete Against Biogenic Sulfuric Acid Corrosion, a New Method for Determination – Proceedings of the 10th International Congress on the Chemistry of Cement, Gothenberg, 1997, 4vi038.

19. SCHMIDT M, HORMANN K, HOFMANN F J, WAGNER E, Concrete with Greater Resistance to Acid and to Corrosion by Biogenous Sulfuric Acid, *Concrete Precasting Plant and Technology*, Vol. 4, 1997, pp. 64-70.

20. VINCKE E, VERSTICHEL S, MONTEN, J, VERSTRAETE W , A New Test Procedure for Biogenic Sulfuric Acid Corrosion of Concrete, *Biodegradation*, Vol. 10, 1999, pp. 421-428.

21. DE BELIE N, MONTENY J, BEELDENS A, VINCKE E, VAN GEMERT D, VERSTRAETE W, Experimental Research and Prediction of the Effect of Chemical and Biogenic Sulfuric Acid on Different Types of Commercially Produced Concrete Sewer Pipes. *Cement and Concrete Research*, Vol. 34, 2004, pp. 2223-2236.

22. FOURIE C W, Biologically Induced Sulphuric Acid Attack on Concrete Samples in the Experimental Sewer Section at Virginia. Department of Civil Engineering, University of Cape Town, 2002.

23. ALEXANDER M G, GOYNS A., FOURIEC. Experiences with a full-scale experimental sewer made with CAC and other cementitious binders in Virginia, South Africa – Calcium Aluminate Cement : Proceedings of the Centenary Conference, Avignon, 30 June – 2 July 2008, pp. 279-292. Fentiman CH, Mangabhai RJ and Scrivener KL. (editors). IHS BRE Press, 2008, EP94. ISBN 978-1-84806-045-6.

24. GOYNS A., ALEXANDER M G, FOURIE C. Applying experimental data to concrete sewer design and rehabilitation – Calcium Aluminate Cement: Proceedings of the Centenary Conference, Avignon, 30 June – 2 July 2008, pp. 293-308. Fentiman CH, Mangabhai RJ and Scrivener KL. (editors). IHS BRE Press, 2008, EP94. ISBN 978-1-84806- 045-6.

25. POMEROY R D, PARKHURST J D, The Forecasting of Sulfide Build-up Rates in Sewers. Conference of International Association of Water Pollution Research, Sydney, 1976.

26. GOYN, A M, Sewer Design Manual, Published by Pipe and Infrastructural Product Division, CMA, Midrand, South-Africa, 2008.

27. EN 14647, Calcium aluminate cement - Composition, specifications and conformity criteria, BS EN 14647:2005/AC, November 2006.

# TOWARDS A NEW GENERATION OF CALCIUM SULFOALUMINATE CEMENTS

**S Skalamprinos** **M Whittaker** **G Jen**

**I Galan** **M S Imbabi** **F P Glasser**

University of Aberdeen

United Kingdom

**ABSTRACT.** The need to reduce $CO_2$ emissions has increased the pressure on the cement research community to develop alternatives to traditional Portland cement. Calcium sulfoaluminate cements, first developed commercially in China in the 1970's, are being investigated as an alternative. Expanding upon current knowledge of calcium sulfoaluminate cements, a new generation incorporating combustion of chemically reduced sulfur has been developed and successfully clinkered to further reduce embodied $CO_2$ in excess of 30% compared to Portland cement. However, some systems set too fast probably because ettringite forms too rapidly.

**Keywords:** Sulfoaluminate, Calcium sulfate, Setting time, Calorimetry, SEM

**Mr Solon Skalamprinos** is a PhD candidate at the University of Aberdeen undertaking research on the hydration of new generation $C\bar{S}A$ cements.

**Dr Mark Whittaker** is a University of Aberdeen post-doctoral Fellow having honed his analytical skills to observing degradation phenomena in cementitious materials.

**Dr Gabriel Jen** is a University of Aberdeen Research Fellow having interests in the performance and durability of high performance cementitious composites.

**Dr Isabel Galan** is a researcher specialized in the field of durability of cement based materials with a background in physics and materials science and engineering.

**Dr Mohammed Imbabi** is an eminent, multi-lingual scientist, professional engineer and innovator in the diverse fields of civil engineering, low energy building and renewable energy technology.

**Professor Fredrik P Glasser** is Professor of Chemistry at the University of Aberdeen.

## INTRODUCTION

About 5% of the total man-made $CO_2$ emissions come from cement production, both directly from calcination of $CaCO_3$ and indirectly by the operational energy required for the plant [1]. The amount of $CO_2$ emitted by the cement industry is nearly 900 kg of $CO_2$ for every 1000 kg of Portland cement (PC) clinker produced. With increasing pressure to reduce $CO_2$ emissions the research community constantly seeks less carbon-intensive cements. An alternative is calcium sulfoaluminate ($C\bar{S}A$) cements which were first commercially developed in China in the 1970's [2].

$C\bar{S}A$ cements are produced by clinkering together limestone, bauxite, clay and calcium sulfate to produce predominantly ye'elimite ($C_4A_3\bar{S}$) and belite ($C_2S$). However, the chemistry of $C\bar{S}A$ cements differs to that of PC such that $CO_2$ emissions may be reduced by around 30% in total. Firstly this is because they require less calcium per kg clinker, thereby reducing the amount of limestone to be decarbonated. Secondly because $C_4A_3\bar{S}$ is formed at temperatures ~1250°C, much lower than the 1400°C needed to stabilise alite ($C_3S$) in PC: reduction of clinkering temperature reduces fossil fuel consumption. Additionally, $C\bar{S}A$ clinkers are more friable than PC clinkers reducing the energy input of grinding, thus reducing the embodied $CO_2$. Furthermore, a variety of $C\bar{S}A$ cements can be manufactured with special characteristics including high early strength, rapid setting, expansive or self-stressing and shrinkage compensating versions [3].

Upon hydration, the main clinker phase, ye'elimite, reacts with water to form calcium monosulfoaluminate hydrate, "monosulfate", and aluminium hydroxide and in the presence of calcium sulfate, ettringite and aluminium hydroxide (Equation 1 & Equation 2). The second major phase, belite, reacts with water and aluminium hydroxide to form strätlingite, a silicate monosulfate- type phase. (Equation 3) [3-6].

$$C_4A_3\bar{S} + 18H \rightarrow C_3A.C\bar{S}.H_{12} + 2AH_3 \qquad \text{Equation 1}$$

$$C_4A_3\bar{S} + 2C\bar{S} + 38H \rightarrow C_3A.3C\bar{S}.H_{32} + 2AH_3 \qquad \text{Equation 2}$$

$$C_2S + AH_3 + 5H \rightarrow C_2ASH_8 \qquad \text{Equation 3}$$

Lack of paradigms regarding the set behaviour of $C\bar{S}A$ cements drove us to extrapolate some knowledge about set behaviours from PC. Both in PC and $C\bar{S}A$ cements, calcium sulfate is typically added to control dimensional stability and to control the initial and final set times. In PC systems, calcium sulfate is added to retard $C_3A$ hydration, preventing flash set. The calcium sulfate dissolution rate is important to avoid anomalous set problems. In its absence, in PC systems a gel-like substance may form within the aqueous phase in pores, producing a low-strength material and releasing large amounts of heat, sometimes giving rise to "flash setting" from which workability cannot be regained [7]. It is also well reported that calcium sulfate speciation can cause another problem regarding setting time. During the grinding process of PC clinker gypsum is added, however due to high temperatures of the mechanical process dehydration to hemihydrate and anhydrite may occur. Upon wetting, hemihydrate converts back to gypsum causing thickening and liberating some heat, although much less compared to the reactions involved during flash setting. In this case though, workability can be regained with further mixing [8, 9].

The main focus of this work was to compare the setting time and behaviour between a commercial $C\bar{S}A$ cement (c. $C\bar{S}A$) imported from China (Shenzhen Chenggong Building Materials Company) and a new generation of $C\bar{S}A$ cements ($C\bar{S}A$ 1, $C\bar{S}A$ 2). This new generation was produced via a novel technology [10,11] validated in a pilot scale rotary kiln operating at a raw–meal feed rate of 25 kg/hr; the setup and operating conditions are described in detail by Hanein et al. [12]. The essential feature of the new process is that sulfur is combusted to produce sulfate thereby reducing consumption of fossil fuel and emitting less $CO_2$ per unit mass of clinker.

The phase composition of all three cements, obtained from Rietveld analysis are compared in Table 1. The commercial $C\bar{S}A$ cement was much richer in ye'elimite compared to the experimental cements; $C\bar{S}A$ 1 and $C\bar{S}A$ 2 were deliberately designed to have a lower ye'elimite content, to reduce dependence on expensive bauxite. Calcium sulfate was not observed in the commercial $C\bar{S}A$ cement while the two experimental cements had 10 percent anhydrite from the clinkerisation process. All cements had minor phases including ferrite, gehlenite and perovskite (other phases).

Table 1 Phase Composition of Commercial $C\bar{S}A$, $C\bar{S}A$ 1 and $C\bar{S}A$ 2 Cements.

| | $C_4A_3\bar{S}$ [%weight] | $C_2S$ [%weight] | $C\bar{S}$ [%weight] | OTHER PHASES |
|---|---|---|---|---|
| c. $C\bar{S}A$ | 58 | 19 | 0 | 23 |
| $C\bar{S}A$ 1 | 36 | 44 | 10 | 10 |
| $C\bar{S}A$ 2 | 35 | 17 | 10 | 38* |

*including ~29% $C_5S_2\bar{S}$, ternesite

In order to understand in depth the influence of cement composition and hydration kinetics upon setting time, isothermal conduction calorimetry, scanning electron microscopy and XRD were used.

## EXPERIMENTAL ANALYSIS

### Setting Time

Due to material limitations, setting time experiments were performed using 20 gram samples. The samples were mixed and placed in a small cylinder with 3.7cm height and 2.5cm diameter. The initial and final setting time was checked using a manual Vicat apparatus. The same water to binder (w/b) ratio was kept constant at 0.485 for all cements.

### Isothermal Conduction Calorimetry

Samples were tested using a Calmetrix I-CAL 4000 to continuously follow early age hydration. Sample materials (water, cement and mixing spoon) were placed in the calorimeter 24 hours prior to testing to allow the constituents to reach thermal equilibrium. All cement pastes were prepared by external mixing of samples having 5 grams of solids and a 0.485 w/b ratio for 20 seconds. The reference mass was also adjusted to match sample heat capacity [13]. The heat release from early-age hydration was monitored for 72 hours at 25 $^{o}$C.

### X-ray Diffraction

Clinker compositions were determined using XRD patterns that were collected using a Philips Empyrean diffractometer in the Bragg Brentano geometry operating at 45 kV and 40 mA, equipped with a Cu K-α X-ray source, a Ge monochromator and a PIXcel1D detector. For analysis, the sample was ground to a fine powder and back loaded in the sample holders to avoid preferred orientation. Each pattern was measured from 5° to 70° 2-theta with a step size of 0.0132°. The stage was set to rotate at a rate of one revolution per 4 seconds, to improve statistics. The Rietveld refinements were carried out using the GSAS software [14]. The relevant crystal files were sourced from the ICSD database and the peaks were fitted using the Pseudo-Voigt profile function with asymmetry correction [15]. Hydrated samples were tested only qualitatively, using Philips X-pert diffractometer. The setup matched exactly that of the Empyrean with the exception that the X-pert was not fitted with a monochromator.

### Scanning Electron Microscopy (SEM)

Scanning electron microscopy (CARL ZEISS EVO MA 10) was used to study phase distribution in the clinkers. Test samples were prepared by mixing the ground clinkers with epoxy and casting them in a cylindrical sample disks. Samples were placed under vacuum for 20 minutes to remove any trapped air and then left to cure at room temperature for 24 hours. The sample surface was polished using diamond paste and water-free solvent to avoid any unwanted hydration. All samples were carbon coated before backscattered electron (BSE) imaging and compositional examination by energy dispersive X-ray spectroscopy (EDX). The accelerating voltage was set at 20KeV.

## RESULTS AND DISCUSSION

Setting times were determined for all cements and are shown in Table 2. Anhydrite with a specific surface area of 7000cm$^2$/g was blended with the commercial C$\bar{S}$A cement in order to match the content of the two experimental cements. Even with this normalization, the commercial C$\bar{S}$A has the longest setting time despite its finer Blaine. It is well known in the cement industry that for the same cement, the finer the grinding the faster the set so the cause of the differences must lie elsewhere. Despite the similarities in ye'elimite and calcium sulfate contents between the two novel cements (see Table 1), the apparent setting times differ greatly (see Table 2). C$\bar{S}$A 2 exhibited a moderate setting time, but C$\bar{S}$A 1 experienced extremely fast thickening.

Table 2 Setting Time of Commercial (c.) C$\bar{S}$A, C$\bar{S}$A 1 and C$\bar{S}$A 2 Cements.

| CEMENT | w/b | C$\bar{S}$ [%weight] | BLAINE [cm$^2$/g] | IST [min] | FST [min] |
|---|---|---|---|---|---|
| c. C$\bar{S}$A | 0.485 | 10 (added externally) | 6500 | 170 | 194 |
| C$\bar{S}$A 1 | 0.485 | 10 | 4000 | 1 | 2 |
| C$\bar{S}$A 2 | 0.485 | 10 | 4000 | 90 | 110 |

IST = initial setting time, FST = final setting time

Figure 1 follows the heat evolution rate of all 3 cements. Calorimetric results revealed a large exothermic peak in the first 15 minutes of hydration for C$\bar{S}$A 1 whose intensity was approximately 6 and 100 times that of those measured in C$\bar{S}$A 2 and the commercial C$\bar{S}$A, respectively. This ordering, in which the cumulative heat of the C$\bar{S}$A 1 remains the highest of the three samples, persists through 14 hours of hydration at which point it is overtaken by the commercial C$\bar{S}$A (Figure 2). A unifying feature of each of the three cements is the dormant period after initial wetting, where activity was minimal preceding an increase in exothermic reactivity. This induction period was longest in the case of C$\bar{S}$A 1, however, the identified point of calcium sulfate consumption (see Figure 1) occurred one hour earlier than in either the commercial cement or C$\bar{S}$A 2.

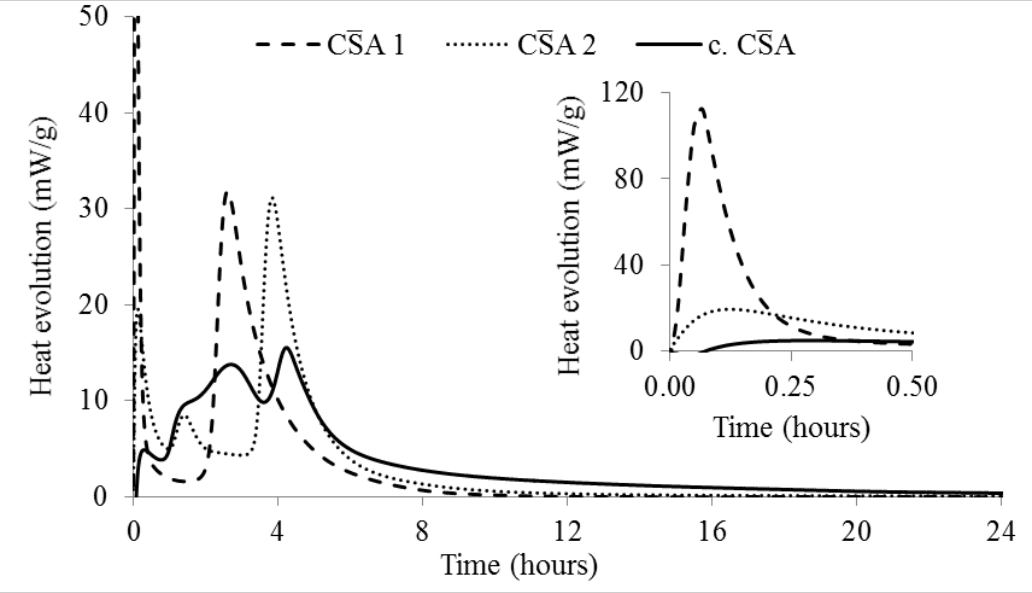


Figure 1 Heat Evolution Rates of Commercial C$\bar{S}$A Cement, with C$\bar{S}$A 1 and C$\bar{S}$A 2. The inset shows heat evolutions at the earliest stages.

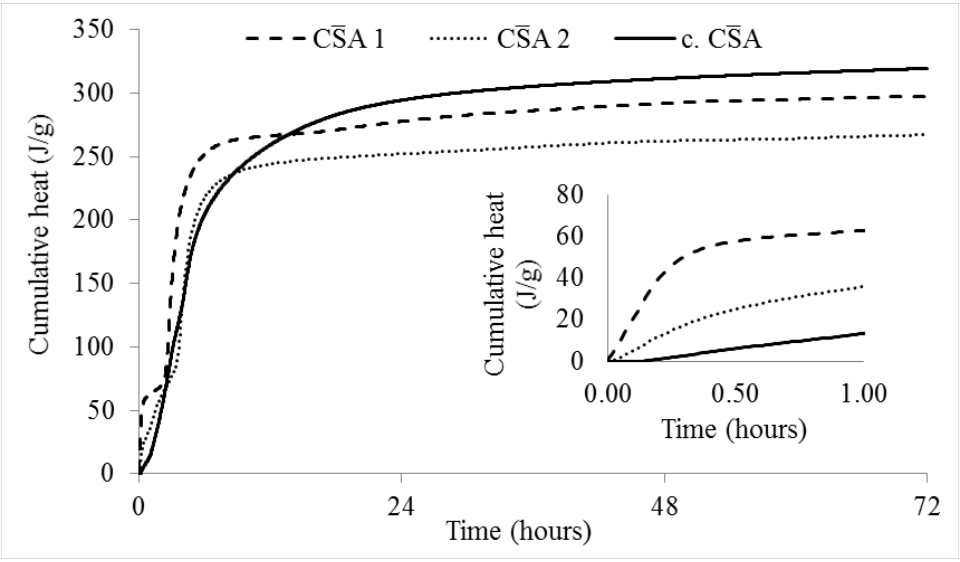


Figure 2 Total Heat Release of Commercial C$\bar{S}$A Cement, with C$\bar{S}$A 1 and C$\bar{S}$A 2. Cumulative releases at short ages are shown in the inset.

To determine why C$\bar{S}$A 1 sets so fast, and to distinguish between false and flash set, a paste with w/b of 0.65 was prepared. Upon mixing by hand, the sample was noticeably easier to mix than at w/b = 0.485 but exhibited similar stiffening after 2 minutes. During mixing, heat radiating from the sample could be felt through the plastic container in which the paste was mixed. With continuous mixing the paste initially remained stiffer than normal consistency but regained workability after 4 minutes.

To understand the impact of hydrate formation on the early stiffening behaviour observed in the first stages of hydration of C$\bar{S}$A 1, seven pastes were prepared, continuously mixed by hand, with a w/b 0.65. Hydration was subsequently stopped after 0.5, 1, 2, 4, 6, 8 and 10 minutes by solvent replacement. A few grams of each paste were washed twice in excess acetone (1:200 solids:acetone for the first wash, and 1:100 for the second wash). Excess acetone was dried off at 40°C. The dried pastes were then qualitatively observed by XRD.

The XRD patterns, highlighting the changes in intensity of the peaks associated with ye'elimite, calcium sulfate and ettringite, are reproduced in Figure 3. Observing the results between 30 seconds and 10 minutes, the initial reactivity of ye'elimite and calcium sulfate was high. Ettringite started to form within the first minute and reached a maximum after 4 minutes of hydration. Both the main peaks of ye'elimite and calcium sulfate showed the same trend, *i.e.* a fast dissolution up to the 4$^{th}$ minute.

Unlike PC, false setting could not be attributed to the conversion of anhydrite to gypsum as the latter was never observed. The formation of early ettringite agrees with the calorimetric observations as its formation is highly exothermic ($\Delta_f H^o_{ettringite}$ = -13,970.95 J/g [16]). The early formation of copious amounts of ettringite is suggested to be the underlying cause of the rapid stiffening. Only by mechanical action could this network be broken, allowing the paste to regain some fluidity.

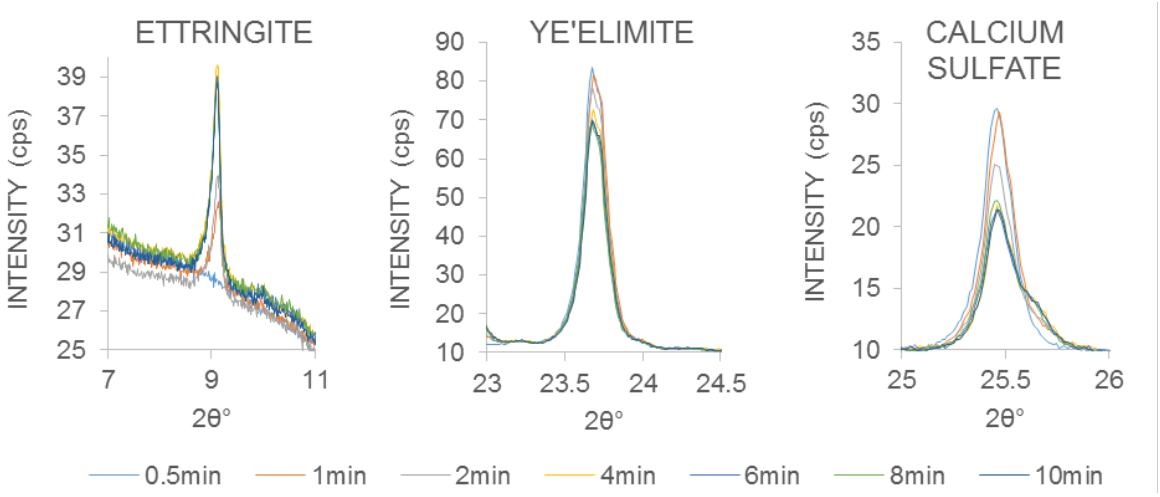


Figure 3 Rapid Formation of Ettringite and Rapid Dissolution of Ye'elimite and Calcium Sulfate during the First 10 Minutes of C$\bar{S}$A 1.

SEM analysis of the commercial C$\bar{S}$A cement grains (Figure 4) shows a smooth surface having distinct internal structure arising from the several solid phases crystals and a high density. Three separate grey levels were observed.

The whitest areas (reflective) were Fe and Ti-rich areas, possibly revealing the presence of ferrite and perovskite, while light grey areas were richer in Si and Ca, which were confirmed by EDX analysis to be belite crystals (marked as B). Finally, the darker shade of grey containing Al, Ca and S were found to be ye'elimite crystals (marked as Y). Both belite and ye'elimite crystals were small in size, around 10 μm.

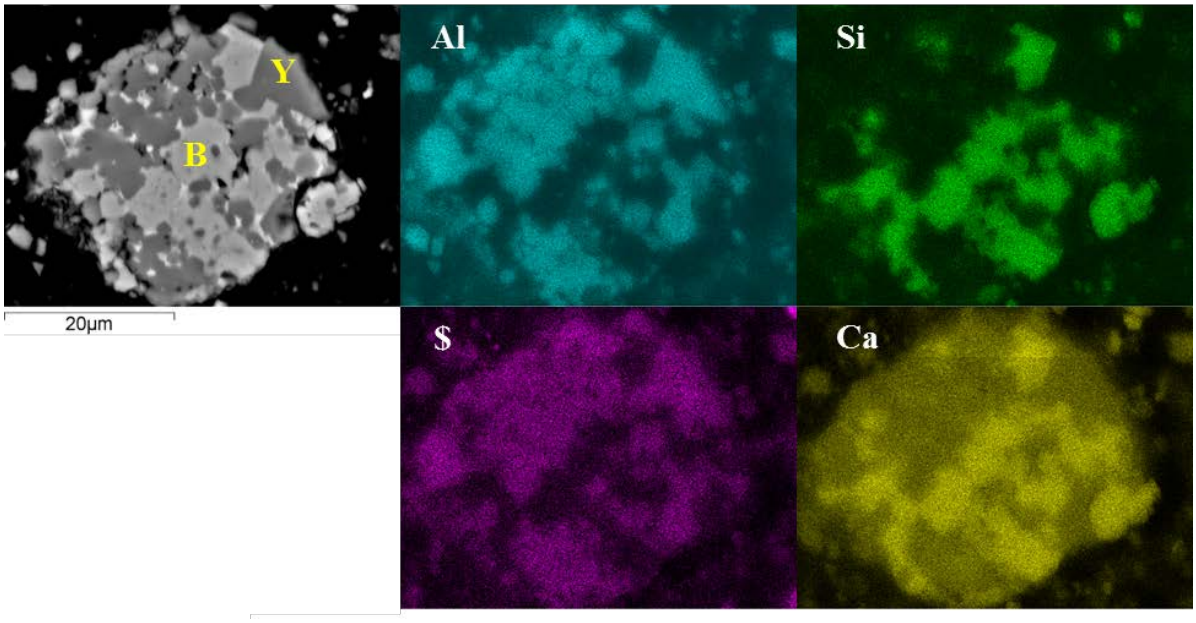


Figure 4 BSE Micrograph of the Commercial C$\bar{S}$A Clinker Grains with Selected Elemental Maps.

C$\bar{S}$A 1 cement grains (Figure 5) had a much rougher surface and were relatively porous in comparison to the commercial C$\bar{S}$A. Three grey levels can be identified albeit with difficulty. The brighter areas (white) were rich in Ti and Fe. The next darker zones were difficult to associate with a known clinker phase. However, a combination of elemental maps more readily revealed the presence of belite (marked as B), rich in Ca and Si, and gehlenite (marked a G), and rich in Ca, Si and additional Al. Finally the darkest areas were rich in Al, S and Ca, and were most likely ye'elimite (marked as Y). While a possible calcium sulfate crystal can be identified, marked by the arrow on the sulfur map, the bulk of the calcium sulfate was unidentifiable due to homogeneity of elements. This was suggestive of an intermixing of minute crystallites within the clinker grains. Calcium sulfate crystallite size was, on some occasions, around 1 μm in size making EDX spot analysis unreliable.

Finally C$\bar{S}$A 2 (Figure 6), had a similar surface roughness and porous structure as was observed with C$\bar{S}$A 1. As with C$\bar{S}$A 1, the three grey levels can be distinguished with difficulty. The brightest areas remained Ti and Fe rich zones. Similarly to C$\bar{S}$A 1, the differentiation between ye'elimite, belite and gehlenite by greyscale alone proved challenging. Unlike C$\bar{S}$A 1, 10 to 30μm vein-like calcium sulfate crystals in length were observed according to the sulfur map and were subsequently confirmed by EDX analysis.

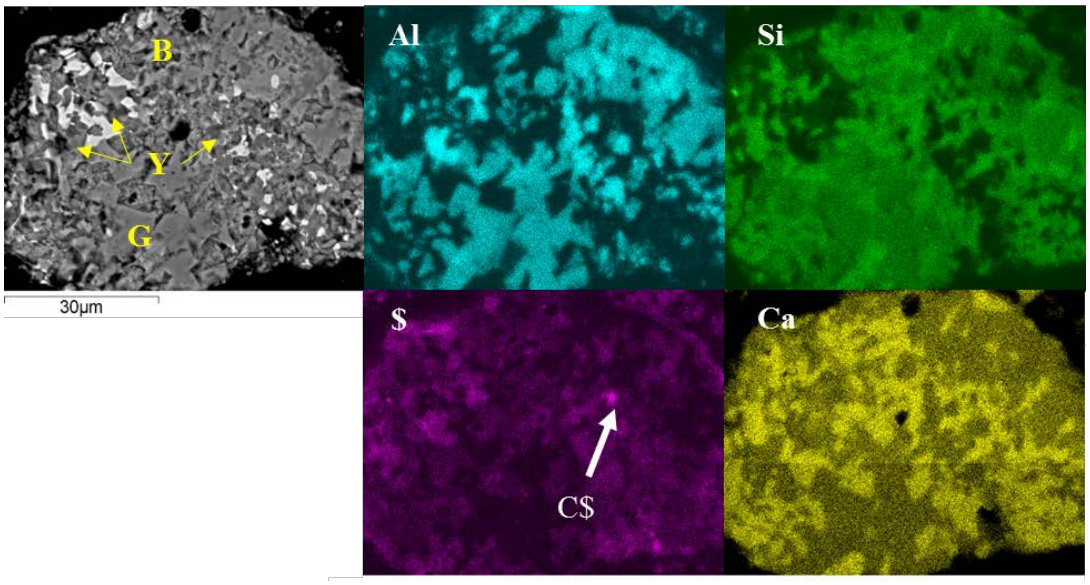


Figure 5 BSE Micrograph of a C$\bar{S}$A 1 Clinker Grain with Selected Elemental Maps.

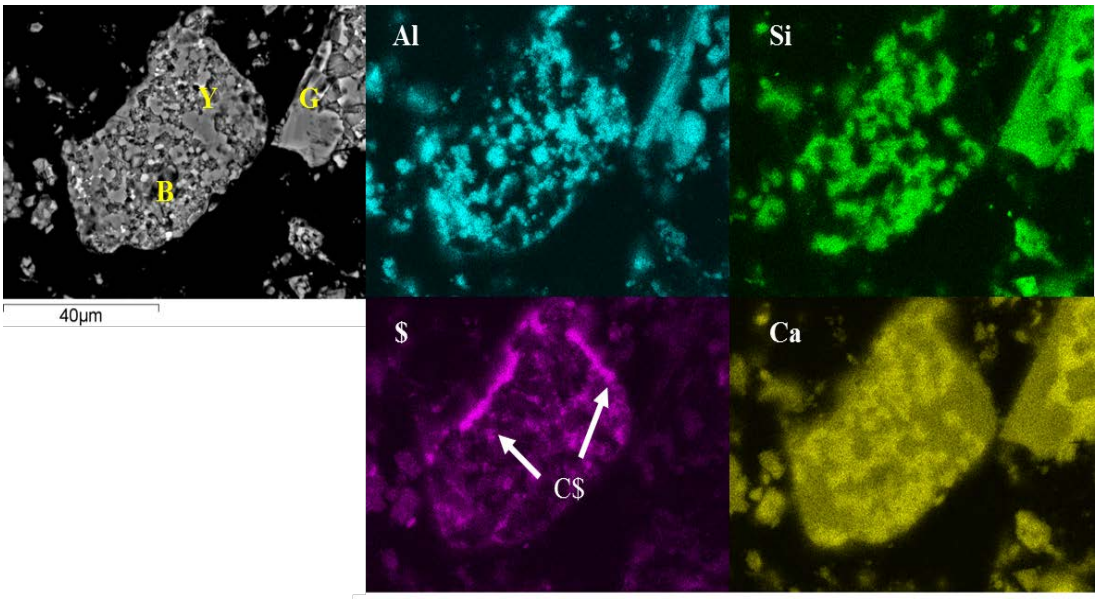


Figure 6 BSE Micrograph of a C$\bar{S}$A 2 Clinker Grain with Selected Elemental Maps

It is unclear exactly why the individual clinker phases formed in the 2 experimental C$\bar{S}$A cements cannot be identified by greyscale alone as can be done in the commercial C$\bar{S}$A cement. This effect may likely be due to the fact that the crystallite size in these systems are small in size. Furthermore, C$\bar{S}$A 1 differs from C$\bar{S}$A 2 by having very fine calcium sulfate crystals. Because of their overall small crystal size, in the case of C$\bar{S}$A 1, it may be that ye'elimite dissolves rapidly with anhydrite to form ettringite (Figure 3) to which the undesirable stiffening of the paste is attributed (Table 2); at the same time, a large amount of heat is released (Figure 1 and Figure 2). However, the network of ettringite crystals can be broken by prolonged mechanical mixing. This false set like behaviour was not observed in C$\bar{S}$A 2 likely because of the larger anhydrite crystals restricting its early dissolution.

Recent progress in relating phase constitution to chemistry has shown that it is possible to control the phase content of $C\bar{S}A$ with the same accuracy as for Portland cement. However the phase chemistry can be more complex: for example, sulfur can be removed by volatilisation from the clinkering batch but it can also be added by controlling the kiln atmosphere. Sulfur, if present, appears in low- alkali PC as $CaSO_4$ but in $C\bar{S}A$ clinkers it can appear as anhydrite, ternesite and ye'elimite. This means that it is desirable to use computer modelling, informed by a phase development model, to relate chemistry to mineralogy.

But the model will still not predict clinker microstructure. The title paper shows that clinkers can be developed with different availability of $CaSO_4$ in the course of early hydration and this can strongly influence set in the example clinkers. False set results from ettringite formation commencing within the first minute of hydration. False set is encouraged by the presence and amount of reactive anhydrite at or near grain surfaces. It is thus desirable to produce clinkers with low free anhydrite contents, especially if the anhydrite is reactive during early hydration. While retarder systems can be developed to reduce rheological problems arising from an excess of reactive anhydrite, it is a problem best avoided by controlling clinker mineralogy and the spatial distribution of $CaSO_4$. If $CaSO_4$ is needed to control set time and dimensional stability in the post hardening period, this is best done at the grinding stage such that the amount and reactivity of the $CaSO_4$ product can be controlled.

## CONCLUSIONS

Experimental analysis revealed a unique phenomenon of morphology dependant set time where:

- $C\bar{S}A$ 1 cement was found to have small crystallites of anhydrite, much more so than the commercial $C\bar{S}A$ and $C\bar{S}A$ 2.
- Ettringite was identified after a minute of hydration, this formation caused the rapid set.
- This differs from false set observed in PC where water deficient calcium sulfate rehydrates to gypsum as prismatic needles causing stiffening of the paste.
- The initial network of ettringite can be worked to regain some plasticity, and we can qualify this setting as 'false-like'.
- This false-like set behaviour was not observed in the commercial $C\bar{S}A$ and $C\bar{S}A$ 2 where the anhydrite crystals were more consequent in size.

## ACKNOWLEDGEMENTS

The authors gratefully acknowledge the financial support provided by the Gulf Organization for Research and Development, Qatar, through research grant number RGG11757-10.

## REFERENCES

1. Low Carbon Technology Partnerships initiative, The World Business Council for Sustainable Development (WBCSD), (2015).

2. F.P. GLASSER, L. ZHANG, High-performance cement matrices based on calcium sulfoaluminate–belite compositions, Cem. Concr. Res. 31 (2001) 1881-1886.

3. MORIN V., WALENTA G., GARTNER E., TERMKHAJORNKIT P., BACO I., CASABONNE J.M., Hydration of a Belite-Calcium Sulfoaluminate-Ferrite cement:AetherTM, Proceedings of the 13th International Congress on the Chemistry of Cement, Madrid, Spain (2011).

4. L. ZHANG, F.P. GLASSER, Hydration of calcium sulfoaluminate cement at less than 24 h, Advances in Cement Research. 14 (2002) 141-155.

5. W. LAN, F.P. GLASSER, Hydration of calcium sulphoaluminate cements, Advances in Cement Research. 8 (1996) 127-134.

6. F. WINNEFELD, S. BARLAG, Calorimetric and thermogravimetric study on the influence of calcium sulfate on the hydration of ye'elimite, Journal of Thermal Analysis and Calorimetry. 101 (2010) 949-957.

7. H.F.W. TAYLOR, Hydration of Portland cement, in: Cement Chemistry, Second ed., Thomas Telford Publishing, London, 1997, pp. 218.

8. F. W. LOCHER, W. RICHARTZ, S. SPRUNG, Setting of Cement Part II: Effect of Adding Calcium Sulfate, Zement-Kalk-Gips (1980) 33, 271-277.

9. P G.C.BYE, Portland Cement, Thomas Telford, 2007.

10. I. MOHAMMED, F. P. GLASSER, I. GALAN, A method for producing cement, International Publication Number WO 2014/177858 A1, November 2014.

11. I. GALAN, F.P. GLASSER, A. ELHOWERIS, S. TULLY, A. MURDOCH, Novel process for Calcium Sulfoaluminate Production, 34th Cement and Concrete Conference (CCSC). (2014).

12. T. HANEIN, I. GALAN, A. ELHOWERIS, S. KHARE, S. SKALAMPRINOS, G. JEN, M. WHITTAKER, M.S. IMBABI, F.P. GLASSER, AND M.N.

13. BANNERMAN, Production of Calcium SulfoAluminate cement using sulfur as a fuel and as a source of clinker sulfur trioxide: Pilot kiln trial. Submitted to Advances in Cement Research.

14. L. WADSÖ, Operational issues in isothermal calorimetry, Cem. Concr. Res. 40 (2010) 1129-1137.

15. A.C. LARSON, R.B. VON DREELE, General structure analysis system (GSAS), Los Alamos Laboratory, Rep.No.LA-UR. 86 (2004).

16. M.A. ARANDA, G. ÁNGELES, L. LEÓN-REINA, Rietveld quantitative phase analysis of OPC clinkers, cements and hydration products, Reviews in Mineralogy and Geochemistry. 74 (2012) 169-209.

17. B. LOTHENBACH, T. MATSCHEI, G. MÖSCHNER, F.P. GLASSER, Thermodynamic modelling of the effect of temperature on the hydration and porosity of Portland cement, Cem. Concr. Res. 38 (2008) 1-18.

# LOW-ENERGY CEMENTS: THEIR PRODUCTION AND UTILIZATION

**T Staněk**

**M Boháč**

Research Institute for Building Materials

Czech Republic

**ABSTRACT.** Term “low-energy cements” describes cements that can replace ordinary Portland cement in at least some applications and can also reduce energy consumption during the production process. An expansion of these cements could lead in both lower costs of binders production and lower emissions, $CO_2$ especially. Belite cements are part of low-energy cements. Pure belite clinkers with interstitial matter comprising $C_3A$ and $C_4AF$ are not produced, since they yield materials with insufficient strength. Currently, sulfoaluminate-belite cements, low-energy cements doped with fluorine and chlorine as well as undoped high-belite cements are produced in limited volumes in China. Results of hydraulic activation of high-belite clinker by sulfate anions are also given in this work. A principle of activation is the preparation of belite clinker with increased Ca:Si ratio in the structure of dicalcium silicate at substitution of $SiO_4^{4-}$ by $SO_4^{2-}$. Cements prepared from these high-belite content clinkers with alite content up to 25% that were burned at 1350°C display the same technological properties including early strengths as ordinary alite Portland cements.

**Keywords:** Low-energy cement, Belite clinker, Hydraulic activation, Sulfate anion.

**Theodor Staněk** is the Manager of Department of Mortars and Physical Chemistry at the Research Institute for Building Materials in Brno.

**Martin Boháč** is the researcher in Department of Mortars and Physical Chemistry at the Research Institute for Building Materials in Brno.

## INTRODUCTION

The research and the production of hydraulically active low-energy cements, especially of those based on high belite clinkers, is again highly topical and for the future of cementitious binders highly prospective. It is expected to be one of the possible main directions of the development of world cement industry.

Mass production of low-energy cements would mean considerable decrease in total expenses on their production in comparison to the currently common Portland cement with high alite content, along with overall decrease of the environmental impact of cement production. The production of low-energy cements allows to decrease the temperature of burning by 100 – 300°C, what along with economical benefits brings also lowering of $CO_2$ and $NO_x$ emissions. Further decrease of $CO_2$ emissions is brought by the composition of the raw meal for the production of low-energy clinkers, as they require less CaO and thus lesser consumption of $CaCO_3$. This approach also means high quality raw materials resources saving, above all pure limestones, and utilization of less valuable natural materials with lower $CaCO_3$ content, and especially of various secondary and waste products from other industrial productions.

Belite in common Portland clinker has considerably lower hydraulic activity than alite [1] and contributes significantly only to strengths after 28 days of hydration. This led to efforts to stabilize hydraulically active forms of belite, above all its high-temperature modifications. A chemical stabilization by suitable admixtures, usually complemented by extremely fast cooling [2, 3, 4, 5] is one of possibilities. Newer method of belite hydraulic activation is a utilization of the so called remelting reaction [6, 7] or sol-gel method [8, 9]. Such methods can be realized only under conditions outside the possibilities of currently used industrial technologies. The research of the mechanism and kinetics of belite clinker formation has shown, that quickly formed belite clinker has (in contrary to original expectations) lower hydraulic activity than longer burned, recrystallized belite clinker [10].

### Production and Utilization of Low-energy Cements

Basic category of low-energy belite cements:

- Sulfobelite (especially sulfoaluminate-belite (SAB))
- Belite-aluminate (porsal cements)
- Fluor-aluminate belite
- Fluor-sulfoaluminate belite
- Alumina-ferrite and sulfo-ferrite belite
- Belinite

Production of sulfoaluminate-belite (SAB) cements is performed in limited extent, as these cements show appropriate properties [11, 12]. Experiments with industrial production of sulfo-aluminate-ferrite belite clinker (SAFB) and high-Fe belite clinker (HFBC) were realized, which yielded satisfactory strengths after 28 days of hydration, but low short-term strengths [13].

China makes great progress in testing such technologies with industrial production of SAB and also fluoraluminate belite cements and highly belite Portland cements with 20-30 wt. % alite [14]. Chinese authors describe 6 types of produced low-energy cements.

**System of $CaO$-$SiO_2$-$Al_2O_3$ (NA)**

Content of CaO in the system is such that only minerals with low content of CaO such as CA, $CA_2$ and $C_2S$ are formed. Clinker is burned at 1400°C from raw mix of limestone, quartz and high quality $Al_2O_3$.

**System of $CaO$-$SiO_2$-$Al_2O_3$-$CaCl_2$ (LC)**

$CaCl_2$ considerably decreases the temperature of sintering. Clinker contains alinite that is stable from 1050 to 1250°C, phase $11CaO{\cdot}7Al_2O_3{\cdot}CaCl_2$ that is formed from 750°C and it is stable up to 1300°C and $C_2S$. Sintering temperature is 1300°C and clinker is produced from limestone, fly ash and alkali slag.

**System of $CaO$-$SiO_2$-$Al_2O_3$-$CaF_2$ ($\overline{F}A$)**

$CaF_2$ significantly decreases the sintering temperature. Clinker consists of $11CaO{\cdot}7Al_2O_3{\cdot}CaF_2$ and $C_2S$ a can contain $3CaO{\cdot}SiO_2{\cdot}CaF_2$, $C_3A$ and $C_3S$. The raw mix of limestone, bauxite and fluorite is used for clinker production. Sintering temperature is 1300°C.

**System of $CaO$-$SiO_2$-$Al_2O_3$-$CaSO_4$ ($\overline{S}A$)**

Clinker consists mainly of $C_4A_3\overline{S}$ and $C_2S$, and can contain of $C_{12}A_7$, CA and $C\overline{S}$. Clinker is burnt from mixture of gibbsite, limestone and gypsum. Sintering temperature is 1350°C.

**System of $CaO$-$SiO_2$-$Al_2O_3$-$Fe_2O_3$-$CaSO_4$ (FA)**

This clinker contains ferrite phase (solid solution $C_2F$ – $C_6A_2F$) same as ferrite phase from Portland cement clinker. Furthermore it contains $C_4A_3\overline{S}$, $C_2S$ and $C\overline{S}$. Clinker is prepared from raw mix of limestone, Fe-Al slag and gypsum at sintering temperature of 1300°C.

**System of $CaO$-$SiO_2$-$Al_2O_3$-$Fe_2O_3$-$CaSO_4$-$CaF_2$ (HCA)**

In this system, unlike in the system without fluorite, $C_3S$ can be formed. Clinker may contain $C_3S$, $C_4A_3\overline{S}$, $C_6A_2F$ and $C_{11}A_7{\cdot}CaF_2$ or $C_3A$. The raw mix contains limestone, clay, gypsum and fluorite (or slag). Sintering temperature is 1300°C.

These cements have generally very high initial strengths (24-hour strength is comparable to 28-day strength of PC) and are used for special purposes. Cement $C\overline{S}$ may be used in winter concreting at temperatures down to -25°C. Rapid setting FA cements have high resistance to sea water and are used for quick repairs and constructions in marine environments. NA and FA cements are used for the repair of airport runways. Slightly expansive cements $\overline{S}A$ and FA were used to repair damaged cellars. Cements $\overline{S}A$ and FA may be applied during shotcreting. Self-expanding cements NA, $\overline{S}A$ and FA are used for the production of pressure pipes of different diameters.

The main problem to be solved is the production of hydraulically active belite cement, with properties like those of standard “alite” Portland cement, using the existing technological lines. The principle of activation is a formation of belite clinker with increased ratio of CaO : $SiO_2$ in the structure of dicalcium silicate by substitution of $SiO_4^{2-}$ anions by $SO_4^{2-}$ anions.

## PREPARATION AND METHODS

The raw materials used for the preparation of experimental raw meals were pure limestone (L1), limestone with increased $SiO_2$ content (L2), clay shale (CS), iron correction (Fe) and FGD gypsum (EG). The composition and expected chemical parameters of the raw meals are given in Table 1. The planned experiments involved burning of two belite clinkers with about 4 wt. % of $SO_3$ and different lime saturation index, the reference low-saturation belite clinker, and reference alite clinker without $SO_3$ addition.

6 kg of each raw meal were ground to fineness characterized by - 0.09 mm fraction of about 12 wt. %. The raw meals were pressed into tablets 4 cm in diameter, weighing about 80 g. All belite clinkers were burned in a superkantal oven in the following regime: rate of temperature rise 15°C/min, final temperature 1400°C, isothermal dwell 40 min. The alite clinker was burned at 1450°C for 120 min.

Table 1 The composition of raw meals in wt. % and expected basic chemical parameters

| RAW MEAL | RM-B | RM-B80S4 | RM-B90S4 | RM-A |
|---|---|---|---|---|
| L1 | 55.27 | 48.82 | 52.74 | 64.41 |
| L2 | 19.59 | 18.92 | 17.51 | 14.1 |
| CS | 23.72 | 22.96 | 20.57 | 20.62 |
| Fe | 1.42 | 1.37 | 1.26 | 0.87 |
| EG | - | 7.92 | 7.92 | - |
| LSF | 80 | 80 | 90 | 96 |
| SR | 2.6 | 2.6 | 2.6 | 2.6 |
| AR | 1.4 | 1.4 | 1.4 | 1.6 |

Annotation: LSF – lime saturation factor after Lea - Parker, SR – silica ratio, AR – alumina-iron ratio

The representative portion of clinker needed for the determination of phase composition was crushed and sieved to obtain 0.045 – 1 mm grain size fraction, which was then mounted in epoxy resin and polished for observation in optical microscope. To enable the perfect distinction of clinker phases, the polished section was etched in acetic acid fumes [15]. Thus prepared polished and etched sections were point counted [16]. To obtain accurate volume proportions of clinker phases, 2000 points were registered. For the recalculation from volume to weight percentages, following densities were used: $C_3S$ – 3.15, $C_2S$ – 3.28, $C_3A$ – 3.03, $C_4AF$ – 3.77, free CaO – 3.35 $g.cm^{-3}$.

After repolishing, the sections were analyzed with electron microprobe (CAMECA SX100 with 5 crystal spectrometers) to determine the chemical composition of clinker minerals. The quantitative spot analyses were performed under the following analytical conditions: accelerating voltage 15 kV, probe current 20 nA, spot size 2 microns; all elements were analyzed on Kα lines.

The qualitative determination of $SO_3$-phases in clinkers was performed by X-ray diffraction. XRD analysis was performed with diffractometer Bruker D8 Advance, using Cu anode in the range 6-80° of 2 Θ angle. β-$C_2S$ unit cell parameters were refined by the Rietveld method using the Topas 3 software.

Subsequently, cements with approximately the same specific surface were prepared from all clinkers, to which 4 wt. % of natural gypsum were added as controller of setting. The cements were subjected to technological tests according the European standards of the EN 196 series. The determination of the released hydration heat was done by the dissolution method according to EN 196-8 after 2, 7, 28, 56 and 90 days of cement paste hydration, compressive strengths according to EN 196-1 after the same times of cement mortar hydration.

## RESULTS AND DISCUSION

### Composition of Clinkers

The results of quantitative phase composition of all clinkers are given in Table 2, total content of $SO_3$ and real LSF in Table 3. An example of diffractogram of belite clinker doped with $SO_3$ is shown on Figure 1 and the comparison of unit cell parameters of belite without and with $SO_3$ doping is demonstrated in Table 4.

The chemistry of belite grains were determined by electron microanalysis. The results are given in Table 5. Calculations of atomic ratios of elements filling the Ca site (i.e. Ca, Mg, Na, K) versus elements filling the Si site (Si, S, P, Al, $Fe^{3+}$, Ti) have shown that they are close to stoichiometric 2 : 1.

Table 2 Phase composition of clinkers in wt. %

| CLINKER | S-B | S-B80S4 | S-B90S4 | S-A |
|---|---|---|---|---|
| $C_3S$ | 0.2 | 0.0 | 8.3 | 66.7 |
| $C_2S$ | 79.3 | 81,3 | 71.5 | 12.2 |
| $C_3A$ | 4.0 | 2.6 | 4.1 | 12.3 |
| $C_4AF$ | 16.5 | 14.6 | 13.6 | 7.8 |
| $C_{free}$ | 0.0 | 0.0 | 0.0 | 0.9 |
| $C\bar{S}$ | 0.0 | 1.5 | 2.5 | 0.0 |
| $C_4A_3\bar{S}$ | 0.0 | trace | trace | 0.0 |

Table 3 Total content of $SO_3$ in wt. % and real lime saturation factor in clinkers

| CLINKER | S-B | S-B80S4 | S-B90S4 | S-A |
|---|---|---|---|---|
| $SO_3$ tot | 0.06 | 4.44 | 4.43 | 0.03 |
| LSF | 70.4 | 77.0 | 82.7 | 93.5 |

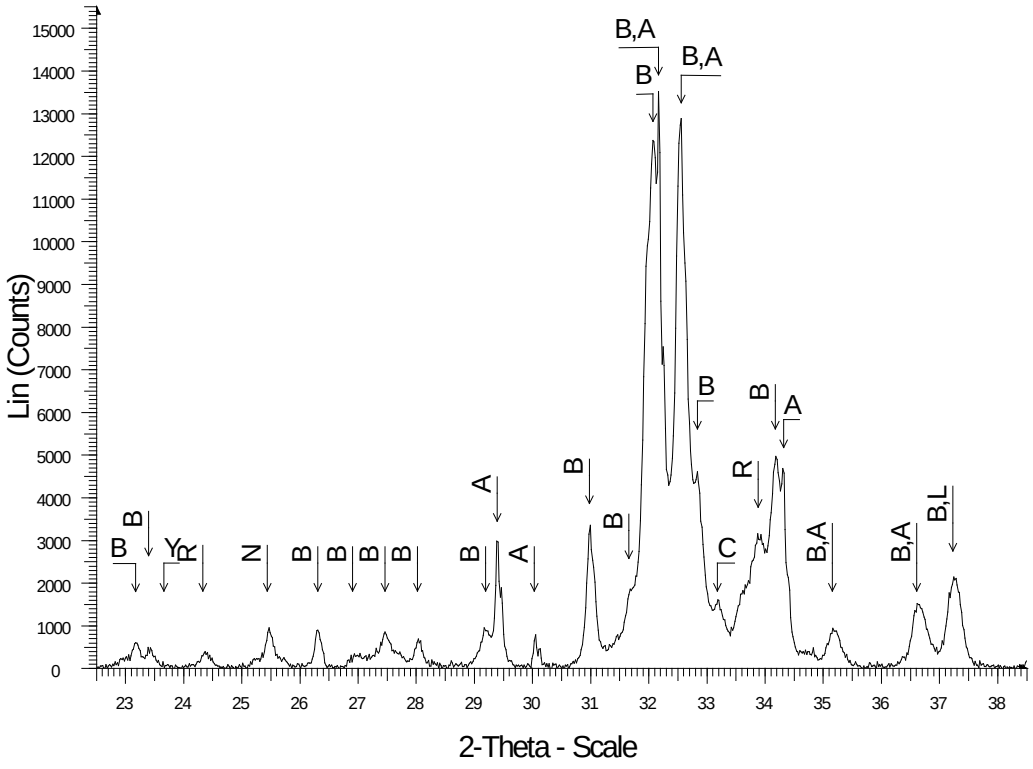


Figure 1 Diffractogram of clinker S-B90S4 (B=β-$C_2S$, A=$C_3S$, R=$C_4AF$, C=$C_3A$, L=free lime, N=anhydrite II, Y=yeelimite)

Table 4 Unit cell parameters of belite

| CLINKER | S-B | S-B90S4 |
|---|---|---|
| a (Å) | 5.5034 | 5.5215 |
| b (Å) | 6.7622 | 6.7747 |
| c (Å) | 9.3306 | 9.3492 |
| beta (°) | 94.085 | 94.331 |
| Volume (Å$^3$) | 346.36 | 348.72 |

Table 5 Average chemical composition of belite grains determined by electron microprobe in wt. %

| CLINKER | S-B | S-B80S4 | S-B90S4 | S-A |
|---|---|---|---|---|
| $SiO_2$ | 32.01 | 30.56 | 28.80 | 31.01 |
| $TiO_2$ | 0.21 | 0.22 | 0.22 | 0.28 |
| $Al_2O_3$ | 0.96 | 1.81 | 2.76 | 1.62 |
| $Fe_2O_3$ | 1.14 | 1.17 | 1.76 | 1.48 |
| $P_2O_5$ | 0.09 | 0.10 | 0.09 | 0.07 |
| MnO | 0.05 | 0.06 | 0.07 | 0.07 |
| MgO | 0.38 | 0.25 | 0.61 | 0.32 |
| CaO | 63.23 | 63.74 | 65.36 | 63.72 |
| $Na_2O$ | 0.26 | 0.11 | 0.15 | 0.37 |
| $K_2O$ | 0.79 | 0.10 | 0.14 | 0.93 |
| $SO_3$ | 0.06 | 1.61 | 3.09 | 0.07 |
| $CaO:SiO_2$ (atomic) | 2.12 | 2.24 | 2.43 | 2.20 |
| (Ca+K+Na+Mg):(Si+S+P+Al+Fe+Ti) (atomic) | 2.04 | 1.97 | 1.99 | 2.06 |

**Cement Properties**

The specific surface (Blaine) and density of prepared cements are given in Table 6. The principal technological property of cements is their strength; that was measured according to EN 196-1 and results are given on Figure 2. The released hydration heat, determined by the dissolution method (according to EN 196-8) is given on Figure 3.

Table 6 Density (in $kg/m^3$) and specific surface (in $m^2/kg$) of prepared cements

| CEMENT | C-B | C-B80S4 | C-B90S4 | C-A |
|---|---|---|---|---|
| Density | 3230 | 3261 | 3191 | 3179 |
| Specific surface | 435 | 436 | 438 | 437 |

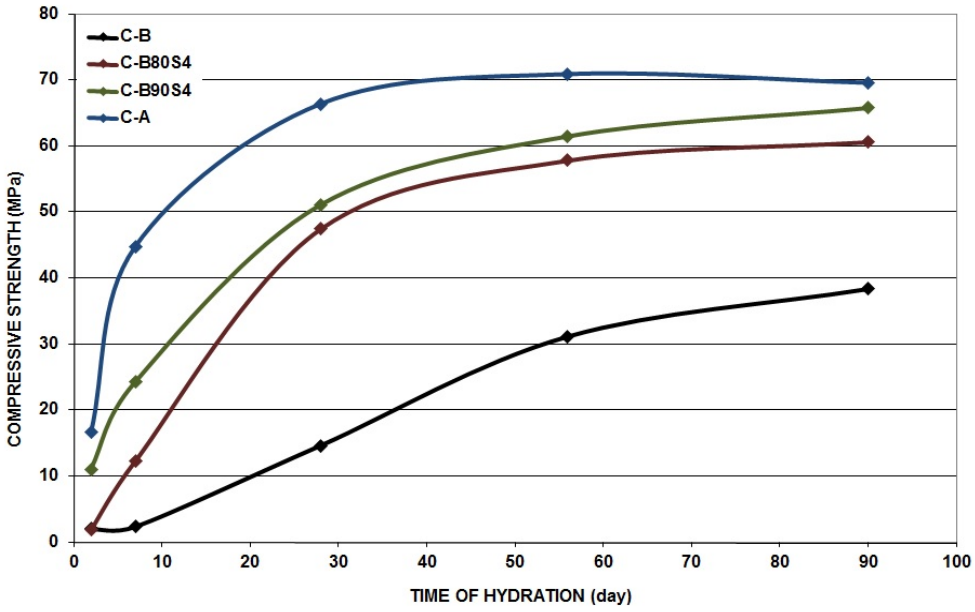


Figure 2 The development of compressive strength in prepared cements

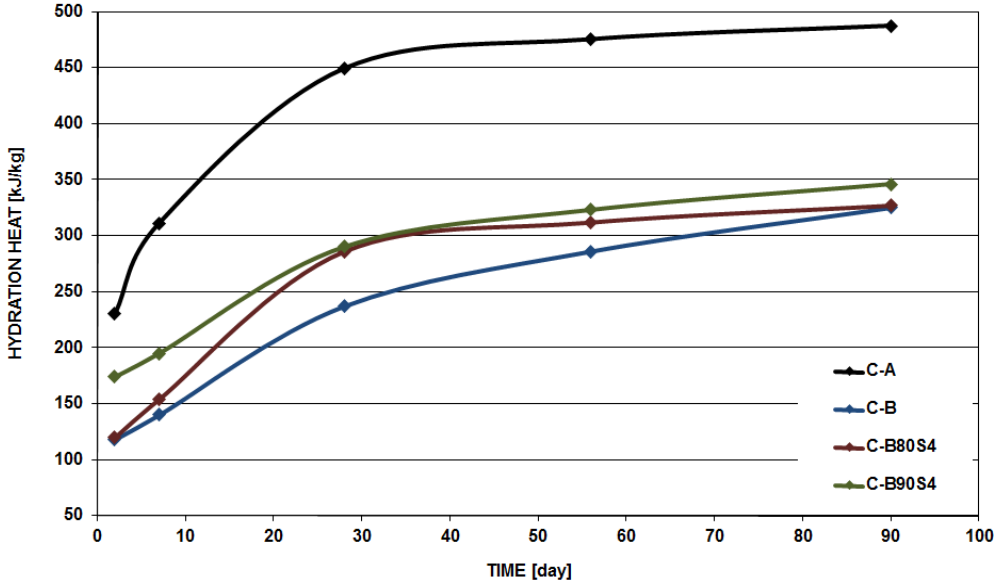


Figure 3 The development of hydration heat in prepared cements

## Optimization of "Sulfobelite" Cements

The optimization of "sulfobelite" cements was done through a series of experiments, varying the chemical composition of raw meals, the burning regime with the aim of achieving as high as possible strengths in all hydration times. To prepare the raw meals, common cement-making raw materials were used; the source of $SO_3$ was industrial FGD gypsum. The fundamental characteristics of chosen clinkers and belite cements prepared from them are given in Table 7, together with reference cements. For comparison, the first three columns give parameters of clinkers prepared without $SO_3$ addition (B – purely belite, B81S0 – belite with 25 % alite content and A97S0 – high alite clinker).

Table 7 Properties of cements prepared from belite clinkers doped with $SO_3$ and reference cements

| CEMENT | B | B81S0 | A97S0 | B80S4 | B92S8 | B89S6 | B92S6 |
|---|---|---|---|---|---|---|---|
| Phase | Phase composition of used clinker [wt. %] | | | | | | |
| $C_3S$ | 0.2 | 24.5 | 75.8 | 0.0 | 10.0 | 17.0 | 33.6 |
| $C_2S$ | 79.3 | 58.4 | 6.9 | 81.3 | 71.5 | 65.0 | 50.8 |
| $C_3A$ | 4.0 | 6.5 | 11.0 | 2.6 | 3.7 | 3.5 | 4.0 |
| $C_4AF$ | 16.5 | 10.0 | 5.8 | 14.6 | 11.4 | 10.1 | 8.8 |
| $C_{vol}$ | 0.0 | 0.5 | 0.5 | 0.0 | 1.9 | 1.6 | 0.8 |
| $C_4A_3\bar{S}$ | 0.0 | 0.0 | 0.0 | trace | 0.0 | 0.0 | 0.0 |
| $C\bar{S}$ | 0.0 | 0.0 | 0.0 | 1.5 | 1.5 | 2.8 | 2.0 |
| Parameter | Chemical parameters of used clinker [wt. %] | | | | | | |
| $SO_3$ (wt. %) | 0.06 | 0.07 | 0.02 | 4.44 | 6.77 | 4.18 | 5.48 |
| LSF (%) | 70.4 | 79.9 | 96.2 | 77.0 | 89.4 | 88.6 | 92.1 |
| SR | 2.88 | 3.00 | 2.57 | 2.63 | 3.12 | 3.09 | 3.31 |
| AR | 1.41 | 1.28 | 1.41 | 1.49 | 1.45 | 1.57 | 1.33 |
| Parameter | Clinker burning parameters [°C, min] | | | | | | |
| Temperature | 1400 | 1350 | 1450 | 1400 | 1350 | 1350 | 1350 |
| Burning time | 40 | 50 | 120 | 40 | 30 | 50 | 60 |
| Parameter | Cement parameters [wt. %, $kg/m^3$, $m^2/kg$] | | | | | | |
| Gypsum | 4.0 | 3.0 | 4.0 | 4.0 | 3.0 | 3.0 | 3.0 |
| Density | 3230 | 3225 | 3172 | 3261 | 3231 | 3201 | 3191 |
| Specific surface | 435 | 397 | 398 | 436 | 402 | 406 | 410 |
| Hydration time | Compressive strength [MPa] | | | | | | |
| 2 days | 2.0 | 4.5 | 21.6 | 1.8 | 16.9 | 20.1 | 31.7 |
| 7 days | 2.3 | 12.8 | 49.3 | 12.2 | 26.1 | 39.4 | 51.6 |
| 28 days | 14.6 | 63.5 | 66.9 | 47.4 | 36.4 | 59.1 | 64.7 |
| 90 days | 38.3 | 81,1 | 72,7 | 60.6 | 64.9 | 67.6 | 76.2 |

## CONCLUSIONS

Chemical activation of belite by sulfate anions has significant impact on its hydraulic activity. The incorporation of $SO_3$ into the belite structure, where it substitutes $SiO_2$, enables to widen this substitution also for other oxides, above all $Al_2O_3$ a $Fe_2O_3$. In this way, the CaO : $SiO_2$ ratio in belite is distinctly higher than in belite without the $SO_3$ incorporation. This phenomenon is more pronounced in belite clinker with higher lime saturation factor. Unit cell volume of belite doped with $SO_3$ is slightly larger than that of belite without doping of $SO_3$, which is in accordance with earlier findings of Morsli et al. [17].

This „sulfobelite“ clinker burned at temperature by 100 °C lower than in common Portland clinker has at the content of alite around 20 wt. % and technological parameters similar to that of high content alite clinker. Moreover, it develops much less hydration heat, what can be very favorable in certain applications.

In contrast to pure belite clinker doped with $SO_3$, a small amount of alite distinctly supports the growth of early strengths, because this alite is present in its more hydraulically active $M_1$ modification [18], which is stabilized just by $SO_3$.

The relatively high lime saturation (yet still about 10 % lower than in common Portland clinker) in this belite clinker ensures at the reaction with water formation of higher amounts of portlandite ($Ca(OH)_2$) and increases the overall alkalinity, accelerating thus the course of hydration.

Hydraulic activation of this „sulfobelite“ clinker is therefore caused on one hand by the disturbance of the belite crystal structure and its “contamination” by foreign ions, on the other hand by relatively high CaO content in clinker and probably also by the presence of small amounts of anhydrite II, which, as was found, has positive impact on the development of cement strength [19].

This activated belite clinker could be used with regard to its good hydraulic properties for the production of self-contained sulfobelite cement, or for blending with OPC for production of special cements. In working practice it would be advantageous to use the existing kiln lines for alternating production of “sulfobelite” and classical alite clinker. The lower burning temperature and very short clinkering zone during the belite clinker burning would enable to use the sticking from the preceding burning of the alite clinker, because the sticking from belite burning is probably insufficiently stable.

The increase in lime saturation causing formation of up to 20 – 30 wt. % alite would contribute to the increase of hydraulic activity as well as to improvement of parameters of burning and grindability.

The obtained results indicate the possibility of separate industrial production of special low-energy active belite clinker alongside with the production of common alite clinker and the production of economically and ecologically expedient blended Portland cements, possessing suitable technological properties, or goal-directed preparation of special cements with properties tailored according to the intended use. Introduction of this cement into the cement making industry would lead to a decrease of energy consumption, saving of high quality limestone and at the same time lowering of $CO_2$ emissions.

## ACKNOWLEDGEMENTS

This research was done within the project No. 16-08959J, financed by the Czech Science Foundation.

## REFERENCES

1. SHARARA, A M, EL-DIDAMONY, H, EBIED, E, ABU EL-ALEEM. Hydration characteristic of β-$C_2S$ in the presence of some pozzolanic materials, Cement and Concrete Research, Vol. 24, No. 5, 1994, pp 966-974.

2. CHATTERJEE, A. High Belite Cements–Present Status and Future Technological Options: Part I., Cement and Concrete Research, Vol. 26, No. 8, 1996, pp 1213-1225.

3. EMANUELSON, A LANDA-CÁNOVAS, A R, HANSEN, S. A comparative study of ordinary and mineralised Portland cement clinker from two different production units Part II: Characteristics of the calcium silicates. Cement and Concrete Research, Vol. 33, No. 10, 2003, pp 1623-1630.

4. GIES, A, KNÖFEL, D. Influence of alkalis on the composition of belite-rich cement clinkers and the technological properties of the resulting cements, Cement and Concrete Research, Vol. 16, No. 3, 1986, pp 411-422.

5. JOST, K H, SEYDEL, R, MÜLLER, A, STARK, J. Relationship between phase-composition, cooling rate and $Na_2O$ content in belite clinkers, Zement-Kalk-Gips, Vol. 41, No. 4, 1988, pp 169 – 170.

6. FUKUDA, K, MAKI, I, ITO, S. Remelting reaction within belite crystals during cooling, Journal of the American Ceramic Society, Vol. 75, No. 10, 1992, pp 2896-2898.

7. FUKUDA, K, WAKAMATSU, N, ITO, S. Improvement in hydration reactivity of alpha-phase belite by remelting reaction, Journal of the American Ceramic Society, Vol. 84, No. 3, 2001, pp. 639-641.

8. CHRYSAFI, R, PERRAKI, T, KAKALI, G. Sol-gel preparation of $2CaO.SiO_2$, Journal of the European Ceramic Society, Vol. 27, No. 2-3, 2007, pp 1707-1710.

9. KURDOWSKI, W, DUSZAK, S, TRYBALSKA, B. Belite produced by means of low-temperature synthesis, Cement and Concrete Research, Vol. 27, No. 1, 1997, pp 51-62.

10. STANĚK, T. Influence of preparation parameters on properties of belite clinker, Advanced Materials Research, vol. 897, 2014, pp. 3-8.

11. BROWN, A D R. In Commercial, production, composition and properties of a calcium sulfoaluminate cement, Int. Conf. on Cements for the Future - Calcium sulphoaluminates, London, 1992, pp 3.

12. MOJUMDAR, S C, JANOTKA, I. Thermophysical properties of blends from Portland and sulfoaluminate-belite cements, Acta Physica Slovaca, Vol. 52, No. 5, 2002, 435-446.

13. POPESCU, C D, MUNTEAN, M, SHARP, J H. Industrial trial production of low energy belite cement, Cement and Concrete Composites, Vol. 25, No. 7, 2003, pp 689-693.

14. SUI, T, WEN, Z, WANG, J, FAN, L. Development of belite based cements in China, Cement Combinations for Durable Concrete, Proceedings of the International Conference held at the University of Dundee, Eds. R K Dhir, T A Harrison and M D Newlands, 2005, pp 323-328.

15. CHROMÝ, S. Anfärben des freiem CaO und Silikate in anschliffen von Portlandklinker, Zement-Kalk-Gips, Vol. 27, No. 2, 1974, pp 79-84.

16. CHROMÝ, S. Accuracy and precision of microscopic quantitative phase analysis of Portland clinkers (in Czech), Silikáty, Vol. 22, No. 3, 1978, pp 215-226.

17. MORSLI, K, DE LA TORRE, Á G, ZAHIR, M, ARANDA, M A G. Mineralogical phase analysis of alkali and sulfate bearing belite rich laboratory clinkers, Cement and Concrete Research, Vol. 37, No. 5, 2007, pp 639-646.

18. STANĚK, T, SULOVSKÝ, P. The influence of the alite polymorphism on the strength of the Portland cement, Cement and Concrete Research, Vol. 32, No. 7, 2002, pp 1169-1175.

19. STANĚK, T, TOMANCOVÁ, L. The influence of the forms of calcium sulfate on the properties of cement (in Czech), Silika, Vol. 18, No. 1-2, 2008, pp 41-44.

# ACCELERATED AGING STUDIES OF A CALCINED CLAY-BASED GEOPOLYMER BINDER

**J A McIntosh** **D Jose** **M N Soutsos**

Queen's University Belfast

**S E Lawther**

banah UK Ltd

United Kingdom

**ABSTRACT.** Geopolymer binders have emerged as a more eco-friendly and more durable alternative to Portland cements. They are generally formed by reacting a powdered aluminosilicate precursor with an alkali silicate activator. The most promising research to date has concentrated on using calcined clays containing dehydroxylated kaolin (metakaolin) as the main aluminosilicate source. However, detrimental structural changes in the microstructure of certain metakaolin-based geopolymers causing a reduction in compressive strength during accelerated aging tests have been reported. In this study, testing was carried out using the same experimental methodology on geopolymer pastes and mortars formulated with a ferruginous kaolinitic clay precursor. The samples were characterised from a structural and microstructural point of view where effects on compressive strength and change in crystallinity were examined and a correlation between the two proposed. Preliminary studies have found that geopolymers based on multi-mineral calcined clays do not undergo the dramatic changes seen in previous studies by other researchers who used high-purity metakaolin. It has been shown that the increase in crystalline structure and decrease in compressive strength caused by accelerated aging at 95°C and 99 % RH over a period of time was minimal and therefore will have little impact on the service life of concretes and mortars formulated using this binder.

**Keywords:** Accelerated ageing, Metakaolin-based geopolymer, Amorphous to crystalline phase conversion, Microstructure.

**Mr John A McIntosh** is the Director of Research for banah UK Ltd, based in Coleraine, Northern Ireland.

**Dr Deepa Jose** is a Research Scientist with banah UK Ltd. She is currently working on the further development of geopolymer materials within banah UK.

**Dr S E Lawther** is a KTP Associate with banah UK Ltd and Queens University Belfast.

**Professor Marios Soutsos** is Professor at the School of Planning, Architecture and Civil Engineering at Queen's University, Belfast.

## INTRODUCTION

Research on the development of geopolymer binders or alkali activated cementitious materials (AACM) has been gaining traction since interest was re-ignited almost 40 years ago [1]. It is claimed that by using these materials as an alternative to Portland cement, more eco-friendly and more durable concretes and mortars can be obtained [2]. Geopolymers are typically formed from the reaction of an amorphous aluminosilicate powder with an alkali silicate solution. Powders based on calcined clays containing dehydroxylated kaolin (metakaolin) as the main aluminosilicate source show the greatest potential in terms of sustainable supply and consistent performance. Research has shown that use of these new binders makes it possible to manufacture concretes with superior resistance to sulfate attack, improved performance in fire and reduced carbon emissions during manufacture [3].

A key characteristic of a hardened geopolymer matrix is that the microstructure formed is x-ray amorphous. It has been stated that from a thermodynamic viewpoint, geopolymers can be considered as 'metastable' [4]. This is in contrast to zeolites which, although possessing a similar alkali aluminosilicate composition, have a highly developed crystalline structure. Whether a given alkali-aluminosilicate mixture forms a zeolite or a geopolymer depends on the relative ratios of each of the main components and the processing conditions applied during manufacture. Due to this similarity, concerns have been raised that the meta-stability of geopolymers can result in the slow development of crystalline structures within the geopolymer matrix over time [5]. Should geopolymers undergo an amorphous to crystalline phase change, this has the potential to have negative implications for the long term durability of structures.

To date, various studies have been carried out in this area. In 2004, Schmücker et al studied the changes in a sodium polysialate siloxo geopolymer subjected to elevated temperatures for a short period of time. They found that after heating to both 300°C and 1200°C for 4 hours the geopolymer retained its x-ray amorphous structure. The only exception was that areas of mullite formed where relics of unreacted metakaolinite remained [6]. On the other hand, work carried out by Duxson et al has shown that when metakaolin-based geopolymer pastes were heated to temperatures of up to 1000°C, changes did take place in the microstructure. This was identified as densification and formation of crystalline phases which was greatly influenced by the alkali cation used and the ratio of Si/Al [7, 8]. It was found that as the Si/Al ratio increased, the tendency to form zeolites decreased, but also that the densification of Na-based geopolymer occurred at a lower temperature than that of K-based geopolymer [9].

Further studies were carried out by Lloyd et al comparing the effects of accelerated ageing on metakaolin and fly ash-based geopolymers. Building on previous research and the fact that geopolymer binder systems have been described as zeolite precursors, this work was carried out to assess whether meta-stable geopolymer systems would undergo a phase change causing densification and loss in strengths similar to the conversion process described for calcium aluminate cements (CAC) [10]. The conclusion of this work was that although metakaolin-based geopolymer experienced a small strength gain in the first day of accelerated aging, significant conversion of amorphous geopolymer phases to crystalline zeolite phases occurred after 5 days of curing at 95°C in a sealed environment. This was accompanied with a strength loss of 60% of the original cured value. When fly ash-based geopolymer was subjected to the same procedure the development of new crystalline phases were also observed. Unlike the metakaolin-based binder this was not accompanied with a strength loss. Lloyd concludes that metakaolin-based geopolymers should not be used in applications where strength regression would have dangerous repercussions, such as in structural concrete.

banah UK Ltd was formed in 2008 with the aim of researching and developing a commercially viable geopolymer binder system for the construction industry. Research concentrated on the use of a laterite, known as lithomarge, found in large quantities as part of the Interbasaltic Formation – a geological feature found in Northern Ireland. As a result of this work a geopolymer binder was developed and is currently marketed as banahCEM.

Given the importance of long-term durability of concrete structures to the construction industry and the need to ensure public safety, investigations were carried out to determine whether conversion also occurs in calcined clay-based geopolymer binder systems. As existing research is contradictory and it has been shown that the chemical composition of the geopolymer matrix is highly influential, the effect of accelerated ageing on physical properties was examined and evolution of the microstructure determined over a range of metakaolin-based geopolymer systems.

This paper presents initial results from research carried out by banah UK Ltd and Queen's University, Belfast, which form part of a larger on-going research project.

## EXPERIMENTAL PROGRAMME

### Materials

Testing was carried out on a range of geopolymer mortars. In each case the binder was a 2-part system comprising a powder component principally based on a calcined kaolinite-rich clay and a liquid component based on an aqueous solution of alkali silicate.

Two calcined ferruginous lateritic clays with an identical mineralogical composition, but produced to differing specifications, were used in this study. The minerals present in the clays prior to calcination were: kaolinite, gibbsite, goethite, hematite and anatase. C1 was calcined and milled to a particle size distribution with d90 = 56 µm. C2 was calcined and milled to have a finer particle size distribution to comply with the proprietary banah specification. As a further variation in the composition of the powder components Ground Granulated Blastfurnace Slag (GGBS) was added as a main constituent. This was introduced to reflect practices seen in literature for similar compositions [11]. GGBS was sourced from Lafarge UK. As a comparison to the calcined ferruginous clay a high purity metakaolin, Metamax, was sourced from BASF. This material had a d50 = 1.3µm.

One liquid activator was used in this work. This was an aqueous solution of potassium silicate obtained from PQ Corporation and modified to banah's proprietary chemical composition.
The filler used was a 0/4mm natural pit sand from Tobermore Concrete Products Ltd.

### Mortar Preparation and Equipment

Geopolymer mortars were prepared according to the ratios shown in Table 1 using 5L laboratory mixers. Powder/activator ratios were calculated based on the relative content of active material present in each binder system. The flow of each mortar was measured according to BS EN 1015-3:1999 with a target value of 175mm. Test specimens were cast in nylon moulds with dimensions 50mm x 50mm x 50mm and cured for 24 hours at 20°C, covered with an acetate sheet.

After removing from moulds, the specimens were cured for 28 days at 20°C in a sealed environment to prevent moisture loss. To enable clarity in microstructural examination geopolymer pastes were also prepared according to the same formulation, but without the inclusion of sand.

Table 1 Geopolymer mortar composition.

| VARIABLE | MIX CODE | | | | | |
|---|---|---|---|---|---|---|
| | C1 | C1G | C2 | C2G | M | MG |
| Powder/Activator Ratio | 1.346 | 1.349 | 1.347 | 1.349 | 0.60534 | 0.618 |
| Water/Binder Solids Ratio | 0.396 | 0.395 | 0.305 | 0.305 | 0.389 | 0.389 |
| Paste volume ($L/m^3$) | 0.473 | 0.473 | 0.440 | 0.440 | 0.405 | 0.405 |
| %GGBS in powder | 0 | 12.6 | 0 | 12.6 | 0 | 12.6 |

Compressive strength testing was performed using an Impact 2000kN compression test machine. During accelerated ageing curing, specimens were stored in a sealed environment within a Genlab laboratory oven as described below. Powder X-ray diffraction (XRD) measurements were carried out on both a PANalytical X'pert PRO MPD at Queen's university, Belfast and on a PANalytical X'pert3 PRO at banah UK Ltd. Analysis was performed using Highscore software. Simultaneous thermal analysis using a Netzsch STA-449 F5 was carried out at banah UK Ltd. Polished paste specimens were examined by scanning electron microscopy (SEM) using a FEI Quanta FEG –Environmental SEM (E-SEM) at Queen's University, Belfast.

### Test Methodology

Following initial casting and subsequent ambient temperature curing for 28 days, 3 mortar specimens were tested for compressive strength. The remainder of the cubes were then placed in a sealed plastic container on a wire mesh that was raised off the base of the container. Water was placed in the base of the container to provide humidity and maintained at such a level such that the test specimens did not come into contact with the water. The complete container was then placed in an oven heated to 92°C ± 3°C.

Specimens were removed for testing at 14, 28 and 90 days of high temperature curing. Mortars were tested for compressive strength and pastes analysed by x-ray diffraction to monitor the development of crystalline phases.

## RESULTS AND DISCUSSION

### Compressive Strength

Evolution of the compressive strength of mortar specimens throughout testing is shown in Figure 1. During the first 14 days of high temperature curing, all mixes showed an increase in compressive strength with the exception of C1G. By 28 days of high temperature curing, mean compressive strength values of C1 and C1G mortars had decreased significantly from the original 28 day ambient curing value. C2 and C2G compressive strengths varied slightly, but are within an acceptable coefficient of variation for a mortar specimen.

Mortars based on the pure metakaolin, M and MG, undergo a strength increase that is then maintained to 90 days accelerated ageing.

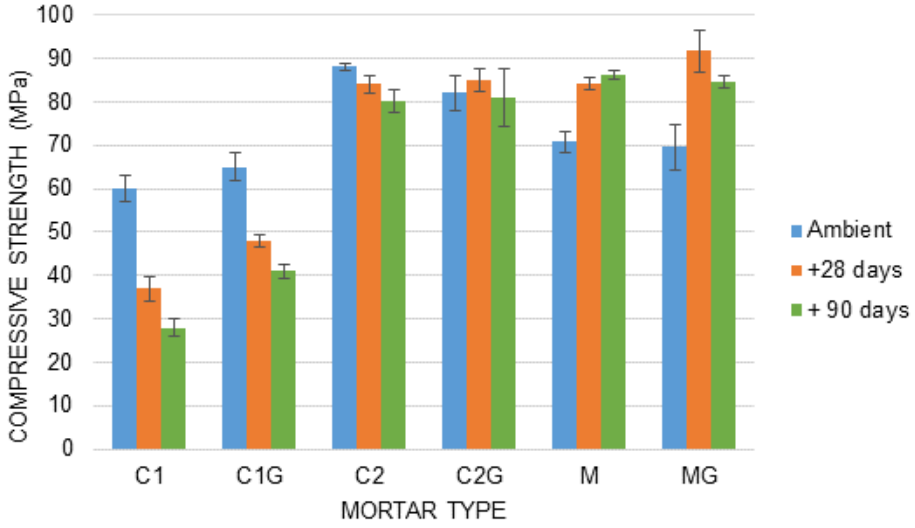


Figure 1 Compressive strength development of mortars before and during accelerated ageing.

It is apparent from Figure 1 that some mortars – specifically those based on C1 and C1G - undergo compressive strength regression during continued high temperature curing. The strength loss is most significant with C1 where up to 50% of the 28 day ambient compressive strength is lost at 90 days. However, compressive strength profiles are not the same across all binder types. It can be seen that for mortar C2 the maximum strength reduction is less than 10% and when error is taken into account, this becomes negligible. Mortar C2G undergoes a slight strength increase followed by a return to original ambient strengths by 90 days of ageing. For mortars M and MG, the profile is different in that an initial strength gain is seen followed by stabilisation.

Figure 1 shows that both strength loss and strength gain occurred regardless of whether GGBS was present or not. It can also be seen that although C1 and C1G mortars had the same binder solids content, these mortars developed significantly lower compressive strengths after 28 days ambient curing compared to the other mortars. This is due to a requirement for increased water content needed to achieve the target flow.

**Powder X-Ray Diffraction (XRD)**

Powder XRD analysis was used to identify any change in the crystallinity of each paste after 28 days ambient curing and then after 14, 28 and 90 days of accelerated curing. The diffractograms are shown in Figure 2. All of the pastes display the amorphous ‘hump’ centred around 28 degrees 2Θ - typical of a metakaolin-based geopolymer binder system [2]. For pastes based on calcined ferruginous clay, this hump is interspersed with peaks showing the presence of hematite and quartz or calcite. The presence of quartz and calcite in the calcined ferruginous clay specimens is due to contamination introduced during bulk processing of the powder prior to calcination. Specimens based on white metakaolin display peaks that indicate the presence of quartz.

During the first 28 days of accelerated ageing, no new peaks were observed in any of the samples. This indicates that minimal change has taken place within the amorphous structure of the geopolymer matrix (Figure 2a-f).

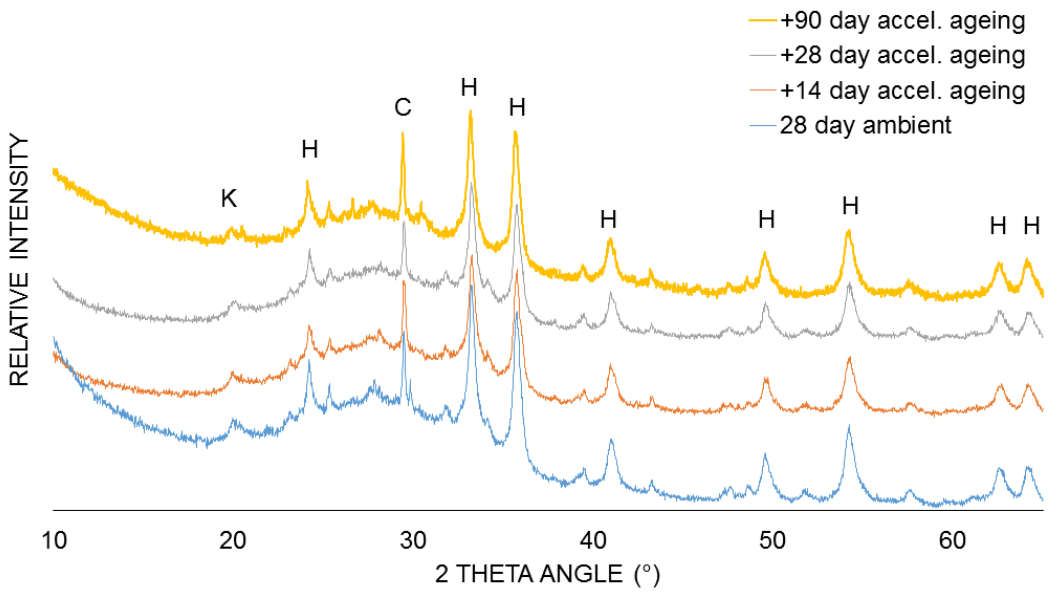


Figure 2a X-ray diffractogram of paste C1

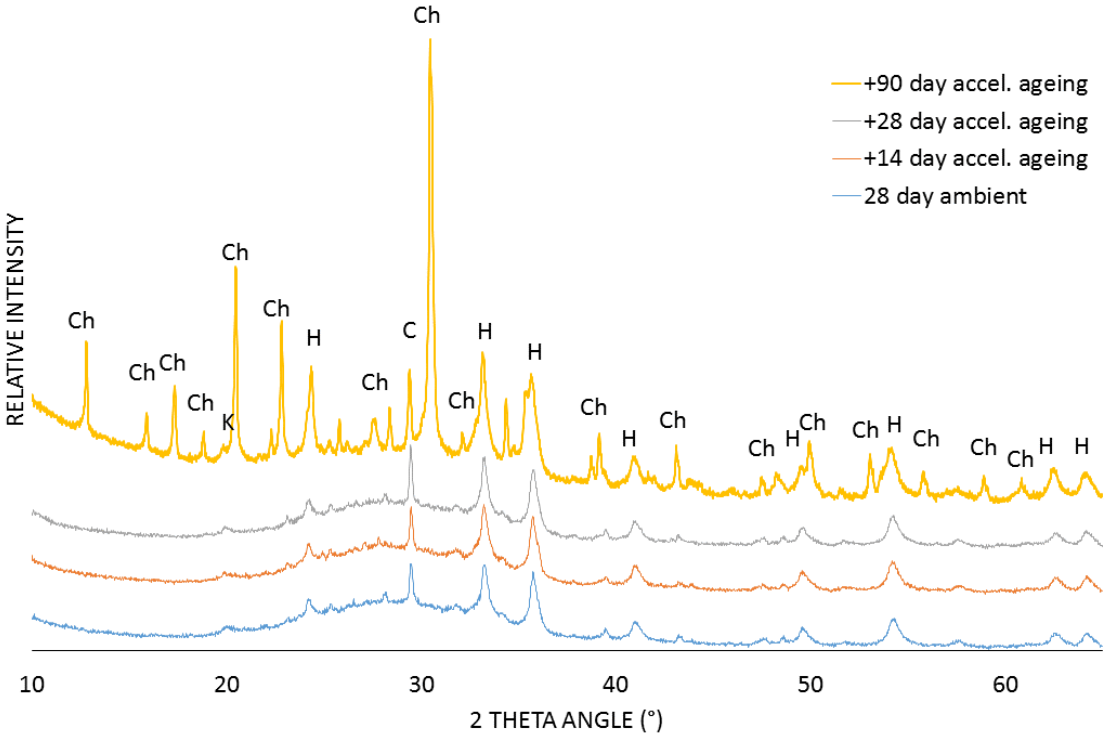


Figure 2b X-ray diffractogram of paste C1G

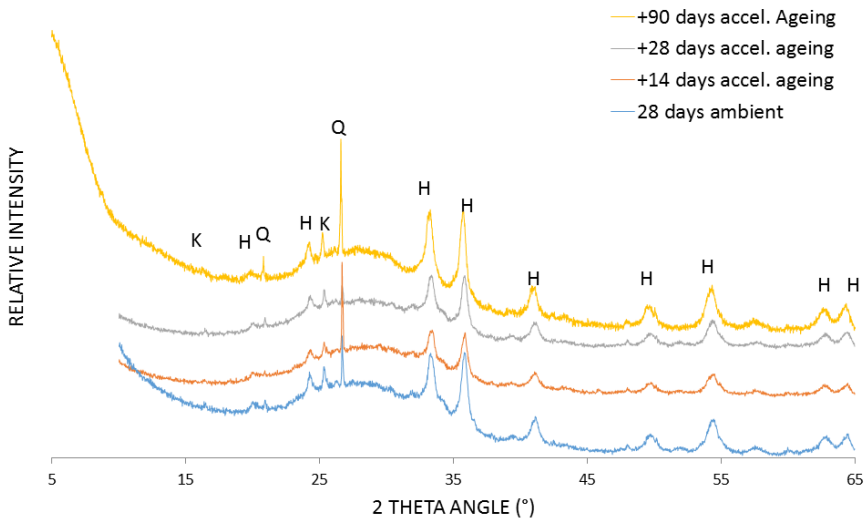


Figure 2c X-ray diffractogram of paste C2.

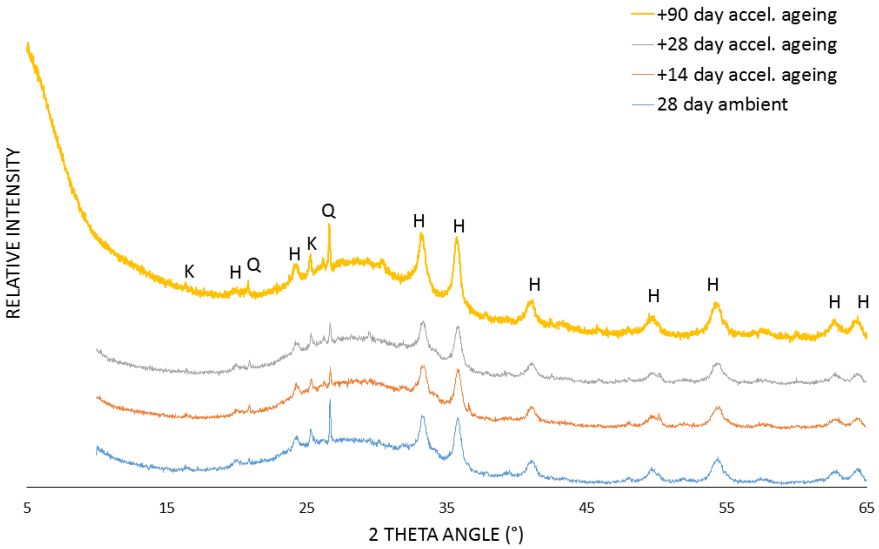


Figure 2d X-ray diffractogram of paste C2G.

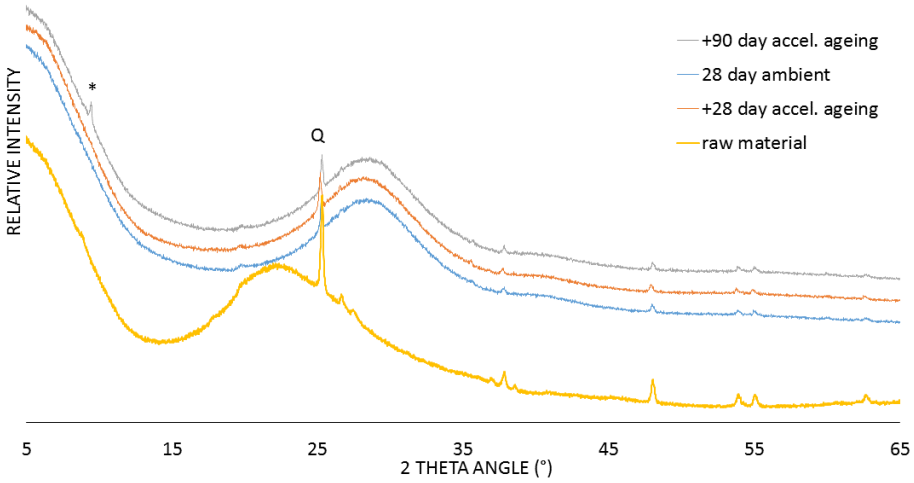


Figure 2e X-ray diffractogram of paste M.

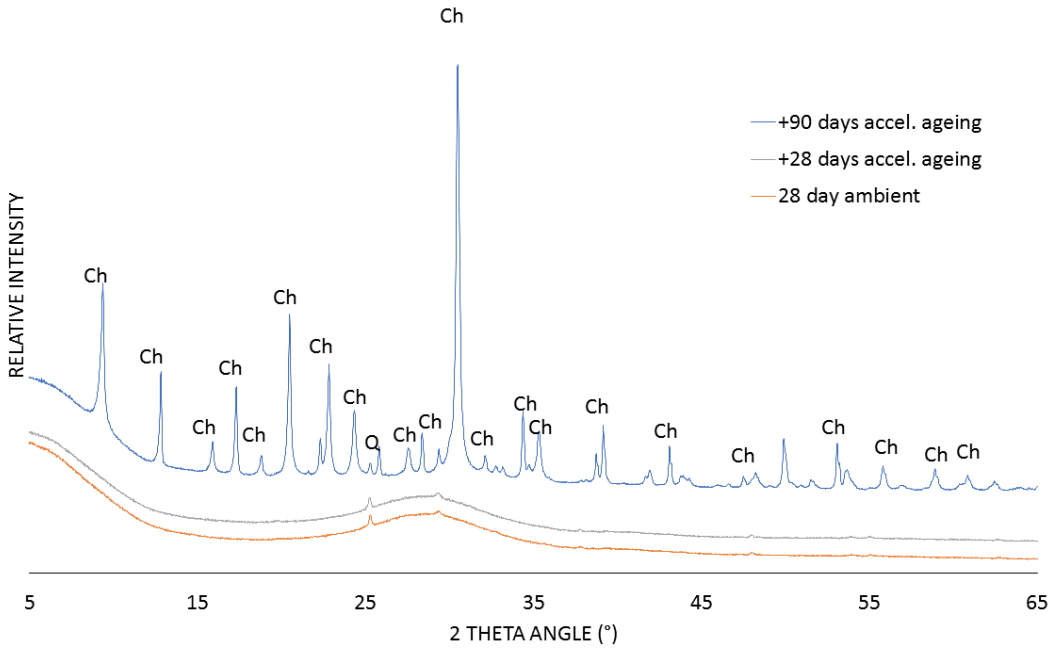


Figure 2f X-ray diffractogram of paste MG.

Key: H – hematite; K – kaolin; Q – quartz; C – calcite; Ch – (Ca,K)-chabazite; * - unidentified phase

As accelerated aging continued to 90 days, a change to the diffraction pattern of both C1G and MG indicated the presence of new crystalline phases. Analysis of the peaks concluded that they could be attributed to the presence of the alkali aluminosilicate hydrate, Chabazite. This mineral forms part of the zeolite group. The pastes contained both calcium and potassium sources in the form of GGBS and aqueous alkali silicate respectively, therefore the chabazite formed is most likely Ca/K-enriched.

No change was observed in the X-ray diffraction pattern for C2 after 90 days ageing showing that the amorphous structure of the geopolymer remains stable. For paste M after 90 days, the emergence of a small peak at 9.4 °2Θ was observed. Identification of this peak was not possible, but as compressive strengths were unaffected, it is not considered to be detrimental. C1 and C2G appear to be developing a small peak at 29.4 °2Θ after 90 days. Analysis of this peak suggest the presence of a K-zeolite, but the quantities involved are small. Further analysis after 180 days will be necessary.

Comparison of C1G, C2G and MG X-ray diffraction patterns show that the development of crystallinity is largely due to the presence of GGBS. However, when the compressive strengths are then considered, the development of this crystallinity does not imply a resultant strength loss.

**Simultaneous Thermal Analysis**

Simultaneous Thermal Analysis (STA) can be used to help differentiate between free moisture present in the paste and ‘interstital’ or hydroxyl water weakly bound within the geopolymer structure. This is performed by examining mass loss and calorimetric effects at increasing temperatures [12]. Unlike free moisture, interstitial water will not evaporate under normal ambient conditions, but when measured using thermal decomposition techniques can give an indication of changes within the microstructure.

In an effort to build understanding of the cause of variation in performance of C1 mortars when compared to C2 and M, paste samples were subjected to thermal decomposition analysis yielding both thermogravimetric (TG) and calorimetric analysis (DSC) (Figure 3). Samples containing GGBS were omitted from this study for clarity.

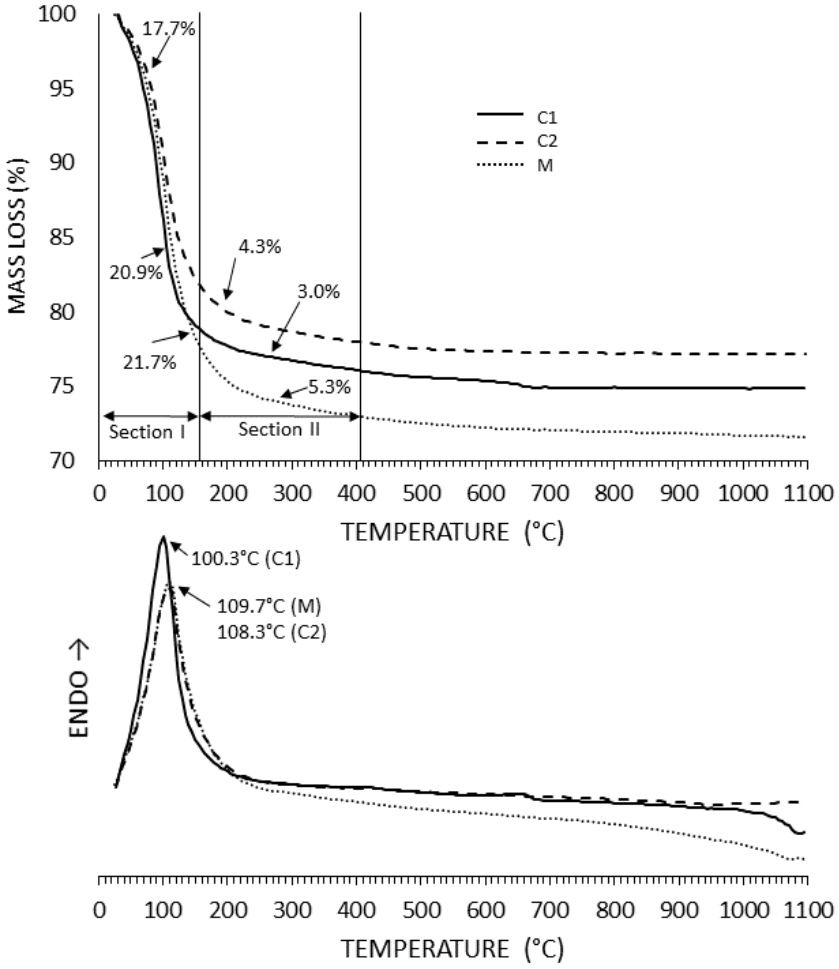


Figure 3 Comparison of C1, C2 and M Pastes using TG (upper) and DSC (lower).

It can be seen from the TG trace that although the majority of the mass loss in all samples occurs between ambient and 400°C, there is a difference in the scale and profile of that mass loss for each material. For C1, 88% of the total mass loss occurs up to 150°C (Section I) and 12% between 150°C and 400°C (Section II). For pastes C2 and M, 80.3% of the total mass loss takes place in Section I and 19.7% in Section II. When compared with C1, a greater proportion of the total mass loss for C2 and M pastes occurs in Section II of the TG trace.

As the specimens tested were not pre-treated under identical conditions, the figures for Section I are highly dependent on the moisture content of the paste at the time of testing and therefore may not be directly comparable.

DSC offers an alternative method for comparison. Traces show an endotherm peak for C1 occurs at 100.3°C, followed by C2 (108.3°C) and M (109.7°C). This indicates geopolymers M and C2 have a higher proportion of bound water and therefore a more fully developed geopolymer structure.

## Scanning Electron Microscopy (SEM)

To further examine the effects of accelerated aging on the microstructure of geopolymer paste, sections from each paste formulation were polished and studied using an environmental SEM. For the purposes of this paper, a comparison is made of C1G (aged and unaged), C2G (aged and unaged) and C2 (aged and unaged) (Figures 4, 5 and 6)

The images show that before ageing, C1G already has a large number of voids present. This could be due to excess free water evaporating out of the matrix. Areas around the slag particles have a well formed, dense matrix and iron-rich particles are larger in size than in C2 formulations. Following 90 days of accelerated ageing (Figure 4, right), the matrix had degraded significantly with large areas of open voids visible. GGBS particles seemed to retain a 'halo' of dense matrix, but these are generally surrounded with open space.

Figure 4, 5 & 6 Key: 1 – GGBS Particle; 2 – Metakaolin relic; 3 – Hematite Particle; 4 – Geopolymer Matrix.

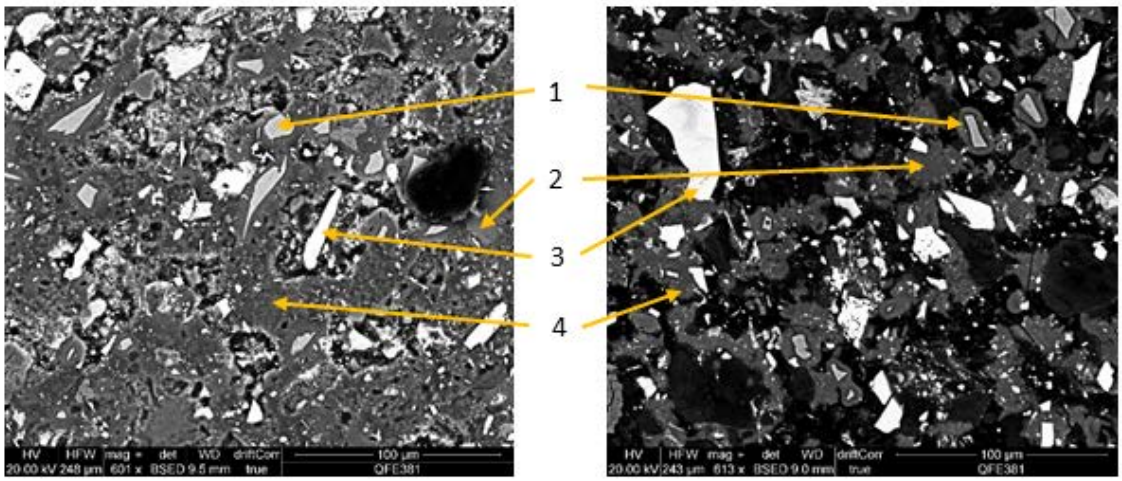


Figure 4 SEM image of C1G ambient (left) and C1G after 90 days accelerated ageing (right).

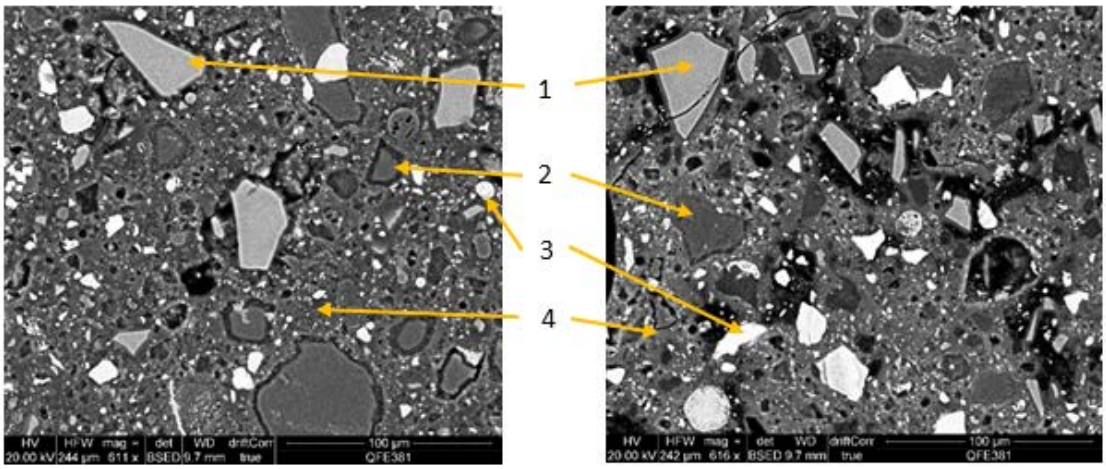


Figure 5 SEM image of C2G ambient (left) and C2G after 90 days accelerated ageing (right).

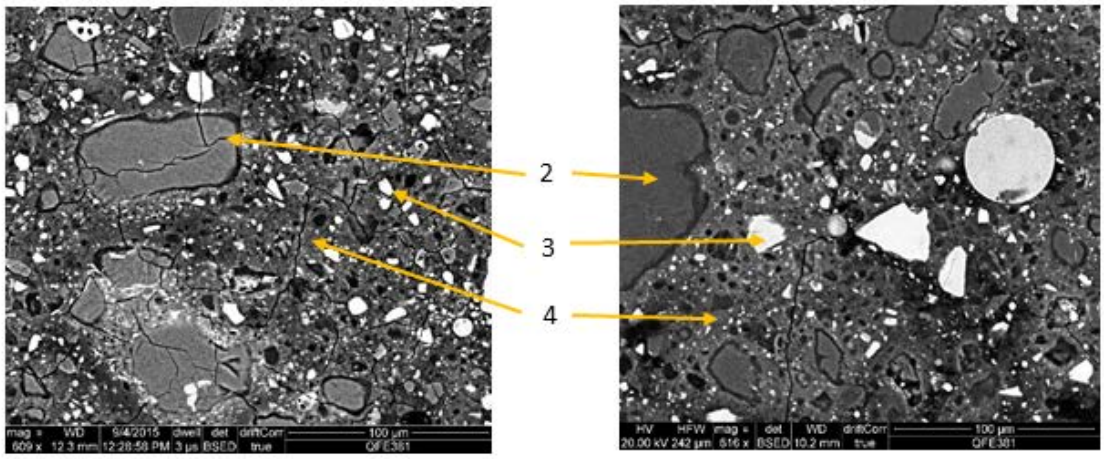


Figure 6 SEM image of C2 ambient (left) and C2 after 90 days accelerated ageing (right).

Figure 5 shows a much denser matrix with GGBS particles present. Prior to accelerated ageing, small porous areas can be seen around some GGBS particles. Following accelerated ageing for 90 days, these voids become much more predominant, although there is still sufficient matrix present to prevent significant strength loss.

SEM images of C2 paste can be seen in Figure 6. There is no GGBS present in this material and little difference can be observed between the two images. The sample examined in Figure 3c (left) was prepared as a thin section resulting in extensive cracking. However, the morphology of the particles in the specimen has remained stable.

## CONCLUSIONS

The work published in this paper is the result of an initial study on the effects of accelerated ageing on a calcined clay geopolymer, with and without GGBS. The study also included a geopolymer based on a pure metakaolin for comparison. This work was prompted by existing publications that have cast doubt on the stability of the amorphous structure of metakaolin-based geopolymers.

Contrary to the findings of other researchers, it has been found that all metakaolin-based geopolymers do not undergo strength degradation under high temperature/high humidity conditions. However, it has been shown that it under certain circumstances and depending on a number of variables, some strength degradation may be experienced.

It has been shown that for the formulations which do develop crystalline structures, the time taken for conversion to commence under accelerated ageing is much longer than previously reported. In addition, this phase change is not always associated with a corresponding strength loss.

Following ambient curing, geopolymer pastes containing GGBS were found to have formed small voids around many particles. After accelerated ageing these voids had increased significantly in volume, but in the majority of cases sufficient matrix remained to prevent any strength loss. It has been found that the presence of GGBS may accelerate the development of crystalline phases when a high water/binder solids ratio is used.

Metakaolin-based geopolymer systems formulated with a fine particle size distribution was found to be more resistant to both strength loss and crystalline phase formation than those made using a coarse ground powder.

Examination of the effects of accelerated ageing is continuing. Each of the pastes will again be examined after 180 days exposure to elevated temperature and humidity and the development of new crystalline phases will be monitored. Due to the differences observed between C2G and MG in powder x-ray diffraction, the influence of minerals other than kaolinite present in the ferruginous laterite will be investigated. Further work will also take place examining the influence of varying the water/binder solids ratio.

Based on the results from this work, it has been proven that the statement ‘geopolymers based on metakaolin must be considered unsuitable for use in construction and building materials’ does not apply to the majority of metakaolin-based geopolymers. As with other cements - raw material preparation, binder formulation and mix design all play a significant role in the stability of a geopolymer concrete. Understanding how each of these variables influence the end product will build confidence in these new materials.

## REFERENCES

1. DAVIDOVITS, J. World-wide increase in geopolymer research, 2010. [Online]. Available at http://www.geopolymer.org/science/worldwide-increase-in-geopolymer-research (accessed 20 March 2013)

2. DUXSON, P, FERNANDEZ-JIMENEZ, A, PROVIS, J L, LUKEY, G C, PALOMO, A, VAN DEVENTER, J S J. Geopolymer Technology: the current state of the art, Journal of Material Sciences, Vol. 42, No. 9, 2007, pp 2917-2933

3. KONG, D L Y, SANJAYAN, J G. Effect of elevated temperatures on geopolymer paste, mortar and concrete, Cement and Concrete Research, Vol. 40, No. 2, 2010, pp 334-339

4. KRIVEN, W M, GORDON, M, BELL, J L. Geopolymers: nanoparticulate, nanoporous ceramics made under ambient conditions, Microscopy and Microanalysis '04, Proc. 62nd Annual Meeting of the Microscopy Society of America, Vol. 10, 2004, pp. 404–405
5. DE SILVA, P, SAGOE-CRENSTIL, K. Medium-term phase stability of Na2O-Al2O3-SiO2-H2O geopolymer systems, Cement and Concrete Research, Vol. 38, No. 6, 2008, pp 870-876

6. SCHMUCKER, M, MACKENZIE, K J D. Microstructure of sodium polysialate siloxo geopolymer, Ceramics International, Vol. 31, 2005, pp 433-437

7. DUXSON, P, LUKEY, G C, VAN DEVENTER, J S J. Evolution of gel structure during thermal processing of Na-Geopolymer Gels, Langmuir, Vol. 22, No. 21, 2006, pp 8750-8757

8. DUXSON, P, LUKEY, G C, VAN DEVENTER, J S J. Thermal evolution of metakaolin geopolymers: Part 1 – Physical Evolution, Journal of Non-Crystalline Solids, Vol. 352, No. 52-54, 2006, pp5541-5555

9. DUXSON, P, LUKEY, G C, VAN DEVENTER, J S J. Thermal evolution of metakaolin geopolymers: Part 2 – Phase Stability and Structural Development, Journal of Non-Crystalline Solids, Vol. 353, No. 22-23, 2007, pp 2186-2200

10. LLOYD, R R. Accelerated ageing of geopolymers, Geopolymers: Structure, Processing, Properties and Industrial Applications, 2009, Elsevier, pp 139-166.

11. DAVIDOVITS, J. Geopolymer Chemistry and Applications, 2011, Institute Geopolymere, p 201

12. LIZCANO, M, GONZALEZ, A, BASU, S, LOZANO, K, RADOVIC, M. Effects of Water Content and Chemical Composition on Structural Properties of Alkaline Activated Metakaolin-Based Geopolymers, Journal of the American Ceramic Society, Vol 95, No.7, 2012 pp 2169-2177

# ALKALI-REACTION PHENOMENON 'AAR' IN STRUCTURAL ELEMENTS PRODUCED WITH CONCRETE AND REINFORCED CONCRETE

**M F Habita** **F Bouabdallah**

**R Daoud** **N Rehamnia**

Annaba University University of Oum El Boughi

Algeria

**ABSTRACT.** Serious physical and mechanical damages threaten the sustainability of reinforced concrete structures in the Civil Engineering field: dams, water towers, bridges and viaduct pillars.... The physical changes in the length (expansion), thus textural damages by concrete discoloration, with the gel exudation, the de-cohesion (Aggregate-Cement), oriented cracks or polygonal cracking-checking, strains, affect the structures. In this effect, the mechanical performance of the material (concrete) is substantially achieved. Hence, the commissioning and the life and sustainability of the structures are severely reduced. These results are due to the presence of the most severe chemical reaction, which occurs when the aggregates are reactive with a high alkalinised medium in hydraulic concrete. That's the alkali Aggregate reaction 'AAR' a pathology that threatens the structure's life and known for a century. It requires a high rate of the humidity (RH> 80 to 85%), a granular high reactivity and an over-alkalinization in the concrete interstitial matrix (pH> 13). Our study is elaborated to identify the 'AAR' aggressiveness rate with the local Algerian materials with structural simulation: according to ASTM, CSA, AFNOR and NBRI requirements standards, in the laboratories of Annaba University and "EmirLabo". In the presence of the favourable factors to the 'AAR', the structural elements of concrete and reinforced concrete are produced using (limestone and dolomite) aggregates and (CPJ) cement. The obtained results are unequivocal; highly reactive aggregates were detected with a very destroying effect on concrete elements

**Keywords:** Alkali, Reaction, Concrete, Structure, Alteration.

**Professor Mohamed Fouzi Habita** is Director of his Building Materials laboratory (Emir-Labo) at City of Annaba. He is the president of National Research Project entitled Pathology and Eco-materials at Civil engineering laboratory of UBMA (Algeria). **Fouzia Bouabdallah** is a senior lecturer in the University of Oum El Boughi and a member of National Research Project entitled Pathology and Eco-materials at Civil engineering laboratory of UBMA. These researches presented the detection of the first cases of reactive aggregates in our country. She has published on concrete and mortar with the alkali reactive pathology. **Nadjette Rehamnia** is an Engineer in the public sector of El Tarf City and a member of National Research Project entitled Pathology and Eco-materials at Civil engineering laboratory of UBMA. **Rabiaa Daoud** is senior lecturer in the University of Oum El Boughi. She has published on hydraulic concrete pathologies and on the other fields.

## INTRODUCTION

The concrete structures are exposed to the important risks. Their performance and functionality are targeted: dams, water towers, bridges and infrastructures ...etc. Concrete is a living material and contains moving microscopic particles; in which internal chemical reactions can occur between its components: basic minerals hydrated in the exposition environment (ionisation) and aggregates potentially reactive. It caused a microstructure changes in the concrete matrix conducting to pathological symptoms this hard material.

The 'AAR' is a concrete disease; it occurs only with three conditions: High level of granulate reactivity, important alkalinity in the medium when PH is more than 13 and moisture superiorof85%. Moreover, this pathology had favourable factors providing to the progress of reaction speeds and the damages degree as: temperature effect, compound rates in cement, reactant types ...etc. When 'AAR' started, harmful transformations take place in concrete structural elements. Gel exudation in surface and internal moisture zones formed, strains and expansions can be measured. Permanent crack networks and evolution cracks were propagated, exfoliation was equally appeared. To understand the relationship between these pathologic symptoms, many searchers were involved to study the 'AAR' mechanism. Several universal results were found; theories were thinking about and put. But multiple points must be cleared for (AAR) tests which are note completely standardized. Because of this chemical issue which is complex; and the multi-scenario of its mechanism disorders. These tests were to detect 'AAR' phenomena on specimens produced in laboratories or samples taken from structures damages by 'AAR'. The American standards ASTM were the mainly tests used in this field. The standards of BS, ACNOR, NBRI, AFNOR and JIS were based on ASTM standards but the modifications are continuing.

Nowadays; civil engineering prevention rest without a radical solution for the concrete affected which lose its initial performance. Treatments in 'AAR' field are timid comparing with the degradation rates. For the existent structures attacked by 'AAR'; prevention resided only in reactant separation by using the water-tightness system on the one hand. On the other hand, for the future structures the vigilance to decrease damage resides in taking away the reactive granulate or using the mineral additions as Blast furnace slag, fly ash, silica fume ...etc.

Our research team is the first one to declare that our country is threatened with 'AAR' pathology. The Algerian authorities must start work programmes against this serious issue, especially when our national quarries produce high reactive aggregate as in Guelma quarries: Heliopolis, Bouhachana [1]. In this article we have intention to simulate 'AAR' damages experimentally with local materials. In our experiments established in Algerian laboratories of UBMA and Emir-Labo, the requirements of international standards of ASTM, ACNOR, NBRI and AFNOR were used. The accelerated test was done with structural elements with concrete and reinforced concrete in favourable conditions during storage time. The response time of these tests is then 4 to 8weeks. When comparing the reference concrete and concrete affected by 'AAR' that allows us to detect the degradation rates. We had studied the new physical and mechanical characteristics of our local material after 'AAR' attacks. We had equally used the microscopic scale to scout the existing microstructure and the distribution of components in the concrete matrix.

**Abbreviations used in this paper:** ACNOR-CSA: Canadian Association for Standardization. AFNOR: French Association for Standardization. ASTM: American Standard Testing Materials. AAR: Alkali Aggregate Reaction. BS: British Standard. NBRI: National Building of Research Institute. DLC/ Canada: Laboratory Roadway Direction/ Canada. LCPC: Recommendation for damage prevention due to alkali-reaction, and central laboratory of roads and bridges (LCPC) - 1994. JIS: Japanese Industrial Standards. UBMA: University of Badji Mokhtar- Annaba (Algeria).

## EXPERIMENTAL INVESTIGATIONS

### Materials

The cement used: Portland cement CPJ-42.5 grade, according to ASTM and ACNOR standards; produced by Hadjar-Essoud cement work (Skikda) situated in the North-East of Algeria (Skikda). The chemical compositions of our cement were in Table 1.

Table 1 Chemical, physical and mechanical characteristics of cement used [2]

| CHEMICAL CHARACTERISTICS | | | PHYSICAL CHARACTERISTICS | | | MECHANICAL CHARACTERISTICS | |
|---|---|---|---|---|---|---|---|
| AFNOR standard | Element | Mass % | National standards | | | National standards & strength in (MPa) | |
| NF P15-467 FL UOX | NA 235 PAF 975°C | 1-5 | NA230 | Normal consistency | ≥ 25 | NA 442 | Compression test |
| | | | NA230 | Initial setting time | ≥ 60 | | 2 days ≥12,5 |
| | | | NA230 | Final setting time | 150-270 | | 7 days 25-35 |
| | | | NA232 | Lime expansion | ≤ 10 mm | | 28 days 42.5-52.5 |
| | | | NA231 | Blaine cm²/g | 3200-4000 | | |
| | | | NA231 | Density g/cm³ | 0.05-3.12 | | |
| | | | INSTR | Cumulated passing 45 µm | 18-28 | | |
| | | | | | | NA 234 | Bending test |
| | | | | | | | 2 days 3.0-4.0 |
| | | | NA440 | Mortar shrinkage µm/m | ≤ 800 | | 7 days 5.0-7.0 |
| | | | | | | | 28 days 6.2-8.5 |
| | CaO | 55-65 | Bogue compounds, % | | | Compounds | % |
| | $SiO_2$ | 19-28 | | | | | |
| | $Al_2O_3$ | 4-6 | | | | | |
| | $Fe_2O_3$ | 2.5-3.6 | | | | | |
| | MgO | 1-2 | | | | | |
| | $K_2O$ | 0.3-0.6 | | | | | |
| | $Na_2O$ | 0.1-0.16 | | | | | |
| | $SO_3$ | 1.8-3 | | | | | |
| Glycol NF P15-467 FLUOX | CaOL | 0.5-2.5 | $C_3S$ | 55-65 | | Clinker | ≥ 74 |
| | $Cl^-$ | 0-0.02 | $C_2S$ | 10-25 | | Gypsum | 4-6 |
| | | | $C_3A$ | 8-12 | | Limestone | 0 |
| | | | $C_4AF$ | 7-13 | | Slag | ≤ 20 |

Alkalis could be with high rates to activate internal chemical reactions between (Alkali and Reactive aggregates). Alkalis in concrete came from two sources as shown in Table 2.

Table 2 Alkali sources of alkali reactive concrete, prepared in the laboratory

| ALKALI SOURCES | MATERIAL TYPES | DESCRIPTION |
|---|---|---|
| Source 1 | Cement | weak content 0.3% $Na_2O_{eq}$ = 0.3%.(Table 01) |
| Source 2 | Concrete matrix | Additional alkalis of Sodium-Potassium solutions to the water for mixing. NaOH and KOH according to AFNOR-587 [3]; AFNOR-585 [4]; AFNOR-594 [5] and ACNOR-14A [6] and equivalency formula (1): $Na_2O_{eq}$ (%) = [$Na_2O$+0.658$K_2O$] (%) (1) |

Coarse and fine aggregates used in our mix design of concrete were highly reactive; they are tested with accelerated tests for 'AAR' detection on mortar bars in our previous research works in UBMA laboratory. These granulate were Limestone rock origin from the Bouhachana quarry of Guelma town; they were natural and crushed their grading curve was in Figure 1 according to AFNOR standards. They satisfied the physical test codes: AFNOR-301[7]; AFNOR-304 [8]; AFNOR-309 [9]; AFNOR-554 [10]; AFNOR-555 [11] and AFNOR.EN-933.2 [12]; they were distributed in three classes:

- Gravel (15-25) mm
- Gravel (5-15) mm
- Sand (0-5) mm, with a fineness modulus FM = 2.75

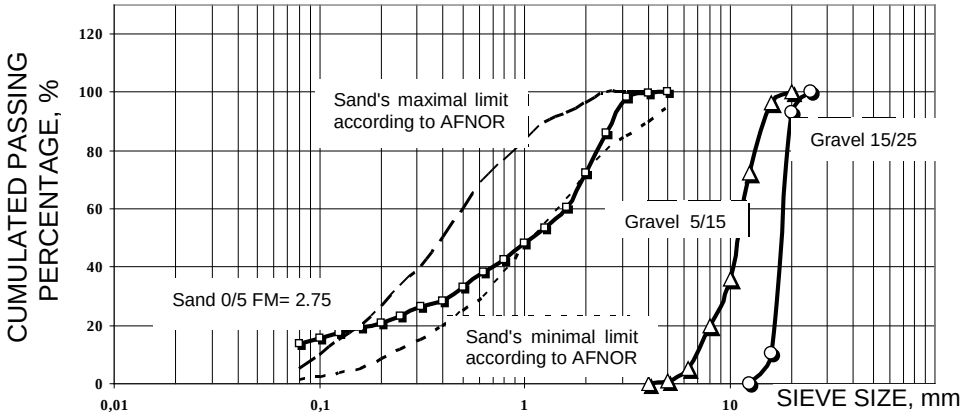


Figure 1 Grading curve

Our mix design was chosen adequately to Dreux Method for ordinary concrete which was selected with our concretes (A, B and C). Concrete reference (A) was without alkali addition and (B, C) concretes with alkalis addition; for both concrete types: concrete and reinforced concrete. Casted concrete was applied according to slump test AFNOR-451 [13] or ACNOR-5C [14]. Then 24 to 48 hours after casting we had demoulded structural elements; and cured them for 30 minutes at 23°C according to AFNOR-405 [15]. The specimens were stored, resealed and heated to 20°, 38° and 48°C; and the moisture was 100% (Table 3). For samples, initial lengths were measured just before storage (reference length).

To accelerate 'AAR' attacks, our concrete elements were stored in following conditions:

[Reference Concrete (A): 0.3% $Na_2O_{eq}$; RH=100%; T=20°C]
[Reactive Concrete (B): 1.25% $Na_2O_{eq}$; RH=100%; T=38° and 48°C];
[Reactive Concrete (C): 2.5% $Na_2O_{eq}$; RH=100%; T=48°C]; alkalis adding in concordance with (formula 1).

Table 3 Mix-design of concretes chosen and conditions storage for all specimens and beams

| CONST Concrete | SAND 0-5 kg/m³ | GRAVEL kg/m³ | | CEMENT kg/m³ | RATIOS | | $H_2O$ l/m³ | ALKALIS kg/m³ | | STORAGE CONDITION (°C, %) | |
|---|---|---|---|---|---|---|---|---|---|---|---|
| | | 5-15 | 15-25 | | w/c | c/a | | NaOH | KOH | T | RH |
| Concrete (cylinders and beams) | | | | | | | | | | | |
| A | 740 | 430 | 715 | 420 | 0.4 | 1 / 2.25 | 157 | - | - | 20 | 100 |
| B & C | | | | | | | | 2.00 | 3.04 | 38 | 100 |
| Reinforced concrete ( cylinders and beams) | | | | | | | | | | | |
| A | 740 | 430 | 715 | 420 | 0.4 | 1 / 2.25 | 157 | - | - | 20 | 100 |
| B | | | | | | | | 2.00 | 3.04 | 48 | 100 |

The establish programme tests were described in (Table 4) in order to investigate the new material which is attacked by alkalis. We compared concrete (B and C) with reference concrete (A).

Table 4 Structural elements used with concretes (A, B and C)

| CONCRETE TPYES | CONCRETE ELEMENTS, cm | | REINFORCED CONCRETE ELEMENTS, cm | AGE, week | ALKALI $Na_2O_{eq}$, % | NUMBER | TOTAL |
|---|---|---|---|---|---|---|---|
| REFERENCE CONCRETES | | | | | | | |
| 2A | Cylinder (3) H=22, dia=11 | Beam (3) 120×20×15 | Beam (3) 120×20×15 | 8 | 0.3 | 9 | 48 |
| 3A | Cylinder (3) H=22, dia=11 | Beam (3) 120×20×15 | Beam (3) 120×20×15 | 4 | | 9 | |
| AKALI REACTIVE CONCRETES | | | | | | | |
| 2B | Cylinder (3) H=22, dia=11 | Beam (3) 120×20×15 | Beam (3) 120×20×15 | 8 | 1.25 % | 9 | |
| 3B | Cylinder (3) H=22, dia=11 | Beam (3) 120×20×15 | Beam (3) 120×20×15 | 4 | | 9 | |
| 2C | Cylinder (3) H=22, dia=11 | Beam (3) 120×20×15 | - | - | 2.50 % | 6 | |
| 3C | Cylinder (3) H=22, dia=11 | Beam (3) 120×20×15 | - | - | | 6 | |

As shown in Table 5 specimen forms were cylindrical specimens and beams; the cylinders were prepared with the tests for measuring length variations due to the (AAR) and compression test according to standards ASTM, ACNOR and AFNOR. Beams were produced according to the test of flexural strength of concrete.

Table 5 Preparation of specimen forms according to standards ASTM, ACNOR and AFNOR

| SPECIMEN TYPES, cm | PREPARATION ACCORDING TO AFNOR AND ACNOR ASTM STANDARDS | TESTS |
|---|---|---|
| Cylinders H=22, dia=11 | AFNOR-400 [16] AFNOR-406 [17] or ACNOR-2C [18] ACNOR-3C [19]; ACNOR-1D [20]; ACNOR-14A and AFNOR-587 | Length changes test due to 'AAR' and Compression test |
| Beams: Concrete and reinforced concrete 120×20×15 | ASTM C78-94 [21]; ACNOR-8C [22] | Test of flexural strength of concrete, this test is adapted for concrete and reinforced concrete |

Reinforced concrete beams were produced for concretes (A and B), we had put in each upper and lower layer two rows of longitudinal reinforcement with 2Ø10 (HA, FeE400). These were hidden by stirrups Ø10 with 15 cm space. In Figure 2 the fresh concrete was cast in three equal layers, vibrating, and the cylinders and beams being kept uncharged during storage.

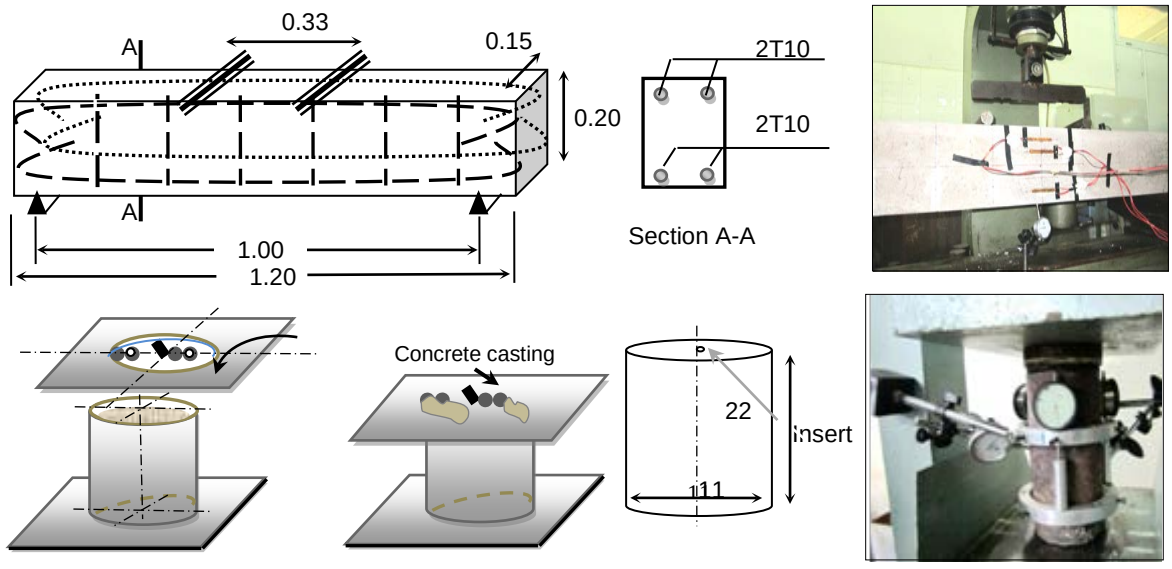


Figure 2 Bending test, by 4 points of beams 120×20×15 cm and compression test for cylindrical samples (Ø=11, H=22) cm

**Tests**

In literatures we can accelerate the chemical reaction 'AAR' when we have high levels of reactivity in aggregates, high alkalinity and when favourable factors were present (T, HR) [23, 24 and 25]. In our experiments we had studied various aspects: physical and textural aspect (AR alterations); mechanical aspect and micro-structural aspect.

## Investigation of 'AAR' alterations in concretes

Textural study of 'AAR' alteration mainly is established by monitoring symptoms: discoloration in concretes, cracks with their form and evolution during the storage time, development of checking-cracks and networks. Then we have represented cracks by (Opening cracks-Time) curves; checking-cracks by (Mesh per surface-Time) curves and discoloration by Photography method [26, 27].

The expansion measures take place almost each week, according to requirement of standard codes: AFNOR-587, ASTM C1105-95 [28] and ACNOR-14A. This test is established for prisms 7 cm × 7 cm × 28 cm, we had adapted it for cylindrical specimens (Ø=11, H=22) cm equipped with inserts in the longitudinal direction. Expansion test was with cylinders except beams; for concrete types (A, B and C). We have used in these tests the retractometer device for length measurements; it is provided with a digital comparator (1/1000) mm. After calibration, the measurements are made at 1, 2, 4, 8 weeks in the storage conditions up to 2 months which cited previously. Comparing lengths measured in samples with the initial measurements at regular intervals; we could identify length variation by (Expansion-Times) curves. After each expansion measurement, alterations were monitoring: photos were taken for discoloration, opening crack measurement were done, and formed mesh were counting.

## Mechanic characteristics

In this article, we have intention to restrain the mechanical study by evaluation of the most important characteristic in concrete for our two specimen types (cylinders and beams). First ones, cylinders were chosen for compression tests according to standard codes AFNOR-406 and ACNOR-9C [29]. The same specimens of retractometer tests with (A and B) concretes were tested for compression behaviour (failure).

Then, beams elements were tested with bend testing (four points) in concordance with (ACNOR-8C or ASTM C78-94) to identify indirectly the tensile and compression failure strength. This test is established for concrete with prismatic section, we had adapted it for reinforced concrete also (Table 5).

## Microscopic examination

At the moulded surface where 'AAR' alterations were manifested; concrete samples were examined by polarized optical microscopy (POM) in the geology laboratory of UBMA. It was, according to petrography method with a thin section (45 × 30 × 1.5) mm referenced by Brot-Geology taken from samples of concretes (A and B) after expansion test. Our microscopic study is limited at 28 days of storage age; based on:

- Description of pure rock which is the aggregate origins.
- Examination of both concretes (A and B), we have selected:

- Fine aggregate
- Coarse aggregate
- Cement paste
- Adherence zones (cement- aggregate)

# RESULTS AND DISCUSSION

## Concretes and 'AAR' Alterations

When monitoring concrete types, we mention that reference concrete (A) rest always without 'AAR' alteration, with healthy texture in concrete skin for all element structures.

## Concrete expansion

In general, the results of Expansion-Time curves present expansion for all structural elements tested with noted (B and C) concretes. However, the reference concretes (A) remain healthy aspect with shrinkage (Figure 3).

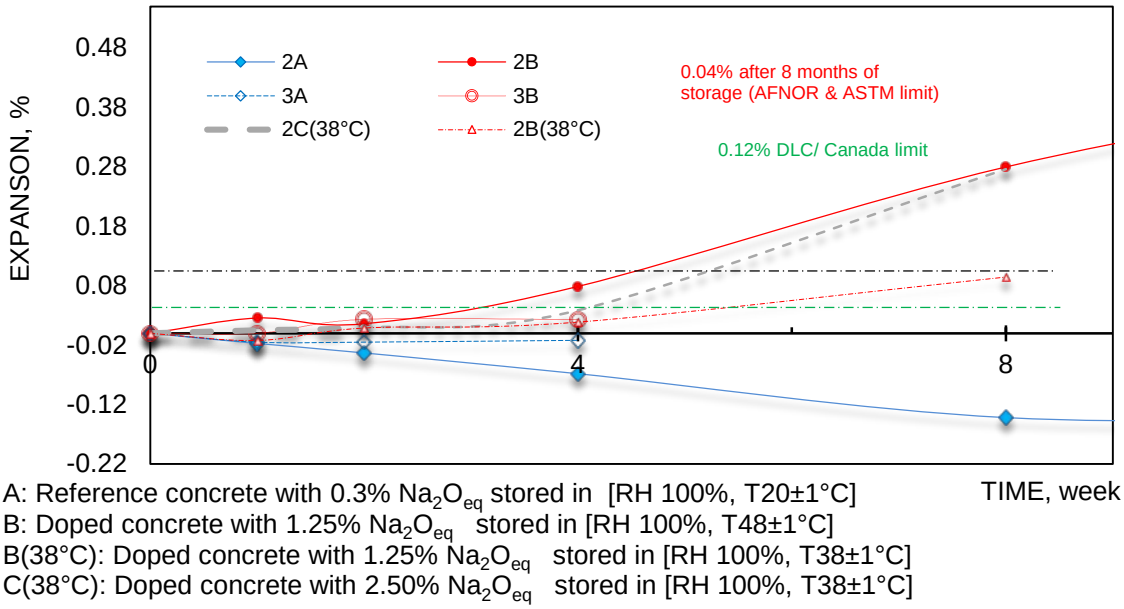


Figure 3 Expansion test in Alkali Reactive Concretes with cylindrical specimens (Ø11, H22) cm after 2 months of storage

After 2 months of conservation in expansion test, cylindrical specimens (dia=11, H=22) cm expansion is higher than samples which were more doper and more heated. We had measured (0.28 and 0.27%) expansion rates in concrete (B and C) which were heated in 48°C and doped 2.5% in $Na_2O_{eq}$. These values decreased by 65.5% in concrete (B) stored in 38°C temperature.

When, we had measured -0.14% shrinkage in reference concretes (A). We confirmed that our aggregates are classified as "Reactive" according requirements of ASTM-1105.95 and AFNOR-587. Moreover, they are classified as "High reactivity" according to DLC- Canada.

According to the method of three tangents; the Expansion-Time curves retain always the Larive shape "S" in all specimens in doped concretes (Figures 3 and 4). The extracted data when comparing Expansion test curves with three tangents method for the cylinders were tabulated in Table 6.

Table 6 Extracted data by comparing Expansion test curves with three tangents method for the cylinders (Ø11, H22) cm after 2 months of concretes storage

| CYLINDERS, cm CURVE DATA | PHASE I | | | PHASE II | | | PHASE III | | | PHASE IV | | |
|---|---|---|---|---|---|---|---|---|---|---|---|---|
| | B(38°C) | C(38°C) | B(48°C) | B(38°C) | C(38°C) | B(48°C) | B(38°C) | C(38°C) | B(48°C) | B(38°C) | C(38°C) | B(48°C) |
| Time (weeks) | 1-3 | | | 3-8 | | | - | - | - | - | - | - |
| Reaction speed (%) | >50 | | | >50 | | | - | - | - | - | - | - |
| Phase Description | Early | | | Slow (not finished) | | | - | - | - | - | - | - |

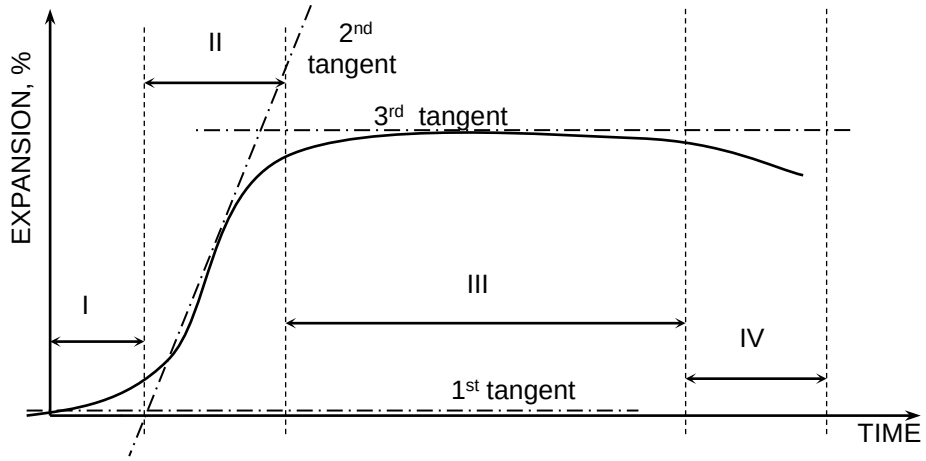


Figure 4 Three-tangents-method, the general form of Expansion-Time curve in Alkali-reactive concrete [30, 31]

**Concrete discoloration and gel exudation**

In concrete attacked by 'AAR', expansion was appeared combined with discoloration after a few days of storage only in concrete (B and C). White spots appear in the external concrete skin at early ages of storage for all specimens and beams. These spots propagated in external concrete surface as a function of time; it is the 'AAR' gel that fills the pores. Then it comes in skin as a white powder (very fine powder) lesser than 0.08 mm, and later it moves in large amounts through cracks (Figure 5). In affected concretes, element faces became whitest as a function of time comparing with the reference concrete (A) during 2 months of tests.

**Concrete cracks**

Expansion with concrete discoloration were illustrate few days after storage only in concrete (B and C). Crack started after few weeks of conservation; they became clearly seen during the storage time. These cracks had (Y) form with an angle of 120° (Isle of Man); which noted by crack form of 'AAR'. These permanent cracks were propagated at concrete surfaces in all directions, even in depth. These progressive cracks were joined to give us the polygonal form of checking cracks of 'AAR' (Meshing). The first crack was seen after one month of tests at the corner and at insert boundary, but its real birth moment was ignored (Figure 5).

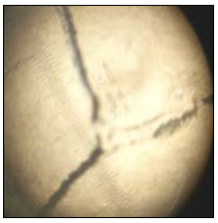
1

2


3

4

(1) (AR) crack with (Y) form (Isle of Man) in cylinder (Ø11, h=22) cm in (B) concrete [$Na_2Oeq$= 1.25%, T=38°C & HR=100%].
(2) (AR) crack in insert boundary of specimens.
(3) & (4) (AR) Polygonal form of checking crack in cylinder (Ø11, h=22) cm and beam 120 cm × 20 cm × 15 cm produced with (B) concrete.

Figure 5 Alterations in affected concretes by (AR)

For the (Open crack - Time) curves of concretes stored in (38°C) (Figure 6). Although, the affected concrete (C) was more doper in alkalis, but the bigger opening cracks measured by fissurometer were associated with (B) concrete. We have found in these curves, from the third week until the end of test concrete orders was: B(Beam), B(Cylinder), C(Cylinder) and C(Beam). At 8 weeks, extreme opening cracks were in concrete (B): 0.7 mm in beams and 0.65 mm in cylinders. These values decreased in concrete (C) with 78.57 and 43.03% for beam and cylinders respectively. The variation in $Na_2O_{eq}$ content is the main cause of these decreasing values, which provide a different volume effect in our structural elements.

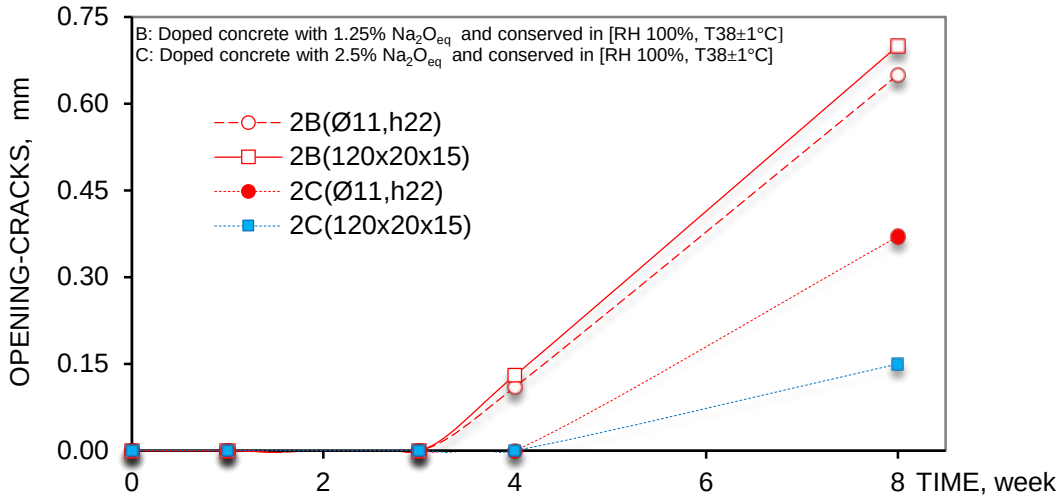


Figure 6 Opening-cracks evolution in concretes (B and C) with cylinders (Ø11, H22) cm and beams 120 cm × 20 cm × 15 cm, after 2 months of storage

For concrete and reinforced concrete (B) which was conserved in (48°C) (Figure 7). These concretes were affected by 'AAR' with discoloration, expansion and cracks since the first week of storage. We have found in the Opening cracks-Time curves, from the second week to the end of test concrete an order: Beam then the cylinder with rates of (0.47), and (0.25) mm. The maximum opening cracks measured until 8weeks monitoring was 0.7mm in concrete beams (B), it's neither the most doper in alkali nor the more heated. It was clear that Cylinders (B conserved at 38°C) were more cracked comparing with those which were highly heated and doped with alkali. They were nearer to the extreme crack of beam (B) without reinforcement.

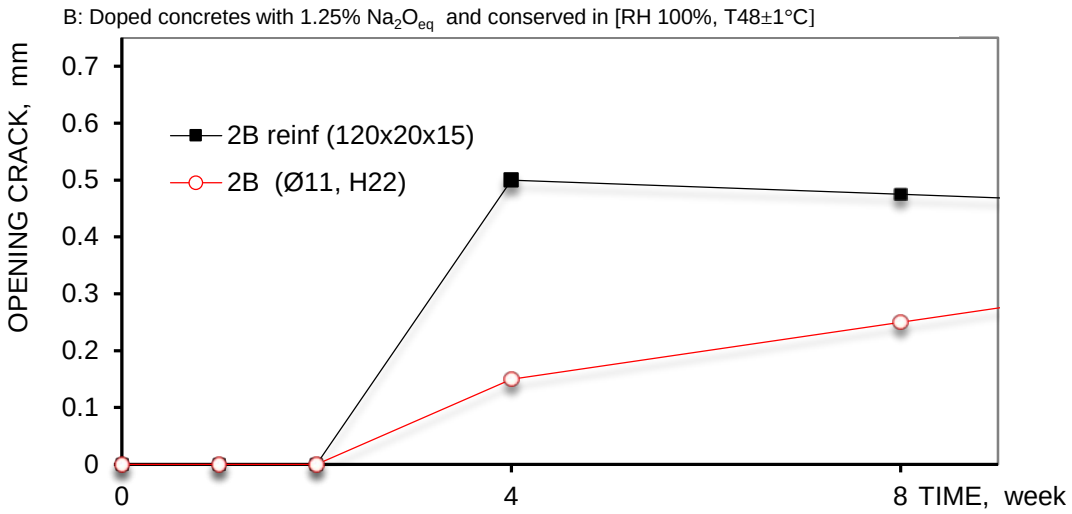


Figure 7 Opening-cracks evolution in concrete and reinforced concrete (B) with beams 120 cm × 20 cm × 15 cm and cylinder (Ø11, H22) cm, after 2 months of storage

## Concrete checking cracks

After expansion and gel exudation, cracks stated and propagated until to give us the polygonal meshing. This was the chronology of 'AAR' alterations which was the same for all structural elements with concretes (B and C).

Expansion curves progressed after a few days, cracks curves started before 1 month approximately. And the last one was meshing curves which took place after 4 weeks. Really, at 1 or 2 months of conservation mesh monitoring was difficult; due to undersize of opening cracks and high amount of gel exudation. In (Mesh-Time) curves for concretes conserved at 38°C, curves of (C) concrete were higher than (B). The order was from the fourth week until the end of test at 8 weeks: C(Cylinder), C(Beam), B(Cylinder) and B(Beam) with 524.45, 281.48, 161.82 and 94.44 Mesh/m² respectively. We could see that in checking crack curves, the effect volume was completely different than in crack curves (Figure 8).

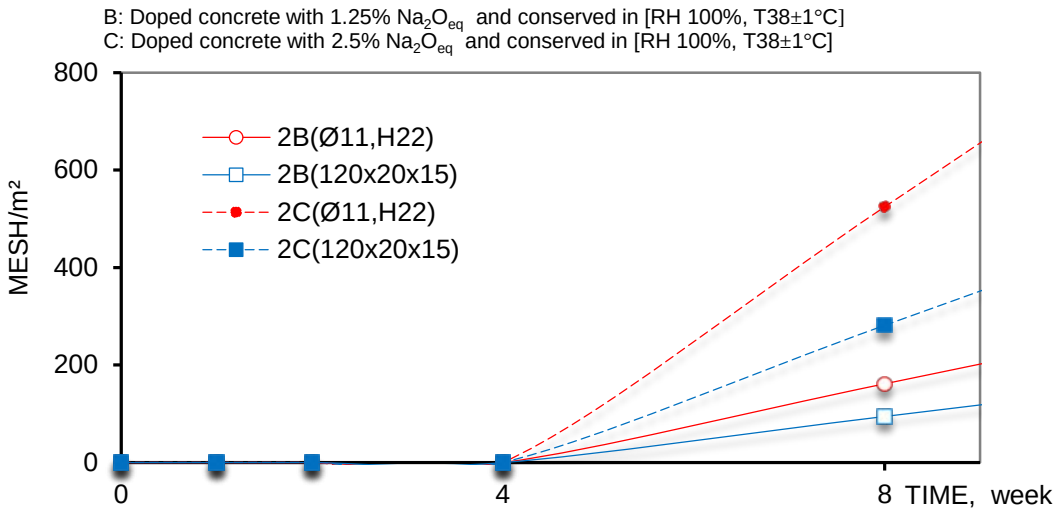


Figure 8 Checking-cracks evolution in concretes (B and C) with cylinders (Ø11, H22) cm, and beams 120 cm × 20 cm × 15 cm, after 2 months of storage

For concrete and reinforced concrete (B) which was conserved in (48°C) (Figure 9). We have found in the Checking cracks-Time curves, as in crack curves from the second week to the end of test concrete order was: Beam then the cylinder with values of (8937.14), and (559.26) mm. There is a big divergence between the two elements due to material types (reinforced concrete and concrete). The reinforced material presented extreme meshing 8937.14 Mesh/m². However, concretes were not enormously influenced by various conditions of: temperature, $Na_2O_{eq}$ content and form. They had a limited interval of meshing [94.44; 559.26] Mesh/m².

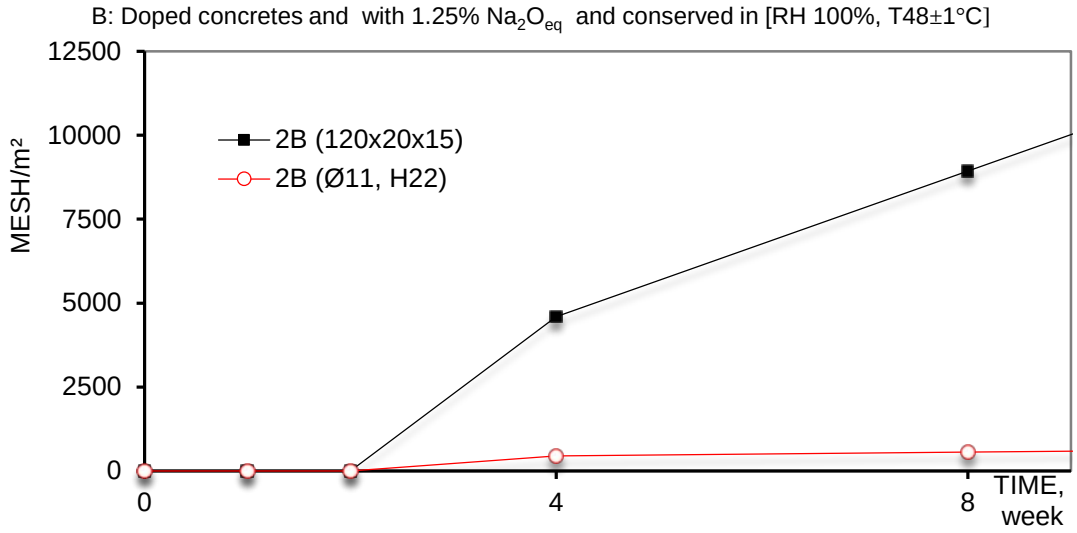


Figure 9 Checking cracks evolution in concrete and reinforced concrete (B) with structural beams 120 cm × 20 cm × 15 cm and cylinder (Ø11, H22) cm, after 2 months of storage

## Mechanical Characteristics of Concretes

In this article, we have intention to restrain the mechanical study by evaluation of the most important characteristic in concrete for our two element types (cylinders and beams). First ones, cylinders were chosen for compression tests according to standard codes AFNOR-406 and ACNOR-9C. The same specimens of retractometer tests with (A and B) concretes were tested for compression behaviours (failure).

Then, beams elements were tested with bend testing (four points) in concordance with (ACNOR-8C or ASTM C78-94) to identify indirectly the tensile and compression failure strength. This test is established for concrete with prismatic section, we had adapted it for reinforced concrete (Table 5).

The curves of compressive and tensile failure strengths presented a progress of strength in the first 28days. After that, they stabilised for all structural elements with both materials (concrete and reinforced concrete). These strength curves increased differently from the first day to the end of the test; until to obtain a clear divergence in force values after 4weeks. This is mainly due to differences in the form, material types and storage conditions which varied comparing with cracking or meshing of these concrete elements (Figures 10 and 11).

For the compression behaviour, we could see cylinders classified first with an important superiority of (A) specimens then (B and C) with 31.00, 17.00 and 14.39MPa. The stronger cylindrical samples (B) were weaker in alkali and less heated. After cylinders we could find secondary beams with reinforced concrete; they had a strength value nearer to the doped cylinders. This convergence was due to the (AR) effect and reinforcement in beams; although the compressive height was different. Third one was beams without reinforcement; they were the weaker elements with nearer values of (A), (B) and (C) concretes (2.50, 1.92 and 1.17 MPa). Reinforcement effect was higher than the temperature and alkali effects which was less in this case.

For the traction behaviour, we found the same order of compression in beams reinforced concrete, then concrete without reinforcement with the extreme value in reinforced beam -6.3 MPa. In concrete beams we had order: (A), (B) then (C) with -1.5, -1.15 and -0.7 MPa. Reinforcement effect was higher as in compression.

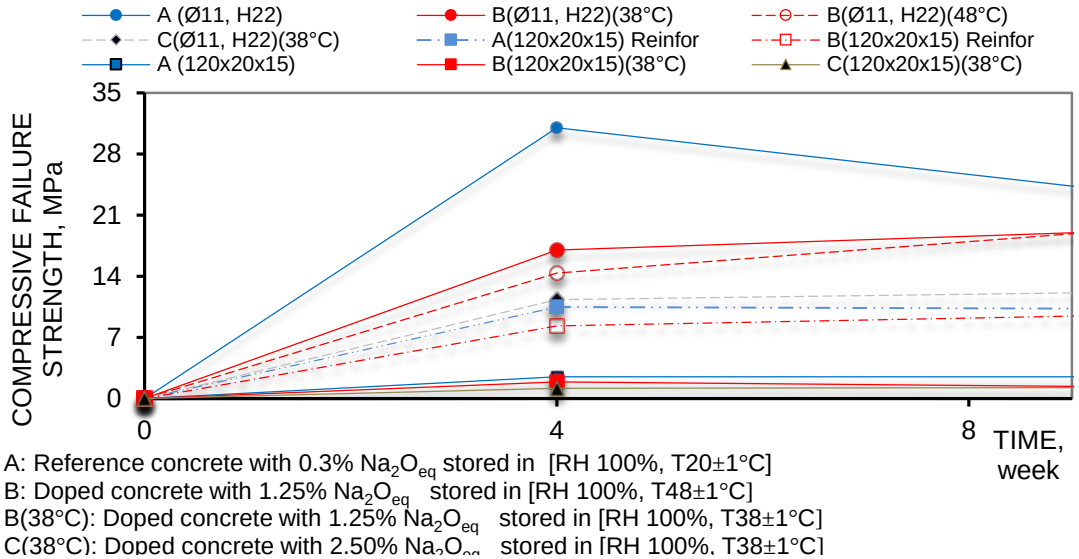


Figure 10 (Compressive failure strength – Time) curves after 2 months of storage with cylindrical specimens (Ø11, H22) cm, beams (120 cm × 20 cm × 15 cm) with concrete and reinforced concretes (A, B and C)

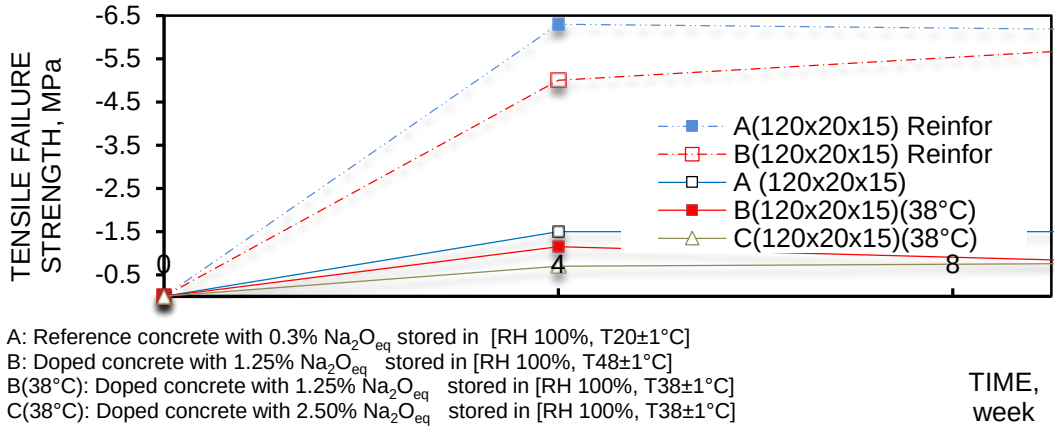


Figure 11 (Compressive failure strength –Time) curves after 2 months of storage with cylindrical specimens (Ø11, H22) cm, beams (120 cm × 20 cm × 15 cm) with concretes and reinforced concretes (A, B and C)

## Microscopic Examination

For microscopic examination, the petrography method was chosen on samples which was a thin section (45 × 30 × 1.5) mm referenced by Brot-Geology. They were prepared from specimens of expansion test. Precisely, from the moulded surface in where 'AAR' alterations were manifested. We had limited our material detection of the microstructure only for concretes of 4weeks age due to the important changes of the mechanical characteristics. For these reasons we had used (POM) polarized optical microscopy, which was in the geology department at UBMA. We want to monitor our granulate evolution before 'AAR' begging (Natural rock), then during this reaction (Doped concrete) comparing with granulate without 'AAR' attacks.

Origin rock analyses was macroscopically a massive rock black and without cracks. Microscopically, in our thin section of this stone we had three component types. First one was a Marly Limestone rock with clear fine beds of calcified microfossils (60%) and dark layers Clay minerals $SiO_4$ (Silicate) (40%). and Iron Pyrite ($FeS_2$) (Figure 12). The second component was a clear granulate of Limestone poor in fossil and rich in microcrystalline Calcite ($CaCO_3$) about (90%) as in Figure 13. Third element was a Calcite grain and rare grain of Quartz with crystal and circular form (Figures 14 and 15).

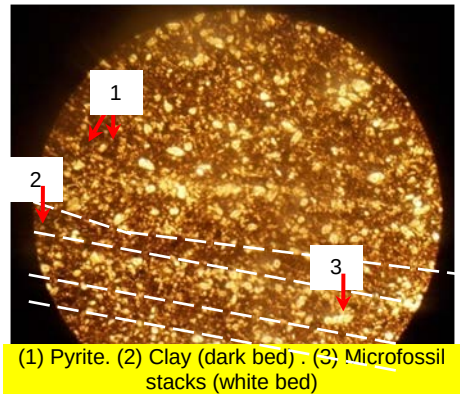


Figure 12 Sedimentary stratification aspects [NL, G5X]

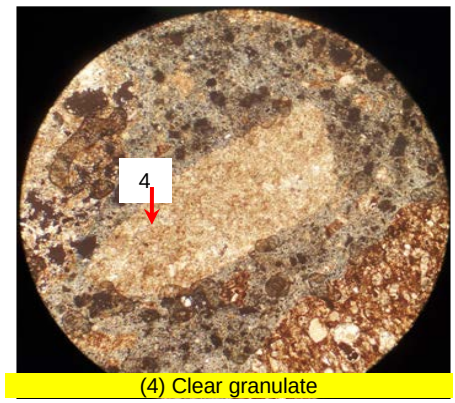


Figure 13 Clear Granulate [PL, G10X]

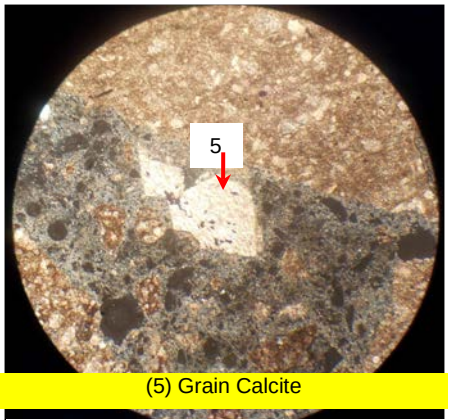


Figure 14 Calcite grain [PL, G10X]

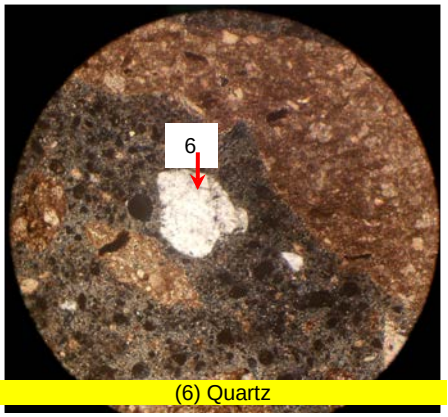


Figure 15 Quartz grain with circular or angular form [PL, G10X]

The moulded surface of concrete (A), the gravels were irregularly broken and filled with Pyrite coming from the origin rock. We had seen also a parallel cracks filled with Calcite ($CaCO_3$) (Figure 16). In concrete (B), this coarse granulate was composed of Marly Limestone and Limestone in angular form inferior to 15 mm and rich in microfossil which lesser then 50%. It also contained grey binder which attached the other components.

At the gravel boundary in concrete (A), the granulate-cement adherence zone is noted by (Transition zone). For Marly Limestone component, this zone was clear with about 60µ of width. But, it had empty cracks in limestone component (Figure 17). In concrete (B) this zone was clear with circular pores and cracks in cement paste (Figure 18).

The sand grain in concrete (A), was without cracks with unclear due to drowning grains in cement paste. In concrete (B), this granulates composed of various stones (Figure 19): circular and angular grains of Quartz about; angular grains of Limestone. It equally composed of grey binder which attached the other rock components. In the fine aggregate boundary, the transition zone was clear with circular pores in cement paste.

In the doped concretes, the gel was absent from granulate and cement; It equally absent from cracks and pores in moulded surface.

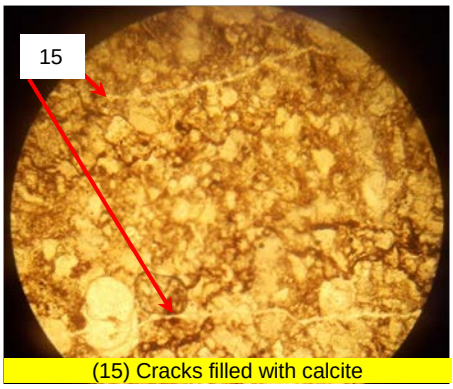


Figure 16 Parallel cracks filled with Calcite [NL, G20X]

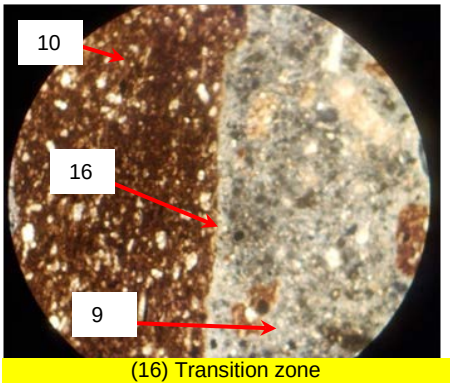


Figure 17 Clear bounder of granulate (>5mm) – Cement pate [PL, G20X]

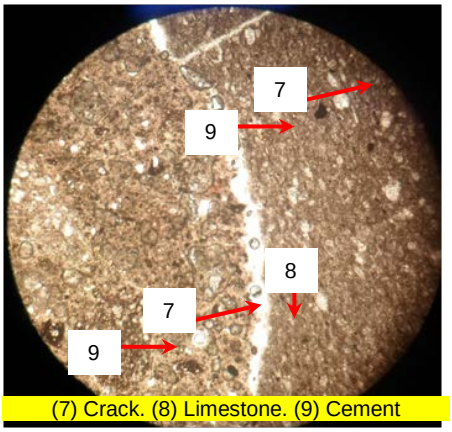


Figure 18 Cracking between Limestone granulates - Cement [NL, G5X, Ø4mm]

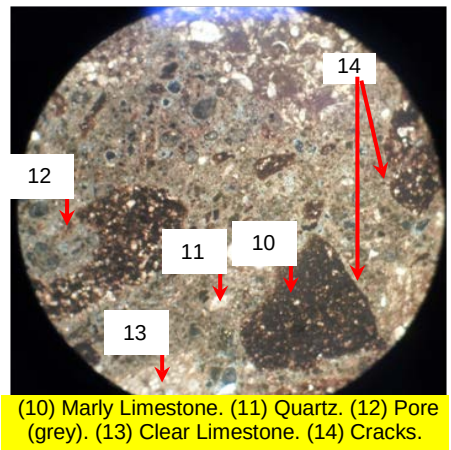


Figure 19 Concrete components (3B) [PL, G5X]

# CONCLUSIONS

During two months of storage in favourable conditions to 'AAR'; we test the reactivity of local aggregates. The cylindrical specimens (Ø11, H22) cm and beams 120 cm × 20 cm × 15 cm with alkali-reactive concrete and Alkali-reactive reinforced concretes had shown:

**Reference concretes: concretes and reinforced concrete (A)**

This concrete was without additional alkalis and conserved at ordinary temperature; it illustrates a healthy aspects and normal texture (absent 'AAR' alteration in skin).

**Doped concretes: concretes and reinforced concrete (B and C)**

i. Physical damages:

- High reactivity of our local aggregates is confirmed according to standards (ASTM, AFNOR, ACNOR and DLC). The expansion values were highly superior to the limit standards.
- Reinforcement in concrete, doping in alkali and structural element form affect highly on the results of mechanical proprieties and physical damages: expansion, opening crack, discoloration.
- The discoloration was detected in the external faces in all concretes and structural elements.
- Expansion and cracks of 'AAR' are found at early ages in our elements for all concrete types also. Cracks were both directional, even in depth; with (Y) form.
- The more cracked concrete was (B) in: Beam then cylinders.
- The more meshed concrete was (C) we had found an order in reinforced concrete: Beam then cylinder which was the contrary to the concretes without reinforcement.

ii. The mechanical characteristics:

For compression and traction (failure strengths) which presented a progress of strength in the first 28 days. Then we have the stability for the both behaviours for all structural elements with both materials (concrete and reinforced concrete). At 4 weeks, strengths were highly diverged due to differences in the form, material types and storage conditions which varied with different manner than cracking or meshing.

iii. Microstructure

- Granulate transformation has been examined microscopically at 28 days of concrete age and in moulded surface; on samples which was a thin section (45 × 30 × 1.5) mm using (POM) polarized optical microscopy of geology. Granulate evolution was studied before 'AAR' begging with Natural rock (Bouhachana granulate). Then during this reaction Doped concrete (B & C) comparing with granulate without 'AAR' attacks of Reference concrete (A).
- The moulded surface analyses of concretes (A and B) in rock origin, coarse and fine aggregates, boundary aggregates, and at cement paste had shown different chemical components. There is a good micro-structure (no important deteriorations) which explains the strength progress at the first month of tests for both materials (A and B); it's the reactive phase of the components before physical material degradation.

## REFERENCES


1. HABITA M.F., BOUABDALLAH F. and REHAMNIA N. Detection of aggregate reactivity at the Algeria east, by autoclave test and that of ACNOR (CSA) (2), INVACO2: International seminar, Innovation & recovery in civil engineering & construction materials, Rabat- Morocco, No. 2, 2011, p- 072.

2. AFNOR NF P15-467. X Fluorescence, elemental analysis of cement. French association for standardization.

3. AFNOR NF P18-587. Aggregates: Dimensional establishes in alkaline field- Test for Concrete. French association for standardization, Dec 1990.

4. AFNOR NF P18-585. Dimensional establishes in alkaline field- Test for Mortar. French association for standardization, 1990.

5. AFNOR NF P18-594. Aggregates - Test methods of reactivity to alkalis. French association for standardization, Feb 2004.

6. ACNOR CSA A23.2-14A. Potential expansively of aggregates (procedure for length change due to alkali- aggregate reaction in concrete prisms at 38°C. Canadian standard association, Oct 1994.

7. AFNOR NF P18-301. Aggregates - Natural aggregates for hydraulic concrete (E). French association for standardization, Dec 1983.

8. AFNOR NF P18-304. Granulometry of aggregates (E). French association for standardization, Dec 1973.

9. AFNOR NF P18-309. Aggregates - Rotary-Furnace made expanded clay or shale aggregates for making concrete (E). French association for standardization, Dec 1982.

10. AFNOR NF P18-554. Aggregates - Measurements of mass per unit volume, porosity, coefficient of absorption and contain in water of chippings and pebbles (E). French association for standardization, Dec 1979.

11. AFNOR NF P18-555. Aggregates - Measurements of mass per unit volume, coefficient of absorption and contain in water of sands (E). French association for standardization, Apr 1980.

12. AFNOR NF EN 933-2. Tests Method for geometrical properties of aggregates. French association for standardization, 1996.

13. AFNOR NF P18-451. Concretes- Slump test (E). French association for standardization, Dec 1981.

14. ACNOR CSA A23.2-5C. Concrete slump determination. Canadian standard association, Oct 1994.

15. AFNOR NF P18-405. Concretes data test manufacturing and samples conservation (E). French association for standardization, Dec 1981.

16. AFNOR NF P18-400. Concretes- Moulds for cylindrical and prismatic specimens (E). French association for standardization, Dec 1981.

17. AFNOR NF P18-406. Concretes - Compression test. French association for standardization, Dec 1990.

18. ACNOR CSA.A23.2 2C. Concrete mixture manufacturing in the laboratory. Canadian standard association, Oct 1994.

19. ACNOR CSA.A23.2 3C. Manufacturing and cure of Concrete samples destined for compression and bend tests. Canadian standard association, Oct 1994.

20. ACNOR CSA.A23.2 1D. Moulds for manufacturing of cylindrical test of the vertical. Canadian standard association, Oct 1994.

21. ASTM C78-94. Flexural Strength of Concrete (Using Simple Beam with Third-Point Loading). American society for testing materials, Philadelphia PA, USA.

22. ACNOR CSA A23.2-8C. Flexural Strength of Concrete (Using a Simple Beam with Third Point Loading). Canadian standard association, Oct 1994.

23. CARLSON R.W. Discussion of Expansion of concrete through reaction between cement and aggregate. Proceedings of the American Society of Civil Engineers, Vol. 47, 1942, pp. 265–266.

24. VIVIAN H.E. Some Effects of temperature on mortar expansion, Australia, Journal of Applied Science, Vol. 2, 1951, pp. 114–122.

25. CHEN H. The effect of cement composition on alkali-aggregate reaction, final report, Institute for Research in Construction, National Research Council, Ottawa, Canada, DSS Contract N°1SQ84-00349, No. DSS, Contract N°1SQ84-00349, 1988.

26. MOHAMED I. Contribution to the study of alkali reactive concrete containment by composite materials (epoxy carbon). Thesis for obtaining of doctorate diploma, UCBL France, 2004, pp. 77–237.

27. PLUMIER A. Pathology and structural repairs of buildings, Characterization of an existing structure, Faculty of applied sciences, department of Architecture, geology, environment and constructions, Liege university, Belgium, Part 02, 2006.

28. ASTM C1105-95. Standard Test Method for Length Change of Concrete Due to Alkali-Carbonate Rock Reaction. American society for testing materials, Philadelphia PA, USA.

29. ACNOR CSA A23.2-9C. Compressive Strength of cylindrical concrete specimens. Canadian standard association, Oct 1994.

30. LARIVE C. Combined contribution of experimental and modelling to the understanding of the alkali reaction and its mechanical effects, Thesis for obtaining of doctorate diploma, National school of roads and bridges, France, 1997, 327 p.

31. LI K., ULM F., COUSSY D., LARIVE C. and FAN L. Chimioelastic modeling of alkali-silica-reaction in concrete, 11th international conference on Alkali-Aggregate reaction, Canda, 2000, pp. 989–1008.

# HYDRAULIC LIME – POZZOLANS: PROPERTIES, USES AND RESEARCH NEEDS

**E R Grist**
**K A Paine**
**A Heath**
University of Bath
United Kingdom

**ABSTRACT.** Concerns with the harmful environmental impact of Portland cement manufacture on a global scale, has prompted an extensive search for clinker replacement materials and alternative low $CO_2$ cements. Amidst the development of radical new binder technologies there has been some resurgence in interest in Portland-cement's predecessor – hydraulic lime. This paper describes recent collaborative research, conducted by multidisciplinary engineering consultancy Ramboll and researchers at the BRE Centre for Innovative Construction Materials at the University of Bath, to develop modern, structural-grade, hydraulic-lime concretes. The paper details work to identify the pozzolanic additions, and combinations thereof, which result in structural strength concrete; and the results of a suite of tests to assess the structural and durability properties of the most-promising hydraulic-lime pozzolan concretes. The environmental credentials of hydraulic-lime pozzolan concretes in comparison with Portland cement-based concretes is then considered. In relation to these results the paper discusses the ways in which hydraulic-lime pozzolan concretes can be used, including case studies, and methods to adapt the mix proportions to optimise the properties for uses as varied as conservation of historic structures to engineered reinforced concrete construction. Finally, the paper discusses the future research that is needed to fully realise the potential of this new concrete.

**Keywords:** Hydraulic lime, Pozzolan, Low-carbon concrete

**E R Grist** is a practising structural engineer at Fenton Holloway. She was formally a research engineer at Ramboll, and was awarded an EngD by the Industrial Doctorate Centre in Systems, a collaboration between Ramboll and the Universities of Bath and Bristol. She has published on both lime-pozzolan technology and innovation management.

**K Paine** is a Reader in civil engineering and Deputy Director of the BRE Centre for Innovative construction Materials at the University of Bath. His research focusses on low carbon, smart and nanotechnology-enhanced concretes.

**A Heath** is a Professor of geomaterials at the BRE Centre for Innovative construction Materials at the University of Bath.

## INTRODUCTION

Until recently lime-based materials have been understood to be weak and slow to set and have consequently been regarded as unsuitable for modern construction. The research described in this paper has, however, demonstrated the feasibility of producing modern, structural-grade concretes based on naturally hydraulic lime. Furthermore this research has demonstrated the potential for hydraulic lime-pozzolan concretes (HLPCs) as low-$CO_2$ alternatives to Portland cement (PC) concretes.

These innovative HLPCs should not be confused with 'Limecrete', or other commercially available lime-concretes, which are appropriate for the repair of historic buildings but not as alternatives to PC for structural applications.

### Historical Context

Before the advent of PC, lime was the predominant binder for use in construction. Lime binders have a long and rich history and a lime-concrete floor slab discovered in Southern Israel in 1985 was dated back to 7000BC [1]. The practice of 'gauging' lime mortars and concretes with pozzolanic materials to improve performance is credited to the Greeks who used volcanic tuff with lime [2]. The Romans similarly utilized the volcanic ash from Pozzuoli, at the base of Mount Vesuvius. The technique then spread across Europe with the expansion of the Roman Empire, with lime-pozzolan concretes used to construct walls, floors, domes, bridges, aqueducts, harbours and cisterns [3]. By the middle ages the technology had been largely lost.

In the 19th century there was a revival in lime-pozzolan concrete technology and it was at this time that the first attempts to scientifically understand the properties of hydraulic-lime binders was undertaken by Smeaton (1724-92) and Vicat (1786-1861). Their work was followed by relatively rapid advances in binder technology and in 1824 Joseph Aspdin was granted the patent for a new artificial stone based on an improved binder he named Portland-cement. This 19th century 'proto-Portland cement' [2] was a forerunner of modern Portland-cements, which are now a mainstay of global human development. The development of PC meant that lime-pozzolans as a binder technology for concrete disappeared. Figure 1 depicts the three ages of lime-pozzolan concrete technology.

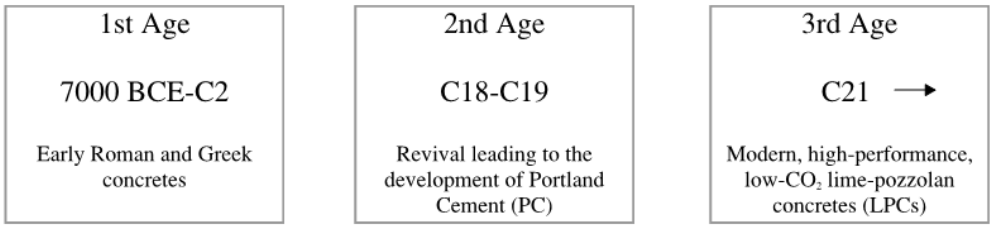


Figure 1 The three ages of lime-pozzolan concrete

Although this work was informed by historic practice and inspired by the durability of ancient concrete structures, these innovative HLPCs do not represent a return to a former technology as they utilise modern industrial waste ashes and exploit the advanced performance of the latest generation of admixtures.

### Initiation of the Research

In November 2008 Ramboll was contacted by an architectural practice interested in designing an eco-house with a doubly-curved concrete shell roof. The aspiration was to reduce the embodied impact of the structure by utilising a lime-based, as opposed to a PC-based, concrete. It was acknowledged that both the technical feasibility and the environmental desirability of this novel solution were contingent upon the structural capacity a concrete based on lime. The potential use of lime-concrete as an alternative to PC concrete for structural components was highlighted by Holmes and Wingate in 1997, but they acknowledged 'the science has not yet been developed' [3].

Prior to this research programme the only significant modern research on HLPC was that undertaken at the University of Aveiro, Portugal between 2009 and 2011 where HLPCs were being shown to attain 28-day compressive cube strengths ($f_{c28}$) of 11 MPa, with 20% of the hydraulic lime replaced with a waste residue of expanded clay production [4]. Subsequently, Cachim et al. demonstrated a maximum $f_{c28}$ of 17 MPa could be attained with 20% of the hydraulic lime replaced with a metakaolin [5]. However, Cachim et al made no further attempts to improve strength as their principal interest was the sustainable use of local materials. Although compressive strengths of around 10-15 MPa were ostensibly attainable, it was anticipated that compressive strengths in excess of 30MPa were going to be necessary to make the proposed HLPC shell roof both a feasible and desirable structural solution.

## RESEARCH TO DATE

### Phase 1- Relative Efficiency of Binary and Ternary Lime-Pozzolan Binders

In the absence of a definitive source of information on hydraulic lime-pozzolan (HLP) binders, the initial phase of testing was a systematic study of the compressive strength development of HLP mortars prepared with NHL5, conforming to BS EN 459-1 [6], and a range of aluminosilicate mineral additions. In total 22 different mortar types were prepared and tested. The aim of this preliminary laboratory research was to identify a small number of additions, and/or combinations thereof, with the potential to result in structural strength HLPCs when scaled up from mortars to concretes.

The results showed that a ternary combination of 50% natural hydraulic lime (NHL5), 25% silica fume (SF) and 25% ground granulated blastfurnace slag (GGBS) resulted in a mortar with an average $f_{c28}$ of 28 MPa, at a water-to-binder (w/b) ratio of 0.5 [7]. This was eight times the strength of an equivalent mortar prepared with NHL5 alone and broadly speaking comparable with that of a low-heat cementitious mortar.

The results of this study allowed the pozzolanic additions, and combinations thereof, to be ranked from low to high efficacy, when used in conjunction with NHL5. The ternary combination of NHL5, SF and GGBS was shown to result in the greatest overall pozzolanic efficacy ($PE(\%)_{28d}$), attaining a maximum value of 94%. The four most promising combinations of additions, resulting in the highest strength mortars, which were chosen to be scaled up to HLPCs in the subsequent phase of testing, were:

| | |
|---|---|
| 70% NHL5, 15% FA & 15%MK, | (i) |
| 50% NHL5, 25% SF & 25% GGBS, | (ii) |
| 70% NHL5 & 30%SF, | (iii) |
| 50% NHL5, 25% SF & 25% FA | (iv) |

Figure 2 shows the compressive strength development of HLP combinations (i) to (iv) in comparison to 100% NHL5 and that of a proprietary formulated lime mortar (NHL-PC).

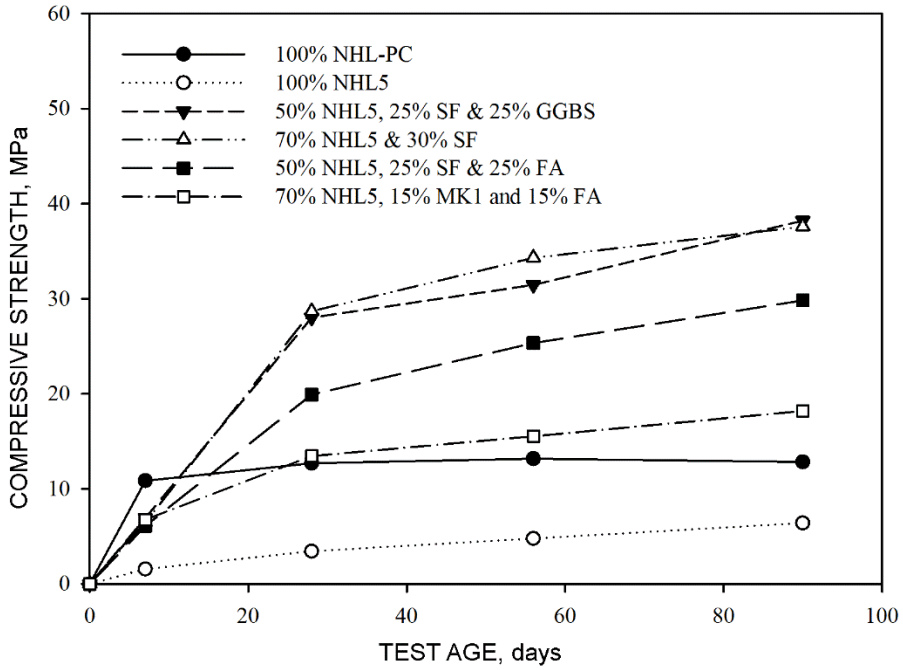


Figure 2 Compressive strength development of key mortars

**Phase 2 - Preliminary Hydraulic Lime-Pozzolan Concretes**

The aim of the second phase of testing was to investigate the structural and durability characteristics of four preliminary HLPCs. The compressive strength development, elastic modulus, linear shrinkage and rate of carbonation of the HLPCs were tested in comparison with Portland cement (PC) and blastfurnace cement (CIII/A) control concretes. Each concrete was prepared at three w/b ratios to investigate the effect of w/b ratio on the resultant properties of the hardened concretes. Additionally, the impact of curing conditions on compressive strength development was assessed by curing test specimens either in air (20 ± 0.5°C, 60-65% RH) or in a water bath (20 ± 0.5°C, 100% RH) [8].

The maximum $f_{c28}$ of the four HLPCs was 35MPa, attained by combining NHL5 (70% by mass) with SF (30% by mass) and curing the resultant concrete in water. The $f_{c28}$ of the equivalent air-cured concrete was 21MPa, 40% lower. Elastic modulus results demonstrated that the elasticity-compressive strength equation in Eurocode 2 for PC concretes, substantially overestimated the elastic modulus of the HLPCs.

The carbonation resistance of HLPCs was observed to be low in comparison to PC concretes. The results suggested that a HLPC incorporating 25% SF & 25% GGBS should provide sufficient protection for steel reinforcement for around 130 years. Increasing the depth of cover from 40 to 50mm increased this to over 200 years

The observed drying shrinkage of the HLPCs tested was, in the vast majority of cases, broadly in line with that of the PC-based control concretes over a 20 week period. SF was shown to be effective in minimising the impact of w/b ratio on the linear shrinkage of the resultant concretes. The HLPC comprising 70% NHL5, 15% FA & 15% MK was found to be highly sensitive to the variation in w/b ratio, raising concerns about the suitability of this ternary combination in practice.

As well as wanting to explore the mechanical characteristics of a range of HLPCs, a key aim of this industry-led research programme was to comment on the feasibility of constructing the lime-concrete dome that initiated the research. With $f_{c28}$ in excess of 30MPa having been shown feasible in the laboratory, the focus of the research shifted to converging on single HLPC appropriate for this project.

In this study the mechanical properties of the four alternative HLPCs were compared at a w/b ratio of 0.65. The greatest initial and long term strength gain, the highest strain at the maximum compressive strength ($\varepsilon_{c1}$), the greatest carbonation resistance and the least drying shrinkage, was exhibited by a HLPC comprising 50% NHL5, 25% SF and 25% GGBS [8]. As a result this ternary combination was selected for further investigation in Phase 3.

As well as successfully converging on a single ternary combination, this testing was effective in highlighting a number of practical considerations which were to inform the subsequent phase. For example, the results showed that the strongest and most durable HLPCs were produced at low w/b ratios. Having been unable to compact the HLPCs at low w/b ratios it was clear that a suitable superplasticiser (SP) needed to be identified going forward.

It was also recognised that the high dosage of SF used in Phases 1 & 2 of this study (25-30% by mass), might be untenable in future HLPCs due to commercial and legislative constraints. It was decided at this juncture to limit the use of SF to 10% of the total binder as is the case in PC based concretes [9].

**Phase 3 – An Innovative Concrete by Design**

This phase of testing sought to address to fundamental question about this novel concrete technology. Firstly, could a HLPC be cast into structural elements with an appearance and surface finish similar to PC concrete? Secondly, could HLPC elements be designed to Eurocode 2 (EC2)?

The laboratory testing conducted during this phase comprised a sequence of experiments, aiming to explore and enhance the fresh behaviour and mechanical performance of a ternary combination of NHL5, GGBS and SF. Figure 3 illustrates the fresh behaviour of HLPC before and after the addition of a SP.

Figure 3 HLPC before and after the addition of SP

By varying the mix proportions and experimenting with different proprietary SPs a HLPC with an $f_{c28}$ of 49MPa and an $f_{c90}$ excess of 60MPa was produced. This phase of testing culminated with the production and flexural testing of two reinforced HLPC beams. The failure load of the two beams was as predicted by EC2 (with due consideration of partial safety factors). The load-displacement behaviour of the two HLPC beams, in comparison to that of two identical PC beams is shown in Figure 4. Beams A_LP and A_ PC were under-reinforced and failed in a ductile manner whereas beams B_LP and B_PC were over-reinforced and failed suddenly when the compressive strength of the concrete was reached, as commonly observed in over-reinforced beams.

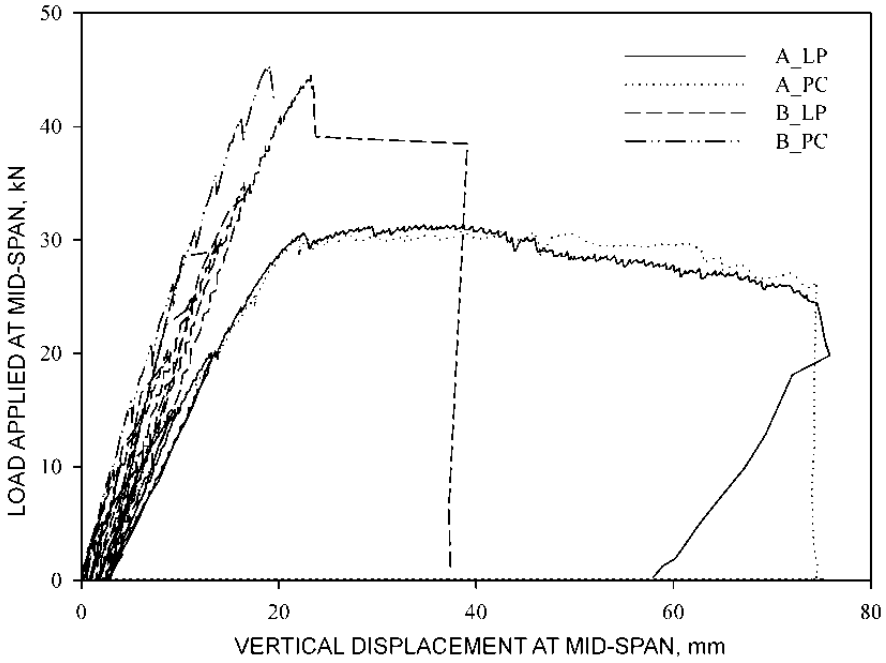


Figure 4 Load-displacement behaviour of under- and over-reinforced HLP and PC beams

**Phase 4 – So it can be done, but is it worth doing?**

The aim of this phase of the research was to assess whether these novel HLPCs were, or could be, desirable alternatives to PC concrete, particularly in the context of the industry wide search for low-$CO_2$ cements. Specifically, the embodied $CO_2$, embodied energy and binder intensity of a selection of these novel HLPCs were compared with PC concretes of the same $f_{c28}$. This included a laboratory study investigating the influence of the total binder content on the eco-efficiency of the resultant HLPCs.

This study demonstrated that the use of GGBS and SF in combination with NHL5 could realise savings in environmental impact, but that the potential savings were highly dependent on the boundaries of the analysis [10]. Specifically, the choice of allocation procedure was shown to have a profound effect on the selection of the 'greenest' binder when comparing PC and HLP concretes. Whereas in the case of GGBS it has been shown that economic allocation procedures maintain environmental benefits in comparison to PC [11], both mass and economic allocation procedures were shown to have a very detrimental effect on the environmental credentials of SF, see Figure 5.

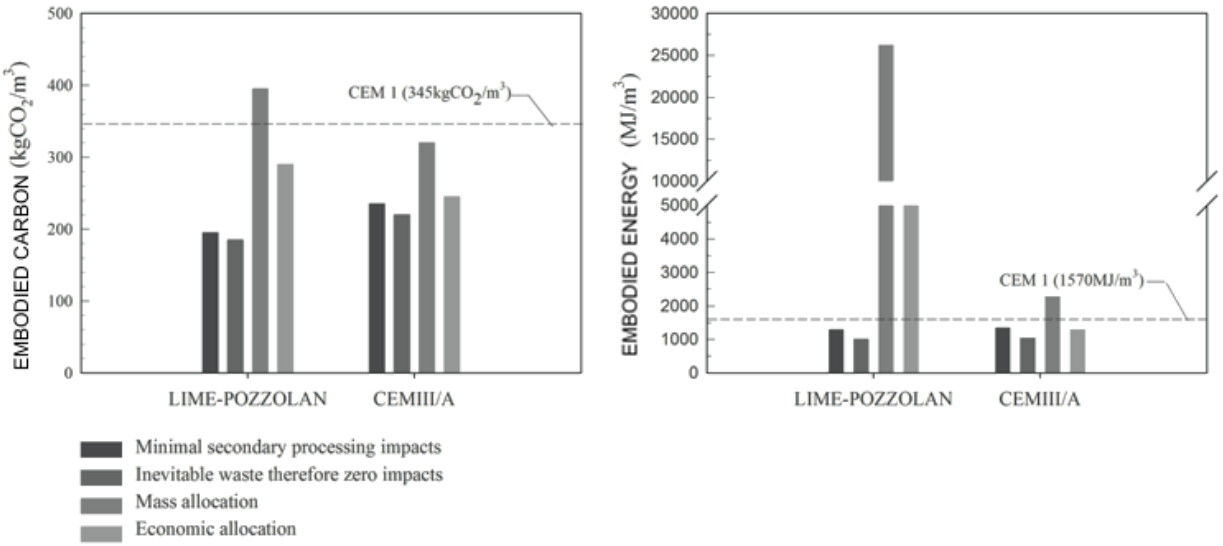


Figure 5 Influence of allocation methodology on the EC and EE of HLPC and CEMIII/A concretes

Assuming a 'waste' allocation and considering only the impacts associated with the secondary production of GGBS and SF, a HLPC with a binder comprising 50% NHL5, 40% GGBS & 10% SF and a $f_{c28}$ of 49MPa has an embodied $CO_2$ 43% less than a PC concrete of equivalent strength. The embodied $CO_2$ of this concrete is also 17% less than an equivalent strength CEMIII/A concrete. The embodied energy of this HLPC is 17-24% lower than that of the CEMI concrete (depending on inclusion of SP) and is 3-12% that of the CEMIII/A concrete.

## APPLICATION OF THIS TECHNOLOGY

In seeking to develop a HLPC suitable for reinforced structural elements, the research programme to date has tried to minimise differences between HLP and PC concretes. To maximise the impact of this material research and to exploit the potential environmental benefits of this binder technology, subsequent research will need to identify and amplify differential properties, which will open up the market for these alternative concretes. Whilst this research was initiated by a specific real-world project, for which a single structural-grade concrete was sought, the significance of innovation in binder technologies is the multifarious family of concretes that a new binder could bring about.

Potential early-adopter interest in this novel, low-$CO_2$ concrete technology created the opportunity to develop a second project-specific HLPC 'product' during the research programme. This real-world project was used as a case study for exploring the feasibility of a distinctly different application of this novel technology. In this case, keen to expose the innovative concrete in the building, the client sought a polished HLPC floor finish. This decorative screed incorporated oolitic limestone aggregate extracted from the site for which this flooring was developed. Although there is little recent precedence for polishing lime-concrete floors, examples of this technique, such as the decorative terrazzo floor at the Villa Saraceno, Italy laid in 1612, provided historical precedence for this solution [3].

This case study project was effective in addressing a number of questions about the possible application of this novel binder technology [12]. Development of the bespoke floor solution in conjunction with a specialist contractor demonstrated that HLPC can be diamond polished after two weeks, as per PC concrete and sealed with proprietary sealants. The embodied $CO_2$ of a 100mm thick polished HLPC floor was shown to be 45% less than a typical 100mm thick polished PC-concrete floor and 25% less than a conventional vinyl floor makeup. The embodied energy of a 100mm thick polished HLPC floor was 21% less than a typical 100mm thick polished PC-concrete floor and 37% less than a conventional vinyl floor makeup. The steel reinforcing mesh specified in the HLPC floor slab was shown to account for 43% of the embodied energy per $m^2$.

## DISCUSSION AND FUTURE RESEARCH DIRECTIONS

It is recognised that different applications and markets will require different material properties, leading to differentiation of the binder itself. For example in the conservation of historic buildings, lime-based materials are preferred as they exhibit a number of favourable characteristics that differentiate them from PC-based alternatives and make them preferable for the repair and maintenance of historic buildings, specifically breathability, permeability and flexibility. On this basis research is needed to understand the porosity, capillarity and elastic behaviour of HLPCs and importantly how these characteristics are affected by the nature and proportion of aluminosilicate additions in the binder. It is thought that a high proportion of SF in the binder may be detrimental in this respect. Similarly, lime-mortars are also advocated for autogenous-healing; the ability for free lime to carbonate in microcracks leading to self-healing mechanism. Whether or not HLPCs are also capable of being self-healing will depend on the long-term availability of free lime in the binder. These application-specific benefits might favour HLPCs with a low-pozzolanic content.

## Sustainability

In the 'green' building field the opposite may be true. Initial results suggest that the eco-efficiency of future HLPCs might be improved by increasing the proportion of pozzolanic materials in the binder (assuming the environmental impact of these materials is deemed lower than that of the NHL5 they replace). Testing has shown that a concrete prepared with a lower proportion of lime in the total binder (23% NHL5, 65% GGBS and 12% SF) has a $f_{c28}$ 3-4MPa greater than a concrete prepared with a higher proportion of lime in the total binder (53% NHL5, 35% GGBS and 12% SF), suggesting that the optimum dosage of aluminosilicate mineral additions, with respect to compressive strength, may exceed 77%. A substantial proportion of aluminosilicate mineral additions in the binder composition thus may prove beneficial from both an environmental and economic perspective.

## Durability

Lime-pozzolan concretes have a long history of use in marine structures; Pozzuoli Bay (Baianus Sinus), constructed in the first century BC, being just one example [13]. Although testing is still required to compare the performance of HLP and PC based concretes subject to aggressive exposure conditions, it is hypothesised that a high pozzolanic content may also be advantageous in HLPCs in aggressive environments, such as marine and sub-structural applications. Rapid Chloride Permeability Testing is needed to model the chloride ion diffusion coefficient of HLPCs. The high permeability of the HLPCs which are desirable for conservation and some other purposes can have a detrimental effect on some durability properties.

Other physical-chemical effects that warrant further performance testing and pre-qualification in the case of whether HLPCs are resistant to sulfate attack and alkali-silica reactions (ASR). The risk of the ettringite form of sulfate attack in HLPCs is thought to be low because of the low content of tricalcium aluminate ($C_3A$) in the binder and consequently the low amount of the AfM phase monosulfate in the concrete. However, it is acknowledged that there are several mechanisms of sulfate attack, including direct attack on $Ca(OH)_2$, which needs further investigation, before the sulfate resistance of HLPCs can be substantiated. The risk of ASR in HLPC is also thought to be low because NHL has a low sodium ($Na^+$) and potassium ($K^+$) ion content. Any $Na^+$ and $K^+$ present would be expected to react with the highly reactive pozzolanic materials, leaving no free $Na^+$ and $K^+$ in the system. Substantiation of the resistance of HLPCs to ASR would open up the possibility for HLPCs with a high recycled glass content.

## Alternative Aluminosilicates

The combination of aluminosilicate additions that have been investigated in this research to date, may be currently deemed appropriate for the UK construction industry, but are unlikely to be the only, or the most appropriate, combination in other regional markets. There are indications that GGBS, FA and SF are becoming increasingly difficult to source in the UK [10]. Based on the results of laboratory testing of ternary HLPCs, there is substantial scope for broadening this field of enquiry into the testing and development of regional HLPCs that exploit locally available materials. Alternative mineral additions include industrial ashes, naturally occurring pozzolanic deposits, calcined clays and low-cost agro wastes.

Industrial waste ashes that may warrant further consideration in the development of future HLP cements include paper sludge ash [14], sewage sludge ash [15], municipal solid waste ash [16] and oil shale ash [17; 18]

Low-cost agro-wastes are also being investigated as partial PC replacement materials because of their pozzolanic properties. These materials might also warrant further investigation in the development of regional HLPCs: rice-husk ash [19], sugar cane bagasse [20], saw dust ash [21], corn cob ash [22], coconut husk ash [23], wheat straw ash [24], locust bean pod ash [25], palm oil fuel ash [26], cassava waste ash [27], olive waste ash [28] and periwinkle, oyster and snail shell ash [29]. Of this selection of waste ashes rice husk ash (RHA) is particularly interesting in the dialogue about future HLPCs, because of its wide scale availability and its high content of amorphous silica, which makes its oxide composition not dissimilar from that of SF.

### 'Cement' Chemistry

The potential diversification of HLPC technology makes an in-depth study of the reaction chemistry and microstructure of HLP binders imperative. The insight gained from such an analysis will be hugely valuable in limiting the list of candidate pozzolanic mineral additions, and combinations thereof, and enable a design-led approach to the development of future HLPCs.

## FUTURE RESEARCH

In depth micro analysis is required to investigate the reaction kinetics and hydration products. Techniques identified as appropriate for such a study include isothermal conduction calorimetry, x-ray diffraction, thermal gravimetry and Fourier transform infrared spectrometry. Other techniques that might be valuable in studying the pore structure and phase assemblages of HLPCs include scanning electron microscopy, mercury intrusion porosimetry and x-ray computed tomography. General physiochemical results are needed, not only to explain the empirical results attained to date, but to refine and optimise future HLPCs.

### Choice of Application

A design-led approach to the development of a range of tailored application- or region-specific concretes has the potential to improve the sustainability of the concrete industry. Such an approach puts emphasis on identifying specific requirements in-use and conducting testing at the front end. This might be expected to result in a shift focus, from generalised results to specialist testing and certification for use of HLPCs in different applications. For example, although this research has shown that HLPCs can be polished [12], the implementation of this material in floor systems will inevitably demand further testing to quantify the thermal performance of these novel concretes and their slip, stain, chemical and wear resistance in use.

## SUMMARY

This research programme was initiated by a real-world project aspiration and was required to converge on a single concrete, which represented a recommended and realisable solution to a specific design problem. The objective of the research presented in this paper was not, however, to discover a unique formula for a new marketable product, which might at some level compete with PC, but rather to push the boundaries of lime technology and where possible to create design space for future lime-based construction materials. 28-day compressive strengths in excess of 45MPa are boundary pushing, representing a step-change in our understanding of the potential strength, and rate of strength gain, associated with lime-based binders.

The results attained to date are recognised to be incomplete, with physiochemical analysis required to explain the phenomena observed laboratory. It is hoped that the research outlined in this paper, and detailed elsewhere, will inspire and inform a number of subsequent research projects and that the work to date might prove to be a platform for future research and development on HLPCs.

## ACKNOWLEDGEMENTS

This work was supported by the EPSRC funded Industrial Doctorate Centre in Systems (Grant EP/G037353/1), Ramboll and the Universities of Bath and Bristol.

## REFERENCES

1 BENSTED, J & COLEMAN, N. Cement and Concrete - 7000BC to 1900AD, Cement-Wapno-Beton, Vol.3, 2003, pp 134-142.

2 BLEZARD, RG. Reflections on the history of the chemistry of cement, Lecture Paper Series, Vol.0104, 2000.

3 HOLMES, S & WINGATE, M. Building with Lime: A practical introduction, 1997, ITDG Publishing.

4 VELOSA, AL & CACHIM, PB. Hydraulic-lime based concrete: Strength development using a pozzolanic addition and different curing conditions, Construction and Building Materials, Vol.23, No.5, 2009, pp 2107-2111.

5 CACHIM, P, VELOSA, AL & ROCHA, F. Effect of Portuguese metakaolin on hydraulic lime concrete using different curing conditions, Construction and Building Materials, Vol.24, No.1, 2010, pp 71-78.

6 BS EN 459-1, Building Lime - Definitions, specifications and conformity criteria, 2010, BSI.

7 GRIST, ER, PAINE, KA, HEATH, A & NORMAN, J. Compressive strength of binary and ternary lime-pozzolan mortars, Materials and Design, Vol.52, 2013, pp 514-523.

8 GRIST, ER, PAINE, KA, HEATH, A, NORMAN, J & PINDER, H. Structural and durability properties of hydraulic lime–pozzolan concretes, Cement and Concrete Composites, Vol.62, 2015, pp 212-223.

9 BS EN 197-1, Cement Part 1: Composition, specifications and conformity criteria for common cements, 2011, BSI.

10 GRIST, ER, PAINE, KA, HEATH, A, NORMAN, J & PINDER, H. The environmental credentials of hydraulic lime-pozzolan concretes, Journal of Cleaner Production, Vol.93, 2014, pp 26-37.

11 CHEN, C, HABERT, G, BOUZIDI, Y, JULLIEN, A & VENTURA, A. LCA allocation procedure used as an incitative method for waste recycling: An application to mineral additions in concrete, Resources, Conservation and Recycling, Vol.54, No.12, 2010, pp 1231-1240.

12 GRIST, ER, PAINE, KA, HEATH, A, NORMAN, J & PINDER, H. Innovative solutions please, as long as they have been proved elsewhere: The case of a polished lime-pozzolan concrete floor, Case Studies in Construction Materials, Vol.1, 2014, pp 33-39.

13 JACKSON, MD, CHAE, SR, MULCAHY, SR, MERAL, C & TAYLOR, R. Unlocking the secrets of Al-tobermorite in Roman seawater concrete, American Mineralogist, Vol.98, 2013, pp 1669-1687.

14 BAI, J, CHAIPANICH, A, KINUTHIA, JM, O'FARRELL, M, SABIR, BB, WILD, S & LEWIS, MH. Compressive strength and hydration of wastepaper sludge ash–ground granulated blastfurnace slag blended pastes, Cement and Concrete Research, Vol.33, No.8, 2003, pp 1189-1202.

15 CYR, M, COUTAND, M & CLASTRES, P. Technological and environmental behaviour of sewage sludge ash (SSA) in cement-based materials, Cement and Concrete Research, Vol.37, No.8, 2007, pp 1278-1289.

16 AUBERT, JE, HUSSON, B & VAQUIER, A. Use of municipal solid waste incineration fly ash in concrete, Cement and Concrete Research, Vol.34, No.6, 2004, pp 957-963.

17 SMADI, MM & HADDAD, RH. The use of oil shale ash in Portland cement concrete, Cement and Concrete Composites, Vol.25, No.1, 2003, pp 43-50.

18 GAO, G-M, ZOU, H-F, GAN, S-C, LIU, Z-J, AN, B-C, XU, J-J & LI, G-H. Preparation and properties of silica nanoparticles from oil shale ash, Powder Technology, Vol.191, No.1, 2009, pp 47-51.

19 CHAO-LUNG, H, ANH-TUAN, BL & CHUN-TSUN, C. Effect of rice husk ash on the strength and durability characteristics of concrete, Construction and Building Materials, Vol.25, No.9, 2011, pp 3768-3772.

20 CORDEIRO, GC, TOLEDO FILHO, RD, TAVARES, LM & FAIRBAIRN, EMR. Pozzolanic activity and filler effect of sugar cane bagasse ash in Portland cement and lime mortars, Cement and Concrete Composites, Vol.30, No.5, 2008, pp 410-418.

21 ELINWA, AU & MAHMOOD, YA. Ash from timber waste as cement replacement material, Cement and Concrete Composites, Vol.24, No.2, 2002, pp 219-222.

22 ADESANYA, DA & RAHEEM, AA. Development of corn cob ash blended cement, Construction and Building Materials, Vol.23, No.1, 2009, pp 347-352.

23 ETTU, LO, EZEH, JC, IBEARUGBULEM, OM, ANYA, UC & NJOKU, KO. Strength of Binary Blended Cement Composites Containing Coconut Husk Ash, International Journal of Science and Research, 2013, India.

24 BIRICIK, H, AKÖZ, F & TULGAR, AN. Study of pozzolanic properties of wheat straw ash, Cement and concrete research, Vol.29, No.5, 1999, pp 637-643.

25 ADAMA, AY & JIMOH, YA. Effect of Locust Bean Pod Ash on Strength Properties of Weak Soils, AU Journal of Technology, Vol.16, No.1, 2012, pp 27-34.

26 TANGCHIRAPAT, W, SAETING, T, JATURAPITAKKUL, C, KIATTIKOMOL, K & SIRIPANICHGORN, A. Use of waste ash from palm oil industry in concrete, Waste Management, Vol.27, No.1, 2007, pp 81-88.

27 ETTU, LO, EZEH, JC, IBEARUGBULEM, OM, ANYA, UC & NJOKU, KO. Strength of Binary Blended Cement Composites Containing Cassava Waste Ash, International journal of Emerging Technology and Advanced Engineering, Vol.3, No.4, 2013, pp 15-20.

28 CRUZ-YUSTA, M, MÁRMOL, I, MORALES, J & SÁNCHEZ, L. Use of olive biomass fly ash in the preparation of environmentally friendly mortars, Environmental Science & Technology, Vol.45, No.16, 2011, pp 6991-6996.

29 ETUK, BR, ETUK, IF & ASUQUO, LO. Feasibility of Using Sea Shells Ash as Admixtures for Concrete, Journal of Environmental Science and Engineering, Vol.1, No.1, 2012, pp 123-129.

# EVOLVING LOW CARBON SUSTAINABLE BUILDING MATERIAL: MAKING CASE FOR CEMENT-LIME COMPOSITES

**S A Olaniyan**

**A J Klemm**

**F C R Almeida**

Glasgow Caledonian University

United Kingdom

**ABSTRACT.** Portland cement is unquestionably the primary cementitious material used in construction. Its massive production and usage contributes 2.83 billion tonnes of $CO_2$ emissions (roughly 2.3% of the total emissions) worldwide in 2008 alone and 5-7% to the global anthropogenic $CO_2$ emissions in general. Considering this environmental situation with its attendant large energy consumption, this study seeks to evolve a low carbon composite construction material in form of cement-lime mortar with cement serving as a partial replacement for lime. It aims at evolving acceptable combination ratio(s) of cement and lime for emergence of possible sustainable composite material in new construction works. The research is focused on mortars with same binder/aggregate mix ratios using five different compositions of cement/lime binder (i.e. 1:1, 1:2, 1:3, 3:1 and 2:1). The methodology involves comparative evaluations of each composition's mechanical characteristic connections enhanced by their microstructural features (MIP method) at one and six months of curing. In maximising their sustainable performance synergy, the results of this study suggest appropriate volumetric combination ratios of the composite materials, keeping in mind the final desirable effect of strength development or quickening hardening process. This in effect, would further facilitate lime usage revival, minimise carbon emissions and ultimately, protect natural environment from construction standpoint.

**Keywords:** $CO_2$-emissions, Porosity, Composite, Microstructure, Mortar, Sustainable

**Sule A Olaniyan** is currently undertaking a PhD on Lime Mortar Performance Assessment at Glasgow Caledonian University. With background in Sustainable Architectural Studies, his research interest lies in sustainable building materials.

**Dr Agnieszka J Klemm** is a Reader in construction materials in the School of Engineering and Built Environment, at the Glasgow Caledonian University. She is a Fellow of the Institute of Concrete Technology, Member of the Chartered Institute of Building and a Fellow of the Higher Education Academy. .

**Fernando C R Almeida** is a PhD researcher in the School of Built Environment (Glasgow Caledonian University – UK). He possesses MSc in Structures and Civil Construction (Federal University of São Carlos – Brazil), and Civil Engineer (Federal University of São Carlos – Brazil, with academic exchange at University of Coimbra – Portugal).

## INTRODUCTION

Prior to the beginning of this century, lime based mortar dominance as a building material was incontrovertible as reminiscence of this is reflected in many buildings of historic references which stand till date. This is premised on lime's durability features predominantly attributed to its flexibility, plasticity, breathability, autogenous healing property, relatively low carbon dioxide emissions (during its manufacture) and its carbon dioxide adsorption (in the course of its carbonation), among others [1; 2; 3]. Despite these sterling qualities, introduction of Portland Cement (PC) in the late 19th century put lime use into decline. The overwhelming acceptance of PC was consequent upon characteristic lime mortars shortcomings, inclusive of its low mechanical strength, poor internal cohesion and some exhibited volumetric changes [4; 5]. However, PC mortar which is characterised with high mechanical strength and short 'setting and hardening' periods exhibits negligible plastic deformation under load and fails by brittle fracture, a situation which can lead to the development of large internal stresses, often dissipated by the formation of unsightly cracks and subsequent reduction in the overall integrity of the structure. This, coupled with large cement related $CO_2$ emissions (approximately 5-8% per tonne) constitute major drawbacks for the PC mortar application [2; 6; 7].

Considering this background, coupling with the need to protect the natural environment, researchers have been making significant efforts at integrating and maximising these materials' (i.e. lime and cement) individual sterling qualities at the expense of their identified drawbacks. In this regard, efforts have been directed at evolving composite lime-cement mortars for enhanced structures' (i.e. masonry) durability. Along this direction, previous studies involving investigations into effects on: pore structure and vapour transport [8], viscosity [4], mechanical properties and drying shrinkage [9; 10], air influence [11], capillary porosity [12], silica fume addition [13], dewatering [14], among others, are worthy of mentioning.

However, much of these efforts have been directed at performance interventions on restoration works of the cultural heritage [15; 16; 17; 18; 19] as less attention is given to modern constructions. Besides, there is little specific information as to the manner in which processing variables such as constituents or mixing ratios influence the final properties of the composite, which, in turn, play a significant role in the actual behavioural pattern of the material. Obviously, limited knowledge concerning lime technology constitutes the main stumbling block to achieving a standardized application as low cement content is added to lime-based mixes just to minimize inconveniences, such as long hardening and setting times, in many restoration works [8]. For this purpose, this paper assesses the effect of cement on the microstructure of lime-based mortars with a view to determining the influence of specific proportions of cement on the properties and performance of lime based mortars over a 6-month curing period. In doing this, specific attention is given to the evaluation of the constituents' mix ratios, to arrive at the right proportion between cement and lime in order to adequately and economically promoting the hardening reactions by the cement hydration on one hand, and strength developments on the other. In the face of threatening adverse effects of Climate Change and on-going global calls for environmental consideration as a factor in design and material selection, this research aims at developing sustainable lime based composites as potential alternatives to predominant polymer based cementitious products, without undermining compliance with the current regulations.

## EXPERIMENTAL PROCEDURE

### Materials and Mortar Preparation

Materials used for the present research have been products commercially available in the market. The lime is Natural Hydraulic Lime, NHL-5.0 (St Astiers, United Kingdom). This lime type (NHL-5) was chosen on the basis of its relatively shorter setting time for optimal strength yield [18] and the need to maximise performance behaviour of the material being investigated. The cement used is CEM I 52.5 [20] (Hanson Cement, United Kingdom). Siliceous fine kiln dried sand obtained from Fife Silica Sands (United Kingdom) constituted the aggregates. Materials chemical compositions (by elements) as determined by Energy Dispersive X-rays analysis (EDX) are given in Table 1 while Figure 1 indicates the sand particle size distributions.

Table 1 Chemical Composition of the materials

| MATERIAL | ELEMENTAL CHEMICAL COMPOSITION OF THE MATERIALS, by % weight of the dry specimen | | | | | | | | | | | |
|---|---|---|---|---|---|---|---|---|---|---|---|---|
| | Ca | O | Si | C | Sb | Al | Fe | Mg | S | K | Na | Ti |
| Lime | 47.6 | 37.6 | 5.2 | 4.4 | 3.3 | 0.7 | 0.5 | 0.5 | 0.2 | - | - | - |
| Cement | 75.6 | 9.2 | 4.7 | - | 5.7 | 1.1 | 0.3 | 0.4 | 1.8 | 1.2 | 0.1 | - |
| Sand | 0.2 | 53.5 | 43.0 | - | - | 1.6 | 0.4 | - | - | 1.1 | | 0.2 |

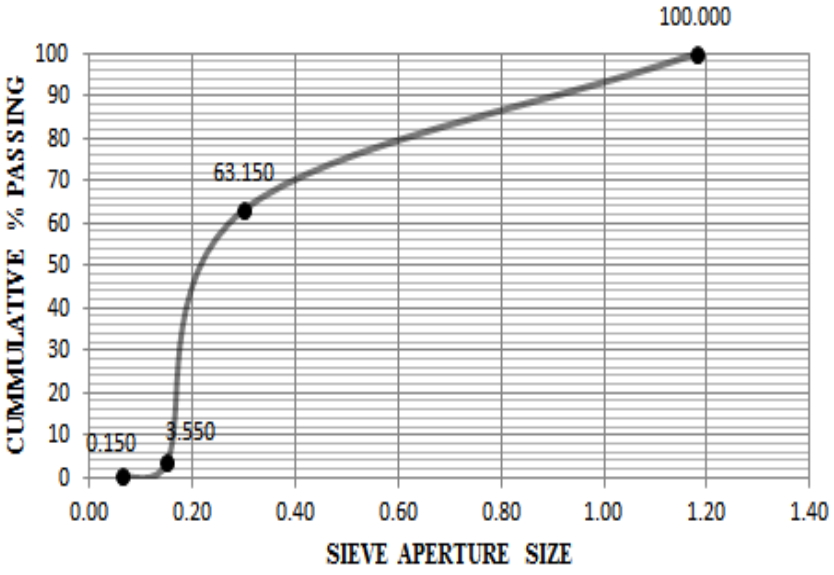


Figure 1 Grain size distribution of the aggregate

The mortars were prepared in accordance with the standard, BS-EN 1015-11 [21]. The binder-aggregate (B/A) ratio was maintained at 1:3 by volume, chosen from the commonest dosage reported in the literature [22]. Volume proportions of components were converted to weights, to avoid measurement imprecision during batching processes. Mortar mixtures were

prepared using the correct amount of water required to obtain adopted workability of 145±5mm (measured by the flow table test – BS EN1015-3) [23] as BS EN 1015-6 [24] specifies a flow value of '140-200mm' for 'plastic mortar'. Arising from visual and physical assessments of the mixes during the trial experimentation however, a flow value of 140 – 150mm (i.e. 145±5mm) was adopted. As observed, either higher or lower value tends towards stiffness or fluidity respectively. This was determined in accordance with BS EN 1015-3 [23]. Using the stated B/A ratio (i.e. 1:3), each mortar formulation was prepared with progressively increasing/decreasing cement contents as indicated in Table 2.

Table 2 Composition of mortars

| ID | LIME | CEMENT | SAND | W/B |
|---|---|---|---|---|
| Group I: Increasing Cement Order | | | | |
| LC10 | 1 | 0 | 3 | 1.52 |
| LC11 | 1 | 1 | 6 | 1.17 |
| LC12 | 1 | 2 | 9 | 1.23 |
| LC13 | 1 | 3 | 12 | 1.16 |
| Group II: Decreasing Cement Order | | | | |
| LC11 | 1 | 1 | 6 | 1.17 |
| LC21 | 2 | 1 | 9 | 1.81 |
| LC31 | 3 | 1 | 12 | 1.95 |

Mixing was done in the laboratory mixer of 30 litres maximum capacity. The mixing procedure was performed in a number of stages: aggregates were placed first, followed by other dry materials (i.e. lime and cement, pre-mixed earlier, where applicable) and these were blended consistently for 60 seconds as best practice dictates that the NHL powder should be thoroughly mixed through the dry sand, ensuring batch colour consistency prior to gradually adding water.

Water was then added slowly during 30 seconds and mixing continued for another 30 seconds. Mixing was stopped for 90 seconds as mortar adhering to the wall and bottom of the mixer bowl was scraped off. Mixing then resumed to obtain consistent mixture. The entire mixing period lasted about 5minutes.

For every mortar mix, minimum of three prismatic specimens of 40×40×160 mm were prepared, the average value of which represented the 'actual value' for consideration during the specimen evaluations afterwards. The specimens were compacted with a vibration table after mould filling in prismatic casts (according to BS-EN 459-2) [25], removed from the moulds 2 days later and left to cure at the laboratory ambient conditions of 21±4ºC (temperature) and 40±5% (relative humidity), until the test dates of 1 and 6 months.

## EXPERIMENTAL TECHNIQUE

### Microstructural Characteristics

Microstructural characteristics of the mortar samples were evaluated in terms of the total porosity (%), median pore diameter (by volume), bulk density and pore size distribution, using Mercury Intrusion Porosimetry (MIP) technique. This was achieved with AutoPore IV 9500 by Micrometrics (with pressure range up to 60000 psi). The test was carried out with samples of approximately 1.5g that were extracted from the core of the crushed prisms. Under short term loading and at a relatively low rate of load application (approximately 2mm/min), the chance of micro crack propagation is very limited [26]. These samples were obtained at the test ages of one and six months, and dried in an oven at temperature of 75 ± 1 ºC for 24 hours before the test.

### Mechanical Properties

The mechanical properties were evaluated with regard to the three-point flexural tests, and compressive strength. While the flexural strength tests were performed on the ELE AutoTest 2000 apparatus with a load application pace of 50 N/s, compressive strength tests were conducted on the two fragments of each specimen (resulting from the preceding flexural test) using INSTRON 3367, with 30kN load capacity moving at a loading rate of 2mm/min. The results reported in this work were all taken as an average value of six similar specimen fragments. In addition, mortars' deformation tendencies relative to their moduli of elasticity' definitions were extrapolated based on the previous studies [27; 17].

## RESULTS AND DISCUSSION

### Microstructural Characteristics

Figures 2a & 2b compare the mercury intrusion curves (i.e. intrusion pore volume as a function of pore diameter) for different mortars at 1 and 6 months, with regard to their microstructural characteristics, hence, their behavioural performances.

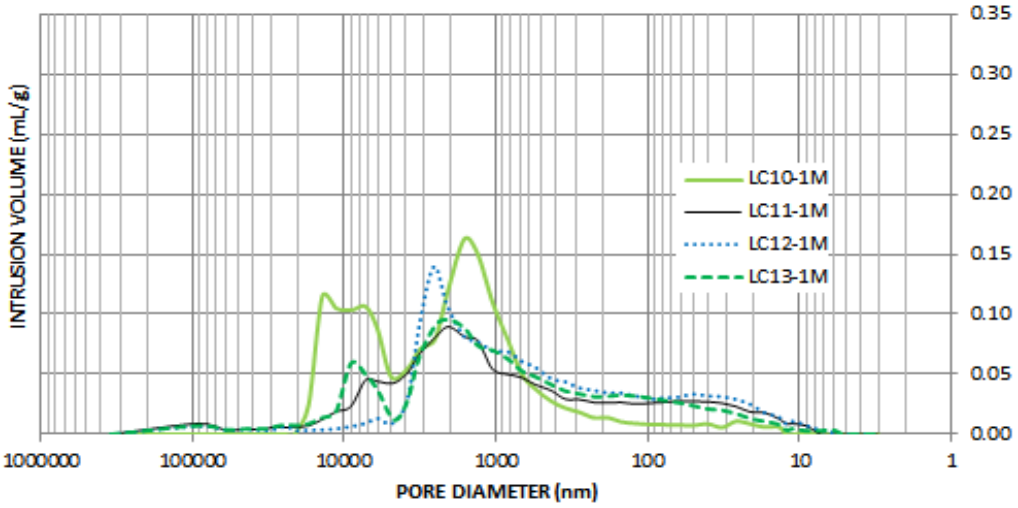


Figure 2a 1-month Pore size distribution of mortars (Increasing Cement Order)

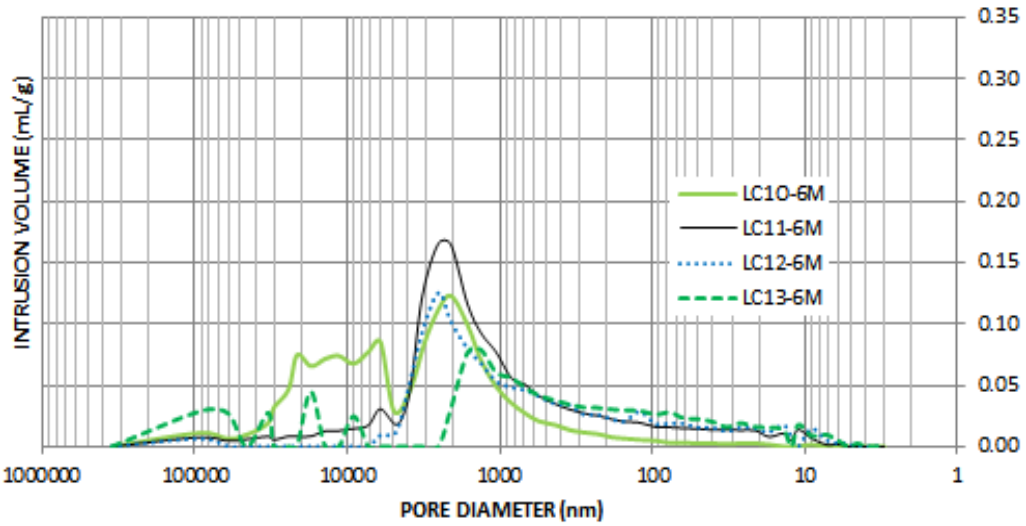


Figure 2b 6-month Pore size distribution of mortars (Increasing Cement Order)

With lime only (i.e. 0% of cement content), the graph indicates a bi-modal pore size distribution at 28 days of curing at 1800nm and 10000nm pore diameters (figure 2a), with porosity of 27% (Table 3) and bulk density of 1.74g/ml. This trend which was maintained even after 6 months of curing, with the graph shifting slightly towards the left (figure 2b) as well as a slightly lower bulk density value (i.e. 1.71g/ml) indicates substantial presence of mortar matrix containing varying higher pore diameters of about 2000nm and 20000nm.

However, addition of cement in equal volumetric composition with lime (i.e. 50-50, lime-cement composition), at 1-month of curing induces modification of the mortar microstructures with a reduction in porosity value recorded at 24.3%. Further to this, when the cement volumetric contents were doubled (i.e. LC12) and tripled (i.e. LC13), more impacts on the microstructural distribution of the pastes with decrease in total intrusion pore volume were observed, a situation which is assumed to be the result of filling of larger pores by the formation of more C–S–H gel [28]. Consequently, value for bulk density is raised in each case. Here, a correlation between the total intruded pore volume and the strength development profiles is observed, though not in corresponding ratios.

Table 3 Results from Mercury Intrusion Porosimetry

| ID | TOTAL POROSITY, %% | | BULK DENSITY AT 0.52 psia, g/Ml | |
|---|---|---|---|---|
| | 1-month | 6-months | 1-month | 6-months |
| LC10 | 27.77 | 23.42 | 1.7448 | 1.7169 |
| LC11 | 24.35 | 25.67 | 1.8297 | 1.8663 |
| LC12 | 25.51 | 20.81 | 1.8566 | 1.9213 |
| LC13 | 24.64 | 21.45 | 1.8608 | 1.8954 |
| LC21 | 27.54 | 23.43 | 1.7824 | 1.8395 |
| LC31 | 29.17 | 22.79 | 1.7749 | 1.7998 |

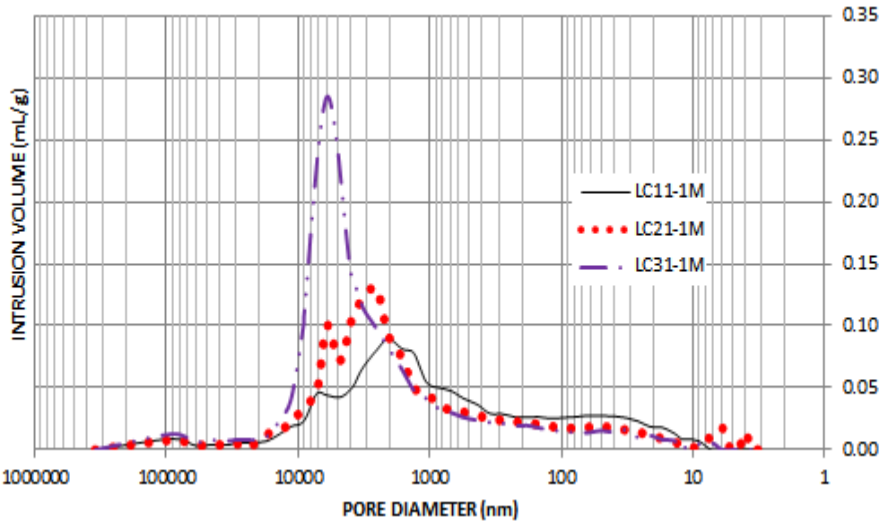


Figure 3a 1-month Pore size distribution of mortars (Decreasing Cement Order)

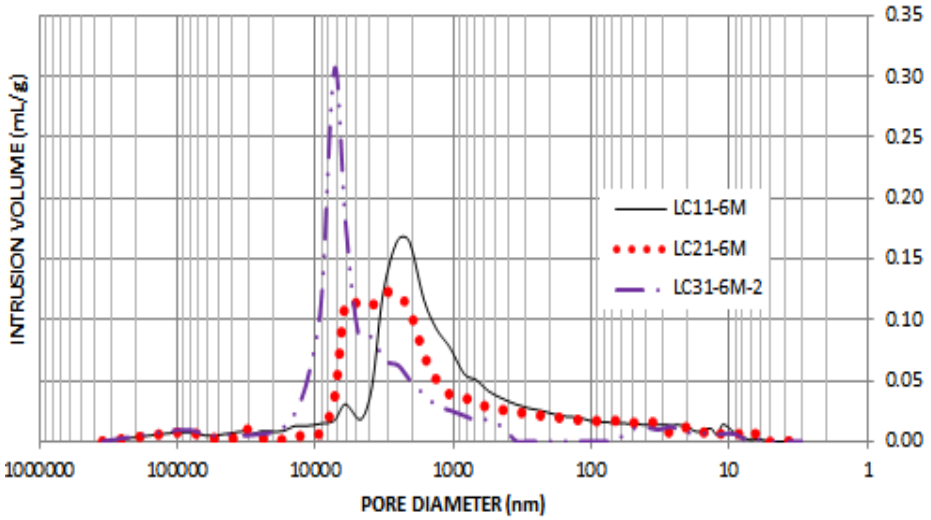


Figure 3b 6-month Pore size distribution of mortars (Decreasing Cement Order)

Further drop in the porosity value was also obtained in each case, but with LC12 higher (i.e. 25.51%) relative to LC11 (24.35%). In explaining this, Arandigoyen & Alvarez [12] observe that porosity varies with the composition of the paste in a wide range which can be attributed to the amount of kneading water employed in the preparation of the pastes in order to get a similar consistency for all the pastes, as in this study. Usually, kneading water decreases with increasing percentage of cement content in the paste because of the swelling of the structure produced as a consequence of the hydration of the calcium silicates that diminishes the porosity. Notwithstanding, it has been established that the amount of kneading water does not modify the complexity of the pore system (at least in lime pastes), but changes the porosity [10; 29]. In order words, with higher Water/Binder (W/B) ratio in LC12 (W/B ratio of 1.23 – Table 2), the porosity recorded at 28 days was higher (i.e. 25.51%). At the end of 6 months of curing, there was a porosity reduction in each of the mixes with the exception of the mix with equal volumetric lime-cement content (i.e. 24.35% to 25.66% in LC11). This indicates a minimal or less pronounced impact of cement addition on porosity of the emerging lime-cement composite mortar at equal volumetric composition.

On the other hand, a progressive decrease in cement content (i.e. increase in lime content) results in higher W/B ratio (Table 2), and corresponding higher porosity value (Table 3) as well as higher maximum continuous pore diameter, over 28 days curing period (figure 3a). The mix with highest lime content recorded highest W/B ratio and hence, highest porosity value (i.e. 29.16%) as earlier pointed out. After six months of curing, slightly higher pore diameter (with slight shift of the intrusion curve to the left – figure 3b) and reduction in porosity value were observed in each case with the exception of LC11 as stated earlier. To expound these results, various physical and chemical phenomena that take place during the setting and hardening processes of a mortar (as a function of the binder composition) need to be reviewed as follows [10]: in lime-based mortars, the drying of the kneading water takes place, together with a certain degree of shrinkage [30].

The carbonation process starts when the water content of the mortar does not hinder the diffusion of the air through the material; in cement-based mortars however, the setting is a consequence of the hydration of the calcium silicates, which starts quickly owing to the hydration of the $C_3S$ and continues more slowly because of the hydration of the $C_2S$. The hydration of both compounds gives strength to the mortar [11; 14]. The carbonation process which also takes place slowly, is a reaction of the basic compounds of hydrated cement (essentially $Ca(OH)_2$ and CSH) with carbonic acid. These may account for the behavioural patterns exhibited by the mixes with the exception of LC11 in this case. In general, Mosquera et al [8] observe that intruded pore volume of composite lime-cement mortar exhibits decreased pore volumes with more cement contents over the curing ages of 1-6 months, thereby enhancing the pore distribution for durable material performance [31].

The results obtained in this study is in agreement with a previous study [8] with the exception of the mix containing equal lime-cement volumetric ratio (i.e. LC11) which is characterised with higher porosity over a curing period of 6 months. For practical purpose, the implication of these results is its usefulness when considering the impact of cement on lime-cement composite mortar with regard to potential mix-ratios, as equal volumetric combination will impact less on improving porosity of the composite mortar.

Higher mix ratio (double or triple) of the cement volumetric content would facilitate a remarkable effect on improving the composite mortar microstructural property for overall durability. This is in line with the position of Lanas et al [10] who affirm in contrast, that addition of just 25% of lime content impacts negatively on cement based mortar pore distribution with a net decrease in its mechanical strength by 50%. However, this result may be subjected to further investigations particularly maintaining same B/A ratio with coarse aggregate, as varying aggregates grains distribution may impact on the observed trend.

## Mechanical Properties

Results of the two mechanical parameters – flexural and compressive strengths, for 1 and 6 months of curing have a similar evolutionary trend as shown in Figures 4 and 5. With lime only (i.e. 0% of cement content- LC10), the graphs indicate 0.54N/mm$^2$ and 0.49N/mm$^2$ for both flexural and compressive values respectively, at the curing age of 1 month. These values marginally increased to 0.63N/mm$^2$ and 0.68N/mm$^2$ respectively at 6 months curing age. At this stage, carbonation predominates as the hardening progresses, so the mechanical strengths increase in parallel, relative to the carbonation process [10]. This is usually slow and marked with micro-cracking. Nevertheless, provided any subsequent micro-cracking is not extensive,

the compressive strength of the mortar will be enhanced over time as the slow carbonation reactions might encourage autogenous healing of such micro-crack [18; 32]. However, progressive addition of cement in equal, double and triple volumetric compositions relative to lime contents returned the flexural strength value of 2.91, 4.14 and 4.41N/mm$^2$, and compressive strength value by 6.58, 10.99 and 12.77 respectively, at 6 months of curing (Figures 4 and 5). In this case, mortar with highest cement binder content shows the highest compressive strength, as large amount of binder give more Calcium Silicates Hydrate phases, thus increasing the strength [33]. One practical usefulness of these results is the marginal strength increment recorded between doubling (i.e.LC12) and tripling (i.e. LC13) the volumetric cement contents in the composite mortar which puts LC12 more economically advantageous. In this regard, where mechanical strength quotient is the primary consideration, doubling volumetric contents of cement (i.e. LC12) in the composite mix ratio is considered appropriate economically. Consequently, less cement, which translates to better economic value and less environmental impact is adopted.

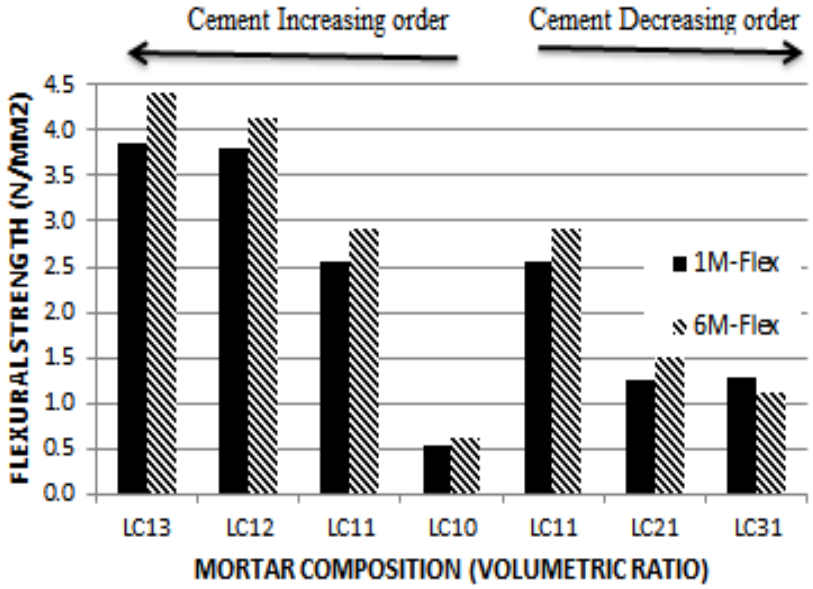


Figure 4 1 & 6 months Mortar Flexural Strength Developments

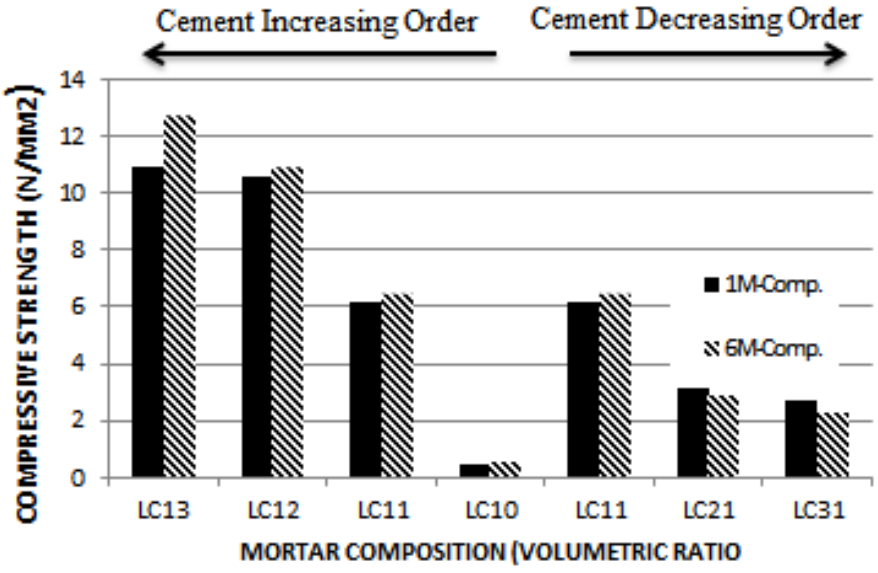


Figure 5 1 & 6 months Mortar Compressive Strength Developments

Conversely, a progressive decrease in cement content (i.e. increase in lime content) results in low composite mortar flexural and compressive strength developments as the mortar with highest lime volumetric content (i.e. LC31) recorded marginal increase in values (i.e. flexural - 1.13N/mm$^2$; compressive - 2.38N/mm$^2$) relative to LC10 (i.e. 0.63 & 0.68N/mm$^2$ respectively) at the end of the 6 months curing period. This is as indicated in figures 4 & 5.

Despite varying cement compositions in the emerging composite mortars, each mortar presents a low ratio of compressive to flexural strength ($f_c/f_f$), which suggests that the evolving composites are characterized by elastic behaviours comparable with the basic lime-based mortar (i.e. LC10), as obtained in their ($f_c/f_f$) values. This position is supported by a research carried out by Briccoli and Rovero [27] as corroborated by Moropoulou [17], where the former found that the ratio $f_c/f_f$ of similar materials is proportional to the modulus of elasticity (E), for mortars' mechanical measurements from 1 to 6 months. The authors conclude that a low $f_c/f_f$ ratio corresponds to a low modulus of elasticity, which was determined for lime mortars [27].

However, standard procedure needs to be adopted to determine actual value for the elastic modulus in each case. This assertion [27] can be related to the Stress-Strain curves of figures 6a & 6b, where the curve representing LC10 behavioural pattern defines the least slope to the horizontal, a factor which corresponds to its approximate modulus of elasticity value (lowest), as that of LC13 indicates the highest slope (i.e. approximate highest modulus value).

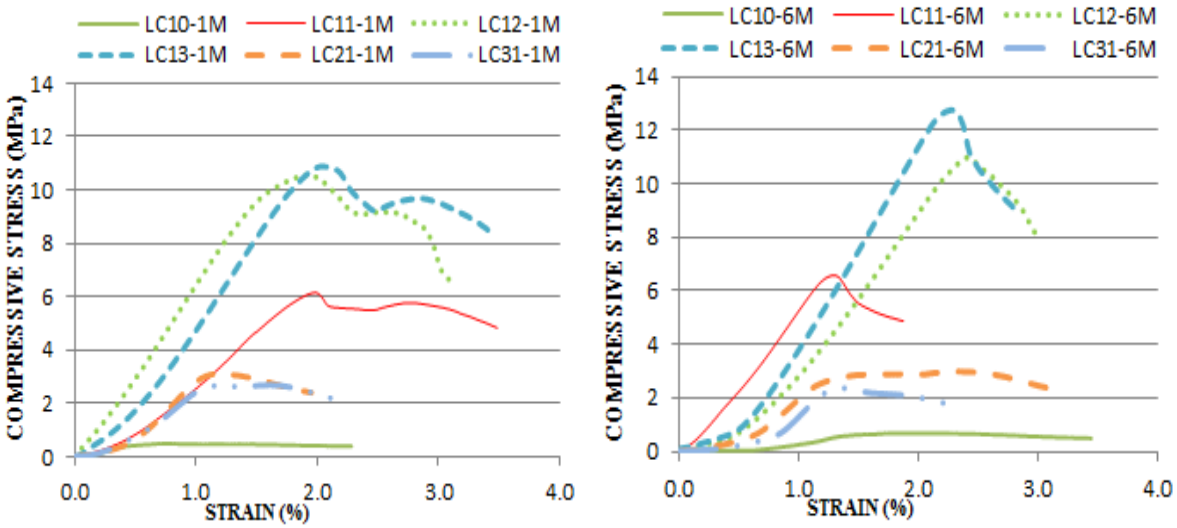


Figure 6 (a) 1-month compressive Stress/Strain curve (b) 6-months compressive Stress/Strain curve

Despite their varying compositions, the stress-strain curves in general suggest that the mortars are characterised by elastic behaviours, which is a measure of their deformation absorption [10]. The mortars therefore, possess varying degrees of flexibility and deformation absorption potentials, and therefore capable of accommodating movements of masonry units to varying proportional extents. This property would enhance structures' overall durability.

## SUMMARY AND CONCLUSIONS

Lime based mortar allows movements within the mortar joints while maintaining its structural stability. Structures erected with it can tolerate seasonal and minor structural movements without damage to the masonry units or joints as any movement experienced is taken up by minute adjustments within the flexible mortar beds over many courses of bricks or other masonry units. The hairline cracks that may occur are subsequently resealed by the so-called 'autogenous healing'. Further to this is the greater environmental awareness of its advantages in terms of relatively low carbon dioxide emissions released during manufacture and the adsorption of carbon dioxide during carbonation [1; 2]. However, this type of mortar is slow to harden and weak in compressive strength, thereby hindering rapid construction progress.

In addressing these shortcomings, cement is added to lime based mortar with a view to modifying latter's microstructural properties, thereby quickening the evolving composite hardening process and increasing its mechanical strength. Effort in this direction is an attempt to determine the influence of specific proportions of cement on the properties and performance of lime based mortars over a 6-month curing period, by evaluating required constituents' mix ratios. This is to arrive at the right proportion between cement and lime, in order to adequately and economically promoting the hardening reactions by the cement hydration on one hand, and strength developments on the other.

For this purpose, the results of this study suggest that:

(i) lime-based mortars reduces both their porous volume and their pore size as cement content in the mix increases;

(ii) equal volumetric addition of cement to lime based mortar (i.e. LC11) impacts less on the final properties of the evolving composite mortar;

(iii) where mechanical strength increment is the primary consideration, doubling cement volumetric ratio (i.e. LC12) is considered appropriate and economically logical; and

(iv) where the need for shortening the hardening process is of utmost desirability, lime-cement combination ratio of 3:1 (i.e. LC31) would serve the purpose.

For practical considerations however, it should be noted, that aggregates varying grains distribution may impact on mortar behavioural pattern as demonstrated in previous studies [9; 34; 5]. The results may therefore require further investigations particularly, maintaining same B/A ratio (i.e. 1:3) and equal workability range (as in this study i.e. 145$\pm$5mm), but with 'coarse aggregates'.

Conclusively, in the face of threatening adverse effects of Climate Change and on-going global calls for environmental consideration as a factor in design and material selection, this research aims at developing sustainable lime based composites as potential alternatives to predominant polymer based cementitious products. This effort would facilitate lime revival, diminish direct cement applications and consequently minimise impacts on the environment.

## ACKNOWLEDGEMENTS

The authors gratefully acknowledge the financial supports from: *TETFUND AST&D Scheme*, an educational development organ of The Federal Government of Nigeria, and *Conselho Nacional de Desenvolvimento Cientifico e Tecnologico (CNPq)*, Brazil. Thanks are also due to *Hanson Cement, United Kingdom*, for the provision of the cement used for this work.

## REFERENCES

1. LACHLAND MCDONALD. Hydraulic lime mortar for the house of the future, The Structural Engineer Volume 78/No79, 2000.

2. BALL, R J, ALLEN, W J, NICHOLSON, J A. Deformation of NHL3.5 and CL90/PC hybrid mortars, Proceedings of the ICE - Construction Materials, Volume 162, Issue 1, 2009, pp 29-35.

3. OLANIYAN, S A, KLEMM, A J. Current Trends in Development of Lime Based Composites, Building Physics in Theory and Practice, Volume VII, No.3, 2015, pp 49-54.

4. SÉBAÏBI, Y, DHEILLY, R M, QUÉNEUDEC, M. A study of the viscosity of lime–cement paste: influence of the physico-chemical characteristics of lime, Construction and Building Materials, 18(9), 2004, pp 653-660.

5. LANAS, J, PÉREZ BERNAL, J L, BELLO, M A, ALVAREZ GALINDO, J I. Mechanical properties of natural hydraulic lime-based mortars, Cement and Concrete Research, 34(12), 2004, pp 2191-2201.

6. KEUN-HYEOK YANG, AH-RAM CHO, JIN-KYU SONG, SANG-HO NAM. Hydration Products and Strength Development of Calcium Hydroxide-Based Alkali-Activated Slag Mortars, Construction and Building Materials 29, 2012 pp 410-419

7. ESCALANTE-GARCIA, J I, ESPINOZA-PEREZ, L J, GOROKHOVSKY, A, GOMEZ-ZAMORANO, L Y. Coarse Blast Furnace Slag as a Cementitious Material, Comparative Study as a Partial Replacement of Portland Cement and as an Alkali Activated Cement, Construction and Building Materials 23, 2009 pp 2511-2517

8. MOSQUERA, M J, SILVA, B, PRIETO, B, RUIZ-HERRERA, E. Addition of cement to lime-based mortars: Effect on pore structure and vapor transport, Cement and Concrete Research, 36(9), 2006 pp 1635-1642.

9. POZO-ANTONIO, J S. Evolution of mechanical properties and drying shrinkage in lime-based and lime cement-based mortars with pure limestone aggregate, Construction and Building Materials, 77, 2015, pp 472-478.

10. ARANDIGOYEN, M, ALVAREZ, J I. Pore structure and mechanical properties of cement–lime mortars, Cement and Concrete Research, 37(5), 2007, pp 767-775.

11. SIMINA, M, MOLNAR, L, MANEA, D, ARDELEAN, I. Monitoring the air influence on Cement–Lime mortar hydration using low-field nuclear magnetic resonance relaxometry, Applied Magnetic Resonance, 43(3), 2012, pp 443-450.

12. ARANDIGOYEN, M, ALVAREZ, J I. Blended pastes of cement and lime: Pore structure and capillary porosity, Applied Surface Science, 252(23), 2006 pp 8077-8085.
13. GLEIZE, P J P, MÜLLER, A, ROMAN, H R. Microstructural investigation of a silica fume–cement–lime mortar, Cement and Concrete Composites, 25(2), 2003, pp 171-175.

14. EL-TURKI, A, BALL, R J, CARTER, M A, WILSON, M A, INCE, C, & ALLEN, G C. Effect of dewatering on the strength of lime and cement mortars, American Ceramic Society, Journal of the American Ceramic Society, 93(7), (2010, pp 2074.

15. KLEMM A J, WIGGINS D E. Chapter 89: The role of material microstructure in the durability of historic buildings, Concrete Solutions, Proceedings of the 5th International Conference on Concrete Repair, Ed. Grantham M, CRC Press/Balkema, Leiden, the Netherlands, 2014, pp 637-644.

16. KLEMM A J, WIGGINS D E. Microstructural characteristics of modern repair materials vs. the performance requirements of historic lime mortar, Proceedings of the 11th International Symposium on Brittle Matrix Composites, Ed. Brandt A M, Rilem, Bagneux, France, 2015 (in press).

17. MOROPOULOU, A, BAKOLAS, A, MOUNDOULAS, P, AGGELAKOPOULOU, E, ANAGNOSTOPOULOU, S. Strength development and lime reaction in mortars for repairing historic masonries, Cement and Concrete Composites, 27(2), 2005, pp 289-294.

18. STARINIERI, V, HUGHES, D C, WILK, D. Influence of the combination of roman cement and lime as the binder phase in render mortars for restoration, Construction and Building Materials, 44, 2013 p 192.

19. GREEN, K M, CARTER, M A, HOFF, W D, & WILSON, M A. The effects of lime and admixtures on the water-retaining properties of cement mortars, Cement and Concrete Research, 29(11), 1999, pp 1743-1747. 19

20. BS EN 197-1:2011. Cement. composition, specifications and conformity criteria for common cements, 2011, British Standards Institute.

21. BS-EN 1015-11: 1999. Methods of test for mortar for masonry Part 11: determination of flexural and compressive strength of hardened mortar, A Standard publication of the British Standards Institution.

22. VENTOLA, L, VENDRELL, M, GIRALDEZ, P. Newly-designed traditional lime mortar with a phase change material as an additive, Construction and Building Materials, 47, 2013, pp 1210-1216.

23. BS-EN1015-3: 2000. Methods of test for mortar for masonry Part 3: determination of consistence of fresh mortar (by flow table), A Standard publication of the British Standards Institution

24. BS-EN 1015-6: 1999. Methods of test for mortar for masonry. Part 6: determination of bulk density of fresh mortar, A Standard publication of the British Standards Institution
25. BS-EN 459-2: 2010. Building lime Part 2: Test Method, A Standard publication of the British Standards Institution.

26. CHOQUETTE M, B´ERUB´E M A, LOCAT J. Mineralogical and microtextural changes associated with lime stabilisation of marine clays from eastern Canada, Applied Clay Science 2, 1987, pp 215-232.

27. BRICCOLI B S, ROVERO L. Gli additivi per malte usati nell' antichita, Ed. Mascolo G, Materiali e tecniche per il Restauro Cassino, Idea Stampa Editore AIMAT, INISM, 1997

28. GRILO, J, FARIA, P, VEIGA, R, SILVA, A S, SILVA, V, VELOSA, A. New natural hydraulic lime mortars – physical and microstructural properties in different curing conditions, Construction and Building Materials, 54, 2014, pp 378-384.

29. ARANDIGOYEN, M, BERNAL, J L P, LÓPEZ, M A B, & ALVAREZ, J I. Lime-pastes with different kneading water: Pore structure and capillary porosity, Applied Surface Science, 252(5), 2005, pp 1449-1459.

30. LANAS, J, ALVAREZ-GALINDO, J I. Masonry repair lime-based mortars: Factors affecting the mechanical behaviour, Cement and Concrete Research, 33(11), 2003, pp 1867-1876.

31. RAMLI, M, TABASSI, A A, HOE, K W. Porosity, pore structure and water absorption of polymer-modified mortars: An experimental study under different curing conditions, Composites Part B, 55, 2013, pp 221.

32. Yurtdas, I, Peng, H, Burlion, N, & Skoczylas, F. Influences of water by cement ratio on mechanical properties of mortars submitted to drying, Cement and Concrete Research, 36(7), 2006, pp 1286-1293.

33. MARAVELAKI-KALAITZAKI, P. Hydraulic lime mortars with siloxane for waterproofing historic masonry, Cement and Concrete Research, 37(2), 2007, pp 283-290.

34. KALAGRI, A, KARATASIOS, I, KILIKOGLOU, V. The effect of aggregate size and type of binder on microstructure and mechanical properties of NHL mortars. Construction and Building Materials, 53, 2014, pp 467-474.

# HYBRID ALKALINE CEMENTS - DEVELOPMENT AND PERSPECTIVE OF PRACTICAL EXPERIENCES

**V Bílek**
ZPSV a.s
Czech Republic
**A Palomo**
Instituto Eduardo Torroja (CSIC)
Spain
**J Hurta L Zidek P Done**
VSB - TU Ostrava
Czech Republic

**ABSTRACT.** Hybrid cements represent a relatively new type of binders which includes some advantages of Ordinary Portland Cement, the application of mineral admixtures – especially secondary materials (fly ash, slag,) and alkali activation. The paper is focused on the study of the properties of concretes prepared from hybrid cements with a different composition of powder. Concretes prepared from cements based on OPC + fly ash and those based on hybrid cements were prepared. Their properties are compared from the point of view of strengths (compressive and flexural), modulus of elasticity and fracture properties. This makes it possible to select an optimum concrete for a specific practical application

**Keywords:** Hybrid cement, Alkali activation, Fly ash

**Dr Vlastimil Bílek** is a Research Engineer at the ZPSV a.s. and a senior lecturer at VSB Technical University in Ostrava. His research interests include alkali activated materials, concretes with mineral admixtures and the durability of concrete.

**Prof Angel Palomo PhD** Chemistry. CSIC professorial fellow with the Eduardo Torroja Institute (IETcc). His expertise has been specialized in the chemistry of cement for over 20 years.

**Jan Hurta** works as a senior lecturer at the TU VSB of Ostrava,. He is dedicated to building materials testing and the diagnostics of building structures.

**Libor Zidek** works as Head of the Laboratory of Building Materials His research interests are the diagnostics of buildings, the rehabilitation of concrete structures and the development of construction materials.

**Petra Done** is a senior lecturer at VSB TU Ostrava, Czech Republic. She is particularly interested in the testing of building materials, especially their durability

## INTRODUCTION

Concrete is still a very important material for industry all over the world. Sometimes concrete is considered an environmentally not very friendly material, but it is still very good in comparison with some other materials, such as steel, or also burned bricks [1]. But to find some new ways to make concrete even more environmentally friendly is still necessary. One of the more progressive ways is concrete with ternary binders [1,2] or concrete with hybrid cements [3, 4].

The aim of this paper is a comparison of some properties of concrete made from OPC only, with concrete with an increasing replacement of cement with fly ash, and also with concrete prepared with the use of alkali activated hybrid cements, containing 75 - 85 % of fly ash. These hybrid cements were ground for finer granulometry for better performance.

## EXPERIMENTAL PROCEDURES

Ordinary Portland cement CEM I 52.5 N (see EN 197) was used as well as fly ash (FA) originated from brown cool of good quality burnt in power plant Chvaletice, matakaoline Metaver I (M) and ground granulated blast furnace slag (GBFS). For the chemical analysis of this composition see Table 1.

Table 1 Chemical composition of compounds [%]

| | $CaO$ | $SiO_2$ | $Al_2O_3$ | $Fe_2O_3$ | $MgO$ | $K_2O$ | $Na_2O$ | $TiO_2$ | $SO_3$ |
|---|---|---|---|---|---|---|---|---|---|
| CEM | 64.2 | 20.0 | 3.8 | 3.2 | 0.9 | 0.76 | 0.16 | - | 3.1 |
| FA | 3.6 | 49.7 | 24.9 | 14.7 | 1.15 | 1.9 | 0.6 | 1.4 | 1.3 |
| GBFS | 41.5 | 37.7 | 6.5 | 0.4 | 10.1 | 0.4 | 0.6 | - | 0.8 |
| M | 0.4 | 52.5 | 41.0 | 1.5 | 0.3 | 1.6 | 0.1 | 0.8 | - |

Some pre-activated binders (PAB) were made by common grounding of CEM, FA and GBFS and M. The PAB1 and PAB1n contain FA, CEM and M, PAB2 and PAB 2n contain FA, CEM and GBFS and PAB3 and PAB3n FA and CEM. Amount of FA was minimum 75 % and content of CEM was maximum 15 % per mass. Some granulometry characteristics are recorded in Table 2. Composition of mixtures is shown in Table 3.

Table 2 Characteristics of pre-activated binders

| | $x_{50}$ [mm] | $x_{90}$ [mm] | $x_{99}$ [mm] | $S_v$ [m] |
|---|---|---|---|---|
| PAB1 | 6.07 | 33.61 | 73.79 | |
| PAB2 | 9.30 | 39.53 | 89.01 | |
| PAB1n | 7.84 | 34.75 | 77.40 | 1402 |
| PAB2n | 7.63 | 27.94 | 52.67 | 1381 |
| PAB3n | 8.61 | 31.38 | 61.34 | 1279 |

Mixtures were mixed in a laboratory mixer in volume up to 30 litres. Cubes of 150 mm were produced for compressive strengths $f_c$ measurement and beams 80 x 80 x 480 mm were used for other tests - bending strengths $f_b$, flexural strength on notched beams $f_r$, modulus of elasticity E, fracture toughness $K_{IC}$ and fracture work $W_F$. The setup of tests was this: firstly beams were notched 220 mm from one of the ends. The depth of the notch was 1/3 of the height of the beam. Fracture tests in three point bending with the span of 400 mm were performed

with a continuous recording of *load vs. deflection* curve. After the test a fragment of the beam with the length of 260 mm was used for bending strength measurement with the span of 220 mm. This means that from one beam, besides both flexural strengths $f_b$ and $f_r$, $K_{IC}$ and E was computed in accordance to Karihaloo and Nallathambi model [5] and $W_F$ was computed in accordance to RILEM method [6,7]. Also flexural strength on notched beams and flexural strength were computed. The presented values are average values from three beams.

Table 3 Composition of concretes ($1m^3$) - all masses are in kg

| | B1 | B2 | B3 | B4 | B5 | B6 | B7 | B11 | B12 | B13 |
|---|---|---|---|---|---|---|---|---|---|---|
| CEM I | 308 | 262 | 231 | 154 | - | - | - | - | - | - |
| FA | - | 46 | 77 | 154 | - | - | - | - | - | - |
| PAB1 | - | - | - | - | 308 | - | - | - | - | - |
| PAB2 | - | - | - | - | - | 308 | - | - | - | - |
| PAB3 | - | - | - | - | - | - | 308 | - | - | - |
| PAB1n | - | - | - | - | - | - | - | 308 | - | - |
| PAB2n | - | - | - | - | - | - | - | - | 308 | - |
| PAB3n | - | - | - | - | - | - | - | - | - | 308 |
| water | 168.5 | 168.5 | 168.5 | 168.5 | 168.5 | 168.5 | 168.5 | 168.5 | 168.5 | 168.5 |
| ChP 760 | 3.5 | 3.5 | 3.5 | 3.6 | 3.5 | 3.0 | 3.5 | 3.5 | 3.0 | 3.5 |
| sand 0/4 | 645 | 645 | 645 | 645 | 645 | 645 | 645 | 645 | 645 | 645 |
| agg. 4/8 | 225 | 225 | 225 | 225 | 225 | 225 | 225 | 225 | 225 | 225 |
| agg8/16 | 990 | 990 | 990 | 990 | 990 | 990 | 990 | 990 | 990 | 990 |
| slump | 95 | 85 | 85 | 80 | 95 | 150 | 90 | 100 | 100 | 85 |

## RESULTS AND DISCUSSION

Compressive strengths at the ages of 24 hours, 48 hours and 28 days are shown in Figure 1. It is evident that concretes with 0 up to 50% CEM replacement by fly ash show much higher strength than concretes with hybrid cements. Hybrid cement with GBFS shows the best results of all hybrid cements. The effect of finer granulometry is positive - see B7 and B13, for example.

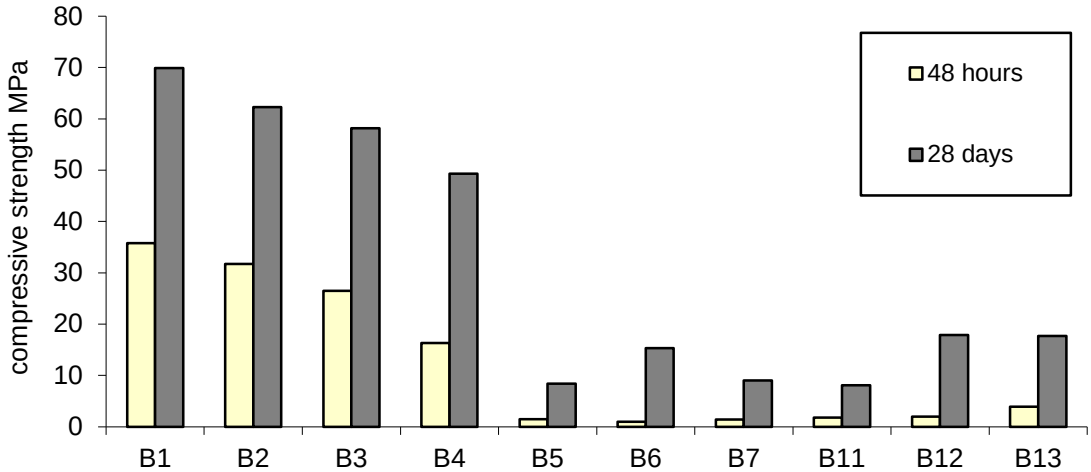


Figure 1 Compressive strength of concrete (cubes 150 mm)

The flexural strength of un-notched beams of concretes with CEM and FA is higher than that of concrete with CEM only up to FA content of 25 %. It is interesting that the flexural strength of notched beams shows a different development - it decreases continuously with FA content increase. The strength of un-notched beams reflects especially the properties of surface while the strength of notched beams reflects the properties of the central area of the cross-section. Also the strength of notched beams influenced by the stress concentration near the end of the notch. The stress intensity factor which characterises the stress field, shows a similar development as the flexural strength of notched beams. Both of the flexural strengths are much lower for hybrid cements. But the ratio *compressive strength / flexural strength* is much lower for hybrid cements. For example, for the concrete B2 the ratio is 8.0 and for concrete B12 it is only 3.7 . The brittleness of the hybrid cements seems to be lower.

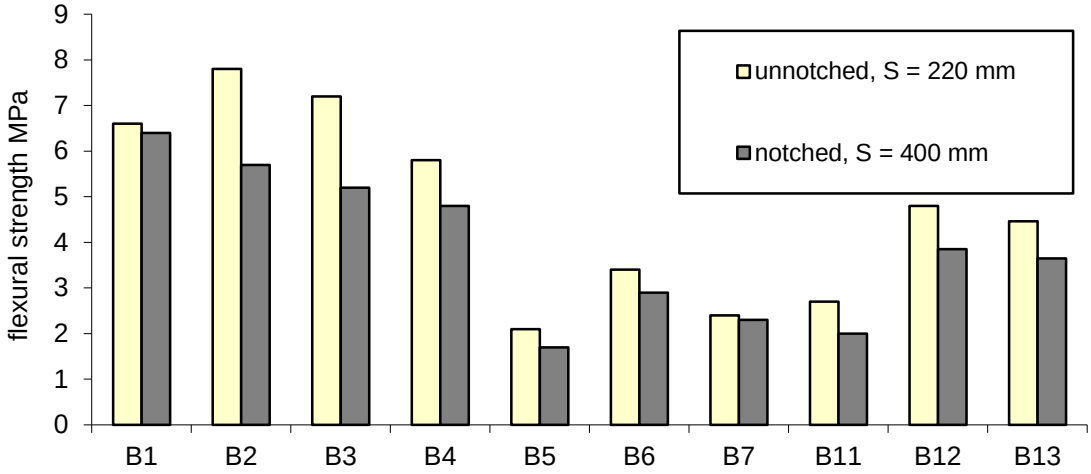


Figure 2 Flexural strength of concrete on unnotched fragments (spam 220 mm) and notched beams (spam 400 mm)

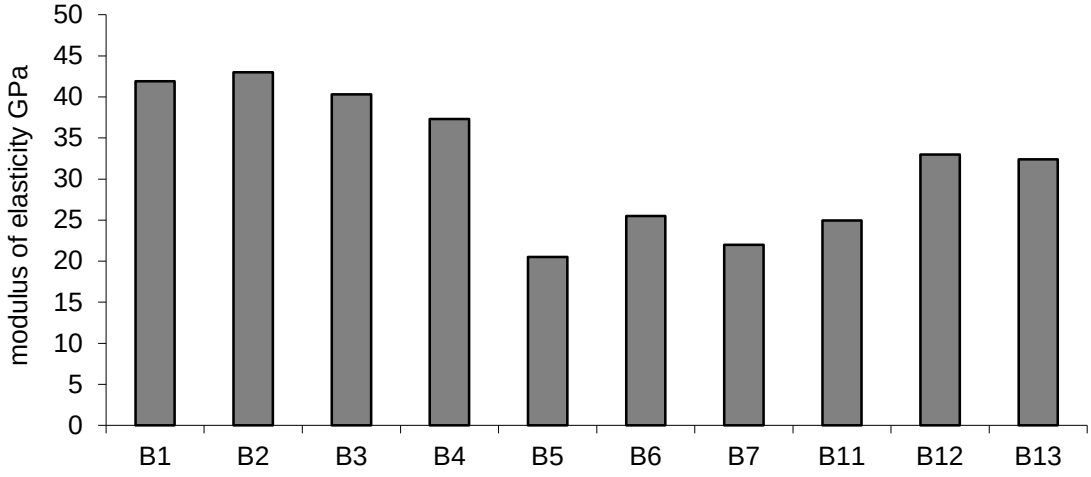


Figure 3 Modulus of elasticity in three-point bending of notched beams

The modulus of elasticity of concretes with CEM and CEM + FA reaches relatively high values and they are similar to the predicted value for the concrete with corresponding compressive strength with granite [8]. The modulus of elasticity of concretes with hybrid cements - concrete B12 and B13 - is comparable with that, but the compressive strength of these concretes is significantly lower. This means that it might be possible to reach better modules of elasticity for concrete with hybrid cement.

This result is interesting also from the point of view that concretes with alkali activated slag show a much lower modulus of elasticity although they reach a very high compressive strength [9].

Conclusions similar to those can also be made for fracture toughness and fracture work, Figures 4 and 5, as these characteristics are not related to compressive strength. The fracture properties of concretes with good hybrid cements are good and after some optimisation they can provide better properties of these concretes with comparable a compressive strength as the strength of usual concrete from CEM or CEM + FA.

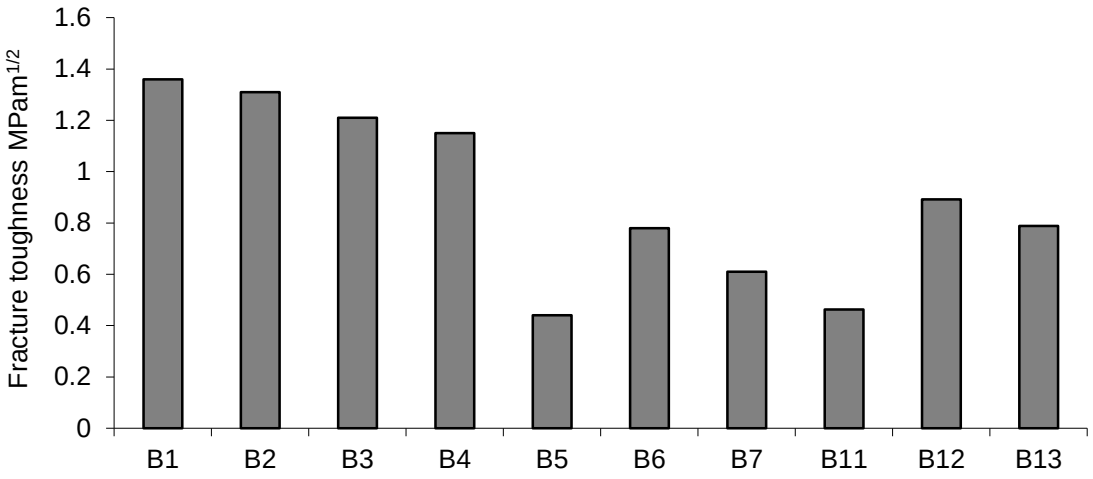


Figure 4 Fracture toughness of concretes

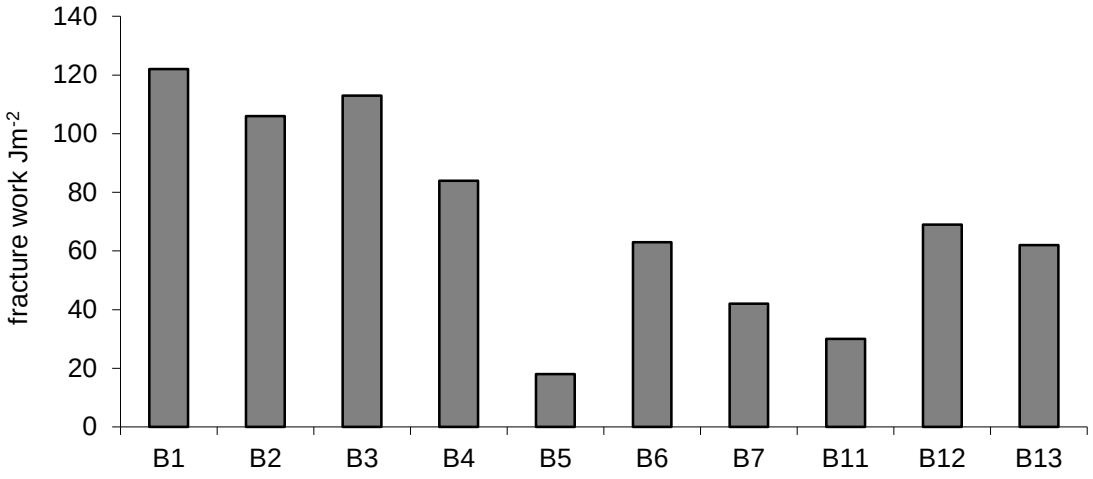


Figure 5 Fracture work of concretes

**Practical application**

Hybrid cement was used for the production of light inserts into ceiling panels for a newly developed subtle skeleton for energetically efficient buildings [10]. As commonly produced hollow core panels can be much more productive, for better acoustic properties some inserts with a volume mass of around 500 kg/m$^3$ are required. Different materials were designed for the production of lightening inserts. The first alternative is inserts from a light cellular concrete from expanded clay (Liapor). The second alternative is the use of new material Stered® , which is recycled material from different textiles, especially from car upholstery. For better fire

resistance, inserts from Stered® are finally designed as a sandwich structure from Stered® and from cellular concrete with hybrid cement similar as in concrete B12 (see Table 3). A view of the insert is shown in Figure 6. The production of inserts proceeded without problems and the application of hybrid cement for this purpose seems to be convenient.

Figure 6 Ceiling inserts from Stered® and cellular concrete from hybrid cement and expanded clay

## CONCLUSIONS

Some concretes with hybrid cements were prepared and their properties were compared with those of the concrete with OPC and OPC with fly ash. Sodium chloride was used as the activator of hybrid cements, which makes them cheaper and – with regards to content of secondary materials - very environmentally friendly. Naturally, the use of these concretes is limited, thanks to chloride ions content. On the other hand, some positive effect of hybrid cements was found in terms of brittleness, modulus of elasticity and fracture properties. Ongoing optimisation of the composition of hybrid cement and also the optimisation of their granulometry can brings a positive effect which can result in a promising new kind of concrete.

## ACKNOWLEDGEMENTS

The contribution has been created with the financial support from the budget of the Moravian-Silesian region within the frame of program Backing of the science and research in the Moravian-Silesian Region, number of the program: RRC/07/2014.

## REFERENCES

1. SCRIVENER, K. L. Options for the future of cement, The Indian Concrete Journal, July 2014, pp.11 - 21

2. BILEK, V. Development and properties of concretes with ternary binders, Cement, Wapno, Beton, 6/2013, pp.343-352, ISSN-1425-8129

3. SANITSKII, M.A., Alkaline portland cements, Proceeding of 2nd International Conference Alkaline Cements and Concretes, P.V. Krivenko (Ed.), Kyiv (Ukraine) 1999, pp. 315 - 336.

4. GARCIA-LODEIRO, I., PALOMO, A., FERNÁNDEZ-JIMENEZ, A., Hybrid alkaline cements: Hydration kinetics study during the early reaction stages, Proceeding of 5th International conference Non-traditional Cements and Concretes, V. Bilek and Z. Kersner (Eds.), Brno (Czech Republic) 2014, pp.59-62

5. KARIHALOO, B.L., NALLATHAMBI, P. An improved effective crack model for determination of fracture toughness of concrete, Cem. Concr. Res., Vol.19, pp.603-610

6. RILEM TC-50 FMC (Recommendation) Determination of fracture energy of mortar and concrete by means of three-point bend test on notched beams, Mater. Struct. Vol.18 (107), 1985, pp.285 - 290

7. ELICES, M., GUINEA, G.V., PLANAS, J. On the measurement of concrete fracture energy using three-point bend test, Mater. Struct., Vol.30 (1997), pp 375-376

8. CIKRLE, P., BILEK, V. Modulus of elasticity of high strength concretes, BETON TKS, No. 2, 2010, pp. 40-44 (in Czech)

9. BILEK, V., ZIDEK, L., HURTA, J., MEC, P. Searching for durable and friendly, alkali activated concrete for building elements, Adv. Mater. Res. 1098, 126—131.

10. BILEK, V., FIALA, C., HAJEK, P., HEJL, J., RUZICKA, J., NOVOTNA, M. Light subtle sceleton for environmentally efficient buildings, Proc. of 2nd Int. Conf. Advances in Cement and Concrete Technology in Africa (ACCTA), Tanzania, 2016, pp. 561-566

# INFLUENCE OF LIMESTONE POWDER ON THE REACTION KINETICS AND MECHANICAL PROPERTIES OF SODIUM CARBONATE ACTIVATED SLAG

**B Yuan**

**Q L Yu**

**H J H Brouwers**

Eindhoven University of Technology

The Netherlands

**ABSTRACT.** The effects of limestone powder (LP) on the performance of Portland cement based composites have been extensively studied, considering that LP not only acts as nuclei, but that it is also chemically involved in the hydration process, which improves the reaction degree at the early age. In high calcium containing alkali activated system, the function of LP is considered as inert filler, probably due to the low solubility of calcium carbonate. However, the role of LP may differ in sodium carbonate activated slag (AAM) with respect to the initial precipitated calcium carbonate sharing the same chemical composition to LP. By replacing the solid ingredient ground granulated blast furnace slag (GGBS) with LP at different levels (5%-30% by mass of slag), the reaction kinetics and compressive strength of sodium carbonate activated slag-LP blends were studied. The results show that the reaction of sodium carbonate activates is slightly accelerated when the content of LP is below 5%. When increasing the LP content further, the reaction process is gradually delayed. Besides, the intensity of the reaction as shown by calorimetric measurement is increased with up to 10 % of LP. On the other hand, the compressive strength of mixtures benefits from the incorporation of LP up to 15%, and then decreases 2.4% when 30% LP is used. Furthermore, the highest strength was achieved with 10% replacement of LP, which is in line with the calorimetric results, indicating that the incorporation of LP accelerates the reaction of sodium carbonate activated slag.

**Keywords:** Limestone powder, Sodium carbonate, Ground granulated blast furnace slag, Reaction kinetics, Mechanical properties.

**B Yuan** received his master's degree from Wuhan University of Technology, China. He is currently working as a PhD student in the Department of Built Environment, Eindhoven University of Technology.

**Q L Yu,** received his Ph.D. degree from Eindhoven University of Technology, the Netherlands. He is currently assistant professor of Building Materials in the Department of the Built Environment, Eindhoven University of Technology

**Prof Dr Ir H J H Brouwers** is professor of Building Materials in the Department of the Built Environment, Eindhoven University of Technology.

## INTRODUCTION

Limestone powder has been widely applied in Portland cement based building materials because of its low price and good performance [1–5]. The effect of limestone powder on the hydration of cement has been extended from the earliest filler effect only to the chemical reactions involved with cement components such as $C_3S$ and $C_3A$ [6–9]. However, the effects of limestone powder on the reaction of alkali activated materials have not been systematically established yet. Up till now, only a few concerns [10–12] have been paid to this topic partly because of the complex characteristics of the activators and raw materials applied compared to Portland cement systems [13–15].

In the low-calcium containing alkali activated metakaolin system, Cwirzen et al. [10] studied the potential chemical involvement of limestone powder, and reported that limestone powder is dissolved in the sodium hydroxide solution releasing $Ca^{2+}$ and its presence enhances the release of Al and Si ions from metakaolin, leading to the formation of layered calcium carboaluminates. However, the contribution of limestone powder is limited to a low level as all samples were below 7 MPa after 28 d of curing. While in the high-calcium containing alkali activated slag system, the effect of limestone powder is not known yet because the hydrolysis of calcium carbonate is detained due to the fact that slag will release sufficient $Ca^{2+}$ ions. Besides, slag does not contain the chemical components like $C_3S$ or $C_3A$ in the cement that can chemically react with limestone powder [6–8]. In this case, the effect of LP in the alkali activated slag system is more likely to act as an inert filler. Using waterglass as an activators, Gao et al. [11] studied the effect of both fly ash and limestone on the reaction and strength development of slag based AAM system, and found that limestone powder shows a good filler effect in terms of strength development. However, no sign of chemical reactional involvement was observed.

However, the role of limestone powder may differ in the sodium carbonate activated slag system due to the initial precipitated calcium carbonate [16, 17]. It has been identified that the main reaction products of sodium carbonate activated slags are calcium carbonate ($CaCO_3$), gaylussite ($Na_2Ca(CO_3)_2 \cdot 10H_2O$), hydrotalcite ($Mg_6Al_2CO_3(OH)_{16} \cdot 4H_2O$), etc. As a result, limestone powder could be potentially involved in the reaction, leading to a modified strength development.

This paper aims to study the filler effect of limestone powder on the reaction kinetics and mechanical properties of sodium carbonate activated slag. Applying an isothermal calorimeter (TAM AIR Calorimeter), the heat release of mixtures containing different levels of LP up to 30% was measured. The compressive strength of samples was measured at the curing ages of 7 d and 28 d, respectively.

## MATERIALS AND EXPERIMENT

### Materials

Ground granulated blast furnace slags (GGBS) and limestone powder (LP) were applied as raw materials. Table 1 presents the chemical compositions of these two materials, as determined by XRF. The particle size distributions are shown in Figure 1 with the d(0.5) of 19.37 μm and 10.30 μm, respectively, measured by a Mastersizer 2000. Before sample preparation, sodium carbonate was firstly dissolved in the water followed by cooling down to room temperature.

Table 1 Chemical compositions of raw materials

| CHEMICAL COMPOSITION | SLAG, % | LIMESTONE, % |
|---|---|---|
| $SiO_2$ | 35.50 | 0.84 |
| CaO | 38.60 | 53.96 |
| $Al_2O_3$ | 13.60 | 0.24 |
| MgO | 10.20 | 1.01 |
| $Fe_2O_3$ | 0.48 | 0.32 |
| $SO_3$ | 1.27 | |
| $K_2O$ | 0.48 | 0.34 |
| $TiO_2$ | 1.01 | |
| Cl | 0.01 | |
| L.O.I. | | 43.01 |
| Specific density (g/cm³) | 2.93 | 2.71 |
| Blaine fineness (m²/kg) | 373 | 546 |

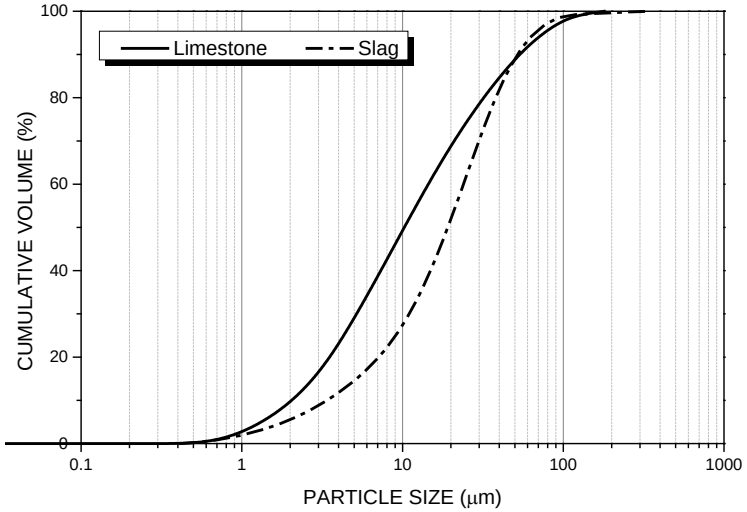


Figure 1 Particle size distributions of raw materials

## Experiments

The reaction kinetics of samples are studied by applying an 8 channels' isothermal calorimeter (Tam Air Calorimeter) set at 20ºC. The heat releases of sodium carbonate activated slag-limestone powder blenders were measured up to 180 hours. Before loading to the instrument, the samples were firstly manually mixed and transferred to an ampoule. It should be noted that the heat release at the first 5 min was not recorded because of the sample preparation procedure. Due to the preparation process, the heat release at the first 5 min was not recorded. It should be noted that the first hour of the recorded data is also questionable due to the unstable condition of the calorimeter disturbed by the loading process. The calorimetry data were normalized by the total amount of materials.

According to the suggestion of EN 196-1, the samples were prepared with a mortar mixer. Then the fresh pastes were cast into plastic moulds ($40 \times 40 \times 160$ $mm^3$) with manual vibration before sealed with plastic foils to prevent the moisture loss. The samples were demoulded at the ages of testing.

## RESULTS

### Reaction Kinetics

Figure 2 presents the heat evolution of sodium carbonate activated slag with different replacement levels of limestone powder. It is clear that the reaction process of SCAS incorporating LP is similar to that of cement hydration or other alkali activated materials [18–20], which can be generally divided into five stages. Similar to the previous researches [16, 17], the dormant period of the mixtures is relatively long due to the initial precipitation of calcium carbonate. As depicted in Figure 2, the intensities of the heat evolution is firstly increased till 10 % replacement of LP and then gradually decreases, which is in line with the strength development (Figure 3). It should be noted that, the reaction process of SCAS is slightly accelerated when the dosage of LP is 5%, while the time to reach the reaction peak (TTRP) is significantly delayed when further increasing the LP content. On the other hand, the accumulated heat release of the mixtures containing within 10% LP is gradually increased, while further increasing the LP content the total heat release is decreased probably due to the dilution effect.

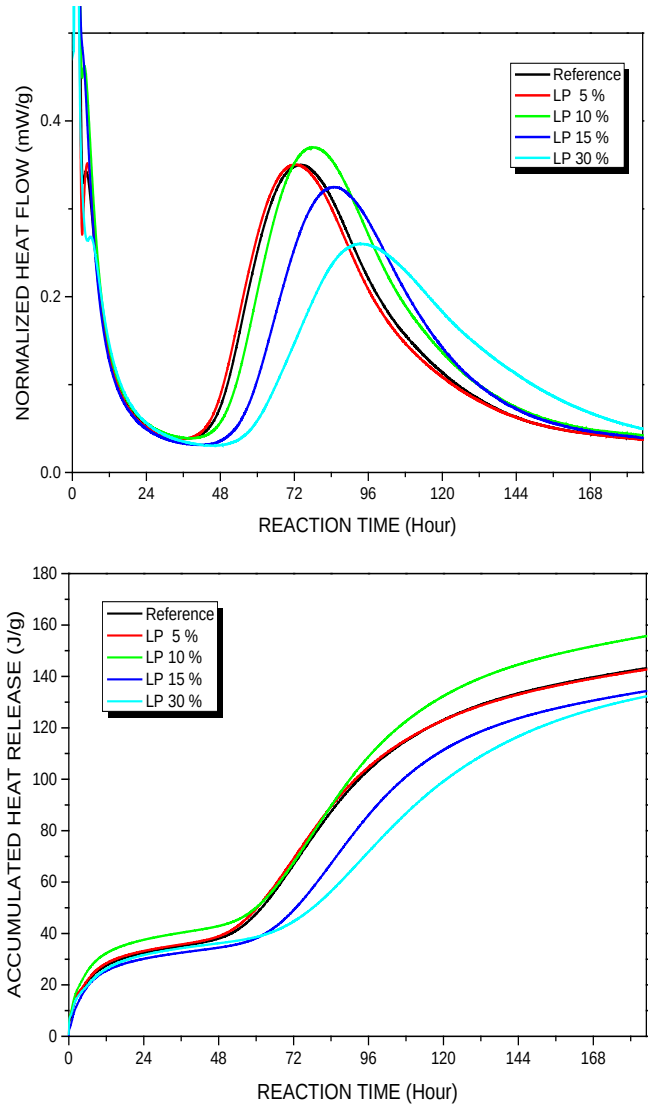


Figure 2 Heat release of the mixtures containing different levels of limestone powder: normalized by the mass of materials (top) and accumulated heat release (bottom)

In cement based system, the incorporation of LP has been reported to possess an accelerating effect on the cement hydration [6], and both intensity and TTRP were improved when cement/$C_3S$ were blended with LP. The similar results were obtained by Zajac et al. [21] who studied the influence of limestone on the hydration of cements, and found that a mixture with 4% of LP shows slight faster and intensive reaction than pure cement mixture. As shown in Figure 2, the same trends were found in the sodium carbonate activated slag-LP blends when the LP content is lower than 5%. When the LP content is higher than 5%, different behaviours were observed between cement and sodium carbonate activated system, indicating the different functions of LP on these two system.

## Compressive Strength

The compressive strengths of the mixtures containing different levels of LP is shown in Figure 3. As can be seen, the strength firstly gradually increases with the increase of limestone contents up to 10%, and then decreases. A strength of 38.1 MPa and 54.5 MPa at the curing ages of 7 d and 28 d was achieved, respectively, in the mixture with 10% LP replacement. However, it should be noted that even with 30% replacement of limestone powder to slags, the compressive strength does not significantly reduce compared to the references sample.

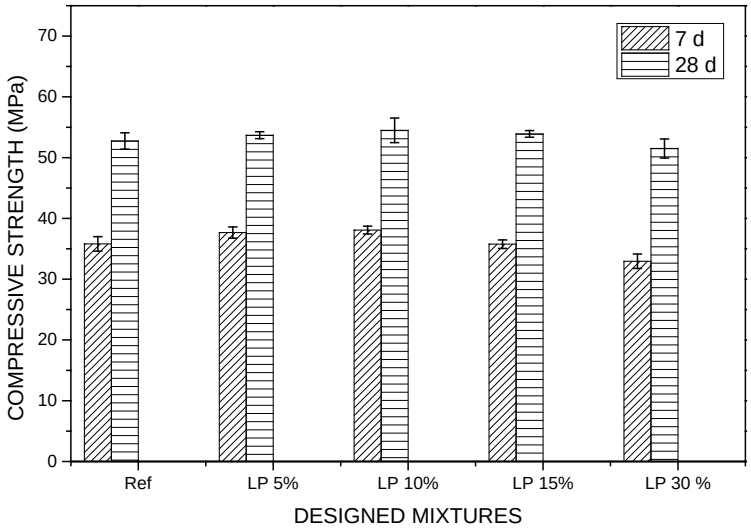


Figure 3 Compressive strength of the mixtures containing different levels of limestone powder at the curing ages of 7 d and 28 d

During the last decades, the benefits of incorporating limestone powder on the cement hydration have been well established and its dilution effect on the strength development is also widely studied. Kumar et al. [5] reported that with 5% replacement of limestone powder, the strength of mixtures will not be weakened. However, when further increasing the LP content, the compressive strength decreases roughly linearly. With 30% LP replacement, the compressive strength was decreased approximate 32 % compared to its reference. Ramezanianpour [3] also reported that samples with up to 10% LP replacement show competitive properties to cement concrete.

In this case, it is clear that limestone powder shows a good filler effect, by giving an excellent strength development at a higher replacement level and showing comparative properties. Similar result was observed by Gao et al. [11] who characterized the reaction kinetics and compressive strength of waterglass activated slag-fly ash-limestone powder blends.

## DISCUSSION

In general, the incorporation of limestone powder can provide both positive and negative effect on the reaction of sodium carbonate activated slag: acting as nuclei sites similar to inert fillers or diluting the binder content leading to a reduction on the strength development. However, it should be noted that LP shares the same chemical composition to the initial precipitated calcium carbonate generated at the early ages of sodium carbonate activated slag [22]. Bernal et al. [16] reported that the concentration of $CO_3^{2-}$ anions in the pore solution controls the reaction process. Also in the previous research [17], we have concluded that the transformation of precipitated calcium carbonate to other phases dominates the reaction process. As a result, the incorporated limestone powder could potentially involve in the reaction, influencing the formation of gaylussite and hydrotalcite.

In the current study, the samples with different contents of LP were characterized and the benefits on the reaction of sodium carbonate activated slag are evaluated. It is clear that up to a 10% LP content, it will not weaken the compressive strength of the mixtures, while in the cement system the same condition this is around a 5-10 % LP content [2,3]. It is indicated that the incorporation of limestone powder within 10% positively affects the reaction of sodium carbonate activated slag. It is clear that LP powder can behave better in the sodium carbonate activated slag system than in cement or waterglass activated slag systems. However, further investigation is required for a deeper understanding the potential chemical involvement of limestone powder.

## CONCLUSIONS

This study investigated the effect of limestone powder on the reaction kinetics and compressive strength of sodium carbonate activated slag. Based on experimental results and discussion above, the following conclusions can be drawn:

1. The incorporation of limestone powder within 5% accelerates the reaction of sodium carbonate and 10% LP content gives the highest reaction intensity.

2. A LP replacement level of up to 10% increases the compressive strength of the mixture and a slight 2.4% reduction is observed when the LP content is increased to 30%.

## ACKNOWLEDGEMENTS

This research was carried out under the fund of China Scholarship Council and the Department of The Built Environment of Eindhoven University of Technology. The authors wish to express their gratitude to the following sponsors of the Building Materials research group at TU Eindhoven: Rijkswaterstaat Grote Projecten en Onderhoud, Graniet-Import Benelux, Kijlstra Betonmortel, Struyk Verwo, Attero, Enci, Rijkswaterstaat Zee en Delta - District Noord, Van Gansewinkel Minerals, BTE, V.d. Bosch Beton, Selor, GMB, Icopal, BN International, Eltomation, Knauf Gips, Hess AAC Systems, Kronos, Joma, CRH Europe

Sustainable Concrete Centre, Cement&BetonCentrum, Heros, Inashco, Keim and Sirius International.

## REFERENCES

1. TENNIS P D, THOMAS M D A, WEISS W J. State-of-the-Art Report on Use of Limestone in Cements at Levels of up to 15 %, 2011, pp 1–78.

2. DIAB A M, ABD ELMOATY A E M, ALY A A. Long term study of mechanical properties, durability and environmental impact of limestone cement concrete. Alexandria Eng J, 2016. doi:10.1016/j.aej.2016.01.031.

3. RAMEZANIANPOUR A A, GHIASVAND E, NICKSERESHT I, MAHDIKHANI M, MOODI F. Influence of various amounts of limestone powder on performance of Portland limestone cement concretes. Cem Concr Compos, Vol. 21, 2009, pp 715–720. doi:10.1016/j.cemconcomp.2009.08.003.

4. VOGLIS N, KAKALI G, CHANIOTAKIS E, TSIVILIS S. Portland-limestone cements. Their properties and hydration compared to those of other composite cements. Cem Concr Compos, Vol. 27, 2005, pp 191–196. doi:10.1016/j.cemconcomp.2004.02.006.

5. KUMAR A, OEY T, KIM S, THOMAS D, BADRAN S, LI J, FERNANDES F, NEITHALATH N, SANT G. Simple methods to estimate the influence of limestone fillers on reaction and property evolution in cementitious materials. Cem Concr Compos, Vol. 42, 2013, pp 20–29. doi:10.1016/j.cemconcomp.2013.05.002.

6. PERA J, HUSSON S, GUILHOT B. Influence of finely ground limestone on cement hydration. Cem Concr Compos, Vol. 21, 1999, pp 99–105. doi:10.1016/S0958-9465(98)00020-1.

7. KAKALI G, TSIVILIS S, AGGELI E, BATI M. Hydration products of $C_3A$, $C_3S$ and Portland cement in the presence of $CaCO_3$. Cem Concr Res, Vol. 30, 2000, pp 1073–1077. doi:10.1016/S0008-8846(00)00292-1.

8. IPAVEC A, GABROVSEK R, VUK T, KAUCIC V, MacEK J, MEDEN A. Carboaluminate phases formation during the hydration of calcite-containing Portland cement. J Am Ceram Soc, Vol. 94, 2011, pp 1238–1242. doi:10.1111/j.1551-2916.2010.04201.x.

9. TSIVILIS S, CHANIOTAKISB E, BADOGIANNIS E, PAHOULASA G, ILIAS A. A study on the parameters affecting the properties of Portland limestone cements. Cem Concr Compos, Vol. 21, 1999, pp 107–116. doi:10.1016/S0958-9465(98)00031-6.

10. CWIRZEN A, PROVIS J L, PENTTALA V, HABERMEHL-CWIRZEN K. The effect of limestone on sodium hydroxide-activated metakaolin-based geopolymers. Constr Build Mater, Vol. 66, 2014, pp 53–62. doi:10.1016/j.conbuildmat.2014.05.022.

11. GAO X, YU Q L, BROUWERS H J H. Properties of alkali activated slag–fly ash blends with limestone addition. Cem Concr Compos, Vol. 59, 2015, pp 119–128. doi:10.1016/j.cemconcomp.2015.01.007.

12. MOSESON A J, MOSESON D E, BARSOUM M W. High volume limestone alkali-activated cement developed by design of experiment. Cem Concr Compos, Vol. 34, 2012, pp 328–336. doi:10.1016/j.cemconcomp.2011.11.004.

13. PACHECO-TORGAL F, CASTRO-GOMES J, JALALI S. Alkali-activated binders: A review. Constr Build Mater, Vol. 22, 2008, pp 1305–1314. doi:10.1016/j.conbuildmat.2007.10.015.

14. RASHAD A M. Alkali-activated metakaolin: A short guide for civil Engineer – An overview. Constr Build Mater, Vol. 42, 2013, pp 751–765. doi:10.1016/j.conbuildmat.2012.12.030.

15. PROVIS J L, BERNAL S A. Geopolymers and Related Alkali-Activated Materials. Annu Rev Mater Res, Vol. 44, 2014, pp 299–327. doi:10.1146/annurev-matsci-070813-113515.

16. BERNAL S A, PROVIS J L, MYERS R J, SAN NICOLAS R, Van DEVENTER J S J. Role of carbonates in the chemical evolution of sodium carbonate-activated slag binders. Mater Struct, Vol. 48, 2014, pp 17–29. doi:10.1617/s11527-014-0412-6.

17. YUAN B, YU Q L, BROUWERS H J H. Time-dependent characterization of $Na_2CO_3$ activated slag. Cem Concr Compos 2015, Under review.

18. RAVIKUMAR D, NEITHALATH N. Reaction kinetics in sodium silicate powder and liquid activated slag binders evaluated using isothermal calorimetry. Thermochim Acta, Vol 546, 2012, pp 32–43. doi:10.1016/j.tca.2012.07.010.

19. HAHA M B, LOTHENBACH B, Le SAOUT G, WINNEFELD F. Influence of slag chemistry on the hydration of alkali-activated blast-furnace slag - Part II: Effect of $Al_2O_3$. Cem Concr Res, Vol. 42, 2012, pp 74–83. doi:10.1016/j.cemconres.2011.08.005.

20. BERNAL S A, NICOLAS R S, MYERS R J, De GUTIÉRREZ R M, PUERTAS F, Van DEVENTER J S J, PROVIS J L. MgO content of slag controls phase evolution and structural changes induced by accelerated carbonation in alkali-activated binders. Cem Concr Res, Vol. 57, 2014, pp 33–43. doi:10.1016/j.cemconres.2013.12.003.

21. ZAJAC M, ROSSBERG A, Le SAOUT G, LOTHENBACH B. Influence of limestone and anhydrite on the hydration of Portland cements. Cem Concr Compos, Vol. 46, 2014, pp 99–108. doi:10.1016/j.cemconcomp.2013.11.007.

22. JIMENEZ A F, PUERTAS F. Setting of alkali-activated slag cement. Influence of activator nature. Adv Cem Res, Vol. 13, 2001, pp 115–121. doi:10.1680/adcr.2001.13.3.115.

# HYDRATION AND COMPRESSIVE STRENGTH OF SLAG BASED BINDER ACTIVATED WITH RECYCLED CONCRETE FINE: EFFECTS OF POLY-ALUMINIUM CHLORIDE

**Wei Chen**

**Bo Li**

**Jian Tian** **Ning Zhang**

Wuhan University of Technology

China

**ABSTRACT.** Effects of poly-Aluminium chloride (PAC) on the hydration of blastfurnace slag (BFS) based binder activated with recycled concrete fine (RCF) are studied in this research. The RCF is simulated by calcining hardened cement paste at 600 $^{o}$C followed by grinding. The research shows that the binder prepared from the RCF and BFS has comparable mechanical performance to the ordinary cement if PAC is added with a dosage of 1~2% by weight. The microstructural analysis shows the PAC provides polymeric aluminium- oxyhydroxide units with high positive charge that promotes the reaction of slag, resulting in enhanced strength of the binder.

**Keywords:** Dehydrated phase, Poly-aluminium chloride, Microstructure, Blastfurnace slag

**Professor Wei Chen** is the Dean Associate of the School of Materials Science and Engineering at Wuhan University of Technology. He is member of ACI and RILEM since 2003, and is committee member of Materials Analysis and Testing Council, The Chinese Ceramic Society. His research interests cover cement chemistry, development of novel high performance concrete, and recycling concrete in new construction projects. He is author of more than 150 research papers and PI of over 50 research projects funded by the Chinese Government and companies.

**Mr Bo Li** is a phd candidate at School of Materials Science and Engineering, Wuhan University of Technology. His research field is the micro-structure characterization and properties of C-A-S-H.

**Mr Jian Tian** is postgraduate student at School of Materials Science and Engineering, Wuhan University of Technology. His research interest is application of industrial waste and recycled concrete fine.

**Miss Ning Zhang** is also at School of Materials Science and Engineering, Wuhan University of Technology. She is interested in the research on preparation and properties of amorphous silica based materials

## INTRODUCTION

Ecology and green concrete have been paid much attention to in recent years for environmental concerns expressed by new legislation and commercial trends. It has been aid to push the concrete industry toward minimizing its environmental impact, and natural resources (such as limestone and gypsum) consumed in producing cement and concrete [1]. On the other hand, waste concrete has accumulated to great amount due to the demolishment of buildings, bridges and roads world widely. The recycling of components from waste concrete is a major concern in regard to the development of concrete industry for the coming years.

Anastasiou identified that construction and demolition waste, high calcium fly ash and electric arc furnace slag can be combined to produce environmentally friendly concrete [2]. Recycled concrete fine (RCF) is the fine powder obtained from waste concrete in the process of separating aggregate from the matrix, which is mainly hardened cement paste. RCF has been studied for its environmental friendly property and low cost, especially those thermally activated. The experimental by Zhonghe Shui indicated that the compressive strength of the activated fly ash/RCF depends on the value of the theoretical Ca/Si radio in the mixture [3].

Poly-aluminum chloride (PAC) is a recently developed inorganic coagulant for water treatment that is wildly used due to its higher efficiency than the traditional coagulant, such as aluminum sulfate and alunite [4]. Polymeric Al-oxyhydroxide is actually a series of intermediates during the hydrolyzation and polymerization reaction of aluminum salts at different pH [5,6,7]. The most stable form is $Al_{13}$ ($[Al_{13}O_4(OH)_{24+n}]^{(7-n)+}$) with a Keggin-13 structure and a hydrated monomeric radius of 10~20 Å. Since the large number of active groups and high negative charge, PAC enable particle precipitation via adsorption bridging and charge neutralization [8].

In this study, the enhanced effect of polyaluminum chloride to slag based binder activated with RCF obtained from calcining hardened cement paste at 600$^o$C is investigated. Not only the high negative charge in the particle surface but also the large number of active aluminum-oxyhydroxide groups of PAC produces significant contributions by modifying the cohesion of particles. The experiments reveals that the binder prepared from the recycled fine and BFS has comparable mechanical performance with the ordinary cement if PAC is added with a dosage of 1~2% by weight.

## EXPERIMENTAL METHODS

### Materials And Sample Preparation

RCF is synthesized by calcining hardened cement paste at 600 $^o$C. The harden cement paste is prepared by mixing Ordinary Portland cement of P.O 42.5 grade conforming to the specifications of GB 175-2007 of China with a water to cement radio is 0.5 and hardens for 3 months. The hardened paste is crushed, ball milled and sieved to obtain particles smaller than 150 μm.

The chemical composition of GGBFS, PAC and RCF are listed in Table 1, obtained by PANalytical B.V. Axios advanced X-ray fluorescence. The slag with a specific surface area of 420 $m^2$/kg is supplied by Wuhan Iron and Steel group co., LTD. PAC is provided by Lantianyuzhou Chemical reagent co., LTD. The XRD patterns of the PAC are shown in Figure 1, and the functional group of the PAC identified in the Fourier transform-infrared (FTIR) spectrum (Thermo Nicolet Nexus) are shown in Figure 2.

The spectrum reveals that the PAC is mainly in the amorphous state containing large number of Al-OH and Al-OH-Al.

The compressive strength of mortar samples is tested according to the Chinese standard GB/T 17671-1999. The mass ratio of sand to binder (all powders) is 3.0 in mortar and the water to binder ratio of mortar and pastes are 0.50. The mass ratio of RCF to slag is 2:3 in the binder. All samples (4×4×16 cm) are cured at 30±2 ºC for 3, 7 and 28 days. Three groups specimens are prepared with 0, 1% and 2% PAC by weight added in the mixtures. The recipes of mortar and neat paste are listed in Table 2.

Table 1 Oxide composition of materials

| CONTENTS | RCF | SLAG | PAC |
|---|---|---|---|
| $Na_2O$ | / | 0.33 | 5.91 |
| MgO | 1.71 | 7.34 | 1.80 |
| $Al_2O_3$ | 5.05 | 14.31 | 22.0 |
| $SiO_2$ | 21.04 | 34.22 | 1.43 |
| $P_2O_5$ | 0.10 | 0.04 | 0.03 |
| $SO_3$ | 1.82 | 2.40 | 0.35 |
| $K_2O$ | 0.44 | 0.57 | 0.26 |
| CaO | 58.79 | 38.59 | 1.11 |
| $Fe_2O_3$ | 2.68 | 0.66 | 0.85 |
| Cl | 0.04 | / | 16.32 |
| LOI | 7.71 | -0.77 | 49.97 |

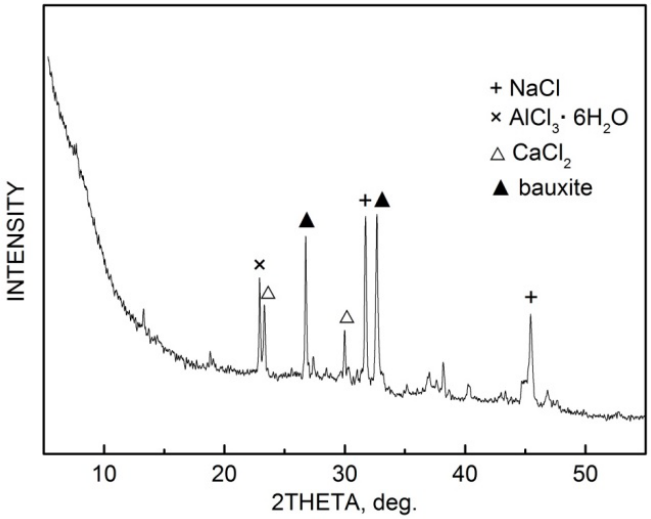


Figure 1 XRD patterns of PAC

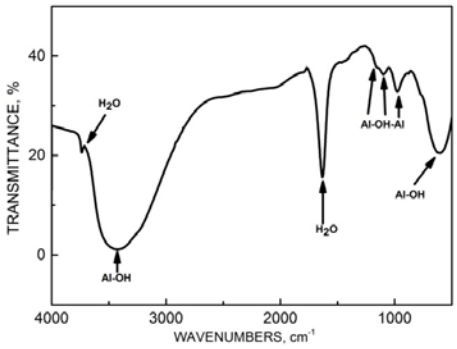


Figure 2 FTIR spectrum of the PAC

Table 2 Recipes of mortar and neat paste

| SPECIMEN | NUMBER | RECYCLED CEMENT (g) | SLAG (g) | SAND (g) | PAC (%) | WATER (g) |
|---|---|---|---|---|---|---|
| Paste | 1 | 120 | 180 | / | 0 | 120 |
| | 2 | 120 | 180 | / | 2 | 120 |
| mortar | 3 | 180 | 270 | 1350 | 0 | 180 |
| | 4 | 180 | 270 | 1350 | 1 | 180 |
| | 5 | 180 | 270 | 1350 | 2 | 180 |

### Analytical techniques

The XRD patterns of the samples at different ages are obtained by D8 Advance powder X-ray diffractometer with a Cu Kα (λ=1.54 Å) incident radiation. ULTRA PLUS-43-13 Scanning Electron Microscope (SEM) is employed for the morphology of hydration product of cement paste and interfacial contact between sand and paste.

The porosity of the hardened mortar prepared with the binder from the RCF, slag and PAC is measured by using the methanol exchange method.

## RESULTS AND DISCUSSION

### Compressive strength

The compressive strength of mortar presented in Figure 3 showed that adding poly-aluminum chlorides increases the compressive strength at the age of both 7d and 28d. The 7d compressive strength of mortar without PAC is 18 MPa and is increased to 30.5 MPa with 2% of PAC. The 28d compressive strength of the mortar reference and with PAC is 23.6 MPa and 35.8 MPa, respectively. However it is also observed that strength increase of the mortar is not significant at 3d, as shown in Figure 3.

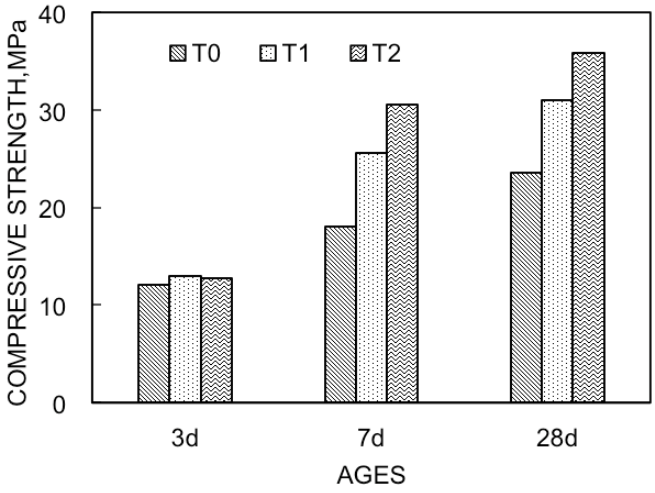


Figure 3 Compressive strength of mortar specimens.

The porosity of the hardened mortar at different ages is listed in Table 3. In general the effects of PAC on the porosity of the mortar are marginal. Link between the porosity and the compressive strength shown in Figure 3 is weak.

Table 3 Porosity of hardened mortar at 7d and 28d (%)

| AGES | REF (WITHOUT PAC) | 1% PAC | 2% PAC |
|---|---|---|---|
| 7d | 9.5 | 9.3 | 8.7 |
| 28d | 7.8 | 8.1 | 7.5 |

**Phase identification with XRD pattern**

The XRD patterns of the cement paste with 2% PAC and the reference at 28d are shown in Figure 4. The main crystalline phase in hydration product is AFm phase, and calcite. There is no new phase identified in the hydration products if comparing both specimens. But, the structure and amount of AFm phase are changed.

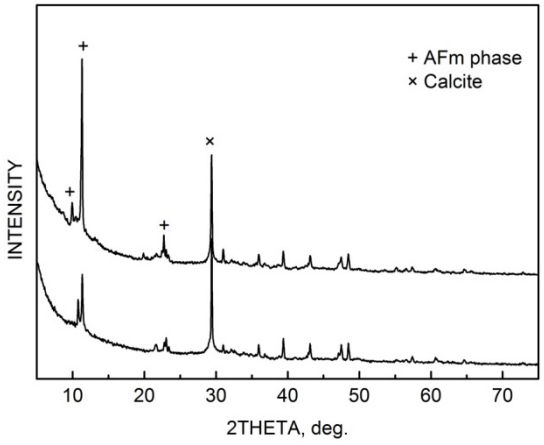


Figure 4 The XRD patterns of neat paste cured for 28d

Table 3 showed the detailed value of the 2theta and corresponding interlayer spacing (d). The interlayer spacing of AFm phase is 8.16 Å, 3.86 Å, 2.63 Å without PAC, and it changes to 8.01 Å, 4.00 Å, 3.84 Å, 2.89 Å with the incorporation of 2% PAC. The change of the d space indicates new AFm phase formed by the corporation of PAC. It indicated that chlorines brought with PAC enters into the interlayer of AFm phase and replaces the hydroxyl, leading to part of hydroxy-AFm transform to Friedels' salt [9,10]. The d spacing increases from 2.63 Å to 2.89 Å.

Table 4 Interlayer spacing of AFm phases

| | INTERLAYER SPACING (Å) | | | |
|---|---|---|---|---|
| T0 | 8.150 | 3.865 | 2.627 | -- |
| T2 | 8.031 | 4.006 | 3.858 | 2.888 |

**Microstructural observations with SEM**

SEM images of the paste are shown in Figure 5. Some unreacted slag is observed in the samples of all ages. The image of paste cured for 3d with 2% PAC is similar to the one without PAC at 3d, which is consistent with the strength data at 3d. Hydration product such as plate-like AFm phase, hexagonal plate-like portlandite and disordered gel phases, as shown in XRD patterns, are clearly observed in the figures.

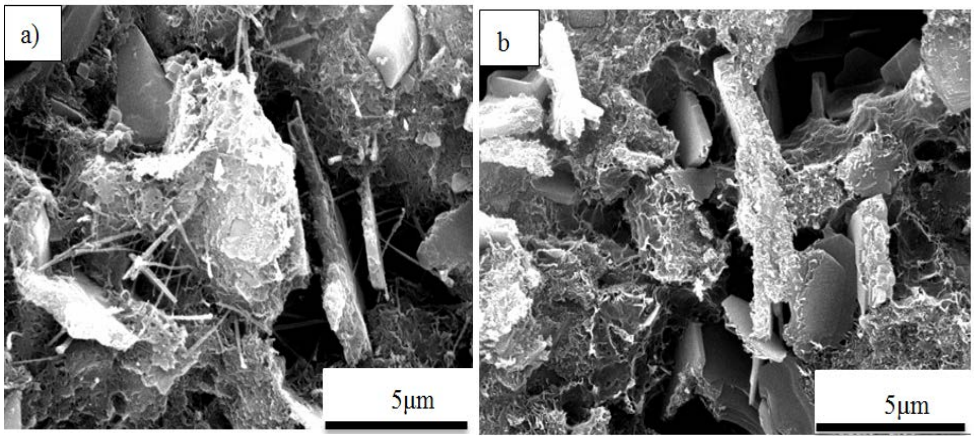


Figure 5 SEM images of hardened cement paste cured for 3d; a) Reference b) with 2% PAC.

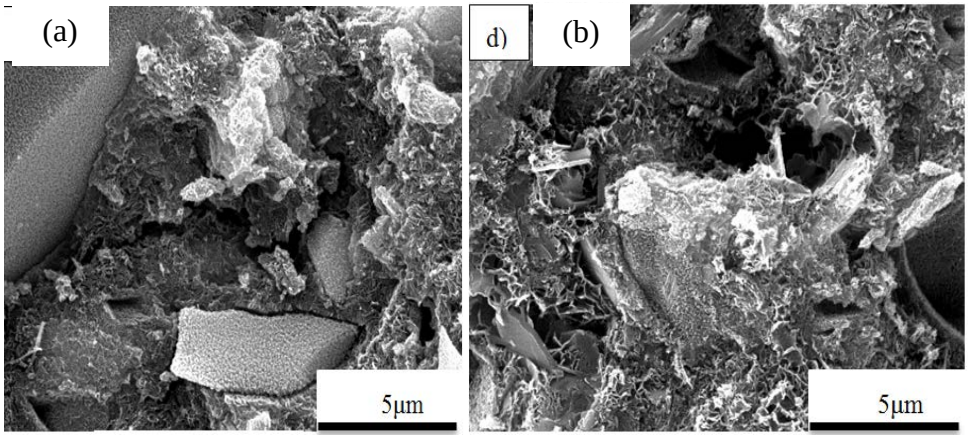


Figure 6 SEM images of hardened cement paste cured for 7d; a) Reference b) with 2% PAC.

However, the images at 7d shown in Figure 6a and 6b indicate some changes over the curing time. The regularly shaped crystalline product identified in the XRD patterns (AFm phase and portlandite) is hardly discerned in the images. Semi-crystalline C-A-S-H with disordered frameworks of short-range order bonding is seen together with anhydrous slag particles. A gap is obvious between the hardened paste and the anhydrous slag in the blank reference, while in the paste with 2% PAC, the transition zone in between is dense. Surface of the anhydrous slag is also obviously modified with PAC, indicating accelerated reaction of slag. If PAC is mixed water, it depolymerizes with high positive surface charge and is adsorbed onto particles quickly through bridging and charge neutralization. The improved interfacial contact due to PAC could be interpreted by absorption of PAC to slag surface and the enhanced hydration.

## CONCLUSIONS

RCF is obtained from calcining hardened cement paste at 600$^{o}$C. The binder prepared from the recycled paste and BFS has comparable mechanical performance with the ordinary cement if PAC is added with a dosage of 1~2% by weight. The main conclusions drawn from the study are presented below:

1. The compressive strength increase of the binder with PAC is not related to the porosity but the modification of the transition zone between hydration products and the anhydrous slag particle.

2. PAC provided a lot of polymeric Aluminum-oxyhydroxide units with high positive charge in the space between slag and cement particles, resulting in high dissolution and reaction rate of slag.

3. The incorporation of PAC can accelerate the reaction rate of slag and the structure of AFm phase is partly transformed from hydroxyl-AFm to Fridels' salt.

## ACKNOWLEDGEMENTS

This research is financially supported by the Fundamental Research Funds for the Central Universities (WUT:142201001).

## REFERENCES

1. P. E. ULLA-MAIJA MROUEH, JUTTA LAINE-YLIJOKI, Life-cycle impacts of the use of industrial by-products in road and earth construction, Iste Management vol. 21, 2001, pp. 271-277,.

2. E. ANASTASIOU, K. GEORGIADIS FILIKAS, AND M. STEFANIDOU, Utilization of fine recycled aggregates in concrete with fly ash and steel slag,Construction and Building Materials, vol. 50, 2014, pp. 154-161,.

3. Z. SHUI, R. YU, AND J. DONG, Activation of fly ash with dehydrated cement paste," ACI Materials Journal, vol. 108, 2011.

4. CHENGHONG FENG, ZHE BI, XIAOHONG WU. The flocculation morphology and coagulation flocculation mechanism of Polymeric Aluminum-oxyhydroxide, Beijing 2015.

5. J, F.J., F, V.C., H, B.,Structure of alumunum cations in aqueous solutions.Journal of Physcial Chemistry, vol. 7, 1965(7)

6. W, A.J., A, F.,New $^{27}$Al NMR studies of the hydrolysis of aluminum(III) cation, J Magn Reson,1978(3):

7. J, B., N, P., W, H.,Importance of speciation mothods in analyticcal control of water treament processes with application to fluoride removal from iste water Water Res,1985(1):

8. YINING, Y., LIYUAN, C., ZHIHUI, Y., YINGPING, L., XINHUI, D., SHUJUAN, Z.,Application of polymeric aluminum salts in remediation of soil contaminated by Pb,Cd,Cu and Zn.Jounral of CentSouth Univ,2013(20):

9. T. MATSCHEI A, B. LOTHENBACH B, F.P. GLASSER A, The AFm phase in Portland cement., Cement and Concrete Research vol. 71, pp. 118-130, 2007.

10. F.P. GLASSER *, S.A. STRONACH, Stability and solubility relationships in AFm phases Part I. Chloride, sulfate and hydroxide, Cement and Concrete Research, vol. 29, pp. 861-866, 1999

# EFFECT OF CURING METHOD ON ALKALI ACTIVATED FLY ASH

**X Huang**

**F Z Wang**

**W Q Zhang P Liu**

Wuhan University of Technology

China

**ABSTRACT.** This paper studies the properties of alkali activated fly ash (AAFA) pastes cured by standard curing, heat curing and microwave curing method, and resulting compressive strength, Na-leachability, composition and microstructure compared against different curing methods are discussed. The compressive strength results displayed that AAFA pastes gained the highest compressive strength under microwave curing which is mainly contributed to the uniform energy and efficiency of absorbed energy provided by microwave. Na-leachability results showed that microwave curing AAFA pastes leached least Na+ concentration, which implied highest hydration degree and demonstrated the results of compressive strength. The XRD and FT-IR results revealed there was no new crystal phase generated in hydration products under heat and microwave curing. In addition, FT-IR test implied that the hydration products possessed greater polymerization and more orderly molecular arrangement after thermal curing. The SEM showed that AAFA pastes by microwave curing formed the most compact structure compared to other curing methods. Microwave curing was one of the most suitable thermal curing patterns to AAFA.

**Keywords:** Alkali activated fly ash, Curing method, Na-leachability, Hydration products

**Dr Xiao Huang** is a candidate of school of materials science and engineering, Wuhan University of Technology, Wuhan, China. He is committed to the field of environmental and sustainable construction materials.

## INTRODUCTION

Portland cement (PC) and concrete are central to modern civilization, with their reliance on the built environment to provide a high quality of life. Given its ubiquitous use in civil construction, the very high PC production volume required to generate enormous quantity of concrete introduces significant environmental issues [1]. Each year, the concrete industry produces approximately 12 billion tonnes of concrete and uses about 1.6 billion tonnes of PC worldwide [2]. Indeed, with the manufacture of 1 tonne of cement approximately 0.94 tonnes of $CO_2$ are launched into the atmosphere [3]. The cement industry accounts for 5–8% of worldwide $CO_2$ emission [4]. $CO_2$ emissions from cement manufacture are mainly due to the thermal decomposition of calcium carbonate to generate the reactive calcium silicate and aluminate phases, and also the combustion of fossil fuels [5]. Not only releases $CO_2$ from cement manufacture, but also $SO_3$ and $NO_x$ which can cause the greenhouse effect and acid rain release from cement manufacture [6, 7]. As global society produces ever-increasing quantities of concrete to meet the infrastructure needs of the developing world [8], there is an urgent need for the development and commercialization of alternative cement-like binders, which will enable the provision of housing and infrastructure to billions of people without excessive damage to the Earth's atmosphere and seas.

Alkali-activated materials (AAMs) [9] are a high-profile example of the alternative binders being discussed and developed with a view toward obtaining environmental savings in the construction industry. The main binding phases are derived by the reaction of aluminosilicates sourced from industrial by-product or other inexpensive material [10]—with an alkaline activator that accelerates the reaction process and induces the formation of strong, insoluble binding phases [9], usually being a concentrated aqueous solution of alkali hydroxide, silicate, carbonate or sulfate [11, 12].

Alkali activated fly ash (AAFA) is a typical kind of AAMs, using fly ash as raw material which is a by-product from coal power plant and produced on a large scale each year, but more than 65% of fly ash is stockpiled at coal power plants or disposed of in landfills, which have negative impact on the environment [13]. Although fly ash has been used as an addition in blended cements to replace part of the Portland cement, such as CEM II and CEM IV in the current European standard, at the early-age strength of concrete is usually low with high replacement level of fly ash [14,15], which has caused concerns in industrial applications of fly ash.

AAFA, a non-clinker cementitious material, considered as a potential alternative to replace PC in certain industrial applications [16, 17, 18] which can not only reduce $CO_2$ emission remarkably but also recycle fly ash more effectively, receives increasing attention and interest in a worldwide scale. It has been proposed that the reaction process of AAFA is a chemical process which involves two main stages, namely, dissolution and polymerization [19]. In the dissolution stage, the reactive silica and alumina components in fly ash are dissolved under strong alkaline condition [16], whilst in the polymerization stage, the dissolved reactive silica and alumina polymerize to produce the main reaction product, sodium aluminosilicate hydrate along with a small quantity of zeolites [17], leading to the formation of a well-compacted cementitous binding material. Compared to PC system, it has been claimed that AAFA produces lower $CO_2$ emission, consumes less energy and possesses superior durability [18, 20, 21].

However, the strength development of AAFA is very slow under room temperature and thermal curing has been considered essential for the initiation of the chemical reaction and subsequent

strength development [22, 23, 24]. Conventional heat curing techniques deliver thermal energy to the surface of the material by radiant or convective heating. This creates thermal gradients in the material and thus non-uniform heating that might result in less than desirable properties. An alternative curing technique is microwave curing method, where microwave energy is delivered directly to the material through the interactions at the molecular level with the electromagnetic field. Microwaves penetrate the material and provide energy, resulting in volumetric heating. The electromagnetic energy is converted to thermal energy which is used to enhance the reaction kinetics and accelerate the strength development. Hence microwave curing relies on energy conversion rather than heat transfer [25, 26]. Since the energy transfer does not rely on diffusion of heat from the surfaces, rapid and uniform heating is possible [27]. Previous studies [13, 28] into microwave-cured AAFA indicated that microwave irradiation can accelerate hydration rate, leading to a more rapid strength development.

It is generally believed that the extra energy provision is beneficial for reaction process of AAFA. This paper focuses on response of AAFA pastes to different energy delivery pattern, including conventional heat curing and microwave curing method. The compressive strength, Na-leachability, composition and microstructure of AAFA pastes under heating curing and microwave curing comparing against standard curing are also provided.

## EXPERIMENTAL PROGRAMME

### Raw materials and Specimen preparation

#### Fly ash

The fly ash used in this study was supplied by self-provided power plant of Wuhan Iron and Steel Corporation, China. The chemical composition of the fly ash used was determined by X-ray fluorescence (XRF) analysis (PANalytical.B.V, Netherlands), with the results shown in Table 1.

Table 1 Chemical composition of fly ash

| CHEMICAL COMPOSITION, % | | | | | | | | | | | |
|---|---|---|---|---|---|---|---|---|---|---|---|
| Fly ash | $SiO_2$ | $Al_2O_3$ | $Fe_2O_3$ | MgO | CaO | $Na_2O$ | $K_2O$ | $SO_3$ | $TiO_2$ | $P_2O_5$ | Loss |
| | 53.58 | 27.11 | 3.85 | 0.55 | 4.08 | 0.27 | 1.23 | 0.87 | 1.50 | 0.55 | 6.00 |

#### Alkali solution

Reagent grade NaOH produced by Sinopharm Chemical Reagent Corporation, China, and water glass ($Na_2SiO_3$) produced by Hubei Seven Eight Nine Chemical Corporation was used as the alkaline activator. The purity of the NaOH was more than 99% and the water glass consisted of 28.5% $SiO_2$, 11.2% $Na_2O$ and 49.0% $H_2O$. The modulus ratio (mass ratio of $SiO_2$ to $Na_2O$) of alkaline solution used in this study was selected to 1.0 which had been tested to gain highest mechanical property [29], and was cooled to room temperature prior to the mixing of the AAFA.

**Specimen preparation**

The AAFA pastes was produced by mixing the fly ash with concentration of 5M $Na_2O$ alkaline solution of modulus radio 1.0, and water to fly ash ratio of 0.35. Requisite amount of the alkaline activator solution was gradually added while mixing until the components were homogenized. The pastes was filled in cubical steel molds of 40 mm size, and compacted using a table vibrator. The specimens were cured for 24±2 h in the molds at 20±1 °C, and then demolded and subjected to the different curing regime.

**Curing methods**

Standard curing method: Standard curing method implied that the demolded specimens were placed in a circumstance where the temperature maintained consistently at 20±1 °C and humidity above 95%.

Heat curing method: Some studies showed that increasing curing temperature would enhance the dissolution of silica and alumina from fly ash, leading to better activation [16,17]. This study employed 90°C temperature and 48 hours curing time as heat curing. The demolded specimens would immediately undergo heat curing, and then gone to standard curing situation.

Microwave curing method: The microwave oven (P70F23P-G5, Galanz) with an adjustable power ranging from 0 to 700W at a frequency of 2.45 GHz was utilized in this work. According to some research [13,28], this study chose 280W of microwave heating power and 1 hour of heating time to cure demolded specimens promptly, then moved specimens to standard curing condition.

Following heat curing and microwave curing, all the samples were cooled down to room temperature prior to the compression test or put into other condition. Selected debris from the compression tests and soaked the debris in alcohol for three days in order to arrest further reaction. The debris was then put into vacuum drying oven at temperature of 65 °C for at least 24 hours. After this, some of the debris was partly ground into fine powder and the particles passed 75μm sieve was used for further chemical analysis. The rest of the debris was well kept for further microstructures analysis.

**Analysis techniques**

For each curing AAFA samples, $40\times40\times40$ $mm^3$ cubes were prepared and three specimens were tested at the ages of 3, 7, and 28 days to determine the average compressive strength.

The ground powder passed 75μm sieve was characterised by means of Na-leachability test, X-ray Diffraction (XRD), Fourier Transform Infrared Spectroscopy (FT-IR), and the treated debris was analysed through Scanning Electron Microscopy (SEM).

In Na-leachability test, 5.000g±0.0001g of powder was added to 50 mL of deionized water in a covered container. After 18h±2h vibration in oscillator, the mixed solution was filtered to remove solid powder with collecting the filtered solution. The filtered solution was given suitable $Na^+$ concentrations for inductive coupled plasma optical emission spectrometer (ICP-OES, Optima4300DV, PerkinElmer) analysis.

The XRD patterns were obtained with D8 Advance (BRUKER AXS GMBH) using monochromatic CuKα radiation and running with 2θ in the range of 10°-70° at a speed of 0.1°/min.

The FT-IR spectra were obtained on a Thermo Nicolet 6700 (Thermo Electron Scientific Instruments) over the range of 4000cm$^{-1}$ and 400cm$^{-1}$. Specimens were prepared using the KBr pellet technique through mixing 1 mg of AAFA powder sample with 300 mg of KBr. A FEI Quanta FEG450 SEM was used to examine the morphology of the hydration products.

## RESULTS AND DISCUSSION

### Compressive strength

The compressive strength of AAFA pastes through three curing methods at the ages of 3, 7 and 28 days is shown in Figure 1. Using microwave cure AAFA pastes obtained the highest compressive strength (13.0 MPa) at curing age of 3 days, approximately double to the compressive strength (7.4 MPa) of AAFA pastes under heat curing, while standard curing AAFA pastes only reached 1.3MPa at the age of 3 days. With curing age growth, microwave curing samples displayed mild fluctuation about 13.0 MPa, and heat curing samples declined slightly to 7.1 MPa at age of 28 days. Meanwhile, standard ones maintained continuously development of compressive strength to 4.1 MPa at age of 28 days.

After only an hour microwave curing, AAFA specimens obtained prominent mechanical property, for microwave curing provides volumetric heating to the specimen, which enhanced the reaction kinetics [28]. Both thermal curing methods could significantly improve the compressive strength of AAFA specimens compared to standard curing method, indicated that providing additional energy was very essential to AAFA hydration progress and resulted in accelerating hydration reaction rate and increasing formation of hydration products.

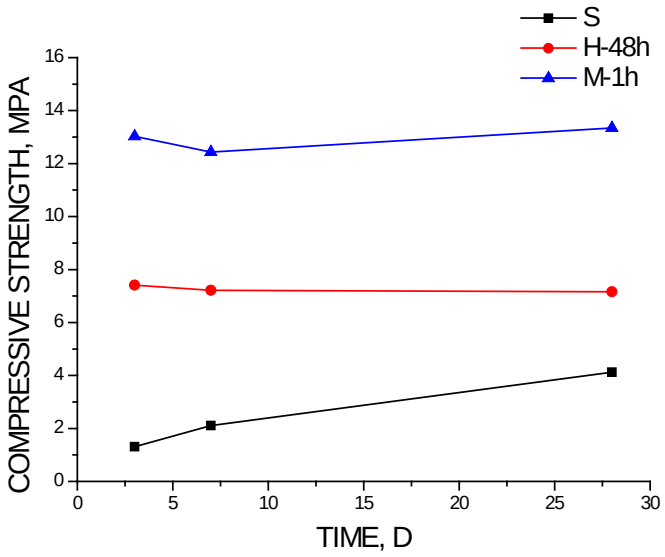


Figure 1 Effect of curing method on compressive strength

## XRD results

Figure 2 presents the XRD spectra of the raw FA and AAFA pastes at curing age of 3 days through three kinds of curing methods. It displayed that the raw FA mainly consisted of two crystal phases, quartz and mullite. After the alkali activation under various curing, XRD spectra had little change, especially under standard curing almost coinciding with the raw FA, for that FA was poorly reacted with alkali solution in this situation leading to the lowest compressive strength. And with energy supplied by heat and microwave curing, the diffraction peak corresponding to mullite slightly decreased particularly at 25–27° 2Theta indicated that mullite phase was partly dissolved in AAFA pastes and brought a better development of compressive strength.

Some researches [13,16,28] reported that zeolite-like phases appeared in AAFA after heat curing and microwave curing, however this study did not discover that experimental phenomenon possibly due to the different raw materials or alkali concentration.

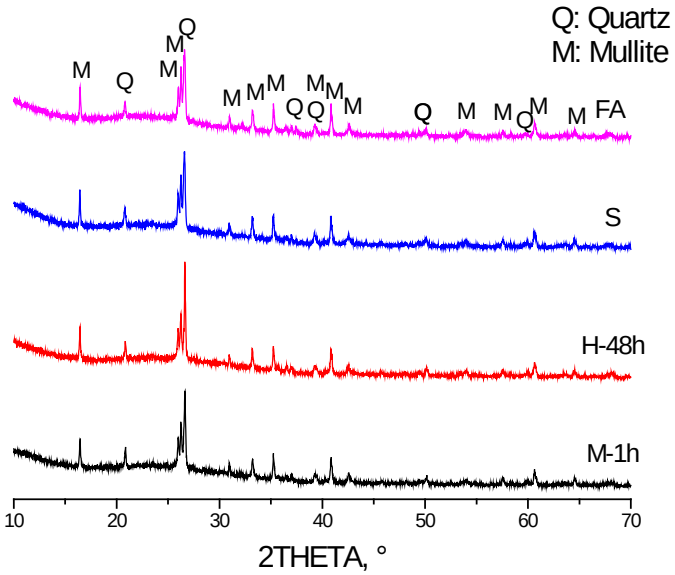


Figure 2 XRD spectra of FA and AAFA at curing age of 3days after various curing methods

## FT-IR results

The FT-IR spectra of the raw FA and three AAFA specimens after various curing are exhibited in Figure 3. The bands at 795 $cm^{-1}$ and 554 $cm^{-1}$ were corresponded to the crystalline phases of quartz and mullite respectively in the raw FA, which showed scare change under diverse curing and were consistent with the XRD results, suggesting that quartz and mullite hardly participated in the reaction of alkali activation. A wide band at 1094 $cm^{-1}$ associated with T-O (T=Al, Si) asymmetric stretching vibrations was observed in the raw FA. This band which had been regarded as the fingerprint of the formation of alkaline aluminosilicate gel [13] in AAFA pastes at curing age of 3 days shifted to lower frequencies at 1079 $cm^{-1}$ for standard curing, 1035 $cm^{-1}$ for heat curing and 1028 $cm^{-1}$ for microwave curing, revealing the process of hydration reaction in AAFA samples and generation of the sodium aluminosilicate gel polymerizing to various extent which was primary hydration product, with the lower frequencies implying the greater polymerization and more orderly molecular arrangement [24]. Therefore it explained why AAFA pastes under thermal curing could get higher compressive strength.

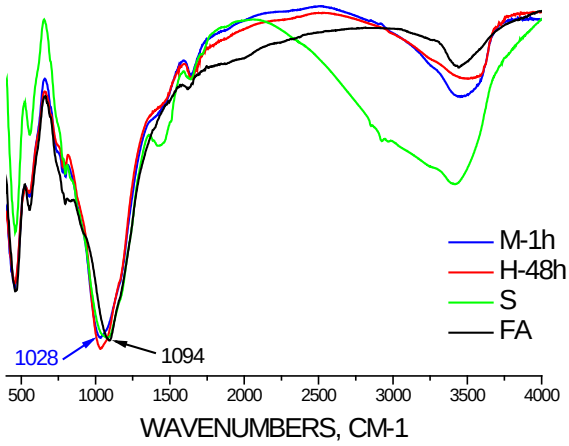


Figure 3 The FT-IR spectra of FA and AAFA at cutting age of 3 days after various curing

**Na-leachability**

Na-leachability test results are displayed in table 2. As results shown in the table, standard curing specimen leached maximum $Na^+$ concentration (1.792 g/L) with accounting for 48.3 percentages to mass $Na^+$ concentration in AAFA pastes at curing age of 3 days. After thermal curing, $Na^+$ leaching concentration remarkably decreased to 1.146 g/L and 0.825 g/L, corresponding to heating curing pastes and microwave curing pastes respectively, with occupying 30.9 percentages and 22.2 percentages to mass.

Some research revealed that the main hydration product of AAFA was a kind of amorphous three-dimension network alkali aluminosilicate (N-A-S-H) gel， with highly crosslinked and disordered pseudo-zeolitic structure [1,30,31]. Due to some $Si^{4+}$ was replaced by $Al^{3+}$ in the N-A-S-H structure, $Na^+$ weakly bond around $Al^{3+}$ to balance electron valence state [32]. So the reduction of $Na^+$ leaching concentration implicated that the more hydration products were formed in the AAFA pastes or some amorphous formative N-A-S-H gel converted to crystalline structure with binding $Na^+$ firmly [33]. But from results of XRD and FT-IR, there was no new crystal phase to be detected. Therefore it was considered that AAFA hydration degree was enlarged and more hydration products were formed by thermal curing. This explanation also supported the results of compressive strength.

Table 2 Effect of curing method on Na-leachability

| EFFECT OF CURING METHOD ON NA-LEACHABILITY, 3 days | | |
|---|---|---|
| | $Na^+$ leaching concentration, g/L | Proportion to mass $Na^+$ concentration, % |
| S | 1.792 | 48.3 |
| H-48h | 1.146 | 30.9 |
| M-1h | 0.825 | 22.2 |

### SEM results

Figure 4 shows SEM images of FA and AAFA at curing age of 3 days after various curing. The microstructure of the raw FA shown in Fig 4(a) was composed of nonuniform sizes of sphere. When FA had experienced alkali activation under 3 days standard curing, there were many flocculent and granulated hydration products formed and surrounded around the surface region of FA particles as seen in Fig 4(b). In Fig 4(c), AAFA pastes under heat curing formed continues structure which the hydration products crossed, accumulated and entirely wrapped up the surface area of FA particles. In addition, the more compact and densifying texture with several FA spheres been imbedded was observed in AAFA pastes under microwave curing shown in Fig 4(d). Overall, the distinct microstructure crucially effected and decided macro-properties of AAFA pastes, and more compact microstructure which corroborated to the results obtained by compressive strength test implied better macro-properties.

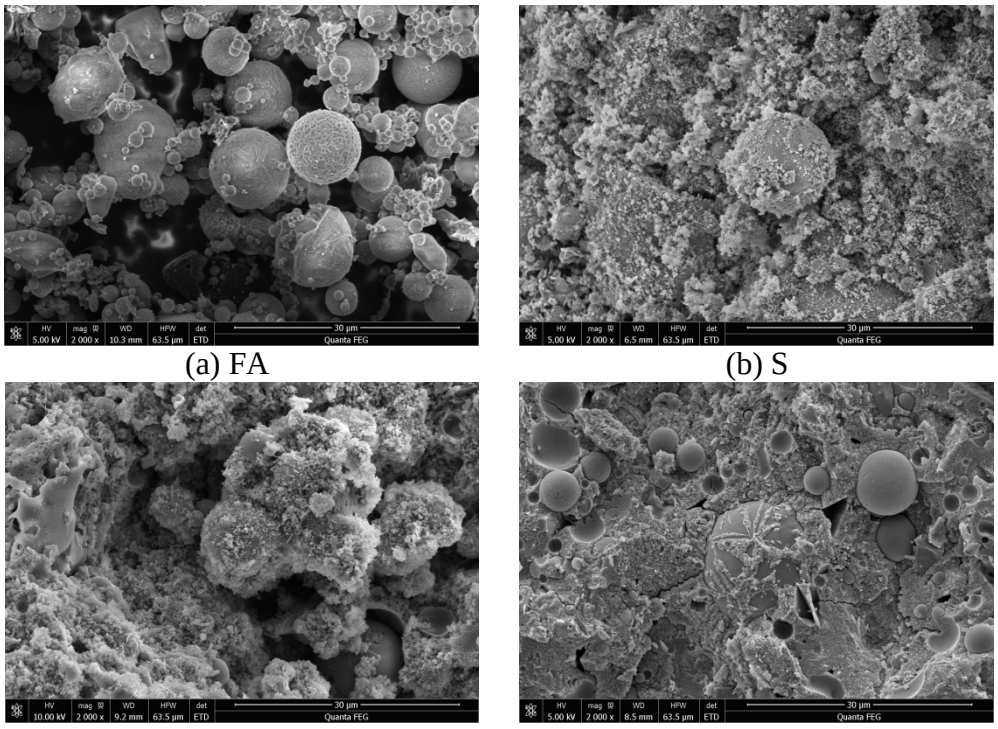

(a) FA (b) S

(c) H-48h (d) M-1h

Figure 4 SEM images of FA and AAFA at cutting age of 3 days after various curing

## CONCLUSIONS

This study focused mainly on the compressive strength development, composition, Na-leachability, and microstructure of AAFA pastes through various curing methods. The following conclusions, pertaining to the range of parameters considered, were drawn from this study. As curing time went on, the compressive strength of AAFA pastes maintained slight change by heat and microwave curing methods, while AAFA samples with standard curing kept sustaining increase. It was found that 1 hour of microwave curing AAFA samples resulted in compressive strength were higher than those heat cured at 90 °C for 48 h, and both these two pastes by thermal curing methods were superior to standard curing samples.

Microwave curing provided volumetric heating and the absence of thermal gradients, as well as potentially microwave energy efficiently assimilated by AAFA pastes, resulted in better compressive strengths. In addition, supplying extra energy was very essential to the development of compressive strength.

The XRD and FT-IR results demonstrated that there were no new crystalline hydration products generated in AAFA pastes undergoing the three kinds of curing methods. Furthermore, the FT-IR test displayed that the thermal cured AAFA samples obtained higher degree of polymerization of sodium aluminosilicate gel which was the prime reaction product, and microwave cured samples get highest polymerization degree. According to Na-leachability test, AAFA pastes under thermal curing leached lower $Na^+$ concentration, implying superior hydration degree and more hydration products formed, and AAFA pastes under microwave curing leached lowest $Na^+$ concentration. Thermal cured AAFA pastes showed more compact microstructure observed in SEM images and microwave cured AAFA pastes also possessed the most compact microstructure. In general, thermal curing methods highly improved the hydration degree of AAFA pastes and formed a densifying microstructure. Compared to heat curing method, microwave curing method was a better thermal curing method for AAFA pastes.

## REFERENCES

1. PROVIS JOHN L. AND BERNAL, SUSAN A. Geopolymers and Related Alkali-Activated Materials. Annual Review of Materials Research. 2014; 44:299–327.

2. MALHOTRA VM, METHA PK. High performance, high volume fly ash concrete. Supplementary cementing materials for sustainable development. 2nd ed. Ottawa: ONT; 2005.

3. GARTNER E. Industrially interesting approaches to low-$CO_2$ cements. Cement and Concrete Research, 2004; 34: 1489–98.

4. SCRIVENER KL, KIRKPATRICK RJ. Innovation in use and research on cementitious material. In: 12th International congress of chemistry of cement, Montreal, Canada; 2007.

5. GARTNER E. Industrially interesting approaches to "low-$CO_2$" cements. Cement and Concrete Research, 2004; 34:1489–98.

6. RASHAD ALAA M, ZEEDAN SAYIEDA R. The effect of activator concentration on the residual strength of alkali-activated fly ash pastess subjected to thermal load. Construction and Build Material, 2011; 25: 3098–107.

7. PARK SANG-SOOK, KANG HWA-YOUNG. Characterization of fly ash-pastess synthesized at different activator conditions. Korean J Chem Eng 2008; 25(1):78–83.

8. TAYLOR M, TAM C, GIELEN D. Energy efficiency and $CO_2$ emissions from the global cement industry. Presented at Workshop, Energy Efficiency and $CO_2$ Emission Reduction Potentials and Policies, Int. Energy Agency, Paris, 2006, Sept. 4–5.

9. PROVIS JL, VAN DEVENTER JSJ, eds. Alkali-Activated Materials: State-of-the-Art Report, RILEM TC 224-AAM. Dordrecht, 2014, Neth.: RILEM/Springer.

10. DUXSON P, PROVIS JL. Designing precursors for geopolymer cements. J Am Ceram Soc. 2008; 91(12):3864–3869.

11. PROVIS JL, VAN DEVENTER JSJ, eds. Alkali-activated materials: State-of-the-Art Report, RILEM TC 224-AAM. Springer/RILEM, Berlin, 2013.

12. PROVIS JL. Activating solution chemistry for geopolymers. In: Provis JL, van Deventer JSJ (eds) Geopolymers: structure, processing, properties and industrial applications. Woodhead, Cambridge, 2009, pp 50–71.

13. SHI, S. BAI, Y. eds. Comparative Study of Alkali-Activated Fly Ash Manufactured Under Pulsed Microwave Curing and Thermal Oven Curing. 4th International Conference on the Durability of Concrete Structures, Purdue University, West Lafayette, Indiana, USA, 2014.

14. DURÁN-HERRERA, A., JUÁREZ, C. A., VALDEZ, P., & BENTZ, D. P. Evaluation of sustainable high-volume fly ash concretes. Cement and Concrete Composites, 2011; 33, 39–45.

15. FELEKOGLU, B. Utilisation of Turkish fly ashes in cost effective HVFA concrete production. Fuel, 2006; 85, 1944–1949.

16. BAKHAREV, T. Geopolymeric materials prepared using Class F fly ash and elevated temperature curing. Cement and Concrete Research, 2005b; 35, 1224–1232.

17. PALOMO, A., GRUTZECK, M. W., & BLANCO, M. T. Alkali-activated fly ashes - A cement for the future. Cement and Concrete Research, 1999; 29, 1323–1329.

18. MIRANDA, J. M., FERNANDEZ-JIMENEZ, A., GONZÁLEZ, J. A., & PALOMO, A. Corrosion resistance in activated fly ash mortars. Cement and Concrete Research, 2005; 35, 1210–1217.

19. FERNANDEZ-JIMENEZ, A., PALOMO, A., & CRIADO, M. Microstructure development of alkali-activated fly ash cement: A descriptive model. Cement and Concrete Research, 2005; 35, 1204–1209.

20. BAKHAREV, T. Durability of geopolymer materials in sodium and magnesium sulfate solutions. Cement and Concrete Research, 2005a; 35, 1233–1246.

21. FERNANDEZ-JIMENEZ, A., GARCÍA-LODEIRO, I., & PALOMO, A. Durability of alkali-activated fly ash cementitious materials. Journal of Materials Science, 2006; 42, 3055–3065.

22. PUERTAS, F., AMAT, T., FERNANDEZ-JIMENEZ, A. & VAZQUEZ, T. Mechanical and durable behaviour of alkaline cement mortars reinforced with polypropylene fibres. Cement and Concrete Research, 2003; 33, 2031-2036.

23. KATZ, A. Microscopic study of alkali-activated fly ash. Cement and Concrete Research, 1998; 28, 197–208.

24. CRIADO, M., FERNANDEZ-JIMENEZ, A., & PALOMO, A. Alkali activation of fly ash: Effect of the $SiO_2/Na_2O$ ratio Part I: FTIR study. Microporous and Mesoporous Materials, 2007b; 106, 180–191.

25. S. DAS, A.K. MUKHOPADHYAY, S. DATTA, D. BASU, Prospects of microwave processing: an overview, Bulletin of Material Science, 2009; 32, 1–13.

26. D.K. AGRAWAL, Microwave processing of ceramics, Current Opinion in Solid State and Materials Science, 1998; 3, 480–485.

27. THOSTENSON, E.T. CHOU, T.-W. Microwave processing: fundamental and applications, Composites: Part A, 1999; 30, 1055–1071.

28. SOMARATNA, J., RAVIKUMAR, D. & NEITHALATH, N. Response of alkali activated fly ash mortars to microwave curing. Cement and Concrete Research, 2010;40, 1688–1696.

29. XIE, Z. XI, Y. Hardening mechanisms of an alkaline activated class F fly ash. Cement and Concrete Research, 2001; 31:1245–1249.

30. PROVIS, J.L. VAN DEVENTER J.S.J. (Eds.), Alkali-Activated Materials: State-of-the-Art Report, RILEM TC 224-AAM, Springer/RILEM, Dordrecht, 2014.

31. PROVIS, J.L. LUKEY, G.C. VAN DEVENTER, J.S.J. Do geopolymers actually contain nanocrystalline zeolites? — A reexamination of existing results, Chem. Mater. 2005; 17:3075–3085.

32. SZKLORZOVÁ H, BÍLEK V. Influence of alkali ions in the activator on the performance of alkali-activated mortars. In: Bílek V, Keršner Z, editors. 3rd International symposium on non-traditional cement and concrete. Czech Republic: Brno; 2008. p. 777–84.

33. ZHANG Z, PROVIS JL, REID A, WANG H. Fly ash-based geopolymers: the relationship between composition, pore structure and efflorescence. Cement and Concrete Research, 2014; 64:30–41.

# REDUCING THE ENVIRONMENTAL IMPACT OF ALKALI-ACTIVATED CONCRETES

**M Kovtun**
University of Pretoria
South Africa

**ABSTRACT.** Alkali-activated concretes are considered as a low carbon alternative to Portland cement concretes. Technical grade chemicals are normally used to activate a precursor to produce alkali-activated concretes. These chemicals are responsible for the major part of mix cost and greenhouse gas emissions associated with alkali-activated concretes. Industrial alkaline wastes can be used in production of alkali-activated concretes to decrease the cost and greenhouse gas emissions. In this paper, industrial alkaline brine was used to activate granulated blast furnace and Corex slags, producing alkali-activated slag concretes with compressive strength up to 56 MPa at 28 days. Basic estimation showed that up to 20% reduction in greenhouse gas emissions was achieved by using the industrial alkaline brine instead of technical grade sodium carbonate solution. The cost was reduced on 11-17%.

**Keywords:** GBFS, Corex slag, Alkali-activated concrete, Greenhouse gas emissions, Waste utilization.

**Doctor M Kovtun** is the researcher of the Civil Engineering Department at the University of Pretoria. His current research focus is alkali-activated materials.

## INTRODUCTION

Concrete is the most commonly used construction material. Ordinary Portland Cement (OPC) is normally used as the binder in concretes. About 0.85 tonne of $CO_2$ is released during the production of one tonne of OPC [1]. Taking into account current consumption of concrete across the globe, OPC production is one of the major industrial activities, contributing considerably to greenhouse gas emissions. Annually, the production of OPC contributes approximately 5-7% of $CO_2$ equivalent ($CO_2$-e) emissions [2, 3], which can increase to nearly 10% of total anthropogenic $CO_2$-e emissions in the near future due to a world-wide increase in the demand for OPC [4].

Significant efforts are being made in cement industry to reduce $CO_2$-e emissions. Blended cements, comprising of OPC and supplementary cementitious materials (e.g., granulated blast furnace slag (GBFS), fly ash etc.), can reduce $CO_2$-e emissions by 13-22%, depending on local conditions [5]. Alkali-activated materials (AAM) have been considered as a promising low $CO_2$ alternative to OPC [6]. Several studies were done on the estimation of environmental impact of AAM [4, 6-10]. $CO_2$-e emissions associated with AAM can be 44-64% lower in comparison to OPC [8]. However, the environmental impact of AAM strongly depends on many factors, like transportation, utilisation of specific raw materials, mix design and the actual production in a given location [7, 8, 11]. Most of the studies show that the activators used in AAM contribute the most to the $CO_2$-e emissions and cost, which means that AAM mixes must be designed carefully, aiming for a minimal activator content [4, 6-8, 10, 11].

The objective of this study was to investigate if an industrial alkaline waste can be used for AAM production instead of technical grade chemicals, providing satisfactory strength and reduction in cost and $CO_2$-e emissions of AAM.

## MATERIALS AND METHODS

### Materials

Granulated blast furnace slag and Corex slag were used as the binders in this study. The specific density of the GBFS and Corex slag was 2900 kg/m$^3$ and 3000 kg/m$^3$ respectively. The chemical compositions of the GBFS and Corex slag are given in Table 1.

Table 1 Chemical composition of binders

| CHEMICAL COMPOSITION OF BINDERS (%) | | | | | | | | | | | |
|---|---|---|---|---|---|---|---|---|---|---|---|
| Slag | $SiO_2$ | $TiO_2$ | $Al_2O_3$ | $Fe_2O_3$ | MgO | CaO | $Na_2O$ | $K_2O$ | $SO_3$ | other | LOI |
| GBFS | 35.36 | 1.13 | 12.74 | 0.80 | 8.46 | 33.25 | 0.38 | 1.74 | 2.80 | 1.61 | 1.73 |
| Corex | 30.96 | 0.51 | 13.92 | 1.52 | 11.06 | 37.72 | 0.17 | 0.81 | 2.09 | 1.91 | -0.67 |

The binders were activated by sodium carbonate solutions and industrial alkaline brine. Technical grade sodium carbonate in the form of powder with 98% purity was used to prepare the activator solutions. The industrial alkaline brine had a specific density of 1025 kg/m$^3$. The chemical composition of dry residue of the industrial alkaline brine is presented in Table 2. Mineralogical composition of the dry residue is mostly represented by thermonatrite (≈68%) and trona (≈32%).

Table 2 Chemical composition of dry residue

| CHEMICAL COMPOSITION OF DRY RESIDUE (%) | | | | |
|---|---|---|---|---|
| $Na_2O$ | $SO_3$ | Cl | other | LOI |
| 44.20 | 0.04 | 0.03 | 0.03 | 55.70 |

Crushed dolomite stone with a maximum size of 9.5 mm was used as the coarse aggregate. The fine aggregate was crushed dolomite sand with a fineness modulus of 3.86 and 9% passing the 75 μm sieve. The specific gravity of the aggregates was 2860 kg/m$^3$.

**Mix Designs and Curing Procedure**

Slag content of 500 kg/m$^3$ was used to produce alkali-activated slag (AAS) concretes [12]. The alkaline solution-to-binder ratio was kept constant at 0.36 *l*/kg for all mixes. The amount of sodium carbonate varied from 29.3 kg/m$^3$ to 37.9 kg/m$^3$ to produce alkaline solutions with different concentration. The industrial alkaline brine was beneficiated by evaporation to increase the alkali concentration. The brine was evaporated to specific densities of 1150 kg/m$^3$ and 1210 kg/m$^3$. Fine-to-total aggregate ratio was fixed at 0.35 by mass. Final mix designs are given in Table 3.

Table 3 Mix designs

| MIX DESIGNS (kg/m$^3$) | | | | | | | |
|---|---|---|---|---|---|---|---|
| Mix | Binder | | Activator | | Water | Fine aggregate | Coarse aggregate |
| | GBFS | Corex slag | $Na_2CO_3$ | Brine | | | |
| G1 | 500 | | 29.7 | | 177.3 | 648 | 1204 |
| G2 | 500 | | 33.8 | | 176.8 | 648 | 1204 |
| G3 | 500 | | 37.9 | | 176.3 | 648 | 1204 |
| C1 | | 500 | 29.7 | | 177.3 | 654 | 1215 |
| C2 | | 500 | 33.8 | | 176.8 | 654 | 1215 |
| C3 | | 500 | 37.9 | | 176.3 | 654 | 1215 |
| GW1 | 500 | | | 184.5 | | 648 | 1204 |
| GW2 | 500 | | | 207.0 | | 648 | 1204 |
| GW3 | 500 | | | 217.8 | | 648 | 1204 |
| CW1 | | 500 | | 184.5 | | 654 | 1215 |
| CW2 | | 500 | | 207.0 | | 654 | 1215 |
| CW3 | | 500 | | 217.8 | | 654 | 1215 |

Concrete mixes were prepared in a pan mixer and cast in 100 mm cubic moulds. All mixes were precured for 2 h at 25 °C. After the precuring, moulds were placed into a steam bath and heated up to 80 °C at 15 °C/h. The duration of the heating phase and isothermal curing was 16 hours. Samples were demoulded immediately after the steam curing without a gradual cooling phase and kept in a room at a temperature of 25±2 °C and 55±5% relative humidity till testing.

### Cost and $CO_2$-e Emissions

Prices used in estimation of mix cost, are given in Table 4. It is important to note that the prices are listed for Gauteng province as of September 2015, and they serve as an indication, as actual prices will depend on many factors (e.g., volume of purchase, special agreements with producer, type of aggregates used, transportation costs etc.). Handling cost was included in the industrial alkaline brine price.

Table 4 Prices

| PRICES ($/t) | | | | | | |
|---|---|---|---|---|---|---|
| GBFS | Corex slag | $Na_2CO_3$ | Brine | Water | Dolomite stone | Dolomite sand |
| 75 | 115 | 390 | 5 | 2 | 17 | 17 |

Calculations of greenhouse gas emissions are limited to emissions associated with concrete mix components [8, 10, 13] and the steam curing [9], which are presented in Table 5. Effect of transportation of concrete components and final concrete products, which can be a significant $CO_2$-e contributor [8], was not considered in this study.

Table 5 Greenhouse gas emissions

| GREENHOUSE GAS EMISSIONS (kg $CO_2$-e/kg) | | | | | | | |
|---|---|---|---|---|---|---|---|
| GBFS | Corex slag | $Na_2CO_3$ | Brine | Water | Stone | Sand | Steam curing[a] |
| $2.65 \cdot 10^{-2}$ | $2.65 \cdot 10^{-2}$ | $4.15 \cdot 10^{-1}$ | 0 | $1.96 \cdot 10^{-4}$ | $7.5 \cdot 10^{-3}$ | $2.6 \cdot 10^{-3}$ | $3.997 \cdot 10$ |

[a] – kg $CO_2$-e/$m^3$ of concrete [9]

It should be noted that transportation mode and distances will significantly affect the prices and, as mentioned earlier, $CO_2$-e emissions [8]. Thus, accurate calculations shall be done in each specific case, and the results of this study only serves to show potential benefits of using local industrial alkaline brine in production of AAM.

## RESULTS AND DISCUSSION

### Compressive Strength

Compressive strength of AAS concretes activated by technical grade sodium carbonate solutions is presented in Figure 1. As expected, an increase in concentration of sodium carbonate solution increases compressive strength of the AAS concretes at all ages. The compressive strength of the AAS concretes containing Corex slag increased by 18% (compare C3 to C1 mix, Figure 1), while the compressive strength of the AAS concretes containing GBFS increased by only 11% (compare G3 to G1 mix, Figure 1), when the concentration of the sodium carbonate solution was increased. It is important to note that Corex slag gives significantly lower compressive strength in comparison to GBFS despite the fact that Corex slag is a higher quality slag (the basicity, activity and quality coefficients of Corex slag are higher than the coefficients of GBFS) [14].

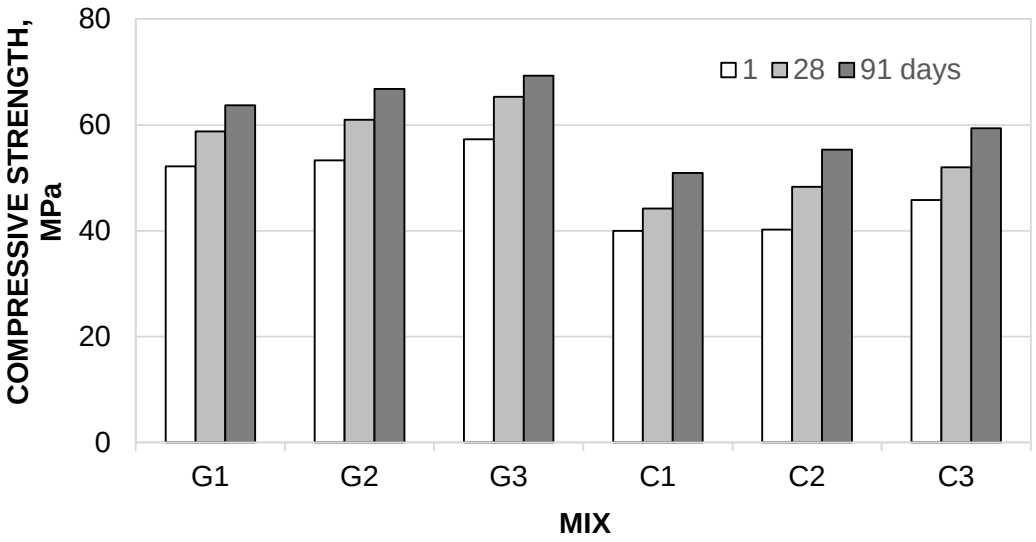


Figure 1 Strength development of AAS concretes activated with sodium carbonate solutions

Compressive strength development of AAS concretes activated with the industrial alkaline solution is shown in Figure 2.

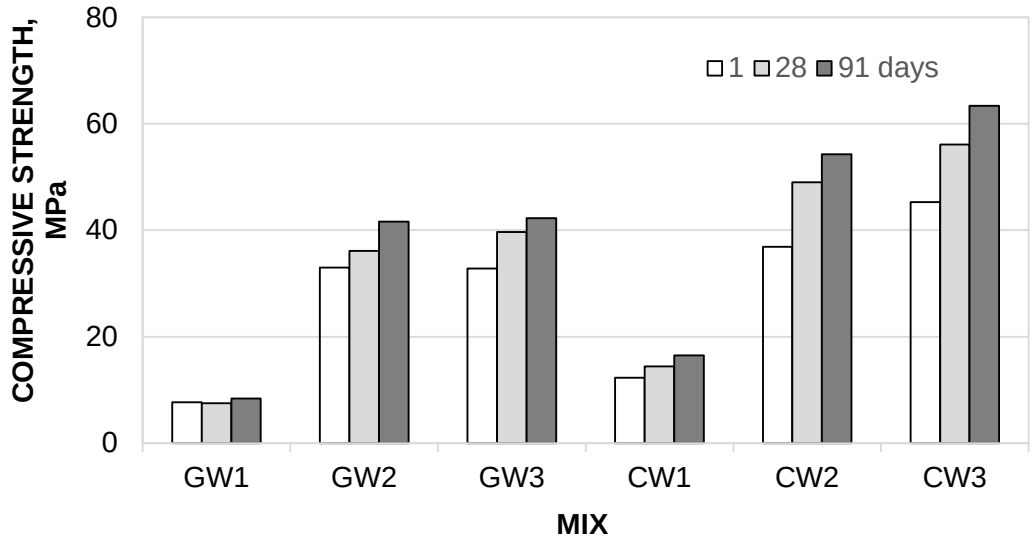


Figure 2 Strength development of AAS concretes activated with the industrial alkaline brine

It can be seen that beneficiation of the brine by evaporation significantly improve compressive strength development of the AAS concretes, regardless of slag type used. Compressive strength of GBFS and Corex slag concretes increased at 28 days from 7.5 to 39.7 MPa and from 14.4 to 56.1 MPa respectively. Important to note that the AAS concretes containing Corex slag developed higher compressive strength in comparison to the GBFS concretes, exceeding the strength of the Corex AAS concretes activated with technical grade sodium carbonate solution (Figure 1). The results show that industrial alkaline wastes can be used for activation of AAS concretes, providing comparable or even exceeding compressive strength when compared to AAS concretes activated with technical grade chemical solutions.

## Basic Estimation of the Cost and $CO_2$-e Emissions

Estimation of the cost and $CO_2$-e emissions of the AAS concretes is shown in Table 6. $CO_2$-e emissions of the studied AAS concretes are considerably lower in comparison to the values for AAM available in scientific literature [7-10]. It should be emphasised that transportation was not considered in this study, which can contribute significantly to $CO_2$-e emissions [8].

The low $CO_2$-e emissions are also caused by the use of sodium carbonate (G1-G3, C1-C3 mixes, Table 6) which has significantly lower environmental effects than sodium hydroxide and sodium silicate frequently used in production of AAM [4, 7, 8, 13]. Utilization of the industrial alkaline brine makes the $CO_2$-e emissions even lower, decreasing the environmental impact of the AAS concretes by 16-20% (GW1-GW3, CW1-CW3 mixes, Table 6).

Cost of the AAS concretes decreases up to 17% when the technical grade sodium carbonate solutions are replaced by the industrial alkaline brine. However, location of AAS concrete production in relation to the industrial alkaline brine source will significantly influence the costs. Thus, the results indicate the possibility of cost reduction but careful cost estimation should be done for each specific project.

Table 6 Cost and $CO_2$-e emissions of AAS concretes

| COST AND $CO_2$-e EMISSIONS OF AAS CONCRETES | | | | |
|---|---|---|---|---|
| Mix | Cost ($/m$^3$) | Cost/$f_c$[a] ($/m$^3$/MPa) | $CO_2$-e (kg/m$^3$) | $CO_2$-e/$f_c$[a] (kg/m$^3$/MPa) |
| G1 | 80.92 | 1.38 | 76.30 | 1.30 |
| G2 | 82.52 | 1.35 | 78.00 | 1.28 |
| G3 | 84.12 | 1.29 | 79.70 | 1.22 |
| C1 | 101.21 | 2.29 | 76.39 | 1.73 |
| C2 | 102.81 | 2.13 | 78.09 | 1.62 |
| C3 | 104.41 | 2.01 | 79.80 | 1.53 |
| GW1 | 69.91 | 9.32 | 63.93 | 8.52 |
| GW2 | 70.02 | 1.94 | 63.93 | 1.77 |
| GW3 | 70.07 | 1.77 | 63.93 | 1.61 |
| CW1 | 90.20 | 6.26 | 64.03 | 4.45 |
| CW2 | 90.31 | 1.84 | 64.03 | 1.31 |
| CW3 | 90.36 | 1.61 | 64.03 | 1.14 |

[a] – compressive strength of the mix at 28 days.

Table 6 also contains cost and $CO_2$-e emission values normalized to compressive strength of the AAS concretes. It is interesting to note that only two mixes containing Corex slag (CW2 and CW3, Table 6) show better performance in cost and $CO_2$-e emissions in comparison to mixes activated with technical grade sodium carbonate solution (C2 and C3 mixes, Table 6) when the results are normalized to the strength.

## CONCLUSIONS

The results of the study show that industrial alkaline wastes can be successfully used in production of alkali-activated slag concretes. Depending on slag chemistry, alkaline wastes can provide better strength development in comparison to technical grade chemical solution, whilst providing considerable savings in cost and $CO_2$-e emissions. However, cost and $CO_2$-e emissions due to transportation of raw materials and concrete products should be considered in each specific project. Utilization of hazardous alkaline wastes in production of alkali-activated materials should be included in an estimation of the environmental impact.

## ACKNOWLEDGEMENTS

This work is based on the research supported by The National Research Foundation.

## REFERENCES

1. VAN OSS, H G, PADOVANI, A C. Cement manufacture and the environment, Part II: Environmental challenges and opportunities, Journal of Industrial Ecology, Vol. 7, No. 1, 2003, pp 93-126.

2. ALLWOOD, J M, CULLEN, J M, MILFORD, R L. Options for achieving a 50% cut in industrial carbon emissions by 2050, Environmental Science and Technology, Vol. 44, No. 6, 2010, pp 1888-1894.

3. FRIEDLINGSTEIN, P, HOUGHTON, R A, MARLAND, G, HACKLER, J, BODEN, T A, CONWAY, T J, CANADELL, J G, RAUPACH, M R, CIAIS, P, LE QUÉRÉ, C. Update on $CO_2$ emissions, Nature Geoscience, Vol. 3, No. 12, 2010, pp 811-812.

4. HABERT, G, D'ESPINOSE DE LACAILLERIE, J B, ROUSSEL, N. An environmental evaluation of geopolymer based concrete production: reviewing current research trends, Journal of Cleaner Production, Vol. 19, No. 11, 2011, pp 1229-1238.

5. FLOWER, D J M, SANJAYAN, J G. Green house gas emissions due to concrete manufacture, The International Journal of Life Cycle Assessment, Vol. 12, No. 5, 2007, pp 282-288.

6. DUXSON, P, PROVIS, J L, LUKEY, G C, VAN DEVENTER, J S J. The role of inorganic polymer technology in the development of 'green concrete', Cement and Concrete Research, Vol. 37, No. 12, 2007, pp 1590-1597.

7. HEATH, A, PAINE, K, MCMANUS, M. Minimising the global warming potential of clay based geopolymers, Journal of Cleaner Production, Vol. 78, 1 September, 2014, pp 75-83.

8. MCLELLAN, B C, WILLIAMS, R P, LAY, J, VAN RIESSEN, A, CORDER, G D. Costs and carbon emissions for geopolymer pastes in comparison to ordinary portland cement, Journal of Cleaner Production, Vol. 19, No. 9-10, 2011, pp 1080-1090.

9. TURNER, L K, COLLINS, F G. Carbon dioxide equivalent ($CO_2$-e) emissions: A comparison between geopolymer and OPC cement concrete, Construction and Building Materials, Vol. 43, June, 2013, pp 125-130.

10. YANG, K-H, SONG, J-K, SONG, K-I. Assessment of $CO_2$ reduction of alkali-activated concrete, Journal of Cleaner Production, Vol. 39, January, 2013, pp 265-272.

11. PROVIS, J L, PALOMO, A, SHI, C. Advances in understanding alkali-activated materials, Cement and Concrete Research, Vol. 78, Part A, 2015, pp 110-125.

12. RAVIKUMAR, D, PEETHAMPARAN, S, NEITHALATH, N. Structure and strength of NaOH activated concretes containing fly ash or GGBFS as the sole binder, Cement and Concrete Composites, Vol. 32, No. 6, 2010, pp 399-410.

13. U.S. ENVIRONMENTAL PROTECTION AGENCY. Inventory of U.S. Greenhouse Gas Emissions and Sinks: 1990-2013. Annual Report, 2015.

14. KOVTUN, M N, KEARSLEY, E P, SHEKHOVTSOVA, J A. Producing alkali-activated concrete in South Africa, Cement Combinations and Durable Concrete, Proceedings of UKIERI Concrete Congress: Innovations in Concrete Construction, Jalandhar, India, 2013, pp 919-928.

# banahCEM – COMPARISON OF PROPERTIES OF A LATERITE-BASED GEOPOLYMER WITH CONVENTIONAL CONCRETE

**J Kwasny** **M Soutsos**
**D J Cleland**
Queen's University Belfast
**J A McIntosh**
banah UK Ltd
United Kingdom

**ABSTRACT.** This paper presents the overview of a project, as well as selected results from the experimental work aimed at direct comparison of the physical and durability properties of room temperature cured geopolymer and Portland cement concretes (GPCs and PCCs, respectively). Geopolymer binder was formed by reacting low purity geologically-originated lateritic clay, banahCEM(a), with an alkali silicate activator, banahCEM(b). Economical and "industry friendly" mix design of GPCs was developed to satisfy common medium and high strength applications. In order to allow a like-for-like comparison, both GPCs and PCCs were proportioned with equivalent paste volume and characteristic compressive strength. It was found that in the first 24 hours after mixing the GPCs achieved 55–75% of their 28-day strength, while equivalent PCCs gained 37–43%. Selected durability properties of developed geopolymer mortars, such as acid (solutions of $H_2SO_4$ and HCl) and sulfate (solutions of $Na_2SO_4$ and $MgSO_4$) resistance have been found to be better than those of Portland cement systems. Room temperature curing and reported engineering properties make this geopolymer binder most suitable for harsh environment applications, where rapid strength gain is of essence, *e.g.* repair applications, pre-cast industry (fast mould turnover), tunnel or mine linings.

**Keywords:** Acid attack, Geopolymer concrete and mortars, Setting time, Strength development, Sulfate attack.

**Dr Jacek Kwasny** is a research fellow in the School of Planning, Architecture and Civil Engineering at Queen's University, Belfast.

**Professor Marios Soutsos** is Professor at the School of Planning, Architecture and Civil Engineering at Queen's University, Belfast.

**Mr John A McIntosh** is the Director of Research for banah UK Ltd, based in Coleraine, Northern Ireland and is currently undertaking PhD research with Queen's University, Belfast.

**Professor David Cleland** is Professor of Civil Engineering at Queen's University, Belfast. David Cleland is a Civil Engineer with research interests in the behaviour of reinforced concrete structures and the durability of concrete.

## INTRODUCTION

Geopolymer-based concretes are a novel class of construction materials, where the cementitious binder is replaced with typically low carbon geopolymer alternatives. Geopolymer binders are produced by reacting an alumino-silicate precursor (often a waste or a by-product material) with an alkali-silicate solution, also called chemical activator [1]. An inorganic polymerisation reaction results in the formation of hardened material with three dimensional amorphous microstructure. Thanks to unique, ceramic-like microstructure, geopolymer-based materials have been reported to have potentially superior/equivalent physical and durability properties when compared to conventional materials made with Portland cement [2]. However, where the concrete/construction industry is concerned, the geopolymer concrete still has to be proven to be more user-friendly and cost-efficient, and comply with specific engineering properties in order to gain more popularity.

Recognising the benefits of geopolymer binders, a Northern Irish company banah UK Ltd, which was established in 2008, undertook a challenge to develop and commercialise such a binder for the UK market. Development of a novel, low-carbon geopolymer binder system, called banahCEM, was the result of an intensive five-year R&D programme undertaken by the company. As shown in Figure 1, this binder consists of two components: a powder precursor – banahCEM(a) and a chemical activator – banahCEM(b), and by mixing with water and aggregates, it can be used to produce concretes and mortars. The powder precursor is based on an aluminosilicate, namely altered basalt (lithomarge) sourced from the Interbasaltic Formation of the Antrim Lava Group (Northern Ireland) [3,4]. The precursor is manufactured by lithomarge calcination at *ca.* 750 °C, followed by grinding. The chemical activator is an aqueous solution of alkali silicate.

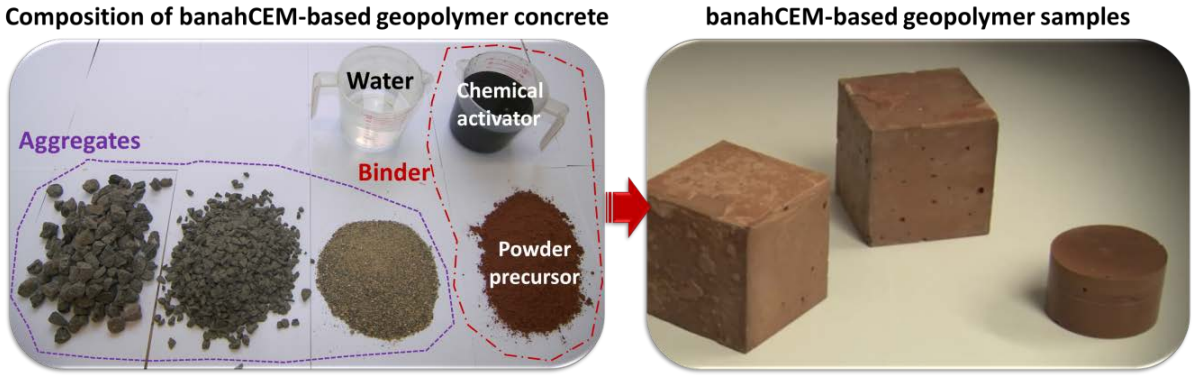


Figure 1 Materials required for banahCEM geopolymer concretes and mortars

In order to commercialise the product, the initial effort led to a three-year R&D Invest Northern Ireland funded project, which started in February 2014, involving banah UK Ltd and Queen's University Belfast. The aim of this ongoing project is to provide strong proof to designers, specifiers, clients and developers, *via* extensive testing programme, that the novel geopolymer-based binder system (banahCEM) can be produced and placed with similar ease as Portland cement concretes (PCCs) and mortars (PCMs). Concrete mix designs and quality control systems are being developed to assist in the larger scale production of the binder and commercialisation of the banahCEM-based geopolymer concretes (GPCs) and mortars (GPMs) for a range of products (Phase 1a). Low energy GPC and GPM mixes are being optimised to investigate the practicalities of producing mixes similar to those currently used in construction, *i.e.* having characteristic compressive strengths of 37.5 and 60 MPa

(Phase 1b). These mixes are being comprehensively tested to provide reassurance that the new binder will have fresh, mechanical and durability properties at least as good, if not better, than those of Portland cement.

Specifically, this is being achieved by checking whether design strength of geopolymer mixes can be obtained whilst having acceptable fresh and early age properties, *i.e.* workability and setting time, required for casting structural elements (Phase 2). In addition to ease of placement, values of structural properties such as strength in compression and tension, thermal expansion, modulus of elasticity, creep, shrinkage, permeability and fire resistance of these new concretes and mortars are being measured (Phase 3). The durability of these new systems is being evaluated by testing their resistance to freeze-thaw action, acid attack, sulfate attack and alkali-silica reaction (Phase 4). Moreover, chloride ion ingress and corrosion of reinforcement steel is being tested to evaluate the protective properties of banahCEM-based materials.

Finally, conventional PCC and PCM mixes, with the same paste content and characteristic strength as corresponding geopolymer mixes, are being designed and tested using the same experimental programme as outlined above. This allows for a like-for-like comparison of banahCEM and Portland cement systems.

This paper presents results obtained from the ongoing research project. Objectives of this part of work were to characterise the materials used in this research, and to study the strength development, setting time, as well as selected durability properties, *i.e.* resistance to acid and sulfate attack, of nominated geopolymer mixes. The results were benchmarked against analogous cement mixes.

## EXPERIMENTAL PROGRAMME

### Materials

Geopolymer binder was based on a two component system produced by banah UK Ltd: banahCEM(a), being the powder component, and banahCEM(b), the liquid component. As described earlier, banahCEM(a) is an aluminosilicate precursor [3,4]. Aqueous solution of alkali silicate with water content of 41.2% was used as a chemical activator. The solution had a specific gravity of 1.57. Portland cement CEM I 42.5N, produced by Quinn Cement in Northern Ireland and conforming to the requirements of BS EN 197-1:2011 [5], was used in conventional cement concretes.

Chemical compositions of banahCEM(a) and Portland cement, determined using X-ray fluorescence spectrometry, are shown in Table 1. A polycarboxylate-based superplasticiser Chemcrete HP3 produced by Larsen Building Products, with specific gravity of 1.1 and solid content of 35%, was added to conventional concretes. Water from the mains supply (17 ±1 °C) was used as the mixing water, throughout.

Table 1 Chemical composition and physical properties of banahCEM(a) and Portland cement

| ELEMENTAL COMPOSITION [%] | banahCEM(a) | PORTLAND CEMENT |
|---|---|---|
| $SiO_2$ | 32.04 | 20.21 |
| $Al_2O_3$ | 24.99 | 4.79 |
| $Fe_2O_3$ | 25.21 | 2.78 |
| CaO | 7.78 | 63.01 |
| MgO | 1.71 | 1.93 |
| MnO | 0.37 | 0.08 |
| $TiO_2$ | 3.17 | 0.27 |
| $Na_2O$ | 0.36 | 0.19 |
| $K_2O$ | 0.15 | 0.59 |
| $SO_3$ | 0.22 | 2.60 |
| $P_2O_5$ | 0.14 | 0.12 |
| LOI [%] | 3.08 | 3.16 |
| Specific gravity [-] | 2.89 | 3.13 |

Three aggregates, *i.e.* 0–5 mm concrete sand, 4–10 mm crushed basalt and 10–20 mm crushed basalt, were sourced in Northern Ireland. The oven-dry particle density and water absorption (tested according to BS 812-2:1995 [6]) of all aggregates are reported in Table 2.

Table 2 Basic physical properties of used aggregates

| AGGREGATE NAME | PARTICLE DENSITY ON THE OVEN-DRY BASIS [kg/m$^3$] | 1-H WATER ABSORPTION [%] | 24-H WATER ABSORPTION [%] |
|---|---|---|---|
| 0–5 mm concrete sand | 2695 | 0.9 | 1.1 |
| 4–10 mm crushed basalt | 2790 | 1.4 | 2.2 |
| 10–20 mm crushed basalt | 2751 | 1.2 | 2.1 |

**Mix Composition**

An extensive experimental programme was undertaken to develop the mix design of banahCEM GPCs and GPMs. Geopolymer mixes were proportioned by varying two of the mix proportion parameters, *viz.* paste volume and water to solid (w/s) ratio. Two GPC mixes, with slump of 50−100 mm (determined according to the procedure described in BS EN 12350-2:2000 [7]) and 28-day specific characteristic compressive strengths ($f_{c,28}$) of 37.5 and 60 MPa (referred to as GPC-37.5 and GPC-60, respectively), were selected for further examination. Their proportions are given in Table 3. For comparison, two cement-based concretes (PCC-37.5 and PCC-60), having the same paste volume, workability and $f_{c,28}$ as the corresponding GPCs, were designed following the BRE mix design guidelines [8] – mix proportions are also given in Table 3. Importantly, a superplasticiser was added to PCC mixes during mixing process to obtain the essential workability.

Table 3 Proportions of geopolymer and Portland cement concrete mixes

| MATERIALS [kg/m$^3$] | MIX CODE | | | |
|---|---|---|---|---|
| | GPC-37.5 | GPC-60 | PCC-37.5 | PCC-60 |
| banahCEM(a) | 265 | 363 | - | - |
| banahCEM(b) | 188 | 258 | - | - |
| Portland cement | - | - | 336 | 468 |
| Superplasticiser | - | - | 1.2 | 0.6 |
| 0–5 mm concrete sand | 794 | 739 | 794 | 739 |
| 4–10 mm crushed basalt | 476 | 443 | 476 | 443 |
| 10–20 mm crushed basalt | 714 | 665 | 714 | 665 |
| Water for aggregate 1h absorption | 23 | 21 | 23 | 21 |
| Total added water | 87 | 57 | 191 | 197 |
| Free water content[kg/m$^3$] | 141 | 142 | 169 | 176 |
| Binder content [kg/m$^3$]* | 376 | 515 | 336 | 468 |
| Total paste content [kg/m$^3$] | 517 | 656 | 503 | 643 |
| Total paste content [L/m$^3$] | 275 | 325 | 275 | 325 |
| w/s ratio [-] | 0.375 | 0.275 | - | - |
| w/c ratio [-] | - | - | 0.502 | 0.376 |

* – for geopolymer mixes it represented banahCEM(a) and solid part of banahCEM(b)

To achieve the required $f_{c,28}$ of 37.5 and 60 MPa, mortar mixes were designed with different w/s ratios for GPMs (0.375 and 0.275, respectively) and w/c ratios for PCMs (0.60 and 0.42, respectively). Paste volume of all mortars was kept constant at 500 L/m$^3$, so the effect of aggregates on the properties of mortars could be ignored.

Variability in concrete and mortar production was also taken into consideration, in accordance with the guidelines of BRE for design of normal concrete mixes [8]. Therefore, concrete and mortar mixes were designed with the 28-day target mean strength ($f_{m,28}$) of 50.6 MPa and 73.1 MPa (margin of 13.1 MPa was added to each $f_{c,28}$).

**Mix Preparation**

To ensure that no other parameters influenced the results, all constituent materials were stored in dry locations at room temperature (20 ±2 °C) prior to batching. Before mixing, all aggregates were oven-dried (at 105 ±5 °C) for more than 48 hours, until a constant mass was reached, subsequently cooled and stored in plastic bags until mixing. All mixes were batched following exactly their pre-determined mix proportions, *i.e.* no additional water (other than what is given in the mix design) was added during mixing to adjust the workability.

The concrete mixes were prepared in a Croker RP50XD, 82 kg capacity rotating pan mixer, in 18 L batches. The mixing procedure consisted of the following steps:

Step 1 − Pre-saturation of aggregates started 30 minutes before the actual concrete mixing (Step 2). Dry aggregates were placed in the mixer's pan with ½ of the total water (free + pre-saturation water) and mixed for 1 minute.

Step 2 – The dry portion of binding material, *i.e.* banahCEM(a) or Portland cement, was introduced into the mixing pan followed by 1 minute of mixing.

Step 3 – The remaining water (free + pre-saturation water) and the chemical activator (in the case of GPCs), or the superplasticizer (in the case of PCCs), were added to the mix. This was followed by 6 minutes of mixing. The beginning of this step is referred to as time zero.

The mortar mixes were made in a Hobart mixer in 3.5 L batches using similar procedure to that described above.

**Sample Casting, Demoulding and Conditioning**

All specimens were cast in two layers. Each layer was compacted on a vibrating table. After casting, the moulds with samples were covered with polythene plastic sheets and placed in the conditioning room (RH > 95% and 20 ±1 °C). Samples were demoulded at 24 ±0.5 hours, counting from the time zero, and placed in plastic boxes on 15 mm plastic supports. Boxes were filled with water to the height of 5 mm, then covered with tightly fitting lids and stored in the conditioning room (20 ±1 °C). This procedure allowed the conditioning of the samples at RH of > 95% and prevented unintentional carbonation of the samples, and leaching of alkalis.

**Test Techniques**

Compressive strength of concrete specimens at given ages (3-hour, 6-hour, 12-hour, 24-hour, 3-day, 7-day, 28-day, 91-day, 182-day and 365-day) was determined by crushing three 100×100×100 mm cubes each time (at a constant loading rate of 200 kN/min). The average of three measurements is reported in MPa.

Initial and final setting times of concretes were determined with penetration resistance method described in ASTM C 403 [9]. A wet-sieve method, using a 5 mm sieve, was used to sieve out coarse portion of aggregates and obtain a mortar sample. Mortar samples were cast in plastic moulds (150 mm size cubes) and compacted. Samples were left in the conditioning room at 20 ±1 °C and between experiments were covered to prevent water evaporation. Penetration resistance results were plotted against time. For each mix, the times of initial and final setting (counting from the time zero) were determined as the times when the penetration resistance equalled 3.5 and 27.6 MPa, respectively. Setting time results are reported in minutes.

Resistance to inorganic sulphuric ($H_2SO_4$) and hydrochloric (HCl) acid attack was tested based on the general guidelines provided in ASTM C 267 [10]. After five weeks of curing, sets of four 50×50×50 mm mortar cubes from each mix were placed in plastic boxes containing acid solutions (20 ±1 °C) with concentrations of 0.10, 0.31 and 0.51 moles of $H_2SO_4$ or HCl per kg of solution. Every 7 days, any loose material was removed from the samples by gentle brushing under a stream of tap water. Subsequently, the mass of each cube was recorded, and they were returned to the boxes holding fresh acid solutions. This procedure was repeated for 8 consecutive weeks. To exemplify acid resistance of tested specimens, the mean cumulative percentage of mass loss (for 4 cubes) during 8 weeks of testing for samples immersed in acid of concentration of 0.51 mol/kg solutions (which corresponds to 5% $H_2SO_4$ and 1.9% HCl by weight of solution) is reported in this paper.

Sulfate attack resistance was tested similarly to the procedure described in ASTM C 1012 [11]. After five weeks of curing, sets of three 25×25×285 mm mortar bars from each mix, equipped with 6 mm stainless steel balls at each end of the bar, were placed vertically in

plastic boxes containing 0.352 moles of $Na_2SO_4$ or $MgSO_4$ per litre of solutions. Samples were kept in the solutions (20 ±1 °C) for 52 weeks during which their length was measured at specific intervals (every week for the duration of the first 4 weeks, then every two weeks for the duration of 8 weeks, and for the remaining 40 weeks they were tested every 4 weeks). During the first 12 weeks of testing, sulfate solutions were renewed every 2 weeks, and every 4 weeks afterwards. The mean length change (for three bars) at week 32 of measurements, given in microstrains, is reported in this paper.

## RESULTS AND DISCUSSION

### Concrete Strength Development

Strength development of GPC and PCC mixes over the period of one year is shown in Figure 2. As designed, all mixes achieved their 28-day target mean strength. As expected, mixes with lower w/s ratio (for GPC) or lower w/c ratio (for PCCs) had higher compressive strength.

In comparison to PCC mixes, GPCs had very high initial strength. At the age of 3 hours, it was possible to demould and test the GPC samples (the 3-hour strength was *ca.* 7.5 MPa for GPC-37.5 and *ca.* 15 MPa for GPC-60), while PCC samples were still soft, as they have not reached their initial setting time yet (see next section). At the age of 24 hours, GPC-37.5 had strength 1.5 times higher than PCC-37.5, while GPC-60 strength was almost double that of PCC-60. Up to the age of 28-days the strength gap between the corresponding GPC and PCC mixes decreased, with clear strength crossover effect, in favour of PCC mixes, at 28 days.

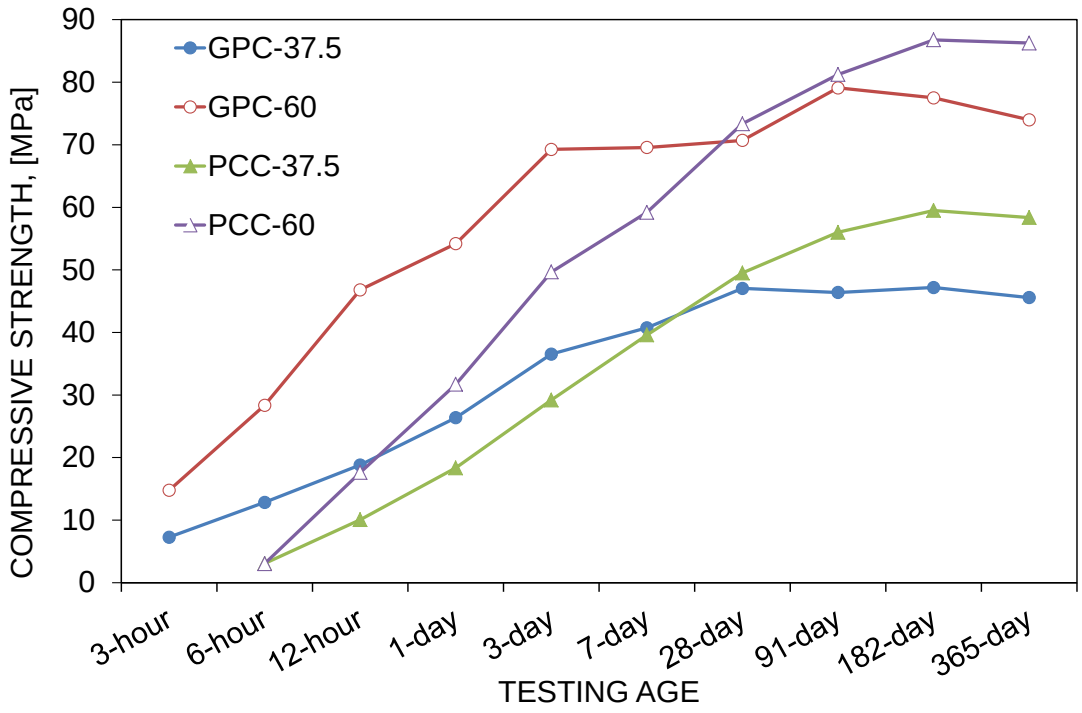


Figure 2 Strength development of geopolymer and Portland cement concretes

The strength gain of GPCs was very rapid up to the age of 3 days. Afterwards, the strength development was relatively slow in comparison to PCCs. Beyond the 28-day mark, there was no noticeable change in the strength of GPC mixes, indicating that the geopolymer reaction was nearly completed at this age. On the other hand, cement hydration continued, resulting in further increase in strength of PCCs. Importantly, in the first 24 hours, the GPCs achieved 55–75% of their 28-day strength, while equivalent PCCs gained 37–43%.

## Setting Time

The initial and final setting times found for selected concrete mixes are shown in Figure 3. GPMs showed relatively shorter initial and final setting times than those obtained for cement mixes. The ratio of initial setting time between PCC-37.5 and GPC-37.5 was 1.9, while for stronger grades it was 2.5. Similar ratios were obtained for final setting times.

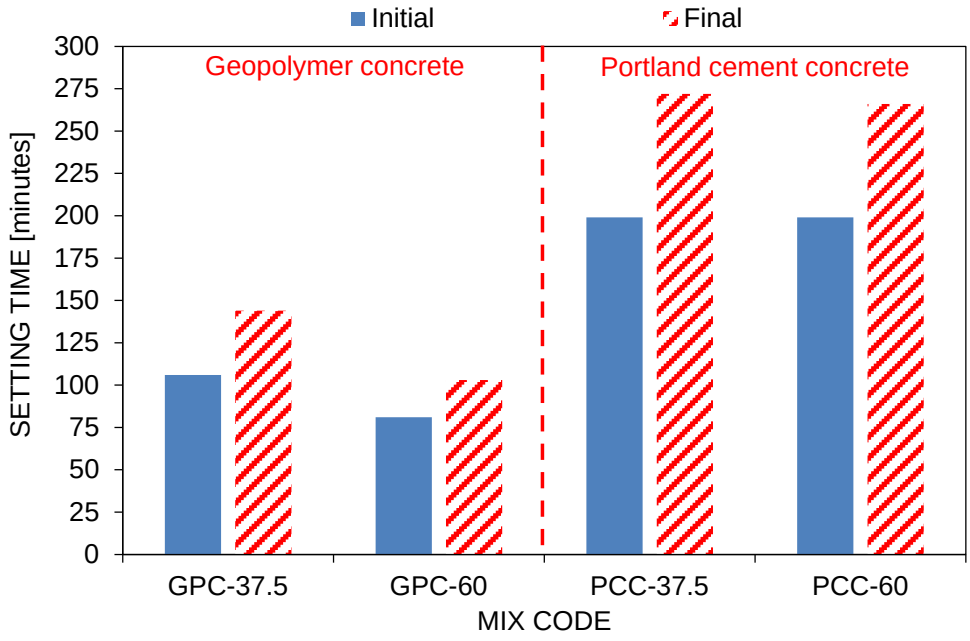


Figure 3 Setting time of geopolymer and Portland cement concretes

Where GPCs are concerned, both setting times increased with an increase in w/s ratio (setting times of GPC-37.5 were higher than those of GPC-60). For lower strength grade PCC mixes, the initial and final setting times were only marginally higher than those of PCC-60. This was unexpected, since the setting times of Portland cement systems are known to increase with an increase in w/c ratio [12]. However, superplasticiser was used in both PCC mixes, which might have affected the setting times [12]. The difference between initial and final setting increased with an increase in the w/s ratio or w/c ratio.

## Acid Attack Resistance

The cumulative mass losses obtained for mortar samples during 8 weeks of immersion in acid solutions are shown in Figure 4. When GPM mixes are compared to PCMs of the same strength grade, it is clear that geopolymer-based ones lost less mass than the conventional mixes, hence showing better resistance to $H_2SO_4$ and HCl acid attacks.

Irrespective of the binder used and strength grade, $H_2SO_4$ attack caused larger mass loss than that of HCl (*ca.* 1.5 times larger for GPMs and at least 2.3 times larger for PCMs). Where Portland cement is concerned, both acids have a dissolution effect on hardened cement paste caused by hydrogen ions (primarily dissolution of portlandite and decalcification of C-S-H and C-A-S-H phases) [13]. Indeed, as the pH of the solutions was periodically measured, a rise in the pH over the period of seven days (one cycle) was clearly observed. In addition, $H_2SO_4$ acid leads to sulfate attack. Expansive acid reaction products (gypsum and, later on, ettringite) can precipitate on the samples' surface and within pores of already degraded near-surface layer, leading to microcracks and sprawling caused by induced tensile stresses [14]. In the case of HCl, chloride ions penetrate into the cement matrix, causing monosulphate to react forming Friedel's salt and ettringite [13]. For banahCEM mortars, the mechanisms of the matrix destruction caused by these two acids are uncertain, but they appear to be distinctly different, and this requires further detailed investigation. As reported by Gao *et al.* [15], immersion in HCl solution of metakaolin-based geopolymer samples, made with potassium activator, caused leaching of KOH, $KHCO_3$ and $K_2CO_3$. The increase in pH of the acid solution used for banahCEM seems to support these findings.

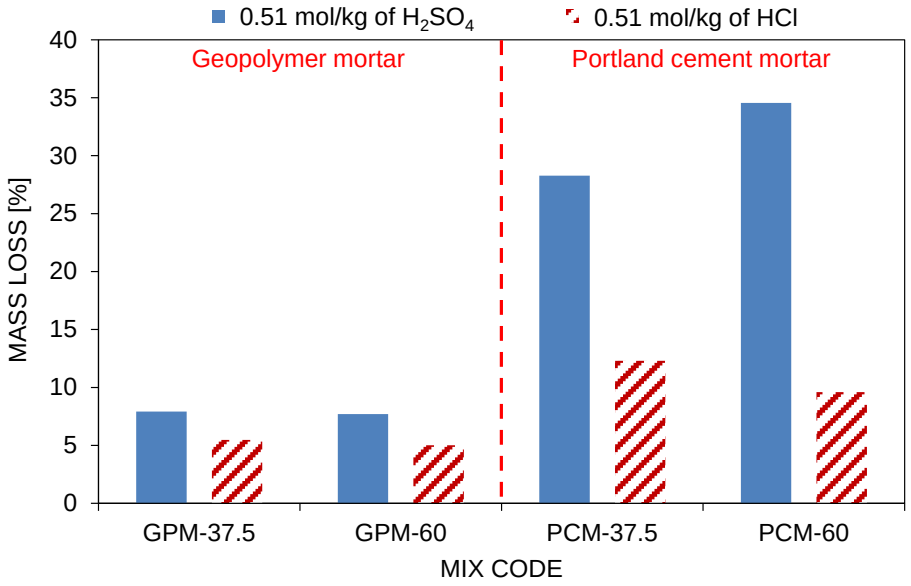


Figure 4 Mass loss of GPM and PCM samples due to the acid attack

**Sulfate Attack Resistance**

Regardless of strength grade, up to the age of 32 weeks, samples of GPM mortars proved to be stable in sulfate solutions, exhibiting relatively small change in length (shrinkage/elongation below 200 microns for both $Na_2SO_4$ and $MgSO_4$ solutions). As expected, attacked by sulfate ions, PCM mixes showed large expansions [16]. Mix PCM-37.5 immersed in $Na_2SO_4$ was already disintegrating at 32-week, while PCM-60 had expansion exceeding 1200 microstrain (cracks can be observed at samples of both PCM mixes, while PCM-37.5 bars showed large curvature – see Figure 5). For $MgSO_4$ PCM-37.5 and PCM-60 had expansion at the level of more than 4500 and 700 microstrain, respectively.


Figure 5 Samples of GPMs and PCMs after 32 weeks of exposure to $Na_2SO_4$ solution

### General Remarks

Presented results are very promising for designers and producers of concrete, both ready-mix and precast. It appears that it is possible to use banahCEM to cast structural elements and demould them as quickly as 3–12 hours later, potentially without providing any external sources of heat to speed up the strength development. Rapid development of strength could enable fast mould turnover on the work site. The binder could revolutionise the precast concrete production by allowing for as many as four concrete castings a day. This would lead to maximised use of moulds, concrete factory production assets, and space, providing precast producers with substantial savings on one hand and increased production capacity on the other. Reported durability properties, *i.e.* resistance to acid and sulfate attack, makes this geopolymer binder most suitable for harsh environment applications, where rapid strength gain is of essence, *e.g.* repair applications, tunnel or mine linings.

## CONCLUSIONS

Geopolymer concrete and mortar mixes were designed with 28-day characteristic strength of 37.5 and 60 MPa to satisfy common medium and high strength structural applications. Their physical and durability performance were compared with performance of equivalent Portland cement mixes (having the same paste volume and 28-day compressive strength). Based on the selected results, obtained during the ongoing research project, the following conclusions have been reached:

- GPCs showed very rapid compressive strength development, achieving 55–75% of their 28-day strengths within the first 24 hours after mixing. Corresponding PCCs gained 37–43% within this time.

- In general, GPCs had shorter initial and final setting times than the equivalent Portland cement mixes. Setting times of GPCs increased with a decrease in strength grade (increase in w/s ratio). Since superplasticiser was added to PCCs, setting times of lower grade mix (with higher w/c ratio) was only slightly longer.

- GPM samples exhibited lower mass lost than the conventional cement mixes, hence showing better resistance to attack of both tested acids ($H_2SO_4$ and HCl). Irrespective of the binder used and strength grade, $H_2SO_4$ attack caused larger mass loss than that of HCl. It was recognised that further work is required to explain the action of these acids on GPMs.

- After 32-weeks of immersion, geopolymer mortars showed superb resistance to attack by sodium and magnesium sulfate salt solutions, irrespective of the strength grade of the mortar mix. PCM mixes were found to expand in these two media, with the lower grade mixes being more prone to the sulfate attack. Larger expansion was recorded for PCM samples stored in $Na_2SO_4$ solution.

## ACKNOWLEDGEMENTS

The work reported here is part of the ongoing Invest Northern Ireland funded research project (Ref. No.: RDO212970 – Development and commercialisation of banahCEM geopolymer binder) at Queen's University Belfast. The authors are grateful to the School of Planning, Architecture and Civil Engineering for the facilities provided and to the Invest Northern Ireland for the financial support. The authors greatly appreciate the help of Mr. Timothy Aiken, PhD student at Queen's University Belfast, with acid attack tests.

## REFERENCES

1. PROVIS, J L, BERNAL, S A. Geopolymers and Related Alkali-Activated Materials, Annual Review of Materials Research, Vol. 44, pp 299-327.

2. RILEM TC 224-AAM. Alkali-Activated Materials: State-of-the-Art Report, RILEM State-of-the-Art Reports Volume 13, Eds. J L PROVIS and J S J van DEVENTER, 2014, Springer/RILEM, Dordrecht, p. 396.

3. MCINTOSH, J A, KWASNY, J, SOUTSOS, M N. Evaluation of Northern Irish Laterites as Precursor Materials for Geopolymer Binders, 34th Cement and Concrete Science Conference, Sheffield, UK, 14-17 Sep 2014, p 6.

4. MCINTOSH, A, LAWTHER, S E M, KWASNY, J, SOUTSOS, M N, CLELAND, D, NANUKUTTAN, S. Selection and characterisation of geological materials for use as geopolymer precursors, Advances in Applied Ceramics, 2015, DOI: 10.1179/1743676115Y.0000000055.

5. BRITISH STANDARDS INSTITUTION. BS EN 197-1:2011 – Cement. Composition, specifications and conformity criteria for common cements, BSI, London, UK, 2011.

6. BRITISH STANDARDS INSTITUTION. BS 812-2:1995 – Testing aggregates. Methods for determination of density, BSI, London, UK, 1995.

7. BRITISH STANDARDS INSTITUTION. BS EN 12350-2:2009 – Testing fresh concrete. Slump-test, BSI, London, UK, 2009.

8. TEYCHENNE, D C, FRANKLIN, R E, ERNTROY, H C. Design of normal concrete mixes: second edition, BRE Report 331, 2nd edition, BREPress, 1997.

9. ASTM INTERNATIONAL, ASTM C403/C403M-08 – Standard Test Method for Time of Setting of Concrete Mixtures by Penetration Resistance, Annual Book of ASTM Standards, ASTM International, West Conshohocken, United States, 2008.

10. ASTM INTERNATIONAL, ASTM C267-01 – Standard Test Methods for Chemical Resistance of Mortars, Grouts, and Monolithic Surfacings and Polymer Concretes, Annual Book of ASTM Standards, ASTM International, West Conshohocken, United States, 2001.

11. ASTM INTERNATIONAL, ASTM C1012/-04 – Standard Test Method for Length Change of Hydraulic-Cement Mortars Exposed to a Sulfate Solution, Annual Book of ASTM Standards, ASTM International, West Conshohocken, United States, 2004.

12. SPIRATOS, N, PAGÉ, M, MAILVAGANAM, N P, MALHOTRA, V M, JOLICOEUR, C. Superplasticizers for Concrete: Fundamentals, Technology, and Practice, Supplementary Cementing Materials for Sustainable Development Inc., Ottawa, Canada, 2003, 322 pp.

13. GUTBERLET, T, HILBIG, H, BEDDOE R E. Acid attack on hydrated cement – Effect of mineral acids on the degradation process, Cement and Concrete Research, Vol. 74, 2015, pp 35-43.

14. ATTIOGBE, E, RIZKALLA, S. Response of concrete to sulfuric acid attack, ACI Material Journal, Vol. 85, No. 6, 1988, pp 481-488.

15. GAO, X X, MICHAUD, P, JOUSSEIN, E, ROSSIGNOL, S. Behavior of metakaolin-based potassium geopolymers in acidic solutions, Journal of Non-Crystalline Solids, Vol. 380, 2013, pp 95-102.

16. SANTHANAM, M, COHEN, M D, OLEK, J. Sulfate attack research – whither now? Cement and Concrete Research, Vol. 31, No. 6, 2001, pp 845-851.

# SULFATE-ACTIVATED CLASS C FLY ASH BASED CEMENTS

**T Y Duvallet  A E Oberlink**

**R B Jewell  T L Robl**

University of Kentucky

United States of America

**ABSTRACT.** Supplementary cementitious materials (SCMs), which are materials such as fly ash, slag, silica fume, or natural pozzolans, are blended with ordinary Portland cement, as a way to improve concrete production and performance (reduce $CO_2$ emissions/costs, and/or improve workability/durability/strength). However, these SCMs, such as GGBS and Class C fly ash, can present cementitious properties on their own, or by way of activation. For example, developing strength by activation of the alumina and silica phases of the materials using strong alkalis, such as sodium or potassium silicate in combination with sodium or potassium hydroxide. Drawbacks from the use of these strong alkalis occurs which include: erratic setting, either lack of, or very slow setting or flash setting; slow strength development that may require curing at elevated temperatures or grinding slag at higher fineness; rheological problems with the concrete or mortars themselves, i.e. they become "sticky"; worker safety issues since high levels of sodium hydroxide exposure are dangerous; and long-term issues with surface efflorescence. Another way to activate slag is by sulfation activation, which consists of mixing approximately 85 wt % slag with 10-15 wt.% anhydrous calcium sulfate (anhydrite) and 5 wt.% OPC. This type of activation was thought to be a phenomenon restricted to ground granulated blast furnace slag (GGBFS) cement. A recent discovery, demonstrated that a supersulfated cement (SSC) can be based entirely on Class C fly ash instead of GGBFS. Through this new approach, the challenges from the alkali activation can then be overcome, which would potentially lead to a new generation of low energy, low $CO_2$ emissions mortars and concretes.

**Keywords:** Fly Ash, Supersulfated cements, Compressive Strength, Particle Packing, Hydration process

**Tristana Y Duvallet** is a Research Engineer Senior in the Materials Group at the University of Kentucky Center for Applied Energy Research (CAER).

**Anne E Oberlink** is a Research Scientist Senior in the Materials Group at the University of Kentucky Center for Applied Energy Research (CAER).

**Robert B Jewell** is a Research Engineer Senior in the Materials Group at the University of Kentucky Center for Applied Energy Research (CAER).

**Thomas L Robl** is a Senior Technical Fellow in the Materials Group at the University of Kentucky Center for Applied Energy Research (CAER).

## INTRODUCTION

As a way to reduce the carbon dioxide emitted by the production of cement (5% of the anthropogenic $CO_2$ emissions worldwide [1]), supplementary cementitious materials, or also called SCMs, are used as a substitute for ordinary Portland cement (OPC) in cement and concrete, resulting in a reduction of both cost and carbon dioxide emissions. These SCMs include fly ash, slags, and natural pozzolans, which have little to no cementitious properties by themselves when mixed with water, but, when reacted with calcium hydroxide, can gain cementitious properties [2].

As the substitution of OPC with SCMs increases, the early compressive strength may decrease, and the setting times may be delayed. Activation methods are thus applied to improve the hydraulic properties of SCMs, and consequently the mechanical properties of blended cements at specifically early ages, without degrading the late mechanical properties. These activation methods, which by definition is the process of curing and strength development, include thermal (elevated curing temperature) [2], mechanical (grinding materials to higher fineness) [3], [4], and chemical activations (use of specific chemical activators). [5] In particular, alkali-activated cement made from pozzolans are very popular, as they gain their mechanical and chemical properties through a chemical reaction between an alkali and a pozzolan (silica-alumina-rich product). The alkali acts as an activator and can be an alkali silicate solution (e.g. sodium silicate, also called waterglass), sodium hydroxide, lime, etc. [6] However, drawbacks result from all these activation methods. High temperature curing and mechanical grinding methods are both high energy demand processes. Similarly, the production of alkali-activated cements also present drawbacks: efflorescent issues caused by the leaching out of alkalis, which react with $CO_2$ to form alkali carbonates [6], [7]; erratic set times, which is caused by over/under dosage of the strong alkali activators [8]; difficulty to work with as they become “sticky” due to high viscosity observed overtime which is more prominent than in standard cement pastes [8]; and worker safety with use of strong alkalis as they are corrosive and can cause a lot of damage if not handled properly.

A highly effective method for chemical activation of slag is based on supersulfated cement, which is a cement that is activated through chemical reactions, by means of calcium sulfates and an alkaline activator of OPC. Supersulfated cement is composed of more than 75 wt.% granulated blast furnace, 5-20 wt.% calcium sulfate, 0-5 wt.% OPC, and 0-5 wt.% of other constituents. [9] They present advantages compared to OPC: superior resistance to sulfate attack, and lower heat of hydration than OPC. [9], [10] Not all slags may be suitable for use as supersulfated cement; it highly depends on their reactivity, which thus relies on their chemical composition and glass content. The higher the contents of lime, alumina, and glass are in slags; the higher their hydraulic properties are. [11], [12] Sulfation activation of GGBFS involves sulfates reacting with aluminium oxides in the glassy phase to produce ettringite ($3CaO{\cdot}Al_2O_3{\cdot}3CaSO_4{\cdot}32H_2O$), which is a mineral present as rod-like crystals and contributes to early strength development. Supersulfated cements are exclusively based on slag [11], and no previous research, known by the authors, has been directed on supersulfated cements based entirely on class C fly ash. Previous work focused on the activation of class F fly ash/cement blends with calcium sulfates with replacements from 30 to 60 wt.% of OPC with fly ash. [13], [14]. In general, a Class C fly ash is much lower in calcium oxide than a typical GGBFS (Table 1); and calcium oxide is considered critical in “activating” the cementitious reaction in a sulfated system. However, also very important as mentioned earlier, is the amount of aluminium oxide available in the system, which is what the sulfates need in sulfate activation to produce ettringite.

Table 1 Chemical compositions of a typical slag and class C fly ash [15]

| COMPOSITION, wt.% | CaO | $SiO_2$ | $Al_2O_3$ | $Fe_2O_3$ | $SO_3$ | $Na_2O$ | $K_2O$ |
|---|---|---|---|---|---|---|---|
| A typical Ground Slag | 40 | 35 | 12 | 1 | 9 | 0.3 | 0.4 |
| A typical class C fly ash | 21 | 35 | 18 | 6 | 4.1 | 5.8 | 0.7 |

This paper presents some preliminary work of supersulfated cements based on class C fly ash. Several activation methods are tested: optimization of particle packing, addition of admixtures, and reduction of water/cement ratio. The reduction of the water/cement ratio and the addition of water reducer (as admixture) are proven to increase compressive strength of cement. Addition of sodium sulfate (as admixture) serves a dual purpose: alkali activation with the "sodium-side", and sulfation activation with the "sulfates-side". Additions of sodium sulfate to slag and lime-pozzolan blend increased early and late compressive strengths. [16]–[18] By adjusting the water to cement ratio, admixtures compositions and concentration, and optimizing the particle packing formulation, the possibility of formulating supersulfated cements based on class C fly ash is studied.

## MATERIALS, EQUIPMENT AND PROCEDURES

### Materials

The materials used for this project are the following:

- cementitious materials: OPC type I, Type C fly ash "A", anhydrous calcium sulfate (anhydrite), and reagent chemical calcium oxide (97+% pure from Acros Organics);
- admixtures: water reducer and reagent chemical sodium hydroxide (99% pure from Fisher Scientific);
- and aggregates: river sand of different particle sizes (1000 by 500 μm, 500 by 250 μm, 250 by 125 μm, 125 by 63 μm, and under 63 μm), quartz flours (with particle size d(50) of 3 and 11 μm), and ultrafine limestone.

Their chemical compositions and particle size distributions are presented in Table 2 and Figure 1, respectively.

Table 2 Chemical compositions obtained by X-Ray fluorescence of OPC type I, Type C fly ash "A", anhydrite, and ultrafine limestone

| COMPOSITION, % | CaO | $SiO_2$ | $Al_2O_3$ | $Fe_2O_3$ | $SO_3$ | MgO | $Na_2O$ | $K_2O$ | $P_2O_5$ | $TiO_2$ |
|---|---|---|---|---|---|---|---|---|---|---|
| OPC Type I | 61.95 | 21.89 | 6.23 | 2.53 | 2.96 | 2.85 | 0.11 | 0.71 | 0.1 | 0.26 |
| Type C Fly Ash "A" | 23.57 | 33.63 | 22.34 | 4.81 | 3.86 | 4.46 | 1.64 | 0.59 | 1.39 | 1.15 |
| Anhydrite | 42.26 | <0.01 | <0.2 | <0.2 | 53.36 | 0.18 | <0.01 | <0.1 | <0.5 | <0.1 |
| Ultrafine limestone | 96.88 | 0.12 | 0.2 | 0.57 | <0.1 | 0.95 | 0.06 | 0.06 | 0.04 | <0.1 |

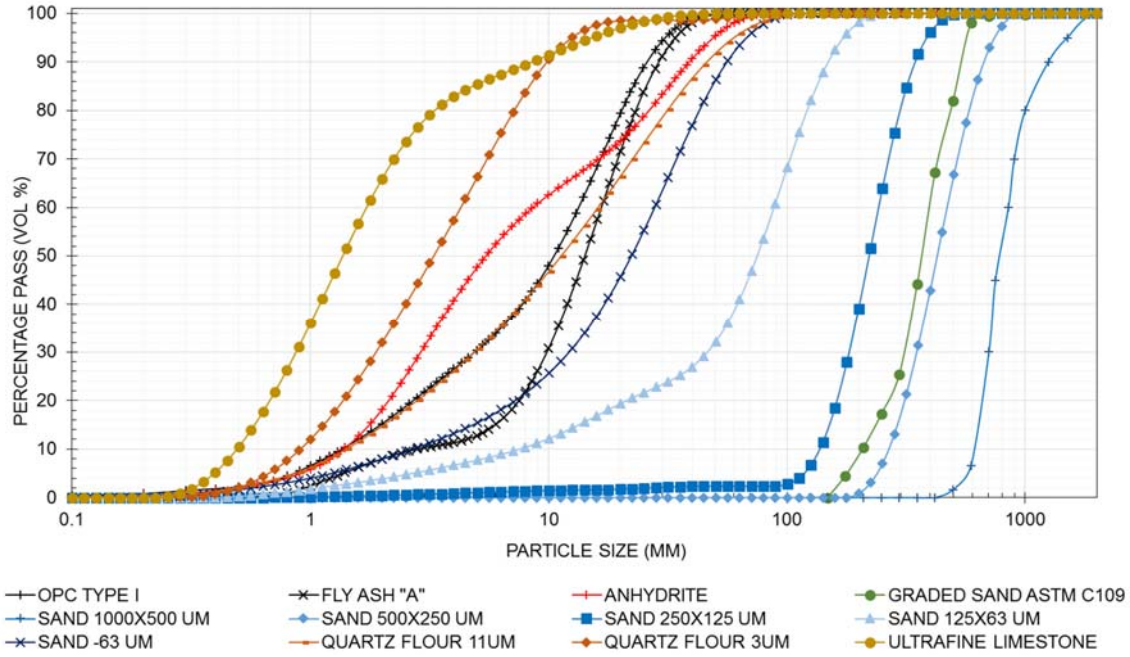


Figure 1 Particle size distributions of all raw materials

## Equipment and Procedures

Chemical compositions of the raw materials was determined by X-ray fluorescence, following the standard test method ASTM C4326-13 [19].

The mechanical properties were determined by measuring the compressive strength of mortar cubes after 1, 7, 28, and 56 days. The production of mortar cubes followed both ASTM C305 [20] and C109 [21], except for some minor modifications. ASTM C305 was modified as the cementitious materials were dry blended altogether with the aggregates, and then mixed with deionized water for 60 seconds at low speed in a Hobart mixer, while the rest of procedure was identical to the ASTM C305. ASTM C109 was modified as the mortar cubes were not cured in lime saturated water, but in a curing room at 25°C and 100% relative humidity. The use of a vibrating table was necessary for some compositions, as some of them were a very thick paste.

The hydration process was followed by three complementary methods: calorimetry, X-ray diffraction (XRD), and thermogravimetric analyses (TGA). For all methods, cement pastes were produced by mixing cementitious materials, admixtures, and deionized water. The water/cement ratio was kept constant at 0.50 for all cement pastes. Cement pastes were placed in an I-Cal 8000 Isothermal Calorimeter, at 23°C, and the hydration process was followed for 300 hours. Cement pastes made for X-ray diffraction and thermogravimetric analyses were prepared and stored in a tightly closed plastic bottle with a wet paper in it (to keep humidity at 100%) and at 25°C. After 1, 7, 28, and 56 days, fragments from cement pastes were retrieved, crushed in a mortar and pestle, and immersed in acetone to stop the hydration process. The subsequent powder, with the acetone, were then placed in an oven at 45°C until dry, and finally stored in a desiccator until XRD and TGA analyses were performed. All XRD analyses were performed with a Philips X'Pert diffractometer (model PW3040-PRO), operating at 45 kV and 40 mA, and utilizing Cu K-α radiation. Prior to analyses, the samples were mechanically

ground in a small shatter box, and if necessary were also ground by hand with a ceramic mortar and pestle. The samples were dry mounted in aluminium holders and front loaded. The step size was set at 0.017 ° at 0.035 °/second, over 8 to 60 ° 2θ. For qualitative XRD, the crystalline phases were identified with an International Centre for Diffraction DATA (ICDD, Newton Square, Pennsylvania, USA) powder diffraction (PDF) database. TGA analyses were performed with a TA Instruments SDT Q600. Approximately 10-20 mg of sample were placed into an alumina pan, and fired from 50 to 1000 °C, at a heating rate of 20 °C/min, under a continuous flow of nitrogen at 100 mL/min.

The particle packing of mortar samples was optimized by following the modified Andreassen equation [22], [23], and by using the EMMA software. [23] This particle packing theory has demonstrated to significantly improve the mechanical properties in both early and late compressive strengths, when compared with non-packing compositions. [24] All particle size distributions measured for each raw material were imported into the EMMA software. A model was created by setting the minimal and maximal particle sizes of the system at 0.35 and 1500 µm, respectively, into the modified Andreassen equation:

$$CPFT = \left[\frac{(d^q - d_0^q)}{(D_0^q - d_0^q)}\right] * 100$$

CFPD = cumulative (volume) percent finer than
d = particle size
$d_0$ = minimum particle size of distribution
$D_0$ = maximum particle size of distribution
q = distribution coefficient or exponent, set at 0.25

The modified Andreassen model is represented in red in Figure 2. As a way to optimize the particle packing of the composition fly ash/anhydrite (80/20 percent by weight), the amounts of aggregates were varied until the blue curve (Figure 2) was as close as possible to the modified Andreassen model. The optimal composition, presented in Table 3, was then defined. The ratio cementitious materials to aggregates was kept at 1 to 2.75, to be able to compare with graded sand from ASTM C109.

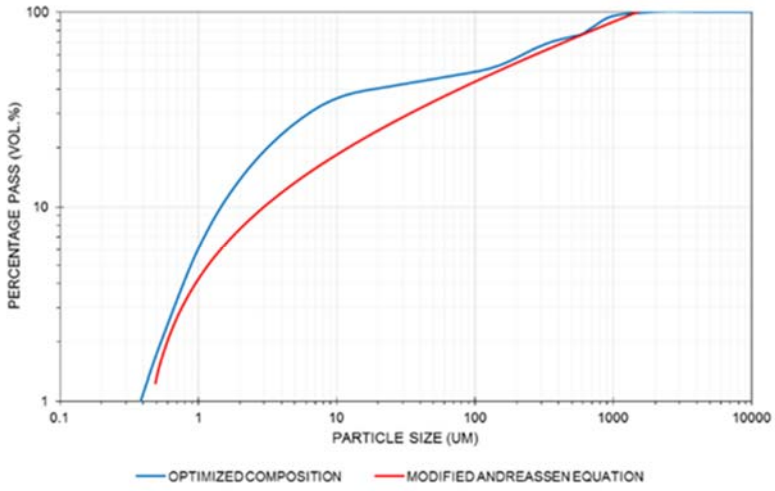


Figure 2 Particle size distribution of the optimized composition and the modified Andreassen equation (q-value of 0.25, maximal particle size of 1500 µm, and minimal particle size of 0.35 µm)

Table 3 Optimized particle packing for composition #1, with a cement/aggregates ratio of 1:2.75 (similar to ASTM C109)

| MATERIALS | PARTS BY WEIGHT |
|---|---|
| Anhydrite | 0.2 |
| Fly Ash “A” | 0.8 |
| River Sand 1000 by 500 µm | 0.9 |
| River Sand 500 by 250 µm | 0.3 |
| River Sand 250 by 125 µm | 0.7 |
| River Sand 125 by 63 µm | 0.3 |
| River Sand under 63 µm | 0.2 |
| Quartz Flour 11 µm | 0.08 |
| Quartz Flour 3 µm | 0.02 |
| Ultrafine Limestone | 0.25 |
| OPC type I | - |

## RESULTS

### Influence of particle packing

Mortar cubes, composed of 80 wt.% Class C fly ash “A” and 20 wt.% anhydrite, were produced with two different particle packings: 1) with graded sand defined as “no optimized packing”, as described in the standard test method ASTM C109, and named RefAsh; and 2) with the “optimized particle packing” described in Table 3, named composition 1. For both compositions, whether the packing is optimized or not, the water/cement ratio was set up at 0.31. The flow for composition RefAsh seemed appropriate for making mortar cubes, however the water/cement ratio was not sufficient for composition 1, as the mixture was too dry to easily work with. As a result, the amount of water was increased to reach a water/cement ratio of 0.34 for composition 1, even though the composition was still dry, but wet enough to make mortar cubes.

Compressive strength of composition RefAsh after 1 day is lower than of composition 1, which may be explained either by the dry mixture, or by the optimized particle packing. However, after 7, 28, and 56 days, RefAsh had compressive strengths higher than composition 1. Another explanation for these results may be that the optimized particle packing contained aggregates that are larger than the graded sand. Indeed, as it can be seen on Figure 1, river sand 1000 x 500 and 500 x 250 µm are coarser than graded sand.

Table 4 Compressive strengths of compositions "RefAsh" and "1" without (use of graded sand from ASTM C109) and with optimized particle packing, respectively

| SAMPLE | FLY ASH "A" | SLAG | ANHYDRITE | PACKING | W/C RATIO | FLOW | COMPRESSIVE STRENGTH, MPa at day | | | |
|---|---|---|---|---|---|---|---|---|---|---|
| | | | | | | | 1 | 7 | 28 | 56 |
| Ref Ash | 0.8 | - | 0.2 | No | 0.31 | Good | 9.0 | 16.4 | 23.3 | 29.4 |
| 1 | 0.8 | - | 0.2 | Yes | 0.34 | Dry | 9.7 | 12.4 | 14 | 19.6 |

## Influence of admixtures on Ash/Anhydrite compositions

### Mechanical studies

The influence of admixtures (water reducer, sodium sulfate, and OPC) was studied on fly ash/anhydrite compositions, with optimized particle packing for all compositions. The original water/cement ratio was originally set at 0.31, but depending on the aspect of the compositions while being made in the Hobart mixer, water/cement ratio was increased, and the final values are reported in Table 5. The addition of water reducer, between compositions 1 and 2, improved the workability of the mortar cement by increasing its fluidity. As a result, the compressive strengths of 2 are lower than of 1. The addition of sodium sulfate, between compositions 1 and 3, and between compositions 2 and 6, did not significantly have any effect.

Table 5 Compressive strengths of compositions

| PROPERTY | MORTAR CUBES | | | | | |
|---|---|---|---|---|---|---|
| | 1 | 2 | 3 | 4 | 5 | 6 |
| Paste equivalent | Ref | 2 | 3 | 4 | 5 | 6 |
| OPC | 0 | 0 | 0 | 0.05 | 0.05 | 0 |
| Fly ash "A" | 0.8 | 0.8 | 0.8 | 0.76 | 0.76 | 0.8 |
| Anhydrite | 0.2 | 0.2 | 0.2 | 0.19 | 0.19 | 0.2 |
| WR* | 0 | 0.01 | 0 | 0 | 0.01 | 0.01 |
| SS$ | 0 | 0 | 0.01 | 0 | 0.01 | 0.01 |
| TOTAL | 3.75 | 3.76 | 3.76 | 3.75 | 3.77 | 3.77 |
| Actual w/c | 0.34 | 0.31 | 0.35 | 0.35 | 0.31 | 0.31 |
| Flow | Dry | Liq | Dry | Dry | Liq | Liq |
| Compressive Strength, MPa | | | | | | |
| 1-day | 9.7 | 6.4 | 9.8 | 6.0 | 3.6 | 5.4 |
| 7-day | 12.4 | 9.2 | 13.6 | 12.7 | 13.8 | 8.7 |
| 28-day | 14 | 12.8 | 17.9 | 18.2 | 20.0 | 11.4 |
| 56-day | 19.6 | 17.6 | 19.0 | 24.4 | 22.8 | 13.9 |

*water-reducer, $ sodium sulfate

The addition of OPC, between samples 1 and 4, and between 5 and 6, increased the late compressive strengths, after 7, 28, and 56 days. However, composition 1 with no OPC showed a compressive strength of 9.7 MPa after 1 day, compared to 6.0 MPa with OPC, for sample 4. Same remark is available for 5 and 6, where the compressive after 1 day are 3.6 and 5.4 MPa, and after 28 days are 22.8 and 13.9 MPa for 5 and 6, respectively.

The mortar cement for compositions 1 and 3 are both dry and the compressive strengths are highly similar to each other, with 9.7 and 9.8 MPa after 1 day, and 19.6 and 19.0 MPa after 56 days, for mortar cubes 1 and 3, respectively. With water reducer in samples 2 and 6 and same water/cement ratio of 0.31, the addition of sodium sulfate did not increase the compressive strengths as expected, in the contrary: 6.4 and 5.4 MPa after 1 day, and 17.6 and 13.9 MPa after 56 days, for mortar cubes 2 and 6, respectively.

**Hydration studies**

The hydration process and the influence of each admixture in cement pastes Ref through 6 was followed by calorimetry, as presented in Figure 3. The addition of water reducer, between curves Ref and 2, decreased the heat of hydration; while the addition of sodium sulfate, between curves Ref and 3, increased the heat flow.

The addition of OPC as an admixture into samples 4 and 5 inhibited the appearance of a second peak after 30 minutes, like seen previously for all the other samples, but generated a peak after approximately 50 and 100 hours for sample 4 and 5, respectively, which may be due to the hydration of anhydrous calcium sulfate (anhydrite – $CaSO_4$) to calcium sulfate dihydrate (gypsum – $CaSO_4.2H_2O$).

By comparing the thermogravimetry analyses from Figure 4, ettringite was formed after 1 day in all cement pastes, which is represented by a peak at around 100°C. More ettringite is present in cement paste 5 after one day, than in any other pastes. Therefore, we would expect that the compressive strength of composition 5 would be the highest after one day than the other samples, which was not observed as mentioned in Section “Mechanical studies”. The mortar cubes 1 with no OPC exhibited higher compressive strength than composition 4 with OPC after one day. After 56 days, all cement pastes had similar thermogravimetry curves, with the formation of gypsum observed at around 160°C.

From Figure 4, the peaks present at around 400, 600, and 900°C after one day may be due to the presence of water reducer, as these peaks appeared only in cement pastes 2, 5, and 6, where water reducer had been introduced. The peak present at around 700°C is related to the presence of anhydrite in the samples.

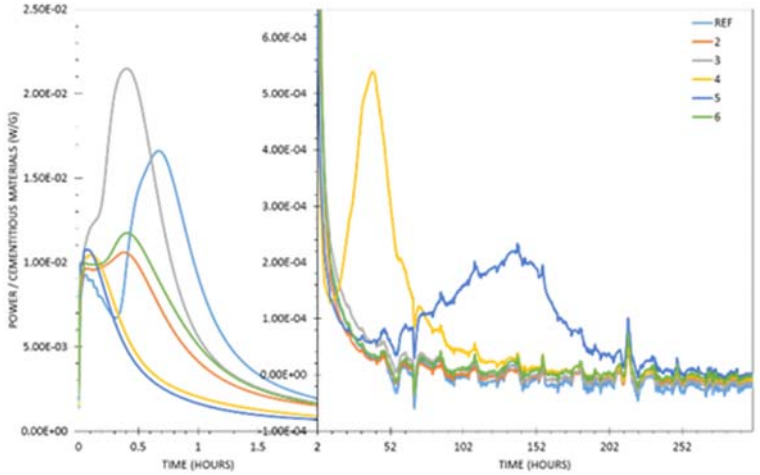


Figure 3 Calorimetry results of cement pastes Ref through 6, for the first 300 hours of the hydration process

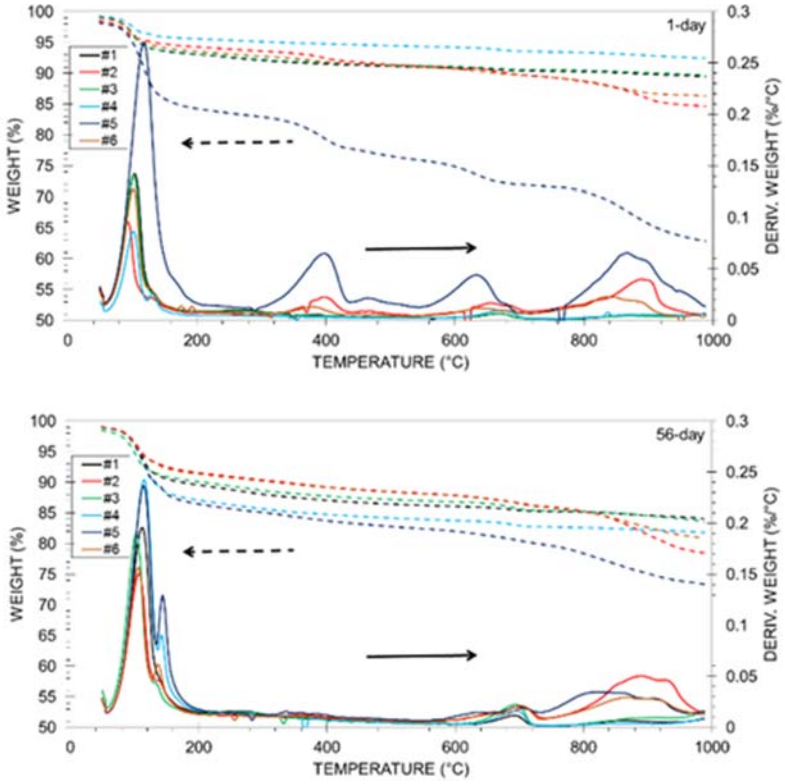


Figure 4 Thermogravimetry analyses of cement pastes Ref through 6 after 1 and 56 days

## Optimization (reduction of water/cement ratio, and OPC content)

Three methods were investigated in optimizing the compositions fly ash A with anhydrite: the reduction of water/cement ratio from 0.31 to 0.25; the reduction of OPC from 0.05 to 0.01; and the replacement of OPC with calcium oxide. The results of the compressive strengths of mortar cubes made from these compositions are presented in Table 6.

The influence of the reduction of the water/cement ratio, between compositions 5 and 7, and between 6 and 9, significantly increased both early and late compressive strengths. The addition of OPC to the compositions 7, 9, and 10 differs depending on the amounts added. In mortar cubes 10 with 1 wt.% OPC added, the compressive strength are lower at all days compared to when no OPC was added as in samples 9. However, the addition of 5 wt.% OPC in samples 7 only increased late compressive strengths (7, 28, and 56 days) compared to samples 10 with no OPC.

Mortar cubes 10 exhibited the highest compressive strength after 1 day with 16.4 MPa, compared to 13.4 and 11.0 MPa for 7 and 10, respectively. The replacement of OPC with calcium oxide in composition 11, compared to 10, significantly increased both early and late compressive strengths.

Table 6 Compressive strength of optimized compositions 7, 9, 10, and 11, compared to previous compositions 5 and 6, by reduction of water/cement ratio, reduction of OPC content, and replacement of OPC with calcium oxide.

| PROPERTY | MORTAR CUBES | | | | | |
|---|---|---|---|---|---|---|
| | 5 | 6 | 7 | 9 | 10 | 11 |
| Paste equivalent | 5 | 6 | 5 | 6 | 10 | 11 |
| OPC | 0.05 | 0 | 0.05 | 0 | 0.01 | - |
| Lime (CaO) | - | - | - | - | - | 0.01 |
| Fly ash "A" | 0.76 | 0.8 | 0.76 | 0.8 | 0.792 | 0.792 |
| Anhydrite | 0.19 | 0.2 | 0.19 | 0.2 | 0.198 | 0.198 |
| WR* | 0.01 | 0.01 | 0.01 | 0.01 | 0.01 | 0.01 |
| SS$ | 0.01 | 0.01 | 0.01 | 0.01 | 0.01 | 0.01 |
| TOTAL | 3.77 | 3.77 | 3.77 | 3.77 | 3.77 | 3.77 |
| Actual w/c | 0.31 | 0.31 | 0.25 | 0.25 | 0.26 | 0.25 |
| Flow | Liq | Liq | Liq | Liq | Liq | Liq |
| Compressive Strength, MPa | | | | | | |
| 1-day | 3.6 | 5.4 | 13.4 | 16.4 | 11.0 | 15.4 |
| 7-day | 13.8 | 8.7 | 35.9 | 23.6 | 14.4 | 23.6 |
| 28-day | 20.0 | 11.4 | 49.2 | 30.8 | 23.3 | 33.2 |
| 56-day | 22.8 | 13.9 | 61.4 | 37.2 | - | - |

*water-reducer, $ sodium sulfate

## CONCLUSIONS

Based on this work, the possibility of producing supersulfated cements based on class C fly ash has been confirmed, for example, with compressive strengths of approximately 36 MPa after 7 days, and 49 MPa after 28 days for composition 7. The strengths are higher than the ones described as a requirement in ASTM C150-12 [25] for Portland cements, or in the European Standard EN 15743:2010 [9] for supersulfated cements made from slags.

Several activation methods were tested to improve the compressive strength development of supersulfated cements based on class C fly ash. The optimization of the particle packing presented in this paper did not improve the strength development, which may be due to the selection of the aggregates, which are, for some, larger than the graded sand used in ASTMs C305 and C109. The use of sodium sulfate did not improve the strength development, while the use of water reducer significantly improved the workability of the mortar compositions, and also allowed for a high reduction of the water-cement ratio, thus an improved strength development. The use of OPC as admixtures did not improve early strength development at after one day, but did improve long term strength development (after 7, 28, and 56 days).

## ACKNOWLEDGEMENTS

The authors would like to thank Kevin Henke, Gerald Thomas, and Shelley Hopps for their help during this project. This work was supported by funding from a seed grant from the University of Kentucky Center for Applied Energy Research.

## REFERENCES

1. WORRELL, E, PRICE, L, MARTIN, N, HENDRICKS, C AND MEIDA, L O, “Carbon dioxide emissions from the global cement industry 1,” Annu. Rev. Energy Environ., vol. 26, pp. 303–329, 2001.

2. HEWLETT, P C AND MASSAZZA, F, Lea’s Chemistry of Cement and Concrete. 2003.

3. KUMAR, S, KUMAR, R, BANDOPADHYAY, A, ALEX, T C C, RAVI KUMAR, B, DAS, S K K AND MEHROTRA, S P P, “Mechanical activation of granulated blast furnace slag and its effect on the properties and structure of portland slag cement,” Cem. Concr. Compos., vol. 30, no. 8, pp. 679–685, Sep. 2008.

4. SAJEDI, F, “Mechanical activation of cement–slag mortars,” Constr. Build. Mater., vol. 26, no. 1, pp. 41–48, Jan. 2012.

5. SHI C AND DAY R L, “Comparison of different methods for enhancing reactivity of pozzolans,” Cem. Concr. Res., vol. 31, no. 5, pp. 813–818, May 2001.

6. SHI C, KRIVENKO P V, AND ROY D M, Alkali-Activated Cements and Concretes. 2006.

7. DELAWARE QUARRIES, “Efflorescence causes, removal, and prevention.” [Online]. Available: 4. http://www.delawarequarries.com/cleaners/efflorescence.html. [Accessed: 01-Jan-2015].

8. PACHECO-TORGAL, F, LABRINCHA, J A, LEONELLI, C, PALOMO, A AND CHINDAPRASIRT, P, Handbook of Alkali-Activated Cements, Mortars and Concretes. Elsevier, 2015.

9. BRITISH STANDARDS INSTITUTION, “BS EN 15743:2010 - Supersulfated cement — Composition , specifications and conformity criteria Contents,” London, 2010.

10. WOLTRON, G“The utilisation of GGBFS for advanced supersulfated cements,” World Cem., 2009.

11. KAPUR, P. C. C, MEHROTRA, V. P, SAI, A. S. R., AND P. C. C. KAPUR, “Plaster of Paris activated supersulfated slag cement,” Cem. Concr. Res., vol. 12, no. c, pp. 463–473, Jul. 1982.

12. FUENTES A. F., AND GOROKHOVSKY A., “Early and late hydration of supersulphated cements of blast furnace slag with fluorgypsum,” Mater. Constr., vol. 65, no. 317, pp. 1–13, 2015.

13. POON, C., KOU, S., LAM, L AND LIN, Z, “Activation of fly ash/cement systems using calcium sulfate anhydrite (CaSO4),” Cem. Concr. Res., vol. 31, no. 6, pp. 873–881, May 2001.

14. AIMIN X. AND SARKAR S., “Microstructural study of gypsum activated fly ash hydration in cement paste,” Cem. Concr. Res., vol. 21, no. 6, pp. 1137–1147, 1991.

15. WILSON M. L. AND KOSMATKA S., “Fly Ash , Slag , Silica Fume , and Natural Pozzolans,” in Design and Control of Concrete Mixtures, 15th Ed., Portland Cement Association, 2011.

16. RASHAD A. M., BAI Y., M. BASHEER P. A., MILESTONE N. B., AND COLLIER N. C., “Hydration and properties of sodium sulfate activated slag,” Cem. Concr. Compos., vol. 37, pp. 20–29, Mar. 2013.

17. SHI C. AND DAY R. L., “Pozzolanic reaction in the presence of chemical activators Part I. Reaction kinetics,” Cem. Concr. Res., vol. 30, no. 1, pp. 51–58, Jan. 2000.

18. SHI C. AND DAY R. L., “Pozzolanic reaction in the presence of chemical activators Part II. Reaction products and mechanism,” Cem. Concr. Res., vol. 30, no. 4, pp. 607–613, Apr. 2000.

19. ASTM INTERNATIONAL, “ASTM D4326-13 - Standard Test Method for Major and Minor Elements in Coal and Coke Ash By X-Ray Fluorescence,” in Book of Standards Volume: 05.06, 2013.

20. ASTM INTERNATIONAL, "ASTM C305 - Standard Practice for Mechanical Mixing of Hydraulic Cement Pastes and Mortars of Plastic Consistency," in Book of Standards Volume: 04.01, 1999.

21. ASTM INTERNATIONAL, "ASTM C109-13 - Standard Test Method for Compressive Strength of Hydraulic Cement Mortars (Using 2-in. or [50-mm] Cube Specimens)," 2013.

22. MANGULKAR M. AND JAMKAR S., "Review of Particle Packing Theories Used For Concrete Mix Proportioning," Int. J. Sci. Eng. Res., vol. 4, no. 5, pp. 143–148, 2013.

23. ELKEM, "EMMA - Particle packing program." [Online]. Available: http://www.elkem.com/en/silicon-materials/support/software-emma/.

24. DUVALLET T., FROUIN L., AND ROBL T., "Effect of fly ash particle packing on performance of OPC-activated GGBS slag," in World of Coal Ash (WOCA), 2015.

25. ASTM INTERNATIONAL, "ASTM C150-12 - Standard Specification for Portland Cement," West Conshohocken, PA, 2012.

# CEMFREE – THE DEVELOPMENT OF SUSTAINABLE NON-PORTLAND CEMENT BASED CONCRETES*

**P C Hewlett**

David Ball Group Ltd and University of Dundee

**M Liska**

David Ball Group Ltd

United Kingdom

**ABSTRACT.** This paper presents a hydraulically active binder that is a sustainable and environmentally responsible alternative to Portland cement. In addition it addresses the problems of transferring an innovation into adopted best practice and presents possible solutions. The paper reports on both laboratory and site trial investigations into Cemfree with strength values and characteristics of practical relevance. Performance characteristics are presented and the indications are that those concretes, based on Cemfree, are of similar or better performance than their Portland cement (PC) equivalents. Cemfree is an innovation and as such has to become accepted by and integrated into best practice. The options available are described and their relevance to all innovations in the construction materials sector are discussed.

**Keywords:** Concretes, Activator, Slag, Performance, Carbon, Superplasticisers

**Peter Hewlett** is Group Technical Consultant at David Ball Group and is regarded as a global figure in construction materials, with several hundred publications and various patents to his name. He was awarded an honorary Doctor of Laws degree for his work on admixtures and concrete durability at the University of Dundee, where he is also a visiting Industrial Professor in the Division of Civil Engineering. In 2006 he was awarded the U.K. Concrete Society Gold Medal, and in 2000 was given the Polish honour "Officer's Cross of Merits" for excellence in Science and Technical Cooperation. Three times President of UK Concrete Society and Past President of the Institution of Concrete Technology.

**Martin Liska** obtained his PhD in the Department of Engineering at the University of Cambridge, where he studied the fundamental properties of reactive magnesia cements. Martin joined David Ball Group as a Research and Development Manager in 2011. His primary role within the group is to develop further generations of existing products as well as new ones; addressing engineering performance, economics and sustainability criteria. Martin is the author/co-author of 13 journal papers, 12 conference papers and 4 patents. He is a graduate member of the Institution of Civil Engineers, and member of the Institute of Concrete Technology.

## INTRODUCTION

Portland cement (PC) based concrete has become institutionalised by way of standards, specifications and good practice. That is understandable because Portland cements are used to make concretes, mortars, renders and grouts and these materials are used to build, protect and stabilise things. These things, usually constructions and products, need to have a legacy of performance and well-being. However, that is not how such usage of Portland cement started and its development roots were in commercial opportunity and the replacement of an expensive commodity called masonry.

The present concerns about environmental and sustainability issues have created opportunity to innovate and challenge conventions. In the last 20 years the concerns over global CO2 emissions and energy use and the contribution from cement manufacture and use have become apparent and the need to reduce their impact has been accepted, both politically, socially and technically.

In recent reviews [1, 2, 3] concerned with finding an alternative to Portland cement [4], some facts are mentioned that cannot be ignored. These are;

1. Portland cement manufacture accounts for 6-7% of global and anthropomorphic CO2.
2. In the last 200 years, CO2 levels have risen from 200ppm to 365ppm (2010) [5], and rising.
3. The rate of increase of CO2 has gone up by a factor of ~2.3 from 0.55ppm per year to 1.25 ppm per year.
4. It is projected that by 2025 the cement industry will be producing approximately 3.5 billion tonnes of CO2 per year. That is about the same as the total CO2 from Europe in 2010/11 [5].
5. Globally, the demand for construction seems insatiable and much of it will be based on concrete and that leaves one thinking that there has to be an alternative to Portland cement in some form.

In a paper given by Glasser at the 2012 ICT Symposium [6] it was inferred that practical changes to production issues, i.e. using less energy, carbon capture, etc. have probably reached their practical benefit limit.

Ironically, and for more than 100 years alternative binders based on ground granulated blast furnace slag (GGBS) have been worked upon [7] and well-reviewed technically [9,10]. The technical literature and patents are extensive. [[11] and references of 9-11 of [12]] deal extensively with GGBS derivatives. Whilst GGBS is used as a supplementary cementing material (SCM) its use as a 100% replacement is still not established although publicised attempts are appearing [13,14]. Interestingly, a parallel development of a Portland cement alternative based on pulverised fuel ash (PFA) [15] is also finding cautious acceptance due in part to a complicated quantification of the total CO2 legacy.

Standards and specifications are tolerant of rather than committed to using alternatives to PC with practical examples not exceeding 50:50 GGBS:PC with the occasional exception [16]. For instance BS 8500 [17] and BS EN 197-1:2000 [18] and BS 4246: 1996 [19] do not recognise 100% replacement of PC by GGBS notwithstanding potential good durability and high chemical resistance [11] reduced chloride and sulphate intrusion [20], but some results are contradictory [21].

Most product Standards record current practice and reflect the state of the art at time of writing the Standard. Input to standards also reflect the interest of those making and using the products in question. Designers and specifiers look for product compliance with Standards written for existing products rather than new and innovative alternatives. This is a problem at both national and international level.

A possible solution would be a performance based standard rather than a product based. If the product meets the performance required it should not matter what comprises the product. This problem will be enlarged upon at the end of the paper.

It is relevant and perhaps telling that the ASTM have produced a performance based Standard – C1157 [22] that is not dependent on defined materials, so opening up the prospect of showing conformity to one of the stated performance categories that should allow specifiers to recognise the role of non PC based concretes and mortars. Additionally, the American Concrete Industry, building code requirements for structural concretes [23] allows the use of hydraulic cements conforming to ASTM C1157 in lieu of Portland cement.

It is usual but not necessary to incorporate some PC when making GGBS based concretes. For instance BS EN 197[18] allows up to 95% GGBS (but rarely if ever specified) but with a minimum of 5% PC. PC is added to generate some alkali that acts as a stimulant to the hydraulic latency of the GGBS. Some 5% "minor constituents" are also allowed but not at the expense at the PC. It is the chemical stimulation of the GGBS and the level of structure building that controls the strength/time/temperature properties of the resulting concretes and to some extent their durability. It is the comparison with the Portland cement concretes that has limited the applications and committed development of alternatives. However, is such a comparison entirely justified if one is genuinely concerned about reducing clinker use, and making best use of the environmental legacy of such materials as GGBS?

This paper is concerned with what is called Cemfree – the development of concretes containing no PC and stimulated in such a way as to yield strengths of practical application and with durability characteristics that are comparable to and in some aspects an improvement on PC based concretes. Cemfree is basically available in three forms namely; White (standard), Super (higher strength) and Econ (reduced cost). However, there are various options depending on aggregate type and conditions surrounding particular applications. This paper reports primarily on the White grade with some comments relating to Super and Econ.

There are three fundamental stages to this development, namely

1. The stimulation and activation of GGBS
2. Maximising the level of activity by reducing internal spacing between hydraulically active centres and enhancing nucleation while maintaining acceptable levels of workability.
3. Providing the means of getting acceptance of a new product.

None of these stages is entirely original, but the combination would appear to overcome substantially the known limitations of high GGBS/non PC based concretes. The developments are subject to international and British patent applications [24, 25].

## Activation of the Hydraulic Latency of GGBS

GGBS is the product of blast furnace iron making [26], but that from steel making can sometime be used [27] and as a result can vary both physically and chemically. Activity depends upon the chemical composition, glass content and fineness resulting in a range of hydraulic indexes [28, 29]. There are many different types of slag and some intermediate examples known as basic oxygen slag (BOS) [30, 31]. Slags from different origins can have different reactivities and performances [32]. Best strengths are obtained if the Al2O3 content is 15-20% and the CaO 40-50%, therefore selection is important. As a result of rapid quenching, slag forms an encapsulating glassy sheath containing predominantly calcium silicates and aluminates. A typical analysis of usable GGBS from two sources is given in Table 1 [33].

Table 1 Chemical Composition of Two Sources of GGBS.

| LOCATION | BULK OXIDE, % by mass | | | | | | | | | | |
|---|---|---|---|---|---|---|---|---|---|---|---|
| | $SiO_2$ | $Al_2O_3$ | $Fe_2O_3$ | CaO | MgO | MnO | $TiO_2$ | $SO_3$ | $Na_2O$ | $K_2O$ | LOI |
| 1 | 36.17 | 11.93 | 0.39 | 39.38 | 8.12 | 0.68 | 0.24 | 0.98 | 0.29 | 0.6 | 0.76 |
| 2 | 35.54 | 12.81 | 0.31 | 39.47 | 8.38 | 0.37 | 0.78 | 0.48 | 0.21 | 0.62 | 0.96 |

In order for GGBS to become hydraulically active, the glassy encapsulation has to be broken down and the products of hydration depend on the manner of activation [34, 35].

Various activators are used with various degrees of success. The range of activators varies from Portland cement, a range of alkalis [36] and alkaline earths [37] such as lime, sodium sulphate [38], sodium carbonate and various forms of sodium silicate. Most result in CSH (Calcium silicate hydrate) formation with some CASH (Calcium alumina silicate hydrate $C_2ASH_8$, $C_4ASH_{13}$) depending on the Ca:Si and Al:Si molar ratios, i.e. Ca:Si ~1 yileds CSH but Al:Si~0.1 yields CASH. Hydration is different to PC in that little or no CH (Calcium hydroxide) is produced [39]. If sodium salts are used as activators, then other derivatives such as AFm and Hydrotalcite (Natural mineral $Mg_6Al_2O_3(OH)_{15}\cdot 4H_2O$) are also formed[40] as well as NASH (sodium aluminium silicate hydrate) [41].

A list of activators includes sodium hydroxide, calcium hydroxide, calcium sulphate, sodium carbonate, sodium sulphate and sodium silicate [28, 42], that can be classified into six groups according to chemical composition [43, 44].

In this work the Cemfree activator and other components are the subject to current PCT patent applications [24].

The mechanism of the GGBS activation is considered to consist of three stages namely

1. The dissolution of the glass network that itself consists of $SiO_4$ tetrahedra in a three dimensional network with a bond strength of 335 kJ/mol (80.4 kcal/mol). This is quite substantial and explains the low reactivity without some stimulation by what are sometimes called network modifiers[21] that helps to depolymerise the encapsulation (210 kJ/mol). Sodium, potassium and calcium containing entities are such modifiers

resulting in monomeric and oligomeric Al and Si species [1,11]. This phase is also referred to as destruction and coagulation [1]. By means of electron donation from the alkali ($OH^-$) the

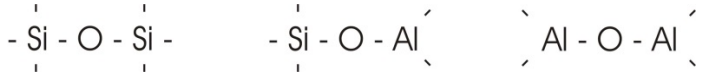

bonds are broken forming $Al(OH)_4^-$ and $Al(OH)_6^{3-}$ as well as $Si(OH)_4$ entities depending on the pH. In general, the higher the pH the higher the activation. However, the stronger the alkali restricts the practical use of such alkalis from a health and safety point of view [42, 45]. In addition the cost of using caustic alkalis can be expensive, some 6-7 that of alternatives.

2. Precipitation and condensation phases. This state depends on the calcium content of the GGBS and results in the coming together of the dissociated species resulting in polycondensation.

3. Condensation/crystallisation. This stage is complex and depends on the nature of the reactants to begin with. The oligomers (polysialates) 46 in the agglomeration phase are thought to condense in large networks with water being incorporated.

When other materials such as fluidifiers are added to GGBS based concretes regard has to be taken of the surface charge resulting from the GGBS in contact with water. This charge might be negative (-20mV), neutral (+1 mV) or positive (+17mV) [47,48]. Such changes may be manipulated to aid the adsorption of the fluidifiers [49] – such is the case with Cemfree [48].

It is fair to say that the detailed chemistry and structural composition is somewhat complicated and confused due to compositional variation and physical circumstances surrounding methods of curing. In that regard, proven outcomes are a good engineering starting point. After all we still discuss, if not argue about, the physical chemistry related to PC hydration and durability some 180 years after its invention.

Therefore let us present some laboratory and field trial comparative results concerning Cemfree types of concretes.

## EXPERIMENTAL

### Laboratory Testing

The following issues were considered relevant and addressed. Workability, setting time, temperature increase, compressive, flexural and tensile strength, dimensional stability, water absorption and hydraulic permeability, resistance to chemical attack, chloride penetration, carbonation, freeze-thaw, abrasion resistance and alkali silica reaction. In addition, some early comment on microstructure, composition and durability is offered.

### Test Methods Used and Background

Concrete samples were prepared and tested for various properties according the following listed standards:
Preparation of specimens (100mm cubes) – BS EN 12390-2:2009
Sampling of ready mixed concrete delivered to site – BS EN 12350-1:2009
Setting time of cement paste: BS EN 196-3:2005
Setting time of concrete - BS EN 13294: 2002
Workability of concrete determined by measuring its slump - BS EN 12350-2:2009 (test method) and BS EN 206-1:2010 (classification according to resulting consistence)
Compressive strength - BS EN 12390-3:2009
Flexural strength - BS EN 12390-5:2009
Tensile strength – BS EN 12390-6:2000
Drying shrinkage – ASTM C426-10
Initial surface absorption - BS 1881-208:1996
Permeability - BS EN 12390-8:2009
Freeze-thaw - DD CEN/TS 12390-9:2006
Carbonation depth – BS DD CEN/TS 12390-10:2007
Chloride ion penetration test - ASTM 1202-12
Abrasion resistance – BS 13892-4:2002, BS 8204-2:2003 +A2:2011

Resistance to chemical attack – This test was a comparative evaluation of Cemfree concrete against PC based concrete, both exposed to a range of chemical solutions. These were sulphuric acid (0.5M), Hydrochloric acid (0.5M), Acetic acid (0.5M) and Magnesium sulphate (10wt%). Samples (prisms 40x40x160 mm) were initially water cured for 28 days at 21°C, then they were exposed to the aggressive solutions with pH inspected on a weekly basis and replaced as required. Control systems were exposed to water throughout the duration of the test. After twelve months, samples were tested for flexural strength according to BS EN 12390-5:2009.

Temperature development during hydration – This parameter was determined using a set of five thermocouples placed in the middle of a polystyrene insulated box (1m x 1m x 0.4m) containing Cemfree concrete. A further 3 thermocouples were fixed outside the system to record the ambient temperature. The thermocouples were connected to a computer so that a continuous record of the temperature was achieved over 14 days of hydration.
Dealing with each aspect in turn.

**Workability/Rheological Properties**

Concretes with slumps in a range S1 (10-40mm) – S3 (100-150mm) were the norm. The workability of all four classes as per BS EN 12350 – 2:2009 was achieved by suitable selection and dosage of appropriate admixtures, all at relatively low water: binder ratios, 0.3-0.35. The resulting system was then somewhat more sensitive to correct dosing of components, however, practical utilisation of such a procedure is proven as demonstrated below. The level of control over water content and correction of moisture in stored sand and aggregates has to be assessed with more care than for PC based mixes.

Cement pastes based on Cemfree binder using PCE as a fluidifier exhibit shear thickening. As the paste is stirred rather the viscosity decreasing it increases at higher shear rates. This has been observed previously with mixtures containing PCEs. These admixtures are relatively large molecules that when adsorbed onto the surface of GGBS can interfere with one another. At low shear rate these attached entities can slip by one another with expected viscous response but at

high shear rates the PCEs attached to the GGBS can obstruct one another resulting in higher viscous drag.

## Setting Time of Paste And Concrete

The setting time for the Cemfree binder paste according to BS EN 197 was 3.5 and 5.5 hours for initial and final respectively. Despite attempts to measure the setting times of Cemfree concretes according to BS EN 13294:2002 the method proved unsuitable due to the apparent thixotropic properties of such concretes rather than the effect of stiffening of the binder resulting from hydration. There is a possible need to develop an instrument that can differentiate between rheological stiffening and actual setting since the standard method has limitations.

## Temperature Development During Hydration

According to ASTM C1157 [22] Cemfree concretes may be described as “low heat”. Under real, but approximately adiabatic conditions on a well-insulated slab measuring 1 x 1 x 0.3 m. The temperature increased by a maximum of 2-8°C which represents a promising result since temperature differentials due to hydration of cements in concrete not exceeding 20°C are considered safe from early age thermal shrinkage point of view [49,50].

In addition Cemfree paste temperature measurements rose by a maximum of 5°C after some 50 hours under adiabatic conditions. Parallel work indicated a heat output of 55 kJ/kg after 40 hours. Corresponding outputs for CEM I and 70:30 GGBS:PC pastes were 350 and 180 kJ/kg, respectively.

This would indicate Cemfree is well within the requirements of ASTM C1157 that require not more than 250-290 kJ/kg at 28 days.

However, it has to be born in mind that the thermal behaviour of the concrete is dependent on the ambient condition and the geometry of the concrete element[48] and some heat losses are likely to occur in practice so the thermal output is also likely to be reduced further.

## Compressive, Tensile and Flexural Strength

Compressive strength development of Cemfree type concretes progress over long periods of time. As demonstrated in Figure 1 the strength reached 45 MPa at 28 days and continues to rise to 70 MPa at 12 months at a temperature of 21 °C. For comparison, the same figure shows a minimum strength requirement for high GGBS concrete according to BS 4246[19]. It is evident that from strength point of view Cemfree concrete show satisfactory performance.

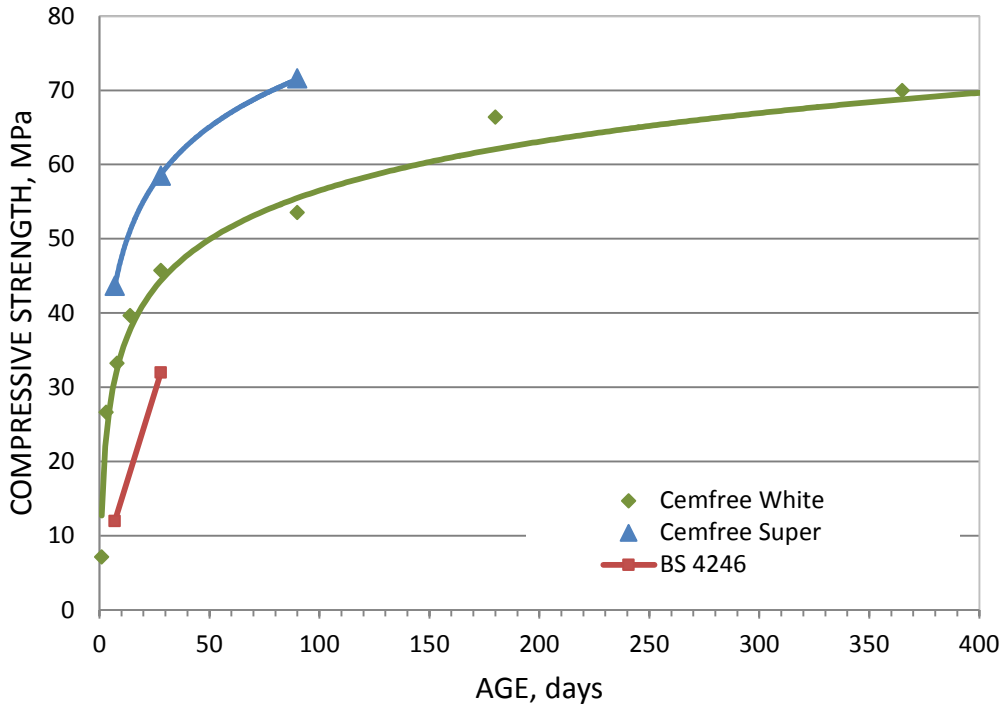


Figure 1 Compressive Strength of Cemfree Concrete (10 and 20mm Granite), Compared With Minimum Strength Requirements of BS 4246.

It is well known that the strength development of high GGBS concretes is affected by the curing temperatures and Cemfree concretes are no exception. Figure 2 demonstrates such responses with curing temperatures around 10 °C substantially lowering the hydration process. On the other hand, the opposite effect is seen if the curing temperature is increased to 30 °C. The end applications will determine if the temperature dependence is important.

A rapid strength increase to over 17 MPa after 12 hours was observed when Cemfree White was subjected to an elevated temperature curing at 45°C as demonstrated in Figure 3. Such an outcome demonstrates the suitability of Cemfree for operations taking advantage of raised temperature curing conditions that are commonplace in precasting.

Tensile strength of Cemfree concrete, presented in Figure 4, approached 3 MPa at 28 days and continued to rise further to exceed 3.5 MPa at 56 days.

A relatively steep increase in flexural strength (Figure 5) was seen up to 28 days when it reached 4 MPa after which the rate slowed down reaching 4.5 MPa at 56 days.

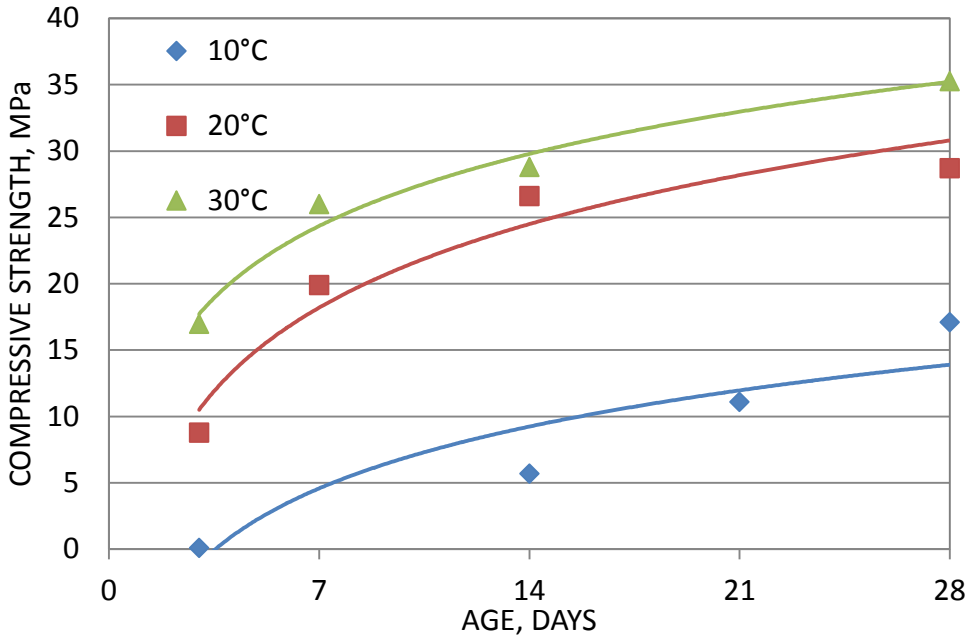


Figure 2 Effect of curing temperature on compressive strength of Cemfree concretes (20 mm angular gravel).

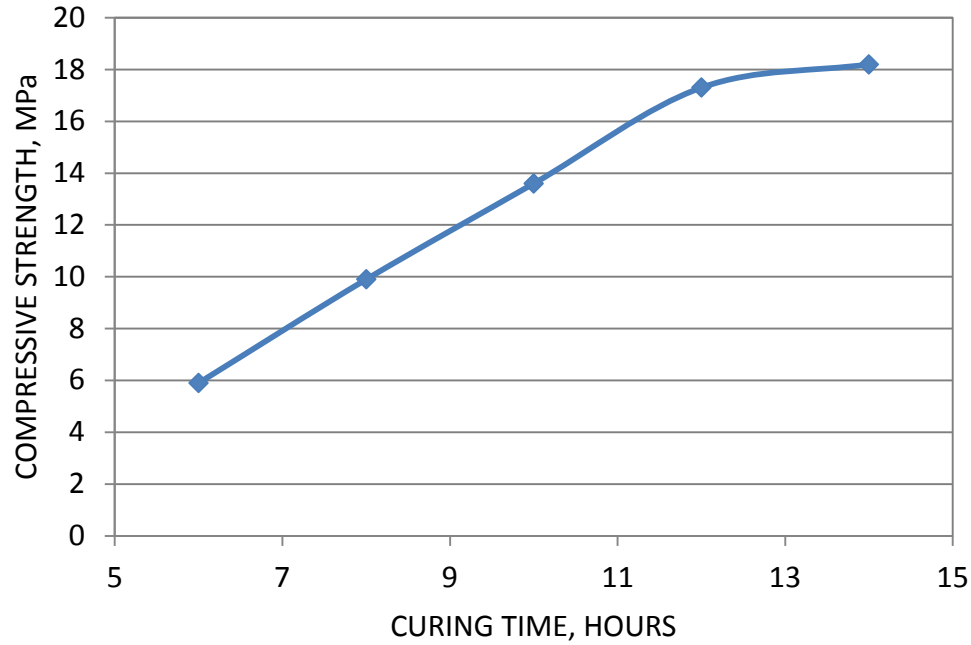


Figure 3 Compressive strength development of Cemfree white cured at 45°C.

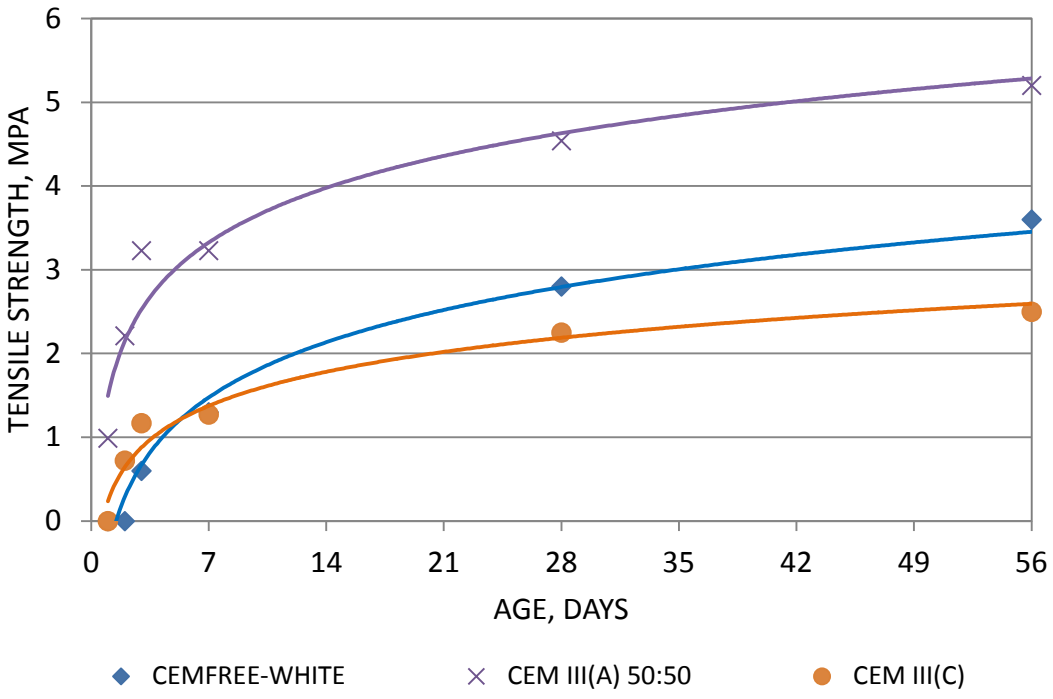


Figure 4 Tensile strength of Cemfree White concrete and PC based comparators.

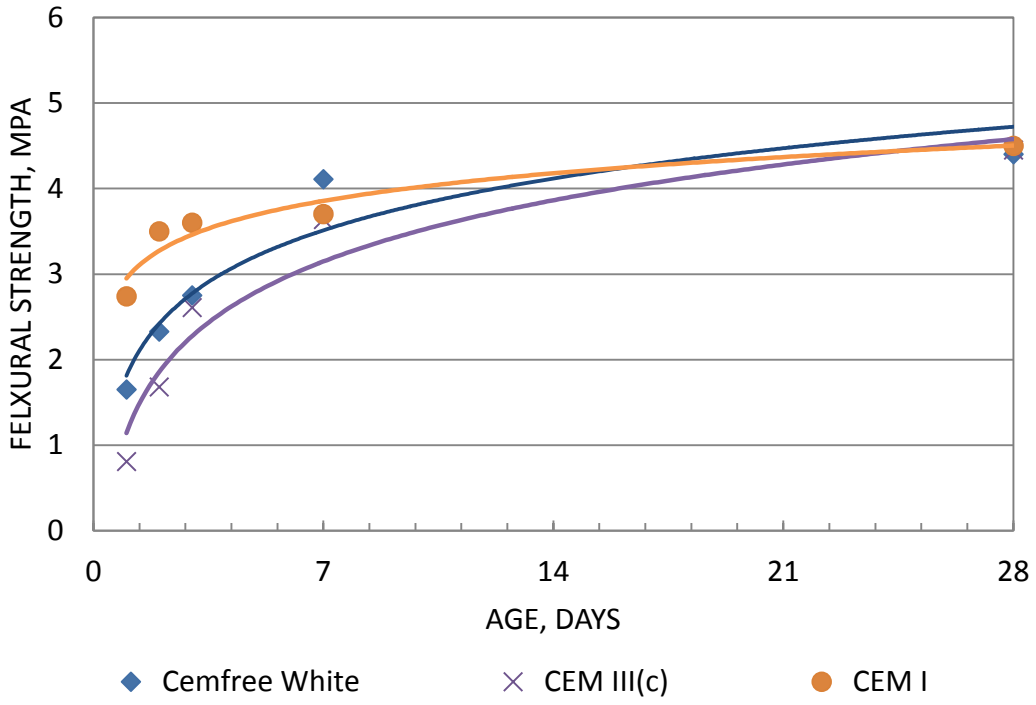


Figure 5 Flexural strength of Cemfree concrete.

## Dimensional Stability

Drying shrinkage was measured using the ASTM as listed.

Similar shrinkage behaviour of both Cemfree White, CEM I and CEM III(A) concretes was observed. The data is presented in Figure 6 from which it is evident that both the level attained (~300 microstrains at 6 weeks of drying) as well as the rate of shrinkage was very similar for all the concrete types.

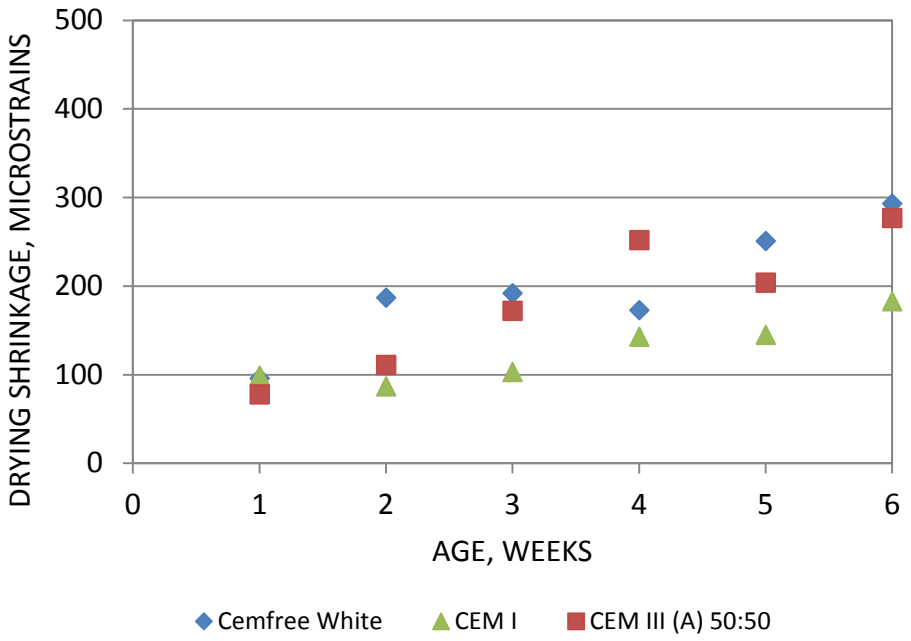


Figure 6 Drying shrinkage of Cemfree concrete compared with that of CEM I and CEM III (A).

## ISAT + Hydraulic Permeability (measured as given in section on test methods)

The ISAT gave the following results:

10 minutes: 0.05 ml/m$^2$.s

30 minutes: 0.04 ml/m$^2$.s

60 minutes: 0.03 ml/m$^2$.s

According to Concrete Society report TR31[51] such performance signifies low absorptivity. The permeability was measured as presented in the Test Methods section and after 72 hours no water had penetrated within the sample indicating a very low permeability of the concrete. This has a direct impact on durability whereby the ingress of adverse substances is inhibited. Results for gas permeability and the deduced hydraulic values will be published at a later date.

## Resistance to Chemical Attack

The resistance of Cemfree and PC control concretes to Acetic acid, Sulphuric acid and Magnesium Sulphate was tested. The initial results obtained after 12 months of exposure are presented in Figure 7 by means of flexural strength of the exposed samples relative to the control cured in water during the same time period. The effect of both the acids is evident in the decreased strength of all the exposed systems as demonstrated in Figure 7. The best resistance to the organic acid (acetic acid) was shown by CEM III(A) (~80% retained strength), followed closely by Cemfree White (~65% retained strength).

Better performance of the Cemfree White concrete in the inorganic acid (sulphuric) was clearly seen (~70% retained strength) followed by the CEM III(C) mix (~60% retained strength). The remaining two mixes exhibited the highest reduction in strength to ~40%. The effect of magnesium sulphate solution on all the tested concretes was minimal at this stage of testing for both the Cemfree concretes as well as CEM III(A). A strength reduction to 70% is evident for CEM III(C). These tests are on-going.

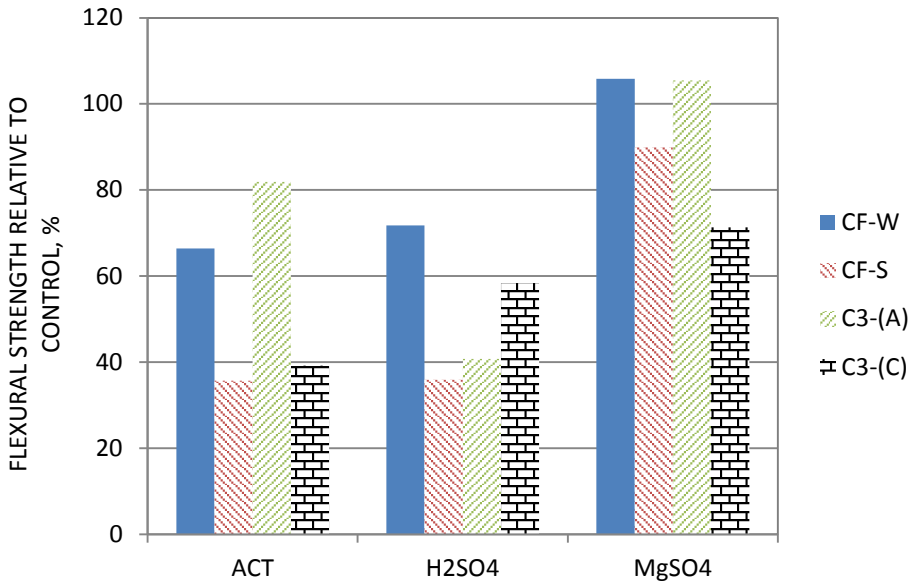


Figure 7 Relative strength performance of Cemfree and PC based concretes exposed to aggressive solutions to their respective controls. ACT: Acetic acid, CF-W: Cemfree White, SF-S: Cemfree Super, C3-(A): CEM III(A), C3-(C): CEM III(C).

## Chloride Ion Penetration Test

The chloride penetration test is an important parameter for the protection of the reinforcing steel. The parameter was determined using ASTM 1202-12. The authors are aware that the test has been criticised when used in concretes where part of the binder was replaced with GGBS. However, this test is still widely used. It was found that the passed charge of 196 Coulombs corresponds to a very high resistance of the concrete to chloride penetration as shown in Table 2 reproduced from [52]. This suggests a beneficial environment for the protection of the reinforcing steel. At time of writing this paper, alternative test procedures are being considered [53, 54].

Table 2 Interpretation of Passed Charge Values in Terms of Chloride Ion Penetrability (reproduced from ASTM C1202-12)

| PASSED CHARGE, coulombs | CHLORIDE ION PENETRABILITY |
|---|---|
| >4000 | High |
| 2000-4000 | Moderate |
| 1000-2000 | Low |
| 100-1000 | Very Low |
| <100 | Negligible |

**Freeze-Thaw**

The mechanism of freeze-thaw response is well established as is the alleviating role of air entrainment. As such, Cemfree concretes without air entrainment are likely to be similar to OPC concretes, also without air entrainment as far as freeze-thaw response is concerned. However, the compatibility of the air entrainment admixtures with Cemfree is the subject of current corroboration. Non air entrained Cemfree concretes are not expected to perform differently to non-air entrained PC concretes. However, work to establish the performance relative to both types as well as the compatibility with air entraining admixtures [55].

**Depth of Carbonation**

The depth of carbonation (in mm) was measured on two Cemfree and two Portland cement concretes. The measured values after 6 and 12 months of exposure to ambient conditions are shown in Table 3. They demonstrate a similar behaviour of all the concretes with high GGBS content (8.5 – 12mm). No carbonation was seen for CEM III(A) mix (50:50) at this stage of testing. Accelerated carbonation (1%) indicates similar performance up to 28 days.

Table 3 Carbonation depth (in mm) of Cemfree and PC based concretes.

| AGE | CARBONATION DEPTH, mm | | | |
|---|---|---|---|---|
| | Cemfree White | Cemfree Super | CEM III (A) | CEM III (C) |
| 6 months | 8.5 | 9 | 0 | 10 |
| 12 months | 10 | 12 | 0 | 12 |

There is evidence to show that standard accelerating carbonation tests yield figures indicating higher carbonation than that from natural exposure and raises questions about the test methods themselves. The predominant gel (CASH) from alkali activated GGBS de-calcifies under higher $CO_2$ concentrations whereas the NASH gels derived from activated PFA remains largely unchanged [46].

## Comment on Alkali Silica Reaction

Testing the propensity of Cemfree concrete to alkali silica reaction problem is in hand. However, the literature indicates repeatedly good alkali silica performance as a result of using GGBS [57]. The relationship between high alkali and the potential to alkali silica reaction problems is known [58]. Given the moderate pH level of ~12 of the Cemfree concrete it is likely that the risk of adverse reactions due to the presence of alkali sensitive aggregates should be minimised.

## Microstructure – Durability Prognosis

The character of the hydration products of Cemfree binder was studied independently [59, 60] using microstructural analysis (SEM with EDX). Figure 8 (a) shows an example of the analysed Cemfree paste (cured for 28 days) showing GGBS (bright particles) surrounded by hydration products. Since these are mostly intermixed, plotting elemental ratios aids identifying them. The analysis revealed that the main hydration product was CSH with Ca:Si ratio of around 1.6 with very limited amount of Portlandite (see Figure 8 (b)). The sulphur was present mainly as AFm (monosulphate) with a very limited amount of AFt (trisulphate/ettringite) (Figure 8(c)). Figure 8(d) indicates the presence of hydrotalcite and some AFm. All of these hydration products were very similar to a GGBS:PC (70:30) paste also analysed as part of this work for comparison purposes.

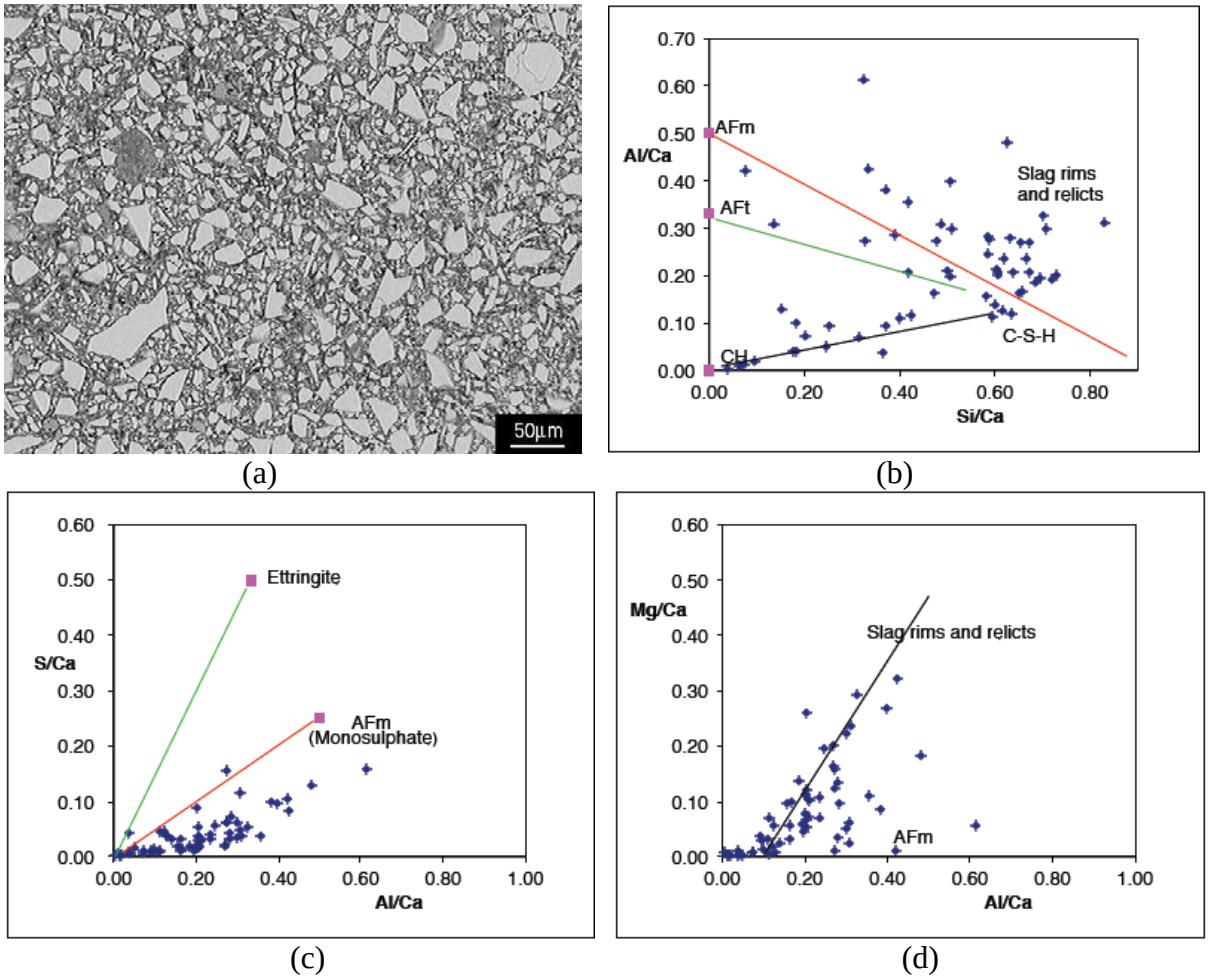


Figure 8 (a) SEM of Hydrated GGBS, (b)-(d) Elemental Ratios of EDX Data.

### Durability Considerations

The long term performance as well as performance in aggressive environments of any binder is always of paramount importance for widespread acceptance to occur. Very often a design life of 120 years is required. However, such stringent, but understandable, requirements often hinder innovation as it is not possible to realistically test novel systems in all possible scenarios for the required amount of time. Accelerated testing is often questionable due to yielding results which in fact do not represent the real long term behaviour of the tested system [61].

In order to overcome this shortcoming, we decided to compare the hydration products to a well-established binder system such as Portland cement with high GGBS content. There is a plethora of evidence that such blends exhibit markedly improved durability when compared to pure Portland cement. The durability of a system depends partially on the physical characteristics of the concrete (i.e. porosity and permeability) and also on the chemical speciation of the system [62] (i.e. presence of compounds which readily take part in expansive reactions, such as Portlandite and sulphates). Given the close similarity of the hydration products of Cemfree (including the dense nature of the paste) and the PC-GGBS blend it is not unreasonable to assume that their long term behaviour would be very similar as well.

## FIELD TRIALS

Full scale trials have been performed over the last two years and are ongoing both privately and in collaboration with interested parties. Field trials comprised casting over 600 $m^3$ of Cemfree concretes in approximately 50 pours comprising various sized slabs, large warehouse floor, feature staircase and the casting of a large free standing wall. The purpose was to optimise and scale up the Cemfree production process in terms of batching, transport, placing, finishing and performance. Typical slab sizes were 5m by 3m by 0.2m.

### Batching

Cemfree requires close control over the specified w:b ratio. This in turn requires control over stored sand and aggregate free water/moisture content and carries forward a correction to the added water when making and mixing. Once this requirement was appreciated, consistent supply was achieved. It is fair to say that PC concretes are more tolerant to water content variations and its consequences seem more readily accepted. Mixing efficiency is also a relevant factor. Where dry batching takes place, i.e. all the materials are placed in the concrete truck where the mix is then homogenised, it was recognised that the internal arrangement of the mixing blades within the barrel have a significant impact on the mixing efficiency and thus the quality of the resulting concrete. The ideal mixing blades appeared to be curved on the ends as opposed to being flat which are not capable of exerting the same mixing efficiency.

### Transportation

Since the Cemfree concrete mix contains a fluidifier, it is important to ensure that the travel time does not exceed the effective workability time of the mix. This is dependent on the ambient temperature and would reflect normal concrete practice. In the case of the trials the transport time was between 30 and 40 minutes and during this time no loss in workability was experienced. Nevertheless, if that were to occur, it was better to re-establish the workability by adding more fluidifier rather than more water.

## Placing Characteristics

Cemfree concrete showed somewhat different characteristics to what is known to the skilled person as ordinary concrete. Although the mix was very dense, its slump characteristics were classed as S3 and higher despite it appearing to be “dry”. A relatively limited amount of energy exerted on the concrete increased the workability substantially. The placing characteristics of Cemfree concretes are well within the experience and skills of most operatives, but normal controls should be exercised.


Figure 9 Typical Cemfree that approaches self-compacting concrete.

## Finishing and Surface Quality (Abrasion Resistance)

Although this is relevant only to surfaces which are to be exposed in service, it is important to note that very good surface quality can be obtained with Cemfree concrete. Due to its high density, the energy input during finishing the surface is increased compared to conventional concrete. Various surface finishing techniques were tested such as hand trowelling, beam tamping (Figure 10(a)), vibratory beam (Figure 10(a)), roller beam and also a large scale laser screeder (Figure 10(b)).


(a) (b)

Figure 10 Slabs cast with Cemfree with different placing and surfacing techniques.

The slab in Figure 11(a) was cast during hot weather and cured using a curing membrane. Post cure abrasion resistance testing[62] was performed to BS 8204 Part 2: 2003 resulting in a value of 0.10 mm categorising the concrete as AR1/DF-heavy duty. As with all good concrete practice, Cemfree needs to be properly cured. Failure to do so can result in reduced surface quality as indicated in Figure 11(b).

(a) (b)

Figure 11 (a) Excellent abrasion resulting from good cure and surface finish and (b) poor abrasion resulting from inadequate cure and finishing technique.

## Curing

As with PC concretes normal good curing conditions must be applied[63] in order to obtain a high quality concrete when using Cemfree. Due to the extended setting characteristics, Cemfree concrete is more at risk to drying with the potential for plastic shrinkage and cracking. However, this is easily overcome by using a curing agent (membrane) together with covering the freshly poured slabs with tarpaulin to prevent moisture loss from evaporation. As a result, high quality surfaces are attainable as demonstrated in Figure 11(a) above.

## Workability Attainment and Retention

As mentioned earlier, the workability can be adjusted to any requirement i.e. S1 – S4. However, the most commonly used consistence class was S3. The inadequacy of the slump test was recognised during this work and despite the concretes exhibiting high slump values the yield stress was substantially higher than what would be expected from a mix of that slump class.

## Setting Behaviour

The setting characteristics of concretes with high GGBS binders are typically extended and it was the case for Cemfree types concretes. In any case, the dense nature of the concrete gives the impression of a set concrete after a very limited time of approximately 1 hour, i.e. the concrete is stiff enough to be walked upon. However, if further energy is supplied say by way of vibration, the workability is restored to some extent.

## Compressive Strength Development

During the various trials, samples (100mm cubes) were cast for subsequent compressive strength testing from the same mix as used for the trials themselves. The samples were then covered with a plastic foil and placed in close proximity to the placed structure to ensure similar curing conditions of both samples and placed concretes. Actual curing temperatures varied with the prevailing weather conditions. Various concretes and their associated compressive strength that were used during the trials are given in Table 3.

Table 3 Range of concrete compressive strengths placed during the field trials.

| COMPRESSIVE STRENGTH, MPa | | |
|---|---|---|
| Age | | |
| 7 days | 28 days | 90 days |
| 28 | 39 | 47 |
| 22 | 41 | 52 |
| 18 | 34 | 42 |

## Coring

A number of hardened concretes were cored and these are showed in Figures 12 (a) and (b). They show well distributed aggregates with minimum voids and a close contact with rebar demonstrating that good quality concrete was obtained.

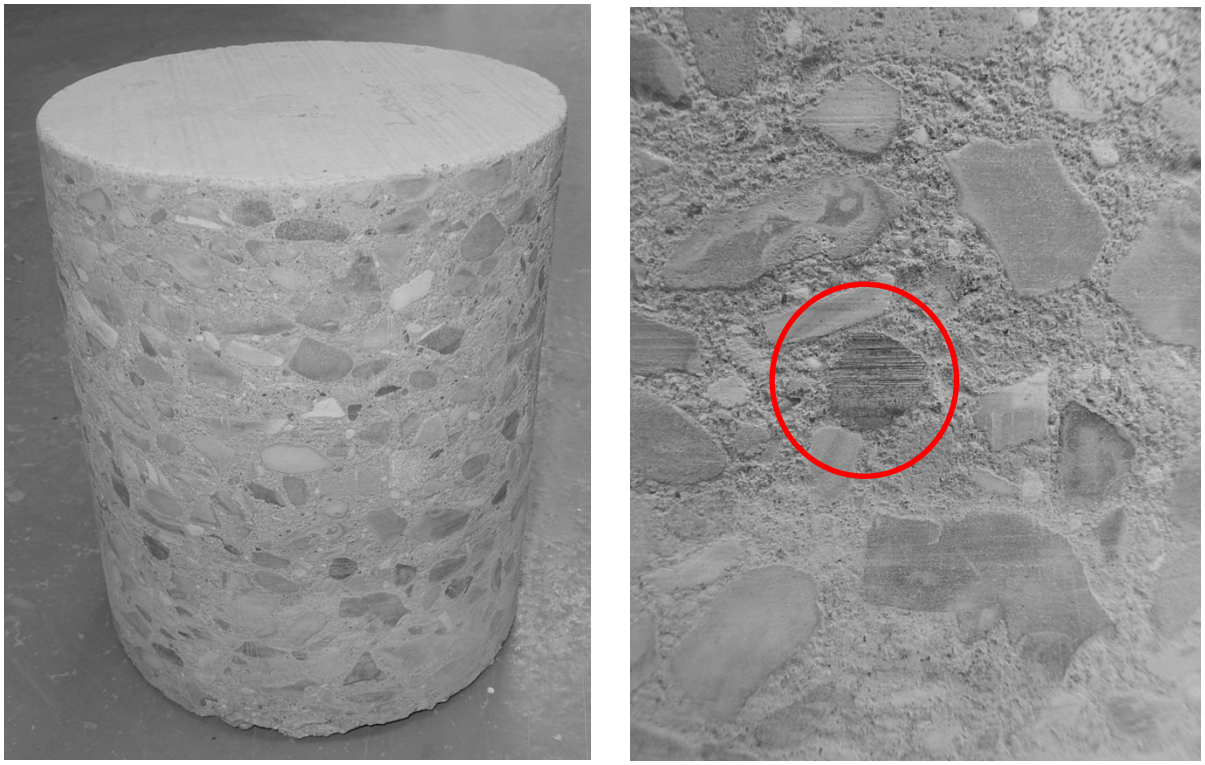

Figure 12 (a) Well Compacted Cemfree Concrete and (b) Cored Sample Showing Compaction Around Rebar in Red.

## Practical Applications

Noted below are several examples of recognisable structures resulting from the use of Cemfree concrete.
Example 1. This comprised a wall measuring 30m x 2.5m x 0.3m, containing 22.5 $m^3$ of Cemfree concrete. The entire wall was constructed in one day and consisted of several different surface finishes. The stages of construction are shown in the three figures below.

Mix design as used:
GGBS (Hanson Purfleet) 380 kg/m³
Cemfree Activator (David Ball Group) 20 kg/m³
4-20mm gravel (Hanson Needingworth) 1079 kg/m³
0-4mm sand (Hanson Needingworth) 801 kg/m³
Water 120 kg/m³

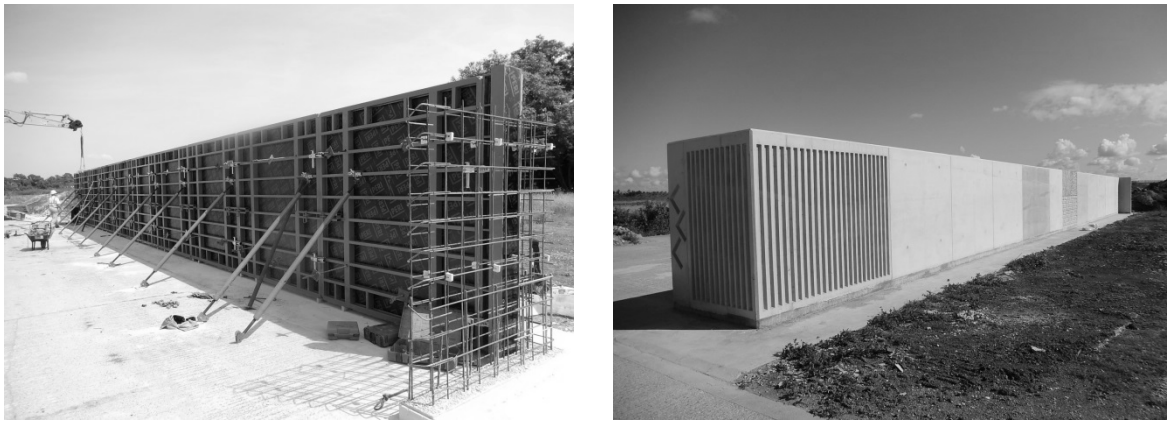

Figure 13 (a) Shuttering/reinforcement of one side of a wall and (b) finished wall showing a range of surface profiles.

Example 2. Functional decorative staircase at David Ball Group Ltd Head Quarters. The steps were pre-cast individually and integrated by way of pre-located reinforcement.

Figure 14 Decorative staircase and reception area. Staircase from separate precast units and the floor from self-compacting Cemfree concrete.

Example 3. Warehouse floor at David Ball Group Head Quarters measuring 36m by 24m and using 220 $m^3$ of Cemfree concrete (Figure 15). The entire floor was laid in one day and finished with using power floats the following day, with no joints cut. The method of placing and levelling was performed using a laser screeder. The mix design was the same as for Example 1.

Figure 15 Warehouse floor after power floating within 24 hours after placing.

Example 4. Pumpable version of Cemfree concrete used for a client in Chester, UK, to construct foundations for an extension to an existing office block. The compressive strength achieved 21.7 at 3 days, 25.7 MPa at 7 days and 30.6 MPa at 15 days.

Figure 16 Self compacting pumpable concrete for footings.

## TRANSFERING INNOVATIVE CONSTRUCTION MATERIALS INTO BEST PRACTICE

New materials often cannot comply with established specifications since by their nature may offer something new and a departure from established norms. In the case of Cemfree and other alkali activated products this problem is being addressed in conjunction with the UK's National Standardisation Body (BSI) to produce what is called a Publically Available Specification (PAS) which at time of writing this paper is at final draft stage with an intended publication date of March 2016[64]. The document identifies performance requirements set against appropriate PC based controls. The performance has to be equal to or better than.

The PAS may well become a National Standard in time but should help designers and specifiers to consider using these innovative materials. One issue that is difficult to predict with confidence is the long term durability, but usage of these new concretes has been reported in one way or another for over 50 years and indications are that such concretes have a good prognosis [65].

## CONCLUSIONS

- This work has shown that practical concretes can be made using the Cemfree activator concept based on GGBS and other precursors to geopolymers used in combination, but continuing no Portland cement. There has been much published work on high GGBS concretes containing some PC and caustic alkalis as activators, but little at 100% GGBS and less caustic alkalis [27, 37].

- Such concretes have a low carbon footprint. For instance 1 m3 of Cemfree based concrete at a binder level of 400 kg/m3 would be equal to 17.3 kg of CO2. The near equivalent for OPC based concrete would be 365 kg of CO2, a factor of 21 times.

- To make Cemfree concrete in a consistent manner may require tighter control over some common practices. This could also benefit PC based concretes.

- The issue of durability can only be addressed over time. However, there are many case histories of GGBS based concretes that have indicated comparable or better durability to PC concretes. The work using SEM and EDX has indicated strong similarities between the hydrated material in Cemfree concretes and that comprising GGBS/PC mixes, therefore the prognosis for durability is likely to be similar.

- Combinational mixes of GGBS/PFA showed increased strength over what can be obtained from GGBS alone. Such mixed comprise Cemfree Super.

- In the construction material sector whilst sustainability is desirable any additional cost is resisted. If the environmental issues associated with Portland cement are to be tackled seriously the cost burden has to be acknowledged and accepted.

- To bring materials innovation in construction as recognised good practice the manner in which materials are specified has to be reconsidered. Designers, consultants and clients wish to reduce risk associated with new materials that do not have a legacy of established use. As a consequence specifiers demand new materials comply with

standards or their accepted equivalents. Such standards usually relate to existing products and not to the innovations. This incompatibility can only be resolved by having performance based standards and specifications. How the performance is achieved becomes less relevant, current example of such a standard is ASTM C1157/C1157M-11 [22].

- In the case of Cemfree and other alkali activated potentially hydraulically active materials this change is happening in the UK via the British Standard Institution (BSI) by means of what is called a Publically Available Specification (PAS) [64]. The emergence of such an approach could assist the adoption of responsible innovation.

- Cemfree represents a significant advance towards durable and practical concretes having a very low carbon footprint as well as advantageous characteristics.

- Future work will concentrate on alkali-silica reactivity, freeze-thaw response and use of Nord Tests [53, 54] to monitor chloride ingress. In addition and expansive programme is in hand dealing with an extended range of mix designs, creep and exposure classes to mention some.

## REFERENCES

1. SHI C, JIMÉNEZ F, and PALOMO A, New Cements for the 21st Century, the Pursuit of Alternatives to Portland Cement, Cement and Concrete Research 41, 2011, p750-763.

2. SANJAYAN, J Non-Portland cement based concretes, Concrete in Australia, Vol 38, No1, p34-39, 2012.

3. HOSSEIN M. M., KARIM M. R., HOSSEIN M. K., ISLAM M. N., ZAIN M.F.M., Durability of mortar and concretes containing alkali-activated binder with pozzolans: a review., Construction and Building Materials 93, 2015, pp 95-109.

4. SCRIVENER, K.L., Options for the future of cement, The Indian Concrete Journal, 2015, July, Vol 88, Issue 7, pp11-21.

5. INTERNATIONAL ENERGY AGENCY, http://www.iea.org

6. GLASSER F.P, 40 Years of Cement and Concrete, ICT Yearbook 17th edition 2012/13, p17-24.

7. KÜHN K, Slag Cement and a Process of Making the Same, USA Patent 900939, 1908.

8. ROY D M, Alkali-Activated Cements, Opportunities and Challenges, Cement and Concrete Research, 29, 1999, p249-254.

9. PROVIS, J. L. Geopolymers and Other Alkali Activated Materials: Why, How and What?, Materials and Structures, 2014, 47,p11-25.

10. PROVIS, J.L., Green concrete or red herring – future of alkali-activated materials, Advances in Applied Ceramics, 2014, Vol 113, No8, pp472-477.

11. TÄNZER R, Concrete Based on Alkali-Activated Granulated Blast Furnace Slag (Part 1), Betontechnologie BFT International 03, 2012, p25-33.

12. DUNSTER A, QUILLAN K, ABORA K, Alkali-Activated Binder Concretes in Construction IP4/11,BRE May 2011 pp8, ISBN978-1-84806-189-7.

13. UNIVERSITY OF BRIGHTON, News and Events, 20th of May 2013. Contact z.osmond@brighton.ac.uk

14. UNIVERSITY OF QUEENSLAND, Global Change Institute Architecture and Design, 13th of September 2013.

15. TURENER L and COLLINS F, Geopolymers: A Greener Alternative to Portland Cement, Concrete in Australia, 39, No.1, p49-56.

16. TOMSON A, HOUSTON D, LEMMENS B, The Shart – Europe's Tallest Building, ICT Yearbook 2012-13, 17th edition, p52-58.

17. BS 8500-1:2006 + A1: 2012 (Complementary Standard to BS EN 206-1:2010)

18. BS EN 197-1:2011, Cement: Composition, Specification and Conformity Criteria for Common Cements.

19. BS 4246: 1996, Specification for High Slag Blast Furnace Cements.

20. CHI M, Effects of Dosage of Alkali-Activated Solution and Curing Conditions on the Properties of Durability of Alkali-Activated Slag Concrete, Construction and Building Materials, 35, 2012, p240-245.

21. LAW D W and ADAM A A, Durability Assessment of Alkali Activated Slags (AAS), Materials and Structures 45, 2012, p1425-1437.

22. ASTM C1157/C1157M-11, Standard Performance Specification for Hydraulic Cement, October 2011.

23. ACI, Building Code Requirements for Structural Concrete and Commentary, ACI 318-08 Section 3.2.1, 2008.

24. DAVID BALL GROUP LTD (Named inventors: David M. J. Ball, Martin Liska and Peter C. Hewlett). 2014. Cementitious binders, activators and methods of making concrete. UK Patent GB2504904.

25. DAVID BALL GROUP LTD (Named inventors: David M. J. Ball, Martin Liska and Peter C. Hewlett). Jan 2015. Activator Composition and Method for making Concrete. UK Patent Application No 1501173.7.

26. CONNELL M D, The Production of Ground Granulated Blast Furnace Slag, Concrete, September/October, 25, No6 1991, p11-16.

27. MIN SIK KIM, YUBIN JUN, CHANGHAN LEE, JAY EUN OH, Use of CaO as an activator for producing a price competitive non-cement structural binder using ground granulated blast furnace slag, Cement and Concrete Research, 54, 2013, p208-214.

28. SHI C, KRIVENKO P V, ROY, D M, Alkali-Activated Cements and Concretes, Taylor and Francis, 2006, pp376.

29. TANZA R., BUCHWALD A., STEPHAN D., Effect of slag chemistry on the hydration of alkali-activated blast-furnace slag, Materials and Structures, 2015, 48, pp629-641.

30. JALULL G., GANJIAN E., SADEGHI-POUYA H., Using ground granulated blast-furnace slag and mineral wastes to reduce cement in paving block. Construction Materials, 2014 (April), Vol 167, Issue CM2, pp91-103.

31. TSAI C.-J., HUANG R., LIN W.-T., CHIANG H.-W., Using GGBOS as the alkali activator in GGBS and GGBOS blended cements. Construction and Builiding Materials, 2014, 70, 501-507.

32. BOUGARA A., LINSDALE C., MILESTONE N. B., Reactivity and performance of blast furnace slags of different origin. Cement and Concrete Composites, 2010, 32, pp319-324.

33. PRIVATE COMMUNICATION, Hanson plc, 2013.

34. MORANVILLE-REGOURD M, Cements Made From Blast Furnace Slag, Chapter 11 in Lea's Chemistry of Cement and Concrete, 4th edition, edited by P C Hewlett, Butterworth-Heinemann, 2001, p637-678.

35. GARTNER E M and MACPHEE D E, A Physico-Chemical Basis for Novel Cementitious Binders, Cement and Concrete Research, 41, 2011, p736-749.

36. ESCALANTE-GARCIA J. I., PALACIOS-VILLANEUVA V.M., GOROKHOVSKI A.V., MENDOZA-SUAEZ G., AND FUENTES A.F. Characteristics of NaOH – activated blast furnace slag blending with a fine particle silica waste. Journal of American Ceramic Society, 85(7), 2002, p1788-92.

37. GRIST E.R., PAINE K.A., HEATH H., NORMAN J., PINDER H., Structural and durability properties of hydraulic lime – pozzolan concretes. Cement and Concrete Composites, 2015, 62, pp212-223.

38. RASHAD, A.M., BAI, Y., BASHEER, PAM, MILESTONE, M.D., COLLIER N.C., Hydration and properties of sodium sulphate activated slag. Cement and Concrete Composites. 37, 2013, p20-29.

39. THOMAS J F, ALLEN A J and JENNINGS H M, Density and Water Content of Nanoscale Solid CSH Formed in Alkali Activated Slag (AAS) Paste and Implications for Chemical Shrinkage, Cement and Concrete Research, 42, 2012, p377-383.

40. WANG S-D and SCRIVENER K L, Hydration Products of Alkali Activated Slag Cement, Cement and Concrete Research, 25, No3, 1995, p567-571.

41. RUIZ-SANTA QUITERIA C, SKLBSTED J, FERNANDEZ-JIMENEZ A and PALOMO A, Alkaline Solution/Binder Ratio as a Determining Factor in the Alkaline Activation of Alumino Silicates, Cement and Concrete Research, 42, 2012, p1242-1251.

42. DAIMON M, Mechanism and Kinetics of Slag Cement Hydration, 7th International Conference on the Chemistry of Cement (Paris 1980), Sub-Theme III-Z, p1-9.

43. GLUCHOVSKY V D, SILIC IND, 48 (10) 1983, p197-200.

44. GLUCHOVSKY V D, ROSTOVSKAJA G S and RUMYNA G V, 7th International Conference of the Chemistry of Cement (Paris 1980), Sub-Theme III-V, p164-168.

45. FALACIOS M and PUERTAS F, Effect of Superplasticiser and Shrinkage Inducing Admixtures on Alkali-Activation on Slag Pastes and Mortars. Cement and Concrete Research 35, 2005, p1358-1367.

46. KRIVEN W.M. Inorganic polysialates or “geopolymers”. American Ceramic Society Bulletin, Vol89, no4, 2010, pp34.

47. HABABA A. AND PLANK, J. Surface chemistry of ground granulated blastfurnace slag in cement pore solution and its impact on the effectiveness of polycarboxylate superplasticisers. Journal of American Ceramic Society, 95 (2) 2012 p768-775.

48. KASHANI, A. PROVIS, J. L. QILO, J.J. VAN DEVENTER J.S. J. The interrelationship between surface chemistry and rheology of alkali activated slag paste. Construction and Building Materials, 65,2014, p583-591.

49. BAMFORTH P B, Concreting Large-Volume (Mass) Pours, Chapter 13 from Construction of Deep Lifts and Large Volume Pours from BAMFORTH P B and PRICE W F, CIRIA, 1995, pp47.

50. CIRIA ,Control of Contraction Induced Cracking in Concrete, C660, 2007, p17-19.

51. CONCRETE SOCIETY, Permeability Testing of Site Concrete, a Review of Methods and Experience, CSTR31 Concrete Society, Table 19, 1987, pp75.

52. ASTM C1202-12, Standard Test Method for Electrical Indication of Concretes Ability to Resist Chloride Ion Penetration.

53. NORD TEST METHOD, NT.Build 492, 1999-11.

54. NORD TEST METHOD, NT.Build 443, 1995-11.

55. BERNAL, S.A. PROVIS, J.L. WALKLEY, B. SAN NICOLAS, R.. GEHMAN, J.D BRICE, D.J. KILCULLEN, A.R. DUXON P.AND VAN DEVENTER J.S.J.. Gel structure in alkali activated binders based on slag and fly ash and effects of accelerated carbonation. Cement and Concrete Research, 53, 2013, p127-144.

56. FREARSON J and SIMS I, Sandberg on Slag, Concrete, September/October 1991, 25, No 6, p37-40.

57. TÄNZER R, BOHNE T, STEPHAN D, Investigation on the Resistance of Alkali Activated GGBS to Alkali-Silica Reaction, First International Conference on the Chemistry of Construction Materials, October 7-9 2013 Berlin, GDCh-monograph, Vol 46, 9-12.

58. WINTER N B, WHD Report 1591, Cemfree Paste Samples, 31st October 2013, pp13.

59. REVIE W A, Certificate of Analysis 18/19.12.13 and 8/10/13.01.14 pp12, Construction Materials Consultancy Ltd.

60. PROVIS J L, First International Conference on the Chemistry of Construction Materials, October 7-9 2013 Berlin, GDCh-Monograph, Vol 46, 9-12.

61. REPORT DB-ABR-210613, Aston Services, June 2013, pp8.

62. CONCRETE SOCIETY, Curing, No 6, Concrete on site, Concrete Society 2010.

63. THE BRITISH STANDARD INSTITUTION, Draft PAS 8820:2016. Publically Available Specification. Construction materials – Alkali-activated cementitious material – Specification. The British Standard Institution, Expected publication date: January 2016.

64. EVANS I., GGBS its durability benefits. Concrete. 2015 (September), pp15-16.

# CARBONATION OF A LOW CALCIUM FLY ASH GEOPOLYMER CONCRETE

**M S H Khan** **A Castel** **A Noushini**

University of New South Wales

Australia

**ABSTRACT.** This paper investigates the carbonation resistance of a blended slag and low calcium fly ash (FA) geopolymer concrete. The geopolymer binder is composed of 90% low calcium FA and only 10% ground granulated blast furnace slag (GGBFS). The alkalinity of the pore solution plays a pivotal role in carbonation progression and subsequent corrosion initiation. pH profiles were measured to assess the pore solution alkalinity. Phenolphthalein indicator was used to measure the carbonation depth. X-ray diffraction (XRD) and quantification were carried out to identify and quantify the carbonation products. The obtained pH profiles illustrated a wider semi-carbonation zone in the geopolymer specimens although pH drop was insignificant in most cases. XRD revealed that nahcolite mainly formed at 3% $CO_2$ concentration and led to a significant drop in pH values. The results further demonstrated that 1% accelerated carbonation well replicated the natural carbonation process where only natron was identified as a carbonation product. This work contributes to the assessment of the risk of carbonation-induced reinforcement corrosion in low calcium FA geopolymer concrete.

**Keywords:** Geopolymer concrete; Carbonation; pH profile; XRD; Class F fly ash.

**M S H Khan** is a Research Associate at the School of Civil and Environmental Engineering, The University of New South Wales, Sydney.

**Professor A Castel** is Associate Professor in the School of Civil and Environmental Engineering at the University of New South Wales. He received his PhD from the University of Toulouse in France. His research expertise includes investigation of durability of construction materials, low carbon concrete, the performance and service life design of reinforced/prestressed concrete affected by steel corrosion.

**A Noushini** is a PhD candidate at the School of Civil and Environmental Engineering, The University of New South Wales, Sydney.

## INTRODUCTION

The increasing potential threats to environment imposed by $CO_2$ and the growing demand for concretes have promoted the development of inorganic polymer binder called 'geopolymer' which involves the reaction between solid aluminosilicate materials with alkaline solutions [1-3]. With the introduction of geopolymer concrete (GPC), the industrial by-products such FA and GGBFS, have been proposed and researched as aluminosilicate source materials due to their low cost and widespread availability.

GPC has the potential to be a suitable alternative to Ordinary Portland Cement (OPC) concrete; however, its long term durability is yet to be established [4]. Carbonation process plays a detrimental role to concrete as $CO_2$ diffuses through pore structure and reduces the alkalinity of the pore solution [5]. This may lead to the depassivation of reinforcing steel leaving them prone to corrosion. To date, there is relatively little existing knowledge on carbonation process in low calcium FA geopolymer concrete. Bernal et al. [6] carried out a detailed microstructural analysis to investigate the effects of accelerated carbonation on alkali activated FA and slag. It is important to mention that their study only focussed on powder samples allowing understanding some important and fundamental aspects of carbonation chemistry but the results were unlikely to represent the performance of concrete under natural exposure condition. Law et al. [4] measured the pH of the extracted pore water in geopolymer mortar specimens exposed to 5% accelerated carbonation and recommended a pH value of 11 to protect the reinforcing steel following carbonation. However, the pore solution extraction method is unlikely to provide the pore solution composition at the vicinity of the steel to assess the degree of depassivation. This necessitates an accurate measurement of pH profile along the depth of geopolymer concrete cover under natural and accelerated carbonation conditions.

This paper presents a wide range of pH profiles of low calcium FA geopolymer concrete exposed to natural and accelerated carbonation. XRD was carried out to identify and quantify the carbonation products. A correlation was established between natural and accelerated carbonation. The pH profile along with the identification and quantification of the carbonation products provide a precise evaluation of the degree of carbonation of low calcium FA geopolymer concrete.

## EXPERIMENTAL PROGRAM

### Materials

Low calcium FA (class F), ultra-fine FA also known as Kaolite high performance ash (HPA) and GGBFS were used in this study as aluminosilicate sources. Low calcium FA and Kaolite HPA were obtained from Eraring Power Station in New South Wales and Callide Power Station in Queensland, Australia, respectively, while GGBFS was obtained from Blue Circle Southern Cement Australia. The chemical compositions of these supplementary cementitious materials are available in Noushini et al [7]. A mixture of sodium hydroxide (NaOH) solution and sodium silicate ($Na_2SiO_3$) solution were used with the ratio of 1:2.5 (by mass) according to Hardjito and Rangan [8]. The technical grade NaOH pellets obtained from Ajax Finechem were used to prepare NaOH solution and 361 g of NaOH pellets were dissolved into 639 g of Sydney tap water in order to obtain 12M NaOH solution. The $Na_2SiO_3$ solution was obtained from PQ Australia and has a chemical composition of $Na_2O$ = 14.7%, SiO2 = 29.4% and H2O = 55.9% (by mass) with a modulus ratio (Ms) of 2 (Ms = $SiO_2/Na_2O$ = 2). It is to be noted that the activator solutions were mixed together 24 hours prior to usage.

Sydney sand with specific gravity of 2.65 and water absorption of 3.5% was used as fine aggregate. The coarse aggregate was 10 mm nominal size crushed basalt with specific gravity of 2.8 and water absorption of 1.6%. To accurately adjust the mix water, all aggregates were oven dried to drive away the moisture content.

### Geopolymer concrete mix design and batching procedure

The geopolymer concrete mix detail is presented in Table 1. The solid contents except GGBFS were mixed dry for 5 minutes which followed further 15 minutes mix while gradually adding the alkaline solution and then the free water. To avoid rapid setting, GGBFS was added at the end and the mixing was continued for another 5 minutes. The moulds were filled in three layers and compacted using a vibrating table. The obtained slum and air content of the freshly mixed concrete were 120 mm and 3.5% respectively.

Table 1 Mix details for geopolymer concrete

| MATERIALS | PROPORTION, kg/m$^3$ |
|---|---|
| Coarse aggregate | 1221.2 |
| Fine aggregate | 620.8 |
| Fly ash | 271.6 |
| Kaolite HPA | 77.6 |
| GGBFS | 38.8 |
| NaOH solution | 55.3 |
| $Na_2SiO_3$ solution | 138.7 |
| Free water | 13.3 |
| $Na_2SiO_3$ / NaOH | 2.5 |
| Molarity of NaOH solution | 12 M |

### Curing and $CO_2$ exposure conditions

In a previous study by Noushini et al. [7], the influence of 12 different heat-curing regimes on mechanical properties of a FA GPC was investigated. The curing regimes included three temperatures of 60, 75 and 90°C, and four curing durations of 8, 12, 18 and 24 h. The optimum heat-curing regime for GPC, combining best performance and energy efficiency, was found to be 75°C for 18 h. Therefore, in this study, the sealed samples were placed in an oven at 75°C for 18 hours for heat curing and the samples were then demoulded. To achieve a uniform moisture redistribution, the samples were kept in an environmental chamber for two weeks at a constant temperature of 23 ± 2°C and 55% relative humidity. After the dry conditioning, 25 mm section was removed from top and bottom of each cylinder and remaining segment was cut into 50 mm sections for subsequent carbonation testing. 50 mm discs were sealed using aluminium tapes along the perimeter leaving top and bottom sides exposed for $CO_2$ diffusion. For natural carbonation, the specimens were kept in a controlled environmental room. For accelerated carbonation, the specimens were placed in a carbonation chamber with a $CO_2$ concentration of 1% and 3%. It is to be noted that the exposure temperature and relative humidity, in all cases, were 23°C and 55% respectively. The carbonation depth, pH profiles and the microstructure analysis were performed after 2, 4 and 6 weeks of exposure. Some of the specimens exposed to the natural carbonation were analysed after 6 and 18 months to establish a correlation between natural and accelerated carbonation.

### pH profile and carbonation depth

pH profiles were obtained by combining water extraction method [9] and pore solution extraction method [10]. For water extraction method, concrete powder was sampled every 1 mm over 25 mm depth of the GPC specimen by using a Profile Grinder PF-1100 purchased from Germann Instruments. The powder was then mixed with de-ionised water with a solid to liquid ratio of 1:1 and the pH of the solution was measured using a pH probe. Water extraction method always overestimates the pH value [9]. As a result, the trend provided by the pH profile is accurate but not the pH values. To overcome this effect, pore solution was extracted from uncarbonated paste samples (having the same mix design and curing condition as the GPC) [10]. The pH of the extracted pore solution was directly measured by using a calibrated pH probe and then compared to the one obtained by using water extraction method for uncarbonated specimen. The difference between these two pH values were then deducted from all water extracted pH values in order to obtain the calibrated pH profile. To assess the carbonation depth, each specimen was split and 1% phenolphthalein was sprayed on the fractured surface.

### Identification and quantification of the carbonation products in geopolymer concrete

X-ray diffraction (XRD) was carried out in this study to identify and quantify the carbonation products in the geopolymer specimens. 50 mm cube specimens were cast with geopolymer paste having the same mix design and curing conditions as the GPC. Samples were collected from the surface of the cube for the XRD analysis. The paste samples were ground to powder and the powder were analysed using X-ray diffractometer Phillips X'Pert Pro Multi-purpose (MPD) system housed at the Mark Wainwright Analytical Centre at the University of New South Wales, Australia. This used Cu-Kα radiation with wavelength of 0.15418 nm and operated at 45 kV and 40 mA, scan range 5-65$^o$ and 0.026$^o$ 2θ step size. The scan results were interpreted using the software package HighScore Plus for phase identification. The crystalline phases were also quantified by using the software package HighScore Plus that is based on Rietveld method [11].

## RESULTS AND DISCUSSIONS

The average compressive strength and the elastic modulus of the GPC samples at 28 days were 55.7 MPa and 23.8 GPa respectively.

### Identification and quantification of carbonation products by using XRD

XRD patterns of geopolymer pastes exposed to natural, 1% accelerated carbonation (AC) and 3% AC are shown in Figures 1, 2 and 3 respectively. Figure 1 shows that natron ($Na_2CO_3.10H_2O$) was identified after 6 weeks of natural carbonation and this was the only carbonation products under natural conditions. It is interesting to note that the same carbonation product was observed for 1% AC. Figure 3 reveals that the elevated $CO_2$ concentration led to the formation of nahcolite ($NaHCO_3$) even after 2 weeks of exposure. It is important to mention that Bernal et al. [6] observed nahcolite in the powder sample even at 1% AC after 1 week of exposure. This indicates that GPC powders exposed to accelerated carbonation are likely to suffer a higher extent of carbonation reaction compared to GPC specimens.

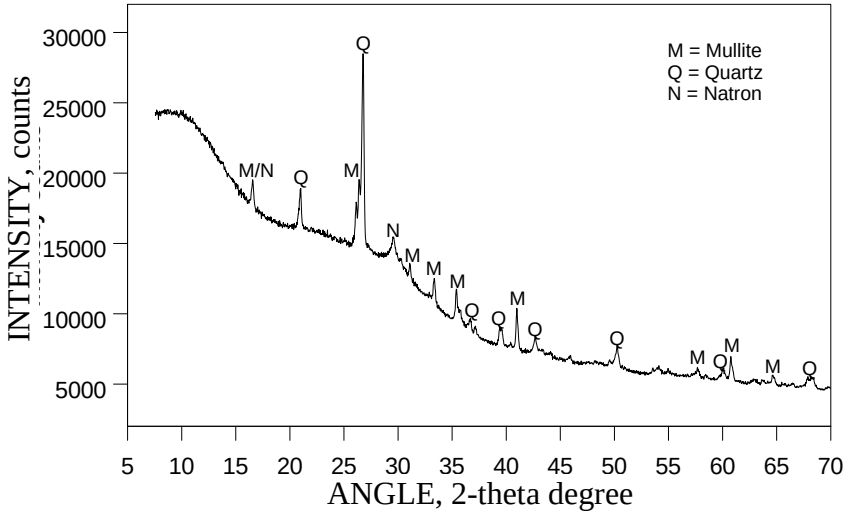


Figure 1 XRD traces of geopolymer pastes exposed to natural carbonation for 6 weeks

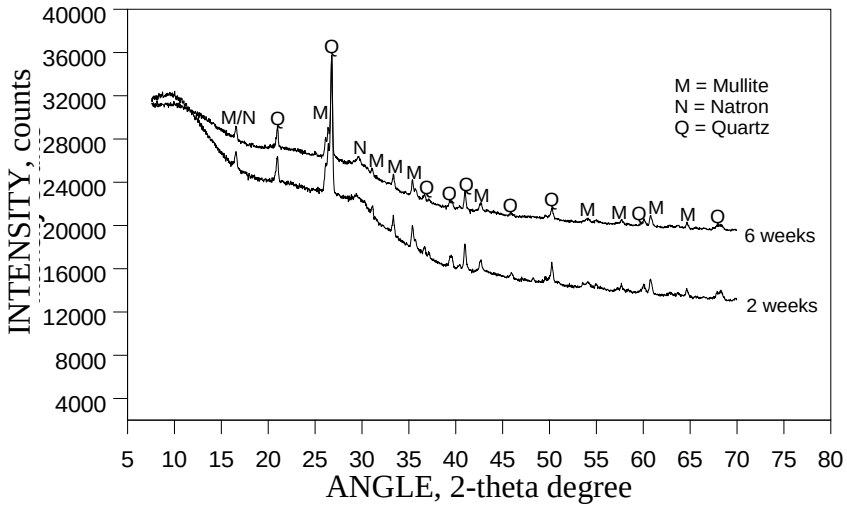


Figure 2 XRD traces of geopolymer pastes exposed to 1% AC for 2 & 6 weeks

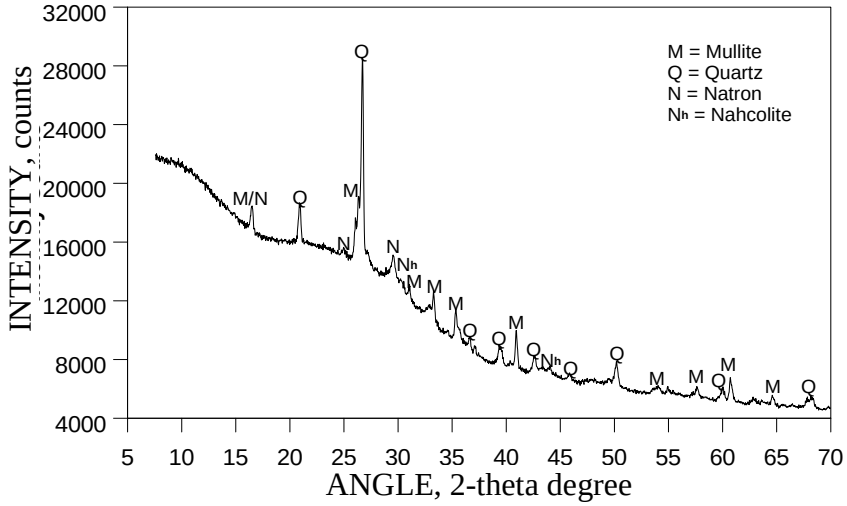


Figure 3 XRD traces of geopolymer paste exposed to 3% AC for 2 weeks

Table 2 shows the quantification of the crystalline phases formed in the geopolymer pastes exposed to carbonation. Table 2 reveals that natron comprised almost one-fourth of the crystalline phases in the specimens after 6 weeks natural carbonation and 2 weeks 1% AC respectively. Its proportion increased to 29.4 wt.% after 6 weeks 1% AC. However, it can be seen that the proportion of nahcolite was 17.4 wt.% while the proportion of natron decreased to 6.3 wt.% after 2 weeks of 3% AC. This shows that high $CO_2$ concentration (>1%) can lead to the transformation of natron to nahcolite.

Table 2 Quantification of the crystalline phases formed in pastes exposed to $CO_2$

| EXPOSURE CONDITION | MULLITE, wt.% | QUARTZ, wt.% | NATRON, wt.% | NAHCOLITE, wt.% |
|---|---|---|---|---|
| Natural carbonation – 6 weeks | 42.2 | 33.8 | 24.0 | - |
| 1% AC – 2 weeks | 42.6 | 33.0 | 24.3 | - |
| 1% AC – 6 weeks | 38.5 | 32.2 | 29.4 | - |
| 3% AC - 2 weeks | 41.4 | 34.9 | 6.3 | 17.4 |

**pH profile and carbonation depth in GPC**

The pH values obtained from pore extraction and water extraction method for an uncarbonated specimen were 11.46 and 12.13 respectively. This difference of 0.67 was deducted from each water extracted value to obtain the calibrated pH profiles. The split uncarbonated GPC specimen sprayed with phenolphthalein indicator and the pH profile are shown in Figure 4. As expected, the dark pink colour throughout the fractured surface of the specimen indicates no carbonation. Figure 4 also shows that the pH values of uncarbonated GPC is close to 11.5 which has also been previously reported by other researchers, showing that pH value can range from 11.5 to 12.5 in GPC [12]. In the case of OPC concrete, the pH value is greater than 12.5 in the uncarbonated zone and around 8.5 in the fully carbonated zone. The pH value of 8.5 in carbonated OPC concrete is due to the formation of calcium carbonate [12-14]. These two values were considered in this study to compare to the alkalinity of GPC exposed to carbonation.

Figure 5 illustrates the pH profiles of GPC exposed to natural carbonation. Up to 6 weeks exposure, the maximum drop in pH value was about 0.46 and all the profiles converged to uncarbonated profile at about 6 mm depth. The pH profiles suggest that for natural carbonation, 6 weeks exposure may not be sufficient to assess the durability and therefore GPC specimens were exposed for extended period to evaluate their resistance against natural carbonation. It can be seen that the minimum pH value was 10.76 after 6 months exposure. The minimum pH values were 10.2 and 9.8 for specimen 1 and 2 respectively after 18 months exposure although the pH values reached above 10.5 beyond 3 mm depth.

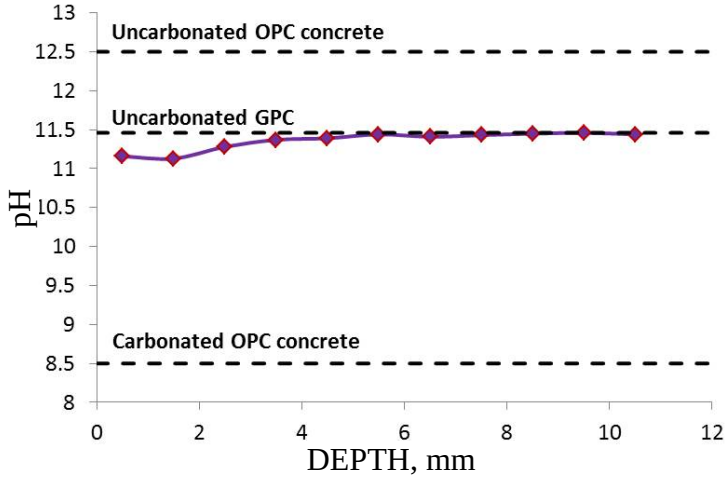


Figure 4 pH profile of uncarbonated GPC

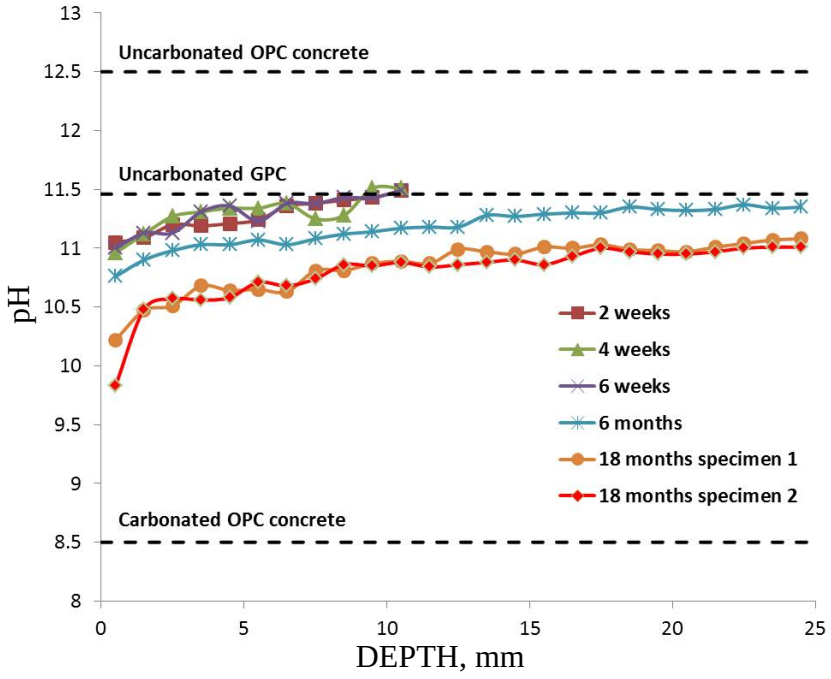


Figure 5 pH profiles of GPC exposed to natural carbonation

Figure 6 shows the pH profiles for GPC exposed to 1% AC. It can be seen that the profiles were very similar after 2 and 4 weeks exposure while the profile after 6 weeks exposure experienced a higher drop in pH. In all cases, the pH value dropped below 10 at 1mm depth and then gradually converged to uncarbonated zone. Pore blockage plays a vital role in controlling the diffusion of $CO_2$ through concrete.

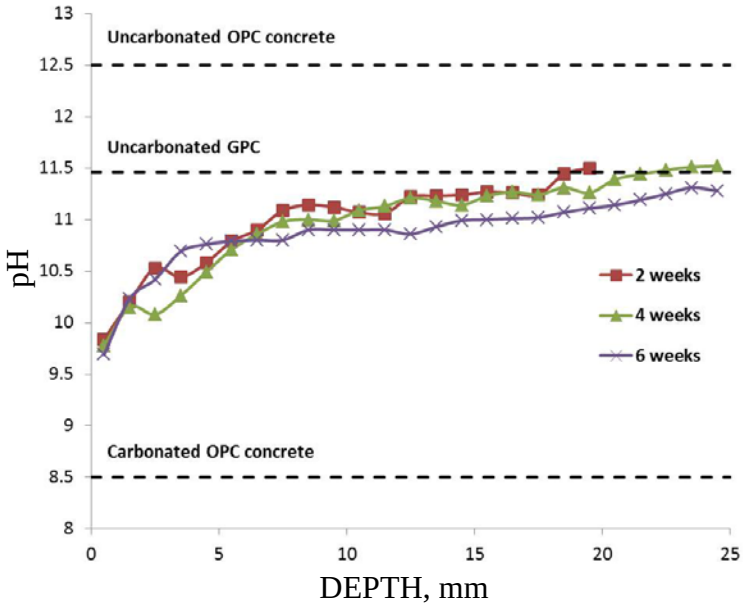


Figure 6 pH profiles of GPC exposed to 1% AC

Natron has a very large molar volume (196.56 $cm^3$/mol) compared to nahcolite (38.66 $cm^3$/mol) and calcite (36.93 $cm^3$/mol) (www-mincryst - IEM Databases). Therefore, natron fills a large pore space, and thus provides a significant degree of pore blockage in carbonated low calcium FA GPC [15]. The significant amount of natron formed in 1% AC specimens might have slowed down $CO_2$ diffusion by enhancing the degree of pore blockage, and thus the pH profiles did not experience a significant drop compared to the pH profiles obtained with 3% AC (Figure 7).

Figure 7 shows the pH profiles of GPC specimens exposed to 3% AC. Each of the profiles experienced a significant drop in pH and attained a fully carbonation stage with pH values ranging between 9.25 to 9.45. After 2 weeks exposure, the fully carbonated depth was 8mm and beyond that point, the pH values gradually increased and converged to uncarbonated profile at around 25 mm depth. After 4 and 6 weeks of exposure, the fully carbonation depth extended further and none of them could reach uncarbonated pH at 25 mm depth.

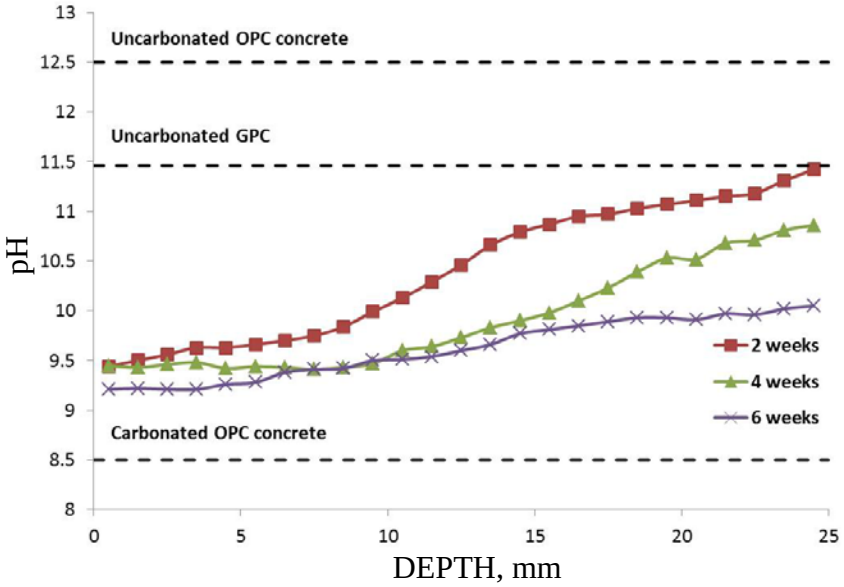


Figure 7 pH profiles for GPC exposed to 3% AC

The quantification revealed that a significant amount of nahcolite formed even after 2 weeks of exposure. The molar volume of nahcolite is five times smaller than that of natron. This fills less space and thus provides lower degree of pore blockage which might have inspired $CO_2$ diffusion to a greater extent. Furthermore, the alkalinity of nahcolite is much lower than that of natron (http://www.engineeringtoolbox.com/). Therefore, nahcolite formation is the most possible reason for the significant lower pH values measured in the specimens exposed to 3% AC compared to natural and 1% AC conditions.

## Carbonation depth of GPC

Figures 8 and 9 show the pH profile and the split specimen sprayed with phenolphthalein indicator after 18 months natural carbonation and 6 weeks 1% AC respectively. It is to be noted that the specimen exposed to 18 months natural carbonation was sealed in bottom side only.

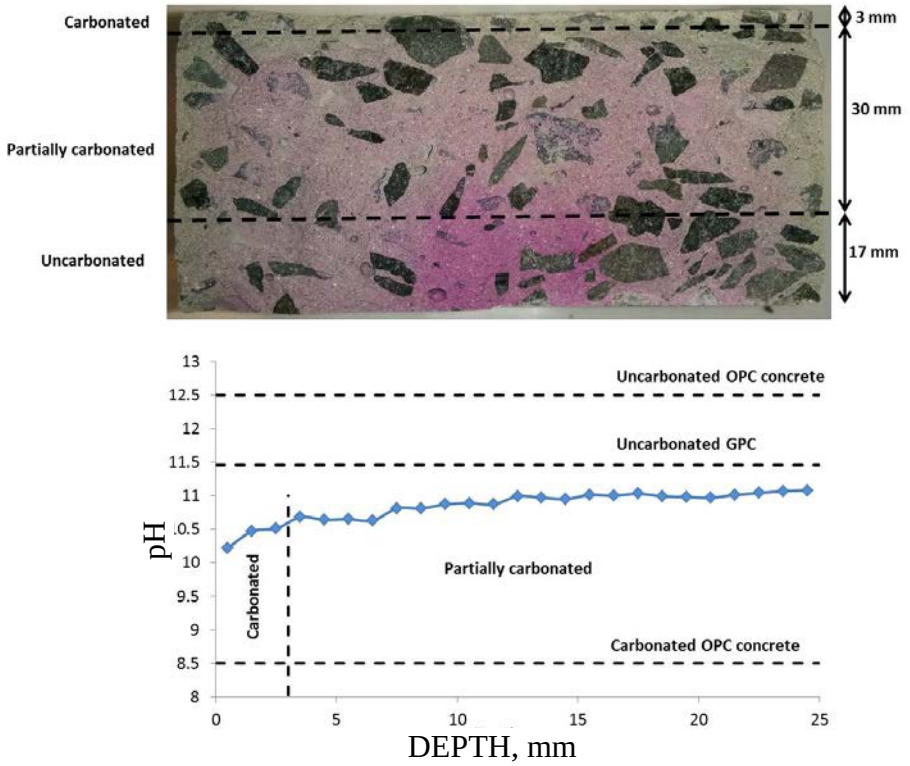


Figure 8 pH profile and carbonation depth of GPC exposed to natural carbonation for 18 months

Three stages were observed in all specimens: carbonated (colourless), partially carbonated (faded colour) and uncarbonated (coloured). Figure 8 reveals that after 18 months natural carbonation, the fully carbonated depth was only 3 mm. The faded colour zone was about 30 mm and beyond 33 mm depth, the concrete was uncarbonated. After 6 weeks 1% AC, the colourless depth was only 2 mm and the faded colour zone was 21 mm. OPC concrete usually displays a clear border between the coloured and colourless zone when sprayed with phenolphthalein indicator [5] and the pH profile shows a narrow partially carbonated zone [13]. However, this was not the case of GPC in this study where faded colour was scattered throughout an elongated depth. The pH profiles suggest that the pH value did not drop below 10.5 in the partially carbonated zone after 18 months natural carbonation. Furthermore, the minimum pH value was 10.42 after 6 weeks 1% AC in the faded region (Figure 9). These

results indicate that this partially carbonated zone may still provide chemical protection against corrosion. Therefore, it may not be appropriate to consider the faded colour region or the partially carbonated zone as an integral part of the carbonation depth in GPC. Instead, the colourless depth offered a range of pH values that, in some case, may be inadequate to sustain the passivity of steel bar and it would be more appropriate to consider this colourless depth as carbonation depth in low calcium FA GPC. To provide a more precise and conclusive result in this matter, experiments are in progress to measure the corrosion current of steel bar embedded in similar concrete.

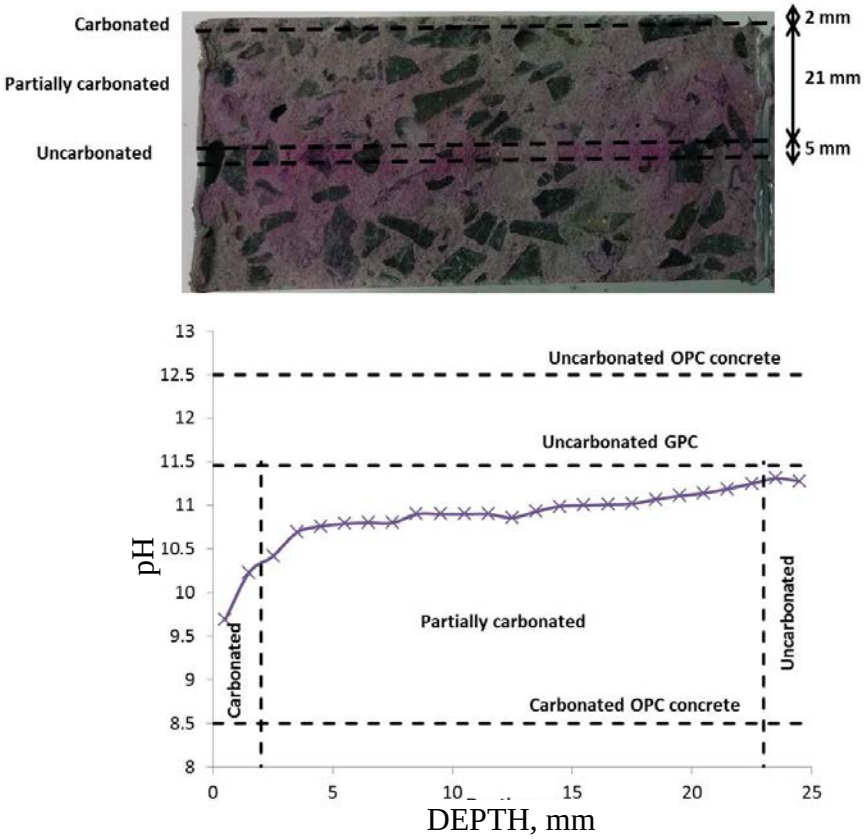


Figure 9 pH profile and carbonation depth of GPC exposed to 1% AC for 6 weeks

**Correlation between natural and accelerated carbonation**

The natural carbonation process may last more than tens of decades. To assess the long term performance of concrete structures, it is desirable to accelerate the carbonation process to curtail the duration. If an accelerated carbonation test would accurately replicate the natural carbonation conditions, a correlation between natural and accelerated carbonation could be established [15]. However, the $CO_2$ concentration used during the accelerated testing strongly affects the pore structure and the composition of pore solution in alkali activated concrete. It is therefore not recommended to carry out accelerated carbonation testing of alkali activated binders at $CO_2$ concentration exceeding 1% [16]. It can be seen from Figure 10 that both pH profiles of 18 months natural carbonation reasonably converged to the pH profile of 6 weeks 1% AC. This indicates that the carbonation products so as the pore solution composition might have been similar in both cases. It is therefore reasonable to conclude that 6 weeks 1% AC is likely to replicate what is happening after 18 months natural carbonation of low calcium FA GPC. Thus 1% AC test is likely to provide an accurate service life prediction of low calcium FA GPC.

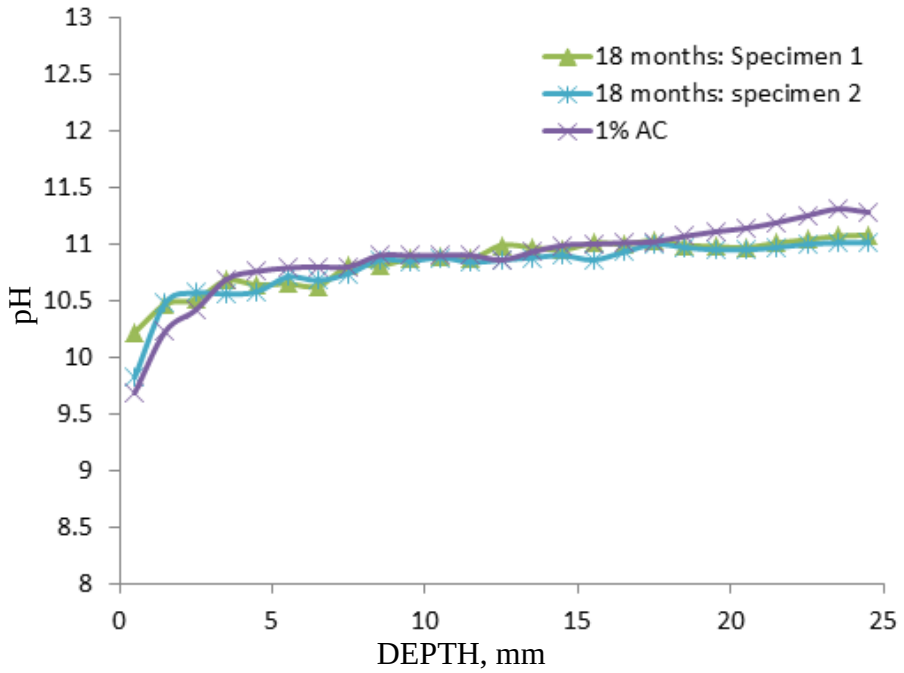


Figure 10 Correlation between natural and accelerated carbonation in GPC

## CONCLUSION

XRD results revealed that natron was the only carbonation product in the specimen exposed to natural and 1% AC for 6 weeks. Quantification showed that natron is about one-fourth of the crystalline phases in both exposure conditions. On the other hand, nahcolite started to form just after 2 weeks of 3% AC and its crystalline proportion was 17 % (wt.) while the proportion of natron was only 6.3 % (wt.).

Under natural and 1% accelerated carbonation exposure, the pH values did not experience a significant drop and none of the pH profiles showed a clear indication of a fully carbonation zone due to the formation of natron only. On the other hand, the specimens exposed to 3% AC experienced significant drop in pH values and the pH profiles offered an extended fully carbonated zone.

The phenolphthalein indicator test showed faded colour throughout an elongated depth although the pH values did not drop significantly. Therefore, this faded colour region may not be an integral part of the carbonation depth in low calcium fly ash geopolymer concrete. Instead, colourless depth would be more appropriate to consider as carbonation depth in geopolymer concrete.

The results demonstrated that 1% AC for 6 weeks replicated 18 months natural carbonation and thus 1% AC is likely to provide an accurate natural carbonation prediction of geopolymer concrete.

## ACKNOWLEDGEMENT

This research is funded by the CRC for Low Carbon Living Ltd supported by the Cooperative Research Centres program, an Australian Government initiative.

## REFERENCES


1. DAVIDOVITS J. Properties of geopolymer cements. Proceedings of the First International Conference on Alkaline Cements and Concretes, Ukraine, 1994.
2. DUXSON P., FERNANDEZ-JIMENEZ A., PROVIS J.L., LUKEY G.C., PALOMO A. and Van DEVENTER J.S.J. Geopolymer technology: the current state of the art. Journal of Material Science, Vol. 42, 2007, pp. 2917–2933.
3. DAVIDOVITS J. Geopolymer chemistry and application, Institut Géopolymère, Saint-Quentin, France, 2011.
4. LAW D.W., ADAM A.A., MOLYNEAUX T.K., PATNAIKUNI I. and WARDHONO A. Long term durability properties of class F fly ash geopolymer concrete. Materials and Structures, Vol. 48, 2014, pp. 721–731.
5. CHANG C-F. and CHEN J-W. The experimental investigation of concrete carbonation depth. Cement and Concrete Research, Vol. 36, 2006, pp. 1760–1767.
6. BERNAL S.A., PROVIS J.L., WALKLEY B., NICOLAS R.S., GEHMAN J.D., BRICE D.G., KILCULLEN A.R., DUXSON P. and Van DEVENTER J.S.J. Gel nanostructure in alkali-activated binders based on slag and fly ash, and effects of accelerated carbonation. Cement and Concrete Research, Vol. 53, 2013, pp. 127–144.
7. NOUSHINI A., BABAEE M. and CASTEL A. Suitability of heat-cured low-calcium fly ash-based geopolymer concrete for precast applications. Magazine of Concrete Research, 2015, DOI: 10.1680/macr.1615.00065.
8. HARDJITO D. and RANGAN B.V. Developments and properties of low calcium fly ash based geopolymer concrete, Curtin University of Technology, Perth, Australia, 2005.
9. HAQUE M.N. and KAYYALI O.A. Free and water soluble chloride in concrete. Cement and Concrete Research, Vol. 25, No. 3, 1995, pp. 531–542.
10. BARNEYBACK R.S. and DIAMOND S. Expression and analysis of pore fluids from hardened cement pastes and mortars. Cement and Concrete Research, Vol. 11, 1981, pp. 279–285.
11. RIETVELD H.M. A profile refinement method for nuclear and magnetic structures. Journal of Applied Crystallography, Vol. 2, 1969, pp. 65–71.
12. DAVIDOVITS J. Geopolymer chemistry and sustainable development. The Poly(sialate) terminology: a very useful and simple model for the promotion and understanding of green-chemistry. Proceedings of the World Congress Geopolymer, Saint Quentin, France, 2005.
13. JI Y-S., YUAN Y-S., SHEN J-L., MA Y. and LAI S. Comparison of concrete carbonation process under natural condition and high $CO_2$ concentration environments. Journal of Wuhan University of Technology, 2010, pp. 515–522.
14. JI Y-S., WU M., DING B., LIU F. and GAO F. The experimental investigation of width of semi-carbonation zone in carbonated concrete. Construction and Building Materials, Vol. 65, 2014, pp. 67–75.
15. BERNAL S.A., PROVIS J.L., BRICE D.G., KILCULLEN A., DUXSON P. and Van DEVENTER J.S.J. Accelerated carbonation testing of alkali-activated binders significantly underestimates service life: The role of pore solution chemistry. Cement and Concrete Research, Vol. 42, 2012, pp. 1317–1326.
16. PROVIS J. and Van DEVENTER J.S.J, Eds. Alkali Activated Materials: State-of-the-Art Report RILEM TC 224-AAM, 2014.

# DURABILITY OF ALKALI-ACTIVATED FLY ASH AND SLAG CONCRETE

**K Arbi**

**M Nedeljković**

**Y Zuo G Ye**

Delft University of Technology

The Netherlands

**ABSTRACT:** The aim of this study is to provide new insights on durability properties of AAM and to assess their resistance under severe conditions. For that purpose, concrete specimens have been exposed to accelerated carbonation (varying the curing and the exposure times from 7 to 28 days). After 28 days curing, their chloride resistance has been assessed using the non-steady-state chloride migration experiments following the NordTest method (NT Built 492). Prior to durability test, the compressive strength of investigated mixtures was determined at early ages (1, 7 days) and after 28, 56, 90 days curing. The slag-rich mixtures have shown high compressive strength values (~45MPa after 1 day and ~80MPa after 28 days curing). Excellent mechanical properties have been also found for the fly ash-rich mixtures at early and late curing ages (15MPa after only 1 day and ~50MPa after 28 days curing). From carbonation test, it has been found that the carbonation depth increases as increasing fly ash/slag ratio or the exposure time. However when curing time is increased, a decrease on carbonation depth was observed. When the concrete specimens were exposed to chloride ingress, a high chloride permeability associated with higher concrete porosity was found for fly ash-rich mixtures with a chloride penetration depth of 18mm and chloride migration coefficient near 15-17×$10^{-12}$$m^2s^{-1}$. These parameters decreased considerably as increasing slag content reaching values near 5mm and 2×$10^{-12}$$m^2s^{-1}$, respectively.

**Keywords:** Geopolymer, Alkali-activated materials (AAM), Durability, Fly ash, slag.

**Dr Kamel Arbi** is a Postdoc researcher at the department of Materials and Environment (Microlab), Faculty of Civil Engineering & Geosciences, Delft University of Technology. He is a member of the RILEM Technical Committee TC DTA-247 (Durability Testing of Alkali-activated materials). **Marija Nedeljković** is a PhD student in the Faculty of Civil Engineering and Geosciences, Delft University of Technology. **Yibing Zuo** is a PhD student in the Faculty of Civil Engineering and Geosciences, Delft University of Technology. **Dr. Guang Ye** is associate professor at Microlab/Section Materials and Environment, faculty of Civil Engineering and Geosciences, Delft University of Technology. He is member of a few RILEM Technical Committees and fib workgroups.

## INTRODUCTION

The growing demand for concretes with high performances, lower cost and reduced environmental impact when compared to those produced with conventional Portland cements has promoted the development of clinker-free or almost free alternative cementitious materials. Among them, alkali-activated materials (AAM) [1-6] and those classified as geopolymers [7, 8], are a high-profile example able to produce cement and concrete with the advantages of Portland cements but with a large reduction in $CO_2$ emissions and general aspects of good performances such as high mechanical strength at early ages of curing, high stability in aggressive environments and resistance to elevated temperatures, among others [9-13]. The bulk application of these new binders is still limited because there are still some uncertainties regarding their durability and degradation mechanisms under severe conditions [14-17]. The effect of chloride diffusion and $CO_2$ exposure on the concrete structure is probably the most extensively observed and assessed aspect of concrete durability as both attacks lead to the degradation of embedded steel reinforcing and account for over 50% percent of the deterioration of concrete structures [18]. However, there is limited existing knowledge about these phenomena in concretes based on AAM despite the increasing interest on durability issues of these new binders along the past few years. In most published works dealing with AAM resistance either to carbonation or to chloride ingress, there is no general agreement whether these materials exhibit better, similar or worse durability performances than conventional cements. There are also some contradictory conclusions regarding the evolution of carbonation rate, the effect of carbonation on mechanical properties or even the correlation between natural and accelerated carbonation of AAM [19-25]. From thermodynamic calculations related to pore-solution chemistry, Bernal et al. [21] stated that if an alkali-activated concrete and a Portland cement concrete show the same carbonation depth in an accelerated test, the AAM will suffer less carbonation under natural conditions, and thus the service life would be much longer. Low et al. [19] found that the carbonation of alkali activated slag was higher than that of blended slag-Portland cement, and Portland cement based concrete. Hakkinen [22] observed 40% higher compressive strength after 22 months of accelerated carbonation compared to the same materials after 28 days of curing; however Bernal et al. [23, 24] found that these materials decrease notably in compressive strength with accelerated carbonation. Bakharev et al. [20] reported higher strength reduction and higher susceptibility to carbonation in alkali-activated slag concrete than in ordinary Portland concretes. Conversely, Deja [25] reported that alkali-activated slag mortars and concretes showed carbonation depths comparable to those obtained for reference samples of Portland cement, along with increased compressive strengths as increasing exposure time to $CO_2$. These results were associated with a refinement of the pore structure, as carbonates precipitated during the carbonation reaction. It has been reported [26] that AAM demonstrate better performance against chloride ingress, according to both accelerated (NordTest NT Build 492) and ponding (ASTM C1543) methods; but Law et al. [19] concluded that alkali-activated slag concretes exhibited lower durability properties (water sorptivity, chloride and carbonation resistance) than Portland cement and blended concretes.

Considering the current state-of-the-art, there are still some uncertainties and lack of consensus regarding the durability performances of AAM mostly when compared to Portland cement under carbon dioxide or chloride ingress. The present study reports an investigation on durability performances of alkali-activated fly ash and slag concretes. The aim of this work is to provide new insights for a better understanding of durability properties of AAM and to assess their resistance under accelerated carbonation and chloride ingress.

## MATERIALS AND METHODS

### Materials

Solid precursors used for the preparation of concretes are a class F fly ash (according to ASTM C618-12a [27] from VLIEGASUNIE BV and a blast furnace slag (BFS) supplied by ORCEM (The Netherlands). FA has a specific gravity of 2440 kg/m$^3$ and 82% of particles with size less than 45µm, compared to 2890 kg/m$^3$ and 95% of particles with an average size of 45µm for BFS. The chemical compositions of the FA and BFS determined by X-ray fluorescence (XRF) spectroscopy are shown in Table 1. Gravel is crushed granite with nominal sizes of 4-16 mm and a specific gravity of 2640 kg/m$^3$. Fine aggregate is natural sand having a specific gravity of 2620 kg/m$^3$ and particle size of 0-4 mm. All mixtures were activated using a multi-compound activator solutions (low concentration) formulated by blending a commercial sodium silicate solution (27 wt% $SiO_2$, 8 wt% $Na_2O$ and 65 wt% $H_2O$), and NaOH solution. The $Na_2SiO_3$ solution supplied by BRENNTAG (Netherlands) has a specific gravity of 1350 kg/m$^3$ and a modulus ratio Ms=3.37.

Table 1 Chemical composition of FA and BFS as deduced from XRF data

| Oxide | $SiO_2$ | $Al_2O_3$ | CaO | MgO | $Fe_2O_3$ | $SO_3$ | $Na_2O$ | $K_2O$ | $TiO_2$ | $P_2O_5$ | L.O.I |
|---|---|---|---|---|---|---|---|---|---|---|---|
| BFS | 34.40 | 11.53 | 39.17 | 7.81 | 1.42 | 1.60 | 0.23 | 0.58 | - | - | 1.15 |
| FA | 54.28 | 23.32 | 4.23 | 1.62 | 8.01 | 0.64 | 0.85 | 1.97 | 1.23 | 0.54 | 3.37 |

### Concrete preparation

Concrete specimens were produced in a 40 L laboratory pan mixture by mixing first the coarse and fine aggregates for 2 min followed by the precursors for additional 3 min to get a homogenous mixture and the premixed alkaline activator solution (prepared one day before casting) was then added gradually and the mixing continued further for about 3-5 min. The concretes were produced in 150 mm cubic moulds with binder content of 400 kg/m$^3$, activator solution to binder ratio of 0.50 and a binder to aggregates ratio of 1:4.3 by weight. After casting, The specimens were sealed and cured in laboratory conditions for 24 h, then demoulded and stored in a curing chamber (99%RH, 20 ± 2 C) until testing. Three mixtures with the following FA/BFS ratios 70:30, 50:50, 30:70 named respectively S30, S50 and S70 have been prepared.

### Testing methods

The concrete carbonation resistance was assessed according to a slightly modified form of the standard EN 13295:2004 [28]. After the desired curing is achieved (7, 14, 21 and 28 days) the specimens were removed from the humidity chamber, and then the cylinders needed for carbonation test ($\phi$= 75±1 mm, h = 150±1 mm) are drilled from cubic specimens. Drilled samples are dried for 24h in laboratory condition (55±5% RH, 20±2°C) and immediately transferred to the carbonation chamber for carbonation testing. This procedure was applied to all samples regardless their curing period.

Concrete specimens of different mixtures were exposed during 7, 14, 21 and 28 days to 1±0.1% $CO_2$, at a temperature of 21±2°C and RH of 60±5%. Specimens were removed from the chamber after achieving the desired exposure time, and the corresponding carbonation depth was measured by treating the surface of a freshly cleaved specimen with a 1 % solution

of phenolphthalein in alcohol. Depending on the alkalinity of concrete contact area with the phenolphthalein, purple-red coloration (noncarbonated) and colourless region (carbonated) can be distinguished. The carbonation depth was measured in 6 different points per sample using four replicate samples for each mixture.

The rapid chloride migration (RCM) test was conducted following the NordTest method NT Build 492 [29] using cylindrical specimens with a diameter of 100 mm and a thickness of 50 mm, sliced from drilled cores of ϕ100x150 $mm^2$ after 28 days of curing. A 0.1 M silver nitrate ($AgNO_3$) solution was applied to freshly split samples to determine chloride penetration depth. $AgNO_3$ reacts with both chloride and hydroxyl ions to form white silver chloride and dark brown silver oxide, respectively. Chloride penetration depth is measured as the visible boundary between white precipitation of silver chloride when chloride ion is present, and precipitation of brown silver oxide.

## RESULTS AND DISCUSSIONS

### Compressive strength

The dependence of compressive strength on curing ages of investigated concrete mixtures is shown in Figure 1. It can be observed that the compressive strength increases as increasing slag content reaching values close to 100 MPa for S70 after 90 days of curing. It can be also deduced that all mixtures exhibit high early age strength even for fly ash-rich mixture (S30) which has about 15 MPa after 1 day and near 40 MPa after one week of curing. It is important to highlight that the compressive strength of this mixture after 56 and 90 days of curing are practically the same. This indicates that the fly ash-rich mixture has already reached its maximum strength. Contrarily, concrete mixtures with slag amount ≥50% are still developing additional strength during the same curing period but with strength gain compared to early age strength development.

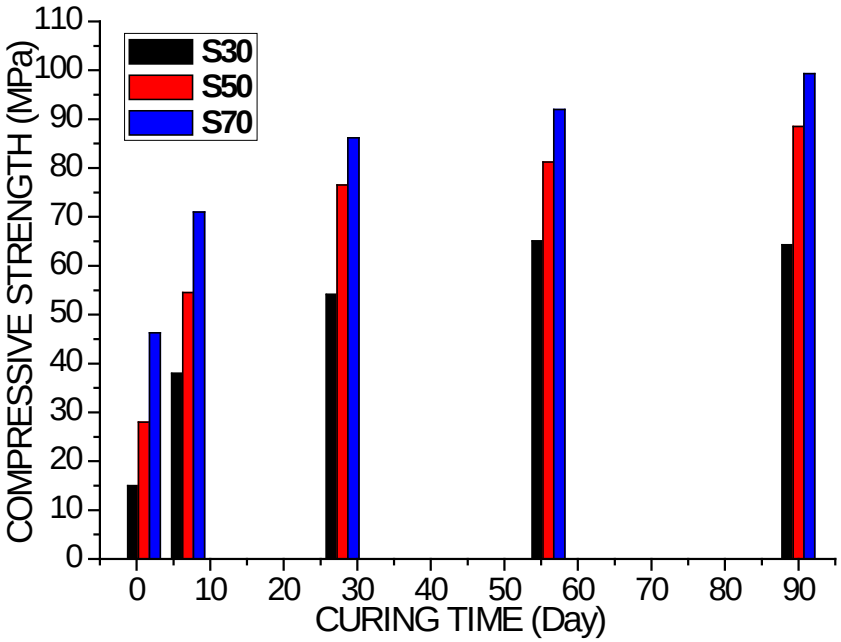


Figure 1 Compressive strength of the indicated concrete mixtures after 1, 7, 28, 56 and 90 days of curing

## Carbonation resistance

The investigated concretes have been cured at different ages and then exposed to 1% $CO_2$. Their carbonation resistance has been assessed through the evaluation of the carbonation depth measured by mean of the phenolphthalein test. The effects of the exposure time, the fly ash to slag ratio as well as the curing time on carbonation depth are shown in Figure 2 and 3.

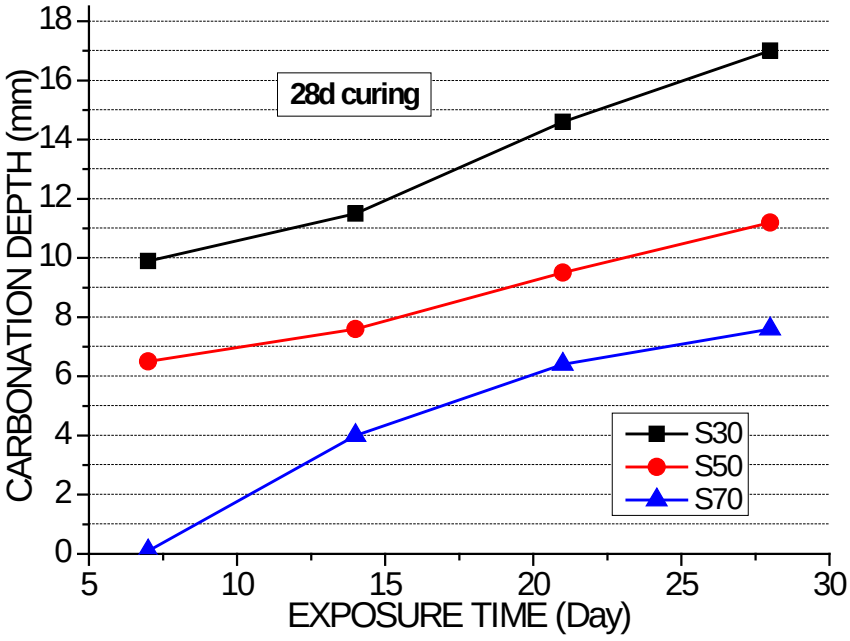


Figure 2 Effect of exposure time on carbonation depth of S30, S50 and S70 after 28d curing.

It can be observed from Figure 2 that, regardless the exposure time, the fly ash-rich mixture exhibits the highest carbonation depth and the slag-rich mixture the lowest one. This trend could be related to the higher porosity of concrete with high fly ash content [26]. An increase of the slag content produced a refinement of the concrete pore structure making difficult the penetration of $CO_2$. After 7 days exposure, S70 was not carbonated whereas S50 and S30 show a carbonation depth of about 7 and 10 mm, respectively. As increasing the exposure time, all mixtures are carbonated but keeping the tendency already mentioned previously i.e. the slag-rich mixture was less carbonated than the porous concrete containing higher fly ash amount. After 28 days exposure, the carbonation depth of S30 reaches 17 mm which is about 1.5 times higher than for S50 and more than 2.5 times higher than that of S70. A comparison of the observed slopes shows that the mixture S30 shows a higher carbonation rate than S50 and S70. Based on these findings it could be expected that for reinforced fly ash/slag based concretes, the passivating layer will be damaged first in S30 then in S50 and finally in S70. Consequently S70 could exhibit the longest service life among the 3 mixtures.

The effect of curing time on carbonation resistance of the 3 investigate mixtures is shown in figure 2. At all curing ages, the increase of fly ash to slag ratio increases the carbonation depth. At early age of curing (7, 14 days), all samples are carbonated with a carbonation depth ranging from 6 to 18 mm. When the curing time is increased, a decrease on carbonation depth was observed. This decrease is induced by the refinement of the pore structure and the densification of concrete matrix as the geopolymirization process continues. After 28 days of curing, the slag-rich concrete exhibits a very low permeability. This mixture is not carbonated

after 7 days of $CO_2$ exposure and its carbonation depth does not exceed 8 mm after 28 days exposure. At 7 and 14 days of curing, the slopes of the exposure time dependence of the carbonation depth are practically similar indicating that the carbonation rate of the 3 mixtures is quite similar as the gel maturity (responsible for hardening and densification of the concrete) is not enough to prevent a high-rate $CO_2$ penetration. At increased curing ages (21 or 28 days), The slopes in S50 or S70 are lower than that of S30 due to the higher slag content which in turn improves the density and reduces the concrete chloride permeability.

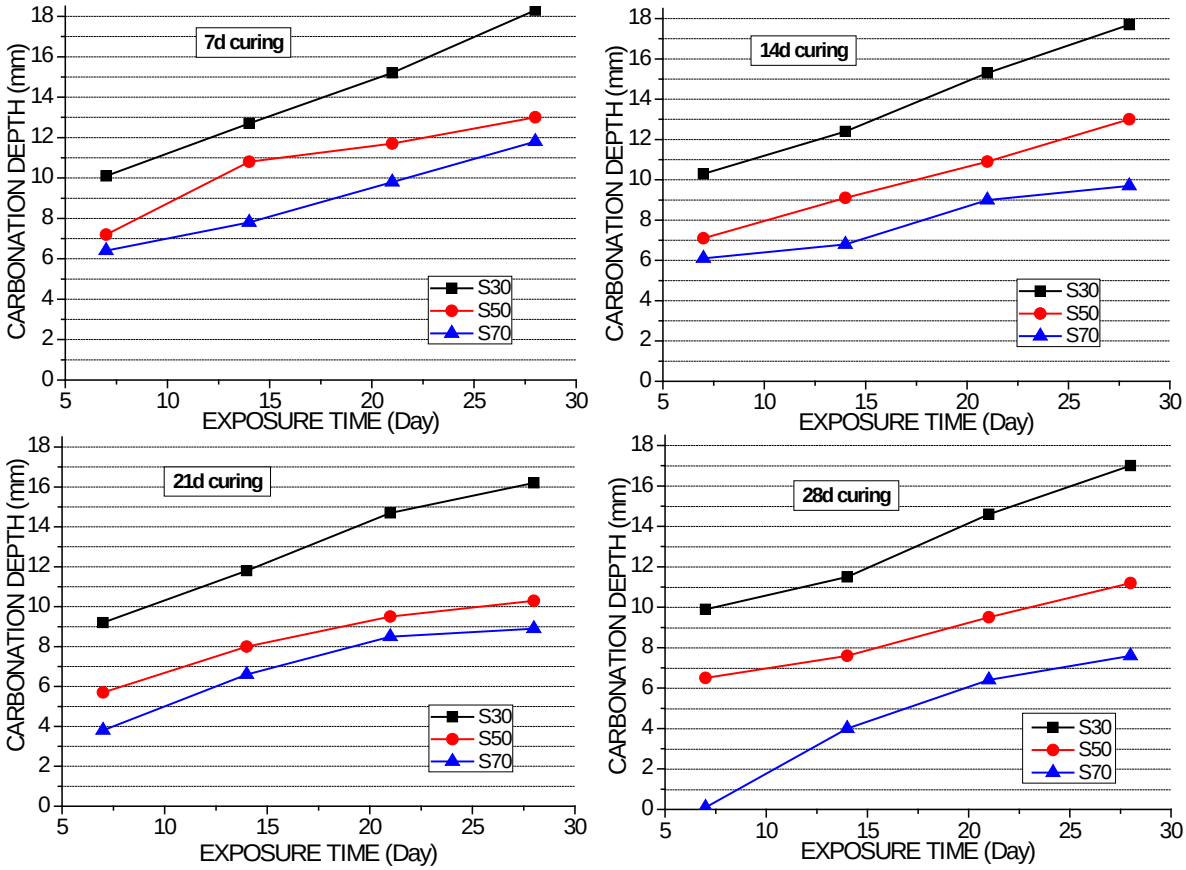


Figure 2 Effect of curing time on carbonation depth of S30, S50 and S70.

On the other hand it can be deduced that despite the lower carbonation depth mostly observed in slag rich concrete, these values are very high compared to those reported in aging structures (In Russia, Ukraine and Poland) where a carbonation rate of aged structures between 12 and 40 years does not exceed 1mm/year [5]. The divergence of these results open a new debate on the correlation between natural and accelerated carbonation resistance of alkali activated materials. The curing time before starting the accelerated carbonation test could be one of the parameters that affect the nature of the reaction products formed after carbonation as it is directly related to the microstructure development and gel maturity. According to Bernal et al. [21], the influence of gel maturity is essential when analysing the results of accelerated carbonation. During the exposure to natural carbonation the binder structure evolution lasts long term of period (years), while accelerated tests are applied on relatively young concretes for short time of period (weeks).

## Chloride resistance

The rapid chloride migration test (RCM) according to NT Build 492 standard has been used to evaluate the resistance of the investigated mixtures to the chloride ingress. For sake of comparison, the chloride resistance of Portland cement concrete (CEM I 42.5 R) used as reference has been also assessed. From Figure3, it can be deduced that the chloride resistance in alkali activated concretes is higher than that of CEM I which has a carbonation depth close to 25 mm. These results are in a good agreement with those reported by Ismail et al. [26]. Among the 3 investigated concretes, S30 exhibits the highest chloride penetration depth (~18 mm) and S70 the lowest one (~5mm) which indicates that the increase of slag content increases the concrete resistance to the chloride ingress. The non-steady-state migration coefficients deduced from the chloride penetration depth (Equation 4 in ref. 29) are 17.6, 4.4 and $1.91\times10^{-12}m^2s^{-1}$ for S30, S50 and S70, respectively.

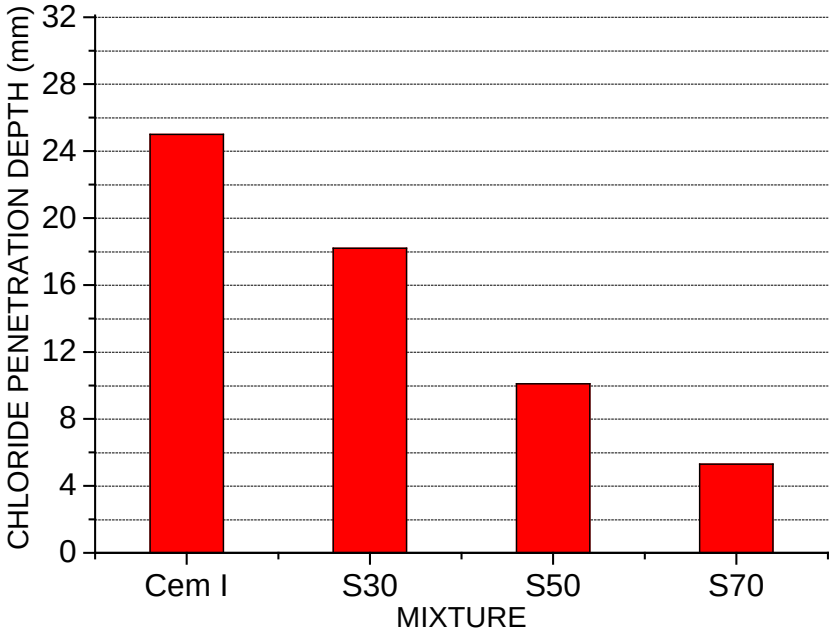


Figure 3 Evolution of the chloride penetration depth of Cem I, S30, S50 and S70 at 28 days of curing.

The initial current values obtained during the RCM test (applying a voltage of 30V conforming to NT Build 492 standard) are 85, 162.3, 52.3 and 33.8 mA for CEM I, S30, S50 and S70, respectively. This parameter could provide preliminary information about the concrete porosity. Taking into account that the measured current results from the migration of mobile species through the concrete pores, it can be deduced that S30 has an open pore structure (higher porosity) in comparison with S50 or S70 where the concrete matrix becomes denser as increasing the slag content. Therefore the chloride ingress will be easier in S30 than S50 or S70 which is in a good agreement with the measured chloride penetration depth values (see figure 3). However this trend is not observed when comparing CEM I with S30. CEM I has a lower initial current but higher chloride penetration depth. Several possible reasons could explain this behaviour: i) Despite the higher porosity of S30 in comparison to that of CEM I, the critical pore size may not be favourable for an optimum chloride mobility in the fly ash-rich concrete. The accommodation of mobile chloride species in the conduction

paths connecting the pores is not suitable because they may spend more time between the wall-paths (zigzag movement) of bigger pores before crossing the specimen section in S30 than in CEM I. In accordance with this hypothesis, it has been reported [30] that the critical pore size in alkali silicate powder activated slag concretes is more influential than porosity in determining the chloride transport properties. ii) At a given initial voltage (30 V here), the measured initial current will define the applied voltage for each RCM test. As in the fly ash-rich mixture the measured initial current could involve chlorides and other mobile species, this could underestimate/affect the value of the resulting applied voltage before starting the RCM test leading to a lower chloride penetration for S30 than CEM I. finally these results could rise some concerns regarding the suitability of the RCM test for the evaluation of chloride resistance in alkali activated materials and the need for new standards.

## CONCLUSIONS

The carbonation and chloride resistance of alkali activated fly ash and slag concretes have been examined in this study. It can be concluded that the carbonation depth is increased as increasing the fly ash to slag ratio or the $CO_2$ exposure time but decreases with increasing the curing age. Slag rich-concrete exhibits better durability performances than fly ash-rich mixture either against $CO_2$ or under chloride ingress. CEM I shows higher chloride penetration than alkali activated concretes even when compared with a high-volume fly ash concrete (S30). This behaviour was mainly related to the concrete porosity especially the pore distribution/connection and the critical pore size within the concrete matrix. The conventional testing protocols used to evaluate the durability of Portland cement are not necessary suitable for the assessment of durability performances in AAM.

## ACKNOWLEDGEMENTS

This research was carried out under the project S81.1.13498 in the framework of the Partnership Program of the Materials innovation institute M2i (www.m2i.nl) and the Technology Foundation STW (www.stw.nl), which is part of the Netherlands Organisation for Scientific Research (www.nwo.nl).

## REFERENCES

1. VAN DEVENTER, J SJ. Alkali activated materials. Ed. PROVIS, J L. Springer, 2014.
2. PALOMO, A, GRUTZECK, M W, BLANCO, M T. Alkali-activated fly ashes: a cement for the future, Cement and concrete research, Vol. 29, No. 8, 1999, pp 1323-1329.
3. PUERTAS, F. Cementos de escoria activados alcalinamente: situación actual y perspectivas de futuro, Materiales de Construcción, Vol. 45, No. 239, 1995, pp 53–64.
4. ROY, D. Alkali-activated cements – opportunities and challenges, Cement and Concrete Research, Vol. 29, No 2, 1999, pp 249–254.
5. SHI, C, ROY, D M, KRIVENKO, P V. Alkali-activated cements and concretes, 2006, Taylor & Francis, Abingdon (UK).
6. WANG, S D, PU X C, SCRIVENER, K L, PRATT, P L. Alkali-activated slag cement and concrete: a review of properties and problems, Advances in Cement Research, Vol. 7, No 27, 1995, pp 93–102.

7. DAVIDOVITS J. Geopolymers - Inorganic polymeric new materials. Journal of Thermal Analysis and Calorimetry, Vol. 37, No 8, 1991, pp 1633-1656.
8. DAVIDOVITS J. Geopolymer Chemistry and Applications. Institut Géopolymère, Saint-Quentin, France, 2008.
9. GUERRIERI, M, SANJAYAN J G. Behavior of combined fly ash/slag-based geopolymers when exposed to high temperatures. Fire and Materials, Vol. 34, No 4, 2010, pp163–175.
10. SUGAMA, T, BROTHERS, L E, VAN DE PUTTE TR, Acid-resistant cements for geothermal wells: sodium silicate activated slag/fly ash blends, Advances in Cement Research Vol. 17, No 2, 2005, pp 65–75.
11. ISMAIL, I, BERNAL, S A, PROVIS, J L, HAMDAM, S, VAN DEVENTER, J S J. Microstructural changes in alkali activated fly ash/slag geopolymers with sulfate exposure, Materials and Structures, Vol. 46, 2013, pp 361–373.
12. KOMLJENOVIĆ, M, BAŠČAREVIĆ, Z, MARJANOVIĆ, N, NIKOLIĆ, V. External sulfate attack on alkali-activated slag. Construction and Building Materials, Vol. 49, 2013, pp 31–39.
13. BAKHAREV, T. Durability of geopolymer materials in sodium and magnesium sulfate solutions. Cement and Concrete Research, Vol. 35, 2005, pp 1233-1246.
14. PACHECO-TORGAL. F, ABDOLLAHNEJAD, Z, CAMOES, A F, JAMSHIDI, M, DING, Y. Durability of alkali-activated binders: A clear advantage over Portland cement or an unproven issue? Construction and Building Materials, Vol. 30, 2012, pp 400–405.
15. PROVIS, J L, PALOMO, A, SHI, C. Advances in understanding alkali-activated materials.. Cement and Concrete Research, Vol. 78, 2015, pp 110-125.
16. SHI, C, SHI, Z, HU, X, ZHAO, R, CHONG, L. A review on alkali-aggregate reactions in alkali-activated mortars/concretes made with alkali-reactive aggregates. Materials and Structures, Vol. 48, No 3, 2015, pp 621-628.
17. ARBI, K, NEDELJKOVIĆ, M, ZUO, Y, YE, G. A review on the durability of alkali activated fly ash/slag systems: Advances, issues and perspectives. Industrial and Engineering Chemistry Research, Vol. 55, No 19, 2016, pp 5439–5453.
18. Tilly G P, Jacobs J. Concrete Repairs: Performance in service and current practice. CONREPNET Project Report, IHS BRE Press, 2007, Watford, UK.
19. LAW, D W, ADAM, A A, MOLYNEAUX, T K. PATNAIKUNI, I. Durability assessment of alkali activated slag (AAS) concrete. Materials and Structures, Vol. 45, 2012, pp 1425-1437.
20. BAKHAREV, T, SANJAYAN, J G, CHENG, Y B. Resistance of alkali-activated slag concrete to carbonation. Cement and Concrete Research, Vol. 31, 2001, pp 1277-1283.
21. BERNAL, S A, PROVIS, J L, BRICE, D G, KILCULLEN, A, DUXSON, P, VAN DEVENTER, J S J. Accelerated carbonation testing of alkali-activated binders significantly underestimates the real service life: The role of the pore solution. Cement and Concrete Research, Vol. 42, 2012, 1317-1326.
22. HAKKINEN, T. The permeability of high strength blast furnace slag concrete. Nordic Concrete Research, Vol. 11, No 1, 1992, pp 55-66.

23. BERNAL, S A, MEJIA DE GUITIERREZ, R, PROVIS, J L, Engineering and durability properties of concretes based on alkali-activated granulated blast furnace slag/metakaolin blends. Construction and Building Materials, Vol. 33, 2012, pp 99-108.
24. BERNAL, S A, PROVIS, J L, MEJIA DE GUITIERREZ, R, VAN DEVENTER, J S J. Accelerated carbonation testing of alkali-activated slag/metakaolin blended concretes: effect of exposure conditions. Materials and Structures, Vol. 48, 2015-I, pp 653-669.
25. DEJA, J. Carbonation aspects of alkali activated slag mortars and concretes. Silicates Industriel. 2002, Vol. 67, 37-42.
26. ISMAIL, I, BERNAL, S A, PROVIS, J L, NICOLAS, R S, BRICE, D G, KILCULLEN, A R, HAMDAN, S, VAN DEVENTER, J S J. Influence of fly ash on the water and chloride permeability of alkali-activated slag mortars and concretes. Construction and Building Materials, Vol. 48, 2013, 1187-1201.
27. ASTM International. Standard specification for coal fly ash and raw or calcined natural pozzolan for use in concrete (ASTM C618–12a), 2012
28. EN 13295:2004, Products and systems for the protection and repair of concrete structures—test methods—determination of resistance to carbonation
29. NordTest. NT Build 492, Chloride migration coefficient from non-steady state migration experiments, 1999.
30. RAVIKUMAR, D, NEITHALATH, N. An Electrical impedance investigation into the chloride ion transport resistance of alkali silicate powder activated slag concretes. Cement and Concrete Composites, Vol. 44, 2013, pp 58-68.

# STUDY OF THE EFFECTS OF SILICA FUME, CALCIUM NITRATE AND TRISOPROPANOLAMINE ON SOME OF THE SHORT-TERM PROPERTIES OF CEMENT PASTES

**M Cheikh-Zouaoui**

University of Saad Dahlab - Blida

**N Chikh**

University of Mentouri Constantine

Algeria

**ABSTRACT.** The purpose of this work is to investigate the on the effects of triisopropanolamine, silicate fume used alone and in combination with calcium nitrate on the setting and hardening process of cement pastes. Tests were performed on specimens from various mixes considering cement with normal tri calcium silicate content. The results obtained indicate that triisopropanolamine performed well as a hardening accelerator at all ages. Silicate fume produced a continuous compressive strength increase with time but slowed down the initial setting. The use of calcium nitrate in combination with triisopropanolamine leads at very early age to significant results with respect to both setting and hardening acceleration. The incorporation of silicate fume in combination with calcium nitrate and triisopropanolamine had little effect on the setting times. However, early strength improvement was very important though the joining effect of hardening from the combined action of triisopropanolamine and silicate fume was not important as expected.

**Keywords:** Cement paste, Triisopropanolamine, Silica fume, Setting time, Strength,

**Dr Mustapha Cheikh-Zouaoui** is Reader at the University of Saad Dahlab, Department of Civil Engineering. His main research fields include: use of admixtures in concrete technology, properties of concrete, reinforced and pre-stressed concrete.

**Dr Nasr-Eddine Chikh** is Professor at the University of Mentouri Constantine, Department of Civil Engineering His main fields of research include: properties of concrete, durability of constructions, repair and strengthening of concrete structures with composites materials.

## INTRODUCTION

Modern concrete is more than simply a mixture of cement, water, and aggregates; modern concrete contains more often mineral components, chemical admixtures, fibers, etc. [1]. Various admixtures have been used to get a concrete with sufficient strength at a very early age. Dodson [2] presented a review of non-chloride, non-corrosive set accelerating salts. It was established that the calcium nitrate can be used as a set accelerator and was found to be a very effective corrosion inhibitor for metal imbedded in concrete. Various studies [3, 4] indicate that the calcium nitrate (CN) used alone (1%) acts mainly as a setting accelerator and may improve the compressive strength at 24hrs. However, in the long term, its strength increase is not significant so as to be considered as a hardening accelerator. In another hand, the triethanolamine (TEA) combined with calcium nitrate was proposed in 1981 like non-corrosive concrete accelerator for concretes. Authors' results [5] show that triethanolamine within the range of 0.05-010% performed well as a hardening accelerator at all ages. It was found that initially calcium nitrate acted as a setting accelerator then triethanolamine took over by accelerating mainly the hardening phase. The combination of both additives resulted in their joining effects with time, translated by a reduction in the initial and final setting times and a significant strength enhancement at all ages of the cement pastes [6]. The addition of small amounts of higher tertiary alkanolamines, such as triisopropanolamine (TIPA) resulted in interesting increases in the strengths of cement pastes at different ages [7, 8]. Another study carried out on the strength enhancing mechanism of TIPA presented compressive strength data for 10 Portland cements tested as cement paste and found a substantial strength improvement.

In recent years, mineral additives due to the advantages such as evaluation of waste for ecological balance, improving the physical and mechanical properties of cement or concrete a wide field of use is found [9–12]. One of the waste materials is silica fume (SF) which is a pozzolanic material that is a byproduct of the silicon melting process. Pozzolanic materials are generally able to combine with the hydrated calcium hydroxide [Ca(OH)2] forming the hydrated calcium silicate (C-S-H), which is the principal responsible for the strength of hydrated cement pastes. SF is a pozzolanic material that is known to produce a high-strength concrete and is used in two different ways: as a cement replacement to reduce the cement content (usually for economic reasons) and as an additive to improve concrete properties (in both fresh and hardened states). The use of SF decreases the permeability, thereby increasing the resistance of concrete against corrosion and chemical attack, improving its strength and durability [13–15].

The present work investigates the effects of TIPA, SF used alone and in combination with CN on the setting and hardening process of cement pastes. Tests were performed on specimens from various mixes proportions considering cement with normal tri calcium silicate content. The purpose of the present work is to find combinations of CN with other compounds so as to fulfil the criteria for both a setting and a hardening accelerator. However, as silica fume is a quite expensive mineral component, an alternative is considered by using milled recovered silica sand (SS) as additive by making it homogenous with the cementitious composite through a grinding process.

## EXPERIMENTAL STUDY

### Materials

The cement used in all the mixtures was Portland cement CPJ, CEM II/A 42.5, with normal tri calcium silicate content, supplied by Ain Touta cement plant (Algeria). It has an absolute density of 3100 kg/m³ and a specific surface (Blaine) of 3200 cm²/g. Its mineralogical composition is given in Table 1.

Table 1 Mineralogical composition of the clinker (Bogue).

| MINERALS | $C_3S$ | $C_2S$ | $C_3A$ | $C_4AF$ |
|---|---|---|---|---|
| % | 51.28 | 24.68 | 8.33 | 8.94 |

The general formula of the calcium nitrate (CN) used is: $X.NH_4\ NO_3\ Y.Ca(NO_3)_2\ Z.H_2O$. The coefficients X, Y and Z values are respectively X=0.092, Y=0.500 and Z=0.826, which correspond to 19.00% $Ca^{2+}$, 1.57% $NH^{4+}$, 64.68% $NO_3$ and 14.10% $H_2O$. The chemical formula of the triisopropanolamine (TIPA) added was $N(CH_2CH_2CH_2OH)_3$ $[C_9H_{21}O_3N]$, corresponding to a developed spatial molecular structure. The chemical composition of the used silica fume is indicated in Table 2, its loss on ignition (LOI) is 2.2%.

Table 2 Chemical composition of silica fume sample.

| | $SiO_2$ | $Al_2O_3$ | $Fe_2O_3$ | CaO | MgO | $K_2O$ | $SO_3$ | $NA_2O_3$ | Si |
|---|---|---|---|---|---|---|---|---|---|
| % OXIDES | 89 | 0.3 | 0.9 | 0.3 | 1.5 | 1.7 | 0.3 | 0.6 | 3.2 |

These chemical and mineral components were used for the purpose of providing the hardening criteria to the blend admixture. The w/c ratio for the various mixtures investigated is 0.3. The characteristics of theses mixes proportions are summarised in Table 3.

Table 3 Various mixes proportions investigated.

| MIXTURE | CN % | TIPA % | SF % |
|---|---|---|---|
| M1 | 0.00 | 0.00 | 0.00 |
| M2 | 0.00 | 0.05 | 0.00 |
| M3 | 0.00 | 0.10 | 0.00 |
| M4 | 0.00 | 0.00 | 7.50 |
| M5 | 0.00 | 0.00 | 10.0 |
| M6 | 1.00 | 0.05 | 0.00 |
| M7 | 1.00 | 0.10 | 0.00 |
| M8 | 1.00 | 0.05 | 7.50 |
| M9 | 1.00 | 0.10 | 7.50 |
| M10 | 1.00 | 0.05 | 10.0 |
| M11 | 1.00 | 0.10 | 10.0 |

### Setting times

The setting test on the cement pastes was performed using a Vicat apparatus and following EN196-3 procedure. The setting is registered by penetrating a needle of a fixed cross section and with a constant force into the cement paste. The initial setting time is determined to be when full depth intrusion of the needle is not obtainable, while the final setting time is taken when the needle no longer penetrates the cement paste at all.

### Compressive strength

The hardening criteria were determined through simple compressive strength tests on cubic specimen 50x50x50mm3. These latter were cast in metallic moulds and kept for 24 hours at 20±1°C and at 55±5% RH. They were then demoulded and conserved in water at 20°C until required for testing. Using a hydraulic testing machine, compressive strength tests were carried out according to the French code NF18-406. Each compressive strength value represents the average of the results from 3 specimens.

## TEST RESULTS AND DISCUSSION

The purpose of this work is to investigate the effects of using triisopropanolamine and silicate fume alone and then combined with calcium nitrate on the cement pastes setting process and hardening. Tests were carried out on specimen at the age of 1, 3 and 7 days. The results regarding setting times and compressive strength, are given in Table 4 and Figure 1 and 2.

Table 4 Experimental results.

| MIXTURE NAME | SETTING TIME (min) | | COMPRESSIVE STRENGTH (MPa) | | |
|---|---|---|---|---|---|
| | Initial | Final | 1 day | 3 days | 7 days |
| M1 | 137 | 205 | 18 | 25 | 38 |
| M2 | 140 | 210 | 32 | 48 | 80 |
| M3 | 130 | 210 | 40 | 52 | 88 |
| M4 | 210 | 247 | 16 | 32 | 60 |
| M5 | 200 | 255 | 14 | 34 | 56 |
| M6 | 75 | 110 | 36 | 48 | 80 |
| M7 | 75 | 100 | 44 | 52 | 82 |
| M8 | 140 | 240 | 26 | 50 | 72 |
| M9 | 130 | 235 | 32 | 52 | 73 |
| M10 | 130 | 235 | 22 | 46 | 85 |
| M11 | 120 | 220 | 27 | 56 | 80 |

### Effect of Triisopropanolamine

The use of respectively 0.05% and 0.1% TIPA (M2, M3) had a small effect on the initial and final setting times. However, it produced a significant improvement on the compressive strength at all ages. With 0.05% TIPA, the increase in strength in relation to the control mix (M1) was about 80% at 1 day, 90% at 3 days, and 110% at 7 days.

The influence was further enhanced with 0.10% TIPA where the recorded increase was about 120% at 1 day, 110% at 3 days and 130% at 7 days. These results show that TIPA performed well as a hardening accelerator and the increase in strength was not important from using 0.05% to 0.10% TIPA.

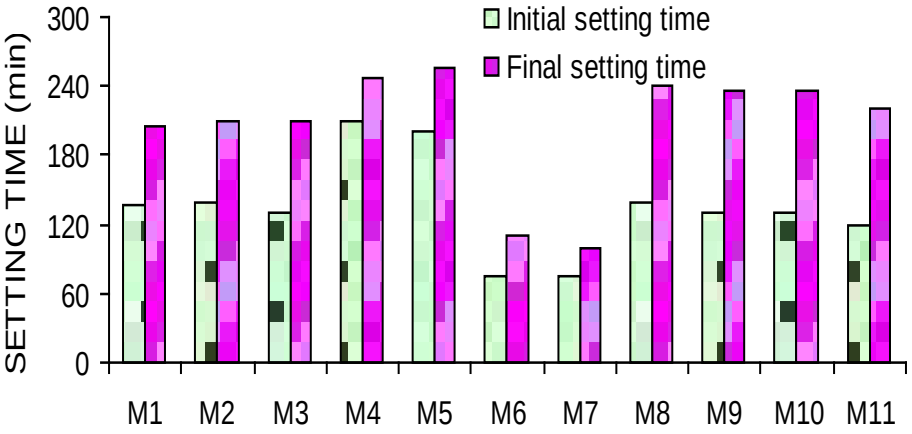


Figure 1 Initial and final setting times of cement pastes.

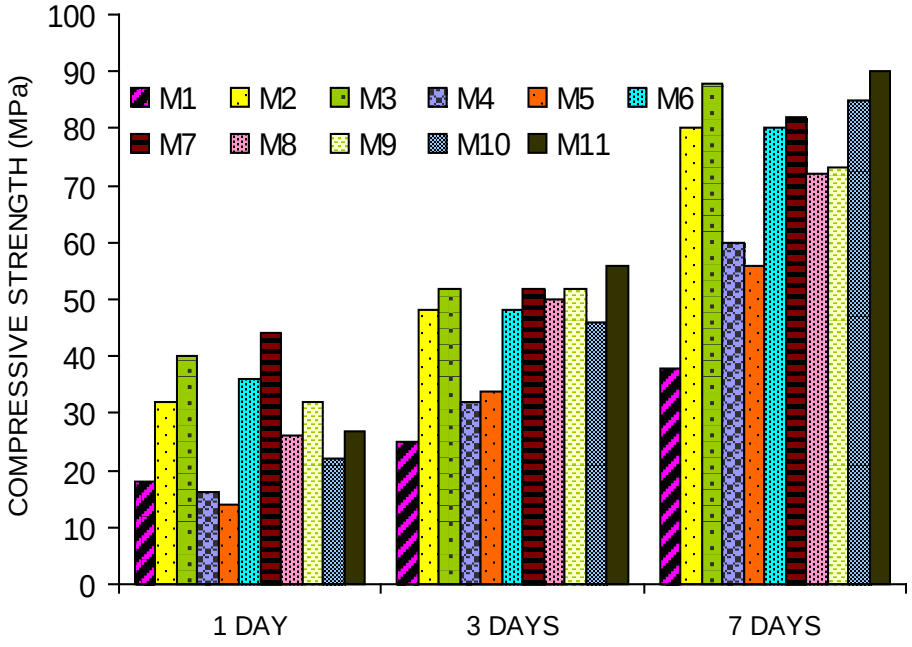


Figure 2 Compressive strength of cement pastes.

**Effect of Silica Fume**

The variation of setting times of cement pastes with SF substitution (M4, M5) is shown in Figure 1. It was observed that for the SF percentages considered, both the initial and final setting times increased respectively by 45% and 25%.

Thus the pozzolanic reaction of SF seems not to be very active at early hours of hydration. Regarding the compressive strength, it can be seen a decrease of cement pastes containing SF at 1 day. However, the strength exceeded the control mix at both 3 and 7 days by respectively 30% and 55%. It should be noted that the variation of SF content from 7.5% to 10% by weight of cement did not have significant effects on both setting times and compressive strength.

**Effect of Calcium Nitrate combined with Triisopropanolamine**

Combining calcium nitrate with triisopropanolamine (M6, M7) resulted in their joining effects. The initial and final setting times compared with the control mix (M1) values were reduced respectively to 45% and 50% for 0.1 % TIPA. The compressive strength increase for early and long term ages was respectively more than 90% and 45%. However, it is worth indicating that the increase in strength produced with 0.05% TIPA compared to 0.0% TIPA was far more important than that produced from using 0.10% TIPA with respect to 0.05% TIPA. The dosage of 0.05% TIPA seems to be close to the optimum dosage. These results clearly show that calcium nitrate combined to triisopropanolamine leads at the early ages to very interesting and promising results in terms of accelerating both setting and hardening.

**Effect of Calcium Nitrate combined with Triethanolamine and Silica Fume**

Table 4 shows that the initial setting times of mixtures M8, M9, M10 and M11 are slightly different to control mix, within a range of 7÷14%, despite the presence of the setting accelerator CN. This is due to the inverse effect of SF which slows down the initial setting. However, their final setting times indicate a small improvement resulting in an increased time setting. The compressive strength development presented in Figure 2 shows that mixtures M8, M9, M10 and M11 increase significantly by time with respect to control mix. Early strength improvement was more than 25% at 1 day, 85% at 3 days, and 90% at 7 days. However, the expected joining effect of hardening from the combined action of TIPA and SF was not important.

**Alternative for Silica Fume**

As silica fume is a quite expensive mineral component, an alternative is considered by using milled recovered silica sand (SS) as additive by making it homogenous with the cementitious composite through a grinding process. The characteristics of theses mixes proportions are indicated in Table 5. The results are presented in Table 6 and graphically in Figures 3 and 4.

Table 5 Various mixes proportions investigated for SS samples.

| MIXTURE | CN % | TIPA % | SS % |
|---|---|---|---|
| M12 | 0.00 | 0.00 | 7.50 |
| M13 | 0.00 | 0.00 | 10.00 |
| M14 | 1.00 | 0.05 | 7.50 |
| M15 | 1.00 | 0.10 | 7.50 |
| M16 | 1.00 | 0.05 | 10.00 |
| M17 | 1.00 | 0.10 | 10.00 |

It was observed that both the initial and final setting times for M12 mix were delayed respectively by 68 min and 50 min compared to control mix, but in the case of M13 mix they remain close to control mix values. Unlike the effect of SF on setting times, the presence of SS in cement pastes in combination with CN and TIPA did not slow down the setting accelerant action of CN. Thus, both initial and final setting times of mixtures M14, M15, M16 and M17 decreased significantly by 30÷50% compared to control mix, resulting in times settings greatly shortened.

Table 4 Experimental results for SS samples.

| MIXTURE NAME | SETTING TIME (min) | | COMPRESSIVE STRENGTH (MPa) | | |
|---|---|---|---|---|---|
| | Initial | Final | 1 day | 3 days | 7 days |
| M1 | 137 | 205 | 18 | 25 | 38 |
| M12 | 210 | 255 | 20 | 36 | 44 |
| M13 | 150 | 200 | 20 | 30 | 42 |
| M14 | 80 | 125 | 28 | 60 | 76 |
| M15 | 80 | 110 | 32 | 68 | 88 |
| M16 | 95 | 120 | 32 | 48 | 60 |
| M17 | 90 | 105 | 36 | 56 | 72 |

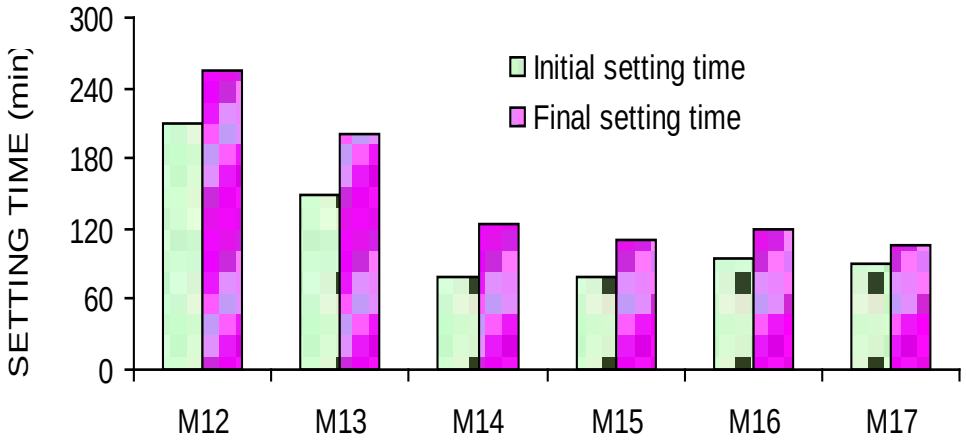


Figure 3 Initial and final setting times of cement pastes with SS.

The replacement of SF by SS in cement pastes M12 and M13 produced also increases in strength at all ages, more than 10%, 20% and 15% at respectively 1 day, 3 days and 7 days. The performance was even better when used in combination with CN and TIPA. The compressive strength evolution illustrated by Figure 4 shows that mixtures M14, M15, M16 and M17 increase significantly with respect to control mix, more than 55% at 1 day, 90% at 3 days, and 60% at 7 days.

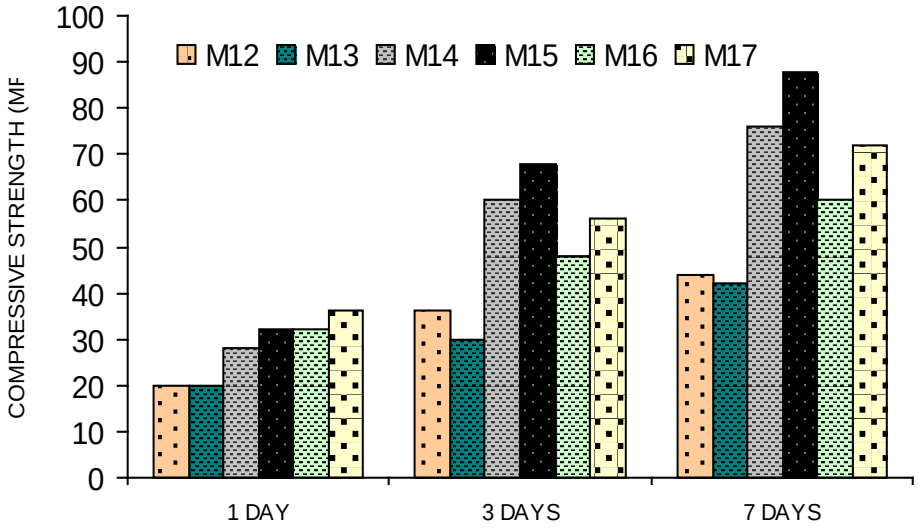


Figure 4 Compressive strength of cement pastes with SS.

## CONCLUSIONS

Tests have been carried out on cement pastes specimens to investigate the effect of using as additives the calcium nitrate, the triisopropanolamine and the silicate fume as cement replacement on the setting time and compressive strength evolution. The main results show that:

- TIPA has a small effect on setting times and performed well as a hardening accelerator at all ages. Best results were obtained with 0.10% TIPA content.

- The pozzolanic reaction of SF was not very active at early hours of hydration. However, it produces continuous strength increases in strength with time. The effect of the variation of SF content from 7.5% to 10% by weight of cement was not important on both setting times and compressive strength.

- The combination of both CN and TIPA results in their joining effects with time, translated by a reduction in the initial and final setting times by more than 40% and a significant strength enhancement, more than 45%, at all ages of the cement pastes. Initially, CN acts as a setting accelerator then TIPA takes over by accelerating mainly the hardening phase.

- The incorporation of SF in combination with CN and TIPA had little effect on the setting times. However, early strength improvement was more than 25% at 1 day, 85% at 3 days, and 90% at 7 days though the joining effect of hardening from the combined action of TIPA and SF was not important as expected.

- Unlike SF, the presence of SS in cement pastes in combination with CN and TIPA did not slow down the setting accelerant action of CN and important decreases (30÷50%) of both initial and final setting times occurred. The performance on the compressive strength improvement with time is close to that of SF.

## REFERENCES

1. AITCIN, P C. Cements of yesterday and today: Concrete of tomorrow, Cement and Concrete Research, Vol. 30, No. 8, 2000, pp. 1349-1359.

2. DODSON, V H. Concrete Admixtures, 1990, V.N. Reinhold, New York.

3. JUSTNES, H, NYGUARD, E C. The influence of technical calcium nitrate additions on the chloride binding capacity of cement and the rate of chloride induced corrosion of steel embedded in mortars, Proceedings of International Conference on Corrosion and Corrosion Protection of Steel in Concrete, Sheffield, UK, 1994, pp. 491-502.

4. JUSTNES, H, NYGUARD, E C. Technical calcium nitrate as set accelerator for cement at low temperatures, Cement and Concrete Research, Vol. 25, No. 8, 1995, pp. 1766-1774.

5. CHEIKH-ZOUAOUI, M, AGGOUN, S, CHIKH, N, DUVAL, R. Effets du nitrate de calcium et de la triethanolamine sur le temps de prise et de l'évolution des résistances mécaniques au jeune âge des pâtes de ciment, Revue Européenne de Génie Civil, Vol. 10, No. 4, 2006, pp. 475-485 (French).

6. CHEIKH-ZOUAOUI, M, AGGOUN, S, CHIKH, N, DUVAL, R. Effect of some admixtures on the setting time and strength evolution of cement pastes at early ages, Construction and Building Materials, Vol. 22, No. 82, 2008, pp. 106-110.

7. GARTNER, E, MYERS, D. Influence of tertiary alkanolamines on Portland cement hydration. Journal of the American Ceramic Society, Vol. 76, No. 6, 1993, pp. 1521-1530.

8. SANDBERG, P G, DONCASTER, F. On the mechanism of strength enhancement of cement paste and mortar with triisopropanolamine, Cement and Concrete Research, Vol. 34, 2004, pp. 973-976.

9. BOUDCHICHA, A, CHEIKH-ZOUAOUI, M, GALLIAS, J L. Analysis of the effects of mineral admixtures on the strength of mortars, Journal of Civil Engineering and Management, Vol. 13, No. 2, 2007, pp. 87-96.

10. GALLIAS, J L, KARA ALI, R, BIGAS, J P. The effect of fine mineral admixtures on water requirement of cement pastes, Cement and Concrete Research, Vol. 30, 2000, pp. 1543-1549.

11. NEDHI, M, MINDESS, S, AITCIN, P C. Rheology of high performance concrete: effect of ultra fine particles, Cement and Concrete Research, Vol. 28, 1998, pp. 687-697.

12. FERRARIS, C F, OBLA, K H, HILL, R. The influence of mineral admixtures on the rheology of cement pastes and concrete, Cement and Concrete Research, Vol. 31, 2001, pp. 245-255.

13. DUVAL, R, KADRI, E H. Influence of silica fume on the workability and the compressive strength of high performance concretes, Cement and Concrete Research, Vol. 28, No. 4, 1998, pp. 533-547.

14. QING, Y, ZENAN, Z, DEYU, K, RONGSHEN, C. Influence of nano-SiO2 addition on properties of hardened cement paste as compared with silica fume, Constructions and Building Materials, Vol. 24, 2010, pp. 315-321

15. SONG, H W, PACK, S W, NAM, S H, JONG, J C, SARASWATHY, V. Estimation of the permeability of silica fume cement paste, Constructions and Building Materials, Vol. 24, 2010, pp. 315-321.

# EFFECT OF ENTRAINED AIR AND SMALL SIZED BALLOON COMPONENT ON THE SALT SCALING RESISTANCE OF CONCRETE BY FREEZING AND THAWING WITH SODIUM CHLORIDE DEICER

**S Hanehara**

**T Oyamada Y Tanakadate**

Iwate University

**K Igarashi**

Denka Co. Ltd

Japan

**ABSTRACT.** The increase of entrained air in concrete may be effective for reducing salt scaling deterioration of concrete. Two kinds of microballoon admixtures, namely admixture A consisting of graded coal fly ash, and admixtures B consisting of balloons foamed from polyvinylidene chloride, were used mixed with cement mortar in this study. The effectiveness of the addition of these two kinds of microballoon admixtures in terms of the salt scaling resistance of mortar was evaluated compared with air-entrained mortar, using the small sized sample test method for the salt scaling test proposed by the author previously. In the case of AE agent use, 20% of air content was lost during transportation, placing, compaction and setting of fresh concrete. Admixture A was found not to be effective in reducing salt scaling because the shell thickness of component A is too thick to deform in the same way as entrained air voids. Admixture B was found to be effective in increasing durability of concrete in terms of resistance to salt scaling, because component B with thin shell thickness responds to pressure in a similar way to entrained air voids. The addition of component B is more effective for retaining air content in concrete, because component B does not excape during transportation, placing, compaction and setting of fresh concrete.

**Keywords:** Salt scaling, AE concrete, Microballoon admixture, Freeze-thaw resistance, Sodium sulfate, Salt scaling, freeze and thaw, Small sized balloon component, Deicer

**S Hanehara** is Full Professor of Concrete Laboratory, Civil and Environmental Engineering Department, Faculty of Engineering, Iwate University.

**T Oyamada** is Associate Professor of Concrete Laboratory, Civil and Environmental Engineering Department, Faculty of Engineering, Iwate University.

**Y Tanakadate** is student of graduate school, Civil and Environmental Engineering Department, Faculty of Engineering, Iwate University.

**K Igarashi** is manager of Technical section, Special cement additive department, Infrastructure & Inorganic Materials, Denka Co. Ltd.

## INTRODUCTION

The use of deicer causes scaling deterioration of concrete, a recognized phenomenon that is called salt scaling. The introduction of independent fine air bubbles (entrained air) through the use of AE agent has been shown to be effective to a certain extent for reducing salt scaling [1]. The introduction of entrained air through the use of AE agent is also known to promote air content reduction when concrete is transported, placed, and compacted, and thus the effective introduction of air bubbles has arisen as a new issue that needs to be addressed.

The present study prepared mortars using two types of admixture consisting of hollow spheres (balloons) of small diameter (20 μm to 150 μm) equivalent to that of entrained air bubbles, and evaluated their resistance to salt scaling. The two admixtures used were admixture A consisting of graded hollow fly ash microballoons, and admixture B consisting of foamed polyvinylidene chloride microballoons. The effectiveness of these admixtures was evaluated by comparing the mortars prepared with these microballoon admixtures with mortars using conventional AG agent and plain mortar.

## SAMPLES AND EXPERIMENTAL METHODS

### Microsphere admixtures

The microballoon admixtures used were admixture A, consisting of hollow fly ash microballoons graded by elutriation (E-SPHERES of Taiheiyo Cement Corporation), and admixture B produced by foaming a material consisting mainly of polyvinylidene chloride (FTP of Denka Company Limited). Table 1 lists the respective characteristics of each admixture, and Figure 1 shows the shape of the balloons. Admixture A consists of hollow fly ash microballoons ranging in size between 20 μm and 300 μm, with an average particle size of 130 μm, but it is of high bulk density owing to the thick shells of the balloons. Admixture B, on the other hand, is comparatively more uniform in particle size, with somewhat smaller particles of 100 μm owing to the foaming conditions. Admixture B has also lower bulk density owing to thinner shells. Both admixtures have the advantage that the air content of the hardened mortar can be adjusted by the admixture dosage

Table 1 Characteristics of small sized balloon for blending component

| NAME | COMPONENTS | SIZE RANGE, μm | MEAN SIZE , μm | DENSITY, g/l |
|---|---|---|---|---|
| A | $SiO_2$-$A1_2O_3$ glass phase | 20-300 | 130 | 392 |
| B | Polyvinylidene chloride | 10-100 | 40 | 20 |

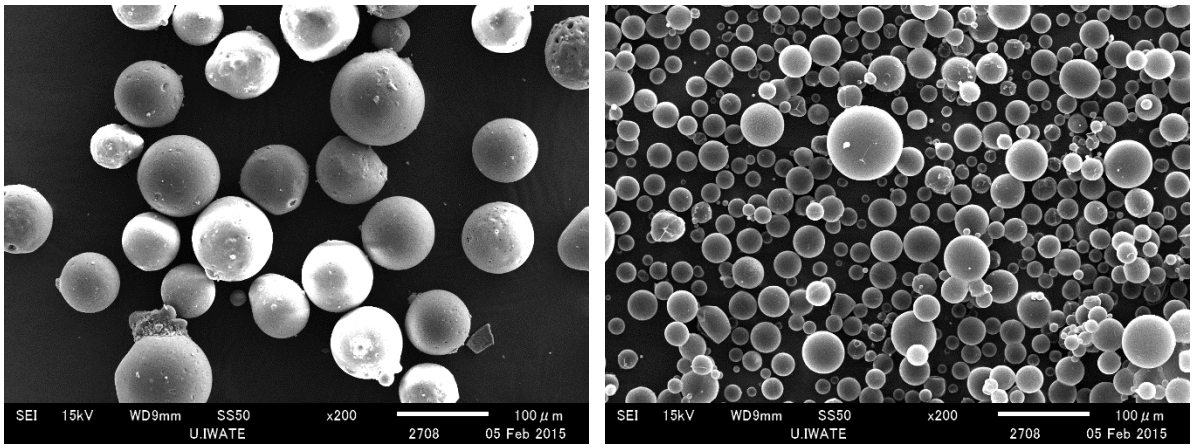


Microballoon A Microballoon B

Figure 1 SEM images of microballoon A and B

**Fabrication of the specimens**

The cement used was Ordinary Portland cement, and the fine aggregate consisted of crushed sand from Kurokawa, Morioka City, Japan. Keeping the mortar content of concrete in mind, the mortar specimens were prepared with water-cement ratio of 0.55 and sand-cement ratio of 2.8. Regarding the admixture dosage, the exact dosages were determined to obtain air content of 4%, 6%, and 8%.. For admixture A, the volume ratio of air voids in the hollow microballoons was calculated based on the bulk density and the true density of fly ash, to arrive at respective admixture dosages of 60 g, 90 g, and 120 g per liter of mortar. For admixture B, dosages of 1.5 g, 3.0 g, and 4.5 g per liter of mortar were used. For comparison, generic AE agent using alkyl ether sulfates was used to prepare AE mortar with 6% air entrainment. Plain mortar without any admixture was also prepared. JIS mortar specimens measuring 4 × 4 × 16 cm were prepared and water cured to the age of 28 days.

**Measurement of air content**

Air content before curing was measured using the air chamber pressure method. Mortar specimens measuring 4 × 4 × 16 cm were cut perpendicularly to the longitudinal direction to yield 4 × 4 × 1 cm test pieces, whose cut faces were polished, and the air content and the air-void spacing factor were measured through the area ratio method of image processing [2].

**Salt scaling evaluation tests**

Salt scaling evaluation was done using the evaluation method using test pieces proposed by the authors [3] [4]. Sets of three 8-mm sided cubes (weighing approximately 4 g) cut using a diamond cutter were subjected to one free-thaw cycle per day using a 3% solution of NaCl (deicer) in a 100 ml polypropylene container, until the prescribed number of freeze-thaw cycles was reached. Following the prescribed number of free-thaw cycles, the test pieces were cleaned of debris and dried and the mass residual ratio was obtained from 2.5 mm piece of retained material. Based on the residual mass ratio, the scaling durability index (SDI) was calculated. The calculation of SDI is as follows.

SDI = Residual mass ratio (%)
If residual mass ratio is less than 60%

SDI = P × N / M
P = 60 (%)
N = Number of cycles when residual mass ratio = P (times)
M =Total cycles of Freezing and thawing (times)
(M = 5 in this report)

Comparison of this test method using small-sized test pieces with other salt scaling evaluation test methods such as the ASTM C672 method showed the proposed test method to have a certain degree of consistency [5] making it valid for scaling evaluation.

## EXPERIMENTAL RESULTS AND DISCUSSION

### Air content and distribution of air voids in mortar

Regarding the effects of admixture use, Table 2 lists the test results for air content in fresh and hardened mortar, Figure 2 show the changes in air content in fresh mortar, and Figure 3 shows the relationship between air content in fresh and hardened mortar. In the case of the microballoon admixtures, the dosage was set to obtain air content of 4%, 6%, and 8% in the hardened mortar, but the air content of the fresh mortar for admixture A remained unchanged even when the admixture dosage was increased, showing a value around 3%, equivalent to that of plain mortar. In the case of admixture B, the admixture dosage and air content of the fresh mortar were proportional, with the air content increasing in line with the dosage, and air content of 7.5% secured compared with the targeted air content of 8%. The air content of the fresh mortar was obtained using the pressure method. This method consists in increasing the air pressure on the concrete inside an air chamber and measuring air content from the pressure difference that arises due to volume change, which is proportional to the total void volume. The measured air content of the mortar obtained using admixture A was almost the same as that of plain concrete. This indicates that the admixture did not deform under the effect of the pressure in the air chamber, demonstrating the rigidity of microballoon admixture A. On the other hand, as described later, the air content of hardened mortar using admixture B was almost the same as that of fresh mortar, indicating that the elasticity of the microballoon admixture itself deforms to the same extent as air voids under the same pressure. The air content resulting from admixture B was determined using an air meter.

Table 2 Air content in fresh and hardened specimens

| Balloon and others | Mark | Amount of addition (g/L) | Air content(%) | | Air void spacing factor (μm) |
|---|---|---|---|---|---|
| | | | Fresh | Hardened | |
| A | A4 | 57.9 | 2.8 | 4.4 | 166 |
| | A6 | 86.7 | 3.1 | 6.7 | 118 |
| | A8 | 115.7 | 3.3 | 7.1 | 120 |
| B | B4 | 1.6 | 3.9 | 4.2 | 149 |
| | B6 | 3.1 | 5.8 | 5.9 | 106 |
| | B8 | 4.6 | 7.5 | 7.1 | 101 |
| AE agent | AE6 | 0.021 | 5.8 | 4.3 | 185 |
| Plain | Plain | - | 3.2 | 1.5 | 335 |

In addition to the air content introduced in the fresh and hardened concrete through the use of AE agent, the relationship between the air contents of fresh and hardened mortars was also examined. As previously mentioned, the use of AE agent causes the air content of mortar to drop. The drop measured in this study was 1.5%, thus a decline of about 20%. In the case of admixture A, air content was not measured before curing and was the same as that of plain mortar, but was found to have increased after curing, in proportion to the addition of admixture A. Admixture B showed almost no effect in terms of the difference in air content before and

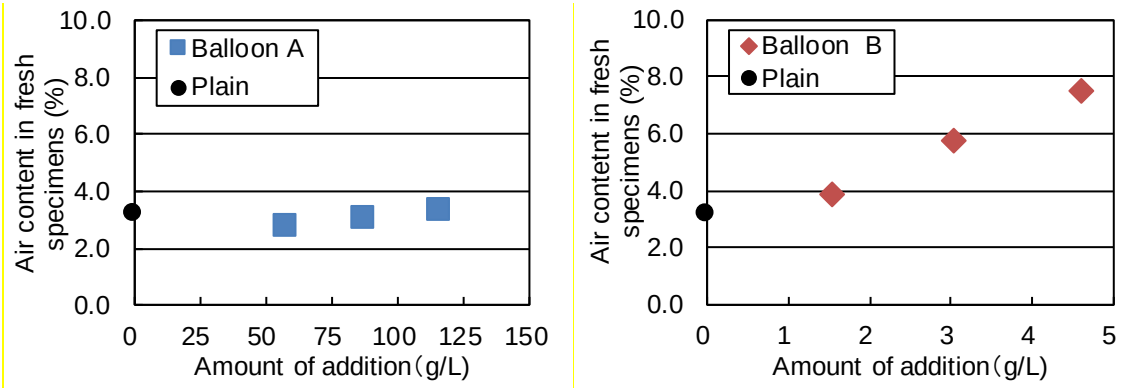


(a) Microballoon A (b) Microballoon B

Figure 2 Relationship between added amount of microballoon and air content in fresh

after curing. In the case of actual concrete, transportation, placing and compacting causes air voids to move upward, coalescing with other small-diameter voids to form larger voids, which can move upward more easily, resulting in loss of air content reported to be on the order of 2% or 3%6). In the case of admixture B, which does not result in a change in air content before and after curing, air voids do not coalesce and remain present in the concrete as small-diameter voids. In other words, through the various construction processes, air voids do not decrease, and the air content increases in proportion to the admixture dosage.

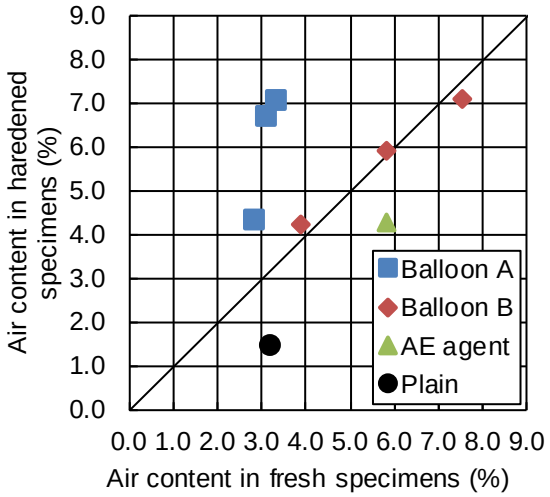


Figure 3 Relationship between air content in fresh and hardened mortar

Figure 4 shows SEM images of air voids in hardened mortar. The recesses are the cross-sections of air voids and admixture. They range in diameter between 50 μm and 100 μm. In hardened AE mortar with AE agent, the air voids are spherical in shape and precipitate of calcium hydroxide and other substances can be seen inside. In the case of hardened mortar containing

microballoon admixture A, examination of the shell part at the interface between the microballoon wall and the cement paste shows that the microballoon is sphere shaped and that the thickness of the shell is 10 μm or more. Inside the shell, smaller air voids 1 μ or less in diameter can be seen. The shell consists of fly ash and is believed to be $SiO_2$-$A1_2O_3$ in the glass phase. The shell being thick, it has high rigidity and thus is unlikely to become deformed within the pressure range of the pressure method. The air voids in hardened mortar containing admixture B are substantially the same as those in mortar containing AE agent, and the boundary between the cement paste and admixture cannot be confirmed.

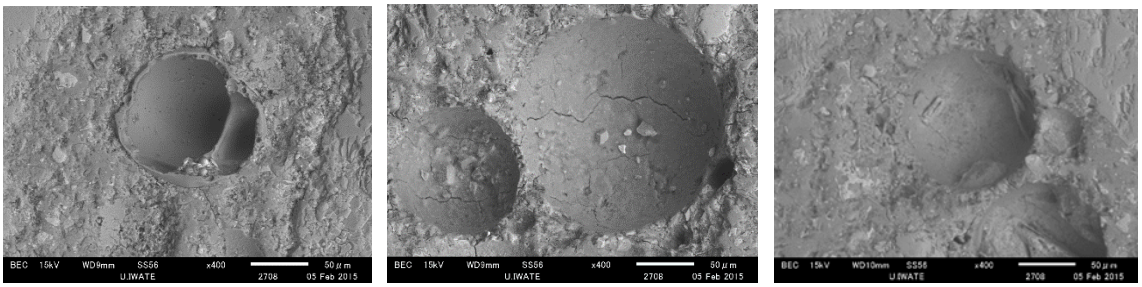

In balloon A In balloon B In AE mortar

Figure 4 SEM image of air void in hardened specimens

Figure 5 shows the distribution of air void diameters in hardened mortars. In the case of plain mortar, the peak diameter shared by most of the air voids in the mortar is about 100 μm, but the curve has a broad base indicative of a large range of air void sizes. Considering the particle sizes of AE agent and microballoon admixtures, the measurement range of 20 μm to 300 μm was adopted.

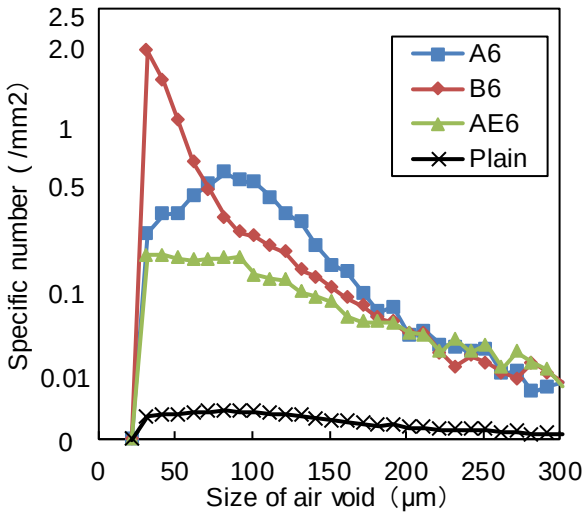


Figure 5 Size distribution of air void

Most AE agent particles range in size between 20 μm and 150 μm, and the peak is 50 μm. In the case of microballoon admixture A, the peak diameter is 80 μm in a similar air void range as for AE agent, which indicates larger air voids than AE agent. Given that the air void diameter distribution curve for microsphere admixture B peaks at 30 μm and air voids 80 μm or smaller in diameter account for a large percentage of air voids, admixture B can introduce smaller air bubbles than entrained air. These findings are consistent with the results of SEM observation in Figure 1.

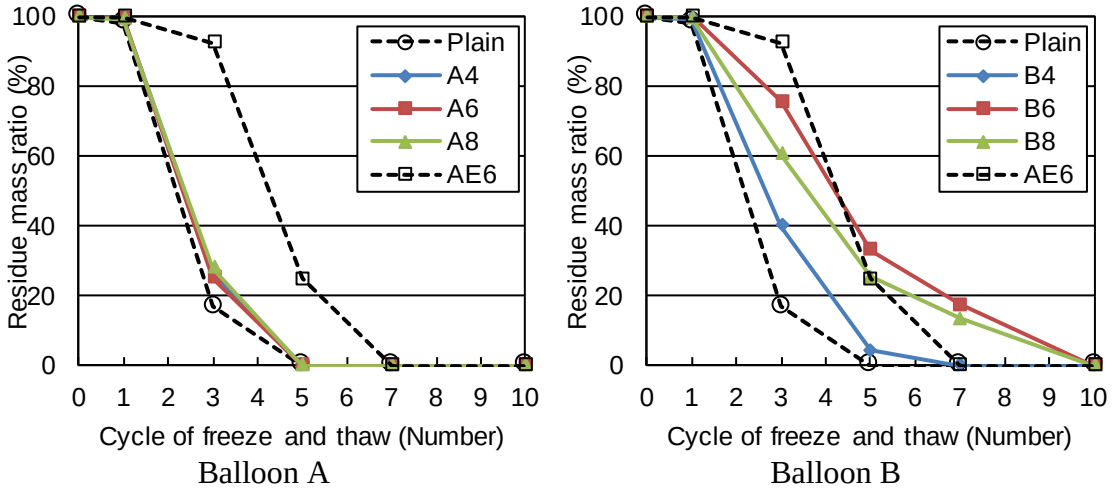


Figure 6 Change of residue mass ratio with cycles of freeze and thaw

**Scaling resistance**

Figure 6 shows the test results for scaling resistance of mortars using microballoon admixtures. In addition to the results for admixture A mortar and admixture B mortar, this figure shows also the results for plain mortar and AE mortar as dotted lines.

Admixture A mortar shows scaling resistance equivalent to that of plain mortar, regardless of the dosage of admixture A. In the case of admixture A, which introduces small air voids, the air content after curing is secured, but this has almost no effect in terms of boosting scaling resistance. In terms of freeze - thaw resistance, entrained air bubbles ranging in diameter between 30 $\mu$m and 100 $\mu$m are pointed out to be effective, but we can see that although admixtures such as admixture A cause the inclusion of air voids, these air voids have thick shells that impede the movement of water, making such admixtures ineffective for improving freeze - thaw resistance.

In the case of admixture B, as shown in Figure 6, the residual mass ratio increases according to the admixture dosage. At the third cycle, the residual mass ratio is 40% for B4, 60% for B8, and 75% for B6 compared with 20% for Plain. Air content is lowest for B4 at 4%, a level comparable with that of AE agent. B6 and B8 show residual mass ratios comparable to that of AE6, indicating scaling resistance on the same order as that obtained through the introduction of air content of 6% through the use of AE agent.

Figure 7 shows the observed change in appearance of the test pieces at each cycle as obtained with the test method using small test pieces with air content of 6% through the use of AE agent or microballoon admixture. Since the examination looked at the shapes of test piece residue in a 2.5 mm sieve, the white cells in Figure 7 indicate that all the test pieces were smaller than 2.5 mm for the cycle in question. At the first cycle, none of the test pieces showed scaling of any sort. Scaling degradation progresses from the surface toward the inside, causing progressive disintegration, regardless of whether AE or microballoon admixture is used. Since the corners break down in the early stages of deterioration, the test pieces gradually become round in shape. In the case of AE6 and B6, scaling of the surface begins at the third cycle, and from the fifth cycle, the test pieces become scaled down to half or less of their original size.

Figure 8 shows the relationship between the air-void spacing factor of all the hardened mortars and their scaling resistance. The air-void spacing factor can be obtained by measuring the air

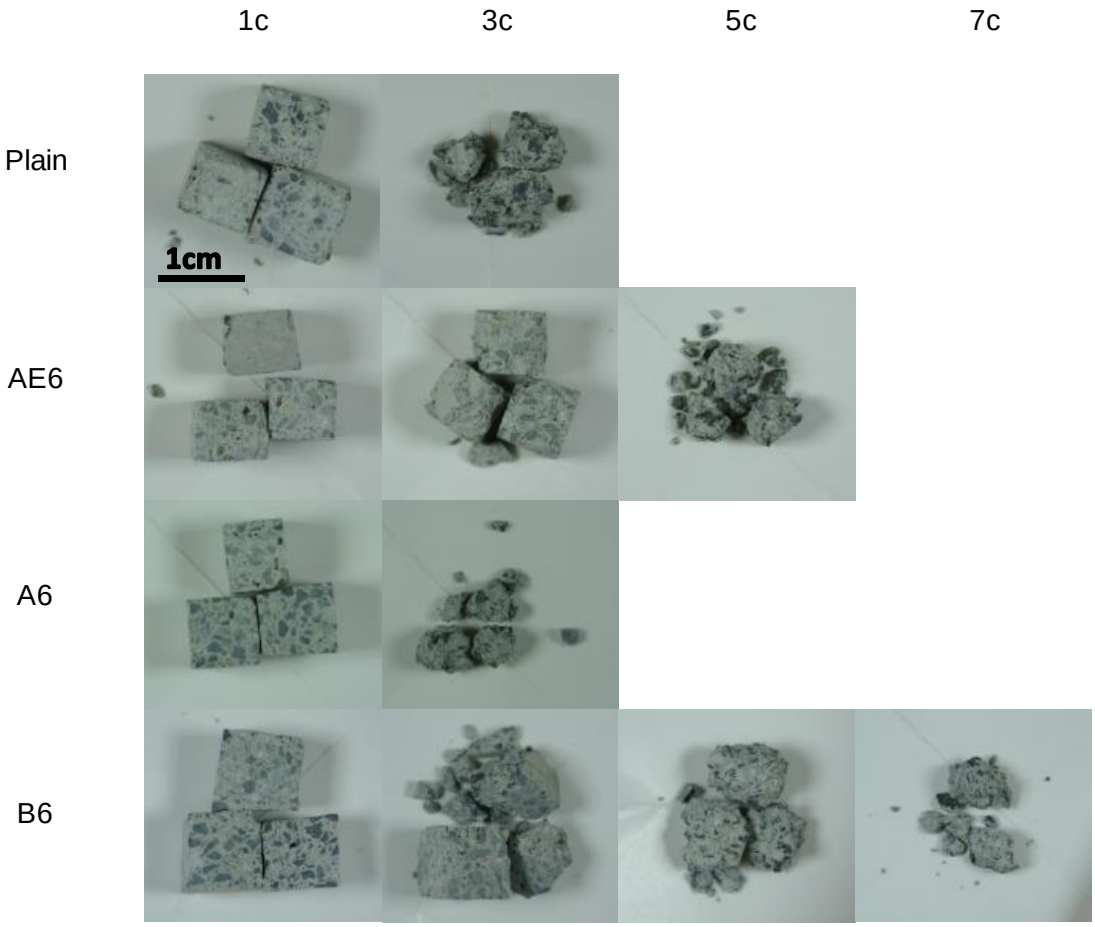


Figure 7 Appearance of specimens of 2.5mm over as the freeze-thaw cycles

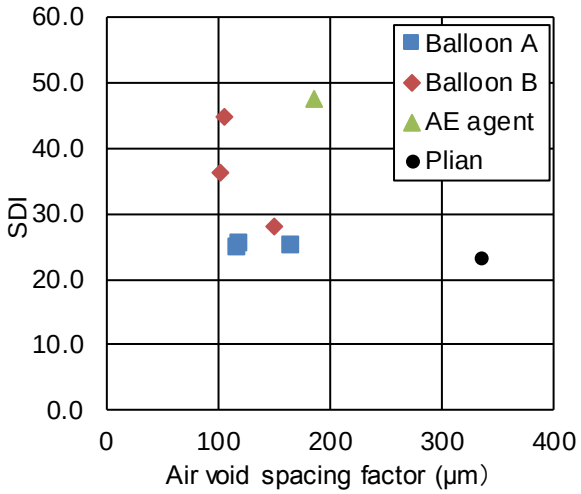


Figure 8 Relationship between air void spacing factor and SDI at 5cycles.

content (amount of air voids) of hardened mortar. With regard to the air-void spacing factor and scaling durability index (SDI), the air-void spacing factor, which is an indicator of freeze-thaw resistance, was 250 μm or less when microballoon admixture or

AE agent was used. Admixture A has a smaller air-void spacing factor than 6% air content using AE agent, and although the distance between air voids is smaller, SDI is only about half. Moreover, the SDI value is on the same order as that of plain mortar, which has an air-void spacing factor that is two or more times larger. Based on the above, admixture A is not effective in terms of the air voids is provides. On the other hand, admixture B is shown to improve scaling resistance if the air-void spacing factor is in the order of 100 μm. When hollow microballoon admixture is used, the relationship between the air-void spacing factor and scaling resistance does not necessarily hold.

The evaluation of scaling by using a method that uses small test pieces revealed that the introduction of entrained air through the use of AE agent does have some effect on suppressing scaling deterioration. Even microballoon admixtures are effective for introducing small air bubble corresponding to entrained air, but in the case of admixture A, where the shell itself has rigidity and does not lend itself to measurement by the pressure method, there is no scaling inhibition effect, whereas admixture B, which has the ability to deform similarly to entrained air, exhibits a scaling inhibition effect similar to that of AE. Moreover, the average diameter of air voids being smaller than that of entrained air, the air content is characterized by the fact that it remains unchanged before and after curing, a characteristic not exhibited by AE agent. Going forward, admixture B shows promise as a new material capable of delivering improved scaling resistance.

## CONCLUSIONS

The present study examined changes in air content before and after curing and salt scaling resistance through the use of AE agent and two types of microballoon admixture. The findings of this study are given below.

- In the case of AE agent, about 20% of air content is lost during the curing process, but salt scaling resistance is increased by the increase in air content.
- Admixture A, which features thick shells of $SiO_2$-$A1_2O_3$, did not offer salt scaling resistance.
- Admixture B consisting of foamed polyvinylidene chloride showed little loss of air content through processes such as molding and thus high air content retention, offering salt scaling resistance equivalent to that of entrained air introduced through the use of AE agent.

## REFERENCES

1. SEKIGUCHU C, OYAMADA T, HANEHARA S, HAYASAKA Y, Influence of air void and capillary pore in concrete on the scaling deterioration, TOHOKU division annual meeting of technology of JSCE(Japanese Society of Civil Engineering), Sendai, 2013, V-16.

2. NISIYAMA T, MAEKAWA S, KUSAKABE Y, NAKANO K, Dyeing and observation of air void structure in hardened concrete by use of cyanoacrylate, Cement Science and Concrete Technology, Vol. 42, 1988, pp.212-214.

3. OYAMADA T, HAMEHARA S, TAKAHASHI T, TAKAHASHI S, Study on the new test method for freeze-thaw resistance with de-icing chemicals, Proceeding of the Japan Concrete Institute, Vol. 33, No.1, 2011pp. 935-940.

4. HANEHARA S, OYAMADA T, KANNO H, NAKAMURA D, Influence of type of deicer on salt scaling of frost damage, Cement Science and Concrete Technology, Vol.67, 2013, pp.95-101.

5. KANNO H, HANEHARA S, OYAMADA T, ECHIGO T, Relationship between existing freeze-thaw test and new test method with small sized sample, Cement Science and Concrete Technology, Vol.68, 2014, pp.419-425.

6. OYAMADA T, FANG X, HANEHARA S, SAITO K, Relationship between air void structure and resistance against the salt scaling of concrete, JCI TC Symposium on The role and control of air void system in concrete (JCI-C86), 2015.6, pp.49-52.

# LABORATORY INVESTIGATION OF THE POTENTIAL USE OF PHOSPHOGYPSUM AS EMBANKMENT CONSTRUCTION MATERIAL

**A Anagnostopoulos**

**G Gaidajis**

Democritus University of Thrace

**M Papachristoforou**

Aristotle University of Thessaloniki

Greece

**ABSTRACT.** In order to reduce the annually deposited large quantities of phosphogypsum in natural environment an extensive research is underway, investigating the potential use of the material in embankment construction and environmental rehabilitation by filling large voids. In this context a laboratory investigation of the geomechanical properties of phosphogypsum material as samples taken from a deposition site in Greece, has been performed by the authors. The investigation included various tests to evaluate physical properties of the raw material and to measure the engineering behaviour of the compacted material. From the results of the investigation it is clear that the compacted phosphogypsum exhibits an excellent engineering performance at a very large spectrum of water content (high strength and low deformability). Moreover, the material was subjected to leaching test and it was shown that the concentrations of hazardous metallic elements were 2-3 times lower than those of the acceptable limits. However, as it is mentioned in the literature, the long-term behaviour of the compacted material in moisture saturated conditions should be monitored and further investigated in order to conclude about its potential unconditional use in embankment construction. Nevertheless, it is clear from the findings that the compacted material can be compacted easily and can be used as core material for various types of embankments, provided that it is protected satisfactorily from the percolating water.

**Keywords:** Industrial by-product utilization, Phosphogypsum, Geomechanical properties, Laboratory investigation, Embankment construction

**Argyrios Anagnostopoulos** graduated from the Department of Production and Management Engineering at Democritus University of Thrace. Currently he is a postgraduate student on Renewable Energy Systems Engineering at University of Surrey, UK.

**Assistant Professor Georgios Gaidajis** is the Director of the Environmental Management and Industrial Ecology Laboratory at the Department of Production and Management Engineering, at Democritus University of Thrace. He is a specialist in environment protection and sustainable development.

**Dr Michalis Papachristoforou** is post-doctoral researcher at the Laboratory of Building Materials of the Civil Engineering Department of Aristotle University of Thessaloniki.

## INTRODUCTION

Phosphogypsum is a waste by-product of the phosphoric acid production procedure at the phosphate fertilizers production industries, where phosphate rock is processed by dry thermal or wet acid method. It consists mainly from calcium sulphate hydrate, ($CaSO_4.2H_2O$) which is produced from the following chemical reaction:

$$Ca_3(PO_4)_2+3H_2SO_4+6H_2O \rightarrow 2H_3PO_4+3CaSO_4.2H_2O$$

This method, although is financially attractive, has a serious side effect, the production of large quantities of phosphogypsum.

Only a small percentage (in the order of 15%) of the international phosphogypsum production (100-300 Mt) is recycled and it is used as an alternative raw material in the construction and building industry, as fertilizer and for soil stabilization amendment in agriculture and as a set controller in Portland cement production industry [1].

The rest of the phosphogypsum quantity is mostly disposed, in most cases without any treatment, usually by depositing in very large stockpiles, close to phosphoric fertilizer plants covering large areas. The uncontrolled deposition can cause very serious environmental impact (e.g. in surface and underground water and in air quality). For these reasons an extensive research is internationally underway, investigating the potential use of the material in other applications, where on one hand a serious financial benefit will exist and on the other hand a lot of environmental pollution problems will be eliminated. A much promising section seems to be the embankment construction and environmental rehabilitation by filling large voids.

The present study is part of this investigation and presents the results of the laboratory tests performed at phosphogypsum samples, in order to measure and evaluate the geomechanical properties of the material ant its suitability for filling and compaction works.

## PHYSICAL PROPERTIES OF THE MATERIAL

### Introduction

The laboratory tests were performed in samples prepared using phosphogypsum raw material, supplied by “HELLENIC FERTILIZERS –ELFE” S.A. They took place at Soil Mechanics and Building Materials Laboratories of Civil Engineering Department at Aristotle University of Thessaloniki, Greece.

The investigation programme included the measurement and evaluation of the following:

a) The physical properties of the material (i.e. natural water content, particle size distribution and Atterberg limits)
b) The measurement of the engineering properties of the material (i.e. strength, deformability, compactness)

In order to be dried the raw material was spread on disks and was put in an oven with 105°C temperature.

## Measurement of Physical Properties

### Natural water content

The water content of the raw material was measured at five samples according to ASTM D2216-90 [2] and was found of the order of 27%.

### Grain size analysis

From the raw material three samples were taken and a grain size analysis test was performed at each sample according to ASTM D422-63-07 [3]. The grain size analysis included the sieve analysis for the coarser part of the soil sample and the hydrometer analysis for the finer part. The characteristic limit between finer and coarser part of the material was considered the opening of sieve #200 (0.074 mm) according to ASTM D2487-11 (USCS, [4]).

In the beginning the sieve analysis was performed with the dry method, i.e. at dried material and with vibration of the sieves. The fines content of the material was found to be between 55-61%. From the inspection of the material it was found that agglomerations which were not broken with the vibration, were developed between the grains, and thus the sieve analysis was performed again with the wet method.

From the results of the sieve analysis, presented at Figure 1, the fines content was of the order of 70%, which is well compared with the findings of other researchers [5, 6, 7].

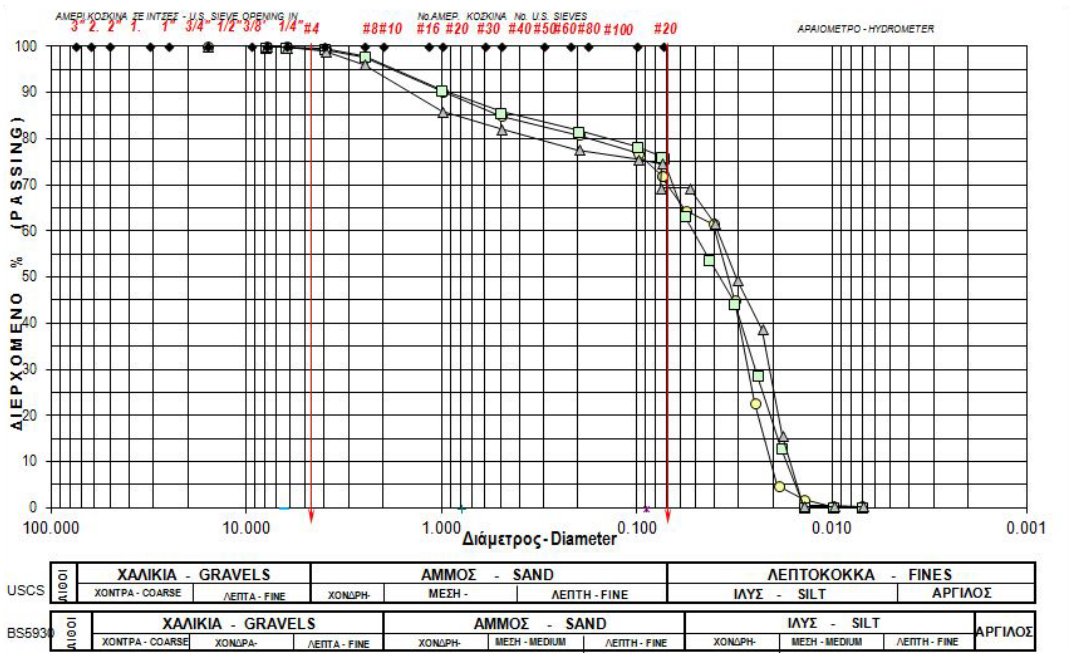


Figure 1 Particle size distribution curves

It is obvious that the apparent diameters of the grains of the finer part of the sample are almost equal (the curve is almost vertical) and the percentage in clay area is zero. Thus the material is classified as a coarse sandy silt according to BS5930 [8].

### Atterberg limits

The plasticity and the liquidity of the fines part were measured at three samples according to ASTM D4318-2010 [9]. In all cases they were found equal to zero. According to ASTM D2487-2011 [4] the material is classified as silt of low plasticity (ML). Similar evaluations have been presented from other researchers [5, 7].

### Suitability of the material for embankment material based on physical properties

According the AASHTO M145 [10], taking into account that the fines content of the material is equal to 70% and the plasticity of fines is zero, the material is classified as an A-4 (8) material. This material is characterized as "fair" and thus can be used for the construction of low to mid height (H<10 m) embankment bodies, provided that there are not more suitable materials in the area and the material can be compacted at the 90% percentage of the optimum density obtained according to modified Proctor compaction test.

According to USCS (ASTM D4217, [4]) and BS 6031 [11], [12] the A-4 materials are classified as "poor to fair", as far as their suitability for construction of motorway embankment bodies is concerned, whereas, as far as their compressibility behaviour is considered, they are classified as "of medium quality".

Finally, according to Greek National Specifications [13] the utilization of A-4 materials is allowed for motorway embankments, but due to high percentage of gypsum contained, the specific material considered as not acceptable.

## ENGINEERING PROPERTIES OF THE MATERIAL

### Compaction Tests

The compaction tests were performed according to the standard Proctor laboratory compaction test ASTM D698 [14] and the modified Proctor laboratory compaction test, (ASTM D1557 [15]). The results of the two test series are presented at Figure 2. For the case of standard Proctor compaction tests the optimum water content was found equal to w=15.4%, whereas the corresponding maximum dry density is equal to $\gamma d$=1.26 g/cm$^3$. For the case of the modified Proctor compaction test (which is the most often used in practice) the optimum water content was found equal to w=13.1% whereas the corresponding maximum dry density is equal $\gamma d$=1.44 g/cm$^3$.

The results of present study are presented and compared with the results from other researchers at Table 1.

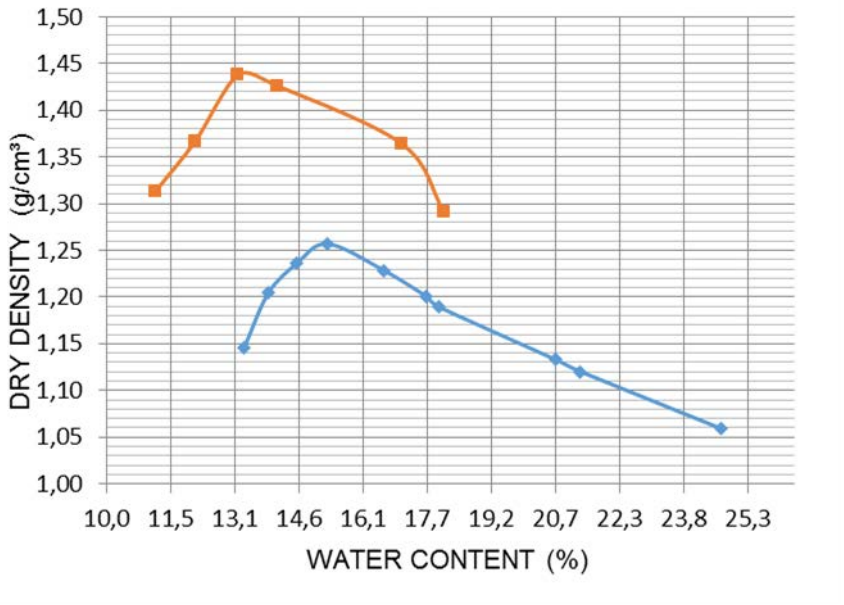


Figure 2 Compaction tests - Water content - dry density curves

Table 1 Values of maximum dry density / optimum water content

| RESEARCHER | MODIFIED PROCTOR | STANDARD PROCTOR |
|---|---|---|
| | $\gamma_{dmax}$ - $w_{opt}$ | $\gamma_{dmax}$ - $w_{opt}$ |
| Ho et al. [16] | 1.51 g/cm$^3$ - /16.3% | 1.42 g/cm$^3$ - /18.1% |
| Dapena et al. [17] | 1.56 g/cm$^3$ - /16.9% | 1.43 g/cm$^3$ - /19.1% |
| Moussa et al. [18] | 1.40 g/cm$^3$ - /18% | 1.27 g/cm$^3$ - /22% |
| FHWA-RD-97 [6] | 1.50 g/cm$^3$ - /17.5% | 1.27 g/cm$^3$ - /22% |
| Present study | 1.44 g/cm$^3$ - /13.1% | 1.26 g/cm$^3$ - /15.4% |

Since the natural water content is around to 27%, much higher than the optimum water content, it was decided to investigate the ability to compact satisfactorily the raw material with a water content percentage higher than 27%. For this a series of modified Proctor compaction tests was performed with water contents varied from 32% to 42%. These values of water content permit the easiest compaction of the raw material in the filed without drying.

As can be seen from Figure 3, where all the diagrams are presented, the optimum water content is equal to w=35%, whereas the corresponding maximum dry density is equal to $\gamma_d$=1.31 g/cm$^3$. From the comparison it can be deduced that the maximum dry density obtained from the modified Proctor test is 14% bigger than the obtained from the one obtained with the standard compaction test. It can also be concluded that for the whole spectrum of the examined values of water content with the modified Proctor tests (10%-42%) the minimum value of the dry density is not lower than the 85% of the obtained maximum dry density of 1.438 g/cm$^3$. Moreover, if the area of 12-16% , where the local maximum is appeared, it seems that the water

content does not has significant influence the value of maximum dry density. The same conclusion has been declared from other researchers [19]. The above lead to the basic conclusion that the raw phosphogypsum can be compacted in the field under various meteorological conditions (from completely dry to very wet).

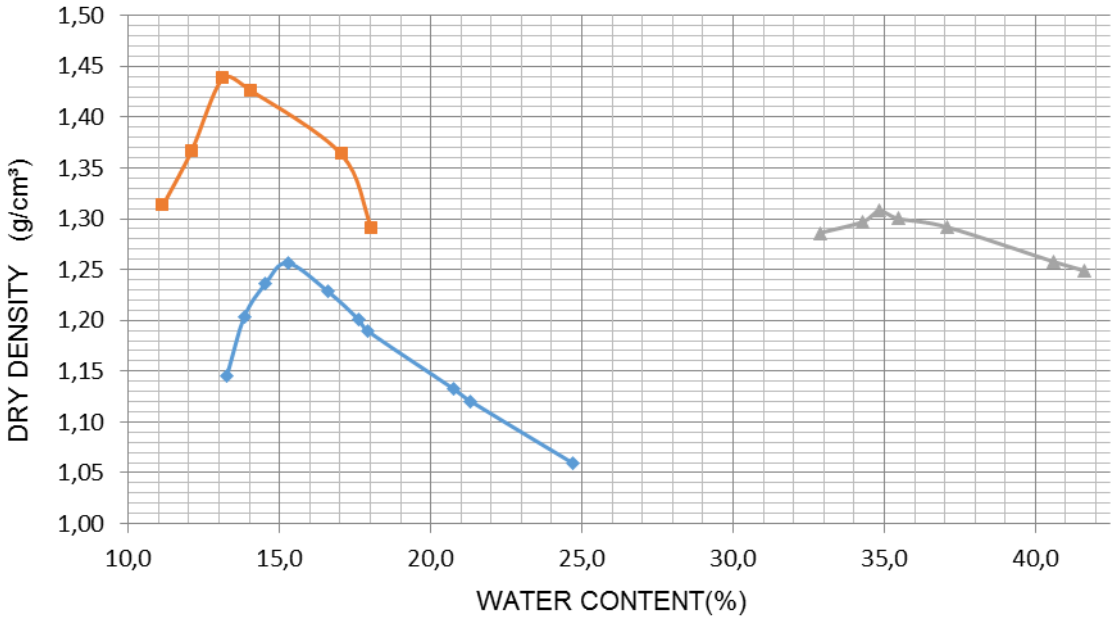


Figure 3 Compaction test in the 10-42% area

**CBR Bearing Capacity Tests**

In order to evaluate the bearing capacity of a stratum from compacted phosphogypsum, a CBR (California Bearing Ratio) test was performed according to the relevant ASTM D1883 – 2007 Specification [19]. The specimens were prepared with a water content of 15% and with a number of blows of 30 and 65. The results are presented at Figure 4. The resulted CBR value was found equal to 260, an impressive high value. The specimen of 30 blows was tested in a unconfined compression test and gave a $q_u$=4.97 MPa, which is also a very high value. From the results of the test it can be easily concluded that the compacted (near to the optimum water content) phosphogypsum exhibits very satisfactory bearing capacity.

**Triaxial Compression Tests – Measurement of Compressive Strength**

In order to measure the strength and the deformability of the compacted phosphogypsum two triaxial UU compression tests (unconsolidated and undrained) according to ASTM D2850/87 [20] were performed, for three values of lateral confining stress of 50, 100 and 200kPa. The tests were performed at specimens with a H/D =70mm/35mm ratio, which were constructed with water content around 15% (optimum water content according to modified Proctor compaction test ASTM D1557 [15]). The three specimens of the first test were unsaturated, where the three specimens of the second test ere saturated with water under pressure. The results of the test with saturated specimens are presented at Figures 5 and 6 and they concern the calculation of strength and deformability.

For the case of saturated test the undrained shear strength was calculated equal to $c_u$=720 kPa, whereas for the unsaturated test the values of the strength parameters were calculated equal to φ=42°και c=185 kPa. The values of the deformation modulus were calculated equal to E=50 MPa and 25 MPa, respectively.

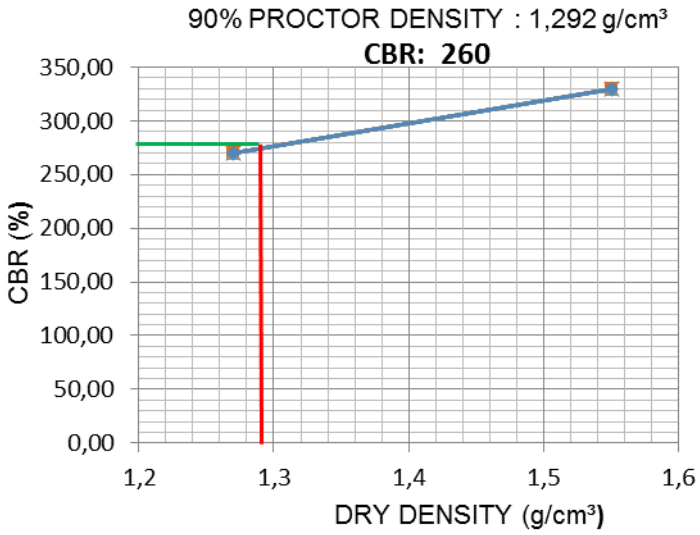


Figure 4 CBR test results

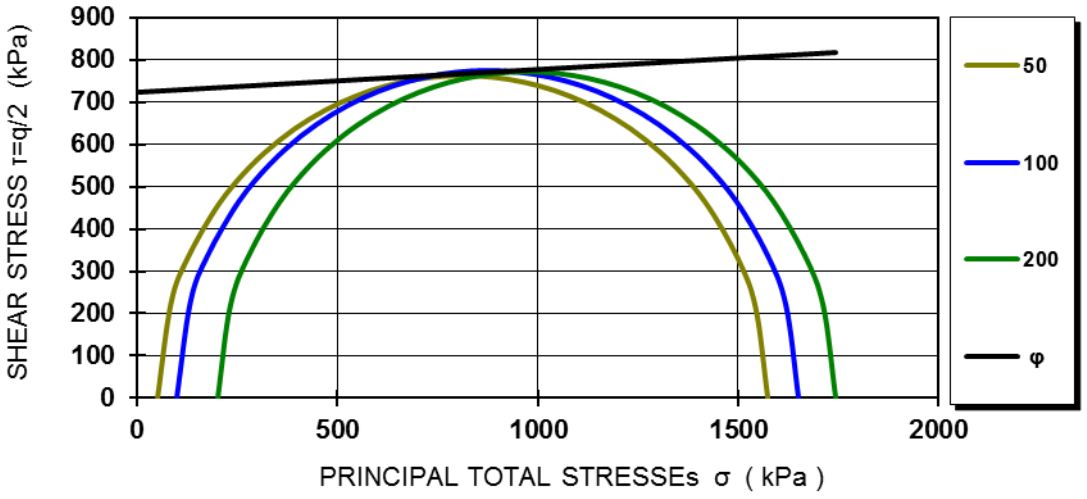


Figure 5 Shear strength of saturated test

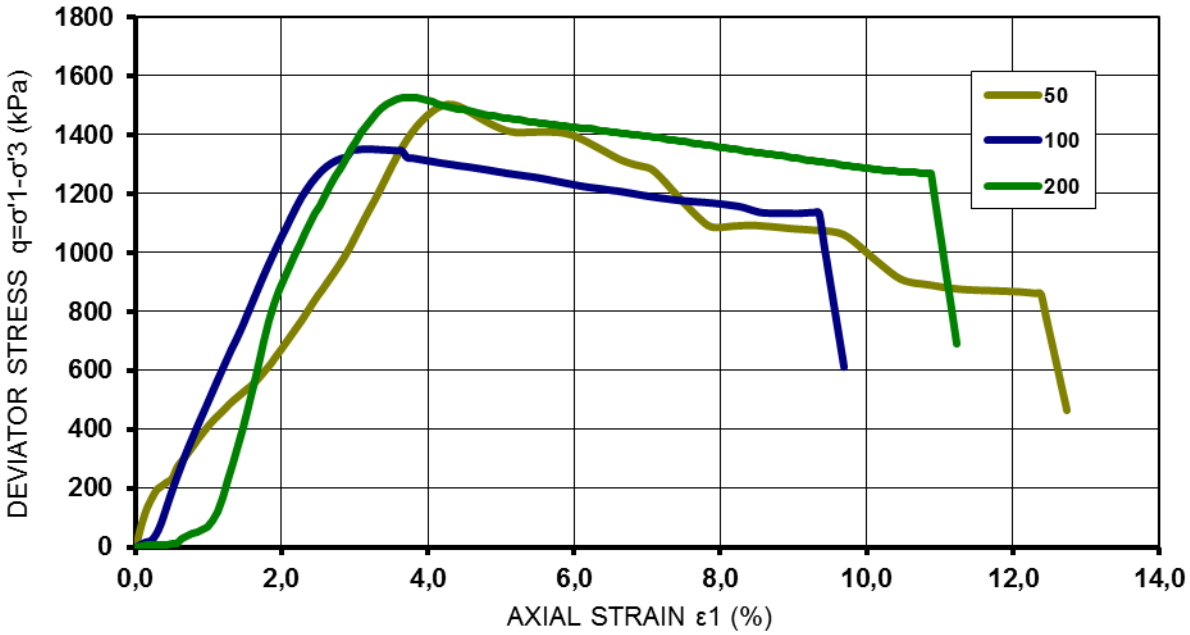


Figure 6 Stress-strain curve for the saturated test

**Consolidation Test – Compressibility and Permeability Measurement**

In order to measure the compressibility and the permeability of compacted phosphogypsum a consolidation test was performed according to ASTM D2435-11[21].The test was performed at a specimen prepared with water content around 15% (optimum water content according to modified Proctor compaction test) as in the case of the triaxial tests. The main results of the experiments are presented in brief at Figures 7 and 8.

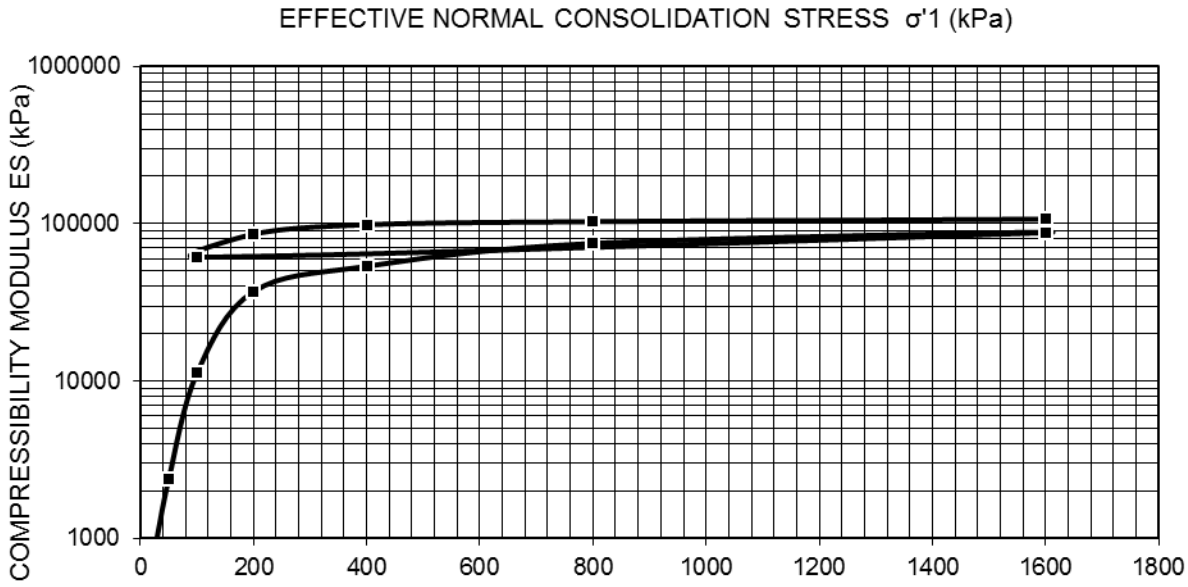


Figure 7 Consolidation Test Compressibility Modulus vs normal consolidation stress curve

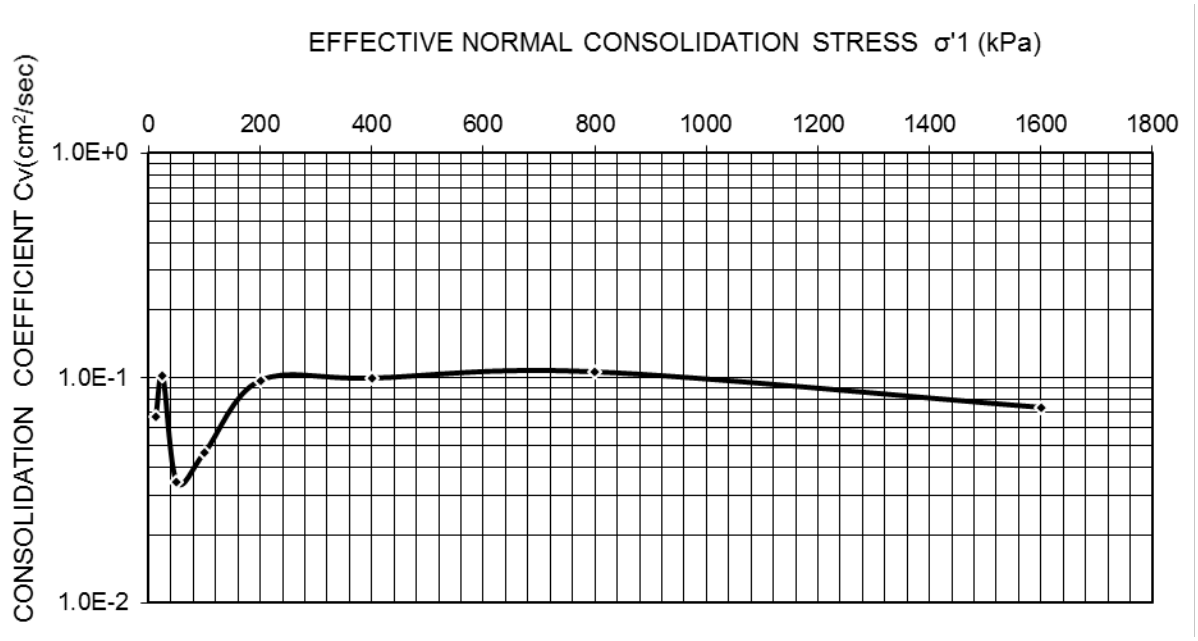


Figure 8 Consolidation Test – Consolidation coefficient vs normal consolidation stress curve

As it is clear from Figure 7 the compressibility modulus $E_S$ varies from 11 to 90 MPa, whereas in the case of recompression has a constant value of 100 MPa. This means that phosphogypsum, when compacted around its optimum water content, becomes a very "hard" material and exhibits a very small compressibility, even in low vertical stresses, especially if it has been compacted with high stresses.

The consolidation coefficient $C_V$, according to Figure 8, has an almost constant value of $1.10^{-1}$ cm²/s, which gives a coefficient of permeability in the order of $2.5\times10^{-7}$ cm/s (0.022 cm/day). This value is very low and means that the compacted material is practically impermeable but it must be remembered that the result comes from a small specimen compacted in the optimum water content. Thus the conclusion must be confirmed from a more detailed investigation in more and larger specimens, compacted in various water contents.

## LEACHING TEST

Since from the previous presented results the construction of various kind of embankments in the field seems to be a much promising potential solution for the environmentally friendly disposal of phosphogypsum, it was decided to check the quality of the leachates. This was done with a procedure which simulated the disposal of the material to the expected environmental conditions, using a TCLP test (Toxicity Characteristic Leaching Procedure, EPA Test Method 1311, [22]). From the results, which are summarized at Table 2 , it is obvious that the concentrations of basic elements and heavy metals at the leachate are lower at 2-3 orders of magnitude from the corresponding proposed environmental safe limits. So, it was concluded that, in an initial level, the examined material is compatible with the proposed potential uses of the material and it is not expected to cause any relevant environmental problems.

Table 2 TCLP test results and maximum allowable concentration of contaminants for the toxicity characteristic (US EPA, 2003)*

| EPA WW No** | ELEMENT | RESULTS | LIMIT VALUE, mg/l |
|---|---|---|---|
| D004 | As | 0.021 ±0.005 | 5.0 |
| D005 | Ba | 0.07 ±0.003 | 100.0 |
| D006 | Cd | 0.004 ±0.0005 | 1.0 |
| D007 | Cr | 0.014 ±0.001 | 5.0 |
| D008 | Pb | 0.034 ±0.005 | 5.0 |
| D010 | Se | <0.1 | 1.0 |
| D011 | Ag | <0.01 | 5.0 |

*US EPA (2003) Toxicity Characteristic, Table 1-Maximum concentration of contaminants for the toxicity characteristic. Title 40 Code of Federal Regulations, Part 261.24, Edition 7-1-03, 59-60.
**Hazardous Waste Number.

## DISCUSSION AND CONCLUSIONS

According to the results of the presented extensive laboratory investigation the phosphogypsum raw material can be easily compacted, achieving very satisfactory values of strength and deformability, even when it has been wetted.

As it is reported from other researchers [17] the compacted phosphogypsum, when it has been saturated and is under continuous loading, exhibits significant increase of its deformability in the long term conditions. According to Moussa [18] the settlement of a compacted phosphogypsum sample, loaded in a consolidation apparatus, was continued to settle for three months. So, before definitive conclusions for the feasibility of the compacted phosphogypsum application in embankment construction are drawn, the further and more detailed investigation of the long term behaviour of compacted saturated phosphogypsum is inevitable. This investigation should include a more detailed laboratory investigation programme and a pilot test in the field similar to described by Gaidajis et al. [26]. At this investigation project the compliance of the leachates quality to the specific environmental criteria should be included.

Nevertheless it should be mentioned that the excellent engineering behaviour of the non-saturated compacted phosphogypsum has been definitely well documented. This means that when the compacted material is protected from the percolating water by using various waterproofing techniques (e.g. the well-known geotextile/geomembrane system), it is an excellent material for construction of any kind of embankment. So it can be applied in cases of environmental rehabilitation (e.g. fill of cavities) and as a core at embankment of secondary roads etc. Thus enormous quantities of phosphogypsum can be used in a sustainable way.

Another relative possible use of the phosphogypsum is the construction of embankments by compacted phosphogypsum mixed with small quantities of cement, fly ash and lime. It is obvious that this idea should also be thoroughly examined.

Finally it is important to be remembered that by using extensively the by-product of phosphogypsum, the cost of the protection projects against the environmental threatening from the uncontrolled deposition in stockpiles becomes very much lower. Moreover, when the dramatic consequences of an environmental destruction of the stockpiles due to an earthquake or due to a flood are considered, the need for the urgent confrontation of the problem becomes very clear. According to these remarks the potential use of the compacted phosphogypsum as a material for various types of embankments should be strongly encouraged and thus extensively investigated.

## ACKNOWLEDGEMENTS

The authors would like to express their gratitude to the personal of the Soil Mechanics and Building Material Laboratories of the Civil Engineering Department of Aristotle University of Thessaloniki for their valuable assistance at the performance of the laboratory tests. They would like also to acknowledge “HELLENIC FERTILIZERS – ELFE” S.A. for the raw material supplied and its permission to publish the results of the investigation.

## REFERENCES

1. TAYIBI H., CHOURA M., LOPEZ F. A., ALGUACIL F. J., LOPEZ-DELGADO A. (2009). Environmental impact and management of phosphogypsum, Journal of Environmental Management, Vol. 90, pp. 2377–2386.

2. ASTM D2216-10 (2010).Standard Test Methods for Laboratory Determination of Water (Moisture) Content of Soil and Rock by Mass, American Association of State and Highway Transportation Officials.

3. ASTM D422-63 (2007). Standard Test Method for Particle-Size Analysis of Soils, American Association of State and Highway Transportation Officials.

4. ASTM D2487-11 (2011). Standard Practice for Classification of Soils for Engineering Purposes (Unified Soil Classification System), American Association of State and Highway Transportation Officials.

5. VALVERDE P. I, VALVERDE E. I., FUENTES G.R., MORALES M.M (2011). Geotechnical Risk and Environmental Impact: the Stability of Phosphor-Gypsum Embankments in SW Spain, Electronic Journal of Geotechnical Engineering, http://www.ejge.com/2011/Ppr11.143/Abs11.143.htm

6. FHWA-RD-97-148 Report. (1997). User Guidelines for Waste and By-product Materials in Pavement Construction http://www.fhwa.dot.gov/publications/research/infrastructure/structures/97148/nfs1.cfm

7. DESHPANDE, P.S. (2000).The determination of appropriate phosphogypsum: class c fly ash: Portland type ii cement compositions for use in marine applications**,** Thesis submitted to Louisiana State University.

8. BS 5930:1999+A2 (2010). Code of practice for site investigations, British Standards, BSI.

9. ASTM D4318 -10 (2010). Standard Test Methods for Liquid Limit, Plastic Limit, and Plasticity Index of Soils, American Association of State and Highway Transportation Officials.

10. AASHTO M145-91 (2012). Standard Specification for Classification of Soils and Soil-Aggregate Mixtures for Highway Construction Purposes, American Association of State and Highway Transportation Officials.

11. BS 6031 (2009). Code of practice for earthworks, British Standards, BSI.

12. NICOLAIDES, A. (2015), Highway Engineering Pavements, Materials and Control of Quality, CRC Press.

13. GREEK SPECIFICATIONS PETEP 1501-02-07-01-00 (2009). Embankment construction with appropriate excavation products www.ggde.gr/dmdocuments/02-07-01-00.pdf

14. ASTM D698-12 (2012). Standard Test Methods for Laboratory Compaction Characteristics of Soil Using Standard Effort (12.400 ft-lbf/ft$^3$ (600 kN-m/m$^3$)), American Association of State and Highway Transportation Officials.

15. ASTM D1557-12 (2012). Standard Test Methods for Laboratory Compaction Characteristics of Soil Using Modified Effort (56,000 ft-lbf/ft$^3$ (2,700 kN-m/m$^3$)), American Association of State and Highway Transportation Officials.

16. HO, ROBERT K.H. & ZIMPFER (1985). Comments on the Investigation of Phosphogypsum for Embankment Construction. Proceedings of the Second Workshop on By-Products of Phosphate Industries. The Florida Institute of Phosphate Research, May 1985, pp.182-213.

17. DAPENA E., SANTAYANA F.P. AND FLORES E.D. (2009). Characteristics of phosphogypsum for utilisation in roadwork fills, Proceedings of the 17th International Conference on Soil Mechanics and Geotechnical Engineering, M. Hamza et al. (Eds.) pp.116-119.

18. MOUSSA D. CRISPEL J.J., LEGRAND AND THENOZ B. (1984). Laboratory study of the structure and compactibility of Tunisian phosphogypsum (SFAX) for use in embankment construction, Resources and Conservation, Vol. 11 (1984), pp. 95-116.

19. ASTM D1883–14 (2014). Standard Test Method for California Bearing Ratio (CBR) of Laboratory-Compacted Soils, American Association of State and Highway Transportation Officials.

20. ASTM D2850-03a (2007). Standard Test Method for Unconsolidated-Undrained Triaxial Compression Test on Cohesive Soils, American Association of State and Highway Transportation Officials.

21. ASTM D2435-11 (2011). Standard Test Methods for One-Dimensional Consolidation Properties of Soils Using Incremental Loading, American Association of State and Highway Transportation Officials.

22. EPA Test Method 1311 (1992). TCLP - Toxicity Characteristic Leaching Procedure, Environmental Health & Safety Online, www.ehso.com.

23. USEPA (2003). U.S. Environmental Protection Agency. National Primary Drinking Water Regulations; Radionuclides; Washington, D.C., Office of Water, U.S. Environmental Protection Agency Report EPA-815-2-00-003.

24. USEPA (2002). U.S. Environmental Protection Agency. National Emission Standards for Hazardous Air Pollutants, Subpart R.

25. USEPA (1993). Diffuse NORM Wastes-Waste characterization and Preliminary Risk Assessment. Prepared by S. Cohen and Associates, Inc. and Rogers & Associates Engineering Corp., for the U.S. Environmental Protection Agency Office of Radiation and Indoor Air.

26. G. GAIDAJIS, E. MYLONA, K. ADAM, E. GAZEA (2004). Pilot scale field performance of a reclamation scheme for sulphidic waste rock, The European Journal of Mineral Processing and Environmental Protection, Vol. 4, No.2, I303-0868, pp. 152-161.

# ULTRA HIGH PERFORMANCE FIBRE REINFORCED CONCRETE FOR INFRASTRUCTURE CONSTRUCTION

**W Wilson**

**T O'Flaherty**

Institute of Technology Sligo

Ireland

**ABSTRACT.** Sustainable development requires that infrastructure, such as bridges, are not only designed to be fit for purpose but also take account of the environmental impact of the whole life cycle of the structure, from 'cradle to grave'. The performance and durability of the materials used in their construction, such as concrete, must be improved. Ultra-high performance fibre reinforced concrete (UHPFRC) is used worldwide to improve the structural performance of bridges, extend their working life and reduce environmental impact. UHPFRC is an encouraging development in concrete technology as it exhibits much higher strength than conventional concrete. As a result thinner structures are constructed leading to reductions in the structure's self-weight and the volume of concrete and natural raw aggregates used in their construction. A drawback to UHPFRC is that it results in a significant rise in initial costs over normal and even high performance concretes, and the cost-efficiency and sustainability of this material must be improved. These costs are significantly higher in Ireland due to the lack of availability of certain materials such as quartz flour used in its design. The research reported here discusses the developments in designing a new type of UHPFRC using locally sourced materials, where possible, to produce a sustainably viable material for the Irish construction industry. Using mix design calculations and experimental testing of cylinders in compression and beams in flexure , two different mixes consisting primarily of rapid hardening high strength cement, silica fume, sand and high strength steel fibres are proposed. Results indicate that using a steel fibre volume of 2%, both mixes exhibit cost savings in comparison to similar strength UHPFRCs available based on the cost of the individual constituents used in the mix design.

**Keywords:** Fibre reinforced concrete, Infrastructure, Sustainable construction, Ultra high performance concrete.

**Mr William Wilson** is a PhD Candidate in the Department of Civil Engineering & Construction at the Institute of Technology Sligo. His research is focused on ultra high performance fibre reinforced concrete and numerical modelling of concrete.

**Dr Tomas O'Flaherty** is a lecturer in the Department of Civil Engineering & Construction at the Institute of Technology Sligo.

## INTRODUCTION

High Performance Concrete (HPC) has achieved the maximum compressive strength in its traditional mix design of coarse aggregate, fine aggregate, cement and water. However, at such a level of strength, as the compressive strength of the concrete mix has exceeded the compressive strength of the coarse aggregate, the coarse aggregate becomes the weakest constituent in concrete. In order to increase the compressive strength of concrete even further, the only way is to remove the strength of the coarse aggregate. This philosophy has been employed in UHPFRC [1]. In UHPFRC the coarse aggregate is replaced by ultra-fine particles which are stronger than the coarse aggregate. Ultra-fine particles also allow a superior packing of the constituents to occur which reduces the number of voids within the concrete. A high amount of silica fume is included in the mix typical 20 – 35% the weight of cement, this value is generally less than 10% in conventional concrete. Similarly, a high dosage of superplasticiser in the region of 4 – 6% the weight of cement is used in comparison to less than 2.5% in conventional concrete. The water cement (w/c) ratio is generally less than 0.25 [2]. Like other fibre reinforced concretes, high energy dissipating capacity is an advantage of UHPFRC that is useful when dynamic loading, such as bridge loading, is applied. UHPFRC is generally cured with heat and or pressure treatments to enhance its properties and to accelerate the hydration reaction of the binder. UHPFRC can be used in-situ or as a precast unit. Compressive strengths can be in excess of 150 MPa and flexural strength over 30 MPa [3]. With this increase in strength higher loads can be supported and conventional structural components can be reduced in size and weight.

The main characteristics of UHPFRC are self-consolidating workability, very high mechanical properties, and low permeability. To achieve this, the mix design of UHPFRC is more complex than that of normal strength concrete. The mix design plays an important part of the process in concrete and ultimately decides the 28 day strength of a mix. Typically a normal concrete mix is designed using a series of tables and graphs in accordance with BS 5328 or a similar design code specific to each country or region. There are limits on sizes of aggregates and w/c ratios depending on the final strength that is required. However these calculations can only be used for normal and high strength concrete up to 90MPa. There are currently no standards available that facilitates the design of a specific strength of UHPFRC. Trial and error tests and published literature are used to obtain a new UHPFRC strength and mix design.

### UHPFRC Mix Design Properties

Ultra high performance concrete mix designs are based on high strength concrete mix designs with changes in the quantities of cement and water with additions of admixtures and micro fillers such as silica. The water/binder ratio is further lowered from that used in a high strength concrete mix with further additions of admixtures such as superplasticiser to increase the workability. The addition of fibres to the concrete greatly increases the flexural toughness [4]. The traditional coarse aggregates in normal concrete are replaced by smaller and stronger aggregates such as fine sand and ultra-fine particles of silica fume and quartz flour in UHPFRC. Generally the maximum particle size is less than 7mm and in most mixes less than 1mm. According to the Japan Society of Civil Engineers [5] by using aggregates of less than 2.5mm the size of microcracks formed in the interfacial transition zone (ITZ) can be greatly reduced. This in turn reduces the shear stresses within the concrete when the load is applied [1]. The smaller the aggregates used the smaller the weak link or ITZ is within the concrete. By utilising the smaller difference between the stiffness of the aggregates and the cement

paste in UHPFRC a more homogenous material can be achieved in comparison to normal strength and high performance concretes. The quantity of cement in the concrete mixture is also large, usually close or above 1000 kg/m$^3$ [6]. However, recent studies have shown that products such as ground granulated blast furnace and silica fume can be used as partial cement replacements [7] [8].

**Concrete Mix Design Tools**

There are several tools and methods available for the design of concrete mixes. Due to the properties of multimodal, discretely sized particles three different approaches were developed and improved for concrete mix designs called the Linear Packing Density Model (LDPM), Solid Suspension Model (SSM) and Compressive Packing Model (CPM) [9][10]. These methods are based on the packing fraction of the individual components of the mixture and their combinations. These methods are unreliable where a large volume of fines are used and as a result it is extremely challenging to obtain the packing fraction of the fine particles used in UHPFRC using these design tools. A different approach, which dates back 100 years, is to use integral particle size distribution of continuously graded mixes; this method allows very fine particles to be integrated. It has been illustrated that aggregate packing affects the properties of the hardened concrete and that a geometric continuous grading of the aggregates will improve concrete properties [11]. Based on this study, and another investigation by Andreasen & Andersen [12], a minimal porosity can be theoretically obtained using the optimal particle size distribution (PSD) of all the individually applied particle materials used in the mix. This equation is known as the Andreasen and Andersen Equation shown in EQN (1). The disadvantage of using this equation is that the minimum particle size is not included in the calculation matrix. To overcome this a modified model was developed that takes account of this and is known as the modified Andreasen and Andersen model [13], as shown in EQN (2).

$$P(D) = \left(\frac{D}{D_{max}}\right)^q \tag{1}$$

$$P(D) = \frac{D^q - D_{min}^q}{D_{max}^q - D_{min}^q} \tag{2}$$

where:

P(D) is a fraction of the total solids smaller than size D.
D is the particle size (μm).
Dmax is the maximum particle size.
q is the distribution modulus.
$D_{min}$ is the minimum particle size (μm).

This approach has already been effectively applied to optimisation algorithms for the mix design of normal and lightweight concrete [14]. The value of the distribution modulus q determines the proportion between coarse and fines in the mix, hence by changing this value different types of concrete can be obtained. High values ( q > 0.5) will lead to a coarse mix while low values (q < 0.25) shall result in a mainly fine concrete mix [15]. While it has been shown that a distribution value of 0.0 – 0.28 would result in optimal packing of the particles [16], a further study demonstrated that a value in the region of 0.22 – 0.25 should be used for self-compacting concrete which is a property of UHPFRC [17].

A previous study on UHPFRC using a coarse sand with a maximum particle size of 2000μm, including a large portion of fine particles used a q value of 0.23 [18].

### Developing a new UHPFRC for Ireland

The purpose of this research is to develop a UHPFRC mix suitable for the Irish construction industry and to do this it is required to use aggregates which are easily accessible in Ireland. Constituents which were calculated to be expensive or required a large volume of materials to be imported and as a result increase the costs and environmental footprint of UHPFRC where not considered in the mix design. One of the constituents excluded from the mix design was the filler material quartz flour which is used throughout the world in UHPFRC. Two UHPFRC's are presented in this research, one using a coarse sand and one using a fine sand. The fibre content used in both mixes was 2% by volume, this dosage was selected as it is the typically fibre dosage in UHPFRCs. A plain mix with no fibre reinforcement was also designed for both mixes to illustrate the effect of fibres on the characteristics of ultra-high performance concrete.

## METHODLOGY

Particle Size Distribution curves in conjunction with the modified Andreasen and Andersen model and the Elkem Materials Mix Analyser software (EMMA) are used to design the UHPFRC mixes. EMMA is an application that calculates and displays the particle size distribution of a mixture of components. For the mix containing coarse sand a value of the distribution modulus q of 0.23 was selected as the distribution modulus as determined using previous literature [18], this value was reduced to 0.22 for the fine sand mix as the aggregate size is smaller and to stay within the limits of 0.22 – 0.25 for self-compacting concrete.

### Materials

Rapid Hardening Portland Cement (RHPC) CEM I Class 42.5R was used as it achieves a higher rate of strength development in comparison to normal cement due to the increased product fineness. The Microsilica used in this research is Elkem 920D as it improves the early age and final strength, density and durability of the concrete, which is accomplished by the highly active pozzolanic materials reacting with the free lime produced by the hydration process. A coarse and a fine sand with particles size distributions in the range of 50μm - 3000μm and 10μm - 550μm were used in the coarse mix and fine mix respectively with both sands obtained from a local limestone based quarry. Sika ViscoCrete Premier was selected as the accelerating high range water reducing/superplasticiser admixture. This admixture is specifically used for the production of concrete with high early strength development, high water reductions and excellent flowability which makes it an excellent material to achieve the early age and final strength properties of UHPFRC. The steel fibres used in this research are Dramix OL 13/.20. These fibres have a length of 13mm and a diameter of 0.20mm with a tensile strength of 2600MPa. They are typically used in high dosages in high strength and brittle concrete which make them an ideal fibre type in UHPFRC. Figure 1 presents the various materials used in the mixes reported here.

Figure 2 demonstrates the particle size distribution of the individual constituents used in each mix and the target curves based on the calculations conducted using the modified Andreasen and Andersen model and the EMMA mix design software. The final mix design for each

plain and fibrous mix can be viewed in Table 1. Each concrete batch was denoted in two parts, the first part was UHPC or UHPFRC to illustrate a plain or fibre mix respectively, this was followed by the letter C or F to illustrate if a coarse of fine sand was used, e.g., UHPFRC-F symbolises a fine sand mix with 2% fibres. The quantities used were determined by varying the percentage of each material which would add up to give a volume of $1m^3$ and which gave a composed PSD curve that best matched the target curve for the two graphs in Figure 2. The embodied energy and the cost of each constituent used within the four mix designs are presented in Table 2 and the reader should note that the given costs were accurate in as of December 2015.

Table 1 Material quantities of each mix

| MATERIAL QUANTITIES OF EACH MIX | | | | |
|---|---|---|---|---|
| Material | UHPC-C ($kg/m^3$) | UHPC-F ($kg/m^3$) | UHPFRC-C ($kg/m^3$) | UHPFRC-F ($kg/m^3$) |
| Cement CEM I 42.5R | 685 | 810 | 685 | 810 |
| Microsilica (Elkem 920D) | 137 | 203 | 137 | 203 |
| Coarse Sand (50μm - 3000μm) | 1317 | 0 | 1317 | 0 |
| Fine Sand (10μm - 550μm) | 0 | 1022 | 0 | 1022 |
| Superplasticiser (Viscocrete Premier) | 40 | 40 | 40 | 40 |
| Water | 162 | 178 | 162 | 178 |
| Steel Fibres (Dramix OL13/.20) | 0 | 0 | 155 | 155 |
| Total Binder Content | 822 | 1013 | 822 | 1013 |
| Water/Cement Ratio | 0.24 | 0.22 | 0.24 | 0.22 |
| Water/Binder Ratio | 0.20 | 0.18 | 0.20 | 0.18 |
| Cost €/$m^3$ (Dec 2015) | 619 | 825 | 1,022 | 1,228 |
| Embodied Energy MJ/$m^3$ | 3,832 | 4,438 | 9,412 | 10,017 |

Table 2 Embodied energy and cost of constituents used

| EMBODIED ENERGY AND COST OF CONSTITUENTS USED | | |
|---|---|---|
| Material | Embodied Energy (MJ/kg) | Material Cost (€/Tonne) |
| Cement CEM I 42.5R | 4.900 | 121.50 |
| Microsilica (Elkem 920D) | 0.036 | 2,550.00 |
| Coarse Sand (50μm - 3000μm) | 0.083 | 21.50 |
| Fine Sand (10μm - 550μm) | 0.080 | 18.00 |
| Superplasticiser (Viscocrete Premier) | 9.000 | 4,230.00 |
| Water | 0.010 | - |
| Steel Fibres (Dramix OL13/.20) | 36.000 | 2,600.00 |

(a) (b) (c) (d) (e)

Figure 1 Materials used to design the UHPFRC mixes (a) Cement CEM 42.5R, (b) microsilica, (c) coarse sand, (d) fine sand and (e) micro steel fibres OL13/.20

**Particle Size Distribution Curves**

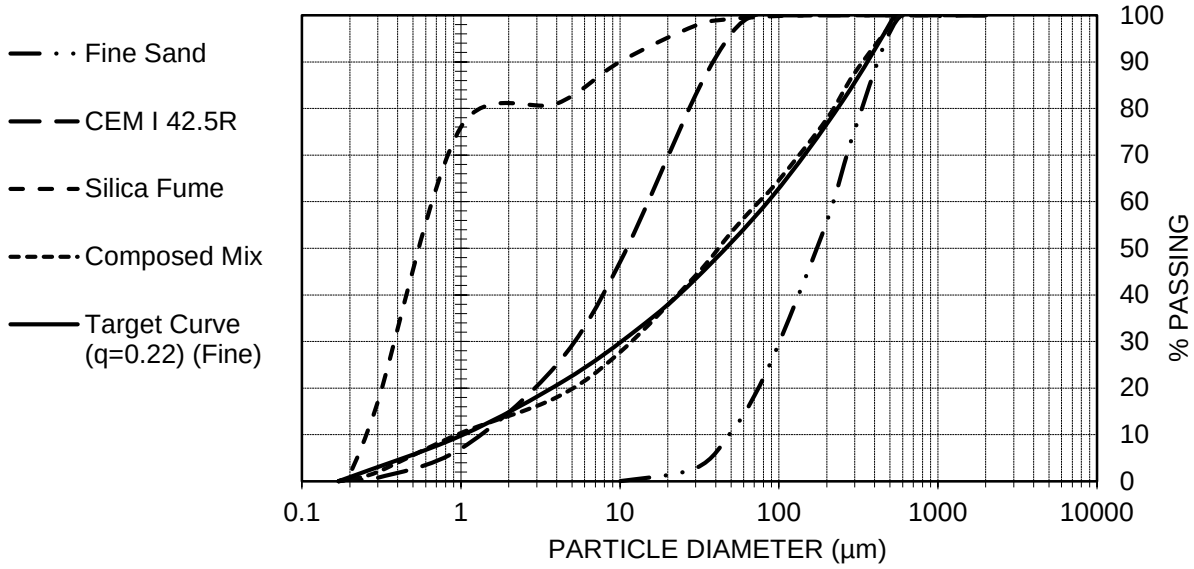


(a)

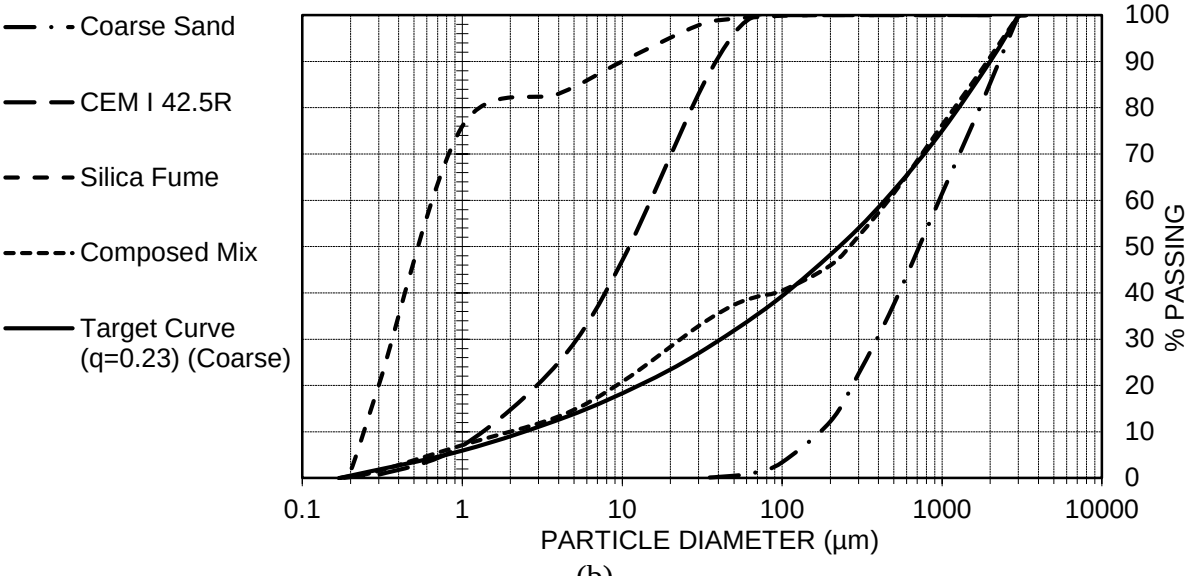


(b)

Figure 2 PSDs of the mix constituents, the target curve and the resulting integral grading line of the composed mix for (a) UHPC-F, and (b) UHPC-C

## EXPERIMENTAL TESTING

Compression and flexural tests were conducted using cylinder and beam specimens respectively. Specimens for the four batches were tested at 28 days after casting. Careful consideration was taking during casting, striking, curing and testing to eliminate variations in results. In particular, the same equipment and procedures for casting and testing were used at all times. The test program involved using existing and developing novel test methods to accurately measure the pre and post cracking behaviour of UHPFRC including the stress-strain curves in compression and the load-deflection behaviour in flexure.

### UHPFRC Mixing and Curing Procedure

The mixing time and procedure of UHPC and UHPFRC can vary depending on the type and speed of mixer used with typical values ranging from 10 – 25 minutes. In this research mixing was conducted using a Creteangle Multiflow 56 litre horizontal pan mixer. Firstly the sand and silica fume is dry mixed for 3 minutes, next the cement was added and the dry particles were mixed for a further 5 minutes until a uniform dry powder mix was achieved. Over a period of 2 minutes the water and superplasticiser, which were previously mixed together, were added to the dry mix. In approximately 4-5 minutes a significant change from dry to wet occurred known as “the turn”. In a further 3 minutes a wet paste concrete was achieved. At this point the plain UHPC mixes are ready, specimens are then cast into the various moulds and placed on a vibrating table for compaction. For the UHPFRC mixes, the steel fibres were added by hand to mix over a period of 1 minute and mixing occurs for a further 3 minutes until a uniform fibre distribution was obtained. UHPFRC specimens were cast and vibrated in a similar fashion to the UHPC specimens. Total mixing time is approximately 18 and 22 minutes for the UHPC and UHPFRC respectively. All specimens were covered with a damp hessian cloth and polythene sheets and kept at a constant temperature of 20°C for 24 hours at which time demoulding occurred. All specimens are then placed in a curing tank at 20°C ± 2°C until testing.

### Compression Testing

The compressive strength and associated stress-strain curve was determined using cylindrical specimens with a diameter of 100mm and a height of 200mm. Linear Variable Displacement Transducers (LVDT’s) with accuracy of 0.1 μm and a total travel of 10mm were used to measure the deflection. It should be noted that if load control was used to determine the stress-strain curve, the sudden failure of the specimen would not facilitate recording of the post-peak behaviour of the specimen. To overcome this specimens are first loaded using load control to 85% of the expected failure load which was pre-determined by loading a cylinder specimen under load control at a rate of 0.5MPa/s. At this point the load control is switched to displacement loading using three LVDT’s attached to the machine and loading continues at a rate of 1μm/s. The three LVDT’s are at equal distances apart to ensure the correct displacement is obtained as demonstrated in Figure 3(a). Therefore, when peak load is reached the sudden failure of the UHPFRC specimens is prevented and the post-peak behaviour can be recorded accurately. The plain ultra high performance specimens will still portray an explosive failure but using displacement loading the change in stiffness at peak strength was recorded more accurately. Three cylindrical specimens are tested using this method and the compressive stress-strain curve is taken as the average of the three results.

### Flexure Testing

The beam flexure test is an indirect tensile test. A two point loading method was selected for this research as this provides an even distribution of maximum stress over the middle section of the beam or prism. The testing was carried out in accordance with BS EN 14488-3:2006 [19], although some modifications to this standard have been made. The purpose of this test was not just to determine peak tension stress but to also find the residual strength given by the fibres after first cracking occurred. The test is initially conducted at a speed of 2µm/s with servo feedback from the average of two deflection LVDT's placed on either side of the specimen. The test speed is increased to 8µm/s when peak strength has been reached. Due to testing machine limitations the specimens selected for this test have a span of 300mm and a breath and height of 100mm as illustrated in Figure 3(b). A strain gauge was attached to the underside of the beam to measure the associated strain with increasing stress.

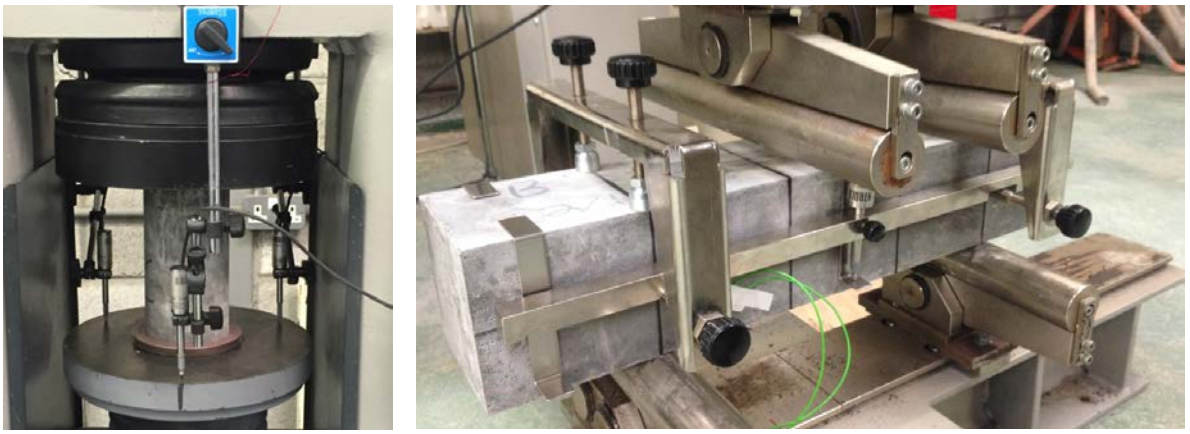

(a) (b)

Figure 3 Experimental testing arrangements for (a) cylinders in compression and (b) beams in flexural

## RESULTS AND DISCUSSION

### Compression Tests

The average compressive strengths at 28 days of the cylindrical specimens are presented in Figure 4. Firstly, it can be observed that by adding 2% fibres to both mixes the peak strength of the specimens increased from 117MPa to 131MPa for the coarse sand mix and from 126MPa to 147MPa for the fine sand mix. As the total binder content in the fine mix was 191kg/m$^3$ higher than the coarse sand mix it was expected that the UHPC-F and UHPFRC-F mixes would obtain higher strengths than the UHPC-C and UHPFRC-C mixes respectively. However, this strength increase was only 8% for the UHPC mixes and 12% for the UHPFRC mixes. The water/binder ratio in the UHPC and UHPFRC is less than 0.2, which indicates the degree of hydration is relatively small. This is portrayed in the results for the fine sand mix as not all cement particles are hydrated and are instead used as filler material, by physical inspection of the tested UHPC-F specimens non-hydrated cement particles were evident.

The results illustrate that for UHPC and UHPFRC in compression, adequate particle packing contributes more to the strength than a high binder content and as a result filler materials are used to reduce the cement content. Both sands used in this research have a high volume of small particles, which act as the filler material in both mixes.

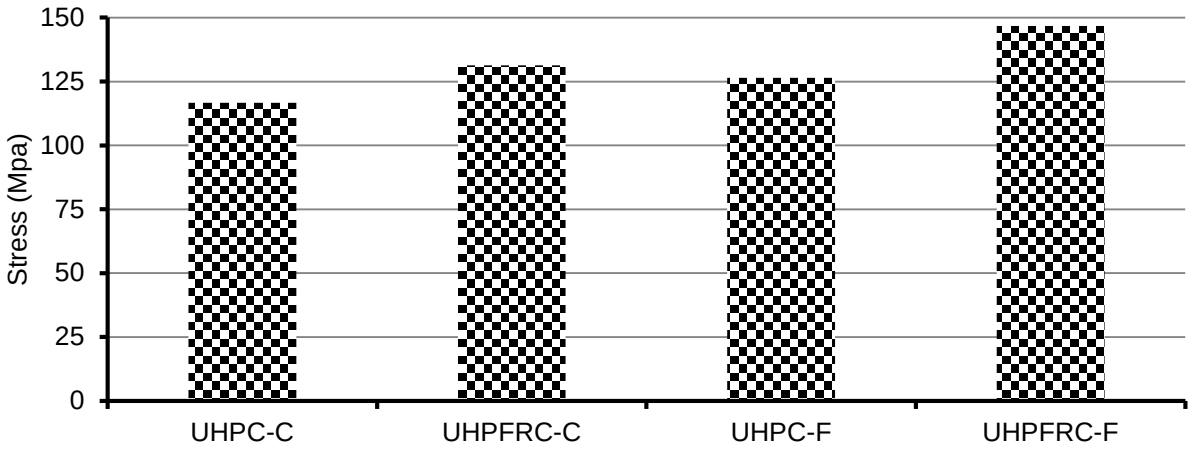


Figure 4 Average compressive cylinder strength of the four mixes at 28 days

The failure modes for the four mixes are presented in Figure 5. For the UHPC specimens it was found that both concretes failed in a similar manner. Once the first crack is recorded the cylinders fail suddenly and explosively. If the UHPFRC specimens are examined it is observed that although failure has occurred with significant cracking visible, the fibres have bridged the cracks and prevented an explosive failure. This demonstrates that although the steel fibres may only contribute a minor increase in peak strength of UHPFRC, they do eliminate the explosive nature of the failure of UHPC.

(a) (b) (c) (d)

Figure 5 Compression failure modes of: (a) UHPC-C, (b) UHPFRC-C, (c) UHPC-F and (d) UHPFRC-F cylinders

**Flexure Tests**

The flexure strength of the beams tested at 28 days is given in Figure 6. Similar to the cylinder results for the plain mixes, the fine sand mix only exhibited a minor increase of strength of 7%, from 14.1MPa to 15.1MPa, over the coarse sand mix.

If both UHPFRC mixes are considered it is observed that the coarse sand mix shows a strength increase of 33%, from 14.1MPa to 18.7MPa and the fine sand mix shows a significantly higher strength increase of 75%, from 15.1MPa to 26.5MPa over the plain mixes. This illustrates that the inclusion of steel fibres in ultra high performance concrete has a substantially higher impact on the flexure strength than the compressive strength.

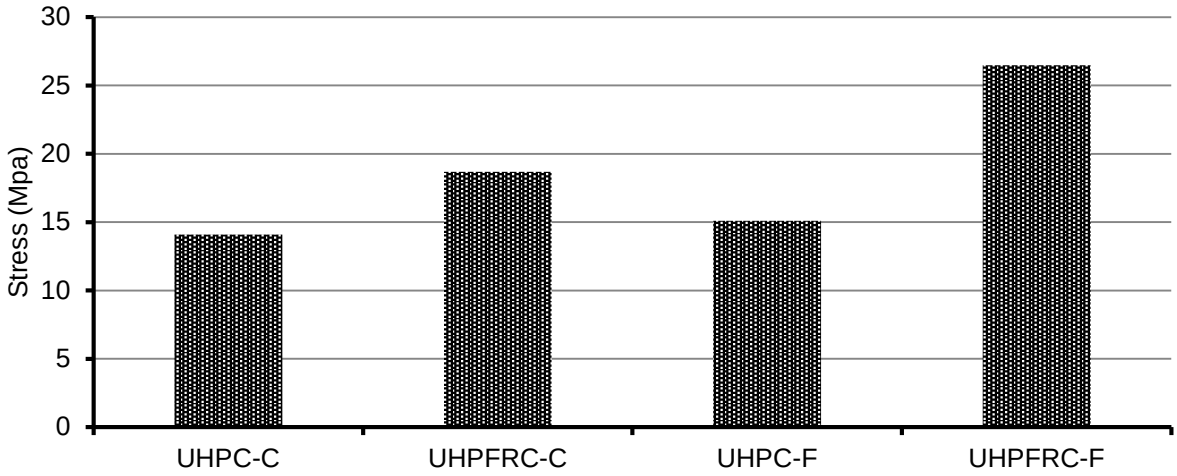


Figure 6 Average flexural strength of the four mixes at 28 days

Due to the self-compacting and flowability nature of UHPFRC as the mix is placed in the moulds it flows so that the steel fibres align themselves with the direction of the flow which is perpendicular to the flexural stresses obtained in beams. As the fibres are stronger in tension, by including the steel fibres in the UHPC mix both the pre-cracking and post-cracking strength and behaviour of the concrete is enhanced. From the tested UHPFRC beam specimens investigated it was noted that the fine sand mix had a higher percentage of fibres aligned with the direction of the flow in comparison to the coarse sand mix. This illustrates why the fine sand fibre reinforced mix had the higher percentage increase in strength of the two fibre reinforced mixes in comparison to the plain mixes. It can be concluded that the smaller particle size in the fine sand mix allowed the fibres to align in an improved manner with the direction of flow. By giving careful consideration to how UHPFRC is placed in structural members such as beams and slabs, the fibres can be aligned to give maximum performance and strength. Numerical modelling methods are currently being used to extrapolate the experimental results to produce prediction models that will be used to modify existing bridge design guidelines for use with UHPFRC.

Figure 7 Failure mode of a UHPFRC-F specimen illustrating fibre alignment

### Cost and Embodied Energy Analysis

From the tests conducted on the four mixes it is clear that by adding a steel fibre dosage of 2%, by volume, the cost and embodied energy of the mix is increased by 57% and 136% respectively as calculated from the data given in Tables 1 and 2. This is expected as steel fibres cost approximately €2,600/tonne and have an embodied energy of 36MJ/kg. However, due to the increased strength characteristics of the UHPFRC mixes, and in particular flexural strength, these figures are offset by the savings made on the reduction of conventional steel reinforcement required. The results also indicate that due to the increase in the binder content by 23% in the fine sand mix in comparison to the coarse sand mix the cost and embodied energy of the fibre reinforced fine sand mix increased by 20% and 6% respectively. In a similar manner to the plain versus fibre mixes the rise in these values is offset by the superior strength which results in a reduction in the volume of material required, as thinner and lighter structures may be used. If other UHPFRCs available on the market are considered for use in Ireland they may obtain similar or higher strength mixes but costs would increase, although embodied energy values would be similar. It must be noted that the strength of the mixes investigated in this research could further be increased by 15% through the use of early age steam curing.

## CONCLUSIONS

This paper presents the findings of a new type of ultra-high performance fibre reinforced concrete mix, which is made more sustainably viable in terms of strength, cost and environmental impact by reducing or removing the inclusion of filler materials such as quartz flour. The following conclusions can be drawn based on the results:

- It is possible to design dense UHPFRC mixes with low air void ratios using the Andresen & Anderersen model based on the maximum and minimum particle size used excluding fibre size.
- By using a fibre volume of 2% the compressive strength of the coarse sand and fine sand UHPFRC mixes was increased by 13% and 16%, respectively, which illustrates that the steel fibre volume has a moderately small effect on the pre-cracking compressive strength of UHPFRC.
- The flexural strength of the UHPFRC coarse sand and fine sand mixes were increased by 33% and 75% respectively, by using a steel fibre volume of 2%. This illustrates the advantage of using steel fibres in UHPFRC for structural members such as bridge decks.
- The inclusion of steel fibres by 2% volume increases the cost and embodied energy of UHPFRC on average by 57% and 136% respectively. However, these figures are offset due to the superior strength characteristics leading to a large reduction in the use of conventional steel reinforcement.
- The binder content was increased by 23% by using a fine sand mix in comparison to a coarse sand mix. This lead to an increase in cost and embodied energy of the UHPFRC mixes by 20% and 6%, respectively for the fibre reinforced fine sand mix. These increases are offset by the superior physical and mechanical characteristics.
- Both UHPFRCs investigated are more economical for use in Ireland in comparison to using other typical UHPFRCs available on the international market. Although, other UHPFRC may have superior strength characteristics. It is necessary to conduct further tests on the UHPFRC mix designs including steam curing which should further increase the strength by approximately 15%.

## ACKNOWLEDGEMENTS

The authors appreciatively acknowledge the following companies for sponsoring the materials for this research, Bekaert, Kerrigan's Quarry, Irish Cement and Sika Ireland. The research is funded under the Institute of Technology, Sligo President's Bursary Award.

## REFERENCES

1. P. RICHARD AND M. CHEYREZY, "Composition of reactive powder concretes," Cem. Concr. Res., vol. 25, no. 7, pp. 1501–1511, 1995.

2. A. A. AL-AZZAWI, A. S. ALI, AND H. K. RISAN, "Behavior of Ultra High Performance Concrete Structures," ARPN J. Eng. Appl. Sci., vol. 6, no. 5, pp. 95–109, 2011.

3. B. GRAYBEAL AND J. L. HARTMANN, "Strengh And Durability Of Ultra-High Performance Concrete," Concr. Bridg. Confrenece, 2003.

4. N. CAUBERG, J. PIÉRARD, AND O. REMY, "Ultra High Performance Concrete : Mix design and practical applications," pp. 1085–1088, 2008.

5. JAPAN SOCIETY OF CIVIL ENGINEERS, "Recommendations for Design and Construction of Ultra High Stregth Fiber Reinforced Concrete Structures (Draft~)," Tokyo, 2006.

6. S. H. PARK, D. J. KIM, G. S. RYU, AND K. T. KOH, "Tensile behavior of Ultra High Performance Hybrid Fiber Reinforced Concrete," Cem. Concr. Compos., vol. 34, no. 2, pp. 172–184, 2012.

7. A. M. T. HASSAN, S. W. JONES, AND G. H. MAHMUD, "Experimental test methods to determine the uniaxial tensile and compressive behaviour of ultra high performance fibre reinforced concrete ( UHPFRC )," Constr. Build. Mater., vol. 37, pp. 874–882, 2012.

8. A. S. EL-DIEB, "Mechanical , durability and microstructural characteristics of ultra-high-strength self-compacting concrete incorporating steel fibers," Mater. Des., vol. 30, no. 10, pp. 4286–4292, 2009.

9. F. DE LARRARD AND T. SEDRAN, "Optimization of ultra-high-performance concrete by the use of a packing model," Cem. Concr. Res., vol. 24, no. 6, pp. 997–1009, 1994.

10. T. SEDRAN, "Mixture-proportioning of high-performance concrete," vol. 32, pp. 1699–1704, 2002.

11. W. B. FULLER AND S. E. THOMPSON, "The Laws of Proportioning Concrete," Trans. Am. Soc. Civ. Eng., vol. LIX, no. No. 2, pp. pp. 67–143, 1907.

12. A. H. ANDREASEN AND J. ANDERSEN, “Ueber die Beziehungen zwischen Kornabstufungen und Zwischenraum in Produkten aus losen Körnern (mit einigen Experimenten),” Kolloid-Zeitschrift, vol. 50, no. 3, pp. 217–228, 1930.

13. J. E. FUNK AND D. R. DINGER, Predictive Process Control of Crowded Particulate Suspensions: Applied to Ceramic Manufacturing. Boston: Kluwer Academic Publishers, 1994.
14. Q. L. YU, P. SPIESZ, AND H. J. H. BROUWERS, “Development of cement-based lightweight composites – Part 1: Mix design methodology and hardened properties,” Cem. Concr. Compos., vol. 44, pp. 17–29, 2013.

15. G. HÜSKEN AND H. J. H. BROUWERS, “A new mix design concept for earth-moist concrete: A theoretical and experimental study,” Cem. Concr. Res., vol. 38, no. 10, pp. 1246–1259, 2008.

16. H. J. H. BROUWERS, “Particle-size distribution and packing fraction of geometric random packings,” Phys. Rev. E, vol. 74, no. 3, p. 031309, 2006.

17. M. HUNGER, “An integral design concept for ecological self-compacting concretee,” Eindhoven Univeristy of Technology, 2010.

18. R. YU, P. SPIESZ, AND H. J. H. BROUWERS, “Mix design and properties assessment of Ultra-High Performance Fibre Reinforced Concrete (UHPFRC),” Cem. Concr. Res., vol. 56, pp. 29–39, 2014.

19. BS EN 14488-3:2006, “Testing sprayed concrete - Part 3: Flexural strengths (first peak, ultimate and residual) of fibre reinforced beam specimens,” vol. 24, no. 6, p. 248, 2006.

# PERFORMANCE OF CONCRETE WITH RECYCLED PLASTIC AS A PARTIAL REPLACEMENT FOR SAND

**J Thorneycroft**

**P Savoikar**

**J Orr R Ball**

University of Bath

United Kingdom

**ABSTRACT.** Environmental concerns have led to severe restrictions on dredging for sand in much of India, including in the state of Goa, leading to direct impacts on the economics of concrete construction. At the same time, waste plastic is rarely recycled across India, with a large proportion of plastic simply exposed of into landfill presenting further environmental concerns. This paper describes a study seeking a solution to both problems by utilising processed waste plastic as a partial replacement for fine sand in concrete mixes. This initial work was supported through project funding from the British Council under the UKIERI (United Kingdom India Educational Research Initiative) programme. The compressive strength and performance of concrete mixes with plastic have been tested, and suggestions for suitable replacement percentages are proposed. Parameters including the size and aspect ratio of the plastic particles replacing the san aggregate and effects of chemical treatment are addressed. Results show that replacing sand with recycled plastic is viable and by using a suitable mix design the impact on the compressive strength of the concrete mix can be kept at acceptably low levels.

**Keywords:** Sand replacement, Recycled plastic, Mix design, Performance.

**Mr James Thorneycroft** is a researcher in the Department of Architecture and Civil Engineering at the University of Bath. His research has been funded by a British Council UKIERI Project 'Development of structural concrete with the help of plastic waste as partial replacement for sand' (ICB/13-14/047).'

**Professor Purnanand Savoikar** is currently Professor of Civil Engineering at the Goa Engineering College, Farmagudi, India and coordinator for PG course in Foundation Engineering and is the Principal Investigator (India) for the British Council Project ICB/13-14/047.

**Dr John Orr** is an EPSRC Early Career Fellow and Lecturer (Assistant Professor) in the Department of Architecture and Civil Engineering at the University of Bath.

**Dr Richard Ball** is a Senior Lecturer in the Department of Architecture & Civil Engineering. His research is primarily in the area of low-carbon building materials, specialising in lime based materials, nano-materials and photocatalytic coatings.

## INTRODUCTION

Cement manufacture in India reached 280Mt in 2014 [1], second only to China. India exports only small volumes of cement, with internal demand for concrete being driven by a growing economy, growing population, and rising living standards [2]. Mass extraction of sand, usually via river dredging, has been a problem in India for a number of years and is mainly fed by construction demand. A high court ruling in 2010 put a stop to sand dredging [3] and has led to severe supply problems within much of India.

The Indian central pollution control board (CPCB) reported in 2008 that approximately 15,000 tons of plastic waste is dumped every day in India [4]. Non-biodegradable plastic waste is inert and breaks down very slowly once buried in landfill. Even if all of this plastic could be recycled, by-products of the recycling process such as polyethylene terephthalate (PET) sand are still required to be sent to landfill. A solution to both of these problems is proposed by substituting sand in concrete mixes with processed waste plastic, which would otherwise remain as waste in landfill. This would not only encourage the collection and use of waste, but would provide alternative sources of fine material in place of sand in novel concrete mixes

## PLASTIC AS A REPLACEMENT FOR SAND IN CONCRETE

The majority of the research undertaken to date has studied the changes in concrete physical properties attributable to the addition of plastic waste. Variables such as the plastic replacement ratio, the type, size, shape and surface texture of plastic, the concrete mix design and curing conditions all have the potential to modify the concrete properties when plastic is used as a replacement for sand.

### Compressive Strength and Bonding Performance

Initial research on the effects of plastic aggregate substitution on concrete compressive strength was undertaken by Al-Manaseer and Dalal [5]. The effect of an increasing proportion of angular waste plastic particles on cylinder strength for three different w/c ratios was explored. It was found that the compressive strength decreased when the plastic aggregate content increased, with the loss in strength attributed to poor bond characteristics between plastic and cement paste. The plastic was seen to pull out of the sample, rather than to split in tension during compressive testing.

Saikia and de Brito [6] tested concrete mixes containing three different sized and shaped particles: 1) large course particles 2) shredded flaky fine sized particles and 3) cylindrical pellet shaped particles. Each of these were tested over a series of replacement ratios, ranging from 0% to 15% of sand. It was found that the higher the replacement ratio of plastic for sand, the lower the concrete's compressive strength, which was attributed to the lack of interaction between the PET aggregate and cement paste. This study concluded that the interfacial transition zone in concrete containing PET aggregate is weaker than that of standard concrete.

Albano *et al* [7] tested different sized PET particles for two different w/c ratios over a range of plastic replacement quantities. The PET particles used in the mixes were irregularly shaped, and were all between 2.6mm and 11.4mm in size. The compressive strength reduced with increases in the proportion of plastic, implying that plastic particles acted as defects within the internal structure of the concrete. Mix designs containing all large plastic particles were substantially weaker compared to mixes containing smaller particles.

Formation of a honeycomb of cavities and pores was observed and attributed to the low workability affecting the compaction of the concrete.

As the fine aggregate that is used for concrete is normally graded Frigione [8] decided to use granulated PET that was graded very similarly to the siliceous sand that was to be replaced in the mix. It was found that the compressive strength decreased, however, the reduction in compressive strength was only in the order of 0.5 to 2%, when a replacement ratio of 5% was used. However, this is still favourable compared to the 12% loss seen by Saikia and de Brito [6] when 5% sand was replaced with plastic pellets. This indicates that although the use of plastic will cause a decrease in compressive strength because of a poorer bond to the cement compared to the sand, the loss can be limited by appropriate mix design and choice of plastic.

Another possible reason for a lower compressive strength being achieved when plastic is introduced was provided by Ismail and Al-Hashmi [9], when concrete containing a mixture of PET and polystyrene was tested. They explained that the trend can not only be attributed to the decrease in adhesive strength between the surface of the waste plastic and the cement paste, but also because plastic is considered to be a hydrophobic material. Therefore movement of the water required for hydration through the concrete is hindered leaving isolated volumes of unhydrated cement.

Saikia and de Brito [6] found that as with compressive strength, there was a loss of tensile performance when plastic aggregate was introduced into the concrete, and the more plastic added, the greater the loss. Coarser plastic aggregate exhibited lower performance, followed by fine particles and then the smooth pellets. The loss of tensile strength was attributed to the characteristics of the plastic, primarily its smooth surface, but also the presence of free water at the plastic surface causing a weak bond to the cement. Microscopic studies of failed specimens revealed that the most common form of failure was de-bonding at the plastic – concrete interface.

Albano *et al* [7] also found that the behaviour under tension was similar to that under compression, and the loss was attributed to the same reasons. It was found that the introduction of waste PET reduced the tensile strength of the concrete, and then when higher proportions were added there was a significant drop due to number of voids present in the concrete. It was therefore noted that when a 50/50 mix of small and large plastic particles were used, a higher tensile strength was recorded compared to when either just small or just large particles were used. Frigione [8] also observed a loss of tensile strength when granulated PET particles were used, and once again, only a very minimal loss in the range of 2% was observed. It was concluded that the loss of compressive strength could be correlated to the loss of tensile strength.

**Treatment of Particles**

To improve the bond between plastic particles and surrounding matrix, chemical or physical treatment of the plastic prior to concrete mixing has been proposed. Naik *et al* [10] subjected shredded high-density plastic waste to treatment with (i) 5% Hypochlorite Solution and (ii) 5% Hypochlorite Solution + 4% Sodium Hydroxide in an attempt to improve bonding with the cementitious matrix. It was stated that in general plastics do not form chemical bonds with cementitious materials, only physical bonds. However, by being treated with oxidising chemicals or treatments the polymer chains would react with the chemicals modifying the surface functional groups. Rather than having fairly stable hydrogen ions bonded to the carbon,

hydroxide and oxygen ions would be bonded as well. As these ions are more unstable it is easier for the calcium in the cement matrix to bond with them to create calcium oxides or calcium hydroxide. Hence, a partial chemical bonding between cement and plastic could be possible. It was found that compared to the concrete containing untreated plastic, both mixes had an increased compressive strength, however, the alkaline bleach was the strongest and therefore the most effective at reducing the loss of compressive strength.

Choi *et al* [11] cut waste PET bottles into fractions in the range of 5-15mm and coated them in ground granulated blast-furnace slag (GGBS) to solidify the surface of the aggregate. This aimed to facilitate the reaction of GGBS to form a pozzolanic material, strengthening the interfacial zone between cement paste and aggregate. It would also improve the workability, the resistance to chemical attack and reduce the heat of hydration. By using a SEM it was shown that hydrates densely covered the surface of the plastic aggregate, which indicates the GGBS on the plastic does react with the calcium hydroxide in the cement to form a chemical bond. It can be seen that the percentage loss of strength in the concrete containing the GGBS is considerably smaller than the loss of strength found by other researchers who didn't use GGBS to coat their plastic, even though large sized particles were used. However, no tests were done by Choi et al. (2005) on concrete containing plastic aggregate that had not been treated, and so it is not possible to make a direct comparison of the effect that the GGBS had. However, it can probably be assumed the addition of the GGBS improves the bonding between the plastic and cement and hence increases the achievable compressive strength.

**Summary**

The substitution of waste plastic for sand in a concrete mix reduces the compressive strength, and the higher the plastic replacement ratio the greater the loss of strength. The loss of strength is either due to a loss of bonding between the plastic aggregate and the cement paste, the presence of excess water in the mix and hence an increase in voids, or a failure of the plastic. The use of smaller plastic particles reduces the loss of compressive strength in comparison to large particles. However, grading the size of the particles to include some small and some large can be equally effective as more efficient packing of the particles can be achieved.

By treating the plastic particles before they are added to the concrete stronger bonding between the plastic and cement can be achieved, and hence the loss in compressive strength can be minimised. This treatment can include changing the physical and chemical properties of the surface. The performance of concrete in compression is intrinsically linked to its performance in tension [12] and so if one concrete mix has a lower tensile strength than another, it is likely that it will also have a lower compressive strength. This relationship appears true when plastic is included in the mix.

Figure 1 shows a combination of the compressive strength results obtained by each of the pieces of research studied in the literature review. As they all had different mix designs, the compressive strength of the reference concretes were all different. For this reason the proportion of plastic has been plotted against strength loss. The spread of results is attributed to the number of variables, and hence differences there are between the mixes. These include the w/c ratio, and the type, size, shape, surface texture and treatment of the plastic. To balance substituting significant volumes of sand with plastic, while not having a considerable loss of compressive strength, this research will use a replacement ratio of 10%.

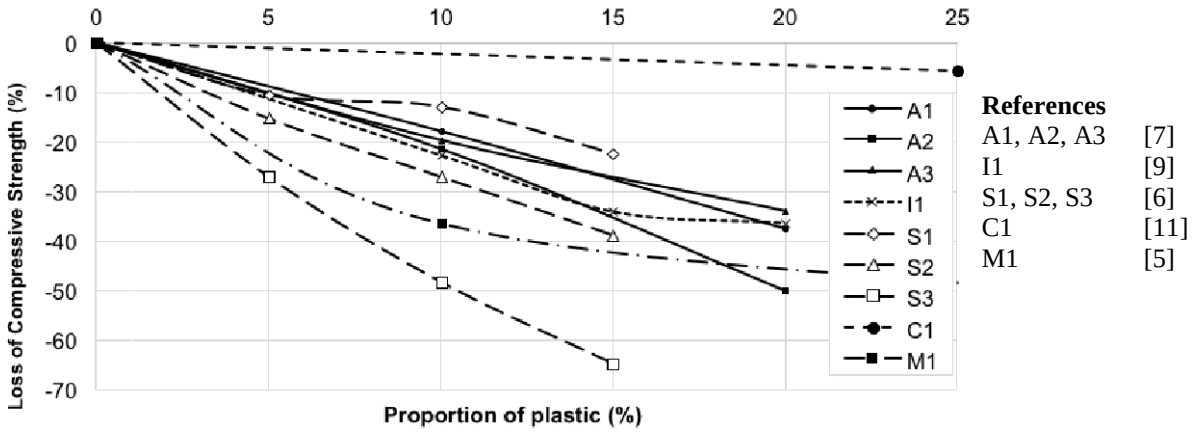


Figure 1 The relationship between plastic replacement and loss in compressive strength in different pieces of literature

## TEST METHODOLOGY

This experimental research compares different forms of plastic, and attempts to identify the optimum form or shape that provides the most efficient performance in terms of strength. A number of different mixes will be made, each containing a different plastic sample as the only changing variable, and then tested for both compressive and tensile strength.

### Characterisation of materials

A total of 5 different plastics were used in the test regime, referenced in Table 2 and described below:

1. Recycled polyethylene terephthalate (PET) drinks bottles, washed, shredded and blended. The plastic is ungraded, with particles ranging from 15mm to 0.05mm in diameter. Fourier transform infrared spectroscopy (FTIR) was used to confirm the type of plastic by sampling a random selection of particles;
2. Virgin 3mm diameter smooth finished spherical high density polypropylene (PP) pellets;
3. Recycled, high-density polyethylene (HDPE) carrier bags shredded into plates between 500mm$^2$ and 5mm$^2$;
4. Virgin polypropylene multifilament fibres, 20mm length, diameter 0.05mm;
5. Virgin polypropylene strips, 20mm long, 3mm wide, triangular in cross section.

### Mix Design

A concrete mix was designed according to [13]. Coarse Aggregate was angular, maximum 10mm diameter crushed gravel; Fine Aggregate was uncrushed, mixed coarse and fine sand, graded, percentage finer than 0.6mm was 30% and density was 1.66g/cm$^3$. For the concrete with plastic, 10% by volume of the fine sand in the reference mix was replaced with plastic materials, as shown in Table 1 (10% by volume of sand in this case is 0.047m$^3$).

Table 1 Mix proportions

| MIX REFERENCE | CEMENT CEM I 42.5R | WATER | AGGREGATE | | PLASTIC | PLASTIC, % |
|---|---|---|---|---|---|---|
| | | | FINE | COARSE | | |
| | kg/m³ | | | | | |
| R1 | 550 | 220 | 780 | 780 | 0 | 0 |
| P1 | 550 | 220 | 702 | 780 | 0.047 | 10 |

Ten mixes with plastic were used, with a replacement volume of 0.047m$^3$. One reference mix (R1) was cast. The description of each mix is given in Table 2. All preparation, mixing and casting was undertaken in accordance with BS EN 12390-2:2009 [14].

Table 2 Mix descriptions

| MIX NUMBER | BASE MIX DESIGN | PLASTIC TYPE | MIX DESCRIPTION |
|---|---|---|---|
| 1 | R1 | NA | None – Reference mix |
| 2 | P1 | 1 | PET bottle fragments graded to match the sand replaced |
| 3 | P1 | 2 | Smooth spherical pellets uniform in size and shape |
| 4 | P1 | 3 | Shredded carrier bags passing through a 4mm sieve |
| 5 | P1 | 4 | Virgin polypropylene fibres (aspect ratio 400) |
| 6 | P1 | 5 | Plastic strips (aspect ratio 6.7) |
| 7 | P1 | 1 | PET bottle fragments between 2 and 4mm in size and treated with sodium hydroxide and sodium hypochlorite |
| 8 | P1 | 1 | PET bottle fragments between 2 and 4mm in size |
| 9 | P1 | 1 | PET bottle fragments between 0.5 and 2mm in size |
| 10 | P1 | 1 | PET bottle fragments between 2 and 4mm in size and treated with sodium hydroxide and sodium hypochlorite and washed |
| 11 | P1 | 4 | 0.64% substitution of sand with virgin polypropylene fibres |

**Testing**

Three 100mm concrete cubes were tested 14 days after casting in compression for each mix listed in Table 2. Compressive testing was performed in accordance with BS EN 12390-3:2009 [15]. Three 100mm diameter concrete cylinders for each mix listed in Table 2 were tested in a split cylinder following BS EN 12390-6:2009 [16] 14 days after casting.

## RESULTS, ANALYSIS AND DISCUSSION

A summary of test results for each mix is provided in Table 3, with each mix being described in detail in Table 2. Figure 2 summarises the percentage changes in compressive and tensile strength for each mix. Figure 3 and Figure 4 show the mean average strength for each concrete mix in either compression or tension. The range of results obtained from the samples tested can be seen by the error bars, which show the highest and lowest recorded results.

Table 3 Summary of test results for tensile and compression testing

| MIX NO | AVERAGE DENSITY, kg/m³ | AVERAGE COMPRESSIVE STRENGTH, N/mm² | % CHANGE IN COMPRESSIVE STRENGTH | AVERAGE TENSILE STRENGTH, N/mm² | % CHANGE IN TENSILE STRENGTH |
|---|---|---|---|---|---|
| 1 | 2300 | 53.8 | - | 3.26 | - |
| 2 | 2273 | 54.4 | +1.2 | 4.07 | +25.0 |
| 3 | 2244 | 47.0 | -12.5 | 3.05 | -6.3 |
| 4 | 2242 | 45.6 | -15.1 | 3.77 | +15.8 |
| 5 | 2111 | 33.5 | -37.7 | 3.77 | +15.7 |
| 6 | 2266 | 52.2 | -2.9 | 2.41 | -26.0 |
| 7 | 1861 | 11.8 | -78.1 | 1.55 | -52.4 |
| 8 | 2282 | 51.6 | -4.1 | 3.31 | +1.5 |
| 9 | 2272 | 51.8 | -3.7 | 3.70 | +13.7 |
| 10 | 2269 | 52.7 | -1.9 | 2.88 | -11.5 |
| 11 | 2288 | 54.5 | +1.5 | 4.04 | +24.0 |

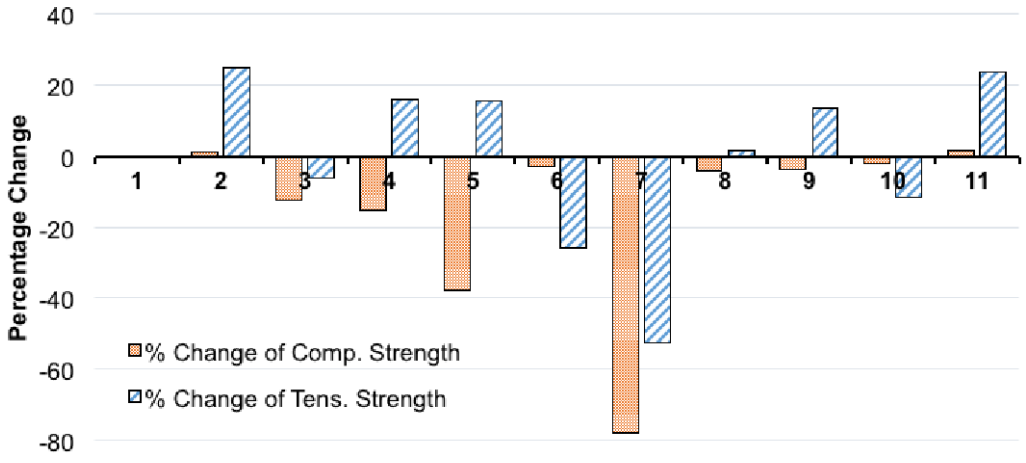


Figure 2 Percentage change in strength of each mix compared to the reference mix

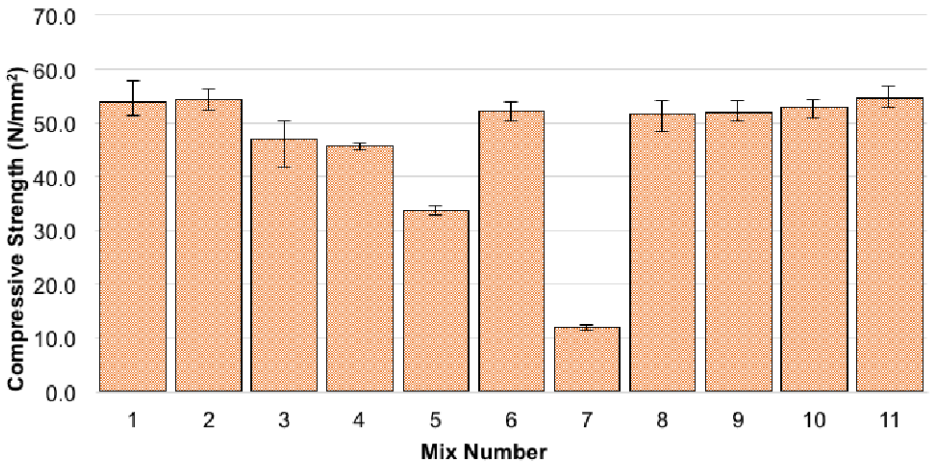


Figure 3 Comparison between the average compressive strength achieved with each mix after 14 days

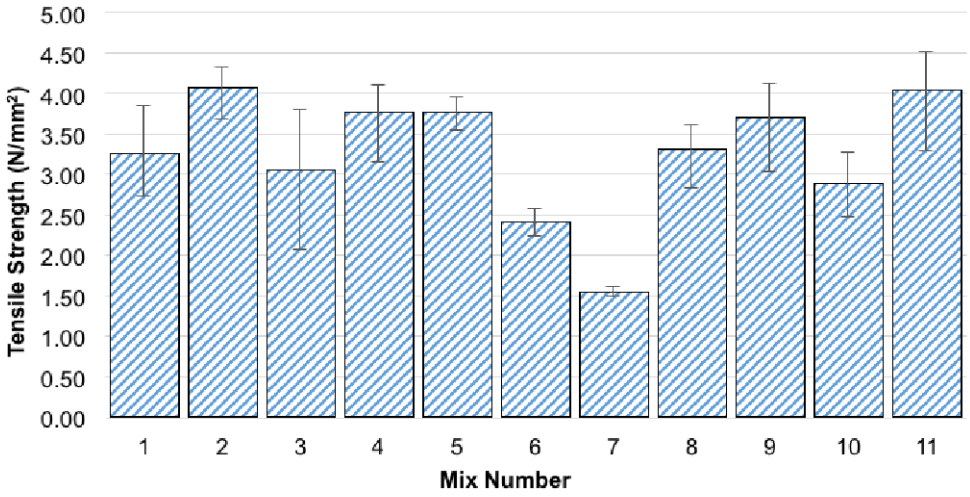


Figure 4 Comparison of the average tensile strength achieved with each mix after 14 days

**Mixtures containing PET bottle fragments (Mixes 2, 8, and 9)**

Mix numbers 2, 8 and 9 had different plastic size distributions (Table 2). The three mixes gave compressive strengths that were very close in value (Table 3). Mix 2, containing plastic graded according to the sand it replaced, achieved the best performance (+1.2%). The improved packing in such a situation supports work by Albano *et al* [7] and shows that a 10% replacement has negligible effect on the concrete strength achieved. Mixes 8 and 9 achieved almost identical performance in compression, showing that particles up to 4mm in size can feasibly be used as replacement aggregates. The loss in compressive strength shown by Mix 8 (4.1%) is less than that reported seen in the literature for similar sized particles. All mixes performed well in tension, with Mix 2 achieving a 25% increase, proving the addition of this type of plastic improves the tensile properties of the concrete. This may also explain why the concrete achieved better compression results than expected.

### Mix containing spherical 3mm diameter pellets (Mix 3)

Mix 3 contained smooth spherical pellets, whereas the plastic used in Mix 8 was approximately the same size but had a more irregular surface geometry. It can be seen that Mix 3 achieves a significantly lower compressive strength than Mix 8, and the same trend is seen for tensile strength. These results confirm that a smoother surface and more regular shape of plastic aggregate create a weaker bond between the cement and plastic. The weaker the bond between the particles and cement, the lower the strength of the concrete.

### Mixture containing shredded plastic bags (Mix 4)

Mix 4, which utilises shredded plastic carrier bags, had a 15% lower compressive strength than the reference mix, whilst the tensile strength was 15% higher. During tensile testing, failure was more gradual compared to Mixes 1 or 2. HDPE, which the carrier bags are made from, has a very low ultimate tensile strength compared to either PP or PET, however, it can elongate up to 500% before failing completely, compared to around 100% for the other two types of plastic used. Therefore, rather than the sudden failure observed with samples from Mix 2, where at a particular load the bond between particles and cement fails, in this mix the plastic reaches its yield point before a load sufficient enough to cause de-bonding is reached. The plastic then continuously deforms until the point of fracture. Hence, this concrete had a different failure mechanism to previous mixes, as the plastic failed rather than its bonding.

### Mixtures containing plastic fibres and strips (Mixes 5, 6, and 11)

Mixes 5, 6, and 11 used plastic strips with a higher aspect ratio than in other mixes (Table 2). The fibres used in Mix 5 resulted in a 38% loss in compressive strength, but a 16% improvement in tensile strength. The large drop in compressive strength is attributed to the large volume of the fibres used, which made the mix unworkable and resulted in numerous voids. During tensile testing, a gradual failure mode was again noted caused by the presence of the fibres crossing the failure plane. The high drop in compressive strength led to a new mix design, Mix 11, which used the same fibres as Mix 5 but in a reduced replacement quantity of just 0.64%, following the work of Bayasi and Zeng [17]. As seen in Table 3, this improved the performance of the mix, but the small volume of fibres used represents only a very small reduction in sand use, negating the aim of the research. These fibres would also be difficult to manufacture from recycled plastic. Mix 6 used 3mm diameter plastic strips in an attempt to mimic the same tensile strength improvements that the fibres had, while being of a size that shouldn’t reduce workability as much. Mix 6 saw a loss of compressive strength of only 2.9% compared to the reference, a considerable improvement on Mix 5. However, there was a large decrease in tensile strength between the fibres and the strips.

### Mixture containing PET bottle fragments treated with chemicals (Mixes 7 and 10)

Mix 7 used the same plastic as Mix 8 (Table 2) but was undertaken to investigate methods to improve bond between PET bottle fragments and the cement matrix through the use of chemical treatment. The PET in Mix 7 was treated with a solution of sodium hydroxide and sodium hypochlorite before being dried. However, it can be seen in Table 3 that it performs very badly in both compression (-78%) and tension (-52%) when compared to the reference concrete. It is proposed that after the plastic was subjected to the chemical solution and dried, excess solution on the surface of the plastic crystallised. When the plastic was added to the concrete mix these crystals reacted with the water and cement to produce oxygen bubbles. It

can be seen in Table 3 that the average density of Mix 7 after 14 days is significantly lower than all other mixes, due to the large number of voids present in the concrete. A modified method (Mix 10) of chemical washing was then utilised, in which the plastic was washed first in bleach and sodium hydroxide, and then in water, before being dried. The results show that Mix 10 achieved a compressive strength only 1.9% lower than the reference mixture, but perhaps more importantly 2.1% higher than Mix 8, which used the same, but untreated, plastic.

## CONCLUSIONS

This research was undertaken to explore the potential for using recycled waste plastic in a concrete mix. If this could work on a commercial level then vast quantities of waste plastic could be used in situations where recycling is not yet practical, rather than being disposed of in landfill. This would reduce sand demand from the construction industry, and as a result provide environmental benefits through a reduction in sand dredging. It is generally seen that substituting plastic into a concrete mix causes a decrease in compressive and tensile strength due to a reduction in bond strength between the plastic and cement. This paper has investigated several ways in which this loss of strength could be limited, including size, shape, grading, and treatment of the plastic. The use of a graded PET plastic matched to the size of the sand particles it replaces, and at a replacement of 10% by volume, gave the most promising overall performance.

A reduction in strength when plastic is added to a concrete mix is generally due either to the de-bonding of the plastic from the cement matrix, or a failure of the plastic itself. This failure mode is dependent on the shape, type and texture of the plastic. High aspect ratio fibres perform well, but are more difficult to produce from waste material. Random cut or fragmented particles are more likely to fail by de-bonding from the surrounding matrix and large plate like particles introduce failure planes. The performance of concrete with partial replacement of sand using plastic could also be improved through chemical treatment of the plastic aggregate to promote the formation of chemical bonding with the cement. An improved bond will mitigate against failure by premature de-bonding, and as a result lead to an increase in compressive strength of the concrete.

By testing different forms of plastic, it has been easy to see that the most efficient plastic aggregate used in a concrete mix should have a rough surface, be irregular in shape, and be sufficiently small so as to not create a significant failure surface, but also be graded similar to the sand it replaces. Concrete strength can also potentially be further enhanced by the treatment of the plastic to improve the bond to the cement. The results strongly indicate that no significant reduction in strength will occur (Table 3) and small increases in strength can be achieved.

## RECOMMENDATIONS FOR FUTURE WORK

Further investigations are needed before plastic can be considered for use in structural concrete on a commercial level. More investigation is required to understand the bond performance with the plastic, the potential for higher replacement percentages beyond 10%, effect on bonding with steel reinforcement, different mix designs and cement types, and the effect that plastic has on durability, workability, fire performance, and construction cost.

## ACKNOWLEDGEMENTS

This paper was supported by British Council UKIERI Project ‘Development of structural concrete with the help of plastic waste as partial replacement for sand’ (ICB/13-14/047).’

## REFERENCES

1. VAN OSS HG. CEMENT. In: USGS, editor. US Geological Survey, Mineral Commodity Summaries, January 2015: USGS; 2015.

2. WORLD BANK. India | Data. 2015. Online. http://data.worldbank.org/country/india (Accessed 10/01/2016)

3. ZEENEWS. Sand mining ban in Maharashtra threatens mega projects. 6/10/10. Online. http://zeenews.india.com/news/maharashtra/sand-mining-ban-in-maharashtra-threatens-mega-projects_659907.html (Accessed 10/01/2016).

4. ANON. 60 cities generate over 15,000 tonnes of plastic waste per day. Times of India. 30/04/2015. Online. http://timesofindia.indiatimes.com/home/environment/pollution/60-cities-generate-over-15000-tonnes-of-plastic-waste-per-day/articleshow/47110633.cms (Accessed 10/01/2016).

5. AL-MANASEER AA, DALAL TR. Concrete containing plastic aggregates. Concrete International, 1997, Volume 19, pp.47-52.

6. SAIKIA N, DE BRITO J. Mechanical properties and abrasion behaviour of concrete containing shredded PET bottle waste as a partial substitution of natural aggregate. Construction and Building Materials. 2014, Vol. 52, pp.236-44.

7. ALBANO C, CAMACHO N, HERNANDEZ M, MATHREUS A, GUTIERREZ A. Influence of content and particle size of waste pet bottles on concrete behaviour at different w/c ratios. Waste Management. 2009, Vol 29, pp.2707-16.

8. FRIGIONE M. Recycling of PET bottles as fine aggregate in concrete. Waste Management. 2010, Vol 30, pp.1101–6.

9. ISMAIL Z, AL-HASHMI E. Use of waste plastic in concrete mixture as aggregate replacement. Waste Management. 2008, Vol 28, pp.1041-2047.

10. NAIK TR, SINGH SS, HUBER CO, BRODERSEN BS. Use of post-consumer waste plastics in cement-based composites. Cement and Concrete Research. 1996, Vol 26, pp.1489-92.

11. CHOI YW, MOON DJ, CHUMG JS, CHO SK. Effects of waste PET bottles aggregate on the properties of concrete. Cement and Concrete Research. 2005, Vol 35, pp.776–81.

12. EYRE JR, NASREDDIN HS. Tension strain failure criterion for concrete. Magazine of Concrete Research. 2013, Vol 65, pp.1303-14.

13. TEYCHENNE DC, FRANKLIN RE, ERNTROY HC. Design of normal concrete mixes - second edition. Watford: Building Research Establishment, 1997.

14. BSI. BS EN 12390-2. Testing hardened concrete Part 2: Making and curing specimens for strength tests. London: BSI, 2009.

15. BSI. BS EN 12390-3. Testing hardened concrete Part 3: Compressive strength of test specimens. London, UK: BSI, 2009.

16. BSI. BS EN 12390-6. Testing hardened concrete Part 6: Tensile splitting strength of test specimens. London, UK: BSI, 2009.

17. BAYASI Z, ZENG J. Properties of polypropylene fibre reinforced concrete. ACI Materials Journal. 1993, Vol 90-M61.

# EFFECTS OF VARIOUS SURFACE TREATMENT AND GRADING OF RUBBER AGGREGATE ON THE STRENGTH OF RUBBERISED CONCRETE

**I Pocklington**

**H Kew**

Kingston University London

United Kingdom

**ABSTRACT.** In the UK alone over 55 million waste tyres are produced each year according to the Environmental Agency. In 2010, just over 30 per cent of waste tyres were turned into crumb, 18 per cent were used in energy recovery, nearly 20 per cent were re-used (in the UK or abroad), 16 per cent were specifically used in landfill engineering and 11 per cent were re-treaded. The European landfill directive means that this type of waste disposal would be illegal in Europe. Since 2006, EU rules have banned the disposal of tyres in landfill sites, leaving about 480,000 tonnes of recyclable shredded rubber each year. To alleviate this issue, high volume applications must be found which can best utilise recycled rubber. One such promising civil engineering application is that of rubberised concrete safety/crash barriers for highways. The current project involves modification of concrete properties through rubber aggregate substitution by volume, producing rubberised concrete. This material takes advantage of the inherent enhanced toughness and impact absorption characteristic of recycled rubber tyres. A control mix of C40 was designed and tested. A series of subsequent mixes containing either coarse, fine or mixed (both coarse and fine) rubber aggregates at various percentage replacements by volume of the natural aggregate were produced. Compressive strengths tested at 7, 14 and 28 days were analysed. To further increase the benefits and minimise detriments to the concrete mix due to the addition of rubber aggregates, plain rubber was either water washed, coated with cement paste or surface treated with Sodium Hydroxide (NaOH), respectively. It was observed that the reduction in strength of the concrete mix very much depended on the grading of the rubber aggregate, the type of surface treatment the rubber aggregate was subjected to, as well as the percentage replacement of the natural aggregate.

**Keywords:** Rubber, Rubberised, Concrete, Sustainability, Compressive.

**Mr I Pocklington** is a PhD student at Kingston University, London.

**Dr H Kew** is an Associate Professor in Civil Engineering at Kingston University since 2015 and holds referee positions at international journals. His research interest includes innovation in concrete for structural applications, recycling and reuse of waste materials in concrete and self-healing concrete.

## INTRODUCTION

Waste recycled rubber tyres are a significant worldwide problem with hundreds of millions more being produced annually. Their disposal and management is a major environmental concern in many countries. Aesthetic problems incurred by their storage must be considered along with health concerns to local populations. Their storage may result in significantly expanded breeding grounds for a variety of vermin and mosquitoes. Waste tyres also pose a substantial fire hazard which can result in both ground pollution and toxic fumes given off as emission from combustion [1], [2]. To alleviate this issue, high volume engineering applications must be found which can best utilise recycled rubber.

Rubber particles have been used in the past [3], [4] to increase concrete properties such as impact resistance, energy absorption and toughness whilst reducing the unit weight of the concrete. Properties, such as tensile, flexural and compressive strengths are all known to suffer as a result of increased rubber content [4], [5], [6]. Workability is also thought to reduce with increased rubber content [7], [8], though not all research attests this [9].

The objective of this study is to analyse and compare the differences between using coarse, fine or a combination of both rubber aggregates in a given mix design. The data included will range from 0-30% with data points at intervals of every 5%. Future data to be added aims to include a range up to 70% aggregate replacement by volume with correspondingly sized rubber particles with data points at every 10%.

## EXPERIMENTATION

### Mix Design and Testing Materials

A control mix with a target compressive strength of 40 MPa designated ‘Mix Design A’ as displayed in Table 1 was used in order to be compatible with future mixes involving the use of different rubber aggregate sizes. Sand <4 mm diameter and coarse Thames Valley aggregate graded 12-20 mm was used, along with rubber aggregate ranging from 12-20 mm (although certain rubber aggregates are considered elongated in nature) as well as fine rubber ranging in size of approximately 1-4 mm. Super Plasticiser ADVA 650 was used at a ratio of 8.57 ml/kg of cement consistently throughout all samples.

Table 1 Concrete Mix Design

| CONCRTE MIX DESIGN | | | | | |
|---|---|---|---|---|---|
| Cement | Fine Aggregate | Coarse Aggregate | Water | Super Plasticiser | Volume |
| 375 kg | 710 kg | 1110 kg | 180 kg | 3215 ml | 1 $m^3$ |

The rubber used as a replacement for the natural aggregates in the control mix has a significantly lower density than that of the natural aggregates it substitutes, with a $G_s$ of 1.14 compared to $G_s$ 2.6 for coarse and 2.7 for fine aggregates, respectively. As such, it was decided to replace the natural aggregates by relative volume with the correspondingly graded rubber aggregates. Surface treatment included cement paste coating, water washing and sodium hydroxide (NaOH) treating as a means to improve the properties of rubberised concrete. Their usage range in mix designs can be categorised as a set of 8 batches, displayed in Table 2.

Table 2 Concrete batch designation based on the rubber aggregates used

| CONCRETE MIX BATCHES | | | | |
|---|---|---|---|---|
| Aggregate Size | Surface Treatment | | | |
| - | Plain (P) | NaOH (N) | Cement Paste Coated (C) | Water Washed (W) |
| Coarse (A) | AP | AN | AC | AW |
| Fine (B) | BP | BN | - | - |
| Mixed (C) | CP | CN | - | - |

Abbreviated designations for concrete mixes will correspond to those given in Table 2. For instance: a mix utilising coarse, plain rubber aggregates will be designated ‘Mix AP’ whilst a mix using fine, sodium hydroxide treated rubber aggregates is designated ‘Mix BN’.

Compressive strength tests were carried out on 100 mm concrete cubes after curing periods of 7, 14 and 28 days. Natural aggregates were replaced with rubber ranging from 0% (control) to 30% aggregate replacement by volume at increments of 5%. Table 3 displays examples of sample coding in relation to the batch designations of Table 2.

Table 3 Sample coding examples

| CONCRETE SAMPLE CODING | | | |
|---|---|---|---|
| Aggregate Size | Rubber replacement by volume | Surface Treatment | Mix Designation |
| A | 0% | C | A0C |
| A | 5% | W | A5W |
| B | 15% | N | B15N |
| C | 30% | P | C30P |

The example of C30P given in Table 3 is a percentage replacement relative to the overall volume of relative constituents in the concrete mix. As such, it denotes the replacement of both 15% coarse aggregates and 15% of fine aggregates in a mix, resulting in the overall volume of rubber being relative to 30% total rubber content. This makes the quantity of rubber and expected compressive strength of the mix to be directly comparable to both coarse and fine samples coded as A30P and B30P, respectively.

### Rubber Aggregate Preparation

#### Sodium hydroxide surface treatment

All surface treatments of rubber aggregates were carried out prior to their introduction to the concrete mix. The sodium hydroxide treated aggregates were prepared by immersing them in a large 400 l container of prepared NaOH solution at a concentration of 10%/wt.

Once the rubber was suitably treated, the NaOH was drained and diluted whilst the rubber was thoroughly washed for an extended period of time in order to remove any excess NaOH solution from the rubber before being left to dry. This was done to ensure both user safety when handling the rubber post surface treatment as well as to remove a variable, namely chemical reactions between NaOH residue and the concrete mix.

#### Cement paste coating surface treatment

To coat the surface of coarse rubber with cement paste, a ratio of 1 kg cement, 0.3 kg water and 1.5 kg of surface dry rubber was used. All components were placed in a standard concrete mixer which ran for 2-4 minutes until the rubber aggregates were thoroughly coated, leaving no visible excess cement paste. The rubber was then spread out on a plastic covered board and left to dry for 24 hours before being stored.

The cement paste coated rubber aggregates were left for a minimum of 28 days in storage prior to use. A particle density test revealed that cement paste coating the rubber aggregates increases the mass of the rubber particles, resulting in a new $G_s$ of 1.54. This 35% increase in particle density can result in significant changes in the overall volume of the concrete mix if not accommodated for in the mix design.

#### Water washing surface treatment

Aggregates that underwent water washing were saturated in water for approximately 20 minutes and disturbed with a metal rod to dislodge surface contaminants. The water was then drained and the remaining aggregates were spread out in a sieve with apertures of <10 mm. They were then thoroughly washed with a hose for another 3-5 minutes. Note that the rubber aggregates could not be oven dried post washing due to laboratory health and safety requirements.

## TEST RESULTS AND DISCUSSION

Figure 1 shows batch AC providing the most promising results on average when compared to all other coarse aggregate batches. The trend continued across all days of testing, with only the control and 5% replacement of cement paste coated aggregate yielding lower results than other coarse mixes. The increase in compressive strength can be attributed to the increased stiffness modulus between the rubber particles and the concrete matrix [10].

The water washed AW batch was worst performing between A0W to A15W at 7 days, however at 20% replacement onwards, it either matched or exceeded the compressive strength of the NaOH treated coarse aggregates at all ages (see Figures 1 and 4).

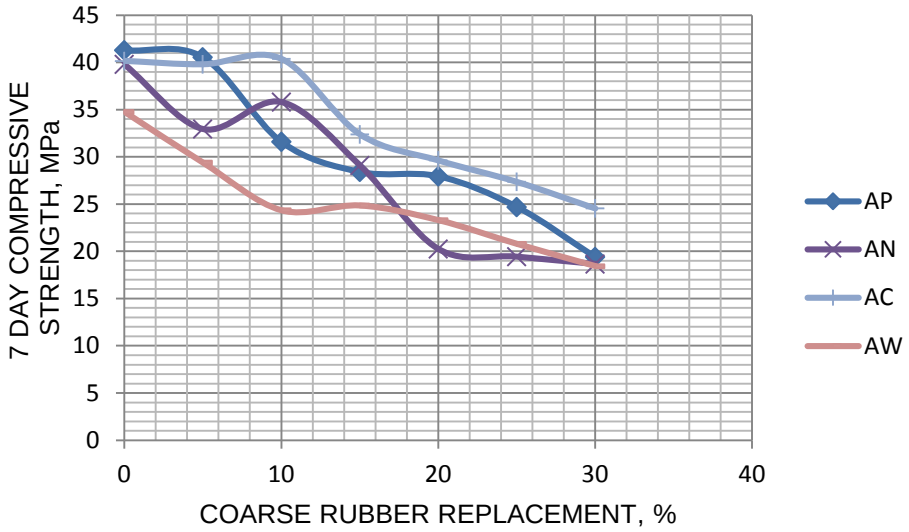


Figure 1 Effects of surface treatment on coarse rubber aggregate in concrete at 7 days

At 7 days curing, plain coarse rubber batch AP performed consistently with the exception of the significant drop in compressive strength between A5P and A10P. As can be seen in Figure 2, the drop in compressive strength between A5P and A10P is least at 14 days, however further developmental increase is minimal at the 28 day compressive strength test. This is most likely due to hydrocarbon contamination of the sourced coarse rubber aggregates [10].

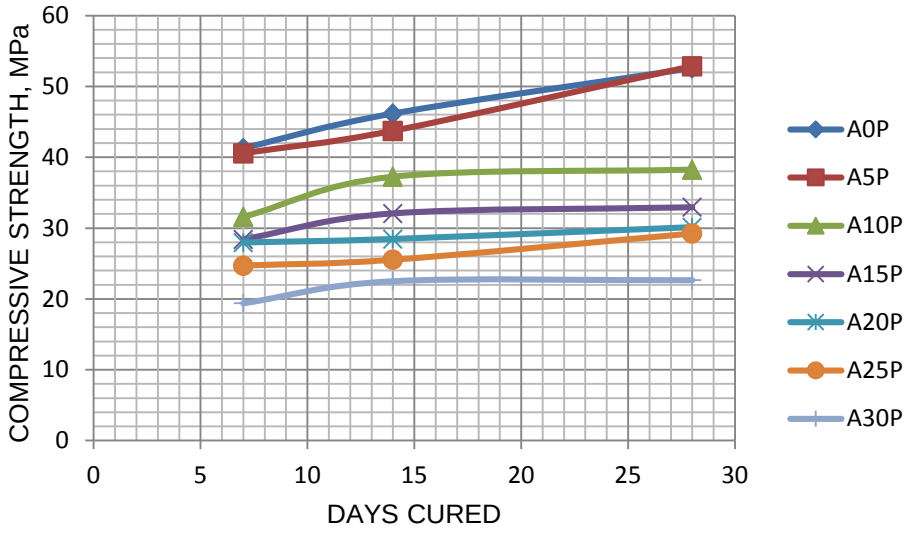


Figure 2 Developed strength of coarse plain rubberised concrete over 28 days

The most significant difference between plain and NaOH treated coarse rubber is on the 7 day test shown in Figure 1. Reasons for Coarse NaOH treated rubber not performing as well could be due to residual NaOH solution on the surface of coarse rubber aggregates influencing the hydration process of concrete. For instance, [11] discovered that strong alkaline substances in certain instances are known to significantly retard both the initial and final setting time of concrete such as sodium bicarbonate ($NaHCO_3$) although others such as sodium carbonate ($Na_2CO_3$) are thought to accelerate this.

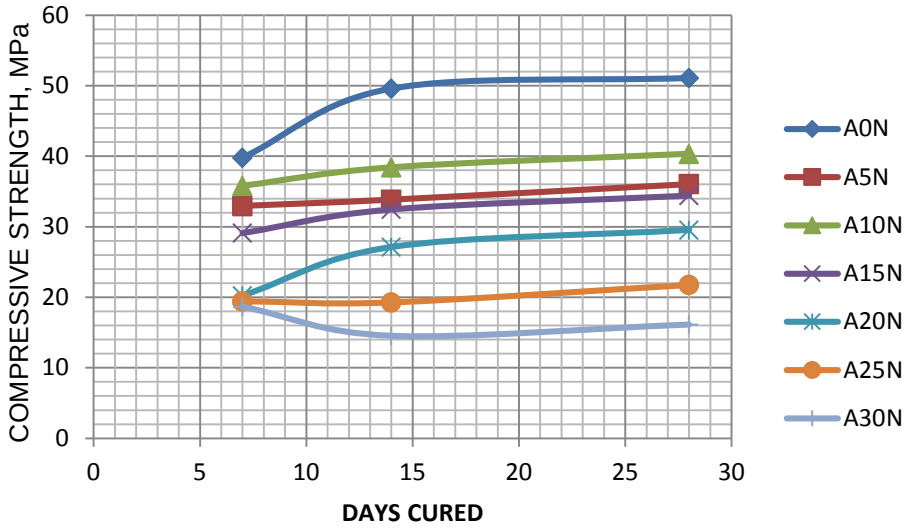


Figure 3 Developed strength of coarse NaOH treated rubberised concrete over 28 days

Figure 3 shows a small, linear increase in compressive strength over time for the A5N series. Furthermore, the data gathered for A5N was extremely consistent showing little variation between samples tested. As such, an explanation for the more significant drop in compressive strength at A5N shown in both Figure 1 and 4 could be due to the proportion of rubber to NaOH residue. It is possible that the amount of NaOH being introduced to the concrete would have a negative effect on the compressive strength if present on the rubber particles in high enough concentration. Conversely, the etching of the rubbers surface along with the removal of other contaminants should have an increase in the compressive strength of the concrete, although an increase in this regard is not considered likely according to [12]. At only 5% rubber content however, any potential increase in compressive strength due to physical changes in the rubber would most likely be outweighed by the negative effects of the presence of NaOH.

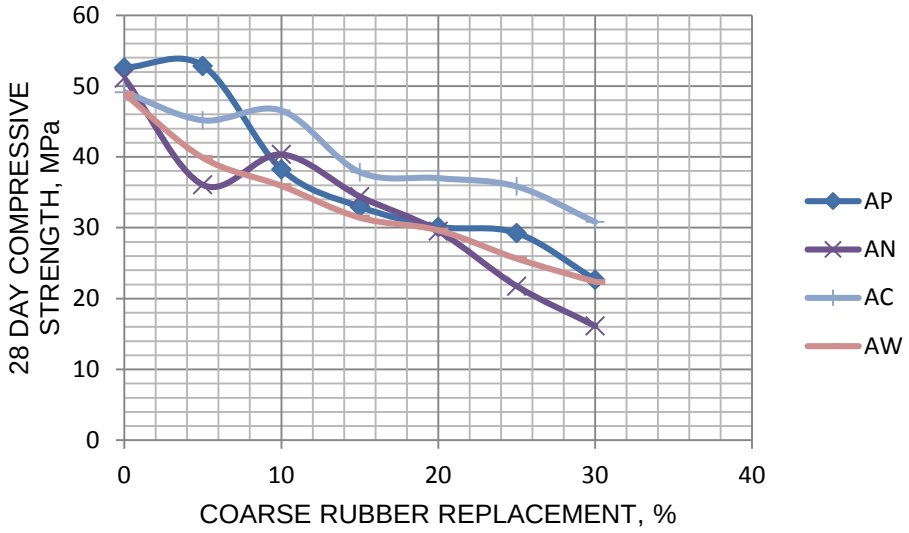


Figure 4 Effects of surface treatment on coarse rubber aggregate in concrete at 28 days

At 28 days, Figure 4 shows that between 10-20% replacement, concrete using NaOH treated coarse rubber can match or exceed the strength of plain coarse rubber aggregates, but not by a significant amount to justify its use when combined with it underperforming plain coarse rubber batch AP at levels of replacement both less and greater than this.

Based on [13] it may be beneficial to leave some residual NaOH on the rubber to increase the compressive strength, but it would have to be within a molar value of 8 M and 12 M. A 10% solution of NaOH should have a molarity of approximately 2.75 M, which in itself is significantly lower than the threshold for negative influence. Whilst [13] does not cover the effects of lower concentrations relative to a control, the current study has the possibility of variations of NaOH present on rubber particles. Whilst draining the NaOH solution from the container, it is possible that some NaOH pellets had not fully dissolved. With a reducing water level, the remaining solution may have become more concentrated, resulting in rubber at the lower levels of the container being subjected to sodium hydroxide of an increased concentration. If some solution at any time exceeded a concentration of 30%/wt, it would produce NaOH with a molarity in excess of 12 M. Due to the large scale and quantities of material involved in the manufacture of NaOH treated rubber for this project, this being a suitable explanation for instances of significant strength variance in compressive strength of concrete using NaOH treated coarse rubber aggregate merits a degree plausibility.

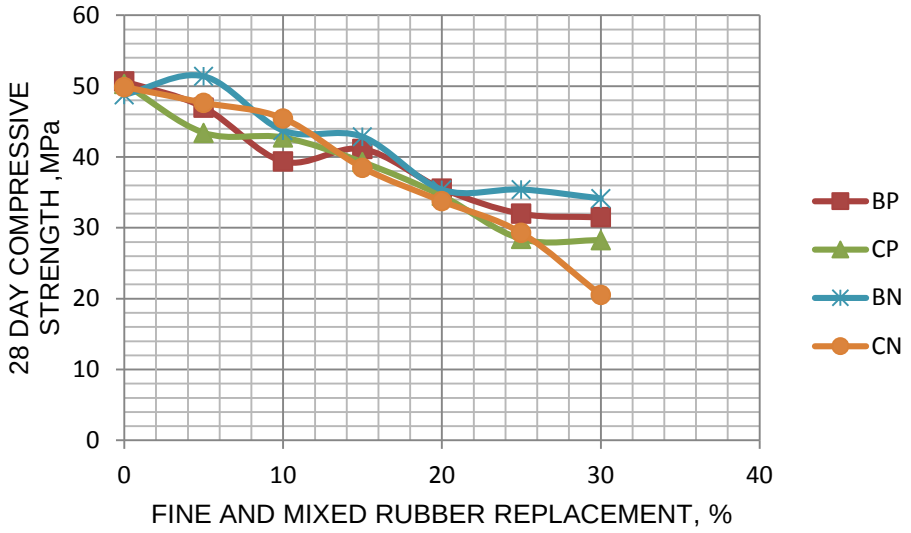


Figure 5 Effects of surface treatment on fine and mixed aggregate in concrete at 28 days

Throughout 7, 14, and 28 days, NaOH treated fine rubbers (BN) proved to be on average a superior mix when compared to plain fine rubbers (BP). This result is consistent with the previous findings of [12] as alkaline surface treatment on fine rubber proved more effective than the same treatment on coarse rubber aggregates when it came to improving their compressive strength relative to plain, untreated rubbers (Figure 5).

When both coarse and fine aggregates were present in rubber, the graphical trend of strength decline was relatively stable. This could be a result of improved grading of the rubber content, resulting in a more even distribution of rubber particles throughout the concrete matrix. Whilst mixed rubber aggregates CP and CN showed minor improvement over plain, fine mix BP at 10% replacement, they both produced weaker results from 15% onwards at 28 day strength.

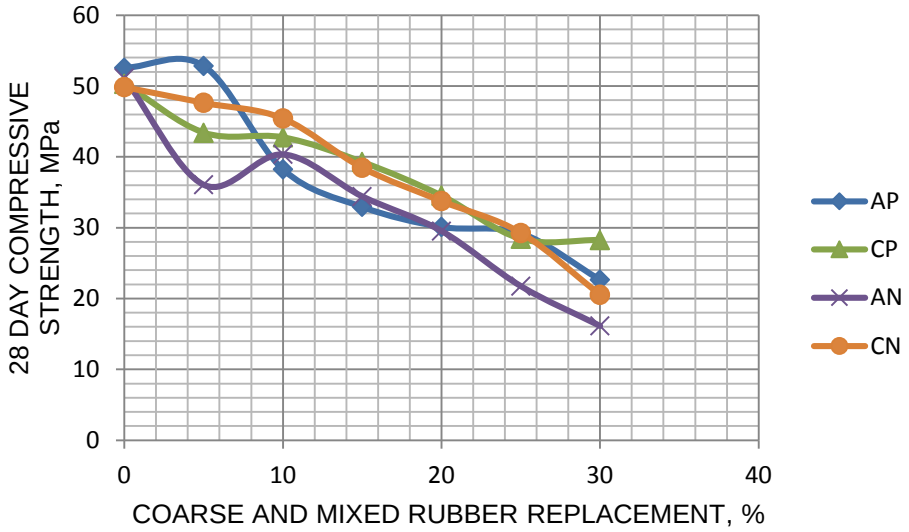


Figure 6 Effects of surface treatment on coarse and mixed rubber aggregate in concrete at 28 days

With the exception of 5% rubber replacement, CP and CN both produced stronger results across the majority of data when compared to their coarse equivalents as shown in Figure 6. At 25% and 30% replacement, they yielded similar results to AP. Again, AN did not perform well and was weaker across the whole range when compared to CP and CN. Whilst the increase relative to the control of A5P could be considered an outlier in the data, a similar increase at 5% was noted in [14]. Furthermore BN (Figure 5) also displays a minor increase in compressive strength, indicating that inclusion of rubber at low percentages has the potential to increase the compressive strength of concrete. The majority of data sets in this paper however note a consistent decline in compressive strength upon any inclusion of rubber. Negligible strength reduction supplemented by variance in the standard deviation of the control compressive strength of the mix could be considered a probable cause of this increase. More tests involving minimal natural aggregate replacement with rubber is recommended in order to clarify this.

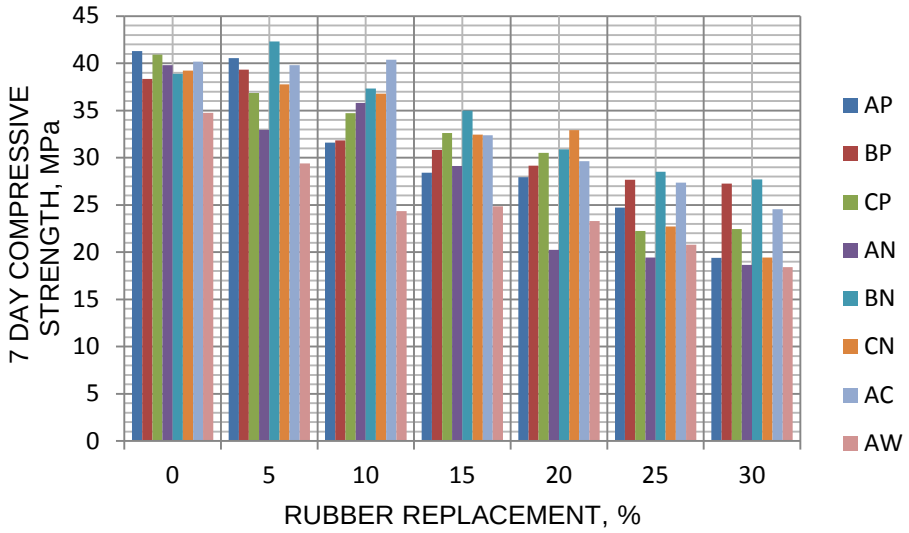


Figure 7 Influence of rubber replacement by volume on 7 day compressive strength of concrete

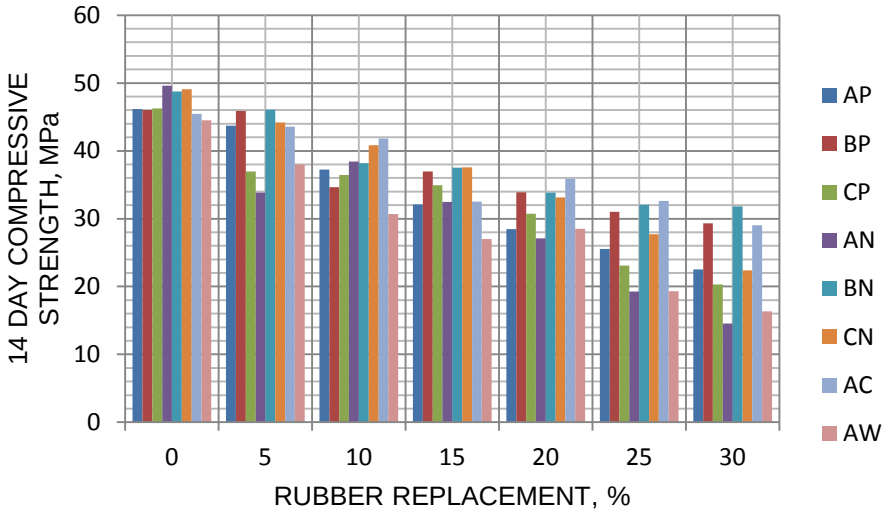


Figure 8 Influence of rubber replacement by volume on 14 day compressive strength of concrete

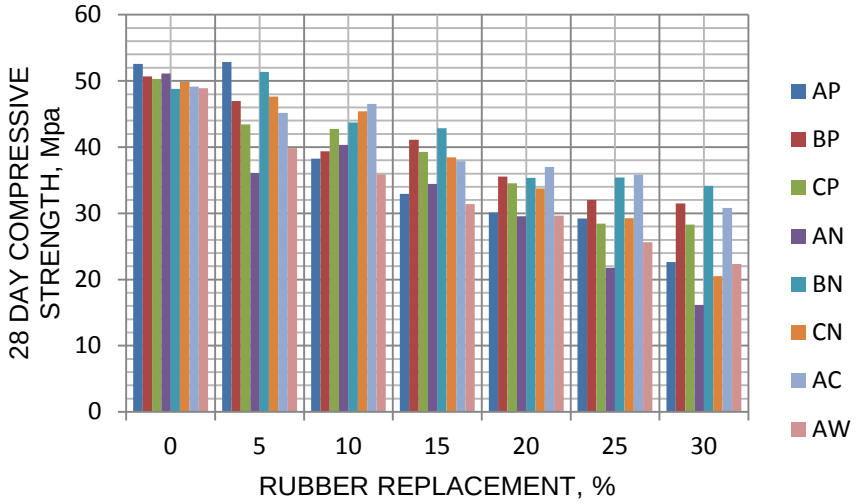


Figure 9 Influence of rubber replacement by volume on 28 day compressive strength of concrete

Figure 10 confirms the majority of data from Figure 9 as being strongly representative of the actual decline in compressive strength relative to each batches the control samples at 28 days testing. What is more apparent is the negligible increase in compressive strength for A5P. Due to the increase in compressive strength being as small as 0.49%, one cannot confidently state that 5% natural aggregate replacement by coarse rubber will have any noticeable benefits to the concrete. However, B5N is noted to have an increase in compressive strength of 5.3%. Whilst this is still negligible, the reduction in compressive strength relative to increased percentages of fine aggregate replacement is consistent for this series of data. Fine rubber treated with NaOH was on average approximately 8.4% stronger at all 28 day tests than its plain counterparts. Bearing in mind the batch BP showed an increase in compressive strength at 7 days testing of approximately 1 MPa and only a minor decrease of 0.38 MPa at 14 days, one could conclude that the increase in compressive strength for B5N at 28 days is likely to be quantifiable.

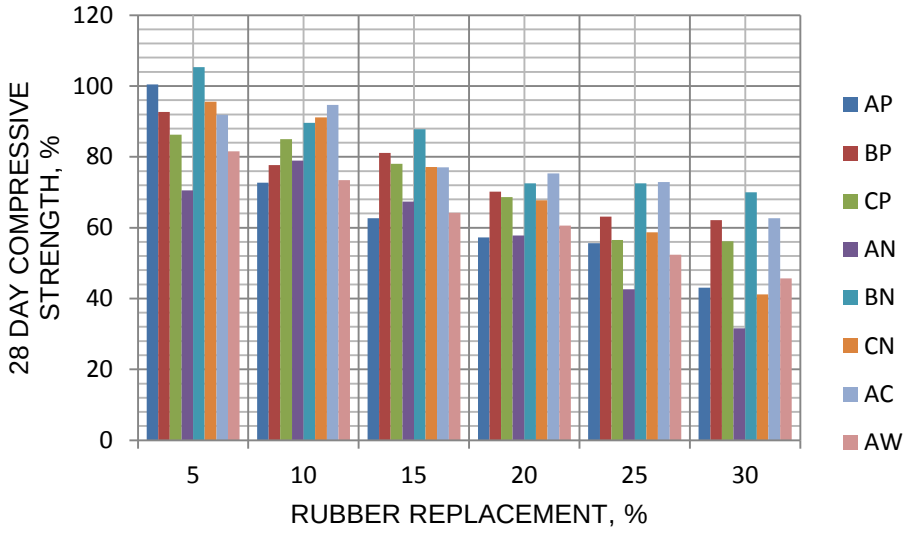


Figure 10 Effect of rubber aggregate substitution on compressive strength of 28 day concrete relative to control samples

Furthermore whilst NaOH treated coarse rubber had in general a negative effect when compared to plain coarse rubber, the use of NaOH on fine rubber had a positive effect. This is explained as a result of the increased surface area of the fine rubber aggregates relative to the same mass of coarse aggregates. This results in more surface contact with the cement and hence an increase in the positive effects of the NaOH surface treatment [12].

When comparing the compressive strength of concrete using plain rubber aggregates as a volumetric replacement of its natural aggregates, the highest strength obtained was from the replacement of fine rubbers whilst coarse rubbers proved to be the weakest. This indicates that the inclusion of coarse rubber aggregates in CP and CN limited its compressive strength to below that of BP, whilst remaining higher than AP.

When comparing A10P to C20P, there is only a 4.09% reduction in strength, and a 6.45% reduction in strength between A15P and C30P. This reduction in strength is relatively small considering a 10% and 15% respective increase in fine rubber content. With a reduction in strength of only 5.97% between B30P and C30P, this mix is still a viable option due to the fairly minimal reduction in compressive strength, but a sizeable increase in rubber content.

## CONCLUSIONS

For plain rubber aggregate, the least reduction in compressive strength was obtained when using fine rubbers. CP is recommended for maximising rubber usage due to low reductions in strength relative to BP whilst utilising 28% more rubber due to its replacement of both fine and coarse rubber aggregates.

Water washing rubber aggregates did not prove beneficial to the compressive strength of rubberised concrete utilising coarse rubber aggregate. Any benefit that may have come from removing surface contaminants would be negligible enough to be undermined by potential increased water content from the surface of the washed rubbers.

One can conclude that the best performing rubberised concrete using coarse aggregate was cement paste coated rubber (AC), displaying an increase in compressive strength of almost 20% at a rubber content of 30% volume of coarse aggregate. This can be attributed to increased compatibility in stiffness between rubber and cement paste.

The best performing mix utilising fine rubber aggregate was that of sodium hydroxide treated fine rubber aggregate – mix BN. This is can be attributed to enhanced hydrophilic properties of rubber due to the treatment with NaOH resulting in reduced negative effects of the rubber on the hydration process of the cement in the concrete matrix [15]. The treatment of coarse rubber aggregates with NaOH is not recommended.

Concrete cubes at strength class C30 can comfortably be achieved using either Cement paste coated coarse rubber (AC) or Sodium hydroxide treated fine rubber (BN) at replacement levels of up to 25% by volume of natural aggregates.

## REFERENCES

1. KHALOO, A R, DEHESTANI, M, RAHMATABADI, P. Mechanical properties of concrete containing a high volume of tire-rubber particles, Waste Management, Vol. 28, 2008, pp 2472-2482.
2. ELCHALAKANI, M, High strength rubberized concrete containing silica fume for the construction of sustainable road side barriers, Structures 1, 2015, p 20-38.
3. LIU, F, CHEN, G, LI, L, GUO, Y, Study of impact performance of rubber reinforced concrete, Construction and Building Materials, No. 36, 2012, pp 604-616.
4. ATAHAN, A, SEVIM, U, Testing and comparison of concrete barriers containing shredded waste tire chips, Materials Letters, No. 62, 2008, pp 3754-3757.
5. ELDIN, N, SENOUCI, A, Rubber-tyre particles as concrete aggregate, Journal of Materials in Civil Engineering Vol. 5, No. 2, 1993, pp 478-496.
6. GESOGLU, M, GUNEYISI, E, KHOSHNAW, G, IPEK, S, Abrasion and freezing-thawing resistance of pervious concretes containing waste rubbers, Construction and Building Materials, No. 73, 2014, pp19-24.
7. KHATIB, Z, BAYOMY, F, Rubberised Portland Cement Concrete, Journal of Materials in Civil Engineering, Vol. 11, No. 3, 1993, pp 206-213.
8. ELDIN, N, SENOUCI, B, Measurement and prediction of the strength of rubberised concrete, Cement & Concrete Composites, Vol. 16, 1994, pp 287-298.
9. MORONEY, C, The use of granulated rubber from used tyres in concrete, PhD thesis, University of Dundee, UK, 2003
10. POCKLINGTON, I, KEW, H, DONCHEV, T, LIMBACHIYA, M. Compressive strength and mix behaviour of rubberised concrete, International conference of composite materials, 2015.

11. REDDY, V V, RAO, H S, JAYAVEERA, K N. Influence of strong alkaline substances (sodium carbonate and sodium bicarbonate) in mixing water on strength and setting properties of concrete, Indian Journal of Engineering & Materials Sciences, Vol. 13, 2006, pp 123-128.

12. LI, G, STUBBLEFIELD, M A, GARRICK, G, EGGERS, J, ABADIE, C, HUANG, B. Development of waste tyre modified concrete, Cement and Concrete Research, Vol. 34, 2004, pp 2283-2289.

13. MEMON, F A, NURUDDIN, M F, KHAN, A, SHAFIQ, N, AYUB, T. Effect of sodium hydroxide concentration on fresh properties and compressive strength of self-compacting geopolymer concrete, Journal of Engineering Science and Technology, Vol. 8, No. 1, 2013, pp 44-56.

14. GANJIAN, E, KHORAMI, M, MAGHSOUDI, A A, Scrap-tyre-rubber replacement for aggregate and filler in concrete, Construction and Building Materials, Vol. 23, No. 5, 2009, pp 1828-1836.

15. LU, L H C C, CHANG, J, LEE, M T. Use of waste rubber as concrete additive, Waste Management & Research, Vol. 25, 2007, pp 68-76.

# PERFORMANCE OF STRUCTURAL CONCRETE CONTAINING MARBLE DUST AS PARTIAL REPLACEMENT FOR RIVER SAND

**R Kishore**

University College of Engineering Osmania University

India

**ABSTRACT.** The paper present the results of experimental investigation carried out to understand the mechanical properties of concrete containing marble dust. Two grades of concrete viz. M25 and M35 have been considered for investigation. For each grade of concrete five replacement percentages of sand viz. 5%, 10%, 15%, 20% and 25% by marble dust have been considered. In all, 12 concrete mix cases including two control concrete mixtures have been studied to understand the key properties such as Compressive strength, Modulus of elasticity, Modulus of rupture and Split tensile strength. Development of Compressive strength is also investigated. In general, the results of investigation indicated improved performance of concrete mixture containing marble dust. About 21% increase in Compressive strength is noticed for concrete mixtures containing 20% marble dust and 80% river sand. An overall assessment of investigation results pointed towards high potential for marble dust as alternative construction material coming from waste generated in marble industry.

**Keywords:** Construction material, Partial replacement, Marble dust, Compressive strength, Modulus of elasticity, Modulus of rupture, Split tensile strength.

**Prof. Ravande Kishore** is presently Dean, Faculty of Engineering at Osmania University, Hyderabad, India. He has 33 years of teaching and research experience at the Department of Civil Engineering at Osmania University. Prof. Kishore has carried out four Research Projects funded by National agencies and published several research papers in the National and International Journals/ conference. His research interests are Recycle Aggregate Concrete, Geoploymer Concretes, Non-destructive Testing, Retrofitting and Rehabilitation of Structures including Health Monitoring, Cost Effective and Environment friendly Housing etc. He is a member of several Professional Societies and widely travelled abroad on Profession Assignments.

## INTRODUCTION

Marble stone has found a prominent place in building industry with its intense use for flooring and other architectural needs in buildings. Since ancient times, it is known to be a material of architect's choice for several heritage buildings both in India and across the world. Taj-Mahal, one of the Seven Wonders of the World is a historic structure made purely out of marble. The quarrying of marble stone generates lot of coarse and fine waste. However, the mechanization of cutting and dressing besides very fine chiseling of marble to make it ready for the desired application such as flooring, cladding and other architectural needs results in production of about 25% of the original mass in the form of powder and dust. Hence utilization of marble dust or safe disposal has been a key issue for environmentalist. Utilizations being always a better option to disposal, the researchers in the field of Civil Engineering are considering it as an alternate construction material as a partial replacement for cement and/or fine aggregate. While production of cement contributes to the carbon dioxide emissions causing serious environmental hazards, scarcity of good quality of river sand has been a serious problem for construction industry. This research investigation undertaken by the Author is an attempt to solve the twin problem of disposal and utilization. The paper presented here is the narration of research investigation carried out and discussion of results obtained and conclusions drawn from the investigation.

## OBJECTIVES

Disposal of marble waste and conservation of scarcely available river sand is the key objective of this investigation. The present research investigation aims at evaluating the influence of partial replacement of river sand by marble dust on mechanical properties of M25 and M35 grade concrete. It also aims at finding out the optimum replacement percentage of river sand by marble dust, thus, giving the maximum technical advantage to the concrete mixtures.

## SCOPE

Predominantly used M25 and M35 grades of concrete in most of the structural elements in India, were considered for the present investigation. Five replacement percentages of sand viz; 5%, 10%, 15%, 20%, 25% by marble dust were considered. In all 10 concrete mixtures containing marble dust and two control concrete mixtures were studied for evaluating the influence of marble dust on mechanical properties of concrete. Five ages of curing viz; 3 days, 7 days, 28 days, 56 days and 90 days of curing periods were considered for evaluating the compressive strength-the principal property of concrete. The other properties considered for testing at 28 days age of curing were Modulus of elasticity, Modulus of rupture and Split tensile strength.

## MATERIALS AND PROPERTIES

### Conventional Materials

Ordinary Portland Cement (OPC) of 53 grade was used. Necessary test were conducted to satisfy the requirements of OPC confirming to IS 12269 (BIS,1999).Locally available river sand was used as one of the constituents of fine aggregate. Required tests were conducted on fine aggregate to ascertain its characteristics in conformity with IS 383 (BIS,1997).Coarse aggregate of size 20mm down were used in manufacturing the required grade of concrete.

Necessary tests were conducted to check the properties of aggregate and the test results were verified for the requirements as per IS 383 (BIS, 1997). The potable water available in the Institute laboratory was used for experimental work of the present investigation program.

### Marble Dust

Marble powder/dust was collected from local vendor wherein the cutting and dressing of marble stone is carried before its delivery to the customer. The marble dust passing through 300 micron sieve was considered as a replacement material. The physical and chemical properties of marble dust used for the investigation satisfy the requirements and match with some of the investigators.

## MOULDING AND CURING OF SPECIMENS

Various constituents of concrete mixtures were weigh batched accurately. After thorough dry mixing, required quantity of water was added to the dry mixture. The mixture is then overturned and mixed well to obtain a homogeneous concrete mixture. The cube, cylinder and prism moulds were filled in three layers and each layer was poked thoroughly with tamping rod and finally compacted on vibratory table. Temperature and humidity conditions at the time of mixing concrete and moulding the specimens were recorded. Demoulding was done after 24 hours and the labeled specimens were moved to the curing tank. Curing was done for 3, 7, 28, 56, 90 days at the standards temperature and humidity. Procedures and guidelines specified in relevant IS code were followed for concrete mixing, and placing and for curing the specimens.

## TESTING OF SPECIMENS

All the specimens were subjected to mechanical strength tests namely, Compressive strength, Modulus of rupture, Modulus of elasticity, and Split tensile strength as per the procedures documented in relevant Indian Standard Codes of practice. For Compressive strength test, an Universal Testing Machine (UTM) of 1000 kN capacity was used. To ensure uniform load transfer, two packing steel plates were placed at top and bottom of the cube specimens. The load was applied at the rate of 140 kg/sq.cm/min for cube as per IS 516. The loading was continued till the failure of the specimen is noted and the corresponding Compressive strength was calculated. In case of prism specimens, two point loading was applied at the rate of 180 kg/min as per IS 516. The failure pattern of prism specimen was carefully observed and noted. The failure load for the specimens was noted and Modulus of rupture was calculated as per the guidelines given in the relevant Indian Standard Code. Modulus of elasticity was evaluated by subjecting standard cylinder specimen to the test. The specimen was fixed with extensometer with its top and bottom being properly capped. Two cycles of loading and unloading was carried out within the elastic limit and the third cycle was taken through up to failure. The load versus compression data was recorded at appropriate intervals of loading. Standard procedure with respect to rate of loading etc. was adopted as per IS 516.Stress-Strain curve was drawn and the values of Modulus of elasticity was evaluated using the same. As regards to split tension test is concerned, the specimens were placed on the bottom platen of the UTM with two wooden strips at top and bottom for ensuring line loading on the specimen. The loading is applied at the desired speed and failure load is recorded as per IS 5816.

The value of Split tensile strength is computed using the test data. While the test results for cube Compressive strength at various ages of curing are tabulated in Table 1, Table 2, the test results of Modulus of rupture, modulus of elasticity and Split tensile strength are presented in Table 3 .

Table 1 Compressive strength of M25 grade (A) concrete at various ages of curing

| MIX NOTATION | MARBLE CONTENT (% by weight of RS) | COMPRESSIVE STRENGTH (MPa) | | | | |
|---|---|---|---|---|---|---|
| | | 3 days | 7 days | 28 days | 56 days | 90 days |
| AM0 | 0 | 18.8 | 24.4 | 34.6 | 38.2 | 39.8 |
| AM5 | 5 | 20.1 | 26.8 | 38.7 | 43.7 | 46.4 |
| AM10 | 10 | 19.5 | 26.3 | 39.8 | 43.0 | 44.5 |
| AM15 | 15 | 23.2 | 30.3 | 41.5 | 47.3 | 48.5 |
| AM20 | 20 | 21.0 | 30.2 | 42.0 | 45.8 | 47.9 |
| AM25 | 25 | 21.2 | 30.8 | 40.6 | 44.0 | 45.8 |

Table 2 Compressive strength of M35 Grade (B) concrete at various ages of curing

| MIX NOTATION | MARBLE CONTENT (% by weight of RS) | COMPRESSIVE STRENGTH (MPa) | | | | |
|---|---|---|---|---|---|---|
| | | 3 days | 7 days | 28 days | 56 days | 90 days |
| BM0 | 0 | 21.8 | 30.8 | 43.1 | 47.2 | 48.1 |
| BM5 | 5 | 26.6 | 35.2 | 48.5 | 50.6 | 51.8 |
| BM10 | 10 | 25.2 | 34.8 | 49.7 | 52.7 | 54.2 |
| BM15 | 15 | 26.7 | 38.4 | 51.1 | 52.8 | 56.2 |
| BM20 | 20 | 27.8 | 39.8 | 52.3 | 53.5 | 55.4 |
| BM25 | 25 | 19.5 | 28.0 | 40.6 | 44.0 | 44.8 |

Table 3 Twenty eight days mechanical properties of M25 and M35 grade concrete mixes

| MIX NOTATION | MARBLE CONTENT (% by weight of RS) | MECHANICAL PROPERTIES (MPa) | | | | | |
|---|---|---|---|---|---|---|---|
| | | Modulus of Elasticity | | Modulus of Rupture | | Split Tensile Strength | |
| Grade of Concrete | | M25 (A) | M35(B) | M25(A) | M35(B) | M25(A) | M35 (B) |
| AM0/BMO | 0 | 27.5 | 33.1 | 5.6 | 6.6 | 4.2 | 5.3 |
| AM5/BM5 | 5 | 30.6 | 36.4 | 6.3 | 7.2 | 4.8 | 6.1 |
| AM10/BM10 | 10 | 32.3 | 39.3 | 6.9 | 7.7 | 5.3 | 7.2 |
| AM15/BM15 | 15 | 34.9 | 40.8 | 7.7 | 8.4 | 6.0 | 7.5 |
| AM20/BM20 | 20 | 35.8 | 42.0 | 8.3 | 8.9 | 6.3 | 7.9 |
| AM25/BM25 | 25 | 34.3 | 41.0 | 7.1 | 7.5 | 5.7 | 6.8 |

Further, the test results were analyzed and depicted graphically for its better understanding. Figure 1 (1.1 and 1.2) demonstrate graphically the development of Compressive strength of concrete for all the cases of concrete mixtures under investigation. Relative Compressive strength of all the concrete mixtures at 7,28 and 90 days of curing are presented in the form of bar charts through the Figure 2 (2.1 and 2.2).The relative performance of other mechanical properties, namely, Modulus of elasticity, Modulus of rupture and Split tensile strength are illustrated through bar charts shown in Figure 3 (3.1 and 3.2).

## DISCUSSIONS

### Compressive Strength

Development of compressive strength of concrete is an important parameter to be considered whenever the concrete containing new/unconventional material is being developed. Strength development pattern/ profile presented in Figure 1 (1.1 & 1.2) follows the same trend as that of control concrete mixtures (AMO/BMO). Attainment of minimum desired Compressive strength at early ages is also another important requirement. In general, it is desired that about 60 % to 65% of 28 days cube compressive strength is attained at the age of 7 days curing. From Table 1 and Table 2, it is noticed that for all concrete mixtures of both M25 and M35 grade concrete, 66 % to 70% of 28 days Compressive strength is attained which is quite satisfactory. The result indicate that replacement of river sand by marble dust has not influenced the rate of gain of strength for the concrete mixture under investigation. Even in the case of 3 days Compressive strength, most of the concrete mixtures have gained over 50% of 28 days Compressive strength. A glance at Table 1 and Table 2, and Figure 2 (2.1 & 2.2) reveal that, 28 days Compressive strength steadily increases with the increase in marble dust content up to 20%. Although similar trend is noticed at the other ages of curing, it is not consistently same. However, a drop in Compressive strength is noticed for concrete mixtures containing 25% of marble dust for both M25 and M35 grade concrete. Thus, concrete mixtures containing marble dust upto 20% attains gain in Compressive strength in the range of 12 to 21% for both M25and M35 grade concrete. The investigation results, therefore, reveal clearly that the optimum replacement percentage of river sand by marble dust is 20% which is in tune with the results reported by earlier investigator. It is to be noted that, the gain in Compressive strength of concrete up to 21% is a significant achievement. This achievement can be attributed to the fine particles of marble dust with and significantly high filling ability leading to dense concrete.

### Other Mechanical Properties

As described earlier, the two grade of concrete viz; M25 and M35 were evaluated for other mechanical properties, namely, Modulus of elasticity, Modulus of rupture and Split tensile strength. A glance at results tabulated in Table 3 reveals that, mechanical properties of concrete mixtures improved significantly. Bar charts depicted in Fig 3(3.1 & 3.2) further indicated that, while upto 27% increase in Modulus of elasticity is noticed, the increase of the order of 35% to 48% in Modulus of rupture values and upto 50% increase in Split tensile strength values are observed. It is also important to note that maximum gain in all the mechanical properties of concrete mixtures investigated is attained for concrete containing 20% replacement of river sand by marble dust. The improved performance of concrete mixture can be mainly attributed to the production of dense and cohesive concrete.

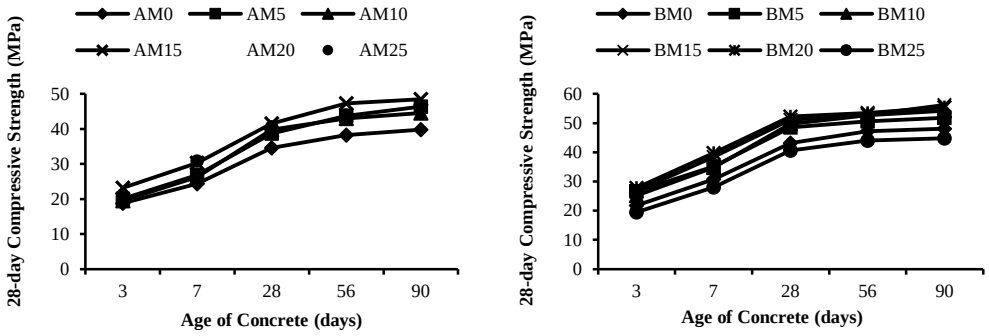


(1.1) M25 Grade (A) (1.2) M35 Grade (B)

Figure 1 Development of compressive strength of concrete with age of curing

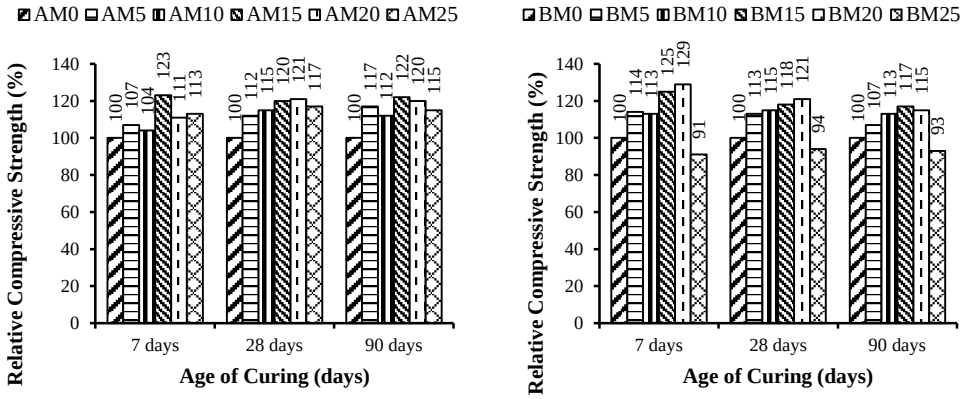


(2.1) M25 Grade (A) (2.2) M35 Grade (B)

Figure 2 Relative compressive strength of concrete at typical ages of curing

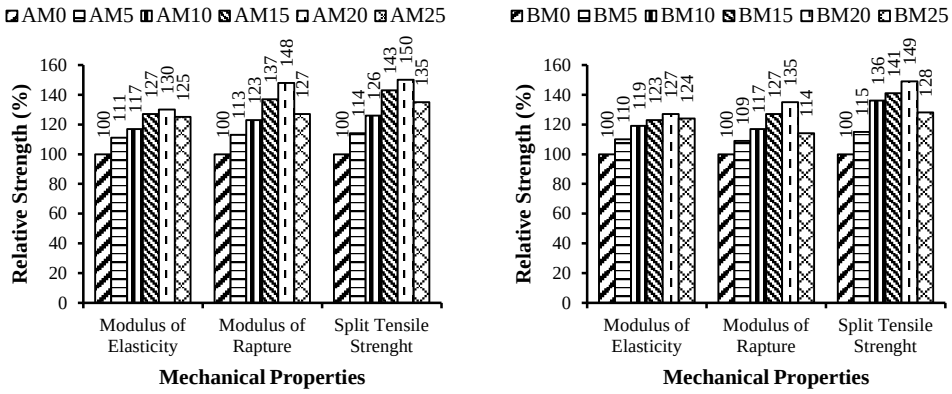


(3.1) M25 Grade (A) (3.2) M35 Grade (B)

Figure 3 Relative mechanical strength of concrete at the age of 28 days curing

## CONCLUSIONS

- Results of investigation clearly indicate the usefulness of marble dust as a substitute material in place of river sand for production of concrete. A significant improvement in all the properties of concrete mixture containing marble dust is consistently observed.
- Twenty percent of replacement of river sand by marble dust in a concrete mixtures is found to be optimum, yielding best performing concrete.
- Rate of gain in compressive strength of concrete mixture containing marble dust more or less remain same as that of control concrete.
- A maximum of 21% increase in compressive strength, 27% gain in Modulus of elasticity, 48% enhancement in modulus of rupture, and 50% increase in Split tensile strength are observed for both M25 and M35 grades of concrete.
- Very fine particles of marble dust and its filling ability contributes to improving the density of concrete considerably, thus leading to overall improvement in the performance concrete mixtures.

## CLOSING REMARKS

The result of investigation successfully demonstrated that marble dust is an alternate construction material, particularly useful as partial replacement for river sand. It is indeed one of the best options available to conserve natural recourses and utilize waste coming from marble industry. Further research investigation can explore the possibility of utilizing marble dust even up to 50% so that natural resources are conserved for future generations and the concept of sustainable development gets promoted.

## REFERENCES

1. BIS, Indian Standard Specification for 53 Grade Ordinary Portland Cement, IS:12269-1963 (reaffirmed1997), Bureau of Indian Standards, New Delhi.
2. BIS, Indian Standard Specification for Coarse and Fine Aggregate from Natural Sources for Concrete, IS:383-1970 (reaffirmed1997), Bureau of Indian Standards, New Delhi.
3. BIS, Indian Standard Method of Test for Strength of Concrete, IS:516-1959, Bureau of Indian Standards, New Delhi.
4. BIS, Indian Standard Test for Splitting Tensile Strength of Concrete Cylinders, IS:5816-1970, Bureau of Indian Standards, New Delhi.
5. HONGOVANA, R., MAHENDRANA, N., AND NAGAMANIB, K. Strength and Durability Properties of Concrete containing Quarry Rock Dust as a Fine Aggregate, APRN Journal,2008.

6. VALERIA CORINALDESI, GIACOMO MORICONI, AND TARUN R,NAIK. Characterization of Marble Powder for its Use in Mortar and Concrete, NMET/ACI International Symposium on Sustainable Development of Cement and Concrete, October 5-7, Toronto, Canada, 2005.

# Theme 4

# Novel, Smart and Multi-Functional Concrete

# PHOTOCATALYTIC CONCRETES: IMPROVED PERFORMANCE THROUGH SUPPORTED CATALYSIS

**A Hakki**

**L Yang**

**D E Macphee**

University of Aberdeen

United Kingdom

**ABSTRACT.** Photocatalytically active $TiO_2$-$SiO_2$ composites have been prepared by different methods; (i) by the thermal hydrolysis (TH) of titanyl sulfate ($TiOSO_4$) in the presence of quartz, (ii) by the hydrolysis of $TiCl_4$ in alkaline media, and (iii) by binding commercial $TiO_2$ (PC105, 100% anatase) to quartz *via* a silica gel binding bridge. The formation of Ti-O-Si linkages was confirmed by means of FTIR spectroscopy and the photocatalytic degradation of NO was followed according to the ISO standard (ISO 22197−1). Methods (ii) and (iii) have shown promising results in terms of coverage of the support and photocatalytic activity. The electron microscope images of the obtained materials showed that sufficient coverage of support surface with the photocatalyst can successfully be achieved. Importantly, in comparison to pure $TiO_2$, $SiO_2$ covered with only 10% $TiO_2$ is sufficient to insure ca. 73% of the photocatalytic activity for the NO abatement which has an economic advantages by decreasing the required amount of the applied photocatalyst. Moreover, excess chemical Ti-O-Si linkages plays an important role in defining reaction selectivity.

**Keywords**: Photocatalysis, $TiO_2$, Binding, Supported catalysis

**Donald Macphee** is Professor of Chemistry at the University of Aberdeen. He is the author or co-author of more than 80 papers in materials chemistry, mostly related to the chemistry of cements but also on photocatalysis and his recent research on photocatalytic concrete. He a Fellow of the Royal Society of Chemistry and is on the editorial boards of the journals ‘Cement and Concrete Research’ and ‘Materiales de Construcción’.

**Dr Lu Yang** is research fellow at the University of Aberdeen. He got his Ph. D degree in Wuhan University of Technology at Dec 2014. His research mainly focus on the modification of photocatalysts and their application in cement and concrete materials.

**Dr Amer Hakki** is Research Fellow at Chemistry Department at the University of Aberdeen. He has been included in different industrial and academic projects dealing with applying photocatalysis for environmental applications and for light energy conversion into chemical energy and he has many publications in these fields.

## INTRODUCTION

Concrete structures are ubiquitous in our society. They are typically associated with our urban centres and their significant surface area represents an interface with the urban atmosphere. Application of photocatalysts to construction materials will introduce additional functionality to the concrete structures benefiting their high surface area[1, 2]. Many important effects related to the nature of the employed photocatalyst had been discovered: (i) the self-cleaning effect as a result of the sunlight promoted redox reactions occur on the surface of the photocatalyst on which the pollutants are attacked[3]; (ii) the photo-induced hydrophilicity caused by the interaction between the photogenerated charges carriers on the photocatalysts' surface and adsorbed water molecules, which also enhance the self-cleaning effect[3]; and (iii) purification of urban atmosphere which today, is typically polluted by vehicle emissions at levels that exceed recommended permissible levels, particularly with respect to NOx[4]. $TiO_2$ is so far the most generally employed photocatalyst in these fields due to its properties including chemical stability, relatively low price, high photocatalytic activity, and more importantly its eco-safety as up-to-date knowledge on $TiO_2$ toxicology indicates[5].

Photocatalytic concretes are well placed to address these air quality issues and have already demonstrated their potential in trial sites throughout Europe and elsewhere. In the last two decades, a lot of scientific works have focused on photocatalytic cementitious materials which predominantly dealt with activity issues[1, 6-9]. For such applications, $TiO_2$ is so far applied in the form of nanoparticles which insure high specific surface area required for higher activity. However, dispersion effectiveness of such nanoparticles is still a challenging topic because of the high tendency of $TiO_2$ nanoparticles to agglomerate influencing the overall photocatalytic performance[9]. Moreover, the major fraction of $TiO_2$ amounts applied to cementitious materials by traditional ways are occupied inside the cement bulk and thus are shielded from the sunlight[1]. This will, again, reduce the available photocatalytically active surface area required for gaseous pollutant adsorption.

Significantly improved performance can be anticipated by engineering more efficient photocatalytic structures. However, the chemical bonding of powdered photocatalysts to exposed construction material surfaces may influence chemical bonding in the near surface region of the photocatalyst, affecting both optical and surface properties of the photocatalyst and therefore its photocatalytic activity/reaction selectivity behaviour. Therefore, the focus of the present work is on effective support of $TiO_2$ nanoparticles, via chemical bonding, on concrete aggregates which will be exposed on concrete surfaces and to investigate the impact of such bonding on the photocatalytic performance. For this purpose, commercial as well as synthesised $TiO_2$ have been bonded, by different methods, onto quartz $SiO_2$ sand (Q; as a simple example of an aggregate).

## EXPERIMENTAL PROCEDURE

### Synthesis of $TiO_2$-$SiO_2$ composites

Quartz (Aldrich) was first ball milled. The powder was then sieved by vibratory sieve shaker to collect quartz with particles sizes in the range 20-100 μm. The powders were then modified with $TiO_2$ by three different methods:

**Method (1):** Q/$TiO_2$ composites were obtained via the thermal hydrolysis of titanyl sulfate solutions into which the quartz was suspended. 50 ml of $TiOSO_4$ aqueous solution (0.4M) were added to 50 ml water in which 5 g of Q was suspended. After 0.5 h stirring at RT, the

suspensions were stirred in a water bath at 90 $^0$C for 4 hours. After the thermal hydrolysis time is finished, the mixtures were cooled to RT and the precipitates were filtered and washed three times with deionized water. The obtained powders were dried at 90$^0$ C overnight and calcined either at 500 $^0$C or 300 $^0$C for 4h. Then, powders were sieved again to collect particles bigger than 20 µm to separate modified quartz from loosely or non-connected $TiO_2$. As reference material, $TiO_2$ was prepared by the same method but in the absence of the quartz employing 500 $^0$C for 4h heat treatment.

**Method (2):** Titanium(IV) tetrachloride ($TiCl_4$) was used as photocatalyst precursor[10]. 5 g of Q powder were slowly added to 200 ml of freshly prepared $TiCl_4$ solution (0.1M in 20% hydrochloric acid) placed in an ice bath under constant stirring. Next, the slurry was continuously stirred at room temperature and 30 vol % $NH_3$ was slowly added to the solution to maintain a condition where pH=9.2. After stirring at RT for an additional 1h, the slurry was transferred to a Petri dish and allowed to dry overnight under ambient conditions and then washed with distilled water and dried at 90 $^0$C overnight. The obtained powders were then calcined at 400 $^0$C for 2h and then sieved to remove the non-connected $TiO_2$.

**Method (3):** In this method, commercial photocatalyst (PC105) was supported on the quartz via a silica gel binder. In this case, tetraethyl orthosilicate (TEOS) was employed to form the binder. TEOS mother solution was prepared by adding the required amount of TEOS into ethanol:water:HCl mixture (1:0.84:0.78x$10^{-3}$ molar ratio) and stirring for 10 days at RT. Then accurate volumes of the obtained solution were added to 100 ml of ethanol, in which 0.2g $TiO_2$ were suspended, to get $TiO_2$:TEOS of 1:1. After gentle stirring at RT overnight, the suspension was added dropwise to 2g of Q with continuous stirring at 80 °C under reduced pressure. The obtained powders were dried at 90 °C overnight followed by heat treatment at 200 °C for 4h.

**Synthesis of gel networks based on Ti-O-Si linkages**

In order to develop an analytical capability for quantifying the important chemical linkage between $TiO_2$ and the quartz substrate, $SiO_2/TiO_2$ composites were prepared by a sol-gel method using tetraethyl orthosilicate (TEOS) and titanium tetraisopropoxide (TTIP) as precursors for Si and Ti, respectively. This method was chosen to maximise the possibility of Ti-O-Si linkage formation. The required amount of TEOS was added dropwise into an ethanol:water:HCl mixture (1:0.84:0.78x$10^{-3}$ molar ratio). After stirring at RT for 1h, the desired amount of TTIP was added and the mixture was stirred at RT overnight. The solution was converted to gel after stirring at 80 $^0$C for 1h. The obtained gel was then heat treated as follows: overnight drying at 90 $^0$C, calcination at 450 $^0$C for 5h, and re-calcination at 500 $^0$C for 5h. Pure $TiO_2$ was also prepared by the same sol-gel method but in the absence of TEOS.

**Characterization**

IR spectra were recorded using a PerkinElmer Spectrum Two equipped with UATR (Single Reflection Diamond). X-ray diffraction (XRD) patterns were obtained using a PAN analytical diffractometer (X'Pert$^3$ Powder) equipped with a CuKa1 1.54 A$^0$ X-ray source. The morphology of the samples was analysed via scanning electron microscopy (SEM) model - ISI-ABT55, equipped with ED X-ray analyser and Link Analytical BSE detector with operating voltage between 10-20kV. The used ED system is LINK ANALYTICAL AN10/55S with LINK ANALYTICAL LZ5 detector. Images were captured with an ISS – I-SCAN 2000 Digital Image Acquisition System. The transmission electron microscopy (TEM) was performed on a JEOL-JEM-2000EX microscope operated with an accelerating voltage of 200kV. Images were captured with a Gatan Erlangshen ES500W camera.

### Photocatalytic performance test

The photocatalytic activities of the prepared materials were tested using the removal of NOx from polluted air. For this purpose, an air-purification test set-up has been established according to ISO 22197-1 (see Figure 1). This set-up consists of, gas supplies (100 ppm NO in $N_2$, and synthetic air, BOC), humidifier, three mass flow controllers (Bronkhorst, UK) by which the volumetric concentration of NO has been adjusted to 1ppmv and the relative humidity of ca. 50%, with laminar volume flow of $5x10^{-5}$ $m^3.s^{-1}$, a photoreactor made of PMMA covered by borosilicate glass, a light source (Ultra-Vitalux 300 W, Osram, Germany) placed above the sample holder at distance that insure 10 $Wm^{-2}$ light intensity reaches the sample. The concentrations of NO, $NO_2$ and total NOx in the outlet gas flow were monitored using a Thermo Scientific Model 42i-HL High Level NO-$NO_2$-NOx Analyzer (Air Monitors Ltd., United Kingdom).

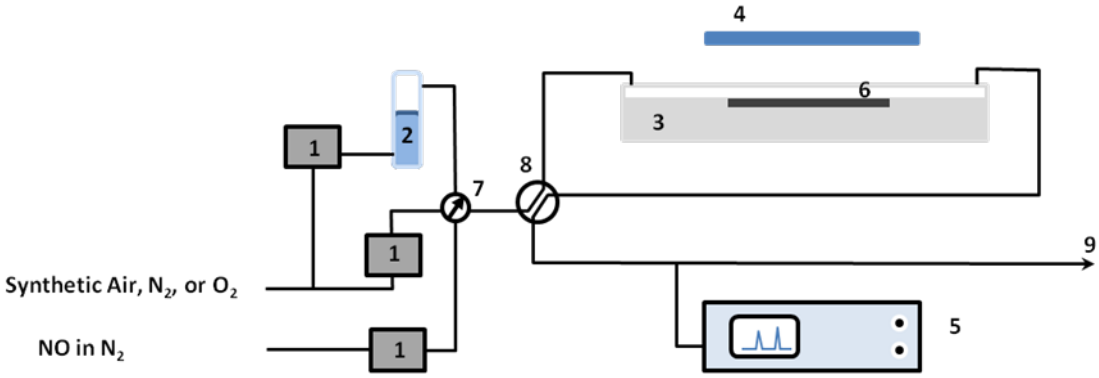


Figure 1 The experimental set-up used for the photocatalytic tests: (1) mass flow controllers, (2) humidifier, (3) photocatalytic reactor, (4) UV(A) light source, (5) NOx analyzer, (6) test sample, (7) and (8) valves, and (9) gas stream outlet.

The test samples were prepared by pressing 0.8 g of the material into a rectangular PMMA holder (height 0.2 cm, width 3 cm, and length 8 cm). The resulting briquettes with a geometric surface area of $2.4 \times 10^{-3}$ $m^2$ were irradiated overnight with UV (320 nm) to remove any organic contaminants adsorbed on their surfaces.

## RESULTS AND DISCUSSION

The X-ray patterns of bare quartz sand and the obtained $TiO_2$-Q composites are shown in Figure 2. The XRD patterns of pure $TiO_2$ samples prepared in the absence of Q are also presented in Figure 2. It is clear from the peaks positions that both $TiO_2$ samples prepared by thermal hydrolysis (method-1) or by sol-gel method are essentially anatase. The typical anatase phase patterns appeared for $TiO_2$-Q composites obtained from different modification methods confirm the formation of this phase on the modified quartz. The differences in the peaks intensities and widths are due to the differences in particle sizes and crystallinity between the different samples. However, the sample prepared by method-1 and calcined only at 300 $^0$C has only shown a very tiny shoulder at Θ around $25.2^0$. This can be attributed either to low crystallinity of this sample or to less amount of $TiO_2$ loaded on quartz under these preparation conditions.

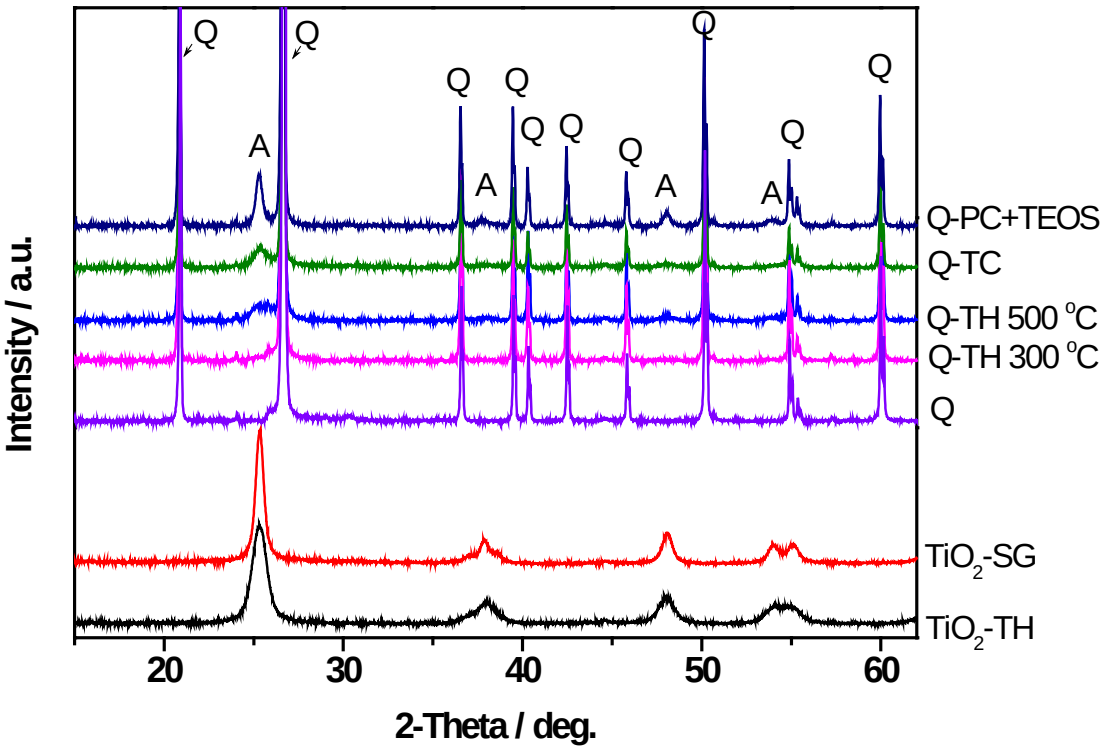


Figure 2 XRD patterns of pure $TiO_2$ and $TiO_2$-Q composites prepared by different methods

In order to identify any chemical interaction between the formed $TiO_2$ and quartz, infrared spectra of the $TiO_2$-Q composites obtained by the employed different methods have been recorded and compared with that recorded for $SiO_2/TiO_2$ mixed oxides prepared by a sol-gel method. The FTIR spectra of the $SiO_2/TiO_2$ mixed oxides samples and of the $TiO_2$-Q composites are shown in Figures 3 (a) and (b), respectively.

As can be seen from Figure 3(a), $SiO_2/TiO_2$ mixed oxides have shown an infrared absorption in the range between 910-950 $cm^{-1}$ assignable to the Si–O–Ti stretching vibrational mode[11], whereas no absorption peak due to this mode was observed for $SiO_2$, $TiO_2$, or physically mixed $TiO_2$ and $SiO_2$. This indicates the interfacial chemical bond formation between $TiO_2$ and $SiO_2$. Since we found that Si–O–Ti linkages can be successfully followed by FTIR spectroscopy, FTIR spectra of the materials obtained via methods 1,2, and 3 were recorded in order to identify any chemical interaction between the formed $TiO_2$ and the quartz. Figure 3(b) shows the FTIR spectra of the obtained material from these methods.

As can be seen from this figure, an obvious shoulder in the range between 920-960 $cm^{-1}$ appears in the IR spectra of $TiO_2$-Q prepared by binding commercial PC105 to Q via silica gel binder indicating the formation of Ti-O-Si bonds between PC105 and the binder. Although no significant peak can be noticed for composites obtained from methods 1 and 2, a flattening of the IR spectra can be clearly noticed in the range between 920-960 $cm^{-1}$ which can be attributed to the very low amount of Ti-O-Si bonds (if formed) in these composites. Tokarsky et al. [12]were also not able to observe a clear evidence, from their recorded IR spectra, for the formation of Ti-O-Si upon modification of sand by $TiO_2$ employing thermal hydrolysis of titanyl sulfate. However, they have proved the presence of such bonds indirectly by computer molecular modeling.

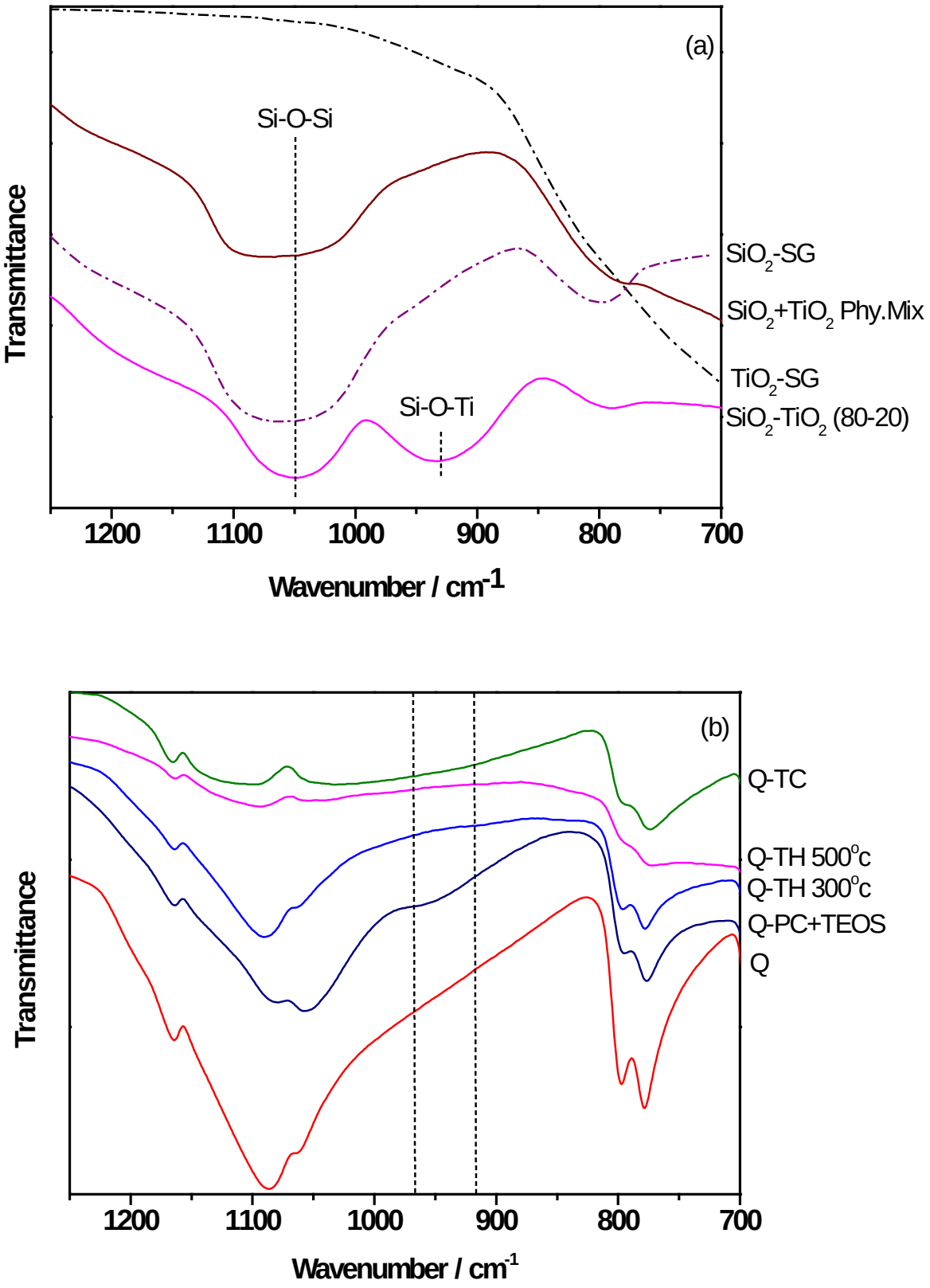


Figure 3 FTIR Transmission spectra of $TiO_2$-$SiO_2$ mixed oxides (a) and of $TiO_2$-Q samples prepared via the employed different methods

On the other side, the adhesion of $TiO_2$ nanoparticles on quartz surface in the sample obtained from method-2 has also been proved by TEM investigation. Figure 4 shows electron transmission micrographs of the Q coated with $TiO_2$ employing $TiCl_4$ precursor. The low magnification view, c.f., Figure 4(a), shows that Q particles are successfully covered with small $TiO_2$ nanoparticle. The particle sizes of the formed $TiO_2$ nanoparticles are between 10-40 nm as can be seen from Figure 4(b).

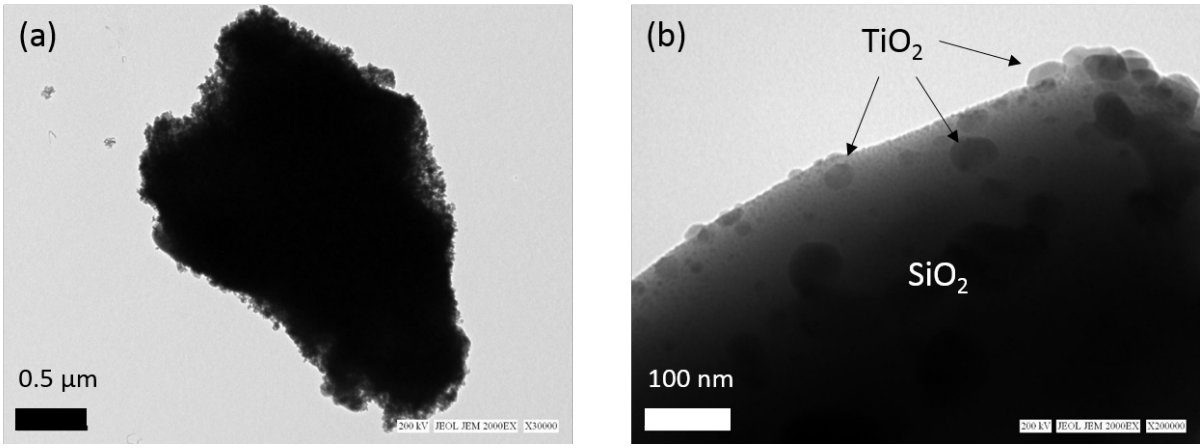


Figure 4 TEM images of the titania-coated quartz prepared via method-2. (a) Low magnification view and (b) the higher magnification view of the same sample shows small $TiO_2$ particles decorating the quartz surface (b).

On the other hand, the homogeneity of the distribution of commercial $TiO_2$ on the quartz prepared via method-3 has been investigated by scanning electron microscopy. Figure 5 shows the SEM-EDS of commercial $TiO_2$ (PC105) loaded onto quartz employing TEOS as a binder in 1:1 molar ratio to $TiO_2$. Due to the shape and morphology of the milled quartz, titania was found to have not been immobilized very homogenously on the grains as some areas remain uncovered. However, it is clear from these images that sufficient amounts of $TiO_2$ are present on the surface.

## Photocatalytic performance

Figure 6 shows an example of the changes in the concentrations of NO, NOx, and $NO_2$ in the gas stream flows over $TiO_2$ (PC105) in the dark and under illumination. When light was switched on, the initial NO concentration drops ca. 48% with a simultaneous formation of $NO_2$, as one of NO oxidation products. Consequently, the concentration of NOx, which reflect the total oxidation of NO to $HNO_3$, is reduced during illumination time. It can also be noticed that the concentration of NO increased slightly and continuously during the entire irradiation time. This can be attributed to the accumulation of photocatalytically generated NO oxidation products which may compete with the initial NO on the available active sites. However, Bloh et al. reported that a steady-state of NO, $NO_2$ and NOx concentrations over illuminated $TiO_2$ is achieved after several hours of illumination meaning that the surface is not blocked with the produced intermediates.

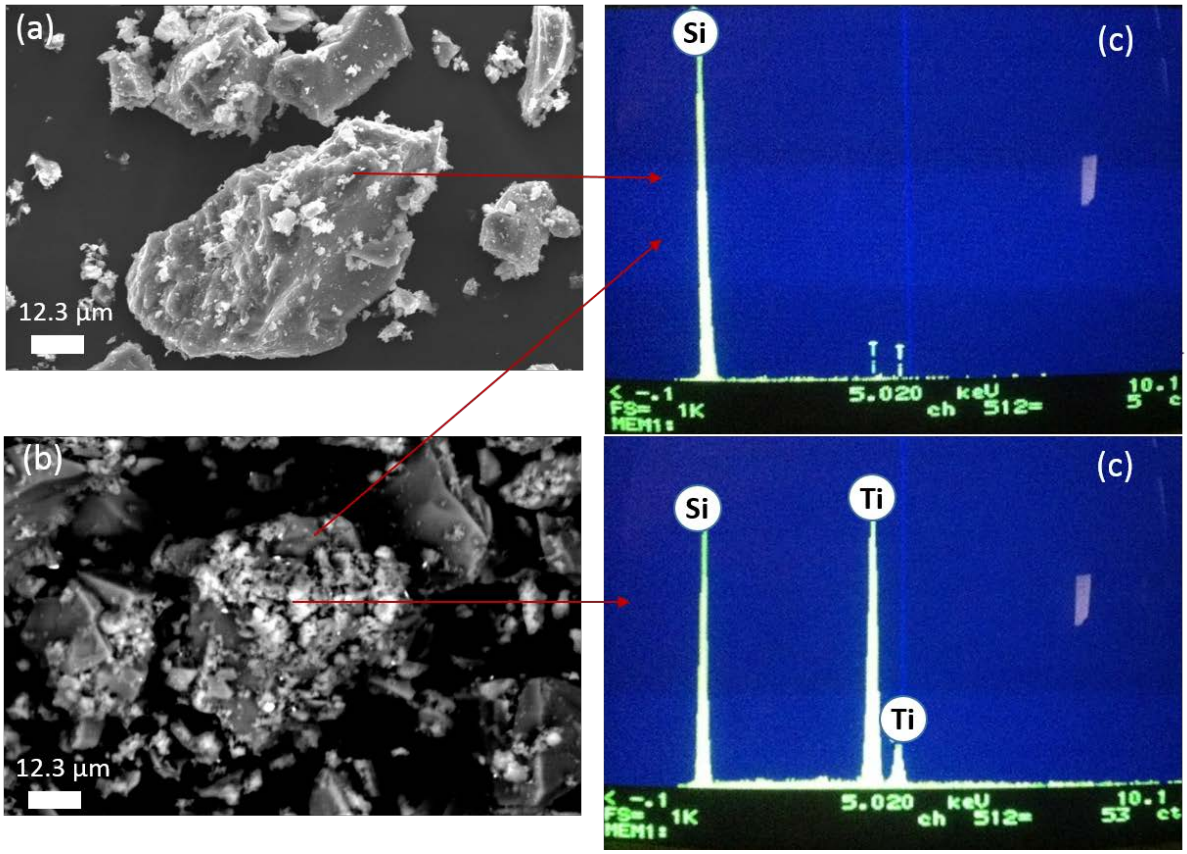


Figure 5 SEM images for (a) bare quartz and (b) $TiO_2$ (commercial PC105) immobilized on quartz via $SiO_2$ binder formed from TEOS

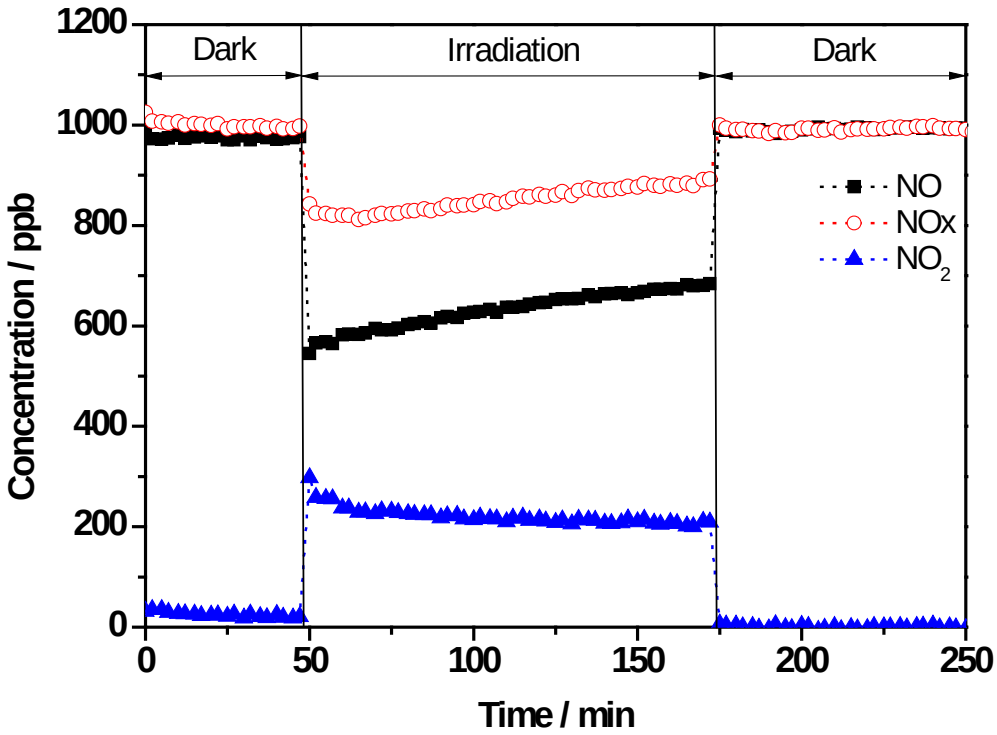


Figure 6 Concentration of NO, $NO_2$, and NOx as a function of time in the presence of commercial PC105 $TiO_2$.

To determine and compare the activities of the obtained $TiO_2$-$SiO_2$ composite powders for the NOx abatement, the photonic efficiencies ($\xi$) for the removal of NO, NOx and the formation of $NO_2$ was calculated and illustrated in Figure 7.

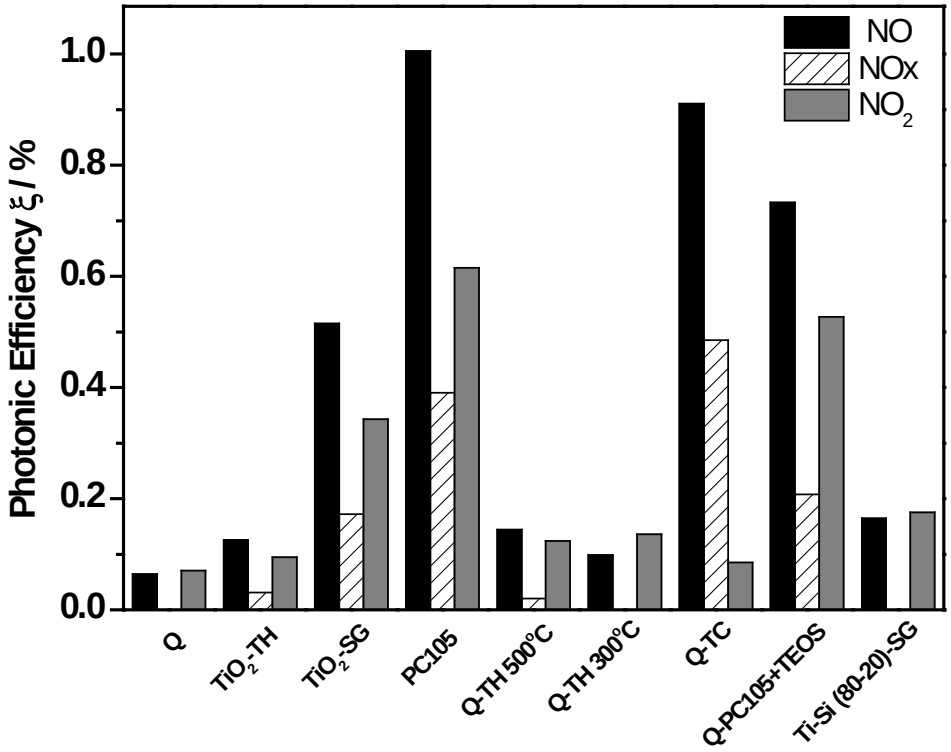


Figure 7 Photonic efficiencies of different $TiO_2$ and $TiO_2$-Q composite powders for NO and NOx removal and for $NO_2$ formation.

$\xi$ is defined as the ratio of the reaction rate and the incident photon flux and was calculated according to eqn (1), where $\dot{V}$ is the volumetric flow rate; $c_d$ the concentration of NO, NOx, or $NO_2$ under dark conditions; $c_i$ the concentration of the same gas under illumination; p the pressure; $N_A$ the Avogadro constant; h is the Plank constant; c is the speed of light; I the incident irradiation intensity, $\lambda$ the employed wavelength assuming monochromatic light (365 nm), A the irradiated area; R the gas constant; and T the absolute temperature.

$$\xi = \frac{\dot{V}\,(c_d - c_i)\,pN_A hc}{I\lambda ART} \qquad (1)$$

As can be seen from Figure 7, loading of $TiO_2$ onto the surface of quartz strongly enhance its activity for NOx abatement. However, this activity differs depending on the immobilizing method. A significant increase in NO removal has been recorded for materials which are prepared from commercial $TiO_2$ as well as from $TiCl_4$ as precursor for $TiO_2$, i.e., methods 2 and 3, as compared to that prepared via thermal hydrolysis of titanyl sulfate according to method 1. On the other hand, bare commercial $TiO_2$ itself has shown 2 to 8 times higher activity for NO removal comparing to that synthesized via sol-gel or thermal hydrolysis method, respectively. This different in the photocatalytic activity can be attributed to the difference in

particle sizes and active surface areas of the studied materials. Interestingly, binding of commercial $TiO_2$ (PC105) to the surface of quartz via silica-gel binder has not affected its photocatalytic performance dramatically. As can be noticed from Figure 7, the photonic efficiency for NO removal has only decreased by factor of 0.3. Taking into account the low amount of $TiO_2$ loaded on Q in this material, i.e., only 10%, the efficiency of $TiO_2$ when supported on quartz, as prepared by this method, is remarkable. These results are in good agreement with the SEM image of this material (c.f., Figure 5) which shows that ca. 70% of the quartz particle surface is covered with $TiO_2$ particles. On the other hand, the composite prepared vie method-2 has also shown a very good activity even higher than that prepared from commercial $TiO_2$. The advantages of this method is the low cost of the used $TiO_2$ precursor, i.e., $TiCl_4$, which make it also a promising method for industrial applications.

## CONCLUSIONS

Silica in form of quartz sand has been successfully modified with $TiO_2$ either via binding the commercial $TiO_2$ utilizing binder from silica gel or via the hydrolysis of different Ti precursors. Both materials which are prepared from commercial $TiO_2$ or from the hydrolysis of $TiCl_4$ have shown high efficiency for the removal of both NO and NOx. Although the photonic efficiency for NO oxidation appears lower for supported $TiO_2$ than that for the unsupported powder, the surface supported $TiO_2$ is more efficient per unit mass since only 10% of the $TiO_2$ mass used in the $TiO_2$-Q composite.

## ACKNOWLEDGEMENTS

The authors are grateful to acknowledge the financial support of EPSRC (Grant No. EP/M003299/1).

## REFERENCES

1. FOLLI, A., ET AL., Engineering Photocatalytic Cements: Understanding TiO2 Surface Chemistry to Control and Modulate Photocatalytic Performances. Journal of the American Ceramic Society, 2010. **93**(10): p. 3360-3369.
2. WANG, F.Z., ET AL., The hierarchical porous structure of substrate enhanced photocatalytic activity of TiO2/cementitious materials. Construction and Building Materials, 2014. **64**: p. 488-495.
3. FATEH, R., R. DILLERT, AND D. BAHNEMANN, Preparation and Characterization of Transparent Hydrophilic Photocatalytic TiO2/SiO2 Thin Films on Polycarbonate. Langmuir, 2013. **29**(11): p. 3730-3739.
4. DILLERT, R., ET AL., Light intensity dependence of the kinetics of the photocatalytic oxidation of nitrogen(II) oxide at the surface of TiO2. Physical Chemistry Chemical Physics, 2013. **15**(48): p. 20876-20886.
5. SHI, H.B., ET AL., Titanium dioxide nanoparticles: a review of current toxicological data. Particle and Fibre Toxicology, 2013. **10**.
6. FREITAG, J., ET AL., Nitrogen(II) Oxide Charge Transfer Complexes on TiO2: A New Source for Visible-Light Activity. Journal of Physical Chemistry C, 2015. **119**(9): p. 4488-4501.

7. MA, J.Z., ET AL., Photocatalytic Removal of NOx over Visible Light Responsive Oxygen-Deficient TiO2. Journal of Physical Chemistry C, 2014. **118**(14): p. 7434-7441.
8. MENDOZA, C., ET AL., TiO2 and TiO2-SiO2 coated cement: Comparison of mechanic and photocatalytic properties. Applied Catalysis B-Environmental, 2015. **178**: p. 155-164.
9. KAMARUDDIN, S. AND D. STEPHAN, Sol-gel Mediated Coating and Characterization of Photocatalytic Sand and Fumed Silica for Environmental Remediation. Water Air and Soil Pollution, 2014. **225**(5).
10. ANDONOVA, S.M., G.S. SENTURK, AND E. OZENSOY, Fine-Tuning the Dispersion and the Mobility of BaO Domains on NOx Storage Materials via TiO2 Anchoring Sites. Journal of Physical Chemistry C, 2010. **114**(40): p. 17003-17016.
11. YAMASHITA, H., ET AL., Characterization of titanium-silicon binary oxide catalysts prepared by the sol-gel method and their photocatalytic reactivity for the liquid-phase oxidation of 1-octanol. Journal of Physical Chemistry B, 1998. **102**(30): p. 5870-5875.
12. TOKARSKY, J., ET AL., A low-cost photoactive composite quartz sand/TiO2. Chemical Engineering Journal, 2013. **222**: p. 488-497.

# DESIGN AND PERFORMANCE OF BACTERIA-BASED SELF-HEALING CONCRETE

**K A Paine** **M Alazhari**
**T Sharma** **R Cooper**
**A Heath**
University of Bath
United Kingdom

**ABSTRACT.** The effect of water-borne contaminants on the durability of concrete is was well-known and cracked concrete is more susceptible to permeation of these contaminants. Consequently, research is attempting to develop concrete that can self-heal cracks, potentially reducing costs of repair and maintenance work on infrastructure projects dramatically. The research described in this paper was carried out to demonstrate the use of microbiologically-induced calcite-precipitation as a means of autonomic self-healing of concrete in a full-scale site trial. The paper describes microbiology and concrete technology investigations carried out to select an appropriate combination of spores and nutrients, and to devise a method for encapsulating these safely within the concrete. It is demonstrated that for the encapsulation method used and the agents chosen it is possible to produce self-healing concrete with similar ealy-age and mechanical properties to that of normal concrete. This self-healing concrete was then used in a reinforced concrete wall, and the initial findings are described.

**Keywords:** Self-healing, Bacteria, Lightweight aggregates, Encapsulation

**Dr Kevin Paine** is a Reader in Civil Engineering and Deputy Director of the BRE Centre for Innovative Construction Materials at the University of Bath. His research focuses on low carbon, smart and nanotechnology-enhanced concretes.

**Mr Mohamed Alazhari** is a PhD candidate in the BRE Centre for Innovative Construction Materials at the University of Bath working on bacteria-based repair of concrete.

**Dr Trupti Sharma** is a Research Associate in the Department of Biology and Biochemistry at the University of Bath. Her research focuses on extremophiles and microbiologically induced calcium carbonate precipitation.

**Dr Richard Cooper** is a Reader in the Department of Biology and Biochemistry at the University of Bath. His research focuses on plant-microorganism interactions.

**Professor Andrew Heath** is Professor of Geomaterials at the University of Bath. His research focusses on low impact earth and concrete construction materials.

# INTRODUCTION

The effect of water-borne contaminants on the durability of concrete is was well-known and cracked concrete is more susceptible to permeation of these contaminants. Consequently, research is attempting to develop concrete that can self-heal cracks; potentially reducing costs of repair and maintenance work on infrastructure projects dramatically. The Materials for Life (M4L) project, a partnership between Cardiff University, University of Bath and the University of Cambridge is aiming to develop self-healing concretes to reduce the repair and maintenance requirements of concrete structures. The project combines research on a number of multi-scale techniques to develop autonomic self-healing within concrete [1, 2].

One approach to autonomic self-healing is the utilization of microbiologically-induced calcite-precipitation. This approach utilises the metabolic activity of bacteria and biomineral precursors embedded within the material to form an inorganic material, usually calcium carbonate ($CaCO_3$), in the form of calcite, as the healing compound.

There are two key pathways for delivering the healing process: (i) enzymatic hydrolysis of urea [3] and aerobic metabolic conversion of calcium salts [4]. The aerobic metabolic conversion pathway was used in this research and the healing occurs because the bacteria act as a catalyst for the conversion of an organic calcium salt (precursor), for example calcium acetate, to calcite under favourable conditions: the presence of water, oxygen and nutrients. The by-products of the conversion of calcium acetate to calcite are carbon dioxide and water which are compatible with concrete (Equation 1). Furthermore, a weak carbonic acid may form that will lead to carbonation of calcium hydroxide within the concrete leading to a form of enhanced autogenous healing. Figure 1 shows the healing of a 0.4 mm crack by impregnation of *Bacillus cohnii*, calcium acetate and yeast extract [5].

$$CaC_4H_6O_4 + 4O_2 \rightarrow CaCO_3 + 3CO_2 + 3H_2O \qquad \text{Eq.1}$$


Figure 1 Precipitation of calcite in a crack as a result of bacterial conversion of calcium acetate [5]

Consequently it is necessary that any ingredient used does not affect the early-age and mechanical properties of the concrete. Once a crack appears the ingredients must become active and form calcite rapidly within the crack without adversely affecting undamaged concrete and steel reinforcement. This restricts the choice of ingredients that may be used.

Furthermore, it is necessary, in order to ensure survival, that the bacteria are added in the form of spores. Consequently upon cracking it is necessary for the spores to germinate.

Laboratory-based experiments have demonstrated the viability of this method for self-healing of concrete in ideal conditions and in controlled environments. However, the implementation of bacteria-based self-healing concrete on a larger scale has not been attempted in Europe and it present a number of challenges: (i) the selection of sufficiently cheap and available microbial self-healing agents, (ii) a means of encapsulating the self-healing agents within the concrete to ensure they survive and do not adversely affect the concrete production process, and (iii) ensuring that the early-age and mechanical properties of the concrete are not significantly affected by the inclusion of the self-healing agents. Research towards meeting these challenges is discussed in this short paper.

## COMPOSITION OF MEDIUM

To ensure complete self-healing from germination to healing to sporulation, Sharma et al [6] have suggested that it is necessary to use a complex healing agent consisting of carbon and nitrogen sources, sporulation and germination aids, proteins and buffer solutions. Indeed, i*n vitro* tests by Sharma et al [5] at the University of Bath have shown that spores can be germinated to cells within approximately 3 hours in a complex medium that includes germination aids (isonine and alanine) and the presence of sodium ions to carry them across the spore wall.

However, further initial microbiology tests, by the authors, have demonstrated that *Bacillus pseudofirmus* spores may germinate and grow adequately in the presence of only yeast extract and that complete germination occurs within 24 hours. Although slower than that with the more complex agent it is appropriate for the application of self-healing concrete.

Tests at the University of Bath have further demonstrated that neither calcium acetate nor yeast extract would affect the setting of the cement or hardening of the concrete provided fewer than 10% of the nutrients were released into the concrete during mixing [7].

For the purposes of further research the composition of the nutrient solution was 300 g/l of calcium acetate and 30 g/l of yeast extract. Both values are close to the maximum solubility of these ingredients in water.

## ENCAPSULATION

Wiktor and Jonkers [4] have previously demonstrated the capability of encapsulating calcium lactate (80g/l), spores of *B. alkalinitrilicus*, yeast extract (1 g/l) in expanded lightweight clay aggregates (Liapor). For the purposes of the trial the nutrients were encapsulated in perlite, a lightweight aggregate commonly used in microbiological applications as a plant growth media. The properties of perlite are given in Table 1. Using a different approach to Wiktor and Jonkers [4], the nutrients (calcium acetate and yeast extract) was encapsulated separately from the bacteria spores (*B. pseudofirmus*) to minimise the potential for germination before a crack is formed.

The perlite were impregnated with the nutrients and bacteria by soaking the perlite in the appropriate volume of solution until all solution was absorbed. . The composition of the perlite is shown in Table 2.

Table 1 Physical properties of uncoated and coated perlite

| | UNCOATED PERLITE | COATED PERLITE |
|---|---|---|
| Apparent density, kg/m$^3$ | 292 | 1050 |
| Loose bulk density, kg/m$^3$ | 122 | 476 |
| water absorption | 146.3 | 15.7 |

Table 2 Composition of uncoated perlite, per g of perlite, after "impregnation" with bacterial agents

| | CALCIUM ACETATE, g | YEAST EXTRACT, g | SPORES (*B. pseudofirmus*) |
|---|---|---|---|
| Perlite with nutrients | 0.3 | 0.03 | - |
| Perlite with spores | - | - | approx. 4.1 x $10^9$ |

To verify the suitability of perlite in terms of its ability to prevent the nutrients from being released into the concrete, initial tests were carried out in which safranin, a dye commonly used to stain microbial cells, was added to the perlite. These stained perlite were then added to mortar. On inspection of cut faces from the hardened faces it was clear that there was substantial leakage of the dye from the perlite. Further trials considered a number of coatings that could be used to prevent leakage of the dye. It was found that a double layer of protection: consisting of a layer of sodium silicate and a layer of Portland fly ash cement prevented leakage of the dye. The sodium silicate coating was applied by soaking the impregnated perlite in sodium silicate solution until the perlite was completely wet. The perlite was then dried at 20°C for 24 hours. A second layer of sodium silicate was then applied to the perlite, as above, followed by the application of dry cement to the wet sodium silicate surface. The perlite was then cured in water for 48 hours. The properties of the coated perlite (in the absence of bacteria and nutrients) are given in Table 1. Based on comparison of the density of the coated and uncoated perlite it was estimated that the mass of the coating was approximately 70% of the overall mass of the coated perlite.

Tests were also carried out to ensure that the viability of spores (ability to germinate) was retained after impregnation in the perlite. Experiments were conducted under sterile/aseptic conditions by crushing perlite impregnated with *B. pseudofirmus* spores at 0, 3, 15 and 30 days. 1g of each sample was obtained at each time period and serially diluted (10-1-10-9) in test tubes. These were then vortexed for two minutes to provide homogeneity. The viability of spores in terms of colony forming units (CFU) was then determined. The results indicated that whilst the number of viable spores may have decreased steadily over a period of 30 days, from approximately 10 x $10^9$ to 2 x $10^9$ (Figure 2), this reduction in viable spores was only around 0.01% of the initial number.

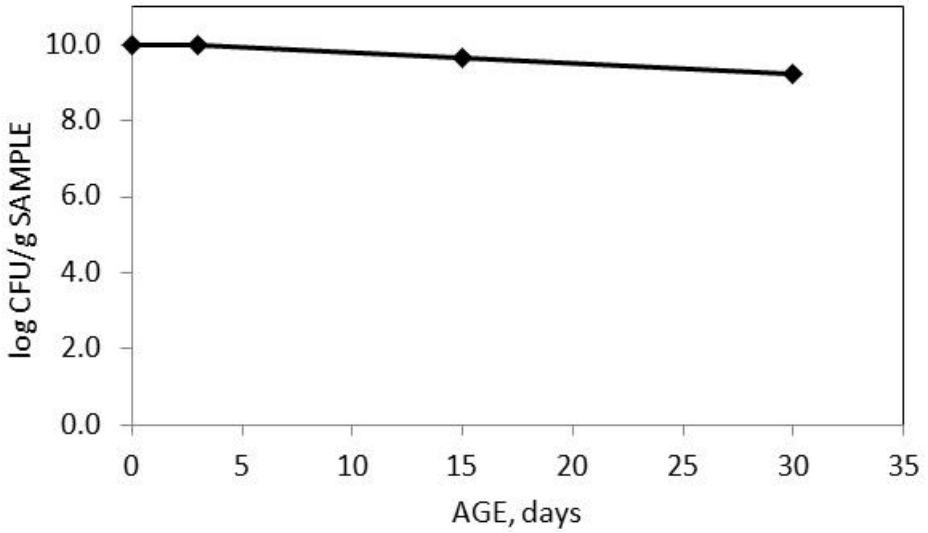


Figure 2 Viability of spores after impregnation in perlite

## PRELIMINARY LABORATORY CONCRETES

Two preliminary concrete mixes were prepared in the laboratories to assess the effect of the coated perlite (containing nutrients) on the properties of the concrete. It was important to ensure that the nutrients were well encapsulated so that they did not affect the early-age or mechanical properties of the concrete, and that the addition of a lightweight aggregate did not adversely influence the compressive strength of the concrete. The mix proportions for both preliminary concretes are provided in Table 3.

The mixes were proportioned to achieve a cube strength of 40 MPa at 28 days. A w/c ratio of 0.40 was used to account for the use of the weak perlite aggregates. The sand (0/4) content of normally designed concrete mixes (without self-healing agents) was reduced to permit the use of perlite as a replacement, despite the fact that the perlite was coated with some unhydrated cement. Superplasticizer was used to obtain a target slump of 100 to 150mm. In terms of the addition of self-healing agents, Mix M1 contained 1.9% calcium acetate by mass of cement and 0.05% yeast extract by mass of cement. M2 contained 3.8% calcium acetate by mass of cement and 0.1% yeast extract by mass of cement. No spores were added to the perlite for these preliminary trials as the intention was to assess the effects on early-age properties and not to assess self-healing. Coated perlite containing spores were used in the full-scale trial described later.

These mixes both gave the necessary degree of consistence and from visual inspection of the fresh concrete there was no damage of the perlite coating. Perlite is a distinct white colour and is clearly visible in concrete when used without a coating. Both concretes set and hardened normally and could be demoulded at one day. The mean seven day strengths were 33.4 MPa and 27.4 MPa for concretes M1 and M2, respectively. The 28-day water-saturated density of M1 and M2 was 2253 kg/m$^3$ and 2240 kg/m$^3$, respectively..

Table 3 Mix designs for preliminary laboratory concretes

| MIX | NUTRIENT CONTENT (% by mass of cement) | CONSTITUENTS, kg/m$^3$ | | | | | |
|---|---|---|---|---|---|---|---|
| | | Water | Cement (CEM II/B-V 32.5N) | 0/4 | 4/10 | Coated perlite (with nutrients) | Coated perlite (for spores) |
| M1 | 2.6 | 185 | 455 | 655 | 930 | 70 | 25 |
| M2 | 5.3 | 175 | 440 | 505 | 895 | 140 | 45 |

Superplasticizer (Glenium® ACE 456) used at a dosage of 1.2 litres per 100 kg of cement in both mixes

After cracking, visual inspection showed uniform distribution of the perlite and it was clear that cracking of the concrete resulted in splitting of the perlite (Figure 3) – thus in practice cracking would lead to release of the self-healing agents This was anticipated and desired as the perlite aggregates were expected to have a lower strength than the paste or conventional aggregates, ensuring cracking would allow access to the self-healing agents.

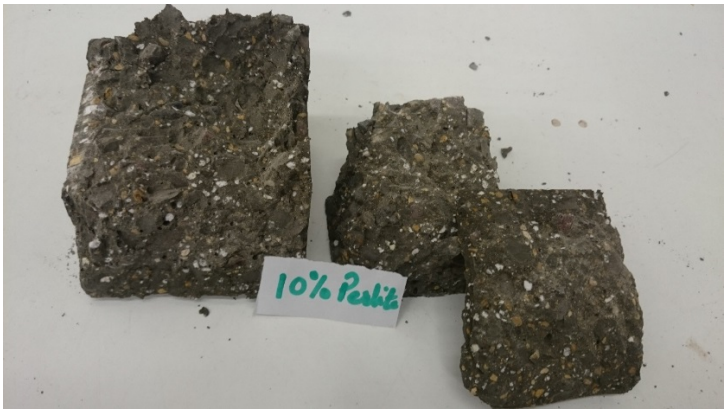


Figure3 Broken cube showing good distribution of perlite (the white spots) in concrete M2

## FULL-SCALE TRIAL

### Overview

For the full-scale trial, five concrete panels were cast on the same day as part of a series of work with Cardiff University and the University of Cambridge under M4L (Figure 4). There was one control panel with no self-healing system, and the other four had different forms of self-healing systems installed, one of which contained the bacterial self-healing mix M2 described above. The trial was carried out at the A465 Heads of the Valleys section 2 project; a £200M contract to upgrade an 8.1km section of the A465 road between Gilwern to Brynmawr in South Wales, UK, from single to dual carriageway. Costain Group Plc was the lead contractor for the project. The project office compound was used for construction of the trial elements.

Figure 4 The five panels cast. The bacteria-based self-healing concrete panel is the third from the left.

The panels were designed to crack at 500 mm above the base slab upon loading by including 16 mm diameter starter bars on the front face up to this point, before changing to an A393 mesh (10 mm diameter bars) to create a weak section in the panel. In addition a capillary network created by a 2D network of 4 mm diameter channels through which healing agents could be pumped under pressure was embedded in the concrete to permit later addition of further nutrients, bacteria or oxygen as necessary (Figure 5). To enable the healing agents to migrate to areas of damage the network was designed for and placed in the zone most susceptible to cracking. The network was created using polypropylene tubes which were removed from the concrete once it had hardened. The network channels were joined using 3D printed joints made from polylactic acid [8].

Figure 5 Embedded capillary network installed prior to casting of the concrete

Because of the size of the panel, bacteria-based self-healing concrete was only added to the panel at the weak section where cracking would occur (Figure 6). As previously stated the concrete mix used was M2 as given in Table 3. The only difference was that spores were also used. Coated perlite impregnated with spores were used at a content of 45 kg/m$^3$. This equated to approximately 4 x 10$^{13}$ spores per m$^3$ of concrete. The other parts of the panel were made of concrete supplied by a ready-mixed concrete producer of design concrete strength C40/50.

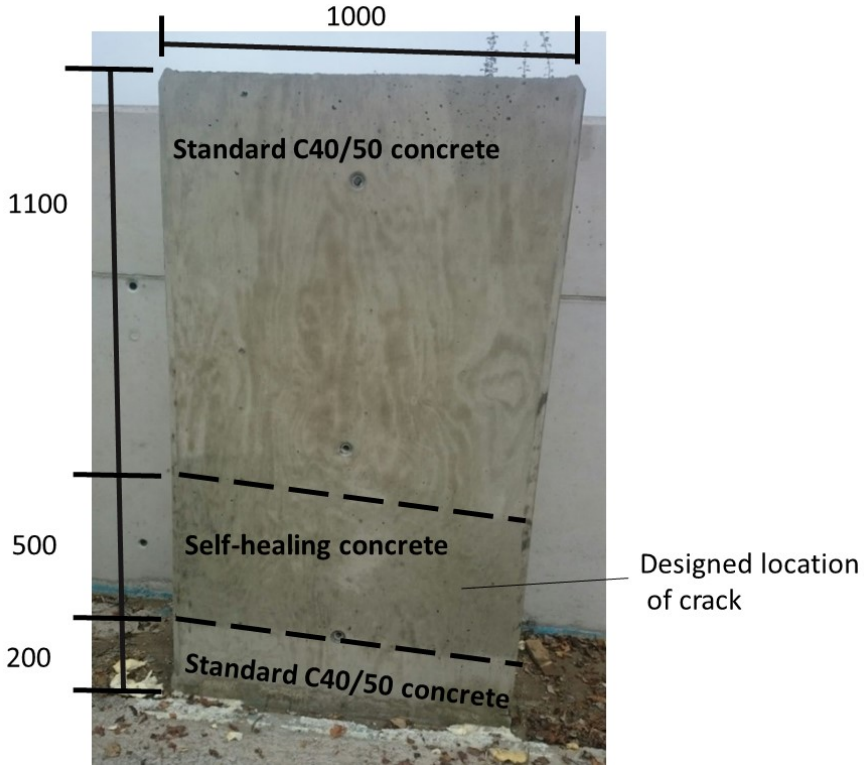


Figure 6 Panel containing bacteria-based self-healing concrete (all dimensions in mm)

The self-healing concrete was made in a 90 litre tilting drum mixer. Due to the type of mixer used it was only possible to add ingredients whilst the drum was revolving. This meant that the constituents were “dry” mixed for longer than anticipated, and much longer than in the preliminary trial.

To monitor crack healing, the panel was cracked at 36 days after casting by applying load through a threaded bar running through the centre of the width of each panel to a reaction wall designed to act against the force produced by the jack. The bars were placed 1.5m above the base slab into each panel and the reaction wall. The procedure is described in full in [8]. Throughout the site trial the crack width, deflections, strains, permeability and applied loading on the panels were all monitored. This was achieved using a combination of DEMEC pips, optical microscopes, linear variable displacement transducers, load cells, on-site permeability apparatus and a digital image correlation system [8].

## RESULTS

The panel was demoulded at two days (Figure 5), which was consistent with the other four panels cast. Although the extended period of mixing had led to damage of the coated perlite through attrition with the coarse aggregates –the perlite being clearly visible due to its white colour in the fresh concrete, there was no noticeable delay in setting or early-age hardening. This suggests that even though the perlite lost its coating during mixing there was insignificant release of nutrients to have an effect on cement hydration. Cubes tested at 7 and 28 days gave mean strengths of 29.1 and 35.1 MPa, respectively. Whilst this was weaker than anticipated it can be perhaps explained by some difficulties with compacting the concrete cubes on site.

The panel was cracked at 36 days and the crack ran through the centre of the self-healing concrete section as designed. Figure 7 shows the initial cracks that occurred upon loading and the residual cracks that remained after unloading. These residual cracks were approximately 0.1 mm in width.

At the time of writing, optical microscope images show a degree of crack healing. However further investigation is required to establish whether this observed crack-healing can be attributed to the incorporation of bacteria, or whether autogenous healing has occurred.

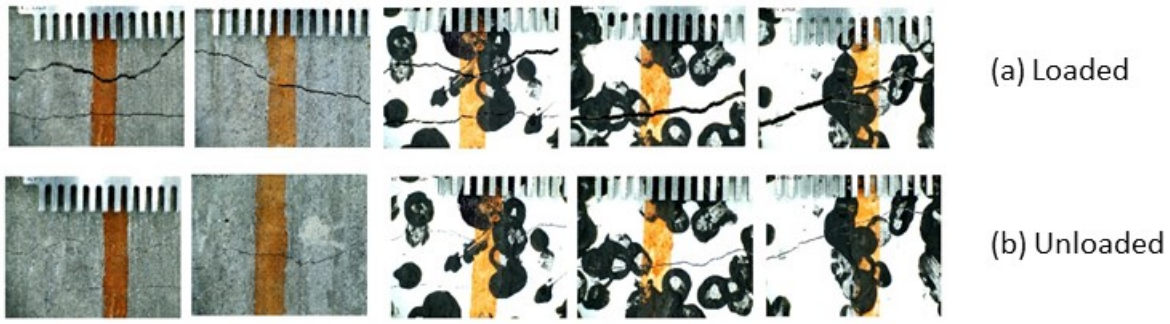


Figure 7 Cracking of the bacteria-based panel: (a) cracks immediately upon loading, and (b) residual cracks after unloading.

## CONCLUSIONS

The following conclusions can be made from the work presented.

1. A combination of bacteria-based self-healing agents have been developed consisting of ingredients that have limited effect on setting and hardening of concrete, but which permit rapid germination and growth of bacterial spores.

2. A coating has been developed that prevents the release of self-healing agents into the concrete prior to cracking.

3. Self-healing concretes cast at full-scale have successfully demonstrated that mechanical properties can be maintained and that setting and hardening is unaffected by the addition of encapsulated self-healing agents.

## ACKNOWLEDGEMENTS

The support of the EPSRC for their funding of the Materials for Life (M4L) project (EP/K026631/1) and Costain Group PLC for providing the site and conventional materials for the trial are gratefully acknowledged. The Libyan Government are acknowledged for the financial support to Mr Alazhari. M4L Colleagues at Cardiff University and University of Cambridge are thanked for their help; particularly Oliver Teall who coordinated the site trials. Fernanda Monsó Salgado Peres is thanked for her assistance with developing the encapsulation techniques.

## REFERENCES

1. LARK, R.J., AL-TABBAA, A., PAINE, K. Biomimetic multi-scale damage immunity for construction materials: M4L Project overview. 4th International Conference on Self-Healing Materials, Ghent, Belgium, June 2013.

2. DAVIES, R., PILEGIS, M., KANELLOPOULOS, A., SHARMA, T. Materials for Life (M4L): Combining multi-scale healing techniques in cementitious materials. 5th International Conference on Self-Healing Materials, Durham, USA, June 2015.

3. VAN TITTELBOOM, K., DE BELIE, N., DE MUYNCK, W., VERSTRAETE, W. Use of bacteria to repair cracks in concrete. Cement and Concrete Research, Vol. 40, 2010, pp157–166

4. WIKTOR, V., JONKERS, H.M. Quantification of crack-healing in novel bacteria-based self-healing concrete. Cement and Concrete Composites, Vol. 33, 2011, pp763–770

5. SHARMA, T., COOPER, R., HEATH, A., PAINE, K. Microbiologically induced calcium carbonate precipitation by extremophilic *Bacillus* species: A potential application as microbial agents for the development of self-healing concrete. BACELL 2015, Amsterdam, The Netherlands, April 2015

6. SHARMA, T., ALAZHARI, M., COOPER, R., HEATH, A., PAINE, K. The Requirements for autonomic microbiologically-induced calcite-precipitation in concrete. 5th International Conference on Self-Healing Materials, Durham, USA, June 2015.

7. PAINE, K. Bacteria-based self-healing concrete: Effects of environment, exposure and crack size. RILEM Conference on microorganism-cementitious material interactions. Delft, The Netherlands, June 2016

8. TEALL, O., DAVIES, R., PILEGIS, M., KANELLOPOULOS, A., SHARMA, T., PAINE, K., JEFFERSON, A., LARK, R., GARDNER, D., AL-TABBAA, A. Self-healing concrete full-scale site trials. 11th FIB International PhD Symposium in Civil Engineering, Tokyo, Japan, August 2016

# IMPROVEMENT ON SELF-HEALING ABILITY OF FLY ASH-CEMENT SYSTEMS BY INTERNAL CURING

**Liu Yunpeng** **Wang Fazhou**

**Nie Shuai** **Hu Shuguang**

Wuhan University of Technology

**Ding Lujing**

China Construction Ready Mixed Concrete Tianjin Co. Ltd.

China

**ABSTRACT.** The internal curing method is employed to provide water for pozzolanic reaction which contributes to self-healing ability of concrete. The effect of w/c ratio, fly ash content and internal curing agent on the self-curing ability was studied. Results show that the 58d compressive strength recovery rate of cement paste with internal curing was higher than that without internal curing, especially with low w/c ratio of 0.24. The increase of fly ash content is a benefit to self-healing ability improvement when with enough water. However, the strength recovery rate of cement paste with w/c ratio of 0.4 and fly ash content of 40% was sharply decreased with SAP addition, which could be contributed to increased defects introduced. BSE image also indicated that fly ash system with high SAP addition has reacted to a greater degree. The addition of activity agent improved the strength of cement paste, but decreased the strength recovery rate.

**Keywords:** Self-healing; Fly-ash-cement system; Internal curing; Cracks.

**Dr Liu Yunpeng** is from State Key Laboratory of Silicate Materials for Architecture at Wuhan University of Technology.

**Prof Wang Fazhou** is the vice director of State Key Laboratory of Silicate Materials for Architecture at Wuhan University of Technology.

**Mrs Ding Lujing** is an engineer from China Construction Ready Mixed Concrete Tianjin Co.

**Dr Nie Shuai** is an Ph.D candidate of Wuhan University of Technology.

**Prof Hu Shuguang** is a renowned researcher and practitioner in the field of concrete technology.

## INTRODUCTION

Cracks can be caused by external loading, shrinkage, time-dependent effect et al, which are unavoidable defects in the concrete structure. Cracks facilitate the ingress of aggressive and harmful substances into concrete and reduce concrete durability [1]. Research on cracks sealing has attracted sound attentions [2].

For the self-healing of cementitious materials, the essence is to provide necessary products which can then fill in the cracks when damage happens [3]. With respect to how to endow composite materials with self-healing property and improve the self-healing efficiency, many experimental studies and explorations have been conducted, which include using hollow fibres to store functional components which will be embedded in the cement matrix [4], using microencapsulation approach incorporating self-healing agent [5]; introduction of repair technique into concrete [6], incorporating functional materials like shaping memory alloy or polymers[7,8], using expansive agents and mineral admixtures [9] etc.

In fact, concrete itself has the ability of self-healing, which has been studied over a decade [10]. Two major hypotheses regarding the reactions in self-healing mechanisms: the hydration of anhydrous cement available in the microstructure of hardened concrete and the precipitation of calcium carbonate $CaCO_3$. Fly ash is a pozzolanic material that reacts with $Ca(OH)_2$ from cement hydration and produces C–S–H gel.[11]. The improvement on the self-healing ability by pozzolanic reaction between CH and fly ash has been reported. Of which, the self-healing ability of cement paste consisted of fly ash has attracted sound attention due to its advantages including good compatibility of the generated healing products with the cement matrix.

From the literature view, in all cases, additional water is essential for the self-healing mechanism. The pozzolanic reaction and cement late hydration contribute to the self-healing performance. Former research have shown that the pozzolanic reaction and self-healing performance with low w/c ratio were worse than that with high w/c ratio [11, 12].

On the other hand, pozzolanic reaction is a late-stage reaction; much water in the early stage is of less use for improvement on self-healing ability. For aboveground structures, the availability of water is limited. Though enough water is needed to improve the self-healing performance, the increase of w/c ratio will also increase the porosity and reduce the concrete strength.

Internal curing is a popular method to reduce the concrete self-shrinkage by the increase of internal humidity due to the release water of internal curing agents. The water release will last a long period. Our former research [13] has shown that the internal curing could retard the humidity decrease speed. So the introduce of internal curing should be benefit to the self-healing performance.

In this paper, the effect of pozzolanic reaction on self-healing performance including mechanical performance (different w/c ratio, different fly ash content) were investigated. The effect of internal curing on the performance improvement was also studied. XRD and TG-DTG methods were employed to evaluate the hydration degree of cement and fly ash to evaluate the self-healing effect. Results hopefully shed some lights on the improvement on concrete self-healing.

## EXPERIMENTAL METHODS

### Raw Materials

Ordinary Portland Cement (OPC, P I 52.5) and fly ash are used in this study. The physical and chemical properties of OPC and the fly ash are shown in Tables 1 and 2, respectively.

Table 1 Physical properties of cement

| SETTING TIME (min) | | FLEXURAL STRENGTH (MPa) | | COMPRESSIVE STRENGTH (MPa) | | DENSITY ($g/cm^3$) | IGNITION LOSS (%) | SURFACE AREA ($m^2/kg$) |
|---|---|---|---|---|---|---|---|---|
| Initial setting | Final Setting | 3d | 28d | 3d | 28d | | | |
| 130 | 185 | 6.6 | 9.4 | 34.3 | 62.6 | 3.14 | 2.6 | 350 |

Table 2 Chemical composition from XRF analysis (mass)

| | CaO | $SiO_2$ | $Al_2O_3$ | $Fe_2O_3$ | MgO | $SO_3$ | $Na_2O$ | $K_2O$ | IGNITION LOSS (%) |
|---|---|---|---|---|---|---|---|---|---|
| OPC | 63.01 | 21.7 | 4.76 | 3.57 | 2.12 | 1.98 | 0.14 | 0.67 | 1.17 |
| Fly ash | 3.16 | 51.31 | 31.95 | 4.14 | 0.66 | 0.78 | 0.33 | 1.66 | 3.72 |

Superabsorbent polymers which were a copolymer of acrylamide and sodium acrylate (particle size 100.0 ± 21.5 μm) were used as internal curing agent. Its water absorption curve was shown in Figure 1. Dry SAP particles were added to the cement and were first dry mixed to ensure a homogenous dispersion in the cement.

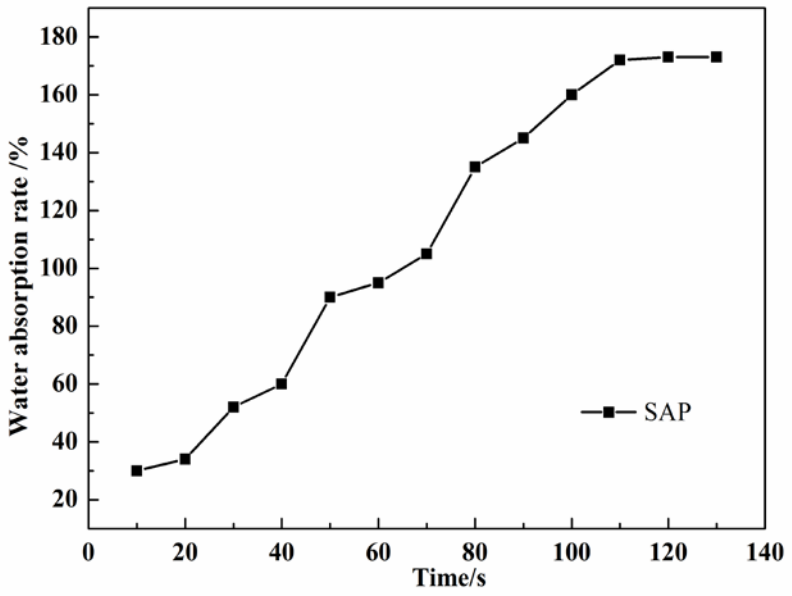


Figure 1 SAP water absorption

(3) Superplasticizer (SP) was polycarboxylic type high performance water reducer with 20.0% solid content and 26.6% water reducing ratio.

Table 3 Mix proportion of cement paste

| SAMPLE | W/C RATIO | FLY ASH CONTENT/% | SP CONTENT/% | INTERNAL CURING AGENT | |
|---|---|---|---|---|---|
| | | | | content/% | Water content/% |
| 0.24-0 | 0.24 | 0 | 1.4 | 0 | 0 |
| 0.24-2 | | 20 | | | |
| 0.24-3 | | 30 | | | |
| 0.24-4 | | 40 | | | |
| 0.30-0 | 0.3 | 0 | 0.9 | | |
| 0.30-2 | | 20 | | | |
| 0.30-3 | | 30 | | | |
| 0.30-4 | | 40 | | | |
| 0.40-0 | 0.4 | 0 | 0.3 | | |
| 0.40-2 | | 20 | | | |
| 0.40-3 | | 30 | | | |
| 0.40-4 | | 40 | | | |
| 0.24-0-S | 0.24 | 0 | 1.4 | 0.2 | 4.32 |
| 0.24-2-S | | 20 | | | |
| 0.24-3-S | | 30 | | | |
| 0.24-4-S | | 40 | | | |
| 0.30-0-S | 0.3 | 0 | 0.9 | | 5.4 |
| 0.30-2-S | | 20 | | | |
| 0.30-3-S | | 30 | | | |
| 0.30-4-S | | 40 | | | |
| 0.40-0-S | 0.4 | 0 | 0.3 | | 2 |
| 0.40-2-S | | 20 | | | |
| 0.40-3-S | | 30 | | | |
| 0.40-4-S | | 40 | | | |

**Experimental Methods**

Mercury intrusion porosimetry: At the required age, the samples were broken into 2.5–5.0 mm pieces by hammer, soaked in acetone to stop the hydration reaction, and further dried at 105°C. A part of each of the samples was kept in a desiccator for mercury intrusion testing. The remaining material was ground in a disc mill until particles smaller than 75 μm were created.

Self-healing behaviour investigation: Two groups cement mortars with dimension size of 160 mm × 40 mm × 40 mm was prepared. It was demoulded after 24h curing under standard curing. Then, it was continued to be curing to 28d and its mechanical properties were tested. Of which, one group mortars was pre-loaded with 30% of 28d compressive strength. The samples were continued to be cured under the standard curing to 58d.

Then, the results were compared with the samples cured under standard condition without pre-loaded. The compressive recovery rate was calculated according to Eq. 1.

$$f' = \frac{Rc'}{Rc} \times 100\% \qquad \text{(Eq.1)}$$

Of which: $f'$ ——Compressive strength recovery rate;

$Rc'$ ——58d compressive strength with 30% pre-loading (MPa);

$Rc$ ——58d compressive strength of controlled sample (MPa).

As for the cracks and/or the porosity formation, it is difficult to precisely measure the position and width of cracks in concrete because a multitude of factors influence the crack formation. Therefore, in this study, the pore modification measured by mercury intrusion porosimetry was used to analyse the cracks and the pore formation.

The amount of cracks was not measured directly but was implied by the amount of total porosity[11].The cement paste structure was moved to the large pore, the average pore diameter increased and small pores decreased (Figure 2).

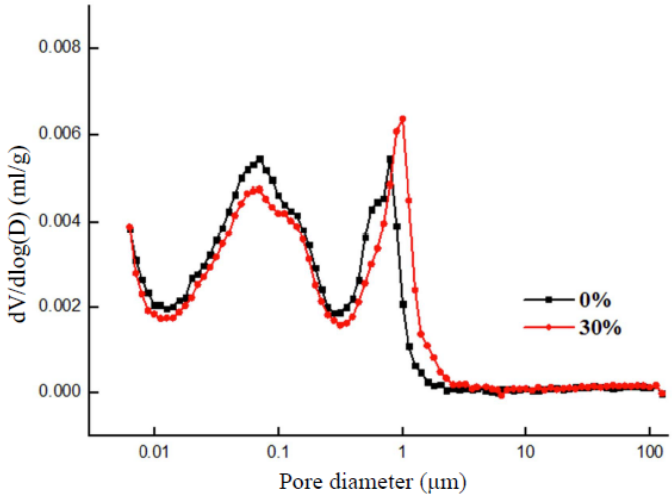


Figure 2 Effect of loading on pore structure of cement paste

## RESUTLS AND DISCUSSIONS

### Effect of w/c Ratio on the Self-Healing Performance

As expected in Figure 3, compressive strength recovery rate of specimens decreases with increasing w/c ratio (from 0.24 to 0.40). This is because the cement paste with high w/c ratio will have more micro-cracks under the pre-loading. The self-curing ability of cement paste is limited which could not contribute to enough strength recovery. However, with the addition of fly ash, it's interesting to note that the compressive strength recovery rate increased with w/c ratio. This is because the pozzolanic reaction of fly ash improved the self-curing ability. The higher w/c ratio created more effective environment for fly-ash hydration. With the addition of SAP, the 58d compressive strength recovery rate has been higher than that of controlled cement paste. Especially under the low w/c ratio (0.24), the self-curing performance has been significantly improved.

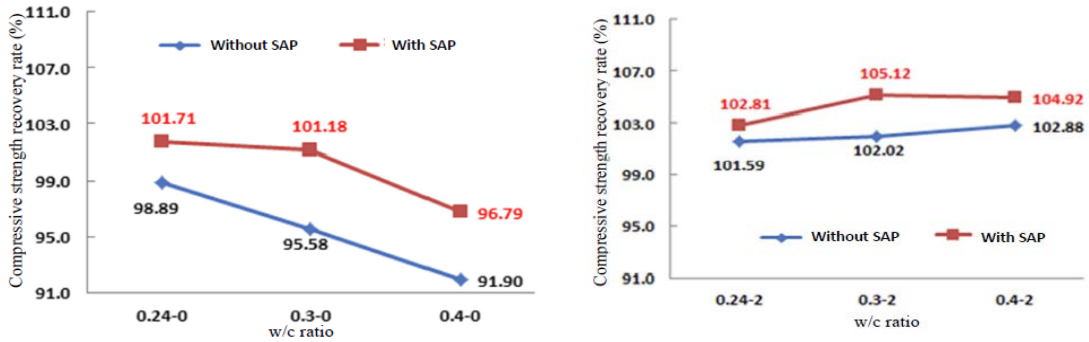


FA=0% FA=20%

Figure 3 Effect of w/c ratio on compressive strength recovery rate of cement paste (FA=0%)
Note: "0" indicated that pre-loading of 0; 30% indicated that pre-loading of 30%; "S"-indicated that cement paste with SAP agent

## Effect of Fly Ash Content on the Self-Healing Performance

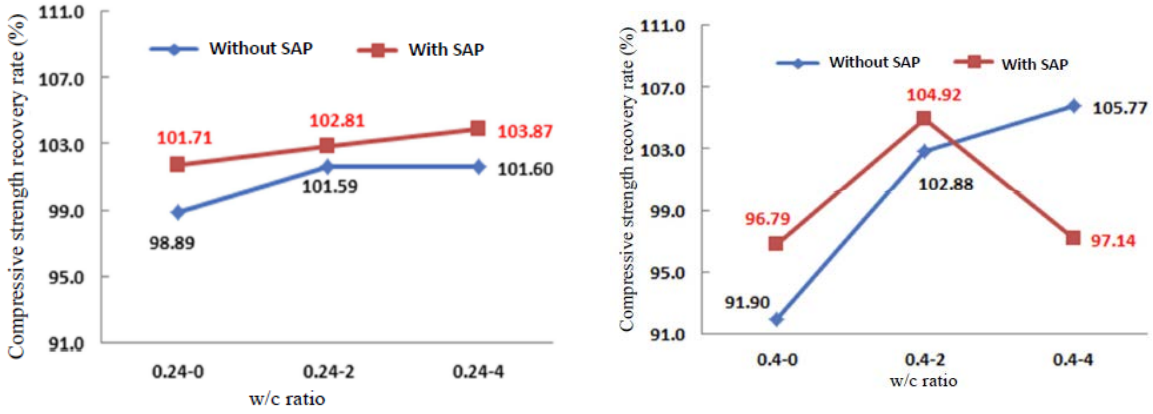


(a)W/C=0.24 (b)W/C=0. 40

Figure 4 Effect of fly ash content on compressive strength recovery rate of cement paste

Note: 0.24, 0.40-indicated w/C ratio of 0.24 and 0.40 respectively; 0,2,4-indicated 0%,20%,40% content fly ash, respectively ; "S"-indicated that cement paste with SAP agent

Figure 4(a) showed the effect of fly ash content on 56day compressive strength recovery rate with the w/c ratio of 0.24. As can be seen, the compressive strength recovery rate increased with the fly ash content which could be attributed to its pozzolanic reaction effect. The strength recovery rate of controlled cement paste (without SAP) is 98.89%. It was over 100% with the fly ash addition. However, the recovery rate increased slowly when the fly ash content increased to 40%. This is because the low w/c ratio could not provide enough for pozzolanic effect of fly ash.

Figure 4(b) showed the effect of fly ash content on 56day compressive strength recovery rate with the w/c ratio of 0.40. This trend was similar with that of Figure 4(a). But the trend that recovery rate increased with fly ash content under high w/c ratio (0.40) was more obvious than that of 0.24. This is because that high w/c ratio provide enough water for fly ash pozzolanic reaction. What should be noted is that the recovery rate of cement paste with fly ash content of

40% was sharply decreased with the SAP addition. This is because cement paste with high w/c ratio and high fly ash content has increased defects (Figure 5). The pores with 0.01~0.1 μm decreased and 0.1~1 μm pores sharply increased. The average pore diameter and pore rate increased. Moreover, the addition of SAP introduce more water which increased the cement pastes defects, which deceased the self-curing performance of cement pastes.

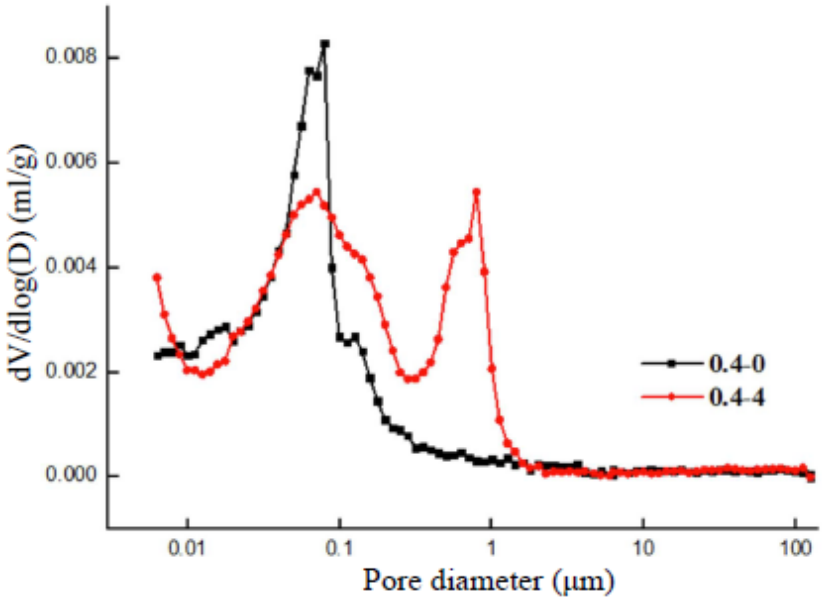


Figure 5 Effect of fly ash content on cement paste pore structure

**Effect of internal curing on self-healing performance**

Table 4 Compressive strength increase rate of cement paste from 28d to 60d

| FA content / w/c ratio | 20% | 30% | 40% | 50% |
|---|---|---|---|---|
| 0.24 | 15.38 | 13.71 | 3.61 | 2.94 |
| 0.3 | 6.49 | 12.05 | 23.14 | 16.53 |
| 0.4 | 9.04 | 14.54 | 23.05 | 14.41 |
| S-0.24 | 16.25 | 14.05 | 13.20 | 7.57 |
| S-0.3 | 22.09 | 22.27 | 23.95 | 25.90 |
| S-0.4 | 10.63 | 18.14 | 27.67 | 32.49 |

Note：“S-” Cement paste with SAP agent

As can be seen in Table 4, the addition of SAP increased compressive strength increase rate of cement paste from 28d to 60d. Though its addition could introduce defects and decrease compressive strength, it also provide enough water to late stage cement hydration and fly-ash pozzolanic reaction, increase hydration degree of cement and fly ash, thus increased late stage compressive strength.

**Microstructure of harden cement paste**

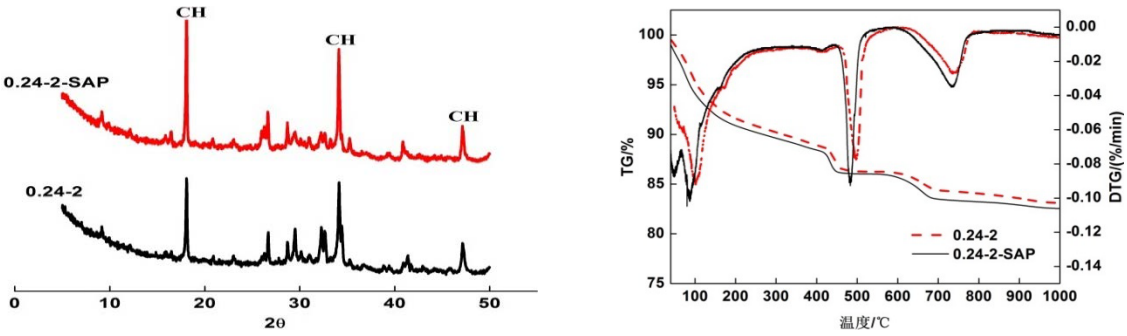


XRD results TG-DSC results

Figure 6 XRD and TG results of cement paste with and without SAP

Figure 6 showed the effect of SAP on the cement hydrate products. As can be seen, CH peaks in both the XRD and TG results were increased with the addition of SAP. This could be attributed to the increased CH and fly ash hydration degree by increased humidity. This also could explain the improved self-healing performance.

Figure 7 showed the microstructure of fly ash surface in the cement paste with the curing age of 28d and 60d. Of which figures c and d is with the SAP internal curing effect. As can be seen, fly ash surface with 28d age show a slight erosion, which means it reaction with CH; the erosion was strengthened when the curing age increased to 60d, which shows a more strengthened ability. Besides, with the addition of SAP, the erosion rate of fly ash is obviously than that without SAP, which explains that the self-curing ability is improved with the addition of SAP.

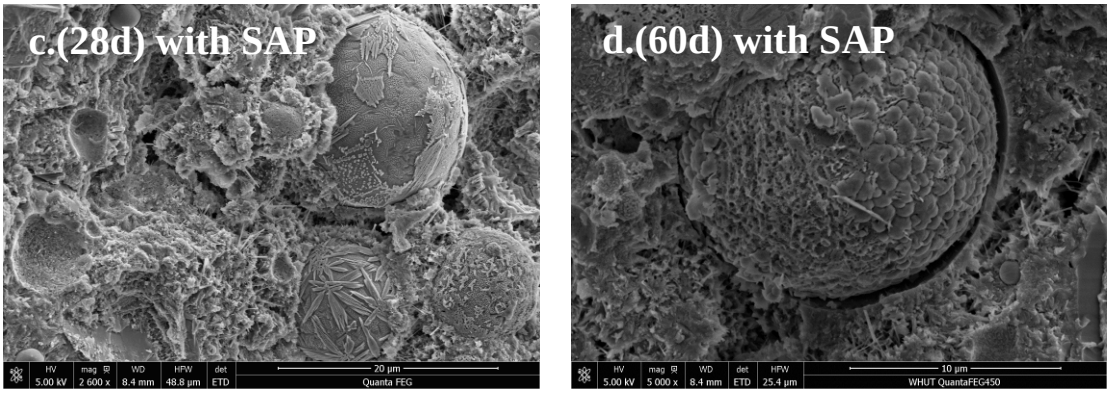


Figure 7 Fly ash surface in cement paste

Figure 8 showed the BSE image of cement paste with SAP addition. Compared with the cement paste (w/c of 0.3, fly ash content of 40%, with addition of SAP). As can be seen, with the microstructure of cement hydration of 28d, the cracks has been reduced, which indicated that the fly ash promoted the hydration and cure the cracks. The results mean that with the addition of SAP, the standard curing improves the strength and strength recovery rate, which improved the self-curing properties.

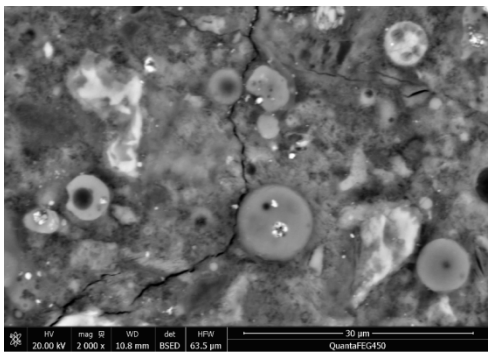


(a) 28d

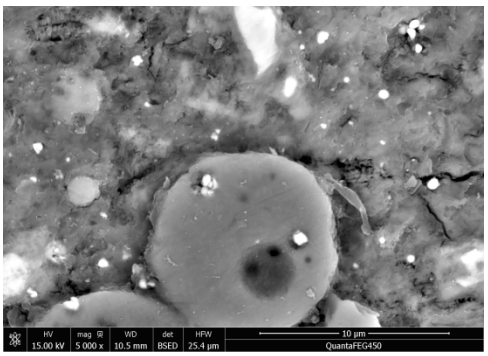


(b) 30d curing after pre-loading 30%

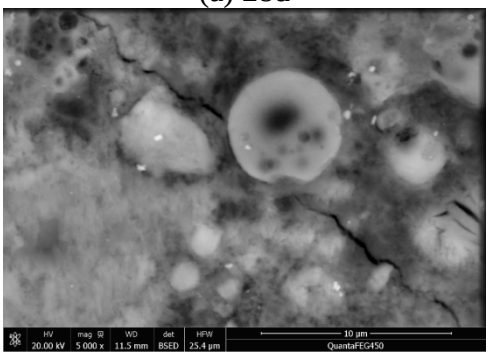


(c) 30d curing after pre-loading 30%

Figure 8 BSE image of cement paste

## CONCLUSIONS

This paper introduced the micro-cracks in the cement paste, with the pozzolanic effect of fly ash. The effect of w/c ratio, fly ash content and internal curing agent on the self-curing effect was studied. The main conclusions were as following:

1) With the high w/c ratio or internal-curing effect, the addition of fly ash is benefit to the improvement on compressive strength of cement paste from 28d to 60d. The late strength development indicated that it is potential in the self-curing improvement. The lower w/c ratio is not benefit for the curing effect of fly ash.

2) With the addition of fly-ash, the improvement on w/c ratio is benefit for the increase of 58d strength recovery rate. The SAP addition could increase mechanical strength recovery rate of cement paste when the w/c ratio was less than 0.4. However, it's not proper to add SAP in the cement paste with a higher w/c ratio (w/c>0.4).

3) The increase of fly ash content is benefit to self-healing ability of cement paste, especially with a higher w/c ratio or with SAP addition.

## ACKNOWLEDGEMENTS

The authors would like to thank the financial supports from the National Natural Science, Foundation of China (NO. 51502223 and 51172173).

## REFERENCES


1. HUANG, H., YE, G., & DAMIDOT, D. Characterization and quantification of self-healing behaviors of microcracks due to further hydration in cement paste. Cement and Concrete Research, Vol. 52, 2013, pp 71-81.

2. YANG, Z., HOLLAR, J., HE, X., & SHI, X. A self-healing cementitious composite using oil core/silica gel shell microcapsules. Cement and Concrete Composites, Vol. 33, No. 4, 2011, pp 506-512.

3. WU, M., JOHANNESSON, B., & GEIKER, M. A review: Self-healing in cementitious materials and engineered cementitious composite as a self-healing material. Construction and Building Materials, Vol. 28, No. 1, 2012, pp 571-583.

4. PANG, J. W. C., & BOND, I. P. A hollow fibre reinforced polymer composite encompassing self-healing and enhanced damage visibility. Composites Science and Technology, Vol. 65, No. (11–12), 2015, pp 1791-1799.

5. BOH B, ŠUMIGA B. Microencapsulation technology and its applications in building construction materials. Mater Geoenviron, Vol. 55, No.3, 2008, pp 329-344.

6. Van TITTELBOOM, K., De BELIE, N., De MUYNCK, W., & VERSTRAETE, W. Use of bacteria to repair cracks in concrete. Cement and Concrete Research, Vol. 40, No. 1, 2010, pp 157-166.

7. GRANGER, S., LOUKILI, A., PIJAUDIER-CABOT, G., & CHANVILLARD, G. Experimental characterization of the self-healing of cracks in an ultra high performance cementitious material: Mechanical tests and acoustic emission analysis. Cement and Concrete Research, Vol. 37, No.4, 2007, pp 519-527.

8. JEFFERSON, A., JOSEPH, C., LARK, R., ISAACS, B., DUNN, S., & WEAGER, B. A new system for crack closure of cementitious materials using shrinkable polymers. Cement and Concrete Research, Vol. 40, No. 5, 2010, pp 795-801.

9. AHN TH, KISHI T. Crack self-healing behavior of cementitious composites incorporating various miner admixtures. Journal of Advanced Concrete Technology Vol. 8, No. 2, 2010, pp 171-186.

10. SISOMPHON, K., COPUROGLU, O., & KOENDERS, E. A. B. Self-healing of surface cracks in mortars with expansive additive and crystalline additive. Cement and Concrete Composites, Vol. 34, No. 4, 2012, pp 566-574.

11. TERMKHAJORNKIT, P., NAWA, T., YAMASHIRO, Y., SAITO, T. Self-healing ability of fly ash–cement systems. Cement and Concrete Composites, Vol. 31, No. 3, 2009, pp 195-203.

12. GRANGER, S., LOUKILI, M., PIJAUDIER-CABOT, G., CHANVILLARD, G., Experimental characterization of the self-healing of cracks in an ultra high performance cementitious material: mechanical tests and acoustic emission analysis. Cement and Concrete Research, Vol.37, No.4, 2007, pp 519-527.
13. WANG, F., ZHOU, Y., PENG, B., LIU, Z., HU, S. Autogenous shrinkage of concrete with super-absorbent polymer. ACI Materials Journal, Vol. 106, No. 2, 2009, pp 123-127.

# MICRO-INDUCED CALCITE PRECIPITATION: CRACK SEALING APPLICATION

**A Richardson**

**K Coventry**

**J Pasley**

Northumbria University

England

**ABSTRACT.** This paper investigates the sealing and healing properties of micro-induced calcite precipitation with regard to surface finish and sealing cracks in cementitious materials. *Sporosarcina pasteurii* has been used to effectively precipitate calcium carbonate in order to seal porous media. The bacteria are fed a nutrient broth mix to create conditions where microbiologically induced calcite precipitation (MICP) can be effectively used. The tests carried out, assessed the effect of MICP on a sample of twenty-four concrete cubes and to what extent the surface has been consolidated. Weight gain was measured and a MOHs hardness test was used to evaluate the surface condition of the treated surface. In addition, three fibre reinforced concrete beams were micro-cracked to evaluate *Sporosarcina pasteurii*'s ability to seal cracks that are common in concrete structures globally. Calcite deposits were observed to be effective at sealing cracks and consolidating the surface finish of the concrete. The treatment is an organic remedial method that has industrial applications.

**Keywords:** Micro-induced calcite precipitation, Sporosarcina *pasteurii*, Concrete, Cracking, remedial methods, Bacteria.

**Alan Richardson** is Reader and a member of RILEM and carries out research into cementitious materials and has approaching 100 publications in the field of concrete technology and sustainable construction.

**Kathryn Coventry** is Director of Programmes and has a wide range of research interests.

**Jack Pasley** contributed towards the operational aspects of this work.

## INTRODUCTION

Concrete is an inherent part of our built environment, but it is not without its long term durability problems. As with any building material, deterioration is an expected occurrence with regards to the service life of structures. Both stone and concrete are susceptible to weathering; a breakdown of the mineral matrix leads to increased porosity of the surface and with it brings numerous issues [1]. The lack of a cost-effective, eco-friendly repair method is a cause for concern: 'In the United States of America, for instance, the annual direct costs for maintenance and repair of concrete highway bridges due to corrosion of the reinforcement is 4 billion dollars' [2]. Steel corrosion is one consequence of moisture penetration resulting from a variety of factors.

Figure 1 depicts the interactions between normal and high quality materials used in infrastructure, and the associated cost and strength performance over a period of time. If natural MICP can be used as a repair agent, lower cost materials can be maintained to an acceptable performance standard.

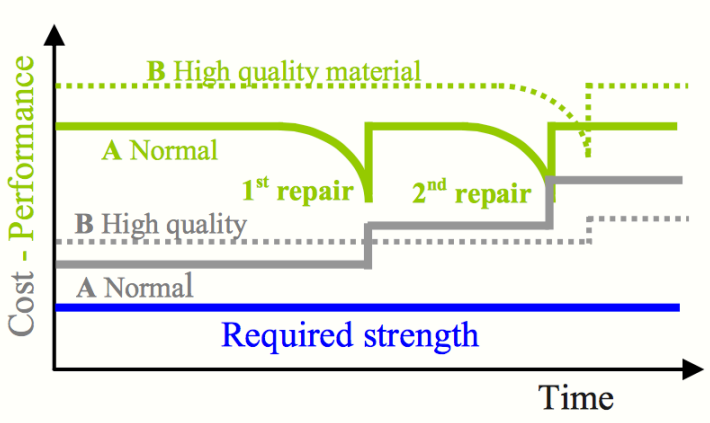


Figure 1 Quality of Infrastructure Materials [3]

With more extreme weather now common place, concrete structures within our built environment are subject to forces which in turn lead to micro scale propagation damage. The porosity of concrete permits micro-cracks to propagate and damage the material. This in turn provides an easy path for the transportation of liquids and gasses that potentially contain harmful substances which may damage the structure [4]. Micro cracks are commonplace in concrete structures, and Eurocode 2 permits design cracks widths up to 0.3mm. Micro cracks need to be sealed in order to stop them propagating and leading to costly repairs. Cracks under 0.05mm are not deemed problematic as concrete can repair itself through swelling of the cement paste, hydration of the remaining un-hydrated cement, precipitation of calcium carbonate ($CaCO_3$) crystals, and crack filling by impurities in water or by debris from the crack surface [5]. The life cycle costs of buildings are under more scrutiny than ever; buildings need to require less maintenance and have longer life spans to become more eco-friendly [6] and in this vein MCIP provides and alternative repair, sealing and reinstatement method using natural eco-friendly component parts.

### Causes of Deterioration and Transport Mechanisms

The durability of concrete is fundamentally dependent on the ease, or difficulty it can repel fluids in either liquid or gas form from permeating its surface. Concrete is a porous material

and the number, type and size of its pores influence its durability [7]. Deterioration of a concrete surface happens in three, chemico-physical stages [8].

1. Initiation
2. Propagation
3. Deterioration
4.

These processes occur due to a variety of mechanisms leading to deterioration. Reinforced concrete is expected to exhibit cracking of up to 0.3mm in normal service conditions [9]. It is susceptible to deterioration in the form of water infiltration, as cracks on both a macro and microscopic level develop under mechanical loading and sorption/desorption cycles [10]. Moisture ingress mechanisms are displayed in Table 1:

Table 1 Moisture Transfer [7]

| METHOD OF TRANSFER | DESCRIPTION |
|---|---|
| Diffusion | The movement of ions, liquid or gases from an area of high concentration to one of low concentration and is a result of the random motion of ions or molecules in solution. |
| Absorption | Concrete is able to intake a fluid which is dictated by the available space in the microstructure. |
| Permeability | The ease with which a fluid passes into and through the body of the concrete under the influence of a pressure differential. |

**Traditional Remedial Methods**

The majority of traditional remedial methods available are largely based on environmentally unfriendly materials such as epoxy systems, acrylic resins or silicone-based polymers [11]. Traditional inorganic coatings consist of calcium-silicate compounds, which exhibit a composition similar to cement [12].

Requirements for the repair of concrete structures are outlined in BS EN 1504. Figure 2 outlines the stages in the repair of a defective concrete structure.

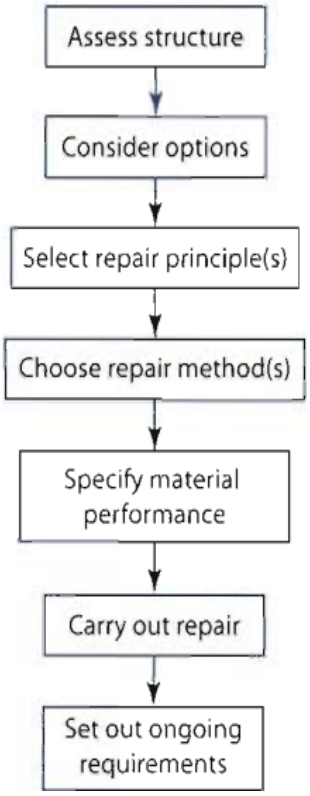


Figure 2 Repairing Concrete Structures (Adapted from BS EN 1504)

The repair of concrete structures falls into three basic categories:

- Structural
- Semi-Structural
- Cosmetic

In the context of this investigation, it is only anticipated to provide solutions to the cosmetic element of remedial works, which is described by The Concrete Society, [13]. as when holes do not surpass the reinforcement with the repair materials used based on lightweight solutions; either a cementitious or polymer binder. These solutions are unlikely to possess the same qualities as the original concrete in terms of elastic modulus, creep and shrinkage [13].

## MATERIALS AND BACTERIA

The mix designs used in this paper are displayed in Table 2. The change in water cement ratio provided varying porosity and surface finish to provide different surface conditions. A steel float finish was provided to the test surface and this was lightly trowelled to provide a textured surface.

Table 2 Mix design

| 0.8 WCR | CONSTITUENT | 0.4 WCR |
|---|---|---|
| 170 kg/m$^3$ | CEM 1 52.2 (R) | 337 kg/m$^3$ |
| 652 kg/m$^3$ | Sand < 4 mm | 482 kg/m$^3$ |
| 1522 kg/m$^3$ | Gravel < 20 mm | 1526 kg/m$^3$ |
| 136 l/m$^3$ | Water | 134.8 l/m$^3$ |

When the bacterial broth is applied to the cubes and beams, it will need to pool on the concrete surface and not run off, a silicone bead was applied around the edge of the cubes to ensure the mixture stays within the desired surface area. Similarly, a retaining bead of silicone will be applied around the induced cracks on the beams to contain the mixture and on the sides to contain the bacterial broth.

**Bacteria**

Bacteria are abundant, incredibly diverse and conduct precipitation of mineral carbonates across a spectrum of natural environments [14]. The majority of bacteria are either spheres or known as cocci or rod shaped and referred to as bacilli [14].

**Bacteria calcite precipitation**

In nature, it is common for microbial mineral plugging to occur in porous media. Bio-calcification or microbiologically induced calcite precipitation (MICP) is a phenomenon concerning the urease enzyme [15]. Microbial $CaCO_3$ has wide scope, as it has a varied range of environmentally friendly applications. It can consolidate damaged materials, especially ones bearing cracks [16]. MCIP is a natural phenomenon which is associated with a range of bacteria species given the right conditions, in particular, an alkaline environment rich in $Ca^{2+}$ ions [17]. The calcite deposition is able to consolidate media and potentially reduce moisture ingress.

**Ureolytic activity**

Bacteria that hydrolyse with urea are the most investigated with regard to calcite production. The following sequence of reactions adapted from Siddique and Chahal [14], demonstrates the process:

$$CO(NH_2)_2 + H_2O \rightarrow NH_2COOH + NH_3 \quad (1)$$

$$NH_2COOH + H_2O \rightarrow NH_3 + H_2CO_3 \quad (2)$$

$$H_2CO_3 \rightarrow HCO_{3-} + H^+ \quad (3)$$

$$2NH_3 + 2H_2O \rightarrow 2NH^{4+} + 2OH^- \text{ (pH increase)} \quad (4)$$

$$HCO_{3-} + H^+ + 2OH^- \rightarrow CO_3^{2-} + 2H_2O \quad (5)$$

$$CO_3^{2-} + Ca^{2+} \rightarrow CaCO_3 \text{ (carbonate precipitation)} \quad (6)$$

$$CO(NH_2)_2 + 2H_2O + Ca^{2+} \rightarrow 2NH^{4+} + CaCO_3 \text{ (overall reaction)} \quad (7)$$

Equation 1 Hydrolysis of Urea [14]

One molecule of urea is hydrolysed intracellularly to 1 molecule of ammonia and 1 molecule of carbonate (Eq. 1), which then spontaneously hydrolyses to form an additional molecule of ammonia and carbonic acid (Eq. 2). In water, the products then form bicarbonate, 2 molecules of ammonium, and 2 molecules of hydroxide ions Eqs. (3) and (4).

The overall reaction is demonstrated in Eq. 7 [14]. It is mentioned by Zamarreño et al. [18]. that a correct temperature of between 22°C and 32°C is required to catalyse the process.

**Microbiologically induced precipitation**

A more complex pathway to derive calcite precipitation is through microbiologically induced precipitation [14]. It relies on bacteria such as *Sporosarcina pasteurii*, urease and a high pH level. The enzyme catalyses and hydrolysis of urea occurs to produce $CO_2$ and ammonia, which, in turn, increases both the pH and carbonate concentration in the bacterial environment [19]. This is chemically expressed as:

$$Ca^{2+} + CO_3^{2-} \rightarrow CaCO_3 \downarrow$$

Equation 2 MICP [14]

**Bioremediation**

A bacterial cell surface can provide a nucleation site to non-specifically induce mineral deposition due to its variety of ions [14]. Bacteria have the largest surface area to volume ratio of any life form [20]. Therefore they are able to harbour calcium carbonate formation as shown in Figure 3.

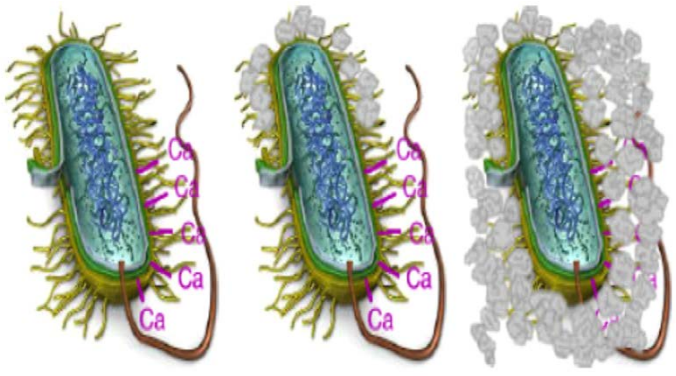


Figure 3 Simplified ureolysis calcite precipitation [1]

**Calcite precipitation in concrete**

Numerous studies have being conducted to assess the effectiveness of calcite precipitation in concrete. As discussed, Stocks-Fischer et al. [21] outlined that such precipitation can plug porous media.

*Sporosarcina pasteurii* (Previously *Bacillus pasteurii*), is able to aid in the urease production which, in turn, hydrolyses urea to ammonia and $CO_2$. Such urease production from *Sporosarcina pasteurii (S. pasteurii)* was witnessed by Sarda et al., [15], stating among the other microbial cultures *S. pasteurii* NCIM 2477 was able to produce the most urease (Figure 4).

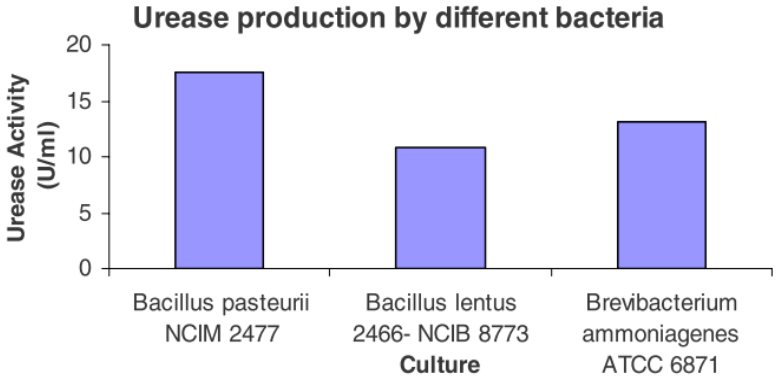


Figure 4 Urease Production by Different Bacteria [15]

It is concluded by Siddique and Chahal (2011) that microbial mineral precipitation is a promising technique with regard to improvements in the compressive strength, permeability, lesser water absorption and reduced chloride ingression. Wiktor and Jonkers [22] support this conclusion; their bio-chemical healing agent consisting of bacterial spores (*Bacillus alkalinitrilicus,* an alkali resistant soil bacterium) and calcium lactate was able to void cracks whilst being submersed in tap water for 100 days. The deposits were then tested using energy dispersive spectroscopy. The results verified the anticipated $CaCO_3$ production as the deposits were a combination of calcium, oxygen and carbon atoms as displayed in Figure 5.

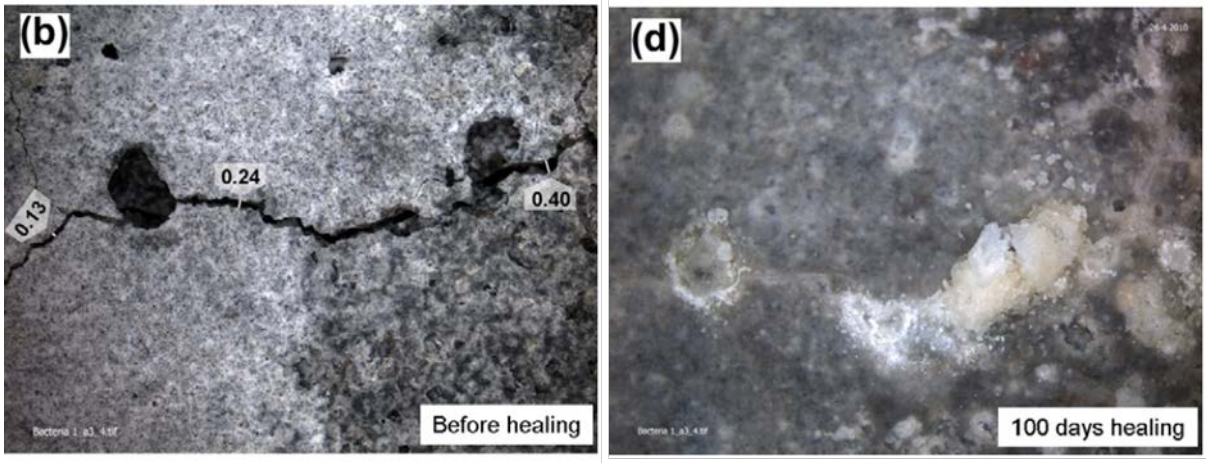


Figure 5 Bio-chemical crack healing ability [22]

*S. pasterurii* is conveyed as consistently being able to produce urease, which is of paramount importance with regards to $CaCO_3$ precipitation. It is apparent, *Sporosarcina pasteurii* appears to be the bacteria of choice throughout the various studies by Bang, Galinat, & Ramakrishnan [23] and Achal & Pan ([17] and will subsequently be the bacteria to be used in this study.

## METHODOLOGY

To assess any changes to surface finish, twenty-four, 100mm concrete cubes were produced. The sample included two water cement ratios (WCR) and different surface finishes in equal numbers (six each). To quantify the calcite deposition, the comparable weights of the dry cubes pre and post treatment were recorded. Three fibre concrete beams were cast and once fully cured, they were cracked under a three point bending system, then a bead of silicone was applied around the cracked area to provide a reservoir to retain the liquid whilst the bacteria fed upon the food source, thus creating calcite as a repair agent.

The process outlined was repeated a total of three times, at 24 hour intervals and this layering effect gave the mixture time to be absorbed by the beams. Once the bacteria and the nutrient broth were mixed together, there was calcite formed almost immediately and this is a key finding in terms of an application process. This effect was noted in an earlier test [24].

### Bacterial Preparation and Application

The *S. pasteurii* cultures were suitably incubated in an orbital incubator at 37°C at a rate of 200 rpm. The cultures were then measured at $OD_{600}$ to see if the cell density is within the desired range (Approx. 0.9-3). A higher OD will provide more nucleation sites for calcite formation.

Once the culture was prepared a100ml aliquot containing the bacterial cultures was added to a 900ml Duran container of nutrient broth with 50 ml $CaCl_2$ (calcium chloride) at a concentration of 1 g/ml. Immediately after mixing the solution, it was applied to the 3 beam sections and cubes. 15 ml of solution per cube was applied followed by 1.5ml of urea to catalyse the reaction and help support the bacteria's hydrolysis, leading to a higher calcite yield.

## RESULTS

The bacterial residue was examined at the surface (foreground) and at the intersection between the calcite and the concrete (background), using an Energy Dispersive Spectroscopy (EDS) image analysis technique and the chemical component parts are displayed in Table 3 and Figure 6.

Table 3 Chemical component parts of calcite deposit

| | OXYGEN (%) | CARBON (%) | CALCIUM (%) |
|---|---|---|---|
| Background | 58.0 | 17.5 | 24.5 |
| Foreground | 60.6 | 13.4 | 26.0 |

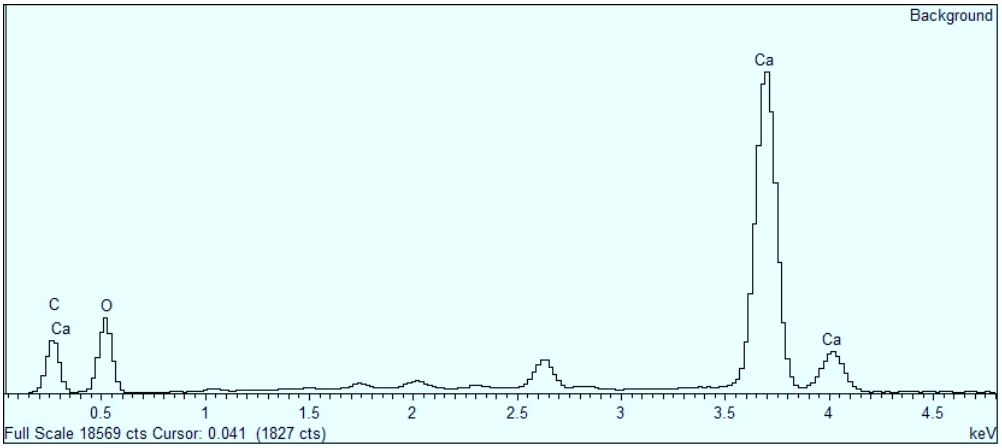


Figure 6 Energy Dispersive Spectroscopy (EDS) image

The Energy Dispersive Spectroscopy (EDS) results were tested alongside a MOH's hardness test and hydrochloric acid test which showed the calcite formation was within normal hardness associated with the formation of calcite and the acid test showed the material to be of an alkaline nature.

Following the treatment, an average oven dry weight increase of 3.6g was recorded. The WCR ratio of the cubes did not affect the average weight gain for the respective samples. The surface treatment levelled the cube face and bound loose particles together.

**Crack Sealing**

The effectiveness of the MICP crack healing properties are displayed in Figures 3 and 4.


Figure 3 Cracked fibre beam (left) and MICP sealing the crack (right)

Figure 4 Cracked concrete beam on left and healed concrete beams to the right.

This study has demonstrated the potential *S. pasteurii* and consequently MICP holds in improving the integrity of finish to concrete, without the use of chemical based sealants.

## CONCLUSIONS

By reaching an average $OD_{600}$ of 2.1 over the three applications, adequate nucleation sites were provided for MICP to occur. The investigation has hereby acted as a 'proof of concept' in that MICP can perform as an organic repair alternative for concrete structures, especially in a time where heavy emphasis is placed on environmentally sustainable building solutions. The layering effect provided visible results on both the cubes and beams which had bonded with the concrete cube surface.

Although the MICP did not penetrate the cube surfaces, the bacteria successfully filled the majority of imperfections and voids on the samples.

Uneven concrete surfaces can also be smoothed using this treatment; although the colour of calcite (white) may not be deemed aesthetically pleasing and therefore require suitable pigmentation additives.

The results, with regard to depth of calcite penetration, demonstrated the near 100% consolidation of the micro cracks to a depth of approximately 20mm. The use of the treatment in such a way could be plausible on a commercial scale as the cracks house the NBU, in turn pooling the solution and leading to MICP. This reduces the reliance on surface pooling which was needed with the cube samples.

The cube surface scans gave a thorough analysis of the calcite formations build up. The comparable scans showed a surface mass increase and a reduction in surface structure deviation, effectively fusing the cubes' surface with the $CaCO_3$. With lessened surface porosity, in theory, the rate of deterioration would slow in a real world application. However, this is reliant on further porosity testing.

## REFERENCES


1. DE MUYNCK, W., DE BELIE, N. AND VERSTRAETE, W. (2010) "Microbial carbonate precipitation in construction materials." *Ecological Engineering*, 36(2), pp. 118–136.
2. SIERRA-BELTRAN, M. G., JONKERS, H. M. AND SCHLANGEN, E. (2014) "Characterization of sustainable bio-based mortar for concrete repair." *Construction and Building Materials*, 67, Elsevier Ltd, pp. 344–352.
3. SCHLANGEN, E. AND SANGADJI, S. (2013) "Addressing infrastructure durability and sustainability by self healing mechanisms - Recent advances in self healing concrete and asphalt." *Procedia Engineering*, 54, Elsevier B.V., pp. 39–57.
4. VAN TITTELBOOM, K., DE BELIE, N., DE MUYNCK, W. AND VERSTRAETE, W. (2010) "Use of bacteria to repair cracks in concrete." *Cement and Concrete Research*, 40(1), Elsevier Ltd, pp. 157–166.
5. STUCKRATH, C., SERPELL, R., VALENZUELA, L. M. AND LOPEZ, M. (2014) "Quantification of chemical and biological calcium carbonate precipitation: Performance of self-healing in reinforced mortar containing chemical admixtures." *Cement and Concrete Composites*. Elsevier Ltd, 50, pp. 10–15.
6. SRINIVASAN, R. S., INGWERSEN, W., TRUCCO, C., RIES, R. AND CAMPBELL, D. (2014) "Comparison of energy-based indicators used in life cycle assessment tools for buildings." *Building and Environment*. Elsevier Ltd, 79, September, pp. 138–151.
7. BASHEER, P. A. M. AND BARBHUIYA, S. A. (2010 "*Pore Structure and Permeability*," pp. 1-2.
8. LAMBERT, P. (2002) "Reinforced concrete - history, properties and durability," *Corrosion Prevention Association*.
9. BRE (2000) "Corrosion of steel in concrete - durability of reinforced concrete structures," *Digest 444(Part 1)* pp. 2–9.
10. ROUCHIER, S., WOLOSZYN, M., FORAY, G. AND ROUX, J.-J. (2013) "Influence of concrete fracture on the rain infiltration and thermal performance of building facades." *International Journal of Heat and Mass Transfer*. Elsevier Ltd, 61, June, pp. 340–352.
11. SIERRA-BELTRAN, M. G., JONKERS, H. M. AND SCHLANGEN, E. (2014) "Characterization of sustainable bio-based mortar for concrete repair." *Construction and Building Materials*, 67, Elsevier Ltd, pp. 344–352.
12. DE MUYNCK, W., DEBROUWER, D., DE BELIE, N. AND VERSTRAETE, W. (2008) "Bacterial carbonate precipitation improves the durability of cementitious materials." *Cement and Concrete Research*, 38(7) pp. 1005–1014.
13. THE CONCRETE SOCIETY (2009) "*Repair of Concrete Structures with Reference to BS EN 1504*."

14. SIDDIQUE, R. AND CHAHAL, N. K. (2011) “Effect of ureolytic bacteria on concrete properties.” *Construction and Building Materials*, 25(10) Elsevier Ltd, pp. 3791–3801.

15. SARDA, D., CHOONIA, H. S., SARODE, D. D. AND LELE, S. S. (2009) “Biocalcification by Bacillus pasteurii urease: a novel application.” *Journal of industrial microbiology & biotechnology*, 36(8) pp. 1111–1115.

16. WANG, J. Y., SOENS, H., VERSTRAETE, W. AND DE BELIE, N. (2014) “Self-healing concrete by use of microencapsulated bacterial spores.” *Cement and Concrete Research*, 56, Elsevier Ltd, pp. 139–152.

17. ACHAL, V. AND PAN, X. (2011) “Characterization of urease and carbonic anhydrase producing bacteria and their role in calcite precipitation.” *Current microbiology*, 62(3) pp. 894–902.

18. ZAMARREÑO, D. V, INKPEN, R. AND MAY, E. (2009) “Carbonate crystals precipitated by freshwater bacteria and their use as a limestone consolidant.” *Applied and environmental microbiology*, 75(18), pp. 5981–5990.

19. CHAHAL, N., SIDDIQUE, R. AND RAJOR, A. (2012) “Influence of bacteria on the compressive strength, water absorption and rapid chloride permeability of concrete incorporating silica fume.” *Construction and Building Materials*. Elsevier Ltd, 37, December, pp. 645–651.

20. FORTIN, D., DAVIS, B. S. AND BEVERIDGE, T. J. (1996) “Mineralization of bacterial surfaces,” *Chemical Geology 132*.

21. STOCKS-FISCHER, S., GALINAT, J. K. AND BANG, S. S. (1999) “Microbiological precipitation of $CaCO_3$” *Soil Biology and Biochemistry*, pp. 31.

22. WIKTOR, V. AND JONKERS, H. M. (2011) “Quantification of crack-healing in novel bacteria-based self-healing concrete.” *Cement and Concrete Composites*, 33(7), Elsevier Ltd, pp. 763–770.

23. BANG, S. S., GALINAT, J. K. AND RAMAKRISHNAN, V. (2001) “Calcite precipitation induced by polyurethane-immobilized Bacillus pasteurii.” *Enzyme and Microbial Technology*, 28(4-5) pp. 404–409

24. RICHARDSON, A. E, COVENTRY, K. A., FORSTER, A., JAMISON, C. (2014) "Surface consolidation of natural stone materials using microbial induced calcite precipitation", Structural Survey, Vol. 32, No. 3, pp 265-278

# MULTI - SCALE CEMENTITIOUS SELF-HEALING SYSTEMS AND THEIR APPLICATION IN CONCRETE STRUCTURES

**R E Davies** **M Pilegis**

Cardiff University

**A Kanellopoulos** **T Sharma**

University of Cambridge University of Bath

**O Teall** **D Gardner**

**T Jefferson** **R Lark**

Cardiff University

United Kingdom

**ABSTRACT.** The Materials for Life (M4L) project team have developed multi-scale self-healing systems for cementitious materials using a range of interdisciplinary technologies. The three-year EPSRC funded project, which began in July 2013, is a collaboration between Cardiff University, University of Cambridge and University of Bath. The project has investigated individual healing techniques, combined these techniques in the laboratory and now used these techniques in the field at the full-scale. This paper will summarise the findings and challenges encountered to date. The individual healing techniques address damage at various length and time scales and include encapsulating healing agents, bacterial healing, crack closure using shape memory polymer (SMP) tendons and vascular networks with the ability to supply healing agents on a repeated basis. Amalgamating these techniques to form a multi-scale healing system has been shown to improve the overall healing efficiency with respect to strength recovery. This work has given an insight into the interaction between the various healing processes and healing trigger mechanisms. The project's primary industrial sponsor, Costain, have built a full-scale concrete structure, which includes a number of wall panels incorporating different combinations of self-healing techniques. The wall panels are loaded to induce cracks after which the recovery of structural properties is monitored over time. The challenges encountered in scaling-up, the feasibility of construction and early performance results are discussed. These field-scale trials have been an important step in evaluating the feasibility of self-healing concrete.

**Keywords:** Multi-scale, Self-healing, Concrete, Cementitious, Site-trials.

**Dr Robert Davies** was a Research Associate working on the M4L project and now a lecturer at the School of Engineering, Cardiff University. He is a Chartered Civil Engineer. **Dr Martins Pilegis** is a Research Associate at Cardiff University working on the M4L project. **Dr Antonis Kanellopoulos** is a Research Associate at University of Cambridge. **Dr Trupti Sharma** is a microbiologist and Research Associate based at University of Bath. **Oliver Teall** is a PhD research student whist remaining a Costain employee. **Dr Diane Gardner** is a senior lecturer and a member of the BRE Institute of Sustainable Engineering in the School of Engineering at Cardiff University. **Professor Tony Jefferson** has spent 10 years in industry and 20 years in academia. His current academic position is sponsored by the finite element company LUSAS. **Professor Bob Lark** is a Chartered Engineer and the Dean of Education and Students for the College of Physical Sciences and Engineering and Deputy Director of Teaching in Engineering at Cardiff University. Bob is the principal investigator on the M4L project.

## INTRODUCTION

The “Materials for Life (M4L): Biomimetic multi-scale damage immunity for construction materials” project [1] addresses a vision of a sustainable and resilient built environment. The new generation of materials and structures developed will continually monitor, regulate, adapt and repair themselves without the need for external intervention. In this way, such self-healing materials and intelligent structures will significantly enhance durability and serviceability, improve safety and reduce maintenance costs [2].

The conglomerate materials that form the basis of the majority of such construction materials (concrete, grouts, mortars, hydraulically bound materials, grouted soils etc), are extremely complex multiphase composites with multi-scale internal structures that exhibit a hierarchy of multi-dimensional, time-dependent damage mechanisms. For example, in cementitious composites nano-scale damage occurs during hydration and the strength development phase, while medium-term damage due to chemical attack also leads to the formation of defects in its structure. Other short-term factors such as residual stresses that arise during curing and compaction or longer-term physical actions, like repeated cycles of freezing and thawing and fatigue loading, can also produce dislocations at the nano-scale. In time, this nano-damage grows to form micro-cracks within the cement paste and these micro-cracks themselves eventually coalesce to form networks of meso-cracks. It is these meso-scale cracks that lead to debonding between the paste and aggregate particles, a network that finally grows to become the discrete number of visible macro-cracks which so often lead to corrosion of the steel reinforcement.

Cracking is inevitable in reinforced concrete structures, indeed it is an inevitable consequence of its response to thermal effects, early-age shrinkage, mechanical loading, freeze-thaw effects or a combination of these factors [3]. It is widely accepted that the design-life of concrete structures is reduced by the development of micro-cracks which allow the ingress of water, carbon dioxide and chlorine ions into the structure. This causes carbonation, sulphate-related degradation of the concrete and corrosion of the reinforcement. This concrete degradation currently results in the requirement for regular repair and maintenance work to concrete structures, which comes with large associated costs. Hence, it is evident that a system is needed that can act at both the different spatial and temporal scales at which the damage can form. The purpose of this research is to identify a cost effective self-healing cementitious composite.

M4L is a three-year EPSRC funded project which began in July 2013. The project consortium, led by Cardiff University and including the University of Cambridge and the University of Bath, has worked alongside industrial partners to bring together the whole supply chain to address the challenges and feasibility of delivering self-healing materials on civil engineering projects in the future. Individual technologies developed, work done on combining self-healing technologies and construction of the first UK self-healing site trial is presented in this paper.

## SELF-HEALING TECHNOLOGIES

The interdisciplinary nature of this project makes use of multi-scale systems that use primarily four main technologies to promote and enable self-healing of construction materials over various timescales. These are: the release of healing agents from microcapsules, the deposition of material in the cracks promoted by bacterial action, crack closure using shape memory polymer tendons, and the repeated supply of healing agents through vascular networks.

### Release of Healing Agents from Microcapsules

Led by University of Cambridge, this element of research focused on embedding microcapsules containing various healing agents into a cement based matrix. Upon crack formation, and when the crack front reaches the microcapsules, the rupturing capsules release healing agents into the crack promoting healing. This action serves to block the ingress of harmful substances and aids the recovery of structural strength.

The work focused on the manufacture of microcapsules and the selection of a suitable cargo. Three shell manufacturing techniques were investigated, i) interfacial polymerisation (ii) complex coacervation and (iii) using a microfluidic device. The microcapsule size varied between 50 μm to 700 μm on average, depending on the technique. Minerals were selected as the preferred healing agent and an experimental series using macro-scale glass capsules showed that all mineral compounds improved substantially the condition of cracked specimens [4]. These water soluble minerals were then successfully encapsulated and the production scaled-up. Figure 1 shows microcapsules approximately 600 μm in diameter made from pig gelatine which contain 50% sodium silicate and 50% oil. Detailed analysis and characterisation of the different microencapsulation systems was carried out and the effect the volume fraction of microcapsules in the cement based matrix has on: healing, the fresh and hardened properties of cement based materials was considered [5].

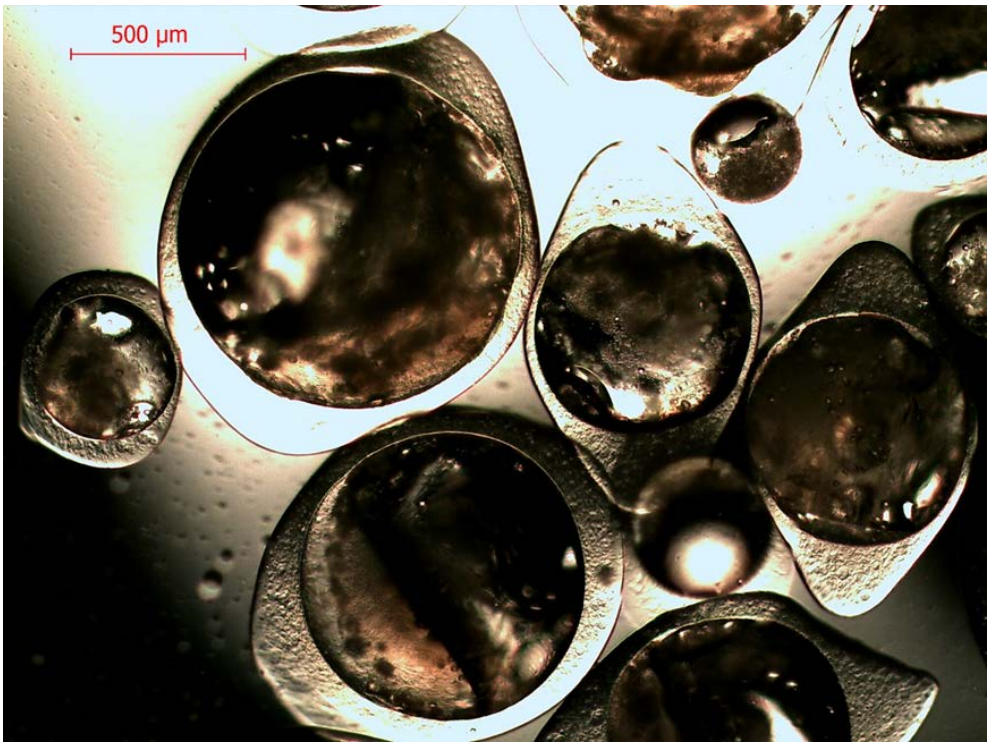


Figure 1 Microcapsules made from pig gelatine and containing 50% sodium silicate and 50% oil (picture courtesy of University of Cambridge)

## Deposition of Material in the Cracks Promoted by Bacterial Action

The University of Bath focused on a bacterial self-healing solution, whereby specially selected bacteria, which can survive in concrete, precipitate calcite in any cracks in concrete. The work involved selection of suitable bacteria that can behave in the necessary way in the extremely hostile environments within concrete. Such considerations led to selecting bacteria that can survive alkaline conditions, form spores, germinate into live bacteria when the conditions are suitable and form calcite. Screening of calcium compounds for calcite production was undertaken and survival of spores under extreme compression was examined [6]. Figure 2 shows magnified calcium carbonate crystals that have been produced by bacteria in-vitro.

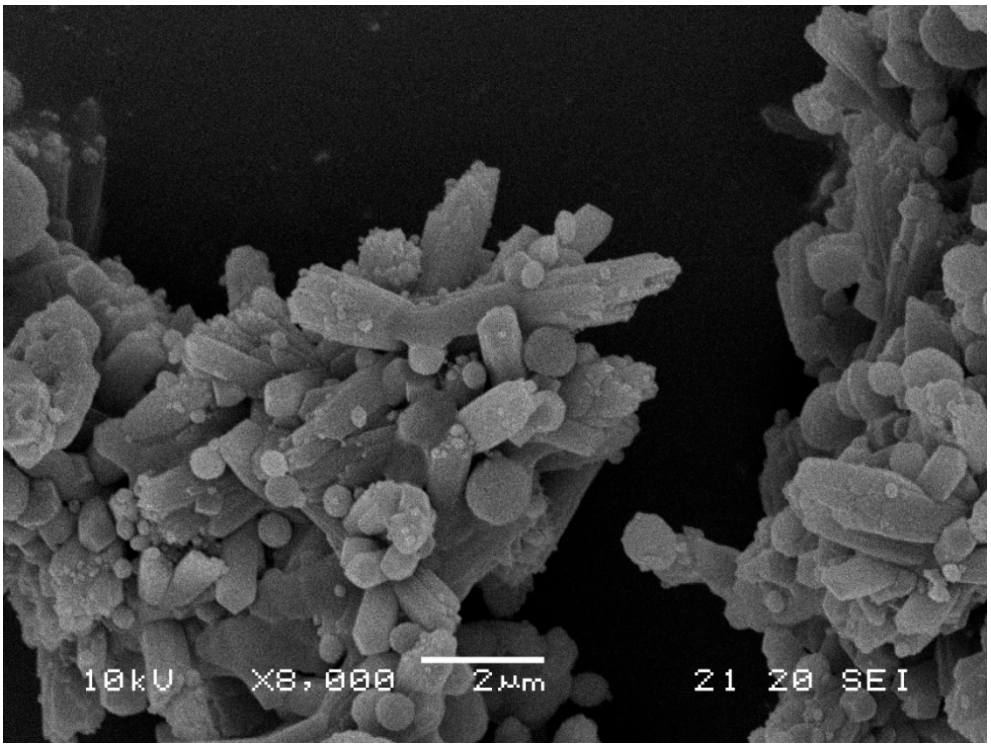


Figure 2 Magnified calcium carbonate crystals the product of bacterial healing (picture courtesy of University of Bath)

## Crack closure using shape memory polymer tendons

Cardiff University developed a solution using shape memory polymers (SMP) as a crack closure mechanism within concrete structures to enhance autogenic healing. This follows on from previous research at Cardiff into the use of polyethylene terephthalate (PET) strips for crack closure [7]. The SMP, upon activation, returns to a built-in shape, or if restrained generates an external stress. One of the key challenges in this work was to scale-up the SMP tendons from small 125 mm long mortar beams to firstly 500mm long beams, then to 1m long beams and finally to full scale in the site trials. The tendons, initially developed using PET strips, and then formed from filaments were designed to create 1 MPa compressive stress at the crack face after activation. A schematic of a SMP tendon is shown in Figure 3. A new testing setup and sequence was developed to characterise the SMP, qualitative evidence of healing was sought and load recovery results were generated. Key indicators for developing filaments with higher stress capabilities were identified and reported by Pilegis et.al. [8].

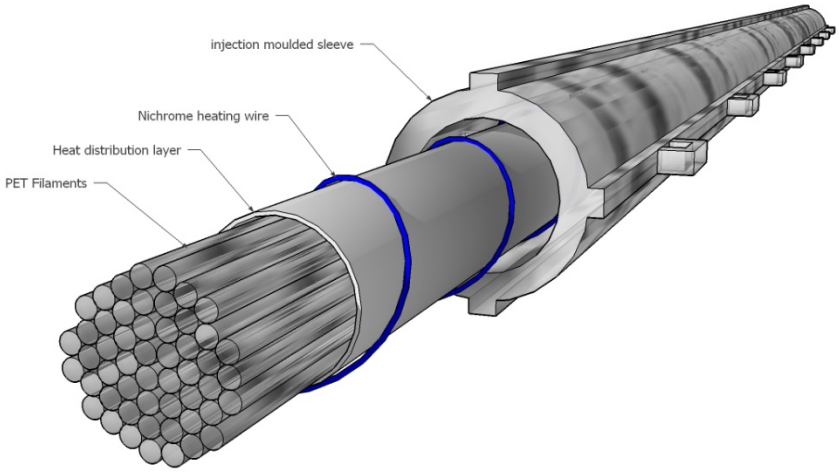


Figure 3 Schematic of a shape memory polymer tendon

**Repeated supply of healing agents through vascular networks**

Cardiff University has also developed a technique for creating vascular networks within concrete structures. The concept is to create a hollow network that can be re-used over the lifetime of a structure, with the primary aim being to enhance and enable multi-scale healing in cementitious materials. Vascular networks in 1D and 2D were created using 4 mm circular diameter channels in beams, slabs and walls. Characterisation of the different properties which influence the flow of the healing agent have been investigated.

To enable the healing agents to migrate to areas of damage the networks were placed in the areas most susceptible to cracking, which is typically the cover zone of concrete subject to tension. A 2D vascular network of channels can be seen in a 600 mm square slab mould prior to casting in Figure 4. The preferred healing agent was sodium silicate, which combines with sodium hydroxide to form Calcium Silicate Hydrate in the cracks [9]. A key finding of the work was that a pressurised vascular network, with externally supplied healing agent is capable of promoting significant strength recovery. When used in combination with the SMP technique, for example, the strength recovery was shown to double from 15% to 30% in 500mm beams with 0.5mm cracks when supplied with sodium silicate.

Figure 4 Vascular network channels before casting 600mm square 100mm deep slab

## SITE TRIALS

One of the aims of the M4L research project was to scale-up from laboratory size and apply these techniques to larger scale concrete structures on a construction site. The design, construction, testing and monitoring of the site structures, are described briefly in this section. The self-healing concrete site trial was built by Costain in October 2015 within the site compound of the A465 Heads of the Valleys section 2 project in South Wales. Costain are the lead contractor on the £200M Welsh Government contract, where 8.1km of existing highway is being upgraded from single to dual carriageway between Gilwern and Brynmawr in South Wales.

### Site trial set-up and constituents

A conventional cantilever wall mimicking a retaining wall was used for the trial, replicating many of the permanent work structures on the highway project. A base, reaction wall and 5 individual panels were cast in concrete, as shown in the schematic in Figure 5. The panels are 1.8m in height, 1m wide and 0.15m in depth. Four panels contain different combinations of self-healing techniques, whilst a fifth panel acts as a control. Table 1 shows the contents of each trial panel and Table 2 shows the basic concrete mix that was used with a design strength of C40/50.

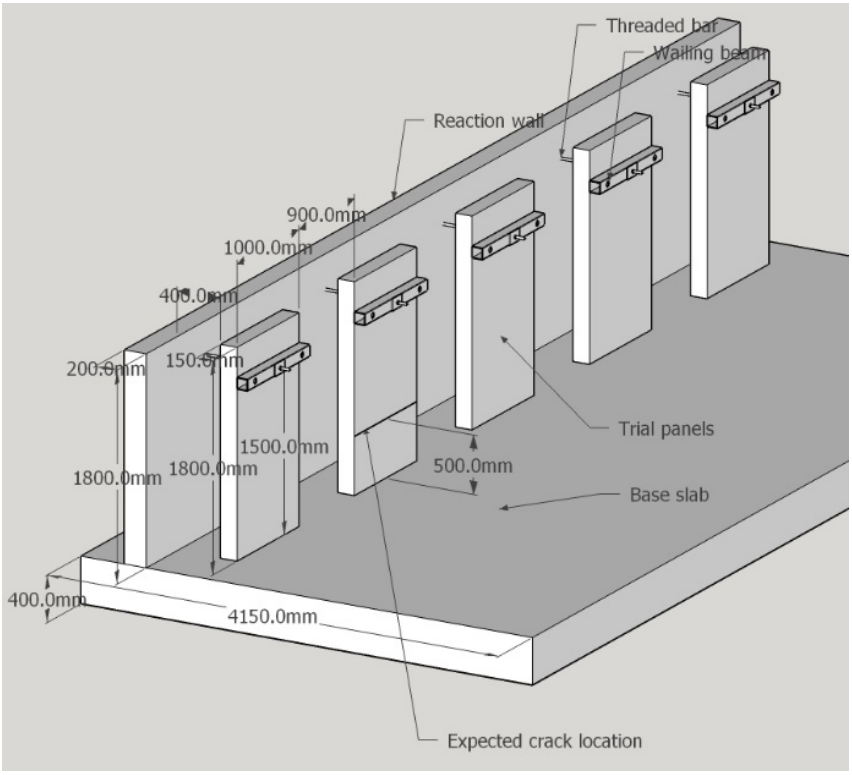


Figure 5 Site trial concept design

Table 1 Trial panel notation and contents

| PANEL | CONTENTS |
|---|---|
| A | Microcapsules and basic mix (microcapsules 8% by weight of cement) |
| B | SMP tendons and flow network with basic mix |
| C | Encapsulated bacterial spores, nutrients and flow networks with equivalent concrete mix |
| D | Control using basic mix |
| E | Control with flow network using basic mix |

In Panel A, the microcapsules, illustrated in Figure 1 at 8% by weight of cement, were manually added to the basic concrete mix on site. In Panel B shape memory polymer ‘tendons’ were tied onto the main reinforcement within the trial structure, these were activated by passing an electrical current through heating wires incorporated in the tendons. A 2D network of 4mm diameter channels was also created using polypropylene tubes, which were removed from the concrete once cured. The tubes were joined using 3D printed joints made from polylactic acid which remained in the wall. The tendons and flow network setup before casting can be seen in Figure 6. In Panel C, the bacteria used was bacillus pseudofirmus, which was infused into lightweight aggregates in the form of perlite. Precursors and nutrients were also included in separate aggregates as a food source for the bacteria. This purpose made bacteria mix with the same design strength as the basic mix was placed in a 500 mm layer at the expected location of the cracking.

Table 2 Basic concrete mix design

| MATERIAL | SSD QUANTITY (kg/m³ unless noted otherwise) | |
|---|---|---|
| Cement (CEM I) | 415 | |
| 10mm Limestone aggregates | 944 | |
| Limestone fines (0-2mm) | 396 | |
| Marine sand | 393 | |
| Water | 179 | |
| Admix: VS100 (SIKA) plasticiser | 0.35 cement | l/100kg |
| Admix: SIKATARD R retarder | 0.1 cement | l/100kg |

Figure 6 Shape memory polymer tendons and vascular network setup before casting concrete

**Site trial testing sequence**

Controlled damage of the walls was initiated between 33 and 36 days after casting, by applying a load to the top of the cantilevered panels. This was achieved via a spreader beam, threaded bar and jack pulling against the reaction wall. The panels were designed to crack on their front face, 500mm from the base, which allowed the majority of the measuring techniques to be focussed on one area of the panel. The peak load applied to the panels was approximately 24KN

which resulted in crack widths on the front surface of the wall of approximately 0.5mm. After the initial loading phase, the tendons in Panel B were activated and a reloading cycle was initiated to assess the effectiveness of the SMP system. Similarly Panel E which was used as a Control for Panel B and was subjected to the same loading and unloading cycle.

Throughout this initial phase of the site trial, the crack width, deflections, strains, permeability and applied loading on the panels were monitored and the results will be compared with a second phase of load testing which is planned for the summer of 2016 when the panels will be 6 months old. The monitoring techniques adopted made use of DEMEC pips, optical microscopes, linear variable displacement transducers (LVDT), load cells, on-site permeability apparatus and a Digital Image Correlation (DIC) system. Following the initial loading, monitoring of the panels was conducted at one month intervals recording microscope images, DEMEC readings and any changes in the LVDT readings. The intention is to flush the flow networks in panels B and E with sodium silicate healing agent 90 days after initial loading.

**Site trial initial results**

This section will provide a brief insight into the initial loading results of the trial panels. Other results will be published in due course when they become available. One of the aims of the M4L project was to scale-up the self-healing techniques for site trials and this has been successfully achieved as evidenced in Figure 7.

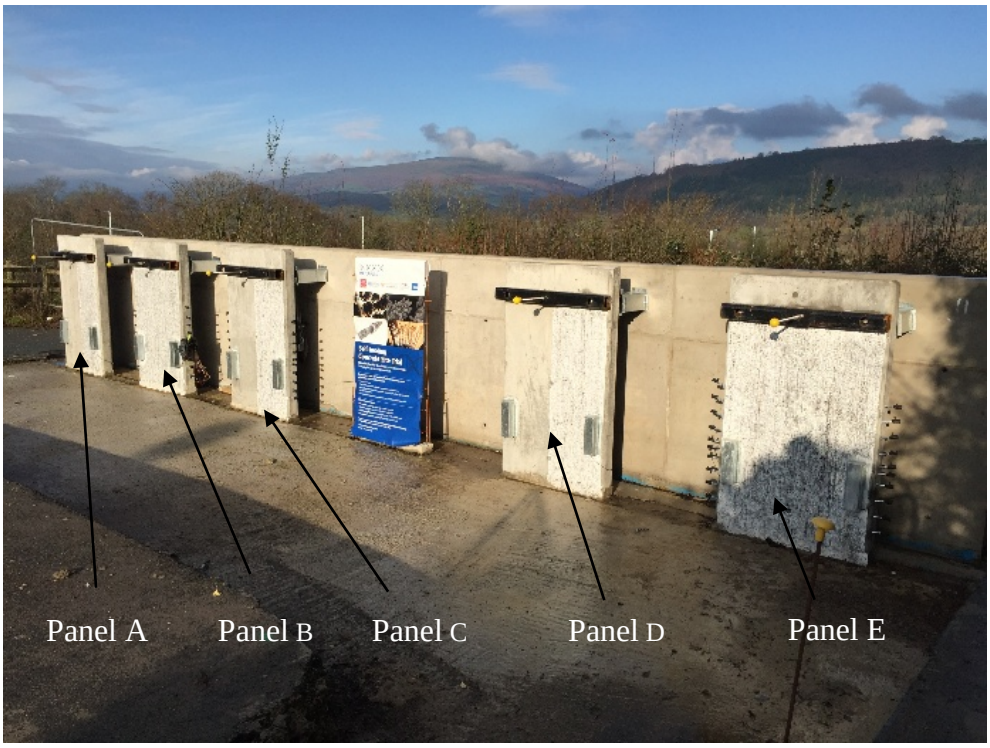


Figure 7: Site trial panels after initial loading

Early visual measurements have shown some crack healing in Panel A when compared with the control Panel D. Mechanical load regain will be assessed upon reloading of the panels at a later stage of the project. The activation of the polymer tendons in Panel B resulted in an average reduction in crack width of around 20% and an increase in stiffness upon reloading of

the panel. Panel C has also demonstrated some evidence of crack healing, although further tests are required to assess whether this healing is due to the presence of bacteria or through the autogenous healing process which naturally occurs in concrete structures.

The load versus the displacement curve for the top of all panels from the initial load cycle is shown in Figure 8. During loading, several cracks were formed as can be seen from the load peaks and troughs in the graph. The formation of the final crack at the expected location, approximately 500 mm above the base, was achieved with a load ranging from 20 to 24kN.

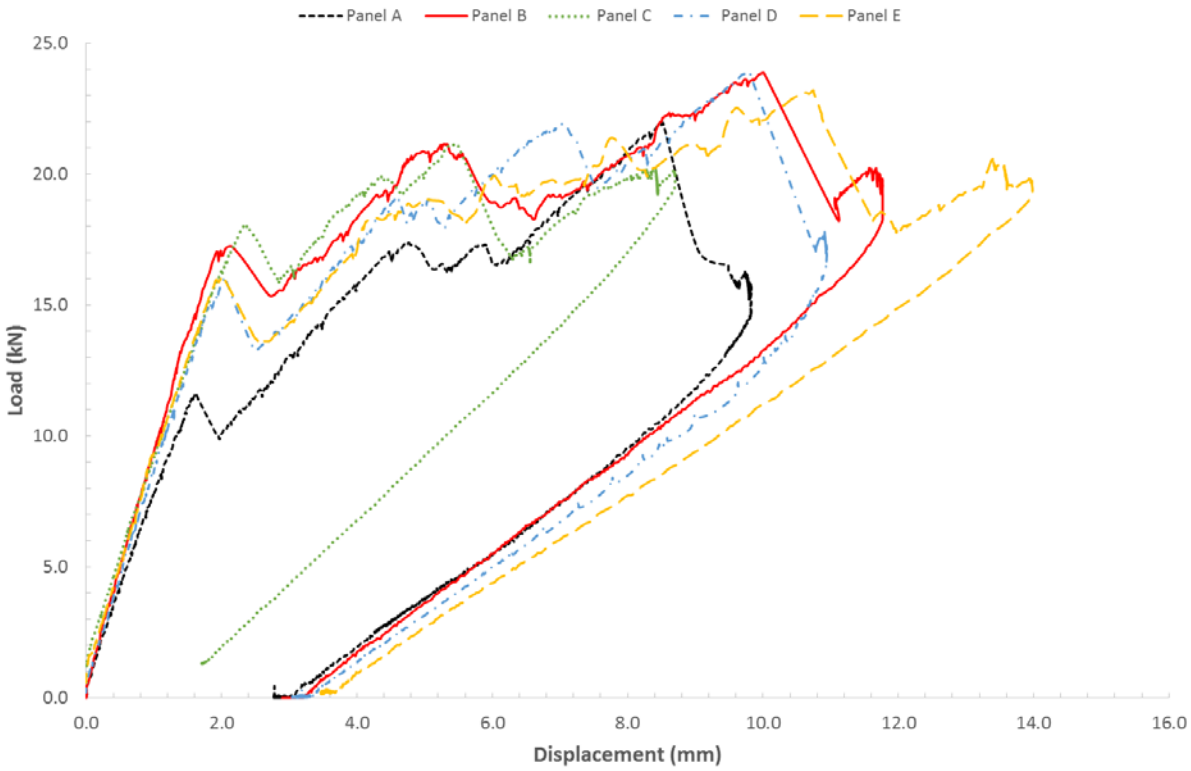


Figure 8: Load versus top of the panel displacement

Figure 9 shows the vertical strain of Panel B after unloading and three cracks can be seen that correspond to the higher peaks in the load displacement graph. The crack at the expected location is wider than the other ones as shown by the DIC in Figure 9. Similar cracking behaviour and the occurrence of the largest crack at 500 mm above the base was observed in all panels.

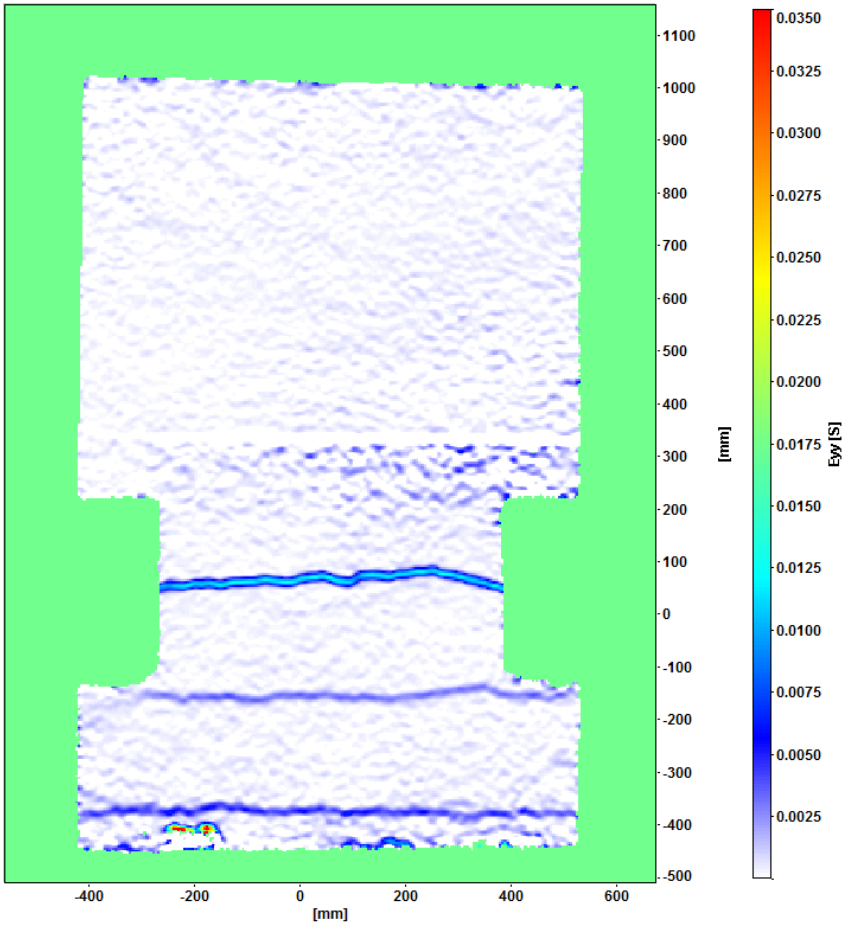


Figure 9: DIC strain plot of Panel B after unloading

The microscope image analysis showed that the residual crack width of the crack 500 mm above the base of all panels ranged from 0.063 mm to 0.161 mm. The site trials are still ongoing and the monitoring is carried out every month as detailed in the testing sequence section. The next site trial event is filling the flow networks with a healing agent and evaluation of the corresponding healing effectiveness. The challenges associated with undertaking these site trials have been significant, but many have been overcome. These included scaling up the techniques, making custom rigs and dealing with inclement weather conditions away from the laboratory. For example, a key requirement for the SMP tendons was the need to develop an electrical activation system. The evaluation of healing will be undertaken after the second phase of load testing which is planned for the summer of 2016.

## CONCLUSIONS

The M4L self-healing concrete trials have been successful in achieving their primary aim, which was to scale-up the four individual healing technologies and implement these in a full-scale structure on a construction site. Each technology works at a different length scale and could respond to the range of damage that can arise in construction materials. The physical implementation has been shown to be a relatively straightforward process. Initial results are sufficiently positive to give confidence that these techniques warrant further investigation, working towards reducing and removing the requirement for inspection, maintenance and repair of concrete structures.

## ACKNOWLEDGEMENTS

The writers gratefully acknowledge the financial support for this study given by the Engineering and Physical Sciences Research Council (EPSRC) (Project Ref. EP/K026631/1). Thank you must be extended to the whole Materials for Life project team whose collaboration made this work possible and to Costain for providing construction support and use of their site for the trial. Further information about the M4L project, its collaboration members, academic publications and outreach activities can be found on the project website http://m4l.engineering.cf.ac.uk.

## REFERENCES

1. LARK, R.J., AL-TABBAA, A., PAINE, K., *Biomimetic multi-scale damage immunity for construction materials: M4L project overview*, in: ICSHM 2013: Proceedings of the 4th International Conference on Self-Healing Materials, Ghent, Belgium, June 16-20, 2013. Ghent University

2. DE ROOIJ, M. R. VAN TITTELBOOM, K. DE BELIE, N. SCHLANGEN, E. *Self-Healing Phenomena in Cement Based Materials*. State-of-the-Art Report of RILEM TC 221-SHC. 2013.

3. RICHARDSON, M.G., Fundamentals of durable reinforced concrete (Modern Concrete Technology). 2002. Spon Press, London.

4. KANELLOPOULOS A., QURESHI T.S. AND AL-TABBAA A. *Glass encapsulated minerals for self-healing in cement based composites*, Construction and Building Materials, Vol. 98, 2015, pp. 780-791.

5. GIANNAROS P., KANELLOPOULOS A. AND AL-TABBAA A. *Sealing of cracks in cement using microencapsulated sodium silicate*, Smart Materials and Structures, 2016, paper accepted (in-press).

6. SHARMA, T., ALAZHARI, M., COOPER, R., HEATH, A. AND PAINE, K., *The requirements for autonomic microbiologically-induced calcite-precipitation in concrete*. Paper presented at the 5th International Conference on Self-Healing Materials, Durham, USA, June 2015

7. ISAACS, B., LARK, R., JEFFERSON, T., DAVIES, R., DUNN, S., Crack healing of cementitious materials using shrinkable polymer tendons. Structural Concrete. doi:10.1002/suco.201200013, 2013.

8. PILEGIS, M. TEALL, O. HAZELWOOD, T. JEFFERSON, T. GARDNER, D. LARK. R. *Delayed concrete pre-stressing with shape memory tendons*. Fib symposium 2015, Copenhagen, Denmark.

9. DAVIES, R., JEFFERSON, T., LARK, R. GARDNER, D, *A novel 2D vascular network in cementitious materials.* Fib symposium 2015, Copenhagen, Denmark.

# THE EFFECTS OF SOL-GEL SILICATES ON HYDRATION KINETICS AND MICROSTRUCTURE OF PORTLAND CEMENT SYSTEMS

**M Shakil**

**J C Holley**

**K A Paine M P Ansell**

University of Bath

United Kingdom

**ABSTRACT:** The effects of sol-gel silicates on Portland cement hydration were investigated. Silica sols were realized by tetraethylorthosilicate, triethoxymethylsilane, ethanol, water and nitric acid or ammonia. Solvent-free sols were also synthesised. The prepared sols were mixed with cement pastes at a w/c of 0.4 or 0.5 at varying doses of 0.5–10% by mass of dry cement. The solvent-free synthesised sol appeared to be a more suitable candidate. This is because observation of the hydration kinetics revealed a shortening of the dormant phase of cement hydration and exhibited a higher power output during this stage, representative of additional nucleation sites created in the system. However, the main peak power output that occurs at the end of acceleratory stage was decreased, further pronounced at higher sol dosages. This can be attributed to the ethoxy-based precursor, which produces ethanol as a by-product of hydrolysis reactions. It is therefore of great interest to investigate possible routes to optimise the sols to limit the alcohol content. SEM analyses on fractured surfaces of 28 day old pastes revealed a distinctive morphology, particularly at higher sol dosages. The development of C-S-H on portlandite was observed, which further suggests that the sol-gel silicates could be providing additional nucleation sites, acting as a seeding agent.

**Keywords:** Silica, Sol-gel, Nanotechnology, Nucleation seeding, C-S-H polymerisation.

**Muzzamil Shakil** is a second year PhD Candidate in Civil Engineering at the BRE Centre for Innovative Construction Materials, University of Bath.

**Dr Juliana Calabria-Holley** is a Lecturer in Architecture within the BRE Centre for Innovative Construction Materials at the University of Bath. Her research focuses on nanotechnology applied to natural building materials and cementitious systems, sol-gel systems for construction materials and surface engineering.

**Dr Kevin Paine** is a Reader in Civil Engineering and Deputy Director of the BRE Centre for Innovative Construction Materials at the University of Bath. His research focuses on low carbon, smart and nanotechnology-enhanced concretes.

**Dr Martin Ansell** is Reader in Materials at the University of Bath and a member of the BRE Centre for Innovative Construction Materials. His research is currently centred on eco-innovative construction materials, including natural fibre composites and photocatalytic coatings for wood-based panel products.

## INTRODUCTION

In light of the overriding imperative to reduce the carbon footprint, research in the recent decades has been underscored to improve the sustainability of cementitious materials. Primarily, this has been focused on limiting the amount of Portland cement (clinker content) in cement-based mixtures through various possible routes. These have included the use of chemical admixtures, inert fillers, supplementary cementitious materials, and optimization of aggregate size and content [1-4]. Enhancing the durability of cementitious materials, which are susceptible to degradation due to moisture ingress, aggressive ions, chemicals, abrasion or weathering, has persisted as another major challenge for material scientists.

Calcium Silicate Hydrate (C-S-H), a micro and nano-porous gel, is the most critical product of cement hydration and the major phase responsible for cohesion. Occupying over 60% by volume of the hydrated cement paste [5-7], it is a major contributor to the mechanical and physical properties, which include strength, shrinkage and permeability. Recent advances in nano-characterization techniques have led to an increased understanding of the nanostructure of C-S-H [6]. This has led to a promising new stream of research focused on the application of nanotechnology to modify and manipulate matter at a near atomic scale in efforts to develop superior and novel C-S-H systems [3, 7-9]. Several researchers have demonstrated that conventional cementitious materials exhibit radically improved properties when engineered at the nanoscale [10].

The term ‘seeding’ agents, or nucleation seeding, often refers to the use of pre-hydrated silicates for the modification of the hydration processes [11]. It has proved to be a useful approach to control the kinetics of cement hydration, most notably for acceleratory effects [12]. More importantly, it has also been recognised as a unique tool to tailor the overall composition of C-S-H and the micro and nanostructure of hydrated Portland cement. In particular, the seeding effect in silica-cement systems is rather well documented, and known to improve the strength, stiffness and the durability characteristics of cement-based materials. In addition to the pozzolanic properties, it is believed that particles of micro and nanosilica serve as nucleation sites for enhanced precipitation of C-S-H [12-19]. Accordingly, a more intricate and denser microstructure of C-S-H networks has been observed for silica supplemented cement systems [18, 20-23].

The important role of silica in the C-S-H framework is irrefutable. Careful examination of silica chemistry shows that the chemical reactions that occur during formation of the basic silicate species follow an almost identical pathway in the case of Portland cement hydration, pozzolanic materials and blended mixtures. It must also be emphasised that cement hydration displays many similarities to the synthesis processes of sol-gel silicates, and may be regarded as a special branch of inorganic polymerisation. Typically, sol-gel synthesis involves the hydrolysis and polycondensation of silicon alkoxide precursors using water, alcohol as a mutual solvent and a catalyst. Careful control of the processing parameters may provide the ability to produce cementitious systems that are low in carbon, more energy efficient and with greater resilience than conventional Portland cement based systems. This can be achieved by tailoring the degree of polymerisation of C-S-H to a higher level, which is expected to facilitate the ‘refinement’ of the micro and nanostructure. In addition, the increase in the silicate chain length within the C-S-H framework would also lead to a more stable matrix. In line with the objectives discussed above, the application of sol-gel technology to cementitious materials opens up the door to endless possibilities, both for research and industry.

In the current work, investigations were carried out to assess the prospect of employing sol-gel material as a seeding agent for Portland cement systems. In this regard, the effects of sol-gel silicates on cement hydration were examined. The parameters of the sol-gel synthesis were explored in order to elucidate the suitable candidates, and to gain an improved understanding with regards to the limitations. The synthesis parameters of importance include the molar ratio of the materials, type of silicon alkoxide precursors, nature and concentration of the catalyst, pH, temperature, amount of water or more specifically the R-value, that is, the molar ratio of $H_2O/Si$, and synthesis duration. These parameters not only affect the sol-to-gel kinetics and the resultant gel structure but also influence the overall behaviour of the sol-gel material as it interacts with Portland cement. In more detail, the kinetics of cement hydration and the effects on the microstructure of cement pastes dosed with sol-gel material were characterised by means of isothermal calorimetry and scanning electron microscopy.

## EXPERIMENTAL

### Synthesis of Sol-gel Silicates

For the synthesis of sol-gel silicates, tetraethoxysilane (TEOS) reagent grade 98% and triethoxymethylsilane (MTES) technical grade 90% supplied by Sigma-Aldrich were the two silicon precursors used. Nitric acid ($HNO_3$) puriss .p.a > 65% and ammonium hydroxide ($NH_4OH$) 28–30% $NH_3$ basis were used as the acid and base catalysts, respectively, also supplied by Sigma-Aldrich. Ethanol (EtOH) puriss. p.a ACS reagent 99.8% was employed as the mutual solvent, supplied by Fluka. Distilled water was used for all sol preparations. The molar ratios of the starting materials, synthesis parameters and duration are presented in Table 1. The formulations and parameters for sol-gel synthesis were adopted on the merits of low and high pH to investigate the two ranges of pH spectrum of the starting sols on cement hydration. The solutions were continuously agitated for the entire duration of the synthesis procedure. The prefix, A, as in the case of sol A1 denotes an acidic medium, and similarly a basic medium for sol B1. In order to mitigate the effects of alcohol on cement hydration, sols A2 and B2 were allowed to age in partially opened containers for one week prior to being used as admixtures. Sol N1 was synthesized without the use of a catalyst and without ethanol.

Table 1 Formulations and parameters for sol synthesis

| DES | TEOS | MTES | EtOH | $H_2O$ | $HNO_3$ | $NH_4OH$ | pH | TEMP | DURATION |
|---|---|---|---|---|---|---|---|---|---|
| A1 | 1 | 0.333 | 4 | 8 | 0.005 | - | 3.00 | 40°C | 1.25 hr |
| B1 | 1 | - | 4 | 10 | - | 0.03 | 9.80 | 40°C | 1.67 hr |
| A2 | 1 | - | 4 | 4 | 0.05 | - | 0.95 | 25°C | 25 hr |
| B2 | 1 | - | 4 | 4 | - | 0.05 | 9.80 | 25°C | 25 hr |
| N1 | 1 | - | - | 4 | - | - | 4.50 | 25°C | 1 hr |

### Sol-gel Enhanced Cement Mixtures

The cement used in the present work was CEMI (BS EN 197-1:2011) with 95% OPC content and 5% minor additional constituents. Table 2 illustrates the mix design of the prepared specimens. Cement pastes were prepared at a predetermined water-to-cement ratio (w/c) of 0.4

or 0.5. The designation is assigned according to the sol that was used and the w/c ratio. For example, A1C1, the prefix indicates that sol 'A1' was used to prepare the cement pastes whereas the suffix 'C1' indicates that the w/c ratio was 0.4. Similarly, for A2C2, sol 'A2' was used and 'C2' represents a w/c of 0.5 Accordingly, the controls are designated simply as C1 or C2. A Standard mortar mixer conforming to BS EN 196-1:2005 was used at blade rotational speed of 285 $min^{-1}$ and planetary movement of 125 $min^{-1}$. Cement quantity was fixed for all cement pastes and the dosage of sol-gel material was varied at doses of 0.5, 1, 3 and 5% by mass of dry cement for sols A1 and B1. Given that the sols A2, B2 and N1 were optimised for lower alcohol content, dosages were increased to 1, 3, 5 and 10% by mass of dry cement. The higher percentage was used to augment the possible effects and to elucidate minor changes in the chemical and the microstructural properties. In some cases, particularly at high dosages, inhomogeneous mixing of the sol-gel material with the cement pastes was observed. In all cases, part of the prepared paste was immediately placed in a sample holder and analysed using isothermal calorimetry. The remainder was cast into 8x40x160 mm moulds for a 24 hour period and subsequently cured for 28 days under water at 20°C until microstructural characterisation.

Table 2 Mix design

| DESIGNATION | SOL | CEMENT | W/C | DOSAGE (% BY MASS OF DRY CEMENT) |
|---|---|---|---|---|
| C1 | - | CEMI | 0.4 | - |
| A1C1 | A1 | CEMI | 0.4 | 0.5, 1, 3 and 5 |
| B1C1 | B1 | CEMI | 0.4 | 0.5, 1, 3 and 5 |
| C2 | - | CEMI | 0.5 | - |
| A2C2 | A2 | CEMI | 0.5 | 1, 3, 5 and 10 |
| B2C2 | B2 | CEMI | 0.5 | 1, 3, 5 and 10 |
| N1C2 | N1 | CEMI | 0.5 | 1, 3, 5 and 10 |

## Instrumentation

The kinetics of cement hydration was followed using a Calmetrix I-Cal 4000 calorimeter. The equipment was set to log data for a 52-hour period, allowing for enough information on early hydration to be collected. Tests were carried out at a temperature of 20°C for all series of investigations.

Morphological changes were investigated using secondary imaging generated by a Joel JSM 6301F field emission scanning electron microscope. The protocol employed to prepare the samples for microstructural characterisation has been described elsewhere [18]. The as-prepared 28-day samples were fractured using a blade and the fracture surface coated with 20nm of chromium. The conductive coating permitted operating at higher accelerating voltages without the effects of 'charging', giving cleaner images at higher magnifications.

## RESULTS

### Kinetics of Cement Hydration (Isothermal Calorimetry)

The hydration kinetics of cement pastes A1C1 and B1C1 are presented in Figure 1 and Figure 2, respectively. In the case of A1C1 (Figure 1), cement pastes with the acid catalysed sol, the 'dormant' phase was extended and the peak power output decreased considerably, as the dosage was increased from 0.5% to 5%. Accordingly, a reduction in the total amount of energy released with increasing dosage during the period of 52 hours was observed. Cement pastes with 3% and 5% dose were significantly retarded.

For B1C1 (Figure 2), cement pastes with the base catalysed sol, as the dosage was increased from 0.5% to 5%, no lengthening of the dormant phase was observed but the main peak power output decreased. The deceleration stage was marginally lengthened. In more detail, an increase in dosage from 0.5 to 1% should have resulted in a further decrease in peak power output. Instead, an increase was noted. Likewise, the power plots for 0.5% and 3% dosages are very similar to each other. Accordingly, the total energy released over the 52 hour period is almost the same for the control and the sample with 1% dose, similarly for 0.5% and 3% dosages. A significantly increased level of activity during the dormant phase was noted when sol dosage was increased to 5%. Two distinct preliminary conclusions could be drawn. (i) Alcohol content in the sol is of primary concern and 'inhibits' cement hydration, that is, reduces the peak power output. (ii) The pH alone is not a limiting factor, the acid may be considered to be of secondary importance, which so far appears to 'delay' hydration, that is, shifts the peak power.

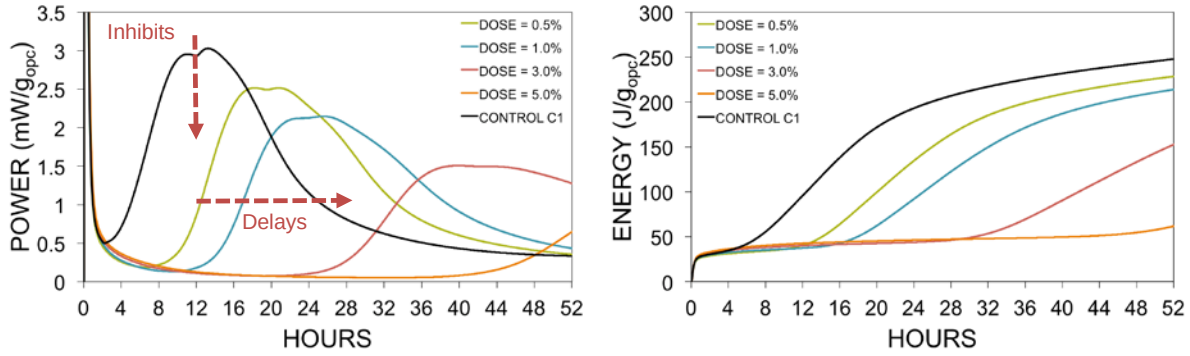


Figure 1 Hydration of cement pastes A1C1, (Left): Power output (Right): Cumulative energy

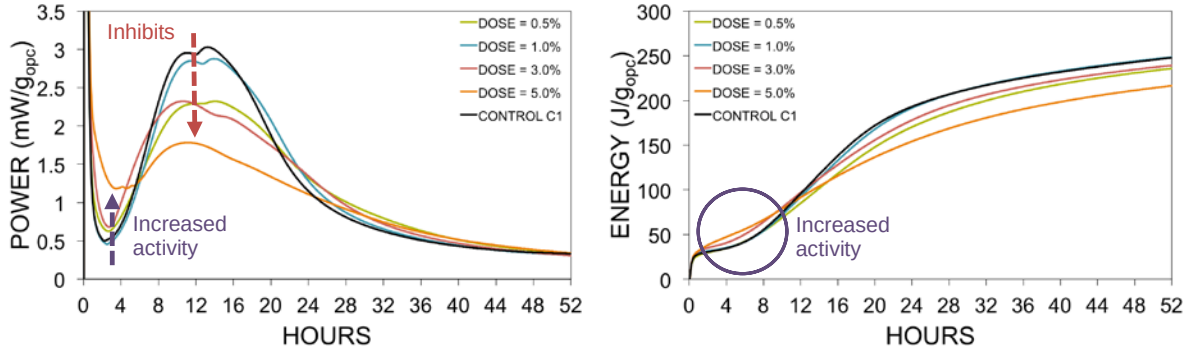


Figure 2 Hydration of cement pastes B1C1, (Left): Power output (Right): Cumulative energy

The hydration kinetics of cement pastes with the optimised sols, A2C2, B2C2 and the solvent–free synthesised sol N1C2 are presented in Figure 3, Figure 4 and Figure 5, respectively. In the case of A2C2, cement pastes with the optimised acid catalysed sol, with increase in dosage from 1% to 10% a reduction in the peak power output was noted in comparison to control C2. Despite the higher sol dosages, the effects were less dramatic compared to A1C1 (Figure 1). Likewise, a lengthening of the dormant phase was observed, which was also less pronounced than A1C1. A significant lengthening of the deceleration stage occurred, particularly at higher doses. Overall, the cumulative energy plots of A2C2 illustrate that the post-synthesis 'optimisation protocol' of the sol A2 (1 week ageing in partially open containers) led to an improvement of cement hydration, when compared to A1C1. This is evident considering the higher energy evolved at the 52-hour mark. Speculatively, if the test continued to run for a longer duration of 72 hours, for 1% dosage, the total energy may have increased beyond that of the control. Further experimentation to validate this hypothesis is required. It is also worth mentioning that a direct comparison between A2C2 and A1C1 is limited to some extent, owing to the rather different formulations employed.

Considering B2C2 (Figure 4), cement pastes with the optimised base catalysed sol, with an increase in dosage from 1% to 10% a reduction in the peak power output was detected in comparison to control C2. These effects were more dramatic in comparison to B1C1 (Figure 2). Interestingly, despite the alkaline pH of the sol, lengthening of the dormant stage occurred, which was more prominent at higher dosages. The paste with 10% dose was considerably retarded. This 'delaying' effect was not observed in the case of B1C1 (Figure 2). A direct comparison between B2C2 and B1C1 is limited to an extent due to the different formulations. It is however worth mentioning that in the case of B2C2, the sol was more concentrated with alcohol, due to the lower R-value ($H_2O$/Si molar ratio) employed; despite the post-synthesis 'optimisation protocol' of the sol B2 (1 week ageing in partially open containers), it had a higher alcohol percentage in the dose applied. Collectively, the aforementioned observations support the initial hypothesis that alcohol 'inhibits' cement hydration and that pH alone is not the dominant limiting factor. The power output plots of A2C2 (acidic sol) in Figure 3 and B2C2 (basic sol) in Figure 4, which can be directly compared owing to similar formulations employed, further support this view.

In the case of N1C2 (Figure 5), cement pastes with the solvent-free non-catalysed sol, as the dosage was increased from 1% to 10% a decrease in peak power output was noted. There were some discrepancies, for example when the sol dosage was increased from 3% to 5%, possibly due to inhomogeneous intermixing with the cement paste. A significant lengthening of the deceleration stage was detected, and more interestingly the extended 'shoulder' observed at the 28–36 hour mark in the case of 5% dose. As a result, the total energy evolved, appeared to increase at later stages. The 1, 3, and 5% dosed pastes exhibited a shortening of the dormant stage with an elevated power output in comparison to control C2, indicating possible additional nucleation of C-S-H. Despite this, the main peak power output at the end of acceleratory stage was markedly reduced for all sol-gel modified cement pastes compared to control C2. The 10% dose led to a completely retarded cement paste, which can be rationalised by the following: (i) due to the short processing time and lack of a catalyst the unhydrolysed silicon precursor molecules were hydrolysed in the highly alkaline pH environment of cement pastes, and the by-product of precursor hydrolysis (alcohol) retarded the paste, (ii) the unhydrolysed silicon precursor molecules were strongly adsorbed onto the clinker or the nucleated particles, preventing further dissolution of the clinker and precipitation of C-S-H. The cumulative energy plot further supports this view where the 10% dose revealed the highest total energy in the early stages (see Figure 5). Two possible methods to further optimise the sol N1 include (i) slightly

longer synthesis duration for increased hydrolysis or employing a dilute catalyst solution, (ii) removal of the alcohol that is produced as a by-product of precursor hydrolysis.

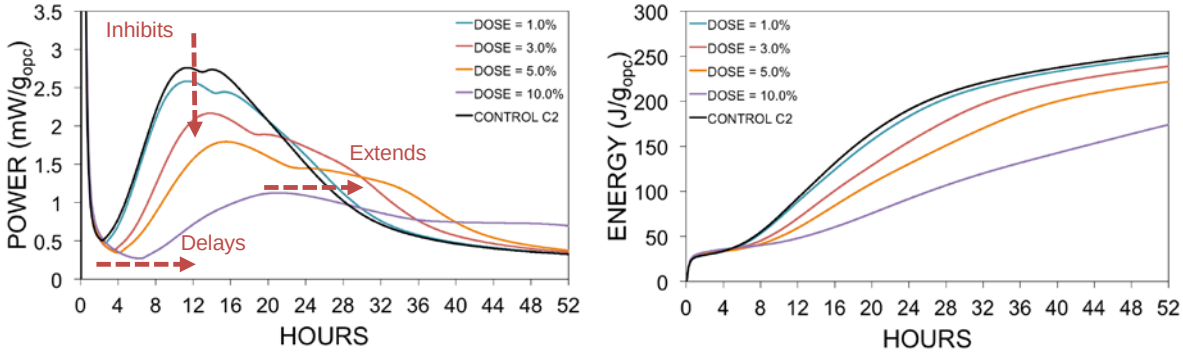


Figure 3 Hydration of cement pastes A2C2, (Left): Power output (Right): Cumulative energy

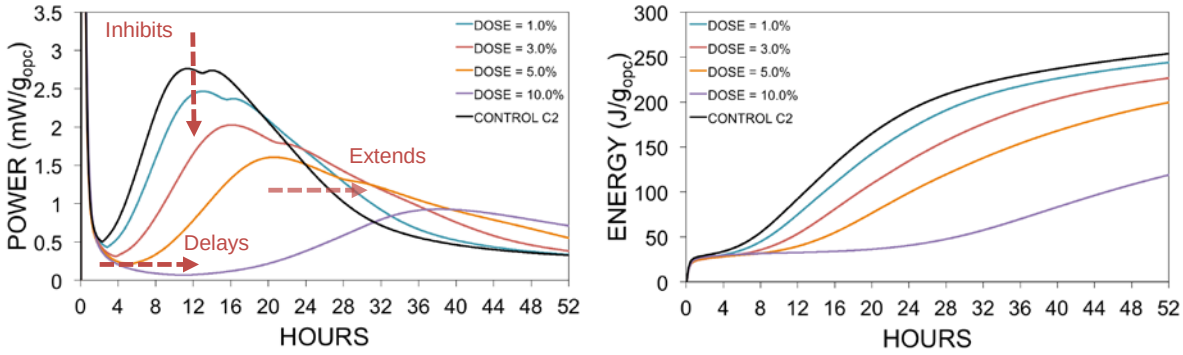


Figure 4 Hydration of cement pastes B2C2, (Left): Power output (Right): Cumulative energy

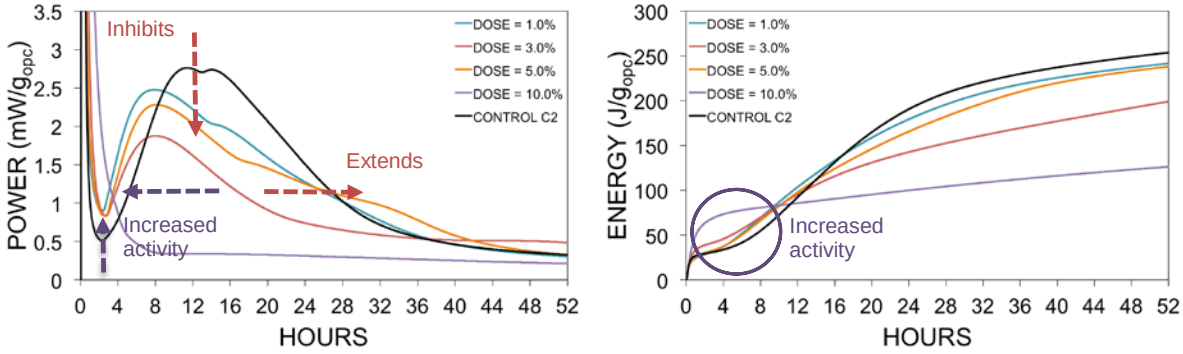


Figure 5 Hydration of cement pastes N1C2, (Left): Power output (Right): Cumulative energy

### Microstructure (scanning electron microscopy)

The microstructure of the sol-gel cement composites was investigated at 28 days to elucidate the differences in morphology of mature cement pastes. Investigations were carried out on all samples at 28 days. However, in light of the observed hydration kinetics that exhibited a shortening of the dormant stage along with an increased level of activity during this stage (see Figure 5), emphasis here is placed on cement pastes with the solvent-free non-catalysed sol (N1C2). At low magnifications no real distinctions could be made. Figure 6 displays SEM micrographs at high magnifications for the control C2 and N1C2 at doses of 1, 5 and 10%.

With an increase in dosage, particularly at 5% and 10%, differences in morphology could be observed along with C-S-H nucleation.

For the control C2 at high magnification (Figure 6a), the long thin needles represent ettringite, whereas C-S-H can be seen as the fine smaller fibre-like structures. The tiny spherical particles were unexpected in the control sample, which can most likely be attributed to the minor additional constituents. The strong resemblance to micro and nanosilica particles is also worth pointing out. The microstructure and morphology for N1C2 dose 1% (Figure 6b) was almost identical to that of control C2, despite the calorimetry data indicating that some form of additional nucleation of C-S-H had occurred. In the case of N1C2 dose 5%, Figure 6c displays what appears to be dense C-S-H gel towards the right hand side of the protruding needles of ettringite.

Closer examination at higher magnifications of the specimen, illustrated in Figure 6d, shows what appears to be C-S-H covered with dense clusters or particles, different than what was observed in Figure 6a and Figure 6b. Given the high percentage of the sol dosage, it could either be silica nanoparticles that precipitated at the high pH, or possibly a granular form of C-S-H observed at very low Ca/Si ratios, as also reported by He et al. [24]. The latter gains further prospect, given the power plot of the calorimetry data (Figure 5) that showed a shortening of the dormant phase with an increased level of heat output, representative of additional nucleation of C-S-H.

Additionally, for N1C2 dose 5%, the C-S-H gel as observed in Figure 6c, or the granular agglomerations of C-S-H as shown Figure 6d, both, appear to form much denser pastes when compared to the control C2 and N1C2 dose 1%. This could lead to enhanced durability characteristics and performance.

The micrograph for N1C2 dose 10%, shown in Figure 6e, displays a very distinct morphology, a reticular form of C-S-H being developed on a portlandite sheet, also intrinsic to low Ca/Si ratio (higher degree of C-S-H polymerisation). These appear to form rather intricate or interconnected networks. A similar observation of another N1C2 sample at 10% sol dosage, shown in Figure 6f, further corroborates these findings. It is worth noting, that the individual elements are bulkier than the thin fibre-like structures of C-S-H observed in Figure 6a and Figure 6b, and should facilitate pore refinement and a stronger paste. The obtained findings strongly suggest the interaction of the sol-gel material with cement, and that it possibly acts as a seeding agent for the nucleation of C-S-H.

Indeed, the energy plot of the calorimetry data (Figure 5) showed the highest amount of total energy evolved at the early stage for the 10% dose, indicative of additional nucleation, but subsequent retardation was noted. Perhaps, the paste ‘recovered’ during the curing process. However, optimising the sol to mitigate the retardation effect could lead to better control over the formation of such a microstructure or perhaps lead to even more unique morphologies.

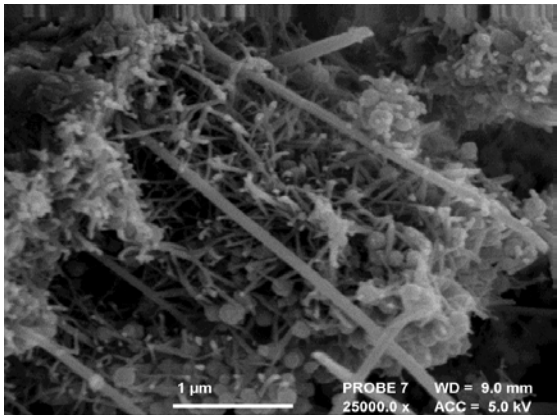


a) Control C2

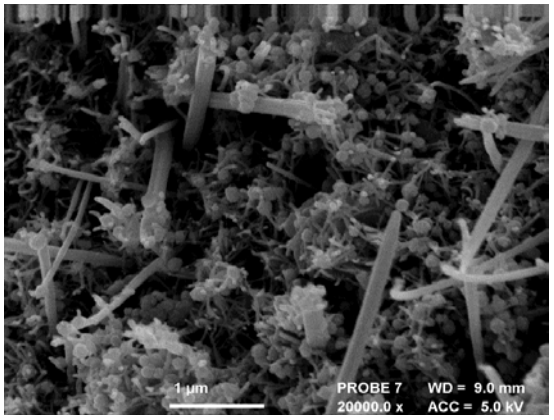


b) N1C2 Dose 1%

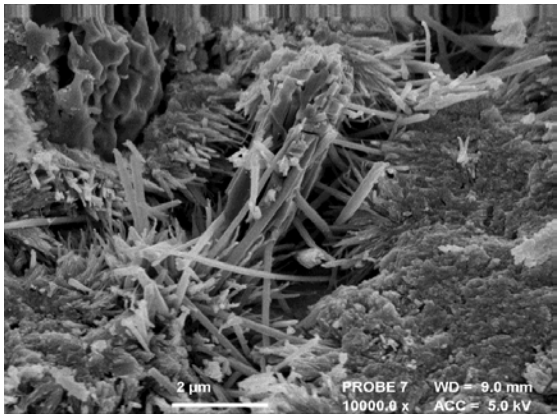


c) N1C2 Dose 5%

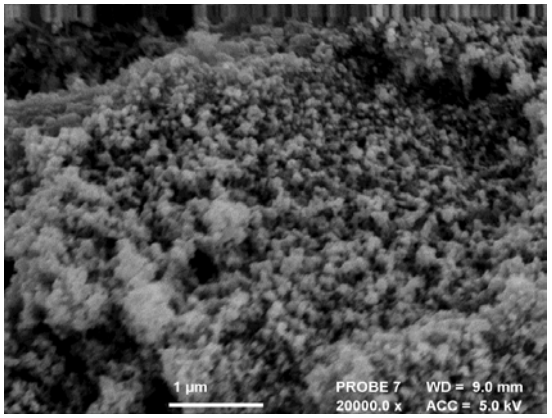


d) N1C2 Dose 5%

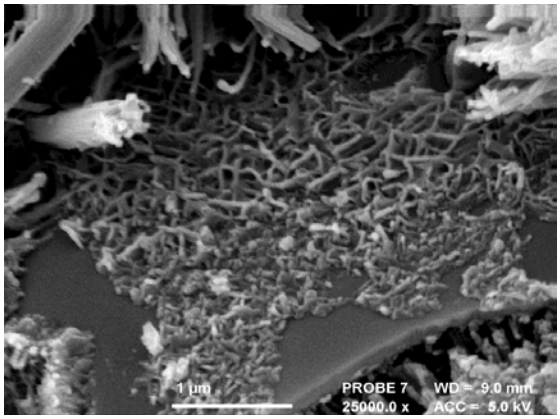


e) N1C2 Dose 10%

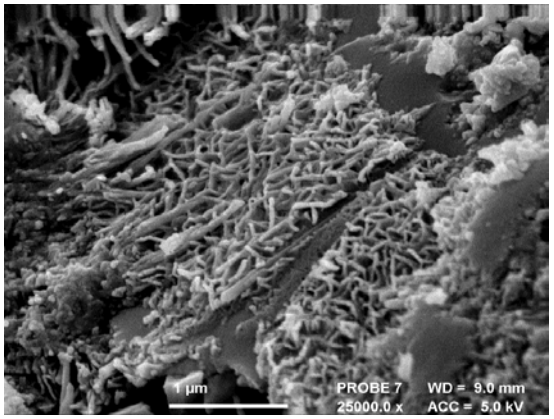


f) N1C2 Dose 10%

Figure 6 SEM micrographs at 28 days showing differences in morphology at high magnification.

## CONCLUSIONS

The effect of sol-gel material on cement hydration was investigated. Initial findings based on calorimetric data suggested that alcohol, either used as a solvent or that which is produced as a by-product of precursor hydrolysis, primarily 'inhibits' cement hydration whereas an acidic sol 'delays' the hydration processes. For cement pastes with the optimised and solvent-free synthesised sols, the data further supports that pH alone is not the limiting parameter. The optimised acidic and basic sols, both, exhibited similar trends concerning early hydration kinetics. The solvent-free synthesised sol appeared to accelerate cement hydration and indicated enhanced nucleation of C-S-H. SEM micrographs showed distinct morphologies of C-S-H, changing from isolated 'thin' fibre-like, to dense granular and lastly to reticular C-S-H structures. The latter being a result of a more intricate network of the silicates, particularly at higher sol dosages. The development of a complex network of C-S-H with bulkier elements than the control was observed on a portlandite crystal. The findings so far suggest that the silicate species introduced by the sol-gel material provided additional nucleation sites for C-S-H precipitation.

## ACKNOWLEDGEMENTS

The authors would like to acknowledge and thank the Engineering and Physical Sciences Research Council for their support via grant EP/L016869/1.

## REFERENCES

1. HOOTON, R D & BICKLEY, J A, Design for durability: The key to improving concrete sustainability, Construction and Building Materials, 67, Part C(0), 2014, pp. 422-430.
2. SCRIVENER, K L & NONAT, A, Hydration of cementitious materials, present and future, Cement and Concrete Research, 41(7), 2011, pp. 651-665.
3. ALIZADEH, R A, Nanostructure and engineering properties of basic and modified calcium-silicate-hydrate systems, PhD Thesis, 2009, University of Ottawa.
4. DAMTOFT, J S, LUKASIK, J, HERFORT, D, SORRENTINO, D & GARTNER, E M, Sustainable development and climate change initiatives, Cement and Concrete Research, 38(2), 2008, pp. 115-127.
5. PAPATZANI, S, PAINE, K & CALABRIA-HOLLEY, J, A comprehensive review of the models on the nanostructure of calcium silicate hydrates, Construction and Building Materials, 74(0), 2015, pp. 219-234.
6. WU, H-C, Re-examination of cement hydration: sol–gel process, Advances in Cement Research, 26(5), 2013, pp. 292-301.
7. RAKI, L, BEAUDOIN, J, ALIZADEH, R, MAKAR, J & SATO, T, Cement and concrete nanoscience and nanotechnology, Materials, 3, 2010, pp. 918-942.
8. SAFIUDDIN, M, GONZALEZ, M, CAO, J & TIGHE, S L, State-of-the-art report on use of nano-materials in concrete, International Journal of Pavement Engineering, 15(10), 2014, pp. 940-949.

9. BIRGISSON, B, MUKHOPADHYAY, A K, GEARY, G, KHAN, M & SOBOLEV, K, Nanotechnology in Concrete Materials: A Synopsis, Transportation Research E-Circular, (E-C170), 2012.

10. KIM, J J, RAHMAN, M K, AL-MAJED, A A, AL-ZAHRANI, M M & TAHA, M M R, Nanosilica effects on composition and silicate polymerization in hardened cement paste cured under high temperature and pressure, Cement and Concrete Composites, 43, 2013, pp. 78-85.

11. ALIZADEH, R, RAKI, L, MAKAR, J M, BEAUDOIN, J J & MOUDRAKOVSKI, I, Hydration of tricalcium silicate in the presence of synthetic calcium-silicate-hydrate, Journal of Materials Chemistry, 19(42), 2009, pp. 7937-7946.

12. LAND, G & STEPHAN, D, The influence of nano-silica on the hydration of ordinary Portland cement, Journal of Materials Science, 47(2), 2012, pp. 1011-1017.

13. LARBI, J, FRAAY, A & BIJEN, J, The chemistry of the pore fluid of silica fume-blended cement systems, Cement and Concrete Research, 20(4), 1990, pp. 506-516.

14. DETWILER, R J & MEHTA, P K, Chemical and physical effects of silica fume on the mechanical behavior of concrete, ACI Materials Journal, 86(6), 1989.

15. WU, Z-Q & YOUNG, J, The hydration of tricalcium silicate in the presence of colloidal silica, Journal of materials science, 19(11), 1984, pp. 3477-3486.

16. BULLARD, J W, JENNINGS, H M, LIVINGSTON, R A, NONAT, A, SCHERER, G W, SCHWEITZER, J S, SCRIVENER, K L & THOMAS, J J, Mechanisms of cement hydration, Cement and Concrete Research, 41(12), 2011, pp. 1208-1223.

17. BJÖRNSTRÖM, J, MARTINELLI, A, MATIC, A, BÖRJESSON, L & PANAS, I, Accelerating effects of colloidal nano-silica for beneficial calcium–silicate–hydrate formation in cement, Chemical Physics Letters, 392(1), 2004, pp. 242-248.

18. HOLLEY, J C, PAINE, K & PAPATZANI, S, Effects of nanosilica on the calcium silicate hydrates in Portland cement–fly ash systems, Advances in Cement Research, 27(4), 2014, pp. 187-200.

19. FLORES-VIVIÁN, I & SOBOLEV, K, 2015. The Effect of Nano-SiO2 on Cement Hydration. Nanotechnology in Construction. Springer, pp. 167-172.

20. SINGH, L, AGARWAL, S, BHATTACHARYYA, S, SHARMA, U & AHALAWAT, S, Preparation of silica nanoparticles and its beneficial role in cementitious materials, Nanomaterials and Nanotechnology, 1(1), 2011, pp. 44-51.

21. JO, B-W, KIM, C-H, TAE, G-H & PARK, J-B, Characteristics of cement mortar with nano-SiO 2 particles, Construction and building materials, 21(6), 2007, pp. 1351-1355.

22. LI, H, XIAO, H-G, YUAN, J & OU, J, Microstructure of cement mortar with nano-particles, Composites Part B: Engineering, 35(2), 2004, pp. 185-189.

23. DOTTO, J, DE ABREU, A, DAL MOLIN, D & MÜLLER, I, Influence of silica fume addition on concretes physical properties and on corrosion behaviour of reinforcement bars, cement and concrete composites, 26(1), 2004, pp. 31-39.

24. HE, Y, LU, L, STRUBLE, L J, RAPP, J L, MONDAL, P & HU, S, Effect of calcium–silicon ratio on microstructure and nanostructure of calcium silicate hydrate synthesized by reaction of fumed silica and calcium oxide at room temperature, Materials and Structures, 47(1-2), 2014, pp. 311-322.

# PUNCHING OF SLABS REINFORCED WITH RECYCLED STEEL FIBRES FROM USED TYRES

**M Bartolac** **D Damjanović** **J Krolo**
**I Duvnjak** **A Baričević**

University of Zagreb
Croatia

**ABSTRACT.** This paper presents an effort to find a new application for sorted recycled tyre steel fibres. Namely, usage of these fibres as reinforcement in concrete slabs loaded in punching has been investigated. Punching of a slab in a building is a rather brittle phenomenon that can lead to progressive collapses of neighbouring slab – column connections. Finally, this domino effect can cause collapse of the entire structure. Punching shear capacity of slabs is traditionally increased by reinforcement in the form of stirrups or headed shear studs. In addition to these methods, industrially manufactured steel fibres have proved to be an effective alternative because of their positive effect on punching load and deformation capacity of the elements concerned. The main objective of the presented research was to test the ability of sorted recycled steel fibres to perform in the same way as industrial steel fibres. Research included investigation of reinforced concrete slabs made of several mixes including plain concrete, a mix with industrial steel fibres and mixes with industrial and recycled steel The obtained results indicate that the usage of hybrid fibres can improve the punching strength and deformation capacity of concrete slabs. Furthermore, the slabs reinforced with hybrid fibres showed better behaviour when compared to slabs reinforced only with industrial steel fibres.

**Keywords:** Fibre reinforced concrete, Flat slab, Punching shear, Recycled tyres, Experimental investigation

**Marko Bartolac** is a postdoctoral researcher and teaching assistant at the Faculty of Civil Engineering, University of Zagreb.

**Domagoj Damjanović** is an Assistant Professor and Head of the Structural Testing Laboratory at the Faculty of Civil Engineering, University of Zagreb.

**Joško Krolo** is an Associate Professor and Head of the Chair of Material Mechanics and Structural Testing at the Faculty of Civil Engineering, University of Zagreb.

**Ivan Duvnjak** is a postdoctoral researcher and teaching assistant at the Faculty of Civil Engineering, University of Zagreb.

**Ana Baričević** is a postdoctoral researcher and teaching assistant at the Department of Materials at the Faculty of Civil Engineering, University of Zagre.

## INTRODUCTION

Because of their construction and architectural advantages, flat slabs are usually used in medium height office buildings, residential buildings and parking garages. This system makes the formwork and reinforcement substantially simpler, also allowing for easy placement and installation of equipment underneath the slab. In addition, it offers lower overall storey heights [1], [2]. Since flat slabs are supported directly on columns, without beams between the columns, they generally transfer a significant concentrated load that affects a relatively small area. The issues in design of flat slabs are mostly governed by quite high deflections in serviceability conditions and punching shear failure in the ultimate limit state [2]. The punching failure mode is generally a brittle failure mode that can lead to progressive collapses because of the adversely redistributed loads. Finally, such an event can lead to the load bearing capacity loss of the entire structure [1]. There are many reinforcement solutions available for increasing the punching shear capacity, such as bent-up bars, stirrups, double headed shear studs, structural steel shear heads, shear bands, lattice shear reinforcement and UFO punching preventers [3]. Furthermore, there are solutions available for increasing the punching shear capacity of existing flat slab systems, i.e. post-installed punching shear reinforcement [4]. In the last couple of decades, the use of steel fibre reinforced concrete (SFRC) for increasing the punching shear capacity of flat slabs has been researched (e.g. [5], [6], [7], [8], [9], [10]). Researches in these studies generally concluded that the use of fibre reinforcement is a viable alternative for increasing the punching shear capacity of slab-column connections.

Furthermore, researchers noticed an increase in deformational capacity of SFRC slabs which was explained by the bridging effect of the fibres after the concrete matrix cracked. Overall, it can be concluded that steel fibres are able to maintain the integrity of the slabs, i.e. to mitigate or even prevent the brittle failure caused by punching shear [11]. Besides industrially manufactured steel fibres (MSF), recycled tyre steel fibres (RTSF) as a by-product in the recycling process of waste car and truck tyres came in focus of the researchers in the last decade (e.g. [12], [13], [14], [15], [16], [17], [18], [19]). The main subject in most of the studies in this area were material properties of concrete reinforced with RTSF or with mixed MSF and RTSF (hybrid fibres – HF; hybrid steel fibre reinforced concrete – HFRC). The latter is assessed as necessary as RTSF alone are not able to bridge macro cracks because of their relatively short length. In HFRC, the amount of RTSF which replaces a certain amount of MSF in SFRC, is advised to be up to 1.5 times larger than the latter [13].

Some studies were also performed in order to assess the practical application of RTSF in the concrete industry (e.g. [20], [21], [22]). Please note that one should differentiate between the unsorted RTSF and sorted (classified) RTSF with known geometrical and mechanical properties. This fact is very important because up to date, unsorted RTSF contaminated with rubber and carbon black present the majority in the RTSF market.

This paper presents an experimental study to evaluate the effect of manufactured and hybrid (mixed manufactured and sorted recycled) steel fibres on the punching shear resistance and deformation capacity of flat slabs. A total of nine small-scale flat slabs were tested using three different concrete mixes: plain concrete mix, SFRC mix and HSFRC. Experimental results are analysed and performance of steel fibres for this kind of application is assessed.

## EXPERIMENTAL PROGRAMME

### Materials and Specimen Geometry

Three concrete mixes were used in the presented research: plain concrete mix (mix id PC), SFRC mix with 40 kg of manufactured steel fibres per m³ of concrete (mix id 40M0R) and HSFRC mix with 10 kg of manufactured and 45 kg of recycled steel fibres per m³ of concrete (mix id 10M45R). The concrete mix composition of the mentioned mixes is shown in Table 1.

Table 1 Composition of the used concrete mixes.

| CONCRETE MIXES COMPOSITION DATA | | | | | | | |
|---|---|---|---|---|---|---|---|
| Concrete mix | Cement (kg/m³) | Water (l/m³) | w/c ratio | Aggregate, total (kg/m³) | Superplasticizer (kg/m³) | MSF (kg/m³) | RTSF (kg/m³) |
| PC | | | | 1840 | | 0 | 0 |
| 40M0R | 370 | 170 | 0.46 | 1790 | 2.22 | 40 | 0 |
| 10M45R | | | | 1790 | | 10 | 45 |

Table 2 Properties of manufactured and recycled fibres used in the research.

| USED MSF AND RTSF DATA | | | | | | |
|---|---|---|---|---|---|---|
| Fibre type | Geometrical shape | Producer | Length L (mm) | Diameter D (mm) | Aspect ratio L/D | Tensile strength (N/mm²) |
| manufactured | straight with hooked ends | ArcelorMittal | 35.0 (+2/-3) | 0.55 (±0.04) | 64 | 1200 |
| recycled, sorted | irregular (wavy) | Twincon | 20.0 (±2.0) | 0.15 (±0.04) | 166 | 2850 |

The following river aggregate fractions were used: 0 – 4 mm crushed, 4 – 8 mm and 8 – 16 mm. The cement type CEM II/A-M 42,5 N was used. Also, superplasticizer was used in order to achieve the target consistency class S4. Properties of the used manufactured and sorted recycled steel fibres are shown in Table 2. Both fibre types are also shown in Figure 1.

Cube specimens with sides of 150 mm were used to determine the compressive strength $f_c$ of concrete according to the standard EN 12390-3:2009/AC:2011 [23]. Cylindrical specimens of 150 mm diameter and 300 mm height were used to determine the splitting tensile strength $f_{ct}$ of concrete according to the standard EN 12390-6:2009 [24]. The obtained average concrete strengths are shown in Table 3. Steel reinforcement bars of 14 mm in diameter and with yield strength $R_{p0.2}$ = 560 MPa, tensile strength $R_m$ = 637 MPa and elastic modulus $E_s$ = 200 GPa was used. Mechanical properties of the used reinforcement bars were determined experimentally according to the standard EN ISO 15630-1:2010 [25].

Figure 1 Manufactured steel fibres (MF) on the left and recycled tyre steel fibres (RTSF) on the right.

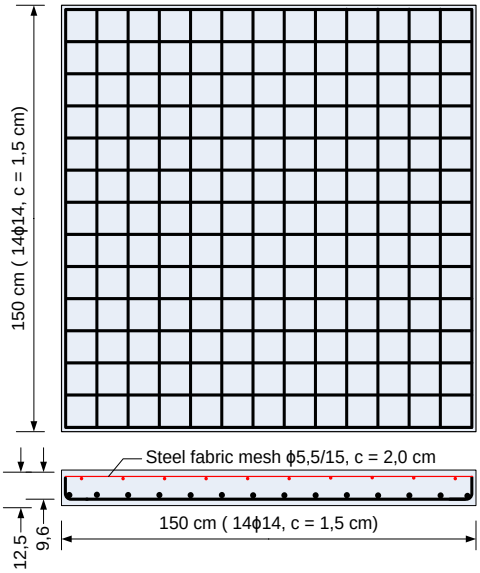


Figure 2 Slab reinforcement

Table 3 List of slab specimens.

| SLAB SPECIMENS MATERIAL PROPERTIES | | | |
|---|---|---|---|
| Slab | Concrete mix | Concrete compressive strength $f_c$ (MPa) | Concrete tensile splitting strength $f_{ct}$ (MPa) |
| S2-1 | PC | 50.4 | 3.5 |
| S2-2 | | 52.8 | 3.2 |
| S2-3 | | 54.1 | 3.1 |
| S3-1 | 40M0R | 43.1 | 3.0 |
| S3-2 | | 42.3 | 3.3 |
| S3-3 | | 44.8 | 2.9 |
| S5-1 | 10M45R | 44.3 | 3.6 |
| S5-2 | | 44.1 | 3.2 |
| S5-3 | | 43.8 | 3.7 |

Each of the three concrete mixes was used to cast three identical slab specimens. Therefore, a total of nine slabs with dimensions of 1.5 m × 1.5 m × 0.125 m were tested. Each slab was casted from different batch, so concrete properties were determined separately for all the batches. Adequate compaction was achieved by using a table vibrator. All the data regarding each particular slab are shown in Table 3. Tensile reinforcement ratio was 1.5 % in all slabs and rebars of 14 mm in diameter were spaced at 11 cm. The steel fabric mesh consisting of 5.5 mm rebars spaced at 15 cm in both directions was placed on the compression side. The protective layer of concrete was 1.5 cm on the tension side and 2.0 cm on the compression side, while the effective depth of the slabs amounted to 9.6 cm. The arrangement of slabs reinforcement in plan and cross-section is shown in Figure 2.

## Punching Tests Setup and Instrumentation

Slabs were supported by eight discrete spatially hinged supports placed on steel columns of circular cross-section, which were distributed in the radius of 75 cm from the slab centre. The slabs were loaded in displacement control mode (v = 0.6 mm/min) using a hydraulic static-dynamic testing machine of 600 kN capacity. Load was applied in the centre of the slabs via steel plate of dimensions 13 cm × 13 cm × 3 cm. To prevent stress concentration in the edges of this plate, a thin high-density fibreboard pad of approx. 850 kg/m³ and of equal plan dimensions was placed between the steel plate and the concrete slab. Figure 3 shows the described test setup.


Figure 3 Test setup: a) view of slab mounted for testing, b) sensors on slab's top face.

The loading force and various other slab behaviour parameters were continuously measured during the testing. Measurement positions are shown in Figure 4. Twelve linear variable differential transformers (LVDTs) were used for measurement of vertical displacements on top and bottom surfaces of the slabs. On the top side, displacements were measured along two axes in one-eighths and one-fourths of the span. To control the displacement symmetry, displacements were also measured in one-fourths of additional two axes. On the bottom side, displacements were measured along one axis only.

Measurement points were located in one-fourths, one-eighths and one-half of the span. Since the LVDTs for displacement measurement were placed on exact distances between each other, these measurements were also used for the calculation of slab's slope. Radial strains were measured on the compression side of the slabs using LVDTs placed on measuring base of 100 mm. Sensors were located along two axis, two sensors per each axis. The occurrence of decompression (reduction of compression strain) on these measurement points is an indicator of development of shear cracks, i.e. of the oncoming punching shear failure.

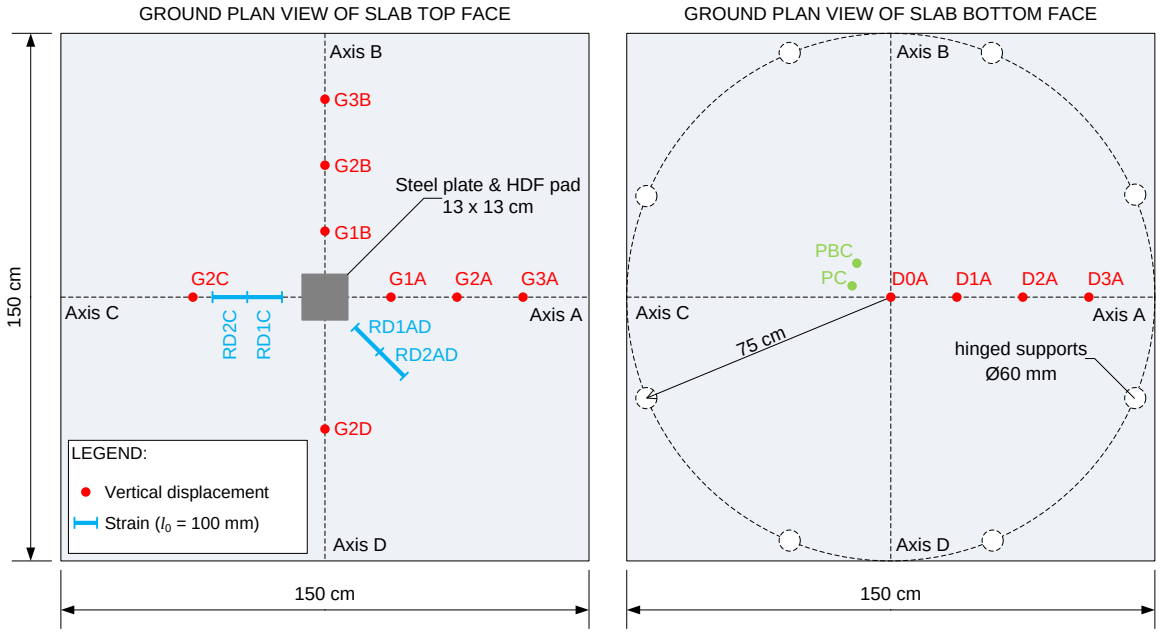


Figure 4 Positions of measurement points on slabs.

## EXPERIMENTAL RESULTS AND DISCUSSION

### Load versus Displacement Response

Figure 5 represents the load versus displacement diagrams for all the tested slabs. Displacement marked D0A was measured in the centre of the bottom side of the slabs (see Figure 4).

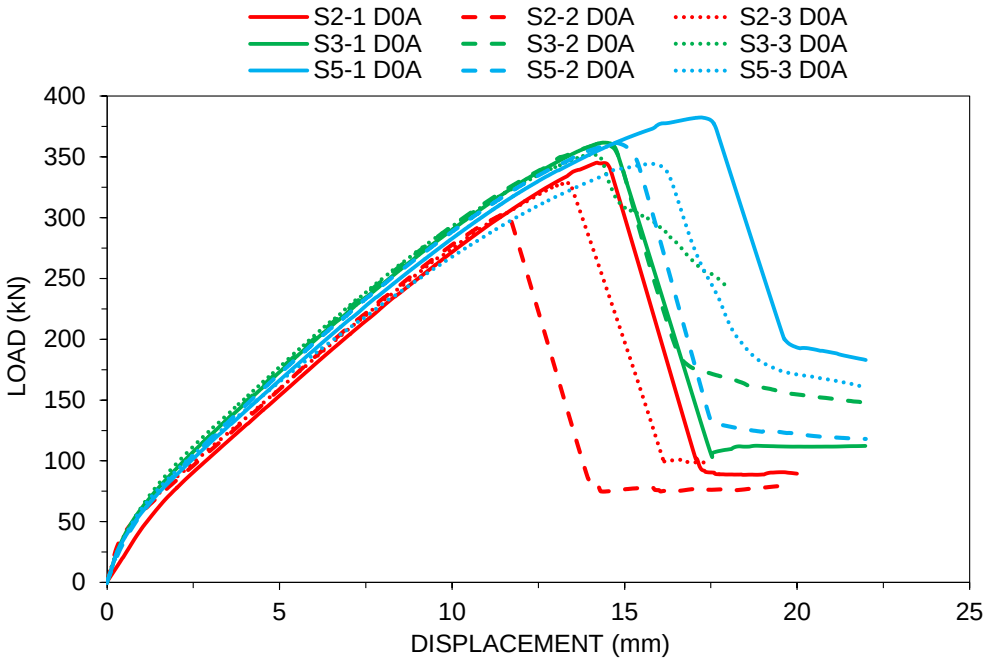


Figure 5 Load – bottom side centre displacement diagrams for all the tested specimens.

Table 4 shows relevant obtained test results, where $F_{max}$ is the maximum applied load (punching load) and $\delta_{Fmax}$ is the corresponding D0A displacement, $F_{max,\,ratio}$ is the ratio between maximum average load for SFRC (HSFRC) slabs and RC slabs, $\delta_{Fmax,\,ratio}$ is the ratio between average D0A displacement at maximum load for SFRC (HSFRC) slabs and RC slabs. The observed failure mode for each slab is also included in Table 4.

Table 4 Maximum load and displacement D0A results obtained in the punching tests.

| PUNCHING TESTS DATA | | | | | | | |
|---|---|---|---|---|---|---|---|
| Slab | $F_{max}$ (kN) | $F_{max,\,av}$ (kN) | $\delta_{Fmax}$ (mm) | $\delta_{Fmax,\,av}$ (mm) | $F_{max,\,ratio}$ | $\delta_{Fmax,\,ratio}$ | Failure mode |
| S2-1 | 345.16 | | 14.20 | | | | |
| S2-2 | 303.33 | 325.62 | 11.54 | 13.04 | - | - | Punching |
| S2-3 | 328.37 | | 13.40 | | | | |
| S3-1 | 361.69 | | 14.38 | | | | |
| S3-2 | 359.86 | 357.89 | 14.40 | 14.27 | 1.10 | 1.09 | Punching |
| S3-3 | 352.14 | | 14.03 | | | | |
| S5-1 | 382.36 | | 17.23 | | | | |
| S5-2 | 361.50 | 362.71 | 14.75 | 15.92 | 1.11 | 1.22 | Punching |
| S5-3 | 344.28 | | 15.77 | | | | |

The following Figure 6 shows average values of bottom face displacements D0A to D3A for each of the three slab groups.

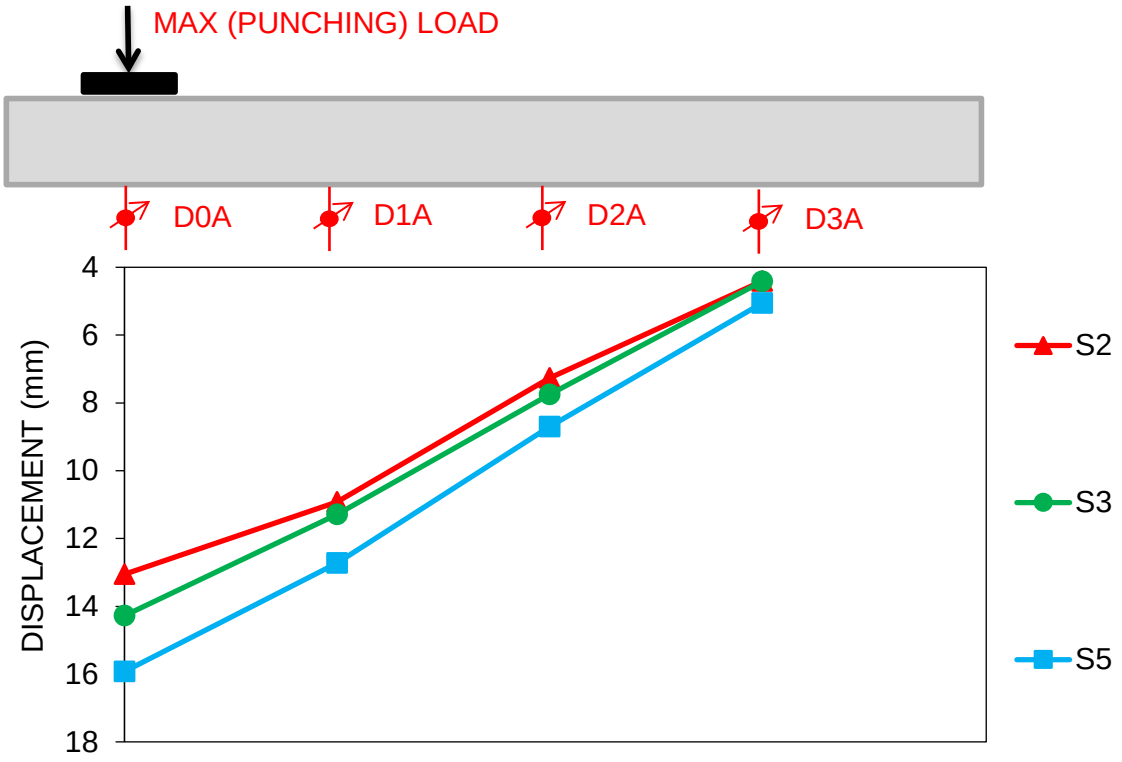


Figure 6 Average bottom face displacements at maximum (punching) load.

The presented results show a clear increase of stiffness and punching capacity with the introduction of steel fibres in the concrete mix. Punching load was higher for both SFRC and HSFRC slabs when compared to referent RC slabs, in average for 10 % and 11 %, respectively. However, due to the relative low content of fibres in this research (40 kg per m³ of concrete), failure of the slabs in punching mode was not prevented, i.e. none of the specimens failed in bending mode.

In terms of centre displacement on the bottom face of the slabs at maximum (punching) load, similar trends were observed as in case of punching capacity of the slabs. This displacement increased for 9 % and 22 % in case of SFRC and HSFRC slabs when compared to referent RC slabs.

Generally, it is worth noting that HSFRC slabs showed somewhat better results than the SFRC slabs, especially regarding the increase in deformation capacity. These results evidence that sorted recycled tyre steel fibres can be used as an equivalent replacement for manufactured steel fibres. Of course, further extensive research is needed in order to study larger spectrum of different HSFRC mixes.

**Load versus Strain and Load versus Slope Responses**

The following Figure 7 and Figure 8 represent load versus strain (mark RD) and load versus slope (mark Ψ) diagrams for all the tested slabs. Position of these measurement points can be seen in Figure 4. Concrete compressive strain decrease presents the advancement of shear cracks in the slab, i.e. the announcement of the oncoming punching failure.

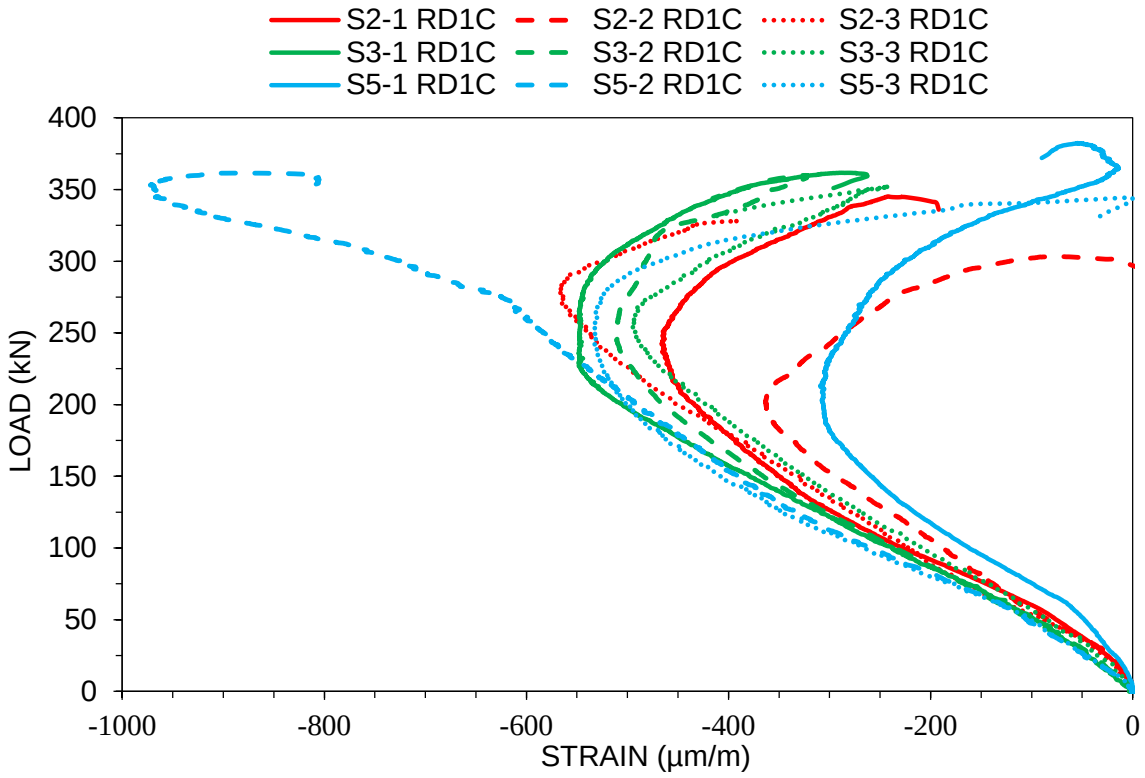


Figure 7 Load – RD1C strain diagrams for all the tested slabs.

Regarding the measured slopes, it is visible that SFRC and HSFRC slabs had bigger slopes (higher deformation capacity) at maximum load, when compared to referent RC slabs. Again, note that HSFRC slabs showed somewhat better behaviour in this respect than the SFRC slabs.

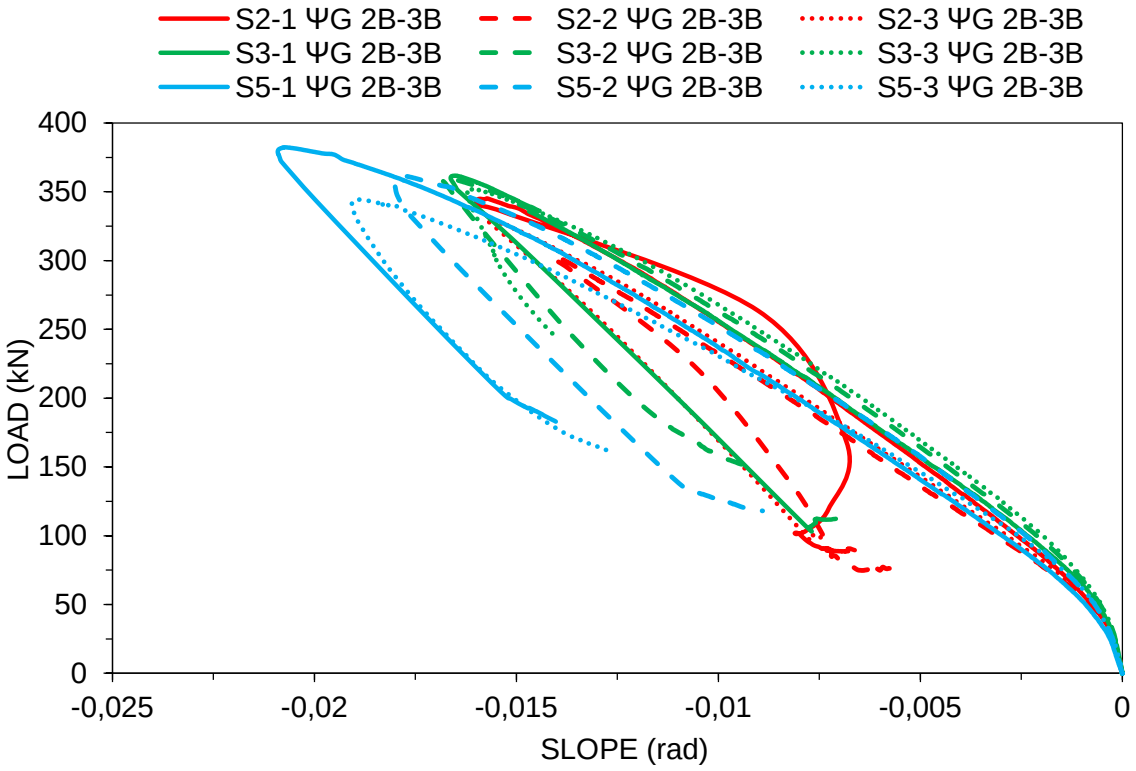


Figure 8 Load – ΨG 2B-3B slope diagrams for all the tested slabs.

**Inspection of the Slabs after Failure**

After failure, each slab was inspected and cracks on the tensile surface were marked in order to study the influence of fibres on crack pattern. Furthermore, one slab per each group (each concrete mix) was saw-cut in order to study the influence of fibres on the shear crack inclination.

Figure 9 shows one slab per each group with its crack pattern where it can be seen that these patterns are somewhat similar, but concrete protective layer on SFRC slab and HFRC slab remained integral unlike the one on the PC slab.


Figure 9 Crack pattern for some of the tested slabs (form left to right): S2-3, S3-1, S5-3.

Figure 10 shows comparison of shear crack inclination between PC, SFRC and HSFRC slab after the slabs were saw cut. Shear crack angles were approximately 36° for PC slab, 24° for SFRC slab and 33° for HSFRC slab. From this data, it is visible that fibres have a tendency of decreasing the shear crack angle and moving it away from the column, i.e. including a larger portion of concrete to resist the punching action. However, this effect is somewhat smaller in the studied HSFRC slab when compared to the studied SFRC slab. This is caused by a relatively small amount of MSF in the HSFRC concrete mix (10 kg per m³ of concrete). Namely, these fibres are crucial for macro-cracks bridging because of their length and hooked ends. RTSF are generally only able to bridge micro-cracks.

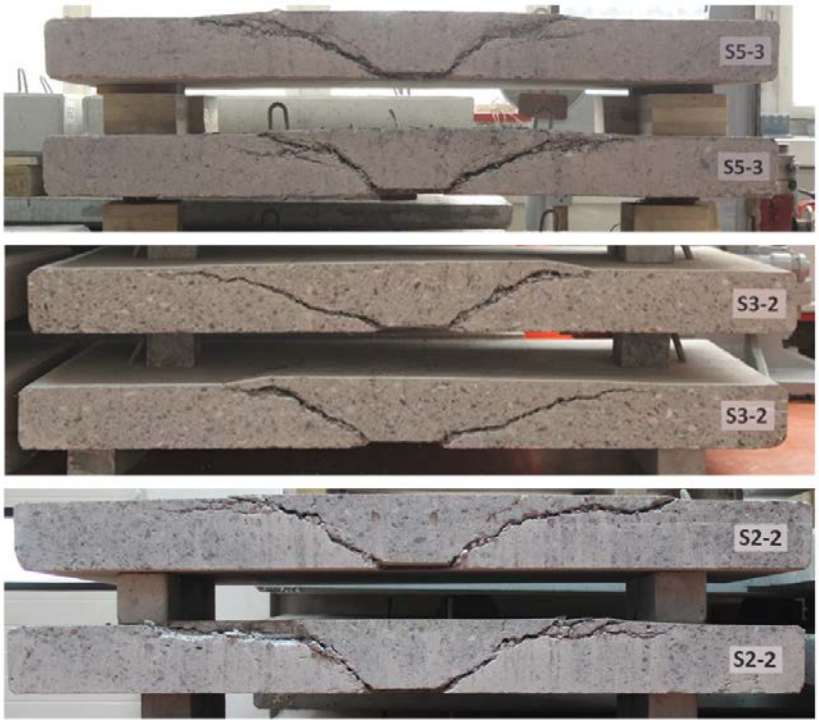


Figure 10 Slabs cut after testing

## CONCLUSIONS

In this study, the results of punching shear tests carried out on flat slabs with different concrete mixes (PC – plain concrete, SFRC – steel fibre reinforced concrete, HSFRC – hybrid steel fibre reinforced concrete) are presented and discussed. Three small-scale slabs were tested per each concrete mix. SFRC mix included 40 kg of manufactured fibres per m³ of concrete while HSFRC mix included 10 kg of manufactured and 45 kg of sorted recycled tyre steel fibres per m³ of concrete.

Steel fibres in SFRC and HSFRC slabs improved the punching shear resistance when compared to PC slabs. In addition, fibres caused higher stiffness and deformation capacity of the mentioned FRC slabs. Furthermore, although the crack pattern was somewhat similar in all types of slabs, slabs with FRC remained integral while the concrete protective layer in PC slabs fell apart in some regions of the slabs.

In addition, after the failure, some of the tested slabs were saw cut in order to study the influence of fibres on the angle of the shear crack. This angle was smaller (relative to the horizontal) in case of SFRC and HSFRC slabs which indicates that fibres have a tendency of moving the shear crack away from the column, i.e. including a larger portion of concrete to resist the punching action. However, this effect is somewhat smaller in the studied HSFRC slab when compared to the studied SFRC slab.

Slabs with HSFRC generally showed somewhat better behaviour than the SFRC slabs in many aspects that were analysed in this research. Therefore, sorted recycled tyre steel fibres have proven to be a quality replacement for a certain amount of manufactured steel fibres in FRC, i.e. to be to be an economical and ecological alternative for this type of fibres. However, extensive research is still necessary in order to study their performance on a large spectrum of different HSFRC mixes (amount of RTSF in total fibre quantity; different MSF types) and applications.

## ACKNOWLEDGEMENTS

The authors wish to acknowledge the financial support of the 7th Framework Programme of European Community “Anagennisi – Innovative Reuse of All Tyre Components in Concrete” under contract number 603722 and all the partners in this project.

## REFERENCES

1. L. F. MAYA, M. FERNÁNDEZ RUIZ, A. MUTTONI, and S. J. FOSTER, “Punching shear strength of steel fibre reinforced concrete slabs,” Eng. Struct., vol. 40, pp. 83–94, 2012.

2. A. MUTTONI, “Punching shear strength of reinforced concrete slabs without transverse reinforcement,” ACI Struct. J., Vol. 105, No. 4, pp. 440–450, 2008.

3. N. SUBRAMANIAN, “Alternative punching shear reinforcement for RC flat slabs,” Indian Concr. J., no. January, pp. 33–44, 2014.

4. J. KUNZ, M. FERNÁNDEZ RUIZ, and A. MUTTONI, “Enhanced safety with post-installed punching shear reinforcement,” in Tailor made concrete structures - new solutions for our society, 2008, pp. 679–684.

5. R. N. SWAMY and S. A. R. ALI, “Punching Shear Behavior of Reinforced Slab-Column Connections Made with Steel Fiber Concrete,” ACI J. Proc., Vol. 79, No. 5, pp. 392–406, 1982.

6. K. K. CHOI, M. M. REDA TAHA, H. G. PARK, and A. K. MAJI, “Punching shear strength of interior concrete slab-column connections reinforced with steel fibers,” Cem. Concr. Compos., Vol. 29, No. 5, pp. 409–420, 2007.

7. I. Y. S. DARWISH and R. NARAYANAN, “Punching shear tests on steel-fibre-reinforced micro-concrete slabs,” Mag. Concr. Res., Vol. 39, No. 138, pp. 42–50, 1987.

8. M. H. HARAJLI, D. MAALOUF, and H. KHATIB, “Effect of fibers on the punching shear strength of slab-column connections,” Cem. Concr. Compos., Vol. 17, No. 2, pp. 161–170, 1995.

9. L. NGUYEN-MINH, M. ROVŇÁK, and T. TRAN-QUOC, “Punching Shear Capacity of Interior SFRC Slab-Column Connections,” J. Struct. Eng., Vol. 138, No. 5, pp. 613–624, 2012.

10. D. D. THEODORAKOPOULOS and N. SWAMY, “Contribution of steel fibers to the strength characteristics of lightweight concrete slab-column connections failing in punching shear,” ACI Struct. J., Vol. 90, No. 4, pp. 342–355, 1993.

11. R. N. SWAMY, “FRC for sustainable infrastructure regeneration and rehabilitation,” in Fifth RILEM Symposium on Fibre-Reinforced Concretes (FRC), 2000, pp. 3–19.

12. D. BJEGOVIĆ, A. BARIČEVIĆ, S. LAKUŠIĆ, D. DAMJANOVIĆ, and I. DUVNJAK, “Positive interaction of industrial and recycled steel fibres in fibre reinforced concrete,” J. Civ. Eng. Manag., Vol. 19, No. sup1, pp. S50–S60, Dec. 2013.

13. A. BARIČEVIĆ, “Contribution to the development of sustainable hybrid fibre reinforced conmcrete using by-products from recycling of waste tyres,” Doctoral thesis, University of Zagreb, 2014.

14. M. BARTOLAC, “Properties of precast constructive elements with reinforcement partially replaced with recycled steel fibres,” Doctoral thesis, University of Zagreb, 2015.

15. D. BJEGOVIĆ, A. BARIČEVIĆ, and S. LAKUŠIĆ, “Innovative low cost fibre-reinforced concrete. Part I: Mechanical and durability properties,” in Concrete Repair, Rehabilitation and Retrofitting III, 2012, pp. 199–203.

16. J. KROLO, D. DAMJANOVIĆ, I. DUVNJAK, D. BJEGOVIĆ, S. LAKUŠIĆ, and A. BARIČEVIĆ, “Innovative low cost fibre-reinforced concrete. Part II: Fracture toughness and impact strength,” in Concrete Repair, Rehabilitation and Retrofitting III, 2012, pp. 204–209.

17. G. CENTONZE, M. LEONE, and M. A. AIELLO, “Steel fibers from waste tires as reinforcement in concrete: A mechanical characterization,” Constr. Build. Mater., Vol. 36, pp. 46–57, Nov. 2012.

18. K. NEOCLEOUS, H. TLEMAT, and K. PILAKOUTAS, “Design Issues for Concrete Reinforced with Steel Fibers , Including Fibers Recovered from Used Tires,” J. Mater. Civ. Eng., Vol. 18, No. October, pp. 677–685, 2006.

19. H. TLEMAT, K. PILAKOUTAS, and K. NEOCLEOUS, “Stress-strain characteristic of SFRC using recycled fibres,” Mater. Struct., vol. 39, no. 3, pp. 365–377, 2006.

20. C. ACHILLEOS, D. HADJIMITSIS, K. NEOCLEOUS, K. PILAKOUTAS, P. O. NEOPHYTOU, and S. KALLIS, “Proportioning of Steel Fibre Reinforced Concrete Mixes for Pavement Construction and Their Impact on Environment and Cost,” Sustainability, Vol. 3, No. 12, pp. 965–983, Jul. 2011.

21. A. G. GRAEFF, K. PILAKOUTAS, K. NEOCLEOUS, and M. V. N. N. PERES, “Fatigue resistance and cracking mechanism of concrete pavements reinforced with recycled steel fibres recovered from post-consumer tyres,” Eng. Struct., Vol. 45, pp. 385–395, Dec. 2012.

22. M. SERDAR, A. BARIČEVIĆ, S. LAKUŠIĆ, and D. BJEGOVIĆ, “Special purpose concrete products from waste tyre recyclates,” J. Croat. Assoc. Civ. Eng., Vol. 65, No. 9, pp. 793–801, 2013.

23. EUROPEAN COMMITTEE FOR STANDARDIZATION, “EN 12390-3:2009/AC:2011. Testing hardened concrete - Part 3: Compressive strength of test specimens.” 2011.

24. EUROPEAN COMMITTEE FOR STANDARDIZATION, “EN 12390-6:2009. Testing hardened concrete - Part 6: Tensile splitting strength of test specimens.” 2009.

25. EUROPEAN COMMITTEE FOR STANDARDIZATION, “EN ISO 15630-1:2010. Steel for the reinforcement and prestressing of concrete - Test methods - Part 1: Reinforcing bars, wire rod and wire.” 2010.

# DISCRETE HOOKED-END STEEL FIBRE SHAPE AND GEOMETRY ON MATERIAL PROPERTIES OF SELF-COMPACTING CONCRETE UNDER BENDING STRESS

**C A O Okeh**
Southampton Solent University
**D W Begg**
**S J Barnett N Nanos**
University of Portsmouth
United Kingdom

**ABSTRACT.** The effect of discrete steel fibres in fibre reinforced concrete has been shown to prevent the propagation of crack(s) as well as bridging crack(s) at crack localisation point(s) accounting for increase in energy absorption and ductility in tension. Steel fibre distribution and alignment is guaranteed when used in self-compacting concrete, hence reduces the scatter of material properties and further improves mechanical performance. The aim of this study is to investigate the effect of new innovative multiple hook ends steel fibres as against existing single hook ends steel fibre on the material properties and scatter when used in self- compacting concrete. A laboratory investigation was carried out using different steel fibre hooked-end shapes and geometries (S1, M1 and M2) at 0.25%, 0.5%, 0.75% and 1% fibre content in self-compacting concrete to obtain material properties. Four point bending test and single fibre pull-out test were used as the test methods. The results show that alterations in the hooked end shape and geometry from single hook to multiple hooks affects the pull-out response by increasing the peak pull-out load and dissipated energy as well as the anchorage coefficient. There is an increase in flexural strength, ultimate flexural strength and fracture energy up to a maximum of 1.7, 2.1 and 11 times respectively when compared to plain concrete. However, the post-cracking response of steel fibre reinforced self-compacting concrete is not only influenced by the alteration of hooked end shape and geometry but also the percentage fibre content and length of steel fibre embedment.

**Keywords:** Steel fibre self-compacting concrete, Single and multiple hooked ends steel fibres, Pull-out load, Dissipated energy, Flexural strength, Fracture energy.

**Clifford A O Okeh** is a PhD Research Student in the Department of Civil Engineering and Surveying at the University of Portsmouth, UK, and a Senior Lecturer in Civil Engineering and Construction Technology at Southampton Solent University, UK. His research interest is in fibre reinforced concrete structures (FRCS).

**Dr David W Begg** is a Senior Lecturer at the University of Portsmouth, United Kingdom.

**Dr Stephanie J Barnett** is a Senior Lecturer at the University of Portsmouth, United Kingdom.

**Dr Nikos Nanos** is a Senior Lecturer at the University of Portsmouth, United Kingdom.

# INTRODUCTION

Self-compacting concrete (SCC) is now widely pronounced within the construction industry due to its ability to flow in formwork, passing through reinforcing bars and other obstacles, flowing and consolidating under the action of its own weight. SCC also minimises the use of skilled labour in placing and finishing concrete which decreases costs and time of the building process over traditional vibrated concrete [1]. However its use with steel fibre reinforcement (SFR) enhances its durability property because of its fragile nature and provides a very adherent matrix for fibres to function effectively [2]. This combination results in fibre distribution that is more uniform within a specimen and an orientation along the casting direction that is very effective depending on the application, thereby enhances the mechanical behaviour in the cracking process [3]. "The first crack load, pre-cracking and post-cracking behaviour, deflection pattern, crack development pattern and ultimate load carrying capacity" of SCC beams improved with steel fibre addition [4].#

The general behaviour of steel fibre reinforced concrete under flexural loads produces a much higher post cracking residual strength than in plain concrete due to fibres bridging the cracks which depends on fibre geometric characteristics, fibre material properties; concrete properties and methods of steel fibre reinforce concrete (SFRC) application [5]. Although past and current studies has also shown that ductility, crack resistance, applied or impact loading, energy absorption increased with steel fibre addition in concrete [5], The bridging efficiency of individual fibre largely depends on the fibre-matrix bond characteristics which contributes to the improvement in the mechanical properties of SFRC [6],

Distinct steel fibre geometry (straight, hooked, twisted, crimpled etc.) presents different bond characteristics when used in concrete thereby influencing the pre and post cracking behaviour [7]. Apart from straight steel fibres, the use of hooked end steel fibres is most common in the construction industry with 67% of sold fibre consisting of hooked type; this is due to its influence on the mechanical behaviour in SFRC application [1]. The use of hooked end steel fibres in concrete is more effective if the embedment length is greater than hooked end length [8] as a result generates an additional frictional force due to straightening of the hooks which leads to higher frictional pull-out resistance [6], in addition to the adhesion with the matrix [2] when compared to straight fibres thereby improving its material properties.

Notwithstanding the benefits of using single hooked end steel fibre to improve the behaviour of concrete in tension when compared to straight steel fibre, the recent introduction of new innovative hooked end steel fibres by manufacturers with multiple hooks, increase in hooked end depths and tensile strengths poses the need to investigate the bridging efficiency and pull-out response (to be discussed in another publication) on the mechanical performance of SFRC for structural application.

It is also important to highlight on the effect of these new steel fibres on the post cracking behaviour and scatter of the material properties when used in self-compacting concrete since designer's lack of confidence to adopt this material model in current practice has been attributed to the high scatter of the material behaviour of conventional SFRC beams allowing for high material safety factors [9].

Therefore this study focused on the effect of new innovative discrete hooked end steel fibres shape and geometry on the material properties when incorporated in self-compacting concrete under bending test and further investigation on the pull-out force and energy.

## EXPERIMENTS

The experimental programme aim to study the effect of different steel fibre hooked end shape and geometry in self-compacting concrete with a compressive strength of 64MPa. Various parameters influencing the behaviour, such as fibre content (0%, 0.25%, 0.50%, 0.75% and 1.0%), number of hooks and depth of the hook end region with respect to material properties under bending is carefully examined. Single pull-out test on individual hooked end steel fibre embedded in self-compacting concrete at depths of 10mm, 20mm and 30mm ($0^0$ inclination angles) was also investigated.

## EXPERIMENTAL PROGRAMME

### Material characteristics and specimen preparation

The parameters and geometry of the macro steel fibres used for the experimental tests are presented in Figure 1 and Table 1; Fosroc Auracast .200 high range water reducing superplasticizer admixture is specified for this mix design. The cement specification used is Portland Cement CEM I 52.5R and the mix incorporated high cement content similar to [10] and [1] for self-compacting concrete (SCC). See Table 2 for material details. The fine aggregate composed of sea-won flint with no fraction of clay or fine silts and coarse aggregate composed of sea-won flint gravel, with maximum size of 6mm and 10mm respectively. The contents of fine and coarse aggregates were fixed to achieve self-compatibility easily by altering the ratio of superplasticiser and water-powder amount [10]. The water/cement ratio of the concrete was 0.27 with 0.69% cement mass of superplasticizer admixture in order to obtain comparable rheological and mechanical parameters. No content of fly ash or silica fume was added to the mix design since the focus was on the effect of various hooked end fibre types within a concrete matrix rather than the use of fly ash and silica fume to compliment the cement in order to prevent variation of physical and chemical properties to improve strength [1].

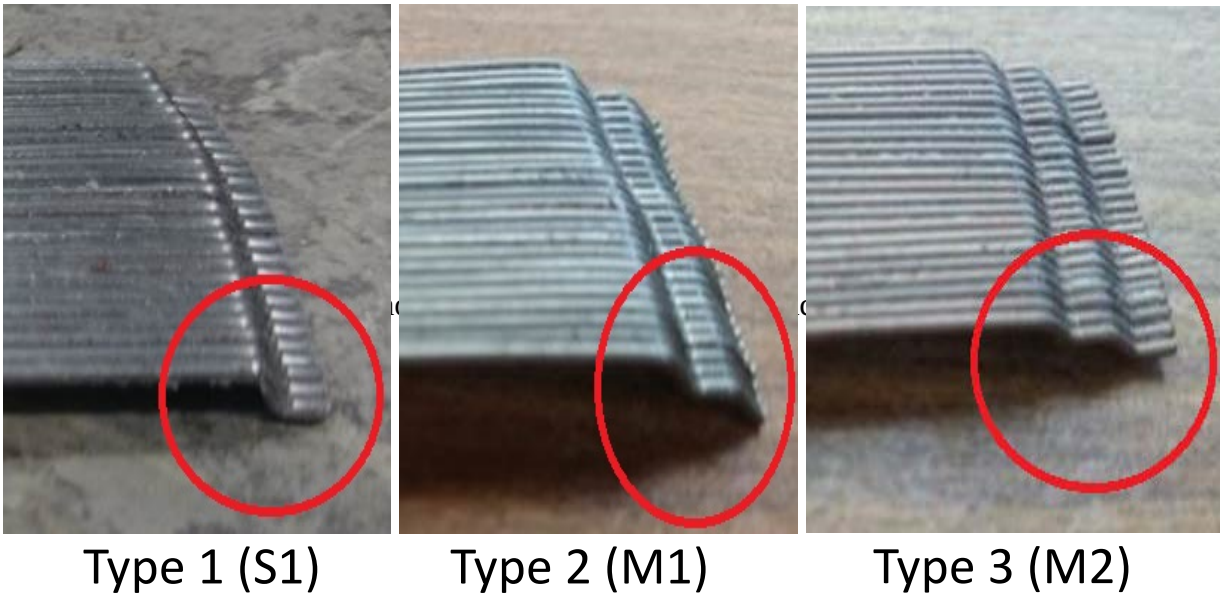


Figure 1: Shape of hooked-end macro steel fibres (Manufactured by Bekaert, 2012)

Table 1 Geometry details and mechanical properties of hooked end steel fibres (S1, M1 and M2)

| FIBRE SHAPE | TYPE | LENGTH (mm) | DIAMETER (mm) | ASPECT RATIO | EFFECTIVE HOOKED-END REGION LENGTH (mm) | DEPTH OF HOOKED END REGION (mm) | TENSILE STRENGTH ($N/mm^2$) | NO OF FIBRES/kg | YOUNG MODULUS $N/mm^2$ |
|---|---|---|---|---|---|---|---|---|---|
| Single Hooked end | S1 | 60 | 0.90 | 65 | 5.66 | 3 | 1.160 (+/-7.5%) | 3.183 | 210 |
| Double Hooked end | M1 | 60 | 0.90 | 65 | 11.22 | 6 | 1.500 (+/-7.5%) | 3.183 | 210 |
| Double Hooked end | M2 | 60 | 0.90 | 65 | 11.66 | 4 | 2.300 (+/-7.5%) | 3.183 | 210 |

Table 2 Self-compacting concrete mix design

| MATERIAL | QUANTITY ($kg/m^3$) |
|---|---|
| Cement | 735.35 |
| Sand | 738.38 |
| Gravel | 761.62 |
| Water | 201.00 |
| Superplasticiser | 5.05 |

## Mixing procedure, manufacture and testing of specimens

Drum tilting mixer has been used for all mixing operation during experimental work. The mixing procedure and time started with 30 seconds wet mixing of coarse aggregate using 70% of measured water. Fine aggregate was added and allowed to mix for a further 1 minute. Cement was then added and mixing carried on for a further 2.5 minutes after which the remaining 30% of water containing superplasticiser was slowly added. Mixing continued for a further 4.5 minutes to allow the effect of the superplasticiser to kick-in followed by the addition of steel fibres within 30 seconds after which a further 4 minutes mixing was allowed to ensure uniform dispersion of the steel fibres and to avoid balling. Total mixing time was 13 minutes. The procedure was adopted throughout.

39 beams and 39 cubes specimens measuring 100mm x 100mm x 500mm and 100mm x 100mm x 100mm were manufactured respectively. Specimens were demoulded after 24 hours and placed in a curing tank at $20^{\circ}C \pm 2$ for 28 days. The Four point beam bending test was carried out using a 250KN Zwick test machine which complied with international standards. Bending test was carried out under closed loop load control operation. The pull-out test was carried out on 27 cubes specimen (100mm x 100mm x 100mm) using a 30kN Lloyd instrument testing machine with suitable grip under closed loop load control operation (2mm/minute speed rate).

## RESULTS AND DISCUSSIONS

The results obtained from tests conducted on fresh and hardened properties is presented and evaluated. Discussions focused on workability, density, compressive strength, flexural strength, ultimate flexural strength, fracture energy, pull-out force and pull-out dissipated energy.

### Workability

Slump flow test were used to measure the fluidity of the self-compacting concrete in accordance to BS EN 12350-8:2010 testing procedures. The measured values obtained for slump flow for all steel fibre types and fibre contents falls within the range of 760mm to 850mm in line with [11] recommendations (SP3) for vertical application in congested structures. The results presented in Figure 2 indicates that addition of steel fibres do affect the slump flow. The increase in percentage steel fibre content reduces the spread of the flow (up to a maximum of 13.2%) for all hooked end steel fibre types when compared to plain concrete. This indicates that workability of the mix decreased with increase in fibre content. However, it was observed during the procedure that as percentage fibre content increases, the segregation of fibres at the centre of the spread after cone removal increased. The results also indicate that the shape of fibre hooked end affects the workability of the mix; the tip section of the hooked end seems to play an important role. A more workable mix is seen with inclined tip and less workable mix with a flat tip when comparing M1 to S1 and M2 steel fibre types. Although when S1 and M2 with flat tip are compared, the results suggest that increasing the number of hooks and depth of the hooked end accounts for the decrease in workability.

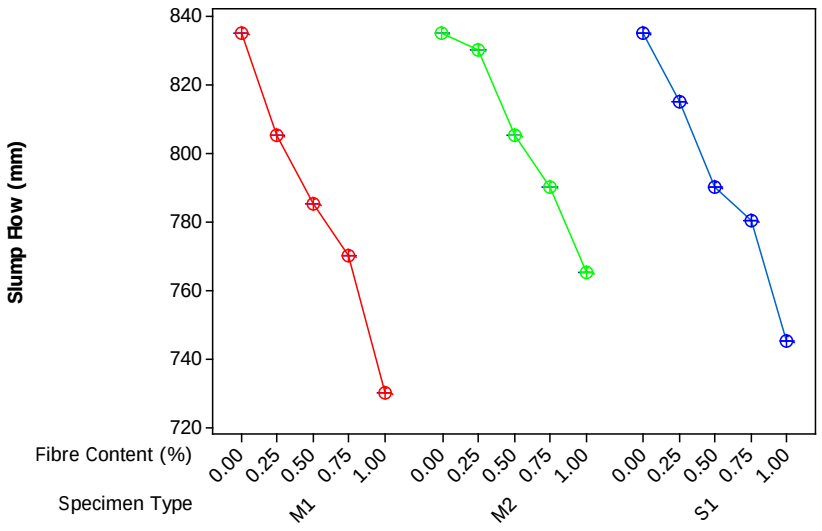


Figure 2 Graph of slump flow against fibre content and specimen types

## DENSITY

Density test result has been obtained from hardened cube specimens as described in BS EN 12390 – 7: 2009. The results indicate that steel fibre addition and percentage increase in steel fibre volume increases the density slightly when compared to plain concrete. Figure 3 shows increase in the density up to a maximum percentage of 2.7% with the addition of steel fibres. The value of density as shown on the graph is between 2375 to 2448 kg/m$^3$ with steel fibre

addition. There is no significant effect by altering the shape of steel fibre hooked end on the density when compared to plain concrete. The discrepancies seen when comparing each fibre type at varying percentage fibre content could be as a result of fibre quantity and coarse aggregate within specific cube samples due to manufacturing.

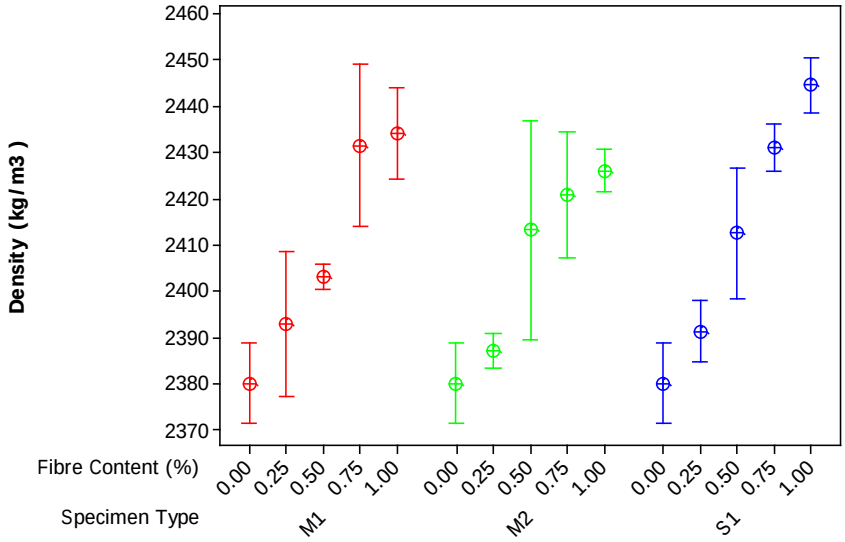


Figure 3 Graph of density against fibre content and specimen types

## COMPRESSIVE STRENGTH

Compressive strength test on hardened cube specimens has been carried out in accordance to BS EN 12390 – 3: 2009. Figure 4 shows no significant difference in the average compressive strength with all hooked end steel fibre types. This again like the density indicates that no significant increase by altering the shape of steel fibre hooked end on the average compressive strength when compared to plain concrete (increase up to a maximum of 17%).

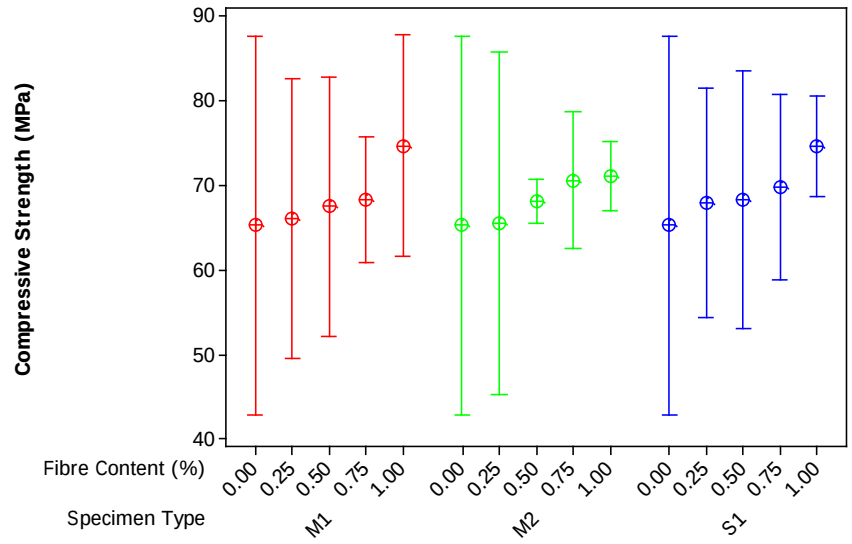


Figure 4 Graph of compressive strength against fibre content and specimen types

## FLEXURAL STRENGTH

The flexural strength has been calculated from the first crack load obtained on a force-displacement curve using formula given in BS EN 14488-3 2006 ($PL/bd^2$). The result shown in Figure 5 clearly indicates that addition of steel fibres increases the flexural strength when compared to plain concrete up to a maximum of 76%. However, there is a large variability in the scatter of the flexural strengths obtained when comparing steel fibre types making it difficult to conclude if different hooked end steel fibres have an effect. This variability could be attributed to fibre volume Figure 7, distribution and orientation within specimens tested. Therefore the result shows no significant effect on the flexural strength with alteration of fibre shape and geometry except at 0.25% steel fibre content based on average values up to a maximum of 17%. This behaviour is because hook influence is more pronounced after initial crack failure when the stress is transferred from the concrete matrix to the steel fibres. This stress transfer prevents brittle failure resulting in toughness increase as a result of increase in the characteristic length attributed to additional anchorage mechanism provided by the hooks. Yet, the result indicates that the maximum fibre content to produce peak flexural strength for S1, M1 and M2 are 0.75%, 1% and 0.5% respectively based on mean values obtained.

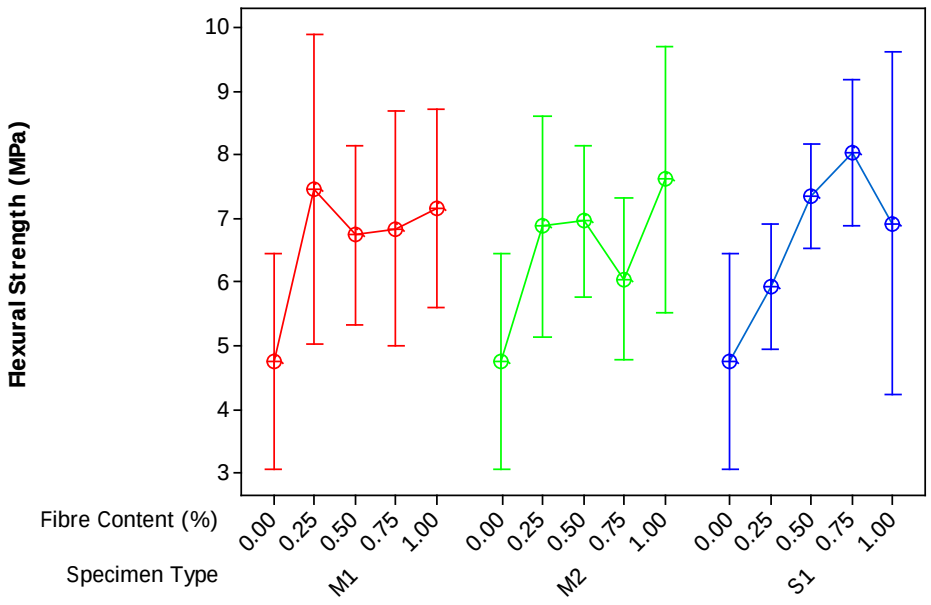


Figure 5 Graph of flexural strength against fibre content and specimen types

## ULTIMATE FLEXURAL STRENGTH

The ultimate flexural strength has been calculated from post peak crack load obtained on a force-displacement curve using formula given in BS EN 14488-3 2006 ($PL/bd^2$). The result in Figure 6 shows an increase in the flexural strength after initial crack localisation to a peak stress (second crack localisation point) termed as the ultimate stress up to a maximum of 74.6% before a gradual degradation of the stress. This increase in flexural strength was only observed at high percentage fibre content of 0.75% and 1% for all steel fibre types. This indicates a hardening behaviour as a result of multiple cracking generated on the test specimen during load action. This failure pattern is as a result of a large amount of fibres bridging the gap aiding the distribution of the stress transferred from the concrete matrix at the cracked section.

A comparison of the bridging efficiency of individual steel fibre types in the post cracking phase when the stress is fully transferred to the fibres is evaluated using the result shown in Figure 6 and 7. Figure 6 does not show a clear correlation with increase in hook number or hook depth to increase in post crack strength when considering the mean values of all fibre types; the trend seen is a result of the number of fibres bridging the crack during stress transfer as shown on Figure 7. At 1% fibre content the number of fibres bridging gap is 85, 77 and 92 for S1, M1 and M2 respectively. This clearly correlates with the trend result on Figure 6 for the ultimate flexural strength.

At fibre content of 0.75%, the results show that S1 fibre produced higher post peak strength compared to M1 and M2 which did not follow the behaviour observed in the pull-out test on Figure 9. This is a result of the number of fibres bridging the crack 86, 62 and 63 for S1, M1 and M2 steel fibres respectively as shown in Figure 7.

Therefore, the influence of the number of fibres bridging the crack makes it difficult to observe the effect of alteration of hooked end steel fibre shape and geometry in the post cracking process as indicated in the pull-out test. It can also be argued that lack of full embedment, of the M1 and M2 hooks at the crack section could have also contributed to this behaviour, thereby not utilising the additional frictional resistance and energy attributed to the increase in hook number.

A comparison between S1 and M1 hooked end steel fibre types at 0.75% fibre content with approximately the same amount of fibres (63 numbers) bridging the crack does clearly show that increase in hook number increases post crack strength. This increase is as a result of additional frictional stress and pull-out dissipated energy generated to straighten the additional hook.

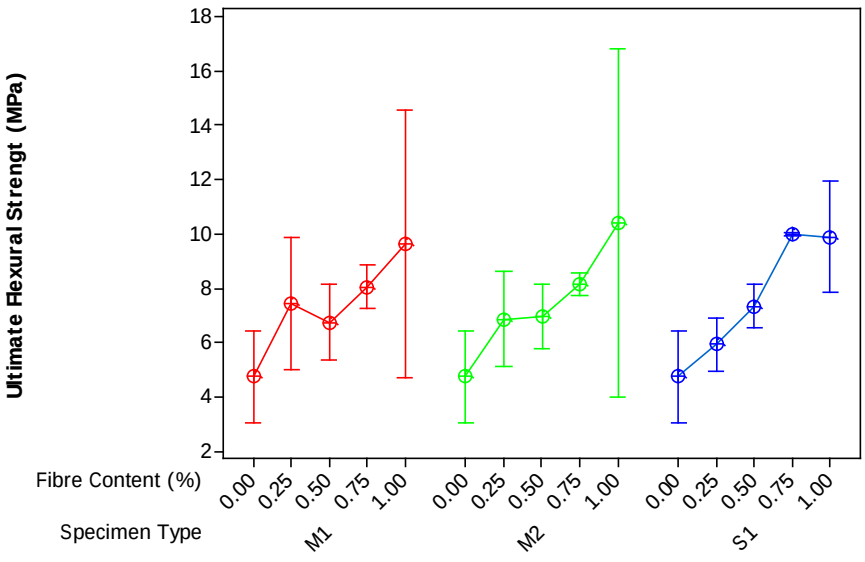


Figure 6 Graph of ultimate flexural strength against fibre content and specimen types

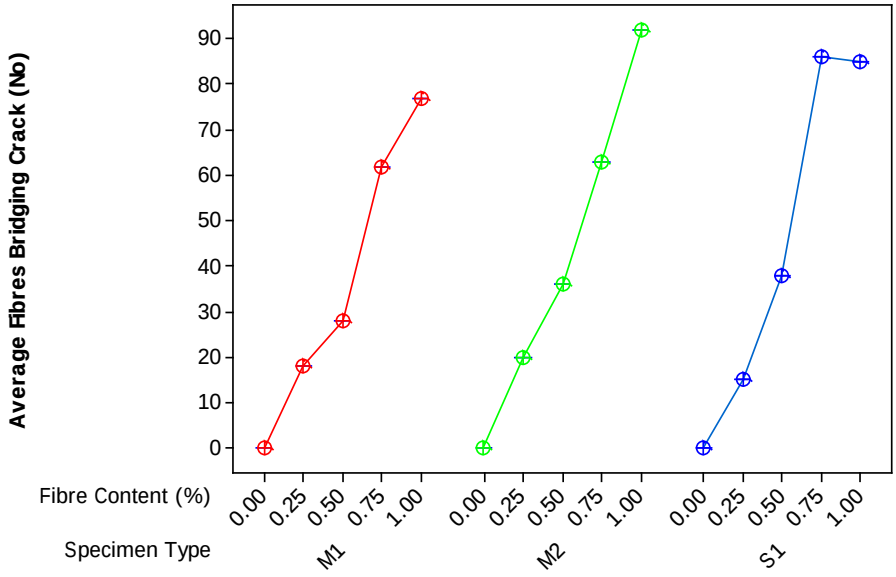


Figure 7 Graph of Average numbers of fibres bridging crack under flexural load against fibre content and specimen types

## FRACTURE ENERGY

The fracture energy was calculated from the load deflection curve as it is a function of the displacement and not strain. This research calculated the fracture energy as the area under the load deflection curve for each specimen. The results obtained as shown in Figure 8 indicate that steel fibre addition increases the fracture energy for all hooked end steel fibre types up to a maximum of 11 times when compared to plain concrete. The graph also suggest that alteration of hook shape and geometry affects the facture energy under bending when S1 steel fibre is compared to M2 due to adhesion of fibres and matrix; and additional frictional resistance generated in straightening the hooks, although on observation of Figure 7, it can be argued that the number of steel fibres bridging the gap could have caused the increase in fracture energy.

However, when S1 is compared to M1 and M2, this behaviour is completely different when considering the mean values. A careful observation of Figure 8 and 7, suggest that the volume of fibre bridging the crack contributed to this un-expected behaviour when consideration is given to the pull-out test result presented in Figure 9. At low fibre content (0.25%), no significant increase in average energy is observed from S1 to M1 as hook number and depth increases however at 0.5%, 0.75% and 1% fibre content S1 steel fibre type is seem to be dissipating more energy than M1 and M2 based on average values. This can be attributed to the higher amount of fibre that is bridging the crack to dissipated energy most especially at 0.5% and 0.75%. It can also be argued that with a high scatter of S1 fibre type in comparison to M1 and M2; this could have affected the mean value, making it difficult to see the effect of alteration of hooked end shape and geometry on energy absorption. This high scatter could be caused by fibre orientation in relation to the applied load and embedment length of the hooks.

At 1%, steel fibre content when the number of fibres bridging the crack is more for M2 compared to S1 but the energy dissipated is seen to be more for S1 when compared to M2. It could be suggested that full embedment of the M2 hooks across the crack was not achieved thereby not utilising fully the additional frictional resistance generated as seen in the pull-out test in Figure 9.

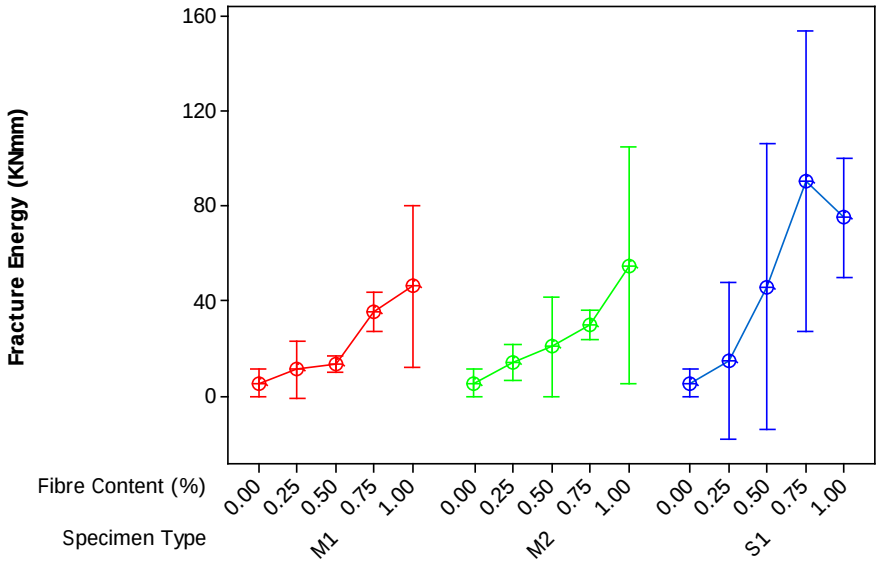


Figure 8 Graph of area under load deflection curve against fibre content and specimen type

## PULLOUT FORCE AND DISSIPATED ENERGY

The pull-out force and pull-out dissipated energy were derived from load displacement curve. The test results as presented in Figure 9 indicates that alteration of steel fibre hooked end shape and geometry by increasing the hook number and adjusting hook depth increases the pull-out force and pull-out dissipated energy up to a maximum of 160% from S1 to M2 hooked end steel fibre types. The result suggests that there is a direct relationship between the pull-out force and pull-out dissipated energy with alteration of hooked end shape and geometry; and embedment length. The behaviour in the pull-out parameters can be assessed based on the bond-slip hardening characteristics with relationship to wedge effect of the abraded particle, scratching of the fibre surface and end deformation of the fibre as suggested by Wille and Naaman (2010).

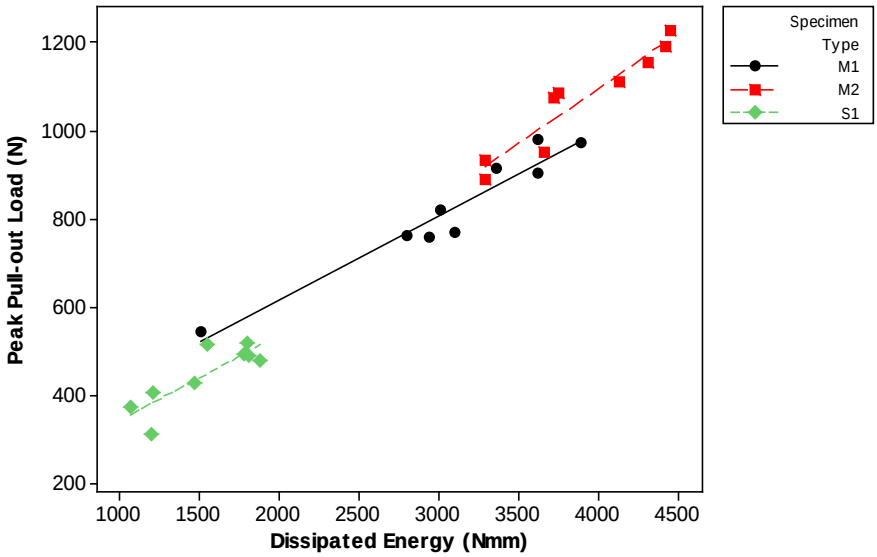


Figure 9 Graph of peak pull-out load against pull-out dissipated energy & fibre type

These improvements obtained in this experiment suggest clearly a link to the effect of the fibre end deformation of the hooked end steel fibre region thereby accounting for additional frictional resistance and bond anchorage interlock between steel fibre and concrete matrix which can only be attributed to hook number, hook depth and steel fibre tensile strength. The additional frictional resistance and anchorage interlock mechanism generated is caused by the bond stresses at the straight and hooked region $\tau_1$ and $\tau_2$ respectively (to be discussed in another publication) as defined by Remigijus and Gediminas (2010). These stresses can be used to determine the hook efficiency from their ratio towards obtaining the anchorage coefficient ($K_{an}$). Therefore it can be argued that the increase in force and energy is as a result of the increase in hook efficiency and the anchorage coefficient ($K_{an}$) for M1 and M2 steel fibre types when compared to S1 steel fibre type.

## CONCLUSIONS

The investigation with particular reference to hooked end steel fibre types (shape and geometry); steel fibre content and pull-out test (embedment depths of 10mm, 20mm and 30mm at $0^0$ inclination angle) on the mechanical properties led to the following conclusions:

- Steel fibre addition to plain concrete affects the flowability of the mix. An increase in steel fibre content decreased workability but increased segregation. Slump flow values above 860mm causes segregation of fibres and aggregates (non-uniform distribution) within the specimen. Fibre content increase reduces segregation.

- There is a direct relationship between pull-out force and energy. An increase in pull-out force and dissipated energy is due to increase in the hook efficiency for multiple hook end steel fibres (M1 & M2) when compared to single hook end fibre (S1).

- The fracture energy increased with alteration of hooked end shape and geometry up to a maximum of 11 times when compared to plain concrete. Apart from the number of fibres bridging the crack which accounts for the increase in fracture energy in the post cracking process, result analysis suggests that orientation and the extent of embedment of the individual hooks across the crack section influences the efficiency of different hooked end steel fibre shape and geometry on the fracture energy.

- There is an increase in the flexural strength up to a maximum of 76% with addition of steel fibres when compared to plain concrete. No significant difference in strength when comparing hooked end steel fibre types. However, the optimum flexural strength was obtained at 0.75%, 1% and 0.5% for S1, M1 and M2 steel fibre types respectively.

- Ultimate flexural strength increased at 0.75% and 1% fibre content for all hooked end steel fibre types up to a maximum of 74.6% when compared to the flexural strength. The number of steel fibres bridging the crack accounts for the amount of increase in ultimate flexural strength making it difficult to account for the efficiency of the different hooked end steel fibre types in generating additional frictional resistance and energy as observed during the pull-out test. However, the improved efficiency of alteration of hooked end steel fibre shape and geometry on the ultimate flexural strength is observed between M1 and M2 at 0.75% fibre content.

## REFERENCES


1. PAJAK, M., AND PONIKIEWSKI, T. (2013). Flexural behaviourof self-compacting concrete reinforced with different types of steel fibres. Construction and Building Materials; Vol. 47, pp397-408.

2. BENAICHA, M., JALBAUD, O., HAFIDI, A. A., AND BURTSCHELL, Y. (2013). Rheological and mechanical characterisation of fibre-reinforced self-compacting concrete, International Journal of Engineering and Innovative Technology; Vol 2, Issue 7.

3. CUNHA, V. M. C. F., BARROS, J. A. O., SENA-CRUZ, J. M. (2010). Tensile behaviour of steel fibre reinforced self-compacting concrete, ACI Committees 544 and 237, pp 51-68.

4. JEENU, G., REJI, U., AND PRAKASH, V. (2007). Flexural behaviour of hybrid fibre reinforced self-compacting concrete, CI-Premier PTE LTD. 32 Conference on Our World in Concrete & Structures; Singapore.

5. SORELLI, L. G., MEDA, A., AND PIZZARI,G. A. (2006). Steel fibre concrete slabs on ground: A structural matter, ACI structural journal, Technical Paper, Title no. 103-S58.

6. BREITENBÜCHER, R., MESCHKE, G., SONG, F., ZHAN, Y. (2014). Experimental, analytical and numerical analysis of the pull-out behaviour of steel fibres considering different fibre types, inclinations and concrete strengths. Structural Concrete Journal of the fib; Vol 15, Issue 2, pp 126-135.

7. LOK, T. AND PEI, J. (1998). Flexural behaviour of steel fibre reinforced concrete. *Journal of Materials in Civil Engineering*

8. ROBINS, P., AUSTIN, S., AND JONES, P. (2002). Pull-out behaviour of hooked steel fibres. Material Structures. 35 (251), 434-442.

9. ABBAS, A., MOHSIN, S., COTSOVOS, D. (2010). Numerical modelling of fibre reinforced concrete, Nottingham University Press, UK.

10. OKAMURA, H., AND OUCHI, M. (2003). Applications of Self-Compacting Concrete in Japan. Proceedings of the 3rd International RILEM Symposium on Self-Compacting Concrete, RILEM Publications, pp. 3 – 5.
11. EFNARC., (2005). The European Guidelines for Self-Compacting Concrete Specification, Production and Use.

12. WILLE, K., AND NAAMAN, A. E., (2010). Bond stress-slip behavior of steel fibers embedded in ultra-high performance concrete", 18$^{Th}$ European Conference on Fracture, Gruppo Italiano Frattura.

13. REMIGIJUS, S., AND GEDIMINAS, M. (2010); Influence of fibre shapeon the strength of steel fibre reinforced concrete. Proceedings of the 10$^{th}$ International Conference on Modern Building Materials, Structures and Techniques, Vilnius, Lithuania.,

# PROPERTIES OF HYBRID STEEL FIBRE REINFORCED ALKALI ACTIVATED SLAG-FLY ASH COMPOSITES

**X Gao Q L Yu**

**R Yu H J H Brouwers**

Eindhoven University of Technology

The Netherlands

Wuhan University of Technology

China

**ABSTRACT.** Alkali activated materials have attracted great attention in recent years due to their excellent mechanical properties, durability, thermal stability; as well as the much lower carbon emission and energy costs compared to Portland cement. However, these also suffers from their relatively low flexural strength and high shrinkage compared to Portland cement system. On the other hand, the application of steel fibre in Portland cement systems has proved its advantages in improving the flexural strength, fracture toughness, impact and the efficiency of reducing the shrinkage behaviour of the brittle matrix. The purpose of this study is to design high performance alkali activated slag-fly ash composites that are modified by steel fibres. Mixtures are designed by applying the modified Andreasen & Andersen particle packing model, in order to achieve a condensed matrix. The influences of the fibre length and dosage, as well as the utilization of hybrid fibres on the workability, compressive strength, flexural strength and drying shrinkage are investigated. Additionally, the reaction products of this blended alkali binder are identified by using Fourier transform infrared spectroscopy.

**Keywords:** Mix design, Alkali activation, Slag-fly ash blends, Hybrid steel fibre, Shrinkage.

**H J H Brouwers** is professor of Building Materials in the Department of the Built Environment at Eindhoven University of Technology.

**Qingliang Yu** is currently working as an assistant professor of Building Materials in the Department of the Built Environment, Eindhoven University of Technology.

**Rui Yu** is currently working as an assistant professor in the State Key Lab of Silicate Materials for Architectures, Wuhan University of Technology, China.

**Xu Gao** is currently working as a Ph.D. student in the chair Building Materials in the Department of the Built Environment, Eindhoven University of Technology, the Netherlands. His research interests include the modification, modelling and application of alkali activated materials.

## INTRODUCTION

In order to reduce the negative environmental impacts, the utilization of alkali activated materials (AAMs) as a substitute has been extensively studied in recent years. This type of materials usually exhibits excellent performance together with low environmental impacts compared to Portland cement [1, 2]. Recently, growing attention is paid to the blended alkaline system that is prepared by mixing calcium enriched precursors and low calcium ones, due to the modified properties such as setting times, workability, shrinkage, mechanical properties and durability [3, 4]. The reaction products in the blended system are mainly stably coexisting C-(A)-S-H and N-A-S-H type gels [5]; the large amount of available calcium and aluminate affects the original structure of N-A-S-H and C-(A)-S-H gels to some extent [6]. Besides, the influences of key synthesizing factors on reaction kinetics, gel characteristics, mechanical properties and durability issues were also intensively investigated.

However, even though excellent performance can be achieved from the blended alkaline systems, the relatively high drying shrinkage due to the nature of both raw materials and activators is still a remaining issue. Besides, the application of steel fibres in Portland cement systems has proven its advantages in improving the flexural strength, fracture toughness, impact and fatigue resistance; as well as the efficiency of reducing the shrinkage behaviour of the brittle matrix. Besides, steel fibres with different lengths play distinct roles in inhibiting the cracks. Those improved properties may also indicate the potential of using steel fibre in alkali activated systems. Bernal et al. [7] applied steel fibres in waterglass activated slag, the results showed that the flexural strength was largely improved and there was a reduction in compressive strength when increasing the fibre content; also water absorption and permeable porosity were reduced. Aydin et al. [8] used long and short steel fibres with the volume fraction up to 2% in waterglass activated slag-silica fume blends, and they reported that as the fibre content increases, there is a reduction in drying shrinkage; while mixes with a higher fibre content and longer length exhibit higher compressive and flexural strength. However, they present limited mechanism study and performance evaluation regarding the effect of hybrid steel fibre on the blended alkaline system.

The objective of this study is to design a high performance alkali activated slag-fly ash composite that is modified by steel fibres. Mixtures are designed by applying the modified Andreasen & Andersen particle packing model. The influences of fibre length and dosage, as well as the utilization of hybrid fibres on workability, mechanical properties, porosity and drying shrinkage are investigated. Additionally, the reaction products of this blended alkali binder are identified by using Fourier transform infrared spectroscopy (FTIR).

## EXPERIMENTS

### Materials

The solid precursors used in this study were ground granulated blast furnace slag and Class F fly ash. Their major chemical compositions are shown in Table 1. Limestone powder was used as filler; two types of sand were used as fine aggregates: a micro sand (0-1 mm) and a normal sand (0-2 mm). Besides, two types of straight steel fibres were applied: (1) fibre length of 13 mm with a diameter of 0.2 mm; (2) fibre length of 6 mm with a diameter of 0.16 mm. For the alkaline activators, a mixture of sodium hydroxide (analytical level of 99 wt.%) and a commercial sodium silicate solution (27.69% $SiO_2$, 8.39% $Na_2O$ and 63.92% $H_2O$ by mass) was used.

Table 1 Major chemical composition of slag and fly ash, wt. %

| OXIDES | FLY ASH | SLAG |
|---|---|---|
| $SiO_2$ | 54.62 | 30.23 |
| $Al_2O_3$ | 24.42 | 12.58 |
| CaO | 4.44 | 40.51 |
| MgO | 1.43 | 9.05 |
| $Fe_2O_3$ | 7.21 | 0.60 |
| $Na_2O$ | 0.73 | - |
| $K_2O$ | 1.75 | 0.43 |
| $SO_3$ | 0.46 | 3.47 |
| LOI | 2.80 | 1.94 |

## Mix Design Methodology

In order to maximize the packing of the granular solid materials, the mixes were designed using the modified Andreasen and Andersen (A&A) model. The applied packing model, works as a target function for the subsequent granular optimization of the individual solid materials.

$$P(D) = \frac{D^q - D_{\min}^q}{D_{\max}^q - D_{\min}^q} \tag{1}$$

where P(D) is a fraction of the total solids materials that are smaller than the particle size D (μm), $D_{max}$ is the maximum particle size (μm), $D_{min}$ is the minimum particle size (μm) and q is the distribution modulus. The distribution modulus (q) in the model is used to determine the proportion between the fine and coarser particles in the mixture. In order to achieve an ideal workability, the value of q is fixed at 0.23 for all mixtures in this study, based on the previous experiences [9]. By using an optimization algorithm based on the Least Squares Method (LSM), the proportions of each individual material in the mix are adjusted until an optimum fit between the composed mix grading curve and the target curve is reached. Therefore, the optimized mixture will possess a compact matrix due to the optimal packing. The particle size distributions of the raw materials, the target curve and the resulting integral grading curve of the mixture is shown in Figure 1. Additionally, the fibre contents up to 1% by volume are added internally in the original system; its effect on the packing is not considered in this case but will be investigated in a future study.

## Sample Preparation

The activator used in this study has an equivalent sodium oxide ($Na_2O$) content of 5% by mass of the binder and an activator modulus of 1.4. The water/powder ratio was kept constant as 0.4 in all mixtures. A slag/fly ash ratio of 80/20 by mass is used in all mixtures. Steel fibre contents up to 1% (by volume) with an interval of 0.25% are applied, and mixes with long/short fibre ratios of 80/20, 60/40, 40/60 and 20/80 are studied. All mortar specimens were prepared in a laboratory mixer; the fresh mortar was then poured into plastic moulds of 40 × 40 × 160 $mm^3$ and vibrated for 1 min, covered with a plastic film on the top surface for 24 h; finally all specimens were demoulded and cured at a temperature of 20°C and a relative humidity of 95% until their testing age.

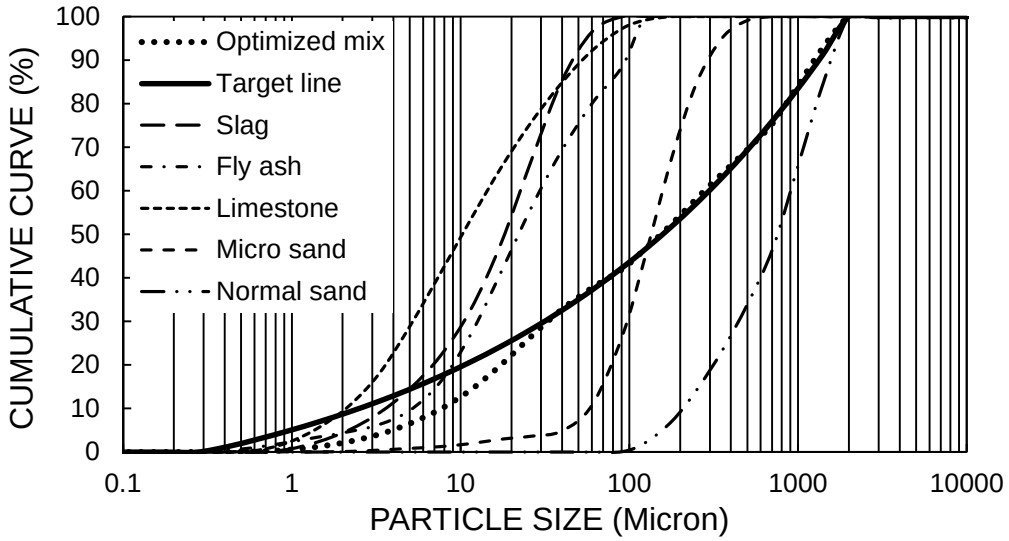


Figure 1 Particle size distributions of the raw materials, the target curve and the resulting integral grading line of the mixture

## Testing Methods

The workability of mortar samples was tested by the mini spread-flow test according to EN 1015-3. The compressive strength testing was carried according to EN 196-1. The flexural strength was tested under three-point loading using displacement control. A testing machine controlled by an external displacement transducer was used; the specimen mid-span deflection rate is 0.10 mm/min with a span of 100 mm. FTIR measurements were performed with the wavenumbers ranging from 4000 to 600 $cm^{-1}$ at a resolution of 1 $cm^{-1}$. The samples for drying shrinkage test were cast in moulds with dimensions of 40 × 40 × 160 $mm^3$ and cured in sealed condition at a temperature of 20°C. After 24 h of curing, specimens were exposed in a cabinet with a temperature of 20°C and relative humidity of 50%, also the initial length ($L_0$) was measured at that time. Afterwards, the length ($L_n$) was measured daily until the age of 28 d.

# RESULTS AND DISCUSSION

## Flowability

The slump flows of the fresh mortars with fibre additions are depicted in Figure 2. It is shown that as the steel fibre content increases, the slump flow exhibits a gradual decrease in general, and the long steel fibre shows a more significant effect on the slump flow than the short ones. In samples without fibre addition, the slump flow is 25.9 cm; and it slightly decreases to 23.1 cm when the short fibre content increases to 1%. Similar trends are also shown in mixes containing long steel fibres but with a higher decrement when compared to the short fibre. This result is in line with the previous researches that the steel fibre addition presents a negative effect on flowability in both Portland cement system and alkali activated system [10, 11]. It is suggested that the decrease of slump flow is due to the increased surface area and the resulting higher cohesive forces within the matrix. And long steel fibres have a relatively significant influence on this cohesive force. The slump flows of samples with 1% fibre content and different long/short fibre ratios are also tested, those values are all in between of the samples with 1% pure long and short fibres (20.6 and 23.1 cm), following the tendency that a higher long/short fibre ratio exhibits a relatively low slump flow.

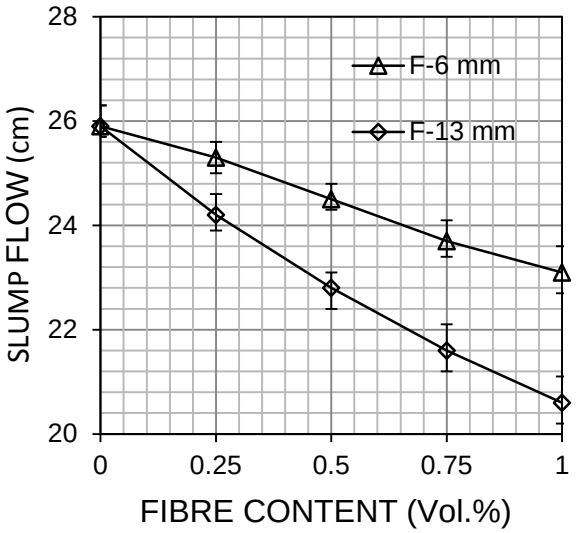


Figure 2 Slump flow of AA slag-fly ash composites with steel fibre addition

**Compressive Strength**

The 7 and 28 d compressive strengths of mixtures with different long and short fibre contents are presented in Figure 3(a). For the reference sample, the compressive strength is 65.4 MPa at 7 d, and it increases to 81.1 MPa after 28 d of curing. When short fibres with a dosage of 0.25% are added, the compressive strength increases to 71.6 MPa and 85.8 MPa at 7 and 28 d, respectively. It indicates that although steel fibres are well known for improving the tensile or flexural strength, they can also bridge the cracks and retard their propagation to some extent during the compression loads. Further increment of the fibre content from 0.25% to 1% leads to a gradual increase of strength up to 73.35 MPa at 7 d and 89.9 MPa at 28 d, respectively. The mixes with 0.75% and 1% fibre content do not show significant difference in strength, which may reveal that there is a limitation in contributing the compressive strength for steel fibres. The incorporation of long fibres leads to a relatively sharp increase with a dosage of 0.25%, followed by a continuous but slight increase of strength up to around 1%. It is important to notice that mixes with long fibres present higher strengths than the short fibre in general, this is due to the higher efficiency of long steel fibres in inhibiting the growth of macro-cracks.

A total fibre content of 1% is chosen for investigating the effect of hybrid steel fibres. Mixtures with four different long/short fibre ratios (80/20, 60/40, 40/60 and 20/80 vol.%) are applied and the results are presented in Figure 3(b). It can be seen that with a fixed total amount of fibre dosage, the compressive strength firstly increases when lowering the long/short fibre ratio, reaching the maximum strength in mixes with long/short ratio of 60/40, and then followed by a gradual decrease. This result indicates the beneficial effect of using hybrid steel fibre on compressive strength, by doing so a higher strength can be achieved with the same fibre content; and a certain fraction of long/short fibres may exhibit the optimum performance. Additionally, the relatively high strength for all mixes in general is also due to the utilization of particle packing methodology.

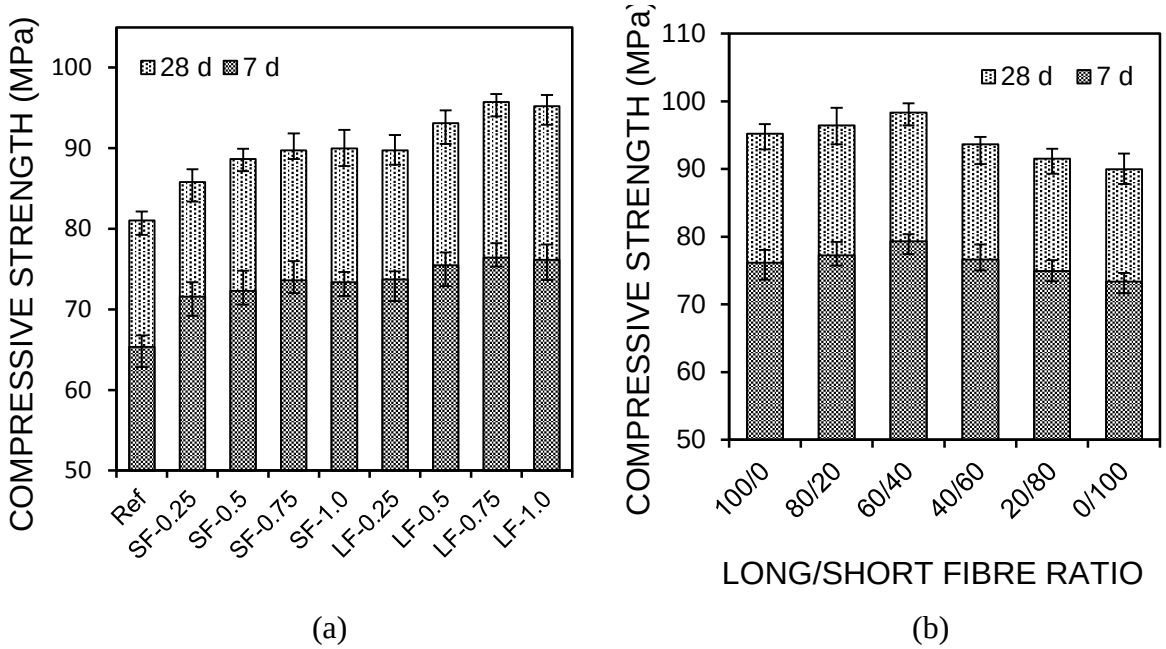


(a) (b)

Figure 3 7 and 28 d compressive strength of AA slag-fly ash composites with fibres (a: single fibre, b: hybrid fibre)

**Flexural Strength**

The 28 d stress-strain curves of mixtures with long and hybrid steel fibres are shown in Figure 4. The addition of short steel fibres slightly increases the ultimate flexural strength from 8.5 MPa to 11.2 MPa (not shown in the Figure), and the fracture mode of the mixtures with short fibres remains the same as the reference sample: the brittle fracture. This is attributed to shape of this fibre, the relatively short length and diameter makes this fibre capable of inhibiting the micro cracks under flexural loads, thus the flexural strength is increased as a result; while as the loading continues, the micro cracks develop and merge into larger ones and short fibres become less effective in macro crack bridging due to their limited length, and finally brittle fracture occurs. Compared to the effect of short fibres, a more significant increment in ultimate flexural strength and plastic fracture are presented when long fibres were added. The flexural strength continuously increases from 8.5 MPa to 13.5 MPa with the increasing fibre content up to 1%. It can be observed that with the same fibre dosage, mixes with long fibres always present a higher strength, indicating that long fibres are more effective in improving the flexural strength. This is probably due to the longer size of long fibres which makes them more oriented between two imaginary borders, thus a better capacity of preventing the growth of macro cracks can be achieved.

The influence of hybrid steel fibres on flexural strength is presented in Figure 4(b). The fibre content for all mixes is fixed at 1% and samples with only long or short fibres are used as references. As the long fibre fraction increases, mixes show generally a higher energy absorption capacity and a lower stress drop rate after reaching the stress peak; which shows again the higher efficiency of long fibres in bridging the macro-cracks and therefore a more stable post-peak response. The highest flexural strength is shown in mixes with a short/long fibre ratio of 40/60. It confirms that the ultimate flexural strength is not well linked to the toughness; the proportions between the long and short steel fibres exhibit a synergetic effect and result in the occurrence of optimum flexural strength.

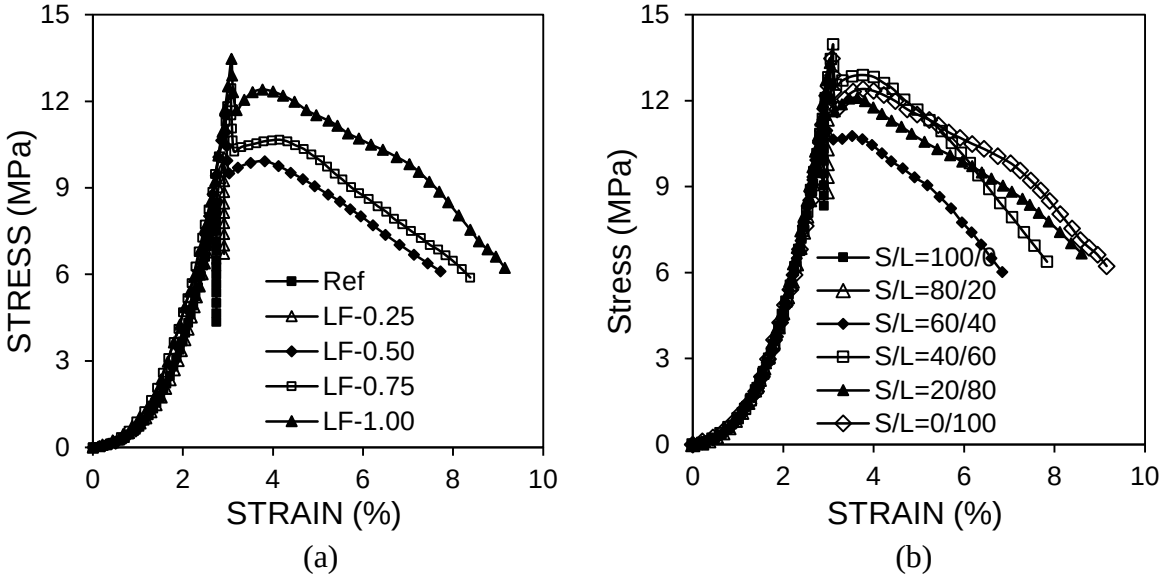


Figure 4 Stress-strain curve of AA slag-fly ash composites with fibre addition (a: long fibre, b: hybrid fibre)

**Gel Structure**

The infrared spectra of the unreacted slag and fly ash, as well as the reaction products after 1, 7 and 28 d of curing are given in Figure 5. For the starting materials, a main vibration band at around 900 $cm^{-1}$ and a small shoulder at around 670 $cm^{-1}$ are shown in the original slag, which is assigned to the vibration of terminal Si-O bonds and T-O groups [12], respectively. As for the fly ash, a main absorption band at around 1020 $cm^{-1}$, indicating the presence of large amount of the bridge Si-O-T bonds [13].

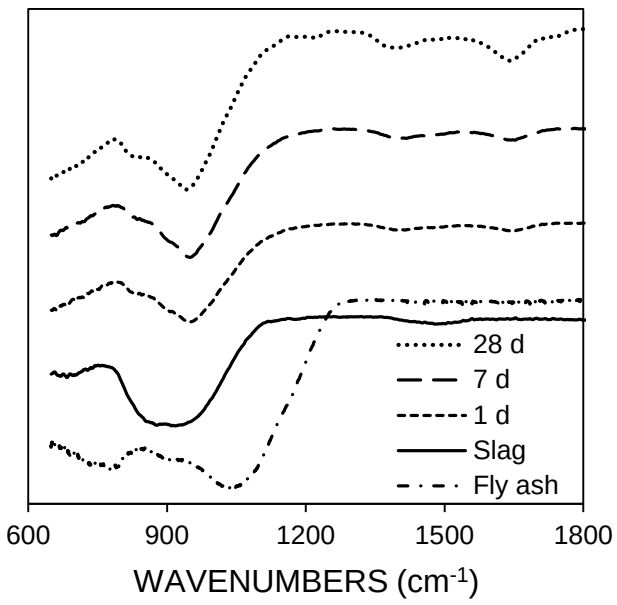


Figure 5 FTIR spectra of the starting materials and AA slag-fly ash blends at 1, 7 and 28 d

After activation, the main absorption band shifts to around 940 $cm^{-1}$ that is assigned to the non-bridging Si-O bonds [14], showing that the main reaction products exhibit a chain structure; and they are generally regarded as C-A-S-H type gels. When compared to the starting materials, the location of the main absorption band shows an increase for slag (from 900 to 940 $cm^{-1}$) while a decrease for fly ash (from 1020 to 940 $cm^{-1}$), implying that the original Si-O networks in slag experienced a certain degree of polymerization while the high cross-linked bridging Si-O bonds in fly ash seems to be decomposed to some extent. The slight shoulder at around 815 $cm^{-1}$ together with the absorption band at 1400 $cm^{-1}$ reveal the presence of carbonates, and the absorption bands at 1640 $cm^{-1}$ and around 3200 $cm^{-1}$ (not shown in the figure) are assigned to the vibration of bound water. Concerning the gel structure development, no significant structural changes were observed between the curing age of 1, 7 and 28 d.

## Drying Shrinkage

Figure 6 depicts the drying shrinkage results of mixes with only long or short steel fibres until 28 d; each value is an average of two measurements. It is apparent that the reference sample exhibits an obvious length change over time, especially during the first few days, and the addition of both long and short fibre can reduce the drying shrinkage to some extent. It is commonly known that the drying shrinkage is caused by the evaporation of free water from the pores of the hardened matrix [15], and a generally higher drying shrinkage is usually shown in alkali activated materials compared to the Portland cement based materials.

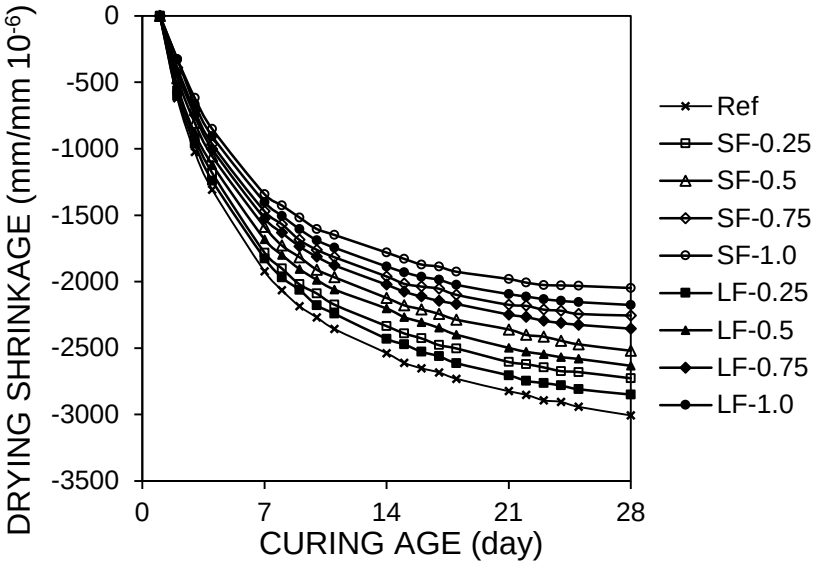


Figure 6 Drying shrinkage of AA slag-fly ash mortars with different fibre lengths

It can be seen that the drying shrinkage decreases with the increasing steel fibre content up to 1%. For a fixed fibre dosage, mixes with long fibre present relatively high values when compared to the ones with short fibre, indicating that the long fibre is slightly less effective than short fibre in inhibiting the shrinkage; but a long fibre addition of 1% still exhibits a shrinkage reduction rate of 27.6% compared to the reference sample. The evaporation of free water from the matrix can result in a reduction of the absolute volume, and meanwhile tensile stresses may arise from the resulted internal restraints. When steel fibre is incorporated, the generated tensile stresses will be imposed on the fibre (on the matrix as well), due to the high elastic modulus and bridging effect of steel fibre, the influence of this inner force on shrinkage

can be suppressed to some extent. The effect of hybrid fibre is not shown in the figure, but the results show that samples with higher short fibre contents exhibit a slightly lower shrinkage, while all mixtures present a similar level of drying shrinkage in general, indicating that the fibre content possesses a more significant influence, and the utilization of hybrid fibre seems not to show any synergetic effect.

## CONCLUSIONS

This paper investigates the performance of alkali activated slag-fly ash composites that are reinforced by long and/or short steel fibres, and the mortar samples are designed by applying the modified Andreasen & Andersen particle packing model. The results show that both long and short fibre additions decrease the slump flow, and the utilization of long steel fibres presents a more significant effect. The compressive strength is increased by 10.3%/16.8% when a short/long steel fibre content of 1% is incorporated, respectively. The hybrid usage of long and short fibres presents a synergetic effect and resulting in the presence of an optimum strength. The addition of long fibres with contents higher than 0.25% by volume changes the fracture mode from brittle into plastic; while the addition of short fibres increases the flexural strength moderately. Synergetic effect of long and short fibres is also shown in flexural strength results. The main reaction product of this blended alkali binder is a chain structured C-A-S-H type gel and remains stable after 1 d of curing. The utilization of long and short steel fibres at the dosage of 1% effectively reduces the shrinkage (by 27.6% and 31.9%, respectively) due to their ability of suppressing the generated inner force.

## ACKNOWLEDGEMENTS

This research was supported by China Scholarship Council and the Department of the Built Environment at Eindhoven University of Technology. The authors gratefully thank Mr. P. de Vries (ENCI B.V., the Netherlands) and Mr. J. van Eijk (Knauf Insulation, the Netherlands) for the materials supply. Furthermore, the authors wish to express their gratitude to the following sponsors of the Building Materials research group at TU Eindhoven: Rijkswaterstaat Grote Projecten en Onderhoud; Graniet-Import Benelux; Kijlstra Betonmortel; Struyk Verwo; Attero; Enci; Rijkswaterstaat Zee en Delta-District Noord; Van Gansewinkel Minerals; BTE; V.d. Bosch Beton; Selor; GMB; Geochem Research; Icopal; BN International; Eltomation; Knauf Gips; Hess AAC Systems; Kronos; Joma; CRH Europe Sustainable Concrete Centre; Cement & Beton Centrum; Heros and Inashco (in chronological order of joining).

## REFERENCES

1. WANG S D, SCRIVENER K L, PRATT P L. Factors affecting the strength of alkali-activated slag, Cem Concr Res, Vol. 24, No. 6, 1994, pp 1033-1043.

2. FERNÁNDEZ-JIMÉNEZ A, GARCÍA-LODEIRO I, PALOMO A. Durable characteristics of alkali activated fly ashes, J Mater Sci, Vol. 42, 2007, pp 3055-3065.

3. LEE N K, LEE H K. Setting and mechanical properties of alkali-activated fly ash/slag concrete manufactured at room temperature, Constr Build Mater, Vol. 47, 2013, pp 1201-1209.

4. SUGAMA T, BROTHERS L E, Van de PUTTE T R. Acid-resistant cements for geothermal wells: sodium silicate activated slag/fly ash blends, Adv Cem Res, Vol. 17, No. 2, 2005, pp 65-75.

5. YIP C K, LUKEY G C, Van DEVENTER J S J. The coexistence of geopolymeric gel and calcium silicate hydrate at the early stage of alkaline activation. Cem Concr Res, Vol. 35, 2005, pp 1688-1697.

6. GARCÍA-LODEIRO I, FERNÁNDEZ-JIMÉNEZ A, BLANCO M T, PALOMO A. FTIR study of the sol-gel synthesis of cementitious gels: C-S-H and N-A-S-H, J Sol-Gel Sci Techn, Vol. 45, 2008, pp 63-72.

7. BERNAL S, GUTIERREZ R D, DELVASTO S, RODRIGUEZ E. Performance of an alkaliactivated slag concrete reinforced with steel fibers, Constr Build Mater, Vol. 24, 2010, pp 208-214.

8. AYDIN S, BARADAN B. The effect of fiber properties on high performance alkali-activated slag/silica fume mortars, Compos Part B: Eng, Vol. 45, 2013, pp 63-69.

9. HÜSKEN G, BROUWERS H J H. Earth-moist concrete: application of a new mix design concept, Cem Concr Res, Vol. 38, pp 1246-1259.

10. RASHAD A M. A comprehensive overview about the influence of different additives on the properties of alkali-activated slag-A guide for Civil Engineer, Constr Build Mater, Vol. 47, 2013, pp 29-55.

11. YU R, SPIESZ P, BROUWERS H J H. Mix design and properties assessment of Ultra-High Performance Fibre Reinforced Concrete (UHPFRC), Cem Concr Res, Vol. 56, 2014, pp 29-39.

12. KOVALCHUK G, FERNÁNDEZ-JIMÉNEZ A, PALOMO A. Alkali-activated fly ash: Effect of thermal curing conditions on mechanical and microstructural development - Part II, Fuel, Vol. 86, 2007, pp 315-322.

13. HAJIMOHAMMADI A, PROVIS J L, Van DEVENTER J S J. Time-resolved and spatially resolved infrared spectroscopic observation of seeded nucleation controlling geopolymers gel formation. J, Colloid Interface Sci, Vol. 357, 2011, pp 384-392.

14. ZHANG Z H, WANG H, PROVIS J L, BULLEN F, REID A, ZHU Y C. Quantitative kinetic and structural analysis of geopolymers. Part 1. The activation of metakaolin with sodium hydroxide, Therm Acta, Vol. 539, 2012, pp 23-33.

15. MA Y W. Microstructure and engineering properties of alkali activated fly ash, PhD Thesis, 2013, Delft University of Technology, Delft, The Netherlands.

# FRESH BEHAVIOUR OF ULTRA-HIGH PERFORMANCE CONCRETE (UHPC): AN INVESTIGATION ON THE EFFECT OF SUPERPLASTICIZERS AND STEEL FIBRES

**P P Li** **Q L Yu**

**H J H Brouwers**

Eindhoven University of Technology

The Netherlands

**R Yu**

Wuhan University of Technology

China

**ABSTRACT:** To decrease the porosity and increase the strength of Ultra-High Performance Concrete (UHPC), lower water-to-powder ratios and high contents of steel fibres are usually used, which lead to a reduced workability of fresh UHPC. In the present research, the effects of different superplasticizers and steel fibres on the fresh behaviour of UHPC were investigated. The initial and final setting times of the UHPC pastes containing 4 different superplasticizers (SP) were measured by Vicat needle tests. The effects of SP type and dosage on the spread flow were analysed for both paste and UHPC. The spread flows of UHPC with saturation dosages of SP were measured up to 2 hours to analyse the slump life and retention effect. Furthermore, the effects of 4 types steel fibres on the fresh behaviour of UHPC were investigated by using different fibre volume contents. The results show that the dispersing ability, retardation and retention effect of SP differed with different chemical constituents and structures, which greatly influenced the mixture's setting time, spread flow and slump life. The workability of UHPFRC was affected by the steel fibres' geometric characteristics and coating type, and it decreased continuously with the increase of the fibre content.

**Keywords:** Ultra-High Performance Concrete; Steel fibres; Superplasticizers; Fresh behaviour

**P P Li** is currently working as a PhD student in the Department of Built Environment, Eindhoven University of Technology.

**Dr Q L Yu**, received his Ph.D. degree from Eindhoven University of Technology, the Netherlands. He is currently assistant professor Building Materials in the Department of the Built Environment, Eindhoven University of Technology.

**Dr R Yu**, received his Ph.D. degree from Eindhoven University of Technology, the Netherlands. He is currently associate professor in the Faculty of Materials Science and Engineering, Wuhan University of Technology.

**Prof Dr Ir H J H Brouwers** is professor Building Materials in the Department of the Built Environment at Eindhoven University of Technology.

## INTRODUCTION

Ultra-High Performance Concrete (UHPC) is a relatively new building material, which has been fabricated since 1990s. Compared to conventional concrete, it has superior mechanical strength, durability and impact resistance [1, 2, 3]. These excellent material properties can be achieved by certain methods, such as eliminating the coarse aggregate to increase the homogeneity, optimizing the grain-size distribution of the raw materials to improve compactness, utilizing a special heat curing and compressing treatments, etc. [4]. Besides those principles, adding high content of steel fibres and limiting the porosity by using low water-to-powder ratios for concretes are probably the mostly convenient and efficient ways to realize those superior material properties.

Superplasticizers (SP) are used to increase the fluidity of concrete with relatively low additions of water. Since their introduction in the 1930s, they have been used as critical chemical admixtures for modern concrete. The molecules are adsorbed onto particles, which are then physically separated by opposing their attractive forces with steric and/or electrostatic forces [5]. As the first generation water reducers, the Lignosulfonates (LS) can only limit the water content by about 10%. The polymelamine sulfonate (PMS) and sulfonated melamine formaldehyde condensate (PMS) have been produced as the second generation dispersant since 1960s, with a water-reduction ability of about 20-30%. The new generation of superplasticizers polycarboxylic ethers (PCEs), developed in 1980s, can achieve up to 40% water reduction. The properties of those PCE polymers are mainly determined by the following parameters: chemistry and length of the backbone, number and length of the side chains, amount of anionic and ionic groups, bond type between backbone and side chain, and overall charge density [5, 6, 7]. Therefore, different types of SP certainly show different effects on the fresh behaviour of UHPC.

The addition of steel fibres can significantly improve the performance of UHPC in the hardened state, especially the ductility, impact resistance, tensile strength and fatigue strength [8, 9, 10]. Nevertheless, steel fibres can also decrease the workability of UHPC to some extent at the same time. Nowadays, the available steel fibres in the market have various types with different length, diameter, coating category, as well as straight, twist and hook ended shapes. Those different characteristics of steel fibres have different degrees of influence on the workability reduction. Hence, it is necessary to investigate the effect of steel fibres on flowability of UHPC before their utilization.

The objective of this study was to investigate and understand the SP type and dosage effects on the setting times, spread flow of paste and UHPC, slump life and retention effect. Furthermore, the effects of steel fibres with different geometric and coating characteristics on the flowability were also investigated.

## EXPERIMENTS

### Materials

The raw materials used in this study were Portland Cement CEM I 52.5R (OPC), limestone powder (LP), nanosilica (nS), microsand 0-1 (MS), sand 0-2 (S), water (W), superplasticizers (SP) and steel fibres (SF). The specific densities of those ingredients are shown in Table 1. The particle size distributions of the used materials were measured by the sieve and laser diffraction analyses, shown in Figure 1.

Four PCE-type superplasticizers with different dispersing and retarding abilities were used in the pastes and UHPC. Steel fibres with different geometric and coating characteristics, with the tensile strength of 1100 MPa, were utilized to produce the Ultra-High Performance Fibre Reinforced Concrete (UHPFRC). The detailed information of superplasticizers and steel fibres are shown in Tables 2 and 3, respectively.

Table 1 Specific densities of raw materials

| MATERIALS | OPC | LP | MS | S | nS | W | SP | SF |
|---|---|---|---|---|---|---|---|---|
| Specific density (g/cm³) | 3.15 | 2.71 | 2.22 | 2.72 | 2.64 | 1.00 | 1.05-1.14 | 7.80 |

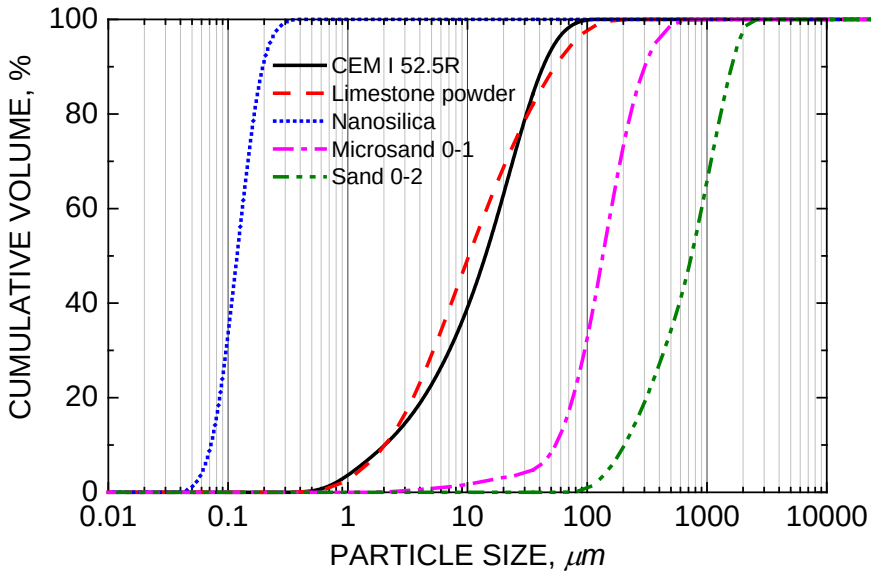


Figure 1 Particle size distribution of raw materials

Table 2 Product information of SP

| NO. | DRY MATTER | SHAPE/COLOUR | DENSITY (g/ cm$^3$) | pH | CHLORIDE CONTENT | ALKALI CONTENT |
|---|---|---|---|---|---|---|
| SP1 | 35% | Amber liquid | 1.082-1.142 | 7 | ≤ 0.1% | ≤ 3% |
| SP2 | 25% | Light brown liquid | 1.05 | 5 - 8 | ≤ 0.1% | ≤ 1.5% |
| SP3 | 35% | Translucent yellowish liquid | 1.07 | 5.0 ± 1.5 | ≤ 0.1% | ≤ 0.5% |
| SP4 | 40% | Yellowish liquid | 1.09 | ca.4 | ≤ 0.1% | ≤ 1% |

Table 3 Characteristics of utilized steel fibres

| NO. | FIBRE TYPE | LENGTH (mm) | DIAMETER (mm) | ASPECT RATIO | COATING |
|---|---|---|---|---|---|
| 1 | Short straight steel fibre (SSF) | 6 | 0.16 | 38 | Copper |
| 2 | Long straight steel fibre (LSF) | 13 | 0.20 | 65 | Copper |
| 3 | Short hook ended steel fibre (SHF) | 29 | 0.65 | 45 | Nickel |
| 4 | Long hook ended steel fibre (LHF) | 31 | 0.45 | 69 | Copper |

## Mixture Proportions

The nanosilica-to-binder ratio, limestone-to-powder ratio and water-to-powder ratio were fixed at 4%, 30% and 0.2, respectively, in all mixtures, following previous research [8]. The totally used water included the water in the nanosilica slurry and SP. In the setting time tests of pastes, the dosages of SP were at constant of 0.4%, 0.8% and 1.2%, dry matter by weight of powder. In the flow tests of pastes, the dosages of SP were varied from 0.4% to 2.0%, dry matter by weight of powder. In the flow tests of UHPC, the microsand-to-powder ratio and sand-to-powder ratio were fixed at 0.25 and 1.2, respectively, with the dosages of SP varying from 1.0% to 3.0%. After obtaining the relationship between the spread flow and SP dosages, the flow tests of UHPC were conducted at the saturation dosages of SP. In the flow tests of UHPFRC, the contents of steel fibres were from 0 to 3% by volume of mixture at the saturation dosages of each SP. The recipe of the UHPC reference admixture in this study is shown in Table 4.

The mixing of pastes lasted about 5 min using a 5-liter Hobart mixer, using the following procedure: dry mixing (cement and limestone) for 30s at the low speed, sequentially adding nanosilica slurry, 80% water, SP slurry, and remaining water for about 2 min at the low speed, followed by mixing the paste for 2 min at the low speed and 30 s at the medium speed. The adding order of components in mixing procedure of UHPC was similar to that of paste, whereas the total time is about 8 min (30 s for dry mixing, 180 s for adding slurries and water, another 150 s at the low speed and 120 s at the medium speed).

Table 4 Recipe of UHPC reference mixture

| PRODUCTS | OPC $kg/m^3$ | LP $kg/m^3$ | MS $kg/m^3$ | S $kg/m^3$ | nS $kg/m^3$ | W $kg/m^3$ |
|---|---|---|---|---|---|---|
| Mass | 611.3 | 272.9 | 227.4 | 1091.6 | 25.5 | 181.9 |

## Testing Methods

The setting times of pastes were evaluated by using the manual Vicat apparatus based on EN 196-3: 2005. The spread flow of pastes and concretes were measured by using a truncated conical mould (Hägermann cone: height 60 mm, top diameter 70 mm, bottom diameter 100 mm), in accordance with EN 1015-3: 2007. To evaluate the slump life of the fresh UHPC, the spread flow of UHPC were also measured in 2 hours. The lab ambient temperature while mixing and testing was relatively constant, about 21°C.

# RESULTS AND DISCUSSION

## Setting Time and Flow of Paste

Figure 2 presents the initial and final setting times of pastes incorporating SP1, SP2, SP3 and SP4. From the figures it is obvious that the setting times are affected by both SP types and dosages. For all those 4 SPs, high dosages always increase the setting times. It indicates that those SPs have a retardation effect on the hydration of pastes, and the retardation effect is higher with the increase of SP dosages. It is also clear that pastes with SP1 have the longest setting times, reaching at about 7 h of initial and 8.9 h of final setting time at a dosage of 1.2%. It means that SP1 is not suitable to obtain a high early age strength for paste or concrete due to

the high retardation effect. The pastes with SP2 show the shortest setting times, which are approximately 1.42 h (2.67 h), 2.75 h (4.58 h) and 3.58 h (5.42 h) of initial (final) setting time respectively at the dosages of 0.4%, 0.8% and 1.2%. The low retardation effect of SP2 makes it possible to achieve a relatively high early age strength for paste or concrete. Compared with SP1 and SP2, medium setting times are observed for the pastes containing SP3 and SP4.

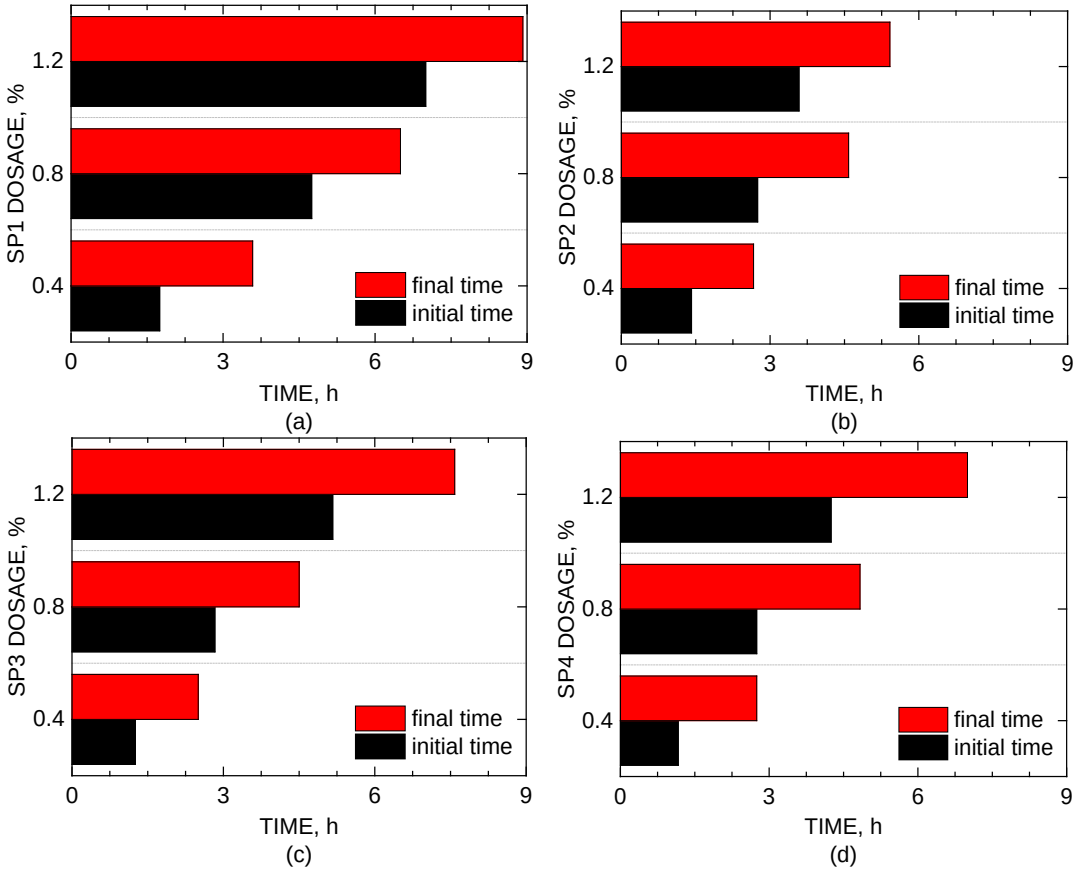


Figure 2 Setting times of pastes

Figure 3 shows the time differences between the initial and final settings at different SP dosages. The time differences of SP1 maintain at a stable level (approximately 75-175 min). SP2 shows a similar pattern at dosages of 0.8% and 1.2%, however it is shorter than that of SP1 at the dosage of 0.4%. The time difference of SP3 shows a nearly same increasing tendency with the increase of SP dosage to SP4, with about 20 min earlier than that of SP4.

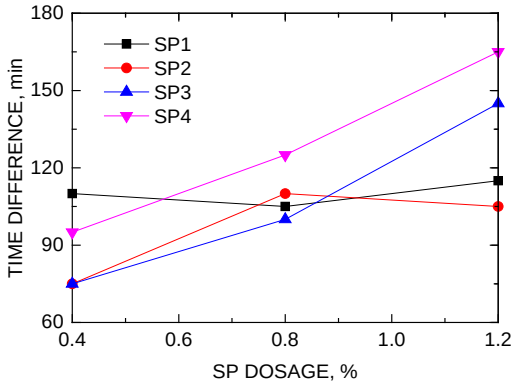


Figure 3 Time difference between initial and final settings

Figure 4 depicts the spread flow of pastes incorporating different types and dosages of SP. Generally, the flow diameters are increased with the increasing SP dosages at relatively low SP dosages. Nevertheless, the spread flows are kept at stable levels above the saturation dosages. This typical plateau at high dosages can be also observed from the relationships between SP adsorption on particles and SP dosages in some other researches [5, 7, 11]. It manifests that SP works only after the adsorption on the particles, which corresponds to surface coverage, similarly to the results in other studies [4, 12]. When the used SP exceeds the saturation dosage, a complete surface coverage will be obtained. Then the dispersing ability of SP will not increase anymore, which results in the occurrence of the typical plateau at high dosages.

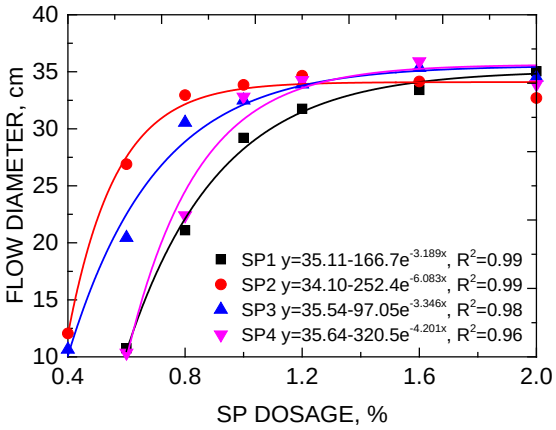


Figure 4 Spread flow of pastes

It is clear that the maximum flow diameters of pastes with different SP types are approximately 35 cm. The critical (saturation) dosages of SP1, SP2, SP3 and SP4 for paste are approximately 0.6% (1.4%), 0.4% (0.8%), 0.6% (1.2%) and 0.4% (1.2%), respectively. It can be concluded that SP2 and SP3 have a much higher dispersing ability for pastes with dosages ranging from 0.4% to 1.2%. However, with the increase of SP dosages, the dispersing ability of SP3 and SP4 are only a bit higher than that of SP2 and SP1. The following mathematical model is proposed to express the relationships between the spread flow and SP dosage:

$$y = y_0 - ae^{-bx} \tag{1}$$

where $y$ is the flow diameters of pastes, $x$ is the dosage of SP. $y_0$ is the maximum flow diameter (plateau). $b$ represents the velocity to approach the plateau with the increase of SP dosage. $a$ is related to the dispersing ability of SP, when $b$ is fixed, a larger $a$ means a higher increasing velocity of flow at a certain SP dosage.

**Flow of UHPC**

Figure 5 presents the spread flows of UHPC incorporating different types and dosages of SP. The spread flows of UHPC with SP2, SP3 and SP4 show a typical plateau at high dosages, which are similar to that of pastes. However, the SP1 presents a linear increase, which indicates that SP1 increases the flow ability very slowly at a relatively low dosage. All the critical dosages of SP2, SP3 and SP4 for UHPC are close to 1.0%, meanwhile all the saturation dosages are near to 2.2%. And the critical dosage of SP1 for UHPC is approximately 1.0%, but it does not show a clear saturation dosage till 3.0%. In conclusion, SP3 and SP4 have a higher dispersing ability than SP1 and SP2 for UHPC.

All relationships between the spread flow of UHPC and SP dosage can be also subjected to the exponential model $y = y_0 - ae^{-bx}$, which is similar to that of paste. It is worth to point out, the curve of SP1 is more likely to a linear model. In the case of SP1, the $y_0$ is just a 'theoretical' maximum flow diameter, which maybe not be possible in practice. It indicates that SP1 has a poor adsorption effect in UHPC, which may be incompatible with UHPC in this study.

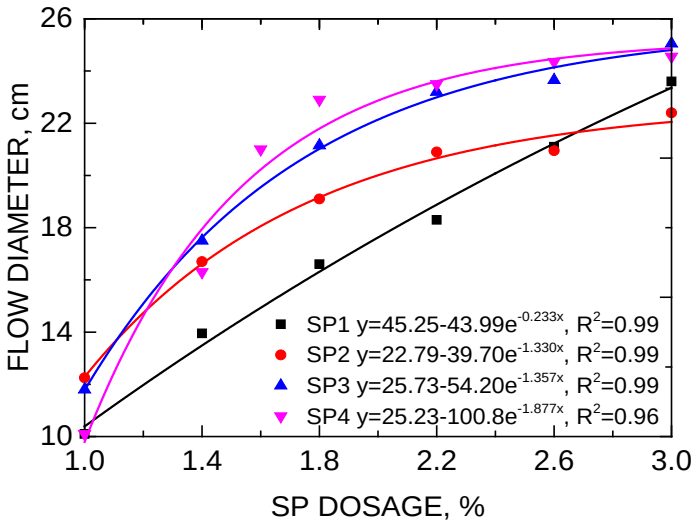


Figure 5 Spread flow of UHPC

**Slump Life and Retention Effect**

Figure 6 presents the slump life of fresh UHPC in 2 hours. Fresh concrete is well known to lose its workability with time, which is called 'slump loss' [4]. The previous researches imply that slump loss involves chemical and physical processes, which is mainly attributed to the physical coagulation of particles rather than to chemical processes [13]. Therefore, UHPC with SP1 has a shortest slump life, even though SP1 show the highest retardation effect on the paste setting. The possible reason is that SP1 has a low adsorption ability, which induces an uncompleted surface coverage. Uncompleted surface coverage (below saturation dosage) results in a rapid stiffening of the concrete [7]. UHPC with SP2 has a poor slump life probably due to its weak retardation effect on paste hydration and uncompleted surface coverage. UHPC with SP3 shows a perfect slump life in the whole testing time (2 h), which even has a slight increase of flow diameter before 80 min. UHPC with SP4 can maintain a good slump life before 40 min, which experiences a sharp decrease after that time.

Generally, UHPCs with SP1 and SP2 have a short slump life, which have a linear decrease relationship between the flow and elapsed time. UHPC with SP3 can just keep a good slump life within 40 min. UHPC with SP4 presents the best slump life, nearly without any slump flow loss in 2h.

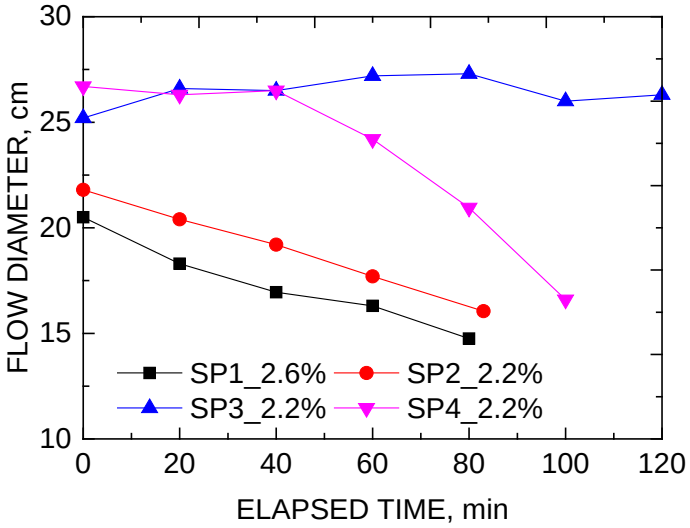


Figure 6 Slump life (2 h) of UHPC

## Effect of Steel Fibres on Flowability

Figure 7 shows the effect of steel fibre on the spread flow of UHPFRC. Obviously, fibre types and contents affect the characteristics of UHPFRC in the fresh state. As needle-like particles, those steel fibres decrease the flow of UHPFRC due to two reasons: mechanical interaction (cohesive and anchoring forces) between fibres and grains, and interlock of fibres.

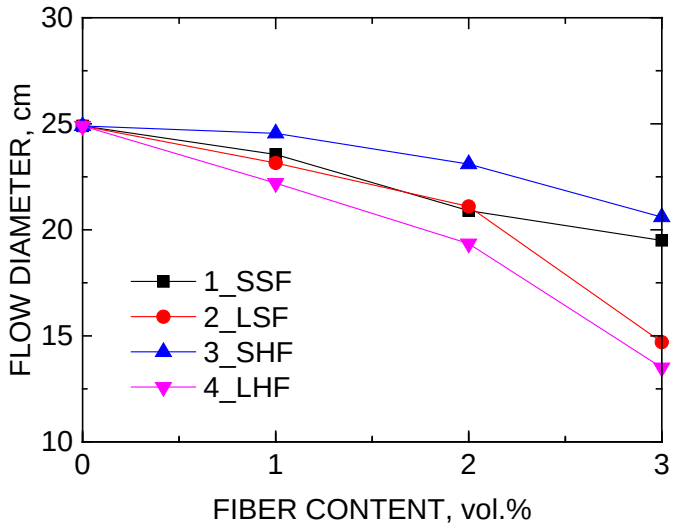


Figure 7 Spread flow with steel fibres

The characteristics of the utilized steel fibres are shown in Table 2. 1-SSF, 2-LSF and 4-LHF are copper coated steel fibres, while 3-SHF is coated with nickel. Compared to 1-SSF, the 2-LSF is more elongated, which contributes to a higher internal mechanical interaction in matrix, especially at high fibre contents. The hook ended characteristic of 4-LHF leads to a higher anchorage and interlock than 1-SSF and 2-LSF, which results in a larger resistance to the flow of UHPFRC. Even though, 3-LSF has a bigger anchoring and interlock effect than 1-SSF and 2-LSF, its cohesive forces are much less pronounced due to the minimum surface area per volume and unique coated surface.

## CONCLUSIONS

This paper investigates the effect of superplasticizers and steel fibres on the fresh behaviour of UHPC. Both paste and concrete mixtures are designed to analyse the setting and flowability. Based on the obtained results, the following conclusions can be drawn:

- The type and dosage of SP have an obvious effect on the setting times which will be longer at higher dosages. The SP1 contributes to the longest setting times of pastes due to the largest retardation effect on the hydration, whereas the SP2 results in the shortest ones. The time differences between the initial and final settings are nearly to 75-175 min.
- The flowabilities of paste and UHPC are greatly influenced by the types and dosages of SP, which is related to the different adsorption abilities due to the different chemical constituents and structures. After obtaining a complete surface coverage of particles above the saturation dosage of SP, the dispersing ability of dosage will not increase anymore, which results in the occurrence of the typical plateau at high dosages. An exponential model$y = y_0 - ae^{-bx}$ is proposed to describe the relationships between the spread flow and SP dosage, which also presents that the SP3 and SP4 have a better dispersing ability than SP1 and SP2 for UHPC.
- The UHPCs with SP3 and SP4 have longer slump life, namely longer than 120 min and 40 min respectively. Whereas UHPCs with SP1 and SP2 present a poor slump life, with a linear decrease relationship between the flow and elapsed time. The slump loss and retention effect mainly depend on the physical coagulation of particles, as well as chemical processes to same extent.
- Geometric characteristic, coating type and volume content of steel fibres affect the flowability of UHPFRC. Generally, high volume content, elongated type, hooked ended type and copper-coated type of steel fibres contribute to a lower flow, due to the higher mechanical interaction and interlock.

## ACKNOWLEDGEMENTS

This research was carried out under the fund of China Scholarship Council and the Department of the Built Environment of Eindhoven University of Technology. The authors wish to express their gratitude to the following sponsors of the Building Materials research group at TU Eindhoven: Rijkswaterstaat Grote Projecten en Onderhoud, Graniet-Import Benelux, Kijlstra Betonmortel, Struyk Verwo, Attero, Enci, Rijkswaterstaat Zee en Delta - District Noord, Van Gansewinkel Minerals, BTE, V.d. Bosch Beton, Selor, GMB, Icopal, BN International, Eltomation, Knauf Gips, Hess AAC Systems, Kronos, Joma, CRH Europe Sustainable Concrete Centre, Cement&BetonCentrum, Heros, Inashco, Keim and Sirius International.

## REFERENCES

1. RICHARD, P, CHEYREZY, M. Composition of reactive powder concretes, Cement and Concrete Research, Vol. 25, No. 7, 1995, pp 1501-1511.

2. WANG, W, LIU, J, AGOSTINI, F, DAVY, C A, SKOCZYLAS, F, CORVEZ, D. Durability of an Ultra High Performance Fiber Reinforced Concrete (UHPFRC) under progressive aging, Cement and Concrete Research, Vol. 55, 2014, pp 1-13.

3. YU, R, VAN BEERS, L, SPIESZ, P, BROUWERS, H J H. Impact resistance of a sustainable Ultra-High Performance Fibre Reinforced Concrete (UHPFRC) under pendulum impact loadings, Construction and Building Materials, Vol. 107, 2016, pp 203-215.

4. WANG, D, SHI, C, WU, Z, XIAO, J, HUANG, Z, FANG, Z. A review on ultra high performance concrete: Part I. Raw materials and mixture design, Construction and Building Materials, Vol. 101, No. 1, 2015, pp 741-751.

5. FLATT, R J, SCHOBER, I. Superplasticizers and rheology of concrete, 2011, Woodhead Publishing Limited.

6. YAMADA, K, TAKAHASHI, T, HANEHARA, S, MATSUHISA, M. Effects of the chemical structure on the properties of polycarboxylate-type superplasticizer, Cement and Concrete Research, Vol. 30, No. 2, 2000, pp 197-207.

7. WINNEFELD, F, BECKER, S, PAKUSCH, J, GÖTZ, T. Effects of the molecular architecture of comb-shaped superplasticizers on their performance in cementitious systems, Cement and Concrete Composites, Vol. 29, No. 4, 2007, pp 251-262.

8. YU, R, SPIESZ, P, BROUWERS, H J H. Development of Ultra-High Performance Fibre Reinforced Concrete (UHPFRC): Towards an efficient utilization of binders and fibres, Construction and Building Materials, Vol. 79, 2015, pp 273-282.

9. KIM, D J, PARK, S H, RYU, G S, KOH, K T. Comparative flexural behavior of Hybrid Ultra High Performance Fiber Reinforced Concrete with different macro fibers, Construction and Building Materials, Vol. 79, No. 11, 2011, pp 4144-4155.

10. KANG, S T, KIM, J K. The relation between fiber orientation and tensile behavior in an ultra high performance fiber reinforced cementitious composites (UHPFRCC), Cement and Concrete Research, Vol. 41, No. 10, 2011, pp 1001-1014.

11. ZHANG, Y, KONG, X. Correlations of the dispersing capability of NSF and PCE types of superplasticizer and their impacts on cement hydration with the adsorption in fresh cement pastes,Cement and Concrete Research, Vol. 69, 2015, pp 1-9.

12. KIRBY, G, LEWIS, J A, MATSUYAMA, H, MORISSETTE, S, YOUNG, J F. Polyelectrolyte effects on the rheological properties of concentrated cement suspensions, Journal of the American Ceramic Society, Vol. 83, No. 8, 2000, pp 1905-1913.

13. CHANDRA, S, BJÖRNSTRÖM, J. Influence of superplasticizer type and dosage on the slump loss of Portland cement mortars - Part II, Cement and Concrete Research, Vol. 32, No. 10, 2002, pp 1613-1919.

# ULTRA HIGH PERFORMANCE SHOTCRETE FORMULATIONS

**T Robl**

**A Oberlink**

**R Jewell T Duvallet**

University of Kentucky

**P Mills**

Minova USA, Inc.

United States of America

**ABSTRACT.** This effort was focused on the development of fibre reinforced ultra-high performance (FR UHPC) shotcrete formulations designed to restore structural integrity to shock damaged infrastructure. The FR UHPC mixes are a "single bag" dry design. The mix formulations were based on Type III Portland cement (OPC III), calcium sulfoaluminate cement (CSA) and aggregates with gradations that extended from the nano-scale to 0.50 mm top size. Both novel short (6mm) and conventional (12 mm) high tensile steel fibres were used. Three aggregate types were used and mixes also contained ultra-fine (UF) quartz flour and silica fume. Successful mixes had W/C ratios of ~0.25 and steel fibre contents of 3.5% or more. Compressive strengths as high as 188 MPa and post-cracking flexural strengths up to 18.8 MPa were recorded.

**Keywords:** Shotcrete, Gunite, Short steel fibres, Ultra-high strength, Rapid setting

**Thomas L Robl** is the Associate Director for the Environmental and Coal Technologies group (ECT) at the University of Kentucky Center for Applied Energy Research (CAER). He is a member of the University of Kentucky Graduate Faculty and is a Director of the American Coal Ash Association and Co-Chairman of the World of Coal Ash International Symposium. He received his PhD from the University of Kentucky in 1977 in Geology. **Anne E Oberlink** is a Research Scientist Senior in the Environmental and Coal Technologies group (ECT) at the University of Kentucky Center for Applied Energy Research (CAER). She received her Master of Science in Chemistry from the University of Kentucky in 2010. **Robert B Jewell** is a Research Engineer Senior in the Environmental and Coal Technologies group (ECT) at the University of Kentucky Center for Applied Energy Research (CAER). He received his MS in geology, and his PhD in Civil Engineering from the University of Kentucky. **Tristana Y Duvallet** is a Research Engineer Senior in the Environmental and Coal Technologies group (ECT) at the University of Kentucky Center for Applied Energy Research (CAER). She received her PhD in Materials Science and Engineering from the University of Kentucky in 2014. **Peter S. Mills** is the Technology Leader for Minova USA Inc based in Georgetown, Kentucky. He has numerous patents to his name and has been instrumental in developing many life saving and productivity enhancing products for the world's mining and tunnelling industries.

# INTRODUCTION

## Background

The overarching goal of this work is to develop useful tools to rapidly repair critical infrastructures damaged by natural (e.g. earthquake, tsunami) or manmade activities (shelling, bombing). Very rapid strength development and high bonding strength are critical when applied to infrastructure repair and stabilization. Shotcrete mixes were develop through collaboration among researchers at the University of Kentucky, Center for Applied Energy Research, USA, the University of Dundee, Concrete Technology Unit (CTU), Scotland, UK and Minova, Inc. USA that meet those objectives.

That effort resulted in the development of PVA fibre reinforced mixes designed for dry shotcrete applications. Those formulations were based in part on calcium sulfoaluminate cement (CSA). A commercial version of this material is currently offered as Minova's Tekcrete Fast® product [1] which has been successfully deployed in the mining industry.

## Purpose and Scope of This Research

The objective of this research is to produce a shotcrete formulation that extends beyond stabilization and can be used to restore the structural integrity of damaged infrastructure. Our challenge is to develop mix formulations that are very strong, with a 28 day compressive strength that exceed 172 MPa (25 KSI); and tough, with a post cracking tensile strength of 5.0 MPA (0.72 KSI) or more.

Our approach to product design is the development of "single bag" dry mixes that are entirely self-contained, can be rapidly transported anywhere in the field or underground, and be deployed using simple equipment. Dry mix eliminates issues relevant to high shear water mixing, as water is added in the form of a mist at the point of delivery; thus low W/C can be achieved. However, as there is no onsite mixing, the product must have a high degree of inherent homogeneity.

One of the challenges for a successful dry mix shotcrete is the blending and homogeneity of the fibres. Even steel fibres as short as 12 mm, the current state of the art for shotcrete, can cause problems with dry blending. High loadings of these fibres can cause flow and bridging problems both at the mixing plant and in the field. Polyvinyl alcohol (PVA) fibres in dry mixes can form balls which result in holes and weakness in the final shotcrete product. The approach used was to work with suppliers Nycon and N.V. Bekaert to further reduce the size of the fibres, in an effort to create a mix that was more free flowing and stable, i.e. less prone to segregate in the bag during transport and storage.

Several novel approaches are taken to aggregate selection, as discussed below, including crushed calcium aluminate clinker (active aggregate), calcined bauxite as well as more conventional silicate aggregate. Aggregate gradations using the practices of ultra-high performance concrete (UHPC) were used to maximize packing and minimize void volume. Finally to achieve rapid strength development, both fast setting type III Portland cement (OPC III) and ultra-rapid setting calcium sulfoaluminate (CSA) were used in the mix designs.

## METHODS, PROCEDURES AND ASSUMPTIONS

The development of fibre reinforced (FR) UHPC formulations for shotcrete application was an exploratory effort that included the formulation and testing of a large number of mixes. More than 80 mixes were created in the course of the study and more than 600 specimens were moulded and tested for compressive strength. Even with this amount of effort, a number of simplifying assumptions had to be made due to the complexity of FR UHPC, which contains 10 to 12 components, or more, making the design of a test matrix rather formidable.

### Methods

The lab work was conducted at the University of Kentucky CAER. Only conventional laboratory equipment was used, for example Hobart paddle type mixers as described in ASTM C 305 procedures. [2] Test specimens were cured at standard temperature (25 °C).

Standard 50x50x50 mm (2x2x2 inch) mortar test cubes were prepared in accordance with ASTM C 109 procedures. [3] This approach provides a large number of test specimens per volume of mix. Flow testing was not conducted on most mixes because of the very rapid set time of some of the materials and the lack of relevance to dry-mix shotcrete.

Post-crack strength testing was conducted on 76x76x305 mm (3x3x12 inch) bar specimens prepared and moulded in accordance with ASTM C 192 which utilized the same mix formulations as the 50 mm cubes. [4] ASTM methods C 1609 and C 1399 were used to evaluate the post-cracking strength of the various test mixes; the strengths determined by C 1609 reflect the behavior of fibre-reinforced concrete under static flexural loading. [5,6] ASTM C 1399 was modified by following the procedure described in the ASTM C 1609 protocol for testing the post-cracking strength, i.e. residual strength.

ASTM C 1399 is a fairly new standard based on determining the post-crack strength after initiating a controlled crack at a deflection of 0.20 mm in the test specimen. The ASTM standard states that if a crack has not occurred at a deflection of 0.20 mm the test is invalid. However, due to the unique performance of the FR UHPC matrix the first crack occurs beyond a deflection of 0.20 mm. ASTM C 1609 does not require producing a first crack before evaluating for the post-crack strength, and has been reported to result in more reproducible data. Research has indicated that the results from ASTM C 1399 are on average 6.4% lower than by the procedure of test method C 1609. [7]

Durability testing included both dry shrinkage bars (ASTM C596) and expansion bars (ASTM C 157). [8,9] These tests give the most information on dimensional stability and durability in a short time frame.

### Procedures

Batches of materials were blended using a V-blender modified with high speed counter–rotating knifes. This apparatus provided very homogenous test materials. The thorough blending of very fine materials with coarser aggregate is a challenge for less aggressive mixers. This approach also mitigated the need to use high shear apparatus later in the procedure. The dry mixes were blended with water in a Hobart paddle mixer and then moulded into 50 mm brass moulds. The initial efforts included work with paste rich formulations which are relatively easy to mould. The use of high loadings of very fine materials resulted in batches

that were viscous. These were moulded with the help of a vibrating table. The filled moulds were stored overnight at 25°C and 100% humidity and the test specimens were removed from the moulds the following morning. Compressive strength was measured according to ASTM test procedure (C-109), at intervals of 1, 3, 7 and 28 days. Late in the program a 14 day break was added. The early test breaks were conducted to assess the rate of strength development, a parameter of interest. Due to the frequency of tests, two specimens rather than three were used and in some of the 1 and 3 day tests only one specimen was tested.

It was found necessary to polish the test specimens on a wet lap wheel with 120 grit wet carbide paper, as even the smallest surface irregularities caused early failure at the very high compressive strengths measured.

Post cracking flexural strength is another critical parameter of the study and a minimum target of 5 MPa (0.72 KSI) was chosen. This test was performed on moulded bars which utilized the final design mixes of the study. The post cracking test (ASTM C1609) measures material strength against forces that are both tensional and compressional in nature. The deflection of a specimen is monitored along with load, which is applied at a slow rate (900 N/minute). The load at the deflection equal to the span length/600 and the deflection equal to the span length/150 is used to calculate the measured strength which is reported as an average of the two measurements. For the bars of this study and our apparatus, the L/600 deflection was equal to 0.44 mm and the L/150 deflection was equal to 1.76 mm. The results from this test are summarized in Table 1, all of the test bars exceeded the minimum strength requirements by very large margins.

**Assumptions and Limitations**

Shotcrete mix design provides some challenges in the laboratory. Shotcrete is best tested at scale using appropriate equipment and test batches of 50 kilograms or more. This approach, for a study such as this, which entails a large number of exploratory mixes, would require years and high levels of funding. Thus our experimental design was a compromise between time, money and applicability of results.

For a dry mix shotcrete, issues such as set time, paste flow and water demand are not as relevant as in other laboratory test work. The high velocity provided by the shotcrete system produces excellent compaction and uniformity of materials, which are difficult to replicate in small batch exploratory testing conducted in the laboratory.

To illustrate some of these issues, the calcium sulfo-aluminate cement (CSA) which we used in the test work is ideal for dry mix design as it develops strength very rapidly. To work with this material at all in the laboratory we had to use relatively high dosages of retarder, i.e. sodium citrate at the level of 1wt% of cement. Without the retarder this material sets up in the mixing bowl within a minute or two. This is not a problem in dry mix shotcrete, but in a wet mix can rapidly create a paste so stiff as to be impossible to mould.

The problems in laboratory testing using wet mixes generally contribute to weaker test specimens. Errors for this kind of testing are not normally distributed, but rather tend to be asymmetric.

The error associated with the actual measurement of compressive strength, which is normally distributed, is very small compared to errors of technique in specimen moulding which contribute to loss of strength through the incorporation of voids or planes of weakness from irregular packing or preferred orientation of fibres. Thus the implicit assumption is that if a material reaches a given strength in the laboratory it will do so in shotcrete field trials.

## MATERIALS

Fibre reinforced UHPC has many more components than ordinary concrete, due primarily to its gradation. The materials are graded from coarse (mm) to ultra-fine (nm) to obtain the highest solid particle density. There are a number of computer algorithms available to calculate optimum packing density. These programs give similar, but never identical results. We used the Elkem EMMA program based on the Andreassen equations. This program is easy to use and is publically available free of charge [10] and produces useful results.

We divided the materials into four categories: cement, the primary bonding material; cementitious, that is materials that are both a filler and reactive to form secondary bonding materials; fibre, critical reinforcing materials; aggregate, non-cementitious matrix materials; and admixes, chemicals used to affect the properties of the mix including water demand, air entrainment and set time.

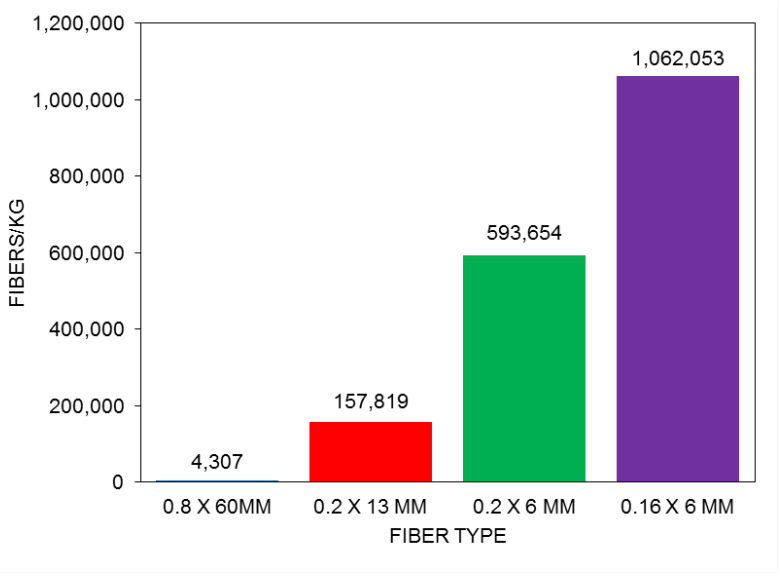


Figure 1 Comparison of the number of steel fibres per kg

### Cement

The cements used consisted of calcium sulfo-aluminate cement (CSA). We used two different batches, initially one that we had in stock, and a fresh second batch received a few weeks into the study. Likewise, we used Type III OPC from three different venders.

### Cementitious Materials

Cementitious materials used in the study included two very high quality fly ash samples, representing both Class C and Class F fly ash (ASTM C-618), and both fumed silica, a primary manufactured product, and silica fume, an industrial byproduct. The potassium and sodium silicate listed are spray dried versions of PQ Corporation's liquid products.

### Admixtures

A high range water reducer was used in the mixtures at a rate of 0.1% to cement by weight.

### Aggregates

The aggregates listed include very fine quartz, as well as three aggregate types representing three different approaches to shotcrete mix design:

*Conventional Quartz Sand Aggregate.* This included graded Ohio River sand in the 35x60 mesh (500 x 250 µm), 60x120 (250 x 125 µm), 120x230 (125 x 62.5 µm) and <230 (62.5 µm) mesh sizes. ASTM C778 quartz sand was substituted for the 35x60 mesh river sand in some tests.

*Active Aggregate.* This is a research trial aggregate formulation consisting of 35x60, 60x120 and 120x230 mesh aggregate made from calcium aluminate cement clinker. When not milled to cement particle sizes, calcium aluminate is both hard and stable. However because the surfaces of the aggregate have hydraulic properties, they present to the cement an "active" bonding site which may improve the overall strength development of the concrete and make it a "smart" material capable of self- healing under the proper circumstances.

*High Strength Aggregate.* This is an aggregate formulation consisting of 35x60, 60x120, 120x230 mesh, <230 mesh aggregate made from bauxite calcined at 1,500 °C. Calcining the bauxite at high temperature converts the bulk of it to corundum, which give it high strength.

### Fibres

*Steel.* Fibres with 0.2 mm x 6 mm dimensions were obtained from Nycon, Inc and Bekaert N.V. provided 0.16mm x 6 mm fibres for the study. In addition, test work was conducted using more conventional 0.2 mm x 12 mm steel fibres.

The shorter 6 mm fibres were simpler to mix and feed and are less prone to bridging. This results in an ability to effectively handle higher loadings, providing better performance and more flexible applications.

The smaller sized fibres provide some performance advantage. All of the steel fibres have strengths in the 830 to 1,100 MPa range, well above what is needed for these materials and their elongation and breakage is not an issue. Thus the number of fibres, or fibre density, per unit volume of the UHPC is of importance. In general, higher fibre density improves both compressive strength and material toughness (Figure 1).

## RESULTS AND DISCUSSION

The test program was divided into three phases which progressed from simple formulations to more complex. First using simple paste rich mortar mixes, parameters such as water cement ratio (W/C), cementitious component additions, cement blends and admixture concentrations were varied and compressive strength measured. The purpose of these tests was to weigh the importance of parameters to the final mix designs. Later aggregates were introduced and optimized and finally fibres were introduced.

**Successful mix designs and components based on OPC Type III**

*Low W/C.* Water to cement ratios for the successful designs ranged from 0.25 to 0.29, somewhat higher than the <0.24 typical needed for UHPC materials. All three of the aggregate types had mix formulas that achieved the target of 172 MPa (25 KSI) when used with Type III OPC; including the conventional quartz sand aggregate, the aggregate armor and the calcium aluminate. The highest strength recorded was 188.4 MPa (27.3 KSA) for mix 61 of the aggregate armor design. A summary of data for some of the successful mixes is presented in Table 1.

The successful mixes had the following elements in common: *Steel Fibres.* The use of steel fibres was found to be critical to achieve the high strength target in the mix designs. Both the 12 mm, and the 6 mm steel fibres were used in successful mixes. Steel loadings of ~3.4% by volume were used in most of the tests. However we found that even higher loadings of the 6mm fibres were feasible as they blended easily and the dry mix had good flow properties.

The addition of the steel fibres changes the material properties substantially. For example the identical mixes with the exception of one had the addition of 3.2% (by volume) steel fibres. Without the fibres a compressive strength of 153 MPa was achieved in 28 days, with fibres, 170.8 MPa was achieved for an overall strength increase of 11%. More significantly however is the change in material behavior. The mixes without the fibres demonstrates a strong but brittle behavior with rapid failure following the initial break which occurs at peak load at the end of the elastic zone of deformation. The addition of fibres induced a considerable amount of plastic deformation after the initiation of failure and sustaining its peak load in the region of plastic deformation. This is a demonstration of toughness that is imparted by the fibres

A mix with higher steel fibre loadings (Mix 67) of 0.57 weight/cement was prepared to determine the effect of higher loadings on material properties compared to a mix of otherwise similar composition (mix 59) was found to have both a faster rate of strength development as well as higher overall strength (183 MPa vs 174 MPa).

*Ultrafine Materials.* Most of the successful mixes had 2 μm quartz flour and silica fume at weight ratios of ~0.25 each to total cement.

**Successful mix designs and components based on CSA**

Over much of the test work the performance of CSA based cement considerably lagged that of OPC III.

The strength development of CSA was found to be clearly inhibited by highly reactive silica admixes such as fumed silica and silica fume. Also the data indicated that the 1:1 blend of CSA and OPC is not the optimum, but that CSA or OPC III alone may develop the highest strength.

Table 1 Data summary of compressive and post cracking strengths for successful mixes (SF = Silica Fume, Qtz = Quartz, * Also contained PVA Fibres in equal volume.

| MIX | CEMENT TYPE | AGG TYPE | U FINE TYPE | FIBRES WT-LENGTH | L/600 (N) | L/150 (N) | L/600 (MPa) | L/150 (MPa) | AVE. (MPa) | FLEX. (MPa) | COMP STRENGTH (MPa) | FLEX/ COM (%) |
|---|---|---|---|---|---|---|---|---|---|---|---|---|
| 59 | III OPC | Qtz Sand | Qtz/SF | 0.34-12 | 32099 | 21975 | 17.2 | 11.8 | 14.5 | 15.8 | 174 | 9 |
| 60 | III OPC | Ca-Al | Qtz/SF | 0.34-12 | 22160 | 18176 | 12.6 | 10.3 | 11.5 | 12.4 | 165 | 8 |
| 61 | III OPC | C. Baux | Qtz/SF | 0.34-12 | 36191 | 28331 | 18.9 | 14.8 | 16.9 | 19.8 | 172 | 11 |
| 67 | III OPC | Qtz Sand | Qtz/SF | 0.36-6 | 36929 | 16457 | 21.9 | 9.7 | 15.8 | 21.5 | 184 | 12 |
| 68 | III OPC | Ca-Al | Qtz/SF | 0.35-6 | 30692 | 14583 | 17.9 | 8.5 | 13.2 | 17.9 | 176 | 10 |
| 71 | CSA | Qtz Sand | Qtz/SF | 0.35-6 | 24949 | 10198 | 15.2 | 6.2 | 10.7 | 15.5 | 133 | 12 |
| 72 | CSA | C. Baux | Qtz/SF | 0.35-6 | 32004 | 14347 | 18.7 | 8.4 | 13.6 | 18.8 | 155 | 12 |
| 81 | CSA | C. Baux | SF | 0.35-6 | 21980 | 7751 | 13.0 | 4.6 | 8.8 | 13.0 | 145 | 9 |
| 82 | CSA | C. Baux | Qtz/SF | 0.35-6 | 26066 | 8585 | 15.2 | 5.0 | 10.1 | 15.4 | 148 | 10 |
| 83 | CSA | C. Baux | Qtz/SF | 0.35-6 | 26688 | 11706 | 15.6 | 6.8 | 11.2 | 15.4 | 148 | 10 |
| 84 | CSA | C. Baux | Qtz/SF | 1.0-6 | 39182 | 28523 | 23.1 | 16.8 | 19.9 | 24.2 | 179 | 14 |

**Post Cracking Flexural Strength.**

The deformation behavior of cementitious composites such as concrete, fibre reinforced concrete (FRC), and fibre-reinforced ultra-high performance concrete (FR UHPC) is typically distinguished according to their tensile stress-strain characteristics, in particular, the post-cracking response.

Brittle matrices, such as plain mortar and concrete, lose their tensile load-carrying capacity almost immediately after formation of the first matrix crack. The addition of fibres in conventional FRC can increase the toughness of cementitious matrices, however, their tensile strength especially strain capacity beyond first cracking are not enhanced. FR UHPC can be defined by an ultimate strength higher than their first cracking strength and the formation of multiple cracking during the inelastic deformation process. [11]

While the cracking strength of the composite is primarily influenced by the strength of the matrix, the post-cracking strength is solely dependent on the fibre reinforcing parameters and the bond at the fibre-matrix interface. [12] Thus, improving the post-cracking strength is key to the success of the FR UHPC.

Figure 2 depicts the load/deflection curves of three bar specimens with different reinforcing mechanisms. Mix 59c/d contains the 12 mm steel fibres at 3.4% volume, while Mix 67 contains the 6 mm steel fibres at 5.6% by volume. The addition of short steel fibres (6 mm) at an increased volume loading produced a specimen that exhibited an increased cracking threshold in addition to an extended inelastic region; this translates to a better distribution of fractioning stresses moving from the fibre/matrix bond surface into the surrounding matrix. However, due to the length of the shorter fibres (6 mm versus 12 mm) the L/150 post-cracking strength was decreased due to the inability of the shorter fibres to bridge the opening crack as the deflection of the specimen increased.

The formulation for Mix 61B contains calcined bauxite which was proven to strength in the matrix under compressive loading. The same strengthening was seen in flexural loading as compared to Mix 59c/d, which contains the same 12 mm steel fibres at 3.4% volume loading. The stronger matrix yielded less to deflection under loading and delayed the transition into the

inelastic zone, where multiple cracking occurs. This allowed for a higher load to be obtained before crack opening occurred. The ability for the 12 mm fibres to bridge the opening crack in tandem with the calcined bauxite matrix produced a shallow-sloping curve on the softening-frictional tail of the load/deflection curve (Figure 2).

Overall, formulations loaded with the short-steel fibres achieved higher loading values before the development of cracking. The ability for the short steel fibres to produce a desired multiple cracking throughout the matrix was exceptional; as seen by the extended inelastic zone beyond first crack (L/600) and before wider crack opening occurred (L/150). Post-cracking strengths reached levels well beyond what were targeted at the onset of the project. The inclusion of short-steel fibres in combination with the incredibly strong matrix yielded a material that will easily withstand sustained loading after experiencing some type of damage.

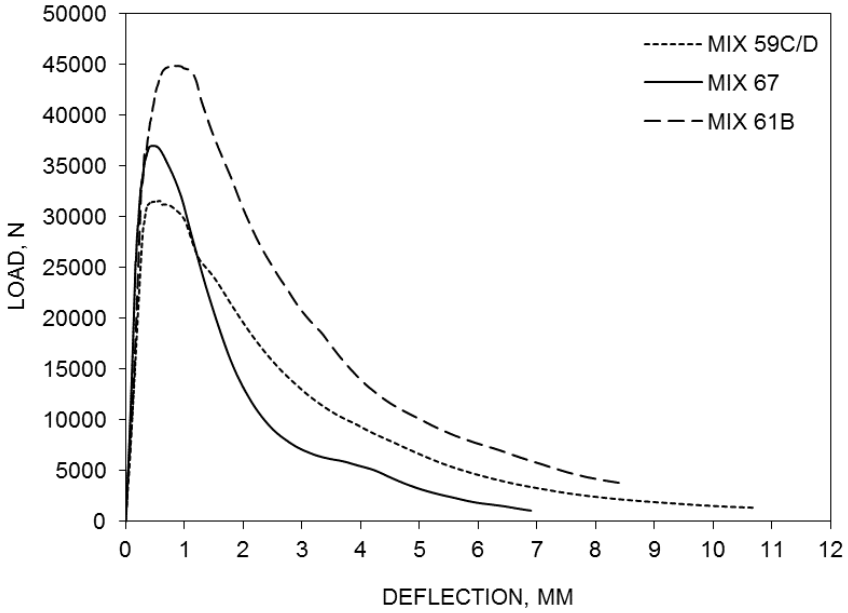


Figure 2. Load/deflection curves for three different mixes. Mix 59c/d contains 3.4% 12 mm steel fibres; Mix 67 contains 5.6% 6 mm steel fibres; Mix 61B contains 3.4% 12 mm steel fibres in addition to calcined bauxite.

**Technical problems and issues.**

In addition to the successful mix designs, it is of value to also discuss the materials and elements of the study that did not work or did not work as expected. It was attempted to incorporate some geopolymer cementitious materials into the study based on other work in this area. [13] Technical issues included problems in grinding and blending these materials due to their hygroscopic nature. Also, the Wollastonite proved not to contribute to the compressive strength at the level expected. It clearly increased the water demand when used in substantial quantities. It was used in several early mix designs and later tested as an addition to one of the successful mix designs with only small benefit noted.

An important observation was the negative affect of highly reactive silica such as fumed silica and silica fume of CSA performance. The addition of materials with very small particle sizes is an essential component in FR UHPC. Fumed silica and silica fume serve both as fillers and reactive cementitious components and are one of the most common of the ultrafine additives.

## CONCLUSIONS

This effort established lab scale proof-of-concept for several FR UHPC shotcrete formulations that meet or exceeds the compressive strength target of 174 MPa (25 KSI) and greatly exceeds the post cracking tensile strength target of 5 MPa (0.72 KSI).

To achieve these strengths all of the formulations required: steel fibre loadings that exceeded 3% by volume; water to cement ratios (W/C) of 0.25 to no more than 0.29; silica fume, quartz flour in combination at weight rations of 0.5 to that of the cement. The formulations include: one based on highly graded conventional silicate aggregate, including Type III Portland cement, 6mm or 12 mm steel fibres, silica fume and ultra-fine calcium carbonate or quartz flour; formulations based on highly graded calcined bauxite containing high concentrations of the mineral corundum, including type III Portland cement, 6 or 12 mm steel fibres, silica fume and quartz flour; and formulations based on calcined bauxite aggregate or conventional aggregate, including CSA cement, 6 or 12 mm steel fibres, and quartz flour.

In addition to being very strong, these FR UHPC mixes are very tough, demonstrating very high levels of post cracking strength. All of the formulations are “single bag” dry mixes and thus could be easily stored and rapidly transported anywhere and applied with conventional shotcrete equipment.

## ACKNOWLEDGEMENTS

This work was supported in part by a grant from the Defense Threat Reduction Agency (DTRA), United States Department of Defense.

## REFERENCES

1. ORICA AMERICAS, http://www.minovausa.com/

2. ASTM STANDARD C 305, 2011, Standard Test Method for Mechanical Mixing of Hydraulic Cement Pastes and Mortars of Plastic Consistency, ASTM International, West Conshohocken, PA, 2006

3. ASTM STANDARD C 109, 2011, Standard Test Method for Compressive Strength of Hydraulic Cement Mortars (Using 2-in. or [50-mm] Cube Specimens), ASTM International, West Conshohocken, PA, 2008

4. ASTM STANDARD C 192, 2008, Standard Practice for Making and Curing Concrete Test Specimens in the Laboratory, ASTM International, West Conshohocken, PA, 2007

5. ASTM STANDARD C 1609, 2008, Standard Test Method for Flexural Performance of Fibre-Reinforced Concrete (Using Beam with Third-Point Loading), ASTM International, West Conshohocken, PA, 2007

6. ASTM STANDARD C 1399, 2008, Standard Test Method for Obtaining Average Residual-Strength of Fibre-Reinforced Concrete, ASTM International, West Conshohocken, PA, 2007a

7. BANTHIA, N. AND DUBEY, A., Measurement of Flexural Toughness of Fibre Reinforced Concrete Using a Novel Technique, Part I: Assessment and Calibration, Materials Journal, American Concrete Institute, Vol. 96, Issue 6, 1999, pp 651-656.

8. ASTM STANDARD C 596, 2011, Standard Test Method for Drying Shrinkage of Mortar Containing Hydraulic Cement, ASTM International, West Conshohocken, PA, 2009

9. ASTM STANDARD C 157, 2008, Standard Test Method for Length Change of Hardened Hydraulic-Cement Mortar and Concrete, ASTM International, West Conshohocken, PA, 2006

10. ELKEM, EMMA User Guide Version 2, last accessed on January 26th 2016, https://www.elkem.com/documents/software/emma-user-doc.pdf

11. NAAMAN, A.E. AND REINHARDT, H.W., Characterization of High Performance Fibre Reinforced Cement Composites-HPFRCC, in Proc. of High Performance Fibre Reinforced Cement Composites 2 (HPFRCC 2), 1995, Ed. A.E. Naaman and H.W. Reinhardt, pp 1-23

12. NAAMAN, A.E., Engineered Steel Fibres with Optimal Properties for Reinforcement of Cement Composites, Journal of Advanced Concrete Technology, Vol. 1, No. 3, 2003, pp 241-252.

13. DAVIDOVITS, J., Geopolymer, Chemistry and Applications, 2011, 3rd ed., Institut Geopolymere, 16 rue Galilee, F-021000 Saint-Quentin, France, 612 p.

# PROPERTIES OF FOAMED CONCRETE WITH SISAL FIBRE

**Amarnath Y**
Madanapalle Institute of Technology and Science (MITS)
**Ramachandrudu C**
Srinivasa Ramanujan Institute of Technology (SRIT)
India

**ABSTRACT.** Tensile properties in concrete can be incorporated using fibres. Different fibres like glass, polypropylene and carbon have been in use to improve properties of concrete. However, use of natural fibres in concrete could be a useful option to make concrete as sustainable material. Several natural fibres like sisal, coir, jute, palm etc. also have been used in concrete to investigate properties. However, use of natural fibres in foamed concrete was found scarce in the literature. Therefore, in this investigation sisal fibre was used in foamed concrete and studied properties of the foamed concrete. Foamed concrete of density 1200kg/$m^3$ with cement, water, fine aggregate and foam quantities of 250kg/$m^3$, 125kg/$m^3$, 825kg/$m^3$ and 24kg/$m^3$ respectively was made. Sisal fibre of length 30mm was used in the foamed concrete mix and the fibre quantities was varied from 0.67 - 2% with weight of the cement. Slump, stability, density, compressive strength, split tensile strength, water absorption and moisture migration tests were conducted to ascertain foamed concrete properties using sisal fibre. The test result show that use of sisal fibre into foamed concrete can improve performance of foamed concrete.

**Keywords:** Compressive strength, Foamed concrete, Lightweight concrete, Natural fibre, Sustainability.

**Dr Amarnath Y** is Head of the Department of Civil Engineering, Madanapalle Institute of Technology (MITS). Member of Indian Concrete Institute. His research interests include sustainable construction and light weight concrete.

**Dr Ramachandrudu C** is Head of the Department of Civil Engineering, Sri Ramanujam Institute of Technology (SRIT). His research interests include ferrocement.

## INTRODUCTION

Foamed concrete, a light weight concrete in which air-voids are entrapped in mortar by suitable foaming agent. Although the material was first patented in 1923 [1], its construction applications increasing to diverse fields in the last few years owing to its advantages like possibility to produce wide range of densities (1600– 400 kg/m$^3$); high workability; light weight; high thermal insulation and flexibility to use waste materials, such as fly ash, slag, sludge, palm oil fuel ash etc. Its applications include high volume void backfills, bridge abutments, arch bridge infills, road sub-bases, floor and roof screeds, soil stabilization, grouting tunnel walls, thermal and acoustic insulation, sacrificial cladding and as a semi structural material [2,3].

Inferior qualities of concrete like poor fracture toughness, poor resistance to crack propagation and low impact strength can be improved by using fibres in concrete. Further, fibres can arrest cracks formation and propagation and improve strength and ductility [4,5,6]. Many researchers used different fibres like steel, glass, carbon and polypropylene in concrete to understand behaviour of concrete. Although there is a little difficulty in incorporating fibres in foamed concrete due to presence of foam bubbles, in recent years researchers have produced foamed concrete with fibres to enhance mechanical properties of foamed concrete. Glass fibres, polypropylene, steel, kenaf, oil palm fibre and basalt fibres have been used in foamed concrete and reported improved properties of foamed concrete with the addition of fibres, as in normal concrete [7,8].

In comparison to the most common synthetic reinforcing fibres, natural fibres require less energy to produce and are the ultimate green products. Therefore, using such natural fibre in concrete in place of regular fibres could be an alternate option to make concrete more sustainable.

Many researchers have used natural fibres in concrete to study properties of concrete. Table 1 shows details of different natural fibres used in concrete by different researchers. From the Table it is clear that there are range of natural fibres available to use in concrete. In this investigation sisal fibre was used, sisal fibre is a natural fibre and is very easily cultivated. It has short renewal times and grows wild in the hedges of fields and railway tracks [9]. In the present investigation foamed concrete was produced by incorporating sisal fibre and tested the foamed concrete for fresh, mechanical and durability characteristics.

### Materials and Mix Proportions

The constituent materials used in this investigation were procured from local sources. Ordinary Portland cement of C53 grade conforming to both the requirements of IS: 12269 [15] and ASTM C 642-82 type I [16] was used. Chemical compositions of the material was found to satisfy the requirements of both ASTM C 618 and IS: 3812–1981 [17,18], and is given in the Table 2. Well-graded river sand finer than 2.36 mm was used. Fine aggregate grading is shown in Figure 1. Grading of the fine aggregate is within the range of Zone-II as per IS 383 [19]. Locally available potable water was used for mixing and curing. Vegetable protein based surfactant was used and locally available sisal fibre was used, the properties of the fibre are: Specific gravity-1.21; Water absorption-165%; Tensile strength -352MPa; Diameter-0.32mm; Elongation-5%.

Table 1 Literature summary of properties of natural fibres used in concrete

| FIBRE TYPE | SPECIFIC GRAVITY, kg/m$^3$ | WATER ABSORPTION, % | TENSILE STRENGTH, MPa | MODULUS OF ELASTICITY, GPa | DIAMETER | ELONGATION, % | REFERENCE |
|---|---|---|---|---|---|---|---|
| Sisal | 1170-1370 | 110-200 | 347-378 | 15,2 | NA | 6 | [10,11] |
| Coconut | 1177 | 93,8 | 95-174 | 19-26 | 0.1-0.4 | 10'-25 | [10,12] |
| Bamboo | 1158 | 145 | 73-505 | 10-40 | NA | NA | [10] |
| Hemp | 1500 | 85-105 | 310-1110 | 34 | NA | NA | [10,13] |
| Caesarweed | 1409 | 182 | 300-500 | 10-40 | NA | NA | [10] |
| Banana | 1031 | 407 | 384 | 20-51 | 0.154 | 5.2 | [10,12] |
| Piassava palm | 1054 | 34-108 | 143 | 5,6 | NA | NA | [10,12] |
| Date palm | 1300-1450 | 60-84 | 70-170 | 2,5-7.8 | NA | NA | [14] |
| Sugarcane | NA | NA | 170-290 | 15-19 | 0.2-.0 | NA | [12] |
| Wheat straw | NA | NA | 30-40 | NA | NA | NA | [13] |
| Elephant grass | NA | NA | 180-260 | NA | NA | NA | [13] |
| Jute fibre | 1000 | 281 | 60.14 | NA | NA | 13.1 | [11] |
| Coir fibre | 1000 | 180 | 51 | NA | NA | 17.6 | [11] |
| Hibiscus Cannebinus | 0.71 | 285 | 76.08 | NA | NA | 6.7 | [11] |

NA-Data not available

Table 2 Chemical composition and physical characteristics of cement

| CHEMICAL | COMPOSITION, % |
|---|---|
| Silica ($SiO_2$) | 21.8 |
| Alumina ($Al_2O_3$) | 6.6 |
| Ferric oxide ($Fe_2O_3$) | 4.1 |
| Calcium oxide (CaO) | 60.1 |
| Magnesium oxide (MgO) | 2.1 |
| Sodium oxide ($Na_2O$) | 0.4 |
| Potassium oxide ($K_2O$) | 0.4 |
| Sulphuric anhydride ($SO_3$) | 2.2 |
| Loss on ignition (LOI) | 2.4 |
| Physical Characteristics | |
| Blaine Fineness, $m^2/kg$ | 307 |
| Standard consistency, % | 33 |
| Normal consistency, % | 28 |
| Specific gravity | 3.15 |
| Initial setting time, min | 205 |
| Final setting time, min | 287 |
| Compressive strength | $N/mm^2$ |
| 1 day | 24 |
| 3 days | 37.5 |
| 7 days | 49.5 |
| 28 days | 65 |

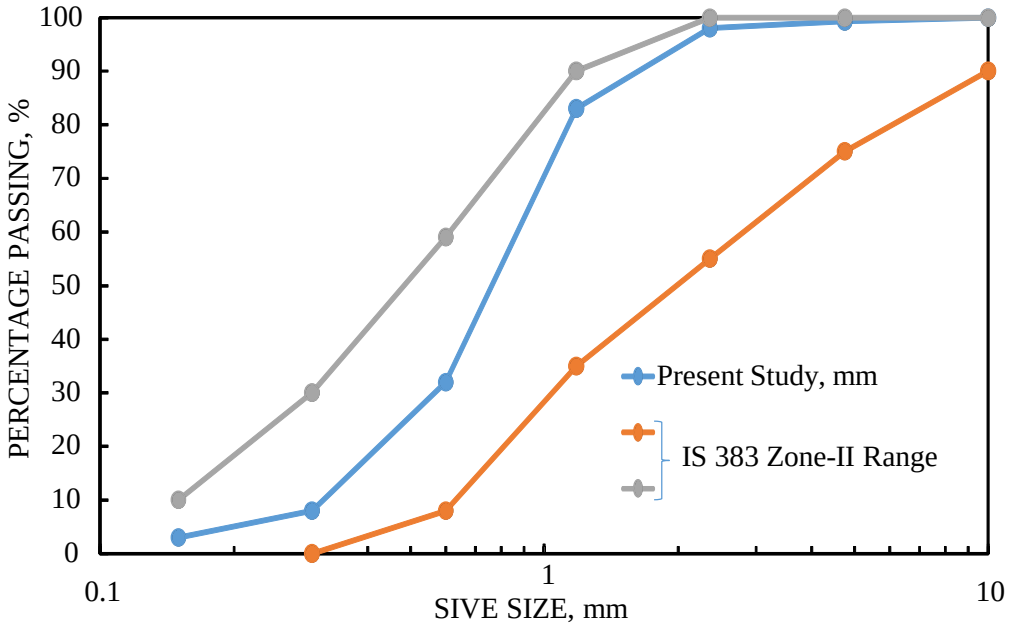


Figure 1 Aggregate grading

Mix proportioning method used in this investigation was developed at the University of Dundee (Equation 1) [20] and is described below. For a given cement content and water/cement (w/c) ratio, the fine aggregate content was calculated by equating the sum of solids and water content to the target plastic density value.

$C + W + F = D$ Equation 1

Where: C = cement (PC and FA) content, kg/m$^3$

W = water content, kg/m$^3$

F = fine aggregate (sand and/or RSA) content, kg/m$^3$

D = target plastic density, kg/m$^3$

Adjustments were then made to sand and water contents (as with normal weight concrete) to take account of their water absorption and laboratory air dry condition. The level of water contained in the foam is minimal and, therefore, was not considered in the calculations. Although it is recognised that foam collapse occurs during mixing, the actual w/c ratio of the mix is slightly higher than the batched quantity.

In order to establish the theoretical foam quantity required to achieve the target plastic density, the volume of air in the mix was calculated by considering a unit volume (Equation 2), as shown below:

$V_c + V_w + V_f + V_{foam} = 1m^3$ i.e. $\frac{C}{\rho_C} + W + \frac{F}{\rho_F} + \frac{M_{foam}}{\rho_{foam}} = 1$ Equation 2

where $\rho_C$ = density of cement, kg/m$^3$

$\rho_F$ = particle density of fine aggregate, kg/m$^3$

$M_{foam}$ = quantity of foam, kg/m$^3$

$\rho_{foam}$ = density of foam, kg/m$^3$

For the mixes, the target plastic density of the FC was selected as 1200kg/m$^3$. The cement content was selected as 250kg/m$^3$ and the w/c ratio 0.50. Mix proportions of the FC are given in Table 3. Fibres of 20 – 30mm length were used as shown in table.

Table 3 Mix proportions of the foamed concrete

| MIX | CEMENT, kg/m$^3$ | W/C | SAND, kg/m$^3$ | FOAM, kg/m$^3$ | FIBRE, % * |
|---|---|---|---|---|---|
| Mix1 | 250 | 0.5 | 825 | 24 | 0.0 |
| Mix2 | 250 | 0.5 | 825 | 24 | 0.5 |
| Mix3 | 250 | 0.5 | 825 | 24 | 1.0 |
| Mix4 | 250 | 0.5 | 825 | 24 | 1.5 |
| Mix5 | 250 | 0.5 | 825 | 24 | 2.0 |

*-fibre percentage was added with weight of cement content

FC production in the laboratory was conducted in a rotary drum (free-falling action) mixer. This apparatus is more suitable for incorporating foam in the base mix than a typical horizontal force action pan mixer.

Mixing of the concrete was carried out in the sequence. Dry materials that is cement and fine aggregate and part of the designed water were combined in the mixer for half a minute. Remaining quantity of water was then added and mixed with the dry materials for four minutes, or until a homogeneous mortar or grout with no lumps of undispersed cement was obtained. Following this, fresh property tests were carried out on the base mix. Pre-formed foam was then produced by the foam generator and the approximate quantity (calculated by the mix proportions) added to the mix, immediately after preparation. This was combined with the mortar or grout for at least two minutes, until all foam was uniformly distributed and incorporated in the mix. The plastic density of the mix was then measured and values within ±50 kg/m³ accepted. If the density was higher, additional foam was prepared and added incrementally until the target value was achieved, followed by further mixing. Mixes with densities lower than the range of acceptable values were rejected and the mix repeated. Fresh property tests (slump flow) were conducted and sampling of FC began soon thereafter, in accordance with BS EN 12350-1 [21]. Sisal fibre was then added into the foam mix rotated the mixer until uniform mix. Mix densities and slump flow was measured. Finally, concrete was poured into oiled moulds but no compaction was provided as this would cause collapse of the pre-formed foam. Left for 24 hrs and then the specimens were kept in tank for normal water curing until test age.

## Test Program

Main objective of the present investigation was to study performance of foamed concrete with sisal fibre. Performance of the concretes was assessed through: fresh properties, compressive strength, split tensile strength, stress strain behavior, water absorption and sorption.

## Plastic density

Plastic density of FC was assessed in accordance with BS EN 12350-60 [22]. A container with known volume was used to measure the density of FC. The container was filled with plastic FC and the excess amount of sample at the top of the container was removed by using a trowel and the top surface was levelled, without any vibrations. The container was then carefully weighed and the plastic density was determined by using the Equation 3.

$$\rho_m = \frac{M_2 - M_1}{V} \qquad \text{Equation 3}$$

Where:

$p_m$ = measured plastic density, kg/m$^3$
$M_2$ = combined mass of container and sample, kg
$M_1$ = mass of empty container, kg
V = volume of container, m$^3$

## Consistence

The consistence of FC was assessed in terms of slump flow. The slump flow test is effectively the measurement of the diameter of a sample after a collapse slump has been obtained [23], and is thought to reflect trends of yield stress in concrete [24,25]. The fresh fibre reinforced foamed concrete was placed into a mould in the shape of a frustum of a cone, conforming to BS EN 12350-2 [26]. When the cone is withdrawn upwards, the distance that the FC has spread over a flat horizontal surface is measured Figure 4.


Figure 4 Measurement of slump spread

**Compressive strength**

Water cured cube specimens of 150x150mm size were tested for compressive strength in accordance with BS EN 12390-3 [27]. The cubes tested for 1, 7 and 28 days to understand strength behaviour of fibre reinforced foamed concrete. Two cubes for each mix was tested, however, if the results of the cubes vary more than 10% the third cube was tested and the average of the two cubes with nearer results was reported as a cube strength. The rate of loading was gradually increased manually during the testing, until cube failure. Immediately after noticing the cube failure the failure load was recorded and cube strength was calculated by using the Equation 4 The compressive strength of the specimen was calculated to the nearest 0.1N/mm$^2$.

$$\text{Compressive strength} = \frac{Load\ at\ failure}{Cross\ sectional\ area\ of\ specimen} = \text{to nearest } 0.1\text{N/mm}^2 \quad \text{Equation 4}$$

**Split tensile strength**

Split tensile strength test was conducted in accordance with ASTM C496 [28]. Cylinders of 100 x 200 mm size were used for this test, the test specimens were placed between two platens with two pieces of 3 mm thick and approximately 25 mm wide plywood strips on the top and bottom of the specimens. Split tensile strength test was conducted on specimens after 28 days of curing. The strength was found as per Equation 5.

$$f_t = \frac{2.P}{\pi.d.L}$$

Equation 5

### Water absorption

An absorption study was conducted to understand the relative porosity permeable void space of the concretes, in according to ASTM C 642-82 [29]. The specimens removed from the oven were allowed to cool to room temperature. These specimens were then completely immersed in water and weight gain was measured until a constant weight was reached. The final absorption for all the concretes was observed to be at 72 h.

### Sorption

The sorption test was conducted on the concretes in order to characterize the rate of moisture migration of water into the concrete pores. 100x200mm cylinder specimens. As explained in the water absorption test, the specimens were oven-dried. They were then allowed to cool down to the room temperature. After cooling, the cubes were placed in water on the wedge supports to make sure that only the bottom surface of the specimens was in contact with the water. A cotton cloth was covered on top of the wedge supports to ensure the specimens are in contact with water throughout the test period. Weight of the cylinders was measured at regular intervals.

## Results and Discussion

### Plastic density and consistence

Fresh properties of the concretes were assessed based on visual observations, measuring plastic density and through slump spread test. During mixing and mould preparation, visual observations were carried out. From the observations it was noticed that the mixes were uniform and has no bleeding. It was also observed that sisal fibre distributed uniformly within the mix. Further, it was observed that uniform bubbles within the mix. Densities of the fresh concretes is shown in Table 4. Densities of the concretes after demoulding also measured, no big variation was observed, this observation suggests that no collapse of bubbles within the mix. Slump spread values shown in Figure 5 suggest that there is no marked difference in workability with the addition of sisal fibre in concrete mixes, when compared with the base mixes. All mixes were easily flowable. Distribution of sisal fibre in hardened concretes was examined on failure specimens of compression and split tensile strength, the observations suggests that the bubbles and sisal fibre uniformly distributed across the specimens in all the concretes.

Table 4 Plastic densities of fibre foamed concrete

| MIX | FRESH DENSITY, kg/m³ |
|---|---|
| Mix-1 | 1180 |
| Mix-2 | 1210 |
| Mix-3 | 1205 |
| Mix-4 | 1195 |
| Mix-5 | 1187 |

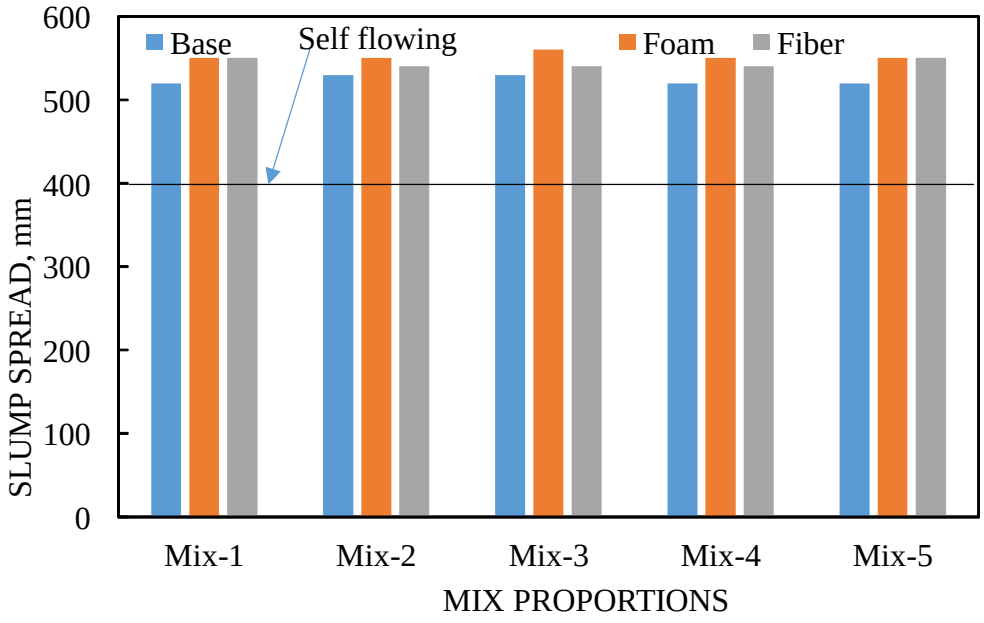


Figure 5 Slump spread of base, foam and fibre concretes

## Compressive strength

Results of compressive strength test for 1, 7 and 28 days are shown in Figure 6. When compared with Mix1 increase in strength was observed in sisal fibre concretes. This observation suggests that addition of sisal fibre increases compressive strength of foamed concrete, this can be attributed to composite action that exists such that the fibres bridge the matrix cracks and transfer the loads, allowing a distributed microcrack owing to tensile nature of sisal fibre. From the result it is clear that maximum strength can be obtained at 2 % sisal fibre addition.

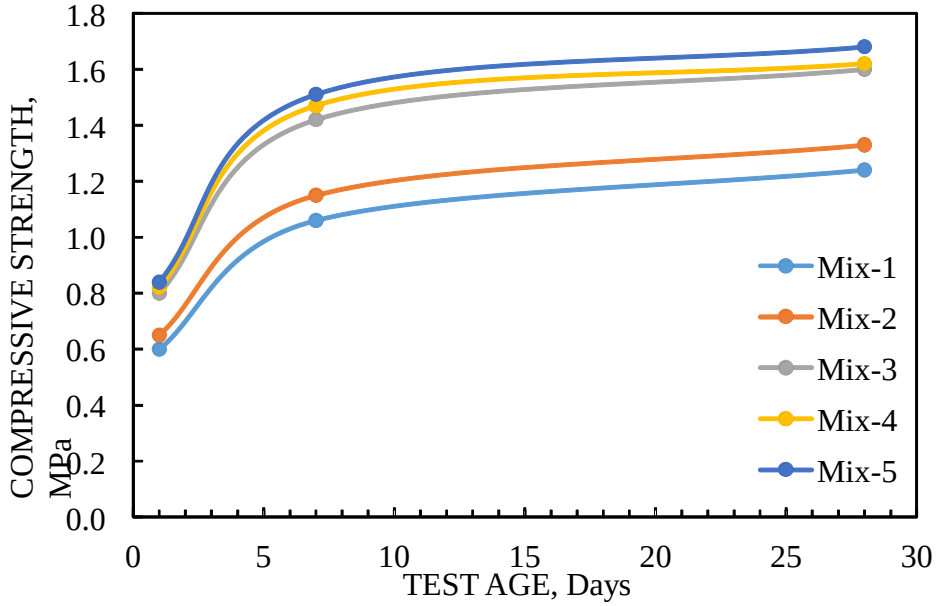


Figure 6 Strength gain with age

However, maximum rate of strength gain is between 0.5 to 1% and further increase in sisal fibre did not show any big variation (Figure 7). Strength of all the concretes increased with curing age. The strengths at 28 days are 2 times higher than corresponding concretes one day strengths.

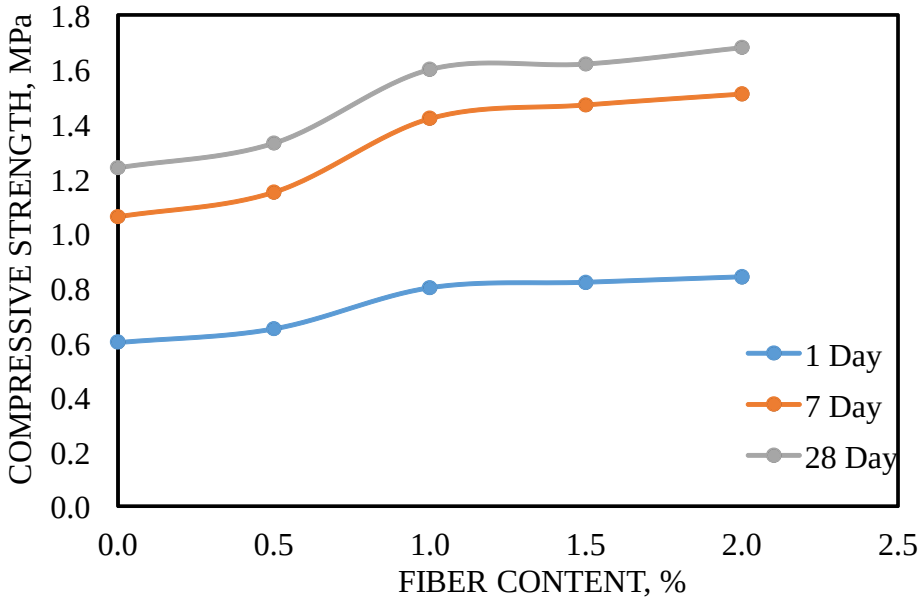


Figure 7 Relationship between compressive strength and fibre content

**Split tensile test**

Figure 8 shows relationship between split tensile strength and fibre percentage. From Figure 8 it is clear that split tensile strength increased with fibre percentage. Figure 9 shows relationship between compressive strength and split tensile strength, from the figure it can be observed that, as compressive strength increased split tensile strength also increased.

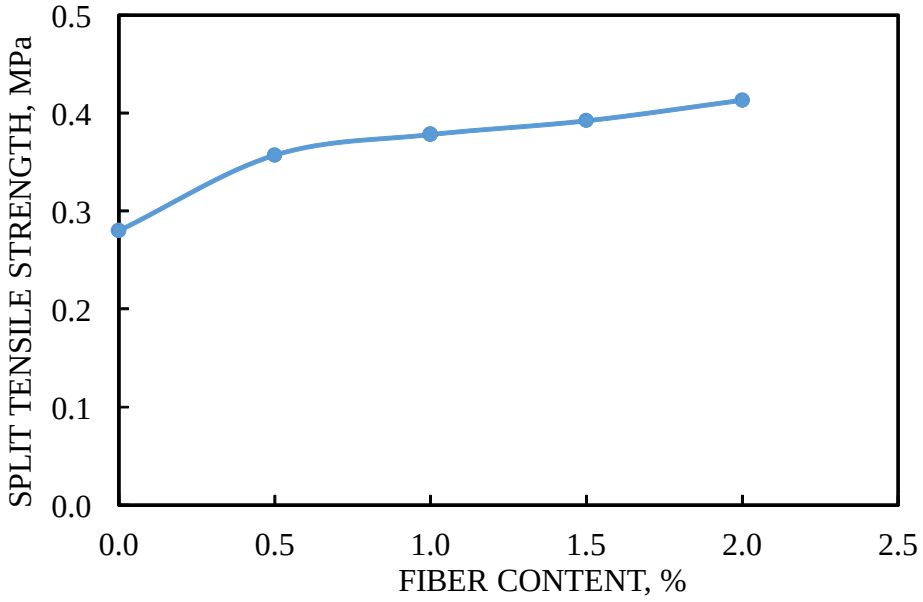


Figure 8 Relationship between fibre content and split tensile strength

A good power relationship was observed between the variables with regression coefficient of 0.82. There exist various empirical relationships to relate the compressive strength of concrete to its tensile strength. Equation suggested by FIP, 1991[30] for light weight aggregate concrete is shown in Figure 9 to compare the present study. It can be observed that for same compressive strength increased tensile strength in fibre reinforced foamed concrete. Equation 3 shows regression equation for present data.

$f_t=0.23(f_{cu})^{0.67}$ Equation 6

$f_t=0.24(f_{cu})^{1.2}$ Equation 7

where $f_t$ is splitting strength and $f_{cu}$ is compressive strength measured on cubes both in MPa.

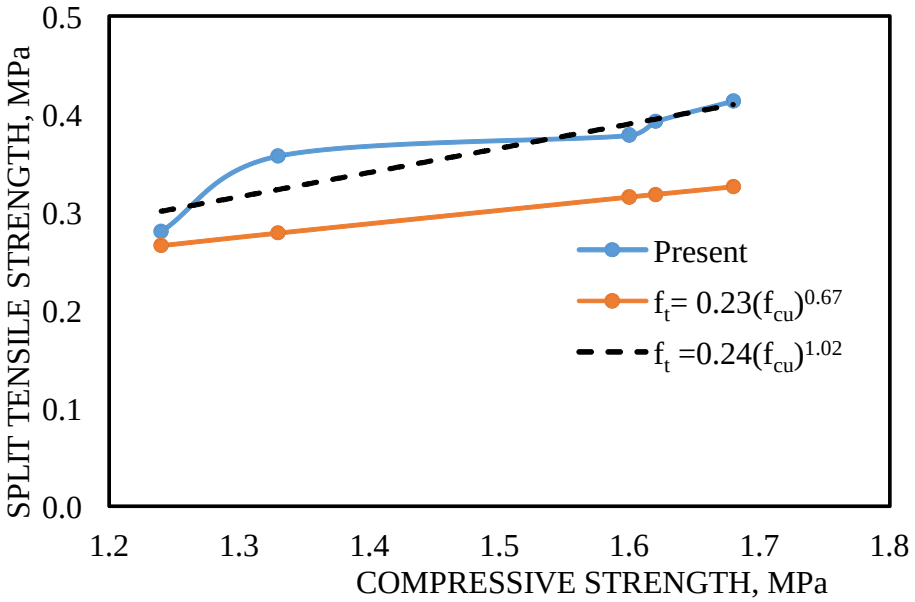


Figure 9 Relationship between split tensile strength and compressive strength

**Bond between fibre and concrete matrix**

Bond between the sisal fibre and concrete matrixes was assessed on the specimens failed in compression and split tensile strength tests. The bond strength was arbitrarily assessed by pulling the exposed fibres with fingers on surfaces of failed specimens. Few fibres were broken suggesting a good bond between the matrix and few fibres slipped from the matrix could be due to weak bond or insufficient embedded length of fibre. Further research is clearly needed to understand bond between sisal fibre and concrete matrix.

**Permeable voids and water absorption**

Variation of water absorption with time for the concretes is shown in Figure 10. From the figure it can be observed that within 30mts the water absorption is very high in all the concretes, after thirty minutes the rate of water absorption is gradual. From the figure it can also be observed that the water absorption is low for Mix 3 and for Mix 1, Mix 2 and Mix 5 have similar water absorption.

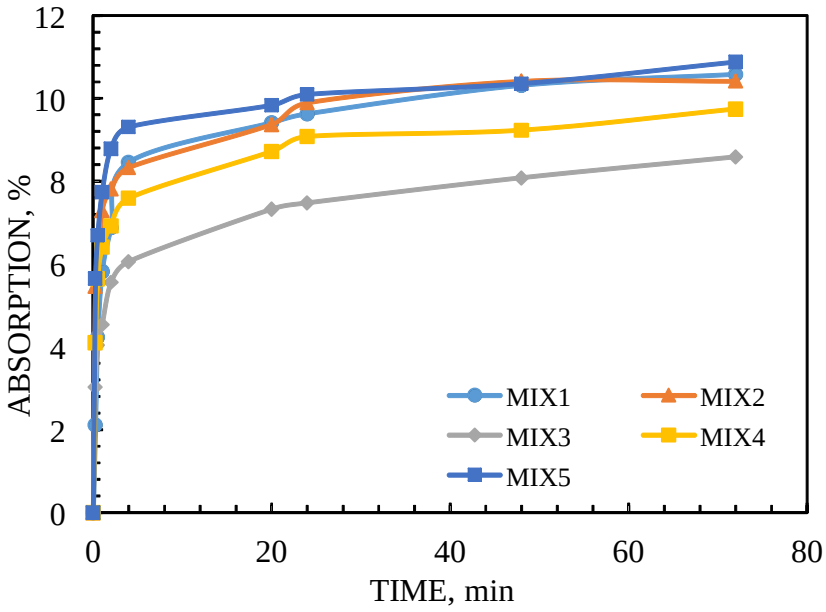


Figure 10 Variation of water absorption with time

**Sorptivity – capillary water absorption**

Variation of water sorption with time for the concretes is shown in Figure 11. From the figure it can be observed that similar to water absorption, the sorption is also high within 30mts. After that the rate of water sorption is gradual. From the figure it can also be observed that the sorption is low for Mix4 and nearly equal for Mix2 and Mix3. Further, it can be noticed that sorption is higher for Mix1 and Mix5.

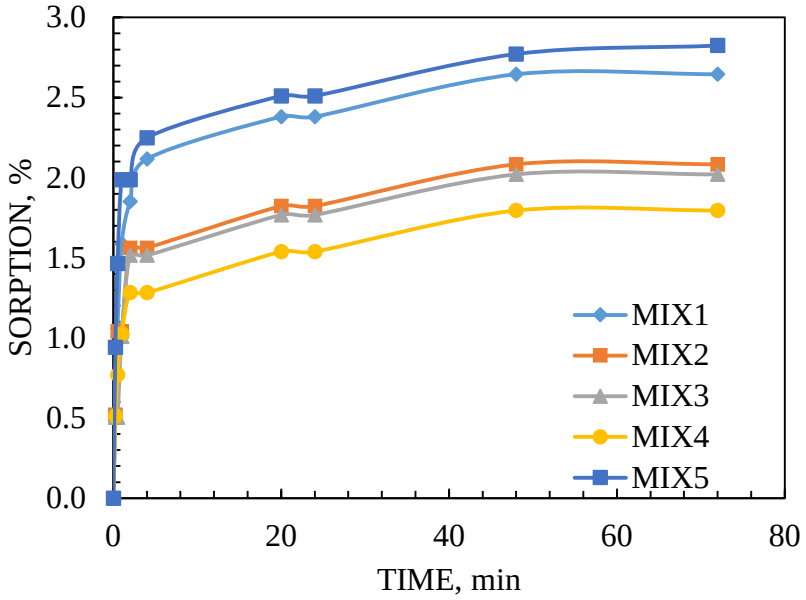


Figure 11 Weight change due sorption with time

## CONCLUSIONS

The data show that use of sisal fibre improve foamed concrete properties. Addition of sisal fibre has no influence on workability and foamed bubbles in the concretes. Sisal fibre in foamed concrete increased compressive and split tensile strength. Further, addition of sisal fibre into foamed concrete improved absorption properties.

## REFERENCES

1. VALORE, R C. Cellular concrete part 1 composition and methods of production. ACI J 1954; 50:773–96.

2. AMARNATH, YERRAMALA, JONES, M R. Environmental effects on heat of hydration in foamed concrete, Role for concrete in global development, Edited by Ravindra K Dhir, Peter C Hewlett, Laszlo Csetenyi and Moray d Newlands, 8-10 July 2008, pp 863-872.

3. ZHAO, H, YU, H, YUAN, Y, ZHU, H. Blast mitigation effect of the foamed cement-base sacrificial cladding for tunnel structures, Construction and Building Materials Vol. 94, 2015, pp710–718.

4. NAHHAS, T M,. Flexural behavior and ductility of reinforced lightweight concrete beams with polypropylene fibre. J. Constr. Eng. Manage. Vol. 1, No. 1, 2013, pp 4–10.

5. BAGHERZADEH, R, PAKRAVAN, H R, MASOUD L, MERATI, A A,. An investigation on adding polypropylene fibres to reinforce lightweight cement composites (LWC). J. Eng. Fibres Fabr, Vol. 7 No. 4, 2012, pp13–21.

6. MEHTA, P K, MONTEIRO, P J M. Concrete: Microstructure, Properties and Materials, third ed. McGraw-Hill, New York, 2006.

7. KHAN M I. Experimental investigation on mechanical characterization of fibre reinforced foamed concrete, MS thesis. 2014, pp142.

8. AWANG, H, HMAD, M H. Durability Properties of Foamed Concrete with Fibre Inclusion, World Academy of Science, Engineering and Technology International Journal of Civil, Environmental, Structural, Construction and Architectural Engineering Vol:8, No:3, 2014.

9. YAN, L I, MAI, Y, LIN, Y E.. Sisal fibre and its composites: a review of recent developments Composites Science and Technology, 60, 2000, pp2037-2055.

10. SAANDEEPANI, V, MURTHY, N N K, Study on addition of the natural fibres into Concrete, international journal of scientific & technology research, Vol. 2, No. 11, 2013, pp213-218.
11. RAMAKRISHNA, K, SUNDARARAJAN, T. Impact strength of a few natural fibre reinforced cement mortar slabs: a comparative study, Cement & Concrete Composites Vol. 27, 2005, pp547–553.

12. REIS, Fracture and flexural characterization of natural fibre-reinforced polymer concrete, Construction and Building Materials, Vol. 20, 2006, pp673–678.

13. MERTA, TSCHEGG, Fracture energy of natural fibre reinforced concrete, Construction and Building Materials, Vol. 40, 2013, pp991–997.

14. COOKE, The measurement and significance of green sheet properties for the properties of hardened fibre cement, Cement & Concrete Composites, Vol. 27, 2005, pp604–610.

15. IS: 12269-1987. Specification for 53 grade ordinary Portland cement.

16. ASTM C 642–82. Test method for specific gravity, absorption and voids in hardened concrete. Annual book of ASTM standards, Vol. 4. No.2, 1995.

17. ASTM C 618. Standard specification for coal fly ash and raw or calcined natural pozzolan for use in concrete. Annual book of ASTM standards, Vol. 04.02; 1995.

18. IS: 3812-1981. Specification for fly ash for use as pozzolana and admixture.

19. IS 383-1970 indian standard specification for coarse and fine aggregates from natural sources for concrete.

20. DHIR R K, JONES M R and NICOL L A. Development of Structural Grade Foamed Concrete, Final Report, DETR Research Contract 39/3/385, February 1999, pp84.

21. BS EN 12350-1: Testing fresh concrete. Sampling, 2000.

22. BS EN 12350-6: Testing fresh concrete. Density, 2000.

23. DOMONE P L J. The slump flow test for high-workability concrete, Cement and Concrete Research, Vol. 28, No. 2, pp177-182.

24. TATTERSALL G.H. Workability and Quality Control of Concrete, E & FN Spon. London. 1991, pp262.

25. MARRS D L and BARTOS P J M. Development and testing of self-compacting low strength slurries for SIFCON, Proceedings of the International RILEM Conference 'Production methods and workability of concrete (Ed P J M Barots, D L Marrs and D J Cleland), E and FN Spon, London, pp199-208.

26. BS EN 12350-2. Testing fresh concrete

27. BS EN 12390-3 Testing hardened concrete. Compressive strength of test specimens, 2002.

28. ASTM C496 Standard Test Method for Splitting Tensile Strength of Cylindrical Concrete Specimens

29. ASTM C 642–82. Test method for specific gravity, absorption and voids in hardened concrete. Annual book of ASTM standards, Vol. 04.02; 1995.

30. FIP, Manual of Lightweight aggregate concrete, 2nd EDn. Surrey University press. 1983 pp259.

# ULTRA-LIGHTWEIGHT CONCRETE: FROM RESEARCH TO PRACTICAL APPLICATION

**Q L Yu**

**H J H Brouwers**

Eindhoven University of Technology

**P Spiesz**

ENCI HeidelbergCement Benelux

The Netherlands

**ABSTRACT.** The present study addresses the properties of ultra-lightweight concrete, including such as the durability concerning the alkali silica reaction (ASR) in concrete, the stability of the mixture properties during long transport time and the heat release/temperature increase due to the cement hydration during massive concrete element production for its potential practical engineering application. The accelerated ASR test following the guideline RILEM TC 106-AAR shows that there is no ASR in the developed concretes. The workability of the previously developed ultra-lightweight concrete remains stable during the testing time (up to 80 min), indicating it can be transported without causing any problems within a reasonable distance. The semi-adiabatic heat release tests show a high temperature increase (about 60°C in the centre) within the concrete matrix, and a solution to this issue from the materials point of view is proposed and positively verified.

**Keywords:** Ultra-lightweight concrete, Durability, Mechanical properties, Heat release, Thermal conductivity.

**Dr Q L Yu** is Assistant Professor of Building Materials in the Department of the Built Environment, Eindhoven University of Technology.

**Dr P Spiesz** obtained his PhD degree at Eindhoven University of Technology and is currently senior researcher at ENCI HeidelbergCement Benelux.

**Prof Dr Ir H J H Brouwers** is Professor of Building Materials in the Department of the Built Environment, Eindhoven University of Technology.

## INTRODUCTION

In previous research [1], the design methodology of an ultra-lightweight concrete with a good balance between the mechanical properties and thermal properties was investigated. An ultra-lightweight concrete with excellent thermal properties (e.g. a very low thermal conductivity of about 0.12 W/(m·K)) while retaining a reasonable strength (a compressive strength of about 10.0 N/mm² at 28 days) was designed and tested. This design concept indicates that a monolithic concrete structure will be in reach. The monolithic concrete structure concept leads to the following advantages: 1) cost saving, due to the exemption of extra insulation installations; 2) provides architects and structural engineers with more flexibility for the building design; 3) sustainability, since the monolithic structure will ensure a relatively easy maintenance requirement and is much easier to recycle.

In the present study, effort is spent on investigating the developed ultra-lightweight concrete for its potential engineering application. The durability concerning the alkali silica reaction in concrete is studied. The so-called alkali silica reaction (ASR) is a deleterious reaction, which takes place in hardened concrete. This reaction appears when there is a certain minimum amount of alkalis present in the pore solution of concrete and reactive silica such as tridymite, cristobalite, chalcedony or opal present in the aggregates [2]. As the lightweight aggregates applied here are made from waste glass [1, 3], which indicates potentially the aggregates could cause ASR in the concrete. The lightweight aggregates possess very low densities, ranging between 300 to 800 kg/m³, which could possibly cause stability problem especially during the long time transport. Besides, the very low densities of the used aggregates lead to a very low thermal conductivity, which in turn might cause great self-insulating of the concrete in its fresh state especially considering the massive concrete production and this might cause significant problems such as cracks. Therefore, the stability of the mixture during the long transport time, including its fresh properties and resulted hardened properties, and the heat release/temperature increase during the massive concrete elements production were studied.

## ALKALI SILICA REACTION

The alkali silica reaction mechanism can be described as follows: first the alkalis react with water, producing alkali hydroxides. Then, the hydroxide ions ($OH^-$) in the cement paste attack the reactive silica and cause it slow dissolution. Subsequently, the dissolved silica reacts with the alkali hydroxides ($Na^+$ and $K^+$) and as a result, an unstable, viscous alkali-silica gel is formed (sodium silicate, potassium silicate). This gel has the ability of imbibing water and swelling to a volume greater than that of the initial substrates. The water absorbed by the gel may originate from for instance the pore solution, rainwater or air moisture. With more water, the creation of the gel is enhanced. As the water flows continuously, the gel continues to swell and expand. When the pressure generated by the swelling is larger than the tensile strength of concrete, cracks occur. The mechanical properties and the lifespan of concrete can be affected by the reaction. However, the reaction is not affected directly by the alkali ions and siliceous aggregates, but by the formation of hydroxide ions which react with the aggregates. It is reported that the alkalis contribute initially to the high concentration of hydroxide ions in the pore solution and later on to the formation of the alkali silica gel [4].

## Alkali Silica Reaction Test

For the alkali silica reaction test, RILEM TC 106-AAR guideline is followed. This test method is used to determine rapidly the alkali-reactivity of aggregates through the evaluation of the expansion of concrete prisms, immersed in NaOH solution at 80°C for continuous 14 days. Concrete prisms are cast in steel moulds, with two metal pins inserted. The metal pins are used for the measurement of the expansion as they are not reactive. The prisms are demoulded after 24 hours, and the length of the prisms is measured (accuracy of 2 µm). The samples are then placed in a container with water, immersing them completely and transferred to an oven at 80°C for 24 hours. Then, the samples are removed from the water and the length of the prisms is measured immediately before the temperature has dropped substantially (zero reading, $L_0$) with a length comparator, where the values are always compared with the same reference wooden bar for verification. Subsequently, the prisms are placed in a container with 1 M NaOH solution in the oven at 80°C. The length measurements ($L_n$) of the prisms are then taken periodically until 14 days.

The ASR-induced expansion is obtained by calculating the difference between the length of the prism $L_n$ (where n is the each measurement time) and the zero measurement ($L_0$), divided by the gauge length (distance between inner ends of the metal pins, measured to the nearest 1 mm). The ASR-induced expansion is considered deleterious for the lifespan of concrete, if after 14 days of submersion in 1 M NaOH solution the expansion of the prism is higher than 0.1%.

## Results Analysis

Two concrete mixtures are tested in the present study, with the first one using CEM III/A 52.5 N as the binder and the second one using CEM I 52.5 N. The aim is to investigate, besides the possible reactive potential of the used lightweight aggregates, also the influence of the applied cement type (e.g. the slag in the used cement) in concrete on the ASR potential. The ASR-induced expansion results are shown in Figure 1. As clearly shown, in both cases, the expansion rate is about zero, meaning that no alkali silica reaction in the tested concrete matrix occurred. Under even very extreme condition, i.e. with a high porosity (density of 800 kg/m³), the ASR test does not show any expansion, indicating that the used lightweight aggregates can be applied to any lightweight concrete without possible alkali silica reaction.

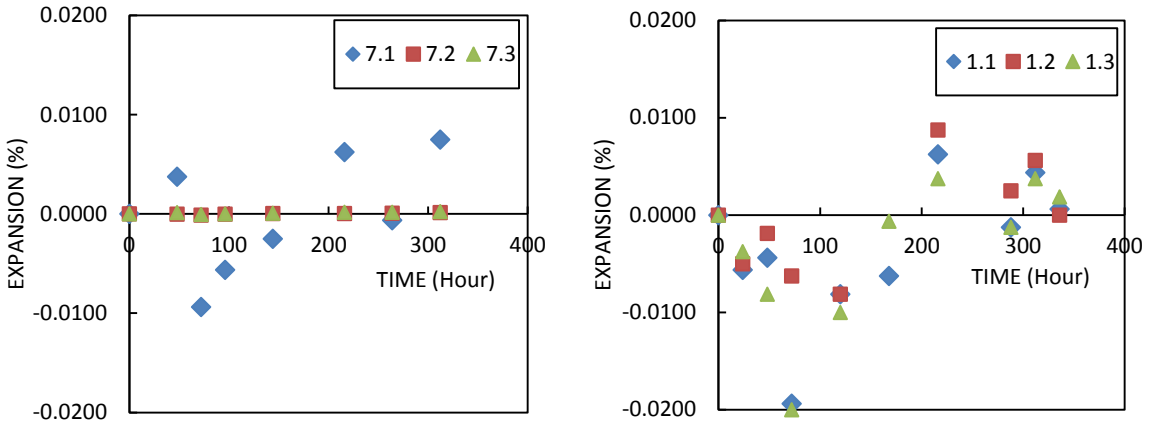


Figure 1 Expansion of concrete prisms due to the ASR:
Left: CEM I 52.5 N as binder; right: CEM III/A 52.5 N as binder

## STABILITY DURING THE LONG TIME TRANSPORT

### Introduction

In practice, concrete must keep a desired workability during the transport from the concrete plant to the construction site. In another word, the concrete should have a sufficient open time, especially taking into account possible traffic jams in highly populated places or other causes of delay. In the present study, the stability of the previously designed concrete (Mix A) [1] is investigated in the case of a long time mixing, and a 80 min mixing time is applied as a reasonable long transport time. The properties of the concrete, including the fresh state behaviour such as slump, flow and fresh density and hardened state properties such as compressive strength, are investigated. The fresh properties are measured every 20 minutes during the whole mixing time (a low mixing speed is applied to simulate the real mixing during the transport), namely after the first normal mixing at 13 min, at 40 min, at 60 min and at 80 min, respectively. The hardened properties are determined on the samples of two batches, with the first one cast after normal mixing time (i.e. 13 min) and the second one at the end of mixing (i.e. 80 min). All the experiments are carried out following the relevant EN standards [5, 6, 7].

### Results Analysis

Table 1 shows the fresh state properties of the mixture after mixing different time. One can see that during the first 40 min, the flow ability remains the same while the slump values decrease slightly; then until 80 min, the flow ability slightly reduces but the slump remains relatively stable, indicating an excellent consistency of the fresh concrete. Especially, during the whole 80 mins' mixing, the fresh density of the mixture keeps very stable, from 779 kg/m$^3$ at the beginning to 781 kg/m$^3$ at the end of the mixing. To summarize, the relatively stable values from these three different tests show that up to 80 min mixing, the resulted mixture has relatively stable fresh properties, meaning that it can be transported within a reasonable distance without any problems. Moreover, in case more time is needed for transport, suitable admixtures can be applied accordingly to slightly adjust the workability and open time.

Table 1 Fresh state properties of Mix A during the long time mixing

| | MIXING TIME, min | | | |
|---|---|---|---|---|
| | 13 | 40 | 60 | 80 |
| Fresh density, kg/m³ | 779 | 778 | 766 | 781 |
| Flow, mm | 465 | 465 | 438 | 445 |
| Slump, mm | 210 | 180 | 180 | 173 |

Table 2 shows the hardened properties of the concrete cast at two different mixing time of 13 min and 80 min, respectively. It can be seen that the hardened densities at these two batches remain the same, indicating the constant properties of samples, which is also confirmed by the results in the fresh state conditions. The other properties, including the thermal conductivity, compressive strength and E-modulus, also stay rather similar after long time mixing, as can be seen from Table 2.

Table 2 Hardened properties of Mix A cast at different mixing time

| | MIXING TIME, min | |
|---|---|---|
| | 13 | 80 |
| Density, kg/m³ | 759 | 760 |
| Thermal conductivity, W/(m·K) | 0.131 | 0.135 |
| Compressive strength (7-day), MPa | 8.4 | 8.4 |
| Compressive strength (28-day), MPa | 8.7 | 9.0 |

To conclude, the properties of the mixture remains rather stable after long time mixing (up to 80 min). This confirms that the developed ultra-lightweight concrete can be practically handled in commercial concrete plants, as firstly no other specific mixing methods besides normal concrete mixing are needed and secondly the concrete can be transported within a reasonable distance (time) with the same properties.

## HEAT RELEASE DURING THE HYDRATION

The temperature of fresh concrete changes due to the hydration of binders (released heat) and heat exchange between the concrete and surrounding environmental. It is normally unwanted if the temperature of concrete reaches too low (low hydration speed, poor strength development) or too high (fast hydration, potential induction of thermal micro cracks). In the case of ultra-lightweight concrete, there is a potential risk that the temperature of fresh concrete can reach high values, as the heat originating from the hydrating cement is kept within the material and dispersed very slowly to the surrounding environment due to the very low thermal conductivity of the resulted concrete.

In a fresh cement paste system (cement and water), the heat (Q) needed to change the temperature by a certain value can be obtained by considering the ingredients individually:

$$Q = C_{p-c} m_c \Delta T + C_{p-w} m_w \Delta T \tag{1}$$

where: $C_{p\text{-}c}$ – specific heat of cement [J/(kg·K)], $m_c$ – mass of cement [kg], $C_{p\text{-}w}$ – specific heat of water [J/(kg·K)], $m_w$ – mass of water [kg] and $\Delta T$ – temperature change [°C].
Assuming adiabatic conditions in the system (no heat exchange between the cement paste and surrounding), the heat generated in the system is equal to the heat released upon the cement hydration ($Q_g$):

$$Q_g = m_c H_c = C_{p-c} m_c \Delta T + C_{p-w} m_c \, {}^{w}\!/_{c} \, \Delta T \tag{2}$$

where: $H_c$ – enthalpy of cement hydration [J/g] and $w/c$ – water to cement ratio (i.e. $m_w = m_c \cdot w/c$).

With a known cement hydration enthalpy, specific heat of cement and w/c ratio, assuming full cement hydration, the maximum temperature increase in a hydrating system can be calculated from:

$$\Delta T = \frac{H_c}{C_{p-c} + w/c \cdot C_{p-w}} \tag{3}$$

Considering a system composed of cement paste and lightweight aggregates, Eq. (3) can be re-written as follows:

$$\Delta T = \frac{H_c}{C_{p-c} + w/c \cdot C_{p-w} + LWA/c \cdot C_{p-LWA}} \tag{4}$$

where: *LWA/c* – mass ratio between the lightweight aggregates and cement and $C_{p\text{-}LWA}$ – specific heat of lightweight aggregates [J/(kg·K)].

**Enthalpy of Cement Hydration**

The enthalpy of cement hydration depends upon the phase composition of cement, as each phase contributes differently to the total generated heat. Additionally, cement can be composed of not only Portland cement clinker but also other supplementary cementitious materials (SCM) such as ground-granulated blast furnace slag (GGBS) of fly ash (FA). An expression for the total enthalpy of cement and SCM hydration reads [8]:

$$H_{total} = H_c \cdot M_c + 461 \cdot M_{GGBS} + 1800 \cdot M_{CaO(in\ FA)} \cdot M_{FA} \tag{5}$$

where: $H_{total}$ – total enthalpy of hydration [J/g], $H_c$ – enthalpy of cement hydration [J/g], $M_c$ – mass fraction of cement in the total binders amount, $M_{GGBS}$ - mass fraction of GGBS in the total binders amount, $M_{CaO(in\ FA)}$ – mass fraction of CaO in fly ash and $M_{FA}$ – mass fraction of fly ash in the total binders amount.

The hydration heat of Portland cement, taking into account its phase composition, can be calculated as follows [8]:

$$H_c = 500 \cdot M_{C_3S} + 260 \cdot M_{C_2S} + 866 \cdot M_{C_3A} + 420 \cdot M_{C_4AF} + 624 \cdot M_{SO_3} + 1186 \cdot M_{free\_CaO} + 850 \cdot M_{MgO} \tag{6}$$

where: *M* – mass fraction of a phase in the total cement amount and subscripts: $C_3S$, $C_2S$, $C_3A$, $C_4AF$, $SO_3$, free_CaO and MgO refer to alite, belite, aluminate, alumino-ferrite, sulphate, free lime and magnesium oxide, respectively. The phase composition of the cement used in this study (CEM I 52.5 N) is presented in Table 3.

By applying Eq. (6) and data presented in Table 3, the hydration enthalpy of the cement used in this study is computed and yields $H_c$ = 475.0 [J/g or kJ/kg].

Table 3 Phase composition of CEM I 52.5 N [9]

| CEM I 52.5 N | Mass, % |
|---|---|
| $C_3S$ | 58.67 |
| $C_2S$ | 17.05 |
| $C_3A$ | 3.24 |
| $C_4AF$ | 10.26 |
| $SO_3$ | 2.98 |
| Free CaO | 0.97 |
| MgO | 0.97 |

## OPC-Based Ultra-Lightweight Concrete

Assuming adiabatic conditions and a complete hydration of cement, the temperature increase of fresh ultra-lightweight concrete can be estimated using Eq. (4). An ultra-lightweight concrete developed in the previous project (Mix A) is analyzed here for the temperature increase during the hydration [1, 10]. The mass proportions of the ingredient in Mix A are shown in Table 4.

Table 4 Composition of ultra-lightweight concrete [1]

| MATERIAL | Mass, kg/m³ |
|---|---|
| CEM I 52.5 N | 431.7 |
| LWA (total) | 154.1 |
| Water | 201.0 |

The data used to estimate the temperature increase in the concrete is presented in Table 5.

Table 5 Data used in the calculation of the temperature increase (1 [11]; 2 [12])

| *w/c* | 0.5 |
|---|---|
| $C_{p\text{-}c}$ | 0.92 [kJ/(K·kg)][1] |
| $C_{p\text{-}w}$ | 4.184 [kJ/(K·kg)] |
| $C_{p\text{-}LWA}$ | 0.84 [kJ/(K·kg)][2] |
| $H_c$ | 475.0 [kJ/kg] |
| *LWA/c* | 0.36 |

The temperature increase ($\Delta T$) in such a system, following Eq. (4), would yield 149.9°C, meaning that an initial temperature of all the ingredients of 20°C, the final temperature would reach about 170°C, provided that no heat is lost from the system.

## OPC-FA Blend Ultra-Lightweight Concrete

As shown in the previous section, the heat released upon OPC hydration can be high, leading to technical problems with a proper concrete curing. Supplementary cementitious materials (especially fly ash) can decrease the hydration heat, as can be seen from Eq. (5). Considering the fact that the hydration of fly ash is relatively slow under normal conditions, the increased temperature of concrete can be advantageous, accelerating the fly ash pozzolanic reaction. Nevertheless, the temperature of the cement-based system should not be too high so that the thermally-induced cracks can be avoided. Here, a final temperature of 60°C is used as the target temperature, fulfilling these criteria. Therefore, assuming the initial temperature of concrete ingredients of 20°C, such an enthalpy of hydration is needed which would increase the temperature further by 40°C.

In the case of applying fly ash in concrete, Eq. (4) can be re-written, as follows:

$$\Delta T = \frac{\alpha H_{total}}{C_{p-c} + {}^{w}\!/\!_{b} \cdot C_{p-w} + {}^{LWA}\!/\!_{b} \cdot C_{p-LWA}} \tag{7}$$

where: *w/b* – water-binder ratio (including cement and fly ash as binders), *LWA/b* – ratio between the amounts of lightweight aggregates an binder in concrete mixture, $H_{total}$ – total enthalpy of cement and fly ash hydration (see Eq.(5)) and α – cement hydration degree. A complete hydration degree of cement is assumed in the calculations shown in the previous section. Nevertheless, for more realistic calculations, an un-complete hydration should be assumed, therefore a hydration degree is also incorporated in Eq. (7) and a value of 0.8 is applied.

For the computation of the released heat and temperature increase the data presented in Table 6 is applied. The amount of water, binder and LWA is the same as specified in Table 4 (the binder here is composed of cement and fly ash). The estimated heat release and corresponding temperature increase for adiabatic conditions for different OPC-FA blends ultra-lightweight concrete are shown in Table 7.

Table 6 Data used in the calculation of the temperature increase [13]

| | |
|---|---|
| *w/b* | 0.5 |
| $C_{p\text{-}c}$ | 0.92 [kJ/(K·kg)] |
| $C_{p\text{-}w}$ | 4.184 [kJ/(K·kg)] |
| $C_{p\text{-}LWA}$ | 0.84 [kJ/(K·kg)] |
| $H_c$ | 475.0 [kJ/kg] |
| *LWA/b* | 0.36 |
| $M_{CaO(in\ FA)}$ | 0.1[1] |
| $\alpha$ | 0.8 |

Table 7 Heat release and temperature increase in OPC-FA based ultra-lightweight concrete.

| $M_c$ | $M_{FA}$ | ΔH, kJ/kg | ΔT, °C |
|---|---|---|---|
| 1 | 0 | 380.01 | 119.96 |
| 0.9 | 0.1 | 356.41 | 112.51 |
| 0.8 | 0.2 | 332.81 | 105.06 |
| 0.7 | 0.3 | 309.21 | 97.61 |
| 0.6 | 0.4 | 285.60 | 90.16 |
| 0.5 | 0.5 | 262.00 | 82.71 |
| 0.4 | 0.6 | 238.40 | 75.26 |
| 0.3 | 0.7 | 214.80 | 67.81 |
| 0.2 | 0.8 | 191.20 | 60.36 |
| 0.1 | 0.9 | 167.60 | 52.91 |
| 0.05 | 0.95 | 155.80 | 49.18 |
| 0 | 1 | 144.00 | 45.46 |

It can be seen in Table 7 that in order to increase the temperature of concrete by about 40°C in adiabatic conditions, theoretically the cement should be completely replaced by fly ash. This is however not realistic from the practical point of view, as the cement is needed in the system to activate the pozzolanic reaction of fly ash. Nevertheless, for instance in the case of 70% OPC replacement with FA, the maximum temperature increase is estimated to be about 68 °C (adiabatic conditions), while in non-adiabatic or semi-adiabatic conditions this would result in a much lower temperature increase, yet high enough to accelerate the hydration of fly ash. Therefore, in the present study, a partial replacement of cement (CEM II/B-V 42.5 N) with fly ash (50% by mass) is applied to study its effect on the temperature change during the hydration.

## Experimental Investigation

An experimental set-up is built in the present study to measure the temperature increase due to the hydration of binders. The wooden mould ($30 \times 30 \times 30$ $cm^3$) is insulted by applying EPS and mineral-wool. Additionally, a plastic container is used for embedding them. Two temperature sensors are used, by inserting them to the fresh concrete right after casting, to measure the temperature change at different locations inside the concrete. Then a wooden lid is used to cover the opening of the mould and finally a larger wooden panel is used to cover completely the plastic container after the temperature sensors are connected to the data log system.

Two concrete mixtures are produced here to investigate the temperature change during the hydration. The first one is Mix A, which was produced in the previous study [10], and the second mixture (namely Mix f-1) has the same composition as Mix A by only replacing 50% of cement (CEM II/B-V 42.5 N) by mass with fly ash (meaning that the binder is composed of approximately 25% of OPC and 75% of fly ash). The temperature measurement in the first test lasts for 24 hours and during the second test lasts for about 60 hours considering the potentially slower reaction of fly ash. Two temperature sensors are used in the test of Mix A, while one is embedded in the centre of the concrete cube and the other one is embedded in the side of the

cube to check the difference. Two temperature sensors are also used in the test of Mix f-1, but both sensors are embedded in the centre of the concrete cube to check if the measurement is representative. The results are shown in Figure 2.

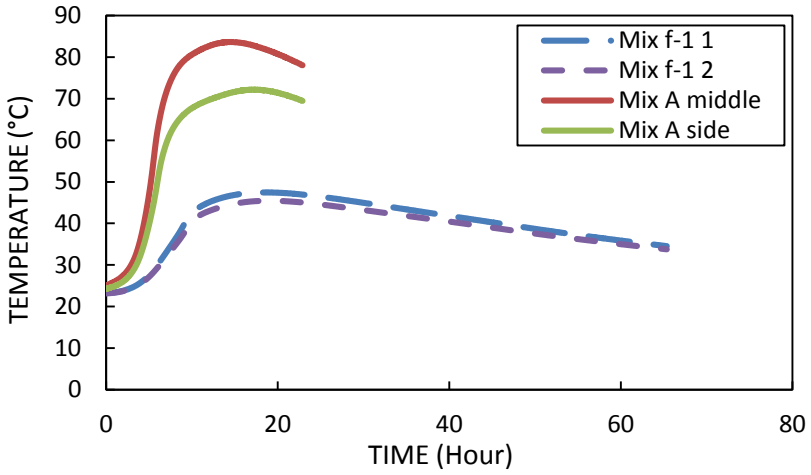


Figure 2 The temperature development measured in the concrete cubes

It can be clearly seen that the experimental set-up is only semi-adiabatic as the temperature first reaches a peak value and then decreases. This however also reflects the realistic condition as in reality no concrete is applied in adiabatic environment. Moreover, the better insulation here compared to real application to some extent compensates the smaller volume of concrete cast in the present study (27 l) compared to massive production in real application.

The temperature in Mix A increased maximally to about 85°C in the centre of the concrete cube, which is lower than the theoretical calculation (about 120°C, assuming the used cement CEM II/B-V 42.5 N is simply composed of 75% of CEM I and 25% fly ash and a room temperature of 20°C, see Table 7). The temperature in Mix f-1 increased maximally to about 48°C in the centre of the concrete cube, which is lower than the theoretical calculation (about 80°C, assuming a room temperature of 20°C, see Table 7). This can be explained by two reasons, while the first one is that the generated heat is partly released from the set-up and the second one is that the hydration degree at the testing period is lower than the assumed value (i.e. 0.8, see Eq. (7)). The temperature increase in Mix f-1 is much lower compared to that in Mix A, indicating a very positive role the fly ash plays, i.e. on the one hand the sustainable application of industrial by-products and on the other hand the solution of the potential problem related to the high temperature increase in the special case of ultra-lightweight concrete.

To verify the hardened properties of Mix f-1, additional measurements are performed, including the compressive strength and the durability in terms of water penetration under pressure. The 7-day compressive strength of Mix f-1 reaches 8.5 N/mm², which is lower than the 7-day compressive strength of Mix A (10.1 N/mm², see [1]), while the 28-day compressive strength of Mix f-1 reaches 10.1 N/mm², which is very comparable to the 28-day compressive strength of Mix A (10.3 N/mm², see [1]). The lower 7-day compressive strength of Mix f-1 can be explained by the low hydration speed of the used fly ash. The very comparable 28-day compressive strength of Mix f-1 and Mix A shows that the replacement of OPC by up to 75% of fly ash does not cause any negative effect on the strength.

## CONCLUSIONS

The present research aims at a deeper understanding of the previously designed ultra-lightweight concrete concerning its potential engineering application. The durability, in terms of the potential alkali silica reaction, is studied. The temperature increase during the hydration in the massive LWAC production is investigated as potentially it can cause problems due to the very good self-insulating effect caused by its very low thermal conductivity. The workability as well as the open time during the long time mixing is investigated considering a long time transport needed in some practical applications. Based on the performed study, the following conclusions can be reached:

- There is no alkali silica reaction risk in the developed lightweight aggregates concrete;
- The temperature increase due to the cement hydration reaches up to 87 °C in the semi-adiabatic experiments, which potentially could cause problems to the concrete such as micro cracks;
- From the material point of view, a solution to partly replace the cement by fly ash is proposed and investigated, as fly ash reacts slower than cement. The results show very positive effect concerning the lower temperature increase in the concrete; moreover up to 75% of OPC replacement by fly ash does not show negative effect on the 28-day compressive strength;
- The long-time mixing (up to 80 min) to simulate the long-time transport of the developed LWAC concrete does not show any negative effects on both fresh and hardened properties;

## ACKNOWLEDGEMENTS

The authors wish to express their gratitude to Materials innovation institute (M2i) particularly to Mrs. Dr. Ir. V. Savran, to Dr. M. van Leeuwen from CRH Europe Sustainable Concrete Centre, and Mr. H. Köhne from Cement&BetonCentrum for sponsoring this project (project number: MA. 13275), as well as to Dr. M. Hunger from ENCI B.V., HeidelbergCement Benelux for the cement supply.

## REFERENCES

1. YU, Q L, SPIESZ, P, BROUWERS, H J H. Ultra-lightweight concrete: Conceptual design and performance evaluation, Cement and Concrete Composites, Vol. 61, 2015, pp 18-28.

2. PREZZI, M, MONTEIRO, P J, SPOSITO, G. The alkali-silica reaction, Part I: use of the double-layer theory to explain the behavior of reaction-product gels. ACI Mater J, Vol 84, 1997, pp 10-17.

3. YU, R, VAN ONNA, D V, SPIESZ, P, BROUWERS, H J H. Development of Ultra-Lightweight Fibre Reinforced Concrete applying expanded waste glass, Journal of Cleaner Production, Vol. 112, 2016, pp 690-701.

4. THOMAS M. The effect of supplementary cementing materials on alkali-silica reaction: A review. Cement and Concrete Research, Vol. 41, 2011, pp 1224-1231.

5. BS-EN 12390-3. Testing hardened concrete - Compressive strength of test specimens. British Standards Institution-BSI and CEN European Committee for Standardization. 2009.

6. BS-EN 12350-2. Testing fresh concrete - Part 2: Slump-test. British Standards Institution-BSI and CEN European Committee for Standardization. 2009.

7. BS-EN 12350-5. Testing fresh concrete - Part 2: Flow table test. British Standards Institution-BSI and CEN European Committee for Standardization. 2009.

8. POOLE, J L, RIDING, K A, FOLLIARD, K J, JUENGER, M C G, SCHINDLER, A K. Hydration study of cementitious materials using semi-adiabatic calorimetry. ACI Special Publication 2007; 241.

9. YU, Q L. Personal communication with M. Hunger. 3-9-2012.

10. YU, Q L, SPIESZ P, BROUWERS HJH. Ultra-lichtbeton voor monoliete gevelconstructies. Cement 7, pp 34-39. 7-11-2013. Netherlands, Cement.

11. http://www.engineeringtoolbox.com/specific-heat-solids-d_154.html 2013

12. http://hyperphysics.phy-astr.gsu.edu/hbase/tables/sphtt.html 2013

13. GOODARZI, F. Characteristics and composition of fly ash from Canadian coal-fired power plants. Fuel, Vol. 85, 2006, pp 1418-1427.

# BUBBLE STRUCTURE, STABILITY AND RHEOLOGY OF FOAMED CONCRETE

**M R Jones** **L Zheng**
University of Dundee
United Kingdom
**M Mohammad**
Public Works Department
Malaysia

**ABSTRACT:** Foamed concrete has been identified as a versatile construction material with excellent properties that include being highly flowable, light, and durable, which are mainly own to its large volume of spherical bubbles. However, improper bubble structure in foamed concrete could result in stability problem unexpectedly on-site during its application and cause it to collapse. In this study, the bubble structure of foamed concrete was examined to establish links with its stability and rheology properties. Mixes with plastic densities ranging from 300 to 1400 kg/m³ were produced with CEM I, CSA and fine fly ash cement combinations. Water-cement (w/c) ratios varied from 0.4 to 0.8 and two types of surfactant were used. The bubble size of foamed concrete was found to be a function of its density, w/c ratio, the material fineness and surfactant types. The bubble diameters were shown to range between 0.1 to 0.5 mm. The stability was improved with increase in density. Reducing w/c ratio and fineness of constituent materials was also beneficial. The hardening time had a significant effect for stability of low density mixes and stable mixes with 300 kg/m³ density were achieved by using cement combinations of CSA with CEM I R or CSA with fine fly ash. A relationship was also established between bubble structures and the rheological values. Bubble sizes reduced when the yield stress increased. Changing the densities exhibited significant variance in the rheological values due to the changes in total bubble content. Altering the w/c ratio also had a considerable variation in the rheological values due to the changes in consistence of base mixes.

**Keywords:** Foamed Concrete, Bubble Structure, Stability, Rheology.

**Professor M Rod Jones** is the Director of the Concrete Technology Unit at the University of Dundee. A renowned practitioner in the field of concrete technology, he is a member of numerous national and international technical committees and has published extensively on many aspects of concrete technology, cement science and sustainable construction.

**Dr Li Zheng** is a Research Fellow in the Concrete Technology Unit, University of Dundee.

**Dr Maziah Mohammad** is the senior principal assistant director in the Public Works Department (JKR), Malaysia, heading the structural forensic division.

## INTRODUCTION

Foamed concrete has been identified as a versatile construction material with excellent properties that include being light, durable, simple to use, environmentally sustainable and versatile without being restricted by factory requirements [1]. It has the advantage of high flowability with its capacity to flow readily to fill restricted and irregular cavities, and its ability to be pumped successfully over vertical and horizontal distances [2]. This is mainly own to its large volume of spherical bubbles which provide the ball bearing effect. Air content of the foamed concrete are typically varying from 40 to 80 % of the total volume while size of the bubbles varying from 0.1 mm to 1.5 mm in diameter [3]. Ideal bubble structure provides foamed concrete with not only a good flowability, but also improved strength and reduced thermal conductivity [3, 4]. It also endows foamed concrete excellent anti-impact property [5]. However, improper bubble structure in formed concrete could result in stability problem unexpectedly on-site during its application and cause it to collaps [6, 7]. Hypothesis of stability and instability of foamed concrete based on laboratory studies and site observations was proposed to develop an empirical understanding of the factors that have been identified as being critical to bubble stability [8]. It was concluded that the underlying cause of instability is considered to be the buoyancy force of the bubbles and the use of rapid-setting cement combinations is the best method of overcoming this.

The study presented in this paper was carried out with an effort to understand in-depth the effects of the constituent materials and mix proportions on the bubble structure of foamed concrete and its relationships to its stability and rheology. For the study, foamed concrete mixes with plastic densities ranging from 300 to 1400 kg/m³ were produced with CEM I, CSA and fine fly ash cement combinations. Water-cement ratios varied from 0.4 to 0.8 and two types of surfactant were used.

## INTRODUCTION

The aim of this study was to examine the bubble structure in relation to constituent materials, densities, water-cement (w/c) ratios and surfactant admixtures. Stability in foamed concrete was examined with the record of the drop after 24 hours in the surface level of the specimen for each mix. The hardened specimens were split open and the digital images were taken and analysed. The rheology was studied in terms of the empirical values of yield stress and plastic viscosity of different mixes using a Brookfield Viscometer. Details of materials, foamed concrete mixes and test methods are described as follows.

### Materials and Foamed Concrete Mixes

The cements used for foamed concrete mixes were:

(i) Portland cement (CEM I, BS EN 197-1). CEM I, 42.5N grade was used for all mixes with densities above 600 kg/m³ while CEM I, 52.5R used for 300 kg/m³ mixes.
(ii) Calcium sulphoaluminate (CSA) cement, labelled QuickCem from Castle cement Ltd. It was used for 300 kg/m³ mixes.
(iii) Fine fly ash ($FA_f$, BS EN 450-1) with 45 μm sieve retention of 7.5% and loss on ignition of 5.0%. It was used to replace CEM I 42.5N at 30% by mass in 600 and 1000 kg/m³ mixes and to replace CSA at 40%, 50% and 60% by mass in 300 kg/m³ mixes.

The chemical compositions of cements are given in Table 1.

Table 1 Chemical composition of cements, % by mass

| COMPOUND | CEM I | | CSA | $FA_f$ |
|---|---|---|---|---|
| | 42.5N | 52.5R | | |
| CaO | 62.7 | 66.7 | 42.25 | 7.19 |
| $SiO_2$ | 21.3 | 19.9 | 10.96 | 51.22 |
| $Al_2O_3$ | 5.9 | 4.8 | 29.93 | 27.30 |
| $Fe_2O_3$ | 3.6 | 3.1 | 3.01 | 3.60 |
| MgO | 2.4 | 1.1 | 1.45 | 1.35 |
| $TiO_2$ | 0.3 | - | - | 1.38 |
| $K_2O$ | 0.7 | 0.7 | 1.02 | 1.55 |
| $Na_2O$ | 0.2 | 0.3 | 0.23 | 0.58 |
| $SO_3$ | 2.99 | 2.7 | 8.82 | 1.30 |

The fine aggregate conforming to BS EN 12620 was used for 600, 1000 and 1400 kg/m³ mixes, which was natural sand and sieved through a 2.36 mm sieve. In the study of rheology, a finer size, sieved through a 1 mm sieve was used to accommodate the apparatus used. In addition, coarse fly ash ($FA_c$) with a 45µm sieve retention of 36.0% and conforming to BS EN 450-1 was used as 50% and 100% replacement for sand.

The foam added to the base mortar-mixes (or paste for 300 kg/m³ mixes) was produced by commercial protein-based and synthetic surfactants diluted with water using a laboratory-scale foam generator. The concentration of the surfactant solution used for the production of foam was typically 60 g per litre of water to produce foam of 50 ± 5 kg/m³ density.

The mix design, described in [1], gave foamed concrete with plastic densities of 300, 600, 1000 and 1400 kg/m³ was produced with different w/c ratios varying from 0.4 to 0.8. A cement content of 300 kg/m³ was maintained for all mixes with densities above 600 kg/m³. Table 2 gives the foamed concrete mixes for 600, 1000 and 1400 kg/m³ densities and Table 3 for 300 kg/m³ mixes.

Table 2 Foamed Concrete Mix Proportions for 600, 1000 and 1400 kg/m³ mixes

| TARGET PLASTIC DENSITY, kg/m$^3$ | w/c | MIX CONSTITUENT PROPORTIONS*, kg/m$^3$ | | | AIR %, Vol |
|---|---|---|---|---|---|
| | | Free Water | Sand | Foam | |
| 600 | 0.40 | 120 | 180 | 55.9 | 71.6 |
| | 0.50 | 150 | 150 | 54.4 | 69.8 |
| | 0.60 | 180 | 120 | 53.0 | 67.9 |
| 1000** | 0.40 | 120 | 580 | 44.0 | 56.4 |
| | 0.50 | 150 | 550 | 42.6 | 54.6 |
| | 0.60 | 180 | 520 | 41.1 | 52.7 |
| | 0.70 | 210 | 490 | 39.6 | 50.8 |
| | 0.80 | 240 | 460 | 38.2 | 49.0 |
| 1400 | 0.40 | 120 | 980 | 32.1 | 41.2 |
| | 0.50 | 150 | 950 | 30.7 | 39.4 |
| | 0.60 | 180 | 920 | 29.2 | 37.5 |

* CEM I 42.5 N = 300 kg/m$^3$.

** For 1000 kg/m³ mixes, additional CEM I/FA mix was made with 30% $FA_f$ used to replace CEM I.

Table 3 Foamed Concrete Mix Proportions for 300 kg/m³ mixes

| MIX CODE | MIX CONSTITUENT PROPORTIONS*, kg/m$^3$ | | | | | Air %, Vol |
|---|---|---|---|---|---|---|
| | Free Water | CEM I 52.5 R | CSA | $FA_f$ | Foam | |
| 100PC | 100 | 200 | 0 | 0 | 38.5 | 83.6 |
| $20CSA_P$ | | 160 | 40 | 0 | 38.4 | 83.5 |
| $40CSA_P$ | | 120 | 80 | 0 | 38.4 | 83.5 |
| $50CSA_P$ | | 100 | 100 | 0 | 38.4 | 83.4 |
| $60CSA_F$ | | 0 | 120 | 80 | 37.8 | 82.1 |
| $50CSA_F$ | | 0 | 100 | 100 | 37.7 | 81.8 |
| $40CSA_F$ | | 0 | 80 | 120 | 37.5 | 81.6 |
| $30CSA_F$ | | 0 | 60 | 140 | 37.4 | 81.3 |

* w/c = 0.5

The plastic density of the foamed concrete was measured during mixing in accordance with BS EN 12350-6 by weighing a foamed concrete sample in a pre-weighed container of a known volume. A tolerance on plastic density was set at ± 50 kg/m³ of the target value, which is typical of industry practice for foamed concrete production. If the density was higher, additional foam was prepared and added incrementally until a density within the accepted range was achieved. However, mixes with densities lower than the range of acceptable values were discarded and the whole mixing process was repeated.

**Test Methods**

**Stability:**

There is no standard test to investigate the stability of foamed concrete and normally it was examined by visual observation of the consistency of mix [1, 7]. Adopting this in the current study, a drop in the surface level was also measured to quantify the stability of foamed concrete. The specimens were cast in ø80 × 500 mm cylinder moulds lined with plastic 'cling' film to avoid the foamed concrete from adhering to the mould surface and the amount of drop in level over 24 hours was used as indicator for stability. The hardened specimens were then sealed-cured at 20°C to 28 days and split longitudinally for bubble structure analysis.

**Bubble structure:**

To date, there has been no standard method for the study of the microstructure of foamed concrete. Several indirect methods have been used by other researchers [9] based on the ASTM C457. This method required rigorous surface preparation involved surface grinding and polishing. It was not suitable for foamed concrete since the air voids tended to coalesce and the fragile thin walls between the voids could be damaged during the processing.

Kearsley and Visagie [10] and Nambiar and Ramamurthy [11] adopted a method using a high resolution digital camera and image analysis software. Taking cognisance of their work, the current study adopted a similar approach to investigate the microstructure of foamed concrete. The image analysis software employed was 'ImageJ' [12].

From the longitudinal specimens, the cylinder was 'divided' into four sections which enabled the study of microstructure varying along the height. After split, the specimens were cleaned with compressed air to remove loose deposits. Only the specimens with an excellent quality surface were subjected to the image analysis. A total of two clear images were selected from each section of the specimen. The parameters obtained from the image analysis included bubble counts over a fixed area (5 × 6.7 mm), equivalent mean bubble diameter (=d50), as shown in Figure 1, and bubble size distribution, expressed as d10, d50 and d90.

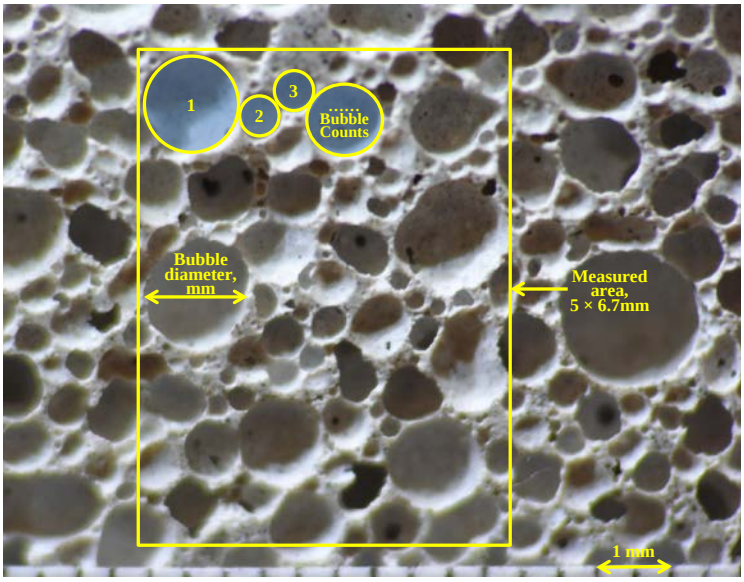


Figure 1 Image analysis of bubble structures of foamed concrete

**Rheological properties:**

Since foamed concrete behaves more Bingham-like in nature, the rheological properties can be characterised with two parameters, i.e. yield stress and plastic viscosity. In this study, Brookfield Viscometer was used to determine the empirical values of yield stress and plastic viscosity, following the method developed by Domone et al [13]. The freshly mixed foamed concrete was put into a beaker to half fill and the torque was measured with T-bar spindles and a Helipath stand at different rotational speeds. The results of torque against rotational speed were then plotted and a best fit line was drawn.

$$T = g + hN \quad (1)$$

Where, T = torque (viscometer reading), N.mm
g = empirical value of yield stress (function of yield value $\tau_0$)
h = empirical value of plastic viscosity (function of plastic viscosity $\eta$)
N = rotational speed, rev/s

The empirical values of yield stress g and plastic viscosity h were determined from the intercept value and slope of the line and used in this study. Please note that g and h are functions of yield value $\tau 0$, N.mm, and plastic viscosity $\eta$, N.mm.s. However, the units for g and h are unknown.

## RESULTS AND DISCUSSION

### Bubble Structure

Figure 2 shows the bubble counts and bubble diameter varying with densities at w/c ratios of 0.4, 0.5 and 0.6. It can be seen that there was an increase in bubble count with increase in density (Figure 2a). However, the bubble count decreased with increase in w/c ratio. In Figure 2b, the (mean) diameter decreased with increase in density. For each density, the diameter reduced with decreased in w/c ratio. However, in any density, the variation in bubble diameter is not clearly defined, which accounts for the small variation in Figure 2b. Increase in density is related to increase in solids for the same volume. The higher volume of solids reduced the spaces for the bubble size increasing and amalgamation, hence small bubble diameter was observed. The average diameter of mixes in the higher w/c ratio was bigger than that in the mixes of lower w/c ratio. This trend was similar to all the densities. The bubbles in density 1400 kg/m³ were very small, the smallest being the lowest w/c ratio at 0.4. This bubble density accounts for the stable mix.

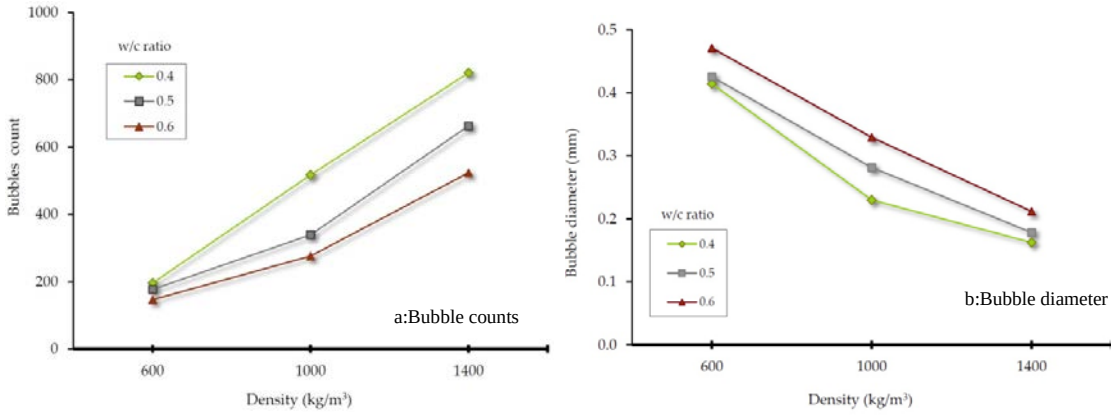


Figure 2 Bubble counts and bubble diameter varying with densities of foamed concrete

Figure 3 shows bubble diameter varying with w/c ratio for 1000 kg/m³ CEM I and CEM I/30%$FA_f$ foamed concrete. Again it illustrates an increase in bubble size with w/c ratio for both mixes. It can be seen that CEM I/30%$FA_f$ mixes had smaller bubble sizes than correspond CEM I mixes, which mainly due to the fineness improvement. It has been observed that bubbles less than 0.35 mm in diameter corresponded to stable mix.

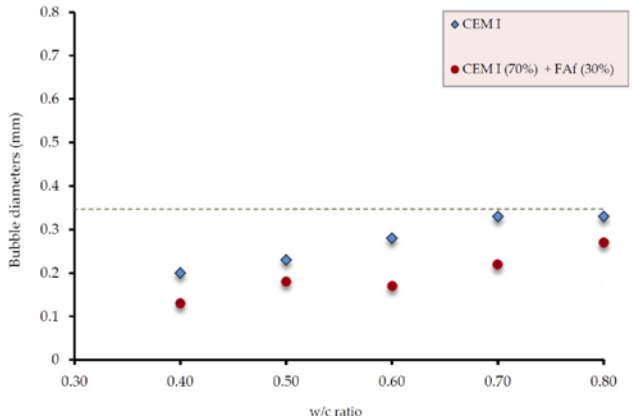


Figure 3 Bubble diameter varying with w/c ratio for CEM I and CEM I/30%$FA_f$ foamed concrete (Plastic density = 1000 kg/m³).

Results for $FA_c$ replacing sand filler also indicate the similar tendency as shown Figure 4. Bubble size distribution for 600 kg/m³ mixes with w/c =c 0.50 was analysed in this case, which again indicates that bubble size reduced with fineness of the mixes and the reduction is mainly in the large bubble range (d90) and few changes in small bubbles (d10). With 50% fine aggregate replacement, the d90 value was reduced to more than half and with 100% total replacement, to a third compared to the sand only mix.

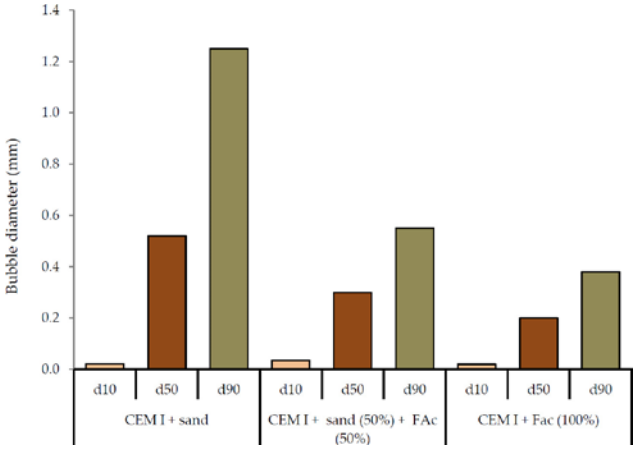


Figure 4 Bubble size distribution varying with $FA_c$ replacing sand in foamed concrete (Plastic density = 600 kg/m³ and w/c = 0.50).

The comparisons in bubble count and diameter between the top and bottom sections of a specimen are shown in Figure 5. The difference in bubble count was not distinctive in all densities, as shown in Figure 5a as well as bubble diameter in Figure 5b. Only a slight increase in bubble size from top to bottom for 600 kg/m³ was observed.

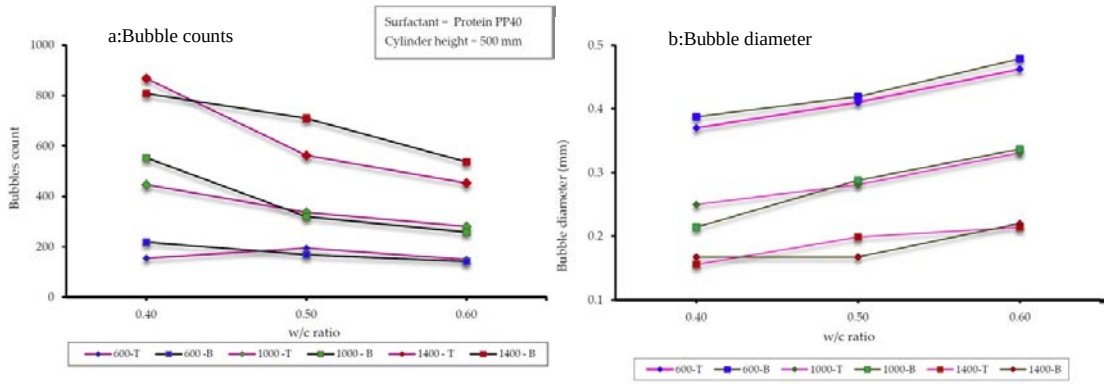


Figure 5 Bubble counts and diameter varying with height of specimens (T=Top, B=Bottom)

All the above results were obtained from the specimens, which were produced using protein-based surfactant. When synthetic-based surfactant was used, large size open bubbles were produced as compared with protein-based surfactant in Figure 6. The bubbles appear to have 'holes' or 'bubbles inside the bubbles' for specimens produced with synthetic-based surfactant (Figure 6b). Bubble count and diameter calculation using image analysis were impossible for these specimens.

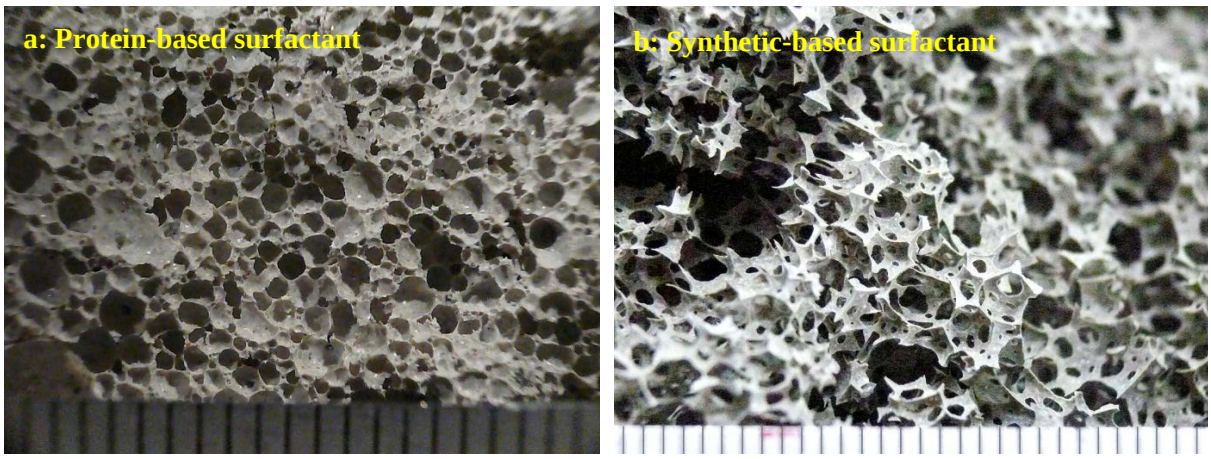


Figure 6 Comparison of the bubble structures of foamed concretes produced with different types of surfactants. (a) protein-based surfactant and (b) synthetic-based surfactant (Plastic density = 600 kg/m³ and w/c = 0.50)

For ultra-light foamed concrete with 300 kg/m³, only visual observation was carried out in current study as shown in Figures 7 and 8. Figure 7 shows bubble structure varying with different CEM I/CSA ratios. In the 100% CEM I 52.5R, the bubbles were clearly defined and spherical (Figure 7a). With 20% CSA replacement, the bubbles became smaller in size, although the sphericity was still obvious (Figure 7b). The bubbles became less distinctive with additional replacement of CSA; a total of 40% (Figure 7c). With further replacement totalling to 50% of CSA, the bubbles appeared to have reduced in number and seemed less spherical (Figure 7d). However, in all four cement combinations, the foamed concrete mixes remained stable, which will be discussed in the following section.

Figure 8 shows bubble structure for CSA/$FA_f$ combinations at different proportions. The CSA/$FA_f$ at ratios of 60:40 to 30:70 was found to have produced stable foamed concrete mixes. On their microstructural characteristics, there was no distinct characteristic difference in the various proportions of the mixes (Figures 8a to d). In all the mixes, the bubbles appear small and barely spherical. These were repeated in all w/c ratios.

**Stability**

Instable foam causes the bubbles to collapse which alters the density of the concrete, and consequently, affects both the fresh and the hardened properties. Except the external environmental factors, e.g. temperature, humidity, alkalinity or acidity, a number of internal factors can affect the stability of foamed concrete, such as its density and the type of surfactant used, chemical admixtures, w/c ratios and other constituent materials like fly ash [3]. Since these internal factors affected the bubble structure as discussed above, relationship between bubble structure and stability of foamed concrete can be established.

Figure 9 shows a relationship between stability and bubble size of foamed concrete. The decrease in drop in level indicates an increase in stability, which corresponds to smaller bubble diameters. The drop in level was less in higher densities means the stability increasing with density of foamed concrete. Correspondingly, the bubble sizes reduced with increased density. The stability also increased with the reduction of w/c ratio especially for the low density foamed concrete but less significant for high density specimens.

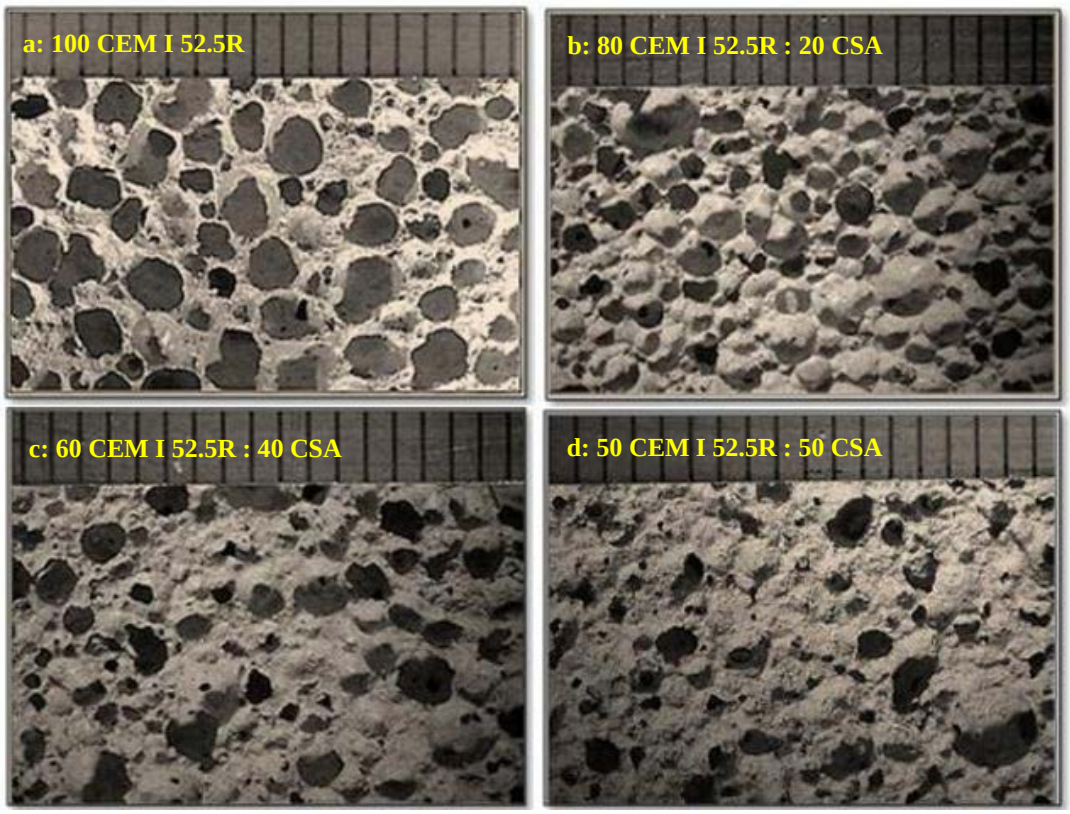


Figure 7 Comparison of the bubble structures of foamed concretes produced with different CEM I/CSA ratios (Plastic density = 300 kg/m³ and w/c = 0.50)

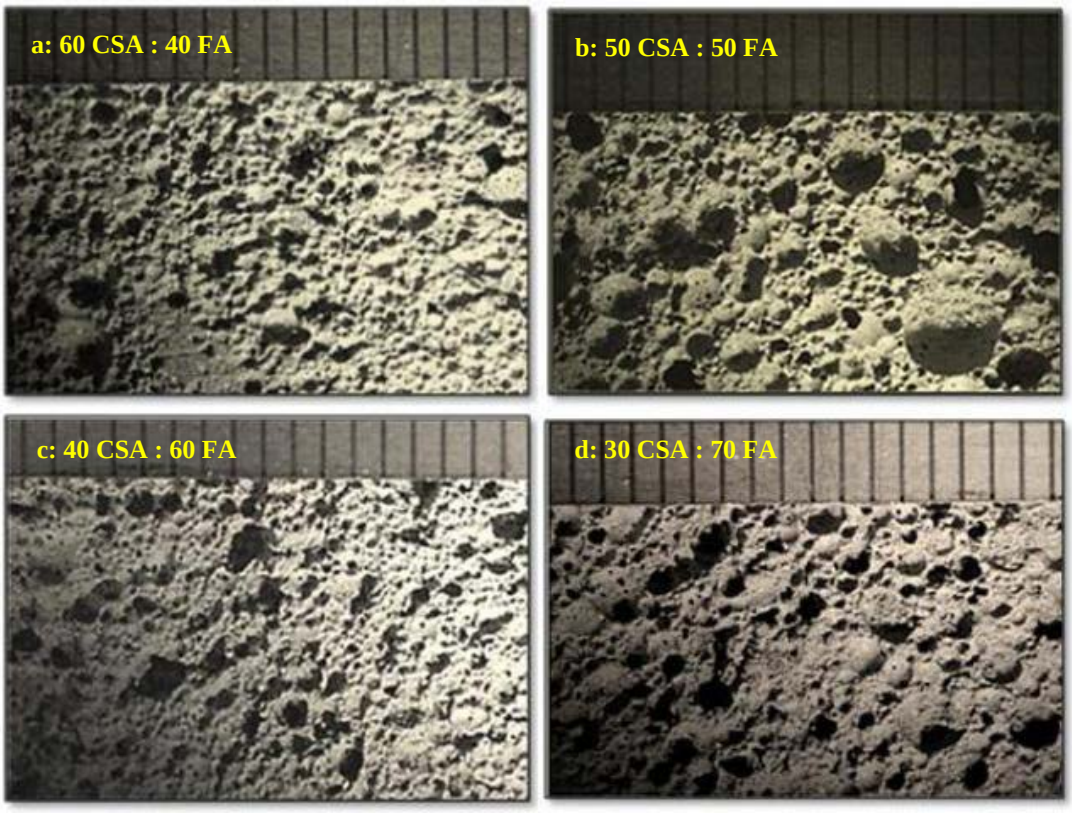


Figure 8 Comparison of the bubble structures of foamed concretes produced with different CSA/$FA_f$ ratios (Plastic density = 300 kg/m³ and w/c = 0.50)

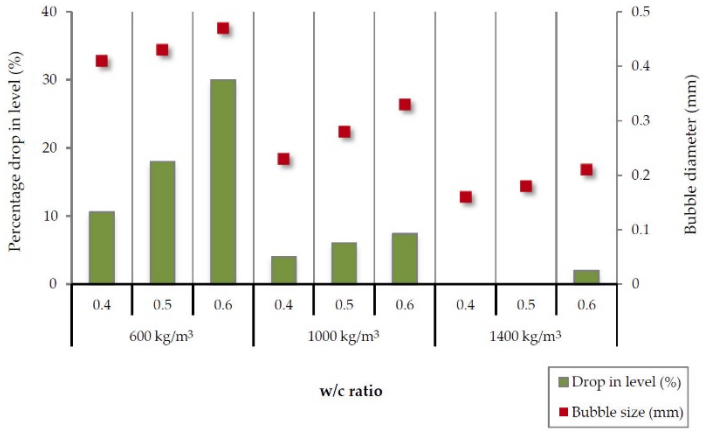


Figure 9 Relationship between stability and bubble size of foamed concrete

Figure 10 shows drop in level varying with w/c ratio for 1000 kg/m³ CEM I and CEM I/30%$FA_f$ foamed concrete. It can be seen that the stability reduced with w/c ratio for both mixes. The CEM I/30%$FA_f$ mixes were more stable than correspond CEM I mixes (Figure 10a), due to the reduced bubble size as indicated in Figure 3. When coarse fly ash used to replace sand, stability was also improved for mixes with w/c $\leq$ 0.5 (Figure 10b) in relation to the reduction in bubble size as shown in Figure 4. However, for w/c $\geq$ 0.6, 100% replacement mixes had reduced stability compared to 50% replacement mixes.

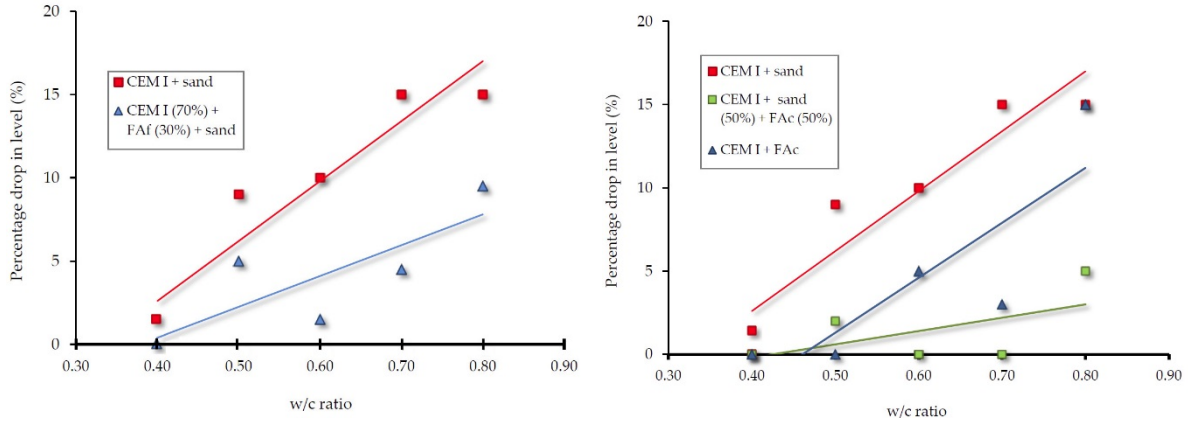


Figure 10 Stability varying with w/c ratio for foamed concrete (a) $FA_f$ replacing CEM I; and (b) FAc replacing sand. (Plastic density = 1000 kg/m³).

Stability of foamed concretes produced with two different types of surfactants is compared in Figure 11. There is no significant difference for 1400 kg/m³ mixes and all of them exhibited stable with drop in level less than 1%. Stability was much improved for low density mixes with w/c ratios $\leq$ 0.5 by using protein-based surfactant, which also attributed the bubble structure difference as indicated in Figure 6.

For foamed concrete with very low densities, e.g. 300 kg/m³, it required a rapid hardening cement to obtain a stable mix and then CEM I 52.5R and CSA cement were used. Two sets of cement combinations were explored. The first was CEM I 52.5R with CSA and the second was CSA with $FA_f$. All combinations had 0 to 5 % drop in level and indicated stable mixes, while the same density mix with CEM I 42.5N was collapsed with more than 50% drop in level.

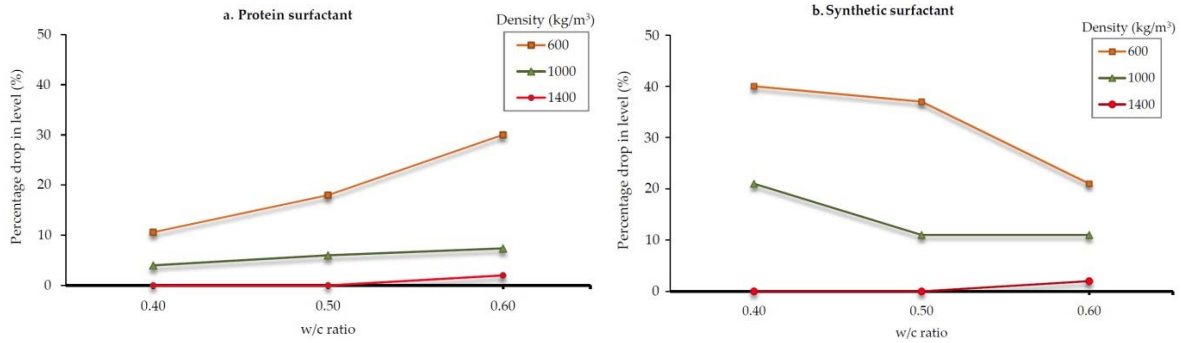


Figure 11 Comparison of the stability of foamed concretes produced with different types of surfactants. (a) protein-based surfactant; and (b) synthetic-based surfactant

## Rheology

Rheological properties in the fresh state of foamed concrete play a critical role in the maintenance of the ideal bubble structures and stability as well as the development of foamed concrete in the hardened state. Significant changes to the rheological behaviour were found when using different constituent materials [1]. The rheological properties of foamed concrete were also found varying with air content (i.e. density of foamed concrete) and w/c ratio [14].

The empirical values of yield stress and plastic viscosity, together with their bubble sizes, are given in Table 4 and schematic shown in Figure 12. In general, increase in yield stress and plastic viscosity reduced the bubble sizes although the effect of yield stress is more significant. Large volume of ideal spherical bubbles provided the ball bearing effect, which significantly improved the rheological properties of foamed concrete and, therefore, yield stress and plastic viscosity reduced with the density of foamed concrete (via increasing bubble volume). Reduced bubble size could increase the total bubble numbers and enhance stability of the bubbles and therefore improve the rheology. However, it was not the case when the bubble size reduced due to reducing w/c ratio, which reduced consistence of base mixes. An increasing in w/c ratios could improve rheological properties, which, was through the improvement of consistence of base mixes. Figure 13 shows yield stress varying with w/c ratio for 1000 kg/m³ CEM I and CEM I/30%$FA_f$ foamed concrete. It indicates that the yield stress reduced with w/c ratio for both mixes. The CEM I/30%$FA_f$ mixes had smaller values than correspond CEM I mixes, due to the reduced bubble size as indicated in Figure 3. However, Figure 3 also indicates an increase in bubble size with w/c ratio and stability was also reduced with w/c ratio as shown in Figure 10. All of these indicate that foamed concrete is a complex system.

Table 4 Relationship between bubble sizes and rheological properties

| w/c ratio | PLASTIC DENSITY, kg/m$^3$ | | | | | | | | |
|---|---|---|---|---|---|---|---|---|---|
| | 600 | | | 1000 | | | 1400 | | |
| | Yield stress, empirical value | Plastic viscosity, empirical value | Bubble diameter, mm | Yield stress, empirical value | Plastic viscosity, empirical value | Bubble diameter, mm | Yield stress, empirical value | Plastic viscosity, empirical value | Bubble diameter, mm |
| 0.4 | 7.6 | 0.11 | 0.41 | 16.8 | 0.66 | 0.23 | 52.8 | 1.18 | 0.16 |
| 0.5 | 3.7 | 0.09 | 0.43 | 11.0 | 0.33 | 0.28 | 43.6 | 1.07 | 0.18 |
| 0.6 | 1.8 | 0.08 | 0.47 | 2.6 | 0.29 | 0.33 | 21.8 | 0.85 | 0.21 |

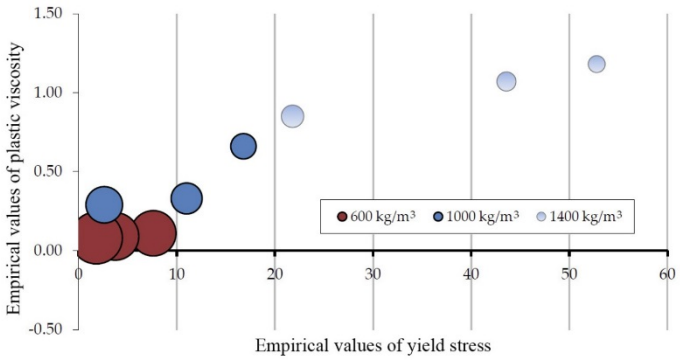


Figure 12 Schematic bubble sizes for varying yield stress and plastic viscosity

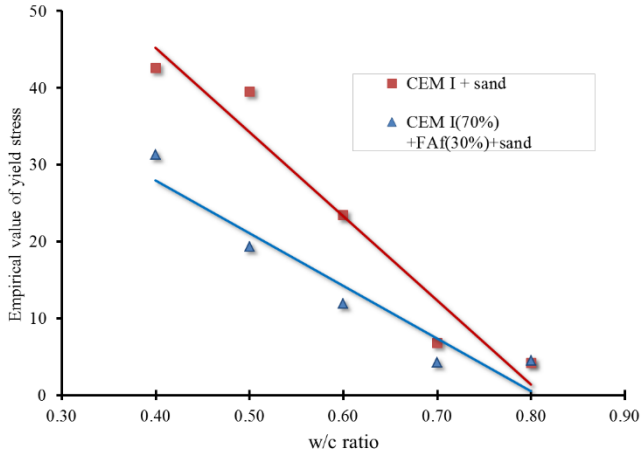


Figure 13 Yield stress varying with w/c ratio for CEM I and CEM I/30%FAf foamed concrete (Plastic density = 1000 kg/m³).

## CONCLUSIONS

- The bubble size of foamed concrete was found to be a function of its density, w/c ratio, the material fineness and surfactant types. The bubble diameters were shown to range between 0.1 to 0.5 mm. Bubbles less than 0.35 mm in diameter corresponded to stable mix with a drop in level of less than 15% in height in densities of 1000 kg/m$^3$ and higher and the big bubbles linked to unstable mixes.

- In examining the stability, it was found that it improved markedly with increase in density. Reducing w/c ratio and fineness of constituent materials was also beneficial to the stability of foamed concrete. The hardening time had a significant effect for stability of low density mixes, as it was evidenced by the use of CSA compared to CEM I 42.5N cement. Stable mixes with 300 kg/m$^3$ density were achieved by using cement combinations of CSA with CEM I 52.5R or CSA with fine fly ash.

- A relationship was also established between bubble structure and the rheological values. Bubble sizes reduced when the yield stress increased. Changing the densities exhibited significant variance in the rheological values due to the changes in total bubble content. Altering the w/c ratio also had a considerable variation in the rheological values due to the changes in consistence of base mixes.

It was found that the three aspects, i.e. bubble structures, stability and rheology of foamed concrete, in this study were correlated and constrained mutually. For example, reduced bubble size could be beneficial to both stability and rheology. However, if this was simply done by reducing air content (i.e. increasing density) or w/c ratio, stability could be improved but rheology would tend to worse. Using fly ash to partially replace CEM I or sand filler to reduce the bubble size could improve both stability and rheology.

## ACKNOWLEDGEMENTS

The support and technical advice is gratefully acknowledged from Propump Engineering Ltd and CALTRA Nederland BV are thanked for their support with the supply of CSA.

## REFERENCES

1. JONES, M R, MCCARTHY, A. Preliminary views on the potential of foamed concrete as a structural material, Magazine of Concrete Research, Vol. 57, No. 1, 2005, pp 21-31.

2. JONES, M R, MCCARTHY, A, KHARIDU, S, NICOL, L. Foamed Concrete – Development and applications, Concrete, Vol. 39, No. 8, 2005, pp 41-43.

3. BRADY, K C, WATTS, G R A, JONES, M R. Specification for Foamed Concrete, Prepared for Quality Services, Civil Engineering, Highway Agency, Application Guide AG39, Transport Research Laboratory (TRL) Limited, 2001, p 62.

4. JONES, M R, GIANNAKOU, A. Thermally Insulating Foundations and Ground Slabs Using Highly-Foamed Concrete, Journal of ASTM International, Vol. 1, No. 6, 2004, DOI: 10.1520/JAI11879.

5. JONES, M R, ZHENG, L. Energy absorption of foamed concrete from low velocity impacts, Magazine of Concrete Research, Vol. 65, No. 4, 2013, pp 209-219.

6. JONES, M R, MCCARTHY, A. Heat of hydration in foamed concrete: Effect of mix constituents and plastic density, Cement and Concrete Research, Vol. 36, No. 6, 2006, pp 1032-1041.

7. NAMBIAR, E K K, RAMAMURTHY, K. Fresh state characteristics of foam concrete, Journal of Materials in Civil Engineering, Vol. 20, No. 2, 2008, pp 111-117.

8. JONES, M R, OZLUTAS, K, ZHENG, L. Stability and instability of foamed concrete, Magazine of Concrete Research, 2015, DOI: 10.1680/macr.15.00097.

9. ALIGIZAKI, K K. Pore Structure of Cement-based Materials, Taylor and Francis, 2006, pp 286-331.

10. KEARSLEY, E P, VISAGIE, M. Micro-properties of foamed concrete, Specialist techniques and materials for concrete construction, Proceedings of the International Conference ‘Creating with concrete’ (Ed R K Dhir and N A Henderson), University of Dundee, Scotland, 1999, Thomas Telford, pp. 173-184.

11. NAMBIAR, E K K, RAMAMURTHY, K. Air-void characterisation of foam concrete, Cement and Concrete Research, Vol. 37, No. 2, 2007, pp 221-230.

12. FERREIRA, T, RASBAND, W. ImageJ User Guide, IJ 1.46r, http://imagej.nih.gov, accessible in November, 2012.

13. DOMONE, P L, YONGMO, X, BANFILL, P F G. Developments of the two-point workability test for high-performance concrete, Magazine of Concrete Research, Vol. 51, No. 3, 1999, pp 171-179.

14. CHIA, K S, ZHANG, M H. Workability of air-entrained lightweight concrete from rheology perspective, Magazine of Concrete research, Vol. 59, No. 5, 2007, pp 367-375.

# GEOPOLYMERIC THERMAL CONDUCTIVITY SENSORS FOR SURFACE-MOUNTING ONTO CONCRETE STRUCTURES

**M Perry**
University of Strathclyde
**M Saafi**
University of Lancaster
**G Fusiek** **P Niewczas**
University of Strathclyde
United Kingdom

**ABSTRACT:** In this work, we present a novel, geopolymer temperature-sensing patch which can be heated using induction and used to infer thermal conductivity of the surrounding medium. The sensor patches, applied to concrete specimens, were fabricated by loading a geopolymer binder with 0 - 60 wt% ground magnetite. The magnetite content allowed the patches to be heated using an induction coil, while temperature profiles were monitored via changes in patch electrical impedance. Sensor patches were left uncoated, or were coated in surface-water, soil and sand. Each material provided a unique thermal signature which, with simple signal processing, could be used to reliably detect whether the patch was buried.

**Keywords:** Geopolymer, Sensors, Thermal, Conductivity, Deburial.

**Marcus Perry** is a Research Fellow in Civil and Environmental Engineering at the University of Strathclyde. He has broad expertise in the areas of electronic and fibre optic sensing, structural health monitoring, materials science and signal processing. He has seven years of project experience in delivering concrete monitoring solutions for industrial collaborators.

**Mohamed Saafi** is a Professor and Chair in Structural Integrity and Materials at the University of Lancaster. His research focuses on the development of Functional Materials and Smart Sensors for Energy and Civil Infrastructure. He developed several structural integrity monitoring tools using MEMS, graphene and carbon nanotubes. Professor Saafi holds a USA patent (Smart Paint) for structural integrity monitoring of civil infrastructure.

**Grzegorz Fusiek** is a Research Associate in the department for Electronic and Electrical Engineering at the University of Strathclyde. His research interests include the development of fibre optic sensors, systems and interrogators for applications in the energy industry.

**Pawel Niewczas** is a Reader at the Institute for Energy and Environment, in the department for Electronic and Electrical Engineering at the University of Strathclyde. He is leading the Advanced Sensors Team within the Institute for Energy and Environment in the same department. His main interests centre on the advancement of optical sensing methods in applications that lie predominantly in the fields of power industry and energy systems.

## INTRODUCTION

Deburial and scouring can degrade the stability of any large civil structure. Structures subjected to large dynamic loads or changing water levels, such as wind turbines and bridges, are particularly affected [1]. Traditional automated scour monitoring methods and instrumentation are often expensive to install and maintain, so there is keen interest in developing new deburial monitoring systems.

Several methods have been proposed for deburial detection, including solutions based on fibre optics and micro-electromechanical system (MEMS) devices [2]. Unfortunately, the technical challenge of providing robust packaging for fibre and MEMS sensors can present a barrier to their widespread use [3, 4].

Geopolymer binders are a novel class of chemically stable, low shrinkage piezoresistive materials, which are highly suited to civil applications. Unintrusive and easy to apply, geopolymer binders provide excellent adhesion to concrete structures [5]. Once cured, the binders form a tough ceramic-like resin that can be used to detect environmental parameters via changes in electrical impedance [6].

In this preliminary work, geopolymer binders are doped with a ferromagnetic mineral and then applied to concrete surfaces. The doping allows the patches to be heated using an induction coil, while the electrical impedance of the patches is interrogated to monitor patch temperature during heating and cooling. Thermal decay signatures are then used to detect whether the sensor is surrounded by air, soil, sand, or a mixture of these materials. It is proposed that these geopolymer sensor patches may provide a new method of detecting deburial of concrete assets.

## THEORY OF OPERATION

### Geopolymer Binders

Adhesive geopolymer gels can be created by mixing fly ash with an alkaline activator. When the gel is exposed to elevated temperatures, it cures over several hours to form a solid, ceramic-like binder. On the microscale, geopolymers are amorphous materials, comprised of a matrix of long, cross-linked chains of tetrahedral $AlO_4$ and $SiO_4$ units [7]. Free alkali ions, such as $Na^+$, reside within this matrix to balance its electrical charge. These residual ions act as charge carriers, allowing geopolymers to behave as fast ionic conductors, with conductivities of order $10^{-6}$ S/cm [8].

When an alternating current, *I*, is applied across a geopolymer, the measured voltage, *V*, is dependent on the specimen's impedance, *Z*:

$$\frac{V}{I} = Z = \frac{L}{\sigma A} \tag{1}$$

Here, $\sigma$ and *L* are the conductivity and length of the geopolymer sample, while *A* is the contact area between the geopolymer and the electrodes. If it is assumed that the contact area remains reasonably constant, then partial differentiation of (1) reveals the temperature, *T*, dependence of the impedance:

$$\frac{1}{Z}\frac{\partial Z}{\partial T} = \alpha_L - \frac{1}{\sigma}\frac{\partial \sigma}{\partial T} \tag{2}$$

where $\alpha_L = (1/L)(\partial L/\partial T) \approx 10^{-6}$ °C$^{-1}$, is the geopolymer's coefficient of thermal expansion [9]. The dependence of ionic conductivity on temperature is governed by the Arrhenius equation, parameterised by a constant $B$ [10]:

$$\sigma \propto e^{-B/(T-T_g)} \tag{3}$$

where $T_g \approx 800$ K is the geopolymer glass transition temperature [11]. The parameter $B$ is proportional to the activation energy of the alkali ions in the geopolymer, and typically takes a value ~$10^4$. Note that below $T_g$, geopolymer conductivity increases with temperature because the alkali charge carriers become more mobile as the sample is heated. Differentiation of equation (3) and substitution into (2) shows that the temperature sensitivity of the impedance takes the form:

$$\frac{\Delta Z}{Z} = \left(\alpha_L - \frac{B}{(T-T_g)^2}\right)\Delta T \tag{4}$$

where $B/(T-T_g)^2 \gg \alpha_L$. Below $T_g$, fractional shifts in the measured impedance take unique values. If the geopolymer patch remains close to room temperature, then $T_g \gg T$, and equation (4) is approximately linear:

$$\frac{\Delta Z}{Z} \approx \left(\frac{B}{T_g^2}\right)\Delta T \tag{5}$$

Characterisation of this equation allows geopolymer patches to be used as thermometers

### Induction Heating

Alternating the current within an induction coil sets up a local, temporally changing magnetic field. This can initiate Eddy currents at the surfaces of nearby conductors, resulting in Joule heating. While geopolymers may experience some Joule heating, their electrical conductivities are ~$10^{12}$ times lower than most metals, so the Eddy currents generated are small.

To enhance heating, geopolymer gels may be doped with ferromagnetic materials prior to curing. Ferromagnets possess an inherent magnetisation, designated by the vector $\boldsymbol{M}$. Application of the induction coil's external field, $\boldsymbol{H}$, causes the magnetic domains within the ferromagnet to expand and contract along the axis of $\boldsymbol{M}$. During one cycle of the H-field, the friction produced by this movement generates additional heat.

## SENSOR MANUFACTURE AND TESTING

### Overview

The configuration of the geopolymer patch sensor is shown in Figure 1a. A magnetite-doped geopolymer sensing patch is applied to the surface of a small concrete cube (each side approximately 3 cm) and protected with a thin layer of epoxy. Four electrical probes are embedded into the geopolymer layer. An alternating current, $I$, is applied across the two outer probes using a current source, while the voltage, $V$, is measured over the two inner probes. Impedance, $Z$, is then calculated using equation (1). Separation of the electrodes allows for more accurate impedance monitoring as it reduces contact and lead resistances.

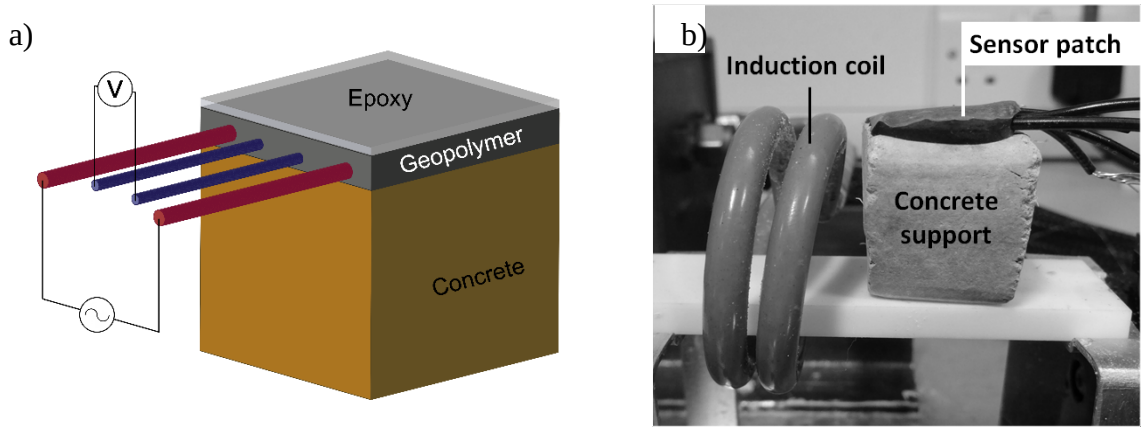


Figure 1 The configuration of the geopolymer patch sensor, shown in a), and the induction heating set up, shown in b).

The patch sensor was left uncovered in air or covered with surface water, dry sand, wet sand or wet soil. The instrumented concrete block was then heated by a two-turn induction coil, as shown in Figure 1b. The current within the coil was driven at 100 – 200 A amplitude and 350 kHz frequency for 15-20 seconds.

For initial characterisation, patches of varying magnetite content were heated in air for 20 seconds while sensor impedance was monitored. Temperature measurements from a fibre Bragg grating thermometer were used to verify that impedance shifts were indeed a result of geopolymer patch heating [12]. Finally, a patch with 35 wt% magnetite content was sequentially tested while uncovered and while covered in surface water, dry sand, wet sand, or wet soil. Impedances were monitored for each case during 15 seconds of induction heating and ~80 seconds of cooling.

## Manufacturing Method

The geopolymer gel was fabricated by combining 72 wt% low-calcium, class-F fly ash, with 20 wt% sodium silicate solution ($Na_2SiO_3$, with 29.4 wt% SiO2 and 14.7 wt% $NaO_2$, in water) and 8 wt% of 10 M sodium hydroxide solution.

Batches of geopolymer gel, each 2 – 3 grams, were mixed with varying quantities of crushed magnetite – a ferromagnetic mineral containing iron oxides. Magnetite contents in each batch varied from 0 – 60 % by weight. Each doped geopolymer gel batch was applied to the surface of a separate concrete cube, prior to curing in an oven for 3 days at 40 ˚C. After curing, a thin layer of epoxy was applied over the patches to protect them from mechanical abrasion and changing chemical contamination, as these factors may lead to spurious impedance signals.

## Interrogation

Alternating currents of 30 – 80 µA amplitude were applied across the outer-probes of the sensor, while the voltage over the inner probes was measured using a data acquisition card. The typical voltage noise was 2 mV and the interrogation rate was ~10 kHz. High-frequency alternating currents at 1 kHz frequency were used during impedance monitoring as this reduces the effects of capacitance and false polarisation potentials at the sensor electrodes [13].

## RESULTS

### Initial Characterisation

Figure 2 shows the evolution of patch temperature (as measured by the fibre gauge) and its electrical impedance during 20 seconds of induction heating and one minute of cooling. Profiles for magnetite contents of $W$ = 10, 20, 30 and 35 wt% are shown. For $W$ < 30 wt%, the maximum temperatures achieved are approximately linear with magnetite content. Beyond this, temperature saturation occurs as the induction heating rate cannot overcome heat losses.

The temperature and impedance profiles match, which confirms that the impedance is providing a measurement of heating and cooling. As the geopolymer sensor is more sensitive to temperature than the fibre gauge, the impedance signal provides a low-noise, high resolution measurement.

The peaks in temperature and impedance shifts from Figure 2 are plotted against each other in Figure 3. This is a graphical representation of equation (5), and so the parameter $B = 5\times10^4$ can be estimated from the slope of the linear fit. This is of the same order ($10^4$) as that suggested by underlying ionic conductor theory.

Note that, while the results are not presented here, sensors with magnetite contents as high as 60 wt% were briefly tested. The higher contents yielded little or no improvement to induction heating. Furthermore, as with any cementitious substance, as more aggregate (magnetite) was added to the geopolymer, its flow and adhesion decreased. This decreased the robustness of the patches, so geopolymer gels with 35 wt% magnetite were used for the remainder of this work.

### Deburial Sensing

The 35 wt% patch sensor was left uncovered or covered in water, soil or sand and then induction heated for 15 seconds. The impedance profiles for the various materials tested are shown in Figure 4. Note that two separate cases for air are provided to demonstrate sensor repeatability.

While there are minor differences in the temperature rise portions of the graphs, the temperature decays provide a more distinct signature for each material. Temperature decays are slower for air and sand due to their lower thermal conductivities (<1 W/m.K). Wet soil and wet sand have much higher thermal conductivities (1-4 W/m.K) and so provide the most rapid temperature decays.

In this work, a simple algorithm was written to allow software to distinguish between the impedance-shift signatures for each material. The line labelled *air* in Figure 4 provides a set of reference impedance-shift values. These are denoted $Air_i$, for $i$ = 1… $N$. Any other line, such as *dry sand*, can be denoted by a different set, $G_i$. The difference between $G_i$ and $Air_i$ is calculated on a point-by-point basis, and the difference is then integrated numerically:

$$f(G) = \frac{\Delta t}{2}\sum_{i=1}^{N}(G_i - Air_i) + (G_{i+1} - Air_{i+1}) \qquad (6)$$

where Δt is the time interval between measurement points.

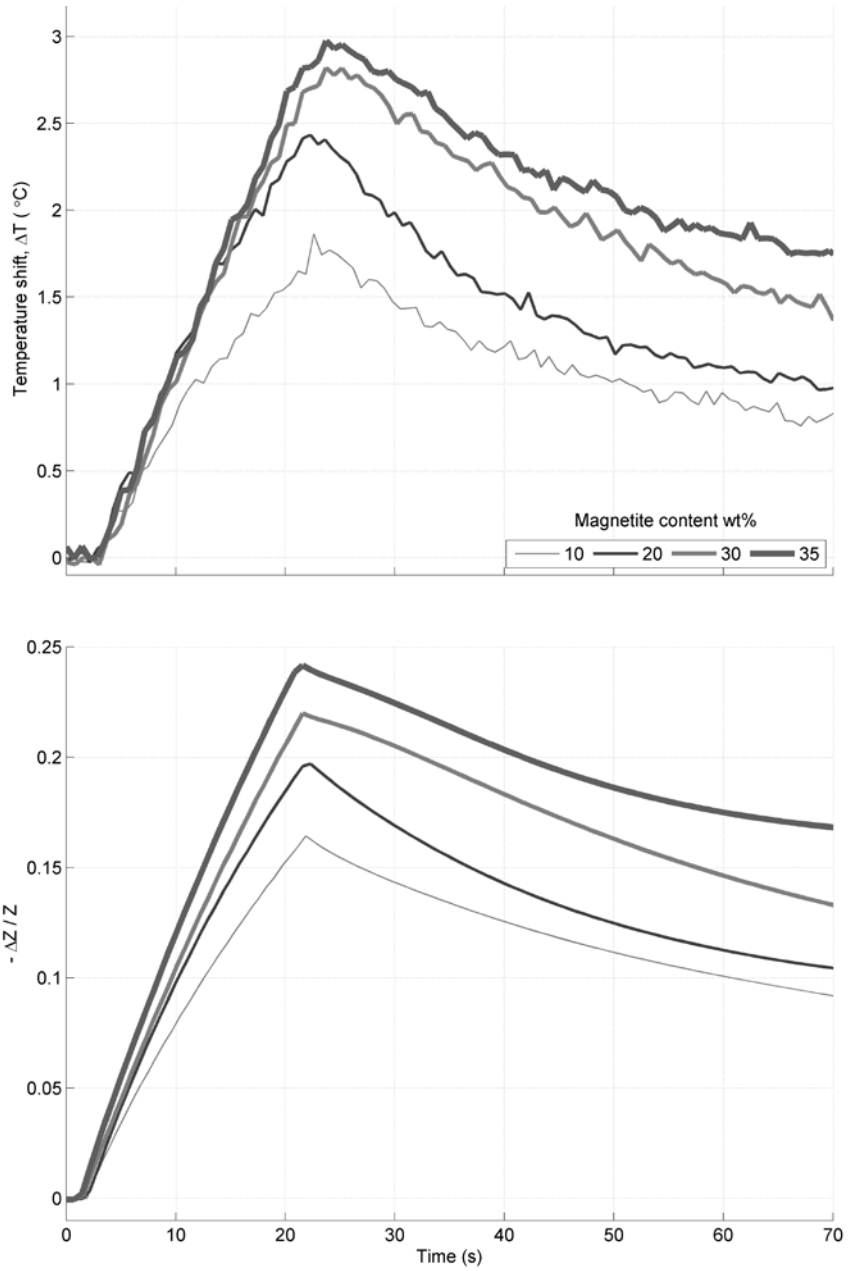


Figure 2 Temperature and impedance evolution of doped magnetite geopolymer specimens during 20 seconds of induction heating.

Values for |f(G)| for each of the materials tested are provided in Figure 5. Each of the materials is clearly distinguishable from air, so it the sensor is able to detect deburial. There are limitations to the approach, however. While water and dry sand signatures are clearly distinguishable in Figure 4, the difference is less obvious in Figure 5. Distinguishing between these, and a wider variety of materials at different ambient temperatures in real applications, may require more sophisticated machine learning approaches.

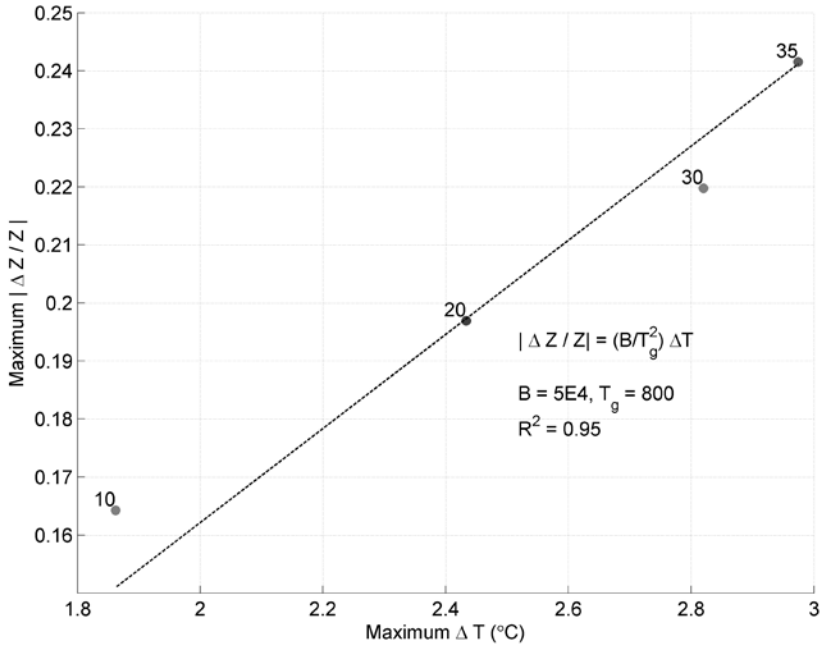


Figure 3 Relationship between maximum geopolymer temperature and impedance shift. Magnetite contents (wt%) are labelled.

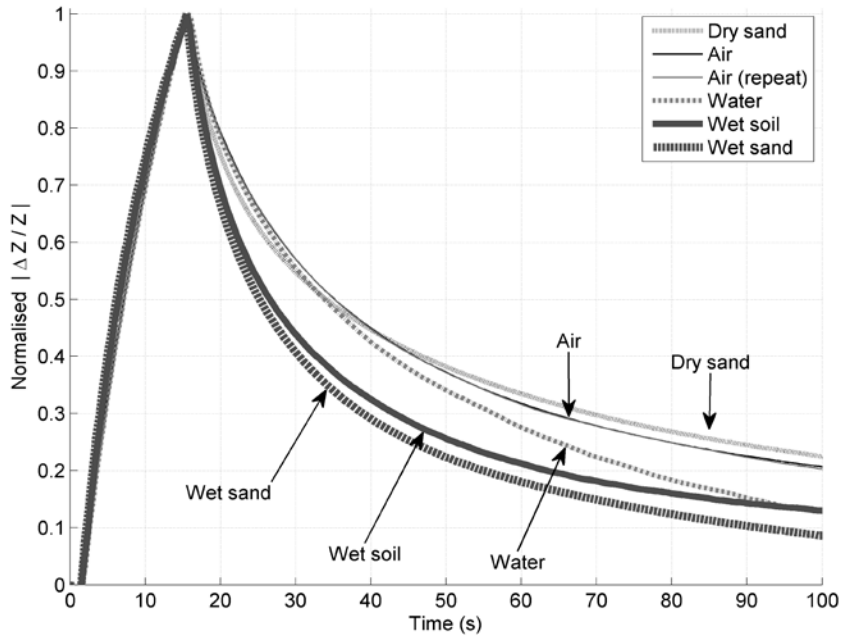


Figure 4 Patch (35 wt% magnetite) response during 15 seconds of induction heating. The sensor was covered in dry sand, nothing (air), water, wet soil and wet sand. The impedance response has been normalised by its maximum value.

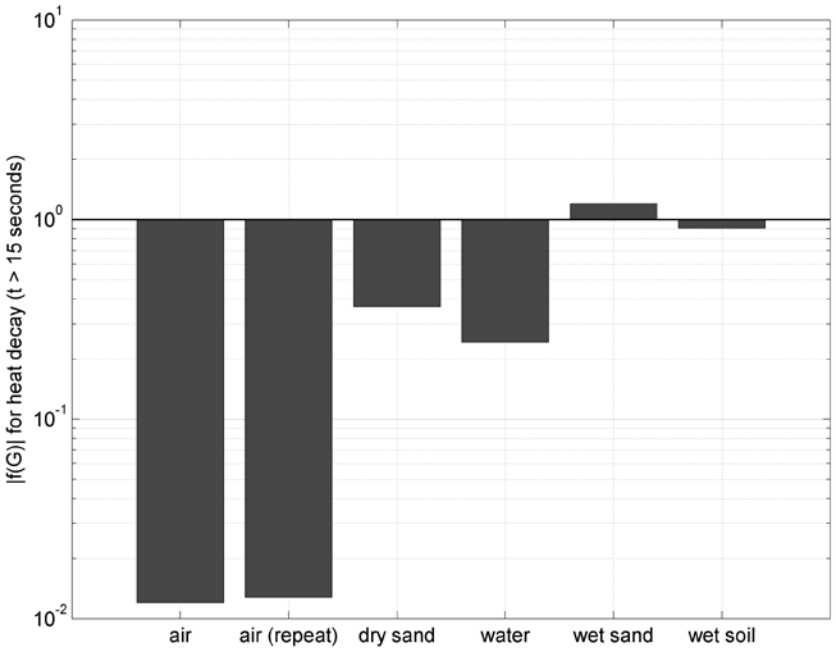


Figure 5 Values of |f(G)| for the impedance decay of each line from Figure 4.

## CONCLUSIONS

Thermal conductivity sensor patches have been fabricated by doping geopolymer binders with ground magnetite. When the geopolymer's magnetite content was less than 35 wt%, it retained its adhesion and flow characteristics, allowing it to be painted on to concrete surfaces prior to curing. Once cured, the magnetite doping allowed the patches to be heated by up to 3 °C within 20 seconds using a 100 A induction coil. Temperature changes in the patch were monitored via changes in its electrical impedance. In this preliminary work, sensor patches were able to distinguish between the presence of air, surface water, dry sand, wet sand and wet soil, as each material provided a unique thermal signature. Crucially this allows the sensor to detect whether it is buried. With further development, these sensors may be used to monitor scouring of wind turbine foundations, deep sea cables and bridges.

## REFERENCES

1. WHITEHOUSE, R.J.S, HARRIS, J.M., REES, J., The nature of scour development and scour protection at offshore windfarm foundations, Marine Pollution Bulletin, 62`1): 73-88, 2011.

2. PENDERGAST, L.J. AND GAVIN, K., A review of bridge scour monitoring techniques, Journal of Rock Mechanics and Geotechnical Engineering, 6(2): 138-149, 2014.

3. MILLER, J.W. AND MENDEZ, A., Fiber Bragg Grating Sensors: Market Overview and New Perspectives, Fiber Bragg Grating Sensors: Recent Advancements, Industrial Applications and Market Exploitation, 8: 313-320, 2014.

4. JIANG, L. AND SPEARING, S.M., A reassessment of materials issues in microelectromechanical systems (MEMS), Journal of the Indian Institute of Science, 87(3): 363-385, 2007.

5. PACHECO-TORGAL, F., CASTRO-GOMES, J. AND JALALI, S., Alkali-activated binders: A review, Construction and Building Materials, 22(7): 1305-1322, 2008.

6. SAAFI, M., TANG, L., FUNG, J., RAHMAN, M., SILLARS, F., LIGGAR J. AND ZHOU, X., Graphene/fly ash geopolymeric composites as self-sensing structural materials, Smart Materials and Structures, 23(6), 2014.

7. HANJITSUWAN, S., CHINDAPRASIRT, P., AND PIMRAKSA, K., Electrical conductivity and dielectric property of fly ash geopolymer pastes, International Journal of Minerals, 18(1): 94-99, 2011.

8. CUI, X., ZHENG, G, HAN, Y., SU, F. AND ZHOU, J., A study on electrical conductivity of chemosynthetic Al2O3–2SiO2 geoploymer materials, Journal of Power Sources, 184(2):652-656, 2008.

9. DAVIDOVITS, J. Geopolymer Chemistry and Applications 2nd Edition. Saint-Quentin: Institut Geopolymere, 2011.

10. DANIEL, C. AND BESENHARD, J.O., Handbook of Battery Materials 2nd Edition. New York: John Wiley & Sons, Inc, 2011.

11. PAN, Z. AND SANJAYAN, J.G., Stress-strain behaviour and abrupt loss of stiffness of geopolymer at elevated temperatures, Cement and Concrete Composites, 32(9): 657-664, 2010.

12. HILL, K.O. AND MELTZ, G., Fiber Bragg grating technology fundamentals and overview, Journal of Lightwave technology, 15(8): 1263-1276, 1997.

13. SAIPRASAD V. AND ALLOUCHE, E.N., Experimental evaluation of electrical conductivity of carbon fiber reinforced fly-ash based geopolymer, Smart Structures and Systems, 7(1): 27-40, 2011.

# STATE OF THE ART OF THE USE OF BAMBOO STICKS TO REPLACE STEEL REINFORCEMENT IN REINFORCED CONCRETE

**A Moh'd Khatib**

**G Nounu**

University of West of England

United Kingdom

**ABSTRACT.** The paper provides a literature review showing (i) the properties of bamboo and how it lends itself towards its use in reinforced concrete: Bamboo has high tensile strength, cheap, available in places where steel is not affordable, a renewable resource, and a non-polluting material, (ii) the limitations and the issues with using bamboo as reinforcement: bamboo's low modulus of elasticity, bamboo's weak bond with concrete, its durability inside of concrete, (iii) mechanical properties for different bamboo species: There are about 1200 bamboo species around the world with different mechanical properties, as a reinforcing material, species with high tensile strength and high modulus of elasticity are desirable. There are some data on the mechanical properties of few species in literature, the results vary significantly for the same species between different researchers, and this can be attributed to two reasons as follows: different testing methods and different properties of bamboo culms used by different researchers, (iv) bamboo's high tensile strength encouraged many researchers to study its use as bending reinforcement. The results found by the different researchers varied significantly, but generally lower than expected from using a material with bamboo tensile strength. The researchers have presented the experimental bending strength at failure. However what the researchers presented does not inform if the bamboo reinforcement tensile strength has been fully utilised, and does not inform how the beams compare to steel reinforced beams. This paper compares the bending capacity of bamboo reinforced beams to the theoretical bending capacity of steel reinforced beams and shows that the tensile strength of bamboo is not fully utilised when it is used as reinforcement.

**Keywords:** Reinforced Concrete, Bamboo, Tensile test, Bending capacity.

**Abdullah Moh'd Khatib** is a PhD research student in the University of the West of England, Bristol, UK

**Ghassan Nounu** is a senior lecturer at the University of the West of England, Bristol, UK

## INTRODUCTION

Steel has excellent mechanical properties, but it is not available and affordable in some parts of the world, it has high embodied energy, and it is not a renewable resource. Iron ore (the main component of steel) reserves equal 230 billion tonnes worldwide [1]. Iron ore production increased from 274 million tonnes in 1950 to 1554 million tonnes in 2005. Iron ore production in 2014 around the world according to the U.S. Geological Survey [2] equals 3220 million tonnes. At the current level of production, it will last about 50 years. The global annual $CO_2$ emissions from steel production from the different manufacturing routes are estimated to be 3169 million tonnes by 2020 [1].

Bamboo has high tensile strength comparable to that of mild steel (table 1), bamboo is cheap, available in places where steel is not affordable, a renewable resource, a non-polluting material and it can help against flooding. Bamboo is much cheaper than steel: an approximate price is US$ 105 per cubic metre of bamboo [3]; where hot rolled steel prices during 2014 were between US$ 765 – 621 [2], which is equivalent to US$ 5814 – 4720 per cubic metre. Bamboo exists mostly in developing countries, which makes it available in places where steel is not affordable [4, 5], and it does not require high technology or big industry for production. Bamboo is a rapidly renewable resource: bamboo can be harvested ideally at the age of three to four years while wood takes decades to mature. Bamboo improves the local climate through photosynthesis (photosynthesis produces Oxygen and consumes $CO_2$) [6], and sequesters more carbon per hectare than trees [30]. Bamboo helps prevent erosion and flooding because of its root system [6].

Bamboo's high tensile strength makes it desirable to use as a sustainable replacement of steel. There are some factors that need to be studied and taken into consideration, in order to decide if bamboo can be used safely and economically as reinforcement. These factors are bamboo's low modulus of elasticity relative to steel's (Table 1), its durability inside concrete, and its bond with concrete.

## MECHANICAL PROPERTIES OF BAMBOO

Bamboo species can be divided into two groups as follows: woody (lignified) stems bamboos, which belongs to the tribes Arundinarieae (temperate) and Bambuseae (tropical); and non-woody bamboo which belongs to the tribe Olyreae (temperate) [8]. Woody bamboo is the one that is more familiar and has many uses in industry. Woody bamboo has high tensile strength (Table 1) which is sometimes (depending on species, age and moisture content) comparable to that of mild steel. Fibres are responsible for the materials high tensile strength. Their distribution within the culm is not uniform. The fibre content increases from the inner surface towards the outer surface, and the fibre content increases with height [9].

There are about 1200 bamboo species in the world [7]. These species have different mechanical properties. Table 1 shows the tensile strength and the tensile modulus of elasticity for a few species. The existence of nodes within specimens weakens them as it can be seen from Table 1.

Table 1 Bamboo tensile strength and modulus of elasticity data

| BAMBOO TENSILE STRENGTH & MODULUS OF ELASTICITY | | | | | | |
|---|---|---|---|---|---|---|
| Bamboo species | Age (year) | Thickness (cm) | Tensile strength / No node (MPa) | Modulus of Elasticity / No node (GPa) | Tensile strength / one node (MPa) | Modulus of Elasticity / one node (GPa) |
| Bambusa multiplex raeusch[4] | - | 0.35 | 124.7 | 11.2 | 95.3 | 10.05 |
| Bambusa tuldoidis[4] | - | 0.60 | 119.5 | 11.93 | 104.00 | 9.27 |
| Dendrocalamus Giganteus[4] | - | 1.1 | 135.0 | 14.5 | 119.02 | 11.75 |
| Bambusa vulgaris[4] | - | 0.80 | 134.4 | 7.76 | 48.05 | 6.05 |
| Bambusa vulgaris[5] | - | | 200 | - | 145 | - |
| Phyllostachys edulis[10] | - | - | - | - | 125.1 | 7.94 |
| Bambusa vulgaris[11] | 3 | 1.0–1.5 | 335 | - | - | - |
| Dendrocalamus asper Backer[12] | 3 | - | 224 | - | - | - |
| Dendrocalamus giganteus[13] | - | - | 277 | 23.75 | - | - |
| Melocanna bambusoides[14] | 3-5 | - | - | - | 185.9 | 24.5 |
| Dendrocalamus strictus[15] | 3 | - | 321 | 20 | - | - |

The data in the literature on bamboo tensile strength vary significantly for the same species, e.g. the Bambusa Vulgaris species was tested by three different researchers and their results ranged between 126-335 Mpa. There are a few factors that cause this variation as follows: bamboo tensile strength increases with height, and it increases towards the outer region of the culm cross-section [9]; different moisture contents: an increase in moisture content will yield lower tensile strength and lower modulus of elasticity; age affects the tensile strength: bamboo strength peaks at the age of 3-4 years; different growing environment; and the testing method is very important in achieving accurate results.

Bamboo specimens can be crushed under the testing machine grip before it reaches ultimate tensile strength because of bamboo's low compressive strength perpendicular to the grain. The International Organization for Standardization [16] produced a standard for testing bamboo physical and mechanical properties, the standard requires the end of specimens to be shaped in a way to ensure the failure in the gauge area; however it does not specify how.

In order to prevent the bamboo tensile specimens from being crushed under the machine grip the researchers followed different methods: Lima Jr *et al.* [13]; Agarwal *et al.* [14]; Schneider *et al.* [10] and Kute and Wakchaure [15] used Aluminium tabs with epoxy (Figure 2.5). The tabs (1-3 mm thick) were glued to the specimens in the grip area using the epoxy. The researchers explained that the taps with the epoxy can prevent the splints from being crushed by distributing the load: the epoxy fills the gaps that result from the curvature of the specimen (Figure 1), which allows the epoxy to transfer some of the compressive load to the specimen in the area where there is no direct contact with the tabs. Adewuyi *et al.* [11], and Kute and Wakchaure [15] did not reduce the section in the gauge area. Lima Jr *et al.* [13] reduced the section in the gauge area to 1:5 ratio (width in the gauge area:width in the grip area).

Figure 1 Bamboo sample section curvature

Figure 2 Tensile test specimen with tabs and epoxy

The reduction of the specimen width in the gauge area relative to the grip area reduces the compression on the specimen ends significantly, e.g. a reduction to a ratio of 1:3 (gauge width:grip width) reduces the compressive force from the machine by a factor of 3 for the same tensile stress. The problem with using this reduction is that the weighted value for each specimen is reduced since the section of the tested material is reduced, so more specimens would be needed to determine accurately the tensile strength of the bamboo culm. The effectiveness of each testing method needs to be established and compared to see if there are significant differences between the different methods the researchers used, and to find out the best method that ensures the failure occurs in the gauge area.

## DURABILITY AND LONG TERM BEHAVIOUR OF BAMBOO

### Durability

Wood is the oldest construction material. The durability of wood depends largely on the environment surrounding it. Under the right conditions, wood service life has been known to exceed 500 years [17]. The biological decay of wood can be caused by fungi, insects, marine borers and bacteria [18]. When bamboo is used as reinforcement the environment of bamboo is completely different from the environment of wood structures: bamboo reinforcement is subjected to the alkalinity of concrete, but it is protected from weathering, insects, and marine organisms.

Bamboo has been shown to be durable against the alkalinity of concrete. Lima Jr *et al.* [13] tested bamboo after it was immersed in a pH 12.8 solution of calcium hydroxide, and tested bamboo that was embedded in concrete prisms that were submerged in tap water. The bamboo was tested after 60 cycles of 24 hours. The strength of bamboo was not affected by the severe conditions. However, more research on bamboo durability inside concrete for long term behaviour is needed.

Bamboo reinforcement can be decayed by fungi. Fungi require oxygen, moisture and appropriate temperatures. All of these are available for fungi to decay bamboo reinforcement; however, fungi require at least a water content of 22% to decay wood [17]. The use of a water-repellent treatment can protect against fungi. Some bamboo species are more durable against fungi than the others but generally bamboo is durable against most fungi strains. Wei, Schmidt and Liese [19] tested 6 bamboo species in accordance with the European standards EN 350-1, EN 350-2 and EN 113. The researchers investigated 10 strains of fungi that belong to Brown-rot fungi, white-rot fungi, and soft-rot fungi. All the bamboo species that the researchers tested were durable against most of the strains: for most of the strains, the species were classified into class II (durable according to the European 5 scale standard). For one strain of soft-rot fungus the bamboo species were grouped into class II and class III (moderately durable), for another strain of white-rot the bamboo species were grouped into class II, class III, and class IV (little durable).

### Treatment

To increase the design life of bamboo, it can be treated with preservatives or protective finishes and coatings. Preservatives are restricted to within certain concentrations in a growing number of countries because they are toxic and can contaminate the environment during usage or disposal [17]. Protective finishes and coatings improve bamboo durability by protecting it from

moisture. Some types of finishes or coatings form a thin film on the surface of wood; others penetrate the surface of wood. By penetrating the surface of wood the water is repelled more effectively and the moisture content is kept low which protects the wood from biological attack [17], also, the repelling water treatment helps against concrete high alkalinity and limits volume variation by preventing bamboo from absorbing water from the concrete.

Heat treatment improves bamboo durability against insects and fungi greatly: 90 minutes of heat treatment at 180$^{o}$ and 220$^{o}$ C reduced weight loss due to biological attack in a test based on BS 7282: 1990 [20] from 48% to 11% and 5% respectively [21]. The problem with heat treatment is that it affects the mechanical properties of bamboo negatively, e.g. 90 minutes of treatment at 180$^{o}$ C and 220$^{o}$ C reduced the modulus of rupture from 174 Mpa to 152 Mpa and 132 Mpa respectively [21].

### Creep

There are some data in the literature on bamboo creep behaviour under flexure, but nothing found on bamboo creep behaviour under tensile stress. Bamboo specimens subjected to flexure show stable secondary creep behaviour [22]. The average fractional deflection (the rate of deflection at day 90 of loading relative to instant deflection) of Bamboo under flexure is equal to 1.29 [22], which is less than 2.0 the maximum acceptable fractional deflection [23]. Bamboo's creep behaviour under tension is yet to be investigated.

## BAMBOO BOND WITH CONCRETE

The bond between reinforcement and concrete is critical: weak bond with concrete causes the two materials to deform independently and causes the member to collapse at a low load. Steel reinforcement has an excellent bond with concrete. This bond is the result of the projections (ribs) on the steel surface, steel chemical adhesion with concrete, and the roughness of the steel surface. For deformed reinforcement bars, the bond is mainly developed because of the mechanical interlock with concrete that is caused by the projections (ribs) [24]. Bond is also affected by the strength of concrete: the bond is improved with higher concrete strengths. Adequate concrete cover is important for a strong bond. The timing of the test affects the results: allowing the specimens more time before testing improves the bond [24].

Table 2 shows that bamboo without bonding treatment has a weak bond with concrete. This is attributed to two reasons as follows: 1- When the concrete is cast, the bamboo absorbs water from the concrete, this makes it expand inside of the concrete, and when the concrete is cured the bamboo loses its moisture causing it to shrink and lose contact with the concrete [31]. 2- Bamboo has a smooth surface. This causes the bamboo reinforcement to slip without the development of a strong bond with the concrete. In order to achieve a better bamboo bond with concrete, some researchers (table 2) waterproofed bamboo, to prevent it from absorbing water, and roughened the surface of bamboo: they sprinkled sand on the surface and sometimes wrapped it with steel wires. This resulted in significantly higher bond results in the pull-out tests: the use of Negrolin + fine sand + wiring improved the bond by 87% relative to untreated bamboo bond with concrete. The presence of a node improved the bond significantly which suggests that a treatment that utilises mechanical interlock with concrete could improve the bond greatly. However, even with the treatment, bamboo's bond with concrete is not strong enough to prevent failure at a low load (table 3). Bamboo's weak bond with concrete is an important factor in using it as reinforcement.

Table 2 Bamboo bond strength with concrete data

| BOND STRENGTH OF BAMBOO WITH STEEL AND BAMBOO | | | |
|---|---|---|---|
| Description of treatment | Average Bond stress (Mpa) | Embedment Length (mm) | Concrete Compressive strength (Mpa) |
| Mild steel (ms)[15] | 1.79 | 150 | 20 |
| TMT steel (tmt) [15] | 2.87 | 150 | 20 |
| Untreated (unt) [15] | 0.73 | 150 | 20 |
| Untreated node inside[15] | 0.90 | 150 | 20 |
| Untreated, notched, node inside[15] | 0.92 | 150 | 20 |
| Nailed[15] | 0.90 | 150 | 20 |
| Nailed node inside[15] | 1.09 | 150 | 20 |
| Binding wire wound[15] | 1.06 | 150 | 20 |
| Binding wire wound, node inside[15] | 1.25 | 150 | 20 |
| Oil painted[15] | 0.48 | 150 | 20 |
| Oil painted, node inside[15] | 0.69 | 150 | 20 |
| Oil painted, with zeolite powder[15] | 0.71 | 150 | 20 |
| Oil painted, with zeolite powder, node inside[15] | 0.93 | 150 | 20 |
| Black Japan[15] | 0.66 | 150 | 20 |
| Black Japan, node inside[15] | 0.86 | 150 | 20 |
| Black Japan, with zeolite powder[15] | 1.06 | 150 | 20 |
| Black Japan, with zeolite powder, node inside[15] | 1.19 | 150 | 20 |
| Untreated[14] | 0.127 | 100 | 20 |
| Araldite[14] | 0.232 | 100 | 20 |
| Araldite with wire[14] | 0.539 | 100 | 20 |
| Tapecrete P 151[14] | 0.315 | 100 | 20 |
| Anti Corr RC[14] | 0.159 | 100 | 20 |
| Sikadur 32 Gel[14] | 0.588 | 100 | 20 |
| No treatment (NT)[4] | 0.52 | 100 | 19* |
| Negrolin + fine sand[4] | 0.73 | 100 | 19* |
| Negrolin + fine sand + wiring[4] | 0.97 | 100 | 19* |
| Untreated[25] | 0.404 | 152 | 28 |
| Untreated[25] | 0.208 | 305 | 28 |
| Untreated[25] | .202 | 457 | 28 |
| Untreated[25] | 0.195 | 610 | 28 |

[14] The results are on the low side when compared to other researchers work, it was reported that some splints failed as a result of eccentricity in the experiment.
* Lightweight concrete (17 kN/M$^3$)

All of the research on bamboo bond with concrete was done using the pull-out test, which does not estimate bamboo's bond with concrete in structural elements. The pull-out test can be used to compare the bond between different treatments; this is the reason for using it to test the bond of steel and FRP reinforcement with concrete. The pull-out test overestimates the bond with concrete because the concrete in the pull-out test is under compression while in beams the

concrete around the reinforcement is under tension; and because the rebar embedment length inside concrete elements is much higher than the embedment length in the pull-out test. The data in table 2 show a significant difference between the average bond results for different embedment lengths: the average bond for 152 mm embedment is twice that of the average bond for 304 mm embedment.

## BENDING ELEMENTS

Bamboo reinforced beams bending capacity has been investigated by a number of researchers [4,5,14,26,27]. The researchers have presented the experimental bending strength at failure, beam dimensions, bamboo strength, and reinforcement area. However what the researchers presented do not inform if the bamboo reinforcement tensile strength have been fully utilised, and they do not inform how the beams compare to steel reinforced beams, in order to do that the researcher calculated the theoretical bending strength of steel reinforced beams that have steel reinforcement with an equal tensile strength to the bamboo reinforcement in the corresponding bamboo reinforced beams. These steel-reinforced beams also have the same geometry, same effective depth, and the same concrete strength as the corresponding bamboo reinforced beams.

Bamboo was investigated as reinforcement by the researchers because it has high tensile strength; however the tensile strength of the bamboo reinforcement was not fully utilised in the beams they tested. Table 3 shows the bending capacity of a few bamboo reinforced concrete beams. Table 3 also shows the theoretical strength of the equivalent steel reinforced beams. These beams have steel reinforcement with an equal tensile strength to the bamboo reinforcement in the corresponding bamboo reinforced beams. It can be seen from table 3 that the bamboo reinforced concrete beams have much lower bending strength than the corresponding steel reinforced beams. There are two factors that can be the cause of bamboo reinforcement not reaching ultimate tensile strength as follows: bamboo reinforcement losing bond with concrete, and bamboo's lower modulus of elasticity to steel's.

The theoretical strength of the equivalent steel reinforced concrete beams is found using the stress block analysis of ACI code [28].

$$M = T \times (d - a/2)$$

Where:

$a = (T)/(0.85 \times f_c \times b)$
M: Moment capacity
T: Tensile strength of reinforcement
b: Beam width
d: Effective depth
a: depth of stress block.
$f_c$: concrete compressive strength

Table 3 Bamboo reinforced beams VS steel reinforced beams

| Beam | Area of reinforcement ($mm^2$) | Tensile strength (Mpa) | Equivalent steel RC beam (ES) (KN.M) | Experimental Capacity (EC) (KN.M) | EC/ES | Bond Treatment | Bamboo species |
|---|---|---|---|---|---|---|---|
| A2[5] | 881 | 200 | 29.60 | 18.75 | 0.633 | Water glass | Bambusa vulgaris |
| A3[5] | 893 | 200 | 29.64 | 18.75 | 0.633 | Bitumen + Sand | Bambusa vulgaris |
| B4[5] | 1273 | 200 | 42.23 | 25.2 | 0.597 | Water glass | Bambusa vulgaris |
| B5[5] | 1302 | 200 | 42.87 | 30 | 0.700 | Bitumen + Sand | Bambusa vulgaris |
| C6[5] | 1362 | 200 | 44.03 | 15 | 0.341 | Water glass | Bambusa vulgaris |
| C7[5] | 1361 | 200 | 44.52 | 20.5 | 0.460 | Bitumen + Sand | Bambusa vulgaris |
| D8[5] | 1374 | 200 | 44.26 | 19.5 | 0.441 | Water glass | Bambusa vulgaris |
| D9[5] | 1367 | 200 | 44.30 | 18 | 0.406 | Bitumen + Sand | Bambusa vulgaris |
| BBR1[29] | 1030 | 126.7 | 9.69 | 4.2 | 0.434 | Not treated | Bambusa vulgaris |
| BBR2[29] | 1162 | 126.7 | 10.35 | 6.6 | 0.638 | Not treated | Bambusa vulgaris |
| BBR3[29] | 1072 | 126.7 | 9.91 | 7.2 | 0.727 | Not treated | Bambusa vulgaris |
| BBR4[29] | 1045 | 126.7 | 9.77 | 6 | 0.614 | Not treated | Bambusa vulgaris |
| BBR5[29] | 1421 | 126.7 | 23.21 | 6 | 0.259 | Not treated | Bambusa vulgaris |
| BBR6[29] | 1381 | 126.7 | 22.76 | 14.7 | 0.646 | Not treated | Bambusa vulgaris |
| BBR7[29] | 1207 | 126.7 | 20.67 | 15.3 | 0.740 | Not treated | Bambusa vulgaris |
| BBR8[29] | 1364 | 126.7 | 22.56 | 10 | 0.443 | Not treated | Bambusa vulgaris |
| BB1[29] | 1092 | 126.7 | 7.68 | 2.4 | 0.313 | Not treated | Bambusa vulgaris |
| BB2[29] | 1049 | 126.7 | 7.63 | 6.6 | 0.865 | Not treated | Bambusa vulgaris |
| BB3[29] | 1018 | 126.7 | 7.59 | 7.2 | 0.949 | Not treated | Bambusa vulgaris |
| BB4[29] | 1009 | 126.7 | 7.58 | 6.6 | 0.871 | Not treated | Bambusa vulgaris |
| BB5[29] | 983 | 126.7 | 16.89 | 12 | 0.710 | Not treated | Bambusa vulgaris |
| BB6[29] | 1031 | 126.7 | 17.50 | 13.3 | 0.760 | Not treated | Bambusa vulgaris |
| BB7[29] | 1078 | 126.7 | 18.06 | 14 | 0.775 | Not treated | Bambusa vulgaris |
| BB8[29] | 917 | 126.7 | 16.03 | 12.7 | 0.792 | Not treated | Bambusa vulgaris |
| VB1[4] | 1200 | 135 | 37.78 | 14 | 0.371 | Negrolin + Sand | Dendrocal-amus giganteus |
| VB2[4] | 1800 | 135 | 51.59 | 10 | 0.194 | Negrolin + Sand | Dendrocal-amus giganteus |

In Sharma's [5] work, the beams experimental strength averaged 53% of the theoretical strength, the beams treated with water glass (Sodium silicate) averaged 50% of the theoretical strength, and the beams treated with Bitumen + sand averaged 55% of the theoretical strength. Mark and Russell's [29] beams averaged 65% of their equivalent steel beams theoretical strength. Beams with steel stirrups averaged 80%, beams with no stirrups averaged 43%, beams with bamboo stirrups averaged 73%, and beams with cane stirrups averaged 68%. The type of stirrups affected the results of Mark and Russell's [29] beams significantly which suggests that at least some of the beams had shear failure. Ghavami's [4] beams averaged 28% of the equivalent steel beams theoretical strength.

Ghavami [4] presented the strain ($\epsilon$) at the level of the reinforcement. The strain at the level of reinforcement for the bamboo reinforced beams is above 2%, this amount of strain is enough for bamboo to reach its ultimate strength, but the bamboo reinforced beams failed at a much lower load relative to the capacity that the beam would have achieved if the full tensile strength of reinforcement had been utilised. The only explanation is a loss of bond between bamboo and concrete which allowed the two materials to deform independently resulting in failure.

Improving bamboo's bond with concrete is expected to improve the behaviour of bamboo reinforced concrete beams, the bamboo's low modulus of elasticity issue can be mitigated by the use of a higher percentage of bamboo in the beam section, since bamboo is much cheaper than steel the use of a higher percentage of bamboo is not expected to increase the cost of the member significantly.

## REFERENCES

1. YELLISHETTY, M, RANJITH, P, THARUMARAJAH, A. Iron ore and steel production trends and material flows in the world: Is this really sustainable?, Resources, Conservation and Recycling, Vol. 54, No. 12, 2010, pp 1084-1094.

2. USGS Mineral Commodity Summaries, National Minerals Information Center, 2015.

3. INTERNATIONAL NETWORK FOR BAMBOO AND RATTAN. Designing and Building with Bamboo. Technical Report No. 20, 2000.

4. GHAVAMI, K. Ultimate load behaviour of bamboo-reinforced lightweight concrete beams, Cement and Concrete Composites, Vol. 17, No. 4, 1995, pp 281-288.

5. SHARMA, A. Bamboo-reinforced concrete beams, International Association for Bridge and Structural Engineering Reports, Vol. 60, 1990, pp 677-682.

6. KHATIB, J M. Sustainability of Construction Materials, 2009, Woodhead.
7. LOBOVIKOV, M, PAUDEL, S, PIAZZA, M, REN, H, WU, J. World Bamboo Resources: A Thematic Study Prepared in the Framework of the Global Forest Resources Assessment 2005, 2007, Food and Agriculture Organization of the United Nations.

8. KELCHNER, S A, BAMBOO PHYLOGENY GROUP. Higher level phylogenetic relationships within the bamboos (Poaceae: Bambusoideae) based on five plastid markers, Molecular Phylogenetics and Evolution, Vol. 67, No. 2, 2013, pp 404-413.

9. VERMA, C S, CHARIAR, V M, PUROHIT, R. Tensile strength analysis of bamboo and layered laminate bamboo composites, International Journal of Engineering Research and Applications, Vol. 2, No. 2, 2012, pp 1253-1264.

10. Schneider, N, Pang, W, Gu, M. Application of bamboo for flexural and shear reinforcement in concrete beams, Proceedings of Structures Congress 2014, Eds. G R, Bell and M A, Card, 2014, pp 1025-1035.

11. ADEWUYI, A P, OTUKOYA, A A, OLANIYI, O A, OLAFUSI, O S. Comparative Studies of Steel, Bamboo and Rattan as Reinforcing Bars in Concrete: Tensile and Flexural Characteristics, Open Journal of Civil Engineering, Vol. 5, 2015, pp 228-238.

12. LEELATANON, S, SRIVARO, S, MATAN, N. Compressive strength and ductility of short concrete columns reinforced by bamboo, Sonklanakarin Journal of Science and Technology, Vol. 32, No. 4, 2010, pp 419-424.

13. LIMA JR, H C, WILLRICH, F L, BARBOSA, N P, ROSA, M A, CUNHA, B S. Durability analysis of bamboo as concrete reinforcement, Materials and Structures, Vol. 41, No. 5, 2008, pp 981-989.

14. AGARWAL, A, NANDA, B, MAITY, D. (2014) Experimental investigation on chemically treated bamboo reinforced concrete beams and columns. Construction and Building Materials, Vol. 7, 2014, pp 610-617.

15. KUTE, S, WAKCHAURE, M. Performance Evaluation for Enhancement of Some of the Engineering Properties of Bamboo as Reinforcement in Concrete, Journal of the Institution of Engineers (India): Series A, Vol. 94, No. 4, 2013, pp 235-242.

16. THE INTERNATIONAL ORGANIZATION FOR STANDARDIZATION. ISO 22157-1 Bamboo - Determination of Physical and Mechanical Properties - Part 1: Requirements, 2004, The International Organization for Standardization.

17. BIJEN, J. Durability of Engineering Structures: Design, Repair and Maintenance, 2003, Woodhead.

18. BRITISH STANDARDS INSTITUTE. BS EN 335 Durability of Wood and Wood-Based Products. Use Classes: Definitions, Application to Solid Wood and Wood-Based Products, 2013, British Standards Institute.

19. WEI, D., SCHMIDT, O. AND LIESE, W. Durability test of bamboo against fungi according to EN standards. European Journal of Wood and Wood Products, Vol. 71, No. 5, 2013, pp 551-556.
20. BRITISH STANDARDS INSTITUTE. BS 7282 Field Test Method for Determining the Relative Protective Effectiveness of a Wood Preservative in Ground Contact, 1990, British Standards Institute.

21. WAHAB, R, MOHAMAD, A, SAMSI, H W, SULAIMAN, O. Effect of heat treatment using palm oil on properties and durability of Semantan bamboo, Journal of Bamboo and Rattan. Vol. 4, No. 3, 2005, pp 211-220.

22. GOTTRON, J, HARRIES, K A, XU, Q. Creep behaviour of bamboo. Construction and Building Materials, Vol. 66, 2014, pp 79-88.

23. ASTM INTERNATIONAL. ASTM D6815-09 Standard Specification for Evaluation of Duration of Load and Creep Effects of Wood and Wood-Based Products, 2015, ASTM International.

24. AREL, H S, YAZICI, S. Concrete–reinforcement bond in different concrete classes, Construction and Building Materials, Vol. 36, 2012, pp 78-83.

25. CHIEF OF ENGINEERS OFFICE, US ARMY. Expedient Reinforcement for Concrete for use in Southeast Asia. Technical Report No. 3, 1970.

26. KHAN, I K. Performance of Bamboo Reinforced Concrete Beam, International Journal of Science, Environment, and Technology, Vol. 3, No. 3, 2014, pp 836-840.

27. TERAI, M, MINAMI, K. (2012) Research and Development on Bamboo Reinforced Concrete Structure, Proceedings of 15th World Conference on Earthquake Engineering.

28. AMERICAN CONCRETE INSTITUTE. Building Code Requirements for Structural Concrete (ACI 318-08) and Commentary, 2008, American Concrete Institute.

29. MARK, A, RUSSELL, A O. A comparative study of Bamboo reinforced concrete beams using different stirrup materials for rural construction. International Journal of Civil & Structural Engineering, Vol. 2, No. 2, 2011, pp 407-423.

30. LOBOVIKOV, M, SCHOENE, D, YPING, L. Bamboo in climate change and rural livelihoods, Mitigation and Adaptation Strategies for Global Change, Vol. 17, No. 3, 2012, pp 261-276.

31. GHAVAMI, K. Bamboo as reinforcement in structural concrete elements, Cement and Concrete Composites, Vol. 27, No. 6, 2005, pp 637-649.

# FLEXURAL FATIGUE OF PLAIN AND GLASS FIBRE REINFORCED POLYMER CONCRETE COMPOSITES

**R Bedi**

**S P Singh**

**R Chandra**

Dr B R Ambedkar National Institute of Technology

India

**ABSTRACT.** Results of flexural fatigue of epoxy resin based polymer concrete composites with and without glass fibres as reinforcement are reported. Three point flexural fatigue tests were conducted on polymer concrete specimens using MTS servo controlled cyclic load test setup to obtain the fatigue lives at different stress levels. One hundred and eighty four specimens of size 40 x 40 x 160 mm were tested in flexural fatigue. Fifty Seven static flexural tests were also conducted to facilitate fatigue testing. It has been observed that the probabilistic distribution of fatigue life of polymer concrete composite (PCC) and glass fibre reinforced polymer concrete composite (GFRPCC), at a particular stress level, can be modelled by the two-parameter Weibull distribution, with statistical co-relation coefficient values exceeding 0.90. The fatigue strength prediction models, particularly representing S-N relationships, have been examined and the material coefficients have been obtained for! PCC as well as GFRPCC containing 0.5%, 1.0% glass fibres. The two million cycle endurance limits for PCC and GFRPCC containing different amount of glass fibres have been obtained and it has been observed that the addition of fibres enhances the endurance limit of PCC.

**Keywords:** Polymer concrete composites, Flexural fatigue performance, Two-million cycles Fatigue strength.

**R Bedi** is an Associate Professor of Mechanical Engineering at Dr B R Ambedkar National Institute of Technology Jalandhar, India. His research interests are evaluation of mechanical and fatigue behaviour of Polymer concrete composites.

**S P Singh** is a Professor of Civil Engineering at Dr B R Ambedkar National Institute of Technology Jalandhar, India. His research interests are fatigue behaviour of concrete composites and recycling of materials in concrete.

**R Chandra** is a Professor of Mechanical Engineering at Dr B R Ambedkar National Institute of Technology Jalandhar, India. His research interests are evaluation of mechanical and fatigue behaviour of Polymer concrete composites.

## INTRODUCTION

Polymer concrete composite (PCC) is a material which results from polymerization of a monomer/aggregate mixture. The polymerized monomer acts as binder for the aggregates and the resulting composite is called “Polymer Concrete”. For a given type of PCC, the properties are dependent upon binder content, aggregate size distribution, nature and content of the microfiller, curing conditions etc[1]. Use of PCC in machine tool applications has been reported since late 70’s wherein these have been used to replace materials including metals like cast iron for machine tool bases[2–8]. These applications inevitably call for cyclic loading of the material resulting in its fatigue failure.

Large variability usually exists in the fatigue strength/life results obtained through experimental investigations at a given stress level, even under carefully controlled test procedures. The same was taken care of by providing higher safety factors earlier. However, optimum design requirements these days require accurate characterization of this variability for the materials. The dispersion of fatigue life has, therefore, been a subject of statistical analysis by various researchers[9–12].

Studies on fatigue of PCC are restricted in number, wherein compression fatigue[13], Flexural fatigue[14,15] has been characterized to a very limited extent. Very small number of specimens have been tested at different stress level in these studies[14] and therefore, accurate characterization of fatigue life distributions of PCC is not available till date. Fatigue life has been related to the applied stress level using various linear, exponential and power law relationships. All these equations are deterministic in nature and can only predict the mean number of cycles to failure. As the fatigue life data of PCC exhibit a large scatter, even at carefully controlled and identical loading conditions, it is necessary to incorporate the probability of failure ($P_f$) into equations describing fatigue life[15]. A S-N-$P_f$ relationship given by McCall[16] has been used earlier to predict the flexural fatigue strength of PCC for different probabilities of failure[14,15].

To the best of the knowledge of the authors, no study on fatigue performance of fibre reinforced polymer concrete composite (FRPCC) is reported in literature. It has been observed in case of conventional cement concrete that addition of fibres enhances the fatigue strength/life of the material[9–11,17,18]. Therefore, a comprehensive investigation has been planned to study the flexural fatigue performance of PCC and FRPCC containing different types and content of fibres. The result reported in this paper are part of the investigation with reference to fatigue of PCC and glass fibre reinforced polymer concrete composite (GFRPCC).

## EXPERIMENTAL PROCEDURE

### Materials and Methods

Aggregate grading plays an important role in the final properties of PCC and therefore an optimized aggregate mix suggested in literature has been used in this study[19]. Locally available crushed gravel has been used as aggregate in PCC. The aggregate mix had been optimized based upon the least void content criteria. Epoxy resin, LAPOX- B47 along with hardener LAPOX- K46 supplied by Atul Ltd., Mumbai has been used in this investigation. The hardener and resin have been mixed in the ratio of 1:2 by weight. The particular grade of epoxy resin is chosen because of its low viscosity which results in better workability of the mix. Resin

dosage of 10-14% by weight of PCC has been reported in literature when using coarse aggregates[4,20,21] whereas higher resin dosages up to 20% have reported when using only sand as aggregate material[22]. Resin dosage of 12% by weight of PCC has been used in this investigation.

A microfiller is also often added to PCC mix to reduce the void content in aggregate mixture and thereby increase the strength of PCC. Fly ash is a by-product of the coal burning in power plants and is used as a filler because of its easy availability and because its usage in PCC is reported to yield better mechanical properties as well as reduced water absorption[23]. Addition of fly ash also improves the workability of fresh PCC mix resulting in products with excellent surface finish[24]. F-type fly ash has been used in the ratio of 10% by total weight of PCC in this study.

Addition of glass fibers in PCC is reported to enhance the flexural strength, compressive strength etc. of the resulting material[25,26]. Alkali resistant macro glass fibres (Anti Crak-HP 67/36) supplied by Owens Corning India were added in PCC. The glass fibre dosage was kept at 0.5% and 1.0% by weight of PCC. The glass fibres had an average length of 12 mm. Details of the materials used in this study are provided in Table-1.

Table 1 Materials used for PCC and GFRPCC

| AGGREGATE ( Crushed Gravel ) | |
|---|---|
| Particle Size (mm) | Quantity (as percentage of total aggregate weight) |
| 4.76- 9.52 | 39.6% |
| 2.38-4.36 | 33.5% |
| 0.15- 0.3 | 26.9% |
| **RESIN & HARDENER SYSTEM** | |
| Description | Quantity (as percentage of total weight of polymer concrete) |
| (LAPOX- B47 & K-46) | 12 % |
| **MICROFILLER** | |
| Description | Quantity (as percentage of total weight of PCC) |
| F –Type Fly Ash | 10% |
| **GLASS FIBRE REINFORCEMENT (Only for GFRPC)** | |
| Description | Quantity (as percentage of total weight of PCC) |
| Owens Corning- Anti Crak –HP 67/36 | 0.5%, 1% |

Table 2 Static Flexural Strength for PCC and GFRPCC

| MATERIAL | STATIC FLEXURAL STRENGTH (MPa) |
|---|---|
| PCC | 24.41* |
| GFRPCC-0.5% | 28.16** |
| GFRPCC-1.0% | 30.47** |

***** *Average of 15 specimens, ** Average of 14 specimens*

The specimens of 40x40x160 mm size were cast on a vibratory table using the materials listed above. The specimen size has been chosen as per RILEM PC-2 –TC113 and has been used by a number of researchers in their work on polymer concrete[22,27]. Aggregate material and fly ash was dried before preparation of samples to reduce moisture content below 0.5 % as it has been reported that moisture content of aggregates has a deleterious effect on the properties of polymer concrete[28]. The specimens were cured at room temperature for 7 days before conducting the fatigue tests as per method adopted by a number of other researchers[29–31].

The estimation of static flexural strength ($f_r$) of the test material is a pre-requisite for the selection of maximum and minimum loads to be applied in particular fatigue test. The static flexural strength of the PCC and GFRPCC specimens was, therefore, evaluated prior to fatigue testing. Generally 4-5 specimens from a particular batch were randomly selected and tested to determine their static flexural strength. The results are listed in Table-2. It is observed that the addition of glass fibres enhances the static flexural strength of PCC. An increase of 15% in static flexural strength is observed by addition of 0.5% glass fibres by weight when compared to PCC, whereas, addition of 1.0% glass fibres resulted in an increase of the static flexural strength to the tune of 25%.

All the fatigue tests were carried out on a 100 kN MTS- Cyclic load testing facility in three point bending mode. The loading span was taken as 100 mm. A stress ratio of R = 0.1 was used in fatigue testing. The tests were carried out at a frequency of 10 Hz. The minimum fatigue stress ($f_{min}$) and maximum fatigue stress ($f_{max}$) to be applied was selected from $f_r$ and a particular stress level 'S' ($f_{max}/f_r$). For each mix, the first test was conducted at the highest possible stress level and the number of cycles to failure was noted as fatigue life 'N'. Subsequent tests were conducted by lowering the stress levels in a systematic manner. Since fatigue testing is a time consuming and expensive process and a large number of specimens were proposed to be tested, an upper limit of number of cycles to be applied was fixed depending upon the availability of testing equipment and time constraints. A particular test was terminated when the failure of the specimen occurred or the upper limit was reached, whichever was earlier.

## ANALYSIS AND DISCUSSION OF FATIGUE TEST RESULTS

### Fatigue life distributions of PCC and GFRPCC

A number of mathematical models have been employed to study the statistical dispersion of fatigue life. One of the popular model being the logarithmic-normal (lognormal) distribution function[32]. The lognormal distribution was thus extensively used for this purpose. However, it was pointed out later that the hazard function or risk function of lognormal distribution decreases with increasing life or time[33], which violates the basic physical phenomenon of progressive deterioration of engineering materials resulting from fatigue .

Weibull distribution function has proved to be useful and versatile means of describing fatigue behaviour of cement concrete[11,34] as well as other composite materials[12]. This is because the probability density function of the Weibull distribution has a wide variety of shapes. For example when the shape parameter of the distribution is equal to 1, it becomes the two parameter exponential distribution. For shape parameter nearing 3, the function is capable of approximating a normal distribution. Thus because of physically valid assumptions, sound

experimental verification, relative ease in its use and better developed statistics, the Weibull distribution is being used extensively for statistical description of fatigue life data.
Some data points obtained in the laboratory fatigue life data may deserve consideration for rejection as outliers. Chauvenet's criterion[35] was applied to the data points at all the stress levels tested in this investigation, and data points meeting this criterion for rejection were identified and excluded from further analysis. A few other researchers have also used the same criterion for rejection of outliers in their work on fatigue [11,12].

**Analysis of fatigue life data by graphical method**

A two-parameter Weibull distribution function which is characterized by a probability density function (PDF), $f(n)$; and the cumulative distribution function (CDF), $F(n)$ as follows:

$$f(n) = \frac{\alpha}{u}\left(\frac{n}{u}\right)\exp\left[-\left(\frac{n}{u}\right)\right] \quad (1)$$

$$F(n) = 1 - \exp\left[-\left(\frac{n}{u}\right)^{\alpha}\right] \quad (2)$$

in which $n$ = specific value of the random variable N; $\alpha$ = shape parameter or Weibull slope at stress level $S$ and $u$ = scale parameter or characteristic life at stress level $S$.

The probability of survival, $L_R(n)$, may be defined as $L_R(n) = 1 - F(n)$, and substituting this value of $F(n)$ in equation (2) it is modified to:

$$L_R(n) = \exp\left[-\left(\frac{n}{u}\right)^{\alpha}\right] \quad (3)$$

taking the logarithm twice of both sides of equation (3), it can be rewritten as

$$\ln\left[\ln\left(\frac{1}{L_R}\right)\right] = \alpha\ln(n) - \alpha\ln(u) \quad (4)$$

Equation (4) represents a linear relationship between $\ln[\ln(1/L_R)]$ and ln(n). In order to obtain a graph from equation (4), the fatigue-life data corresponding to a particular stress level are first arranged in ascending order of cycles to failure and the empirical survivorship function $L_R$ for each fatigue-life data at a given stress level is obtained from the following relation[35]:

$$L_R = 1 - \frac{i}{k+1} \quad (5)$$

where $i$ denotes the failure order number and k represents the number of data points in a data sample under consideration at a particular stress level $S$. The empirical survivorship function in the form of $\ln[\ln(1/L_R)]$ for each fatigue-life data is then plotted on a graph with the corresponding fatigue lives ln(N). If a linear trend is established for the data points, the best fit line is drawn using method of least squares. It can then be assumed that fatigue-life data for that particular stress level follows the two-parameter Weibull distribution. The slope of the line provides an estimate of shape parameter $\alpha$ and the characteristic life $u$ can be obtained as that value of $n$ which corresponds to $L_R = 0.368$.

Figure 1 presents the fatigue life data for few selected stress levels plotted as described above for PCC. The approximate straight line plot in this figure with statistical correlation coefficients "$r$" exceeding 0.9, indicate that the two-parameter Weibull distribution is a reasonable assumption for the statistical distribution of fatigue-life for PCC. Similar

results have been obtained at all the stress levels in this investigation. The estimated parameters thus obtained are listed in Table-3.

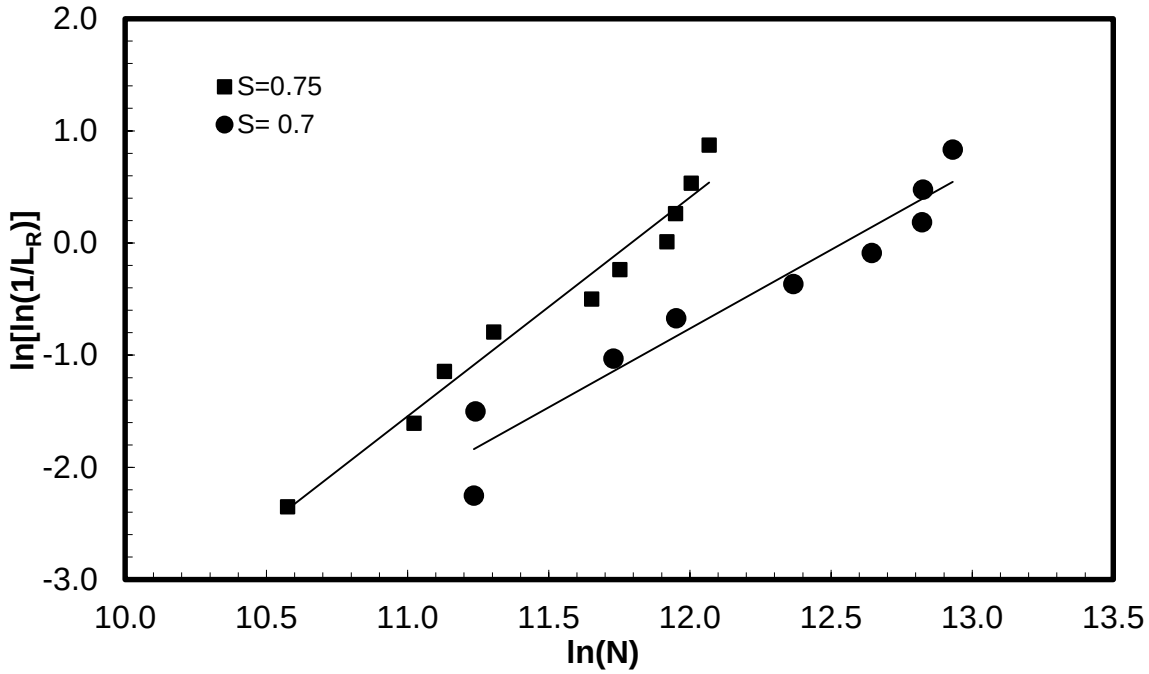


Figure 1 Graphical analysis of fatigue life data for PCC

Table 3 Parameters of Weibull distribution for PCC and GFRPCC

| POLYMER CONCRETE COMPOSITE (PCC) | | | | | | |
|---|---|---|---|---|---|---|
| Stress Level "S" | Graphical Method | | Method of Moments | | Average | |
| | $\alpha$ | $U$ | $\alpha$ | $u$ | $\alpha$ | $u$ |
| 0.8 | 2.43 | 8331 | 2.77 | 8204 | 2.60 | 8267 |
| 0.75 | 1.93 | 132242 | 2.51 | 127809 | 2.22 | 130025 |
| 0.7 | 1.40 | 281252 | 1.84 | 266577 | 1.62 | 273914 |
| 0.65 | 1.23 | 585252 | 1.56 | 556060 | 1.39 | 570656 |
| GLASS FIBRE REINFORCED POLYMER CONCRETE COMPOSITE (GFRPCC-0.5%) | | | | | | |
| Stress Level "S" | Graphical Method | | Method of Moments | | Average | |
| | $\alpha$ | $U$ | $\alpha$ | $u$ | $\alpha$ | $u$ |
| 0.85 | 2.10 | 4505 | 2.46 | 4404 | 2.28 | 4455 |
| 0.8 | 2.02 | 29482 | 2.31 | 28146 | 2.17 | 28814 |
| 0.75 | 1.69 | 221010 | 1.83 | 215809 | 1.76 | 218410 |
| 0.7 | 1.42 | 520972 | 1.64 | 502165 | 1.53 | 511568 |
| GLASS FIBRE REINFORCED POLYMER CONCRETE COMPOSITE (GFRPCC-1.0%) | | | | | | |
| Stress Level "S" | Graphical Method | | Method of Moments | | Average | |
| | $\alpha$ | $U$ | $\alpha$ | $u$ | $\alpha$ | $u$ |
| 0.85 | 1.98 | 31088 | 2.19 | 30469 | 2.08 | 30779 |
| 0.8 | 1.62 | 141795 | 1.63 | 137363 | 1.63 | 139579 |
| 0.75 | 1.31 | 492291 | 1.64 | 470856 | 1.48 | 481754 |

| | | | | | | |
|---|---|---|---|---|---|---|
| 0.7 | 1.15 | 1095935 | 1.58 | 1050287 | 1.37 | 1073111 |

**Kolmogorov-Smirnov test for goodness-of-fit**

In the preceding sections, graphical method has been employed to show that the statistical distribution of fatigue-life of PCC and GFRPCC, at various stress levels, can approximately be described by the two-parameter Weibull distribution. The Kolmogorov-Smirnov test [35] has been applied to validate the results, which can be carried out by using the following equation:

$$D_i = \max_{i=1}^{k}\left[\left|F^*(x_i) - F(x_i)\right|\right] \qquad (6)$$

where $F^*(x_i) = i / k$ = observed cumulative histogram, $i$ = order number of the data point, $k$ = total number of data points in the sample under consideration at a given stress level and $F(x_i)$ = hypothesized cumulative distribution given by equation (2). The value of $D_i$ thus obtained is compared with $D_c$ values for each data set obtained from Kolmogorov-Smirnov Table. If $D_i < D_c$ The model is acceptable with 5% significance level. This goodness-of-fit test was applied to fatigue life data of PCC and GFRPCC at all the stress levels and it was found that the model was acceptable at 5% level of significance. The results are compiled in Table-4.

Table 4 Results of Kolmogorov-Smirnov test for PCC and GFRPCC

| POLYMER CONCRETE COMPOSITE (PCC) | | | |
|---|---|---|---|
| Stress Level | $D_i$ | $D_c$ | Remarks |
| S=0.80 | 0.1334 | 0.41 | Accepted |
| S=0.75 | 0.1820 | 0.41 | Accepted |
| S=0.70 | 0.1801 | 0.435 | Accepted |
| S=0.65 | 0.1497 | 0.435 | Accepted |
| GLASS FIBRE REINFORCED POLYMER CONCRETE COMPOSITE (GFRPCC-0.5%) | | | |
| Stress Level | $D_i$ | $D_c$ | Remarks |
| S=0.85 | 0.1164 | 0.41 | Accepted |
| S=0.80 | 0.1598 | 0.41 | Accepted |
| S=0.75 | 0.1455 | 0.41 | Accepted |
| S=0.70 | 0.1116 | 0.41 | Accepted |
| GLASS FIBRE REINFORCED POLYMER CONCRETE COMPOSITE (GFRPCC-1.0%) | | | |
| Stress Level | $D_i$ | $D_c$ | Remarks |
| S=0.85 | 0.1509 | 0.41 | Accepted |
| S=0.80 | 0.1954 | 0.41 | Accepted |
| S=0.75 | 0.1055 | 0.41 | Accepted |
| S=0.70 | 0.1453 | 0.41 | Accepted |

**Fatigue strength prediction models**

**S-N relationships**. Fatigue life or fatigue strength estimates have traditionally been based on test data expressed in terms of the S-N curves which is a relationship between a non-dimensional term, $S$ and corresponding number of cycles to failure, $N$ also termed as

fatigue life. The S-N relationships facilitate designers in estimating the fatigue life of a structure subjected to a particular stress history or, provide an initial estimate of fatigue life for design purpose. Several fatigue models or equations have been in use to characterize the S-N relationships for modelling of fatigue strength. Most of the researchers have used a S-N relationship represented by Eq (7), as mentioned below which is also known as the Wholer equation-

$$S=\frac{f_{max}}{f_r} = a + b\ log_{10}(N) \qquad (7)$$

Where *a* and *b* are material constants, which can be determined by regression from the fatigue test data for PCC and GFRPCC. Figures-2,3 and 4 present the test results in the form of S-N curves obtained in this study for PCC, GFRPCC with 0.5% glass fibres and GFRPCC with 1.0% glass fibres respectively. Linear regression is carried out by method of least squares to determine the values of coefficient *a* and *b*. The values of coefficients obtained are listed in Table-5.

Another form of the fatigue equation used by researchers is a modification of the Wholer equation that incorporates a stress ratio *R*, which is the ratio of minimum fatigue stress $f_{min}$ to the maximum fatigue stress $f_{max}$ into the Wholer equation. The *R*-term is included to simulate the loading conditions in actual structures where the minimum value of the repeated stress is not zero. The modified equation takes the following form

$$S=\frac{f_{max}}{f_r} =1-\beta(1-R)log_{10}(N) \qquad (8)$$

where $\beta$ is an experimental coefficient. This equation can be used for $0 \leq R \leq 1$ but not for stresses that vary between tension and compression. The material coefficient $\beta$ in Eq. (8) can be obtained from the test data to make Eq. (8) applicable to PCC and GFRPCC. Using the values of stress level *S* (that is, $f_{max}/f_r$), *R* and $\log_{10}(N)$ the values of the coefficient $\beta$ are determined for each test for PCC and GFRPCC. The values of coefficients obtained are listed in Table-4.

Table 5 Coefficients *a* and *b* for Eq.9 and coefficient $\beta$ for Eq.8

| MATERIAL | COEFFICIENT *a* | COEFFICIENT *b* | COEFFICIENT $\beta$ |
|---|---|---|---|
| PCC | 1.0606 | -0.0679 | 0.06138 |
| GFRPCC-0.5% | 1.0773 | -0.0646 | 0.05104 |
| GFRPCC-1.0% | 1.1184 | -0.0665 | 0.04581 |

**Two million cycle endurance limits**

To examine the flexural fatigue performance, the Figs.-2,3 and 4 have been used to determine the two-million cycle endurance limits of PCC and GFRPCC. For PCC, the two-million cycle endurance limit has been found to be approximately 62% of the corresponding static flexural strength, whereas for GFRPCC containing 0.5% and 1.0% glass fibres, the endurance limit have been found to be 66% and 70% respectively of their corresponding static flexural strength.

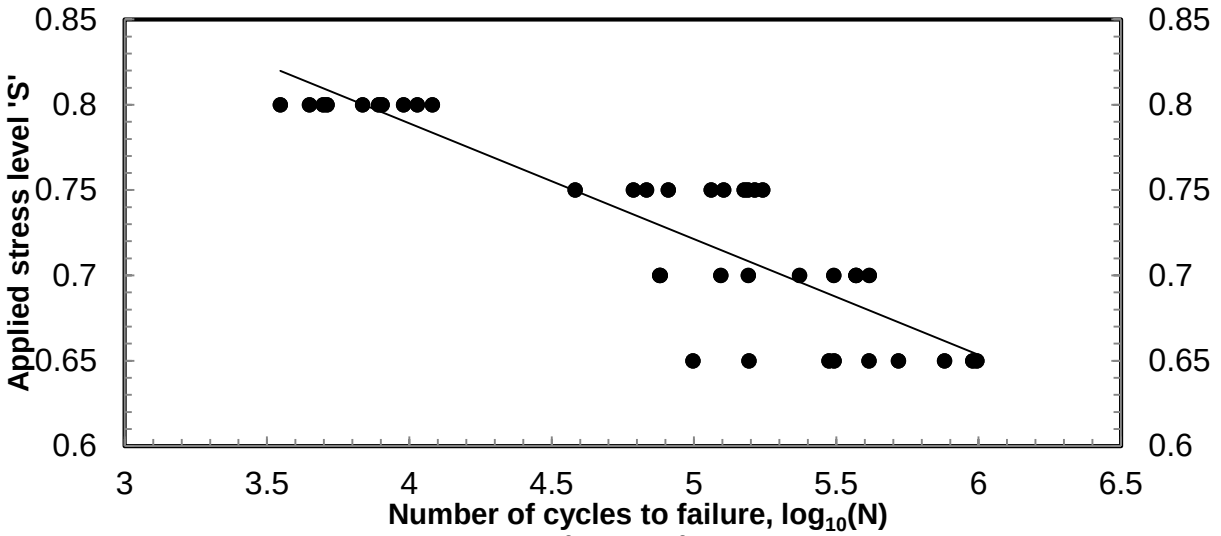


Figure 2 S-N relationship for PCC from experimental data

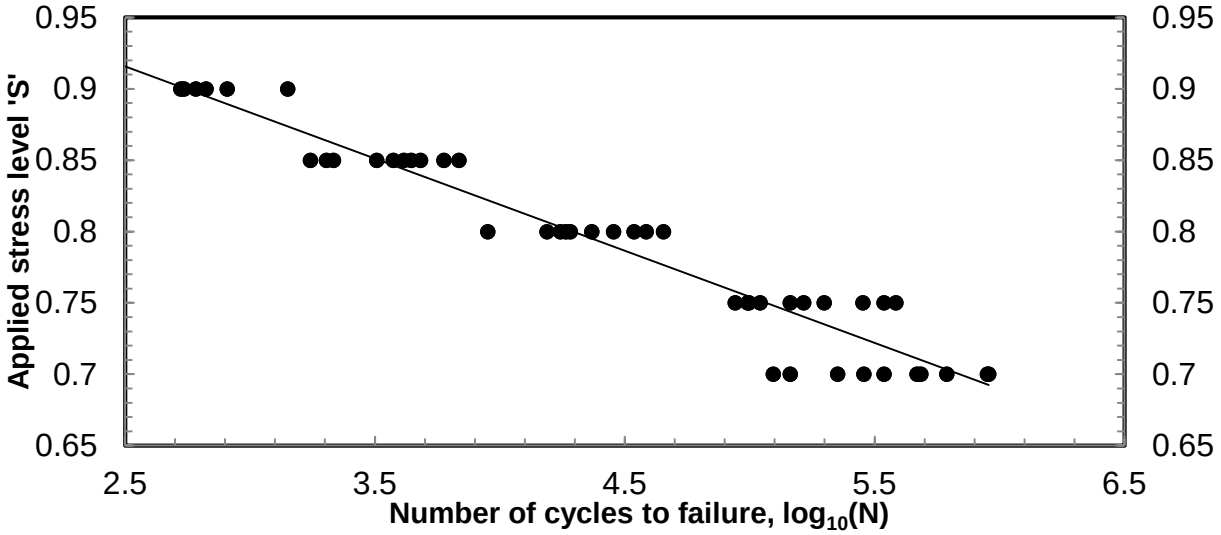


Figure 3 S-N relationship for GFRPCC- 0.5% from experimental data

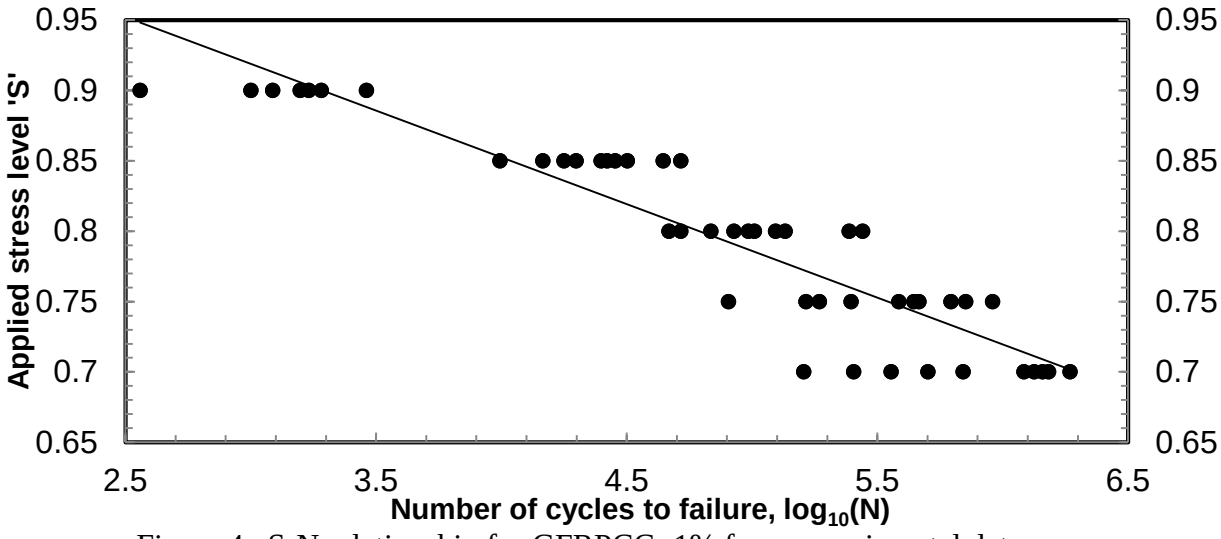


Figure 4 S-N relationship for GFRPCC- 1% from experimental data

## CONCLUSIONS

Experimental investigation has been carried out to obtain the fatigue lives for PCC and GFRPCC specimens containing different contents of glass fibres. Flexural fatigue life data of PCC as well as GFRPCC have been obtained in this investigation corresponding to different stress levels. It has been observed that the fatigue life distributions for these materials, at any stress level, approximately follow two parameter Weibull distribution. Parameters of Weibull distribution have been obtained by graphical as well as method of moments. The values of the shape parameter for GFRPCC have been found to be considerably lower than those for PCC, indicating higher variability in the fatigue life data of GFRPCC compared to PCC. The test data has been used to generate S-N curves for PCC and GFRPCC and equations have been proposed to predict the flexural fatigue strength of these materials. The proposed equations can be used to predict the flexural strength of these materials using the appropriate coefficients obtained in this investigation. The endurance limit of GFRPCC has been found to be higher than that of PCC.

## REFERENCES

1 KIRLIKOVALI E. Polymer/Concrete Composites- A review. Polym Eng Sci 1981;21:507–9.

2 MCKEOWN P, MORGAN G. Epoxy granite: a structural material for precision machines. Precis Eng 1979;1:227–9. doi:10.1016/0141-6359(79)90104-1.

3 SALJE E, GERLOFF H, MEYER J. Comparison of Machine Tool Elements Made of Polymer Concrete and Cast Iron. CIRP Ann - Manuf Technol 1988;37:381–4. doi:10.1016/S0007-8506(07)61659-X.

4 CORTES F, CASTILLO G. Comparison between the dynamical properties of polymer concrete and grey cast iron for machine tool applications. Mater Des 2007;28:1461–6. doi:10.1016/j.matdes.2006.03.012.

5 ORAK S. Investigation of vibration damping on polymer concrete with polyester resin. Cem Concr Res 2000;30:171–4. doi:10.1016/S0008-8846(99)00225-2.

6 TANABE I, TAKADA K. Thermal deformation of machine tool structures using resin concrete. JSME Int J 1994;37:384–9.

7 TANABE I. Development of ceramic resin concrete for precision machine tool structures. JSME Int J 1993;36:494–8.

8 TANABE I, TAKADA K, NAKAMURA A. Thermal and mechanical characteristics of epoxy resin concrete used in machine tool structures. JSME Int J 1990;56:236–43.

9 SINGH SP, MOHAMMADI Y, MADAN SK. Flexural fatigue strength of steel fibrous concrete containing mixed steel fibres *. J Zhejiang Univ Sci A 2006;7:1–7. doi:10.1631/jzus.2006.A0155.

10 SINGH SP, KAUSHIK SK. Flexural Fatigue Analysis of Steel Fiber-Reinforced Concrete. ACI Mater J 2001;98:306–12.

11 SINGH SP, KAUSHIK SK. Flexural Fatigue Life Distributions and Failure Probability of Steel Fibrous Concrete. ACI Mater J 2000;97:658–67.

12 BEDI R, CHANDRA R. Fatigue-life distributions and failure probability for glass-fiber reinforced polymeric composites. Compos Sci Technol 2009;69:1381–7. doi:10.1016/j.compscitech.2008.09.016.

13 KOBAYASHI K, OHAMA Y, ITO T. Fatigue Properties of Resin concrete under repeated compression loads. Seisan Kenkyu 1974;26:116–8.

14 WOELFL G, MCNERNEY M, CHANG C. Flexural Fatigue of Polymer Concrete. Cem Concr Aggregates 1981;3:84. doi:10.1520/CCA10209J.

15 VIPULANANDAN C, MEBARKIA S. Fatigue crack growth in polyester polymer concrete. California: 2001.

16 MCCALL JT. Probability of fatigue failure of plain concrete. ACI J 1958;55:233–44.

17 SINGH SP, MOHAMMADI Y, KAUSHIK SK. Flexural Fatigue Analysis of Steel Fibrous Concrete Containing Mixed Fibers. ACI J 2005;102:438–44.

18 SINGH B, SINGH SP, KAUSHIK SK. Probability of fatigue failure of steel fibrous concrete. Mag Concr Res 2005;57:65–72. doi:10.1680/macr.2005.57.2.65.

19 MUTHUKUMAR M, MOHAN D, RAJENDRAN M. Optimization of mix proportions of mineral aggregates using Box Behnken design of experiments. Cem Concr Compos 2003;25:751–8. doi:10.1016/S0958-9465(02)00116-6.

20 FATTAH A, EL-HAWARY M. Flexural behavior of polymer concrete. Constr Build Mater 1999;13:253–62.

21 REBEIZ K, SERHAL SP, CRAFT A. P. Properties of Polymer Concrete Using Fly Ash. J Mater Civ Eng 2004;16:15. doi:10.1061/(ASCE)0899-1561(2004)16:1(15).

22 FERREIRA AJM. Flexural Properties of Polyester Resin Concretes. J Polym Eng 2000;20:459–68.

23 VARUGHESE K. Fly ash as fine aggregate in polyester based polymer concrete. Cem Concr Compos 1996;18:105–8. doi:10.1016/0958-9465(95)00006-2.

24 GORNINSKI JP, DAL MOLIN DC, KAZMIERCZAK CS. Study of the modulus of elasticity of polymer concrete compounds and comparative assessment of polymer concrete and portland cement concrete. Cem Concr Res 2004;34:2091–5. doi:10.1016/j.cemconres.2004.03.012.

25 BROCKENBROUGH TW. Fiber reinforced methacrylate polymer concrete. ACI J 1982;july:322–5.

26 REIS J. Mechanical characterization of fiber reinforced Polymer Concrete. Mater Res 2005;8:357–60. doi:10.1590/S1516-14392005000300023.

27 RIBEIRO M, TAVARES CML, FIGUEIREDO M, FERREIRA AJM, FERNANDES AA. Bending characteristics of resin concretes. Mater Res 2003;6:247–54. doi:10.1590/S1516-14392003000200021.

28 OHAMA Y. Mix proportions and properties of Polyester Resin Concretes. 1973.

29 REBEIZ K. Time-temperature properties of polymer concrete using recycled PET. Cem Concr Compos 1995;17:119–24. doi:10.1016/0958-9465(94)00004-I.

30 TAWFIK ME. Polymer Concrete from Marble Wastes and Recycled Poly(ethylene terephthalate). J Elastomers Plast 2006;38:65–79. doi:10.1177/0095244306055569.

31 OHAMA Y, DEMURA K. Relation between curing conditions and compressive strength of polyester resin concrete. Int J Cem Compos Light Concr 1982;4:241–4. doi:10.1016/0262-5075(82)90028-8.

32 ASTM SPECIAL PUBLICATION 91-A, A guide for fatigue testing and the statistical analysis of fatigue data. 1963.

33 GUMBLE EJ. Parameters in the distribution of fatigue life. J Eng Mech ASCE 1963;October:45–63.

34 GOEL S, SINGH SP, SINGH P. Fatigue Analysis of Plain and Fiber-Reinforced Self-Consolidating Concrete. ACI Mater J 2012;109:573–82.

35 KENNEDY J, NEVILLE A. Basic Statistical Methods for Engineers and Scientists. A Dun-Donnelley Publishers; 1986.

# Theme 5

# Durability, Serviceability and Reliability

Keynote Paper

# HEAL THE PONT ADOLPHE

**A E C Borderon**
Valbruna stainless steel
Italy

**ABSTRACT.** Emblematic feature of the City of Luxembourg, the Adolphe Bridge was designed by Paul Séjourné as an arch bridge and built between 1900 and 1903. With four lanes, one to the Upper City reserved for public transport, and three reserved for individual traffic going towards the Central Station, the bridge has a 1.80 metre wide pavement on each side, separated from the road by a traffic barrier. Inspections have shown that the ”Pont Adolphe” is in a state of advanced decay. Faced with this finding and the increasing use of the bridge, far-reaching rehabilitation measures were taken before restrictions on service. In accordance with the wishes of UNESCO, the rehabilitation techniques used are designed to preserve in the best way possible the architecture of Séjourné. The project provides for taking down the present deck and then constructing a new one. It will be wider (2 x 0.75 m each side) and thicker and will also constitute a watertight cover for the underlying ma! sonry which for a long time suffered from the abundant run off of infiltrations of water and brine, despite previous rehabilitations in 1990 and 2004. One of the main objectives of the project is to permanently strengthen the main arches against delamination and to avoid corrosion of the connecting parts. The new deck of the Adolphe Bridge, which has been expanded for the integration of two new tracks for the tram and two lanes for cars/buses with sidewalks on both sides, cannot accommodate a cycle track. The proposed solution is to insert a new gateway between the two arcs below the rebuilt deck of the Pont Adolphe. Extensive use of stainless steel was mandatory to secure 120 years service life of Luxembourg City's main tourist attraction.

**Keywords:** Concrete, Rehabilitation, Extended service life, Increased bearing capacity, Stainless steel.

**A E C Borderon** is specialist in Concrete durability at Valbruna Spa. He is Architect DLPG from France and Structural engineer from UK, and has published several articles on the topic of concrete durability and the use of non-corrosive reinforcement materials.

## INTRODUCTION

The protection of properties belonging either to the State or to the City of Luxembourg or individuals is governed primarily by the Law of 18 July 1983 relating to the conservation and protection of national sites and monuments, and Old Quarters and Fortifications area where the Pont Adolphe is located, are part of UNESCOs world heritage. The requests are therefore to ensure durability of the bridge despite greater loading and changed configuration with larger deck and underlying cycle track.

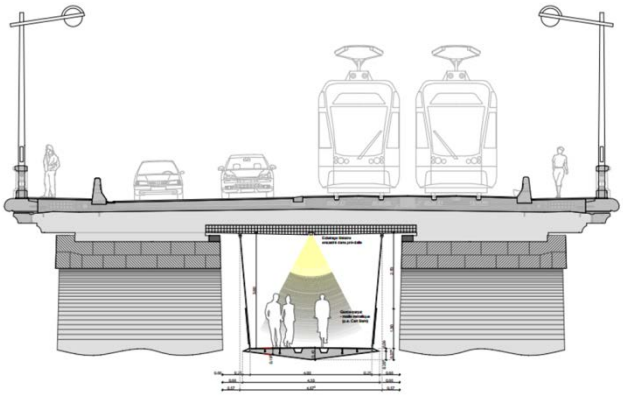

Figure. 1 New bridge configuration for the Pont Adolphe

## WATER PENETRATION AND CRACKS

In the 90´s, the administration had commissioned a full investigation of the situation of the bridge. Visual control had shown loose masonry (Figure 2) and cross section cracks in both directions. Detachment of the stones was also observed as well as leakage of the deck.

As ice melts are used in the winter period to keep the road above ice free, the melted ice now containing salts seeps into the structure through the mortar joints. Penetration of chloride filled water through the deck was observed as masonry clearly showed mortar flaking and efflorescence. (Figure. 3).

Figure 2 Efflorescence on piers

Figure 3 Mortar flaking on the piers

Efflorescence occurs when moisture migrates to the surface, bringing with it salts from within the concrete and depositing them on the surface. The primary material that is brought to the surface is calcium hydroxide, but there are many other salts that can also come to the surface.

## Cracks

Following the visual control on site, a full investigation (Figures4-5) was needed to clarify the structural status of the bridge. Mortar flaking and cracks were investigated by georadar technology to clarify the actual bearing capacity of the structure in order to design the strengthening required for the new configuration.

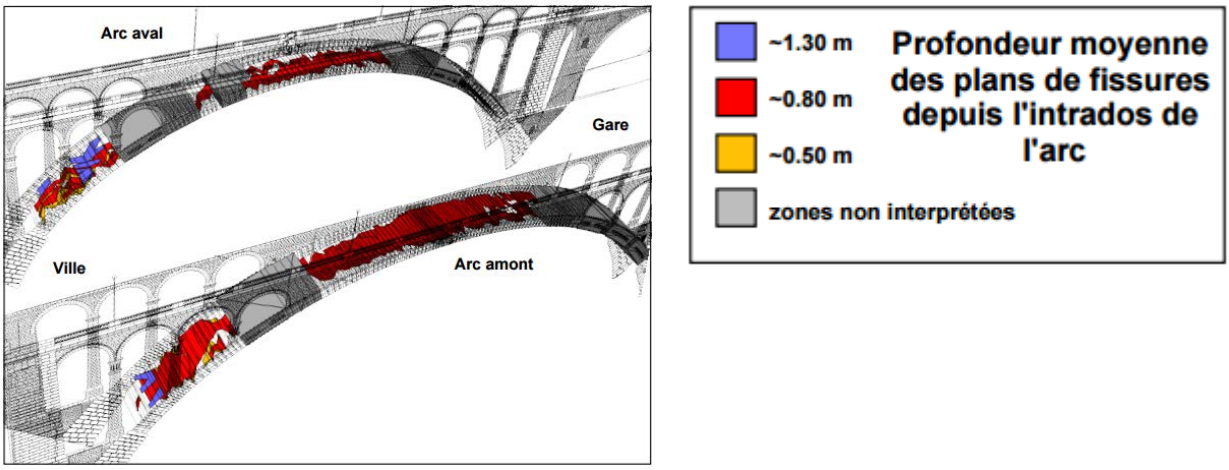


Figure 4 Crack depth in arches

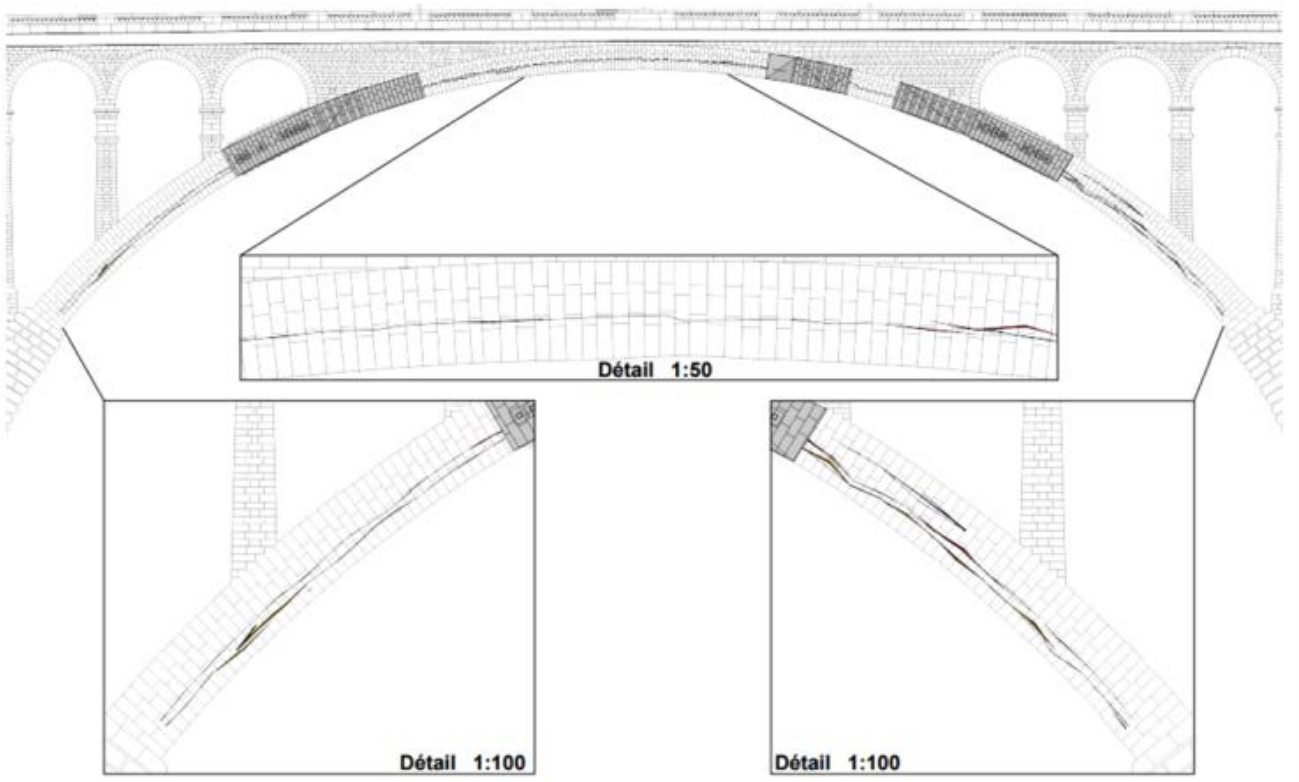


Figure 5 Longitudinal cracks in the arches

## CONSTRUCTIVE STRENGTHENING OF THE BRIDGE

The investigation was followed by a constructive design of the necessary strengthening of the bridge at accommodate the new loads and secure durability.

The measures are stabilization of the piers by 40 mm thick concrete steel rebar and connection of the masonry with the new concrete deck through steel anchors to increase stiffness in the structure. (Figure 6)

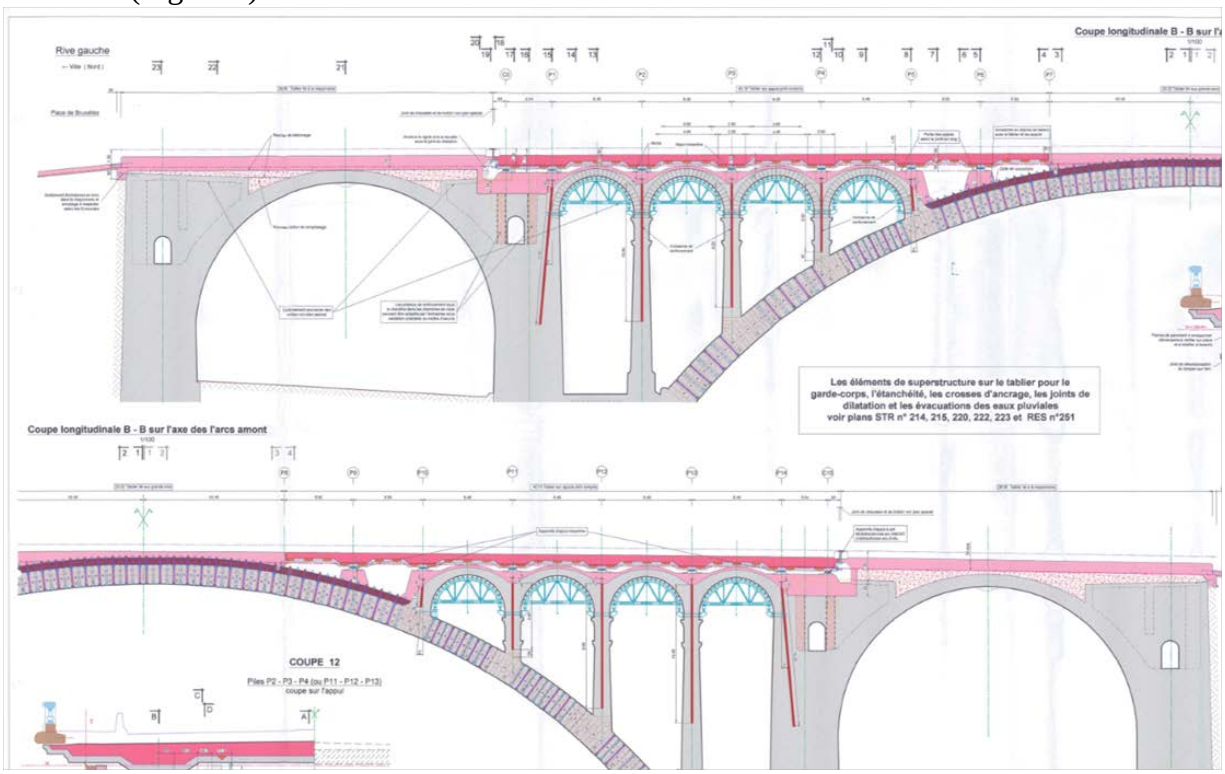


Figure 6 Structural strengthening of the piers using ø40 mm rebar.

To meet the required durability of the solutions, materials should demonstrate their ability to resist corrosion in time. It was therefore necessary to address the topic of corrosion threshold to choose the adequate material.

### Corrosion Threshold

To choose the right reinforcing material, the chloride ingress in the structure over time had to be evaluated and predicted using a known model of chloride ingress into concrete based on mathematical solutions of Fick´s second law:

$$C(x,t) = C_i + C_o\left(1 - erf\left(\frac{0.1 \cdot x}{2\sqrt{D \cdot t}}\right)\right)$$

where $C_{(x,t)}$ chloride content in concrete at time t;
$C_i$ inital chloride content in concrete;
$C_o$ chloride content at concrete surface;
x depth of reinforcement;
D diffusion factor;
t time.

Given the necessary data, calculation was done with the following results:

| | | | |
|---|---|---|---|
| C | Cement content | 400 kg/$m^3$ | |
| x | Concrete cover | 30 mm | |
| D | Diffusion coefficient | 6,22E-11 $m^2$/s | (PC) |
| T | Time | 120 years | |
| $C_{cr}$ | Surface chloride content ratio in % mass of cement | 0,8% | |
| $C_s$ | Surface chloride content | 3,2 kg/$m^3$ | |
| $C_o$ | Initial concrete chloride content | 0,6 kg/$m^3$ | (EN 206) |
| $C_t$ | Chloride content at x at t | 1,7 kg/$m^3$ | |

The chloride content surrounding the reinforcement would probabilistically achieve 1,7 kg / $m^3$ of concrete. As the corrosion threshold of carbon steel is 0,71, it became obvious other types must be considered to avoid early corrosion damages.

In that particular project, under the supervision of UNESCO, any risk of corrosion was to be eliminated at design stage.

Table 1 Corrosion threshold of available reinforcing products.

| **Reinforcement type** | **Corrosion threshold kg of $Cl^-/m^3$ concrete** |
|---|---|
| Carbon steel | 0,71 |
| Galvanized steel | 1,52 |
| Composite rebar | - |
| Stainless steel | 10,8 |

## STONE-MORTAR INTERACTION

### Exposure and Risks

As the masonry is anchored to the deck through steel connectors, there is a risk of corrosion in time, and ultimately cracking of the stones as corroded steel would increase its volume. To prevent any risk, the use of non-corrosive rebar was mandatory for all connectors.

### Choice of Reinforcement

Different types of reinforcement products were considered in the design phase, such as stainless steel, FRP, and epoxy-coated carbon steel.

The specifications stipulated a solution of workable material, which could be processed similarly to carbon steel and with a high degree of reliability in time. FRP and epoxy-coated steel were accordingly removed as options, and stainless steel remained the obvious option, especially due to the fact that stainless steel can be bend onsite without affecting its non-corrosive performance.

The choice of the grade of stainless steel (Figure 7) was made according to durability requirements.

Figure 7 Stainless steel anchors to masonry stones.

## Structural Strengthening

### Requirements

The 40 mm diameter rebar used for structural strengthening of the arches were designed as rebar with welded plates on top. The plates were expected to be welded to the bars through the all contact surface. The best way to ensure total contact between bar and plate was friction welding.

### Production

Friction welding is a rotary, inertia friction welding process, which generates heat through mechanical friction between work pieces in relative motion to one another, with the addition of a lateral force called "upset" to plastically displace and fuse the materials. Force was in this particular case 30 tons, leaving a welded thickness of 6 mm. (Figure 8).

## DURABILITY

### Pitting Corrosion

The passive layer on stainless steel can be attacked by certain chemical species, in the case of this bridge, the chloride ion Cl- in deicing salts. Corrosion if any on stainless steel begins with pitting, that is localized corrosion of the surface confined to a point or small area, which takes the form of cavities. Pitting corrosion is avoided by choosing a grade of steel which is more resistant to attack. The pitting corrosion resistance can be assessed using the Pitting Resistance Equivalent Number calculated from the alloy content.

Figure 8 Friction welded plates and Stainless steel bars.

**PREN Numbers**

The Pitting Resistance Equivalent Number (PREN) is a measure of the relative pitting corrosion resistance of stainless steel in a chloride-containing environment. Higher PREN values indicate greater corrosion resistance. The formula for PREN is:

PREN = %Cr + 3.3*%Mo + 16*%N

This formula suggests that molybdenum is 3.3 times more effective than chromium at improving pitting resistance, which is true within limits. Chromium must always be present in stainless steel to provide basic corrosion resistance. Molybdenum cannot provide this basic resistance, but it significantly enhances a stainless steel's corrosion resistance, as the formula shows. The table shows ferritic, austenitic and duplex stainless steels with different levels of pitting resistance, for available reinforcing steels.

**Choice of Grade**

Given the likely chloride content at 120 years, decision was made for Duplex grade 1.4462 for all steel of the project. 1.4462 has the highest PREN value of available stainless steel reinforcing bars, and would avoid any risk in time of corrosion inside the structure , where monitoring and maintenance are impossible once the deck is poured.

Table 2 PREN Numbers stainless steels.

| Common ferritic, austenitic and duplex stainless steels | | | | | | | |
|---|---|---|---|---|---|---|---|
| **EN** | **AISI** | **UNS** | **Cr** | **Mo** | **Ni** | **N** | **PREN** |
| **Ferritic grades** | | | | | | | |
| 1.4526 | 436 | S43600 | 17.5 | **1.25** | | | 21.6 |
| **Austenitic grades** | | | | | | | |
| 1.4301 | 304 | S30400 | 18.1 | | 8.3 | | 18.1 |
| 1.4401 | 316 | S31600 | 17.2 | **2.1** | 10.2 | | 24.1 |
| 1.4539 | 904L | N08904 | 20 | **4.3** | 25 | | 34.2 |
| **Duplex grades** | | | | | | | |
| 1.4362 | 2304 | S32304 | 23 | **0.3** | 4.8 | 0.1 | 25.6 |
| 1.4462 | 2205 | S32205 | 22 | **3.1** | 5.7 | 0.17 | 35 |

## CONCLUSIONS

The overall cost of selectively choosing stainless steel rebar to ensure concrete durability over the 120 years' service life of the bridge, is less than 0,5 % of the total project budget and cheaper than scaffolding.

The challenge has been concentrated on the right choice of reinforcing material, as prediction of the chloride threshold at rebar at 120 years was and still is very uncertain.

Most tests found in related literature are conducted at a maximum period of 4 years, leaving any calculation with a high level of variation.

## REFERENCES

1. EDVARDSEN C., SLOTH M. ENGELUND S., Service Life Estimation and Durability Design of Concrete Structures Subject to Destructive Mechanisms, 1999
2. GJORV, OE, Durability Design of Concrete Structures in Severe Environments, CRC Press, Boca Raton, USA, 2014
3. KWAN AKH, WONG HHC, Durability of Reinforced Concrete Structures: Theory vs Practice, Proceedings of the Hong Kong Government Standing Committee on Concrete Technology Annual Concrete Seminar, Hong Kong, 2005
4. HURLEY MF, SCULLY JR, Chloride threshold levels in clad 316L and solid 316LN stainless steel rebar, Corrosion 2002, National Association Of Corrosion Engineers, Paper No.02224, 2002, 24pp
5. MARKESET G, ROSTAM S, KLINGHOFFER O, Guide for the Use of Stainless Steel Reinforcement in Concrete Structures, Nordic Innovation Centre project 04118, Norwegian Building Research Institute, 2006
6. www.Healtheadolphebridge.lu

# HIGH TENSILE LAMINATED FERROCEMENT AS PERMANENT SHUTTERING FOR MARINE STRUCTURES

**J M Pemberton**

**T Tucker M Pullan**

Trafalgar Marine Technology Ltd

United Kingdom

**ABSTRACT.** This paper will describe the recent development of High Tensile Laminated Ferrocement Plates for application as permanent shuttering for the construction of marine structures. Recent Patent Applications relate to improvements in Laminated Ferrocement construction technologies to reduce the costs of Marine Structures for the extraction of renewable energy from the Oceans. The new Laminated Ferrocement manufacturing techniques offer reduction in CAPEX and OPEX for Marine Structures. “If you put steel into the Ocean – then better to wrap the steel in quality concrete (Ferrocement) – otherwise the costs of maintaining the steel (painting both inside and out) – will dissipate the revenue earned from the structure and deplete the ‘bottom line’.” “This applies to all steel in the Ocea Ships, Wind Turbine Towers, Wind Turbine Foundations and any wave or tidal energy device constructed in steel.”

**Keywords:** Renewable Energy. Marine structures. Ferrocement. Permanent shuttering.

**Michael Pembertonn** is the Managing Director of Trafalgar Marine Technology Ltd.

**Tony Tucker** is a Naval Architect and Marine Surveyor.

**Martin Pullan is** member of the Engineering Council, member of the Institution of Engineering and Technology and associate member of the Institute of Concrete Technology.

## INTRODUCTION

### What Is Ferrocement?

"Ferciment," or ferrocement, is truly the first invention of reinforced concrete, the most used construction material in the world. The main difference between them is mostly in scale. Reinforced concrete used larger sized reinforcing bars instead of wires or meshes, and a concrete binder, which, unlike cement paste and mortar, contains larger size aggregates. Ferrocement is a thin composite made with a cement-based mortar matrix reinforced with closely spaced layers of small diameter wire mesh. The mesh may be made of metallic or other suitable materials. Since advanced fibre reinforced polymeric meshes, such as carbon, Kevlar, Spectra and the like are becoming increasingly available for use in its construction, Ferrocement can also be considered a high performance laminated cementitious composite. The fineness of the cementatious matrix is designed to allow full encapsulation of the reinforcing mesh system, and will limit the size of the largest sand grains used. The thickness of Ferrocement is generally smaller than 25mm but in some cases reaches up to 50mm." [1]. Figure 1 shows Joseph Louis Lambot and his first Ferrocement boat on the lake of his estate. You can see in the photograph the stone copings at the lake edge, the lilies of his lily pond and, in the background, the yellow roses above the copings, which he was known to cultivate.

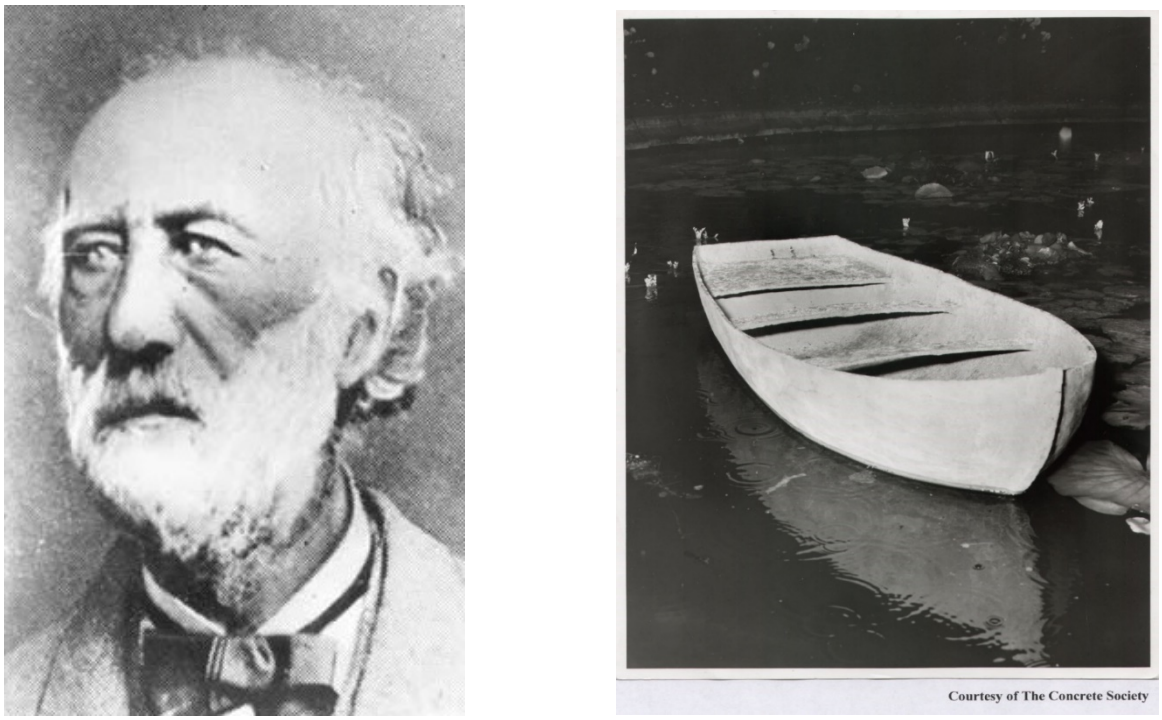


Figure 1 Joseph Louis Lambot Inventor of Ferrocement and his boat

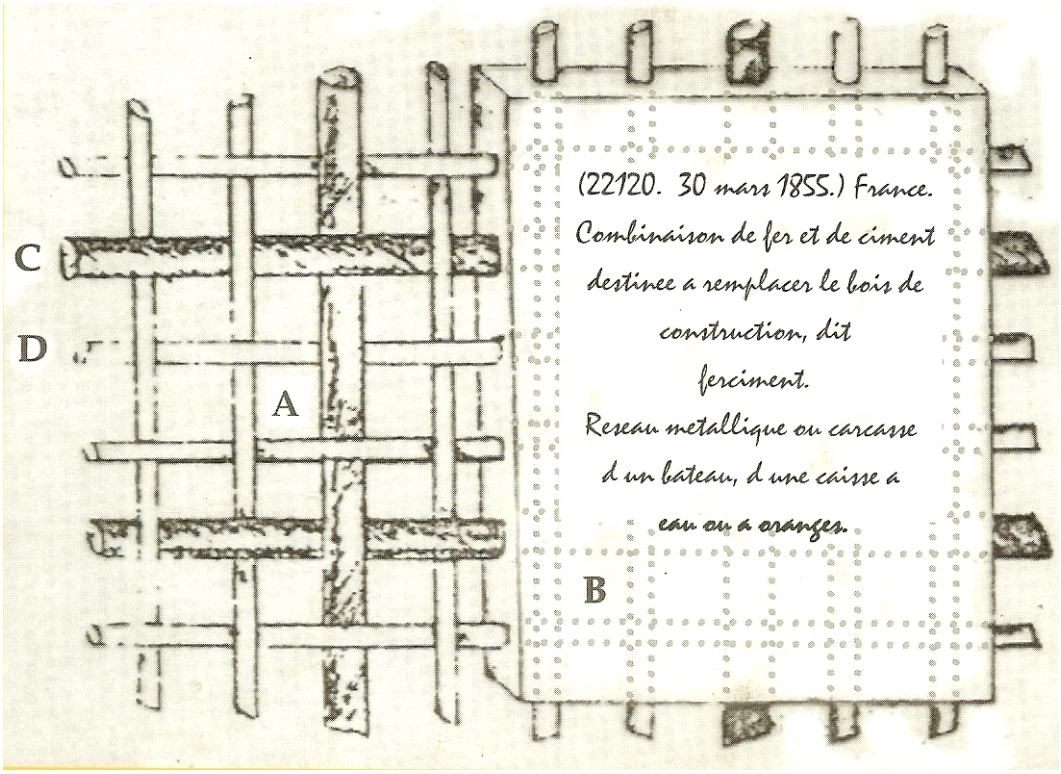


Figure 2 Lambots' Patent 1855 [2]

Figure 2 shows Lambots' Patent in 1855. Can you see the similarity with today's reinforced concrete? This is the first patent for 'ferciment', perhaps the first Patent for reinforced concrete! Has the concrete industry forgotten its roots? We think so!

Ferrocement has been widely used for boat and yacht building since the invention of 'ferciment' by Lambot and other pioneers including Pier Luigi Nervi who called the material 'Ferrocemento'. It was popular after WW11 and up to the 1980's for building boats and yachts but because the armature and hand plastering traditional method of construction was too laborious it was superseded by GRP and Ferrocement application declined except in the third world where it became useful for various utility products.

The use of Ferrocement in the marine environment is well proven. The use of Ferrocement in marine renewable energy structures remains to be proven.

**What Is Laminated Ferrocement?**

Figure 3 shows an analogy of typical concrete construction. Figure 4 shows a typical concrete cross section. Figure 5 show an analogy of laminated ferrocement concrete. Figure 6 shows a typical laminated ferrocement construction.

Fish = Concrete,
Chips = Reinforcements
Salt and vinegar = Additives.

Figure 3 Typical Concrete Analogy

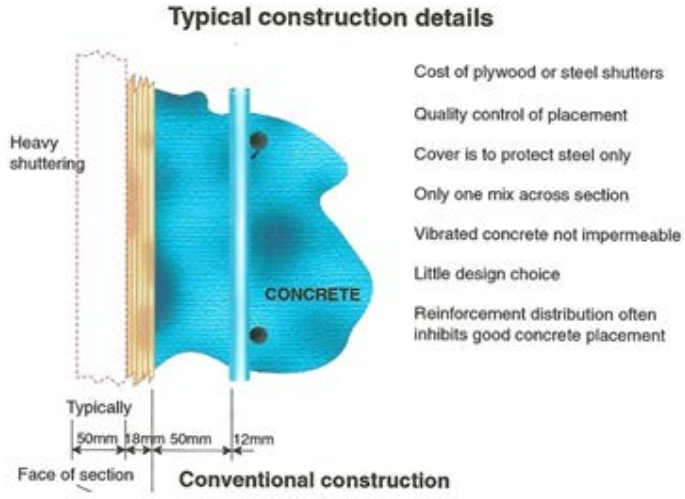


Figure 4 Typical Concrete Construction

Choice of layers of food
Choice of types of food in layers
Choice of where to put layers of food.

Figure 5 Laminated Ferrocement Analogy.

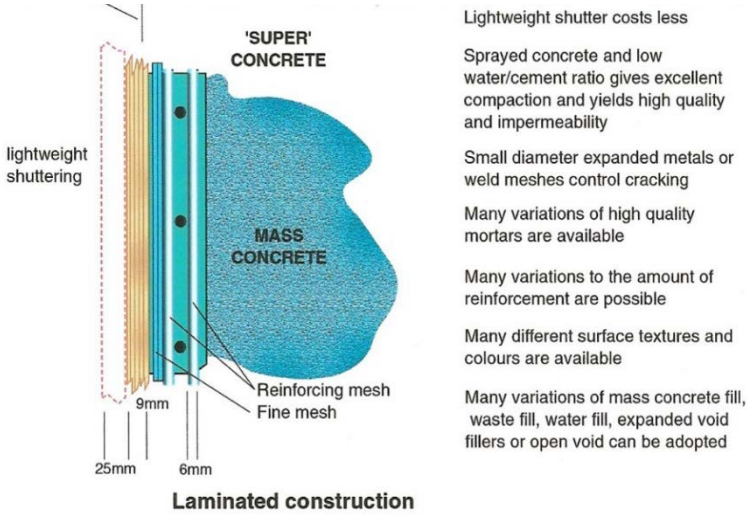


Figure 6 Laminated Ferrocement Construction

**So Why Do We Laminate Ferrocement?**

There are several ways of constructing ferrocement and over the years methods have been found to increase productivity. The original and traditional method of making an armature of wire and hand plastering has been used since Lambot's invention in 1848 and Patent of 1855 but is now far too laborious to be commercial. The application of positive displacement mixers and 'mono' type pumps to convey the mortar permits spraying of mortar onto a mould. This type of machine provides an efficient means to mix and convey mortar.

The embedding of reinforcements into a plastic mortar is the essential methodology of the laminating techniques invented by Iorns and Watson in California in the 1960s.

This was proved to be the best method to manufacture the roof leaves for the DeMenil project in 1985 and subsequently for the manufacture of sewer lining systems. So why does the spray and laminating technology produce the best in quality ferrocement?

1) Firstly, the mixing of mortar in a positive displacement mixing machine and then passing that mortar through a mono type pump is almost self-controlling.
2) A ferrocement mortar mix of 2 to 1 sand/cement ratio of plastering sand and cement with the appropriate plasticisers, produces a mortar with <.40 water cement ratio which can be pumped through a pipe and sprayed.
3) Using flat sheet reinforcements of expanded metal and flat sheets of reinforcing meshes is the most efficient way of handling the reinforcing materials and placing them into a plastic (wet) mortar.
4) There is no need to roll out and flatten rolls of small mesh materials and there is no need to wire together the small meshes to an armature.
5) There is no need to work by hand plastering to force mortar into an armature and worry about the correct penetration and total encapsulation of the wires.
6) The spray and laminating technology can be used for both vertical walls and horizontal casting.
7) The spraying of mortar produces excellent compaction against the mould surface. Thus replicating the features of that mould surface when demoulded.
8) The spraying process drives out any excess moisture and therefore delivers an excellent low water-cement ratio with good compaction at the mould surface. This also provides the impermeable ‘gel coat’.
9) Surface cracking is controlled by two layers of expanded metal which is set next to the gel coating. These three layers - of gel coat plus expanded metals (1) and expanded metals (2) provides an impermeable barrier with crack control and yet might also be regarded as a ‘sacrificial layer’ protecting the subsequent layers of reinforcements.
10) IMPORTANT – Expanded Metal meshes dissipate surface cracking whereas round wire meshes of a square welded mesh concentrate cracks along the wires.
11) IMPORTANT - These three layers of super quality ferrocement - forming the first 8 - 10 mm of the section are the essential barrier to chloride penetration and crack control.

IF…repeat…IF…. the surface of ‘gel coat’ is damaged and corrosion starts to form on the bare metal where expanded metal is sheared in manufacturing, the oxidation is minimal and is restricted to the cut ends of the sheared metal.

The sheet metal used to manufacture the expanded metal is galvanised in the first place!
“The process of oxidation (rusting) of the fine wire ends of expanded metal sheeting is never stronger than the surrounding matrix of quality mortar so ‘spalling’ as known in normal poor concrete work, does not occur in this type of quality ferrocement. In fact, the slight expansion of fine wire oxidation actually ‘tightens’ the matrix in the area and further oxidation is prevented. A ‘gel coat’ and expanded metal crack control form a perfect protective layer.”

12) IMPORTANT - The placing of ‘steel reinforcement’ closer to the outside of any element cross section and away from the ‘neutral’ axis provides a more efficient use of steel.
13) IMPORTANT - We have found that 2 to 3 mm of cover of sprayed mortar is adequate to prevent moisture penetration and two layers of expanded metal can be regarded as a ‘sacrificial layer’ protecting the more important reinforcements subsequently added into the section.

The concrete industry appears not to recognise the very simple ferrocement truths described here as it creates rules and regulations requiring cover of concrete to reinforcing bars. Perhaps the industry has ignored the benefits of ferrocement in their self-interest to sell the maximum amount of sand cement and aggregate when in fact a more careful use of a better quality material (ferrocement) has been ignored, or possibly forgotten for the commercial interests of the sand, cement aggregate industry with their desire to sell more volume / tonnage of material? It is hard for conventional concrete workers and engineers to understand and realise that a cover of 2 – 3 mm of quality sprayed concrete as opposed to a more usual 20 – 30 mm – of poured and vibrated concrete is impermeable in the marine environment. [3]

## PRESENT SITUATION

### Current Methods of Construction

At the moment Ferrocement as a structural material has largely been forgotten, except where enlightened architects have used Ferrocement for unusual structures. Recent examples include deMenil Museum, Houston, Yanbu’al Bahr Cement Plant, Saudi Arabia and the recently completed Ferrocement Solar Roof structure to the Stavros Niarchos Cultural Centre, Athens.

Engineers tend to think only of steel when designing marine structures. Steel has the problems of maintenance against corrosion and the costs of maintenance dissipate revenue earned from the structure.

The structures are created on land, transported to the coast, loaded onto ships, towed or carried out to site, lifted into the water and secured in place. This is a very expensive and inefficient method of installing wind, wave and tidal structures into the Ocean.

We can make concrete float - so why go to the expensive of lifting it about?

### Proposed Future Methods of Construction

A more cost effective method would be to use Ferrocement as the main construction material for these wind, wave and tidal structures.

The ideal material is a combination of steel and concrete (Ferrocement), which does not require excessive maintenance. The structures could be created in a dry-dock and floated out to site. They could then be sunk into position and secured onto the seabed with ballast. Once the device has reached its end of life, then the structure could then be de-ballasted and re-floated to be towed away for recycling.

By using horizontal casting of Ferrocement plates – used as a permanent shuttering – cellular structures can be built and filled with concrete or ballast as required by design.

By incorporating this material and new techniques, cost of maintenance would be lower, cost of production and transport would be lower and cost to the environment would be better.

“Our objective is to produce more with less.” For the benefit of all.

## DEVELOPMENTS/PATENTS/TESTING

Trafalgar Marine Technology Ltd. are developing High Tensile Laminated Ferrocement Plates (Patents Pending), which are horizontally casted to make permanent shuttering.

These ‘innovative and disruptive ‘construction methods offer reduced CAPEX and OPEX for marine renewable energy structures.

We have a system (Patent Pending) whereby horizontally casted plates can be offered together in a self-locking system to form a cross section of cellular structure and void areas through which additional stressing wires can be installed through that structural cross section and the whole cross section or void can subsequently be filled with self-compacting concrete. This system will offer considerable savings in construction costs, producing a very high quality structure that requires little maintenance.

Recent Testing of Laminated Ferrocement beams and plates is being funded under an EU Innovation Futures programme at Sheffield Hallam University.

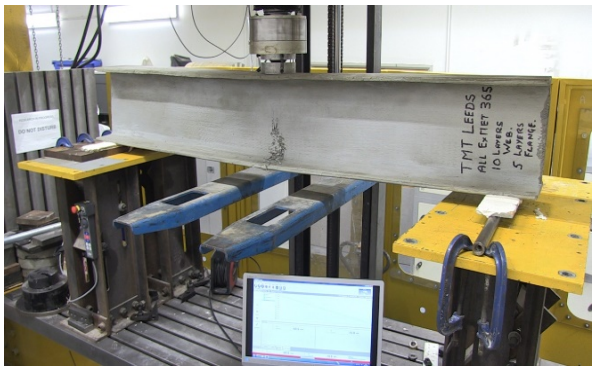


Figure 8 Exmet beam under test

Figure 9 Exmet Plate under test

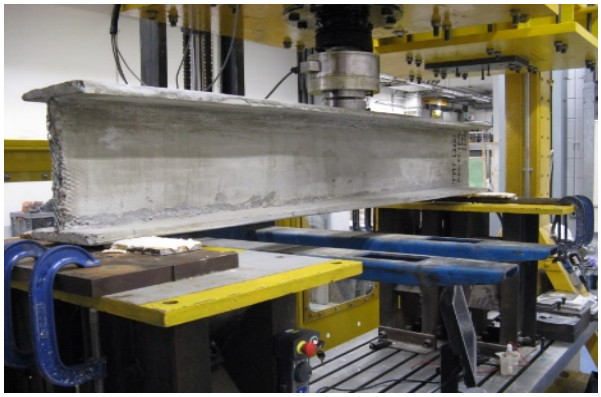

Figure 10 Exmet & A142 Beam under test

Figure 11 Exmet & A142 plate under test

Note the cracking mechanisms of the beam under test and the bending of the Ferrocement plates shown in Figures 8, 9, 10 & 11.

Ferrocement does not collapse in a catastrophic break - it tears - as the stresses pull apart the Multi-layers of small meshes in the laminate.

## MARKETS

For concrete to play its part in combating global warming, and to tackle the ever increasing excessive climate change weather events and to generally reduce our production of CO2 we need to do more with less……..

The cement industry has made great efforts to reduce CO2 production from cement manufacturing process and to blend many materials to extend and improve ordinary portland cement. These improvements in cement chemistry and production, together with the application of super plasticisers to produce self-compacting concretes, can equally be applied to self-compacting mortars and used with multi-reinforced Ferrocement Laminate to produce a material more akin to steel plate than has been previously produced.

By joining plates of Laminated Ferrocement with a sprayed concrete/mortar we can ‘Concrete weld’ flat plates together to form cellular structure.

By applying High Tensile Steel materials into a relatively thin cross section of Laminated Ferrocement we produce a truly remarkable construction material incorporating all the benefits of steel and concrete - the most widely used construction material in the world.

The application of High Tensile Laminated Ferrocement in permanent shuttering construction systems offers the world wide construction business and the growing markets for marine renewable energy structures, an innovative but disruptive method to improve construction performance across the board.

Wind Turbine Gravity Bases and Turbine Towers. Tidal energy device structures. Floating. Turbine support structures. Wave energy devices. Ships and large pontoon structures.

Engineers presently use steel, which has to be maintained, because we have a lack of knowledge about the potential applications of Ferrocement.

Our objectives at Trafalgar Marine Technology Ltd are to demonstrate and market our systems to the construction industry and we seek co-operations with academia and the industry to bring about all round improvements so that Construction UK can best exploit our vast marine energy resources to power our Nation.

## SUMMARY

The original reinforced concrete material (Ferrocement) can be considerably improved by the application of innovative and disruptive technology, the product of recent improvements in cement manufacture and chemistry, to reduce costs and improve productivity.

The application of these innovations into High Tensile Laminated Ferrocement will produce a material more akin to steel and provides considerably more benefit to the construction of marine renewable energy structures than steel.

We need now to amend the University Engineering Curriculum and to teach again the History of Ferrocement to better understand the ‘roots’ of our construction industry.

Then we need to apply recent developments in ‘innovative and disruptive ‘systems to reduce cost of manufacturing / production.

We need to produce more with less and to produce better quality by application of knowledge - it is possible.

“If you put steel into the Ocean, best you wrap the steel in quality concrete (Ferrocement) Otherwise the costs of maintaining the steel (painting both inside and out) will dissipate the revenue earned from the structure and this will deplete the ‘bottom line”.

## REFERENCES

1. NAAMAN A.E. Ferrocement & Laminated Cementitious Composites, 2000, ISBN 0-9674939-0-0, p xiii.

2. NAAMAN A.E. Ferrocement 6 Lambot Symposium, University of Michigan, 1998, front cover.

3. PEMBERTON J.M. PULLAN M. TUCKER T. Ferro-11 Proceedings of the 11th International Symposium on Ferrocement and 3rd ICTRC International conference on Textile Reinforced Concrete, Ferro-Past and Ferro-Future, 2015, pp407-415.

# REQUIREMENTS AND POSSIBLE SIMPLIFICATIONS FOR MULTIONIC TRANSPORT MODELS – CASE OF CONCRETE SUBJECTED TO WETTING-DRYING CYCLES IN MARINE ENVIRONMENT

**A Soive**
Cerema

**V Baroghel-Bouny**
IFSTTAR
France

**V-Q Tran**
Ecole Centrale de Nantes

**ABSTRACT.** In this paper, a physically and chemically based model, which describes coupled ion-moisture transport, is used to simulate chloride ingress in concrete elements subjected to wetting-drying cycles in marine environment. Various assumptions are tested, in order to quantify the influence of taking into account thermochemistry such as Friedel's and Kuzel's salts precipitation on the ingress kinetics or to underline the differences between complex model and very simple one (assuming saturated conditions in the latter case). Numerical simulations are compared to experimental chloride concentration profiles, obtained on OPC concrete specimens exposed to 6 h / 6 h seawater wetting-drying cycles in lab (where RH and T are controlled). The results show that when the initial amounts of hydration products are known, the assessment of the chloride binding parameters is not needed. In addition, including thermochemistry in the model improves the predictions, in particular with regard to pH value that can be used as rebar depassivation evaluation criterion. Moreover, the "intrinsic" permeability value and the boundary layer thickness that reflects the evaporation kinetics are not important parameters for the studied concretes. Updating at each time step the transport properties in order to account for dissolution / precipitation of mineral species hardly affects the chloride profiles. Simulations carried out in saturated conditions provide good results compared to those obtained when accounting for wetting-drying cycles, notwithstanding such simulation avoids the problematic assessment of the "intrinsic" permeability. The results require further analyses for higher or smaller permeabilities and for different wetting-drying cycle frequencies to predict RC service life.

**Keywords:** Chloride ingress, Wetting-drying cycles, Thermochemical model, Concrete

**Anthony Soive** is a researcher at Cerema, a new public body in support of national and local authorities in the field of sustainable development. His research field covers RC durability.

**Véronique Baroghel-Bouny** is the Director of the Mix-design, microstructure, modelling and durability ($FM^2D$) Laboratory at IFSTTAR. She is in charge of various research projects and working groups. Her research field covers microstructure of cement-based materials and various aspects of RC durability with special interest in new concretes.

**Van-Quan Tran** is a PhD student at Ecole Centrale de Nantes, France. He works on thermochemical model for simulating corrosion initiation in concrete subjected to seawater.

## INTRODUCTION

The main deterioration cause for reinforced concrete structures exposed to marine environment is the corrosion induced by chloride penetration into concrete. Owing to the expensive costs of repair and maintenance it is highly requested to develop reliable models intended to predict the chloride concentration profiles in tidal zone where the corrosion is occurring faster than in the other zones in the structure.

Many studies have been dedicated to the modelling of chloride transport through unsaturated concrete by taking into account diffusion and convection. Some are based on an approach that describes moisture ingress as a pure Fickian process [1]–[5]. They used semi-empirical laws found by fitting experimental data to get the relationship between moisture diffusivity and the chloride diffusion coefficient. Others are coupled moisture-multionic transport models that take into account advection and diffusion process for liquid and gas [6], [7]. However, these models have a number of limitations. First, they cannot be applied to all types of concrete since they use empirical relationship for the chloride binding isotherm. Few models take into account both Friedel's salt precipitation and "physical" binding onto C-S-H [8], [9] but they do not have been used with seawater. Second, pH calculation is often missing. However, the aim of chloride transport modelling is to lead to a better understanding of the mechanisms and to a better estimation of the time needed to reach a given critical or threshold value, which induces depassivation, at the first layer of reinforcement. Several threshold expressions need the hydroxide concentration [10], [11]. Then chloride ion propagation models involve the evolution of the pH in the cementitious material.

Furthermore, transport in unsaturated concrete involves many complex mechanisms. The number of parameter that describes the various phenomena involved can be significant. The modelling requires taking into account the transport of liquid water and that of the gas phase (air and water vapour), and the transport of the ions contained in seawater. With regard to moisture transport, a number of studies have been performed on the drying process and how to model it [12]–[15]. They show that, in addition to water vapour sorption isotherm and to the conventional parameters related to transport ("intrinsic" permeability, and diffusion coefficient), it is necessary to estimate an evaporation layer thickness over which diffusion occurs [16].

Faced with this situation, the main objectives of the study described in the paper is to evaluate the influence of several parameters dedicated to in order to identify possible simplifications and requirements for transport models in concrete subjected to wetting-drying cycles in marine environment. A numerical simulation program for chemically reactive non-isothermal flows of multiphase fluids in porous and fractured media [17], has been used. The interaction between chlorides and monosulfate are deduced from the modelling of the precipitation of salts, such as Friedel's or Kuzel's salts [18], [19]. With regard to the chloride binding onto the C-S-H surface [20], a linear adsorption that depends on the initial C-S-H amount is adopted here by sake of simplicity. The influence of a number of parameters is then evaluated, as the "intrinsic" permeability, the evaporation layer thickness, updating porosity and permeability. The numerical results have been compared to experimental data measured concrete samples subjected to wetting-drying cycles in lab. The differences between a complex model and a very simple one (assuming saturated conditions in the latter case) are also evaluated.

In the present paper, section 1 describes the experimental set-up used for exposing concrete specimens to wetting-drying cycles with natural seawater and controlled environmental conditions. Section 2 depicts the governing equations used to simulate moisture and ionic transport in non-saturated cementitious materials. Section 3 introduces the predicted and experimental chloride concentration profiles.

## EXPERIMENTAL STUDY

### Concrete Mixtures

The experimental study was carried out on one normal-strength OPC concretes submitted to wetting/drying cycles with seawater in lab (BO). The mix proportions of this concrete are summarized in Table 1. The aggregates are composed of limestone gravel and calcareous and silico-calcareous sand. The cement used is a CEM I 52.5 PM ES CP2. The mix-design principles of these concretes are explained in [21].

Table 1. BO concrete mix-design [21]

| LIMESTONE GRAVEL 4/20, kg/m³ | CALCAREOUS AND SILICO-CALCAREOUS SAND 0/5, kg/m³ | CEMENT CEM I 52,5, kg/m³ | WATER, kg/m³ | w/c |
|---|---|---|---|---|
| 1192 | 744 | 353 | 152 | 0.43 |

### Experimental Procedure

The BO concrete was cast in cylindrical specimens (thickness = 100 ± 1 mm; diameter = 110 mm). After demould, the non-curved surfaces were polished to have plane and clean surfaces. The specimens were immersed into water during 1.5 years. Then, a dense epoxy coating was applied to lateral surface and one face, leaving an exposed plane surface to ensure a one-dimensional flow inside the cylinders.

The samples were submitted to 72-h vacuum saturation with a 0.1 N NaOH solution prior to exposure to wetting and drying cycles. Each specimen was exposed to 2 daily cycles of 6 hours of seawater penetration (seawater extracted from the bay of Saint-Brieuc in northern France) and drying for 6 hours. During drying, a fan ensured a well-mixed atmosphere in the chamber. BO samples were exposed during 90 and 180 days. Temperature (T = 20±1°C) and relative humidity (RH = 65±5%) were controlled thanks to an air-conditioning system.

### Measurements

Total and free chloride concentration profiles have been measured on cores at given depths. A Profile Grinder was used to extract powder (< 80 μm) from the samples over a 50 mm disk and allows a 2 mm penetration increment. The total chloride concentration (resp. free chloride concentration) has been assessed by means of nitric acid (resp. water) extraction and potentiometric titration (by using a 0.01 N $AgNO_3$ solution), according to the AFPC-AFREM procedure [22].

## MODELLING APPROACH

A physically and chemically based model, which describes coupled ion-moisture transport, is used to simulate chloride ingress in concrete elements subjected to wetting-drying cycles in marine environment. The transport equations for moisture are first exposed. Ionic transport and dissolution / precipitation of mineral species follow.

### Moisture Transport

The mass balance equation used can be written in a general form (Equation 1 [23]).

$$\frac{d}{dt}\int m^i\,dV = \int J^i.ndS + \int q^i\,dV \qquad 1$$

Which leads to 2 by applying Gauss divergence theorem:

$$\frac{d}{dt}m^i = -div(J^i) + q^i \qquad 2$$

Where *m* represents mass per volume, *J* mass flux, *q* sinks and sources and *i* labelling the components (water, air). The mass accumulation term and mass fluxes read:

$$m^i = \phi \sum_\beta S_\beta \rho_\beta X_\beta^i \qquad 3$$

$$J^i = \sum_\beta X_\beta^i \left[-k\frac{k_{r_\beta}\rho_\beta}{\mu_\beta}\left(\nabla P_\beta - \rho_\beta g\right)\right] - \sum_\beta \rho_\beta D_\beta^i \nabla X_\beta^i \qquad 4$$

Where $\phi, S_\beta, \rho_\beta, k, k_{r_\beta}, \mu_\beta, P_\beta$ are the porosity accessible to water, degree of saturation, density, "intrinsic" permeability, relative permeability of phase $\beta$, dynamic viscosity and pressure of phase $\beta$, respectively. $X_\beta^i$ is the mass fraction of component *i* present in phase $\beta$ and $D_\beta^i$ the diffusion tensor.

The relative permeabilities to liquid and gas is assumed to be expressed as a function of liquid saturation, as proposed by Van Genuchten (Equation 5) [24]., and Corey (Equation 6) [25], respectively.

$$k_{r_l} = \sqrt{\tilde{S}}\left[1 - \left(1 - \tilde{S}^{1/\lambda}\right)^\lambda\right]^2 \qquad 5$$

with $\tilde{S} = \left(S_l - S_{l_r}\right)/\left(S_{l_s} - S_{l_r}\right)$

$$k_{rg} = (1 - S^*)^2\left(1 - S^{*2}\right) \qquad 6$$

with $S^* = (S_l - S_{lr})/\left(1 - S_{lr} - S_{gr}\right)$

where $S_{lr}$ and $S_{gr}$ are residual liquid and gas saturation, respectively.

The liquid pressure is a function of the capillary pressure, Pc, and the gas pressure (Equation 7). The capillary pressure is assumed to be expressed as a function of liquid saturation, as proposed by Van Genuchten (Equation 8) [24]:

$$\boldsymbol{P_l = P_g - P_c} \quad 7$$

$$\boldsymbol{P_c = -P_0 \left( \left[ \tilde{S} \right]^{-1/\lambda} \right)^{1-\lambda}} \quad 8$$

In this system of equations, the gaseous phase is assumed to be the result of the mix between two ideal gases (dry air and water vapour). The mix is also considered as ideal leading to the fact that the total gas pressure is equal to the sum of the pressures of the two gases described before. The vapour adsorption and desorption are described by the same parameters that result from equation 10 and the Kelvin equation that express capillary pressure as a function of relative humidity. Skeleton is incompressible and non-expansive.

In addition, several hypotheses were done in order to simplify the system of equations. First, gravity forces are negligible compared to forces due to pressure. Second, relative humidity and liquid pressure are supposed to be independent of the concentration of ions in the solution. This point will be discussed further in the results section. Finally, dynamic viscosity and density are supposed to be independent of the NaCl amount [26].

**Ionic Transport**

In unsaturated porous media, the species transport in the material is driven by convection and diffusion. At a local scale two fluxes are then associated: a diffusive and an advective flux. Fick's first law can approximate the first one where each species has the same diffusion coefficient. This assumption insures the electroneutrality of the system. Fick's first law is preferred here to Nernst-Planck approach since it is simpler and its less computing-time consuming. In addition, in Nernst-Planck approach only primary species (e.g. $Na^+$, $Cl^-$, $SO_4^{2-}$ etc.) are supposed to propagate. However, primary species react in the solution to form aqueous complexes (that reactive geochemical transport modelling are able to simulate). Such reactions lead to electronic charges that can be very different from primary species generally used. The advective flux depends on fluid velocity that is calculated by moisture transport model. The total flux is given by the sum of the two fluxes (Equation 9):

$$\boldsymbol{J = -D_e \nabla C + u_l C} \quad 9$$

where $\boldsymbol{J}$ is the total flux (kg/m²s), $\boldsymbol{\nabla}$ is the gradient operator, $D_e$ a tensor of second order which represents the effective ionic diffusion coefficient in the porous media (m²/s), C the concentration of ions in the solution (kg/m³ of solution) and $u_l$ the water velocity vector.

In addition, chloride ions can be bound to the concrete matrix. Nevertheless, in order to avoid the use of empirical parameters for binding isotherm, a thermochemical model is used. Such a model allows one to simulate the precipitation of mineral species (e.g. Friedel's salt). This is described in the next section. For the chloride binding on C-S-H, the model should describe the Stern double layer [27]. However, by sake of simplicity, a linear adsorption is supposed and calculated from the initial C-S-H amount.

Finally, although several ionic species present in the seawater are taken into account in the model, one unique and constant effective diffusion coefficient was adopted. It is considered as a function of tortuosity, τ, porosity, and pure diffusion coefficient of species, $D_0$ in water:

$$\boldsymbol{D_e = \Phi \tau S_l D_0} \qquad 10$$

The ionic species in the liquid phase are not supposed to diffuse in the gas phase.

**Dissolution / Precipitation of Mineral Species**

When the solution is not equilibrium state, one can calculate the ion activity product $Q$ for one mineral species that is the product of the species concentration formed divided by the product of the species concentration consumed. This equilibrium is controlled by the law of mass action. The ratio between $Q$ and the thermodynamic solubility product $K$, enters the definition of the saturation index $IS$, expressed as:

$$\boldsymbol{IS = log_{10}\left(\frac{Q}{K}\right)} \qquad 11$$

When $IS = 0$, equilibrium is reached. When $IS < 0$, the solution is undersaturated and the mineral species should dissolve. On the contrary, when $IS > 0$ the solution is supersaturated and the mineral species should precipitate. Hence, at each time step, $Q$ is calculated for each mineral species and compared to its solubility product.

The geochemical reactions rate is supposed to be large with respect to the ionic and fluid transport processes. In this particular case, the local chemical equilibrium was assumed to be preserved throughout the porous system. This hypothesis is usually valid in most practical cases involving the diffusion of ions in fluid saturated systems [28], [29].

## NUMERICAL METHODS AND INPUT DATA

**Boundary Conditions**

During drying, strong capillary forces are present as a result of the gradient between the vapour partial pressures in the material and in the atmosphere. Schlünder [12] and other [13]–[15] works have shown that evaporative fluxes from wet porous surfaces are constrained by the saturation degree of the material and transport properties of the porous medium, and by the vapour transport across the boundary air layer adjacent to the surface [12]–[15].

Under typical natural conditions (airflow velocity U1< 4 m/s), Haghighi et al. showed that the contribution of advection is relatively minor compared to diffusion porous media (pore sizes < 1000 mm) [15]. Nevertheless, in such an approach, it is necessary to estimate an evaporation layer thickness over which diffusion takes place. Gezzehei et al. suggested values between 5 and 20 mm by inverse analysis [30].

From a numerical point of view, the most mechanistic approach to simulate evaporation is to define an air-mass fraction in the atmosphere that corresponds to the relative humidity value, and then actually simulate vapour diffusion from the material surface through the laminar boundary layer (the thickness of which depends on surface roughness and wind velocity etc.) to the well-mixed atmosphere [30], [31].

However, by sake of simplicity and recognizing that both relative humidity and capillary pressure reflect a "water potential", evaporation is approximated by imposing a capillary suction in the boundary element. This capillary suction corresponds to the relative humidity in the atmosphere thanks to Kelvin's equation. Then the boundary layer thickness may be an important factor for evaporation kinetics. Unfortunately, this thickness is very difficult to assess. Gezzehei et al. suggested values between 5 and 20 mm [30] by inverse analysis. These extreme values will be tested in this study.

During wetting, 100% HR is imposed and the concrete is in contact with seawater. The ionic species concentration present in the Atlantic Ocean seawater and adopted here are given in Table 4. By sake of simplicity and due to convergence difficulties of the wetting-drying model, dissolved $CO_2$ is not considered in the seawater composition.

Table 2. Seawater ionic composition for the Atlantic Ocean, mol/l

| $Cl^-$ | $Ca^{2+}$ | $SO_4^{2-}$ | $K^+$ | $Mg^{2+}$ | $Na^+$ |
|---|---|---|---|---|---|
| 0.546 | $9.97\ 10^{-3}$ | $2.76\ 10^{-2}$ | $9.71\ 10^{-3}$ | $5.22\ 10^{-2}$ | 0.459 |

## Hydrated concrete properties and mineral species

The use of a coupled transport/thermochemical model, in order to model the propagation of ions in concrete permits to avoid the use of empirical parameters such as binding isotherm parameters that are dependent of the concrete mix-design. Nevertheless, the initial amount of the various hydration products in the concrete is required as input data. A model of hydration is used, based on Thiery et al. work [32] in order to assess such data (Table 3).

Table 3. BO phase results with hydration model

| PHASE | FORMULATION | VOLUME FRACTION OF SOLID |
|---|---|---|
| $C_3AH_6$ | $Ca_3Al_2(OH)_{12}$ | $5.88\ 10^{-3}$ |
| Jennite | $Ca_{1.67}SiO_2(OH)_{3.33}{:}\,H_2O$ | $1.31\ 10^{-1}$ |
| Ettringite | $Ca_6Al_2(SO_4)_3(OH)_{12}{:}\,26H_2O$ | 0 |
| Monosulphate | $Ca_4Al_2(SO_4)(OH)_{12}{:}\,6H_2O$ | $1.63\ 10^{-2}$ |
| Portlandite | $Ca(OH)_2$ | $4.34\ 10^{-2}$ |

A database has been built according to [33]. The C-S-H (assumed here as jennite) was considered as a single phase gel. Table 4 shows a part of the database where the mineral phases were supposed to react.

Table 4. Thermodynamic properties at T=25°C for the hydrated products and mineral species that may precipitate

| MINERAL | log(K) |
|---|---|
| $C_3AH_6 + 12H^+ \rightarrow 3Ca^{2+} + 2Al^{3+} + 12H_2O$ | 80.88 |
| Jennite $+ \ 18H^+ \rightarrow 9Ca^{2+} + \ H_4SiO_4(aq) + \ 8H_2O$ | 147.34 |
| Ettringite $+ 12H^+ \rightarrow 2Al^{3+} + \ 6Ca^{2+} + 3SO_4^{2-} + \ 38H_2O$ | 56.67 |
| Monosulphate $+ 12H^+ \rightarrow 4\ Ca^{2+} + 2Al^{3+} + \ {SO_4}^{2-} + \ 18H_2O$ | 72.44 |
| Portlandite $+ 2H^+ \rightarrow Ca^{2+} + \ 2H_2O$ | 22.76 |
| Halite $\rightarrow Na^+ + Cl^-$ | 1.60 |
| Friedel_Salt $+ 12.05H^+ \rightarrow 2Al^{3+} + \ 4Ca^{2+} + 1.95Cl^- + 16.05H_2O$ | 76.14 |
| Kuzel_Salt $+ 12H^+ \rightarrow 2Al^{3+} + \ 4Ca^{2+} + 1Cl^- + 0.5{SO_4}^{2-} + 18H_2O$ | 73.24 |

### Numerical procedure

The simulations were performed in 1D, due to the symmetry of the system. A simple mesh composed of one 100-element row was used and represented the length of the sample. Calculations are managed with a code developed in Python [34]. This allows one to apply wetting-drying cycles by 1-hour time step without effort. At each time step a restart is running with the previous time step results.

## NUMERICAL RESULTS AND COMPARISON WITH EXPERIMENTAL DATA

### Friedel's and Kuzel's Salts

A simulation has been carried out on BO concrete with the proposed model. Figure 1 shows the precipitation and dissolution of concrete mineral species as a function of depth after 90 wetting-drying cycle days. It indicates that Friedel's salt and halite (NaCl) do not precipitate. Only Kuzel's salt is able to precipitate by consuming monosulfate and $C_3AH_6$. This can be explained by the presence of sulphate in seawater. The model also predicts precipitation of ettringite in the first millimetres. The pH remains basic (between 12 and 14, Figure 1) due to the presence of portlandite, except in the first millimetres due to leaching of the concrete and the total dissolution of portlandite. This leaching also leads to the important decrease of the Kuzel's salt amount (see also Figure 2 b).

### Influence of the "Intrinsic" Permeability Value

The influence of the "intrinsic" permeability value is evaluated by calculating free chloride concentrations as a function of depth with several permeability values (cf. Figure 2). Three permeability values are tested here: $3.10^{-21}$, $8.10^{-21}$ and $3.10^{-20}$ $m^2$. The first two were assessed by indirect method and Katz-Thomson formula [35], while the third one is 10 times the first one in order to test a concrete that may be micro-cracked.

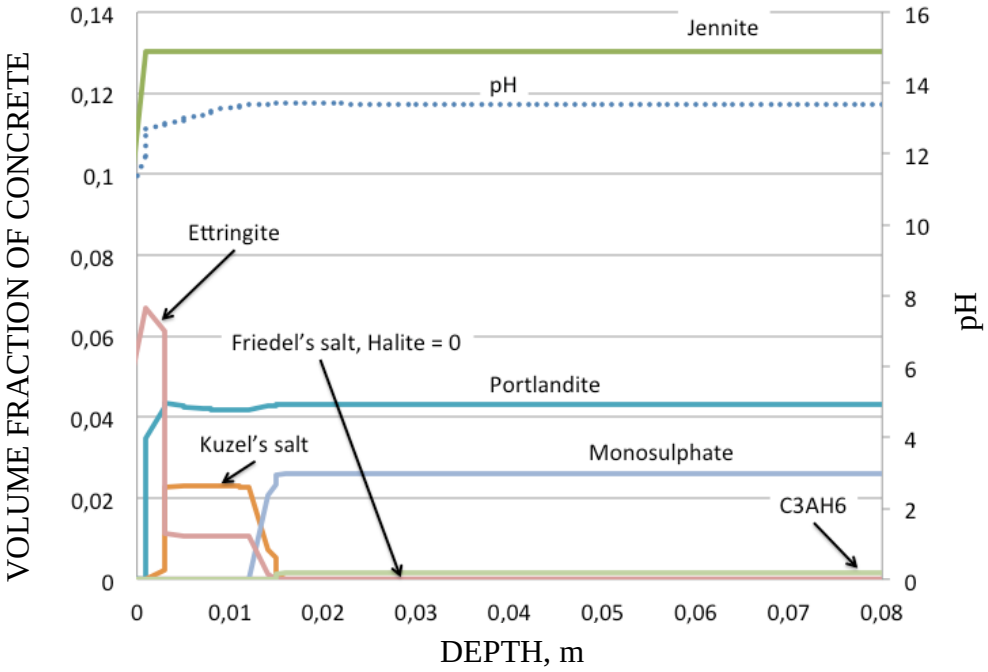


Figure 1. Precipitation and dissolution of concrete mineral species as a function of depth after 90 wetting-drying cycle days

Figure 2 a) shows that regardless of the permeability values the free chloride concentration profiles are very close to each other and provides quite good results compared to the experimented one. This can be explained by drawing the "drying depth" as a function of the permeability values after 90 days of exposure and time (Figure 3 a and b, respectively). This depth can be defined as the depth over which drying and wetting profiles are the same.

Figure 3 b) shows that the saturation profiles after only 2 days are very close to profiles after 90 days. Furthermore, the saturation profiles for various permeability values (Figure 3 a) show that the greater the permeability value the greater the drying depth. This result was expected since the liquid water transport is easier for more permeable material. The drying depth values are 10 mm, 20 mm and 30 mm for permeability values of $3.10^{-21}$, $8.10^{-21}$ and $3.10^{-20}$ $m^2$, respectively.

Total chloride concentration profiles are not satisfying since they are not close to experimental data (Figure 4). The main explanation is that the amount of ettringite is overestimated (Figure 1) since the sulphate is not adsorbed onto C-S-H in the model. Hence, Kuzel's salt dissolves in the first millimetres. Other explanations can be given. First, kinetics of precipitation are not taken account in this study, in particular for Kuzel's salt. However, the required thermodynamic data are missing in the literature to the author's knowledge. Second, adopting a linear "physical" adsorption isotherm in order to approximate adsorption isotherm onto the C-S-H leads to an underestimation of the bound chlorides for low free chloride concentration and to an overestimation for the high concentration compared to Freundlich or Langmuir isotherms. Third, the leaching in the first millimetres is probably overestimated since the model does not account for the presence of dissolved $CO_2$ in seawater. Hence the possible precipitation of monocarbonate that is more stable than monosulfate should limit the dissolution monosulfate amount.

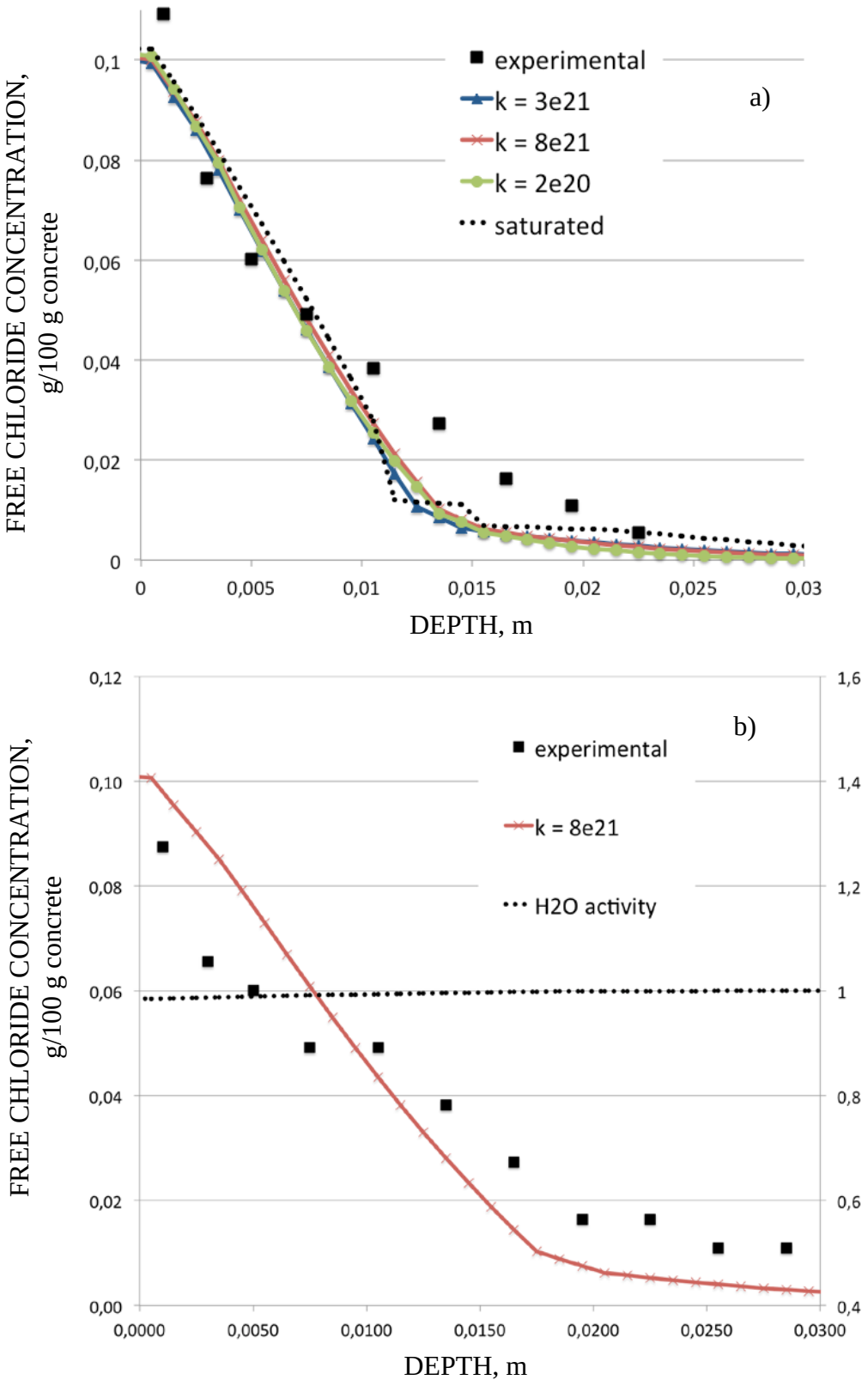


Figure 2. Free chloride concentration as a function of the depth, for BO
a) in various cases (several permeability values and the case of saturated concrete) after 90 days of exposure and
b) 180 days for k = 8 $e^{-21}$ $m^2$

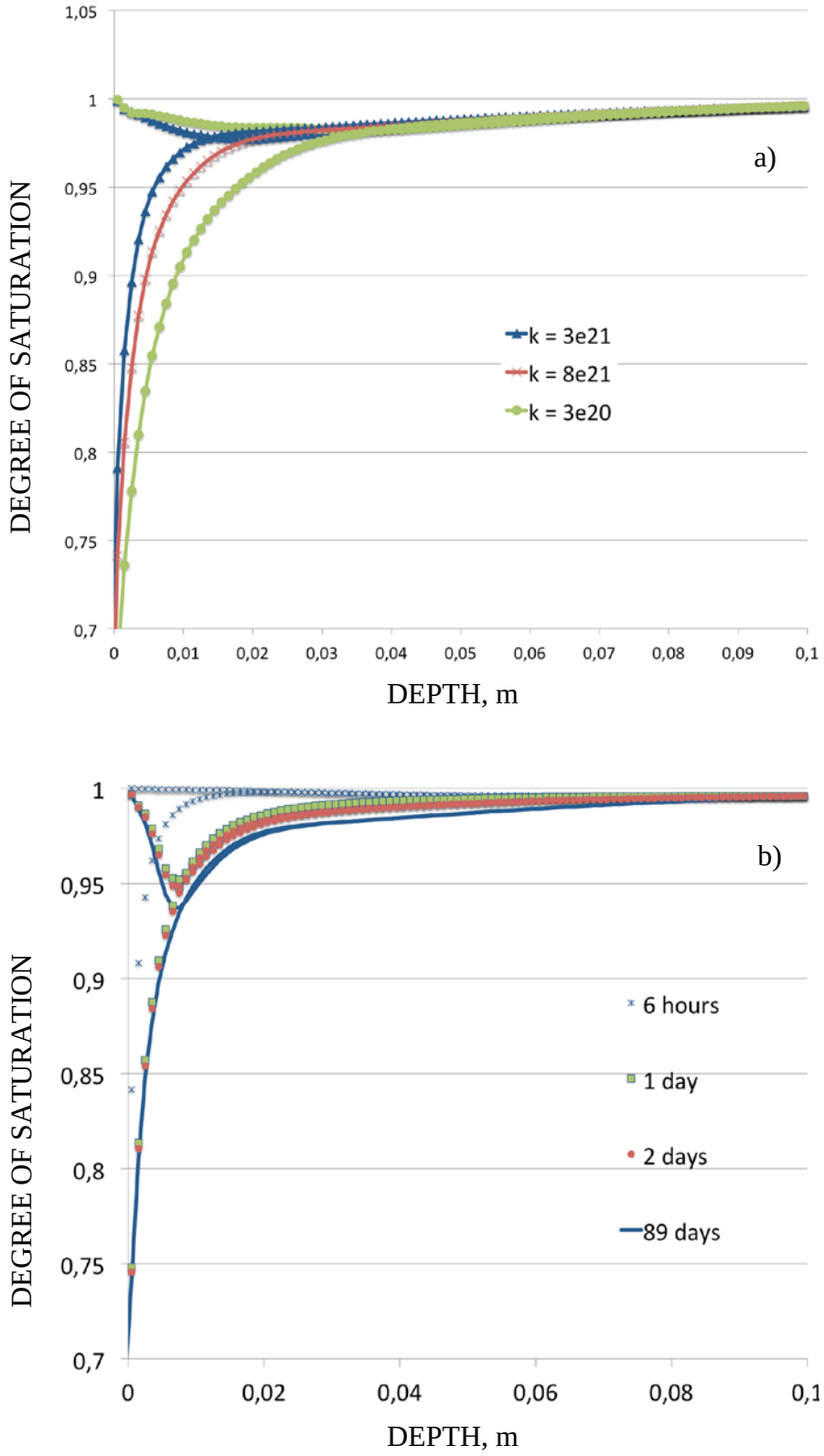


Figure 3. Evolution of saturation degree vs depth for
a) several "intrinsic" permeability values and
b) time evolution (intrinsic permeability = 8 $10^{-21}$)

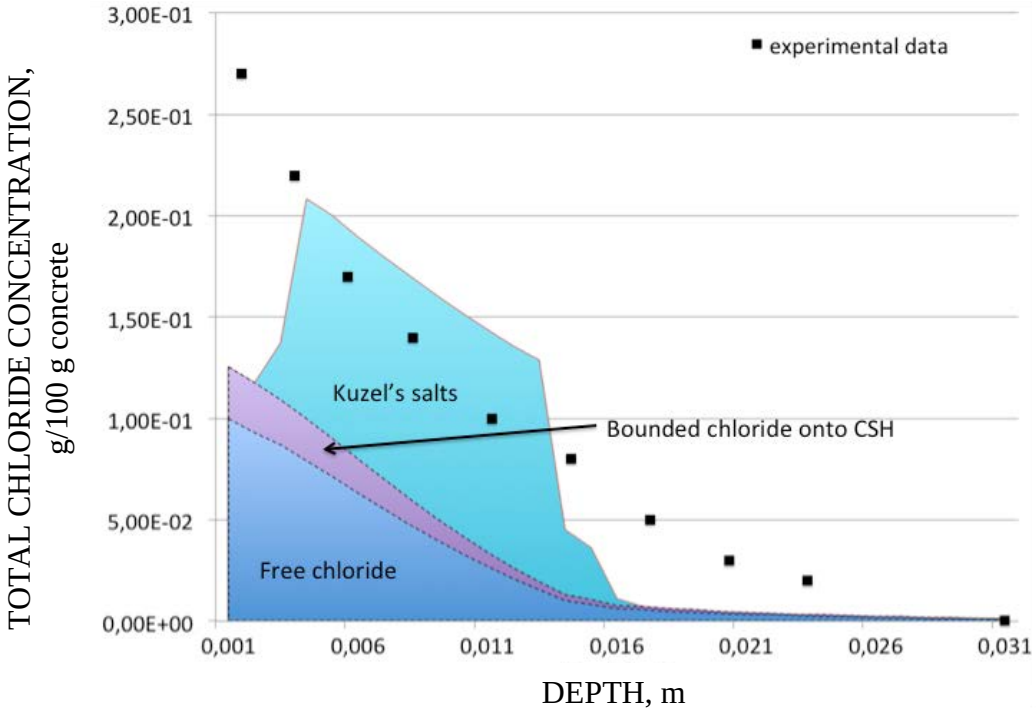


Figure 4. Total chloride concentration as a function of the depth for BO after 90 days of exposure

It should be noted that the vapour-pressure lowering caused by dissolved salts is not taken into account. The pore solution is considered as a dilute solution. This hypothesis is confirmed by the calculation of the chemical activity of water which remains very close to 1 (Figure 2 b).

**Influence of the Boundary Layer Thickness**

The values of the boundary layer thickness calculated by Ghezzehei et al. [30] have been tested. They correspond to different environmental conditions in which specimens are exposed: wind are present (d=5 mm) or not (d=20 mm). Despite the presence of a fan in the chamber the specimens are not exposed to ventilation, since the surface in contact with seawater is the bottom of the specimens. A value of 20 mm should rather be chosen.

The results show that free chloride concentration profiles are not very sensitive to the thickness of the boundary layer (Figure 5). This can be explained by the fact that the wetting-drying cycle frequency is relatively high and that the drying depth is small as explained in the previous section (Figure 3).

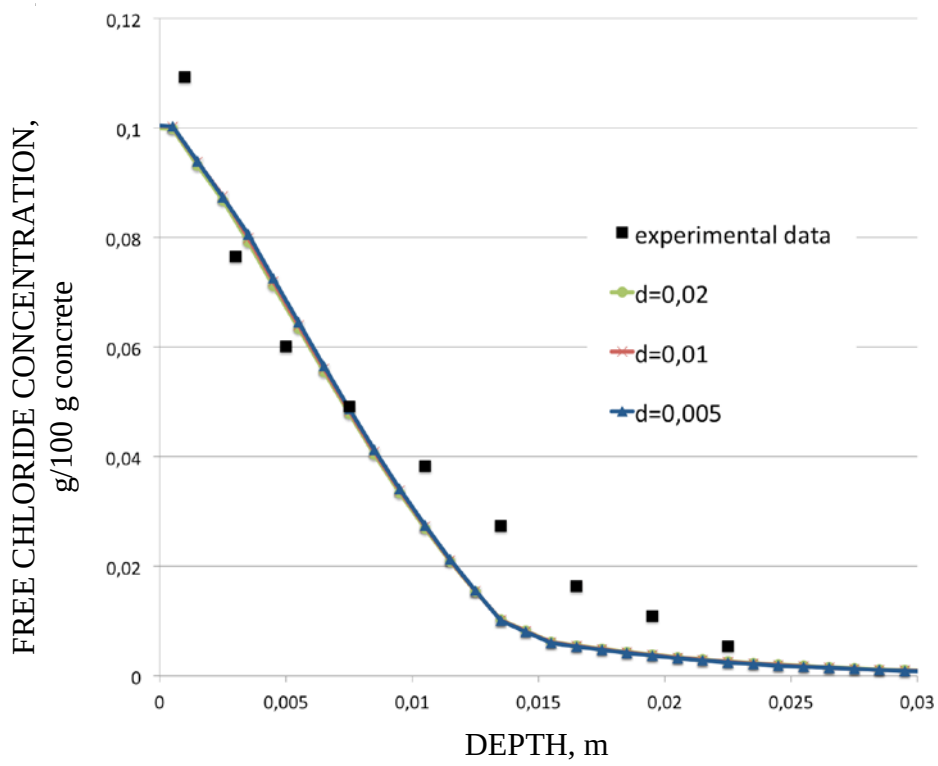


Figure 5. a) Free chloride concentration and b) total chloride concentration as a function of the depth for BO after 90 days of exposition and for various boundary layer thickness values (intrinsic permeability = 8 $10^{-21}$)

**Wetting-Drying Cycles vs. Saturated**

Considering the high frequency of the wetting-drying cycles, it can be relevant to compare the results provided by the model described here to those obtained by means of a simpler model assuming saturated conditions. Such a model is less time consuming and the number of parameters is smaller. Figure 2 a) shows that the free chloride profile is close to experimental results. Hence, it is reasonable, in the case considered, to assume that the concrete is permanently saturated. Such an assumption have to be further discussed for higher and lower intrinsic permeability value and for other wetting-drying cycle frequencies.

**Effect of Discounting Transport Properties**

Transport properties can be updated by calculating the material porosity $\phi$ as a function of the volumes of dissolved and precipitated mineral species (Equation 12). Hence, the permeability can be expressed thanks to Carman-Kozeny [36] empirical law (Equation 13).

$$\boldsymbol{\phi = 1 - \sum_{i=1}^{n} f_{r_i}} \qquad 12$$

where $n$ is the number of minerals, $f_{r_i}$ is the volume fraction of mineral m in the material (Vmineral/Vmedium, including porosity).

$$k = k_i \frac{(1-\phi_i)^2}{(1-\phi)^2}\left(\frac{\phi}{\phi_i}\right)^3 \qquad 13$$

The results show that the effect of the permeability updating is limited. Nevertheless, such an updating needs to be used with caution. First, the change of average porosity is an approximation of the poral distribution one. Second, the actual relationship between porosity and permeability is still an open debate.

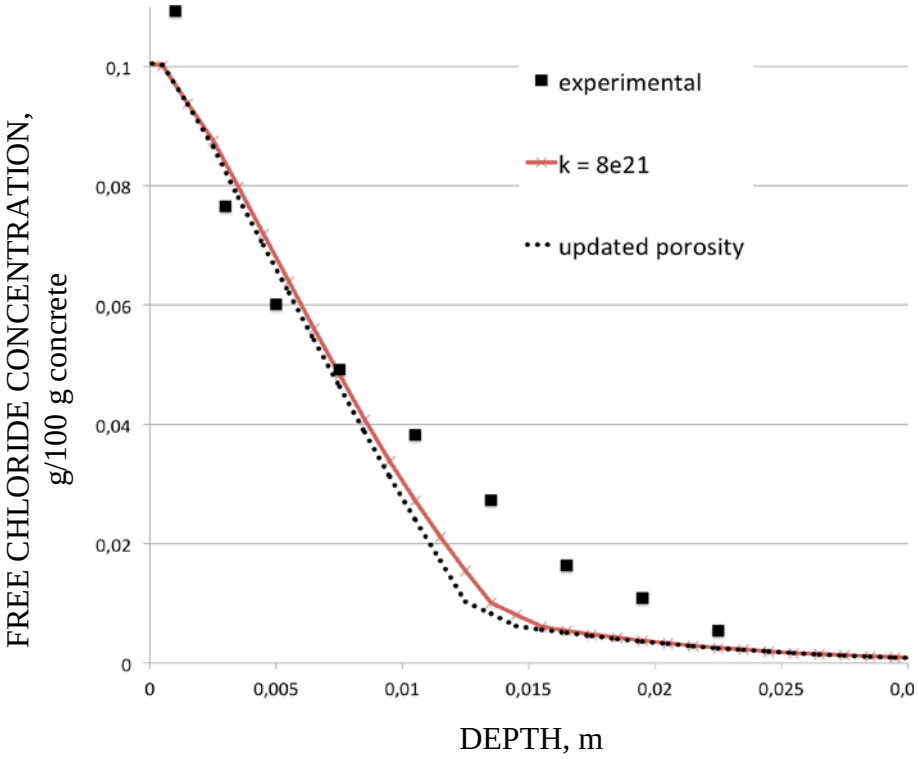


Figure 6. a) Free chlorides concentration as a function of depth for BO after 90 days of exposure. Comparison between profiles with and without properties actualization

## CONCLUSIONS

The main objective of the study was to evaluate the influence of several parameters in order to identify possible simplifications and requirements for transport models in concrete subjected to wetting-drying cycles in marine environment. A physically and chemically based model, which describes coupled ion-moisture transport, was used to simulate chloride ingress in concrete elements subjected to wetting-drying cycles in marine environment.

The influence of a number of parameters is then evaluated, such as the “intrinsic” permeability, the boundary layer thickness, updating porosity and permeability. Numerical simulations were compared to experimental chloride concentration profiles obtained on an OPC concrete specimen exposed to 6 h / 6 h seawater wetting-drying cycles in lab (where RH and T are controlled).

The results show that the “intrinsic” permeability value and the boundary layer thickness that reflects the evaporation kinetics do not play a significant role on the chloride propagation kinetics and the drying depth value. Updating at each time step the transport properties in order to account for dissolution / precipitation of mineral species does not change very much the chloride profiles as well.

Furthermore, simulations carried out in saturated conditions provide good results compared to those obtained when accounting for wetting-drying cycles for the studied concrete. This result is interesting since such a simulation avoids the problematic assessment of the “intrinsic” permeability.

Nevertheless, these results have to be further discussed for higher or smaller value and for different wetting-drying cycle frequencies in order to predict RC service life. Finally, including reactive geochemical modelling in the model improves the predictions, in particular with regard to pH value that can be used as rebar depassivation evaluation criterion.

However, the model needs further improvements such as a complete description of the adsorbed ionic species onto mineral species such as C-S-H and the introduction of kinetics of mineral dissolution and precipitation.

Furthermore, the effect of $CO_2$ has to be considered since it reacts with monosulfate to precipitate monocarbonate that is more stable than monosulfate in the presence of chloride.

## REFERENCES

1. SAETTA A.V., SCOTTA R. and VITALIANI R. Analysis of chloride diffusion into partially saturated concrete, ACI Mater. J., Vol. 90, No. 5, 1993, pp. 441–451.

2. ABABNEH A., BENBOUDJEMA F. and XI Y. Chloride penetration in non saturated concrete, J. Mater. Civ. Eng., Vol. 15, No. 2, 2003, pp. 183–191.

3. SAMSON E., MARCHAND J., SNYDER K.A. and BEAUDOIN J.J. Modeling ion and fluid transport in unsaturated cement systems in isothermal conditions, Cem. Concr. Res., Vol. 35, No. 1, 2005, pp. 141–153.

4. MEIJERS S.J.H., BIJEN J., BORST R. and FRAIIJ A. Computational results of a model for chloride ingress in concrete including convection, drying- wetting cycles and carbonation, Mater. Struct., Vol. 38, No. 2, 2005, pp. 145–154.

5. IQBAL P.O. and ISHIDA T. Modeling of chloride transport coupled with enhanced moisture conductivity in concrete exposed to marine environment, Cem. Concr. Res., Vol. 39, No. 4, 2009, pp. 329–339.

6. BAROGHEL-BOUNY V., THIÉRY M. and WANG X. Modelling of isothermal coupled moisture–ion transport in cementitious materials, Cem. Concr. Res., Vol. 41, No. 8, 2011, pp. 828–841.

7. BAROGHEL-BOUNY V., THIÉRY M. and WANG X. Performance-based assessment of durability and prediction of RC structure service life : transport properties as input data for physical models, Mater. Struct., Vol. 47, 2014, pp. 1669–1691.

8. SAMSON E and MARCHAND J. Modeling the effect of temperature on ionic transport in cementitious materials, Cem. Concr. Res., Vol. 37, 2007, pp. 455–468.

9. NGUYEN T.Q. Modélisations physico-chimiques de la pénétration des ions chlorures dans les matériaux cimentaires., Ecole Nationale des Ponts et Chaussées, 2007.

10. HAUSMANN D.A. Steel corrosion in concrete. How does it occur?, Mater. Prot., Vol. 6, 1967, pp. 19–23.

11. GOUDA V.K. Corrosion and corrosion inhibition of reinforcing steel. I. Immersed in alkaline solutions, Br. Corros. J., Vol. 5, 1970, pp. 198–203.

12. SCHLÜNDER E-U. On the mechanism of the constant drying rate period and its relevance to diffusion controlled catalytic gas phase reactions, Chem. Eng. Sci., Vol. 43, No. 10, 1988, pp. 2685–2688.

13. LEHMANN P., ASSOULINE S. and OR D. Characteristic lengths affecting evaporative drying of porous media, Phys. Rev. E, Vol. 77, 056309, 2008.

14. SHAHRAEENI E., LEHMANN P. and OR D. Coupling of evaporative fluxes from drying porous surfaces with air boundary layer: Characteristics of evaporation from discrete pores, Water Resour. Res., Vol. 48, 2012, pp. 1–15.

15. HAGHIGHI E., SHAHRAEENI E., LEHMANN P. and OR D. Evaporation rates across a convective air boundary layer are dominated by diffusion, Water Resour. Res., Vol. 49, 2013, pp. 1602–1610.

16. ROHSENOW W.M. and CHOI H. Heat, mass and momentum transfer, Prentice Hall, 1961.

17. XU T., SPYCHER N. and SONNENTHAL E. TOUGHREACT User's Guide: A Simulation Program for Non-isothermal Multiphase Reactive Transport in Variably Saturated Geologic Media, version 2.0, Lawrence Berkeley, October. 2012.

18. KUZEL H. Röntgenuntersuchung im system $3CaO.Al_2O_3.CaSO_4.nH_2O$-$3CaO.Al_2O_3.CaCl_2.nH_2O$-$H_2O$, Neues Jahrb. für Mineral. Monatschefte, Vol. 13, 1966, pp. 193–200.

19. GLASSER F.P., KINDNESS A. and STRONACH S.A. Stability and solubility relationships in AFm phases Part I. Chloride, sulfate and hydroxide, Cem. Concr. Res., Vol. 29, 1999, pp. 861–866.

20. BEAUDOIN J.J., RAMACHANDRAN V.S. and FELDMAN R.F. Interaction of chloride and C-S-H, Cem. Concr. Res., Vol. 20, 1990, pp. 875–883.

21. BAROGHEL-BOUNY V., DIERKENS M., WANG X., SOIVE A., SAILLIO M., THIÉRY M. and THAUVIN B. Ageing and durability of concrete in lab and in field conditions: investigation of chloride penetration, J. Sustain. Cem. Mater., Vol. 2, No. 2, 2013, pp. 67–110.

22. CHAUSSADENT T. and ARLIGUIE G. AFREM test procedures concerning chlorides in concrete: extraction and titration methods, Mater. Struct., Vol. 32, No. 217, 1999, pp. 230–234.

23. XU T., SONNENTHAL E., SPYCHER N., ZHENG L., MILLER N. and PRUESS K. TOUGHREACT V3.0-OMP Reference Manual: A Parallel Simulation Program for Non-Isothermal Multiphase Geochemical Reactive Transport. Lawrence Berkeley National Laboratory, Berkeley, 2014.

24. Van GENUCHTEN M.T. A Closed-form Equation for Predicting the Hydraulic Conductivity of Unsaturated Soils 1, Soil Sci. Soc. Am. J., Vol. 44, 1980, pp. 892–898.

25. COREY A.T. The Interrelation Between Gas and Oil Relative Permeabilities, Prod. Mon., 1954, pp. 38–41.

26. ARCHER D. and CARTER R. Thermodynamic Properties of the NaCl + $H_2O$ System. 4. Heat Capacities of $H_2O$ and NaCl(aq) in Cold-Stable and Supercooled States, J. Phys. Chem. B, Vol. 104, 2000, pp. 8563–8584.

27. DZOMBAK D.A. and MOREL F.M.M. Surface complexation modeling, Wiley Inte. New York, 1990.

28. SAMSON E. and MARCHAND J. Modeling the transport of ions in unsaturated cement-based materials, Comput. Struct., Vol. 85, 2007, pp. 1740–1756.

29. BARBARULO R., MARCHAND J., SNYDER K.A. and PRENE S. Dimensional analysis of ionic transport problems in hydrated cement systems Part 1. Theoretical considerations, Cem. Concr. Res., Vol. 30, 2000, pp. 1955–1960.

30. GHEZZEHEI T.A., TRAUTZ R.C., FINSTERLE S., COOK P.J. and AHLERS C.F. Modeling Coupled Evaporation and Seepage in Ventilated Cavities, Vadose Zo. J., Vol. 3, 2004, pp. 806–818.

31. FINSTERLE S. and PRUESS K. Solving the estimation-identification problem in two-phase flow modeling, Water Resour. Res., Vol. 31, No. 4, 1995, pp. 913–924.

32. THIERY M., PLATRET G., MASSIEU E., VILLAIN G. and BAROGHEL-BOUNY V. Un modèle d'hydratation pour le calcul de la teneur en portlandite des matériaux cimentaires comme donnée d'entrée des modèles de carbonatation, in Journées Ouvrages d'Art du réseau des L.P.C., 2005.

33. BLANC P., LASSIN A. and PIANTONE P. Thermoddem: a database devoted to waste minerals, Orléans, France, 2007.

34. Van ROSSUM G., Python tutorial, Amsterdam, 1995.

35. BAROGHEL-BOUNY V. Water vapour sorption experiments on hardened cementitious materials. Part II: Essential tool for assessment of transport properties and for durability prediction, Cem. Concr. Res., Vol. 37, No. 3, 2007, pp. 438–454.

36. BEAR J. Dynamics of fluids in porous media. New York: Dover Publication, 1972.

# CEMENTS FOR MARINE ENVIRONMENTS

**C Bartolome**

**M Á Sanjuán**

Spanish Institute of Cement and its Applications (IECA)

Spain

**ABSTRACT.** This paper presents the deterioration mechanisms of concrete structures within marine environments and it addresses the most appropriate cements for seawater constructions among the cements included in the European standard EN 197-1. The paper analyses separately sulphate and magnesium attack to concrete and chloride attack to reinforcing steel. The combined effect when both ions (sulphate and chloride ions) are present in the surrounding environment is also discussed. Once these deterioration mechanisms are described, it is shown how cement composition selection can help to extend the service life of concrete structures when exposed to marine environments. The benefits of supplementary cementitious materials (SCMs), such as fly ash, natural pozzolans and slag, among others, are also described. Reinforcement corrosion protection in marine environments is addressed according to the European concrete standard EN 206:2013 and the Spanish regulation on structural concrete, EHE-08, where two methods for evaluating the service life of a concrete structure are set: deemed to satisfy rules and modelling by performance. Finally, the paper gives some recommendations about the most appropriate cement types for marine environments and about concrete mix design.

**Keywords:** Seawater concrete, marine environment, sulphate resistant cement, calcium aluminates, concrete service life.

**César Bartolome** is the Director of the Innovation Area at the Spanish Institute of Cement and its Applications (IECA). A renowned practitioner in the field of concrete technology, he is a member of numerous national and international technical committees.

**Dr Miguel A Sanjuán** is the Head of the Cements and Mortars Department at the Spanish Institute of Cement and its Applications (IECA). He is a member of several national and international technical committees related to cement and concrete technology and he also has published extensively on many aspects of concrete durability and cement science.

## INTRODUCTION

Concrete durability is considered an important subject by society for sustainable reasons. Economically, the repairing cost sometimes exceeds the value of a new construction. Moreover, the rise in durability involves an environmental issue related to the preservation of natural resources [1].

Reinforced concrete durability may be defined as the ability of the concrete and the embedded reinforcing steel to maintain their physical properties and mechanical performance in satisfactory safety conditions during the prescribed service life of the structure in the expected working conditions [2].

In marine environments, the sources of deterioration of concrete and reinforcing steel are linked to the direct influence of the external aggressive ions such as sulphates, chlorides, magnesium and so on. In consequence, the concrete permeability is a crucial factor strongly related to the quality of the concrete mix. Another important factor to be considered is the potential reactivity of the cement constituents with such aggressive ions.

This work presents the main causes of concrete deteriorations in marine environments and emphasises the challenges of an adequate cement selection as an unavoidable step to enhance the durability of concrete structures in marine environments and hence to fulfil the need for a sustainable built environment.

The aim of this work is to adequately quantify the increase/decrease of the concrete service life due to the use of cements considered sulphate-resistant in the European one EN 197-1 or in the Spanish standard UNE 80303-1 or considered marine-resistant in the UNE 80303-2.

### Common Portland Cements in Marine Environments

Traditionally sulphate-resistant common Portland cements are recommended to be used in marine environments. However, a limiting $C_3A$ value of 5% is preferable than 0% or 3% due to the presence of chloride ions in the seawater. Such ions react with $C_3A$ forming Friedel salt. Chloride ion is one of the main aggressive agents that cause corrosion in reinforced concrete structures, which is present mainly in marine environments.

### Blended Cements in Marine Environments

Another possible way to improve the concrete mix design, aiming to increase the service life of a reinforced concrete structure in marine environments, is the use of blended cements. Then, it is important to take into account some topics about the performance of these seawater resistant cements in this type of aggressive environment.

### Concrete Permeability

Concrete permeability is directly influenced by the mixing proportions. It can be reduced by decreasing the quantity of mixing water and dosing an adequate cement amount, and hence, reducing the porosity leading to a compact and dense microstructure. This way to minimize external aggressive agents to penetrate deeper inside can be enhanced by using the most appropriate type of cement in each case.

Low permeability in concrete helps keep aggressive ions out of the concrete and slows down the leaching of lime from the concrete. In consequence, any design and construction measures that reduce permeability will improve concrete durability. In this sense, an adequate amount and type of cement will play positively in this general objective better protecting reinforcing steel from corrosion.

## MARINE ENVIRONMENT EFFECTS ON REINFORCED CONCRETE

Marine environment with regard to concrete durability normally is classified in the European standard EN 206:2013 into three exposure zones: atmospheric (XS1), fully submerged (XS2) and splash (XS3). The concrete in the submerged zone is continuously covered by seawater, in the splash zone is subjected to wetting and drying and, finally, the concrete exposed to the atmospheric zone is located above the splash zone but sometimes is subjected to seawater spray. Concrete in the submerged zone is not as vulnerable as concrete in the splash zone.
Concrete in marine environment suffers some processes that cause damage that promote an increase in the concrete's permeability. This effect makes the concrete more susceptible to deterioration. Concrete exposed to seawater may deteriorate from the combined effects of chemical (Sulfate attack, Leaching of calcium hydroxide, alkali-aggregate expansion and embedded reinforcing steel corrosion) and physical (salt crystallization, freezing and thawing, erosion and abrasion) processes. On the other hand, most seawaters around the world are similar in composition, containing about 3.5% soluble salts by weight, mainly chlorides and sulphates (Figure 1), and the pH of seawater varies from 7.5 to 8.4, averaging about 8.1.

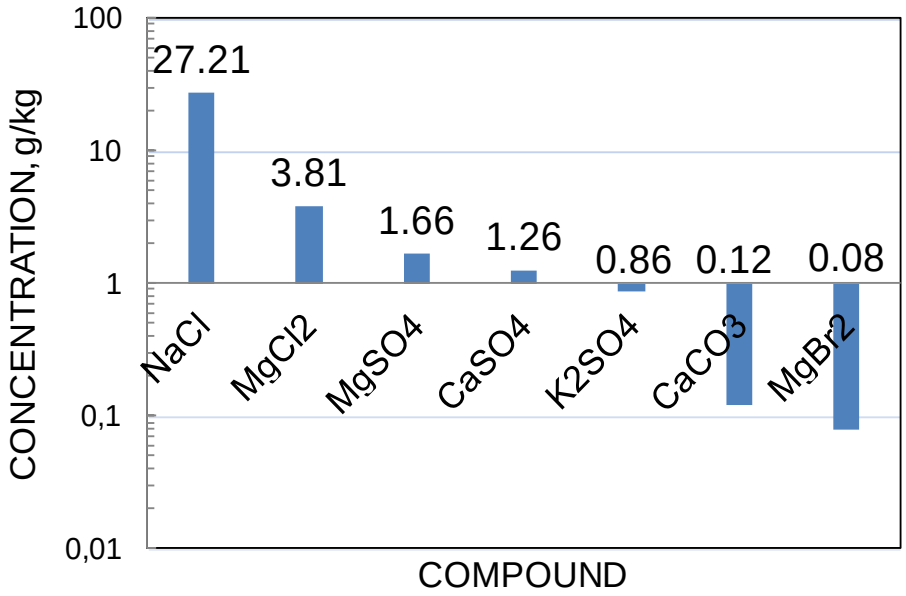


Figure 1 Seawater average chemical composition (g/kg)

### Reinforcement Corrosion Protection in Marine Environments

According to the Spanish regulation on structural concrete, EHE-08 [2], two methods for evaluating the service life of a concrete structure are set:

- Deemed to satisfy rules, i.e. provisions for the concrete composition (maximum water/cement ratio and minimum cement content) and for the minimum reinforcement cover, in dependence of the exposure class.
- Modelling by performance.

The first one is the traditional system (see Tables 1 and 2), while the modelling by performance is intended for the estimation of the lifetime which outcome is directly related to certain characteristics or concrete performance. Designer has to choose the right values (exposure class, reinforcement cover, concrete type) from the tables given in the Spanish national regulation [2].

For corrosion protection the Spanish regulation on structural concrete, EHE-08 [2] provides a maximum water-cement ratio and minimum cement content for the different exposure zones (Table 1). EHE-08 [2] requires the maximum water-cement ratio to be 0.50, 0.50 or 0.45 and the minimum cement content of 300, 325 or 350 for reinforced concrete exposed to seawater depending on the exposure zones: atmospheric (XS1), fully submerged (XS2) and splash (XS3), respectively. For prestressed concrete, EHE-08 requires the maximum water-cement ratio to be 0.45 for all the exposure zones. Also, minimum compressive strengths of 30 or 35 $N/mm^2$, depending on durability requirements, are recommended by EHE-08 (Table 2).

EHE-08 allows the use of a pozzolanic cements but it is not required. Spanish engineers commonly include pozzolanic cements in concrete exposed to seawater which can provide some benefits such as reduced permeability and better durability in that environments [3, 4].

Fly ash, natural pozzolans, blast-furnace slag and silica fume are the most common pozzolanic cement constituents used in concrete mixtures for marine environments in Spain.

Silicon from the pozzolanic cement constituents combines with the calcium hydroxide and water in the mix to form hardened cementitious products which increase the strength and reduce the permeability of the concrete.

Table 1 Maximum water/cement ratio and minimum cement content specified in EHE-08 according to the general and specific types of exposure [2]

| PARAMETER | CONCRETE TYPE | EXPOSURE CLASS | | | | | | |
|---|---|---|---|---|---|---|---|---|
| | | X0 | XC1 | XC4 | **XS1** | **XS2** | **XS3** | XD |
| Maximun water/cement ratio | Mass | 0.65 | - | - | - | - | - | - |
| | Reinforced | 0.65 | 0.60 | 0.55 | **0.50** | **0.50** | **0.45** | 0.50 |
| | Prestressed | 0.60 | 0.60 | 0.55 | **0.45** | **0.45** | **0.45** | 0.45 |
| Minimum cement content ($Kg/m^3$) | Mass | 200 | - | - | - | - | - | - |
| | Reinforced | 250 | 275 | 300 | **300** | **325** | **350** | 325 |
| | Prestressed | 275 | 300 | 300 | **300** | **325** | **350** | 325 |

Table 2 Minimum recommended strengths according to EHE-08 depending on durability requirements [2]

| PARAMETER | CONCRETE TYPE | EXPOSURE CLASS | | | | | | |
|---|---|---|---|---|---|---|---|---|
| | | X0 | XC1 | XC4 | **XS1** | **XS2** | **XS3** | XD |
| Minimum strength ($N/mm^2$) | Mass | 20 | - | - | **-** | **-** | **-** | - |
| | Reinforced | 25 | 25 | 30 | **30** | **30** | **35** | 30 |
| | Prestressed | 25 | 25 | 30 | **30** | **35** | **35** | 35 |

**External sulphate attack**

The external sulphate attack induced damage is determined by the chemical interaction of a sulphate ions present in seawater with the cement paste. Ettringite and gypsum formation is associated with expansion and some hypotheses of these products related expansion have been advanced [5].

Anhydrous cement is composed by calcium silicates, $C_3S$ and $C_2S$, tricalcium aluminate, $C_3A$, and tetracalcium ferroaluminate, $C_4AF$. Calcium silicates are hydrated forming tobermorite, CSH gel) and portlandite (calcium hydroxide, CH) according to equations (1) and (2) or, considering both of them, according to equation (3).

$$C_3S + 3\ H \rightarrow CSH + 2\ CH \quad (1)$$
$$C_2S + 2\ H \rightarrow CSH + CH \quad (2)$$
$$C_3S + C_2S + 5\ H \rightarrow 2\ CSH + 3\ CH \quad (3)$$

Portlandite, CH, in contact with seawater reacts, firstly, with sulphate ions, Š, and water, H, to form calcium sulphate dihydrate, $CaSO_4 \cdot 2H_2O$, with a low solubility of 16 mmol/l:

$$CH + Š + H \rightarrow CŠH_2 \quad (4)$$

This is promoted because the electrolytic dissociation balances of the portlandite, Ca(OH) (Equation 5) and calcium sulphate, $CaSO_4$ (Equation 6) tilts rightward caused by the higher calcium sulphate insolubility (16 mmol/l) and lower one of the portlandite (25 mmol/l). Then, the chemical balance shown in Equation (7) and gypsum crystallization according to Equation (8) are produced.

$$Ca(OH)_2 \leftrightarrow Ca^{2+} + 2\ OH^- \quad (5)$$
$$Ca^{2+} + SO_4^{2-} \leftrightarrow CaSO_4 \quad (6)$$
$$Ca(OH)_2 + SO_4^{2-} \leftrightarrow CaSO_4 + 2\ OH^- \quad (7)$$
$$CaSO_4 + 2\ H_2O \rightarrow CaSO_4 \bullet 2H_2O \quad (8)$$

All these processes can be summarized in a global process shown in Equation (9).

$$Ca(OH)_2 + SO_4^{2-} + 2H_2O \rightarrow CaSO_4 \bullet 2H_2O + 2\ OH^- \quad (9)$$

Gypsum crystallization puts pressure on the cement paste and it spoils the aggregate-paste adherence and, finally, cracking the concrete.

On the other hand, anhydrous cement has also calcium aluminate, $C_3A$, forming hydrated calcium aluminate, $C_4AH_{13}$, in the cement hydration process:

$$C_3A + CH + 12\ H \rightarrow C_4AH_{13} \quad (10)$$

Another alternative way to the gypsum formed according to Equations (4), (8) or (9) is the reaction between the hydrated calcium aluminate, $C_4AH_{13}$, with sulphate ions, Š, to produce ettringite, $C_3A + 3C\check{S} + 32H$ (or $C_6A\check{S}_3H_{32}$), also named as Candlot salt [6]. As a result, portlandite is regenerated (Equation 11). Ettringite is the mineral name for calcium sulfoaluminate, which is normally found in Portland cement concretes.

$$3\ C\check{S}H_2 + C_4AH_{13} + 14H \rightarrow\ C_6A\check{S}_3H_{32} + CH \quad (11)$$

The formation of ettringite in the fresh, plastic concrete is the mechanism that controls stiffening. When ettringite occurs in the hardened concrete stage, causes a significant harmful stress and a disruptive action. This type of ettringite is called ‘‘secondary’’ ettringite as opposite to ‘‘primary’’ ettringite which occurs in the plastic stage of the concrete and does not produce any significant harmful stress. The structural formula of ettringite is $[Ca_6Al_2(OH)_{12}\bullet 24H_2O]^{6+}[3(SO_4)\bullet 2H_2O]^{6-}$, where the first bracket corresponds to the columns and the second to the channels.

**Magnesium Attack**

Magnesium hydroxide can crystallize in cement-based materials in contact with seawater. Indeed, the $Mg^{2+}$ cation is the second most abundant cation in seawater, just behind $Na^+$ and before $Ca^{2+}$. The mechanisms of deterioration due to magnesium attack in Portland cements have been reported elsewhere [5], whereby the mode of magnesium attack is predominantly controlled by the generation of magnesium hydroxide, $Mg(OH)_2$, being nearly insoluble ($Mg(OH)_2$ solubility is 0.01 g/l compared to 1.37 g/l for calcium hydroxide, $Ca(OH)_2$). However, magnesium hydroxide has a low solubility in water large enough that it will partially dissolve to produce ions in the solution. Magnesium hydroxide in a saturated solution has a pH of about 10.5. Therefore, it destabilizes both ettringite, $C_6A\hat{S}_3H_{32}$, and calcium silicate hydrates, CSH. Therefore, magnesium sulphate ($MgSO_4$) attack on C-S-H is not directly related to ettringite formation. The magnesium attack mechanisms are generally represented by the reactions shown in Equations (12-19). Portlandite reacts with magnesium ions from the seawater to form magnesium hydroxide or brucite, MH (Equation 12). Because brucite is a swelling mineral, it causes volumetric expansion.

$$CH + M \rightarrow MH + C \quad (12)$$

This can be justified because of the electrolytic dissociation balances of the portlandite, $Ca(OH)_2$, (Equation 13) and magnesium hydroxide, $Mg(OH)_2$, (Equation 14) shifts rightward caused by the higher magnesium hydroxide insolubility (1.5 mmol/l) leading to the balance shown in Equation (15), whereby brucite is precipitated. Then, brucite can be easily precipitated from supersaturated solutions at ambient temperatures.

$$Ca(OH)_2 \leftrightarrow Ca^{2+} + 2\ OH^- \quad (13)$$

$$Mg^{2+} + 2\ OH^- \leftrightarrow Mg(OH)_2 + Ca^{2+} \quad (14)$$

$$Ca(OH)_2 + Mg^{2+} \leftrightarrow Mg(OH)_2 + Ca^{2+} \quad (15)$$

This process could be considered as a cationic exchange, calcium for magnesium, whereby the most insoluble salt is formed, i.e. magnesium hydroxide or brucite. Firstly, brucite crystallizes in the concrete pores in contact with seawater filling them and leading to a compressive strength increase. Secondly, a local volumetric expansion is produced, which is responsible for tensile stress in concrete. This leads to the formation of cracks promoting concrete degradation in seawater.

Magnesium-tobermorite interaction can be explained by an exchange of bases according to Equations (16) and (17) or cationic exchange, where calcium ions have been replaced by magnesium according to Equations (18) and (19), where the left-hand side is the calcium tobermorite and the right-hand side is the magnesium tobermorite.

$$CSH + M \leftrightarrow MSH + C \quad (16)$$

$$2\,CSH + M \leftrightarrow CMS_2H_2 + C \quad (17)$$

$$C_{1.5}SH_{2.5} + Mg^{2+} \rightarrow C_{0.5}\,MgSH_{2.5} + Ca^{2+} \quad (18)$$

$$2\,C_{1.5}SH_{2.5} + 2\,Mg^{2+} \rightarrow CM_2S_2H_{2.5} + 2\,Ca^{2+} \quad (19)$$

This exchange process may be total (Equation 16) or partial (Equation 17), (Equation 18) and (Equation 19), which generates the magnesium tobermorite by removing calcium and incorporating magnesium. As the magnesium tobermorite is not hydraulic, a decrease in strength and loss of cement paste-aggregate adherence is found.

**Combined Effect of Several Ions Present in Seawater**

Seawater environment is considered as the most harmful with regard to the steel corrosion of reinforced concrete by chloride ions. Taking into account only the chloride effect on reinforced concrete and the sulphate attack of the concrete, CEM I according to the European standard EN 197-1:2011would be the most adequate cement. CEM I provides a high pH to the concrete pore solution maintaining the alkaline reserve, calcium hydroxide, keeping the steel passive layer. Moreover, hydrated calcium aluminates, $C_4AH_{13}$, will form choroaluminate salt or Friedel salt, partly immobilizing chloride ions (Equation 20) but liberating calcium hydroxide and water, leading to a porosity increase. It has been reported that $C_4AH_{13}$ or $C_3A$ only fixes chloride ions after an initial period which is longer than the one corresponding to the absorption process [7].

$$2\,Cl^- + Ca^{2+} + C_4AH_{13} \rightarrow C_3A{\bullet}CaCl_2{\bullet}H_{10} + CH + 2H \quad (20)$$

Rarely anhydrous calcium aluminates are present in concrete, thus their reaction with chlorides is unexpected (Equation 21).

$$CaCl_2 + C_3A + 10H \rightarrow C_3A{\bullet}CaCl_2{\bullet}H_{10} \quad (21)$$

Chloride ions ingress to the concrete faster than sulphate ions due to their smaller atomic radius. We further submit that the cement recommendation would fail to define the relevant durability aspects correctly, by not considering the sulphate ions penetration to the concrete.
The external sulphate attack takes time and produced a great damage when the cement has a high level of hydrated calcium aluminates, $C_4AH_{13}$, because secondary ettringite is formed (Equation 22).

$$3SO_4^{2-} + 3Ca^{2+} + C_4AH_{13} + 20H \rightarrow C_3A\,(CaSO_4)_3 \bullet H_{32} + CH \qquad (22)$$

Equation (23) shows the unexpected reaction of anhydrous calcium aluminates with sulphates.

$$3CaSO_4^{2-} + C_3A + 32\,H \rightarrow C_3A \bullet (CaSO_4) \bullet H_{32} \qquad (23)$$

Also sulphate ions react with portlandite producing calcium sulphate and increasing the alkalinity of the pore solution (Equation 24). Then, the calcium sulphate hydrates according to Equation (25) or produces ettringite according to Equation (22).

$$SO_4^{2-} + Ca^{2+} + 2\,OH^- \rightarrow CaSO_4 + 2\,OH^- \qquad (24)$$

$$CaSO_4 + 2H_2O \rightarrow CaSO_4 \bullet 2H_2O \qquad (25)$$

Finally, the external sulphate ions and the formed calcium sulphate (Equation 25) get in contact with the Friedel salt producing expansive secondary ettringite and chloride ions will ultimately leak into the pore solution and cause damage to the reinforcing steel (Equation 26).

$$3CaSO_4\,(3Ca^{2+}+3SO_4^{2-}) + C_3A \bullet CaCl_2 \bullet H_{10} + 22H \rightarrow C_3A \bullet (CaSO_4)_3 \bullet H_{32} + CaCl_2\,(Ca^{2+}+2Cl^-) \qquad (26)$$

Blastfurnace, pozzolanic and composite cements have been demonstrated to reduce the potential for deleterious expansion due to ettringite and the chloride penetration.

## MOST ADEQUATE CEMENTS FOR MARINE CONCRETE STRUCTURES

The most adequate cements for marine concrete structures; this will then provide the basis for supporting the proposal of seawater-resisting cements.

### Resisting Cements to the Sulphates Present in the Seawater

The most resisting cements to the sulphate ions present in the seawater are those with a lower amount of weak components which are easily attacked by sulphate ions. Such weak components are portlandite, tobermorite and tricalcium aluminate. Below, common Portland cements according to EN 197-1:2011 are evaluated.

### Common Portland cements, CEM I

Common Portland cements CEM I have more than 95% of clínker. Then, CEM I would be more resistant to the seawater when less portlandite (CH) and tobermorite (CSH) are formed during the cement hydration. This is the case in low $C_3S + C_2S$ clinkers. Also, the lesser tricalcium aluminate, $C_3A$, is, the lesser possibility of ettringite formation will be.

### Portland-composite cement, CEM II

Portland composite cements CEM II have more than 65% of clínker and also contain mineral additions described in EN 197-1:2011 (from 6 to 20% -subtype A- or from 21 to 35% - subtype B-. The lesser clinker in the cement, the higher sulphate resistance will be. With regard to the

addition, the most beneficial are blastfurnace slag (S), natural pozzolan (P), silicious fly ash (V) and silicafume (D). They are rank up in merit order.

**Blastfurnace, pozzolanic and composite cements, CEM III, CEM IV and CEM V, respectively**

Blastfurnace cements CEM III, pozzolanic cements CEM IV and composite cements CEM V follow the same criteria used for Portland composite cements CEM II. Blastfurnace slags are hydraulic and could be activated by sulphates and hydroxyl anions leading to an increase in compressive strength and a formation of hydration products less susceptible to adverse attack by the usual elements present in the seawater (sulphates or magnesium salts). Pozzolanic cement constituents such as fly ash, natural pozzolan and silicafume, react with calcium hydroxide to form secondary tobermorite which is more stable and less assailable than the primary one.

Summing up, Table 4 gives a list of common Portland cements (EN 197-1:2011) which are resistant to sulphate ions present in the seawater. Relevance ranked proposal returns a list of recommended cements in the order of most relevant to least relevant from the top to the bottom.

**Magnesium Attack Resisting-Cements**

The most resisting cements to the magnesium salts present in the seawater are those with a lower amount of weak components, which are portlandite and tobermorite. The aim is to avoid the brucite and magnesium tobermorite formation. Below, common Portland cements according to EN 197-1:2011 are evaluated.

Table 4 Common Portland cements (EN 197-1:2011) which are resistant to sulphate ions present in the seawater (From the top to the bottom)

| RECOMMENDED CEMENTS | |
|---|---|
| Notation | Main Type |
| Blastfurnace cements | CEM III/C<br>CEM III/B<br>CEM III/A |
| Composite cements | CEM V/B<br>CEM V/A |
| Pozzolanic cements | CEM IV/B<br>CEM IV/A |
| Portland composite cements | CEM II/B-S<br>CEM II/B-P<br>CEM II/B-V<br>CEM II/A-S<br>CEM II/A-P<br>CEM II/A-V<br>CEM II/A-D |
| Portland cement | CEM I |

### Common Portland cements, CEM I

The less portlandite (CH) and tobermorite (CSH) formation during the cement hydration, the more seawater-resistant CEM I.

### Portland-composite cement, CEM II

Pozzolanic cement constituents react with portlandite forming secondary tobermorite with a lower calcium/silicon ratio than the primary one. Therefore, it improves the chemical characteristics: It decreases the cationic exchange capacity (calcium-magnesium) and it recovers insoluble forms.

Also, the lesser clinker in the cement, the higher magnesium resistance will be. With regard to the addition, the most beneficial are natural pozzolan (P) or silicious fly ash (V), blastfurnace slag (S) and silicafume (D), in this order of priority.

### Blastfurnace, pozzolanic and composite cements, CEM III, CEM IV and CEM V, respectively

Blastfurnace cements CEM III, pozzolanic cements CEM IV and composite cements CEM V follow the same criteria used for Portland composite cements CEM II.
Summing up, Table 5 gives a list of common Portland cements (EN 197-1:2011) which are resistant to the magnesium ions present in the seawater sorted by relevance. At the top of the list are the most magnesium-resisting cements.

Table 5 Common Portland cements (EN 197-1:2011) which are resistant to the magnesium ions present in the seawater (From the top to the bottom)

| RECOMMENDED CEMENTS | |
|---|---|
| Notation | Main Type |
| Pozzolanic cements | CEM IV/B<br>CEM IV/A |
| Composite cements | CEM V/B<br>CEM V/A |
| Blastfurnace cements | CEM III/C<br>CEM III/B<br>CEM III/A |
| Portland composite cements | CEM II/B-V<br>CEM II/B-P<br>CEM II/B-S<br>CEM II/A-P<br>CEM II/A-V<br>CEM II/A-S |
| Portland cement | CEM I |

Table 6 Recommended common Portland cements (EN 197-1:2011) to be used in concrete structures subjected to seawater atmospheric environments (XS1)

| TYPE OF CONCRETE | RECOMMENDED CEMENTS | |
|---|---|---|
| Mass concrete | Highly recommended cements | CEM IV/A, CEM IV/B, CEM V/A, CEM V/B, CEM III/A, CEM III/B, CEM III/C, CEM II/B-S, CEM II/B-M, CEM II/B-V, CEM II/B-P |
| | Recommended cements | CEM II/A-S, CEM II/A-M, CEM II/A-V, CEM II/A-P, CEM II/A-L, CEM II/A-LL |
| | Usable cements | CEM II/A-D, CEM I |
| | Unusable cements | The rest of cements |
| Reinforced concrete | Highly Recommended cements | CEM II/A-P, CEM II/A-V, CEM II/A-M, CEM II/A-S, CEM II/A-D, CEM I |
| | Recommended cements | CEM II/B-V, CEM II/B-P. CEM II/B-M, CEM II/B-S, CEM IV/A, CEM III/A |
| | Usable cements | CEM IV/B, CEM V/A, CEM V/B, CEM III/B, CEM II/A-L, CEM II/A-LL |
| | Unusable cements | The rest of cements |
| Prestressed concrete | Usable cements | CEM II/A-D, CEM I, CEM II/A-V, CEM II/A-P, CEM II/A-M (V, P) (They should be at least /MR)* |
| | Unusable cements | The rest of cements |

* Seawater-resisting cement (/MR) according to the Spanish standard UNE 80303-2:2011.

Table 7 Recommended common Portland cements (EN 197-1:2011) to be used in concrete structures fully submerged in seawater (XS2)

| TYPE OF CONCRETE | RECOMMENDED CEMENTS | |
|---|---|---|
| Mass concrete | Highly recommended cements | CEM III/B, CEM III/C, CEM V/A, CEM V/B, CEM IV/B, CEM II/B-S, CEM II/B-M, CEM II/B-V, CEM II/B-P |
| | Recommended cements | CEM III/A, CEM IV/A, CEM II/A-M, CEM II/A-V, CEM II/A-P |
| | Usable cements | CEM II/A-D, CEM II/A-L, CEM II/A-LL, CEM I |
| | Unusable cements | The rest of cements |
| Reinforced concrete | Highly recommended C. | CEM III/A CEM V/A, CEM IV/A, CEM II/B-S, CEM II/B-M, CEM II/B-V, CEM II/B-P |
| | Recommended cements | CEM III/B, CEM IV/B, CEM II/A-S, CEM II/A-M, CEM II/A-V, CEM II/A-P |
| | Usable cements | CEM II/A-D, CEM II/A-L, CEM II/A-LL, CEM I |
| | Unusable cements | The rest of cements |
| Prestressed concrete | Usable cements | CEM II/A-D, CEM I, CEM II/A-V, CEM II/A-P, CEM II/A-M (V, P) (They should be at least /MR)* |
| | Unusable cements | The rest of cements without any exception |

Table 8 Recommended common Portland cements (EN 197-1:2011) to be used in concrete structures in the splash seawater zone (XS3)

| TYPE OF CONCRETE | RECOMMENDED CEMENTS | |
|---|---|---|
| Mass concrete | Highly recommended cements | CEM IV/B, CEM V/B, CEM III/B, CEM III/C, CEM IV/A, CEM III/A, CEM II/B-S, CEM II/B-M, CEM II/B-V, CEM II/B-P |
| | Recommended cements | CEM II/A-S, CEM II/A-M, CEM II/A-V, CEM II/A-P |
| | Usable cements | CEM II/A-D, CEM II/A-L, CEM II/A-LL, CEM I |
| | Unusable cements | The rest of cements |
| Reinforced concrete | Highly recommended C. | CEM IV/A, CEM V/A, CEM III/A CEM II/B-S, CEM II/B-M, CEM II/B-V, CEM II/B-P |
| | Recommended cements | CEM II/A-S, CEM II/A-M, CEM II/A-V, CEM II/A-P |
| | Usable cements | CEM II/A-D, CEM II/A-L, CEM II/A-LL, CEM I |
| | Unusable cements | The rest of cements |
| Prestressed concrete | Usable cements | CEM II/A-D, CEM I, CEM II/A-V, CEM II/A-P, CEM II/A-M (V, P) (They should be at least /MR)* |
| | Unusable cements | All the rest of cements without any exception |

* Seawater-resisting cement (/MR) according to the Spanish standard UNE 80303-2:2011.

**Combined Effect of Magnesium and Sulphate Salts Present in Seawater**

Taken into account that:

i) The sulphate ion concentration in the seawater is double than that of magnesium.
ii) Both of them attack the portlandite and tobermorite, but only sulphate ions attack tricalcium aluminate, $C_3A$.
iii) The magnesium ion produces expansive brucite, but sulphates produce two expansive products: gypsum and ettringite.
iv) The powerful forces of expansive gypsum and ettringite are stronger than brucite ones.
v) Magnesium-calcium cationic exchange in the primary tobermorite is a second-order effect, particularly, in the cements showed at the top of the list shown in Tables 5 and 6. Such cements not only have less primary tobermorite, but also secondary tobermorite is produced which is more resistant to the magnesium ions.

Therefore, considering than both ions, magnesium and sulphate, are present in the seawater, Table 4 prevails over Table 5 in marine environments.

**Recommended Cements According to the Environmental Exposure**

Finally, Tables 6-8 list the recommended cements for concrete structures exposed to seawater depending on the exposure zones: atmospheric (XS1), fully submerged (XS2) and splash (XS3), respectively. The atmospheric zone (XS1) is submitted to carbonation and chloride attack, whereas the fully submerged (XS2) rarely is carbonated but suffer magnesium and sulphate ions attack. Finally, the splash zone (XS3) is the most damaged area.

## REFERENCES

1. MEHTA, K. Reducing the Environmental Impact of Concrete. Concrete International, Vol. 23, No.10, 2001, pp 61-66.

2. SECRETARÍA GENERAL TÉCNICA DEL MINISTERIO DE FOMENTO (SPAIN). EHE-08: Instrucción Española del Hormigón Estructural, 2008, Centro de Publicaciones de la Secretaría General Técnica, p 722.

3. ANDRADE, C, WHITING, D A. Comparison of chloride ion diffusion coefficients derived from concentration gradients and non-steady state accelerated ionic migration, Materials and Structures, Vol. 29, No.192, 1996, pp 476-484.

4. CASTRO, P, DE RINCON, C T, PAZINI, E J. Interpretation of chloride profiles from concrete exposed to tropical marine environments, Cement Concrete Research, Vol. 31, No. 4, 2001, pp 529–537.

5. CALLEJA, J. Durability. Proceedings of 7$^{th}$ International Congress on Chemistry of Cement. Editions Septima, Paris, 1980, Sub-Theme VII-2, 1, pp VII:2/1-VII:2/48.

6. CANDLOT, E. Sur les propriétés des produits hydraulique, Bull. Soc. Encourage Ind. Natl. Vol. 89, No. 682, 1890, pp 685–716.

7. SANJUÁN, M A. Electrochemical method to assess the absorption of NaCl solutions in OPC and SRPC mortars, Building and Environment, Vol. 35, No. 7, 2000, pp 595–601.

# MIX DESIGN AND PERFORMANCE EVALUATION OF CONCRETE WITH ULTRA-LOW PERMEABILITY

**Z Qu**

**Q Yu**

**H J H Brouwers**

Eindhoven University of Technology

The Netherlands

**ABSTRACT.** This paper presents the mix design and properties assessment of a low permeability concrete (LPC) with high volume fly ash and nanosilica. The LPC is designed by using the modified Andreasen and Andersen particle packing model. The workability, porosity, mechanical properties and permeability of the designed LPC are measured and analyzed. The results of the RCM test present an ultra-low permeability with a DRCM of 1.64, which indicates that an ultra-low permeable concrete can be achieved by utilizing this packing model.

**Keywords:** Mix design, Concrete, Ultra-low permeability, Nanosilica, Fly ash.

**Zhengyao Qu** is currently working as a Ph.D. student in the Department of the Built Environment, Eindhoven University of Technology. His research interests include concrete durability and design of multi-functional concrete system.

**Dr Qingliang Yu** is assistant professor of Building Materials in the Department of the Built Environment, Eindhoven University of Technology.

**Prof Dr Ir H J H Brouwers** is professor of Building Materials in the Department of the Built Environment, Eindhoven University of Technology.

## INTRODUCTION

Concrete durability in different environments has been intensively investigated over decades [1, 2]. The majority of concrete durability issues is closely relevant to porosity and permeability to fluids, as the transport of fluids into the concrete takes place through the interconnected pore system of concrete. Among the fluids which bring deterioration to concrete, those containing aggressive ions, carbon dioxide and oxygen are most frequently taken into account. Therefore, the reduction of the permeability of concrete is of vital importance to achieve the design and construction requirement for safety and durability. Concrete permeability is highly related with capillary porosity, pore structure and the interfacial transition zone (ITZ) between the cement phase and reinforcement. An efficient and simple way to reduce concrete permeability is through decreasing the water/cement ratio or water/powder ratio as it decreases the amount of free water which results in lower porosity in the concrete structure. Recently applying low water/cement ratios with pozzolanic admixture has become an efficient way to prepare low permeable concrete (LPC) with desirable durability and fly ash, which is produced in coal-burning power plants, has presented a considerable potential to improve the durability of concrete. Owing to the high content of reactive glassy $SiO_2$ phase and high specific surface area, fly ash is reactive in alkaline environments and once in contact with $Ca(OH)_2$, generated during the process of hydration of Portland cement (PC), further C-S-H gel will be produced. This gel can modify the micro-structure of concrete by filling the capillary voids and reducing the capillary porosity. Together with this process, due to the high alumina content in FA, Friedel's salt is produced, which also ameliorates the pore structure of concrete.

Besides the chemical modification effect, FA can also play a role as a micro filler (micro-sized aggregate), water reducing agent (the "ball-bearing" effect of spherical FA particles creates a lubricating action in fresh concrete) and prevent the formation of micro-cracks at early ages (slow release of the hydration heat). Ampadu [3] found that, due to the slow reaction, concrete containing fly ash at early ages represents higher permeability compared with PC concrete with the same w/c ratio, but shows advantages in reducing chloride diffusivity at later ages and a level of 40% replacement was the best. Thomas [4] found that when a replacement proportion is less than 35%, the initiation of corrosion of steel rebars in fly ash concrete decreased with the same w/c ratio. A low w/c ratio also resulted in a better performance in terms of the resistance against the intrusion of chlorides.

The effect of nano-silica (nS) has been widely investigated in cement and concrete research. The application of nano-silica involves both physical and chemical effects. Due to its very fine particle size, nano-silica can fill the voids in concrete and increase its packing density. Furthermore, the pozzolanic reaction between silica and calcium hydroxide results in more C-S-H gel formation in the reaction process. Both of these effects can refine the pore structure and improve the chloride binding ability of concrete. Zhang [5] has used nano-silica to reduce the setting time and increase the early strength of concrete with high volumes of fly ash. Due to the extremely fine particle size of the nano-silica and highly reactive pozzolanic property, this may contribute to reducing setting times and increasing early strength. Said [6] found that the incorporation of nano-silica could improve the overall performance of concrete with and without fly ash. Due to the pronounced effect on reducing the conductivity and refining the pore structure of the cementitious matrix, the application of nano-silica can decrease the permeability of concrete significantly. Although it is beneficial to employ nano-silica in concrete design, the maximum level of addition is limited to 5%-10% based on the weight of cement [16]. A higher proportion of nano-silica results in higher autogenous shrinkage attributed to self-desiccation.

Brouwers and Radix [7] concluded that by optimization of the PSD in nanometer range, the total performance of concrete could be improved. Consequently, in this research, the continuous geometric random packing of the poly-disperse particles model is accepted to design low permeability concrete. Often the Rapid Chloride Migration test (RCM) is applied to investigate the ion permeability of concrete.

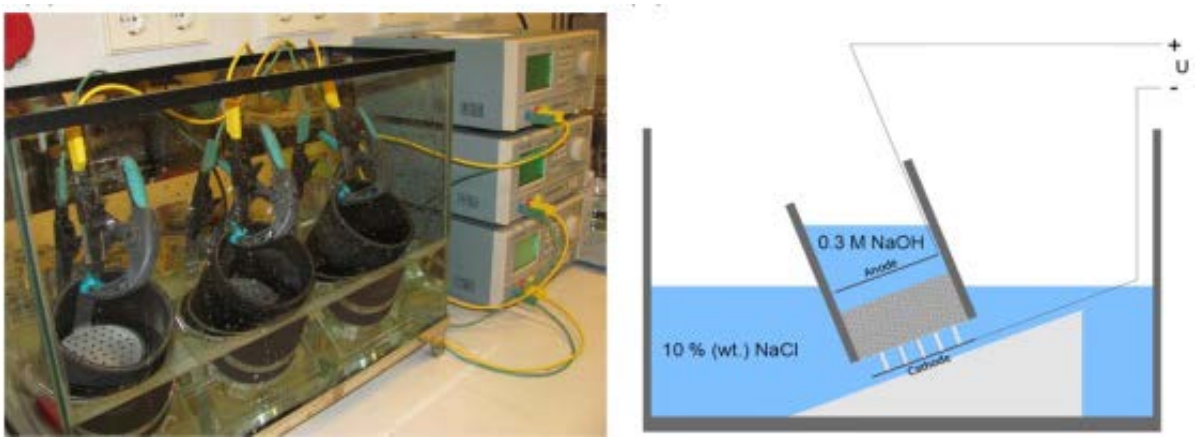


Figure 1 Rapid chloride migration (RCM) test set-up (left) and scheme (right)

## MATERIALS AND METHODS

### Materials

The cement used in this study was Portland Cement (PC) CEM I 52.5 R, provided by ENCI (the Netherlands). A polycarboxylic ether based superplasticizer (MasterGlenium 51, BASF) was used to adjust the workability of the designed LPC. A Class F FA was used to replace cement. One type of nano-silica slurry (AkzoNobel, Sweden) was selected as a high active pozzolanic material in this study. Two types of sand were used, one normal sand with the fractions of 0-2 mm and the other one microsand with the fraction 0-1 mm (Graniet-Import Benelux, the Netherlands). The physical properties and chemical composition of the used materials are shown in Tables 1-3.

Table 1 Material types and densities

| MATERIALS | SPECIFIC DENSITY (kg/m$^3$) |
|---|---|
| CEM 1 52.5R | 3150 |
| FA | 2300 |
| Fine sand (0-1) | 2720 |
| Coarse Sand (0-2) | 2640 |
| Superplasticizer | 1050 |
| Nano-silica | 1.40 |

Table 2 General characteristics of the employed nano-silica

| PROPERTY | NS |
|---|---|
| Type | Colloidal |
| Specific density (g/cm$^3$) | 1.39 |
| Bulk density (g/cm$^3$) | 1.40 |
| pH | 9-11 |
| Solid content (% w/w) | 50 |
| Viscosity (mPa.s) | <50 |
| BET (m²/g) | 50 |
| PSD by LLS (nm) | 50-300 |
| Mean particle size (μm) | 0.12 |

Table 3 Oxide composition of cement, FA, nS

| CHEMICAL COMPOSITION (%) | CEMENT | FA | NS |
|---|---|---|---|
| CaO | 64.60 | 4.46 | 0.08 |
| $SiO_2$ | 20.08 | 55.32 | 98.68 |
| $Al_2O_3$ | 4.98 | 22.45 | 0.37 |
| $Fe_2O_3$ | 3.24 | 8.52 | - |
| $K_2O$ | 0.53 | 2.26 | 0.35 |
| $Na_2O$ | 0.27 | 1.65 | 0.32 |
| $SO_3$ | 3.13 | 1.39 | - |
| MgO | 1.98 | 1.89 | - |
| $TiO_2$ | 0.30 | 1.17 | 0.01 |
| $Mn_3O_4$ | 0.10 | 0.11 | - |
| $P_2O_5$ | 0.74 | 0.76 | 0.15 |

## Experimental Methodology

### Mix design

In this study, the modified Andreasen and Andersen model is applied to design all the concrete mixtures, which reads as follows:

$$P(D) = \frac{D^q - D_{\min}^q}{D_{\max}^q - D_{\min}^q} \tag{1}$$

where D is the particle size (μm), P(D) is a fraction of the total solids being smaller than size D, $D_{max}$ is the maximum particle size (μm), $D_{min}$ is the minimum particle size (μm) and q is the distribution modulus.

As presented in the literature [2, 7, 9, 13, 17], different types of concrete can be designed using Eq. (1) by applying different values of the distribution modulus q, as it determines the proportion between the fine and coarse particles in the mixture. As recommended in, considering that a high amount of fine particles is utilized to produce the LPC, the value of q is fixed at 0.22 in this study.

The modified Andreasen and Andersen model (Eq. (1)) acts as a target function for the optimization of the composition of mixture of granular materials. The proportions of each individual material in the mix are adjusted until an optimum fit between the composed mix and the target curve is reached, using an optimization algorithm based on the Least Squares Method (LSM), as presented in Eq. (2). When the deviation between the target curve and the composed mix, expressed by the sum of the squares of the residuals (RSS) at defined particle sizes, is minimized, the composition of the concrete is considered the best one (optimized packing).

$$RSS = \sum_{i=1}^{n} (P_{mix}(D_i^{i+1}) - P_{tar}(D_i^{i+1}))^2 \tag{2}$$

where $P_{mix}$ is the composed mix, and the $P_{tar}$ is the target grading calculated from Eq. (1). Four recipes were designed in the present study. The PSDs of the used materials and the composed mix are shown in Figure 2. The detailed mix proportions are listed in Table 4.

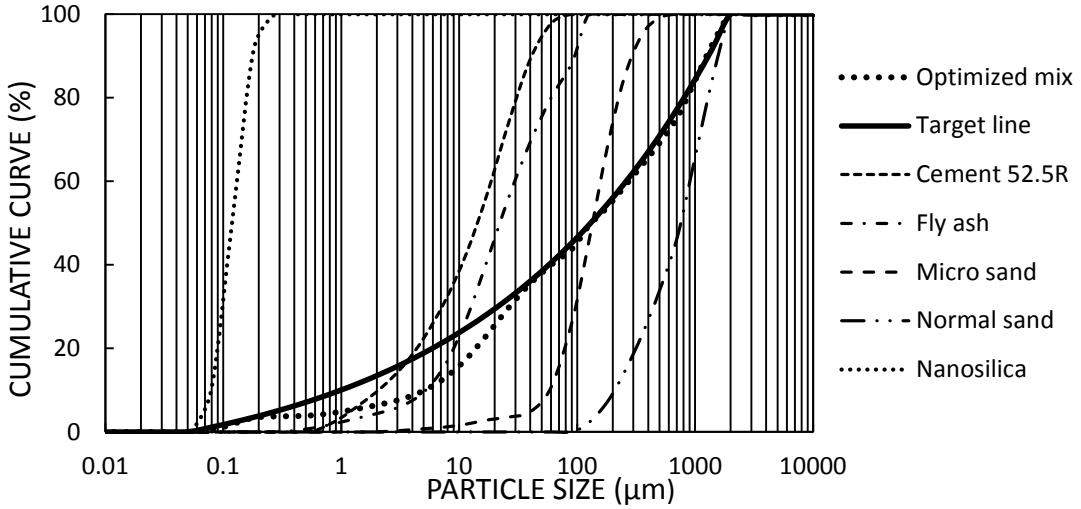


Figure 2 Particle size distributions of the material used, target and optimized grading curves of the designed concrete

Table 4 Mix proportions of the concrete

| MIX | PROPORTION (kg/m³) | | | | | | | W/B | SP/B |
|---|---|---|---|---|---|---|---|---|---|
| | C | FA | S | MS | W | NS | SP | | |
| LPC-0.18 | 445.78 | 424.63 | 998.43 | 212.37 | 156.67 | 42.13 | 34.82 | 0.18 | 0.04 |
| LPC-0.20 | 438.48 | 417.68 | 982.08 | 208.90 | 171.23 | 41.38 | 34.25 | 0.20 | 0.04 |
| LPC-0.22 | 430.34 | 409.92 | 963.84 | 205.11 | 184.86 | 40.67 | 33.61 | 0.22 | 0.04 |
| M-ref | 452.20 | 430.91 | 1014.90 | 258.11 | 158.96 | 0 | 35.32 | 0.18 | 0.04 |

**Flowability**

All powders and sands are added into a laboratory mixer and mixed for 30 s at a low speed; then, around 75% of water is added into the mixer. After mixing for 90 s, the mixer is stopped for 30 s. Afterwards, the remaining water and SP are added and then mixed at the same speed for 180 s. Finally the mixture is mixed at a high speed for 120 s.

To evaluate the flowability of LPC, the flow table tests are performed following EN 1015-3 [8]. During the test, the cone is lifted vertically in order to allow a free flow of the mixture without any jolting (following suggestions from [9]). In the test, two diameters perpendicular to each other ($d_1$ (mm) and $d_2$ (mm)) are determined. Their mean is employed to compute the relative slump ($\Gamma$) via:

$$\Gamma = \left( \frac{d_1 + d_2}{2d_0} \right)^2 - 1 \tag{3}$$

where $d_0$ represents the base diameter of the used cone (mm), i.e. 100 mm in the case of the Hägermann cone.

**Mechanical properties**

After preforming the flowability tests, the fresh concrete is cast in molds with the dimensions of 40 mm × 40 mm × 160 mm covered. The prisms are demolded 24 h after casting and then cured in water under room temperature. The flexural and compressive strengths of the specimens are tested according to EN 196-1[10] at the ages of 7 and 28 days, respectively.

**Water-permeable porosity**

The water-permeable porosity of the designed LPC is measured applying the vacuum-saturation technique, which is referred to as the most efficient saturation method. The saturation is carried out on at least 3 samples (100 mm × 100 mm × 20 mm) for each mix, following the description given in NT Build 492 [11] and ASTM C1202 [12]. The water permeable porosity is calculated from:

$$\varphi = \frac{m_s - m_d}{m_s - m_w} \times 100 \tag{4}$$

where $\varphi$ is the water permeable porosity (%), $m_s$ is the mass of the saturated sample in surface-dry condition measured in air (g), $m_w$ is the hydrostatic mass of water-saturated sample (g) and $m_d$ is the mass of oven-dried sample (g).

**RCM test**

For RCM test, the designed concrete were cast in cubes (150 mm side length). One day after casting, the specimens were demolded and cured in water until the age of 26 days, when the RCM test samples were extracted from the cubes by drilling and cutting. At the age of 28 days the RCM test (NT Build 492) is performed. 12 cores (d=100 mm) were extracted from the prepared mortar cubes. From these cores 12 specimens of 50 mm in height were sliced for the RCM test (one specimen from each core, 10-20 mm of the outermost surfaces of each core

were cut off) and stored in water. One day prior to the RCM test, each series of the test samples were saturated with limewater under vacuum conditions. The vacuum-saturation was performed following the procedure described in [11]. Surface-dry samples were placed vertically in a desiccator connected to a vacuum-pump and a pressure of 40 mbar was applied for 3 h. Then, with the vacuum pump still running, the desiccator was slowly filled with limewater to immerse all the samples completely. After that, for an additional hour, the vacuum was maintained before allowing air to re-enter the desiccator. The samples were kept in the solution for about 18 h.

After the vacuum-saturation process, the samples were placed in tightly clamped rubber sleeves, as shown in Figure 1. At the end of the 24 h time period in which voltage was applied, the sample was rinsed with distilled water and the surface was wiped with a cloth. The sample was then split into two pieces and 0.1 mol/l silver nitrate solution is sprayed on the fractured surface of the sample. The chloride penetration depth is measured at 10 locations across the section which are then used to determine an average depth of penetration. The chloride non-steady state migration coefficient ($D_{nssm}$) was calculated using:

$$D_{nssm} = \frac{0.0239(273+T)\cdot L}{(U-2)\cdot t}\cdot\left(x_d - 0.0238\sqrt{\frac{(273+T)\cdot L\cdot x_d}{U-2}}\right) \quad (5)$$

where $D_{nssm}$ is the non-steady state migration coefficient ($10^{-12}$ $m^2/s$), U is the absolute value of the applied voltage (V), T is the average value of the initial and final temperatures in the solution (C), L is the thickness of the specimen (mm), $x_d$ is average value of the average chloride penetration depth (mm) and t is the test duration (h). Three specimen was tested for each mortar mixture at each testing age.

## RESULTS AND DISCUSSION

### Fresh Behavior

Table 5 presents the fresh state properties of the mortars. As can be seen, with an increase of the water amount, the flow slump of the concrete mixtures increases. The LPC-0.18 presents the lowest flowability with $\Gamma$ =10.4. In this study, it can be noticed that the flowability is better than that in a previous study [12], which reported a relative slump of 9.5 for an UHPC designed applying the modified A&A model using a water /powder ratio of 0.18 and also a relatively high content of fly ash. Moreover, the fresh concrete mix here used a less SP dosage compared to [12]. This could be attributed to the following reason: the higher volume of fly ash used in this study improves the workability of the concrete mixture. In the dense concrete packing system, FA plays a role of a micro filler (mirco-sized aggregate) as shown in Figure 2, which contributes to the grading of the particles and results in but also to the densification of transition zone between the paste-sand, which leads to the refinement of hydration products via a so called nucleation mechanism. Furthermore, due to the “ball bearing” effect of spherical fly ash particles which creates a lubricating action in fresh concrete, partial replacement of the cement with fly ash results in the improvement of the workability of concrete. Li et al. [14] have investigated the effect of fly ash on the workability of the concrete and the replacement proportion of fly ash. A higher volume fly ash addition leads to a better workability.

Table 5 Fresh state properties of the mortars

| MIXTURE | FLOW (mm) | | Γ |
|---|---|---|---|
| LPC-0.18 | 335 | 340 | 10.4 |
| LPC-0.20 | 360 | 355 | 11.8 |
| LPC-0.22 | 370 | 373 | 12.8 |
| Ref | 371 | 380 | 11.5 |

## Hardened State Properties

Table 6 Hardened state properties of mortar mixes after 7 and 28 days, averaged

| MIXTURE | $R_{t,7}$ [MPa] | $R_{t,28}$ [MPa] | $R_{c,7}$ [MPa] | $R_{c,28}$ [MPa] | $\Phi_7$ [%] | $\Phi_{28}$ [%] |
|---|---|---|---|---|---|---|
| $w/c_{0.18}$ | 7.87 | 11.10 | 52.54 | 78.55 | 10.4 | 9.3 |
| $w/c_{0.20}$ | 7.37 | 9.68 | 49.95 | 68.03 | 11.4 | 10.3 |
| $w/c_{0.22}$ | 6.91 | 8.44 | 43.50 | 58.60 | 12.2 | 11.4 |
| Ref | 7.27 | 8.35 | 48.77 | 66.20 | 13.4 | 11.8 |

Where $R_{t,7}$ — flexural strength after 7 days, $R_{c,7}$ — compressive strength after 7 days, $\Phi_7$ — porosity after 7 days, $R_{t,28}$ — flexural strength after 28 days, $R_{c,28}$ — compressive strength after 28 days, $\Phi_{28}$ — porosity after 28 days.

## Mechanical properties

An overview of the determined mechanical properties of the prepared mortars is shown in Table 6. The compressive and flexural strengths development is presented in Fig. 3, from which it can be noticed that both flexural and compressive strength results at 28 days indicate that there was significant improvement in strength beyond the age of 7 days for all the four groups and the increase in strength from 7 to 28 days was between 15% and 41%. It also shows that both on 7 days and 28 days, LPC-0.18 develops the highest strengths among the prepared mortars and a trend of strength decrease can be observed when the water/binder ratio increases from 0.18 to 0.20. This is mainly because that the excessive water enhances the porosity of concrete [15], the strength of concrete gradually decreases with an increase of the water amount and the permeable porosity measurement has proved this. Furthermore, it can be found here the mixture with the addition of nano-silica has superior mechanical properties than the mortar without ns at both 7 and 28 days. This can be attributed to the pozzolanic properties of nano-silica which results in a finer C-S-H gel and densified microstructure. Comparing the mechanical properties of the high volume fly ash concrete designed in a previous study [18], LPC present better properties due to the denser packing system and the addition of nanosilica.

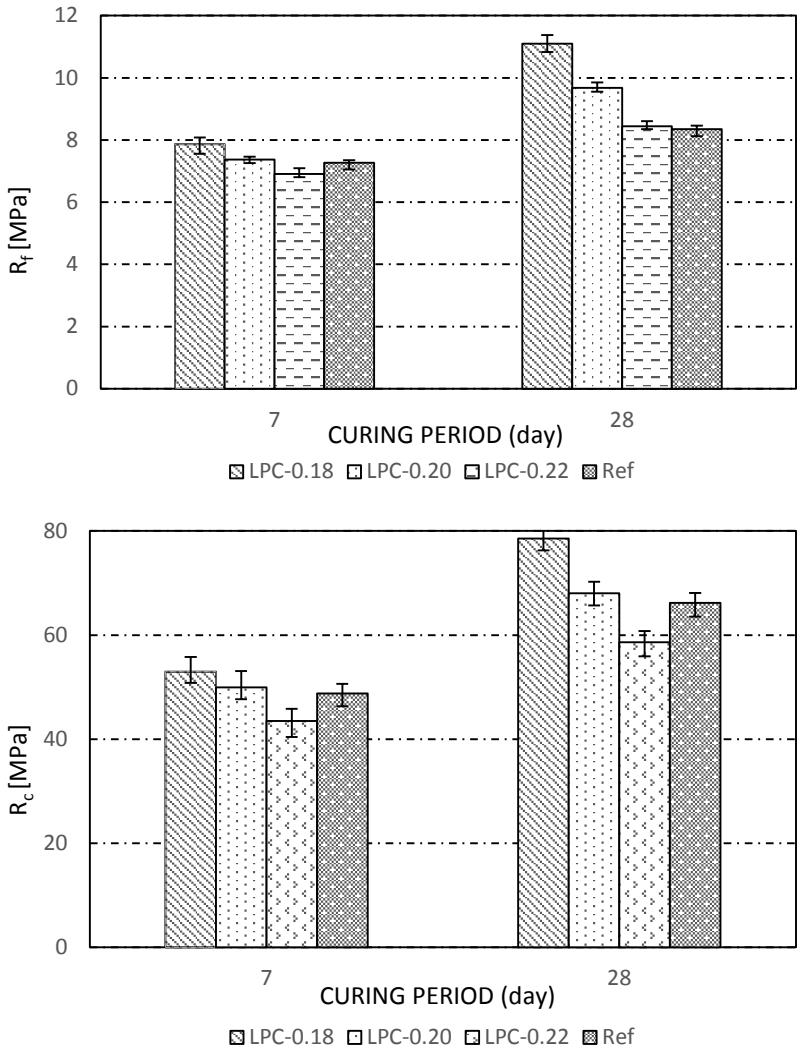


Figure 3 (a) flexural and (b) compressive strengths of mortars mixes at 7 and 28 days

## Porosity

The porosity of hardened UHPC show an obvious tendency related with the w/c ratio. With the increase of water amount, the porosity of LPC increases. In this study, the porosity of reference sample is 13.4% and 11.8% separately after 7 and 28 days. Comparing the LPC-0.18 and Ref samples, it can be seen that the total porosity is significantly decreased both after 7 and 28 days with the addition of nanosilica. This phenomenon should be attributed to the positive effect of nano-silica on the cement hydration.

As commonly known, due to the nucleation effect of nano-silica, the formation of C–S–H phase is no longer restricted on the grain surface alone, which causes that the hydration degree of cement is higher and more pores can be filled by the newly generated C–S–H. It should be noted that the addition of high volume of fly ash results in lower porosity when compared to a study base on the same raw materials [13] who reported a porosity of higher than 10%. This is due to the application of fly ash provides more nucleation sites for the precipitation of cement hydration products thus the hydration of fly-ash forms products and fills the already formed pore structure.

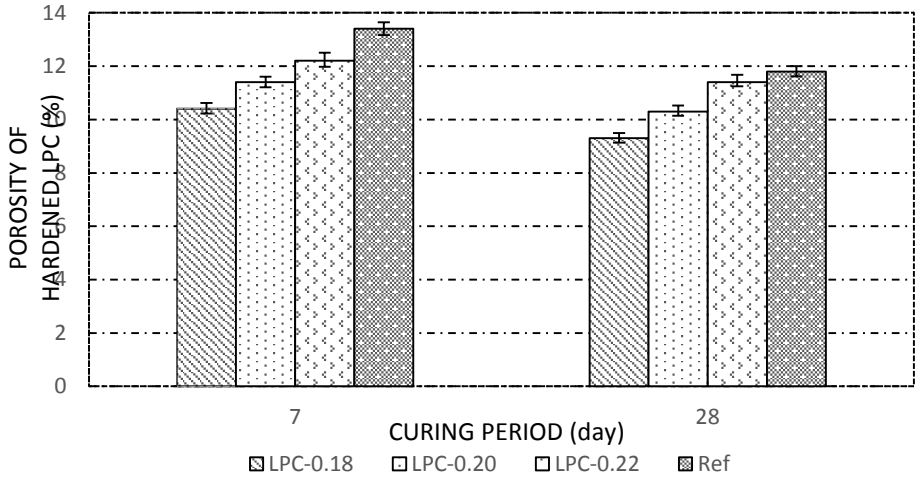


Figure 4 Water permeable porosity of the concrete at 7 and 28 days

**Chloride penetration depth and $D_{RCM}$**

After performing the RCM test, the colorimetric indicator for chlorides ($AgNO_3$ solution) is sprayed onto freshly split mortar samples to determine the chloride penetration depth. The colorimetric boundary between the regions with and without chlorides is clearly visible due to the chemical reaction of $Ag^+$ with $Cl^-$ or $OH^-$ and formation of white or dark precipitate regions. Subsequently, an average chloride penetration depth $x_d$ is measured and used for the calculation of $D_{RCM}$ (Eq. 5), as reported in Table 7. It may be observed that the chloride diffusion coefficients for mortars LPC-0.18 and LPC-0.20 are reduced compared to the two other mortars, and this can be attributed to the lower water/cement ratio, which results in lower amounts of free water in the system and in turn reduces the porosity of the hardened cement paste. It also shows that the addition of nano-silica into concrete could reduce the 28-days $D_{RCM}$ by 3.71 compared to the Ref-0.18 mixture. Due to the pozzolanic reaction of nano-silica, an additional amount of dense C-S-H gel is produced in the capillary pores. This densified microstructure of concrete is less water permeable and mechanically stronger compared to the Ref-0.18 mixture. At an early age, high volume fly ash concrete always present higher chloride migration coefficient due to the slow pozzolanic reactivity of fly ash. However, the addition of nanosilica modifies the pore structures and fills the space inside the concrete [16]. The $D_{RCM}$ of LPC-0.18 is lower than the ns containing concrete mix in a previous study [17] by a factor of 2 due to the decrease of water amount.

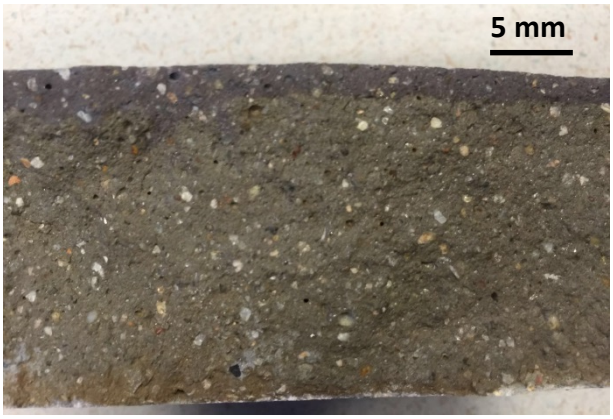


Figure 5 Chloride penetration depths in the LPC-0.18

Table 7 RCM test conditions and results for 28 days

| MIXTURE | SAMPLE | APPLIED VOLTAGE (V) | INITIAL CURRENT (mA) | TEST DURATION (h) | $X_d$ (mm) | $D_{RCM}$ ($\times 10^{-12} m^2 s^{-1}$) average |
|---|---|---|---|---|---|---|
| LPC-0.18 | 1 | 30 | 42.2 | 24 | 4.6 | 1.64 |
| | 2 | | | | 4.3 | |
| | 3 | | | | 3.9 | |
| LPC-0.20 | 1 | 30 | 46.3 | 24 | 4.4 | 1.73 |
| | 2 | | | | 4.8 | |
| | 3 | | | | 4.2 | |
| LPC-0.22 | 1 | 30 | 60.2 | 24 | 5.8 | 2.40 |
| | 2 | | | | 6.5 | |
| | 3 | | | | 5.5 | |
| Ref-0.18 | 1 | 25 | 82.0 | 24 | 11.1 | 5.35 |
| | 2 | | | | 12.6 | |
| | 3 | | | | 12.8 | |

## CONCLUSIONS

1. The designed concretes show excellent low permeability, indicated by a very low chloride diffusion coefficient. Chloride diffusion is reduced in the mixture containing nS. A lower w/c ratio results in a lower $D_{RCM}$.
2. The designed concretes show excellent workability, attributed to the higher fly ash dosage.
3. The designed concretes show very good mechanical properties. The addition of nano-silica results in a significant increase of the mechanical strength of the mortars.

## ACKNOWLEDGEMENTS

This research was carried out under the fund of China Scholarship Council and the Department of the Built Environment of Eindhoven University of Technology. The authors wish to express their gratitude to the following sponsors of the Building Materials research group at TU Eindhoven: Rijkswaterstaat Grote Projecten en Onderhoud, Graniet-Import Benelux, Kijlstra Betonmortel, Struyk Verwo, Attero, Enci, Rijkswaterstaat Zee en Delta - District Noord, Van Gansewinkel Minerals, BTE, V.d. Bosch Beton, Selor, GMB, Icopal, BN International, Eltomation, Knauf Gips, Hess AAC Systems, Kronos, Joma, CRH Europe Sustainable Concrete Centre, Cement&BetonCentrum, Heros, Inashco, Keim and Sirius International.

## REFERENCES

1. GJØRV, E. Durability Design of Concrete Structures in Severe Environment, 2009.
2. YU, Q L, SPIESZ, P, BROUWERS, H J H. Development of cement-based lightweight composites –Part 1: mix design methodology and hardened properties. Cement and Concrete Composites, Vol. 44, 2013, pp 17-29.
3. AMPADU, K O, TORII, K, KAWAMURA, M. Beneficial effect of fly ash on chloride diffusivity of hardened cement paste, Cem. Concr. Res. Vol. 29, 1999, pp 585–590. doi:10.1016/S0008-8846(99)00047-2.

4. THOMAS, M. Chloride thresholds in marine concrete, Cem. Concr. Res. Vol. 26, 1996, pp 513–519. doi:10.1016/0008-8846(96)00035-X.

5. ZHANG, M-H, ISLAM, J. Use of nano-silica to reduce setting time and increase early strength of concretes with high volumes of fly ash or slag, Constr. Build. Mater. Vol. 29, 2012, pp 573–580. doi:10.1016/j.conbuildmat.2011.11.013.

6. SAID, A M, ZEIDAN, M S, BASSUONI, M T, TIAN, Y. Properties of concrete incorporating nano-silica, Constr. Build. Mater. Vol. 36, 2012, pp 838–844. doi:10.1016/j.conbuildmat.2012.06.044.

7. BROUWERS, H J H, RADIX, H J. Self-Compacting Concrete: Theoretical and experimental study, Cem. Concr. Res. Vol. 35, 2005, pp 2116–2136. doi:10.1016/j.cemconres.2005.06.002.

8. BS-EN-1015-3. Methods of test for mortar for masonry - Part 3: Determination of consistence of fresh mortar (by flow table). British Standards Institution-BSI and CEN European Committee for Standardization; 2007.

9. HUNGER, M. An integral design concept for ecological self-compacting concrete. PhD thesis. Eindhoven University of Technology, Eindhoven, the Netherlands; 2010

10. BS-EN-196-1. Methods of testing cement - Part 1: Determination of strength. British Standards Institution-BSI and CEN European Committee for Standardization; 2005

11. NT Build 492. Concrete, mortar and cement-based repair materials: Chloride coefficient from non-steady-state migration experiments. Nordtest method, Finland; 1999.

12. ASTM C1202. Standard test method for electrical indication of concrete's ability to resist chloride ion penetration. In: Annual book of ASTM standards, Vol. 04.02. American Society for Testing and Materials, Philadelphia, July 2005.

13. YU, R, SPIESZ, P, BROUWERS, H J H. Development of an eco-friendly Ultra-High performance Concrete (UHPC) with efficient cement and mineral admixtures uses. Cement and Concrete Composites, Vol. 55, 2015, pp 383-394.

14. LI, G, WU, X. Influence of fly ash and its mean particle size on certain engineering properties of cement composite mortars. Cement and Concrete Research, Vol. 35, No. 6, 2005, pp 1128-1134.

15. MacGREGOR, J G. Reinforced concrete: mechanics and design. Upper Saddle River, NJ: Prentice Hall, 1997.

16. QUERCIA, G, HÜSKEN, G, BROUWERS, H J H. Water demand of amorphous nano silica and its impact on the workability of cement paste. Cement and concrete research, Vol. 42, No. 2, 2012, pp 344-357

17. QUERCIA, G, SPIESZ, P, HÜSKEN G, BROUWERS, H J H. SCC modification by use of amorphous nano-silica. Cement and Concrete Composites, Vol. 45, 2014, pp 69-81.

18. GERT, B. Physico-chemical Interactions in Portland Cement - (High Volume) Fly ash Binders. PhD thesis. Gent University, Gent, the Belgium; 2009.

# INFLUENCE OF PRE-EXPOSURE FATIGUE LOADING ON CHLORIDE PENETRATION IN CONCRETE SPECIMENS WITH EPOXY-COATED REINFORCEMENT

**X-H Wang**

**D V Val**

Heriot-Watt University

United Kingdom

**ABSTRACT.** The paper presents results of an experiment study of chloride penetration into concrete specimens with epoxy-coated reinforcement. The test specimens were made of ordinary Portland Cement (PC) concrete with w/c ratio of 0.44 and reinforced with uncoated and epoxy-coated reinforcing bars. For the latter two nominal coating thicknesses: 200 μm and 600 μm, were chosen. The specimens were divided into three groups and then the specimens from two groups were subjected to different fatigue loads. After that all specimens were repeatedly fully immersed in 3.5%~ 5% NaCl solution and dried; these wetting/drying cycles simulating seawater attack continued for388days. Four ϕ100×120-mm cylinders were then drilled out from the bottom side of the central 300-mm long zone of each specimen. The cylinders were used to measure chloride profiles within the concrete cover. Results of the measurements are presented in the paper. The apparent chloride diffusion coefficient and surface chloride concentration of each sample were estimated by fitting a solution of Fick's 2$^{nd}$ law of diffusion to the measured chloride profiles. It can be concluded that the chloride content at the bar level and the apparent chloride diffusion coefficient are influenced by pre-exposure fatigue loads, especially in the specimens with epoxy-coated reinforcement. It is also interesting to note that according to the test results undamaged specimens with epoxy-coated reinforcement had lower chloride diffusivity than those with uncoated reinforcing bars.

**Keywords:** Fatigue loading, Wetting/drying cycles, Total chloride content, Chloride diffusion coefficient, Epoxy-coated reinforcement

**Dr Xiao-Hui Wang** is a Marie-Curie Research Fellow at Heriot-Watt University. Previously, she worked in Department of Civil Engineering, Shanghai Jiao Tong University as an Associate Professor. She has published over 30 papers on various aspects of bond modelling of corroded reinforcing bars, strength of corroded RC elements, ITZ in steel fibre reinforced mortar and durability performance of RC elements with epoxy-coated reinforcement.

**Professor Dimitri V Val** is Professor of Infrastructure Safety and Reliability in the Institute for Infrastructure and Environment at Heriot-Watt University. His research interests are in the area of quantitative/probabilistic risk assessment of infrastructure systems with emphasis on reliability assessment of existing structures and inter-infrastructure risks due to various natural and man-made hazards including effects of changing climate.

## INTRODUCTION

Corrosion of reinforcing steel in reinforced concrete (RC) structures due to penetration of chloride ions from in-service environments is one of the main causes of deterioration of these structures. In the past decades, a large amount of research has been carried out to study the chloride penetration into sound and cracked concrete [1-5].A particular attention has been paid to the influence on this phenomenon of flexural loading and induced by it concrete cracking [6-8], including the effect of flexural cyclic loading on the chloride diffusivity of plain concrete [9]. Research on chloride penetration in RC structures with epoxy-coated reinforcement has been mainly focused on field surveys [10-12]. For example, based on concrete samples obtained from 44 bridge decks with epoxy-coated reinforcement it was determined that the chloride concentration at the bar level in most cases were above the threshold level of corrosion initiation in black steel; its average value was 2.1kg/m$^3$with the highest of 6.8kg/m$^3$ [10].

Another field study of six bridge decks in West Virginia showed that the average chloride content in the decks with epoxy coated reinforcement was similar to that in the decks reinforced with uncoated bars [12]. Since epoxy-coating affects the bond between reinforcing steel and concrete it also influences cracking of the concrete cover under loading, in particular under fatigue (i.e., cyclic) loading. In its turn, the concrete cover cracking affects chloride penetration into concrete. Thus, it may be worth to specifically investigate the effect of fatigue loading on chloride penetration in RC elements with epoxy-coated reinforcement.

The paper presents results of an experiment study of chloride penetration into RC specimens with uncoated and epoxy-coated reinforcing bars. The specimens were cast from ordinary Portland cement (PC) concrete with w/c ratio of 0.44. After 28-day curing, the specimens were divided into three groups and then the specimens from two groups were subjected to fatigue loads (500,000 cycles with two different load ranges).

After that all specimens were repeatedly fully immersed in 3.5%~ 5% NaCl solution and dried; these wetting/drying cycles simulating an environmental attack continued for388days. Four 100-mm diameter and 120-mm long ($\phi$100×120-mm) cylinders were then drilled out from the bottom side of the central 300-mm long zone of each specimen. The cylinders were cut into 10-mm thick slices, which were oven-dried and grounded into powder for measuring the total chloride content.

The apparent chloride diffusion coefficient and surface chloride concentration in the specimens were then estimated by fitting the error function solution of Fick's 2$^{nd}$ law of diffusion to the measured chloride profiles.

## EXPERIMENTAL PROGRAM

### Specimen Details and Materials

All test specimens had a rectangular cross section with the following intended dimensions: width =300 mm, height = 120 mm, overall length =1500mm (Figure1). The actual dimensions could slightly deviate from the intended ones. The specimens were reinforced with three 12-mm diameter deformed bars in the longitudinal direction and 8-mm diameter plain bars in the transverse direction.

Commercial ordinary PC concrete with w/c ratio of 0.44 from a single batch was used to cast all the test specimens to ensure that they had the same concrete properties. Portland cement P Ⅱ 52.5 with micro furnace slag and coarse aggregate with maximum aggregate size of 25mm were used in the concrete mixture.

The slump of the concrete was 140±20mm. Concrete mix proportion of the water: cement: sand: aggregate: superplasticizer: admixture = 180:320:770:1020:4.51:90. The compressive strength of a 150×150×150-mm concrete cube at 28 days was 50 MPa. The specimens were designated with letters and numbers. The letters 'E' and 'FE' indicate the type of exposure and loading to which the specimens were subjected, namely the Environmental attack and Fatigue load & Environmental attack, respectively. The first letter 'E' with the following number '0.2' or '0.6' (i.e., E0.2 or E0.6) denotes the specimens with epoxy-coated reinforcement, where the numbers represent the nominal thickness of the epoxy coating, 200μm or 600μm, respectively.

The final number in the designations indicates the specimen number. There were in total 9 specimens, which were divided into three groups: Group 1 (E1, E0.2E2 and E0.6E2) was subjected only to an environmental (i.e., simulated seawater) attack, Group 2 (FE1, E0.2FE3 andE0.6FE3) and Group 3 (FE2, E0.2FE5 andE0.6FE5) were initially subjected to fatigue loading and then to an environmental attack.

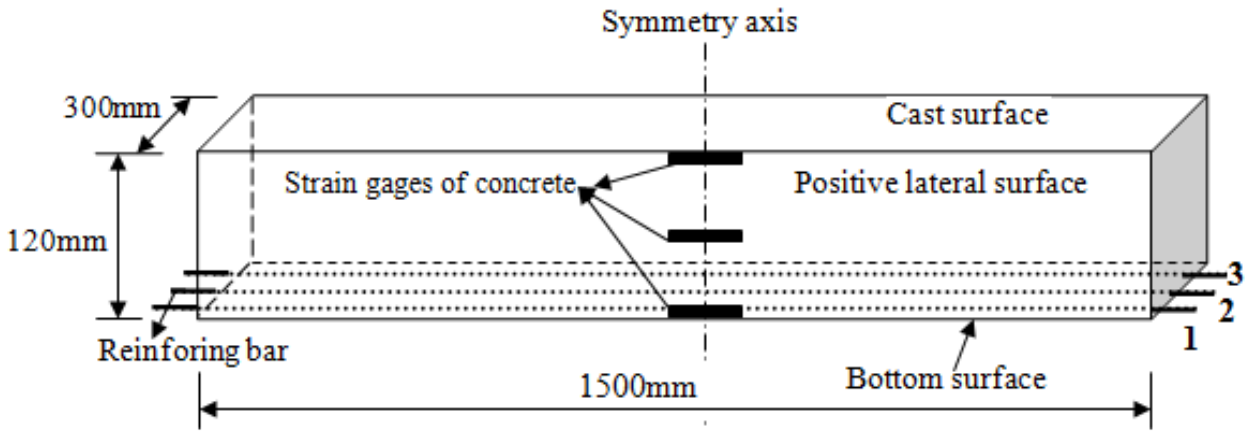


Figure 1 Test specimens [13]

**Pre-Exposure Fatigue Loading**

After 28-day curing, the specimens in Groups 2 and 3 were subjected to fatigue loading. A three-point loading setup with span of 1100 mm was used for this purpose. Loads were created by a 100-kN pulse fatigue testing machine. The specimens from Group 2 were subjected to 500,000 cycles of loads in the range of 5.4 to 18 kN, Group 3 – 500,000 cycles and the load range 2.8~14 kN. Displacements at mid-span and two pivots of the supports of each test specimen were measured by displacement transducers.

A load cell was used to control and record the magnitudes of fatigue loads [13]. For the test specimens subjected to 500,000 fatigue loading with 4 Hz frequency, when the number of cycles reached 50,000, 100,000, 300,000 and 500,000, the fatigue load was unloaded to zero; during each load stopping, developments of the cracks were observed and the corresponding

numbers of the load cycles were recorded at the cracking tips. Then, test specimen was reloaded to the upper limit of the fatigue load and the developments of the cracks and the maximum cracking widths were recorded again.

**Exposure Conditions**

All test specimens were subjected to a simulated environmental attack: from Group 1 straight after curing, from Groups 2 and 3 after loading. Initially, the specimens were turned upside down, horizontally placed and their bottom surfaces were covered by sponges, which were wetted with 3.5%~ 5% NaCl solution simulating seawater. Plastic sheets were then placed over the sponges. Two weeks later, the plastic sheets and sponges were removed and the specimens were air-dried for one week. The three weeks constituted one cycle of wetting and drying. After four such wetting-drying cycles, in order to accelerate the tests, the specimens were fully immersed in 3.5%~ 5% NaCl solution.

A 4m×5m pool was specifically built for this purpose. After one month of the full immersion, the NaCl solution was discharged and the specimens were air-dried for one month. In total, three such wetting-drying cycles were performed. The simulated environmental attack continued for 388 days.

**Location of Drilled-out Cylinders in Test Specimens**

To measure chloride content in the test specimens, four ϕ100×120-mm cylinders were drilled out from the bottom side of the central 300-mm long zone of each specimen after the simulated environmental attack had been completed. The location of the cylinders is shown in Figures 2-4. The cylinders were labelled with numbers: the first digit indicated the number of the longitudinal bar (1 or 3) under which the cylinder was drilled out, the second just distinguished two different positions.

**Sample Preparation for Measuring Chloride Content in Concrete**

After the cylinders were drilled out and labelled, they were transported to a laboratory of the Shanghai Research Institute of Building Science CO., LTD for measuring the chloride content in concrete. Since the concrete cover to the longitudinal reinforcing bars in each specimen was 40mm, four 10-mm thick slices were cut from each cylinder between its bottom surface and the surface of a reinforcing bar. The slices were then put in an oven for drying and after that grounded to powder. From each slice, 1.5 g of fully-mixed powder were taken to measure the chloride content in the slice.

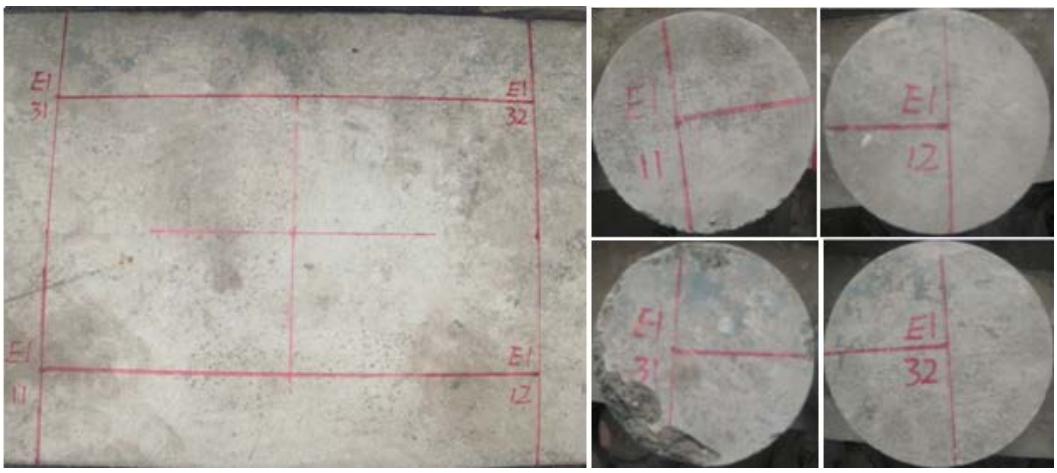

(a) Specimen E1

(b) Specimen E0.2E2

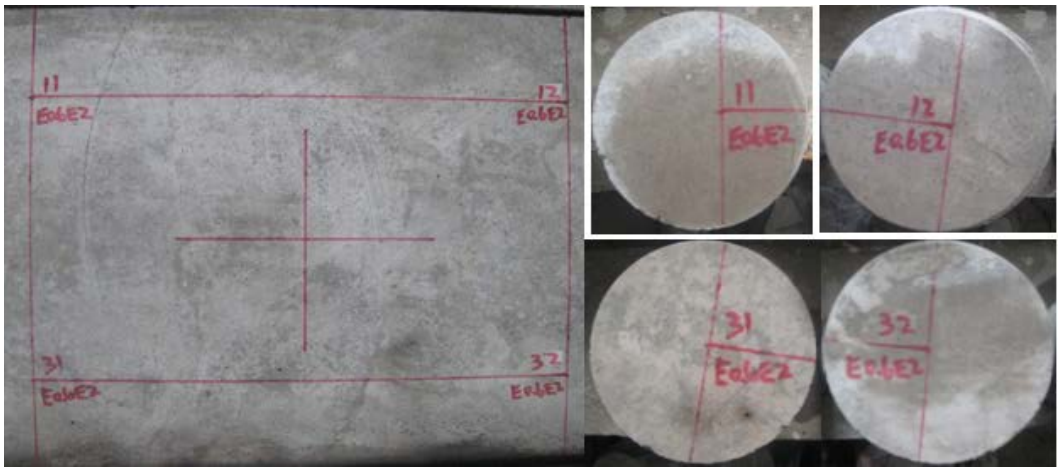

(b) Specimen E0.6E2

Figure 2 Position of cylinders on the bottom side of test specimens in Group 1 and the drilled-out cylinders


(a)Specimen FE1


(b) Specimen E0.2FE3

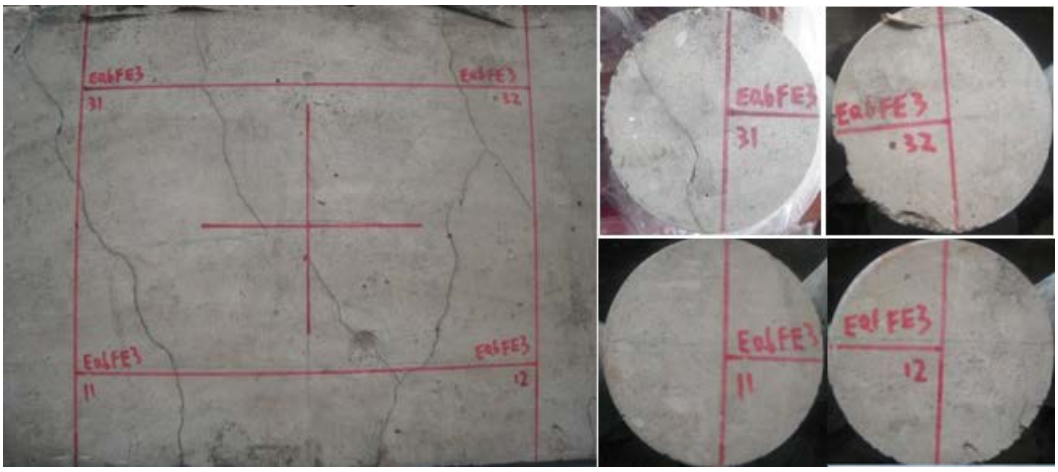


(c) Specimen E0.6FE3

Figure 3 Position of cylinders on the bottom side of test specimens in Group 2 and the drilled-out cylinders

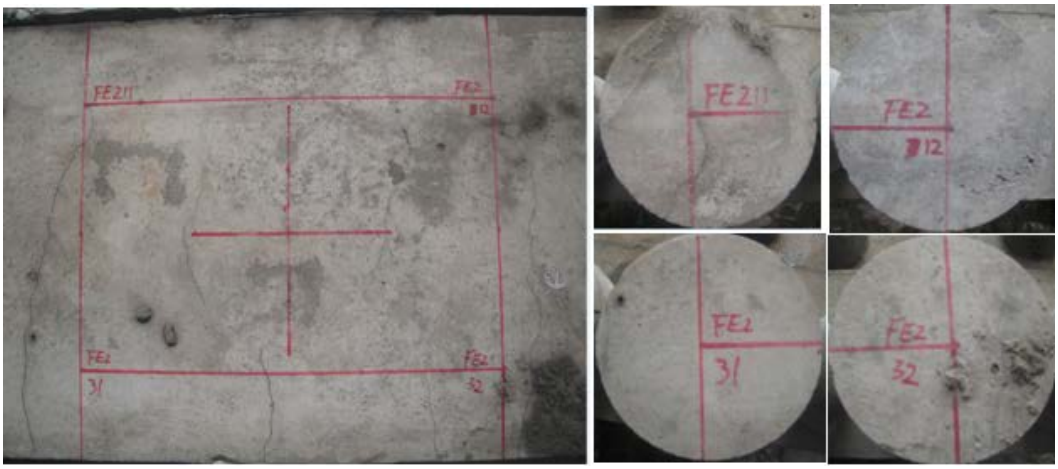


(a)Specimen FE2


(b) Specimen E0.2FE5


(c) Specimen E0.6FE5

Figure 4 Position of cylinders on the bottom side of test specimens in Group 3 and the drilled-out cylinders

## TEST RESULTS

Results of the measurements of the chloride content in the concrete cover of the test specimens are presented in Figures 5 to 7. As described above, the 40-mm concrete cover zone of each cylinder was cut into four 10-mm thick slices. Thus, it is assumed that the chloride content obtained for each slice corresponds to the depth from the surface to the midpoint of the slice, i.e., the measured chloride contents correspond to the depths of 5, 15, 25 and 35 mm. The chloride content, especially at the level of reinforcement, is needed in order to determine the time of corrosion initiation. The common approach is that corrosion starts when the chloride content at the surface of a reinforcing bar exceeds the so-called threshold concentration, $C_{crit}$. There is still no general agreement on how to set the value of the latter because it depends on too many different factors [14]. Moreover, $C_{crit}$ has been presented in different forms, e.g., by total or free chloride content expressed as absolute value or relative to the weight of cement or concrete, or as chloride to hydroxyl concentration ratio ($Cl^-/OH^-$). Based on data presented in [14], $C_{crit}$ for uncoated reinforcement in the specimens tested in this study should be the range of 0.04-0.75% by the weight of binder or 0.007-0.129% by the weight of concrete (the binder content in the specimens' concrete was 17.2%). For epoxy-coated reinforcement values of $C_{crit}$ in the range 0.03-0.19% by the weight of concrete (or 0.73-4.56 kg/m$^3$) have been reported [15]. The tests carried out in the present study do not allow to estimate $C_{crit}$ because the chloride content was measured only after completion of the simulated environmental attack. Thus, only a comparison of the final chloride content at the reinforcement level with the above values of $C_{crit}$ is possible. The measured chloride content is % relative to the weight of concrete.

### Chloride Penetration into the Bottom Concrete Cover of Test Specimens in Group 1

The measured chloride profiles for the test specimens from Group 1 are shown in Figure 5. In most cases, the chloride content gradually decreases with the concrete cover depth except of at the 5-mm depth in the cylinders 11/E1 (Figure 5a) and 32/E0.2E2 (Figure 5b). The reason for that is that the chloride content within the external layer of concrete (the so-called "skin layer") is mainly controlled by convection of the pore water, i.e., chlorides move in and out of the concrete with moisture [16]. Comparing the chloride profiles for the three specimens from this group a noticeable difference can be observed between the ones obtained for the specimen E1 with uncoated reinforcement and those for the E0.2E2 and E0.6E2 with epoxy-coated reinforcing bars. The chloride contents in the E1 are lower near the concrete surface but higher near the reinforcing steel. This indicates that the chloride diffusion coefficient in the E1 was higher than in the E0.2E2 and E0.6E2. Since no cracks were observed in the three specimens (see Figure 2) it could be explained by differences in the concrete compaction of the specimens. Another possible reason will be discussed further in the paper. The chloride content at the level of reinforcement in the E1 varied between 0.027% and 0.093% by the weight of concrete, i.e., well within the range of the $C_{crit}$ values mentioned above, and corrosion at the end of the tests was observed in both bars. In the E0.2E2 and E0.6E2 the chloride content near the reinforcing bars was below 0.03% by the weight of concrete (except of the cylinder 31/E0.6E2, where it was 0.035%). After the tests, none of the epoxy-coated bars showed signs of corrosion.

### Chloride Penetration into the Bottom Concrete Cover of Test Specimens in Group 2

The measured chloride profiles for the test specimens from Group 2 are shown in Figure 6. The chloride content gradually decreases in all specimens except of at the 5-mm depth in the cylinders 31/FE1 (Figure 6a) and 32/E0.2FE3 (Figure 6b); a possible reason for that has been explained previously.

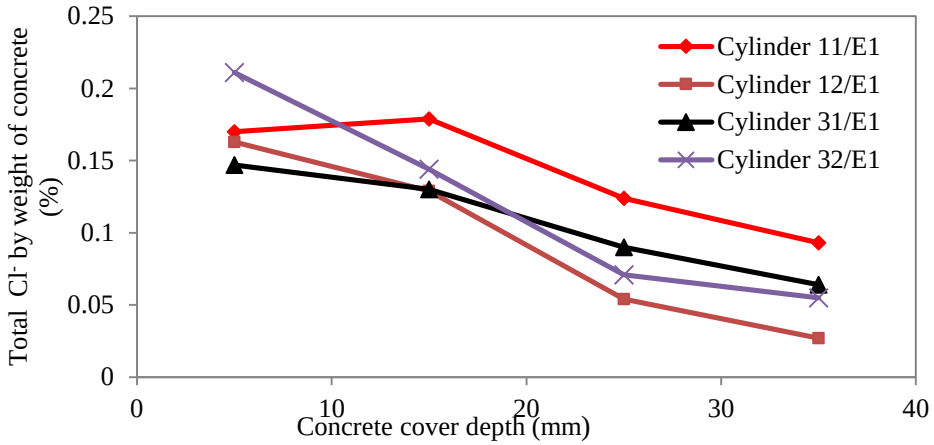


(a) Specimen E1

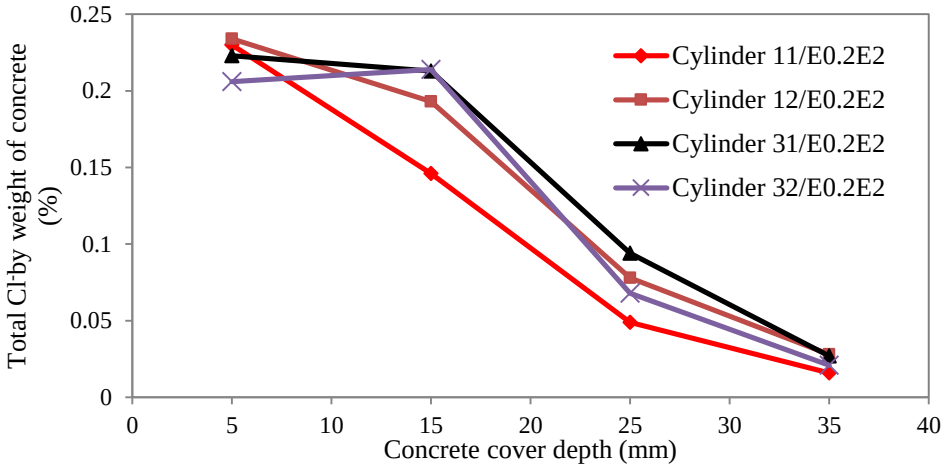


(b) Specimen E0.2E2

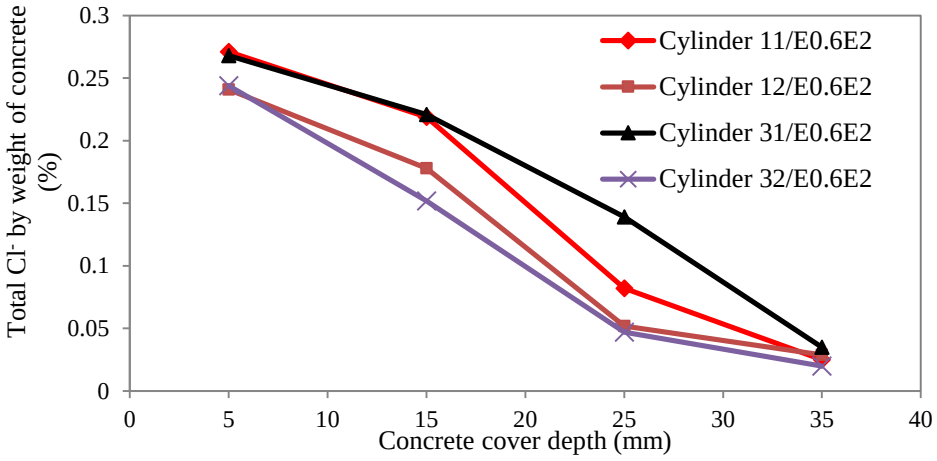


(c)Specimen E0.6E2

Figure 5 Measured chloride profiles in the test specimens from Group 1

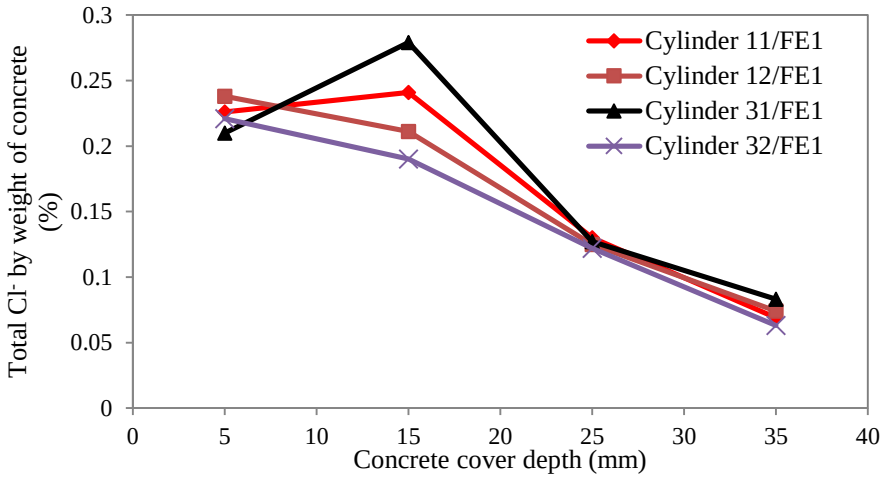


(a) Specimen FE1

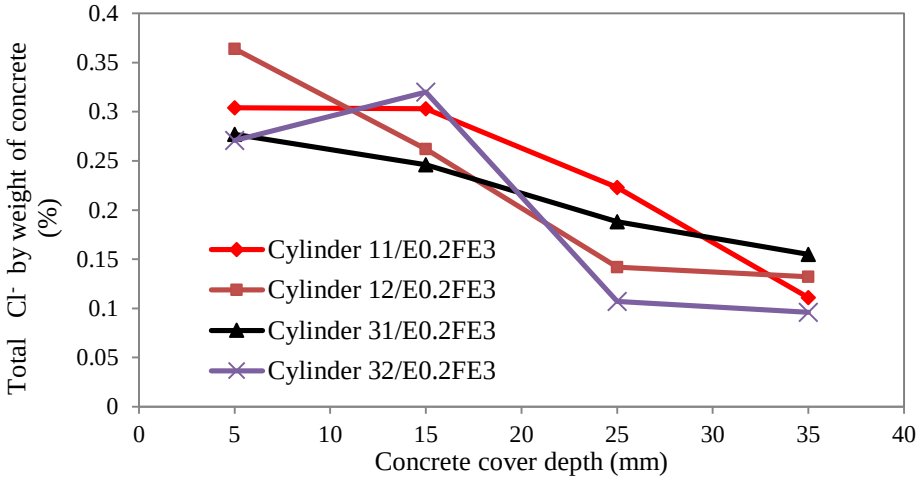


(b) Specimen E0.2FE3

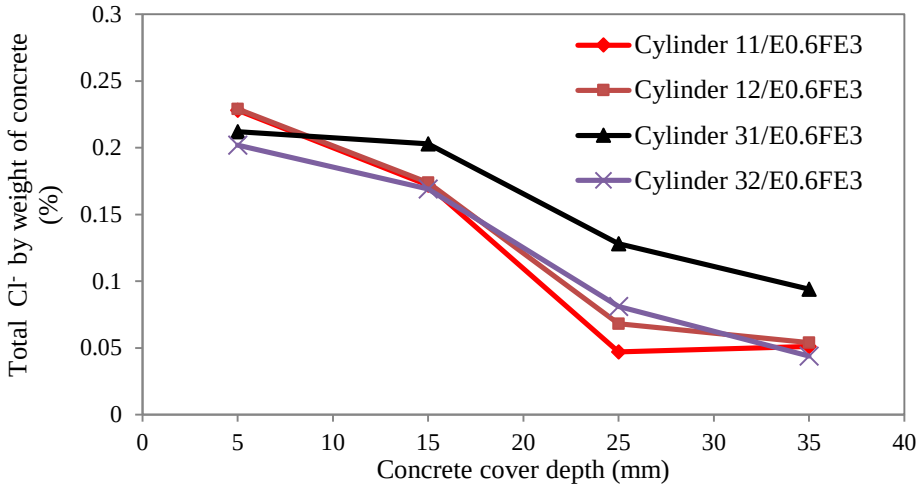


(c) Specimen E0.6FE3

Figure 6 Measured chloride profiles in the test specimens from Group 2

The specimens in this group were subjected to pre-exposure fatigue loading that induced damage to the concrete in the form of visible cracks and invisible but much more numerous micro-cracks. This led to an increase in the concrete diffusivity and as a result of that an increase in the chloride content at the level of reinforcement compared to the specimens from Group 1.

In the FE1 the chloride content near the uncoated reinforcing bars varied between 0.063% and 0.083% by the weight of concrete and corrosion was observed in both bars. In the specimens with epoxy-coated bars, E0.2FE3 and E0.6FE3 the increase in the chloride concentration near the reinforcing bar compared to those from Group 1 was even more significant, especially in the cylinders with visible cracks. The chloride content at the depth of 35 mm in the cylinder 31/E0.2FE3 was 0.155% by the weight of concrete and in 31/E0.6FE3 – 0.094%, i.e., about five and three times, respectively, greater than in the similar specimens from Group 1. Signs of corrosion were observed in the epoxy-coated bars.

**Chloride Penetration into the Bottom Concrete Cover of Test Specimens in Group 3**

The measured chloride profiles for the test specimens from Group 3are shown in Figure 7. The chloride content gradually decreases in all specimens except of at the 5-mm depth in the cylinder 12/E0.6FE3 (Figure 6b); a possible reason for that has been explained previously.

Like the specimens in Group 2, the specimens from this group were subjected to pre-exposure fatigue loading but with the slightly lower magnitude of applied loads. The chloride content at the level of reinforcement in practically all cases was higher compared to that in the specimens from Group 1, except of the results for the two cylinders without visible cracks, 11 and 31, from the specimen E0.6FE5, for which very low values of the chloride content, 0.021% and 0.017% by the weight of concrete were obtained (see Figure 7c).

At the same time, the chloride concentrations in the specimens with epoxy-coated reinforcement, E0.2FE5 and E0.6FE5, were lower than those in the similar specimens from Group 2. In the specimen FE2 the chloride content was higher compared to that in the FE1 from Group 2 due to the higher concentrations in the surface layer. Corrosion was observed in the uncoated bars in the FE2 and also in the epoxy-coated bars with the thinner coating, i.e., in E0.2FE5.

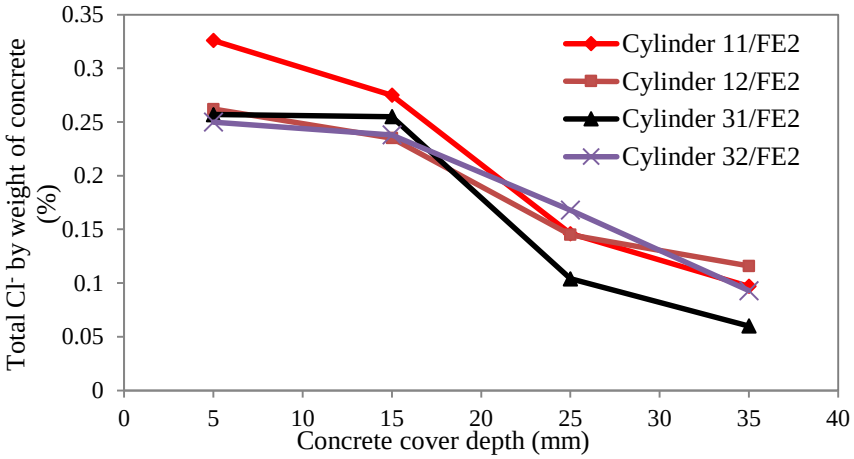


(a) Specimen FE2

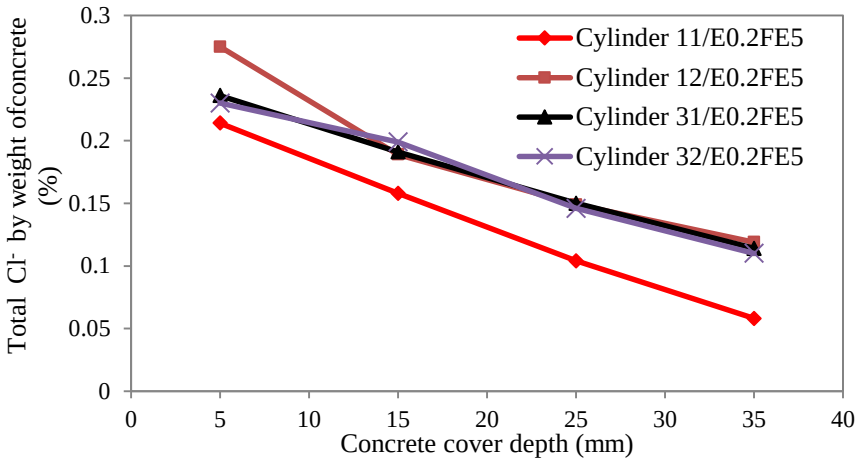


(b) Specimen E0.2FE5

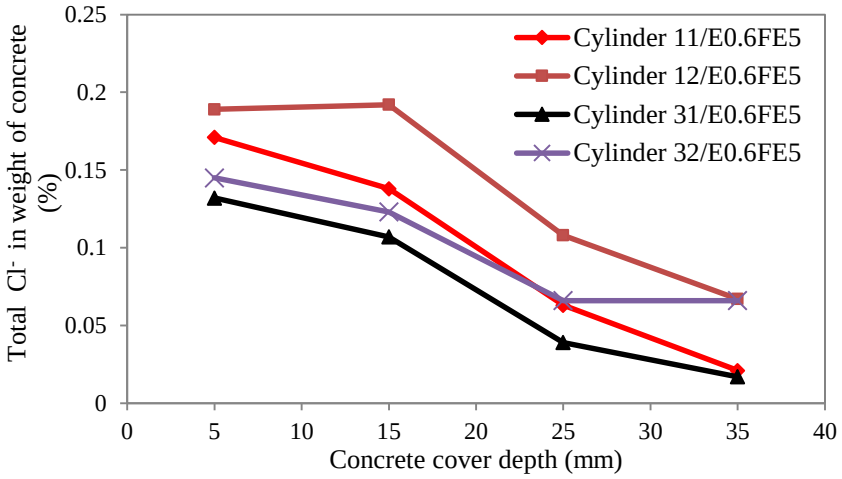


(c) Specimen E0.6FE5

Figure 7 Measured chloride profiles in the test specimens from Group 3

## ANALYSIS AND DISCUSSION

Chloride profiles in concrete are commonly described by the error function solution of Fick's 2nd law of diffusion (e.g., [1, 16])

$$C(x,t) = C_0\left[1 - \mathrm{erf}\left(\frac{x}{2\sqrt{Dt}}\right)\right] \quad (1)$$

where $C(x,t)$ is the chloride content at the depth $x$ and time $t$ from the beginning of exposure,$C_0$the surface chloride concentration, $D$ the apparent chloride diffusion coefficient and erf(.) the error function.

The values of $C_0$ and $D$ are determined by fitting this solution to measured data using a nonlinear regression analysis. In this study MatlabR2014b was employed for this purpose. The values of $C_0$ and $D$ obtained using the data shown in Figures 5-7 ($t$ = 388 days) are presented in Table 1. In the case of several uncracked cylinders drilled out from the same specimens the values $C_0$ and $D$ were estimated once using the data for all these cylinders. When the chloride content at the 5-mm depth was lower than those at larger depths in the same cylinder this data point was excluded from the analysis [16].

Comparing the values of the apparent diffusion coefficient for similar specimens from different groups the following observations can be made. Firstly, damage caused by the pre-exposure fatigue loading led to an increase in the chloride diffusivity. This is especially noticeable for the specimens with epoxy-coating reinforcing bars when the damage was presented in the form of visible cracks. The maximum increase in $D$ compared to its value for the corresponding specimen from Group 1 is 4.90 for the E.02 specimens (i.e., 200-μmepoxy coating) and 3.25 for the E.06 specimens (i.e., 600-μm epoxy coating). Both these results are for the cracked cylinders from Group 2. The increase for Group 3 is lower: 3.59 for the E.02 specimens and 2.62 for the E.06 specimens. The magnitude of cycling loads applied to the specimens from Group 2 was slightly higher compared to those from Group 3 that might lead to larger damage and the more significant increase in the chloride diffusivity. For the specimens with uncoated reinforcing bars, the maximum increase in $D$for Groups 2 and 3 compared to Group 1 is much smaller and practically the same for both groups: 1.40 for Group 2 and 1.45 for Group 3. This difference between the specimens with uncoated and epoxy-coated reinforcing bars can be explained by worse bond between the epoxy-coated bars and concrete that resulted in larger damage caused by fatigue loading and, subsequently, the larger increase in the chloride diffusivity. For uncracked cylinders from Group 2 and 3, an increase in $D$ is only observed for the E.02 specimens: 1.77 for Group 2 and 1.61 for Group 3. Secondly, it can be observed that the undamaged specimens with epoxy-coated reinforcement had lower chloride diffusivity than the one with uncoated reinforcing bars (Group 1). This observation is also valid for the uncracked cylinders from the E.06 specimens in Groups 2 and 3. As noted previously, it can be caused, e.g., by differences in the concrete compaction. However, there is another possible explanation. It is known that concrete under a bottom reinforcing bar is more porous because the bar obstructs plastic settlement of the concrete after casting. Since the epoxy coating decreases the surface adhesion between the reinforcing bar and concrete it also decreases this obstruction that may lead to reduction of the concrete porosity under the bar. The thicker the coating is the greater this effect. Of course, this is just a hypothesis and further research is needed to check it.

Table 1 Comparison of the model parameters for reinforcing bars in four groups

| TEST GROUPS | SPECIMENS | CYLINDERS AND CRACK INFORMATION (see Figures 2-4) | $D\times10^{-4}$, $m^2$/year | $C_{0,}$ % by concrete weight |
|---|---|---|---|---|
| Group 1 | E1 | No cracks | 5.157 | 0.2194 |
| | E0.2E2 | No cracks | 2.688 | 0.2904 |
| | E0.6E2 | No cracks | 2.484 | 0.3260 |
| Group 2 | FE1 | 11: one middle crack (<0.15mm) | 5.705 | 0.2861 |
| | | 12: one edge crack (<0.1mm) | 5.215 | 0.2852 |
| | | 31: one edge crack (0.15 mm) | 7.229 | 0.2851 |
| | | 32: no crack | 5.118 | 0.264 |
| | E0.2FE3 | 11: one edge crack (<0.15mm) | 8.05 | 0.3682 |
| | | 12, 32: no crack | 4.752 | 0.3834 |
| | | 31: one middle crack (0.15mm) | 13.16 | 0.3043 |
| | E0.6FE3 | 11, 12, 32: no crack | 2.258 | 0.2710 |
| | | 31: one middle crack (0.2mm) | 8.071 | 0.2486 |
| Group 3 | FE2 | 11: one middle crack (0.16mm) | 4.458 | 0.3899 |
| | | 12 and 32: one edge crack (0.16mm) | 7.470 | 0.2998 |
| | | 31: one edge crack (0.22 mm) | 3.904 | 0.3284 |
| | E0.2FE5 | 11: no crack | 4.330 | 0.2489 |
| | | 12: one middle crack (0.2mm) | 7.065 | 0.2945 |
| | | 31: one middle crack (0.2mm) | 9.660 | 0.2584 |
| | | 32: one edge crack (0.08mm)+ side crack | 9.427 | 0.2576 |
| | E0.6FE5 | 11 and 31: no crack | 2.715 | 0.1921 |
| | | 12: one middle crack (0.12mm) | 6.247 | 0.2324 |
| | | 32: one middle crack (0.14mm) | 6.517 | 0.1645 |

## CONCLUSIONS

Results of the experimental study of chloride penetration into RC specimens with uncoated and epoxy-coated reinforcing bars have been presented. A part of the specimens were subjected to pre-exposure fatigue loading. According to the results, the loading led to an increase in the chloride diffusivity of the specimens, especially the ones with epoxy-coated reinforcement. It was also observed that the chloride diffusivity of the undamaged specimens with epoxy-coated reinforcement was lower than that of the specimens with uncoated reinforcing bars. However, due to the limited number of specimens that were tested this issue requires further research.

## ACKNOWLEDGMENTS

The authors gratefully acknowledge the support provided by the National Natural Science Foundation of China (No. 51178266).

## REFERENCES

1. KONIN, A, FRANÇOIS, ARLIGUIE G. Penetration of chloride in relation to the microcracking state into reinforced ordinary and high strength concrete, Materials and Structures, Vol.33, 1998, pp 310-316.

2. RODRIGUEZ, O G, HOOTON, R D. Influence of cracks on chloride ingress into concrete, ACI Materials Journal, Vol.100, No. 2, 2003, pp 120-126.

3. DJERBI,A, BONNETS, KHELIDJ, A, BAROGHEL-BOUNY, V. Influence of traversing crack on chloride diffusion into concrete, Cement and Concrete Research, Vol.38, No.6, 2008, pp 877-883.

4. ANDRADE, C, PIETRO, M, TANNER, P, TAVARES, F, D'ANDREA, R. Testing and modelling chloride penetration into concrete, Construction and Building Materials, Vol. 39, 2013, pp 9-18.

5. BENTZ, D P, GARBOCZI, E J, LU, Y, MARTYS, N, SAKULICH, A R, WEISS, W J. Modeling of the influence of transverse cracking on chloride penetration into concrete, Cement & Concrete Composites, Vol. 38, 2013, pp 65-74.

6. GOWRIPALAN, N, SIRIVIVATNANON, V, Lim, C C. Chloride diffusivity of concrete cracked in flexure, Cement and Concrete Research, Vol. 30, No. 5, 2000, pp 725–730.

7. SAHMARAN, M. Effect of flexure induced transverse crack and self-healing on chloride diffusivity of reinforced mortar, Journal of Material Science, Vol. 42, No. 22, 2007, pp 9131–9136.

8. WANG, L C, WANG, J Z. Mesoscale simulation of chloride diffusion in concrete subjected to flexural loading, Advances in Structural Engineering, Vol. 17, No. 4, 2014, pp 561-572.

9. TRAN, V M, BOONCHAI, S, TOYOHARU, N. Prediction of chloride diffusion coefficient of concrete under flexural cyclic load, Computers and Concrete, Vol. 8, No. 3, 2011, pp 343-355.

10. SMITH, J L, VIRMANI, Y P. Performance of epoxy-coated rebars in bridge decks, Public Roads, Vol.60, No.2, 1996, pp 6-12.

11. CUSSON, D, QIAN S, CHAGNON, N, BALDOCK, B. Corrosion-inhibiting systems for durable concrete bridges. I: five-year field performance evaluation, Journal of Materials in Civil Engineering, Vol.20, No.1, 2008, pp 20-28.

12. LAWLER, J S, KRAUSS, P D, KURTH, J, MCDONALD, D. Condition survey of older West Virginia bridge decks constructed with epoxy-coated reinforcing bars, Transportation Research Record: Journal of the Transportation Research Board, Vol. 2220, 2011, pp57-65.

13. WANG,X-H, CHEN, B,GAO, Y, WANG, J, GAO L. Influence of external loading and loading type on corrosion behavior of RC beams with epoxy-coated reinforcements, Construction and Building Materials,Vol.93, No. 15, 2015, pp 746-765.

14. ANGST, U, ELSENER, B, LARSEN, C K, VENNESLAND,Ø, Critical chloride content in reinforced concrete–A review, Cement and Concrete Research, Vol.39, No.12, 2009, pp1122-1138.

15. FANOUS, F S, WU, H-C. Service life of Iowa bridge decks reinforced with epoxy-coated bars. Proceedings of the Mid-Continent Transportation Symposium, Iowa State University, USA, 2000, pp 259-262.

16. ANDRADE, C, CLIMENT, M A, DE VERA, G. Procedure for calculating the chloride diffusion coefficient and surface concentration from a profile having a maximum beyond the concrete surface, Materials and Structures, Vol. 48, No. 4, 2015, pp 863-869.

# THE EFFECT OF CURING REGIME ON THE COMPRESSIVE STRENGTH OF ULTRA HIGH PERFORMANCE CONCRETE

**S Vatannia**

**E Kearsley**

**D Mostert**

University of Pretoria

South Africa

**ABSTRACT.** Curing regime plays an important role on the properties of concrete especially on the compressive strength of Ultra High Performance Concrete (UHPC). It is common to cure UHPC in hot water at temperatures of more than 70°. In order to get 200MPa compressive strength, different curing durations were considered with the samples kept in 85°C water. The days which the samples were cured in the heat treatment were: 1, 3 and 6 days. After the heat curing samples were kept in 24°C water up to 28 days. Abnormal behaviour was seen in the results with the 28-day compressive strengths being lower than the 7-day results. In this study, the reason for the reduction in the strength is investigated. Different curing regimes and procedures are taken into account. Different water temperatures for heat treatment were considered: 65°C, 85°C and 92°C. After the heat treatment, half of the samples were kept in water at 24°C and the other half were kept in a humid room at 99% RH till testing. The compressive strength of cubes was investigated after 7, 28 and 90 days of curing.

**Keywords:** UHPC, Compressive strength, Curing regime, Heat treatment.

**Sharifeh Vatannia** is a PhD candidate at University of Pretoria.

**Elsabe Kearsley** is a professor in Civil Engineering at the University of Pretoria where she has been involved with cement and concrete research for more than 20 years. She holds a PhD from the University of Leeds, UK.

**Derek Mostert** is a Concrete Technologist with an ACT diploma from City and Guilds and a Master's degree in advanced concrete technology from the University of Belfast.

## INTRODUCTION

Ultra High Performance Concrete (UHPC) is known for its high compressive strength (more than 150 MPa) and ductile behaviour under tension in the presence of steel fibers [1]. Curing regime plays an important role on the properties of concrete especially on the compressive strength of UHPC. It is common to cure UHPC in hot water at temperatures of more than 70°, as UHPC mostly contains cement extenders and there is a belief that high temperatures accelerate the pozzolanic reaction in concrete.

Various investigations have been published referring to various curing regimes with different procedures in order to reach to the highest possible compressive strength [1-4]. These different curing regimes include hot air curing, steam curing, water curing and autoclaving at different temperatures and durations. Richard and Cheyrezy [5] suggested heat treatment as one of the basic principles used to increase the compressive strength of PRC (Powder Reactive Concrete) which is also known as UHPC. In their study the compressive strength of concretes were enhanced from 170MPa to 230MPa by heating samples from 20°C to 90°C, respectively. Larrard and Sedran [6] observed that 7-day compressive strength improved from 120.6 MPa to 235.8 MPa. This improvement was achieved by changing the curing regime from normal water curing to thermal curing at 90°C for 48 hours. Heat treatment is considered as a curing regime in most of the UHPC studies [7-10].

In a previous study by the authors, the properties of UHPC for different curing regimes were investigated. The properties include compressive strength, direct tensile strength and flexural strength (MOR). Hook-ended steel fibers as well as steel micro fibers reinforced the UHPC. The samples were submerged in 24°C water immediately after removing them from the 85°C water. The direct tensile and flexural strengths were studied for samples which were kept in 85°C water for 6 days followed by storing the samples in 24°C water. Curing the samples in 24°C water for 28 days was considered as well. The 7-day and 28-day strengths of reinforced and non-reinforced UHPC were measured. Figure 1 shows the 28-day results of direct tensile and flexural strength for different curing regimes. The graph shows that the new generation 5 fibers are nearly as good as the micro fibers for both bending and direct tension. These fibres can thus be a suitable replacement for the very expensive steel micro fibers that is often used to reinforce UHPC.

The compressive strength was studied for samples which were kept in 85°C water for different durations (1, 3 and 6 days). The results showing the effect of curing regime on the compressive strength of Ultra High Performance Fiber Reinforced Concrete (UHPFRC) is presented in Figure 2. The graph shows that the 28-day compressive strength is lower than the 7-day strength for the UHPC containing no fiber and that reinforced by generation 5 hook-ended fiber while the other strengths was only affected marginally. The strength loss can be either the result of the curing regime or the glue used to make it easier to mix in this type of fibers. There is thus a concern that the glue might affect the compressive strength, especially when high fiber contents are used.

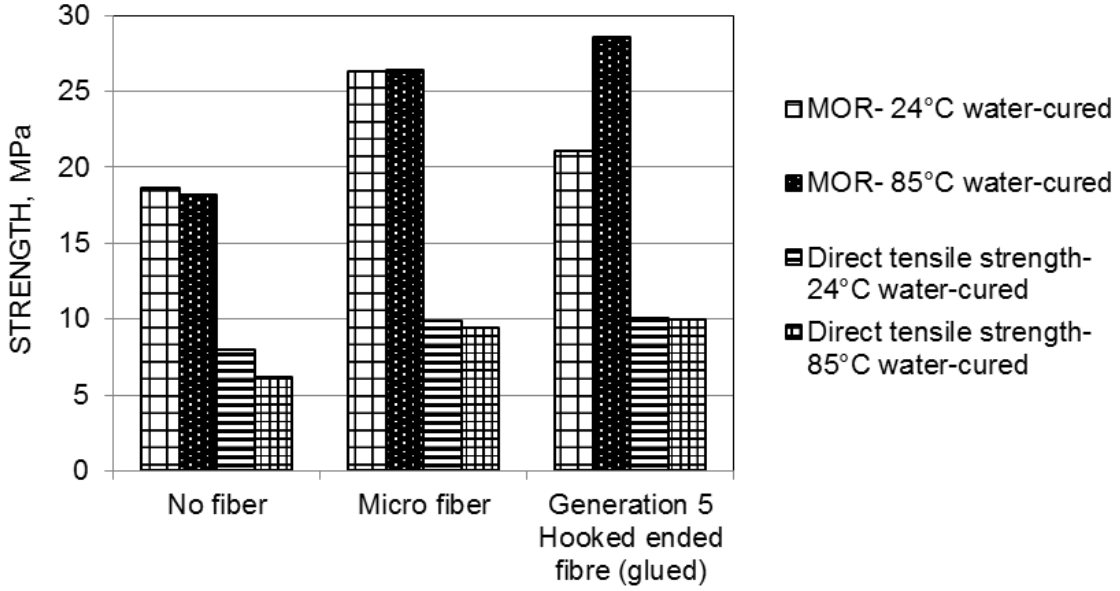


Figure 1 Direct tensile and flexural strength for different curing regimes

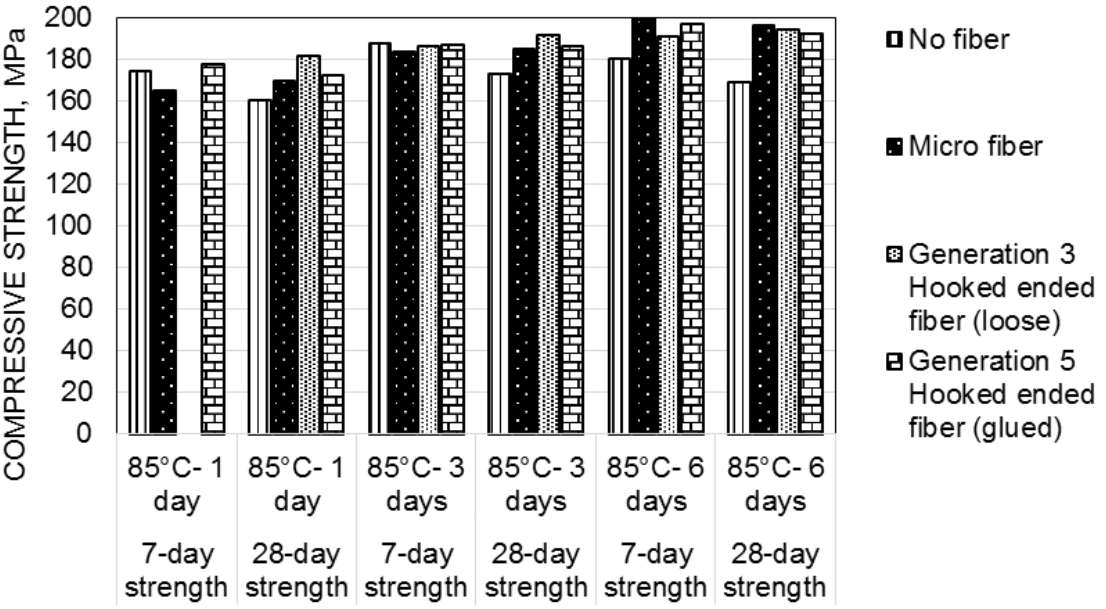


Figure 2 Compressive strength of UHPFRC for the different curing regimes

These results indicate the possibility of thermal shocking (as a result of high heat gradient) during the curing procedure. This phenomenon can happen either when cubes are placed in 85°C water after 24 hours curing at room temperature or at the time of moving cubes from 85°C to 24°C water. In addition, these results show the possible effect of glue. In this paper the effect of thermal shocking (with different heat gradients) on the compressive strength of UHPC as well as the possible effect of glue is studied.

## EXPERIMENTAL PROGRAMME

In this study, two different curing regimes with different procedures were investigated. Firstly, the effect of different heat gradients on the compressive strength of UHPC was studied where after cubes were cured in a way that no thermal shocking occurred during the curing time. For compressive strength testing 100 mm cube samples were used. It is noteworthy that these studies were carried out on UHPC containing no fiber as the effect of thermal shocking is more pronounced for UHPC containing no fibers. Secondly, UHPC was reinforced with fibers. The compressive strength of UHPFRC which experienced no thermal shocking during the curing process was investigated.

### Materials

Undensified silica fume (USF), Ground Granulated Blast Furnace Slag (GGBS) and cement were considered as the cementitious materials. A CEM I52.5N with a relative density of 3.14 was chosen as cement. USF and GGBS had relative densities of 2.2 and 2.93, respectively. The chemical composition of the cementitious materials is given in Table 1. A retarder was used to keep the mix workable for longer. Andesite with maximum size of 4.75mm and 6.7mm was chosen as a fine aggregate and coarse aggregate respectively. The Particle Size Distribution (PSD) of these materials is shown in Figure 3. No sieving was done for aggregates and they were used in the mix as they were provided.

Table 1 Chemical compositions of cement, USF and GGBS

| MATERIAL | CHEMICAL COMPOSITIONS, % | | | | | | | | | |
|---|---|---|---|---|---|---|---|---|---|---|
| | $SiO_2$ | MgO | $Al_2O_3$ | $SO_3$ | $K_2O$ | CaO | $Fe_2O_3$ | $TiO_2$ | $Na_2O$ | LOI |
| Cement | 31.6 | 1.39 | 3.75 | 3.4 | 0.18 | 54.75 | 4.09 | 0.27 | <0.01 | 1.77 |
| USF | 84 | 1.08 | 0.75 | 0.09 | 3.34 | 2.22 | 1.96 | 0.03 | 0.17 | 5.56 |
| GGBS | 34.87 | 8.03 | 14.38 | 1.96 | 0.72 | 37.05 | 0.89 | 0.72 | <0.01 | 0.16 |

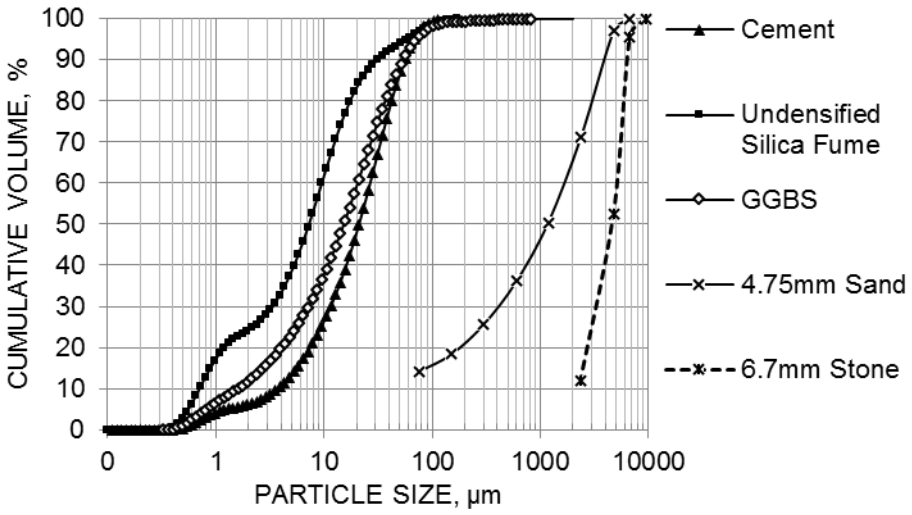


Figure 3 The Particle size distribution of the materials

## Mix Design

The main idea of the mix design in this study was to reduce the cost as well as making it practical and providing optimal properties at the same time. The water to cement ratio was kept constant at 0.25. The content of retarder was 2.5% of the cementitious materials weight. The ratio of total aggregate to cement (by weight) was taken as 2.5. Hook-ended steel fibers with a length of 45 mm and a diameter of 0.45 mm were used in those mixes containing fibers. The tensile strength of these fibers is 2500 MPa. A fiber content of 2% (by volume) was considered. The mix design can be seen in Table 2.

Table 2 Mix design

| COMPONENTS, $kg/m^3$ | | | | | | | |
|---|---|---|---|---|---|---|---|
| Cement | USF | GGBS | Stone-6.7 mm | Sand-4.75 mm | Water | Retarder | Detrainer |
| 605 | 182 | 121 | 455 | 1057 | 151 | 22.7 | 1.5 |

## Casting and Curing Procedure

All the dry materials except USF were mixed together for 1 minute. Water and admixtures were added to the mix. Then, USF was added. The reason for adding it later was that this material is undensified and therefor it flies away during dry mixing. After 5 minutes, the mix had a uniform texture and was ready for casting. The casting was done on a vibrating table and the cube moulds filled with UHPP (Ultra High Performance Paste) were vibrated for 1 minute. The cubes were covered with plastic sheets while they were kept in a laboratory at 24°C and 98% relative humidity for 48 hours, followed by demoulding.

In the first part of the study, 9 cubes were submerged in 24°C water and experienced no heat-treatment. In addition, 45 cubes were divided into three groups with each group of cubes experiencing different temperatures of heat curing in water. These temperatures were 65°C, 85°C and 92°C. The cubes were kept in the heat curing regime for 5 days. Half of each group of cubes was moved immediately to 24°C water to thermally shock them, while the other half was stored under plastic sheets in a laboratory room at 24°C and 98% relative humidity. The cubes stayed in these conditions till the day of testing. The compressive strength of all cubes was measured at 7, 28 and 90 days after the casting day.

In the second part of the study, steel fibers were added to the mix design in two different conditions in two batches. In one batch the fibers were added to the mix while they were glued as they were provided from the supplier and in the other batch the fibers were added after washing all the glue from the fibres. From each batch 6 cubes were cast. These 12 cubes were kept in 85°C water for 3 days. After the heat treatment, they were stored in 24°C water till the day of testing. In this study, the rising and falling of the water temperature was controlled to avoid thermal shocking. The temperature of the water bath was gradually increased from room temperature to 85°C. At the end of heat treatment, the temperature of the water was controlled to fall gradually to room temperature. The cubes were then stored in the 24°C water. The compressive strength of the cubes was measured at 7 and 28 days after the casting day.

## RESULTS

### The Effect of Heat Gradient on the Compressive Strength of UHPC

Figure 4 presents the compressive strength of UHPC where heat treatment was followed by 24°C water curing. A drop in strength can be observed from the 7-day strength to the 28-day strength at curing temperatures of 65°C and 92°C. Interestingly, the 90-day compressive strength increases in a way that exceeds the 7-day strengths. It seems that the pozzolanic reaction has continued resulting in the strength enhancement. It is worth noting that the reductions in the compressive strength from 7-day to 28-day strength were not significantly affected by the different heat gradients. At the highest heat gradient one may expect the higher reductions in the compressive strength, but this reduction is the same as the one observed for the lowest heat gradient.

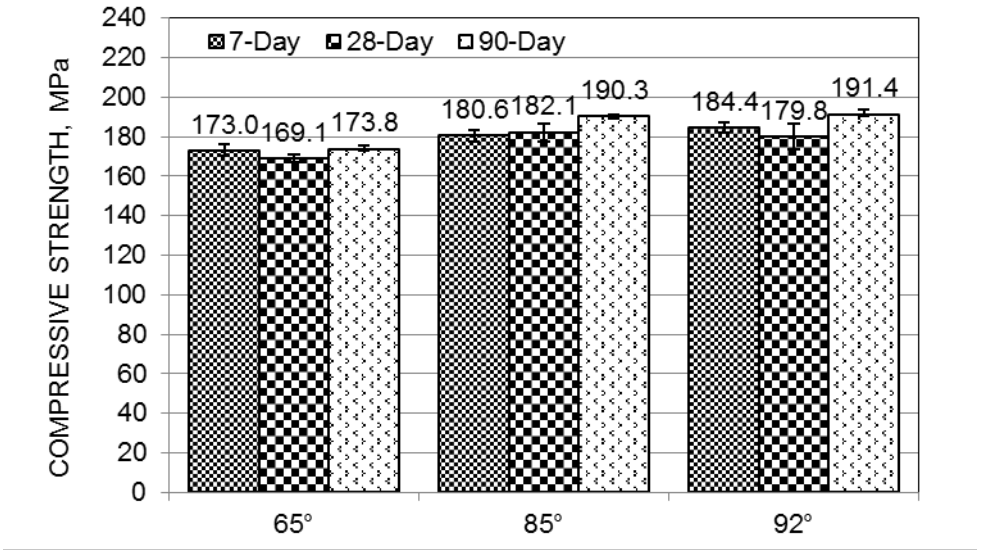


Figure 4 Compressive strength of UHPC cured at different temperatures

Figure 5 compares the effect of different curing temperatures on 7, 28 and 90-day strengths of UHPC placed in 24°C water after the heat treatment. It shows that increasing the temperature of heat treatment from 65° to 92°C leads to an increase in 7-day strength from 173 to 184.4 MPa while this trend is not observed for 28-day strengths. The 28-day compressive strength of UHPC exposed to 92°C was lower than the strength of cubes exposed to 85°C heat treatment. An enhancement in 90-day compressive strength is observed for increased temperature of heat treatment.

The compressive strength of non-heat treated UHPCs (cured only in 24°C water) is shown in Figure 6. These results indicate that the 28-day compressive strength of UHPC cured at 24°C has the same strength than the concrete that experienced heat treatment at 65°C and higher strength was achieved at 90 days. In other words, heat treatment at 65°C is not an economical curing regime. The same 28-day strength, and higher 90-day compressive strength is achievable by applying the normal curing regime.

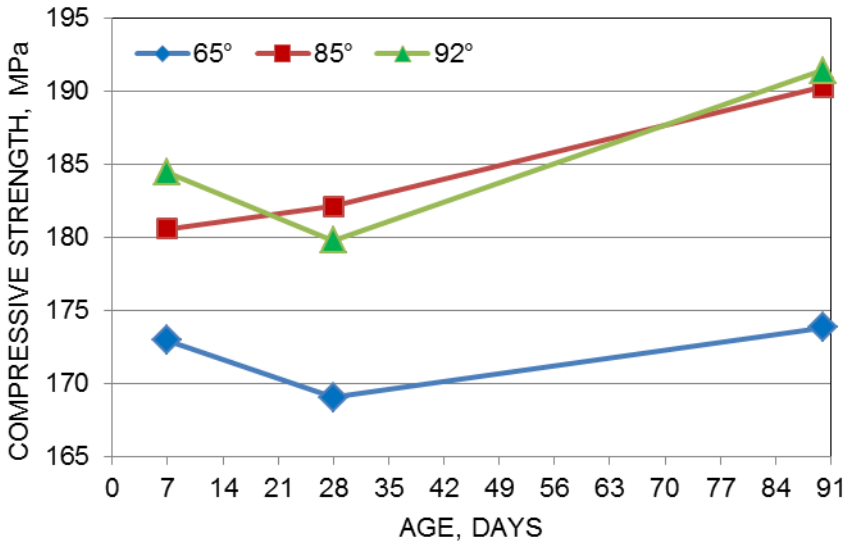


Figure 5 The effect of heat curing temperature on compressive strength

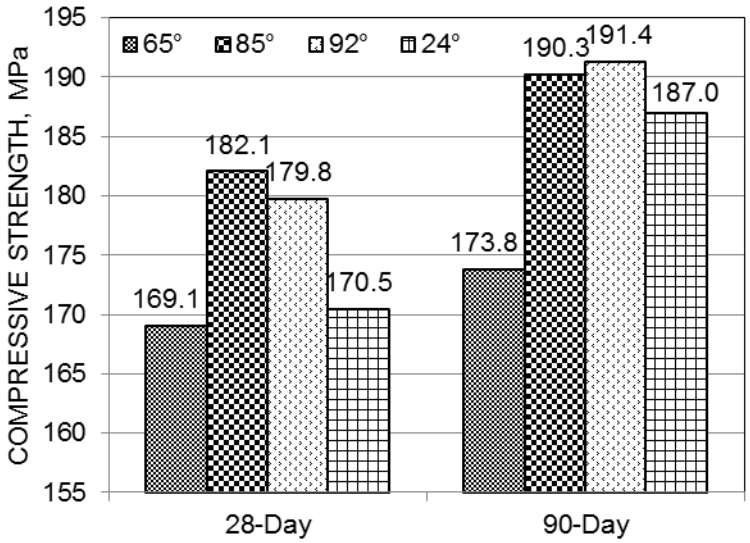


Figure 6 Comparison between normal curing and heat curing

**The Compressive Strength of UHPC Cured in Room at 24°C After Heat Treatment**

According to Figure 7, UHPC cured in a laboratory room at 24°C after the heat treatment, showed no reduction from 7-day to 28-day strength. This can be attributed to the fact that the samples did not experience thermal shocking during the curing process. However, it seems that curing the samples in the laboratory room at 24°C adversely affected the 90-day compressive strength. A 2.4% and 5.5% reduction were observed in the compressive strength of cubes which experienced 85°C and 92°C heat treatment, respectively. No reduction in 90-day compressive strength occurred in samples that experienced 65°C heat treatment.

It seems that the reason for strength loss at 90 days for the samples exposed to 85°C and 92°C can be attributed to either "self-desiccation" or "crossover effect" or the combination of both effects. The self-desiccation gives autogeneous shrinkage and a RH-drop without any

moisture leaving the concrete. The rate and final relative humidity (RH) level depends only on the water cement ratio, type of cement and temperature conditions during curing. The autogeneous shrinkage might be high enough to cause internal cracking and therefore decreased the strength. Crossover phenomena occur in samples exposed to high temperature at early ages. This phenomena cause strength loss at later ages as a result of non-uniform distribution and rapid formation of the Calcium Silicate Hydrate crystals within the pores and the hardening paste.

Since the crossover effect can only occur in those samples that experienced a temperature exceeding 65-70°C at early ages [12], the strength loss did not occur in the samples exposed to 65°C while it happened in samples that experienced higher temperatures. It seems that self-desiccation can also amplify the strength loss. Since the samples cured in the laboratory room after heat treatment did not have access to water, the self-desiccation affected the 90-day strength and led to the strength loss. The reason that no strength loss was observed at 90 days in the samples cured in water after the heat treatment is the access of samples to water, despite the crossover effect. Curing the samples in water after heat treatment helps them to suck up water, thus compensating the low water to cement ratio, resulting in more hydration taking place.

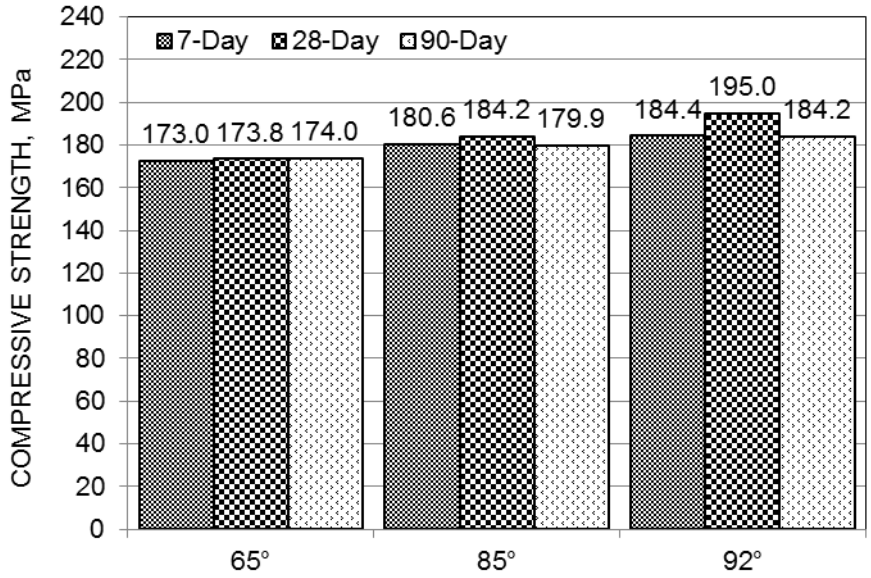


Figure 7 Compressive strength of UHPC cured at different water temperatures followed by 24°C laboratory room

Figure 8 presents the effect of different curing temperatures on 7, 28 and 90-day strengths of UHPC placed in the 24°C laboratory room after the heat treatment. It shows that increasing the temperature from 65°to 92°C leads to compressive strength enhancement at 7, 28 and 90 days. The strength loss for the samples exposed to 92°C heat-treatment indicates that self-desiccation still remains a problem. In order to avoid that, it is recommended that the samples that experienced 92°C heat-treatment should be stored in water after.

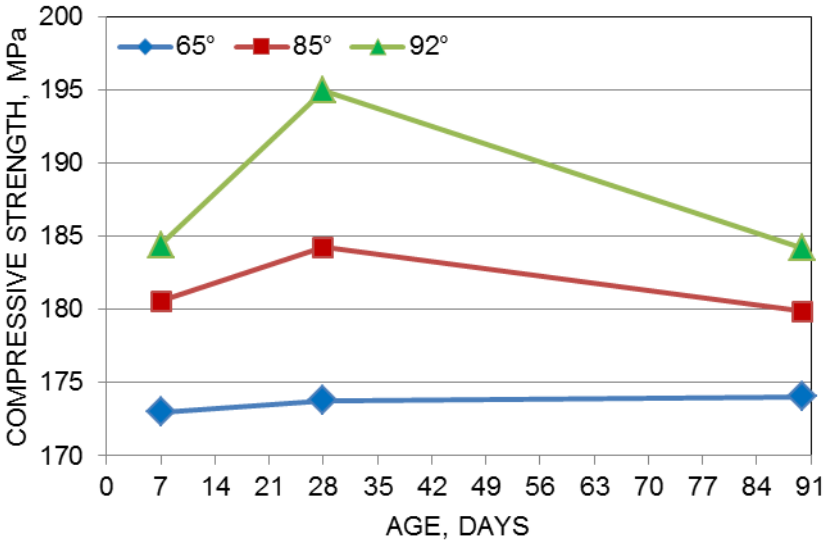


Figure 8 The effect of temperatures on the compressive strengths of UHPC placed in 24°C laboratory room

**The Effect of Glue on the Compressive Strength of UHPFRC**

Figure 9 shows the compressive strength of UHPFRC samples containing hooked ended fibres. The inclusion of fibres does not significantly affect the compressive strength of the matrix but although no reduction is observed in the compressive strength of UHPC containing washed fibers, a 2.6% reduction occurred in the compressive strength of UHPC reinforced with glued fibers. It seems that the glue has a negative effect on the compressive strength of UHPC.

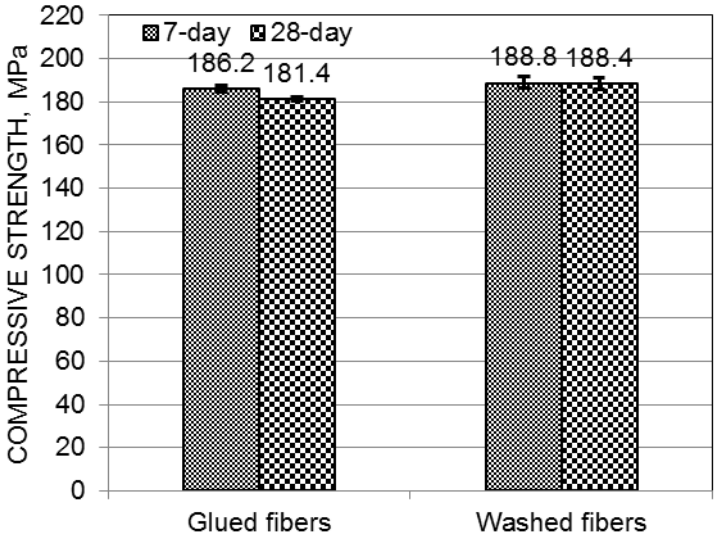


Figure 9 The effect of glue on the compressive strength of UHPFRC

The effect of glue on the compressive strength of UHPFRC requires more investigation to confirm the negative influence observed in this study. In addition, the compressive strength of UHPC at later age needs to be investigated in order to confirm the crossover effect.

## CONCLUSIONS

In this study, two different curing regimes were considered. In UHPC cured in water after the heat treatment, a reduction in compressive strength from 7-day strength to 28-day strength was observed. It seems that thermal shocking has a negative effect on the compressive strength. It is worth mentioning that the reduction in strength was not significantly affected by the different heat gradients and did not continue at older ages as the 90-day compressive strengths exceeded the 7-day strengths.

In UHPC cured in the laboratory at room temperature after the heat treatment, no reduction was observed from 7-day to 28-day strength. These samples did not experience thermal shocking. However, strength reductions occurred in the 90-day compressive strength in comparison to the 28-day strength of samples that experienced 85°C and 92°C heat treatment, respectively. The samples are not only exposed to the high temperatures (more than 65°C) at early ages, but the water to cement ratio is also low. The reason for strength loss at 90 day can be attributed to the either “self-desiccation” or “crossover effect” or the combination of both effects. Storing UHPC in water after the heat-treatment eliminates the self-desiccation phenomena, but avoiding that the samples experience thermal shocking has to be taken into account.

UHPC containing washed fibers showed no reduction in the compressive strength from 7-day to 28-day strength. However, a reduction was observed in UHPC reinforced with glued fibers. It seems that glue used to make it easier to mix fibers into concrete could have a negative effect on the compressive strength of UHPC. Additional research is needed to confirm this negative influence.

## REFERENCE

1. FRENCH ASSOCIATION OF CIVIL ENGINEERING-FRENCH AUTHORITIES OF CIVIL ENGINEERING STRUCTURE DESIGN, AND CONTROL (AFGC-SÉTRA). "Ultra high performance fibre-reinforced concretes." Interim recommendations, Bagneux, France,2002

2. YANG, S. L., ET AL. "Influence of aggregate and curing regime on the mechanical properties of ultra-high performance fibre reinforced concrete (UHPFRC)." Construction and Building Materials 23.6 (2009): 2291-2298.

3. AHLBORN, T. M., ET AL. "Durability and strength characterization of Ultra-High Performance Concrete under variable curing regimes." proceedings, second international symposium on ultra-high performance concrete, Kassel, Germany (2008): 197-204

4. SCHACHINGER, I., HILLBIG, H. AND STENGEL, T. "Effect of curing temperature at an early age on the long-term strength development of UHPC." proceedings, Second international symposium on ultra-high performance concrete, Kassel, Germany (2008): 205-212

5. AY, L. "Curing tests on the ultra-high strength plain and steel fibrous cement based composites." proceedings, International symposium on ultra-high performance concrete, Kassel, Germany (2004): 695-701

6. RICHARD, P., AND CHEYREZY, M. "Composition of reactive powder concretes." Cement and concrete research 25.7 (1995): 1501-1511.

7. DE LARRARD, F. AND SEDRAN, T. "Optimization of ultra-high-performance concrete by the use of a packing model." Cement and Concrete Research 24.6 (1994): 997-1009.

8. YANG, I. H., JOH, C. And KIM, B. S. "Structural behavior of ultra high performance concrete beams subjected to bending." Engineering structures 32.11 (2010): 3478-3487.

9. YOO, D. Y., LEE, J. H. And YOON, Y. S. "Effect of fiber content on mechanical and fracture properties of ultra high performance fiber reinforced cementitious composites." Composite Structures 106 (2013): 742-753.

10. VOO, Y. L., FOSTER, S. J., And GILBERT, R. I. "Shear strength of fiber reinforced reactive powder concrete prestressed girders without stirrups." Journal of Advanced Concrete Technology 4.1 (2006): 123-132.

11. HASSAN, A. M. T., JONES, S. W., And MAHMUD, G. H. "Experimental test methods to determine the uniaxial tensile and compressive behaviour of ultra high performance fibre reinforced concrete (UHPFRC)."Construction and Building Materials 37 (2012): 874-882.

12. TÜRKEL, S., And ALABAS, V. "The effect of excessive steam curing on Portland composite cement concrete." Cement and Concrete Research35.2 (2005): 405-411.

# WAYS TO REDUCE SHRINKAGE OF HIGH STRENGTH CONCRETE

**Drago Saje**
University of Ljubljana
Slovenia

**ABSTRACT.** The laboratory investigation on the autogenous and total shrinkage of high strength concrete, and the ways of its reduction, are presented. Such concretes demonstrate significant autogenous shrinkage, which should, however, be limited in the early stages of its development in order to prevent the occurrence of cracks. The following ways for reducing concrete shrinkage were investigated and analysed: the use of low-heat cement, steel fibres, pre-moistened polypropylene fibres, and pre-soaked lightweight aggregate. In the case of the use of pre-soaked natural lightweight aggregate, with a fraction from 2 to 4 mm, the shrinkage of 28-days old high strength concrete decreased by about 48%, with no change to the concrete's compressive strength in comparison with that of the reference concrete.

**Keywords:** High strength concrete, Autogenous shrinkage, Drying shrinkage, Fibres, Lightweight aggregate.

**Drago Saje** is Assistant professor at the Faculty of Civil and Geodetic Engineering, University of Ljubljana and a member of IABSE and its alternate delegate.

## INTRODUCTION

Shrinkage of concrete causes cracks in the material. It is one of the most detrimental properties of concrete, which affects the long-term strength and durability.

The shrinkage of concrete consists of autogenous shrinkage, as well as shrinkage due to drying, plastic shrinkage, shrinkage due to temperature changes, and shrinkage due to carbonation. Autogenous shrinkage, which is specially pronounced at low water-binder (w/b) concrete, is caused by self-desiccation in the pore system of the hardened cement paste, when water is consumed during the cement hydration process. During the chemical reaction between the cement and the water heat is released, which causes an increase in the temperature of the concrete, and thus deformation of the latter due to this temperature change.
Low hydration cements, which contain a predominant amount of belite, can be used, in which case the cement hydration process is less intense than that which occurs in the case of alite hydration. This is expressed by a lower level of released energy and lower water consumption [1, 2].

If the low w/b high strength concrete has internal reservoirs of water, then the water from the fine capillary pores can be consumed, during the hydration process, later - in concrete that already has higher stiffness. The idea of using internal reservoirs is that the water from the reservoirs replenish the water which is consumed by hydration. Thus, the effect of self-desiccation of low w/b concrete is mitigated. Such reservoirs can be provided by means of pre-soaked lightweight aggregate, pre-moistened polypropylene fibres, and super-absorbing polymers [3, 4].

The results of experimental investigations and their numerical simulations performed by various researchers [5, 6, 7, 8] have shown that, by adding short strengthening fibres to the concrete, it is possible to improve the mechanical properties, as well as some other important properties, in comparison with comparable plain concrete. Bayasi and Zeng [5], who investigated the influence of dry polypropylene fibers on the compressive strength of fiber-reinforced normal-strength concrete, found that concrete compressive strength increased by 15% when reinforced with 1.27-cm-long dry polypropylene fibers with a volumetric content of 0.1% and by 19% in the case of a volumetric content of 0.3%, whereas at a volumetric content of 0.50% it decreased by 2.5% compared with concrete having no reinforcing fibers. Through the addition of steel fibres, according to Paillere et al. [6] an increase of approximately 15% in the compressive strength of the composite can be obtained, whereas according to Thomas and Ramaswamy [7] a 10% increase can be obtained, compared with the compressive strength of a comparable concrete without fibres. Swamy [8] has indicated that, as well as causing an increase in compressive strength, the contained steel fibres also improve the deformation capacity of the composite when compared that with the reference concrete without fibres.

The autogenous shrinkage of high strength concretes usually makes up about half of the total shrinkage, with more than one half of the final autogenous shrinkage occurring during the first 24 hours after mixing of the concrete [2, 9]. Thus, the greatest effect on reducing the total concrete shrinkage is obtained in the case when the early autogenous shrinkage is reduced. So, the reduction of early autogenous shrinkage of high strength concrete is the primary focus of this paper.

## MATERIALS

### Cement

Three different types of cement were used to make the experimental concrete mixes: rapid hardening Portland slag cement CEM II/A-S 42.5R, rapid hardening Portland cement CEM I 52.5R, and a Portland cement with a low heat of hydration, CEM I 42.5LH, all of which are produced at the same cement factory. The composition of the clinker in these cements is shown in Table 1.

Table 1 The mineral composition of the used types of cement clinker (Bogue)

| CEMENT | BLAINE | CLINKER MINERALS | | | |
|---|---|---|---|---|---|
| | [$m^2$/kg] | $C_3S$ (alite) % | $C_2S$ (belite) % | $C_3A$ % | $C_4AF$ % |
| CEM II/A-S 42.5R | 355 | 64 | 15 | 9 | 9 |
| CEM I 52.5R | 440 | 64 | 15 | 9 | 9 |
| CEM I 42.5LH | 367 | 34 | 46 | 1.5 | 15 |

### Aggregates

The test specimens of all the investigated concretes were prepared from washed and crushed limestone aggregate, with a maximum nominal grain size of 16 mm, with the addition of fine silica sand. The silica sand, the aggregate fraction 0-2 mm, the aggregate fraction 2-4 mm, the aggregate fraction 4-8 mm and the aggregate fraction 8-16 mm represent 15%, 18%, 27%, 15% and 25% of the total volume of the aggregate used, respectively. The densities of limestone aggregate and silica sand amounted to 2700 kg/$m^3$ and 2710 kg/$m^3$, respectively. The compressive strength and modulus of elasticity of the stone aggregate amounted to 178 MPa and 243 GPa, respectively.

### Steel fibres

The properties of the steel fibres which were added to some of the concrete mixes are given in Fig. 1 and Table 2. The influence of steel fibres on the shrinkage of steel fibre reinforced concrete, with a water-to-binder ratio of 0.36, was investigated at a fibre volume content of 0.75%.

Figure 1 The steel fibre IRI 50/30. Steel fibres were added to some of the concrete mixtures.

Table 2 Properties of the used steel fibres

| STEEL FIBRES | FIBRE LENGTH mm | EQUIVALENT FIBRE DIAMETER mm | FIBRE TENSILE STRENGTH MPa | FIBRE CLASS (ASTM A 820) |
|---|---|---|---|---|
| IRI 50/30 | 30 | 0.5 | 900 | Type 1 |

**Polypropylene fibres**

Some of the other concrete mixes were reinforced by previously-moistened polypropylene fibres, as shown in Fig. 2. The properties of these fibres are presented in Table 3.

Table 3 Properties of the used polypropylene fibres

| DENSITY g/cm$^3$ | LENGTH mm | CROSS-SECTION μm | TENSILE STRENGTH MPa | MODULUS OF ELASTICITY MPa |
|---|---|---|---|---|
| 0.91 | 12 | 35 × (250-600) | 340-500 | 8500-12500 |

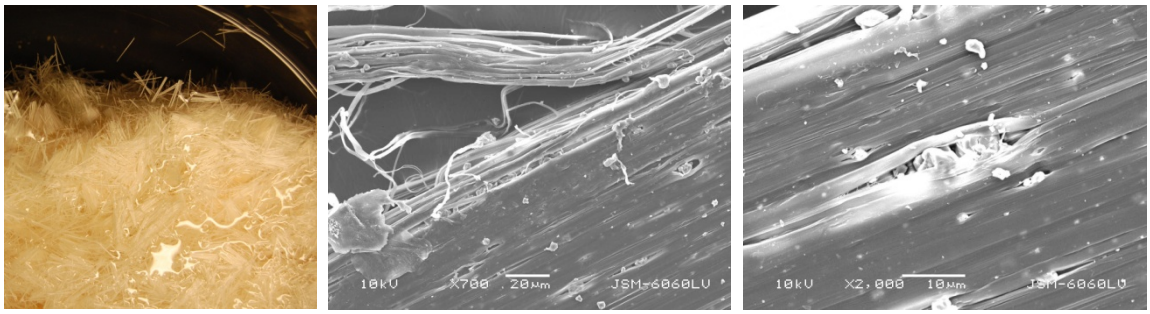


a) Moistening of fibres b) Microimage of a fibre c) A furrowed fibre surface

Figure 2 The polypropylene fibres which were added to some other concrete mixes

**Lightweight aggregate**

As internal reservoir of water, contributing 12% of the total volume of the aggregate, i.e. pre-soaked natural lightweight aggregate "Lehnjak", with fractions from 0-2 mm or 2-4 mm, was used. The porosity of this aggregate, which is of sedimentary origin, was between 10% and 15%. Its bulk density amounted to 1440 kg/m$^3$.

**Chemical admixtures**

In order to ensure adequate workability F2 [10] at a relatively low water-to-binder ratio, a naphthalene or polycarboxylate type of superplasticizer was used. The naphthalene based superplasticizer was in a dry state with a density of 2.2 kg/dm$^3$ and the polycarboxylate based superplasticizer was in a liquid state with its density of 1.05 kg/dm$^3$.

## TESTING PROCEDURES

The test specimens were made from five different mixtures of high strength concrete, designated M1 to M5, and three mixture of a comparable concrete, designated C1 to C3. The total content of the binder in each of the mixtures was 400 kg per $m^3$ of the composite, 90% of which was cement (360 kg/$m^3$) and 10% silica fume (40 kg/$m^3$). Mixture M1 contained the low heat cement, mixture M2 the steel fibres, mixture M3 the previously moistened polypropylene fibres (immersed for 24 hours in water), mixture M4 the pre-soaked lightweight aggregate fraction 0-2 mm (immersed for 24 hours in water), and mixture M5 the pre-soaked lightweight aggregate fraction 2-4 mm (immersed for 24 hours in water) and cement CEM I 52.5R. The compositions and properties of the fresh and hardened concretes are given in Table 4.

Table 4 Mix proportions of the composites

| MIXTURE | C1 | M1 | C2 | M2 | M3 | M4 | C3 | M5 |
|---|---|---|---|---|---|---|---|---|
| Fine aggregate 0-4 mm (kg/$m^3$) | 1130 | 1138 | 1138 | 1126 | 1126 | 911 | 1138 | 911 |
| Coarse aggregate 4-16 mm (kg/$m^3$) | 752 | 758 | 758 | 750 | 750 | 758 | 758 | 758 |
| Lightweight aggregate 0-2 mm (kg/$m^3$) | - | - | - | - | - | 121 | - | - |
| Lightweight aggregate 2-4 mm (kg/$m^3$) | - | - | - | - | - | - | - | 121 |
| Type of cement | RII | LH | RII | RII | RII | RII | RI | RI |
| Steel fibres (% by volume) | - | - | - | 0.75 | - | - | - | - |
| Polypropylene fibres (% by volume) | - | - | - | - | 0.75 | - | - | - |
| Water-to-binder ratio | 0.40 | 0.40 | 0.36 | 0.36 | 0.36 | 0.36 | 0.36 | 0.36 |
| Naphthalene based superplasticizer (% by weight of the binder) | - | - | 2.05 | 2.05 | 2.05 | 2.05 | 2.05 | 2.05 |
| Polycarboxylate based superplasticizer (% by weight of the binder) | 3.70 | 3.70 | - | - | - | - | - | - |

Key: CEM I 52.5R (RI), CEM II/A-S 42.5R (RII), CEM I 42.5LH (LH)

### Preparation of the specimens

Measurements of autogenous concrete shrinkage were performed on three sealed prisms, however measurements of total shrinkage were performed on three prisms exposed to drying, from each mix. Each prism being of size: 10 × 10 × 40 cm, whereas the compression strength of the investigated concrete was determined on test cubes with edges of 15 cm (at least three cubes for each mix). The autogenous and drying shrinkage measurements were performed in a climatic chamber at a constant temperature of 22 ± 3°C and at a relative humidity of 70 ± 5%.

### Autogenous and total shrinkage tests

Computer-controlled measurements of the early autogenous shrinkage of the sealed test specimens were performed, from the beginning of concrete hardening onwards, in accordance with the provisions of the corresponding Japanese standard [11, 12], by means of an electronic displacement transducer with a precision of $10^{-3}$ mm (Fig. 4). A polytetrafluorethylene sheet was inserted between the test specimen and the base in order to reduce the friction between the two surfaces (Fig. 3).

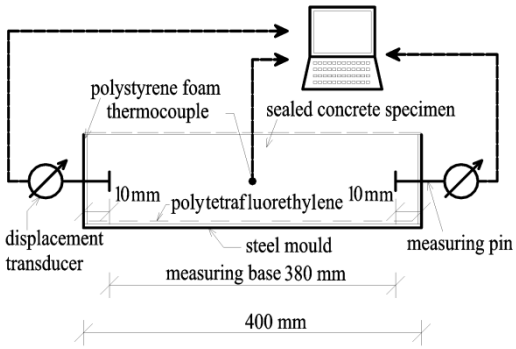


Figure 3 Schematic representation of the method of measurement of test specimen shrinkage

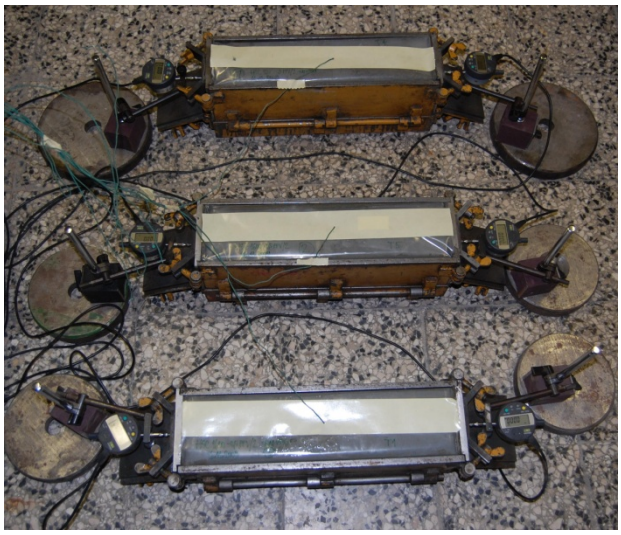

Figure 4 Measurement of the autogenous shrinkage of a test specimen

The moulds for the preparation of the test specimens for the measurement of autogenous shrinkage, over the first 24 hours, were adapted so that holes were bored through their front steel plates for the insertion of shrinkage measurement pins. The latter were inserted in such a manner that the length of the measuring base was 380 mm. The temperature in the middle of the specimen was measured by means of a thermocouple.

The development over time of the autogenous shrinkage of a test specimen ($\varepsilon_{ca}$) is determined by the sum of the development over time of the measured deformations ($\varepsilon_c = \Delta L/L$) and the temperature expansion ($\varepsilon_{(\Delta T)} = \alpha_T \cdot \Delta T$) of the specimens due to variations, over time, in temperature. The temperature of the test specimens varied significantly during the first 24 or 48 hours, i.e. during the period of rapid setting of the cement, but was later in equilibrium with the ambient temperature of the environment. The variations in the length of the test specimen over time, due to the varying temperature during the period of rapid setting of the cement, were determined analytically, taking into account the temperature expansion coefficient of the concrete and the measured variations, over time, of the temperature. A value of $\alpha_{T,f} = 1.48 \cdot 10^{-5}$, which had been determined by separate measurements [2], was assumed as the temperature expansion coefficient of the fresh concrete, and a value of $\alpha_{T,h} = 1.0 \cdot 10^{-5}$, was assumed as the temperature expansion coefficient of the hardened concrete [12]. The concrete was considered fresh until the temperature of the specimen began to rise ($\alpha_T = \alpha_{T,f}$), which roughly corresponded to the start of the rapid hardening of the concrete. After rapid hardening had been completed, i.e. from around the 24$^{th}$ hour onwards, the concrete was regarded as hardened

($\alpha_T = \alpha_{T,h}$). During the intermediate period of time, when the temperature of the test specimens changed more rapidly, the temperature expansion coefficient was determined by linear interpolation between the values for fresh concrete ($\alpha_{T,f}$) and hardened concrete ($\alpha_{T,h}$).

The total shrinkage of the fibre reinforced concrete was measured on the test specimens which were exposed, during all the time after casting, to a constant RH of 70% ±3% and a temperature of 22°C ±3°C. During the first 24 hours, the specimens in moulds were coverd by polyethylene foil in order to prevent them from drying out. It was assumed that within the first 24 hours the autogenous shrinkage of the specimens was equivalent to that of the sealed specimens. The total shrinkage of the composite was measured on test specimens which were, for the first 24 hours, in moulds, and which were removed from the moulds after 24 hours and exposed to drying. The shrinkage due to drying, was determined as the difference between the total shrinkage and the autogenous shrinkage measured on the sealed test specimens.

## TEST RESULTS AND DISCUSSION

In Tables 5 to 7, values of the autogenous shrinkage of the high strength concrete measured at an age of 24 hours and 28 days, $\varepsilon_{ca,\ 24\ hours}$ and $\varepsilon_{ca,\ 28\ days}$, values of the total shrinkage at an age of 28 days, $\varepsilon_{ct,\ 28\ days}$, and values of the compressive strength of the concrete at an age of 28 days, $f_{cm,\ 28\ days}$ are compared.

Table 5 Comparison of the autogenous and total shrinkage of 1 day, 2 and 28 days old concretes which differed according to the type of cement, and their associated 28-day compressive strengths

| CONCRETE MIX | ADDITIONAL MEASURE | $\varepsilon_{ca,\ 24\ hours}$ ‰ | $\varepsilon_{ca,\ 48\ hours}$ ‰ | $\varepsilon_{ca,\ 28\ days}$ ‰ | $\varepsilon_{ct,\ 28\ days}$ ‰ | $f_{cm,\ 28\ days}$ MPa |
|---|---|---|---|---|---|---|
| C1 | / | -0.216 | -0.205 | -0.358 | -0.503 | 80.6 |
| M1 | Use of a low-heat cement | below detection level | -0.027 | -0.121 | -0.207 | 74.0 |

After 24 hours the contraction of concrete M1, which contained the low-heat cement, could not be detected by the used measuring technique. After 48 hours this concrete developed approximately one-eighth (13%) of the shrinkage measured on the comparable concrete C1 (Table 5). The autogenous shrinkage of the comparable concrete C1 was, after 48 hours, even slightly less than that measured after 24 hours due to thermodynamic effects. This physical phenomenon is the result of the thermodynamic equilibrium in the pores of the hardened cement paste. As the temperature in the concrete begins to fall, the concrete shrinks because of its linear coefficient of thermal expansion, resulting in a decrease in the volume of the closed pores within the hardened cement paste. Due to the reduction in the volume of the closed pores, the relative humidity inside them increases according to the laws of thermodynamics. Thus, if there is a reduction in the tensile forces acting on the pore walls, then there is a decrease in the autogenous shrinkage of the concrete. Because of the drop in the air temperature inside the closed pores at thermal equilibrium, the relative air humidity rises, which results in a further decrease in the autogenous shrinkage of the concrete.

The measured 28-day compressive strength of concrete M1, which contained the low-heat cement, represented 92% of the 28-day compressive strength of the comparable concrete C1. The autogenous shrinkage of the concretes containing low-heat, mainly belite cement CEM I 42.5LH, was less than that of the concrete containing rapid-hardening, predominantly alite cement CEM II 42.5R, due to the fact that less water is consumed in the hydration of belite [1, 2]. Reduced water consumption means less self-desiccation in the cement paste pores, and smaller forces acting on the pore walls, resulting in lower autogenous shrinkage of the concrete.

Table 6. Comparison of the autogenous and total shrinkage of 1 day and 28 days old non-reinforced and fibre-reinforced concretes, and their associated 28-day compressive strengths

| CONCRETE MIX | ADDITIONAL MEASURE | $\varepsilon_{ca,\,24\ hours}$ ‰ | $\varepsilon_{ca,\,28\ days}$ ‰ | $\varepsilon_{ct,\,28\ days}$ ‰ | $f_{cm,\,28\ days}$ MPa |
|---|---|---|---|---|---|
| C2 | / | -0.203 | -0.401 | -0.536 | 81.4 |
| M2 | Added steel fibres | -0.165 | -0.403 | -0.494 | 92.1 |
| M3 | Added pre-moistened polypropylene fibres | -0.064 | -0.272 | -0.362 | 78.1 |

In the case of the concrete M2, which contained steel fibres, about four-fifths (81%) of the shrinkage developed over a period of 24 hours compared to that which was measured on the comparable concrete C2 (Table 7). The 28-day compressive strength of this steel-fibre reinforced concrete amounted to 113% of the 28-day compressive strength of the comparable concrete C2.

In the case of young composites, the stiffness and load-bearing capacity of the steel fibres are relatively high in comparison with those of the, as yet not hardened, cement paste. For this reason they affect the general properties of the young steel-fibre reinforced concrete. The fibre forces are transferred from the fibres into the concrete through the bond along the stress transfer lengths and through the snubbing zones at the cracks and additionally through the end-hooks by the steel fibres [13]. This is the reason for the reduction in autogenous shrinkage which occurs in the case of concretes that are reinforced with steel fibres.

In the case of the concrete M3, which contained previously moistened polypropylene fibres, about one-third (32%) of the shrinkage developed over a period of 24 hours compared to that which was measured on the comparable concrete C2 (Table 7). The 28-day compressive strength of the concrete which was reinforced with saturated polypropylene fibres amounted to 96% of the 28-day compressive strength of the comparable concrete C2.

The polypropylene fibres, which had been previously immersed in water for 24 hours, act in concrete as internal reservoirs of water. Taking into account the fact that the wetting angle of the propylene fibres is less than 90° [14], it can be assumed that these fibres are not absolutely hydrophobic. Apart from this, 3-dimensional pores are formed between individual fibres within bunches of fibres [3]. Due to the capillary osmotic pressure, these 3-dimensional pores or channels between the fibres pick up the water due to soaking, which causes significant attractive forces between the soaked fibres, even in the case when the wetting angle is considerably greater than 0° but less than 90° [15].

The attractive forces between the fibres retain water during the mixing of the concrete, but the cement hydration process starts to consume this water as soon as the free water available for mixing is consumed. If the hydrating binder continues to be supplied with water then the development of larger autogenous shrinkage can be prevented.

Table 7 Comparison of the autogenous and total shrinkage of 1 day and 28 days old concretes, containing natural crushed stone aggregate or with added pre-soaked lightweight aggregate, and their associated 28-day compressive strengths

| CONCRETE MIX | ADDITIONAL MEASURE | $\varepsilon_{ca,\ 24\ hours}$ ‰ | $\varepsilon_{ca,\ 28\ days}$ ‰ | $\varepsilon_{ct,\ 28\ days}$ ‰ | $f_{cm,\ 28\ days}$ MPa |
|---|---|---|---|---|---|
| C2 | / | -0.203 | -0.401 | -0.536 | 81.4 |
| M4 | Added pre-soaked lightweight aggregate, fraction 0-2 mm | -0.186 | -0.342 | -0.441 | 89.1 |
| C3 | / | -0.293 | -0.455 | -0.590 | 83.0 |
| M5 | Added pre-soaked lightweight aggregate, fraction 2-4 mm | -0.028 | -0.196 | -0.306 | 84.4 |

In the case of the concrete M4, which contained natural crushed stone aggregate to which a pre-soaked lightweight aggregate of fraction 0-2 mm had been added, about ten-elevenths (92%) of the shrinkage developed over a period of 24 hours compared to that which was measured on the comparable concrete C2, which contained only natural crushed stone aggregate (Table 7). The 28-day compressive strength of the concrete M4 amounted to 109% of the 28-day compressive strength of the comparable concrete C2.

In the case of the concrete M5, which contained natural crushed stone aggregate to which a pre-soaked lightweight aggregate of fraction 2-4 mm had been added, about one tenth (10%) of the shrinkage developed over a period of 24 hours compared to that which was measured on the comparable concrete C3, which contained only natural crushed stone aggregate (Table 7). The 28-day compressive strength of the concrete M5 amounted to 102% of the 28-day compressive strength of the comparable concrete C3.

The increased porosity of the lightweight aggregate of fraction 2-4 mm made possible the capturing of larger amounts of water than the lightweight aggregate of fraction 0-2 mm. The finer lightweight aggregate contained fewer appropriate capillaries and more dust particles.

In the case of concrete containing pre-soaked light-weight aggregate, the formation of a better-quality transition zone between the grains of the aggregate and the hardened cement paste apparently makes it possible for this type of concrete to be able to transfer compressive stresses which even slightly exceed the load-carrying capacity of comparable concretes. It is remarkable that the comparable concrete contains the same proportion of aggregate as the investigated concrete, and that its aggregate consists of just natural crushed stone whose strength exceeds that of the lightweight aggregate.

## CONCLUSIONS

Autogenous shrinkage of high strength concrete is an essential part of the total shrinkage. The development of autogenous and consequently total shrinkage can be limited by various measures. During the cement hydration process in concretes which are made from predominantly belite cements, less water is consumed. The addition of steel fibres increases the stiffness of the concrete matrix. The use of previously moistened fibrillated polypropylene fibres or pre-soaked lightweight aggregate can provide reservoirs of water during the cement hydration process.

The total shrinkage of the 28-days old investigated high strength concretes which were internally cured by means of pre-soaked lightweight aggregate was 18 to 48% less than that of the comparable concrete made with ordinary aggregate, and their compressive strengths were between 2 and 9% higher than that of the latter.

Inside the concrete pre-soaked fibrillated polypropylene fibres occur in bundles, in which there is a pore system which retains water. The autogenous shrinkage of a 28-days old concrete which contained 0.75% of previously moistened polypropylene fibres was 32% less and the total shrinkage at the same concrete age was also 32% less than that of a comparable concrete without fibres.

Hooked steel fibres, due to their stiffness and good bonding properties, strengthen the concrete, and have a favourable impact on shrinkage and compressive strength. In the case of the investigated concretes, which contained 0.75% steel fibres with a length of 30 mm, the total shrinkage at an age of 28 days was 8% less, and their compressive strength was 13 % greater than that of the comparable concrete without fibres.

The use of low-heat cement in concrete slows down the process of hydration. The total shrinkage of the investigated concrete, which contained a low-heat, mainly belite cement, was, after one day, below the detection limit, whereas after 28 days it was 59% less than that of the comparable concrete, which contained ordinary predominantly alite cement. The compressive strength of the 28 days old concrete made with a predominantly belite cement was 8% less than that of a comparable concrete made with predominantly alite cement.

## REFERENCES

1. NEVILLE, A M. Properties of Concrete, 1995, Longman, Harlow, p 844.

2. SAJE, D. Compressive Strength and Shrinkage of High Strength Concrete, PhD thesis, 2001, Faculty of Civil and Geodetic Engineering, University of Ljubljana, Slovenia, p 157.

3. SAJE, D, BANDELJ, B, ŠUŠTERŠIČ, J, LOPATIČ, J AND SAJE, F. Shrinkage of polypropylene fibre reinforced high performance concrete. Journal of Materials in Civil Engineering, Vol. 23, No. 4, 2011, pp 941-952.

4. AÏTCIN, P C. Internal Curing. 3rd International Symposium Non-Traditional Cement & Concrete, Eds. V Bílek and Z Keršner , Brno, 2008, pp 1-7.

5. BAYASI, Z AND ZENG, J. Properties of polypropylene fibre reinforced concrete, ACI Materials Journal, Vol. 90, No. 6, 1993, pp 605–610.

6. PAILLERE, A M, BUIL, M AND SERRANO, J J, Effect of fiber addition on autogenous shrinkage of silica fume concrete, ACI Materials Journal, Vol. 86, No. 2, 1989, pp 139-144.

7. THOMAS, J, RAMASWAMY, A. Mechanical Properties of Steel Fiber-Reinforced Concrete. Journal of Materials in Civil Engineering, Vol. 19, No. 5, 2007, pp 385- 392.

8. SWAMY, R N. Fiber Reinforcement of Cement and Concrete. Materials and Structures, Vol. 8, No. 3, 1975, pp 235-254.

9. KOVLER, K, JENSEN, O M. Internal curing of concrete. RILEM TC 196-ICC: State-of-the-Art Report, 2007.

10. EN 206. CONCRETE - Specification, performance, production and conformity, CEN Brussels, Belgium, 2000.

11. JIS A 1129-1. Methods of test for length change of mortar and concrete, JIS Standards, Tokyo, 2001.

12. TAZAWA, E. Autogenous shrinkage of concrete, E&FN Spon, London, 1999, p 411.

13. FOSTER, S J. The application of steel-fibres as concrete reinforcement in Australia: from material to structure, Materials and Structures, Vol. 42, No. 9, 2009, pp 1209-1220.

14. FELEKOGLU, B, TOSUN, K AND BARADAN, B. A comparative study on the flexural performance of plasma treated polypropylene fiber reinforced cementitious composites, Journal of Materials Processing Technology, Vol. 209, No. 11, 2009, pp. 5133-5144.

15. SMOLEJ, V AND PEJOVNIK, S. Some remarks on the driving force for liquid-phase sintering, Zeitschrift fuer Metallkunde, Vol. 67, No. 9, 1976, pp 603-605.

# EARLY AGE AND MECHANICAL PROPERTIES OF ENVIRONMENTALLY FRIENDLY ULTRA-HIGH PERFORMANCE CONCRETE (UHPC)

**O M Abdulkareem** University of Nantes
**A Ben Fraj** CEREMA
**M Bouasker** Polytech' Orléans
**A Khelidj** University of Nantes
France

**ABSTRACT.** This paper addressed the development of an environmentally friendly ultra-high performance concrete (UHPC) containing high volumes of Blast Furnace Slag (BFS) with desired early-age properties. Three levels of replacement of cement by BFS are used (30%, 50% and, 80%). To improve early age performance of blended UHPC, BFS was activated chemically by KOH with different concentrations. Results showed that the compatibility between the superplasticizer and the couple system of cement-silica fume affects greatly the workability of UHPC. The addition of BFS particles, acting as nucleation sites, results in a change of superplasticiser content, to ensure the same workability. This nucleation effect is noticed for low BFS content (30%), which induces an acceleration of hydration reaction of cement. For BFS contents of 50 and 80%, the hydration reaction is decelerated and the heat flow peak decreased. BFS addition also affects the strength development. At 3 days, the strength decreased by 26 and 66% for the UHPC mixtures containing, respectively, 50 and 80% of slag, while with 30% of BFS there is a slight increase of 3%. The addition of KOH activator, increases pH and accelerates hydration of UHPC with high BFS content. For the third concentration of KOH ($[KOH]_3$), alkalis cause slag's dissolution and reaction, which improves the compressive strength of UHPC containing 80%, by 42% and 11%, at 3 and 7 days, respectively.

**Keywords:** Ultra-high performance concrete, Blast Furnace Slag, Chemical activation, Hydration, Compressive strength.

**Omar M Abdulkareem** is PhD student at the University of Nantes in France and lecturer at the University of Mosul, Department of Environmental Engineering, Iraq. His research work concerns sustainable Ultra High Performance Concrete, its early age, microstructure and durability properties.

**Amor Ben Fraj** is PhD and researcher at Eco-Materials Laboratory of Cerema. His interests include mineral admixtures, valorisation of alternative materials, waste management and durability of concrete.

**Marwen Bouasker** is PhD and researcher at Polytech' Orléans. His research topics are early age properties of cementitious materials, mineral admixtures and their effects on physico-chemical properties of cementitious matrix and historical materials.

**Abdelhafid Khelidj** is professor at the University of Nantes and the head of Interaction-Water-Geomaterials team. His topics are early age properties of cementitious materials, durability of concrete and transport phenomena.

## INTRODUCTION

Compared to ordinary and high strength concretes, ultra high performance concrete (UHPC) exhibits much denser microstructure with no capillary porosity. The use of finer particles improves its matrix packing and confers high mechanical and durability properties [1]. Introduced by Richard and Cherezy [2], UHPCs have high superplasticizer content and low water-to-binder ratio, which result in self compacting concrete with a compressive strength of about 150 MPa.

Despite of exceptional mechanical and durability properties of UHPCs, their high cement content (800-100 kg/m³) affects their production costs and has negative effects on environment. To reduce the economic and environmental disadvantages of UHPC, the use of mineral admixtures could be considered as promising alternative. Many researchers studied their effects and showed the improvement of concrete properties, particularly in log term, when these by-products are added. Blast Furnace Slag is particularly used in aggressive environment. BFS contains silica, alumina, and lime, with a composition close to that of Portland cement. It can be substituted for Portland cement at proportions varying from about 25% to 85%. The use of BFS in concrete results in low porosity and high bound capacity of aggressive agents [1, 3, 4]. However, the properties of concrete at early age remains a critical point, when BFS is incorporated. Indeed, the reaction of slag is very slow and it depends greatly on produced portlandite, by the reaction of cement. This reaction increases pH and promotes BFS reaction. This problem can be overcome by activation the BFS chemically in order to accelerate hydration and evolve strength development [5].

Alkali activated slag (AAS) is considered as effective pattern of chemical activation, promoting the BFS reactivity during hydration, leading to quite quick development of mechanical performance, and high durability. In AAS, the main hydration products found are C-S-H with a low Ca/Si ratio and depending on the structure of BFS and the kind of used activator. AAS reaction is impacted by numerous parameters such as fineness and chemical composition of BFS, water/binder (w/b) ratio of the mixture, temperature or the pH of the alkaline solution. The chemical activation affects greatly the hydration characteristics in terms of reaction heat and kinetic which involves the porosity and consequently the strength [4].

To address the aforementioned research needs, our research work aims at the formulation of environmentally-friendly UHPCs with different slag contents and controlled workability, and characterising their heat reaction and compressive strength. Besides, we will highlight the effect of the chemical activation, using KOH, on cited properties.

## EXPERIMENTAL PROGRAM

### Materials Used

Materials used in this study are of local origin (France). The cement used is a CEM I 52.5 N PM ES (Le Teil´s plant). Its chemical composition is provided in Table 1. It contains 97% of clinker and 2.8% of gypsum. The mass percentages of principal constituents of main clinker phases, given by Bogue's formula are: 67.8% of $C_3S$, 16.6% of $C_2S$, 4.0% of $C_3A$ and 7.2% of $C_4AF$. In the present study, two types of mineral admixtures have been considered: Blast Furnace Slag (BFS) and Silica Fume (SF). BFS comes from Ecocem's plant and Silica fume is commercialised by Condensil, as S95 B DM. Their main physical properties and chemical composition are given in Table 1.

Crushed Quartz (CQ), used as a partial substitution of SF, comes from Sibelco and commercialised as C500. It contains more than 99.1% of $SiO_2$ and its specific area and density are 10435 cm²/g and 2.65, respectively.

Quartz Sand (QS), containing more than 99% of $SiO_2$, comes from Sibelco and commercialised as CV32. Its specific area and density are 124 cm²/g and 2.65, respectively.

Table 1 Chemical compounds (mass percentage), fineness and density of the used materials

| | CEMENT | SILICA FUME | BLAST FURNACE SLAG |
|---|---|---|---|
| CaO | 65 | 0.3 | 43.9 |
| $SiO_2$ | 22 | 95 | 37.4 |
| $Al_2O_3$ | 2.78 | - | 10.9 |
| $Fe_2O_3$ | 2.42 | - | 0.7 |
| $K_2O$ | 0.17 | - | 0.24 |
| MgO | 0.76 | - | 6.5 |
| $Na_2O$ eq | 0.24 | 0.08 | 0.46 |
| $SO_3$ | 2.2 | 0.06 | 0.1 |
| MnO | 0.01 | - | - |
| $TiO_2$ | 0.17 | - | 0.5 |
| Cl- | <0.1 | 0.1 | 0.01 |
| $S^{2-}$ | <0.1 | | 0.8 |
| Specific area, cm²/g | 3555* | 250000** | 4450* |
| Density, g/cm³ | 3.17 | 2.24 | 2.9 |

*Blaine method; **BET method

In the present study, an acrylic copolymer superplasticizer (Sika Viscocrete Krono 20 HE) is used. It is produced by Sika and its density and dry extract are 1.085 and 41%, respectively. To activate slag, KOH was used. When cement is substituted with BFS, KOH is added to compensate the decrease of alkalis normally provided by cement. Thus, $[KOH]_1$ is the original concentration of added KOH for each mixture to provide the same $[Na_2O]_{eq}$ if only cement is used. As the slag content changes (0%, 30%, 50% and 80%), the quantity of added KOH changes, even for the same concentration. The concentrations $[KOH]_2$, $[KOH]_3$ and $[KOH]_4$ are, respectively, two, three and four times $[KOH]_1$.

**Manufacturing of UHPC Mixtures**

The considered reference mix of UHPC is designed by Cheyrezy et al. [6] and Mounanga et al. [7]. In their studies, authors have used white silica fume and a water-to-cement ratio of 0.16. As this kind of SF is no longer commercialised in France, grey silica fume is used in our research. Therefore, a preliminary study to optimise water-to-cement ratio and superplasticizer's type and content was suggested. The proposed new mix design is provided in Table 2.

Table 2 Constituents of reference UHPC mixture

| | CEM I 52.5 PM ES | QS | SF | CQ | SP | WATER |
|---|---|---|---|---|---|---|
| Mass ratio | 1 | 1.1 | 0.25 * 3/4 | 0.25 * 1/4 | 1.8% | 0.175 |

To reduce the environmental impact of UHPC, cement is partially substituted with slag. Three levels have been explored and provided in Table 3. These levels are volume percentages. SF, QS, CQ and water contents are kept constants. SP content was adjusted to obtain the same concrete workability.

Table 3 UHPCs mix proportion

| Mix designation | $UHPC_1$ | $UHPC_2$ | $UHPC_3$ | $UHPC_4$ | $UHPC_5$ |
|---|---|---|---|---|---|
| Cement, % | 100 | 70 | 50 | 20 | 20 |
| Slag, % | 0 | 30 | 50 | 80 | 80 |
| [KOH] | - | - | - | - | $[KOH]_3$ |

**Testing Methods**

The concretes were prepared by first mixing the solid components (cement, SF, CQ, BFS and QS) during 30 s. Solution of dissolved superplasticizer and water was then added at ambient temperature and the mixture was mixed for 3 min. An intensive Eirich mixer was used, providing high mixing energy and allowing more cohesion of particles. At the end of the mixing phase, the workability of different concretes was measured through mini-slump test, as shown in Figure 1. Fresh density and hydration kinetic were also measured.

Hydration test consists on measuring the temperature and heat of hydration of concretes by means of semi-adiabatic calorimetry, also known as the Langavant method. This method is described in European Standard NF EN 196-9: a freshly made concrete (approximately 1900 g) is introduced in an insulated flask, which is placed into calorimeter (Figure 2) in order to determine the quantity of heat emitted in accordance with the development of the temperature. Temperature is measured with platinum resistance thermometer.

Figure 1 Mini slump flow test

Figure 2 Semi-adiabatic calorimeter for hydration test

For mechanical properties, fresh concrete is introduced in steel moulds, which were stored for 24 h, before demoulding. Then 4 cm × 4 cm × 16 cm specimens were plastic-wrapped, avoiding any drying and stored in fog room at 20°C. At 3, 7 and 28 days, compressive strength was measured by means of 300 kN load-machine.

## RESULTS AND DISCUSSION

### Fresh Properties

Firstly, different types of superplasticizers (polycarboxylate, polycarboxylate and phosphonate, acrylic copolymer) are examined and their effect on mini slump flow (Ø cm) of reference UHPC was measured. Considered as acrylic polymer, Sika Viscocrete Krono H20 gives the highest Ø. For this type of superplasticizer, the polymer adsorption itself rather than the electrostatic repulsion is responsible for the dispersion of large agglomerates of cement particles into smaller ones, resulting in a remarkable increase of the fluidity of UHPC mix compared to the other types [8].

Then, in order to reach a fixed slump flow (Ø = 30 cm), different contents of SP (0.5- to 4.5%) were investigated to determine the saturation point (1.8%). The saturation point is the the dosage beyond which there is any improvement of the workability. Below it, the workability decreases due to the friction at the increased surface area [9] (Figure 3).

Concerning the blended mixtures, and for slump flow of 30 cm, the superplasticizer dosages are 0.75, 1.6 and 1.8% for the BFS contents of 30%, 50% and 80%, respectively (Table 4). When small quantity of BFS is added, there is more mixing water available to the CEM I, which explains the low dosage of SP. For high BFS content, smooth slag particles adsorb SP in its porous structure, resulting in more demand of SP to reach the required workability [10].

Table 4 UHPCs mix proportion

| Mix designation | $UHPC_1$ | $UHPC_2$ | $UHPC_3$ | $UHPC_4$ | $UHPC_5$ |
|---|---|---|---|---|---|
| Slag, % | 0 | 30 | 50 | 80 | 80 |
| SP, % | 1.8 | 0.75 | 1.6 | 1.8 | 1.8 |
| Density, kg/m³ | 2465 | 2461 | 2446 | 2398 | 2344 |

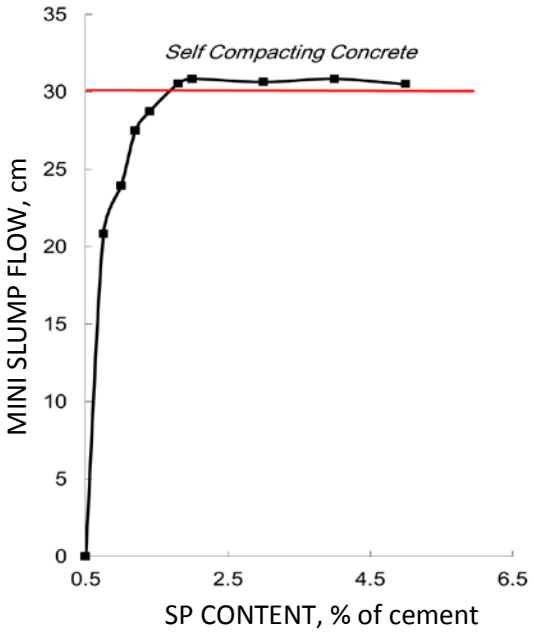


Figure 3 Saturation point of the superplasticizer

As shown in Table 4, density decreases when slag content increases. Indeed, for constant volume, added slag's mass is lower than cement, which induces lower concrete's density. The alkaline activation (KOH) is water consumer and has great influence on concrete packing and rheology, which explains the drop of density for $UHPC_5$.

**Hydration Reaction and Heat Flow**

Figure 4 gives the variation of the reaction heat for the UHPC mixtures while the reaction heat flow measured for these mixtures is presented in Figure 5. Also Table 5 summarizes the main measured and normalized characteristics values of the semi-adiabatic hydration curves, where $t_{max}$ is the time of maximum heat flow and $I_{max}$ is the maximum intensity of heat flow. As shown, the replacement of cement with BFS causes a reduction in the magnitude of heat reaction and the peak of heat flow. This phenomenon is related to the dilution effect of BFS and the fact that hydraulic and pozzolanic reactions release less heat than Portland cement hydration.

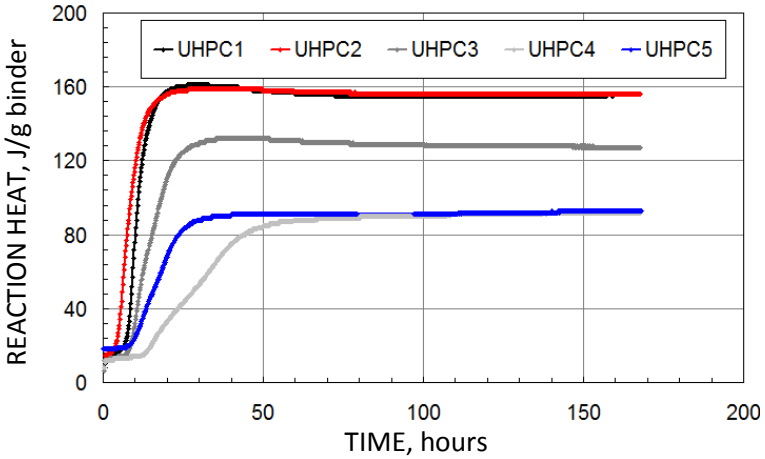


Figure 4 Reaction heat of studied UHPC

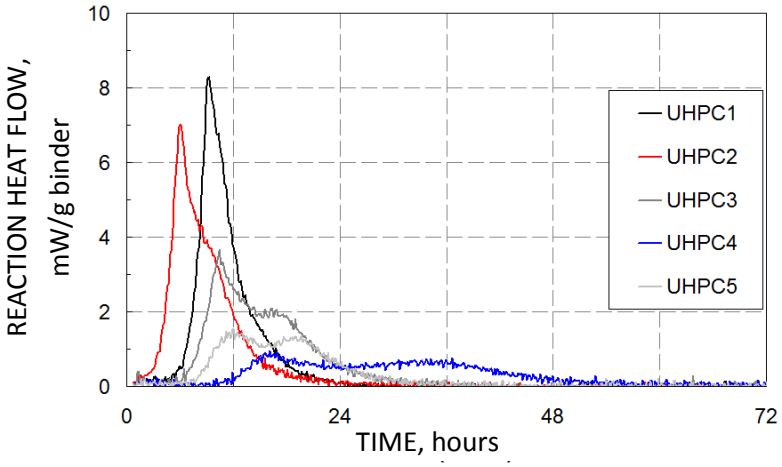


Figure 5 Reaction heat flow of studied UHPC

For $UHPC_1$ mix (0% slag), the maximal heat reaction and the peak of heat flow are, respectively, 161 J/g and 8.29 mW/g. The influence of low BFS content on hydration seems rather low and profile of hydration characteristics of the $UHPC_2$ (30% slag) shows a closed behaviour to the $UHPC_1$. Indeed, the maximal heat reaction is 159 J/g and is reached after 1595 min. By adding slag, the heat reaction of binder decreases, but also there is more water available to cement reaction, inducing the formation of $Ca(OH)_2$. This product reacts with BFS and promotes its reaction with water to generate the insoluble cementitious phase of C-S-H gel. Thus, the hydration kinetic is promoted due to the nucleation centers for C–S–H precipitation during the acceleration period of hydration [11]. As a result of this phenomenon, heat flow peak of $UHPC_2$ appears 177 min earlier than that of $UHPC_1$. Such effect is also amplified by the high SP content of $UHPC_1$. The increase of BFS content decreases the reaction heat of UHPC and extend the hydration reaction. For 50% and 80% of cement substitution, the reaction heat of UHPC decreases by 18% and 43%, respectively. Its maximal magnitude is reached after 2109 min and 3241 min for $UHPC_3$ and $UHPC_4$, respectively. Figure 5 shows clearly the remarkable change of reaction sequences for high BFS contents. Indeed, two peaks appear: the first peak is related to cement reaction and the second one is related to BFS phases hydration. The peaks appear at 10 and 16 hours for $UHPC_3$ and at 16 and 32 hours for $UHPC_4$. As both concretes contain the same or more SP than $UHPC_1$, the slow behaviour could be attributed to the low cement content, which limits the rate of portlandite. In fact, as explained above, the cement reaction results in portlandite production, which induces an increase of pH. This phenomenon promotes BFS solubility and reactivity [12, 13].

From Figure 4, it is noticed the great influence of KOH solution with $[KOH]_3$, on the reaction heat kinetic, without affecting its magnitude. The maximal reaction heat measured on $UHPC_4$ and $UHPC_5$ is 91 J/g. The addition of chemical activator accelerates hydration reaction and decreases by 26% the time to reach the maximal heat reaction. The same effect is observed on Figure 5, showing the earlier apparition of both peaks, in comparison to $UHPC_4$. The first peak, related to the cement reaction appears 4 hours earlier. The second peak, related to BFS reaction is more pronounced and is accelerated by 16 hours. Thus, the chemical activation accelerates the cement reaction, and promotes the reaction of BFS by supplying sufficient alkalis. Indeed, these alkalis accelerate the dissolution of Si and Al ions by breaking the Si-O-Si, Al-O-Al, Ca-O, Mg-O, and Al-O-Si bonds in the slag glass structure, which is related to the initial peak, and then a second family of peak occurs due to the formation of a Si-Al layer all over the surface of the slag grains [14, 15].

Table 5 Hydration characteristics of UHPC mixtures

| MIX | REACTION HEAT | | TIME OF MAXIMUM HEAT FLOW-$T_{MAX}$ | | MAXIMUM INTENSITY OF HEAT FLOW-$I_{MAX}$ | |
|---|---|---|---|---|---|---|
| | Measured value $Q_{max}$, J/g of binder | Time of maximum reaction time, min | Measured value $t_{max}$, min | Normalized value $\frac{t_{max}}{t_{max}(UHPC1)}(-)$ | Measured value $I_{max}$, mW/g of binder | Normalized value $\frac{I_{max}}{I_{max}(UHPC1)}(-)$ |
| $UHPC_1$ | 161 | 1572 | 552 | 1 | 8.29 | 1 |
| $UHPC_2$ | 159 | 1595 | 375 | 0.68 | 6.94 | 0.84 |
| $UHPC_3$ | 132 | 2109 | 629 | 1.14 | 3.66 | 0.44 |
| $UHPC_4$ | 91 | 3241 | 966 | 1.75 | 0.96 | 0.12 |
| $UHPC_5$ | 91 | 2401 | 721 | 1.31 | 1.55 | 0.19 |

## Compressive Strength

Figure 6 provides the test results on compressive strength of different studied UHPC at 3, 7 and 28 days with air curing. Every result is the average of three tests.

Compared to $UHPC_1$ mix, it is exhibited that a substitution of 30% of cement by BFS improves slightly the strength for all ages. As BFS reacts in long term, this increase of compressive strength could be explained by a physical effect, consisting on the improvement of matrix packing. For high contents of BFS (50 and 80%), there is a remarkable drop in the strength at 3, 7 and 28 days. Compressive strength decrease is 26 and 12% for $UHPC_3$ and 66 and 37% for $UHPC_4$, at 3 and 7 days, respectively. Since slag hydrates more slowly than Portland cement, the early rate of strength development of slag concretes is slower, the higher slag content the slower strength development. This is confirmed by Figures 4 and 5, which indicate that the increase of the concentration of the portlandite leads to promotion of the slag reaction, which simultaneously causes that more heat can be released and the mechanical performance can be enhanced [3]. At 28 days, compressive strength is lower for blended mixtures with high content of slag, which explains the non-sufficient water, totally consumed at early ages by the cement hydration.

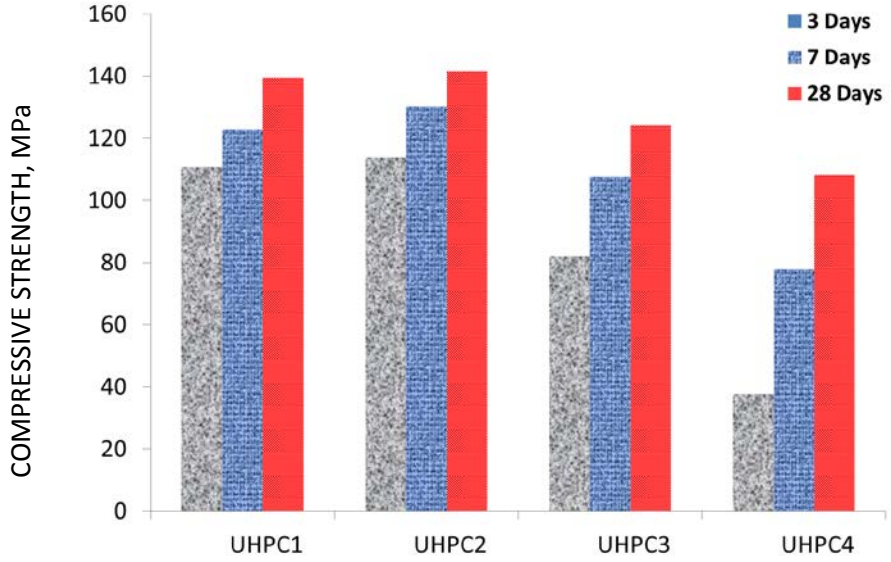


Figure 6 Compressive strength of studied UHPC at 3, 7 and 28 days

To improve the compressive strength of concretes with high BFS content, KOH was added with two concentrations for $UHPC_3$ and with three concentrations for $UHPC_4$. For every concentration, we have to ensure the same slump flow (30 cm). Figures 7 and 8 show the resulted compressive strength of studied mixtures at 3 and 7 days. From Figure 7, it is noted that alkaline activation does not improve compressive strength of $UHPC_3$. Indeed, for a BFS content of 50% the added basic solution (KOH) doesn't increase greatly pH, which should promote the hydration of slag and the formation of hydrates.

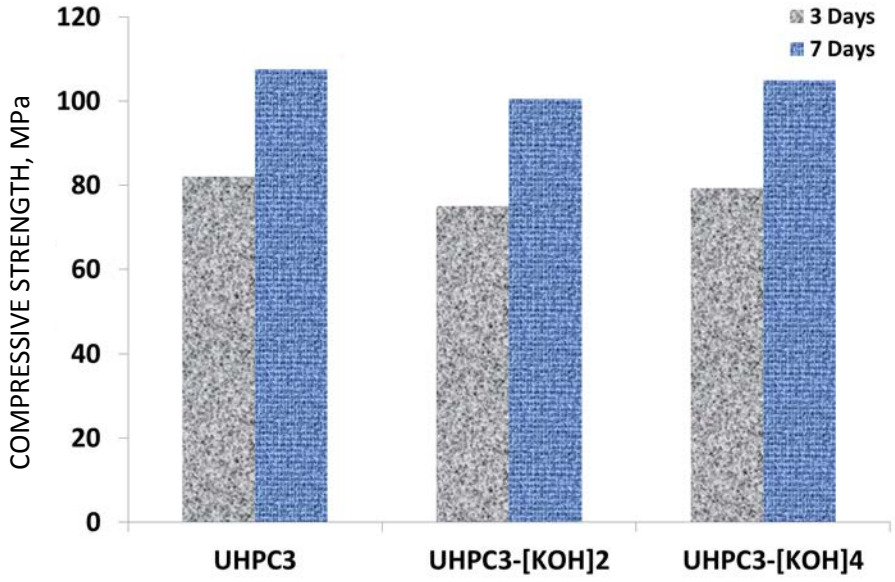


Figure 7 Compressive strength of $UHPC_3$ with activated slag by different concentrations at 3 and 7 days

This effect is more noticed when BFS content is high. As shown in Figure 8, the compressive strength at 3 days increases by approximately 7%, 25% and 42%, for $[KOH]_1$, $[KOH]_2$ and $[KOH]_3$, respectively.

The addition of KOH in $UHPC_4$, with concentration $[KOH]_3$ (i.e. $UHPC_5$), improves the compressive strength by 42 and 11% at 3 and 7 days, respectively. For high concentration of KOH, the pH of alkaline solution increases, which destroys the constraints of Si–O and Al–O, and consequently facilitates the dissolution of the slag glass structure. As a result, the hydration promotes [16].

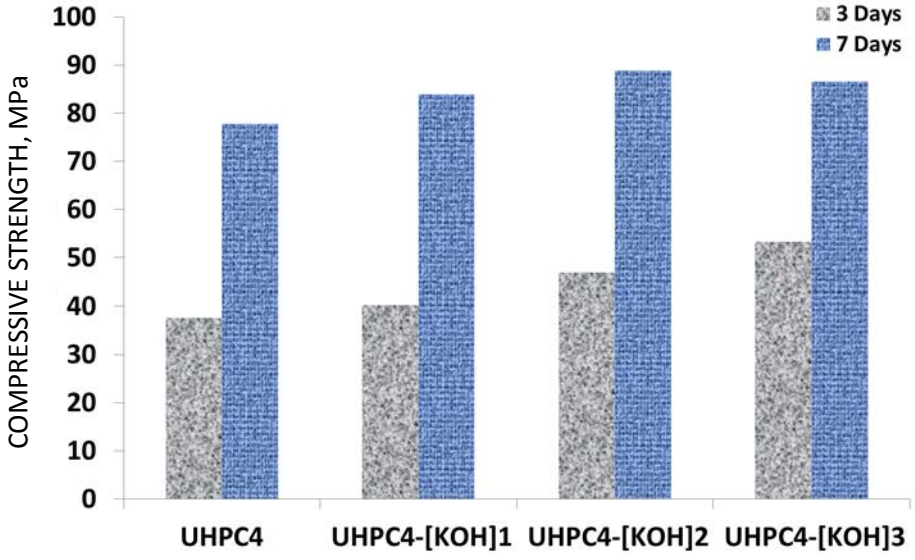


Figure 8 Compressive strength of $UHPC_4$ with activated slag by different concentrations at 3 and 7 days

## CONCLUSIONS

Based on the results of this experimental investigation, these conclusions are drawn:

1. The use of acrylic copolymer SP ensures the best concrete workability, with an optimum dosage of 1.8%. When BFS is added, and for a controlled workability (Ø = 30 cm), the SP dosage decreases. This decrease depends on BFS content.

2. The slag affects the hydration (phase development) quantitatively and kinetically: for $UHPC_2$, the low BFS content involved a faster production of the portlandite by nucleation site effect, which promotes BFS reaction. For $UHPC_3$ and $UHPC_4$, the high BFS content decreases greatly the heat reaction and the curves of heat flow show clearly two peaks. The first one is related to the production of $Ca(OH)_2$. The production of portlandite increases pH and promotes BFS reaction, which corresponds to the second peak. The addition of KOH solution accelerates by 4 hours and 16 hours, the first and second peak, respectively, for a BFS content of 80%. Indeed, the chemical activator, supplies sufficient alkalis, which promotes the dissolution of slag glass structure and its reaction.

3. The slag content affects the strength development of UHPC: the low content of slag ($UHPC_2$) improves matrix packing, which increases slightly the compressive strength at early age and in long term. For high BFS content, the slow hydration reaction affects greatly the strength development and particularly the compressive strength at 3 days. This result could be explained by the insufficient $Ca(OH)_2$, necessary to activate BFS and promote its reactivity. To resolve this problem, KOH was added, supplying sufficient alkalis and increasing pH, necessary to the reaction of BFS, which improves by 42% the compressive strength of $UHPC_5$, at 3 days, in comparison with $UHPC_4$.

## ACKNOWLEDGEMENTS

Authors acknowledge the technical help in concrete manufacturing of M. Carriat Jérôme.

## REFERENCES

1. AÏTCIN P.C. Binders for Durable and Sustainable Concrete, 2008, Taylor and Francis Group, 500 p.

2. RICHARD P. and CHEYREZY M. Composition of Reactive Powder Concretes, Cement and Concrete Research, Vol. 25, No. 7, 1995, pp. 1501–1511.

3. YU R., SPIESZ P., BROUWERS H.J.H. Development of an Eco-Friendly Ultra-High Performance Concrete (UHPC) with Efficient Cement and Mineral Admixtures Uses, Cement & Concrete Composites, Vol. 55, 2015, pp. 383–394.

4. BEN FRAJ A., BONNET S. and KHELIDJ A. New approach for coupled chloride/moisture transport in non-saturated concrete with and without slag, Construction & Building Materials, Vol. 35, 2012, pp. 761–771.

5. MOUNANGA P., KHOKHAR M.I.A., EL HACHEM R. and LOUKILI A. Improvement of the early-age reactivity of fly ash and blast furnace slag cementitious systems using limestone filler, Vol. 44, No. 2, 2011, pp. 437–453.

6. CHEYREZY M., MARET V. and FROUIN L. Microstructural Analysis of RPC (Reactive Powder Concrete), Cement and Concrete Research, Vol. 25, No. 7, 1995, pp. 1491–1500.

7. MOUNANGA P., CHERKAOUI K., KHELIDJ A., COURTIAL M., NOËLLE DE NOIRFONTAINE M. and DUNSTETTER F. Extrudable Reactive Powder Concretes: Hydration, Shrinkage and Transfer Properties, European Journal of Environmental and Civil Engineering, Vol. 16, No. 1, 2012, pp. 1–20.

8. COLLEPARDI S., COPPOLA L., TROLI R. and COLLEPARDI M. Mechanisms of Action of Different Superplasticizers of High-Performance Concrete, ACI Special Publication, Vol. 186, 1999, pp. 503–523.

9. DASHTI RAHMAT ABADI M.A., HAJI KAZEMI H., SHAHABIAN F. Effects of Different Water and Super Plasticizer Amount, Pre-Setting and Curing Regimes on the Behavior of Reactive Powder Concrete, Civil Engineering Infrastructures Journal, Vol. 47, No. 2, 2014, pp. 291–304.

10. LING W., PEI T. and YAN Y. Application of Ground Granulated Blast Furnace Slag in High-Performance Concrete in China, China Building Materials Academy, Proceedings of International Workshop on Sustainable Development and Concrete Technology, 2004, pp. 309–317.

11. JUENGER M.C.G. and SIDDIQUE R. Recent Advances in Understanding the Role of Supplementary Cementitious Materials in Concrete, Cement & Concrete Research, Vol. 78, 2015, pp. 71–80.

12. CINCOTO M.A., MELO A.A. and REPETTE W.L. Effect of Different Activators Type and Dosages and Relation to Autogenous Shrinkage of Activated Blast Furnace Slag Cement, Proceedings of the 11th International Congress on the Chemistry of Cement (ICCC), 2003, pp. 1878–1886.

13. FUJII A.L., Dos REIS TORRES D., De OLIVEIRA ROMANO R.C., CINCOTTO M.A. and PILEGGI R.G. Impact of Superplasticizer on the Hardening of Slag Portland Cement Blended with Red Mud, Construction and Building Materials, Vol. 101, 2015, pp. 432–439.

14. TORGAL F.P., GOMES J.C. and JALALI S. Alkali-Activated binders: A Review Part1. Historical Background, Terminology, Reaction Mechanisms and Hydration Products, Construction and Building Materials, Vol. 22, 2008, pp. 1305–1314.

15. VANCE K., AGUAYO M., DAKHANE A., RAVIKUMAR D., JAIN J. and NEITHALATH N. Microstructural, Mechanical, and Durability Related Similarities in Concrete Based on OPC and Alkali-Activated Slag Binders, International Journal of Concrete Structures and Materials, Vol. 8, No. 4, 2014, pp. 289–299.

16. BOUGARA A., LYNSDALE C. and EZZIANE K. Activation of Algerian in Mortars, Construction and Building Materials, Vol. 23, 2009, pp. 542–547.

# EFFECT OF NANO-SILICA AND AGGREGATE TYPE ON PROPERTIES OF ULTRA HIGH PERFORMANCE CONCRETE

**K Janković**
IMS Institute

**S J Stanković**
Vinča Institute of Nuclear Sciences

**M Stojanović** **D Bojović** **L Antić**
IMS Institute
Serbia

**ABSTRACT.** The aim of this investigation is to develop ultra high performance concrete (UHPC) for multipurpose - higher mechanical and ionizing radiation protection. The effect of nano-silica replacement (2 or 5%) on the properties of UHPC was compared with the referent concrete by testing compressive and flexural strength. As nano-silica influences cement hydration and modifies the pore structure, qualitative and quantitative analysis of pores was done using a device RapidAir 457. The second objective of this paper is to evaluate the influence of different aggregates on concrete properties. Two types of aggregate were used: quartz and barite. One of the most important characteristics of the concrete for protection against gamma and X radiation is its Total Attenuation Coefficient $(\mu/\rho)_{tot}$.

**Key word*:*** Nano-silica, UHPC, Barite, Radiation protection.

**Ksenija Janković,** senior research fellow is Head of Laboratory for Concrete at IMS Institute, Belgrade, Serbia. Her research interests include ultra high performance concrete, utilization of by-products and recycled waste materials in concrete and concrete durability. She has published about 140 papers.

**Srboljub J Stanković**, MSc EE, research assistant is working in the Department of Radiation and Environmental Protection at Vinča Institute of Nuclear Sciences, University of Belgrade, Serbia. He is a PhD candidate at the School of Electrical Engineering at Belgrade University. He is especially interested in nuclear engineering, physical properties of materials, radiation protection and ionizing radiation.

**Marko Stojanović**, MSc CE, research assistant is working in the Laboratory for Concrete at IMS Institute. He is a PhD student at the Faculty of Civil Engineering, Subotica at Novi Sad University. His research interests are SCC and ultra high performance concrete.

**Dragan Bojović**, MSc CE, research assistant is working in the Laboratory for Concrete at IMS Institute. He is a PhD candidate at the Faculty of Technical Sciences at Novi Sad University. His research interests focus on ultra high performance concrete, SCC, concrete fracture and concrete quality control in situ.

**Lana Antić**, MSc CE is working in the Laboratory for Concrete at IMS Institute.

## INTRODUCTION

Modern construction industry required building materials with improved properties. Ultra high performance concrete is one of them. Significant increases in mechanical properties of cementitious materials have been achieved by incorporating nano-silica [1]. By replacing a part of cement content with nano-silica it is possible to produce concrete with high performance and it can also reduce $CO_2$ emission.

Land and Stephan studied the way different nanoparticles affect cement hydration [2]. The acceleration of cement hydration was dependant on the total surface size of added nano-silica particles [3]. The pore size distribution also showed that nano-silica refined the large capillary pores, due to the combined contribution of the nano-filler effect and the pozzolanic reaction [4]. The fact that pore-size distribution was becoming finer, reduced pore volume and improved physico-mechanical properties of the mortars after the addition of nano-powders could be explained by the filler effect or the amount of hydration products of cement [5].

By adding between 3% and 10% w/w of colloidal silica suspension in the fiber-cement composites, the pullout of the fibers increased significantly [6]. Compressive strength and transport properties of UHPC also increased with the addition of nano-silica. For best performance, the optimum amount of nano-silica for cement replacement in the cement paste was 3 wt.% [7]. The results showed that up to 3% increase in the nano-silica content resulted in the increase in compressive and flexural strength of UHPC, and when the nano-silica content was more than 3% the mechanical properties decreased slightly due to agglomeration of nano-silica particles. The addition of nano-silica accelerated the hydration process. By increasing the nano-silica content the average pore diameter and porosity decreased. The microstructure was more homogenous and dense for nano-silica specimens when compared to the control specimen [8].

By using new nanomaterials higher temperatures will be allowed and hence a more efficient operation of power plants will be achieved, and the development of new energy production systems based on solar, nuclear and renewable sources will be enabled [9]. Ultra high performance concrete can be used in nuclear power plants and defensive facilities due to its dynamical behavior [10].

Barite aggregate is used to produce heavyweight concrete which is used for shielding in nuclear facilities and hospitals. Concrete with barite powder used as sand substitution in range between 0% and 25% decreased the compressive strength at 28 days just by 10% [11]. The grading curve of barite was modified by mixing process at a higher extent than for other aggregates. This influenced the properties of concrete by increasing workability, but decreasing compressive strength and the modulus of elasticity [12]. The basic characteristics of ordinary concrete and heavy-weight concrete with barite were studied for the application in shielding from gamma radiation [13, 14].

Also, one of the goals is the implementation of appropriate numerical calculations for obtaining the total mass attenuation coefficient value in the energy range 10 keV - 150 MeV of gamma and X radiation, depending on the changes in the concrete type in UHPC concrete with specially defined mechanical properties.

## EXPERIMENTAL WORK

The design of ultra high performance concrete is different than ordinary concrete. High amount of fine particles is used for UHPC manufacturing. Their properties are shown in Table 1.

Table 1 Properties of powder materials and sand

| | CEMENT | SILICA FUME | QUARTZ POWDER | QUARTZ SAND | BARITE SAND |
|---|---|---|---|---|---|
| $SiO_2$, % | 20.51 | 92.52 | 97.54 | 97.54 | 11.13 |
| $Al_2O_3$, % | 6.15 | 0.64 | 0.52 | 0.52 | 2.24 |
| $Fe_2O_3$, % | 2.80 | 0.31 | 0.57 | 0.57 | 1.55 |
| CaO, % | 63.41 | 0.38 | 0 | 0 | 0.18 |
| MgO, % | 1.85 | 0.44 | 0 | 0 | 0 |
| $Na_2O$, % | 0.29 | 0.32 | 0 | 0 | 0.86 |
| $K_2O$, % | 0.79 | 0.87 | 0.24 | 0.24 | 0.72 |
| $SO_3$, % | 2.69 | 0.22 | 0 | 0 | 28.05 |
| Ba, % | 0 | 0 | 0 | 0 | 53.15 |
| Cr, % | 0 | 0 | 0 | 0 | 0.4 |
| Sr, % | 0 | 0 | 0 | 0 | 1.72 |
| Specific density, kg/m³ | 3100 | 2200 | 2695 | 2695 | 3770 |
| Bulk density, kg/m$^3$ | | | | 1650 | 2260 |

Concrete was made with ordinary Portland cement CEM I 42.5 R. Also, silica fume (SF) and nano-silica (nS) with average particle size of 7 nm were pozzolanic materials. Quartz powder (Qp) with average particle size of 50 μm and quartz sand (Qs) or barite sand (B) up to 4 mm were used as aggregate. A modified polycarboxylates based superplasticizer allowed high water reduction. Brass coated steel fibers with 8 mm length and a diameter of 0.15 mm were used (5% by volume). Six types of concrete were made with varying percent of nano-silica (0%, 2% and 5%) and aggregate type (quartz and barite). Composition of concrete mixtures are shown in Table 2.

Table 2 Concrete mixture composition, kg/m³

| | K0f5 | K2f5 | K5f5 | B0f5 | B2f5 | B5f5 |
|---|---|---|---|---|---|---|
| C | 950 | 931 | 902.5 | 950 | 931 | 902.5 |
| SF | 200 | 200 | 200 | 200 | 200 | 200 |
| nS | 0 | 19 | 47.5 | 0 | 19 | 47.5 |
| Qp | 350 | 350 | 350 | 335 | 335 | 335 |
| Qs | 570 | 570 | 570 | 0 | 0 | 0 |
| B | 0 | 0 | 0 | 810 | 810 | 810 |
| Water | 230 | 250 | 250 | 230 | 250 | 250 |
| Superplasticizer | 55 | 55 | 55 | 55 | 55 | 55 |
| Fibers | 390 | 390 | 390 | 390 | 390 | 390 |

## NUMERICAL CALCULATIONS OF TOTAL MASS ATTENUATION COEFFICIENT

Total Mass Attenuation Coefficient $(\mu/\rho)_{tot}$ is one of the most important concrete characteristics for protection against gamma and X radiation.

The definition of Total Mass Attenuation Coefficient for mixture is given by:

$$\left(\frac{\mu}{\rho}\right)_{tot} = \sum_j w_j \cdot \left(\frac{\mu}{\rho}\right)_j \tag{1}$$

where $(\mu/\rho)_j$ and $w_j$ are the weight fraction and mass attenuation coefficient of the constituent element j.

The numerical calculations included two steps: 1. The composition of each type of concrete from Table 2 was determined in accordance with the nomenclature of chemical elements and chemical compounds, 2. Interactive use of the XCOM program [15], where the known composition of individual types of concrete determines the total mass attenuation coefficient depending on the change of energy photon radiation.

XCOM program enables the calculation of interaction coefficients for the following processes: Compton (incoherent) and Rayleigh (coherent) scattering, photoelectric absorption, and pair production in the fields of the atomic nucleus and atomic electrons. The mean free paths between scatterings, between photo-electric absorption events, or between pair production events are the reciprocals of partial interaction coefficients. The total attenuation coefficient is calculated as the sum of the interaction coefficients for the individual processes.

## RESULTS AND DISCUSSION

Samples for testing the mechanical properties were prepared in molds 4 cm × 4 cm × 16 cm by the vibration on vibro-table for 60 s. Next day, specimens were demoulded and put into water and cured up to testing.

The results of compressive strength of concrete with quartz were given in Figure 1 and for UHPC with barite aggregate were shown in Figure 2.

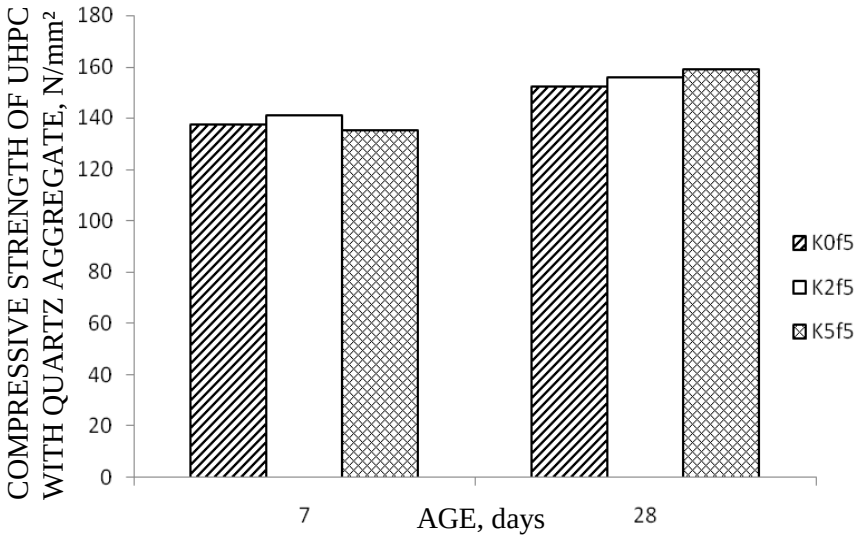


Figure 1 Compressive strength of UHPC with quartz aggregate

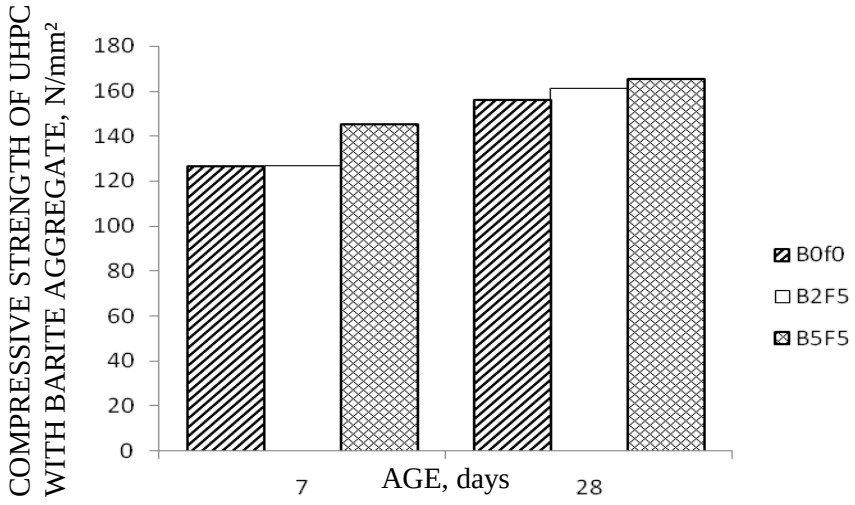


Figure 2 Compressive strength of UHPC with barite aggregate

Obtained values of flexural strength of all concrete types are shown in Table 3.

Table 3 Flexural strength of concrete, N/mm²

| | K0f5 | K2f5 | K5f5 | B0f5 | B2f5 | B5f5 |
|---|---|---|---|---|---|---|
| 7 days | 26.1 | 29.4 | 25.0 | 25.0 | 34.0 | 24.8 |
| 28 days | 28.0 | 37.4 | 27.3 | 31.1 | 38.9 | 32.0 |

By comparing concrete made with different aggregate it can be seen that the concrete made with barite aggregate had better results than concrete made with quartz aggregate. For compressive strength, the difference is about 4% for concrete with nano-silica and 3% for concrete without nano-silica. Flexural strength of concrete with barite sand and 5% of nano-silica is 17% higher, for UHPC without nano-silca is 11% higher, while concrete made with 2% nano-silica had only 4% higher flexural strength when compared to concrete made only with quartz aggregate.

Comparing concrete made with the same type of aggregate we can see that its compressive strength increases with the addition of nano-silica. For barite concrete, the difference is 3% for concrete with 2% nano-silica and 6% for concrete with 5% nano-silica related to UHPC without nano-silica. Concrete with quartz sand and 2% nano-silica had only 2% higher compressive strength and with 5% nano-silica had 4% greater compressive strength comparing to mixture without nano-silica. Influence of 2% nano-silica had positive effect on flexural strength. It increased 34% for quartz concrete and 25% for barite concrete. With 5% nano-silica flexural strength slightly decreased for concrete with quartz aggregate, while it slightly increased for concrete with barite aggregate when compared to UHPC without nano-silica.

Pore-size distribution was tested by RapidAir 457 device. With the increase in the nano-silica content pore-size distribution became finer. Results for concrete with barite sand are given in Table 4.

Table 4 Test results by device RapidAir 457

| CONCRETE | B0f5 | B2f5 | B5f5 |
|---|---|---|---|
| Air Content, % | 3.35 | 3.30 | 2.64 |
| Specific Surface, $mm^{-1}$ | 24.14 | 30.17 | 68.61 |
| Spacing Factor, mm | 0.421 | 0.278 | 0.164 |
| Void Frequency, $mm^{-1}$ | 0.202 | 0.400 | 0.454 |
| Average Chord Length, mm | 0.166 | 0.133 | 0.058 |

For a selected value of the nano-silica content (2%) calculations for the mass attenuation coefficients were carried out and their dependence on energy photon radiation is shown in the Figure 3.

Larger values of mass attenuation coefficient for concrete B2 in relation to the K2 concrete due to the presence of barium (Ba) as a component of the aggregate with which the concrete B2 was made (Figure 3). Especially it can be observed the influence of the presence of barium in the concrete type B2 because it significantly increases its capability for absorption of X and gamma rays with energies below 300 keV.

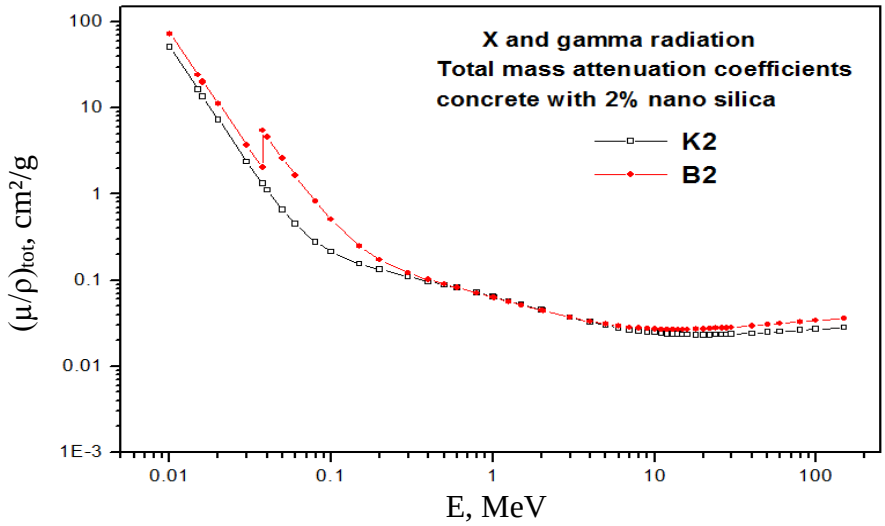


Figure 3 Total mass attenuation coefficients for concrete with 2% nano-silica

## CONCLUSIONS

If we compare concrete made with the same type of aggregate, it can be concluded that cement replacement with nano-silica in the amount of 2% has a positive impact on both the compressive and flexural strength. The flexural strength decreased, but the compressive strength increased when the nano-silica content was 5%.

Concrete with barite aggregate had better mechanical properties than concrete with quartz aggregate. Type of used aggregate has a much greater influence on flexural strength than on the compressive strength, e.g. for mixtures with 5% nano-silica content, concrete made with barite sand had 4% greater compressive and 17% greater flexural strength than concrete with quartz sand.

Based on the results of the corresponding graphs for Total Mass Attenuation Coefficient it can be concluded that in the range of energy of gamma and X radiation from 10 keV to 150 MeV, concrete with barite sand has greater protective power than concrete with quartz sand. From the aspect of compressive, flexural strength and radiation protection UHPC with barite sand and 2% cement replacement with nano-silica is optimal.

## ACKNOWLEDGEMENTS

The work reported in this paper is a part of the research project TR 36017 supported by the Ministry of Education, Science and Technological Development, Republic of Serbia.

## REFERENCES

1. SINGH L.P., KARADE S.R., BHATTACHARYYA S.K., YOUSUF M.M. and AHALAEAT S. Beneficial role of nanosilica in cement based materials – A review, Constr Build Mater, Vol. 47, 2013, pp. 1069–1077.

2. LAND G. and STEPHAN D. Controlling cement hydration with nanoparticles, Cem Concr Comp, Vol. 57, 2015, pp. 64–67.

3. LAND G. and STEPHAN D. The influence of nano-silica on the hydration of ordinary Portland cement, J Mater Sci, Vol. 47, 2012, pp. 1011–1017.

4. DU H., DU S. and LIU X. Durability performances of concrete with nano-silica, Constr Build Mater, Vol. 73, 2014, pp. 705–712.

5. OLTULU M. and SAHIN R. Pore structure analysis of hardened cement mortars containing silica fume and different nano-powders, Constr Build Mater, Vol. 53, 2014, pp. 658–664.

6. SANTOS S.F., De ANCHIETA RODRIGUES J., TONOLI G.H.D., De SOUZA ALMEIDA A.E.F. and SAVASTANO H. Jr. Effect of colloidal silica on the mechanical properties of fiber–cement reinforced with cellulosic fibers, J Mater Sci, Vol. 49, 2014, pp. 7497–7506.

7. GHAFARI E., COSTA H., JULIO E., PORTUGAL A. and DURAES L. The effect of nanosilica addition on flowability, strength and transport properties of ultra high performance concrete, Mater Des, Vol. 59, 2014, pp. 1–9.

8. RONG Z., SUN W., XIAO H. and JIANG G. Effects of nano-$SiO_2$ particles on the mechanical and microstructural properties of ultra-high performance cementitious composites, Cem Concr Comp, Vol. 56, 2015, pp. 25–31.

9. CHATURVEDI S. and DAVE P.N. Design process for nanomaterials, J Mater Sci, Vol. 48, 2013, pp. 3605–3622.

10. LAI, J, SUN, W. Dynamic behaviour and visco-elastic damage model of ultra-high performance cementitious composite, Cem Concr Res, 39(11), 2009, pp 1044–51

11. SAIDANI K., AJAM L. and OUEZDOU M.B. Barite powder as sand substitution in concrete: Effect on some mechanical properties, Constr Build Mater, Vol. 95, 2015, pp. 287–295.

12. GONZALEZ-ORTEGA M.A., CAVALARO S.H.P. and AGUADO A. Influence of barite aggregate friability on mixing process and mechanical properties of concrete, Constr Build Mater, Vol. 74, 2015, pp. 169–175.

13. AKKURT I., BASYIGIT C., KILINCARSLAN S., MAVI B. and AKKURT A. Radiation shielding of concretes containing different aggregates, Cem Concr Comp, Vol. 28, 2006, pp. 153–157.

14. AKKURT I., BASYIGIT C., KILINCARSLAN S. and MAVI B. The shielding of gamma – rays by concretes produced with barite, Prog Nucl Energy, Vol. 46, No. 1, 2005, pp. 1-11.

15. BERGER M.J., HUBBELL J.H., SELTZER S.M., CHANG J., COURSEY J.S., SUKUMAR R., ZUCKER, D.S. and OLSEN K. XCOM: Photon Cross Section Database (version 3.1). http://www.nist.gov/pml/data/xcom/index.cfm, NBSIR 87-3597. National Institute of Standards and Technology, Gaithersburg, MD, 2010.

# COMBATING ASR TO ENABLE USAGE OF LOCAL AGGREGATES IN TURKEY

**R C Lewis**
Elkem Silicon Materials
United Kingdom
**E Bayrak**
KGM
Turkey

**ABSTRACT.** This paper looks at the use of silica fume to negate the high reactivity of aggregates in Turkey. Reference is made to initial testing for ASR resistance in the early 1970's, then to local research by KGM in 2013/2014 and further testing in Iceland in 2015. The paper will show that the addition of silica fume in the area of 8% by weight of cement will control the ASR within the specified limits and enable the use of local aggregates, with known reactivity potential, in major concrete construction. Further research is expected to establish levels at which even higher reactivity aggregate may be safely used.

**Keywords:** Alkali-silica reaction (ASR), Pozzolans, Silica fume, Expansion values.

**R Lewis** is the Technical Marketing Manager at Elkem Silicon Materials. Currently he provides technical support to Elkem's International concrete market.

**E Bayrak** is a senior engineer at KGM, part of the Government Highways Department (DLH) of Turkey, based in Ankara. She works in the R&D section of KGM.

## INTRODUCTION

Turkey is at the junction of the European and Asian continents (Figure 1) – a crossover for travelers for millennia – and to maintain that "fulcrum point of the world", is looking to improve its infrastructure and communications. To do this means a lot of building from scratch and a lot of upgrading, including airports (Figure 2), dams, roads, bridges, tunnels, ports and and power services.

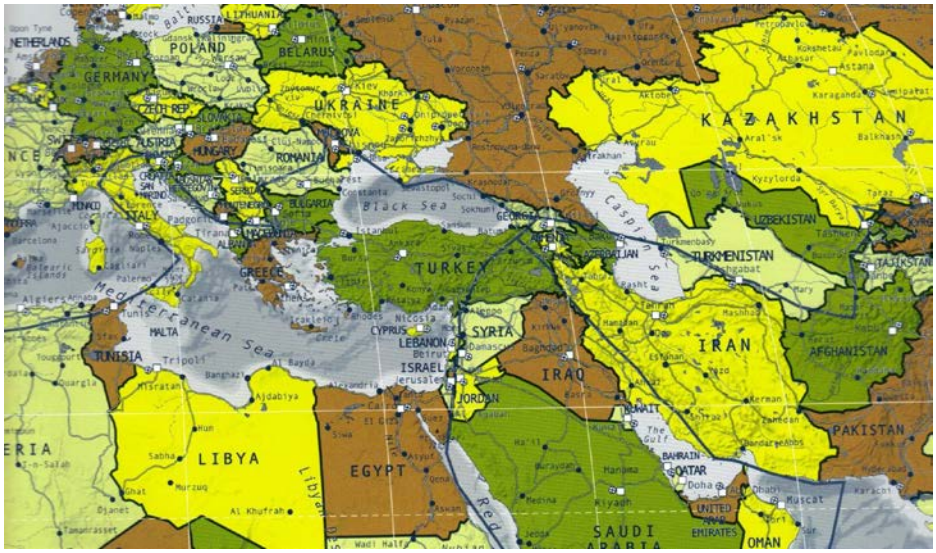


Figure 1 A central position – from ancient times to the modern world.

Such construction will use huge quantities of concrete, nominal and high performance, which will in turn mean vast tonnages of aggregates. The drawback to this is the reactivity level of the majority of aggregate in Turkey. The potential for Alkali Silica Reaction (ASR) from these aggregates means that a number of precautionary steps must be taken to prevent the reaction happening and causing damage and possible failure of structures. The alternative is to ship in low reactivity aggregates to blend with local materials and thus reduce the potential for ASR. With the aggregate tonnages being registered in many tens of millions, such action would be costly and unfriendly to the environment. Readymix Concrete production volumes for the past few years have been approximately:

- 2010 ~ 80 million $m^3$
- 2011 ~ 91 million $m^3$
- 2012 ~ 93 million $m^3$
- 2013 ~ 100 million $m^3$
- 2014 ~ 110 million $m^3$

At roughly 1,800kg of aggregate per cubic metre, the last couple of years have approached some 200 million tonnes of aggregate consumption. At even a 50:50 blend with a low reactivity aggregate, the import potential would be around 100 million tonnes. The use of pozzolans has long been known to combat ASR with silica fume being widely acknowledged as the highest effectiveness in resisting this form of concrete deterioration. The target behind the research discussed in this paper is that being able to control the ASR potential, using silica fume, will mean that more local aggregates can be used, negating the need for import and thus reducing both the cost of the construction and the damage to the environment.


Figure 2 The airport network alone is a huge system to upgrade (from Turkish Airlines)

## HISTORY

Since the early 1970s when large scale filtering meant that sufficient volumes of silica fume were available for the concrete industry, research has been conducted on how to make the best use of its pozzolanic action. The superfine nature and high silicon dioxide content of the silica fume gave it two advantages in combating the ASR attack.

The small size and perfect spherical particles gave both a packing effect – filling the voids between cement grains – and a ball bearing effect to give cohesion but also a thixotropic effect. Once the calcium hydroxide was produced by the cement hydration, the pozzolanic reaction took over filling the void space with calcium silicate hydrates adding more bond within the matrix and blocking the pores in the cement. This meant a dense concrete with high water resistance and the pozzolanic action mopped up excess alkalis ions and calcium hydroxide (Figure 3).

Thus, three parts of the quartet required for ASR were greatly reduced or negated and thus the ASR was controlled. It was in 1979 that Iceland, with its highly reactive aggregates and high alkali cement ruled that all concrete made with local materials must contain 7 to 8% silica fume to combat the ASR (Figure 4).

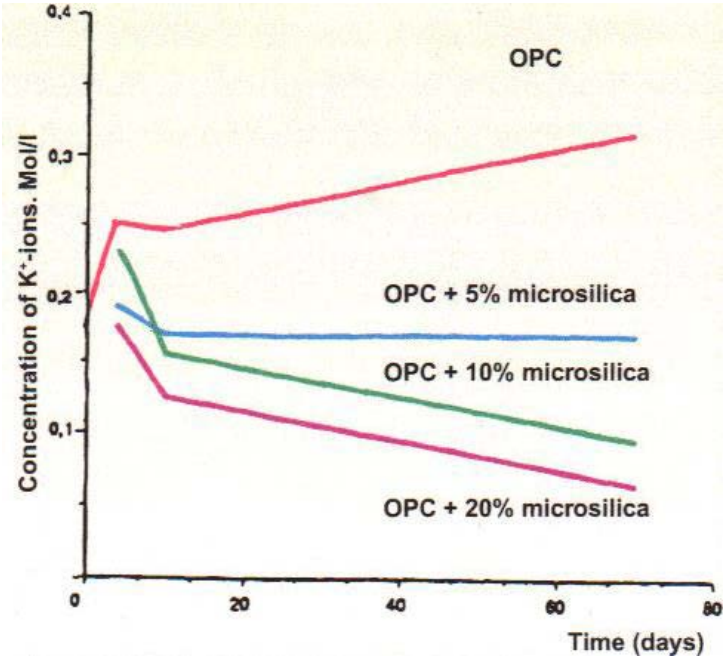


Figure 3 Reduction in Alkali ions with the addition of silica fume [1]

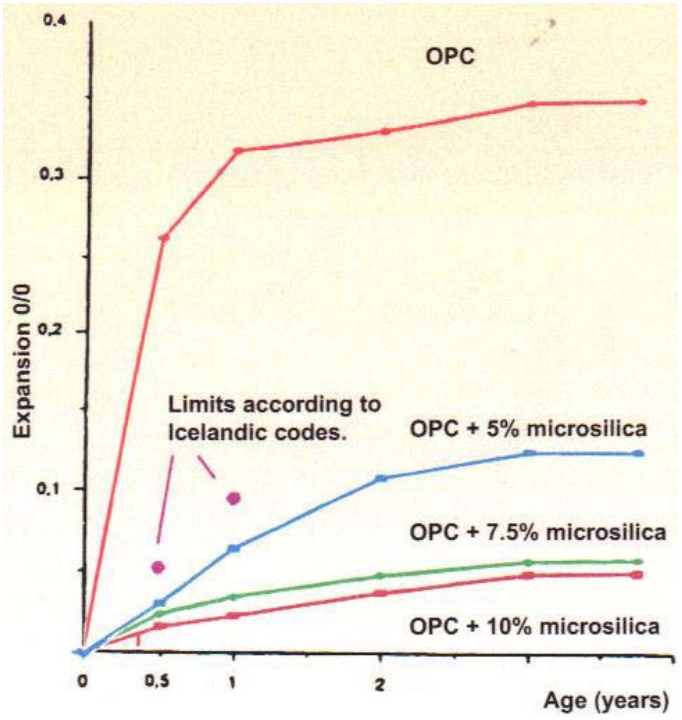


Figure 4 Reduction in Expansion with the addition of silica fume [2]

## RESEARCH IN TURKEY

The use of concrete for roads and bridges and similar infrastructure in Turkey is covered by the current Highways Manual. The limitation on ASR expansion in this manual is 0.20% to allow aggregates to be used. As many of the local aggregates are around 0.30% to 0.50% expansion this becomes a difficult target. With some aggregates tested at around 0.80% expansion, the need for a solution to be able to use these increases. The Government Authority, DLH, through the KGM Highways department decided in 2013 to run some testing on the use of silica fume as an addition to concrete to combat the potential ASR with local materials. Using the Standard 14 day test and measuring the expansion for a series of silica fume dosages, the KGM research showed a very effective pattern of suppressing the ASR expansion, Table 1.

Table 1. Expansion values (%) by age and addition of silica fume. Ref 3.

| | SILICA FUME CONTENT, % by mass | | | | |
|---|---|---|---|---|---|
| AGE | 0 | 8% | 10% | 12% | 14% |
| 3 days | 0.051 | 0.016 | 0.014 | 0.016 | 0.013 |
| 7 days | 0.161 | 0.015 | 0.010 | 0.008 | 0.004 |
| 14 days | 0.334 | 0.060 | 0.025 | 0.014 | 0.008 |

The values obtained showed that the use of silica fume at an 8% addition (by weight of cement) would limit the expansion of this level of reactive aggregate (0.30~0.40%) down to below 0.10%. This is half the target maximum of the Highways Manual. The values also showed that for each additional 2% of silica fume, the expansion at 14 days reduced by 50% from the previous level. The findings suggest that it may even be possible to use a dosage of between 8 and 10% silica fume to control reactive aggregates with values of 0.60 to 0.80%, reducing that expansion down to below 0.1%. A graph of the data is shown in Figure 5.

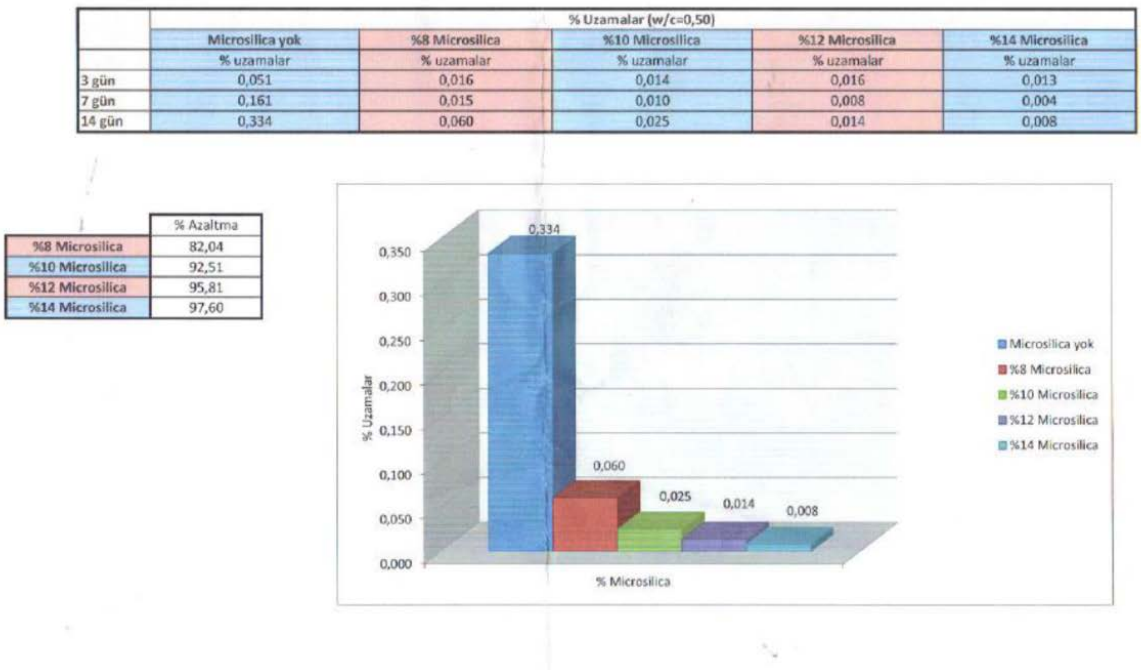


Figure 5 Tables and graph reproduced from KGM data [3]

The research at DLH / KGM is continuing to refine the levels of addition of silica fume needed for different types of reactive aggregates. The work may also include the use of other pozzolans such as fly ash or slag – also known to provide a level of resistance to ASR. The combination of these supplementary cementitious materials can achieve very high durability as well as numerous improvements to the concrete quality. It is hoped that this research will lead to the adoption of silica fume use within the Highways Manual.

## WORK IN ICELAND

Although Iceland uses silica fume to suppress the ASR, it is known that new sources of aggregates can require changes in the addition rate to maintain a level of confidence in the concrete quality. Over the years since 1979, the stipulated addition rate of silica fume (7.5%) has been 'trimmed' back – with the use of other materials and better superplasticisers – to around 6% by cement weight. Like Turkey, the idea is to blend high and low reactivity aggregates to get the best environmental sustainability and use the silica fume to ensure low expansion. A new sand source (Stokksnessandur) became available recently and testing showed that this had a potential expansion of between 0.40 and 0.50%. A 50% blend of this sand with a relatively inert sand (Raudamelssandur) would be the normal method of helping to control the ASR with the use of silica fume. Tests run at the Innovation Centre Iceland's 'Rheocenter' showed that, even at the 50% blend, the addition of silica fume would have to be increased to approximately 8% (Figure 6, Ref 4.). To use the Stokksnessandur sand at 100%, rather than 50:50, would require an addition of silica fume at 9% to stay below 0.20% expansion or 11% to reach less than 0.10% expansion.

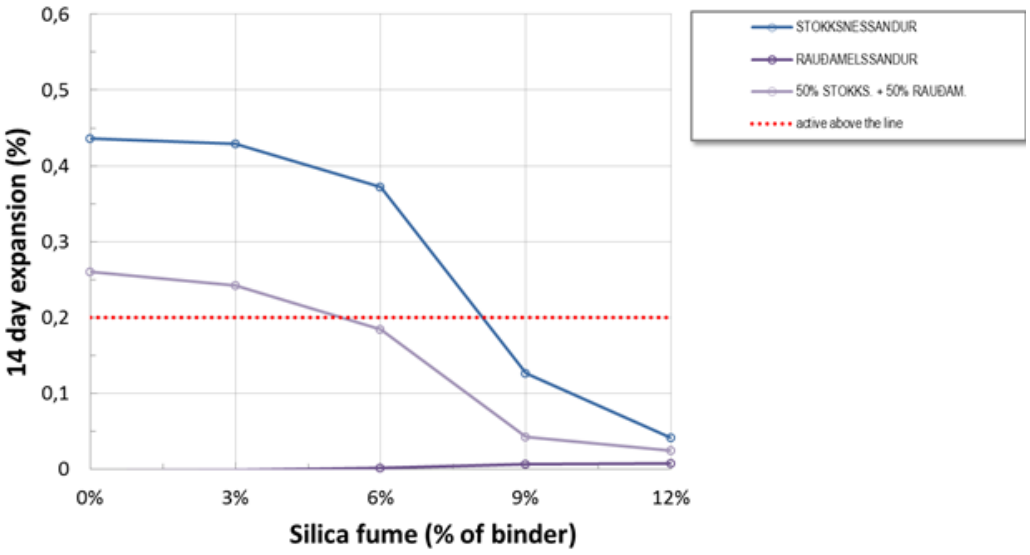


Figure 6 Expansion of individual and blended sand mixes with increasing silica fume [4].

## COMBINING THE RESULTS.

With the two sets of results achieving similar numbers for the usage of the silica fume, it was interesting to plot all the numbers on a single graph (Figure 7, Turkish results in orange). This emphasised the fact that 7.5% value was well set as a minimum for keeping expansion below 0.2% (large red arrow). It can be seen from the combined graph that the target for moderately reactive aggregates should be 7 to 8% silica fume for an expansion of less than 0.1%. For higher reactivity aggregates, this value should rise to 11% (short red arrow) or more, depending on the actual reactive potential of the aggregate. For Iceland, the implication is that they should return to the 7.5% rate that was specified back in 1979, to ensure control of the potential ASR with the aggregates there.

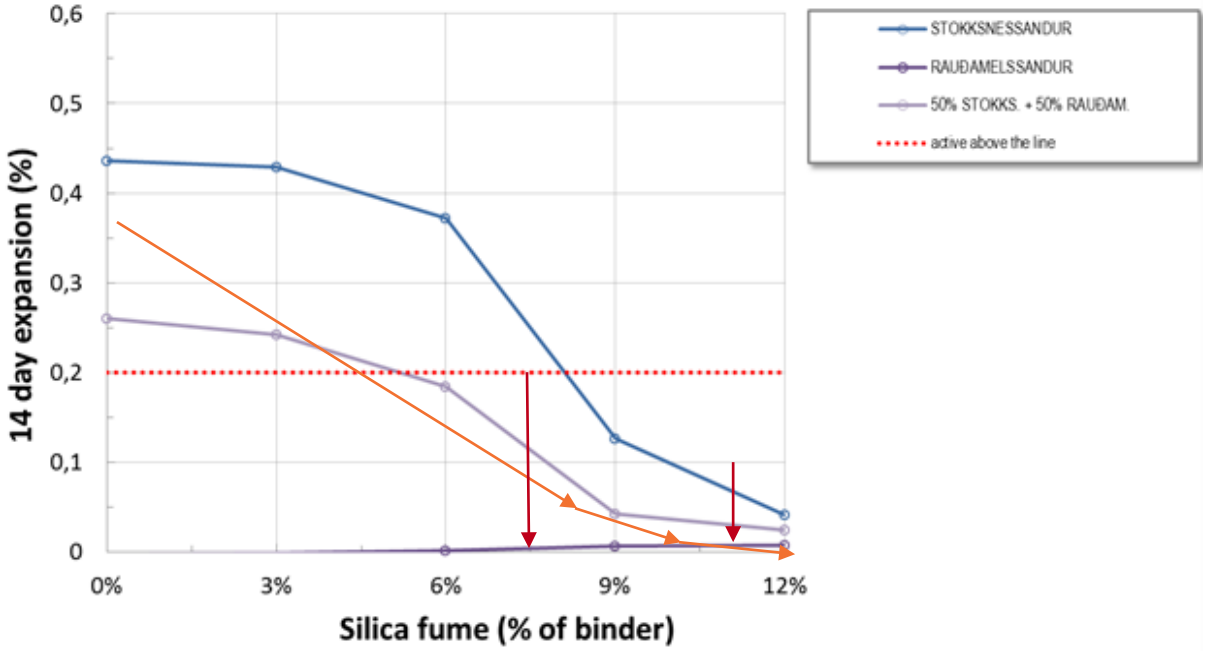


Figure 7 Combined Turkish and Icelandic results

## SUMMARY

The current work in both Iceland and in Turkey substantiate the early results from the 1970s and 1980s. This shows that ASR can be resisted using silica fume as an addition to concrete. With 'moderately reactive' materials (0.30~0.40% expansion), this addition rate is around 8% by weight of cement. Higher reactivity aggregates can also be controlled in this manner, by using around 9% silica fume, although test runs should be made to determine the optimum addition of silica fume.

The use of other supplementary cementitious materials, such as fly ash and slag has not been considered in this work. The combinations of such, into triple blends with silica fume, may give additional benefits, such as reduced heat in large volume pours and provide better economics on cost.

The use of silica fume in concrete in Turkey should be highly considered by the authorities, in order to allow previously ‘unusable’ aggregates to be used, thus saving costs, energy and the environment, by not importing less reactive materials.

## ACKNOWLEDGEMENTS

The primary author wishes to thank Elif Bayrak and the team at KGM and the DLH authority for their work on the research in Turkey, and for allowing him use of the results so far achieved.

Additional information has been taken from Elkem Microsilica datasheet C3-05, Alkali Silica Reaction. This can be found on the web-site www.elkem.com

## REFERENCES

1. DIAMOND S, Effects of microsilica on pore solution chemistry of cement pastes, Journal of the American Ceramic Society, Vol. 66, 1983, pp. 82-81.

2. ASGEIRSON, H, Silica fume in cement and silane for counteracting of alkali-silica reactions in Iceland, Cement and Concrete Research; Vol. 16, 1986, pp. 423-428.

3. BAYRAK E and team, ongoing research, unpublished, KGM, Ankara

4. WALLEVIK and HJARTARSON, ongoing research, unpublished, ICI, Iceland

# CORROSION RESISTANCE OF FERROCEMENT MORTAR WITH ALTERNATIVE CEMENTITIOUS MATERIALS AND SYNTHETIC FIBRES

**M Papachristoforou**

**I Papayianni**

Aristotle University of Thessaloniki

Greece

**ABSTRACT.** Ferrocement is a mortar with steel mesh encapsulated in it that is used widely for flat or corrugated roofing sheets on which photovoltaic cells are often supported. The mortar should be of high fluidity, in order to be injected on the steel mesh, apart from high strength and durability requirements needed for steel mesh protection. However, the thin ferrocement sheets do not adequately protect the steel mesh and corrosion due to chloride penetration often causes deterioration of them, particularly in areas near the sea. In order to improve the performance to chloride ingress of ferrocement mortar, Calcareous Fly Ash (CFA) and Ladle Furnace Slag (LFS) were incorporated in the matrix as well as synthetic fibres. Their addition ranged from 0,10 to 0,20 cementitious/cement ratios and fibres content 0,7 to 0,9% by volume of the total mixture. Apart from mechanical and elastic characteristics of the alternative ferrocement mortars, toughness and shrinkage deformations were also been measured. In addition, the alternative ferrocement mortars were tested for chloride penetration and compared with control cement mixtures. Up to 20% cement replacement by cementitious materials and addition of fibres 0,7-0,8% by volume provide comparable or higher strength ferrocement matrix with significant reduction of shrinkage and chloride penetration. These positive results in combination with low cost and sustainability aspects of this alternative ferrocement make it interesting for in situ precast cement products.

**Keywords:** Ferrocement, Calcareous fly ash, Ladle furnace slag, Synthetic fibres, Compressive strength

**Dr Michalis Papachristoforou** is post-doctoral researcher at the Laboratory of Building Materials of the Civil Engineering Department of Aristotle University of Thessaloniki. His research actions aim towards the utilization of by products in concrete for specific applications.

**Professor Ioanna Papayianni** is the Director of the Laboratory of Building Materials at the Department of Civil Engineering, at Aristotle University of Thessaloniki. She is a specialist in concrete technology and sustainable development.

## INTRODUCTION

Ferrocement is a cement product that could be defined as reinforced mortar with multiple layers of steel mesh (often galvanized) encapsulated in the mortar matrix [1]. It is can be used to construct various structural components such as housing units, water tanks, grain silos, flat or corrugated roofing sheet and it seems to be a good alternative for roofing elements supporting photovoltaic cells, providing convenience and short time constructional solutions. In this case, the ferrocement could be applied by injection contributing to bonding of the matrix with mesh. This process requires mortar mixture of high fluidity which will last a logical period of time to finish application. A robust self compacting mortar, rich in cementitious materials which fulfill strength and durability requirements imposed in each application could be used as ferrocement matrix.

One of the most important factors affecting the durability of ferrocement is the corrosion of wire meshes. This phenomenon is magnified in corrosive environments. The corrosion of the wires leads to a reduction in diameter, loss of effective strength and deterioration of the bond between the matrix and the reinforcement [2]. Even though the measures to insure durability on conventional reinforced concrete can also be applied to ferrocement, the thin coating of the metallic mesh, the large surface area of the structure and the extreme environmental conditions that ferrocement is usually subjected makes it prone to deterioration [3]. For this reason, the wire mesh reinforcement used in ferrocement is also available to galvanized form. Since this matrix is prone to shrinkage deformations including autogeneous shrinkage (which is favored in rich in cement and low water/cement ratios mixtures), any improvement of the matrix to this direction will be beneficial to its service life. Other measures to improve the corrosion resistance of ferrocement are the use of mineral admixtures in concrete such as fly ash, blast furnace slag or silica fume [2], [4], [5] or low water-to-cement (w/c) ratio [6]. In ACI 549 1R-2, the use of pozzolanic admixtures for a part replacement of fine aggregates as well as of synthetic fibres is also recommended.

In this paper, the research work aimed to improve the ferrocement matrix by adding supplementary cementitious materials as substitute for cement and fines and also polypropylene fibres to increase toughness of the matrix. Greek calcareous fly ash of relative high lime content and ladle furnace slag were used as cementitious materials since they had been proven effective constituents of self compacting mixtures in reducing early shrinkage and increasing fluidity respectively [7, 8].

## EXPERIMENTAL PROGRAMME

River sand of 2,650 g/cm³ density tested according to ASTM C 128-01 (Standard Test Method for Density, Relative Density and Absorption of Fine Aggregate) and 3% moisture content according to ASTM C 566-97 (Standard Test Method for Total Evaporable Moisture Content of Aggregate by Drying) was used as aggregate. The nominal maximum aggregate size of river sand was 2 mm. Type I 52.5N cement was used, following the ASTM C150 or ASTM C595 for conventional concrete, as proposed by ACI Committee 549. The two pozzolanic admixtures that were added in the mixtures were either Fly Ash (FA) or Ladle Furnace Slag (LFS). Fly ash, with 9-10% $CaO_{free}$ and 5-6% $SO_3$, is coming from a lignite combustion power plant while ladle furnace slag is originated from a steel industry. The retained material at the 45μm sieve (R45) was 38,5% for FA and 21,0% for LFS. Corrugated polypropylene fibres of 50mm length and 0,8mm diameter and super plasticizer of carboxylic origin (Glenium SKY 645) were also

added in the mixtures. The characteristics of the 14 mixtures that were prepared in the laboratory are presented in Table 1. In half of the mixtures, polypropylene fibres were used and the fibre volume content was 0,7, 0,8 or 0,9% by volume of the total mixture. Mixture C and fibrous mixture CF are the control mixtures in which no pozzolanic admixtures were added.

Table 1 Basic characteristics of ferrocement mixtures produced in the laboratory

| CONTROL FERROCEMENT MIXTURES C, CF AND MIXTURES WITH FA | | | | | | | | |
|---|---|---|---|---|---|---|---|---|
| | C | CF | CA1 | CAF1 | CA2 | CAF2 | CA3 | CAF3 |
| Binding materials, kg/m³ | 660 | 660 | 660 | 660 | 660 | 660 | 660 | 660 |
| LFS/ Cement ratio | - | - | - | - | - | - | - | - |
| FA/ Cement ratio | - | - | 0,10 | 0,10 | 0,15 | 0,15 | 0,20 | 0,20 |
| Water/Cement ratio | 0,35 | 0,35 | 0,36 | 0,36 | 0,37 | 0,37 | 0,38 | 0,38 |
| Fibre volume content, % | - | 0,8 | - | 0,7 | - | 0,8 | - | 0,9 |
| Plasticizer/cementitious, % | 2 | 2 | 2 | 2 | 2 | 2 | 2 | 2 |
| FERROCEMENT MIXTURES WITH LFS | | | | | | | | |
| | CS1 | CSF1 | CS2 | CSF2 | CS3 | CSF3 | | |
| Binding materials, kg/m³ | 660 | 660 | 660 | 660 | 660 | 660 | | |
| LFS/ Cement ratio | 0,10 | 0,10 | 0,15 | 0,15 | 0,20 | 0,20 | | |
| FA/ Cement ratio | - | - | - | - | - | - | | |
| Water/Cement ratio | 0,35 | 0,35 | 0,35 | 0,35 | 0,39 | 0,39 | | |
| Fibre volume content, % | - | 0,7 | - | 0,8 | - | 0,9 | | |
| Plasticizer/cementitious, % | 1,0 | 1,5 | 1,5 | 1,5 | 2,0 | 2,0 | | |

The two by-products, FA and LFS, replaced cement at 10, 15 or 20% of the cement mass in plain and fibrous ferrocement mixtures. The moisture of the aggregates was taken into account so the amount of water was modified properly. The proportions of all the mixtures are shown in Table 2.

Table 2 Mix proportions of ferrocement mixtures (kg/m³)

| CONTROL FERROCEMENT MIXTURES C, CF AND MIXTURES WITH FA | | | | | | | | |
|---|---|---|---|---|---|---|---|---|
| | C | CF | CA1 | CAF1 | CA2 | CAF2 | CA3 | CAF3 |
| Cement I 52,5N | 660 | 660 | 594 | 594 | 561 | 561 | 528 | 528 |
| Water | 245 | 245 | 261 | 261 | 281 | 281 | 301 | 301 |
| FA | - | - | 66 | 66 | 99 | 99 | 132 | 132 |
| River sand | 1360 | 1360 | 1360 | 1360 | 1360 | 1360 | 1360 | 1360 |
| Glenium SKY 645 | 13,60 | 13,60 | 14,52 | 14,52 | 15,18 | 15,18 | 15,84 | 15,84 |
| Polypropylene fibres | - | 7,20 | - | 6,30 | - | 7,20 | - | 8,10 |
| FERROCEMENT MIXTURES WITH LFS | | | | | | | | |
| | CS1 | CSF1 | CS2 | CSF2 | CS3 | CSF3 | | |
| Cement I 52,5N | 594 | 594 | 561 | 561 | 528 | 528 | | |
| Water | 254 | 254 | 266 | 266 | 309 | 309 | | |
| LFS | 66 | 66 | 99 | 99 | 132 | 132 | | |
| River sand | 1334 | 1334 | 1334 | 1334 | 1334 | 1334 | | |
| Glenium SKY 645 | 7,26 | 10,89 | 11,39 | 11,39 | 15,84 | 15,84 | | |
| Polypropylene fibres | - | 6,30 | - | 7,20 | - | 8,10 | | |

The apparent specific densities of fresh ferrocement mixtures are shown in Figure 1. The measurements for fluidity of the mixtures immediately and 1h after mixing are given in Table 3.

No compaction was applied during the casting since the fluidity of the mixtures was sufficient. The specimens cast for determining the properties of each ferrocement mixture were six cylinders 150x300 mm (for measuring the characteristic compressive strength and modulus of elasticity), two cylinders 102x200 mm (for measuring the chloride ion penetration), two beams 150x150x550 mm (for measuring the flexural strength) and two beams 100x100x400 mm to measure the early shrinkage deformation. All specimens were cured at 20° C and 95% RH for 28 days. Additionally, the flexural behavior of notched beams was tested by recording load-Crack Mouth Opening Displacement (CMOD) curves (Figure 2). From the analysis of these curves, the toughness levels were estimated by calculating the Fracture Energy $G_f$ according to JCI-S-001-2003 Standard [10].

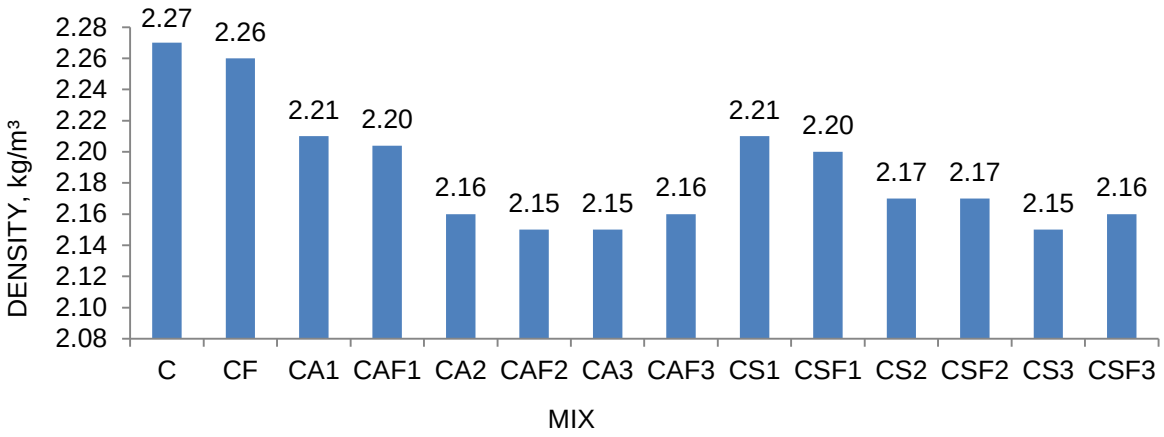


Figure 1 Density of fresh ferrocement

Table 3 Plasticity of fresh mortar according to ASTM C 1611-09 [9]

| CONTROL FERROCEMENT MIXTURES C, CF AND MIXTURES WITH FA | | | | | | | | |
|---|---|---|---|---|---|---|---|---|
| | C | CF | CA1 | CAF1 | CA2 | CAF2 | CA3 | CAF3 |
| Immediately after mixing | | | | | | | | |
| Time for 50cm Expansion, sec | 19 | 14 | 20 | 23 | 10 | - | - | - |
| Final expansion, cm | 52 | 52 | 51 | 54 | 50 | 43 | 44 | 41 |
| 1 hour after mixing | | | | | | | | |
| Time for 50cm Expansion, sec | 22 | - | - | 50 | - | - | - | - |
| Final expansion, cm | 50 | 48 | 46 | 50 | 49 | 33 | 37 | 36 |
| FERROCEMENT MIXTURES WITH LFS | | | | | | | | |
| | CS1 | CSF1 | CS2 | CSF2 | CS3 | CSF3 | | |
| Immediately after mixing | | | | | | | | |
| Time for 50cm Expansion, sec | 9 | 4 | 8 | 15 | 3 | 7 | | |
| Final expansion, cm | 55 | 74 | 58 | 53 | 65 | 60 | | |
| 1 hour after mixing | | | | | | | | |
| Time for 50cm Expansion, sec | 10 | 3 | 13 | 60 | 8 | 15 | | |
| Final expansion, cm | 50 | 72 | 54 | 50 | 55 | 51 | | |

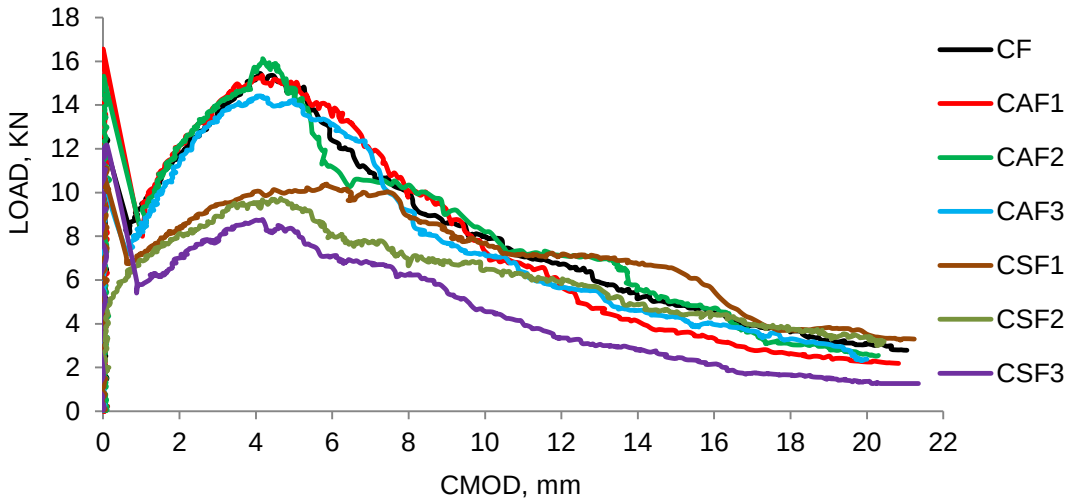


Figure 2 Load-CMOD curves of all the fibrous mixtures

## RESULTS AND DISCUISSION

The properties of hardened ferrocement matrices are shown in Table 4 and Figures 3 to 5. Regarding 28-d compressive strength, for mixtures with up to 0,2 FA/cement ratio the same or higher level of strength has been achieved in comparison to control mixtures C (without fibres) and CF (with fibres).

Mixture CAF1 presented the best results, reaching 50,33 MPa, with fibre volume content 0,7% and FA/cement ratio 0,10. Flexural strength (MPa) and Modulus of Elasticity (GPa) follow in general the mode of compressive strength. However, it could be said that as the content of fly ash increases, these mechanical characteristics are shifted to lower values in relation to control.

Fracture energy values of mixtures with fly ash are comparable to those of control mixtures. Considering early shrinkage deformation, they are significantly lower in mixtures with fly ash, even in those without fibres, as shown in Figure 5. It is obvious that fly ash additions improve the ferrocement matrix. However, the fluidity for FA/cement ratios higher than 0,15 is reduced although superplasticizer has been used. This is a negative phenomenon especially in the case of mixtures with fibres.

When LFS is used from LFS/cement ratio 0,10 to 0,20, the 28-d strength development is lower or of the same level compared to control mixtures. Fracture energy values follow the strength pattern and early shrinkage deformations are lower than those of control mixtures. Flexural strength and Modulus of Elasticity are not developed as compressive strength and are lower compared to control ferrocement. The best composition is CSF1 with LFS/cement ratio 0,1 and 0,7% fibre volume content. What is very advantageous is the reduction of time for initial fluidity (measured by expansion according to relative EFNARC regulative frame) and the higher final expansion (cm) 1 hour after mixing. For chloride ion penetration, the procedure of ASTM C1202-97 was followed.

The method consists of monitoring the amount of electrical current passed through concrete cylindrical slices (51mm thick and of 102mm diameter). Mixtures CA1, CA3 with FA/cement ratio 0.1 and 0.2 respectively and CS1, CS3 with LFS/cement ratio 0.1 and 0.2 respectively were compared with reference mixture C and results are shown in Figure 6. The addition of FA and LFS increases the resistance of chloride penetration in comparison to reference mixture [11],[12],[13]. Lower chloride ion penetrability is also observed when the FA or LFS/cement ratio increases and when FA is used instead of LFS.

Table 4 Properties of hardened matrix

| CONTROL FERROCEMENT MIXTURES C, CF AND MIXTURES WITH FA | | | | | | | | |
|---|---|---|---|---|---|---|---|---|
| Properties | C | CF | CA1 | CAF1 | CA2 | CAF2 | CA3 | CAF3 |
| Density, kg/m³ | 2185 | 2163 | 2174 | 2171 | 2140 | 2132 | 2122 | 2045 |
| Flexural strength, MPa | 4,23 | 4,51 | 4,31 | 4,45 | 3,65 | 3,77 | 3,08 | 3,71 |
| Modulus of elasticity, GPa | 24,6 | 24,3 | 24,5 | 23,3 | 22,0 | 20,0 | 19,1 | 20,5 |
| 28-d early shrinkage, μstrain | 1150 | 1100 | 875 | 850 | 788 | 843 | 775 | 745 |
| FERROCEMENT MIXTURES WITH LFS | | | | | | | | |
| Properties | CS1 | CSF1 | CS2 | CSF2 | CS3 | CSF3 | | |
| Density, kg/m³ | 2180 | 2150 | 2120 | 2150 | 2140 | 2150 | | |
| Flexural strength, MPa | 3,87 | 4,20 | 3,10 | 3,83 | 2,87 | 3,02 | | |
| Modulus of elasticity, GPa | 23,3 | 24,2 | 22,6 | 25,1 | 17,6 | 19,8 | | |
| 28-d early shrinkage, μstrain | 875 | 825 | 850 | 825 | 775 | 763 | | |

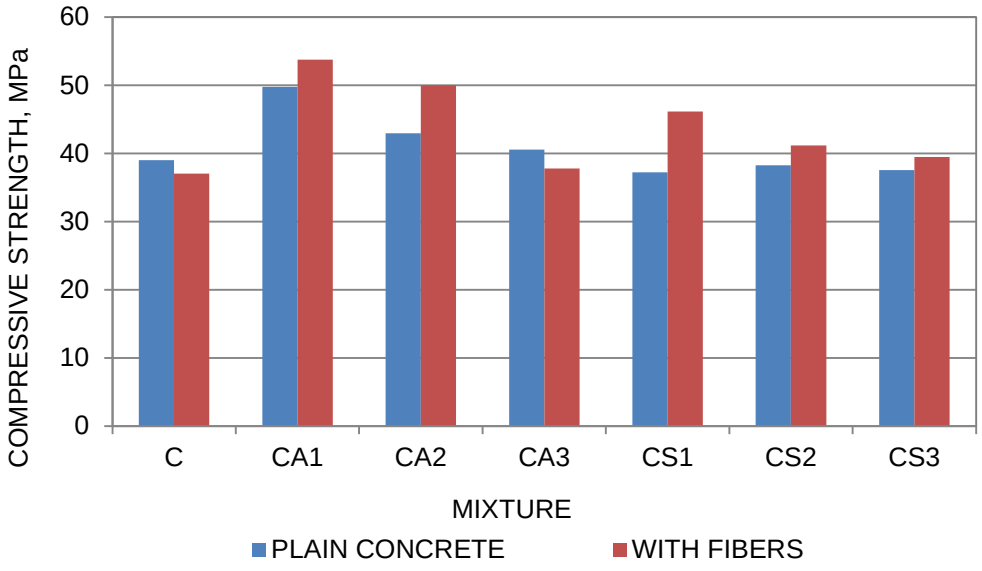


Figure 3 Compressive strength of the ferrocement mixtures

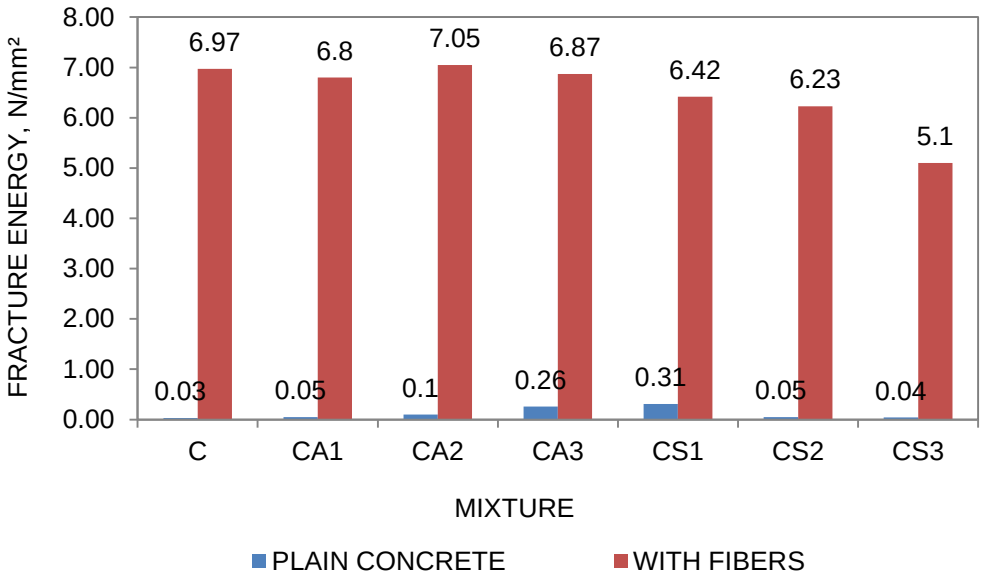


Figure 4 Fracture Energy of all the mixtures as obtained from the Load-CMOD curves

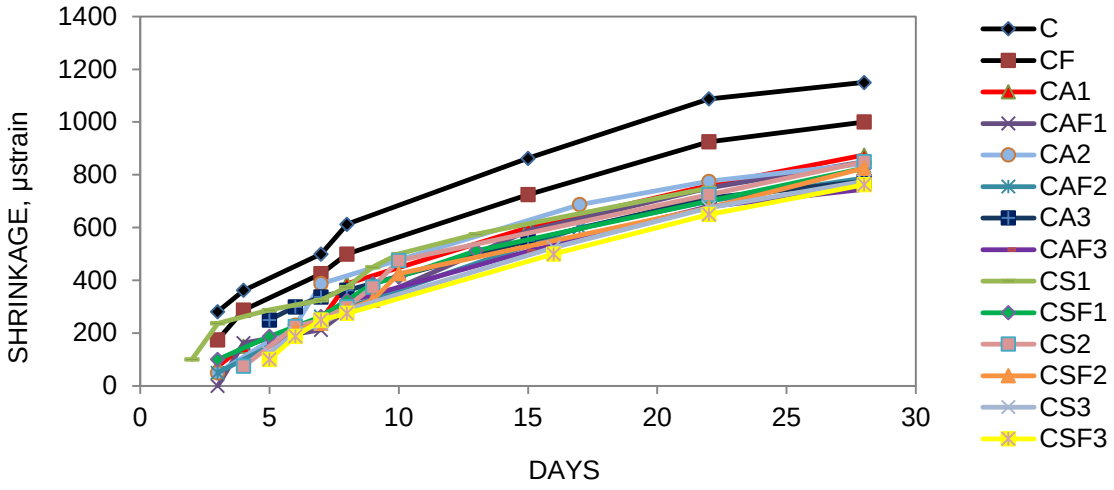


Figure 5 Early shrinkage deformation of all the mixtures

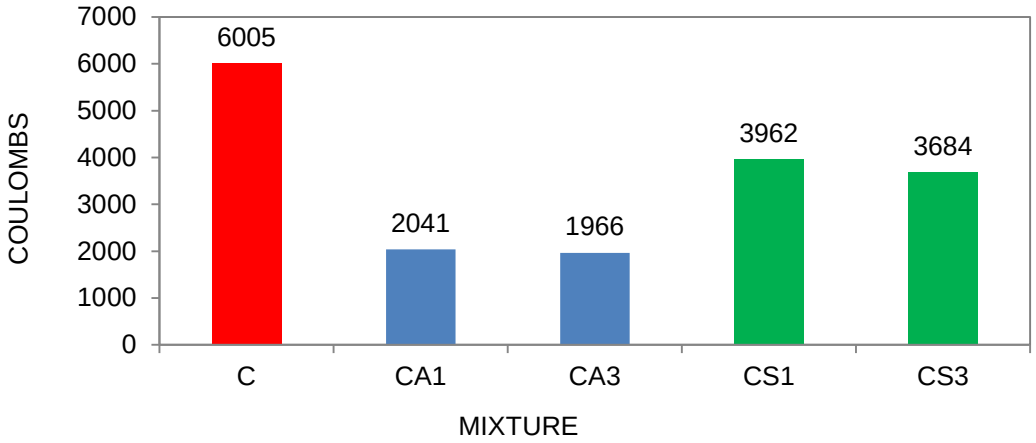


| CHARGE PASSED coulombs | CHLORIDE ION PENETRABILITY |
|---|---|
| >4000 | High |
| 2000-4000 | Moderate |
| 1000-2000 | Low |
| 100-1000 | Very Low |
| <100 | Negligible |

Figure 6 Chloride ion penetration

The pros and cons of FA and LFS addition to ferrocement mixtures seem to limit their addition towards low FA or LFS/cement ratios such as 0,10 and 0,15. Comparing the effectiveness of fibre volume content, it seems that the 0,7 and 0,8% presented the best results in both series of

mixtures with FA and LFS. Regarding durability of ferrocement and inparticular, resistance to chloride ingress and corrosion. The results of mixtures with LFS and FA showed improved performance compared to the control mixture.

## ACKNOWLEDGEMENTS

TITAN cement industry is acknowledged for the free supply of cement used in this work. Thanks are also expressed to students of Civil Engineering of AUTH participating in the experimental work under author's supervision.

## REFERENCES

1. ACI COMMITTEE 549 1R-93, *Guide for the Design, Construction and Repair of Ferrocement*, 1999.

2. VICKRIDGE, I G, NAKASSA, A S, TURNER, M. *High durability ferrocement*, Proceedings of 6th International Symposium on Ferrocement, University of Michigan, Ann Arbor, USA, 1998, pp 297-312.

3. SHANNAG, M J, *Bending behavior of ferrocement plates in sodium and magnesium sulfates solutions*, Cement & Concrete Composites 30, 2008, pp 597-602.

4. KILLOH, D G, PARROT, L J, PATEL, R G, *Influence of curing at different relative humidities on the hydration and porosity of a Portland/fly ash cement paste*, Proceedings of Third International Conference on Fly Ash, Silica Fume, Slag and Natural Pozzolans in Concrete, Trondheim, ACI Spec. Publ. (114), 1989, pp 157-174.

5. MASOOD, A, ARIF, M, AKHTAR, M, HAQUIE, M. *Performance of ferrocement panels in different environments*, Cement and Concrete Research 33, 2003, pp 555-562.

6. VICKRIDGE, I G, RANJBER, M M. *The effect of an aggressive environment on the flexural performance of ferrocement*, Proceedings of 6th International Symposium on Ferrocement, University of Michigan, Ann Arbor, USA, 1998, pp 313-328.

7. PAPAYIANNI, I, ANASTASIOU, E. *Development of self compacting concrete (SCC) by using high volume of calcareous fly ash*, Proc. Of World of Coal Ash WOCA 2011, Denver, Colorado, May 9-12 2011, CD proceedings.

8. PAPAYIANNI, I, ANASTASIOU, E, PAPACHRISTOFOROU, M. *Effect of polypropylene fibres on the performance of SCC incorporating calcareous fly ash*, CD proceedings of Conf. Concrete in the Low Carbon Area, Dundee, 9-1 July 2012, pp 866-877.

9. ASTM C1611 / C1611M-09, *Standard Test Method for Slump Flow of Self-Consolidating Concrete.*

10. JCI-S-001-2003, Method *of test for fracture energy of concrete by use of notched beam*, Japan Concrete Institute Standard, 2003.

11. TORI, K, KAWAMURA, M. *Chloride induced corrosion of steel reinforcement made with various mineral admixtures*, Trans Jpn Concrete Ins, 1990, pp 183-90.

12. PAPADAKIS, V, TSIMAS, S. *Effect of supplementary cementing materials on concrete resistance against carbonation and chloride ingress*, Cement and Concrete Research, Vol 30, 2000, pp 291-299.

13. PAPADAKIS, V, TSIMAS, S. *Supplementary cementing materials in concrete. Part 1; efficiency and design*, Cement and Concrete Research, Vol 32, 2002, pp 1525-1532.

# STUDY OF DURABILITY OF MORTAR REINFORCED BY FIBRES IN AGGRESSIVE ENVIRONMENTS

**A H M Belhadj**
Univ Ctr of Ain Temouchent
**A Mahi**
University of Sciences and Technology of Oran
**R Derbal B Ammraoui**
Univ Ctr of Ain Temouchent
Algeria

**ABSTRACT.** The high compressive strength, good fire resistance, thermal and sound insulation, flexibility employment and the abundance of raw materials make concrete the most used material in all areas of construction. Despite these advantages, the concrete is a material which is characterized by a low resistance to traction, a poor resistance to the shock and cracking; harmful properties that affect the durability and safety of structures. In an attempt to remedy these harmful aspects, several methods have been used such as reinforced concrete, prestressed concrete … etc. Today, the fibre reinforced concrete is a very ingenious process. The objective of this study is to define the behaviour of fibre-reinforced mortar in aggressive environment. The work involves the preparation of several series of specimens using three types of fibres: polypropylene, polyethylene and metallic, with a ratio W/C = 0.49. The mortar samples have dimensions as 4x4x16mm is immersed in two strong acids: hydrochloric acid (HCl) and sulfuric acid ($H_2SO_4$). Other samples have undergone treatment in a weak acid: acetic acid ($CH_3COOH$). Other series of samples were kept in a basic solution (NaOH). Tests of mass loss, the compressive strength to 7, 14 and 28 days are made. The results showed that the fibre-reinforced mortar, preserved in acidic environment, have a resistance drop to compression relative to the mortar without fibres. a clear improvement of the compressive strength is observed for the same samples even in the presence of aggressive agents.

**Keywords:** Mortars, Durability, Polypropylene fibres, Metallic fibres, Polyethylene fibres.

**Mrs MOHAMMED BELHADJ Ahlem Houaria** is Assistant professor and member of Smart Structures Laboratory (Univ Ctr of Ain Temouchent, Algeria), working on the durability of concrete, and the promotion of local materials (products) in the concrete. **Pr MAHI Abdelkader** is professor and member of the soils laboratory materials and thermal(LMST, university of science and technology Oran ,Algeria) and Chairman of the Scientific Council of the department. **Mr DERBAL Rachid** is Assistant professor and member of Smart Structures Laboratory (Univ Ctr of Ain Temouchent, Algeria), working on the earthquake engineering and construction materials **Mr AMMRAOUI Benamar** is PHD student and member of Smart Structures Laboratory (Univ Ctr of Ain Temouchent, Algeria), working in the field of geotechnical engineering.

## INTRODUCTION

In recent years, the construction industry has shown significant interest in the use of fibre-reinforced concrete due to the advantages it offers over traditional plain concrete. The use of fibres as reinforcement in plain concrete not only enhances the tensile strength of the composite system but also reduces cracking under serviceability conditions. Further, steel-fibres improve resistance to material deterioration as a result of fatigue, impact, shrinkage and thermal stresses [1] [2].

The concept of using fibres or as reinforcement is not new. Fibres have been used as reinforcement since ancient times. Historically, horsehair was used in mortar and straw in mud bricks. In the 1900s, asbestos fibres were used in concrete. In the 1950s, the concept of composite materials came into being and fibre-reinforced concrete was one of the topics of interest [3] [4]. Once the health risks associated with asbestos were discovered, there was a need to find a replacement for the substance in concrete and other building materials. By the 1960s, steel, glass (GFRC), and synthetic fibres such as polypropylene fibres were used in concrete. Research into new fibre-reinforced concretes continues today [5] [6].

Nataraja [7] investigated the splitting tensile strength of steel fibre reinforced concrete (SFRC) using a typical 100 mm cube specimen. The results of flexural, compression and splitting tensile tests indicated that the splitting tensile strength of SFRC was 0.67 times the flexural strength, and 0.09 times the compressive strength. Fibre-reinforced concrete can be used to improve the performance of concrete structural members such as deep beams, columns and floors on grade in terms of crack-reduction, toughness and ductility [8]. Similarly, Lee [8] [9] discovered that a larger volume of longer fibres would give better mechanical performance to concrete if it is uniformly distributed. However, there could be an increased problem of workability and uniform distribution with increasing volume and length of fibres [10] [11].

Concrete is a widely used material in all areas; under certain conditions, it may be faced with aggressive media, these aggressive environments can change certain physical and chemical factors and cause a significant danger to the concrete [12] [13].

Acidic environments likely to be aggressive for concrete start at pure waters extend to fresh water, little or much loaded with carbon dioxide and acid rain, and ended with inorganic and organic acids, including y wastewater [4] [6]. Effluent kilns using rich fuels suffer and effluents from chemical may contain sulfuric acid. The decomposition of organic matter in sewage, silos or in storage tanks can lead to the formation of $H_2S$ gas that can be converted into sulfuric acid by the bacterial activity. This type of acid is very vulnerable for concrete [4] [6].

In this paper we presented the results of our study on the contribution of fibre on the durability of mortars in various aggressive environments at a young age of mortar specimens, going strong acids such sulfuric and hydrochloric acid and low acid acetic acid and passing through a basic medium, sodium hydroxide.

The tests were performed on dimensions of mortar 4×4×16 cm specimens and we varied the types of fibres metal fibres, polypropylene and polyethylene in to see the mechanical behavior and durability of fibre reinforced mortar in various aggressive environments.

After 7, 14 and 28 days of conservation in the different environments, the mechanical characteristics of the samples were determined by the 3-point bending on specimens 4×4×16 $cm^3$, and by the compression on cubes of 4×4×4 $cm^3$ mortars fibre reinforced. The durability characteristics were determined by mass loss measurements mortars.

## EXPERIMENTAL PROGRAM

### Mortar composition and specimens preparation

The choice of local Algerian materials was based on their abundant availability and their moderate cost.

### Cement

The study was conducted on ordinary concrete, using local materials. It was made with Portland Composite Cement (CEM II/A 42.5) from the factory of Beni-Saf (west of Algeria), according to the Algerian standard NA 442. This cement is well suited to the most common uses of building in west region of Algeria. The chemical and mineralogical compositions of this cement are presented in Table 1 (LI: Loss in ignition) and 2 and its physical characteristics are summarized in Table 3. The analysis of the chemical and mineralogical compositions of Bogue was performed in the cement laboratory, while the studies of the physico-mechanical characteristics were performed in SSL laboratory (Univ Ctr of Ain Temouchent, Algeria).

Table 1 Chemical compositions of cement

| $SiO_2$ | CaO | $Al_2O_3$ | $Fe_2O_3$ | MgO | $SO_3$ | LI | insolubles | Total |
|---|---|---|---|---|---|---|---|---|
| 23.65 | 56.80 | 5.52 | 3.22 | 1.03 | 2.45 | 2.42 | 4.6 | 99.69 |

Table 2 Mineralogical (Bogue) compositions of cement

| BOGUE COMPOSITION (%) | | | | |
|---|---|---|---|---|
| $C_3S$ | $C_2S$ | $C_3A$ | $C_4AF$ | Free CaO |
| 51.74 | 24.50 | 8.78 | 10.51 | 0.91 |

Table 3 Physical composition of cement

| CEMENT POWDER | | | CEMENT PASTE | | |
|---|---|---|---|---|---|
| Apparent Gravity $g/cm^3$ | Mass absolute Gravity $g/cm^3$ | Surface BLAINE $Cm^2/g$ | Refusal sieves0.063 mm (%) | initial setting | End of setting |
| 1.14 | 3.17 | 38.40 | 80.90 | 2h15 min | 3h30- 4h30 |

### Sand

The aggregates (sand of sea) used were from TERGA quarry that belongs to the National Company of Aggregates (ENG) in Terga (Province of Ain Temouchent). This choice was determined by the fact that it is the main quarry that supplies the entire region.
The results of physical properties, made according to the Algerian standard NA 451 are worn on the table 4.

Table 4 Physical properties of sand

| | |
|---|---|
| Apparent density | 1.46 g/cm$^3$ |
| Absolute density | 2.70 g/cm$^3$ |
| Equivalent sand (ES) | 97 % |
| Water content | 0.009 % |

### The mixing water

Mixing water is the total water added to the dry mortar mixture, it is necessary for hydration of the binder, the wetting of the aggregates and facilitates implementation.

### Adjuvant

The adjuvant used is named "SIKA VISCOCRETE TEMPO 12" is a super high adjuvant versatile plasticizer water reducing new generation uncolored based acrylic copolymer.

### Fibres

The fibres used to prepare various samples of bundles mortars are three types: polypropylene fibres, metal fibres and polyethylene fibres. Their properties are summarized in Table 5.

Table 5 Fibres properties

| FIBRE TYPE | POLYPROPYLENE | METALLIC | POLYETHYLENE |
|---|---|---|---|
| Length (mm) | 6 | 30 | 50 |
| Diameter (mm) | 0.05 | 0,5 | 0.3 |
| Density (g/cm$^3$) | 0.900 | 7.85 | 0.935 |
| Tensile strength (MPa) | 600 | 1700 | 350 |
| Modulus of elasticity (GPa) | 5-10 | 150-200 | 5 |
| Elongation at break (%) | 10-20 | 3-4 | 3-80 |


Picture 1 Type of fibres

**Mortar mix**

The mortars were prepared using different type of fibres. The mix proportions of mortar tested in this study are given in table 6 (M0: without fibres ; MF1: with polyethylene fibres ; MF2: with Metallic fibres ; MF3: with Polypropylene fibres).

Table 6 Mix proportion of the mortar mixtures per cubic meter

| MORTAR | M0 | MF1 | MF2 | MF3 |
|---|---|---|---|---|
| Cement (kg) | 450 | 450 | 450 | 450 |
| Sand (kg) | 1350 | 1350 | 1350 | 1350 |
| Water (L) | 220 | 220 | 220 | 220 |
| Adjuvant (kg) | 5.4 | 5.4 | 5.4 | 5.4 |
| Fibres (%) | 0 | 0.11 | 0.51 | 0.67 |
| W/C | 0.49 | 0.49 | 0.49 | 0.49 |

**Curing specimens**

The form stripping is done after 24 hours of molding. Then the conservation of specimens in various harsh environments while maintaining control samples with each series of mortar is realized. To ensure the preservation of samples in a constant PH, measurements are made every 7 days using the PH meter, there by changing solutions is mandatory following a significant difference.

Table 7 Chemical solution

| SOLUTION | CONCENTRATION (%) | AMOUNT/10 LITRES OF WATER | OBSERVATION |
|---|---|---|---|
| HCl | 5 | 1300ml/10 L | strong acid |
| $H_2SO_4$ | 5 | 520ml/10 L | strong acid |
| $CH_3COOH$ | 5 | 500ml/10 L | weak acid |
| NaOH | 10 | 13g/10 L | Basic |

## RESULTS AND DISCUSSION

### Loss of mass

We followed a comparative setting durability of our samples: losses masses. Measuring mass loss was made on three samples identified for this purpose, previously wiped and cleaned three times with distilled water to remove surface solution and mortar altered. We used the following equation (1) to calculate mass loss:

$$ML = \left(\frac{Mt-Mi}{Mi}\right) \times 100 \quad (1)$$

Where *Mt* is the mass (g) at time t and *Mi* is the mass initial (g)

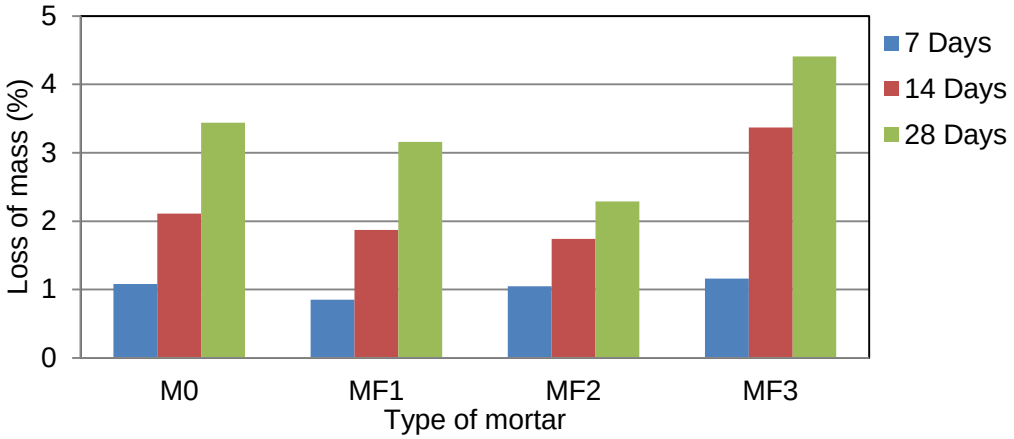


Figure 1 Mass loss of reference specimens.

In this figure 1, we can see that the mass loss of 2% to 4% mortars references stored in the open air is a result of evaporation of the interstitial water.

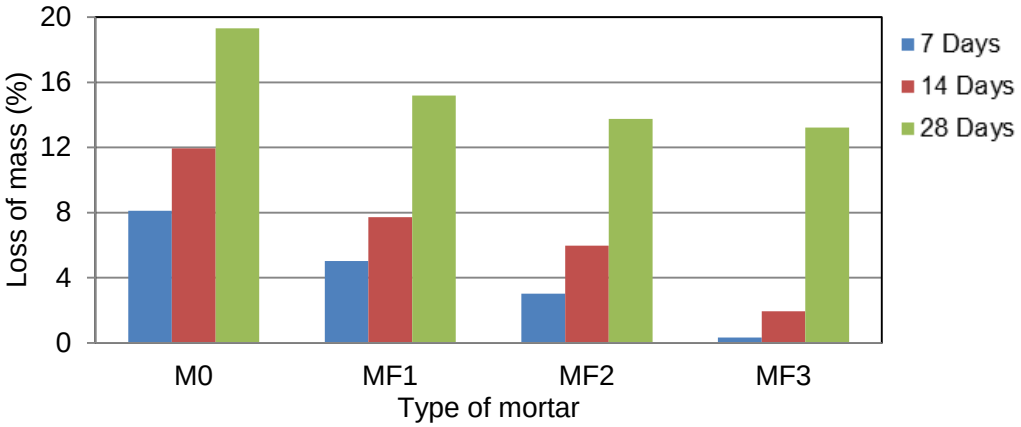


Figure 2 Mass loss of samples stored in Hcl

From Figure 2 we observe that there are significant mass losses caused by hydrochloric acid (Hcl), from 13% to 19.33% after 28 days of immersion. The incorporation of fibres in the mortar to give a 6% improvement compared to the reference mortar.

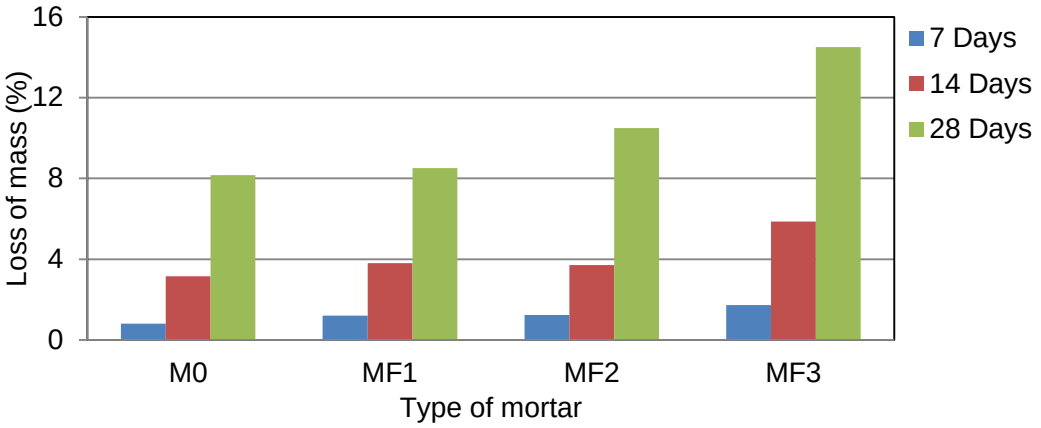


Figure 3 Mass loss of samples stored in $H_2SO_4$

The results of Figure 3 show a significant loss of mass is caused by the sulfuric acid $H_2SO_4$, which ranges from 8% to 15%. Sulfuric acid reacts with components in a cement matrix, mainly with hydrates of calcium aluminate, to form voluminous reaction products. Which causes the gypsum and ettringite formation according to the following reactions:

$$H_2SO_4 + Ca(OH)_2 \rightarrow CaSO_4.2H_2O \qquad \text{gypsum} \qquad (2)$$

$$3CaSO_4 + 3CaO.Al_2O_3.6H_2O + 25H_2O \rightarrow 3CaO.Al_2O_3.3CaSO_4.31H_2O \quad \text{Ettringite} \qquad (3)$$

The gypsum is formed due to the reaction between the acid and portlandite sulfuric (eq 2). The deposited gypsum is then leached, which explains the white color of the solution from the second week. The degradation of cementitious materials in these environmental conditions is characterized by the complete passage in solution of the portlandite and by the progressive decalcification of HSCs, and in other proportions of ettringite and monosulfoaluminate(eq3) [14]. Mortar MF1 had less loss of mass than others mortars with fibres. No improvement seen following the addition of the fibres.

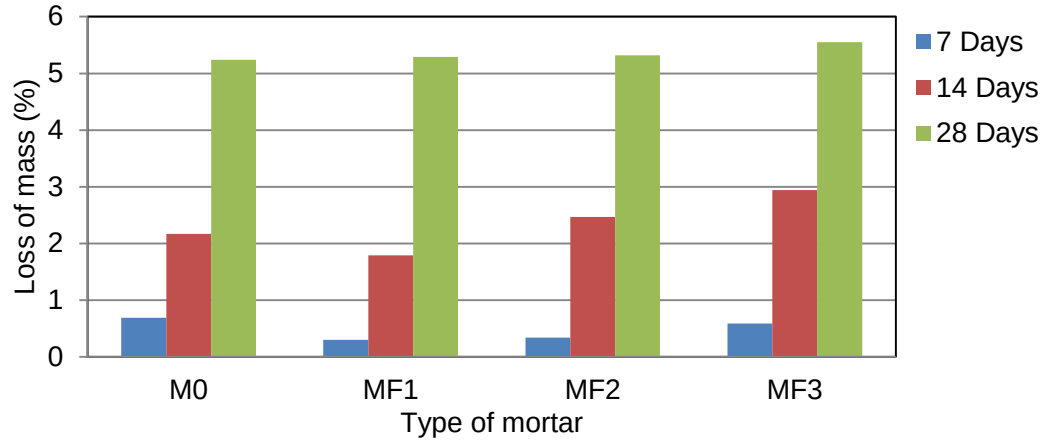


Figure 4 Mass loss of samples stored in $CH_3COOH$.

The results of the weight loss of the specimens preserved in $CH_3COOH$ which are of the order of 5% to 28 days for the different types of mortar (see figure 4), signifies that acetic acid is less aggressive compared to Hcl and $H_2SO_4$ .

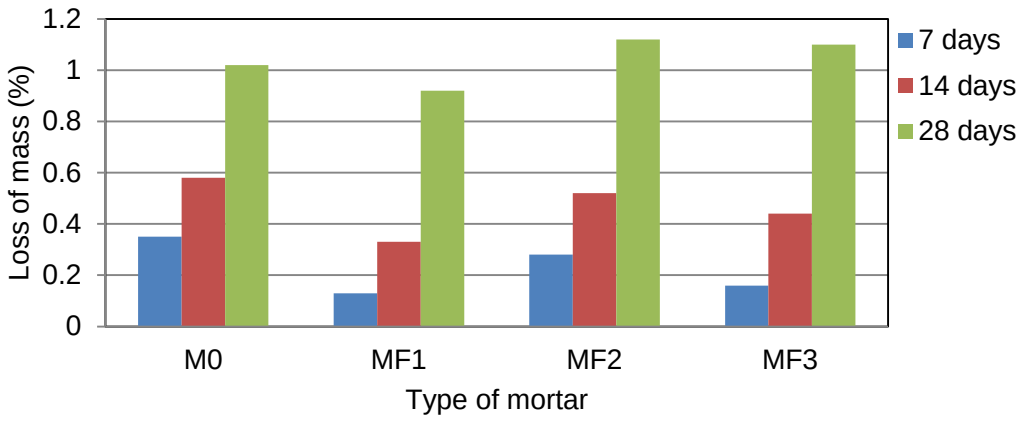


Figure 5 Mass loss of samples stored in NaOH.

The results of the immersion of the four types of mortars in the sodium hydroxide NaOH 10% concentration show that the basic solutions present no risk of aggression on mortars and concretes. The mass losses were slightly exceeded 1% (figure 5).

**The compressive strength**

The mortar specimens are subjected to simple compression .The results of tests on ordinary mortar and fibres reinforced mortar specimens are given in following figures.

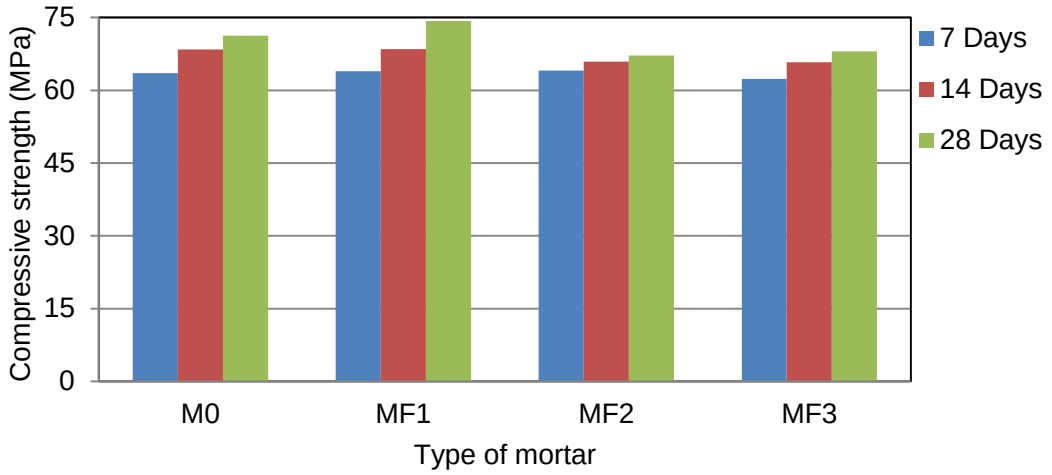


Figure 6 Evolution of the compressive strength for specimens references.

We note that the compressive strengths of the specimens evolve over time, for all studied mortars. As can be seen in Figure 6, but for MF2 we observed a small evolution.

Based on results we observe clearly in Figure 7 a drop in compressive strength of 22% between the resistor 7 days and for 28 days. A decrease in resistance of 18% compared to the reference mortar is observed

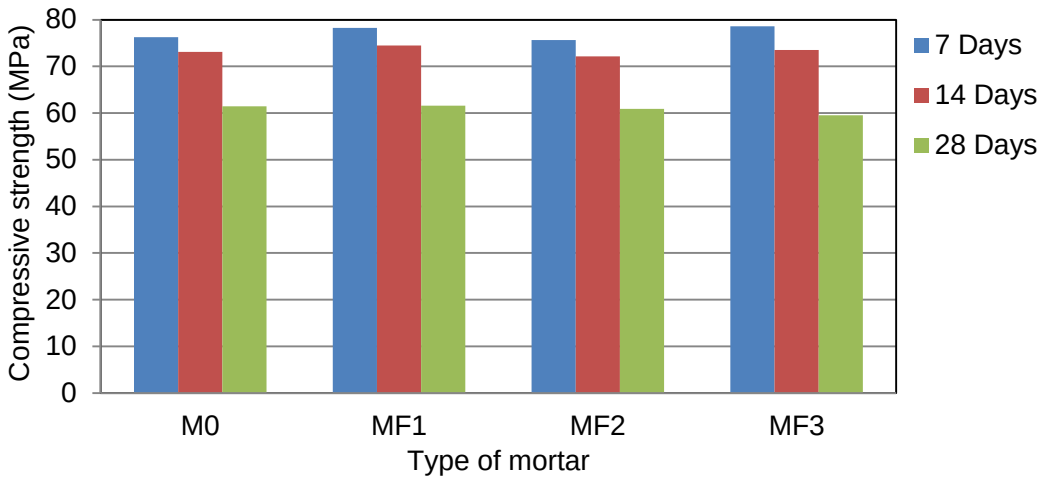


Figure 7 Compressive strength of the specimens preserved in Hcl

In Figure 8 we can see that under the effect of $H_2SO_4$, the compressive strength has not advanced in the time for the mortar reinforced polypropylene fibre (MF1) with a decrease of 6% between the resistor 7 and 28 days for another type of mortar. It is of import to note that the mortars reinforced by MF2 and MF3 fibres have given higher results from normal mortar (12% increases).

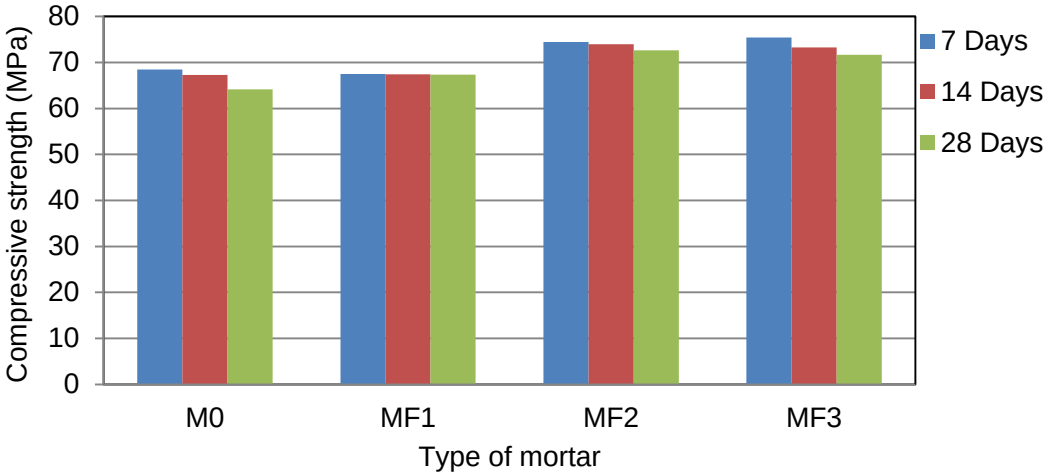


Figure 8 Compressive strength of the samples stored in $H_2SO_4$

From the results shown in Figure 9, we see that the resistance of specimens preserved in CH3COOH increased 3% to 6%, this observation is valid for the four types of mortars. for the compression tests on samples stored in NaOH (basic medium) we can note a compressive strength of evolution according to age MF1 by mortar against the other types of mortars we do not find this behaviour is not a change in resistance between 7, 14 and 28 days (see in the Figure 10).

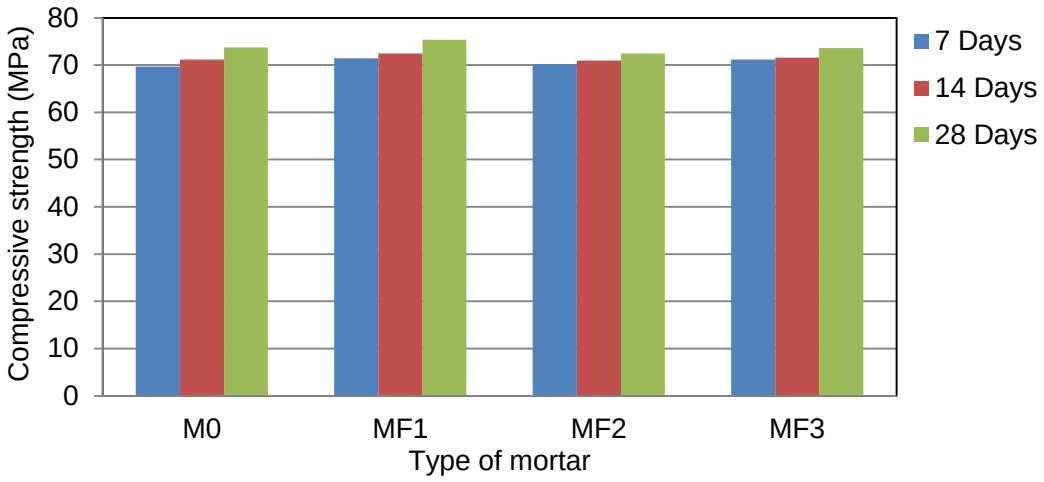


Figure 9 Compressive strength of the samples stored in $CH_3COOH$

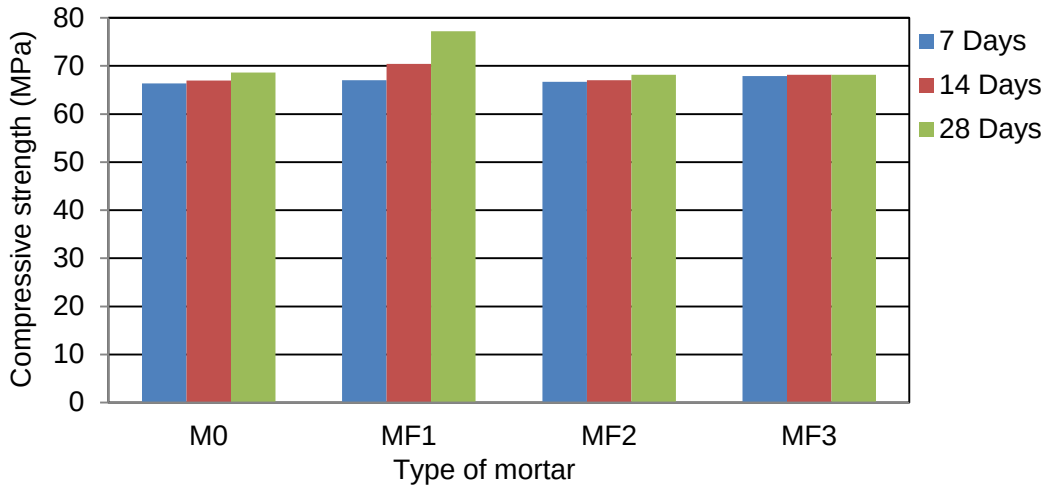


Figure 10 Compressive strength of the samples stored in NaOH

## CONCLUSION

In this work we try to make a comparison between the different types of fibres used in the mortar and see their behaviour in aggressive environments knowing that worked with mortar at a young age, because in reality once demoulded concrete faces directly to the various aggressive agents, of course we accelerated the phenomenon we use a 5% concentration of different acids and 10% of the basic medium.

Experimental work allowed us to draw the following conclusions that mortars exposed to sulfuric acid H2SO4 have a big loss of mass compared to normal mortar (M0) this is due to the gypsum formations and ettringite. Two highly soluble elements. This explains the loss of mass. Mortars with fibres have good behaviour towards the acid hydrochloric HCl compared to no fibres mortar.

We also observed that mortar $MF_1$ have the best resistance to compression relative to other mortars we can say that the addition of polyethylene fibres is beneficial to compressive strength. Both media acids Hcl and $H_2SO_4$ are more aggressive with respect to other media by respective weight losses (% de13% A19) and (8% to 15%) and compressive strength.

We see a different behaviour for mortars kept in the NaOH especially for the $MF_3$ mortar based fibre polypropylene, an analysis of the mortar microstructure is recommending a fine understanding of this behaviour.

## REFERENCES


1. LIE, T T and KODUR, V K R. Mechanical properties of fibre-reinforced concrete at elevated temperatures, Internal Report No. 687, February 1995, Institute - Bev Creighton Analyse.

2. KALIFA, P, CHENE, G, GALLE, C H, High-temperature behavior of HPC with polypropylene fibres from spalling to microstructure, Cement and Concrete Research, Vol. 31, 2001, pp. 1487–1499.

3. BHARGAVA, A, BANTHIA N, Permeability of concrete with fiber reinforcement and service life predictions, Materials and Structures, Vol. 41, 2008, pp. 363–372.

4. FEDAOUI-AKMOUSSI, O, MOLEZ, L, KACI, S, JAUBERTHIE, R, Etude du comportement mécanique et de durabilité des bétons fibrés dans un milieu agressif, Rencontres Universitaires de Génie Civil, Mai 2015, Bayonne, France.

5. DUPONT, D, VANDEWALLE, L, Distribution of steel fibres in rectangular sections, Cement and Concrete Composites, Vol. 27, 2005, pp. 391-398.

6. TULLIANI J M, MONTANARO L, NEGRO A, COLLEPARDI, M, Sulfate attack of concrete building foundations induced by sewage waters, Cement and Concrete Research, Vol. 32, No. 6, 2002, pp. 843-849.

7. NATARAJA, M C, DHANG, N, GUPTA, A P, Splitting tensile strength of SFRC, Indian Concrete Journal, Vol. 75, 2001, pp. 287-290.

8. AWOYERA, P O, IJALANA, J K, BABALOLA, O E, Influence of Steel and Bamboo Fibres on Mechanical Properties of High Strength, Concrete Journal Materials and Environmental Sciences, Vol. 6, No. 12, 2015, pp. 3634-3642, ISSN : 2028-2508.

9. LEE, S, Handbook Composites Reinforcements, Wiley-VCH, 1993.

10. KHERBACHE, S, BOUZIDI, N, BOUZIDI, M A, MOUSSACEB, K, TAHAKOURT, A K, The behavior of the concretes and mortars reinforced by metallic fibres wastes as substitution of cement, Journal of Materials, Environment and Sciences, Vol. 7 No. 1, 2016, pp. 18-29, ISSN : 2028-2508.

11. PARK, S H, RYU, G S, KOH, K T, KIM D J, Effect of shrinkage reducing agent on pullout resistance of high-strength steel fibres embedded in ultra-high-performance concrete, Cement and Concrete Composites, Vol. 49, 2014, pp. 59-69.

12. DUBOSE A, ESCADEILLAS G, BLANC P J, Characterization of biological stains on external concrete wallsand influence of concrete as underlying material, Cement and Concrete Research, Vol. 31 No. 11, 2001, pp. 1613-1617.

13. GARCÍA-SANTO, A, RINCÓN, J M, ROMERO, M, TALERO, R, Characterization of a polypropylene fibreed cement composite using ESEM, FESEM and mechanical testing, Construction and Building Materials, Vol. 19, No. 5, 2005, pp. 396-403.

14. PERLOT C, VERDIER J, CARCASSÈS M, Influence of cement type on transport properties and chemical degradation: Application to nuclear waste storage, Materials and structures, Vol. 39, No. 5, 2006, pp. 511-523.

# ENHANCING DURABILITY OF PLAIN CEMENT CONCRETE BY INCORPORATING GGBS

**U V Dave**

**B R Sojitra**

Nirma University

India

**ABSTRACT.** With increased industrialization, the quality of air, water and soil deteriorates. The demand for durable structural concrete to resist aggressive environments is increasing. The state of Gujarat in India has over 1000 km coastline, with the surrounding areas suffering from salinity and other issues in soil, as well as sulphates and chlorides in water. Cement companies have started to explore the use of GGBS to overcome these problems in Gujarat recently, replacing clinker up to 40-50%. Hence, an attempt has been made to explore the potential of using GGBS in concrete up to 60% of OPC to protect concrete during various durability tests of M25 grade concrete, as evaluated in the present study. Three mixes were prepared with 0%, 40% and 60% GGBS. Compressive strength of such concrete was determined after curing for 28 days. The resistance to acid, sulphate and chloride was measured after exposures up to 90 days. Acid exposure test results showed greater weight and compressive strength loss for control concrete than those of slag concrete. The sulphate and chloride exposure test results showed that the slag concrete mixes matched the weight change as well as the compressive strength recorded for control concrete. It has been observed from the accelerated corrosion test that with increased slag content, the rate of corrosion decreased for the concrete mixes. Slag concrete performed excellent as compared to that of control concrete for the RCPT. Overall, it can be stated that an increase in GGBS dosage results in better performance of concrete with respect to various durability properties attempted in the present investigation.

**Keywords:** OPC, GGBS, Chemical attack, Accelerated corrosion, Rapid chloride penetration test.

**Dr Urmil Dave,** BE (Civil), ME (Structures), PhD (Civil), is a Professor at Nirma University, Ahmedabad. He has 19 years of teaching experience. His research areas are concreting materials and techniques, non-destructive testing of structures & repair and rehabilitation of structures. He has published a number of papers at national and international conferences and journals. He has been invited for giving expert talks in various programmes by industries and academic institutions. He has organized different short term training programmes, seminars and conferences. He has been actively involved in consultancy and testing work related to concreting materials and Repair & Rehabilitation of Structures.

**Bhautik R. Sojitra** is a Post Graduate Student in Computer Aided Structural Analysis and Design at the Nirma University of Ahmedabad, India.

## INTRODUCTION

Considering the environmental aspects for Gujarat's coastal region, slag concrete has the potential for making structures more durable. From several research it is found that the addition of GGBS in concrete helps enhancing its durability properties. Gujarat is one of the major producers of steel manufacturing units which have potential for the production of GGBS indirectly. The state of Gujarat has witnessed establishment of cement plants producing Portland slag cement using 40% of replacement of OPC with slag. This strategy is considered to be useful to reduce costs, conserve energy, and reduce waste volumes. Elahia et al. [1] observed that the addition of GGBS up to 50% and collaborative use of other supplementary cementitious materials like fly ash and silica fume performed well in enhancing the durability of concrete. O'Connell et al. [2] investigated 50% and 70% dosage of GGBS and concluded that the resistance of Portland cement binders against sulphate attack and acid attack enhanced greatly. Gadpalliwar et al. [3] investigated durability properties through acid tests with 1% sulphuric acid and 3% hydrochloric acid, revealing that 22.5% GGBS + 7.5% RHA replaced for cement and 60% quarry sand replaced for natural sand in concrete made it more durable than the control mix. Pavia and Condren [4] explored the effect of 30% and 50% replacement of GGBS in concrete on sulphate attack in $MgSO_4$ solution. It was observed that increasing the percentage of GGBS in the mix enhanced performance of concrete on exposure to sulphate. Topçu and Boğa [5] carried out an impressed current technique on concrete containing 0%, 25%, 50% GGBS and observed that the 25% mix performed best among all mixes. Aldea et al. [6] observed the effect of cement replacement by GGBS at 0%, 25%, 50%, 75% by a rapid chloride penetration test (RCPT). It was observed that chloride permeability and penetrability significantly decreased with an increase in slag replacement.

## NEED OF STUDY

Cement manufacturers in India are currently exploring the use of slag up to 40% as clinker replacement. It is envisaged that further increase in replacement of clinker would facilitate concrete to be more durable. Present investigation is aimed at ascertaining the performance of concrete mixes containing GGBS as replacement for OPC at 40% and 60% dosage. It is attempted to compare the performance of slag concrete mixes with that of a plain concrete mix of M25 grade by various durability tests.

## EXPERIMENTAL PROGRAMME

### Materials

Physical and chemical properties of cement and GGBS are presented in Tables 1 and 2.

Table 1 Physical and chemical properties of Portland cement

| PARAMETERS | PORTLAND CEMENT | REQUIREMENT IS 12269 [7] |
|---|---|---|
| Loss on ignition | 1.87 | 4.0 max. |
| Specific gravity | 3.18 | - |
| Fineness ($m^2/kg$) | 300 | 225 min. |
| Magnesia (%) | 3.6 | 6.0 max. |
| Chloride content (%) | 0.05 | 0.1 max. |
| Lime saturation factor (%) | 0.92 | 0.8 to 1.02 |
| Alumna iron ratio (%) | 1.25 | 0.66 min. |

Table 2 Physical and chemical properties of GGBS

| CHARACTERISTIC | TEST RESULTS | REQUIREMENT IS 12089 [8] |
|---|---|---|
| Colour | white | - |
| Specific surface area ($m^2$/ kg) | 379 | 275 min. |
| Loss of ignition (%) | 0.6 | 3 max. |
| $SiO_2$ | 36.8 | - |
| $Al_2O_3$ | 17.12 | - |
| CaO | 34.4 | - |
| $Fe_2O_3$ | 0.92 | - |
| Glass content | 92.5 | 85 min. |
| Specific gravity | 2.91 | - |
| Pozzolanic Activity Index (%) [9] | 90.9 | 80 min. |

Physical properties of coarse and fine aggregate were evaluated as per IS 383-1970 [10] and are presented in Table 3. The sand used was of zone II category throughout the investigation.

Table 3 Physical properties of coarse and fine aggregates

| PARAMETERS | FINE AGGREGATE | COARSE AGGREGATE | |
|---|---|---|---|
| | | 10 mm downside | 20 mm downside |
| Compacted bulk density, kg/$m^3$ | 1670.49 | 1508.51 | 1600.93 |
| Loose bulk density, kg/$m^3$ | 1531.37 | 1347.52 | 1541.30 |
| Specific gravity | 2.57 | 2.73 | 2.73 |
| Fineness modulus, % | 2.79 | 6.03 | 7.29 |

## Concrete Mix Design

Mix design for M25 grade concrete was carried out as per the provision of IS 10262 [11]. The stipulations for such mix were considered as OPC of 53 grade, maximum size of coarse aggregate 20 mm, minimum & maximum cement content 320 kg/$m^3$ & 450 kg/$m^3$, respectively, maximum water/cement ratio 0.50, slump for ordinary concrete 100 mm & good degree of supervision. The details of mix design for 1 cubic meter of concrete produced are presented in Table 4. Dosage of superplasticizer of 0.7% by weight of cement was finalized based on Marsh cone test. The polycarboxylate ether based superplasticizer was utilized for concrete mixes to achieve a desired strength and workability. Notations used throughout this paper for various concrete mixes include M25-1 representing concrete with 0% GGBS, as well as M25-2 and M25-3 representing 40% and 60% replacement of OPC by GGBS, respectively.

Table 4 Mix proportions for 1 cubic meter of concrete

| CONSTITUENTS | | | | | |
|---|---|---|---|---|---|
| Cement (kg) | Fine aggregate (kg) | Coarse aggregate (kg) | | Water (kg) | Admixture (kg) |
| | | 10 mm down side | 20 mm down side | | |
| 350 | 700 | 378 | 567 | 140 | 2.14 |

## Testing Procedures

### Acid resistance test (IS 4456) [12]

Acid resistance of concrete mixes was evaluated by measuring the residual compressive strength and change in mass after the acid exposure. Cubes of 150 mm × 150 mm × 150 mm were cured for 28 days and then immersed in 5% $H_2SO_4$ solution for 30, 60 and 90 days. The pH of the acid was maintained at 3 and checked every 15 days.

### Sulphate resistance test (IS 4456) [12]

Sulphate resistance of concrete mixes was evaluated by measuring the compressive strength and change in mass after completion of sulphate exposure. Cubes of 150 mm × 150 mm × 150 mm were cured for 28 days and then immersed in 5% $Na_2SO_4$ solution for 30, 60 and 90 days. The pH of the solution was maintained at 8 and checked every 15 days.

### Chloride resistance test (IS 4456) [12]

Chloride resistance of concrete mixes was evaluated by measuring the compressive strength and change in mass after completion of chloride exposure. Cubes of 150 mm × 150 mm × 150 mm were cured for 28 days and after that immersed in 5% NaCl solution for 30, 60 and 90 days. The pH of the chloride solution was maintained at around 7 and checked every 15 days.

### Accelerated corrosion test [5]

Concrete cylinders of 150 mm diameter and 300 mm length were cast for this test using one HYSD bar of 8 mm diameter and one stainless steel bar of the same diameter. The cylinders of concrete mixes were submerged in a tank of 5% NaCl solution. The HYSD bar was connected with the positive terminal of a DC voltmeter which served as anode. The stainless steel bar was connected with the negative terminal which served as cathode as shown in Figure 1. The DC supply was set to 30 V. Current readings were monitored and recorded for each concrete specimen on a regular basis using a multi-meter. The specimens were removed from the tank immediately after observing a drop in the current readings. The concrete cylinders were placed in a compression testing machine and split into two parts by applying a nominal compressive load. The effect of corrosion in reinforcement was measured through visual observation and the reduction in diameter of the reinforcement for cylinders of all concrete mixes.

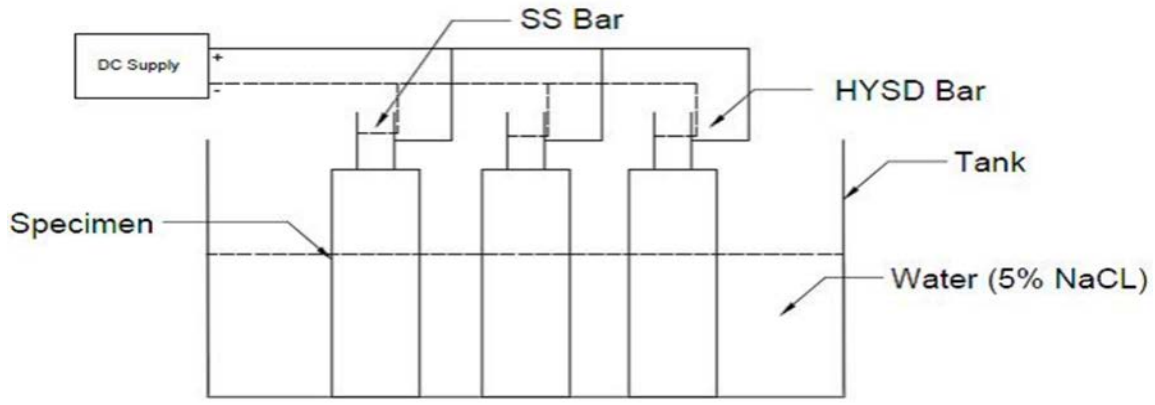


Figure 1 Accelerated corrosion test setup

### Rapid chloride penetration test (ASTM C1202) [13]

Three cylinders of 150 mm diameter and 50 mm height per concrete mix were removed from the tank after 28 days of water curing. The excess water was removed from the cylinders by means of a cloth and the specimens were kept in a chamber at 95% humidity for 2 hours. The specimens were removed from the humidity chamber and all exposed surfaces were covered with an impermeable paint to restrict the moisture movement.

The cylindrical specimen was kept between the Applied Voltage Cell (two symmetric polymethyl methacrylate chambers) as shown in Figure 2. Each chamber contained an electrically conductive mesh and external connectors. Sealant was applied between the specimen and the voltage cell to avoid leakage. The side of the cell containing the top surface of the specimen was filled with 3.0% NaCl solution.

The said side of the cell was connected to the negative terminal of the power supply. The other side of the cell was connected to the positive terminal of the power supply and filled with 0.3 N NaOH solution. Lead wires were attached between the cell banana posts & the voltmeter and 60 V voltage was applied. An initial current reading was recorded for each specimen. Results of concrete specimens were recorded at every 30 minute interval up to a total duration of 6 hours.

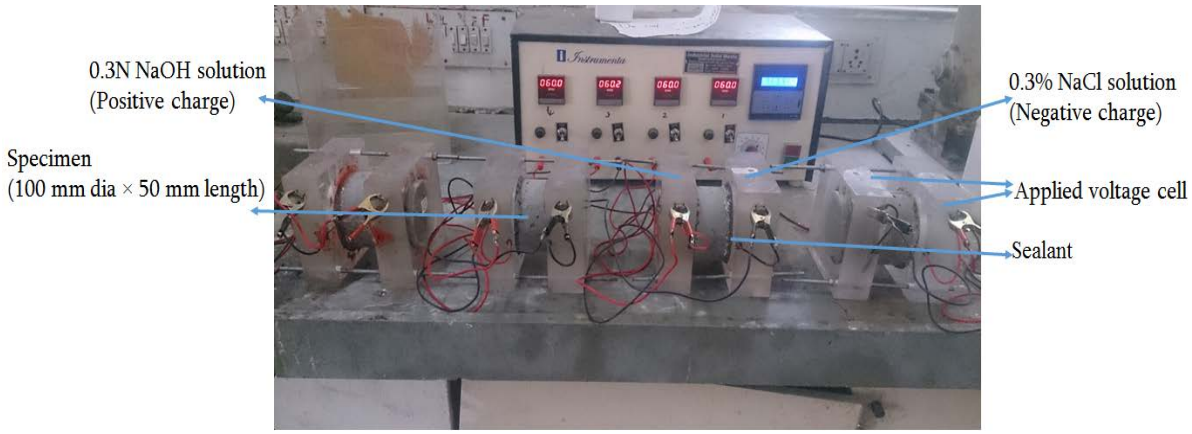


Figure 2 Rapid chloride penetration test setup

## TEST RESULTS AND DISCUSSION

### Acid Resistance Test

The results of change in weight for each concrete mixes due to acid exposure of different durations are presented in Table 5.

The highest weight loss of 11.53% has been observed for the control concrete at 90 days of acid exposure. The M25-3 mix showed a very small weight loss at each exposure ranging from 2% to 5%, respectively. It was observed that with an increase in age, weight loss increased and with an increase in GGBS dosage, the weight loss decreased for all concrete mixes.

Table 5 Percentage change in weight of concrete specimens due to acid exposure

| | EXPOSURE CONDITION | | | | | |
|---|---|---|---|---|---|---|
| | 30 days | | 60 days | | 90 days | |
| | Before | After | Before | After | Before | After |
| | 8.58 | 8.12 | 8.54 | 8.02 | 8.62 | 7.64 |
| M25-1 | 8.44 | 8.01 | 8.45 | 7.85 | 8.51 | 7.52 |
| | 8.41 | 7.96 | 8.51 | 7.81 | 8.46 | 7.48 |
| Average (kg) | 8.48 | 8.03 | 8.50 | 7.89 | 8.53 | 7.55 |
| % change in weight | 5.27% | | 7.14% | | 11.53% | |
| | 8.62 | 8.22 | 8.11 | 7.11 | 8.58 | 7.81 |
| M25-2 | 8.56 | 8.35 | 7.85 | 8.02 | 8.71 | 7.85 |
| | 8.53 | 8.29 | 8.19 | 7.85 | 8.64 | 7.62 |
| Average (kg) | 8.57 | 8.29 | 8.05 | 7.66 | 8.64 | 7.76 |
| % change in weight | 3.31% | | 4.84% | | 10.22% | |
| | 8.61 | 8.42 | 8.60 | 8.40 | 8.65 | 8.25 |
| M25-3 | 8.65 | 8.54 | 8.65 | 8.35 | 8.54 | 8.27 |
| | 8.58 | 8.38 | 8.71 | 8.41 | 8.7 | 8.11 |
| Average (kg) | 8.61 | 8.45 | 8.65 | 8.39 | 8.63 | 8.21 |
| % change in weight | 1.93% | | 3.08% | | 4.87% | |

Table 6 presents compressive strengths of concrete specimens before acid exposure i.e. 28 days of water curing and after acid exposure of 30 days, 60 days and 90 days, respectively.

Table 6 Percentage reduction in compressive strength of concrete due to acid exposure

| | EXPOSURE CONDITION | | | | | |
|---|---|---|---|---|---|---|
| | 30 days | | 60 days | | 90 days | |
| | Before | After | Before | After | Before | After |
| | 33.62 | 29.24 | 34.52 | 27.21 | 35.87 | 22.65 |
| M25-1 | 32.66 | 29.84 | 33.64 | 26.55 | 33.92 | 21.45 |
| | 31.54 | 30.21 | 32.78 | 26.39 | 35.42 | 23.14 |
| Average (MPa) | 32.61 | 29.76 | 33.65 | 26.72 | 35.07 | 22.41 |
| % reduction in compressive strength | 8.72% | | 20.60% | | 36.09% | |
| | 32.48 | 29.57 | 34.69 | 28.56 | 35.91 | 25.28 |
| M25-2 | 32.73 | 30.02 | 34.55 | 28.31 | 36.54 | 24.86 |
| | 31.48 | 29.38 | 33.48 | 27.06 | 35.12 | 26.15 |
| Average (MPa) | 32.23 | 29.66 | 34.24 | 27.98 | 35.86 | 25.43 |
| % reduction in compressive strength | 7.98% | | 18.29% | | 29.08% | |
| | 32.65 | 30.86 | 34.55 | 28.95 | 35.84 | 26.55 |
| M25-3 | 32.08 | 29.73 | 34.26 | 29.58 | 36.61 | 25.84 |
| | 31.11 | 30.42 | 33.25 | 29.24 | 34.41 | 27.12 |
| Average (MPa) | 31.95 | 30.34 | 34.02 | 29.26 | 35.62 | 26.50 |
| % reduction in compressive strength | 5.04% | | 14.00% | | 25.59% | |

The control concrete specimens were significantly deteriorated as compared to those of slag concrete. From the test results, it was observed that the slag concrete performed well compared to the control concrete in terms of retention of the compressive strength. The M25-3 concrete mix performed better than the M25-2 mix in terms of compressive strength. With an increase in GGBS dosage, the resistance of the concrete against the acid attack improved.

**Sulphate Resistance Test**

Table 7 represents the changes in compressive strength of concrete mixes due to sulphate exposure up to 90 days. An increase in weight up to 1% has been observed for all concrete mixes due to ingress of sulphate ions during the sulphate exposure.

Table 7 Percentage change in compressive strength of concrete due to sulphate exposure

| | EXPOSURE CONDITION | | | | | |
|---|---|---|---|---|---|---|
| | 30 days | | 60 days | | 90 days | |
| | Before | After | Before | After | Before | After |
| M25-1 | 33.62 | 33.24 | 34.52 | 34.21 | 35.87 | 34.85 |
| | 32.36 | 31.84 | 33.64 | 33.55 | 33.92 | 33.45 |
| | 31.54 | 31.21 | 32.78 | 32.39 | 35.42 | 34.74 |
| Average | 32.51 | 32.10 | 33.65 | 33.38 | 35.07 | 34.35 |
| % reduction in compressive strength | 1.26% | | 0.78% | | 2.06% | |
| M25-2 | 32.48 | 32.57 | 34.69 | 33.56 | 35.91 | 35.28 |
| | 32.73 | 32.02 | 34.55 | 35.31 | 36.54 | 34.86 |
| | 31.48 | 31.38 | 33.48 | 33.06 | 35.12 | 36.15 |
| Average | 32.23 | 31.99 | 34.24 | 33.98 | 35.86 | 35.43 |
| % reduction in compressive strength | 0.74% | | 0.77% | | 1.19% | |
| M25-3 | 32.65 | 31.86 | 34.55 | 33.95 | 35.84 | 36.55 |
| | 32.08 | 32.03 | 34.26 | 34.58 | 36.61 | 35.84 |
| | 31.11 | 31.42 | 33.25 | 33.24 | 34.41 | 34.12 |
| Average | 31.95 | 31.77 | 34.02 | 33.92 | 35.62 | 35.50 |
| % reduction in compressive strength | 0.55% | | 0.28% | | 0.33% | |

Overall, a reduction in compressive strength has been observed for all concrete mixes after sulphate exposure. A higher reduction was observed for the control concrete as compared to the slag concrete mixes. The M25-3 mix performed better because of the least reduction in compressive strength. No significant effect of sulphate exposure has been observed on concrete mixes due to the incorporation of slag. A higher dosage of GGBS in the concrete mix yielded an improvement in its sulphate resistance.

**Chloride Resistance Test**

A minor increase in weight has been observed for concrete specimens due to the immersion in chloride solution. Such tendency was more pronounced with the increase in exposure duration for all concrete mixes. The increase in weight can be considered as due to the ingress of chloride ions in the concrete specimens.

Table 8 Percentage change in compressive strength of concrete due to chloride exposure

| | EXPOSURE CONDITION | | | | | |
|---|---|---|---|---|---|---|
| | 30 days | | 60 days | | 90 days | |
| | Before | After | Before | After | Before | After |
| M25-1 | 33.62 | 33.34 | 34.52 | 33.85 | 35.87 | 34.74 |
| | 32.46 | 31.84 | 33.64 | 33.58 | 33.92 | 33.57 |
| | 31.54 | 31.39 | 32.78 | 32.48 | 35.42 | 34.69 |
| Average | 32.54 | 32.19 | 33.65 | 33.30 | 35.07 | 34.33 |
| % reduction in compressive strength | 1.08% | | 1.02% | | 2.10% | |
| M25-2 | 32.48 | 32.57 | 34.69 | 33.47 | 35.91 | 35.32 |
| | 32.73 | 32.52 | 34.55 | 35.19 | 36.54 | 34.65 |
| | 31.48 | 31.28 | 33.48 | 33.26 | 35.12 | 36.03 |
| Average | 32.23 | 32.12 | 34.24 | 33.97 | 35.86 | 35.33 |
| % reduction in compressive strength | 0.33% | | 0.78% | | 1.46% | |
| M25-3 | 32.45 | 31.96 | 34.55 | 33.75 | 35.84 | 35.51 |
| | 32.08 | 32.03 | 34.26 | 34.08 | 36.61 | 35.88 |
| | 31.11 | 31.22 | 33.25 | 33.42 | 34.41 | 34.37 |
| Average | 31.88 | 31.74 | 34.02 | 33.75 | 35.62 | 35.25 |
| % reduction in compressive strength | 0.45% | | 0.79% | | 1.03% | |

Table 8 represents the compressive strength of concrete specimens before chloride exposure i.e. 28 days of water curing and after chloride exposure of 30, 60 and 90 days, respectively. Compressive strength of slag concrete mixes were at par with that of the control concrete. No significant change in their compressive strength has been observed for slag concrete mixes as compared to that of the control concrete. The slag concrete performed well in terms of compressive strength retention against chloride exposure. A higher dosage of GGBS in the concrete mix exhibited higher chloride resistance.

**Accelerated Corrosion Test**

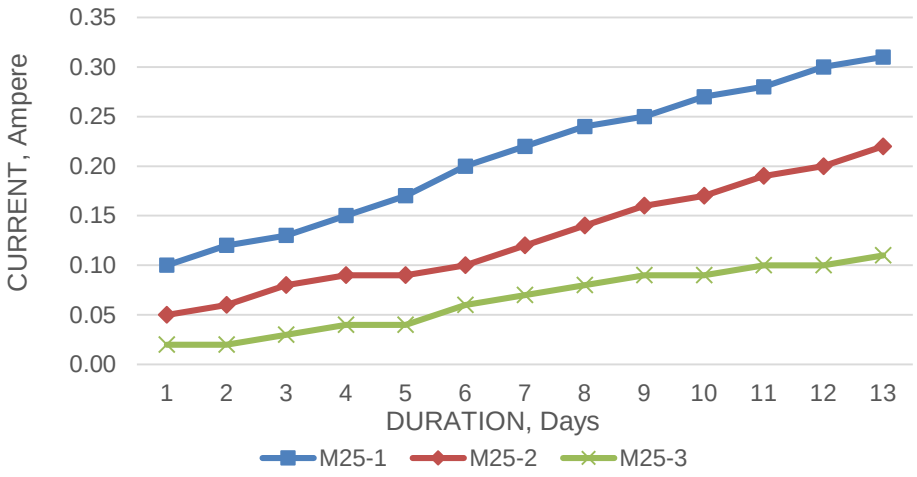


Figure 3 Current readings for concrete mixes during accelerated corrosion test

Figure 3 shows the current readings passing through the concretes for the duration of the test, 13 days. The current was measured every day for all concrete mixes. It was observed that the current passing through the control concrete was higher than that for the slag concrete mixes. A higher current reading is indicative of less resistance to corrosion for the respective concrete specimen. Based on this consideration, the M25-3 concrete mix performed superior to the other two mixes.

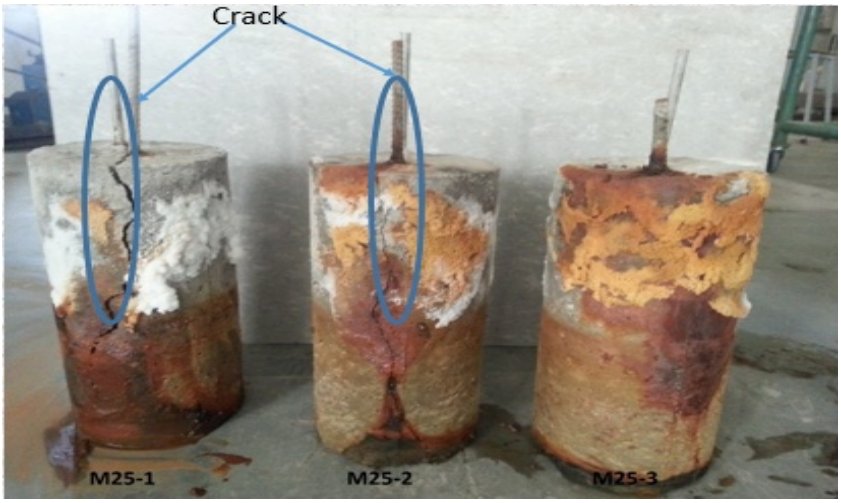


Figure 4 Specimens after accelerated corrosion test

Figure 4 shows the visual appearance of specimens of all three concrete mixes after the completion of the test. The M25-1 mix specimen was severely damaged and had wide cracks compared to the specimens of the other two slag concrete mixes. The M25-3 performed better in terms of resistance against corrosion as no visible cracks were observed. Thus, it is observed that slag concrete performs well as compared to control concrete.

Table 9 represents the reduction in reinforcement diameter of cylinders of all concrete mixes after completion of the test. It has been observed that the diameter of the reinforcement reduced by 2.21 mm in the case of the control concrete. The M25-3 mix performed well as it showed the least reduction in diameter of only 0.26 mm among the three concrete mixes.

Table 9 Measurement of reduction in diameter of reinforcement

| READING POSITIONS | DIAMETER (mm) | | |
|---|---|---|---|
| | M25-1 | M25-2 | M25-3 |
| Top | 7.72 | 8 | 8 |
| Middle | 6.24 | 7.68 | 8 |
| Bottom | 3.41 | 6.42 | 7.21 |
| Average | 5.79 | 7.37 | 7.74 |

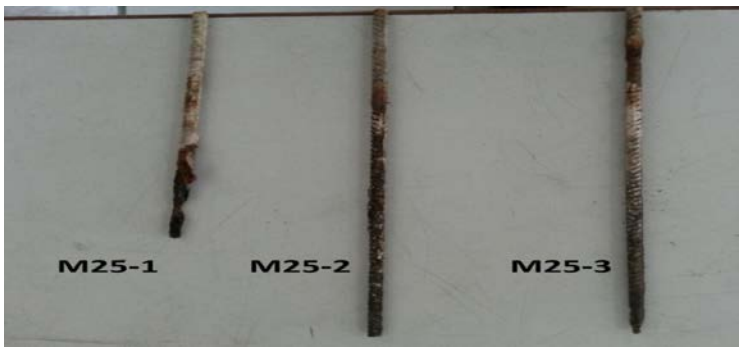


Figure 5 Visual appearance and condition of reinforcement after accelerated corrosion test

Figure 5 indicates that the reinforcement for control concrete was completely corroded. The outer surface of the reinforcement bar of the M25-2 concrete mix corroded throughout the length as is visible from Figure 5. No corrosion effect is visible for the reinforcement of the M25-3 concrete mix. Based on these observations, it can be said that the M25-3 slag concrete mix performed better compared to the other two concrete mixes.

**Rapid Chloride Penetration Test**

Figure 6 shows current versus time results in the form of separate curves for concrete mixes. The current for concrete mixes was recorded at every thirty minute time intervals.

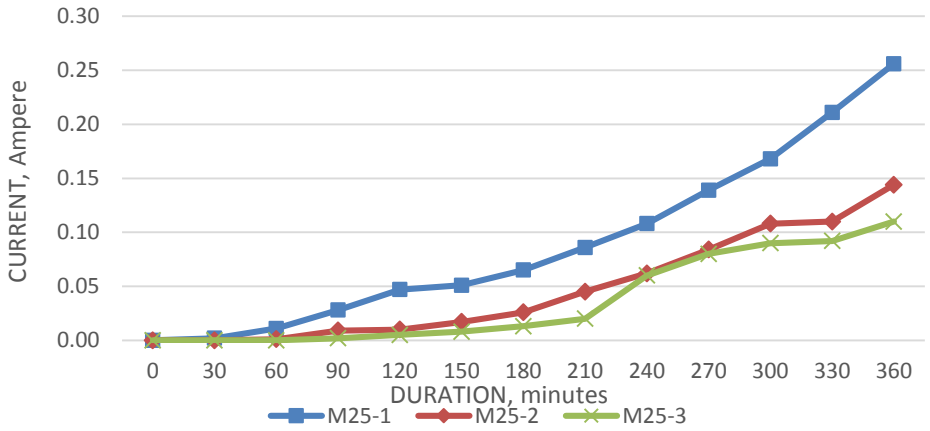


Figure 6 Chloride ion permeability test results for concrete mixes

The area under the curve of current versus duration gives the total charge passing through the respective concrete specimens. The said charge is calculated by the trapezoidal rule, given in Equation 1.

$$Q = 900\ (I_0 + 2I_{30} + \ldots. + 2I_{300} + 2I_{330} + 2I_{360}) \quad (1)$$

where,
Q = charge passed (Coulombs)
$I_o$ = current immediately after voltage is applied (Ampere)
$I_t$ = current at t minute after voltage is applied (Ampere)

Table 10 presents qualitative measures of the rapid chloride penetration test for concrete mixes. It is observed that slag concrete mixes offered higher resistance to chloride penetration as compared to that of control concrete. The M25-3 mix exhibited very small chloride penetration as compared to that of mix M25-2.

Table 10 Qualitative measures for chloride penetrability

| GRADE | M25-1 | M25-2 | M25-3 |
|---|---|---|---|
| Coulombs | 2109 | 1108 | 864 |
| Condition (ASTM C1202 [13]) | Moderate | Low | Very low |

## CONCLUSIONS

Based on the experimental results presented herewith, the following conclusions are drawn:

1. Acid exposure for the control concrete shows higher weight loss and larger reduction in the compressive strength. The concrete mixes with replacements of 40% and 60% of OPC by GGBS performed exceedingly well against acid exposure. A higher GGBS dosage also led to better performance of concrete in terms of the acid exposure.
2. Sulphate exposure has resulted in an increase in the weight of concrete specimens. The compressive strength of slag concrete mixes was at par with the results of control concrete. A higher GGBS dosage in concrete mixes also maintained the performance of the concrete subjected to sulphate exposure.
3. An increase in weight of all concrete mixes has been observed after completion of chloride exposure. The results of compressive strength of slag concrete were at par with the results of the control concrete. Slag concrete mixes exhibited better resistance against chloride exposure as compared to control concrete. A higher dosage of GGBS further improved the performance of concrete against chloride exposure.
4. It was observed during the accelerated corrosion test that the current passing through the reinforcement for control concrete specimens was higher than that for slag concrete specimens. This phenomenon resulted in a larger reduction of reinforcement diameter for the control concrete as compared to the slag concrete mixes. Such behaviour depicted that the corrosion resistance increases with increased GGBS level in concrete.
5. Charge passing through the slag concrete was smaller than that for the control concrete as evidenced from the results of the RCP test. Thus better resistance to chloride ion penetration was observed for slag concrete than for the control. A reduction in chloride ion penetration was observed with an increase in the slag content of concrete.

From all the results and observations, it can be concluded that slag concrete mixes performed better as compared to the control concrete. The increase in GGBS dosage led to superior performance of concrete regarding long-term durability.

## Acknowledgements

We are thankful to the Director of the Institute of Technology, Nirma University, Ahmedabad, India for giving the necessary permission for conducting the present investigation and

presenting the work. We are thankful to Hi-bond cement, Ahmedabad, India for technical support throughout the work. We are also thankful to Stallion energy ltd., Rajkot, India for providing GGBS material for the present investigation.

## REFERENCES

1. ELAHIA A, BASHEERB P A M, NANUKUTTANB S V, KHANA Q U Z. Mechanical and durability properties of high performance concretes containing supplementary cementitious materials, Construction and Building Materials, Vol. 24, Issue 3, 2010, pp 292–299.

2. O'CONNELL M, MCNALLY C, RICHARDSON M G. Performance of concrete incorporating GGBS in aggressive wastewater environment, Construction and Building Materials, Vol. 27, Issue 1, 2012, pp 368–374.

3. GADPALLIWAR S K, DEOTALE R S, ABHIJEET R N. To Study the Partial Replacement of Cement by GGBS & RHA and Natural Sand by Quarry Sand In Concrete, Journal of Mechanical and Civil Engineering, Vol. 11, 2014, pp 69-77.

4. PAVIA S, CONDREN E. Study of the Durability of OPC versus GGBS Concrete on Exposure to Silage Effluent, Journal of Materials in Civil Engineering, Vol. 20, No. 8, 2008, pp 313-320.

5. TOPÇU İ B, BOĞA A R. Effect of ground granulated blast-furnace slag on corrosion performance of steel embedded in concrete, Material and Design, Vol. 31, Issue 7, 2010, pp 3358-3365.

6. ALDEA C, YOUNG F, WANG K, SHAH S. Effects of curing conditions on properties of concrete using slag replacement. Cement and Concrete Research, Vol. 30, Issue 3, 2000, 465-472.

7. BUREAU OF INDIAN STANDARDS, Specification for 53 grade ordinary Portland cement, No. 12269, 1987.

8. BUREAU OF INDIAN STANDARDS, Specification for Granulated slag for the manufacture of Portland slag cement, No. 12089, 1987.

9. BUREAU OF INDIAN STANDARDS, Method of test for Pozzolanic materials, No. 1727, 2009.

10. BUREAU OF INDIAN STANDARDS, Specification for coarse and fine aggregates from natural sources for concrete, No. 383, 1970.

11. BUREAU OF INDIAN STANDARDS, Concrete mix proportion guidelines, No. 10262, 2009.

12. BUREAU OF INDIAN STANDARDS, Methods of test for chemical resistant mortars, No. 4456-1, 1967

13. AMERICAN SOCIETY FOR TESTING AND MATERIALS, Standard Test Method for Electrical Indication of Concrete's Ability to Resist Chloride Ion Penetration. C1202.

# SWISS REQUIREMENTS FOR THE CARBONATION RESISTANCE OF CONCRETE FOR THE EXPOSURE CLASSES XC3, XC4 AND XD1

**F Hunkeler**
TFB AG
Switzerland

**ABSTRACT.** In the past, many reinforced concrete structures have shown cracking and spalling due to the carbonation of the concrete and subsequent corrosion of the reinforcement. The carbonation rate was high because of the use of concrete that was too porous (high porosity and high water/cement ratio, respectively) and due to an insufficient concrete cover of the reinforcement, very often not conforming to the national standards. Due to changes in the cement and concrete market, the durability of concrete came into the focus of research and standardisation. The overall goal is to establish a performance-based concept for requirements and testing. This paper will provide an overview of extensive Swiss research work on the carbonation resistance of concrete. The correlation between carbonation under accelerated conditions and carbonation at normal atmospheric levels of $CO_2$ with a variety of concrete mixes was investigated, as well as the influence of cement type, water/cement (w/c) ratio, curing, preconditioning (pre-treatment) and relative humidity. Furthermore, some results of $CO_2$ measurements at different locations in Switzerland, including a road tunnel, will be presented. Based on the results of these studies, a Swiss standard for an accelerated carbonation test (4% $CO_2$) was elaborated and published in 2013. Since then concrete producers have to check within the factory production control that they fulfil the limiting values for carbonation resistance (carbonation coefficient) defined by the Swiss concrete standard for the exposure classes XC3, XC4 and XD1. Both the test method (including precision) and the limiting values will be explained.

**Keywords:** Carbonation resistance, Accelerated carbonation test method, Natural and field exposure, Curing, Modelling.

**Fritz Hunkeler** is senior consultant at TFB AG in Wildegg. Until 2011 he was CEO of this company. His activities are focused on the durability of reinforced concrete structures (corrosion of reinforcement, deterioration of concrete). He is involved in national and international technical committees.

## INTRODUCTION

In the 1950s and 1960s, corrosion due to carbonated concrete was a significant focus of practice and research. The insights gained at the time led to a requirement for more compact concretes (lower w/c ratios), for a control of the fresh concrete properties and for an increase of the concrete cover. This was ultimately reflected in the corresponding standards. In Switzerland and in Europe, the cement and concrete market is changing at a rapid rate (new cement types, concrete recycling). Whereas in 1995 the proportion of CEM I cements was still about 90% of total Swiss cement usage, in 2015 it was only about 10%. The CEM I cements were initially replaced by CEM II/A cements (mainly CEM II/A-LL) and in recent years increasingly with CEM II/B cements. The CEM II/A cement achieved a maximum of 73% of total usage in Switzerland in 2010.

Linked to these changes is the reduction of the clinker content (clinker factor) of the cements. This trend leads to potentially higher carbonation rates. The driving force behind these changes is the demand for sustainable construction and concrete structures. This is reasonable and necessary, but it requires a re-evaluation of the durability of concrete. In particular, it has to be checked whether the previous requirements for concrete composition (w/c ratio, cement content) are still adequate. These questions were the starting point for various research works in Switzerland, which are presented in summary below.

## INFLUENCE OF THE $CO_2$ CONTENT ON THE CARBONATION OF CONCRETE

A comprehensive experimental study examined the influence of $CO_2$ content, concrete composition (cement type, w/c ratio) and curing on the rate of carbonation [1]. The aim of this work was to establish a basis for a rapid testing of the carbonation resistance of concretes.

### Experimental

In the first phase of the project, studies were carried out with a natural $CO_2$ content and at 1, 10 and 100% $CO_2$. In the second phase, just 1% and 4% $CO_2$ were used for the accelerated carbonation. The results of the carbonation tests are presented below. The results of the further tests carried out (fresh concrete properties, compressive strength, gas permeability, water permeability, porosity, sodium/potassium/calcium content) are given in the final report. Some results were also published in [2].

The concrete mixes AGB11 and AGB12 (Table 1) were used for phase 1, the other concrete mixes for phase 2. The concrete specimens were cured according to table 2. Before the start of the rapid carbonation, they were pre-conditioned for 14 to 27 days in a climatic room (20°C, 70% RH). In phase 1B, after curing and before the carbonation test, the specimens were pre-dried in addition for 18 days at 60°C. The carbonation conditions are summarised in Table 3. Prisms (120 x 120 x 360 mm) were used for the tests. In Switzerland, this type of specimens is used for shrinkage measurements in accordance with the standard SIA 262/1 [3]. Special testing chambers have been developed for the accelerated carbonation, in which the $CO_2$ content and the relative air humidity can be varied [4]. While the increased $CO_2$ contents could be kept constant in the testing chambers, the natural $CO_2$ content in the climatic room fluctuated widely, as this room was also used for other work. When storing young concrete test specimens, the $CO_2$ content decreases, whereas it increases rapidly to over 1000 ppm when people are present (Figure 1).

Table 1 Designation and composition of the concrete mixes

| MIX NO. | EXPOSURE CLASS | CEMENT | | w/c ratio | AIR ENT-RAINING ADMIXTURE |
|---|---|---|---|---|---|
| | | Type | Content, kg/m$^3$ | | |
| AGB11 | XC4 | CEM I 42,5 N | 300 | 0.50 | no |
| AGB12 | XC4 | CEM III/B 42,5 L-LH SR | 300 | 0.50 | no |
| AGB21 | XC3 | CEM I 42,5 N | 280 | 0.60 | no |
| AGB22 | XD3, XF4 | CEM III/B 42,5 L-LH-SR | 320 | 0.45 | yes |
| AGB24 | XC4 | CEM II/A-LL 42,5 N | 300 | 0.50 | no |
| AGB25 | XD3, XF4 | CEM II/A-LL 42,5 N | 320 | 0.45 | yes |
| AGB26 | XC3 | CEM II/B-LL 32,5 R | 280 | 0.60 | no |
| AGB27 | XC4 | CEM II/B-LL 32,5 R | 300 | 0.50 | no |
| AGB28 | XD3, XF4 | CEM II/B-LL 32,5 R | 320 | 0.45 | yes |
| AGB29 | XC3 | CEM II/B-M (T-LL) 42,5 N | 280 | 0.60 | no |
| AGB30 | XC4 | CEM II/B-M (T-LL) 42,5 N | 300 | 0.50 | no |

Table 2 Curing conditions and pre-conditioning

| ABBR. | CURING | PRE-CONDITIONING IN A CLIMATIC ROOM (20 °C, 70% RH) | AGE AT START OF TEST |
|---|---|---|---|
| NB 1d | 1 d in the mould | 27 d | 28 d |
| NB 7d | 1 d in the mould, 6 d in water | 21 d | 28 d |
| NB 28d | 1 d in the mould, 27 d in water | 14 | 42 d |

Table 3 Carbonation conditions (ACC: Accelerated carbonation)

| ABBR. | TEMP (average), °C | RELATIVE HUMIDITY (average), % | AVERAGE $CO_2$ CONTENT (variation), ppm |
|---|---|---|---|
| Natural | 20.2 | 69.0 | 0.032 (0.01 to 0.11) |
| ACC 1% | 20.3 | 59.8 | 0.99 (0.95 to 1.05) |
| ACC 4% | 20.6 | 61.8 | 4.02 (3. 9 to 4.1) |

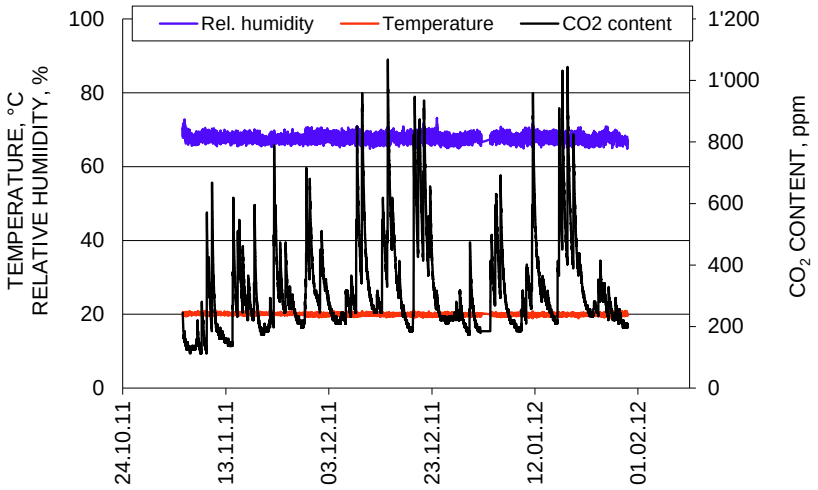


Figure 1 Temperature, relative humidity and $CO_2$ content over time

**Influence of the $CO_2$ content**

Figure 2 is used as an example to show the effect of the $CO_2$ content on the carbonation of the concrete AGB22 with a curing of 1 day. The accelerating effect of $CO_2$ can be taken into account according to equation 1. In Figure 3 all values, converted to 320 ppm $CO_2$, are compared.

$$K_{SN} = \frac{K_S}{\sqrt{\frac{[CO_2]_S}{[CO_2]_N}}} \qquad \text{Eq. 1}$$

$K_{SN}$ Carbonation coefficient measured under accelerated conditions and converted to the natural or reference $CO_2$ content
$K_S$ Carbonation coefficient under accelerated carbonation conditions
$[CO_2]_N$ Natural $CO_2$ content (or reference content)
$[CO_2]_S$ $CO_2$ content for accelerated carbonation

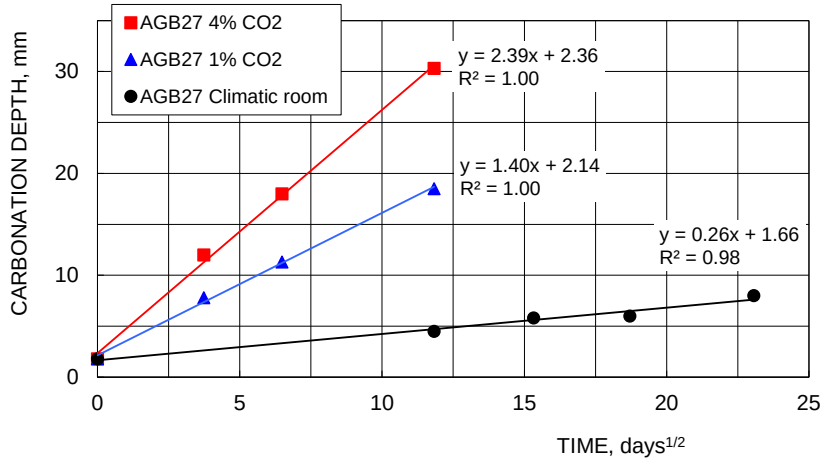


Figure 2 Carbonation of concrete mix AGB22 under natural and accelerated carbonation

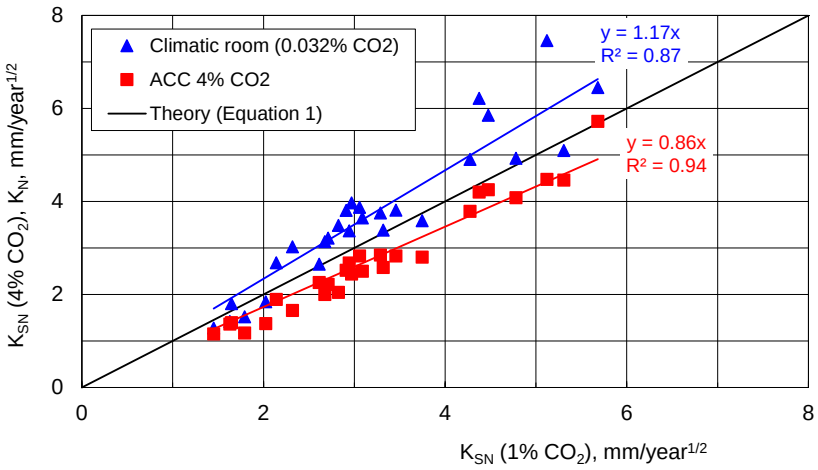


Figure 3 Carbonation coefficient under natural $K_N$ (0.032 % $CO_2$) and accelerated conditions $K_{SN}$ (4 % $CO_2$, converted to 0.032 % $CO_2$) vs. $K_{SN}$ (1 % $CO_2$, converted to 0.032 % $CO_2$)

If the carbonation coefficient is determined under accelerated, as well as natural conditions, the effective acceleration can be calculated with the ratio $K_{SN}/K_N$ (equation 2).

$$K_{Rel} = \frac{K_{SN}}{K_N} \qquad \text{Eq. 2}$$

$K_{Rel}$ Relative carbonation coefficient

If $K_{Rel} = 1$, the effect of the elevated $CO_2$ content corresponds exactly to the theoretical acceleration. If $K_{Rel} < 1$, the effect of the $CO_2$ content is weaker than the theoretically expected value. $K_{Rel}$ cannot be greater than 1, if the reference value is the lowest studied or observed $CO_2$ content. This is mostly the natural content. The results of this study, as well as of some other research work, are shown in Figure 4.

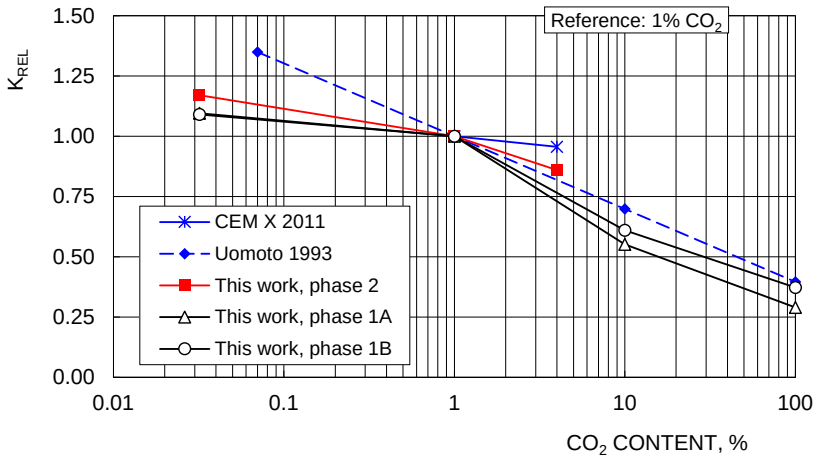


Figure 4 Relative carbonation coefficient ($K_{rel}$ acc. to Eq. 2) as a function of $CO_2$ [1]. CEM X 2011 = [5]; Uomot0 1993 = [6].

Table 4 Influence of the $CO_2$ content on the relative carbonation coefficient [1]

| $CO_2$ CONT. , VOL. -% | RELATIVE CARBONATION COEFFICIENT | | |
|---|---|---|---|
| | Phase 1A | Phase 1B | Phase 2 |
| 0.032 | 1.10 | 1.09 | 1.17 |
| 1.0 | 1.00 | 1.00 | 1.00 |
| 4.0 | - | - | 0.86 |
| 10 | 0.55 | 0.61 | - |
| 100 | 0.29 | 0.37 | - |
| Ratio "0.032" to "4" | - | - | **1.36** |
| Ratio "0.032" to "100" | 3.77 | 2.93 | - |
| | 3.35 | | |

**Influence of curing**

The influence of the duration of curing is clearly dependent on the type of cement (Figure 5). On average, the effect is scarcely dependent on the CO2 content (Table 5). The dependency from Gehlen [7] used for the modelling of the carbonation resistance classes is outside of this range. In the Swiss standard [3], a curing duration of 3 days has been fixed, since the curing of concrete is often not as long as it should be. The duration of 3 days is a compromise between several requirements and aspects (e.g. slowly reacting cements).

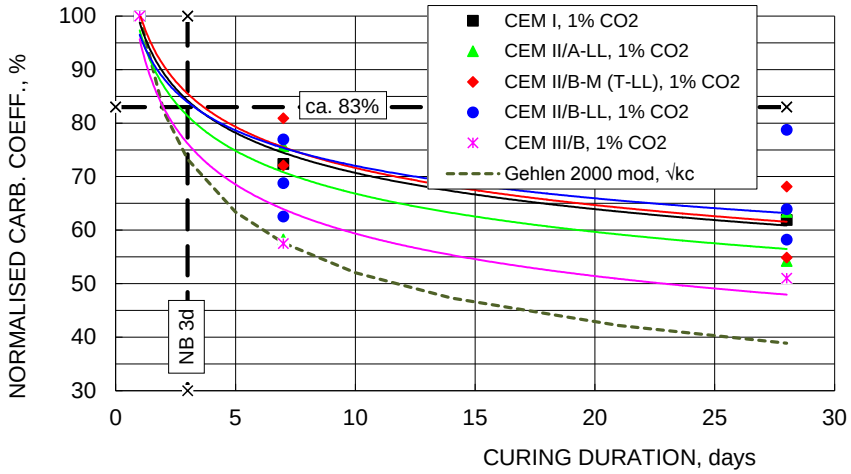


Figure 5 Normalised carbonation coefficient as a function of curing duration [1]

Table 5 Relative Effect of Curing on Carbonation

| $CO_2$ Content, Vol. -% | Relative effect of curing | | |
|---|---|---|---|
| | NB 1d | NB 7d | NB 28d |
| 0.032 | 1. 00 | 0.69 | 0.63 |
| 1. 0 | 1. 00 | 0.69 | 0.63 |
| 4. 0 | 1. 00 | 0.69 | 0.63 |

## SWISS TESTING STANDARD FOR CARBONATION RESISTANCE

Based on the research work, a testing standard was developed for determining the carbonation resistance with 4 vol.-% $CO_2$. Testing details can be found in [1,2]. Equation 3 is used for calculating the carbonation coefficient from the accelerated carbonation test.

$$K_{N,ACC} = c \bullet K_{SN} = a \bullet b \bullet c \bullet K_S = 2.60 \bullet K_S \qquad \text{Eq. 3}$$

| | | | |
|---|---|---|---|
| $K_{N,ACC}$ | Carbonation coefficient from the accelerated carbonation test converted to 400 ppm $CO_2$, and corrected with the correction factor c, mm/year$^{1/2}$ | | |
| $K_{SN}$ | Carbonation coefficient measured under accelerated conditions and converted to the reference $CO_2$ content of 0.04 vol.-% (400 ppm), mm/year$^{1/2}$ | | |
| $K_S$ | Carbonation coefficient under accelerated carbonation condition, mm/day$^{1/2}$ | | |
| a | Conversion factor for time: 1 day to 1 year: | (365/1)1/2 = | 19. 10 |
| b | Conversion factor for $CO_2$: | $(0.04/4.\ 0)^{1/2}$ = | 0.10 |
| c | Correction factor (see Table 4) | | 1. 36 |

Concrete producers have to test the concrete for the exposure classes XC3, XC4 and XD1 in accordance with this testing standard (valid since 01.08.2013) and to demonstrate that they meet the required carbonation resistance (see next chapter).

A Swiss round robin test with 18 laboratories [8] and 4 concrete mixes demonstrated the high reliability of the test procedure given in [2] (Figure 6). The results of a smaller RRT [] are included in this Figure.

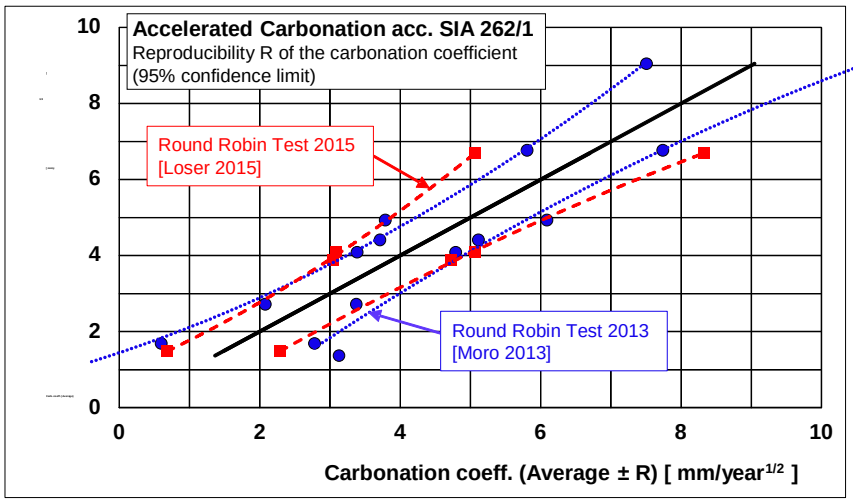


Figure 6 Average carbonation coefficient vs. carbonation coefficient ± R (reproducibility). Data taken from [8,9].

## SWISS REQUIREMENTS FOR THE CARBONATION RESISTANCE

As part of the research project [1], the results of various long-term studies were analysed. The following procedure can only be used when the carbonation depths were measured under laboratory (indoor) and outdoor conditions at the same time and over an extended period of time. The $CO_2$ contents should be similar. There are only very few such publications available.

At first it is assumed that the √t law is valid under laboratory or indoor conditions (time exponent b = 0.5). In order to assess the influence of the type of exposure, the carbonation depths of the (unweathered/sheltered and weathered) outdoor storage are compared to the carbonation depths in the laboratory. The relationship between "outdoor storage" and "laboratory storage" carbonation depths can be described by equation 4.

$$\frac{d_{KA}}{d_{KL}}(t) = \frac{K_A\ t^{b(A)}}{K_L\ t^{0.5}} = \frac{K_A}{K_L}\ t^{b(A)-0.5} \qquad \text{Eq. 4}$$

$d_{KA}$ Carbonation depth under outdoor conditions, mm
$d_{KL}$ Carbonation depth under laboratory conditions, mm
$K_A$ Carbonation coefficient under outdoor conditions, mm/year$^{b(A)}$
$K_L$ Carbonation coefficient under laboratory conditions (normal $CO_2$ content), mm/year$^{0.5}$
b(A) Time exponent for outdoor conditions
t Time, years

Figures 7 and 8 show the results of the analysis of data from Wierig [7]. The following conclusions can be drawn:

- The ratio $K_A/K_L$, i.e. the relative carbonation coefficient, is between 70 and 100% for the sheltered outdoor storage. The lower the w/c ratio, the lower this ratio is.
- The exponent ´b(A) – 0.5´ is around -0.10. The time exponent b(A) is therefore around 0.40 (= -0.10 + 0.50). The influence of the w/c ratio is minimal.

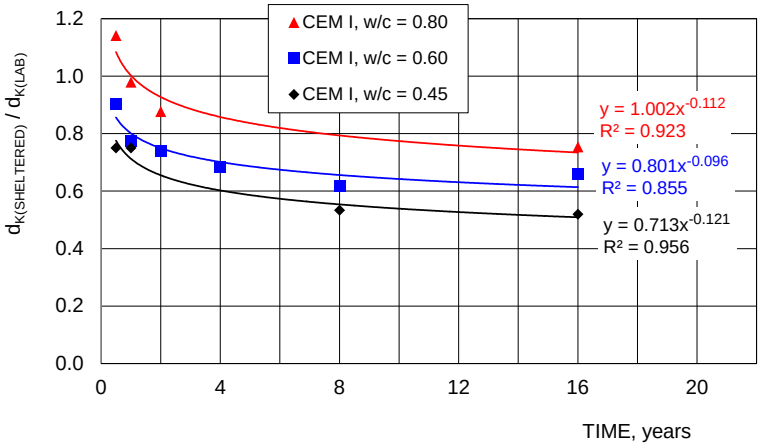


Figure 7 Ratio $d_{KA}$ (outdoor sheltered) to $d_{KA}$ (laboratory) as a function of time. Data taken from [10].

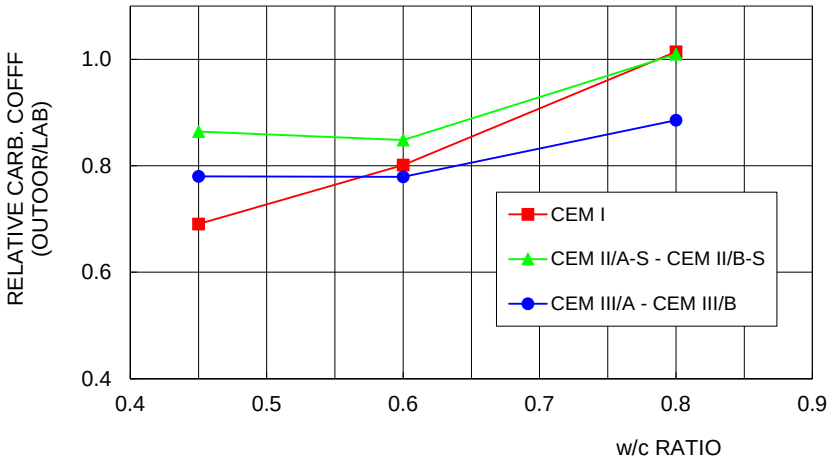


Figure 8 Influence of the exposure condition and the w/c ratio on the normalised carbonation coefficient [1]. Data taken from [10].

Based on these results, equation 5 was derived and used for calculating the limiting values for the carbonation coefficient (carbonation resistance).

$$d_{K,Max} \leq r_K \; K_{SN} \; t^{0.40} = 0.80 \; K_{SN} \; t^{0.40} = K_{Max} \; t^{0.40} \qquad \text{Eq. 5}$$

$d_{K,Max}$ Maximum allowable carbonation depth [mm]. $d_{K,Max}$ can be set as e.g. 80% of the minimum concrete cover ($c_{min}$) according to SIA 262 [11].
$r_K$ Factor for considering the influence of the relative humidity [-]
$K_{SN}$ Carbonation coefficient from testing according to SIA 262/1 [3], appendix I [mm/year$^{0.40}$]. Reference for $CO_2$ content: 400 ppm.
$K_{Max}$ Maximum allowable carbonation coefficient [mm/year$^{0.40}$]
t Time (service life), [years].

For fixing the limiting values for $K_{Max}$, in principle several further influences can be taken into consideration:

1) The two- and three-dimensional diffusion of $CO_2$ leads to significantly deeper carbonation in corner and edge areas. According to our studies, the interaction coefficient with a cover of 20 mm is about 1.2 [1].
2) The maximum carbonation depth can be greater than the average value up to a factor of 1.2 or more [1].
3) The corrosion of the reinforcement can start already if the carbonation depth determined by phenolphthalein has reached 80% of the concrete cover of the reinforcement [1].
4) The $CO_2$ content is constantly increasing worldwide. In the “unpolluted” air on the Jungfrauhoch at 3580 metres above sea level it has increased over the last 10 years by appr. 2 ppm per year. At the end of 2014 it reached appr. 400 ppm [12].
5) The end of the service life has not been reached when the carbonation depth has reached the reinforcement. It then still takes a certain time until the corrosion of the reinforcement leads to cracks in the concrete (and later on to spalling), i.e. the time it takes until a certain critical corrosion attack has been reached can be further taken into account. For conventional concrete the critical corrosion loss is between 10 and 100 µm [1].

The aim of being able to fix a single limiting value for a service life of 50 years and both exposure classes XC3 and XC4 (and XD1) made it necessary that the mentioned influences could only partially be taken into account. The limiting values, valid since 2013, are listed in Table 6. The concrete cover is given in [11].

Table 6 Limiting values for carbonation resistance according to [13]

| PARAMETER | SERVICE LIFE, YEARS | EXPOSURE CLASS | |
|---|---|---|---|
| | | XC3 | XC4 |
| Concrete cover $c_{min}$, mm | | 25 | 30 |
| Limiting values for $K_{max}$ | 50 | 5.0 mm/year$^{1/2}$ | 5.0 mm/year$^{1/2}$ |
| | 100 | 4.0 mm/year$^{1/2}$ | 4.5 mm/year$^{1/2}$ |

## CORRELATION BETWEEN CARBONATION UNDER NATURAL AND ACCELERATED CONDITIONS

Experience has shown that the carbonation rate is at its greatest within a humidity level of between about 50 and 70%. Completely water saturated concrete practically does not carbonate, as the diffusion speed of $CO_2$ in the pore solution is about 3 to 4 times lower than in dry or scarcely moist concrete. Very dry concrete does not carbonate, since free water, necessary for the carbonation reaction, is not available.

Within another research project [14] concrete mixes with CEM II/A-LL (300 kg/m³) with a w/c ratio of 0.65, 0.60 and 0.50 without and with partial replacement of the cement with limestone filler were studied with the accelerated carbonation test method (NB 1d.). Figure 9 shows that the carbonation coefficient decreases with increasing relative air humidity. The w/c ratio has a strong influence. This finding can be explained by the different adsorption isotherms of the concrete mixes. Figure 9 also contains the curve from Gehlen [7] used for the modelling of the carbonation resistance classes. It does not cover the behaviour of less carbonation resistant concrete mixes as they are often used for buildings.

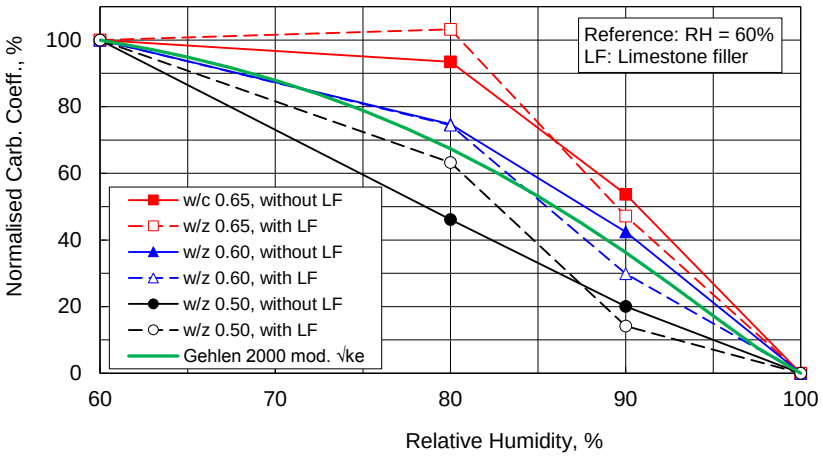


Figure 9 Influence of relative air humidity and the water/cement ratio on the normalised carbonation coefficient [14]. Gehlen 2000 = [7].

Specimens of same concrete mixes were stored for up to 2 years also under natural conditions in a climatic room (20°C, 70% RH) and in the Stevenson Screen in Wildegg (temperature and RH average 2012: 10.3 °C, 75 % RH). Figure 10 shows the influence of the relative humidity

(RH) and of the storage conditions on the carbonation coefficient. The results of the outdoor storage in the Stevenson Screen are similar to those of the rapid carbonation at 80% RH. The results from the climatic room and the accelerated carbonation tests are in good agreement. Further, it was found, that the time exponent b under sheltered outdoor conditions remained at 0.50, i.e. no decrease to 0.40.

In the light of these new results, the assumptions for the calculation of the limiting values for carbonation resistance (see Eq. 5) must be questioned critically.

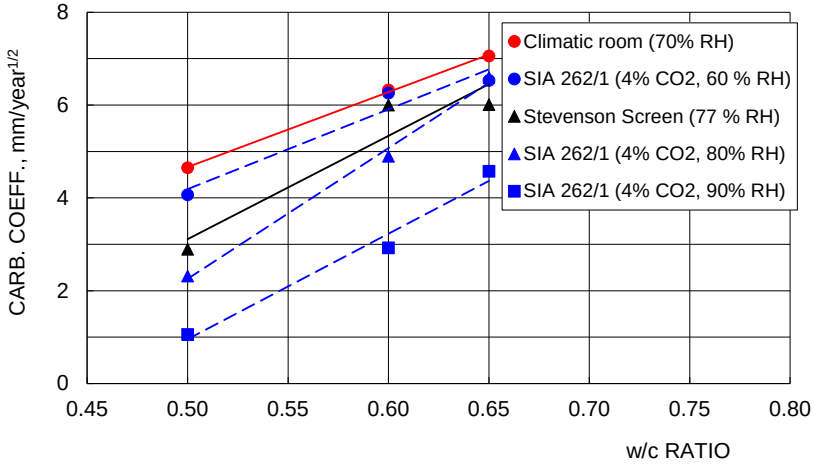


Figure 10 Influence of the exposure conditions and the water/cement ratio on the normalised carbonation coefficient [14]

## ONGOING RESEARCH

In 2014, a new research programme, funded by the Federal Roads Office and cemsuisse, was launched with the goals detailed in Table 7. All these topics are of fundamental importance for a correct long-term modelling. WP 1 and 2 are intended to provide answers to the questions raised in the previous chapter.

Table 7 Goals of the ongoing research

| WORKING PACKAGE (WP) | | INFLUENCE ON | NEED FOR RESEARCH |
|---|---|---|---|
| 1 | Influence of RH on the carbonation rate | Carbonation coefficient, factor $r_K$ | Measurements of various concrete mixes (e. g. slow reaction concrete) |
| 2 | Time exponent b | Carbonation rate over time | Long-term field studies under sheltered outdoor conditions (5 to 10 years) |
| 3 | Actual $CO_2$ content in natural air and in tunnels | Carbonation coefficient | Monitoring of $CO_2$ at different locations and in two Swiss road tunnels |
| 4 | Influence of RH on the corrosion rate of the reinforcement | Corrosion time until cracks and spalling appear | Corrosion rate measurements on different reinforced concrete specimens |

In the Swiss midlands, the average $CO_2$ content already significantly exceeds the reference value of 400 ppm. In Wildegg the average $CO_2$ content during the summertime is around 400 ppm and in the winter season around 550 ppm (Figure 11). The average value from June 2014 to June 2015 was 492 ppm (±76 ppm). This causes an increase in the carbonation coefficient of around 11% (see equation 1). As part of WP 3, in addition to Wildegg further monitoring systems were installed in summer 2015 at several locations in Switzerland. Preliminary results in the ca. 3.18 km long road tunnel Belchen, a part of the motorway between Basle and Lucerne, show again much higher $CO_2$ contents (Figure 12). The $CO_2$ content depends not only on the day time and day of the week, but also on the location of the measurement in the tunnel. The location Q2 is about 700m from the entrance to the tunnel, Q6 about 2300m.

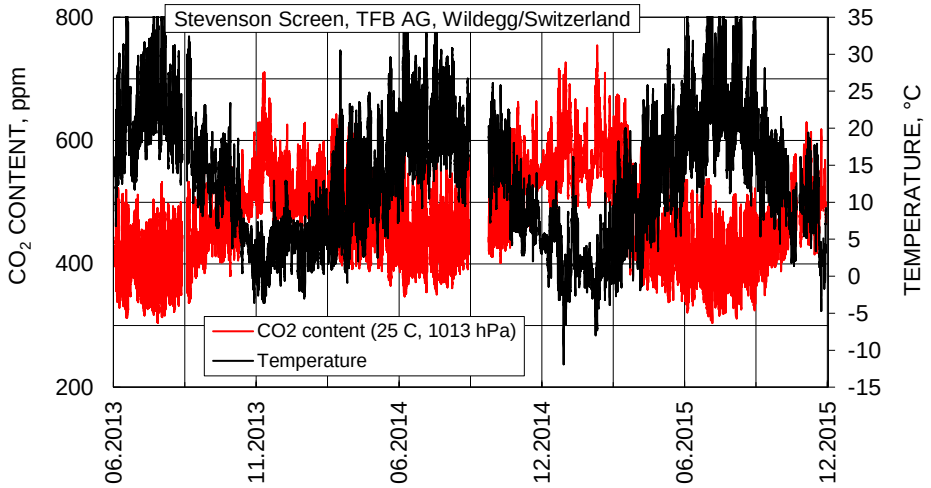


Figure 11 $CO_2$ content (normalised to standard conditions) of air in Wildegg

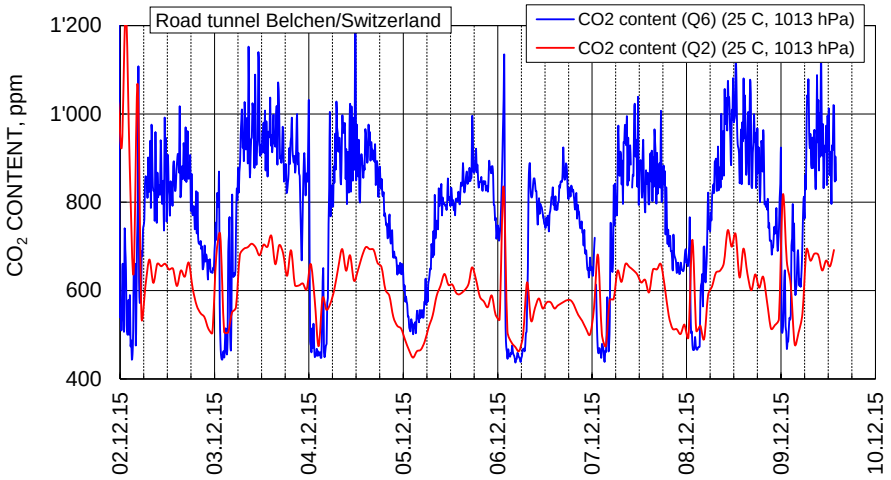


Figure 12 $CO_2$ content (normalised to standard conditions) in the road tunnel Belchen/Switzerland at the two locations Q2 and Q6

WP 4 focuses primarily on the question of whether the reinforcement corrosion under XC3 conditions is sufficiently small so that no cracking or spalling of the concrete can occur for 50 or 100 years. If this can certainly be excluded with some safety margin, then the requirements on concrete for XC3 could be dropped.

For old, reinforced and pre-carbonated test specimens that have been stored for several years in the Stevenson Screen (sheltered outdoor storage), the corrosion loss in summer 2015 was around 1 µm/year or lower (Figure 13).

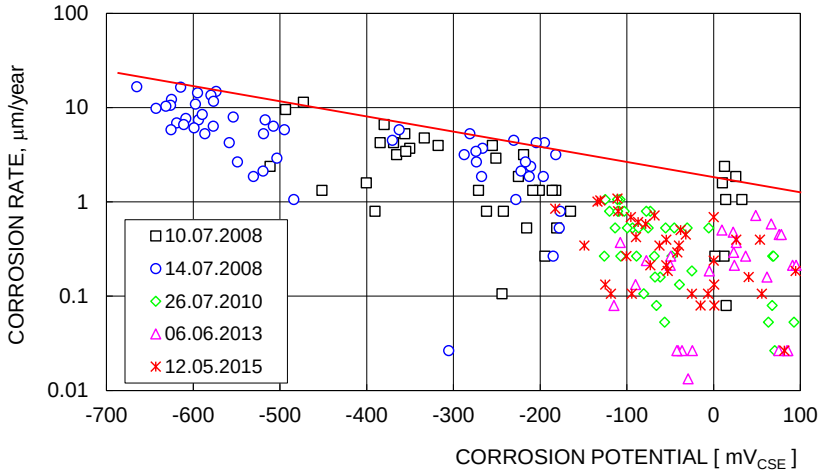


Figure 13 Dependence of the corrosion rate, calculated from the macroelement current between common and stainless steel reinforcement, on the corrosion potential. On 14 July 2008, the specimens were soaked with water. Since then they have been stored in a Stevenson Screen in Wildegg, where the yearly average RH lies between 75-80%.

## ACKNOWLEDGEMENTS

The author thanks the Working Group “Bridge Research” of the Federal Roads Office, cemsuisse (Swiss Association of Cement Manufacturers) and TFB AG for the financial support of these studies.

## REFERENCES

1. HUNKELER, F, LAMMAR, L. Anforderungen an den Karbonatisierungswiderstand von Betonen (Requirements for the carbonation resistance of concrete mixes). Research project AGB 2008/012, Report VSS No. 649, November 2012. Download: http://www.tfb.ch/de/Publikationen.html.

2. HUNKELER, F. Einfluss des $CO_2$-Gehaltes, der Nach- und Vorbehandlung sowie der Luftfeuchtigkeit auf die Karbonatisierungsgeschwindigkeit von Beton. Beton- und Stahlbetonbau, Vol. 107, Issue 9, 2012, pp 613-624.

3. SIA 262/1. Betonbau – Ergänzende Festlegungen (Concrete Structures – Supplementary specifications). Swiss Society of Engineers and Architects (SIA), Swiss standard, 2013.

4. TFB DS AG. Accelerated carbonation reactor, http://www.tfb-diagnostic.ch/ds/Produkte/Carbonator-english.html.

5. GERMAIN, O, PIERRE, C, BROUARD, E, CHONIER, M A. Development of new ternary cements with reduced clinker content. CEN/TC 51/WG 6 Ad Hoc Group “CEM X”, Prestandardisation Research, “CEM X program”, Joint report CRIC – Lafarge, October 2011.

6. UOMOTO, T, TAKADA, Y. Factors affecting concrete carbonation ratio. Concrete Library of JSCE, No. 21, June 1993, pp 31-43.

7. GEHLEN, CH. Probabilistische Lebensdauerbemessung von Stahlbetonbauwerken, Zuverlässigkeitsbetrachtungen zur wirksamen Vermeidung von Bewehrungskorrosion. Deutscher Ausschuss für Stahlbeton, Beuth Verlag GmbH, Berlin, 2000.

8. LOSER, R. Round Robin Test «Carbonation Resistance of Concrete according SIA 262/1, Annex I», Final Report 2-1-040-02. 15a, 16.2.2015. Swiss Association of Accredited Testing Laboratories of Building Materials.

9. MORO, F, HUNKELER, F, NYGAARD, P, CUCHET, S. Carbonation resistance: Accelerated determination and limiting values based on Swiss standard method. RILEM International workshop on performance-based specification and control of concrete durability 11 - 13 June 2014, Zagreb, Croatia.

10. WIERIG, H-J. a) Long-term studies of the carbonation of concrete under normal outdoor exposure. Proc. of the RILEM Seminar on the Durability of Concrete, Hannover (Germany), 26-29 March, 1984, pp 239-249. b) Structures under Normal Outdoor Exposure. Institut für Baustoffkunde und Materialprüfung, Universität Hannover, 1984.

11. SIA 262. Betonbau (Concrete Structures). Swiss Society of Engineers and Architects, Swiss standard (SIA), 2013.

12. UNIVERSITY OF BERN, Physics Institute, Climate and Environmental Physics, Berne/Switzerland, http://www.climate.unibe.ch/?L1=research&L2=NRT.

13. SN EN 206 (incl. NAD), Concrete – Specification, performance, production and conformity. Swiss Society of Engineers and Architects (SIA), Swiss standard, 2nd Edition, 2016.

14. HUNKELER, F, SCHULTHEIS, U. Karbonatisierung von Hochbaubetonen (Carbonation of concrete for buildings). Project cemsuisse 201103, Report TFB AG U 113002, 5.9.2013, unpublished.

# ACID MEDIA-INDUCED LEACHING IN ALKALI-ACTIVATED PASTES EFFECT OF FLY ASH NATURE

**C Varga**

**M Alonso F Puertas**

Eduardo Torroja Institute for Construction Sciences (IETcc-CSIC)

Spain

**ABSTRACT.** Chemical attack on Portland cement pastes in $NH_4NO_3$ acid media has been widely studied and shown to induce changes in their microstructure that translate into a loss of mechanical strength. Acid attack on alkali-activated slag (AAS) likewise generates microstructural effects, modifying the main reaction products (C-A-S-H gels). The impact of this aggressive solution on alkali-activated fly ash (AAFA) is insufficiently understood, however. This study consequently explored leaching in early age (3-21 days) AAFA pastes in a concentrated $NH_4NO_3$ solution to determine the effect of the nature and composition of the starting material on the process. Two AAFA pastes of different origins and compositions were prepared, along with control OPC pastes. The findings showed that this aggressive 6M-$NH_4NO_3$ solution had a much more moderate effect on AAFA than OPC or AAS paste strength. Whilst small amounts of calcium and magnesium leached out of the former material, the leachate contained no aluminium, a component of its main reaction product, N-A-S-H gel. NMR and FTIR studies showed that the gels forming because of the attack had higher silicon content. The chemical composition of the starting materials and particularly their loss on ignition were determinants in their reactivity and hence in their mechanical behaviour and durability.

**Keywords:** Alkali-Activated Cements, durability, microstructure, acid attack, leaching

**Dr Celia Varga** is expertise in Cement and Concrete chemistry and technology. She has papers and communications in this field.

**Dr Mar Alonso** is the Responsible of Cement Chemistry labs in Eduardo Torroja Institute in Madrid. She is expertise in chemical admixtures and alkaline cements. She has papers and communications in this field.

**Prof Francisca Puertas** is Research Professor at Eduardo Torroja Institute in Madrid. She is member of numerous national e international committees and has published more than 130 papers in cement and concrete technology. She is Editor in Chief of “Materiales de Construccion” Journal.

## INTRODUCTION

Portland cement paste resistance to acid attack has been studied and described by a number of authors [1-3]. Such studies showed that the hydrates in OPC pastes (Portlandite, C-S-H gels and ettringite) dissolve or decompose in acid media with the concomitant leaching of (primarily $Ca^{2+}$ and $OH^-$) ions into the aqueous phase. Alkali-activated materials (AAMs) are known to be much more stable in acid media than Portland cement systems [4-9]. In alkali-activated slag (AAS) pastes, such higher performance is due primarily to the composition and structure of the main reaction products (C-A-S-H gels). The C-A-S-H gels present in AAS exhibit low Ca/Si ratios, longer mean chain lengths (MCL) and denser cross-linking than C-S-H gels. Varga et al [8] found that the chemical composition of the starting slag, particularly $Al_2O_3$ and MgO contents, conditioned the structure of the C-A-S-H gel formed, as well as the number of secondary reaction products (hydrotalcite) and consequently its resistance to acid attack. Komljenovic et al [10] reported that AAS cement pastes were more decalcification-resistant than OPC under the same conditions.

Very few studies have been published studying the acid resistance in alkali-activated fly ash (AAFA) pastes and mortars. Bascarevic et al. [11] observed that acid attack with accelerated 6-M $NH_4NO_3$ solution lowered mechanical strength and induced alkaline and alkaline-earth metal leaching, as well as alterations in the N-A-S-H gel structure that explained the differences in mechanical performance observed. No studies have been carried out studying the effect of fly ash nature in the acid resistant behaviour. An understanding of the short-term interaction between 6-M $NH_4NO_3$ and these fly ashes activated pastes and mortars, as well as of the characteristics of early-age leaching and decalcification, is therefore deemed to be needed.

## EXPERIMENTAL WORK

CEM I 52.5R (OPC) commercial cement was used as a reference for comparison to two types of fly ash, FA-1 and FA-2. The chemical composition of these materials is given in Table 1.

Table 1 Chemical characteristics of raw materials

| | $SiO_2$ | $Al_2O_3$ | $Fe_2O_3$ | CaO | MgO | $SO_3$ | $Na_2O$ | $K_2O$ | $TiO_2$ | LoI |
|---|---|---|---|---|---|---|---|---|---|---|
| OPC | 18.0 | 4.2 | 2.2 | 64.0 | 3.2 | 4.5 | 0.5 | 1.0 | 0.2 | 1.8 |
| FA-1 | 54.4 | 27.5 | 6.4 | 2.7 | 1.5 | -- | 0.5 | 3.1 | 1.3 | 2.1 |
| FA-2 | 53.7 | 21.5 | 4.5 | 0.8 | 0.6 | 0.6 | -- | 1.4 | 1.0 | 14.7 |

| | Vitreous phase | Reactive $SiO_2$ | Reactive $Al_2O_3$ | $SiO_2/Al_2O_3$ |
|---|---|---|---|---|
| FA-1 | 61.1% | 45.1% | 18.0% | 2.5 |
| FA-2 | 50.3% | 44.8% | 13.2% | 3.4 |

LoI: loss on ignition

OPC pastes were prepared mixing with water and AAFA pastes were prepared using waterglass solutions as alkaline activator. Two different molar ratios were used to activate the fly ashes: FA-1: $SiO_2/Al_2O_3$ = 3.6, $Na_2O/SiO_2$ = 0.3 and FA-2: $SiO_2/Al_2O_3$ = 6.0, $Na_2O/SiO_2$ = 0.3. They were used according previous studies [12].

Prismatic specimens 1x1x6 cm were prepared from the three pastes prepared with a liquid/solid ratio of 0.40. For the first 24 hours, the moulded specimens were stored in air-tight receptacles containing distilled and decarbonated water (to ensure a humid atmosphere and prevent

carbonation as far as possible) at a temperature of 22±2 °C and a relative humidity of approximately 99 %. They were subsequently removed from the moulds, wrapped in aluminium foil and cured in the container under the same conditions for another 27 days. All these operations were conducted in an "atmosbag" that afforded a nitrogen (inert) atmosphere.

The paste specimens cured as described above were suspended (to ensure a uniform attack) in a 6-M solution of $NH_4NO_3$ at a pH of 5.2 [13] weighing 10 times the weight of the specimens. The test times were 3, 9 and 21 days. The pH remained within the range described in the procedure throughout the test with no need to renew the $NH_4NO_3$ solution.

The $t_0$ or pre-exposure (throughout this paper: refers to exposure time, not to curing time, which was 28 days for all specimens) as well as the $t_3$, $t_9$ and $t_{21}$ specimens were compressive-strength tested on an IBERTEX Autotest 200/10 test frame. The elemental composition of the ions dissolved in 20-mL aliquots of solution was determined on a VARIAN 725 ES-ICP inductively-coupled plasma optical emission spectrometer. Specimen microstructure was studied at each test time (on samples submerged in acetone/ethanol to detain the reaction) on a NICOLET 6700 FTIR spectrometer and a $^{29}Si$ and $^{27}Al$ MAS NMR spectra.

## RESULTS AND DISCUSSION

Figure 1 shows the strength in the three systems at the various test times. Table 2 gives the residual strength in the pastes at the three test ages as a percentage of pre-exposure specimen strength.

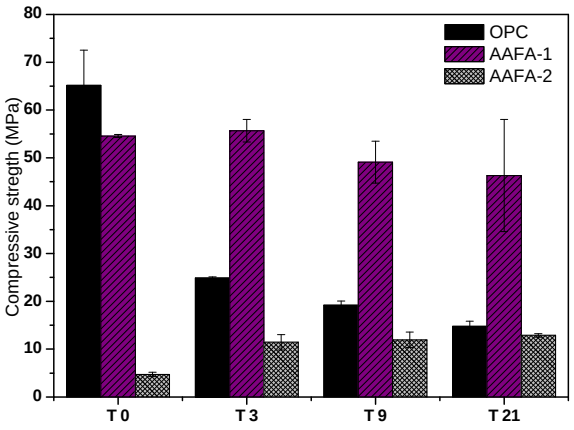


Figure 1 Compressive strength results

Table 2 Residual strength (%) after AAFA paste exposure to a 6-M $NH_4NO_3$ solution

| | Residual strength (relative to $t_0$) | | |
|---|---|---|---|
| | 3 d | 9 d | 21 d |
| OPC | -62 | -70 | -77 |
| AAFA-1 | +2 | -10 | -15 |
| AAFA-2 | +143 | +154 | +173 |

Compressive strength in pre-exposure ($t_0$) AAFA-1 and AAFA-2 specimens was respectively 16 and 92 % lower than in OPC. The explanation for these findings lies in the compositional differences between the two types of fly ash (see Table 1), particularly respecting loss on ignition (2.1 % in FA-1 and 14.7 % in FA-2), and the $SiO_2/Al_2O_3$ moduli used for alkaline activation [14].

According to the results showed in Figure 1 and Table 2 AAFA pastes were much more resistant to the 6-M $NH_4NO_3$ medium than the OPC materials. After just 3 days of interaction, when OPC paste compressive strength had declined by 62 %, the value was practically

unaltered in the AAFA-1 pastes and rose by 143 % in the AAFA-2 pastes. After 3 days, the AAFA-1 pastes began to be impacted by exposure to the acid medium, with $t_{21}$ strength declines of 10-15 %, although these values were much smaller than observed for OPC (see Table 2). AAFA-2 paste compressive strength, in turn, continued to rise with reaction time: the $t_{21}$ values were 173 % higher than the strength recorded prior to interaction with the acid medium ($t_0$).

Aliquots of the leachates/aggressive solution were analysed by ICP to determine the proportion of ions that had leached out of the pastes. The percentage of leached cations ($Ca^{2+}$, $Al^{3+}$ and $Mg^{2+}$) was calculated from the chemical composition of the starting materials (FA-1 and FA-2) and the percentage of their reaction products at $t_0$. The percentage of reaction product was calculated by attacking the pastes with 1:20 (v:v) HCl [15], which separates the reaction products (zeolites and N-A-S-H gel) dissolved in the acid from the unreacted fly ash and non-reactive phases such as quartz and mullite, which remain in the insoluble residue. According these results the percentage of reaction products obtained in AAF-1 pastes were 32.9% and 40.6% in AAFA-2 pastes.

Table 3 lists the percentages of the $Ca^{2+}$, $Al^{3+}$ and $Mg^{2+}$ cations that leached into the 6-M $NH_4NO_3$ solution at the three test ages, as well as the percentages of the same cations leaching out of the OPC as reported by Puertas et al. [1].

Table 3 Cations in the leachate by reaction time (wt%)

| | Time | $Ca^{2+}$ | $Al^{3+}$ | $Mg^{2+}$ |
|---|---|---|---|---|
| OPC | 9 days | 70.00 | n.d | n.d. |
| | 21 days | 82.00 | n.d | n.d. |
| AAFA-1 | 3 days | 7.47 | < 0.1 | 0.88 |
| | 9 days | 13.40 | < 0.1 | 2.04 |
| | 21 days | 18.90 | < 0.1 | 3.69 |
| AAFA-2 | 3 days | 2.59 | < 0.1 | 0.03 |
| | 9 days | 7.00 | < 0.1 | 0.11 |
| | 21 days | 5.97 | < 0.1 | 0.13 |

n.d.: not determined

According to the results shown in Table 3 more cations leached out of the OPC than the AAFA pastes after exposure to the 6-M $NH_4NO_3$ solution. Specifically calcium leaching data quite different in OPC and AAFA pastes. Those findings should be interpreted in context, however: the CaO content in fly ash FA-1 was 2.7 % wt and in FA-2 0.8 % wt, in OPC was 64.0 % wt. The amount of $Ca^{2+}$ cations leaching out of the AAFA-1 pastes was about 50-70 % higher than found for the AAFA-2 pastes, although these amounts never exceeded 20 % of the total in the former or 7 % in the latter, compared to 82 % in OPC. Less than 4 % $Mg^{2+}$ (with higher leaching in AAF-1 pastes) and less than 0.1% $Al^{3+}$ leached out of either of the pastes.

For explaining the mechanical and leaching behaviour of AAFA pastes in 6M- $NH_4NO_3$ solutions a deep mineralogical and microstructural study of pastes by FTIR and NMR-MAS has been carried out.

The FTIR spectra for pastes AAFA-1 and AAFA-2 before and after exposure to the aggressive $NH_4NO_3$ solution are reproduced in Figure 2.

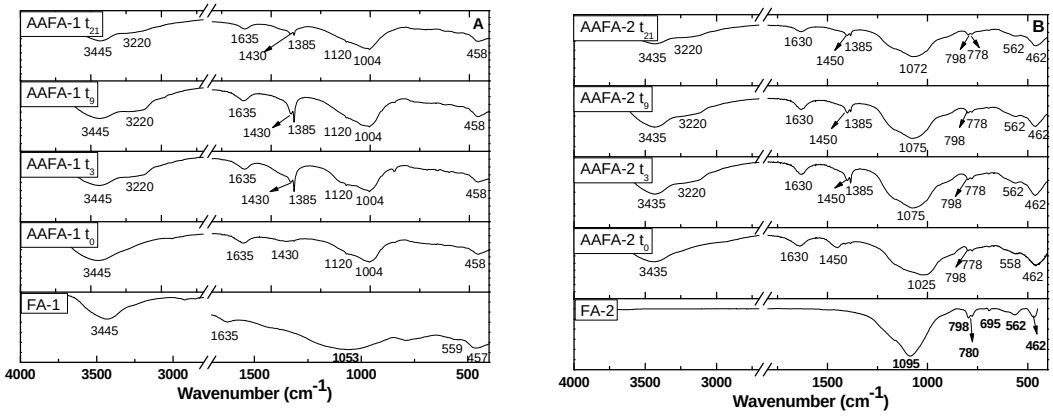


Figure 2 FTIR spectra for anhydrous samples and pastes after exposure to an aggressive medium for 0, 3, 9 and 21 days ($t_0$, $t_3$, $t_9$ and $t_{21}$):
A) FA-1 and AAFA-1;
B) FA-2 and AAFA-2

The IR spectra exhibited bands at 3 435 and 1 635 $cm^{-1}$ assigned to asymmetric stretching ($\nu_3$ H-O-H) and bending ($\nu_4$ H-O-H) vibrations in $H_2O$ molecules, respectively. Traces of carbonates were also detected as the wide band at around 1 430 $cm^{-1}$ attributed to the ($\nu_3$ O-C-O) asymmetric stretching vibrations in $CO_3^{2-}$ functional groups. The intensity of the carbonate group bands failed to rise throughout, confirming the effectiveness of the atmosbag to minimise contact with atmospheric $CO_2$.

The wide band at around 1 053 and 1 095 $cm^{-1}$ on the spectra for FA-1 and FA-2, respectively was assigned to the $\nu_3$ asymmetric stretching vibrations in T-O-T (T = Si, Al). Alkaline activation of the fly ash induced a shift in this band to lower wavenumbers: 1 004 and 1 025 $cm^{-1}$, respectively, due to the formation of N-A-S-H gels, the main product of fly ash alkaline activation. The exact position of that band was determined by the Si/Al ratio in the reaction products (N-A-S-H gel) and more specifically by the number of $Al^{3+}$ atoms [16]. By reducing the angle in the T-O-T bond, the replacement of $Si^{4+}$ with $Al^{3+}$ induced a shift in the respective band to lower wavenumbers.

The different positions of the $\nu_3$ asymmetric stretching band in the T-O-T (T = Si, Al) bonds in the two pastes implied that the N-A-S-H gels formed had different Si/Al ratios. In the AAFA-2 pastes, the band was centred over 1 025 $cm^{-1}$, denoting a larger number of Si-O bonds and therefore a higher-Si gel than formed in the AAFA-1 pastes. The 1 004 $cm^{-1}$ for the latter denoted a higher proportion of Al-O bonds. The band at 457-462 $cm^{-1}$ in the anhydrous pastes, assigned to T-O stretching vibrations, barely changed with alkaline activation. This band is indicative of sample amorphisation: although the amount of amorphous material in the initial fly ash declined, as it was replaced by amorphous material in the N-A-S-H gel, the position of the band remained essentially unvaried [16]. On the contrary, the wide band at 800-500 $cm^{-1}$ in FA-1 and 800-562 $cm^{-1}$ in FA-2, associated with the vibrations in Si-O-Al or Si-O-Si tetrahedra and fragments of aluminosilicates, was affected by alkaline activation. It disappeared in FA-1 and shifted to lower wavenumbers in FA-2 due to the aforementioned changes induced in this type of structures by alkaline activation.

This technique revealed no changes in the AAFA-1 pastes after contact with the aggressive solution. The T-O-T (T = Si, Al)-generated $\nu_3$ asymmetric stretching band did not shift, confirming the ICP-OES observations: i.e., that the 6-M $NH_4NO_3$ solution was unable to extract aluminium from N-A-S-H gels. On the contrary, changes were observed in the $\nu_3$ asymmetric stretching band for T-O-T (T = Si, Al) bonds on the spectra for the AAFA-2 pastes. After the first 3 days of interaction with the aggressive solution, the band was found to shift from 1 025 $cm^{-1}$ ($t_0$) to 1 075 $cm^{-1}$ ($t_3$ and $t_9$) and 1 072 $cm^{-1}$ ($t_{21}$), denoting the formation of a larger number of Si-O bonds in the gel.

The mechanism governing the rise in silicon content in the N-A-S-H gel may have been similar to the process described for zeolite 'de-aluminisation'. The $NH_4^+$ in the aggressive solution would induce gel protonation, followed by the release of gaseous ammonia. Such protonation would weaken the Al-O bonds, so that in the presence of water Al ions would migrate from the crystalline network as aluminium hydroxide hydrates. The voids in the network would be occupied by silicons either migrating from other positions or taken up from the pore solution [17].

Figure 3 A) and B) depicts the $^{27}Al$ MAS NMR spectra for pastes AAFA-1 and AAFA-2. Two distinct regions were observed on the spectra for the two types of ash: a first at 50 to 80 ppm, containing the bands attributed to tetrahedrally coordinated aluminium ($Al_T$); and a second at 20 to -10 ppm, with bands assigned to octahedrally coordinated Al ($Al_O$). $Al_T$ was associated with the aluminium in the reaction products (N-A-S-H gel and zeolites), while $Al_O$ was associated with the element present in mullite.

The $^{27}Al$ MAS NMR spectra for the pre-exposure pastes ($t_0$ pastes) revealed the presence of both tetra- and octahedrally coordinated aluminium as bands centred over 57.93 (blue signal) and 0 (grey signal) ppm, respectively, associated with the aluminium in the reaction products and in mullite. The presence of the latter was also detected on FTIR spectra. After leaching process, the band attributed to $Al_T$ barely shifted throughout the test in either type of ash (see Figure 3), again confirming that although the gel structure changed, the aluminium remained tetrahedrally coordinated. Two signals on the spectra for the AAFA-2 pastes attributable to octahedral aluminium were observed: one at 0 ppm, associated with mullite, and another, a new signal, at -2 ppm, related to the presence an aluminium hydroxide [18].

Figure 3 C) and D) depicts the deconvoluted $^{29}Si$ MAS NMR spectra, while Table 4 lists the ppm values and attributions for the 0-, 3-, 9- and 21-day fly ash pastes.

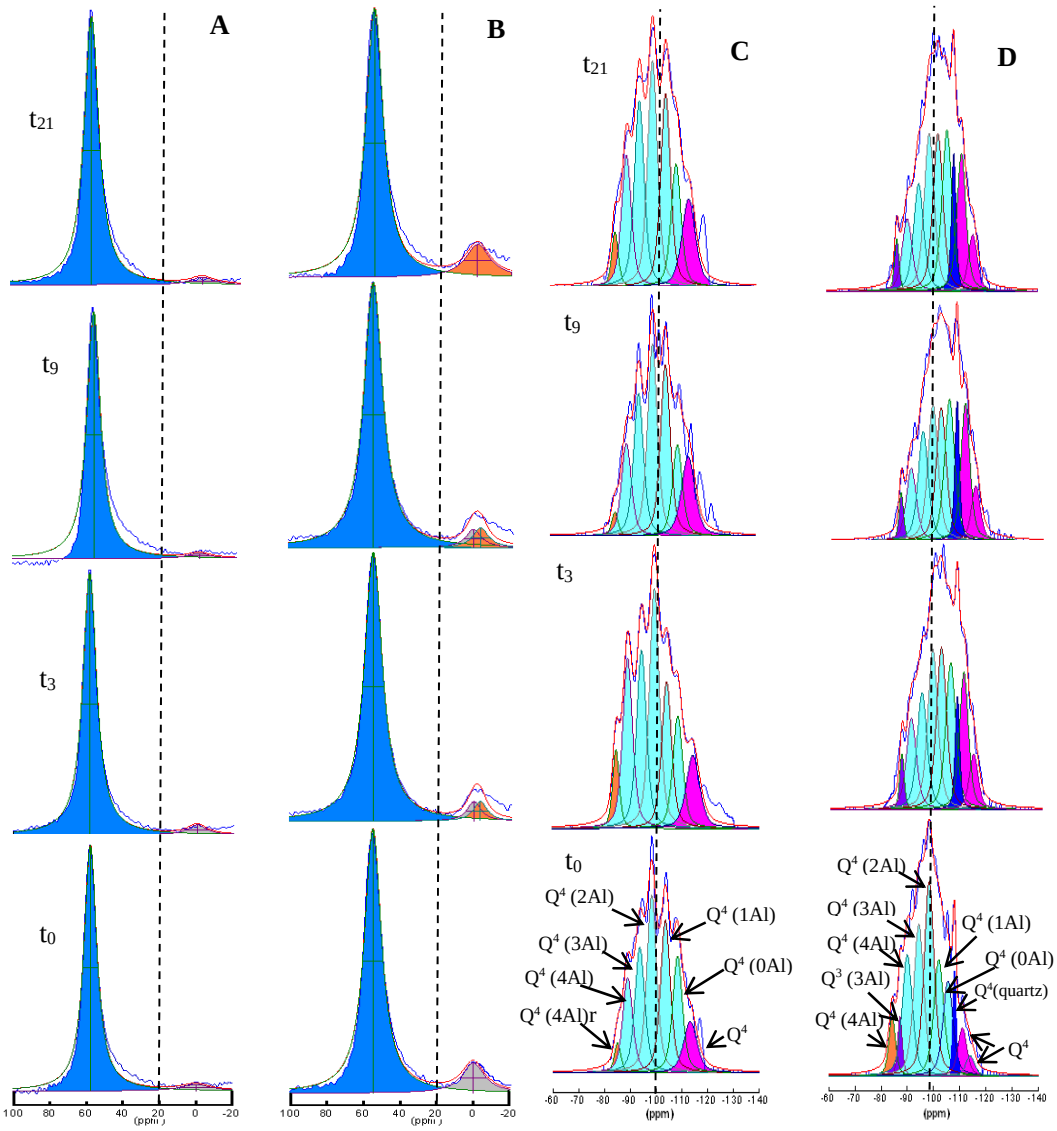


Figure 3 MAS NMR spectra for A) $^{27}$Al AAFA-1, B) $^{27}$Al AAFA-2, C) $^{29}$Si AAFA-1 and D) $^{29}$Si AAFA-2

The deconvoluted $^{29}$Si MAS NMR spectra for the AAFA pastes exhibited no new signals after contact with the acid solution, but rather merely variations in the existing signals (see Table 4).

Five signals appeared on the $^{29}$Si MAS NMR spectra for the two AAFA pastes at $t_0$, centred over -89.0, -95.0, -99.0, -104.0 and -109.0 ppm. These signals were attributed to five possible species with $Q^4$ (mAl) units (m = 4, 3, 2, 1 or 0) in the aluminosilicate N-A-S-H gels generated during the alkaline activation of fly ash [19]. Four other signals were also present. The first was centred over -85.0 ppm, attributed to less condensed species present in the system or even to residual silanol groups [19]. The second, centred over -87.5 ppm, was assigned to the $Q^3$ (3Al) units in the mullite present in fly ash FA-2. The third, at -108.0 ppm, characteristic of the $Q^4$ units in quartz, was associated with that mineral. Lastly, the group of signals between -111.0 and -115.0 ppm was associated with the $Q^4$ (0Al) units present in high-silicon, silica gel-like reaction products [11, 19].

Table 4 Deconvolution of bands on $^{29}$Si MAS NMR spectra for pastes AAFA-1 and AAFA-2

| | t | | $Q^4$ (4Al)r | $Q^3$ (3Al) | $Q^4$ (4Al) | $Q^4$ (3Al) | $Q^4$ (2Al) | $Q^4$ (1Al) | $Q^4$ (0Al) | $Q^4$ (Quartz) | $Q^4$ (Silica gel) |
|---|---|---|---|---|---|---|---|---|---|---|---|
| AAFA-1 | 0 | ppm | -85.8 | | -89.7 | -94.5 | -99.1 | -104.4 | -109.1 | | -114.1 |
| | | W | 3.0 | --- | 4.5 | 4.5 | 4.5 | 4.5 | 4.5 | --- | 4.0 |
| | | I | 2.7 | | 12.7 | 16.7 | 23.8 | 20.3 | 16.8 | | 6.9 |
| | 3 | ppm | -84.8 | | -89.3 | -94.7 | -99.6 | -104.4 | -108.7 | | -114.5 |
| | | W | 3.0 | --- | 4.5 | 4.5 | 4.5 | 4.5 | 4.5 | --- | 4.0 |
| | | I | 5.4 | | 17.3 | 18.1 | 24.4 | 14.7 | 12.6 | | 7.5 |
| | 9 | ppm | -85.5 | | -90.0 | -94.7 | -100.1 | -105.1 | -109.8 | | -114.0 |
| | | W | 3.0 | --- | 4.5 | 4.5 | 4.5 | 4.5 | 4.5 | --- | 4.0 |
| | | I | 2.0 | | 11.6 | 17.9 | 24.1 | 21.3 | 13.6 | | 9.4 |
| | 21 | ppm | -85.5 | | -89.9 | -94.9 | -100.0 | -105.1 | -109.1 | | -114.0 |
| | | W | 3.0 | --- | 4.5 | 4.5 | 4.5 | 4.5 | 4.5 | --- | 4.0 |
| | | I | 3.7 | | 13.2 | 18.6 | 22.7 | 19.1 | 14.0 | | 8.7 |
| AAFA-2 | 0 | ppm | -84.3 | -87.2 | -90.0 | -94.4 | -98.3 | -102.0 | -105.5 | -108.0 | -111/-114 |
| | | W | 3.0 | 2.0 | 4.5 | 4.5 | 4.5 | 4.5 | 4.5 | 2.0 | 4.0 |
| | | I | 4.7 | 3.2 | 14.4 | 18.0 | 23.1 | 13.8 | 11.3 | 4.2 | 7.3 |
| | 3 | ppm | | -87.0 | -90.6 | -94.6 | -98.7 | -102.0 | -105.5 | -108.0 | -110/-114 |
| | | W | --- | 2.0 | 4.5 | 4.5 | 4.5 | 4.5 | 4.5 | 2.0 | 4.0 |
| | | I | | 2.7 | 9.9 | 12.6 | 17.3 | 17.5 | 15.9 | 5.5 | 18.6 |
| | 9 | ppm | | -86.7 | -90.5 | -95.0 | -98.7 | -101.8 | -105.0 | -107.9 | -111/-115 |
| | | W | --- | 2.0 | 4.5 | 4.5 | 4.5 | 4.5 | 4.5 | 2.0 | 4.0 |
| | | I | | 2.5 | 8.6 | 12.9 | 16.1 | 15.7 | 16.7 | 7.3 | 20.2 |
| | 21 | ppm | | -86.7 | -90.6 | -95.0 | -99.0 | -102.3 | -105.8 | -108.3 | -111/-115 |
| | | W | --- | 2.0 | 4.5 | 4.5 | 4.5 | 4.5 | 4.5 | 2.0 | 4.0 |
| | | I | | 2.6 | 7.9 | 11.7 | 17.2 | 17.2 | 17.6 | 6.7 | 19.0 |

r: residual silanol groups [18]; W = width; I = intensity

The N-A-S-H gels in the AAFA-1 pastes had 29.4 % $Q^4$(4Al) + $Q^4$(3Al) units compared to 44.1 % $Q^4$(2Al) + $Q^4$(1Al) units. These differences in intensity in high-aluminium and high-silicon units are consistent with observations reported by Criado et al. [19]. The proportions were more balanced in the AAFA-2 pastes, at 32.4 versus 36.9 %. Nonetheless, since the FTIR analyses (see Figure 2) assigned the vibration band centred over 1 025 $cm^{-1}$ to T-O (T = Si, Al) units, identified with N-A-S-H gel formation, and since at that position these units would be closer to a silica gel, the large proportion of high-aluminium units in these pastes may have been due to the presence of unreacted fly ash and the formation of an aluminium-low N-A-S-H gel.

The centre of gravity on the spectra for the $t_0$ pastes was located at -100 ppm in the AAFA-1 pastes and at -98 ppm in the AAFA-2 pastes. While no variation was observed in the AAFA-1 pastes after exposure to 6-M $NH_4NO_3$, in the AAFA-2 pastes it shifted by 2 ppm, i.e., toward higher-silicon gels. This was consistent with the FTIR findings (see Figure 2), where the vibration band characteristic of the T-O units (T = Si, Al) remained invariable throughout the 21 days of the trial in the AAFA-1 pastes but shifted toward higher values closer to silica gel in the AAFA-2 pastes.

Whilst the number of high-silicon units ($Q^4$ (mAl) (m=1 or 0)) grew in the AAFA-1 pastes with the decline in the high-aluminium units ($Q^4$ (mAl) (m = 4 or 3)), the variations in intensity in these signals amounted to no more than around 10 %. The intensity of the signal at -114 ppm,

associated with the $Q^4$ units in silica gel, rose by 30 %. This rise in the silica gel units, an indication of the degradation of N-A.S-H gel, is related to the decline in mechanical strength in these pastes as the trial advanced. The intensity of the signals on the spectra for the AAFA-2 pastes changed more significantly between $t_0$ and $t_{21}$. The intensity of the units with high aluminium contents ($Q^4$(4Al), (3Al) and (2Al)) dropped by 55 to 75 %, whereas the $Q^4$(1Al) and (0Al) units rose by 25 and 56 %, respectively, denoting the formation of a gel with a higher silicon content. Moreover, the intensity of the signals between -111 and -114 ppm, associated with the $Q^4$ units in silica gel, rose by 160 %. This gel might induce phase agglutination, which would explain the slight rise in the mechanical strength observed in these pastes with reaction time.

## CONCLUSIONS

The main conclusions extracted from the present study are:

- AAFA pastes were altered slightly when exposed to a 6-M $NH_4NO_3$ solution, the alterations were much less intense than in OPC and AAS pastes under the same experimental conditions. The explanation lies in the compositional and structural differences between the C-S-H and C-A-S-H gels in OPC and AAS pastes and the N-A-S-H gels in AAFA pastes.
- No aluminium leached out of the N-A-S-H gel in any of the pastes after exposure to the 6-M $NH_4NO_3$ aggressive solution. Further to NMR and FTIR analysis, the direct effect of the attack on AAFA pastes was the formation of higher-silicon N-A-S-H gels.
- The chemical composition of the starting fly ash is a determinant in its reactivity and therefore in the structure of the N-A-S-H gels formed as well as in their stability in the presence of an acid medium.

## ACKNOWLEDGEMENTS

This research was funded by the Spanish Ministry of Economy under project BIA2013-47876-C2-1-P.

## REFERENCES

1. PUERTAS, F, GOÑI, S, HERNÁNDEZ, M S, VARGA, C, GUERRERO, A. Comparative study of accelerated decalcification process among $C_3S$, grey and white cement pastes, Cement and Concrete Composites, Vol. 34, No. 3, 2012, pp 384 - 391.
2. HARRIS, A W, MANNING, M C, TEARLE, W M, TWEED, C J. Testing of models of the dissolution of cements-leaching of synthetic CSH gels, Cement and Concrete Research, Vol. 32, 2002, pp 731 – 746.
3. HAGA, K, SUTOU, S, HIRONAGA, M, TANAKA S, NAGASAKI, S. Effects of porosity on leaching of Ca from hardened ordinary Portland cement paste, Cement and Concrete Research, Vol. 35, 2005, pp 1764 - 1775.
4. SHI, C, STEGEMANN, J A. Acid corrosion resistance of different cementing materials, Cement and Concrete Research, Vol. 30, 2000, pp 803 - 808.

5. PUERTAS, F. Cementos de escorias activadas alcalinamente: Situación actual y perspectivas de future, Materiales de Construcción, Vol. 45, No. 239, 1995, pp 53 - 64.
6. PALOMO, A, BLANCO-VARELA, M T, GRANIZO, M L, PUERTAS, F, VAZQUEZ, T, GRUTZECK, M W. Chemical stability of cementitious materials based on metakaolin, Cement and Concrete Research, Vol. 29, No. 7, 1999, pp 997 – 1004.
7. BERNAL, S A, RODRÍGUEZ, E D, MEJÍA DE GUTIÉRREZ, R, PROVIS, J L. Performance of alkali-activated slag mortars exposed to acids, Journal of Sustainable Cement-Based Materials, Vol. 1, No. 3, 2012, pp 138 – 151.
8. VARGA, C, ALONSO, M M, MEJÍA DE GUTIERREZ, R, MEJÍA, J, PUERTAS, F. Decalcification of alkali-activated slag pastes. Effect of the chemical composition of the slag, Materials and Structures, Vol. 48, 2015, pp 541 - 555.
9. PALOMO, A, KRIVENKO, P, GARCIA-LODEIRO, I, KAVALEROVA, E, MALTSEVA, O, FERNANDEZ-JIMENEZ. A, A review on alkaline activation: new analytical perspectives, Materiales de Construcción, Vol. 64, No. 315, 2014, pp 1 - 24.
10. KOMLJENOVIC, M M, BASCAREVIC, Z, MARJANOVIC, N, NIKOLIC, V. Decalcification resistence of alkali-activated slag, Journal of Hazardous Materials, Vol. 233 – 234, 2012, pp 112 - 121.
11. BASCAREVIC, Z, KOMLJENOVIC, M M, MILADINOVIC, Z, NIKOLIC, V, MARJANOVIC, N, ZUJOVIC, Z, PETROVIC, R. Effects of the concentrated $NH_4NO_3$ solution on mechanical properties and structure of the fly ash based geopolymers, Construction and Building Materials, Vol. 41, 2013, pp 570 – 579.
12. VARGA, C. Cementos activados alcalinamente. Comportamiento reológico y durable en medio ácido". PhD Thesis. Universidad Autónoma de Madrid. 2015 (In Spanish)
13. HEUKAMP, F H, ULM, F J, GERMAIN, J T. Mechanical properties of calcium-leached cement pastes. Triaxial stress states and the influence of the pore pressures, Cement and Concrete Research, Vol. 31, 2001, pp 767 - 774.
14. MASSIOT, D, FAYON, F, CAPRON, M, KING, J, LE CALVE, S, ALONSO, B, DURAND, J O, BUJOLI, B, GAN, Z, HOATSON, G. Modelling one and two dimensional solid state NMR spectra, Magnetic Resonance in Chemistry, Vol. 40, 2002, pp 70 - 76.
15. CRIADO, M, FERNÁNDEZ-JIMÉNEZ, A, DE LA TORRE, A G, ARANDA, M A G, PALOMO, A. An XRD study of the effect of $SiO_2/Na_2O$ ratio on the alkali activation of Fly ash, Cement and Concrete Research, Vol. 37, 2007, pp 671 - 679.
16. FERNÁNDEZ-JIMÉNEZ, A, PALOMO, A. Mid-infrared spectroscopic studies of alkali-activated fly ash structure, Microporous and Mesoporous Materials, Vol. 86, 2005, pp 207 - 214.
17. ENGELHARDT, G, MICHEL, D. High resolution solid-state of silicates and zeolites, John Wiley and Sons Ed, 1987.
18. PENA, P, RIVAS MERCURY, J M, DE AZA, A H, TURILLAS, X, SOBRADOS, I, SANZ, J. Solid-state $^{27}Al$ and $^{29}Si$ NMR characterization of hydrates formed in calcium aluminate-silica fume mixtures, Journal of Solid State Chemistry, Vol. 181, 2008, pp 1744 - 1752.
19. CRIADO, M, FERNÁNDEZ-JIMÉNEZ, A, PALOMO, A, SOBRADOS, I, SANZ, J. Effect of the $SiO_2/Na_2O$ ratio on the alkali activation of fly ash. Part II: $^{29}Si$ MAS-NMR survey, Microporous Mesoporous Materials, Vol. 109, 2008, pp 525 - 534.

# EMBEDDED SENSORS FOR THE CORROSION MONITORING AND CONTROL IN MARINE STRUCTURES

**C Bartolomé**

Spanish Institute of Cement and its Applications

**C Andrade**

Instituto of Construction Science Eduardo Torroja

Spain

**ABSTRACT.** Reinforcement corrosion induces several structural damages which affect the serviceability and the safety of concrete structures. The use of sensors can help to control and optimize the life cycle and indicate the best time to undertake repair at the lower cost. Monitoring by embedded is not a new technology as there are an increasing number of concrete structures that are being monitored. However, results are scarce on the interpretation of the values obtained due the difficulty to link them to the climatic changes in temperature and humidity. On the parameters to be monitored and evaluated, temperature and corrosion potential are the most common although there are other which are also very important regarding the prediction of future durability. Thus, strains, concrete resistivity (liquid water content) and corrosion rate seems also necessary to be monitored if accurate predictions are necessary. In present paper, an example of a marine structure, the super-harbour of Langosteira in La Coruña is presented in order to illustrate the difficulties of placing electrodes and equipments in during the fabrication of the structures. A central unit able to collect powered by batteries has been developed the data are transmitted via radio and shown in a web site were the data will be analyzed and introduced in models of service life.

**Keywords:** Sensor, Resistivity, Durability, Harbour, Chloride, Corrosion.

**Mr César Bartolome** is the Director of the Innovation Area at the Spanish Institute of Cement and its Applications (IECA).

**Dr Carmen Andrade** is a scientist studying the durability of buildings, with particular attention at the phenomenon of corrosion of steel in reinforced concrete.

## INTRODUCTION

The need to predict the reinforcement corrosion is increasing the demand to use embedded sensors (1) during the construction of the structures or to install them in existing ones. These sensors can measure several parameters being the usual: the corrosion potential, the galvanic current between a more external and a more internal steel coupon and the concrete resistivity, all together with the temperature. Less common are sensors to measure the corrosion rate (2) due to this technique needs to account for the amount of polarized area of the reinforcement.

The use of sensors present three main problems in the opinion of the authors: 1) the cabling whose avoidance has promoted in the last few years the use of wireless technologies, that however have the inconvenience of the short duration of the batteries. This is due to the relatively high demand of energy by the corrosion sensors which need to be activated for the measurement (resistivity and polarization resistance), 2) the interpretation of the results, because they are very numerous and demand to be expertise for their translation into useful information for the manager of the structure, 3) finally, the survival of the sensor to the construction phase of the structure. In present case this phase is very potentially damaging, because the concrete placement is by using slipping formwork and enormous cranes and machinery are operating.

In present paper the description of a long duration sensor with wireless technology is presented. This corrosion sensor has been embedded in several harbour caissons in order to anticipate possible future corrosion of the reinforcements. The results of the sensor are being sending to a web site in which the results, not only are plotted but they are used to calculate the time to corrosion of reinforcements. The sensor and the recording of data have been developed within the frame of a national project (3) in which several technologies are being studying for a better control of the deterioration in harbour structures.

## EXPERIMENTAL PROGRAMME

The site were the sensors have been applied is the new super-harbour of Langosteria- La Coruña in the Atlantic northwest of Spain. A view of the harbour in its present state of construction is given in Figure 1. The concrete production planned is of around 3.5 million tons. The main structures being built are: the caissons for a dock Figure 2, the breakwater composed of a wall and disordered very large concrete cubes (named concrete blocks), Figure 3.

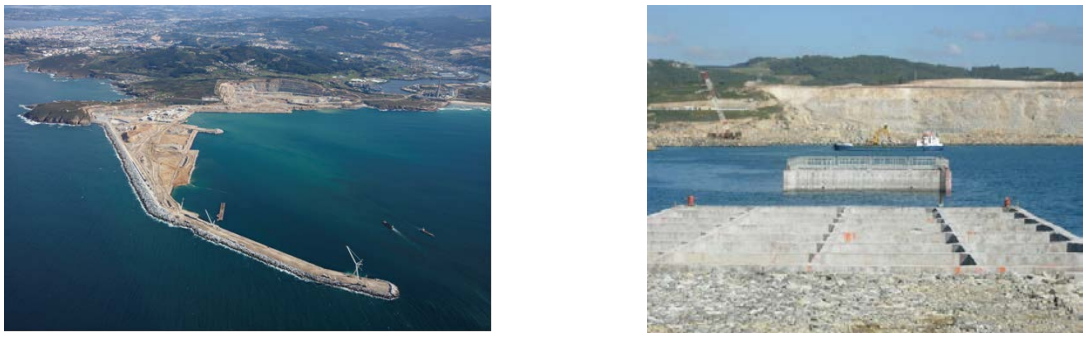

Figure 1 View of the super-harbour Langosteira and a detail of the caissons being placed aligned for the dock.

Figure 2 Several aspects during the construction of the caissons where the sensors are embedded

Figure 3 Concrete blocks and their placement for the breakwater.

**Description of sensors**

It is called sensor the set of elements from the electrodes to collect the data to the device able to transmit them. Several attempts were made to optimize the design. Finally, the sensor consists in four bodies: 1) the electrodes that are placed embedded in the concrete, Figure 4, 2) the central device which has the hardware with the techniques, also registers the results and transmits them via radiofrequencies, Figure 5, 3) the collector-transmitter via internet of the signal (Figure 7 and 4) the web site in which the results are plotted and analysed.

**Electrodes embedded**

Two kinds of sensors were used: passive sensors, which do not need any current to work, and active sensors, which need an electrical current for measuring.

Passive sensors:

- Corrosion potential: consisting in a $Mn/MnO_2$ reference electrode.
- Temperature: consisting of a commercial thermistor.

Active sensors:

- Corrosion rate: consisting of two coupons of reinforcing bar for measuring the Polarization Resistance, Rp. A connection to the main reinforcement is also made for the sake of comparing its potential to that recorded in the two small bar coupons.
- Resistivity: by means of a two parallel stainless steel bars

Figure 4 Aspect of the electrodes fabricated to collect data and during its placement attached to the reinforcement of the caisson.

Additionally, sensors for the detection of chloride anions were also placed. This device consisted of two bars with different covers, so that they begin to corrode (measured by detecting changes in the corrosion potential) at different time. As the distance between both bars is known, measuring the lapse of time between the corrosion initiation between them, the rate of chloride penetration can be calculated.

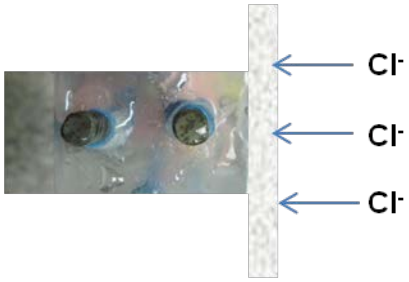


Figure 5 Sensor for chloride detection

**Techniques**

The small central body having the hardware is shown in figure 5. It carries out all the mentioned techniques: corrosion potential, polarization resistance by means of a galvanostatic pulse registering the potential during 30 seconds and resistivity through the ohmic drop of the galvanostaic pulse. It has autonomy for several years. Also this body can measure other techniques as the temperature and the deformation (vibrating wires or accelerometers). It is connected to a single set of electrodes.

Figure 6 In the left the central unit having the hardware and in the right the collector of data by means of radio-frequency which is connected to a computer.

This central unit of the sensor has a datalogger and it is able to transmit by radio the collected results when requested from a second unit (shown in the right photo of Figure 5) which is connected to a computer that transmit the data to a web-site via internet.

**Placement of sensor central unit**

The fabrication of the caissons represents a big risk for survival of the sensors and of the central sensor unit due the operation of the finger for the concrete pumping (Figure 7 left) and dumpers (Figure 7 right) all during the fabrication and after it for the filling of the alveolus of the caissons.


Figure 7 Left: concrete pumping and right dumper filling the alveolus of teh acisson after its fabrication.

In order the sensors to survive, the cables of the electrodes were attached to the reinforcements and made to arrive to the surface of the caisson where the central unit was introduced in a box (Figure 8), that was made watertight. A mechanixcally resistant cap (Figure 8 right) was placed on the surface of this box in order to protect it from the machinery.As soon as the concrete has hardened, the cap is removed and the cables are taken and extended. The central unitis then was intoduced in another box (see Figure 9) a bit elevated from the caisson surface in order to mantain it not accessible for the dumpers and also elevated from the sea water.

Figure 8 left: Box embedded in the concrete during concrete setting and right the cap to protect this box from machinery

Figure 9 Left: the box in which the central unit of Figure 5. In the centre the aspect at the border of the caisson and in the right the access to it after the concrete has hardened.

### Position of sensors

Sensors were placed in two different positions within the dock:


Figure 10 Position of sensors inside the harbor

Two sensors of every type were placed in each position in order to guarantee at least one measurement for both points.

## RESULTS

### Temperature

The first problem to face when building the caissons was the temperature increase during the setting due the large size of the structure. Micro cracking caused by temperature gradient should be avoided to guarantee the durability of the structure.

For these reason, CEM IV/A-V according to European standard EN 197-1 was chosen. This cement has a high contain of fly ashes (between 11 and 35%), which defers in time cement hydration, thus reducing the peak temperature reached inside concrete.

The maximum permitted temperature was established in 60ºC. Under this temperature, micro cracking was considered not to be relevant for durability. The measured temperatures inside concrete, given by temperature sensors, are shown in Figure 11. Maximum temperature resulted to be permanently under the limits.

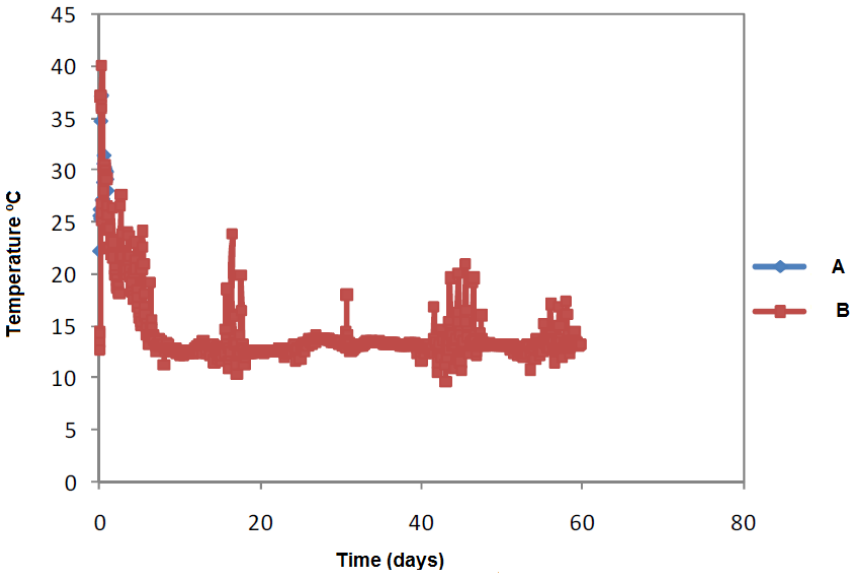


Figure 11 Temperature inside caisson when concrete hardening

## Corrosion rate

When designing the structure, an alert system was defined for creating a durability strategy. The following values were decided:

- When Icorr < 0,2 µA/cm$^2$, the structure was considered not to have any durability risk.
- When 0,2 µA/cm$^2$ > Icorr > 0,5 µA/cm$^2$, in situ inspections shoud be carried out.
- When Icorr > 0,5 µA/cm$^2$, repair actions are necessary.
-

Figure 12 shows the corrosion rate measured for both positions:

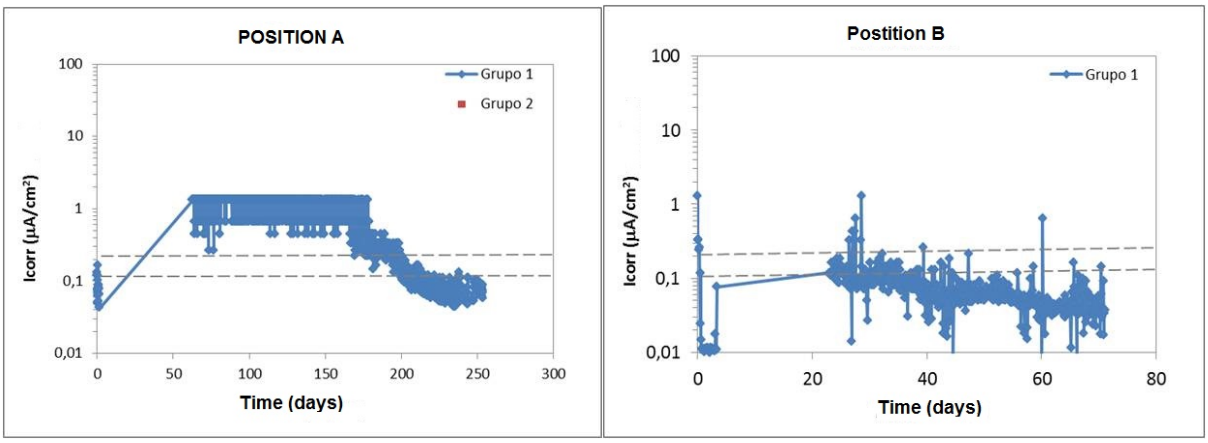


Figure 12 Corrosion rate measured by sensors in positions A and B

Just after construction, these values were over the limit, which was not reasonable. As the uncertainty about battery capacity was high, very short polarization times were programmed. When battery was checked to last for several months, polarization time was changed into a time of 100 seconds. From that moment, corrosion rate values decreased under the limit value of 0,2 µA/cm$^2$.

**Resistivity and durability model**

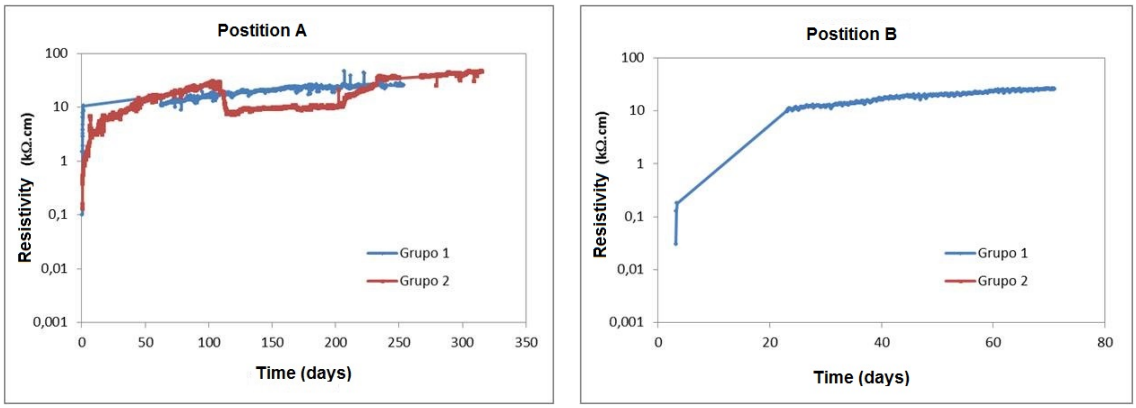


Figure 13 Resistivity measurements

The main novelty of this work is the application of a durability model based on resistivity. As it is continuously measured by means of a non-destructive method, the model can be updated constantly to predict the exact moment when the reinforcement will be despassivated.
The mathematical expression of the model is:

$$t_L = \frac{c^2 \cdot \rho}{F_{exp}} \cdot r_{Cl}$$

Where:

- $t_L$ = despassivation time
- c = cover
- $\rho_e$ = resistivity
- $F_{exp}$ = coefficient depending on exposure class
- $r_{Cl}$ = chloride-cement reaction coefficient
-

Caisson values are listed in Table 1.

Table 1 Specific parameters of the caisson for durability model

| | |
|---|---|
| Cover, x | 5 cm |
| chloride-cement reaction coefficient ($r_{Cl}$) (cement type IV) | 1,6 |
| F exp (exposure class IIIc according to Spanish code) | 20 cm$^3$kΩ/year |

Applying the durability model, corrosion of reinforcing steel will begin after 50 years.

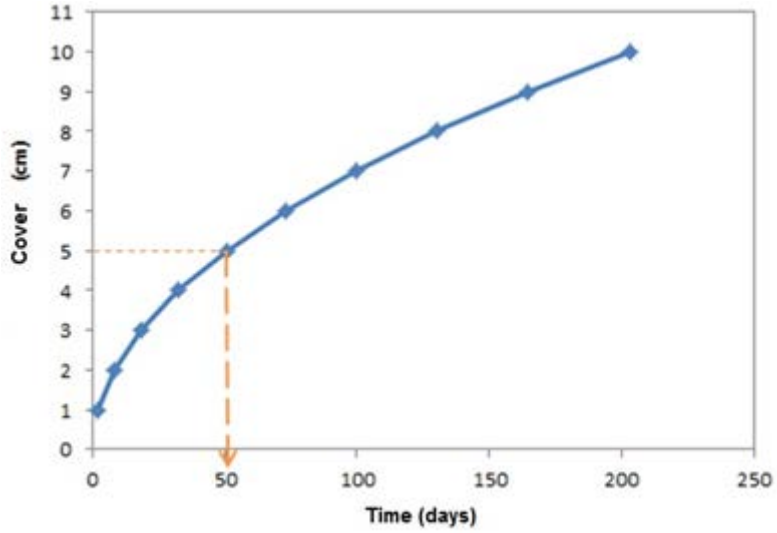


Figure 14 Durability law for caissons, service life

## CONCLUSIONS

It can be concluded from the experience that:

1. One of the most critical steps in the placing sensors in structures is the concreting time because the cables need to survive to the ad hoc operations and machinery. The placement has to be then very well planned and designed.
2. Wireless technologies from the concrete structures until a central measuring unit are much more adequate than to use cables. These wireless technologies need also to be well planned in order not to be perturbed by other signals and storms.
3. The amount of data to record has to be rationalized in order to take few but critical intervals. This will help to save energy and to facilitate the analysis of data.

Additionally, durability model based on resistivity permits predicting the service life of the structure.

## ACKNOWLEDGEMENTS

The authors are grateful to the funds provided by the Ministry of Science and Innovation in Spain in the project DYNAPORT. They are also grateful to the construction companies: DRAGADOS, SATO and COPASA, working as joint venture for the construction of the harbor and to the Port Authority of La Coruña for the collaboration provided.

## REFERENCES

1. Ø. VENNESLAND Æ M. RAUPACH Æ C. ANDRADE -Rilem Recommendation of TC 154-EMC: ‘‘Electrochemical techniques for measuring corrosion in concrete’’—measurements with embedded probes“. Materials and Structures (2007) 40:745–758

2. C. ANDRADE ET AL,- Rilem Recommendation of TC 154-EMC, "Test methods for on-site corrosion rate measurement of steel reinforcement in concrete by means of thepolarization resistance method, *Materials and Structures*, vol 37, November 2004, pp 623-643.

3. B. ELSENER ET AL.- Rilem Recommendation of TC 154-EMC, "Half-cell potential measurements. Potential Mapping on reinforced concrete structures". Materials and Structures vol 36 ag-sept. 2003 pp 468-471.

4. C. ANDRADE, I. MARTÍNEZ, M. CASTELLOTE, P. ZULOAGA, Some principles of service life calculation of reinforcements and in situ corrosion monitoring by sensors in the radioactive waste containers of El Cabril disposal (Spain). Journal of Nuclear Materials. 358 (2006) 82-95.

5. EHE-08, Spanish Structural Concrete Code

6. Ø. VENNESLAND, Electrochemical parameters of repaired and non repaired concrete at Gimsoystrauman Bidge. Solvaer-Norway, May 1997, p.253-262.

7. ANDRADE, C., SARRÍA, J., ALONSO, C., Corrosion rate evolution in concrete structures exposed to the atmosphere. Cement and Concrete Composites 24 (2002) 55-64.

# ELECTROCHEMICAL ASSESSMENT OF A WELDED JOINT BETWEEN CARBON STEEL ASTM A 615 AND STAINLESS STEEL 304L EMBEDDED IN CONCRETE

**R Hernández-Leos**

**R Antaño-López J**

Centro de Investigación y Desarrollo Tecnológico en Electroquímica S.C

**T Pérez-Quiroz**

Instituto Mexicano del Transporte

México

**ABSTRACT.** Corrosion in reinforced carbon steel concrete structures invokes the need for constant repairs if the same steel is used to rehabilitate the concrete structures. Therefore, a material to reduce maintenance costs and extend the lifetime of existing structures is sought. Research has shown that the corrosion resistance of stainless steel is higher than that of carbon steel even in aggressive media. It is also confirmed that galvanic corrosion to electrically connect stainless steel to carbon steel is negligible compared to that generated by carbon steel with corroded carbon steel. This work utilised electrochemical techniques in alkaline and neutral saline media and explored the possibility of using carbon steel conforming to ASTM A615 welded to 304L stainless steel for the rehabilitation of concrete structures. Corrosion potential, linear polarization resistance and Impedance Spectroscopy were performed at different time periods to characterize the possible corrosion products at the welded junction of stainless steel - carbon steel. The results so far suggest the feasibility of using stainless steel to rehabilitate concrete structures.

**Keywords:** Stainless Steel, Concrete Structures Rehabilitation, Galvanic Corrosion.

**R Hernández-Leos** is a doctoral student in the Centro de Investigación y Desarrollo Tecnológico en Electroquímica S.C. Her research interest is in the field of corrosion, with special emphasis on durability of reinforced concrete structure, electrochemical techniques to determine the steel corrosion kinetics. She has participated in national and international Congresses and published in the journal Anticorrosion Methods and Materials.

**J T Pérez-Quiroz** is a researcher at the Instituto Mexicano del Transporte in the field of concrete technology. He is a member of several national and international technical committees and has published extensively on many aspects of concrete technology, cement science and sustainable construction.

**R Antaño-López** is a researcher at the Centro de Investigación y Desarrollo Tecnológico en Electroquímica S.C. His main research interest is the study of corrosion processes by electrochemical techniques, especially by Impedance Spectroscopy, which he has been using for more than 20 years.

## INTRODUCTION

The trend to corrosion of embedded metal in concrete is the prime cause of the majority of structural deterioration [1]. Two conditions can break down the passivating environment in concrete without attacking the concrete first. One is carbonation and the other is chloride attack. Once the passive layer breaks down then areas of rust will start appearing on the steel surface.

Carbonation is the result of the interaction of carbon dioxide gas in the atmosphere with the alkaline hydroxides in the concrete. The depassivation mechanism for chloride attack is somewhat different. The initial mechanism appears to be sorption, especially when the surface is dry [2].

Corrosion of concrete reinforcement can be prevented by changing the material used as reinforcement, replacing carbon steel with stainless steel. The better performance of stainless steel compared to carbon steel is mainly due to the presence of chromium generating a protective passivating layer [3].

Some researchers, like Bertolini et al. [4], used stainless steel reinforcement for diminishing corrosion and extend life cycle in comparison with concrete structures reinforced with carbon steel. In the same way, Hunkeler [5] and Jones [6] found that the use of stainless steel reinforcement in concrete extended the life cycle without maintenance.

Pérez Quiroz [7] and Qian Qu [8] found insignificant galvanic corrosion in the electrical junction between stainless steel 304 and carbon steel in alkali solution. They concluded that the electrical connection did not increase the corrosion rate.

Some specifications concerning durability have suggested the use of stainless steel reinforcement in coastal structures: in the tidal zone, splash zone or selects areas in the structure [9].

Previous research works focused on stainless steel and obtained better corrosion resistance. No studies have been reported in which a welded junction between stainless steel and carbon steel has been used in a concrete structure.

It is reported that joining metals by welding has an important advantage, the possibility of joining top to top with better load distribution enables making light structures; easily bonded with the same mechanical resistance; rigid junctions, homogeneous and continuous structures [10]. A special zone for a welding joint is the heat affected zone which experiences higher temperatures and that causes microstructural changes in the base material during welding solidification [11].

Due to the above in this paper we make use of electrochemical techniques to monitor welded stainless steel/carbon steel junctions embedded in concrete immersed in saline solution.

## EXPERIMENTAL PROCEDURE

### Sample Preparation

For preparing the samples, five carbon steel A615 and five stainless steel 304L specimens were cut, 1:1 area ratio, arc welded using a 309L electrode, making 30° angle bevel beforehand. The samples were embedded in concrete with a water to cement (w/c) ratio of 0.45. At the same time another specimen was made of a carbon steel bar, embedded in 0.45 w/c concrete, and used as control. After curing the concrete cylinders immersed in water for 28 days, they were immersed in 3.5% NaCl solution.

Table 1 shows the chemical composition of stainless steel 304L, carbon steel A615 and 309L electrode, using the Schaffler diagram to obtain a microstructure that does not generate corrosion.

Table 1 Chemical composition of materials

| CHEMICAL COMPOSITION, % | | | | |
|---|---|---|---|---|
| | C | Cr | Ni | Fe |
| A615 | 0.24 | 0.07 | 0.07 | 98.3 |
| 304L | 0.01 | 18.3 | 8.07 | 74.1 |
| 309L | 0.02 | 23.0 | 13.0 | 13 |

### Electrochemical Techniques

To characterize the possible corrosion at the Stainless Steel - Carbon Steel welded joint, linear polarization resistance (LPR) and Electrochemical Impedance Spectroscopy measurements were performed at different time periods.

A Gamry Interface 1000 potentiostat was used for all the measurements. Each test was performed using carbon steel-stainless steel welded joint rebar or carbon steel as a working electrode, stainless steel mesh as a counter electrode and Ag/AgCl as a reference electrode.

For corrosion potential monitoring, a Fluke multimeter was used. Each test was performed using carbon steel-stainless steel welded joint rebar or carbon steel as a working electrode and $Cu/CuSO_4$ as a reference electrode.

## RESULTS AND DISCUSSION

### Corrosion Potential

Figure 1 shows the potential values obtained in carbon steel (C) and stainless steel/carbon steel welded joint (SC) embedded in concrete immersed in saline solution. The results show positive values to -200 mV, indicating passive behaviour in SC according to ASTM C876 Standard [12], remarking that the C specimens get more negative potential, thus found in active state.

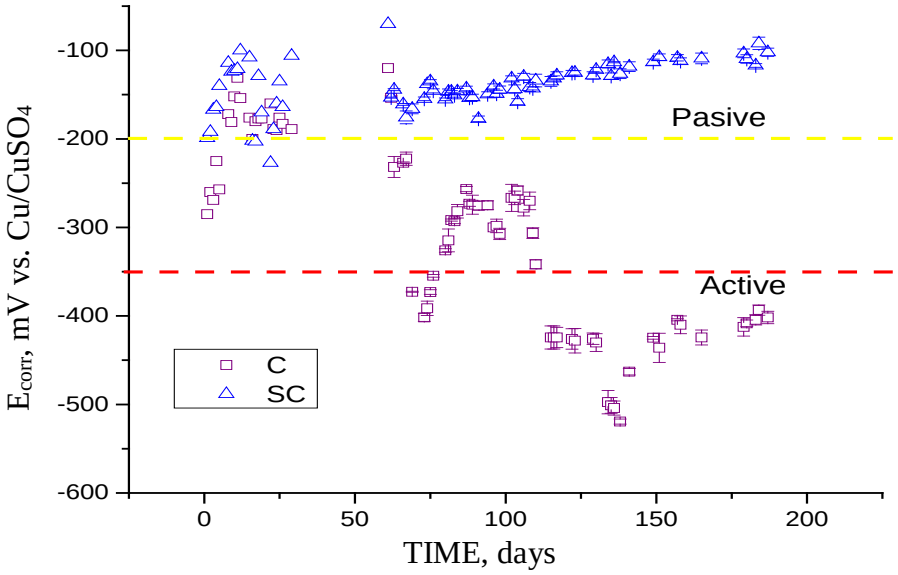


Figure 1 Corrosion potential versus time for carbon steel and stainless steel/carbon steel welded joint embedded in w/c 0.45 concrete and immersed in saline solution

Figure 2 shows potential values obtained in carbon steel (C) and stainless steel/carbon steel welded joint (SC) embedded in w/c 0.65 concrete immersed in saline solution. The results show positive values to -200 mV indicating passive behaviour in SC according to ASTM C876 Standard [12], and remarking that the carbon steel specimens get more negative potential, so they are in active state. These results show better behaviour (less corrosion probability) with specimens in concrete with a w/c 0.45 ratio (Figure 1) than with w/c 0.65 ratio (Figure 2).

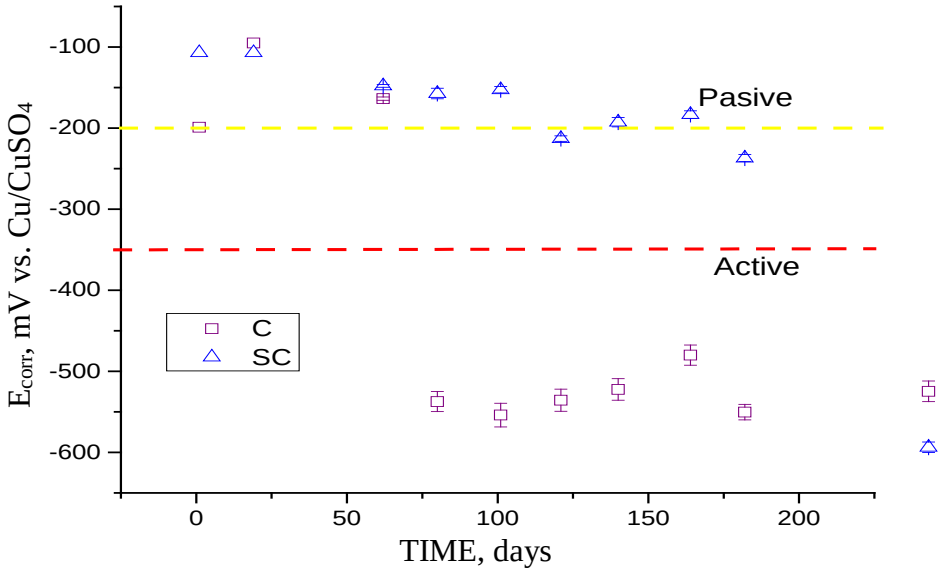


Figure 2 Corrosion potential versus time for carbon steel and stainless steel/carbon steel welded joint embedded in w/c 0.65 concrete and immersed in saline solution

## Polarization Resistance

Figure 3 shows results for polarization resistance (Rp) of stainless steel/carbon steel welded joint (SC) and carbon steel (C) embedded in concrete immersed in saline solution. Larger Rp values were found for SC than for C. According to ASTM G102 [13] and the Stern-Geary equation, this indicates smaller corrosion rate for SC than for C

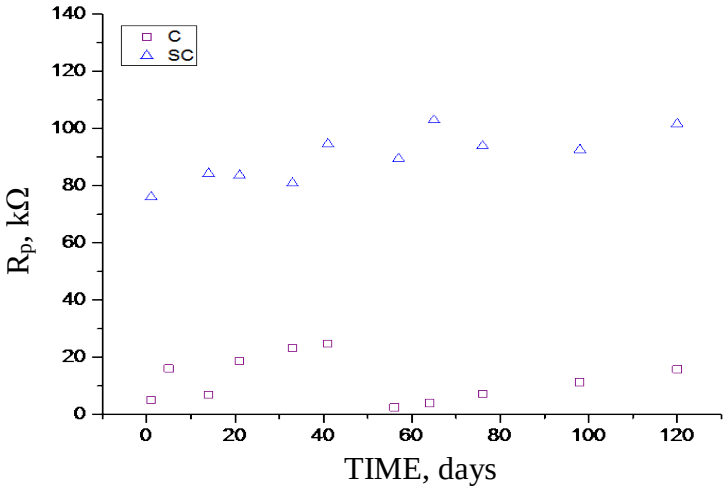


Figure 3 Polarization resistance versus time for carbon steel and stainless steel/carbon steel welded joint embedded in w/c 0.45 concrete and immersed in saline water

Figure 4 shows results for polarization resistance (Rp) of stainless steel/carbon steel welded joint (SC) and carbon steel (C) embedded in concrete immersed in saline solution. Larger Rp values were found for SC than for C. According to ASTM G102 [13] and the Stern-Geary equation this indicates smaller corrosion rate for SC versus C. It is worth noting that higher corrosion rates were found in specimens with w/c 0.65 ratio than with w/c 0.45 ratio.

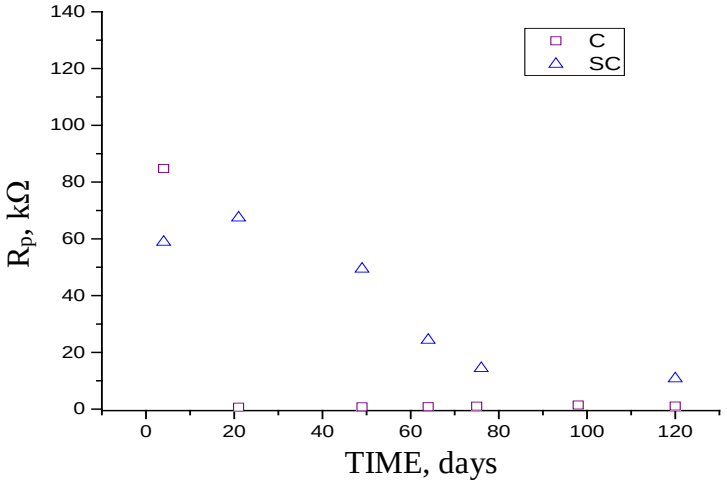


Figure 4 Polarization resistance versus time for carbon steel and stainless steel/carbon steel welded joint embedded in w/c 0.65 concrete and immersed in saline water

## Electrochemical Impedance Spectroscopy

Figure 5 shows Nyquist and Bode diagram obtained for carbon steel (C) embedded in concrete immersed in saline solution, Nyquist diagram shows a resistance (Rs = 77 Ω) associated to electrolyte resistance and has a trend to form a semicircle whose diameter represents the charge transfer resistance (Rct = 2207 Ω·cm²). It is noted that Rct increases with time. This suggests resistive behaviour involving an active interface where the charge transfer resistance will be small, allowing the passage of current, and indicating a high rate of corrosion.

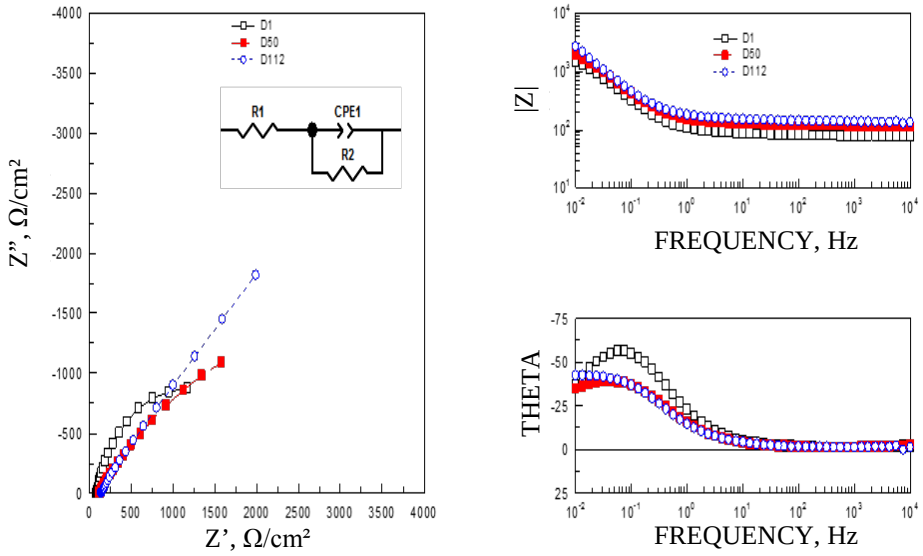


Figure 5 Nyquist and Bode Diagram for carbon steel embedded in w/c 0.45 concrete

Figure 6 shows the Nyquist and Bode diagram obtained for carbon steel (C) embedded in w/c 0.65 concrete immersed in saline solution. The Nyquist diagram shows a resistance (Rs = 102 Ω) associated to electrolyte resistance, has a trend to form a semicircle whose diameter is related to Rct (Rct = 1055 Ω·cm$^2$), and increases with time. This suggests resistive behaviour leaving to the same conclusions as before.

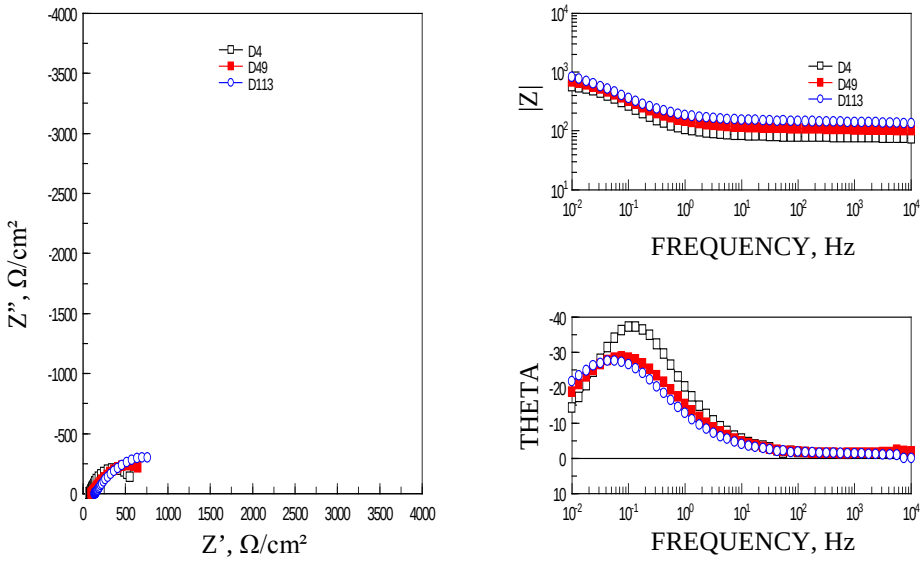


Figure 6 Nyquist and Bode Diagram for carbon steel embedded in w/c 0.65 concrete

Figure 7 shows results obtained in EIS, where the Nyquist diagram at high frequency has a solution resistance (Rs = 102 Ω) and Rtc in low frequency (Rtc = 14554 Ω·cm$^2$), showing a diffusive behaviour at a very low frequency. It may be related to oxygen diffusion (corroborated with the Bode diagram) as this step may be the rate limiting corrosion, because oxygen has to be dissolved in water before reaching the concrete reinforcement, generating small corrosion rates. According to the Rct value, we find smaller corrosion rate in SC/C welded joint (Figure 7) than in C (Figure 5).

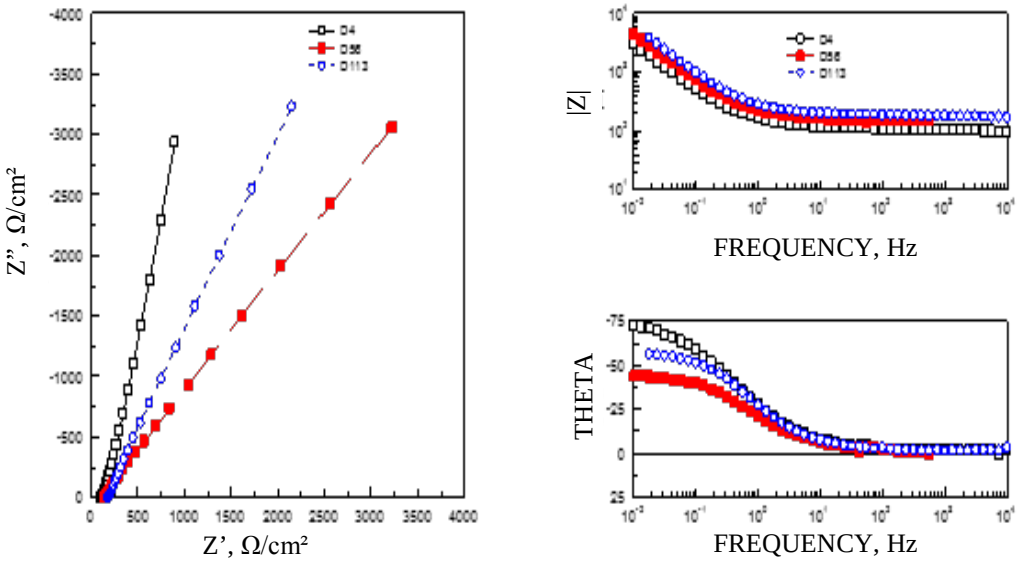


Figure 7 Nyquist and Bode Diagram for stainless steel /carbon steel welded joint embedded in w/c 0.45 concrete

Figure 8 shows results obtained in EIS, where the Nyquist diagram at high frequency has a solution resistance of Rs = 113 Ω and Rct a charge transfer resistance of Rct = 5411 Ω·cm$^2$. The spectra show a diffusive behaviour at very low frequency that may be related to oxygen diffusion (corroborated with the Bode diagram) and this step may be the rate limiting corrosion, because oxygen has to be dissolved in water before reaching the concrete reinforcement, generating small corrosion rates. According to the obtained Rct, we find smaller corrosion rate in SC/C welded joint (Figure 8) than in C (Figure 6).

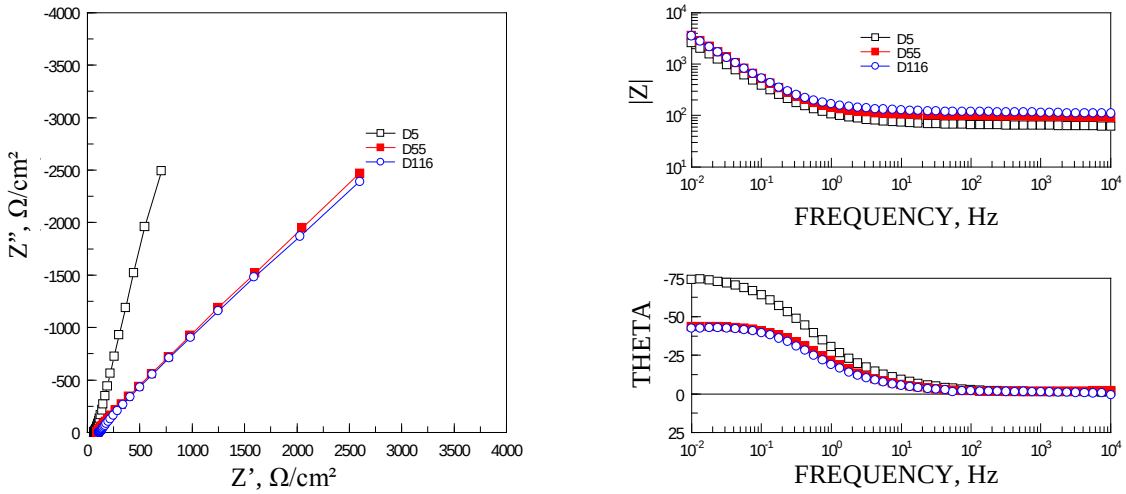


Figure 8 Nyquist and Bode Diagram for stainless steel /carbon steel welded joint embedded in w/c 0.65 concrete

## CONCLUSIONS

The results show that the potentials SC/C welded joint has less probability for corrosion in comparison with C embedded in w/c 0.45 or 0.65 concrete immersed in saline solution. The Rp results allow corroborating smaller corrosion rate for SC/C welded joint in comparison with C embedded in w/c 0.45 or 0.65 concrete immersed in saline solution. The EIS diagrams show resistive behaviour for C (corrosion higher) than SC/C welded joint embedded in w/c 0.45 or 0.65 concrete immersed in saline solution in the same way as Rp.

All results point out to better corrosion resistance in specimens embedded in concrete with a water to cement ratio of 0.45 than for specimens embedded in concrete of w/c 0.65. The results suggest that it is more recommendable to use SC/C welded joint embedded in w/c 0.45 concrete immersed in saline solution than C to obtain better corrosion resistance.

## ACKNOWLEDGEMENTS

The authors would like to thank CONACYT, CIDETEQ and IMT for the support granted for the development of this research.

## REFERENCES

1. MAYS G. Durability of concrete structure, E&FN Spoon, USA 2003, p 9.
2. BROOMFIELD P.J. Corrosion of steel in concrete, E&FN Spoon, New York 2007, pp 7, 61.
3. BASTIDAS D.M. and MEDINA E. Armaduras de acero inoxidable, CEDINOX, España 2013, p. 68.
4. BERTOLINI L., BOLZONI F., PASTORE T. and PEDEFERRI P. Behaviour of stainless steel in simulated concrete pore solution, British Corrosion Journal 1996, Vol. 31, No. 3, pp. 218–222.
5. HUNKELER F. Use of stainless steel rebars for reinforced concrete structures, TFB CH-5103 Wildegg, Switzerland 2001, pp. 1–5.
6. JONES C.D. The viability of 3Cr12 reinforcing bar, 3CR12CROMWELD, Stainless steel, No. 01, 2001, pp. 1–14.
7. TRINIDAD P.Q.J. Evaluación de acero inoxidable para la rehabilitación de estructuras de concreto reforzado, Tesis Doctoral, UNAM 2009, pp. 1–167.
8. QU Q. Galvanic effect induced by coupling of stainless steel and carbon steel reinforcements, 14th Asian Pacific corrosion control conference, Shanghai, China, Oct 2006, pp. 1–6.
9. BRUCE W. Public Works engineering, October/November 2002, pp. 28–32.
10. ÁLVARO P.I. Medios de unión de estructuras metálicas, Jornada Nacional de Investigación en Edificación, Universidad Politécnica de Madrid, mayo 2007.
11. MELGAREJO M.I., MARTIN C.R. and CHAPARRO W.A.A. Determinación de las causas de falla en la ZAC de una acero ASTMA36 soldado con proceso SMAW, INGECUC, Vol. 9, No. 2, 2013, pp. 75–82.
12. ASTM C 876-09 Standard Test Method for Half-Cell Potentials of Uncoated Reinforcing Steel in Concrete pp. 1–6.
13. ASTM G 102-04 Standard Practice for Calculation of Corrosion Rates and Related Information from Electrochemical Measurements, p 1.

# CONCRETE CARBONATION PROTECTION PERFORMANCE OF FINISHING MATERIALS CONTAINING SLAKED LIME POWDER

**Y Kitsutaka**

**S Kusumi K Matsuzawa**

Tokyo Metropolitan University

Japan

**ABSTRACT.** For long-time use of reinforced concrete structures, the concrete surface layer needs to have high shielding performance against carbonation. A protection effect of carbonation of concrete surface is improved by applying a finishing material which has a chemical reaction with carbon dioxide in the atmosphere. In this study, we focused on the concrete carbonation protecting ability of a finishing material containing slaked lime powder for the use of building wall finishing. Carbonation accelerating tests were performed for mortar specimens coated with various finishing materials by using a carbonation accelerating test apparatus. Finishing materials containing an appropriate amount of slaked lime powder showed carbonation inhibition effect because of the protection effect caused by the chemical reaction with carbon dioxide and calcium contained in slaked lime powder.

**Keywords:** Concrete, Durability, Carbonation, Finishing materials, Slaked lime powder.

**Yoshinori Kitsutaka** is a Professor in the Department of Architecture and Building Science at Tokyo Metropolitan University, Japan. He received his Eng. Dr. from Tokyo Institute of Technology in 1986. His research interest includes aesthetics of building finishes, durability of building materials, new concrete material, fracture mechanics of structural materials. His research these received the 2001 prize of Architectural Institute of Japan. He is a president of Japan Society for Finishing Technology.

**Shinzo Kusumi** is a graduate student in the Department of Architecture and Building Science at Tokyo Metropolitan University, Japan.

**Koichi Matsuzawa** is an Assistant Professor in the Department of Architecture and Building Science at Tokyo Metropolitan University, Japan. He received his Eng. Dr. from Tokyo Metropolitan University in 2016.

## INTRODUCTION

Carbonation of concrete proceeds from its surface by reaction with carbon dioxide ($CO_2$) in the atmosphere. When carbonation reaches the depth of reinforcement, its passive film is destroyed to cause corrosion, resulting in cracking and losses in the load-bearing capacity of concrete. While a large number of studies have been conducted on various surface finishing materials for carbonation protection of concrete [1], there have been few studies that deal with the carbonation-inhibiting effect of slaked lime (calcium hydroxide) applied to concrete as a surface finishing material, though it has long been used as a construction material. For instance, application of plaster containing slaked lime is reported to inhibit carbonation. Slaked lime powder binds to $CO_2$ in the atmosphere to form calcium carbonate, contributing to further hardening. This process can reduce the amount of $CO_2$ that acts on concrete. In other words, the presence of slaked lime on the surfaces causes sacrificial carbonation, thereby inhibiting carbonation of internal concrete.

This study is intended to elucidate the carbonation-inhibiting effect of finishing materials containing slaked lime powder.

## EXPERIMENT OVERVIEW

### Outline of Specimens

Figure 2 and Table 1 show the test flow and the outline of the finishing materials, respectively. The finishing materials under study are a cement paste (CP) and an exterior thin-painting finish coating material (RE) containing different percentages of slaked lime (CH). Fibres were added to each finishing material at a ratio of 1% by weight of CH to prevent shrinkage.

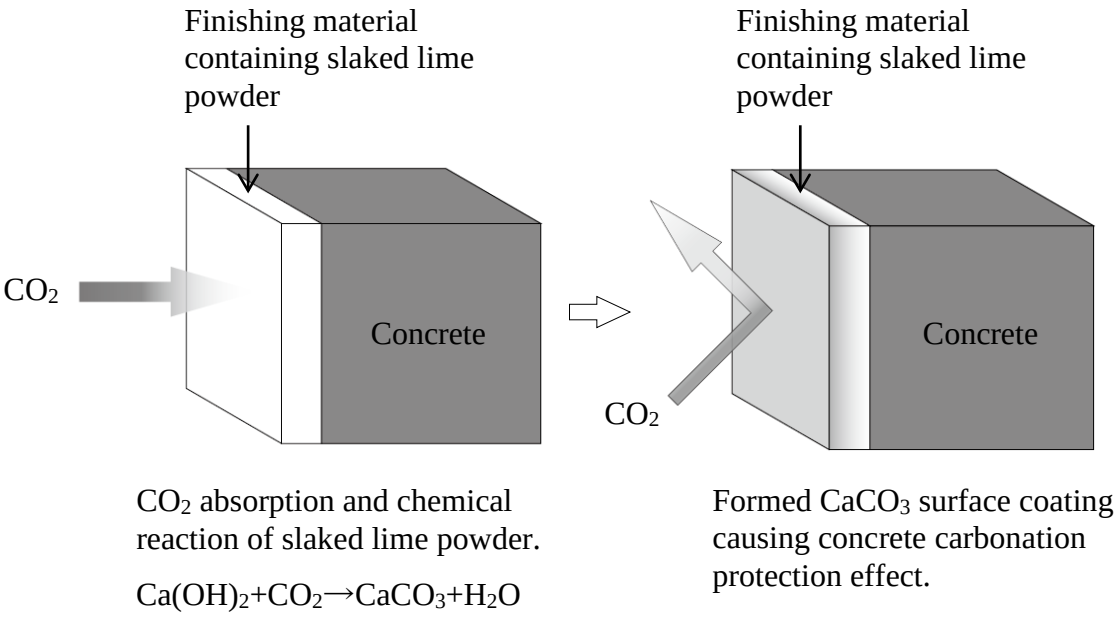


Figure 1 Conceptual diagram of the present study

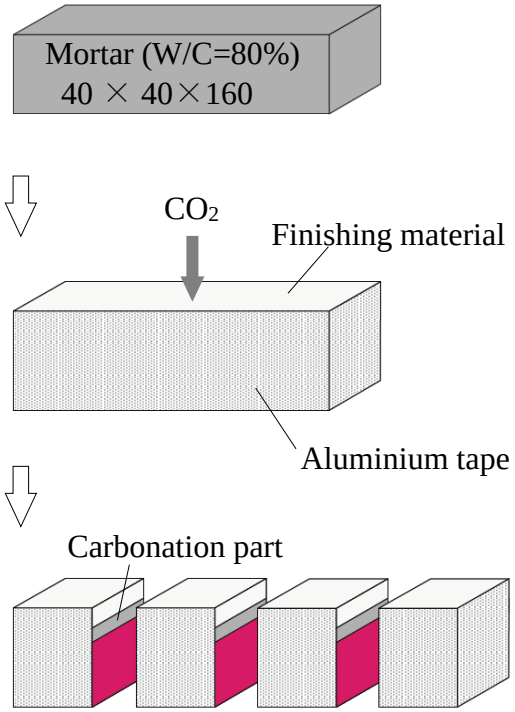


Figure 2 Test flow

1. Mortar substrate specimen

W/C=80%, S/C=4.3, size=40 mm × 40 mm × 160 mm. Demoulded after 8 days.

Water curing for 1 day.

2. Mortar specimen with finishing material

5 sides were sealed by aluminium tape.

Finishing material was applied for one side.

Finishing material was sealed and cured for 5 days, then cured in air for 2 days (20°C, 60% RH)

3. Accelerated carbonation test

Test period was 4 weeks.

(20°C, 60% RH, $CO_2$ concentration 5%)

4. Carbonation depth measurement

Each specimen was cut for four cubes.

Carbonation depth was measured,

5 points on 3 cut surfaces were measured and an average of 15 points was calculated for each specimen.

Table 1 Outline of finishing materials

| SYMBOL | CP | RE |
|---|---|---|
| Combination | Cement paste + Slaked lime powder | Exterior thin-painting finish coating material + Slaked lime powder |
| Water/Binder (W/B), % | 30 | 33 |
| $Ca(OH)_2$/Binder (CH/B), % | 0, 25, 50, 75, 100 | 0, 25, 50, 75, 100 |
| Fibre CH×x, % | 1.0 | 1.0 |
| Coating thickness, mm | 3 | 3 |

For cement paste, the water-powder ratio (W/B) was kept constant at 30%. The ratios of CH were 0%, 25%, 50%, 75%, and 100% in place of the powder content. Due to the low W/B, an air-entraining and high-range water-reducing admixture was used. The coating thickness was 3 mm for all specimens. The exterior thin-painting finish coating material was a thin-painting finish coating material of a common acrylic resin emulsion type. The W/B was kept constant at 33%, with the CH content being 0%, 25%, 50%, and 75% in place of part of the powder content. The coating thickness was 3 mm for all specimens.

Tables 2 and 3 give the materials used and the mixture proportions of the finishing materials, respectively. The base mortar to which the finishing materials were applied was produced with a W/C of 80% and S/C of 4.3, placed in moulds measuring 40 by 40 by 160 mm, demoulded at an age of 8 days, and water-cured for 1 day. The finishing materials were applied to one of the four sides of each specimen, with the other sides and ends being sealed with aluminium tape. The base mortar was wetted with water before applying the coating materials. The specimens were then seal-cured at 20°C and 60% R.H. for 5 days, and air-cured for 2 days. A single specimen was prepared for each set of conditions.

Table 2 Materials used for the test

| | MATERIAL | SYMBOL | PROPERTY |
|---|---|---|---|
| Cement | Portland cement | C | Density 3.16 g/cm³ |
| Fine aggregate | hard sandstone crushed sand (Sagamihara production) | S | Saturated-surface-dry density 2.61 g/cm³<br>Absolute dry density 2.56 g/cm³<br>Water absorption rate 2.15%<br>Coarse grain rate 3.25% |
| Fibre | Vinylon fibre | VF | Density 1.3 g/cm³ |
| Admixture | Polycarboxylic acid-based high performance water-reducing agent | SP | Density(at 20°C 1.05～1.09 g/cm³ |
| Slaked lime | Slaked lime | CH | Density 2.21 g/cm³ |
| Exterior thin-painting finish coating material | Synthetic resin emulsion | RE | Density 1.11 g/cm³ |

Tables 3 Mixture proportions of the finishing materials

| | | CP | | | | | RE | | | |
|---|---|---|---|---|---|---|---|---|---|---|
| Symbol | | CP100 | CP75 | CP50 | CP25 | CP0 | RE75 | RE50 | RE25 | RE0 |
| Coating thickness | mm | 3.0 | 3.0 | 3.0 | 3.0 | 3.0 | 3.0 | 3.0 | 3.0 | 3.0 |
| W/B | % | 32.5 | 31.9 | 31.2 | 30.6 | 30 | 32.5 | 32.5 | 32.5 | 32.5 |
| Unit mass kg/m³ | W | 416 | 431 | 447 | 466 | 487 | 233 | 139 | 62.7 | 0 |
| | SP | 63.9 | 50.4 | 35.3 | 18.6 | 0 | 42.3 | 25.2 | 11.4 | 0 |
| | C | 0 | 345 | 726 | 1149 | 1622 | - | - | - | - |
| | S | - | - | - | - | - | - | - | - | - |
| | CH | 1279 | 1007 | 707 | 373 | 0 | 846 | 504 | 228 | 0 |
| | VF | 12.8 | 10.1 | 7.1 | 3.7 | 0 | 8.5 | 5 | 2.3 | 0 |
| | RE | - | - | - | - | - | 376 | 673 | 913 | 1110 |

## Accelerated Carbonation Test

Specimens were subjected to accelerated carbonation for 4 weeks in an environment with the air temperature, relative humidity, and $CO_2$ concentration of 20°C, 60%, and 5%, respectively according to the Japanese Industrial Standards (JIS A 1153 : 2012) [2]. Each specimen was then cleft into four equal parts to measure the carbonation depth and finish coating thickness. Measurements were made at 5 points on each of the 3 cleft surfaces to calculate the average of the 15 points for each specimen.

Figure 3 Accelerated carbonation testing machine

## RESULTS AND DISCUSSION

Figure 4 shows the results of the carbonation depth measurement of CP specimens. The carbonation depth of specimens coated with the finishing material is smaller than that of the uncoated specimen (N), proving that the application of a finishing material can inhibit carbonation.

This is presumably because the finish coating reduces the amount of $CO_2$ permeating into mortar. The carbonation depth was smallest in the specimen coated with cement paste containing 0% lime.

On the other hand, the carbonation depth was largest in the specimen coated with lime and no cement. This is presumably because finishing only with lime is prone to surface cracking. The addition of lime generally led to no appreciable effect on carbonation protection.

This is presumably due to the strong carbonation-inhibiting effect of cement paste, which forms hydrates, while the addition of lime can adversely cause air voids in the hydrates. It is therefore considered that, for a finishing material in which the permeability of the matrix is low, the addition of lime leads to no clear effect of carbonation protection.

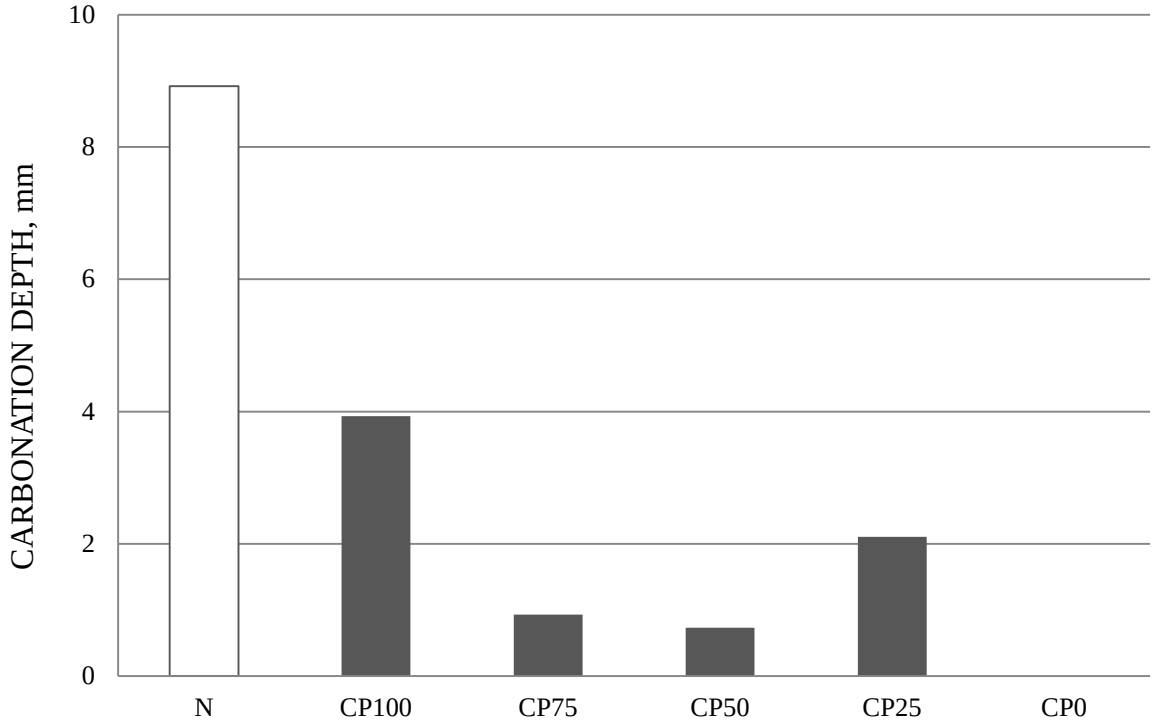


Figure 4 Carbonation depth measurements of CP specimens

Figure 5 shows the results of carbonation depth measurement of RE specimens. Similarly to CP, the carbonation depth of specimens coated with RE is smaller than that of the uncoated specimen (N). As to the effect of lime, the carbonation depth of specimens coated with RE containing 75% lime tends to be smaller than those coated with RE containing no lime, though 25% and 50% lime led to no appreciable changes. In this case, lime was presumably carbonated as a component of the coating material with a high $CO_2$ permeability, thereby reducing the action of $CO_2$ on the mortar base. It is therefore considered that a carbonation-inhibiting effect can be obtained by an appropriate amount of lime added to a finishing material comprising a highly permeable matrix.

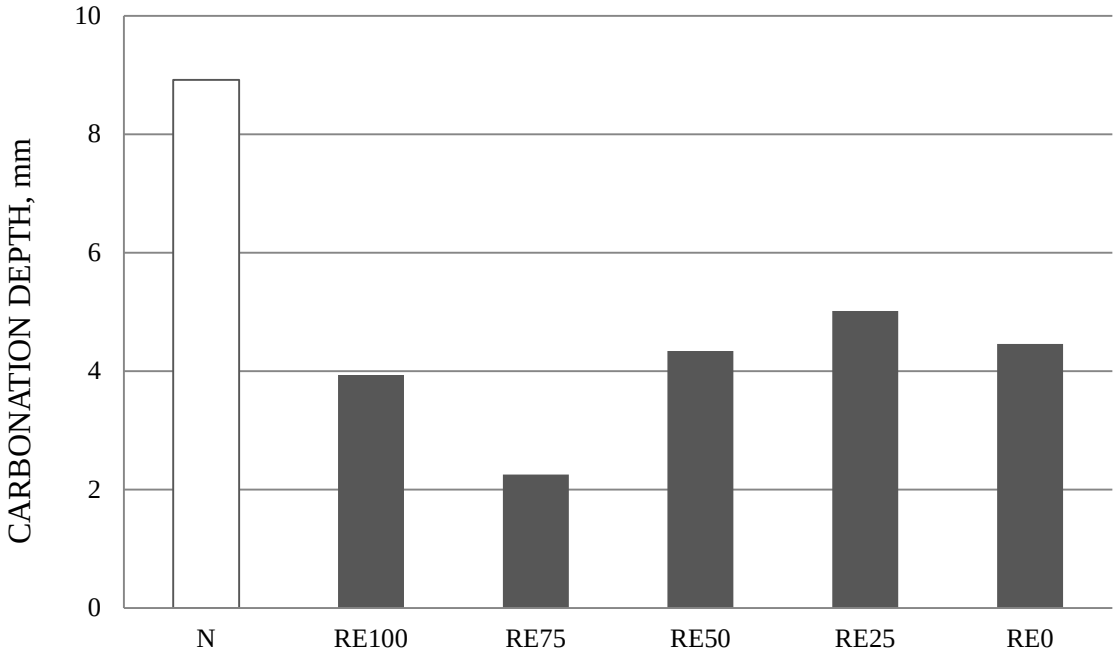


Figure 5 Carbonation depth measurement of RE specimens

## CONCLUSIONS

The following were found in this study:

(1) A finishing coat on mortar has a carbonation-inhibiting effect in comparison with no coating.
(2) The carbonation-inhibiting effect of slaked lime is not clearly observed when added to cement paste as a coating material with a low permeability.
(3) A carbonation-inhibiting effect is obtained by adding an appropriate amount of slaked lime to a thin-painting finish coating material with a high permeability.

## ACKNOWLEDGEMENTS

We thank Nippon Plaster Co., Ltd. And Kaken Material Co., Ltd. for giving us materials and cooperation during our research.

## REFERENCES

1. UCHIMURA Y., HIRAMOTO Y. and MOTOHASHI K. Neutralization behaviour of plaster coating materials and plaster under various environmental conditions, Summaries of Technical Papers of Annual Meeting, Japan Society for Finishing Technology, Vol. 24, No. 144, 2012, pp. 207–210.

2. JIS A 1153:2012, Method of Accelerated Carbonation Test for Concrete, Japanese Industrial Standards.

# FUNDAMENTAL EXPERIMENT ABOUT THE LONG-TERM CARBONATION CONTROL EFFECT OF THE ELASTIC PAINT FOR HOUSING BASE CONCRETE

**M Sugiyama**
Hokkai Gakuen University
Japan

**ABSTRACT.** This paper considers the influence of elastic paint (modified silicone resin emulsion paint) applied to the surface of concrete has on carbonation. First, heat deterioration of the elastic coating was conducted. Next the concrete specimens were exposed to an accelerated carbonating atmosphere. The conditions of accelerated carbonation were 20 °C, 60% relative humidity, in an atmosphere of 5% carbon dioxide. The experiment examined the heat deterioration conditions of three kinds of elastic paint: (1) with no heat deterioration, (2) after ten weeks held at 23 °C, (3) after ten weeks held at 80 °C. Exposure to the carbonating atmosphere ran over a period of two years (114 weeks). The elastic paint prevented carbonation even after heat deterioration at 80 °C.

**Keywords:** Housing base concrete, Carbonation, Elastic paint, Durability

**M Sugiyama** is a Professor of the Faculty of Engineering, Hokkai Gakuen University of Sapporo, Japan. He is a member of ACI, RILEM, AIJ, JCI and JSCE.

## PURPOSE

This research examines the influence of heat degradation of elastic paint on a carbonation of concrete used in housing applications. Initially, heat deterioration of the paint coatings was conducted, followed by exposure of the coated concrete specimens to an accelerated carbonating atmosphere.

The experiment examined the effect of heat deterioration of the paint coating using three conditions:

1) with no heat deterioration.
2) after ten weeks at 23 °C .
3) after ten weeks at 80 °C.

Exposure of the specimens to the carbonating atmosphere was conducted for a maximum period of two years (114 weeks).

## EXPERIMENTAL DESIGN

The experimental programme is summarised in Table 1. Experiment number 1 used concrete specimens that were not painted. Experiments 2 and 3 were painted concrete specimens. The painted surface of the specimens in Experiment 2 were cured for ten weeks at a temperature of 23 °C. The specimens in Experiment 3 underwent heat deterioration for ten weeks at 80 °C.

The experiment compared the carbonation depth of the specimens. Measurements of carbonation depth were conducted at four, eight, 13, 26, 66 and 114 weeks. A commercially available modified silicone emulsion paint was used (40% paint, 22 % synthetic resin, plus other constituents). Application in a conventional manner achieved a coverage of 1100 g/m$^2$. Based on this, the theoretical film thickness is 786 μm.

Table 1 Experimental programme

| № | COATING | HEAT DETERIORATION | SPECIMENS |
|---|---|---|---|
| 1 | None | - | 3 pieces×6 period |
| 2 | Done | Normal temperature (23 deg.) / 10weeks | 3 pieces×6 period |
| 3 | Done | Heat deterioration (80 deg.) / 10weeks | 3 pieces×6 period |

## TEST METHOD

### Concrete Specimens

In order to avoid any batch difference, ready-mixed concrete was used to make the specimens. A water cement ratio of 0.55, slump of 18 cm, and a maximum aggregate size of 20 mm was specified. The strength of the concrete cubes at an age of four weeks was 24 N/mm$^2$. Portland cement was used as the cement.

The specimens were 150x150x150 mm concrete cubes. Demoulding was conducted one day after the mix was produced. Curing consisted of curing in water for six days, followed by three weeks of air-drying (20 °C and 60 % RH).

### Heat Deterioration

There exists the potential for paint coatings to be damaged by exposure to elevated temperatures. This aspect was explored as part of the study through exposure to different temperature regimes prior to carbonation. The specimens were coated with the paint which was left to dry for a period of one week. After drying, the specimens for Experiment 2 continued to be held at ambient temperature (23 °C ) for ten weeks, whilst the Experiment 3 specimens were held at 80 °C for the same period. The coat which underwent heat deterioration was cut into a 150-mm angle, it used epoxy resin for the end of the both sides of a concrete test piece, pasted up, and was covered.

### Accelerated Carbonation

Accelerated carbonation was conducted under conditions of 20 °C, 60% relative humidity, and in an atmosphere of 5% carbon dioxide. The test method followed the measuring method of the carbonation depth of the concrete of JIS A 1153. The carbonation depth measurements used phenolphthalein solution (1 % concentration) applied to the split faces of cubes removed at the required age. Carbonation depth was measured using digital slide calipers.

## EXPERIMENTAL RESULTS

The result of a carbonation of 114 weeks (two years) of promotion is shown in Figure. 1. The result of a promotion carbonation examination is shown in Figure 2.

Figure 1 Test results of 114 weeks (from left, Experiment 1, 2 and 3)

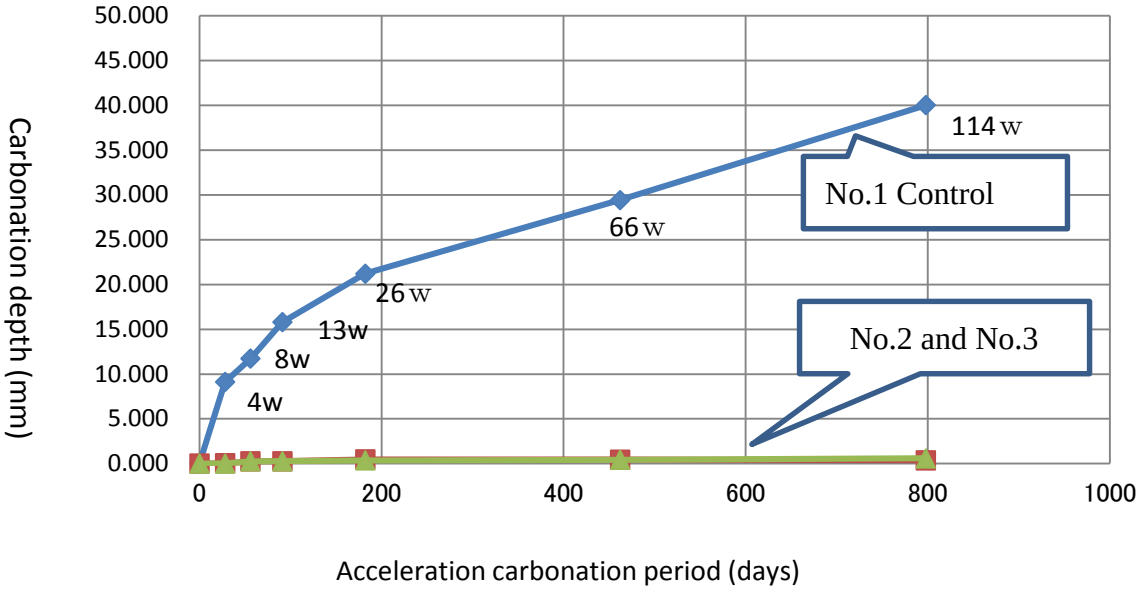


Figure 2 Result of the acceleration carbonation test

(1) The carbonation depth of the Experiment 1 specimens was 21.2 mm at 26 weeks and 40.0-mm at 114 weeks. On the other hand, the carbonation depth of the Experiment 2 specimens was 0.5 mm at 26 weeks, and 0.4 mm at 114 weeks. Thus, under these conditions carbonation control was effective.

(2) The carbonation depth of the Experiment 3 specimens which carried out heat deterioration of the coat in 80 °C. heat environment was 0.4 mm at 26 weeks, and 0.6 mm at 114 weeks. These results are comparable to those obtained for Experiment 2.

## CONCLUSIONS

The modified silicone resin emulsion paint studied displayed excellent carbonation control under accelerated carbonating conditions over a period of two years.

## REFERENCES

KAZUO H, AKIRA F, SUGIYAMA M, Fundamental study on durability improvement of the housing base concrete, part 1~10, Architectural Institute of Japan: Summaries of Technical Papers of Annual Meeting, 2014, pp381-382

# EFFICIENCY IN MODELLING HEAT DEVELOPMENT IN LONG-SPAN CONCRETE CONTAINING GGBS AS A PARTIAL REPLACEMENT OF CEMENT

**K Tang**

University of Wolverhampton

United Kingdom

**ABSTRACT.** Isothermal calorimetry, semi-adiabatic calorimetry tests and finite element modelling (FEM) are commonly used methods to study the early-age heat development in cast-in-place concrete. The continuous curing conditions of mass concrete or long-span concrete structures can be simulated using a well-insulated box, inside which a concrete cube specimen is cured under a semi-adiabatic condition. The volumes of the specimens used for such tests varied significantly based on a review of literature. This paper investigates the effects of concrete specimen sizes on the heat development in concrete. The curing conditions of suspended concrete slabs were found to be better simulated with a semi-adiabatically cured concrete specimen of a reasonable size in addition to sufficient insulations. FEM investigations, validated by the semi-adiabatic calorimetry tests, indicate a beneficiary effect of using GGBS as a partial replacement of CEM I cement in structural concrete with reduced thermal loading (or T1 values). With 50% of CEM I replaced with GGBS, thermal loading reduced by 30% at an elevated curing temperature of 38°C, which represents hot climatic conditions in south Asian cities such as Shanghai.

**Keywords:** Concrete, Early-age, Thermal loading, GGBS, FEM

**Kangkang Tang** is a senior lecturer of the Faculty of Science and Engineering at the University of Wolverhampton. He is a chartered civil engineer (CEng) and a member of the Institution of Civil Engineers (MICE).

## INTRODUCTION

As the most ubiquitous construction material in China, 2.2 billion cubic meters of concrete were produced per annum and this accounts for about 50% of global production [1]. Early-age expansion and subsequent contraction takes place in concrete as a result of the exothermic hydration process. Significant resultant internal stresses will build up in structural concrete such as beams and slabs if these movements are externally restrained. Contraction in these suspended concrete elements against external restraints leads to tensile stresses which may cause deleterious tensile cracking in concrete. The restraint to large volume concrete pours normally arises internally as a result of the temperature and strain differentials which is different from that of suspended concrete slabs and beams [2]. The heat development from cement containing ground granulated blast furnace slag (GGBS) as a partial replacement of CEM I cement is slower than that of the CEM I only mixes. As a result, the peak temperature in fresh GGBS concrete is lower and this will result in a reduced thermal contraction. There is therefore scope to use GGBS in long-span concrete structures for crack mitigation purposes.

Cheng et al. [3] reported that the peak hydration temperature reduced by 36%, with up to 70% of cement replaced with GGBS. Bamforth [2] and Zheng et al. [4] quantified this effect by introducing a short-term temperature difference value T1 (°C) which defines the difference between the peak temperature during the early-age cement hydration reaction and the ambient temperature at the time of casting. T1 values were measured when the concrete casting temperature was at 20°C and 35°C respectively. Higher T1 values were obtained at 35°C and this indicates that an accelerated hydration of both cement and GGBS mixes.

High ambient temperature alongside insufficient curing however has a detrimental effect on the strength of concrete. ACI 305R [5] recommends that the maximum ambient temperature shall be determined based on a case-by-case investigation, because “a maximum ambient or concrete placing temperature that will serve a specific case may be unrealistic in others”. GB 50204-92 [6], Chinese standard for concrete structures, advises a maximum concrete casting temperature of 28°C. GB 50204-92 was superseded by GB 50204-2002 [7] in 2002 and the maximum ambient or casting temperature was not constrained further. In summer in Shanghai, it is not unusual that the ambient temperature exceeds 38°C. In this project, the maximum ambient temperature was set at 38°C which represents the typical summer climatic conditions in Shanghai [8]. For comparison, an ambient temperature of 20°C was used to measure the heat development under standard curing conditions.

It is important to determine the heat development during cement hydration, especially for large volume concrete pours. Semi-adiabatic calorimetry and isothermal calorimetry tests are common methods to investigate the rate of cement hydration. Both tests, although under different curing conditions, can be used to monitor and predict the cast-in-place concrete heat development. Da Silva [9] successfully predicted the peak hydration temperature in a 1050 $m^3$ concrete foundation based on the temperature data obtained in a 1 $m^3$ concrete cube specimen under a semi-adiabatic curing condition. The volumes of the specimens used for semi-adiabatic calorimetry tests vary significantly from 0.027 $m^3$ [10], 0.1 $m^3$ [11] and 1 $m^3$ [12] based on a review of literature. The effects of specimen sizes on the concrete heat development however have not been sufficiently investigated. The actual curing conditions of structural concrete slabs are different to those of mass concrete due to heat losses from both the top and underside of the slabs. The peak hydration temperature determined under a conventional semi-adiabatic curing condition may therefore be an overestimate. In contrast to the semi-adiabatic calorimetry test where the concrete temperature rises during curing, the

isothermal calorimetry test directly measures the heat output rate (W/g) of cement at a constant temperature. Bougara et al. [13] investigated the hydration heat output of cement and GGBS using an isothermal calorimeter. In addition to experimental methods, FEM becomes an important tool nowadays to predict the heat development within hydrating concrete specimens. Lawrence et al. [12] successfully predicted the core temperatures of mass concrete specimens using commercial FEM software DIANA.

## EXPERIMENTAL PROCEDURES

This paper reports an ongoing project which investigated the potential of using GGBS in structural concrete elements such as beams and slabs to minimise the use of more expensive crack control reinforcement. The objective was to determine an 'optimum' GGBS mix proportion which could yield lower thermal loading or T1 values and thus an associated saving in crack control reinforcement. Concrete slab specimens were cast under a semi-adiabatic condition to simulate cast-in-place floor slab curing conditions.

### Materials, Concrete Mix Proportions and Strength Test

The cement used for this project was supplied in bags. It conformed to the requirements of the Chinese Standard GB175-2007 [14] for P·O 42.5 cement (CEM I 42,5). The GGBS used for this project was class S93 according to GB/T 18046-2008 [15]. The coarse aggregate used for this study was 5-40 mm graded crushed gravel supplied by a local quarry with a water absorption value of 0.88%. The fine aggregate was well-graded medium sand with a water absorption value of 2.62%. The particle density of gravel and sand was 2680 kg/m$^3$ and 2450 kg/m$^3$ respectively. Following concrete mixes (Table 1), with up to 50% CEM I replaced with GGBS, were developed to investigate the effect of partial replacement of CEM I with GGBS on the strength and heat development of concrete. The target strength of 0% GGBS mix was to achieve C30/37 concrete with a suitable workability for floor slab casting according to BS 8500-1 [16].

Table 1 Mix proportions

| | TOTAL BINDER CONTENT, kg/m³ | FREE W/B | TOTAL AGGREGATE CONTENT, kg/m³ |
|---|---|---|---|
| 0% GGBS | 398 | 0.49 | 1782 |
| 15% GGBS | 398 | 0.51 | 1782 |
| 30% GGBS | 398 | 0.50 | 1782 |
| 50% GGBS | 398 | 0.51 | 1782 |

### Semi-adiabatic Calorimetry Test

The purpose of the semi-adiabatic calorimetry test was to simulate the slab concrete hydration heat liberation process in the laboratory. Concrete slab specimens, 350 mm × 250 mm × 300 mm, were cast inside an insulated plywood box to simulate the 300 mm thick flat slab curing conditions (Figure 1). Four sides of the specimen were insulated with 2 cm thick expanded polystyrene sheets. The sides of the slab mould were made of 17 mm plywood. The underside of the specimen was in contact with a 17 mm plywood formwork and the top surface was exposed to air. This allows heat losses to occur differently from both

the top and underside of concrete. Concrete slab specimens, inside the insulated plywood box, were placed in an environmental cabinet immediately after casting. The environmental cabinet temperature was set either at 20°C or 38°C. Thermocouples, with an accuracy of ±0.1°C, were embedded into the concrete slab specimens. In order to verify that the laboratory semi-adiabatic conditions can simulate the curing conditions of a continuous concrete slab, additional thermocouples were placed at the boundary between concrete and insulation materials. The actual temperature of the environmental cabinet has been monitored and it was found to be generally within ±1°C of the prescribed temperature. Temperature data were recorded every 10 minutes for 3 days. Standard concrete cube specimens, 150 mm × 150 mm × 150 mm, were cast alongside the slab specimen and cured at a room temperature, i.e. approximately 20°C. Within 24 hours of casting, the cube specimens were demoulded and placed inside two water curing tanks which were set at 20°C and 38°C respectively. The testing ages for the cube specimens were 3 days and 28 days.

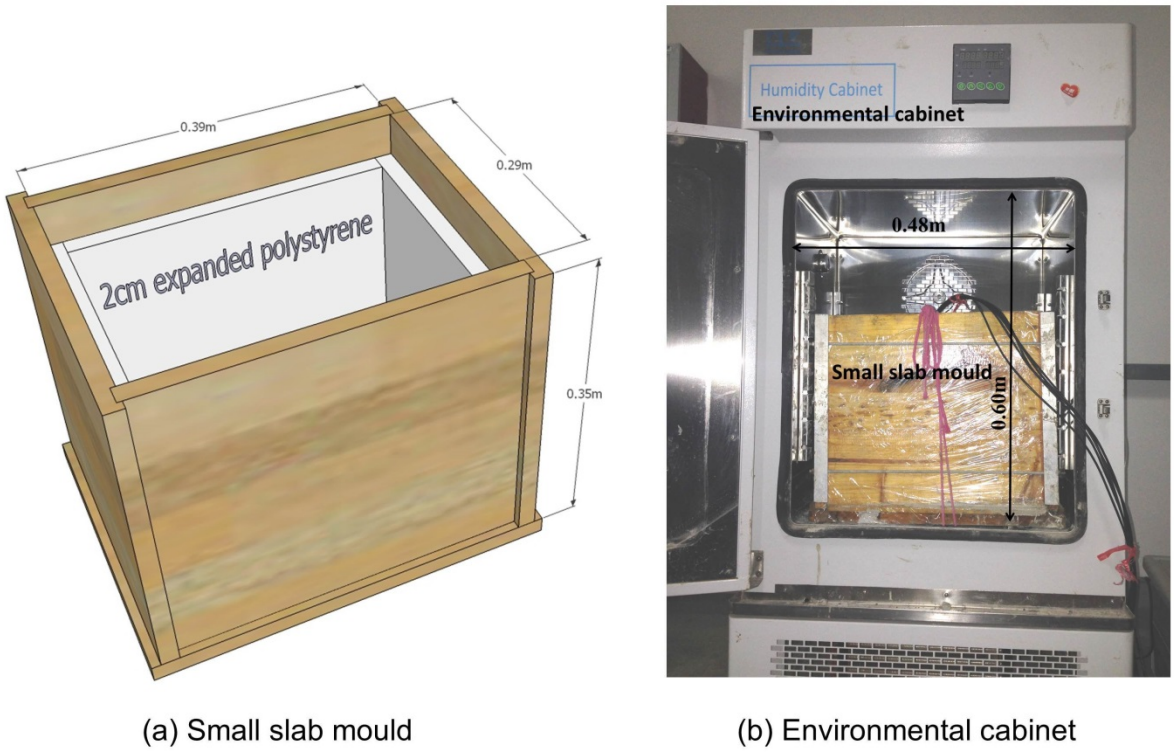


(a) Small slab mould (b) Environmental cabinet

Figure 1 Small slab mould and environmental cabinet [17]

In order to investigate the effect of concrete specimen sizes on the heat development in concrete, a larger concrete slab specimen, 660 mm × 460 mm × 300 mm, was cast and tested inside an environmental room (Figure 2). The large concrete slab specimen was insulated on four sides by 2 cm thick expanded polystyrene sheets. The sides of the slab mould were made of 100 mm thick timber boards, which not only provided better insulation but also ensured the integrity of the specimen during concrete compaction. The underside of the concrete was in contact with a 50 mm timber board sitting on two timber beams. The top surface was exposed to air. Concrete slab specimens placed in an environmental room immediately after casting. The entire experimental setup provides a good experimental modelling of the expected thermal conditions of suspended floor slabs cast upon timber formwork. The actual temperature of the environmental chamber was found to be more variable than that of the environmental cabinet.

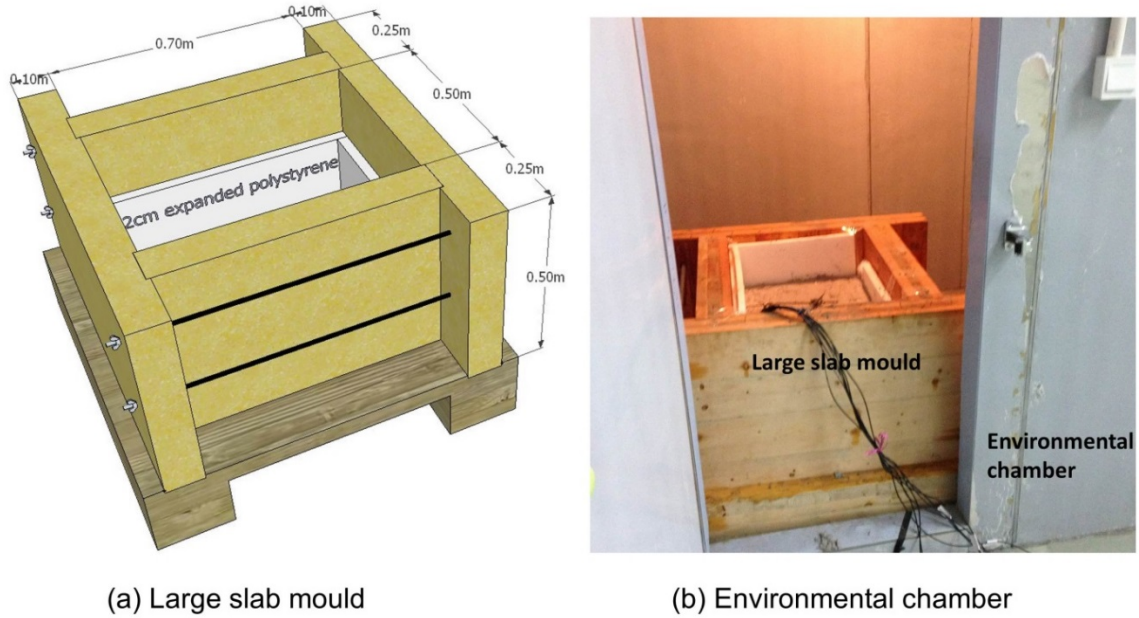


(a) Large slab mould (b) Environmental chamber

Figure 2 Large slab mould in an environmental chamber [17]

**Isothermal Calorimetry Test**

An isothermal calorimetry test directly measures the heat output rate (W/g) of cementitious materials curing at a constant temperature. A TAM Air isothermal calorimeter was used in this project and it is capable of measuring heat flow rate in the mW range. This calorimeter comprises 8 channels and each channel can test one sample and one reference sample made from an inert material. Approximately 10g of samples was prepared according to the proportions between CEM I and GGBS used in 0% GGBS and 50% GGBS mixes at different curing temperatures:

- 0% GGBS at 20°C
- 0% GGBS at 38°C
- 50% GGBS at 20°C
- 50% GGBS at 38°C

Each sample was inserted into a 20 ml glass ampoule. Water was weighed and added to the ampoules to give the same W/B ratio as the concrete mixes presented in Table 1. This allows the results to be applicable for the heat generated in the equivalent concrete mixes. The isothermal calorimeter measured the heat outputs at 20°C and 38°C respectively. The heat output rate, or the thermal power, was recorded every 20 seconds for 3 days.

The isothermal calorimeter recorded the heat output rate in Watts and this was then converted into a heat output rate per g of binder according to the weight of the specimens, Figure 3 (a). The accumulated heat output (J/g) was calculated according to Figure 3 (a) and presented in Figure 3 (b). The presence of GGBS contributes to a reduced heat output rate (W/g) and a reduced overall heat output (J/g). The heat output rates of GGBS blended cement samples were found to be more sensitive to the curing temperatures. Early-age heat output rates of 50% GGBS samples increased significantly at 38°C. Furthermore, less time was required to reach the peak of heat output rate by replacing CEM I with GGBS and this finding agrees with Ballism et al. [18].

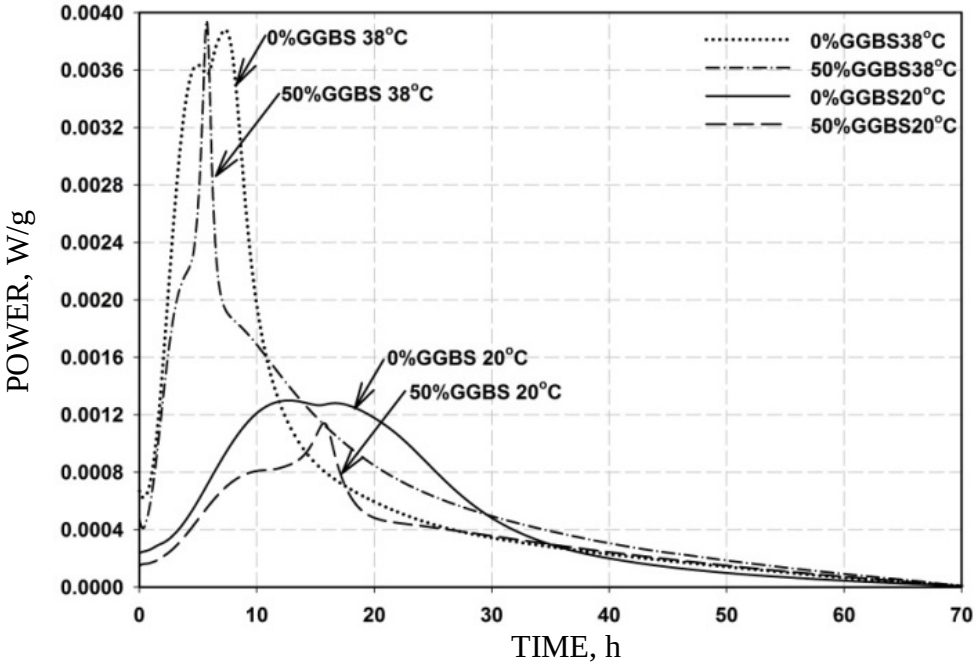


(a) Hydration heat output rate, W/g

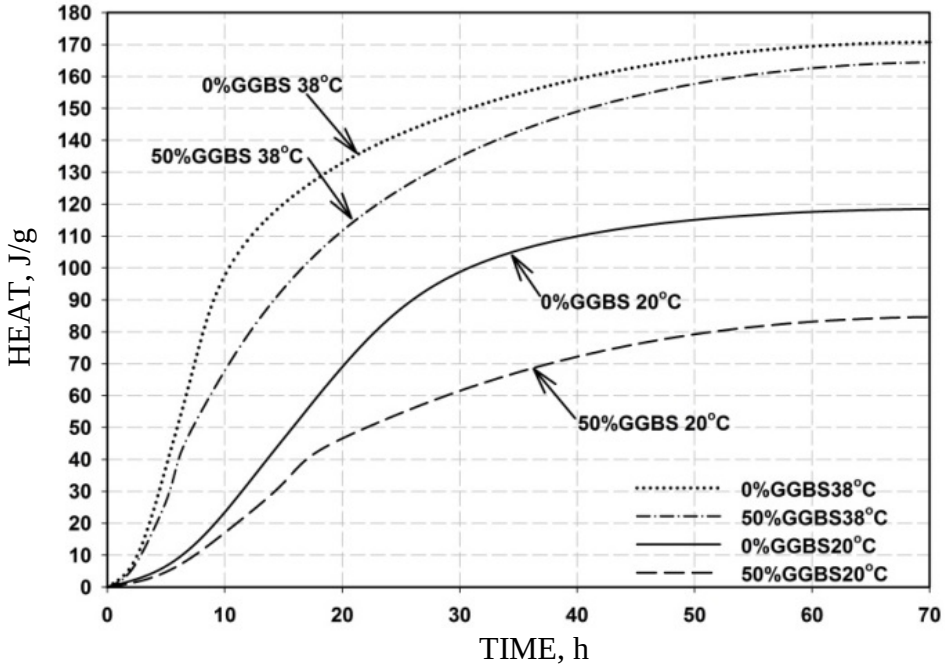


(b) Accumulated heat output, J/g

Figure 3 Isothermal calorimetry test results [17]

## FEM PROCEDURES

Numerical simulations of concrete heat development from cement hydration were conducted using ANSYS, a general multi-physics finite-element software package. The purpose was to verify that FEM is an effective tool in predicting the concrete temperature development in concrete slabs which were experimentally investigated using the semi-adiabatic calorimeter.

The temperature rises during concrete construction are primarily due to the heat release from the hydration of cementitious materials, i.e. CEM I and GGBS. The heat outputs of the cementitious materials used in the computer modelling were calculated by converting the isothermal calorimeter recordings displayed in Figure 3 (a) into a concrete heat output rate per cubic metre [17].

The Pre-processor supplied with ANSYS enables the generation of 8-node hexahedron solid elements, SOLID70, for thermal analysis. Both large and small concrete slabs (③ in Figure 4) were meshed into 10 mm × 10 mm × 10 mm SOLID70 elements. One fourth of the semi-adiabatic model was generated by taking advantage of the symmetry of the whole model about its two vertical planes. The same mesh density has been followed to mesh the expanded polystyrene and mould outside it. The ambient temperature was set to be identical to the temperature histories measured during the semi-adiabatic tests.

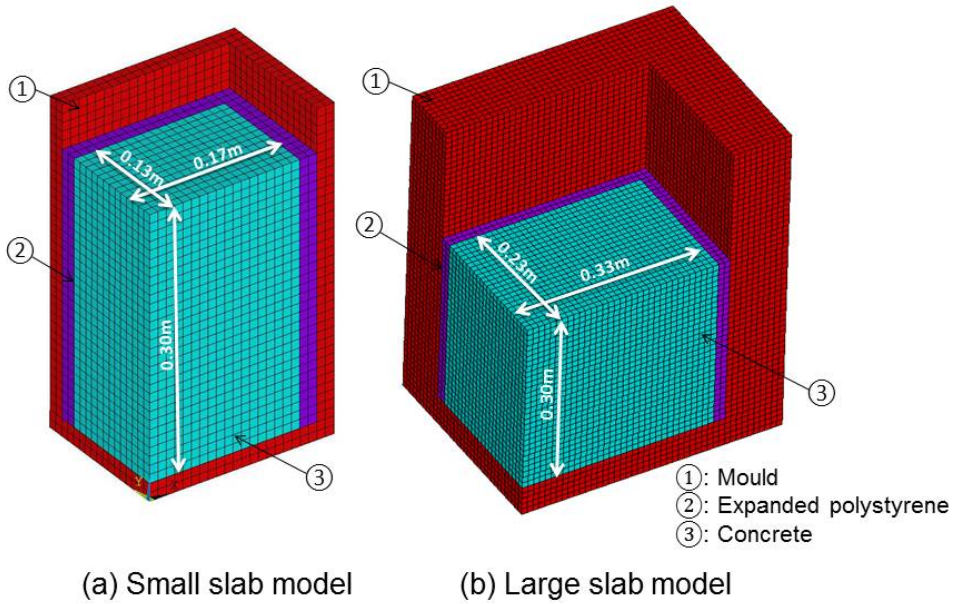


Figure 4 Finite element model (a quarter model) [17]

The thermal and physical properties required in the FEM include the thermal conductivity and specific heat capacity and the density. The properties of principal materials used in the semi-adiabatic calorimetry tests, i.e. concrete, expanded polystyrene, plywood and timber mould, were obtained from literature sources [12, 19]. A constant convection factor of 5.6 W/m²·°C, obtained from the literature [12], was used to define the heat loss into the air from the upper surface of the concrete.

## RESULTS AND DISCUSSION

Partial replacement of CEM I with GGBS was observed to have a detrimental effect on the early-age strength of concrete under the standard curing temperature regime of 20°C. Figure 5 indicates that the 3-day compressive strengths of all GGBS concrete mixes were lower than that of CEM I concrete. With 50% of CEM I replaced with GGBS, the 3-day compressive strength reduced from 22.3 N/mm$^2$ to 12.2 N/mm$^2$.

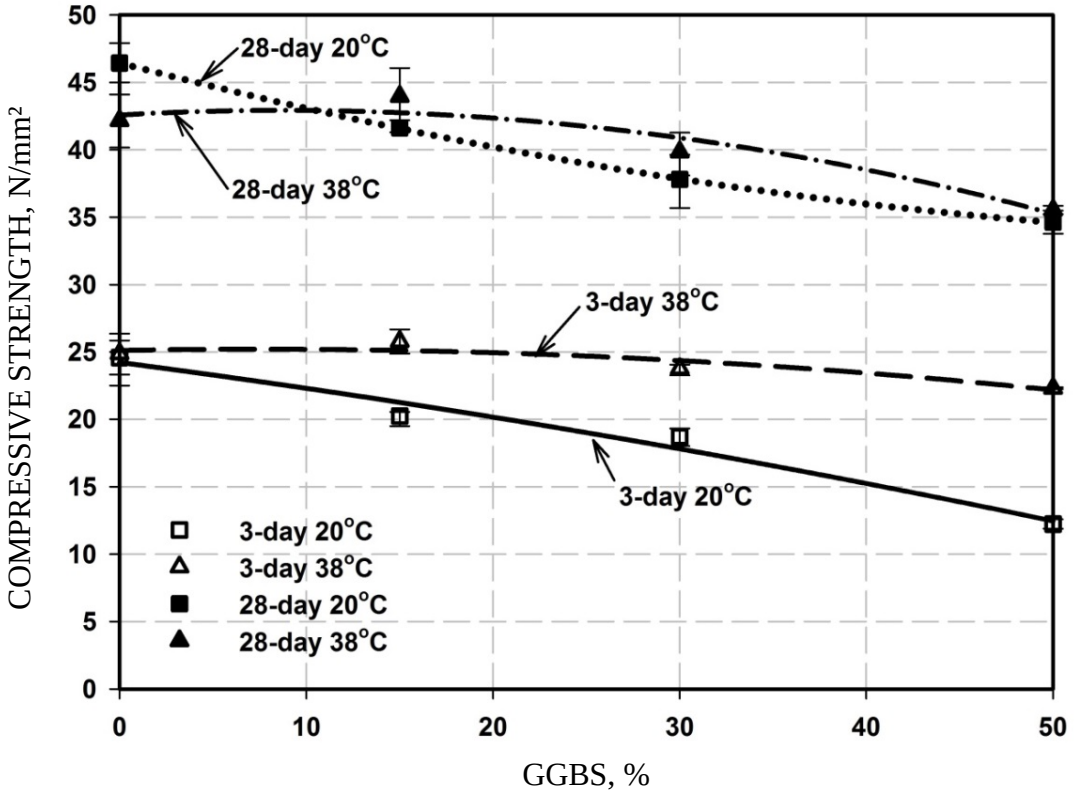


Figure 5 3-day and 28-day compressive strengths [17]

This shows the retardation effect of GGBS, which may prevent is application in structural concrete in winter when the ambient temperature is less than 20°C. This detrimental effect however becomes less significant at a higher curing temperature, 38°C. The average 3-day compressive strength of 50% GGBS mix was 22.3N/mm$^2$, which was not much lower than the 3-day compressive strength of 0% GGBS mix, 24.9 N/mm$^2$.

Both the predicted and the measured concrete core temperatures in the small slab model are presented in Figure 6a and 6b. As the GGBS content increases, the rate of hydration decreases. The predicted peak temperatures were observed to be lower than the measured values, with a maximum error of 5°C. At 38°C curing, the hydration rates of both 0% GGBS and 50% GGBS mixes were observed to be much higher than those at 20°C. This indicates that a higher curing temperature accelerated the hydration of both CEM I and GGBS mixes.

The FEM simulations gave more accurate predictions of the temperature history curves in the large slab model (Figure 7). The predicted peak temperatures were almost identical to the experimental results. This might be attributed to the larger specimen size and the greater insulation thickness which prevented the heat ingress from side boundaries at an early age. In conclusion, the curing conditions of concrete floor slabs can be better modelled with a semi-adiabatically cured concrete specimen of a reasonable size alongside a sufficient insulation thickness.

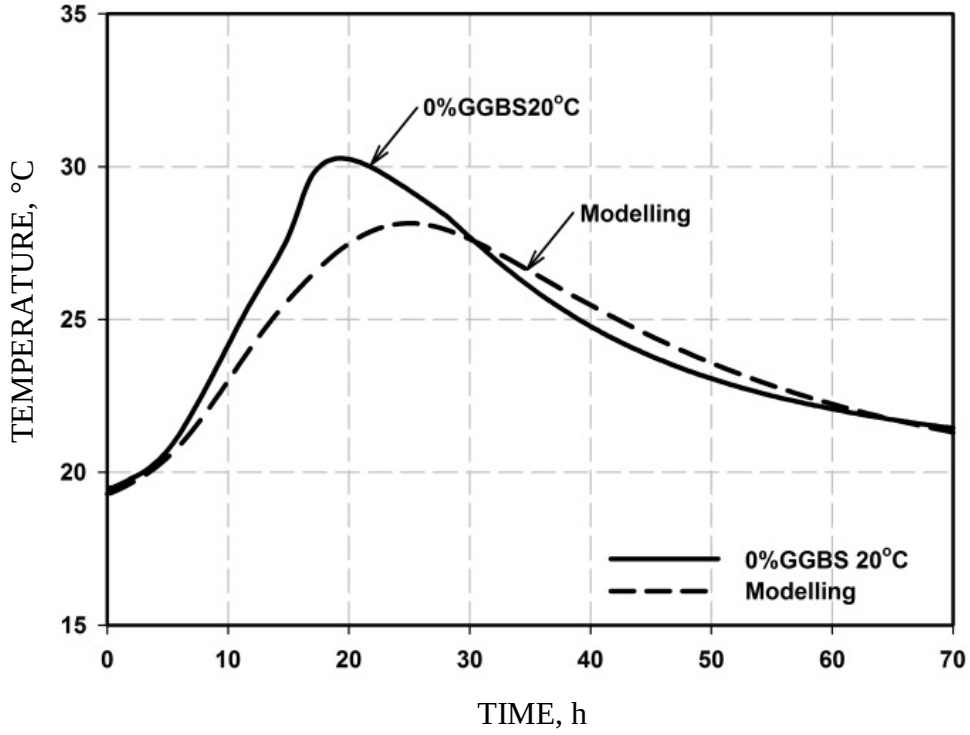


(a) 0% GGBS 20°C curing

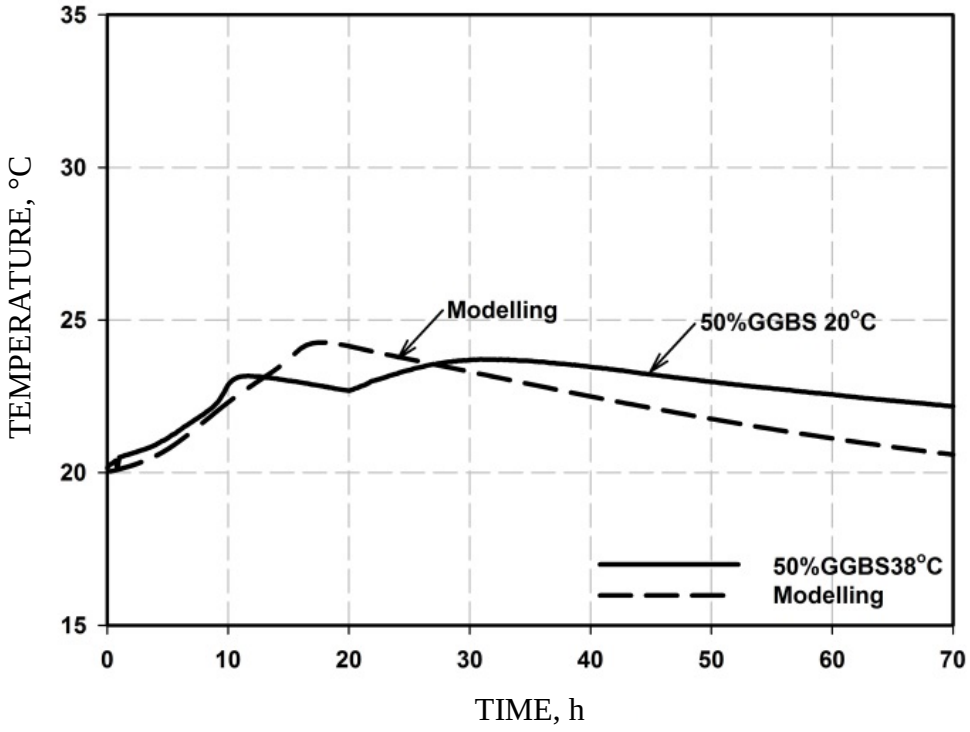


(b) 50% GGBS 20°C curing

Figure 6a Semi-adiabatic test and FEM temperature simulation results (small slab model) [17]

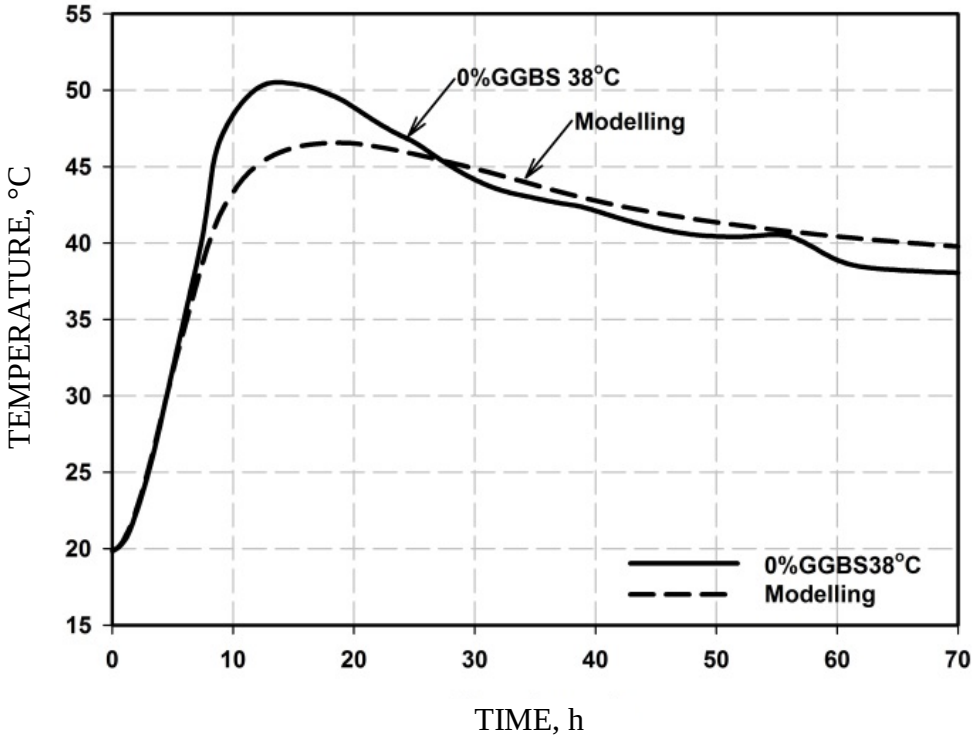


(c) 0% GGBS 38°C curing

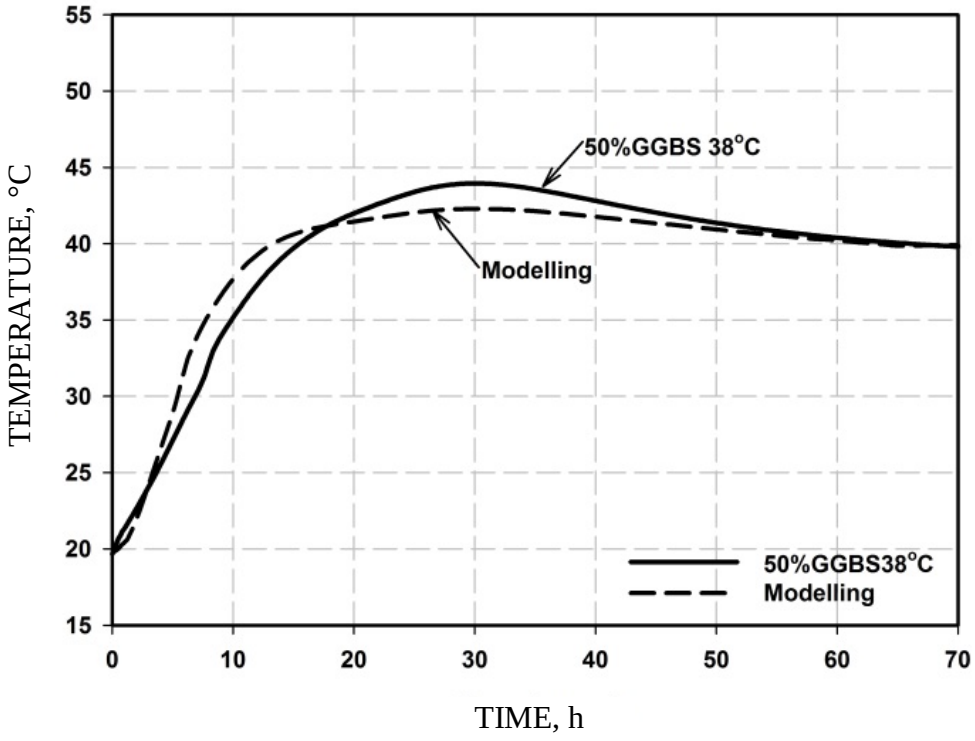


(d) 50% GGBS 38°C curing

Figure 6b Semi-adiabatic test and FEM temperature simulation results (small slab model) [17], continued

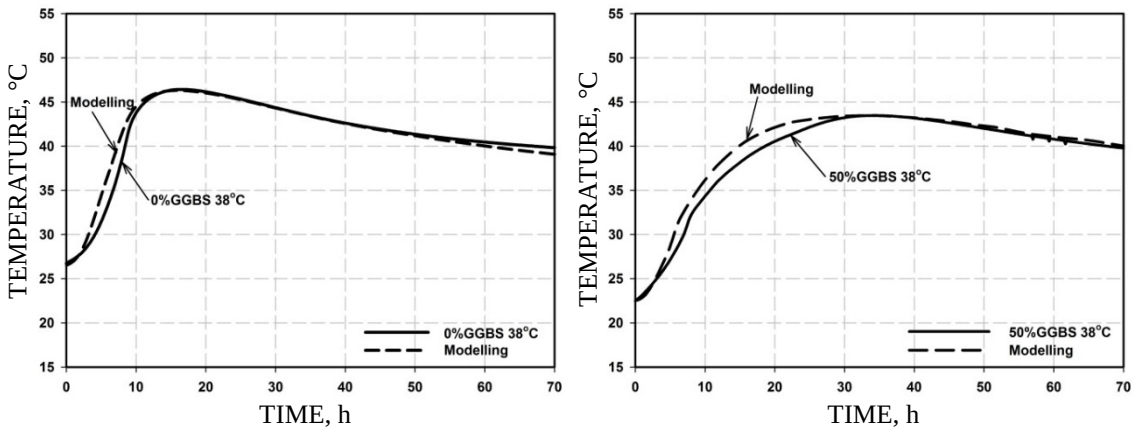


(a) 0% GGBS 38°C curing (b) 50% GGBS 38°C curing

Figure 7 Semi-adiabatic test and FEM simulation results (large slab model) [17]

## CONCLUSIONS

Partial replacement of cement with GGBS may have a retardation effect on the early-age strength of concrete. Based on the experimental study, partial replacement of CEM I with GGBS has a detrimental effect on the early-age strength of concrete at a standard curing temperature regime of 20°C. This retardation effect may prevent the application of GGBS in structural concrete in winter when ambient temperature is 20°C or lower. This detrimental effect however becomes less significant at a hot climatic condition. The average 3-day compressive strength of 50% GGBS mix was almost same as the 3-day compressive strength of 0% GGBS mix at 38°C curing, which represents hot climatic conditions in Shanghai.

Isothermal calorimetry, semi-adiabatic calorimetry tests and FEM were conducted in this project to investigate the heat development in GGBS concrete. The results obtained from the isothermal calorimetry tests were used to simulate to the hydration heat liberation process in concrete floor slabs. FEM results, validated by the semi-adiabatic calorimetry tests, show a beneficiary effect of using GGBS in concrete structures in summer. With 50% of CEM I replaced with GGBS, thermal loading (or T1 values) reduced by 30%.

## REFERENCES

1. CHINACONCRETES. Commerical concrete production in China 2013, 2014, Available from: http://www.cnrmc.com/news/show.php?itemid=92151 [cited 18/8/2014].
2. BAMFORTH P.B. CIRIA C660 Early-age Thermal Crack Control in Concrete, London, CIRIA 2007, ISBN 978-8-86107-660-2.
3. CHENG F., WEI R. and LI H. Utilization of GGBS in China, Journal of Xi'an University of Architecture & Technology, Vol. 42, No. 3, 2010, pp. 446–450.
4. ZHENG L., PAINE K.A. and DHIR R.K. Early-Age Temperature Rises in GGBS Concrete: Part 1: Determination of T1 Values, Proceedings of International Congress - Global Construction: Ultimate Concrete Opportunities, 2005, Editors: Dhir RK, Harrison TA, Newlands MD, London, Thomas Telford, ISBN 0727733877, p 173–182.

5. ACI. ACI 305R Hot weather concreting, ACI, 1999.
6. PRC MINISTRY OF CONSTRUCTION. GB 50204-1992 Code for construction and acceptance of concrete structures, 1992.
7. PRC MINISTRY OF CONSTRUCTION. GB 50204-2002 Code for construction and acceptance of concrete structures, 2002.
8. CHINA METEOROLOGICAL ADMINISTRATION. Chinese ground temperature monthly data (1961 to 1990), 2004, Available from: http://www.cma.gov.cn/ [cited 15/12/2014].
9. DA SILVA W.R.L., SMILAUER V. and STEMBERK P. Upscaling semi-adiabatic measurements for simulating temperature evolution of mass concrete structures, Materials and Structures, Vol. 48, No. 4, 2013, pp. 1031–1041.
10. KIM G.Y., LEE E.B., NAM J.S. and KOO K.M. Analysis of hydration heat and autogenous shrinkage of high-strength mass concrete, Magazine of Concrete Research, Vol. 63, No. 5, 2011, pp. 377–389.
11. AZENHA M., FARIA R. and FERREIRA D. Identification of early-age concrete temperatures and strains: Monitoring and numerical simulation, Cement and Concrete Composites, Vol. 31, No. 6, 2009, pp. 369–378.
12. LAWRENCE A.M., TIA M., FERRARO C.C. and BERGIN M. Effect of early age strength on cracking in mass concrete containing different supplementary cementitious materials: experimental and finite-element investigation, Journal of Materials in Civil Engineering, Vol. 24, No. 4, 2012, pp. 362–372.
13. BOUGARA A., KHATIB J. and KHELLAFI H. Some parameters affecting the heat of hydration of blast-furnace slag cement, in 1st International Conference on Sustainable Built Environment Infrastructures in Developing Countries. 2009: ENSET Oran, Algeria, pp. 9–16.
14. PRC MINISTRY OF CONSTRUCTION. GB 175-2007 Common portland cement, General administration of quality supervision, inspection and quarantine of the People's Repulic of China, 2007, ISBN 155066130308.
15. PRC MINISTRY OF CONSTRUCTION. GB/T 18046-2008 Ground granulated blast furnace slag used for cement concrete, General administration of quality supervision, inspection and quarantine of the People's Repulic of China, 2008, ISBN 155066131017.
16. BSI. BS 8500-1: 2006 Complementary British Standard to BS EN 206-1. Method of specifying and guidance for the specifier British Standards Institution (BSI), 2006.
17. TANG K., MILLARD S. and BEATTIE G. Early-age heat development in GGBS concrete structures, Structures and Buildings, Vol. 168, No. 8, 2015, pp. 541–553.
18. BALLIM Y. and GRAHAM P.C. The effects of supplementary cementing materials in modifying the heat of hydration of concrete, Materials and Structures/Materiaux et Constructions, Vol. 42, No. 6, 2009, pp. 803–811.
19. BAMFORTH P., CHRISHOLM D., GIBBS J. and HARRISON T. Properties of concrete for use in Eurocode 2, The Concrete Centre, London, UK, 2008, ISBN 978-1-904482-39-0.

# PROPERTIES OF RECYCLED AGGREGATE CONCRETE AFTER 16 YEARS OF EXPOSURE TO REAL CONTINENTAL CONDITIONS

**K Janković D Bojović M Stojanović**

**L Lončar L Antić**

IMS Institute

Serbia

**ABSTRACT.** It has been observed from the literature that the recycled aggregate concrete (RAC) shows better freeze-thaw resistance than the conventional concrete because recycled aggregate is more porous. Laboratory tests have shown that air entrained concrete made up of crushed bricks as aggregate has very good frost resistance. In this paper compressive and flexural strength after 16 years under real continental conditions were tested. Concrete exposed to freezing changes its characteristics both in terms of strength and in terms of the structure. The aim of this study is to determine how to modify the structure of the concrete after real cold climate conditions. Changing the structure of concrete was evaluated by qualitative and quantitative analysis of pores using the device RapidAir 457.

**Keywords:** Recycled aggregate concrete, Durability, Pores, RapidAir 457

**Ksenija Janković,** senior research fellow is Head of Laboratory for Concrete at IMS Institute, Belgrade, Serbia. Her research interests include ultra high performance concrete, utilization of by-products and recycled waste materials in concrete and concrete durability. She has published about 140 papers.

**Dragan Bojović MSc CE,** research assistant is working in the Laboratory for Concrete at IMS Institute. He is a PhD candidate at the Faculty of Technical Sciences at Novi Sad University. His research interests focus on ultra high performance concrete, SCC, concrete fracture and concrete quality control in situ.

**Marko Stojanović, MSc CE,** research assistant is working in the Laboratory for Concrete at IMS Institute. He is a PhD student at the Faculty of Civil Engineering, Subotica at Novi Sad University. His research interests are SCC and ultra high performance concrete.

**Ljiljana Lončar, BSc CE** is working in the Laboratory for Concrete at IMS Institute. She is especially interested in concrete quality control, control of concrete factory and production of precast elements. She is a part of the team for implementation of new EN in that field.

**Lana Antić, MSc CE** is working in the Laboratory for Concrete at IMS Institute.

## INTRODUCTION

Generally concrete durability performance is a measure of concrete permeation characteristics, as well as integrity of concrete against aggressive agents in the environment, for example sulphate, acids, chlorides, oxygen, carbon dioxide, etc. Investigations of the RAC have shown that, the durability performance of RAC is poorer than that of conventional concrete. The poor durability performance of RAC is connected with the inferior quality of RA due to the presence of numerous cracks and fissures and pores inside the aggregate, which makes it more susceptible to permeation [1, 2]. RAC microstructure is porous due to the presence of old adhesive mortar around the RA and high water absorption characteristics of RA, which also influences the permeability characteristics of RAC. The controlling factor for better durability performance of RAC is the porosity of RA. Because of that RAC needs special treatment so that the open path for foreign agents would be blocked. On the other hand, one of the major difficulties with RA is the variability in their properties due to processing, composition, contents and proportions which are extensively linked to the original source of debris.

Permeation, that is, the movement of various foreign agents through the concrete happens not only by the flow through the porous system but also by sorption and diffusion. Therefore, the first essential step for studying the durability of concrete made with RA is the evaluation of concrete water absorption. In case of RAC, water absorption of concrete is directly related to the water absorption of RA. Thus, if the water absorption value of RA is high, it imposes a high risk towards the durability of RAC. Various research works show that the water absorption of RAC is significantly higher than that of natural aggregate concrete [2-5]. Concrete made up of RA shows better freeze and thaw resistance than the conventional concrete, although RA is more porous [6, 7].

The waste which appears when the burning process is not adequately performed during the industrial production of brick and tiles can successfully be used for the production of smaller concrete prefabricated elements [8, 9]. Concrete based on crushed brick aggregate has satisfactory compressive and tensile strength and thermal insulating properties but weaker resistance to water and frost action and has greater shrinkage by 20-60% when compared to ordinary concrete [10, 11].

The resistance of concrete to frost action can be performed on the macro and mezzo level structures of concrete. In the case of macro level concrete is tested by exposing it to traditional cyclic freezing and thawing. In this case all testing was performed in accordance with SRPS norms. Concrete resistance to mezzo level is determined by the quantity and quality of entrained air. The factor of pore spaces (Power`s spacing factor) is taken as a measure of the resistance of concrete to frost.

In the case of intake aggregate of recycled bricks for questioning at the macro level there is no difference in the approach to testing. During the testing at the mezzo level it is necessary to pay attention to the characteristics of the applied unit. The primary characteristic of crushed bricks aggregate is great water absorption, which indicates that there are many pores in its structure. During the testing at the mezzo level the properties of crushed bricks aggregates can lead to different results of tests obtained by testing fresh concrete. It would not be possible to compare testing on fresh concrete, testing at the macro level and testing at mezzo level if it weren’t for this fact which is necessary to somehow incorporate the obtained test results.

## EXPERIMENTAL WORK

Four out of twelve representative concrete samples from the previous investigation [11, 12] were tested. All concrete mixtures were made using by ordinary Portland cement (CEM I 42.5R). Two types of concrete (A and H) had 350 kg/m$^3$ and two of them (E and J) had 250 kg/m³ cement content. Two kinds of concrete (A and E) were made using recycled bricks as aggregate and two kinds of concrete (J and H) were made using a combination of river sand and recycled bricks. Concrete mixtures E and H were modified by an admixture of polymer. Mixture composition of concrete is shown in Table 1.

Table 1 Quantities of component materials of concrete

| TYPE OF CONCRETE | | A | E | J | H |
|---|---|---|---|---|---|
| Cement, kg/m³ | | 350 | 250 | 250 | 350 |
| River sand, kg/m³ | 0/4 | - | - | 574 | 532 |
| | 0/4 | 469 | 487 | - | - |
| Recycled bricks | 4/8 | 161 | 167 | 197 | 182 |
| Aggregate, kg/m³ | 8/16 | 214 | 222 | 262 | 243 |
| | 16/32 | 496 | 514 | 607 | 562 |
| Water, kg/m³ | Absorbed | 224 | 232 | 177 | 164 |
| | Free | 76 | 38 | 33 | 61 |
| Polymer, kg/m³ | | - | 21.11 | - | 29.55 |

Laboratory tests have shown that air entrained concrete made up of crushed bricks as aggregate had very good frost resistance [11-15]. In this paper testing results of specimens after 16 years under real continental conditions are shown. Average temperatures for the last two years [16] are given in Table 2.

Table 2 Average temperatures, °C

| YEAR | I | II | III | IV | V | VI | VII | VIII | IX | X | XI | XII | ANNUAL |
|---|---|---|---|---|---|---|---|---|---|---|---|---|---|
| 2013. | 2.5 | 3.6 | 5.8 | 13.0 | 17.3 | 20.0 | 22.1 | 22.8 | 15.9 | 13.6 | 8.4 | 1.3 | 12.2 |
| 2014. | 3.8 | 5.7 | 9.1 | 12.8 | 16.1 | 20.3 | 21.4 | 20.6 | 17.1 | 13.2 | 8.5 | 3.0 | 12.6 |

For the reference period 1981-2010 mean annual air temperature was in the range 10.1-12°C, the number of days with temperature up to 0°C was 11-22, the number of frosty days was 71-90 and the average relative humidity was 76.4%.

## RESULTS AND DISCUSSION

### Specimens Description

Referent concrete cured in laboratory conditions for 16 years is shown in Figure 1.

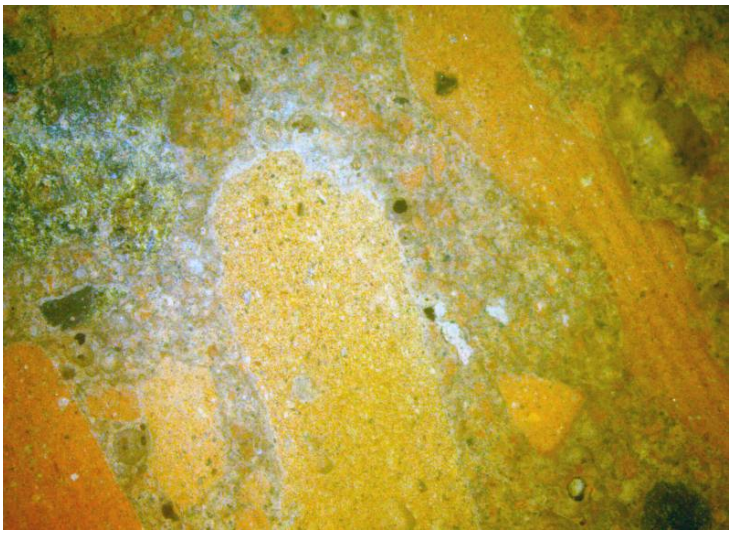

Figure 1 Concrete cured in laboratory conditions – stereo-microscope 6.5×

The sample was pale ochre reddish colour. Pores that are more or less round in shape and below 1 mm in size occasionally appear on the outer side. Parts of crushed brick which was used as aggregate can be found on the inner side. Transition zone recycled brick - mortar can sometimes have pores and cracks on it. Pores on the whole sample are frequent, varying in shape and size that is about 2 mm and originated primarily.

Concrete with recycled bricks as aggregate exposed to real conditions for 16 years is shown in Figure 2.

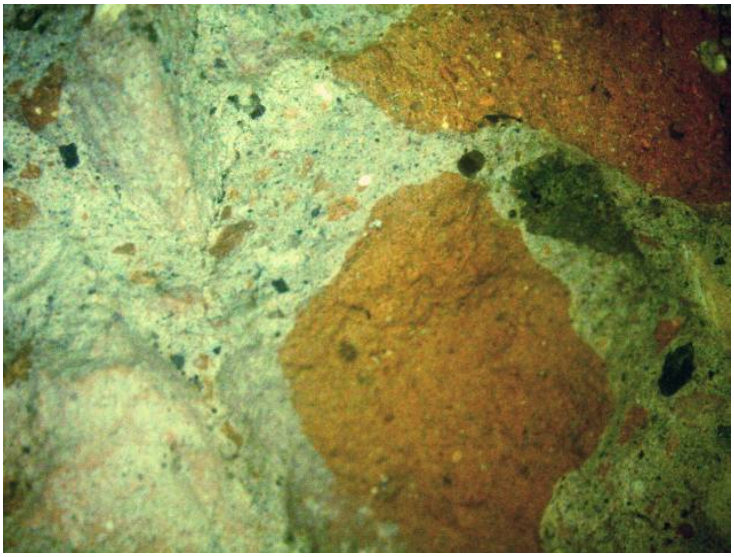

Figure 2 Recycled bricks concrete cured in real conditions – stereo-microscope 6.5×

The appearance of the sample without aggregate on the outer side – The sample is grey with a green shade and it reflects some kinds of wear and tear due to the weather. There is discoloration, i.e. the change of the original colour to grey and green and the occurrence of ruptures and small cracks on the surface of the sample. The changes followed due to the effect of microclimate, that is, the exposure of the sample to the influence of aggressive urban environment, where the water is the main cause of the physical and chemical disintegration. The grey colour comes from the dirtiness of the sample with particles from the air - soot. The green colour comes from its biocolonization by lower plants-algae.

The sample on the inner side - The sample is composed of crashed bricks and mortar. There are pores that are more or less round in shape and of different sizes. The edge of brick grain can occasionally have small pores and cracks on it.

Concrete with recycled bricks as coarse aggregate and river sand exposed to real conditions for 16 years is shown in Figure 3.

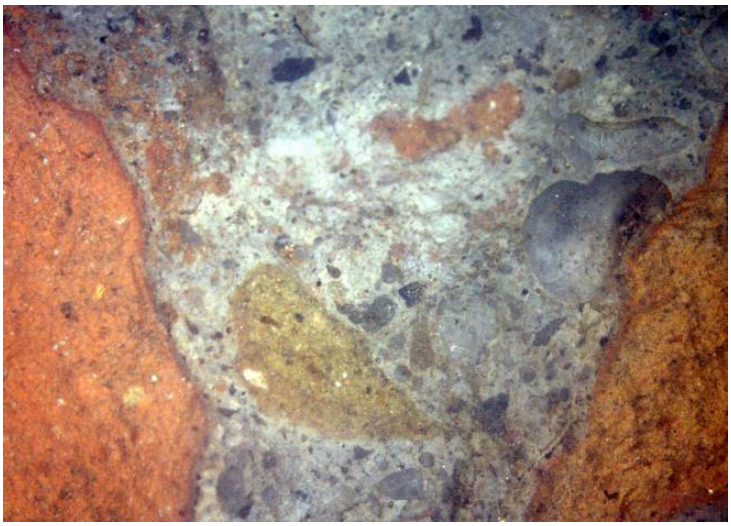

Figure 3 Concrete with recycled bricks and river sand cured in real conditions – stereo-microscope 6.5×

The appearance of the sample with aggregate from the outer side – The sample is dirty grey. The original light grey colour has turned into a dark grey due to the action of agents from the atmosphere. This primarily happened due to the impact of soot and moisture. Rainwater purifies the atmosphere and rinses the aerosols and dissolves gases, creating acid rains which are corrosive.

A sample from the inner side – The sample consists of crashed brick and natural aggregate (mainly quartz sand). Besides the primary pores and rare small cracks on the aggregate-mortar transition zone, the subsequent secondary changes, which could occur due to exposure of sample to the action of external agents, were not noticed.

## Compressive and Flexural Strength

Compressive and flexural strength of specimens cured up to 2 years in laboratory conditions and after 16 years under real continental conditions are given in Tables 3-4.

Table 3 Compressive strength, N/mm²

| SAMPLE | AGE | | | | |
|---|---|---|---|---|---|
| | 28 days | 6 months | 1 year | 2 years | 16 years |
| A | 28.4 | 31.7 | 31.4 | 31.7 | 28.69 |
| E | 20.3 | 26.4 | 25.8 | 25.0 | 24.11 |
| J | 21.6 | 27.5 | 29.9 | 29.0 | 40.26 |
| H | 27.0 | 30.2 | 31.7 | 33.4 | 42.26 |

Table 4 Flexural strength ($N/mm^2$)

| SAMPLE | AGE | | | | |
|---|---|---|---|---|---|
| | 28 days | 6 months | 1 year | 2 years | 16 years |
| A | 1.9 | 3.0 | 3.2 | - | 2.86 |
| E | 2.2 | 3.1 | 3.1 | - | 3.12 |
| J | 2.6 | 4.0 | 4.4 | - | 6.25 |
| H | 3.1 | 3.6 | 4.4 | - | 7.18 |

By analysing results of compressive and flexural strength of specimens cured up to 2 years in laboratory conditions it can be seen that there are no significant changes in the values of concrete exposed to real continental conditions for 16 years, for concrete with recycled bricks as aggregate (A and E). Concrete with river sand (J and H) had an increase in strength. As one can see in Fig.3 for this type of changes in the structure were not observed. These results were expected considering that the laboratory tests have shown that recycled bricks aggregate concrete had resistance to freezing and thawing [11-15].

## Pore Size Distribution

Air content of fresh concrete varied from 2.6 % to 3.2 %. Testing of concrete samples was done with the RAPID AIR 457 equipment in order to obtain the results of the total amount of pores in samples and spacing factor of pores in concrete. Experimental results are given in Table 5 and Figure 4.

Table 5 Experimental results

| Testing | A | E | J | H |
|---|---|---|---|---|
| Density of hardened concrete, kg/m³ | 1707 | 1707 | 1920 | 1897 |
| Spacing factor, mm | 0.137 | 0.184 | 0.151 | 0.117 |
| Rapid Air 457, % of air | 4.12 | 4.06 | 3.46 | 3.73 |

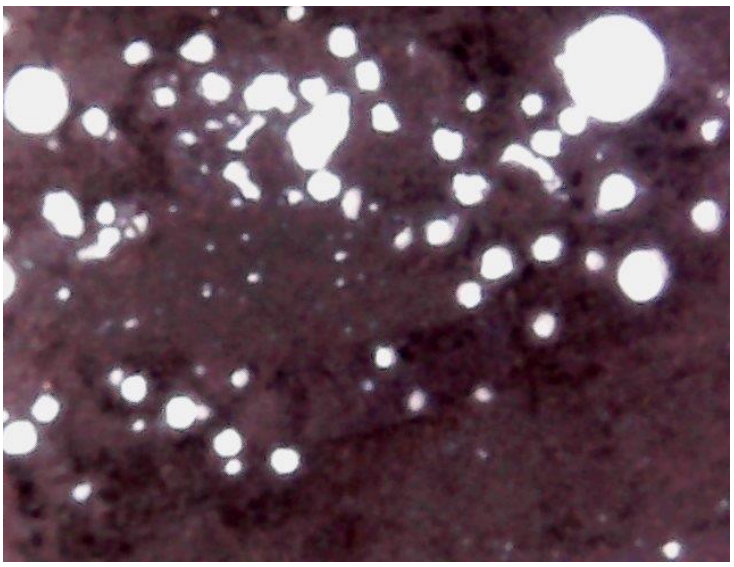

Figure 4 Sample of concrete with recycled bricks and river sand as aggregate (H) for testing by Rapid Air 457

## CONCLUSIONS

Based on the microscopic analysis it can be concluded that the exposure of sample to alternating wetting, drying, temperature change on daily and annual basis and frost action besides the deterioration on the outer side have not led to greater disintegration in the interior.

The samples of concrete with only recycled bricks as aggregate exposed for 16 years to conditions of continental climate have not had a significant decrease in values of compressive and tensile strength. These findings confirmed the results of the testing of frost resistance obtained under laboratory conditions.

The resistance is not surprising, having in mind that the spacing factor done by Rapid Air 457 device is very low in all specimens. Small value of spacing factor is partly caused by the use of aggregates from recycled bricks. This aggregate is rich with pores that affect the properties of the concrete.

## ACKNOWLEDGMENTS

The work reported in this paper is a part of the investigation within the research project TR 36017 "Utilization of by-products and recycled waste materials in concrete composites in the scope of sustainable construction development in Serbia: investigation and environmental assessment of possible applications" supported by the Ministry of Education, Science and Technological Development, Republic of Serbia. This support is gratefully acknowledged.

## REFERENCES


1. OLORUNSOGO F.T. and PADAYACHEE N. Performance of recycled aggregate concrete monitored by durability indexes, Cement and Concrete Research, Vol. 32, 2002, pp. 179–185.
2. KOU S.C. and POON C.S. Enhancing the durability properties of concrete prepared with coarse recycled aggregate, Construction and Building Materials, Vol. 35, No. 10, 2012, pp. 69–76.
3. RAO M.C., BHATTACHARYYA S.K. and BARAI S.V. Influence of field recycled coarse aggregate on properties of concrete, Materials and Structures, Vol. 44, 2011, pp. 205–220.
4. WIRQUIN E., HAHDJEVA-ZAHAARIEVA R. and BUYLE-BODIN F. Use of water absorption by concrete as a criterion of the durability of concrete – application to recycled aggregate concrete, Materials and Structures, Vol. 33, 2000, pp. 403–408.
5. LEVY S.M. and HELENE P. Durability of recycled aggregates concrete: a safe way to sustainable development, Cement and Concrete Research, Vol. 34, No. 11, 2004, pp. 1975–1980.
6. ACI committee 201.2R-01. Guide to durable concrete. Farmington Hills: American Concrete Institute; 2000:1–41.
7. GOKCE A., NAGATAKI S., SAEKI T. and HISADA M. Freezing and thawing resistance of air-entrained concrete incorporating recycled coarse aggregate: the role of air content in demolished concrete, Cement and Concrete Research, Vol. 34, No. 5, 2004, pp. 799–806.
8. DEBIEB F. and KENAI S. The use of coarse and fine crushed bricks as aggregate in concrete, Construction and Building Materials, Vol. 22, 2008, pp. 886-893.
9. POON C.S. and CHAN D. Paving blocks made with recycled concrete aggregate and crushed clay brick, Construction and Building Materials, Vol. 20, 2006, pp. 69–577.
10. CACHIM P.B. Mechanical properties of brick aggregate concrete, Construction and Building Materials, Vol. 23, 2009, pp. 1292–1297.
11. JANKOVIĆ K. Polymer modified concrete based on recycled brick, Ph.D. thesis, 1998, University of Belgrade, Faculty of Civil Engineering, Belgrade (in Serbian).
12. JANKOVIĆ K. Using recycled brick as concrete aggregate, Proceedings of the international congress “Challenges of concrete construction”, Book “Sustainable Concrete Construction”, 2002, Dundee, UK, pp. 231-240.
13. JANKOVIĆ K., BOJOVIĆ D., NIKOLIĆ D., LONCAR Lj. and ROMAKOV Z. Frost Resistance of Concrete with Crushed Brick as Aggregate, Facta Universitatis, Series: Architecture and Civil Engineering, Vol.8, No 2, 2010, 155 - 162
14. JANKOVIĆ K., NIKOLIĆ D. and BOJOVIĆ D. Concrete Paving Blocks and Flags Made with Crushed Brick as Aggregate, Construction and Building Materials, Vol. 28, 2012, pp. 659–669.
15. JANKOVIĆ K., STANKOVIĆ S., NIKOLIĆ D., BOJOVIĆ D. and LONČAR, Lj. Determination of Recycled Aggregate Concrete Degradation by Resonance Frequency Analysis, Romanian Journal of Materials, Vol. 41, No.1, 2011, 22–25.
16. http://www.hidmet.gov.rs

# NOVEL METHOD FOR MONITORING OF CONCRETE STRUCTURES BY MEANS OF COMPOSITE TENSOMETERS

**R Cechmanek**
Research Institute for Building Materials
Czech Republic

**ABSTRACT:** The paper informs about an ongoing research on using carbon-based composite tensometers for monitoring of concrete structures under loading to prevent them to unexpected collapsing. For this reason it was necessary to design special fibre-cement elements able to transfer any mechanical impulse to an electrically-measured signal detected as a change in electrical resistance with computer outputs. Regarding previous research studies it was concluded that special fibre-cement composites are able to conduct electric current under specific conditions. This property is ensured by using of various kinds of carbon materials. Though carbon fibres are less conductive than metal fibres, composites with carbon fibres were evaluated as better current conductors than the composites with metal fibres. The level of electric conductivity is monitored by means of impedance measurement of designed samples. These composites could be used for a range of applications such as heating of trafficable surfaces or shielding of electro-magnetic fields. By means of various kinds of carbon particles and fibres it is possible to design cement composites with an ability to monitor changes in electrical conductivity of concretes. As a typical element for laboratory testing there were chosen a concrete column and a longitudinal beam, which were repeatedly subjected to load by simple pressure with continual monitoring of changes in electrical properties.

**Keywords:** Carbon, Conductivity, Loading, Monitoring.

**R Cechmanek** graduated at the Brno University of Technology in 2000 and since that year he has worked in the Research Institute for Building Materials, currently as a head of the department Applied research and development with the special aim to fibre-cement composites and utilization of industrial waste materials.

## INTRODUCTION

Nowadays, characteristics of composite materials based on cement include also other applications, among others for construction of self-monitoring buildings, bridges, etc. Besides monitoring the usual properties (mechanical stability over the period of time, environmental resistance, design limits or economic profitability) it becomes to be more important and significant for construction of buildings.

One of the most common structural materials used in engineering construction is cement and its mixtures (concrete and mortar). Cement is slightly conducting material, but its electrical conductance, Electro-magnetic interference (EMI) shielding effectiveness and wave absorbing properties are very poor. In order to increase the ability of cement materials to transfer electrons, additional conductive components have to be added. Smart Concrete (SC) could be considered as a material of the future. Due to its attractive features, SC can be used as a strain-sensing element.

The strain-sensing properties are achieved by a proper volume amount of conductive filler. In this system, the matrix is made of cementitious material with small amount of silica fume, fly ash, and fine aggregates [1]. Different conductive fillers were tested considering the best strain-sensitivity/material price ratio. Previous research proved carbon black and graphite particles to be the best choice in terms of price. The best strain-sensitivity is achieved near the percolation threshold of filler particles [2].

Strain properties of the composite can be evaluated by impedance changing. The impedance changing sensitivity regarding deformation can be widely affected by a proper choice of concrete admixtures [3]. The real part of impedance is strongly affected by deformation and can be used for measurements.

Conventional DC techniques for resistance measurements cannot be used. Electrode system of a sensing element could be damaged by electrolytic corrosion in this case. Square-wave AC technique with an excitation frequency of 1 kHz and an excitation voltage of 1 V were experimentally set [3]. In the light of new knowledge about materials, a necessity to a simple, relatively inexpensive and portable device has been raised.

The Research Institute for Building Materials focuses on cement-based building materials reinforced with fibres almost for 20 years. The main interest is in glass-fibre reinforced concrete (GFRC), which is used for the range of applications, such as light-weight facing panels and various architectural elements up to channels for deposition of high-voltage cables in tunnels of the Prague Underground. The other utilization of fibres is for cement-based composites for high-temperature application. In this case carbon fibres are successfully used.

Recently a research team in co-operation with experts from the Faculty of Electrical Engineering and Communication in the Brno University of Technology developed modified cement matrixes with effective amount of carbon particles and fibres for a design of electrically conductive elements for special purposes.

Proposed applications were heating of trafficable surfaces and shielding of electro-magnetic fields between cables of different voltage.

These outputs are utilized also for a new aim to monitor internal states connecting to mechanical strains in concrete structures under mechanical loading. For this reason it was necessary to design special fibre-cement elements able to transfer any mechanical impulse to an electrically-measured signal detected as a change in electrical resistance with computer outputs.

As carbon particles there were used expanded or micronized graphite, fibres were on the base of polyacrylnitril (PAN) or pitch. The optimal variants were used for preparation of one-dimensional specimens most suitable for measurement of simplified impact of stress and strain.

## MATERIALS AND METHODS

### Carbon Materials for Concrete Conductivity Improvement

Glass fibre reinforced concrete was taken as a standard and modified with an addition of carbon particles and other suitable materials to enhance its electrical conductivity and broaden application possibilities of thin-walled fibre-reinforced inorganic composites for elimination of electromagnetic field effect, heating of concrete trafficable surfaces and monitoring of building structures.

In the course of searching for suitable components there were selected mainly various kinds of micronized or expanded graphite with particle size in micro- or nanometers, which is characterized by excellent electrical properties as well as good compatibility with a cement matrix, except for higher demand of batch water due to its bulk specific surface.

Carbon black with similar properties as micronized graphite was used as well. Carbon black has elementary particles generally in a range from 10 to 100 nanometers, but during the production process individual spherical particles agglomerate in chains or clusters. Micronized graphite has carbon content above 80%; carbon black has high carbon content (99%). Expanded graphites have lower carbon content (60 – 96%).

Considering an application based on a relation between electrical behavior and mechanical strain and reverse deformation of concrete elements, two types of fibre reinforcement (carbon and metal) were chosen too.

### Composite Mixtures with Carbon Particles and Fibres

All mixtures were prepared in a mixer with a stationary drum and forced movement of paddles. Standard fine-grained matrix consisting of cement, sand and fine filler with 3% of dry mixture weight reinforcement by alkali-resistant glass fibres with length 12 mm was chosen for further modifications.

The addition of carbon particles induces good electrical properties in cement-based composites. Though carbon fibres are less conductive than metal fibres, composites with carbon fibres were evaluated as better current conductors than the composites with metal fibres. It is supposed that this is due to extremely fine size of carbon fibres which provides more effective inter-fibre continuity. Thus further research was carried out with carbon particles and carbon fibres.

During the tests suitability of fine-grained particle and fibre combination was confirmed. The proportion of carbon particles was expressed as a percentage of a dry mixture weight (cement + sand + fine filler) as a substitution of a part of sand in range of 4 – 10% by mass. Carbon fibres with diameter 18 μm and length 10 mm substituted for glass fibres up to 2% by mass.

Basic components stated in Table 1 are as follows: carbon fibre CF, micronized graphite MG, expanded graphite EG and nickel-coated expanded graphite EG/Ni. Carbon particles suitable for given applications have size from 0.01 to 100 μm.

Table 1 Basic mixture compositions

| BASIC MIXTURE COMPOSITIONS | | | | |
|---|---|---|---|---|
| Mixture components | CF | MG | EG | EG/Ni |
| Cement binder | 54% | 54% | 54% | 54% |
| Silica filler | 40% | 34% | 36% | 35% |
| Fine filler | 3% | 3% | 3% | 3% |
| glass fibre | 1% | 1% | 1% | 1% |
| Carbon fibre | 2% | 2% | 2% | 2% |
| Micronized graphite | - | 6% | - | 3% |
| Expanded graphite | - | - | 4% | - |
| Nickel-coated expanded graphite | - | - | - | 2% |

**Influence on Workability**

Fibre-cement mixtures were prepared in order to achieve optimal workability and minimal impedance, i.e. maximal electrical conductivity. To compare an influence of the type of carbon matter on impedance of the cement-fibre composite, each carbon powder always replaced the same proportion of dry components.

Carbon origin as well as particle size both affect impedance properties of the final composites, and as well the particle size affects workability of fresh mixtures. It was found that the finer carbon powder, the lower was the impedance and the worse mixture workability.

Carbon particles should be properly dispersed among other mixture components without bleeding during transport and molding. With carbon fibres the perfect defibering and ideal anchoring in binder should be reached [4].

**Mixture Optimization**

Within the optimization process fine fillers were withdrawn from the composition. Despite the positive effect on dense structure and better mechanical characteristics of composites, pozzolanic admixtures increase electric resistance of concrete mixtures [5].

All samples were cured in laboratory conditions close to real manufacture conditions with temperature 25°C and humidity 55%.

The physical-mechanical properties of composites were tested on standard samples for thin-walled GFRC elements with dimensions 250 mm $\times$50 mm $\times$10 mm in the age of 28 days. Higher water/cement ratio causes significantly higher absorption and lower bulk density, associated with low flexural strength and impact strength of the final composites.

### Measurement of Electrical Properties

Ions in pore solutions cause conducting of electric current in concretes. Conduction of electrical current in cements and concretes is essentially electrolytic. In order to avoid problems of polarization, alternate currents are often used for determining resistivity of electrolytes and therefore also of cements and concretes [6]. Therefore electrical resistance of composite materials is expressed as impedance.

Percolation threshold expresses minimal concentration of the certain component that creates the first conductive way through the whole volume of measured composite [4]. In the end percolation threshold of carbon fibres was determined to 0.75% of the dry mixture weight.

In order to optimally assess the electrical parameters an influence of voltage and A.C. frequency was observed. The influence of voltage was evaluated as non-relevant. The influence of A.C. frequency on the calculated values of impedance was found to be reasonably significant. The impedance decreased dramatically with increase in the applied frequency. Consequently, frequency of 20 kHz was adopted as the measurement frequency and the calculated impedance was assumed equal to the resistance.

## APPLICATION OF PROPOSED ELEMENTS

### Electro-Magnetic Shielding

Electro-magnetic field is assumed to be a problem in the so called “sick house syndrome”. External electro-magnetic fields can cause problems both in human health and in industry, where it can interfere with production of electronic equipment.

Standard glass fibre reinforced concrete inhibits electro-magnetic field up to approximately -5 dB but our modified fibre-cement composite is able to achieve a level up to -35 dB. In comparison to a massive steel reinforced concrete the same shielding effect is achieved with using of incomparably less structural thickness.

In order to approach real conditions as much as possible the measurement was carried out in a special electro-magnetic chamber. Shielding efficiency was proven by the non-availability of any communication network inside the chamber [7].

A modified fibre-cement mixture was used for manufacturing of a concrete channel to demonstrate the application of electro-magnetic shielding. It contains three chambers to separate electric cables with different voltage so that they do not interfere with each other.

### Concrete Heating

Electric heating of pavements and other surfaces is carried out by using of heating cables built into a concrete panel or a sand bed under a pavement made of asphalt or cobble-stone.

Heat is generated along the whole cable body by means of direct electric energy transformation in their cores. Within accumulation systems electric input 180 – 250 W/m$^2$ is needed. According to our measurements it has been concluded that for direct heating systems only about 1 third or 1 half (80 – 130 W/m$^2$) is sufficient for the equal heat output.

A trafficable steel reinforced concrete panel was made with the ability to thaw snow cover or to defrost ice for reduction of slipping hazard on pavements or access ramps in front of buildings. The proposed element combines advantages of the solid bearing steel reinforced concrete and those of a thin fibre-cement slab with the required heating capacity.

## MONITORING OF CONCRETE STRUCTURES

Smart concrete can be used for sensing the load of concrete elements and structures mainly for measurements which use strain gauges. A strain gauge is a device used to measure strain on the surface part by means of mechanical stress (tension, compression, etc.). In fact the strain gauge measures the relative deformation. Mechanical stress cannot be measured directly, and thus converted from the measured deformation.

Composite material with carbon particles is sensitive to load changes [3]. This sensitivity is manifested by a rapid change of the measured impedance. Generally, in all types of carbon admixtures, the impedance of component is affected by the deformation and can be used to detect the changes. Appropriately selected admixture has an effect on the relative size of the impedance changes depending on the pressure. The voltage level of the measuring voltage depends on used copper electrodes. These electrodes have a high resistance to corrosion in an alkaline environment.

The aim of the present research was to design an element with the ability to monitor internal processes in building structures and prevent them from collapsing. Any change in mechanical loading is immediately recognized and transferred into a measurable electric signal with a computer output.

For monitoring of concrete elements under loading there are used mostly tensometers. Tensometer actually measures only relative deformation.

It was concluded that cement composites with carbon fibres are suitable for monitoring of transition actions caused by change of strain, stress, temperature or humidity. Electrical resistance monitoring is a suitable way for characterization of cracks in concrete structure [8].

Besides ceiling panels, columns or foundations these elements could be implemented into the overloaded parts of bridge constructions.

Within experimental tests on flexural strength selected samples with effective carbon addition provided measurable changes in the impedance. For the purpose of monitoring in conditions close to a real application a model of steel reinforced concrete structure was made. The model was used for evaluation of electrical properties of the embedded element as well as an influence of a concrete mass on these properties.

## Description of the Measuring Device

The device function is based on 16-bit microcontroller and it is equipped with the Secure Digital (SD) card, which can be inserted into a side slot, for saving the measured data. SD card communicates with the microcontroller via Serial Peripheral Interface (SPI). A special feature of used microcontroller is built in Universal Serial Bus (USB) interface connection for transferring the measured data into PC. Microcontroller contains complete physical layer of USB communication device. Specialized software developed together with the device is able to receive this data and display it in a graph.

Dynamic measurements of specimens bring problems such as dusty environments, mechanical vibrations, EMI interferences and temperature stress. Mechanical design of the device is based on requirements for battery powered laboratory instrument which must be robust and environmentally resistant.

Under cover, there is a very well readable display panel. Four control buttons are placed from the front. The opposite side is equipped with eight connectors for measuring probes and four connectors for digital sensors. On the left side, there is the main switch and a connector for charging. The right side includes a water and dust proof USB connector with a rubber plug.

## Selection of the Proper Composition for Conductive Composites

The aim was to design a cement-based composite with the ability to change its electrical properties in dependence on mechanical stress and strain by means of modified cement matrix. For this purpose there was a search for suitable inorganic additives. 25 carbon materials of different origin were tested, including micro-milled graphites, expanded graphites or high conductive carbon black.

For the selected set of carbon particles an optimization process was carried out to reach the percolation threshold, i.e. the proper amount of an additive, for which no significant changes of electrical properties do not take place in the final composite.

Concerning results gathered within static as well as dynamic measurements, the most suitable additives – carbon black and carbon fibres and their dosing were selected. The final composition consists of 50-60% of high-valuable cement, 30-45% of fine aggregate, up to 10% of carbon particles and up to 2% of carbon fibres (in weight %).

## Testing of Modified Samples

Planar samples were evaluated as inconvenient for monitoring of electrical response in individual directions of building elements for the reason of combined impact of stress and strain. Therefore the elements were designed in the shape of prisms with one dominant dimension comparing to others to avoid multi-parametrical loading effect.

These specimens were made in two dimensions 40 mm × 40 mm × 160 mm or 20 mm × 20 mm × 100 mm. In one set there was 1 element with 2 copper contacts ca. 2-5 mm from the end as shown in Figure 1. The other 2 elements were intended for testing of physical-mechanical characteristics, i.e. compressive, flexural and tensile strength, bulk density and absorptivity.

Cement-based tensometers are prepared from fresh mixture containing all the particular components listed above in accordance with required technological process. The mixture is filled into molds, copper contacts are inserted into it and an isolated part sticks out of it. After 28 days of curing in water the isolation is taken out and the tensometers are provided with long electrical outlets for connection to the measuring device.

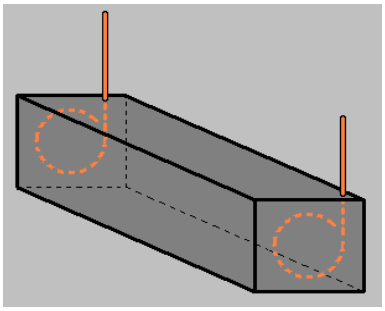

Figure 1 Design of modified sample

The tensometers are placed into molds for reinforced structural elements by means of electrically non-conducting straps according to the assembly drawing (Figure 2).

Impedance measurement of individual samples was conducted under following conditions: alternate voltage 1 V and frequency 1 kHz were set to avoid corrosion of used copper electrodes, because cement composites adopt behavior of solutions due to their internal moisture. Maximal loading 1 kN was set within the measurements to avoid unexpected damage of samples.

**Design of Concrete Column**

Relation of deformation to impedance of composite elements has been already verified [6]. The next logical step was evaluation of this relation in the practical utilization.

For evaluation of utilization of integrated composite elements in concrete or reinforced concrete column a model in standard cross section was designed. For the purpose of loading simulation in the column by means of hydraulic press machine it was necessary to shorten its length. Therefore the final dimensions were 300 mm × 300 mm × 500 mm. There were 2 variants – the first column without steel reinforcement and the second one with steel reinforcement for comparison (see Figure 2).

In both variants 3 composite elements were put into the model column. The first one was placed vertically in the column centroid, the second one was placed horizontally above the first one and the third one was placed again vertically at the side of the column next to steel reinforcement. The similar placement was used for the variant without reinforcement. The aim was to compare effect of the steel reinforcement and a different position of individual composite elements.

A mold from water-proof plywood was made according to common praxis of the column production in the horizontal position. The composite elements were fixed in the mold by the means of plastic strips to distance elements for the steel reinforcement (see Figure 3). The concrete models were made from concrete C30/37 XC4 S4 D22 compacted by inner vibrators.

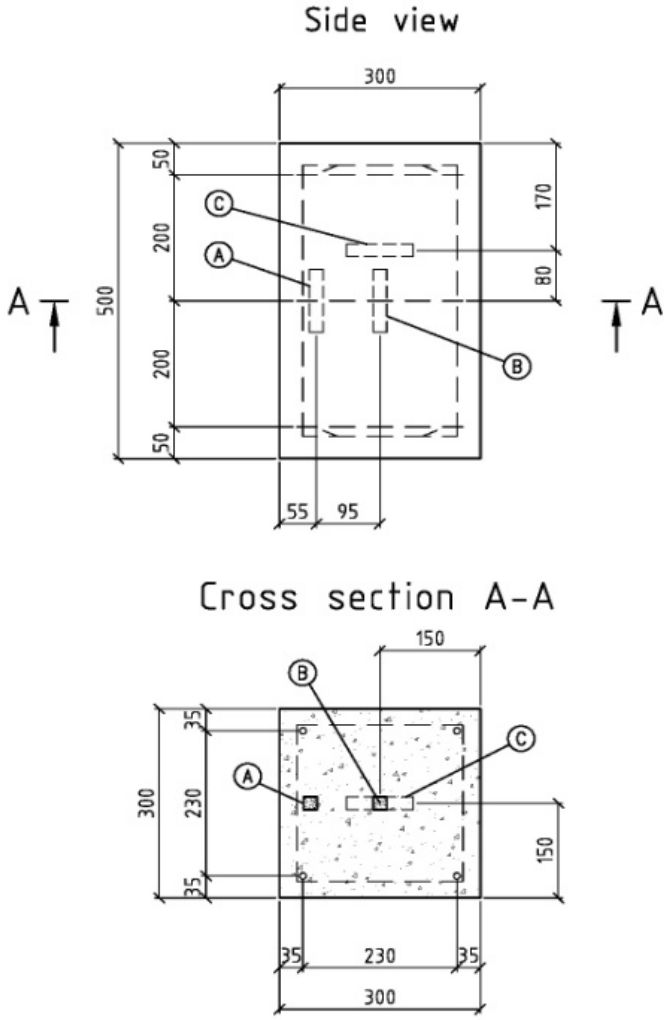


Figure 2 Design of the concrete column with element placement and steel reinforcement

Figure 3 Mold with the composite elements and steel reinforcement

## Measurement of Impedance and Deformation during Loading

Model columns were supplemented by plugs for deformation measurement. Digital deviation indicators were fixed to the plugs [10]. Digital impedance detectors with generated alternate voltage of 1 V were fixed to cable outlets of the composite elements.

Loading of the model columns was simulated by means of the hydraulic press machine (Figure 4). Applied force reached values of 0 to 1,500 kN, which corresponds with pressure 16.7 MPa.

Impedance of the composite elements and strain in the model columns was monitored in the course of loading in time of reaching 200 kN (2.2 MPa) by hand operation and 5x 1,500 kN (16.7 MPa) in automatic mode and again de-loading to 200 kN.

In the achieved graphs it is possible to see clear impedance change of the composite elements corresponding with changes of unit strain in the model columns.

Figure 4 The model column in the hydraulic press machine connected to the equipment monitoring changes in deformation and impedance

The subsequent measurement of relation of mechanical loading of a horizontal element and electrical properties of the composite tensometers was carried out in the specialized testing room (Figure 5) without negative effects of the environment (effect of temperature and humidity).

The element with dimensions 150×150×3400 mm was subjected to 4-point bending. The course of cyclical increase and decrease of the force F = 0-50 kN, the induced deflection and the values of impedance during measurement were depicted in graphs.

The impedance of tensometers was significantly changed in the case of overloading, when an accumulation of microcracks occurred on the tested element. This state we can describe as the emergency state of the structural elements, when it is necessary to send signal for evacuation of the building.

Figure 5 The longitudinal beam in the hydraulic press machine subjected to bending

## CONCLUSIONS

It was concluded that special fibre-cement composites are able to conduct electric current under specific conditions. This property is ensured by using of various kinds of carbon materials in a form of dispersive particles or fibres. Electric conductivity is monitored by means of impedance measurement of the designed samples. These composites could be used for heating of trafficable surfaces or shielding of electro-magnetic fields.

It is also possible to monitor internal processes in building structures and prevent them from collapsing. For this application it is necessary to design one-dimensional elements to simplify the combined loading in the structures.

Relation of impedance of the composite elements to unit strain in the model columns was successfully verified thereof. Positions of the composite elements in the models did not significantly affect monitored changes in impedance. It connected only to the absolute change of impedance, but not to the sensitivity to change detection.

The ability to transform unit strain to change in impedance seemed to be a material parameter independent on shape and orientation of the composite elements. The steel reinforcement could affect impedance of the composite elements only in some cases.

## ACKNOWLEDGEMENTS

The research was conducted under the project FR-TI3/485 Engineering structure state monitoring by means of electrically conductive elements with modified cement matrix supported by the Ministry of Industry and Trade of the Czech Republic.

## REFERENCES

1. XIE, N, SHI, X, FENG, D, KUANG, B, LI, H. Percolation backbone structure analysis in electrically conductive carbon fiber reinforced cement composites, Composites Part B: Engineering, Vol. 43, Issue 8, 2012, pp 3270-3275.

2. LI, H, XIAO, H, OU, J. Effect of compressive strain on electrical resistivity of carbon black-filled cement-based composites, Cement and Concrete Composites, Vol. 28, Issue 9, 2006, pp 824-828.

3. CECHMANEK, R, JUNEK, J, NESPOR, B, STEFFAN, P. Carbon-Based Composites Enable Monitoring of Internal States in Concrete Structures, International Journal of Civil, Structural, Construction and Architectural Engineering, Vol. 8, No.10, Part I, 2014, pp 70-75.

4. VOSSOUGHI, F. Electrical resistivity of carbon fiber reinforced concrete, CE241: Concrete Technology, Berkeley, 2004.

5. HOSSEINI, P, MORADIAN, M. Performance of pozzolanic admixtures on mechanical and durability properties of concrete, Microstructural-related Durability of Cementitious Composites, Amsterdam, 2012, pp 86.

6. NIKKANEN, P. On the Electrical Properties of Concrete and Their Application, 1962, Valtion Teknillinen Tiedotus, Rakennus.

7. http://www.computer.org/portal/web/csdl/doi/10.1109/ICONS.2010

8. PACHECO, J, SAVIJA, B, SCHLANGEN, E, POLDER, R B. Relationship between cracking and electrical resistance in reinforced and unreinforced concrete, Microstructural-related Durability of Cementitious Composites, Amsterdam, 2012, pp 61.

9. MACHAN, L, STEFFAN, P. A New Laboratory Equipment for Characterization of Smart Concrete Materials, ICONS 2013 The Eighth International Conference on Systems, pp 123-126.

10. TECHNICAL AND TEST INSTITUTE FOR CONSTRUCTION PRAGUE. Test protocol No. 060-038, 2013.

# REHABILITATION OF REINFORCED CONCRETE BEAMS WITH INSUFFICIENT LAP-SPLICE LENGTH USING FRP SHEETS

**T El-Rakib**

Housing and Building National Research Center

**E-T M El-Tony**

Alexandria University

Egypt

**ABSTRACT:** Insufficient reinforcement lap-splice is one of the defects that negatively affect the structural behaviour of reinforced concrete beams. Experimental investigation was carried out to study the efficiency of transverse FRP sheets on enhancing the structural behaviour of RC beams that had defected lap splice zones with normal and low concrete strength. Eight RC rectangular beams were tested in positive bending, four of them were strengthened by transverse FRP wraps in the defected lap splice region and the other four beams were kept unstrengthened and considered as control specimens. The main parameters were concrete compressive strength, type of FRP sheets and the retrofitting length as a percentage of the defected lap splice length. The cracking behaviour, failure modes, load-deflection relationships and the strains in longitudinal steel were investigated. It was concluded that the transverse FRP confining system provided a new mechanism whereby most bars over the spliced region could be used more effectively in the stress transfer between steel and concrete leading to a more ductile failure mode combined with a noticeable increase in the ultimate load.

**Keywords:** FRP, Beams, Lap-splice, Rehabilitation

**Ass. Professor Tamer Elrakib** is a member of the Reinforced Concrete Department at the Housing and Building National Research Center, Egypt. He is also a member of the committees of the Egyptian Code of Practise for concrete structures, ECP 203. His research interests include rehabilitation and strengthening of concrete structures using FRP composites.

## INTRODUCTION

Previous experimental researches reported in the literature have shown that there are mainly two effective methods for enhancing the bond strength in the lap splice regions of beams. Harjli [1] showed that the use of steel fibers in the concrete matrix increased both of the tensile strength and toughness of normal strength concrete resulting in higher bond strength and leading to a considerable improvement in ductility. Research conducted by Najjar [2] showed that the use of transverse reinforcement in the form of hoop stirrups can cause higher bond strength levels and more ductile bond behaviour leading to adequate bond strength with a relative shorter lap splice length. On the other hand, FRP composites have been used widely for repairing of deteriorated RC elements and they are also used to strengthen the existing structures against shear and flexural failures. FRP-laminated composites present significant advantages such as high-strength/weight ratio, lightweight, ease of handling and application, faster construction rates, Ashour [3] and Baha [4]. However, a limited number of studies were conducted to investigate strengthening RC beams defected in lap splice zone with FRP sheets. Hamed [5] et al have experimentally and analytically studied the effect of confinement provided by FRP on bond strength of tension lap splice anchored in high strength concrete beams. Although the strengthened beams have shown more ductile response in comparison with control beams, the final mode of failure was splitting of the concrete cover. Reinforced concrete beams have defects in both of their compressive strength and steel reinforcement lap splice length are currently faced in considerable number of structures constructed under soft quality control procedures. This study evaluates the efficiency of FRP sheets as an alternative and efficient tool to enhance the bond strength of defected lap splice reinforced concrete beams.

## TEST PROGRAM

The experimental test program involved eight RC beams 150x300x2200 mm designated as B1 to B8. Control beams B1 and B2 had full lap splice length according to ECP (2007). Beams B3 and B4 had shortage in the lap splice length. Beams B5 to B8 were retrofitted with U-shaped FRP sheets with different schemes in the defected lap splice region.

Table 1 and Figure 1 show the details of the tested beams. The modulus of elasticity, tensile strength and thickness of the used CFRP sheets were 240 GPa , 3900 MPa and 0.11 mm respectively while they were 65 GPa , 1700 MPa and 0.135 mm for the GFRP sheets.

Table 1 Details of the tested beams

| BEAM NO. | $F_{cu}$ N/mm$^2$ | LAP SPLICE LENGTH $L_s$, mm | FRP Configuration | RETROFITTING LENGTH, mm |
|---|---|---|---|---|
| B1 | 35 | 750 | Control | ---- |
| B2 | 19 | 960 | Control | ---- |
| B3 | 35 | 300 | Control | ---- |
| B4 | 19 | 380 | Control | ---- |
| B5 | 35 | 300 | U-shaped CFRP layer | 100%$L_s$=300 |
| B6 | 19 | 380 | U-shaped CFRP layer | 100%$L_s$=380 |
| B7 | 19 | 380 | U-shaped GFRP layer | 100%$L_s$= 380 |
| B8 | 19 | 380 | U-shaped CFRP layer | 200%$L_s$=760 |

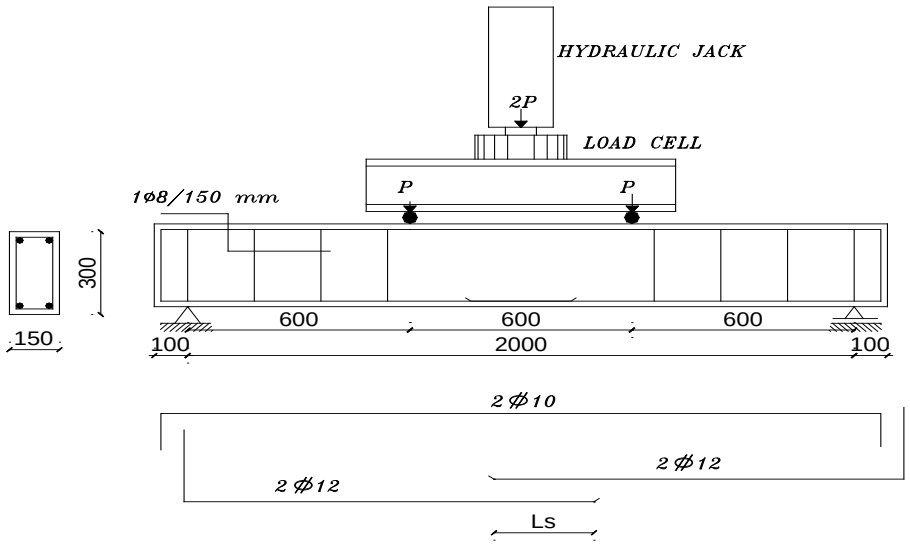


Figure 1 Test setup and reinforcement details of tested beams, mm

## TEST RESULTS AND ANALYSIS

### Mode of Failure and Load-Deflection Behaviour

The test beams were loaded to failure and the observed behaviour in terms of cracking, modes of failure and load-deflection response were recorded. Generally, for all the control beams (B1 to B4) two major flexural cracks initially appeared at the critical sections adjacent to the end of the lap splice zone and extended vertically by the increase of load up to failure. In addition to the two major cracks minor diagonal tension cracks appeared. For the control beams B1 and B2 failure occurred by yielding of tension reinforcement followed by splitting the concrete cover within the lap splice zone. Beams B3, B4 with inadequate lap splice length, failure occurred suddenly and accompanied with loud sound after the formation of longitudinal splitting cracks in the bottom cover of the tension side. The failure of beams B3 and B4 could be classified as pronounced sudden and brittle mode of failure. Beams B5, B6, and B7 with transverse FRP sheets showed a noticeable enhancement in the overall structure behaviour as they exhibited a more ductile failure mode. For those beams, two major vertical cracks appeared at the two ends of the splice zone followed by noticeable sings of longitudinal splitting cracks in the bottom and side concrete cover within the splice region. The clamping force developed by the FRP sheets delayed the propagation of the longitudinal splitting cracks and force the beams to carry additional load. After reaching the peak load, the load dropped gradually with increasing deflection. Beam B8 with FRP sheet cover 200% of the defected splice zone has showed similar mode of failure. The appearance of some of the tested beams after testing is shown in Figure 2. Ultimate load $P_u$, deflection at failure $\Delta_f$, defection at yield $\Delta_u$, steel strain at ultimate load $\varepsilon_u$ are shown in Table 2. On the other hand, the applied load was plotted against the vertical deflection measured at midspan for all tested beams as shown in Figure 3 (a,b). For beams B1, B3 and B5, a noticeable increase in the ultimate load and deflection of the strengthened beam B5 compared with the control beams B3 was found. The load deflection relationships for beams B2, B4 and B6, lead to the same observations.


Figure 2 Mode of failure of beams B1 and B5

### Stiffness, Ductility and Strains in Longitudinal Steel Reinforcement

The stiffness of each beam was evaluated as the slope of the linear ascending part of the load deflection curve and presented in Table 2. It can obviously noticed that the unstrengthened control beams (B3, B4) had relatively lower stiffness compared with those with full lap splice length (B1 and B2). Meanwhile, beams with U-shaped CFRP sheets (B5, B6 and B8) had

approximately the same stiffness compared with unstrengthened control beams (B3, B4) indicating that the use of transverse FRP sheets did not affect the flexural stiffness of the strengthened beams. On the other hand, many authors adopted the displacement ductility index, $\mu_\Delta$ , to evaluate the ductility level of RC beams, Ashour [3] and Baha [4].

Displacement ductility index, $\mu_\Delta = \Delta_f/\Delta_y$ (1)

Where $\Delta_f$ = Deflection at 80% of the ultimate load on the descending branch of the load-deflection curve, $\Delta_y$ = Deflection at yield load was calculated from the load-deflection curve as the corresponding displacement of the intersection of the secant stiffness at a load value of 80% of the ultimate lateral load and the tangent at the ultimate load. Regarding Table 2, beams with U-shaped FRP sheets had a meaningful increase in the ductility indexes compared with B3 and B4. Also, it was noted that the longitudinal steel strain values for all tested beams, except for B3, are much higher than the yield strain $\varepsilon_y$=2000 μs indicating that the longitudinal reinforcing steel of these beams reached the hardening range leading to ductile behaviour.

Table 2 Experimental results of the tested beams

| BEAM | ULTIMATE LOAD, $P_u$ (kN) | $\Delta_f$ mm | $\Delta_y$ mm | STEEL STRAIN AT ULTIMATE LOAD, $\varepsilon_u x10^{-6}$ | STIFFNESS N/mm | DUCTILITY RATIO $\mu_\Delta=\Delta_f/\Delta_y$ |
|---|---|---|---|---|---|---|
| B1 | 57.00 | 24.4 | 8.56 | 5100 | 6670 | 2.85 |
| B2 | 59.00 | 26.5 | 8.69 | 4000 | 6700 | 3.05 |
| B3 | 41.60 | 12.5 | 7.14 | 1993 | 6100 | 1.75 |
| B4 | 37.05 | 8.5 | 6.58 | 2712 | 5900 | 1.29 |
| B5 | 49.10 | 18.3 | 7.46 | 4334 | 5800 | 2.45 |
| B6 | 47.05 | 13.6 | 6.32 | 3370 | 6000 | 2.15 |
| B7 | 45.15 | 14.3 | 6.36 | ---- | 5400 | 2.25 |
| B8 | 59.50 | 23.5 | 8.55 | 4200 | 6300 | 2.75 |

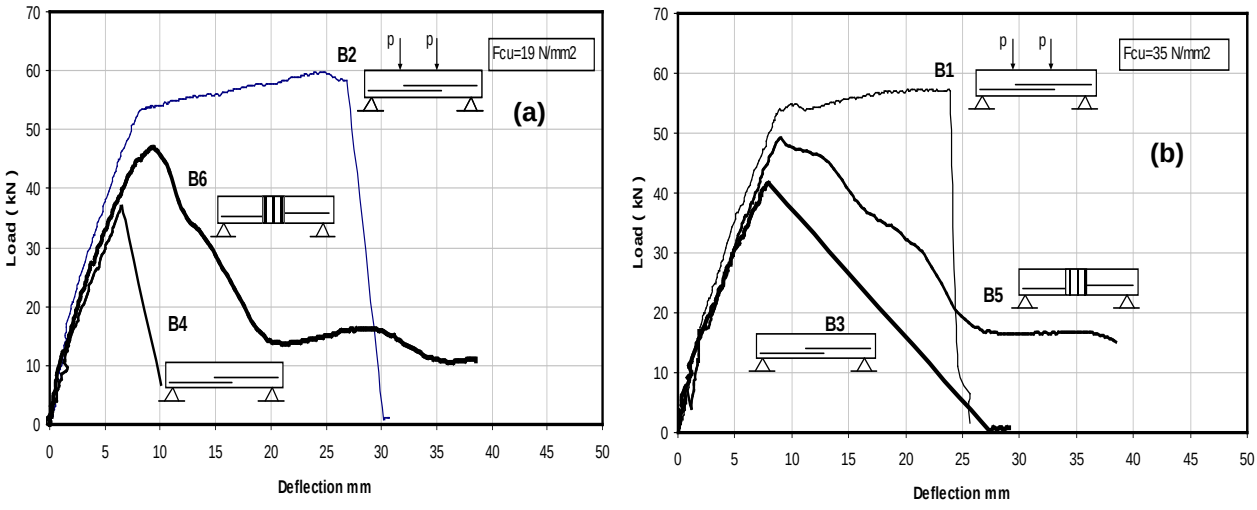


Figure 3 Load deflection relationship: (a) Beams B2, B4, and B6,
(b) Beams B1, B3, and B5

As shown in Table 2, the difference in the steel strain values between the control specimen B1 and the strengthened one B5 was approximately small and the strain of both recorded about 5000 μs while the maximum strain of B3 hardly reached 1993 μs indicating that using FRP wraps allowed steel bars along the splice zone to participate more effectively in the stress transfer within the lap splice zone.

## EFFECT OF KEY PARAMETERS

### Effect of Type of FRP

Figure 4 (a) and Table 2 show that the ultimate load of B6 and B7 was 27% and 22% higher than that of the control beam B4 and lower than the ultimate load of control beam B2 by 20% and 23% respectively. The displacement ductility indexes of B6 and B7 were increased by 66.66% and 74.42% respectively compared with that of the defected beam B4. The overall structural behaviour of beams B6 and B7 showed that the type of FRP sheets, glass or carbon, confining the splice zone had no significant effect on load-deflection behaviour or mode of failure.

### Effect of Length of the Strengthened Zone

Figure 4 (b) presents the load deflection relation for B6 with a strengthened zone equal to 100% of lap splice length and B8 with strengthened length equal to 200% of the same lap splice length. The ultimate load of the strengthened beams B6 and B8 were higher than that of the defected beam B4 by 27% and 60% respectably. In addition, the ultimate load of beam B6 was lower than that of the control beam B2 by 20% whereas, the ultimate load of the strengthened beam B8 was almost identical to the ultimate load of the control beam B2.

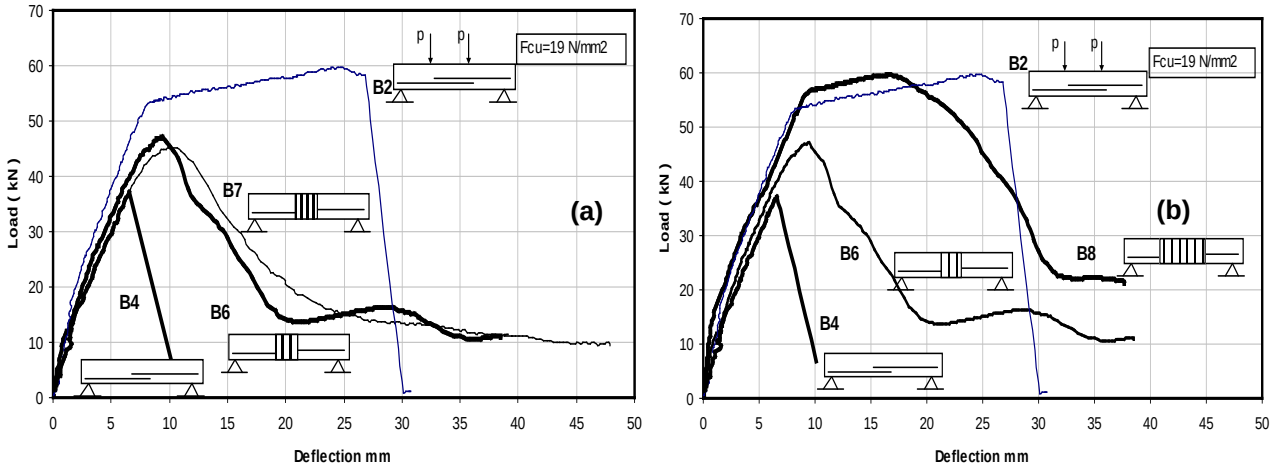


Figure 4 Load deflection relationship: (a) Beams B2, B4, B6, and B7, (b) Beams B2, B4, B6 and B8

Table 2 shows that the ultimate load and ductility index of beam B8 were higher than that of beam B6 by 26% and 27% respectively. The pronounced improved behaviour of beam B8 in comparison with beam B6 indicate that the negative effect of the defected splice zone on the

beam behaviour is practically extends beyond the lap splice area and the extension of the U-shape FRP wraps is practically required to restore the structural behaviour of the defected beam.

**Effect of Concrete Compressive Strength**

Figure 5 (a) shows the load deflection relation of beams B1, B2, B3, and B4. Beams B1 and B2 represents the control beams which had reinforcement lap splice lengths according to the provisions of the Egyptian code while, beams B3 and B4 represent the defected beams which had 40% of the lap splice lengths assigned for beams B1 and B2, respectively. In addition, Figure 5 (b) shows the load deflection of the retrofitted beams B5 and B6 in comparison with the control beams B1 and B2. Although the compressive strength of beam B2 (19 MPa) was lower than that of B1 (35 MPa) by 45.70%, the ultimate load was slightly higher than that of beam B1 by 3.50% in clear contradiction with the expected behaviour. The previous behaviour could be attributed to two reasons; first is the lap splice length of beam B2 which equal to 960 mm longer than the distance between the two-points load (600 mm) and consequently the beam actually contained four longitudinal steel bars at the constant moment region, the second is due to the fact that concrete compressive strength has minor effect on the ultimate strength of the flexural members. The load deflection responses of the defected beams B3 and B4 were approximately similar. However, beam B4 was more negatively affected by the shortage of lap splice length regarding the ultimate load and ductility. Reducing the concrete compressive strength by 45.70% for beam B4 in comparison with B3 resulted in reduction of ultimate load and ductility by 10.90% and 26.30% respectively, which could conclude that Egyptian Code equation of calculating lap splice length is conservative for low quality concrete. The load deflection relations of the retrofitted beams B5 and B6 shown in Figure 5 (b) support the previous conclusion. As shown in Figure 5 (b), the retrofitted beams B5 and B6 had almost the same behaviour although the ductility of beam B6 was slightly lower than that of beam B5 by 12%.

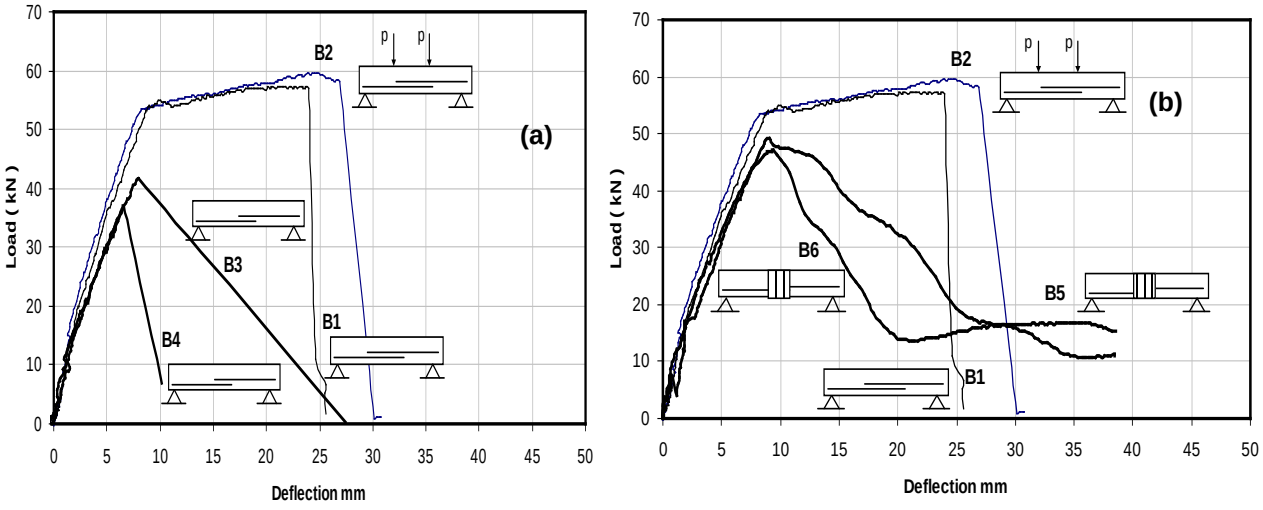


Figure 5 Load deflection relationship: (a) Beams B1, B2, B3, and B4

(b) Beams B1, B2, B5, and B6

## CONCLUSIONS

Based on the presented experimental test results, the following conclusions could be drawn:

1) Wrapping the insufficient lap splice length zone of reinforced concrete beams having either normal or low concrete strength by FRP is highly effective in enhancing both of the ultimate load and mode of failure. Ductile mode of failure instead of brittle mode was observed for all wrapped beams. In addition, the load deflection flexural stiffness was almost the same for all the tested beams.

2) None of the FRP U-shaped strengthened beams had experienced debonding or separation of the sheet at the end of the U-shape and based on the results of the tested beams, no special anchorage system is needed for bonding the FRP sheets on the concrete faces.

3) Wrapping the beams in the lap-splice zone by GFRP has comparable structural performance in comparison with those beams wrapped by CFRP. In both cases, the mode of failure changed from brittle mode to ductile one and the enhancement in ultimate load and ductility were approximately the same. In addition, increasing the FRP strengthening length beyond the defected lap splice length zone completely restores the beam performance including ultimate load and ductility.

## REFERENCES

1. HARAJLI, M, HAMED, B, JUMAA, G. Effect of fiber reinforcement on bond strength of tension lap splice in HSC, ACI Structural Journal, Vol. 98, No. 5, Nov.2001, pp. 638-647.
2. NAJJAR, S, HAMED, B. Evaluation of the role of transverse reinforcement in confining tension lap splices in HSC, Materials and Structures Journal, Vol.35, 2002, pp. 219-228.
3. ASHOUR, A F, El-REFAIE, S A, GARRITY, S W. Flexural strengthening of RC Continues Beams using CFRP Laminates Cement and Concrete Composites Journal, Vol.26, Mars 2004, pp. 765-775.
4. BAHA, T, KHAFAGA, M. Strengthening of Continuous RC Beams Using CFRP Laminates, The 7th International Conference on Multi-Purpose High Rise Towers and Tall Buildings, Dec. 2005, Dubai, UAE.
5. HAMED, B, SOUDKI, K, HARAJLI, M. RTEIL, A. Experimental and Analytical Evaluation of Bond Strength of Reinforcement in Fiber-Reinforced Polymer-Wrapped High Strength Concrete Beams, ACI Structural Journal, Vol. 101, No. 6, July 2004, pp. 747-754.
6. ECP 203, Egyptian Code of the Design and Construction of Reinforced Concrete Structures, Housing and Building National Research Center, 2007, Egypt.

# PARAMETRIC STUDY USING FEM FOR RC BEAMS RETROFITTED IN BENDING WITH FRP SHEETS

**A M Morsy**

**N H El-Ashkar**

**I S Mattar**

Arab Academy for Science, Technology, and Maritime Transport

Egypt

**ABSTRACT.** In order to analyse plane stress members such as RC beams strengthened/retrofitted with FRP, a nonlinear finite element model has been prepared. The FE model is based upon using the FE software package ABAQUS CAE 6.11-3. Experimentally verified numerical material models are used to obtain unavailable material properties. For the purpose of model verification, the developed modelling procedure has been applied to specimens upon various experimental procedures performed. Agreement between FE model results and the results obtained from previously performed experimental procedures indicate that the developed modelling procedure is suited for modelling RC beams retrofitted with FRP in bending. Finally, a parametric study is carried out in order to study the effect of sheet length, sheet width and number of FRP layers.

**Keywords:** ABAQUS, Fibre reinforced polymer (FRP), Finite element, Retrofitted, Strengthening

**Alaa M Morsy** is an associate professor, Construction, and Building Depart., college of Engineering & Technology. He has received his Ph.D. in Structural Engineering from Alexandria University, Egypt; where his research work included usage Advanced Composite Materials (FRP) in Repair and Strengthening of R.C., Heat Transfer and fire Protection, and Use Finite Elements Software's in Modelling. He has fifteen years of experience in Structural engineering, practice and research. He is currently posted as Vice Dean and Manager of Education and Training department, at Port Training Institute, AASTMT.

## INTRODUCTION

Reinforced concrete structures may need upgrading due to various factors affecting the structure over long periods of time. Such factors may be increased loads, corrosion of reinforcement steel, earthquakes, construction accidents or deficient design. In the recent years, the use of FRP for strengthening/retrofitting reinforced concrete structures. FRP act with concrete in a composite manner to carry the applied loads. Although the use of FRP has some drawbacks such as de-bonding issues and also being a linear elastic material with high material cost. However, such issues are neglected in comparison with the enhanced flexural and shear performance for structural elements strengthened/retrofitted with FRP. Accordingly, throughout this research, modelling of FRP retrofitted beams in bending using the finite element method shall be illustrated.

Throughout this research, FE modelling for reinforced concrete beams retrofitted with FRP in bending will be carried out .The developed modelling procedure is verified through its application to specimens upon which various experimental procedures were performed. Finally a parametric study is carried out in order to emphasize the effect of various parameters included in the retrofitting process.

## MATERIAL MODELS

### Concrete

Stress-Strain curve for concrete under compression is obtained based upon an experimentally verified numerical model (Hsu and Hsu 1994). The model obtains stress-strain curve under uni-axial compression up to 0.3 characteristic strength ($f_{cu}$) in the descending portion based upon maximum compression strength $f_{cu}$. Such model is also characterized by having a linear Stress-Strain relationship in accordance with HOOK's Law till $0.5f_{cu.}$The stress strain relation-ship based on the numerical model is shown in Figure 1. Equations (1-4) emphasize the use of the model to obtain the stress-strain curve for concrete.

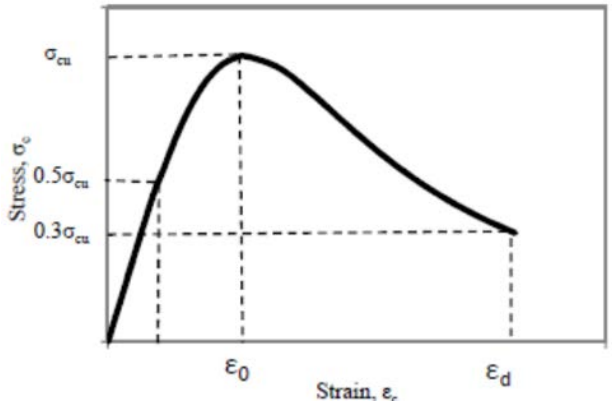


Figure 1 Compressive Stress-Strain relationship for concrete (Hsu and Hsu 1994)

$$\sigma_c = \left[\frac{(\eta * \beta) * (\varepsilon_c/\varepsilon_c)}{(\eta * \beta) - 1 + (\varepsilon_c/\varepsilon_c)^{(\eta * \beta)}}\right] * \sigma_{cu} \quad (1)$$

$$\beta = \frac{1}{1 - [\sigma_{co}/(\varepsilon_o * E_o)]} \quad (2)$$

$$\varepsilon_o = (8.9 * 10^{-5} * \sigma_{cu}) + 2.114 * 10^{-3}$$

$$E_o = (1.2431 * 10^{2} * \sigma_{cu}) + (3.28312 * 10^{3})$$

***Where:***

β : A material parameter which depends on shape of stress-strain diagram

$\varepsilon_o$ : Strain at peak stress

$E_o$ : Initial tangential modulus (Kip/in²)

$\varepsilon_d$ : Strain at 0.3 $f_{cu}$ in the descending portion and is iteratively calculated using equation (1) at $s_c = 0.8 * s_{cu}$

$s_c$ : Compressive strength (Kip/in²)

$s_{cu}$ : Ultimate compressive strength (Kip/in²)

(1 MPa = 0.145037743 Kip/in²)

n:Material parameter which depends on $s_{cu}$

$0 < s_{cu} < 62$ MPa → n = 1

62 MPa ≤ $s_{cu}$ <76 MPa → n = 2

76 MPa≤ $s_{cu}$ <90 MPa → n = 3

90 MPa≤ $s_{cu}$ → n = 5

In order to represent the softening behavior of concrete under tension model [2] is used as shown in Figure 2. Concrete assume a linear elastic behavior till maximum tensile stress ($f_{ct}$) after which tensile softening follows the curve in Figure 2.

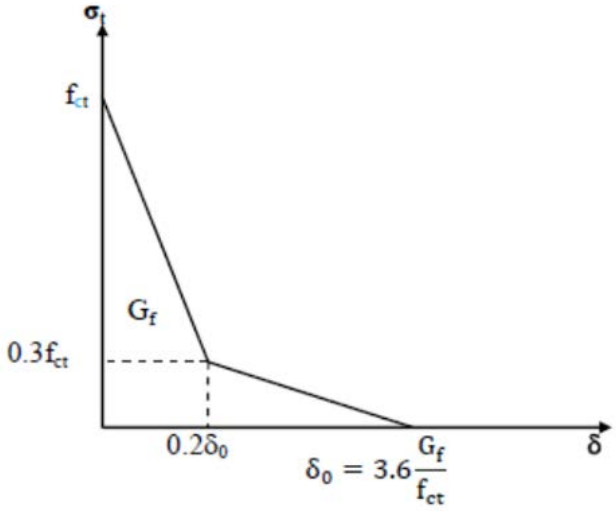


Figure 2 Softening curve for concrete under uni-axial tension (Hillerborg, 1985)

Values for $f_{ct}$ (in MPa) can be obtained by referring to (CEB-FIP, 1993) where upper, lower bounds as well as mean value are specified as by the equations (5-7)

$$f_{ctk,min} = 0.95 * (0.1 * f_{ck})^{2/3} \quad (5)$$

$$f_{ctk,m} = 1.4 * (0.1 * f_{ck})^{2/3} \quad (6)$$

$$f_{ctk,max} = 1.85 * (0.1 * f_{ck})^{2/3} \quad (7)$$

***Where:***

$f_{ck}$: Concrete compressive strength (MPa)
$f_{ctk,min}$: Minimum value for tensile strength (MPa)
$f_{ctk,m}$ : Mean value for tensile strength (MPa)
$f_{ctk,max}$: Maximum value for tensile strength (MPa)
$\delta_{\circ}$: Crack opening displacement (mm)
$G_f$: Fracture energy (Nmm/mm²), energy required to propagate a tensile crack of unit surface area projected in a plane parallel to the crack direction.

Values for $G_f$ (Nmm/mm²) can be obtained by referring to [6] by using equation 8, where the resulting deviations in value of $G_f$ are up to ± 30% (CEB-FIP, 1993)

$$G_f = G_{fo} * (0.1 * f_{ck})^{0.7} \quad (8)$$

Where:

$f_{ck}$: Concrete compressive strength (MPa)

$G_{fo}$: Base value for fracture energy (Nmm/mm²) and depends on maximum aggregate size as shown in table 1.

Table 1 Base Values for fracture energy (CEB-FIP, 1993)

| $d_{max}$, mm | $G_{fo}$, Nmm/mm² |
|---|---|
| *8* | 0.025 |
| *16* | 0.030 |
| *32* | 0.058 |

## Reinforcement

Reinforcement is considered elastic-perfectly plastic behaviour identical in tension and compression as shown in Figure 3.

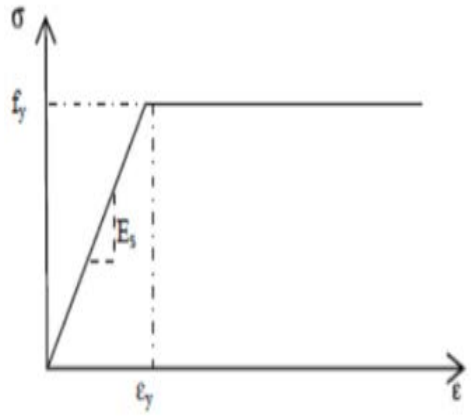


Figure 3 Stress –Strain behavior for reinforcement

## Fibre Reinforced Polymer

FRP is modelled as a linear elastic isotropic material till failure. Although FRP is an orthotropic material yet since the composite is mainly stressed in fibre direction, thus the modulus in fibre direction is more important.

## Adhesive

The cohesive zone model developed by (Lu et al., 2005) is used to model the adhesive as shown in Figure 4.

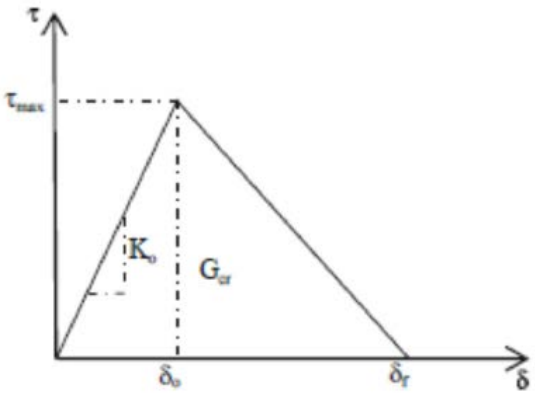


Figure 4 Bilinear model for bond slip curve (Lu et al., 2005)

## FINITE ELEMENT MODELLING

Simulation for R.C, is done with C3D4 mesh elements emphasized in Figure 5a while mesh elements used for FRP are C3D8R mesh elements shown in Figure 5b. Also it should be noticed that concrete is modelled using concrete damaged plasticity model. Reinforcement steel is modelled as wire elements of mesh element type T3D2 as shown in Figure 5c. The interaction between R.C. and reinforcement is achieved using the embedded element constraint. Regarding numerical analysis, three-dimensional nonlinear analysis has been carried out using Newton's method (Simulia, 2011).

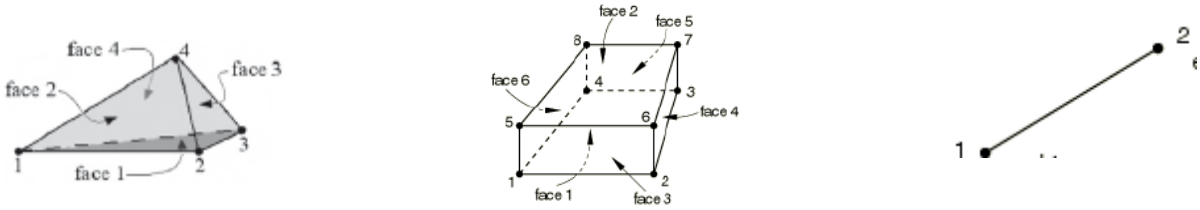


Figure 5 (a) 4-node linear tetrahedral element, (b) 2-node linear displacement truss elements, (c) 2-node linear displacement truss elements (Simulia, 2011).

## EXPERIMENTAL DATA USED FOR MODEL VERIFICATION

Experimental data used for model verification are obtained from specimens used in the experimental procedure performed by (Obaidat et al., 2011) as shown in Figure 6 Where design for such specimens ensures shear failure at weak side.

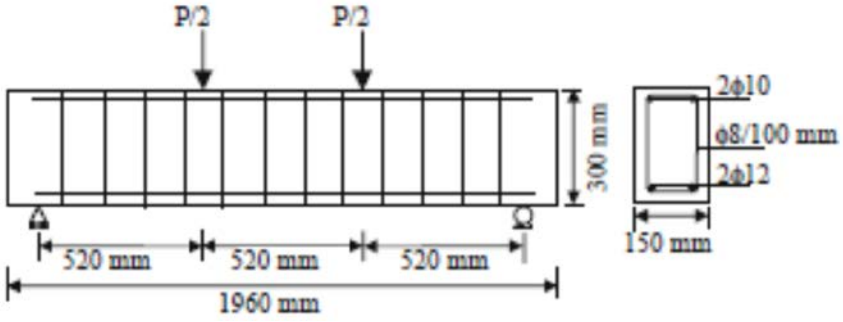


Figure 6 Geometry and arrangement of reinforcement for control specimen (Obaidat et al., 2011)

Figures 7 -9 show the Retrofitting schemes for the tested specimens by (Obaidat et al., 2011) showing the different lengths used in bending retrofitted.


Figure 7 Retrofitted beam RB1 (Obaidat et al., 2011)

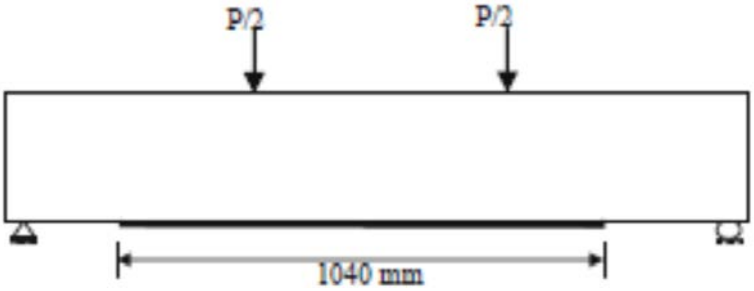


Figure 8 Retrofitted beam RB2 (Obaidat et al., 2011)

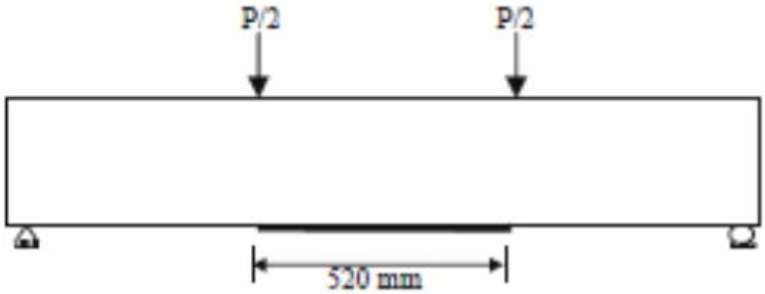


Figure 9 Retrofitted beam RB2 (Obaidat et al., 2011)

## MODEL VERIFICATION

### Load Displacement Curves

Load displacement curves for control specimens and retrofitted specimens are in agreement with results obtained from FE model as shown in Figures 10-13. Such results indicate that the FE model is suited for modelling R.C beams retrofitted with FRP in bending. In addition, the numerical models used to model various components of the model have proven to be suitable for the modelling process.

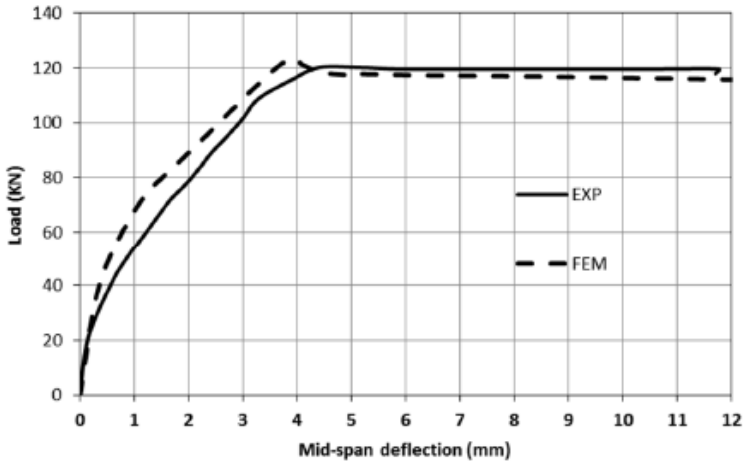


Figure 10 Load – Displacement curve for control specimen CB

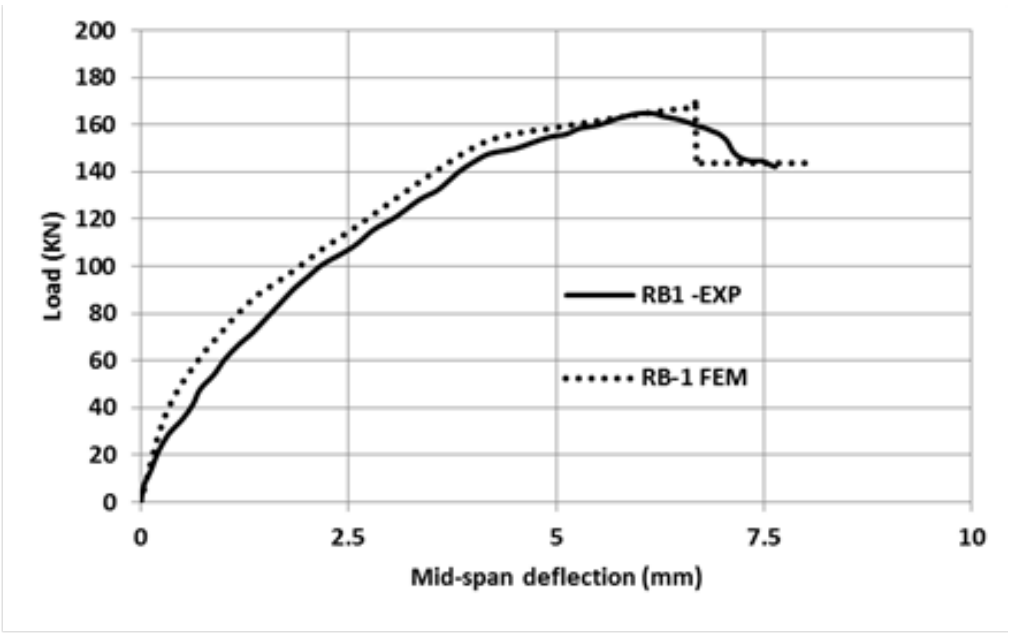


Figure 11 Load – Displacement curve for specimen RB 1

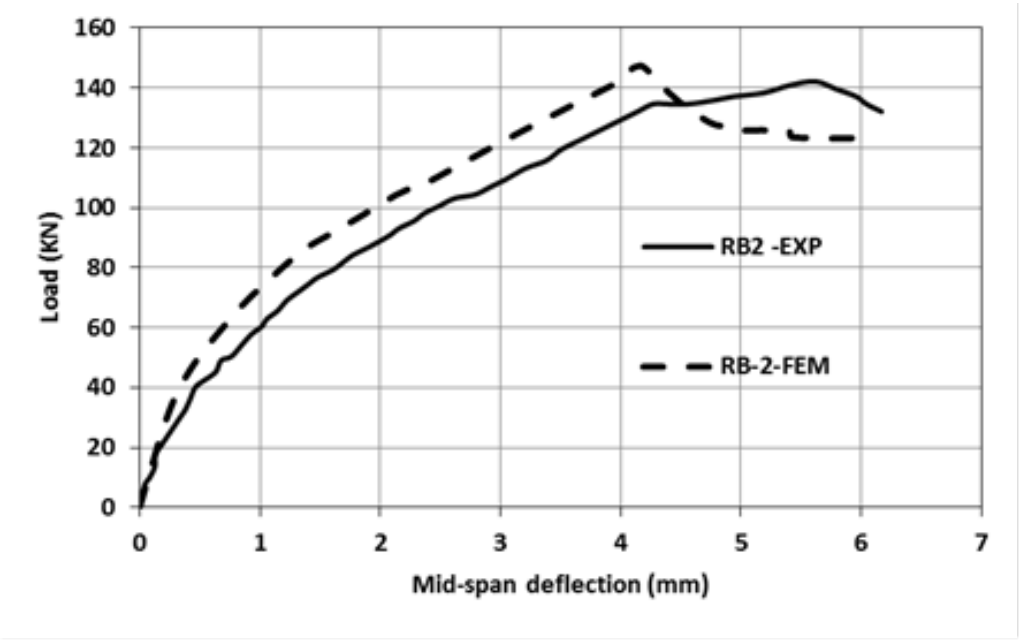


Figure 12 Load – Displacement curve for specimen RB 2

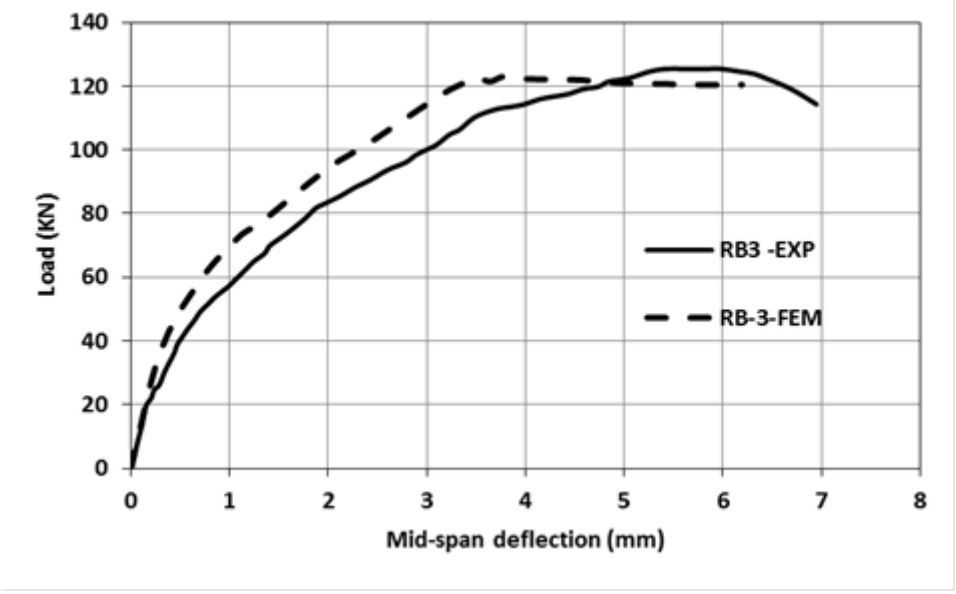


Figure 13 Load – Displacement curve for specimen RB 3

## Cracking Pattern

The concrete damaged plasticity model in ABAQUS does not have a notation for cracks, however, it is assumed that cracking initiates at the points where the maximum principal plastic strain is positive (Lubliner et al., 1989). The direction of the vector normal to the crack plane is assumed to be parallel to the direction of the maximum principal plastic strain (Simulia, 2011). Cracking patterns as well as direction of the vector normal to the cracking plane are in shown in Figure 14 and Figure 15. Upon Comparing FEM to cracking patterns obtained from experimental results**.** It is noted that the FEM cracking pattern is in good agreement with experimental results which indicates that the FEM can capture the fracture mechanism.

Figure 14 Failure for control specimen CB

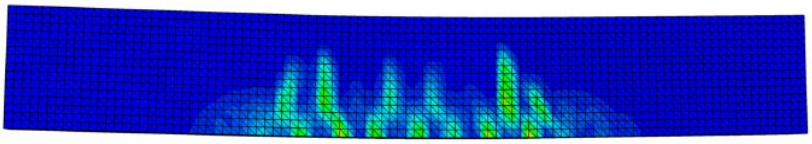

Figure 15 Cracking pattern obtained from FEM for control specimen CB

## PARAMETRIC STUDY

In order to study the effect of sheet width and sheet length, a number of simulations were performed on specimens RB1, RB2 and RB3. Specimens RB1a and RB1 b were modelled with sheet widths 100 mm and 150 mm respectively. Specimens RB2a and RB2b were modelled with sheet widths 100 mm and 150 mm respectively and also specimens RB3a and RB3 b were modelled with sheet widths 100 mm and 150 mm respectively. Results for such simulations are shown in Figure 16. Where the obtained results indicate that sheet length is a more effective parameter than sheet with, in addition increasing sheet width is effective at longer sheet lengths where there is longer anchorage length outside the maximum moment region. The effect of increasing sheet width at lower sheet length is barely noticed.

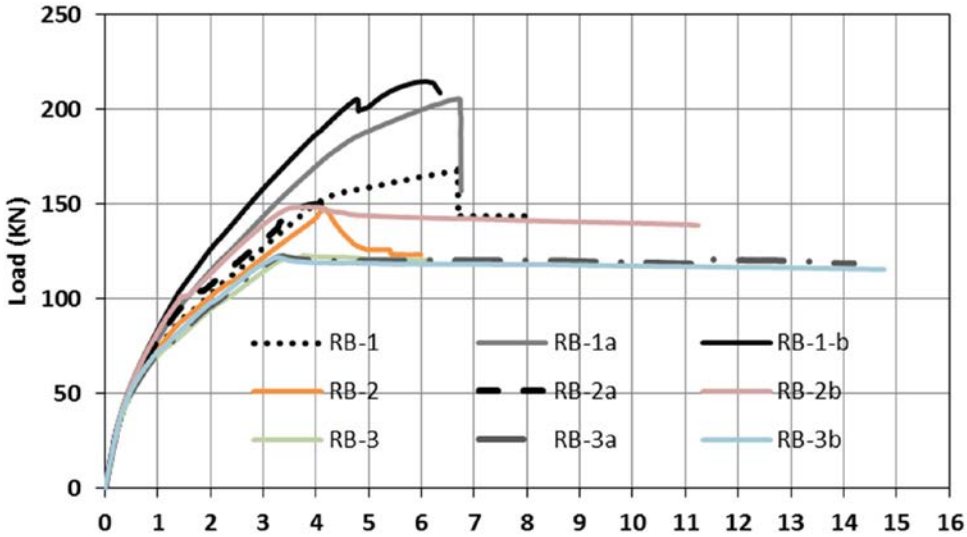


Figure 16 Load-displacement curve for s various simulations performed on retrofitted specimens

For the purpose of studying the effect of number of layers, a number of simulations were performed on specimen RB1. RB -1t, RB – 2t and RB-3t are modelled with single, double and triple layers. Results for such simulations are shown in Figure 17, where such simulations indicate that the number of layers had a noticeable effect on ductility and a slight effect on peak load.

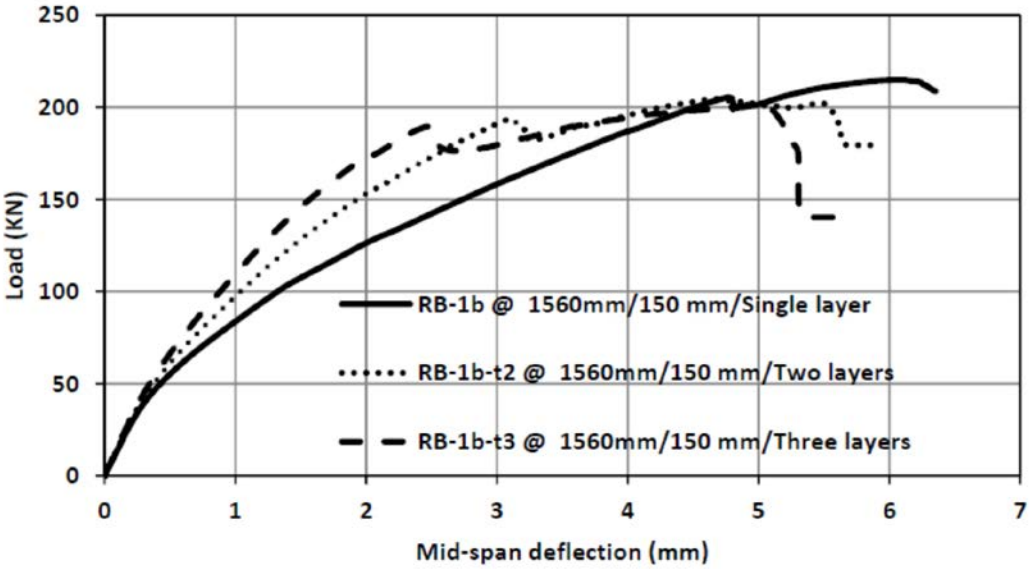


Figure 17 Load-displacement curve for specimen NSM upon varying laminate width

## CONCLUSIONS

A Finite element modelling process is carried out on a number of specimens using the FE software package ABAQUS-CAE 6.11-3 where the behaviour of such specimens has been experimentally examined. Finally a parametric study is carried out to study effect of various retrofitting parameters on the element behaviour. Upon examining the FEM results the following conclusions are drawn:

1. Upon comparing the load-displacement curve as well as the cracking pattern obtained from FEM with those obtained from experimental procedure only a slight deviation is noticed which indicates that the FEM model can properly capture the fracture mechanism.

2. Increasing sheet length is more effective than increasing sheet width regarding increased load carrying capacity, where the effect of increasing sheet width is only noticed at longer sheet lengths.

3. Increasing the number of FRP layers had a noticeable effect on ductility and a slight effect on peak load.

## REFERENCES


1. HSU, L.S., & HSU, C.-T.T. (1994). Complete stress-strain behavior of high-strength concrete under compression. Magazine of Concrete Research, 46(169), 301-312.

2. HILLERBORG, A. (1985). The theoretical basis of a method to determine the fracture energy $G_f$ of concrete. Materials and Structures, RILEM 50-FMC, 108, pp 291-296.

3. GORINEVSKY, D., BOYD, S., STEIN, G., Optimization-based tuning of Beton, C. E.-I. (1993), CEB-FIP Model Code 1990 (CEB-FIP MC90), Bulletin D'Information, No. 215, Lausanne.

4. LU, X., TENG, J., YE, L. & JIANG, J. (2005). Bond–slip models for FRP sheets/plates bonded to concrete. Engineering Structures, 27, 920-937.

5. LUBLINER J, OLIVER J, OLLER S, ONATE E. (1989). A plastic-damage model for concrete. Int J Solids Struct, 25:299–329.

6. DASSAULT SYSTÈMES SIMULIA CORP. ABAQUS Theory manual, User manual, Analysis manual and Example Manual, Version 6.11. Providence, RI; 02909–2499.numerical simulation of various engineering applications.

7. OBAIDAT, Y., HEYDEN, S., DAHLBLOM, O., (2011). Retrofitting of reinforced concrete beams using composite laminates. Construction and Building Materials, 25, 591-597.

8. MORSY, A.M., EL-ASHKAR, N., HELMI, K. (2011). “A Comparative Study for Shear Strengthening Techniques of Reinforced Concrete Beams Using FRP”. Fourth international conference on concrete repair with cooperation by technical university Dresden. Germany.

9. MORSY, A.M., MAHMOUD, E.T. (2013). “Bonding techniques for flexural strengthening of RC beams using CFRP laminates”, Ain Shams Engineering Journal, Elsevier, Vol. 4, No. 3, 369-374.

# INFLUENCE OF CEMENT TYPE ON THE EFFICIENCY OF ELECTROCHEMICAL CHLORIDE EXTRACTION

**S Bond**

**C Osmani**

**N Holmes B Norton**

Dublin Institute of Technology

Ireland

**ABSTRACT.** The corrosion of steel in concrete due to chlorides is well established. Concrete structures are susceptible to chloride ions ingress when exposed to de-icing salts or seawater which pass through the cover zone to the embedded steel. Erosion of the passive layer leads to corrosion, a reduction in cross-sectional area, cracking and a loss of structural capacity. Electrochemical Chloride Extraction (ECE) has been shown to reduce the chloride concentration in concrete. However, previous work has demonstrated that improper application of the electrical charge has led to adverse side effects such as loss of bond strength and cracking around the steel/concrete interface. This paper presents the effect of a constant voltage and current density on three different cement types and the subsequent rate of chloride ion removal from the cover zone and deeper in the concrete. The findings show how appropriate electrical energy can lead to improved and efficient ECE treatments.

**Keywords:** Electrochemical Chloride Extraction, Cement, Reinforced Concrete, Current density, Voltage

**Sean Bond** graduated with an Honours degree from the Dublin Institute of Technology Bolton Street in 2015. He is currently a PhD student in the School of Civil and Structural Engineering at DIT Bolton Street where he is researching electrochemical chloride extraction and its efficiency.

**Chahrazed Osmani** graduated with an Honours degree in Civil Engineering from the Dublin Institute of Technology in 2013 and a Masters in Sustainable Infrastructure (also DIT) in 2015.

**Niall Holmes** is Assistant Head of the School of Civil and Structural Engineering at DIT Bolton Street. His research interests in concrete lie in concrete durability and electrical properties, cement science and developing sustainable concrete using waste materials. He is also a Fellow of Engineers Ireland.

**Brian Norton** is the President of Dublin Institute of Technology. He is the author or co-author of over 400 papers principally in solar energy research including nearly 170 in major international learned journals He has supervised forty doctorates and serves as Editor-in-chief of Foundations and Trends in Renewable Energy, Associate Editor of Solar Energy - the premier international journal in the field and serves on four other editorial boards.

## INTRODUCTION

The aim of this work is to investigate how the performance of Electrochemical Chloride Extraction is effected by different cement types. In order to speed up treatment, a slightly higher current than recommended was used. By analysing how different cement types respond to the treatment in terms of chloride concentration through the depth, a better understanding of the appropriate applied current for each cement type can be achieved.

Reinforced concrete is one of the most widely used materials in the world due to the availability of raw materials. Since concrete is permeable, it is susceptible to the penetration of dissolved chloride ions from the environment such as exposure to a marine environment, salty groundwaters or de-icing salts during cold spells. There are many ways that chloride ions can ingress into a reinforced concrete (RC) structure including capillary action, absorption, hydrostatic pressure and diffusion [1].

Chloride ions are considered to be the major cause of premature corrosion of reinforced concrete structures as they lead to a reduction in the cross-sectional area due to pitting. Chloride ions accumulate near the rebar until they reach a concentration that is sufficient to initiate corrosion (e.g. 0.2% to 1.5% by weight of cement [2]). Local disruption of the passive oxide film that protects the steel in a high alkaline environment may occur on the steel surface [3].

Until recently, rehabilitating concrete bridge decks and piers, subjected to corrosion or chloride ingress, involved the removal of affected damaged concrete and patching. However, this practice was found to lead to the introduction of new electrochemical cells between the new chloride-free concrete following the repair. In turn, these new cells accelerated corrosion often within a few years of the repair [4]. As steel corrosion is an electrochemical process, the most effective means to stop it are electrochemical techniques, such as chloride extraction (ECE) which protects the structure by removing the chloride ions in the vicinity of the reinforcement.

ECE is based on the principle that negatively charged chloride ions may be migrated toward a positive anode positioned on the surface of the concrete. The process turns the concrete and embedded reinforcement into an electrochemical cell, powered externally. The direct current power supply for the system is typically provided using diesel generators. Treatment times for ECE generally last around 6 to 8 weeks depending on the cement type and chloride levels. A schematic diagram of the typical migration of chloride ions in the concrete is shown in Figure 1.

A suitable conductive anode may be a stainless steel or a titanium mesh submerged in an electrolyte or a cement paste placed on the concrete surface. The positive terminal of the power supply is connected to the external anode and the negative terminal to the reinforcement (cathode), embedded within the concrete. Since the electrons are repelled from the negative terminal towards the reinforcement, the cathode becomes negative due to the electrons negative charge. The chloride ions being negative ions are therefore migrated towards the positive anode located at the surface of the concrete via the pore water solution.

This causes the concentration of chlorides inside the concrete located around the reinforcement to be reduced. The speed of the chloride removal is largely dependent on the magnitude of the applied current. The higher the current can be set, the more intensive the chloride movement will be. The treatment usually utilizes a current density of 1-5 $A/m^2$ and a potential difference of less than 41V for safety reasons [2].

The work here was carried out on concrete blocks containing embedded reinforcement with different cement types. The ECE treatment was measured by analysing concrete dust samples collected through the depth in the concrete to trace the movement over time.

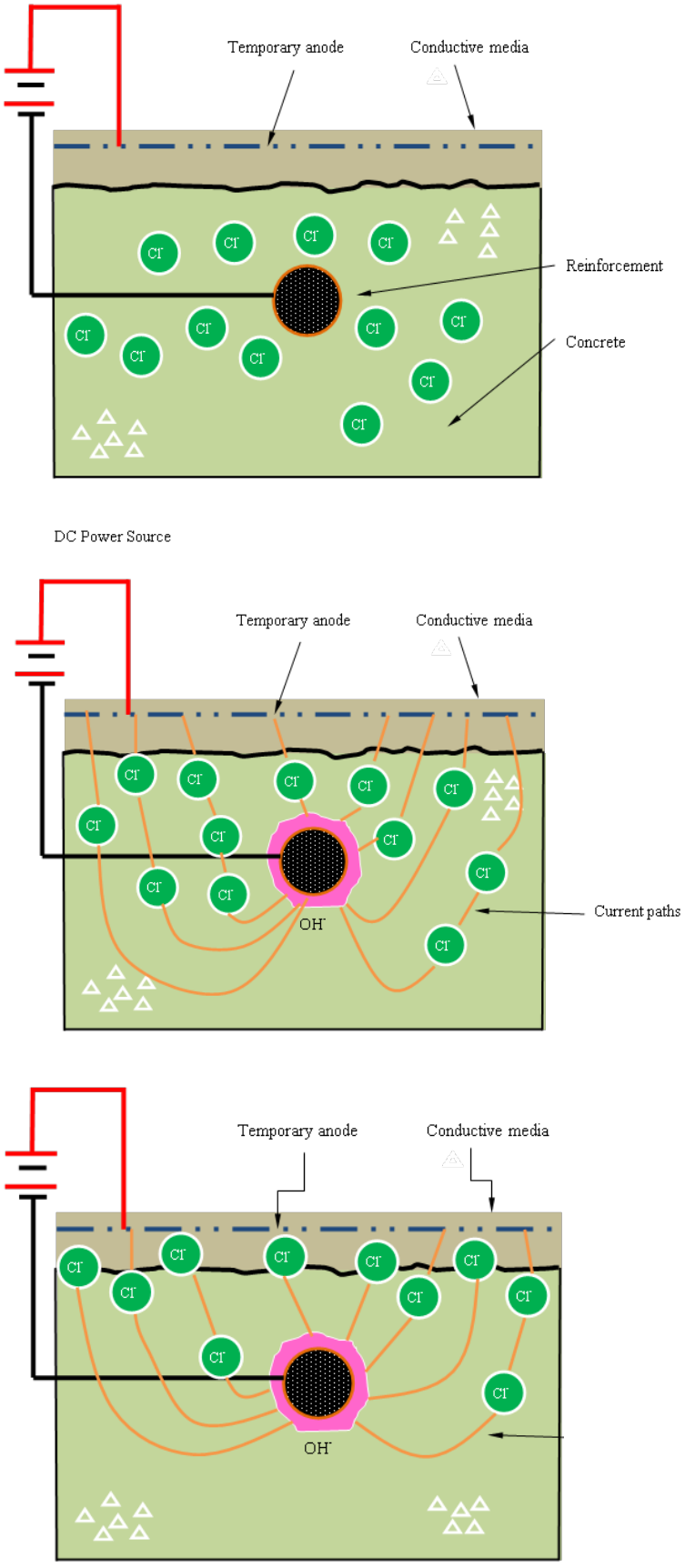


Figure 1 Chloride ions migration in the concrete

## LITERATURE REVIEW

The efficiency of ECE relies on the availability of free chlorides in the pore water solution. Chlorides are present in concrete in either a free or bound state. The free chloride ions exist in the pore water solution and the bound in the concrete mix (cement, aggregate, sand, add-mixtures). With continuous ECE treatment, the concentration of the free chlorides will decrease over time and the chloride extraction efficiency will also decrease. At the end of the treatment, only the bound chlorides remain in the concrete. [5] By switching-off the current, a balance between the free and bound chloride will take place in the concrete with the bound chlorides dissolving into the pore water solution until equilibrium is re-established [5/6].

Laboratory studies were carried out by Angst [7], in which a current-off treatment period was used on two concrete blocks with dimensions of 320 mm × 245 mm × 70 mm and w/c ratio of 0.5 and 0.6. The specimens were contaminated with chlorides sodium solution and steel reinforcement was embedded at an average depth of 50 mm. Sensors were embedded in the concrete at different depths to measure the free chloride content in the pore solution. The current density applied was 2 $A/m^2$ by the steel surface in a discontinuous manner, as shown in Table 1.

The results of this study, in terms of chloride concentrations are shown in Figure 2. The ECE treatment was most efficient in the early stage of the treatment and became inefficient over-time. Overall, both specimens showed a complete removal of the free chloride ions present in the pore solutions within a few days.

As seen in Figure 2, due to the complete elimination of free chlorides, the release of bound chlorides into the pore solution occurred in the first few days of the current-off period, and the equilibrium between the bound and free chloride was re-established, followed by a gradual decrease during the current-off period.

The results show that by switching the current off for a period it allows the chloride extraction to be more effective by promoting the release of the bound chlorides than continuous application of the electric current field.

In work carried out by Elsener [6] a field study was performed on the durability of ECE in Switzerland. The ECE process was applied as a rehabilitation method on an abutment of an underpass under a highway that had been exposed to deicing salt. The cover depths of the concrete varied between 25 mm and 35 mm, and the concrete quality reported as good [6]. A titanium mesh anode was used during the treatment and the process was applied using a voltage of 36 – 40 V in two stages; a continuous current of 0.3 to 0.75 $A/m^2$ by concrete surface was applied for 60 days [9]. An intermittent current was applied six months later to treat the areas with high chloride concentrations (more than 1% of the cement weight) with current densities of 1 to 0.7 $A/m^2$ for 60 days. The intermittent current was applied for two weeks on followed by one week-off [2, 6].

Table 1 Schedule of the ECE [7].

| PERIOD | DURATION, days |
|---|---|
| Phase I – On | 7 |
| Phase II – Off | 12 |
| Phase III – On | 4 |
| Phase IV – Off | 3 |
| Phase V – On | 7 |

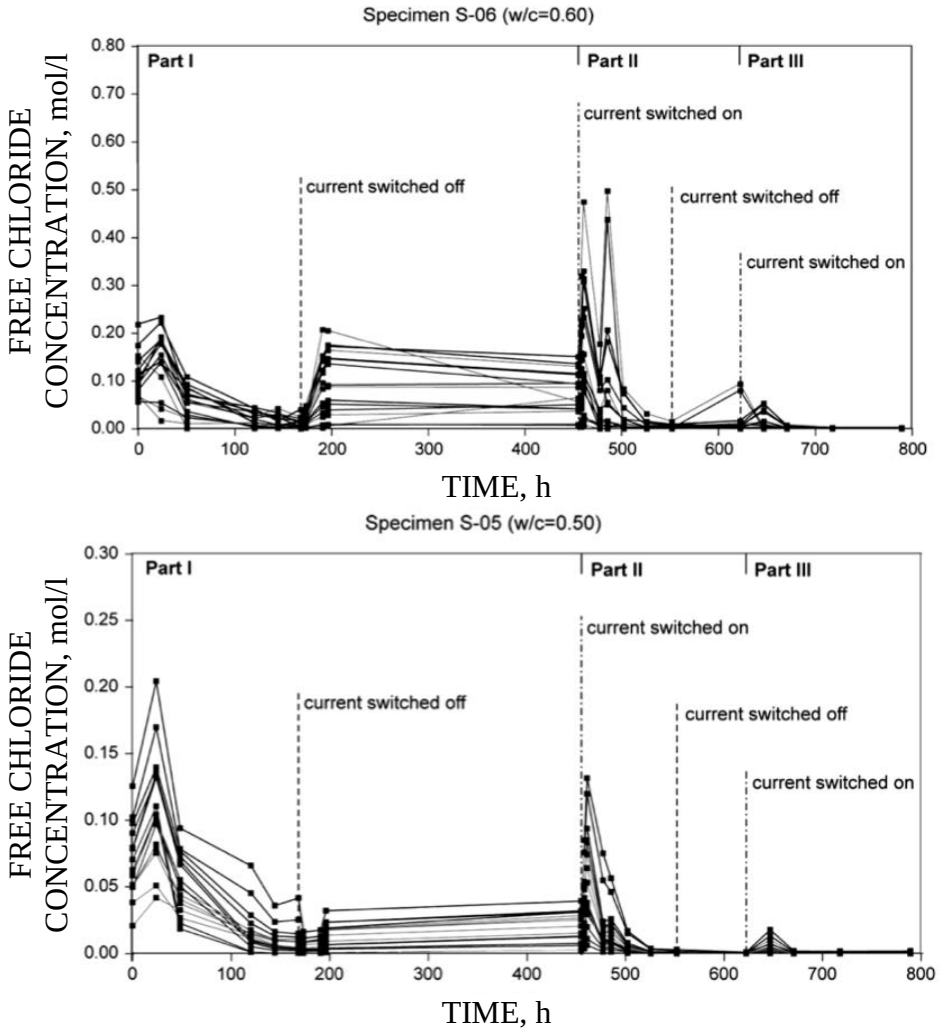


Figure 2 Change in free chloride content in concrete structure with time [7]

After 6-8 weeks, it was found that 50% of the total chloride contents were extracted in each stage of the treatment and the intermitted ECE treatment was found to be more effective in areas with high chloride contents [2, 6]. It was concluded that the current-off treatment was more beneficial than the continuous current treatment, due to its ability to rebalance the chloride ions [6].

## EXPERIMENTAL WORK

### Preparation of Specimens

Specimens S1, S2 and S3 were cast with Ordinary Portland Cement (CEM I), CEM I with 30% Pulverised Fuel and CEM II only respectively. In order to achieve sufficient chloride concentration and ensure an even distribution, a NaCl solution of 2.2 % (by cement weight) was added during mixing. By adding the NaCl solution to the mix, simulation of externally exposed concrete may be achieved by pre-saturating the concretes. It is not identical to normal chloride ingress but it allows the processes of interest to be studied. The mix proportions of the concretes cast are presented in Table 2 and a description of each specimen in Table 3. Each specimen was covered with a 50% cement:sand mix. All cements conform to EN-197.

Table 2 Concrete compositions in kg/m³

| MIX ID | CEM I | CEM II | PFA | WATER | W/C | FA | CA | |
|---|---|---|---|---|---|---|---|---|
| | | | | | | | 10 mm | 20 mm |
| S1 | 524.8 | - | - | 224.9 | 0.43 | 586.8 | 521.4 | 521.4 |
| S2 | 367.3 | - | 157.4 | 224.9 | 0.43 | 586.8 | 521.4 | 521.4 |
| S3 | - | 524.8 | - | 224.9 | 0.43 | 586.8 | 521.4 | 521.4 |

- FA – Fine Aggregate, CA – Coarse Aggregate, PFA – Pulverised Fuel Ash

Table 3 Description of specimens

| MIX ID | DESCRIPTION |
|---|---|
| S1 | CEM I cement only |
| S2 | 70 % CEM I cement and 30% PFA |
| S3 | CEM II cement only |

Figure 3 shows a schematic of the specimens and the depths at which dust samples were taken. In each specimen, a 10 mm diameter bar was cast into the concrete at a depth of 50 mm. The samples were mixed in the laboratory using a concrete mixer and were cast in the moulds, shown in Figure 4. The fresh concrete was vibrated on a vibrating table to remove trapped air. They were then stored for 24 h after which they were de-moulded and stored in a curing tank for one month until testing.

**Setup of Electrochemical Chloride Treatment**

A titanium mesh was placed on the surface of the specimens (Figure 5a) and covered with a cementitious material (Figure 5b), to serve as the electrolyte. A direct current (DC) power source was used to power the treatment (Figure 6).

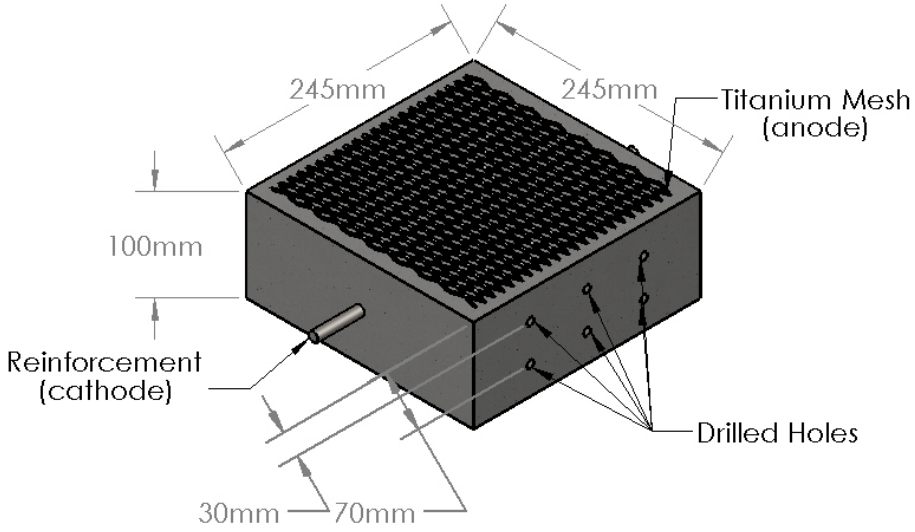


Figure 3 Schematic of the concrete slab cast

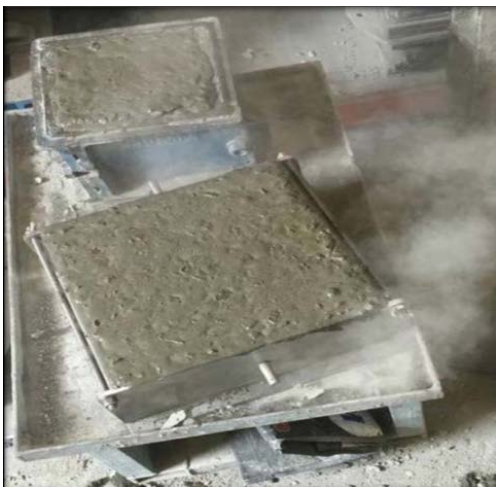

Figure 4 Specimens cast into moulds

(a) (b)

Figure 5 (a) Titanium mesh on surface of concrete (b) Cementitious media placed over mesh

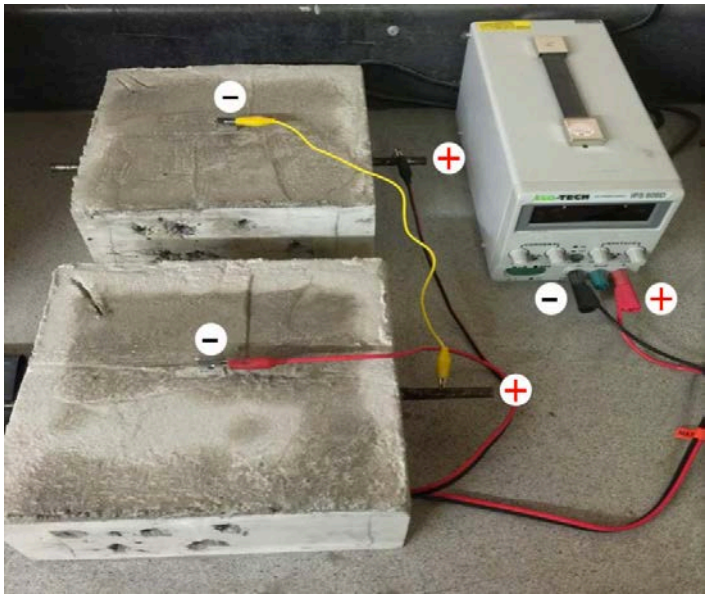


Figure 6 DC power supply connected to steel and titanium mesh

ECE began with the application of a D.C. current, in which the anode and the embedded steel in the concrete were connected to the two terminals of a DC power supply: the positive terminal was connected to the titanium mesh and the negative terminal was connected to the embedded steel. The specimens were connected in series to a DC supplier to regulate the current. The sides of each specimen was painted to ensure chlorides only moved vertically upwards.

### Applying ECE Treatment

The current density used in this work depended on the voltage used and the concrete resistivity. A constant voltage of 30 V was maintained, and the current densities were an average of 4.5 A/m² by steel surface for four weeks corresponding to charge densities of 2600 and 3300 Ah/m². The specimens were kept moist by pouring water onto the concrete's surface every four to five days.

Based on previous work in this area, the periods of current application were interrupted by switching-off the treatment to release the bound chlorides. The current was applied in cycles of 14 days on followed by two days off, as shown in Table 4.

Table 4 Schedule of ECE

| PERIOD | DURATION, days |
|---|---|
| Phase I – On | 14 |
| Phase II – Off | 2 |
| Phase III – On | 12 |

Chloride concentration profiles were obtained from concrete samples collected from the test specimens before and during the ECE application. Holes were drilled at depths of 30mm and 70 mm using an 8 mm drill bit. The powdered dust samples were analysed using potentiometric titration using a silver nitrate solution in accordance with (AASHTO T 260- 97, 2005).

## RESULTS

### Cube Tests

Results from compressive strength tests performed on cubes cast from the three concrete mixes are shown in Figure 7. Average 7, 28 and 56 day compressive strengths of 47.4 N/mm$^2$, 57.18 N/mm$^2$ and 58.03 MPa were achieved.

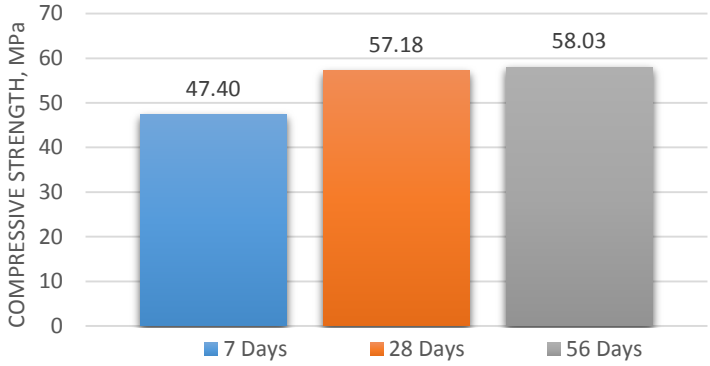


Figure 7 Concrete Cube Test Results

## Chloride concentration

As may be seen in Figure 8, chloride extraction is influenced by the concrete type. For instance, the variation in chloride content with time shows that the removal was faster with S1, with a reduction of 45% achieved at 21 days as opposed to 28 days in S3. The average was computed by comparing the reduction in concentration with the initial chloride content in each specimen.

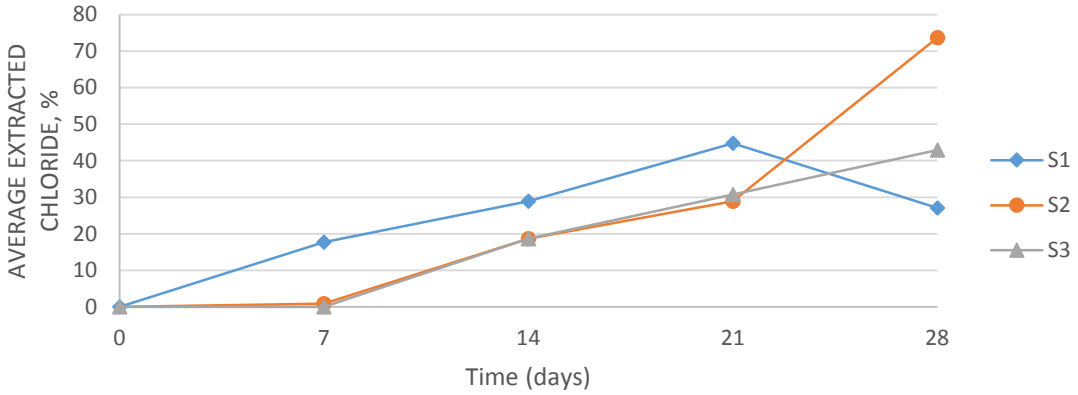


Figure 8 Average extracted chlorides in specimens during ECE treatment

Another observation was the lower amount of chlorides extracted during the first three weeks from S2 and S3. After 7 days, the rate of extraction appears to be similar for all cement types between 7 and 21 days. At four weeks, a significant removal of chlorides (approximately 74%), was observed from S2. However, S3 maintained its extraction rate but slowed in the final week. It can be concluded that CEM I with PFA will allow better removal when compared with CEM II alone. Again CEM I was more effective with chloride removal. This is possibly related to the denser matrix or finer pore structure associated with the CEM II cements which lowers permeability thereby limiting chloride diffusion [10]. The chloride concentrations at 30mm and 70 mm from the surface (FS) are plotted against time in Figures 9 to 11 with the average of all specimens shown in Figure 12.

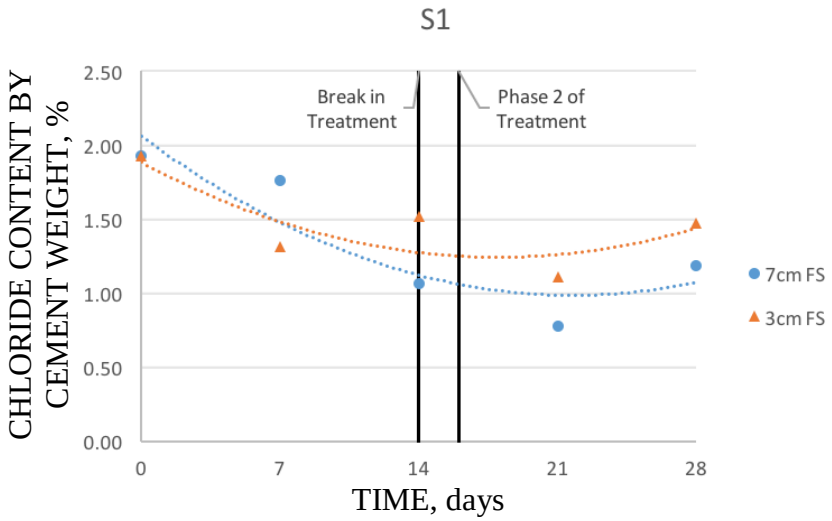


Figure 9 Chloride content in S1 during ECE treatment

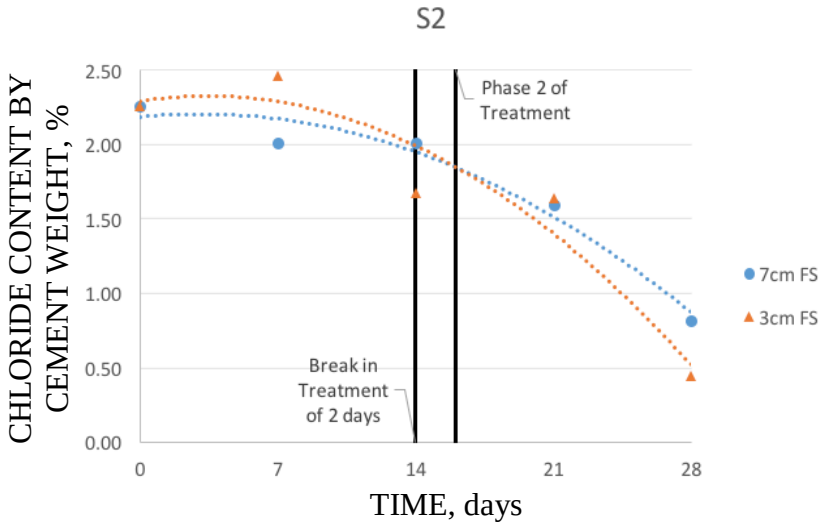


Figure 10 Chloride content in S2 during ECE treatment

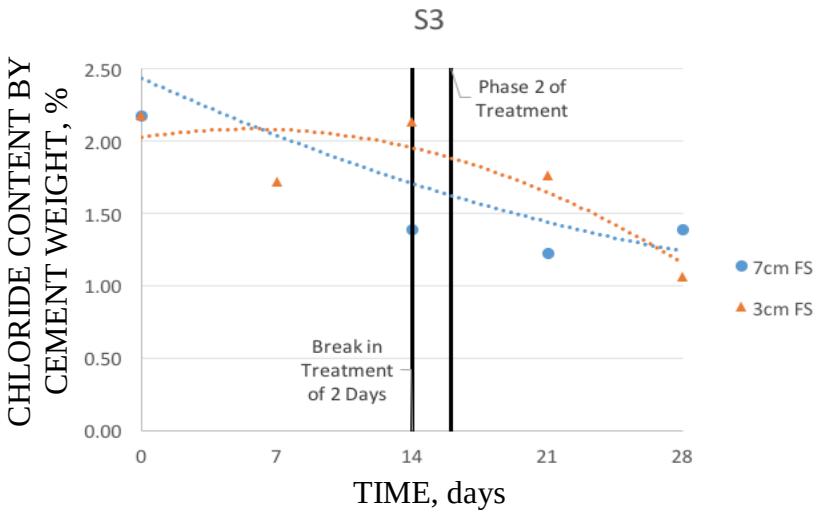


Figure 11 Chloride content in S3 during ECE

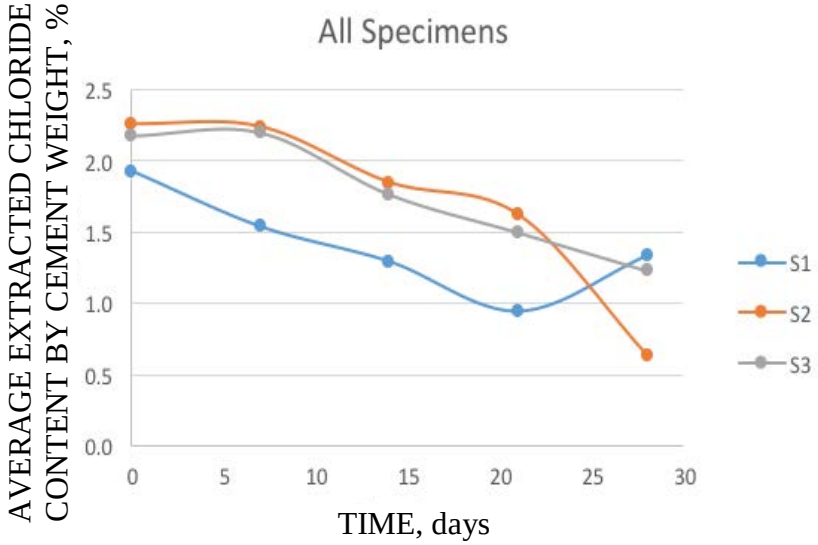


Figure 12 Average Chloride content in S1/2/3 during ECE

As may be seen in S1 (Figure 9), the chloride concentrations at 30 mm FS drop after 7 days. The concentration at 70 mm FS is reduced significantly initially indicating that increased extraction rates are occurring. In S2 (Figure 10), the break in treatment appears to have had a positive effect on the ability to extract chlorides from the concrete.

After the break, the slope of the line increases dramatically at each location. Elsener [7], showed that a break in treatment allows the bound chlorides to be dissolved into the pore solution which may explain the increase in concentrations at 28 days for S1. Following a slow start, S3 showed the most consistent extraction rate while not appearing to benefit from the break in treatment. It appears that the break in treatment has a positive effect on the CEM I with PFA.

## CONCLUSIONS

In light of the results of this research, the following conclusions have been drawn:

1. The efficiency of the ECE treatment increases with permeability. If the concrete surface remained saturated during the ECE process, a significant amount of chlorides could be removed.

2. A stable current density of 4.5 A/m² by steel surface with 30 V makes the duration of the ECE treatment shorter, and it can be the optimal choice for treating concrete with normal reinforcing to avoid negative impacts on the reinforced concrete.

3. A current density of 4.5 A/m² can be used in the CEM I concrete type in order to extract as much as 40% of chloride ions content in the concrete. While CEM II required longer time to extract the same rate.

4. A higher efficiency of the ECE treatment with the CEM I concrete type than with the CEM II and cement fly ash concrete types.

5. The cement fly ash has higher capacities to bind chlorides than the CEM I and CEM II. Therefore, the PFA cement replacement required a longer time to extract a significant amount of the chloride.

## ACHKNOWLEDGEMENTS

The author acknowledges the financial support from the PhD scholarship funded by the College of Engineering and Built Environment at DIT.

## REFERENCES

1. AL-NUMAN B. and CICEK V. Corrosion Chemistry (Vol. 1st Ed.). New Jersey, Salam, Massachusetts: John Wiley & Sons. Scrivener Publishing LLC, 2011.

2. LIU Y. and SHI X. Electrochemical chloride extraction and electrochemical injection of corrosion inhibitor in concrete: state of the knowledge. Corrosion Reviews, Vol. 27, Nos. 1-2, 2009, pp. 53–81.

3. BROOMFIELD J.P. Corrosion of Steel in Concrete. London and New York: Taylor & Francis, 2007.

4. CLEMEÑA G. and Jackson D. Trial Application of Electrochemical Chloride Extraction on Concrete Bridge Components in Virginia. VTRC 00-R18, Virginia Department of Transportation and the University of Virginia, U.S. Department of Transportation Federal Highway Administration, 2000.

5. BERTOLINI L., ELSENER B., PEDEFERRI P., REDAELLI E. and POLDER R.B. Corrosion of steel in concrete. Prevention, Diagnosis, Repair. 2nd ed. Co. KGaA, Weinheim: Wiley, 2013.

6. ARKAN L.H. A study of selecting an efficient procedure for intermittent Electrochemical Chloride Extraction. Master. Norway: Norwegian university of science and technology. 2010.

7. ANGST U. and ELSENER B. Mechanism of electrochemical chloride removal. Corrosion science, Vol. 49, No. 12, 2007, pp. 4504–4522.

8. ELSENER B., MOLINA M.M. and BÖHNI H. The Electrochemical Removal of Chlorides from Reinforced Concrete. Corros. Sci., Vol. 35, 1993, pp. 1563–1570.

9. SHARP S.R., CLEMEÑA G.G., VIRMANI Y.P., STONER G.E. and KELLY R.G. Electrochemical Chloride Extraction: Influence of Concrete Surface on Treatment, 2002.

10. ISMAIL M. and MUHAMMAD B. Electrochemical chloride extraction effect on blended cements. ICE Advances in Cement Research, Vol. 23, No. 5, 2011, pp. 241–248.

# MECHANISM ANALYSIS OF RC SLABS STRENGTHENED WITH PRESTRESSED AND NON-PRESTRESSED FRP

**M Davvari**

**Z J Wu**

**Z Zou**

University of Manchester

United Kingdom

**ABSTRACT.** The behaviour of un-strengthened RC column-slabs and RC column-slabs strengthened with non-prestressed and prestressed FRP sheets are evaluated by use of experimental tests and numerical analyses. The results show a significant increase in the ultimate load capacity for the RC column-slab strengthened with non-prestressed FRP in comparison with the un-strengthened sample and failure mode is changed from flexural failure in the un-strengthened slab to punching failure in the slab strengthened with non-prestressed FRP. The RC specimens strengthened with prestressed FRP sheets, however, cannot reach their expected ultimate load capacity due to debonding of FRP sheets although a proper FRP-steel end plate anchoring system to avoid debonding failure has been applied. The finite element models show that the main reason for FRP debonding is concrete fracture near the FRP end plate which is in turn caused by the enhancement of the tensile stresses in the region of above the steel reinforcement and below the neutral axis. Near the endplate, prestressed FRP sheets create a local compression zone close to the concrete surface and local tension zone above the steel reinforcements. These locally stressed zones are located below the primary neutral axis of the concrete section. The superposition of the tensile stresses of the local tension zone and the tensile stresses produced by applying external load on the column, increase the overall tensile stress level in the area above the steel reinforcements and below the primary neutral axis. The result of this superposition process initiates the flexural cracks which propagate due to shear stresses. The flexural-shear cracks propagation leads concrete fracture near the end plate finally and hence causes the debonding of FRP sheets.

**Keywords**: Strengthening RC slabs, Prestressed FRP, Finite element modelling, Debonding.

**M Davvari** is a Ph.D. student at the University of Manchester. The theme of his research is strengthening RC structures.

**Dr Z J Wu** and **Dr Z Zou** are lecturers in structural engineering at the University of Manchester. Their research interests are composite structures, structural failure.

## INTRODUCTION

Strengthening RC structures with fibre reinforced polymers is a common method to overcome issues such as excessive loading or suffering deterioration due to corrosion attack, fire damage, freezing, thawing and so on. The most common method to increase the maximum load capacity of a RC column-slab is applying FRP sheets on its tension surface. In spite of many researches which have been conducted in the respect of FRP strengthened RC structures such as beams and columns, there is a lack of experimental and numerical investigations in the case of FRP strengthened RC column-slabs, especially in the case of strengthening RC column-slabs with prestressed FRP [1-4]. Abdullah [4] carried on an experimental study to investigate the behaviour of two-way RC slabs strengthened with prestressed and non-prestressed FRP sheets. The load capacity of the sample strengthened with non-prestressed FRP was increased significantly as compared with the control specimen. However, the RC slabs strengthened with prestressed FRP have not shown a considerable enhancement of their maximum load capacity. The reason for such a phenomenon and results are not yet clear from the point of view of traditional prestressed structural analysis. In this paper, a numerical analysis is conducted to explain the behaviour of strengthened RC slabs, mainly to clarify the primary reason for the unexpected behaviour of the RC column-slabs strengthened with prestressed FRP sheets as well as explaining the samples failure process.

## EXPERIMENTAL PROGRAMME

In this section, an experimental investigation in strengthening RC column-slab that is the base of the numerical modelling in this study is described briefly. Our heavy structure laboratory in Manchester University has conducted a programme to consider the effect of strengthening RC column-slabs with prestressed and non-prestressed FRP sheets on the parameters such as load carrying capacity, yielding load, deflection, crack patterns and failure modes experimentally [4]. FRP sheets are bonded to the tension surface of the RC slabs externally. Figure 1 presents the geometric details of the test specimens.

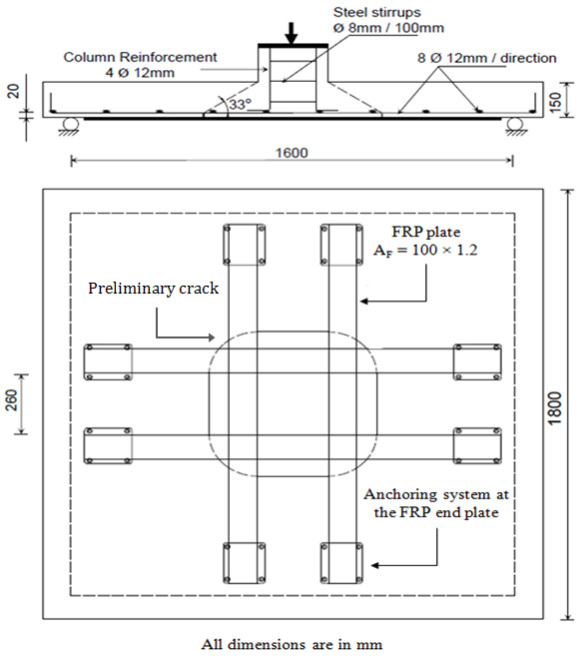


Figure 1 Experimental study layout [4]

The mechanical properties of concrete, FRP and steel bars are the same in all slabs, as indicated in Tables 1 to 3.

Table 1 Concrete properties

| MODULUS OF ELASTICITY (GPa) | COMPRESSIVE STRENGTH (MPa) | TENSILE STRENGTH (MPa) | WATER-CEMENT RATIO | MAXIMUM SIZE AGGREGATE (mm) |
|---|---|---|---|---|
| 31 | 33.10 | 3.39 | 0.48 | 10 |

Table 1 FRP properties

| FIBRE TYPE | DENSITY ($gm/cm^3$) | CROSS SECTION ($mm^2$) | MODULUS OF ELASTICITY (Gpa) | TENSILE STRENGTH (MPa) | RAPTURE STRAIN | VOLUME FRACTION |
|---|---|---|---|---|---|---|
| CFRP | 1.7 | 1.2 × 100 | 172 | 2970 | 0.0168 | 70% |

Table 2 Steel bars properties

| DIAMETER (mm) | YIELD STRENGTH (MPa) | YIELD STRAIN | ULTIMATE STRENGTH (MPa) |
|---|---|---|---|
| 12 | 570 | 0.0034 | 655 |
| 8 | 576 | 0.0030 | 655 |

A low steel reinforcement ratio (0.4%) has been chosen to make a reasonable space for the consideration of the effect of FRP strengthening. Altogether, four slab specimens have been cast (Table 4) in which R0 is an un-strengthened concrete slab (control specimen), R-F0 is a concrete slab strengthened by non-prestressed FRP sheets. R-F15 and R-F30 are the concrete slabs strengthened by 15% and 30% prestressed FRP, respectively. As it can be seen from Figure 2, the slabs were loaded by hydraulic ram acting on the steel frame.

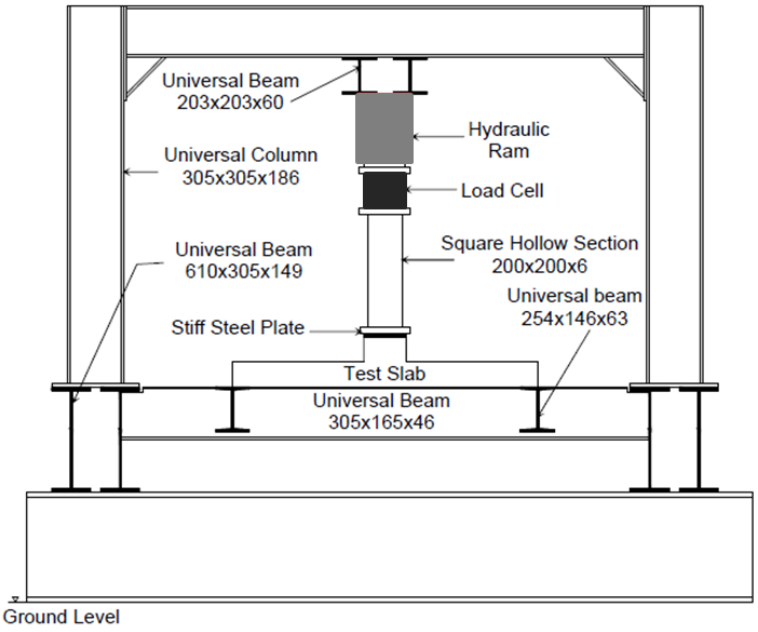


Figure 2 Test setup sketch [4]

The load was a pressure which has been produced by pumping the oil into the ram. The slabs were simply supported on their four edges and free to lift. The relevant test results will be reported, together with the numerical study, as shown in the following section.

## FINITE ELEMENT SIMULATION MODEL

The numerical models have been adopted by using the commercial finite element (FE) ABAQUS software (ABAQUS 6.13 the product of SIMULIA Software Company). In this study, concrete damage plasticity has been considered to simulate the concrete failure due to cracking in tension and crushing in compression. To consider the evolution of concrete failure, the finite element models use tensile and compressive damage variables to observe tensile cracks and compressive crushes. Thanks to the evaluation of compressive and tensile damages, the plastic strains could be observed that is efficacious to compare numerical and experimental crack propagation of samples [5-6]. Since there is no fracture inside the adhesive material in the experimental models, a tie constraint has been assumed between FRP and concrete. The embedded steel reinforcements in the concrete are yielded when the stress in the major axis exceeds the steel yield strength.

The types of the elements that are chosen to simulate the different materials of the samples are as follows. C3D8R (Solid continuum 3-dimensional 8-node element with reduced integration) elements are employed to analyze the linear or nonlinear behaviour of concrete. S4R (Shell 4-node element with reduced integration) elements are applied to model FRP sheets in which their stress variations in their third dimension (the thickness direction) are negligible. Since the main duty of steel reinforcements is transferring the axial forces, T3D2 (Truss 3-dimensional 2-node element) is one of the most applicable elements to model steel bars. Table 4 shows such a comparison between numerical and experimental results. The differences between numerical and experimental results (for all measured parameters such as load and deflection) show a reasonable accuracy in this study.

Table 4 A comparison between numerical and experimental results

| SPEC | YIELD LOAD (kN) | | YIELD DEFLECTION (mm) | | ULTIMATE LOAD (kN) | | ULTIMATE DEFLECTION (mm) | | FAILURE MODE |
|---|---|---|---|---|---|---|---|---|---|
| | EXP | FEM | EXP | FEM | EXP | FEM | EXP | FEM | |
| R0 | 171.6 | 185 | 9.9 | 8.9 | 284 | 247 | 27.3 | 25.1 | Flexural |
| R-F0 | 273.4 | 265 | 14.6 | 12.1 | 405 | 357 | 21.4 | 23.9 | Punching |
| R-F15 | 240 | 275 | 12.0 | 10.7 | 240 | 275 | 15.2 | 17.2 | Debonding |
| R-F30 | 220 | 252 | 14.2 | 10.0 | 220 | 252 | 16.3 | 15.6 | Debonding |

According to the experimental and numerical results, the failure mode of the control specimen (R0) is a flexural failure that happened due to the wide development of the yield lines (that occurs after steel reinforcement yielding) on the tension surface. Park and Gamble [7] also stated that the expected failure mode for RC slabs with low tensile reinforcement ratio (lower than 1%) is a ductile flexural failure. Figure 3 shows the yield lines development with wide flexural cracks which results in a ductile flexural failure.

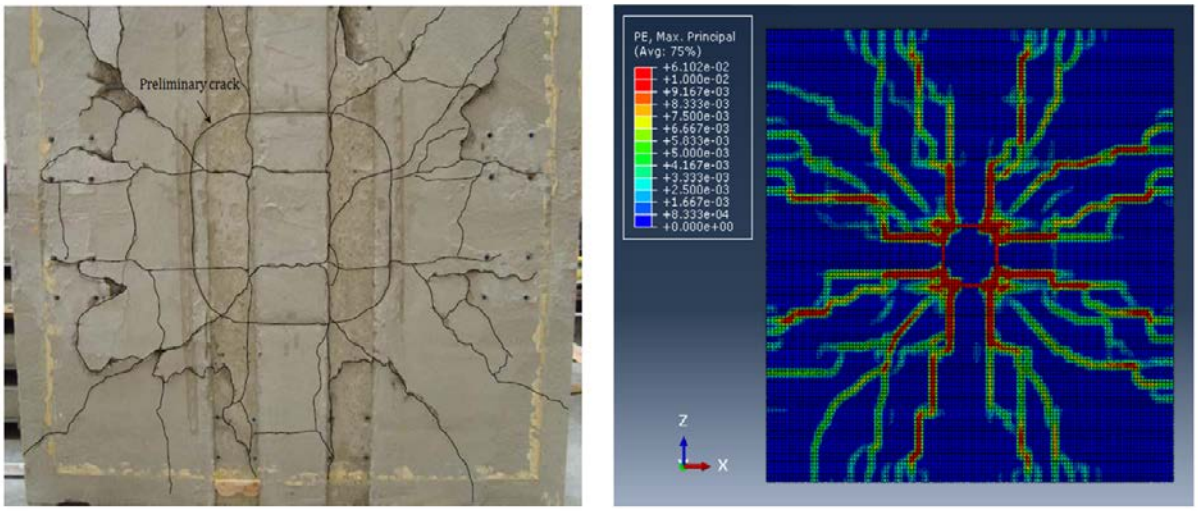


Figure 3 Cracks propagation in R0

The experimental and numerical results show a considerable improvement in the load capacity of the concrete slab strengthened with FRP, however, the ductility of the strengthened sample has been decreased due to the changing of failure mode from flexural failure to punching failure. Figure 4 shows cracks propagation in the finite element and experimental models of R-F0.

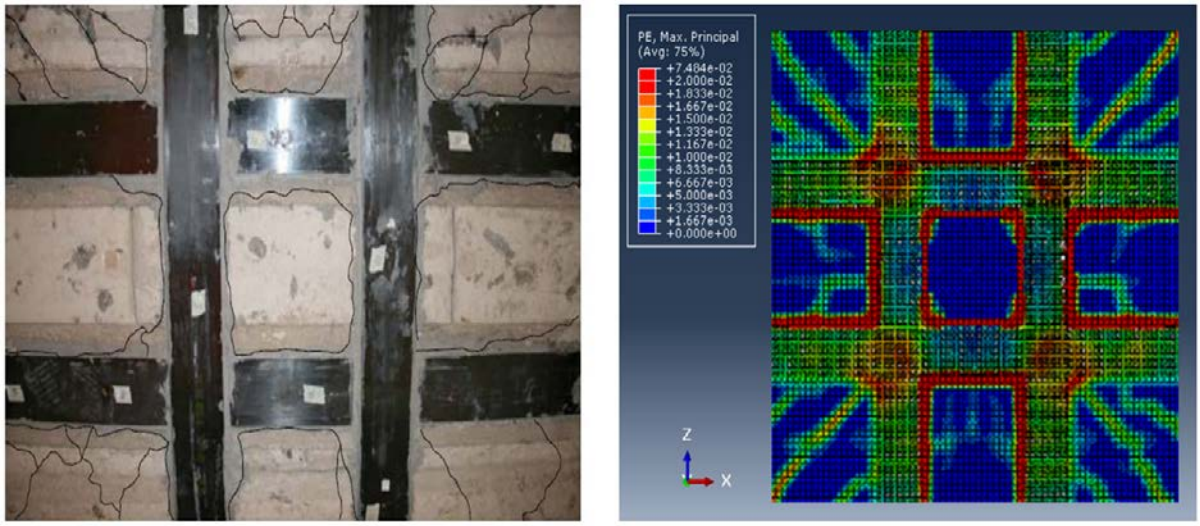


Figure 4 Cracks propagation in R-F0

According to classic theory of structural analysis, prestressing the FRP sheets increases the effective sectional area with tensile residual stress in a slab and would lead more bending resistance of the section caused by the transverse loading compared with non-prestressed FRP in principal. Hence, a remarkable enhancement in the load capacity of the specimens strengthened with prestressed FRP sheets is expected. However, it is noticed in this study that there is no significant increase in the load capacities of R-F15 and R-F30 and both samples failed due to debonding in spite of the expectations. So, numerical and sectional analyses are considered here to clarify the main reason of debonding that is necessary to understand the behaviour of RC samples strengthened with prestressed FRP.

The finite element model has confirmed and illustrated that the primary reason of FRP debonding is caused by concrete fracture near the end plate. The finite element simulation of the samples strengthened with prestressed FRP reveals that the concrete fracture is caused by the enhancement of the tensile stresses in the domain of above steel reinforcement and below the neutral axis (which cannot be avoided by the applied anchorage system). Near the FRP-steel endplate, prestressed FRP sheets develop a local compression zone near the concrete surface and local tension zone above the steel reinforcements and below the primary neutral axis of the concrete section. The superposition of the tensile stresses of the local tension zone and the tensile stresses produced by applying external load on the column increases the overall tensile stress level in that area. Sectional analysis near the FRP end plate (Figure 5) show how the bending stress distribution could lead to such failure mode.

The mentioned process may firstly lead the concrete flexural cracks in the superposition zone of two tensions (global and local) when the overall tensile stresses exceed the concrete tensile strength. Then the cracks are developed due to shear stresses. The cracks propagation causes concrete fracture which in turn leads debonding of FRP sheets. The flexural-shear cracks propagation near the end plate which causes debonding failure has been shown in Figure 6.

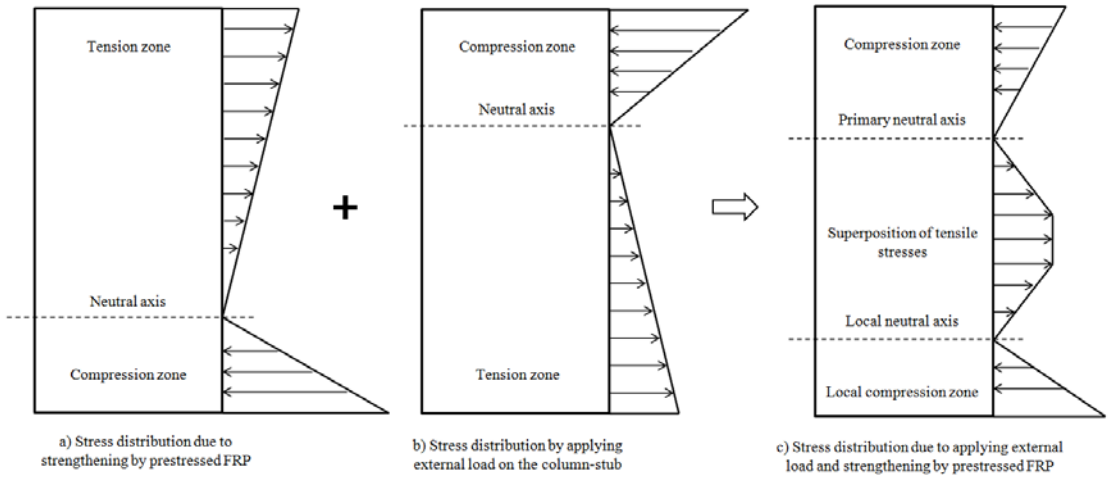


Figure 5 bending stresses distribution in the concrete section near the end plate

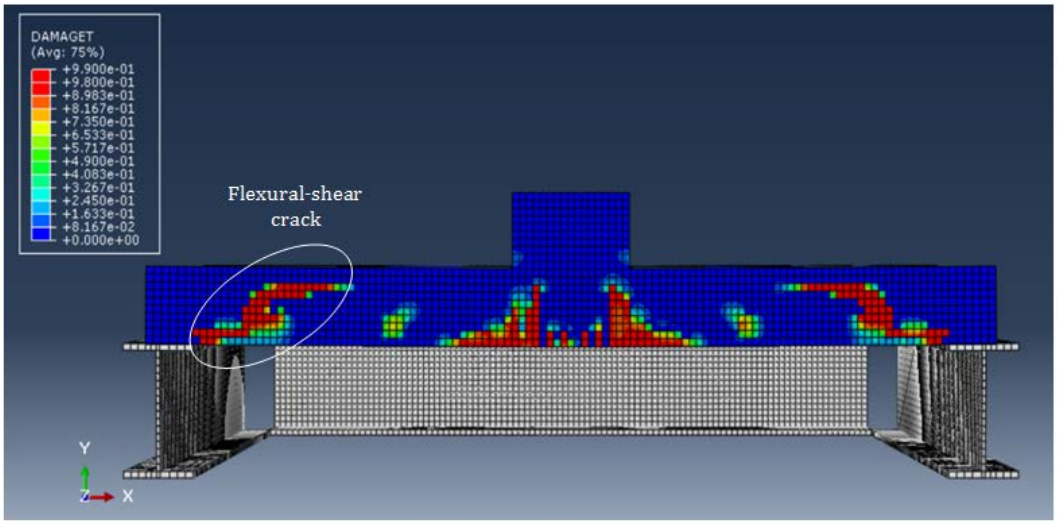


Figure 6 Flexural-shear cracks propagation near the end plate

Figure 7 show cracks propagation and concrete fracture near the end plate in the finite element and experimental models of R-F30.

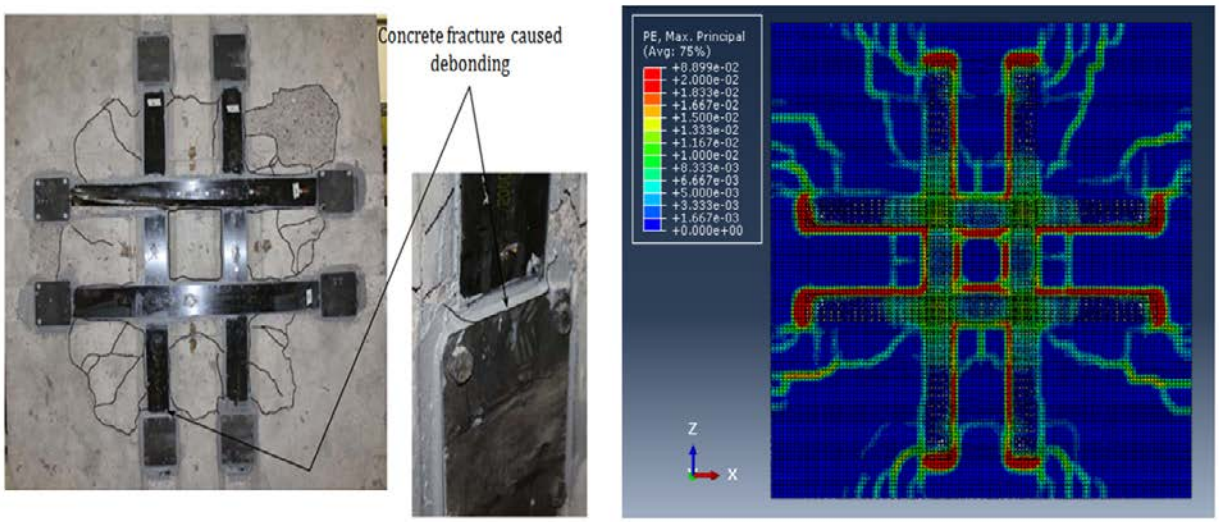


Figure 7 Cracks propagation of R-F30

## CONCLUSIONS

The most possible failure mode of RC slab with low tensile reinforcement ratio is a flexural failure which happens due to the wide development of the yield lines (that occurs after steel reinforcement yielding) on the tension surface.

Strengthening RC slabs with FRP sheets could cause a considerable improvement in the load capacity of the samples; however, the ductility of the strengthened specimens is expected to be decreased.

The finite element models demonstrated that the main reason of FRP debonding is concrete fracture near the end plates for the slabs strengthened with prestressed FRP in this study, while the concrete fracture is initiated by the increment of the tensile stresses in the region of above the steel reinforcement and below the neutral axis. Near the endplates, stress transfer of prestressed FRP sheets creates a local compression zone near the concrete surface and local tension zone above the steel reinforcements and below the primary neutral axis. The superposition of the tensile stresses of the local tension zone and the tensile stresses produced by applying external load on the column-stub increase the overall tensile stress level in that area. This may initiate the concrete flexural cracks which propagate due to shear stresses. The crack propagation causes concrete fracture near the end plate which in turn leads debonding of FRP.

It is notable that the experimental and numerical results in this study do not mean that applying prestressed FRP causes FRP debonding directly but the possibility of earlier debonding failure caused by the concrete tensile fracture inside the slabs increases with the prestress ratio of FRP.

## REFERENCES

1. CRC, Review of strengthening techniques using externally bonded fiber reinforced polymer composites. 2002, CRC Construction Innovation: Brisbane, Australia.

2. EBEAD, U. AND H. MARZOUK, Fiber-reinforced polymer strengthening of two-way slabs. ACI Structural Journal, 2004. **101**(5): p. 650-659.

3. SHARAF, M., K. SOUDKI, AND M. VAN DUSEN, CFRP Strengthening for Punching Shear of Interior Slab–Column Connections. Journal of Composites for Construction, 2006. **10**(5): p. 410-418.

4. ABDULLAH, A.M., Analysis of Repaired/Strengthened R.C. Structures Using Composite Materials : Punching Shear, C.G.S. Bailey, A. University of Manchester. School of Mechanical, and E. Civil, Editors. 2011, Doctor of Philosophy: Manchester, UK.

5. ABAQUS, V., 6.13. Dassault systemes. Pawtucket, 2013.

6. KACHLAKEV, D., ET AL., Finite element modeling of concrete structures strengthened with FRP laminates. Final report, SPR, 2001. **316**.

7. PARK, R. AND W.L. GAMBLE, Reinforced concrete slabs. 2000: John Wiley & Sons.

# PARAMETRIC STUDY FOR RC BEAMS STRENGTHENED IN SHEAR WITH FRP USING NONLINEAR FINITE ELEMENT MODELING

**A M. Morsy**

**N H El-Ashkar**

**I S Mattar**

Arab Academy for Science, Technology, and Maritime Transport

Egypt

**ABSTRACT.** This research aims towards modeling the behavior of RC beams shear-strengthened with fibre reinforced polymer (FRP) using the Finite Element (F.E.) method for the purpose of performing a parametric study on strengthening of beams in shear using different techniques by different FRP materials such as sheets for externally bonding (E.B.), laminates for near surface mounted (N.S.M), and bars for internally embedded reinforcement (I.E.R.). A modeling process is carried out using the F.E. software package ABAQUS CAE 6.11-3. Experimental data for specimens failing in shear and strengthened using different strengthening techniques has been available where an analysis F.E. nonlinear model for each specimen has been prepared based upon loading conditions, material properties and boundary conditions. For the purpose of model verification, the results obtained from the modeling procedure have been compared with the experimental results. The available data was mainly load-deflection curves at mid-span, failure load, and strain as well as cracking pattern, where a slight variation of results has been noticed upon comparison between F.E. results and experimentally results. Finally a parametric study has been carried out so as to study the effect of various parameters in strengthening techniques included in the strengthening process on the beam behavior.

**Keywords**: ABAQUS, Fibre reinforced polymer (FRP), Finite element; near surface mounted; Reinforced concrete; Strengthening

**Alaa M. Morsy** is an associate professor, Construction, and Building Depart., college of Engineering & Technology. He has received her Ph.D. in Structural Engineering from Alexandria University, Egypt; where his research work included usage Advanced Composite Materials (FRP) in Repair and Strengthening of R.C., Heat Transfer and fire Protection, and Use Finite Elements Software's in Modeling. He has fifteen years of experience in Structural engineering, practice and research. He is currently posted as Vice Dean and Manager of Education and Training department, at Port Training Institute, AASTMT.

## INTRODUCTION

Long term behavior of reinforced concrete structures has been one aspect of civil engineering continuously under study for various purposes either repair or maintenance. Various factors such as creep, shrinkage as well as other factors which may be environment induced such as corrosion may cause cracking, reduce the structure's load carrying capacity resulting in failure of the structure system to function properly and may lead to system failure. Accordingly developing new techniques regarding repair and maintenance of reinforced concrete structures has become one necessity which cannot be ignored. From such prospect various techniques for strengthening reinforced concrete structures have been developed in order to prolong the service duration of existing structures as well as preventing their deterioration [1].

One of the most commonly used methods to strengthen existing reinforced concrete structures is the use of FRP through various methods including externally bonded sheets (E.B.), near surface mounted rods (N.S.M.) or internally embedded reinforcement (I.E.R.). Known for their high strength, lightweight as well as being corrosion resistant and highly versatile, FRP represents a highly reliable structural material despite of being linear elastic with high initial material cost [1].

Therefore, many experimental procedures have been carried out in order to study the behavior of FRP strengthened concrete structures so as to further more understand their behavior in order to allow a wider field of application [2-4]. However, the lack of accurate modeling procedures due to the large number of variables included in the model arising from the composite action caused by the interaction between FRP and concrete caused a drawback in predicting the behavior of such structures [5].

While experimental programs for research are extremely useful in obtaining confident information about the composite behavior of FRP and reinforced concrete, the use of numerical models helps in developing a good understanding of the behavior at lower costs and conducting varies tests using parametric study.

Throughout this research, modeling of FRP shear-strengthened reinforced concrete beams using F.E. method will be carried out for the purpose of predicting the future behavior of elements with similar performance. The process is to be carried out through the study of the behavior of a number of beams, modeling them using the finite elements method. The modeling results are to be compared with the experimental data obtained from the modeled beams where such data includes load-deflection curves at mid-span, failure load, strain as well as cracking pattern for each specimen. ABAQUS CAE 6.11-3 finite element package will be used for the modeling process.

Finally a parametric study has been carried out so as to study the effect of various parameters included in the strengthening process on the beam behavior, the tested parameters include three types of shear strengthening as follow which conducted experimentally in other research program [6].

- Shear strengthening using CFRP laminates for near surface mounted (NSM) technique comparing effect of varying both width and spacing of embedded vertical laminates through concrete cover

- Shear strengthening using CFRP rods for internally embedded reinforcement (IER) technique comparing effect of varying spacing between embedded CFRP bars

- Shear strengthening using CFRP sheets for externally bonded sheets (EB) technique comparing effect of varying width of CFRP sheets.

## MATERIAL MODELS

### Concrete

Stress-Strain curve for concrete under compression is obtained based upon an experimentally verified numerical model [7] (Hsu and Hsu 1994). The model obtains stress-strain curve under uni-axial compression up to 0.3 characteristic strength ($f_{cu}$) in the descending portion based upon maximum compression strength $f_{cu}$. Such model is also characterized by having a linear Stress-Strain relationship in accordance with Hook's Law till 0.5fcu.The stress strain relation-ship based on the numerical model is shown in Figure1. Equations (1-4) emphasize the use of the model to obtain the stress-strain curve for concrete

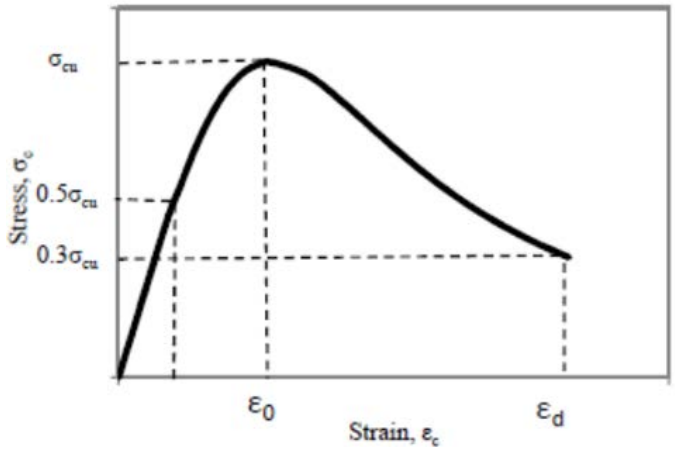


Figure 1 Compressive Stress-Strain relationship for concrete (Hsu and Hsu 1994) [7]

$$\sigma_c = \left[\frac{(\eta * \beta) * (\varepsilon_c/\varepsilon_o)}{(\eta * \beta) - 1 + (\varepsilon_c/\varepsilon_o)^{(\eta*\beta)}}\right] * \sigma_{cu} \quad \text{--------(1)}$$

$$\beta = \frac{1}{1 - [\sigma_{co}/(\varepsilon_o * E_o)]} \quad \text{------(2)}$$

$$\varepsilon_o = (8.9 * 10^{-5} * \sigma_{cu}) + 2.114 * 10^{-3} \quad \text{------(3)}$$

$$E_o = (1.2431 * 10^2 * \sigma_{cu}) + (3.28312 * 10^3) \quad \text{------(4)}$$

Where:

β : A material parameter which depends on shape of stress-strain diagram

$\varepsilon_o$ : Strain at peak stress

$E_o$ : Initial tangential modulus (Kip/in$^2$)

$\varepsilon_d$ : Strain at 0.3 $f_{cu}$ in the descending portion and is iteratively calculated using equation (1) at

$s_c = 0.8 * s_{cu}$

$s_c$ : Compressive strength (Kip/in$^2$)

$s_{cu}$ : Ultimate compressive strength (Kip/in$^2$)

(1 MPa = 0.145037743 Kip/in$^2$)

n:Material parameter which depends on $s_{cu}$

$0 < s_{cu} < 62$ MPa → n = 1

62 MPa ≤ $s_{cu}$ <76 MPa → n = 2

76 MPa≤ $s_{cu}$ <90 MPa → n = 3

90 MPa≤ $s_{cu}$ → n = 5

In order to represent the softening behavior of concrete under tension model [8] is used as shown in Figure 2. Concrete assume a linear elastic behavior till maximum tensile stress ($f_{ct}$) after which tensile softening follows the curve in Figure 2.

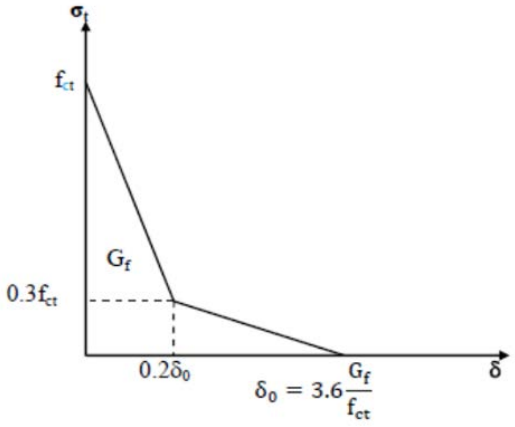


Figure 2 Softening curve for concrete under uni-axial tension (Hillerborg,1985) [8]

Values for $f_{ct}$ (in MPa) can be obtained by referring to (CEB-FIP, 1993) where upper, lower bounds as well as mean value are specified as by the equations (5-7) [9]

$$f_{ctk,min} = 0.95 * (0.1 * f_{ck})^{2/3} \quad (5)$$

$$f_{ctk,m} = 1.4 * (0.1 * f_{ck})^{2/3} \quad (6)$$

$$f_{ctk,max} = 1.85 * (0.1 * f_{ck})^{2/3} \quad (7)$$

Where:

$f_{ck}$: Concrete compressive strength (MPa)
$f_{ctk,min}$: Minimum value for tensile strength (MPa)
$f_{ctk,m}$ : Mean value for tensile strength (MPa)
$f_{ctk,max}$: Maximum value for tensile strength (MPa)
δ◦: Crack opening displacement (mm)

$G_f$: Fracture energy (Nmm/mm$^2$), energy required to propagate a tensile crack of unit surface area projected in a plane parallel to the crack direction.

Values for $G_f$ Fracture energy (Nmm/mm$^2$) can be obtained by referring to (CEB-FIP, 1993) by using equation 8, where the resulting deviations in value of $G_f$ are up to ± 30%

$$G_f = G_{fo} * (0.1 * f_{ck})^{0.7} \quad (8)$$

Where:

$f_{ck}$: Concrete compressive strength (MPa)

$G_{fo}$: Base value for fracture energy (N.mm/mm$^2$) and depends on maximum aggregate size as shown in table 1.

Table 1 Base Values for fracture energy (CEB-FIP, 1993) [9]

| MAXIMUM AGGREGATE SIZE $d_{max}$ (mm) | FRACTURE ENERGY $G_{fo}$ (N.mm/mm$^2$) |
|---|---|
| *8* | 0.025 |
| *16* | 0.030 |
| *32* | 0.058 |

**Reinforcement**

Reinforcement is considered elastic-perfectly plastic behavior identical in tension and compression as shown in figure (3).

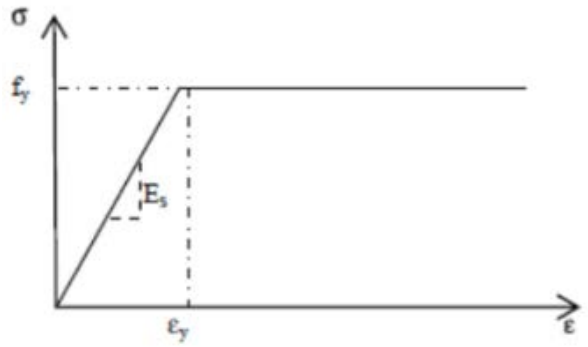


Figure 3 Stress –Strain behavior for steel reinforcement

**FRP**

FRP is modelled as a linear elastic isotropic material till failure. Although FRP is an orthotropic material yet since the composite is mainly stressed in fibre direction, thus the modulus in fibre direction is more important.

## FINITE ELEMENT MODELLING

Simulation for R.C and FRP is done with C3D4 mesh elements emphasized in Figure 4a. Also it should be noticed that concrete is modeled using concrete damaged plasticity model. Reinforcement steel is modeled as wire elements of mesh element type T3D2 as shown in Figure4b. The interaction between R.C. and reinforcement is achieved using the embedded element constraint. Perfect bond is assumed between Concrete and FRP since failure in such strengthening schemes is usually due to concrete cover separation (Lundqvist et al., 2005) [10]. Regarding numerical analysis, three-dimensional nonlinear analysis has been carried out using Newton's method (Simulia, 2011) [11].

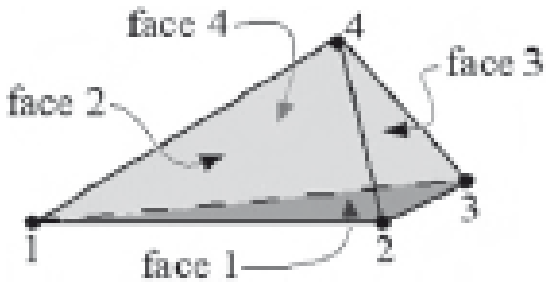


Figure 4a. 4-node linear tetrahedral element [11]

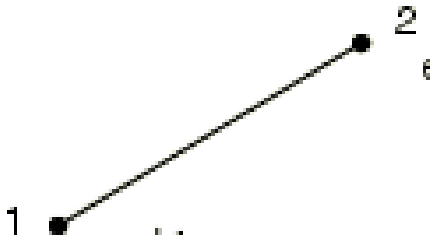


Figure 4b. 2-node linear displacement truss elements[11]

## EXPERIMENTAL DATA USED FOR MODEL VERIFICATION

Experimental data used for model verification were obtained from specimens used in the experimental procedure performed by (Morsy et al, 2011) [6]. That research to study the feasibility of strengthening RC beams in shear using FRP reinforcement internally embedded in holes drilled through the depth of the beam. Five similar beams were tested in this program, a control beam without strengthening, and three beams strengthened using externally bonded CFRP sheets, NSM CFRP strips and embedded CFRP and GFRP rods, where design for such specimens ensures shear failure at weak side. Five reinforced concrete beams were tested in this program.

The specimens had a cross section of 160 mm x 300 mm, and a total length of 2.40 meters. The specimens were designed to fail in shear at one side (The weak side). For flexure reinforcement, four 22 mm deformed bars arranged in two layers were used as bottom reinforcement, while two 22 mm deformed bars were used as top reinforcement. The shear reinforcement for the strong side consisted of 10 mm stirrups spaced at 50 mm, while the shear reinforcement for the weak side consisted of 6 mm bars with a spacing of 150 mm, as shown in Figure 5a – 5b.

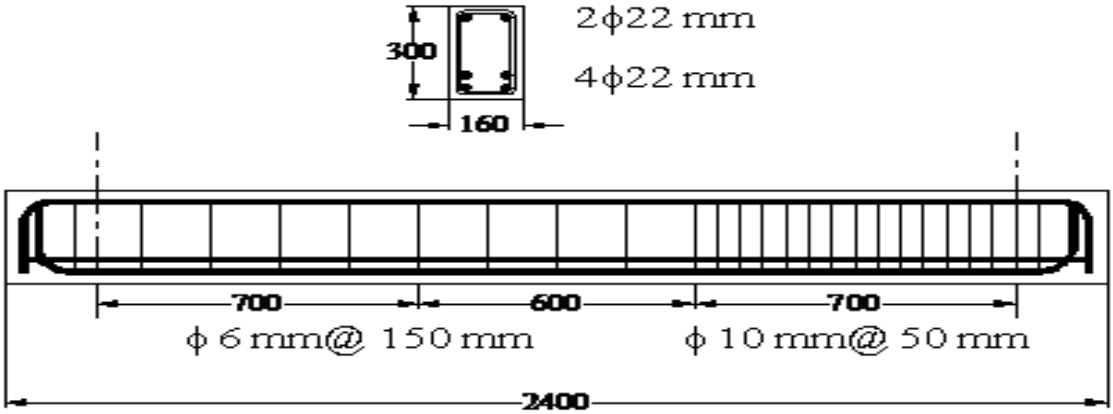


Figure 5a Geometry and arrangement of reinforcement for control specimen (Morsy et al, 2011) [6]

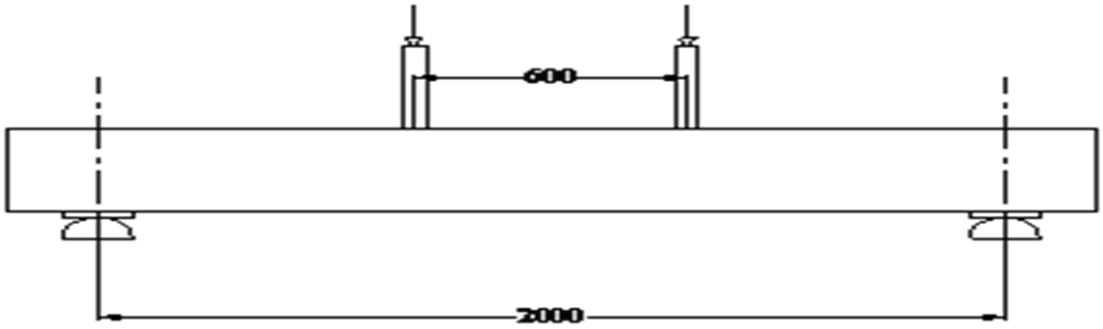


Figure 5.b. Boundary conditions for control specimen (Morsy et al, 2011) [6]

Table 2 provides a summary of the details of the specimens used in that program.

Table 2 Strengthening schemes for specimens examined by (Morsy et al, 2011) [6]

| SPECIMEN | STRENGTHENING TECHNIQUE | STRENGTHENING MATERIAL | MATERIAL DIMENSIONS | SPACING |
|---|---|---|---|---|
| *CB* | None | - | - | - |
| *NSM** | Near surface mounted laminates | CFRP | 1.2 * 15 mm strips | 75 mm |
| *IER*[*] | Internally embedded reinforcement | CFRP | 12 mm bars | 150 mm |
| *EB*[*] | Externally bonded sheets | CFRP | 60 mm sheets | 150 mm |

*Strengthening is only in the weak side along 700mm span.

Table 3 gives full material properties values for the tested specimen.

Table 3 Material properties for tested specimen (Morsy et al, 2011) [6]

| MATERIAL | PROPERTY | VALUE |
|---|---|---|
| General Reinforcement Properties | Modulus of Elasticity | 210000 MPa |
| | Poisson ratio * | 0.3 |
| | Density, t/mm$^3$* | 7850 kg/m$^3$ |
| High Tensile Steel | | |
| *22 mm bars* | Yeild Stress | 360 MPa |
| *10 mm bars* | Yeild Stress | 360 MPa |
| Ordinary Mild Steel | | |
| *6 mm bars* | Yeild Stress | 240 MPa |
| Concrete | Characteristic Strength | 20 MPa |
| | Density* | 2500kg /m$^3$ |
| | Poisson ratio * | 0.2 |
| | Fracture Energy ** | 0.0898 Nmm/mm$^2$ |
| | Modulus of elasticity ** | 25122 MPa |
| | Tensile Strength** | 1.898 MPa |
| *FRP* | Modulus of Elasticity | 165000 MPa |
| | Density, t/mm$^3$ | 1.6 e-9 t/mm$^3$ |
| | Poisson ratio | 0.3 |

* Assumed values as the values for density and Poisson ratio were not specified in the original procedure.

** Material Properties obtained from material models discussed throughout the analytical procedure.

## MODEL VERIFICATION

### Load Displacement Curves

It is noticed that all load- mid span displacement curves obtained from F.E. analysis compared with experimental results could give a good correlation and could capture the experimental behavior for all beams.

Figure (6) shows the load versus mid span displacement curve for control un strengthened specimen (CB) for both finite element and experimental results, it is clearly noticed that the F.E. modeled beam has more stiffness than experimented beam despite of it sustain nearly the same carrying loading capacity it could be related to the perfect bond assumed between reinforcing steel and concrete in the F.E. model and due to excessive free body motion during performing the experimental procedure

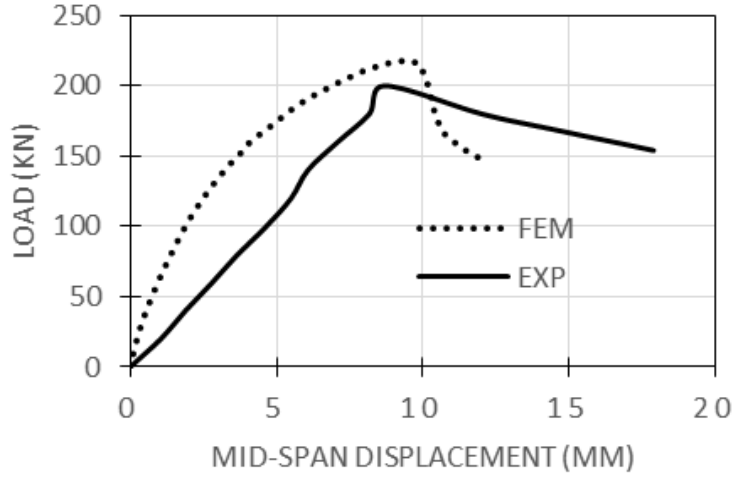


Figure 6 Load – Displacement curve for control specimen CB for both finite element and experimental results.

Figure (7) shows the load versus mid span displacement curve for specimen strengthened using NSM technique for both finite element and experimental results. Also the F.E. modeled beams predict a stiffer behavior than experimentally one, moreover the F.E model could predict the descending curve of the specimen till failure for all specimens which could not be noticed in experimented specimens due to loading conditions.

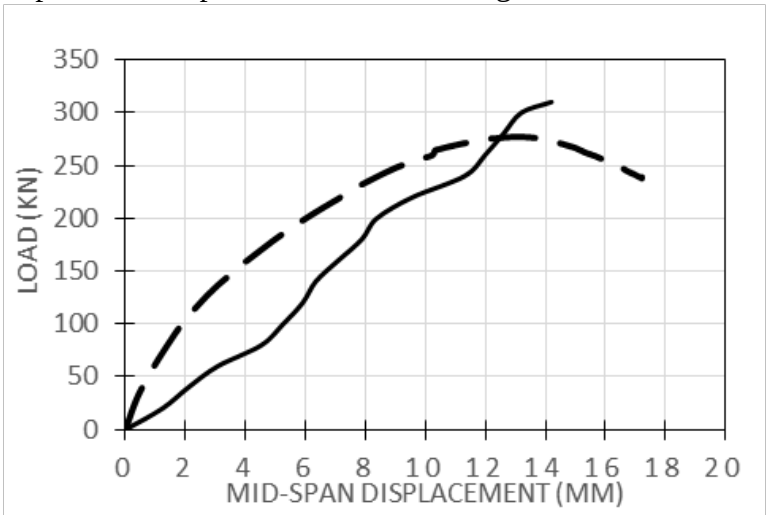


Figure 7 Load – Displacement curve for strengthened specimen using NSM technique for both finite element and experimental results

Figure (8) shows the load versus displacement curve for strengthened specimen using E.B. technique for both finite element and experimental results it is noticed that F.E. model capture the behavior of the experimented beam moreover regarding the load carrying capacity it is noticed that the results are in agreement, where the variation in load carrying capacity is about ±6%.

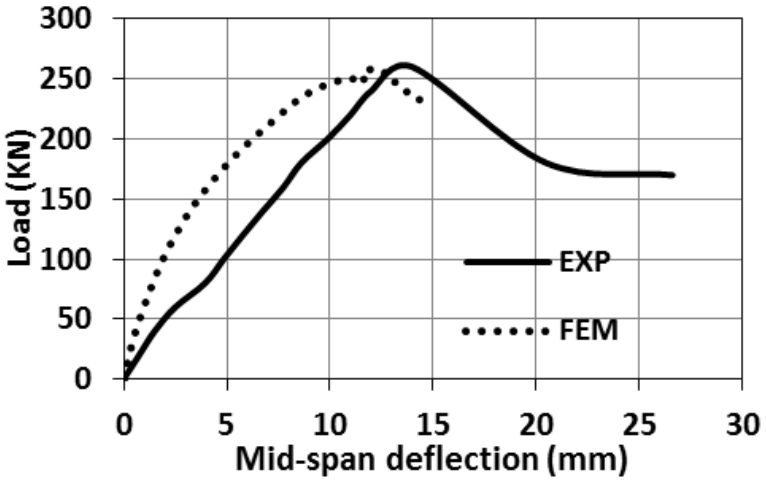


Figure 8 Load – Displacement curve for strengthened specimen using E.B. technique for both finite element and experimental results

Figure (9) shows the load versus displacement curve for strengthened specimen using I.E.R. technique for both finite element and experimental results, the F.E. model predict both elastic and plastic portions of the beam perfectly however the stiffness of the analytical results is also more than that of experimentally results.

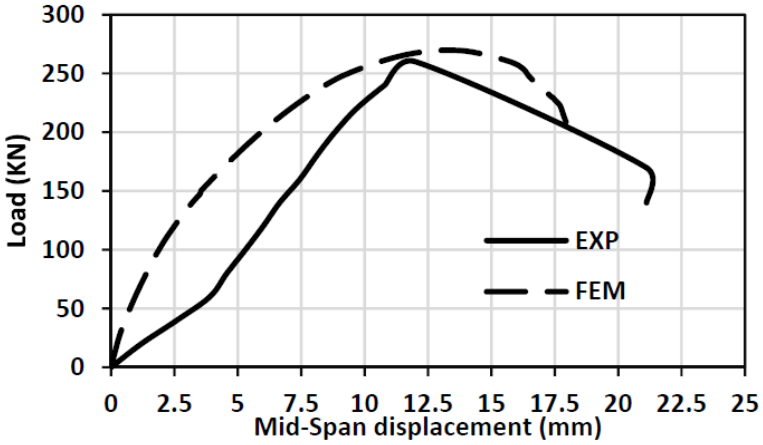


Figure 9 Load – Displacement curve strengthened for specimen using I.E.R. technique for both finite element and experimental results

**Load versus Strain Curves**

The F.E. model also predicts the load versus concrete strain at the position of crack initiation curve as shown in Figure (10) the load versus strain curve for concrete control specimen (CB) at crack location, the model predict the concrete strain till failure better than the experimental results which could not detect the concrete strain till failure due to rupture in strain gauge.

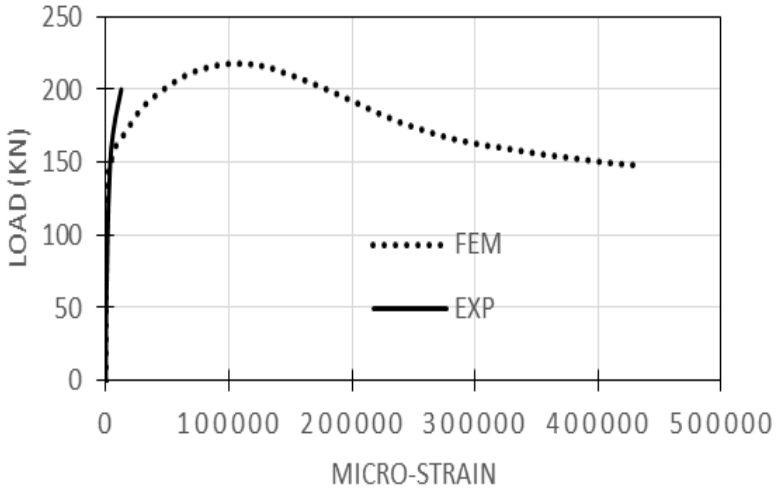


Figure 10 Load – Strain curve for concrete control specimen CB at crack location.

Figures 11, 12, and 13 show the load versus strain at mid-span of lower reinforcement curve for control un-strengthened specimen (CB), specimen strengthened using I.E.R. technique, and specimen strengthened using E.B. technique respectively, it could be concluded that the F.E. model could predict also the reinforcement strain efficiently and both F.E. analysis and experimentally curves almost coincide on each other till failure.

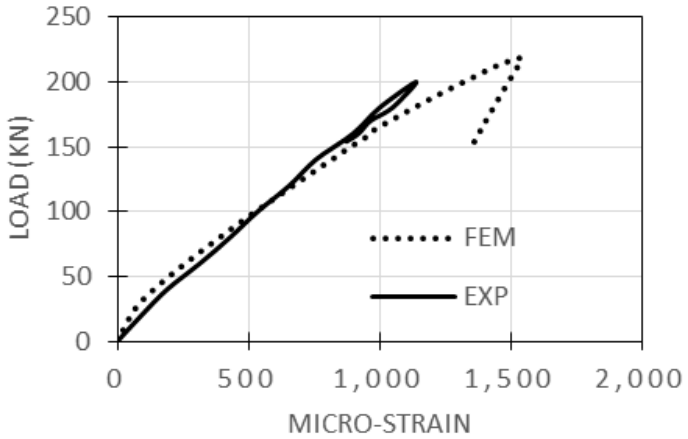


Figure 11 Load – Strain curve for mid-span of lower reinforcement for control un strengthened specimen CB

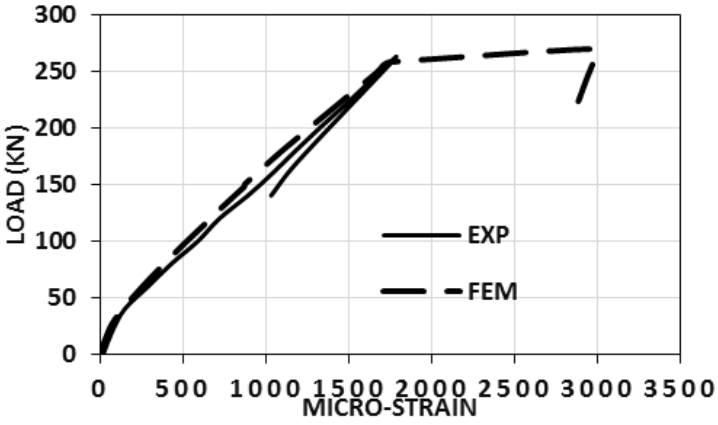


Figure 12 Load – Strain curve for lower reinforcement for specimen strengthened using I.E.R. technique

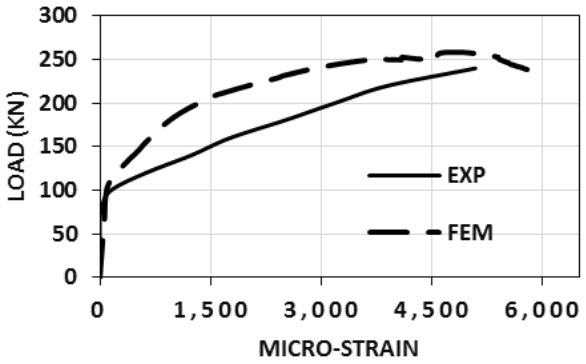


Figure 13 Load – Strain curve for lower reinforcement for specimen strengthened using E.B. technique

Moreover the F.E. model also predict the strain at the vertical part of second stirrup after the support for specimen strengthened using NSM technique efficiently which indicates that the model can capture the behavior of the whole structural element accurately as shown in Figure 14.

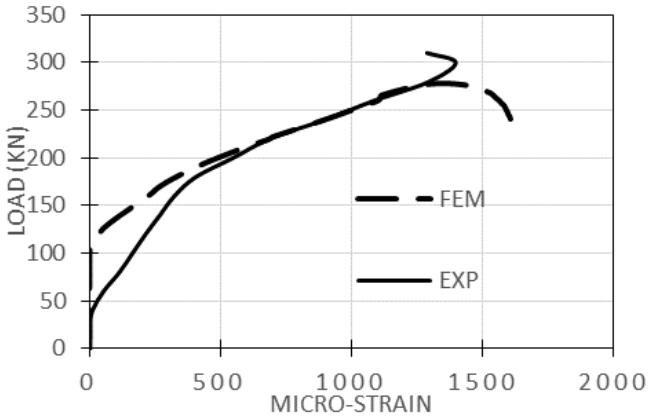


Figure 14 Load – Strain curve for vertical part of second stirrup after the support for specimen strengthened using NSM technique

**Cracking Pattern**

The concrete damaged plasticity model in ABAQUS does not have a notation for cracks, however, it is assumed that cracking initiates at the points where the maximum principal plastic strain is positive. The direction of the vector normal to the crack plane is assumed to be parallel to the direction of the maximum principal plastic strain. Cracking patterns as well as direction of the vector normal to the cracking plane are in shown in Figure (15) which shows the shear failure for control un strengthened specimen (CB) examined experimentally and Figure (16) which shows cracking pattern obtained from FEM for same specimen. Upon Comparing FEM to actual cracking patterns obtained from experimental results**.** It is noted that the FEM cracking pattern is in good agreement with experimental results which indicates that the FEM can capture the fracture mechanism accurately.

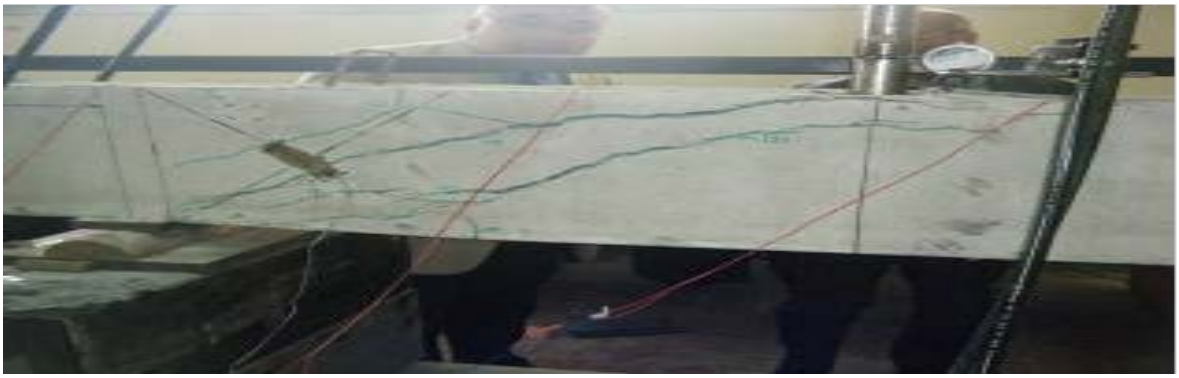

Figure 15 Shear failure for control unstrengthened specimen (CB)

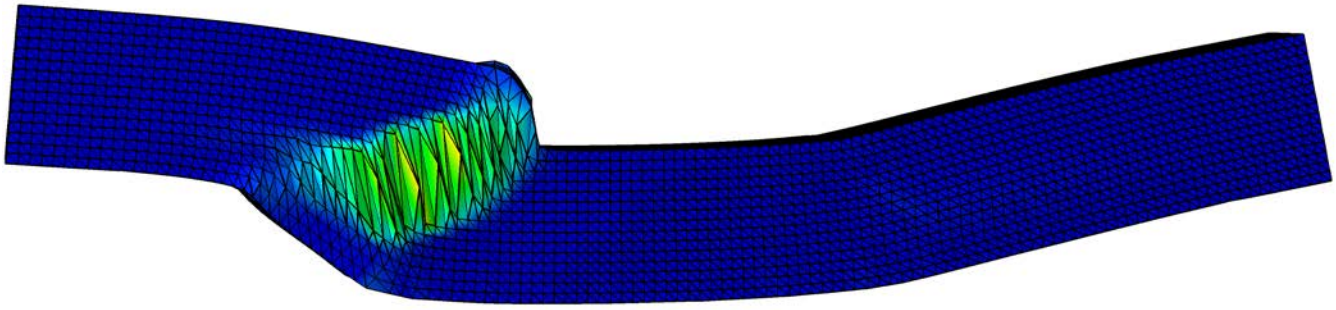

Figure 16 Cracking pattern obtained from FEM for control un strengthened specimen (CB)

**Stress Distribution**

F.E. analysis gives the stress distribution for experimented specimens by (Morsy et al, 2011)[6] as shown in Figure (17), and (18) for un strengthened specimen (CB) and for specimen strengthened using NSM technique respectively. Upon comparing stress distribution diagrams for both experimented specimens with FEM it could be found that both control beam CB and strengthened specimen using NSM technique have a variation in stress distribution in the non-strengthened region is noted which indicates that FRP strengthening has a global effect on the structural element and is not local to the strengthened region only.

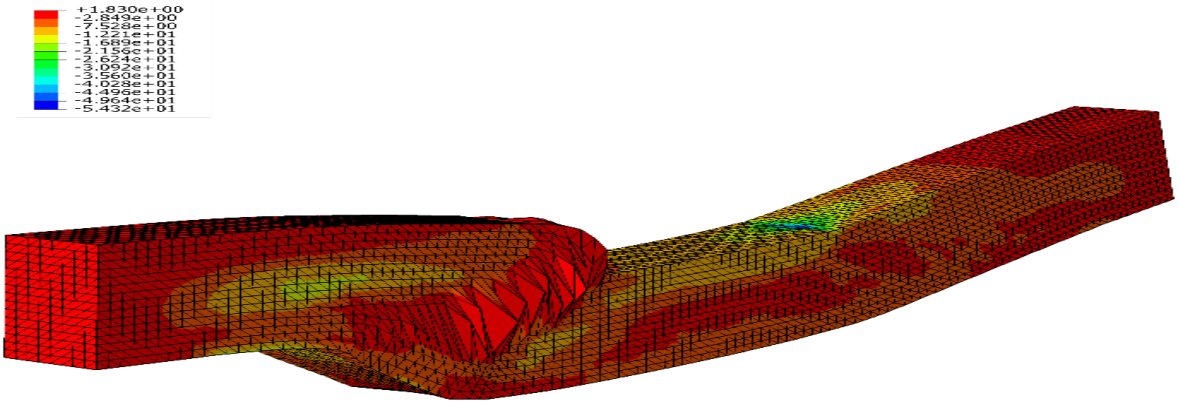


Figure 17 Stress distribution obtained from FEM for control specimen CB

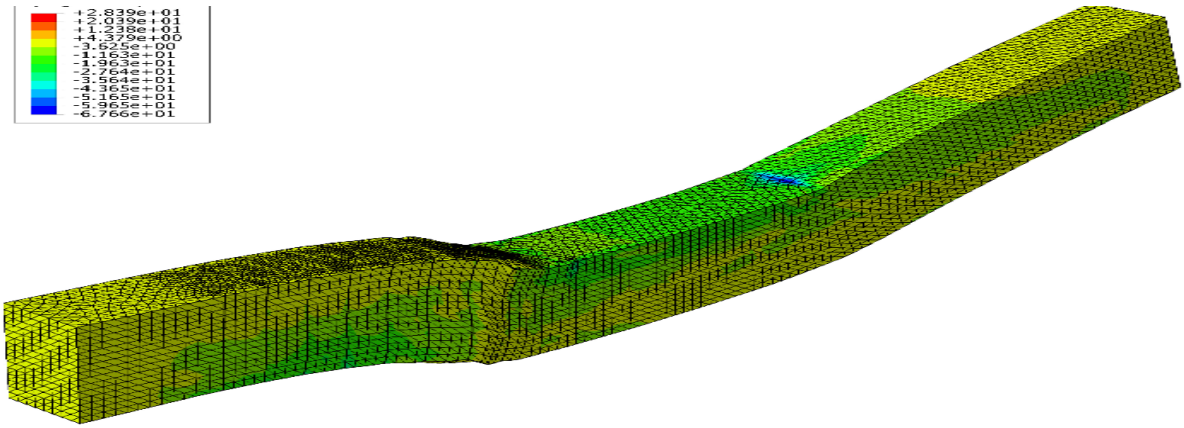

Figure 18 Stress distribution from FEM for specimen strengthened using NSM technique

## PARAMETRIC STUDY

After confirming and verifying that the FEM is suitable and valid for modeling the RC beams shear strengthened with FRP; a parametric study is carried out in order to study the effect of various strengthening parameters on the beam behavior. A parametric study is carried out on specimens experimentally examined by (Morsy et al, 2011) [6] as follows:

### Specimens strengthened by CFRP laminates using near surface mounted (NSM) technique

This research compare the effect of varying the width of CFRP laminate which embedded vertically through the concrete cover (specimens NSM-W1, NSM-W2 and NSM-W3 are modeled with laminate width 10 mm, 20 mm and 25 mm respectively) noticed that the concrete cover in that specimens was 25mm which means that NSM-W3 which represent 25 mm of CFRP laminate fully embedded through concrete cover. Moreover comparing the effect of varying spacing of embedded vertical laminates through concrete cover (specimens NSM-S1, NSM-S2, NSM-S3 and NSM-S4 are modeled with spacing 50 mm, 100 mm, 200 mm and 300 mm respectively).

Finite element analytical results for load versus mid span deflection curve for specimen strengthened with NSM upon varying laminate width and the experimental control specimen have been illustrated in figure 19. It is clearly shown that changing the FRP laminate width had a very slight effect on the carrying loading capacity of the beam however it could slightly enhance the ultimate deflection of the beam. Also it is noticed that there is not any changes in the beam stiffness.

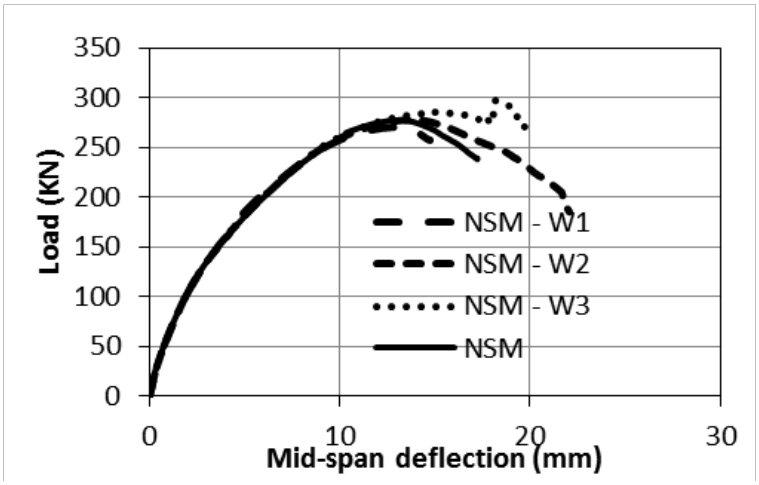


Figure 19 Load-displacement curves for NSM specimens upon varying laminate Width

Figure 20 shows the ratio between analytical ultimate loads of modeled specimens with ultimate load of control un strengthened beam versus the ratio between laminate width with the strengthened shear span length for various laminate width for NSM specimen. It is clearly shown that the NSM technique enhancing the load capacity of the strengthened beams about 20% for laminate width 10 mm till 40% for laminate width 25 mm over the control un strengthened beams.

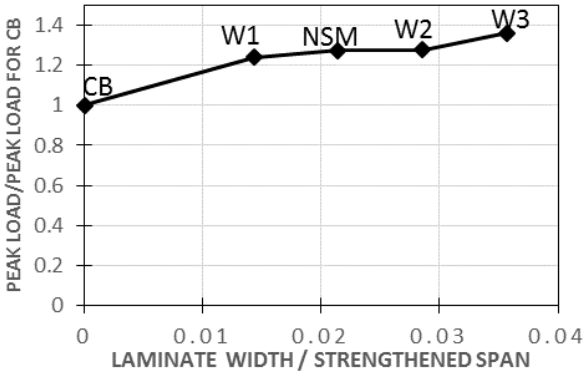


Figure 20 Ratio between ultimate load of specimen with ultimate load of control unstrengthned beam versus the ratio between laminate width with the strengthened shear span length for various laminate width for NSM specimen

Figure 21 shows finite element analytical results for load versus mid span deflection curve for specimen strengthened with NSM upon varying laminate spacing and the experimental control specimen. It is clearly shown that increasing the FRP laminate spacing decrease the carrying loading capacity of and ductility of the beam.

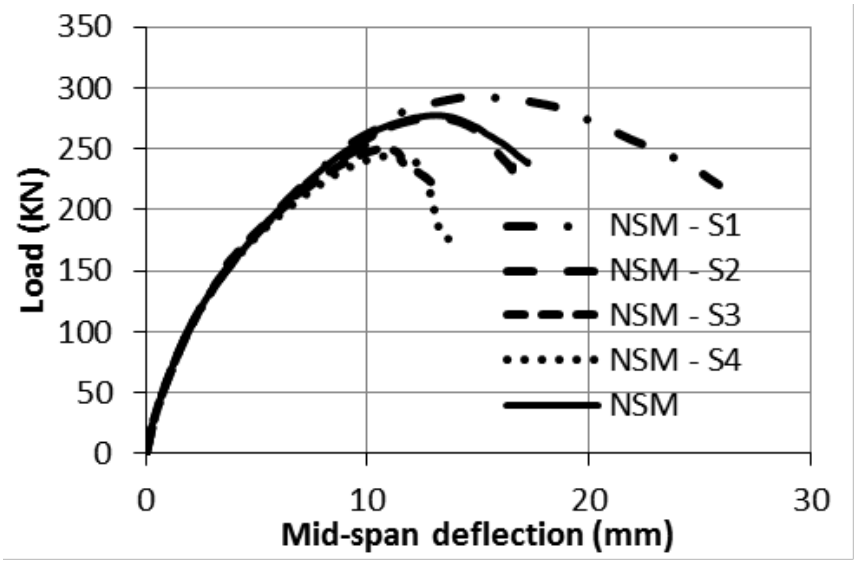


Figure 21 Load-displacement curves for NSM specimens upon varying laminate spacing

Figure 22 shows the ratio between analytical ultimate loads with ultimate load of control un strengthened beam versus the ratio between laminate spacing with the strengthened shear span length for various laminate width for NSM specimen. It is clearly shown decreasing the spacing have great effect on increasing the carrying load capacity of beam, the maximum increase in beam load capacity is about 30% for spacing 50mm till reach 10% when spacing increased to 300mm.

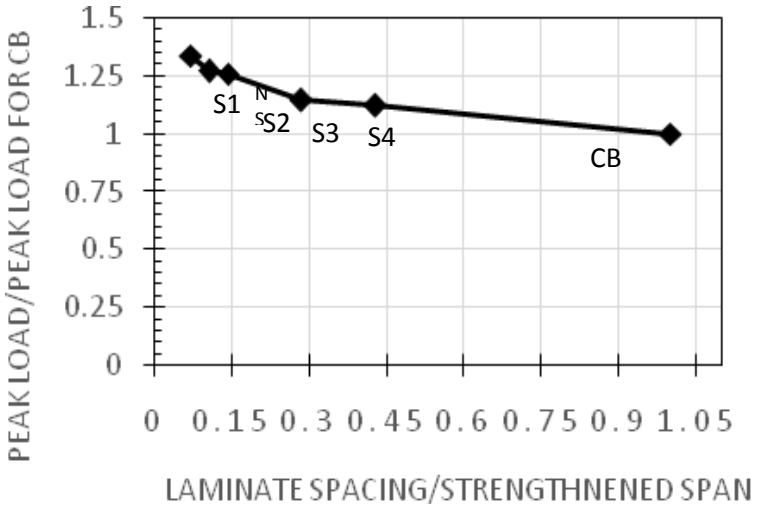


Figure 22 Ratio between ultimate load of specimen with ultimate load of control un strengthened beam versus the ratio between laminate spacing with the strengthened shear span length for various laminate width for NSM specimen

**Specimens strengthened with internally embedded reinforcement CFRP rods (IER) technique**

Comparing effect of varying the spacing between embedded CFRP bars (specimens IER-S1, IER-S2, IER-S3 and IER-S3 are modeled with rod spacing 50m, 100 mm, 200 mm and 300mm respectively). Figure 23 shows finite element analytical results for load versus mid span deflection curve for specimen strengthened with IER upon varying rods spacing and the experimental control specimen. It is clearly shown that increasing the FRP rods spacing decrease the carrying loading capacity of and ductility of the beam.

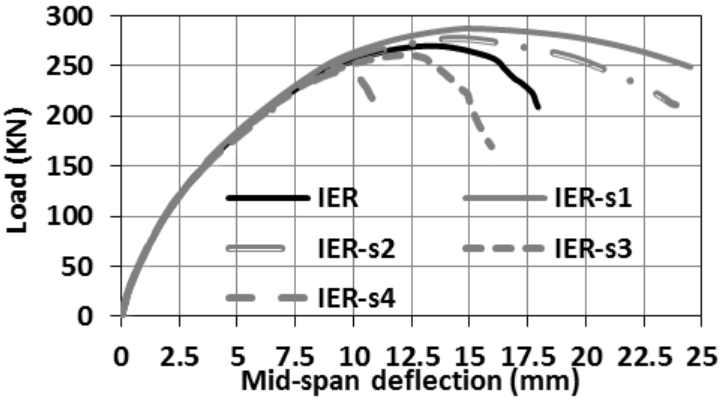


Figure 23 Load versus mid span deflection curve for specimen strengthened with IER upon varying rods spacing

Figure 24 shows the ratio between analytical ultimate loads with ultimate load of control un strengthened beam versus the ratio between rods spacing with the strengthened shear span length for various laminate width for IER specimen. It is clearly shown decreasing the spacing have great effect on increasing the carrying load capacity of beam, the maximum increase in beam load capacity is about 30% for spacing 50mm till reach 20% when spacing increased to 300mm.

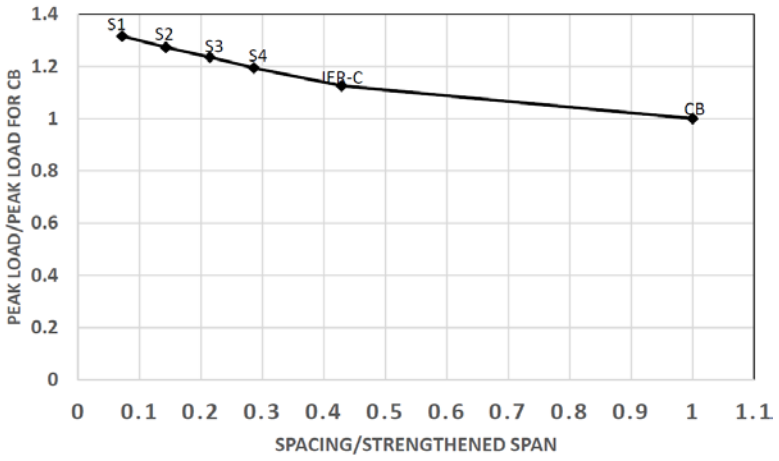


Figure 24 Peak load and rod spacing for specimen IER

**Specimens strengthened with CFRP sheets for externally bonded sheets (EB) technique**

Comparing effect of varying width of CFRP sheets (specimens EB-b1, EB-b2, EB-b3 and EB-b3 are modeled with sheet width 30mm, 90 mm, 120 mm and 700mm respectively). Figure 25 shows finite element analytical results for load versus mid span deflection curve for specimen strengthened with EB upon varying sheets width and the experimental control specimen. It is clearly shown that increasing the FRP sheets width increasing the carrying loading capacity of and ductility of the beam.

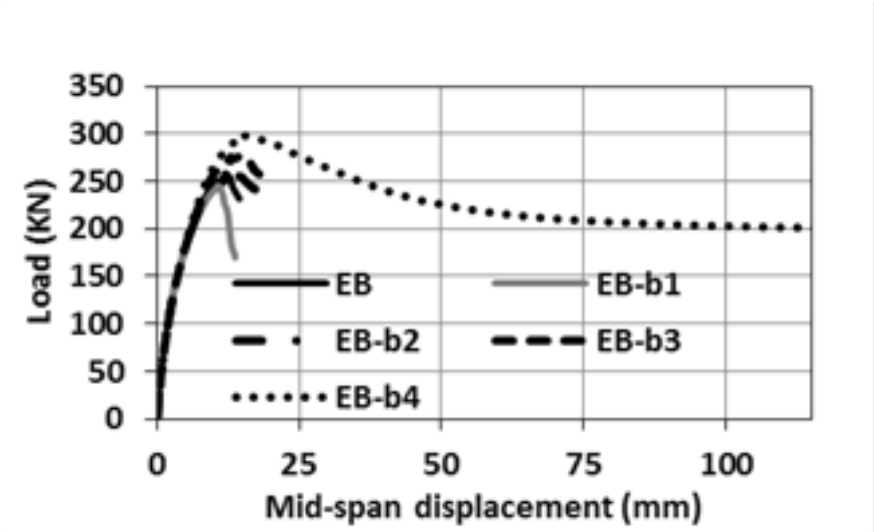


Figure 25 Load-displacement curve for specimen EB upon varying sheet width

Figure 26 shows the ratio between analytical ultimate loads with ultimate load of control un strengthened beam versus the ratio between sheets width with the strengthened shear span length for various sheets width for EB specimen.

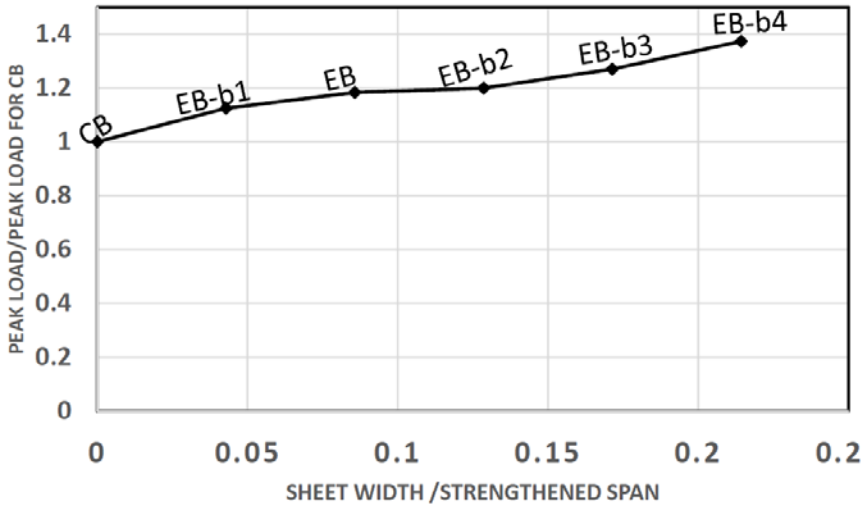


Figure 26 analytical ultimate loads with ultimate load of control un strengthened beam versus the ratio between sheets width with the strengthened shear span length for various sheets width for EB specimen

It is clearly shown increasing the sheets width have effect on increasing the carrying load capacity of beam, the maximum increase in beam load capacity is about 40% for width 700mm till reach 10% when spacing increased to 30mm.

## CONCLUSIONS

A Finite element modelling process is carried out on a number of specimens using the FE software package ABAQUS-CAE 6.11-3 where the behavior of such specimens has been experimentally examined. Finally a parametric study is carried out to study effect of various strengthening parameters on the element behavior. Upon examining the FEM results the following conclusions are drawn:

1. Upon comparing the load-displacement curve, load-strain curve as well as the cracking pattern obtained from FEM with those obtained from experimental procedure only a slight deviation is noticed which indicates that the FEM model can properly capture the fracture mechanism.
2. Upon comparing the stress distribution for strengthened specimen NSM and un-strengthened specimen CB examined by (Morsy et al, 2011) [6] a variation in the stress distribution in the un-strengthened region is noticed which indicates that the strengthening process has a global effect and is not local to the strengthened region.
3. Regarding specimen NSM, the parametric study carried out to study the effect of laminate spacing as well as laminate width on beam behavior indicate an increase ductility and increased load carrying capacity upon decreasing laminate spacing and vice versa. Also increasing laminate width is accompanied by increased load carrying capacity and increased ductility and vice versa.
4. Regarding specimen IER, the parametric study carried out to study the effect of rod spacing on beam behavior indicate an increase ductility and increased load carrying capacity upon decreasing rod spacing and vice versa.
5. Regarding specimen EB, the parametric study carried out to study the effect of sheet width on beam behavior indicate an increased ductility and increased load carrying capacity upon increasing sheet width and vice versa.

## REFERENCES

1. ACI Committee 318. 1999. Building Code Requirements for Structural Concrete and Commentary (ACI 318-99). American Concrete Institute Detroit, MI.

2. ASHOUR, AF, EL-REFAIE, SA & GARRITY, SW. 2004. Flexural strengthening of RC continuous beams using CFRP laminates. Cement & Concrete Composites; 26: 765- 775.

3. ESFAHANI, M., KIANOUSH, M., & TAJARI. 2007. A. Flexural behaviour of reinforced concrete beams strengthened by CFRP sheets. Engineering Structures; 29: 2428-2444.

4. ALAA M. MORSY, ET AL “Bonding techniques for flexural strengthening of RC beams using CFRP laminates”, Ain Shams Engineering Journal, Elsevier, Volume 4, issue 3, page, 369-374

5. OBAIDAT, Y. T., HEYDEN, S., DAHLBLOM, O., ABU-FARSAKH, G. & ABD ELGAWAD, Y. 2011. “Retrofitting of reinforced concrete beams using composite laminates”. Construction and Building Materials, 25, 591-597.

6. ALAA M. MORSY., ET AL.2011 “A Comparative Study for Shear Strengthening Techniques of Reinforced Concrete Beams Using FRP”. Fourth international conference on concrete repair with cooperation by technical university Dresden. Germany.

7. HSU, L.S., & HSU, C.-T.T. (1994). Complete stress-strain behavior of high-strength concrete under compression. Magazine of Concrete Research, 46(169), 301-312..

8. HILLERBORG, A.1985. The theoretical basis of a method to determine the fracture energy $G_f$ of concrete. Materials and Structures, RILEM 50-FMC, 108, pp 291-296.

9. D. GORINEVSKY, S. BOYD, G. STEIN, Optimization-based tuning of Beton, C. E.-I. (1993), CEB-FIP Model Code 1990 (CEB-FIP MC90), Bulletin D'Information, No.215, Lausanne.

10. LUBLINER J, OLIVER J, OLLER S, ONATE E. 1989.A plastic-damage model for concrete. Int J Solids Struct, 25:299–329.

11. DASSAULT SYSTÈMES SIMULIA CORP. ABAQUS Theory manual, User manual, Analysis manual and Example Manual, Version 6.11. Providence, RI; 02909–2499.numerical simulation of various engineering applications.

# Theme 6

# Advances in Structural Modelling

**Keynote Paper**

# CONTROL OF CRACKING CAUSED BY RESTRAINT TO EARLY-AGE DEFORMATION

**I Gilbert**
University of New South Wales
Australia

**ABSTRACT.** Cracks occur in reinforced concrete structures wherever and whenever the tensile stress in the concrete reaches the tensile strength of the concrete. After concrete sets and hardens, tensile stress at any location may be caused by factors such as early-age heat of hydration, applied loads, restrained shrinkage, temperature changes, settlement of the supports and so on. This paper deals with the control of cracking caused by restraint to early-age cooling and shrinkage of concrete. Such cracking is inevitable in many situations and a significant amount of reinforcement crossing each crack is required for crack control. Rational procedures are proposed for determining the degree of restraint and the amount of reinforcement required for the control of cracking. Restraining forces and concrete tensile stresses caused by temperature and shrinkage strains in a variety of situations have been considered, including concrete members subjected to temperature and/or shrinkage differentials, reinforced concrete members containing embedded reinforcement, and reinforced concrete slabs and walls subjected to end-restraint and edge-restraint. Calculation of the width and spacing of cracks caused by any one, or any combination, of these restraining forces is outlined and illustrated by a worked example.

**Keywords:** Cracking, Heat of hydration, Shrinkage, Reinforced concrete, Restraint.

**I Gilbert** is Emeritus Professor of Civil Engineering in the School of Civil and Environmental Engineering at UNSW Australia. He is Deputy Director of the UNSW Centre for Infrastructure Engineering and Safety.

## INTRODUCTION

In many situations, cracking in reinforced concrete structures is inevitable. Cracks occur wherever and whenever the tensile stress in the concrete reaches the tensile strength of the concrete. After the concrete sets and hardens, tensile stress at any location may be caused by many different factors, including early-age heat of hydration, applied loads, restrained shrinkage, temperature changes, settlement of supports and so on. Cracks caused by the internal actions resulting from applied loads are often called *structural cracks*, while cracks caused by restraint to load-independent deformation, including deformations due early-age cooling, shrinkage or ambient temperature changes, are termed *intrinsic cracks*. Often cracks are initiated by a combination of causes. For example, the bending moment at which cracking occurs in a beam or slab may be significantly reduced if tensile stresses caused by restraint to early-age temperature contractions and shrinkage have developed in the member before loading. Shrinkage induced deformation also cause significant increases in crack widths with time.

Many variables influence the width and spacing of cracks, including the magnitude and duration of loading, the quantity, orientation and distribution of the reinforcement crossing the crack, the cover to the reinforcement, the bond characteristics of the reinforcement, the deformational properties of the concrete (including its creep and shrinkage characteristics) and the size of the member. Considerable variations exist in the crack width from crack to crack and in the spacing between adjacent cracks, because of random variations in the properties of the in-situ concrete.

Control of cracking in concrete structures is often achieved by limiting the stress in the bonded reinforcement at the cracked section to some appropriately low value and ensuring that the bonded reinforcement is suitably distributed within the tensile zone. Building codes usually specify the maximum bar spacing for bonded reinforcement and the maximum concrete cover. Some codes specify deterministic procedures for calculating crack widths, with the intention to control cracking by limiting the calculated crack width to some appropriately low value. However, the influence of shrinkage on crack widths is not properly considered in the major building codes and is therefore often not adequately considered in structural design. As a consequence, excessively wide cracks are a relatively common problem for many reinforced concrete structures throughout the world.

This paper deals with the control of intrinsic cracking caused by restraint to early-age cooling and shrinkage of concrete. Rational procedures are proposed for determining the effect of restraint and the development of tensile stresses in the concrete. Guidance is also provided for estimating the maximum width and spacing of cracks in a variety of situations

## EARLY-AGE THERMAL AND SHRINKAGE INDUCED STRESSES AND STRAINS

Heat of hydration in a concrete element in the first day or so after casting rises to a peak value and then dissipates. The peak temperature $T_{peak}$ depends on the cement content, the thickness of the concrete element and the placement temperature. As the concrete element cools, restraint to the early-age contraction may cause cracking in the immature concrete. In many situations, early-age thermal cracking cannot be avoided, but it can be controlled by avoiding excessive heat of hydration, reducing restraint where possible and using an adequate quantity and distribution of reinforcement crossing the cracks.

In concrete elements, calculation of the tensile stresses that initiate cracking is complicated by the changing elastic modulus of the young concrete and the relaxation of stress resulting from tensile creep of the concrete. The change in temperature with time due to heat of hydration in a restrained concrete element is $\Delta T = \pm(T - T_a)$, where $T$ is the temperature at any time and $T_a$ is the mean ambient temperature. $\Delta T$ is taken to be positive for a rise in temperature and negative for a drop in temperature. The corresponding free temperature strain is $\varepsilon_T = \alpha_c \Delta T$, where $\alpha_c$ is the coefficient of thermal expansion for concrete. The actual strain $\varepsilon_{actual}$ measured at a point in the member is significantly different from $\varepsilon_T$ and the difference $\varepsilon_{.r} = (\varepsilon_{actual} - \varepsilon_T)$ is the stress related strain resulting from restraint and consists of elastic and creep strains.

After the temperature has dropped from $T_{peak}$ to $T_a$ at time $t_a$ (i.e. $\Delta T_{max} = T_a - T_{peak}$), the tensile restrained strain due to temperature $\varepsilon_{r.\Delta T}$ is $-\alpha_c \Delta T_{max} R$ where $R$ is a restraint factor that depends on the thickness of the concrete element, the shape of the temperature differential across the member and the restraint provided by embedded reinforcement and by adjacent members and supports (i.e. the external boundary conditions). Determination of the restraint factor $R$ is discussed subsequently.

In the design for early-age crack control, along with the temperature induced strain, it is prudent to include the autogenous shrinkage strain $\varepsilon_{cse}$ and any drying shrinkage strain $\varepsilon_{csd}$ that will have developed at time $t_a$, so that the total restrained strain at time $t_a$ is given by:

$$\varepsilon_r = -(\alpha_c \Delta T_{max} + \varepsilon_{cs}) R \tag{1}$$

remembering that the shrinkage strain $\varepsilon_{cs}$ (= $\varepsilon_{cse}+\varepsilon_{csd}$) is contraction (negative) and so too is $\alpha_c \Delta T_{max}$. Bamforth [1] suggested that for the assessment of early-age cracking, the autogenous shrinkage at age 3 days should be considered.

The stress induced by the restraint to early thermal strains is initially compressive during heating, but due to the low elastic modulus and the high creep strains in the first few hours after initial set when the temperature is rising, the compressive stresses are relatively small. The stress becomes tensile as the concrete cools. Creep also relieves the tensile stress caused by cooling. Provided cracking has not occurred, the restrained strain in Eq. 1 can be expressed in terms of the tensile stress ($\sigma_r$) at time $t_a$ as

$$\varepsilon_r = \varepsilon_{elastic} + \varepsilon_{creep} = (\sigma_r / E_c) + \chi \varphi (\sigma_r / E_c) \tag{2}$$

where $\varphi$ is the tensile creep coefficient associated with the heat of hydration time period and $\chi$ is an aging coefficient to account for the fact that $\sigma_r$ is gradually applied to the concrete. Before cracking, the stress caused by restraint $\sigma_r$ may therefore be determined from the restrained strain (given by Eq. 1) using:

$$\sigma_r = \varepsilon_r \, \overline{E}_e \tag{3}$$

where $\overline{E}_e$ is the age-adjusted effective modulus of the concrete given by:

$$\overline{E}_e = E_c / (1 + \chi \varphi) \tag{4}$$

If cracking occurs, part of the average restrained strain (measured over a gauge length greater than the crack spacing) is relieved by the crack formation. This portion of the restrained strain is termed the *crack-induced strain* $\varepsilon_{r.cr}$ and is important for the calculation of crack widths. The restrained stress at the crack is zero and the average tensile stress between the cracks is now:

$$\sigma_r = (\varepsilon_r - \varepsilon_{r.cr})\overline{E}_e \tag{5}$$

Bamforth [2] suggested that over the early age thermal cycle, creep reduces the stress by about 35%, while others have suggested that the reduction of stress due to creep is up to 50%. Taking $\chi\varphi$ =0.65 in Eq. 4 corresponds to reduction in stress of about 40% due to creep and is recommended here for the assessment of early age cracking at $t_a$ = 3 days.

To avoid early-age thermal and shrinkage cracking, the tensile stress induced by restraint $\sigma_r$ (Eq. 3) must be less than the mean tensile strength of the concrete at time $t_a$, $f_{ctm}(t_a)$, which may be assumed to be 0.5 $f_{ctm}(28)$ at $t_a$ = 3 days, where $f_{ctm}(28)$ is the mean tensile strength of the concrete at age 28 days. Even if early-age thermal cracking does not occur, the stress $\sigma_r$ should not be ignored. Additional stresses caused by restraint to subsequent shrinkage strains (both autogenous and drying shrinkage) may increase the tensile restraining stress to the tensile strength of the concrete and cause cracking. The design process for the control of cracking is the same, whether the tensile stress that causes cracking is caused by restraint to early-age temperature change or restraint to subsequent shrinkage, and the control of such cracking requires an adequate quantity and distribution of steel reinforcement.

## RESTRAINT FACTORS

### Internal Restraint to Early-age Cooling Temperature Differentials

During hydration soon after setting, the temperature rises to its peak value at the centre of the member, dropping to its minimum value at the surfaces of the member. As the temperature rises and the interior expands to a greater extent than at the surface, the surface is subjected to tensile stresses (due to the restrained tensile strain) and the interior of the member is in compression. These restrained stresses, known as *eigenstresses*, are self-equilibrating. If the temperature differential is high enough, cracking may occur at the concrete surfaces and the restrained stresses drop substantially. Even if cracking does not occur, at these elevated temperatures and at this very early age, the elastic modulus of concrete is low, creep is high and the stresses that develop during heating are rapidly relieved.

As cooling takes place, after the peak temperature has been reached, the interior of the member cools and contracts more than the surface and tension develops at the interior of the member, as shown in Figure 1. The concrete is now a little more mature, with a higher modulus, and the concrete stresses are often sufficiently high to cause interior cracks to develop, as shown. The maximum tensile stress that develops at the interior of the member before cracking is

$$\sigma_r = -\alpha_c \Delta T R \overline{E}_e \tag{6}$$

The restrained strain is calculated ignoring autogenous shrinkage which is uniform through the member thickness and does not contribute to the strain differential. In Eq. 6, $\Delta T$ is negative, as it represents a drop in temperature.

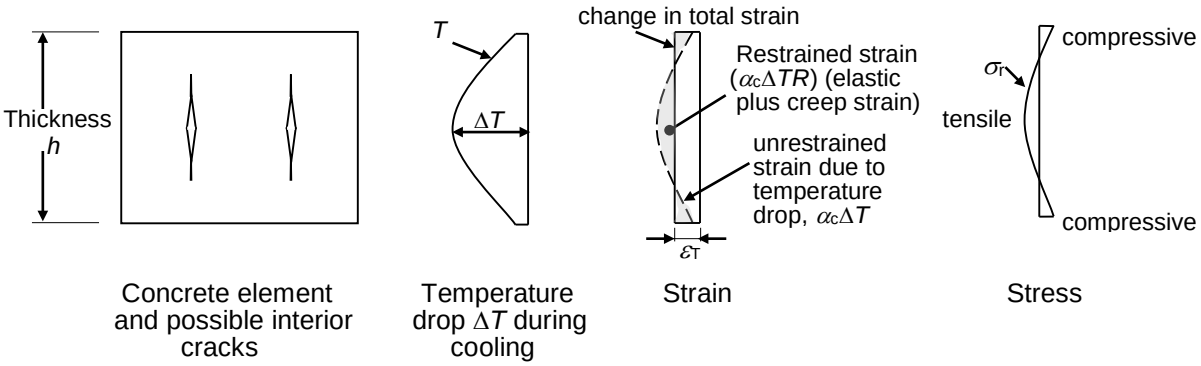


Figure 1 Development of strain, stress and possible cracking due to early-age temperature differentials (cooling)

After cracking, the restrained stress drops, the crack-induced strain $\varepsilon_{r.cr}$ increases and the cracks will open with time due to restrained drying and autogenous shrinkage. Shrinkage may cause the interior cracks and the surface cracks that have developed during the heat of hydration cycle to join, resulting in full depth cracking.

At the interior of the member, where both the temperature drop and the restrained tensile stress is greatest, the restraint factor $R$ is readily determined by simple mechanics and depends on the temperature profile, which in turn depends on the mix characteristics, the member thickness and the environmental conditions. For a parabolic temperature profile, $R = 0.33$. For a triangular temperature gradient, $R = 0.5$. Bamforth [1] recommended that $R$ is taken as 0.42. A value of 0.4 is recommended here.

## Internal Restraint Provided by Embedded Reinforcement

### Symmetrically reinforced sections

Consider the unreinforced and unrestrained concrete member of length $L$ shown in Figure 2a and the symmetrically reinforced concrete member shown in Figure 2b. Except for the inclusion of longitudinal steel reinforcement of area $A_s$ symmetrically placed about the centroid of the cross-section in the second member, the two members are identical.

A gradual compressive strain in the concrete $\varepsilon_{free}$ caused by early age cooling $\varepsilon_T$ (shown in Figure 1) and concrete shrinkage $\varepsilon_{cs}$ would cause the unreinforced member to shorten by an amount $\varepsilon_{free} L = (\varepsilon_T + \varepsilon_{cs})L$, as shown in Figure 2a. If early-age cracking is being considered immediately after the heat of hydration cycle, $\varepsilon_{cs}$ is equal to the autogenous shrinkage at 3 days. If restraint cracking is being investigated at a later time $t$, $\varepsilon_{cs}$ is the sum of the autogenous and drying shrinkage strain components at that time (i.e. $\varepsilon_{cs} = \varepsilon_{cse} + \varepsilon_{csd}$).

The shortening deformation $\varepsilon_{free}$ of the concrete in the reinforced member (Figure 2b), causes a gradual build-up of compression in the bonded reinforcement and this is opposed by an equal and opposite tensile force $\Delta F_t$ applied to the concrete. The gradually increasing tensile force results in tensile elastic strain and tensile creep strain, and the overall shortening of the member is reduced to $(1 - R)\varepsilon_{free} L$ (as shown in Figure 2b), where $R$ is the restraint factor ($0 \le R \le 1.0$), that depends on the amount of reinforcement. The stress in the steel $\sigma_s$ and the compressive force in the steel $F_s$ are:

$$\sigma_s = (1-R)\varepsilon_{free}\, E_s \qquad (7a) \qquad \text{and} \qquad F_s = (1-R)\varepsilon_{free}\, E_s A_s \qquad (7b)$$

where $E_s$ is the elastic modulus of the steel. The reinforced concrete member is shortening, but it is subjected to tensile force that could possibly result in, or contribute to, cracking.

Using the age-adjusted effective modulus method for the time-dependent analysis of the member in Figure 2b, it can be readily shown [3] that the compressive concrete strain $\varepsilon_c$ at time $t$ caused by a free shortening strain of $\varepsilon_{free}$ (= $\varepsilon_T + \varepsilon_{cs}$) and the restraint factor $R$ are given by:

$$\varepsilon_c = (1-R)\varepsilon_{free} = \varepsilon_{free} / (1+\bar{n}_e\, p) \qquad (8) \qquad \text{and} \qquad R = \bar{n}_e\, p / (1+\bar{n}_e\, p) \qquad (9)$$

and the concrete tensile stress $\sigma_{cs}$ at time $t$ induced by the restraint to $\varepsilon_{free}$ is given by:

$$\sigma_{cs} = -\varepsilon_{free} E_s\, p / (1+\bar{n}_e\, p) \qquad (10)$$

where $\bar{n}_e$ is the age adjusted modular ratio (= $E_s / \bar{E}_e$), $p$ is the reinforcement ratio (= $A_s/A_c$), and $\bar{E}_e$ is the age-adjusted effective modulus of the concrete given in Eq. 4.

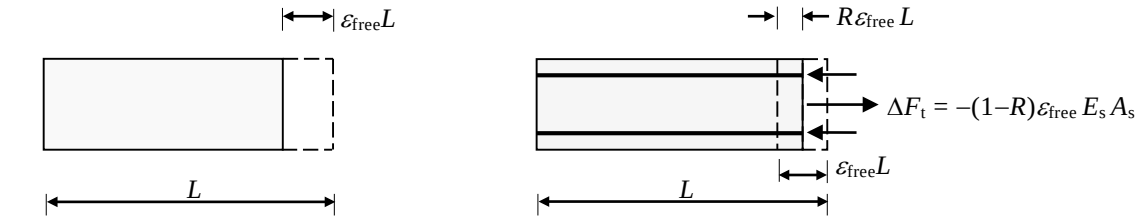


Figure 2 Restraint provided by symmetrically located reinforcement

The creep coefficient for use in Eq. 4 ($\varphi$) is the tensile creep coefficient at time $t$ due to a stress first applied when contraction commenced. As already mentioned, when considering restraint immediately after the heat of hydration cycle, $\chi\varphi$ may be taken as 0.65. When considering the possibility of cracking after say 1 month, $\chi\varphi$ should not be taken greater than about 1.8.

Taking $E_s$ = 200000 MPa, $E_c$ = 20000 MPa, $\chi\varphi$ = 1.625 (typical concrete properties for 30 MPa concrete when considering the possibility of restrained cracking at age 1 month), the restraint factor $R$ is determined using Eq. 9 and is given in Table 1 for a wide range of reinforcement ratios. Also shown in Table 1 is the concrete tensile stress $\sigma_{cs}$ induced by a free strain of $\varepsilon_{free} = \varepsilon_T + \varepsilon_{cs} = -600\times10^{-6}$. Even when these concrete stresses may not initiate cracking in the absence of other actions, such as when $p$ is less than about 2.0%, they will substantially reduce the applied load required to cause cracking.

Of course, this analysis assumes that the concrete is uncracked and that the tensile stress $\sigma_{cs}$ can develop in the concrete. If any early-age cracking occurs at the end of the initial cooling period, the concrete in the vicinity of that crack cannot carry tension and the crack will open due to the subsequent shrinkage.

Table 1 Restraint factors and tensile stresses for symmetrically reinforced sections

| $p = A_s/A_c$ | 0.002 | 0.005 | 0.01 | 0.015 | 0.02 | 0.025 | 0.03 | 0.035 | 0.04 |
|---|---|---|---|---|---|---|---|---|---|
| $R$ | 0.050 | 0.116 | 0.208 | 0.283 | 0.344 | 0.396 | 0.441 | 0.479 | 0.512 |
| $\sigma_{cs}$ (MPa) | 0.23 | 0.53 | 0.95 | 1.29 | 1.57 | 1.81 | 2.01 | 2.19 | 2.34 |

**Unsymmetrically reinforced sections**

If the reinforcement is not symmetrically placed on a section, restraint to early-age thermal and shrinkage contraction will induced a curvature on the cross-section and a concrete tensile stress that may initiate cracking. Consider the singly-reinforced member shown in Figure 3a and the small segment of length, $\Delta z$. The shrinkage/temperature-induced stresses and strains on an uncracked cross-section are shown in Figures 3b. As the concrete shrinks, with a free strain of $\varepsilon_{free} = \varepsilon_T + \varepsilon_{cs}$, the steel reinforcement is compressed and, in turn, the steel imposes an equal and opposite tensile force $\Delta F_t$ on the concrete at the level of the steel. This gradually increasing tensile force, acting at some eccentricity to the centroid of the concrete cross-section produces elastic and creep strains and a resulting curvature on the section. The shrinkage-induced curvature often leads to significant load independent deflection of the member. The magnitude of $\Delta F_t$ (and hence the shrinkage induced curvature) depends on the quantity and position of the reinforcement.

The curvature caused by $\Delta F_t$ obviously depends on the size of the (uncracked) concrete part of the cross-section, and hence on the extent of cracking, and this in turn depends on the magnitude of the applied moment and the quantity of reinforcement. For an uncracked section, the restraint factor depends on the reinforcement ratio. Taking $E_s$ = 200000 MPa, $E_c$ = 20000 MPa, $\chi\varphi$ = 1.625 and $d/h$ = 0.9, the restraint factor $R$ for the uncracked rectangular singly-reinforced cross-section shown in Figure 3b has been determined using the age-adjusted effective modulus method and is given in Table 2 for a wide range of reinforcement ratios $p$ ($=A_s/bD$). The restraint factor $R$, the restraining force $\Delta F_t$ and the extreme fibre concrete tensile stress $\sigma_{cs}$, caused by a uniform free strain of magnitude $\varepsilon_{free} = \varepsilon_T + \varepsilon_{cs}$ may be approximated by:

$$R = \frac{\bar{n}_e\, p(1+\lambda_1)}{1+\bar{n}_e\, p(1+\lambda_1)}\ ; \quad \Delta F_t = \frac{-\varepsilon_{free} E_s A_s}{1+\bar{n}_e\, p(1+\lambda_1)} \text{ and } \sigma_{cs} = \frac{-\varepsilon_{free} E_s\, p(1+\lambda_1\lambda_2)}{1+\bar{n}_e\, p(1+\lambda_1)} \qquad (11a,b,c)$$

where $\lambda_1$ and $\lambda_2$ depend on the geometry of the cross-section and are given by:

$$\lambda_1 = 12\,[(d/h) - 0.5]^2 \qquad \text{and} \qquad \lambda_2 = 0.5h/(d - 0.5h) \qquad (12a, b)$$

Also shown in Table 2 is the extreme fibre concrete tensile stress $\sigma_{cs}$ induced by a uniform free strain of $\varepsilon_{free} = \varepsilon_T + \varepsilon_{cs} = -600\times10^{-6}$.

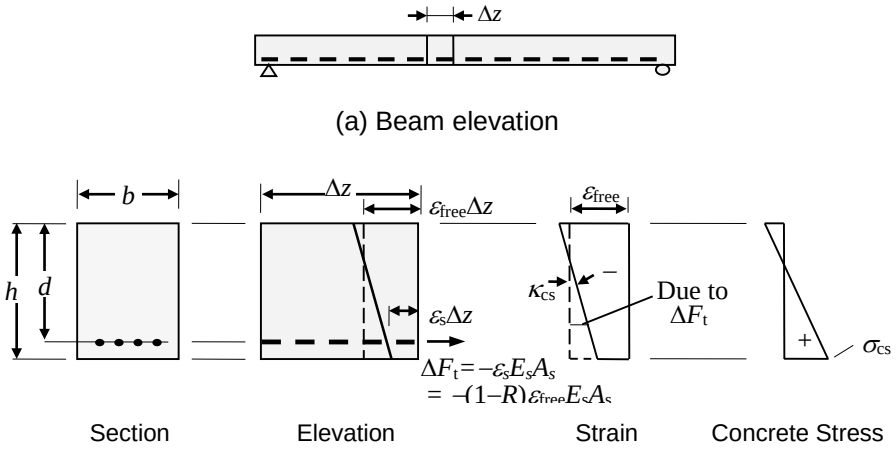


Figure 3 Shrinkage-induced deformation and stresses in a singly-reinforced beam

Table 2 Restraint factors $R$ for an uncracked singly-reinforced section ($d/h$ = 0.9)

| $p = A_s/bh$ | 0.002 | 0.004 | 0.006 | 0.008 | 0.01 | 0.012 | 0.014 | 0.016 |
|---|---|---|---|---|---|---|---|---|
| $R$ | 0.134 | 0.237 | 0.319 | 0.386 | 0.441 | 0.488 | 0.528 | 0.563 |
| $\sigma_{cs}$ (MPa) | 0.711 | 1.260 | 1.697 | 2.053 | 2.348 | 2.598 | 2.811 | 2.995 |

## Edge Restraint in a Slab or Wall

Frequently, walls and slabs are subjected to *edge (or side) restraint*, where shortening due to early-age contraction and shrinkage is restrained on one or more sides of the element. Examples of side restraint are shown in Figure 4. In Figure 4a, contraction in the secondary direction of the one-way slab is restrained by the more massive supporting beams (that will be contracting at a slower rate than the slab). The restraining forces applied to the slab along each supported edge cause a direct tension in the secondary direction of the slab that may cause the cracking shown in the isometric view. The spacing and width of these cracks depend on the amount and distribution of reinforcement in the secondary direction of the slab. Figure 4b shows a wall where contraction ($\varepsilon_{free} = \varepsilon_T + \varepsilon_{cs}$) is restrained on one edge by the footing. The restraint to contraction may result in cracking, initiated at the base of the wall, where the resultant of the tensile restraint force is acting, and then extending the full height of the wall, as shown in the isometric view. A wall restrained on two adjacent edges is shown in Figure 4c, together with crack pattern initiated by restrained shrinkage in the two orthogonal directions. The cracks resulting from restrained shrinkage are direct tension cracks caused by the tensile restraining force(s), $F_t$. They generally extend completely through the restrained slab and, if uncontrolled, can become unserviceable and lead to waterproofing and corrosion problems. They may even compromise the integrity of the member.

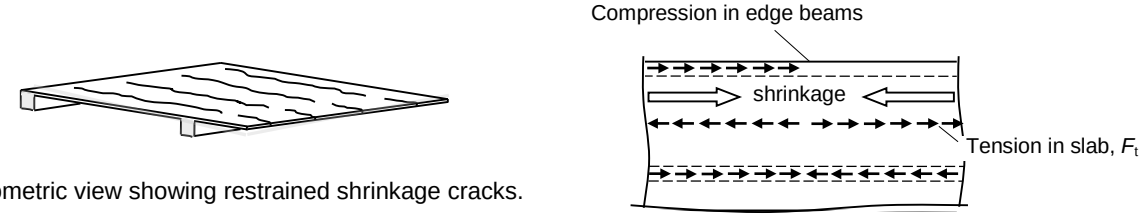


Isometric view showing restrained shrinkage cracks.

(a) Contraction in the secondary direction of a one-way slab.

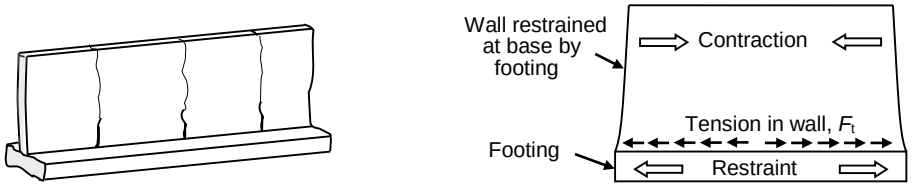


Isometric view showing restrained shrinkage cracks.

Elevation

(b) Contraction in a wall restrained on one edge.

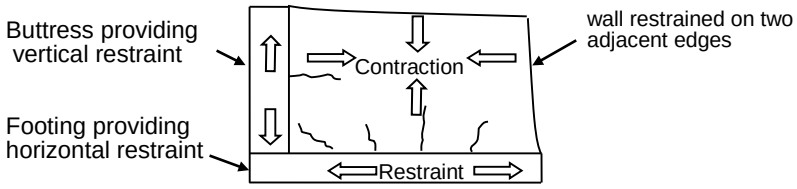


(c) Contraction of wall with two adjacent edges restrained and potential

Figure 4 Typical edge restraint to contraction in beams and slabs

Consider the wall and footing shown in cross-section in Figure 5a. Using the notation specified in the figure, the area, section modulus and second moment of area about the centroid of the wall are $A_1 = b_1h_1$ , $Z_1 = b_1h_1^2/6$ and $I_1 = b_1h_1^3/12$ and, for the footing, $A_2 = b_2h_2$ , $Z_2 = b_2h_2^2/6$ and $I_2 = b_2h_2^3/12$. If the wall is cast at some time after the base, it will be cooling and shrinking at a faster rate than the base. At some time $t$ after the wall is cast, the free contraction strain in the wall is $\varepsilon_{\text{free.1}} = \varepsilon_{\text{T.1}} + \varepsilon_{\text{cs.1}}$, while the contraction of the base is $\varepsilon_{\text{free.2}} = \varepsilon_{\text{cs.2}}$ (where $\varepsilon_{\text{free.2}} < \varepsilon_{\text{free.1}}$). The elastic modulus, creep coefficient, aging coefficient for the wall and base are $E_{\text{c.1}}$, $\varphi_1$, $\chi_1$ and $E_{\text{c.2}}$, $\varphi_2$, $\chi_2$, respectively. The corresponding age-adjusted effective moduli $\overline{E}_{\text{e.1}}$ and $\overline{E}_{\text{e.2}}$ are determined using Eq. 4. The self-equilibrating restraining forces that develop with time, $F_t$ (tensile) in the wall and $-F_t$ (compressive) in the base, act at a distance $\bar{y}$ below the interface between the wall and the base, as shown in the elevation in Figure 5b. The longitudinal strains and stresses are shown in Figures 5c and 5d. It can be readily shown that distance $\bar{y}$ depends on the age-adjusted flexural rigidities of the wall and the base, $\overline{R}_{\text{I.1}} = \overline{E}_{\text{e.1}} I_1$ and $\overline{R}_{\text{I.2}} = \overline{E}_{\text{e.2}} I_2$ , and is given by:

$$\bar{y} = 0.5(h_2\overline{R}_{\text{I.1}} - h_1\overline{R}_{\text{I.2}})/(\overline{R}_{\text{I.1}} + \overline{R}_{\text{I.2}}) \tag{13}$$

The restraining force $F_t$ depends on the age-adjusted axial and first moment rigidities and the difference in free contraction of the wall and base, $\Delta\varepsilon_{\text{free}} = \varepsilon_{\text{free.1}} - \varepsilon_{\text{free.2}}$ and may be obtained by enforcing strain compatibility at the wall-footing interface giving:

$$F_t = -\Delta\varepsilon_{\text{free}} / (\bar{a}_1 + \bar{a}_2 + \bar{z}_1 + \bar{z}_2) \tag{14}$$

where $\bar{a}_{.1} = 1/(\bar{E}_{e.1}A_1)$, $\bar{a}_2 = 1/(\bar{E}_{e.2}A_2)$, $\bar{z}_1 = e_1/(\bar{E}_{e.1}Z_1)$ and $\bar{z}_2 = e_2/(\bar{E}_{e.2}Z_2)$. The terms $e_1$ and $e_2$ are the distances from the line of action of $F_t$ to the centroids of the wall and the base, respectively, i.e. $e_1 = 0.5h_1 + \bar{y}$ and $e_2 = 0.5h_2 - \bar{y}$. The tensile stress at the bottom of the wall caused by the restraining force $F_t$ is:

$$\sigma_{cs} = (F_t / A_1) + F_t(\bar{y} + 0.5h_1)/Z_1 \tag{15}$$

and the restrained strain $\varepsilon_r$ at this point and the corresponding restraint factor $R$ is

$$\varepsilon_r = \sigma_{cs}/\bar{E}_{e.1} \qquad \text{and} \qquad R = -\varepsilon_r/\Delta\varepsilon_{free} = -\sigma_{cs}/(\bar{E}_{e.1}\Delta\varepsilon_{free}) \tag{16a, b}$$

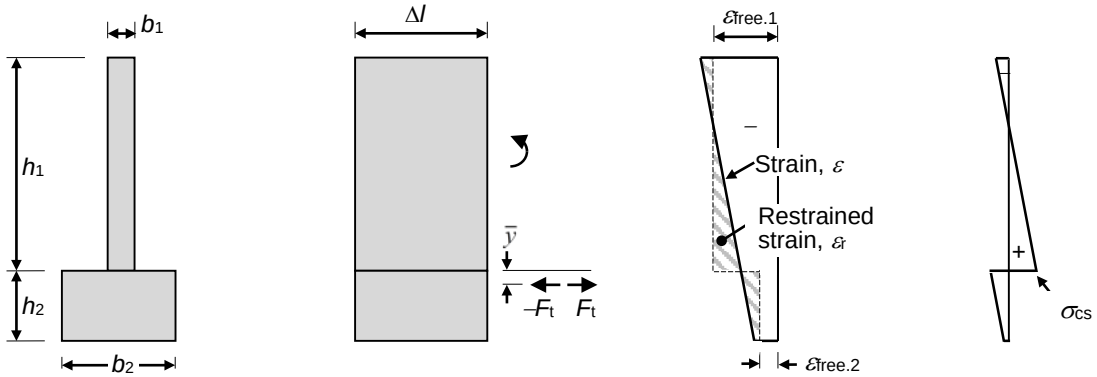


Figure 5 Restraint actions, strains and stresses in an edge-restrained wall

## CRACKING CAUSED BY EDGE RESTRAINT

Before cracking, the deformation resulting from a restraining force $F_t$ over a gauge length $L_o$ is $\varepsilon_r L_o = (\sigma_{cs}/\bar{E}_e)L_o$. When the concrete stress $\sigma_{cs}$ exceeds the tensile strength $f_{ctm}$, cracking occurs. The crack opens and the concrete stress at the crack drops to zero. Either side of the crack, the concrete stress gradually increases due to the steel-concrete bond until at some distance $s_o$ from the crack the concrete stress is unaffected by the crack. It follows that cracks form at a spacing of between $s_o$ and $2s_o$. If the gauge length $L_o$ is long enough to contain $m$ cracks, the deformation caused by restraint $\varepsilon_r L_o$ may now be expressed as:

$$\varepsilon_r L_o = (\varepsilon_{r.cr} + \varepsilon_{r1})L_o \tag{17}$$

where the *residual restrained strain* $\varepsilon_{r1}$ is the sum of the elastic and creep strains caused by the average tensile concrete stress between the cracks and $\varepsilon_{r.cr}$ is the *crack-induced strain* (introduced in Eq. 5). The length $\varepsilon_{r.cr}L_o$ is the sum of the widths of the $m$ cracks within the length $L_o$, i.e.

$$\varepsilon_{r.cr} = \left(\sum_{i=1}^{m} w_i\right)/L_o \qquad \text{and} \qquad \varepsilon_{r1} = \varepsilon_r - \varepsilon_{r.cr} = \frac{\sigma_{av}}{\bar{E}_e} \tag{18a, b}$$

In a member subjected to edge restraint (or a member with restraint provided by eccentric reinforcement), the average spacing between cracks depends on the concrete cover, the bond characteristics between the reinforcement and the concrete, the bar diameter, the ratio of reinforcement area to the effective area of the tensile concrete. The maximum crack spacing $s_{r.max}$ recommended by Eurocode 2 [4] is:

$$s_{r.max} = 3.4c + 0.425 k_1 d_b / p_{p.eff} \tag{19}$$

where $c$ is the concrete cover to the reinforcement; $k_1$ depends on the bond characteristics of the reinforcement and may be taken as 0.8 for high bond bars [4], but when good bond cannot be guaranteed, such as when early-age cracking at $t_a$ = 3 days is being considered, $k_1$ should be increased to 1.14; $d_b$ is the diameter of the reinforcing bars; $p_{p.eff}$ is the ratio of the tensile reinforcement area to the effective area of the tensile concrete (=$A_{st}/A_{c.eff}$). For a wall or slab subjected to edge restraint, $A_{c.eff}$ may be taken as the gross area of the cross-section. For a member in bending, $A_{c.eff}$ is the product of the member width at the tensile steel level and $h_{c.ef}$, where $h_{c.ef}$ is the smaller of (0.5 × member thickness) and 2.5($c$ + $d_b$/2).

The maximum crack width $w_{max}$ is determined from:

$$w_{max} = s_{r.max}\varepsilon_{r.cr} = s_{r.max}(\varepsilon_r - \varepsilon_{r1}) \tag{20}$$

Bamforth [1] conservatively approximated the residual strain $\varepsilon_{r1}$ (given by Eq. 20b) by $f_{ct}/E_c$ and therefore the crack-induced strain $\varepsilon_{r.cr}$ may be taken as:

$$\varepsilon_{r.cr} = \varepsilon_r - \varepsilon_{r1} = \varepsilon_r - (f_{ct}/E_c) \tag{21}$$

**Worked Example**

Determine the stress and strain distribution due to the restraint to early-age contraction and shrinkage of the wall shown in Figure 6a. Also determine the crack spacing and crack width at the base of the wall, if each face of the wall is reinforced with 12mm deformed bars running horizontally at 250 mm centres. The concrete cover to the steel bars is 30 mm and the bond conditions are assumed to be good. Assume that cracking occurs when $f_{ctm}$ = 2.0 MPa. For the wall: $E_{c.1}$ = 20000 MPa, $\varphi_1$ = 2.5, $\chi_1$ =0.65, $\varepsilon_{free.1}$ = –0.0006; and, from Eq. 4, $\overline{E}_{e.1}$ = 7619 MPa. For the footing: $E_{c.2}$ = 35000 MPa, $\varphi_2$ = 1.5, $\chi_2$ =0.65; $\varepsilon_{free.2}$ = –0.0002, and, from Eq. 4, $\overline{E}_{e.2}$ = 17722 MPa.

For the wall, $b_1$= 200 mm and $h_1$ = 4000 mm, and for the base, $b_2$ = 1000 mm and $h_2$ = 600 mm. The age-adjusted rigidities are: $\overline{R}_{A.1} = \overline{E}_{e.1}A_1 = 6.095\times10^9$ N; $\overline{R}_{B.1} = \overline{E}_{e.1}Z_1 = 4.063\times10^{12}$ Nmm; $\overline{R}_{I.1} = \overline{E}_{e.1}I_1 = 8.127\times10^{15}$ Nmm$^2$; $\overline{R}_{A.2} = \overline{E}_{e.2}A_2 = 1.063\times10^{10}$ N; $\overline{R}_{B.2} = \overline{E}_{e.2}Z_2 = 1.063\times10^{12}$ Nmm; $\overline{R}_{I.2} = \overline{E}_{e.2}I_2 = 3.190\times10^{14}$ Nmm$^2$.

From Eq. 13, the distance $\bar{y}$ below the interface between the wall and the base at which the resultant restraining force $F_t$ acts is $\bar{y} = 0.5(h_2\overline{R}_{I.1} - h_1\overline{R}_{I.2})/(\overline{R}_{I.1} + \overline{R}_{I.2}) = 213.1$ mm and, with $\Delta\varepsilon_{free}$ = –0.0004, $e_1 = 0.5h_1 + \bar{y}$ = 2213.1 mm and $e_2 = 0.5h_2 - \bar{y}$ = 86.9 mm, Eq. 14 gives $F_t = -\Delta\varepsilon_{free}/(\bar{a}_1 + \bar{a}_2 + \bar{z}_1 + \bar{z}_2)$ = 452.3 kN.

From Eqs. 15 and 16:

$$\sigma_{cs} = (F_t / A_1) + F_t(\bar{y} + 0.5h_1)/Z_1 = 2.44 \text{ MPa};$$

$$\varepsilon_r = \sigma_{cs} / \bar{E}_{e.1} = +321\times10^{-6}; \text{ and } R = \varepsilon_r / \Delta\varepsilon_{free} = 0.801$$

The longitudinal stress and strain distributions due to restrained contraction are shown in Figures 6b and 6c.

For this example, with $A_{st}$ = 452 mm$^2$/m on each face of the wall, the reinforcement ratio is $p_{p.eff}$ = (2×452)/(200×1000) = 0.00452 and the maximum crack spacing is determined using Eq. 19:

$$s_{r.max} = 3.4\times30 + \frac{0.425\times0.8\times12}{0.00452} = 1005 \text{ mm}$$

Due to the restrained contraction at the base of the wall, $\varepsilon_r = 321 \times 10^{-6}$ and, after cracking, Eq. 21 gives:

$$\varepsilon_{r.cr} = 321\times10^{-6} - \frac{2.0}{20000} = 221\times10^{-6}$$

and the maximum crack width is calculated using Eq. 20:

$$w_{max} = 1005\times221\times10^{-6} = 0.222 \text{ mm}$$

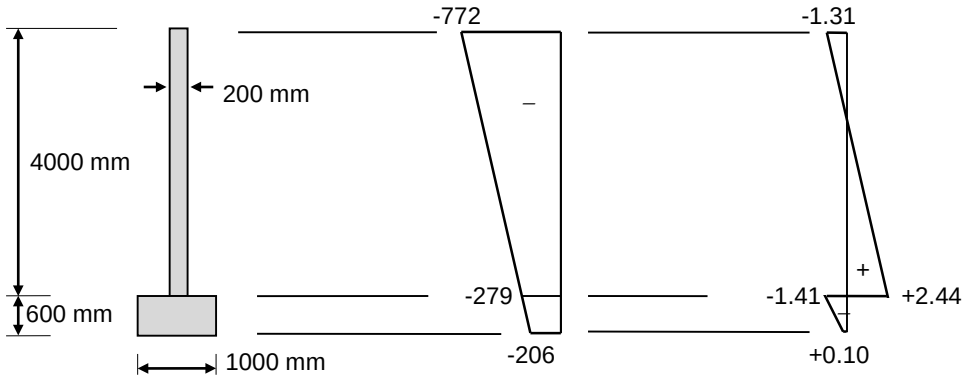


Figure 6 Cross-section of wall and footing and strain and stress distributions due to restrained deformation

## CONCLUSIONS

Rational procedures have been proposed for determining the degree of restraint and the control of cracking caused by early-age cooling and shrinkage of concrete. Restraining forces and concrete tensile stresses caused by temperature and shrinkage strains in a variety of situations have been considered, including concrete members subjected to temperature and/or shrinkage differentials, reinforced concrete members containing embedded reinforcement, and reinforced concrete slabs and walls subjected to edge-restraint. Calculation of the width and spacing of cracks caused by any one or any combination of these restraining forces is outlined and illustrated by a worked example.

## ACKNOWLEDGEMENTS

The work reported herein has been undertaken with the financial support of the Australian Research Council through Discovery Project DP130102966. This support is gratefully acknowledged.

## REFERENCES

1. BAMFORTH P.B. Early-age thermal crack control in concrete, CIRIA C660, London, 1967, p. 112.

2. BAMFORTH P.B. Early-age thermal cracking in concrete, Institute of Concrete Technology, Technical Note TN/2, Slough, 1982.

3. GILBERT R.I. and RANZI, G. Time-dependent behaviour of concrete structures", 2011, Spon press. London.

4. EUROPEAN COMMITTEE FOR STANDARDIZATION, EN 1992-1-1 EUROCODE 2. Design of concrete structures Part 1-1: General rules and rules for buildings, European Committee for Standardization, 2004.

# BOND STRENGTH BETWEEN STEEL REBAR AND CONCRETE

**D Saje**

**J Lopatič**

University of Ljubljana

Slovenia

**ABSTRACT.** The paper deals with the investigation of bond between concrete and steel rebar. The influence of different types of concrete on steel-to-concrete bond strength is presented. Therefore, a series of pull-out tests, based on standard EN 10080:2005, were conducted. In this study, the bond behaviour of rebars in normal strength concrete (48MPa), high strength concrete (81MPa) and two high strength steel fibre-reinforced concretes (84MPa, 89MPa) were tested. The results show that the relationship between bond stress and slip in high strength concrete is form-wise similar to bond stress-slip relationship in normal strength concrete specimens. However, high strength concrete specimens indicated approximately three times larger bond strength compared to normal strength concrete specimens.

**Keywords:** Bond strength, Bond slip, Pull-out test, High strength concrete, Fibre reinforced concrete.

**Drago Saje** is Assistant professor at the Faculty of Civil and Geodetic Engineering, University of Ljubljana. His main research activities are the mechanical and rheological properties of high performance concrete and the design of concrete and timber structures.

**Jože Lopatič** is Associate professor at the Faculty of Civil and Geodetic Engineering, University of Ljubljana. His main research interests include the modelling of nonlinear creep and shrinkage of concrete, design and nonlinear time-dependent analysis of reinforced concrete and timber structures, as well as field testing of structures.

## INTRODUCTION

Applicability of reinforced concrete depends on the compatibility of strains between the reinforcement and the adjacent concrete that enables composite action of both materials. Concrete has large compressive and relatively low tensile strength. Therefore tensile force in reinforced concrete element is normally taken over by steel reinforcement, shaped as bars or welded mesh, where adequate bond between the reinforcement and the surrounding concrete should be provided. Based on adequate bond, acting at the rebar surface area, the force from the rebar is transferred into concrete and vice versa.

Several factors affect the bond behaviour between rebar and concrete, i.e.: anchoring length of the bar, bar diameter, bar position, deformation patterns and rib geometry, corrosion level of the bar, confining reinforcement around the bar, concrete quality, concrete composition, etc. [1, 2, 3]. Metelli and Plizzary [4] report that for a bar diameter increasing from 12 to 50 mm, the reduction in bond strength is about 25%. For bars anchored in normal strength concrete, bottom cast bars have better bond performance then top cast bars [3]. This is due to the increased tendency of bleeding of the concrete around top bars. However, in high strength concrete Azizinamini et al. [5] found that top cast bars have better bond performance than bottom cast bars. The improvement was in the range of 1 to 8%.

One of the tests for the determination of steel-to-concrete bond strength and bond stress-slip relationship is pull-out test, where the bar embedded into a concrete cube is pulled out of its concrete embrace. At the loaded end of the bar the tensile force is measured and at the unloaded end the relative displacement between concrete and the rebar is measured. Standard EN 10080:2005 [6] prescribes the shape and technical properties of the specimen.

## BOND MECHANISM

During the pull-out process in reinforced concrete element the deformed bars are anchored by three bond mechanisms between reinforcement and surrounding concrete i.e. (i) chemical adhesion, (ii) friction at the interface and (iii) bearing of the ribs against the concrete surface. Chemical adhesion assures bond in the beginning, when the bond stress level is still low. After the initial slip of the bar, chemical adhesion is lost. In this moment friction forces at the surface of the bar and bearing forces at the ribs caused by the interlocking action are mobilized [1, 2, 7].

Plain bars without ribs are characterised by poor bond conditions between the bars and concrete, since forces are transferred into concrete only through mechanisms of initial chemical adhesion and friction between the bar and surrounding concrete. Both mechanisms exhibit rather small resistance to pull-out, which is why nowadays plain bars are not used in structural elements. Only ribbed bars are allowed, since ribs provide good anchoring into concrete.

The initial slip of the bar is due to transverse micro-cracks which originate at the tips of the ribs (Figure 1). As slip increases, concrete in front of the ribs starts to crush, which in turns induces a wedging action that increases the normal component of the bearing forces. This normal component is resisted by hoop stresses in the concrete, which cause splitting cracks to develop at the contact with the bar and to propagate radially.

At this stage, the bond resistance is provided by an interlocking mechanism from the concrete struts confined by the undamaged outer concrete ring. In general bond can fail by the splitting of the concrete or pull-out of the bar. The split happens when splitting cracks propagate radially through the concrete towards its external surface. In the case of concrete splitting, the lower bond strengths are achieved compared to pull-out failure mode [1].

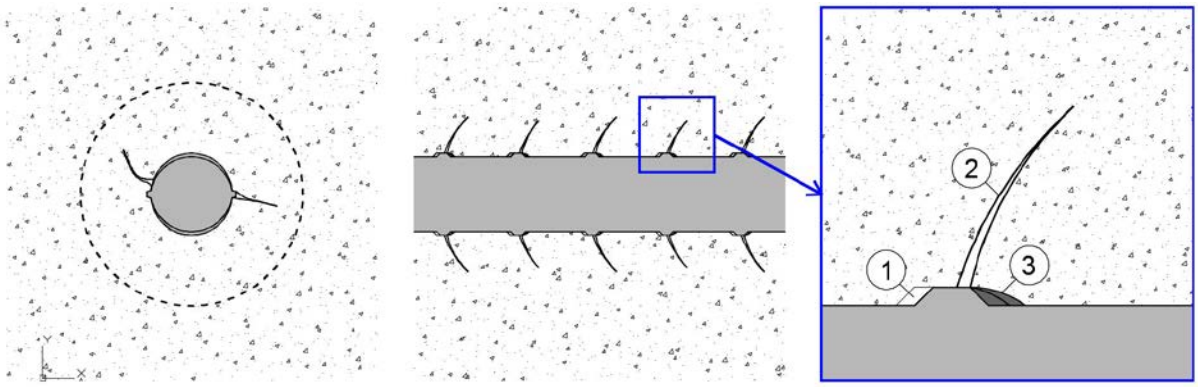


Figure 1 Schematic presentation of contact failure between ribbed rebar and concrete. (1- slip, 2-micro crack, 3-area of crushed concrete) .

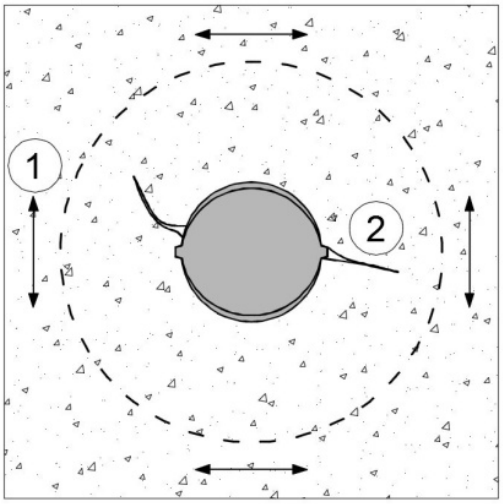


Figure 2 Cross-section, appearance of fracture cracks (2) due to transverse stresses (1).

## EXPERIMENTAL WORK

### Concrete mixtures

The test specimens were made from the mixture of normal strength concrete (NSC), high strength concrete (HSC) and two mixtures of high strength fibre-reinforced concrete (HSC-SF-0.5%, HSC-SF-1.0%). The granulometric composition of the aggregate was kept the same in all four mixes. Washed crushed limestone aggregate with the maximum grain size of 16 mm and fine sand were used. To achieve higher strength and adequate workability (flow class F2) naphthalene based superplasticizer was used. Part of the cement was replaced by silica fume, which additionally increases concrete strength.

The mix proportions of high strength fibre concrete were practically the same to those of high strength concrete, except that in fibre reinforced concretes part of the aggregate were replaced by steel fibres. We used 30 mm long steel fibres IRI, with single hooks at the ends. Volume fractions of fibres used were 0.5% and 1.0%, respectively (Table 1).

Table 1 Composition of concrete mixes.

| MATERIALS | MIX | NSC | HSC | HSC-SF-0.5% | HSC-SF-1.0% |
|---|---|---|---|---|---|
| Aggregate kg/m$^3$ | 0/2 (fine sand) | 264 | 285 | 283 | 281 |
| | 0/4 | 790 | 853 | 847 | 841 |
| | 4/8 | 263 | 284 | 282 | 280 |
| | 8/16 | 439 | 474 | 470 | 467 |
| Cement kg/m$^3$ | CEM II/A-M (LL-S) 42,5 R | 400 | 360 | 360 | 360 |
| Additives | Silica fume kg/m] | 0 | 40 | 40 | 40 |
| | Steel fibres % | 0 | 0 | 0.5 | 1.0 |
| | Water-binder ratio | 0.52 | 0.36 | 0.36 | 0.36 |
| | Density kg/m$^3$ | 2364 | 2449 | 2476 | 2500 |

**Test specimen**

The test specimen for pull-out test was generally a concrete cube 200mm × 200mm × 200mm with a bar embedded coaxially (Figure 4) [6]. Special wooden moulds were fabricated to cast nine specimens in a single batch. The rebars, with a diameter of 12mm and yield strength of 500MPa, were placed horizontally and concrete was cast vertically. Needle vibrator was used to compact the concrete. For each concrete mix three specimens for the pull-out test and three for the concrete compressive strength test (cubes 150mm × 150mm × 150mm) were prepared. The specimens were de-moulded after one day and then cured for 28 days in water at room temperature of 22°C ± 2° till testing.

Figure 3 Mould prepared for concrete casting, bond prevention, bar deformation pattern.

## Experimental setup and testing

The pull-out tests were carried out using the electro-hydraulic testing machine Instron 1345 with capacity ±1000 kN, according to standard EN 10080:2005 [6]. Figure 4 shows the dimensions of the the pull-out test specimen. The standard defines the specimen dimensions regarding the diameter of the used rebar. Dimensions on Figure 4 are valid for the bar with a diameter of 12 mm. The embracing with concrete is provided at a length of 6cm (i.e. 5$\phi$). At the remaining 14 cm bond is prevented by a PVC tube (8). Figure 4 also shows the schematic presentation of the test. The specimen stands on a rubber base (7) and additional steel plate (6). The rebar is clamped in the lower jaw (5) of the testing machine. In the upper jaw (1) the supporting steel cage is clamped. The lower and upper plates of the cage are connected by four steel bars. At the unloaded end of the rebar a digital dial gage with a resolution of 0.001mm (2) was used to measure the relative displacement of the bar related to the upper plane of the concrete cube. The rebar was also equipped with an extensometer (4) to monitor its strain. Loading of test samples was controlled in displacement control mode, with rate of actuator stroke 0.01mm/s. The total movement of 50mm was set as the end value. The test continued until bond area failure or until full range displacement of the hydraulic actuator was reached – whichever occurred first.

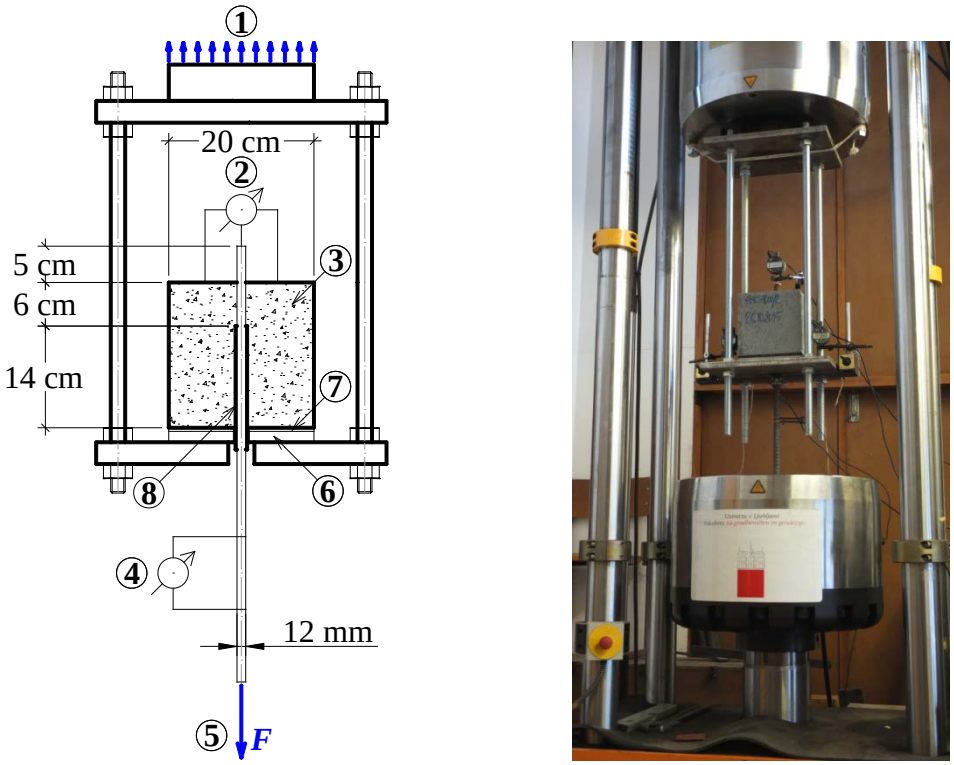


Figure 4 Scheme of pull-out test and specimen dimensions, testing apparatus.

## RESULTS AND DISCUSSION

Using adequate measuring equipment and software for data acquisition, the values of the force and the strain at the loaded end of the embedded rebar and the relative displacement of the unloaded end were obtained. All physical properties (relative displacement, strain and force) were measured and recorded by data acquisition system Dewesoft DEWE 2500.

The notional bond stress is defined as a quotient between the applied force and the nominal surface area of the bar at the anchoring length. Thus the assumption of equal distribution of stresses along the anchoring length was considered.

The measured values of concrete compressive strength and obtained values of the bond strength are shown in Table 3. $f_c$ denotes the average measured compressive strength of individual concrete type. $\tau_{max}$ is the obtained bond strength between concrete and rebar, $\tau_{mean}$. is the average bond strength of three specimens made of same concrete type.

Compared to normal strength concrete (NSC), high strength concrete (HSC) specimens indicated about three times larger bond strength, while the average compressive strength of high strength concrete was only about two times larger than that of normal strength concrete. When comparing HSC and its alternative with steel fibres HSC SF-1.0%, it can be seen that the values of bond strength differ by only a few MPa. The obtained values of bond strength for the HSC and NSC concretes could be compared to the research from literature [2], where a rebar with a diameter of 16 mm and concretes with a 90 day compressive strengths of 54.8 MPa and 83.2 MPa were used. Specimens from the first concrete had on average bond strength of 19.9 MPa, while in specimens from the second concrete it was 29.7 MPa. Compared to our results the difference is rather large, especially in normal concrete with compressive strength of 54.8 MPa. It should be considered that a high level of result variation is typical for pull-out tests. The abovementioned tests were performed in Brazil using Brazilian reinforcing steel and different concrete mix ingredients.

Table 2 Concrete compressive strengths and bond strengths between reinforcement and concrete

| Mix | $f_c$ [MPa] | # | $\tau_{max}$ [MPa] | $\tau_{mean}$ [MPa] |
|---|---|---|---|---|
| NSC | 48,6 | 1 | 9.15 | 9,9 |
| | | 2 | -[2] | |
| | | 3 | 10.70 | |
| HSC | 81,2 | 1 | 30.42 | 28,6 |
| | | 2 | 27.98 | |
| | | 3 | 27.45 | |
| HSC-SF-0.5% | 84.0 | 1 | 31.08 | 30.6 |
| | | 2 | 31.17[1] | |
| | | 3 | 29.62 | |
| HSC-SF-1.0% | 89,0 | 1 | 31.30[1] | 31,5 |
| | | 2 | 31.30[1] | |
| | | 3 | 32.01[1] | |

Note: [1] Contact length between concrete and rebar in specimens amounted to 5$\phi$. In the pull-out test of the rebar from concrete, steel plastification appeared before bond area fails.
Note: [2] Failed measurement

Bond stress-slip relationships for eleven specimens are presented in Figure 5. Large influence of the concrete type on the specimen response during bar pull-out can be seen. The normal and high strength concrete specimens show a behaviour typical for the pull-out test.

In the beginning of the test the diagrams rise steeply. In this range the upper- free end of the bar is almost motionless. Adhesion dominates between concrete and bar. After the initial slip, the first local cracks appear in the concrete specimen and ribs of the bar start to wedge in the concrete. The high strength and normal strength concrete specimens achieve the maximum value of bond stress at approximately the same slip, which is between 1 and 2 mm. After reaching the top of the diagram, both types of concrete behave similarly.

In fibre reinforced concrete (HSC-SF-1.0%), the contact area between concrete and reinforcement did not fail during the test. Strains obtained from extensometer installed on the rebar showed that the steel bar plastified. The movement of the actuator of testing machine was almost the same as the rebar elongation, while the upper-free ends of the bars slipped on average only by 0.35 mm. Also in the high strength concrete specimens the rebars plastified, but during the bar pull-out the concrete crushed in the contact area.

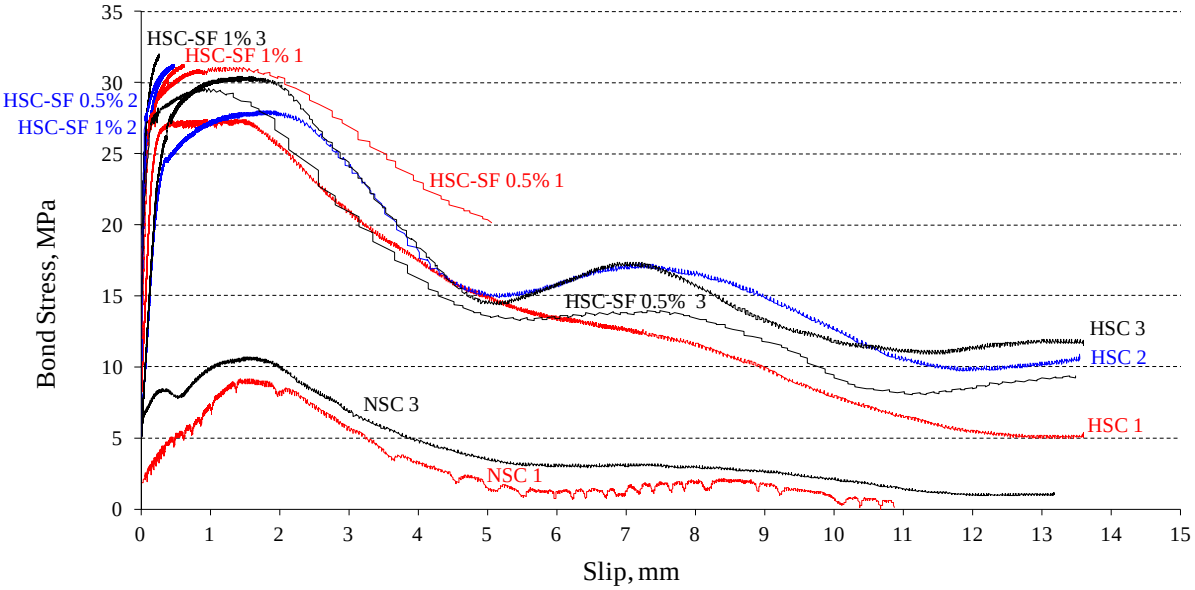


Figure 5 Bond strength-slip relationships for different concrete types.

## CONCLUSIONS

Based on the results of the test of the rebar-to-concrete bond strength of 28 days old concrete cube specimens with embedded steel rebars with a diameter of 12 mm, the following conclusions can be drawn:

The bond strengths of the high strength concrete specimens were on average about three times higher than those of normal concrete specimens. The bond stress-slip relationships are of similar shape for both tested concrete types.

High strength concrete specimens and high strength fibre reinforced concrete specimens had practically the same composition, except that the latter included additional steel fibres. The values of limit bond stress of the specimens from fibre reinforced high strength concrete with 1.0% of volume fraction of fibres are only by about 10% higher than the comparable values for high strength concrete without fibres.

Despite that rebars were anchored only by 6 cm long contact length, plastification of the bar appeared before bond failure occurred, in one high strength concrete specimen and in one high strength fibre reinforced concrete specimens with 0.5% of fibres as well as in all high strength fibre concrete specimens with 1.0% of fibres. This phenomenon could not be noticed in the comparable normal strength concrete specimens.

After plastification of the reinforcement, in both types of high strength concrete specimens, the change in their behaviour was noticed. High strength fibre reinforced concrete with 1.0% of fibres preserved the steel-to-concrete contact, while at concrete without fibres the contact failed and obvious pull-out of the bar from concrete occurred.

High strength fibre reinforced concrete with a volume fraction of 1.0% of steel fibres, indicated 6.0% higher compressive strength compared to high strength fibre reinforced concrete with volumetric fraction of 0.5% of steel fibres, while the pull-out force in the pull-out test was for both concretes approximately the same. This is due to a strong rebar-to-concrete bond at both considered concretes which in turn leads to a plastification of the reinforcement before the contact area fails.

## REFERENCES

1. MURCIA-DELSO, J, STAVRIDIS, A, SHING, B. Modeling the bond-slip behavior of confined large-diameter rebars, Proceedings of the III ECCOMAS Thematic Conference on Computational Methods in Structural Dynamics and Earthquake Engineering, Corfu, Greek, 2011, p 14.

2. BARBOSA, M T G, SÁNCHEZ F S. Investigation of bond stress in pull out specimens with high strength concrete, Global Journal of Researches in Engineering, Vol. 13, Iss. 3, 2013, pp 55-64.

3. FÉDÉRATION INTERNATIONALE DU BÉTON (fib). fib bulletin 10. Bond of reinforcement in concrete, Lausanne, 2000, p 427.

4. METELLI G, PLIZZARI, G. Influence of the relative rib area on bond behaviour. Magazine of Concrete Research, Magazine of Concrete Research, Vol. 66, Iss. 6, 2014, pp 277-294.

5. AZIZINAMINI, A, STARK, M, ROLLER, J J, GHOSH, S K. Bond performance of reinforcing bars embedded in high-strength concrete. ACI Structural Journal, September-October 1993, pp 554-561.

6. EN 10080. Steel for the reinforcement of concrete – Weldable reinforcing steel – General. 2005, p 61.

7. APPA RAO, G, PANDURANGAN, K, SULTANA, F, ELIGEHAUSEN, R. Studies on the pull-out strength of ribbed bars in high-strength concrete, IA-FraMCoS International Association of Fracture Mechanics for Concrete and Concrete Structures, Proceedings of the FraMCoS-6, Catania, Italy, 2007, p 6.

# ANALYSIS OF STRENGTH AND CRACK GROWTH RESISTANCE OF REINFORCED CONCRETE ARCHED STRUCTURES

**Mirzakhid Miralimov Xamitovich**
Tashkent Automobile and Road Institute
Uzbekistan

**ABSTRACT.** Reinforced concrete arched structures are rather perspective type of designs possessing many advantages in comparison with usual designs, widely applied on a network of highway and railway. It is simple, fast technology which can be executed a small brigade and the usual equipment. Installation on distance at half-lengths allows expediting arrangement by means of insignificant means and without traffic restriction. Spans can exceed 15 m, and the height of the top part of an embankment - to be more than 5 m. Imparting to cross-section of arches the folded (triangular, trapezoidal) or wavy shape can achieve a corresponding reduction in the consumption of materials and at the same time maintaining its bearing capacity. Considering above advantage to wide introduction of reinforcement concrete vaulted structures in construction, rather important problem is definition of bearing ability with carrying out of corresponding calculations on strength and crack resistance. The method of calculation is based on the decision of the general equations of structural mechanics of frame systems. The values of loads and impacts, as well as the calculation of the arch on the bearing capacity are carried out under the provisions of the existing building standards.

**Keywords:** Reinforced concrete, Arch structure, Load, Impact, Frame system, Bearing capacity.

**Dr Miralimov M X** is the Associate Professor of the Road Construction Department at the Tashkent Automobile and Road Institute. As recognized expert in the areas of seismic design, design and analysis of reinforced concrete (RC) structures of road buildings, bridges and tunnels, he is a member of numerous national and technical committees. He teaches graduate and undergraduate courses in civil and structural engineering.

## INTRODUCTION

Construction of bridges and overpasses is today one of the most important and complex elements of transport construction system. This system is in a constant dynamic development and requires a sound scientific base during the design, construction and maintenance.

Modern designs of bridges represent the difficult engineering constructions demanding forces and experience of the most various experts - from architects to workers and professionals. Modern technologies of building of bridge designs allow building more and more difficult bridge constructions quickly and qualitatively.

In road construction for the crossing of small and medium watercourses are mainly designed and built short-span girder bridges. During the construction the conical mounds of bridge approaches requires increasing the size of spans. In addition, on the girder bridge the temporary moving load acts directly to the span, which is one of the causes of premature of structure wear. The situation is exacerbated by the introduction high loads from vehicles A14 (140kN), NK-100 (1000kN) according to new design code [1]. In a certain measure the decision of this problem is making structures that are a part of the embankment of the road.

Perspective direction in this case are short-span arch bridges allowing replace culverts and short-span girder bridges, having a totality of advantages of these structures and excluding their disadvantages. Their advantage is also economic efficiency of construction. They can replace usual two- and three span systems that allow reducing nearly on 30 - 40 % of material costs.

Application of backfilled arch bridges made of reinforced concrete vault elements allowing to place at any combination of plan and profile of the road (on the curves in the plane, at presence of vertical curves as convex and concave, and so on) is ensured equal distribution of transport load into the body of road embankment, that greatly reduces the dynamic actions. Prefabricated light weight structures allow using the light-duty cranes, without lifting and handling equipments. It is raised of bearing ability of arched structure giving to cross-section the folded (triangular, trapezoid) or wavy outline.

In order to verify the operational reliability of prefabricated structures they should be examined for its bearing capacity. This article describes the methodology and results of calculations of the arched reinforced concrete structures for strength and crack resistance under the action of permanent and temporary loads.

## DETAILS OF INVESTIGATIONS

### Construction of the Model of Computational Area and Finite-Dimensional Approximation of the Problem

Let’s consider a body defined two-dimensional area XOУ and with border C. Figure 1 shows, the body is fixed in space by reduction to the plane problem and there are acting forces. The computation plane scheme includes arched structure which is represented as a curved bar of arbitrary outline with geometric and strength characteristics for the width of 1.0 m. Suppose that under the action of these forces deformations are small and for them equitable the following basic equations [2]:

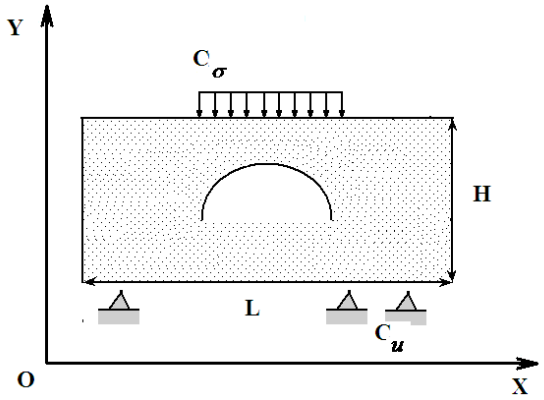


Figure 1 Including arched structure the body is under the actions of forces

1. Equations of equilibrium (static equation) in matrix form:

$$A\vec{\sigma} + \vec{P} = 0 \qquad (1)$$

where $A = \begin{bmatrix} \frac{\partial}{\partial x} & 0 & \frac{\partial}{\partial y} \\ 0 & \frac{\partial}{\partial y} & \frac{\partial}{\partial x} \end{bmatrix}$, $\vec{\sigma} = [\sigma_x \sigma_y \tau]$, $\vec{P} = [\bar{X} \quad \bar{Y}]$

$X$ and $Y$ - body forces.

2. Relationship between strains and displacements (Geometric equation):

$$\vec{\varepsilon} = A^T \vec{U} \qquad (2)$$

where $\vec{\varepsilon} = [\varepsilon_x \quad \varepsilon_y]^T$, $\vec{U} = [u \quad v]^T$

3. Physical equations (Hooke's law):

$$\vec{\varepsilon} = B\vec{\sigma} \qquad (3)$$

where $B = \frac{1}{E}\begin{bmatrix} 1 & -\nu & 0 \\ -\nu & 1 & 0 \\ 0 & 0 & 2(1+\nu) \end{bmatrix}$

Then the equations of theory of elasticity with boundary conditions can be written:

$$\begin{aligned} A\vec{\sigma} + \vec{P} &= 0 \\ \vec{\varepsilon} &= A^T \vec{U} \\ \vec{\varepsilon} &= B\vec{\sigma} \end{aligned} \qquad (4)$$

Kinematic boundary conditions on the contour $C_u$

$$\vec{U} = \vec{U}_u \qquad (5)$$

Static boundary conditions on the contour $C_\sigma$

$$A_c\vec{\sigma} = \vec{P}_\sigma \qquad (6)$$

Here $\vec{U}_u, \vec{P}_\sigma$ - displacement vector on contour $C_u$ and vector of a predetermined force on contour $C_\sigma$, $A_c$ - matrix of direction cosines.

Let us express $\vec{\sigma}$ by second and third equations of the system (4):

$$\vec{\sigma} = B^{-1} A^T \vec{U} \qquad (7)$$

For plane strain Poisson's ratio v is replaced by $\frac{\nu}{1-\nu}$. Substituting the value of $\vec{\sigma}$ in the first equation (4) we obtain the following differential equation of the theory of elasticity in displacements in the matrix form:

$$ADA^T\vec{U} + \vec{P} = 0 \qquad (8)$$

or

$$\begin{aligned} (\lambda+\mu)\frac{\partial \Delta}{\partial x} + \mu\nabla^2 u + P_x = 0 \\ (\lambda+\mu)\frac{\partial \Delta}{\partial y} + \mu\nabla^2 v + P_y = 0 \end{aligned}, \quad \begin{aligned} &\nabla = \varepsilon_x + \varepsilon_y = \frac{\partial u}{\partial x} + \frac{\partial v}{\partial y} \\ &\nabla^2 = \frac{\partial^2}{\partial x^2} + \frac{\partial^2}{\partial y^2}, \lambda = \frac{\nu E}{(1-2\nu)(1+\nu)} \\ &\mu = \frac{E}{2(1+\nu)} - \text{Lame constants} \end{aligned}$$

Now, for the formulation of the variational problem we will use differential equation (8) and corresponding boundary conditions (5-6). Then, according to the Lagrangian variational principle [4], the total potential energy functional ***I*** must take a minimum value. Let's consider that the displacement vector of function *U(x,y)=[u(x,y),v{x,y)]* whicn is minimized the function of the total energy of the system when the loaded condition in the this form:

$$I = \ddot{I} + \bar{A} = \iint_\Omega F(u, v, \frac{\partial u}{\partial x}, \frac{\partial u}{\partial y}, \frac{\partial v}{\partial x}, \frac{\partial v}{\partial y}) dxdy \qquad (9)$$

Under the constraint $\vec{U}\Big|_{C_u} = \vec{U}_u(x, y)$

Here $\bar{A} = \iint_\Omega P_x u + P_y v) dxdy, \quad \ddot{I} = \frac{1}{2}\iint_\Omega (\sigma_x \varepsilon_x + \sigma_y \varepsilon_y + \tau_{xy}\gamma_{xy}) dxdy,$

$\bar{A}$ - potential energy of external forces, *П*- potential energy of the internal forces. Stationarity condition of the functional (9) together with the given boundary conditions should be equivalent to a direct statement of the problem. Then, based on [3], the quadratic functional *F* for two-dimensional problem can be written as follows:

$$F = \mu((\frac{\partial u}{\partial x})^2 + (\frac{\partial v}{\partial y})^2) + \frac{\lambda}{2}(\frac{\partial u}{\partial x} + \frac{\partial v}{\partial y})^2 + P_x u + P_y v \qquad (10)$$

For finding the minimum of functional, equation (10) should be substituted into the Euler equation (11):

$$\frac{\partial F}{\partial u}-\frac{\partial}{\partial x}\frac{\partial F}{\partial u_x}-\frac{\partial}{\partial y}\frac{\partial F}{\partial u_y}=0$$
$$\frac{\partial F}{\partial v}-\frac{\partial}{\partial x}\frac{\partial F}{\partial v_x}-\frac{\partial}{\partial y}\frac{\partial F}{\partial v_y}=0 \qquad (11)$$

So on the basis of [3] can be obtained direct formulation of the problem.

Compliance with such equivalence (variational and direct statement of problem) enables to use the variational approach for solving the finite element method. To obtain a discrete pattern in the area $\Omega$, are introduced a system of piecewise continuous basis functions $\{N_m(x,y)\}$ and nodal displacements $\vec{Z}_m$ [4]. These basis functions are chosen automatically to satisfy the kinematic boundary conditions of the problem at the border $C_u$.

For modeling of soil mass and arched bar are used 4 nodal isoparametric and 2 nodal finite elements. The algorithm is implemented as «Excel-application", i.e. management of all the calculating module is made on Excel tables. Algorithm to division into finite elements, construction of stiffness matrix, solution of equations have been developed in the language TurboPascal-5.5 as a standalone executables. The whole process management solution to the problem was implemented in subprograms of BASIC.

To the table of physical characteristics of the task are entered the following (provided on the basis of geological surveys): (L, H, m) - dimensions of mound, ($E_1$, MPa) - modulus of elasticity, (ν) - Poisson's ratio, (C, MPa) - cohesion force, (φ, °) - angle of internal friction of soil material, (γ, MN/m$^3$) - volume weight of soil, ($E_2$, MPa) - modulus of elasticity of beam material, (I, m$^4$) - moment of inertia of the beam cross section, (F, m$^2$) - cross-sectional area of beam, (l, m), length of beam.

**Algorithmization of Calculation of Arched Structures Taking into Account the Plastic Deformation**

It is known that the relationship between stress and strain in reinforced concrete is significantly different to the stage of its work with cracks and without them. In practical calculations of reinforced concrete structures on the stage of the work without crack effect of linearity deformation to the behavior of the structure is slightly, and the properties of the concrete can be assumed to be isotropic. In the stage of work with crack the nonlinearity is manifested itself quite significantly [3]. Computational method opens a wide prospect in this direction. It is necessary to take notice of fundamental properties of inelastic work of concrete and reinforcement which determine behavior under load.

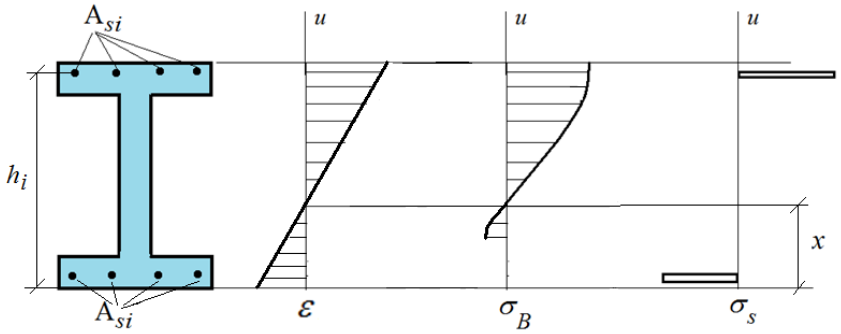


Figure 2 The distribution of strains and stresses in the section of reinforced concrete beam

Figure 2 shows a cross section of reinforced concrete structure and corresponding distribution of stresses in concrete and reinforcement.

a) b)

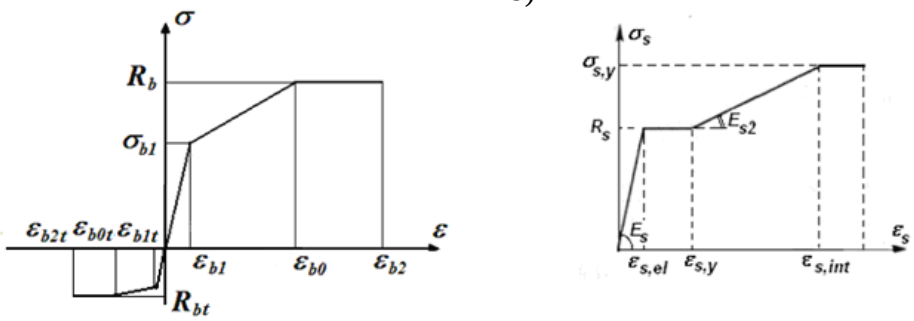


Figure 3 Diagram of deformation for: a) concrete, b) reinforcement

Algorithmization for calculating of reinforced concrete arch structures under load is made up. The program calculates the internal forces (bending moment, shear and axial forces), as well as deflection and deformation in the structure. Structural analysis is performed in the nonlinear formulation. It is used step-by-step method where the load is applied to the structure as portions. For each portion of load increment a solution is searched, then summed with the previous solutions. Using the diagrams of deformation of materials are determined stress and tangent modulus of elasticity (Figure 3). Structure is described by combination of calculated cross sections, each of which is considered consisting of ***n*** layers.

Before loading all layers of design section of a beam have the initial module of elasticity. After the loading start between each load increment for each layer of section modulus of elasticity is determined based on the value of the strain in this layer. Therefore, section bending stiffness $EI$ and compressive stiffness $EF$ are taken as the sum of layers that:

$$EI = \sum_{i=1}^{n} E_i(\varepsilon) I_i \quad EF = \sum_{i=\mathbf{1}}^{n} E_i(\varepsilon) F_i$$

The width of cracks normal to the longitudinal axis of the element, $a_{crc}$, is to be determined in cross section [3] by the formula:

$$a_{crc} = \delta\varphi_1\eta(\frac{\sigma_s}{E_s})20(3{,}5 - 100\mu)\sqrt[3]{d} \quad (12)$$

where δ - accepted factor for eccentric-compressed elements; $\varphi_1$ - accepted factor considering of long action for heavy concrete; η - accepted factor for reinforcement; $\sigma_s$ – calculated stress in reinforcement; μ- percentage of all reinforcements in the cross section; d - diameter of the tension reinforcement. At various diameters of rods its value d is accepted by the formula:

$$d = \frac{n_1 d_1^2 + .... + n_k d_k^2}{n_1 d_1 + .. + n_k d_k}$$

Here $d_1$..., $d_k$ - diameter of rods of the tension reinforcements; $n_1$..., $n_k$ - number of rods in diameters according to $d_1$..., $d_k$.

## NUMERICAL RESULTS AND DISCUSSIONS

### Calculation of Reinforced Concrete Arched Bridge Span

Let consider the solution of the problem. Span of arched bridge is 20,6270 m, rise of arch is 7,5703 m (Figure 4). Arch covered with backfill soil height 0,75 m with volume weight $\gamma$=0,019 MH/m$^3$, on 0,25 m there is asphalt pavement with volume weight $\gamma$ =0,024 MH/m$^3$. Arch is made of concrete with strength class B35. Design strength of concrete according to the norms accepted [2]: $R_b$=17500 kN/m$^2$ - axial compression; $R_{bt}$=1150 kN/m$^2$ - axial tension; $E_b$ =28·10$^6$ kN/m$^2$ - modulus of elasticity of concrete; $\gamma_b$=25 kN/m$^3$ - volume weight of concrete; $\varepsilon_{b1}$=0,0003 - strain of lower branch from diagram of concrete compression; $\varepsilon_{b0}$=0,00092 - strain of upper branch from diagram of concrete compression; $\varepsilon_{b1t}$=0,00016 - strain of lower branch from diagram of concrete tension; $\varepsilon_{b0t}$=0,00075 - strain of upper branch from diagram of concrete compression; $\sigma_{b1}$=9920 kN/m$^2$ - stress of lower branch from diagram of concrete compression; $\sigma_{b1t}$ =500 kN/m$^2$ - stress of lower branch from diagram of concrete tension. In Figure 5 is showed the cross-section of the arch, which is reinforced with longitudinal reinforcement in diameter 20 mm and 25 mm steel class A-III and thus accepted: $R_{pn}$=390000 kN/m$^2$ - regulatory tensile resistance of reinforcement; $E_p$= 2·10$^8$ kN/m$^2$ – modulus of elasticity of reinforcement. In this case are entered the following parameters, F=0,3629469 m$^2$, J=0,009763039 m$^4$ for the computation.

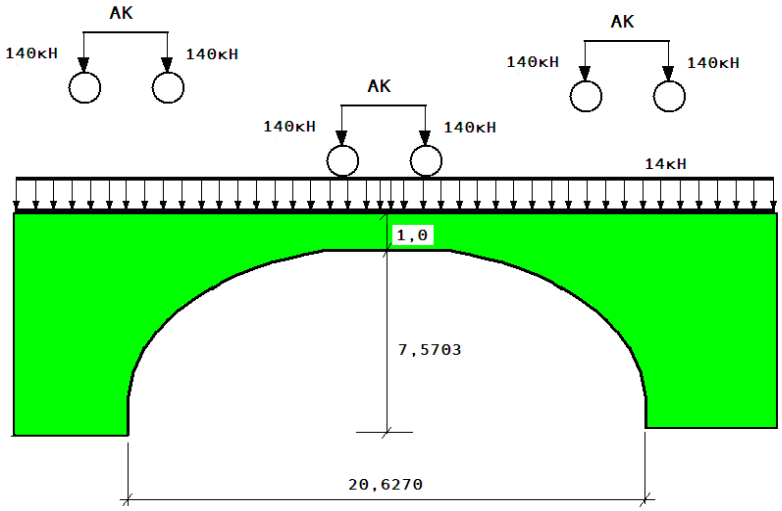


Figure 4 Loaded scheme of arch bridge

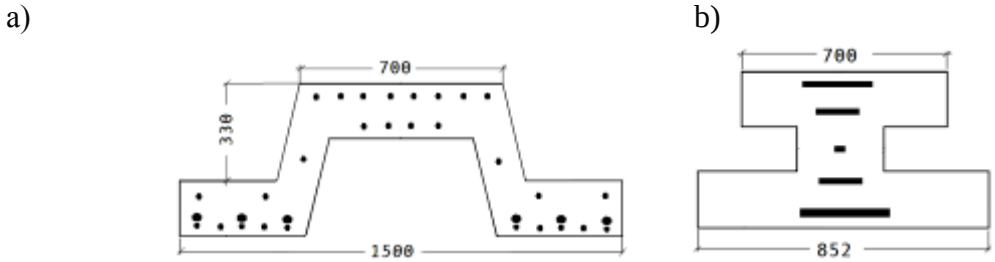


Figure 5 Scheme of cross section of vaulted element: a) existing section, b) reduced section

Figure 6 shows the results of calculation by determining the maximum and minimum principal stresses in the area. In this case, the arch structure accepts the maximum internal forces in its sections. Figure 7 shows the resulting bending moment diagram and deflection.

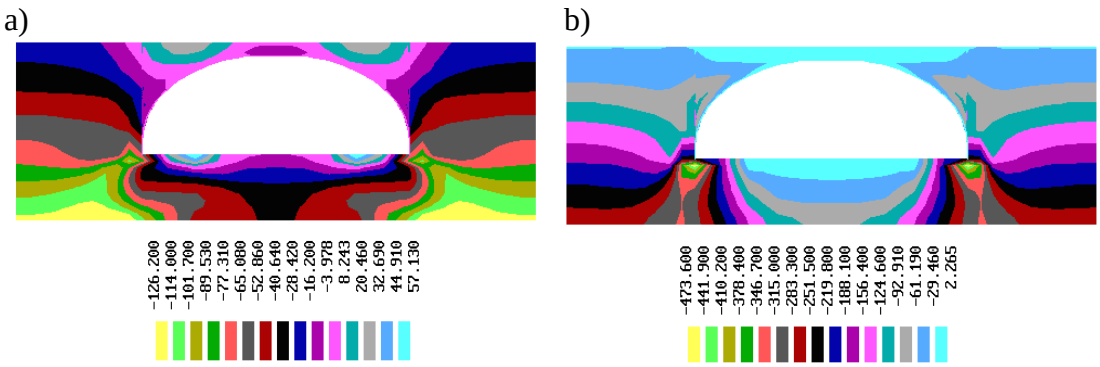


Figure 6 Distribution of principal stresses (MPa): a) maximum, b) minimum

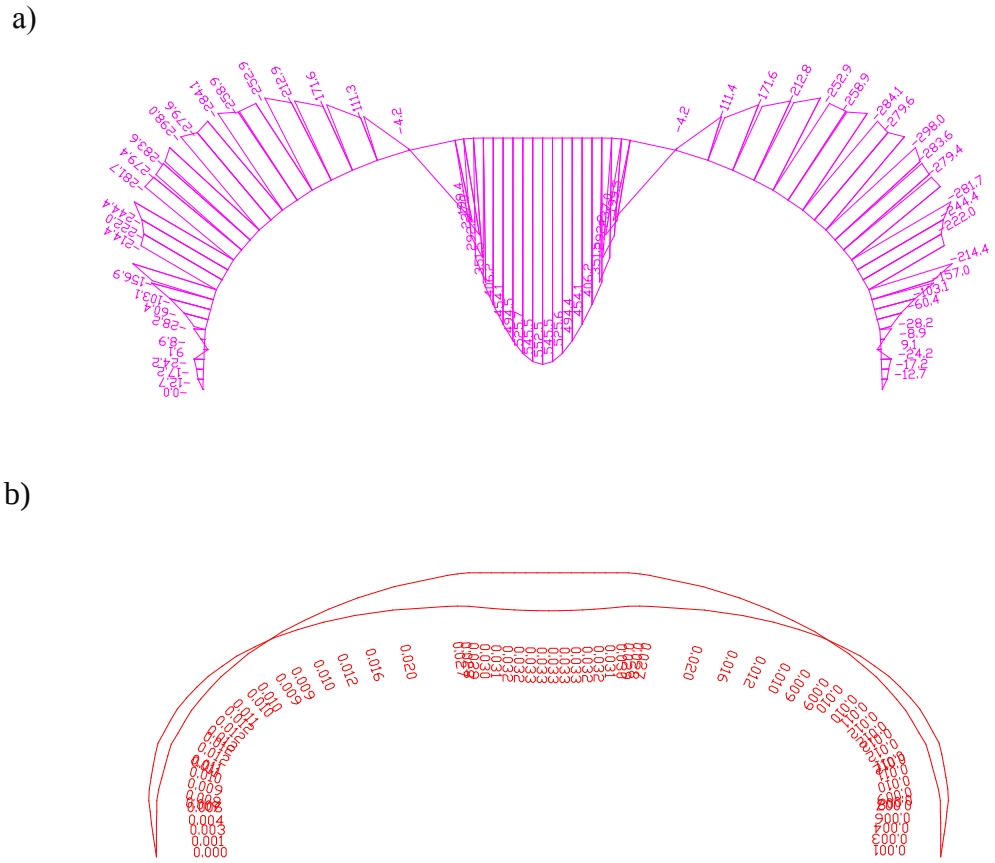


Figure 7 Distribution values: a) bending moment kN·m, b) deflection, m

a)

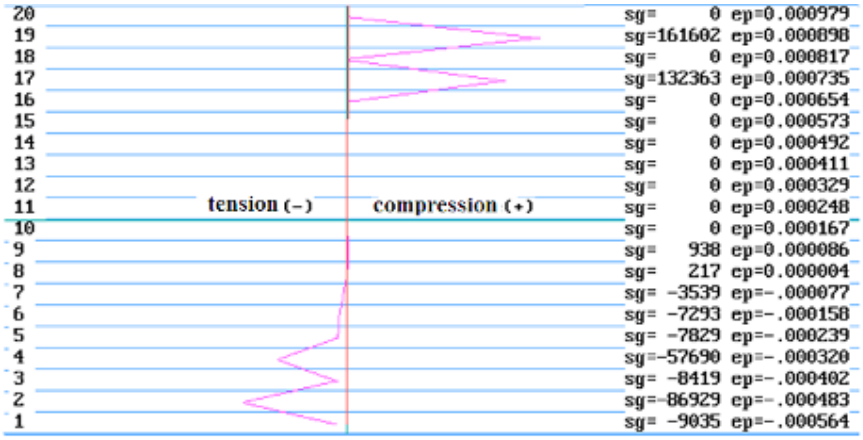


b)

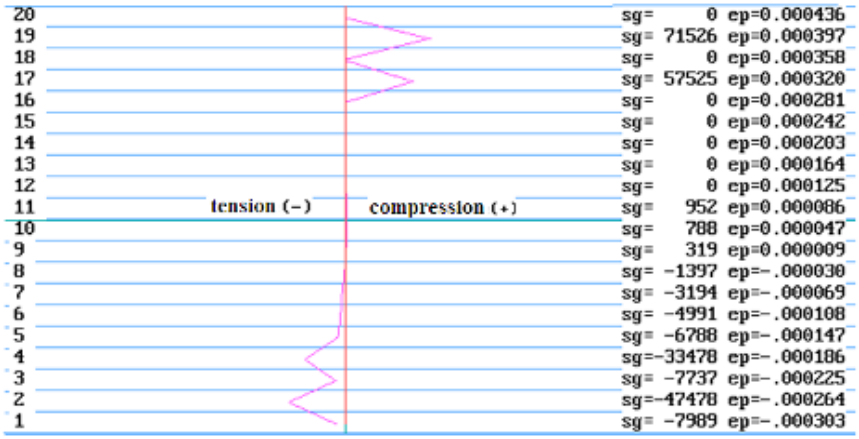


c)

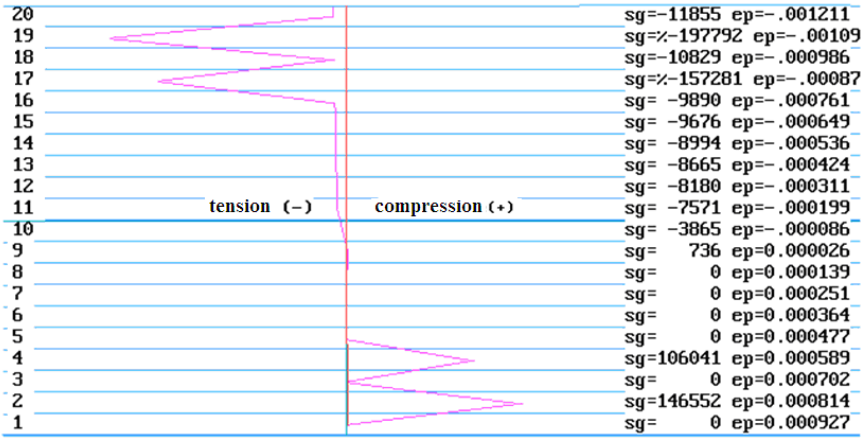


Figure 8. Distribution of stresses and strains in the cross-section of arch span elements on its height: a) element in the bottom left of the arch, b) element in the middle of semi-arch, c) element in the middle of arch

Elastoplastic calculation showed that consideration of nonlinear deformation diagrams of materials is changed stress distribution in the cross sections of the arched span. But in sections of span fracture have not occurred. Reinforcement in the tension zone and concrete in the compression zone are working with a significant margin. Figure 8 shows the results of elastoplastic calculation. Admissible width of disclosing of cracks, normal to a longitudinal axis of an element is equal 0,003 m.

## SUMMARY

In the present work, method and algorithm of analysis of reinforced concrete arched structures interacting with soil with the use of modern aspects of computational mechanics have been developed. Analysis involving a real-world problem was carried out by using the example of stressed-deformed of the reinforced concrete span of arched bridge. The major advantage of the proposed method of calculation consists in the ability to determine of character of deformation of the reinforced concrete arched structures with using of real diagram of deformation of their material. cross-section of arched structure the folded (triangular, trapezoid) or wavy outline.

During numerical investigation in the first phase has been estimated taking into account the dead weight of the arch, the weight of the overlapping pavement and surrounding ground. Then, consider the options, where the temporary motor load is moving in two variants: in the middle of a half-span and span of arch. Analyses show that the most loaded is considered the third variant, i.e. when the motor load is in the middle of the bridge. In this case, the arch structure accepts the maximum internal forces in its sections. Elastoplastic calculation showed that consideration of nonlinear deformation diagrams of materials are changed of the stress distribution in the cross sections of the arch. But in sections of the arch fracture have not occurred. Admissible width of disclosing of cracks, normal to a longitudinal axis of an element was equal 0,003 m.



## ACKNOWLEDGEMENTS

The author would like to acknowledge the support of the Chair of “Applied Mechanics” of TARI.


## REFERENCES


1. MIRALIMOV M. The simulation to model of elastoplastic behaviour of the tunnel heading on computer. Uzbek Journal. Problems of the Informatics and Energy. Informatika va energetika muammolari. Tashkent, № 5, 2001, pp. 47-50

2. MIRALIMOV M., ISHANHODJAEV A. A., SOKOLOV V. N. Bridges and pipes. State Committee of Architecture and Construction of Republic of Uzbekistan, Tashkent, 2012, p. 477

3. BAYKOV S.D. Reinforced concrete structures. M.: Stroyizdat, 1989, p. 423

4. MIRALIMOV M., ISHANHODJAEV A. A., ALMENOV KH., RAUPOV CH. S. Algorithmization of calculation the reinforced concrete structures with assumption of plastic deformation. Proceedings of the Republican scientifically-practical conference of «Saving technologies in rail transport». Tashkent, 24-25 December, 2012, pp. 149-150

# PERIDYNAMICS FOR CONCRETE STRUCTURES: A NEW EXPLICIT ANALYSIS METHOD

**H D Miranda**

**C Williams**

**J Orr**

University of Bath

United Kingdom

**ABSTRACT.** Optimisation of performance and reduction of costs of structures are major issues in engineering. However, this optimisation requires very accurate numerical models to predict the behaviour of the structures that are currently not available for concrete structures after they start cracking. Since concrete may develop cracks, which contradict the classical solid mechanics assumption of a continuum, the results obtained are in general not satisfactory. The classical theory of solid mechanics is formulated in terms of differential equations relying on the basic assumption of material continuity that does not exist in the cracked material. The presented model is based on the existing peridynamics theory which describes the mechanics of materials by employing integral equations, which are valid during cracking. The discretization of the structure in a set of material particles, correspondent interactions and an explicit scheme of integration based on Verlet method are described. Cracks can form by the breaking of interparticle bonds. The capacity of the model to predict the development of discrete cracks in tensile zones was verified with simple numerical tests. This work can provide the basis for more accurate strategies of predicting concrete structures and similar materials behaviour. The main consequences would be the reduction environmental impacts, cost of construction and also the development of new architectonic concepts along with developments in other industries.

**Keywords:** Peridynamics, Concrete, Structures, Explicit methods, Damage mechanics

**Dr H David Miranda** is a Research Fellow in the Department of Architecture & Civil Engineering, at the University of Bath. He's research is dedicated to the development of design tools for materials and structural optimization.

**Dr Chris Williams** is a structural engineer who worked for Ove Arup and Partners prior to joining the Department of Architecture & Civil Engineering, at the University of Bath. Chris has a particular interest in the relationship between geometrical form and structural action as applied to bridges, shells, tension structures and tall buildings.

**Dr John Orr** is an EPSRC Early Career Fellow and Lecturer (Assistant Professor) in the Department of Architecture and Civil Engineering at the University of Bath. His teaching and research are related to sustainable construction, with emphasis placed on concrete, and structural optimisation.

## INTRODUCTION

Research has already shown that concrete is inefficiently used by designers to the extent that significant reductions in material use could be achieved simply through design optimisation. Work by the authors has shown that optimization of reinforced concrete structures can provide material savings of up to 40%, with associated savings in embodied CO2 [1]. These material savings have been achieved by creating structures whose geometry reflects the requirements of their loading envelope.

The detailed structural analysis of reinforced concrete is a continuing challenge for engineers. Optimised structures, whose geometry is often outside the boundaries of existing test data, present additional challenges.

Current techniques for the analysis of reinforced concrete, including codified methods and finite element approaches, often cannot be applied to these non-conventional geometries. Finite element models cannot properly predict the behaviour of complex concrete structures at the ultimate limit state, due to the nature of concrete cracking. The underlying mathematics of the finite element approach assumes that the body being analysed remains continuous as it deforms (thereby allowing partial differential equations to calculate strains). If a crack is to form the material becomes discontinuous, and special techniques are required to continue the analysis.

A completely new approach is required to fully realise the potential of reinforced concrete as a sustainable material. This paper presents a new computational method for modelling concrete, known as peridynamics, which is based on integral equations. This paper will present initial proof of concept work which has shown the new method to be effective at modelling concrete cracking (overcoming a key computational challenge). The new analysis tool has the potential to facilitate robust optimisation of any concrete structure to minimise embodied energy in the built environment.

## MATHEMATICAL FORMULATION

The formulation considered in the presented model is based in the so-called peridynamic theory proposed by Silling [8] and developed in other articles (see for instance [2][3][4]). The theory is appropriate in situations where the continuity of the bodies is disrupted and therefore the classical theory of continuum solid mechanics and the finite element method are not appropriate. The peridynamic theory assumes the body is constituted by a set of particles connected by 'pairwise forces' that each particle develops with other surrounding particles. The interaction force that each pair of particles (1, 2) develop per unit of volume in the eularian configuration $\boldsymbol{f_{12}}$ is a function of their initial positions $\boldsymbol{X_1}$, $\boldsymbol{X_2}$ and their displacements $\boldsymbol{u_1}$, $\boldsymbol{u_1}$ and is given by Eq.(1).

$$\boldsymbol{f}_{12} = \boldsymbol{f}_{12}(\boldsymbol{u}_2 - \boldsymbol{u}_1, \boldsymbol{X}_2 - \boldsymbol{X}_1) \tag{1}$$

A more compact form for Eq.(1) is described in terms of relative positions $\Delta\boldsymbol{X} = \boldsymbol{X_2} - \boldsymbol{X_1}$and relative displacements $\Delta\boldsymbol{u} = \boldsymbol{u_2} - \boldsymbol{u_1}$ according to Eq.(2).

$$\boldsymbol{f}_{12} = \boldsymbol{f}_{12}(\Delta\boldsymbol{u}, \Delta\boldsymbol{X}) \tag{2}$$

This interaction between the generic particles located at $\boldsymbol{X_1}$, $\boldsymbol{X_2}$ among other particles is represented in Figure 1.

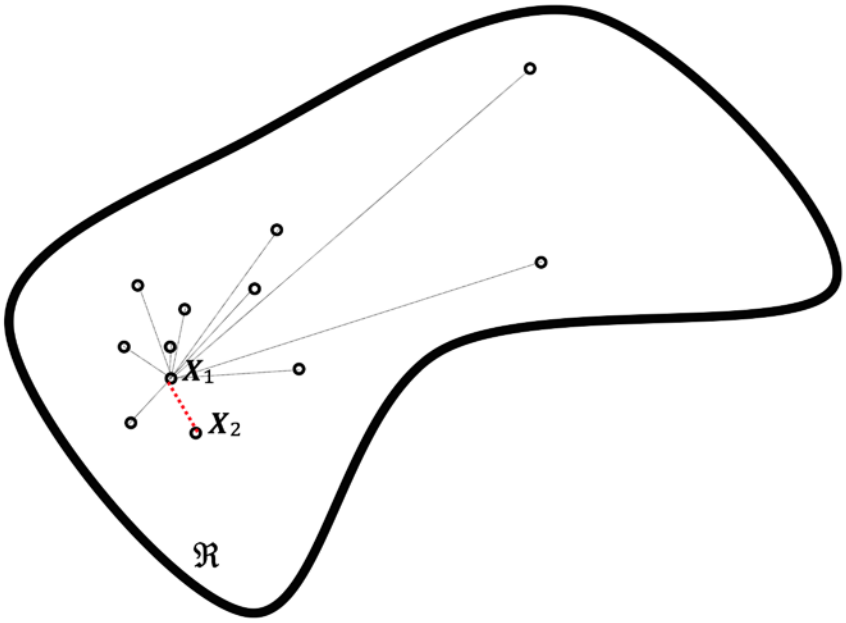


Figure 1 Possible interactions between the particle at $\boldsymbol{X_1}$ and other particles of the body, the interaction with the particle at $\boldsymbol{X_2}$ is highlighted.

If the domain of the body is considered to be a continuum then the resultant of all the interaction per unit of volume $\boldsymbol{l}(\boldsymbol{X})$ acting on a generic particle at the initial position $\boldsymbol{X}$, can be obtained by integration under the domain of the body $\mathfrak{R}$, as given by Eq.(3).

$$\boldsymbol{l}(\boldsymbol{X}) = \int_{\mathfrak{R}} \boldsymbol{f}_{12}(\boldsymbol{u}_0 - \boldsymbol{u}, \boldsymbol{X}_0 - \boldsymbol{X}) d\boldsymbol{X}_0 \tag{3}$$

If a generic point located at coordinates $\boldsymbol{X}$, with mass per unit volume $\rho = \rho(\boldsymbol{X})$, and acceleration $\ddot{\boldsymbol{u}} = \ddot{\boldsymbol{u}}(\boldsymbol{X})$ is actuated through its volume by body forces $\boldsymbol{b} = \boldsymbol{b}(\boldsymbol{X})$, then peridynamic equation of motion [8] is described by Eq.(4).

$$\rho\ddot{\boldsymbol{u}} = \boldsymbol{l} + \boldsymbol{b} \tag{4}$$

A particular case occurs in the absence of body forces, where static equilibrium is simply defined with the Eq.(5).

$$\boldsymbol{l} = \boldsymbol{0} \tag{5}$$

The *initial* configuration is *unstressed*, if the previous condition is achieved, since all the particles are *pairwise equilibrated* in that configuration [8]. This can be derived considering $\Delta\boldsymbol{u} = \boldsymbol{0}$ in Eq.(2), resulting in Eq.(6).

$$\boldsymbol{f}_{12}(\boldsymbol{X})(\boldsymbol{0}, \boldsymbol{X}_0 - \boldsymbol{X}) = \boldsymbol{0} \quad \forall \boldsymbol{X}_0 \in \mathfrak{R} \tag{6}$$

Newtown's third law states that the pair of interaction forces acting on any pair of particles should be symmetrical. Regarding the previous definitions this is expressed according to Eq.(7).

$$\boldsymbol{f}_{12}(\Delta\boldsymbol{u},\Delta\boldsymbol{X}) = -\boldsymbol{f}_{12}(-\Delta\boldsymbol{u},-\Delta\boldsymbol{X}) \tag{7}$$

A condition arising from the conservation of angular momentum is given in Eq.(8).

$$(\Delta\boldsymbol{u}+\Delta\boldsymbol{X})\times\boldsymbol{f}_{12}(\Delta\boldsymbol{u},\Delta\boldsymbol{X}) = 0 \tag{8}$$

Eqs.(7) and (8) imply that the interaction function always develops in the direction of the line connecting the particles. Therefore, the interaction function assumes the form given in Eq.(9).

$$\boldsymbol{f}_{12}(\Delta\boldsymbol{u},\Delta\boldsymbol{X}) = F_{12}(\Delta\boldsymbol{u},\Delta\boldsymbol{X})(\Delta\boldsymbol{u}+\Delta\boldsymbol{X}) \tag{9}$$

In Eq.(9), $F_{12}$ is a scalar valued function, defined so that the property in Eq.(10) is verified.

$$F_{12}(\Delta\boldsymbol{u},\Delta\boldsymbol{X}) = -F_{12}(-\Delta\boldsymbol{u},-\Delta\boldsymbol{X}) \tag{10}$$

Considering any linear operator symmetrical positive defined $\boldsymbol{R}$ (i.e. $\boldsymbol{R} = \boldsymbol{R}^{-T}$ ), then Eq.(11) should hold, for isotropic materials.

$$\boldsymbol{R}(\boldsymbol{f}_{12}(\Delta\boldsymbol{u},\Delta\boldsymbol{X})) = \boldsymbol{f}_{12}(\boldsymbol{R}(\Delta\boldsymbol{u}),\boldsymbol{R}(\Delta\boldsymbol{X})) \tag{11}$$

So far, the interaction function described depends only on the initial and deformed positions of the particles interacting i.e. is independent of the deformation history. However, history dependence can be introduced by employing a state variable $\boldsymbol{\alpha}$ so that the interaction function is defined in Eq.(12).

$$\boldsymbol{f}_{12} = \boldsymbol{f}_{12}(\Delta\boldsymbol{u},\Delta\boldsymbol{X},\boldsymbol{\alpha}) \tag{12}$$

The state variable can be used to describe the internal states of the material such as damage and plasticity.

**Model description**

In the described model the Eqs.(13) to (17), were employed to define the interaction function. Eq.(13) defines a temporary scalar variable called equivalent strain $\tilde{\varepsilon}_{12}$.

$$\tilde{\varepsilon}_{12}(\Delta\boldsymbol{u},\Delta\boldsymbol{X}) = \frac{(\Delta\boldsymbol{X}+\Delta\boldsymbol{u})^2 - \Delta\boldsymbol{X}^2}{2\Delta\boldsymbol{X}^2} \tag{13}$$

The equivalent strain, can also be defined in terms of relative displacements in the initial and final configurations by Eq.(14), which is more convenient for computational implementation.

$$\tilde{\varepsilon}_{12}(\Delta\boldsymbol{x},\Delta\boldsymbol{X}) = \frac{\Delta\boldsymbol{x}^2 - \Delta\boldsymbol{X}^2}{2\Delta\boldsymbol{X}^2} \tag{14}$$

The maximum equivalent displacement is defined with $\kappa_{12}$in Eq.(15).

$$\kappa_{12} = max\{\tilde{\varepsilon}_{12}\} \tag{15}$$

The state variable $\boldsymbol{\alpha}$ is employed to describe the state of the connection between particles according to Eq.(16).

$$\boldsymbol{\alpha} = \alpha = \begin{cases} 1 & if\ \kappa_{12} \leq \tilde{\varepsilon}_{crak} \\ 0 & if\ \kappa_{12} > \tilde{\varepsilon}_{crak} \end{cases} \tag{16}$$

In Eq.(16), $\tilde{\varepsilon}_{crak}$is a scalar material parameter defining the maximum equivalent strain in the connection between particles before the links break down. Therefore, if the link between particles is broken $\alpha = 0$, otherwise $\alpha = 1$.

The general form of the interaction force function mentioned in Eq.(1), was described above. However, the particular form expressed in Eq.(9) was assumed for this function. Furthermore, considering the variables described above in Eqs.(13) to (16), we assume the interaction function to be expressed according to Eq.(17).

$$\boldsymbol{f}_{12}(\Delta\boldsymbol{u}, \Delta\boldsymbol{X}, \alpha) = \alpha K \tilde{\varepsilon}_{12}.(\Delta\boldsymbol{u} + \Delta\boldsymbol{X}) \tag{17}$$

In Eq.(17), $K$ is a scalar material parameter representing the stiffness of the connection. Note that the equivalent strain can be approximated by Eq.(18).

$$\tilde{\varepsilon}_{12}(\Delta\boldsymbol{u}, \Delta\boldsymbol{X}) = \frac{(\Delta\boldsymbol{X} + \Delta\boldsymbol{u})^2 - \Delta\boldsymbol{X}^2}{2\Delta\boldsymbol{X}^2} \approx \frac{|\Delta\boldsymbol{u}|}{|\Delta\boldsymbol{X}|} \tag{18}$$

However, the equivalent shown in Eq.(14) is far more convenient since it does not require the evaluation of square roots, resulting in gains of efficiency. See [5] for more details.

## PSEUDO-CODE

The proposed algorithm is based in the Verlet method [6]. In the following a simple algorithm is proposed to discretize and and solve the peridynamic equations mentioned in the previous sections. Consider a system is composed by a set of $M$ material particles, and a set of $N$ fibres connection pairs of particles. Each particle $j \in [1, \ldots, M]$ consists of:

- position $\boldsymbol{x}_j$
- velocity $\boldsymbol{v}_j$
- resultant interaction force $\boldsymbol{f}_j$
- mass $m_j$

Each fibre $i \in [1, \ldots, N]$ connects two particles 1 and 2 consists of:

- logic flag indicating if the fibre is broken $\alpha_i$
- the numbers of particles that connects 1 and 2

The program starts by initializing the set of particles, the set of fibres and the initial simulation time to zero ($t = 0$). Then the time is increased of $\Delta t$ (time step) until the simulation time $t_f$ is achieved, executing procedure that follows.

(1) **loop**

(2) $t = t + \Delta t$

(3) **forall** fibres $i$ (connecting particles 1 and 2)

(4) update broken fibre flag: $b_i = b(\boldsymbol{x}_1, \boldsymbol{x}_2)$

(5) compute interaction force: $\boldsymbol{f}_i = \boldsymbol{f}(\boldsymbol{x}_1, \boldsymbol{x}_2, \alpha_i)$

(6) sum interaction force to the particles: $\boldsymbol{f}_1 = \boldsymbol{f}_1 + \boldsymbol{f}_i \quad \boldsymbol{f}_2 = \boldsymbol{f}_2 - \boldsymbol{f}_i$

(7) **endfor**

(8) **forall** particles $j$

(9) update velocity: $\boldsymbol{v}_j = \boldsymbol{v}_j + \boldsymbol{f}_j / m_j \,.\Delta t$

(10) **if** $j$ is constrained **then**

(11) set velocity to match the constrain: $\boldsymbol{v}_j = \boldsymbol{v}_{jc}$

(12) **endif**

(13) update position: $\boldsymbol{x}_j = \boldsymbol{x}_j + \boldsymbol{v}_j \,.\Delta t$

(14) reset the interaction force: $\boldsymbol{f}_j = \boldsymbol{0}$

(15) **endfor**

(16) **endloop**

Each time step corresponds to a calculation cycle, where the positions physical and quantities are updated following Newton's laws. The update of the broken fibre flag $b_i$ in line (4) above is given as a function of the positions of the connecting particles. Therefore, if a threshold elongation is achieved the fibre breaks. The computation of the interaction force on line (5) is given as a function of the elongation between the connected particles, and it is set to zero if the fibre is broken according to the expressions (13) to (17) previously mentioned.

## PRELIMINARY RESULTS

### Simple hinged beam

The initial concept described in the previous sections was used to predict the fracture pattern of a simple beam composed by a homogeneous material, with similar elasticity and tensile strength of a simple concrete C16/20, without reinforcement. The Elastic Modulus considered was 20GPa, and the tensile strength 2.0MPa.

The beam has dimensions of 0.3 x 0.4 x 3.0m, and it is constrained by hinged supports located at the edges, while a vertical displacement of 20mm is imposed in the mid-span. The beam

model was discretised with approximately 13.5 thousand particles and 2.71 million fibres connecting the particles. Graphic representation of the results was obtained using the open source software Paraview [7]. Figure 2 shows the deformation for 15% of the maximum displacement, where no damage is visible.

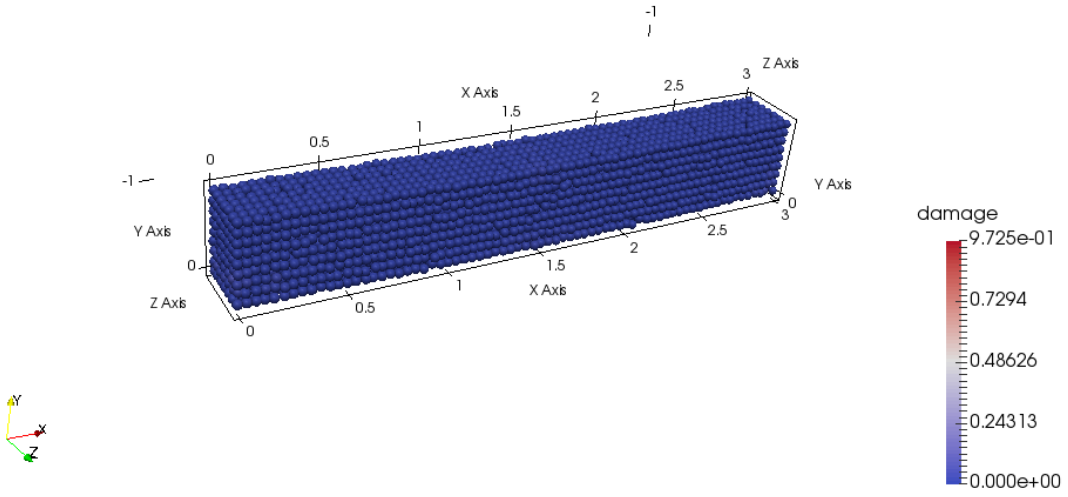


Figure 2 Contour plot of the damage (deformed configuration) for 15% of the maximum displacement.

When the imposed displacement is greater than 15%, a damaged region in bottom at the mid span of the beam becomes apparent, as represented in Figure 3.

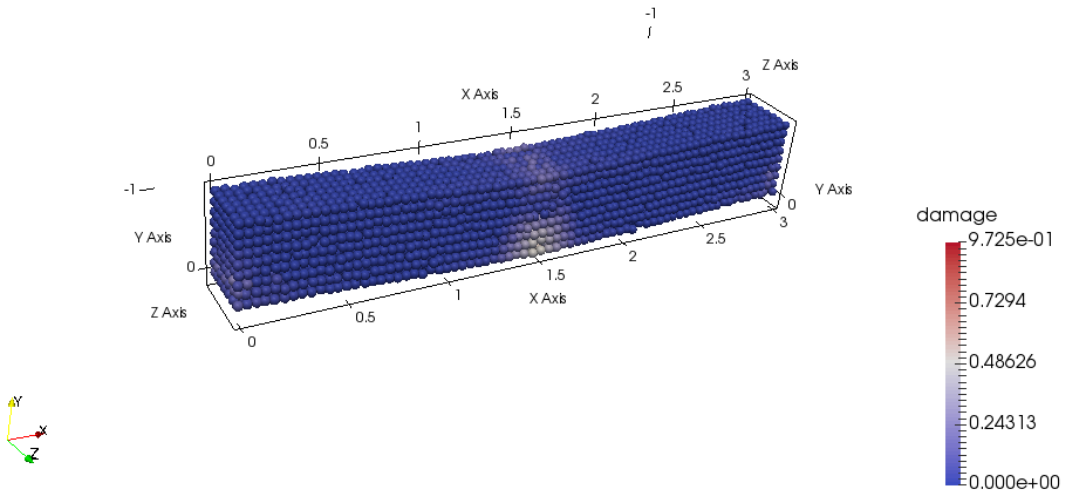


Figure 3 Contour plot of the damage(deformed configuration) for 20% of the maximum displacement.

The development of the crack in the mid span as the imposed displacement progress, results in the total destruction of the element as shown in Figure 4 and Figure 5.

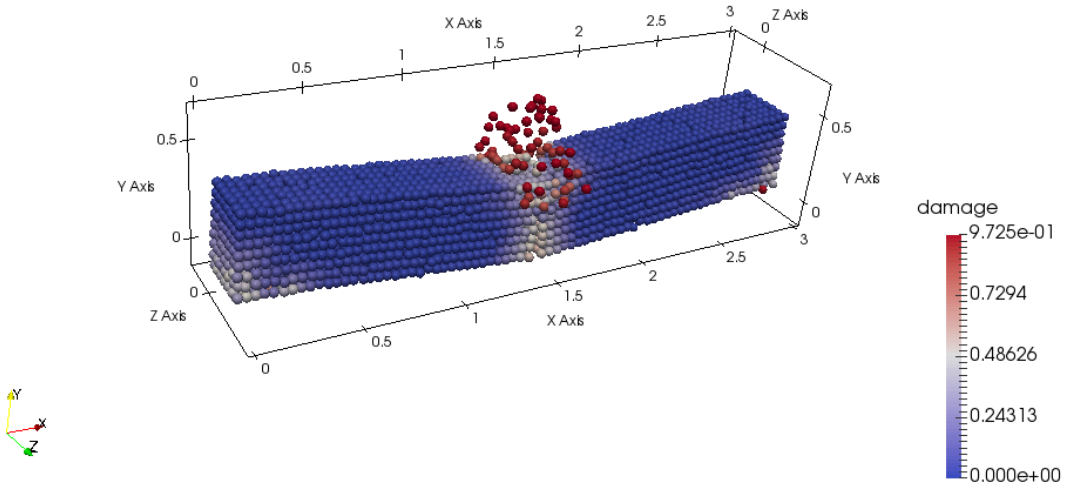


Figure 4 Contour plot of the damage (deformed configuration) for 55% of the maximum displacement.

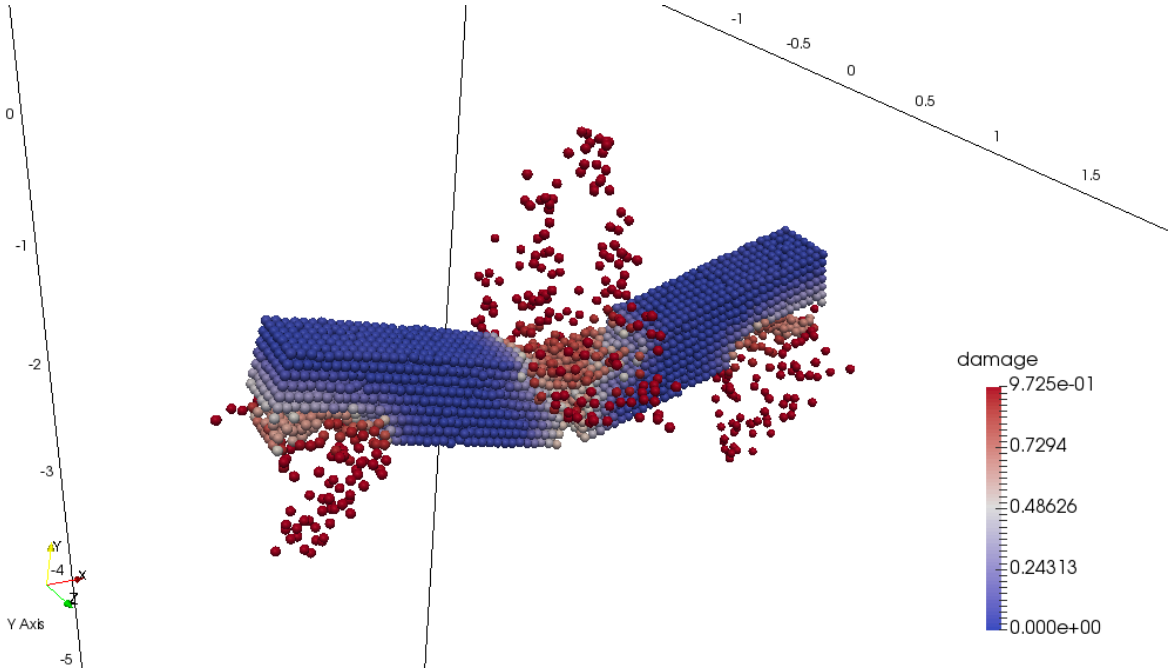


Figure 5 Contour plot of the damage(deformed configuration) for the maximum displacement.

Figure 6 describes the evolution of the moment in the mid-spam as the ratio between applied displacement and total displacement $\delta/\delta_{max}$ increases.

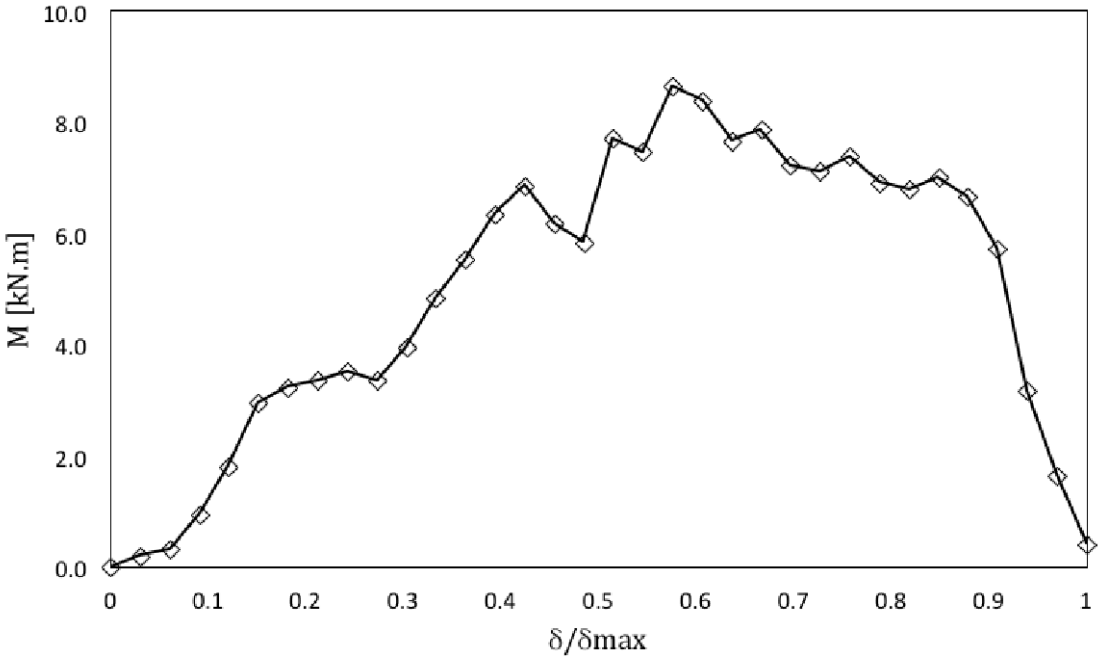


Figure 6 Evolution of the moment in the middle section with the imposed displacement.

**Reinforced beam model**

A model of the previously described beam including reinforcements of a linear elastic material with elasticity modulus 200GPa was considered. The reinforcement consisted of two bars near the top of the beam and two bars near the bottom, each of them with a diameter of 3mm. An increase in the moment capacity was verified. Figure 7 shows the contour plot of the damage obtained for this reinforced beam at 37% of the maximum displacement applied (20mm).

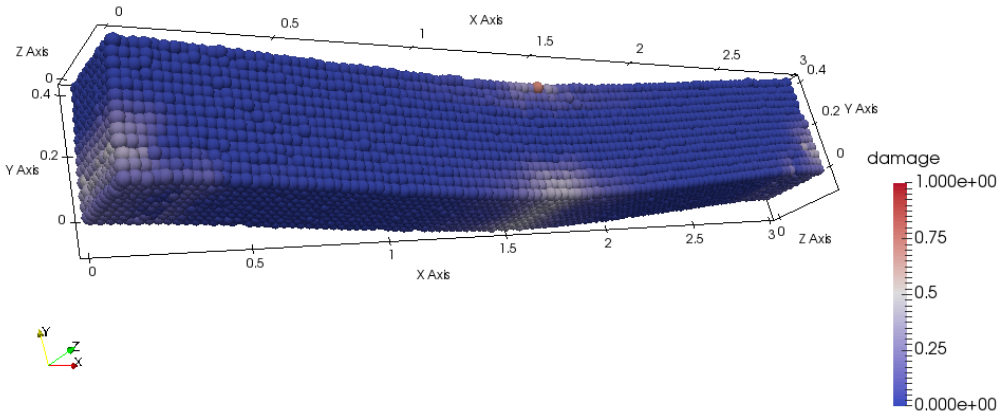


Figure 7 Contour plot of the damage (deformed configuration) for 37% of the maximum displacement.

It was found that damage by spalling, develops in the region where the displacement is applied and near the supports, due to the concentrated forces developed in the absence of distributing reinforcement, as it is apparent in Figure 7. Although, the failure of the beam occurs in shear due to the lack of vertical elements of reinforcement in the model, as shown in Figure 8.

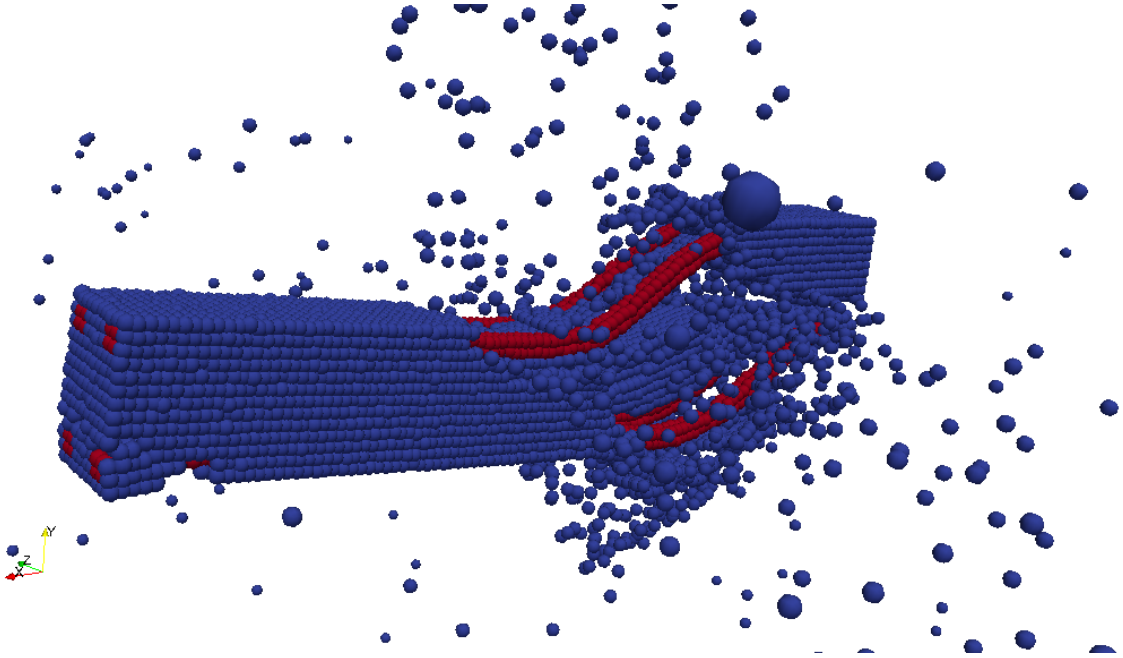

Figure 8 Deformed configuration for 79% of the maximum displacement (bulk material on blue, reinforcement bars on red).

The diagram of Figure 9, represents the evolution of the moment in the mid-span with the imposed displacement ratio $\delta/\delta_{max}$. That diagram describes an initial reduction of the resistant moment followed by a sudden reduction of the resistant moment as the imposed displacement progresses. This sudden reduction corresponds to the brittle failure of the beam depicted in Figure 8.

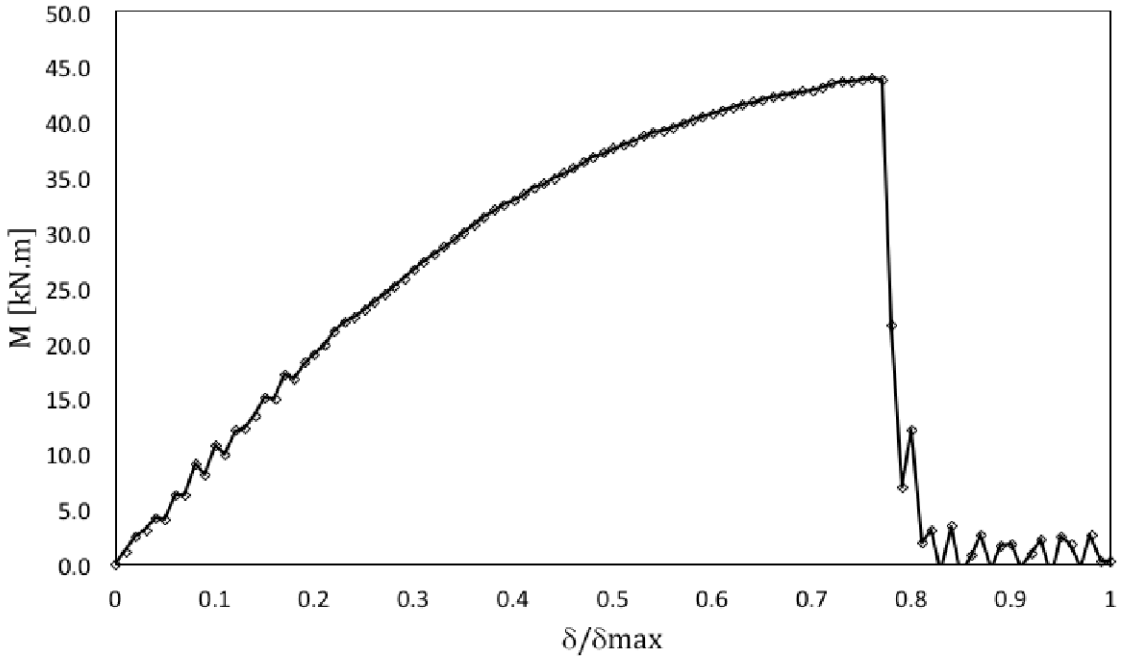


Figure 9 Evolution of the moment in the middle section compared to displacement of the reinforced beam.

## FUTURE WORK AND CONCLUSIONS

The results obtained reveal the potential of the model to reproduce cracking patterns and reduction of load carrying capacity. However, further tests and developments of the model are necessary:

- tests of a beam with longitudinal and shear reinforcement
- calibration of the interaction function and their parameters in comparison with other classical models and laboratorial tests
- improvements of the stability of the method.

However, the explicit scheme presented for the peridynamic equations provide an initial concept to be developed in the future that may lead to better predictions of concrete structures.

## ACKNOWLEDGEMENTS

This research was supported by the project, “Concrete Modelled Using Random Elements “, EP/M020908/1.

## REFERENCES

1. ORR, J. Flexible formwork for concrete structures. 2012. PhD Thesis. University of Bath.

2. SILLING S A., ASKARI E., Meshfree method based on the peridynamic model of solid mechanics, Computers & Structures, June 2005, Volume 83, Issues 17–18, pp1526-1535

3. GERSTLE W., SAU N., SILLING, S A., Peridynamic modeling of concrete structures, Nuclear Engineering and Design, July 2007, Volume 237, Issues 12–13, pp 1250-1258

4. GERSTLE, W.; SAU, N.; AGUILERA, E. Micropolar peridynamic modeling of concrete structures., 2007, Proceedings of the 6th International Conference on Fracture Mechanics of Concrete Structures.

5. WILLIAMS, C J K. Meshfree peridynamic computer modeling of concrete in three dimensions using randomly positioned particles, 2012, International conference on flexible formwork, , Bath, United Kingdom

6. VERLET, L., 1967, Computer “Experiments” on Classical Fluids. I. Thermodynamical Properties of Lennard−Jones Molecules,1967, Physical Review 159: pp.98–103

7. HENDERSON, A. ET AL. The ParaView Guide.2004. Clifton Park, NY: Kitware.

8. SILLING, S A. Reformulation of elasticity theory for discontinuities and long-range forces. Journal of the Mechanics and Physics of Solids, 2000, 48.1, pp 175-209

# EXPERIMENTAL STUDIES ON STATIC AND DYNAMIC MODULUS OF ELASTICITY OF HIGH VOLUMES OF SLAG CONCRETE

**T V Gowri**

BV Raju Institute of Technology Narsapur

**P Sravana P S Rao**

Jawaharlal Nehru Technology University

India

**ABSTRACT.** Ground Granulated Blast Furnace Slag is by-product of steel industry which is considered as waste material. Now-a- days, GGBFS is using as replacement material to cement in both research and application since it consists of cementitious properties, hydraulic property and to avoid the disadvantages of OPC. In the present investigations, Specimens of 150 mm cubes are cast and tested for Compressive strength at 28 Days and 90 Days. Specimens of size 150mm X 300mm cylinders of Ordinary Concrete (OC) and High Volumes of Slag Concrete (cement is replaced with 50% of GGBFS, HVSC) are cast and tested to find Static and Dynamic Modulus of Elasticity at 28 Days and 90 Days. Comparisons are made between OC and HVSC. The relation is made between Compressive Strength and Static Modulus of Elasticity of HVSC. And also other relation is developed between Static and Dynamic Modulus of Elasticity of High Volumes of Slag Concrete. The relations are $E_c = 303*(f_{ck})^{1.2}$ and $E_d = 1.8*(E_c)^{0.98}$ at all the time.

**Keywords:** GGBFS, Ordinary concrete, High volumes of slag concrete, Static and dynamic modulus of elasticity.

**T Vijaya Gowri** is an Assistant Professor in B.V. Raju Institute of Technology, Narsapur, specialized in Transportation Engineering.

**Dr P Sravana** is working as Professor in Jawaharlal Nehru Technology University, Hyderabad, specialized in Transportation Engineering. She has been associated with a number of Design projects, for number of organizations and involved as a key person in Quality control, Mix Designs and Bitumen Emulsion Tests

.

**Dr P Srinivasa Rao** is working as Professor in Jawaharlal Nehru Technology University, Hyderabad, specialized in Structural Engineering. He has been associated with a number of Design projects, for number of organizations and involved as a key person in Quality control and Mix Designs and has 26 years of academic, research and industrial experience.

## INTRODUCTION

Sustainable construction mostly targets at the decrease of undesirable environmental impact that has ensued by the construction industry which is the major consumer of the resources. Energy plays a dynamic role in progress of developing countries like India, in context of low availability of non-renewable energy sources joined with requirements of large quantities of energy to materials like cement, steel etc., the importance of industrial wastes as building materials cannot be undervalued. Over a period of time, waste management has become one of the most intricate and challenging problems in the world, which is distressing the environment. The Ground Granulated Blast Furnace Slag is a waste product of iron industry. It is comparatively most recent pozzolanic material that has acknowledged considerable attention in both research and application. It is now recognized as a desirable ingredient of concrete. Presently, total steel production in India about 72.20 million metric tonnes, but hardly 25% being used typically in cement production.

## LITERATURE REVIEW

The future blended cements appear more attractive due to the expansion in the choice of blending materials, adoption of performance oriented standards, precise tailor-making of niche-products, and improved and flexible manufacturing hardware [1]. Sulfates are commonly present in ground water, soil, sea water and effluent discharges from industry. Damage caused by sulfates has been observed particularly in foundations, sewage systems and marine structures. Sulfates react with calcium hydroxide ($Ca(OH)_2$) thus forming gypsum. Gypsum then may react further with tricalcium aluminate ($C_3A$) present in the concrete forming ettringite and monosulfoaluminate. These reactions cause extensive increase in volume so that subsequent cracking and peeling can occur [2].As slag cement content increases, permeability of concrete decreases. The microstructure of cementitious matrix is changed through the reaction of slag cement with calcium hydroxide and alkalis released during the Portland-cement hydration[3].The percentage level of GGBS in the binder, value of water-binder ratio and curing temperature are the variables considered in studies on strength behavior of mortars containing Portland cement and Ground Granulated Blast-furnace Slag (GGBS). At higher temperatures, all mortars show strength more rapidly and have a lower estimated ultimate strength [4]. The concentration of design mix is on synergistic interaction between Portland cement, slag by a judicious combination of fineness of slag, w/b ratio, level of cement replacement and superplasticizers. Such types of concretes exhibit dense, homogeneous and crack-free microstructure with reduced heat of hydration [5].

Concrete comprise GGBF slag is more vulnerable to poor curing conditions than ordinary concrete without GGBF slag. The strength loss is observed more in high volumes of slag concrete than normal concrete due to improper curing. So, comparatively with plain concrete longer curing duration is suggested for high volume slag cement concrete [6].The growth of compressive strength in case of slag concrete is insignificant at the early age of curing. The improvement in strength occurs at relatively rapid rate at later ages of curing which is depending upon mix proportion of slag with cement [7]. Concrete property can be sustained with advanced mineral admixtures like blast furnace slag powder as 5 to 30% of partial replacement of cement. The Compressive strength behavior of blast furnace slag concrete when cement replaced with different dosage of slag was studied. From experiments it was found that the optimum percentage of replacement of Ground Granulated Blast Furnace Slag Powder is 15%[8].At 28 days, the flexural strength of the together grinding Portland slag cements show

more or less the same values with the separately ground ones for all of the Blaine fineness values. Finally, the flexural strength of the separately ground Portland slag cements show higher values than the together grinding ones again for all of the Blaine fineness values at 90 days[9].Taguchi's approach of optimization is used to estimate effects of aggregates (coarse & fine) are replaced with that of Slag (Crystallized & Granular) on strength properties of concrete. The percentage improvement is observed as 5% to 7% when natural aggregate is replaced with the crystallized slag. At 30% to 50% replacement level, the strength improvements are observed. In all concrete applications, slag could be efficiently utilized as coarse & fine aggregates [10].

The distinct properties like high workability , long slump retention and gradual strength gain properties of MFGGBS has been used beneficially at field by modifying mix proportion of concrete originally designed. High strength Fly Ash based concrete with MFGGBS is highly economical [11].

When slag cement is used as part of the cementitious material in a concrete mixture, it reacts with $Ca(OH)_2$ to form additional CSH, which in turn lowers the permeability of the concrete. The higher percentage of slag cements in concrete mixes reduces the permeability of the concrete [12]. Blended HVFA concrete with individual SF or with equally combination of SF and slag to improve compressive strength and abrasion resistance [13].

Young's Modulus of concrete is studied on the basis of tri-axial compressive experiments. Two Empirical equations were proposed by the authors to calculate its static Young's modulus and dynamic Young's modulus for dynamic Poisson ratio $\mu_d$ varies nearly 0.20. P-wave velocity and elastic modulus varies with similar tendency as letter N. When the rate of loading increases, then $\mu$, $\mu_d$ decrease and $\mu_d$ has a great effect on the parameters $E_d$ and $E_D$ [14]. The fundamental flexural frequency is utilized to measure the dynamic modulus of concrete easily and accurately. It was known that the dynamic modulus of elasticity and the static modulus of elasticity are almost same for the mix design used in this study at similar stress levels below $0.4\ f_c$, where the stress-strain relation showed a linear behavior in that range. This was contrary to the general statement of having the dynamic modulus considerably higher than the static modulus. The dynamic modulus of the plain concrete specimens is lower as compared to reinforced specimens since the presence of micro cracks in plain concrete. The effect of reinforcement in concrete on the fundamental flexural frequency requires further investigations considering more and eccentric bars. The other parameters which affecting the dynamic modulus like moisture content, temperature, and mix proportions need to be investigated [15]. The compressive strength, flexural strength static elastic modulus and the dynamic modulus of elasticity of normal strength of concrete Mix (1) are lower comparing with the high strength of concrete Mix. From results, the influence of the crushed rock aggregate does not perceptible in Mix (1) consequently; the role of coarse aggregate on all properties of high strength concrete is obvious in Mix (2). There is a simple linear relationship between the static and dynamic elastic moduli, which tend to predict static modulus of elasticity using dynamic elastic modulus, may avoid the problems in determining the static elastic modulus of concrete [16]. The dynamic and static modulus tests were carried out at the University of Illinois laboratories confirm that ultrasonic pulse velocity (UPV – ASTM C597) gives longitudinal vibration the lowest and the highest predictions of $E_d$ and the variation of values of $E_d$, depending on method of measurement. In the vibration methods, longitudinal vibration of cylinders (L/D=2) show the least accurate prediction of $E_d$. For longitudinal resonances for cylinders, a modified method (Love's correction) was introduced, which provides more accurate results of $E_d$ that accept with results from the transverse method with an absolute mean error of estimate of 1.10 GPa. UPV may be able to give accurate estimates of E, but the extremely high values of

Poisson's ratio are considered in the calculations. A further study in this area is warranted. It was originate that the transverse method provides higher ($E_d$) estimates than longitudinal method of ASTM C215 for the same sample. As predictable, $E_d$ is always greater than E for concrete; however, this behavior may be because of the composite nature of concrete, rather than non-linear behavior of concrete due to varying strain levels [17]. The effect of percentage of steel fibres and their aspect ratio on the modulus of elasticity of concrete. In this study Hook end steel fibres with aspect ratio of 50 and 71 at volume fractions of 0.5%, 1.0% and 1.5% were used. The optimum fibre volume fraction of 1.5% shows better performance in terms of strength for both the aspect ratios. Fibre with aspect ratio of '71' exhibits better result as compared to fibre with aspect ratio of 50. At a constant aspect ratio of fibre, the modulus of elasticity of Steel Fibre Reinforced Concrete is observed to increase with an increase in the fibre volume fraction. Gain in the ultimate stress and ultimate strain over plain concrete increases with an increase in the fibre content and aspect ratio of fibres [18]. The steel slag without free lime was used as substituting material the coarse aggregates in concrete. The results revealed that the compressive strength and flexural strength for slag concrete was slightly more than the natural gravel concrete. The splitting tensile strength and modulus of elasticity were higher, while drying shrinkage was lower than the natural gravel concrete and no negative effects on short term properties of hardened concrete are observed. The Young's modulus of elasticity E of steel slag aggregates concrete at 28 days was $5 \times 10^6$ Psi (34.3 GPa) while it was $4 \times 10^6$ Psi (27.9 GPa) for gravel concrete. The improvement in strength properties of steel slag aggregate concrete influenced by shape of particles and surface texture which improves adhesion and bond between particles and the cement matrix [19].

## EXPERIMENTAL INVESTIGATIONS

**Cement:** Locally available 53 grade of Ordinary Portland Cement (Ultratech Brand.) confirming to IS: 12269 was used in the investigations. The cement is tested for various properties like Normal consistency, specific gravity, Fineness, Soundness, Compressive Strength, and Specific Surface area were found to be 28%, 3.10, 4%, 0.5 mm, 53Mpa and 3100 $cm^2/g$ in accordance with IS:12269-1987.

**GGBFS:** Ground Granulated Blast Furnace Slag (GGBFS) which is available in local was procured from Steel Plant, Visakhapatnam (Dt.), Andhra Pradesh. The physical requirements in accordance with IS 1727- 1967 (Reaffirmed2008) and chemical requirements in accordance with IS: 12089 – 1987 (Reaffirmed 2008). The GGBFS is tested for various properties like Specific gravity and Fineness were found to be 2.86 and 3500 $cm^2/g$.

**Superplasticizer**: The Super plasticizer utilized was supplied by internationally reputed admixture manufactures. Endure flowcon04 was manufactured by Johnson. Endure flowcon04 is dark brown colored liquid and it is based as sulphonated naphthalene formaldehyde (SNF) super plasticizer. It complies with IS: 9103-1999, BS5075, ASTM C-494 was used. The super plasticizer is tested for properties like density and pH were found to be 1.2 and minimum 6.

**Fine Aggregate:** The locally available river sand is used as fine aggregate in the present investigation. The sand is free from clay, silt, and organic impurities. The sand is tested for various properties like specific gravity, water absorption and fineness modulus of fine aggregate were found to be 2.55,1.72 and 2.74 in accordance with IS:2386-1963.

**Coarse Aggregate:** Machine crushed angular granite metal of 20mm nominal size from the local source is used as coarse aggregate. It is free from impurities such as dust, clay particles

and organic matter etc., the coarse aggregate is also tested for its various properties. The specific gravity, water absorption and bulk density and fineness modulus of coarse aggregate were found to be 2.60, 0.38, 1490 kg/m$^3$ and 7.16 respectively.

**Water:** Locally available water used for mixing and curing which is potable, shall be clean and free from injurious amounts of oils, acids, alkalis, salts, sugar, organic materials or other substances that may be deleterious to concrete or steel.

**Modulus of Elasticity**

The cylindrical specimens 150mm in diameter and 300mm long, cast for various water/binder ratios of ordinary concrete and high volumes of slag concrete were tested in the laboratory for Static Modulus of elasticity, Poisson's ratio and Dynamic Modulus of elasticity.

**Static Modulus of Elasticity and Poisson's Ratio**

Concrete is not a perfectly elastic material and it deforms when load is applied but this deformation does not follow any simple set rule. The deformation depends upon the magnitude of the load, elapsed time after which the observation it made. Modulus of elasticity may be measured in tension, compression or shear. Modulus of elasticity of concrete increases approximately with the square root of the strength. The IS-456 of 2000 gives modulus of elasticity as $E_c = 5000(f_{ck})^{1/2}$. $E_c$ : Short term static modulus of elasticity in N/mm$^2$.

Cylinders of 150mm X 300mm of Ordinary Concrete and High Volumes of Slag Concrete are cast and tested in Universal testing machine for maximum load and axial strain as per IS 9221-1979 (Reaffirmed-1996). The deflections are being taken by using dial gauge. From the observations, stress, axial strain ($\varepsilon_a$) and diametric strain ($\varepsilon_d$) are calculated. Then, Young's modulus and Poisson's ratio have been calculated using above findings.

**Dynamic Modulus of Elasticity**

Dynamic modulus is modulus found out by using Non-destructive testing method. This test is conducted as per IS 13311 (Part-1):1992. In the present investigation Ultrasonic Pulse velocity tester is used for determining the pulse velocity of Cylinders of 150mm X 300mm of Ordinary Concrete and High Volumes of Slag Concrete are cast and tested concrete. The ultrasonic pulse is produced by the transducer which is held in contact with one surface of the concrete member under test. After traversing a known path length (L) in the concrete, the pulse of vibrations is converted into an electrical signal by the second transducer held in contact with the other surface of the concrete member and the electronic timing circuit enables the transit time (T) of the pulse is to be measured. The pulse velocity (V) is given by: V=L/T

The ultrasonic pulse velocity of concrete is mainly related to its density and modulus of elasticity. The quality of concrete in terms of uniformity, incidence or absence of internal flaws, cracks and segregation etc. indicative of the level of workmanship employed, can thus be assessed using the guidelines given in table below which have been evolved for characterizing the quality of concrete in structures in terms of the ultrasonic pulse velocity.

Table 1 Velocity criterion for concrete quality grading

| S NO | PULSE VELOCITY BY CROSS PROBING, km/sec | CONCRETE QUALITY GRADING |
|---|---|---|
| 1 | Above 4.5 | Excellent |
| 2 | 3.5 to 4.5 | Good |
| 3 | 3.0 to 3.5 | Medium |
| 4 | Below 3.0 | Doubtful |
| Note_ In case of 'Doubtful' quality it may be necessary to carry out further tests. | | |

The Dynamic Young's modulus of elasticity (E) of the concrete may be determined from the pulse velocity and Dynamic Poisson's ratio (μ), using the following relationship:

$$\mathrm{E} = \frac{\rho\,(1+\mu)(1-2\mu)}{1-\mu} V^2$$

Where

E = Dynamic Young's Modulus of Elasticity in MPa

$\rho$ = density in kg/m$^3$, and

$V$ = Pulse velocity in m/second.

## RESULTS AND DISCUSSIONS

The quantities of materials for one cubic meter of Ordinary Concrete and High Volumes of Slag Concrete are shown in Table 2. Concrete mixes are designed with the results obtained from the tests on cement, Ground Granulated Blast Furnace Slag, Fine Aggregate and Coarse Aggregate. The workability of different concretes mixes was measured using Slump Cone Apparatus. The test results for Ordinary Concrete and High Volumes of Slag Concrete are given in Table 2.

It can be observed from the table that a medium workability was maintained for almost all the mixes. The superplasticizer was added in required quantities to achieve required workability. Table 3 describes compressive strengths of OC and HVSC for 28 days and 90 days. It was observed that compressive strength of concrete with lower w/c ratio or w/b ratio improved in both the cases of OC and HVSC for 28 days and 90 days.

Table 2 Mix proportions

| W/B RATIO | WATER | CEMENT | GGBFS | Fine Aggregate | Coarse Aggregate | SP*, ml | SLUMP, mm |
|---|---|---|---|---|---|---|---|
| | kg/m³ | | | | | | |
| OPC Mixes | | | | | | | |
| 0.55 | 176 | 320 | 0 | 786 | 1020 | 0 | 80 |
| 0.45 | 176 | 392 | 0 | 743 | 1004 | 1185 | 70 |
| 0.36 | 176 | 488 | 0 | 659 | 1009 | 2470 | 85 |
| 0.27 | 176 | 625 | 0 | 518 | 1025 | 3295 | 120 |
| HVFC Mixes | | | | | | | |
| 0.55 | 176 | 160 | 160 | 763 | 990 | 0 | 75 |
| 0.45 | 176 | 196 | 196 | 715 | 966 | 0 | 65 |
| 0.36 | 176 | 244 | 244 | 625 | 961 | 2122 | 100 |
| 0.27 | 176 | 326 | 326 | 477 | 945 | 4698 | 140 |

*Superplasticizer

Table 3 Compressive strengths of ordinary concrete and high volumes of slag concrete

| W/B RATIO | COMPRESSIVE STRENGTH, MPa | | | |
|---|---|---|---|---|
| | Ordinary Concrete | | High Volumes of Slag Concrete | |
| | 28 days | 90 days | 28 days | 90 days |
| 0.55 | 38.94 | 39.36 | 29.09 | 35.7 |
| 0.45 | 53.24 | 61.76 | 33.90 | 40.31 |
| 0.36 | 64.22 | 76.80 | 42.00 | 51.30 |
| 0.27 | 72.61 | 85.78 | 54.00 | 62.00 |

**Static Modulus of Elasticity and Dynamic Modulus of Elasticity of Ordinary Concrete:**

Static Modulus of Elasticity of Ordinary Concrete exhibits an increasing tendency in its value i.e., from 29091 to 49995 MPa as water-cement ratio varies from 0.55 to 0.27 at 28 Days and the results are shown in Table 4 and Figure 1. The behavior of Dynamic Modulus of Elasticity is showing increasing tendency in its value i.e., from 31100 to 46753 MPa as water-cement ratio varies from 0.55 to 0.27 whereas Poisson's ratio is decreasing, its value from 0.32 to 0.18 for w/c ratios varying from 0.55 to 0.27 at 28 Days and the results are shown in Table 4 and Figure 1. The ratio of Static Modulus of Elasticity ($E_c$) to Dynamic Modulus of Elasticity ($E_d$) of OC varies between 0.94 and 1.07 at 28 days. Static Modulus of Elasticity exhibits an increasing tendency in its value i.e., from 30117 to 51515MPa as water-cement ratio varies from 0.55 to 0.27 at 90 Days and the results are shown in Table 5 and Figure 2. Dynamic Modulus of Elasticity of OC possesses an increasing tendency in its value i.e., from 35651 to 54901MPa as water-cement ratio varies from 0.55 to 0.27 whereas Poisson's ratio of OC is

decreasing, its value from 0.29 to 0.15 for w/c ratios varying from 0.55 to 0.27 at 90 Days and the results are shown in Table 5 & Figure 2. The ratio of Static Modulus of Elasticity ($E_c$) to Dynamic Modulus of Elasticity ($E_d$) of OC varies between 0.84 and 0.95 at 90 days. From the results, it is observed that an increment in Static and Dynamic Modulus of Elasticity and decrease in Poisson's ratio of OC at 90 days is found comparing with 28 Days result.

Table 4 Static modulus of elasticity and dynamic modulus of elasticity of ordinary concrete at 28 days

| NO | w/ c ratio | TIME, µs | PULSE VELOCITY, km/sec | DENSITY, kg/m$^3$ | STATIC MODULUS, $E_c$ MPa | Poisson's ratio, µ | Dynamic Modulus, $E_d$, MPa | $E_c/E_d$ |
|---|---|---|---|---|---|---|---|---|
| 1 | 0.55 | 69.6 | 4.26 | 2451 | 29091 | 0.32 | 31100 | 0.94 |
| 2 | 0.45 | 66.6 | 4.51 | 2464 | 37720 | 0.29 | 38251 | 0.99 |
| 3 | 0.36 | 66.5 | 4.52 | 2469 | 44678 | 0.24 | 42835 | 1.04 |
| 4 | 0.27 | 66.3 | 4.53 | 2474 | 49995 | 0.18 | 46753 | 1.07 |

Table 5 Static modulus of elasticity and dynamic modulus of elasticity of ordinary concrete at 90 days

| NO | w/ c ratio | TIME, µs | PULSE VELOCITY, km/sec | DENSITY, kg/m$^3$ | STATIC MODULUS, $E_c$ MPa | Poisson's ratio, µ | Dynamic Modulus, $E_d$, MPa | $E_c/E_d$ |
|---|---|---|---|---|---|---|---|---|
| 1 | 0.55 | 74.0 | 4.31 | 2515 | 30117 | 0.29 | 35651 | 0.84 |
| 2 | 0.45 | 66.4 | 4.532 | 2635 | 44576 | 0.19 | 49296 | 0.90 |
| 3 | 0.36 | 66.2 | 4.591 | 2643 | 48921 | 0.18 | 51305 | 0.95 |
| 4 | 0.27 | 65.0 | 4.678 | 2649 | 51515 | 0.15 | 54901 | 0.94 |

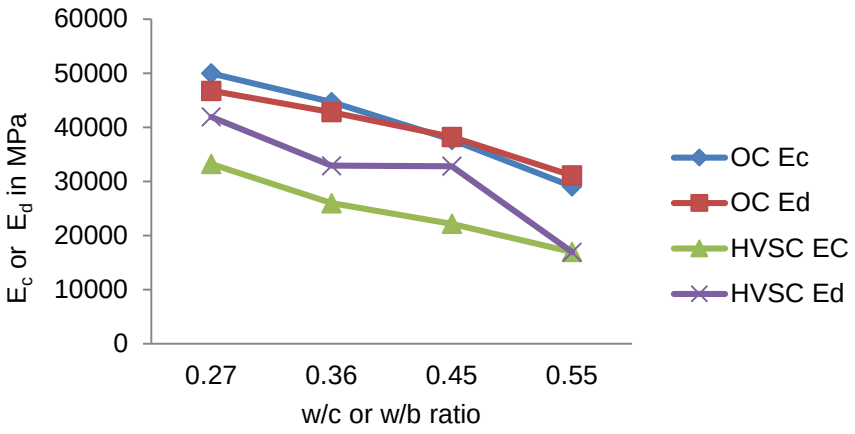


Figure 1 Static and Dynamic Modulus of Elasticity of OC and HVSC at 28 Days

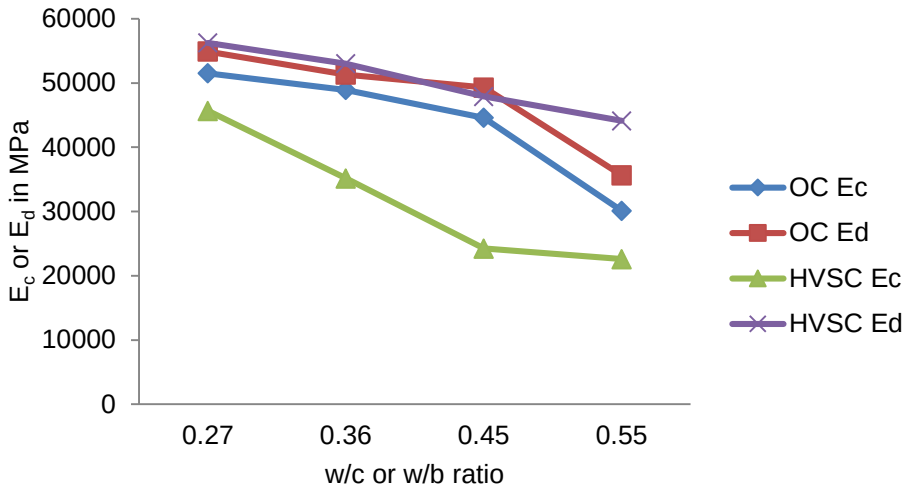


Figure 2 Static and dynamic modulus of elasticity of OC and HVSC at 90 days

**Static Modulus of Elasticity and Dynamic Modulus of Elasticity of High Volumes of Slag Concrete:**

From the Table 6 and Figure 3, it is observed that Static Modulus of Elasticity possesses an increasing tendency in its value i.e., from 16970 to 33239 MPa as water-binder ratio varies from 0.55 to 0.27 whereas Poisson's ratio of HVSC is decreasing, its value from 0.43 to 0.26 for w/b ratios varying from 0.55 to 0.27 at 28 Days. Dynamic Modulus of Elasticity of HVSC shows an increasing tendency in its value i.e., from 16936 to 41939 MPa as water-binder ratio varies from 0.55 to 0.27 at 28 Days and the results are shown in Table 6 and Figure 1. The ratio of Static Modulus of Elasticity ($E_c$) to Dynamic Modulus of Elasticity ($E_d$) of HVSC varies between 0.67 and 1.0 at 28 days.

From the Table 7 and Figure 4, it is observed that Static Modulus of Elasticity of HVSC exhibits an increasing tendency in its value i.e., from 22596 to 45653 MPa as water-binder ratio varies from 0.55 to 0.27 whereas Poisson's ratio of HVSC is decreasing, its value from 0.31 to 0.23 for w/b ratios varying from 0.55 to 0.27 at 90 Days.

Dynamic Modulus of Elasticity of HVSC possesses an increasing tendency in its value i.e., from 44121 to 56250MPa as water-binder ratio decreases from 0.55 to 0.27 at 90 Days and the results are shown in Table 7 and Figure 2. From the results, it is observed that an increment of Static and Dynamic Modulus of Elasticity of HVSC at 90 days is found comparing with 28 Days result.

The ratio of Static Modulus of Elasticity ($E_c$) to Dynamic Modulus of Elasticity ($E_d$) of HVSC varies between 0.51 and 0.81 at 90 days. From the results, it is revealed that the difference in Modulus of elasticity of HVSC is less comparing with OC though it consists of 50% of cement content. The relation of Compressive Strength with Static Modulus of elasticity and Static Modulus of Elasticity with Dynamic Modulus of Elasticity of HVSC are showing non-linear at all Days also.

As per IS 456 the relation between Compressive Strength and Static Modulus of Elasticity is

$E_c = 5000 (f_{ck})^{1/2}$

Similar trend is achieved in the case of High Volumes of Slag Concrete. However, the relations between Static Modulus of Elasticity and Dynamic Modulus of Elasticity of High Volumes of Slag Concrete are also non-linear whereas most of the cases, linear equations were developed for OC by many researchers. Figure 3 shows the relation between Compressive Strength and Static Modulus of Elasticity of HVSC at all the time. Figure 4 shows the relation between Static Modulus of Elasticity and Dynamic Modulus of Elasticity of HVSC at all days.

The relations are

$$E_c = 303.03 *( f_{ck} )^{1.199}$$ with **'$R^2$'** equal to 0.90

Approximately, $E_c = 303 *( f_{ck} )^{1.2}$

and

$$E_d = 1.805*E_c^{0.9768}$$ with **'$R^2$'** equal to 0.99

Approximately, $E_d = 1.8*E_c^{0.98}$ with **'$R^2$'** equal to 0.94

Where

$f_{ck}$ = Characteristic Compressive Strength of High Volumes of Slag Concrete in MPa.

$E_c$ = Static Modulus of Elasticity of High Volumes of Slag Concrete in MPa.

$E_d$ = Dynamic Modulus of Elasticity of High Volumes of Slag Concrete in MPa.

High Volumes of Slag concrete exhibits 'Good and Excellent Quality Grading' when the pulse velocity through the specimens comparing with the standard Table 1 at 28 days and 90 days respectively.

Static Modulus elasticity and Dynamic Modulus of elasticity test setups are shown in Figure 5 to Figure 6 respectively.

Table 6 Static modulus of elasticity and dynamic modulus of elasticity of high volumes of slag concrete at 28 days

| NO | w/ c ratio | TIME, µs | PULSE VELOCITY, km/sec | DENSITY, kg/m$^3$ | STATIC MODULUS, $E_c$ MPa | Poisson's ratio, µ | Dynamic Modulus, $E_d$, MPa | $E_c/E_d$ |
|---|---|---|---|---|---|---|---|---|
| 1 | 0.55 | 61.5 | 4.39 | 2502 | 16970 | 0.43 | 16936 | 1.0 |
| 2 | 0.45 | 61.0 | 4.405 | 2508 | 22174 | 0.33 | 32842 | 0.67 |
| 3 | 0.36 | 60.7 | 4.41 | 2509 | 25991 | 0.33 | 32933 | 0.78 |
| 4 | 0.27 | 59.0 | 4.51 | 2523 | 33239 | 0.26 | 41939 | 0.79 |

Table 7 Static modulus of elasticity and dynamic modulus of elasticity of high volumes of slag concrete at 90 days

| NO | w/ c ratio | TIME, μs | PULSE VELOCITY, km/sec | DENSITY, kg/m$^3$ | STATIC MODULUS, $E_c$ MPa | Poisson's ratio, μ | Dynamic Modulus, $E_d$, MPa | $E_c/E_d$ |
|---|---|---|---|---|---|---|---|---|
| 1 | 0.55 | 68.2 | 4.88 | 2568 | 22596 | 0.31 | 44121 | 0.51 |
| 2 | 0.45 | 68.1 | 4.94 | 2572 | 24226 | 0.29 | 47897 | 0.51 |
| 3 | 0.36 | 68.0 | 4.96 | 2585 | 35144 | 0.25 | 52996 | 0.66 |
| 4 | 0.27 | 67.8 | 5.01 | 2598 | 45653 | 0.23 | 56250 | 0.81 |

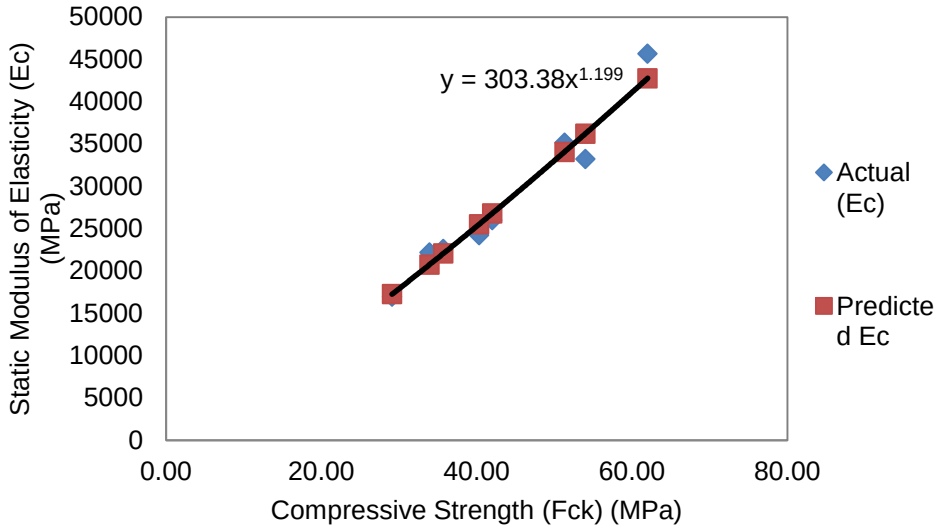


Figure 3 Relation between $f_{ck}$ and Actual $E_c$ and $f_{ck}$ and Predicted $E_c$ at of HVSC at all days.

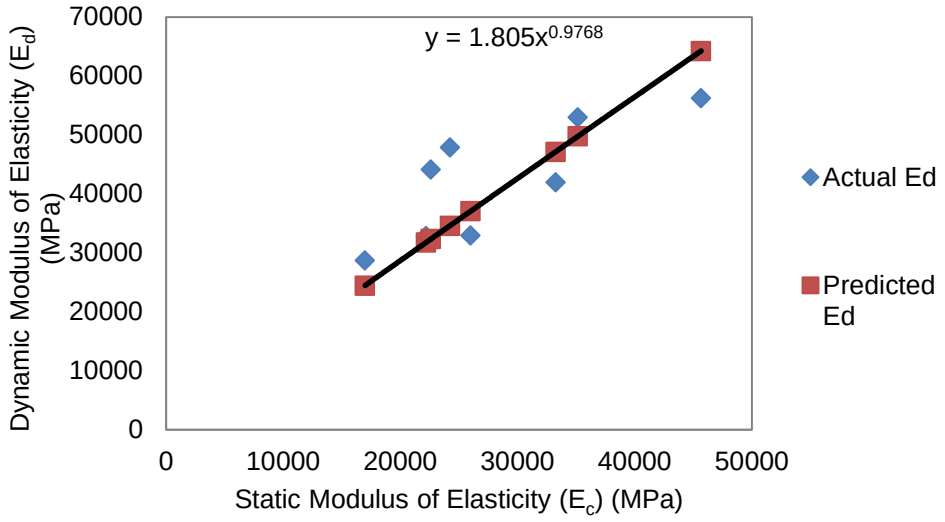

Figure 4 Relations between $E_c$ and Actual $E_d$ and Predicted $E_d$ of HVSC at all days.

Figure 5 Test Setup for finding Young's Modulus

Figure 6 Test setup for Ultrasonic Pulse Velocity

## CONCLUSIONS

The following conclusions are made from the results

- Static Modulus of Elasticity and Dynamic Modulus of Elasticity of HVSC at 90 days is higher when compared to 28 Days result.
- Static Modulus of Elasticity of OC and HVSC increases with increase in Compressive Strength.
- Static and dynamic moduli of elasticity improve with the lower water/binder ratio.

- The relations of Compressive Strength with Static Modulus of elasticity and Static Modulus of Elasticity with Dynamic Modulus of Elasticity of HVSC are non-linear at all times.

- The pulse velocity is observed for the case of High Volumes of Slag concrete from 4.39 km/sec to 5.01km/sec which proves HVSC is good quality concrete.

- The ratio of Static Modulus of Elasticity ($E_c$) to Dynamic Modulus of Elasticity ($E_d$) of OC varies from 0.94 to 1.07 for 28 days and 0.84 to 0.95 for 90 days.

- The ratio of Static Modulus of Elasticity ($E_c$) to Dynamic Modulus of Elasticity ($E_d$) of HVSC varies from 0.67 to 1.0 for 28 days and 0.51 to 0.81 for 90 days.

- The relation between Compressive Strength and Static Modulus of Elasticity of HVSC at all days is $E_c = 303 *( f_{ck} )^{1.2}$ with '$R^2$' equal to 0.90.

- The relation between Static Modulus of Elasticity and Dynamic Modulus of Elasticity of HVSC at all days is $E_d = 1.8*E_c^{0.98}$ with '$R^2$' equal to 0.94.

## REFERENCES


1. CHATTERGEE A.K., "Performance of blended cements – An Indian perspective", The Indian Concrete Journal, Vol.(74)7, 2000, pp.383-393.

2. ELKEM MATERIALS, 2001. www.concrete.elkem.com.

3. RUSSELL T. FLYNN, THOMAS J. GRISINGER AND BRYANT MATHER, "Slag Cement in Concrete and Mortar", Reported by ACI Committee 233, ACI 233R-03.

4. S.J. BARNETT, M.N. SOUTSOS, S.G. MILLARD AND J.H. BUNGEY, "Strength development of mortars containing ground granulated blast-furnace slag: Effect of curing temperature and determination of apparent activation energies", Cement and Concrete Research 36 (2006) 434 – 440.

5. SWAMY R.N, "Sustainable Concrete for 21 Century- Concept of Strength Through Durability", The Indian Concrete Journal, pp.7-15, 2007.

6. SASAN PARNIANI,, MOHD.WARID HUSSIN AND FARNOUD RAHIMI MANSOUR "Compressive strength of high volume slag cement concrete in high temperature curing", Advanced Materials Research Vols. 287-290, 2011, pp 793-796.

7. MD. MOINUL ISLAM, MD.SAIFUL ISLAM, BIPUL CHANDRA MONDAL AND MOHAMMAD RAFIQUL ISLAM "Strength behavior of concrete using slag with cement in sea water environment" Journal of Civil Engineering (IEB), 38 (2), 2010, pp-129-140.

8. ATUL DUBEY AND DR. R. CHANDAK, PROF. R.K.YADAV "Effect of blast furnace slag powder on compressive strength of concrete" International Journal of Scientific & Engineering Research Volume 3, Issue 8, August-2012 1 ISSN 2229-5518.

9. YOUSEF ZANDI AND VEFA AKPINAR M., “An Experimental Study on Separately Ground and together Grinding Portland Slag Cements Strength Properties”Research Journal of RecentSciences, Vol. 1(4), 27-40, April, 2012, ISSN 2277-2502, Res.J.Recent Sci.

10. MOHAMMED NADEEM AND ARUN D. POFALE, “Utilization of Industrial Waste Slag as Aggregate in Concrete Applications by Adopting Taguchi’s Approach for Optimization”, Open Journal of Civil Engineering, 2012, 2, 96-105.

11. C M DORDI , A N Vyasa Rao and Manu Santhanam, “Microfine Gound Granulated Blast Furnace Slag for High Performance Concrete”, Third International Conference Sustainable Construction Materials and Technologies, 2013.

12. SLAG CEMENT ASSOCIATION Printed on recycled paper.© 2013.

13. ALAA M. RASHAD, HOSAM EL-DIN H. SELEEM, AND AMR F. SHAHEEN, “Effect of Silica Fume and Slag on Compressive Strength and Abrasion Resistance of HVFA Concrete”, International Journal of Concrete Structures and Materials, Vol.8, No.1, pp.69–81, March 2014, DOI 10.1007/s40069-013-0051-2.

14. WEN SHI-YOU AND LI XI-BING, Experimental Study on Young's Modulus of Concrete, Vol.7, No.1, March 2000, Article ID: 1005-9784(2000)01-0043-03.

15. ALA MALAIKAH, KHALID AL-SAIF AND RAJEH AL-ZAID, Prediction of the Dynamic Modulus of Elasticity of Concrete Under Different Loading Conditions, International Conference On Concrete Engineering and Technology (2004), Universiti Malaya.

16. MOHAMMED M. SALMAN AND ENG. ALI H. AL-AMAWEE, The Ratio between Static and Dynamic Modulus of Elasticity in Normal and High Strength Concrete, Journal of Engineering and Development, Vol. 10, No. 2, June (2006), ISSN 1813-7822, pp-163-174.

17. JOHN S. POPOVICS, A Study of Static and Dynamic Modulus of Elasticity of Concrete, ACI-CRC Final Report October 2008.

18. MISBA GUL, ALSANA BASHIR, JAVED A NAQASH, Study of Modulus of Elasticity of Steel Fibre Reinforced Concrete, International Journal of Engineering and Advanced Technology (IJEAT), ISSN: 2249 – 8958, Volume-3, Issue-4, April 2014.

19. JIGAR P. PATEL, Broader Use of Steel Slag Aggregates in Concrete, Thesis of Masters of Science in Civil Engineering 2008, Cleveland State University.

# OPTIMIZING THE USE OF CEMENT AND CONCRETE THROUGH HIGH STRENGTH CONCRETE

**E P Kearsley**

**H F Mostert**

University of Pretoria

South Africa

**ABSTRACT:** Cement manufacturers have been working hard at successfully reducing the environmental impact of cement production. The producers of concrete have been optimizing the cost of the mixtures with optimal use of cement extenders and admixtures but they have to produce concrete that meet the requirements and specifications of design engineers. This paper will highlight how lightweight structures manufactured from high strength concrete can be used to reduce the environmental impact of the cement and concrete industry. There is a perception that the material cost of high strength concrete is more than that of the concrete mixtures used in the past, but by increasing the compressive strength and stiffness of concrete, it is possible to reduce the volume of concrete required, reducing both the environmental impact and the total cost of construction. Through the use of fibre reinforced high strength concrete, the need of shear reinforcing can be reduced, resulting in further savings. The actual structural behaviour of traditional concrete beams and slabs will be compared to that of lightweight, high strength fibre reinforced elements with equivalent load carrying capacity. Relevant material properties will be compared.

**Keywords:** Fibre reinforced concrete; high strength concrete; material properties; lightweight concrete structures, pre-cast concrete.

**Professor Elsabe P Kearsley** is a Professor in Civil Engineering at the University of Pretoria in South Africa. For the last 23 years she has been involved with cement and concrete research and her current work is aimed at reducing the environmental impact of the cement and concrete industry through optimal use of materials.

**Mr H F (Derek) Mostert** is a Concrete Technologist with an ACT diploma from City and Guilds and a Master of Science degree in Advanced Concrete Technology from the University of Belfast.

## INTRODUCTION

Cement manufacturers have been working hard at successfully reducing the environmental impact of cement production. The producers of concrete have been optimizing the cost of the mixtures with optimal use of cement extenders and admixtures but they have to produce concrete that meet the requirements and specifications of design engineers. Modern design codes makes it possible to design concrete elements using high strength concrete and it has become standard practice to use concrete strengths of up to 90 MPa in large structures. Well designed and large structures are normally found in developed areas, resulting in optimal use of scarce resources, but the consumption of cement and concrete in the under-developed regions of the world far exceeds that of the first world countries.

In developing countries there is often a dire need for basic infrastructure and large volumes of cement and concrete are used to build relatively small structures on a large scale. Lack of training and knowledge of local builders often result in inferior quality structures being built and these structures are often not fit for purpose, requiring remedial work or even demolition, thus resulting in significant waste of materials with a large environmental footprint. The fact that small structures are built, often means that no design engineers are involved in the material specification, structural design or quality control of the infrastructure built.

Many developing countries face problems with rural infrastructure development as the gap between the knowledge and skill levels in developed and under-developed areas is rapidly increasing and the global availability of modern construction materials and techniques are making it increasingly difficult for inexperienced or untrained builders to enter the construction industry. In countries with large numbers of untrained and unemployed people, the construction industry can be a major source of employment and the cement and concrete industry must find ways of transferring cutting edge knowledge and technology to developing communities thus ensuring that the environmental impact of the cement and concrete industry is minimized.

There is a perception that the material cost of high strength concrete is more than that of the concrete mixtures used in the past, but by increasing the compressive strength and stiffness of concrete, it is possible to reduce the volume of concrete required, reducing both the environmental impact and the total cost of construction. The environmental impact of the construction industry can be limited by manufacturing high strength, fibre reinforced concrete elements for use in rural infrastructure development in a modern pre-cast environment.

In this paper the actual structural behaviour of lightweight, high strength Fibre Reinforced Concrete (FRC) elements for use in structural applications will be investigated. These lightweight applications include Ultra-Thin Continuously Reinforced Concrete Pavements (UTCRCP), surface beds, wall panels, floor slabs and beams as well as permanent shutter systems.

## BACKGROUND

In the past research has proven that it is possible to reduce the cost of structural elements by using high strength fibre reinforced concrete beams instead of conventional reinforced concrete beams [1]. Although the materials used in high strength fibre reinforced concrete are significantly more expensive than the materials used in normal 30 MPa concrete, it is possible to reduce both the own weight and the cost of structural elements by optimizing both the volume of high strength fibre reinforced concrete used and the composition of the fibre reinforced concrete.

With the use of modern admixtures in is possible to make concrete with compressive strengths as high 200 MPa without including any scarce materials or equipment that is not typically available in a normal concrete casting yard. As the concrete compressive strength increases, the material becomes more brittle and fibre reinforcing becomes essential to prevent catastrophic failures. The most appropriate fibre type and content can result in fibre reinforced concrete with an elastic-plastic failure mechanism similar to that of steel [2]. The steel fibres can also be used to provide the shear resistance needed in structural elements, thus eliminating the need for shear reinforcing, resulting in additional savings [1].

In conventional reinforced concrete design it is assumed that the concrete has no tensile strength and only the compressive strength of the concrete is taken into account. Where loads applied to the structural element can result in tensile stresses, steel reinforcing should be provided. Under normal working conditions it is assumed that the behaviour of both the cracked concrete and the steel reinforcing bars follow Hooke's law with increased strain resulting in increased stresses. Reinforced concrete is designed to ensure that at ultimate limit state, when failure occurs, the steel yields in tension before the concrete crushes in compression [3]. The actual dimensions of structural elements are normally standardised and the dimensions and layout of reinforced concrete elements are seldom optimised to minimise the cement and concrete used. Although it has been proven that fibre reinforced high strength concrete can be a cost effective alternative to normal reinforced concrete [1, 4], further reductions in material usage is possible by taking the post-cracking strength provided by the fibre reinforcing into account in optimizing the design of structural elements.

The use of relatively high steel fibre volumes in high strength concrete provides fibre reinforced concrete with sufficient post-cracking strength that plastic hinges can form and bending moments can be re-distributed to minimize the steel reinforcing bars required. The experimental results provided in this paper are used to explain this concept.

## EXPERIMENTAL SETUP

The material properties of high strength fibre reinforced concrete were determined from sets of three samples cast using the mix composition as indicated in Table 1. Both Ground Granulated Blast Furnace Slag (GGBFS) and condensed Silica Fume (SF) were used as cement extenders. The admixture used was a combination of high range water reducing agents, retarders and de-air-entrainers. The steel fibres used were hooked ended drawn wire with a length of 30 mm and a diameter of 0.45 mm. A fibre content of 80 kg/m$^3$ was used which equates to 1% by volume. The effect of fibres was established by casting the same mix composition with and without fibres.

All samples were demoulded 24 hours after casting and then placed in water at 24ºC up to the day of testing. The compressive strength of the concrete was determined 7, 14 and 28 days after casting using both 100 mm cubes and 300 mm high cylinders with a diameter of 150 mm. The moduli of elasticity as well as split cylinder tests were conducted using 150 mm diameter cylinders. The flexural strength of the concrete was measured using Modulus of Rupture (MoR) beams with a 100 mm x 100 mm cross section.

Table 1 Mix composition

| TYPICAL CONCRETE MIX COMPOSITION | | |
|---|---|---|
| Material | Relative density | kg/m$^3$ |
| Cem II 52.5 N cement | 3.14 | 390 |
| Silica Fume | 2.2 | 39 |
| Ground Granulated Blast Furnace Slag | 2.2 | 58 |
| Water | 1 | 175 |
| 6.7 mm Granite stone | 2.65 | 820 |
| Silica sand | 2.65 | 865 |
| Admixture | 1.07 | 9.3 |
| Hooked ended hard drawn steel wire fibre | 7.85 | 80 |
| Polypropylene micro fibre | 1 | 2 |
| w/c ratio | 0.37 | |

As there is a significant known size effect in the flexural strength of concrete [5], flexural samples should have dimensions similar to that of the structural elements they represent. It was thus decided to cast small slabs for flexural testing and these slabs were 55 mm thick, 250 mm wide and 750 mm long.

## EXPERIMENTAL RESULTS

The measured mechanical properties for the concrete and steel used can be seen in Table 2.

Table 2 Material properties

| TYPICALMECHANICAL PROPERTIES | | |
|---|---|---|
| PROPERTY | 7-days | 28-days |
| Compressive Cube Strength, MPa | 108.0 | 122.7 |
| Compressive Cylinder Strength, MPa | 101.6 | 112.0 |
| Modulus of Elasticity, GPa | 46.3 | 49.3 |
| Tensile Cracking Strength (split cylinder), MPa | | 5.7 |
| Ultimate Tensile Strength (split cylinder), MPa | | 6.5 |
| Flexural Cracking Strength (MoR), MPa | | 10.6 |
| Ultimate Flexural Strength (MoR), MPa | | 11.1 |
| Slab Cracking Strength, MPa | | 9.2 |
| Ultimate Slab Strength, MPa | | 12.0 |
| Yield Strength of reinforcing bars, MPa | | 375 |
| Ultimate Strength of reinforcing bars, MPa | | 414 |

The strength development of the concrete can be seen in Figure 1 where the strength of mixtures cast on the same day with and without fibres are compared. It can be seen that although the inclusion of 1% (by volume) steel fibres does not contribute significantly towards the compressive strength of the concrete, the samples containing fibres were marginally stronger than those without.

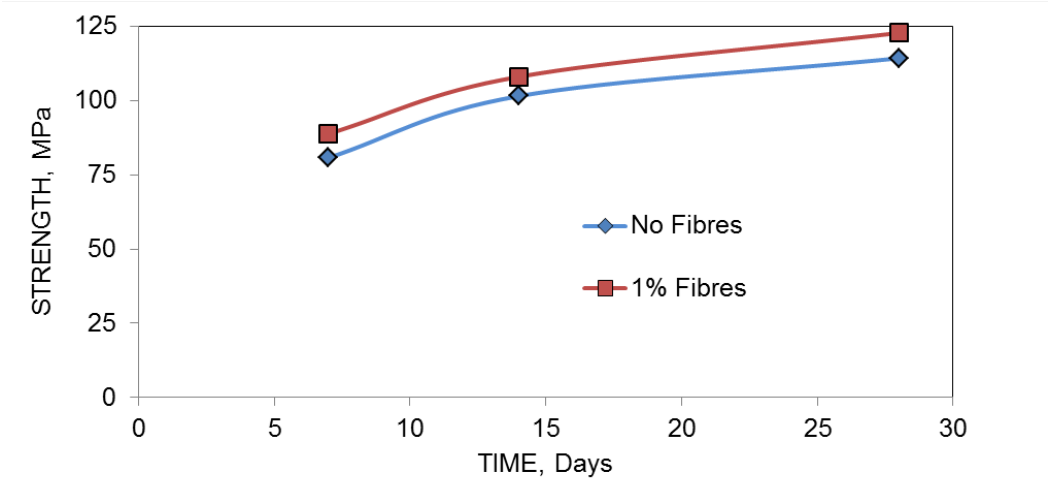


Figure 1 Compressive strength development

As expected the cylinder strengths were lower than the cube strengths but the difference was less than expected with the cylinders having strengths exceeding 90% of the cube strength. The stress-strain behaviour of the cylinders was recorded electronically by placing displacement transducers in a standard E-value collar that measured over the central 167 mm of the cylinders. The modulus of elasticity as indicated in Table 2 was calculated from the slope of the linear section of the stress-strain graphs in Figure 2. These results clearly indicate that the stiffness of the concrete develops rapidly and there is very little increase in concrete stiffness after the first 7 days. As the concrete ages there is less warning of failure with increasing load as can be seen by the constant slope of the stress-strain graph. The limited change in stiffness before failure shows the brittle nature of failures observed in high strength concrete.

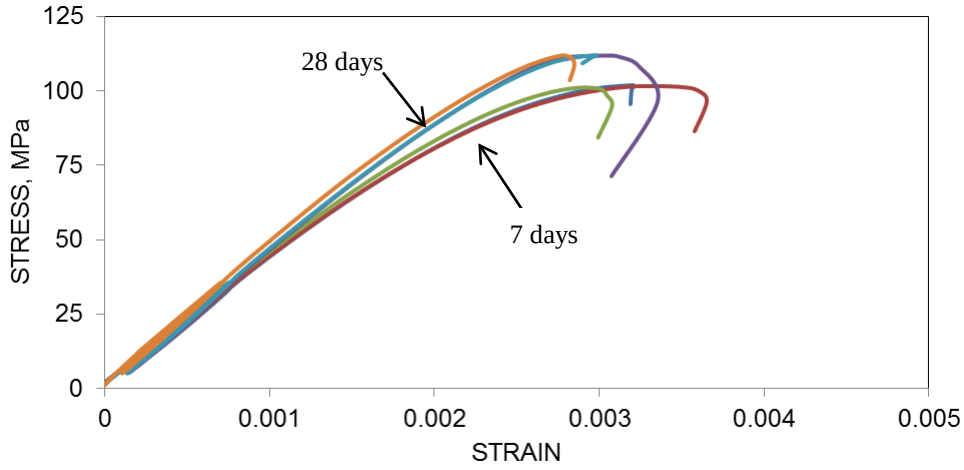


Figure 2 Modulus of elasticity of concrete

The indirect tensile strength of the concrete was measured using split cylinders and the measured values are shown in Table 2. The use of fibres changes the tensile behaviour of the concrete with the fibres providing strength after the concrete has cracked by bridging the cracks that formed. Displacement transducers were used to electronically record the horizontal expansion of cylinders during split cylinder testing and the results can be seen in Figure 3. The concrete cracked at stresses below 6 MPa, where after the cracks opened up, thus straining the fibres bridging the crack to the point where the stress in these fibres was sufficient to transfer the full applied load across the crack.

Figure 3 indicates that there were sufficient fibres in the mixture for the post-cracked strength to exceed the cracking strength of the concrete and after cracking the stress in the sample increased to above 6 MPa for all three samples tested. These results indicate that the tensile failure of the fibre reinforced concrete is no longer brittle and the strength of the material is not affected by the concrete cracking. It would thus be possible to use fibre reinforced concrete for structural elements with structural redundancy (statically indeterminate structural elements) and allow the element to form plastic hinges, by cracking and redistributing the stresses that was caused by applied loads to other parts of the element.

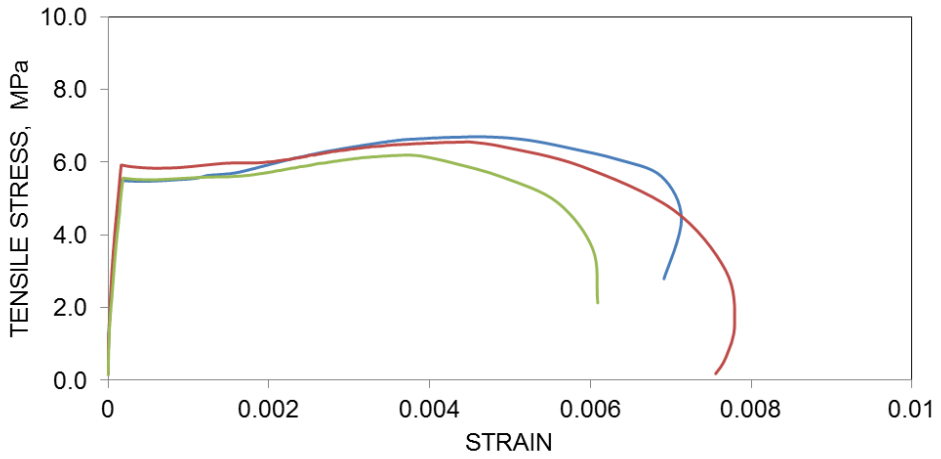


Figure 3 Split cylinder strength of concrete

The stress-strain behaviour of the high strength fibre reinforced concrete as shown in Figure 2 and Figure 3 can be used in material models to mathematically analyse complex structural elements.

The majority of structural concrete elements exposed to loading experience bending and thus the flexural behaviour of fibre reinforced concrete should be taken into account. The indirect tensile strength or Modulus of Rupture (MoR) of concrete is normally determined as the tensile stress at the maximum load that a beam under four point loading can withstand. The test is conducted in load control and the load is increased at a constant rate and only the peak load is recorded. For fibre reinforced concrete this peak load can be the load causing the concrete to crack or the peak load could be the maximum load that the fibres could withstand and there is no way of knowing what contribution the fibres made to the strength if the load-deflection behaviour is not recorded. By testing the MoR beams in deflection control and recording the load as a function of the mid-span deflection it is possible to quantify the contribution of the fibres towards the flexural strength of the fibre reinforced concrete.

The 100 mm x 100 mm beams were supported to span 300 mm and load was applied at third points to obtain the flexural strength results as shown in Figure 4. These graphs clearly show that the concrete cracked at a flexural tensile stress of about 10.5 MPa, but after cracking the steel fibres made it possible for the beam to support loads exceeding the load that caused cracking. These results indicate that the high strength fibre reinforced concrete should be able to handle accidental overloading, where the structural element could be cracked as a result of the load, yet the structural load carrying capacity is not reduced. Although the cracking would reduce the stiffness of the beam, the strength of the beam is not affected by the formation of cracks. The general shape of these graphs indicates elastic-plastic material failure behaviour.

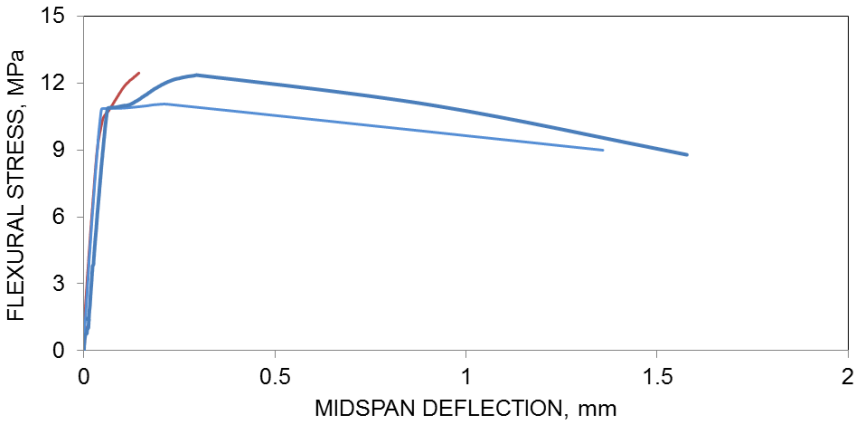


Figure 4 Flexural strength of MoR beams

The 30 mm long fibres are randomly aligned in the 100 mm deep beams, but if at least one of the dimensions of the structural element is not much more than the fibre length, the fibres would align, resulting in increased strength contribution in the length of the elements. This effect can clearly be seen in Figure 5, where the flexural behaviour of 55 mm thick slabs that span 600 mm and are loaded at third points are shown. The strength contribution of the fibres can clearly be seen in this graph. The maximum load for this slab was recorded at a deflection of nearly a 200$^{th}$ of the span, which would indicate that these slender panels would fail by exceeding acceptable deflection limits. If high strength fibre reinforced concrete is used to manufacture lightweight structural elements, care will have to be taken to ensure that deflection limits are not exeeded.

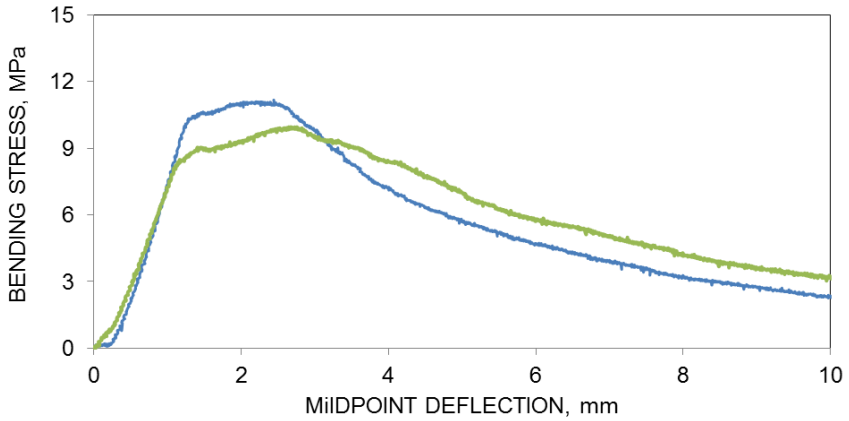


Figure 5 Flexural strength of concrete slabs

The flexural strength of fibre reinforced concrete can further be enhanced by the inclusion of steel reinforcing bars. The small dimensions of the elements means that it is not feasible to have more than one layer of reinforcing and only one layer of steel is placed in the center of the slabs. The steel can act in tension not only when the top of the slab is in compression in the regions of the structure that experience sagging moments, but also when the bottom of the slab is in compression in regions where hogging moments occur.

A steel mesh was made up of 5.6 mm steel bars placed 50 mm apart and this mesh was placed in the 750 mm x 250 mm x 55 mm thick slabs with 15 mm cover to the bottom of the slab. Tensile tests were conducted on the reinforcing bars and the results are shown in Figure 6. Although the steel yielded at a stress of about 375 MPa, some work hardening took place and all six samples tested failed at loads exceeding 400 MPa.

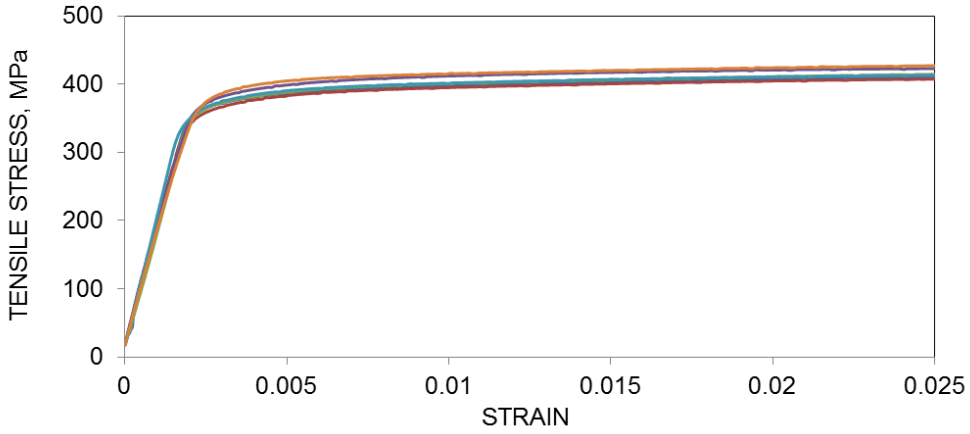


Figure 6 Tensile strength of steel reinforcing bars

The slabs containing mesh were also supported to span 600 mm and loaded at third point. The bending moments that the slabs could resist can be seen as a function of midspan deflection in Figure 7. The steel mesh does not alter the behaviour of the slab up to the point where the slab has cracked and the fibres have reached their capacity. The ultimate failure of the slab is however governed by the behaviour of the steel mesh.

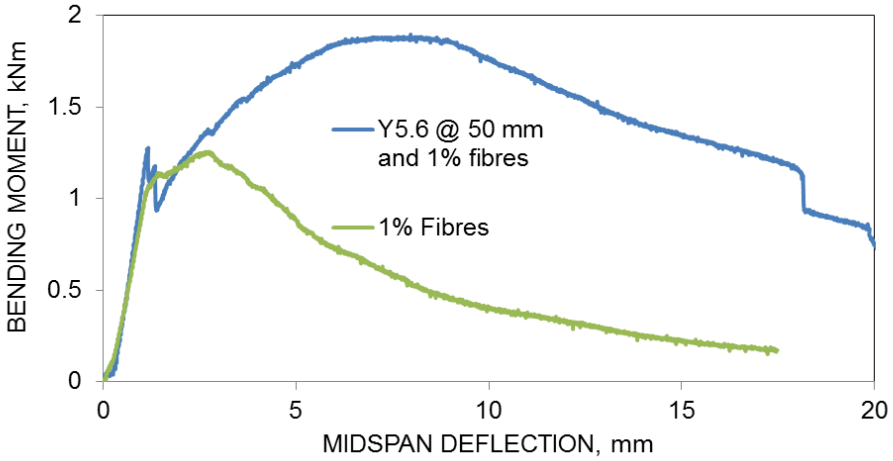


Figure 7 Effect of reinforcing on flexural strength

## CROSS SECTION COMPOSITION AND DESIGN PROPERTIES

The experimental results recorded for the mechanical properties of the high strength fibre reinforced concrete were used to determine whether the standard procedure used for designing reinforced concrete structures [3] could be applied to thin high strength fibre reinforced concrete elements. The assumed internal stresses in the slabs tested are indicated in Figure 8. During normal service the loads on the panel would be such that the concrete would remain un-cracked and linear elastic stress distributions would be present. When the loads increase the concrete would crack and at ultimate limit state, when failure occurs the steel would be yielding and the concrete would behave in a plastic manner, with a compression block under uniform maximum stress. The steel fibres would bridge the cracks in the concrete, thus assisting the steel reinforcing bars in handling the tensile stresses.

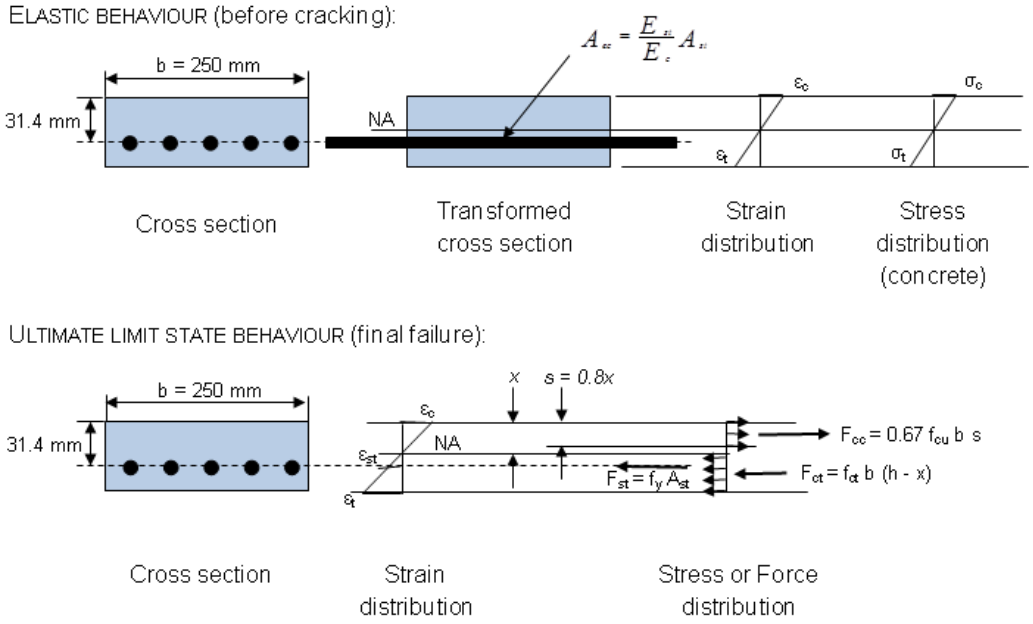


Figure 8 Design principles for fibre reinforced concrete

The mechanical properties as listed in Table 2 were used with the assumptions as indicated in Figure 8 to conduct a theoretical calculation that can be compared to the actual behaviour of the slab containing mesh as shown in Figure 7. The calculated values are listed in Table 3. For the elastic analysis it can be assumed that the concrete cracks when the maximum tensile stress reaches the tensile strength of the concrete as determined from the split cylinder test, then the slab should start cracking at a bending moment of 0.72 kNm. If the flexural cracking strength of the slab without reinforcing (9.2 MPa) is used, the calculated cracking bending moment value increases to 1.17 kNm, which compares well with the values in Figure 7. Using normal reinforced concrete design principles and assuming an ultimate stress in the five 5.6 mm reinforcing bars of 414 MPa the slab section should only have been able to resist a bending moment of 1.54 kNm, which is significantly less than that indicated in Figure 7. At the deflection correlating with the maximum bending moment, the load carrying capacity of the slab containing only fibre reinforcing is already reduced and the contribution of the fibres is less than what it would have been at lower deflections. A uniform tensile stress distribution in the cracked concrete of 1 MPa gives calculated bending moments that matches the actual measured bending moments. Although further work is needed to quantify the exact contribution of the fibres, the load carrying capacity of high strength FRC can be predicted.

Table 3 Design values

| THEORETICAL SLAB BEHAVIOUR | | |
|---|---|---|
| PROPERTY | ELASTIC | ULIMATE LIMIT STATE |
| Depth of netrual axis (x), mm | 27.6 | 3.84 |
| Maximum tensile stress ($\sigma_t$), MPa | 5.7 (9.2) | |
| Maximum bending moment, kNm | 0.72 (1.17) | 1.87 |
| Strain at top of slab ($\varepsilon_c$) | 0.0001165 | 0.0035 * |
| Strain at bottom of slab ($\varepsilon_t$) | 0.0001156 | 0.0461 |
| Tensile stress in FRC ($f_{ct}$), MPa | | 1* |

* Assumed values

## HIGH STRENGTH FIBRE REINFROCED CONCRETE APPLICATIONS

As a result of the dire consequences associated with structural failures, designers of structures tend to be risk evasive and it is difficult to introduce new concept into the marked. The only way to know whether a new system will stand the test of time is to conduct pilot studies where new concepts can be tested at full scale with limited risk. A number of such projects have been undertaken as indicated in Figure 9 to Figure 12. Figure 9 shows pre-cast elements that were developed to assist with providing moveable superstructures to pit latrines for rural sanitation in South Africa, where many households still do not have access to running water or sanitation [4].

Figure 9 Lightweight moveable Ventilated Improved Pit (VIP) superstructure

The photos in Figure 10 were taken when pre-cast lightweight high strength FRC elements (beams and slabs) were used to construct a reservoir (top two photos) and as permanent shutter for a floor slab (bottom two photos). In Figure 11 similar elements were used as permanent shutters to provide emergency access over a river after the bridge was washed away during flooding. In all three these instances the designers assumed that the structural strength of the pre-cast elements would contribute significantly towards the long-term strength of the structure. These elements were thus used as part of a composite system with shear connectors linking the pre-cast elements to the cast in-situ concrete. The volume of concrete required in concrete pavements and surface beds can be significantly reduced as indicated in Figure 12 where the construction of Ultra-Thin Continuously Reinforced Concrete Pavement (UTCRCP) trial sections is taking place.


Figure 10 Lightweight FRC precast elements in water reservoir and floor slab construction

Figure 11 Rural footbridge constructed using high strength FRC permanent shutters

Figure 12 UTCRCP trial section construction

## CONCLUSIONS

High strength fibre reinforced concrete can be used to manufacture pre-cast elements that can be used for rural infrastructure development. These elements become cost effective if they are optimised to minimise the volume of material used and the can be done by taking the post-cracking tensile strength of the fibre reinforced concrete into account. If high strength fibre reinforced concrete is used to manufacture lightweight structural elements, care will have to be taken to ensure that deflection limits are not exeeded. Further research and pilot studies should be conducted to ensure that designers can be confident in designing and using structural elements manufactured from high strength fibre reinforced concrete.

## REFERENCES

1. KEARSLEY, E P, MOSTERT, H F. Comparing the behaviour of high strength fibre reinforced and conventional reinforced concrete beams, Advances in Cement-based Materials, Proceedings of the International Conference on Advanced Concrete Materials, Stellenbosch, South Africa, Taylor & Francis Group, London. November 2009, pp 91- 96.

2. KEARSLEY, E P, MOSTERT, H F. Enabling the effective use of high performance fibre reinforced concrete in infrastructure, Advances in Cement-based Materials, Proceedings of the International Conference on Advanced Concrete Materials, Stellenbosch, South Africa, Taylor & Francis Group, London. November 2009, pp 287-295.

3. MOSLEY, W H, BUNGEY, J H, HULSE, R. Reinforced Concrete Design to Eurocode 2, 2012, 7th ed., Palgrave Macmillan, UK.

4. UNIVERSITY OF PRETORIA. Lightweight moveable superstructure for VIP toilets, Water Research Commission (WRC) Report on project K5/1781/3, March 2010.

5. DENNEMAN, E, KEARSLEY, E P, VISSER A T. Size-effect in high performance concrete road pavement materials. Proceedings of the International Conference on Advanced Concrete Materials, Stellenbosch, South Africa, Taylor & Francis Group, London. November 2009, pp 53-58.

# NUMERICAL AND EXPERIMENTAL ANALYSIS OF THE TRANSFER LENGTH AND ITS INFLUENCE ON THE ANCHORAGE ZONE DESIGN OF PRETENSIONED CONCRETE MEMBERS

**K van Meirvenne**

**W De Corte V Boel**

**L Taerwe**

Ghent University

Belgium

**ABSTRACT.** In order to optimize the end block of a prestressed girder, nonlinear finite element models are frequently used. This way the stresses and possible cracks in the anchorage zones can be predicted in a more reliable manner. However, a preliminary parametric study of nonlinear finite element models has shown that the transfer length has a major influence on the stresses in the concrete and in the reinforcement, and on the crack formation. In this paper this transfer length is examined, firstly by performing a parametric study of the formulations found in literature, secondly by measurements on beams produced at a precast concrete plant. The aim of this parametric study and the experimental research is to get further insight into the transfer length function as required for further numerical analysis of the end zones.

**Keywords:** End Zones, FEM, Pretensioned girders, Transfer length

**Kizzy Van Meirvenne** is a PhD student at the department of structural engineering at Ghent University. She investigates the end zones of prestressed pretensioned concrete girders in collaboration with a Belgian precast company.

**Associate Professor Wouter De Corte** is affiliated to the Department of Structural Engineering at Ghent University. His research interests include design and performance of building parts and civil structures made from steel, concrete and structural composites including static, dynamic and fatigue effects.

**Associate Professor Veerle Boel** is affiliated to the Department of Structural Engineering at Ghent University. Her research is mainly focussed on concrete technology and structural concrete. Veerle was member of RILEM Committees TC 205-DSC and TC 228-MPS.

**Professor Luc Taerwe** is a Senior Full professor of Structural Engineering at Ghent University, Director of the Magnel Lab for Concrete Research and Head of the Department of Structural Engineering. Moreover he is an elected member of the Royal Belgian Academy of Technical Sciences, a High-End Foreign Expert at Tongji University (Shanghai, China) and President of the Royal Flemish Engineering Society. He is recipient of the "Robert L'Hermite Medal 1988" of RILEM and the IABSE Prize 1991, Fellow of the American Concrete Institute and the International Institute for FRP in Construction and also Honorary Life Member fib. Since 2006 he serves as Editor-in-chief of the journal “Structural Concrete” and he is chairman of several national and international scientific and technical committees.

## INTRODUCTION

Pretensioned concrete girders have been used for many years in construction. Nevertheless, optimization is still possible, especially regarding the anchorage zones. These are typically subjected to different types of stresses due to the local transfer of the prestressing force. Generally, the beams are provided with an end block, and are designed by making use of analytical or strut-and-tie models. However, these models lack clarity regarding the reinforcement design, the transfer length, the width of possible cracks, etc. Moreover, the calculated reinforcement does not automatically imply the most economical solution. Furthermore, the need for the end block itself is not obvious. By using a nonlinear finite element model, the stresses in the anchorage zone due to the prestressing forces can be predicted in a more reliable way. Analysing these models shows that the transfer length is the most important parameter. Several transfer length measurements were performed on the production line of a precast beam manufacturer during the prestressing operation. The experimental results are compared with data from literature.

## FINITE ELEMENT MODELING

Nonlinear finite element modelling allows simulating a girder in an accurate way, and the behaviour of the end zone can be analysed directly in 3D with the correct material laws. In order to illustrate the need for an accurate assessment of the transfer length, the results of a nonlinear analysis on a typical prismatic girder without enlarged end zone are shown. The finite element model is based on the contributions of Okumus and Oliva [1,2], and consists of an I-shaped cross-section with a height of 600 mm, a width of 300 mm and 9 seven wire strands of 93 mm² in cross-section (Figure 1).

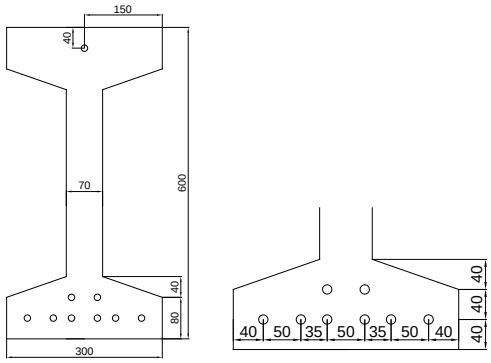


Figure. 1 Front view and detail of the modelled geometry

A reduced length of 4 meter is chosen in order to minimize the calculation time while the remainder of the beam is represented by adequate boundary conditions (Figure 2).

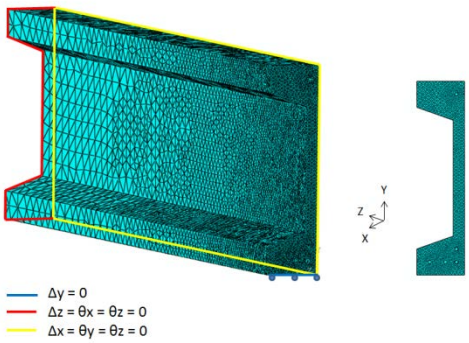


Figure. 2 Boundary conditions

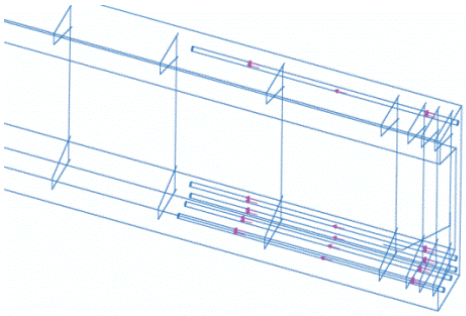

Figure. 3 Modelled reinforcement

The passive reinforcement bars are modelled as linear elastic embedded elements, as they are not expected to yield during the prestress transfer. On the other hand, the strands are modelled as circular holes over the transfer length (Figure 3) [3]. A linearly distributed shear stress is assigned along the outline of the holes. This shear stress has its maximum at the end face and decreases to zero at the end of the transfer length [4].

Regarding the embedded steel, only the density, the modulus of elasticity, and the Poisson's ratio need to be defined. The values of these parameters are given in Table 1.

Table 1 Material properties of steel

| | |
|---|---|
| Density ρ [kg/m³] | 7800 |
| Modulus of elasticity $E_s$ [MPa] | 200000 |
| Poisson ratio $\nu_s$ [-] | 0.3 |

The material parameters of the concrete are based on the concrete damaged plasticity model as provided in the Abaqus material library. This model is appropriate for simulating the nonlinear behavior of concrete in compression as well as in tension. The basic values of the concrete model are given in Table 2.

Table 2 Material properties of concrete

| | |
|---|---|
| Density ρ [kg/m³] | 2500 |
| Poisson $\nu_s$ [-] | 0.2 |
| Dilatation angle [°] | 36 |
| Excentricity [mm] | 0.1 |
| $f_{b0}/f_{c0}$ [-] | 1.16 |
| K [-] | 0.666 |

The nonlinear parameters for the compressed case are determined by using the fib Model Code (2010) [5], in combination with the AASHTO LRFD Bridge Design Specifications [3] for the linear part of the stress-strain diagram. The modulus of elasticity is calculated by using the ASHTOO [3] instead of the Model Code [5]. In the tensile part, the linear part uses the modulus of elasticity mentioned above, whereas the relationship between the concrete tensile stress and the crack opening for concrete in tension is based on the fib Model Code [5] (Figure 4).

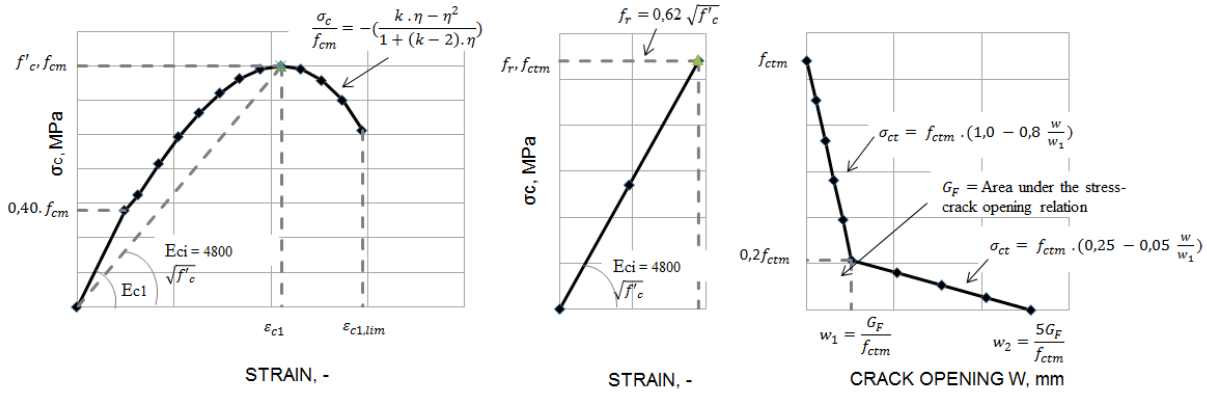


Figure. 4 Constitutive model for concrete in compression (left) and tension (right) [1, 2, 6]

Figure 5 shows a typical result of the principal tensile strains representative for cracked concrete zones in view of the model as represented by Figure 4. Figure 6 displays the corresponding rebar stresses in the stirrups and the oblique rebar.

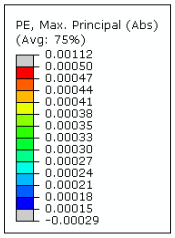


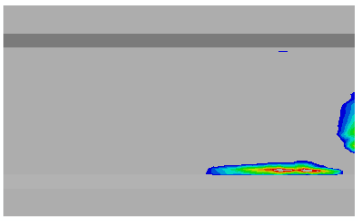

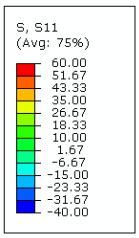


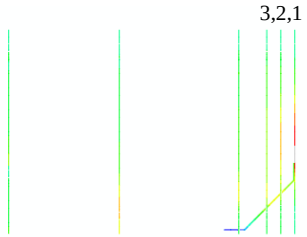


Figure. 5 Maximum principal strains in the concrete Figure. 6 Stresses in the reinforcement

During the analysis different parameters were studied such as the transfer length, the concrete strength, the influence of varying fracture energy, etc. The preliminary conclusion is that the transfer length, which is examined by varying its value from 40 to 80 times the nominal strand diameter, has a major influence on the stresses in the reinforcement. It can be noticed that the rebar stresses increase remarkably when the transfer length is lower than 60 times the strand diameter. For the model presented, the stresses in the stirrups and the oblique rebar show a nonlinear descending trend when increasing the transfer length (Figure. 7).

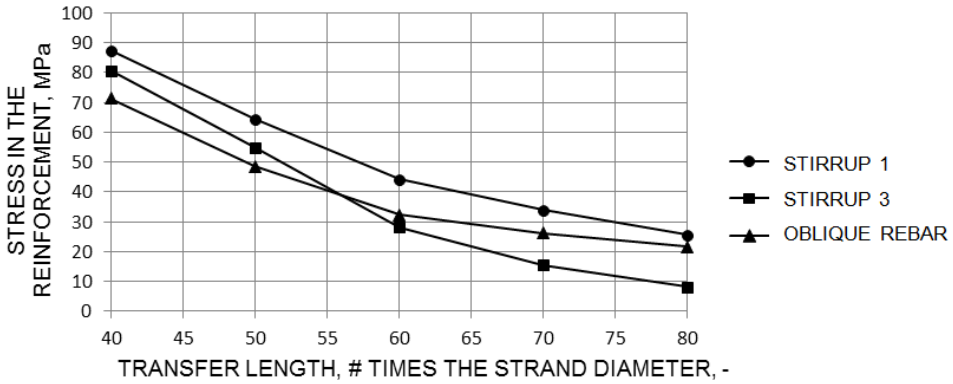


Figure. 7 Transfer length as a function of the stress in the reinforcement

For that reason it is useful to examine the different formulas from literature, in order to gain insight into the different influencing parameters of the transfer length. Moreover the results will be compared with measurements on beams produced at the precast concrete plant.

## PARAMETRIC STUDY OF THE FORMULAS FOR TRANSFER LENGTH ESTIMATIONS FROM LITERATURE

Over the years, the transfer length in a prestressed girder has been examined extensively. In view of the relevance of this transfer length in the end zone reinforcement assessment through nonlinear finite element modeling, a parametric study of formulas from literature is conducted as a matter of comparison with the measured values given further in this paper. The parametric study is based on the work of Pozolo [7] and J.R. Marti-Vargas et al. [8] and compares 16 formulations from 13 sources (See Table 3).

Table 3 Formulas parametric study

| | | | |
|---|---|---|---|
| ACI 318-11 [6] | $L_T = \frac{\sigma_{pcs}\emptyset}{20,7}$ | Balázs [18] | $L_T = \frac{3,15}{\emptyset}\sqrt[5]{\sigma_{pcs}^3/f_{ci}^2}$ |
| Martin and Scott [10] | $L_T = 80\emptyset$ | AASHTO [3] | $L_T = 60\emptyset$ |
| Zia and Mostafa [15] | $L_T = a\frac{\sigma_{pi}\emptyset}{f_{ci}} - b$ | Lane [12] | $L_T = \frac{4\sigma_{pt}\emptyset}{f_c} - 127$ |
| Mitchell et al. [16] | $L_T = \frac{\sigma_{pi}\emptyset}{20,7}\sqrt{\frac{20,7}{f_{ci}}}$ | Kose and Burkett [13] | $L_T = 0,05\frac{\sigma_{pt}(1-\emptyset)^2}{\sqrt{f_c}}$ |
| Shahawy et al. [11] | $L_T = \frac{\sigma_{pi}\emptyset}{20,7}$ | Mahmoud et al. [19] | $L_T = \frac{\sigma_{pi}\emptyset}{\alpha_t f_{ci}^{0,67}}$ |
| Cousins et al. [17] | $L_T = \frac{\sigma_{pcs}A_p}{\pi\emptyset U'_t\sqrt{f_{ci}}} + 0,5\frac{U'_t\sqrt{f_{ci}}}{B}$ | MC 2010 [14] | $L_T = \alpha_{p1}\alpha_{p2}\alpha_{p3}\frac{A_p}{\pi\emptyset}\frac{\sigma_{pi}}{\eta_{p1}\eta_{p2}f_{ctdi}}$ |
| EC2 - 2004 [9] | $L_T = \alpha_1\alpha_2\emptyset\frac{\sigma_{pi}}{\eta_{p1}\eta_{p2}f_{ctdi}}$ | | |

Given the wide range of parameters present in the various formulations, the parametric study was conducted for (seven wire) strands with diameters of 9.3 mm and 12.5 mm, with a gradual and sudden release after 1, 3, and 5 days, and for concrete strengths C55/67 and C60/75. This selection is based on the materials used by the manufacturer and on the beams' manufacturing process. This way the experimental results can be compared with the theoretical estimations based on literature. Table 4 gives the values of the fixed parameters, according to the work of Marti-Vargas et al [8] : $\sigma_{pt} = 0.75f_{pu}$, $\sigma_{pi} = 0.93\sigma_{pt}$, $\sigma_{pcs} = 0.8\sigma_{pt}$ and $\sigma_{pa} = 0.9f_{pu}$. Table 5 shows the variable parameters.

Table 4 Fixed parameters

| | | | |
|---|---|---|---|
| $f_{pu}$ | tensile strength of prestressing strands | 1860 | MPa |
| $\sigma_{pt}$ | initial prestress in prestressing strand prior to release | 1395 | MPa |
| $\sigma_{pcs}$ | effective stress in prestressing strand after all prestress | 1116 | MPa |
| $\sigma_{pi}$ | effective stress in prestressing strand just after prestress transfer | 1297 | MPa |
| $\sigma_{pa}$ | maximum stress in strand at loading | 1674 | MPa |
| s | Coefficient which depends on the cement type | 0.18 | [-] |

Table 5 Variable parameters

| | | |
|---|---|---|
| $f_{ci}$ | concrete compressive strength at time of release [eq. 3.1 of EC2 with s=0,18 for CEM I 52,5 R] | [MPa] |
| $f_{cl}$ | concrete compressive strength at loading [fcl = 1.5fci] | [MPa] |
| $f_{ck}$ | concrete compressive strength at 28 days | [MPa] |
| $f_{ct}$ | concrete tensile strength at 28 days | [MPa] |
| $f_{ctd(i)}$ | concrete tensile strength at time of release | [MPa] |
| Ø | nominal diameter of prestressing strand | [mm] |
| $A_p$ | cross-sectional area of prestressing reinforcement | [mm²] |
| t | time of release | [days] |
| $\beta_{cc}$ | coefficient which depends on the age of the concrete | [-] |
| $P_k$ | choice of prestress force | [kN] |

The choice of parameters given above leads to 12 combinations, for which the calculated transfer lengths are listed in Table 6. For the results at a release time of one day it should be noted that although formulation 3.1 from EC2 [9] for calculating the compressive strength at early age is only valid for ages between 3 and 28 days, the formulation is also used for a concrete age of one day.

From Table 6 it is easily observed that the transfer length foremost depends on the strand diameter with larger transfer lengths corresponding to larger strand diameters. Since the effective stress in the prestressing strands is kept constant for the 4 formulations (ACI [6], Martin and Scott [10], Shahawy et al. [11], AASHTO [3]), the strand diameter is the only parameter. However, as the coefficients in these formulations are not equal they render transfer length predictions differing up to 54% compared to the smallest value. The formulations of Lane [12] and Kose and Burkett [13] consider concrete strength as well. MC 2010 [14], EC2 [9] and Zia and Mostafa [15] also make a distinction in the way of release. Regarding this time dependent effect, and looking at the calculated values of Zia and Mostafa [15], the transfer lengths for sudden release are in 11 of the 12 cases larger than for gradual release, with a maximum difference of 9.5%. The values of MC 2010 [14] and EC2 [9], on the other hand, indicate a 20% larger transfer length in case of sudden release, which is related to the parameter $\alpha_1$. If the time of release is further evaluated, the transfer length decreases with increasing age of the concrete. This is noticeable in every formula except for the 4 equations which depend on the strand diameter, and in the equations by Lane [12] and Kose and Burkett [13]. Finally, when the strand diameter and time of release are kept constant, it can be determined that the transfer length reduces as the concrete strength decreases. In case of a strand diameter of 9.3mm, the largest values exceed the lowest ones by 13%, while for the 12.5mm strand diameter this maximum difference is 12%.

Table 6 Calculated transfer length [mm] based on various sources

| parametric study transfer length | Ø9.3/C55-67/1d | Ø9.3/C55-67/3d | Ø9.3/C55-67/5d | Ø9.3/C60-75/1d | Ø9.3/C60-75/3d | Ø9.3/C60-75/5d | Ø12.5/C55-67/1d | Ø12.5/C55-67/3d | Ø12.5/C55-67/5d | Ø12.5/C60-75/1d | Ø12.5/C60-75/3d | Ø12.5/C60-75/5d |
|---|---|---|---|---|---|---|---|---|---|---|---|---|
| ACI 318-11 [6] | 501 | 501 | 501 | 501 | 501 | 501 | 674 | 674 | 674 | 674 | 674 | 674 |
| Martin and Scott [10] | 744 | 744 | 744 | 744 | 744 | 744 | 1000 | 1000 | 1000 | 1000 | 1000 | 1000 |
| Zia and Mostafa (gradual) [15] | 741 | 417 | 351 | 663 | 375 | 315 | 1016 | 580 | 491 | 910 | 524 | 444 |
| Zia and Mostafa (sudden) [15] | 805 | 431 | 355 | 714 | 382 | 314 | 1123 | 619 | 517 | 1000 | 554 | 462 |
| Cousins et al. [17] | 793 | 620 | 578 | 755 | 594 | 554 | 1051 | 818 | 762 | 999 | 783 | 730 |
| Shahawy et al. [11] | 583 | 583 | 583 | 583 | 583 | 583 | 783 | 783 | 783 | 783 | 783 | 783 |
| Balázs [18] | 583 | 473 | 446 | 559 | 456 | 430 | 784 | 636 | 599 | 752 | 613 | 578 |
| Mitchell et al. [16] | 577 | 445 | 413 | 548 | 425 | 395 | 776 | 598 | 555 | 737 | 571 | 530 |
| Lane [12] | 817 | 817 | 817 | 738 | 738 | 738 | 1141 | 1141 | 1141 | 1036 | 1036 | 1036 |
| Mahmoud et al. [19] | 652 | 460 | 416 | 608 | 432 | 391 | 876 | 618 | 559 | 817 | 581 | 526 |
| Kose and Burkett [13] | 648 | 648 | 648 | 620 | 620 | 620 | 1244 | 1244 | 1244 | 1191 | 1191 | 1191 |
| EC2 - 2004 (gradual) [9] | 851 | 569 | 514 | 812 | 543 | 480 | 1144 | 765 | 690 | 1092 | 730 | 645 |
| EC2 - 2004 (sudden) [9] | 1064 | 711 | 642 | 1015 | 679 | 600 | 1430 | 956 | 863 | 1365 | 912 | 806 |
| MC 2010 (gradual) [14] | 797 | 533 | 481 | 761 | 509 | 449 | 1061 | 709 | 640 | 1012 | 677 | 598 |
| MC 2010 (sudden) [14] | 996 | 666 | 601 | 951 | 636 | 562 | 1326 | 886 | 800 | 1266 | 846 | 748 |
| AASHTO [3] | 558 | 558 | 558 | 558 | 558 | 558 | 750 | 750 | 750 | 750 | 750 | 750 |
| | 1 | 2 | 3 | 4 | 5 | 6 | 7 | 8 | 9 | 10 | 11 | 12 |
| Average | 732 | 573 | 540 | 696 | 548 | 515 | 1011 | 799 | 754 | 961 | 764 | 719 |
| Standard deviation | 159 | 120 | 133 | 145 | 117 | 130 | 222 | 199 | 218 | 202 | 192 | 212 |
| Minimum | 501 | 417 | 351 | 501 | 375 | 314 | 674 | 580 | 491 | 674 | 524 | 444 |
| Maximum | 1064 | 817 | 817 | 1015 | 744 | 744 | 1430 | 1244 | 1244 | 1365 | 1191 | 1191 |
| # times strand diameter | 79 | 62 | 58 | 75 | 59 | 55 | 81 | 64 | 60 | 77 | 61 | 58 |

Figure 8 shows the minimum, maximum, and average transfer length values for the 12 considered scenarios. Clearly there is a big scatter in the results. Given this observation, transfer length measurements were carried out during normal production at the prefab concrete plant.

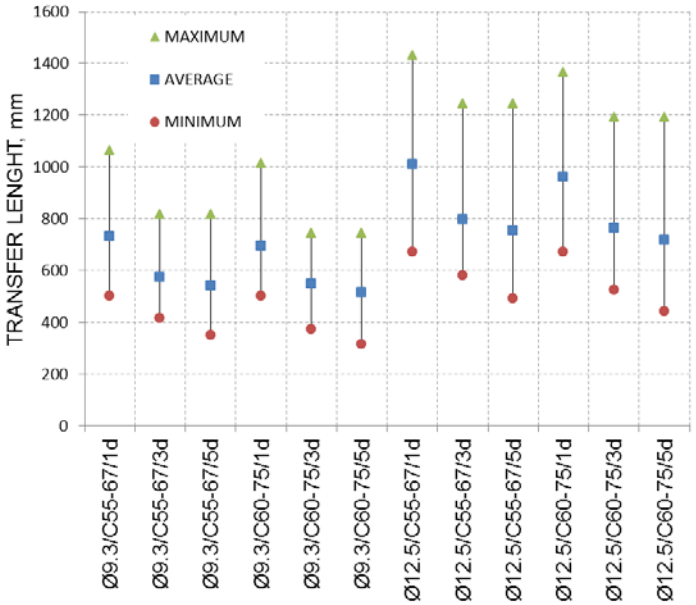


Figure. 8 Summary parametric study

## EXPERIMENTAL WORK

As mentioned in the first part, measurements were conducted on beams produced at the plant during normal production. A non-shrink adhesive was used to attach several measuring points to the concrete's surface at the level of the lower strands. With an invar reference bar, provided with two conical locating points, the measurement points were placed at a fixed distance of 100 mm. Near the end face of the beam the measuring points were placed in overlay, with an intermediate distance of 50 mm in order to obtain more accurate results near the beam end. The distance between the points is measured with a DEMEC mechanical strain gauge, with a resolution of 16 microstrain. The measurements render strain values based on a 100 mm gauge at 50 or 100 mm intervals which are presented hereafter.

Figure. 9 Measurement locations

35 beams, with 4 different geometries and 2 types of concrete, were instrumented and measured over 7 production lines. All the strands were released gradually, except for beams 3 to 6. Equally not every beam was prestressed with the same prestress force (See Table 7).

Although all beams of equal geometry were cast on a single production line, the concrete was made at different days, so the concrete had a different strength at time of release. These exact strength values, however, were not available for most beams. Therefore, the compressive strength was determined on cubes ($f_{ccubm}$) of 150 mm at 28 days (see Table 7).

Table 7 Overview tested beams

| beam | concrete strength class | age concrete [days] | compressive strenght at 28 days [MPa] | prestress force strands lower flange [kN] | prestress force debonded strands lower flange [kN] | beam | concrete strength class | age concrete [days] | compressive strenght at 28 days [MPa] | prestress force strands lower flange [kN] | prestress force debonded strands lower flange [kN] |
|---|---|---|---|---|---|---|---|---|---|---|---|
| I1200/450-1 | C60/75 | 20 | 80.9 | 3875.2 | 553.6 | I1600/600-17 | C55/67 SCC | 7 | 80.3 | 5259.2 | 830.4 |
| I1200/450-2 | | 2 | 78.7 | | | I1600/600-18 | | 2 | 77.5 | | |
| I1200/450-3 | C60/75 | 1 | 94.4 | | | I1600/600-19 | | 8 | 75.4 | | |
| I1200/450-4 | | 1 | 94.4 | | | I1600/600-20 | | 5 | 76.4 | | |
| I1200/450-5 | | 2 | - | | | I1600/600-21 | | 9 | 76 | | |
| I1200/450-6 | | 2 | - | | | I1600/600-22 | | 6 | 76.3 | | |
| I1000/500-7 | C55/67 SCC | 1 | - | 2768 | 553.6 | I1600/600-23 | | ? | 70.4 | | |
| I1000/500-8 | | 2 | 69.9 | | | I1450/600-24 | C60/75 | 2 | 90.9 | 4860.8 | 1107.2 |
| I1000/500-9 | | 3 | 73.9 | | | I1450/600-25 | | 7 | 91.5 | | |
| I1000/500-10 | | 6 | 71.6 | | | I1450/600-26 | | 3 | 92.9 | | |
| I1000/500-11 | | 8 | 73.4 | | | I1450/600-27 | | 8 | 92 | | |
| I1000/500-12 | | 7 | 76 | | | I1450/600-28 | | 4 | 92.1 | | |
| I1400/600-13 | C55/67 SCC | 3 | 73.9 | | | I1450/600-29 | | 9 | 82.1 | | |
| I1400/600-14 | | 7 | 76 | | | I1450/600-30 | C60/75 | 4 | 97.7 | | |
| I1400/600-15 | | 6 | 71.6 | | | I1450/600-31 | | 7 | 93.3 | | |
| I1400/600-16 | | 8 | 73.4 | | | I1450/600-32 | | 5 | 89.7 | | |
| | | | | | | I1450/600-33 | | 10 | 87.5 | | |
| | | | | | | I1450/600-34 | | 6 | 92.1 | | |
| | | | | | | I1450/600-35 | | 11 | 83.8 | | |

From Table 7, it can be concluded that the average value of the cubic compressive strengths ($f_{ccubm}$) at 28 days of concrete class C55/67 is 74.5 MPa. According to EN 206:2014, section 8.2.1.3, this value has to be larger than $f_{ccubk}$ + 4 MPa (71.0 MPa). For this concrete type the specimens' strength meets the requirement of the specified concrete strength class. For the concrete strength class C60/75 these values are 89.3 MPa and 79.0 MPa respectively, so the measured strength exceeds the required strength with 10 MPa. In Figure 10 the measured strain values are shown separately and in Figure 11 all measurements are combined in one graph. Based on the obtained curves it is difficult to determine the actual transfer length. Vertical dotted lines on the graphs in Figure 10 indicate the approximate end of the transfer length, based on the gradient of the curve. In the first graph, two vertical lines can be marked, one at a distance of 480mm from the beam's end, and one at a position of 680mm. These lines indicate the minimum and maximum distance from which the strains remain at a constant level. In the second graph, considering beam 7 up to 12, the transition point is located between 580mm and 680mm. For beams 1 to 12 and 17 to 23 a similar curve shape is noticed, as well. The curves of beam 24 to 35, on the other hand, show an increasing trend until approximately 280mm, then the slope changes and a more slowly ascending trend is observed. The strain values for beam 13 to 16 even keep increasing.

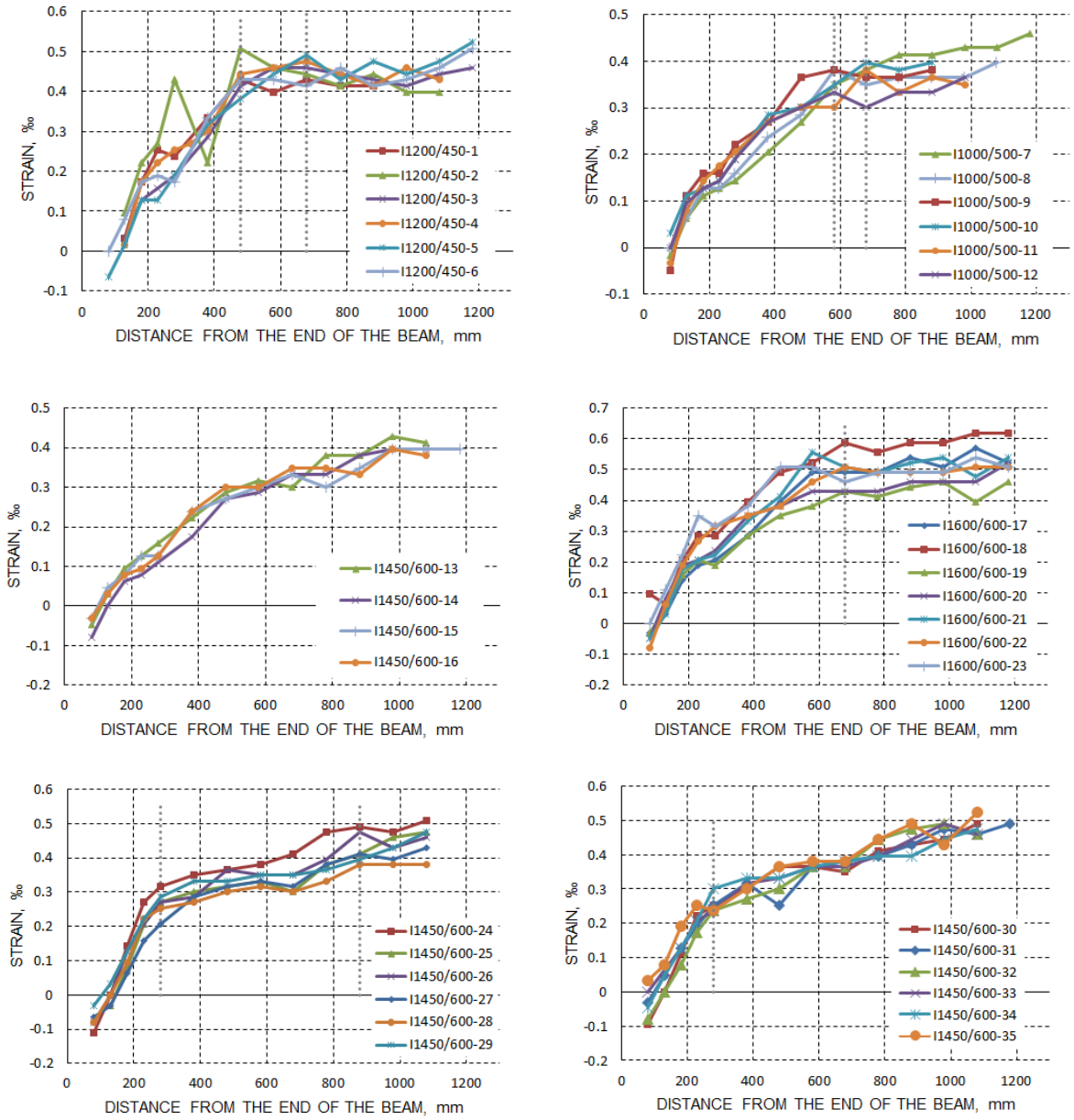


Figure 10 Results of the strain measurements in function of the distance from the end of the beam

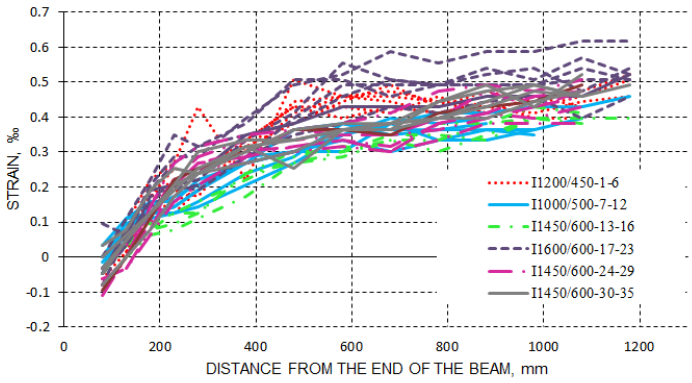


Figure 11 Overview of all the strain measurements in function of the distance from the end of the beam

## Location of the Measuring Points

Regarding the different graphs of the end zone strain measurements (Figure 10), three different shapes of curves can be observed, as mentioned before. This can be explained by the position of the measuring points relative to the centroid of the strands. In order to clarify, the three strand configurations of the beams of equal width, are presented in Figure 12. Considering the group of lower strands, it can be determined that the measurement points of beams 24 to 35 are situated approximately at the level of the centroid of the active strands. Beams 17 to 23 have 3 rows of 12 strands of which 4 debonded strands, and 1 row of 2 strands. The measuring points were attached between the first and the second layer, at 80 mm from the bottom of the beam, and not at the centroid of the active strands, at 110 mm (Figure 12). This is thought to influence the strain measurements, resulting in the different shapes of the curves (Figure 10). Looking at beams 13 to 16, the bottom layer consists of 10 strands, the second one of 8 strands and the top layer of only 2. For these beams the measurement dots were placed at the bottom layer level and not at the centroid of all strands, as the outer strands of this bottom layer are closer to the lateral edges of the lower flange. In general, the evolution of the measured strain in the transfer zone depends on the position of the measuring points. Moreover, for beams 13 to 16, the smaller number of strands and the fact that the strands are located in the central part of the flange cause a lateral dispersion over a longer distance resulting in a slower strain increase. In future measurements, the measuring points will be attached at different distances from the lower fiber to confirm this observation.

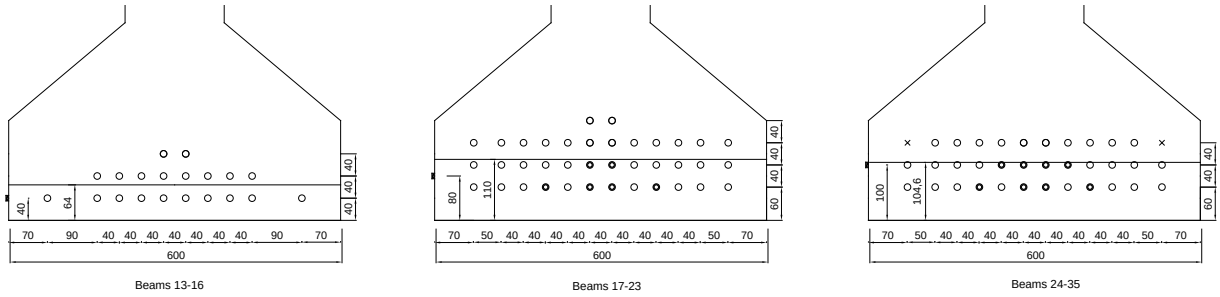


Figure. 12 Strand configuration and location of measuring points

## Validation of the Parametric Study

A parametric study of the transfer length estimation formulas was carried out. The parameters studied showed that the concrete strength class, the time of release, the strand diameter, and the way of prestressing are determining factors for the transfer length. These parameters will be investigated based on the experimental results.

- *Concrete strength*

Two concrete strength classes were used: C60/75 for beams 1 to 6 and C55/67 for beams 7 to 12. Despite these different strengths for beam series with altered geometries and varying prestress forces, the transfer length measurements of the two series can be compared. Analyzing the results of beams 1 to 6 and 7 to 12 (Figure 10) it appears that the graph shape of the first beam series approaches the horizontal asymptote faster. This confirms that a higher concrete strength results in a shorter transfer length.

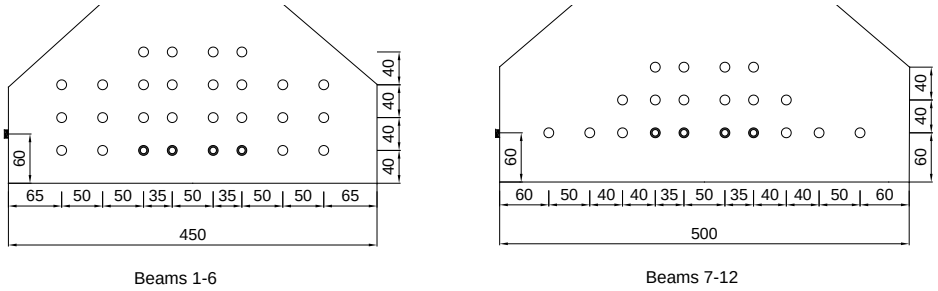


Figure. 13 Position strands beams 1 to 12

- *The time of release*

Only for beams 24 to 29 and 30 to 35, the concrete strength is known at the time of strand release. Figure 14 shows these measured compressive strengths $f_{ccubm}$ at the time of release as well as the early age compressive strength evolution based on the average measured compressive strengths $f_{ccubm}$ at 28 days [3].

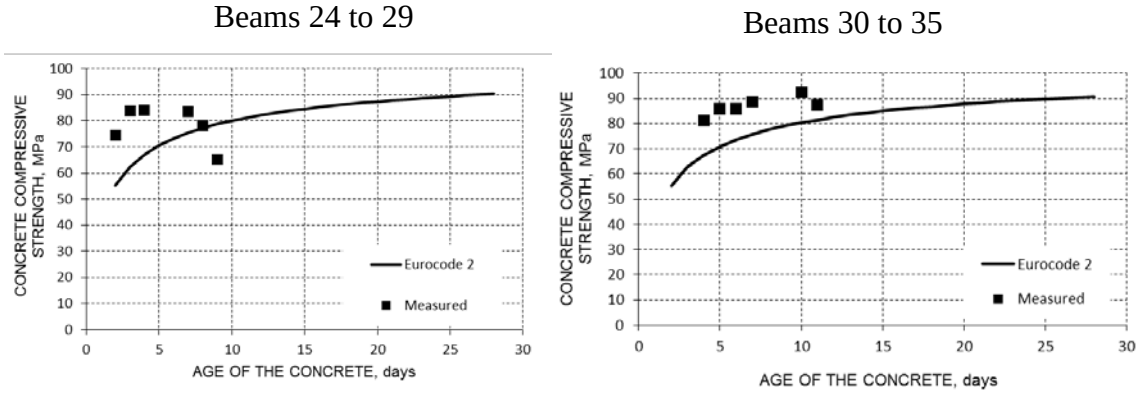


Figure. 14 Measured and calculated compressive strengths at early age

For beam 29 e.g. the average compressive strength is 65.3 MPa, which is the lowest value in its series. The highest average value here is 84.1 MPa and occurred for beam 28. However, this remarkable difference of 18.8 MPa is not reflected in the graphs in Figure 10.

A similar observation is valid for beams 30 to 35 where the difference of 11.2 MPa between the lowest and highest measured compressive strength at the time of release is not reflected in the measured strain in the transfer zone.

In addition, the considered beams' compressive strength at early age is generally higher than estimated based on the measured strength at 28 days. This hinders the use of this important parameter in the assessment of the transfer length.

- *The way of the release and the strand diameter*

Only for beams 3 to 6 the strands are released in a sudden way. Therefore, a clear conclusion regarding the way of release cannot be made. The same can be concluded regarding the strand diameter because nearly all strands are seven wire strands of ½". This will be a subject for further research.

## CONCLUSIONS

The study starts with an FEM of the end zone of a pretensioned girder. The preliminary conclusion is that the transfer length has a major influence on the stresses in the concrete and in the reinforcement. For that reason, a parametric study is conducted, in which different formulations for calculating the transfer length, found in literature, are compared. The study demonstrates that the concrete strength class, the time of release, the strand diameter, and the way of prestressing may be determining factors for the transfer length, but in general a large scatter of the results is observed. Based on this, no unanimous conclusion can be found on how to calculate the transfer length as an input for finite element analysis of an end zone. Therefore, experimental research was carried out on several girders produced in a prefab concrete plant. The results of the strain measurements render a clear influence of the concrete strength, a possible influence of the location of the measurement points, and a certain influence of the concrete strength at early age which is difficult to quantify. The way of releasing the strands seems to have no effect on the transfer length. Further research will consist of extra measurements at different levels at the lateral faces of the beams. From these data and the knowledge of the concrete strength at the time of release, the FEM will be optimized. Such an analysis of the transfer length provides a good reference frame for further research of the end zone of a prestressed girder.

## ACKNOWLEDGMENTS

This research was supported by the Agency for Innovation by Science and Technology (IWT) and the company Structo+, producer of reinforced and prestressed beams, columns, floor and roof elements, and bridge girders. The authors wish to express their gratitude for the support.

## REFERENCES

1. M. G. OLIVA EN P. OKUMUS, "Finite element analysis of deep wide-flanged pre-stressed girders to understand and control end cracking," University of Wisconsin-Madison Civil and Environmental Engineering, (2011), winsconsin.
2. P. OKUMUS, M. G. OLIVA EN S. BECKER, "Nonlinear finite element modeling of cracking at ends of pretensioned bridge girders." Engineering Structures 40, (2012), pp. 267-275.

3. AASHTO LRFD 2012, Bridge Design Specifications, (6), (2012), American Association of State Highway and Transportation Officials, pp. 5-168 - 5-169.

4. G. L. BALÁZS, "Transfer Length of Prestressing Strand as a Function of Draw-In and Initial Prestress," PCI Journal, (1993), pp. 86-93.

5. COMITÉ EURO-INTERNATIONAL DU BÉTON, "CEB-FIP Model Code 2010," T. Telford. (2011), pp. 5-1 - 5-15.

6. ACI Committee 318. Building code requirements for reinforced concrete (ACI 318- 11). Farmington Hills, MI: American Concrete Institute; 2011.

7. POZOLO A, ANDRAWES B. "Analytical prediction of transfer length in prestressed self-consolidating concrete girders using pull-out test results." Constr Build Mater (2011); 25:1026–36.

8. J.R. MARTÍ-VARGAS, P. SERNA, J. NAVARRO-GREGORI, L. PALLARÉS, "Bond of 13 mm prestressing steel strands in pretensioned concrete members." Engineering Structures 41 (2012), pp.403–412.

9. CEN. Eurocode 2: design of concrete structures – Part 1–1: general rules and rules for buildings. European standard EN 1992-1-1:2004: Brussels: Comité Européen de Normalisation; 2004.

10. MARTIN L, SCOTT N. Development of prestressing strand in pretensioned members. ACI Journal (1976); 73:453–6.

11. SHAHAWY M, MOUSSA I, BATCHELOR B. "Strand transfer lengths in full scale AASHTO prestressed concrete girders." PCI Journal (1992); 37(3):84–96.

12. LANE SN. "A new development length equation for pretensioned strands in bridge beams and piles." Research FHWA-RD-98-116. Mclean, VA: Federal Highway Administration;1998.

13. KOSE MM, BURKETT WR. "Formulation of new development length equation for 0.6 in. prestressing strand." PCI Journal, (2005); 50(5):96–105.

14. FIB. Model Code 2010. First complete draft. Fib Bulletin No. 55, vol. 1. Lausanne: International Federation for Structural Concrete (2010).

15. ZIA P, MOSTAFA T. "Development length of prestressing strands." PCI Journal (1977); 22(5):54–65.

16. MITCHELL D, COOK WD, KHAN AA, THAM TH. "Influence of high strength concrete on transfer and development length of pretensioning strand." PCI Journal (1993); 38(3):52–66.

17. TH.E. COUSINS, D.W. JOHNSTON, P. ZIA. "Transfer and development length of epoxy-coated and uncoated prestressing strand." PCI Journal, 35 (4) (1990), pp. 92–103

18. G.L. BALÁZS, G. "Transfer Control of Prestressing Strands." PCI Journal (1992)., Vol. 37, No. 6, p. 60-71.

19. MAHMOUD ZI, RIZKALLA SH, ZAGHLOUL ER. Transfer and development lengths of carbon fiber reinforcement polymers prestressing reinforcing. ACI Struct Journal (1999); 96(4):594–602.

# MODELLING OF PITTING CORROSION IN A REINFORCED CONCRETE ELEMENT

**R Guobys**

**L Chernin**

University of Dundee

United Kingdom

**ABSTRACT:** Chloride-induced corrosion of steel reinforcement is a significant problem in modern concrete infrastructure, which can cause loss of reinforcing bar cross-section, significant reduction of bond between reinforcing steel and concrete, concrete cover failure and eventually structural collapse. Therefore, the understanding of how the chloride-induced corrosion affects surrounding concrete can significantly contribute to early identification and prediction of damage caused by corrosion to reinforced concrete structures. The current paper presents a new numerical (three-dimensional non-linear finite element) approach for the modelling of chloride-induced pits developing on a reinforcing bar surface. In this approach, the expansion of corrosion products is formulated using the thermal analogy method. The contact between concrete and steel bar is modelled using the Coulomb friction model. The non-uniform distribution of corrosion products on a reinforcing bar surface is achieved with an analytical surface function postulated in a cylindrical coordinate system. The developed finite element model of a concrete block with an embedded steel bar was used for the analysis of the effect of the number and position of pits and the sensitivity of the bar pull-out force to the level of pitting corrosion and the number of pits. It was found that both the corrosion level and the pit number increased the pull-out force. The maximum value of the pull-out force depended on the confinement of the corroding bar and was highly affected by concrete cracking. The increase in the number of pits led to an earlier cracking of the concrete block. The mode of cracking depended on the position of the pit on the bar circumference.

**Keywords:** Pitting corrosion; Concrete; Reinforcing steel; Cracking; Numerical modelling.

**Raimondas Guobys** is a PhD student in civil engineering at the School of Science and Engineering of the University of Dundee.

**Dr Leon Chernin** is a lecturer in civil engineering at the School of Science and Engineering of the University of Dundee.

## INTRODUCTION

Chloride-induced pitting corrosion is considered as the most severe type of corrosion affecting the reinforced concrete (RC) infrastructure due to its localised nature and the difficulty to identify it with visual inspection. As a result, it can propagate unnoticed until the bar cross-section is sufficiently consumed to cause sudden structural failure. The sources of chlorides are divers, ranging from seawater and air in the offshore and costal structures to de-icing salts in the onshore structures. The methods for protection of RC structures against chloride-induced corrosion can be too costly or not entirely effective. Therefore, the understanding of the effect of pitting corrosion on surrounding concrete is important for the assessment of structural condition as well as for decision making on steps to be taken regarding structural maintenance.

Detrimental effects of corrosion on RC structures were studied in a number of research works using finite element (FE) method. The expansive action of corrosion products was modelled (i) by applying internal pressure or displacement fields on the concrete without explicitly incorporating a reinforcing bar in the model, e.g. [14, 17], (ii) by the expansion of a reinforcing bar introduced by a thermal load, e.g., [11, 12, 18, 24], or (iii) by strain-induced expansion of a rust layer introduced between the concrete and steel reinforcement, e.g., [10, 22]. One common approach to modelling pitting corrosion is based on an assumption that corrosion develops uniformly around a reinforcing bar, which leads to axisymmetric expansive pressure applied by corrosion products on surrounding concrete, e.g., [3, 9-12, 15, 18, 24]. Such description can only be used to accurately describe corrosion caused by carbonation or chloride-induced corrosion affecting large rebar areas. In the second approach, pitting corrosion is modelled as non-uniform. The obvious difficulty in modelling non-uniform corrosion is the selection an appropriate profile for the distribution of the expansion of corrosion products around a rebar. Du et al. [13] tried to overcome this difficulty by using a distribution of corrosion products observed in tests. The authors found that the pattern of cracks produced by non-uniform corrosion differs from the one produced by uniform corrosion. Jang and Oh [17] investigated the influence of the degree of non-uniformity of the corrosion profile on cracking behaviour of concrete covers. They reported that the cracking pressure decreases when a smaller rebar area was affected by corrosion. To obtain a more realistic chloride concentration profile, Chen and Leung [10] modelled the two-dimensional (2D) diffusion process of chlorides in concrete towards a reinforcing bar using the Fick's second law. The obtained profiles were implemented for studying the development of cracks in RC cross-sections. Ozbolt et al. [19] developed a complex 'chemo-hydro-thermo-mechanical' model of concrete that took into account heat, oxygen, moisture and chloride transport processes and corrosion related chemical reactions coupled with mechanical behaviour of concrete. The authors assumed distribution of anodic and cathodic regions along and around the bar, where the cathodic regions could extend to a quarter or a half of the bar cross-sectional surface. The developed model was implemented for FE simulation of pull-out tests with corroded bars. Good agreement between the patterns of cracks and the deterioration of bond obtained from tests and FE analyses was reported. Tran et al. [22] modelled non-uniform corrosion as uniformly distributed over a quarter or a half of bar cross-sectional area. Corrosion products were formulated as able to penetrate into cracks, which decreased the thickness of the rust layer postponing crack opening.

It is important to note that most of the researches consider the mechanical action of non-uniform corrosion as a 2D process, i.e., occurring in a RC cross-section. In this paper, a new three-dimensional (3D) FE model of pitting corrosion is developed and implemented in the FE package – ABAQUS. The model enables a more realistic representation of the interaction

between a corroding reinforcing bar and surrounding concrete, and allows studying the effect of pits on the bond strength. The 3D pitting model was used for simulation of a RILEM pull-out test with corroding rebar. Only plane bars were considered in this work to isolate the influence of single and multiple pits on cover cracking and the pull-out force. The results yielded by the models with a pitted bar and a uniformly corroded bar were compared.

## PITTING CORROSION MODEL

A 3D model of a pit developing on rebar surface is formulated in this section. In the model, the expansion of corrosion products is simulated using the thermal analogy method, where thermal loading is applied to a region on a reinforcing bar. The non-uniform nature of the bar volumetric expansion is controlled by a temperature field formulated using an analytical surface function, $T(z,\theta)$, in a cylindrical coordinate system, i.e.,

$$T(z,\theta) = T_{max} \cdot \sin^n\left(\frac{\pi z}{l}\right) \cdot \sin^m\left(\frac{\pi\theta}{\zeta}\right) \tag{1}$$

where $z$ is the coordinate along the bar axis, $\theta$ is the angular coordinate, and l and $\zeta$ represent the longitudinal and angular dimensions of a region on the rebar surface where a single pit can develop. The exponents $n$ and $m$ represent the degrees of non-uniformity of the volumetric expansion in the $z$ and $\theta$ directions on the rebar surface, respectively. Larger values of $n$ and $m$ correspond to a pit taking smaller surface area. The parameter $T_{max}$ represents the maximum level of corrosion at the middle of the pit. Eq. (1) can be used to create multiple expansion peaks distributed with the $l$ and $\zeta$ spacings longitudinally and angularly on the bar surface. This feature is used in this paper to study the effect of multiple pits on the bond between the corroding bar and concrete.

The free increase in the rebar radius over the area of a pit, $\Delta r(z,\theta)$, can be accurately estimated as [11]

$$\Delta r(z,\theta) = (\alpha_V - 1) \cdot x(z,\theta) \tag{2}$$

where $\alpha_V$ is the volumetric expansion ratio of corrosion products, $x$ is the corrosion penetration, which can for instance be found using a model from [23], and $r$ is the radius of an intact bar.

In the proposed 3D FE model, the free increase in the rebar radius over the pit area is formulated as

$$\Delta r(z,\theta) = \alpha_T \Delta T(z,\theta) \cdot r \tag{3}$$

where $\alpha_T$ is the coefficient of thermal expansion of steel and $\Delta T(z,\theta)$ is the change in the temperature field that is defined by Eq. (1). Equating the right hand sides of Eqs. (2) and (3) and assuming that $\Delta T(z,\theta) \equiv x(z,\theta)$ yields [11]

$$\alpha_T = (\alpha_V - 1)/r \tag{4}$$

In this study, $\alpha_V$ is assumed equal to 3 in accordance with [4], which leads to $\alpha_T$ = 0.25 for a 8 mm radius bar. Note that $\alpha_T$ is much larger than the real coefficient of the thermal expansion

of steel, which is equal to $10 \times 10^{-6}$. However, any combination of values of $\alpha_T$ and $\Delta T$, giving necessary $\Delta r$, is valid, since the material model of steel implemented in the FE analysis is rate independent.

It is important to mention that the present study focuses solely on the mechanical action of the corrosion products on the concrete cover and bond. Therefore, the proposed pitting corrosion model does not take into account the delay in the built-up of pressure at the corroding-steel-concrete interface caused by the penetration of corrosion products into the porous zone and micro-cracks around a reinforcing bar.

## MODELLING OF PULL-OUT TEST

### FE Model

The influence of pitting corrosion on the bond between concrete and a steel bar was investigated in the present study using a pull-out test partially complying with the RILEM recommendations [20]. The geometry and dimensions of the pull-out test model is depicted in Figure 1. As can be seen, the diameter of the steel bar is $d$ = 16 mm. The face of the concrete block, in which the bar is embedded, is a square with the edge length of 160 mm (= 10$d$). The bar is in contact with the concrete block over whole its thickness of 80 mm (= 5$d$). The bar is 100 mm long. It is placed symmetrically in the block with two ends protruding by 10 mm on each side. Such positioning allows to maintain the connection between the bar and the block over whole 80 mm contact length during the bar pull-out. Only plane bars were used in the model to eliminate the influence of mechanical interlocking on the bond strength.

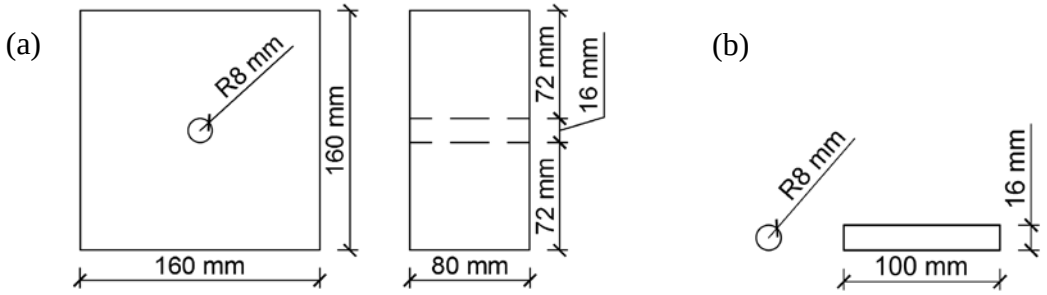


Figure 1 (a) Concrete block, (b) Plain round steel bar

The model was implemented in the FE package – ABAQUS [1]. The capability of ABAQUS to simulate the pull-out test was investigated in [12]. The contact between the bar and concrete was modelled based on the built-in general contact algorithm in the finite sliding formulation. This formulation allows arbitrary separation, sliding and rotation of surfaces in contact. The tangential interaction between the steel and concrete surfaces was defined based on the Coulomb frictional model with linear temperature dependence. The friction coefficient was set to 0.4 for uncorroded areas and 0.6 in the areas highly affected by pitting [7, 12, 19]. The reduction of the friction coefficient with the bar slip was ignored in the present model. The penetration of one surface into another was prevented by enforcing contact constrains through

the penalty method. The surface smoothing was applied to reduce discretisation errors associated with faceted representation of curved surfaces. The concrete block and the steel bar were modelled using 8-node linear brick elements (C3D8R) with reduced integration to prevent over-stiff elements and enhanced hourglass control to avoid spurious deformation mode in the model mesh [1]. The model was analysed using the explicit time integration scheme. The elements were controlled during the analysis to prevent excessive distortion of the mesh. The densities of concrete and steel were increased using the mass scaling function, which enabled significant reduction of the calculation time through the increase in the stable time increment. These minor changes had an insignificant effect on the FE analysis results. The displacement boundary conditions were applied at one square face of the concrete block and at the corresponding outward face of the steel bar. These constrains prevented movements of the block during entire analysis, while allowing for the pull-out of the bar.

The pitting corrosion model, discussed in Section 2, was applied for the simulation of a single pit and multiple pits developing on the bar surface in the zone of contact with concrete. The values of the parameters in Eq. (1) necessary to generate the required shape and number of pits are given in Table 1. An orthotropic thermal expansion coefficient was defined for the steel bar to prevent its thermal elongation.

Table 1 Parameters of Eq. (1) for different number of pits

| NUMBER OF PITS | $n$ | $m$ | $l$ (mm) | $\zeta$ ($^o$) |
|---|---|---|---|---|
| 1 | 10 | 10 | 100 | 90 |
| 2 | 10 | 10 | 50 | 90 |
| 3 | 10 | 10 | 33.3 | 90 |
| 4 | 10 | 10 | 16.7 | 90 |

Apostolopoulos et al. [2] reported based on the experimental study that the pit depth ranged between 0.367÷0.599 mm (with the average equal to 0.477 mm), while the pit area between 0.649÷29.838 mm$^2$. Zhao el al. (2011) [26] found that the thickness of the layer of non-uniform corrosion products can be as large as approximately 0.9 mm. These data were used in the calibration of the model parameters of the temperature field given in Table 1. The maximum depth of a pit and its area were assumed in all FE simulations equal to 0.6 mm and 30 mm$^2$, respectively [2].

Each FE analysis consisted of two steps. In Step 1, a thermal load was applied at the steel bar to simulate the pitting corrosion. In Step 2, a uniform displacement load was applied at the outward face of the steel bar to pull the bar out of the concrete block. The pull-out force and the slip of the bar in the concrete block were recorded.

## Material Models

The expansion of corrosion products introduces tensile circumferential and radial compressive stresses in the concrete around a corroding bar. These stresses are of the same order and thus the tensile behaviour dominates the concrete failure mechanism. The compression behaviour of concrete can be modelled as linearly elastic without a significant loss of accuracy. Therefore, the brittle cracking model incorporated in ABAQUS [1] was used for constitutive modelling of concrete. This is an elastic cracking model with concrete between cracks considered as an isotropic linearly elastic material. In this model, a simple Rankine criterion is used to detect crack initiation. This implies that a crack forms when the maximum principal tensile stress exceeds the tensile strength of the concrete. The crack surface is oriented in the direction normal to the maximum principal tensile stress. Once a crack is formed at a point, its orientation is stored for subsequent calculations. A new crack can form at the same point only in a direction orthogonal to the direction of an existing crack. Such model is called a fixed orthogonal crack model. Cracks are modelled as irrecoverable. They may close and reopen, but remain throughout the rest of the analysis. The tension softening in the direction normal to a crack is described based on the Hillerborg cohesive crack model [16], in which a stress-displacement curve is adopted from CEB-FIP Model Code 2010 [8]. Additionally, the effect of the amount of crack opening on the shear response of concrete is formulated using the shear retention model. In this model, the post-cracked shear stiffness is defined as a power function of the strain across an opening crack, reducing as the crack opens.

The material parameters used for modelling concrete, steel and corrosion products are given in Table 2. The compressive strength of concrete was taken from the pull-out tests on corroding plain round bars [6]. The rest of concrete material properties were calculated based on the recommendations of CEB-FIP Model Code 2010 [8] and Eurocode [21]. The material properties of rust were assumed in accordance with [5, 10]. The reinforcing steel was modelled as linearly elastic. Its Young's and shear moduli were formulated as temperature dependant. This enabled to simulate gradual transformation of the steel in a pit into rust through the local increase in temperature induced by the pitting corrosion model. The temperature dependency was not incorporated into the density of steel. This led to an overestimation of the rust density. However, such inaccuracy did not have any significant influence on the FE analysis, since the volume of rust in a pit is negligible compared with the volume of the steel bar.

Table 2 Material properties of concrete, steel and rust

| MATERIAL | $f_{ck}$ (MPa) | $f_{ct}$ (MPa) | $E$ (GPa) | $G$ (GPa) | $\nu$ | $\rho$ (kg/m$^3$) | $G_F$ (N/m) | $\varepsilon_{ct}$ (‰) |
|---|---|---|---|---|---|---|---|---|
| Concrete | 38.4 | 3.4 | 19.8 | 8.25 | 0.2 | 2500 | 140.8 | 1.904 |
| Steel | - | - | 210 | 81 | 0.3 | 7850 | - | - |
| Rust | - | - | 0.5 | 0.193 | 0.3 | 7850 | - | - |

In Table 2, $f_{ck}$ and $f_{ct}$ are the compressive and tensile strength of concrete, $E$ and $G$ are the Young's and shear moduli, $\nu$ is the Poisson's ratio, $\rho$ the density, $G_F$ the fracture energy, and $\varepsilon_{ct}$ the tensile strain of concrete at cracking.

## ANALYSIS RESULTS AND DISCUSSION

### Model Validation

The developed pull-out FE model was initially checked for mesh sensitivity using three meshes with different levels of refinement. The number of elements in each mesh was in the range of 3000 to 14000. The uniform thermal load was applied to the steel bar to eliminate the effect of non-uniform thermal expansion. Two levels of bar thermal expansion were analysed including $\Delta r_{max}$ = 6.5 μm and 13.0 μm, where $\Delta r_{max}$ is the maximum increase in the bar radius at the middle of a pit. The results of FE simulations indicated that the increase of the number of elements had insignificant influence on the pull-out force. In addition, the insensitivity of the brittle cracking model in the stress-displacement formulation to the element size was investigated elsewhere [24].

Next, the 3D FE model was validated against the results of pull-out tests conducted using corroded plain round bars [6]. Since the corrosion process of the bars in the tests was accelerated using electrical current, a uniform thermal load was applied to the steel bar in the FE model. The results of the FE simulations of Y5 test specimen are given in Table 3. It was reported in [12] that about 95-97% of corrosion products penetrated into the porous zone and micro-cracks in the concrete around the bar. Therefore, the thermal loading was applied until the bar expansion was equal to about 4% of the one obtained in the test. The resulting maximum pull-out force was higher than the one obtained in the test by less than 14%.

Table 3 The estimated and calculated data for tests from [6]

| SOURCE | MAXIMUM PULL-OUT FORCE, kN | BAR EXPANSION, μm |
|---|---|---|
| 3D FE model | 35.9 | 11.5 |
| Y5 specimen [6] | 31.5 | 29.6 |

### Modelling of Pitting Corrosion

### Modelling of a single pit

The numerical investigation of the effect of non-uniform corrosion on the pull-out force starts with the modelling of a single pit on the bar surface. The pit was located at the mid-length of the bar as depicted in Figure 2. Four levels of the localised bar expansion including $\Delta r_{max}$ = 70, 147, 308 and 988 μm were examined. It is important to note that $\Delta r_{max}$ is the maximum confined local expansion (or radius increase) of the bar in the concrete block measured in the middle of the pit at the end of Step 1 of an FE simulation (see Section 3.1 for details on the analysis steps). The confined expansion rather than the free expansion of the bar was used in this study to eliminate the influence of local deformations of concrete and steel on the level of pitting corrosion. In the analysis with $\Delta r_{max}$ = 988 μm, a minor crack appeared in the concrete block at the bar surface at $\Delta r_{max}$ = 353 μm. The crack subsequently reached the outer surface of the block at $\Delta r_{max}$ = 523 μm. The last result falls in the rage of values of the bar expansion observed in the pitting corrosion tests [2]. The location of the pit in the concrete block strongly

influenced the cracking pattern developed. Figure 3a shows that the pit directed towards a side of the block caused its splitting. On the other hand, the pit directed towards a block corner caused corner spalling shown in Figure 3b. Results demonstrate good agreement with chloride-induced corrosion experimental findings [25].

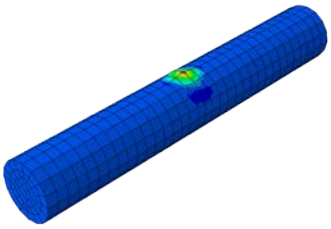

Figure 2 Single pit model

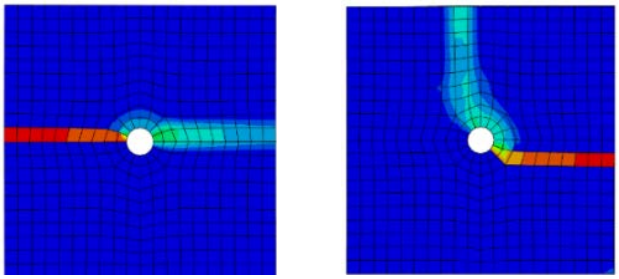

(a) (b)

Figure 3 (a) Block splitting and (b) corner spalling

The curves showing the influence of the corrosion level of a single pit on the pull-out force are presented in Figure 4. As can be seen, the maximum pull-out force increased with the increasing corrosion level due to the growing level of bar confinement in the block. The cracking of the block caused the loss of the confinement and the significant reduction of the force (by more than 65%). The remaining bar confinement in the cracked concrete block at this level of the bar expansion still enabled the pull-out force to develop to the level larger than in the case with $\Delta r_{max}$ = 70 μm.

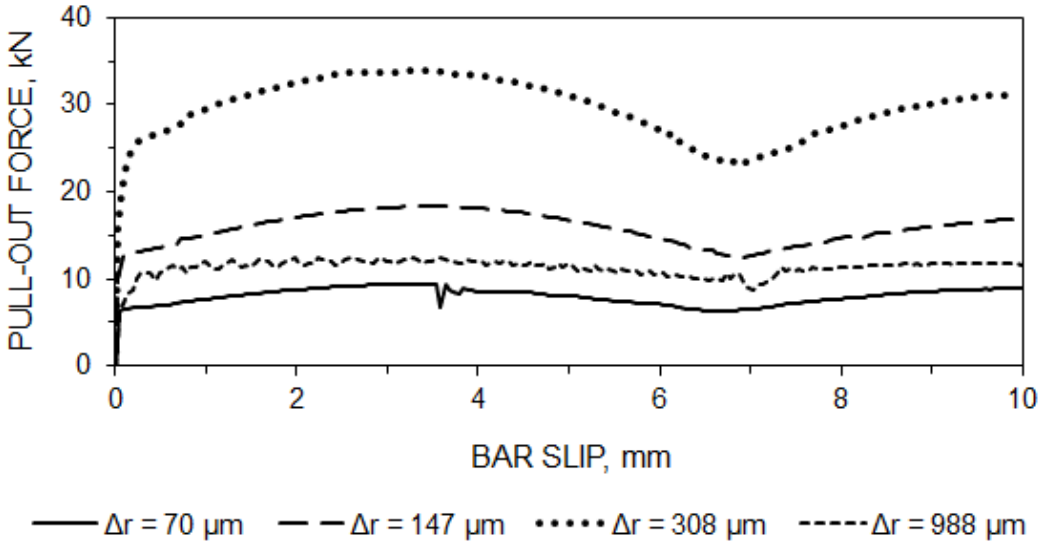


Figure 4 Force-slip diagram for the single pit model

The force-slip curves in Figure 4 have a distinct wave shape after the bar slip occurs. The length of the wave is 6.67 mm, which is equal to the size of the elements of the block along the surface of the contact with the bar. Additionally, the wavelength is not affected by the corrosion level. The wave shape did not disappear when the concrete material model was substituted with a linearly elastic one. This phenomenon was further investigated using the concrete block mesh with 5 mm elements. Figure 5 depicts the force-slip curves obtained with the two meshes. The wave in the case of the FE model with the smaller elements is shorter with the length equal to 5 mm and has a smaller height. Therefore, the wave shape of the force-slip curve is the result of the model discretisation combined with the surface-to-surface formulation of the contact algorithm used in the FE simulations. The waves can further be flattened through decreasing the element size. The wave shape did not develop in the force-slip curve when the uniform expansion was generated in the bar.

As can be seen in Figure 5, the FE model with 5 mm elements produced a lower pull-out force due to a slightly smaller confined bar expansion developed. The difference in the bar expansion levels occurred due to the high sensitivity of the confined expansion to the level of the thermal load applied to the bar.

It is necessary to note that the shape of a local thermal expansion on the bar surface is found to be influenced by the mesh element size. Smaller element size lead to a more accurate representation of the shape but also increased the computational time. Therefore, the elements of 3 mm length along the bar deemed to give a sufficiently accurate approximation and were taken in all FE simulations.

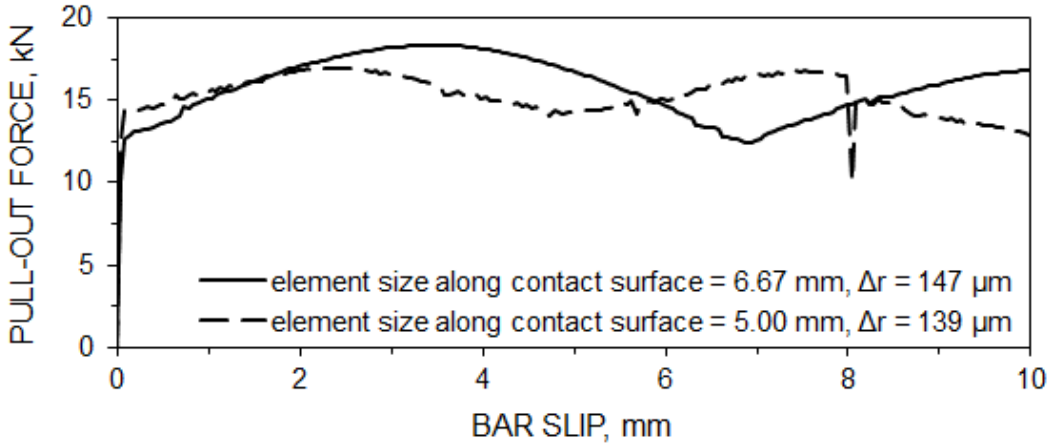


Figure 5 Influence of the concrete block mesh on the force-slip curve

## Modelling of multiple pits

The pitting corrosion model was further to generate 2, 3 and 4 pits on the bar surface as shown in Figure 6. The pits had similar shape and level of corrosion and were located on one line with spacing *l* given in Table 1. It is necessary to note that such similarity of pit shapes and regularity in their spacing is not realistic. However, it allows to conduct a detailed characteristic study on the mechanical behaviour of a steel bar with multiple pits pulled out of a concrete block.

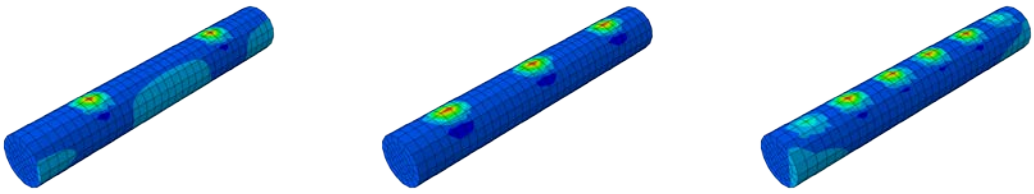

Figure 6 Simulation of 2, 3 and 4 pits

Figure 7 depicts the force-slip curves obtained for single and multiple pit models. The increase in the number of local expansion regions (or pits) on the bar surface did not elimination the wave shape of the force-slip curve. However, it resulted in an increase of the maximum pull-out force by 75%. The maximum increase of the bar radius of the single pit model was different by about 4% from the 2 pit model due to the difficulty of controlling the confined localised bar expansion.

The maximum confined bar expansion of the 3 and 4 pit models was chosen to be higher than that of the 1 and 2 pit models in order to include the influence of the first crack initiation on the pull-out force. The 20% increase in the level of bar expansion combined with the increase in the number of pits led to a larger increase in the pull-out force by about 40%. The loss of the bar confinement in the 4 pit model due to concrete cracking reduced the rate of the force increase with the number of pits by 47%. These observations demonstrate the high interconnection between different factors influencing the confinement of the reinforcing bar in a concrete block.

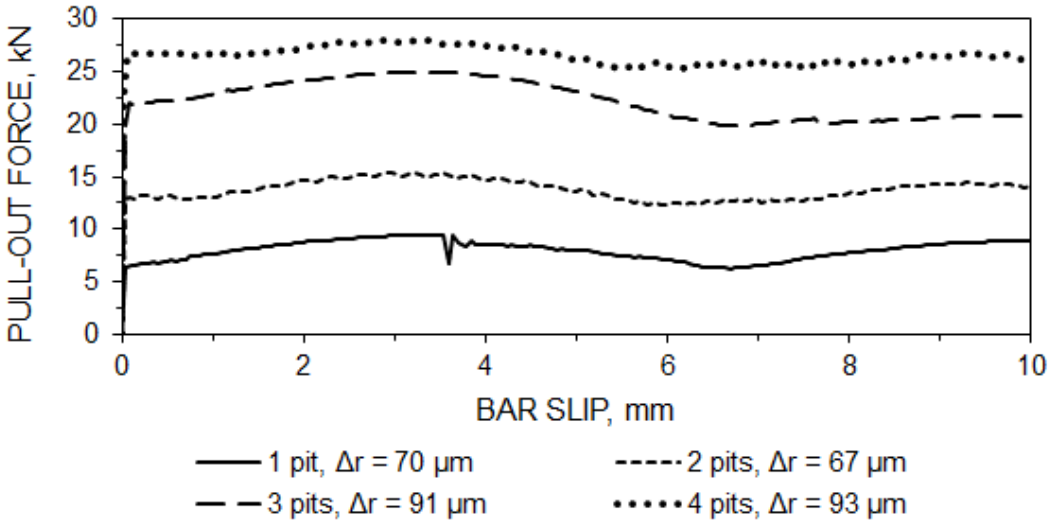


Figure 7 Force-slip curve for 1, 2, 3 and 4 pits

Figure 8 shows that the increase in the number of pits led to a gradual decrease in the maximum confined bar expansion required for cracking of the concrete block. The shape of the curve in the figure suggests that the rate of the decrease of $\Delta r_{max}$ declines with the growing number of pits and $\Delta r_{max}$ gradually converges on the value corresponding to the uniform bar corrosion.

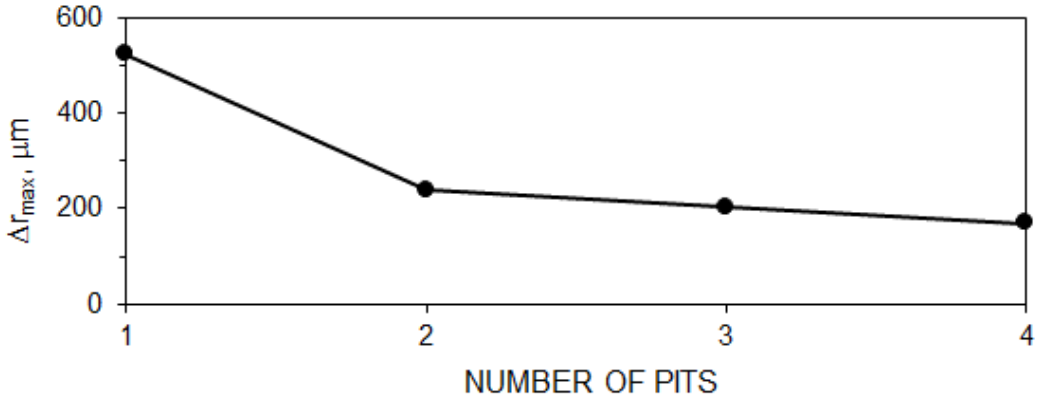


Figure 8 $\Delta r_{max}$ at concrete block cracking vs. number of pits

**Non-uniform vs. uniform corrosion**

The effect of the extent of corrosion of the bar surface area on the pull-out force is analysed using the ratio between the pull-out force and the maximum confined radial expansion of the bar. This normalisation allows to compare the results of FE simulations with different levels of confined bar expansion. Figure 9 depicts the evolution of the force-expansion ratio with the growing of the bar surface area affected by corrosion. Note that the abscissa of the diagram is presented in the logarithmic scale.

As can be seen in Figure 9 that the force-expansion ratio increased with the increase in the area affected by corrosion. It can be concluded that with the increasing number of pits the force-expansion ratio will gradually approach the value corresponding to the uniform corrosion, which is schematically shown by the dashed line in the figure.

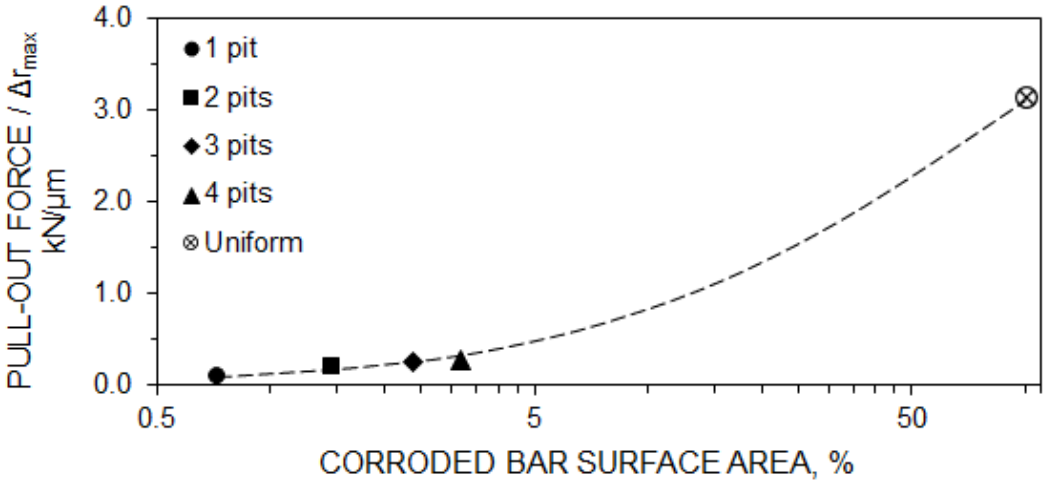


Figure 9 Force-expansion ratio vs. bar surface area affected by corrosion

## CONCLUSIONS

In this paper, a new method for modelling pitting corrosion is presented. It utilises the concept of thermal analogy and allows to achieve localised radial expansion on the surface of a reinforcing bar. A finite element (FE) model of a smooth round steel bar embedded in a concrete block was developed and the proposed method was applied for the simulation of bar pitting corrosion. The contact between the bar and concrete was modelled based on the Coulomb frictional model. The effect of the corrosion level on the steel-concrete contact was taken into account through a gradual increase of the friction coefficient of the affected areas on the bar surface. The FE model was validated against the results of pull-out test with corroding plain round bars. It was shown that the finite element discretisation combined with the surface-to-surface formulation of the contact algorithm used in the FE simulations resulted in a minor inaccuracy in the simulation of the contact between the corroded bar and the concrete. The effects of the level of pitting corrosion and the number of pits on the pull-out force were then investigated. The increase in both the corrosion level and the pit number led to the increase in the pull-out force. A significant decrease in the pull-out forced occurred with cracking of the concrete block due to the loss of bar confinement. With the increasing number of pits, lower corrosion level was required to crack the concrete block. Additionally, the increase in the bar surface area affected by corrosion resulted in the gradual increase in the pull-out force. The location of the pit on the bar surface influenced the mode of concrete block cracking. The pit oriented towards a block side cased splitting, while the pit oriented towards a corner cased its spalling. Finally, it can be concluded that the proposed pitting corrosion model can be efficiently used for studying the mechanical effects of pits on concrete cover cracking and bond between corroded reinforcement and concrete.

## REFERENCES

1. ABAQUS, Abaqus Version 6.13 Documentation, Dassault Systems, 2013.
2. APOSTOLOPOULOS, C, DEMIS, S, PAPADAKIS, V. Chloride-induced corrosion of steel reinforcement – Mechanical performance and pit depth analysis, Construction and Building Materials, Vol. 38, 2013, pp 139-146.
3. BERRA, M, CASTELLANI, A, CORONELLI, D, ZANNI, S, ZHANG, G. Steel-concrete bond deterioration due to corrosion: finite-element analysis for different confinement levels, Magazine of Concrete Research, Vol. 55 No. 3, 2003, pp 237-47.
4. BERTOLINI, L. Corrosion of steel in concrete. Weinheim, Germany: Wiley-VCH, 2013.
5. BOSSIO, A, MONETTA, T, BELLUCCI, F, LIGNOLA, G, PROTA, A. Modeling of concrete cracking due to corrosion process of reinforcement bars, Cement and Concrete Research, Vol. 71, 2015, pp 78-92.
6. CAIRNS, J, DU, Y, LAW, D. Residual bond strength of corroded plain round bars, Magazine of Concrete Research, Vol. 58, No. 4, 2006, pp 21-231.
7. CAIRNS, J, DU, Y, LAW, D. Influence of corrosion on the friction characteristics of the steel/concrete interface, Construction and Building Materials, Vol. 21, 2007, pp 190-197.

8. CEB-FIP. fib Bulletin 55: Model Code 2010 – Final draft, Comité Euro-International du Béton, Lausanne, Switzerland, Vol. 1, 2012.

9. CHEN, D, MAHADEVAN, S. Chloride-induced reinforcement corrosion and concrete cracking simulation, Cement and Concrete Composites, Vol. 30, No. 3, 2008, pp 227-238.

10. CHEN, E, LEUNG, C. Finite element modeling of concrete cover cracking due to non-uniform steel corrosion, Engineering Fracture Mechanics, Vol. 134, 2015, pp 61-78.

11. CHERNIN, L, VAL, D. Prediction of corrosion-induced cover cracking in reinforced concrete structures, Constr. Build. Mat., Vol. 25, No. 4, 2011, pp 1854-1869.

12. CHERNIN, L, VAL, D, CAIRNS, J. A new numerical model of the corroded steel–concrete interface, Magazine of Concrete Research, Vol. 62, No. 6, 2010, pp 415-425.

13. DU, X, JIN, L, ZHANG, R. Modeling the cracking of cover concrete due to non-uniform corrosion of reinforcement, Corrosion Science, Vol. 89, 2014, pp 189-202.

14. DU, Y G, CHAN, A H C, CLARK, L A. Finite element analysis of the effects of radial expansion of corroded reinforcement, Computers and Structures, Vol. 84, 2006, pp 917-29.

15. GRASSL, P, DAVIES, T. Lattice modelling of corrosion induced cracking and bond in reinforced concrete, Cement and Concrete Composites, Vol. 33, No. 9, 2011 pp 918-924.

16. HILLERBORG, A, MODEER, M, PETERSSON, P-E. Analysis of crack formation and crack growth in concrete by means of fracture mechanics and finite elements, Cement and Concrete Research, 1976, pp 773-82.

17. JANG, B, OH, B. Effects of non-uniform corrosion on the cracking and service life of reinforced concrete structures, Cem. Concr. Res., Vol. 40, No. 9, 2010, pp 1441-1450.

18. MOLINA, F J, ALONSO, C, ANDRADE, C. Cover cracking as a function of rebar corrosion. Part 2 – numerical model, Materials and Structures, Vol. 26, 1993, pp 532–48

19. OŽBOLT, J, ORŠANIĆ, F, BALABANIĆ, G. Modeling pull-out resistance of corroded reinforcement in concrete: Coupled three-dimensional finite element model, Cement and Concrete Composites, Vol. 46, 2014, pp 41-55.

20. RILEM/CEB/FIP. Bond test for reinforcing steel: 2. Pullout Test, Recomm. RC 6, 1978.

21. THE BRITISH STANDARDS INSTITUTION. BS EN 1992-1-1:2004. Eurocode 2: Design of concrete structures - Part 1-1: General rules and rules for buildings. London: BSI, 2004.

22. TRAN, K K, NAKAMURA, H, KAWAMURA, K, KUNIEDA, M. Analysis of crack propagation due to rebar corrosion using RBSM, Cement and Concrete Composites, Vol. 33, 2011, pp 906-917.

23. VAL, D, MELCHERS, R. Reliability of Deteriorating RC Slab Bridges, Journal of Structural Engineering, ASCE, Vol. 123, No. 12, 1997, pp 1638-1644.

24. VAL, D V, CHERNIN, L, STEWART, M G. Experimental and numerical investigation of corrosion-induced cover cracking in reinforced concrete structures, ASCE J. Struct. Eng. Vol. 135, 2009, pp 376-385.

25. ZHANG, R, CASTEL, A, FRANÇOIS, R. Concrete cover cracking with reinforcement corrosion of RC beam during chloride-induced corrosion process, Cement and Concrete Research, Vol. 40, No. 3, 2010, pp 415-425.

26. ZHAO, Y, HU, B, YU, J, JIN, W. Non-uniform distribution of rust layer around steel bar in concrete, Corrosion Science, Vol. 53, No. 12, 2011, pp 4300-4308.

# ADVANCED MATERIAL MODELLING OF CONCRETE IN ABAQUS

**M Vilnay**
Abertay University

**L Chernin**
University of Dundee

**D Cotsovos**
Heriot Watt University

United Kingdom

**ABSTRACT.** Abaqus is a complex finite element (FE) package widely used in civil engineering practice. In particular, it is used for modelling of reinforced concrete structures. One of the concrete models incorporated in Abaqus is the brittle cracking model. The main shortcoming of this model is that it assumes linearly elastic behaviour in compression. This paper proposes to eliminate this shortcoming through the use of the user subroutine VUSDFLD. This subroutine allowed to add the nonlinear compressive behaviour into the brittle crack model by introducing the dependency of the modulus of elasticity of concrete on strain. Additionally, the concrete material is modelled to be able to develop damage defined by the maximum strain and damaged elements are deleted from the FE model. The extended brittle crack model is used to examine the strain rate effects and to simulate three benchmark cases with static and blast type loading regimes. The limits of the model applicability are examined. The FE simulation results favourably compared with those observed in experiments. Overall, the extended brittle crack model offers a robust reliable way for modelling of concrete.

**Keywords:** Concrete; Numerical modelling; ABAQUS; User subroutine.

**Margi Vilnay** is a lecturer in structural engineering at the School of Science, Engineering and Technology of Abertay University.

**Dr Leon Chernin** is a lecturer in civil engineering at the School of Science and Engineering of the University of Dundee.

**Dr Demetrios Cotsovos** is a lecturer in structural engineering at the School of Energy, Geoscience, Infrastructure and Society of Heriot Watt University.

## INTRODUCTION

Abaqus is often used by scientists and engineers for modelling of reinforced concrete (RC) structures, e.g., [1-5]. The choice of material models of concrete is limited in Abaqus to the smeared cracking model, the brittle cracking mode and the damaged plasticity model [6]. Each model is designed for a particular type of usage. The smeared cracking model can handle only monotonic loading and low confining pressures. This sufficiently limits the range of its applicability. The damaged plasticity model is by far most complex concrete model incorporated in Abaqus that can be used in any loading regime. However, it is not 'user friendly', includes multiple parameters and its calibration can be very challenging. Additionally, this model does not allow damaged elements to be deleted form the finite element (FE) analysis, which can lead to numerical instability of the solution algorithms. The brittle cracking model can be used in any loading regime and is very 'user friendly' and easy to calibrate. The main disadvantage of this model is that it assumes linear elastic material behaviour in compression. As a result, the model can be reliably used only in the cases where the concrete behaviour is dominated by the tensile failure.

The limited choice of the built-in concrete models combined with their shortcomings often resulted in new models introduced in Abaqus through user-defined subroutines, e.g., [1, 2]. In this paper, the brittle cracking model is extended to include the nonlinear compressive behaviour using the user subroutine VUSDFLD. The new material model is compared with the original brittle cracking model and the damaged plasticity model. It is then used to examine strain rate effects [7, 8] and also to simulate a number of benchmark cases including a three point bending test [9], a standard brittle failure test [10] and an RC column under blast [11]. The limitations of model application are examined.

## EXTENDED BRITTLE CRACKING MODEL

The brittle cracking model is built to work in Abaqus with the explicit time integration scheme [6]. It is an elastic cracking model with concrete between cracks considered as an isotropic linearly elastic material. In this model, the initiation and evolution of individual cracks is not tracked. Instead, a smeared crack method is utilised to present the material discontinuities. The constitutive calculations are independently performed at each material point of an FE element. The presence of cracks affects the stress and material stiffness associated with the material point. A simple Rankine criterion is used to detect crack initiation. Thus, a crack forms when the maximum principal tensile stress exceeds the tensile strength of the concrete. The crack surface is oriented in the direction normal to the maximum principal tensile stress. Once a crack is formed at a point, its orientation is stored for subsequent calculations. A new crack can form at the same point only in a direction orthogonal to the direction of an existing crack. Therefore, this model is called a fixed orthogonal crack model. Cracks are modelled as irrecoverable. They may close and reopen, but remain throughout the rest of the analysis. The tension softening in the direction normal to a crack is described based on the Hillerborg cohesive crack model [12], in which a stress-displacement curve is adopted from CEB-FIP Model Code 2010 [13]. Additionally, the effect of the amount of crack opening on the shear response of concrete is formulated using the shear retention model. In this model, the post-cracked shear stiffness is defined as a power function of the strain across an opening crack, reducing as the crack opens.

The nonlinear behaviour of concrete in compression is incorporated into the brittle cracking model by using the user subroutine VUSDFLD [6]. This subroutine allows to redefine material properties at a material point as a function of a field variable such as stress, strain, temperature, etc. The field variable is updated at each analysis step and the value of the

relevant material property is recalculated. In this study, the nonlinear compressive behaviour of concrete is introduced into the brittle crack model by formulating the modulus of elasticity of concrete ($E_c$) as a function of strain ($\varepsilon_c$). To define the $E_c - \varepsilon_c$ function, the stress-strain ($\sigma_c - \varepsilon_c$) relationship describing the uniaxial compression behaviour of concrete is adopted from CEB-FIB Model Code 2010 [13]

$$\frac{\sigma_c}{f_{cm}} = -\frac{k \cdot \eta - \eta^2}{1 + (k-2) \cdot \eta} \quad \text{for} \quad \varepsilon_c < \varepsilon_{c,lim} \tag{1}$$

where $\eta = \varepsilon_c / \varepsilon_{c1}$ , $\varepsilon_{c1}$ is the strain at the maximum compressive stress $f_{cm}$, $\varepsilon_{c,lim}$ is the strain at crushing of concrete in compression, $k = E_{ci} / E_{c1}$ is the plasticity number, $E_{ci}$ is the initial modulus of elasticity of concrete and $E_{c1}$ is the secant modulus obtained by connecting the diagram origin to the curve peak, i.e., ($\varepsilon_{c1}$, $f_{cm}$). The $E_c - \varepsilon_c$ relationship can be obtained from Eq. (1) taking into account that $E_c = \sigma_c / \varepsilon_c$ and $E_{c1} = f_{cm} / \varepsilon_{c1}$

$$E_c = -\frac{k - \eta}{1 + (k-2) \cdot \eta} \cdot E_{c1} \quad \text{for} \quad \varepsilon_c < \varepsilon_{c,lim} \tag{2}$$

In Eq. (2), $E_c$ is the secant modulus obtained by connecting the diagram origin to a point on the $\sigma_c - \varepsilon_c$ curve. The $\sigma_c - \varepsilon_c$ and $E_c - \varepsilon_c$ curves yielded by Eqs. (1) and (2) are schematically shown in Figure 1.

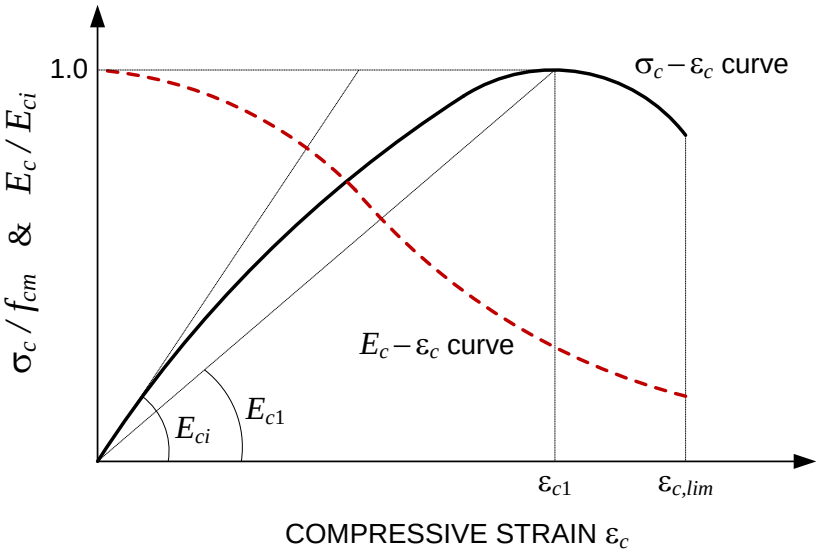


Figure 1 The $\sigma_c - \varepsilon_c$ and $E_c - \varepsilon_c$ curves describing Eqs. (1) and (2)

Additional advantage of the original and extended brittle cracking models is that they can be used together with an algorithm that removes failed elements from the FE model. The failure criterion is defined in this algorithm as the maximum compressive/tensile strain.

## VALIDATION OF THE MATERIAL MODEL

In all FE simulations discussed hereafter, concrete was modelled using 8-node linear brick elements (C3D8R) with reduced integration to prevent over-stiff elements and enhanced hourglass control to avoid spurious deformation mode in the model mesh [6]. The elements were controlled during the analysis to prevent excessive distortion of the mesh.

### Single Finite Element

The efficiency of the extended brittle cracking model was initially examined using a single finite element model representing a 1 m × 1 m × 1 m concrete block. The bottom face of the block was constrained against the vertical movement. Additional constrains where applied at three corners of the block to prevent its rotation and movement in the horizontal plane. Such boundary conditions allowed to avoid the development of an arching effect in the block. A vertical displacement load was applied to the top face of the block in order to stabilise the procedure of the numerical solution. The concrete block had the following material properties: $E_{ci}$ = 30 GPa, Poisson's ratio $\nu$ = 0.2 and the density $\rho$ = 2400 kg/m$^3$.

Three FE models using the extended brittle cracking model, the original brittle cracking model and the damaged plasticity model were compared. The material parameters used in the models are given in Table 1. These parameters correspond to the Abaqus benchmarked solution of a three point bending test [6].

Table 1 Material parameters

| COMPRESSION | | TENSION | | |
|---|---|---|---|---|
| Yield Stress (MPa) | Inelastic Strain | Yield Stress (MPa) | Displacement (m) | Damage Parameter |
| 20 | 0 | 3.33 | 0 | 0 |
| 30 | 0.015 | 0.333 | 7.447e-5 | 0.9 |

Note that only the tensile properties are needed for the brittle cracking models. Additional compressive properties (i.e., the $E_c - \varepsilon_c$ curve) necessary for the extended brittle crack model were obtained based on the $\sigma_c - \varepsilon_c$ curve generated by the damaged plasticity model. This was done in order to exclude the influence of the input data on the material model performance.

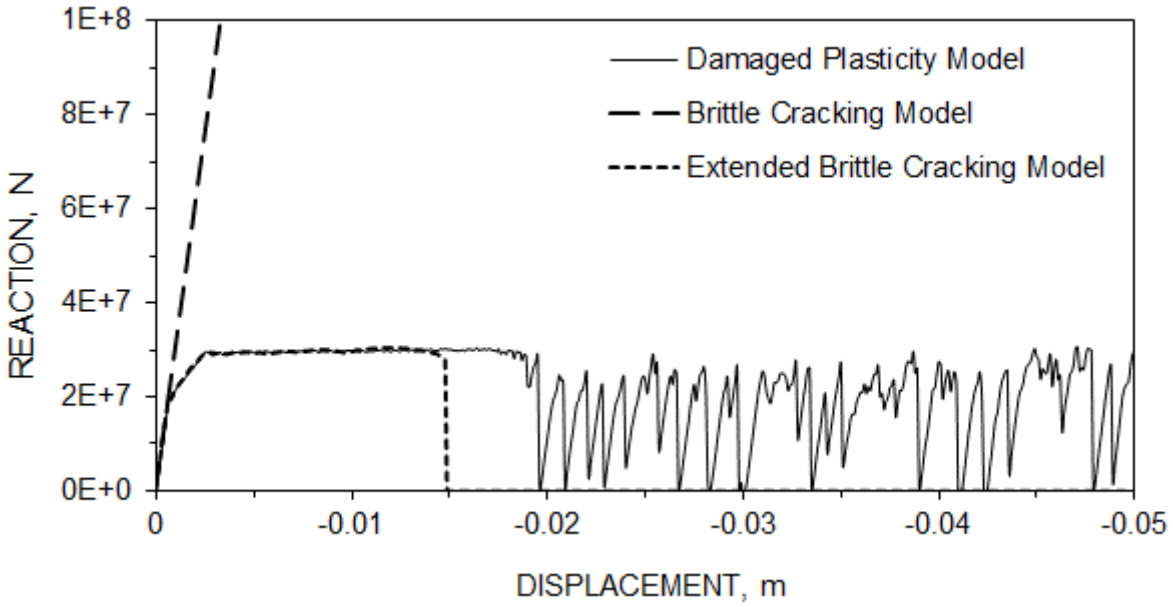


Figure 2 Reaction-displacement curves for compression load

The performance of the three concrete models under uniaxial tension and compression was then examined. All the models behaved similarly under tension with a slight difference between the damaged plasticity model and both the brittle cracking models developing in the part of the curves corresponding to the crack opening. On the other hand, the behaviour of the models highly diverged under compression. Figure 2 shows that the original brittle cracking model exhibited a purely elastic response. The two remaining models behaved similarly until the designated maximum strain of 0.015 (corresponding to the displacement of 0.015 m in the concrete block), when the extended brittle cracking model failed. The damaged plasticity model failed at the strain just under 0.02 (the displacement of 0.02 m in the block). Following its failure, the damaged plasticity model exhibited an unstable response with a series of sharp partial recoveries and failures (see Figure 2). As a result, this model may not be entirely reliable in simulating the post-failure behaviour of concrete structures.

**Strain Rate**

The extended brittle cracking model does not explicitly include the effect of the rate of load application. The sensitivity of this material model to the strain rate was examined using a standard concrete prism with the height of 253 mm and the cross-section of 100 mm by 100 mm [7]. Each edge of the prism cross-section was discretised into 5 elements, while the prism was discretised into 13 elements along its height. This gave 125 elements with the dimensions of 20 mm × 20 mm × 19.5 mm. The uniaxial compressive strength of concrete was assumed to be $f_{cm}$ = 30 MPa, Poisson's ratio equal to $\nu$ = 0.2 and the density to $\rho$ = 2400 kg/m$^3$. The bottom face of the prism was fixed and the load was applied to the top face at different rates.

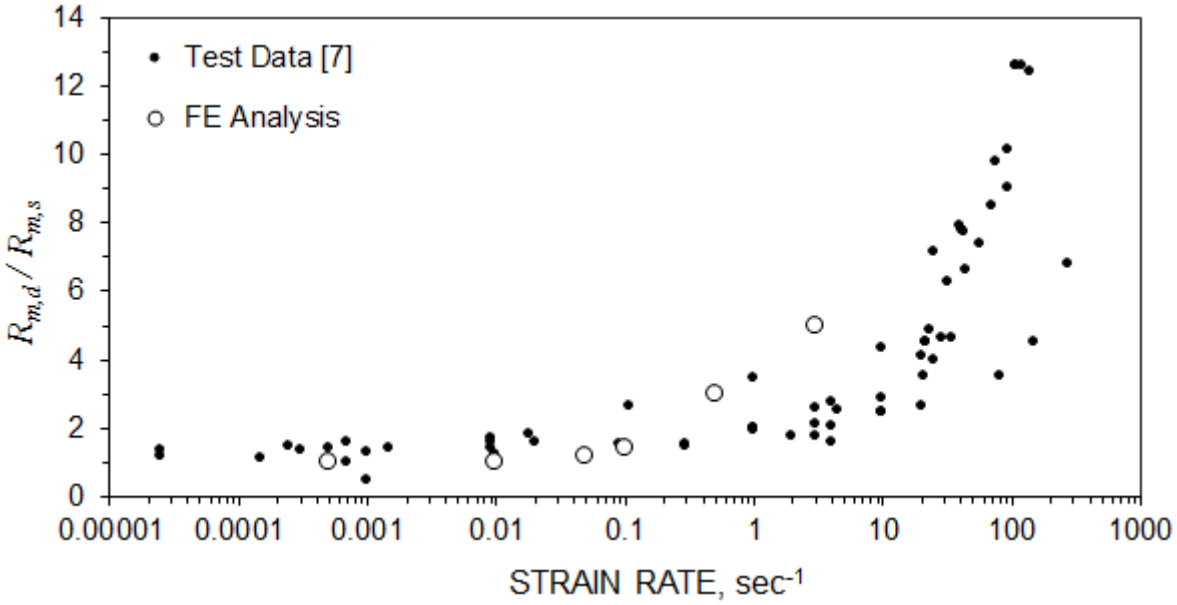


Figure 3 Effect of tensile strain rate

Initially, the effect of the tensile strain rate was examined using a displacement load. The displacement load was selected to stabilise the numerical solution during concrete failure in tension. Six different displacement rates between 10 mm/sec and 20,000 mm/sec (corresponding to the strain rates between 0.0005 sec$^{-1}$ and 3 sec$^{-1}$, respectively) were considered. The increase in the tensile stresses was observed with the growing strain rate.

Figure 3 shows the analysis results plotted together with the existing strain rate experimental data [7]. The abscissa of the diagram in the figure is in a logarithmic scale, and the ordinate is the maximum dynamic reaction force, $R_{m,d}$, at the top face of the prism normalised by the maximum static reaction force, $R_{m,s}$. As can be seen, the numerical results fall within the experimental scatter, and the $R_{m,d}$ / $R_{m,s}$ ratio increases more rapidly for the strain rates larger than 0.1 $sec^{-1}$. It is also necessary to note that the displacement loads with the rates larger than 20,000 mm/sec (corresponding to the strain rate of 3 $sec^{-1}$) caused distortion of the finite elements, rendering the results unreliable.

The effect of the compressive strain rate was examined using the pressure load with the rates between 10,000 MPa/sec and 4,000,000 MPa/sec (corresponding to the strain rates between 0.01 $sec^{-1}$ and 70.8 $sec^{-1}$, respectively). Figure 4 shows the results of numerical simulations as well as the existing experimental data [7]. The abscissa of the diagram in the figure is in a logarithmic scale, and the ordinate is the maximum dynamic pressure, $P_{m,d}$, normalised by the maximum static pressure, $P_{m,s}$. It is evident that the growing strain rate leads to the increase of the $P_{m,d}$ / $P_{m,s}$ ratio and this increase becomes more rapid for the strain rates larger than 0.3 $sec^{-1}$. In addition, the numerical results fall within the experimental scatter.

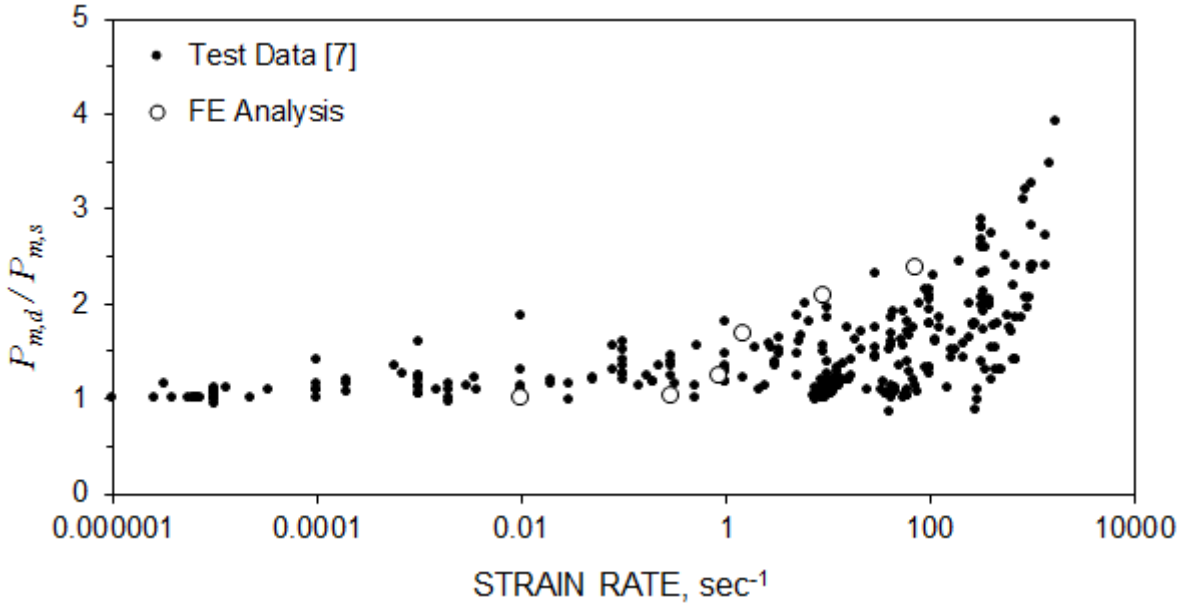


Figure 4 Effect of compressive strain rate

It can therefore be concluded that since the strain rate effect is not incorporated into the extended brittle cracking model, the observed increase in the material strength can only be attributed to the inertia effects occurring at the structural level.

## SIMULATION OF BENCHMARK CASES

The extended brittle cracking model is implemented in this section for simulation of three standard benchmark cases including a notched concrete beam, an RC beam and column.

### Notched Concrete Beam

The 3 point bending tests on a notched unreinforced concrete beam [9] was chosen for the examination of the efficiency of the brittle cracking model in simulating the tensile structural

failure. The simply supported beam had the span equal to 2 m, the depth to 0.2 m and the width to 0.05 m. The midspan notch had the depth of 0.1 m and the width of 0.04 m. The beam was loaded by a knife (line) load at midspan. The concrete had the following material properties: $E_{ci}$ = 30 GPa, $\nu$ = 0.2, the tensile strength $f_{tm}$ = 3.33 MPa, the Mode I fracture energy $G^I_f$ = 124 N/m and $\rho$ = 2400 kg/m$^3$. This benchmark problem was also used for verification of the damaged plasticity model [6], which allowed comparison between the two material models.

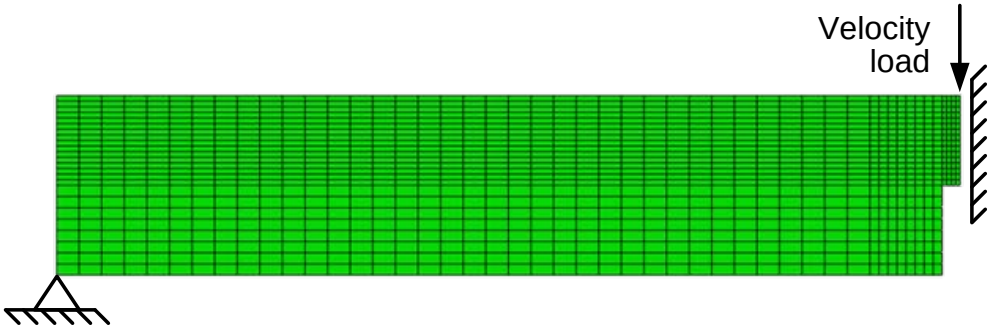


Figure 5 FE model of noted beam

Taking advantage of symmetry, only half of the notched beam was modelled (see Figure 5). The mesh consisted of 1120 three-dimensional elements of the type C3D8R [6]. The mesh around and above the notch was refined to overcome mesh sensitivity due to the possibility of cracking in the out of plane direction.

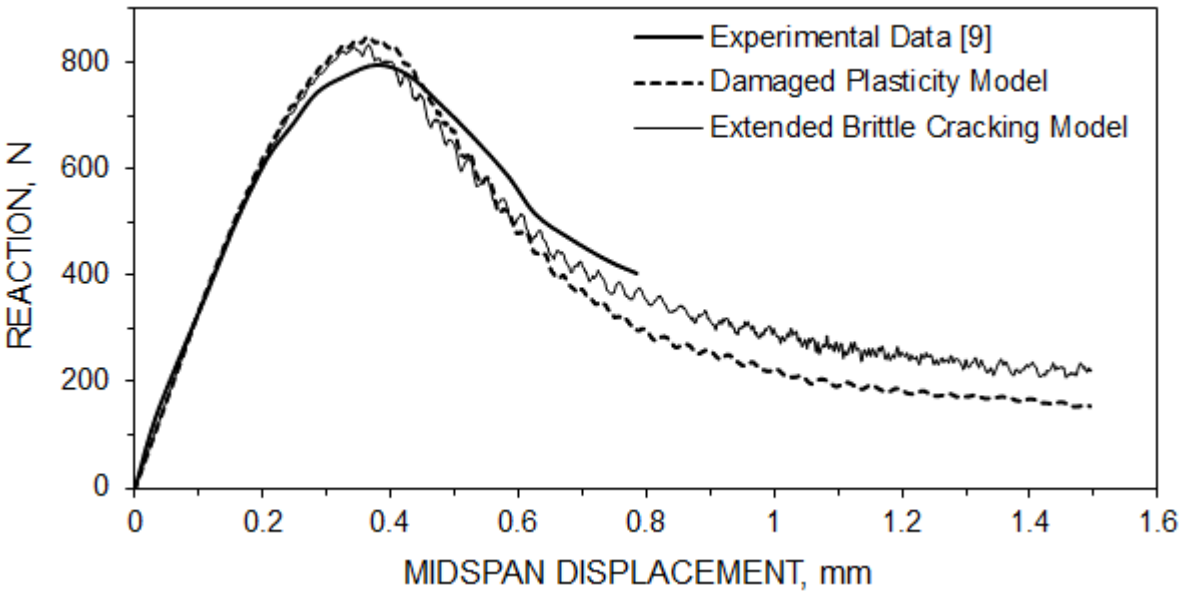


Figure 6 Reaction vs. midspan displacement of noted beam

The analysed beam was expected to fail in a brittle mode with a sudden drop in its load carrying capacity. This behaviour can generally lead to an increase in the kinetic energy content of the numerical response of the beam. Since the FE solution was carried out using

the explicit time integration scheme, the beam had to be kept in the static regime by loading it slowly enough to eliminate significant inertia effects. The static loading regime was achieved by applying a velocity load (see Figure 5) that increased linearly from 0 to 0.06 m/s over a period of 0.05 seconds, which led to the final displacement of 1.5 mm at the beam midspan. This type of loading ensured a quasi-static solution in a reasonable number of time increments, while the kinetic energy in the beam was small throughout the numerical solution. The results of the FE simulations together with a comparison to the experimental data are shown in Figure 6. As can be seen, both material models provide peak and failure responses that agree well with the experimental observations [9]. Although, the extended brittle crack model is slightly more accurate in the failure part of the curve. Small oscillations of the reaction-displacement curves still develop due to the inertial effects before cracking of concrete occurs. The amplitude of the oscillations becomes larger during the failure phase due to amplification of the inertia effect by cracking.

**Reinforced Concrete Beam**

The efficiency of the extended brittle cracking model in simulating the behaviour of a RC beam is examined using the beam C-2 from the experimental series [10]. The simply supported C-2 beam was 4572 mm long with the cross-section presented in Figure 6. The concrete had the following material properties: $E_{ci}$ = 22.924 GPa, $\nu$ = 0.2, $f_{cm}$ = 24.13 MPa and $\rho$ = 2400 kg/m$^3$. The longitudinal reinforcement consisted of 4 bottom #9 bars (28.65 mm diameter) and 2 top #4 bars (12.7 mm diameter). The shear reinforcement consisted of #2 (6.25 mm diameter) stirrups at spacing of 208 mm centres. The concrete cover was equal to 41.3 mm. The material properties of reinforcement are given in Table 2.

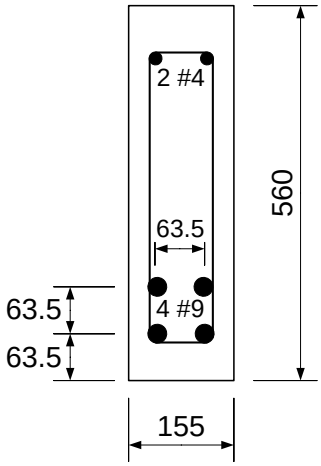


Figure 6 C-2 beam cross-section [10] (all dimension in mm)

The FE model of the whole C-2 beam included 4510 three-dimensional elements of the type C3D8R. All reinforcing bars were modelled using 1178 Timoshenko beam elements (B31) and classic metal plasticity [6]. The reinforcing bar elements were embedded in the concrete elements. This formulation assumed perfect, unfailing bond between steel bars and concrete.

The crack patterns developed in the C-2 beam during a 3 point bending test and the results of the FE simulation are depicted in Figure 7. The FE results show the strain distribution in the concrete. As can be seen, the test beam and the FE model underwent excessive cracking in the same zones. The midspan deflection of the test beam and the FE model are shown in Figure 8. The curves in the figure follow very similar paths till the FE model fails at the 10.1 mm deflection due to numerical instabilities introduced by excessive cracking of concrete. In the case of brittle failure the underestimation of the structural capacity is preferable to its overestimation. Therefore, the extended brittle cracking model provides safe prediction of the beam response.

Table 2 Reinforcement material properties [10]

| STEEL TYPE | ELASTIC MODULUS (GPa) | YIELDING STRESS (MPa) | ULTIMATE STRESS (MPa) |
|---|---|---|---|
| #9 | 205.46 | 551.58 | 932.8 |
| #4 | 201.33 | 345.42 | 603.98 |
| #2 | 189.6 | 325.43 | 429.54 |

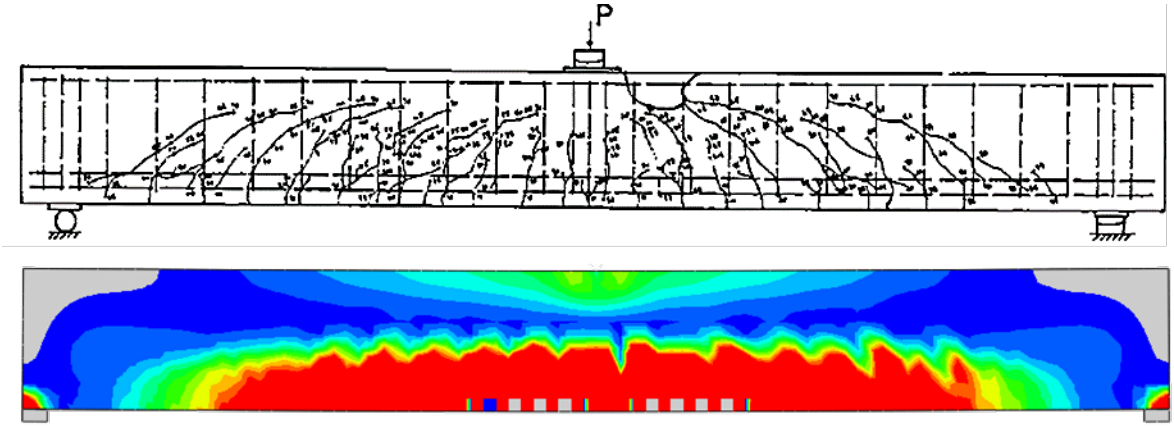


Figure 7 Crack patterns: test beam [10] at the top and FE model at the bottom

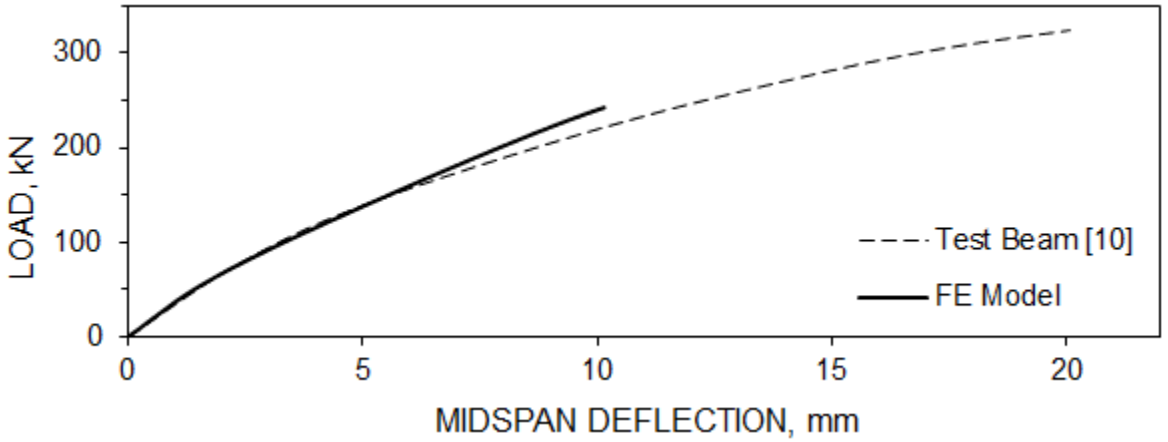


Figure 8 Load-deflection curves

## Reinforced Concrete Column

The efficiency of the extended brittle cracking model in capturing the response of an RC column under a blast load is examined using the Test 7 column from the experimental series [11]. In the tests, the blast load was artificially created using an array of blast generators, each of which was made of an impacting module and a hydraulic actuator. Four blast generators were located over the column height. They impacted the column imparting a controlled blast-like impact. The column was casted with heavily reinforced concrete blocks as its heading and footing. The column footing was fixed to the ground, while a link system applied to the column heading provided lateral and moment restraints while allowing vertical movement only. The column was 3277 mm high and had a 356 mm × 356 mm cross-section. The reinforcement consisted of eight #8 longitudinal bars and #3 hoops spaced at 324 mm centres. The cover depth was 38 mm. The concrete had the following material properties: $E_{ci}$ = 24 GPa, $\nu$ = 0.2, $f_{cm}$ = 40 MPa and $\rho$ = 2400 kg/m$^3$. The yield stress of longitudinal bars was equal to $f_y$ = 335 MPa, while of hoops to $f_y$ = 235 MPa.

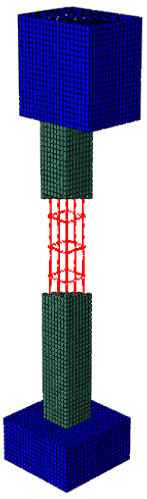

Figure 9 FE model of Tests 7 column [11]

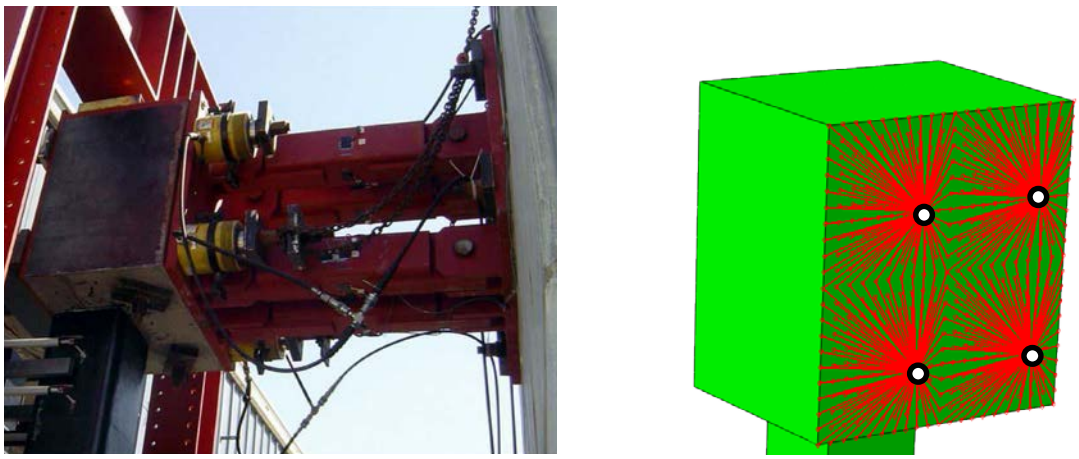

Figure 10 Four link system: test setup [11] on the left and FE model on the right

Figure 9 shows the FE model of the column with the heading, footing and part of the reinforcement exposed. In accordance with the experimental setup, each face of the footing was restrained in the perpendicular direction creating a fixed support. The restraint system at the top of the column was explicitly modelled by applying multipoint constraints between the nodes on one face of the heading and four external nodes. The external nodes were restrained from moving in the horizontal plane, but could move vertically. The experimental setup and the FE model of the heading are shown in Figure 10. Since the footing and heading were confined and heavily reinforced, they were assumed to be linearly elastic in the FE model. The concrete column was modelled using 16224 elements of the type C3D8R. The reinforcing bars were modelled using 1372 Timoshenko beam elements (B31) and classic metal plasticity [6], and were embedded in concrete elements. The blast load was simulated using the equivalent pressure measured in the experiment [11]. The pressure was applied uniformly over a corresponding column face and its intensity was controlled through its amplitude.

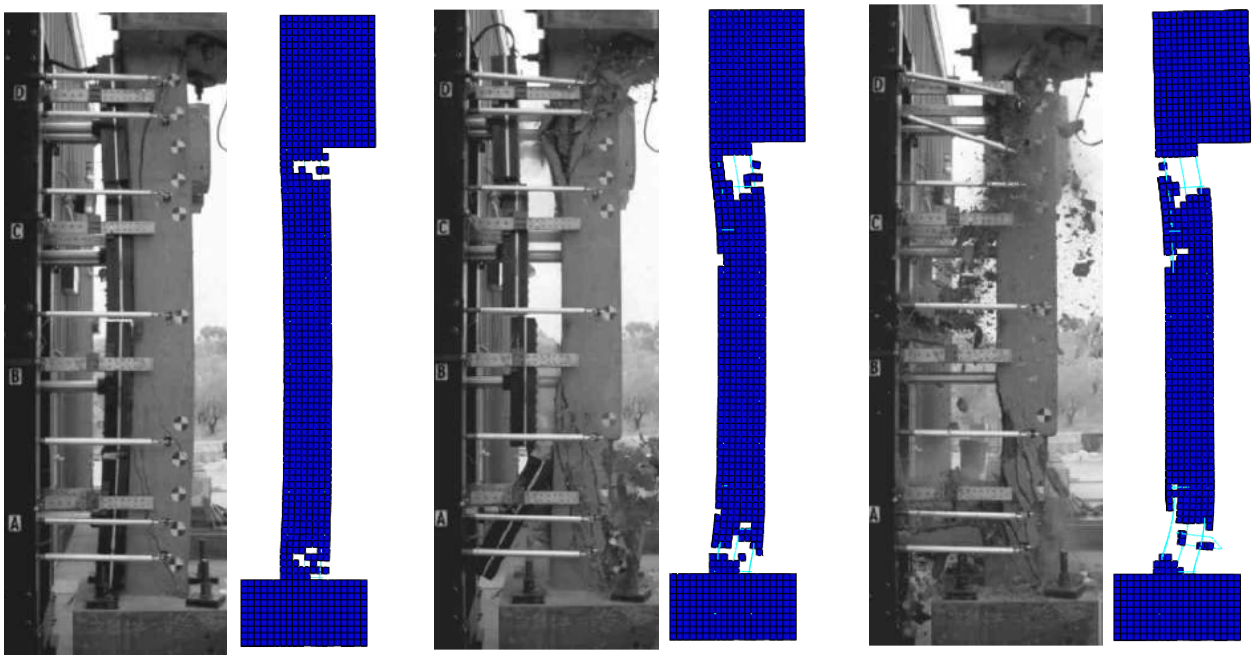

(a) (b) (c)

Figure 11 Test 7 experimental [11] and FE results at (a) 41.7 μsec (b) 84.3 μsec and (c) 558 μsec after blast load application

Figure 11 shows the results of the results of test and FE simulations at different times after blast load application. As can be see, in both cases shear cracks initially developed at both the top and bottom ends of the column (see Figure 11a). This was followed by extensive crashing of concrete (see Figures 11b and 11c). The column eventually failed in both the test and the FE simulation due to the shear failure at both its ends. The peak deflections recorded in the test at 41.7 μsec equalled 122 mm, while in the FE simulation it was equal at 43.2 μsec to 116.3 mm. The residual deflection recorded in the tests was equal to 85 mm, while in the FE simulations to 92 mm. It can be concluded therefore that the numerical analysis closely followed the test and provided an accurate prediction of the evolution of damage and deflections in the column.

## CONCLUSIONS

In this paper, a method for improving the brittle cracking material model incorporated in Abaqus was suggested. This method allowed to introduce nonlinear compressive behaviour into the model using a user subroutine VUSDFLD. This was done by formulating the modulus of elasticity as a function of strain. Additionally, the user subroutine allowed to eliminate failed elements from the finite element (FE) mesh which increased the stability of numerical solution. The extended brittle cracking material model was implemented for modelling concrete. Initially, the performance of the proposed model was compared with other material models built-in in Abaqus using a single FE model. The advantages of the proposed model were clearly outlined. The efficiency of the proposed material model to simulate concrete under high rate loads was then examined using an FE model of a concrete prism. Despite the fact that the strain rate effect was not incorporated into the model formulation, the increase in the tensile and compressive material strength took place with the increase in the rate of loading. The FE results were within the experimental scatter. This behaviour was attributed to the inertia effects occurring at the structural level. Further, the extended brittle cracking material model was implemented for simulation of three standard benchmark cases including a notched concrete beam, a reinforced concrete (RC) beam and an RC column. The beams were subjected to static loads while the column to a blast load. In all examined cases, the extended brittle cracking model showed ability to accurately describe failure modes and evolution of deflection and cracks in a structure.

## REFERENCES

1. CICEKLI, U, VOYIADJIS, G Z, ABU AL-RUB, R K. A plasticity and anisotropic damage model for plain concrete, International Journal of Plasticity, Vol. 23, No. 10-11, 2007, pp. 1874-1900.

2. YU, T, TENG, J G, WONG Y L, DONG, S L. Finite element modeling of confined concrete-II: Plastic-damage model, Engineering Structures, Vol. 32, No. 3, 2010, pp. 680-691.

3. Mohamed, A R, Shoukry, M S, Saeed J M. Prediction of the behavior of reinforced concrete deep beams with web openings using the finite element method, Alexandria Engineering Journal, Vol. 53, No. 2, 2014, pp. 329-339.

4. GENIKOMSOU, A S, POLAK, M A. Finite element analysis of punching shear of concrete slabs using damaged plasticity model in ABAQUS, Engineering Structures, Vol. 98, 2015, pp. 38-48.

5. CHERNIN, L, VAL, D V. Prediction of corrosion-induced cover cracking in reinforced concrete structures, Construction and Building Materials, Vol. 25, No. 4, 2011, 1854-1869.

6. ABAQUS. Abaqus Version 6.13 Documentation, Dassault Systems, 2013.

7. COTSOVOS, D M, PAVLOVIĆ, M N. Numerical investigation of concrete subjected to high rates of uniaxial tensile loading, International Journal of Impact Engineering, Vol. 35, No. 5, 2008, pp. 319-335.

8. COTSOVOS, D M, PAVLOVIĆ, M N. Numerical investigation of concrete subjected to compressive impact loading. Part 1: A fundamental explanation for the apparent strength gain at high loading rates, Computers and Structures, Vol. 86, No. 1–2, 2008, pp. 145-163.

9. PETERSSON, P-E. Crack growth and development of fracture zones in plain concrete and similar materials, Division of Building Materials, Lund Institute of Technology, Lund, Sweden, 1981.

10. BRESLER B, SCORDELIS, A C. Shear strength of reinforced concrete beams, ACI Journal Proceedings, Vol. 60, 1963.

11. RODRÍGUEZ-NIKL, T. Experimental simulations of explosive loading on structural components reinforced concrete columns with advanced composite jackets, PhD Thesis, University of California, San Diego, 2006, p. 252.

12. HILLERBORG A, MODEER M, PETERSSON P-E. Analysis of crack formation and crack growth in concrete by means of fracture mechanics and finite elements, Cement and Concrete Research, 1976, pp. 773-82.

13. CEB-FIP. fib Bulletin 55: Model Code 2010 – Final draft, Vol. 1. Comité Euro-International du Béton, Lausanne, Switzerland, 2012.

# TIME-DEPENDENT BEHAVIOUR OF REINFORCED CONCRETE BEAMS UNDER SUSTAINED LOADING

**S Daud**

**J P Forth**

**N Nikitas**

University of Leeds

United Kingdom

**ABSTRACT.** This paper compares the long term static performance of full scale rectangular normally reinforced concrete beams under sustained loads. Mid-span deflections were monitored for a maximum period of 3 months so that meaningful comparisons could be made between the structural displacements of the beams tested under different load levels. The range of load applied varied from that corresponding to the first cracking moment to that required to produce a stabilised crack pattern. A commercial nonlinear finite element software (Midas FEA) was used to model the experimental tests. The experiments show that the long-term mid-span deflection of the reinforced concrete beams is affected by the number of cracks, specifically the shrinkage curvature portion of the overall deflection. In terms of the numerical modelling, the capacity of the software to separate the shrinkage and creep deflection clearly allows the relationship between number of cracks and shrinkage to be observed, and confirms what was observed in the experimental investigation.

**Keywords:** Cracks, Long-term deflection, Midas FEA, Shrinkage curvature and Sustained loads.

**Sultan Daud** was assistant lecturer in Al Nahrain University, Baghdad, Iraq and is currently with the School of Civil Engineering, University of Leeds, United Kingdom.

**Professor John P Forth** is with the School of Civil Engineering, University of Leeds, United Kingdom.

**Dr Nikolaos Nikitas** is with the School of Civil Engineering, University of Leeds, United Kingdom.

## INTRODUCTION

In reinforced concrete flexural members, at low (pre-cracking) levels of loading, both the concrete and reinforcement act elastically and compositely. As the load increases, such that the applied moment exceeds the cracking moment, primary cracks are produced; the position of these cracks are random due to the variation in the tensile strength of the concrete, but they occur where the tensile strength of the concrete is at its weakest and they occur because the tensile strength has been exceeded by the tensile stress generated by the loading. At stabilized cracking, the bond between the two materials helps to transmit the load; the effectiveness of this load transition depends on the quality of the bond. There are many factors affecting the bond strength such as the strength of concrete, the yield strength, diameter and surface geometry of the steel reinforcement, and the embedded length of the reinforcement inside the concrete [1, 2] As the load increases and cracking is produced by the application of a load and the long-term effects of creep and shrinkage, secondary cracks develop. Chen and Baker [3] found that the crack spacing in reinforced concrete members is influenced by bond slip. However the final crack patterns are different for the case with or without bond-slip. Bakoss [4] assessed the instantaneous and long term deflection predicted by ACI 345 1966 and CP 110 using the experimental results of two simply supported beams and two continuous beams which were subjected to long-term sustained loading. They concluded that both the ACI and CP 110 overestimate the short-term deflection. However, after 500 days, the ACI and CP 110 predicted deflections which were + 16 % and -16 %, respectively. Nie and Cai [5] also conducted an experimental investigation to study the effect of sustained loading on the time-dependent deflection of simply supported beams. Their test results showed that the deflection due to the sustained loading ranged from 0.48 % to 88 % of the elastic deflection over a period of 3 months. However, the work done by Washa and Fluck [6] indicated that the total deflection after 30 months was nearly twice that of the initial deflection for beams with no compression reinforcement, and was ‘slightly greater’ than the elastic deflection in the case of doubly reinforced concrete beams. Similarly, Pillai and Menon [7] showed that the long-term deflection of reinforced concrete members due to shrinkage, creep and temperature could be two to three times the instantaneous deflection.

Recent work carried out by Vakhshouri and Nejadi [8] compared the short and long term-deflections of work published by other researchers. They noticed that the parameters that effect the long term deflection are not the same as those which affect the short-term deflection; thus a linear relationship between short and long term deflection is out of the question. Moreover, Vakhshouri and Nejadi [8] stated that there is no distinct expression to show when the short-term deflection ends and the long-term deflection begins. However, the long-term to initial deflection ratio depends on many factors such as the type of concrete (i.e. normal, high strength or fibre concrete), environmental conditions which enhance the creep and shrinkage, concrete age at the time of loading, and the amount of the sustained loading.

Considering Eurocode 2, the long term predicted curvature appears to depend on the section behaviour rather than the beam behaviour and is based on a weighting factor relating two beam conditions; the elastic uncracked section and the fully cracked section, as presented in equation (1):

$$1/r = \xi(1/r)_{cr} + (1-\xi)(1/r)_{uc} \quad (1)$$

Where

$1/r$ is the average curvature

$(1/r)_{cr}$, $(1/r)_{uc}$ are values of curvature calculated for the cracked and uncracked section, respectively

$\xi$ is the distributed coefficient allowing for tension stiffening given by $\xi = 1 - \beta\left(\frac{M_{cr}}{M_a}\right)^2$.

$\beta$ is the coefficient taking account the duration of loading (0.5 for sustained or cyclic loading and 1 for single short term load)

$M_{cr}$ is the cracking moment

$M_a$ is the applied moment

Eurocode 2 suggests $\xi$ to be $1 - \beta\left(\frac{M_{cr}}{M_a}\right)^2$ when $M_a > M_{cr}$ and $\xi = 0$ when $M_a \leq M_{cr}$. Espion and Halleux [9] noticed that when the applied moment is slightly less than the cracking moment the predicted deflection is imprecise as the deflection is assumed to be purely due to the uncracked section.

A great deal of work has been published on the long term behaviour of reinforced concrete beams under sustained loading. However, the effect of the number of cracks on the long term deflection, specifically the shrinkage curvature, has not yet been considered. Also, it is not really clear when 'long-term loading' begins. In this study, the number of cracks on the long term behaviour will be examined experimentally. In addition the shrinkage curvature predicted by Eurocode 2 and Midas FEA will be verified. Finally the shrinkage curvature will separated numerically.

## EXPERIMENTAL PROGRAMME

Three simply supported reinforced concrete beams were subjected to different magnitudes of sustained load using a 4-point loading arrangement. The first beam was subjected to a load which produced a stabilised crack pattern. The other two beams were subjected to loads of 5 kN and 3 kN, respectively – the calculated load required to produce the initial cracking moment was 3.5 kN. The 5 kN load produced 7 cracks in the constant moment zone while the 3 kN load produced no initial cracks as it was below the load required to produce a cracking moment.

Table 1 Beam Loading Details

| BEAM DESIGNATION | LOADING MAGNITUDE (kN) |
|---|---|
| SUS-19 | 19 |
| SUS-5 | 5 |
| SUS-3 | 3 |

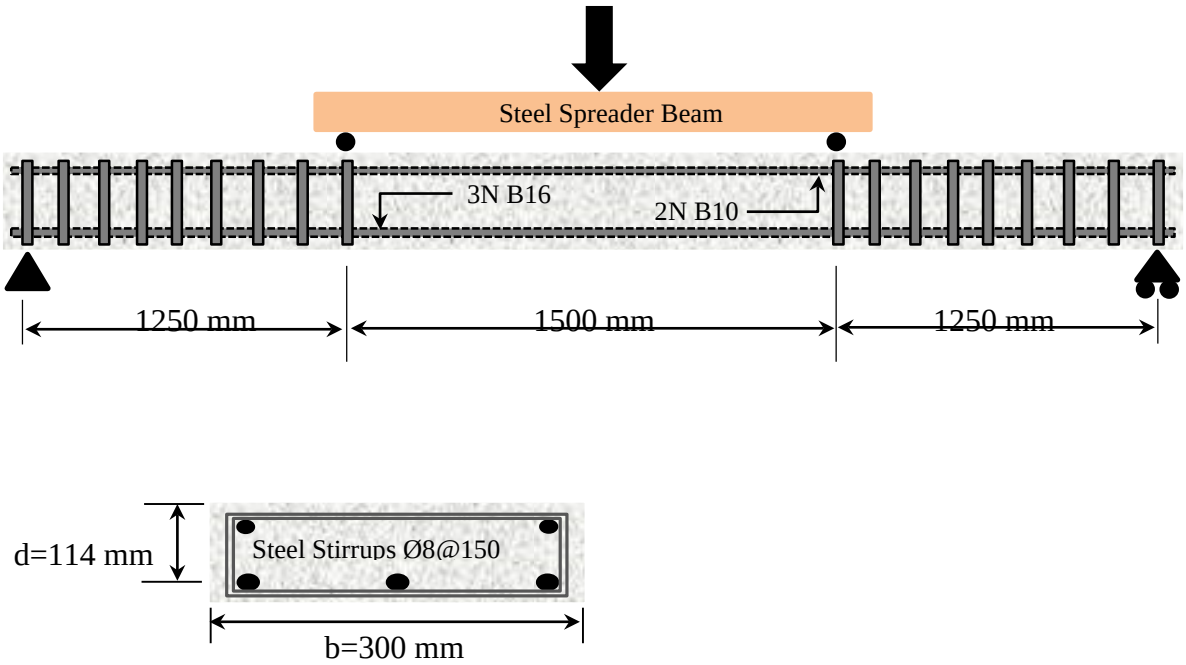


Figure 1 Structural details of the 4200mm beams tested under 4-point loading

For all beams, the mean concrete compressive strength, $f_{\mathrm{ck,cube}} = 55$ MPa (sd 0.56), the mean flexural tensile strength, $f_{ct} = 3.6$ MPa (sd 0.6) and the mean modulus of elasticity, $E_{\mathrm{cm}} = 33.7$ GPa. The beams were 300 mm wide, 150 deep and with a whole span of 4200 mm. Three bars each with a diameter of 16 mm, yield stress of 510 MPa and a modulus of elasticity of 180 GPa were used as the bottom longitudinal reinforcement.

Shear links, 8mm diameter, were placed at 150 mm centre to centre distance outside of the constant moment zone; two 10mm diameter bars, located in the compression face of the beam, were used to support the stirrups. The concrete was cast in two layers, each layer being vibrated; steel formwork was used. After casting, the beams were cured for 1 week in the mould. They were then demoulded and placed in a fog room (99% RH). Three days before the test, the beams were placed in the test rig and prepared for the test. Both sides of the beams were painted white to help monitor the cracks. Four sets of DEMECs were placed on both sides of the beams to monitor the curvature and surface strain. The bottom and top rows of DEMECs were positioned at the level of the reinforcement. Two LVDTs (Linear Variable Differential Transformers) were placed under each beam to monitor the mid-span deflection. At an age of 28 days, the first beam was preloaded to 19 kN to produce a stabilized crack pattern. This level of loading produced 15 cracks in the constant moment zone. The second beam was loaded to 5 kN and 7 cracks were initially produced. While the third beam was loaded to 3 kN. All beams were loaded for 90 days and all readings (i.e. deflection and surface strains) were recorded regularly during the tests.

## NUMERICAL SIMULATION

The reinforced concrete beams were modelled using Midas FEA. The nonlinear analysis was based on material proprieties (i.e. including creep and shrinkage) that were obtained experimentally. For the long term analysis, the construction stage function was used to help define the development in the material properties. In the analysis, the concrete was considered to be elastic in order to use the creep and shrinkage functions. The CEB-FIP model code 1990

suggests that the modulus of elasticity is reduced by 0.85 to reflect the initial plastic strain. The concrete was meshed using 50 mm quadratic map-meshing, while the reinforcement mesh was 50 mm auto-mesh.

## RESULTS AND DISCUSSION

Creep and shrinkage are major parameters which influence long term deflection. Figure 2 illustrates the long term developed deflection of the three reinforced concrete beams tested under different levels of loading. Mu [10] showed numerically that 50 % of the total long term curvature is likely due to creep while the other 50 % is due to shrinkage – this is however dependent on geometry and percentage steel reinforcement. According to this rationale, for the first beam considered here (i.e. SUS-19), the shrinkage curvature should be 9.4 mm (see Figure 2). Similarly it should be 5.5 mm and 5 mm for SUS-5 and SUS-3, respectively. It can be noted that identical beams having a higher number of cracks develop a greater deflection due to shrinkage.

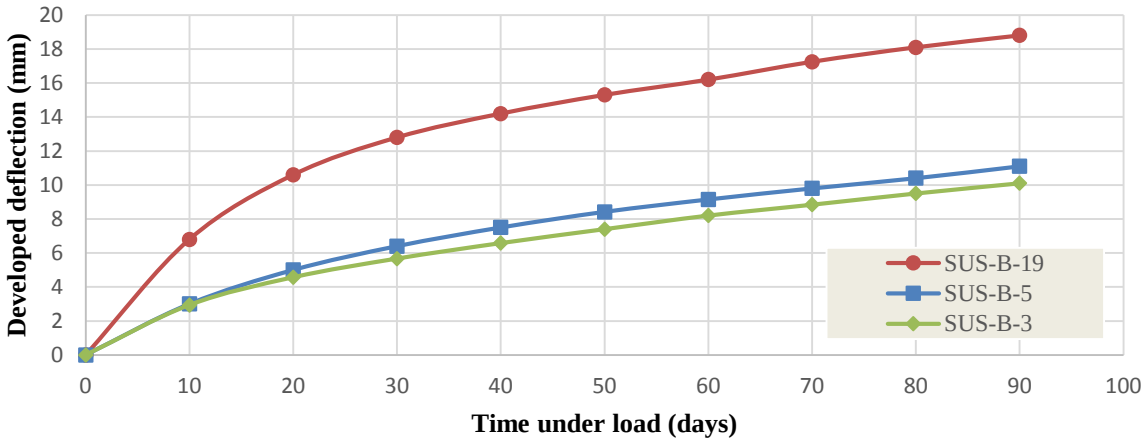


Figure 2 Mid-span developed deflection with time

For the beam with a stabilized crack (i.e. SUS-19) pattern, no more cracks were produced after loading. Whereas in the SUS-5 and SUS-3 cases more cracks were developed during the 90 days testing period. Note that beam SUS-3 was sustained to a load closely below the nominal cracking moment. In this case, the first crack developed the day after the loading was applied. This means that the tensile capacity of the beam was exceeded. As the beam was under constant loading conditions the cracks must be the result of creep and/or shrinkage curvature. As such, 'long-term effects' could apply after only one day.

Midas FEA was employed to simulate the long term deflection of the tested reinforced concrete beams. In Midas FEA, the total long-term curvature results from the summation of the individually calculated creep and shrinkage curvatures; the total long term deflection can therefore be separated into creep and shrinkage deflection. Figure (3a), Figure (3b) and Figure (3c) show the graphical comparison of the experimental and numerical developed mid-span deflection of the selected reinforced concrete beams under 19 kN, 5 kN and 3 kN of sustained loads, respectively. It is clear that the software underestimates the long term developed mid-span deflection in all cases. In the figures it can also be observed that the creep deflection is a function of the sustained load, i.e., the creep deflection in Figure (3a) is higher than that in Figures (3b) and (3c) and the creep deflection in Figure (3b) is higher than that in Figure (3c).

However the shrinkage deflection in all cases, irrespective of load level, is the same. This contradicts the published literature, and the previous assessment of long term deflection being equally due to creep and shrinkage. Previously it was found that the shrinkage curvature depends on the distribution of the cracks [11]. Daud [12] attributed the inability of Midas FEA to correctly predict the long term deflections to the section geometry, pointing out that the reinforced concrete beam, which was modelled as elastic, does not have uniformly distributed shrinkage applied throughout its cross-section.

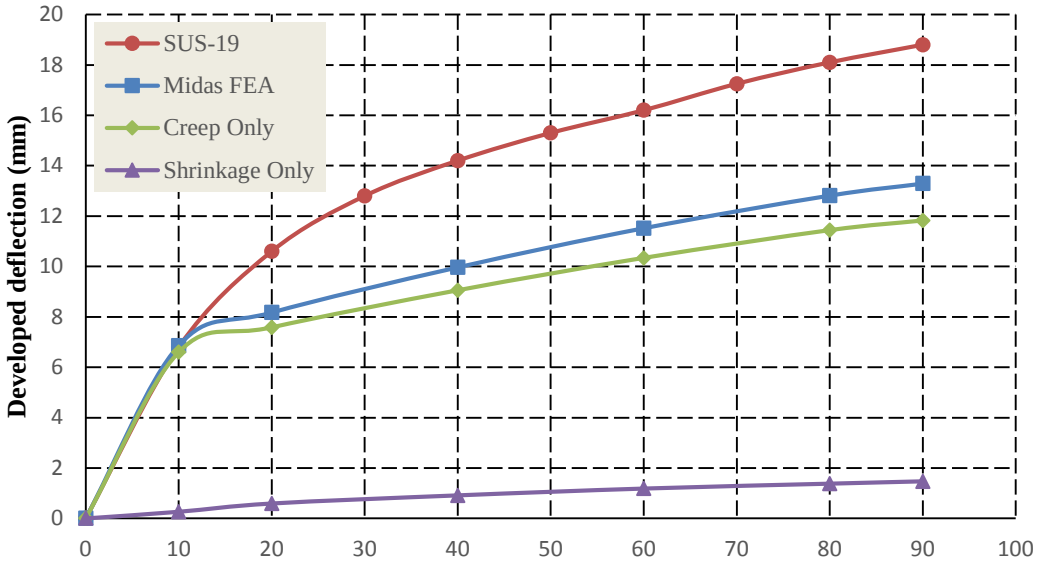


**a)**

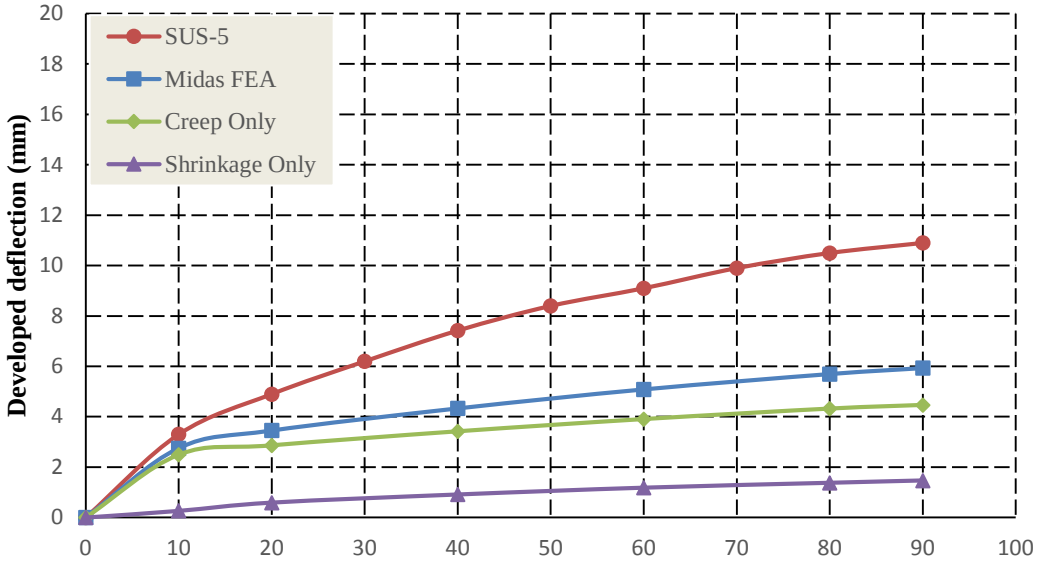


**b)**

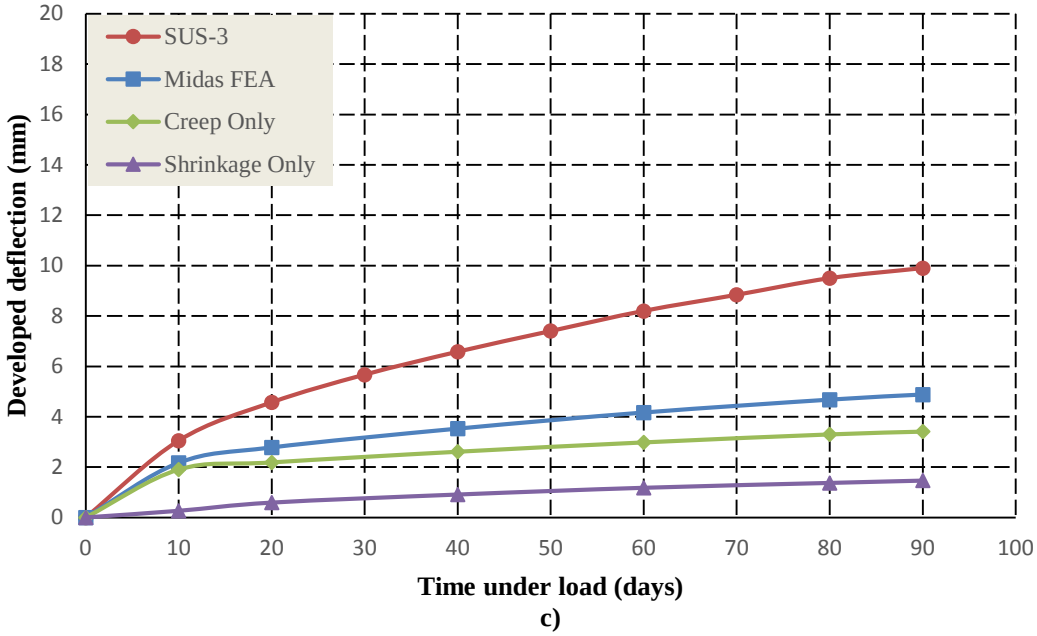


c)

Figure 3 Mid-span developed deflection with time

Figure 4 compares the shrinkage curvature of the three beams as predicted by Midas FEA with that predicted by the Eurocode 2. For the third beam (i.e SUS-3) as the sustained moment was less than the cracking moment, the shrinkage deflection predicted by the Eurocode 2 was only for an uncracked section. It can be seen that the Eurocode 2 predicts the shrinkage deflection by considering the degree of cracking, i.e., the shrinkage deflection for SUS-19 is higher than that in SUS-5 and SUS-3 and the shrinkage deflection of SUS-5 is higher than that in SUS-3. Whereas the shrinkage deflection predicted by Midas FEA is always the same for all cases and always matches the uncracked section because Midas FEA assumes that the concrete is elastic when performing the long term analysis [12].

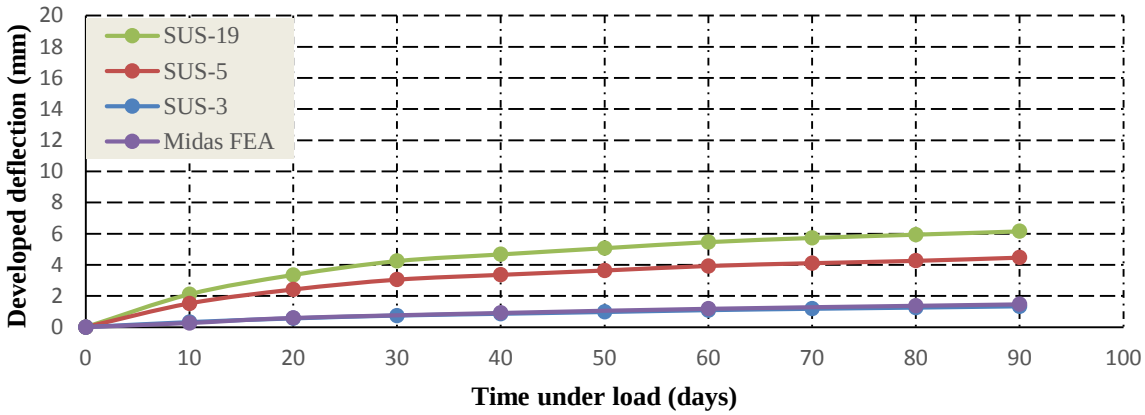


Figure 4 Mid-span shrinkage deflection with time

## CONCLUSIONS

Three identical reinforced concrete beams were tested under various sustained loads in order to study the interplay of cracking with the long term deflection. Using the selected experimental details as input for developing a nonlinear finite element model, comparisons between theory and reality were possible. From the experimental and numerical results derived, the following points can be made:

1. Beams having a greater numbers of cracks develop more deflection with time due to shrinkage.

2. What is broadly recognised as a long term deflection, starts potentially only a single day after the sustained loading has been applied.

3. As expected, creep and shrinkage induced cracks are a function of the sustained applied moment. The higher this sustained moment (i.e. closer to the stabilized crack pattern) the less number of cracks that develop after initial loading.

4. The accuracy of the software is in question as it assumes that the shrinkage curvature is independent of the loading and cracking conditions of the tested beams.

## ACKNOWLEDGMENT

Thank you to “The Higher Committee for Education Development in Iraq” for funding this research. Sincere thanks are expressed to School of Civil Engineering of the University of Leeds for providing the facilities to undertake this research.

## REFERENCES

1. KIM, Y., J. SIM, AND C. PARK, Mechanical properties of recycled aggregate concrete with deformed steel re-bar. J Mar Sci Technol, 2012. **20**(3): p. 274-280.

2. KRISHNAKUMAR, S., et al., Bond strength of concrete containing crushed concrete aggregate (CCA). American Journal of Engineering Research, 2013. **1**.

3. CHEN, G. AND G. BAKER, Influence of bond slip on crack spacing in numerical modeling of reinforced concrete. Journal of Structural Engineering, 2003. **129**(11): p. 1514-1521.

4. BAKOSS, S.L.G., R. I.; FAULKES, K. A.; PULMANO, V. A., Long-term deflections of reinforced concrete beams. Magazine of Concrete Research, 1982. **34**(121): p. 203-212.

5. NIE, J. AND C.S. CAI, Deflection of cracked RC beams under sustained loading. Journal of Structural Engineering, 2000. **126**(6): p. 708-716.

6. WASHA, G. AND P. FLUCK, Effect of compressive reinforcement on the plastic flow of reinforced concrete beams. ACI Journal, 1952. **49**(2).

7. PILLAI, U. AND D. MENON, Reinforced concrete design. 2003: New Delhi: Tata McGraw-Hill.

8. VAKHSHOURI, B. AND S. NEJADI. Limitations and Uncertainties in the Long-Term Deflection Calculation of Concrete Structures. in Second International Conference on Vulnerability and Risk Analysis and Management (ICVRAM) and the Sixth International Symposium on Uncertainty, Modeling, and Analysis (ISUMA). 2014.

9. ESPION, B. AND P. HALLEUX, Long-Term Deflections of Reinforced Concrete Beams: Reconsideration of Their Validity. Structural Journal, 1990. **87**(2): p. 232-236.

10. MU, R.F., JP; BEEBY, AW; SCOTT, R; WALRAVEN, JC; STEELHURST, D, Modelling of Shrinkage Induced Curvature of Cracked Cconcrete Beams. Tailor Made Concrete Solutions (Walraven JC and Steelhurst D (eds)). Taylor & Francis, Abingdon, UK, 2008: p. 573-578.

11. MARÍ, A.R., J.M. BAIRÁN, AND N. DUARTE, Long-term deflections in cracked reinforced concrete flexural members. Engineering Structures, 2010. **32**(3): p. 829-842.

12. DAUD, S.J., P. FORTH,; NIKOLAOS NIKITAS,. Time-Dependent Behavior of Reinforced Concrete Beams under Sustained and Repeated Loading. World Academy of Science, Engineering and Technology, 2015. **106**: p. 156 - 159.

# MODELLING POST-TENSIONED PRECAST CONCRETE SEGMENTAL GIRDER BRIDGES WITH DRY KEYED JOINTS: PRELIMINARY RESULTS

**E Sejkati**

**X Zhou R Shamass**

Brunel University London

United Kingdom

**G Mancini**

Polytechnic University of Turin

Italy

**ABSTRACT.** Precast concrete segmental bridges (PCSBs) have been the most common design technology used in the last decades. It is widely recognized that segmental bridges have better durability, lower life-cycle costs and higher quality for maintenance than other types of bridges. PCSBs with externally prestressed tendons have become very popular in construction because of economical and safety reasons, fast and practical construction, and outstanding serviceability. Moreover, external tendons technique is widely used because it allows to inspect the cables and to replace them or to reinforce the tendons in case of damage while such kinds of actions are difficult to be taken in case of internal prestressing. Therefore, box section is the most common solution due to its aesthetic appeal and elegance that reduces the environmental impact as well due to the convenient maintenance for the tendons. Besides, the hollow concrete box segment can be used for service/electrical cable ducts for bridges. However, there is lack of reliable computational model for analysing behaviour of post-tensioned PCSBs. This research investigates the behaviour of PCSBs with dry keyed joints and external tendons up to failure with the use of finite element method which is validated by comparing experimental results. Deflection, joint opening, tendon slip, stresses of the tendons and the concrete are obtained from numerical analysis with recommendation on further development towards a more accurate numerical model for PCSBs made.

**Keywords:** Dry joint, Keyed joint, Joint opening, Precast concrete segmental bridge, Post-tensioned, Tendon slip

**Mr Edvis Sejkati** holds an MSc degree in Civil Engineering. He has research interests on seismic behaviour of civil structures and post-tensioned precast concrete segmental bridges.

**Dr Xiangming Zhou** is a Reader in Civil Engineering Design at Brunel University London. He has published extensively on concrete science, technology, mechanics and structures.

**Mr Rabee Shamass** is a PhD candidate at Brunel University London. He has research interests on modelling of keyed joints of precast concrete segmental bridges.

**Prof Giuseppe Mancini** is a professor in structural engineering at Polytechnic University of Turin. He has extensive research on concrete structures including concrete bridges.

## INTRODUCTION AND LITERATURE REVIEW

PCSBs are a newly developed bridge construction commonly used during the last decades. The fast construction speed and reduced need to interrupt traffic during construction are the main advantages. Differently from the monolithic type that has a continuous reinforcement in longitudinal direction, the precast segmental type consists in short elements, which are assembled together with externally prestressed tendons through keyed joints rather than continuous reinforcement. Different from pre-tensioned concrete structures, post-tensioning technique is used in PCSBs and the tendons are run outside the original concrete section and its layout cannot follow the parabolic shape. Rather it is linear between two deviation points. With this technique the structure can be prestressed in-situ without the need of transporting to construction site pre-tensioned structural elements, which may be very long, made in factory. Externally prestressed concrete has the advantage, i.e. it allows the maintenance, replacement and strengthening of the tendons. However this is little numerical model available in literature for analysing behaviour of PCSBs with keyed joints.

Ramos and Aparicio [6] proposed a numerical model taking into account material non-linearity of concrete by updating the stiffness matrix at every iteration step, using rigid links between the end nodes of the tendons and the nodes of the bridge structure where the prestressed elements are anchored, and linear elements between the segments of the joint. They obtained very similar results of load-deflection and load-prestressing force curves to experimental ones. However, the model was applied to compare the results of beam test that has much smaller dimensions than a box section of a PCSB in the field. Tandler [7] developed a numerical model by using Abaqus. The results obtained from the model have been compared with the results of Takebayashi T. et al. [5]. He assumed the free slipping of the tendons at the deviator blocks. However, instead of having a lower ultimate load than the actual one as can be expected from the free slipping assumption [6], the results show that the bridge fails at a higher mid-span applied moment. Moreover, the maximum deflection and the maximum joint opening are reached not at the same location of the bridge sample tested. This is due to the position of the applied loads that was not symmetric with respect to the mid-span while the real disposal of the loads was symmetric.

Takebayashi et al. [5] conducted an experimental study on the behaviour of a full span of a PCSB with dry joints and external tendons. The tested bridge was 44.25 m span and 10.20 m wide. The segments length was 3.40 m, except for the diaphragm segments, which were 1.725 m. The box section had a constant height of 2.40 m along the span. The two deviators at the segments 4 and 11 had the same geometry and were named D2, while the deviator at the segment 7 was named D1. The two end diaphragms were the segments 1 and 14. The bridge was prestressed with 12 external tendons: 10 of them formed from 19K15 strands and 2 from 12K15 strands protected with HDPE ducts and cement grout. The tendons are located symmetrically with respect to the longitudinal axis, but not with respect to the mid-span. Tendons from 1 to 5 (19K15) run for the whole span and they are deflected on each of the three deviators, while the tendons 6 (12K15) is anchored between the deviators D2 and it is deflected only at the deviator D1.

Table 1 shows the material properties of the tested bridge. The tested bridge was supported by elastomeric bearings. Their centres are 50 cm far away from the ends of the bridge. It was computed using back calculation that the total tendon force was 38433 kN. It also showed about 12% of losses in tendon force due to creep, shrinkage and relaxation of tendons.

Table 1 Material properties [5]

| MATERIAL | PROPERTIES ITEM | AVERAGE FIGURES [MPa] |
|---|---|---|
| Concrete | Compressive strength | 55 – 62 |
| | Modulus of elasticity | 43000 |
| Re-bars | Tensile strength | 390 |
| Tendons | Breaking strength | 1920 |
| | Modulus of elasticity | 193000 |

## NUMERICAL MODEL

### Geometry

The geometry of the original bridge has been simplified by setting the trial dimension of thickness and width of the slabs and webs, without modifying greatly the original section. The best solution found is detailed in figure 1. As aforementioned, deviators and diaphragms have different geometry from the ordinary segments. The simplified section is the same for each segment including the deviators and diaphragms.

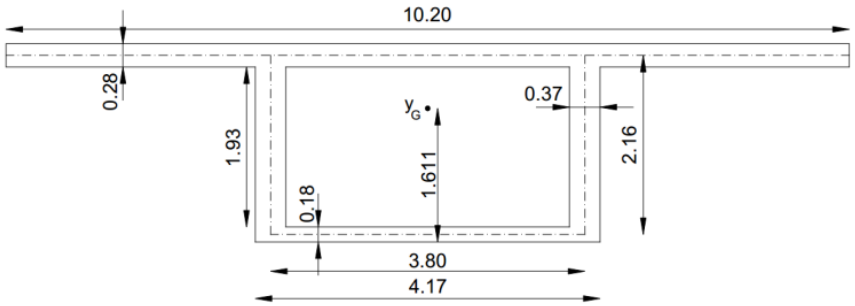


Figure 1 Simplified geometry of the original section with all dimensions in metres

### Material Properties

The analysis has been conducted up to failure for the PCSB span, therefore, a non-linear behavior of the materials has been used for this study. The elastic field is characterized by the elastic modulus and the Poisson's ratio of the material. The Von Mises plasticity model is followed which defines a yield surface that is used to compute the yielding of isotropic materials. The stress-strain relation for the steel reinforcement in the slabs and webs is elastic-perfectly plastic as suggested in EC2. The bilinear behaviour is applied for tension and compression. The value of elastic modulus $E_S$ is assumed 210 GPa and the Poisson's ratio equal to 0.28. The tensile strength of the bars is taken from the value provided by Takebayashi [5], i.e. $f_{yd} = 390\ MPa$.

The non-linear behaviour used for the tendons is similar to the reinforcing bars, except for the values and the elastic-plastic hardening model assumed. The bi-linear model is proposed in the EC2. The value of the elastic modulus of the tendons $E_p$ is 193 GPa, taken from Takebayashi's study and the Poisson's ratio is equal to 0.28 same as reinforcement steel. The breaking strength is also provided from the experimental data and is equal to

$$\frac{f_{pk}}{\gamma_s} = 1920\ MPa$$

The elastic behaviour of the concrete is defined with the Young's modulus and the Poisson's ratio as well. Takebayashi gives a range of concrete compressive strength between 55 and 62 MPa obtained from testing of samples and back calculation [5]. The lower value of the provided range has been used for the analysis. They also measured the elastic modulus of concrete equal to 43 GPa. This value is considered too high even for the upper limit of compressive strength range. Therefore, it is considered appropriate to neglect it and to compute the elastic modulus $E_c$ from the analytical relation with the concrete compressive strength given by EC2.

$$E_c = 22[(f_{cm})/10]^{0.3} = 36.689\ GPa$$

The "Concrete smeared cracking" model in Abaqus is used for modelling the concrete in this research. The smeared cracking concrete model gives a general function to model different structures, including shells as the slabs and webs of the box section [10]. Furthermore, it can be used for reinforced concrete with rebar layer model. The model comprises of an isotropic hardening yield surface in the compressive field and a crack detection surface, which notifies if a node fails by cracking [10]. The two surfaces are independent. The stress-strain relationship for concrete under compression is taken by the EC2 formula. When a crack is detected, it is stored for the following computations, which are affected since a damaged elasticity model is used. The constitutive computations are made for each integration point of the model and the presence of the cracks modifies the material stiffness in that particular point. The crack can open and close. To define the shape of the failure surface of the concrete model, four failure ratios need to be defined. The ratio between the ultimate biaxial compressive stress and the ultimate uniaxial compressive stress is 1.16; the absolute value of the ratio of the uniaxial tensile stress at failure to the ultimate uniaxial compressive stress is 0.09; the ratio of the magnitude of a principal component of plastic strain at ultimate stress in biaxial compression to the plastic strain at ultimate stress in uniaxial compression is 1.28; the ratio of the tensile principal stress at cracking, in plane stress, when the other principal stress is at the ultimate compressive value, to the tensile cracking stress under uniaxial tension is 1/3. This model uses a softening relation between stress and strain after the failure of the concrete in the tensile field. In this case the interaction of the rebar layer with the concrete provides an amount of tension stiffening. It can be assumed that after the failure the stress reduces to a nil value linearly and reach a total strain of about 10 times the strain at failure [10]. The strain at failure tensile stress of the concrete is about $10^{-4}$, therefore, a total strain of $10^{-3}$ is assumed when the tensile stress reduces to zero.

**Element types**

Three element types have been used for this project. Shell elements are set for the concrete slabs and webs of the box section, beam elements model the tendons and gap elements are used for modelling the interaction between the concrete box girder segments. All the elements are deformable except for the gap elements. The thickness of the top slab, bottom slab and webs of the concrete box girder is very small compared with their width and length. Therefore, the shell element in the three-dimensional space is the most suitable element type for this case. The element type S4 is used for the shell parts of the structure. Rebar layer is used to provide reinforcement to the shell elements. The reinforcing steel is used for the material, with 24.2 mm diameter of the rebars, 10 cm of spacing between them and positioned in the middle of the thickness. Two layers of rebar reinforcement have been

assigned to the section. They are mutually orthogonally aligned to the edges of the shell element composing a square mesh. In case of non-linear analysis, the deformation of the underlying shell determines the deformation of the rebar layer. The reinforcement in the web segment where the tendons are anchored is increased for converging the solution and not to cause the failure in these points. The tendons are modelled with three dimensional beam elements. It consists in a wire element between two nodes. A linear integration with just one integration point is chosen since only normal force is acting in the tendons. The element type is called B31. A solid circular section is set for the tendon. The tendons that run along the whole span of the bridge are modelled together in one single tendon. A graphical representation is visible in figure 2. The cross section area of the tendon 19T15 composed by 19 strands of 15 mm diameter is 2850 $mm^2$, while the tendon 12T15 with 12 strands of 15 mm diameter has a cross section area of 1800 $mm^2$ [8]. The modelled long tendons have a radius of 67 mm, while for the short ones it is 24 mm. The tendons are modelled on the plan of the webs. This is a simplified model, however, in reality the tendons are also deviated in transversal direction.

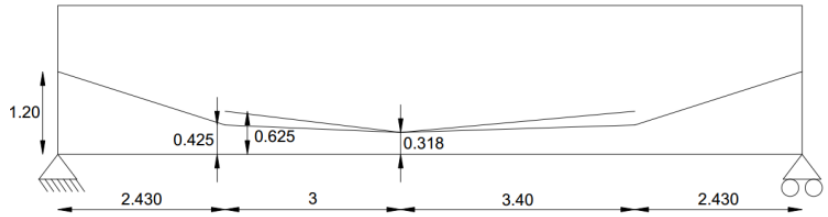


Figure 2 Longitudinal tendon layout with all dimensions in metres

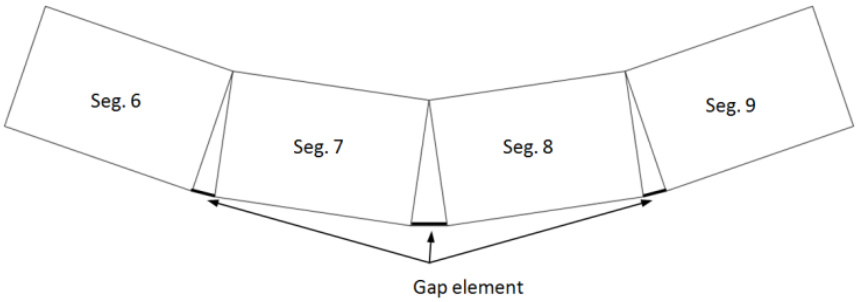


Figure 3 Mid-span segments with gap elements

The interaction between the segments of the bridge has been modelled by using gap elements. Since the slabs and the webs are modelled with shell elements, the interaction between the segments consists only between the edges of the shell and not on a surface interaction, as it would be in reality. For mechanical contact between two nodes GAPUNI elements are chosen. The contact behaviour is defined by the initial separation $d$ of the gap and the direction of the contact **n**. During the loading of the bridge the deflection increases and the keys open starting from the bottom slab. Hence, the rotation around the top slab is allowed in the model (see figure 3). Considering that the segments of the bridge have different rotation from each other, a fixed direction of the gap element cannot be used. To allow the rotation of the gap element, only the distance $d$ is defined in the model. The initial separation distance is set for obvious reason equal to zero since the joint is closed at the beginning. The mesh corresponds to the partition and the nodes created, therefore, in the size control for the mesh definition the unit value is introduced.

## Constrains and Boundary Conditions

The boundary conditions applied in the model are the bridge supports at the end segments and the fixed transversal movement of the tendons at the deviation points. The three translations on one end bearing are fixed, while on the opposite end only longitudinal displacement is allowed. This condition is usually designed in real bridges in order to take into account the displacement due to creep, shrinkage and temperature variation. Four supports are set and the other two have only fixed vertical displacement. The rotation is allowed in all directions. The tendons are anchored to the concrete with tie constraints. The end nodes of the tendons are constrained to have the same motions of the anchorage nodes in the concrete, in other words, of the master nodes. As regards to the tendon deviated points, they are fixed in transversal direction and free to move vertically with the deviator block. Due to the high difficulty of modelling the frictional behaviour of the tendon inside the deviator block, one of these two extreme models has to be chosen: the tendon is blocked with the deviator or the tendon is free to slip. Since one of the required output is the tendon slip, the longitudinal movement of the tendon at the deviated point is allowed. This assumption causes a lower ultimate load and better approximates the stress increment in the tendons [6]. To create the interaction between the tendon and the deviator segment in the way that the tendon moves downwards when the bridge deflects, the multi-point constraint (MPC) of type “link” is used in the model. This constrain is a linear constrain between two nodes selected and provides a pinned rigid link to keep fixed the distance between them. The rigid wire links the deviated points of the tendons to its projection on the centroid level. Figure 4 represents the constraint assumed. In this manner the tendon can freely slip, but it has to deflect as well as the full bridge does.

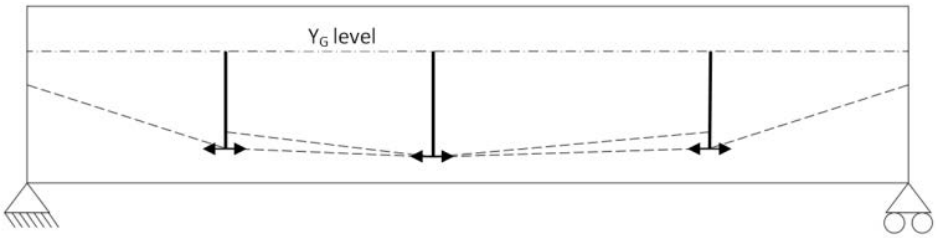


Figure 4 Allowed movement of the tendon at the deviated points

## Load Steps

The initial step is created automatically when the model starts. In this step, the boundary condition and the prestressing force are involved. The load is applied in two further separate steps. The total prestressing computed from back calculation by Takebayashi et al. is 38443 kN. The sum of the cross section areas of 10 tendons 19T15 and 2 tendons 12T15 is 32100 $mm^2$. Hence, the stress in the tendons results to be 1197.60 MPa. In Abaqus the initial stress field is defined to apply the prestress. It is applied uniformly over the beam elements. A local coordinate system is given to the tendons in such a way that the direction of the stress applied can be easily recognized. The first step is a general static step that includes the prestressed force and the dead load. During this stage the materials are still in elastic state and the displacement is small. Therefore, the modified Newton method is sufficient for this step. However, the geometric nonlinearity is activated since this step and it needs to be switched on for the next one when large displacements and material nonlinearity occur. The initial and maximum increment is set equal to 0.1. The dead load is modelled as body force applied to the slabs and webs in vertical direction with a value of 25000 $N/m^3$, which is conventionally

taken as the specific weight for reinforced concrete. During the second step, a static Riks method has been used which is useful to predict unstable, geometrically nonlinear collapse of a structure [10]. This method considers both load magnitude and displacement as unknown. To solve the problem Abaqus uses the "arc length" method. This method is independent from the response, which can be both stable and unstable. The multiple loads applied on the structure are increased and have the same magnitude till the collapse. The solution of load magnitude and displacement are found simultaneously. The method adopted in this paper is based on the Newton one. The load applied in the second step is simplified with respect to the one applied in a real bridge. The distributed load over the top slabs of the six segments 4, 5, 6 and 9, 10, 11 is divided into concentrated forces on the top web nodes of the joints.

## MODEL VALIDATION

The numerical model established in this study is validated by comparing the results optained from the model with the experimental ones in the following aspects.

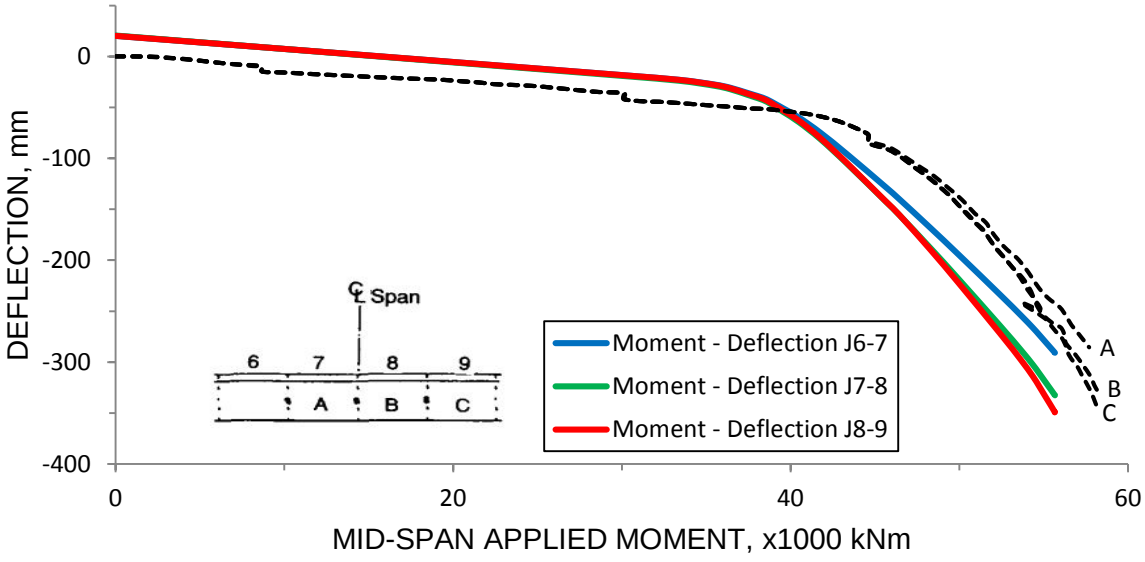


Figure 5 Deflection at the mid-span joints from numerical analysis and experimental test [5]

### Deflection

The load-vertical displacement curve is plotted in figure 5. Deflection is related in the 3 central joints at the height of 1.20 m from the bottom slab of a concrete box girder segment. The plot has a similar trend with the graph provided by Takebayashi from measurement [5]. The modelled bridge fails at a lower load than the real case. This is due to the assumption of free slipping tendon at the deviator points made during the modelling. In fact this leads to a lower ultimate load as it stands in Ramos and Aparicio [6]. The bridge is initially uplifted because of the prestressing force and, therefore, has a positive vertical displacement of about 2 cm. Both graphs have a linear behaviour till the applied midspan moment reaching about 40000 kNm. In the experimental case the local variations is the result of temperature change [5], while in the current model this is not taken into consideration.The maximum vertical displacement in the model, 34.9 cm, is achived in the joint between the segments 8 and 9 while the midspan joint deflection is 33.3 cm. The asymmetric disposal of the tendons causes a lower vertical displacement at the joint between segments 7 and 8.

## Joint Opening

The joint opening between segment 8 and 9 is plotted for different heights from the bottom slab: 1.60 m, 1.20 m, and 0.318 m. The trend of the joint opening versus the midspan applied load is shown in figure 6 for the modelled bridge and for the experimental one. Also, in this case the results are similar except for the load from which the joint starts opening and ultimate load reached. The difference is due to the same reason explained previously. In the model the joint 8-9 starts to open from the bottom, the node at the height 0.318 m from the bottom slab is the first that opens at the loading of 35000 kNm. In the experimental study the same node starts to open at about 40000 kNm. Other two nodes at height 1.20m and 1.60m start to open slightly later and reach respectively a total gap of 17.1 mm and 7.7 mm when the bridge collapse, while the final opening of the lower node is 33.8 mm.

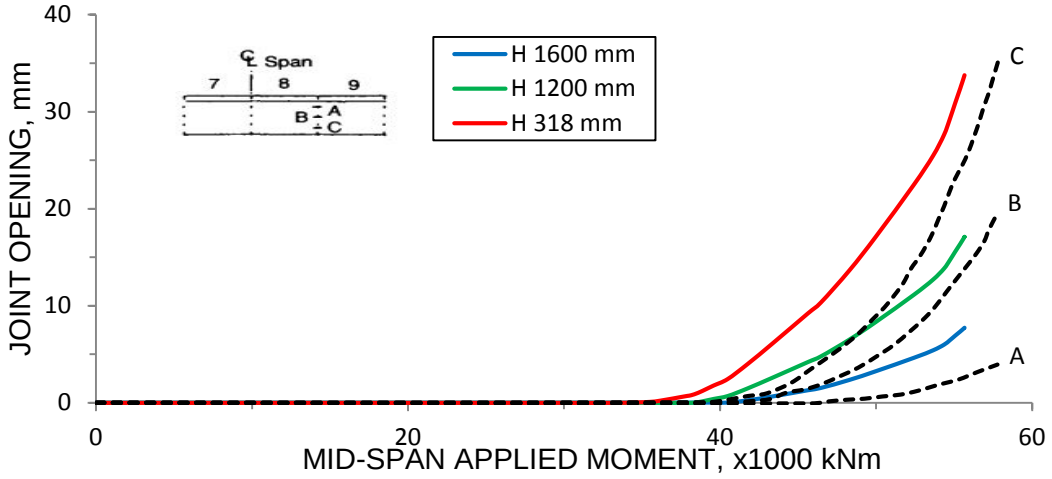


Figure 6 Opening of the joint 8-9 versus mid-span moment from numerical analysis and experimental test [5]

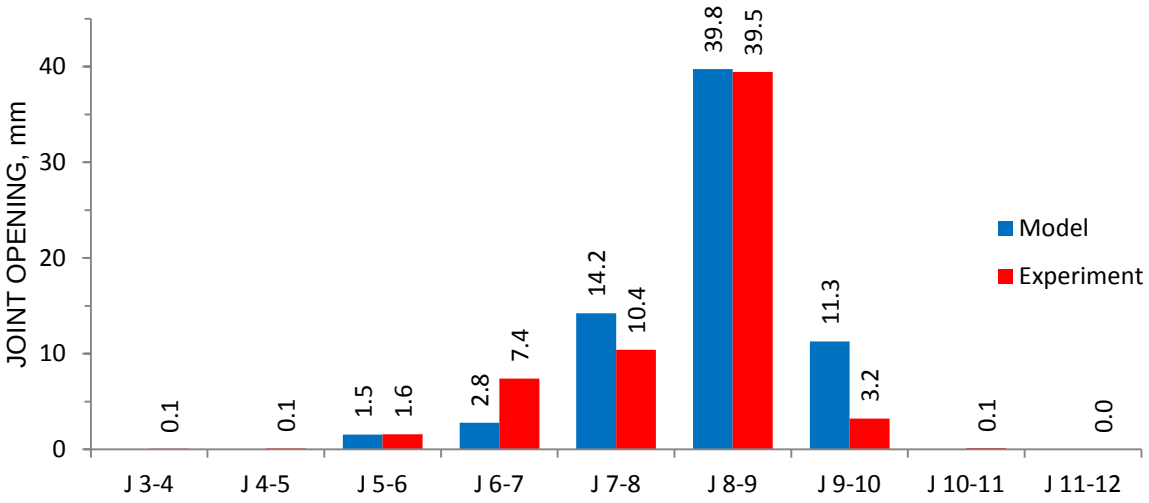


Figure 71 Opening of the joints from numerical analysis and experimental test [5]

The opening is also analysed at the bottom of the web for each joint and plotted in figure 7 from numerical analysis and experimental test. The largest openings are found nearby the mid-span, with the maximum opening at the joint 8-9 of 39.8 mm. The opening values decrease when moving away from the mid-span joint. The joint between segments 6 and 7 has larger opening than the one between segments 9 and 10 in the test, while it is the reverse in the model.

**Tendon Slip**

The tendon slip from numerical analysis are compared with those from experiment. The assumptions made in the model lead to the results of tendon slips shown in Figure 8 and Figure 9 from numerical analysis (continuous lines) respectively for the long and short tendons. The slip at segments 4 and 11 is related to the whole span tendons, while the slip at segment 7 is related to both types of tendons since they are deviated in the same point. The slips are about 13 mm on the side deviators and about 22 mm in the central deviator.

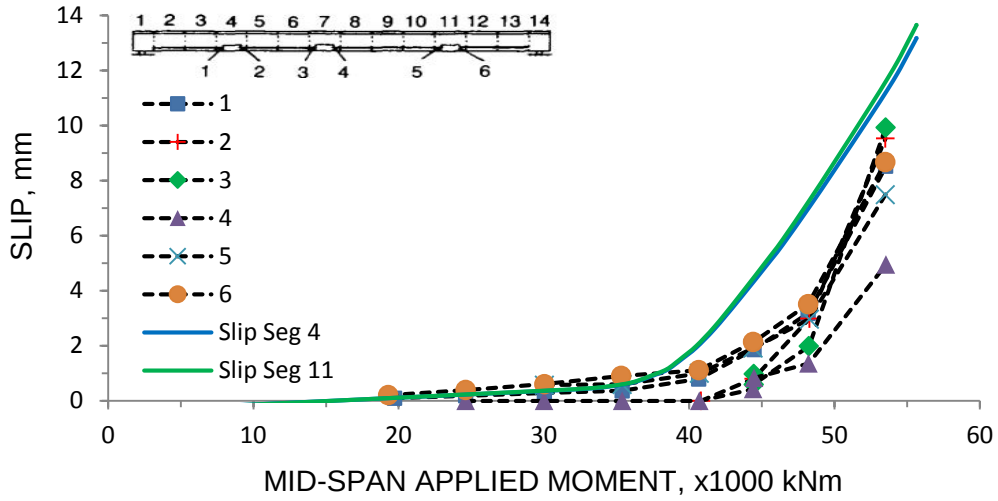


Figure 8 Slip of the long tendon from numerical analysis and experimental test [5]

Comparing the results with those provided by Takebayashi for the tendon 5 and tendon 6 (dashed lines) in figure 8 and figure 9 one can see that the tendon slip from numerical analysis has higher value. For the tendon 5, which runs for the whole bridge, the slips are between 7 mm and 10 mm. In the tendon 6, which has only one deviator at the segment 7, the slippage is about 5.5 mm. This result is very small compared with the value obtained from the numerical analysis in the same deviator. The reason is because the two nodes of the tendons are coupled and the applied prestressing forces are higher in the central deviator node of the model. In order to compare with the tendon slip obtained from numerical analysis, the slippage of the two tendons in the experimental test has to be summed. Hence, a total tendon slip displacement of about 15.5 mm from experiment can be compared with the 22 mm obtained from numerical analysis. The numerical value is larger in any case for every deviator segment and this is due to the free slipping assumption previously mentioned. The slip at the deviators occurs since the beginning of the loading step because of no friction supposed, while in reality the tendons start to move at different load values according to their deviation angle. One can notice that the movement is small during the linear stage and large slippage starts to occur at the loading level between 40000 and 45000 kNm.

This behaviour is observed also in the model but with big displacement starting from about 38000 kNm due to no friction assumption made.

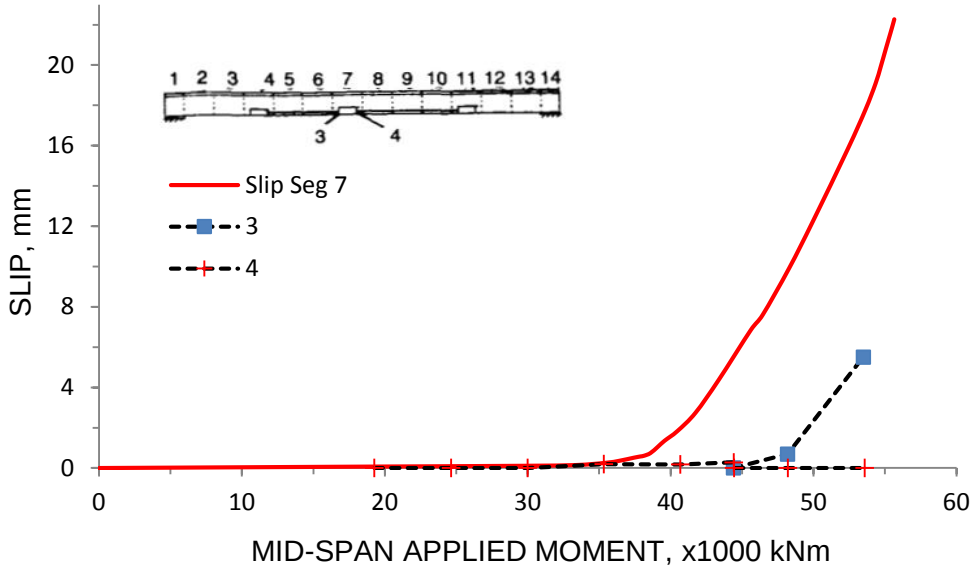


Figure 9 Slip of the short tendon from numerical analysis and experimental test [5]

## SUPPLEMENTAL RESULTS

Some further results of the current study are discussed for better understanding of behaviours of externally prestressed precast segmental bridges with dry joints. Such results as stresses in the concrete and tendons are not obtained from the real test.

### Concrete Stress

The stress in the concrete is plotted for different load steps. In figure 10 it is related to the stage where only the dead load and the prestressing force are applied. It corresponds to the initial condition when the load magnitude is $\lambda = 0$. The vertical displacement is scaled for the factor 20. The bridge is all in compression, except for the end segments where small tensile stress occurs due to the anchorage of the tendons. The maximum compression value is at midspan intrados equal to about 13 MPa.

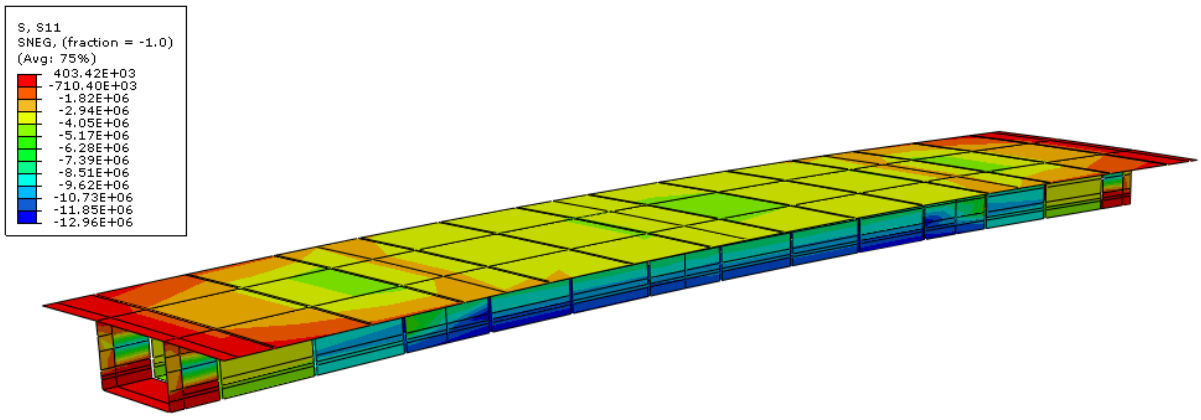


Figure 10 Concrete stress under prestressed force with all dimensions in Pa

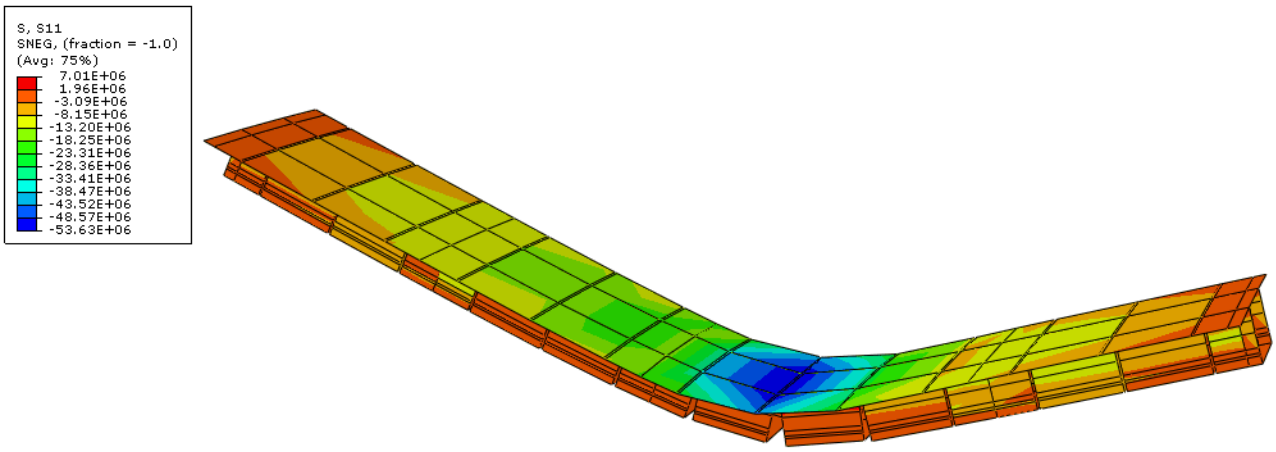


Figure 112 Concrete stress at ultimate load with all dimensions in Pa

The concrete stress at the ultimate load is represented in figure 11. The bridge collapses at the applied midspan bending moment of 55658 kNm. The total applied load on the bridge is 8481 kN. The bridge fails for compression of the top slab, in fact, the stresses reach a value of 53 MPa at the joint 8-9.

**Tendon Stress**

The stresses of the tendon between the ends of the bridge are presented in figure 12, while those of the tendon between the two lateral deviators are shown in figure 13. The initial stress was 1198 MPa and uniformly distributed in both tendons.

The stresses in the long tendon at ultimate load vary from 1429 MPa at the anchorage in segment 1 to 1450 MPa at the central part. The increment is respectively of 231MPa (19%) and 252 MPa (21%). The higher stresses in the central part are due to the larger deflection and concentration of joint opening nearby the mid-span of the bridge. The stresses in the short tendon are 1672 MPa in the part between the segment 4 and 7, while 1602 MPa in the part between segment 7 and 11. They increase respectively of 474 (40%) and 404 (34%) from the initial condition.

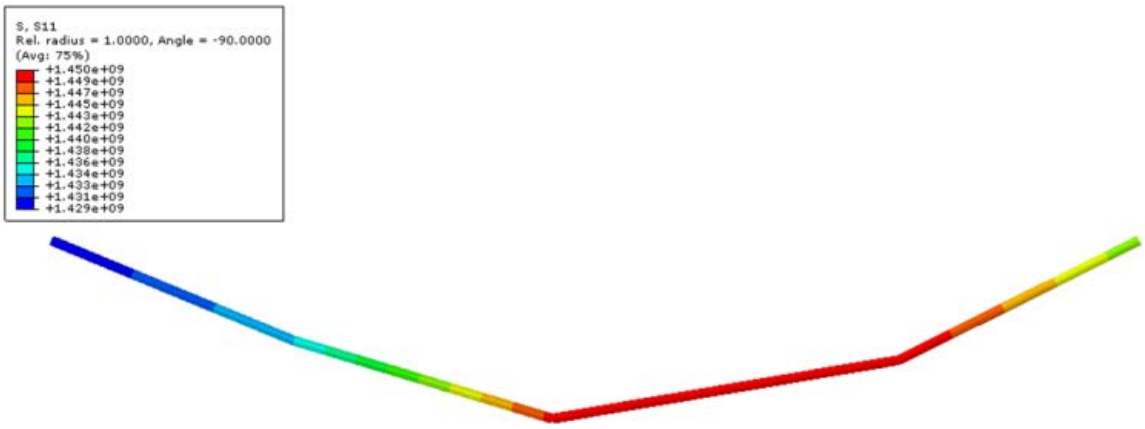


Figure 123 Long tendon stress at ultimate load

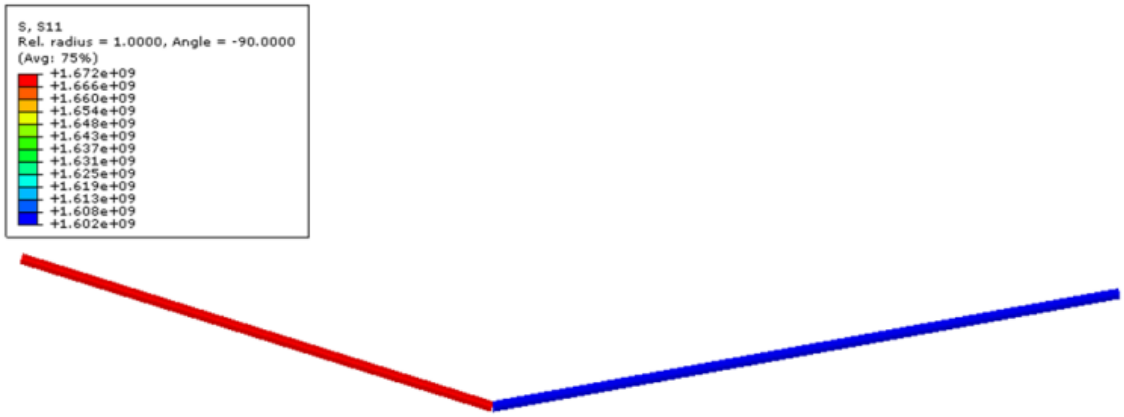


Figure 13 Short tendon stress at ultimate load

## CONCLUSIONS

The behaviour of the precast concrete segmental bridge with external tendons and dry keyed joints is linear in the first loading stage followed by a non-linear one where large displacements occur. All the joints remain close till when about 30000 kNm mid-span moment is applied and all the segments are still in compression. The deflection of about 2 cm at the mid-span of the bridge is also small for this load level. The bridge collapse at 55658 kNm applied midspan moment for flexural failure as experienced during the real test. Crushing of the concrete in the top slab creates a hinge in the midspan and generates the mechanism. The non-linear analysis used in the model well performs the real behaviour of the tested bridge. At the final load level the deflection reaches 35 cm and the opening is 40 mm at joint between segment 8 and 9. The deflection is not symmetric since the layout of the prestressing steel is asymmetric. Considerable warning is given by the large displacements occurred. A higher assumption of concrete strength may increase the loading capacity of the structure. However, a lower ultimate load was expected since no friction was assumed between the tendons and the deviator blocks. If fixed tendon model at the deviators is applied, the structure fails at higher load and the increment of tendon stress is not significant. Better resulting model would be obtained if friction interaction would be used between the nodes of the tendons and those of the concrete at the deviation points.

Concerning the ultimate limit state design, the model does not reach its design limit because of the assumption of free slipping of the tendons. This assumption can be adopted in favour of safety for the design at ULS. If the slippage is denied, the tendon force increases in the central part and the neutral axis drops. Therefore, increasing the friction between the ducts and deviator blocks improve the loading capacity of the structure.

## REFERENCES

1. POSTON, R W, WOUTERS, J P. Durability of Precast Segmental Bridges, NCHRP Web Document 15, National Cooperative Highway Research Program, June 1998, http://www.nap.edu/readingroom/books/NCHRP15/front.html.

2. WIUM, D J W, BUYUKOZTURK, O. Precast Segmental Bridges - Status and Future Directions, Civil Engineering for Practicing and Design Engineers, ACSE, V. 3, 1984, pp 59-79.

3. ZHOU, X, MICKLEBOROUGH, N, LI, Z. Shear strength of joints in precast concrete segmental bridges, ACI Struct. J., 102(1), 2005, pp 3–11.

4. SHAMASS, R, ZHOU, X, ALFANO, G. Finite-Element Analysis of Shear-Off Failure of Keyed Dry Joints in Precast Concrete Segmental Bridges, ASCE J. Bridge Eng., 2014, pp 1-12

5. TAKEBAYASHI, T, ET AL. Full-scale destructive test of a precast segmental box girder bridge with dry joints and external tendons, Proceedings of The Institution of Civil Engineers Structures and Buildings, 1994, pp 297-315

6. RAMOS, G, APARICIO, A C. Ultimate Analysis of Monolithic and Segmental Externally Prestressed Concrete Bridges, Journal of Bridge Engineering, ACSE, V. 1, No. 1, 1996, pp 10-17

7. TANDLER, J. Collapse analysis of externally prestressed structures, 2009, Diplomica Verlag

8. DEBERNARDI, P G. Strutture di calcestruzzo armato e precompresso, 2011, Celid

9. ABAQUS 6.14-4. Computer software. Waltham, MA, Dassault Systèmes

10. ABAQUS Documentation 6.14. Abaqus Analysis User's Guide

11. EN 1992-1-1. Eurocode 2: Design of concrete structures – Part 1-1: General rules and rules for buildings, 2004

12. TURMO, J, RAMOS, G, APARICIO A C. FEM study on the structural behavior of segmental concrete bridges with unbounded prestressing and dry joints: Simply supported bridges, Engineering Structures, 27, 2005, pp 1652-1661

13. EN 1992-2. Eurocode 2: Design of concrete structures – Part 2: Concrete Bridges – Design and detailed rules, 2005

# ASSESSING THE LOAD-CARRYING CAPACITY OF RC BEAMS UNDER IMPACT LOADING

**N Madjlessi**

**P Behinaein D M Cotsovos**

Heriot Watt University

United Kingdom

**ABSTRACT.** Data obtained from drop-weight tests reveals that the response exhibited by reinforced concrete (RC) beam specimens under impact loading differs significantly from that established during equivalent static testing. This shift in structural behaviour predominantly takes the form of an increase in the maximum sustained load as well as a reduction in the portion (span) of the RC beam reacting to the imposed action which tends to concentrate around the area of impact. However, measurements obtained from drop-weight tests concerning certain important aspects of RC structural response (e.g. maximum sustained load or deflection) often correspond to a specimen physical-state characterised by high concrete disintegration in combination with low residual load-bearing capacity and stiffness. This stage of structural response has little practical significance as it depends heavily on post-failure mechanisms for transferring the applied load to the specimen supports. In view of the above, the available test data cannot provide insight into the mechanisms underlying RC structural response nor can it identify the true ultimate limit state of the subject specimens when subjected to impact loading. To achieve insight into the mechanics underlying RC structural response under impact two well established structural analysis packages (ADINA and ABAQUS) are employed in the present study. Both packages are capable of carrying out three-dimensional dynamic nonlinear finite element analysis while realistically accounting for the nonlinear behaviour of concrete and the characteristics of the problem at hand i.e. a wave propagation problem within a highly nonlinear medium. The numerical predictions obtained concerning various aspects of RC structural response are initially validated against relevant data obtained from drop-weight tests. A parametric investigation is then carried out aiming to study the dynamic response exhibited by RC beams when subjected to specific rates and intensities of impact loading. The latter investigation reveals that the true load-bearing capacity is often significantly lower than the maximum sustained load recorded experimentally. In fact, the higher the loading rate and intensity of the impact load the larger the latter difference becomes.

**Keywords:** Reinforced concrete, beams, finite elements, nonlinear dynamic analysis, loading rate, impact, drop-weight tests.

**N Madjlessi** and **P Behinaein** are PhD students at Heriot Watt University investigating experimentally and numerically the mechanics underlying RC structural response under impact loading. **Dr D M Cotsovos** is an Assistant Professor at Heriot Watt University and his research focuses on experimentally and numerically investigating RC structural response under static, seismic and high-rate loading in order to develop suitable design and assessment methods.

## INTRODUCTION

It has been established, experimentally [1-5] and numerically [6-9], that the dynamic response exhibited by reinforced concrete (RC) beams under impact loading exhibits significant departures from that recorded during equivalent static testing as certain thresholds of applied loading rate are surpassed. The analysis of the available published experimental and numerical data reveals that the observed shift in structural response is owed to the combined effect of the inertia forces developing along the element span and the exhibited localised response [6-8]. More specifically, it has been established that the length of the element span (effective length, $L_{eff}$) reacting to the applied load reduces with increasing loading rates. This can be explained when viewing the problem at hand as a wave propagation problem within a highly nonlinear medium. In such cases the deformation exhibited by RC beams when subjected to impact loads is dependent on: (i) the intensity and speed of the stress waves generated during impact, which travel away from the impact region towards the supports of the structural member considered as well as (ii) the level of damage (cracking) sustained which locally reduces the stiffness of the RC element [6-8]. Under high loading rates, structural failure can be exhibited prior to the stress waves reaching the specimen supports resulting in localised response. The higher the loading-rate the more localised the response becomes as the distance within which the stress-waves travel prior to failure gradually reduces, concentrating around the area of impact [6-8]. This reduction of the element span reacting to the imposed load can be used to explain the observed increase in stiffness and load-carrying capacity exhibited by RC beams when subjected to impact loads characterised by increasing loading rates and intensities [6-8].

Present work forms an extension to already published studies investigating numerically the effect of loading rate on the response of RC beams under concentrated loads applied 'monotonically' to failure [6-8]. The aim of this investigation is to determine the '*true*' load-bearing capacity of the RC beam specimens when subjected to specific rates and intensities of impact loading. In an attempt to assess individually the effect of the loading rate and the intensity characterising the imposed impact load on the behaviour of the beams, the form of the latter load is assumed to be described by the simplified force time history shown in Figure1. This function is considered to consist of an ascending and a descending branch in which the rate of loading (associated with the ascending branch) is assumed equal to the rate of unloading (associated with the descending branch). Two well established three-dimensional (3D) dynamic nonlinear finite element analysis (NLFEA) packages are employed (ADINA and ABAQUS) [10,11]which are both capable of realistically accounting for the brittle nature characterising concrete material behaviour as well as the characteristics of the problem at hand: a wave propagation problem with a highly nonlinear medium. Emphasis is presently focused on studying certain important aspects of RC structural response such as the mode of failure as well as the deformation and cracking profiles exhibited throughout the loading process. The predictions obtained from the latter study reveal that the actual load-bearing capacity exhibited under impact loading is often significantly lower than the value of the maximum sustained load recorded experimentally. More specifically, it is observed that the latter difference increases as the loading rate and intensity of the impact load become higher.

## EXPERIMENTAL BACKGROUND

A large number of drop weight tests have been conducted to date on a wide range of RC beam specimens [1-5]. During such tests the load is applied though a steel striker (drop-weight) which is allowed to fall freely onto the mid-span region of the specimen from a predefined height (depending on the desired rate of loading). The layout of the drop-weight testing setup currently employed at Heriot Watt University (HWU) is shown in Figure 2. Different pads (e.g.

steel, rubber, plywood) are usually employed to moderate the level of damage (cracking) sustained locally by the specimen at the impact area and control (to a certain extent) the loading rate and intensity of the contact force generated. During testing measurements concerning the variation of displacement and strain at certain points along the specimen span, the acceleration of the steel impactor, as well as the support reactions and the contact force generated are recorded. In addition, crack formation and propagation up to failure, is closely monitored as it provides an indication of the corresponding internal stress state of the beam throughout the loading process. Typical load-deflection curves obtained from drop-weight tests describing the behaviour of RC beams under impact and equivalent static loading applied at mid-span are shown in Figure3 [5]. These curves reveal that as the rate of loading increases, the beams sustain higher values of loading. In addition, the exhibited crack patterns (see Figure4) suggest that with increasing loading rates the span of the beam mostly affected by the impact load tends to shorten and concentrate around the region where the load is applied (impact region).

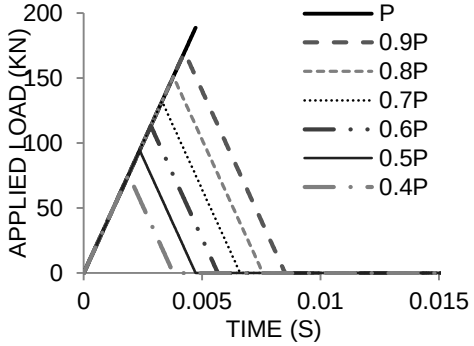


Figure 1 Force time history describing the contact force generated during impact.

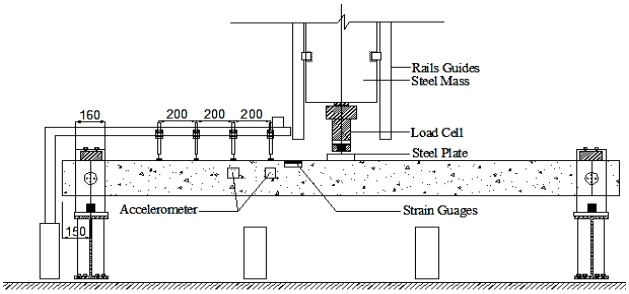


Figure 2 Drop-weight test setup employed at HWU

It should be noted, that drop-weight tests are difficult to conduct as the intensity of the loads generated during impact increase rapidly (in a few milliseconds) from zero to a maximum value (characterised by significantly higher values compared to those recorded during equivalent static testing) often leading to explosive (brittle) forms of failure which can in turn damage the instruments employed. Data obtained from such tests is characterised by a large scatter (see Figure 5) due to a wide range of parameters (associated with the different experimental techniques used, the variation of the size and shape of the impactor and the design details of the RC specimens) which differ from test to test [6-8]. Furthermore, it should be noted that the experimental information available does not usually provide a detailed description of the response exhibited by the RC specimens throughout the loading process. Instead, the available published data, concerning crack patterns and deformation profiles, is usually measured after (and not throughout) the application of the impact load. As a result it is difficult to correlate the measured responses obtained from drop weight tests to the actual physical state of the specimens as the measured maximum value of imposed load frequently corresponds to a specimen physical-state characterised by high concrete disintegration in combination with low residual load-bearing capacity and stiffness. This stage of structural response has little (if any) practical significance as it depends heavily on post-failure mechanisms (e.g. catenary and dowel action) for transferring the applied loads to the specimen supports. Based on the above it appears that the true load-carrying capacity is likely to be significantly lower than the maximum value of the contact force measured during testing. In addition it can be also concluded that the available test data cannot provide detailed insight into the mechanisms underlying RC structural response; it can, however, provide a qualitative description of the effect of loading-rate on certain important aspects of specimen behaviour.

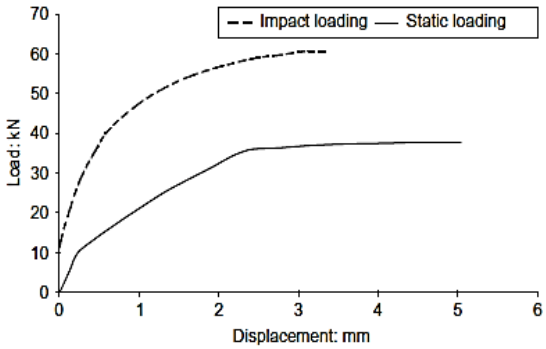


Figure 3 Typical load-deflection curves recorded during static and drop-weight testing of RC beams [5]

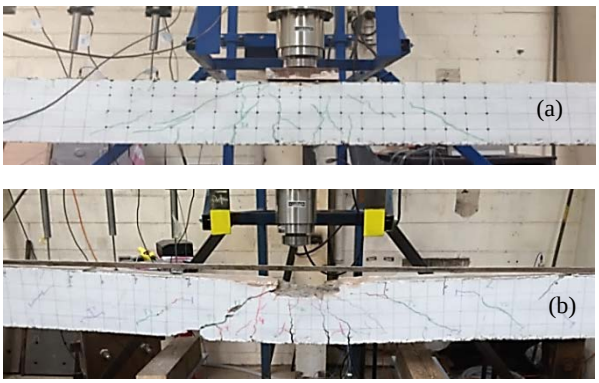


Figure 4 Crack patterns developing on RC beams under different rates of impact loading: (a) 25 kN/ms (b) 100 kN/sec;

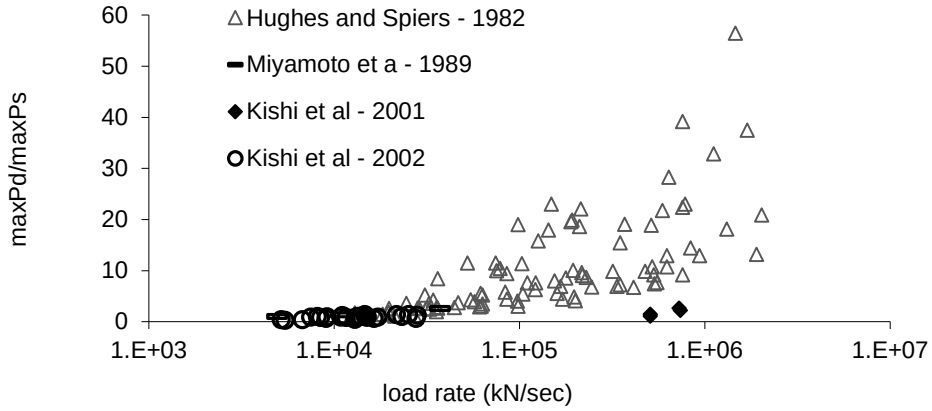


Figure 5 Variation of maximum sustained load during impact ($maxP_d$) normalised by the static load-carrying capacity ($maxP_s$) with increasing values of loading rate

## LIMITATIONS OF EXISTING NLFEA PACKAGES

To date a range of NLFEA packages have been employed to study the RC structural response under impact loading. The use of such packages allows the study of more complex structural forms (compared to the simple structural configurations studied experimentally) while providing a more detailed description of the exhibited response (i.e. stress and strain distribution, deformation profiles, failure modes and crack patterns) throughout the loading process. However, the majority of the available NLFEA packages incorporate models of concrete behaviour, the derivation of which has been based on the regression analysis of test data obtained from static uniaxial compression and tension tests on plain concrete specimens [12-13]. Furthermore, they often assume that concrete material behaviour is strain-rate dependent (sensitive) and employ laws (usually in the form of dynamic increase factors) describing the variation (increase) of key material properties (e.g. modulus of elasticity, concrete compressive and tensile strength, yield and ultimate stress of steel) with strain-rate. The analytical formulation of these material models includes a number of parameters which are mainly linked to post-peak concrete characteristics such as strain softening, tension stiffening, and shear-retention ability. Such parameters are defined at the structural, rather than at the material level and attribute ductile characteristics to concrete behaviour not compatible with its brittle nature and not justified by the available test data [12-13]. As a result, the use of such parameters can affect the objectivity of the numerical predictions obtained since they require recalibration depending on the type of problem investigated.

## GENERAL ASPECTS OF THE FE MODEL PRESENTLY ADOPTED

ADINA[11] shares a number of characteristics with RC-FINEL [14-15]which has been found capable of realistically predicting the response of a wide range of RC structural configurations under static and dynamic loading. In addition, ABAQUS [10] is also employed for purposes of comparison. Both packages are capable of carrying out three-dimensional (3-D) dynamic nonlinear finite element analysis (NLFEA) while realistically accounting for the brittle nature characterising concrete material behaviour and the characteristics of the problem at hand: a wave propagation problem within a highly nonlinear medium. In both cases the equation of motion – which governs structural response – is solved numerically through the use of an implicit Newmark integration scheme. The choice of 3D dynamic NLFEA is dictated by (a) the nonlinear behaviour of concrete under triaxial stress conditions, which invariably develop prior to local failure (i.e. cracking), (b) the introduction of non-homogeneity and stress redistribution after the occurrence of cracking and (c) the development of significant inertia forces.

***Material Modelling:*** The concrete material model employed by ADINA [11] stems from experimental data obtained from tests conducted on concrete cylinders under triaxial loading conditions [14,15]. It realistically accounts for the brittle nature and the triaxiality which characterises concrete material behaviour. Its formulation is characterised by both simplicity (fully brittle, with neither strain-rate nor load-path dependency, fully defined by a single material parameter - the uniaxial cylinder compressive strength $f_c$) and attention to the actual physical behaviour of concrete in a structure. The subject model has been successfully used to predict the behaviour of plain concrete prisms under increasing rates of uniaxial compressive and tensile loading [12,13].The predictions obtained from the latter studies suggest that the observed shift in plain concrete specimen behaviour under high rates of compressive and tensile loading is mainly attributed to parameters associated with structural response (i.e. inertia, the boundary conditions imposed and the geometry of the specimens) as well as the characteristics of the problem at hand (a wave propagation problem within a highly nonlinear medium) rather than to strain-rate sensitivity of the material properties of concrete. In the case of ABAQUS [10] a simple brittle model (termed “brittle cracking model”) is employed for describing concrete material behaviour which is purpose-built for materials the behaviour of which is dominated by tensile cracking. The latter assumption is largely true in the case of RC flexural structural elements where cracks form due to the development of tensile strains within the concrete medium. The predictions of the subject model have been validated for a wide range of RC structural configurations (beams, columns, joints) under static (monotonic and cyclic) loading conditions [16-19]. A simple bilinear elasto-plastic hardening model is employed for describing the behaviour of steel. Finally, concrete and steel material behaviour is assumed to be independent of the loading-rate and full bond is assumed in order to describe the interaction between the two materials.

***Nonlinear Solution Strategy:*** During each time step the equation of motion governing the nonlinear dynamic problem considered is solved as a sequence of equivalent static problems through the use of the Newmark family of approximation methods. At the beginning of each iteration and based on the values of displacement, velocity and acceleration obtained from the previous iteration, the effective stiffness and load matrix are calculated and an equivalent static problem is formulated [15]. The equivalent static problem is solved through an iterative procedure based on the Newton-Raphson method [10, 11, 15]. During the solution process of the equivalent static problem every Gauss point is checked to determine whether loading or unloading takes place and to establish whether any cracks close or form. Depending on the results of the previous checks, changes are introduced to the stress-strain matrices of the individual FE’s and to the global stiffness matrix representing the structure investigated.

Convergence is checked locally at each Gauss point and once the values of the strain and the corresponding stress increments become less than a small predefined value (i.e. convergence criterion) then convergence is accomplished and the solution can move on to the next time step. When the convergence criterion is not achieved, the residual forces are calculated and are then re-imposed onto the FE model of the RC form investigated until convergence is finally achieved.

***Modelling of Cracking:*** The smeared-crack approach is adopted for modelling cracking. A crack forms when the stress developing in a given part of the structure corresponds to a point in the principal stress space that lies outside the predefined failure surface of concrete material. This is then followed by an immediate loss of load-carrying capacity in the direction normal to the plane of the crack. At the same time, the shear stiffness is also reduced drastically to a small percentage (about 5 to 10%) of its previous value (before the occurrence of the crack). However, it is not set to zero in order to minimize the risk of numerical instability during the execution of the solution procedure, as explained elsewhere [15]. It should be noted that each integration point can develop up to three cracks.

## STRUCTURAL FORM INVESTIGATED

The behaviour of the RC beam specimens considered herein (C2, D1, E1) has been experimentally investigated in the past [1] under static and impact loading. The design details of these specimens are presented in Figure6.The elasticity modulus ($E_S$), the yield stress ($f_y$), and the ultimate strength ($f_u$) of both the longitudinal and transverse reinforcement bars are 206 GPa, 460 MPa and 560 MPa, respectively. The uniaxial compressive strength ($f_c$) of concrete is 45 MPa. The subject beams were subjected to drop weight testing at their mid-span. Mild steel, rubber or ply pads were placed on the top face of the specimen in order to prevent or moderate local damage (cracking) in the impact area and to some extent control the rate of loading.

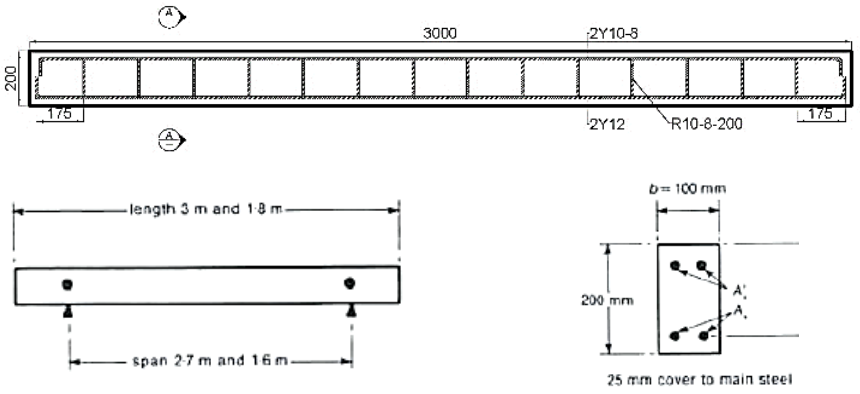


| Beam type | Length | Tensile Steel $A_s$ | Compression Steel $A_{s'}$ | Stirrups |
|---|---|---|---|---|
| C2 | 3m | 2x12Φ | 2x6Φ | 14x6 |
| D1 | 3m | 2x16 | 2x6 | 14x6 |
| E1 | 1.8 | 2x12 | 2x6 | 8x6 |

Figure 6 RC beam investigated [1]

## FE MODELLING OF THE PROBLEM AT HAND

In ADINA [11] concrete is modelled using a mesh of 27-noded brick elements which adopt a 3x3x3 integration rule. In ABAQUS [10] concrete is modelled through the use of a dense mesh of 8-node brick elements the formulation of which adopts a reduced integration scheme to avoid numerical instabilities due to locking. The steel reinforcement bars are modelled as 2-node truss elements of appropriate cross-sectional area which are embedded in the FE mesh representing the concrete medium. Due to the double symmetry of the problem at hand, only a quarter of each beam specimen is modelled with suitable boundary conditions, see Figure 7. The load is assumed to be applied onto the mid-span of the beam through a steel plate. For the case of static loading the load is applied monotonically until failure in the form of displacement increments (displacement control). In the dynamic case studies the load is imposed in the form of load increments applied either monotonically to failure (at a constant rate) or in the form of the pulse described by the force-time histories presented Figure 1.

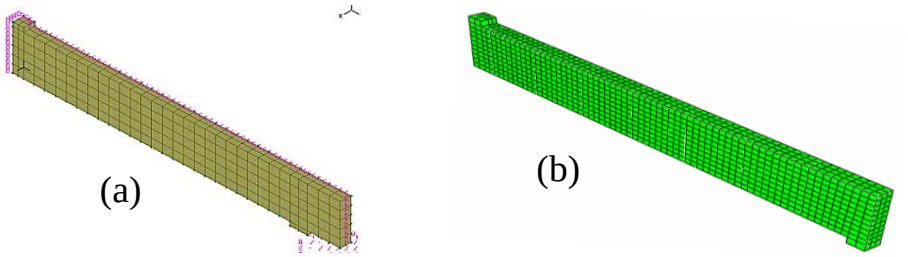


Figure 7 FE mesh adopted (a) ADINA and (b) ABAQUS

## NUMERICAL PREDICTIONS

**Static Case Study:** For the case of static loading the predictions obtained describing the behaviour of the beam specimens are presented in Figure 8a in the form of a load-displacement curves which represent the relation between the applied load and the deflection at the load point (i.e. mid-span). The latter curves are in good agreement with their experimentally established counterparts [1]. Figure8b shows the deformation and cracking profiles predicted for the case of specimen C2 at different stages of the loading process. On the basis of these predictions flexural cracks begin to appear in the mid-span region of the specimen and, as the imposed load increases, they gradually spread towards the supports. Overall, the numerical predictions concerning the response of the RC beam specimens is in generally good agreement with that established experimentally. Both the experimental measurements and their numerically established counterparts show that all beams exhibited ductile behaviour, with failure occurring after yielding of the longitudinal reinforcement bars in the mid-span region of the specimen, resulting in the formation of extensive cracking that, ultimately, leading to loss of load-carrying capacity of the compressive zone at this location.

**Monotonic high rate loading:** The values of the applied loading rates considered in the numerical study range from 1 to 103 kN/ms which is in good agreement with the loading rates achieved experimentally [1]. The predicted load-displacement curves presented in Figure 9a reveal that an increase in the loading rate leads to an increase in stiffness and load-carrying capacity and a reduction of the maximum deflection exhibited at mid-span. As regards the cracking and deformation profiles, Figure 9b indicates that, under relatively low loading rates, beam behaviour is qualitatively similar to that exhibited under static loading. However, as the rate of loading increases, the portion ($L_{eff}$) of the beam essentially affected by the applied load reduces. More specifically, for high rates of loading, $L_{eff}$ extends on either side of the mid-span cross section (area at which the impact load is applied) to a distance marked by the formation of vertical (flexural) cracking initiating at the upper face of the beam and extending downwards

(see Figure9b), whereas the remainder of the beam (extending between the supports and the aforementioned cracking) practically remain unaffected by the applied load. Therefore, under high rates of loading, beam behaviour is essentially controlled by $L_{eff}$. The reduction of $L_{eff}$ under increasing loading rates can explain the experimentally observed increase in stiffness and maximum sustained load. The variation of the dynamic increase factor (*DIF*), i.e. the ratio between the maximum load sustained ($maxP_d$) by the RC beams under high rate loading and the load-carrying capacity determined under static loading ($maxP_s$) ($DIF = maxP_d/maxP_s$), with increasing loading rates is presented in Figure10. The experimentally established values of the *DIF* are in good agreement with their counterparts predicted numerically by ADINA and ABAQUS for all three types of RC beam specimens considered herein.

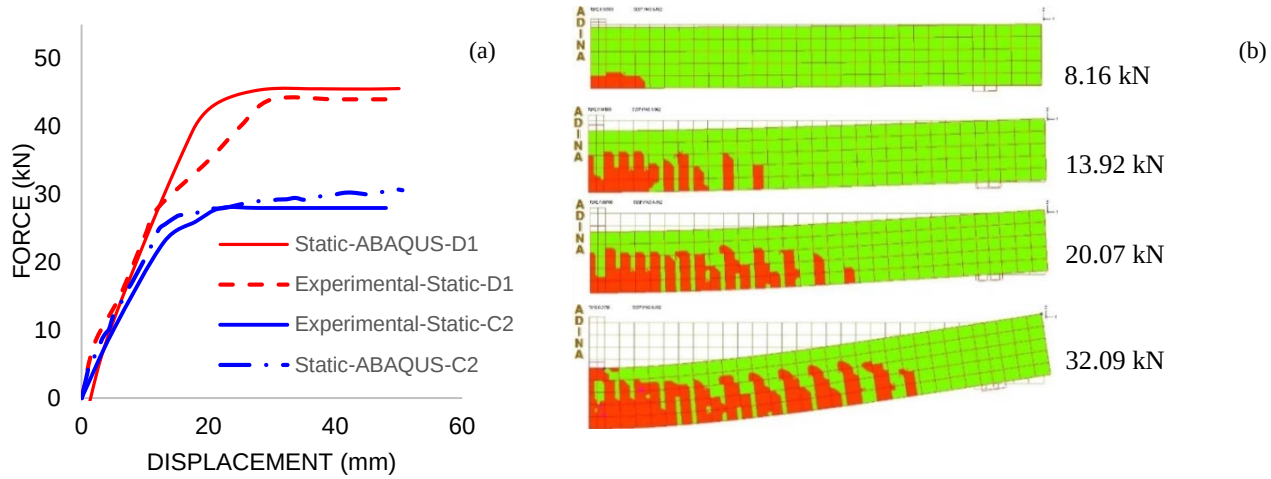


Figure 8 (a) Static load-deflection curves established experimentally and numerically by ABAQUS; (b) deformation and cracking profiles exhibited by beam C2 under static loading predicted by ADINA

**High rate pulse loading:** In an attempt to assess the effect of loading rate and intensity separately, high rate loading is imposed in the form of a concentrated pulse load (see Figure 1) at the mid-span region of the specimens presently considered (see Figure 6). In order to determine the actual load-bearing capacity of the RC beams for a specific value of loading rate ($\dot{P}$) a parametric study is carried out in which the intensity (*peak value*) of the imposed dynamic pulse load is varied as shown in Figure 1. Typical predictions obtained from these parametric studies are presented in Figure 11 for the case of beam C2 [1]. These predictions describe the variation of the mid-span deflection with time when the specimen is subjected to pulse loads characterised by different intensities (peak values) but the same loading rate: $\dot{P}$= 400kN/msec. The latter curves reveal that when the *peak value* of the pulse load is higher than 25% of $maxP_d$ (obtained for the case of monotonic high rate loading) the RC beam fails during unloading. However, when the *peak value* of the pulse load becomes equal or less than 25% $maxP_d$, the RC beam does not fail, but continues to oscillate after unloading takes place. The latter critical value (≈ 25% $maxP_d$) can be considered as the true load bearing capacity of the RC beam for Ṗ= 400kN/msec.

The variation of *DIF* associated with the *peak load* of the pulse load that will not result in failure of the RC beam during unloading ($DIF$ = *peak value*/$maxP_s$) is presented in Figures10(a-c) for different loading rates for all specimens presently considered. These curves are compared to their counterparts established numerically for the case of monotonic high rate loading and experimentally [1]. It is interesting to note that the predictions concerning *DIF* for the case of pulse loading provided by ABAQUS are higher than their counterparts provided by ADINA. This is attributed to the differences in the formulation of the concrete material models

adopted by the two packages, with the ADINA model considered to provide a more realistic description of concrete behaviour. Furthermore, the results obtained from drop-weight testing appear to be in good agreement with their counterparts predicted numerically for the case of the monotonically applied high rate load. This suggests that the relevant tests data are associated with post-failure behaviour and that that the true load-bearing capacity of the RC beams under impact loading is considerably lower than the latter values. The higher the loading rate and intensity of the impact load the larger the latter difference becomes. Figure 12 shows the predicted deformation profiles and the associated crack patterns developing on specimen C2 when subjected to pulse loads with $\dot{P}$= 400kN/msec but different intensities. From these figures it is observed that for a specific loading rate a reduction in the *peak value* of the pulse load applied will result in more global response as a larger portion of the span reacts to the applied load. This suggests that the $L_{eff}$ and the mechanics underlying RC structural response will be affected by both the rate of applied loading and intensity of the imposed impact load.

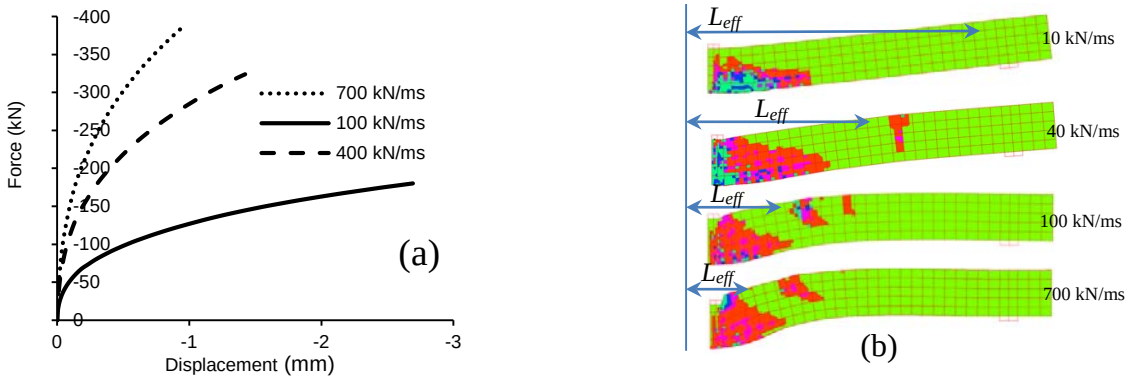


Figure 9 Beam C2 under loading applied at various rates: (a) Load-deflection curves; (b) Deformation and cracking profiles.

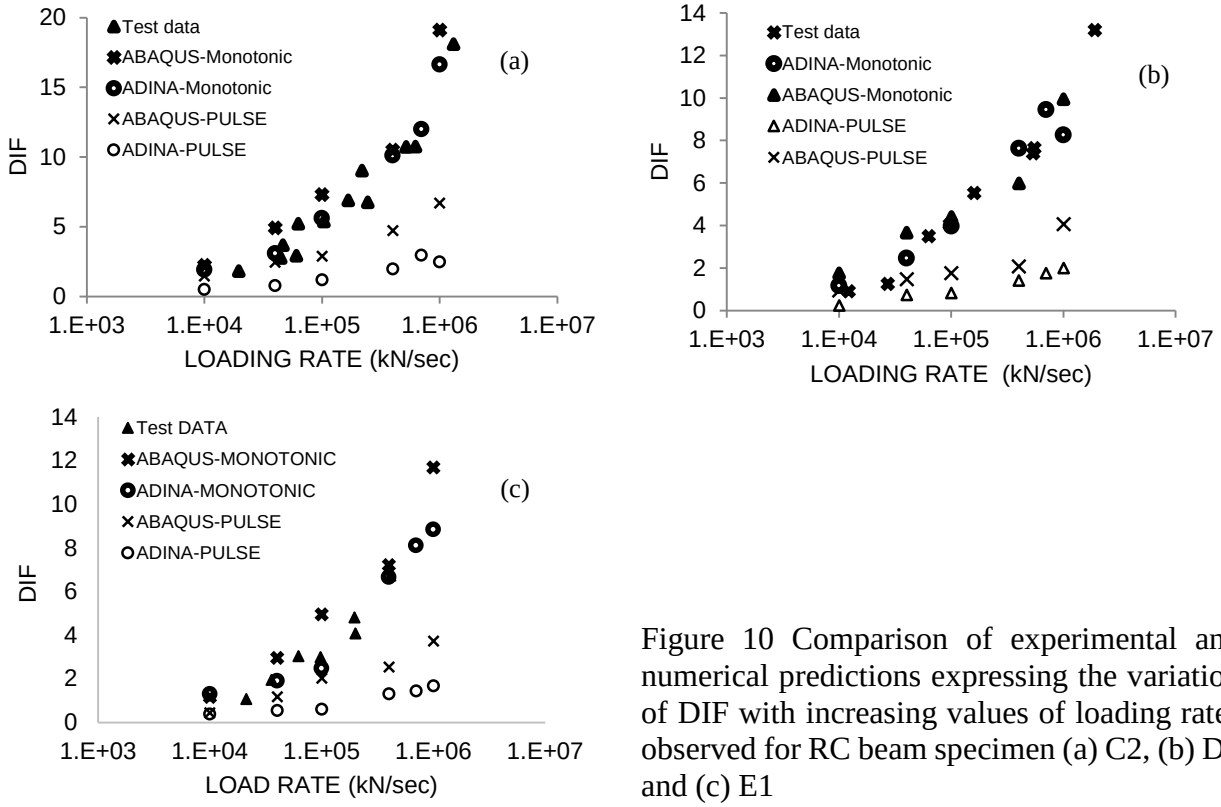


Figure 10 Comparison of experimental and numerical predictions expressing the variation of DIF with increasing values of loading rates observed for RC beam specimen (a) C2, (b) D1 and (c) E1

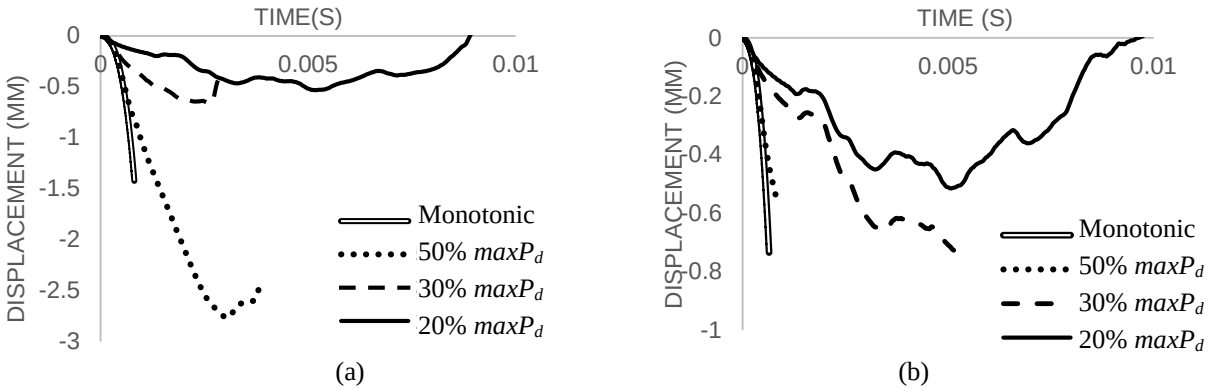


Figure 11 Predicted mid-span displacement time history obtained for pulse loads with $\dot{P}$=400kN/ms but different intensities for (a) Specimen C2 and (b) Specimen E1.

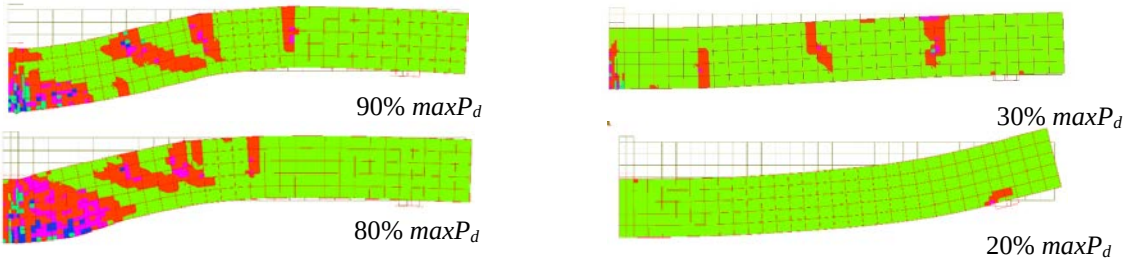


Figure 12 Predicted crack patterns and deformation profiles for specimen C2 for pulse loads with $\dot{P}$=400 kN/ms but different intensities

## CONCLUDING REMARKS

The comparative study between the numerical predictions and their experimental counter parts reveals that the concrete material models presently employed by ADINA and ABAQUS are capable of providing realistic predictions concerning certain aspects of the response exhibited by RC beams under increasing rates and intensities of impact loading. The predictions obtained confirm the findings of previous published numerical studies [6-8] which suggest that effect of loading rate on RC structural response reflects the influence of inertia and the nature of the problem at hand: a wave propagation problem within a highly nonlinear medium. The numerical investigation also reveals that true load-bearing capacity is frequently significantly lower than the maximum sustained load recorded experimentally, the latter being associated with a specimen physical state characterised by considerable concrete disintegration and low residual stiffness and load-bearing capacity. The higher the loading rate and intensity of the impact load the larger the latter difference becomes. Further detailed experimental and numerical studies are currently being conducted in order to consider a wider range of RC structural elements (beams, columns, slabs, walls) and design parameters. The predictions obtained are presently forming the basis for the development of a new method for assessing the performance exhibited by RC structural elements under impact loading.

## REFERENCES

1. HUGHES G., SPIERS D. M. An investigation on the beam impact problem. Cement and Concrete Association, Technical Report 546, 1982.

2. MAY. I. M, CHEN. Y, ROGER. D, OWEN. J, FENG. Y. T, AND THIELE. P. J. Reinforced concrete beams under drop-weight impact loads. Comp.& Conc. 3, (2-3), 2006, pp. 79-90.

3. SAATCI. S., VECCHIO F. J. Effects of shear mechanisms on impact behaviour of reinforced concrete beams. ACI Structural Journal 106 (1), 2009, PP. 78-86.

4. ABBAS, A.A., PULLEN, A.D., COTSOVOS, D.M. Structural response of RC wide beams under low-rate and impact loading. MCR 62(10), 2010, PP. 723-740.

5. MIYAMOTO A, KING M.W, FUJII M. Non-linear dynamic analysis and design concepts for RC beams under impulsive loads. Bulletin of the New Zealand National Society for Earthquake Engineering, (22), 1989, pp.98-111.

6. COTSOVOS DM, STATHOPOULOS ND, ZERIS CH. Behaviour of RC beams subjected to high rates of concentrated loading. J. Struct. Enging ASCE 134(12), 2008, pp. 1839-1851.

7. COTSOVOS DM., PAVLOVIĆ M.N. Modelling of RC beams under impact loading. Proceedings of the ICE-Structures and Buildings 165.2 2012, pp. 77-94.

8. COTSOVOS. D.M. A simplified approach for assessing the load-carrying capacity of reinforced concrete beams under concentrated load applied at high rates. Int. J Imp. Enging 37, 2010, pp. 907-917.

9. THABET. A, HALDANE. D. Three-Dimensional Simulation of Nonlinear Response of Reinforced Concrete Members Subjected to Impact Loading. ACI Structural Journal 97(5), 2000, PP. 689-702.

10. ABAQUS. ABAQUS Standard User's Manual, Version 6.14. Providence, RI (USA): Dassault Systèmes Corp.; 2015.

11. ADINA R & D, Inc: “Theory and Modelling Guide” Volume 1, Report ARD 13-8, Dec. 2013

12. COTSOVOS. D.M., PAVLOVIĆ. M.N. Numerical investigation of concrete subjected to compressive impact loading. Part 1: A fundamental explanation for the apparent strength gain at high loading rates, Comp. & Struct., 86(1-2), 2008a, pp. 145-163.

13. COTSOVOS. D.M., PAVLOVIĆ. M.N. Numerical investigation of concrete subjected to compressive impact loading. Part 2: Parametric investigation of factors affecting behaviour at high loading rates, Comp. & Struct., 86(1-2), 2008b, pp. 164-180.

14. KOTSOVOS. M.D., PAVLOVIĆ. M. N. Structural Concrete: Finite-element analysis and design, 1995, London, Thomas Telford.

15. KOTSOVOS M.D. Finite-Element Modelling of Structural Concrete: Short-Term Static and Dynamic, 2015, Boca Raton, CRC Press

16. ABBAS A.A., MOHSIN S. SYED, COTSOVOS D.M., RUIZ-TERAN A.M., Seismic response of steel fibre reinforced concrete beam-column joints, Enging Struct., 59, pp. 261-283, 2014.

17. ABBAS A.A., MOHSIN S. SYED, COTSOVOS D.M., RUIZ-TERAN A.M., Shear behaviour of SFRC simply-supported beams, ICE Proc. Structures and Buildings, 167, No. SB9, 544-558, 2014.

18. ABBAS A.A., MOHSIN S. SYED, COTSOVOS D.M., RUIZ-TERAN A.M., Nonlinear analysis of statically-indeterminate SFRC columns, Structural Concrete, 15, No. 1, 94-105, 2014.

19. ABBAS A.A., MOHSIN S. SYED, COTSOVOS D.M., RUIZ-TERAN A.M., Statically-indeterminate SFRC columns under cyclic loads, Advances in Structural Engineering, 17, No. 10, 1403-1417, 2014.

# BEHAVIOUR OF HIGH STRENGTH CONCRETE CONTINUOUS DEEP BEAMS WITH OPENINGS

**M E Shoukry** **T I Ebeido** **M A Elnaggar**

Alexandria University

**A A Hamouda**

Kafer Elsheikh University

Egypt

**ABSTRACT.** This paper presents the results of an experimental program on eight reinforced concrete two-span continuous deep beams. All tested beams were fabricated, instrumented and then tested to failure under the effect of two concentrated loads one being placed at each span. Seven beams were made using high strength concrete whereas one beam was made using normal strength concrete. Many significant factors were considered such as: concrete strength, size, shape and location of openings being placed within the interior shear spans. Furthermore, the effect of strengthening of the beams on its behaviour was considered in the case of beams provided with openings. The strengthening technique considered was bonding exterior carbon fibre reinforced polymers (CFRP) in form of strips in the horizontal and vertical directions around the openings. For all tested beams, deflections, strains in the longitudinal flexural reinforcement, and strains in the vertical stirrups were measured and recorded. Also, the initiation and propagation of cracks were recorded. Cracking patterns and failure modes were observed. Test results revealed the significant effect of the concrete strength and the presence of openings on the shear behaviour of tested two-span continuous deep beams. Such behaviour was also affected by the shape and size of the openings. Furthermore, it was found that strengthening of those deep beams with openings by bonding CFRP strips resulted in about 20% enhancement in the beam failure load in comparison to non-strengthened beams. However, the failure load of strengthened deep beams is still less than that of solid beams by about 20%.

**Keywords:** High strength concrete, FRP, Strengthening, Deep beam, Opening.

**M E Shoukry** and **T I Ebeido** are Professors at the Structural Engineering Department, Faculty of Engineering, Alexandria University

**Mohamed A Elnaggar** is Assistant Professor, Structural Engineering Dept., Faculty of Engineering, Alexandria University. He received his Ph.D. in Structural Engineering from Alexandria University, Egypt. His research work includes use of Advanced Composite Materials (FRP) in Repair and Strengthening of R.C. members, Lap Splice, and Use of Finite Elements Method for Modelling of structures. He has twenty years of experience in Structural engineering, practice and research.

**A A Hamouda** is Graduate Teaching Assistant of Civil Engineering Department, Kafer Elsheikh University, Egypt

## INTRODUCTION

Reinforced concrete deep beams are used in structures as load distribution elements such as transfer girders, pile caps, and foundation walls in tall buildings. Although these members commonly have several supports, extensive experimental investigations have brought simple deep beams into focus. The behaviour of continuous deep beams is significantly different from that of simply supported ones. The coexistence of high shear and high moment within the interior shear span in continuous deep beams has a considerable effect on the development of cracks, leading to a significant reduction in the effective strength of the concrete strut, which is the main load transfer element in deep beams. Indeed, few experiments were carried out on continuous deep beams of shear span-to-overall depth ratio (a/h) greater than 1.08 [1]. The results of simple deep beams tested by Tan et al. [2] and Smith and Vantsiotis [3] showed that the relative effectiveness of horizontal and vertical shear reinforcement on controlling diagonal cracks and enhancing load capacity reversed for deep beams having an a/h ratio less than 1.0, that is, horizontal shear reinforcement was more effective for an a/h ratio below 1.0, whereas vertical shear reinforcement was more effective for an a/h ratio larger than 1.0. Therefore, a reasonable evaluation of the influence of shear reinforcement on continuous deep beams having a/h ratio less than 1.0 requires further investigation.

Ashour and Rishi 2000 [4] carried out an experimental work on sixteen testes on reinforced concrete two-span continuous deep beams with web openings to study the behaviour of reinforced concrete continuous deep beams with web openings, The main parameters studied in this experimental work were the size and position of web openings (exterior or interior), and web reinforcement arrangement around openings (horizontal or vertical). The mode of failure depends mainly on the position of the web openings. The web reinforcement arrangement and size of the web openings did not have much influence on the mode of failure. For beams having web openings within interior shear spans, the diagonal cracks that formed at the web opening corners extended both ways towards the edges of the central support and load plates.

The stresses in a deep beam differ radically from stresses predicted by the ordinary theory of beam bending. This difference arises because ordinary beam theory does not account for vertical normal stress induced by the applied loads and supports, not for shearing deformation. Due to their high flexural strength, the strength of deep beams is generally controlled by their shear capacity. The adequate arrangement of the main steel and web reinforcement may change the mode of failure to a ductile one, or at least, the shear capacity will be further increased.

In the construction of modern buildings, transverse openings are often provided through beams for the passage of utility ducts and pipes to better utilize the otherwise dead space below the beam soffit. Such an arrangement of building services leads to a significant reduction in the dead space and results in a more compact and economical design. For multi-storey buildings in particular, the savings in story height thus achieved at each level adds up to a substantial savings in the surface area of partition walls, length of riser ducts, and overall loads on foundation.

The provision of transverse openings will change the continuous beam behaviour into a more complex behaviour. It is obvious that the provision of openings produces discontinuity in the normal flow of stresses, and these results in stress concentration and early cracking around the opening. The ultimate strength of the beam may also be seriously affected. Therefore, special strengthening should be provided around the opening to contain the width of cracks and to prevent possible premature failure of the beam.

The failure loads for some of the deep beams tested in this research were calculated using some of the building codes: ECP 2007 [5], ACI 318-08 [6] and BS 1997 [7] and also using the equations developed by Ashour and Rishi [4] for deep beams with openings. The calculated values were compared to the experimental ones.

## EXPERIMENTAL PROGRAM

The main objective of the present experimental investigation was to study the behaviour of continuous deep beams with interior openings. Also, the study aims to choose the best method and shape of strengthening of such beams by using laminate carbon fibre reinforced polymers (CFRP) around openings. The aim of strengthening was to enhance the behaviour and strength of beams with openings to be close as possible to that of a solid beam without openings.

Eight reinforced concrete continuous deep beams were tested to failure in the present investigation. Seven beams were made of high strength concrete and one beam was made of normal strength concrete. The dimensions of the tested beams were: 150 mm width, overall depth; h = 600 mm and 1740 mm long. The beams were supported on three supports with two equal spans, each span $L_e$ = 720 mm (giving $L_e$ / h ratio of 1.25). All beams were subjected to two increasing concentrated loads, each was applied to mid-span. For all tested deep beams, reinforcement cages were provided at the supports and also at loading positions to prevent premature crushing or bearing failure.

The main variables studied were: the size and shape of openings and strengthening methods by laminate CFRP. The test program consisted of three groups of beams. The first group consisted of four beams, namely; NS, HS0, HS1 and HS4. Beam NS was a normal strength concrete solid beam without any openings. Beam HS0 was a high strength concrete beam without any opening. Beam HS1 had two symmetric square openings, each 200 mm × 200 mm and were formed close to the central support such that the centre of the two openings was exactly at the middle of interior shear span. Beam HS4 had one large rectangular opening 200 mm × 600 mm centred above the central support. The aim of this group was to study the effect of the presence and size of opening on behaviour and strength of high strength concrete deep beams.

The second group consisted of four beams: HS0, HS1, HS2 and HS3. Beams HS2 and HS3 were deep beams with openings and were strengthened around openings by laminate CFRP. Beam HS2 was strengthened by vertical layers of CFRP while beam HS3 was strengthened by horizontal layers of CFRP. The aim of this group was to study the efficiency of the strengthening technique on the behaviour and the strength of the beam with small square opening.

The third group consisted of four beams: HS0, HS4, HS5 and HS6. Beams HS5 and HS6 were deep beams with a large opening and were strengthened around openings by laminate CFRP. Beam HS5 was strengthened by vertical layers of CFRP while beam HS6 was strengthened by horizontal layers of CFRP. The aim of this group was to study the efficiency of the strengthening technique on the behaviour and the strength of the beam with large rectangular opening.

Table 1 gives the properties of the tested beams in all groups while Figures 1 to 4 show dimensions and reinforcement details of beams.

Table 1 Details of tested beams

| BEAM | AVERAGE CONCRETE STRENGTH, $f_{cu}$, N/mm² | OPENINGS SIZE, mm | STRENGTHENING SHAPE (V or H)* & Total fibre width, mm |
|---|---|---|---|
| NS | 32 | Without openings | ---------- |
| HS0 | 70 | Without openings | ---------- |
| HS1 | 112 | 200 × 200 | ---------- |
| HS2 | 65 | 200 × 200 | V & 800 |
| HS3 | 92 | 200 × 200 | H & 400 |
| HS4 | 82 | 200 × 600 | ---------- |
| HS5 | 93 | 200 × 600 | V & 800 |
| HS6 | 90 | 200 × 600 | H & 400 |

*****V = strengthening by vertical layers of CFRP
*H = strengthening by horizontal layers of CFRP

One dial gauges of 0.01 mm accuracy was used to record deflection at the centre of each span of all tested beams. For each beam, five electrical strain gauges were used to measure steel strains, as shown in Figures 2 to 4. Each gauge was 5 mm length and 120+ 0.2Ω gauge resistance.

Each specimen was placed centred and levelled on two roller end supports and hinged support in the middle, as shown in Figure 1. A strong spreader double I beam was rested on the top loading middle points. Test set up is as shown in Figure 1. The load was applied in increments of 100 kN up to 1000 kN then the increment reduced to 50 kN up to failure.

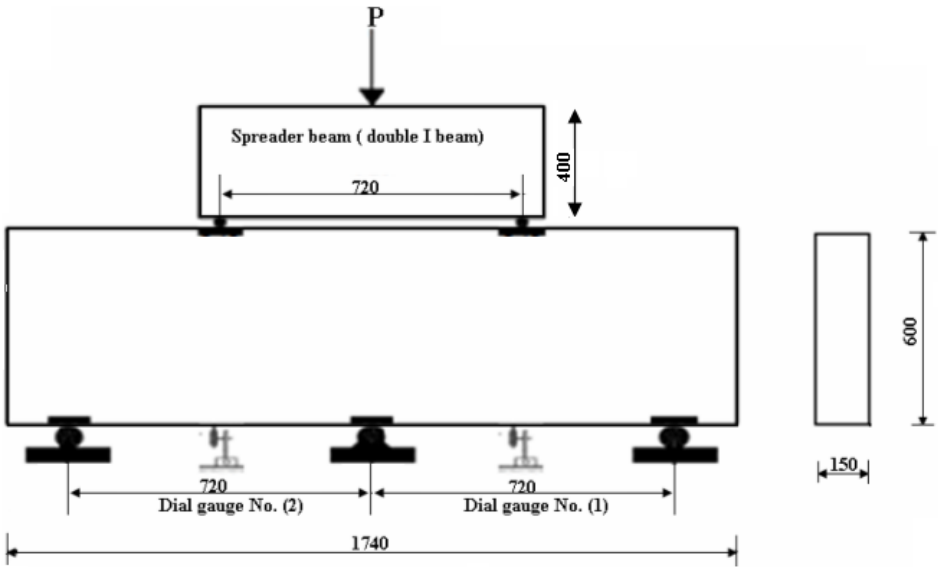


Figure 1 Dimensions and test set up of tested beams (Note: all dimensions in mm)

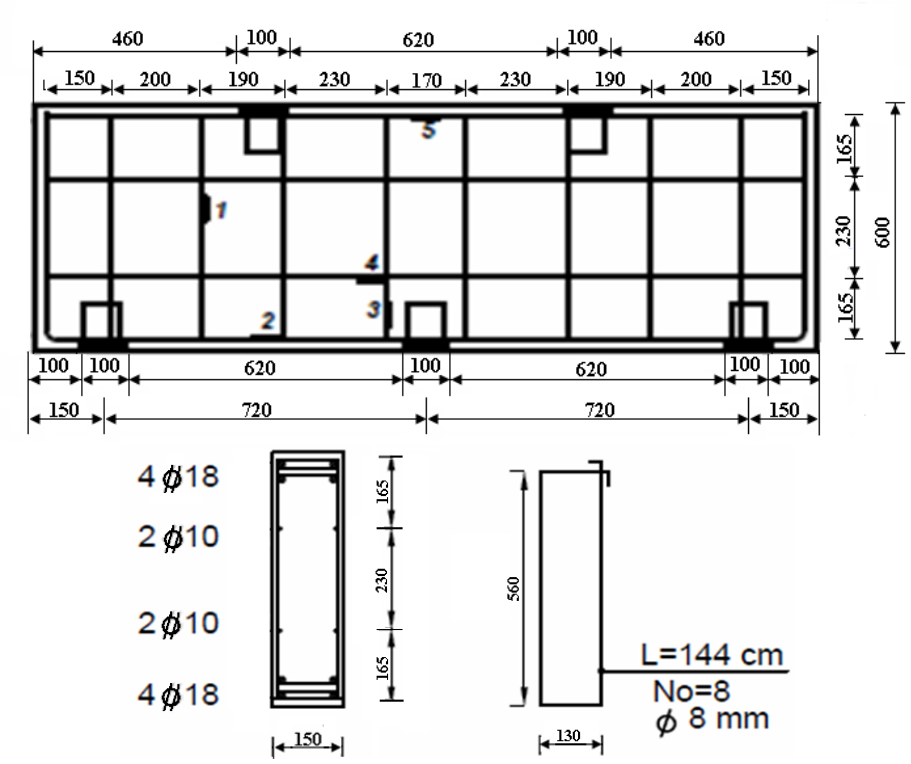


a) Steel reinforcement details and strain gauge positions of NS &HS0

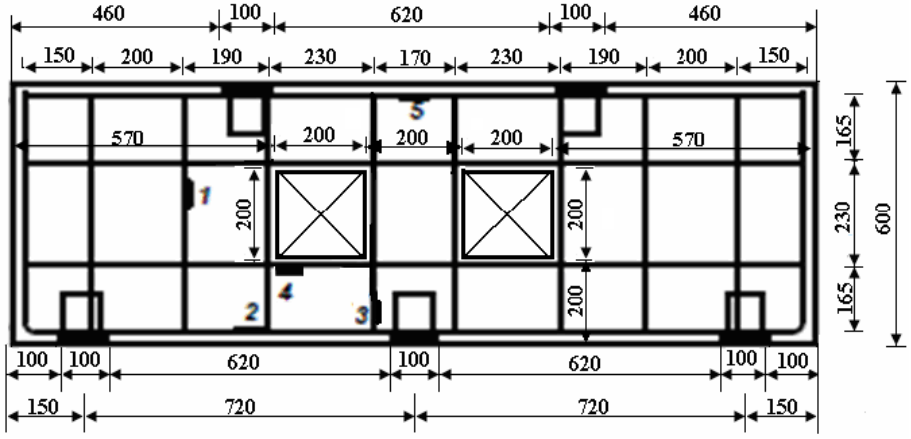


b) Steel reinforcement details and strain gauge positions of HS1

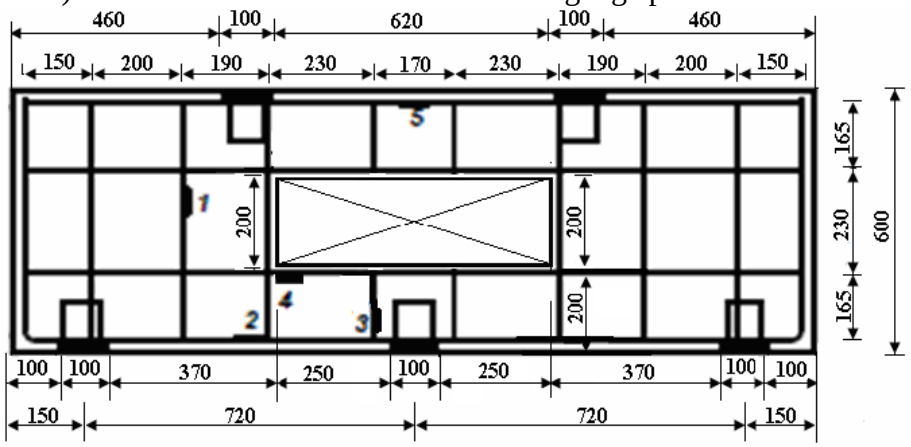


c) Steel reinforcement details and strain gauge positions of HS4

Figure 2 Dimensions and reinforcement details for the beams in the first group (Note: all dimensions in mm)

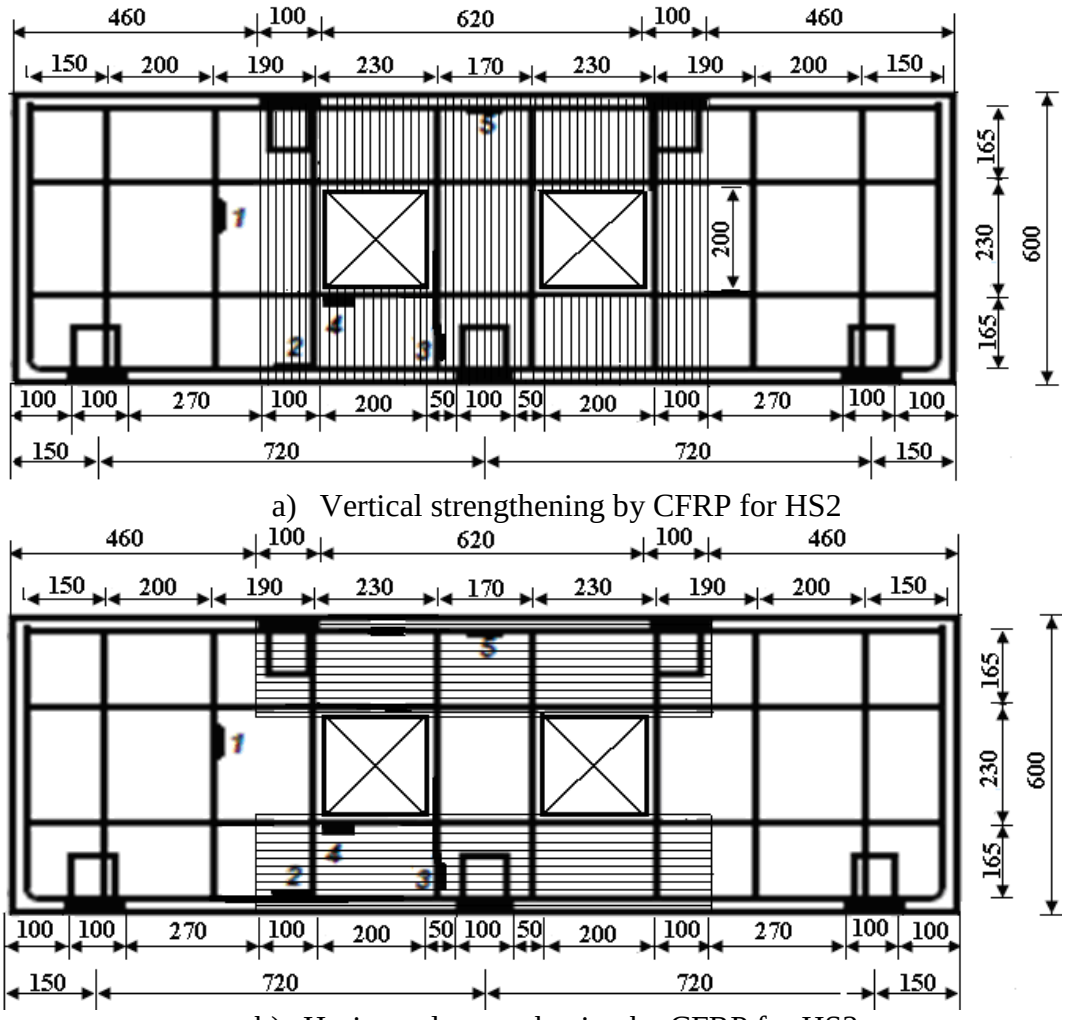


a) Vertical strengthening by CFRP for HS2

b) Horizontal strengthening by CFRP for HS3

Figure 3 Dimensions and reinforcement details for the beams in the second group (Note: all dimensions in mm)

The average value of concrete compressive strength for the normal strength concrete was 32.0 N/mm². The high strength concrete consisted of Ordinary Portland Cement (with content 500 kg/m³), natural siliceous sand, crushed dark basalt of 12.7 mm maximum nominal size and water. The mix proportions by weight were 1: 1.16: 2.4 and w/c ratio was 0.28.

A fine admixture was used by adding to cement with dosage 0.22 in order to reach the required high strength concrete. Also, superplasticizer admixture (sikament – R2002) was used to increase the workability time required for casting and fulfils the limits of ASTM C-494 Type G and BS 5075 Part 3. The average value of compressive strength, obtained from testing standard cubes, $f_{cu}$ of the high strength concrete was 86 N /mm$^2$.

Three kinds of reinforcing steel were used in this work: 18 mm diameter high strength steel agrees with grade 360/520 was used as tension reinforcement, 10 mm diameter high strength steel agrees with grade 360/520 was used for shear resistance in horizontal direction. Plain bars of 8 mm diameter agree with grade 280/450 was used for vertical stirrups.

The laminate fibre was solid strips of carbon fibre reinforced polymers (CFRP) of 100 mm width and thickness 1.2 mm with elastic modulus (E > 165000 N/mm$^2$) and used as strengthening material, the commercial name is Sika Carbodur S.

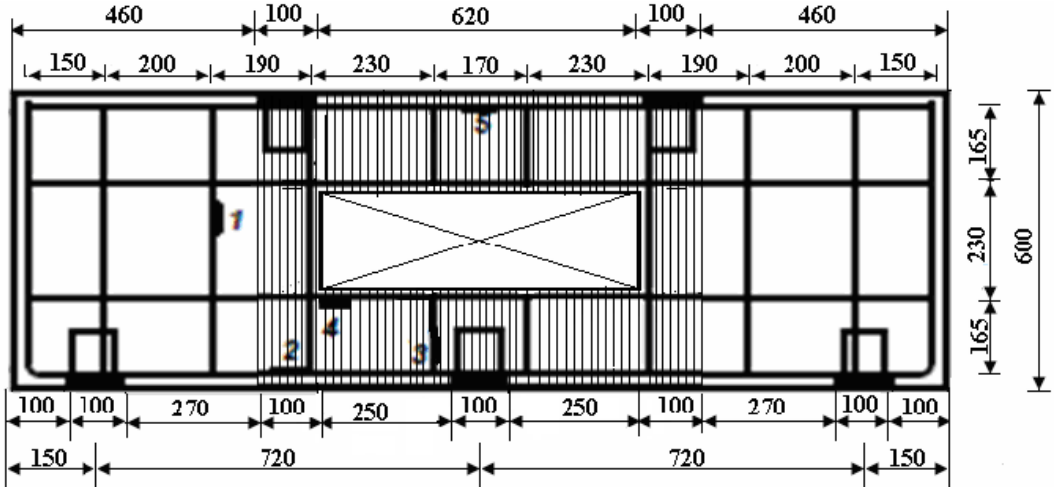


a) Vertical strengthening by CFRP for HS5

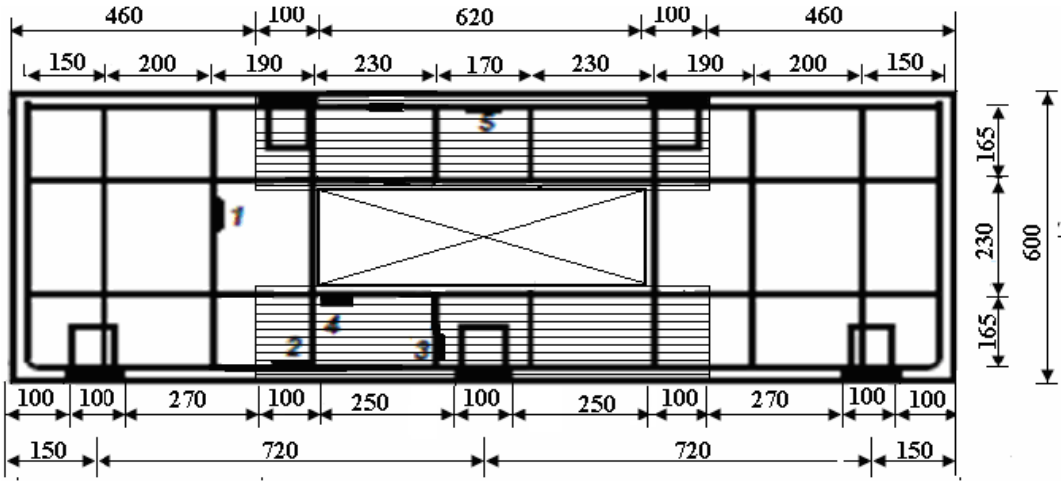


b) Horizontal strengthening by CFRP for HS6

Figure 4 Dimensions and reinforcement details for the beams in the third group (Note: all dimensions in mm)

## TEST RESULTS AND DISCUSSION

Figures 5 to 12 show the crack patterns of the tested beams.

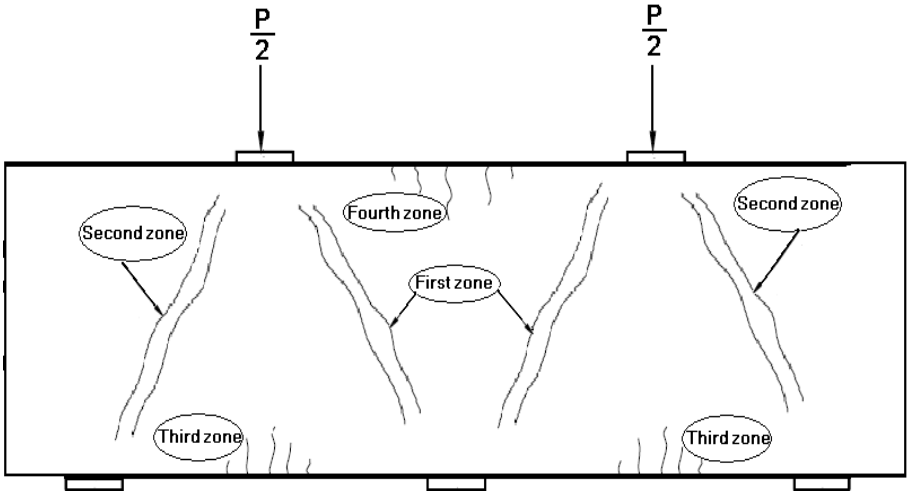


(a)

(b)

Figure 5 Typical cracking of continuous solid deep beams and crack pattern of beam NS

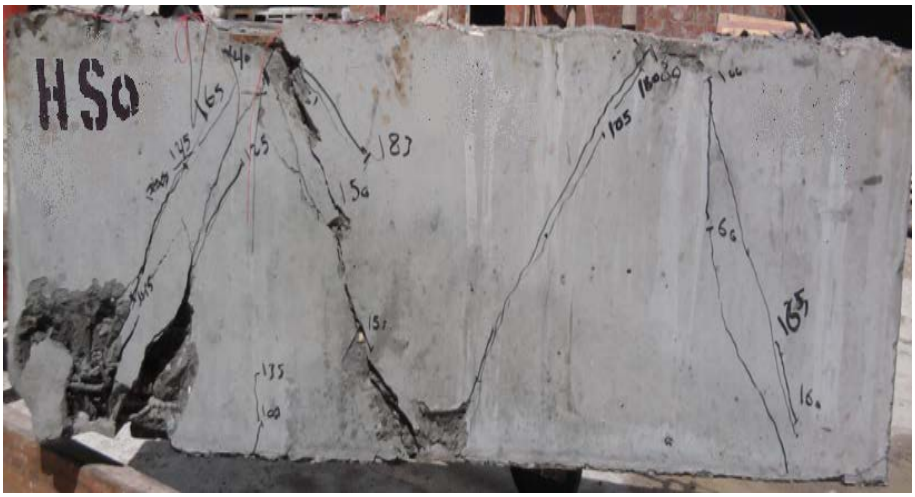


Figure 6 Crack pattern of beam HS0

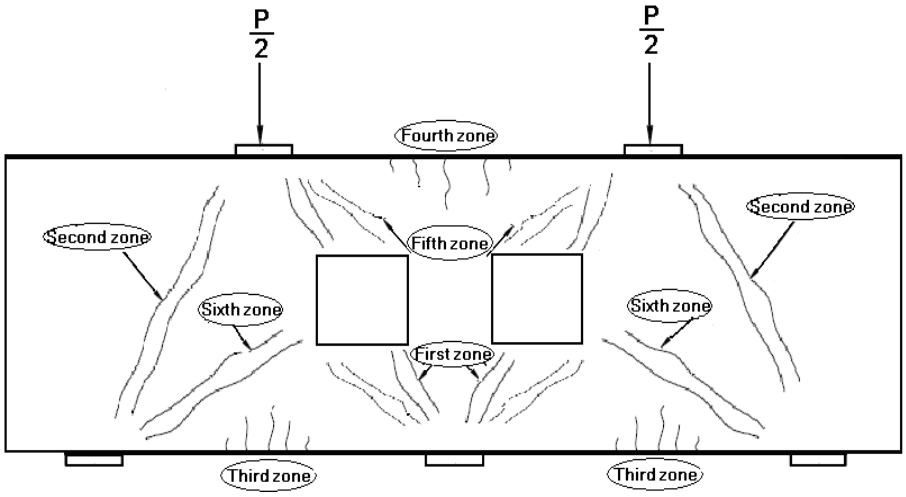


(a)

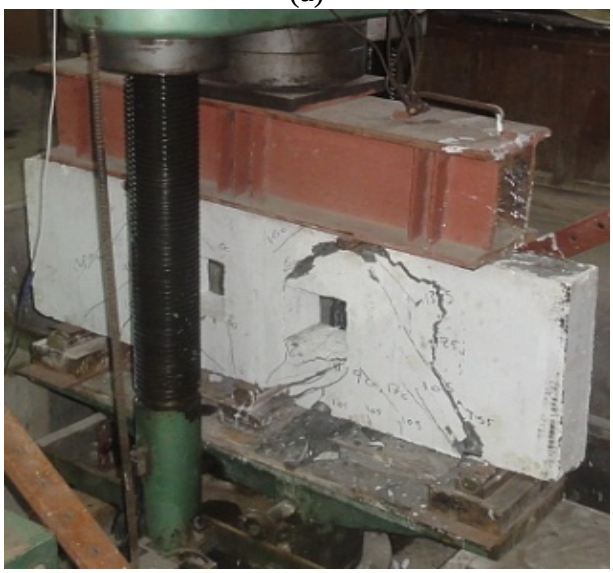

(b)

(c)

Figure 7 Typical cracking of continuous deep beams with two small square openings and crack pattern of beam HS1

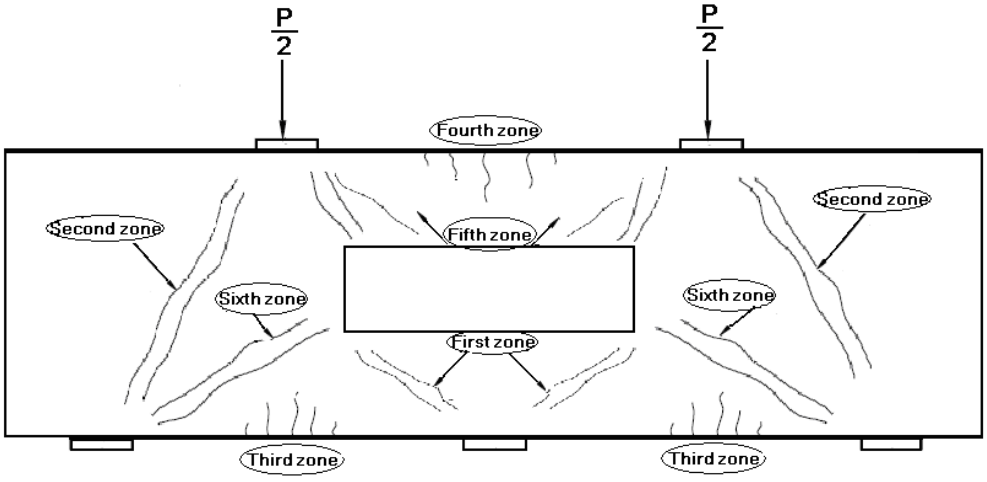


(a)


(b)

Figure 8 Typical cracking of continuous deep beams with two small square openings and crack pattern of beam HS4


Figure 9 Crack pattern of beam HS2


Figure 10 Crack pattern of beam HS3


Figure 11 Crack pattern of beam HS5


Figure 12 Crack pattern of beam HS6

Figures 5-a, 7-a and 8-a show the expected crack patterns for continuous solid deep beams, continuous deep beams with two openings formed near the middle support and continuous deep beam with large rectangular opening centred over the middle support respectively.

Crack patterns of beams at failure indicate that:

- For all beams, flexural cracks did not appear at top surface over the middle support up to failure.
- For solid beams, failure occurred along the diagonal crack extending from the loading point to the exterior end support accompanied by a concrete crushing under the load. The mode of failure is classified as shear failure. It should be noted that the diagonal crack width at mid-height of beam was larger than that at other positions along the diagonal crack.
- For the beam with two square openings with dimensions 200 mm × 200 mm (i.e. height of opening = 1/3 of the beam depth), failure initiated along the strut extending from the load to the inner corner of the opening followed by a sudden failure along the diagonal crack.
- For the beam with a rectangular opening with dimensions 600 mm × 200 mm (i.e. length = 0.85 of shear span each side), sudden failure occurred along the exterior strut extending from the loading plate to the end support accompanied with crushing of concrete under the loading plate.
- For the beams with two square openings and strengthened with vertical strips of CFRP (HS2) or with horizontal layers of CFRP extending the full length of the middle shear spans (HS3), at a load of about 83% of $P_u$, a separation of CFRP strips from concrete started at the strip located under the outer corner of the left opening. This indicated the complete formation of the diagonal crack extending from the middle support to the lower outer corner of the left opening. Sudden failure occurred by crushing of concrete strut extending from the load to top of the left opening with complete debonding of the fibre strips from concrete . After the removal of CFRP strips from the failed zones, it was found that buckling occurred in both horizontal steel located directly above the opening and also in longitudinal top steel above the middle support. Also, diagonal splitting crack occurred at strut extending from the edge of middle support plate to the outer corner of the left opening. At failure the block defined by the diagonal crack from the load to the inner corner of the opening and that from the middle support to the outer corner, rotated about the exterior support and this was observed from the separation of this block from the rest of the beam and buckling of longitudinal bars above the opening. It should be noted that the strips of the fibres under the opening did not have any anchorage length across width due to the type of fibres used. This mode of failure may be classified as shear-compression failure.
- For the beams with large rectangular opening and strengthened with vertical strips of CFRP (HS5) or with horizontal layers of CFRP extending the full length of the middle shear spans (HS6), at a load of about 70 % of $P_u$, a separation of the fibre strips located under the openings started at its left end accompanied with relative movement and separation of fibre strip above the left corner of opening, this strip moved downwards while the other fibres under the opening moved upwards. This may be due to the complete formation of the diagonal crack extending from the middle support to the lower outer corner of the opening. One crack appeared at the line connecting the plate edge of the end support with the outer corner of the bottom surface of the opening at a load of about 38 % of $P_u$. It was obvious that the fibre above the opening did not separate from the concrete surface. Sudden failure occurred along the exterior strut extending from the loading plate to the end support followed by crushing at the concrete. The failure mode was characterized as shear failure.

The values of first shear cracking load $P_{crsh}$ , the ultimate load $P_u$ together with the mode of failure for all beams are given in Table 2.

Table 2 Test results

| SPEC. | CRACKING LOAD | | STEEL YIELD | | FAILURE LOAD | DEFLECTION | | MODE OF FAILURE |
|---|---|---|---|---|---|---|---|---|
| | $P_{cr}$ kN | $P_{crsh}$ kN | $P_y$ kN | $P_{ys}$ kN | $P_u$ kN | $\Delta_{cr}$ mm | $\Delta_u$ mm | |
| NS | 550 | 500 | NY | 1200 | 1400 | 1.44 | 4.20 | shear |
| HSO | 1000 | 600 | NY | 1250 | 2000 | 2.80 | 6.90 | shear |
| HS1 | 1050 | 600 | 1700 | 1000 | 1800 | 2.29 | 5.20 | shear |
| HS2 | ------* | ------* | 1650 | 1100 | 1650 | -------- - | 4.68 | shear-compression |
| HS3 | 1650 | ------* | 1700 | 1000 | 1950 | 4.00 | 5.70 | shear-compression |
| HS4 | 1250 | 400 | NY | 1600 | 1450 | 3.77 | 5.17 | Shear |
| HS5 | 1400 | ------* | 1800 | 1200 | 1850 | 3.04 | 5.54 | Shear |
| HS6 | 1300 | ------* | NY | 1050 | 1900 | 2.30 | 4.71 | shear |

$P_{cr}$ = load at which first flexural cracking occurs (bottom of mid span).
$P_{crsh}$ = load at which first shear cracking occurs (at shear span).
$P_y$ = load at which longitudinal steel yielded (gauge No. 2).
$P_{ys}$ = load at which horizontal or vertical stirrups yielded (gauges No. 1, 3, 4).
$\Delta_{cr}$ = deflection at mid span at $P_{cr}$.
$\Delta_u$ = deflection at mid span at $P_u$.
NY = No Yield.
* Not observed due to the presence of CFRP

Figures 13 - 15 show a comparison of the normalized ultimate load ($P_u/\sqrt{f_{cu}}$) for all the beams tested. Due to the accidental variation in the concrete compressive strength; $f_{cu}$, the values of $P_{crsh}$ are normalized and divided by $\sqrt{f_{cu}}$.

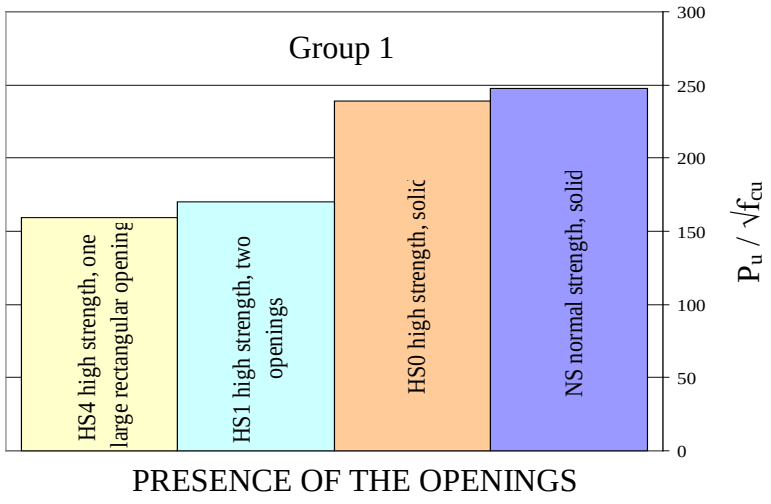


Figure 13 Relation between the normalized ultimate load and the presence of openings

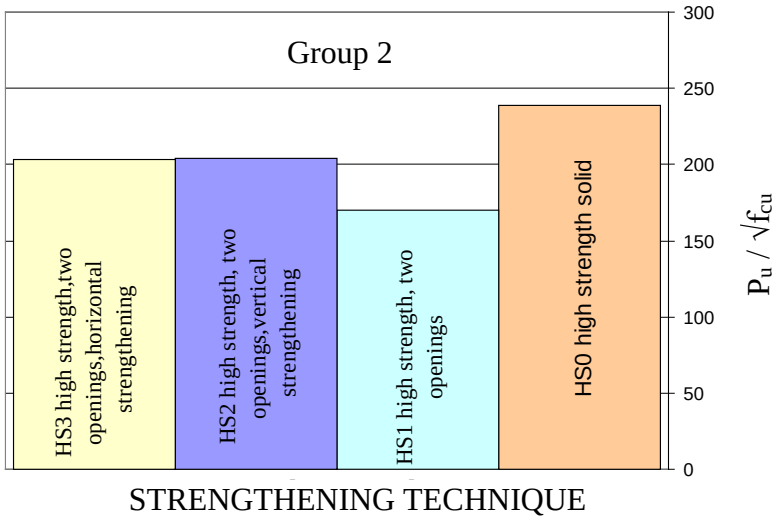


Figure 14 Relationship between the normalized ultimate load and strengthening technique

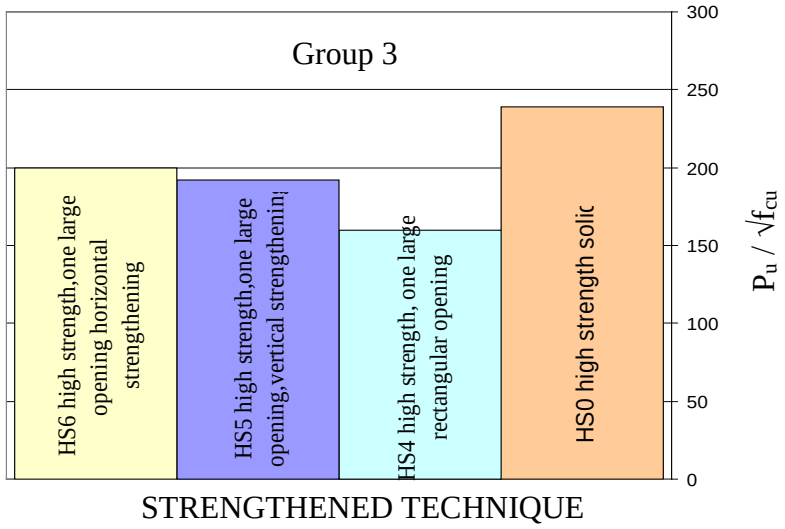


Figure 15 Relationship between the normalized ultimate load and strengthening technique

The results given in Table 2 and shown in Figures 13-15 indicate that:

- The presence of the openings decreased the normalized value of first shear cracking load. However, the ratio of $P_{crsh}$ to $P_u$ was approximately constant and was equal to 30 % for the three beams made of high strength concrete.
- The figures indicate that a 29 % reduction in strength occurred when two square openings were formed at interior shear zones of continuous deep beams. However, when large rectangular opening was formed at middle support, a reduction of strength by 33 % occurred.
- The normalized strength ($\mathbf{P_u/\sqrt{f_{cu}}}$) for both HS2 and HS3 was approximately the same indicating that both techniques of strengthening gave the same enhancement of strength above that of beam HS1 by about 20% as shown in Figure 14. However, the strength of beams strengthened around openings (HS2, HS3) was less than that of a solid beam without

openings (HS0) by about 15%. It was expected that the enhancement of strength using vertical strips of CFRP (beam HS2) would be higher than that when using horizontal strips of CFRP (beam HS3) since, the inclination with the horizontal of the diagonal strut extending from the edge of the middle support plate to outer bottom corner of the opening is less than 45°. However, the poor anchorage of vertical fibre ends under the openings caused some reduction in beam strength.

- As shown in Figure 15, the normalized strength ($\mathbf{P_u/\sqrt{f_{cu}}}$) for both HS5 and HS6 was approximately the same indicating that both techniques of strengthening gave the same enhancement of strength above that of beam HS4 by about 20% for beam HS5 and about 25 % for HS6. However, the strength of beam strengthened around opening was less than that of a solid beam without openings (HS0) by about 20% and 14% for beams HS5 and HS6 respectively.

Figures 16 and 17 show the load-mid span deflection for the four beams in the first group.

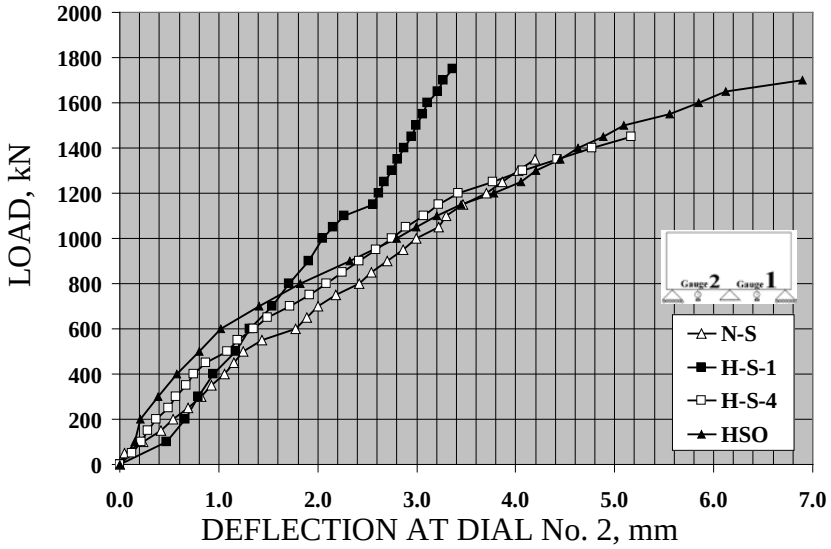


Figure 16 Load-deflection relationship at mid-span – Group 1

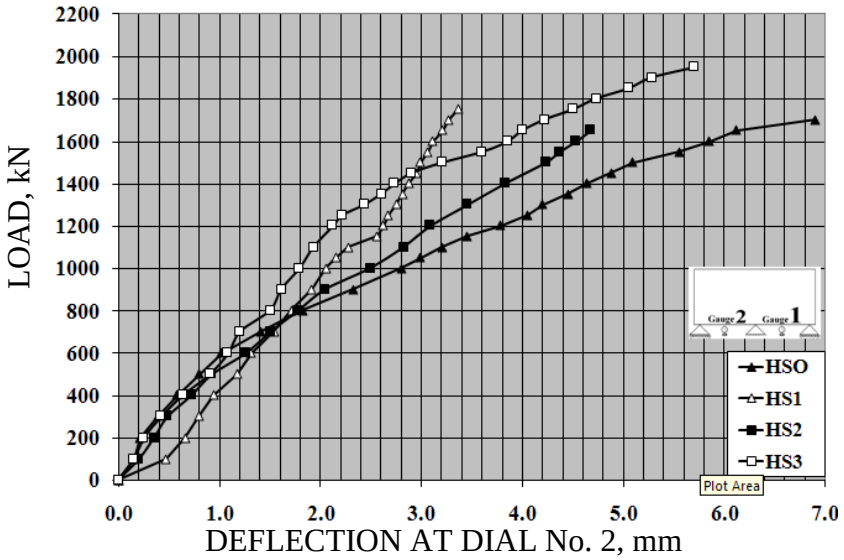


Figure 17 Load-deflection relationship at mid-span – Group 2

Generally, the load - deflection relationship was approximately similar for the four beams. It should be noted that flexural cracking and consequently mid-span deflection for deep beams is not significant since the behaviour is controlled mainly by shear cracking and shear stresses. Also, the value of ($L_e$ / d) in this study was 1.25, which was much smaller than that allowed by the Egyptian code ($L_e$ / d ≤ 2.5) and this may explains small values of measured deflection.

As indicated in Table 2, the value of $\Delta_u$ / $\Delta_{cr}$ was 1.37 for beam HS4, with large rectangular opening, while it was 2.46 for the beam HS0, without opening. This may be due to the small value of shear cracking load for beam HS4 and consequently high value of flexural cracking load. Furthermore, the failure load for beam HS4 was smaller than that of HS0.

Table 2 gives the values of load at which longitudinal steel yielded; $P_y$ together with that at which horizontal or vertical stirrup yielded $P_{ys}$. Figures 18 to 20 show the load-steel strain relationship at all positions of strain gauges (Figure 2).

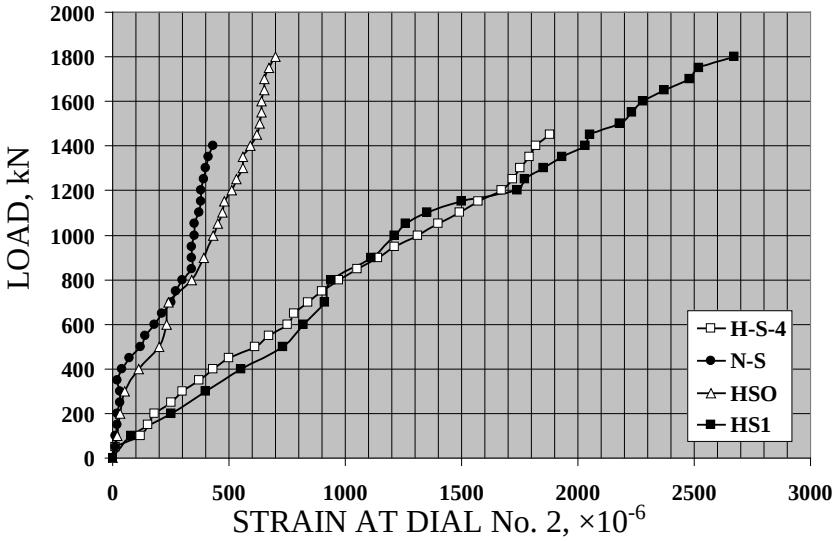


Figure 18 Load – steel strain relationship for longitudinal steel mid-span, Group 1

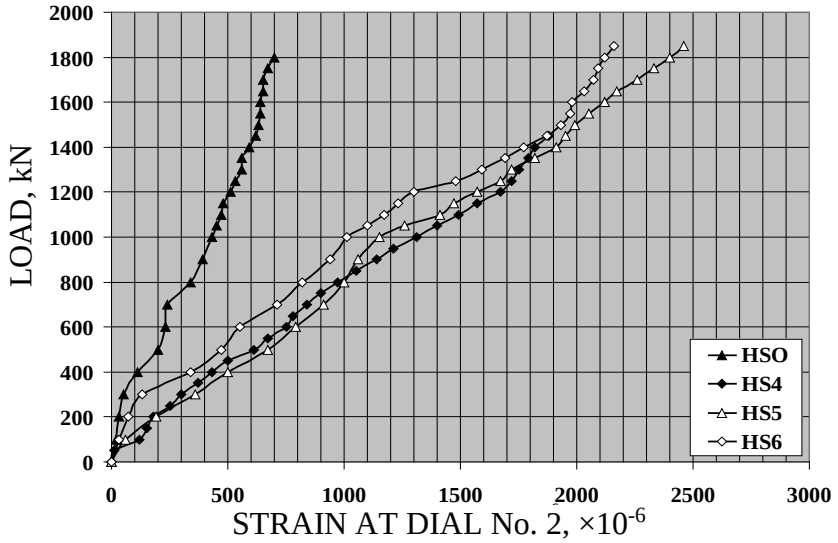


Figure 19 Load – steel strain relationship for longitudinal steel mid-span, Group 3

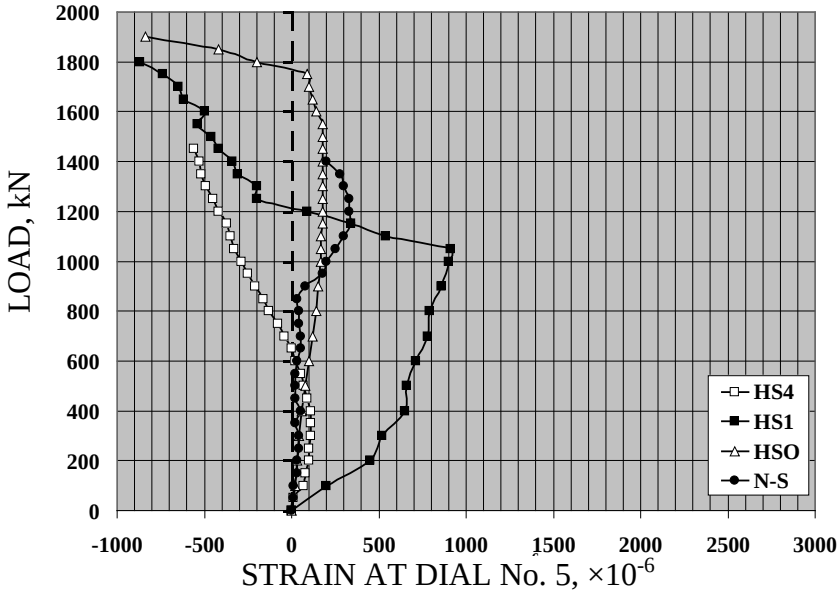


Figure 20 Load – steel strain relationship for top longitudinal steel over middle support, Group 1

Results of steel strains indicated that:

- Yield in bottom mid-span longitudinal steel occurred in all beams with openings, except beam HS4 with large rectangular opening and without strengthening.
- The strain recorded by the gauge mounted on the top longitudinal bars over the middle support was tensile and then reduced gradually and changed to compressive strain up to failure, as shown in Figure 20 for Group 1. This may be due to the progressive occurrence of diagonal cracks around the openings which result in redistribution of forces in the beam and the beginning of the formation of compressive strut at the top surface of the beam between the two loading points.
- For solid beams without opening, the first yield in stirrups occurred in the vertical stirrups at which diagonal crack passed (gauge No.1 at the exterior shear span). For beams with openings the first yield occurred in the horizontal stirrup located below the opening (gauge No. 4) at which cracking of zone one occurred.
- For beams HS3 and HS4 (without strengthening), yield was also recorded in the interior vertical stirrup (gauge No. 3) at interior shear span.

## Comparison of the Experimental Results with Code Predictions

The failure loads for some of the deep beams tested in the present study (beams NS, HS0, HS1) were calculated using some of the building codes (ECP 2007, ACI 318-99 and BS 1997) and also using the equations developed by Ashour and Rishi [4] for deep beams with openings. The calculated values were compared to the experimental ones as given in Table 3.

Table 3 Comparison of test results with code predictions

| BEAM | FAILURE LOAD* $P_{uexp}$ kN | ACI 318-08 [6] | | ECP 203-2007 [5] | | BS 8110-97 [7] | | Ashour and Rishi [4] | |
|---|---|---|---|---|---|---|---|---|---|
| | | $P_{uth}$ kN | $P_{uth}/P_{uexp}$ | $P_{uth}$ kN | $P_{uth}/P_{uexp}$ | $P_{uth}$ kN | $P_{uth}/P_{uexp}$ | $P_{uth}$ kN | $P_{uth}/P_{uexp}$ |
| NS | 1400 | 1484 | 1.06 | 994 | 0.71 | 1134 | 0.81 | ---- | ---- |
| HS0 | 2000 | 1760 | 0.88 | 1020 | 0.51 | 1240 | 0.62 | ---- | ---- |
| HS1 | 1800 | ---- | ---- | ---- | ---- | ---- | ----- | 1404 | 0.78 |

* experimental
$P_{uth}$ = ultimate theoretical shear strength which is less than the flexural strength.

It should be noted that:

- All code equations and equations developed by Ashour and Rishi [4] were recommended for deep beams made of normal strength concrete.
- ACI 318-08 code [6] does not include equations for the shear strength of deep beams, however, the code permits strut-and-tie models as well as methods that take into account the nonlinear distribution of strains for design.
- The limitation of the value given by both the Egyptian code and ACI for $[3.5\text{-}2.5M_u/V_ud]$ was considered 1.9 and 2.5, respectively, this difference resulted in values of shear strength predicted by the Egyptian code smaller than that calculated by ACI.

The results given in Table 3 indicate that:

- For normal strength solid deep beams, the ACI equations predicted well the shear strength of the beams. Both the Egyptian code and BS code recommendations seem to underestimate the shear strength of the beam by 29% and 19% respectively.
- For high strength solid deep beams, the compared codes seem to underestimate the shear strength of the beam. The Egyptian code extremely underestimates the strength by 50%.
- The equations developed by Ashour and Rishi for normal strength deep beams with interior openings underestimate the shear strength by 22%.

Generally, the building codes used for comparisons were conservative in estimating the shear strength of both normal strength concrete beams and high strength beams; however, the ACI code 318-99 gave reasonable predictions for the shear strength of the beams.

## CONCLUSIONS

Based on this study and for the beams considered with ($L_e/d=1.25$), the following conclusions may be drawn:

1. The formation of diagonal cracks in continuous deep beams started at mid-depth along the line connecting the loading plate and the support plate then propagated gradually towards both the loading plate and the supporting plate accompanied by the formation of other lines of parallel diagonal cracks. Finally, for continuous solid deep beams failure occurred by shear along the strut connecting the loading plate with the exterior support plate.

2. For continuous deep beams with central openings, the failure occurred by shear along the exterior strut. Failure took place after the complete formation of wide diagonal cracks under the openings starting from the edge of the centre support plate and was accompanied by wide diagonal cracks starting from the opening corner towards the loading plate.

3. The failure of CFRP strengthened continuous deep beams with small square openings was by shear-compression initiated by diagonal shear failure along the strut connecting the loading plate edge and the inner corner of the square openings. However, the failure of CFRP strengthened continuous deep beam with large rectangular opening was similar to that of the un-strengthened beams.

4. The presence of openings resulted in a significant reduction of the ultimate shear strength of continuous high strength concrete deep beams. Such reduction in the ultimate shear strength was in the range of 29% in the case of two square openings within the interior shear spans and in the range of 33% in the case of large rectangular opening at the middle support region.

5. The application of CFRP strips as a strengthening technique was found to be efficient in enhancing the ultimate shear strength of continuous high strength concrete deep beams with openings. Such enhancement was in the range of 20% in the case of two square openings within the interior shear span and in the range of 25% in the case of large rectangular opening at the middle support region.

## REFERENCES

1. YANG K.H., CHUNG H. and ASHOUR A.F., Influence of Inclined Web Reinforcement on Reinforced Concrete Deep Beams with Openings, ACI Structural Journal, Vol. 104, No. 5, September-October 2007, pp. 580–589.

2. TAN K.H., TONG K. and TANG C.Y., Consistent strut-and-tie modeling of deep beams with web openings, Magazine of Concrete Research, Vol. 55, No. 1, 2003, pp. 572–582.

3. SMITH K.N. and VANTSIOTIS A.S., Shear Strength of Deep Beams, ACI Structural Journal, Proceedings Vol. 79, No. 3, May-June 1982, pp. 201–213.

4. ASHOUR A.F. and RISHI G.R., Tests of Reinforced Concrete Continuous Deep Beams with Web Openings, ACI Structural Journal, Vol. 97, No. 3. May-June 2000, pp. 418–426.

5. ECP 203-2007, Egyptian Code for design and construction of RC buildings, The permanent committee for Egyptian Code, 2007.

6. ACI 318-08, Building Code Requirements for Structural Concrete (318-02), American Concrete Institute, USA, 2008.

7. BSI, BS 8110, Structural Use of Concrete — Part 1: Code of Practice for Design and Construction, British Standard Institute, UK, 1997.

# INFLUENCE OF FIBRE REINFORCEMENT TYPE ON DYNAMIC PROPERTIES OF SLURRY INFILTRATED FIBRE CONCRETE

**M Drdlová** **R Čechmánek**
Research Institute for Building Materials
**R Řídký**
SVS FEM Ltd
Czech Republic

**ABSTRACT.** The contribution is dealing with dynamic characteristics of concrete reinforced with high volume of fibres intended for blast resistant applications. An experimental research aimed at contributing to understanding of the effect of different type of reinforcement on the behaviour of high performance slurry infiltrated fibre concrete (SIFCON) subjected to dynamic load was carried out. SIFCON is a special type of cement-based composite with high fibre volume fraction, extremely strong and ductile. Test specimens were prepared with 7 types of steel fibres (with different shape and mechanical parameters) in four volume fractions (7.5-15 vol. %). High performance fibre-reinforced concrete (HPFRC) has also been cast and tested for comparison purposes. The impact test has been carried out by using an in-house manufactured impact testing machine based on drop test principle. The test results revealed that SIFCON slab with 15 vol. % fibre content exhibits superior energy-absorption characteristics when compared to other slab specimens. Diameter of the fibres plays an important role for both strength and energy absorption capacity of SIFCON - using of low-diameter fibres with higher aspect ratio leads to the best results.

**Keywords:** Steel fibre, Slurry infiltrated fibre concrete, Drop test, Impact loading, Energy absorption.

**Martina Drdlova** is research specialist employed in Research Institute for building materials in Brno, Czech Republic.

**Rene Cechmanek** works in the Research Institute for Building Materials and is a head of the department Applied research and development with the special aim to fibre-cement composites and utilization of industrial waste materials.

**Radek Řídký** is specialist in numerical simulation (FEM) employed in company SVS FEM.

## INTRODUCTION

Concrete structures may be subjected to dynamic loads arising from impact by external projectiles, impulsive loads induced by blast and wind gusts or accidental explosions. The characteristics of the impact load are a high loading rate and very short period that cause high strain rate in the structure.

Mechanical properties of materials are different under impact loading compared to static loading [1]. In the past few years, investigations have been carried out to understand the behaviour of concrete and concrete-based composites under impact loading. Ramakrishnan et al. [2] studied the effect of low volume fraction of steel fibres in fibre-reinforced concrete (FRC) and reported that the impact resistance is about six folds compared to non-fibrous concrete. Song et al. [3] reported the improved performance of static evaluation of impact resistance for steel fibre-reinforced concrete over non-fibrous concrete. Zhang et al. [4] presented the flexural toughness and impact resistance of steel fibre-reinforced light-weight concrete, and the results indicate that the high compressive strength and density are desirable for good impact resistance of plain concrete and also reported that the incorporation of steel fibres improved the impact resistance substantially. Effect of different kinds of fibre reinforcement on blast resistance and mechanical performance of the concrete samples was evaluated in [5].

SIFCON was first developed in 1979 by Lankard Materials Laboratory, Columbus, Ohio, USA, by incorporating large amounts of steel fibres in steel fibre reinforced cement-based composites [6]. It possesses excellent mechanical properties coupled with very good energy-absorption characteristics. The fibre volume fraction of traditional fibre reinforced concrete is limited, because excessive amount of the fibres affects the workability of the fresh concrete in a negative way. This limits the fibre volume $V_f$ to 1 - 5%, depending on the type of fibre used and the required workability of the mixture. SIFCON specimens can be produced with $V_f$ between 5% and 30% [6, 7]. The fibre volume depends on the fibre geometry, length and diameter and vibration of the fibres during their placement process. The other major difference is in the composition and casting process of the composite. SIFCON is prepared by infiltrating pre-placed fibres with fine grain aggregate mortar. It has been reported that SIFCON slab elements exhibit excellent behaviour in flexure and punching shear when compared to HPFRC, reinforced cement concrete (RCC) and plain cement concrete (PCC) slabs [8] and [9]. Due to extraordinary ductility of SIFCON, it seems to be very promising material for applications in structures subjected to impact load, but the literature review reveals only a few studies dealing with the SIFCON under dynamic loading. The results of further presented investigation carried out on SIFCON slab panels under impact loading can bring significant contribution to the current knowledge in the field.

## EXPERIMENTAL

### Raw Materials and Preparation of Specimens

Specimens with various types of dispersed fibre reinforcement were prepared. Fine $SiO_2$ sand with grain size of 0-1 mm, cement CEM 52.5R and water were the main components of the slurry mixture. Superplasticizer Glenium 422 (produced by BASF) was added to achieve good workability with low water/binder ratio.

High dosage of silica fume Elkem 940U (produced by Elkem), with a typical particle size 100–500 nm, was used to create an optimized particle packing density and also for its pozzolanic properties. The mix proportion of the slurry is given in Table 1.

Table 1 Mix proportion of concrete mixture (kg/m$^3$) without fibres

| DESIGNATION | CEMENT CEM 52.5R | FINE AGGREGATE | SILICA FUME | SUPERPLASTICIZER | WATER |
|---|---|---|---|---|---|
| SIFCON | 990 | 670 | 78 | 10 | 320 |
| HPFRC | 929 | 701 | 51 | 9.4 | 303 |

Seven types of steel fibres were used as a reinforcement to determine influence of their shape and mechanical parameters on physico-mechanical properties and responses to impact loading. The fibres with hooked ends (producer KrampeHarex) were selected, as previous studies revealed their best performance in the composite in term of production technology [6, 10]. Table 2 summarizes the shape and strength parameters of the fibres. Steel moulds were used to cast the specimens. Moulds were treated with releasing agent and sealed at the edges by using silicone to prevent any leakage of cement–sand slurry from the mould. Seven types of mixtures with different fibre reinforcement were prepared (the volume fraction of the fibres was kept constant), another 4 types of mixtures were manufactured with different fibre amount: 7.5, 10.0, 12.5 and 15.0 vol. % (the type of fibre DE 50/08 was kept constant). The manufacturing process involved pre-placing of the steel fibres into the mould with subsequent pouring of the slurry over the pre-placed fibres. The mixing procedure of the reference specimen HPFRC was as follows: metallic fibres DE 30/06 N (4 vol. %) were first mixed into the dry mixture of cement, sand and microsilica, then required quantity of water with plasticizer was added. The composition of the mixture is given in Table 1. The test specimens were demoulded after 24 hours and were cured for 28 days in curing water ponds. The overall microstructure of the specimens is shown in Figure 2.

Table 2 Properties of fibres

| DESIGNATION | LENGTH mm | DIAMETER μm | ASPECT RATIO | TENSILE STRENGTH MPa |
|---|---|---|---|---|
| DE 30/06 N | 30 | 0.60 | 50.0 | 1,250 |
| DE 30/08 | 30 | 0.80 | 37.5 | 1,200 |
| RB 80/50 BN | 50 | 0.60 | 83.3 | 1,200 |
| DE 50/08 | 50 | 0.80 | 62.5 | 1,250 |
| DE 60/075 | 60 | 0.75 | 80.0 | 1,200 |
| DE 50/1 | 50 | 1.00 | 50.0 | 1,100 |
| DE 30/06 H | 30 | 0.60 | 50.0 | 2,400 |

### Quasi-static Mechanical Tests and Bulk Density

For the bulk density, compressive and flexural strength investigation the prism specimens 400×100×100 mm were cast. The mechanical parameters were obtained using universal strength testing machine TIRAtest 2710, R58/02. The compressive and flexural load was applied in quasi-static conditions at speed of 5 mm/min. The testing works were performed at the room temperature of 20°C and relative humidity equal to 55%, i.e. within the range of the recommended conditions for testing of composites. The overall results of the quasi-static mechanical test are presented in Table 3 and 4, the average value of five specimens is presented.

Table 3 Physico-mechanical properties of SIFCON with different fibre reinforcement

| DESIGNATION | COMPRESSIVE STRENGTH MPa | BULK DENSITY kg/m$^3$ | FLEXURAL STRENGTH MPa |
|---|---|---|---|
| DE 30/06 N | 126.5 | 2,474 | 30.8 |
| DE 30/08 | 120.9 | 2,485 | 25.7 |
| RB 80/50 BN | 119.5 | 2,477 | 29.5 |
| DE 50/08 | 128.6 | 2,455 | 25.6 |
| DE 60/075 | 120.7 | 2,490 | 29.0 |
| DE 50/1 | 128.9 | 2,470 | 24.6 |
| DE 30/06 H | 122.6 | 2,450 | 31.3 |
| HPFRC | 101.4 | 2,200 | 14.2 |

Table 4 Physico-mechanical properties of SIFCON with different volume fraction of the fibres

| DESIGNATION | COMPRESSIVE STRENGTH MPa | BULK DENSITY kg/m$^3$ | FLEXURAL STRENGTH MPa |
|---|---|---|---|
| DE 30/06 N/7.5 | 122.5 | 2,432 | 25.6 |
| DE 30/06 N/10 | 126.5 | 2,474 | 30.8 |
| DE 30/06 N/12.5 | 135.9 | 2,647 | 32.7 |
| DE 30/06 N/15 | 129.5 | 2,877 | 29.9 |

Compressive strength of SIFCON is not significantly affected by the fibre type (see Table 3), considering the deviations it can be concluded that all specimens perform similarly. With increasing amount of fibres, the compressive strength slightly increases as well up to the 12.5 vol. %. The addition of 15 vol. % of the fibres have not brought further compressive strength enhancement. Flexural strength was affected both by the geometry and amount of the fibres, using of fibres with lower diameter has led to higher values of flexural strength. Regarding the fibre amount, raising of the fibre volume fraction has caused significant increase of the flexural strength, with the maximum at 12.5 vol. %.

**Drop Test Setup and Testing**

The impact test has been carried out by using an in-house manufactured impact testing machine. The detail of test setup used for conducting impact test on slabs can be described as follows. The device has been designed as a massive vertical steel rod with rectangular cross section with two collars, through them a steel rod with the spherical ending is passed. The rod is fitted with the cylindrical weight, which can be freely vertically moved along the guiding rod. During the test, the weight is hitting the centre of the slab specimen (400×400×40 mm) through the sphere end of the steel rod. The test has been adjusted as follows: height of drop 700 mm, weight 25 kg, repeating of the process up to reaching the ultimate failure stage. The total absorbed energy is obtained using the following formula:

$E = m \times a_g \times h \times x$

Where:

E…Total absorbed energy [J]
m…Weight of the impactor [g]
$a_g$…Gravity acceleration [$m \times s^{-2}$]
h…Height of drop [m]
x…Number of the drops [-]

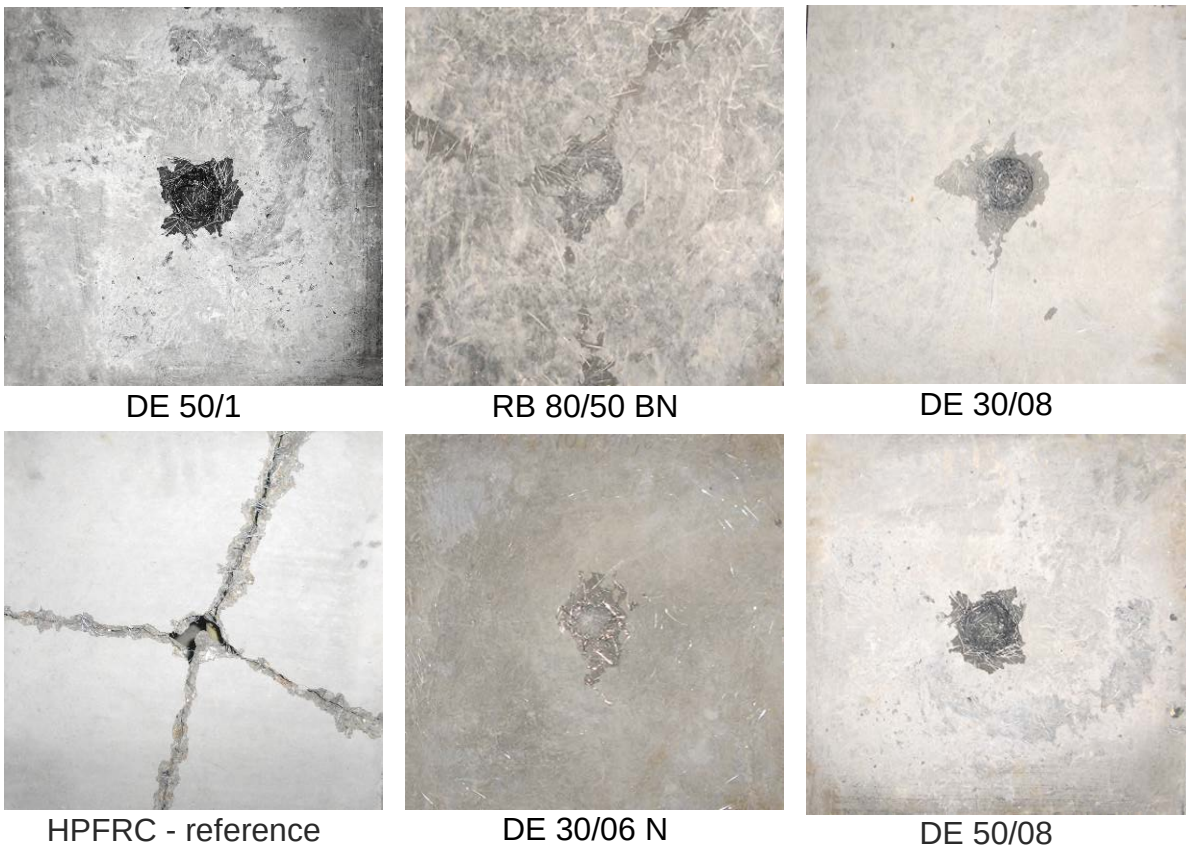


Figure 1 Selected slabs after drop test – different failure modes

A comparison of total energy-absorption capacities of different slab specimens at ultimate impact strength stages is presented in Figure 3. It can be concluded, that the fibre geometry has got significant influence on the impact behaviour of the whole composite and its energy absorption capacity. All the SIFCON slabs has overcome the HPFRC reference specimen with total absorbed energy 95.2 J. The fibre diameter seems to be the most important parameter

which must be taken into consideration when design the SIFCON composite – the lower the fibre diameter, the higher absorbing capacity was measured. The best value of total absorbed energy 19,158.2 J was achieved in the case of RB 80/50 BN specimen (fibre diameter 0.6, aspect ratio 83.3). The other specimens with incorporated fibres of low diameter (DE 30/06 N, DE 30/06 H) performed great as well – the achieved values of total absorbed energy were 18,536.5 and 18,650.4, respectively. The energy of 16,839 J was calculated for the specimen DE 60/075 (fibre diameter 0.75). A comparison of the damage of selected slab specimens under impact loading is presented in Figure 1. Different failure modes were identified, specimens with low-diameter fibres have shown less damage (only cracks and surface damage), when compared to the slabs with high-diameter fibres (hole with disturbance in surrounding of the point of impact). This fact is caused by better reinforcing effect of the fibres with lower diameter – the same volume of fibres contains more fibres, so they are more homogeneously distributed within the concrete. Less areas between the fibres remain unreinforced and thus brittle.

Two specimens reinforced with fibres with the same geometry but different tensile strength were used to assess the influence of the fibre mechanical properties on the impact behaviour of the whole composite. Almost the same values of total absorbed energy were achieved for both specimens and the failure mode was identical as well. It can be concluded, that the response to impact load is not influenced by the fibre tensile strength for tested strain rate, but further tests with more fibres with different tensile strength are necessary to confirm this hypothesis. The investigation of the influence of the fibre tensile strength on the behaviour of SIFCON at very high strain rates (real blast impact) will be conducted as the next step as well.

Table 5 Total absorbed energy as the function of the fibre volume fraction

| DESIGNATION | FIBRE VOLUME FRACTION % | TOTAL ABSORBED ENERGY J |
|---|---|---|
| S7.5 | 7.5 | 3,985 |
| S10.0 | 10.0 | 4,770 |
| S12.5 | 12.5 | 6,216 |
| S15.0 | 15.0 | 8,100 |

Evaluating the effect of the fibre amount, the slab with 15% fibre volume shows least damage and the highest energy absorption capacity compared to the other three, i.e., slabs with 7.5, 10 and 12.5% fibre volume, see Table 5. There is no disturbance surrounding the point of impact on S15.0 specimen. The damage increases with the decrease in the fibre volume content.

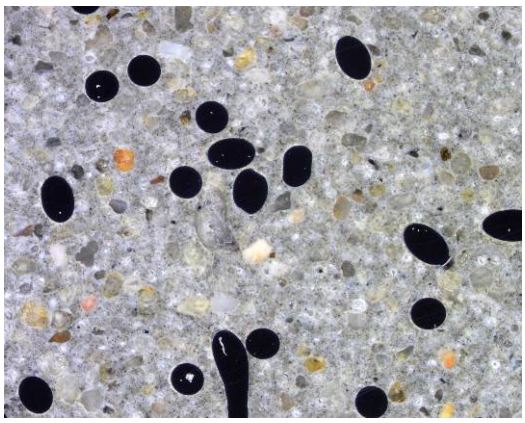

Figure 2 Microstructure of the DE 30/06 spec.

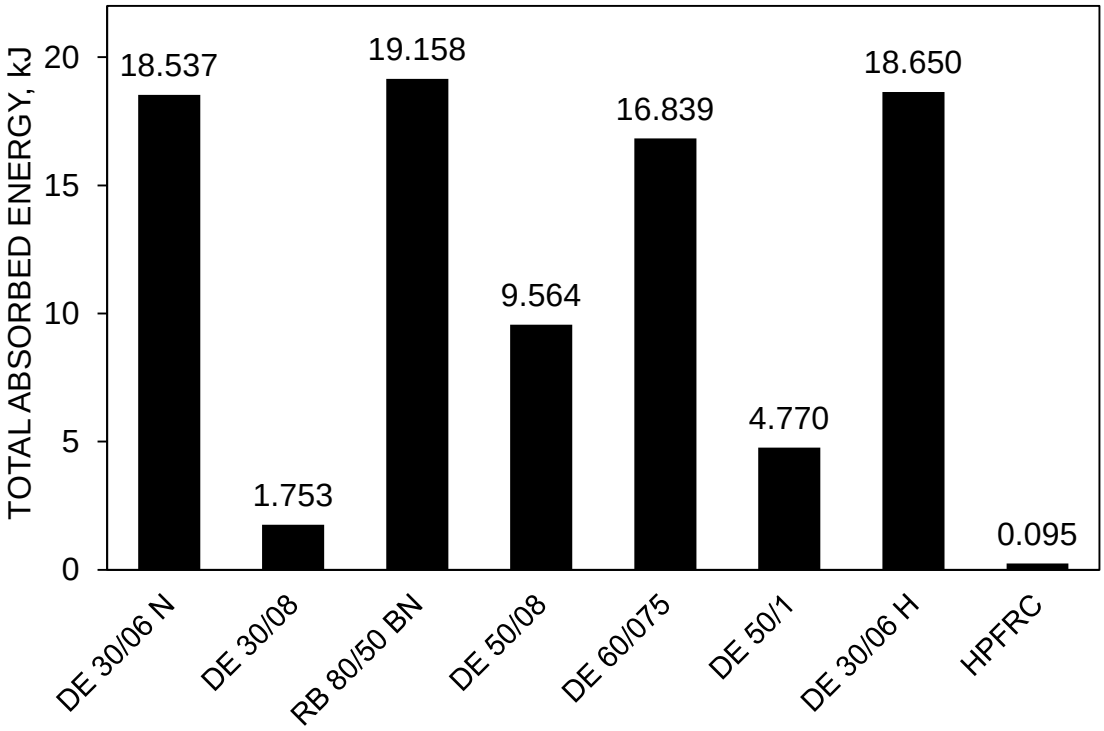


Figure 3 Comparison of total absorbed energy

## CONCLUSIONS AND SUMMARY

This study summarizes the results of the research focused on dynamic behaviour of slurry infiltrated fibre concrete. SIFCON slabs with different fibre geometry, mechanical parameters and volume fractions have been produced and tested under quasi-static and impact loading. The following conclusions can be drawn:

- The superiority of all SIFCON slabs (in term of strength and energy absorption capacity) over HPFRC slab was demonstrated.

- Ascending trend with increasing fibre amount was observed in both quasi-static compressive and flexural strength up to 12.5 vol. %, steeper trend in flexural behaviour was noted in contrast to the compressive failure. Crossing the 12.5 vol. % of fibre, the significant strength drop was observed due to excessive amount of fibres leading to worsen homogeneity of the whole composite.

- Fibre geometry does not affect the compressive strength, but influences the flexural strength significantly. SIFCON with the fibres with lower diameter showed higher values of flexural strength.

- The choice of the fibre geometry is a key factor for achieving a high level of SIFCON impact resistance and energy absorption capacity. Using low-diameter fibres leads to higher total absorbed energy due to better distribution of fibres within the composite.

- There is a relation between the flexural strength of the SIFCON and its total absorbed energy. The higher the flexural strength value, the better is the absorption capacity of the composite.

- Energy-absorption capacity of SIFCON slabs increases with increase of fibre volume.

- The damage in HPFRC slabs is comparatively higher than that in SIFCON slabs, the failure mode of SIFCON slabs under the impact load is possible to be modified by fibre geometry selection.

- Tensile strength of the fibre does not influence both quasi-static and dynamic properties (at the tested strain rates) of the SIFCON. Further investigations will be carried out at higher strain rates (blast tests) to complete data about the dynamic response of SIFCON with different fibre reinforcement.

## ACKNOWLEDGEMENTS

The authors wish to express their gratitude and sincere appreciation to the authority of The Technology Agency of the Czech Republic, project No. **TE02000162** for financial support.

## REFERENCES

1. SUDARSANA, H R, VAISHALI, G G, RAMANA, N V, GNANESWAR, K. Response of SIFCON two-way slabs under impact loading, International Journal of Impact Engineering, Vol 37, No. 4, 2010, p. 452–458.

2. RAMAKRISHNAN, V, COYLE, W V, KULANDAISAMY, V, SCHRADER, E K. Performance charactaristics of fiber reinforced concrete with low fibre content, ACI Journal, Vol. 78, No. 5, 1981, p. 388–394.

3. SONG, P S, HWANG, S, SHEU, B C. Statistical evaluation for impact resistance of steel fibre-reinforced concretes, Magazine of Concrete Research Journal, Vol. 56, No. 8, 2004, p. 437–442.

4. ZHANG, M H, LI, L, PARAMASIVAM, P. Flexural toughness and impact resistance of steel fibre-reinforeced light weight concrete, Magazine of Concrete Research, Vol. 56, No 5, 2005, p. 251–262.

5. DRDLOVÁ, M, BUCHAR, J, KRÁTKÝ, J, ŘÍDKÝ, R. Blast resistance characteristics of concrete with different fibre reinforcement, Structural concrete, Vol. 16, No. 4, 2015, p. 508-517.

6. LANKARD, D R. Preparation, Applications: Slurry Infiltrated Fiber Concrete (SIFCON), Concrete International, Vol. 6, Issue 12, 1984, p. 44-47.

7. HOMRICH, J R, NAAMAN, A E. Stress-Strain Properties of SIFCON in Compression, Fiber Reinforced Concrete - Properties and Applications, ACI SP-105, American Concrete Institute, Detroit, Michigan, 1987, p. 283-304.

8. SUDARSANA RAO, H, RAMANA, N V. Behaviour of slurry infiltrated fibrous concrete (SIFCON) on simply supported two way slabs in flexure, Indian Journal of Engineering Material Science, Vol. 12, 2005, p. 427–433.

9. SUDARSANA RAO, H, RAMANA, N V, GNANESWAR, K. Behaviour of steel reinforced slurry infiltrated fibrous concrete (SIFCON) two way slabs in punching shear, Indian Journal of Engineering Material Science, Vol. 15, 2008, p. 334–342.

10. GILLANI, A D. Various durability aspects of slurry infiltrated fibre concrete, PhD thesis, 2007, School of Natural and Applied Sciences of Middle East Technical University, Ankara, Turkey.

# NON-LINEAR ANALYSIS OF CELLULAR COMPOSITE BEAMS UNDER POSITIVE BENDING

**M Mimoune**

**S Siouane**

**F Z Mimoune**

Constantine University

Algeria

**ABSTRACT.** The behaviour of cellular composite steel-concrete beams depends, most of the interaction between the steel beam and the concrete slab, the presence of openings in the web of the steel beam. These openings according to size and location introduce additional failure modes for typical beams. The connection in the presence of the slip at contact interface greatly influences the global behaviour of the beam, and its modelling in the presence of webs openings is a key issue in the analysis of these composite structures. A finite element model may provide a better understanding of an explicit relation is strongly non-linear between the slip and the shear force given by the connectors. In this article, numerical modelling in 3-D finite element was done to study cellular composite beams simply supported subjected when positive bending due to concentrated loads at mid-span.

**Keywords:** Steel-concrete beams, Cellular composite beams, Finite element modelling, Non-linear analysis

**Professor Mostefa Mimoune,** Professor of Civil Engineering, is interested in steel construction, steel concrete and rehabilitation of construction. Has published on many aspects of steel, steel concrete and rehabilitation.

**Saâd Siouane**, researcher PhD student at the University of Constantine.

**Professor Fatima Z Mimoune,** Professor of Civil Engineering, is interested in steel construction and steel concrete. Has published on many aspects of steel and steel concrete.

## INTRODUCTION

The use of steel-concrete structures results in optimal performance of the two materials (tension in steel and compression in the concrete); but in the design process, it is necessary to evaluate the influence of the connection of the behaviour of the structural members, and therefore, slippage between the steel beam and the concrete slab cannot be neglected, as it is suggested by the most advanced code in steelwork EC-4 [6].

In the cellular composite beams, the discontinuity in the cross section of the metal beam, due to the presence of openings of the web may have a reduction of the flexural capacity of these beams. Therefore, the design of the beams may be based on the concept of partial connection with a transversal rigidity discontinued.
From the preceding, it is evident that:

1. The modelling of the structural behaviour of steel-concrete beams is complex, and must necessarily consider the slip between the concrete slab and the steel beam and the constitutive relationship of the shear connectors, which is strongly non-linear [1].

2. The behaviour in terms of deformability and strength of composite beams depends directly on the distribution of the slip and the consequent interaction force between the slab and the steel beam.

In this work based on the same principles used by Fabbrocino et al. [1] in ordinary composite beams, numerical modelling is proposed for cellular composite beams using software ANSYS v.12.1 [7]. The introduction of the moment-curvature relationship for the perforated cross-section is used to analyse the structural behaviour of composite beams, is varied degree of connection (number of studs) with non-linear properties of materials to optimize design of this type of structure.

This model is validated by similar models ordinary composite beams (solid web profile) existing in the literature [1]; a beam on two supports subjected to a concentrated load at mid-span.

## THE CONSTITUTIVE RELATIONS OF MATERIALS:

Our cellular composite beam is extracted from the test beam "**PI4**" of *Abdel Aziz* [1], this beam is formed by a steel beam the IPE 400 (Oxygen cutting that gives the optimum height of section $h_t$=600mm, with 8 openings), and the reinforced concrete slab of 800x100mm associated with a mechanical connection with the stud head, the geometrical characteristics of the beam is illustrated in Figure 1.

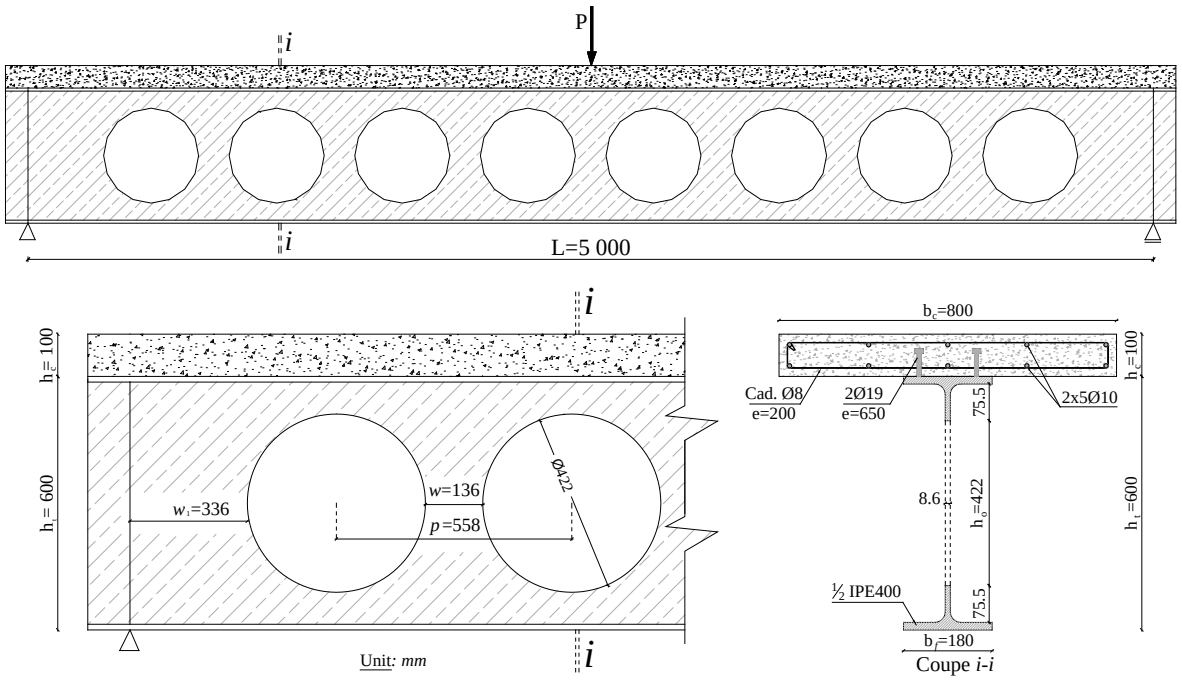


Figure 1 Cellular composite beam.

In this work we choose the same materials used by *Abdel Aziz* in the previous test beam; the steel of the steel beam and the steel reinforcement of the slab have been characterized by the simple three-linear idealization behaviour (Figure 2), with a modulus of elasticity $E_s$=2.1x10$^5$ MPa and Poisson's ratio υ=0.3, the limits of elasticity and ruptures $f_u$ and $f_y$ with their elongations are shown in Table 1.

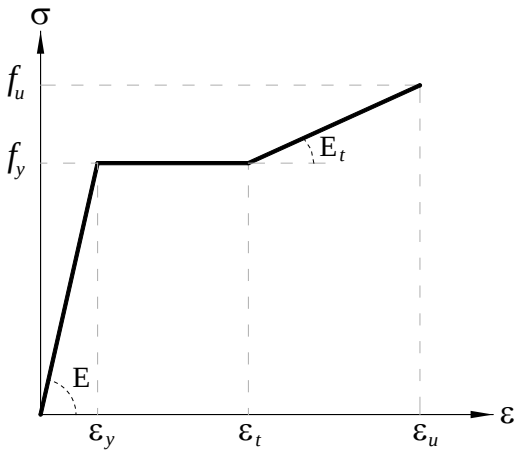


Figure 2 Constitutive relationship for steel.

Table 1 Propriety of steel.

| ELEMENTS | $f_y$ MPa | $f_u$ MPa | $\varepsilon_y$ ‰ | $\varepsilon_t$ ‰ | $\varepsilon_u$ ‰ |
|---|---|---|---|---|---|
| Web (IPE400) | 260 | 372 | 1,24 | 22,28 | 99,0 |
| Flanges (IPE400) | 245 | 361 | 1,17 | 21,0 | 93,36 |
| Reinfor. ϕ=10 | 370 | 375 | 1,76 | 31,68 | 140,8 |

For the concrete slab, the curve behaviour was adopted in classic form "**parabola-rectangle**" (Figure 3) according to Eurocode 2 [5], with a compressive stress $f_c$=35 MPa and modulus elasticity $E_{cm}$=33.5 kN/mm².

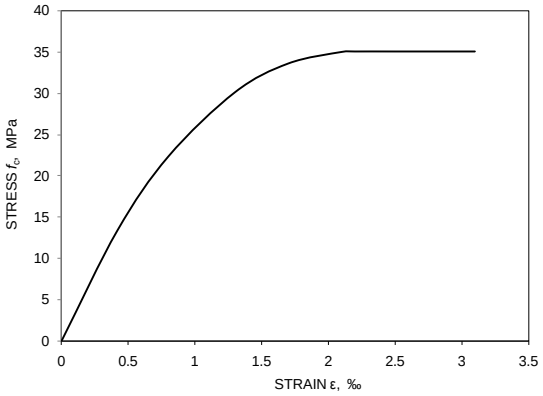


Figure 3 Curve behaviour for concrete.

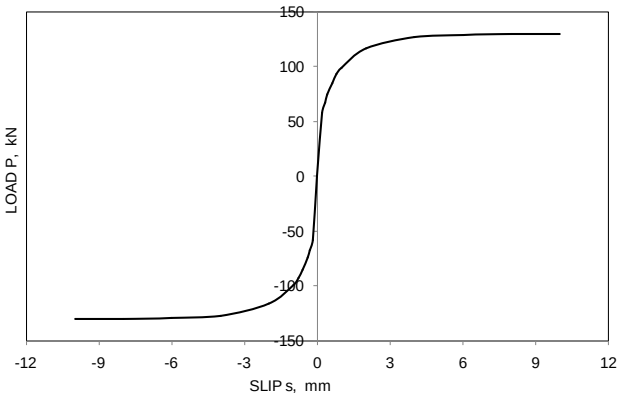


Figure 4 Constitutive relationship for headed connectors.

Regarding the connection that consists of headed studs (type Nilson ϕ=19mm) [1].

The behaviour "**P** *shear force* - **s** *slip*" of a connector is defined by the relationship *Olgaard* [1]; it is characterized by two independent parameters: α and β.

The relationship between shear force $P_j$ and slip $s_j$ to contact interface takes the following form:
$F_j = P_{max}.(1-e^{-\beta.sj})^{\alpha}$

Parameters α and β of controls the initial slope of the curve and shape form, were defined taking into account typical values of the two coefficients found in the literature [8], while the value of $P_{max}$ was measured push-out [1].
In our case; α = 0.4 and β = 0.709$mm^{-1}$ and $P_{max}$= 130 kN (Figure 4).

## NUMERICAL MODELING:

The global finite element analysis 3-D of the existing "PI4" composite beam in the literature was performed and compared with experimental results. The purpose of this analysis is to validate the numerical model for use in the study of cellular composite beams in the presence of circular openings in the web of the steel beam.

### Discretization of elements and the mesh

The modeling of structural system is based on research using software ANSYS 12.1 [7], this software offers a wide range of options such as: the graphic interface, type of elements, behaviour s of materials and controls numerical solutions...

The types of finite elements considered in our model are:

- *Elements of the metal beam (web and flanges)*: modeled by shell elements of four nodes "SHELL43" element having six degrees of freedom for each node with capacity for plastic deformations in large displacement.

- *Concrete slab*: modeled by solid elements "SOLID65" especially for concrete material in the library software, this three-dimensional element of eight nodes having three degrees of freedom for each node with capacity of cracking concrete.

- *Reinforcement of the slab*: modeled by element bar "LINK8", this non-linear element in 3-D is able to support only axial forces of tension or compression, having three degrees of freedom of translation at each node and capacity plastic deformations of large displacement.

- *Connectors*: modeled by non-linear springs "COMBIN39" defined by two nodes, this element is able to present the curve force-slip connector with three degrees of freedom at each node (translations and rotations).

- *Contact steel-concrete:* rigid target surface (upper side of the profile of the flange) modeled by elements "TARGE170", while the contact surface (bottom surface of the slab) modeled by element "CONTA173".

As regards the elements of the mesh; several mesh sizes are tempted to provide the best results of calculation, the choice of mesh size is dictated by the search for better matching of provided and the calculation time results. For shell elements of metal section the size of elements does not exceed 20% of the web height, [4] and the size of solids plan should be similar to the previous size. By reinforcement against the size is limited by the intersection of the reinforcement layers (Figure 5).

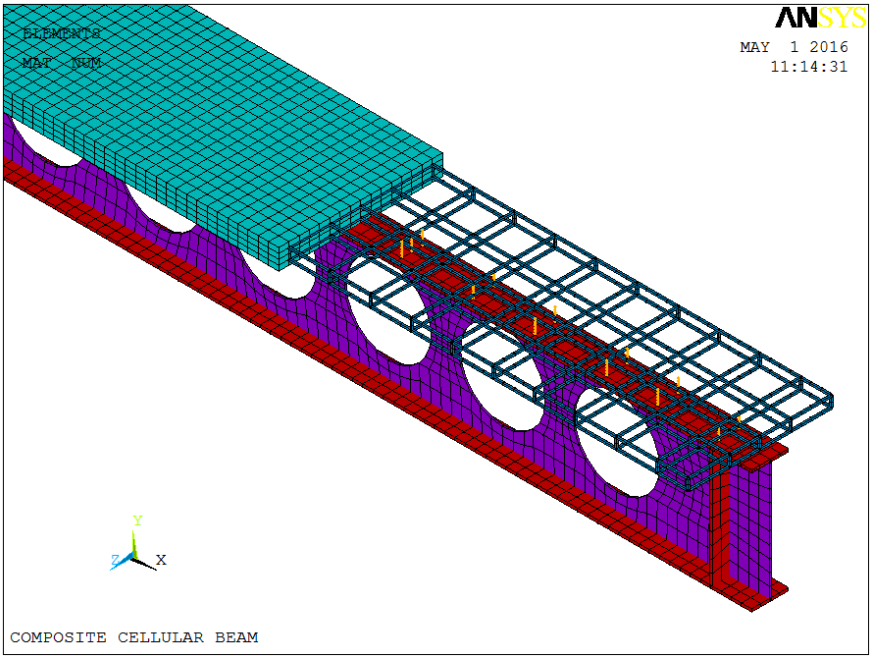


Figure 5 Finite element of cellular composite beam.

**Loading and conditions of support**

The beams considered in this study are simply supported at the ends and held laterally (lateral support), subject to concentrated loads at mid-span; This charge has been applied as a distributed pressure over a 200x200mm surface to avoid stress concentration on the slab (punching of the slab).

## VALIDATION OF THE NUMERICAL MODEL:

The proposed model was validated using different experimental results of "PI4" beam made by *Abdel Aziz* and numerical by *Fabbrocino* et *al*. [1]. Comparison of the results, such as load-deflection relationship, the interface slip of the steel-concrete beam, the derivative of the slip *ds/dx* and curvature ψ; All these results are illustrated in Figures 6 to 10.

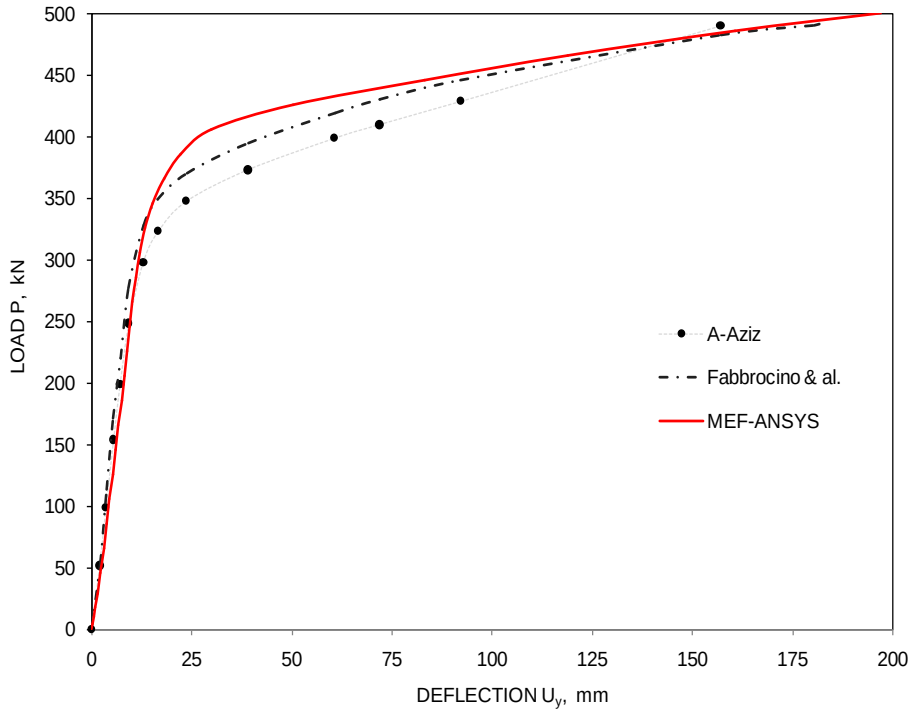


Figure 6 Load-deflection at mid-span.

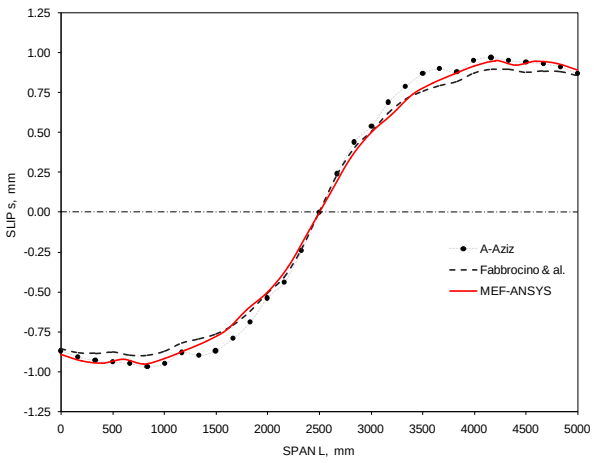


Figure 7 Slip of interface steel-concrete (P=344 kN)

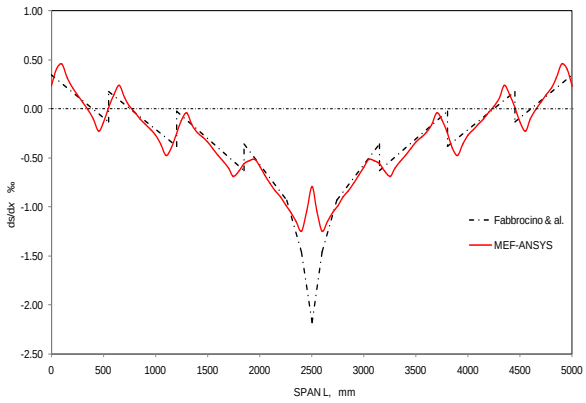


Figure 8 Derivative *ds/dx* (P=344 kN)

It is observed of the peaks in the curves of Fabbrocino et al. in the middle of the beam to the derivative of the slippage ds/dx and ψ curvature. In our opinion this may be an error due to the algebraic sum of the middle of value and that this value neighbouring on both sides.

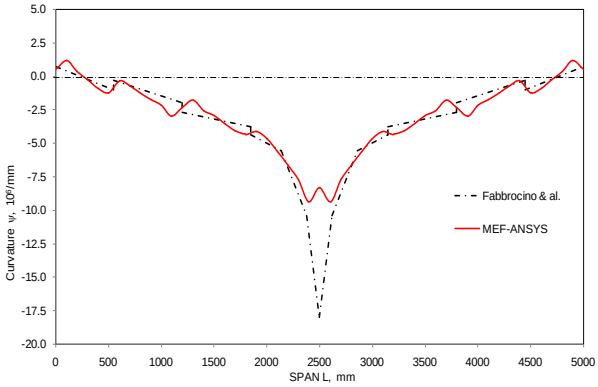


Figure 9 Curvature ψ (P=344 kN)

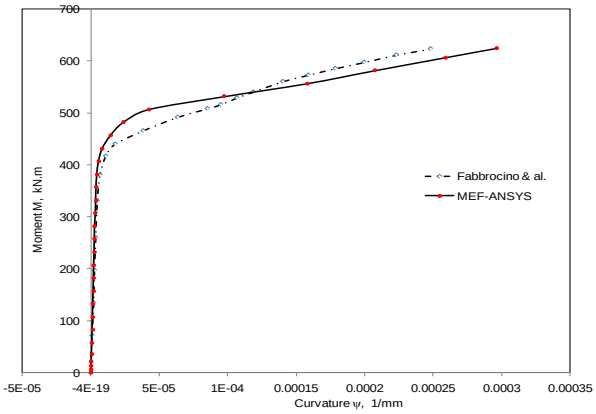


Figure 10 Moment-Curvature ($n_t$=18)

According to the curves shown in the figures above, the following observations can be noted:

- The experimental destruction of the beam "PI4" has been reached for load $P_{exp}$=490 kN, with a deflection equal to 157mm, and the ultimate load calculated by *Fabbrocino* et *al*. $P_{u\text{-}EF}$=488 kN with deflection equal 182mm [1]. For the same load experimental ruins we deflection is 171.7mm, arrow with a relative error equal to 9.4%. Therefore, a slight difference of the elastoplastic area curve is found, it is highly dependent behaviour al relationships both materials and shear connectors.

- Good accord marked on slip curves at the end of the beam, with a maximum error not exceeding 2.5% for the load P = 344kN.

- The mid-span section of the beam is never characterized by the requirement of complete interaction ($ds/dx \neq 0$); the greater the load is, the greater the value of the derivative of the slip in the steel-concrete interface is large (Figure 8).

- An error of 17% is marked on Figure 10, when the failure load is reached for the numerical calculation of the curvature.

## THE STRUCTURAL MODELING:

On the same principles and hypotheses assumptions *Fabbrocino* et *al.* [1], it is indicated by the index *s* for the steel beam and the index *c* to the concrete slab in a monolithic section of the beam, the two components are characterized by the same vertical displacement; in this way both parties have the same rotation and the same curvature.

In the presence of each component slip can be considered an isolated beam, so that the two curvatures may be different, the compatibility of the vertical displacements can be applied in sections containing the shear connectors [1]. Thus, an uprising of the slab may occur; however, this effect is negligible. Shear connectors have been in their actual position along the beam (pair of symmetrically arranged connectors) their action consists of an interaction force applied to a discrete number of sections. The concrete slab is modelled as a conventional reinforced concrete element so that its analysis is based on the following two hypotheses:

- There is no slip between rebar and concrete;
- Concrete in tension is neglected in the calculation.

The analysis of the behaviour of the composite section shows that the reinforced concrete slab work mainly in compression and partly in tension, the steel deformation is small compared to that of concrete. Therefore, the modelling of the slipping between the reinforcements and the concrete is not necessary when the joint section is subjected to bending moment [1]. Evaluation of displacements $u_{(x,y)}$ of the section depends not only on the $\phi$ rotation and the displacement of one of $u_s$ centroids $u_c$, but also on the slip between the slab and the steel beam:

$$s=u_s^t-u_c^b \quad \ldots\ldots\ldots\

The partial translational equilibrium of the concrete slab gives:
$F_c = -F$ …… (5)

The partial translational equilibrium of the steel beam gives:
$F_s = F$ …… (6)

From global translational equilibrium, Eq. (4) can be modified into the more useful form
$F_s = -F_c = F$ …… (7)

So that the global of rotational equilibrium can be rewritten:
$M = M_s + M_c + F.d$ …… (8)

In this way the three independent Eqs. (5), (6), (8) depend on the interaction force F, and the two bending moments acting on the two parts of the composite section.
$F_s$ and $F_c$: normal stresses resulting forces acting on two parts of the section

The connection effect is represented by the term F.*d*; even if the bending moment acting on each part of the section is zero, the composite section is able to bear a total bending moment depending on the interaction force F.

This observation is very important as the strength and the moment-curvature relationship depends on the value of the interaction force.

## RELATIONSHIP MOMENT-CURVATURE OF THE CROSS SECTION:

The global bending moment of the composite section is given by the axial force and bending acting on each part of the section, the value of curvature $\psi$ depends on the derivative of the slip *s*, Eq. (3). Similarly, the global bending moment is directly dependent on the value of the interaction force F, Eq. (8).

To draw a single moment-curvature curve, it is necessary to define a family of curves corresponding to different values of F.

To define this family of curves, on the one hand, the definition of the upper and lower limit of the interaction force F is required. The upper limit of the positive $F_{max}$ interaction force is given by the minimum value (absolute value) between the axial compression forces in the slab and the axial tension forces of the perforated steel beam; this longitudinal shear force is defined force which corresponds the degree of total connection ($N/N_f=1$) according to EC-4. This force is easy to calculate, it is based on the mechanical properties of the reinforced concrete slab and the steel beam, and the lower limit $F_{min}=0$, which matches any force of interaction between steel and concrete ($N/N_f=0$).

The curve corresponding to the slip value equal to zero defines the moment-curvature relationship for the state of the full interaction. Theoretically this curve is the only one compatible with the hypothesis Bernoulli linear deformation of all of the composite cross-section, which occurs when the slip and the derivative to the profiled-slab interface are zero. Against by the moment-curvature relationship of the composite section without interaction

(F=0) in this particular state, the curvature is related to the bending moment by the following relationship:

$$\psi = -\frac{M}{(E_s I_{s-e} + E_c I_c)} \quad \text{..... (9)}$$

where $E_sI_{s\text{-}e}$ and $E_cI_c$ are the flexural rigidities of the equivalent steel cellular beam and of the concrete slab.

## NUMERICAL STUDY RESULTS:

The numerical results of calculation load-deflection, moment-curvature and on slipping along the beam have been summarized in the Figure 11.

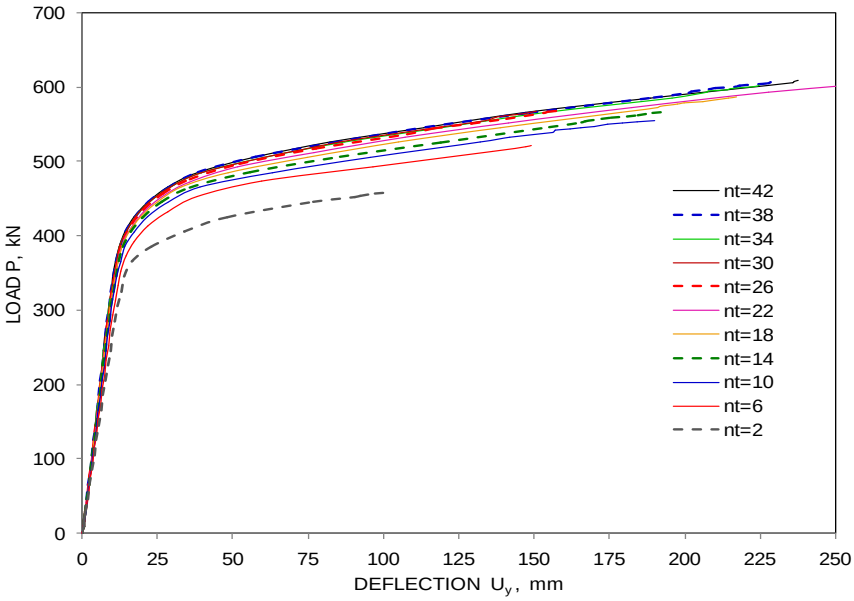


Figure 11 Load P- vertical deflection $u_y$.

The previous figure show that the elastic portion of the beams is between P=0 and P≈350 kN, beyond the last value comprise beams is plastic. To know the forms of slip-like in both areas of deformation, one traces the shift in both intervals for different degrees of connection.

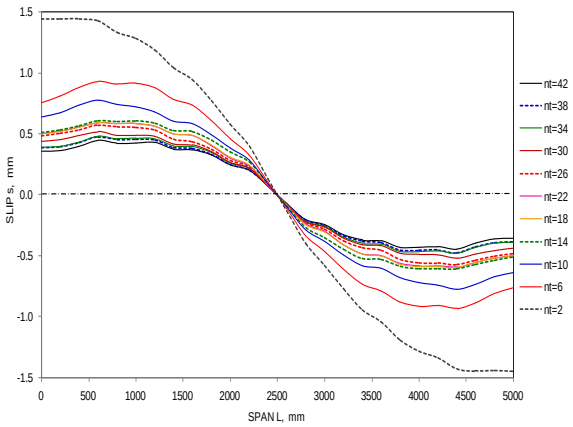


Figure12 Elastic slip *s*, P=300kN.

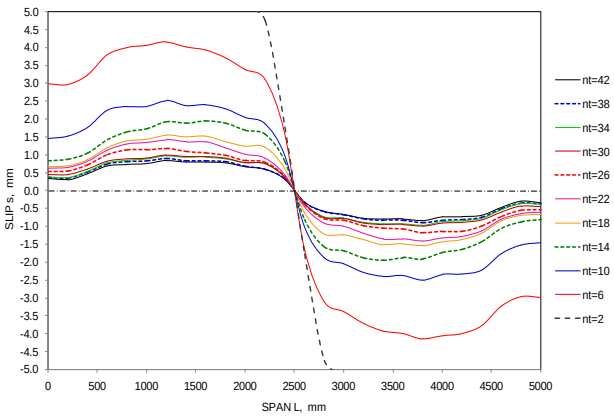


Figure 13 Plastic slip *s*, P=500kN

And the relation curve bending moment is illustrated in Figure 14.

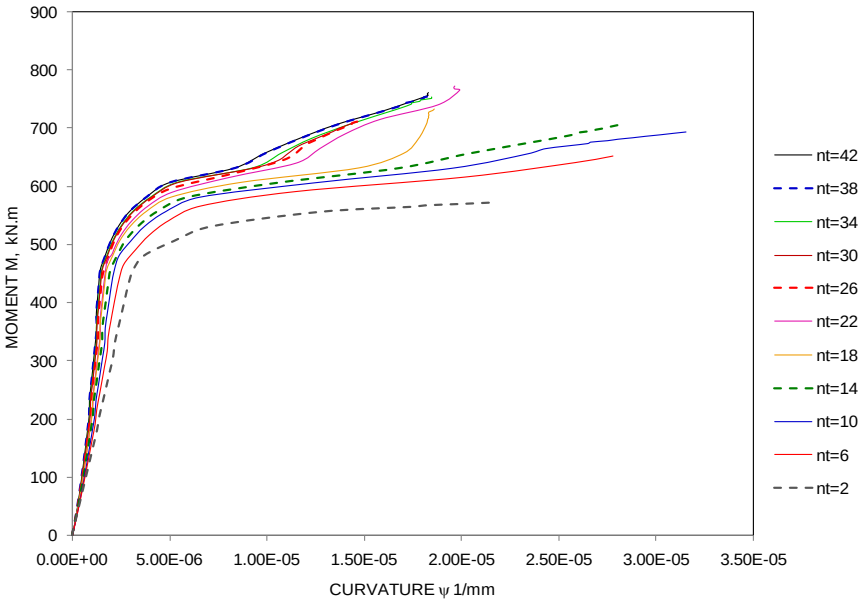


Figure 14 Moment M - Curvature ψ.

## ANALYSIS OF RESULTS

The analysis of the curves plotted in Figures 11, 12, 13 and 14 allows some interesting remarks:

1. The zero slip between the metal beam and slab is practically difficult to achieve by headed studs, as these connecting elements offer a non-zero flexibility despite their considerable number connector (for example, we find s = 0.25mm for a number of connector $n_t$=42 under the load P=500kN).

2. The total or complete connection is matching the number $N_f$ connectors beyond this number (adding additional connectors) cannot increase the resistant of the beam despite the slip at the end of the beam is not zero. We note that the EC-4 does not give the lower limits of the slip but it does suggest that this slip is negligible if its value does not exceed 0.5mm [6].

3. The slip curves in the elastic range are varied regularly along the beam by the same curves against plastic in the area are varied corrugated because in the elastic range of the connection rigidity redistributed between the connectors on the long of the beam, by against the latter is discontinuous by plasticization of the most sought in the future plastic connectors.

4. The maximum slip is measured at the ends of the beam in the elastic domain, and with a distance of 1/5 to 1/4 at the ends in the plastic range.

5. The curvature of the beams increases with decreasing degree of connection because of the connectors provides sufficient slipping which provides adequate ductility of the beam before failure.

6. The failure modes of the beams, which was generally caused by the instability of the web-post central (in concentrated load) which by lifting the slab (Figures 15 and 16).

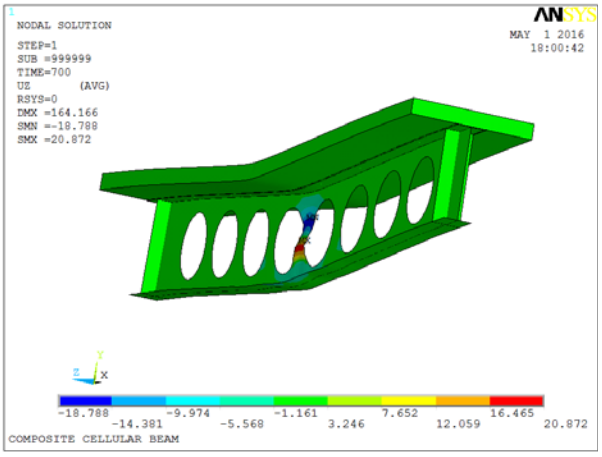


Figure 15 Ruin by instability of central web-post ($n_t$=26).

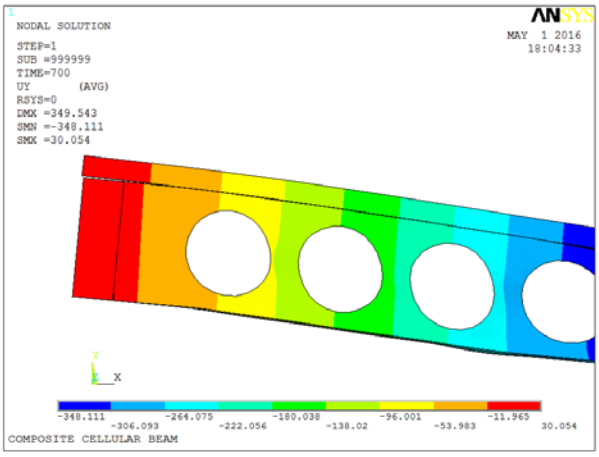


Figure 16 Ruin by slab uprising ($n_t$=6).

## CONCLUSIONS

The modelling of the structural behaviour of composite steel-concrete cellular beams in concentrated static load at mid-span was studied in this paper. In particular, there was presented a numerical 3-D model to provide a clearer understanding of the relationship between the slip and the shear connectors.

The method of calculation by finite element allows us a reliable analysis of this type of composite steel and concrete structure, numerical results show substantial agreement with the experimental test exists in the literature in terms of quantities for composite beams. Nevertheless, one can notice that the estimate of the arrow and curvature seems to be more influenced by the constitutive relations introduced to materials and shear connectors.

This analysis of the structural behaviour of composite beams with a perforated cross section by introducing nonlinear material properties, is a powerful tool for understanding the behaviour of this type of structure and also to perform an optimization of the design in terms of resistance and deformation of composite beams steel-concrete.

## REFERENCES

1. FABBROCINO, G, MANFREDI, G, COSENZA, E. Non-linear analysis of composite beams under positive bending, Computers and Structures, Vol. 70, 1999, pp 77-89.

2. MIMOUNE, M, SIOUANE, S, MIMOUNE, F Z. Elastic buckling of web-post in cellular beams with various opening shapes, World Journal of Engineering, Vol. 9, No. 5, 2012, pp 429-435.

3. MOHEBKHAH, A. The moment-gradient factor in lateral-torsional buckling on inelastic castellated beams, Journal of Constructional Steel Research, Vol. 60, 2004 pp 1481-1494.

4. SWEEDAN, A M I. Elastic lateral stability of I-shaped cellular steel beams, Journal of Constructional Steel Research, Vol. 67, 2011, pp 151–163.

5. EUROCODE 2. Calcul des structures en béton, et document d'application nationale, ENV 1992-1-1, AFNOR 1992, p 18-711.

6. EUROCODE 4. Conception et dimensionnement des constructions mixtes acier- béton, ENV 1994-1-1, AFNOR 1994, p 22-391.

7. ANSYS Mechanical APD, User's manual-version 12.1, 2009

8. BUJNAK, J. Analyse globale de poutres mixtes acier béton - Approche analytique et modélisation non linéaire, Thèse de doctorat, 2007, Ecole doctorale pour Ingénieur, Université de Balaise Pascal –Clermont II, France, p 150

# RAPIDLY DEPLOYABLE SHOTCRETE SYSTEM FOR THE STRUCTURAL STABILIZATION OF SHOCK DAMAGED STRUCTURES

**A Oberlink T Robl R Jewell T Duvallet**
University of Kentucky
**P Mills**
Minova USA, Inc.
**M R Jones**
University of Dundee
United Kingdom

**ABSTRACT.** The University of Kentucky Center for Applied Energy Research, along with Minova USA Inc., and the University of Dundee, developed a rapid strength, high bonding shotcrete system for infrastructure repair and stabilization, at the request of a mandate from the U.S. Department of Homeland Security. This mandate called for development of a material that gains structural strengths very rapidly, as well as the development of a corresponding deployment system to stabilize and repair shock damaged structures to avoid catastrophic failure. Tekcrete Fast® is a material that was developed for this process, and is a specially designed, rapid-setting, and high performance dry-mix shotcrete. This system will stabilize structures like airport runways, tunnels, bridges, and dams that have been shocked and damaged by explosives, or seismic activity, etc. before they fail, by reaching compressive strengths of 41.4 MPa in 3 hours, and 75.8 MPa in 28 days. Additionally, in November 2014, a civil engineering demonstration of Tekcrete Fast® took place in Disaster City, Texas to show that Tekcrete Fast® can help first responders to stabilize building structures.

**Keywords:** CSA cement, Shotcrete, Infrastructure repair.

**Anne Oberlink** is a Scientist at the University of Kentucky Center for Applied Energy Research. She received her second Masters of Science in Chemistry from the University of Kentucky in 2010. **Thomas Robl** is a Scientist at the University of Kentucky Center for Applied Energy Research, Director of the American Coal Association and Co-Chairman of the World of Coal Ash International Symposium. **Robert B Jewell** is an Engineer at the University of Kentucky Center for Applied Energy Research, Lexington, KY. He received his MS in geology and his PhD in Civil Engineering from the University of Kentucky. **Tristana Duvallet** is an Engineer at the University of Kentucky Center for Applied Energy Research. She received an Engineering diploma in Materials Science at Ecole Supérieure d'Ingénieurs de Recherche en Matériaux et Infotronique (ESIREM) at Dijon in France, and a PhD from the University of Kentucky in 2015. **Peter Mills** is the Technology Leader for Minova USA which is part of Orica, the world's largest explosives company. **Professor M Rod Jones** is the Director of the Concrete Technology Unit at the University of Dundee. A renowned practitioner in the field of concrete technology, he is a member of numerous national and international technical committees.

# INTRODUCTION

## Background

The rapid stabilization of shock damaged structures falls outside the purview of normal construction practices, due to the critical time issue and the nature of the damaged structure. The stabilization of damaged structures requires materials and equipment that can be rapidly deployed to place materials that have very rapid strength development. These materials need to be placeable at a distance to provide some degree of safety to the responders. In addition, the materials must be able to adhere to structural surfaces that have not been properly prepared and conditioned, and may also be highly fractured, dusty, wet, and very possibly hot or extremely cold.

The technology for the rapid delivery of large volumes of cementitious materials to vertical or even overhead surfaces currently exists. Pneumatic delivery (shotcreting) has been used in construction for over 100 years [1]. Shotcreting has played a major role in structures like the Washington D.C. Metro subway system and the England to France undersea rail connector ("the Chunnel").

Numerous rapid setting cements are commercially available. They are used for rapid repair of surfaces such as bridge decks, pavements, and commercial floors, as well as structural repairs of vertical and overhead surfaces. Few of these products are specifically marketed for use in shotcrete applications.

The majority of rapid setting cements are based on, or at least contain, Portland cement as a principle component. Other components are added that help provide early strength, such as high alumina cement (HAC), organic polymers, chemical accelerators (which can also be added during concrete batching), and calcium sulfate hemihydrate (e.g. gypsum plaster) [2]. Mortars prepared with some of these cements can achieve compressive strengths of 6.8 – 13.8 MPa (1000-2000 psi) within 1 hour. However, Portland cement mortar and concrete typically require many weeks of proper curing to reach significant levels of their ultimate strengths, even when used with set accelerators. Also, high early strengths require the use of large proportions of Portland cement in the concrete mix, which can lead to high heat evolution, excessive shrinkage of the material, and cracking. The cost also increases substantially with increasing cement content.

Alternatives to Portland cement are also capable of rapid strength development. These include calcium sulfate hemihydrate, and calcium sulfoaluminate (CSA) cements. Unlike Portland cement, these rapid setting cements can gain 75-80% of their strength within 1 day, which means less cement can be used in the mix to achieve comparable early strength [2]. CSA cement and calcium sulfate hemihydrates can also be fabricated, for the most part, from coal combustion by-products (CCB's). These CCB's include fluidized bed combustion spent bed materials and forced air oxidation flue gas desulfurization by-products, i.e. synthetic gypsum, which potentially represents both a cost advantage, as well as an environmental advantage [3].

## Development of Shotcrete

The primary considerations of this project were the rate of strength development (compressive and tensile), short-term dimensional stability, and bonding strength to the

damaged surfaces. Other considerations include heat generation, pumpability, ease of use, stiffness of the set material, and cost.

CSA cements are of interest mainly because they gain strength very rapidly. They also require lower energy to produce, with significantly lower $CO_2$ emissions than Portland cement [2]. CSA-based shotcrete materials can be formulated so that they have lower cement content than Portland-based shotcrete, a higher water to cement ratio, lower viscosity, and yet still achieve very high early strength. This is due to the nature of its principal cementitious hydration product - ettringite. These properties are difficult to achieve with Portland cement-based rapid setting materials.

In addition, the large water/cement ratio of CSA cement shotcrete, coupled with the low heat of hydration of plaster cement, offers a capacity to manipulate the heat of reaction of these materials within a wide band of strength and set parameters. Heat generation is critical in the rapid placement of masses of highly reactive cementitious materials. These cements also offer the potential of lower overall costs. Unlike Portland cement, which gains its strength primarily from the hydration of the calcium silicates "alite" ($Ca_3SiO_5$) and "belite" ($Ca_2SiO_4$), calcium sulfoaluminate (CSA) cements contain Klein's compound which hydrates in the presence of calcium sulfate (e.g. gypsum) to form a cementitious phase called ettringite [4]:

$$\underset{\text{Klein's compound}}{Ca_4Al_6O_{12}SO_4} + 2\underset{\text{Gypsum}}{CaSO_4\cdot 2H_2O} + 34H_2O \rightarrow \underset{\text{Ettringite}}{Ca_6Al_2(SO_4)_3(OH)_{12}\cdot 26H_2O} + 4\underset{\text{Aluminum hydroxide}}{Al(OH)_3}$$

A compound similar to ettringite called "monosulfate" can also form under sulfate-deficient conditions. Belite is often present in CSA cement, but its hydration is slow and only contributes to long-term strength [5, 6]. Because of the rapid rate of formation of ettringite, CSA cements gain strength very quickly. If enough lime ($Ca(OH)_2$) and calcium sulfate is present in the system, additional ettringite can also be formed through reaction with the aluminium hydroxide, a product of the Klein's compound. However, if the system contains excess lime, the cement can induce destructive expansion [4].

CSA cement actually represents a series with a broad range of compositions, from nearly pure Klein's compound, to Klein's compound with belite, calcium ferroaluminate or ($Ca_4(Al_2Fe_2)O_{10}$), free lime (CaO), calcium sulfate ($CaSO_4$) and other minor phases (e.g. $Ca_{12}Al_{14}O_{33}$). Three types of CSA cements were studied and tested during this project to determine which of the three types was the best fit.

**Testing of CSA-Based Shotcrete**

Once the CSA-based materials to be used in the shotcrete were developed and tested, they were used to fabricate shotcrete mortars and concretes. After an initial round of screening, specimens prepared from selected mixes were tested for strength and dimensional stability. When determining what tests to use to evaluate the chosen mixes, it was important to keep in mind that the sprayed-concrete material must provide structural strength within an hour, and bond sufficiently to any substrate or surface under any conditions long enough to provide the necessary assistance to first responders.

ASTM C1140 "Standard Practice for Preparing and Testing Specimens from Shotcrete Test Panels" is typically used for the field testing of the shotcrete compressive and flexural strength [7]. This standard requires the shotcrete be pneumatically projected onto a wooden

form and then samples cored or cut from the sample to be tested. However, because the basis of this research was the study of the interaction of shotcrete and ordinary Portland cement, the aforementioned standard was not used, but instead standards that determine bond strength between different concretes. Therefore, in addition to the standard cement/concrete testing, i.e. compression and stability testing of ASTM standard cubes, cylinders, bars, and cores; flexural strength beam testing; tensile testing; rapid freezing and thawing testing; resistance to carbonation testing, the variations of heat production based on cement thickness, calorimetry measurements for reaction time of CSA cement phases, slant-shear test, pull-off tests, and time-of-set were a few of the additional tests also used during the project [8, 9, 10, 11, 12].

After years of research, Tekcrete Fast® was developed. Worldwide patents have been filed jointly by the University of Kentucky and Minova USA Inc., and received. Tekcrete Fast® can be used in conventional, dry-process shotcrete equipment as a one bag system. As mentioned previously, it also has the ability to adhere to any structural surface, whether it is fractured; dusty, as the dry-mix shotcrete nozzleman will spray water before the Tekcrete Fast® and will thereby quickly remove any dust accumulation; or wet, regardless of temperature. These features are ideal for use by first-responders, as there is usually little time to prep the surface to be sprayed. It can also to be used to repair bridges and roadways, overpasses and runways, etc. Tables 1 and 2 show the average compressive strength and flexural strength for Tekcrete Fast®.

Table 1 Average compressive strength for Tekcrete Fast® in MPa and psi

| COMPRESSIVE STRENGTH, MPa (psi) | | | | | | |
|---|---|---|---|---|---|---|
| 15 min | 30 min | 1 h | 3 h | 1 d | 7 d | 28 d |
| 17.2 (2,500) | 24.1 (3,500) | 31.0 (4,500) | 41.4 (6,000) | 55.2 (8,000) | 62.1 (9,000) | 75.8 (11,000) |

Table 2 Average Flexural Strength for Tekcrete Fast® in MPa and psi

| FLEXURAL STRENGTH, MPa (psi) | | |
|---|---|---|
| 3 h | 1 d | 7 d |
| 17.2 (2,500) | 24.1 (3,500) | 31.0 (4,500) |

## Equipment and Delivery Vehicle Development

We have found that there are many issues to be addressed in determining which shotcrete delivery system to use with the material. Wet-mix systems deliver the material as a paste, and compressed air is used to accelerate the concrete. Strong advantages include the ability to precondition the materials, with a better control of heat, and high delivery rates. However, highly reactive slurries can be difficult to manage and, based on our own experience, flash-set can cause catastrophic equipment failure.

Shotcrete can be reasonably divided into two types or systems - “dry mix” and “wet mix”, and each system has advantages and disadvantages, as Table 3 shows.

Table 3 System Comparisons

| COMPONENT | DRY MIX | WET MIX |
|---|---|---|
| Cost | Low to Moderate, i.e. $10,000's | High, i.e.$50,000 to >$100,000 |
| Production Rate (via Nozzle Person) | Moderate 5 $yd^3/h$ (3.8 $m^3/h$) | High up to 16 $yd^3/h$ (12.2 $m^3/h$) |
| Complexity | Air compressor, water | Pump, Compressor, Water, plus |
| Material Control | Good | Good |
| Single Bag Mix | Yes | Yes |
| Required Clean-Out | Simple, Blast Nozzle with Compressed Air | Must Clean Mixer, Pump, Hose |
| Fibre Capable | Yes | Yes |

Wet mix systems are, as implied, produced with cement and water. The mix is prepared in a mechanical mixer and then the wet concrete is pumped through a hose; the end of which is equipped with a high pressure pneumatic nozzle. The water and cement mixture passes through the hose, and into a mixing nozzle chamber where the nozzle accelerates the mixture to give the high velocity needed for impact consolidation. In dry-mix systems, the dry material is exposed to a water stream at the nozzle, where mixing occurs, and is then given the high velocity it needs for impact consolidation. Several different dry-mix nozzles were investigated and tested throughout the project, and all commercially available nozzles performed very well.

A dry-mix delivery system was determined to be best for the delivery of Tekcrete Fast®, due to the simplicity, the use of single bag product formulations, and the ability to utilize very rapid-setting materials. A variety of dry-mix systems were tested throughout the project, including the Reed SOVA and the Meyco Piccola, and they all worked very well for this process.

Additionally, the delivery system was designed to be a rapidly deployable, low-cost, integrated structure that can be engineered into a facility, or a vehicle deployed by first responders to stabilize damaged structures. Ideally, the system would be maintained in a state of readiness in areas that are considered to be high risk targets, which could include major subway systems, roadways, airports, or other critical infrastructure.
The delivery vehicle is comprised of five essential components: water supply, air supply, cementitious material, a dry-mix shotcrete system, and the inline water heater for use in cold conditions. It has been determined that Tekcrete Fast® will cure much quicker when the water is warm.

The mobile delivery system that has been used previously was deployed on a trailer. The hitch end of the trailer houses the static components, i.e. the air compressor, water tank, and generator (if needed). The working area of the trailer houses the dynamic components that will require operator access, i.e. the dry-mix gun, water booster pump, hose reels, and material supply.

This deployable delivery vehicle includes everything needed for first responders to stabilize shock-damaged structures, all on the back of a flat-bed trailer. In addition, this delivery system will also work in non-emergency situations, allowing for easy deployment of all equipment and material for repairs of any type.

## TEKCRETE FAST® - POST COMMERCIALIZATION

### Additional testing

### Residual strength of sprayed concrete

The deformation behaviour of cementitious composites such as concrete, fibre reinforced concrete (FRC), and fibre-reinforced ultra-high performance concrete (FR UHPC) is typically distinguished according to their tensile stress-strain characteristics, in particular, the post-cracking response.

Friable materials tend to lose their tensile load-carrying capacity very quickly after the development of the first crack in the matrix. Adding fibres to conventional fibre reinforced concrete can increase the toughness of the material. It has been found, though, that the tensile strength of the material, is not enhanced [13].

### Method

Specimens were sprayed in accordance with EN 14488-1, and were tested following BS EN 14488-5 for the determination of energy absorption capacity of fibre reinforced slab specimens under large deflections [14, 15]. The dimensions of the square test panels were 600 mm × 600 mm with a thickness of 100 mm. Specimens were moist cured until testing at 28 days. The panel was loaded with a displacement control at a rate of 1 mm/min at the centre of the slab. The test, Figure 1, was concluded after the central deflection exceeded 30 mm.

The load-displacement results may then be expressed as the energy absorption until a deflection of 25 mm is obtained, Figure 2. The first crack occurred at a maximum load of approximately 80 kN at 6 mm of displacement, followed by a second crack which occurred perpendicular to the first with a peak load of approximately 90 kN at 9 mm of displacement. Due to the shorter length of the 12 mm polyvinyl-alcohol fibre, most of the potential energy absorption was complete after approximately 10 mm of displacement; which provided a toughness of 311.90 J for the shotcrete panel.

Figure 1 Square panel test apparatus

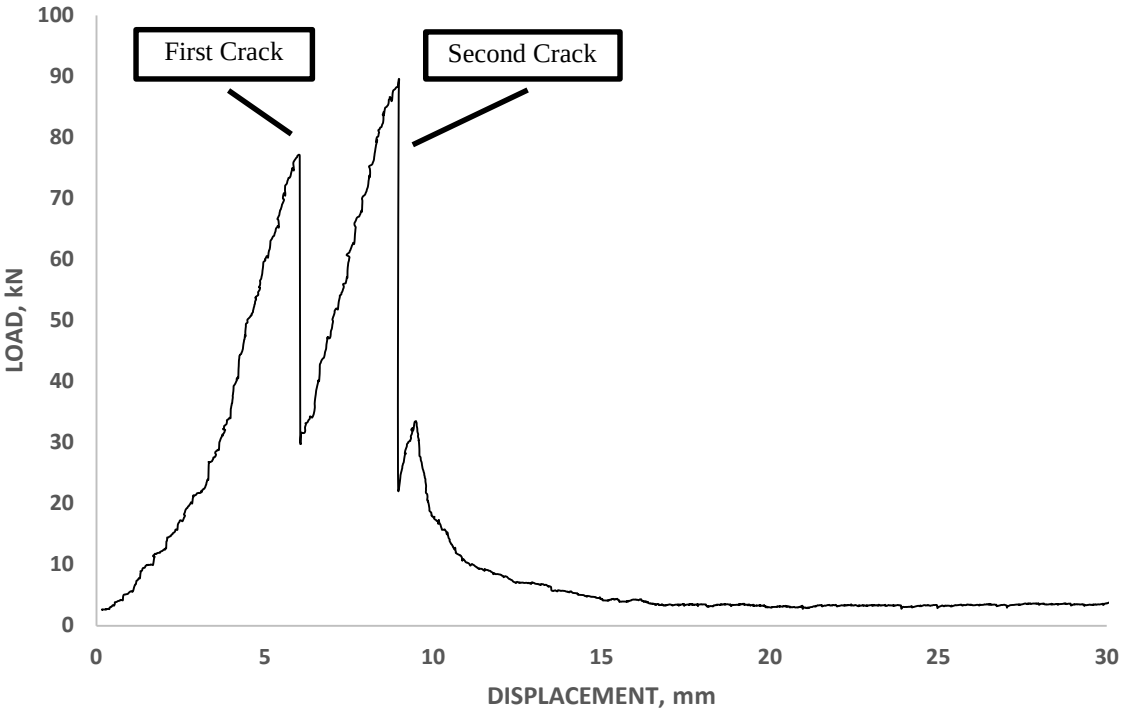


Figure 2 Load-displacement curve for residual strength of sprayed concrete

**Disaster City Demonstration – College City, Texas**

In November 2014, a civil engineering demonstration of Tekcrete Fast® and its dry-mix shotcrete delivery deployment system took place in Disaster City, TX. Disaster City is a 52-acre training facility located in College Station, Texas. It includes an extensive array of disaster scenario simulations for training emergency response professionals. Disaster City includes full-scale, collapsible structures designed to simulate various levels of disaster and wreckage, ranging from shock-damaged structures, to chemical plant fires, and overturned passenger trains, etc., which can be customized for the specific training of any group [16].

The UK CAER and Orica USA Inc., with the help of Mr. Carl Baur, ASA Certified Nozzleman and Examiner with the CCS Group of Millstadt, Illinois; Jeff Saunders, the director of the Texas Task Force 1 of the Texas A&M Engineering Extension Service (TEEX); and Dr. Peter Keating from the Texas A&M Civil Engineering High-Bay Structural & Materials Testing Laboratory, demonstrated the repairing and testing of damaged or wrecked, reinforced concrete vertical beams, simulating catastrophic shocks from an explosion or earthquake to a building or parking garage type structure. The demonstration was to show that Tekcrete Fast® and its dry-mix shotcrete delivery deployment system can help first responders to stabilize such a structure, so they can get in and out quickly and safely, and to bring any victims of said catastrophic wreckage the help they need.

The reinforced concrete vertical beams that were intentionally formed with a missing section, and a purposefully damaged beam, were placed into the ground, and were repaired with Tekcrete Fast®. All concrete beams used in the demonstration had been poured several months in advance of the demonstration to make sure that they were fully cured, and at full strength. The beams had a column cross section that was 12” × 12” (300 mm × 300 mm), with the length of the damaged area on two of the four columns being approximately 18” (450 mm) long. The third column was damaged a day or two before the demonstration by bending it until it cracked. The fourth column was left whole, and used as a control beam during testing.

Once spraying was finished, the repaired beams were immediately removed from the ground and taken directly to the Texas A&M Civil Engineering lab for compressive strength testing. The entire process for this demonstration, including shotcreting the beams, getting the beams out of the ground, and transferring them over to the high bay lab for testing took less than five hours. With less than five hours of curing time for the Tekcrete Fast® section, the beams tested were shown to fail outside of the repaired section, i.e. the original concrete failed while the section repaired with Tekcrete Fast® did not.

## CONCLUSIONS

In conclusion, Tekcrete Fast® and its dry-mix shotcrete delivery system has repeatedly demonstrated that it has an overwhelmingly superior rate of strength development to conventional Portland cement based shotcrete. It has excellent bonding capabilities, and its potential for disaster recovery has been demonstrated. Tekcrete Fast® is an easy, one-bag sand/cement mix, and has been proven to be nozzleman-friendly, with a very wide water range. The set times are very predictable, with no flash set, but with the ability to cure very quickly, within 15 minutes of shotcreting.

## ACKNOWLEDGEMENTS

Thank you to John Wiseman from the University of Kentucky Center for Applied Energy Research, and Carl Baur, ASA Certified Nozzleman and Examiner with the CCS Group of Millstadt, Illinois.

## REFERENCES

1. AMERICAN SHOTCRETE ASSOCIATION. Technical Questions and Answers Archive, 2014, Retrieved from http://www.shotcrete.org/pages/products-services/technical-questions-archive.htm

2. LEA F.M. The Chemistry of Cement and Concrete. New York, NY: Chemical Publishing Co., Inc., 1971.

3. JEWELL R.B., RATHBONE R.F., DUVALLET T.Y., ROBL T.L. and MAHBOUB K.C. Fabrication and Testing of Low-Energy Calcium Sulfoaluminate-Belite Cements that Utilize Circulating Fluidized Bed Combustion By-Products, Coal Combustion and Gasification Products, Vol. 7, 2015, pp 9–18.

4. MEHTA P.K. Mechanism of expansion associated with ettringite formation, Cement and Concrete Research, Vol. 3, No. 1. 1973, pp. 1–6.

5. GLASSER F.P. and ZHANG L. High-performance cement matrices based on calcium sulfoaluminate-belite compositions, Cement and Concrete Research, Vol. 31, No. 12. 2001, pp. 1881–1886.

6. De La TORRE A.G., ARANDA M.A.G., De AZA MOYA A.H., De AZA PENDAS S. and PEÑA P. Belite Portland Clinkers. Synthesis and Mineralogical Analysis, Bulletin of the Spanish Society of Ceramics and Glass, Vol. 44, No. 3, 2005, pp. 185–191.

7. ASTM C1140 / C1140M-11, Standard Practice for Preparing and Testing Specimens from Shotcrete Test Panels, ASTM International, West Conshohocken, PA, 2011, www.astm.org

8. ASTM C192 / C192M-15, Standard Practice for Making and Curing Concrete Test Specimens in the Laboratory, ASTM International, West Conshohocken, PA, 2015, www.astm.org

9. ASTM C109 / C109M-16, Standard Test Method for Compressive Strength of Hydraulic Cement Mortars (Using 2-in. or [50-mm] Cube Specimens), ASTM International, West Conshohocken, PA, 2016, www.astm.org

10. ASTM C78 / C78M-15b, Standard Test Method for Flexural Strength of Concrete (Using Simple Beam with Third-Point Loading), ASTM International, West Conshohocken, PA, 2016, www.astm.org

11. ASTM C293 / C293M-15, Standard Test Method for Flexural Strength of Concrete (Using Simple Beam With Center-Point Loading), ASTM International, West Conshohocken, PA, 2015, www.astm.org

12. ASTM C666 / C666M-15, Standard Test Method for Resistance of Concrete to Rapid Freezing and Thawing, ASTM International, West Conshohocken, PA, 2015, www.astm.org

13. PRISCO M.D., FELICETTI R. and PLIZZARI G. PRO 39: 6th International RILEM Symposium on Fibre-Reinforced Concretes (FRC) – BEFIB, Volume 1. RILEM Publications. 2004.

14. BS EN 14488-1:2005, Testing Sprayed Concrete. Sampling Fresh and Hardened Concrete, British Standards Institution, 2016.

15. BS EN 14488-5:2006, Testing Sprayed Concrete. Determination of Energy Absorption Capacity of Fibre Reinforced Slab Specimens, British Standards Institution, 2016.

16. TEXAS A&M ENGINEERING EXTENSION SERVICE (2015). Disaster City. Retrieved from https://teex.org/Pages/about-us/disaster-city.aspx

# EFFECT OF STEEL FIBRES AND RECYCLED AGGREGATE ON DRYING SHRINKAGE AND CREEP DEFORMATIONS OF CONCRETE

**L Sryh**

**J Forth**

University of Leeds

United Kingdom

**ABSTRACT.** Laboratory tests were carried out to investigate the effect of steel fibres and recycled aggregate on the drying shrinkage and creep deformations of concrete. Steel fibres (Dramix 3D 65/35BG) were added to the mixes and washed construction and demolition wastes (WCD size 20mm) were used as a coarse recycled aggregate. The main variables of this study are the steel fibre contents; $V_f$ = 0, 0.5 and 1.0% and the recycled aggregate replacement percentages; RP= 0, 50 and 100%. Small prisms (75×75×200mm) and bobbins (75×365mm) were cast (for 9 mixes), cured (for 28 days) and tested (for up to 90 days). A fine natural aggregate was used in all mixes and the amount of cement and the water-to-cement ratio was kept constant. The results showed that there are significant increments in drying shrinkage, compressive creep and tensile creep by 18%, 15% and 8% were recorded respectively when 50% of the recycled aggregate was used. However, when 100% of the recycled aggregate was replaced, the following results were achieved 38%, 29% and 15% respectively. In contrast, the effect of adding 0.5% of steel fibres content recorded reductions in these deformations (drying shrinkage, compressive creep and tensile creep) by 7%, 3% and 10% respectively. However, further reductions with percentages of 15%, 5% and 20% respectively were seen when 1.0% of fibre content was added. Interestingly, steel fibres had a significant effect on tensile creep and shrinkage, but little effect on compressive creep.

**Keywords: S**teel fibres, Recycled aggregate, Recycled aggregate concrete, Drying shrinkage, Compressive creep, Tensile creep

**Lamen Sryh** is a PhD Candidate at the School of Civil Engineering, University of Leeds, United Kingdom.

**Professor John Forth** is a Chair in Concrete Engineering and Structures at the School of Civil Engineering, University of Leeds, United Kingdom.

## INTRODUCTION

Concrete structures usually last for several decades but sometimes their demolition is unexpected and unavoidable for reasons such as structural or material deterioration, natural disasters, construction development and war-inflicted damages. Recently, in the USA, the Environmental Protection Agency has estimated that the generation of rubble from construction demolition wastes (CDW) and renovation of buildings is close to 170 million tonnes annually [1]. Whereas, according to Eurostat it is about 850 million tonnes in the EU [2] and it is roughly 110 million tonnes in the UK alone as WRAP presented [3].

These figures have attracted much attention in the research community of civil engineering. The aim is to reuse the CDW as a coarse aggregate in producing a new concrete and thus contribute to greater sustainability in construction. Indeed, extensive scientific research on this subject has been carried out over the last 30 years.

The previous efforts in this topic concluded that in comparison to natural aggregate (NA), the quality of recycled aggregate (RA) is generally poorer. Replacing the NA by RA showed negative effects on the all properties of concrete [4-8]. The noticeable effects are on the time-dependent deformations (i.e. creep and shrinkage) rather than mechanical properties. This makes its use in various construction applications restricted.

All the studies stated that the presence of adhered mortar and other material such as clay bricks and tiles in RA, which are already poorer than the NA, is the main reason of causing these negative effects in the properties of concrete. These materials make RA more porous and more liable to absorb a high amount of water [4-9]. The high porosity and water absorption capacity of recycled aggregate substantially reduces the various properties of the resulting concrete.

However, several researchers [10-18] have found that the use of mineral additions in the production of recycled aggregate concrete (RAC) such as fly ash, silica fume, furnace slag and fibres could enhance the properties of concrete. These studies focused on the mechanical properties more than the time-dependent deformations.

Therefore, this experimental study aims to investigate the effect of adding steel fibres to the RAC on the drying shrinkage and creep deformations. That may be expected to reduce positively the time-dependent deformations of RAC and make it a suitable structural material and increase its use.

## BACKGROUND

In general, according to the literature review, as the replacement level of RA increases, the shrinkage and creep deformations of concrete also increase. The incorporation of RA at low replacement levels, specifically up to 30%, showed the equivalent or negligibly greater shrinkage than the corresponding concrete with NA [4].

Knaack and Kurama [19] carried out an experimental investigation on the creep and shrinkage of normal-strength concrete with recycled concrete aggregates (RCA) as a replacement for coarse natural aggregates. Three RCA sources and two aggregate replacement levels were used. They concluded that the creep and shrinkage strains of concrete increase significantly with increased aggregate replacement percentage (RP). As an average from the test results, the ratios of the total creep strain for RCA concrete to the companion NA concrete after testing up to approximately 7.5 months, were 1.31 and 1.61 for RP = 50% and 100% respectively.

The corresponding average ratios for the shrinkage strain were 1.21 and 1.71 for RP = 50% and 100%.

Fan et al. [20] studied the effect of replacement percentages of NA by recycled aggregate from crushing concrete (RCA) on the creep and shrinkage deformations. The compressive strength of concrete used to produce the RAC was 30MPa and the replacement percentages of the RCA specimens were at the levels of 33%, 66% and 100%. They observed that as the RCA replacement percentage increases, the creep and shrinkage of RCA concrete increase as well. More specifically, it was found that at the day 200 of testing the creep of concrete increases about 28.7%, 75% and 103.3% for the replacement percentages of 33%, 66% and 100% respectively. Moreover, and similarly to creep, the shrinkage deformations of RCA were approximately 2.6, 15.4 and 26.9% higher than that of NAC.

Domingo et al. [21] measured experimentally the creep and drying shrinkage strains of concrete. After 7 days of curing, samples were tested for 180 days. They observed 35%, 42% and 51% higher total creep deformations and 4%, 20% and 70% higher shrinkage strains when 20%, 50% and 100% of NA was replaced by RCA that produced from concrete has 40MP compressive strength. More studies [22-26] indicated percentages similar to these when other factors such as different sources of RA, mixing methods and types of curing were examined.

With regard to the effects of mineral additions, Kou et al. [15] observed an average decrease in shrinkage strains which corresponds to 15-20% in the RAC specimens that are made with 35% of fly ash (by weight of cement) at the age of 112 days compared to that without fly ash. In another study, Sago-Crentsil et al. [16] concluded that concrete produced with 100% RCA and contained ground granulated blast furnace slag (GGBS) showed 25% lower shrinkage. Moreover, Younis and Pilakoutas [17] stated that the addition of recycled tyres steel fibres (RTSF) can enhance the strength of RAC by 30%.

Since the invention of the steel fibres in 1970s, steel fibre reinforced concrete (SFRC) has become a very useful structural material in various construction applications. Adding steel fibres to concrete significantly enhances its mechanical properties and reduces the time-dependent deformations. However, there is currently limited research on the effect of steel fibres on recycled aggregate concrete, namely their effects on the creep and shrinkage.

In another study [18] presented by the same authors of this study showed that the addition of steel fibres enhanced the cube compressive strength, cylinder compressive strength, splitting tensile strength, flexural strength and the modulus of elasticity of the RAC by 1-5%, 5-25%, 11-55%, 16-53% and 4-15%, in comparison to the specimens without fibres.

Mangat and Azari [27] found that deformed fibres could reduce the shrinkage of the conventional concrete by up to 40% and the reduction increases with the increase in the fibre content. They also pointed out that the fibre geometry has a significant effect on the restraint of shrinkage, where deformed fibres are more effective than straight and smooth ones. In 1985, the same authors also showed that steel fibres would be expected to have only a small effect on the creep of concrete [28].

Swamy and Stavrides [29] reported that drying shrinkage of normal and lightweight aggregate concrete was reduced by about 15-20% due to the addition of 1.0% of steel fibres.

Other test results revealed by Chern and Young [30] indicted that the basic creep under uniaxial compression load and shrinkage were all lower for steel fibre concrete than for conventional plain concrete. Tan et al. [31] presented the same concept of effecting the steel fibres on creep and drying shrinkage.

## EXPERIMENTAL PROGRAMME

A total of nine groups of specimens, each consisting of four small prisms (75×75×200 mm) and two bobbins (75×365 mm), were prepared, cast, cured for 28 days and tested for 90 days. The properties of the materials, mixes proportions, specimens preparation, curing and tests method are described in the following sections.

### Materials and mixes proportions

The same high-strength cement (C52.5) was used in the all mixes for casting the specimens of this study and a natural fine aggregate with a maximum particle size of 5 mm was used. As a coarse aggregate, two types were used in this study; un-crushed natural aggregate with a maximum size of 20 mm and crushed washed construction and demolition waste (CDW) with a maximum size of 20 mm, used as a recycled coarse aggregate. The properties of used aggregate are summarised in Table 1 and samples as shown in Figure 1.

Leeds tap drinking water was used as mixing water in the all mixes of this study and a high range water-reducing concrete admixture (Sika®ViscoCrete) was used as a superplasticiser to control the workability requirements for all mixes. Furthermore, glued discontinued hooked-end steel fibres (Dramix 3D 65/35BG) from Bekaert were used in this study as shown in Figure 2. The fibres have an aspect ratio of 65, length of 35 mm and diameter of 0.55 mm.

Table 1 Properties of the aggregate

| PROPERTIES | (FA) | (NA) | (RA) |
|---|---|---|---|
| Specific gravity | 2.64 | 2.62 | 2.48 |
| Bulk density (kg/m$^3$) | 1580 | 1600 | 1360 |
| Water absorption ratio (%) | 1.06 | 0.49 | 4.78 |
| Porosity (%) | - | 38 | 46 |

A total of nine concrete mixes were designed and made with varying fibre contents ($V_f$= 0, 0.5 and 1.0%) and different recycled aggregate replacement percentages (RP = 0, 50 and 100%). All mixes had the same effective water-to-cement ratio (w/c= 0.42). Additional water was added to the RAC mixes to compensate for the high water absorption capacity of RA and achieve the required workability. The amount of the additional water was calculated depending on the amount of aggregate and its water content.

Sika®ViscoCrete as high range water-reducing admixture, was used for steel fibre concrete mixes to control the workability requirements and keep the w/c ratio constant for all the mixes. The details of the mix proportions are summarised in Table 2.

Natural aggregate Recycled aggregate

Figure 1 Samples of natural and recycled coarse aggregate


Figure 2 Hooked-end steel fibres (Dramix 3D)

**Specimens preparation, casting and curing**

The concrete mixing procedure including preparation of materials, batching and mixing was taken place with accordance to BS 1881−125. For each mix, the materials were prepared and weighed in the required proportions. The materials were poured in the drum mixer in the following order: half of the required quantity of coarse aggregate, full quantity of fine aggregate followed by the cement content and finally the remaining quantity of coarse aggregate. These materials were mixed dry for the first minute to homogenise the batch, then water was added and the wet mixing took place for several minutes. The superplasticiser was used if needed to the mix (mixes with steel fibres) and was added to the water prior to pour.

The workability of fresh concrete was evaluated by the slump test and then the concrete was filled in the prepared moulds directly after measuring the slump. The moulds were filled in layers and the compacting process took place immediately after filling each layer using a vibrating table for few seconds to avoid the segregation of concrete.

The specimens were covered by wet mats and plastic sheets to prevent the evaporation of water and left for at least 24 hours. After the following day, the specimens were demoulded and transferred to the controlled fog room to be curried for 28 days until the day of test as shown in Figure 3.

Table 2 Concrete mixes proportions

| MIX | SPECIMEN | W/C | MIX PROPORTIONS (kg/m³) | | | | | | |
|---|---|---|---|---|---|---|---|---|---|
| | | | W | C | FA | CA | RA | SP | SF |
| M1 | NC | 0.42 | 177 | 422 | 754 | 1024 | - | - | - |
| M2 | SFC-0.5 | 0.42 | 177 | 422 | 754 | 1024 | - | 0.5 | 40 |
| M3 | SFC-1.0 | 0.42 | 177 | 422 | 754 | 1024 | - | 1.0 | 80 |
| M4 | RAC-50 | 0.42 | 177 | 422 | 754 | 512 | 512 | - | - |
| M5 | SFRAC-50-0.5 | 0.42 | 177 | 422 | 754 | 512 | 512 | 0.5 | 40 |
| M6 | SFRAC-50-1.0 | 0.42 | 177 | 422 | 754 | 512 | 512 | 1.0 | 80 |
| M7 | RAC-100 | 0.42 | 177 | 422 | 754 | - | 1024 | - | - |
| M8 | SFRAC-100-0.5 | 0.42 | 177 | 422 | 754 | - | 1024 | 0.5 | 40 |
| M9 | SFRAC-100-1.0 | 0.42 | 177 | 422 | 754 | - | 1024 | 1.0 | 80 |

**Note:** W/C = water-to-cement ratio, W = water, C = cement, FA = fine natural aggregate, CA = coarse recycled aggregate, RA = recycled coarse aggregate, SP = superplasticiser, SF = steel fibres.

Figure 3 Casting and curing

## Tests method

After 28 days of curing, two prisms (75x75x200 mm) were prepared and tested for drying shrinkage. Demec points were placed on the two sides of the specimens and a digital hand-held strain gauge was used to take the readings as shown in Figure 4. Specimens were stored in a control room with proper humidifier to ensure constant environmental conditions; 20ºC ±0.5 ºC and 45% ±5% of relative humidity. The final values of shrinkage strains were calculated based on the average of the samples readings.

Figure 4 Shrinkage test

Another two prisms (75x75x200 mm) from each mix were prepared and tested at the age of 28 days for compressive creep. Demec points were fixed on the two sides of specimens in order to measure the deformations over the time. Specimens were subjected to a constant compressive stress that is equivalent to 0.2 $f$c (of control specimen) as shown in Figure 5. The initial elastic strains due to the applied load were measured then the readings over the time were recorded. The compressive creep strains and coefficients were calculated based on the average of the sample readings after taking into account the shrinkage strains.

Figure 5 Compressive creep test

For the tensile creep test, the test rig and concrete bobbins (75x365 mm) were used as shown in Figure 6. Demec points were placed on the sides of specimens and 1 MPa tensile stress was applied. Initial strains due to the applied load were determined and the measurements of deformations over time were recorded. Shrinkage strains were considered in the final calculations of the tensile creep strains.

Specimens of creep tests were cured in a fog room and tested in the controlled room under the same environmental conditions of the shrinkage specimens. In addition, the same digital hand-held strain gauge was used to take the readings.

Figure 6 Tensile creep test

## RESULTS AND DISCUSSION

### Effect on drying shrinkage

Drying shrinkage can be defined as the deformations that occur due to the volume changes of concrete when it is exposed to drying conditions. In this study, shrinkage was measured after 28 days of curing. Figure 7 shows the effect of steel fibres and recycled aggregate on the shrinkage strain variations with time. As the type of aggregate plays an important role in shrinkage, the influence of the percentage of recycled aggregate in concrete can be clearly observed.

There are greater shrinkage deformations as the substitution ratio of RA increased. More specifically, drying shrinkage strains increased by 18 and 38% when 50 and 100% of the aggregate were replaced. This can be attributed to the presence of adhered mortar in RA that causes an increase in the volume of cement paste in the resulting concrete. The increase in cement paste makes the concrete more porous and more liable to absorb the water. This can have an effect on the rapid evaporation of water in concrete and lead to higher shrinkage.

In contrast, adding steel fibres showed reductions in the drying shrinkage strains of normal and recycled aggregate concrete. The drying shrinkage reduced by increasing the fibre volume fraction ($V_f$). The results recorded reductions by 7% and 15% when 0.5% and 1.0% of steel fibres were added respectively. The reason for this can be explained by the ability of steel fibres to restrain the volume changes in concrete and improve the bond between the cement matrix and coarse aggregate.

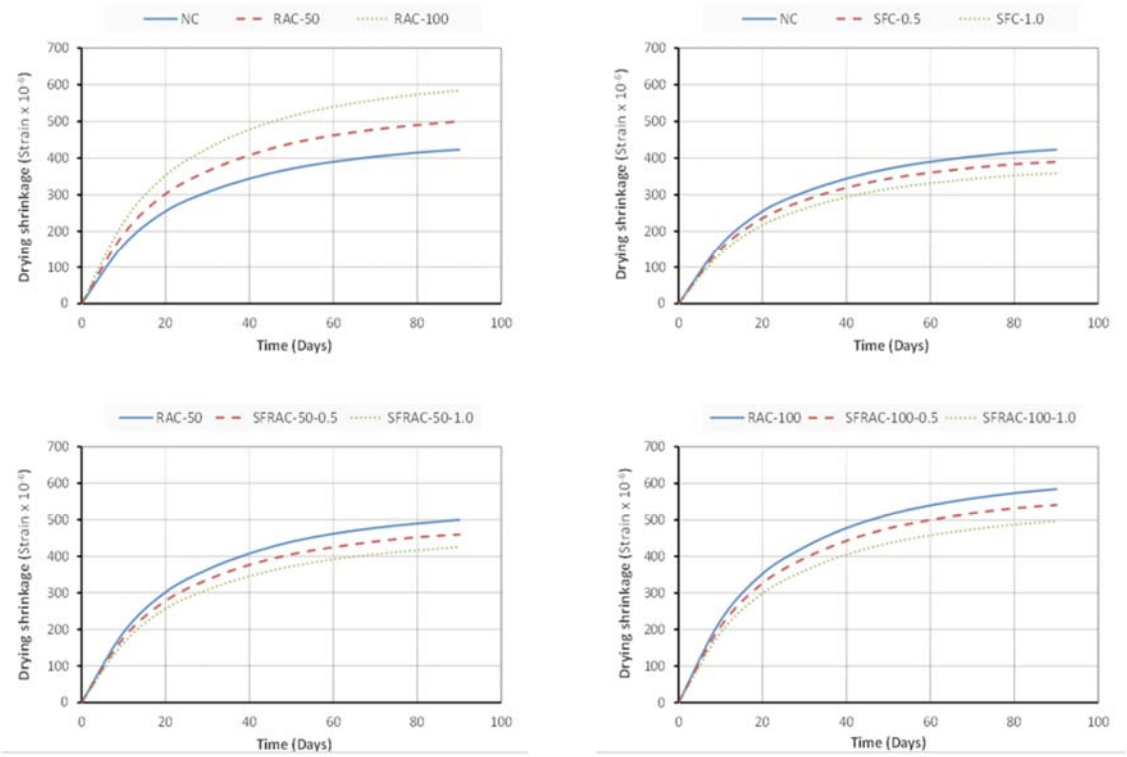


Figure 7 Effect of steel fibres and recycled aggregate on drying shrinkage

## Effect on creep

Creep in concrete is defined as the deformations that occur under sustained loads (compressive or tensile). In this study, specimens were curried for 28 days and then subjected to sustained compressive and tensile stresses as described earlier. In general, the experimental results showed that when the natural aggregate was substituted by the recycled one, the creep deformations increased. The reasons were thought to be that the actual volume of aggregate is reduced due to the presence of adhered cement mortar in the recycled aggregate. This makes the aggregate/cement ratio lower and increases the porosity. Also, the old attached mortar can amplify the Interfacial Transition Zone (ITZ) between the new cement paste and the RA which degrades the properties of concrete and causes more micro cracks in this region under loading over time. Moreover, the elastic modulus of recycled aggregate and the resulting concrete are lower than the natural aggregate and the conventional concrete. All these effects can cause an increment in creep deformations.

Figures 8 and 9 show the effect of adding steel fibres and using recycled aggregate on creep deformations of concrete. Similarly to the shrinkage results, increments of 15% and 8% in the compressive and tensile creep strains were recorded respectively when 50 % of RA was used. However, when 100% of RA was replaced, percentages of 29% and 15% were achieved.

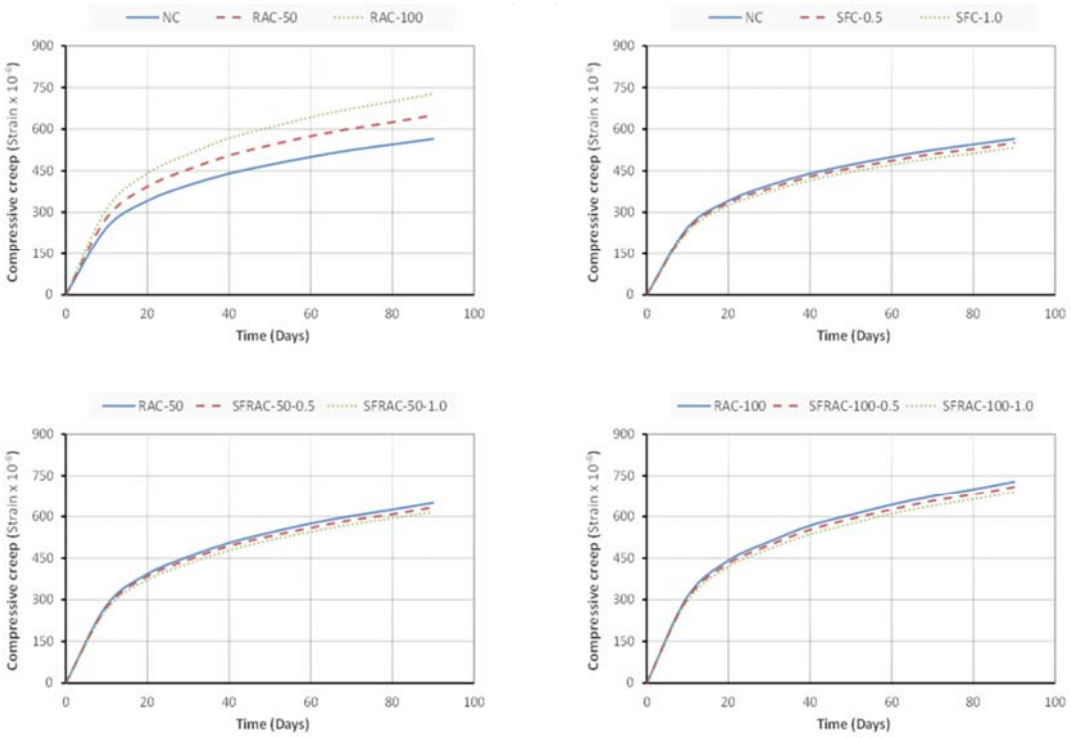


Figure 8 Compressive creep results

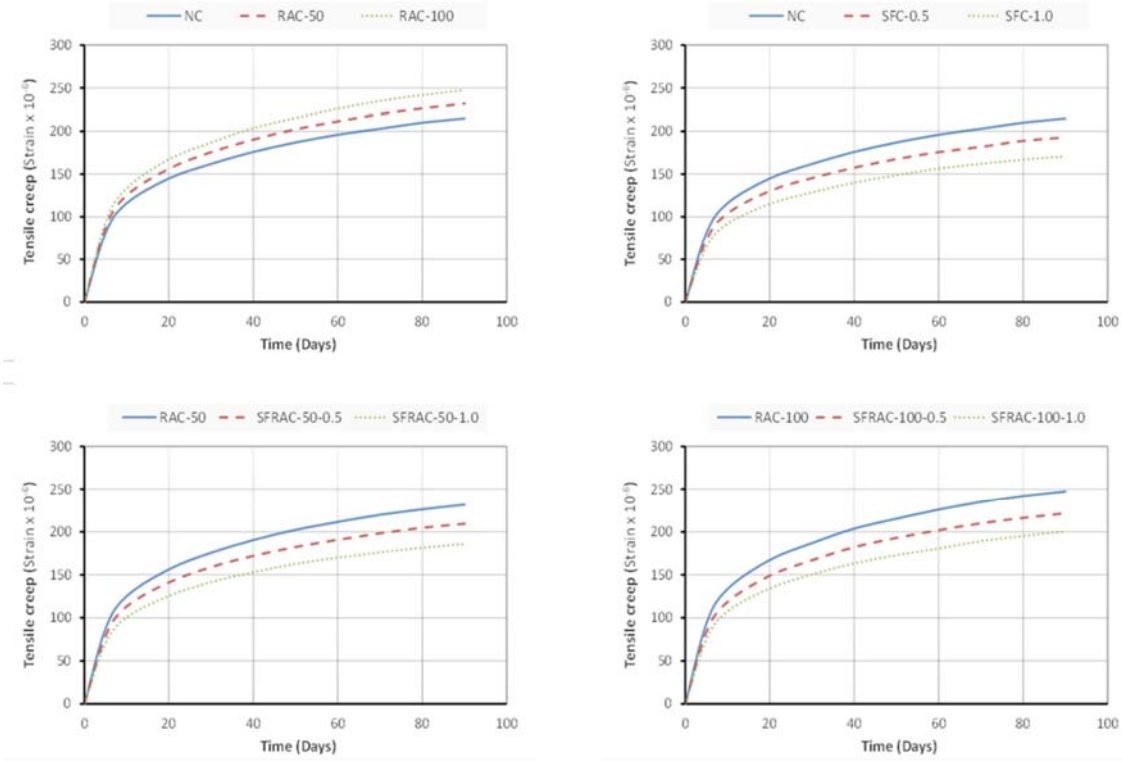


Figure 9 Tensile creep results

On the other hand, and compared to the effect of steel fibres on the drying shrinkage, the results showed there is no significant effect on compressive creep, however, the effect on tensile creep is better. Reductions by 3% and 10% in compressive and tensile creep results respectively were observed by incorporating 0.5% of steel fibre content. However, further reductions with percentages of 5% and 20% respectively were seen when 1.0% of fibre content was added. This can attributed to the role of steel fibres in enhancing the tensile strength of concrete more than the compressive as discussed and presented by the authors somewhere [18]. Adding steel fibres also can contribute in improving the interfacial bonding capacity between the cement matrix and aggregate and enhancing the cracking resistance.

## CONCLUSIONS

The objective of this study was to experimentally investigate the effect of steel fibres and recycled aggregate on creep and drying shrinkage deformations of concrete. Based on the experimental results, the main findings can be concluded as following:

- Replacing the natural aggregate by the recycled one (CDW) indicated negative effects on the drying shrinkage and creep deformations of concrete. The experimental results recorded greater increments due to substituting 50% and 100% of aggregate.

- The results showed that drying shrinkage strains increased by 18% and 38%, compressive creep increased by 15% and 29% and tensile creep increased by 8% and 15% when 50% and 100% of RA were replaced respectively.

- The presence of adhered cement paste and other materials in the recycled aggregate is the main reason to increase the time-dependent deformations of concrete. This can be attributed to the properties of these materials that are lower than the natural aggregate. This causes an increase in the porosity and water absorption capacity and reduces the aggregate/cement ratio and modulus of elasticity of the resulting concrete.

- The old attached mortar also can amplify the Interfacial Transition Zone (ITZ) between the new cement paste and the RA which degrades the properties of concrete and causes more micro cracks in this region under loading over time.

- Adding steel fibres showed significant reductions in the drying shrinkage and tensile creep deformations of concrete. However, its effect on compressive creep was slight. Reductions by 7%, 3% and 10% were observed in the results of drying shrinkage, compressive creep and tensile creep when 0.5% of steel fibre content was added. Further reductions with percentages of 15%, 5% and 20% respectively were seen when 1.0% of fibre content was added.

- In general, it can be concluded that using steel fibres with recycled aggregate in concrete can enhance the mechanical properties of concrete and reduce the time-dependent deformations. This may expand and increase the use of RAC in various structural applications in the future.

## ACKNOWLEDGEMENT

The authors are grateful for the support of the Libyan Embassy in the UK and the School of Civil Engineering at University of Leeds.

## REFERENCES

1. EPA. Environmental Protection Agency. Available in: <http://www.epa.gov> [accessed January 2014].
2. Eurostat. Waste statistics in Europe. Available in: <http://epp.eurostat.ec.europa.eu/> [accessed in July 2014].
3. WRAP. Perfomance Related approach to use recycled aggregates. *Oxon: Waste and Resources Action Programme*; 2007.
4. DE BRITO, JORGE; SAIKIA, NABAJYOTI. Recycled aggregate in concrete; Use of industrial, construction and demolition waste. Springer, London, 2013.
5. RAHAL, KHALDOUN. Mechanical properties of concrete with recycled coarse aggregate. *Building and Environment*, 2007, 42.1: 407-415.
6. YANG, KEUN-HYEOK; CHUNG, HEON-SOO; ASHOUR, ASHRAF F. Influence of type and replacement level of recycled aggregates on concrete properties. *ACI Materials Journal*, 2008, 105.3.
7. XIAO, JIANZHUANG; LI, JIABIN; ZHANG, CH. Mechanical properties of recycled aggregate concrete under uniaxial loading. *Cement and Concrete Research*, 2005, 35.6: 1187-1194.
8. MALEŠEV, MIRJANA; RADONJANIN, VLASTIMIR; MARINKOVIĆ, SNEŽANA. Recycled concrete as aggregate for structural concrete production. *Sustainability*, 2010, 2.5: 1204-1225.
9. DE JUAN, MARTA SÁNCHEZ; GUTIÉRREZ, PILAR ALAEJOS. Study on the influence of attached mortar content on the properties of recycled concrete aggregate. *Construction and Building Materials*, 2009, 23.2: 872-877.
10. JALILIFAR, H., SAJEDI, F. AND KAZEMI, S., 2016. Investigation on the mechanical properties of fiber reinforced recycled concrete. *Civil Engineering Journal*,*2*(1), pp.13-22.
11. NAM, J., KIM, G., YOO, J., CHOE, G., KIM, H., CHOI, H. AND KIM, Y., 2016. Effectiveness of Fiber Reinforcement on the Mechanical Properties and Shrinkage Cracking of Recycled Fine Aggregate Concrete. *Materials*, *9*(3), p.131.
12. KRISHNA, T.S., 2015. An experimental investigation on flexural behavior of recycle aggregate fiber reinforcement concrete.
13. KUMAR, D. NARESH; RAO, T. VENKATESWARA; MADHU, T.; SAROJA, P.L.N.; PRASAD D. S. V. An experimental study of recycled concrete with polypropylene fiber. *International Journal of Innovative Research in Advanced Engineering (IJIRAE)*, ISSN: 2349-2163, Volume 1, Issue 7, August 2014.

14. PRASAD, M.L.V.; KUMAR, P. Rathish. Strength studies on glass fiber reinforced recycled aggregate concrete. *Asian Journal of Civil Engineering (Building and Housing)*, vol. 8, No. 6, 2007, pages 677-690.
15. KOU, S.C., POON, C.S. AND CHAN, D., 2008. Influence of fly ash as a cement addition on the hardened properties of recycled aggregate concrete. *Materials and Structures*, *41*(7), pp.1191-1201.
16. SAGOE-CRENTSIL, K.K., BROWN, T. AND TAYLOR, A.H., 2001. Performance of concrete made with commercially produced coarse recycled concrete aggregate. *Cement and concrete research*, *31*(5), pp.707-712.
17. YOUNIS, K.H. AND PILAKOUTAS, K., 2013. Strength prediction model and methods for improving recycled aggregate concrete. *Construction and Building Materials*, *49*, pp.688-701.
18. SRYH, L.; FORTH, J. Experimental investigation on the effect of steel fibres on the mechanical properties of recycled aggregate concrete. *In Proceedings of: the International Conference on the Fibre Concrete*, Prague, Czech Republic, 2015.
19. KNAACK, A.M. AND KURAMA, Y.C., 2015. Creep and Shrinkage of Normal-Strength Concrete with Recycled Concrete Aggregates. *ACI Materials Journal*, *112*(3).
20. FAN, Y., XIAO, J. AND TAM, V.W., 2014. Effect of old attached mortar on the creep of recycled aggregate concrete. *Structural Concrete*, *15*(2), pp.169-178.
21. DOMINGO, A., LAZARO, C., GAYARRE, F.L., SERRANO, M.A. AND LOPEZ-COLINA, C., 2010. Long term deformations by creep and shrinkage in recycled aggregate concrete. *Materials and structures*, *43*(8), pp.1147-1160.
22. SILVA, R.V., DE BRITO, J. AND DHIR, R.K., 2015. Prediction of the shrinkage behaviour of recycled aggregate concrete: A review. *Construction and Building Materials*, *77*, pp.327-339.
23. FATHIFAZL, G., RAZAQPUR, A.G., ISGOR, O.B., ABBAS, A., FOURNIER, B. AND FOO, S., 2011. Creep and drying shrinkage characteristics of concrete produced with coarse recycled concrete aggregate. *Cement and Concrete Composites*,*33*(10), pp.1026-1037.
24. AJDUKIEWICZ, A. AND KLISZCZEWICZ, A., 2002. Influence of recycled aggregates on mechanical properties of HS/HPC. *Cement and concrete composites*, *24*(2), pp.269-279.
25. KOU, S.C., POON, C.S. AND ETXEBERRIA, M., 2011. Influence of recycled aggregates on long term mechanical properties and pore size distribution of concrete. *Cement and Concrete Composites*, *33*(2), pp.286-291.
26. FERREIRA, L., DE BRITO, J. AND BARRA, M., 2011. Influence of the pre-saturation of recycled coarse concrete aggregates on concrete properties. *Magazine of Concrete Research*, *63*(8), pp.617-627.
27. MANGAT, P.S. AND AZARI, M.M., 1984. A theory for the free shrinkage of steel fibre reinforced cement matrices. *Journal of materials science*, *19*(7), pp.2183-2194.
28. MANGAT, P.S. AND AZARI, M.M., 1985. A theory for the creep of steel fibre reinforced cement matrices under compression. *Journal of materials science*, *20*(3), pp.1119-1133.

29. SWAMY, R.N. AND STAVRIDES, H., 1979, March. Influence of fiber reinforcement on restrained shrinkage and cracking. In *Journal Proceedings* (Vol. 76, No. 3, pp. 443-460).

30. CHERN, J.C. AND YOUNG, C.H., 1990. Factors Influencing the Drying Shrinkage of Steel Fiber Reinforced Concrete. *Materials Journal*, *87*(2), pp.123-139.

31. TAN, K.H., PARAMASIVAM, P. AND TAN, K.C., 1994. Instantaneous and long-term deflections of steel fibre reinforced concrete beams. *ACI Structural Journal-American Concrete Institute*, *91*(4), pp.384-393.

# Additional Papers

# CONCRETE RHEOLOGY AND HOW IT CAN BE NEUTRALISED OR IMPROVED WHEN USING DIFFICULT AGGREGATES

**J Kluegge**
BASF Construction Solutions
Germany
**I Ellis**
BASF Plc
United Kingdom

**ABSTRACT.** Since comb polymers based on PolyCarboxylicEthers (PCEs) have been introduced, they shifted the limits of achievable concrete performance dramatically. Today we are able to build higher, stronger and more durable than ever before. As a consequence of the outstanding water reduction and early strength performance of PCEs the industry was enabled to lower W/C ratios, reduce cement contents and utilize more SCM in the concrete mixes. At the same time the aggregate available for concrete production becomes more and more demanding with regards to its rheological properties. In consequence modern mix designs are often prone to increased concrete viscosity and stickiness of the concrete. We have developed a new superplasticizer technology based on comb polymers featuring aromatic backbones: PolyArylEthers (PAE). Compared to conventional PCE, these new admixtures are able to reduce the thixotropy of concretes. In addition, a good early strength development and outstanding water reduction is maintained. More than 25 years after introducing the first PCE into the industry, PAE provides a breakthrough of rheology performance improvement for concrete. High viscosity of fresh concrete has a big impact on its pump-ability, spray-ability, place-ability and surface finishing. Using PAE based admixtures equip concrete with appropriate rheological properties that help save placing time and labor costs and are therefore highly relevant for the construction industry. The workability of fresh concrete is usually characterized by its slump and slump flow values. However, workers often notice significant differences when handling concrete prepared according to different recipes, even if they exhibit very similar workability. Especially concretes with high SCM content that are treated with PAE are less sticky and can be placed with low effort. This behavior is quantified by comparing yield values, plastic viscosities and thixotropy and is characterized by using V-funnel and rheometer tests. The advantages of this technology are exemplified on mixes optimized for their sustainability and compared with conventional mix designs based on a life cycle assessment.

**Keywords:** Sustainable construction, High range water reducers, Life-cycle analysis, Admixture innovation, Carbon footprint, Concrete performance

**Dr Jan Kluegge** is Head of Marketing Ready-Mix Europe for BASF Construction Solutions, Germany.

**Ian Ellis** is Technical Services Manager - Admixture Systems for BASF Plc, United Kingdom.

## INTRODUCTION

Global warming as a consequence of the increasing emission of carbon dioxide is considered to be a major challenge for mankind. One significant source of human $CO_2$ emission is the production of Portland cement[1]. For every ton of Portland cement produced, approximately 900 kg carbon dioxide is released into the atmosphere[2]. In 2010, around 3.3 billion tons of cement was produced, which corresponds to more than 3 billion tons of $CO_2$ and the demand for cement is expected to continue to grow with the global population and the development of urban centers. It is therefore not surprising that construction industry is experiencing increasing pressure to reduce their $CO_2$ emissions in order to become more sustainable. Consequently, modern concrete technology aims at minimizing the need for Portland cement without sacrificing the strength and the durability of the hardened concrete.

Superplasticizers allow maintaining the workability of fresh concrete with less water and hence help significantly increase the strength after hardening. Stronger concrete allows slimming down structures and thus decreasing the Portland cement consumption. A second important lever to reduce the content of Portland cement in a concrete is the use of supplementary cementitious materials (SCM). However, (partially) replacing Portland cement by SCM often leads to a loss of (initial) strength that is usually compensated by lowering the water cement ratio. The resulting workability drop can again be compensated by the utilization of superplasticizers. However, with high loads of fillers and SCM in the concrete mix design, state of the art PCE based superplasticizers are reaching technical limits: This is and especially problematic when demanding aggregates are used. Although PCE based superplasticizers manage to establish the desired slump and water reduction, the concrete becomes very “sticky” and has a tenacious appearance. The concrete appears viscous and seems to have a higher cohesion, which negatively influences its pump ability, spray ability, place ability and surface finishing. Interestingly, not all superplasticizers have the same negative impact on rheology. Thus, it is very important to choose the right superplasticizer type in order to avoid undesirable stickiness.

This work presents a novel class of superplasticizers, developed by BASF that provides excellent rheological properties even in demanding mix designs. At the same time it maintains known advantages of PCE based superplasticizers like high water reduction capability, high early strength and tune-able slump retention properties. These new dispersants differ from conventional superplasticizers in the chemical nature of their polymer backbones. Like conventional polycarboxylate ethers (PCE), the polymers exhibit a comb structure with polyether side chains; however the acrylate-free backbone has an aromatic rather than aliphatic character and is considered to be more rigid. Moreover, they feature phosphate moieties as anchoring groups. The presence of aromatic units in combination with a very high density of negative charges is believed to increase the affinity to the cement surface, whereas the presence of side chains adds a steric component to the electrostatic component of the inter-particle repulsion forces. These aromatic comb polymers will be called polyaryl ethers (PAE) in order to distinguish them from conventional PCE. They combine some of the beneficial properties of poly(ß-naphthalene sulfonates) (BNS) with the high performance of PCE (Figure 1). The aromatic character of the backbone is believed to induce a much better carbon black dispersion capability, which improves the surface appearance of e.g. fly ash containing concretes.

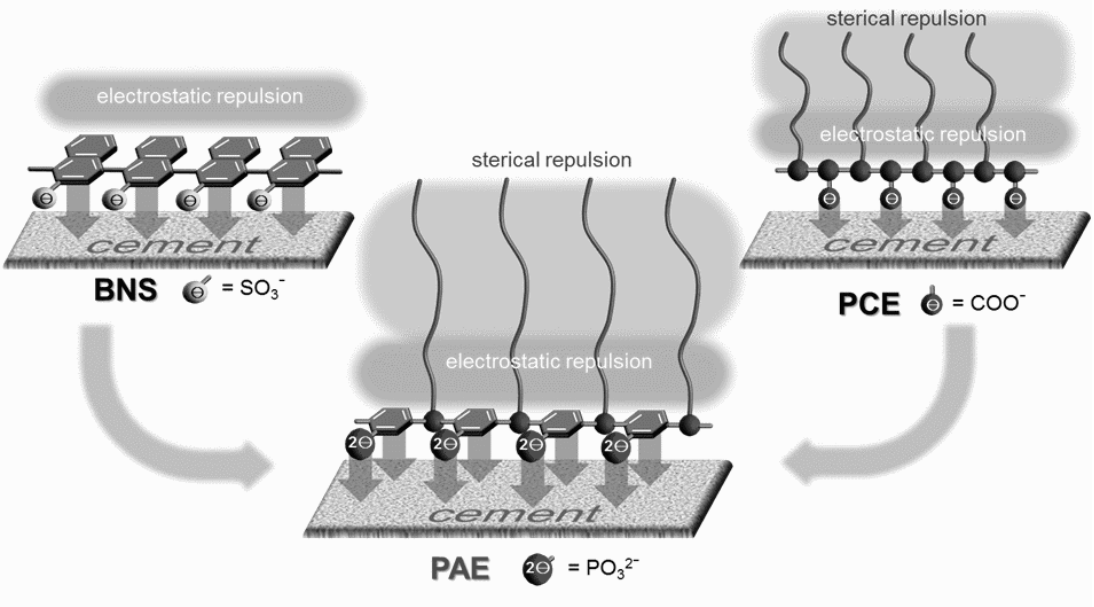


Figure 1 Schematic sketch of the structure of aromatic comb polymers (PAE)

The influence of PAE on the rheology of fresh concrete and mortar is compared with commercially available conventional PCE as well as with laboratory-made small molecule dispersant (SMD). The SMD-type dispersant consists of a single polyether chain that is comparable to those used as side chains in PCE. However, this single polyether chain is not attached to a polymer backbone. Instead, it is functionalized with negatively charged functional groups that serve as anchoring group and thus provide adsorption to concrete (

Figure 2)

Figure 2 Schematic sketch of the structure of a small molecule dispersant SMD

## THEORETICAL BACKGROUND

A Bingham type relation is often used to describe the flow behavior of concrete at low and intermediate shear rates. It describes a linear dependency of shear stress $\tau$ in relation to the applied shear rate $\dot{\gamma}$:

$$\tau = \tau_0 + \mu \cdot \dot{\gamma}$$

In this model, the yield stress $\tau_0$ determines the value when concrete begins to flow under its own mass. This value can be easily measured by the flow test[3]. The flow of concrete or mortar

correlates with yield stress $\tau_0$. On the other hand, the plastic viscosity μ determines the flow time or speed of concrete during molding or pumping. This value indicates how easily the concrete can be placed or filled into forms (knead ability, place ability, spread ability, spray ability, pump ability or flow ability). Furthermore, the flow properties of concrete are also determined by its thixotropy, a shear thinning effect. Due to its thixotropic nature, concrete appears thick (viscous) under static conditions and will start to flow (become thin, less viscous) over time when subjected to mechanical stress (e.g. agitation, shaking, stirring). Upon relieve of the mechanical stress, it takes a certain time for the concrete to return into its previous, more viscous state. Thus, mechanical stress helps to improve the flow ability of fresh concrete.

The flow behavior of concrete is influenced by the water content, type, shape, size and amounts of the solids, viscosity modifying agents (VMA), air entraining agents (AEA) and superplasticizers. *Wallevik et al.* have nicely summarized these influencing factors in form of a rheograph[4]. According to them, dispersants improve the flow ability of concrete mainly by lowering its yield stress. Most superplasticizers have only a minor impact on the plastic viscosity. For some dispersant types a rise of the plastic viscosity can be observed and for others a decrease.

The main application of dispersants, however, is not to improve the flow ability of concrete at a given W/C. More typically, they are used to reduce the water content with the target to achieve a higher compressive strength. The dispersant takes care of maintaining the same flow ability of the concrete by lowering the yield stress compared to the same concrete mix without dispersant.

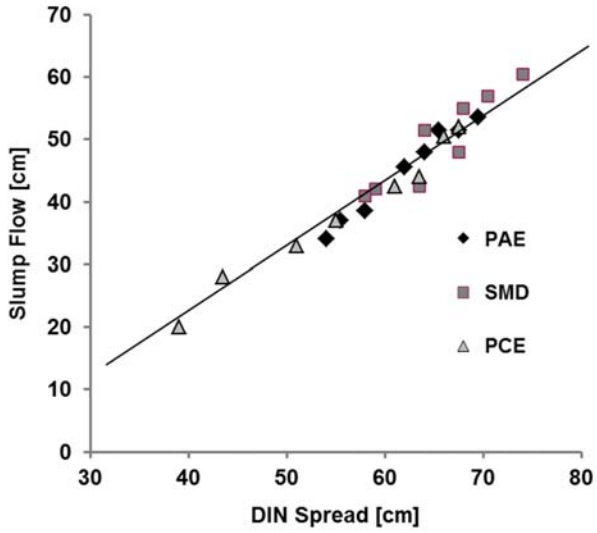


Figure 3 Correlation slump flow and spread (according to DIN EN 12350-5)

The most widely used industrial application test method to characterize the fluidity of concrete is the slump test. The obtained values are based on the flow of concrete under its own weight. However, the concrete is subjected to only minor shear forces during the test. Even the DIN Spread test, a variation of the slump test in which the flow diameter is determined on a shocking table, does not involve substantial shear forces. Thus, the obtained values for slump (remaining height of the concrete pile compared to the test cone), slump flow (flow diameter without

shocking) and DIN spread (flow diameter on a shocking table) are in principle equivalent. If slump values are plotted against slump flow or DIN-spread values, the data show a very good correlation and always fit to the same curve - independent of the concrete mixture, the type of superplasticizer and the age of the fresh concrete. All these values correlate very well with the yield stress. However, plastic viscosity, the other characteristic indicator for the rheology, cannot be assessed by using these methods.

The effect of increasing plastic viscosity becomes obvious in concrete mixture proportions that exhibit a low water to cement ratio and increasing solid volume fractions. These concretes have a sticky appearance to the workers despite exhibiting a normal behavior in slump tests[5]. The increase of the plastic viscosity is related to contact interactions between the fine particles. They are a result of repulsive electrostatic forces, caused by the electric double layers on the surfaces, attractive van der Waals forces and by the steric repulsion caused by the layer of adsorbed superplasticizer. The latter is the dominating force between the fine particles. Due to the steric repulsion caused by the presence of a superplasticizer, agglomerates are getting fractured into smaller particles, which can now be more densely packed compared to the larger agglomerates. This means that the maximum possible solid volume fraction increases. Water that had been stored in interparticle pores becomes displaced and forms a water film around the particles and helps to separate the contact points between the particles. Thus, the mobility of the particles increases and the system becomes more fluid.

The apparent viscosity of a mortar very much depends on the shear rate that is applied. At low shear rates the apparent viscosity is dominated by colloidal interactions and very sensitive to the superplasticizer dosage, because it decreases the stability of the colloidal network. With increasing shear rates (in the range of 3 - 30 $s^{-1}$), the stability of the colloidal network loses significance and viscous interactions start to take over. Finally, at very high shear rates, the liquid interparticle phase loses influence and the system starts to behave like densely packed solid spheres and the apparent viscosity rises again. The best-suited shear rate window for measuring the apparent viscosity is therefore the region around the minimum of the apparent viscosity curves. Artelt et al. have correlated the range of shear forces that typically impact the fresh concrete when applying typical industrial test methods or processing steps.[6] According to them, segregation occurs at virtually non-existent shear rates. At shear rates below around 0.1 $s^{-1}$, concrete stops to flow visibly. For practically relevant concrete processing steps like placement, finishing and handling, the applied shear forces are estimated to be in the range of 10 - 30 $s^{-1}$, which is similar to the shear forces in V-funnel or L-box tests. However, concrete also exhibits a pronounced thixotropic behavior. External shear forces degrade the colloidal network formed in fresh concrete, resulting in a decrease of the viscosity. After a certain time, the network has degraded completely and the viscosity reaches its minimum. However, this thixotropic behavior is reversible. As soon as the concrete is put to a rest, the intercolloidal network starts to reestablish itself. Theoretically, the viscosity should rise until its initial value has been reached. In practice, the final viscosity will be higher than its initial value, due to the ongoing hydrates nucleation[7]. In addition these hydration products increase the surface roughness of the particles, which leads to stronger contact interactions. Consequently, it is only possible to compare values for the plastic viscosities of different concretes if they all have been determined at the same stage of the thixotropic effect, ideally in a stage were all colloidal networks are disrupted.

In a previous work[8] it was reported that PAE and SMD are able to considerably decelerate the colloidal network reformation when compared to PCE. This was proven by applying an experimental setup, in which the colloidal network formation was subsequently completely

destroyed by applying high shear stress followed by a period of rest. After destroying the colloidal network, the sample was always treated with a very low shear rate of 0.5 $s^{-1}$ in order to minimize the plastic viscosity contribution. The shear stress was therefore a more or less pure static yield stress response. The thixotropy can be determined as the first derivative of the yield stress as a function of time. As can be seen in figure 4, the yield stress derived from the shear stress recordings increases over time. However, the slope decreases when comparing the first period of rest (0-30 s) with the second period of rest (30 - 120 s). Moreover, it becomes obvious that PAE exhibits the lowest slope and therefore the lowest thixotropy (Figure 4).

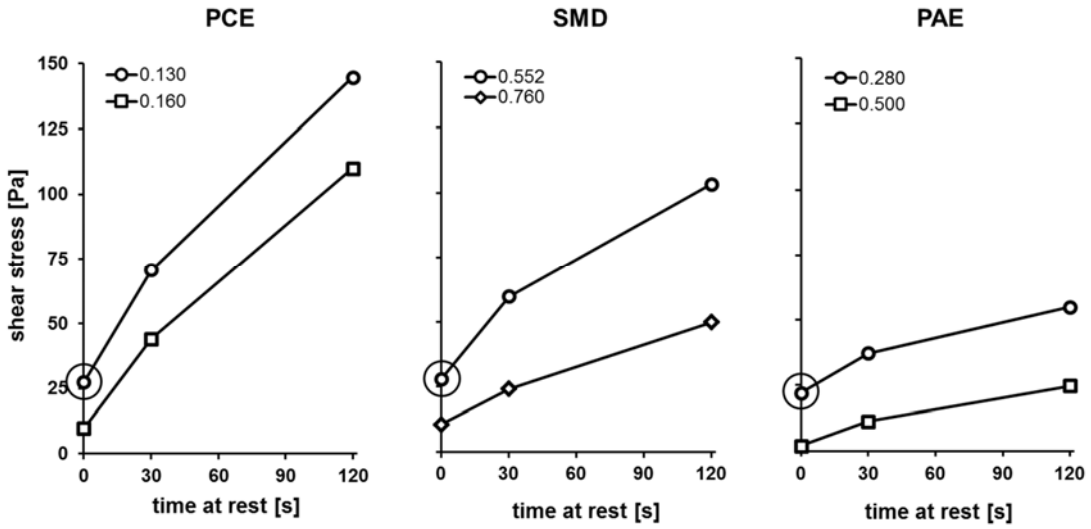


Figure 4 Correlation between shear stress and time at rest for different superplasticizer types, applied at two different dosages

In other words, stiffening of the mortar (increase of the yield stress) over time is much less pronounced if PAE and SMD are used as plasticizers. Both SMD and PAE are able to significantly reduce the thixotropy of mortar and concrete compared to PCE. However, in terms of practical use PAE offers two important benefits: PAE is significantly more dose efficient and, even more important, it is much less retarding compared to SMD. PAE delivers superior early compressive strength: While the 24 h strength could not be tested in case of the SMD-containing concrete (mixture 4), the PAE-containing concrete (mixture 5) already exhibited a compressive strength of 9.9 MPa.

In this work we investigate if the results found for mortar are also valid for concrete. We compare the rheology of concretes prepared with PAE and SMD with PCE by utilizing V-funnel or L-box tests, which give a rather rough qualitative assessment of the plastic viscosity, as well as by employing a concrete rheometer and tribometer. The latter are much better suited for the measurement of the plastic viscosity of concrete, as they allow applying defined shear forces and viscosity measurements without significant time lapse.

## RESEARCH SIGNIFICANCE

The introduction polycarboxylate ethers (PCE) in the mid 1980ies, was the last major technological breakthrough in the field of admixtures and established new “superplasticizer” performance levels for water reduction and workability retention. About 30 years later BASF introduces an entirely new superplasticizer technology: Phosphate-functionalized Polyaryl ethers (PAE) offer state of the art water reduction and outperform most PCE in reducing the stickiness and tenacity of modern SCM based concretes. This work aims toward comparing the influence PAE, SMD and PCE superplasticizers on the rheology of concrete by using industrial V-funnel and L-box as well as a concrete rheometer and a tribometer.

## EXPERIMENTAL INVESTIGATION

### Materials and mixture proportions

All concrete mixture proportions used in this work are summarized in table 1. Ordinary Portland cements were used for the concretes. Aggregate grading was in between grading curve A and B according to DIN EN 1045-2. The maximum grain size $D_{max}$ was 16 mm.

The superplasticizers PCE and PAE were characterized by having relatively short side chains. However, the side charge density was lower in the case of PAE. For comparison a small molecule dispersant (SMD) was also tested. It consisted of a long polyether chain with one chain end being functionalized with four anionic moieties. The admixtures dosages were adjusted to achieve a comparable initial slump flow. All dosages are based on solid content of admixture by weight of cement. The air content has been kept constant in a range of 2 to 2.5%.

Concrete slump flow tests were carried out according to DIN EN 12350-5 and V-Funnel tests according to the EFNARC_SCC Guidelines, May 2005 47-56[9].

Table 1 Overview of the concrete mixture proportions used in this work:

| Mix No. | Cement (Type) | Cement (kg/m³) | Fly ash[1] (kg/m³) | Slag[2] (kg/m³) | Limest. Powder[3] (kg/m³) | Sand/ Aggregates | Water (kg/m³) | W/C | Admixture (type) | Admixture dosage (%)[4] |
|---|---|---|---|---|---|---|---|---|---|---|
| 1 | CEM I 52.5 N | 400 | - | - | - | nat.rounded | 152 | 0.38 | PAE | 0.68 |
| 2 | CEM I 52.5 N | 400 | - | - | - | nat.rounded | 152 | 0.38 | SMD | 0.99 |
| 3 | CEM I 52.5 N | 400 | - | - | - | nat.rounded | 152 | 0.38 | PCE | 0.48 |
| 4 | CEM I 42.5 R | 300 | 75 | 120 | 40 | crushed | 186 | 0.62 | PAE | 0.84 |
| 5 | CEM I 42.5 R | 300 | 75 | 120 | 40 | crushed | 186 | 0.62 | SMD | 1.1 |

[1]Siliceous Fly ash: Blaine 4050 cm²/g, density 2.27 kg/l; [2]Slag: Blaine = 4250 cm²/g, density = 2.91 kg/l; [3]Limestone powder: Blaine = 5750 cm²/g, density = 2.71 kg/l. [4]Admixture dosages are given in % solid content by weight of cement.

For the rheological measurements a simple mortar consisting of 50 wt.% CEM I 52.5 N (see table 1) and 50 wt.% fine quartz sand with a maximum particle size of 0.5 mm was used. The W/C was 0.35.

## Experimental results

Starting point of this work was the observation that concrete prepared with PAE and SMD appeared to be much less sticky and tenacious compared to concrete prepared with a conventional PCE, despite showing the same flow behavior in conventional slump tests. Figure 3 shows a typical concrete test result. They turned out to be quite different for the three superplasticizer types. PCE had the lowest dosage requirement of 0.48% by weight of cement; PAE required 0.68% and the SMD had the highest dosage 0.99%. For the first 10 min, all three admixtures were able to retain the workability at the initial level. After 10 min, the concrete made with PCE started to lose its flow ability, whereas PAE and SMD did not show a drop of workability.

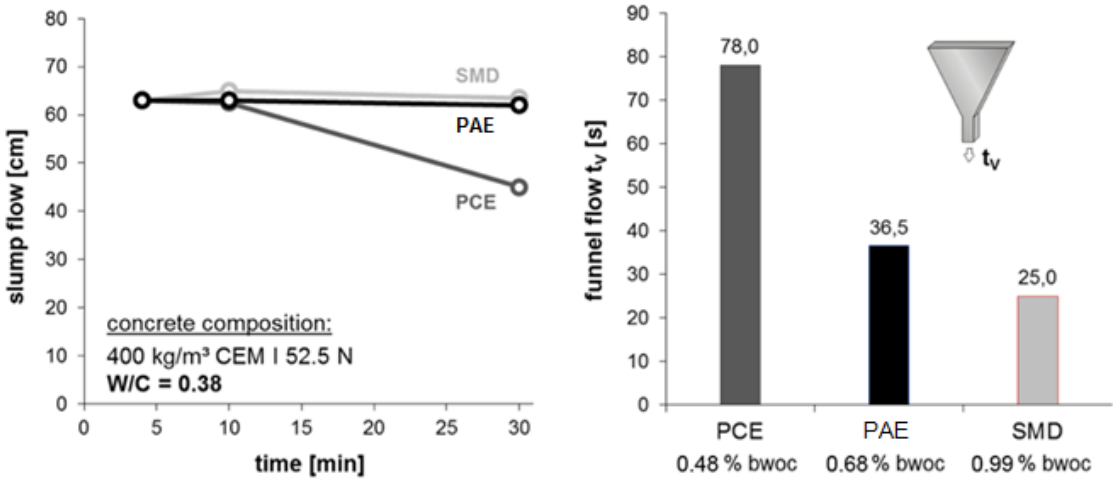


Figure 3 Slump flow behavior and V-funnel times for concrete prepared with PCE, PAE and SMD (concrete mixtures 1, 2, 3)

The lower dose efficiency of PAE compared to PCE can most likely be attributed to its lower charge density, which leads to a slower adsorption. Thus, PAE is able to cover freshly formed surfaces as they appear in the course of the hydration process. In the case of SMD, the adsorption is not sterically hindered since the anionic part is freely accessible, yet the affinity of the SMD to the cement surface is lower compared to PCE and PAE. We believe this can be explained by the fact that PCE and PAE have many more anchoring units per molecule compared to SMD, which leads to a synergistic effect on the strength of adsorption. As long as a polymer is adsorbed by a part of its backbone, it is unable to move away from the surface. The probability of losing the complete surface contact is therefore much lower for a polyelectrolyte (e.g. PCE, PAE) compared to a SMD.

Consequently, SMD require a higher dosage in order to shift the equilibrium between adsorbed and desorbed SMD towards a higher degree of adsorption. As with PAE, the initial surplus of desorbed SMD helps to maintain the flow ability over time.

A first series of experiments was carried out in mortar. The mortar was mixed in an ordinary laboratory mixer. The dry constituents were homogenized for 60 s after which the water and superplasticizer were added and mixed for 90 s. Following a break of 90 s, the mortar was mixed for 60 s. The slump flow was determined immediately after mixing, followed by the

rheological measurement. A rotational rheometer Rheotest RN 4 with vane geometry was used to evaluate the rheological properties. A shear rate profile with linearly increasing shear rate up to 100 $s^{-1}$ over a time of 200 s and afterwards linearly decreasing shear rate over another 200 s was applied.

The yield stress was calculated trough the Bingham model using a typical shear stress versus shear rate plot (
Figure 4). The apparent viscosity was calculated at a selected shear rate of 10 $s^{-1}$ (**Error! Reference source not found.**). Upon increase of the polymer dosage yield stress and apparent viscosity decreases.

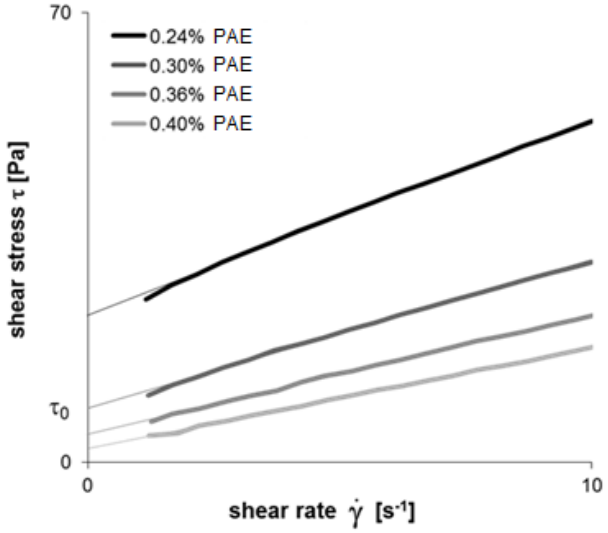


Figure 4 Shear stress of a mortar with different dosages of **PAE** depending on the shear rate.

Like with the concrete tests, the dosages of the admixtures were adjusted to achieve a comparable initial slump flow with the flow-tube (d/h = 3/5 cm) of 13 ± 0.5 cm immediately after mixing. As shown in
, the mortar prepared with PCE exhibited a higher apparent viscosity than the ones prepared with PAE and SMD. However, it must be noted that there is a time gap of approximately 400 s between slump flow and apparent viscosity measurements.

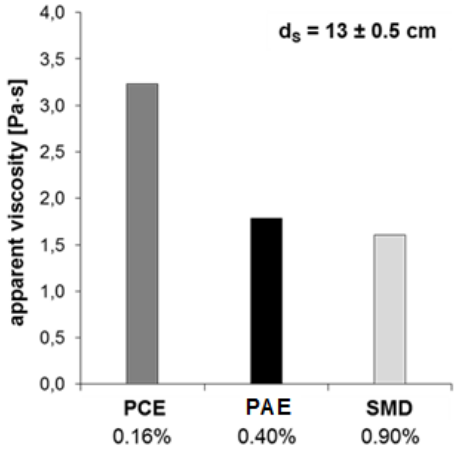


Figure 5 Apparent viscosity at constant slump flow

In order to eliminate the above mentioned time gap, the mortars were compared at the same yield stress (Figure 6, right). Surprisingly, in this experiment all three mortars exhibited virtually the same apparent viscosity at the selected shear rate of 10 $s^{-1}$ (Figure 6, left).

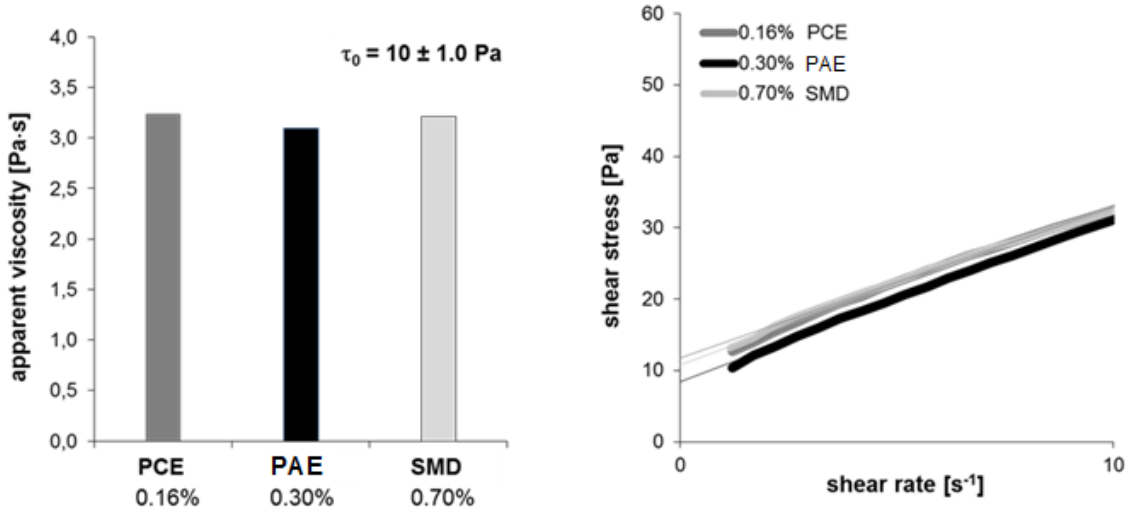


Figure 6: Apparent viscosity at constant yield stress

Now, the question had to be answered why PCE should develop a higher yield stress in comparison to a PAE or SMD within 400 s after showing a constant slump flow. This behavior can be related to two effects that are a consequence of the inevitable time lapse between mixing and testing. In this time gap, only low shear forces occur. The first effect is the partial reestablishment of the colloidal networks that had been deteriorated by mixing (thixotropy of cement paste[7]). A second effect is the consumption of water due to hydration reactions. Both effects lead to a higher yield stress and apparent viscosity. For proving the first hypothesis of thixotropy and observing the formation of a network in time at rest, a second shear rate program was used (Figure 7).

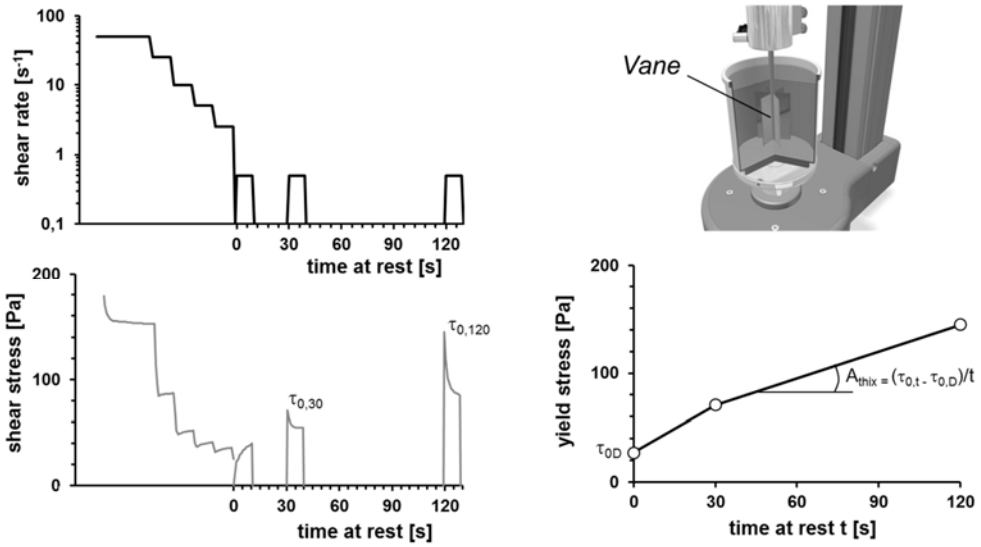


Figure 7 Shear rate profile for detection of shear stress depending on time at rest.

In the first step, the network formation was completely destroyed by applying high shear stress. Then, the sample was treated with a very low shear rate of 0.5 $s^{-1}$ in order to determine the shear stress at the starting point (t = 0 s). Owing to the low shear rate, the measured shear stress is mainly due to the static yield stress of the mortar. The sample was then left at rest for 30 s and the shear stress was again recorded for 10 s. After that, the sample was again allowed to rest until 120 s and again the shear stress was recorded. The first derivative of the yield stress as a function of time is a measure of the thixotropy $A_{thix}$.

As can be seen in the lower right plot of figure 10, the yield stress derived from the shear stress recordings increases over time and exhibits a change in slope from 0 to 30 s compared to 30 - 120 s, due to above mentioned effects. Above described test regime allows now to distinguish the behavior of the three different superplasticizer types (Figure ).

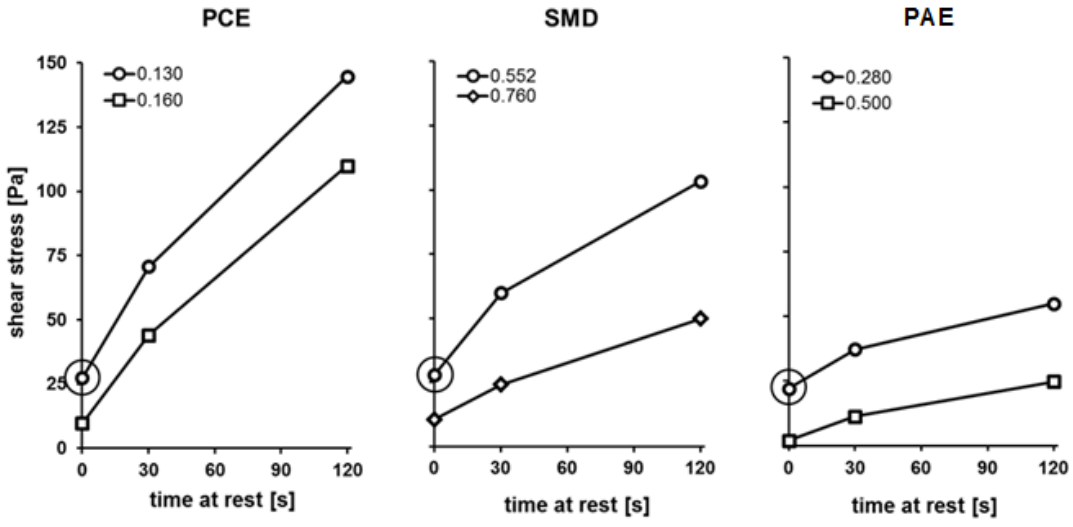


Figure 8 Correlation between shear stress and time at rest for different superplasticizer types

Starting at a shear stress of 25 Pa for all mortar slurries (encircled reading point), the gradient of the slope can now be compared for the three different superplasticizer types. It can be clearly seen that the slope of the curves for different PCE dosages are significantly steeper compared to the curves for SMD and PAE. In other words, stiffening of the mortar (increase of the yield stress) over time is much less pronounced if PAE and SMD are used as plasticizers. Both SMD and PAE are able to significantly reduce the thixotropy of mortar and concrete. However, in terms of practical use PAE offers two important benefits: PAE is significantly more dose efficient and, even more important, it is much less retarding compared to SMD. PAE thus delivers superior early compressive strength: While the 24 h strength was not testable in case of the SMD-containing concrete (mixture 4), the PAE-containing concrete (mixture 5) already exhibited a compressive strength of 9.9 MPa.

## CONCLUSIONS

PAE, a novel class of superplasticizers, has been developed by BASF. PAE features a comb polymer structure like PCE, but exhibits an aromatic backbone. PAEs can be tailored to different customer needs. They can either act as water reducer or workability retainer, depending on what side chain length and charge density have been realized in the comb polymer structure. What really differentiates PAE from conventional PCE is the capability of PAE to significantly reduce the “stickiness” of concrete. Especially concretes with high SCM content, used to improve the carbon footprint of concrete, often appear sticky and tenacious. In combination with difficult aggregates this can lead to instable concrete mixes. In this work we elaborated that the loss off stickiness in case of use of PAE can be traced back to a reduction of the plastic viscosity. This is remarkable, as conventional superplasticizers are only able to reduce the yield stress of concrete. Plastic viscosity of concrete is not properly detectable by using slump flow tests. A full differentiation of yield stress and plastic viscosity is only possible by means of a concrete rheometer.

However, qualitative measurement of rheological properties by tests like by the V-funnel, L-Box and T50 tests clearly support relevance of the rheological measurement for practical applications: Concretes prepared with PAE are easier to place, easier to pump and provide easier surface finishing. For ready mix concrete application these properties can be maintained over extendet times: Workability retention AND rheology retention are achieved in combination with excellent early strength development.

## REFERENCES

[1] HARGREAVES, D.: “International Cement Review”, The Global Cement Report 10th Edition (2013) 8

[2] MAHASENAN, N.; SMITH, S.; HUMPHREYS, K.; KAYA, Y.: “The Cement Industry and Global Climate Change: Current and Potential Future Cement Industry $CO_2$ Emissions”, Greenhouse Gas Control Technologies – 6th International Conference; Oxford, Pergamon (2003) 995-1000

[3] ROUSSEL, N.; STEFANI, C.; LEROY, R.: “From mini-cone test to Abrams cone test: measurement of cement-based materials yield stress using slump tests”, Cement and Concrete Research, 35, 5, 2005, 817-822

[4] WALLEVIK, O.H., WALLEVIK, J.E.: “Rheology as a tool in concrete science: The use of rheographs and workability boxes”, Cement and Concrete Research, 41 (12) (2011) 1279-1288

[5] HOT, J.; ROUSSEL, N.: “Adsorbing polymers and macroscopic viscosity of concentrated cement pastes”, Proceedings of the 7th RILEM International Conference of Self-Compacting Concrete and of the 1st RILEM International Conference on Rheology and Processing of Construction Materials, 2013, p. 197-204

[6] ARTELT, C., GARCIA, E.: “Impact of superplasticizer concentration and of ultrafine particles on the rheological behavior of dense mortar suspensions”, Cement and Concrete Research, 38 (2008) 633-642

[7] ROUSSEL, N.; OVARLEZ, G.; S GARRAULT, BRUMAUD, C.: “The origins of thixotropy of fresh cement pastes”, Cement and Concrete Research, 42 (1) (2012) 148-157

[8] KRAUS, A.; MAZANEC, O; DENGLER, J.; HILLESHEIM, N.; BOKERN, J. “Influence of PAE, SMD and PCE superplasticizers on the rheological properties of mortars and concrete” to be published in RILEM Proceedings (PRO95) International RILEM conference “ Application of superabsorbent polymers and other new admixtures in concrete construction”, 14-17 September 2014, Dresden, Germany

[9] The European Guidelines for Self-Compacting Concrete, 2005, 47-56; http://www.efnarc.org

# CONSISTENCE RETENTION OF MODERN DAY CONCRETES IN BOTH THE READY MIXED AND PRECAST CONCRETE INDUSTRIES

**I Ellis**
BASF Plc
United Kingdom
**J Kluegge**
BASF Construction Solutions
Germany

**ABSTRACT.** Since the use of water reducing admixtures (WRA), & high range water reducing admixtures HRWRA), became accepted as being a normal component of most concrete mixes in the 1980's & 1990's, most users accepted that the workability (consistence) life would be, at best, the same as a similar water/cement ratio concrete, of the same target consistence, or in the majority of instances lower. In the majority of applications, this period was considered to be between 60 minutes & 90 minutes for ready mixed concrete applications, and 30 to 60 minutes for precast applications. For many years, if a longer retention period was required, the normal practice was for the concrete to have a set retarder incorporated, or just a double dose of a lignosulphonate (LNS) based water reducing admixture. The latter was a common approach for concrete being supplied to the piling industry with a target consistence of 175mm. The consistence retention period of the early melamine formaldehyde condensate (MS) & poly(ß-naphthalene sulphonate (NS) based high range water reducing admixtures was often considerably less than 60 minutes, and it wasn't uncommon for these to be added to the truck mixer, at the job site, just prior to discharge. Even the majority of the early poly carboxylate ether (PCE) based admixtures could have similar issues with holding the desired consistence level for much more than 1 hour in normal circumstances, and especially for concretes where a water cement ratio of lower than 0.50 was coupled with a target consistence level of less than 150mm. This paper demonstrates how admixture technology, and in particular, modern PCE based HRWRA products can now provide genuine, multi hour consistence retention periods.

**Keywords:** High Range Water Reducing Admixtures, Consistence Retention, Poly Carboxylate Ether

**Ian Ellis** is Technical Services Manager - Admixture Systems for BASF Plc, United Kingdom

**Dr Jan Kluegge** is Head of Marketing Ready-Mix Europe for BASF Construction Solutions, Germany.

## INTRODUCTION

[(1)]To meet the challenges posed by the modern construction industry, the design engineers and the contractors demand extreme performances of the concrete in its fresh and hardened state. Durability, as mentioned before, is of prime importance.

The parameters which control the durability of concrete structures are design, construction practice, materials properties and exposure conditions.

Besides the quality of the selected materials, a basic requirement for a highly durable concrete is its low permeability which depends upon binder quality, aggregates, water to binder ratio, compaction, degree of hydration, curing and absence or presence of cracks. Effective compaction, related to the workability of the concrete mix and efficient curing is a key point to have a proper degree of hydration and porosity thus obtaining the required durability in place.

Polycarboxylate-based superplasticizers (PCE) are acquiring increasing importance in the production of concrete since they allow the production of high workability concrete with lower water/cement and reduced slump loss, when compared to the old generation superplasticizers like β-naphthalene sulphonate formaldehyde condensate (NS) and melamine formaldehyde condensate (MS).

Consistence retention over time is therefore an essential requirement that has previously been attempted, for many decades, through several methods:

1) Formulation of superplasticizers with retarding admixtures like sugars, corn syrup, chelating agents which may lead to drawbacks such as very low early strength
2) Dosing high amount of superplasticizers or redosing of superplasticizers at the job site with obvious problems derived by managing these operations by personnel not always sufficiently expert and trained
3) Encapsulation techniques which are likely to be expensive and not always reliable, being affected by many uncontrollable parameters of the concrete mix composition and process
4) Partially crosslinked acrylic copolymers able to release effective dispersing molecules over the time under the alkaline environment
5) Addition of water at the jobsite that, despite it represents one of the most serious dangers to the quality and durability of structures, unfortunately it is still a reality even though less and less common

However in recent times the focus has been on the constant improvement of the molecular structure of superplasticizers so as to achieve a consistence retention over a time according to the specific requirements, without any drawbacks both in the fresh and hardened state of concrete and implyng a simple handling and use of the admixture only at the batching plant.

Excellent papers summarize how the mechanism of action of PCE has been profoundly studied investigating the: a) Induced electrostatic repulsion between particles, b) Induced steric hindrance preventing particle-particle contact, c) Reduction of the surface tension of water, d) Lubricating film between cement particles, e) Dispersion of cement grains, releasing water trapped within cement flocks, f) Inhibition of the surface hydration reaction of the cement particles , leaving more water to fluidity the mix, g) Change in the morphology of the hydration products.

Based on these mechanisms, over the last two decades molecular structures have been optimised playing on parameters such as 1) Chain length, 2) Side chain length, 3) Electrical charges, 4) Side chain density, 5) Additional functional groups able to regulate the adsorption kinetics

In addition to the excellence of performance, the construction industry increasingly requires robustness of performance. The use of SCM, recycled aggregates, etc, which is a consequence of the sustainability effort, leads to a higher complexity and variations of the materials used in the concrete.

It can be expected that admixtures designed for excellent performances can present a higher sensitiveness to cementitious materials with respect to less powerful water reducing agents. Therefore it is of extreme interest to predict possible incompatibilities, to understand the reason for those phenomena in order to optimise the polymeric structure of the new superplasticizers and minimise the problems.

## (2) BASIC PCE CHEMISTRY BEHIND CONSISTENCE RETENTION

If we look at the typical properties of a PCE polymer we can see how they impact on the traditional functionalities in a concrete mix:

| | Start Effectivity water reduction | Slump Retention | Early Strength | Rheological Properties |
|---|---|---|---|---|
| increasing charge density | + | - | o | - |
| increasing side chain length | + | o | + | - |
| increasing molecular weight | o | o | o | - |

+: increasing, -: decreasing, o no effect

It is also important to consider the effects of the cement chemistry itself, for instance in general terms it is possible to categorise cement behaviour with a superplasticiser into 3 groups, based on the sulfate content of the cement

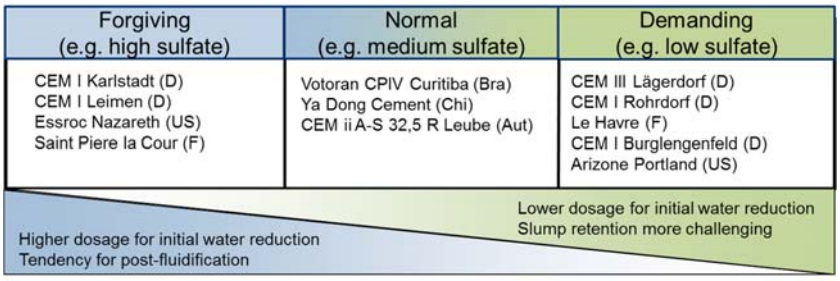


So to achieve consistence retention we need to understand that fresh concrete is a dynamic system, where the hydration processes lead to new cement surface growth. This in itself leads to a time dependant demand of superplasticiser, where there must always be enough superplasticiser available during the entire period of consistence.

This can be achieved by superplasticisers with a low adsorption rate, however, this can lead to a significant part of the dosage not being effective

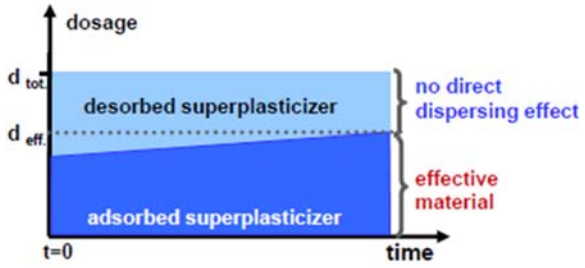


Of course we could always just keep adding additional superplasticiser with a high absorption rate to maintain a constant consistence value, this on a construction site is inconvenient and not really practical. If we added the sum of all these "additions" in one initial dosage, we would see over fluidification & segregation of the mix.

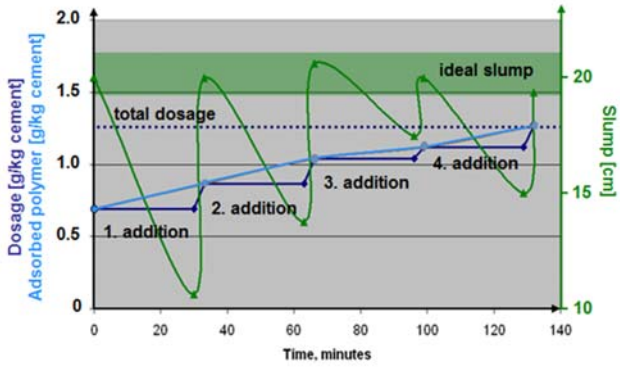


So, in simplistic terms we need to address this issue in a more fundamental polymer design method, and thus basically increase the affinity of the cement to the polymer over time. How has BASF accomplished this with the latest generation MasterGlenium SKY & MasterSure range of admixtures?

By basically developing polymers with latent anchor groups:

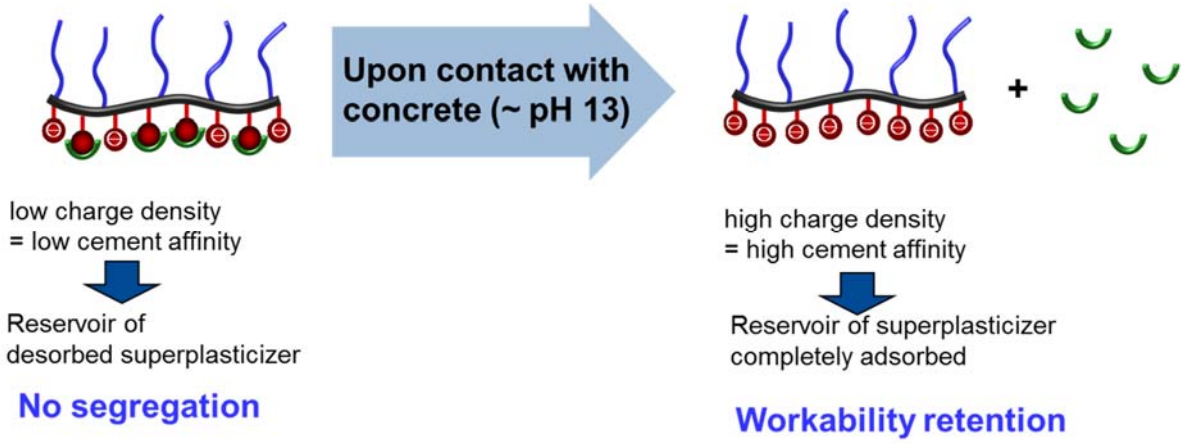

We started to see the availability of these new polymers towards the end of 2007 / 2008, & within our current portfolio, we now have a range of polymers that can be used to provide consistence retention in a wide range of applications. These polymers, because of the way they perform, have been given the internal nickname of “Zombie” polymers.

They can be formulated with carefully selected water reducing polymers to give a 1-component solution, or can be supplied as a pure retention based admixture with minimal water reduction capability, as part of a 2-component system. A 1-component system is easier to handle and more convenient with logistics for the user. A 2-component approach gives additional flexibility in case of changing demands or conditions on site however obviously requires more care to be taken on the concrete batching site. In the UK the preference is for the combined multi-purpose admixture. The remainder of this paper will show some case studies to demonstrate this

## EXAMPLE 1: HINKLEY POINT C

Our first set of work for this project started in January 2010, but the real focus started later that year with some development work performed for AMEC, this then progressed in various stages through to 2013 with the Bouygues / Laing O’Rourke jv (BYLOR). It’s fair to say that the original EDF concrete specification only required consistence retention for a minimum of 2 hours, but this was later increased to 3 hours by the BYLOR requirements. The original target consistence was for a 200mm slump with a criteria that there should be no more than 20mm increase at any time & at the end of the specified retention time the concrete should still be at more than 80% of the original value. This was the first example, in our experience, of detailed limits being placed on concrete performance & basically gave a target consistence window of 200mm +20mm / -40mm for the 3 hour period. BYLOR also requested that some of the mixes had the initial consistence increased to 600mm flow (F5/F6), again with a maximum increase of 20mm & 80% retention at 3 hours but not less than 500mm, giving a range of 620mm to 500mm over the 3 hour period.

A significant period of product development was performed using the materials that were being proposed for use on the contract (even at this early stage). This project also had requirements to develop admixtures that were suitable for use with both CIIB-V & CIIIB cements with & without microsilica. The powder contents typically varied between a 390kg/$m^3$, 0.36 w/c ratio mix (CIIB-V) to a 450kg/$m^3$, 0.35 w/c ratio mix (CIIIB).

The final product developed & recommended for use in the project was MasterGlenium SKY 830.

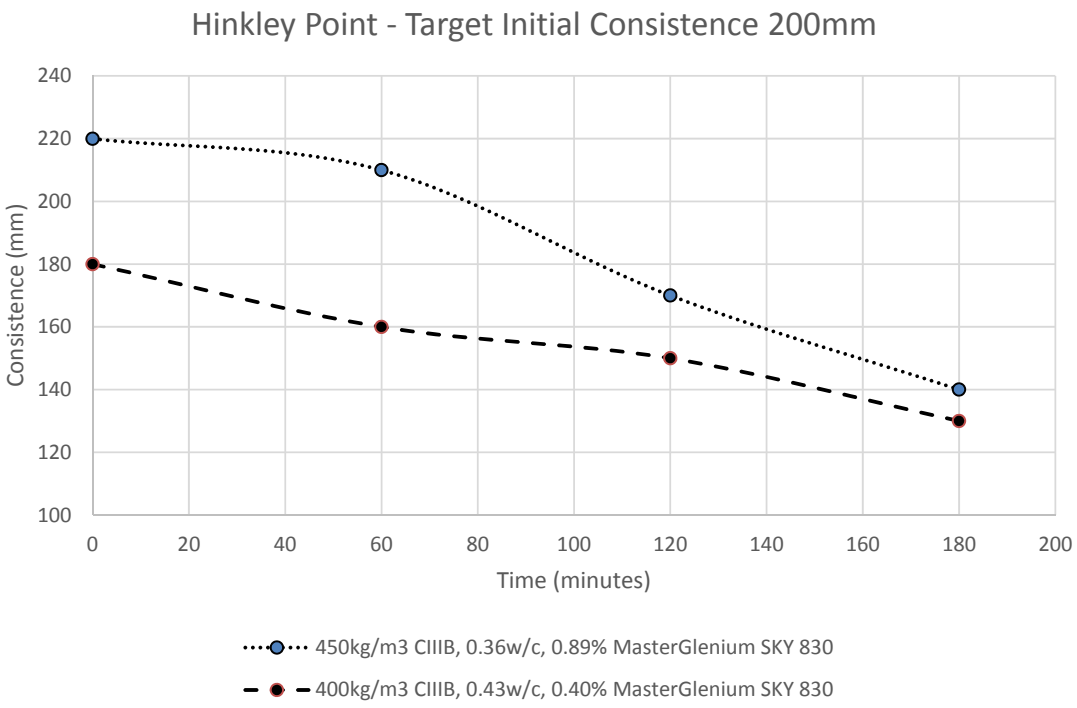
Hinkley Point - Target Initial Consistence 200mm
Consistence (mm)
240
220
200
180
160
140
120
100
0
20
40
60
80
100
120
140
160
180
200
Time (minutes)
450kg/m3 CIIIB, 0.36w/c, 0.89% MasterGlenium SKY 830
400kg/m3 CIIIB, 0.43w/c, 0.40% MasterGlenium SKY 830

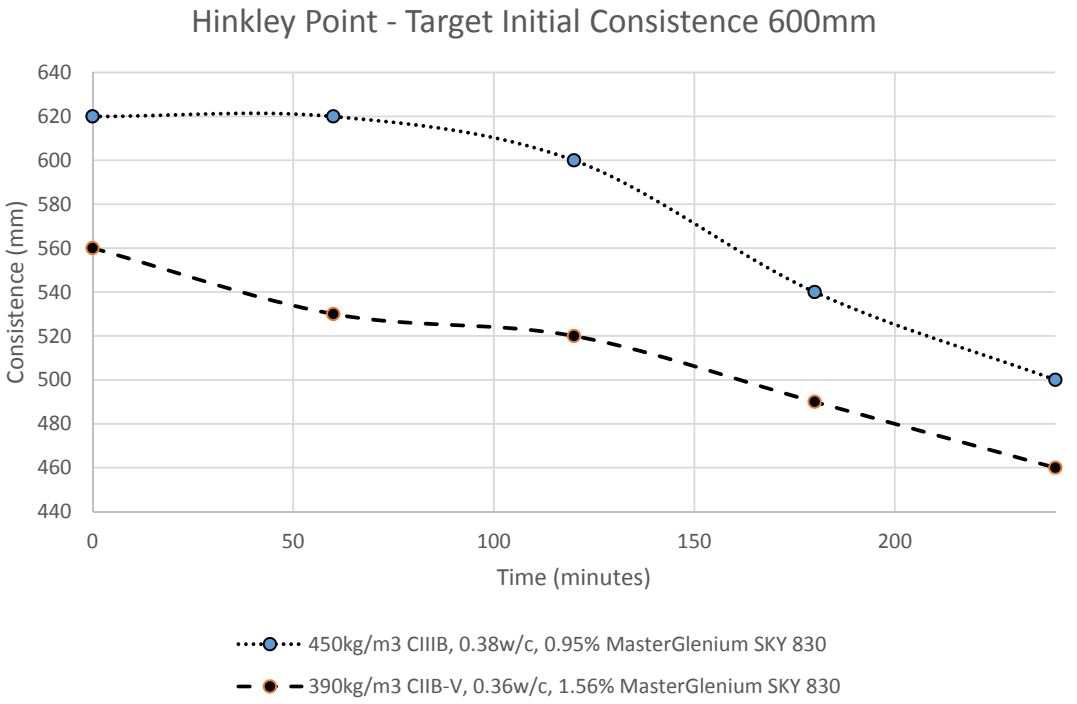
Hinkley Point - Target Initial Consistence 600mm
Consistence (mm)
640
620
600
580
560
540
520
500
480
460
440
0
50
100
150
200
Time (minutes)
450kg/m3 CIIIB, 0.38w/c, 0.95% MasterGlenium SKY 830
390kg/m3 CIIB-V, 0.36w/c, 1.56% MasterGlenium SKY 830

## EXAMPLE 2: FORTH CROSSING (QUEENSFERRY CROSSING) NEW BRIDGE

The second example selected for this paper was the main concrete mix for the Forth Crossing, development of this admixture started in March 2012 and was strongly driven by the methodology of getting the concrete to main structures in the middle of the river Forth. The contractor had chosen to mount truck mixer drums onto barges, with the barge also containing its own concrete pump. The concrete was mixed at the dock side batching plant, it was then transported in conventional truck mixers which then drove to the quay side. The concrete was then pumped from the quay side truck mixers to the static mixers on the barge. The barge then made its way to the relevant discharge location, where the trucks mounted on the barge then discharged into the barge mounted pump for final placement. The net result was a need for a robust concrete that could be pumped twice and had a minimum retention period of 3 hours. It was also a requirement that any retardation was kept to an absolute minimum so that early strengths could be maintained for the construction programme.

The basic main mix was a C50/60 mix, minimum cement content of 380kg/m$^3$ with a maximum water/cement ratio of 0.35. The consistence was specified as being 590mm +/- 50mm. The actual powder content was 480kg/m$^3$ & was comprised of a CIIIA+SR with a ground granulated blast furnace slag percentage of 60%. The admixture developed for this application, & used successfully over the contract duration was MasterGlenium SKY 903.

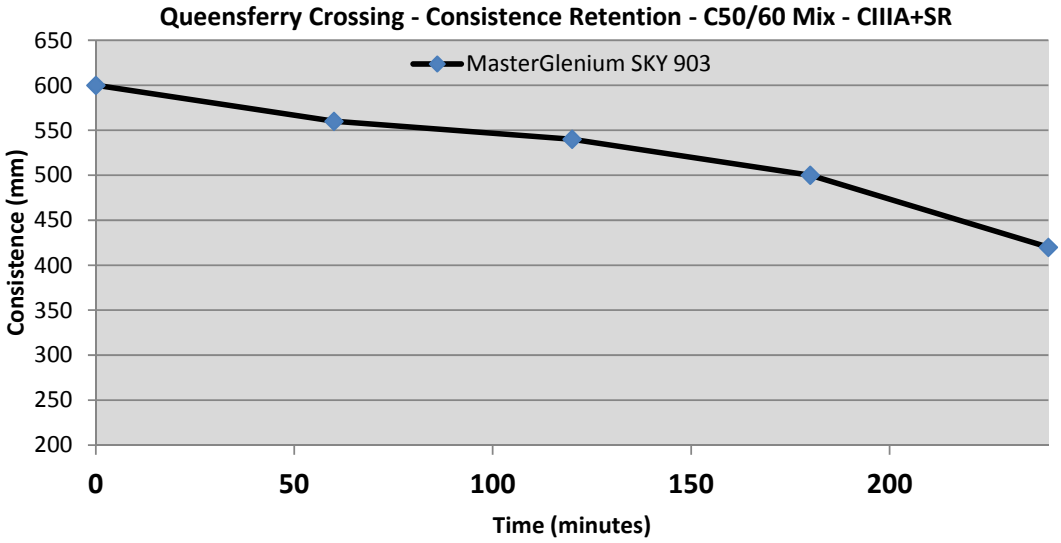


Towards the end of the contract, & when construction of the 3 bridge support pylons were approaching half their maximum height of 207m, concerns were raised regarding the ability of the concrete mix to be pumped to that height, without a significant change to the concrete mix design. To minimise any potential delays due to mix certification requirements, we were asked if we could produce an alternative admixture that would give the existing mix design improved rheological performance, without changing the other constituents or the other properties of the concrete. After a period of development, & using some of the technologies presented during this conference, a revised admixture, MasterEase 3820 was developed & proposed.

Although it wasn't actually used on this contract, it was utilised on a contract on Liverpool docks, where the concrete was required to be pumped horizontally for distances of up to 800m. Of particular note on the attached charts is how the concrete rheology is maintained over the consistence retention period when compared to MasterGlenium SKY 903.

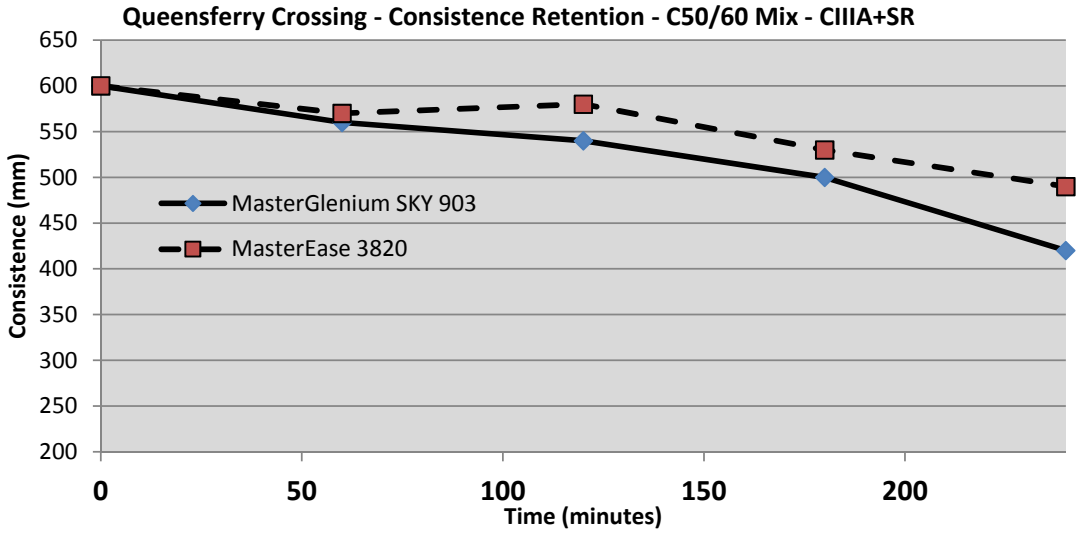


## EXAMPLE 3: LAING O'ROURKE EXTENDED RETENTION REQUIREMENT

During the latter part of 2014, Laing O'Rouke started discussions around changing their basic concrete consistence requirements for all concrete supplied to their sites. Unless circumstances dictated otherwise, all concrete was to be designed & supplied with a target initial consistence of 600 to 650mm. Initially the desired retention period was 2 hours, but this was soon modified to 2 hours, 5 hours & 8 hours.

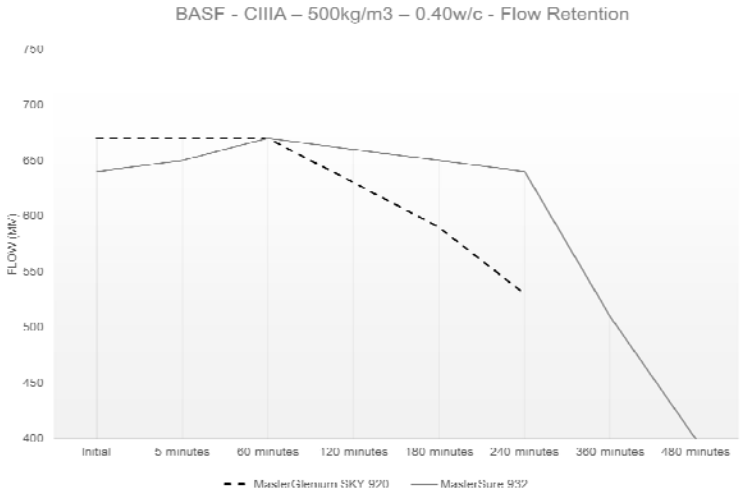

The concrete could show signs of flow increase over the retention period, but this should be limited to as low as possible, & without the concrete showing any signs of segregation. The consistence should not drop below 500mm if the retention period is up to 5 hours & a value of 400mm for retention periods of between 5 & 8 hours. The summary of this work was that for retention periods upto 3 hours, MasterGlenium SKY 920 was the appropriate product, & for greater retention periods, MasterSure 932 is the recommended product to be used.

## CONCLUSIONS

To conclude this paper, it can be seen that the admixtures industry now has the capability to fully satisfy the retention requirements of specifiers, contractors & producers. As long as open communication is had between all involved at as early a stage as possible, then admixtures can be developed to meet the specific project needs. This is not just for the ready mixed concrete industry, but also for the precast industry in situations where a self-compacting concrete requires an extended consistence retention period, without sacrificing the fundamental requirement for early strength development. Although not discussed here, the use of MasterSure in combination with Master X-Seed crystal speed hardening, gives the precast industry a never before seen set of options for high consistence, retention of that consistence, & rapid early strength development for maximum optimisation of the casting process.

Over the last 35 years we have seen a dramatic change in the concrete being specified & supplied, the days of a C40 at 50mm slump being considered high strength concrete are long gone, the concrete industry has shifted from this, to high consistence concretes, frequently with water cement ratios of less than 0.40, & at the same time retaining that consistence for up to 8 to 10 hours. This flexibility has only been possible with the advent of the PCE based admixture, & it’s fair to say that we have probably reached the maximum realistic level of consistence retention.

Although the subject of rheology has only been referenced briefly in this paper, its clear that there is an almost natural synergy between the two subjects of retention & rheology. This is becoming more evident as we deplete the sources of desirable aggregates, and move towards using materials in high quality concretes that we would previously have not used or kept for low grade applications only.

It is also mentioning that the methodology for assessing consistence retention is now clearly defined in BS 8500-1:2015+A1:2016 Appendix B.6

The next stage of concrete evolution, and a fundamental basic concept of the BASF MasterSure product range, is to widen the capacity of these high performance admixtures to cope with the variability of other key raw materials within the concrete mix design. As the demands on concrete are pushed ever further forwards, and the admixture industry rises to these demands, it’s clear that we need to look at the capacity and willingness of the cement industry in particular, to supply products that are more consistent at a clinker chemistry level. Perhaps the time has come to look at defining the source of cement as being the point of clinker production, rather than the current practice of where it is milled. Although the producers take great efforts to ensure that the final cement meets the current standards, should we question if these are now stringent enough to cope with the modern site demands?

[1] MAGAROTTO R., MORATTI F., ZEMINIAN N., ALBRECHT A., FLAKUS S. : “Polycarboxylate Superplasticiser to Ensure Workability Retention & Durability”

[2] TRIEFLINGER, ALBRECHT, DENGLER, KRAUS : “Dispersants for the Future, From classical PCE to new chemistry”

# NEW APPROACHES TO SOURCING FLY ASH FOR CONCRETE CONSTRUCTION IN THE UK

**R A Carroll**
United Kingdom Quality Ash Association
**M J McCarthy** **T A Hope**
University of Dundee
United Kingdom

**ABSTRACT.** Fly ash and furnace bottom ash derived from UK coal-fired power stations are used extensively as constituents within concrete. A decline in the use of coal for electricity generation over the next decade has the potential to reduce the availability of these valuable by-products. The situation is discussed and options to meet current and future demand for concrete manufacture considered. Large amounts of stockpile ash exist in the UK, which if processed effectively, could become a significant source of fly ash for the construction industry. A research project is in progress at the University of Dundee to develop suitable process routes for utilising stockpile ash and initial results from this are reviewed. A case study involving processing at full-scale is also described.

**Keywords:** Concrete, EN 450, Fly ash, Recovery, Stockpile.

**Dr R A Carroll** is Technical Director of the United Kingdom Quality Ash Association. He has over 30 years experience in the concrete industry, including 27 years with Hanson Building Products as Head of Concrete Services. He represents the Association on technical and scientific matters and is a member of several British Standards Committees.

**Dr M J McCarthy** is a Reader in the School of Science and Engineering at the University of Dundee. He has carried out research on a range of topics in concrete materials and construction for the past 25 years. His work on fly ash in concrete has included the use of material (i) to EN 450, (ii) following wet storage, including processing, (iii) at high volumes in cement and (iv) produced from new technologies.

**Mr T A Hope** is a PG Researcher in the School of Science and Engineering at the University of Dundee. He is currently working in the area of recovery and processing of stockpile ash for use in concrete construction.

## INTRODUCTION

In the UK there is considerable demand for fly ash and furnace bottom ash (FBA) as constituents of construction products. There are high utilisation rates for fly ash and FBA due to 50 years of industrial experience, significant technical benefits and the improved sustainability achieved with these valuable by-products. There is a proven history of performance in a wide range of products and this is supported by established product standards and robust technical specifications agreed between suppliers and users.

From 1999 to 2014 the production of fly ash has ranged between 4 to 7 Mt per annum (Figure 1) [1]. Each year 40% to 70% of the fly ash was utilised in beneficial applications and the remaining material deposited in landfills. A further 600,000 to 1,000,000 t of FBA was produced annually and fully utilised, primarily as a lightweight aggregate for concrete with little material sent to landfill.

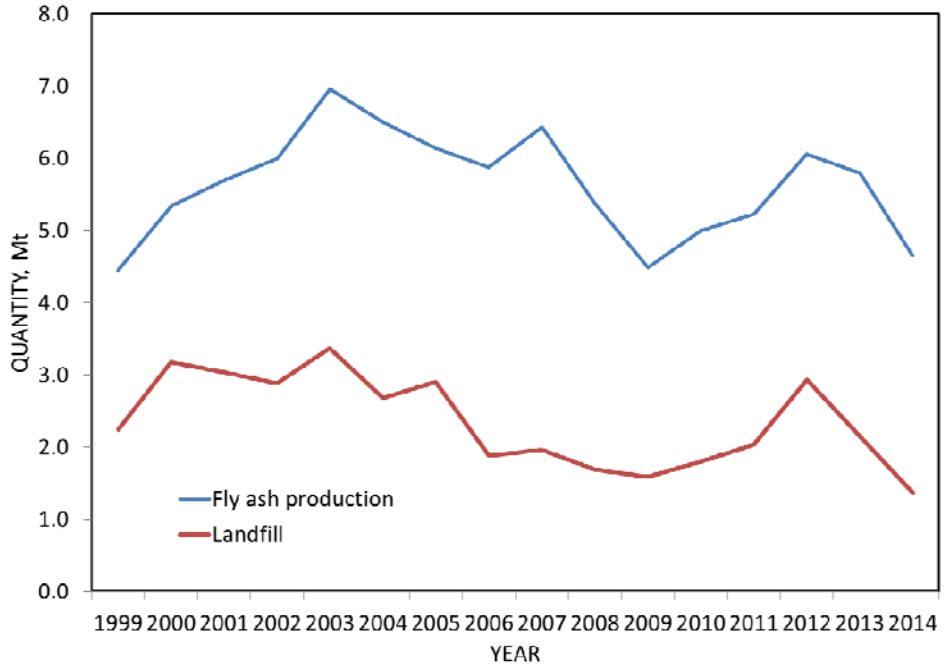


Figure 1 Fly ash production 1999-2014

## USES OF FLY ASH

Fly ash has a wide range of applications within the construction industry (Figure 2) [2]. Uses for fly ash or FBA may be categorised as either bound or unbound. The use of fly ash as an engineering fill and in land reclamation projects are unbound applications. The majority of uses are bound applications, accounting for over 2.5 Mt of fly ash in 2014, or 54% of the annual production. The three major uses for fly ash are in the manufacture of cement, as the siliceous constituents in the manufacture of autoclaved aerated concrete (AAC) and as a Type II addition in precast or ready-mixed concrete. These applications consumed nearly 2 Mt of fly ash in 2014.

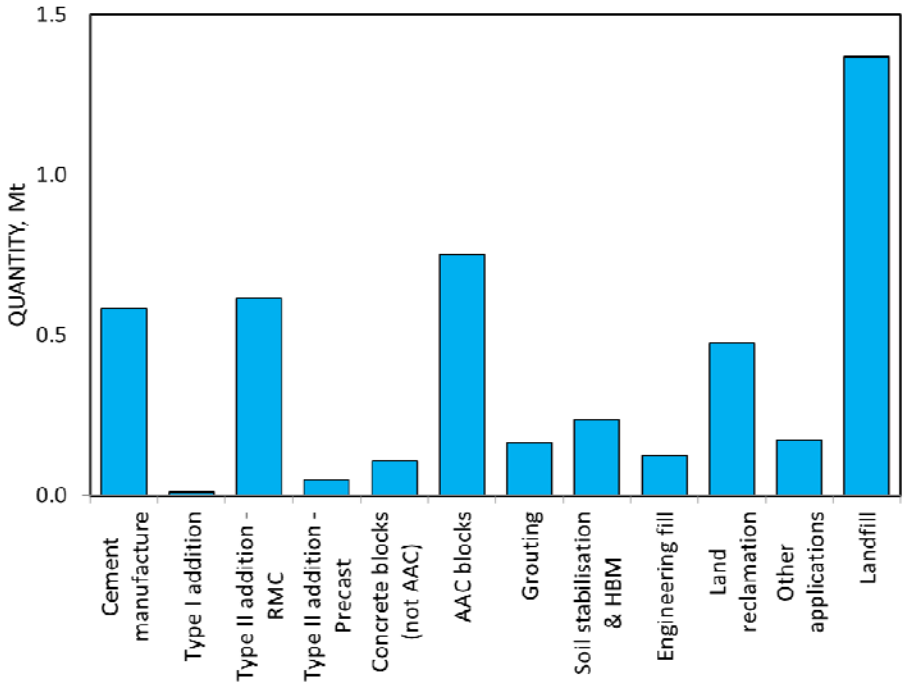


Figure 2 Uses of fly ash in 2014

## FLY ASH IN CONCRETE

### EN 450 Fly Ash

EN 450 [3, 4] is the harmonised European Standard for fly ash used as a Type II addition for concrete. Therefore, the fly ash may be supplied as a pozzolana for concrete in accordance with European Standard EN 206 [5] and the complementary UK Standard BS 8500 [6, 7]. EN 450-1 contains definitions, physical and chemical specifications and the conformity criteria (Table 1). EN 450-2 describes the quality control procedures covering topics such as sampling, autocontrol, auditing and certification. If concrete is specified to EN 206 the EN 450 fly ash is incorporated via a composite cement produced to EN 197-1 [8]. Concrete produced to BS 8500 has the option of adding the fly ash directly to the blending plant with the other constituents.

### Benefits of Fly Ash

Use of EN 450 fly ash as an addition in concrete improves fresh properties, including cohesiveness and bleeding. Less heat is generated from the exothermic reactions during hydration, lowering thermal stresses and the risk of cracking, in particular in large pours. The specified compressive strength will be achieved in 28 days and will generally increase with time, due to continued pozzolanic reaction. As a result, the ultimate compressive strength is usually greater than that of comparable concrete without fly ash. Concrete containing fly ash can also enhance many aspects of durability, e.g. chloride ingress, alkali-silica reaction, thereby potentially extending service life.

Table 1 EN 450-1 specifications for fly ash

| PROPERTY | LIMITS |
|---|---|
| Loss on ignition (LOI) | Category A ≤ 5.0%; Category B ≤ 7.0%; Category C ≤ 9.0% |
| Fineness (45 μm) | Category N ≤ 40.0%; Category S ≤ 12.0% |
| Free calcium oxide | ≤ 1.5% |
| Reactive calcium oxide | ≤ 10.0% |
| Chloride | ≤ 0.10% |
| Sulfate content | ≤ 3.0% |
| Particle density | ± 200 kg/m$^3$ from stated value |
| Activity index | ≥75.0% (28 days) ≥85.0% (90 days) |
| Reactive $SiO_2$ | ≥25.0% |
| Σ $SiO_2$+$Al_2O_3$+$Fe_2O_3$ | ≥70.0% |
| Alkalis | ≤ 5.0% |
| Magnesium oxide | ≤ 4.0% |
| Soluble phosphate | ≤ 100 mg/kg |
| Total phosphate | ≤ 5.0% |
| Initial setting time | ≤ 200% of cement control |
| Water requirement | ≤ 95.0% of cement control (Category S only) |
| Soundness | ≤10 mm (if free lime exceeds ≤ 1.5%) |

Fly ash used as a pozzolana in concrete achieves significant reductions in the amount of Portland cement, the manufacture of which consumes a considerable amount of energy. However, even high fuel efficiency cannot compensate for the substantial quantities of carbon dioxide ($CO_2$) liberated to the atmosphere due to the calcination of limestone or chalk.

Fly ash has low embodied $CO_2$ and low energy associated with its production. Concrete made with a substantial replacement of Portland cement by fly ash has lower embodied $CO_2$ [9]. Less calcareous and siliceous raw material needs to be quarried and fewer fly ash loads are sent to landfill, thereby improving resource efficiency.

## UK COAL-FIRED POWER STATIONS

### Decarbonisation

During the last decade, UK governments have acted to lower emission of greenhouse gases from industry and this has had a particular impact on power generation. In the 2008 Climate Act [10], the UK Government introduced carbon budgets, legally binding limits on $CO_2$ and other greenhouse gas emissions. As a result, there is less reliance on fossil fuels such as coal, with emphasis on renewable sources such as wind, tidal and solar, augmented by nuclear power stations. The percentage of electricity generated from unabated fossil fuel sources is projected to drop from around 60% in 2015 to between 30 to 40% in 2025 [11]. This is a drop in emission

intensity from 400 to 150 $gCO_2e/kWh$. Such an ambitious decarbonisation policy will have a considerable impact on coal use as a primary fuel source. Coal-fired power stations must also comply with the Industrial Emissions Directive (IED) [12], which places stringent limits on the emissions of nitrogen oxides ($NO_x$), sulfur dioxide ($SO_2$) and other pollutants. Utilities must install new abatement procedures which meet the best available technology (BAT) or otherwise close.

There is much ambiguity about the UK energy policy and the operations of its complex incentives. In December 2014 the UK Government held a capacity auction to ensure that sufficient generating capacity is available to the national grid for severe weather events in winter. Several coal-fired power stations received contracts for 2018 to 2021 under the scheme, which means that payments are made for the units on standby during the winter. However, in April 2015 the carbon price floor increased from £9.5/t $CO_2$ to £18/t $CO_2$, making electricity generation from coal-fired power stations considerably more expensive. The UK Government announced plans in November 2015 to close all unabated coal-fired stations by 2025 [13] and in the same month state-funded support of £1billion for carbon capture and storage (CCS) projects was withdrawn [14].

## Status in 2016

The share of electrical generation from coal in 2015 was at a record low of 22.6%, compared with 29.7% in 2014. In contrast, the amount of electricity derived from renewable sources (hydro, wind and bioenergy) increased from 19.1% in 2014 to 24.7% in 2015. Low carbon electricity generation based on renewables and nuclear increased from 37.9% in 2014 to 45.5% in 2015. A total of 29.3 Mt of coal was used to generate electricity during 2015, which compares with 38.4 Mt used in 2014 (24% reduction).

At the end of 2015 there were ten operational coal-fired power stations in the UK with an installed generating capacity of 17,600 MW. In March 2016 stations at Longannet and Ferrybridge closed and Rugeley Power Station closed in June, reducing capacity to around 13,300 MW. Six coal-fired power stations produced EN 450 fly ash in 2015, but this has now reduced to four. By 2020, Department of Energy and Climate Change predictions [15] indicate that around 45 TWh of electricity generation will be derived from coal and will reduce further to around 5 TWh by 2025. If these projections are correct, production of fly ash within the UK will decrease from 4.6 Mt in 2014 to around 2.3 Mt by 2020 and perhaps only 250,000 t by 2025.

Through 2015 and early 2016, concern increased regarding the medium and long-term availability of coal fly ashes for the UK construction market. It must be assumed that the amount of fly ash and FBA obtained directly from UK coal-fired power stations will reduce significantly over the next decade. The mismatch between maximum production in winter but greatest demand in spring and summer, combined with limited dry storage capacity, will exacerbate supply problems. However, there is still strong demand for these valuable by-products which provide substantial technical and sustainability benefits for a range of construction products. The UK Quality Ash Association (UKQAA) and its members are determined to maintain and develop this market by:

1) Maximising the utilisation of fly ash and FBA produced directly from UK coal-fired power stations.

2) Supporting an efficient supply chain for importing fly ash and FBA. Supply of these materials will depend on harmonised product standards and robust technical specifications.

3) Developing processing technologies to extract and recover EN 450 fly ash from stockpiles across the UK.

## STOCKPILE ASH

### Potential Sources

Until the1990's most of the UK's electricity was generated by coal-fired power stations. Large quantities of fly ash were produced but with utilisation rates generally below 50% the surplus material was stored in ash fields or deposited in landfill. Fly ash is conditioned by mixing with a controlled amount of water (10 to 20% w/w) and discharged into tipper trucks. Fly ash may also be slurried with water and pumped to lagoons. Periodically, the lagoons are drained and the partially de-watered ash sent to the ash fields or for disposal at a landfill site operated by the power station.

UK ash fields and landfills may contain up to 50 Mt of stockpile ash and this is a large potential source of raw material for use in construction products. If significant amounts of this material were processed successfully it would be a complementary source of pozzolana for the manufacture of concrete. The demand for EN 450 fly ash as a Type II addition is typically 650,000 to 850,000 tonnes per annum. Several decades of EN 450 fly ash could therefore be supplied to the market if a substantial quantity of the stockpile ash was utilised.

### Current Uses

Generally conditioned ash is extracted from stockpiles for unbound applications, such as engineering fill. The recovery of stockpile ash for the bound applications of grouting and the manufacturing of AAC also occurs.

The particle size distribution of conditioned ash is suitable for grouting applications and sufficient pozzolanic reaction is achieved. Some AAC factories can use conditioned ash and in recent years the recovery of stockpile ash has provided a useful source [16]. Screening occurs to produce a homogeneous feedstock (Figure 3). Efficient dispersal of the ash in slurry will break down many agglomerates. Critically with AAC manufacture the high temperatures and saturated steam conditions in the autoclaves ($\geq$ 180 $^{o}$C) ensure the rapid dissolution of silica, compensating for the reduced surface area of conditioned ash.

Figure 3 Screening stockpile ash for AAC manufacture

**Innovative Processing of Stockpile Ash Project**

The UKQAA and the Engineering and Physical Sciences Research Council are funding a research project at the University of Dundee, investigating processing methods to allow UK stockpile ash to be used as a pozzolana in concrete. Experimental work is underway to characterise the reactions and changes that fly ash undergoes when stored in stockpiles. How reversible are the effects and can the original performance of the fly ash be recovered? This knowledge will guide the selection of appropriate industrial processing methods for recovery. The process route should be capable of transforming stockpile ash into a pozzolana which meets all the requirements of EN 450-1.

Recovery of stockpile ash by utilising its unburnt carbon as a fuel has been developed in the USA [17]. This approach has not been investigated because of adverse effects on $CO_2$, $NO_x$ and $SO_2$ emissions. Wet processing routes have been investigated previously [18] and also commercialised in the Rockton process [19].

Experimental work is concentrating on efficient drying to achieve free-flowing characteristics and de-agglomeration of stockpile ash with the investigation of further particle size reduction techniques. Depending on the loss on ignition (LOI) of the stockpile ash source, it may be necessary to undertake carbon reduction of the dry material by electrostatic separation. Industrial drying plants are operational in France and Germany and material from one of these units is being assessed within the project (see Section 5.5).

**Experimental Work**

Previous work suggests that wet storage of fly ash leads to some agglomeration [20]. This has been found to depend on the free lime content of material, with greatest effects generally noted at moisture levels of around 10 to 20%. An example of the behaviour is shown in Figure 4 for fly ash moistened and stored in the laboratory, which also demonstrates that the process tends

to develop with time, with gradual increases in 45 µm sieve retention over the storage period. For the two fly ashes shown, the fineness exceeds the Category N limit (40%) of EN 450-1 by 90 days.

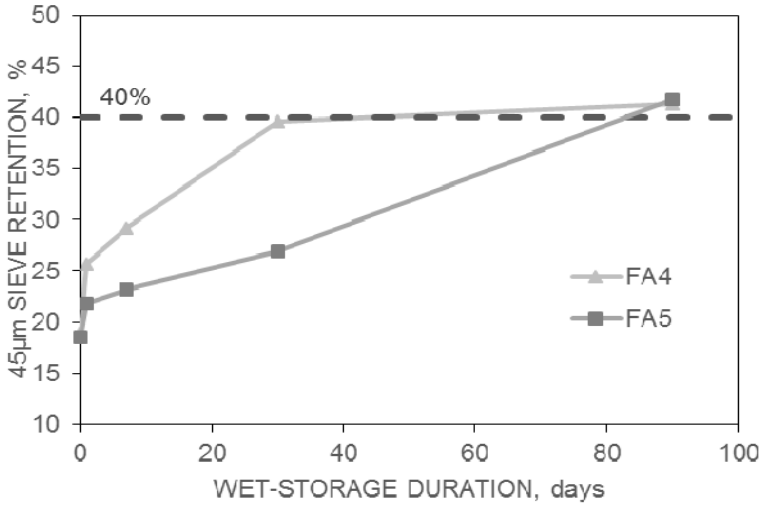


Figure 4 Change in 45µm sieve retention of moistened fly ash with storage time (10% moisture addition, laboratory stored)

As indicated in Figure 5, consistent behaviour has been found between fly ashes, with slightly greater relative changes in finer material and the fineness category of the fly ashes changing with wet storage (12% Category S, 40% Category N). Note variations between 45 µm sieve retention and median particle size data may reflect the difference in test procedures (ultrasonic displacement is used before measurements for the latter, potentially breaking down agglomerates present).

An example showing the typical appearance of low lime dry fly ash and stockpile ash from two power stations is given in the scanning electron microscopy (SEM) images in Figure 6. This illustrates the occurrence of agglomerates in the wet-stored material, with some particle surface roughening also evident.

The effects of moistening on the main chemical composition of laboratory stored fly ash are shown in Table 2. The data indicates that there was little change in the main components during this process. Slight increases in the LOI were generally noted and appear to relate to combined water, held when the fly ash is oven dried at 105 $^{o}$C, but breaking down during ignition.

The presence of calcium sulfate-based products has also been noted with wet storage in earlier work [20] and corresponds to some of the effects observed in the SEM images. Tests for reactivity in terms of activity index suggest that small reductions in this may occur with wet-storage.

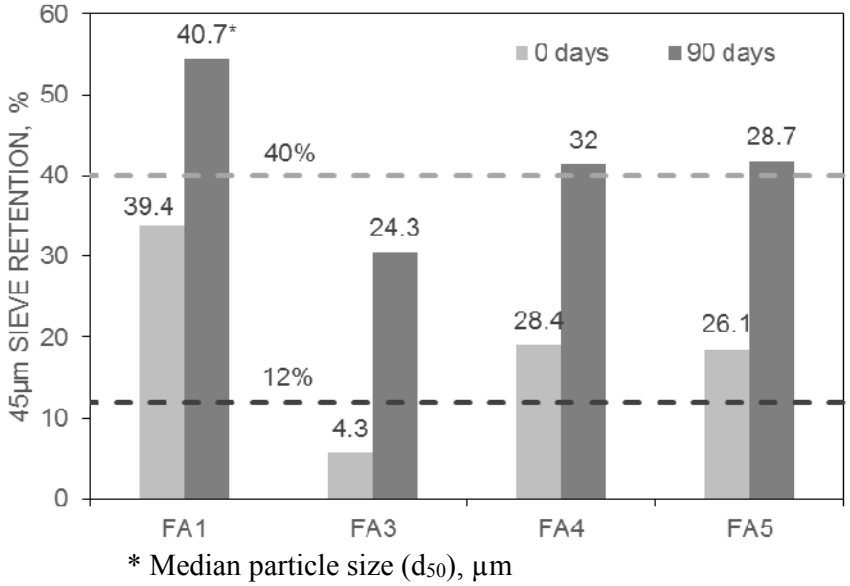


Figure 5 Change in 45μm sieve retention for various fly ashes (10% moisture addition, laboratory stored)

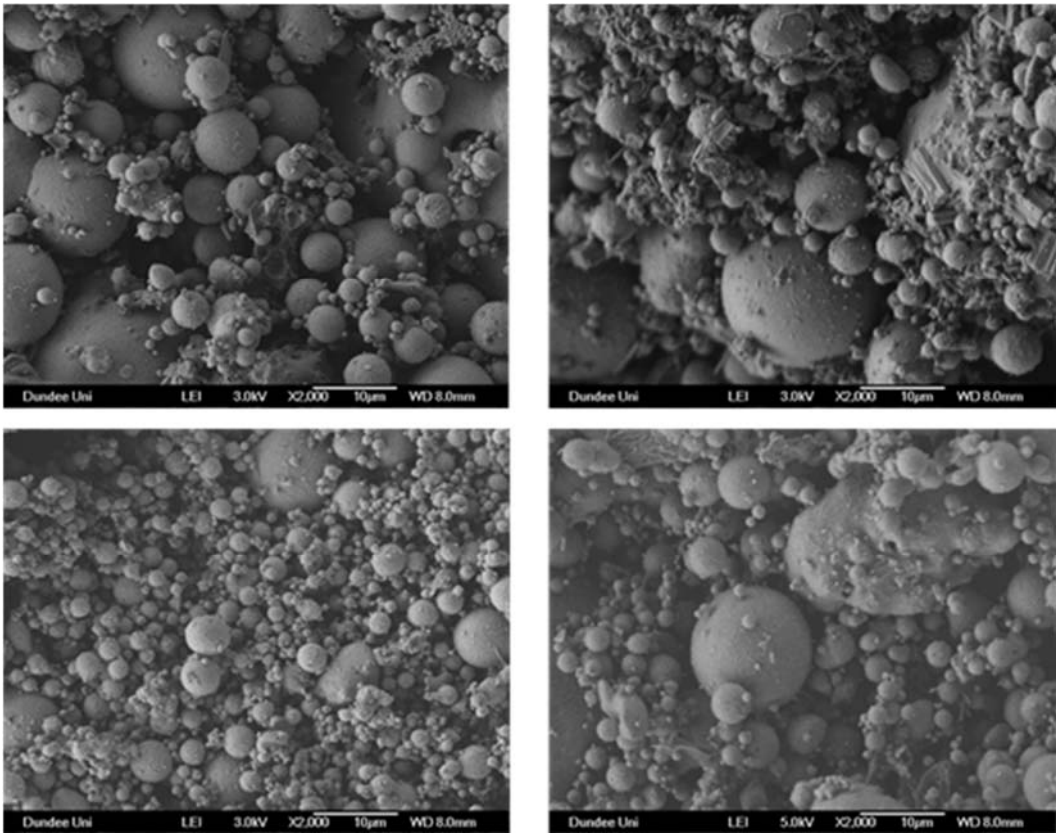

Figure 6 SEM images of dry fly ash (FA1 and FA3, top and bottom left) and stockpile ash (SFA1 and SFA3, top and bottom right)

Table 2 Main chemical properties of dry and wet-stored fly ash (10% moisture addition, laboratory stored)

| COMPONENT, % | LABORATORY WET-STORED FLY ASH | | | | | | | |
|---|---|---|---|---|---|---|---|---|
| | FA1 | | FA3 | | FA4 | | FA5 | |
| | Dry | 90 Days | Dry | 90 Days | Dry | 90 Days | Dry | 90 Days |
| $SiO_2$ | 47.9 | 47.8 | 47.5 | 49.7 | 48.8 | 47.2 | 41.3 | 42.3 |
| $Al_2O_3$ | 20.3 | 20.7 | 21.5 | 22.3 | 17.9 | 16.8 | 23.4 | 23.1 |
| $Fe_2O_3$ | 7.4 | 8.5 | 11.2 | 7.6 | 6.5 | 7.3 | 6.7 | 6.8 |
| CaO | 4.5 | 5.7 | 3.9 | 4.2 | 2.5 | 3.0 | 2.2 | 3.1 |
| $K_2O$ | 2.2 | 2.3 | 2.7 | 2.7 | 2.0 | 1.8 | 2.3 | 2.2 |
| $Na_2O$ | 1.5 | 1.2 | 2.1 | 1.1 | 1.1 | 0.8 | 0.7 | 0.6 |
| LOI | 8.3 | 8.7 | 9.9 | 8.9 | 14.4 | 15.2 | 13.6 | 15.0 |

Laboratory-scale tests have also been made to determine the effects of various processing techniques on the material. These include screening, sieving, grinding, carbon removal and different combinations. Evaluation has involved characterising before and after processing and by testing reactivity and effects on concrete properties. An example of data from grinding of stockpile ash in a laboratory ball mill is shown in Figure 7. The material, which had been dried to enable recovery of handling properties was ground to achieve Category S fineness (12.0%) to EN 450-1.

Use of ground stockpile ash in concrete (w/c ratio 0.5, 30% fly ash) indicates minor benefits in compressive strength (Figure 8). It has been noted in related work that the level of enhancement in stockpile and lagoon ash contribution to concrete properties is influenced by the degree of fineness achieved during processing [21], and this is also being investigated.

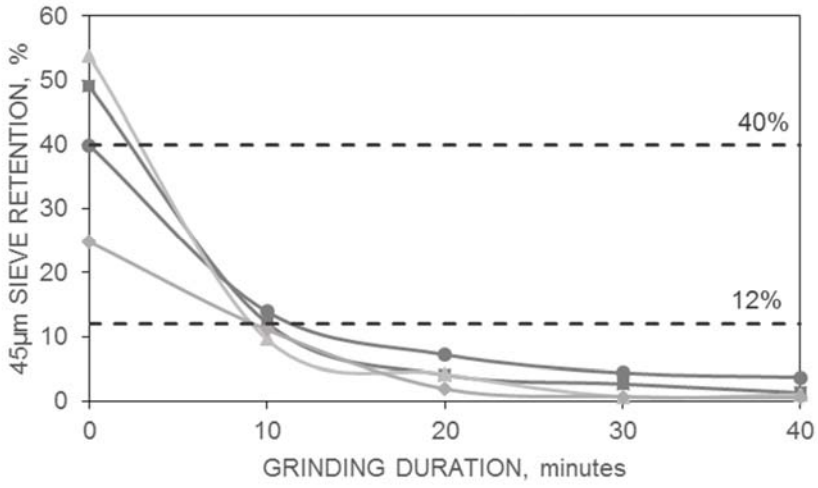


Figure 7 Effect of grinding duration on 45µm sieve retention of various stockpile ashes

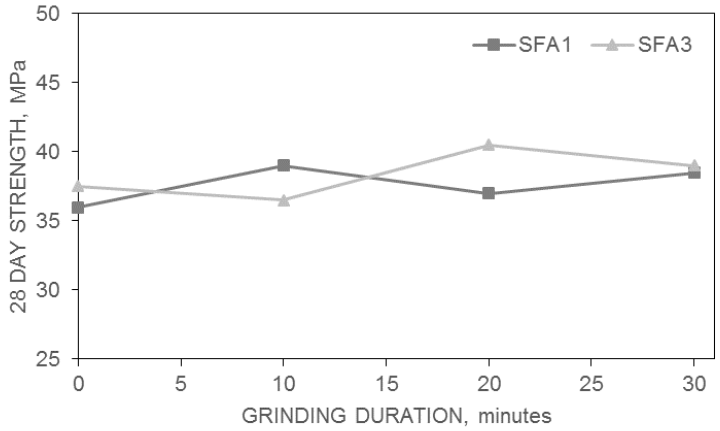


Figure 8 Effect of grinding duration on 28 day cube strength of concrete containing stockpile ash (w/c ratio = 0.5, 30% fly ash in cement)

The project is about to investigate several techniques at pilot-scale to determine if the effects noted in the laboratory with regard to particle size reduction, translate to the processing of larger quantities of material. The final experimental stage will use a full-scale trial to remove carbon and achieve suitable fineness properties. The project will evaluate the practical implications, with regard to the use of processing systems in practice, and will cover issues including, throughput achieved, potential for improvement in stockpile ash properties, environmental impact, economics, etc.

**Case Study: Industrial Processing of Stockpile Ash**

In Germany and France industrial drying plants process stockpile ash and the Authors visited the Lünen Drying Plant in August 2015 to view the facility and obtain samples.

The Lünen Drying Plant (Figure 9) is operated by STEAG Power Minerals and was commissioned in January 2001. Conditioned ash is typically stored for six months on site; stockpiling surplus material from local coal-fired power stations during the winter and drying in the spring and summer are carried out to supply the market at greatest demand. Equivalent to 120,000 tonnes of dry fly ash can be stored on the site. Drying can be achieved at ≤ 20% moisture with wetter material causing significant handling difficulties and reducing the throughput. A Hazemag rapid dryer [22] burning natural gas and designed for processing gypsum is at the core of the Lünen Drying Plant and has an output of up to 50 t/h. The materials are selected with low LOI values which meet the specifications of EN 450-1. Fly ash is conditioned at each of the power stations and delivered in covered tipper trucks.

The stockpile ash is fed into a rectangular drying chamber with two counter rotating horizontal shafts at its base (Figure 10). Ash is transported along the length of the unit within a current of hot air at 120 $^{o}$C. The Hazemag rapid dryer uses uniflow drying which means that hot air meets the wet feed material at the entry zone and passes through the plant in the same direction. This ensures that the hottest air comes into contact with stockpile ash of highest moisture content, improving the drying efficiency. “Throw blades” attached to the rotating shafts promote turbulence and maximise the exposure of material to the warm air (Figure 11). Contact with the “throw blades” and the turbulence within the chamber also de-agglomerates

and causes some particle size reductions. Internal weirs and baffles restrict flow through the main chamber extending the retention time, which also increases drying efficiency. A cyclone classifier delivers ash particles of ≤ 200 μm to a bank of filter bags and any oversize fractions are passed through a hammer mill and returned to the rapid dryer. No coarse material is produced and the only waste occurs when the equipment is cleaned during maintenance.

Figure 9 Lünen Drying Plant, Germany

Figure 10 Main drying chamber

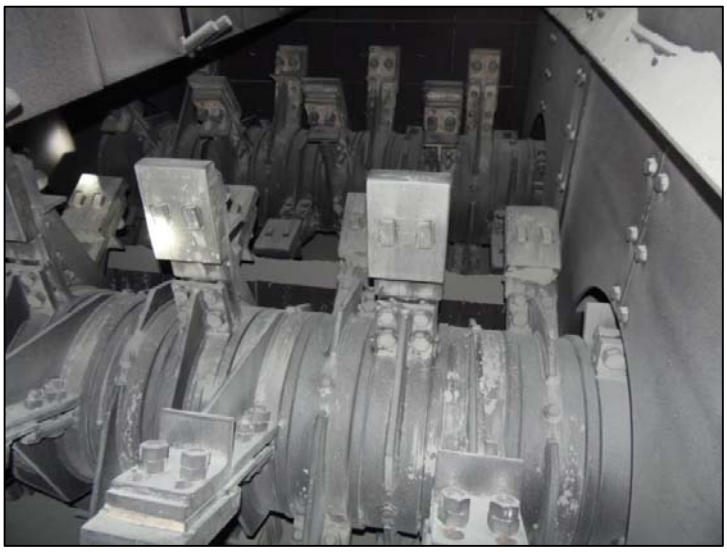

Figure 11 Interior of drying chamber

The product fly ash is controlled to ≤ 0.2% moisture and stored in one of two 1000 $m^3$ capacity silos. Typically the LOI is ≤ 5.0%, of which ~ 0.3% is attributed to combined water from the reaction products which form during wet-storage of the fly ash. The Lünen Drying Plant is certified to manufacture EN 450 fly ash and undertakes CE marking.

A summary of the properties of stockpile ash (SA) and processed fly ash (FA) obtained from the Lünen Drying Plant is shown in Table 3. The process reduced the moisture to very low levels and thereby re-established the flow properties of the fly ash and increased the fineness of the output material. As might be expected, given what has been noted previously, there was little difference in chemical composition and LOI between stockpile (oven dried before testing) and processed materials. The average activity index in autocontrol testing from the last 15 years of operations was 84% at 28 days and 97% at 90 days (cf. EN 450-1 limits, 75% at 28 days and 85% at 90 days).

## CONCLUDING REMARKS

Fly ash is in demand as a constituent of concrete in order to improve performance and achieve technical and sustainability benefits and this is expected to continue, in particular in the case of EN 450 fly ash which is sought after as pozzolana. The likely decline in the amount of dry fly ash available in the UK over the next decade can be compensated for by improving the supply chain of imported fly ash. Since EN 450 is produced to a harmonised European product standard, this is a feasible option.

The research undertaken at the University of Dundee aims to develop stockpile ash as a complementary source of fly ash. This will provide a greater understanding of the effects of wet-storage on the material and will identify suitable processing technology to enable its use in concrete. The case study reviewed, demonstrates the potential for the use of recovered stockpile ash as an EN 450 addition on an industrial-scale.

Table 3 Summary of stockpile ash and processed fly ash properties

| PROPERTY | SA | FA |
|---|---|---|
| Physical | | |
| 45µm sieve retention (range), % | 52.5 - 73.0 | 23.3 - 24.9 |
| Median particle size ($d_{50}$), µm | 29.4 | 23.3 |
| Chemical, % | | |
| $SiO_2$ | 49.6 | 49.8 |
| $Al_2O_3$ | 25.2 | 25.0 |
| $Fe_2O_3$ | 6.2 | 6.3 |
| CaO | 4.3 | 4.1 |
| $K_2O$ | 1.7 | 1.9 |
| $Na_2O$ | 1.1 | 1.0 |
| LOI | 3.5 | 3.4 |

## ACKNOWLEDGEMENTS

The Authors would like to thank Mr Martin Pielke, STEAG Power Minerals GmbH and Mr Ivan Skidmore, Power Minerals Ltd for their help with regard to the case study described.

## REFERENCES

1. UKQAA Ash Availability Report, January 2016 http://www.ukqaa.org.uk/information/statistics/ Accessed 23 June 2016.
2. UKQAA 2014 Ash Utilisation Data http://www.ukqaa.org.uk/information/statistics/ Accessed 23 June 2016.
3. BS EN 450-1: 2012. Fly ash for concrete: Definition, specifications and conformity criteria. British Standards Institution, London, UK.
4. BS EN 450-2: 2005. Fly ash for concrete: Conformity evaluation. British Standards Institution, London, UK.
5. BS EN 206: 2013. Concrete. Specification, performance, production and conformity. British Standards Institution, London, UK.
6. BS 8500-1: 2015+A1: 2016. Concrete. Complementary British Standard to BS EN 206. Methods of specifying and guidance for the specifier. British Standards Institution, London.
7. BS 8500-2: 2015+A1: 2016. Concrete.Complementary British Standard to BS EN 206. Specification for constituent materials and concrete. British Standards Institution, London, UK.
8. BS EN 197-1:2011. Cement. Composition, specifications and conformity criteria for common cements. British Standards Institution, London, UK.
9. Specifying Sustainable Concrete. Understanding the role of constituent materials. The MPA Concrete Centre. ISBN 978-1-908257-01-7. pp 12, London, UK. 2015.

10. Climate Change Act 2008. The Stationery Office, London, UK. 2008.

11. Updated energy and emissions projections 2015. Department of Energy and Climate Change. pp 22-23. London, UK. https://www.gov.uk/government/publications/updated-energy-and-emissions-projections-2015 Accessed 23 June 2016.

12. Directive 2010/75/EU of the European Parliament and of the Council of 24 November 2010 on industrial emissions (integrated pollution prevention and control). Document 32010L0075. Official Journal of the European Union. 17 December 2010.

13. Rt Hon Amber Rudd, Department of Energy and Climate Change. A speech on a new direction for UK energy policy. Institution of Civil Engineers, London, UK, 18 November 2015. https://www.gov.uk/government/speeches/amber-rudds-speech-on-a-new-direction-for-uk-energy-policy Accessed 23 June 2016.

14. Department of Energy and Climate Change. Statement to the London Stock Exchange, 25 November 2015. http://www.londonstockexchange.com/exchange/news/market-news/market-news-detail/other/12597443.html Accessed 23 June 2016.

15. Updated energy and emissions projections 2015. Department of Energy and Climate Change. Annex G Major power producers'generation by source. Reference scenario. London, UK. https://www.gov.uk/government/publications/updated-energy-and-emissions-projections-2015 Accessed 23 June 2016.

16. UKQAA Case Study 19. Tilbury Power Station: Recovery and use of stockpiled PFA. http://www.ukqaa.org.uk/wp-content/uploads/2014/11/Case-Study-19-Tilbury-stockpile-Oct-2014-bullzip.pdf Accessed 23 June 2016.

17. FEDORKA, W. et al. Reclaiming and Recyling Coal Fly Ash for Beneficial Reuse with the STAR™ Process. 2015 World of Coal Ash (WOCA) Conference in Nashville, TN, USA 5-7 May 2015.

18. JONES, M.R. et al. Experiences of Processing Fly Ashes Recovered from United Kingdom Stockpiles and Lagoons, their Characteristics and Potential End Uses. 2009 World of Coal Ash (WOCA) Conference – Lexington, KY, USA, May 4-7, 2009.

19. http://rktron.com/ Accessed 23 June 2016.

20. MCCARTHY, M.J., TITTLE, P.A.J. AND DHIR, R.K. Characterisation of conditioned PFA for use as a cement component in concrete. Magazine of Concrete Research, Vol. 51, No 3, pp 191 - 206, 1999.

21. MCCARTHY, M.J., ZHENG, L, DHIR, R.K. AND TELLA, G. Feasibility of recovery and dry-processing of wet-stored fly ash for use as an addition in concrete. (in preparation), 2016.

22. http://www.hazemag.com/rapiddryers/rapiddryers.htm Accessed 23 June 2016

Keynote Paper

# SUSTAINABLE INNOVATION ON THE ROAD TO MARKET: MOVING FROM THE LAB TO GLOBAL IMPACT FOR THE CEMENT AND CONCRETE INDUSTRIES

**T Schuler**

**N DeCristofaro**

Solidia Technologies®

United States of America

**ABSTRACT.** The production of cement is responsible for 3-5% of total global carbon emissions, making it the world's second largest emitter of carbon dioxide ($CO_2$). Solidia Technologies® is a cement and concrete technology company bringing sustainable innovations to a market that is thousands of years old and in search of a solution. Solidia Cement™ is a low-lime alternative to ordinary Portland cement, and emits 30% less $CO_2$ during its production. Solidia Concrete™, made using Solidia Cement, consumes $CO_2$ in the curing process. Together, these novel technologies reduce the overall carbon footprint associated with the manufacture and use of cement by up to 70%. But we don't lead with the sustainability profile; our primary focus is on the superior performance, the savings of time and costs, and the ease of adoption that our processes offer. To help sustainable innovation gain traction in the marketplace, we advocate changing the conversation, translating our solution as one that directly addresses the industry's current challenges and fits into the way they operate today. The road to market for innovative technologies is paved with risk and potholed with failure. To succeed, you must fail…fail quickly…and recover. It takes a village to shepherd innovation to market: a cast of players, from start-ups to industry giants, investors to academics, all acting out distinct roles based on their resources, market knowledge, technological prowess, and tolerance for risk. The role of the start-up is to learn and then use that understanding to reduce the industry's exposure to risk by rapidly managing the innovation process. As a first step, innovators must learn the market inside and out. Through research and partnership with industry players, innovators must gain firsthand knowledge about how the industry works. Then, by tailoring both the technological approach and commercial strategy to boost performance with minimal change and at the lowest cost, innovators can meet industry where it is today. Solidia Technologies collaborated with industry, government and academic partners to leverage the market's existing equipment, raw materials and processes to make our sustainable technologies easy to adopt. A top priority of our R&D is developing products that offer superior performance over traditional Portland cement-based concrete products. If the worldwide cement industry were to implement Solidia's processes today, it would achieve the Cement Sustainability Initiative of the World Business Council for Sustainable Development's 2050 goals in a matter of years. Solidia Technologies' story is a clear example of how to successfully introduce a sustainable technology into the global concrete market: first make it good business, then make it green.

## INTRODUCTION

Every great success story starts with a story of failure.

Concrete is the most widely consumed man-made material in the world. The production of cement is responsible for 3-5% of total global carbon emissions—the world's second largest emitter of carbon dioxide ($CO_2$). A modern cement plant will release about 810 kg of $CO_2$ per tonne[1] of cement clinker produced.

In an effort to address the large $CO_2$ emissions from the cement industry, the International Energy Agency (IEA) created a roadmap to guide the industry's long-term sustainability efforts. To achieve the IEA goals, the cement industry must reduce its total $CO_2$ emissions from 2.0 Gt in 2007 to 1.55 Gt by 2050. Over this same period, however, cement production is projected to grow from 2.6 Gt to 4.4 Gt.[2,3]

The industry knows this is an issue they must address, and they have set goals to dramatically reduce their carbon footprint. The Cement Sustainability Initiative of the World Business Council for Sustainable Development set 2050 $CO_2$ reduction targets for the global cement industry. For them, it is a matter of survival.

To address this formidable challenge, the cement and concrete industries have adopted both evolutionary and revolutionary strategies. The evolutionary strategies include the implementation of energy-efficient production technologies, the use of alternative fuels, the development of new cement chemistries with low-lime content, and the reduction of the clinker factor in cement. The reduction in clinker factor is achieved by co-grinding cement clinker with supplementary cementitious materials, such as fly ash, slag, natural pozzolanic materials, and fillers, such as limestone. However, even the combined effect of these initiatives is likely to fall far short of the IEA roadmap goals. This roadmap even anticipates revolutionary approaches, including broad implementation of carbon capture and storage technologies that are expensive and, in fact, not yet proven at commercial scale. The industry is left trying to face these challenges with a large and aging infrastructure, complex chemistry, and a conservative market not adept at adapting new technologies.

Attracting investors for new, green technologies is a challenge. Persuading industries to change time-proven practices and products is even harder. Trying to do both as a start-up can be daunting. Leading this change based purely on sustainability will not suffice.

The only way to rapidly introduce a sustainable technology into the cement and concrete markets is to first make it good business, then make it green. To truly bring innovation to the forefront of any industry, especially one resistant to change, the company must demonstrate broad applications and practical, proven benefits of the new technology within it. First fit in, ushering in change with profitability, simplicity and familiarity. Identify the industry's pain point, but don't pile on.

---

[1] All calculations are based on the *tonne*, also known as the *metric ton*, equaling 1,000 kilograms.

[2] *Cement Technology Roadmap 2009*, International Energy Agency., 3 *Cement and Carbon Emissions*, L. Barcelo, J. Kline, G. Walenta & E. Gartner, Materials and Structures, June 2013.

## OVERCOMING OBSTACLES TO DISRUPTIVE INNOVATION

The quickest way to introduce change into a market with longstanding traditions is to work especially hard at making it simple. Simple is hard, really hard. Such a change demands a solution that minimizes cost, maximizes impact and adds value.

Here's our story. Solidia Technologies is a cement and concrete technology company bringing a sustainable innovation to a market that is thousands of years old. The last time this industry embraced a major product innovation was about 200 years ago with the invention of Portland cement. Solidia Technologies created a real solution that was inspired directly by the industry's $CO_2$ challenge.

### Making it Simple is Hard

Solidia doesn't only develop sustainable technologies; we make it possible for industry to adopt them. To drive innovation to market, you need the right people, a compelling vision, collaborators who give you market insight and credibility, and not quite enough time. R&D needs to be quickly focused and directed by market insights and hard data, not theories. To remain competitive, the business itself must be sustainable within the context of the marketplace.

As a leadership team that had worked with disruptive innovation from a variety of angles, we were able to combine our unique perspectives to put Solidia on a more realistic path. Our professional experience includes vantage points critical to commercializing innovation, including that of: the giant global leader (leading global businesses for DuPont in building materials); the technology incubator (directing the Office of Commercial Ventures and Intellectual Property at University of Massachusetts Amherst); and a variety of research and business management roles at Fortune 1000 technology companies in the US and abroad. Joining forces now at a start-up, we shared an appreciation for operating with a deep understanding of the market and set out immediately to place our team in the shoes and mindset of our target industry.

We offer Solidia's roadmap to market and all we've learned as a case history on sustainable innovation. On getting it wrong, until you get it right.

### Understand Your Market

Targeting the estimated US$1 trillion concrete and US$300 billion cement markets, Solidia overcame two of the biggest obstacles to disruptive innovation: ease of implementation and cost of adoption. The technology addressed an urgent, global business and societal need while profitably supporting an industry seeking to improve production methods.

As innovators, to advance sustainability and attract investors, you must first demonstrate that you can sustain yourselves. Above all, the start-up has to prove the technology is commercially viable. First, the innovator must focus on targeting the largest market possible, demonstrating broad applications within the market. To succeed, you have to take the time to understand the industry…intimately and thoroughly.

Our headquarters was full of largely academically trained scientists and engineers who had never spoken to a potential customer in our target market. We had a supportive board; a CTO with vast experience translating technology to markets; an R&D director who knew the science inside and out; and a young team of engineers who really didn't like to be told they couldn't do something. All we had to do was point them in the right direction.

Therefore, the first thing we did as a team at Solidia was move the entire company out of the office for two months to have them go into the industry and learn, with the instruction: "Don't teach. Just listen."

What they learned completely changed the company's direction from both a research and a market perspective.

The team's conclusion was simple: "We have the wrong cement, the wrong curing process and the wrong equipment….but we know exactly what to do!"

Our preliminary technology worked, but we miscalculated the barriers for adoption from a lack of industry knowledge. It wasn't a total failure, per se, but it would have led us to certain failure in the long run. A great indicator of whether R&D organizations are heading down the right track is seeing how they work to bridge the gap between where the target industry is today and where they need it to be to adopt the new technology. Along the way, we discovered through trial and error, as well as supportive guidance from partners, investors, and industry players, that the only way to close that gap is to build the bridge one small section at a time.

**The Solidia Solution: Getting to the Right Cement**

First we had to develop the right cement. By studying the industry closely, we learned that the right cement is made from raw materials that are available everywhere.

Our technology intended to use naturally occurring minerals—wollastonite in particular—as our cement. Our initial narrow view focused on sustainability and the carbon footprint, but it didn't take into account that the product was available only in certain geographies and unavailable in quantities large enough to satisfy this giant market. We had to develop a new cement.

In addition, we spent quite a bit of time trying to understand why other green cements had failed. The answer became very clear, very quickly. Sharing four common characteristics (each had at least one, and most had elements of all), they:

- relied on raw materials that were not ubiquitous.
- relied on investment in expensive new manufacturing equipment.
- produced a concrete that could not meet the physical performance required by the industry.
- tried to bypass industry convention and tried to enter the market on their own terms.

We were faced with developing a new cement that carbonated and could overcome all of these issues. We decided that the cement had to be made on existing kilns using existing raw materials.

No one would invest in an unproven technology, nor would they import new raw materials to their plants that were sited based on raw material availability. Any other solution would be too expensive.

The chemistry needed was apparent. Next we had to find someone willing to make it for us. Our new cement had been successfully made in our own lab kiln, but we needed to demonstrate that it could also be made on a rotary kiln. Most of the research kilns had been decommissioned decades ago, but fortunately we found a lab in Europe that had several we could rent.

We had a few engineers that had run kilns, a group of materials scientists that understood the chemistry, and the money to afford the trials. We selected raw materials that we thought were representative of what you might find at a typical kiln (later learning there are no 'typical' raw materials). Our two-week trial was successful. At this point, we had cement that we could use in trials to prove to potential cement partners and concrete customers that it could be done.

From a technical perspective, we developed Solidia Cement™: a non-hydraulic cement composed primarily of low-lime, calcium silicate phases such as wollastonite / pseudowollastonite ($CaO{\cdot}SiO_2$). This contrasts with the high-lime phases that comprise ordinary Portland cement (OPC). The setting and hardening characteristics of Solidia Cement are derived from a reaction between $CO_2$ and the calcium silicates.

Now we had the chemistry, but who was going to make it?

## LEANING ON THE EXPERTS

Going it alone will get you lost, especially if you're doing it without a map. Large and small industry players have a symbiotic relationship: start-ups often manage risk better than large industry players, while established sector leaders provide real-world, practical market intelligence, R&D support and access.

We needed a partner. But what kind? There were two choices: assemble a network of toll manufacturers that could supply the world, or pick a single partner who was interested in helping us get started and willing to teach others.

The first option wasn't viable. If our new cement was going to be successful, we would have to put in a team of kiln experts to start up new kilns and then define the logistics to move the cement around the world. It was just too complex. We would also have to lead the charge through the code process. Doing that without a partner was impossible.

What kind of partner did we need? Our perfect partner needed a few key characteristics:

- a true commitment to sustainability—not just lip service for their annual report;
- a global footprint (at least in our target geographies);
- a proven track record of research, not just process improvement; and,
- a willingness to work with a start-up.

Beyond that primary relationship with an established industry player with a large global presence, it was clear that we also needed an array of other partners from the public and private sectors and academia who could lend credibility and help shift the discovery from theory to application. Innovators are wise to cultivate third-party, collaborative efforts in applied research, materials testing and characterization, manufacturing logistics and general marketing. (See more on these other R&D partners below.)

Based on our criteria, we chose LafargeHolcim (at the time known as Lafarge, S. A., pre-merger). Fortunately, they also chose us. A world leader in building materials and on research in concrete applications, LafargeHolcim researchers and technical experts worked with Solidia Technologies to demonstrate the feasibility of commercial-scale production in a conventional cement plant. In April 2014, a joint LafargeHolcim and Solidia team validated the reduced carbon footprint and commercial viability of Solidia Cement during a full-scale trial at LafargeHolcim's Whitehall cement plant in the US. Next, we repeated the trials in Europe so that we had a supply plant in each region for early adopters.

Beyond R&D, our industry partners play a vital role helping us enter the market. Central to our commercialization strategy is lining up all the partners and support a customer will need to facilitate adoption.

Next….focus on the concrete and determine the best path to market.

## $CO_2$ CURING: MAKING A COMPLEX TECHNOLOGY SIMPLE

Ordinary Portland cement uses water to cure and releases about 800kg of $CO_2$ for each ton produced. The hydration process involves the hydration reaction between high-lime calcium silicate phases and water to form calcium-silicate-hydrate gel and calcium hydroxide.

It also takes 28 days to reach maximum strength. By contrast, to create Solidia Concrete™ products, water, aggregates and Solidia Cement are mixed, formed into the desired shape and then reacted with gaseous $CO_2$ to produce a durable binding matrix. During the carbonation process, calcite ($CaCO_3$) and silica ($SiO_2$) form and are responsible for the strength development in concrete. In other words, during the curing process, $CO_2$—from waste flue gas—reacts with Solidia Cement to form calcium carbonate. It is permanently transformed from a gas to a solid that resembles natural limestone. The gas could only be released if it were put into a high temperature kiln. The curing process sequesters up to 300 kg of $CO_2$ per tonne of cement used and happens very quickly—certainly less than 28 days. We thought that was enough; we were wrong.

### The Process was Wrong

When we started working together on the leadership team, we were targeting the exterior cladding market using the following approaches:

1. an autoclave, containing a $CO_2$-rich atmosphere;
2. pressurized to 20 psig;

3. heated 90°C; and,
4. maintained for a 72-hour curing cycle.

Through our industry research, we discovered these approaches were all problematic for the industry (see below). And despite our best efforts, the process wasn't uniform, and our results were even more unpredictable. To get to this point, we had simply extended the original experimental process developed in the Material Sciences Department of Rutgers University, where the first generation of the technology was invented. Using pressure and temperature was a time-worn strategy to drive $CO_2$ into cement. People had been doing it for decades with Portland cement. But it was wrong.

At the end of our first week as the CEO/CTO team, we pulled our full leadership team into a room in order to fully understand what the core of our technology was and how we might leverage that to build the business. By the end of the day, the team decided that our current strategy was based on our technical knowledge, not what the market really wanted or needed. It was at this point that we decided to do something radical, as noted above: we stopped all work on our current process, paired technical team members with business team members, and sent them into the market to learn.

We talked to everyone—cement companies, precasters, government officials, architects, and more—anyone that could help us understand how the market worked. There was only one rule: "You can ask questions, but you can't teach, sell, defend or do anything that would keep our discussion partner from opening up."

When the team returned, they had completely changed the R&D strategy. In summary, they identified the following problems within our current approach:

1. **Using the autoclave:** Very few concrete manufacturers used autoclaves, primarily because of their high capital and operating costs. We had to find a simpler, less expensive curing chamber.
2. **72-hour curing cycle:** While the complete curing of concrete takes up to 28 days, most precast concrete manufacturers wanted to load and unload their curing chambers within a 24-hour production cycle (the balance of the 28-day cure cycle occurs outdoors). We had to load, unload and cure in less than 24 hours.
3. **Curing at 90°C:** While 90°C may be the ideal temperature for wollastonite to cure, it was not ideal from an equipment design perspective. Any temperature above 60°C would require specialized hardware that was too expensive. We had to cure Solidia Concrete at a temperature of 60°C or less.
4. **Pressurized curing** (See problem #1!)**:** We knew what our target was. We had spent five years working on a different technical strategy, and now we were going to change everything. How do you completely redirect an organization to chase a different dream, one that they didn't know how to do?

Our leadership team drew a very distinct line: curing at atmospheric pressure, at less than 60°C, in less than 24 hours. No flexibility. Anything outside of those parameters represented failure. If we blinked, the company failed.

Fast forward two months: they did it. Our amazing cohort of scientist and engineers…running the gamut from young to experienced, believers to doubters…met the boundaries that we had established. In doing so, they opened up a completely new patent estate that has defined the company ever since. Give a group of really smart people the resources to do the work and the confidence to succeed, and you get miracles.

Next, we turned to equipment experts to help us design equipment that would allow the $CO_2$ curing process to take place with minimal plant conversion. CDS Group, the world's leading curing and drying specialists, is collaborating with us on the design and manufacture of curing chambers to accommodate the $CO_2$-curing process.

## SUPERIOR PERFORMANCE: THE SAME, PLUS…

Solidia Concrete contains the same raw materials as those used in concrete products made with ordinary Portland cement, namely, fine and coarse aggregate, supplementary cementitious materials, and chemical admixtures. In addition, the manufacturing of Solidia Concrete products is performed using identical mixing and forming processes as those adopted in OPC-based concrete production.

Solidia Concrete can be produced by manufacturers of traditional concretes and designed to address virtually any precast concrete application, and adapted to any concrete formulation, production method and product specification. It outperforms traditional concretes in a range of properties including strength, abrasion resistance and durability. Additionally, the curing of Solidia Concrete can be completed in a matter of hours, allowing for rapid deployment. It is the same, plus.

Our initial technology focus was on unreinforced precast applications, including pavers and blocks. Solidia is now developing commercial processes for reinforced applications, including aerated concrete, railroad ties, architectural panels and hollow core extrusions. Our IP portfolio comprises four US patents and more than 100 patent applications worldwide.

The product strength and durability has been tested and verified according to all market standards: ASTM and AASHTO specification by the CTLGroup, formerly the R&D laboratory of the Portland Cement Association, as well as EN and CSA.

## IT TAKES A VILLAGE TO GET TO MARKET

Don't take our word for it, and certainly never ask customers to do so. Collaboration is key. As noted above, established industry leaders have proffered a wealth of experience, knowledge and reality checks, and have opened doors to potential customers for collaboration and sales.

We sought out eminent authorities respected by the industry who to this day put our innovation through the mill of rigorous testing and analysis. Our R&D is bolstered by the expertise of leading academics at research universities and scientists at national laboratories on the properties of cement and concrete.

Ongoing testing continues in laboratories at Rutgers University, where the original generation of the technology was co-invented by Professor Richard Riman, Ph.D, and Vahit Atakan, Ph.D., who is now Solidia's Chief Scientist. At Purdue University, a team led by Professors Jan Olek, Ph.D., and Jason Weiss, Ph.D., who recently moved to Oregon State University where he continues to test Solidia products, report Solidia Concrete's outstanding performance in freeze-thaw, freeze-thaw with deicing salts and sulfate environments.[4]

At Ohio University's Institute for Corrosion and Multiphase Technology (ICMT), Professors Yoon-Seok Choi, Ph.D., and Srdjan Nesic, Ph.D., are leading a group of scientists examining methods to better passivate the surface of steel rebar. Professor Alberto A. Sagüés, Ph.D., heads a Civil and Environmental Engineering team at the University of South Florida that isaimed at characterizing the corrosion of steel rebar embedded in Solidia Concrete in a variety of service environments. Partnering with academia not only lends credibility through peer review, but also allows new, fresh minds to collaborate on creating a solution.

Public entities offer many programs in support of sustainable technology with targeted needs, from infrastructure to building to reducing air pollution. They offer funding, laboratories, expertise, and conferences where innovators share war stories.

The National Energy Technology Laboratory of the US Department of Energy co-funded a four- year research and development project as part of its $CO_2$ Storage Program. That research has focused in part on improving the understanding of water distribution in Solidia Concrete during the drying and $CO_2$-curing process. The research demonstrated that Solidia Concrete can achieve full hardness in a time comparable to that of Portland cement-based concrete in a controlled curing environment.

Results of research conducted under Phase I of the Small Business Innovation Research (SBIR) Program of the US Environmental Protection Agency confirmed that the incorporation of supplementary cementitious materials can further reduce the carbon footprint associated with the production and use of Solidia Cement. This research demonstrated that waste materials such as ground fly ash and blast furnace slag can be used to replace Solidia Cement by as much as 40% in concrete formulations.

The Federal Highway Administration of the US Department of Transportation supports Solidia with a multi-year Cooperative Agreement to examine transportation infrastructure applications. This joint program includes independent testing of Solidia Concrete at the Turner-Fairbank Highway Research Center.

We have also attracted investors, including Bill Joy, Kleiner Perkins Caufield & Byers (KPCB), Bright Capital, BASF, BP, LaFargeHolcim and Total Energy Ventures, who have elevated sustainability to a core purpose and value social impact as well as profits. Many of our investors offer industry expertise, opportunities for visibility, entrée to other investors, and helpful guidance on bringing innovation to market and building a start-up.

---

4 *Performance of Calcium Silicate-based Carbonated Concretes vs. Hydrated Concretes under Freeze-thaw Environments*, July 2015.

## OH, AND IT'S SUSTAINABLE…

And, the coup de grace: the reduced $CO_2$ emissions associated with the production of Solidia Cement and the $CO_2$ sequestration associated with the curing of Solidia Concrete combine to reduce the carbon footprint of cement and concrete by up to 70%.

Solidia Cement is more sustainable than ordinary Portland cement. The clinker of Solidia Cement is produced at a temperature of about 1200°C, which is roughly 250°C lower than the sintering temperature used in Portland cement clinker manufacturing. Production of Solidia Cement reduces the emission of greenhouse gas-$CO_2$ by 30%.

Solidia Concrete[5] consumes $CO_2$ in the curing process. It sequesters up to 300 kg of $CO_2$ per tonne[6] of cement used.

As water is not consumed during the Solidia Concrete curing process, it can be collected and reused, with recycle rates in excess of 60%, and potentially as high as 100%.[7]

Hypothetically, if the worldwide cement industry were to adopt Solidia's technologies today, it would achieve the WBSCD 2050 goals in a matter of years. Remaining competitive as the industry pivots to a carbon economy will quickly become a much higher priority.

Running businesses has taught us that, if you want to remain competitive, you have to become more sustainable. That said, the fact that Solidia Cement and Solidia Concrete have a vastly superior sustainability profile than anything available in the market today is icing on the cake. More important is that we're making it easy for one of the world's largest industries to go green.

## CONCLUSION: CHANGING THE CONVERSATION

Great technology is not a story about science; it's about the people with the passion, courage humility and staying power required to shepherd it to market.

At Solidia, we have taken a complex technology and made it simple and applicable anywhere in the world. Combined with an innate sense of urgency, our team quickly translates market insight from our industry and other R&D partners with leading-edge technology to produce a credible solution to a problem long sought by the industry. This collaborative approach, along with a focused effort to target individual markets that need a better solution, results in an unusually rapid acceptance by an industry that values performance. The fact that it is sustainable is readily embraced, but it has to work first. It can't just be green; it has to be better.

To open minds to innovation, we need to approach industry first and foremost as a solution to companies looking to survive: namely, how to maintain or boost profitability, how to grow market share, and, for cement manufacturers, how to survive as the world pivots to the carbon economy.

---

[5] Solidia Concrete and Solidia Cement are interdependent materials; Solidia Concrete can only be made with Solidia Cement. All calculations herein are based on trials using Solidia's patented processes. See *Solidia Cement™*, December 2013 and *Solidia Concrete™*, February 2014.

[6] All calculations are based on the *tonne*, also known as the *metric ton*, equaling 1,000 kilograms.

[7] *Water Savings In Concrete Made From Solidia Cement™,* April 2014.

Sustainability cannot lead the conversation; the industry experienced severe setbacks in the past by adopting green cements that were not adequately tested for long-term strength and durability.

Solidia Technologies came up with a vision that informed its business strategy: We are a cement and concrete technology company with a goal of making it easy to adopt sustainable technologies by leveraging the market's existing equipment, raw materials and processes. It has to be profitable from the beginning. And, oh, by the way, it's also green.

Our vision has always been a world where $CO_2$ means green and sustainability is an engine for profitability and growth. For over 50 years, scientists have tried to cure concrete with $CO_2$ knowing the resulting product would be stronger and more durable; Solidia Concrete is the first to become commercially viable. By discovering and successfully commercializing an industrial application for carbon, one of the world's most noxious pollutants, we hope to inspire others to explore problems for solutions.

---

**Thomas (Tom) Schuler, President and CEO, Solidia Technologies, Inc.** With more than 25 years of global leadership experience, including leading two global businesses at DuPont, Tom joined Solidia Technologies in 2011 to lead the company towards global commercialization. He is a frequent guest speaker before international trade and sustainable growth groups in the Americas, Europe and Asia. In 2014, he addressed the CleanTech 100 Summit at the National Press Club in Washington, DC when Solidia was named to the Global Cleantech 100. He was also a panelist at the 2013 Aspen Institute Ideas Festival, the 2014 TomTom Festival at the University of Virginia, the 2013 Cement Sustainability Institute Forum, and the 2013 European Energy Venture Fair. He has appeared on the Bloomberg News program "Money Moves" with Deirdre Bolton and was recently published in Sustainable Business Magazine. He has a Mechanical Engineering degree from the University of Virginia, extensive graduate study in Finance and Marketing, and a mastery of conversational German and French. He serves on UVA's Jefferson Scholarship Foundation's Alumni Advisory Council and national selection committee.

**Nicholas (Nick) DeCristofaro, Ph.D., Chief Technical Officer, Solidia Technologies, Inc.** Nick spearheads both the research and development program and the company's intellectual property strategy. He has extensive experience managing materials science innovation in an industrial context. Throughout his career, Nick has focused on the development and commercialization of advanced materials. He came to Solidia Technologies from the University of Massachusetts Amherst, where he directed the Office of Commercial Ventures and Intellectual Property. Prior to joining UMass, Nick held a variety of research and business management roles over a 28 year period, cumulatively, at AlliedSignal, Honeywell International, and Hitachi Metals in the US and abroad. He has 66 patents and 30 publications to his credit. Nick earned Bachelor's and Master's degrees in metallurgy and a doctorate in materials science and engineering, all from the Massachusetts Institute of Technology.

Solidia Technologies® is a cement and concrete technology company that makes it easy and profitable to use $CO_2$ to create superior and sustainable building and construction materials. Solidia's patented processes start with a sustainable cement, cure concrete with $CO_2$ instead of water, reduce the carbon footprint associated with cement and concrete up to 70%, and recycle 60 to 100% of the water used in production. Using the same raw materials and existing equipment as traditional concretes, the resulting $CO_2$-cured concrete products are higher performing, cost less to produce, and cure in less than 24 hours. Based in Piscataway, N.J. (USA), Solidia's investors include Kleiner Perkins Caufield & Byers, Bright Capital, BASF, BP, LafargeHolcim, Total Energy Ventures, Bill Joy and other private investors. Honors include: 2016 Sustainia 100; 2015 NJBiz Business of the Year; 2014 Global Cleantech 100; 2013 R&D Top 100; 2014 Best Place to Work in NJ; 2014 CCEMC Grand Challenge First Round finalist; 2013 Katerva Award finalist; and MIT's Climate CoLab shortlist. Follow Solidia at www.solidiatech.com and on LinkedIn, YouTube and Twitter: @SolidiaCO2.

# AUTHOR INDEX

**Please enter page number into your pdf reader page navigator to go to paper**

# KEYWORD INDEX

**Please enter page number into your pdf reader page navigator to go to paper**

ISBN 9780957326316